SEE-2016

Second International Conference on Science, Engineering & Environment

Edited by
Zakaria Hossain

21-23 November 2016
International Conference Center
Osaka JAPAN

ISBN: 978-4-9905958-7-6 C3051

SEE 2016 OSAKA, JAPAN
SCIENCE, ENGINEERING AND ENVIRONMENT

PROCEEDINGS OF SECOND INTERNATIONAL CONFERENCE – SEE 2016
SCIENCE, ENGINEERING & ENVIRONMENT OSAKA, JAPAN 21-23 NOVEMBER, 2016

Science, Engineering and Environment

Edited by

Prof. Dr. Zakaria Hossain
Graduate School of Bioresources
Mie University, Japan

THE GEOMATE INTERNATIONAL SOCIETY

Published by:
The GEOMATE International Society
Tsu city, Mie, Japan
E-mail: society@geomate.org
http://www.geomate.org/

ISBN Number: 978-4-9905958-7-6 C3051

Table of Contents

Preface

On behalf of the SEE 2016 Organizing Committee, it is our great pleasure to welcome you to the Second International Conference on Science, Engineering & Environment, held at the Osaka International House Foundation, Japan organized in conjunction with Mie University Research Center for Environmental Load Reduction, The GEOMATE International Society, Useful Plant Spread Society, Glorious International, AOI Engineering, HOJUN, JCK, CosmoWinds and Beppu Construction, Japan.

The conference covers three major themes with many specific themes including:

Engineering	Science	Environment
· Environmental Engineering · Chemical Engineering · Civil and Structural Engineering · Computer Software Web Engineering · Electrical and Electronic Engineering · Energy and Thermal Engineering · Aerospace Engineering · Agricultural Engineering · Biological Engineering and Sciences · Biological Systems Engineering · Biomedical and Genetic Engineering · Bioprocess and Food Engineering · Geotechnical Engineering · Industrial and Process Engineering · Manufacturing Engineering · Mechanical and Vehicle Engineering · Materials and Nano Engineering · Nuclear Engineering · Petroleum and Power Engineering · Forest Industry Engineering	· Environmental Sciences · Chemistry and Chemical Sciences · Fisheries and Aquaculture Sciences · Astronomy and Space Sciences · Atmospheric Sciences · Botany and Biological Sciences · Genetics and Bacteriology · Forestry Sciences · Geological Sciences · Materials Science and Mineralogy · Statistics and Mathematics · Microbiology and Medical Sciences · Meteorology and Palaeo Ecology · Pharmacology · Physics and Physical Sciences · Plant Sciences and Systems Biology · Psychology and Systems Biology · Zoology and Veterinary Sciences	· Environmental Technology · Recycle Solid Wastes · Environmental dynamics · Meteorology and Hydrology · Atmospheric and Geophysics · Physical oceanography · Bio-engineering · Environmental sustainability · Resource management · Modelling and decision support tools · Institutional development · Suspended and biological processes · Anaerobic and Process modelling · Modelling and numerical prediction · Interaction between pollutants · Water treatment residuals · Quality of drinking water · Distribution systems on potable water · Reuse of reclaimed waters

This year we have received many submissions over 70 universities of different countries all over the world including Australia, Georgia, Indonesia, Iraq, Japan, Jordan, Malaysia, Oman, Philippines, Romania, Russia, South Korea, Thailand and United States. The technical papers were selected from the vast number of contributions submitted after a review of the abstracts. The final papers in the proceedings have been peer reviewed rigorously and revised as necessary by the authors. It relies on the solid cooperation of numerous people to organize a conference of this size. Hence, we appreciate everyone who support as well as participate in the joint conferences.

Last but not least, we would like to express our gratitude to all the authors, session chairs, reviewers, participants, institutions and companies for their contribution to SEE 2016. We hope you enjoy the conference and find this experience inspiring and helpful in your professional field. We look forward to seeing you at our upcoming conference next year.

Best regards,

Prof. Dr. Zakaria Hossain, Conference Chairman 

Organization

Scientific Committees:

Honorary Chairman: Dr. Sohji Inoue, E/Prof. Mie University, Japan
Conference Chairman: Dr. Zakaria Hossain, Prof. Mie University, Japan

Conference Organizing Committee:

Dr. Zakaria Hossain, Prof. Mie University, Japan (Chair)
Dr. Satoshi Kaneco, Prof., Mie University, Japan (Co-Chair)
Dr. Sohji Inoue, E/Prof. Mie University, Japan (Co-Chair)
Dr. Toshinori Sakai, Prof. Mie University, Japan (Co-Chair)
Dr. Takamitsu Kajisa, Prof. Mie University, Japan (Co-Chair)
Dr. Masaaki Kondo, A/Prof. Mie University, Japan (Co-Chair)

National & International Advisory Committee:

Dr. Fumio Tatsuoka, Prof., Tokyo University of Science, Japan
Dr. Junichiro Takeuchi, Prof., Kyoto University, Japan
Dr. Kingshuk Roy, Prof., Nihon University, Japan
Dr. Sai Vanapalli, Prof., University of Ottawa, Canada
Dr. Musharraf Zaman, Prof. Univ. of Oklahama, USA
Dr. Rafiqul Tarefder, Prof. University of New Mexico, USA
Dr. M. Bouassida, Prof., National Sch. of Engg. of Tunis
Dr. L.R. Austriaco, Prof., Angles Univ. Found., Philippines
Dr. A.S.M. Abdul Awal, Prof., Univ. Technology Malaysia
Dr. M. Ibn Ibrahimy, Prof., Int. Islamic Univ., Malaysia
Dr. Mohammad Shariful Islam, Prof., BUET, Bangladesh.
Dr. Bujang B.K. Huat, Prof., Univ. Putra Malaysia
Dr. Nemy Banthia, Prof., UBC, Canada
Dr. Ian Jefferson, Prof., Univ. of Birmingham, UK
Dr. John Bolander, Prof., Univ. of California, USA
Dr. Shamsul Chowdhury, Prof., Roosevelt Univ., USA
Dr. Isabel Pinto, Prof., University of Coimbra, Portugal
Dr. Mark Jaksa, Prof., University of Adelaide, Australia
Dr. Jim Shiau, A/Prof., USQ, Australia
Dr. Hj. Ramli Bin Hj. Nazir, A/Prof., UTM, Malaysia
Dr. H.M. Shahin, Prof., Islamic University of Technology, Bangladesh
Dr. Md. Ariful Islam, A/Prof. Dhaka University, Bangladesh
Dr. Md. Nurul Amin, Prof. Dhaka University, Bangladesh
Dr. D.K. Chauhan, Prof. Noida International Univ., India
Dr. Chan Chee-Ming, A/Prof. Universiti Tun Hussein Onn Malaysia
Dr. Ahmed H. A. Dabwan, A/Prof. TATI Univ. College, Malaysia

International Technical Program Committee:

Prof. Adolf Heinrich Horn, Geological Institute - Federa University of Minas Gerais, Brazil
Prof. Bang-Fuh Chen, National Sun Yat-sen University, Taiwan
Prof. Bindeshwar Singh, Kamla Nehru Institute of Technology, India

Prof. Catherine Mulligan, Concordia Institute of Water, Energy and Sustainable Systems, Canada
Prof. Chi-Min Liu Chienkuo Technology University, Taiwan
Prof. Daffalla Rabih, Kenana Sugar Company, Sudan
Prof. Essaid Bilal, Ecole Nationale Superieure Des Mines De Saint Etienne, France
Prof. Hakan Caliskan, Usak University, Faculty of Engineering, Turkey
Prof. Ibrahim Maiyza, National Institute of Oceanography & Fisheries, Egypt
Prof. Loc Nguyen, Sunflower Soft Company, Vietnam
Prof. Marilia Hagen, Indiana University, United States
Prof. Md Najib bin Ibrahim, Universiti Teknologi MARA, Malaysia
Prof. Md. Abdul Baset Mia, BSMR Agri. Univ., Bangladesh
Prof. Mihaela Popescu, University of Craiova, Romania
Prof. Mohamed Abdou, Faculty of Education Department of Mathematics, Egypt
Prof. Mohamed Tahiri, Présidnce de l'Université Hassan II de Casablanca, Morocco
Prof. Nazar Oukaili, University of Baghdad, Iraq
Prof. Radim Cajka, Technical University Ostrava, Faculty of Civil Engineering, Czech Republic
Prof. Rajaraman Jambunathan, AMET University, India
Prof. Saad Farhan Ibrahim Alabdullah, University of Almustansiriyah, Iraq
Prof. Salem Alsanusi, Benghazi, Libya
Prof. Sudhir Kumar Das, Retired Senior Project Manager of Indian Railways, India
Prof. Zachary Senwo, Alabama A&M University, United States
A/Prof. Bindeshwar Singh Kamla Nehru Institute of Technology, India
A/Prof. Hasi Rani Barai, Yeungnam University, South Korea
A/Prof. Jamaluddin Mahmud, Universiti Teknologi MARA, Malaysia
A/Prof. Mohamed Ramadan, University of Hail, Saudi Arabia
A/Prof. Najam Hasan, Dhofar University, Oman
A/Prof. Nosina Krishna Chaitanya, Jawaharlal Nehru Technological University, India
A/Prof. Nurbek Saparkhojayev, Almaty Management University, Kazakhstan
A/Prof. Pandian Vasant, Universiti Teknologi Petronas, Malaysia
A/Prof. Teodor Lucian Grigorie, University of Craiova, Romania
A/Prof. Zawawi Daud, Universiti Tun Hussein Onn Malaysia
A/Prof. Abdull Halim Abdul, OIl and Gas department, Malaysia
A/Prof. Baoping Cai, China University of Petroleum, China
A/Prof. Dariusz Jakóbczak, Koszalin University of Technology, Poland
A/Prof. Edgar Allan Mendoza, University of the Philippines
A/Prof. Lakhveer Singh, Universiti Malaysia Pahang (UMP) Malaysia, Malaysia
A/Prof. Lidia Sas Paszt, Research Institute of Pomology, Poland
A/Prof. Mahmood Barbooti, University of Yechnology, Iraq
A/Prof. Majid Mirzaei, Universiti Tunku Abdul Rahman, Malaysia
A/Prof. Najeh Lakhoua, University of Carthage, Tunisia
A/Prof. Ryan Joseph Calinao, Lyceum of the Philippines University-Laguna
A/Prof. Sarawut Thepanondh, Mahidol University, Thailand
A/Prof. Yasir Al Hussein, Jerash University, Faculty of Engineering, Jordan
Dr. Abolghasem Akbari, University Malaysia Pahang, Malaysia
Dr. Ahmad Safuan A Rashid, Universiti Teknologi Malaysia, Malaysia
Dr. Akinola Johnson Olarewaju, Federal Polytechnic Ilaro, Ogun State, Nigeria
Dr. Alexandre Costa, Federal University of the valleys of Jequitinhonha and Mucuri, Brazil
Dr. Angelo Gallone, Scotland’s Rural College (SRUC), United Kingdom
Dr. Azizul Azhar Ramli, Universiti Tun Hussein Onn Malaysia
Dr. Bashir Dar, University of kashmir Delina Baramulla J&K India, India
Dr. Bassam Abdellatif, National Authority for Remote Sensing and Space Sciences, Egypt
Dr. Binh Phu Nguyen, National University of Singapore, Singapore
Dr. Cazacu Gabriela, S.C. Geotech Dobrogea, Romania
Dr. Chengen Yang, Intel Corporation, United States
Dr. Dayang Norulfairuz Abang Zaidel, Universiti Teknologi Malaysia
Dr. Evgeni Starikov, KIT, Karlsruhe, Germany; Chalmers, Gothenburg Sweden, Germany
Dr. Fatma Khanchel, University of Tunis El Manar, Tunisia
Dr. Hamidreza Khataee, Griffith University, Australia
Dr. Hêriş Golpîra, Islamic Azad University, Iran

Dr. Iskhaq Iskandar, Dept. Physics, University of Sriwijaya, Indonesia
Dr. Jingwei Zhao, University of Wollongong, Australia
Dr. Jitendra Agrawal, Rajiv Gandhi Proudyogiki Vishwavidyalaya, India
Dr. Liza Patacsil, Malayan Colleges Laguna, Philippines
Dr. Mohamed Amine, Ferrag Guelma University, Algeria
Dr. Mohd Afendi Rojan, Universiti Malaysia Perlis, Malaysia
Dr. Mohd Altaf, University of kashmir Delina Baramulla J&K India, India
Dr. Mohd Hairy Ibrahim, Sultan Idris Education University, Malaysia
Dr. Mostafa Khater, Egypt - El sharqia - Zagazig, Egypt
Dr. Najam Hasan, Dhofar University, Oman
Dr. Namir Alkawaaz, University of Almustansiriyah, Iraq
Dr. Nashrul Fazli Mohd Nasir, Universiti Malaysia Perlis, Malaysia
Dr. NaufaL Mansor Kampus Uniciti Alam, Universiti Malaysia Perlis (UniMAP), Malaysia
Dr. Obed Majeed Ali, Northern Technical University, Iraq
Dr. Piyapong Janmaimool, King Mongkhut' University of Technology, Thailand
Dr. Po-Sheng Chiu, National Cheng Kung University, Taiwan
Dr. Prabu Mohandas, Adhiyamaan College of Engineering, India
Dr. Raman Kumar, D A V Institute of Engineering and Technology, India
Dr. Riccardo Colella, University of Salento, Italy
Dr. Rolando Javellonar, Romblon State University, Philippines
Dr. Shikha Agrawal, Rajeev Gandhi Technical University, India
Dr. Stefania Tomasiello CORISA, University of Salerno, Italy
Dr. Sumiyyah Sabar, Universiti Sains Malaysia, Malaysia
Dr. Suphaphat Kwonpongsagoon, Mahidol University, Thailand
Dr. Wei Hong Tan, Universiti Malaysia Perlis, Malaysia
Dr. Yoshiro Fujii, Shin Kobe Dental Clinic, Japan
Dr. Yuk Feng Huang, Universiti Tunku Abdul Rahman (UTAR), Malaysia
Dr. Zongyan Zhou, Monsh University, Australia
Dr. Purnanand Savoikar, Goa Engineering College, India

Conference Correspondence:

Prof. Dr. Zakaria Hossain (Director)
Dept. of Environmental Science and Technology, Mie University, Japan
Mr. Md. Aminul Islam (Secretary)
Dept. of Environmental Science and Technology, Mie University, Japan
E-mail: conference@geomate.org
Tel & Fax: +81-59-231-9578

Editorial and Executive Committee:

Prof. Dr. Zakaria Hossain
Dr. Md. Toriqul Islam
Ms. Siti Hanggita
Mr. Md. Aminul Islam

Note- A: Associate, E-Emeritus

Keynote Paper

Second International Conference on Science, Engineering & Environment,
Osaka City, Japan, Nov.21-23, 2016, ISBN: 978-4-9905958-7-6 C3051

ROCK SLOPE INSTABILITY MECHANISM IDENTIFICATION USING NEW STEREOGRAPHIC METHODS

John V Smith
School of Engineering, RMIT University, Australia

ABSTRACT

There are numerous mechanisms of rock slope instability. The feasible mechanisms can be identified manually by using stereographic projection. The most complex mechanisms involve interactions of multiple planes of weakness within the rock mass. The conventional approach to multiple planes of weakness is to identify the orientation of their lines of intersection relative to known envelopes defined on a stereograph. In the new approach described here, the poles to planes of weakness are joined by great circles on the stereograph. The relationship between the great circles and the daylight envelope of a slope is shown to provide a rapid and accurate assessment of the potential for the wedge sliding instability mechanism. The method is described as the circle method to distinguish it from the conventional 'intersection' method. The circle method also allows the critical slope angle to be identified for each feasible tetrahedral rock wedge. Multi-plane toppling mechanisms are also shown to be readily assessed by use of the circle method. The new methods of stereographic analysis improve the identification and stability analysis of multi-plane weaknesses in rock slopes. The improved assessment technique is beneficial in ensuring that correct methods of stability analysis are applied to each potentially unstable slope. The method is applied to the Guinsaugon landslide in the Philippines and coastal cliff instability in Sydney, Australia.

Keywords: Slope stability, Stereographic analysis, Kinematic analysis, Wedge sliding, Toppling

INTRODUCTION

Large slope failures typically involve the instability of the rock mass and are greatly influenced by the orientation and spacing of discontinuities such as bedding, joints and faults [1-3]. Assessing the risk associated with slope stability hazards slope first requires identification of the potential mechanisms of failure. For the identified mechanisms of failure, slope stability can be analysed by techniques including static methods, limit-equilibrium and finite element methods to find a factor of safety or a probability of failure for that failure mechanism. [4]. It is important to note that the analysis applies only to the mechanism of failure and should not be assumed to demonstrate that the slope is stable unless the possibility of other mechanisms occurring is excluded. Identifying potential instability mechanisms and ensuring that the most problematic mechanisms are carefully analysed is an especially important stage of slope stability analysis.

Appropriate allocation of the resources required to conduct detailed stability analysis requires that the initial assessment of failure mechanisms commonly known as kinematic analysis is completed efficiently and effectively. Kinematic analysis is typically conducted using the stereograph, a graphical tool for recording and comparing orientations of discontinuities [5,6]. The stereograph allows the representation of the orientations of planes by the orientation of the line (known as a pole on the stereograph) perpendicular to the plane and thus is capable of representing large data sets in a clear way [7].

The stereographic method of kinematic analysis is particularly useful for assessment of the stability of pairs of discontinuity planes known as wedges [8] (Fig. 1). The conventional representation and assessment of wedges of rock is by the orientation of the lines of intersection of the pairs of planes [9]. An alternative method of stereographic assessment involves finding the orientation of great circles linking pairs of discontinuity poles [10]. These two methods are referred to here as the intersection method and the circle method, respectively.

This paper demonstrates the application of the circle method of kinematic analysis of wedges to a large rock slide-debris avalanche that occurred in the Philippines and to the coastal rockfall hazard in Sydney Australia. The method is shown to be applicable to wedges with sliding kinematics and toppling kinematics. The main benefits are 1) the circle method is more practical (and less conservative) than the intersection method in identifying feasible wedges and 2) the circle method retains information on the shape of the wedge during the kinematic analysis which is relevant to consideration of the potential stability of the wedge.

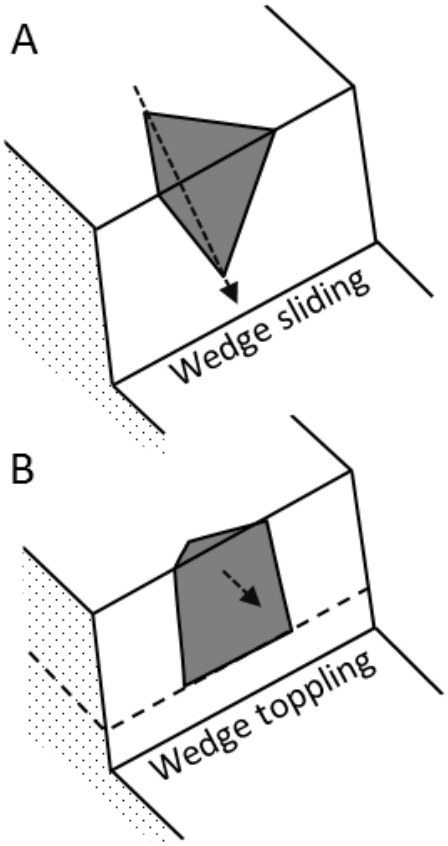

Fig. 1 Schematic diagrams showing wedge blocks susceptible to A) sliding and B) toppling

GUINSAUGON LANDSLIDE

A catastrophic landslide occurred in southern Leyte province in the Philippines on 17 February 2006, burying the village of Guinsaugon with the loss of 1,221 lives. The event was not attributable to a single trigger and was considered to be the result of progressive degradation of the 15 million m^3 rock mass [11]. The failure mechanism and deposit characteristics have been described as a rock slide-debris avalanche [12]. The orientation of joints and faults relative to the ground slope was found to be a critical aspect of the slope failure. The location of the landslide is on an 800 m high east-facing escarpment following the Philippine Fault, a major tectonic feature of the Philippines (Fig. 2).

Structural Data

The beds of sedimentary and volcanic rocks dip at a moderate angle into the escarpment and are not considered to be a major contributor to instability. Structural data collection showed faults and two sets of joints were potential contributors to the instability of the rock mass [12] (Fig. 3A). The distribution of orientations was summarized as ranges of orientations for the structures [12] (Table 1).

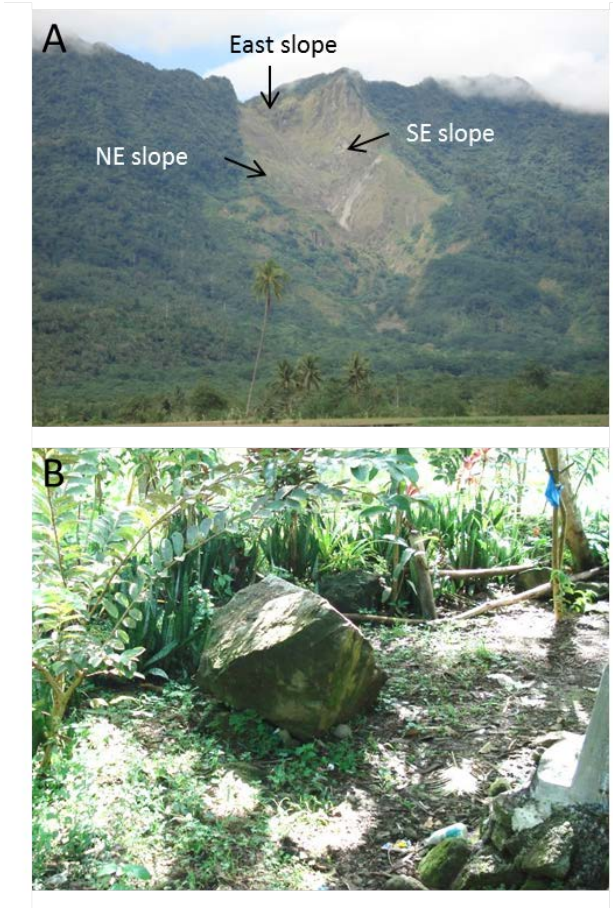

Fig. 2 A) Guinsaugon landslide. B) Block of landslide rock debris. (Photographs from 2010, courtesy of Dr Christian Arnhardt)

Table 1 Structural data at Guinsaugon (Catane et al., 2008)

Structure/Slip surface	Dip (º)	Dip direction azimuth (º)
Bedding	35	252
Fault	45-56	057
Joint set 1 (NE)	80-90	030
Joint set 1 (SW)	65-90	205
Joint set 2	60	009
Slope 1 (SE)	20-75	150
Slope 2 (NE)	35-85	064
Slope 3 (east)	60-80	090

Note: Joint set 1 includes a range of orientations from dipping 80º toward northeast to dipping 65º southwest.

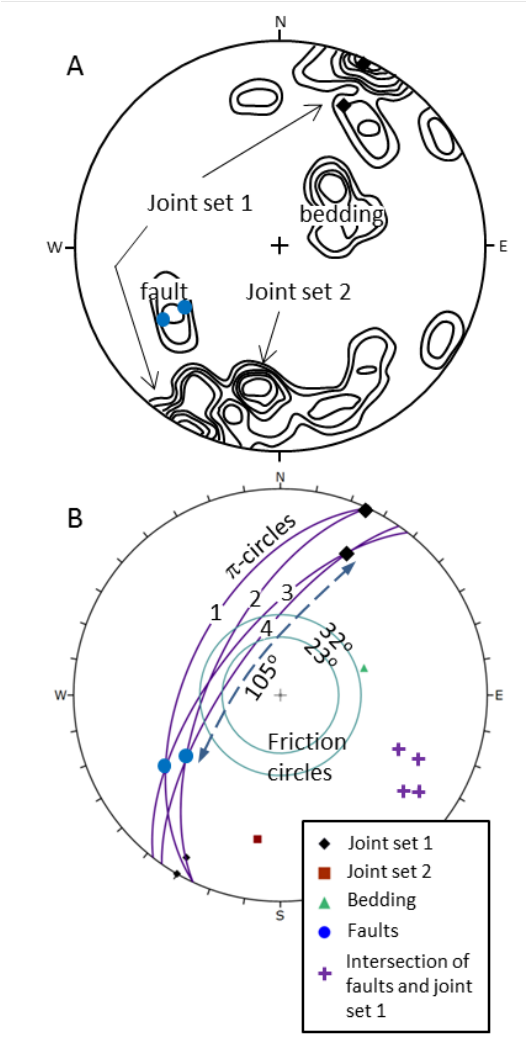

Fig. 3 A) Structural data distributions (Catane et al., 2008). B) Summary of structural orientations. Potential east-sliding wedges shown as great circles known as π-circles. Lower hemisphere, equal area stereographs

Inspection of the stereograph indicates that wedges of rock can form bounded by the north-east dipping faults and vertical to south-west dipping joints of set 1. These two structures intersect in the southeast quadrant of the stereograph making these wedges candidates for sliding from the east-facing slope (Fig. 3). Conventional intersection method focuses on comparing the intersection lines with the friction of the structures and the slope face. The circle method links discontinuities poles together with a great circle which is then assessed relative to the friction angle and slope direction [10]. The term π-circle has been adopted from the structural geology literature to refer to a great circle linking poles. It was noted by Markland in 1972 [9] that "mechanically unstable wedges formed by two poles which lie on the same side of the vertical plane normal to the slope face are in practice extremely unlikely". One of the advantages of the circle method is that these impractical intersections are not generated. Impractical wedge intersections include those formed by planes that are dipping in a similar direction [9] and is extended here to cases where one or both of the planes dip into, rather than out of, the slope face.

The extents of the range of orientation of the fault and south-west dipping joint set 1 populations (Table 1) are shown on the stereograph as individual poles (Fig. 3). For this case example, these data will be analysed as if they were as individual poles. This is a useful form of analysis as it is reasonable to assume that most wedges will have characteristics between these limits. The two fault poles have each been linked to the two joint set 1 poles forming four π-circles (Fig. 3B). The intersection method would generate six intersections rather than four because it would include the intersections of the pair of fault poles and the pair of joint poles. These additional intersections are erroneous as each of these pairs of structures have similar orientation to each other and cannot form practical wedges. This is one of the reasons why the circle method is less conservative than the intersection method.

Wedge Shape

The circle method provides a simple way to include the shape of a wedge in the kinematic analysis. The angle between the two poles comprising the wedge can be subtracted from 180º to give the angle enclosed by the wedge. Therefore the 105º (shown on Fig. 3B) measured between the fault and joint poles of π-circle 4 represents a wedge with an internal angle of 75º. This is a useful feature to observe as the angle between the bounding structures determines the volume of the wedge and also the factor of safety increases as the angle decreases [8].

In the intersection method this block shape information is not retained during kinematic analysis as the orientation of the intersection is considered without reference to the orientation of the contributing poles.

Friction Angle

The friction angle can be considered to be a cone centered on the vertical direction. This cone can be represented on a stereograph as a small circle around the centre point of the stereograph. Any pole plotting within the friction circle would be too shallowly dipping to slide whereas any pole plotting outside the friction circle would be sufficiently steep to slide.

The Mohr-Coulomb model of strength is typically used to represent behavior of soil and rock. That model represents shear strength as a combination of friction and cohesion. If a material or

interface has zero cohesion then its shear strength is represented by the friction angle as represented on the stereograph. Cohesion is more difficult to represent on a stereograph as its contribution to shear strength depends on the scale of the failure surface. The Hoek-Brown model is a methodology for generating strength parameters for rock masses and for translating these into the Mohr-Coulomb model [13]. Barton [14] has argued that cohesion of interfaces is significantly reduced or entirely lost in the initial stages of deformation of a rock mass such that friction is the major, or only, contributor to strength.

The study by Catane et al. [12] used the Hoek-Brown methodology [13] to estimate a range of rock mass strength conditions. They [12] estimated the low end friction angle of the rock mass to be 23º and the high end to be 32º. The total shear strength is also contributed to by cohesion, however, it is instructive to consider the zero cohesion case using the stereograph.

The range of east-plunging wedges represented by the four π-circles (Fig. 3B) can be considered in relation to the friction circle values noted above. If the π-circle passes through the friction circle the wedge is stable because the plunge of the intersection line is less than the friction angle. One wedge is stable for both the low and high friction value, one wedge is unstable for both the low and high friction angles and two wedges are stable for the higher value but unstable for the lower value. This observation is consistent with the finding of Catane et al. [12] that the rock mass was on the limit of stability.

Ground Slope

Kinematic analysis also requires consideration of the angle and direction of the ground slope. The face of a slope is represented as a great circle on the stereograph. For each slope a daylight envelope can be generated. The daylight envelope encloses the poles of planes which dip outward from the slope face; an important requirement for instability. It has been incorrectly stated [3] that poles forming wedges must also be within the daylight envelope. However, it has been shown that wedges can form from poles outside the daylight envelope [10]. That study showed that the relationship between the π-circle and the daylight envelope can be used for kinematic analysis of sliding wedges [10]. If the π-circle passes through the daylight envelope (without passing through the friction circle) the wedge is daylighting and therefore potentially unstable. If the π-circle does not pass through the daylight envelope the wedge is non-daylighting (for that slope) and therefore stable.

Catane et al. [12] considered three slope directions in their analysis of the Guinsaugon slope failure (Table 3). These directions included the east-facing slope at the back of the failure zone and the north-east and south-west slopes that are observable in the failure scar (Fig. 1A). The slope angles are highly variable and the angles shown on Fig. 4 are those also used by Catane et al. [12].

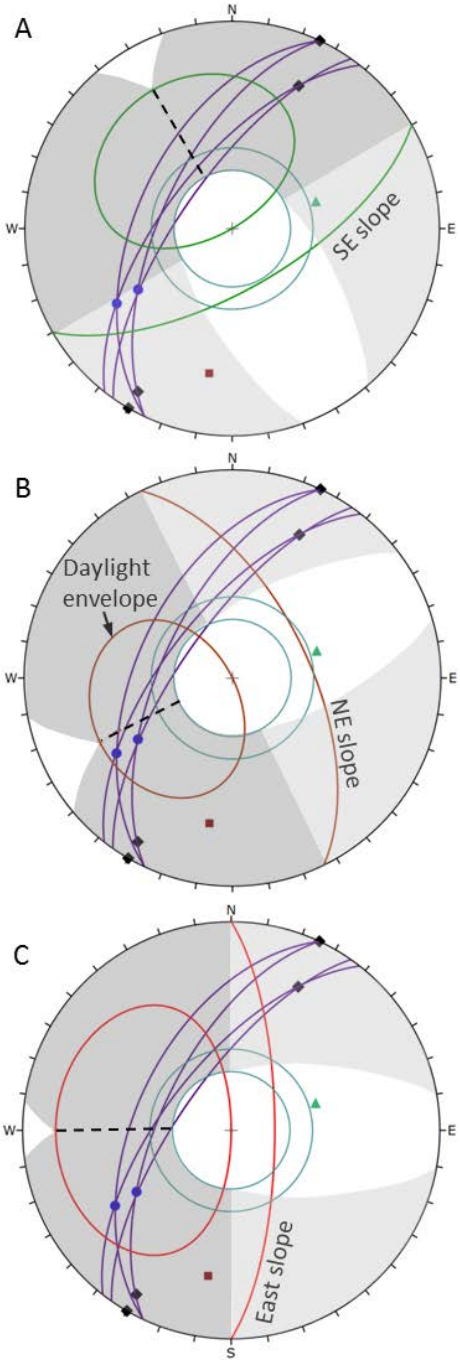

Fig. 4 Stereographic analysis of sliding wedges at Guinsaugon (data collected by Catane, 2008). A) SE slope, B) NE slope and C) east slope. Shaded zones indicate poles which can form part of a wedge for the given slope face for the lower friction angle.

Lower hemisphere, equal area stereographs

In the circle method, the first test for the potential for poles to form a wedge is that the pole lies in the shaded area (valid wedge-forming pole zone) of the stereograph on Fig. 4 [10]. For practical purposes this can be further restricted to the dark shaded of the stereograph (representing planes dipping out of the slope face) on Fig. 4 [10]. Further, a pair of poles must comprise one pole from each of the wedge-forming pole zones on each side of the dashed line (Fig. 4). The planes represented by these poles both dip out of the slope but with opposite apparent dip in the slope. The conventional intersection method does not apply either of these tests and therefore includes many intersection lines that are not representative of practically feasible wedges.

The stereograph of the southeast directed slope shows that the poles to the fault are located within valid wedge-forming pole zone on the boundary between outward and inward dip on the slope face. These planes dip perpendicular to the direction of the slope face (Fig. 4A). For joint set 1 the part of the population which ranges from dipping SSW to vertical is within the practical wedge-forming zone. The NNE-dipping poles to joint set 1 dip into the slope and will not be included in the kinematic analysis. The π-circles which link the fault poles and the SSW-dipping joint set 1 poles represent four potential wedges. The four π-circles pass through the daylight envelope for the slope indicating that the wedges are all kinematically feasible relative to the slope. The influence of friction on their stability was outlined above.

The stereograph of the northeast directed slope shows that the SSW-dipping poles to joint set 1 are outside the practical limits of the wedge-forming pole zone, meaning they actually dip into this face and are not likely to contribute to significant wedges (Fig. 4B). The faults and the NNE-dipping part of the joint set 1 population both lie in the valid wedge-forming pole zone but, as they are in the same half of the zone they have the same apparent dip on the slope face and in practice do not form significant wedges. There are no poles in the other part of the practical wedge-forming pole zone for this slope and therefore wedge failure is not expected from the known structures (Fig. 4B). The stereograph of the northeast directed slope shows that the poles to faults are within the daylight window and close to the dashed line representing the direction opposite to the slope face direction. This relationship indicates that the faults are potentially surfaces of planar sliding (Fig. 4B).

The stereograph of the east directed slope shows that, like the NE slope, the SSW-dipping poles to joint set 1 are outside the practical wedge-forming pole zone and the faults and the NNE-dipping part of the joint set 1 population both lie in the same part of the valid wedge-forming pole zone (Fig. 4C). In contrast to the NE slope, the faults are too oblique to the slope face to be considered significant for planar sliding. Therefore neither wedges nor planar sliding are practical mechanisms on this slope (Fig. 4C).

In summary, the stereographic analysis shows that wedges formed by the faults and joint set 1 are oriented in a manner that is marginally stable for the frictional conditions and the SE slope direction. The NE slope direction has potential for planar sliding of faults but not wedges. The east-facing slope is not kinematically feasible for planar or wedge sliding. The assessment supports the general conclusion of Catane et al. [12] that the rock mass was at the margin of stability with respect to structural failure and that failure occurred by progressive reduction in rock mass strength.

SYDNEY COASTAL CLIFF INSTABILITY

The city of Sydney in the state of New South Wales, Australia is well known for its coastal scenery. This includes numerous areas of coastal cliffs prone to instability [15]. The northern beaches district of Sydney is one such location. The geology comprises Early Triassic Narrabeen Group bedded sandstones and shales and the lower parts of the overlying Middle Triassic Hawkesbury Sandstone which form horizontal strata [15,16]. The orientations of bedding and joints (n=109) were collected in the field for this study (Fig. 5). The orientation of bedding is approximately horizontal and the main joint set strikes northeast-southwest and dips steeply. Joint sets which strike NNW-SSE and WNW-ESE are also present. These steeply dipping and vertical joints are a major influence on the stability of the cliffs of the Sydney northern beaches district. The risk is increased by the many houses built along the cliff tops and the beaches below the cliffs are popular recreation places (Fig. 6).

The stereograph can be used to infer the shapes and orientations of potentially unstable blocks of rock along the coast. The π-circle method will be demonstrated in an assessment of the potential failure mechanisms and the kinematic stability of wedge blocks.

Wedge Sliding

Although toppling is the dominant failure mechanism wedge sliding will be considered first. The orientation of the coastline is variable but an azimuth of 110 (ESE) will be considered for the wedge sliding kinematic analysis. Three sets of joints dip outward relative to this slope direction (Fig. 7). Three π-circles have been constructed, linking the three joint set mean orientations (Fig. 7). Only the two π-circles (wedges) which include the SSE-dipping pole (labeled π1 and π2) meet the

criteria of having each pole with opposite apparent dip on the slope face.

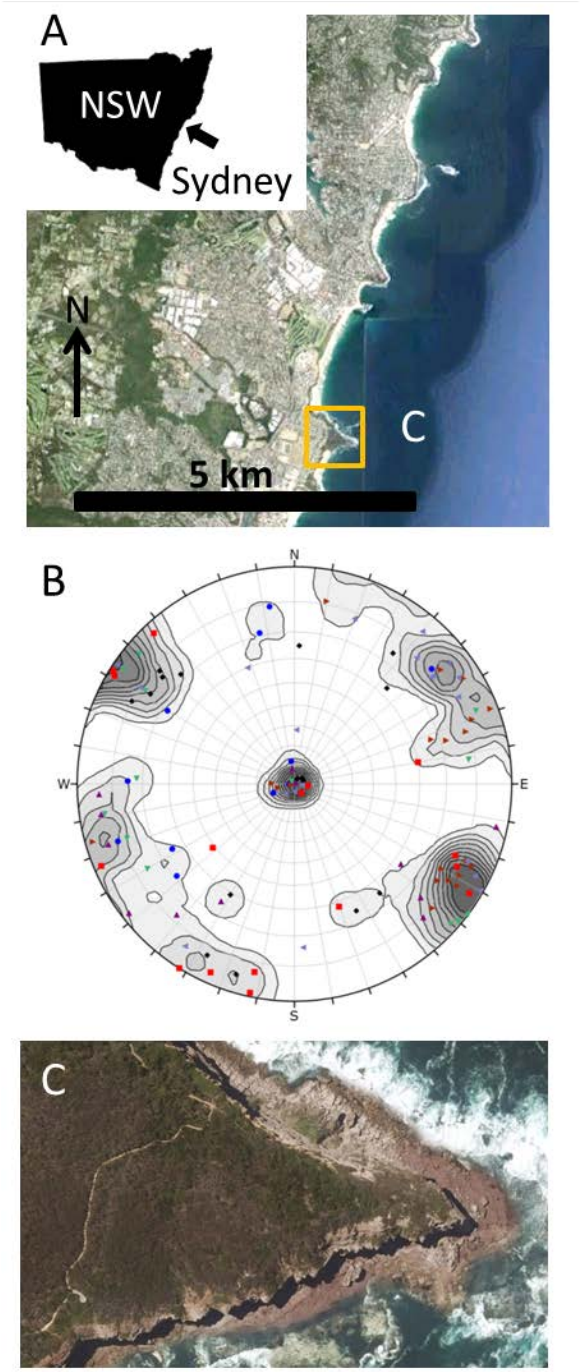

Fig. 5 A) Sydney, New South Wales (NSW), Australia northern beaches district. B) Structural orientations of joints and bedding. Lower hemisphere, equal area stereograph. C) Turrimetta headland showing serrated cliff edges formed by toppling wedges (Google Earth)

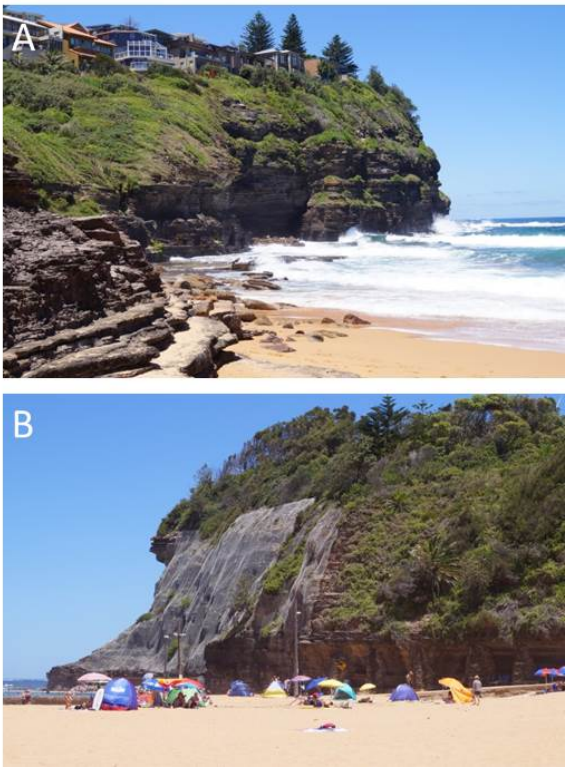

Fig. 6 Coastal cliffs in the study area showing A) houses close to the cliff edges and B) protective drape nets to reduce the rock fall hazard

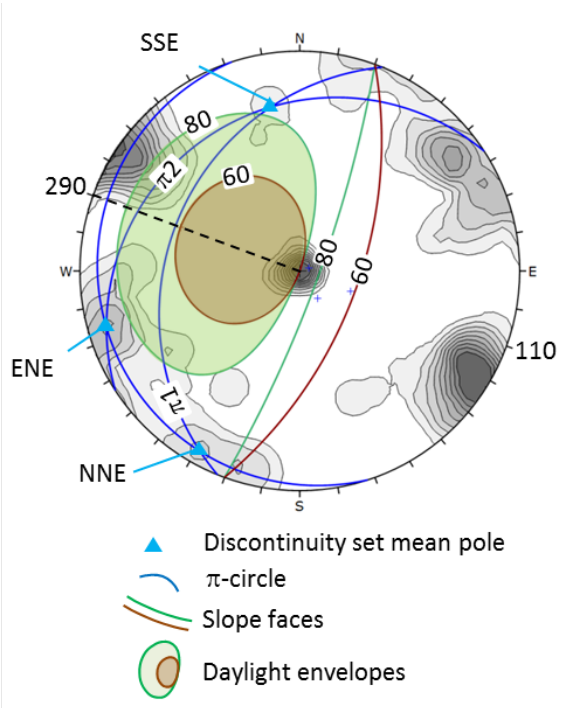

Fig. 7 A) Stereographic analysis of the wedge sliding kinematics using the circle method. Lower hemisphere, equal area stereograph

The daylight envelopes indicate for an 80° slope face the two π-circles each cross the daylight envelope indicating kinematic feasibility of wedge sliding. The daylight envelope for a 60° slope face is also shown on Fig. 7 and it can be observed that neither of the two π-circles cross the daylight envelope indicating wedge sliding is not kinematically feasible for that slope face.

Wedge Toppling

The circle method can also be applied to assessment of toppling failure mechanisms comprising multiple discontinuities. Toppling is considered to be most problematic where discontinuities dip into a steep slope face [1-3]. In the case of a wedge bounded by two discontinuities it is most problematic if the line of intersection of the discontinuities plunges into a steep face [8]. The range of dip angles susceptible to toppling can vary depending on the friction angle of block interfaces, slope face angle, and spacing of discontinuity sets (block size and shape) and has not been directly considered in this study. For the purpose of the case study the range of dips of planes capable of undergoing direct toppling is taken as 60° to 90° in a direction opposing the slope face.

Direct toppling describes the situation of blocks which are free to move out of a slope whereas flexural toppling involves confinement of the layers. The analysis here is restricted to direct toppling. For toppling, the daylight envelope of the slope does not need to be shown so it is possible to consider a wide range of slope directions on a single stereograph. The range of slope face directions being considered is extended a further 90° from each of the slope direction limits to include all poles dipping into the slope (Fig. 8). Although the general direction of the coast is toward ESE (Fig. 5A) the cliff orientations vary locally along the rocky headlands (Fig. 5C). A range of slope face directions from azimuth 030 to 150 has been considered in this analysis. Therefore, the joint set means dipping toward WSW, WNW, SSE and NNE are included in the toppling assessment (Fig. 8).

Before considering the stability of wedge toppling, the stability of planar toppling will be considered. If a discontinuity has a strike within 20° of the strike of the slope it is considered to be susceptible to planar toppling [2]. Therefore this range either side of the WSW- and WNW-dipping set means are marked as planar direct toppling directions (Fig. 8).

Having identified the planar toppling directions, it is necessary to determine if the remaining directions are susceptible to wedge toppling. Using the circle method, this is achieved by observing whether a π-circle passes through that direction and whether that π-circle has a pole on either side of the slope direction being considered.

In this case study, the slope directions between the WSW and WNW set means does indicate potential wedge direct toppling formed by a combination of those two discontinuity sets as shown by the presence of the π-circle (Fig. 8). Wedge direct toppling comprising the WSW- and SSE-dipping set means can occur at the northern limit of the slope direction range. Wedge direct toppling formed by the WNW set mean and the NNE set mean can occur to the south of the slope direction range (Fig. 8).

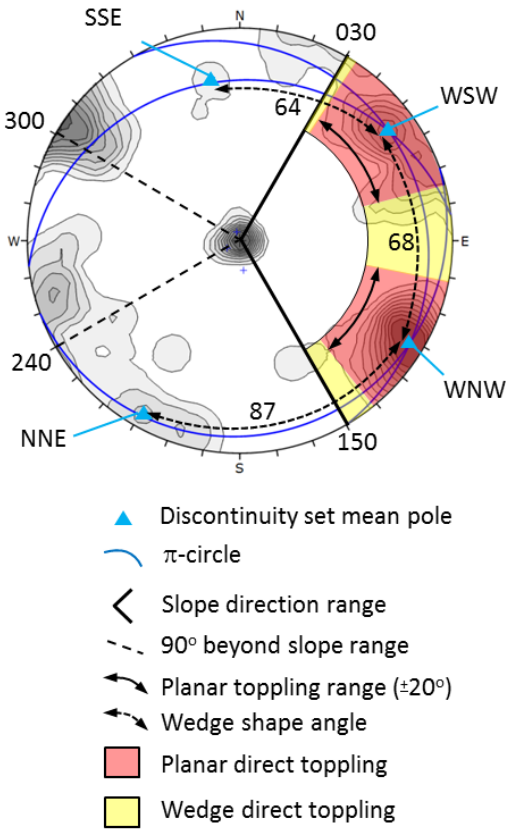

Fig. 8 A) Stereographic analysis of the wedge toppling kinematics. Lower hemisphere, equal area stereograph

The shape of the toppling wedges can be inferred from the information on the stereograph. The shape of the blocks adjacent to the rock face will be the supplement of the angle measured between the poles on the stereograph. For SE facing cliffs, the wedges are approximately right angle blocks. This is illustrated along the southern cliff line of the headland in Fig. 5C. The shape of the toppling wedges on slopes facing east and northeast is between 110 and 120 degrees. Such an obtuse angled block shape is illustrated schematically in Fig. 1B.

CONCLUSION

The circle method is stereographic technique for kinematic analysis of wedges. The method can be applied to sliding and toppling mechanisms. The method has a number of benefits over the conventional intersection method. The circle method excludes intersection formed by near parallel planes or by planes with dip directions not conducive to the practical formation of wedges. These spurious intersections are commonly included in the conventional intersection method.

In addition, the circle method displays the poles and on the connecting great circle (π-circle) and thus retains information about the shape of blocks. These features make the circle method advantageous for assessing the kinematics of potential wedge sliding and wedge direct toppling and the geometry of wedge-shaped blocks capable of producing rockslides in joint-controlled rock masses and rock falls from steep slopes and cliffs.

Although stereographs have been used for many years they have not yet been superseded as a tool for visualizing complex three-dimensional relationships of planar and linear features. The circle method outlined in this paper and other developments such as application of stereographic methods to non-vertical stress trajectories [17] and to flexural toppling [18] indicate that stereographic methods can continue to contribute to advances in geotechnical engineering knowledge.

ACKNOWLEDGEMENTS

RMIT University Research Associate, Dr Christian Arnhardt provided photographs of Guinsaugon landslide from fieldwork he conducted at the site in November 2010 as part of the Environmental and Rural Developement Program - Disaster Risk Management (EnRD-DRM) of the German Society for International Cooperation (GIZ).

REFERENCES

[1] Goodman RE, Introduction to rock mechanics. New York: Wiley; 1989 Jan 17.

[2] Hoek E, Bray JD, Rock slope engineering. CRC Press; 1981 Jun 30.

[3] Wyllie DC, Mah CW, Rock Slope Engineering: Civil and Mining, Spon Press. New York, NY (431pp.). 2004.

[4] Wang YJ, Yin JH, Chen Z, Lee CF, Analysis of wedge stability using different methods. Rock mechanics and rock engineering. 2004 Apr 1;37(2):127-50.

[5] Lucas JM, A general stereographic method for determining the possible mode of failure of any tetrahedral rock wedge. International Journal of Rock Mechanics and Mining Sciences & Geomechanics Abstracts 1980 Feb 1 (Vol. 17, No. 1, pp. 57-61). Pergamon.

[6] Priest SD, Hemispherical projection methods in rock mechanics. Allen & Unwin; 1985.

[7] Lisle RJ, Leyshon PR, Stereographic projection techniques for geologists and civil engineers. Cambridge University Press; 2004 Apr 1.

[8] Hudson JA, Harrison JP, Engineering rock mechanics, vol. I. Pergamon.

[9] Markland JT, A Useful Technique Fro Estimating the Stability of Rock Slopes when the Rigid Wedge Slide Type of Failure is Expected. Imperial College of Science & Technology; 1972.

[10] Smith JV, A method for assessing discontinuity poles for potential wedge sliding. Engineering Geology. 2016 Mar 4;202:55-61.

[11] Guthrie RH, Evans SG, Catane SG, Zarco MA, Saturay Jr RM, The 17 February 2006 rock slide-debris avalanche at Guinsaugon Philippines: a synthesis. Bulletin of engineering geology and the environment. 2009 May 1;68(2):201-13.

[12] Catane SG, Cabria HB, Zarco MA, Saturay Jr RM, Mirasol-Robert AA, The 17 February 2006 Guinsaugon rock slide-debris avalanche, Southern Leyte, Philippines: deposit characteristics and failure mechanism. Bulletin of Engineering Geology and the Environment. 2008 Aug 1;67(3):305-20.

[13] Hoek E, Brown ET, Practical estimates of rock mass strength. International Journal of Rock Mechanics and Mining Sciences. 1997 Dec 31;34(8):1165-86.

[14] Barton N, Shear strength criteria for rock, rock joints, rockfill and rock masses: Problems and some solutions. Journal of Rock Mechanics and Geotechnical Engineering. 2013 Aug 31;5(4):249-61.

[15] Leventhal AR, Kotze GP, Landslide susceptibility and hazard mapping in Australia for land-use planning—with reference to challenges in metropolitan suburbia. Engineering Geology. 2008 Dec 1;102(3):238-50.

[16] Kotze GP, An assessment of rockfall frequency for the coastal cliff-lines of Pittwater local government area, Sydney. Australian Geomechanics. 2007 Mar;42(1):213-9.

[17] Smith JV, A new approach to kinematic analysis of stress-induced structural slope instability. Engineering Geology. 2015 Mar 17;187:56-9.

[18] Smith JV, Self-stabilization of toppling and hillside creep in layered rocks. Engineering Geology. 2015 Sep 28;196:139-49.

Sixth International Conference on Geotechnique, Construction Materials and Environment, Bangkok, Thailand,Nov. 14-16, 2016, ISBN: 978-4-9905958-6-9 C3051

TUNNEL CONSTRUCTION IMPACT ON GROUNDWATER CHEMISTRY OVER 25 YEARS OF OBSERVATION AT MATSUMOTO TUNNEL, MATSUMOTO CITY, JAPAN

Hiroyuki Ii
Professor, Faculty of Systems Engineering, Wakayama University, Japan

ABSTRACT

Construction on the Matsumoto Tunnel north of Matsumoto city, started at the foot of the Matsumoto plateau in 1980. Over the course of 25 years, approximately 11 million m^3 of water inflow in the tunnel was drained. Water inflow in the tunnel during tunnel construction varied from 1 to 8 m^3 per minute decreasing to 1 to 0.6 m^3 per minute between 1993 and 1995. At present, inflow maintains a rate of 0.6 m^3 per minute. ^3H concentration, an indicator of groundwater age during tunnel construction, was less than 0.3 T.U. It has increased and remained less than 1.0 T.U. since 2003. Currently, it remains at 0.6 T.U. and the age of water in flowing into the tunnel has been estimated to be over 30 years old from initial ^3H concentration for surface water which varied from 4 to 10 T.U. As oxygen stable isotope values and HCO_3^- concentration of water inflow in the tunnel were uniform for 25 years, the source of water inflow in the tunnel is not thought to have changed. Roughly 25 to 50 million m^3 water was stored in rocks above the tunnel in the plateau from 10 % porosity measured by rock sample. However, when only 3 million m^3 groundwater, one tenth of porosity was drained, groundwater level decreased widely. Therefore the decrease of groundwater pressure was brought about by drainage of one tenth of total pore. From long term observation, groundwater level increased marginally owing to a decrease of water inflow in the tunnel. An increase in SO_4^{2-} and Ca^{2+} concentrations due to the solubility of the tunnel liner concrete was found.

Keywords: Tunnel construction, Long term drainage, Groundwater level, Tunnel seepage, Groundwater chemistry

INTRODUCTION

Many tunnels have been constructed in Japan. Before the construction of a tunnel, groundwater conditions are researched in detail for evaluating the consequences of tunnel construction. However, following tunnel construction, no long term ongoing studies regarding environmental conditions were reported despite a huge number of tunnels being constructed across the country. In contrast to this, studies focusing on the disposal of radioactive waste using deep underground tunnels were conducted in which groundwater flow and water chemistry over a long term were investigated for Miocene marine sedimentary rock at Horonobe in Hokkaido and for granite at Tono in Gifu [1]. However, it was determined that groundwater condition depended on each area's unique geological and topographical features [1] so information regarding how groundwater flow and water chemistry may have been influenced by tunnel construction over a long period was insufficient. Therefore, in this paper, groundwater condition due to tunnel construction starting in 1990 was researched and studied for over 25 years using water chemistry, groundwater level and flow of water inflow in the tunnel.

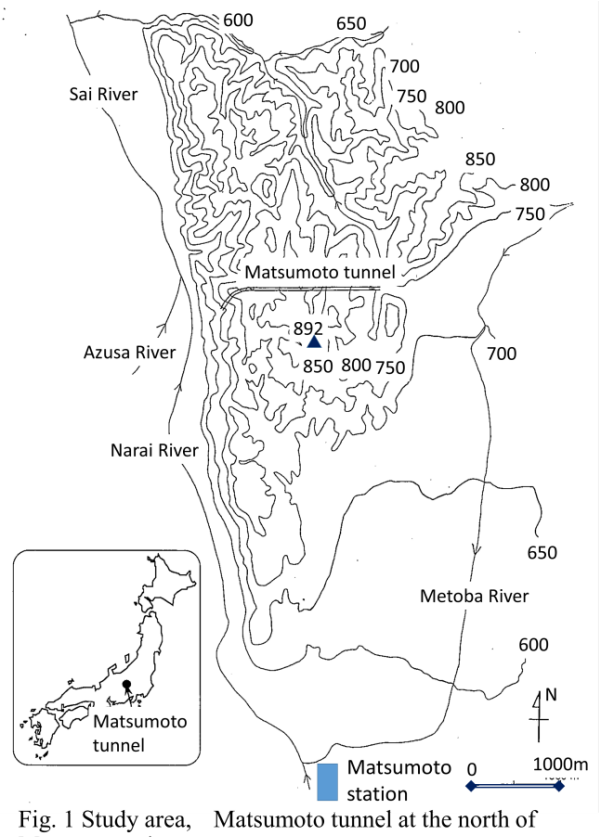

Fig. 1 Study area, Matsumoto tunnel at the north of Matsumoto city

STUDY AREA

The Matsumoto tunnel, approximately 2000 m in length, was constructed within a plateau north of Matsumoto city in central Japan. Tunnel construction began in October 1990 and the tunnel was completed in November 1992 [2]. A Quaternary Period river terrace sedimentary layer is found on the top of the plateau which mainly consists of andesite tuff breccia and sandstone formed in the Miocene period. Water analysis around the tunnel revealed that [1] oxygen and hydrogen isotopes and main soluble substances between water inflow in the tunnel and a dried up

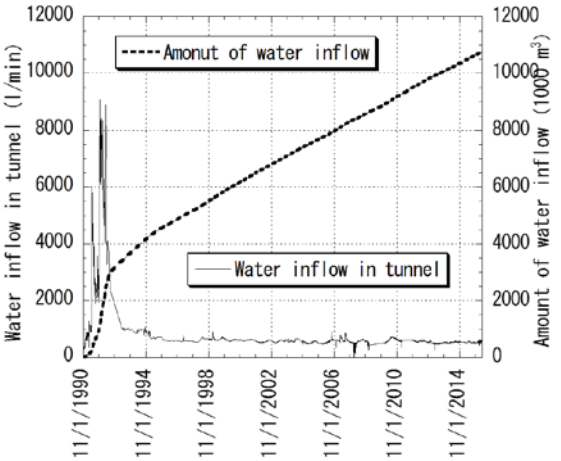

Fig. 2 Water inflow in tunnel and amount of water inflow

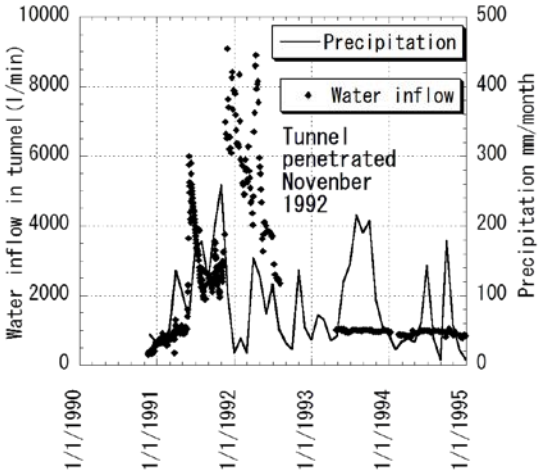

Fig. 3 Water inflow in tunnel and precipitation (1990 to 1995)

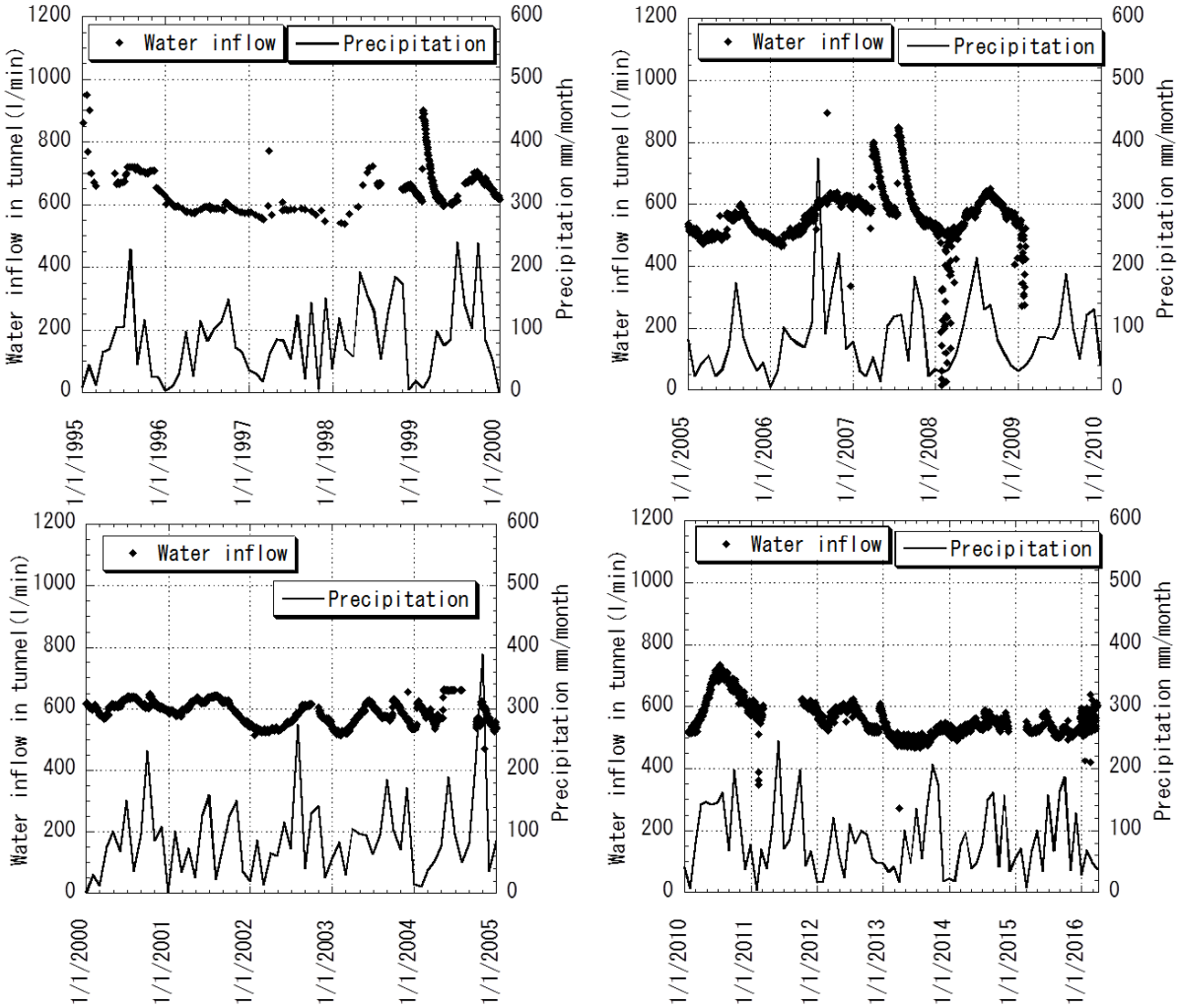

Fig. 4 Water inflow in tunnel and precipitation (1995 to 2016)

spring and well were the almost same. On the other hand, isotope values and main soluble substances for an undried well and spring on the tunnel were different from those for tunnel inflow in the tunnel. Subsequently, water chemistry analysis was able to predict the influence of tunnel construction on the spring and well [2]. During tunnel construction, a tracer test was performed by Br- injection into a borehole and sampling in the tunnel determined effective porosity to be 0.48 % using a three dimensional FEM transport analysis. The effective porosity value was very low relative to porosity, 7 to 15 % for Miocene sedimentary rock [3]. On the other hand, before tunnel construction, effective porosity was measured at 10 % using tritium concentration for water inflow in the tunnel [4]. Groundwater level and water inflow in the tunnel were studied for 5 years [5].

METHOD

Around the Matsumoto tunnel, spring, river, well and cutting face water was sampled during tunnel construction. After the tunnel penetrated was completed, total water inflow in and along the tunnel was sampled. Flow rate for water inflow in and along the tunnel was measured from the beginning of tunnel construction.

Main soluble substances, NO_3^-, Cl^-, Ca^{2+}, and SO_4^{2-} concentrations were measured by ion exchange chromatography. HCO_3^- concentration was measured by titration and ^3H concentration was measured by liquid scintillation counter. The stable hydrogen and oxygen isotopic ratio were measured by mass spectrometer (Sercon Geo Wet System).

RESULTS

Flow rate of water inflow in tunnel

Measurement of water inflow in the Matsumoto Tunnel began from the beginning of construction and has continued until present. Measurements were performed over 25 years with the amount of water inflow in the Matsumoto Tunnel reaching approximately 11 million m^3 as shown in Fig.2. During tunnel construction, storage water in rocks from the cutting face was drained and high water inflow was observed. In November 1992 at the tunnel penetrated (when the tunnel went through completely), the amount of water inflow reached 3 million m^3 when one million m^3 per years was continually drained as water inflow.

Although, uniform flow rate for water inflow in the tunnel as shown in Fig.2 was recognized after the tunnel penetrated, small changes of water inflow in the tunnel were observed as shown in Fig.3. Water inflow in the tunnel varied from 1 to 0.8 m^3 per minute from 1993 to 1994 but decreased to 0.6 m^3 in 1995. Currently, water inflow is stable at 0.6 m^3 per minute. However, after 1993, a small change for water inflow in the tunnel was recognized. A time series for water inflow in the tunnel and monthly precipitation are shown in Fig.4. Monthly precipitation varied from 0 to 400 mm and water inflow was between 500 mm and 700 mm per minute. Peaks and bottoms for precipitation sometimes seemed to coincide with those values in following months for water inflow although abnormal values due to machine trouble for flow mater were sometimes observed.

Cutting face water during construction

During tunnel construction, cutting face water was sampled at the both directions. Main soluble substances, Ca^{2+}, HCO_3^-, and SO_4^{2-}concentrations were shown in Fig.5. The left side was the west entrance and the right side was the east side with 2000m of total tunnel length. SO_4^{2-} concentrations around the entrance of the east side were lower than those at other areas and were observed to be extremely high (1200 m) from the west side, HCO_3^-

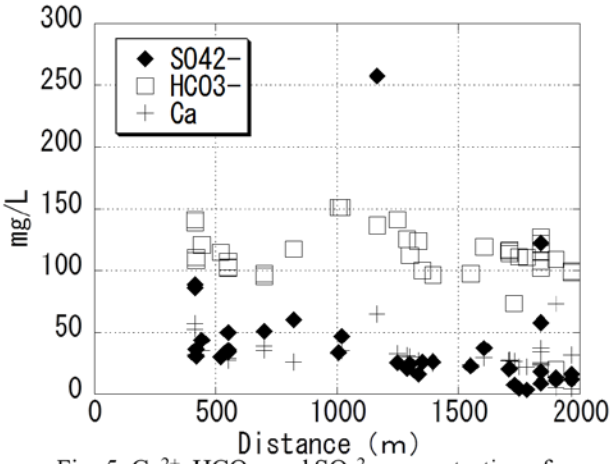

Fig. 5 Ca^{2+}, HCO_3^- and SO_4^{2-} concentration of cutting face

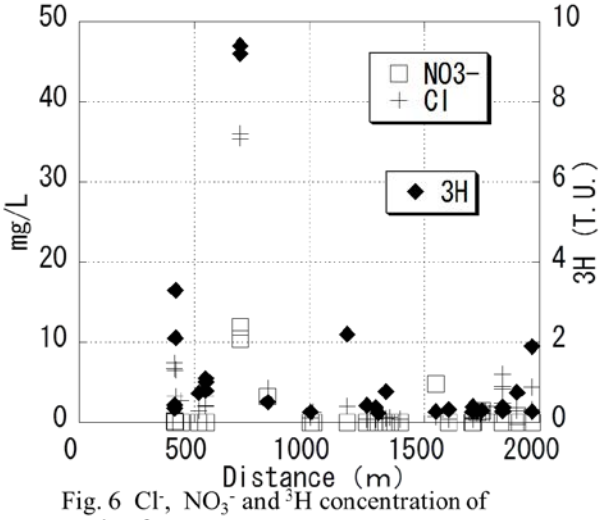

Fig. 6 Cl^-, NO_3^- and ^3H concentration of cutting face

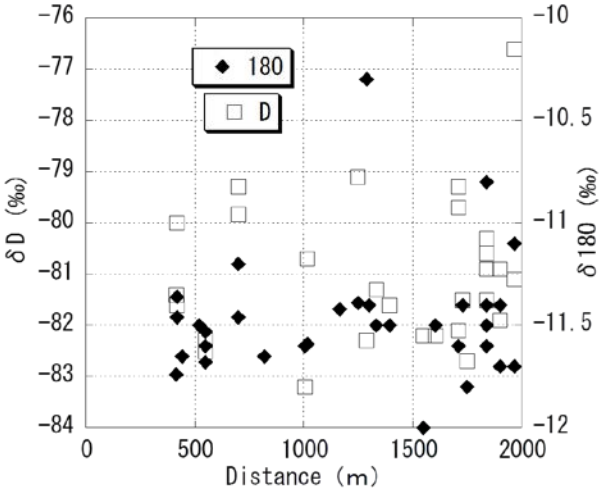

Fig. 7 δD and $\delta^{18}O$ of cutting face

and Ca^{2+} concentrations in contrast were almost the same value.

As farm houses, rice fields and fruit trees were observed on the plateau, surface water contaminated with NO_3^- and Cl^- was suspected. ^3H concentration was an indicator of water age. NO_3^- and Cl^- and ^3H concentrations are shown in Fig.6. Most ^3H concentrations for water inflow in the tunnel were less than 0.3 T.U. therefore it was thought to be old groundwater reserved in rocks. If ^3H concentration for the recharge water is assumed to be 10 T.U., the traveling time for water inflow in the tunnel is over 50 years. Therefore, as the recharge area was thought to be on top of the plateau because the plateau was divided and isolated by a valley and river, surface water on the plateau infiltrated and gradually migrated into the tunnel level. In this process, $NO_3^-$and SO_4^{2-} were thought to be decomposed under a reductive condition and NO_3^- concentration for old groundwater was thought to be under the detection limit and SO_4^{2-} concentration was thought to remain at 50 mg /L.

On the other hand, in some locations, ^3H concentrations were over the detection limit of 0.3 T.U. At a point 700 m from the west side, ^3H concentrations were over 9 T.U. which was the same as surface water, and NO_3^- and Cl^- concentrations were extremely high. Thus surface water on the plateau was thought to flow directly into the tunnel. Similarly at points 450, 1200 and 1900 m, ^3H concentrations were over 2 T.U. At 1200 m from the west side, SO_4^{2-} concentrations were 250 mg/L and at locations 450 and 1900 m from the west side Cl^- concentrations were over 5mg/L relatively higher than the other areas. SO_4^{2-} was also thought to be of agricultural origin because the main fertilizer was $(NH_4)_2SO_4$. Therefore, at specific points 450, 1200 and 1900 m, surface water was thought to mix with old groundwater and the mixed water was thought to flow into the tunnel.

On the other hand, oxygen isotopic ratio values for cutting face water were -11.3 to -11.7 ‰ as shown in Fig.7, uniform although hydrogen isotopic ratios were between -79 and -83 ‰. In general, hydrogen

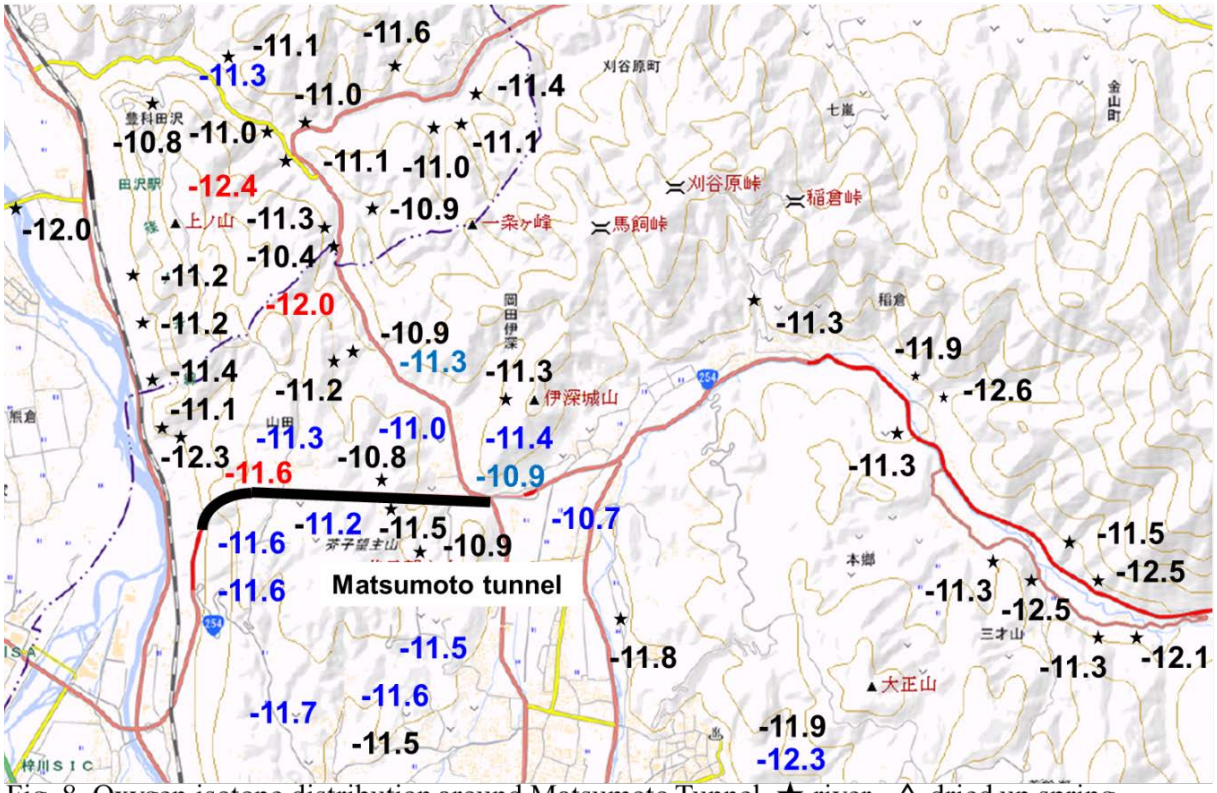

Fig. 8 Oxygen isotope distribution around Matsumoto Tunnel. ★ river, △ dried up spring ◎ non-dried up spring, ○deep borehole

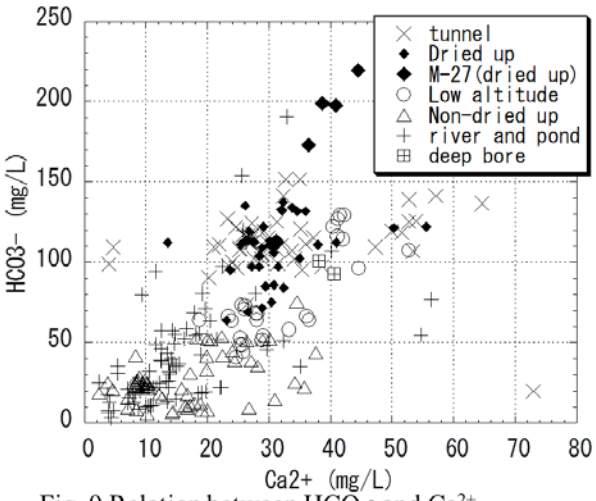

Fig. 9 Relation between HCO_3^- and Ca^{2+} concentrations

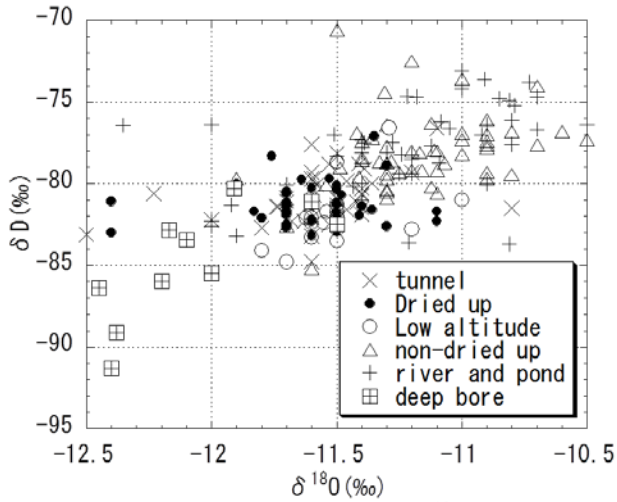

Fig. 10 Relation between δD and $δ^{18}O$

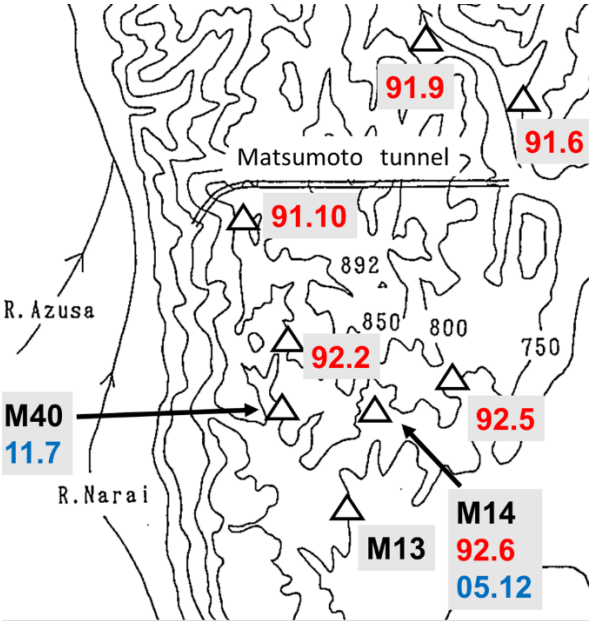

Fig. 11 Dried up springs and wells with the dates of their drying up

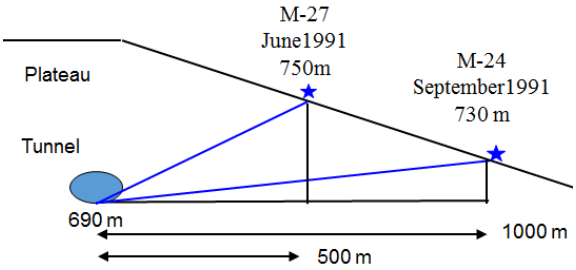

Fig. 12 Estimated groundwater level using spring and well condition at the north of tunnel

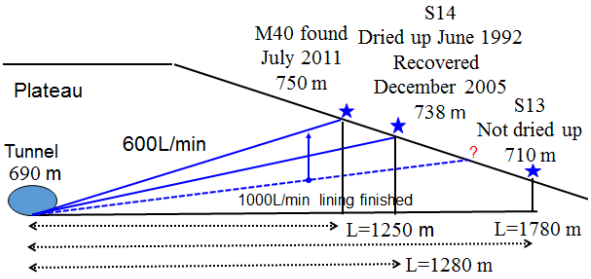

Fig. 13 Estimated groundwater level using spring and well condition at the south of tunnel

isotope values included a large margin of error, but isotope values for cutting face water were uniform.

Dried upspring and well

After the tunnel was completed, some springs and wells around the tunnel dried up. Fig 8 showed wells, springs, rivers and dried up wells and springs around the tunnel with their average oxygen isotope values. Dried up springs and wells were observed within 1.5 km from the tunnel and the altitude was higher than the tunnel level. However, some wells and springs above the tunnel were not dried up. The average oxygen isotope values for river, spring and well varied from -12.4 to -10.8 ‰. In particular, the oxygen isotope values for the dried up springs and wells were -11.7 to -11.3 which coincided with the average value of -11.6 for water inflow in tunnel.

As shown in Fig.6, water inflow in tunnel contained high concentration of Ca^{2+} and HCO_3^-. Ca^{2+} and HCO_3^- concentrations for the cutting face water in the tunnel (tunnel cutting), accumulated water inflow in the tunnel after tunnel construction (total tunnel), dried up spring and well, non-dried up spring and well, and spring and well at the lower altitude than tunnel level (low altitude) are shown as in Fig.9. Although HCO_3^- concentration for dried up spring, M-27 with -11.4 ‰ in Fig.5 at the north of tunnel was over 150 mg/L (extremely high), HCO_3^- concentrations for most dried up springs and wells were the same as those for the total tunnel and tunnel cutting face. On the other hand, most HCO_3^- concentrations for non-dried up springs and wells on

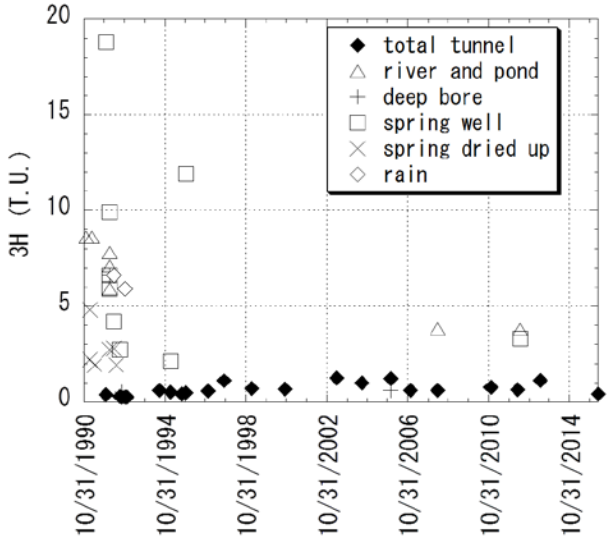

Fig. 14 Time series of ^{3}H concentration

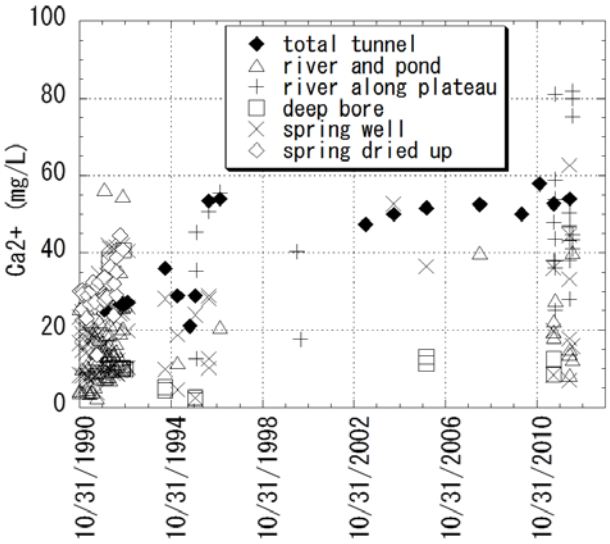

Fig. 15 Time series of Ca^{2+} concentration

the plateau were less than 50 mg/L and Ca^{2+} concentration was also low. Therefore water inflow in the tunnel and dried up spring and well water were thought to be in contact with rocks for a long time.

To determine the recharge area of water inflow in the tunnel, oxygen and hydrogen isotopic ratios for water samples around the tunnel were measured. Fig. 10 showed δD and $\delta^{18}O$ values for sampled water. Isotope values for dried springs and wells coincided with those for water inflow in tunnel. However, isotopic ratios for deep borehole water and non-dried up springs and wells above the tunnel level were different values. Isotopic ratios for non-dried up springs and wells coincided with those for rivers and ponds around the tunnel and these values were higher than those for dried up springs and wells. Isotopic ratios for deep boreholes were lower than those for the dried up springs and wells. From Figs.1 and 3, there are higher mountains at the north east of the tunnel and isotopic ratios for river water at the area were lower than those around the tunnel. From isotopic ratios, the recharge area for water inflow in tunnel and dried up spring and well waters were thought to be the mountain area at the north east of the tunnel. The recharge area for deep borehole water was the higher mountain area at the north east of the tunnel.

Groundwater level and porosity

Fig.11 showed dried up springs and wells with the dates of their drying up. Tunnel construction started on the east side in October 1990 and on the west side in November 1991. At the north of tunnel, two wells dried up in June 1991 and in September 1991 as is shown in Fig.12. At the south of the tunnel, three springs and one well dried up in October 1991, February, May and June 1992 as shown in Fig.13. However the spring M13 and bore hole M40 did not dry up. Groundwater level was estimated from dried up spring and well points and drainage along the whole tunnel line as shown in Figs.12 and 13. The slope of the groundwater level at the N-S direction was 40m/1000m = 0.04 at the north of tunnel and 48m/1280m = 0.038 at the south of tunnel. M14 spring in the south of the tunnel, was recovered in May 2005. M40 bore hole was found in December 2011. The altitude of M40 bore hole was about 750 m and higher than that of M14 spring. Therefore, groundwater level gradually was recovered. From Fig.2, water inflow in the tunnel was 1000L/min when most springs dried up in 1992 however since 1995 water inflow in the tunnel has remained at 600L/min. Following 2005, some springs recovered, and a decrease of water inflow into the tunnel was thought to bring about spring recovery.

The total volume for the unsaturated zone was estimated to be 250 million m^3 (2,000m × 2,500m × 50m) to 500 million m^3 (2,000m × 2,500m ×100m) from the geographical features and the groundwater level. M14 spring, the farthest dried up spring, dried up in June 1992 and at that time the amount of water inflow into the tunnel reached about 3 million m^3 and effective porosity was 0.5 to 1% from volume for the unsaturated zone and total drainage water during that time. On the other hand, effective porosity for rocks at the Matsumoto Tunnel was determined to be 0.48 % by field tracer testing during tunnel construction [3]. Therefore, those effective porosity values were almost the same. Porosities measured from rocks sampled at the Matsumoto Tunnel area were about 10 % [3], [4]. As a result, effective porosity was one tenth of porosity and effective porosity was thought to be due to cracks and main pores connecting with the tunnel. The amount of pore water for the unsaturated zone was calculated to be 25 to 50 million m^3 from 10 % pore value and the volume of the unsaturated zone. At ~~the~~ present, the amount of water inflow into the tunnel is 11 million m^3. If

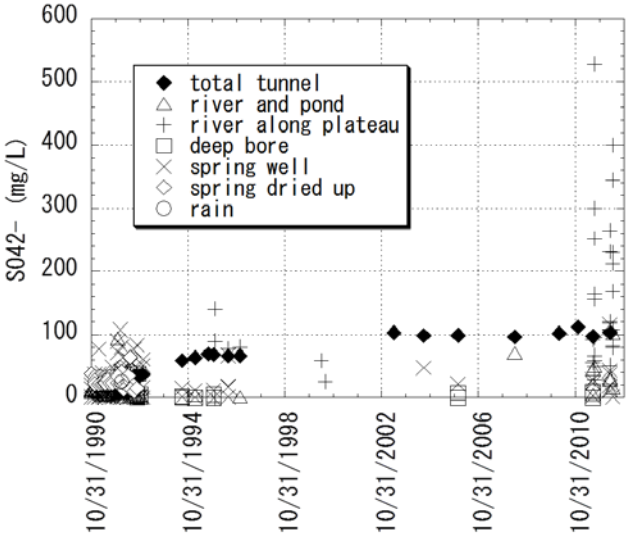

Fig. 16 Time series of SO_4^{2-} concentration

drainage water from the tunnel is assumed to come from pore water for the unsaturated zone, 20 to 40 % of pore water still remains in the unsaturated zone.

Long term changes of water chemistry

For 25 years, ^3H, Ca^{2+} and SO_4^{2-}concentrations and $\delta^{18}O$ values for water around the Matsumoto Tunnel were measured. Fig.14 showed a time series of ^3H concentrations. Although ^3H values at the cutting face were variable, ^3H values at the tunnel remained low, less than 0.6 T.U. The ^3H values of surface water decreased from 10 T.U. to 4 T.U. over 25 years. Furthermore, ^3H values deceased after hydrogen nuclear bomb experiments [6]. Therefore, the age of water inflow into the tunnel was estimated to be over 30 years old from initial ^3H concentration for surface water which varied from 4 to 10 T.U.

Figs.15 and 16 show a time series of Ca^{2+} and SO_4^{2-}concentrations. Ca^{2+} and SO_4^{2-} concentrations for water inflow in the tunnel increased from 25 to 55 mg/L and 40 to 100 mg/L. Both values increased between 1992 and 1994 when the tunnel concrete liner was finished. The concrete contained $CaSO_4$, so the solute of the tunnel concrete liner was thought to have increased Ca^{2+} and SO_4^{2-}concentrations for water inflow in tunnel.

Fig.17 shows a time series of $\delta^{18}O$ values. $\delta^{18}O$ values for water inflow in the tunnel were uniform over 25 years. Therefore the water source for water in the tunnel was thought to not have changed but to have remained the same over 25 years.

DISCUSSION

Judging from water chemistry around the tunnel, flow rate for water inflow in the tunnel and spring and well conditions, groundwater level and groundwater sources were estimated as shown in Fig.18. Before tunnel construction, rock above the tunnel was saturated with water. 2 years later, about 3 million m^3 of groundwater was drained and groundwater level decreased. The total rock volume of unsaturated zone was calculated to be 250 to 500 million m^3 from groundwater level estimated from dried up springs and wells. Therefore, specific yield was 3/500= 0.6 % to 3/250=1.2%. The specific yield coincided with an effective porosity of 0.48 % as determined by tracer test during construction. Effective porosity and specific yield were one tenth of porosity. Thus, effective porosity and specific yield were thought to indicate main pores or cracks. Therefore, pores in the unsaturated zone still retained a lot of groundwater, 25-3=22 to 50-3=47 million m^3 just after tunnel construction. After construction of the tunnel concrete liner, drainage flow rate decreased from 1.0 m^3/min to 0.6 m^3/min. Ca^{2+} and SO_4^{2-} concentrations for water inflow in

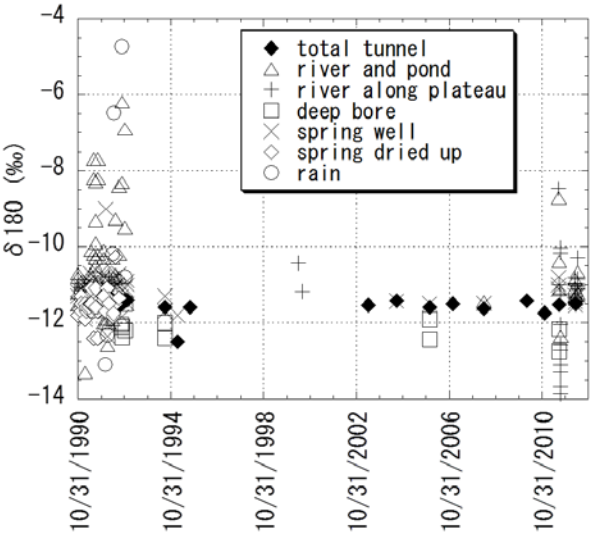

Fig. 17 Time series of $\delta^{18}O$ values

the tunnel increased because of soluble of (solute from?) the concrete liner. Although groundwater level increased marginally and some dried up springs were recovered because of a decrease in flow rate of the water inflow in the tunnel, fundamentally, a big change in groundwater levels was not found. Drainage water have maintained low ^3H concentration until now even when the total volume of water inflow in the tunnel reached 11 million m^3. The drainage water was thought to be old groundwater. Old groundwater for the unsaturated zone was less than 14 to 39 million m^3 as some groundwater was also drained under the groundwater level for maintaining the groundwater level. As stable isotope values for cutting face and water inflow in tunnel were uniform until now, groundwater source is not thought to have changed.

CONCLUSION

In 1980, the Matsumoto Tunnel construction at

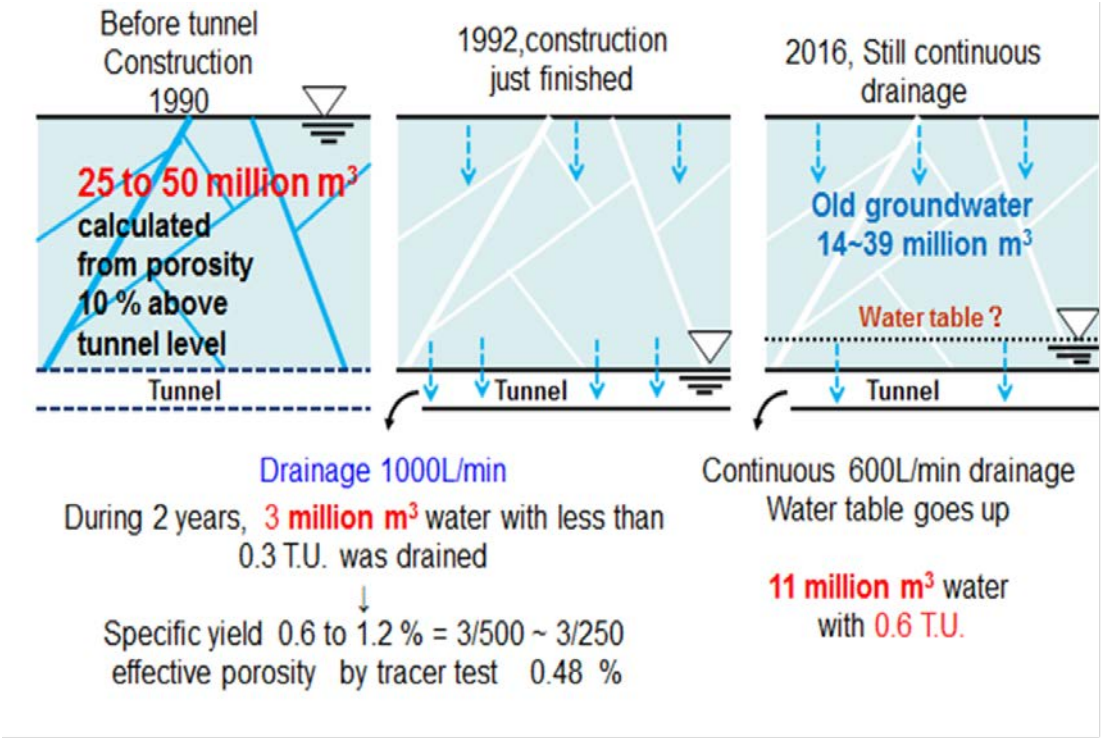

Fig. 18 Schematic diagram for groundwater level changes caused by tunnel construction

the north of Matsumoto city started at the foot of the Matsumoto Plateau which is isolated by surrounding mountains. 11 million m3 of water inflow in tunnel has been drained until present. Water inflow in the tunnel was thought to be derived from precipitation on the plateau. Since 1980, groundwater level and flow rate of water inflow in the tunnel have been measured and then the amount of water inflow in the tunnel from 1980 reached about 11 million m^3 and groundwater level 2km around the tunnel decreased for the first two years but has kept uniform until now.

For 25 years, water inflow in tunnel, river and spring waters around the tunnel have been sampled many times and water chemistry and isotope values have been measured. Water inflow in the tunnel for the first years during tunnel construction varied from 1 to 8 m^3 per minute and from 1993 to 1995 it decreased 1 to 0.6 m^3 per minute. At present inflow is stable at 0.6 m^3 per minute. ^3H concentration, an indicator of groundwater age during tunnel construction was less than 0.3 T.U. It increased and has stayed less than 1.0 T.U. since 2003. On the other hand, ^3H concentrations of river and well water on the plateau were 4 T.U. Therefore, age of water inflow in tunnel was estimated to be over 30 years old from initial ^3H concentrations for surface water which varied from 4 to 10 T.U. Oxygen stable isotope values and HCO_3^- concentration of water inflow in the tunnel were uniform over 25 years. Therefore, as stable isotope values for the cutting face and water inflow in the tunnel was uniform until now, the groundwater source is not thought to have changed.

Effective porosity and specific yield were one tenth of porosity, about 10 % measured by sampled rocks. 25 to 50 million m^3 of water was storage in rocks above the tunnel in the plateau from a 10 % porosity value. However when only 3 million m^3 groundwater, about 1% effective porosity and specific yield, was drained, groundwater level decreased widely. As the water was low ^3H concentration, the drained groundwater was deemed to be old. Therefore, old groundwater in the unsaturated zone was determined to be less than 14 to 39 million m^3. From long term observation, groundwater level increased marginally owing to a decrease of water inflow in the tunnel and a SO_4^{2-} and Ca^{2+} concentration increase was found because of the solubility of tunnel liner concrete.

REFERENCES

[1] Nakao, S, Kikuchi T, and Ishido, T, “Current status of regional hydrogeological, studies and numerical simulations on geological disposal”, Bull. Geol. Surv. Japan, vol. 55(11/12), 2004, p.409 - 415,

[2] Ii H, and Misawa S, “Groundwater chemistry within a plateau neighboring Matsumoto city, Japan”, J. of Environmental Geology, Vol. 24(3), 1994, pp. 166-175.

[3] Ii H, “Effective porosity and longitudinal dispersivity of sedimentary rocks determined by laboratory and field tracer tests”, J. of Environmental Geology, Vol. 25(2), 1995, pp. 71-85.

[4] Ii H, Ohtsuka Y, Mori N, Inagaki T, and Misawa S, “Effective porosity and specific yield of a sedimentary rock determined a field tracer test using tritium as a tracer”, J. of Environmental Geology, Vol. 27(3), 1996, pp. 170-177.

[5] Ii H, and Kagami H, “Groundwater level and chemistry changes resulting from tunnel construction near Matsumoto City, Japan”, J. of Environmental Geology, Vol. 31(1/2) 97, pp. 76-84.

[6] Duvert C., Stewart M.K., Cendón D. I., and Raiber M. ”Time series of tritium, stable isotopes and chloride reveal short-term variations in groundwater contribution to a stream”, Hydrol. Earth Syst. Sci., Vol. 20, 2016, pp.257-277.

Technical Papers

Science

Second International Conference on Science, Engineering & Environment,
Osaka City, Japan, Nov.21-23, 2016, ISBN: 978-4-9905958-7-6 C3051

DILATANCY BEHAVIOR OF WASTE SHELL-SOIL MIXER FOR GROUND IMPROVEMENT

Siti Hanggita Rachmawati and Zakaria Hossain

Graduate School of Bioresources, Mie University, Japan

ABSTRACT

A large amount of waste shell husk has been produced in Japan every year that not only requires a huge amount of money for its disposal but also causing a serious environmental problems. The shell waste has been investigated as recycle aggregate for soil improvement. In this study, shell waste-soil mixture with varying percentage of shell was used to investigate the effectiveness of shell in soil. Dilatancy behavior that controls the performance of earth reinforcement was used as main parameter in this study. Three percentages (10%, 20%, 30%) and control (0%) of shell husk were demonstrated in this study. The water content for all the tests were close to optimum water content (Wopt) or dry side of Wopt to maintain the similarity of the test samples. All the results showed that the vertical displacements increased with the increase in horizontal displacement. This research revealed that the percentage of shell husk could decrease the dilatancy behavior than control which means of ground improvement.

Keywords: Recycle, Shell Waste, Dilatancy Behavior, Soil Improvement

INTRODUCTION

The stability of whole kinds of earth fill structures have to persistent under any circumstances. Natural phenomena such as weathering, erosion, earthquake, and drought reduce the stability then lead to the failure. To tend these problems are required ground improvement that could enhance the stability of earth fill structures [7]. One of main parameters that control the performance of earth reinforcement is dilatancy behavior which explained the volume or shape changing caused by pressure distribution [5]. Previous studies about dilatancy behavior were applied on soil reinforcement that using geosynthetic or geogrid. These grounds reinforcement are commonly used in world wide.

Now-a-days, recycle aggregates are gradually used for ground reinforcement. The aim of recycle aggregate utilizing is one way to apply sustainable development on construction industry including earthwork construction [8], [11], [12]. Recycling principle has benefits which are protecting limited natural resources of aggregates, increasing the abandon waste value and problem solving of waste storage [6], [12]. Many researchers used organic and inorganic materials as recycled aggregates in their investigations. The comparisons between soil without reinforcement and soil with reinforcement have different trends. Previous studied showed that the application of recycle aggregates as ground reinforcement have expected results [3], [7], [9].

Shell husk is one kind of aggregate which has been investigated widely as reinforcing ground. Clamshells have important part in Japanese people dietary and every year in Japan, large quantity of shell husk waste are generated. According to the Japanese Ministry of Forestry, Fisheries and Agriculture, total amount of abandon shell husk is about 151,000 tons/year and nearly 32 million US$ for disposal cost [6].

The present study used abandon shell husk (mactridaes) as ground improvement material. Shear tests under four normal stresses of 40, 60, 80 and 100 kPa were performed to evaluate dilatancy behavior of clayey soil of Mie Prefecture, Japan which was added by three percentages (10%, 20%, 30%) abandon shell husk and also control (without reinforcement). In direct shear test, dilatancy is described as the ratio (δy/δx) of incremental vertical displacement (δy) to incremental horizontal displacement (δx) [2]. Pertinent discussion on the improvement of dilatancy behavior of ground using different percentage of shell husk are made.

PROPERTIES OF GROUND

Properties of soil

Figure 1 illustrates the particle size distribution of clayey soil.

Table 1. Properties of soil

Parameters	Clayey Soil
Dry density (ρ_d)	1.80g/cm^3
Optimum Water Content (W_{opt})	13.29%
Spesific gravity (ρ_s)	2.589
Cohesion (c)	15.66
Angle of internal friction (φ)	77.27
Sand > 75 μm	85.00%
Silt >5-75μm	11.00%
Clay <5μm	4.00%
Liquid limit	39.00%
Plastic limit	26.80%
Plasticity Index	12.20%

Approximately 7 % is coarse gravel, 19% is pebble, 7% is granule, 10% is fine sand, 29% is medium sand, 13% is coarse sand, 11% is silt and 4% is clay. The other properties of soil are shown in Table 1. Plasticity chart given in Figure 2 revealed that this soil contains silt having properties of higher permeability, higher compressive strength, higher dry density and low toughness .

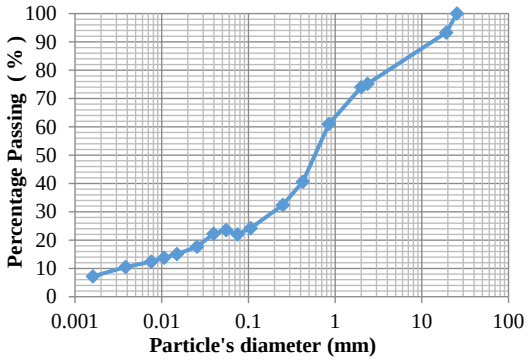

Fig.1 Particle size distribution curve

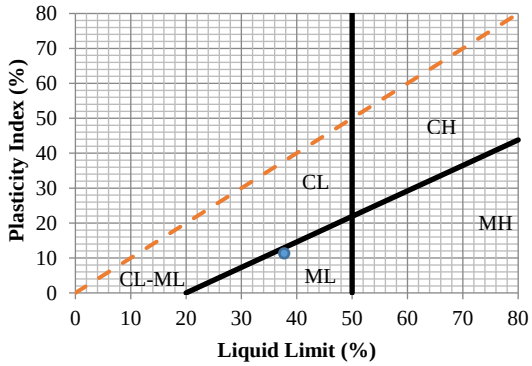

Fig. 2 Plasticity chart of soil

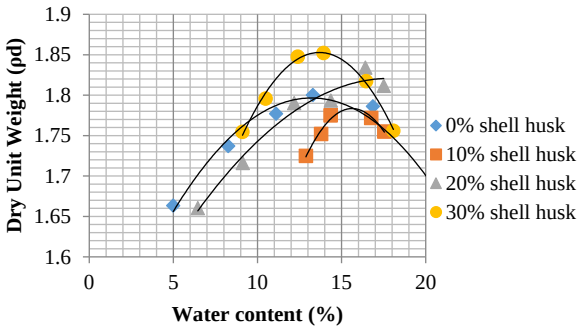

Fig. 3 Compaction curves for soil-shell mixer

Properties of shell husk

The mactridae shell husks waste were collected from the seashore closed to Mie University, Tsu city, Mie Prefecture, Japan. Then the shell husks were graded by performing sieve analysis. The fineness modulus and the maximum size of the abandon shell husks were 4.35 and 4.76 mm, respectively. The shell size distribution curve is shown in Fig.2 and the physical properties in Table 2.

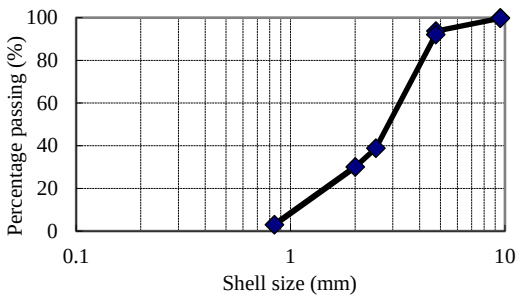

Fig. 4 Shell size distribution curve

Table 2. Physical properties of shell husk

Physical Properties	Values obtained
Water absorption ratio	1.23%
Spesific Gravity	2.723
Unit Weight	1.57

Fig. 5 Shell-soil mixer

EQUIPMENTS AND METHODOLOGY

Description of the testing equipment

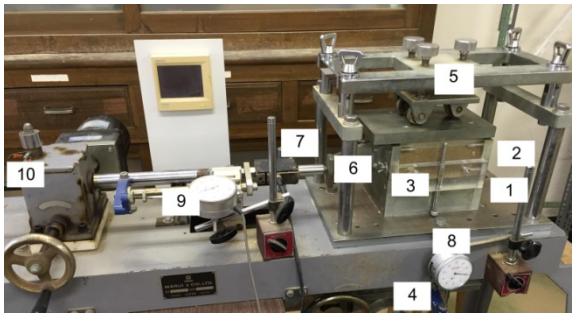

Fig. 6 Pullout and shear testing apparatus

In this study, the apparatus used is able to perform and direct shear test. The shear box with clamping system in outside (6), has rectangular shape of size 150 mm in length, 100 mm in width and 100 mm in height. It consists of fixed lower box (1) and a moving upper shear box (2), both have 50 mm in depth. This apparatus is specifically constructed that the mobility of soil parallel to the shear surface is totally controlled by the four side walls along with its girder during test

(3). The friction between upper box and lower box is removed by using the vertical screws that have been set at both long side of upper box. The normal stress is applied through a lower jack (4) below lower box which is balanced by the opposite stresses of the upper box (5). The data of shear force, horizontal and vertical displacements in this test are recorded by computer software DCS-100 which connected with load cell (7), two dial gages (8,9), through one load cell, and two displacement transducers (one for shear displacement and other for vertical displacement measurement).

Method of testing

This study used 0%, 10%, 20%, and 30 % of Mactridae shell husk as coarse aggregate in the ratio mass of clayey soil. Water was added gradually to the mixture shell husk and clayey soil with water content 9-13%. The water content which were used in this research are slightly less than that of the optimum water content of soil for every percentages (Fig. 3). The reason is to maintain the water content in dry-side of optium and also for field condition with unsaturated soil. Then the mixture between shell, soil and water were filled in shear box by three layers. Every layer had same compaction energy hence the density of soil-shell mixture kept almost stable for every test. The shear load through screw jack (10) was applied after the consolidation by normal stresses reached equilibrium. Screw jack worked under electrically operated constant pressure with a constant speed of 1.0 mm/min and the force was measured using a tension load cell (7). Normal stresses (vertical load) are maintained stable during the test. The specification of this equipment is based on JIS and the Japanese Geotechnical Society (JGS: T941-199X) [4].

RESULT AND DISCUSION

Dilatancy behavior of soil with 0% shell husk

The vertical displacement and horizontal displacement which are known as dilatancy behavior is plotted in Fig. 7. The vertical displacement of 40 and 60 kPa are slightly different on 0-4.7 mm of horizontal displacement
then the range is start increasing till the end of test. On the other hand, the vertical displacement range between 80 and 100 kPa is slightly different after 4-6.7 mm. Also, the vertical displacement for 80 and 100 kPa almost increase two times than other lower stresses. There is not negative displacement for any normal stresses. The maximum vertical displacements are calculated as 6.25, 7.32, 10.07, 11.06 mm for normal stresses of 40, 60, 80 and 100 kPa respectively.

Dilatancy behavior of 10% shell husk

Figure 8 describes the relationship between horizontal displacement and vertical displacement of soil with 10% shell husk as recycled aggregate. The vertical displacement of 60 and 80 kPa for 0-2 mm horizontal displacement are almost similar and after that the vertical displacement of 80 kPa gradually increases higher than 60 kPa. On the contrary with vertical displacement of 40 and 60 kPa which has slightly difference on 5-6.7 mm horizontal displacement and not so much different in the end of the test.

Vertical displacements of 80 and 100 kPa are gradually increase and have similar trends. There is no single number that identified as negative value of vertical displacement. In this part, the highest number of vertical displacements are noted as 6.57, 6.88, 8.01, 8.87 mm for 40, 60, 80 and 100 kPa respectively.

Dilatancy behavior of soil with 20% shell husk

In Fig 9. could be seen the sverticaldisplacement versus horizontal (shear) displacement of soil with 20% shell husk. The dilatancy in term of vertical displacement of 60, 80 and 100 kPa are slightly different on 0-1.5 mm shear (horizontal) displacement then it spreads gradually . For 40 kPa, the vertical displacement gradually increased having moderately wide gap with other normal stresses. The trends between 80 and 100 kPa have similar patterns but quite different on numbers. The similar trends also happen between 40 and 60 kPa, however, the range is higher. In this case, there is not negative value of vertical displacement. The peaks of vertical displacements are recorded 5.57, 7.67, 9.11, 10.86 mm for normal stresses 40, 60, 80 and 100 kPa respectively.

Dilatancy behavior of soil with 30% shell husk

Figure 10 illustrates relationship between vertical displacement and horizontal displacement of soil with 30% shell husk. The vertical displacement trend of 60 and 80 kPa almost similar on 0-2 mm horizontal displacement.

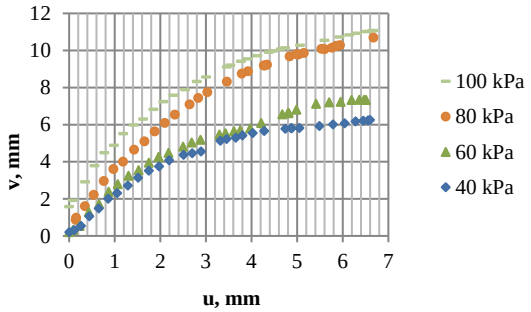

Fig 7. Dilatancy behavior of soil with 0 % shell

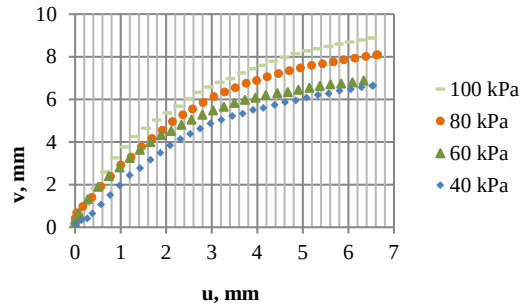

Fig. 8. Dilatancy behavior of soil with 10% shell husk

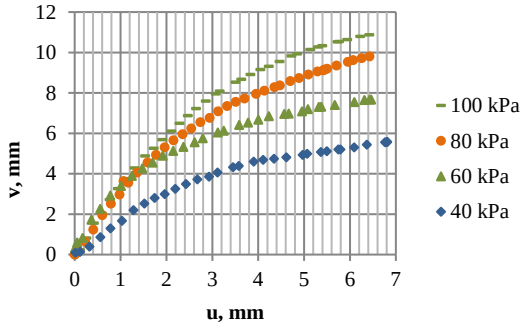

Fig 9. Dilatancy behavior of soil with 20% shell husk

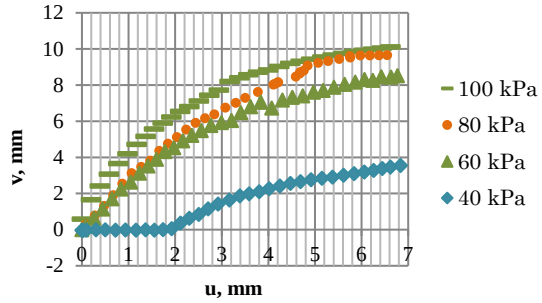

Fig 10. Dilatancy behavior of soil with 30% shell husk

It is shown between the vertical displacement of 40 kPa and other normal stresses has large range. Initially, the dilatancy of 40 kPa has negative value and almost zero on 0-2 mm of shear displacement. The similar trends and value between 60 and 80 kPa are occured on 0-2 mm of vertical displacement. By the end of test, the vertical displacements of 80 and 100 kPa have not much difference. The maximum vertical displacement for normal stresses of 40, 60, 80 and 100 kPa are 3.54, 8.51, 9.64, 10.10 mm, respectively.

Discussion

All the graphs show the vertical displacements are increasing along with the increasing of horizontal displacement. These phenomena are related to volume change by means direct shear test for every type of percentage of shell [2]. Over all data showed that the percentage of shell husk as ground improvement materialhas significant effect to decrease the vertical displacement than soil without shell. It was observed that the mixing of waste shell husk in soil resulted more stress-transfer ability of the ground thereby increased the resisting forces [7]. There are several negative value in the beginning of 30% percentage of shell husk under 40 kPa normal stress which is indicated the increasing volume. It is shown that there is a decrease in the density of clayey soil with the increase of percentage of waste shell husk [9].

CONCLUSIONS

Generally the graphs show the dilatancy (vertical displacement) increase with shear (horizontal) displacement. Soil without reinforcement (zero percent of shell husk) was reached the highest value of vertical displacement. The lowest vertical displacement was obtained by soil with 10% shell husk. It is concluded that shell husk could improve the soil ability.

ACKNOWLEDGEMENTS

Special gratitude and high appreciate for partnership between Mie University, Japan and Sriwijaya University, Indonesia, which contribute to perform this research.

REFERENCES

[1] Andersland OB., Khattak, AS, and Al-Khafaji AWN, “Effect of Organic Ground onSoil Shear Strength”, Laboratory Shear Strength of Soil, ASTM STP 740, Yong RN and Townsend FC, Eds., American Society for Testing and Materials, 1981, pp. 231-232.

[2] Arora KR, Soil Mechanics and Foundation Engineering, Nai Sarak-Delhi: Standard Publishers Distributors, 1978.

[3] Baumgartl Th and Horn R, “Effect of aggregate stability on soil compaction”, J. Soil and Tillage Research, Vol. 19, 1991, pp. 203-213.

[4] Hossain MZ, “Development of a Small-Scale Universal Apparatus for Evaluating Soil-Structure Interaction”, J. of Civil Engineering and Architecture”, Vol. 5, No. 4 (Serial No. 41), April. 2011, pp. 314-321.

[5] Hossain MZ and Inagaki H, “Dilatancy behavior of soil-structure interfaces for farm roads and embankments”, J. of Agricultural Engineering,

Vol 2 (1), 2011, pp.12-17.

[6] Hossain MZ, “Waste Shell Husks Concrete : Durability, Permeability and Mechanical Properties, J. of Building Construction and Planning Research, Vol. 1, September. 2013 pp. 61-66.

[7] Hossain MZ, “Influence of Recycle Aggregate Composites on the Factor of Safety of Earthen Structures”, J. of Geosciences, Vol.4, July. 2013, pp.844-849.

[8] Li X, Zhu Y and Zhang Z, “ An LCA-based environmental impact assessment model for construction processes “, J. Building and Environment, Vol. 45, 2010, pp. 766-775.

[9] Malkawi AIH, Alawneh AS, Abu-Safaqah OT, “Effects of organic matter on the physical and the physicochemical properties of an illitic soil”, J. Applied Clay Science, Vol. 14, 1999, pp. 257-278.

[10] Ng CWW and Menzions B, “Advanced Unsaturated Soil Mechanics and Engineering”, New York: Taylor and Francis, 2007, pp.47

[11] Ortiz O, Castells F and Sonnemann G, “Sustainability in the construction industry: A review of recent developments based on LCA”, J. Construction and Building Materials, Vol. 23, 2009, pp 28-39.

[12] Tam VWY and Tam CM, “ A review on the viable technology for construction waste recycling”, J. Resources Conservation and Recycling, Vol. 47, 2006, pp. 209-221.

Second International Conference on Science, Engineering & Environment,
Osaka City, Japan, Nov.21-23, 2016, ISBN: 978-4-9905958-7-6 C3051

COALBED METHANE EVALUATION OF LOW RANK COALS IN THE AIR LAYA MINING REGION OF SOUTH SUMATRA

Ana Asmina[1], Edy Sutriyono[2], Endang Wiwik Dyah Hastuti[3]
[1]Postgraduate Study Program of Mining Engineering of Sriwijaya University
[2,3]Geology Study Program of Engineering Faculty of Sriwijaya University
Jl. Srijaya Negara, Bukit Besar, Palembang, Indonesia

ABSTRACT

This study was carried out to evaluate the coalbed methane content of coal seams occurring at shallow depths in Air Laya mining area. Tectonically, the region is situated in the Paleogene South Sumatra basin. The present evaluation employed well log and core analysis for different coal seams of Mio-Pliocene Muara Enim sequence. Interpretation of seven log profiles suggests that there are four major layers of coal exposed at depths between 79-264 m. The apparent thickness of individual stratum in each well varies significantly, and average 6.7-13.7 m. Results of core description reveal low rank coals of subbituminous and high volatile bituminous, and there appears an increase in vitrinite reflectance with depth from 0.49% up to 0.59%. These low rank coals contain predominantly huminite, ranging from 56-86 vol. %, and less abundant liptinite and inertinite, ranging from 0.2-12.2 vol. % and 4.2-19.2 vol. % respectively. All samples analyzed consist of a small number of minerals, high moisture content of 2.4-12.6 wt. %, volatile matters of >39 wt. %, and fixed carbons of >43 wt. %. The amount of gas for each coalbed varies from 4.1-5.3 m^3/t, but the resulted estimates tend to increase with depth. The sum of the estimated gas-in-place is approximately 3,019x10^6 m^3. Additionally, the present work suggests that the onset of gas generation within the near surface coals may occur due to biogenic controls during the coal-forming processes, as a result of deeper burial in Pliocene time prior to the subsequent basin inversion commencing in the Plio-Pleistocene.

Keywords: Coalbed Methane, Subbituminous, South Sumatra Basin

INTRODUCTION

Coalbed methane (CBM) has recently become an important unconventional gas resource, especially in the USA as it contributes up to 7% of total natural gas production for the state [1]. This phenomenon to some extent has led initiation of extensive CBM exploration in several other countries, including Indonesia, China, India, and South Africa. The results of exploratory activities for the Indonesian region have been reported for examples by [2]-[9]. Indonesia has been recognized to have at least eleven onshore coal basins with a considerable amount of CBM resources. Studies on deep coal seams (>300 m) suggested that the country has the gas-in-place potential of about 213 tcf [10], [11], approximately 337 tcf [12], and around 453 tcf [13], [14]. These published gas estimates indicate that Indonesia's CBM might have been assessed by less comprehensive analysis. This is in part due to the lack of a data set available for the evaluation, particularly as a result of difficulties in getting access to a package of information on the sub-surface geology, as well as some experimental yields necessitated for the gas measurements remain strictly confidential.

Amongst the Indonesian onshore basins, the South and Central Sumatra basins in Sumatra and the Barito and Kutei basins in Kalimantan are presumably to have the vast amount of CBM resources. This seems likely as the most economically significant coal deposits occur in those areas. More importantly, the deep coal seams in the islands are apparently to be the key reservoir system that currently becomes the main targets for CBM exploration. Based on volumetric calculation, the South and Central Sumatra basins are inferred to have CBM prospectivity of approximately 183 tcf and 145 tcf respectively [13]. Besides, these authors reported that the Barito coal seams hold natural gas of about 120 tcf, and the Kutei basin comprises gas potential of around 51 tcf. Their studies suggested further that the South Sumatra region is the most prospective coalfield for coal seam gas exploration in Indonesia. This scenario is consistent with that proposed by several workers [2], [15], [16].

The present study was aimed at evaluating the CBM content of low rank coals in Air Laya mining area, administratively included in the Muara Enim

Regency that is one of the coal producing areas in South Sumatra Province. This work has employed log observation from seven shallow wells and core analysis for the coal beds of the sequence. The locality of each well is shown in Fig.1.

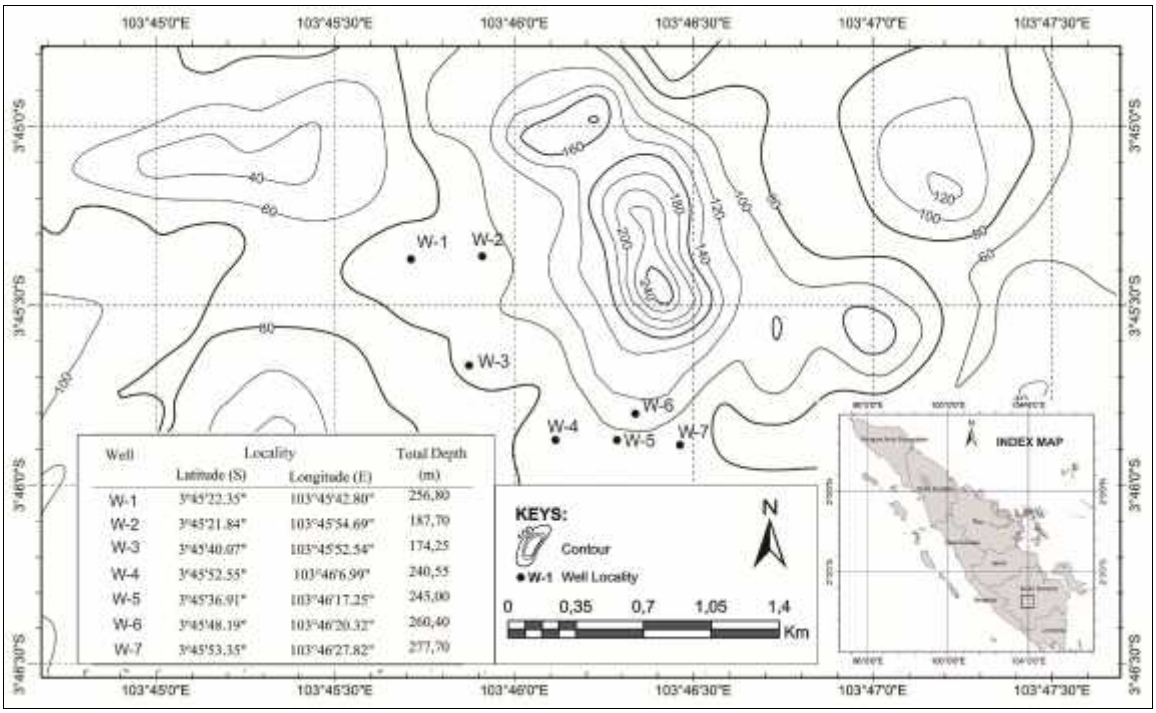

Well	Locality		Total Depth (m)
	Latitude (S)	Longitude (E)	
W-1	3°45'22.35"	103°45'42.80"	256,80
W-2	3°45'21.84"	103°45'54.69"	187,70
W-3	3°45'40.07"	103°45'52.54"	174,25
W-4	3°45'52.55"	103°46'6.99"	240,55
W-5	3°45'36.91"	103°46'17.25"	245,00
W-6	3°45'48.19"	103°46'20.32"	260,40
W-7	3°45'53.35"	103°46'27.82"	277,70

Fig. 1 Topographic map showing the locality of wells studied in the Air Laya mining region of South Sumatra.

Tectonically, the region is situated within the Paleogene South Sumatra basin. The basin is commonly referred to as a graben-like depocenter located in a back-arc setting. The initial development of this basin took place in the Eocene [17], coincident with the inception of tensional regime at the SW margin of Sundaland in the Early Tertiary. The history of sedimentation is generally attributed to two different major events with respect to sea level changes, transgression through Late Oligocene-Early Miocene time and regression during Middle Miocene-Pliocene time. The close of transgressive regime took place in the Middle Miocene, followed by regression in relation to the commencement of regional compressive strain fields in the region. The basin was under the influence of regression up to the early Late Pliocene. The cessation of a regressive phase occurred in conjunction with the onset of regional uplift in response to the Plio-Pleistocene orogeny. The Late Neogene event is considered as the latest tectonic episode responsible for basin inversion, leading to the formation of the present geologic features throughout the region.

The Neogene coal bearing sequence in the basin is the Mio-Pliocene Muara Enim Formation. The thick coal seams are present in this unit. The succession consists mainly of paralic mudstones and sandstones intercalated with siltstones and coals, developed during widespread sea level lowstands in the Late Tertiary. Previous studies suggested that the coal deposits are fluvio-deltaic in origin [18], [19]. The area of an interest of the present study is the coal seams of the Mio-Pliocene rock succession (Fig. 2).

METHODS

This study evaluates the CBM content of low rank coals exposed at shallow depths, using log profiles and core samples derived from seven wells. The wells were drilled and penetrated the coal bearing formation in the Air Laya mining region of South Sumatra. The thickness and depth of coal seams are interpreted primarily on the basis of log data. The lateral continuation and the variety of coal thickness are determined by correlating all logs observed. Analysis of core samples is undertaken to gain the principal

parameters accounted for the gas volume measurements, thus the amount of gas-in-place within the seams. The yielded coal parameters, including maceral content, organic matter, moisture content, fixed carbon, volatile matter and relative density, are utilized for determining the rank of coals.

The gas volume is calculated by following the procedure proposed by [20], but with some necessary modification in order to be more appropriate geologically for the area studied, as carried out by [21]. The modified parameters in calculation are the geothermal gradient value and the approximate surface temperature of the region. The volumetric formula used in the appraisal of gas content generally adopts the geothermal gradient of 1.8°C/100 m and the surface temperature of 11°C. However, the present assessment has employed the temperature gradient of 4.97°C/100 m and the ambient surface temperature of 22°C. In this paper, the sum of gas-in-place within the coal seams has been assessed by adopting the equation of [22].

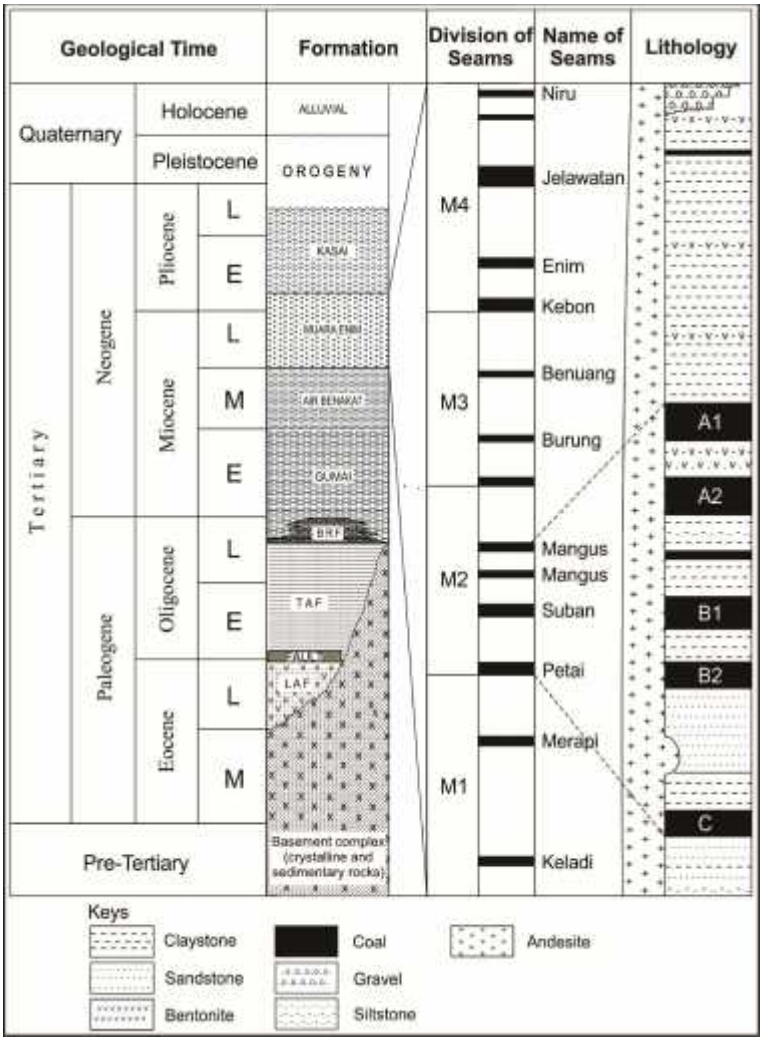

LAF: Lahat Formation; TAF: Talang Akar Formation;
BRF: Baturaja Formation

Fig. 2 Generalized stratigraphy of the Paleogene South Sumatra basin. Also shown is the division of coal seams within the Muara Enim Formation. The coal beds studied in the present work are part of the M2 seam group.

A BRIEF OVERVIEW OF GEOLOGY

The South Sumatra basin has long been recognized as one of oil as well as coal producing areas in Indonesia. The history of the basin began in Early Tertiary, following the initiation of tensional forces in the southwestern margin of Sundaland in Eocene or ~40 Ma [17]. The initial tension allowed the formation of graben-like structures and fault blocks in the pre-Tertiary crystalline rocks underlying the basin. Hence, the pre-Tertiary sequence was fragmented by faults, forming blocky and rough basement topography.

In a regional context, this tectonic stress field is generally considered to have been responsible for the development of back-arc basins extending along the eastern side of Sumatra [17], [23], [24]. The island forms the western section of the amalgamated continental blocks of Sundaland. Evolution of this composite landmass from Late Paleozoic to Late Mesozoic time has been overviewed recently by [25], and it may be beyond the main purpose of the present paper to discuss the development of these continental fragments.

As a tensional event proceeded, the region rifted, the depocenter deepened and widened in the southwestern and central section of the basin, and sea level highstands commenced in the Oligocene [26]. During the rifting period, widespread sedimentation of clastic materials took place from terrestrial to shallow marine environments. The deposition that formed the basal Lahat sequence occurred in the Late Eocene-Early Oligocene. The clastic sediments were sourced principally from the surrounding basement highs, and accumulated in terrestrial environment.

As a rifting event continued and subsidence of the basin accelerated in the Late Oligocene-Early Miocene, the depositional environment shifted from initially smaller and separated to deeper and broader lakes [27]. This regime was followed by a sea level rise, which gradually encroached into basinal area. At this time, sedimentation resulted in the Talang Akar sequence, which is composed mainly of sandstones, siltstones, shales, and few coal seams [23].

Subsequent deposition took place throughout Early-Middle Miocene time as transgression proceeded. This period was the time of extensive sea level highstands in the basinal area. Sedimentation resulted in the predominantly calcareous rocks constituting the Baturaja Formation, and the mainly shales and claystones of the Gumai Formation.

In the late Middle Miocene, the regressive cycle commenced as transgression ended, and sedimentary environments gradually shifted from deeper marine to shallow marine, to transitional or deltaic condition, and eventually to terrestrial sites [23]. This cycle resulted in consecutively the Air Benakat succession, the coal bearing Muara Enim sequence, and the Kasai rock unit. Sedimentation during regression ceased in Plio-Pleistocene time, marked by the deposition of tuffaceous and pumiceous materials sourced from the Quaternary volcanoes. Owing to the Late Neogene orogeny, the basin underwent inversion and uplift, as well as extensive denudation to form the present geologic configuration in the entire region.

RESULTS AND DISCUSSION

Log data used in this study were measured from seven wells with reference number W1-W7 (Fig.1). The W1 and W3 wells were drilled to a total depth (TD) of less than 200 m, and the rest W2, W4, W5, W6, and W7 wells penetrated the TDs ranging from 240-278 m. All wells encountered the coal bearing Muara Enim Formation. The sequence is one of coal bearing successions in the Paleogene South Sumatra basin, containing a large amount of coal deposit, as well as its associated natural gases. The coal seams constitute approximately 10-20% of the whole unit [19].

The correlation of seams on logs implies that lateral continuity of strata is extensive. This interpretation is concordant with that proposed by [13] and [19]. Results of log observation show that there appear at least four major coal beds, known as A1, A2, B, and C seams (Fig. 3). With respect to the regional stratigraphy, layers A1 and A2 are part of Mangus seams, whereas beds B and C are included within Suban and Petai units respectively. However, unless stated otherwise the division names (Mangus, Suban, and Petai) are not used for the simplicity, instead the sorter terms A1, A2, B, and C are utilized throughout this paper.

In the study area, the coal seams of the Muara Enim succession occur at stratigraphic levels between 166-264 m (Table 1). Individual seam determined from each log varies in thickness. Coal bed A1 is 6.9-9.5 m thick with mean 8.2 m. The apparent thickness of layers A2, B, and C ranges between 7.0-10.3 m, 11.5-16.3 m, and 1.3-9.9 m and average 8.6 m, 13.7 m, and 6.7 m, respectively. These data indicate that the B bed is the thickest coal seam, and the C bed is thinnest coal stratum. Maceral analysis reveals that the Air Laya coals are composed predominantly of vitrinite or huminite (73-74 vol. %), but individual seam varies in huminite content, ranging from 56-86 vol. %. Components such as liptinite (3-6 vol. %), inertinite (11-16 vol. %), and mineral matters (6-11 vol. %) are apparently less abundant.

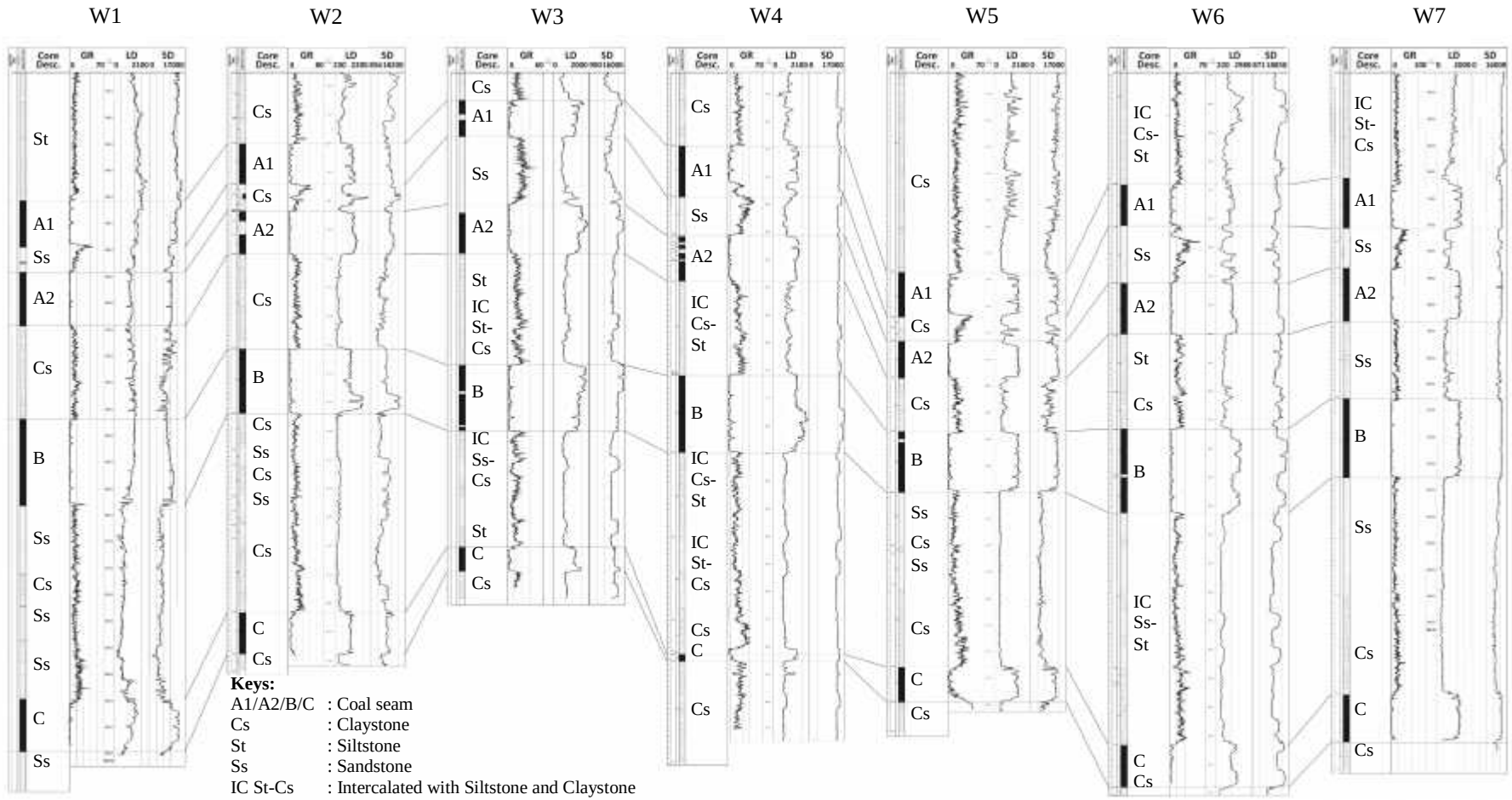

Fig. 3 Correlation of the well logs studied showing a variety of coal thicknesses.

Table 1 Analytical results of CBM evaluation in Air Laya mining area

Observation	Parameters (unit)	Coal Seams								Remarks
		A1		A2		B		C		
		yields	mean	yields	mean	yields	mean	yields	mean	
Log	Depth (m)	79.4-166		100.3-183		126.5-207.5		164.4-263.5		Log analysis
	Thickness (m)	6.9-9.5	8.2	7-10.3	8.6	11.5-16.3	13.7	1.3-9.9	6.7	
Core	Vitrinite (vol. %)	56-86	74.7	65.8-80.6	73.8	64.6-78.8	73.9	65.4-81.4	73.8	Petrographic analysis
	Liptinite (vol. %)	1.2-6.6	3.6	0.2-7.6	3.1	2.2-12.2	5.6	3.4-9.2	5.9	
	Inertinite (vol. %)	4.2-14.8	11.1	9.0-19.2	15.5	14.0-16.4	14.7	6.2-15.8	11.5	
	Minerals (vol. %)	3-30	10.6	2.8-10	7.6	3-9	5.8	5.4-15.0	10.0	
	VR (%)	0.38-0.77	0.49	0.33-0.64	0.49	0.40-0.83	0.52	0.40-0.58	0.59	
	Ash (wt. %)	4.02-30.43	10.77	3.50-9.99	7.28	6.39-7.94	6.11	4.31-12.13	6.78	Proximate analysis
	Moisture (wt. %)	3.90-12.59	7.24	2.75-10.58	6.07	3.85-9.18	6.47	2.36-7.45	4.97	
	FC (wt. %)	32.55-48.95	43.14	42.21-59.35	47.69	43.42-53.23	46.80	43.74-54.32	47.81	
	VM (wt. %)	33.08-42.41	38.84	32.62-42.07	38.94	40.35-41.57	40.47	31.19-43.85	40.44	
	TS (wt. %)	0.62-0.91	0.76	0.20-1.10	0.42	0.23-1.06	0.41	0.60-2.17	1.28	
	CV (cal/g)	4,903-7,150	6,303	5,823-7,524	6,697	6,351-7,319	6,805	6,543-7,350	6,949	
	RD (g/cm^3)	1.23-1.51	1.31	1.23-1.31	1.27	1.22-1.28	1.26	1.22-1.29	1.26	
Gas content[*)] (m^3/t)		3.3-4.8	4.1	4.2-5.6	4.9	4.4-5.4	4.9	4.9-5.7	5.3	Average 4.1-5.3
Gas-in-place[**)] ($x10^6$ m^3)		554		623		1,049		793		Total 3,019

VR: vitrinite reflectance; FC: fixed carbon; VM: volatile matter; TS: total sulphur; CV: calorific value (gross value); RD: relative density; [*)] estimated using the modified formula of [20]; [**)] calculated using the method of [22].

In addition, the results of petrographic analysis in this study are commonly similar to those reported by [28]. Analysis of core sample A1 yielded VR values ranging from 0.38-0.77%, with mean 0.49%. The VR measurements of coals A2, B, and C resulted in 0.33-0.64% with mean 0.49%, 0.40-0.83% with mean 0.52%, and 0.40-0.58% with mean 0.59% respectively. These data suggest that the analyzed coals may be of subbituminous and high volatile bituminous. In addition, the VR yields show that there is an increase in vitrinite reflectance with depth. The values seem slightly higher than those proposed by [19], possibly due to the more locally thermal influence on the coal seams analyzed. The increase in degree of maturation with depth for the South Sumatran coals has also been reported elsewhere [1], [13], [28], [29]. Importantly, the yielded VR may imply that the onset of gas generation within these low rank coals might have occurred due to biogenic processes, as the coal bearing sequence was subjected to the zone of higher paleogeothermal gradient through deeper burial in Pliocene time. The essay on biogenic origin has also been suggested by [19].

The proximate parameters, including ash content, inherent moisture, fixed carbon (FC), volatile matter (VM), total sulphur (TS), calorific value (CV), and relative density (RD), have been analyzed on air dried basis (adb) (Table 1). In order to better understand the characteristics of coals within the region, each of these parameters is compared to the result of proximate analysis reported by [28]. Most of the coal elements are in general akin to those suggested by these authors. The ash content of the A1 samples ranges from 4.0-30.4 wt. % with mean 10.8 wt. %, whereas the A2, B, and C seams have ash composition in that order of 3.5-10 wt. % with mean 7.3 wt. %, 6.4-7.9 wt. % with

mean 6.1 wt. %, and 4.3-12.1 wt. % with mean 6.8 wt. %. Inherent moisture varies among the coal beds, but they are all characterized by high values. To compare with the analytical results published by [28], the Air Laya mining coals are relatively lower in moisture content. Individual coal bed contains fixed carbons that range from 32.6-49.0 wt. % with mean 43.1 wt. % for seam A1, 42.2-59.4 wt. % with mean 47.7 wt. % for seam A2, 43.4-53.2 wt. % with mean 46.8 wt. % for seam B, and 43.7-54.3 wt. % with mean 47.8 wt. % for seam C. The present value is apparently higher than that shown by [28], but remains on the range of values typical for the low rank coals. The VM content obtained from analysis of sample A1 ranges from 33.1-42.4 wt. % with an average of 38.8 wt. %. The other coal specimens result in various VM contents, ranging from 32.6-42.1 wt. % with an average of 38.9 wt. % (seam A2), 40.4-41.6 wt. % with an average of 40.5 wt. % (seam B), and 31.2-43.9 wt. % with an average of 40.4 wt. % (seam C).

Analysis of the sulphur content yields the mean value ranging from 0.4-1.3 wt %. Each coal seam varies in the total sulphur matter. The A1 coal results in 0.6-0.9 wt. % and average 0.8 wt. %, the A2 and B bed possess exactly the same value of 0.2-1.1 wt. % and average 0.4 wt. %, and the C layer has 0.6-2.2 wt. % and average 1.3 wt. %. The calorific data generated from of the analyzed cores indicate that the A1 coal is subbituminous with calories varying between 4,903-7,150 cal/g and average 6,303 cal/g, whereas the A2, B, and C coals are high volatile bituminous with calorific values ranging from 5,823-7,524 cal/g and average 6,697 cal/g, 6,351-7,319 cal/g and average 6,805 cal/g, and 6,543-7,350 cal/g and average 6,949 cal/g respectively. The density of these subbituminous-high volatile bituminous coals is relatively constant with mean of 1.3 g/cm^3.

The average gas volume for the Air Laya mining coals is approximately 4.1-5.3 m^3/t, but each seam has slightly different content. The estimate for the A1 bed ranges from 3.3-4.8 m^3/t with mean 4.1 m^3/t, whilst the A2, B, and C coals comprise natural gas in the range of 4.2-5.6 m^3/t with mean 4.9 m^3/t, 4.4-5.4 m^3/t with mean 4.9 m^3/t, and 4.9-5.7 m^3/t with mean 5.3 m^3/t, respectively. The resulted gas estimates suggest that there is an increase in gas content with depth or temperature gradient (Fig. 4). This implies that the higher coal rank, principally due to the deeper burial, may contain the higher gas volume. Evaluation of gas-in-place in the present study indicates that individual seam possesses distinctive values, but the total gas in all seams is about 3,019x10^6 m^3.

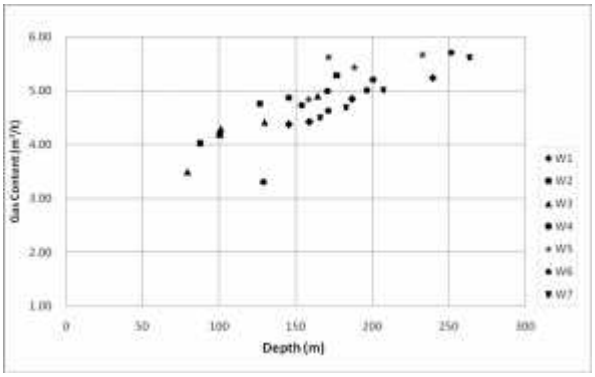

Fig. 4 Diagram displaying the depth vs gas content relation. This graph suggests that the gas content rises as the depth increases.

CONCLUSIONS

In order to conclude the above discussion, some remarks are drawn as the following:

1. The coal seams in Air Laya mining area are subbituminous and high volatile bituminous with various apparent thickness and extensive lateral distribution throughout the region.
2. The average gas content is about 4.1-5.3 m^3/t, and there appears an increase in gas content with depth.
3. The total of gas-in-place is approximately 3,019x10^6 m^3.

ACKNOWLEDGEMENT

The authors would like to take this opportunity to acknowledge PTBA for providing the log data and the core analysis. This paper is published with the permission of the management of PTBA.

REFERENCES

[1] Stevens, S.H. and Sani, K. “Coalbed methane potential of Indonesia: preliminary evaluation of a new natural gas source”, Proceedings of Indonesian Petroleum Association, IPA01-G-063, 2001, pp. 727-738.

[2] Sosrowidjojo, I.B. and Saghafi, A. “Development of the first CBM program in Indonesia: coal seam reservoir properties of the South Sumatra basin”, International Journal of Coal Geology, 2009, v. 79, pp.145-156.

[3] Haris, A., Mujiantoro, A., and Kurniawan, R.E. “Evaluation of coal bed methane potential of Bentian Besar, Kutei basin”, IPA10-G-139, 2010.

[4] Lalean, B. "Launching a first coalbed methane (CBM) project in Indonesia – A case study", Proceedings of Indonesian Petroleum Association, IPA10-BC-189, 2010.

[5] Nurhandoko, B.E.B, Susilo, Ishaq, U.M., Rudiyanto, H., Wiyanto, Y., Sulistyanto, B., Budi, M.L., Triyoso, K., Siahaan, K.R., Abdillah, W.E., and Kusudiharjo, D. "Rock physics study of coal bed methane reservoir rock: case study of Muara Enim coal", IPA12-G-157, 2012.

[6] Sulistiyo, Z.R., Sutanto, A., and Sukhendar, H. "Preliminary study of CBM potential in Jorong – Kintap area, Asem-Asem basin, South Kalimantan", Proceedings of Indonesian Petroleum Association, IPA12-G-009, 2012.

[7] Pitaloka, D.C., Lalean, B., and Hendriyanto, N. "Cracking new CBM potential in South Sumatra: current progress, obstacles, and opportunities", Proceedings of Indonesian Petroleum Association, IPA13-E-061, 2013.

[8] Moore, T.A. and Nas, C."The enigma of the Pinang dome (Kalimantan Timur): a review of its origin, significance and influence on coal rank and coalbed methane properties", Proceedings of Indonesian Petroleum Association, IPA13-G-119, 2013.

[9] Sosrowidjojo, I.B. "Coal geochemistry of the unconventional Muara Enim coalbed reservoir, South Sumatra basin: a case study from the Rambutan field", Indonesian Mining Journal, 2103, v. 16, pp. 71-81.

[10] Nugroho, W. and Arsegianto. "Future prospect of coalbed methane in Indonesia", Proceedings of International Coalbed Methane Symposium, University of Alabama, 1993, pp. 721-726.

[11] Suyartono and Ginting, N. "The possibility of coalbed methane recovery in Indonesia", United Nations International Conference on Coal Bed Methane Development and Utilization, 1995, pp. 187-194.

[12] Stevens, S.H., Sani, K., and Sutarno, H. "Indonesia's 337 tcf CBM resource a low cost alternative to gas", LNG Oil and Gas Journal, 2001, pp. 40-45.

[13] Stevens, S.H. and Hadiyanto. "Indonesia: coalbed methane indicators and basin evaluation", SPE International, SPE 88630, 2004.

[14] Godfrey, P., Ee, T., and Hewitt, T. "Coal bed methane development in Indonesia: golden opportunity or impossible dream?", Proceedings of Indonesian Petroleum Association, IPA10-BC-180, 2010.

[15] Saghafi, A. and Hadiyanto. "Methane storage properties of Indonesian Tertiary coals", Proceedings of the Southeast Asian Coal Geology Conference, 2000, pp. 121-124.

[16] Kurnely, K., Tamtomo, B., Aprilian, S., and Doria, I. "A preliminary study of development of coalbed (CBM) in South Sumatra", Society of Petroleum Engineers, SPE 80518, 2003.

[17] Daly, M.C., Cooper, M.A., Wilson, I., Smith, D.G., and Hooper, B.G.D. "Cenozoic plate tectonics and basin evolution in Indonesia", Marine and Petroleum Geology, 1991, v. 8, pp. 2-21.

[18] Boyd, J.D. and Peacock, S.G. "Sedimentological analysis of a Miocene deltaic system: Air Benakat and Muara Enim Formations, Central Marangin Block, South Sumatra", Proceedings of Indonesian Petroleum Association, 1986, pp. 245-258.

[19] Mazumder, S., Sosrowidjojo, I.B., and Ficarra, A. "The Late Miocene coalbed methane system in the South Sumatra basin of Indonesia", SPE International, SPE 133488, 2010, pp. 1-29.

[20] Kim, A.G. "Estimating methane content of bituminous coalbeds from adsorption data", US Dept. of Interior, Bureau of Mines, RI8245, 1977, pp. 1-22.

[21] Oeke, S., Yunitha, Sukiyah, E., and Sunardi, E. "Prediksi kandungan gas metana batubara berdasarkan formula Kim dengan study kasus di Indonesia bagian barat", Bionatura Jurnal, 2013, v. 15, pp. 139-144.

[22] Mavor, M.J. and Nelson, C.R. "Coalbed reservoir gas-in-place analysis", Gas Research Institute, 1997.

[23] de Coster, G.L. "The geology of the Central and South Sumatra basins", Proceedings of Indonesian Petroleum Association, 1974, pp. 77-110.

[24] Pulunggono, A. "Tertiary structural features related to extensional and compressive tectonics in the Palembang basin, South Sumatra", Proceedings of Indonesian Petroleum Association, 1986, pp. 187-208.

[25] Hall, R. "The origin of Sundaland", Proceedings of Sundaland Resources, MGEI Annual Convention, 2014, pp. 1-25.

[26] Adiwidjaja, P. and de Coster, G.L. "Pre-Tertiary paleogeography and related sedimentation in South Sumatra", Proceedings of Indonesian Petroleum Association, 1973, pp. 89-103.

[27] Sudarmono, Suherman, T., and Eza, B. "Paleogene basin development in Sundaland and its role to the petroleum system in the western Indonesia", Proceedings of the Petroleum System of SE Asia and Australasia

Conference, Indonesian Petroleum Association, 1997, pp. 89-103.

[28] Sanusi, S., Kuswandi, A., Jufri, R.M., and Anggarini, K.S. "Evaluation of coalbed methane potential of Muara Enim Formation in the Muara Enim area, South Sumatra", Proceedings of Sundaland Resources, MGEI Annual Convention, 2014, pp. 467-483.

[29] Amijaya, H. and Littke, R. "Properties of thermally metamorphosed coal from Tanjung Enim area, South Sumatra basin, Indonesia with special reference to the coalification path of maceral", International Journal of Coal Geology, 2006, v. 66, pp. 271-295.

Second International Conference on Science, Engineering & Environment,
Osaka City, Japan, Nov.21-23, 2016, ISBN: 978-4-9905958-7-6 C3051

THE EFFECTS OF WATERING FREQUENCIES AND SLOW-RELEASED-FERTILIZER LEVELS ON THE GROWTH OF *PLATYCERIUM CORONARIUM* IN THE YOUNG SPOROPHYTE PHASE

Sawat Pimsuwan[1], Yaowarat Wongsrisakulkaew[1],
Nadda Jumradjit[1], Patthamawadee Thumsuk[1] and Supawadee Mulmanee[1]
[1] Faculty of Agricultural Technology, Rajamangala University of Technology Thanyaburi, Thailand

ABSTRACT

This study was conducted at the nursery of the Crop Production Department, Faculty of Agricultural Technology, Rajamangala University of Technology, from February to August 2015. The effects of two factors on the growth of *P. coronarium* ferns in the young sporophyte phase were assessed using a factorial in CRD experiment. Factor A consisted of 3 watering frequencies: watered every day, every two days and every three days. Factor B consisted of 4 levels of a commercial slow-released-fertilizer (SRF: 13-13-13, 3 months): 0 g, 1 g, 2 g and 3 g per pot. It was found that the ferns which received water once every three days possessed the highest canopy of 29.47 cm, a sterile leaf width of 14.054 cm, a fertile leaf width of 22.58 cm and a fertile leaf length of 22.20 cm. On the other hand, the fertilizer level of 2 g gave the highest canopy of 27.31cm and a sterile leaf width of 14.63 cm, while the fertilizer level of 3 g gave the biggest fertile leaf width of 21.54 cm and a fertile leaf length of 19.62 cm. However, no interaction between the two factors was demonstrated.

Keywords: watering frequency, fertilizers for staghorn fern, sporophyte, platycerium, slow-released-fertilizer

INTRODUCTION

Ferns are plants that do not have flowers or fruits. They propagate by means of spores. A variety of fern species classifications based on natural habitat is as follows: aquatic ferns named Water Clover (*Marsilea* spp) and Azolla (*Azolla pinnata* R.Br); terrestrial ferns named Tree Fern (Cyatheales), Golden Chicken Fern (*Cibotium barometz*); and epiphyte ferns named Bird's-nest Fern (*Asplenium nidus*) and Staghorn Fern (*Platycerium spp*) [4]. Ferns have a great many uses for humans, for example: wicker from Climbing Ferns (*Lygodium polystachyum* Wall.ex Moore); food from Vegetable Ferns (*Diplazium esculentum*) [13],[16]; and ornamental plants from Oak-leaf Fern (*Drynaria quercifolia*) and Staghorn Fern (*Platycerium* spp).

Many ferns are beautiful and are used as ornamental plants. Ferns' delicate beauty make them ideal for gardens of ornamental plants. Their aesthetics are determined by their foliage color and form [17]. The genus Platycerium is one of the most beautiful ferns among the few epiphytic fern genera. This genus is divided into 18 species by biogeography. There are three main groups consisting of the Java-Australian line, Malayan-Asiatic line and Afro-American line [5],[7].

The popularity of the staghorn fern leaves over other species makes this a good ornamental plant. This fern is a unique adaptation that is very attractive as an epiphyte fern. The stem is a rhizome. There are two types of leaves (fronds), the sterile leaf (shield frond) and the fertile leaf. The sterile leaves are like a basket which gathers organic matter. They turn brown and form layers between which the roots grow. They can then store water like a sponge and protect the rhizome [15]. The fertile leaf form spore patches. In nature, staghorn ferns grow well as they naturally enrich themselves allowing for frequent propagation.

Within the fern genus platycerium, *P. coronarium* has been very popular among ornamental plant growers [12]. It has been referred to as the queen of staghorn ferns. The leaves are dimorphous with unequal base leaves. Fertile leaves are asymmetrical with consecutively forked branches [1]. *P. coronarium* is a distinctive and large fern that frequently grows in the crotches of the tallest trees. In the primitive forests, fertile leaves can reach 200 cm long with suspended dichotomous lobes [2]. There is a relationship between *P. coronarium* and *P. ridleyi* as indicated by the location of their spores which create an appendage resembling a spoon [7].

The process of fern spore germination depends on the time of storage and the conditions of storage, including temperature, humidity and light [2][10]. When the spores are cultured in the nursery, the

important factors affecting propagation are the strength of the wind, humidity, light and temperature. The process of germination transforms the spores into the young sporophyte phase. The spore cultures are kept in plastic containers which maintains constant moisture [11]. The ferns are then able to adapt to these conditions even though they are not natural. When the young sporophytes are ready to be introduced into the external environment, they will be strong enough to adapt.

The important factors that affect the growth of the staghorn fern are moisture and nutrients. The sterile leaves of the staghorn fern retain moisture. There is no need for frequent watering. Normally staghorn ferns get nutrients from natural organic matter. When the ferns grow in the nursery, the necessary nutrients can be added with slow release fertilizers which gradually release nutrients. This method does not pollute the environment and it releases the nutrients in a way that fits plant growth [8]. This experiment wanted to consider how slow release fertilizers might be beneficial to growers working with staghorn ferns in the nursery [9].

The purpose of this research is to study watering frequencies and levels of slow-released-fertilizer on the growth of *P. coronarium* in the young sporophyte phase.

MATERIALS AND METHODS

Materials

This research began with the cultivation of *P. coronarium* spores. Plants were transplanted into plastic containers until they were one year old. The factors that were controlled included moisture, humidity, light and temperature. In the nursery, plants with a similar diameter size of about 27 cm on average were selected. They were then put into 8 x 8 inch plastic pots with plant material. The preparation of plant material involved chopping coconuts and soaking them in water for 1 hour. This absorption of water in the coconut reduces the coconut acidity. These young sporophyte phase ferns were then arranged on the plant bench by Factorial experimental design. The slow release fertilizers were prepared at the different levels of 1 g, 2 g and 3 g with 500 ml of water.

Experimental design and data analysis

Factorial experiment in CRD was used in this experiment. Factor A consisted of 3 watering frequencies: watered every day, every two days and every three days. Factor B consisted of 4 levels of a commercial slow-released-fertilizer (SRF:13-13-13 , 3 months): 0 g, 1 g, 2 g and 3 g per pot with 3 replications. The data was statistically analyzed by ANOVA (Analysis of Variance) and comparisons were made with Duncan at a significance level of 05.

RESULTS

This study found that for Factor A, the frequency of watering every three days resulted in the average following results: a canopy height of 29.47 cm; a sterile leaf width of 14.05 cm; a fertile leaf width of 22.58 cm; and a fertile leaf length of 22.20 cm. There was no statistical difference compared to other watering frequencies. For Factor B, the commercial slow-released-fertilizer weight of 2 grams per pot resulted in the average following results: a canopy height of 27.31 cm; and a sterile leaf width of 14.63 cm. The rate of 3 grams per pot gave the biggest fertile leaf width of 21.54 cm and a fertile leaf length of 19.62 cm. There was no statistical difference compared to the other levels (Table 1 and Fig 1-3).

Table 1 The results of two factors on the growth of staghorn ferns in the young sporophyte phase at 12 weeks

Treatment	Growth of *P. coronarium* ($\bar{X}$/ cm)			
	Canopy Height	Sterile Leaf Width	Fertile Leaf Width	Fertile Leaf Length
Factor A				
Every day	18.98	10.58	13.01	14.38
Every 2 days	23.45	9.87	18.17	16.59
Every 3 days	29.47	14.05	22.58	22.20
CV%	27.23	43.75	36.60	28.17
F-test	ns	ns	ns	ns
Factor B				
SRF 0 g/pot	17.06	7.52	11.93	14.08
SRF 1 g/pot	25.19	11.81	17.38	17.81
SRF 2 g/pot	27.31	14.63	20.83	19.40
SRF 3 g/pot	26.31	11.35	21.54	19.62
CV%	27.23	43.75	36.60	28.17
F-test	ns	ns	ns	ns

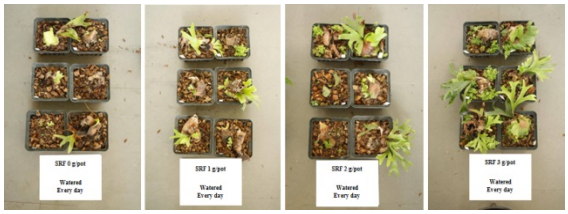

Fig. 1 Watered every day with SRF: 0 g, 1 g, 2 g and 3 g/pot

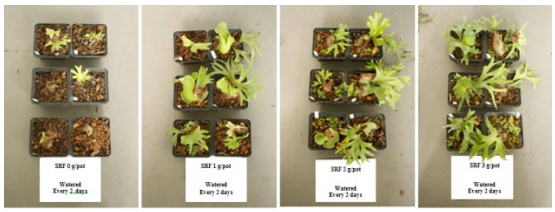

Fig. 2 Watered every 2 days with SRF: 0 g, 1 g, 2 g and 3 g/pot

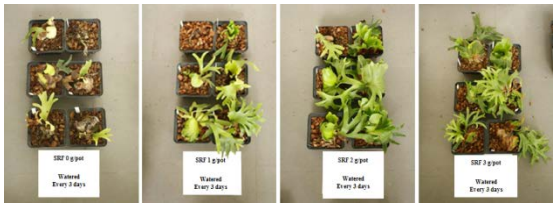

Fig. 3 Watered every 3 days with SRF: 0 g, 1 g, 2 g and 3 g/pot

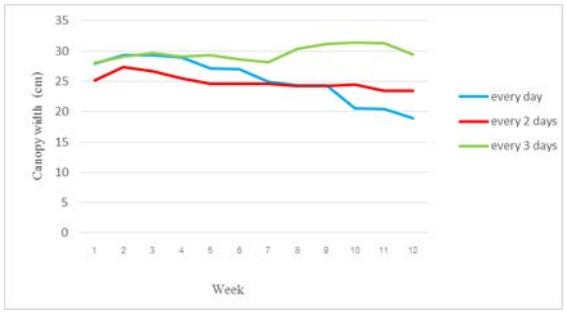

Fig. 4 Canopy width of *P. coronarium* with 3 watering frequencies

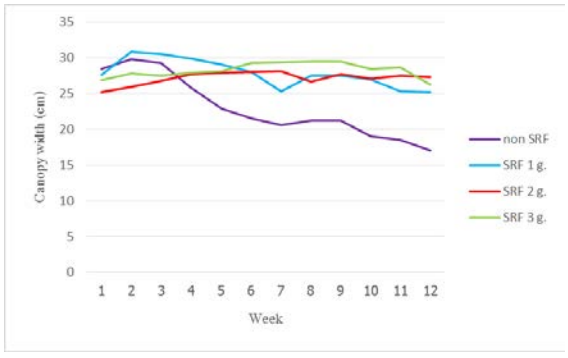

Fig. 5 Canopy width of *P. coronarium* with 4 levels of SRF

Fig. 6 Sterile leaf width of *P. coronarium* with 3 watering frequencies

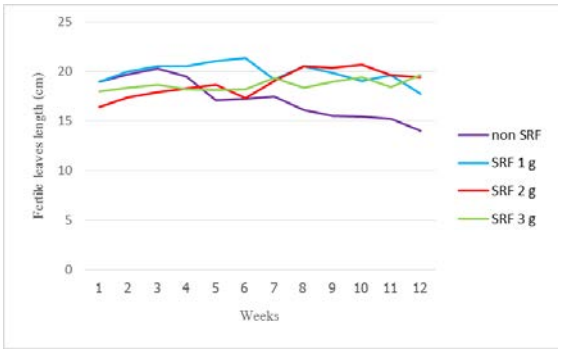

Fig. 7 Sterile leaf width of *P. coronarium* with 4 levels of SRF

Fig. 8 Fertile leaf width of *P. coronarium* with 3 watering frequencies

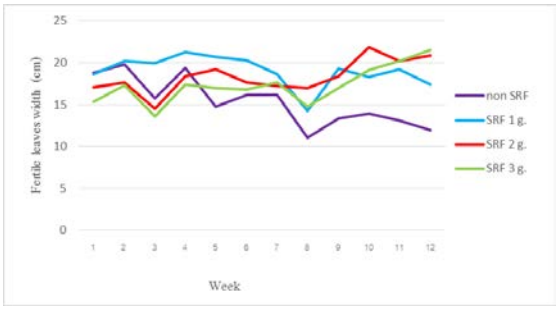

Fig. 9 Fertile leaf width of *P. coronarium* with 4 levels of SRF

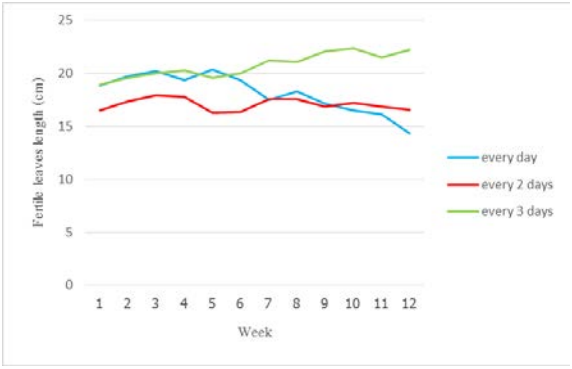

Fig. 10 Fertile leaf length of *P. coronarium* with 3 watering frequencies

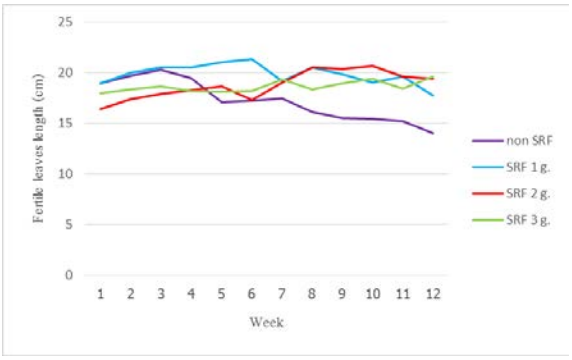

Fig. 11 Fertile leaf length of *P. coronarium* with 4 levels of SRF

DISCUSSION

This research showed a watering frequency of every three days produced the best fern growth (Fig 4, 6, 8 and 10). Roy Vail [15] said that most staghorn ferns only need enough water to be moist. If the ferns are watered until wet, they may die. Some species need far less water. The *P. coronarium* fern can store water easily in the shield frond. However this may create a problem with rot so in the rainy season, watering should be avoided. In the rainy and dry seasons, to minimize problems with the young sporophyte phase of the fern, it must be maintained carefully in a plastic roof house and be moist in the daytime in the dry and hot seasons.

The slow release fertilizers release nutrients more slowly than general release fertilizers, but the rate and duration of the release of nutrients cannot be controlled. The release rate depends on external factors such as soil moisture, the soil reaction, the size of a grain of fertilizer and watering frequency. This research showed the slow release fertilizer level of 2 g produced the best fern growth (Fig 5, 7, 9 and 11). The slow release fertilizer reduces the amount of fertilizer used because the release process reduces nitrogen losses due to volatilization and leaching [6].

Slow release fertilizers are not easily found in normal markets and are expensive. In nature, these epiphyte ferns can grow and have the ability to thrive [14]. As an epiphytic fern, staghorn ferns can grow in tree crotches. The shield fronds gather dry leaves of plants and other dust from which the fern can absorb nutrients as a result of fermentation. Another way is to use bio-fertilizers instead of chemical fertilizers, for example, compost from leaves and manure for the staghorn ferns.

ACKNOWLEDGEMENTS

This research was partially funded by The Faculty of Agricultural Technology, Rajamangala University of Technology Thanyaburi, Thailand. And this text was edited by Dr. Satain Pokul and Mr. Bruce Groening.

REFERENCES

[1] Aspiras R.A. Sporophyte and gametophyte development of *Platycerium coronarium* (Koenig) Desv. and *P. grande* (Fee) C. Presl. (Polypodiaceae) through in vitro propagation. Saudi J Biol Sci. 2010 Jan;17(1): 13–22

[2] Bonomo M.C., Martínez O.G, Tanco M.E., Cardozo R. and Avilés Z. Spores germination and gametophytes of *Alsophila odonelliana* (Cyatheaceae) in different sterile media ΦYTON ISSN 0031 9457, (2013) 82: 119-126

[3] Boonkerd T., Chantanaorrapint S. and Khwaiphan W. Pteridophyte Diversity in the Tropical Lowland Rainforest of Khao Nan National Park, Nakhon Si Thammarat Province, Thailand. The Natural History Journal of Chulalongkorn University 8(2) 2008: 83-97

[4] Dubuisson J., Schneider H. and Hennequin S. Epiphytism in ferns: diversity and history. Science Direct. Vol. 332, Issues 2–3, 2009, P. 120–128

[5] Hoshizaki B.J.. Morphology and Phylogeny of Platcerium Species. Biotropica Vol. 4, No. 2, (Aug., 1972), 93-117 Published by: Association for Tropical Biology and Conservation Stable URL: http://www.jstor.org/stable/2989731 Page Count: 25

[6] Jagadeeswaran R., Murugappan V. and Govindaswamy M., Effect of Slow Release NPK Fertilizer Sources on the Nutrient use Efficiency in Turmeric (*Curcuma longa* L.) World Journal of Agricultural Sciences 1 (1) 2005: 65-69

[7] Kreier H.-P. and Schneider H., Phylogeny and biogeography of the staghorn fern genus platycerium (polypodiaceae) American Journal of Botany 93(2) 2006: 217–225

[8] Ni B., Liu M., Lu S., Xie L, and Wang Y. Environmentally Friendly Slow-Release

Nitrogen Fertilizer. J. Agric. Food Chem., 59 (18) 2011, pp 10169–10175

[9] Pauly D.J., Nyborg M., and Malhi S.S. Controlled-release P fertilizer concept evaluation using growth and P uptake of barley from three soils in greenhouse. Canadian Journal of Soil Science 82, 2002: 201-210

[10] Pérez-García B, Mendoza-Ruiz A., Sánchez-Coronado M.E. and Orozco-Segovia A., Effect of light and temperature on germination of spores of four tropical fern species. Acta Oecologica Volume 32, Issue 2, 2007: 172–179

[11] Pimsuwan S, Hongthong P, Phattraporn, Krangpanich P. and Suwanpinta C. The Effect of Fertilizer on Growth of Staghorn Fern at Seedling Stage. International Journal of GEOMATE, Dec., 2016, Vol. 11, Issue 28, pp. 2879-2882 Special Issue on Science, Engineering and Environment, ISSN: 2186-2990, Japan

[12] Taha R.M., Haron N.W., and Wafa S.N. Morphological and Tissue Culture Studies of Platycerium coronarium, a Rare Ornamental Fern Species from Malaysia. American Fern Journal, 101(4) 2011:241-251

[13] Tongco J.V.V., Villaber R.A.P., Aguda R.M. and Razal R.A. Nutritional and phytochemical screening, and total phenolic and flavonoid content of *Diplazium esculentum* (Retz.) Sw. from Philippines. Journal of Chemical and Pharmaceutical Research, 6(8) 2014:238-242

[14] Uchida T., Furuno M., Minami T., Yamashita S., Uchiyama T., Arase T. and Hayasaka D., Ecological Significance of Masonry Revetments in Plant Biodiversity. Int. J. of GEOMATE, Japan, 2015, Vol. 9, No. 1 (17), pp. 1353-1359

[15] Vail, R. Platycerium Hobbyist's Handbook. Desert Biological Publications. 1984.

[16] Yusuf U.K. Ferns of Malaysian Rain Forest a Journey through the Fern World. Serdang ;Universiti Putra Malaysia Press, 2010.

[17] Zhigila D.A., Sawa F.B.J, Oladele FA. And Muhammad S. Aesthetic Values and Significance of Ferns to Landscaping Industries -A Taxonomic Review. Int. J. Curr. Res. Biosci. Plant Biol. 2(3) 2015: 7-13

Second International Conference on Science, Engineering & Environment,
Osaka City, Japan, Nov.21-23, 2016, ISBN: 978-4-9905958-7-6 C3051

EFFICACY OF STINGLESS BEE *LEPIDOTRIGONA TERMINATA* AS INSECT POLLINATOR OF F_1 HYBRID CUCUMBER

Anchalee Sawatthum[1] Piyaporn Jitake[1] Orapin Rangyai[1]
Rattana Prangprayong[1] Piyaporn Pimboon[1] and Kanokporn Suparit[1]
[1]Faculty of Agricultural Technology, Rajamangala University of Technology Thanyaburi, Thailand
E-mail anchalee_s@exchange.rmutt.ac.th, anchsawat@hotmail.com

ABSTRACT

This research was aimed to study the efficacy of stingless bee *Lepidotrigona terminata* as insect pollinator of F_1 Hybrid cucumber. The experiments were conducted at experimental farm of the Faculty of Agricultural Technology, Rajamangala University of Technology, Thanyaburi. The experiment was divided into two parts. The first part, efficacy study of stingless bee as insect pollinator of F_1 hybrid cucumber was studied. Experimental design used was Randomized Block Design with four treatments and three replications which were opened – pollination, handed – pollination, stingless bee – pollination and closed – pollination. The results revealed that cucumber fruit sets were found only in treatments opened – pollination and handed – pollination, with 9.33 and 12.66 fruits, respectively. While no fruit set was found in another two treatments which were closed and stingless bee – pollinations. Second, species diversity and numbers of insect pollinators which had visited cucumber flowers during 6.00 a.m. – 18.00 p.m. were determined. As a result, four insect species had visited cucumber flower and the most abundant were European bees (*Apis mellifera*) that had visited the cucumber flowers, both male and female, at 09.00 a.m.

Keywords: Stingless bee, Lepidotrigona terminata, Insect pollinator, F_1 hybrid cucumber

INTRODUCTION

Cucumber (*Cucumis sativus* L.) is a plant in the order of Cucurbitales belonging to the Cucurbitaceae family. It is in the group of dicotyledon with stem in the form of creeping vine consisting of yellow flowers. The fruits contain short thorns which will eventually fall off when the fruit reach maturity. Cucumbers have crisp texture, high water content, and can be cultivated all year round. Production is highest during February and March. Propagation is done by planting seeds in which to the duration from planting until harvest is approximately 40 - 60 days. Cucumbers can be consumed raw, fried, pickled, boiled, and steamed as a vegetable or juice. Cucumbers also have an aesthetic value where they are commonly used for plate decoration. Cucumber contains erepsin enzyme that aids digestion of protein. The medicinal properties of cucumbers are aid urination, relief fever, thirst, and diarrhea, and reduce high blood pressure. [1]

Pollination of cucumbers, a Monoecious plant characteristic of containing male flowers and female flowers on the same plant, requires carrier insects such as bees to carry pollen as bee are efficient cucumber pollinators. Bees consist of many species and one of them is a stingless bee. Many researches had been conducted using stingless bees' efficacy to pollinate plants. From several studies on the diversity of insect species that can help pollinate durian flowers, Somnook [2] had found that stingless bees *Lepidotrigona terminata* had a rate of durian flower visits of 80 percent in comparison to all the insects that visited durian flowers. However, the experiment of Wanna [3] had found that stingless bees had only collected nectar and pollen but were not involved in pollination. For the experiment of Janwit et.al. [4], the efficacy of the stingless bee *Trigona pegdeni* to pollinate cucumbers had been studied and was found that by using stingless bee to pollinate cucumber, the fruit set rate was lower than opened pollination. It might be due to the fact that *Trigona pegdeni* stingless bees are smaller than *Lepidotrigina terminata* stingless bees. This study investigated the potential of *Lepidotrigina terminata* stingless bees as pollinators of F1 hybrid cucumbers.

MATERIALS AND METHODS

This research was divided into two parts:

1. The efficacy of stingless bee as insect pollinator of F_1 hybrid cucumber

The experiment was conducted at the Faculty of Agricultural Technology, Rajamangala University of Technology. The F1 hybrid cucumbers were planted at the spacing of 50 x 50 cm per plant. The experiment was designed using Randomized Complete Block Design (RCBD) with three

replicates and four treatments as follows: 1) opened - pollination (the cucumber flower ready for pollination were marked and released for natural pollination). 2) Handed - pollination (male and female flowers that were about to bloom were marked and covered with bags, when the female flowers bloom in the bag, the male flowers were brought to pollinate with the female flowers that bloom then covered with original bags). Closed - pollination (female flowers were covered until they wither to prevent pollination by insects. 4) Stingless bee - pollination (a cage was built around the cucumber plants and stingless bees were introduced into the cage, one hive per cage, for one week and the cucumber flowers that were ready for pollination were marked).

DATA COLLECTION AND ANALYSIS

Fruit set rate was randomized and the characteristics of the fruits were observed through collection of 15 fruits per replicate and the maturation of the fruit was determined. The fruit weight, diameter, and uniformity were measured and were divided into three categories**:** 1) fully-developed fruit, 2) under-developed fruit, and 3) non-uniform fruit. The data was analyzed using analysis of variance, Randomized Complete Block Design **(**RCBD**)** and the difference was compared with Least Significant Difference **(**LSD**).**

2. Diversity of insect species that visited F_1 hybrid cucumber flowers in five days

The number of insects that visited male and female cucumber flowers was counted, five flowers per sex for all three replicates, between 06:00 a.m. – 17:00 p.m. for 10 minutes within five days.

RESULTS AND DISCUSSION

The efficacy of stingless bee as insect pollinator of F_1 Hybrid cucumber

Table 1 and 2 present the results of the four treatments (open, closed, manual, and stingless bee - pollinations) that were conducted in the first part of the study. The results are evaluated using the RCBD experimental design, comparing the efficacy of the stingless bee - pollination to other treatments. It was found that the fruit set of the F1 hybrid cucumbers in opened and handed - pollination were significantly different with the mean fruit set values of 9.33 and 12.66 fruits, respectively. The two treatments are significantly different to the stingless bee and closed - pollination treatments in which both treatments did not exhibit fruit set.

The size of the fruits in opened - pollination were 7.21 cm in length and 3.38 cm in diameter on average. In handed - pollination, the average length and diameter were 6.09 cm and 2.72 cm respectively.

The results showed that the average weight of the cucumber fruits in opened – pollination treatment was 50.73 g. and the average weight for handed – pollination was 34.09 g. The results from the opened and handed – pollinations had shown statistically significant difference that includes the quality of fully-developed fruits from both treatments. Under-developed fruits from opened - and handed – pollinations were also significant different; however, there was no significant difference in non-uniform fruits.

Table 1 Fruit set, size, diameter, and weight of the F1 hybrid cucumbers of the different pollination treatments.

Treatment	Fruit set (fruit)	Length (cm)	Diameter (cm)	Weight (g)
Opened - pollination	9.33 a[1/]	7.21 a	3.38 a	50.73 a
Handed - pollination	12.66 b	6.09 b	2.72 b	12.66 b
Stingless bee -pollination	0 c	0 c	0 c	0 c
Closed - pollination	0 c	0 c	0 c	0 c
LSD 0.01	**	**	**	**
C.V. (%)	4.43	2.74	2.54	8.25

[1/] Means with different superscript within the same row differ significantly (P < 0.01)

Table 2 Quality of F1 hybrid cucumbers from the different pollination treatments

Treatment	Fully-developed fruit (fruit)	Under-developed fruit (fruit)	Non-uniform fruit (fruit)
Opened - pollination	9 a[1/]	2.33 a	3.67 a
Handed - pollination	6.33 b	5.33 b	3.33 a
Stingless bee -pollination	0 c	0 c	0 b
Closed - pollination	0 c	0 c	0 b
LSD 0.01	**	*	**
C.V. (%)	7.15	6.57	8.12

[1/] Means with different superscript within the same row differ significantly (P < 0.01)

Species diversity and numbers of insect pollinators that visited F1 hybrid cucumber flowers

Diversity of insects that visited F1 hybrid cucumber flowers, both male and female flowers, of the five flowers per sex in three replicates over a period of five days were observed. The study period was from 06:00 a.m. - 18:00 p.m. for the duration of 10 min hourly. It was found that insect pollinators had visited both sexes and there were five species present as follows: European bees, dwarf honeybees, stingless bees, beetles, and butterflies at 06.00 a.m. European bees were most common from 07:00 a.m. to 10:00 a.m. and was found most abundant at 09.00 a.m. in both male and female flowers. Stingless bees were found mostly from 10:00 a.m. to 13:00 p.m., and were most abundant in female flowers between 11.00 a.m. and 12.00 p.m. and in male flowers at 11.00 a.m. Other insect pollinators were minimal throughout the day (Figure 1 and 2) and no insect pollinators visited flowers during high-cloud periods.

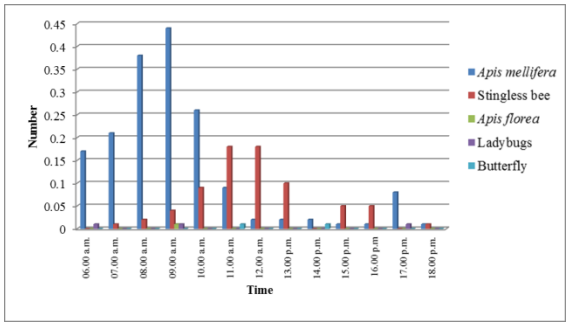

Figure 1. The average number of insect pollinators that visited female cucumber flowers conducted in five-day period between 06:00 a.m. - 18:00 p.m.

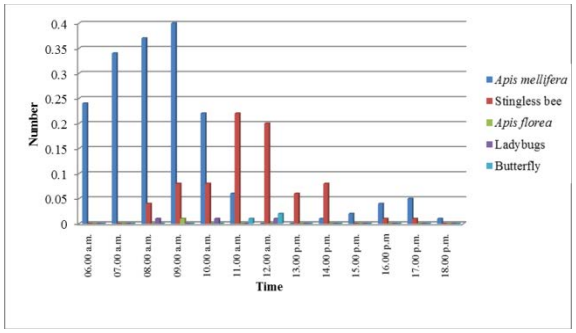

Figure 2. The average number of insect pollinators that visited male cucumber flowers during a five-day period between 06:00 a.m. to 18:00 p.m.

Discussion

Efficacy test of stingless bee as F1 hybrid cucumber pollinator were evaluated using two experiments.

In the study of stingless bees as pollinator, the results showed that fruiting only occurred in opened and handed – pollination treatments which exhibited high significant difference with the stingless bee - and closed –pollination treatments. This shows that stingless bees have lower potential as pollinators for F1 hybrid cucumber than European bees. This result is consistent with the observation by Wanta [3] that in durian, stingless bees were limited to nectar and male pollen collection from durian flowers but did not assist in pollination. European bees are better pollinators than stingless bees [5] because European bees are larger than stingless bees and can collect large quantities of nectar at a time resulting in higher visitation and transfer of male pollen to female pollen rates. On the contrary, stingless bees which are smaller in size exhibited lower transfer rate of male flower to the female flower resulting in no fruit set. The study of species diversity of insect pollinators had shown that insects that visited both male and female flowers were mostly European bees which visited around 06.00 a.m. onwards, and was found most abundant at 09:00 – 10.00 a.m. Stingless bees were found most abundant from 11:00 a.m. - 12:00 p.m. which is outside the optimum timeframe for cucumber pollination.

CONCLUSION

Efficacy of stingless bees *Lepidotrigona terminata* as pollinators of F1 hybrid cucumber is divided into two parts.

1. Efficacy of the stingless bees as pollinators in comparison between opened – pollination and handed – pollination showed that fruit set occurred only in opened and handed – pollination treatments resulting in 9.33 and 12.66 fruits, respectively.

2. The study of diversity of insect species and number that visited cucumber flowers showed that European bees visited most frequently between 06:00 a.m. - 10:00 a.m. and was found most abundant at 09.00 a.m. in both male and female flowers. Stingless bees visited female flowers most during 11.00 a.m. - 12.00 p.m. and visited male flowers most at 11.00 a.m. All other insects were found in minimal quantity throughout the day.

Acknowledgements

Thanks to the Faculty of Agricultural Technology for funding this research.

References

[1] Rapeepan Jaipakdee. 2001. Cucumber Fruit Vegetables Journal, 44(7) : 34

[2] Somnook Boongird. 1989. Durian is the Entomophilous plant. Kehagankaset. 13(17) : 54-57

[3] Wanta Taweepol. 2003. The Studies on Biology of Stingless Bee *Trigona (Lepidotrigona) terminata* Smith and It's Pollinated Efficiency on Durian (Durio zibethinus L.) Cultivar Chanee. Ms. Thesis. Kasetsart University. Bangkok.
[4] Janwit Samoskorn, Noppadol Posri and Piyawat Pantong. 2010. Efficacy of *Trigona pegdeni* for Pollination of F_1 hybrid cucumber. Special Problem of Plant Science, Faculty of Agricultural Technology, Rajamangala University of Technology Thanyaburi.
[5] Sawatthum. A., Sumtha, L., Loylom, N., Chuthapetch, C. and Suparit,K. 2016. Efficacy of European honey bee (*Apis mellifera*) as Insect Pollinator of F1 Hybrid Cucumber. The 4th Academic Science and Technology Conference. 31st May,2016. Bangkok, Thailand.

A LONG WAVES PROPAGATION IN TWO-LAYER FLUID OVER A SUBMERGED HUMP

Fatimah Noor Harun[1] and Muhammad Afiq Ahmad Khairuddin[2]
[1]School of Informatics and Applied Mathematics
Universiti Malaysia Terengganu, 21030 Kuala Terengganu,
Terengganu, Malaysia

ABSTRACT

The study of internal waves has become important because they are associated with the energy transfer mechanism across continental shelf edges. In addition, they also can cause strong localized departures from the surrounding ocean conditions, resulting in increased shear stresses on underwater structures and large variations in acoustic transmission properties of the ocean. Therefore, the internal waves cause problems in many areas such as offshore oil recovery, acoustic propagation in the ocean, and deep water outfall. Hence, this paper is conducted to study the two-layer long-waves propagation through submerged humps using analytical solution. Equation involved in this study are mild slope equation and the methods involve are separation of variables and a series solution. In this study the effect of the geometry of the hump when water waves propagating through the humps are also studied. Besides, the density ratio also give significance effect to the surface wave elevation. An analytical solutions obtained in this study is useful in reviewing applications and condition of the wave amplitude on submerged hump.

Keywords: Internal waves, Two-layer fluid, Mild-slope equation, Long wave, Analytic solution

INTRODUCTION

For almost two centuries, the progression of wave modeling research has intriguing many researchers. With concerns about energy are likely to become extinct, the future energy such as renewable wave energy are become one of the interest. According to [1] there are several types of flows in the ocean, and there is a type of flow which conserves forces and restores it with respect to density in different underwater depth called internal waves. Internal waves is formed by tidal currents propagates seamounts, continental slopes and mid-ocean pits and the waves projects tidal energy. The internal waves contain a large amount of energy, produces noises at the surface of the sea, which eventually causes cusps in the sea-surface spectrum, as discovered by [2]. The study of internal waves is pioneered by Stokes [3], Lamb[4], and Keulegan [5]. The process of wave phenomena such as refraction and diffraction of ocean surface waves can generate the energy. The famous mild-slope equation to study the refraction and diffraction on the ocean wave was introduced by Berkoff [6]. Then, this equation is widely used by [7-10] for single layer fluid and [11-13] for two-layer fluid. Recently, Harun[13] constructed the two-layer fluid for waves propagating over a bowl-pit. By extending[14] to two-layer fluid the analytical solution towards two-layer propagating waves over a submerged hump of variable depths is discussed.

ANALYTIC SOLUTION

This section present the derivation of the long waves propagating in two-layer fluid over a submerged hump of variables depths by utilizing the solution given by Zhu and Harun[12] and Niu and Yu[14]. Consider, a train of plane long waves propagates in two-layer fluids with constant depth, h_1 and h_2 and the densities for upper and lower layer are denoted by ρ_1 and ρ_2 is refracted by an axi-symmetric hump-shaped located on the ocean floor as depicted in Figure 1. The geometry of the hump which located at the lower layer is as described in [14] and defined by

$$h_2(r) = \begin{cases} h_2 & , \quad r > b \\ h_0 + \beta r^{\alpha} , & \quad r \le b. \end{cases} \tag{1}$$

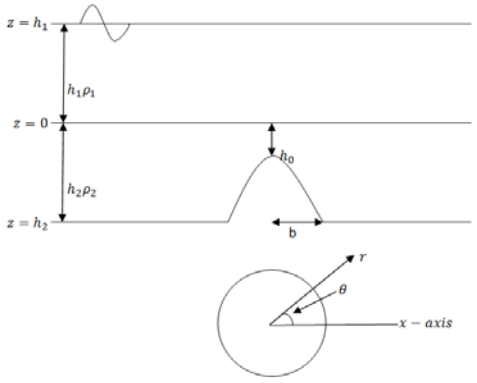

Fig. 1 A definition sketch of a hump located on

the floor in two-layer fluid systems.

Here, b is the radius of the hump in the horizontal plane, α and β are two independent parameters which control the shape of the hump. Here, β must always satisfied the relation $\beta = (h_2 - h_0)/b^{\alpha}$ and α is considered as a rational number defined by

$$\alpha = \frac{p}{q} \tag{2}$$

where p and q are integers and $q \neq 0$ and $p \geq 1$, and $q \geq 2$.

Separation of variables

By extending the solution given by [14] to two-layer fluid, the mild-slope equation in two-layer fluid is used to find the solution. Thus, when the wavelength is much longer than the wave height, the two-layer mild slope equation can be written as [12]

$$\nabla \cdot (\frac{(\rho_2 - \rho_1)h_1 h_2}{\rho_1 h_2 + \rho_2 h_1} \nabla \eta) + \frac{\sigma^2}{g}\eta = 0 \tag{3}$$

where

$$\sigma^2 \cong \frac{gk^2(\rho_2 - \rho_1)h_1 h_2}{\rho_1 h_2 + \rho_2 h_1}$$

and g is the gravitational acceleration, σ is the angular velocity and k is the wave number.

Because our system is axi-symmetric with respect to the z-axis, it is convenient to adopt a cylindrical coordinates system (r, θ, z). Equation (3) can be constructed via separation of variables as

$$\eta = \sum_{n=0}^{\infty} R_n(r)\cos(n\theta) \tag{4}$$

with $R_n(r)$ satisfying

$$r^2(-w_1 r^{2a} - w_2 r^a - w_3)\frac{d^2 R_n}{dr^2} + r(-w_1 r^{2a} - w_{4a} r^a - a_3)\frac{dR_n}{dr} + ((w_{5a} r^{2a} + w_{6a} r^a + w_{7a})\mu r^2 - n^2(a_1 r^{2a} + a_2 r^a + a_3))R_n = 0 \tag{5}$$

where

$$w_1 = (\rho_1 - \rho_2)\beta^2 \rho_1 h_1;$$
$$w_2 = (\rho_1 - \rho_2)(2h_0\rho_1 + h_1\rho_2)\beta h_1;$$
$$w_3 = h_0 h_1(\rho_1 - \rho_2)(h_0\rho_1 + h_1\rho_2);$$
$$w_{4a} = h_1(\rho_1 - \rho_2)(h_1\rho_2 a + 2h_0\rho_1 + h_1\rho_2)\beta;$$
$$w_{5a} = \beta^2 {\rho_1}^2$$
$$w_{6a} = 2\beta\rho_1(h_0\rho_1 + h_1\rho_2)$$
$$w_{7a} = (h_0\rho_1 + h_1\rho_2)^2$$
$$\mu = \frac{\sigma^2}{g}$$

The Frobenius Method

In this paper, we only consider α as a rational number. In order to use the Frobenius method, we have to let $r = s^q$, substitute this to Eq. (5) we have

$$s^2(w_1 s^{2p} + w_2 s^p + w_3)\frac{d^2 R_n}{ds^2} + s(w_1 s^{2p} + w_{4a} s^p + a_3)\frac{dR_n}{ds} + ((w_5 s^{2(p+p)} - w_6 s^{(p+2q)} + w_7 s^{2q}) - q^2 n^2(a_1 s^{2p} + a_2 s^p + a_3))R_n = 0 \tag{6}$$

where

$$w_4 = h_1(\rho_1 - \rho_2)(h_1\rho_2 p + 2h_0\rho_1 + h_1\rho_2)\beta;$$
$$w_5 = -\beta^2 {\rho_1}^2 \mu q^2$$
$$w_6 = -2\beta\rho_1(h_0\rho_1 - h_1\rho_2)\mu q^2$$
$$w_7 = -(h_0\rho_1 - h_1\rho_2)^2 \mu q^2$$

Eq. (6) is only second-order ordinary differential equation, thus, the general solution can be obtained using the Fobenius series method:

$$R_n(s) = \sum_{m=0}^{\infty} a_m s^{m+c} \tag{7}$$

where c is the root to be determined from the indicial equation and a_m are the recurrence relation to be determined and $a_0 \neq 0.$. Substituting Eq. (7) into Eq. (6) results in:

$$\sum_{m=0}^{\infty} a_m s^{m+c}\{[(m+c)^2 - q^2n^2]w_1 s^{2p} + [((m+c)(m+c-1) - q^2n^2)]s^p + [(m+c)^2 - q^2n^2]w_3 + w_5\rho^{2(q+p)} + w_6\rho^{p+2q} + w_7\rho^{2q}\} = 0 \quad (8)$$

Re-indexing Eq. (8), leads to

$$[(m+c-2p)^2 - q^2n^2]w_1 a_{m-2p} + [((m+c-p)(m+c-1) - q^2n^2)w_2 + (m+c-p)w_4]a_{m-p} + [(m+c)^2 - q^2n^2]w_3 a_m + w_5 a_{m-2(q+p)} + w_6 a_{m-(p+2q)} + w_7 a_{m-2q} = 0 \quad (9)$$

where $a_{m-p,}a_{m-2p}, a_{m-2(q+p)}, a_{m-(p+2q)}$ and a_{m-2q} equal to zero with the negative value of subscript. The indicial equation can be obtained by letting $m = 0$ in Eq. (9) and leads to

$$c = \pm nq \quad (10)$$

By the original variable r ,these two distinct roots of the indicial equation lead to two sets of linearly independent solutions:

$$R_{1n}(r) = \sum_{m=0}^{\infty} a_m r^{m/q+n} \quad (11)$$

$$R_{2n}(r) = R_{1n}\ln(r) + \sum_{m=0}^{\infty} b_m r^{m/q-n} \quad (12)$$

Since R_{2n} becomes singular at $r = 0$, it has to be discarded, with the imposition of the condition that water surface elevation must be finite at the origin.

Now, by considering Eq. (11) and when $p < 2q$, $\alpha < 2$, Eq. (9) gives

$a_m = 0$, for $0 < m < p$

$$a_m = -\frac{[((m+nq-p)(m+c-1) - q^2n^2)w_2 + (m+nq-p)w_4]a_{m-p}}{[(m+nq)^2 - q^2n^2]w_3}$$

for $p \le m < 2p$,

$$a_m = -\frac{([((m+nq-p)(m+c-1) - q^2n^2)w_2 + (m+nq-p)w_4]a_{m-p} + [(m+nq-2p)^2 - q^2n^2]w_1 a_{m-2p})}{[(m+nq)^2 - q^2n^2]w_3}$$

for $2p \le m < 2q$,

$$a_m = -\frac{([((m+nq-p)(m+nq-1) - q^2n^2)w_2 + (m+nq-p)w_4]a_{m-p} + [(m+nq-2p)^2 - q^2n^2]w_1 a_{m-2p} + w_7 a_{m-2q})}{[(m+nq)^2 - q^2n^2]w_3}$$

for $2q \le m < p + 2q$,

$$a_m = -\frac{([((m+nq-p)(m+nq-1) - q^2n^2)w_2 + (m+nq-p)w_4]a_{m-p} + [(m+nq-2p)^2 - q^2n^2]w_1 a_{m-2p} + w_7 a_{m-2q} + w_6 a_{m-2q})}{[(m+nq)^2 - q^2n^2]w_3}$$

for $p + 2q \le m < 2(q+p)$,

$$a_m = -\frac{\begin{array}{l}([[(m+nq-p)(m+c-1)-q^2n^2)w_2 \\ +(m+nq-p)w_4]a_{m-p} \\ +[(m+nq-2p)^2-q^2n^2]w_1 a_{m-2p} \\ +w_7 a_{m-2q}+w_6 a_{m-2q}) \\ +w_5 a_{m-2(p+q)}\end{array}}{[(m+nq)^2-q^2n^2]w_3}$$

for $m \geq 2(q+p)$. (13)

Then, when $p > 2q$, $\alpha > 2$, Eq. (9) leads to

$a_m = 0$, for $0 < m < 2q$,

$$a_m = -\frac{w_7 a_{m-2q}}{[(m+nq)^2-q^2n^2]w_3}$$

for $2q \leq m < p$,

$$a_m = -\frac{\begin{array}{l}w_7 a_{m-2q} \\ +[((m+nq-p)(m+nq-1)-q^2n^2)w_2 \\ +(m+nq-p)w_4]a_{m-p}\end{array}}{[(m+nq)^2-q^2n^2]w_3}$$

for $p \leq m < p+2q$,

$$a_m = -\frac{\begin{array}{l}(w_7 a_{m-2q}+ \\ [((m+nq-p)(m+nq-1)-q^2n^2)w_2 \\ +(m+nq-p)w_4]a_{m-p} \\ +w_6 a_{m-(p+2q)})\end{array}}{[(m+nq)^2-q^2n^2]w_3}$$

for $p+2q \leq m < 2p$,

$$a_m = -\frac{\begin{array}{l}(w_7 a_{m-2q}+ \\ [((m+nq-p)(m+nq-1)-q^2n^2)w_2 \\ +(m+nq-p)w_4]a_{m-p} \\ +w_6 a_{m-(p+2q)}+ \\ [(m+nq-2p)^2-q^2n^2]a_{m-2p})\end{array}}{[(m+nq)^2-q^2n^2]w_3}$$

for $2p \leq m < 2(q+p)$,

$$a_m = -\frac{\begin{array}{l}(w_7 a_{m-2q}+ \\ [((m+nq-p)(m+nq-1)-q^2n^2)w_2 \\ +(m+nq-p)w_4]a_{m-p} \\ +w_6 a_{m-(p+2q)} \\ +[(m+nq-2p)^2-q^2n^2]a_{m-2p} \\ +w_5 a_{m-2(p+q)})\end{array}}{[(m+nq)^2-q^2n^2]w_3}$$

for $m \geq 2(q+p)$. (14)

where m denotes the number of recurrence solutions for Frobenius series that we have to find until our solution is converged to a desire point, while n corresponds to the wave propagation modes.

Matched solution

For the general solution in the finite region with variable depth $r < b$, the water surface elevation is given by

$$\eta_2 = \sum_{n=0}^{\infty} C_n R_{1n}(k_0 r)\cos(n\theta) \quad (16)$$

where C_n is a set of complex constant to be determined. In the constant region $r \geq b$ the solution is given by

$$\eta_1 = \eta_l + \eta_s \quad (17)$$

where η_I corresponds to the incident wave and η_S to the scattered wave which defined by:

$$\eta_1 = A_I e^{ik_0 x} = A_I \sum_{n=0}^{\infty} i^n \varepsilon_n J_n(k_0 r)\cos(n\theta)$$

(18)

$$\eta_s = \sum_{n=0}^{\infty} B_n H_{1n}(k_0 r)\cos(n\theta)$$

(19)

in which A_I is the incident wave amplitude, $i=\sqrt{-1}$, k_0 is the wave number in the constant region, J_n is the Bessel function of the first kind, B_n is a set of complex constant to be determined, H_{1n} is the Hankel function of the first kind and ε_n is the Jacobi symbol define by

$$\varepsilon_n = \begin{cases} 1, & n = 0 \\ 2, & n \geq 1 \end{cases}$$

(20)

The solution in these two sub-regions must be matched on the common boundary $r = b$, require

$$\eta_1 = \eta_2 \qquad (r = b)$$

(21)

$$\frac{\partial \eta_1}{\partial r} = \frac{\partial \eta_2}{\partial r} \qquad (r = b)$$

(22)

Therefore, from Eqs. ((16)-(19), the coefficients C_n and B_n can be determined as

$$B_n = \frac{-A_I i^n \varepsilon_n \left[R_{1n}(b) k_0 J_n'(k_0 b) - R_{1n}'(b) J_n(k_0 b) \right]}{R_{1n}(b) k_0 H_{1n}'(k_0 b) - R_{1n}'(b) H_{1n}(k_0 b)} \tag{23}$$

$$C_n = \frac{2A_I i^{n+1} \varepsilon_n}{\pi b [R_{1n}(b) k_0 H'_{1n}(k_0 b) - R'_{1n}(b) H_{1n}(k_0 b)]} \tag{24}$$

in which the prime denote derivatives. By substituting these coefficents back to Eqs.(16)-(19), the water surface elevation for entire domain can be computed.

RESULTS AND DISCUSSION

This section presents a comparison of newly derived solution for a special case by taking $\rho_1/\rho_2 = 0$ with the single-layer equation discussed in Niu and Yu[14]. Then the effect of the density, wave height, and hump shaped to the wave refraction are examined.

Comparison with the single layer fluid

Since the 2-layer fluid model should reduce to single-layer model when $\rho_1 = 0$, it would be interesting to compare both model, as part of verification process. Let $\rho_1 = 0, \rho_2 = 5,$ $h_1 = h_2 = 3, h_0 = 2.8, b/L = 0.5$ and L =120.4. Fig. 2 shows the comparison of the relative amplitudes along x-axis for two- and single-layer fluid models. As expected, both solutions are hardly distinguishable.

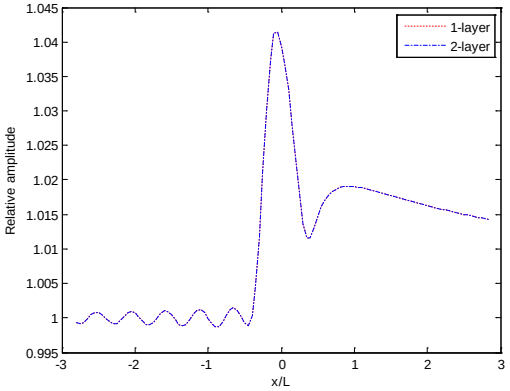

Fig. 2 Relative wave amplitude when ρ_1/ρ_2 are varied.

Effect of the density ratio

The effect of the wave refraction when the ratio of densities ρ_1/ρ_2 are varied while other parameters remain constant is discussed in this section.

Fig. 3 shows the comparisons for each value of ρ_1/ρ_2 along x-axis corresponding to ρ_1/ρ_2 =0, 1/5, 2/5, 3/5 and 4/5 while other parameters being fixed to b/L =0.5, $h_1 = h_2 = 3$. From this figure, it can clearly seen that, the relative wave amplitude increase with the decreasing value of ρ_1/ρ_2. This phenomenon occurs because, when the fluid is denser, the restoring force is weaker, resulting in smaller wave amplitude.

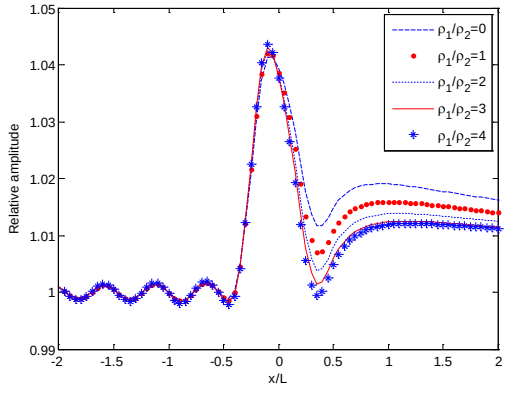

Fig. 3 Relative wave amplitude when ρ_1/ρ_2 are varied.

Effect of the layer thickness

Fig. 4 illustrates the relative wave amplitude for three difference values of h_1 / h_2 with ρ_1/ρ_2 =3/5. We can see that, the depth of the fluid layer also has significance effect to the relative wave amplitude. When, the upper layer is thicker, the wave can amplified more, whereas, when there is less fluid in lower layer, the relative amplitude getting smaller to balance the weight of the upper layer fluid.

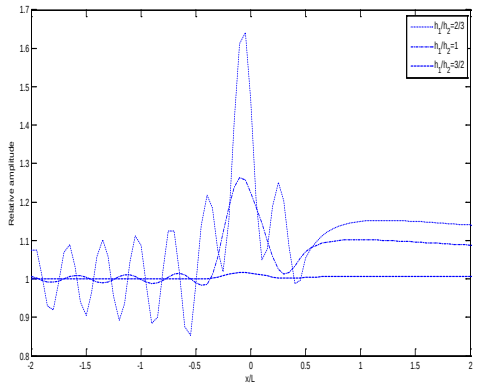

Fig. 4 Relative wave amplitude when ρ_1/ρ_2 =3/5, and h_1 / h_2 are varied.

Effects of the hump profiles

Next, the topographic effect when the hump profiles are changed is studied. In here we set $\alpha = 1/2, 5/2$ and 2. From Fig. 5 we can observed that, the relative wave amplitude is increase with the increasing of the α that control the hump profiles. This is because, when the value of α increase, the area of the hump is expanded.

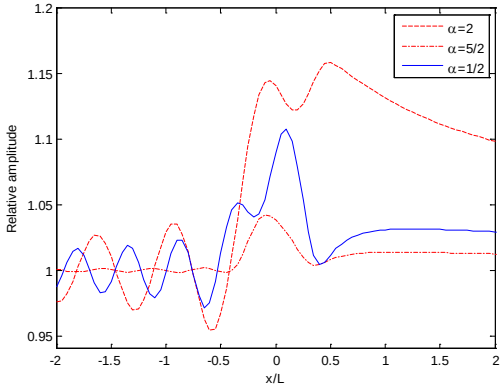

Fig. 5 Relative wave amplitude when $\rho_1/\rho_2 = 2$ and α are varied.

CONCLUSION

A new analytic solution is derived for two-layer fluid model for long waves propagating over a circular hump. The solution is verified with the single layer fluid model when the density of the upper layer, $\rho_1/\rho_2 = 0$. There is also a significance effects to the relative wave amplitude with the addition of the density and the layers. The restoring force between both layers getting weaker with the smaller density difference and when there is more fluid in upper layer, the relative wave amplitude getting smaller to balance the weight of the fluid in the upper layer. For the effect of the hump profiles, the increasing of the α value lead to the increasing of relative wave amplitude. This finding is useful in reviewing applications and condition of the wave amplitude on submerged hump.

ACKNOWLEDGEMENTS

The authors would like to acknowledge the financial support (Vot No: 57105) from Ministry of Higher Education, Malaysia.

REFERENCES

[1] Stewart RH, Introduction To Physical Oceanography. Texas: A&M University, 2008, ch. 7.
[2] Munk WH and Cartwright DE, "Tidal Spectroscopy and Prediction", Phil. Trans. R. Soc. A Mathematical, Physical and Engineering Sciences, Vol. 259,May 1966, pp. 533-581.
[3] Stokes GG, Trans. Camb. Phil. Soc. 8 1847, pp.441-455.
[4] Lamb H., Hydrodynamic, sixth ed., Cambridge University Press, 1932.
[5] Keulegan GH, J. Res. Natl. Bur. Stand 51. 133.1953.
[6] Berkhoff JCW, "Computation of Combined Refraction and Diffraction", Proc. 13th Int Conf On Coastal Eng, July 1972, pp. 471-490.
[7] Mei CC, The Applied Dynamics of Ocean Surface Waves 2nd Edition. World Scientific, Singapore, New Jersey, London, Hong Kong, 1994, ch. 1.
[8] Homma S, "On the Behavior of Seismic Sea Waves around Circular Island", Geophys. Mag.,Vol. 21,1950, pp. 231- 233.
[9] MacCamy RC and Fuchs RA, Wave forces on piles: A diffraction theory, US Army Corps of Engineering Beach Erosion Board Washington DC Technical Memorandum, Vol. 69, Dec. 1954, pp. 1-17.

[10] Massel SR, Extended Refraction-diffraction Equation for Surface Waves, Coastal Eng.,Vol. 19,Jan. 1993, pp. 97-126.
[11] Harun FN, Analytical Solution For Wave Diffraction Around Cylinder, Res. J. Recent Sci., Vol. 2(9), Sept. 2013, pp. 5-10.
[12] Zhu SP and Harun FN, Refraction of interfacial waves by a circular hump, Proc of the Institution of Civil Eng and Comp Mech, 162 (4), 2009, pp.199-213
[13] Harun FN, A Long Waves Propagation in Two-Layer Fluid over a Circular Bowl Pit AIP Conf. Proc. 1750, 2016, pp. 030009-1-030009-10.
[14] Niu x and Yu X, Analytic solution og long waves propogation over a submerged hump, Coastal Eng. 58, 2011, pp 143.150.

Second International Conference on Science, Engineering & Environment,
Osaka City, Japan, Nov.21-23, 2016, ISBN: 978-4-9905958-7-6 C3051

PARASITES OF THREE SPOT GOURAMI (TRICHOGASTER TRICHOPTERUS PALLAS, 1770) IN THE THUNG LAM RESERVOIR AT AMPHOE NANGRONG, BURIRAM PROVINCE, THAILAND

Supamas Sriwongpuk[1]
[1]Faculty of Agricultural Technology, Rajamangala University of Technology Thanyaburi, Thailand.

ABSTRACT

Study on parasites of the Three Spot Gourami *Trichogaster trichopterus* (Pallas, 1770) was conducted using the samples collected from Thung Lam Natural Reservoir in Tumbon Tha-Non Hug, Amphoe Nangrong, Buriram Province, Thailand. For the period of three months collections were made during November 2014 to January 2015. The total number of one hundred and twenty of the Three Spot Gourami were investigated and all of them one hundred percent were found to be prevalenced with the parasites. Three species of parasites in three generas of two phylums were observed. Two species were external parasites found at the gill filaments consisted of monogenetic trematodes or monogenean parasites in phylum Platyhelminthes namely, *Trianchoratus aecleithrium* and *Gyrodactylus* sp. One species was internal parasite found in the intestine consisted of Spiny headed-worm in phylum Acanthocephala namely *Pallisentis nagpurensis.* The highest parasite number of intencity in the Three Spot Gourami was *Trianchoratus aecleithrium* which found to be 64.79 and the least parasite number of intencity in Three Spot Gourami was *Gyrodactylus* sp. which found to be 5.9.

Keywords: Parasites, Three Spot Gourami, Trichogaster trichopterus, Thailand

INTRODUCTION

Three Spot Gourami, *Trichogaster trichopterus* (Fig. 1) also known as the blue gourami or Pla Kra-Dee, is a species of gourami native to southeastern Asia. It has two spots on each side; the third spot is the eye. Its scales are blue colour and it can also called the blue gourami.[1] They are native to standing or slow-moving freshwater habitats in southeastern Asia, ranging from Yunnan (China), through mainland southeastern Asia (Cambodia, Loas, Malaysia, Myanmar, Singapore, Thailand and Vietnam) to Java, Borneo and Sumatra.[2] In Thai is a true native fish of Thailand. It is a traditional diet and the people prefer it salted and sun-dried before serving with rice as deep fry fish.

Fig. 1 Morphology of Three Spot Gourami

Buriram, a representative province of the northeastern region of Thailand is situated at 14°15'N - 15°45'N and 102°30'E - 103°45'E about 410 km from Bangkok. Thung Lam Reservoir is a small natural reservoir which has been renovated into a recreational area with shelters for rest and relaxation. During the dry season, many species of waterfowl can be found at this reservoir. It located at the Ban Hak intersection on highway no.24 about 4 km from Nang Rong District *in Buriram Province.*

Due to Thung Lam Reservoir is important to the economy of Nang Rong District in Buriram province. It is the natural source of water for irrigation, agriculture, fisheries, tourism and the habitat of a variety species of fresh water fish. Most villagers will catch these fish which are smaller to be processed as food protein such as dried fish, fermented fish and fish meal. Nevertheless during the culture peroid, it could experience many serious problems, particularly those caused by parasites which were regarded as a major cause of low production in aquaculture system.

This study, aim to survey and study morphological characterization of the parasites in the Three Spot Gourami from Thung Lam Reservoir in Nang Rong District, Buriram province. This result will be a fundimental data for parasitic study and for prophylaxis this disease causing agents in aquaculture *and* people who consumed those fish for food.

METHODOLOGY

One hundred and twenty of the Three Spot Gourami were obtained from the Thung Lam Reservoir in Nang Rong District, Buriram province during November 2014 to January 2015. Fish were measured and killed. Skin and fin mucous were scraped and examined using compound and phase-contrast microscopy. Gills were removed and scraped into a Petri dish filled with clean water to dislodge the parasites and examined under a stereo microscope. The external parasites found were transferred onto a glass slide and covered with coverslip. The intestines were removed from body cavity and the contents were then examined under the microscope. Parasites were fixed and preserved using the appropriate methods for each group as outlined by Tonguthai *et al*. (1999) [3].

The parasites identification was based on morphological features according to Gelnar (1989) [4], Price and Berry (1996) [5], Sirikanchana (2003) [6] and Paperna (1996) [7]. Prevalence and mean intensity of each parasitic species were determined as in Margolis *et al*. (1982) [8].

RESULTS AND DISCUSSION

Two parasitic groups with a total of three species were collected from one hundred and twenty samples of the Three Spot Gourami. All samples were infected with external and internal parasites (100% prevalence with parasites). There were two monogenetic trematodes or monogenean species found in the gill filaments and one spiny headed-worm species found in the intestine were shown in Table 1.

Table 1. Prevalence and mean intensity of parasites in the Three Spot Gourami collected from Thung Lam Reservoir in Tumbon Tha-Non Hug, Nang Rong District, Buriram province.

Parasite species	Parasite group	Number of fish	Total number of parasites	Prevalence (%)	Mean intensity
Trianchoratus aecleithrium	monogenean	120	219	100	64.79
Gyrodactylus sp.	monogenean	2	20	1.66	5.91
Pallisentis nagpurensis	Acanthocephala	33	99	27.5	29.28

Morphological details of the parasites examined are given below.

1. *Trianchoratus aecleithrium* (Fig. 2-3)

It is a flatworm or monogenetic trematode mainly found on gills of fish, generally elongated and compressed dorso-ventrally. Body: 0.28-0.37 mm long and 0.07-0.09 mm width, covered with smooth and thin cuticle, with two pairs of eye spots in anterior part. Pharynx looked like oval shape, 0.02-0.03 mm in diameter. Opishaptor bilobed, 0.03-0.04 mm long and 0.08 mm width, distinctly separated from body. There are three anchors: dorsal anchor with outer length 0.04 mm, inner length 0.03 mm based width 0.01 mm, point length 0.016 mm, length of inner root 0.017 mm, of outer root 0.008 mm. Ventral anchors with 0.028 mm, inner length 0.026 mm base width 0.015 mm point length 0.018 mm, length of inner root 0.014 mm, of outer root 0.004 mm. Supporting bars of opishaptor lacking. There are 14 marginal hooks, measuring 0.013 in total length. Copulatory organ, measuring 0.04 mm in total length, consists of non-articulated cirrus and accessory piece. Vagina opening laterally and reinforced by weakly sclerotized vaginal tube.

Fig. 2 Copulatory organ of *T. aecleithrium* (arrow) (scale = 0.02 mm)

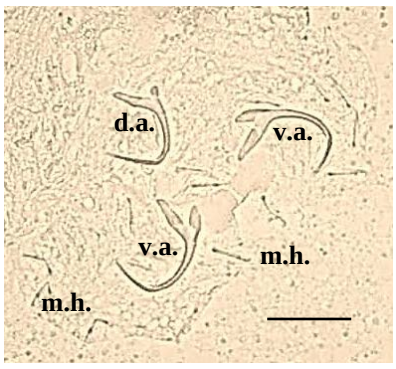

Fig. 3 Opishaptor of *T. aecleithrium* (scale = 0.02 mm) (d.a.= dorsal anchor; v.a.= vental anchor; m.h.= marginal hooks)

The genus *Trianchoratus* has the three well-developed anchors was first described by Price and Berry (1966) [5] from the gills of kissing gourami (*Helostoma rudolfi* Machan) belonging to the family Helostomatidae from south-eastern Asia. *T. aecleithrium* was described by Gelnar (1989) [4] from the gills of *Trichogaster trichopterus trichopterus* from aquarium in Czechoslovakia, which originate from the same geographic region, but belongs to another, though relative family, Belontiidae, extends of the host specificity of the parasite.

2. *Gyrodactylus* sp. (Fig. 4-5)

It is a small (0.2 mm) monogenetic trematode mainly found on fin or external skin of fish, generally elongated and compressed dorso-ventrally. There are two lobes at the anterior end of the head without eye spots. It is viviparous and embryos with well developed hooks may be seen in side the body of adult. The opishaptor armed with a pair of large hooks and sixteen marginal hooks.

Fig. 4 *Gyrodactylus* sp. (scale = 0.02 mm) (op.= opishaptor)

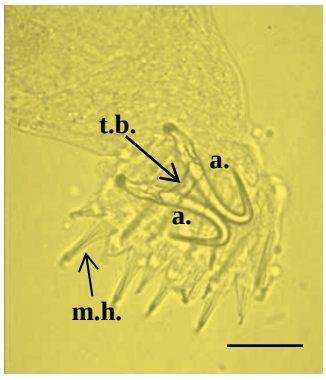

Fig. 5 Opishaptor of *Gyrodactylus* sp. (scale = 0.02 mm) (a.= anchor; t.b.= transverse bar; m.h.= marginal hooks)

The genus *Gyrodactylus* has many species is found worldwide parasitizing mostly that cause infestation in both marine and freshwater fish. [9] Heavy infestations by these parasites can result in destruction of the fin or skin epitheliam due to machanicaldamage caused by the attachment organ.

3. *Pallisentis nagpurensis* (Fig. 6-8)

Body looked like cylindrical 4.1 mm long, 0.3 mm wide. Proboscis large, globular, 0.17 mm long, 0.2 mm wide, armed with 4 circles of 10 fine recurved hooks, similar in shape but different in size. Hooks of first circle stouter and largest, and of basal row smallest. Each hook consists of a recurved blade, a horizontally directed root, handle sunk in proboscis wall. Neck is longer. Proboscis receptacle sac like single layered. Lemnisci tubulars are longer than proboscis receptacle. Body consists of collar and trunk spines. Collar spines arrange in 14-16 transverse circles, each with 16 spines. Trunk spines start after a short non-spiny area having 20 circles, each with 14-16 spines. Anterior and posterior testes are 0.3 mm long and 0.1 wide. Seminal vesicle is 0.3 mm long and 0.06 wide. Cement gland is single, syncytial, cylindrical just behind testes, 0.3 mm long and 0.1 wide. Cement reservoir is 0.2 mm long and 0.1 wide. From each testis a vas deferens runs down in close association with cement gland, cement reservoir and joins bursa.

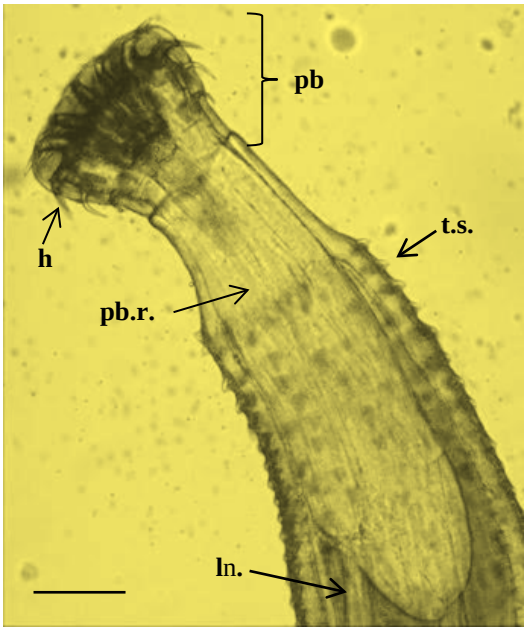

Fig. 6 The head part of *P. nagpurensis* (scale = 0.1 mm) (pb = proboscis; h = hook; pb.r. = proboscis receptacle; ln. = lemnisci; t.s. = trunk spine)

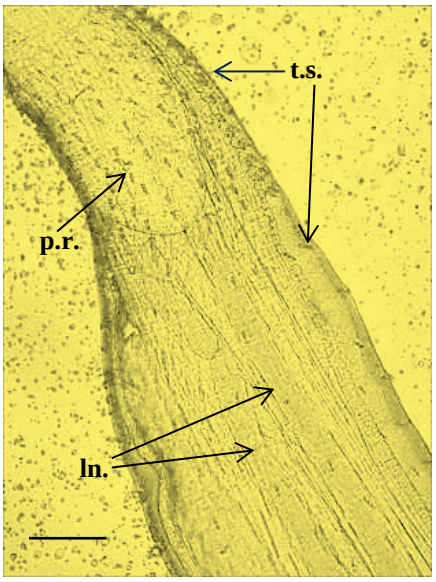

Fig. 7 The trunk part of *P. nagpurensis* (scale = 0.1 mm) (pb.r. = proboscis receptacle; ln. = lemnisci; t.s. = trunk spine)

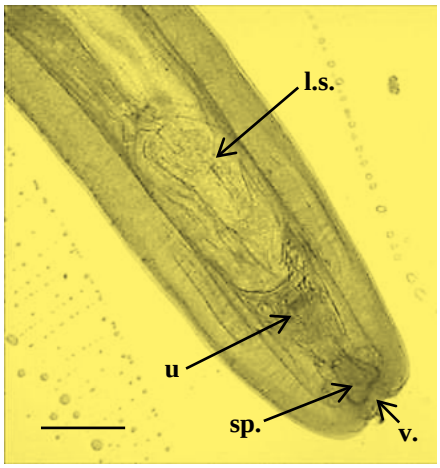

Fig. 8 The tail (end) part of *P. nagpurensis* (female) (scale = 0.1 mm))l.s. = ligament sag; sp. = sphincter; u = uterus; v = vulva(

The genus *Pallisentis* was described by Van Cleave (1928) [10] from an unknown number of specimens collected from Three species of fish at Beijing, China. It was grouped under class Eoacanthocephala [11], order Gyracanthocephala [12], family Quadrigyridae [13] and subfamily Pallisentinae [14]. It is an acanthocephalans. They are intestinal parasites of fishes, amphibians, birds,reptilesmand mammals worldwide distribution, penetrate their thorny proboscis into the intestinal wall of host and absorb nutrition. When a large number of parasites are found, cause occulation of the lumen of stomach and intestine, and even deatg of the fish host.[15] In Thailand *P. nagpurensis* was found in *Ophicephalus striatus* from Sing Buri Province [16] and Bangkok [17]; *Channa striatus* and *C. licius* from Bung Boraphet, Nakhon Sawan Province [18].

CONCLUSSION

This study was found three species of parasites in the Three Spot Gourami *T. trichopterus* collected from Thung Lam Natural Reservoir in Tumbon Tha-Non Hug, Amphoe Nangrong, Buriram Province, Thailand. There were *Trianchoratus aecleithrium*, *Gyrodactylus* sp. and *Pallisentis nagpurensis* with the mean intencity of 64.79, 5.91 and 29.28 respectively.

ACKNOWLEDGEMENTS

The author would like to express the sincere thanks for the participation of the Faculty of Agricultural Technology, Rajamangala University of Technology Thanyaburi and others. We would also say thanks to those who could not be mentioned here for their kindness and encouragement.

REFERENCES

[1] Frankel, J.S. 1992. Inheritance of trunk coloration in the three-spotgourami, Trichogaster trichopterus Pallas. Journal of Fish Biology 41: 663-665.
[2] Vidthayanon, C. 2001. Freshwater Fishes of Thailand. Nanmee Books Co. Ltd., Bangkok. 116 p. (in Thai).
[3] Tonguthai, K., Chinabut, S., Limsuwan, C., Somsiri, T., Chanratchakool, P. and Kanchanakarn, S. 1999. Diagnostic Proceedures for Finfish Diseases, “Blue Book”. Aquatic Animal Health Research Institute. Department of Fisheries, Bangkok.
[4] Gelnar, M. 1989. The morphology of *Trianchoratus aecleithrium* Price et Berry, 1966 (Dactylogyridae, Monogenea) from a new host *Trichogaster trichopterus trichopterus* (Pallas, 1777). Folia Parasitologica 35:7-11.
[5] Price, C.E. and Berry, W.S. 1996. *Trianchoratus*, a new genus of Monogenea. P. Helm. Soc. Wash. 33:201-203.
[6] Sirikanchana, P. 2003. Parasites of Aquatic Animal. 6th edition. Sky Word Advertising Partnership, Bangkok. 270 p. (in Thai).
[7] Paperna, I. 1966. Parasites, infections and diseases of fishes in Africa. An Update. CiFa Technical Paper No. 31. Food and Agriculture Organization, Rome. 220 p.
[8] Margolis, L., Esch, G.E., Holmes, J.C., Kuris, A.M. and Schad, G.A. 1982. The use of ecological terms in parasitology (repoet of an Ad Hoc committee of the American Society of

Parasitologists). J. Parasitol. 68(1): 131-133.
[9] Appleby, C. and Mo, T.A. 1997. Population dynamics of Gyrodactylus salaris (Monogenea) infecting Atlantic salmon, Salmo salar, parr in the river Batnfjordselva, Norway. Parasitology 83(1):23-30
[10] Van Cleave, H.J. 1928. Acanthocephala from China. I. New species and new genera from Chinese fishes. Parasitology 20:1-9.
[11] Van Cleave, H.J. 1948. Expanding horizons in the recognition of a phylum. J parasitol. 34(1): 1-20.
[12] Van Cleave, H.J. 1936. The recognition of a new order in the Acanthocephala. J parasitol. 22(2): 202-206.
[13] Van Cleave, H.J. 1920. Notes on life cycle of two species of Acanthocephala from freshwater fishes. J parasitol. 6(4): 167-172.
[14] Amin, O.M. 1985. Biology of Acanthocephala: Classification, Cambridge University Press, Cambridge, U.K.
[15] Fatima, H. 1988. Seasonal variation and histophatology of nematodes and Acanthocephalan of some edible fishes of Karacho coast. PhD. Thesis, Department of Zoology, University of Karachi, Pakistan. 516 pp.
[16] Sirikanchana, P. (1983). Seasonal variations of parasites in alimentary canal of snake-head fish (*Ophiocephalus striatus* Bloch) from natural waters. Bangkok: Department of Fisheries, Kasetsart University. 22 pp.
[17] Sirikanchana, P. (1988). Some parasites infected fishes from Bung Makkasan, Bangkok. Bangkok: Department of Fisheries, Kasetsart University. 12 pp.
[18] Monrudee, C., Chalobol, W. and Pheravut, W. (2007). Diversity of Helminths Found in Channid Fish from Bung Boraphet. Southeast Asian J Trop Med Public Health 38(suppl 1): 191-193.

Second International Conference on Science, Engineering & Environment,
Osaka City, Japan, Nov.21-23, 2016, ISBN: 978-4-9905958-7-6 C3051

EFFECTS OF BIO-EXTRACTS ON GROWTH AND QUALITY OF LETTUCES

Yaowarat Wongsrisakulkaew[1], Chanpen Chaimongkol[1], Niyom Buaban[1] and Sawat Pimsuwan[1]
[1] Faculty of Agricultural Technology, Rajamangala University of Technology Thanyaburi, Thailand

ABSTRACT

Study on effect of bio-extracts on growth and quality of green oak, red oak, butter head and red coral lettuces. The experimental design was RCBD (Randomized Complete Block Design) with 3 treatments and 4 replications include chemical fertilizer (16-16-16), bio-extract of fish meal and bio-extract of soybean meal. This experiment was conducted at The Division of Crop Production, Faculty of Agricultural Technology, Rajamangala University of Technology Thanyaburi. The result of this study showed that the vegetative yield of butter head and red oak lettuces treated with bio-extract of fish meal and soybean meal was similar to chemical fertilizer. There was no statistically difference on the vegetative yield of red coral and green oak lettuces. Both of Bio-extract of fish meal and soybean meal could increase the color of leaves in red oak and green oak lettuces than chemical fertilizer. Bio-extract of fish meal could increase the color of leaves in red coral and butter head lettuces than bio-extract of soybean meal and chemical fertilizer respectively.
Keywords: Bio-extract, Red Oak, Green Oak, Red Coral, Butter Head

INTRODUCTION

Vegetables are plants which everybody consumes everyday more or less differently. Due to the fact that vegetables are composed of several kinds of essential nutrient. Therefore, vegetables are favored for every household. As we can see in almost every kind of food, there are vegetables as ingredients to flavor better taste of food. They are also used as decoration and make dishes look beautiful and appetizing. As to the value of vegetable consumption of general people is selecting vegetables without traces of worms' destruction or pest, so farmers have to beautify their vegetables to meet the demands of consumers. Once buyers eat those vegetables, they may obtain the danger of toxic residue remained in them. Currently, bio-extract has been used in agricultures in many aspects, especially vegetable and plant production.

Reference [4] shows that bio-extract is fermented water derived from decomposition of remained materials from various parts of plants or animals by the fermenting procedure of anaerobic condition. Microorganisms decomposes plants and animals waste and transforms them to solution as well as uses enzyme generated naturally or adding enzyme to accelerate decomposing [5]. Bio-extract will adjust the condition of acids and bases in soil and water. It helps create plants' hormones and decompose organic matters [6]. To produce numerous quantities of plants, it's necessary to use high chemicals causing hazard to consumers and producers. Using chemicals benightedly of agriculture will affect ecological system both physical and biological ways, especially human's health and life quality [7]. To use chemicals is convenient and easy to find in markets as well as increases products of plants quickly.

On the other hand, using chemicals in agriculture will be slowly decomposed. Therefore, they will be accumulated and spread around which will turn into pollution of environment. They will ruin the balance of soil, water, air and will transmit into food chain. Plus, there will be remained chemicals in agricultural products. The lasted long remained chemicals will enable pest to adjust itself and resist drug action [7],[8]. There will be the dissemination of pest which destroys agricultural products. Agricultural area will be deteriorated. According to these reasons, it's a start-up of making bio-extract to replace chemicals in order to create safety for manufacturers and consumers. Consequently, the study of bio-extract using for lettuce's production may help leverage the capability of vegetable's production safely as well as reduce the cost of vegetable's production because lettuce are popular consuming extensively among groups of people who love their health. The aim of this research was to examine the vegetative yield of lettuces when treated with bio-extracts.

MATERIALS AND METHODS

Experimental details

The experiment was conducted at The Division of Crop Production, Faculty of Agricultural Technology, Rajamangala University of Technology Thanyaburi. To study on effect of bio-extracts on vegetative growth and quality of 4 cultivars lettuces (red oak, green oak, red coral and butter head). The experimental design was RCB with 4 replications and 3 treatments include chemical fertilizer (16-16-

16), bio-extract of fish meal and bio-extract of soybean meal which were applied at 3 weeks after planting. Chemical fertilizer was applied 2 g./pot and both of bio-extracts which were applied 200 ml./plant/week. Sample plants were observed for vegetative growth: plant height, shrub width, number of leaves, fresh weight and color of leaves.

RESULTS

Red oak lettuce

Red oak lettuce grown in media with chemical fertilizer had the widest average of shrub width (26.03 cm.) while the treatments with bio-extract of soybean meal and bio-extract of fish meal showed 25.1 and 24.63 cm. respectively. The maximum number of leaves (14.92) was from treatment with chemical fertilizer, whereas bio-extract of soybean meal and bio-extract of fish meal presented 13.93 and 13.87, respectively. There is no significant difference between three treatments (Table 1). However, comparison of height among three treatments found that the maximum average of height red oak is growing with bio-extract of soybean meal (15.92 cm.), bio-extract of fish meal (14.58) and chemical fertilizer (13.50), respectively.

Table 1 The vegetative yield of red oak lettuce treated with chemical fertilizer, bio-extract of fish meal and soybean meal.

Treatment	Vegetative yield			
	Height (cm)	No.of leaves	Shrub width (cm)	Fresh weight (g)
Chemical fertilizer(16-16-16)	13.50 b	14.92 b	26.03 b	122.20 a
Bio-extract of fish meal	15.92 a	13.87 b	25.21 b	118.37 b
Bio-extract of soybean meal	14.58 ab	13.93 b	24.63 b	117.42 ab
F test	*	ns	ns	*
(CV)%	5.40	16.73	4.67	21.32

Means followed by the same letter at the same column were not significantly different by LSD
* significant at P<0.05 and ns not significant

Treatments with chemical fertilizer and bio-extract did not show color differences of lettuce leaves using necked eyes. However, lettuce leaves had color differences using color chart (RHS) by leaves of red oak with chemical fertilizer showed greyed-orange (166A) and with bio-extracts are greyed-purple(187A) (Fig. 1, Table 2).

Table 2 The color of leaves in red oak lettuce (Greyed-Red Group)

Treatment	Color of leaves
Chemical fertilizer (16-16-16)	Red(Greyed-Orange 166A)
Bio-extract of fish meal	Red (Greyed -purple 187A)
Bio-extract of soybean meal	Red (Greyed -purple 187A)

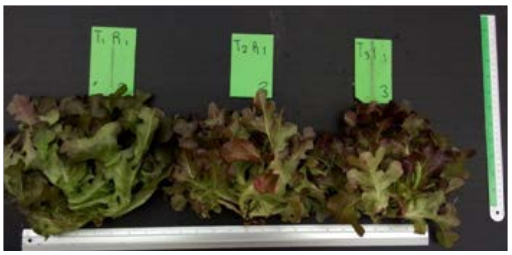

Chemical fertilizer (16-16-16) Bio-extract of fish meal Bio-extract of soybean

Fig. 1 The color of leaves in red oak lettuce treated with chemical fertilizer, bio-extract of fish meal and soybean meal.

Green oak lettuce

Green oak lettuce grown in media with chemical fertilizer had the maximum number of leaves (15.00) , whereas bio-extract of soybean meal and bio-extract of fish meal presented 12.58 and 10.58, respectively. The widest average of shrub width (22.50 cm.) was from treatment with chemical fertilizer while the treatments with bio-extract of soybean meal and bio-extract of fish meal showed 20.46 and 19.79 cm. respectively. There is no significant difference between three treatments (Table 3). However, comparison of fresh weight among three treatments found that the maximum average of fresh weight is growing with chemical fertilizer (55.90 g.), bio-extract of soybean meal (35.96 g.) and bio-extract of fish meal (25.86 g.), respectively.

Table 3 The vegetative yield of green oak lettuce treated with chemical fertilizer, bio-extract of fish meal and soybean meal.

Treatment	Vegetative yield			
	Height (cm)	No. of leaves	Shrub width (cm)	Fresh weight (g)
Chemical fertilizer(16-16-16)	16.42	15.00 a	22.50	55.90 a
Bio-extract of fish meal	15.33	10.58 b	19.79	25.86 b
Bio-extract of soybean meal	16.92	12.58 ab	20.46	35.96 ab
F test	ns	*	ns	*
(CV)%	12.30	16.73	10.03	36.31

Means followed by the same letter at the same column were not significantly different by LSD
* significant at P<0.05 and ns not significant

Treatments with chemical fertilizer and bio-extract did not show color differences of lettuce leaves using necked eyes. However, lettuce leaves had color differences using color chart (RHS) by leaves of green oak with chemical fertilizer showed Yellow-Green group (144 B) and with bio-extracts are Yellow-Green group (145 A) (Table 4, Fig. 2).

Table 4 The color of leaves in green oak lettuce (Green Group)

Treatment	Color of leaves
Chemical fertilizer(16-16-16)	Green (Yellow-Green group 144 B)
Bio-extract of fish meal	Green (Yellow-Green group 145 A)
Bio-extract of soybean meal	Green (Yellow-Green group 145 A)

Chemical fertilizer (16-16-16) Bio-extract of fish meal meal Bio-extract of soybean

Fig. 2 The color of leaves in green oak lettuce treated with chemical fertilizer, bio-extract of fish meal and soybean meal.

Red coral lettuce

Red coral lettuce treated with bio-extract of soybean meal had the widest average of shrub width (27.35 cm.) while the treatments with chemical fertilizer and bio-extract of fish meal showed 21.16 and 20.33 cm. respectively. The maximum number of leaves (10.41) was from treatment with bio-extract of soybean meal, whereas chemical fertilizer and bio-extract of fish meal presented 10.16 and 9.57, respectively. There is no significant difference between three treatments (Table 5). However, comparison of height among three treatments found that the maximum average of height red coral is growing with bio-extract of soybean meal (13.66 cm.), bio-extract of fish meal (12.41) and chemical fertilizer (11.91), respectively. There is no significant difference between three treatments. However, comparison of fresh weight among three treatments found that the maximum average of fresh weight is growing with bio-extract of soybean meal (16.93 g.), chemical fertilizer (15.39 g.) and bio-extract of fish meal (12.01 g.), respectively.

Table 5 The vegetative yield of red coral lettuce treated with chemical fertilizer, bio-extract of fish meal and soybean meal.

Treatment	Vegetative yield			
	Height (cm)	No.of leaves	Shrub width (cm)	Fresh weight (g)
Chemical fertilizer(16-16-16)	11.91a	10.16a	21.16a	15.39a
Bio-extract of fish meal	12.41a	9.57a	20.33a	12.01a
Bio-extract of soybean meal	13.66a	10.41a	27.35a	16.93a
F test	ns	ns	ns	ns
(CV)%	10.59	17.99	18.88	22.94

Means followed by the same letter at the same column were not significantly different by LSD ns= not significant

However, lettuce leaves had color differences using color chart (RHS) by leaves of red coral with chemical fertilizer showed greyed-red (178A) and with bio-extracts are greyed-red (181B and182A) (Table 6, Fig.3).

Table 6 The color of leaves in red coral lettuce (Greyed-Red Group)

Treatment	Color of leaves
Chemical fertilizer (16-16-16)	Red(Greyed-Red 178A)
Bio-extract of fish meal	Red (Greyed -Red 182A)
Bio-extract of soybean meal	Red (Greyed -Red 181B)

Chemical fertilizer (16-16-16) Bio-extract of fish meal meal Bio-extract of soybean

Fig. 3 The color of leaves in red coral lettuce treated with chemical fertilizer, bio-extract of fish meal and soybean meal.

Butter head lettuce

Butter head lettuce grown in media with bio-extract of soybean meal had the widest average of shrub width (27.03 cm.) while the treatments with chemical fertilizer and bio-extract of fish meal showed 21.11 and 20.33 cm. respectively. The maximum number of leaves (19.66) was from treatment with chemical fertilizer, whereas bio-

extract of fish meal and bio-extract of soybean meal presented 15.58 and 15.08, respectively. There is no significant difference between three treatments (Table 7). However, comparison of height among three treatments found that the maximum average of height butter head is growing with bio-extract of soybean meal (22.12 cm.), chemical fertilizer (21.80 cm) and bio-extract of fish meal (18.99 cm), respectively. There was a significant difference between three treatments. However, comparison of fresh weight among three treatments found that the maximum average of fresh weight is growing with bio-extract of fish meal (53.49 g.), bio-extract of soybean meal (50.27 g.) and chemical fertilizer (47.60 g.) , respectively. There is no significant difference between three treatments.

Table 7 The vegetative yield of butter head lettuce treated with chemical fertilizer, bio-extract of fish meal and soybean meal.

Treatment	Vegetative yield			
	Height (cm)	No. of leaves	Shrub width (cm)	Fresh weight (g)
Chemical fertilizer(16-16-16)	21.80a	19.66a	21.16a	47.60a
Bio-extract of fish meal	18.99b	15.58a	20.33a	53.49a
Bio-extract of soybean meal	22.12a	15.08a	27.03a	50.27a
F test	*	ns	ns	ns
(CV)%	5.41	14.14	6.10	12.40

Means followed by the same letter at the same column were not significantly different by LSD ns= not significant

Treatments with chemical fertilizer and bio-extract did not show color differences of lettuce leaves using necked eyes. However, lettuce leaves had color differences using color chart (RHS) by leaves of butter head with chemical fertilizer showed Green group (141 B) and with bio-extracts were Green group (138 A) (Table 8, Fig. 4).

Table 8 The color of leaves in butter head lettuce (Green Group)

Treatment	Color of leaves
Chemical fertilizer(16-16-16)	Green (Green group 141 B)
Bio-extract of fish meal	Green (Green group 138 A)
Bio-extract of soybean meal	Green (Green group 138 A)

DISCUSSION

The availability of nutrients in the bio-extract, for example, available forms of nitrogen ($NO3^-$ and $NH4^+$), available forms of phosphorous (H_2PO^- and HPO_4^{2-}) and available forms of potassium (K^+) could promote plant growth [9]. However, Pathanapibul [10] reported that using only bio-extracts did not enhance plant growth, because the amount of macronutrients and micronutrients in the bio-extract was low and insufficient for plant growth.

In a comparison between the three treatments, produced better growth enhancement. This outcome might be associated with the composition of the available nutrients in the bio-extract of soybean meal suitable for the growth of lettuces. The quantity of nutrients in the bio-extract of soybean meal was quite low and insufficient to support plant growth. In addition, soybean may contain some specific groups of microorganisms that can promote plant growth as plant growth promoting bacteria (PGPB). Several investigations reported that PGPB can produce plant growth regulators, such as indoleacetic acid (IAA), gibberellic acid, cytokinins and gaseous phytohormone (ethylene) [1]. Moreover, some groups of PGPB can fix nitrogen gas, dissolve unavailable phosphate and produce siderophore as an iron chelator, as well as deter plant pathogens [3].

Chemical fertilizer (16-16-16) Bio-extract of fish meal meal Bio-extract of soybean

Fig. 4 The color of leaves in butter head lettuce treated with chemical fertilizer, bio-extract of fish meal and soybean meal.

CONCLUSION

The vegetative growth of red oak lettuce similar to chemical fertilizer with difference statistically significant when treated with bio-extract of fish meal and soybean meal. There were no statistically difference on the vegetative growth of green oak lettuce. Both of Bio-extract of fish meal and soybean meal could increase the color of leaves in red oak, red coral and butter head lettuces than chemical fertilizer. However, the use of bio-extract for cultivation compared to chemical fertilizer is environmentally friendly, low cost and an appropriate way to dispose of agricultural wastes.

ACKNOWLEDGEMENTS

The authors are thankful to Faculty of Agricultural Technology, Rajamangala University of Technology Thanyaburi, for providing the research fund.

REFERENCES

[1] Ahmad, F., I. Ahmad and M.S. Khan. Screening of free-living rhizospheric bacteria for their multiple plant growth promoting activities. Microbiol. Res. Vol.63, 2008, pp. 173-181.

[2] Chaisit, T. and S. Sudprasong. Bio-extract. Thai. Resch. Fund J. Vol.17, No.3, 2000, pp. 48-57.

[3] Compant, S., B. Duffy, J. Nowak, C. Clement and E.A. Barka. Use of plant growthpromoting bacteria for biocontrol of plant diseases: principles, mechanisms of action and future prospects: Minireview. Appl. Environ. Microbiol. Vol.71, 2005, pp. 4951-4959.

[4] Department of land and development. Fish meal. Available online: [http://www.organicthailand.com]. May, 2015.

[5] Division of agricultural chemical. Plant hormone and plant nutrients in bio-extract. Department of agriculture. Ministry of agriculture and cooperative, Bangkok, Thailand, 1999.

[6] Division of soil and water conservation. Production and using of organic fertilizer to improve soil. Department of land and development. Ministry of agriculture and cooperative, Bangkok, Thailand, 1999.

[7] Sassanarakkit, S. Bio-extract. Department of biotechnology. Thailand Institute of Scientific and Technological Research, 1999.

[8] Osotsapa Y. Plant nutrients. Kasetsart University Press. Bangkok, Thailand, 1996, 424 p.

[9] Omsub, N. Bioextract. Entomol. Zool. Gazett. Vol.24, No.2, 2002, pp. 154-158.

[10] Pathanapibul, S. The Efficiency of Bioextract on Some Kinds of Vegetable in Hydroponic System. M.S. Thesis, Kasetsart University, Bangkok, 2003.

Second International Conference on Science, Engineering & Environment,
Osaka City, Japan, Nov.21-23, 2016, ISBN: 978-4-9905958-7-6 C3051

BREAKING SEED DORMANCY OF N.VICTORIA AMAZONICA SOWERBY

Purin Akkarakultron[1], Dowroong Watcharinrat[1], Tongmee Mosom[1] and Yaowamal Noimai[1]
[1]Faculty of Agricultural Technology, Rajamangala University of Technology Thanyaburi, Thailand

ABSTRACT

Giant waterlily (*Victoria amazonica* (Rocpp.) Sowerby; Nymphaeaceae) is the largest leaves with lifting set at the leaf margins and thorny characteristics in whole plant part. Seed production occurs during 50-60 days starting from pollination to broken pod until it was germinated. This research aims to investigate the viable procedure stimulating seed germination rate. Plant materials were grown in the same period. Three stages of seed age were collected after three months of culture, especially 20, 25 and 30 days. Each treatment was performed by the completely randomized design (CRD), including six methods such as without treatment, nicking, soaked within 0.05 % (w/v) gibberellic acid (GA_3) solution for hour, soaked within 0.05% (w/v) GA_3 solution for hour, nicking combined to soak in 0.05% (w/v) GA_3 solution for hour and nicking combined to soak in 0.1% (w/v) GA_3 solution for hour. The results showed that the seed germination was depended on the seed age after pod ripening and combination of nicking and soaking within GA_3 solution. The highest percentage of germination rate (56.5%) was found in seed age of 30 days of pod ripening and then accomplished to break seed coat and soaking in 0.1% (w/v) GA_3 solution for hour after 35 days of culture.

Keywords: Dormancy, N. Victoria, Gibberellic acid

INTRODUCTION

Waterlily (Nymphaea spp. L.) is an important aquatic plant that called “Queen of the Aquarium Plants” and then represented to be the purity, good in the Buddhism and faithful of human being worldwide. Some waterlilies are represented about beautiful floating leaves, fairy flowers and its color change, regarding to an attractive scent. Moreover, some species of the family Nymphaeaceae are occurred as the large size, widespread leaf area and lifting set of leaf margins. Eventually, its venation has been used in the fine and applied arts. At present, many waterlilies are applied to obtain in several fields such as interior decoration, parking, relaxing garden and resort, which are trending on the ecotorism.

Giant waterlily (*Victoria amazonica* (Rocpp.) Sowerby) is now required to cultivate as an ornamental waterlily in the botanic gardens and landscape. This plant is a large emergent aquatic macrophyte and then propagated by seed production after 50 – 60 days of pollination until seed pod ripening in the later. In generals, *ex vitro* propagation is considerable taken time to grow up the seedlings because its seeds are not started to uniformly germinate. Consequently, common seed culture of this waterlily is belated and then affected to loss of mass propagation. In this study, research colleague of Lotus museum in the Plant Genetic Conservation Project under the Royal Initiation of Her Royal Highness Princess Maha Chakri Sirindhorn (RSPG) aimed to demonstrate on breaking seed dormancy of V. amazonica seeds for application of waterlily and lotus planting and plant marketing production in the future.

The procedure used for breaking the dormancy of seeds was composed of seed coat scarification, either rubbed on a sand paper manually, seed coat removal, soaking in warm water and some acidic solutions such as sulfuric acid and nitric acid. The chemical compounds that used to break seed dormancy are available, depending on plant species. Likewise the plant growth regulators are numerous chemical substances, which are profoundly influence on growth and differentiation of plant cells, tissues and organs. Based on the functional mechanism, plant growth regulators act as chemical messengers for intercellular communication throughout the cell signaling and transduction pathway. There are classified into five major groups: for example auxins, gibberellins, cytokinins, abscisic acid (ABA) and ethylene. [1] Previous study, the effective method used for breaking seed dormancy of *Victoria amazonica* was nicking technique. Some experiments have been stimulated seed germination with gibberellic acid (GA_3). The objectives were to investigate about suitable plant materials used for seed germination, and ensure a number of seedlings. Gibberellic acid could make the sprouting faster with GA3: the filiform leaf does not grow, but also improve the germination rate, especially in the unnicked seeds. On the other hands, application of GA_3 on breaking seed dormancy has been demonstrated in several plants. Previously, some experiments were conducted to evaluate GA_3 application on breaking dormancy of ‘Marfona’ potato mini-tubers. The results showed that GA_3 application had significant affected in all traits,

excepting sprout and main stem number. At 160 ppm GA_3 application was reduced the days sprouting to emergence from 100 to 70 days and increase of tuber number per plant from 4 to 7.5, compared to control. [2], reported that the effectiveness of gibberellic acid (GA_3) in breaking seed dormancy in rice. The activity of a-amylase enzyme acts as an indicator of the dormancy level. [3], denoted on the germination response of this species were recognized into various treatments.

Standard germination assay showed that the germination percentage of untreated seeds is 25.8% while chilling treatment at 4 C for 7 days germination percentage reached to 39%. Germination rate of seeds soaked in 100 ppm GA_3 for 36 h was 48%. [4], reported that the highest germination rate of *T. polium* seeds were obtained at concentrations of 500–2500 ppm GA_3. Washing and chilling (at 5 °C) for 14 days were most effective to break seed dormancy in *F. gummosa*. [5] and [6] studied on the seed dormancy and germination characteristics of *A. preissii* by application of GA_3 and smoke-water. GA_3 has been shown to decrease seed dormancy in many plant species, relating to physiological dormancy. However, 50 mg/L GA_3 was only slightly effective to promote seed germination of *Lomandra sonderi* but not stimulate in all dormant seeds.

MATERIALS AND METHODS

This research aims to provide the suitable method used for exiting seed germination and germination rate. Plant materials were grown in the same period. Their seeds were collected after 3 months of culture, including 20, 25 and 30 days of seed age. Each experiment was performed by completely randomized design (CRD) that showed in table 1.

Table 1 Seed pre-treatment of *Victoria amazonica*

Seed age after the pod ripening (days)	Seed Pre-treatment					
	T1	T2	T3	T4	T5	T6
20	30	30	30	30	30	30
25	30	30	30	30	30	30
30	30	30	30	30	30	30

T1: control, T2: Nicking, T3: Soaked substance Gibberellic acid 0.05 % (w/v) GA_3 for hour, T4: Soaked substance 0.05% (w/v) GA_3 for hour, T5: Nicking and soaked substance 0.05% (w/v) GA_3 for hour and T6: Nicking and soaked substance 0.1% (w/v) GA_3 for hour.

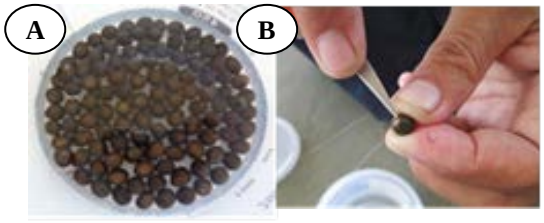

Fig. 1 (A) *V. amazonica* seeds (B) Nicking

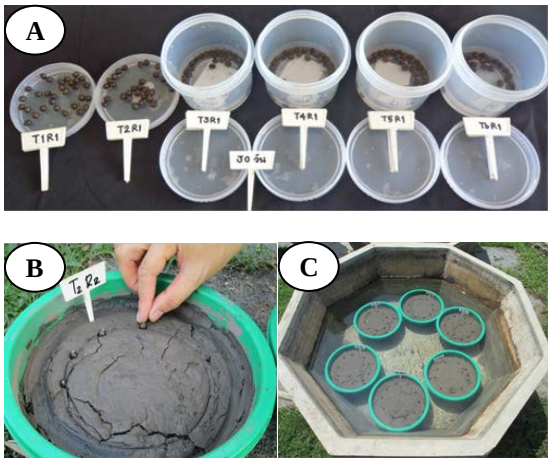

Fig. 2 (A) Pre-treatment of *V. amazonica* seeds from the pods 30 days. (B, C) Seeds planted into nursery trays.

Take the seeds planted into nursery trays, marked the times, treatment and replicate, soak into the cement pond and addition water about 30 centimeters.

Record data times and germination percentages were 7, 14, 21, 28 and 35 days after seeds planted. Statistical analyses by Analysis of Varian, means were compared by the least significance difference Duncan's New Multiple Range Test (DMRT) interval method at $p<0.05$.

RESULTS AND DISCUSSION

In this study, three seed stages (20, 25, and 30 days of ripening) were performed within six treatments. Germination rate of *V. amazonica* seeds at 20 days of ripening showed significantly results after 28 days of culture. Therefore, a mechanical technique to breaks seed coat was combined with different gibberellin concentrations (at 0.05 and 0.1 % (w/v)). Number of germinating seeds cultured with or without soaking in gibberellin solution were 10 and 3.3 seeds, respectively. In case of combination of without breaking seed coat and soaking in different concentrations of gibberellin solution was not effective data, comparing to control. Eventually, the cracking seeds were well grown when compared to other treatments. In this study, a main factor affecting on seed dormancy in *V. amazonica*

was from seed coat imposed dormancy prevents germination. However, these methods might damage onto embryos within seeds, thus should be carefully done. Cracking seed coat in the position of primary growth was more effective to stimulate on growth of *V. amazonica* embryos when compared to without cracking seed coat, soaking in 50 % sulfuric acid or warming water [7]. As table2

Table 2 Germination percentages after the seeds from the pods 20 days.

Days / Treatment	7	14	21	28 1/	35	total
T1	0.0	0.0	0.0	0.0b	3.3	3.3
T2	0.0	0.0	3.3	3.3b	6.6	13.2
T3	0.0	0.0	0.0	0.0b	3.3	3.3
T4	0.0	0.0	0.0	0.0b	3.3	3.3
T5	0.0	0.0	16.6	10.0a	16.6	33.2
T6	0.0	0.0	6.6	10.0a	16.6	33.2
F-test	-	-	ns	**	ns	-
CV%	-	-	207.85	60.61	109.54	-

**significant p<0.01

Among the three seed stages after ripening, combination of cracking seed coat and soaking in 0.1 % (w/v) gibberellin solution gave the highest germination rate after 35 days of culture. Based on the results, seed age at 30 days of ripening gave the highest germination rate, compared to seed age at 20 and 25 days of ripening. The germination percentage in each seed stage showed as 23.3, 20 and 16.6, respectively. In this study, the results showed that factors stimulating on seed germination in *V. amazonica* have been related to seed age after ripening, cracking seed coat and soaking in gibberellin solution. Mazzini, 2003 reported that type of reagents stimulating seed germination and multiplication of seedlings. Gibberellin (GA_3) was suitable treatment used in germination of *V. amazonica* seeds, compared to the others (soil, water and agar media). Although, cultured seeds in gibberellin solution were rapidly produced seedlings from the meristems.

Table 3 Germination rate of cultured seeds from the pods 25 days

Day / Treatment	7	14	21	28 1/	35	total
T1	0.0	0.0	0.0	0.0	3.3	3.3
T2	0.0	0.0	3.3	6.6	10.0	19.9
T3	0.0	0.0	0.0	3.3	6.6	9.9
T4	0.0	0.0	0.0	6.6	10.0	16.6
T5	0.0	0.0	16.6	13.3	16.6	33.2
T6	0.0	0.0	6.6	10.0	20.0	36.6
F-test	-	-	ns	ns	ns	-
CV%	-	-	259.81	70.71	63.64	-

All of *V. amazonica* seed stage investigated during the 35 days of experiment was the same result in total germination rate. In addition, combination of cracking seed coat and soaking in 0.05 – 0.1 % *(*w/v*)* gave the highest percentage of seed germination. *V. amazonica* seeds soaked in gibberellin treatment without cracking seed coat was less effective to germinate than treatment with cracking seed coat, whereas the control was the lowest percentage of seed germination. Summary, the combination of cracking seed coat and soaking in gibberellin treatment was suitable to break seed dormancy in *V. amazonica*.

Table 4 Germination percentages after the seeds from the pods 30 days

Day / Treatment	7	14	21	28 1/	35	total
T1	0.0	0.0	0.0	3.3	3.3	6.6
T2	0.0	3.3	6.6	10.0	30.0	39.9
T3	0.0	0.0	3.3	6.6	10.0	19.9
T4	0.0	0.0	0.0	10.0	13.3	23.3
T5	0.0	6.6	10.0	13.3	20.0	49.9
T6	0.0	6.6	10.0	16.6	23.3	56.5
F-test	-	ns	ns	ns	ns	-
CV%	-	146.97	105.41	49.93	60.86	-

CONCLUSIONS

1. Suitable procedure for stimulating on germination of *V. amazonica* seeds based on seed pod ripening stage and combination of cracking the pericarp and soaking in gibberellin solution.
2. The highest percentage (56.5%) of germination of *V. amazonica* seeds was observed in combination of seed age from 30 days of ripening and soaking in 0.1 % (w/v) gibberellin solution, depending on the total germination rate as approximately 35 days.

Suggestions from this research article

1. Should be study on the germination procedure in *V. amazonica* seeds by increase of soaking period in gibberellin solution for stimulating on germination rate and mass propagation of seedlings.
2. Should be study about the germination of seed age at more than 30 days of seed pod ripening for increasing on germination rate.
3. Recommend on validation of different methods and other effective reagents used for breaking seed dormancy of *V. amazonica* seeds.

ACKNOWLEDGEMENTS

The authors would like to express their sincere thanks for the participated of Faculty of Agricultural Technology and Lotus - Waterlily Musium Rajamangala University of Technology Thanyaburi. We would also say thanks for who could not be mentioned here for their kindness and encouragement.

REFERENCES

[1] Mazzini Renata . 2003. Germination in vitro for the Victoria amazonica sds. Plant Propagation project Course 40 Royal Botanic Gardens.

[2] Shekari Fariborz, Benam Mohammad Bagher Khorshidi, Sardar Germchi and Hassanpanah Davoud. 2010. Effect of GA3 on dormancy breaking of 'Marfona' minitubers under greenhouse conditions.

[3] VieiraI Antonio Rodrigues, VieraII Maria das Gracas Guimaraes Carvalho, Fraga Antonio C., OliveiraII Joao Almir and SantosII Custodio D. dos. 2002. Action of gibberelllic acid (GA3) on dormancy and activity of a-amylase in rice seeds. Rev. bras. Sements vol 2.

[4] HDehghanpour Farashah, RTavakkol Afshari, F Sharifzadeh and S Chavoshinasab. 2011. Germination Improvement and alpha-Amylase and beta-1,3-Glucanase Activity in Dormant and Nondormant Seed of Oregano ('Origanum vulgare'). Australian Journal of Crop Science.Volume 5, Issue 4.

[5] Nadjafia F., Bannayana M., Tabrizia L. and Rastgooa M. 2006. Seed germination and dormancy breaking techniques for Ferula gummosa and Teucrium polium. 542-547p.

[6] Turner S. R., Merritt D. J., ridley E. C., Commander L. E., Baskin J. M., Baskin C. C. and Dixon K.W. 2004. The seed dormancy and germination characteristics of A.preissii. Articles from Annals of Botany are provided here courtesy of Oxford University Press.

[7] Purin Akkarakultron , Dowroong Watcharinrat, Tongmee Mosom and Ausada polpipoon. 2012. Germination of Victoria amazonica Sowerby seed . Faculty of Agricultural Technology, Rajamangala University of Technology Thanyaburi. Pathumtani Province, Thailand.

Second International Conference on Science, Engineering & Environment,
Osaka City, Japan, Nov.21-23, 2016, ISBN: 978-4-9905958-7-6 C3051

GROWTH OF THE EDIBLE MICROALGA *ARTHROSPIRA PLATENSIS* IN RELATION TO BORON SUPPLY

Shotaro Tadama[1] and Hideaki Shiraishi[1]

[1]Graduate School of Biostudies, Kyoto University, Japan

ABSTRACT: *Arthrospira* (*Spirulina*) *platensis* is an edible cyanobacterium that has been consumed worldwide as a nutrient source under the name spirulina. When culturing this microalga, boron is usually added to its growth medium. However, whereas boron is necessary for the N_2-fixation-dependent growth of heterocystous cyanobacteria, boron requirement by *A. platensis*, which is non-heterocystous, has not yet been carefully examined. To examine the effect of boron on *A. platensis*, we prepared a boron-depleted medium in which borate concentration was below a detection limit (0.2 μM), as determined by the spectrophotometric quantitation with H-resorcinol. Using this boron-depleted medium, *A. platensis* NIES-39 was analyzed for changes in growth, dry biomass weight and the protein, chlorophyll *a* and C-phycocyanin contents. Experimental results showed that removal of boron from the growth medium had no detectable effect on them. A control experiment with a heterocystous cyanobacterium *Anabaena* sp. UTEX 2576 showed that the growth of this cyanobacterium was suppressed in a boron-depleted medium. These experiments demonstrated that boron was not required for the growth of *A. platensis*. Our results indicate that boron supply is not necessary for the propagation of *A. platensis* even in the regions where boron deficiency in the soil deteriorates the growth of common crops. Use of boron-free media would also be helpful to improve the reproducibility of sensitive physiological experiments such as metabolome analysis, because precipitation of the insoluble salt manganese borate, which may reduce the concentration of Mn^{2+} in the medium, does not occur in boron-free media.

Keywords: Cyanobacteria, Spirulina, Arthrospira platensis, Boron, H-resorcinol

1. INTRODUCTION

Arthrospira platensis is an edible alkalophilic cyanobacterium that has been consumed worldwide as a nutrient source and food additives [1][2]. Phycobiliproteins from this cyanobacterium are also widely used as natural colorants for foods and cosmetics [2]. Products of *A. platensis* and a closely related species *A. maxima* are usually marketed under the name spirulina, because they had formerly been classified in the genus *Spirulina*.

In the artificial propagation of *A. platensis*, boric acid is usually added to its growth medium [3], as it is well known that boron is required for the growth of many photosynthetic organisms. For example, higher plants require boron for the formation and maintenance of cell wall structures [4]. Therefore, deficiency of boron in the soil causes the development of many symptoms in higher plants [4][5]. Boron is also required for the maintenance of the integrity of heterocyst cells that perform N_2 fixation in heterocystous filamentous cyanobacteria [6][7]. Boron is involved in stabilizing the heterocyst envelope in these cyanobacteria [8]. However, in contrast to higher plants and heterocystous cyanobacteria, many non-heterocystous cyanobacteria are tolerant to boron deficiency [7][9].

Since *A. platensis* is also non-heterocystous, it is possible that boron is not necessary for the growth of this cyanobacterium. However, boron requirement by *A. platensis* has not yet been carefully examined. Knowledge about the boron requirement would be helpful for the agriculture of *A. platensis*, especially in the region where boron deficiency in the soil deteriorate healthy growth of many common crops [5].

Knowledge on the boron requirement by *A. platensis* is also helpful for basic studies of this cyanobacterium. In laboratory-scale experiments, inclusion of boric acid in the growth medium results in the gradual precipitation of the insoluble salt manganese borate [10], possibly causing the change in the Mn^{2+} concentration and gradual depletion of Mn^{2+} in the growth medium. This may reduce the reproducibility of sensitive physiological experiments, *e.g.*, metabolome analysis, because manganese is an essential component of the oxygen-evolving complex in photosystem II [11], as well as many cellular enzymes (*e.g.*, xylose isomerase, glutamine synthetase and phosphoglycerate mutase [12]), and therefore alterations in the manganese concentration may affect cellular physiology. If boron is determined to be dispensable for the growth of *A. platensis*, boric acid can be omitted from the growth medium to improve the

reproducibility of sensitive physiological experiments.

In this study, we prepared a boron-depleted medium, and effects of boron on the growth and some biochemical properties of *A. platensis* were examined to determine whether boron depletion had any effect on this cyanobacterium.

2. MATERIALS AND METHODS

2.1 Reagents

H-resorcinol, or 1-(2,4-Dihydroxy-1-phenyl-azo)-8-hydroxynaphthalene-3,6-disulphonic acid disodium salt, was purchased from Tokyo Chemical Industry Co. (Tokyo). Other chemicals were purchased from Nakalai Tesque (Kyoto) and Wako Pure Chemical Industries (Osaka). All chemicals were reagent grade or better. Water was purified with the Milli-Q Advantage A10 Ultrapure Water Purification System (Merck Millipore, Darmstadt) before use. Polypropylene plasticware was used to prepare reagent solutions, to avoid boron contamination from glassware [13]

2.2 Cyanobacterial strains

A. platensis NIES-39 was obtained from the Microbial Culture Collection at the National Institute for Environmental Studies, Tsukuba (MCC-NIES). *Anabaena* sp. UTEX 2576 was obtained from the Culture Collection of Algae at the University of Texas at Austin (UTEX).

2.3 Growth media and growth conditions

SOT medium and boron-depleted SOT medium for *A. platensis* were prepared as described [14][15], except that the macroelement solution used to prepare the latter medium did not contain boric acid. *Anabaena* sp. UTEX 2576 was cultured either in $BG11_0$ medium [16] or in the boron-depleted $BG11_0$ medium that contained no added boric acid. Cyanobacterial cells were cultured in 250-mL polycarbonate Erlenmeyer flasks (Thermo Scientific Nalgene, Waltham) containing 200 mL each of growth medium. Conditions for light and temperature were as described [15][17]. *A. platensis* NIES-39 was pre-cultured in the boron-containing medium, harvested by filtration on nylon mesh as described [17], and washed on it with boron-depleted medium before inoculation into each growth medium. *Anabaena* sp. UTEX 2576 was cultured in the same way except that pre-cultured cells were collected and washed by centrifugation rather than by filtration.

2.4 Quantitation of boron in the medium

To draw standard curves, 900 µL of 0.11 mM H-resorcinol in 0.65 M ammonium acetate-acetic acid buffer (pH 5.5) was mixed with 100 µL of SOT medium containing various concentrations of boric acid. The mixtures were incubated at 25°C with constant shaking at 140 rpm. After 60 h, optical density at the wavelength of 510 nm (OD_{510}) was determined with a spectrophotometer (Novaspec II, Pharmacia-LKB Biotechnology, Uppsala). Samples for quantitation were reacted with H-resorcinol in the same way, and OD_{510} was determined. Means and the standard errors of means were determined from 4 samples.

2.5 Determination of growth curves

Cyanobacterial cells were cultured in four polycarbonate flasks for each set of culture conditions. The means and the standard deviations of the OD_{730} values and the trichome concentrations were determined over time. The numbers of trichomes in cultures were determined as described [18].

2.6 Determination of the amounts of biomass, protein, chlorophyll *a*, and C-phycocyanin

Samples were taken from cultures during the late logarithmic phase when the OD_{730} values of the cultures were approximately 1.0–1.2. Data were obtained from four independent cultures for each set of culture conditions, and the means and the standard deviations were determined.

To determine the amount of biomass, 10 mL of cultures were centrifuged at 4°C for 20 min at 3,000 *g*, and the collected biomass was washed with 1 mL each of distilled water for 5 times. The washed biomass was dried at 85°C for 72 h, cooled down, and weighed.

To determine the amount of proteins, cells in 1 mL of samples were collected by centrifugation as above and washed five times with 1 mL each of 25 mM Tris-HCl (pH 7.4), 138 mM NaCl, 2.68 mM KCl (Tris-buffered saline). Then, they were disrupted by the Mini-Beadbeater-1 (Biospec Products, Bartlesville) using the 0.1 mm diameter glass beads. In the disruption, shaking the samples on the equipment for 30 sec and cooling them on ice for 1 min were repeated 7 times. Protein concentrations in these samples were determined by Bradford's method [19] using Bio-Rad Protein Assay kit (Bio-Rad Laboratories, Hercules). As a standard for protein determination, bovine γ-globulin (Bio-Rad Laboratories) was used.

Concentrations of chlorophyll *a* and C-phycocyanin were determined from the OD_{620} and OD_{678} values of the cultures as described [20].

3. RESULTS

3.1 Quantitation of boron concentration in the growth medium

In the experiments to follow, *A. platensis* was propagated in the medium with no added boric acid. However, it is known that considerable amount of boron is released from borosilicate glass into water when solutions are stored in glassware [13]. Therefore, the medium and all solutions were prepared in plasticware to avoid boron contamination from glassware. Even with this care, it was still possible that reagents used to prepare the medium were contaminated with boron. Therefore, boron concentration in the prepared growth medium was examined before performing the main experiments. To determine boron concentration, a spectrophotometric quantitation method with H-resorcinol was employed. This reagent forms a 1:1 complex with boron under weakly acidic conditions with an optimum at pH 5.5, and the complex can be determined spectrophotometrically at 510 nm [21]–[23].

Results of the boron quantitation in the boron-depleted medium and in the usual medium (SOT medium) are shown in Fig. 1. As shown in the upper left panel, experiments to draw a calibration curve showed that the standard solutions containing as low as 0.2 µM boric acid (12.4 ng mL^{-1}) exhibited significant OD_{510} values, indicating that detection limit for boric acid with this method was lower than 0.2 µM. In contrast, samples prepared with the boron-depleted medium exhibited hardly detectable absorption at 510 nm (Fig. 1, upper right panel). Therefore it was clear that boric acid concentration in this medium was far lower than 0.2 µM. In this respect, it has been reported that, when water was stored in glass bottles, concentration of boron released from glass into water reached 5.2 µM in 73 days [13]. Therefore, the boron level in the boron-depleted medium (<0.2 µM) was far lower than the residual level of boron in water stored in glass bottles. Concentration of boric acid in the SOT medium used in this study was also examined and determined to be approximately 45 µM (Fig. 1, lower panels).

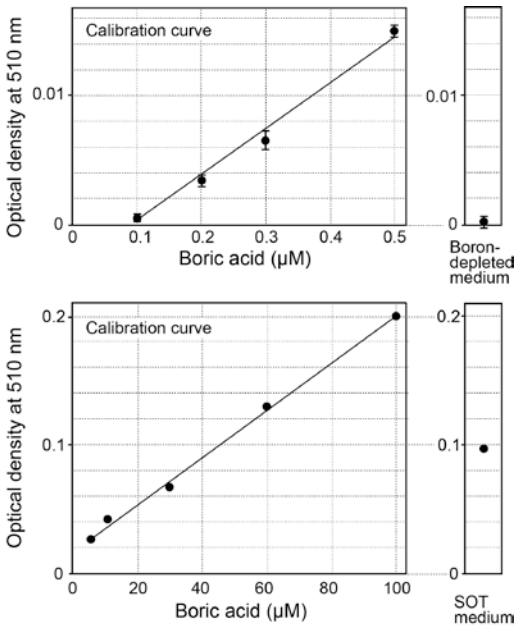

Fig.1 Quantitation of boron concentrations

3.2 Effect of boron depletion on the growth of *A. platensis* NIES-39 and *Anabaena* sp. UTEX 2576

To examine the effect of boron on the growth of *A. platensis*, *A. platensis* NIES-39 was cultured in the usual SOT medium and in the boron-depleted medium prepared as above. Trichome concentrations and the OD_{730} values were determined over time, and growth curves were drawn. As shown in Fig. 2, there were no significant differences between the growth curves determined in the presence and absence of boron,

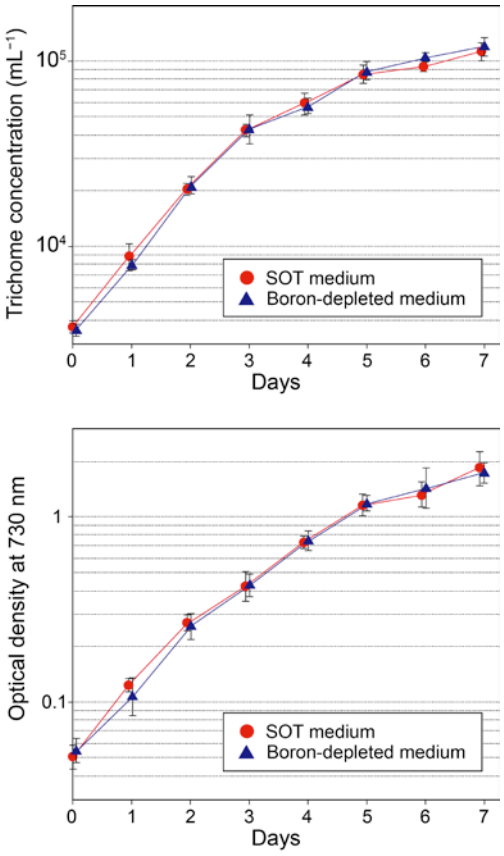

Fig. 2 Growth of *A. platensis* in relation to boron

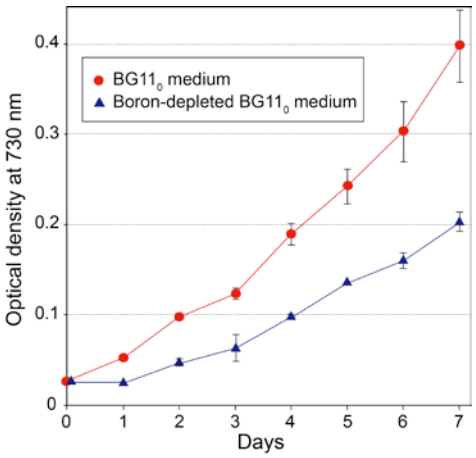

Fig. 3 Growth of *Anabaena* sp. in relation to boron

indicating that boron depletion had no detectable effect on the growth of *A. platensis* NIES-39.

As a control experiment, a heterocystous cyanobacterium *Anabaena* sp. UTEX 2576 was cultured in the boron-containing medium ($BG11_0$ medium) and in the boron-depleted $BG11_0$ medium. As shown in Fig. 3, growth of this cyanobacterium was suppressed in the boron-depleted medium. Statistical analysis by the Student's *t*-test indicated significant differences ($P<0.05$) between the cultures in the $BG11_0$ medium and in the boron-depleted $BG11_0$ medium at and after 24 h. This control experiment confirmed that boron had been effectively depleted in the boron-depleted media prepared in this study. It is worth noting that the culture of *Anabaena* sp. UTEX 2576 grown in the boron-depleted medium exhibited a yellowish color, similar to other heterocystous cyanobacteira grown under boron-depleted conditions [6][7]. In contrast, the culture of *A. platensis* NIES-39 had the usual blue-green color even when it was propagated in the boron-depleted medium.

The experiments in Fig. 2 and Fig. 3 clearly indicated that boron depletion had no detectable effect on the growth of *A. platensis* whereas it deteriorated the growth of *Anabaena* sp. that requires boron for the N_2-fixation-dependent growth.

3.3 Effect of boron depletion on the biomass and the protein, chlorophyll *a*, and C-phycocyanin contents

A. platensis trichomes propagated in the boron-depleted medium were visually indistinguishable from those propagated in the usual SOT medium, when their morphologies were observed under a dissecting microscope. To examine whether there were any differences in their cellular physiology, some biochemical properties were determined next.

Fig. 4 shows the amount of biomass and the protein content of *A. platensis* NIES-39 propagated

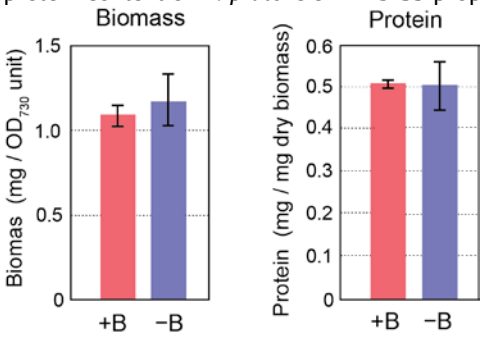

Fig.4 Biomass and the protein content

in the presence and absence of boron. There were no significant differences between them as analyzed by the Student's *t*-test with significance level set at 0.05. The protein content of *A. platensis* NIES-39 was approximately 50% (w/w) both in the presence and absence of boron (Fig. 4, right panel). These values were comparable to the values (50–55%) that had been determined with another *A. platensis* strain [24].

The Chlorophyll *a* and C-phycocyanin contents were also determined and compared (Fig. 5). Analysis by the Student's *t*-test with significance level set at 0.05 indicated that there were again no significant differences in their contents between the cells cultured in the presence and absence of boron.

4. Discussion

The boron requirement by *A. platensis* has not been carefully examined. Whereas there has been a report that boron can be omitted from the growth medium to culture *A. platensis* PCC 8005, experiments in that study were performed using a glass fermenter [25]. Since water becomes contaminated with boron when stored in glass containers and that the boron release from glass is accelerated under alkaline conditions [13], it was possible that the boron released from the glass vessel into the alkaline-leaned medium for *A.*

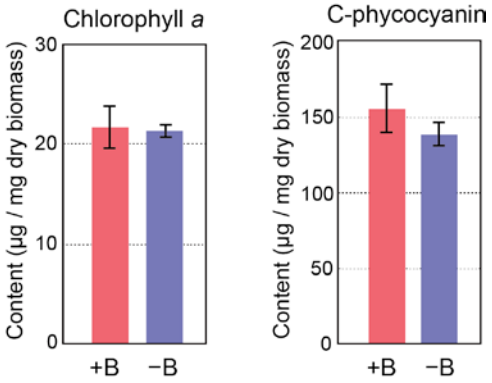

Fig. 5 Chlorophyl *a* and C-phycocyanin contents

platensis was sufficient to support the normal growth of *A. platensis* in that study. In contrast, our study was carefully performed using plasticware to avoid boron contamination. Our experimental results clearly demonstrated that even a residual amount of boron is not necessary for the growth of *A. platensis* (Fig. 2). In addition, there were no detectable differences in the biochemical properties of the cells grown in the presence and absence of boron (Fig. 4 and Fig. 5).

It has been reported that the C-phycocyanin content of many *Arthrospira* strains significantly increased when they were cultured in a medium that was not supplemented with microelements (Fe, B, Mn, Zn, Cu, Mo) [26]. This effect was most likely caused by the limitation of the element(s) other than boron, since our study demonstrated that boron depletion had no significant effect on the C-phycocyanin content.

A. platensis has been used for commercial propagation. In addition to commercial usage, it has also been used as a small-scale crop providing nutritional supplements for the communities where the staple diet is poor or inadequate [27][28]. The results of our study suggest that *A. platensis* can be an excellent crop that can be grown without boron supplementation even in the region where boron deficiency in the soil deteriorates the healthy growth of many common crops.

In the studies of *Arthrospira*, growth media used in biological experiments have been usually supplemented with boric acid [3][14]. However, boric acid gradually forms an insoluble salt manganese borate [10], since the growth media contain manganese ion. Formation of the precipitate of manganese borate may gradually deplete manganese ions in the media during prolonged storage. This may affect the results of sensitive physiological experiments, *e.g*., metabolome analysis, because manganese is an essential cofactor of many metabolic enzymes [11][12]. Since our study showed that boron is not necessary for the growth of *A. platensis*, the use of boron-free media is recommended in sensitive physiological studies of *A. platensis*.

4. CONCLUSION

Boron depletion had no detectable effect on the growth and biochemical properties of *A. platensis*. This result indicates that boron supply is not necessary for the propagation of *A. platensis* even in the regions where boron deficiency in the soil deteriorates the growth of common crops. Since boron is not necessary for the growth of *A. platensis*, the use of boron-free media is recommended when performing sensitive physiological experiments, to avoid the precipitation of manganese borate that may reduce effective concentration of manganese ions in the media.

5. ACKNOWLEDGEMENTS

This work was supported by the Grant-in-Aid for Challenging Exploratory Research from the Japan Society for the Promotion of Science [JSPS KAKENHI Grant Number 26660063] and the Management Expenses Grants for National University Corporations from the Ministry of Education, Culture, Sports, Science and Technology of Japan.

6. REFERENCES

[1] Belay A, “Biology and industrial production of *Arthrospira* (*Spirulina*)”, Handbook of Microalgal Culture: Applied Phycology and Biotechnology, 2nd ed. Richmond A and Hu Q, Eds. West Sussex: Wiley-Blackwell, 2013, pp. 339–358.

[2] Grewe CB and Pulz O, “The Biotechnology of Cyanobacteria”, Ecology of Cyanobacteria II: Their Diversity in Space and Time. Whitton BA, Ed. Dordrecht: Springer, 2012, pp. 707–739.

[3] Zarrouk C, Contribution à l’étude d’une cyanophycée. Influence de divers facteurs et chimiques sur la croissance et la photosynthèse de *Spirulina maxima* Geilter. PhD thesis, Université de Paris. Paris, 1966.

[4] O’Neill MA, Ishii T, Albersheim P and Darvill AG, Rhamnogalacturonan II: Structure and function of a borate cross-linked cell wall pactic polysaccharide. Annu. Rev. Plant. Biol. Vol. 55, 2004, pp. 109–139.

[5] Shorrocks VM, The occurrence and correction of boron deficiency. Plant and Soil, Vol. 193, 1997, pp. 121–148.

[6] Mateo P, Bonilla I, Fernández-Valiente E and Sanchez-Maeso, Essentiality of boron for dinitrogen fixation in *Anabaena* sp. PCC 7119. Plant Physiol. Vol. 81, 1986, pp. 430–433.

[7] Bonilla I, Garcia-González M and Mateo P, Boron requirement in cyanobacteria: Its possible role in the early evolution of photosynthetic organisms. Plant Physiol. Vol. 94, 1990, pp. 1554–1560.

[8] Garcia-Gonzalez M, Mateo P and Bonilla I, Boron requirement for envelope structure and function of Anabaena PCC 7119 heterocysts. J. Exp. Bot. Vol. 42, 1991, pp. 925–929.

[9] Martinez F, Mateo P, Bonilla I, Fernandez-Valiente E and Garate A, Growth of *Anacystis*

nidulans in relation to boron supply. Israel J. Botany, Vol. 35, 1986, pp. 17–21.

[10] The Merck Index: An Encyclopedia of Chemicals, Drugs and Biologicals, 13th ed. O'Neil MJ, Smith A, Heckelman PE and Budavari S., Eds. Whitehouse Station: Merck and Co. Ltd., 2001.

[11] Yachandra VK, Sauer K and Klein MP, Manganese cluster in photosynthesis: Where plants oxidize water to dioxygen. Chem. Rev. Vol. 96, 1996, pp. 2927–2950.

[12] Penner-Hahn JE, "Manganese proteins with mono- & dinuclear sites", Encyclopedia of Inorganic Chemistry, 2nd ed, Vol. V, King RB Ed. West Sussex: Wiley, 2005, pp. 2922–2932.

[13] Green GH, Blincoe C and Weeth HJ, Boron contamination from borosilicate glass. J. Agric. Food Chem. Vol. 24, 1976, pp. 1245–1246.

[14] Ogawa T and Terui G, Studies on the growth of *Spirulina platensis*. (I) On the pure culture of *Spirulina platensis*. J. Ferment. Technol. Vol. 48, 1970, pp. 361–367.

[15] Shiraishi H and Tabuse Y, The *Apl*I restriction-modification system in an edible cyanobacterium, *Arthrospira* (*Spirulina*) *platensis* NIES-39, recognizes the nucleotide sequence 5'-CTGCAG-3'. Biosci. Biotechnol. Biochem. Vol. 77, 2013, pp. 782–788.

[16] Rippka R, Deruelles J, Waterbury JB, Herdman M and Stanier RY, Generic assignments, strain histories and properties of pure cultures of cyanobacteria. J. Gen. Microbiol., Vol. 111, 1979, pp. 1–61.

[17] Shiraishi H, Association of heterotrophic bacteria with aggregated *Arthrospira platensis* exopolysaccharides: Implications in the induction of axenic cultures. Biosci. Biotechnol. Biochem. Vol. 79, 2015, pp. 331–341.

[18] Shiraishi, H, Cryopreservation of the edible alkalophilic cyanobacterium *Arthrospira platenisis*. Biosci. Biotechnol. Biochem. 2016. doi:10.1080/09168451.2016.1189320

[19] Bradford MM, Rapid and sensitive method for the quantitation of microgram quantities of protein utilizing the principle of protein-dye binding. Anal. Biochem. Vol. 72, 1976, pp. 248–254.

[20] Arnon DI, McSwain BD, Tsujimoto HY and Wada K, Photochemical activity and components of membrane preparations from blue-green algae. I. Coexistance of two photosystems in relation to chlorophyll *a* and removal of phycocyanin. Biochim. Biophys. Acta, Vol. 357, 1974, pp. 231–245.

[21] Capelle K, Microdosage colorimétrique du bore en milieu aqueux, au moyen de réactifs a groupement azoïque ou imine dérivés des acides H et K. Anal. Chim. Acta, Vol. 24, 1961, pp. 555–572.

[22] Tôei K, Motomizu S, Oshima M and Onoda M, Spectrophotometric determination of boron by flow injection analysis. Bunseki Kagaku, Vol. 35, 1986, pp. 344–348.

[23] Motomizu S, Oshima M and Jun Z, Anion-exchange chromatographic behaviour of the complex of boron with H-resorcinol: sensitive determination of boric acid. Analyst, Vol. 115, 1990, pp. 389–392.

[24] Anusuya Devi M, Subbulakshmi G, Madhavi Devi K and Venkataraman LV, Studies on the proteins of mass-cultivated, blue-green alga (*Spirulina platensis*). J. Agric. Food Chem. Vol. 29, 1981, pp. 522–525.

[25] Cogne G, Lehmann B, Dussap C-G and Gros J-B, Uptake of macrominerals and trace elements by the cyanobacterium *Spirulina platensis* (*Arhtrospira platensis* PCC 8005) under photoautotrophic conditions: Culture medium optimization. Biotech. Bioengineer. Vol. 81, 2003, pp. 588–593.

[26] Tarko T, Duda-Chodak A and Kobus M, Influence of growth medium composition on synthesis of bioactive compounds and antioxidant properties of selected strains of *Arthrospira* Cyanobacteria. Czech J. Food Sci. Vol. 30, 2012, pp. 258–267.

[27] Jeeji Bai N, Seshadri CV, Small scale culture of *Spirulina* (*Arthrospira*) as food supplement for rural households–Technology development and transfer. Algol. Stud. Vol 50–53, 1988, pp. 565–572.

[28] Habib MAB, Parvin M, Huntington TC and Hasan MR, A review on culture, production and use of spirulina as food for humans and feeds for domestic animals and fish (FAO Fisheries and Aquacultre Circular No. 1034). Rome: Food and Agriculture Organization of the United Nations, 2008.

Second International Conference on Science, Engineering & Environment,
Osaka City, Japan, Nov.21-23, 2016, ISBN: 978-4-9905958-7-6 C3051

EFFECTS OF COURT-TYPE THAI TRADITION MASSAGE VERSUS STRETCHING EXERCISE ON UPPER BACK PAIN ASSOCIATED WITH MYOFASCIAL TRIGGER POINTS: A PILOT STUDY

Phanida Wamontree
School of Health Science, Mae Fah Luang University ChiangRai, Thailand

ABSTRACT

The study aim to immediately verify the effects of court-type Thai traditional massage (CTTM) versus stretching exercise on upper back pain associated with myofascial trigger points (MTrPs). Twenty-four participants who had been diagnosed with MTrP in the upper back were randomly allocated in a massage group and exercise group. CTTM was applied to experimental group for 20 minutes and exercise group for 10 minutes. The visual analog scale of pain intensity (VAS), pressure pain threshold (PPT) and tissue hardness were assessed before and immediately after of treatment. Results of massage group had significant improvement in VAS, PPT except tissue hardness $p<0.05$). Similar changes were observed in exercise group ($p<0.05$) except PPT. In conclusion, CTTM , it could be an alternative treatment for patients with MTrPs.

Keywords: Court-type Thai traditional massage, Stretching exercise, Myofascial trigger point, Upper back

1. INTRODUCTION

Myofascial trigger points (MTrPs) are a common illness among people in their working age, who usually experience referred pain affecting a wide area without being able to identify its original location. 66-71**%** of the patients visit the doctor as a result of such a complaint at least once during their lifetime [1]. The level of pain from varies from person to person. Some may feel occasional mild pain that heals over time without treatment, whereas others may suffer from severe pain that aggravates their movement ability. MTrPs is often found to recur with accompanying upper back pain [2]. Treatment is purposed at relieving or eliminating trigger points including pharmacological approach and non-pharmacological approach.

Stretching is an important treatment to relieve TrP. The advantages of this exercise are increase in muscle blood flow to relax the muscles and reduce muscles pain, also increase range of motion, flexibility and strength of muscles [3]. While stretching, the mechanism called Autogenic inhibition was happened to inhibit muscle tightness. When the muscle have adequate tension, the brain will inhibit nerve impulse to that muscles and restrain muscle stretch, result in muscle relaxation and prevent muscle strain [4].

Court type Thai Traditional Massage (CTTM) is an ancient Thai remedy, it uses only hands and fingers to press the TrP. Also the therapist have a good manners from Thai custom. In the past, CTTM is used only in the palace for royal highness. The pressure is gradually increased until mild pain is felt, maintained for 5-10 seconds, and then released [5]. According to study found that Thai massage can reduce pain as well as exercise in patients with MTrPs neck and upper back pain [6]. Moreover, CTTM have an effectiveness to relieve pain and increase the range of motion in patients with upper trapezius muscle pain [7].

Although massage and stretching exercise are an effective treatment, it has not been study to the effect of court-type Thai traditional massage. So that, the aim of this research was preliminarily verify the effects of CTTM compare with stretching exercise in patients with upper back pain associated myofascial trigger points.

2. SUBJECTS AND METHODS

2.1 Design

The study was a randomized controlled trial, pilot study. It was conducted at Mae Fah Luang University Hospital. Participants received information on the research through announcement during September 2015 and December 2015.Written consent to participate in the study was obtained before enrollment. The School of Health Science's review board approved this study.

2.2 Subjects

2.2.1 Inclusion Criteria

The patients included in the study were male or female aged 18- 35 years old diagnosed with upper back pain with at least 1 TrP lasting at least 3 months. Following the diagnosis involved the presence of taut bands, nodules and spot tenderness.

2.2.2 Exclusion Criteria

The patient exclude from the study were those with shoulder or lower neck pain with other accompanying complaints, such as adhesive capsulitis, cervical spondylosis, herniated muscles pulposus, and movement difficulties caused by deformed joints or scoliosis, having receiving operative treatment within before the participation of the present study.

2.3 Intervention

Twenty-four patients aged 18-35 years who were diagnosed with MTrPs according to the criteria. They were randomly allocated into a CTTM group and exercise group. After diagnosis, the randomization, and signing of the consent form, the patients were given each treatment according to the group to which group belonged. The details are as follows.

The 12 patients who were randomly allocated in the treatment group received the CTTM. The CTTM was done by two licensed applied Thai traditional medical practitioners who have had experience with CTTM more than five years.

In details, the method for alleviating MTrPs using CTTM comprised of two steps lasting 20 minutes, starting from the shoulders (10 minutes), both sides of the upper back (5 minutes), the area connecting the neck and the shoulders (5 minutes).

The other 12 patients who were randomly allocated into the exercise group were given stretching exercise lasting 10 minutes. Stretching was carried out for 10 minutes for treatment.

In details, the waist: Stand with the feet and around shoulder-length apart. Then put one hand on the waist and lift the other hand as high as possible. After that, incline to the side opposite the hand and maintain the posture for five seconds. Repeat the exercise for the other side of the waist and repeated ten times. The waist, shoulders and hips. Stand with the feet around should-length apart. Next, lift the arm to the shoulder level and angle the elbows at approximately 90º. Finally, twist the body to the left and then to the right with each posture maintain for five seconds and then repeated ten times.

2.4 Outcome Measures

Pain intensity by visual analogue scale (VAS): Patients were asked to indicate the average intensity of pain by pointing to a point along a 10-cm line; 0-cm indicating no pain and 10-cm severe pain. The pressure pain threshold (PPT) was the point where the patient started to experience pain by using a tissue hardness meter/algometer (OE-220, Japan). The measurement of tissue hardness meter/ algometer equipped with a 10-cm diameter plastic disc. Pressure was exerted vertically on the painful pressure point to be examined, and tissue hardness was automatically recorded.

All outcome measures were evaluated by physio therapist who was not informed of subject's group assignment. Assessments were done before and immediate after of treatment sessions.

2.5 Statistical Analysis

Characteristic data were as mean± (SD) and percentage. An unpaired t-test was used to compare differences of massage group and exercise group. The significance was set at an alpha level of 0.05.

3. RESULTS

Details of demographic data and health characteristics were shown in (Table 1). The average age of CTTM group and control group were 21.58±0.51 years. The demographic data were equally balanced between two groups. Clinical characterization of the patient's upper back pain after the treatments showed that there were no significant differences between the groups in regard to any of these measures.

Table 1 Demographic and characteristic

	CTTM (N=12)		Exercise (N=12)	
	Mean	SD	Mean	SD
Age (years)	21.58	0.51	21.58	0.51
Weight (kg)	56.58	9.3	62.50	15.85
Height (cm)	162.75	7.56	165.50	9.56
VAS	5.58	0.79	5.00	1.04
PPT	1.65	0.63	1.97	0.59
Tissue hardness	42.01	9.24	45.01	10.92

Table 2 Outcome measure pre-test and post-test assessments in the CTTM and control group (paired t-test)

Outcome	Group	Pre-test	Post-test	P-value
Pain intensity (VAS)	CTTM	5.5±0.7	3.5 ±1.4	<0.5
	Control	5.0±1.0	3.5 ±0.9	<0.5
Pressure pain threshold (kg/cm2)	CTTM	1.6 ±0.6	1.9 ±0.7	<0.5
	Control	1.9±0.5	1.5±0.6	<0.5
Tissue Hardness	CTTM	42.0±9.2	43.5±9.8	>0.5
	Control	45.0±10.9	44.2±7.9	>0.5

Note: Differences were considered as significant when $P < 0.05$.

Table 3 Comparison of outcome measures between the CTTM and Exercise at pretest-posttest

Outcome	Post-test (Mean ±SD)			
	CTTM	Control	Difference (95%CI)	P-value
Pain intensity (VAS)	0.8±0.8	1.8±1.3	-1.1(-1.6 to 0.6)	<0.05
Pressure pain threshold (kg/cm2)	3.9±0.6	2.5±0.4	1.3 (1.1 to 1.5)	<0.05
Tissue hardness (%)	38.13±7.67	44.5±6.5	-7.9(-9.7 to -6.1)	<0.05

Note: Differences were considered as significant when $P < 0.05$.

4. DISCUSSION

The results of this study provide evidence that CTTM is effectiveness treatment reducing pain and improving upper back pain in patients with MTrPs. The finding of this study suggest that CTTM on upper back area was effective in decreasing pain intensity with MTrPs can reduced immediately after treatment with either CTTM or stretching exercise. This finding consistent with previous studies the effects of royal traditional Thai massage in patients with myofascial pain syndrome in upper trapezius muscle found comparable results. The author reported reducing pain intensity immediately after of treatment [7]. In addition to the study of Hantan use ischemic pressure and stretching exercise to treat upper back pain and reported a reduction in present pain of treatment [6]. This reported similarity from the study of Wamontree who applied CTTM localized at the MTrPs and found an improvement in the PPT immediately after treatment for patients with upper back pain [8]. Moreover, the present study finding support the study of Buttagate use Thai traditional massage (TTM) and stretch exercise in patients with MTrPs on upper back pain at which revealed PPT immediately increasing at the end of treatment [9]. When the patients received treatment with CTTM on the upper back area, PPT significantly increased immediately after the treatment. The present study demonstrated that tissue hardness was reduced after treatment when two groups were compared. This indicated that the treatment by CTTM was effective in decreasing tissue hardness, consistent with the results of previous study which found that use of deep massage on upper back pain. The researchers reported reduction in tissue hardness after treatment [8].

5. CONCLUSION

The findings demonstrate the effectiveness of CTTM in treatment of patients with upper back pain. A comparison of the CTTM and stretching exercise was statistically significantly decreased in VAS. The pressure pain threshold was significantly increased. Based on the present finding, CTTM and passive stretching could be an alternative therapy for the patients with myofascial pain syndrome on upper back pain. Further research should determine long term effects and larger the sample size, because the present study only determine the immediate effect and long-term effects of these treatments are unknown.

ACKNOWLEDGEMENTS

The main author would like to acknowledge the School of Health Science Mae Fah Luang University, Thailand for supporting the research. Finally we would like to express our sincere gratitude and appreciation to all patients for their generosity and willingness to participate in this study.

REFERENCES

[1] Travell J.G. and Simons D.G. “Myofacial pain and dysfunction: the trigger point manual,” Baltimore: Williams & Wilkins, 1983.
[2] Gerwin R.D., “Muscle Pain: Diagnosis and Treatment”. Springer: London, 2010.
[3] Berg K. “Stretching Fundamentals”. United States of America: United Graphics, 2011.
[4] Wilmor J.H., Costill D.L., Kenney W.L. “Physiology of Sport and Exercise”, Champaingn, IL; Human Kinetics, 2008.
[5] Ayurved Thamrong School. Thai Traditional Medicine in the Faculty of Medicine Siriraj Hospital. Bangkok: Supavanich Press, 2009.
[6] Mongkol S., Sawangjaithum K., Netwera V. “The effect of royal traditional Thai massage in patients with myofascial pain syndrome at upper trapezius muscle: a pilot study”. Journal of medical technology and physical therapy, vol.25, no.1, pp. 87-95, 2013.
[7] Hantan W.P., Olson S.L., Butls N.L., Nowicki A.L. “Effectiveness of a home program of ischemic pressure followed by sustained stretch for treatment of myofascial trigger points” Journal of Physical Therapy, vol.80, no. 10 pp. 997-1003, 2000.
[8] Wamontree P, “Conference proceedings”, in Proc. 1st Int. Conf. on GEOMAT, 2015, pp. 8-13.

Second International Conference on Science, Engineering & Environment,
Osaka City, Japan, Nov.21-23, 2016, ISBN: 978-4-9905958-7-6 C3051

PHYSIOLOGICAL SPECIALIZATION OF PSEUDOPERONOSPORA CUBENSIS AND SCREENING TECHNIQUE FOR DOWNY MILDEW RESISTANCE IN GHERKIN CUCUMBER

Piyavadee Charoenwattana[1], Januluk Khanobdee [2] and Arit Udomyotin [3]

[1]Faculty of Agricultural Technology, Rajamangala University of Technology Thanyaburi, Thailand;
[2,3] Agricultural Technology Research Institute**,** Rajamangala University of Technology Lanna, Thailand

ABSTRACT

Downy mildew (*Pseudoperonospora cubensis*) causes significant losses in cucurbitaceous crops worldwide. *P. cubensis* isolates were obtained from infected cucumber leaves in Lampang province during 2010-2012 in order to determine the downy mildew virulence. Isolates were tested for the presence of highly compatible reactions on specific hosts and identified as pathotype 3. This study focused on developing the screening method to identify resistance whose technique is discussed for screening gherkin cucumber lines (*Cucumis sativus* L.) resistant to downy mildew under greenhouse and field conditions. It has been used to improve resistance in inbred lines, varieties and hybrid parents. Eight selected gherkin cucumber lines obtained from pedigree method gave an average disease resistance score of less than or equal to 2.4 at 40 days after transplanting using the screening technique. Plant disease management requires a successful disease resistance breeding program to develop host resistance that can adequate control downy mildew. Host plant resistance is the most efficient downy mildew management. The technique is expected to improve the cucumber resistance to downy mildew pathogen.

Keywords: Downy mildew, Pathotype, Gherkin, Screening, Resistance

INTRODUCTION

Downy mildew [*Pseudoperonospora cubensis* (Berk.& Curt.) Rostov.] is an economically important disease in cucumber production, especially in the world' humid regions [1]. The disease developed in temperate and tropical areas with either high or low rainfalls and sufficient leaf wetness periods, usually by dew. Inadequate control measures can cause major losses to outputs of cucumber, melon, squash, pumpkin, watermelon, and other cucurbits [2]. The host range of *P. cubensis* is reported to include 50 species in approximately 20 genera of the Cucurbitaceae family [3]. Pathotypes can be differentiated by observing physiological reactions on a diverse set of cucurbit genera. Six pathotypes of *P. cubensis* were analyzed based on their compatibility with specific hosts [4], [5]. The identification of host specificities of downy mildew provided useful information for the characterization of the pathogen [4].

Breeding programs were conducted to increase the level of resistance to downy mildew in cucumber. Gherkin cucumber (*Cucumis sativus* L.) is the cucurbitaceous vegetables for slicing and pickling [6]. It is difficult to improve resistance to downy mildew in cucumber due to environmental variability and a narrow genetic base in cucumber [1]. Efficient and accurate pathogenicity tests for measuring resistance are important for a successful disease resistance breeding program. Reference [7] screened 155 cucumber cultivars for downy mildew using intensity of sporulation as the method for determining resistance. Plant breeders commonly use a rapid method with visual evaluation using a subjective rating scale [8] to determine sporulation for selection of families resistant to downy mildew. A set of 65 diverse cultivars was evaluated in the field using sporulation and other leaf and vine traits for resistance to downy mildew [9]. Downy mildew requires 4 to 12- day sporulation under controlled conditions [10].

An efficient screening was used to identify downy mildew resistance through the selection of gherkin cucumber lines using three methods (inbred line selection, pedigree and backcross methods). The result is expected to be useful to increase the resistance of cucumber to downy mildew. All experiments were conducted at the Agricultural Technology Research Institute (ATRI), Rajamangala University of Technology Lanna, Lampang province during May 2010 – August 2012 to identify and improve resistance in inbred lines, varieties and hybrid parents for durable resistance and management.

OBJECTIVE

This study determined the pathotype of downy mildew isolates collected at ATRI, Lampang province. It screened selected gherkin cucumber lines in a field highly infested with *P. cubensis* to increase

resistance to the pathogen.

METHODOLOGY

Fungal Isolate, Plant Growth and Host Specificity Testing

The isolates of *P. cubensis* collected from downy mildew lesions on heavily infected cucumber leaves at ATRI, Lampang province (Lampang isolate) to determine host specificities of the pathogens [4]. Inoculations were made to 15 cultivars representing 8 species within 5 genera of the family Cucurbitaceae, with 12 plants per cultivar per assay and repeated twice (Table 1). Plants were grown in a greenhouse in 9 cm^2 plastic pots using sterilized planting materials (Krassmann KTS2, Germany) composed of peat moss and vermiculite; watered twice daily and fertilized as needed. Once they reached a two-expanded-cotyledon stage, adaxial and abaxial leaves' surfaces were inoculated with a suspension of *P. cubensis* (10^4 sporangia ml^{-1}) by spraying until incipient run-off. Inoculated plants were placed in the dark at 20 °C with high humidity for 21 hours. Subsequently, they were transferred to the greenhouse with a temperature of 24-28 °C and relative humidity of 80-90%. The plants were observed daily for symptom development. Inoculated plants were evaluated for the presence of lesions and sporulation intensity. Sporulation was rated qualitatively as compatible or incompatible (Table 1). The disease reactions of the host plants were recorded on Day Seventh after inoculation. The host plants without fungal inoculation were used as a control.

Screening Gherkin Cucumber Lines for Resistance to *P. cubensis* under Greenhouse and Field Conditions

To improve resistance to *P. cubensis* in gherkin cucumber lines, F_2-F_5 generation of gherkin cucumber lines were tested and screened, along with gherkin varieties, commercial varieties of cucumber and downy mildew resistant varieties using Pedigree selection. The pathogenicity test in this study originated from 196 gherkin cucumber lines of F_2 generation. The disease resistance in F_3 and F_4 generation were tested and screened in the greenhouse. The Completely Randomized Design was replicated twice with 12 plants per cultivar per assay. The plants were inoculated with a suspension of *P. cubensis* (Lampang isolate) as described above. The disease reactions of the plants were recorded on the 3rd, 5th and 7th day after inoculation. The host plants without fungal inoculation were used as a control.

F_2-F_5 generation of gherkin cucumber lines were tested and screened under field condition. The experiment deployed a Randomized Complete Block Design. Then 20 plants from each variety were transplanted in fields without using artificial inoculum. During the growing season, the fields were exposed to natural epidemics encouraged by a border row of susceptible varieties in each field to help monitor and spread the inoculum by overhead irrigation. The disease reactions were recorded on the 20th, 30th and 40th day after transplanting.

All cucumber lines and varieties were rated for resistance to downy mildew after inoculation for foliar lesions with a 0-5 visual rating scale (0 – no foliar symptoms, 1 – 1-20 % symptoms, 2 – 21-40 % symptoms, 3 – 41-60 % symptoms, 4 – 61-80 % symptoms, 5 – 81-100 % symptoms) with some modifications of [11] for greenhouse and field assessment.

Statistical Analysis

An analysis of variance (ANOVA) was carried out to compare quantitative data and morphological variations and these were analyzed using Duncan's New Multiple Range Test (DMRT).

RESULTS AND DISCUSSION

Disease symptoms first appeared as small, slightly chlorotic to bright yellow areas on the upper leaf surface. Later, the lesions expanded; they remained chlorotic or yellow or became necrotic and brown. The morphology of Lampang isolate visualized under a light microscope and scanning electron microscope (Fig. 1) provided morphology of the pathogen.

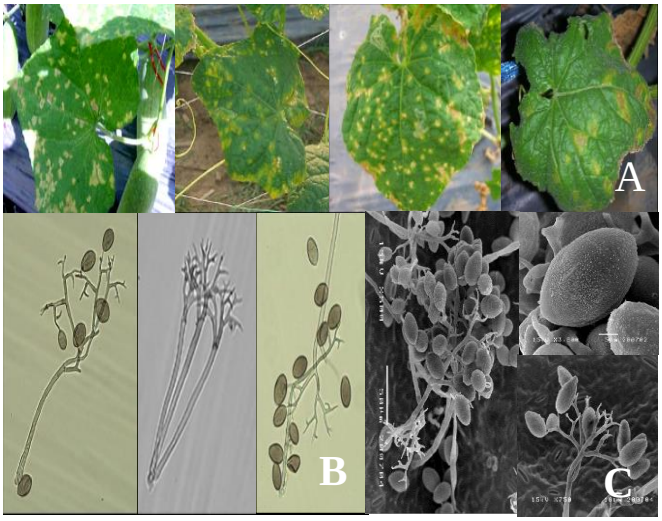

Fig. 1 Disease symptoms and morphology of *P. cubensis* (Lampang isolate) (A) Disease symptoms on leaves,(B) Sporangiophores and sporangia under a light microscope, and (C) visualized by scanning electron microscope.

Physiological Specialization of Downy Mildew

Inoculations to 15 cultivars representing 8 species within 5 genera of the Cucurbitaceae family reveal physiological specialization of Lampang isolate and it was classified as pathotype 3. This isolate was highly compatible with *Cucumis sativus, C. melo* var. *reticulatus, C. melo* var. *conomon* and *C. melo* var. *acidulous* (Table 1 and Fig. **2)**. A pathogenicity test showed that the host specificity of *P. cubensis* isolate could be used to identify downy mildew in cucumber. In 1987, Thomas found five pathotypes of *P. cubensis* including pathotype 1 and 2 in Japan, pathotype 3 in Israel, and pathotype 4 and 5 in the USA. The pathotype 6 was reported in Israel as a new pathotype by Thomas et al. [5]. The resistance of these hosts varied according to locations, suggesting that different pathotypes were present in the various locations.

Table 1 Reactions of selected cultivars of cucurbit host species to *P. cubensis*

Species	Cultivar	Reaction [1/]
Cucumis sativus	C1	+
	Malai 759	+
	Toto	+
	Ranthong	+
Cucumis melo	Singto	+
var.*reticulatus*	Chiatai	+
Cucumis melo	Kamini	+
var.*conomon*	PI420149*	+
	PI420150*	+
	PI532830*	+
Cucumis melo var.*acidulus*	PI200819*	+
Citrullus lanatus	Blackwater melon	-
Cucurbita maxima	Singto	-
Lagenaria vulgaris	Advance	-
Luffa acutangula	Angle luffah	-

** The seeds were obtained from National Plant Germplasm System, GRIN USDA*

[1/] Based on the presence of a highly compatible reaction between P. cubensis and the most susceptible host genotype. + is highly compatible; - is incompatible, very low compatible, or lowly compatible.

Screening for Downy Mildew Resistance under Greenhouse and Field Conditions

The pathogenicity test of downy mildew resistance in greenhouse of gherkin cucumbers distinguished the F_4 generation into two groups: 92 and 36 lines. The test results showed that 54 lines (out of 92) have mildew resistance score of less than or equal to 2.3 after inoculation for 7 days and that 28 lines (out of 36) have mildew resistance score of less than or equal to 1.5 after 7 days. Then, the downy mildew resistance of these F_4 generation was tested and screened in field condition. The test results showed that the 5 highly resistance lines (out of 24) exhibited resistance score of 0.9-1.2 after 40 days of transplanting.

The pedigree selection in F_5 generation in the field yields 8 lines of gherkin cucumber with mildew resistance score of 1.2-2.4 after 40 days of transplanting that can be used as parental lines to generate hybrid variety and perform combining ability test. The F_5 generation yields average output 26.9 tons per hectare and 32.6 fruits per plant, compared to the yields of gherkin cucumber varieties (23.1 tons per hectare and 27.5 fruits per plant). The result indicated that the higher downy mildew resistance can increase the yield of gherkin cucumber lines, thus consistent with Celetti et. al.'s findings [12] that disease reduced the quantity and quality of outputs by 30%-100%. In sum, the pedigree selection of four generation found the gherkin cucumber lines with mildew resistance score of less than or equal to 2.4.

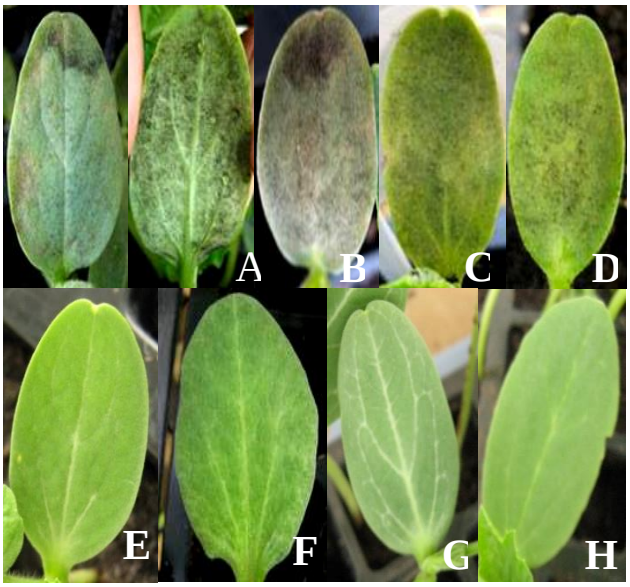

Fig. 2 The disease reaction of *P. cubensis* (Lampang isolate) on cucurbit host species (A) *Cucumis sativus;* (B) *Cucumis melo* var. *reticulatus;* (C) *Cucumis melo* var.*conomon;*(D) *Cucumis melo* var. *acidulous;* (E) *Citrullus lanatus;* (F) *Cucurbita maxima;*(G) *Lagenaria vulgaris;* and (H) *Luffa acutangula* under greenhouse conditions at 7th day after inoculation

CONCLUSION

The cucumber downy mildew (*P. cubensis* - Lampang isolate) was identified as pathotype 3 for the presence of highly compatible reactions on four specific cucurbit host species. Eight selected gherkin cucumber lines obtained from pedigree method gave an average disease resistance score of less than or equal to 2.4 after 40 day of transplanting. The screening under greenhouse and field conditions provides an efficient technique for developing gherkin cucumber lines with high resistance to downy mildew.

ACKNOWLEDGEMENTS

This study was financed by a research grant from the National Center for Genetic Engineering and Biotechnology (BIOTEC), Ministry of Science and Technology, Thailand and their assistance is gratefully acknowledged.

REFERENCES

[1] Palti J. and Cohen Y., 1980. Downy mildew of cucurbits (*Pseudoperonospora cubensis*): the fungus and its hosts, distribution, epidemiology and control. Phytoparasitica 8: 109-147.

[2] Thomas C. E., 1998. Downy mildew. In: Compendium of Cucurbit Diseases (T. A. Zitter, ed.): 25-27. APS PRESS, Minnesota.

[3] Palti J., 1974. The significance of pronounced divergences in the distribution of *Pseudoperonospora cubensis* on its crop hosts. Phytoparasitica 2: 109-115.

[4] Thomas C.E., Inaba T. and Cohen Y., 1987. Physiological specialization in *Pseudoperonospora cubensis.* Phytopathology 77: 1621-1624.

[5] Cohen Y., Meron I., Mor N. and Zuriel S., 2003. A New Pathotype of *Pseudoperonospora cubensis* Causing Downy Mildew in Cucurbits in Israel. Phytoparasitica 31 (5): 458-466.

[6] The Colonial Williamsburg Foundation, 2002. Melons and cucumbers. [On-line]. Available: http://web.archive.org/web/20051211215927/http://georgetown.u47.k12.me.us/history/CWLand/resrch6.cfm**,** September 20, 2012.

[7] Lebeda, A. and Prasil, J. 1994. Susceptibility of *Cucumis sativus* cultivars to *Pseudoperonospora cubensis*. Acta Phytopathol Entomol Hung 29: 89-94.

[8] Jenkins, S. F. and Wehner, T. C. 1983. A system for measurement of foliar diseases in cucumbers. Cucurbit Genet Coop Rpt 6: 10-12.

[9] Criswell, A. D., Wehner, T. C., Klosinska, U. and Kozik, E. 2008. Use of sporulation and other leaf and vine traits for evaluation of downy mildew in cucumber. p. 433-439. *In* Proceedings of the IXth EUCARPIA meeting on genetics and breeding of Cucurbitaceae. May 21-24th, 2008. INRA, Avignon, France.

[10] Zitter, T. A. Hopkin, D. L. and Thomas, C. E. (eds.) 1996. Compendium Cucurbit Diseases. APS Press, St. Paul (MN, USA) pp 25-27.

[11] Thompson, D. C. and Jenkins, S. F. 1985. Pictorial assessment key to determine concentrations that control anthracnose development on cucumber cultivars with varying resistance levels. Plant Disease 69: 833-836.

[12] Celetti, M., Roddy, E. and Pitblado, R. 2007. Downy Mildew in Cucurbits. Ministry of Agriculture, Food and Rural Affairs, Ontario. [On-line]. Available: http://www**.** Omafra.govReferences**.**on.ca/English/crops/facts/downy-mildew-a.htm, June 28, 2011.

Second International Conference on Science, Engineering & Environment,
Osaka City, Japan, Nov.21-23, 2016, ISBN: 978-4-9905958-7-6 C3051

EFFECTIVENESS OF USING RIVER INSECT LARVAE AS AN INDEX OF CU, ZN AND AS CONTAMINATIONS IN RIVERS, JAPAN

Hiroyuki Ii[1] and Akio Nishida[2]
[1]Faculty of Systems Engineering, Wakayama University, Japan; [2] Kyoei High School, Japan

ABSTRACT

Analysis of Dobsonfly larvae for concentrations of Cu and Zn was found to be an effective method of determining levels of Cu and Zn contamination of rivers in metal mine areas and non-metal mine catchments. Metal concentration in Dobsonfly larvae was used as an index of metal contamination because the amount of metal concentration in Dobsonfly larvae decreased with the dry weight of the larvae and also on the degree of metal present in the river water. Dobsonfly makes an excellent tool for contamination evaluation because of their easy classification, wide distribution and commonness. Furthermore, due to their relatively lengthy 2-3 year lifespan, river contamination assessment over a long term could be performed. In this study, Cu, Zn and As concentrations in river insect larvae in metal mine areas were found to be higher than those in non-mine catchments.

Keywords: Mine waste, Dobsonfly, ecotoxicology, heavy metal, insect larvae

INTRODUCTION

Many papers concerning metal concentration in river insect larvae and the high concentration factor of heavy metal found in many kinds of insects have been published [1], [2], [3]. In particular, the influence of metal from waste water or mine tailings on river insects and the relation between metal concentrations in soil and water and metal concentration on insects have been studied [4], [5]. As a result, metal concentrations in river insect larvae were found to be very high relative to non-contaminated areas. The actual mechanism of metal accumulation was studied using nitrogen and carbon stable isotope [6]. Although monitoring water and soil is important for evaluating contamination, it requires taking numerous samples over a long term in order to determine average values of metal concentrations as water and soil metal concentrations vary with time and place. Some insect larvae live in rivers for several years and derive their food from points upstream to their living point therefore they can provide considerable information regarding metal contamination. Measuring metal concentrations in insect larvae is more useful than measuring contamination in water and soil in terms of time, area and concentration.

Dobsonfly is distributed widely in Japan, southern and eastern Asia, South and North America, South Africa, Madagascar, Australia, and New Zealand [7]. Dobsonfly is carnivorous with large jaws and lives in rivers for 2 to 3 years. Metal concentrations in Dobsonfly and Caddisfly are thus thought to provide information for wide areas over a long term. In Japan, metal concentrations in Caddisfly were measured and this metal concentration was used as an indicator of environmental pollution [8], [9]. However, Caddisfly has many kinds of species and classifying each species is difficult. Dobsonfly however, has just two main species, Protohermes grandis and Parachauliodes continentalis in Japan. Dobsonfly is thus thought to be more useful than Caddisfly for classification. Although metal concentrations of dobsonfly were measured [10], these values were not compared with other insects at the same river. The purpose of this study was therefore to evaluate the possibility of using Dobsonfly as an indicator of the degree of metal environmental pollution comparing other river insects.

Fig.1 Study area. Mine area: Waidani, non-mine area: Taisyakukyo, Yada, Kino and Kirime Rivers

MATERIALS AND METHODS

River insect larvae were sampled at both mine and non-mine catchments and metal concentrations were measured. The Waidani area was selected for mine waste water catchments in Okayama Prefecture as shown in Fig.1. The Waidani area is a typical closed small scale copper mine area operated until 70 years ago and its tailing containing ores and slag were disposed of along the top of a local valley with no protection. Pyrite FeS_2, spharelite ZnS, chalcopyrite $CuFeS_2$ and arsenopyrite FeAsS were found in the tailings and Zn, Cu and As contamination was suspected. River water originated from the tailings seepage. River insect larvae were sampled along the downstream of the valley in May, June, November, December 2013 and January 2015. River water was sampled and flow rate was measured from December 2011 to January 2015.

River water and insect larvae in non-mine catchments were sampled along the Taishaku Valley in a limestone valley in Hiroshima Prefecture, the Yada River with volcanic sediments in Hyogo Prefecture, the upstream of the Kino River with sedimentary rocks, basic and felsic metamorphic rock and limestone in Nara Prefecture and the Kirime River with sedimentary rocks as shown in Fig.1. Sampling dates for river water and river insect larvae was in August 2013 at the Taishaku Valley, in July and December 2012 at the Yada River composed of three branch rivers, in December 2013 and December 2014 at the upstream of Kino River with three sampling points and in October 2014 at the Kirime River. Sampled insect larvae were dried then dissolved with concentrated nitric acid solution. The solution after filtration with 0.45 micrometer was analyzed for metal concentration by ICP-AES (Inductively Coupled Plasma Atomic Emission Spectroscopy). River water was also analyzed by ICP-AES.

RESULTS

Table 1 shows pH, EC, Cu, Zn, and As concentrations of river water along the valley for the Waidani area. At the top of the valley, there are large tailing places from which the south and north rivers originated. The upstream, middle and downstream of the south river are SR U, SR M and SR D and the length was 3 km. The sampling points from the upstream to downstream of the north river are NR UP, NR UM, NR MD and NR D and the length was 3 km. The sampling points, SR U, NR UP and NR UM were next to the tailing place.

Although most mine waste water contains high concentrations of H^+ and SO_4^{2-}, EC values were low and pH values were high indicating that in this area waste water was not treated by neutralization and precipitation. Zn, Cu and As concentrations in upstream river water were high relative to the downstream subsequently mine tailings were thought to be metal source along the rivers. Cu, Zn and As loads reached approximately 20, 150 and 10 kg per year. Metal load was not small for these small catchments of only 3 km in length. In particular, As concentration at the SR U and Zn concentrations at the NR UP and NR UM were high.

Table 1 pH, EC, Cu, Zn, and As concentrations of river water

	pH	EC (ms/m)	Cu (mg/l)	Zn (mg/l)	As (mg/l)
SRU	6.7 ~ 7.6	15.7~ 18.8	0.010~ 0.143	0.247~ 0.543	0.127~ 0.178
SRM	6.9 ~ 8.0	8.6~ 9.8	0.007~ 0.086	0.031~ 0.273	0.022~ 0.046
SRD	7.0 ~ 7.5	8.0~ 12.2	0.008~ 0.028	0.026~ 0.051	0.017~ 0.053
NRUP	6.5 ~ 7.5	9.8~ 13.0	0.063~ 0.198	1.047~ 1.914	0.011~ 0.039
NRUM	6.2 ~ 7.7	9.2~ 15.3	0.052~ 0.182	0.831~ 1.429	0.002~ 0.073
NRMD	6.6 ~ 7.5	8.2~ 12.1	0.011~ 0.037	0.308~ 0.637	N.D.~ 0.045
NRD	6.6 ~ 7.7	9.0~ 11.8	N.D.~ 0.014	0.125~ 0.205	N.D.~ 0.026

Fig. 2, 3, and 4 shows Cu, Zn, and As concentrations under dry weight samples for all sampled river insect larvae. Although Cu concentrations in river insect larvae in the Waidani north and south areas were variable values, several 10 to several 1000 ppm, they decreased from upstream to downstream. Cu concentration in river insect larvae was thought to depend on river Cu concentration. Cu concentrations in river insect larvae in the Taisyakukyo, Yada, Kino and Kirime Rivers, were uniform, 10 to 100 ppm but Cu concentrations in river insect larvae in the Waidani

area were 10 times higher than those in non-mine catchments. Cu concentrations for river insect larvae in the Waidani area even 3 km downstream were higher than those in non-mine catchments. Cu concentration of river water in the Waidani area was within the Japanese Effluent Standard. Thus, the high Cu concentration in river water in the Waidani area was thought to increase Cu concentration in river insect larvae. Therefore, the Cu concentration value of the Japanese Effluent Standard was thought to be too high judging from the high Cu concentration in river insect larvae. Cu concentration in river insect larvae depended on the environment's Cu concentration. Then, river insects were thought to be effective as Cu contamination indicators. Dobsonfly was expected to be useful as a metal index because Dobsonfly was found widely, however Cu concentrations in Dobsonfly larvae in the Waidani area were very variable, several 10 to several 1000 ppm. Stenopsyche mamorata is a kind of Caddisfly and very common in Japan. However, Stenopsyche mamorata was not found in the Waidani area although it was very abundant in non-mine catchments. Dragonfly, Caddisfly and Stonefly were found in the Waidani area and were higher than those in non-mine catchments although each concentration had a wide range. In this study, there were 18 species of Stonefly, 13 species of Mayfly and 13 species of Caddisfly and excluding Dobsonfly, many species were thought to bring out variable concentration values because each species was thought to have each concentration character.

Although Zn concentrations in river insect larvae in the Waidani south and north areas were variable values, 100 to 10,000 ppm, they decreased from upstream to downstream. Zn concentration in river insect larvae was thought to depend on river Zn concentration. Although Zn concentrations in the Taishakukyo were variable values, 100 to several 1000 pm as well as mine areas, Zn concentrations in the Kino and Kirime River were several 10 to several 100 ppm and Zn concentrations in the Yada River were several 100 ppm and then Zn concentrations in river insect larvae in mine areas were higher than those in non-mine catchments.

Effluent Regulations although it was under the Japanese Effluent Standard. Thus, the high Zn concentration in river water in the Waidani area was thought to increase Zn concentration in river insect larvae. Therefore, Zn concentration in the Japanese Effluent Standard was thought to be too high judging from high Zn concentration in river insect larvae. Zn concentration in river insect larvae depended on the environment Zn concentration because Zn concentration in river insect larvae in the Waidani area decreased down the stream and Zn concentration in river insect larvae in the Waidani area was higher than those in non-mine catchments. Therefore river insect larvae were thought to be

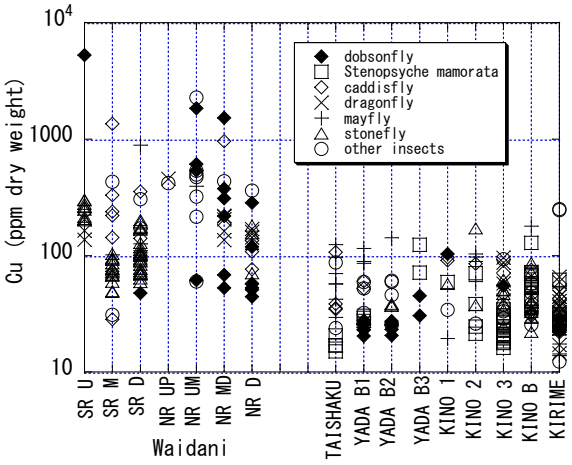

Fig. 2 Cu concentrations under dry weight samples for all sampled river insect larvae.

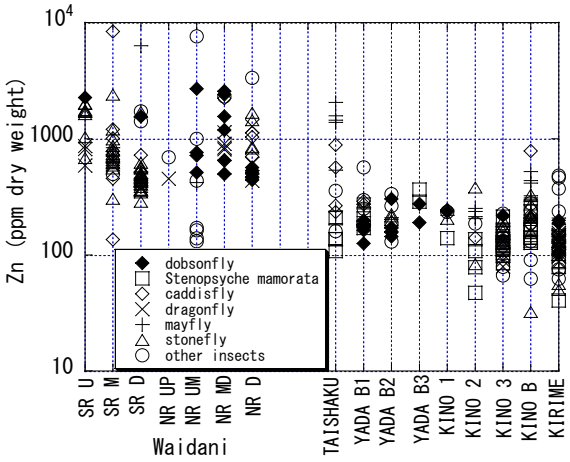

Fig. 3 Zn concentrations under dry weight samples for all sampled river insect larvae.

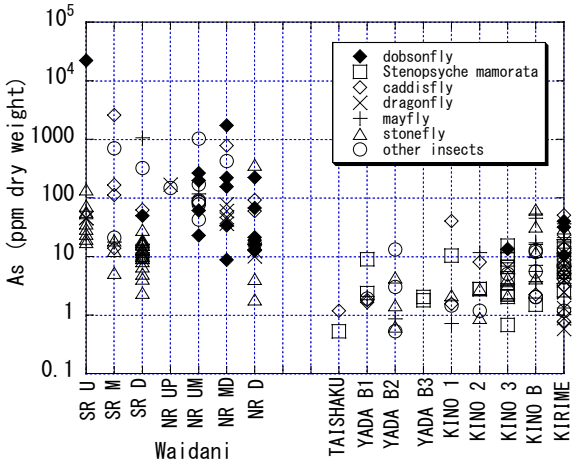

Fig. 4 As concentrations under dry weight samples for all sampled river insect larvae.

effective as a Zn contamination indicator. Zn concentration in Dobsonfly larvae in the Waidani area was 10 times higher than those in non-mine catchments as well as Stonefly although Zn

concentrations in Dobsonfly larvae were variable.

Although As concentrations in river insect larvae in the Waidani south and north areas were variable values, several to several 1000 ppm, they decreased from upstream to downstream. As concentration in river insect larvae was thought to depend on river As concentration. As concentrations in insect larvae in non-mine catchments were several 0.1 to several 10 ppm and As concentrations in river insect larvae in the Waidani area were 10 to 100 times higher than those in non-mine catchments. The high As concentration in river in the Waidani area was thought to increase As concentration in river insect larvae. As concentration in river insect larvae depended on the environmental As concentration because As concentration in river insect larvae in the Waidani area decreased going downstream and was higher than those in non-mine catchments. Therefore river insect larvae was thought to be effective as an As contamination indicator. As concentration in Dobsonfly larvae in the Waidani area was 10 times higher than those in non-mine catchments as well as Stonefly although As concentrations in Dobsonfly larvae had a wide range.

Fig.5, 6, and 7 show the relation between Cu, Zn, and As concentrations in river insect larvae and dry weight in river insect larvae because metal concentrations in insect larvae were thought to change with insect growth. Cu concentration in river insect larvae in both the Waidani area and non-mine catchments decreased with dry weight in insect larvae. Although Cu concentration in river insect larvae had a wide range, Cu concentration for each weight had a narrow range. In particular, Dobsonfly was found to show a good relation between dry weight and concentration while other insects such as Stonefly were not as clear. Other insects had many species and each species was thought to have its own character. Decrease (log(Cu)/log(weight)) in Cu concentration with dry weight for Dobsonfly was about -0.5 log(ppm) /log(g) in the Waidani area and about -1/3 log(ppm) /log(g) in non-mine catchments. At the condition in 0.01 g for dry weight (a common dry weight in river insect larvae), Cu concentration in Dobsonfly larvae in the Waidani area and non-mine catchments were several 100 and several 10 ppm and then Cu concentration in Dobsonfly larvae in the Waidani area was 10 times higher than those in non-mine catchments. Therefore, Cu concentrations in Dobsonfly under the uniform dry weight condition could be useful as an index of Cu contamination.

Zn, as well as Cu concentrations in river insect larvae in both the Waidani area and non-mine catchments decreased with dry weight in river insect larvae. Although Zn concentrations in river insect larvae had a wide range, Zn concentrations for each weight had a narrow range. In particular, Dobsonfly was found to have a good correlation between the

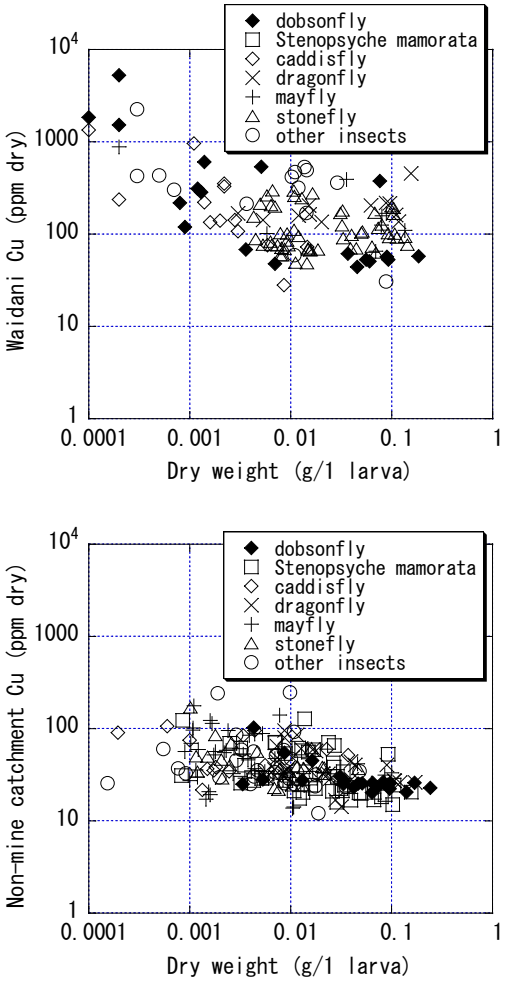

Fig. 5 the relation between Cu concentrations in river insect larvae and dry weight in river insect larvae, upper: Waidani, lower: non-mine catchments

dry weight and Zn and Cu concentrations although other insects such as Stonefly were not clear. Decrease (log(Zn)/log(weight)) in Zn concentration with weight for Dobsonfly was about -1/3 log(ppm) /log(g) both in the Waidani area and non-mine catchments however Zn concentration in river insect larvae in the Waidani and non-mine catchments were different. At the condition in 0.01 g for dry weight, Zn concentration in Dobsonfly larvae in Waidani area and non-mine catchments were 1000 ppm and several 100 ppm and then Zn concentration in Dobsonfly larvae in Waidani area was about 10 times higher than those in non-mine catchments. Therefore, Zn concentration in Dobsonfly under the uniform dry weight condition could be useful as an index in Zn contamination.

As concentration in river insect larvae in both the Waidani area and non-mine catchments decreased with dry weight in insect larvae as well as Cu and Zn. Although As concentration in river insect larvae had a wide range, As concentration for each weight had a narrow range. Dobsonfly was only found to have a good relation between the dry weight and concentration in the Waidani area. Most in As

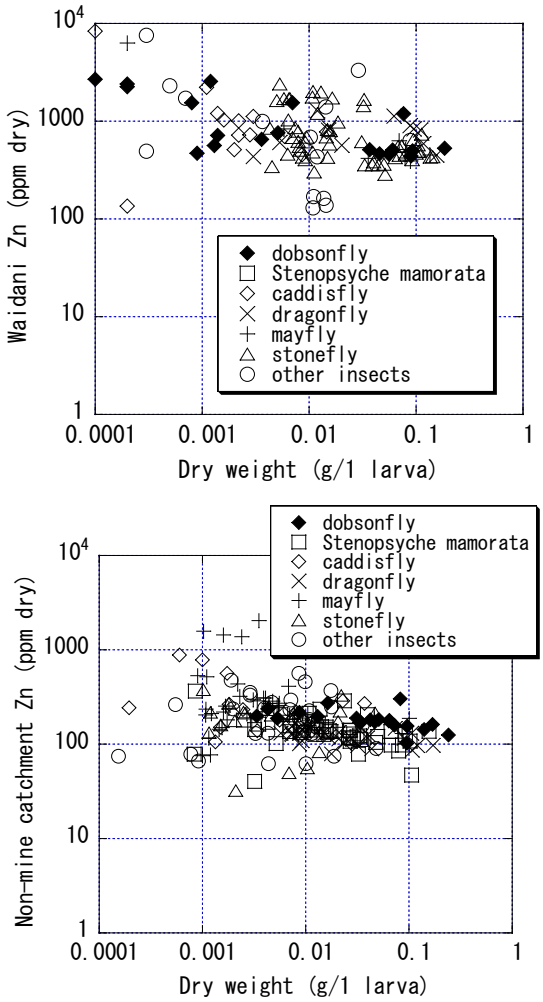

Fig. 6 the relation between Zn concentrations in river insect larvae and dry weight in river insect larvae, upper: Waidani, lower: non-mine catchments

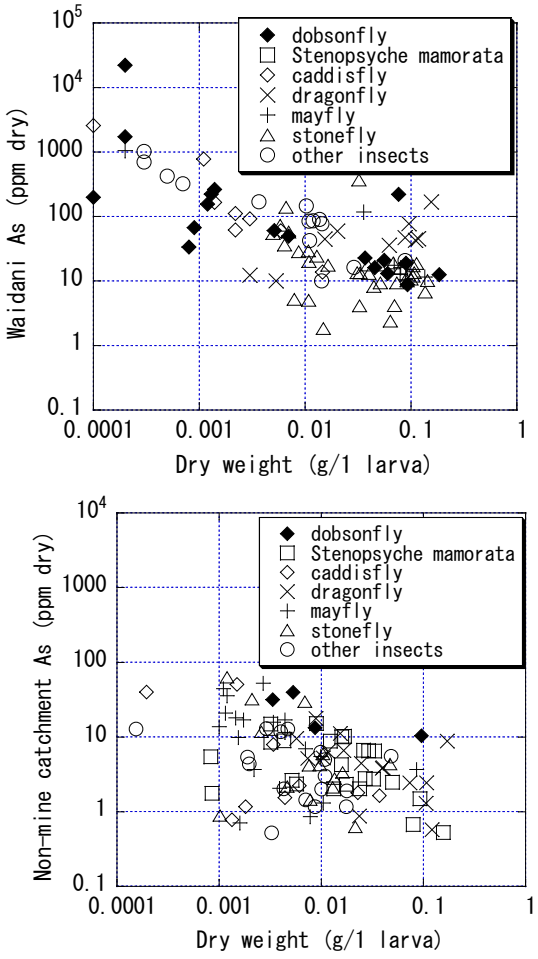

Fig. 7 the relation between As concentrations in river insect larvae and dry weight in river insect larvae, upper: Waidani, lower: non-mine catchments

analysis for river insect larvae in the non-mine catchment was under the detection limit in ICP and there were only 4 samples for Dobsonfly. The relation between concentration and dry weight in both the Waidani area and non-mine catchments was on the same line, decrease (log(As)/log(weight))in As concentration with weight for Dobsonfly was -0.5 log(ppm) /log(g). At the condition in 0.01 g for dry weight, As concentration in Dobsonfly larvae in the Waidani area and non-mine catchments were several 10 ppm and then As concentration in Dobsonfly larvae in the Waidani area and non-mine catchments was the same. On the other hand, As concentration in other river insect larvae in the Waidani area were higher than those in non-mine catchments. Therefore, As concentration in Dobsonfly under the uniform dry weight condition was not thought to be satisfactory as an index in As contamination probably because of a lack of data for Dobsonfly.

DISCUSSION

Dobsonfly larvae are being considered as an index in metal contamination because they are easy to classify, have a wide distribution, are very common, live 2 or 3 years in rivers, and are carnivorous (top of the insect food chain). Metal concentrations in river insect larvae in mine areas and non-mine catchments were measured. Metal concentrations in insect larvae in mine areas were higher than those in non-mine catchments although they were very variable, by as much as two or three orders. However Cu, Zn, and As concentrations in river insects were still variable values, one or two orders at the same area, mine area or non-mine catchments, because the concentrations decreased with weight and depended on species. Then, at the same weight condition, the concentrations for one species, Dobsonfly larvae indicated uniform values, one order, however other insect larvae maintained wide ranges, over one order because these insects had many species and each species had its own concentration character. Concentration in Dobsonfly decreased with dry weight in Dobsonfly under the

same river metal condition and the relations, decreases in metal concentration with weight for Cu, Zn, and As were different values and Cu and Zn concentration in Dobsonfly was thought to depend on river metal condition. However, As concentration in Dobsonfly was not thought to depend on river metal condition because As concentration in Dobsonfly under the same dry weight was the same in the Waidani area and non-mine catchments although As concentration in river insect larvae in the Waidani area was lower than those in non-mine catchments in spite of scarce data on As concentration in Dobsonfly in non-mine catchments. Therefore, metal contamination was estimated from the relations for Dobsonfly excluding As. For example, metal concentration in Dobsonfly at the same dry weight was thought to become an index in metal contamination. Dobsonfly is distributed on a world scale and is very common but limited in its number of species in Japan.

Generally, metal is accumulated in body over time with growth. However, the relation between metal concentration and weight showed reverse results. Elimination ability for metal was thought to increase with growth or during ecdysis, the insect was thought to release metal. Decrease in metal concentration with weight was low for Zn and Cu. It was also thought to depend on toxicity in metal.

Main river water resource at the upstream in the Waidani area, mine area was seepage from the tailings. Therefore, river water was partly mine effluent water. River insect larvae in the upstream were assumed to have grown up in effluent water. From Cu, Zn and As concentration and weight for Dobsonfly, Cu, Zn and As concentration in Dobsonfly in the Waidani, mine area had high concentrations relative to the non-mine catchments.

CONCLUSION

Comparing metal concentrations in river water and river insect larvae in mine areas and non-mine catchments, Cu, Zn and As concentrations in river insect larvae were higher than those in non-mine catchments. However, the metal concentrations had wide ranges and river water metal concentration, insect species and larvae weight made wide ranges. Then, using one species, the Dobsonfly larvae which have a wide distribution, are very common, have long lives and are carnivorous, river metal concentration was evaluated from the relation between metal concentration and weight for Dobsonfly because the relation between metal concentration and dry weight for Dobsonfly was very clear. The metal concentration decrease with weight for Cu, and Zn was different and also depended on river water metal concentration.

REFERENCES

[1] Hickey C.W. and Golding L.A. “Response in macroinvertebrates to copper and zinc in a stream mesocosm”, Environ. Toxicol. Chem., Vol. 21, 2002, pp. 1854-1863.

[2] Tochimoto H., Oshida Y., Kikuchi Y., Sasano H., Nakamura H. and Matsumoto M. “Aquatic Insects in Streams as Biological Monitors in Heavy Metal Pollution”, Ann. Rep. Tokyo Metr. Res. Lab. P.H., Vol. 32(1), 1981, pp. 296-303.

[3] Hatakeyama S., Sugaya Y., Satake K., Miyashita M. And Fukushima S. “Macroinvertebrate communities in heavy metal-polluted rivers in the Shikoku district in Japan”, Verh. Internat. Verein. Limnol, Vol.24, 1990, pp. 220-227.

[4] Hatayama N. “Determination in acceptable copper concentration for macroinvertebrate communities based on field investigations on metal-polluted rivers around abandoned mines in Japan” Japan J. Environ. Toxicol., Vol. 14(1), 2011, pp. 57-68.

[5] Leland H.V., Fend S.V., Dudley T.L. and Carter J.L. “Effects in copper on species composition in benthic insects in a Sierra Nevada, California, stream”, Fresh-water. Biology, Vol. 21, 1989, pp. 163-179.

[6] Watanabe K., Yamamoto N., Kusano H. And Omura T. “ Elucidation in Mechanisms in Heavy Metal Accumulation in Stream Aquatic Insects by Nitrogen and Carbon Stable isotope analysis”, Journal in Japan Society on Water Environment., Vol. 28(12), 2005, pp. 737-744..

[7] Yoshinori T, Takuzou Y, “The life history in Parachauliodes continentails in Sugihara river, Hyogo”, Hyogo Inland Water Living Thing, Vol. 50, 1999, pp. 7-13.

[8] Aizawa S., Kakuta K., Akatsuka M., Inoue S. and Akaiwa H. “Evaluation in Caddisfly as an indicator organism for environmental pollution by heavy metals”, Japan Analyst, Vol.43(11), 1994, pp. 865-871.

[9] Aizawa S., Kakuta A., Yasuda S., Kakuta K. and Itabashi H. “Concentrations in Heavy Metals in Caddisfly Larvae in the Tone River System and Their Seasonal Variations”, Japan Analyst, Vol. 58(4), 2009, pp. 273-285.

[10] Fujino A. and Ii H., “Importance of corydalidae as an index of metal contamination of river”, International Journal of GEOMATE, Dec., 2015, Vol. 9(2), pp. 1483-1490.

Second International Conference on Science, Engineering & Environment,
Osaka City, Japan, Nov.21-23, 2016, ISBN: 978-4-9905958-7-6 C3051

EFFECT OF NIR-ABSORBING OPTICAL FILTERS ON THE PHOTOSYNTHETIC RESPONSE IN *Synechocystis* sp. PCC6803 UNDER SOLAR SIMULATING ARTIFICIAL LIGHT

Kota Oshita, Ayaka Hara, Takuya Suzuki and Tomonori Kawano[1],
[1]Graduate School of Environmental Engineering, The University of Kitakyushu, Japan

ABSTRACT

Solar simulating light (SSL) has been widely used for evaluating the action of photovoltaic cells. For studying the natural photosynthesis, several groups employed SSL in place of natural sun light. Photosynthesis in green plants/algae utilizes the visible light, after harvesting photons through antenna pigments such as chlorophylls. Therefore, the bands of light corresponding to the absorption by chlorophylls mostly contribute to photosynthesis. In contrast, the light components not targeting such pigments hardly energize photosynthesis. However, when the plants were exposed to chlorophyll-targeting red light together with the light with wavelength greater than 680 nm (peaking at around 700 nm), higher rate of photosynthesis can be induced (as known as Emerson effect). In fact, SSL contains a wide range of light components from UV to near infrared (NIR). In the present study, we examined the roles of NIR components in SSL during photosynthetic O_2 evolution in *Synechocystis* sp. PCC6803, by selectively cutting the long wavelength light using several NIR-absorbing optical filters. Here, the effects of intact SSL spectrum and the optical fiter-modified SSL spectra lacking NIR light longer than 690, 710, 750, or 810 nm were compared. We observed that removal of light with wavelength longer than 750 nm resulted in lowered maximal photosynthetic velocity (P_{max} value) whereas cutting of light with wavelength longer than 810 nm showed no significant change. We concluded that the 750-810 nm band may contain the photosynthesis-stimulating NIR component acting differently from the Emerson effect. Contrary, *Synechocystis* regained the photosynthetic performance by eliminating the most NIR (wavelengths, $\geqq$ 710 nm), suggesting that 710-750 nm band may include NIR components inhibitory to photosynthesis possibly corresponding to the absorption band for bacterial phytochrome. There preliminary data must be exposed to further examination.

Keywords: Near infrared, Photosynthesis, Solar simulating light,

INTRODUCTION

Solar simulators were designed to emit the light with spectral features mimicking the sunlight by combining various optical filters and xenon lamp-based light sources. Solar simulating light (SSL) has been frequently employed for evaluating the performance of photovoltaic cells [1] or photocatalysts [2], [3]. Since the photovoltaic cells and photocatalysts are mostly sensitive to ultraviolet (UV) and visible (VIS) lights regions, most SSL are designed to reproduce the spectra of solar ray in these regions. However, spectral features of most SSL developed to date, failed to reproduce the NIR spectrum found in solar ray as shown in Figure1.

For studying the natural photosynthesis, several groups employed SSL in place of natural sun light [4]. Photosynthesis in green plants/algae utilizes the VIS light, after harvesting photons through antenna pigments such as chlorophylls. Therefore, the bands of light corresponding to the absorption by chlorophylls (i.e. 665 nm and 430 nm for chlorophyll *a* and 465 nm and 645 nm for chlorophyll *b*) mostly contribute to photosynthesis. In contrast, light components not targeting such pigments hardly energize the photosynthesis. Although both the spectra of solar ray and SSL ranging between 400 and 700 nm shows broad intensive peaks, the action spectra for photosynthesis suggests that only limited bands reflecting the absorption spectra for chlorophylls are utilized by photosynthesis [4]. Interestingly, when the plants were exposed to chlorophyll-targeting red light together with the light with wavelength greater than 680 nm (peaking at around 700 nm), higher rate of photosynthesis can be induced (as known as Emerson effect) [5]. In the present study, we examined the roles of NIR components in SSL during photosynthetic O_2 evolution in *Synechocystis* sp. PCC6803, by selectively cutting the long wavelength light using several NIR-absorbing optical filters.

MATERIALS AND METHODS

Photosynthetic bacteria

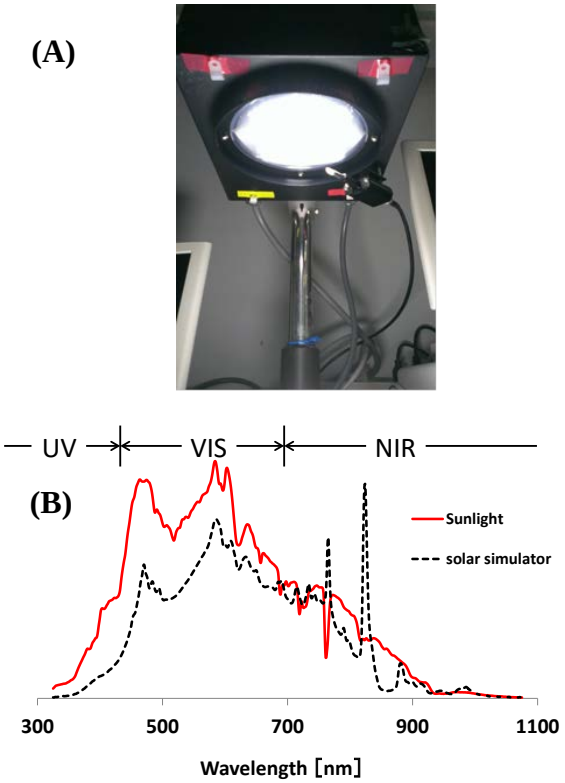

Fig. 1. Comparison of solar spectrum and SSL spectrum. (A) Cell tester YSS-50 (Yamasita Denso, Tokyo, Japan) used here. (B) Spectra of solar ray recorded in Kitakyushu city and that of SSL.

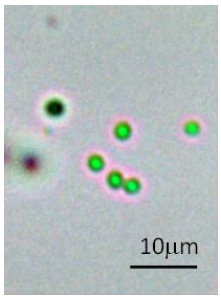

Fig. 2. Cell of PCC6803 used in this stady.

As a simplest model photosynthetic organism, a cyanobacterium would be one of the best materials since the photosynthetic apparatus in this organism is simple but equivalent to the one found in plants [6].

Among cyanobacteria, *Synechocystis* sp. PCC6803 (Fig. 2) was chosen since it is one of the most widely studied strains capable of growth under both autotrophic and heterotrophic conditions [7]. In addition, this strain was used as a model for studying the evolutionary emergence of photosynthetic eukaryotes through symbiosis development between cyanobacteria and protozoa [8]. Cells of PCC6803 were pre-cultured in BG-11 medium (at 23 ±1 °C) under a continuous fluorescent natural-white light at *ca*. 3000 lux. Culture was renewed at 2-week intervals.

Prior to experiments, cells were harvested by centrifugation at 3000 rpm for 10 minutes, then re-suspended in fresh medium and the optical density (OD) of the cell suspension was monitored at 680 nm by a spectrophotometer UV-1800 (Shimadzu Co., Kyoto, Japan). OD was adjusted to be 1.0, at which cellular density can be prepared to be approximately at 10^8 cells/ml. The cell suspension was then kept in darkness for 30 min.

Irradiation by solar simulating light

The light source used was a solar simulator (Cell Tester YSS-50, Yamashita Denso, Tokyo). The spectrum of the light source was measured using a portable NIR field spectro-radiometer (FieldSpec HandHeld 2, ASD Inc., Atlanta, GA, USA). Spectral pattern found in SSL emitted by the above equipment was almost identical to the shape of the spectrum of sunlight especially in the UV-VIS regions (Fig. 1). Four optic short-pass filters shown to cut long wavelength light (>690, 710, 750, or 810 nm) (Asahi Spectra Co., Ltd.) were used and their performance was confirmed with a spectral irradiance meter (KONICA MINOLTA, Tokyo, Japan).

The intensity of the light was scored as photosynthetic photon flux density (PPFD, μmol/m2). The light intensity was adjusted by the layers of black-colored plastic meshes (pore size, 1mm).

Monitoring of disolved O_2 concentration in the cyanobacterium culture

For monitoring the evolution of O_2 from the cyanobacterium culture, a Clerk-type oxygen electrode (Oxygraph Plus System, Hansatech Instruments Ltd., Norfolk, United Kingdom) was used with some modification of oxygen electrode chamber as previously described (Nagasawa et al, 2015.). The electrode chamber was covered with black cardboard with an opening (optical window; diameter, 10 mm). Instead of a plastic lid of the electrode chamber, a transparent acrylic plug was used, so that radiation from LEDs positioned above the oxygen electrode directly reaches the level of algal cell suspension through the optical window. For each measurement of O_2 evolution by living cells, except for dark control, the cell suspension was subjected to a dark cycle of 300 sec followed by a light period of 600 sec.

Kinetic evaluation

Simulation of light response curves (PI-curves)

In 1976, two British marine ecologists [9] have documented their evaluations of several candidate photosynthetic equations and selected one equation adapting a well-known Michaelis-Menten equation (MME) which was originally proposed for studying the velocity of enzyme reaction (V) as a function of substrate concentration ([S]), involving two additional factors, namely V_{max} and K_m representing the maximal V and Michaelis constant, respectively [10]. As below, Platt-Jasby equation (to be designated as PJE) derived from the well-established MME is shown (eq. 1). In fact, most PI-kinetic models are derivatives of MME. Today, MME-derived PJE remains the standards for generation of PI-curves [4], [11].

$$P = \frac{P_{max} \cdot J}{K_J + J} \qquad (1)$$

where P is the rate of gross photosynthesis, P_{max} is maximal photosynthetic rate, J is the intensity of light, and K_j is the Michaelis constant for light.

Determination of coefficients

We have recently performed eco-toxicological simulations of lethal impacts of contaminating chemicals based on limited data size or data points from model experiments using the cells of green paramecia (*Paramecium bursaria*) exposed to various toxic metal ions [12]. In our approach, problem with apparently incomplete curves for toxicity response due to limited experimental data points was overcome by using practically arranged Hill-type equation. For curve fitting, determination of LC_{50} and Hill coefficient was performed with newly proposed method designated as graphical elucidation of Gauss-Newton algorithm (GEGNA). By definition, Gauss-Newton algorithm iteratively finds the value of the variables which minimizes the residual sum of squares (RSS) as often applied to determination of variables (V_{max} and K_m) for MME [13]. RSS is the sum of the squares of the difference between the recorded and the simulated values as shown below.

$$RSS = \sum_{i=1}^{m} \left(y_i - f_n(x_i)\right)^2 \qquad (2)$$

By analogy, PJE was converted to Hill-type equation as below (eq. 3)

$$P = \frac{P_{max} \cdot J^{\alpha}}{K_j^{\alpha} + J^{\alpha}} \qquad (3)$$

where α is Hill coefficient and other variables are identical with PJE.

RESULTS AND DISCUSSION

Effect of light intensity on O_2 evolution

Typical results for measurements of light intensity-dependent O_2 evolution under SSL are shown (Fig. 3).

Here, the effects of intact SSL spectrum and the optical fiter-modified SSL spectra lacking NIR light longer than 810, 750, 710, or 690 nm were compared, as the SSL-dependent PI-curves simulated after the obtained data with and without optical filters are shown (Fig. 4). In Figure 5, parameters for photosynthetic curves expressed by Hill-type photosynthetic equation are compared. Notably, we observed that removal of light with wavelength longer than 750 nm resulted in lowered maximal photosynthetic velocity (P_{max} value) and lowered Michaelis constant for light (K_j value) whereas cutting of light with wavelength longer than 810 nm showed no such significant change.

We concluded that the 750-810 nm band may contain the photosynthesis-stimulating NIR component acting differently from the Emerson effect. Contrary, *Synechocystis* regained the photosynthetic performance by eliminating the most NIR (wavelengths, ≧710 nm), suggesting that 710-750 nm band may include NIR components inhibitory to photosynthesis possibly corresponding to the absorption band for bacterial phytochrome [14].

At present, preliminary data were obtained as shown above. We need to repeat and further examine the phenomena in the future research.

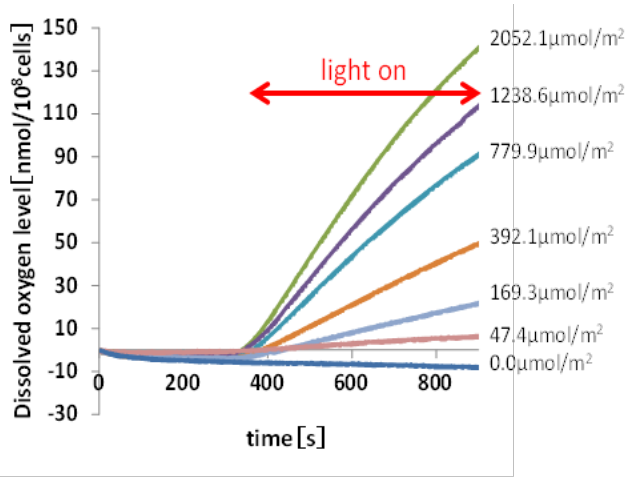

Fig. 3. Effect of SSL light intensity for induction of O_2 evolution by PCC6803 cells.

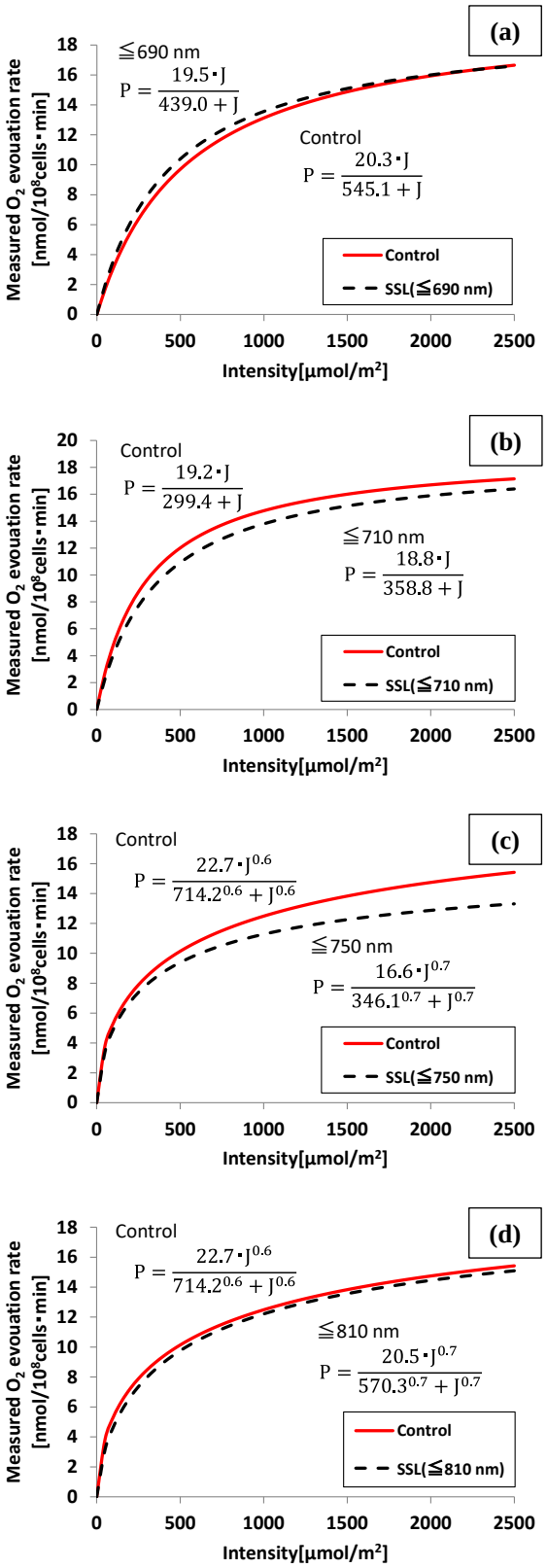

Fig. 4. Effect of optical filters or photosynthetic performance of PCC6803 cells under solar simulating light. Effect of 4 short-pass optical filters (≦690 nm, ≦710 nm, ≦750 nm, and ≦810 nm) were compared with in fact control.

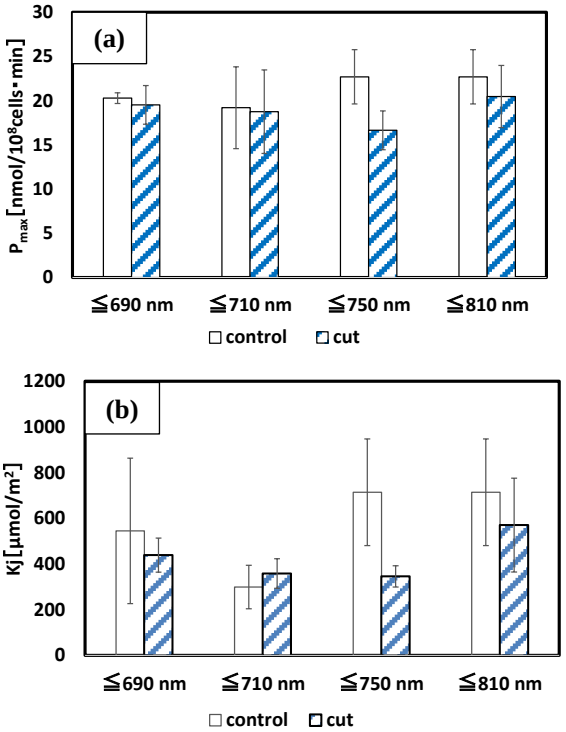

Fig. 5. Effect of optical filters on two photosynthetic parameters, P_{max} and Michaelis constant for light requirement.

ACKNOWLEDGEMENTS

This work was supported by a grant of Regional Innovation Strategy Support Program implemented by Ministry of Education, Culture, Science and Technology (MEXT), Japan.

REFERENCE

[1] Senadeera, G. K. R., Nakamura, K., Kitamura, T., Wada, Y., and Yanagida, S. (2003) Fabrication of highly efficient polythiophene-sensitized metal oxide photovoltaic cells. Appl. Phys. Lett. 83: 5470-5472.

[2] Yu, J., Zhang, Y., and Kudo, A. (2009) Synthesis and photocatalytic performances of BiVO4 by ammonia co-precipitation process. J. Solid State Chem. 182: 223-228.

[3] Sakai, S., Kuroki, S., Oba, T., and Suzuki, T. (2016) Synthesis optimization and characterization of visible-light responsive Ce-doped titanate nanotubes for enhanced degradation of polluting dyes in aqueous environment. Environ. Control Biol. 54:71-74.

[4] Nagasawa, K., Iwase, J., Comparini, D., and Kawano, T. (2015) Empirical and simulative evaluations of white fluorescence-type light emitting diodes as algal growing light sources

based on the photosynthetic oxygen evolution by *Synechocystis* spp. PCC6803. Environ. Cont. Biol. 53: 169-173.

[5] Govindjee, R., Thomas, JB., and Rabinowitch, E. (1960) “Second Emerson Effect" in the Hill reaction of *Chlorella* cells with quinone as oxidant. Science 3424: 421

[6] Jarvis, P. (2004) Organellar proteomics: chloroplasts in the spotlight. Curr. Biol. 14: 317-319.

[7] Ohkawa, H., Pakrasi, H.B., and Ogawa, T. (2000) Two types of functionally distinct NAD(P)H dehydrogenases in *Synechocystis* sp. strain PCC6803. J. Biol. Chem. 2000; 182: 31630–31634.

[8] Ohkawa, H., Hashimoto, N., Furukawa, S., Kadono, T., and Kawano, T. (2011) Forced symbiosis between *Synechocystis* spp. PCC 6803 and apo-symbiotic *Paramecium bursaria* as an experimental model for evolutionary emergence of primitive photosynthetic eukaryotes. Plant Signal. Behav. 6: 773-776.

[9] Platt, T. and Jasby, A. D. (1976) The relationship between photosynthesis and light for natural assemblages of coastal marine phytoplankton. J. Phycol. 12: 421-430.

[10] Michaelis, L. and Menten, M. L. (1913) Die kinetic der Invertinwirkung Biochem. Z. 49: 333-369.

[11] Marra, J., Heinemann, K., and Landriau, G. Jr. (1985) Observed and predicted measurements of photosynthesis in a phytoplankton culture exposed to natural irradiance. Mar. Ecol. 24: 43-50.

[12] Takaichi, H. and Kawano, T. (2016) Expanded and practical use of logistic equations in eco-toxicity evaluation: cases of lethal metal toxicity curves in green paramecia with minimal-sized experiments. J. Adv. Comput. Intellig. Intellig. Inform. (in press).

[13] Björck, A. (1996) Numerical methods for least squares problems. SIAM, Philadelphia.

[14] Igamberdiev, A. U., Eprintsev, A. T., Fedorin, D. N., Popov, V. N., (2014) Phytochrome-mediated regulation of plant respiration and photorespiration. Plant Cell Environ. 37: 290-299.

Second International Conference on Science, Engineering & Environment,
Osaka City, Japan, Nov.21-23, 2016, ISBN: 978-4-9905958-7-6 C3051

HOME BASED PHYSICAL ACTIVITY INTERVENTION PROGRAMME IN WAR-TORN COUNTRY LIKE IRAQ

Jian Abdullah Noori[1, 2], Soh Kim Geok[1, 3], Norhaizan Mohd Esa[4], and Nabeel Abdulwahab Ahmed[2]

[1]Faculty of Education Studies, University Putra Malaysia, Malaysia.[2]Faculty of Basic Education, Al-Mustansiriya University, Iraq. [3]Sports Academy, University Putra Malaysia, Malaysia.[4]Faculty of Medicine and Health Sciences, University Putra Malaysia,

ABSTRACT

The unsuitable conditions as the result of a decade of war had made it difficult to raise the level of physical activity among the youth in Iraq. Lack of awareness, as well as misconceptions about diets and the concept of physical activity among young people and the society in general especially pertaining women involvement in sports had made this matter worsen. Hence, designing home-based intervention program to enhance the physical activity level among the sedentary undergraduate female students in Iraq is crucial. The home based intervention program consists of simple exercises to be carried out at home and some nutrition information on balance diet. Forty-four sedentary undergraduate female students aged 18-22 years old were selected as subjects in this study. They were randomly selected from Northern Region of Iraq. The subjects completed a 12-weeks home based intervention program that combining simple exercises and diet information. Their daily physical activity level was measured using a pedometer. The results showed that there were a significant difference between the steps counts from pre-test to post-test1 (6-weeks) and pre-test to post-test2 (12-weeks) ($p<0.001$) in the experimental group. The mean steps increased by 6825.73 steps from pre-test to post-test1, and 9007.71 steps from pre-test to post-test2. Additionally, the results of these two groups were different in test (time) pre, post1 and post2 ($F(2, 84)= 713.00$, $P<0.05$, $\eta 2= .944$). Based on these results, it was concluded the 12-weeks home based intervention program was effective in enhancing physical activity level among sedentary undergraduate female students in Iraq.

Keywords: Home based intervention program, Physical activity, Undergraduate, Female,

INTRODUCTION

Physical inactivity has been identified as one of the important public health concerns for the youth [1]. Al-Tamimi [2], mentioned that decreased level of physical activity in life is among the most important causes of increase in the percentage of global deaths from non-infectious diseases which are estimated at 60%. Low physical activity cause 310,000 to 580,000 deaths per year and is the main contributor to disabilities resulting from diabetes, osteoporosis, obesity, and stroke [3]. The rate of physical activity begins to decline noticeably in adolescence [4], [5] and continues throughout adulthood [5]-[6]. This trend of declining in physical activity has continued among college students especially in recent years, wherein up to 50% of college students are found to be not physically active at the recommended levels [7]-[8]. In tracking physical activity participation in early college years, Racette, Deusinger, Strube, Highstein, and Deusinger [9] found that 30% of students did not report any exercise during their freshman year. Furthermore, Sengupta, Chaudhuri, and Bhattcharya [10] conducted obesity screening of undergraduate female students and found that almost one of four female students (24 out of 100 participants) was overweight/ obese which was associated with poor to moderate physical activity and higher energy expenditure. This phenomenon has raised a serious concern among the educators because it is associated with the incidence of diseases [11]-[12].

Mirkin [13] indicated that Iraq has about 50% of the population under the age of 19. However, poor security conditions and the instability have made maintenance of health and active life a difficult task to achieve". Despite a significant number of evidence regarding the benefits of being physically active, unfortunately, insecure society forces students to stay at home most of the time which contributes to students' poor participation in sports activities in the university. As a result, parents do not usually encourage their daughters to engage in sports teams and social clubs due to the security situation which could endanger the lives of their children. The other key factors are lack of adequate academic- attributed encouragement and heavy load of academic work. In addition, United Nations

Assistance Mission for Iraq (UNAMI) has repeatedly reported that in society's perception, women's involvement in sport is an indecent phenomenon [14]. This negative society image of women involved in sport has further hindered women participation in sport in Iraq. Furthermore, the World Health Organization (WHO) indicated in its report that the percentages of physically inactive and overweight females in Iraq are 51.3% and 65.1%, respectively [15].

Walking programs are considered safe and effective ways to increase physical activity, decrease body weight, body mass index, and percentage of body fat and resting diastolic blood pressure in previously sedentary adults [16]-[17]-[18]. Physical activity is important in everyday life and low levels of physical activity are independent risk factors for chronic diseases and premature mortality among adults [19]. According to Adams [14], regular physical activity is associated with prevention of morbidity because low level of physical activity increases the risk of cardiovascular, stroke, and coronary events. Sugiyama, Healy, Dunstan, Salmon, and Owen [20] demonstrated that engaging in 150 minutes (2 ½ hours) of moderate intensity physical activity in a weekly basis consistently reduces the risk of many chronic diseases and other adverse health outcomes such as heart disease, coronary heart disease, stroke, some cancers, type 2 diabetes, osteoporosis, and depression and even death". Therefore, introducing walking as an important and easily accessible fitness activity to individuals' daily activities seems to be appropriate and helpful in improving the overall physical activity level and health of an individual especially if it has done at home. The walking activity is easy, fun and will be more acceptable than jogging or other hard activities. Therefore, it will be a suitable way for sedentary people who want to increase their physical activity level. Indeed, the protective effects of physical activity on cardiovascular disease start at moderate levels of this regular activity [21]-[22].

There are many types of intervention that can help to improve individuals' health but a combination of physical activity and dietary intervention programs were found to be more effective to maintain regular physical activity and diet [23]. Good intervention program consisting of a combination of physical activity and dietary awareness can enhance the level of physical activity during daily life behavior [23]-[24]-[25]-[26]-[27]-[28]-[29]. These studies differed according to whether the implementation of the intervention program were at home or outside. However, they were similar to each other in that they were conducted in countries that were safe and secure focusing on patients as the participants of the study. Thus, the current study was conducted to address the gap in the literature on the effect of home based intervention with the combination of physical activity and dietary awareness on sedentary undergraduate female students in Iraq.

METHODS

Ethics Statement

This study was approved by the ethical approval committees in University Putra Malaysia-Malaysia, and the Scientific Committee in the College of Education in Soran University - Kurdistan Regional - Iraq, and all participants provided their written informed consent prior to the intervention.

Participants

One hundred and six freshman female students in the academic year 2014-2015 agreed to participate in this study. They were demographically screened and their physical activity level and health were assessed based on inclusion and exclusion criteria (i.e., being healthy, not associated with any medication or treatment, not pregnant, willing and able to adhere to the intervention program). At the end of the screening, 44 individuals were randomly chosen and were equally divided into 2 groups: an experimental group and a control group.

Assessments Pre, Post1, Post2-Intervention

Physical activity level was measured by the Yamax Digi-Walker® SW-200 pedometer (Yamax Corp. Tokyo, Japan). The SW-200 is a small (2.0 in. x 1.5 in. x 0.75 in.), lightweight (0.75 oz.) pedometer worn on a waistband or belt to measure the daily level of physical activity based on step count. The number of steps was recorded for 3 days a week and the average was calculated for pre-test (week 1), post-test1 (week 6), and post-test2 (week 12) respectively.

THE INTERVENTION PROGRAM

Duration of the treatment for this study was 12 weeks. Five weekly sessions of exercise and 2 weekly sessions of food awareness were conducted. The students allocated to the control group maintained their regular and daily activities during the 12 normal week intervention. At the end of week- 6 and week- 12 intervention, the same test was offered to the experimental and control groups again.

Exercise Intervention

The students were required to practice some of the simple and easy exercises at home. This exercises involved activities like using home

equipment (chair, table, stairs (to move. Besides movement such as walking and walking at a place adapted from well-known physical activity guidelines [16] was also included. The students practised the schedule as follows: each session was 150 minute from week 1 to 4 (Brisk walk exercises, muscle strengthening, 5 times per week), which increased to 225 minutes from week 5 to 8 (brisk walk exercises, muscle strengthening, 5 times per week) which increasing in time practising for each day from 30 minutes to 45 minutes. Finally the progression from week 9 to 12 was 250 minutes (brisk walk exercises, muscle strengthening, 5 times per week) in which practice time for each day gradually increased from 45 minutes to 50 minutes and the distance for physical activity program was extended from 3 miles to 4 miles.

Nutritional Intervention

Two- time- per - week sessions were included in the intervention, emphasis was given to increase the knowledge of the importance and the effect of good diet on life. Students had nutritional lessons during their free time through the 12-week duration of the experiment. Lesson included a variety of topics such as food pyramid, healthy food and a balanced diet, 5 most important points that they must know in dietary, weight control, and food should increase and food should reduce. This information was adapted from the dietary guidelines for Americans, 2010 [30].

RESULTS

No significant differences were found in pre-test between the experimental group, M= 3905.25, SD =483.73 and the control group, M =4136.37, SD =631.54. The results of repeated measures ANOVA on PA showed that the interaction between group and test was statistically significant ($F(2, 84) =731.01$, $P<0.05$, $\eta 2=0.944$) therefore to test the related hypothesis, post hoc test (Bonferroni) was applied to compare the mean scores. After the12 week home-based intervention, significant differences were found between the groups at post-test1 and post-test2 (Table II).

In order to show the efficacy of home based intervention, pre, post1 and post-test2 in both the experimental and control groups were compared. The result of post hoc test (Bonferroni) revealed that the difference between pre-test and post-test1, post1and post-test2 in physical activity score among experimental group was significant. The mean score of physical activity in experimental group increased to 9007.71 steps. While the result for the control group did not show a significant result. The mean score in control group increased to 386.31 steps and there was not a significant difference in physical activity between post-test1 and post-test2 in control group as shown in Table III.

Table II: Physical activity difference between experimental and control groups in pre-test, post-test1 and post-test2

Time	(I) Group	(J) Group	Mean Difference (I-J)	SE	P value	η^2
Pre-test	EXP	CON	-231.12	169.60	0.180	0.04
Post-test1	EXP	CON	6832.33*	206.25	0.001	0.96
Post-test2	EXP	CON	9162.91*	180.15	0.001	0.98

Based on estimated marginal means
* The mean difference is significant at 0 .05 level.
Adjustment for multiple comparisons: Bonferroni

Table III: The difference of physical activity scores between tests in experimental and control groups

Group	(I) time	(J) time	Mean Difference (I-J)	SE	P valve	η^2
EXP	Pre	Post1	-6825.73*	156.53	0.001	
	Pre	Post2	-9007.71*	183.04	0.001	0.99
	Post1	Post2	-2181.96*	206.58	0.001	
CON	Pre	Post1	237.73	156.53	0.409	
	Pre	Post2	386.32	183.04	0.122	0.12
	Post1	Post2	148.59	206.58	1.000	

Based on estimated marginal means
* The mean difference is significant at 0.05 level.
Adjustment for multiple comparisons: Bonferroni

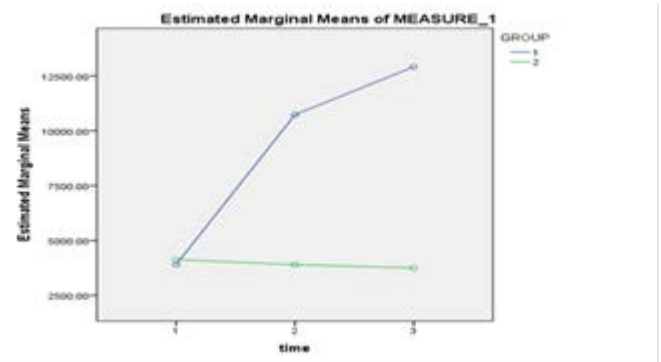

Figure I: Plot of physical activity score in both experimental (1) and control (2) groups

As it can be seen in (Figure I) for experimental group the score of physical activity increased from week 1to week 12, in post-test1 (week 6) and the post-test2 (week 12), however, for control group it did not increase in post-test1 and post-test2. This shows that home-based intervention positively affected physical activity level. In another word, for the control group deterioration in physical activity level was reported during post-test1 (week 6) and further deterioration was reported in the end of post-test2 (week 12). The results indicate that in reality, Iraqi women will remain inactive if they are not encouraged to exercise.

DISCUSSION

Several studies demonstrated that intervention program with moderate intensity of physical activity such as walking, cycling, or participating in sports and diet has significant benefits for health. For

instance, it can reduce the risk of cardiovascular diseases, diabetes, colon and breast cancer, and depression [31]-[32]-[33]-[34]. Low physical activity and dietary awareness contributes to health risks among female undergraduates in Iraq highlighting the importance of physical activity and dietary awareness indicators to find out the humans physical improvement. This study demonstrated significant differences between the experimental and control groups after 6 weeks and 12 weeks of the combined home- based physical activity and diet intervention program, post-test1 ($p<0.05$, $\eta 2=0.963$) and post-test2 ($p<0.001$, $\eta 2=0.984$). Many studies confirm that intervention program with the combination of physical activity and diet can make significant differences in physical activity level [25]-[35]-[36]. Likewise, the physical activity level increased for the experimental group from week1 to week 6 (6825.72 steps), from week 7 to week 12 (2181.98 steps) which is supported by previous studies [7]-[28]-[37]. Thus, increasing the level of physical activity could be regarded as an intervention effect. The results showed that moderate to vigorous physical activity increased the physical activity level for the experimental group compared with the control group.

According to Ferreira et al. [28], physically active women significantly increased their physical activity level after engaging in (physical activity and diet) intervention program for 12 weeks. Accordingly Burke et al. [25], confirmed that physical activity level increased following changes in daily life behavior adopting a low-cost, accessible, home- based physical activity and nutrition intervention program. The results showed that both groups differed significantly in physical activity level. The same results somehow repeated in this study which show the effectiveness of the 12 -week dietary awareness home- based intervention program to increase the physical activity level for sedentary undergraduate female students. The increase in physical activity level suggests that home- based physical activity and diet interventions program and their strategy is an affective way and appropriate means to improve individual's physical activity and eliminate inactive lifestyle.

On another hand, Mostert and Kesselring [38] reported that the physical activity level did not improve during a short-term exercise training intervention program". The intervention in their study consisted of 30-minute bicycle exercise sessions with individualized intensity 5 days per week over 3–4 weeks. They attributed these contradictory findings to two reasons: First, the intervention strategies such as the compliance to the training program were quite low, which affected the result of the research. While, in the current study the subjects were very energetic, however, they could not exercise due to security issues in Iraq. Second, the level of physical activity was recorded lower than it was expected, which was due to the short period of training that lasted four weeks compared with 12 weeks in the current study. Panel of researchers emphasized that when intervention programs were conducted for longer duration it would show positive result regarding physical activity despite the difference in the type of the intervention program [39]-[40]-[41]-[42]. This study also indicated that there were significant differences in physical activity between pre-test, post-test1, and post-test 2 after 12 weeks home- based intervention for the experimental group ($p<0.001$) as well as significant differences in physical activity between experimental and control groups ($p<0.001$).

CONCLUSION

In summary, this study suggested that 12-week home-based physical activity and dietary awareness intervention program was effective in enhancing and improving physical activity level among sedentary undergraduate female students in Iraq. The improvement of the level of physical activity in the experimental group at post-test2 reveals the importance of home- based intervention program and it is a positive step toward a change in the sedentary undergraduate female students' life.

ACKNOWLEDGEMENTS

This study was funded by UPM Putra Grant (Project ID - GP-IPS/2015/9442800). The authors are grateful to UPM Lab assistants and staff from Soran University. Thanks are also due to the subjects who had participated in this study.

REFERENCES

[1] Strong WB, Malina RM, Blimkie CJ, Daniels SR, Dishman RK, Gutin B, et al. Evidence based physical activity for school-age youth. The Journal of Pediatrics. 2005. 146(6): pp. 732-7.

[2] Al-Tamimi YA. Sports and social development goals. Journal of Physical Education Sciences. 2007. 2(5): pp. 143-5.

[3] Pribis P, Burtnack CA, McKenzie SO, Thayer J. Trends in body fat, body mass index and physical fitness among male and female college students. Nutrients Journal. 2010. 2(10): pp. 1075-85.

[4] Caspersen CJ, Pereira MA, Curran KM. Changes in physical activity patterns in the

United States, by sex and cross-sectional age. Medicine and Science in Sports and Exercise Journal. 2000. 32(9): pp. 1601-9.

[5] Malina RM. Physical activity and fitness: Pathways from childhood to adulthood. American Journal of Human Biology. 2001. 13(2): pp.162-72.

[6] Dwyer JJM, Wilson K, Limarzi L, Callaghan B, Croskery L. Physical activity among female adolescents of indian and polish origin in mississauga, ontario: An examination of shared and ethno-cultural barriers. Revue phénEPS/PHEnex Journal. 2013. 4(3): pp. 14.

[7] Jackson, Howton A. Increasing walking in college students using a pedometer intervention: Differences according to body mass index. Journal of American College.

[8] Leslie E, Fotheringham MJ, Owen N, Bauman A. Age-related differences in physical activity levels of young adults. Medicine and Science in Sports and Exercise Journal. 2001. 33(2): pp. 255-8.

[9] Sallis JF, Calfas KJ, Nichols JF, Sarkin JA, Johnson MF, Caparosa S, et al. Evaluation of a university course to promote physical activity: Project GRAD. Research Quarterly for Exercise and Sport Journal. 1999. 70(1): pp. 1-10.

[10] Sengupta P, Chaudhuri P, Bhattacharya K. Screening obesity by direct and derived anthropometric indices with evaluation of physical efficiency among female college students of Kolkata. Annals of Medical and Health Sciences Research Journal. 2014. 3(4): pp. 517-22.

[11] Lowry R, Galuska DA, Fulton JE, Wechsler H, Kann L, Collins JL. Physical activity, food choice, and weight management goals and practices among US college students. American journal of preventive medicine. 2000. 18(1): pp. 18-27.

[12] Racette SB, Deusinger SS, Strube MJ, Highstein GR, Deusinger RH. Weight changes, exercise, and dietary patterns during freshman and sophomore years of college. Journal of American College Health. 2005. 53(6): pp. 245-51.

[13] Mirkin B. Population Levels, Trends and Policies in the Arab Region: Challenges and Opportunities. UN United Nations Development Programme, Regional Bureau for Arab States; 2010.

[14] Adams MA. A Pedometer-Based Intervention to Increase Physical Activity: Applying Frequent, Adaptive Goals and a Percentile Schedule of Reinforcement. United State of America: University of California, San Diego; 2009.

[15] Al-Tamimi YA., Armstrong, T., Cowan, M., & Riley, L. Noncommunicable Diseases Country Profiles 2011. 2011. France: World Health Organization.

[16] Committee PAGA. Physical activity guidelines for Americans. Washington, DC: US Department of Health and Human Services 2008. pp. 15-34.

[17] Cooper K, Hancock C. Review: The Benefits of Physical Activity for Health and Well-being. UK: C3 Collaborating for Health, 2011.

[18] Kassavou, Aikaterini, Andrew Turner, and David P French. "Do Interventions to Promote Walking in Groups Increase Physical Activity? A Meta-Analysis." *International Journal of Behavioral Nutrition and Physical Activity* 10, no. 1 (2013): 18. Health 2008. 57(2): pp. 159-64.

[19] Katzmarzyk PT. Physical activity, sedentary behavior, and health: Paradigm paralysis or paradigm shift? Diabetes Journal. 2010. 59(11): pp. 2717-25.

[20] Sugiyama T, Healy GN, Dunstan DW, Salmon J, Owen N. Joint associations of multiple leisure-time sedentary behaviours and physical activity with obesity in Australian adults. International Journal of Behavioral Nutrition and Physical Activity. 2008. 5(1): pp. 35.

[21] Arroll B, Beaglehole R. Does physical activity lower blood pressure: A critical review of the clinical trials. Journal of Clinical Epidemiology. 1992. 45(5): pp. 439-47.

[22] Kelley G, McClellan P. Antihypertensive effects of aerobic exercise a brief meta-analytic review of randomized controlled trials. American Journal of Hypertension. 1994. 7(2): pp.115-9.

[23] Dunn AL, Marcus BH, Kampert JB, Garcia ME, Kohl III HW, Blair SN. Comparison of lifestyle and structured interventions to increase physical activity and cardiorespiratory fitness: A randomized trial. Jama Journal. 1999. 281(4): pp. 327-34.

[24] Artinian NT, Fletcher GF, Mozaffarian D, Kris-Etherton P, Van Horn L, Lichtenstein AH, et al. Interventions to promote physical activity and dietary lifestyle changes for cardiovascular risk factor reduction in adults a scientific statement from the american heart association. Circulation Journal. 2010; 122(4). pp. 406-41.

[25] Burke L, Lee AH, Jancey J, Xiang L, Kerr DA, Howat PA, et al. Physical activity and nutrition

behavioural outcomes of a home-based intervention program for seniors: A randomized controlled trial. International Journal of Behavioral Nutrition and Physical Activity 2013. 10(1): pp.14.

[26] Collins TC, Lunos S, Carlson T, Henderson K, Lightbourne M, Nelson B, et al. Effects of a home-based walking intervention on mobility and quality of life in people with diabetes and peripheral arterial disease a randomized controlled trial. Diabetes Care Journal. 2011. 34(10): pp. 2174-9.

[27] Esposito K, Pontillo A, Di Palo C, Giugliano G, Masella M, Marfella R, et al. Effect of weight loss and lifestyle changes on vascular inflammatory markers in obese women: A randomized trial. Jama Journal. 2003. 289(14): pp. 1799-804.

[28] Ferreira M, Matsudo S, Matsudo V, Braggion G. Effects of an intervention program of physical activity and nutrition orientation on the physical activity level of physically active women aged 50 to 72 years old. Revista Brasileira de Medicina do Esporte Journal. 2005. 11(3): pp. 172-6.

[29] Morey MC, Snyder DC, Sloane R, Cohen HJ, Peterson B, Hartman TJ, et al. Effects of home-based diet and exercise on functional outcomes among older, overweight long-term cancer survivors: Renew: A randomized controlled trial. Jama Journal. 2009. 301(18): pp. 1883-91.

[30] Agriculture USDo, Services USDoHaH. Dietary Guidelines for Americans, 2010. In: Services USDoAUSDoHaH, editor. 7th ed. Washington, DC: U.S. Government Printing Office; 2010. pp. 112.

[31] Amine E, Baba N, Belhadj M, Deurenbery-Yap M, Djazayery A, Forrester T, et al. Diet, Nutrition and the Prevention of Chronic Diseases: Report of a Joint WHO/FAO Expert Consultation. Switzerland, Geneva: World Health Organization, 2002. 924120916X.

[32] Health UDo, Services H. Physical activity and health: a report of the surgeon general. Atlanta, GA: US Department of Health and Human Services, Centers for Disease Control and Prevention. National Center for Chronic Disease Prevention and Health Promotion. 1996. pp. 147.

[33] Loprinzi PD, Smit E, Mahoney S. Physical activity and dietary behavior in US adults and their combined influence on health. Perceptual and Motor Skills Journal. 2014. 89(22): pp. 190-8.

[34] McDowell MA, Fryar CD, Ogden CL, Flegal KM. Anthropometric Reference Data for Children and Adults: United States, 2003-2006. No. 10: Hyattsville, MD: National Center for Health Statistics, 2008.

[35] Harrison RL. Weight to Life: A Combined Lifestyle Intervention of Diet, Physical Activity, and Behavioral Strategies. USA: University of Missouri--St. Louis; 2007.

[36] Minhas M. Interaction of Physical Activity, Diet, Health Locus of Control and Quality of Life among Finnish University Students. Finland: University of Jyväskylä; 2013.

[37] Dunlap AN. The Impact of a Intervention Program on The Knowledge and Behaviors of School-age Children in Alabama Regarding Nutrition and Physical activity [Graduate Theses and Dissertations]. Ames, Iowa: Iowa State University; 2012.

[38] Mostert S, Kesselring J. Effects of a short-term exercise training program on aerobic fitness, fatigue, health perception and activity level of subjects with multiple sclerosis. Multiple Sclerosis Journal. 2002. 8(2): pp. 161-8.

[39] Calfas KJ, Sallis JF, Nichols JF, Sarkin JA, Johnson MF, Caparosa S, et al. Project GRAD: Two-year outcomes of a randomized controlled physical activity intervention among young adults. American Journal of Preventive Medicine. 2000. 18(1): pp. 28-37.

[40] Epstein LH, Wing RR, Thompson JK, Griffin W. Attendance and fitness in aerobics exercise the effects of contract and lottery procedures. Behavior Modification Journal. 1980. 4(4): pp. 465-79.

[41] Lock RS. College women's decision-making skills relating tovoluntary participation in physical activity during leisure time. Perceptual and Motor Skills Journal. 1990. 71(1): pp. 141-6.

[42] Sallis JF, Calfas KJ, Nichols JF, Sarkin JA, Johnson MF, Caparosa S, et al. Evaluation of a university course to promote physical activity: Project GRAD. Research Quarterly for Exercise and Sport Journal. 1999. 70(1): pp. 1-10.

Second International Conference on Science, Engineering & Environment,
Osaka City, Japan, Nov.21-23, 2016, ISBN: 978-4-9905958-7-6 C3051

NUCLEOPHILIC SUBSTITUTION REACTIONS OF BUTYL METHYL CHLOROPHOSPHATE WITH SUBSTITUTED ANILINES AND DEUTERATED SUBSTITUTED ANILINES IN ACETONITRILE

Hasi Rani Barai[1*], Sang Woo Joo[1] and Seog K. Kim[2,*]
[1]*School of Mechanical Engineering and* [2]*Department of Chemistry, Yeungnam University, Gyeongsan 38541, Korea*

ABSTRACT

The general optimized method for the synthesis of butyl methyl chlorophosphate (**2**) under mild conditions is described. The target compounds were characterized by ^{1}H-nuclear magnetic resonance (NMR), ^{13}C-NMR, and ^{31}P-NMR spectroscopy, as well as mass spectroscopy (MS). The nucleophilic substitution reactions of (**2**) with X-anilines ($XC_6H_4NH_2$) and deuterated X-anilines ($XC_6H_4ND_2$) were investigated kinetically in MeCN at 55.0 °C. The free energy relationship with X in the anilines appeared biphasic concave upwards with a break point at X = H, giving large negative ρ_X and small positive β_X values. The deuterium kinetic isotope effects (DKIEs) were secondary inverse (k_H/k_D < 1: 0.702-0.918) and the magnitudes, (k_H/k_D), increased when the nucleophiles were changed from weakly basic to strongly basic anilines. A concerted mechanism with a rate-limiting leaving group departure from the intermediate is proposed based on the selectivity parameters and the variation trend of the DKIEs with X.

Keywords: Phosphoryl transfer reaction, concerted mechanism, butyl methyl chlorophosphate, Hammett and Brönsted constants, deuterium kinetic isotope effects

INTRODUCTION

Phosphoryl and thiophosphoryl transfer reactions have been studied extensively because of their importance in biochemistry and organometallic chemistry as well as their usefulness in synthesis. Two main types of mechanisms, the stepwise mechanism involving a trigonal bipyramidal pentacoordinate (TBP-5C) intermediate and the concerted mechanism through a single pentacoordinate transition state (TS), occur in neutral phosphoryl and thiophosphoryl transfer reactions. The experimental (anilinolysis,[1-21] pyridinolysis,[22] and benzylaminolysis[23]) and theoretical [24] studies of the phosphoryl and thiophosphoryl transfer reactions of various substrates have been studied extensively. In this work, the phosphoryl transfer reactions of butyl methyl chlorophosphate (2) with substituted anilines ($XC_6H_4NH_2$) and deuterated anilines ($XC_6H_4ND_2$) were investigated kinetically in acetonitrile (MeCN) at 55.0 ± 0.1 °C (Scheme 1). The kinetics are discussed based on the selectivity parameters and deuterium kinetic isotope effects (DKIEs). This study examined the substituent effects, the attacking direction of the nucleophiles to the reaction center, DKIEs and the mechanism of the phosphoryl transfer reactions. The novelty of this work is to synthesize the butyl methyl chlorophosphate (2) in a mild condition and to determine the mechanism kinetically with respect to nucleophilic substitution reactions with substituted anilines ($XC_6H_4NH_2$) and deuterated substituted anilines ($XC_6H_4ND_2$) in MeCN.

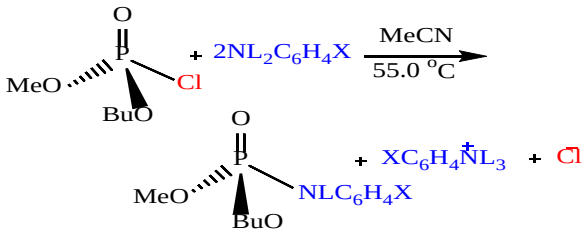

L = H, D & X = 4-MeO, 4-Me, 3-Me, H, 3-MeO, 4-Cl, 3-Cl

Scheme 1. Studied reactions of butyl methyl chlorophosphate (**2**) with $XC_6H_4NH_2(D)_2$ in MeCN at 55.0 °C.

EXPERIMENTAL

Materials and synthetic procedure of deuterated anilines

Butylphosphonic dichloride (98%), HPLC grade acetonitrile (water content < 0.005%), methanol (99.8%), and anilines were purchased from Sigma Aldrich and used without further purification. Ethyl acetate (extra pure grade, 99.0%), diethyl ether (extra pure grade, 99%), and n-hexane (HPLC grade 99.5%) were obtained from DUKSAN and used as received. $MgSO_4$ (extra pure reagents, ≥97%) was supplied by YAKURI Pure Chemicals Co. Ltd./Osaka, Japan. Deuterium oxide (99.999 atom% D) was acquired from Sigma Aldrich and used as received. Deuterated anilines were synthesized using the procedure reported elsewhere[1-21]. Deuterated anilines were synthesized by refluxing anilines in deuterium oxide (99.999 atom% D) with a few drops of HCl as a catalyst at 90 °C for 72 h, and collected

after numerous attempts. The anilines were more than 98% deuterated, as confirmed by ^{1}H- NMR.

Kinetic measurements

The rates and selectivity parameters were calculated as described previously. [1-21] The rates were measured conductometrically using the conductivity bridge, which was a self-made computer-automated A/D converter conductivity bridge. The pseudo-first-order rate constants (k_{obsd}) were calculated by curve fitting analysis of the decay profiles in the origin program 8.5. The concentrations used in this study were [substrate] = 5 × 10^{-3} M and [X-anilines] = (0.10-0.30) M. The k_{obsd} values were an average of at least three runs, which were reproducible within ± 3%. The second-order rate constants, $k_{H(D)}$, were calculated from the slope of a plot of k_{obsd} vs. [X-anilines]. The selectivity parameters, $\rho_{X(H/D)}$, were obtained from the slope of the plot of log $k_{H(D)}$ vs. σ_X and $\beta_{X(H/D)}$ from the slope of the log $k_{H(D)}$ vs. pK_a(X) plot.

***Synthesis of substrate, butyl methyl chlorophosphate* (2)**

The substrate, butyl methyl chlorophosphate (2), was synthesized by reacting butylphosphonic dichloride (98%) with excess methanol at –20°C for 8 hr.[25] The reaction mixture was separated by filtration from the insoluble part. The remaining mixture was treated with water and diethyl ether for work up. The organic layer of diethyl ether was dried over anhydrous $MgSO_4$ for 1-2 hr. The product mixture was separated by column chromatography (silica gel, ethyl acetate/n-hexane, 60%) and dried under reduced pressure. The substrate was characterized by spectral analysis, TLC, ^{1}H-NMR, ^{13}C-NMR, ^{31}P-NMR, and GC-MS, as follows (see electronic supplementary materials):

Butyl methyl chlorophosphate [(C_4H_9O, CH_3O)P(=O)Cl]**:** Colorless liquid; ^{1}H-NMR / ppm (600 MHz, $CDCl_3$ & TMS): δ 0.91-0.93 (m, 3H), 1.39-1.42 (m, 2H), 1.57-1.59 (m, 2H), 1.72-1.78 (m, 2H), 3.73-3.75 (m, 3H) (m, multiple). ^{13}C-NMR / ppm (150 MHz, $CDCl_3$ & TMS): δ 13.5, 23.7, 24.3, 24.8, 52.3. ^{31}P-NMR / ppm (243 MHz, $CDCl_3$ & TMS): δ 35.96 (1P, s, P=O) (s, singlet). GC-MS (EI): m/z 186 [M^+].

Synthesis Procedure of Product Analysis

Butyl methyl chlorophosphate (**2**) was reacted with excess aniline for more than 15 half-lives at 55.0 °C in MeCN. The solvent was evaporated under reduced pressure. The product mixture was treated with diethyl ether by a work-up process with dilute HCl and dried over anhydrous $MgSO_4$. The product was then isolated by column chromatography (30% ethyl acetate/n-hexane) and then dried under reduced pressure. The analytical and spectroscopic data of the product gave the following results (see electronic supplementary materials):

[$C_5H_{12}O_2P$(=O)NHC_6H_5]: Colorless liquid. ^{1}H-NMR / ppm (600 MHz, $CDCl_3$ & TMS): δ 0.91-0.93 (m, 3H), 1.44-1.45 (m, 2H), 1.71-1.73 (m, 2H), 4.12-4.16 (m, 3H), 4.31-4.39 (m, 2H), 5.47 (d, J = 6 Hz, 1H, -NH), 6.78-7.14 (m, 5H) (m, multiple; d, doublet). ^{13}C-NMR / ppm (75 MHz, $CDCl_3$ & TMS): δ 13.6, 30.9, 32.2, 32.3, 66.5, 126.2, 128.4, 130.9, 132.1. ^{31}P-NMR / ppm (243 MHz, $CDCl_3$ & TMS): δ 33.1(1P, s, P=O) (s, singlet). GC-MS (EI): m/z 243 [M^+].

***Theoretical studies of butyl methyl chlorophosphate* (2)**

The B3LYP/6-311+G(d,p) geometry, bond angles, and natural bond order (NBO) charges of **2** in the gas phase [26] were calculated using the B3LYP/6-311+G(d,p) level in the Gaussian 09 program and are shown on the optimized structure of **2** (figure 1). The ground state (GS) structure of **2** does not have a symmetry plane because it has two different ligands, giving the difference in the negative charges of the methoxy and butoxy oxygen atoms. The MO theoretical structure shows that the three oxygen atoms and one chlorine atom have a distorted tetrahedral geometry with the phosphorus atom at the reaction center. The details of the optimized structure of **2** is given in Table S1 and figure S9.

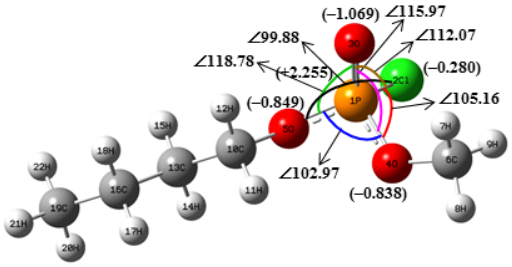

Figure 1. B3LYP/6-311+G(d,p) geometry of butyl methyl chlorophosphate (2) in the gas phase.

RESULTS AND DISCUSSION

The observed pseudo-first-order rate constants, k_{obsd}, were calculated using eq. (1) for all reactions under the pseudo- first-order conditions with a large excess of aniline as a nucleophile. The k_0 values in acetonitrile were negligible ($k_0 \approx 0$). The second-order rate constants ($k_{H(D)}$) were determined from at least five concentrations of anilines. The linear plots of eq. (1) suggest that there are no base-catalysis or noticeable side reactions and that the whole reaction can be described by Scheme 1.

$$k_{obsd} = k_0 + k_{H(D)}[XC_6H_4NH_2(D_2)] \qquad (1)$$

Table 1 summarizes the second order rate constants, k_H with X-anilines, k_D with deuterated X-anilines, the DKIEs (k_H/k_D), selectivity parameters for Hammett $\rho_{X(H\text{ and }D)}$ and Brønsted $\beta_{X(H\text{ and }D)}$. The p$K_a$(X) values of the X-anilines in water were used to obtain the Brønsted β_X values in MeCN; this procedure could be justified both experimentally [1-22] and

theoretically.[24] The pK_a(X) and σ_X values of the deuterated X-anilines were assumed to be identical to those of the X-anilines. Perrin et al. reported that the basicity of the β-deuterated analogs of benzylamine, *N*,*N*-dimethylaniline, and methylamine increase by approximately 0.02 pK_a units per deuterium atom, and that these effects are additive.[27-29] Therefore, the pK_a(X) values of deuterated X-anilines may be slightly higher than those of X-anilines, but the difference was too small to be taken into consideration.

Figures 2 (log $k_{H(D)}$ vs. σ_X) and 3 (log $k_{H(D)}$ vs. pK_a(X)) show the Hammett plots and the Brönsted plots for the substituent variations in the nucleophiles, respectively. The stronger nucleophile leads to a faster rate, as observed in a typical nucleophilic substitution reaction with positive charge development at the nucleophilic N atom (ρ_X < 0) in the transition state (TS). On the other hand, both the Hammett and Brönsted plots exhibit biphasic concave upward free energy correlations for substituent X variations in the nucleophiles with a break point at X = H. The magnitudes of the $\rho_{X(H \text{ and } D)}$ ($\rho_{X(H)}$ = –7.57 and $\rho_{X(D)}$ = –7.38) and $\beta_{X(H \text{ and } D)}$ ($\beta_{X(H)}$ = 2.60 and $\beta_{X(D)}$ = 2.54) values with more basic anilines (X = 4-MeO, 4-Me, 3-Me, H) are much greater than those ($\rho_{X(H)}$ = –2.58, $\rho_{X(D)}$ = –2.41, $\beta_{X(H)}$ = 0.895 and $\beta_{X(D)}$ = 0.834) with less basic anilines (X = H, 3-MeO, 4-Cl, 3-Cl). The magnitudes of the ρ_X and β_X values with the anilines are greater than those with the deuterated anilines, suggesting greater sensitivity to the substituent effects of the anilines compared to the deuterated anilines and a change in the reaction mechanism from the strongly basic to weakly basic anilines. The DKIEs investigated are secondary inverse (k_H/k_D <1) and the magnitudes of the DKIEs decrease constantly as the nucleophile is changed from a more electron-donating to a more electron-withdrawing substituent X: e.g., X = 4-MeO (k_H/k_D = 0.918) to X = 3-Cl (k_H/k_D = 0.702).

Table 1. Second-order rate constants ($k_{H(D)} \times 10^3$/M^{-1} s^{-1}), selectivity parameters (ρ_X and β_X),[a] and DKIEs (k_H/k_D) of the reactions of butyl methyl chlorophosphate (**2**) with $XC_6H_4NH_2(D_2)$ in MeCN at 55.0 °C

X	$k_H \times 10^3$	$k_D \times 10^3$	k_H/k_D
4-MeO	345 ± 1[b]	376 ± 1[b]	0.918 ± 0.001[g]
4-Me	58.8 ± 0.1	68.9 ± 0.1	0.853 ± 0.002
3-Me	9.68 ± 0.01	11.7 ± 0.1	0.827 ± 0.002
H	3.22 ± 0.01	3.95 ± 0.01	0.815 ± 0.001
3-MeO	1.65 ± 0.01	2.11 ± 0.01	0.782 ± 0.001
4-Cl	0.818 ± 0.002	1.09 ± 0.01	0.747 ± 0.001
3-Cl	0.362 ± 0.001	0.516 ± .001	0.702 ± 0.001
$-\rho_X$	7.57 ± 0.13[c,d]	7.38 ± 0.11[c,i]	
β_X	2.60 ± 0.19[c,e]	2.54 ± 0.18[c,j]	
$-\rho_X$	2.58 ± 0.04[f,g]	2.41 ± 0.03[f,k]	
β_X	0.895 ± 0.052[f,h]	0.834 ± 0.051[f,l]	

[a]The σ values were taken from ref. [30]. The pK_a values of X-anilines in water were taken from ref. [31]. [b]Standard deviation. [c]For X = 4-MeO, 4-Me, 3-Me, H. [d]Correlation coefficient, r = 0.999. [e]r = 0.983. [f]For X = H, 3-MeO, 4-Cl, 3-Cl. [g]r = 0.999. [h]r = 0.990. [i]r = 0.999. [j]r = 0.984. [k]r = 0.999. [l]r = 0.989. [g]Standard error {= $1/k_D[(\Delta k_H)^2 + (k_H/k_D)^2 \times (\Delta k_D)^2]^{1/2}$} from ref. [32].

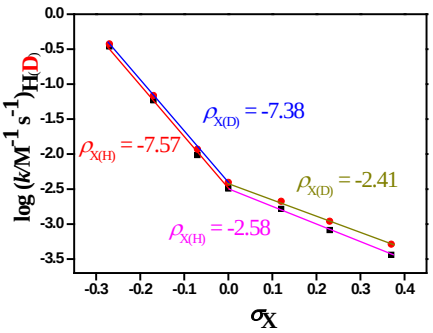

Figure 2. Hammett plots (log $k_{H(D)}$ vs. σ_X) with X of the reactions of butyl methyl chlorophosphate (**2**) with $XC_6H_4NH_2(D_2)$ in MeCN at 55.0 °C.

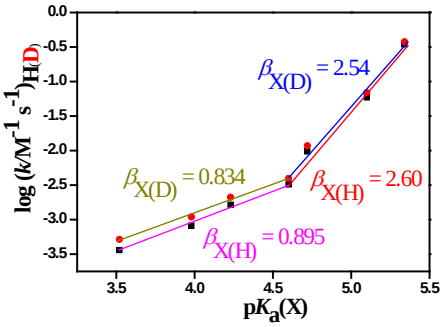

Figure 3. Brönsted plots [log $k_{H(D)}$ vs. pK_a(X)] with X of the reactions of butyl methyl chlorophosphate (**2**) with $XC_6H_4NH_2(D_2)$ in MeCN at 55.0 °C.

Table 2 lists the second-order rate constants (k_H) with unsubstituted aniline, natural bond order (NBO) charges at the reaction center P atom [B3LYP/6-311+G(d,p) level of theory] in the gas phase,[26] Brönsted coefficients ($\beta_{X(H)}$), and DKIEs (k_H/k_D) of the reactions of **1**-**6** with $XC_6H_4NH_2(D_2)$ in MeCN. Counting the magnitudes of the positive charges at

the reaction center P atom, the anilinolysis rate should be **4** > **2** > **5** > **3** > **6** > **1** but the observed sequence of the rate, **1** > **2** > **3** > **5** > **6** > **4** does not follow the expected sequence regarding the electronic influence of the two ligands. Therefore, the positive charge at the reaction center P atom does not play a major role in determining the reactivity and mechanism of the phosphinic chloride systems.

The second order rate constants for the anilinolyses of the mentioned phosphinic chlorides are k_H = 4.28 × 10^{-3} M^{-1} s^{-1} for **1**, k_H = 3.22 × 10^{-3} M^{-1} s^{-1} for **2**, k_H = 2.82 × 10^{-3} M^{-1} s^{-1} for **3**, k_H = 0.710 × 10^{-3} M^{-1} s^{-1} for **4,** k_H = 2.06 × 10^{-3} M^{-1} s^{-1} for **5**, and k_H = 2.00 × 10^{-3} M^{-1} s^{-1} for **6**, giving relative rate ratios of 6.03(**1**): 4.54(**2**): 3.97(**3**): 1.00 (**4**): 2.90 (**5**): 2.82 (**6**) in MeCN at 55.0 ºC. From the observed rate ratio, the anilinolysis rate, **1** > **2** > **3** > **5** > **6** > **4**, does not follow the sequence according to the sizes of the two ligands of the phosphinic chloride system [33,35]: (EtO, PhO) **6**> (BuO, BuO) **5** > (MeO, BuO) **2** > (*i*-PrO, *i*-PrO) **4** > (EtO, EtO) **3** > (MeO, MeO) **1**.

Table 2. Summary of the second-order rate constants (k_H × 10^3/M^{-1} s^{-1}) with $C_6H_5NH_2$, NBO charges at the reaction center P atom, Brönsted coefficients ($\beta_{X(H)}$), and DKIEs (k_H/k_D) for the reactions of **1**-**6** with $XC_6H_4NH_2(D_2)$ in MeCN

substrate	k_H × 10^{3a}	charge at P	$\beta_{X(H)}$[b]	k_H/k_D	ref
1: $(MeO)_2P(=O)Cl$	4.28[c]	2.226	0.96	0.80-0.98[d]	[7]
2: (MeO)(BuO)P(=O)Cl	3.22[c]	2.255	2.60	0.70-0.92[d]	This work
3: $(EtO)_2P(=O)Cl$	2.82[c]	2.236	1.06	0.71-0.92[d]	[7]
4: (*i*-PrO)2P(=O)Cl	0.710[c]	2.269	1.10	0.71-0.95[d]	[18]
5. $(BuO)_2P(=O)Cl$	2.06[c]	2.239	1.11	0.86-1.10[d]	[33]
6: (EtO)(PhO)P(=O)Cl	2.00[c]	2.233	1.13	1.07-1.28[d]	[6]

[a]The values with unsubstituted aniline at 55.0ºC. [b]Strongly/weakly basic anilines. [c]Experimental kinetic value. See ref. [6], ref. [7], ref. [18] and ref. [33]. [d]Values at 55.0 °C.

The DKIEs (k_H/k_D) is a strong tool for clarifying the reaction mechanism. When the k_H/k_D values are greater than unity, primary normal (k_H/k_D > 1.0), the partial deprotonation of aniline occurs as the a rate-limiting step by hydrogen bonding (e.g., front side attack transition state (TSf) in Scheme 2).[4,34,35] On the other hand, the DKIEs are only secondary inverse (k_H/k_D < 1.0) when an increase in the steric congestion occurs in the bond-making process (e.g., back side attack transition state (TSb) in Scheme 2). This is because the N–H(D) vibrational frequencies increase upon going to the TS. [1-22] Therefore, DKIEs provided a useful means of determining the TS structures in nucleophilic substitution reactions; in particular, changes in the substituents altered the TS structures. The incorporation of deuterium in the nucleophile has an advantage in that the α-DKIEs resemble only the degree of bond formation, especially for secondary inverse DKIEs. Therefore, the greater the extent of bond formation, the greater the steric congestion, and the k_H/k_D values become smaller.

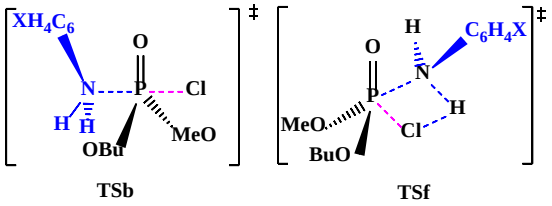

Scheme 2. Backside attack involving in-line-type TSb and front side attack involving a hydrogen bonded, four-center-type TSf.

The authors proposed a concerted mechanism involving a dominant backside attack TSb based on the secondary inverse DKIEs for the anilinolyses of **1**(k_H/k_D = 0.80-0.98)[7] and **3**(k_H/k_D = 0.71-0.92)[7]. The authors proposed a concerted mechanism involving predominant backside attack TSb based on the secondary inverse DKIEs for the anilinolyses of **4**(k_H/k_D = 0.71-0.95)[18] . The authors proposed a concerted mechanism with a backside nucleophilic attack transition state for strongly basic anilines and with a front side attack involving a hydrogen-bonded four-center-type transition state for weakly basic anilines based on the secondary inverse and primary normal, and variation trends of the k_H/k_D values with X.[33] The authors proposed a concerted mechanism involving a partial front side attack through a hydrogen-bonded, four-center-type transition state for the anilinolysis of **6**.[6] Nevertheless, there was no correlation between the k_H/k_D and β_X values. In the present work, the DKIEs are secondary inverse with all the anilines listed in table 1. The secondary inverse DKIEs are strengthened by backside nucleophilic attack involving in-line-type TSb (Scheme 2). The intermediates (TS) are very rapidly changed from the attacking direction of the nucleophiles. The magnitudes of the k_H/k_D values decrease constantly as a more electron-withdrawing substituent X (4-MeO →3-Cl) is present in the nucleophiles. This means that steric congestion in the TS invariably increases as the aniline becomes weakly basic. In other words, the lower reactivity of the nucleophile results in a greater degree of bond formation. Accordingly, the value of k_H/k_D (0.70-

0.92) indicates very severe steric congestion in the TS, suggesting a great extent of bond formation.

Table 3. [a]Activation parameters for the reactions of butyl methyl chlorophosphate (**2**) with anilines in acetonitrile

t/°C	$k_H \times 10^3$/ M^{-1} s^{-1}	$\Delta H^{\ddagger}$/kcal.mol^{-1}	$-\Delta S^{\ddagger}$/cal.mol^{-1}. K^{-1}
35	1.57 ± 0.01		
45	2.32 ± 0.01	6.9	49
55	3.22 ± 0.01		
65	4.74 ± 0.01		

[a]Eyring equation.

Activation parameters, enthalpies and entropies of activation, are summarized in table 3. The enthalpies of activation are relatively low (6.9 kcal/mol) and entropies of activation are relatively large negative value (-49 cal/mol/K). The relatively low value of activation enthalpy and large negative value of activation entropy are typical for the aminolyses of P=O systems. Therefore, the clarification of the reaction mechanism by means of the activation parameters is wretched for the aminolyses of P=O (and P=S) systems.

CONCLUSION

The nucleophilic substitution reactions of butyl methyl chlorophosphate (2) with substituted anilines ($XC_6H_4NH_2$) and deuterated anilines ($XC_6H_4ND_2$) were investigated kinetically in MeCN at 55.0 °C. The magnitudes of the secondary inverse deuterium kinetic isotope effects (k_H/k_D) increased when the nucleophiles changed from weakly basic to strongly basic anilines. A concerted mechanism involving the rate-limiting departure of a leaving group from the intermediate was proposed based on the selectivity parameters and variation trend of the DKIEs with X. The linear free energy relationship in the present work suggests that the attacking direction of the aniline changes gradually from a backside with the strongly basic anilines to a front side involving a hydrogen-bonded four-center-type TSf with weakly basic anilines.

Supplementary Materials

The analytical and spectroscopic data obtained from characterization of the substrate and product are available on the Journal's website, including ^{1}H NMR (Figs. S1 and S5), ^{13}C NMR (Figs. S2 and S6), ^{31}P NMR (Figs. S3 and S7), mass spectrometry spectra (Figs. S4 and S8), the B3LYP/6–311þG(d,p) geometry of butyl methyl chlorophosphate (2) in the gas phase (Fig. S9 and Table S1).

ACKNOWLEDGMENT

This study was supported by Yeungnam University Research Fund.

REFERENCES

[1] Guha, A. K.; Lee, H. W.; Lee,"Kinetics and mechanism of the aminolysis of phenyl substituted phenyl chlorophosphates with anilines in acetonitrile" I. *J. Chem. Soc., Perkin Trans.* 1999, *2*, 765-769.

[2] Lee, H. W.; Guha, A. K.; Lee, I., "Kinetics and mechanism of the reaction of para-chlorophenyl aryl chlorophosphates with anilines in acetonitrile", *Int. J. Chem. Kinet.*2002, *34*, 632-637.

[3] HOQUE, M. E. U.; DEY, S.; GUHA, A. K.; KIM, C.K.; LEE, B. S.; LEE, H. W., "KINETICS AND MECHANISM OF THE AMINOLYSIS OF ARYL PHENYL CHLOROTHIOPHOSPHATES WITH ANILINES", *J. ORG. CHEM.* 2007, *72*, 5493-5499.

[4] Hoque, M. E. U.; Lee, H. W., "Kinetics and Mec hanism of the Aminolysis of Diphenyl Phosphinic C hloride with Anilines" *Bull. Korean Chem. Soc.* 200 7, *28*, 936-940.

[5] HOQUE, M. E. U.; GUHA, A. K.; KIM, C. K.; LEE, B. S.; LEE, H. W., "CONCURRENT PRIMARY AND SECONDARY DEUTERIUM KINETIC ISOTOPE EFFECTS IN ANILINOLYSIS OF *O*-ARYL METHYL PHOSPHONOCHLORIDOTHIOATES", *ORG. BIOMOL. CHEM.* 2009, *7*, 2919-2925.

[6] HOQUE, M. E. U.; DEY, N. K.; KIM, C. K.; LEE, B. S.; LEE, H. W., "KINETICS AND MECHANISM OF THE AMINOLYSIS OF ARYL ETHYL CHLORO AND CHLOROTHIO PHOSPHATES WITH ANILINES", *ORG. BIOMOL. CHEM.* 2007, *5*, 3944-3950.

[7] Dey, N. K.; Hoque, M. E. U.; Kim, C. K.; Lee, B. S.; Lee, H. W., "Kinetics and mechanism of the anilinolysis of dimethyl and diethyl chloro(thiono)phosphates", *J.Phys. Org. Chem.* 2008, *21*, 544-548.

[8] Lumbiny, B. J.; Lee, H. W., "Anilinolysis of S-Aryl Phenyl Phosphonochloridothioates in Acetonitrile", *Bull. Korean Chem. Soc.* 2008, *29*, 2065-2068.

[9] Dey, N. K.; Hoque, M. E. U.; Kim, C. K.; Lee, B. S.; Lee, H. W., "Kinetics and mechanism of the aminolysis of dimethyl and methyl phenyl phosphinic chlorides with anilines", *J. Phys. Org. Chem.* 2009, *22*, 425-430.

[10] Dey, N. K.; Kim, C. K.; Lee, H. W., "Kinetics and Mechanism of the Aminolysis of Dimethyl Thiophosphinic Chloride with Anilines ", *Bull. Korean Chem. Soc.* 2009, *30*, 975-978.

[11] Dey, N. K.; Han, I. S.; Lee, H. W., "Anilinolysis of Diphenyl Thiophosphinic Chloride and Theoretical Studies on Various R_1R_2P(O or S)Cl†", *Bull. Korean Chem. Soc.* 2007, *28*, 2003-2008.

[12] Dey, N. K.; Lee, H. W., " Anilinolysis of Diethyl Phosphinic Chloride in Acetonitrile", *Bull. Korean Chem. Soc.* 2010, *31*, 1403-1406.

[13] DEY, N. K.; KIM, C. K.; LEE, H. W., "KINETICS AND MECHANISM OF THE ANILINOLYSES OF ARYL DIMETHYL, METHYL PHENYL ANDDIPHENYL PHOSPHINATES", *ORG. BIOMOL. CHEM.* 2011, *9*, 717-724.

[14] Barai, H. R.; Lee, H. W., "Kinetics and Mechanism of the Anilinolysis of Bis(aryl) Chlorophosphates in Acetonitrile", *Bull. Korean Chem. Soc.* 2011, *32*, 1939-1944.

[15] Hoque, M. E. U.; Lee, H. W., "Kinetics and Mechanism of the Anilinolysis of Dicyclohexyl Phosphinic Chloride in Acetonitrile", *Bull. Korean Chem. Soc.* 2011, *32*, 1997-2002.

[16] Hoque, M. E. U.; Lee, H.W., "Kinetics and Mechanism of the Anilinolysis of Diethyl Thiophosphinic Chloride in Acetonitrile", *Bull. Korean Chem. Soc.* 2011, *32*, 2306-2310.

[17] Adhikary, K. K.; Lumbiny, B. J.; Dey, S.; Lee, H. W., "Transition State Variation in the Anilinolysis of *O*-Aryl Phenyl Phosphonochloridothioates in Acetonitrile", *Bull. Korean Chem. Soc.* 2011, *32*, 2628-2632.

[18] Hoque, M. E. U.; Lee, H. W., "Kinetics and Mechanism of the Anilinolysis of Diisopropyl Chlorophosphate in Acetonitrile", *Bull. Korean Chem. Soc.* 2011, *32*, 3245-3250.

[19] Barai, H. R.; Lee, H. W., "Kinetics and Mechanism of the Anilinolysis of 1,2-Phenylene Phosphorochloridate in Acetonitrile", *Bull. Korean Chem. Soc.* 2011, *32*, 3355-3360.

[20] Barai, H. R.; Lee, H. W., "Kinetics and Mechanism of the Anilinolysis of Bis(2,6-dimethylphenyl) Chlorophosphate in Dimethyl Sulfoxide", *Bull. Korean Chem. Soc.* 2011, *32*, 3783-3786.

[21] Hoque, M. E. U.; Lee, H. W., " Kinetics and Mechanism of the Anilinolysis of Diisopropyl Thiophosphinic Chloride in Acetonitrile", *Bull. Korean Chem. Soc.* 2011, *32*, 3880-3886.

[22] (A) GUHA, A. K.; LEE, H. W.; LEE, I., "PYRIDINOLYSIS OF PHENYL-SUBSTITUTED PHENYL CHLOROPHOSPHATES IN ACETONITRILE", *J. ORG. CHEM.* 2000, *65*, 12-15. (B) LEE, H. W.; GUHA, A. K.; KIM, C. K.; LEE, I. , "TRANSITION-STATE VARIATION IN THE NUCLEOPHILIC SUBSTITUTION REACTIONS OF ARYL BIS(4-METHOXYPHENYL) PHOSPHATES WITH PYRIDINES IN ACETONITRILE", *J. ORG. CHEM.* 2002, *67*, 2215-2222.

[23] (a) Adhikary, K. K.; Lee, H. W., "Kinetics and Mechanism of the Benzylaminolysis of O,O-Diphenyl S-Aryl Phosphorothioates in Dimethyl Sulfoxide", *Bull. Korean Chem. Soc.* 2011, *32*, 1625-1629. (b) Adhikary, K. K.; Lee, H. W., "Kinetics and Mechanism of the Benzylaminolysis of *O,O*-Diethyl *S*-Aryl Phosphorothioates in Dimethyl Sulfoxide", *Bull. Korean Chem. Soc.* 2011, *32*, 3587-3591.

[24] (A) LEE, I.; KIM, C. K.; LI, H. G.; SOHN, C. K.; KIM, C. K.; LEE, H.W.; LEE, B. S., "ACYL-TRANSFER MECHANISMS INVOLVING VARIOUS ACYL FUNCTIONAL GROUPS: >X ═Y WITH X = C, S, P AND Y = O, S", *J. AM. CHEM. SOC.* 2000, *122*, 11162-11172. (B) HAN, I. S.; KIM, C. K.; LEE, H. W., "THEORETICAL STUDY OF PHOSPHORYL TRANSFER REACTIONS", *BULL. KOREAN CHEM. SOC.* 2011, *32*, 889-893.

[25] Wadsworth, W. S., Jr.; Wilde, R. L. *J. Org. Chem.* 1976, *41*, 2635.

[26] Hehre W J, Random L, Schleyer P V R, Pople J A, *Ab Initio Molecular Orbital Theory* 1964, Chapter 4(Wiley: New York).

[27] PERRIN C I, ENGLER R E, „SECONDARY HYDROGEN/DEUTERIUM KINETIC ISOTOPE EFFECT OF DISSOCIATION OF AQUEOUS AMMONIUM ION", *J. PHYS. CHEM.*1991, *95*, 8431-8433.

[28] PERRIN C I, OHTA B K, KUPERMAN J, B-DEUTERIUM ISOTOPE EFFECTS ON AMINE BASICITY, "INDUCTIVE" AND STEREOCHEMICAL", *J. AM. CHEM. SOC.* 2003, *125*, 15008-9.

[29] PERRIN C I, OHTA B K, KUPERMAN J, LIBERMAN J, ERDELYI M, „STEREOCHEMISTRY OF B-DEUTERIUM ISOTOPE EFFECTS ON AMINE BASICITY", *J. AM. CHEM. SOC.* 2005, *127*, 9641-9647.

[30] HANSCH C, LEO A, TAFT R W, "A SURVEY OF HAMMETT SUBSTITUENT CONSTANTS AND RESONANCE AND FIELD PARAMETERS", *CHEM. REV.* 1991, *91*, 165-195.

[31] Streitwieser A J, Heathcock C H, Kosower E M, *Introduction to Organic Chemistry* (4th ed.) Macmillan (New York) 1992, p 735.

[32] Crumpler T B, Yoh J H, *Chemical Computations and Errors*; John Wiley (New York) 1940, p 178.

[33] Hoque, M. E. U.; Lee, H. W., "Kinetics and Mechanism of the Anilinolysis of Dibutyl Chlorophosphate in Acetonitrile", *Bull. Korean Chem. Soc.* 2012, *33*, 663-669.

[34] Dey N K, Hoque M E U, Kim C K, Lee H. W., "Kinetics and mechanism of the pyridinolyses

of dimethyl and diethyl chloro(thiono)phosphates in acetonitriley", *J. Phys. Org. Chem.* 2010, *23*, 1022-1028.

[35] Barai H R, Lee H. W., "Kinetics and Mechanism of the Pyridinolysis of 1,2-Phenylene Phosphorochloridate in Acetonitrile", *Bull. Korean Chem. Soc.* 2012, *33*, 270-274.

Supplementary Materials

Substrate : $[C_5H_{12}O_2P(=O)Cl]$

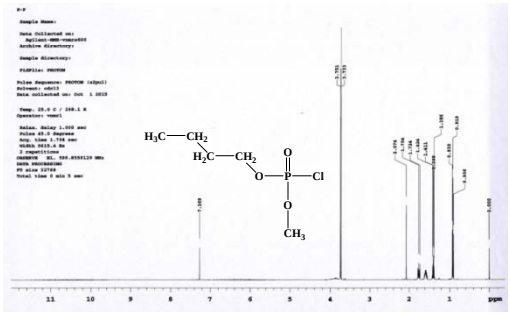

Figure S1. The ^{1}H-NMR spectrum of $[(C_4H_9O, CH_3O)P(=O)Cl]$.

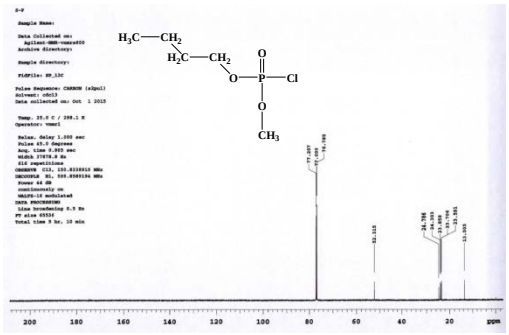

Figure S2. The ^{13}C-NMR spectrum of $[(C_4H_9O, CH_3O)P(=O)Cl]$.

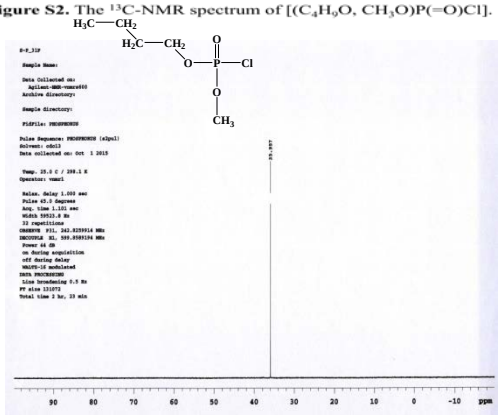

Figure S3. The ^{31}P-NMR spectrum of $[(C_4H_9O, CH_3O)P(=O)Cl]$.

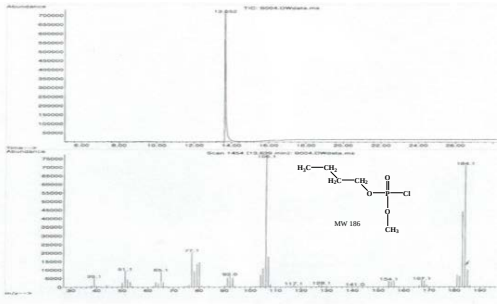

Figure S4. The GC-MS spectrum of $[(C_4H_9O, CH_3O)P(=O)Cl]$.

Product : $[C_5H_{12}O_2P(=O)NHC_6H_5]$

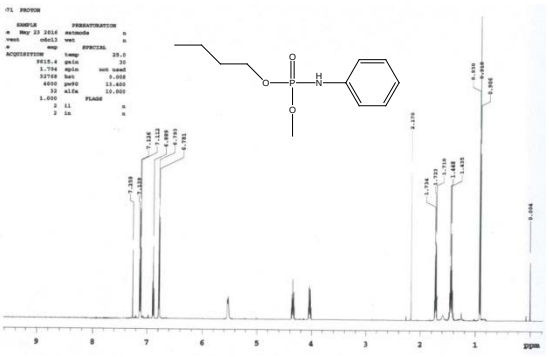

Figure S5. The ^{1}H-NMR spectrum of $[C_5H_{12}O_2P(=O)NHC_6H_5]$.

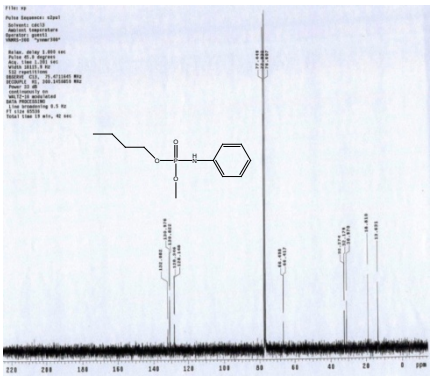

Figure S6. The ^{13}C-NMR spectrum of $[C_5H_{12}O_2P(=O)NHC_6H_5]$.

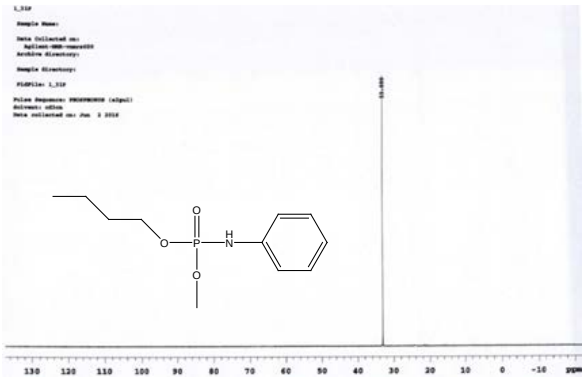

Figure S7. The ^{31}P-NMR spectrum of $[C_5H_{12}O_2P(=O)NHC_6H_5]$.

Table S1. The geometry of butyl methyl chlorophosphate (**2**) in the gas phase by Gaussian 09 Program, B3LYP Level of Theory 6-311+G(d,p) Basis set.

Summary of Natural Population Analysis:

			Natural Population			
Atom	No	Natural Charge	Core	Valence	Rydberg	Total
P	1	2.25550	9.99854	2.59327	0.15269	12.74450
Cl	2	-0.28057	9.99975	7.26751	0.01331	17.28057
O	3	-1.06993	1.99980	7.05918	0.01095	9.06993
O	4	-0.83825	1.99974	6.82225	0.01625	8.83825
O	5	-0.84851	1.99973	6.83133	0.01745	8.84851
C	6	-0.20443	1.99928	4.18877	0.01638	6.20443
H	7	0.19393	0.00000	0.80458	0.00149	0.80607
H	8	0.20315	0.00000	0.79583	0.00102	0.79685
H	9	0.19034	0.00000	0.80842	0.00124	0.80966
C	10	-0.01656	1.99914	3.99784	0.01958	6.01656
H	11	0.19133	0.00000	0.80622	0.00245	0.80867
H	12	0.19267	0.00000	0.80515	0.00218	0.80733
C	13	-0.40768	1.99927	4.39115	0.01726	6.40768
H	14	0.20553	0.00000	0.79206	0.00241	0.79447
H	15	0.20559	0.00000	0.79200	0.00241	0.79441
C	16	-0.38654	1.99930	4.37438	0.01285	6.38654
H	17	0.19563	0.00000	0.80222	0.00215	0.80437
H	18	0.19567	0.00000	0.80219	0.00214	0.80433
C	19	-0.57370	1.99937	4.56516	0.00917	6.57370
H	20	0.19663	0.00000	0.80175	0.00162	0.80337
H	21	0.20356	0.00000	0.79528	0.00116	0.79644
H	22	0.19667	0.00000	0.80171	0.00162	0.80333
* Total *		0.00000	35.99394	61.69826	0.30780	98.00000

Natural Population		
Core	35.99394 (99.9832% of	36)
Valence	61.69826 (99.5133% of	62)
Natural Minimal Basis	97.69220 (99.6859% of	98)
Natural Rydberg Basis	0.30780 (0.3141% of	98)

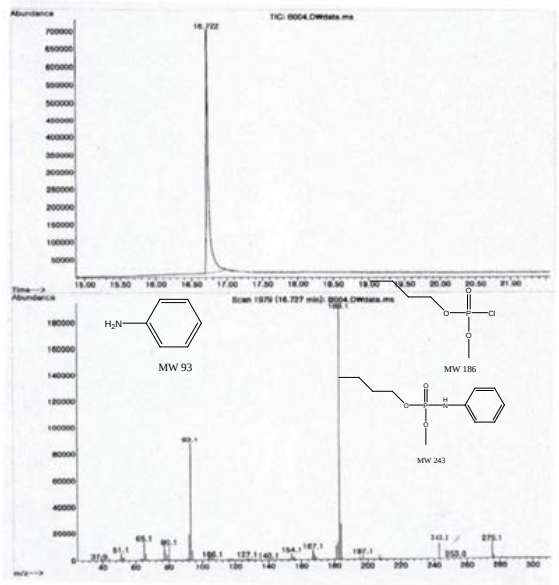

Figure S8. The GC-MS spectrum of $[C_5H_{12}O_2P(=O)NHC_6H_5]$.

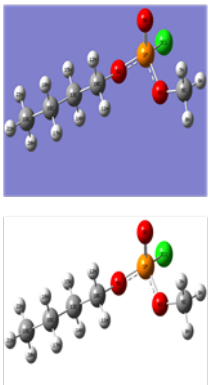

Lengths In Å
P-O_3 = 1.48005
P-O_4 = 1.59321
P-O_5 = 1.58413
P-Cl_2 = 2.05666
O_4-C_6 = 1.45472
O_5-C_{10} = 1.47413

Energies in Hartree
E_0 = -1225.078198
E_t = -1225.064740
H_0 = -1225.063795
G_0 = -1225.120835
S_0 = 120.050 (Cal./mol·K)
HF = -1225.2546373

Angles in Degree
∠O_3PCl_2 = 112.06772
∠O_3PO_4 = 115.97198
∠O_3PO_5 = 118.77524
∠Cl_2PO_4 = 105.16097
∠O_4PO_5 = 102.97069
∠O_3PCl_2 = 99.88009

Dhd∠$Cl_2PO_5C_{10}$ = -177.57007
Dhd∠$Cl_2PO_4C_6$ = 85.46780
Dhd∠$O_3PO_4C_6$ = -38.93244
Dhd∠$O_3PO_5C_{10}$ = -55.51478

Figure S9. The geometry of butyl methyl chlorophosphate (**2**) in the gas phase calculation by Gaussian 09 Program, B3LYP Level of Theory 6-311+G(d,p) Basis set, CPCM method, acetonitrile continuum model.

EFFECTS OF A STAGE-BASED INTERVENTION ON EXERCISE SELF-EFFICACY

Zeinab Ghiami[1], Kim Geok Soh[2], Samsilah Roslan[3], Kim Lam Soh[4]
[1, 2, 3] Faculty of Educational Studies, Universit Putra Malaysia, Malaysia; [4] Faculty of Medicine, Universiti Putra Malaysia, Malaysia

ABSTRACT

Studies on the changes of physical activity patterns demonstrated that physical activity rates decline sharply in adolescence and goes on well into adulthood. Psychological readiness, not physical readiness and facilities, is likely to be the main barrier to activity for most of the people. This seems to signify the importance of designing interventions to improve psychological factors related to exercise behavior willingness. This study evaluated the effect of an intervention contained strategies related to psychological factors of exercise behavior. Fifty-six sedentary adolescents completed an assessment at baseline, 2 months, and 4 months. Experimental group participants received the intervention lasting for 16 weeks and consisting of a 30-minute session every week with the aim of raising learners' awareness about the factors affecting intention to physical activity. Control group attended physical education classes based on the guidelines of the Ministry of Education. Changes in psychological variables were compared between groups using analysis of two-way repeated measure ANOVA. The interaction between group and test was statistically significant, F (2, 108) =127, P =.01, η2=702). There was a significant difference between the scores of self-efficacy in the 3 times measurements in the experimental group. It can be concluded that the stage-based intervention had a significant positive effect on self-efficacy hence enhancing sedentary students' intention towards physical activity.

Keywords: Physical activity, Sedentary, Self-efficacy, Transtheoretical Model.

INTRODUCTION

Health behavior refers to any activity undertaken by an individual for the purpose of promoting, protecting, or maintaining health as well as preventing or detecting diseases [1]. Accordingly, regular physical activity can be also regarded as a health behavior , because this behavior helps individuals maintain and promote their physiological health through improving cardiovascular endurance, as well as improve immune system function [2-4]. Strong evidence showed that physical activity influences individuals' psychological health as well [5] such as enhancing self-esteem, cognitive functioning and reducing anxiety, stress and depression [6].

Despite the benefits of regular physical activity for health, more than 60% of the world's population were considered sedentary, failing to be active for at least 30 minutes daily doing moderate intensity physical activity [7]. Studies on the changes in physical activity patterns showed that physical activity rates decline sharply in adolescence to 75% inactivity and they continue to be low throughout adulthood [8, 9]. This seems to signify the importance of designing interventions for adolescents in order to improve their intention to engage in exercise behavior.

In the context of Iran, patterns of sedentary behavior bear some similarity to the rest of the world, and adolescents constitute a major portion of the society (81.5%) that is not sufficiently physically active [8, 10]. The study by Kelishadi, Razaghi, Gouya, Ardalan, Gheiratmand, Delavari, Motaghian, Ziaee, Siadat and Majdzadeh [11] on elementary, middle, and high school students showed a significant decrease in physical activities among the girls during high school. Moreover, studies have been confirmed sedentary behavior among Iranian adolescent girls [10, 12] and they showed that only 35.9% of girls but 64.1% of boys were in the action or maintenance stages of physical activity.

Psychological readiness, not physical readiness and facilities, is likely to be the main barrier to activity for most people [13]. Many people consider the idea of starting a performance or an action, but they usually fail to realize it. Some people might engage in some physical activity but have not quite figured out how to make it a habit of sufficient frequency and duration. The significance of assessing psychological constructs of change becomes more salient when a researcher attempts to determine what can encourage the unmotivated individuals to consider leading a more active lifestyle [13].

Behavioural change related to physical activity have been studied by numerous cognitive behaviour models [14]. The most important factors to consider in changing physical activity behaviour probably include beliefs related to physical activity, attitudes and self-efficacy, motivations and barriers, and formulation of self-perceptions and identity related to physical activity. However, the issue of behavior change has not been tackled sufficiently as most of the intervention studies on adolescents have

not been successful since they have not identified the root causes of inactivity among adolescents.

According to the transtheoretical model (TTM), which is a combination of several theories of psychotherapy related to behavior change [15], self-efficacy is one of the several psychological constructs contribute to behavior change among individuals. Within the framework of the TTM, since people have different motivation levels, or change readiness, they require different interventions. For this study, the stages of change are considered in conjunction with the constructs of processes of change, decisional balance and self-efficacy in terms of both intervention content and outcomes. The stages of change represent specific collections of intentions, attitudes and behaviors which are related to one's change cycle status [15].

Self-efficacy describes the degree of confidence one has in the ability to perform a certain physical activity [16]. Sedentary students did not possess or make use of these essential psychological factors to improve their intention to change their sedentary behavior, engage in physical activities, and maintain a more active lifestyle [8, 12].

The public health community is becoming increasingly interested in the potential contributions of school physical education to child health. School physical education is seen as an ideal site for the promotion of regular physical activity because up to 97% of students participate in some sort of physical education program. For maximal public health benefit, school physical education programs should prepare children for a lifetime of physical activity.

A number of interventional studies used stages of change to assess changes in individuals' physical activity behavior because of implementing various psychological strategies. Although the number of intervention studies on adolescents' willingness to engage in physical activity in the context of school and physical education courses is very limited. This seems to signify the need to conduct more stage-based intervention studies on psychological constructs in school settings to motivate students to engage in physical activity.

Therefore, this study aimed to design an intervention based on TTM in the school context to evaluate the effect of the psychological strategies on the exercise self-efficacy (SE) among Iranian sedentary students.

METHODS

Participants

Prior to the beginning of this research project, a pre-screening survey was conducted using the stages of change questionnaire to identify the population of sedentary students from a high school in Mashhad, Iran. This research was conducted in the first semester of 2014 on Automn. Based on the result of given questionnaire, 247 of students were in precontemplation, contemplation and preparation stages (sedentary stages) who were considered as the population of the current study (female, M_{age} = 16 years (SD = 1)). Fifty-six students (15% more that the estimation of G-Power) were randomly selected as the participants and were assigned into experimental and control groups with 28 students in each group, respectively. This study assessed students' current exercise behavior, their intention to engage in regular physical activity, and Self-efficacy related to physical activity. A consent forms (parental consent forms for those younger than 18 years) were obtained for all subjects.

Procedure

At the onset of the study, the stages of change questionnaire [13] was given as pre-test to all participants in order to determine their stages of physical activity as well as possible differences between the participants in the groups in terms of their stages of change before starting the treatment phase of the study. Self-efficacy questionnaires were also given to participants at pre-test in order to determine any psychological differences prior to the treatment phase of the study.

Subsequently, the participants in the experimental group received a TTM stage-based intervention lasting 16 weeks and consisting of a 30-minute session every week for the duration of the treatment. The intervention was designed based on guidelines by Marcus and Forsyth [13]. It involved consciousness-raising assessed by awareness-raising questions, discussions, and speeches about the benefits of being physically active; watching film segments and discussing the importance of physical activity; and modeling activities with the aim of raising learners' awareness about the factors affecting intention to physical activity as well as the strategies and processes used to improve students' willingness to become physically active.

The participants in the control group attended physical education classes based on the guidelines provided by the Ministry of Education that did not contain any awareness-raising activities about physical activity. After two months from the beginning and also at the end of the treatment phase at four month, two post-tests were administered to the learners in both groups to determine their stages of physical activity and related psychological factors. The results obtained from the pre-tests, post-test 1, and post-test 2 were analyzed to determine the effect of the treatment on sedentary students' self-efficacy related to physical activity.

Instruments

A set of questionnaires was used divided into two parts. The first part contained questions assessing the demographic profile of sedentary high school students while part two contained TTM questionnaires on stages of change and self-efficacy.

Stages of change questionnaire were used to assess participants' current stage of change measured on a dichotomous scale with *No* = 0 and *Yes* = 1, based on previous work in the areas of exercise studies [13]. According to the stages of change algorithm, If (question 1=0 and question 2=0), then they are at stage 1. If (question 1=0 and question 2=1), then they are at stage 2.If (question 1=1 and question 3=0), then they are at stage 3.If (question 1=1 and question 3=1, and question 4=0), then they are at stage 4.If (question 1=1 and question 3=1, and question 4=1), then they are at stage 5.

A five-item measure of self-efficacy [17] was also administered to assess participants' involvement in exercise. It was designed to measure one's confidence in his/her ability to exercise in various situations. Higher mean score of physical activity self-efficacy can determine whether an individual attempts an activity; the degree of persistence extended when difficulties are encountered, and ultimate success. Reliability analysis was done on all the items in the instrument which used Likert scale measurement. The Alpha coefficient for the instruments of the pilot test (answered by 20 local females, age 15 to 17) ranged from 0.858 to 0.927. The applicability of the questionnaire was confirmed. For the present study, feedback was requested from the advisory committee regarding readability, Persian language, clarity, and redundancy of items. The feedback provided by the pilot participants was also used to revise the instrument and provided content validity for the instrument.

Statistical Analysis

The Statistics Package for Social Science (SPSS) for Windows version 21 was used to analyze the data. Firstly, data was tested for normal distribution with the Kurtosis and Skewness test and for homogeneity of variances with Levene's test [18, 19]. Two-way repeated measures ANOVA design was conducted to analyze the data in order to compare the mean difference to measure whether there was any improve in the psychological variables and stages of change during intervention in the experimental group.

RESULTS

The main objective of this study was to evaluate the effect of a stage-based intervention on students' self-efficacy, as measured by self-efficacy of exercise inventory at baseline, two months, and four months. The results of two-way repeated measure ANOVA on self-efficacy score showed that the interaction between group and test was statistically significant $F_{(2, 108)} = 84.9$, $P = .01$, $\eta^2 = 611$) therefore to test the related hypothesis post hoc test (Bonferroni) was applied to compare the mean scores (Table 1).

Table1. Result of ANOVA within – between subject effects

	Source	MS	F	P value	Partial Eta Squared
Self-efficacy	Test	6.83	24.18	0.00	0.309
	Group	18.8	36.09	0.00	0.401
	Test* group	24.1	84.97	0.00	0.611

In order to show the efficacy of intervention, pre, post 1 and post-test 2 in both the experimental and control were compared. The result of post hoc test (Bonferroni) revealed that the difference between pre and post-test 1 in self-efficacy score among experimental group was significant ($p = .01$) .The mean for the self-efficacy in experimental group increased 1.15 unit in post-test 1 and also there was significant difference between self-efficacy mean between post 1 and post-test 2 ($p = .01$). While the result for control group was not significant between pre-test and post-test 2 ($p = .08$). There was no significant difference between self-efficacy mean between post-test 1and post-test 2 ($p = .08$) in control group (Table 2). According to the results, the students who received stage-based intervention improved more remarkably in their self-efficacy compared to those who received no specific intervention in the control group.

Table 2 Result of Bonferroni Post Hoc test

Group	(I) TEST	(J) TEST	Mean Difference	SE	P value	Partial Eta Squared
Self-efficacy	1	2	.300	0.127	.06	
		3	.614	0.159	.08	0.218
Control	2	3	.314	0.139	.08	
	1	2	-1.15	0.127	.00	
Experimental		3	-2.00	0.159	.00	0.754
	2	3	-.850	0.139	.00	

The significant difference between the mean scores of the experimental group and the control group showed that the intervention improved students' confidence in their ability to successfully perform a particular activity, and improve in their perceptions that they can perform physical activity successfully increased their engagement in physical activity.

DISCUSSION

In the current study, students in the intervention group reported significantly higher self-efficacy at two months and four months compared to participants in the control group. These findings are similar to the previous work that reported an increase in self-efficacy from pre-test (M = 3.4) to post-test (M = 3.8) in sedentary individuals after a brief intervention [20]. In the current study, the mean of self-efficacy improved from 2.3 in the pre-test to 4.3 in the post-test 2. Considering that acquiring and changing attitudes and behaviors can be a long and complicated process (Marcus and Forsyth, 2009), the more improvement in the current study could be because of the duration of intervention, which was longer that the study by Pinto, Lynn, Marcus, Judith and Goldstein [20] who developed six-week intervention. The results suggest that longer duration of intervention (more than 3 months) might be required to encourage change in motivational readiness for physical activity.

The findings of this study are in contrast with those of Boonchuaykuakul [21] who reported that self-efficacy did not improve during the stage-based intervention. This lack of change in self-efficacy may have emerged because the intervention strategies for precontemplators, contemplators, and preparers did not strongly focus on improving engagement on physical activity rather than the cognitive aspect of self-efficacy. It has been demonstrated that using the four information sources of self-efficacy, including verbal encouragement, performance accomplishment, vicarious learning, and physiological and affective responses, have a positive effect on confidence to initiate and maintain physical activity (Lee et al., 2007). The results of the present study is also in contrast with the results of a study by Nelson [22], which indicated that the intervention group made no significant improvements in self-efficacy from pre-test to post-test.

According to [22], the intervention and control groups did not differ in self-efficacy because they became conditioned to particular responses on the questionnaires from previous testing. The measures used were short; hence, it would not have been difficult to remember the answers from one session to the next. The length of time of the study may have also affected the study results. Behavior change is a time-dependent variable and the duration of four months may not have been a long enough to result in significant changes in behavior, especially in self-efficacy.

CONCLUSION

The findings of this study would be useful for physical education teachers Ministry of Education, and researchers. They can undertake stage-based intervention in the physical education course in order to motivate sedentary students to put more time and effort into doing that activity. Moreover, it can encourage sedentary students to be more persistent when they encountered difficulties, which can help them achieve the ultimate success towards changing their sedentary behavior and engaging in physical activity.

REFERENCES

[1] World Health Organization, "The world health report 2002: reducing risks, promoting healthy life," 2002.

[2] M. Cecchini, F. Sassi, J. A. Lauer et al., "Chronic diseases: Chronic diseases and development 3 tackling of unhealthy diets, physical inactivity, and obesity: Health effects and cost-effectiveness," Lancet, vol. 376, no. 9754, pp. 1689-1698, 2010.

[3] A. Gaeini, A. Fallahi, and F. Kazemi, "Effects of aerobic continuous and interval training on rate pressure product in patients after CABG surger," The Journal of sports medicine and physical fitness, 2014.

[4] M. Kargarfard, A. Shariat, B. S. Shaw et al., "Effects of Polluted Air on Cardiovascular and Hematological Parameters After Progressive Maximal Aerobic Exercise," Lung, pp. 1-7, 2015.

[5] Y. Netz, M.-J. Wu, B. J. Becker et al., "Physical activity and psychological well-being in advanced age: a meta-analysis of intervention studies," Psychology and Aging, vol. 20, no. 2, pp. 272, 2005.

[6] R. Rueggeberg, C. Wrosch, and G. E. Miller, "The different roles of perceived stress in the association between older adults' physical activity and physical health," Health Psychology, vol. 31, no. 2, pp. 164, 2012.

[7] World Health Organization, "Physical Inactivity: A Global Public Health

Problem," International Journal of Epidemiology, 4, 2008, pp. 1107-1107.

[8] H. Sanaeinasab, M. Saffari, M. Nazeri et al., "Descriptive analysis of Iranian adolescents' stages of change for physical activity behavior," Nursing and Health Sciences, vol. 15, no. 3, pp. 280-285, 2013.

[9] C. J. Caspersen, M. A. Pereira, and K. M. Curran, "Changes in physical activity patterns in the United States, by sex and cross-sectional age," Medicine and Science in Sports and Exercise, vol. 32, no. 9, pp. 1601-1609, 2000.

[10] A. Pirasteh, A. Hidarnia, A. Asghari et al., "Stages of changes for physical activity among Iranian adolescent girls," World Academy of Science, Engineering and Technology, vol. 5, pp. 1146-8, 2011.

[11] R. Kelishadi, E. M. Razaghi, M. M. Gouya et al., "Association of physical activity and the metabolic syndrome in children and adolescents," Hormone Research in Paediatrics, vol. 67, no. 1, pp. 46-52, 2006.

[12] P. Taymoori, S. Niknami, T. Berry et al., "Application stage of change exercise behavior among Iranian adolescents," Eastern Mediterranean Heath Journal, vol. 15, no. 5, pp. 785-795, 2009.

[13] B. H. Marcus, and L. H. Forsyth, Motivating people to be physically active, 2nd ed., Champaign, IL: Human Kinetics, 2009.

[14] S. J. Biddle, and N. Mutrie, Psychology of physical activity: Determinants, well-being and interventions, UK: Routledge, 2007.

[15] J. O. Prochaska, J. Norcross, and C. C. DiClemente, Changing for Good, New York: Avon Books, 1994.

[16] P. Callaghan, F. F. Eves, P. Norman et al., "Applying the transtheoretical model of change to exercise in young Chinese people," British Journal of Health Psychology, vol. 7, no. 3, pp. 267-282, 2002.

[17] B. H. Marcus, V. C. Selby, R. S. Niaura et al., "Self-efficacy and the stages of exercise behavior change," Research Quarterly for Exercise and Sport, vol. 63, no. 1, pp. 60-66, 1992c.

[18] J. Pallant, SPSS survival manual: A step by step guide to data analysis using SPSS, Melborn: McGraw-Hill International, 2010.

[19] L. S. Meyers, G. Gamst, and A. J. Guarino, Applied multivariate research: Design and interpretation, p.^pp. 68-70, London: Sage, 2006.

[20] B. M. Pinto, H. Lynn, B. H. Marcus et al., "Physician-based activity counseling: intervention effects on mediators of motivational readiness for physical activity," Annals of Behavioral Medicine, vol. 23, no. 1, pp. 2-10, 2001.

[21] J. Boonchuaykuakul, "Effectiveness of applying the transtheoretical model to improve physical activity behavior of university students," Oregon State University, 2005.

[22] M. S. Nelson, "A stage matched physical activity intervention in military primary care," University of Maryland, USA, 2000.

Second International Conference on Science, Engineering & Environment,
Osaka City, Japan, Nov.21-23, 2016, ISBN: 978-4-9905958-7-6 C3051

CLARIFICATION OF SHEAR ZONE DEVELOPMENT IN A GOUGE LAYER RELATED TO SLIP INSTABILITY

Momoko Hirata[1], Jun Muto[1], and Hiroyuki Nagahama[1]
[1]Department of Earth Science, Tohoku University, Japan

ABSTRACT

Earthquakes are typical phenomena of frictional slip in nature. To evaluate slip instability, shear zone development in a gouge layer produced by fault slip has been investigated. However, previous works have not revealed the quantitative relationship between slip instability and shear zone development because of difficulty in quantitative observation of microstructures. Hence, we aim to describe shear zone development in a gouge layer energetically and discuss the relation between shear zone development and slip instability. To this end, we estimated shear angles by utilizing experimental data. As a result, our study revealed that shear bands become low angles or almost parallel to rock-gauge boundaries toward the occurrence of unstable slip. Under a low confining pressure, heterogeneous localized shears trigger unstable slip. On the other hand, under a high confining pressure, rapid sliding of the whole samples with internal homogeneity of gouge structure can be considered. Clarification of shear development of fault materials is useful for assessment of the occurrence of other natural phenomena such as slope failures.

Keywords: Earthquake, Slip instability, Shear zone development, Frictional slip

INTRODUCTION

Earthquakes or slope failures are typical phenomena of frictional instability of geomaterials in nature. These natural phenomena often lead to serious physical damage to our society (e.g., humans, structures, and infrastructures). In general, frictional slip can be categorized into two types; stable slip and unstable slip. The former is a stationary motion without stress drop. On the other hand, the latter is accompanied with dynamic stress drop. To prevent or mitigate damages of unstable slip (i.e., earthquakes or slope failures), assessment for the occurrence of unstable slip is significantly important. With respect to earthquakes, various researchers have tackled on the evaluation of fault instability for earthquake generation, and proposed (1) a friction parameter $a - b$ [1]–[3] and (2) importance of fault gouge generated by a repetition of fault slip [4]–[15].

Frictional parameter $a - b$ is generally derived from a spring-slider model (e.g., [1], [2]) for the assessment of slip instability [2], [3]. The friction parameter derived from the empirical law called rate and state dependent friction law indicates velocity dependence of friction [2], [3]. The positive values of the friction parameters lead to stable slip (velocity strengthening). On the other hand, the negative values of the friction parameters lead to unstable slip (velocity weakening).

In regard to fault gouge, shear zone development in a gouge layer has been focused to assess slip instability. Particularly, transition from the oblique R1-shears formed after peak stress to Y-shears developed parallel to the rock-gouge boundary seems to trigger unstable slip [9], [12]. Reference [11] also shows that degrees of R1-shears with respect to the rock-gouge boundary progressively decrease with shear. Based on these observations, [14] empirically proposed the change in frictional parameter of rock with shear.

In fact, quantitative observation of shear structures developed in a granular material at high pressure is significantly difficult. However, [16] proposed an index to describe deformation process of granular materials based on their energy ratio (e.g., glass and quartz). The index (i.e., the energy ratio) depends on an internal friction angle. The internal friction angle is related to a coefficient of friction. Based on the Rowe's energy relation [16], we had revealed that slip instability of simulated fault gouge could be assessed by the energy ratio [17].

Because the internal friction angle can be related to angles of shear planes developed in granular materials, quantitative assessment of shear zone development is possible. Therefore, the purpose of this study is to clarify quantitatively the process of shear zone development toward the occurrence of unstable slip and to discuss the relationship between slip instability and shear zone development energetically. Through our experimental analysis of friction experiments with simulated fault gouge, we clarify shear zone development in a gouge layer under high confining pressures quantitatively. Results have possibility for evaluating other unstable slip such as slope failures.

EXPERIMENTAL ANALYSIS

Materials and Methods

In this paper, we utilize data of friction experiments with simulated fault gouge published elsewhere [17]. According to [17], friction experiments were conducted by a gas-medium apparatus under confining pressures of 140, 160, and 180 MPa. A sample was composed of gabbroic forcing blocks and simulated fault gouge (quartz). The forcing brocks were cut at oblique angle of 50º to the longitudinal axes. Quartz gouge was sandwiched between two gabbroic blocks. Strain gauges were settled onto a gauge layer to record values of stress and strain rate in the major and minor compressive axes; σ_1, σ_3, $\dot{\varepsilon}_1$, and $\dot{\varepsilon}_3$, respectively. Based on these values, energy ratio K proposed by [16] could be calculated to describe deformation of granular materials as shown in Eq. (1),

$$K = \frac{\sigma_1 \dot{\varepsilon}_1}{2\sigma_3 \dot{\varepsilon}_3}. \quad (1)$$

Experimental Results

Figure 1 shows a representative change in the energy ratio K during multiple loading cycles toward unstable slip (the 4th run under a confining pressure of 140 MPa, see [17] in detail). The increase in energy ratios could be confirmed at all strain gauges until between H1 and H2, between H2 and H3, or between H3 and H4 for top, middle, or bottom strain gauges. After that, all strain gauges showed decrease toward the occurrence of unstable slip. Especially, the bottom strain gauge showed the significant reduction in the energy ratio before the occurrence of unstable slip.

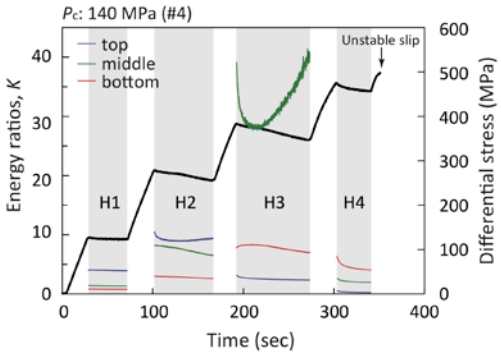

Fig. 1 Change in energy ratios K of fault gouge at a confining pressure of 140 MPa. Notice that the data was obtained from 4th run. Different colors show data obtained from different strain gauges; blue, green, or red results correspond to data of strain gauges settled at top, middle, or bottom of a sample, respectively. The black arrow means the occurrence of unstable slip. The gray shaded areas (H1–H4) indicate the holding periods of differential stress shown in black lines. Only results of energy ratios at the holding periods were displayed.

The sequence data of energy ratios under confining pressures of 140, 160, and 180 MPa is shown in Fig. 2. After the final holding period (H4), all strain gauges showed the significant decreases in energy ratio just before unstable slip. The drops of K in final stages just before the occurrence of unstable slip (L5 stage) were confirmed under all confining pressures.

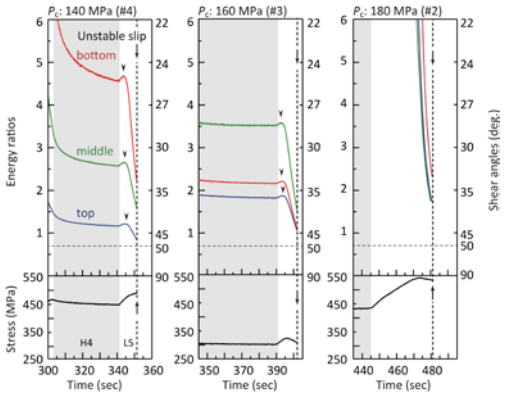

Fig. 2 The sequence data of energy ratios toward the occurrence of unstable slip at all confining pressures. Black marks indicate the drops in energy ratio K at confining pressures of 140 and 160 MPa. Vertical broken lines correspond to the occurrence of unstable slip. Color legends are same as Fig. 1. Right vertical axes indicate Riedel shear angles in a gouge layer.

On the other hand, there were time lags for the sudden drop in K depending on the position of strain gauges. Time lags decrease with increasing confining pressures: 1.6 or 1.3 seconds at 140 or 160 MPa, respectively. Degrees of internal heterogeneity of gouge structures also depend on confining pressures; gouge shows internal heterogeneity of gouge structures at a low confining pressure or internal homogeneity of gouge structures at a high confining pressure.

DISCUSSION

Estimates of Riedel Shear Angles

The energy ratio K expressed as Eq. (1) as

mentioned above can be rewritten as follows,

$$K = \tan^2\left(\frac{\pi}{4}+\frac{\phi}{2}\right), \quad (2)$$

where ϕ is the internal friction angle [16], [18]–[20]. Thus, the change in energy ratios observed during friction experiments indicates the change in internal friction angles. The ϕ can also be connected to Riedel shear (e.g., R1-sehars) angles [5], [21] by

$$\theta = \frac{\pi}{4}-\frac{\phi}{2}, \quad (3)$$

where θ is the angle of Riedel shears with respect to the major compressive axis. Therefore, Riedel shear angles developed in a gouge layer can be estimated based on Eqs. (2) and (3) by utilizing the energy ratios. Right vertical axes in Fig. 2 showed the estimated Riedel shear angles. According to [5], [21], change for clockwise direction is taken to be positive. In Fig. 2, shear angles of 50º (horizontal broken lines) correspond to the angle of rock-gouge boundaries. Fig. 2 indicates that Riedel shear angles gradually change toward the occurrence of unstable slip.

Figure 3 illustrates development of Riedel shears in a gouge layer based on the calculations of Riedel shear angles. Under all confining pressures, Riedel shears develop at lower angles to the rock-gouge boundaries with shear toward the occurrence of unstable slip (blue to red lines). Particularly, under a confining pressure of 140 MPa, the top of samples shows almost parallel (~ 3º) to the rock-gouge boundary at the occurrence of unstable slip. As a general trend, Riedel shears at the middle part tend to develop at higher angles than those at other two parts except for the result under a confining pressure of 140 MPa. The observed development of Riedel shears in low angles near the rock-gouge boundaries is consistent with [11].

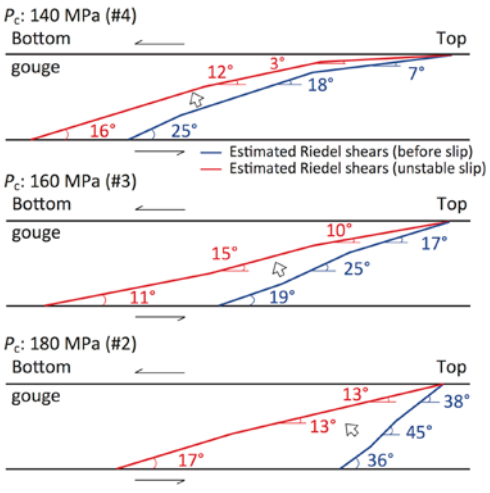

Fig. 3 Development of Riedel shears in a gouge layer under all confining pressures. Blue or red lines indicate the estimated Riedel shears at the beginning of last loading (L5) or at the occurrence of unstable slip shown with black arrows in Fig. 2. The right side corresponds to top of samples. The upper or lower receives shear to left side or right side, respectively. The angles mean the differences between Riedel shear angles and the rock-gouge boundaries which is given by 50º - θ.

Variation in Riedel shear angles is smaller at the high confining pressure than those at lower confining pressures (140 and 160 MPa). This tendency reflects the degree of internal homogeneity of gouge structures derived from energy ratios depending on confining pressures as mentioned above. The internal heterogeneity of gouges is large at lower confining pressures. Therefore, it is considered that development of localized shear (e.g., the top of sample under a confining pressure of 140 MPa) triggers unstable slip at lower confining pressure, while the whole of sample with internal homogeneity of gouge structures slides rapidly under a high confining pressure.

Dependence of Riedel Shear Angles on Energy Ratios

From Eqs. (2) and (3), relationship between Riedel shear angles θ and energy ratios K can be described as follows,

$$\theta = \frac{\pi}{2}-\tan^{-1}\sqrt{K}. \quad (4)$$

According to [17], energy ratios K tend to be larger with confining pressures ($K > 0$). Riedel shear angles range from 0 to 90º. Thus, Riedel shear angles become small with confining pressures. Small values of Riedel shear angles indicate that Riedel shears develop at high angles to rock-gouge boundaries in our experimental set up. Therefore, as shown in Fig. 3, shear bands develop at high angle to the rock-gouge boundaries under high confining pressures. On the other hand, shear bands develop at low angle, or almost parallel to the rock-gouge boundary under a low confining pressure.

However, Riedel shear angles depend not only σ_3 but also other factors (i.e., σ_1, $\dot{\varepsilon}_1$, and $\dot{\varepsilon}_3$) because the energy ratio is a function of these four factors (Eq. (2)). With respect to σ_1, the effect of σ_1 on Riedel shear angles can be considered as slight. If Riedel shear angles depend on σ_1 strongly, Riedel shear angles should become similar values in experiments with similar differential stresses, e.g.

500 MPa and 450 MPa for the results of confining pressures of 140 MPa and 180 MPa, respectively. However, their energy ratios and Riedel shear angles under a confining pressure of 140 MPa are different from those under a confining pressure of 180 MPa as shown in Fig. 2. Additionally, if Riedel shear angles depend on σ_1, Riedel shear angles become large with σ_1 based on Coulomb-Navier's failure criterion. However, in fact, Riedel shear angles are not always increase with differential stress under confining pressures of 140 and 160 MPa (Fig. 2).

In regard to strain rates, variation in the values of strain rates observed through local strain gauges influences the energy ratios as well as Riedel shear angles strongly. Even though samples were applied to under same confining pressures, strain rates near a main slip plane become large locally, and the values of Riedel shear angles become large (i.e., shears develop at lower angles to the rock-gouge boundaries). The top of samples under a confining pressure of 140 MPa showed the representative result. Consequently, strain tends to localize under low confining pressures. Localized strain leads to increase in Riedel shear angles.

Finally, internal friction angle is related to plasticity index I_P of soils with water [22]–[25],

$$\phi = \alpha I_P^{-\beta}, \tag{5}$$

where α and β are constants. From Eqs. (2) and (5), assessment of unstable slip based on energy ratios can take effect of water into consideration. Thus, this study focusing on earthquakes can be useful in assessment of other unstable slip such as slope failures.

CONCLUSION

We investigated energy ratios of simulated fault gouge obtained from previous works and calculated Riedel shear angles based on energy ratios. From our analysis, it is clear that shears develop at low angles to rock-gouge boundaries toward the occurrence of unstable slip. Under a low confining pressure, gouge shows heterogeneous structures and localized shear triggers unstable slip. On the other hand, under a high confining pressure, the whole of samples with homogeneous structures slips. The evaluation of frictional instability by shear angles through energy ratio leads to quantitative assessment of fault instability. Finally, clear understanding of Riedel shear development is also useful for estimation of slip planes of slope failures.

ACKNOWLEDGEMENTS

This study was supported by JSPS KAKENHI grant number 15J02421 and Inter-Graduate School Doctoral Degree Program on Science for Global Safety of Tohoku University.

REFERENCES

[1] Rice JR and Ruina AL, Stability of steady frictional slipping, J. App. Mech., Vol. 50, Jun. 1983, pp. 343–349.
[2] Ruina A, Slip instability and state variable friction laws, J. Geophys. Res., Vol. 88, Dec. 1983, pp. 10359–10370.
[3] Dieterich JH, Modeling of rock friction: 1. Experimental results and constitutive equations, J. Geophys. Res. Vol. 84, May 1979, pp. 2161–2168.
[4] Scholz CH, Wyss M, and Smith SW, Seismic and aseismic slip on the San Andreas fault, J. Geophys. Res., Vol. 74, Apr. 1969, pp. 2049–2069.
[5] Byerlee J, Mjachkin V, Summers R, and Voevoda O, Structures developed in fault gouge during stable sliding and stick-slip, Tectonophysics, Vol. 44, Jan. 1978, pp. 161–171.
[6] Logan JM, Friedman M, Higgs N, Dengo C, and Shimamoto T, Experimental studies of simulated gouge and their application to studies of natural fault zones, Proc. Conf. VIII, Analysis of Actual Fault Zones in Bedrock, U. S. Geol. Surv., Open File Rep., 79-1239, 1979, pp. 305–343.
[7] Marone C and Scholz CH, The depth of seismic faulting and the upper transition from stable to unstable slip regimes, Geophys. Res. Lett., Vol. 15, Jun. 1988, pp. 621–624.
[8] Marone C, Raleigh CB, and Scholz CH, Frictional behavior and constitutive modeling of simulated fault gouge, J. Geophys. Res., Vol. 95, May 1990, pp. 7007–7025.
[9] Logan JM, Dengo CA, Higgs NG, and Wang ZZ, Chapter 2 Fabrics of experimental fault zones: Their development and relationship to mechanical behavior, Fault Mechanics and Transport Properties of Rocks, Int. Geophys. Ser., Vol. 51, A Festschrift in Honor of Brace WF, Evans B, and Wong T-f, Ed. Academic Press, 1992, pp. 33–67.
[10] Marone C and Kilgore B, Scaling of the critical slip distance for seismic faulting with shear strain in fault zones, Nature, Vol. 362, Apr. 1993, pp. 618–621.
[11] Gu Y and Wong T-f, Development of shear localization in simulated quartz gouge: Effect of cumulative slip and gouge particle size, Pure Appl. Geophys., Vol. 143, Mar. 1994, pp. 387–423.
[12] Marone C, Laboratory-derived friction laws and their application to seismic faulting, Annu. Rev. Earth Planet. Sci., Vol. 26, May. 1998, pp. 643–696.

[13] Wong T-f, Baud P, and Klein E, Localized failure modes in a compactant porous rock, Geophys. Res. Lett., Vol. 28, Jul. 2001, pp. 2521–2524.
[14] Ikari MJ, Marone C, and Saffer DM, On the relation between fault strength and frictional stability, Geology, Vol. 39, Jan. 2011, pp. 83–86.
[15] Onuma K, Muto J, Nagahama H, and Otsuki K, Electric potential changes associated with nucleation of stick-slip of simulated gouges, Tectonophysics, Vol. 502, Mar. 2011, pp. 308–314.
[16] Rowe PW, The stress-dilatancy relation for static equilibrium of an assembly of particles in contact, Proc. R. Soc. Lond. A, Vol. 269, Oct. 1962, pp. 500–527.
[17] Hirata M, Muto J, and Nagahama H, Experimental analysis on Rowe's stress-dilatancy relation and frictional instability of fault gouges, Episodes, Vol. 37, Dec. 2014, pp. 303–307.
[18] Niiseki S and Satake M, The instruction and consideration of Rowe's principle on the minimum energy ratio, in Proc. 36th Annu. Conf. JSCE, Vol. 3, 1981, pp. 5–6 (in Japanese).
[19] Morinaga K and Niiseki S, Consideration about Rowe's stress-dilatancy relation according to variational method, in Proc. 38th Annu. Conf. JSCE, Vol. 3, 1983, pp. 33–34 (in Japanese).
[20] Niiseki S, Formulation of Rowe's stress-dilatancy equation based on plane of maximum mobilization, in Proc. 4th Int. Conf. Micromech. Granular Media (Powders and Grains), 2001, pp. 213–216.
[21] Morgenstern NR and Tchalenko JS, Microscopic structures in kaolin subjected to direct shear, Géotechnique, Vol. 17, Dec. 1967, pp. 309–328.
[22] Kenny TC, Geotechnical properties of glacial lake clays, J. Soil Mech. Found. Eng. Div., Vol. 85(SM3), Jun. 1959, pp. 67–79.
[23] Voight B, Correlation between Atterberg plasticity limits and residual shear strength of natural soils, Géotechnique, Vol. 23, Jan. 1973, pp. 265–267.
[24] Kanji MA, The relationship between drained friction angles and Atternberg limits of natural soils, Géotechnique, Vol. 24, Dec. 1974, pp. 671–674.
[25] Dewoolkar MM and Huzjak RJ, Drained residual shear strength of some claystones from front range, Colorado, J. Geotech. Geoenviron. Eng, Vol. 131, Dec. 2005, pp. 1543–1551.

Second International Conference on Science, Engineering & Environment,
Osaka City, Japan, Nov.21-23, 2016, ISBN: 978-4-9905958-7-6 C3051

EXTRACTION OF ESSENTIAL OILS FROM FROZEN LEMON PEELS USING LIQUEFIED DIMETHYL ETHER

Ayano Nakamura, Yuki Hara and Tomonori Kawano[*1]
[1] Graduate School of Environmental Engineering, The University of Kitakyushu, Japan

ABSTRACT

Essential oils (EOs) can be obtained from specific plant organs/tissues such as flower petals and fruit peels in specific species such as rose and citruses. Bulky plant tissues are often required for extraction of, even a single drop of, an EO. Use of an organic solvent such as hexane is one of commonly employed protocols for extraction of EOs. In this case, heat- and vacuum-enhanced separation of EOs from the recovered solvent is required. However, some EOs are sensitive to heat and thus it is favorable to complete the all extraction procedures under controlled low-temperature conditions. In the last decade, dimethyl ether (DME), use of a novel organic solvent substitute, which can be liquefied from gaseous form under low temperature or high pressure has been proposed. Since the liquefied DME behaves similarly to most organic solvents, one may expect that it could be used for extraction of EOs from plant tissues under freezing temperature. Here, we performed the extraction of EOs from flavedo (yellow colored outer peels) of lemon using liquefied DME. The favedo slices (20 gfw) were sealed inside the pressure-resistant extraction chamber kept at -30°C, with *ca*. 50 g of liquefied DME, for 2 to 24 hrs. After fifth renewal of the solvent, 41 mg/gfw tissue of crude EOs were obtained. The major components in DME-extracted crude EOs from lemon peel were determined and quantified with GC-MS/GC-FID, to be limonene (40.4%, w/w), β-pinene (10.4%, w/w), and γ-terpinene (6.9 %, w/w).

Keywords: extraction, dimethyl ether, DME, frozen plant tissues, lemon peels

INTRODUCTION

Dimethyl ether (DME), which is the simplest ether with the formula CH_3OCH_3, is well-known as a useful precursor to other organic chemicals such as liquefied petroleum gas (LPG) [1], [2] and low molecular hydrocarbons [3] by catalytic systems [4]-[6]. Today, DME is also known as an alternative fuel replacing the roles for conventional diesel fuels [7]. In addition to the diesel engine, many types of gas turbines and petrol engines can be fuelled with DME through high-efficiency combustion with reduced emission of NO_x, SO_x, and particulate matter [8]. Furthermore, efficient reformation of DME into H_2 gas at low temperatures can be achieved [8]. While various fuels have serious issues with toxicity, production, infrastructure, or transportation, DME does not seem to have any such problem [8].

Apart from its use as a fuel or a precursor to other organic chemicals, liquefied form or subcritical form of DME attracts the attentions by scientists and engineers since DME in these forms behaves as an solvent. Accordingly, subcritical DME acts as an effective media for extraction of medicinal, flavoring and pungent agents from spices such as ginger, black pepper, and chili powder [9]. In addition, DME can be used as a low-temperature extraction solvent applicable to laboratory procedures for extraction of bio-oils from food wastes such as rice brans [10], pigments from plant tissues [11], and some organic molecules from algal green mass[12], [13].

Citrus fruits form a group of major pomological products cultivated in Japan [14]. Next to the fresh use, citrus fruits are used primarily in juice production [15]. As a results, a huge amount of citrus residues chiefly peels are discarded although citrus peels still have useful components such as essential oils (EOs) and vitamin C [16]. Accordingly, disposal of citrus peels requires the removal of a large amount of water that contained in peels [17]. Therefore, dewatering and extraction of useful components from citrus peels must be performed at once. In fact, liquefied DME can be also used as a dewatering solvent actively removing watery phase from plant tissues [18].

Generally, EOs in citrus peels can be obtained by cold-press or steam distillation method. However, there are problems in both procedures. The yield of EOs in cold-press is likely low because many EOs reminds in citrus peels [19]. By steam distillation method, the components of EOs are readily modified by heat because the method is often carried out at high temperature between 130 and 150℃. On the other hand, during the extraction of oils using liquefied DME, the solvent can be evaporated without heating [12], [13]. Therefore, the use of liquefied DME is one of the most attractive approaches for extraction of EOs.

In the present study, we attempted to develop a

simple protocol for extraction of EOs using low-temperature liquefied DME. Frozen lemon peel (flavedo) was chosen as a model plant material for extractions of EOs.

MATERIALS AND METHODS

Handling of DME was basically achieved according to [10]. With some modifications, batch-type extraction system was employed here. The system consisted of a DME cryo-liquefaction unit and an extraction unit. The DME cryo-liquefaction unit consisted of DME gas cylinder obtained from a local gas vender (Air-Gases Kitakyushu Inc.) and cooling units (liquid collection cylinder incubated with ice (Fig. 1).

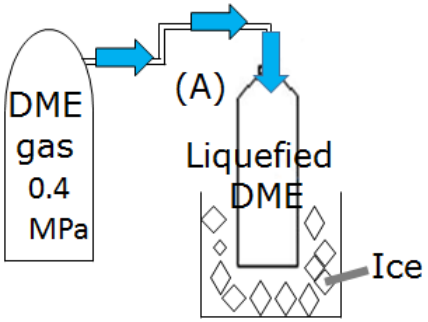

Fig. 1 Equipments for Cryo-liquefaction of DME.

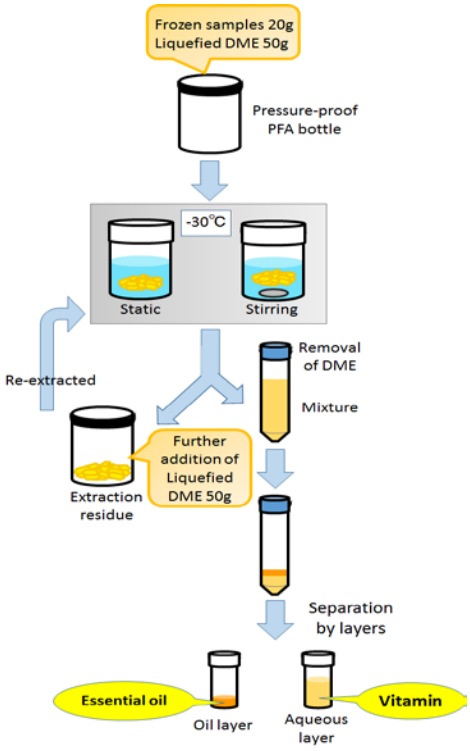

Fig. 2 Procedures for cryo-liquefied DME-based dewatering and extraction of biological components from plant materials. When required, extraction by DME should be repeated until the completion of extraction process.

Supply of gaseous DME was made through aluminum capillaries at 0.5 MPa. Then cryo-liquefied DME was supplied to the pressure-proof bottles made of PFA (Tetrafluoroethylene-perfluoroalkyl vinyl ether copolymer) resin used as the extraction unit (Fig. 2, Fig. 3B). Within the extraction unit, a magnetic stirring bar was used for enhancing the extraction process when required.

Extraction and separation of oily phase and watery phase were performed as illustrated in Fig. 2. Here, lemon peels were used as model plant materials. Lemon fruits were purchased at a local market in Kitakyusyu city.

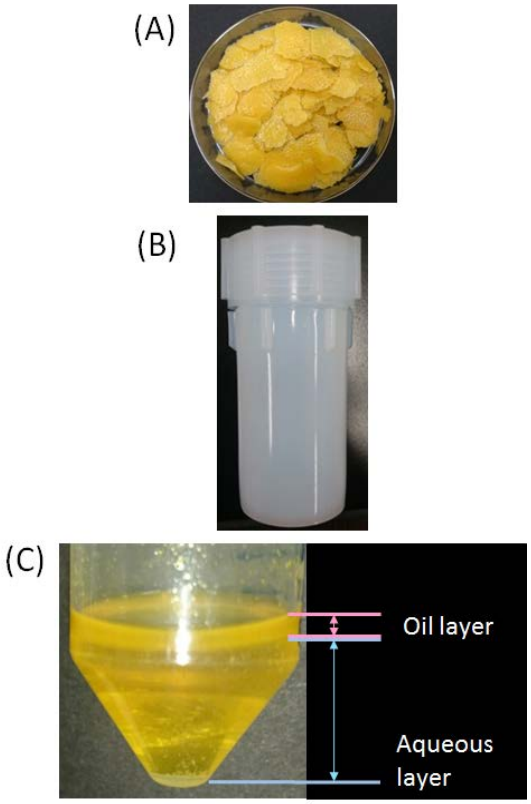

Fig. 3 Extraction of EOs from lemon peels (flavedo) under -30°C. (A) Excised lemon peels used here. (B) Pressure-proof PFA bottle. (C) Layer of EOs above aqueous layer obtained after extract of total liquefied cold DME.

RESULTS AND DISCUSSION

We have chosen the frozen lemon peels as model materials for performing the extraction of EOs using liquefied DME.

Extraction of EOs from the lemon peels was successfully performed at cryo-preservative condition at -30˚C (Fig. 3). We performed the

extraction of EOs from flavedo (yellow colored outer peels) of lemon using liquefied DME. The favedo slices (20 gfw) were sealed inside the pressure-resistant extraction chamber kept at -30°C, with ca. 50 g of liquefied DME, for 2 to 24 hrs.

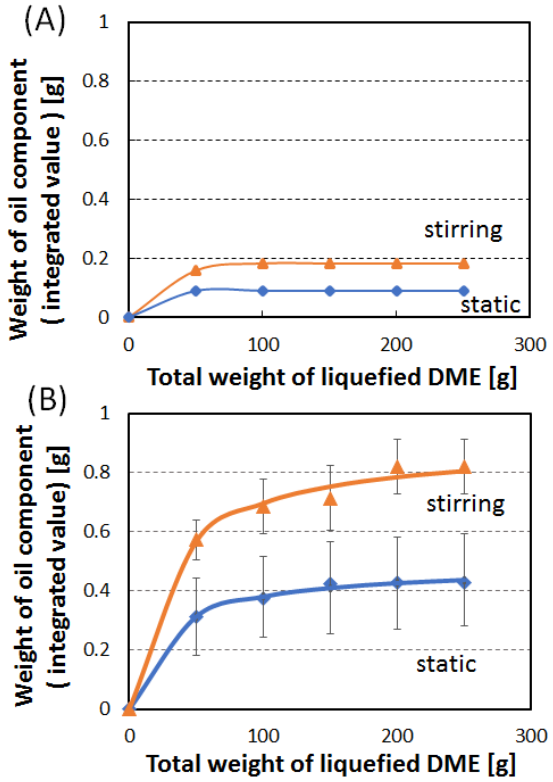

Fig. 4 The amount (weight) of EOs extracted from 20g of frozen lemon peels using cold liquefied DME. (A) Extraction in 2 hours. (B) Extraction in 24 hours.

Analysis of EO components using GC-MS and GC-FID was outsourced to the Mie Prefecture Environmental Conservation. The major components in DME-extracted crude EOs from lemon peel were determined and quantified with GC-MS/GC-FID to be limonene (40.4%, w/w), β-pinene (10.4%, w/w), and γ-terpinene (6.9 %, w/w) as shown in Fig. 5.

CONCLUSION

In the present study, extraction of EOs from frozen lemon peels accompanying the dewatering process using cold liquefied DME was performed.

ACKNOWLEDGEMENTS

This work was supported by a grant of Regional Innovation Strategy Support Program implemented by Ministry of Education, Culture, Sports, Science and Technology (MEXT), Japan; and also by a grant from Tonen General Sekiyu Research/Development Encouragement & Scholarship Foundation.

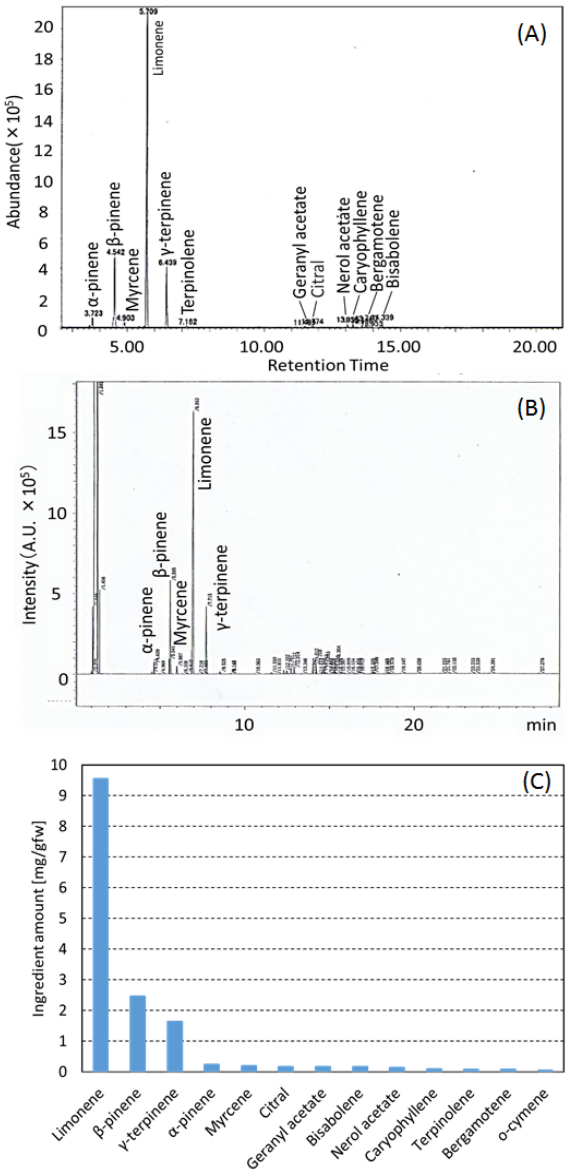

Fig. 5 Composition of lemon peel EOs extracted with cold liquefied DME. Chromatograms for DME-extracted lemon EOs after GC-MS (A) and GC-FID (B) are shown. Yield of EOs in lemon peel extracts are summarized (C).

REFERENCES

[1] Jin, Y., Asaoka, S., Li, X., Asami, K., and Fujimoto, K. “Synthesis of liquefied petroleum gas via methanol/dimethyl ether from natural gas.”, Fuel Processing Technol. 85, 2004 pp. 1151-1164.

[2] Zhu, W., Li, X., Kaneko, H. and Fujimoto, K., “LPG synthesis from DME with semi-direct method”, Studies of Surface Science and Catalysis, Vol. 167, 2007, pp.355-360

[3] Zhu, W., Li, X., Kaneko, H. and Fujimoto, K., "Selective transformation of dimethyl ether into small molecular hydrocarbons over large-pore beta zeolite.", Catalysis Letter, 120(1-2), 2008, pp. 95-99.
[4] Shikada, T., Fujimoto, K., Miyauchi, M. and Tomonaga, H. "Vapor phase carbonylation of dimethyl ether and methyl acetate with nickel-active carbon catalysts.", Appl. Catalysis 7 , 1983, pp. 361-368.
[5] Fujimoto, K., Asami, K., Shikada, T. and Tomonaga, H. "Selective synthesis of dimethyl ether from synthesis gas.", Chem. Lett. 13, 1984, pp. 2051-2054.
[6] Yagita, H., Asami, K., Muramatsu, A. and Fujimoto, K. "Oxidative dimerization of dimethyl ether with solid catalysts.", Appl. Catalysis 53, 1989, pp. 5-9.
[7] Gupta, K., Rehman, A. and Sarviya R., "Bio-fuels for the gas turbine: A review.", Renew. Sustain. Ener. Rev., 14, 2010, pp. 2946.
[8] Semelsberger, T. A., Borup, R. L., and Greene, "Dimethyl ether (DME) as an alternative fuel.", H. L. J. Power Sources 156, 2006, pp. 497-511.
[9] Catchpole, O. J., Grey, J. B., Perry, N. B., Burgess, E. J., Redmond, W. A. and Porter, N., "Extraction of Chili, Black Pepper, and Ginger with Near-Critical CO2, Propane, and Dimethyl Ether: Analysis of the Extracts by Quantitative Nuclear Magnetic Resonance.", J. Agric. Food Chem., 51, 2003, pp.4853.
[10] Hara, Y., Kikuchi, A., Noriyasu, A., Furukawa, H., Takaichi, H., Inokuchi, R., Bouteau, F., Chin, S., Li X., Nishihama, S., Yoshizuka, K., and Kawano, T., "Batch extraction of oil from rice bran with liquefied low temperature dimethyl ether.", Solv. Extr. Res. Dev. Japan 23(1), 2016, pp. 87-99.
[11] Noriyasu, A., Kikuchi, A., Furukawa, H., Takaichi, H., Bouteau, F., Li X., Nishihama, S., Yoshizuka, K., and Kawano, T. "Use of liquefied cold temperature dimethyl ether for extraction of pigments from fresh vegetable tissues.", Adv. Hort. Sci. 29, 2015, pp. 48-52.
[12] Kanda, H. and Li, P., "Simple extraction method of green crude from natural blue-green microalgae by dimethyl ether.", Fuel 90, 2011, pp. 1264-1266.
[13] Kanda, H. and Makino, H., "Energy-efficient coal dewatering using liquefied dimethyl ether.", Fuel, 89, 2010, pp. 2104–2109.
[14] Yamamoto M., "Progress on studies for seedless breeding of critus in Japan.", Adv. Hort. Sci. 28, 2014, pp. 64-72.
[15] Sudo, M., "Current trends and issues with citrus extraction in Ehime.", Nippon Shokuhin Kagaku Kogaku Kaishi 61, 2014, pp. 382-385.
[16] Mandalari G., Bennett R., Bisignano G., Saija A., Dugo G., et al., "Characterization of flavonoids and pectins from bergamot (Citrus bergamia Risso) peel, a major byproduct of essential oil extraction.", J Agric Food Chem 54, 2006, pp. 197-203
[17] Braddock, R. and Crandall, P., "Properties and recovery of waste liquids from citrus pectin pomace manufacture.", J Food Sci 43, 1978, pp. 1678-1679
[18] Furukawa, H., Kikuchi, A., Noriyasu, A., Bouteau, F., Nishihama, S., Yoshizuka, K., Li X., and Kawano, T., "Use of liquefied dimethyl ether for the extraction of proteins from vegetable tissues.", Solv. Extr. Res. Dev. Japan 23, 2016, 127-135.
[19] Suetsugu T., Tanaka M., Iwai H., Matsubara T., Kawamoto Y., et al., "Supercritical CO2 extraction of essential oil from Kabosu (Citrus sphaerocarpa Tanaka) Peel.", Flavour 2, 2013, pp. 18.

Second International Conference on Science, Engineering & Environment,
Osaka City, Japan, Nov.21-23, 2016, ISBN: 978-4-9905958-7-6 C3051

ELECTROCHEMICAL TECHNIQUE FOR 1,3-DICHLORO-2-PROPANOL ANALYSIS

Kanokwan Rudisirisak, Nittaya Ngowattana
Department of Chemistry, Faculty of Science and Technology Rajamangala University of Technology, Thunyaburi, Pathumthani, Thailand.
kanokwan_r@rmutt.ac.th, nittaya_n@rmutt.ac.th

ABSTRACT

Soy sauce is widespread as food seasoning for many type of food, especially Thai and Chinese food. Vegetable acid hydrolysis is the rapid process for seasoning production, but the process cause toxic contaminants such as 3-MCPD and 1,3-DCP that are the epichlorohydrin group. In soy sauce, 1,3-DCP is lower than 3-MCPD in ratio 1:20, so we decided to examine 1,3-DCP. The normal method to analyse 1,3-DCP is GC-MS technique that is high expense, using high purified sample and taking a long time. Our purpose was to reduce expenses and time. Therefore, this research focused on improvement of 1,3-DCP analysis methodology by using electrochemical technique. We produced the carbon paste electrode and used as working electrode. We studied the suitable condition for analysis by using voltammetry technique; electric potential and NaOH in oxidation reaction of 1,3-DCP; and amperometry technique; interval time of reaction at electrode surface(5 and 10 minutes), stirring rate(100,300 and 500 rpm). It was found that the electric potential and the interval time of oxidation reaction for 1,3-DCP analysis were 1.33 V. and 5 minutes interval, respectively. Moreover, we found that 4.0 M NaOH and 100 rpm stirring rate were suitable for this analysis. The result of our research were 0.02 mg/dm^3 of detection limit, 81.27 % recovery, 13.339 ppm of sensitivity, 0.67-4.67 ppm of linear range, 6.95 % RSD of solution preparation, 3.95 % RSD of injection and 5.15 % RSD of produced working electrode.

Keywords: 1,3 Dichloro-2-propanol, Soy sauces, Electrochemical technique, halohydrin, ephichlorohydrin,

INTRODUCTION

Seasoning sauce is produced by acid hydrolyzed vegetable protein [1] that is defat by hydrochloric acid at high temperature. The production process cause the concentration of chloropropanol compounds for example 3-monocholropropane1,2-diol (3-MCPD) and 1,3-Dichloropropanol (1,3-DCP), that are toxic and carcinogen.[6] 1,3-DCP and 3-MCPD have been found in soy sauce and other seasoning sauce. When 3-MCPD were co-occurred in sauce, the amount of 3-MCPD was always higher than that of 1,3-DCP by ratio 3-MCPD:1,3-DCP was 20:1. Therefore, if we found 1,3-DCP in sauce we could find 3-MCPD too. 1,3-DCP is usually analyse by GC-MS.[4] This research was interested to use electrode technique to analyse 1,3-DCP. So,we initiated this technique using carbon paste electrode to examine the reaction capacity.

EXPERIMENT

Reagent and Materials

1,3-Dichloropropanol (1,3-DCP) 98 % and other reagent were purchased from Aldrich. All the solutions were prepared with analytical grade reagents and Milli-Q water

Electrode preparation

The working electrode was prepared by thoroughly hand-mixing 5 g graphite powder and 1mL of silicone oil in a mortar with pestle. This paste was placed in a cavity on electrode body (glass tube ϕ 5 mm) in contact with a copper wire and smoothed on clean paper until it had a shiny appearance.

Apparatus

All voltammetric measurements were performed using VA Stand 663 Voltametric analyzer (Metrohm,Herisau,Switzerland),Potentiostat (Autolab model PGSTAT 20). Three electrodes assembly cell consisted of carbon paste electrode as working electrode, an Ag/AgCl in 3 mole/L KCl as a reference electrode and platinum wire as an auxiliary electrode.

Procedure

Cyclic voltammetry of 1,3-DCP

To consider the suitable potential in oxidation-reduction reaction.

To examine the effect and concentration of sodium hydroxide to oxidation current.

Amperometric Determination of 1,3-DCP

Effect of time and rotation rate in 1,3-DCP analysis.

Analytical parameters for 1,3-DCP determinations

Detection limit, % recovery, sensitivity, linear range, % RSD of injection and % RSD of produced working electrode.

RESULTS AND DISCUSSION

Cyclic voltammetry of 1,3-DCP

The suitable potential in oxidation-reduction.

It was found that cyclic voltammogram of 2,000 ppm of 1,3-DCP as it clear in the Fig1. the complete disappearance of oxidation and reduction peak**.**

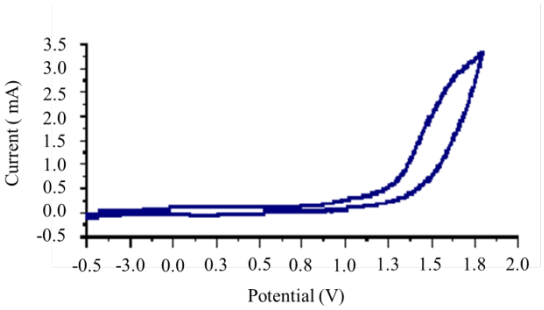

Fig. 1 Cyclic voltammogram of 2,000 ppm 1,3-DCP in water on carbon paste electrode with condition : scan range from -0.5 to 2.0 V, scan rate of 1 V/sec.

The halohydrin react with sodium hydroxide solution to cause an epoxide [9] 1,3-DCP is one of halohydrin compound, so it can reacts with sodium hydroxide to produce epichlorohydrin sodium chloride and water. The reaction can be observed from the following equation [10].

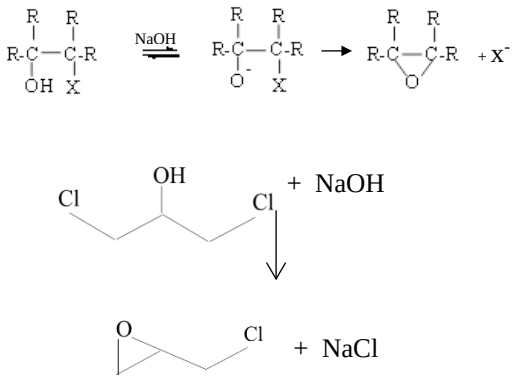

The effect and concentration of sodium hydroxide to oxidation current

Cyclic voltammogram showed the peak anodic current of 2,000 ppm 1,3-DCP in 0.1 M NaOH solution on carbon paste electrode between -0.5 to 2.0 V with scan rate of 1V/sec. The anodic current peak present about 1.45 V as shown in Fig.2 [3]

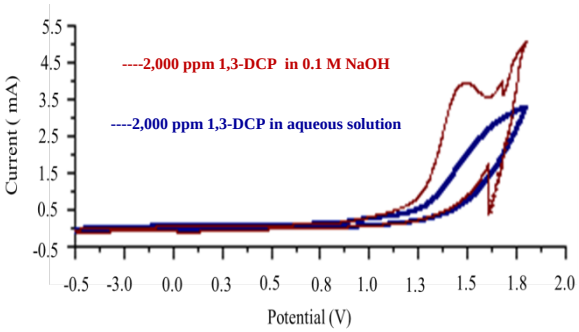

Fig.2 Cyclic voltammogram of 2,000 ppm 1,3-DCP on carbon paste electrode with condition : scan range from -0.5 to 2.0 V,Scan rate of 1 V/sec, with NaOH (red line) and without NaOH (Blue line).

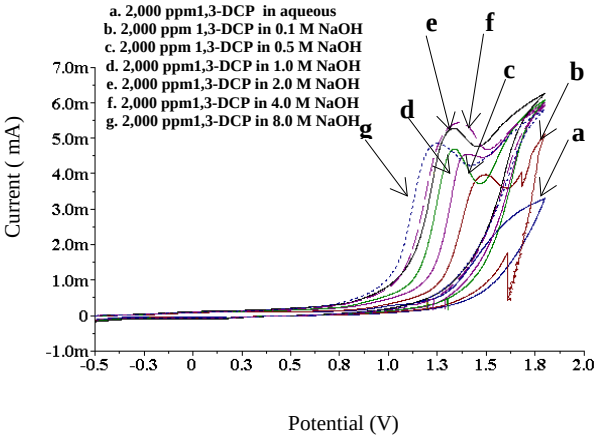

(a.)

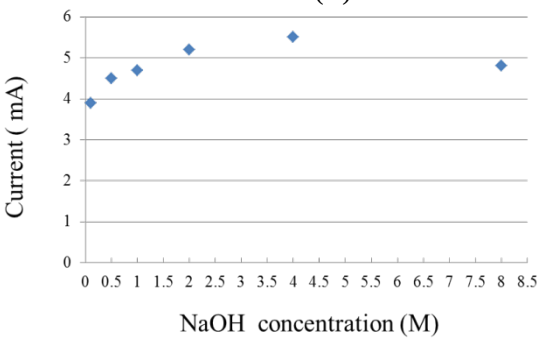

(b.)

Fig.3 (a) The cyclic voltammograms on carbon paste electrode of 2,000 ppm 1,3-DCP in different concentrations of NaOH on carbon paste electrode with condition : scan range from -0.5 to 2.0 V scan rate of 1V/sec.

(b) Maximum current of 0.1-8.0 M NaOH

Cyclic voltammogram of 2,000 ppm.1,3-DCP in 0.1-8.0M NaOH showed oxidation peak that changed in range 1.3-1.5 V. The effect of sodium hydroxide concentration observed through oxidation current as shown in Fig.3(a).

Fig.3(b) showed the comparison between the highest current and 0.1-8.0 M NaOH. We found that the optimum concentration of sodium hydroxide induced anodic current was 4.0 M while potential was fixed throughout at 1.3 V for amperometric experiment.

Amperometric Determination of 1,3-DCP

Fig.4(a,b)showed that the amperometric response obtained by continuous addition 10 µL 20,000 ppm of 1,3-DCP in 4 M NaOH into reservoir at 5 and 10 minute interval, respectively. We found that the sensitivity of the two intervals was nearby, but the r^2 of 5 minute interval was higher than r^2 of 10 minute interval as shown in Fig 4.(c) Therefore we selected the 5 interval for next experiment.

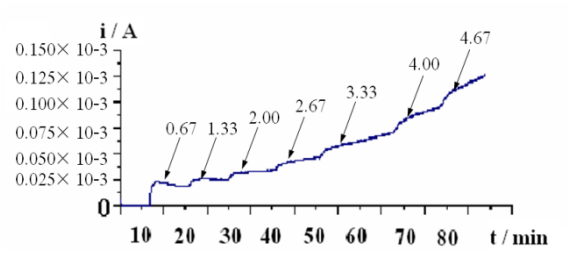

(a) 5 min interval

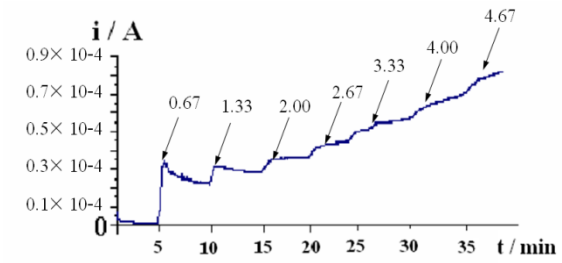

(b) 10 min interval

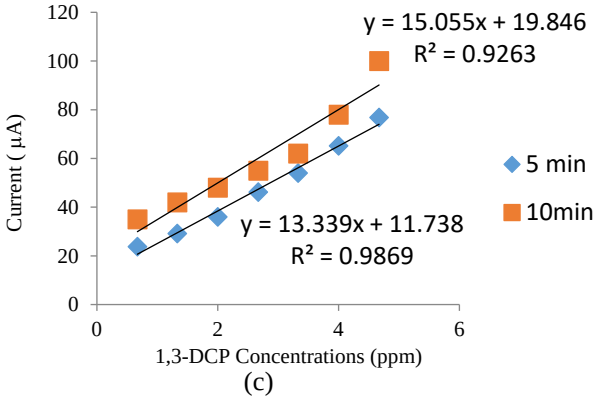

(c)

Fig.4 Amperometric response and analytical curve obtained for 5 and 10 minute addition intervals of 1,3-DCP 20,000 ppm. Experimental conditions: E = 1.3 V, rotation speed 100 rpm .

Amperometric response of continuous addition 1,3-DCP 20,000 ppm at 5 minutes interval using 100 200 and 300 rpm rotation speed. We found that the 100 rotation speed was the highest sensitivity as shown in Fig. 4

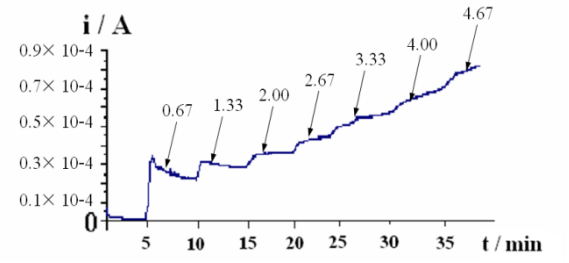

(a) 100 rpm

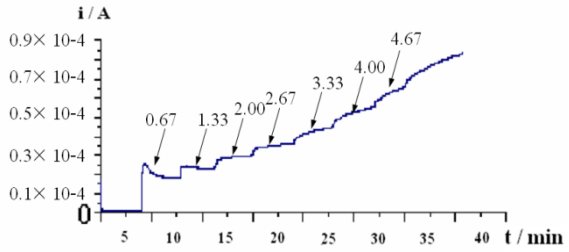

(b) 200 rpm

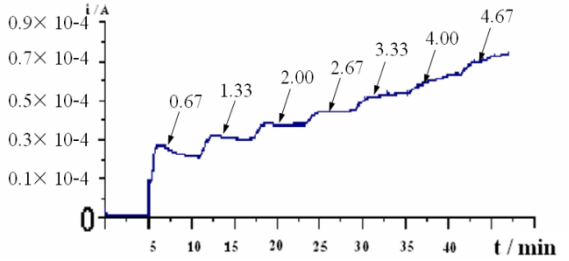

(c) 300 rpm

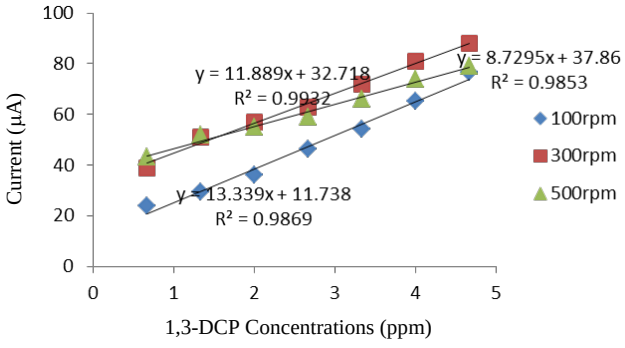

(d)

Fig.5 Amperometric response of continuous addition 1,3-DCP 20,000 ppm at 5 minutes interval, E=1.3 V using 100 200 and 300 rpm rotation speed.

Analytical parameters for 1,3-DCP determinations

The suitable conditions of experiment were 5 minutes interval of addition 1,3-DCP and 4 M

NaOH, appling potential 1.3 V and 100 rpm rotation speed. The results were 0.02 ppm of detection limit, 81.27% recovery, 13.339 ppm of sensitivity, 0.67-4.67 ppm of linear range, 6.95% RSD of solution preparation, 3.95% RSD of injection and 5.15% RSD of produced working electrode.

This experiment could detect 1,3-DCP at 0.02 ppm that was lower than detection in ppb level by GC-MS Headspace.[7]. Contamination amount of 1,3-DCP that is allowed in Thailand is 1 ppm. LOD of 1,3-DCP in this experiment was 0.02 ppm, so we can examine 1,3-DCP and 3-MCPD in other samples because 1,3-DCP was found 20-fold less than 3-MCPD. However we expect to use other materials, such as Glossy carbon, as working electrode to improve result.

CONCLUSION

In this research we could analyse 1,3-DCP by using reaction of halohydrin to epoxide that caused anodic current and then detected with electrochemical technique.

REFERENCES

[1] Wenzl et al.(2007) " 1,3-dichloro-2-propanol",IARC monographs, 375-390.

[2] Eduardo Vicente, et al. "Level of 3-monochloro propane-1,2-diol (3-MCPD) in selected processed food from the Brazilian market", Food Research International. 77 (2015) 310-314.

[3] Kwok Onn Wong,et al..3-monochloprpane-1,2-diol (3-MCPD) in soy and oyster sauces: Occurrence and dietary in take assessment. doi:10.1016/i.foodcont.005.01.010.

[4] Jeong,JH,Sin et al.(2007).1,3-dichloro-2-propanol induced cell damage.J Environ Sci (China),16:229-225.

[5] Abu-EI-Haj S, Bogusz Mj, Ibrahim Z et al.(2007).Rapid and simple determination of chloropropanols (3-MCPD and 1,3-DCP) in food products using isotope dilution GC-MS.Food Contr,18 :81-90.

[6] Scott A. " 1,3-Dichloro -2-propanol Review of Toxicology". Interated Laboratory System, Inc. Research Triangle Park. North Carolina,2005.

[7] Hasnip S. et al. " Determination of 1,3-Dichloropropanol in soy sauce and related products by headspace gas chromatography with mass spectrometric detection inter-laboratory study J AOAC Int. 2005 Sep-Oct;88(5):1404-12.

[8] Food and drug administration,Thailand , http://www.smelawservice.com/service/128/ (25 January 2013).

[9] William H.Brown,Brent L.lverson,Eric Anslyn, Chistopher S. Foote.organic chemistry. ForoMac.com ISBN:1285426509.

[10]Naoya Kansai, Toshio Suzuki, Yoshiro Furukawa. "Chiral C3 epoxides and halohydrin : Their preparation and synthetic application Journal of Molecular Catalysis B:Enzymatic. 1998, vol.4(5) :237-352.

Second International Conference on Science, Engineering & Environment,
Osaka City, Japan, Nov.21-23, 2016, ISBN: 978-4-9905958-7-6 C3051

SOME PROPERTIES OF THE PRODUCT OF (P,Q) – FIBONACCI AND (P,Q) - LUCAS NUMBER

Alongkot Suvarnamani * and Mongkol Tatong
Faculty of Science and Technology, Rajamangala University of Technology Thanyaburi, Thailand
*E-mail address: kotmaster2@rmutt.ac.th

ABSTRACT

Some mathematicians study the basic concept of the generalized Fibonacci sequence and Lucas sequence which are the (p,q) – Fibonacci sequence and the (p,q) – Lucas sequence. For example, Singh, Sisodiya and Ahmad studied the product of the k-Fibonacci and k-Lucas numbers. Moreover, Suvarnamani and Tatong showed some results of the (p; q) - Fibonacci number. They found some properties of the (p,q) – Fibonacci number and the (p,q) – Lucas number. There are a lot of open problem about them. Moreover, the example for the application of the Fibonacci number to the generalized function was showed by Djordjevicand Srivastava. In this paper, we consider the (p,q) – Fibonacci sequence and the (p,q) – Lucas sequence. We used the Binet's formulas to show that some properties of the product of the (p,q) – Fibonacci number and the (p,q) – Lucas number. We get some generalized properties on the product of the (p,q) – Fibonacci number and the (p,q) – Lucas number.

Keywords: Fibonacci sequence, Lucas sequence, (p,q) – Fibonacci number, (p,q) – Lucas number, Binet's formula

INTRODUCTION

Koshy [6] and Vajda [10] explained the Fibonacci number and Lucas number in their comprehensive works. The Fibonacci number F_n is the term of the sequence $\{F_n\}$ where each term is the sum of the two previous terms beginning with the initial values $F_0 = 0$ and $F_1 = 1$. The Fibonacci sequence $\{F_n\}$ is $\{0,1,1,2,3,5,8,...\}$. The Lucas number L_n is the term of the sequence $\{L_n\}$ where each term is the sum of the two previous terms beginning with the initial values $L_0 = 2$ and $L_1 = 1$. The Lucas sequence $\{L_n\}$ is $\{2,1,3,4,7,11,18,...\}$.

Falcon and Plaza [2] introduced the k-Fibonacci sequence $\{F_{k,n}\}$ which is defined as $F_{k,0} = 0$, $F_{k,1} = 1$ and $F_{k,n+1} = kF_{k,n} + F_{k,n-1}$ for $k \geq 1$ and $n \geq 1$. If $k = 1$, we get the classical Fibonacci sequence $\{0,1,1,2,3,5,8,...\}$. And we get the Pell sequence $\{0,1,2,5,12,29,70,...\}$ for $k = 2$.

Falcon [5] studied the k-Lucas sequence $\{L_{k,n}\}$ which is defined as $L_{k,0} = 0$, $L_{k,1} = 1$ and $L_{k,n+1} = kL_{k,n} + L_{k,n-1}$ for $k \geq 1$ and $n \geq 1$. If $k = 1$, we get the classical Lucas sequence $\{2,1,3,4,7,11,18,...\}$. If $k = 2$, we get the Pell-Lucas sequence $\{2,2,6,14,34,82,198,...\}$.

The Binet's formulas for k - Fibonacci and k - Lucas numbers, see [1, 2, 5], are given by $F_{k,n} = \frac{r_1^n - r_2^n}{r_1 - r_2}$ and $L_{k,n} = r_1^n + r_2^n$ where $r_1 = \frac{k + \sqrt{k^2+4}}{2}$ and $r_2 = \frac{k - \sqrt{k^2+4}}{2}$ are roots of the characteristic equation $r^2 - kr - 1 = 0$. We note that $r_1 + r_2 = k$, $r_1 r_2 = -1$ and $r_1 - r_2 = \sqrt{k^2+4}$.

In 2007, Falcon and Plaza [3] studied the k-Fibonacci sequence and the Pascal 2-triangle. Next, they considered the 3-dimensional k-Fibonacci spiral in [4]. Then Thongmoon [8,9] found some properties of the Fibonacci and Lucas numbers in 2009. In 2014, Singh, Sisodiya and Ahmad [7] studied the product of the k-Fibonacci and k-Lucas numbers.

In 2015, Suvarnamani and Tatong [11] showed some results of the (p,q)-Fibonacci number. Next Suvarnamani [12] proved some properties of the (p,q)-Lucas number in 2016. Moreover Raina and Srivastava [13] showed a class of numbers

associated with the Lucas number in 1997. Moreover, the example for the application of the Fibonacci number to the generalized function was showed by Djordjevic and Srivastava [14] in 2006. In this paper, we find some properties of the product of (p,q) Fibonacci and (p,q) Lucas numbers.

THEORITICAL BACKGROUND

1. The (p,q) - Fibonacci number

The (p,q) - Fibonacci sequence $\{F_{p,q,n}\}$ is defined as $F_{p,q,0}=0$, $F_{p,q,1}=1$ and $F_{p,q,n}=pF_{p,q,n-1}+qF_{p,q,n-2}$ for $p\geq 1$, $q\geq 1$ and $n\geq 2$. So, the (p,q) - Fibonacci number is the each term of the (p,q) - Fibonacci sequence.

2. The (p,q) - Lucas number

The (p,q) - Lucas sequence $\{L_{p,q,n}\}$ is defined as $L_{p,q,0}=2$, $L_{p,q,1}=p$ and $L_{p,q,n}=pL_{p,q,n-1}+qL_{p,q,n-2}$ for $p\geq 1$, $q\geq 1$ and $n\geq 2$. So, the (p,q) - Lucas number is the each term of the (p,q) - Lucas sequence.

3. The Binet's formula

The Binet's formula for (p,q) - Fibonacci number $F_{p,q,n}$ is given by $F_{p,q,n}=\frac{r_1^n-r_2^n}{r_1-r_2}$ where $r_1=\frac{p+\sqrt{p^2+4q}}{2}$ and $r_2=\frac{p-\sqrt{p^2+4q}}{2}$ are roots of the characteristic equation $r^2-pr-q=0$. And the Binet's formula for (p,q) - Lucas number $L_{p,q,n}$ is given by $L_{p,q,n}=r_1^n+r_2^n$. We note that $r_1+r_2=p$, $r_1r_2=-q$ and $r_1-r_2=\sqrt{p^2+4q}$. We prove the Binet's formulas for (p,q) - Fibonacci number and (p,q) - Lucas number by mathematical induction.

THE PRODUCT OF (P,Q) - FIBONACCI NUMBER AND (P,Q) - LUCAS NUMBER

Theorem 1. Suppose that p, q, m and n be positive integers. We get

$$F_{p,q,m+n}L_{p,q,m}=F_{p,q,2m+n}+(-q)^mF_{p,q,n}.$$

Proof. Let p, q, m and n be positive integers. We have

$$\begin{aligned}
&F_{p,q,m+n}L_{p,q,m}\\
&=\left(\frac{r_1^{m+n}-r_2^{m+n}}{r_1-r_2}\right)\left(r_1^m+r_2^m\right)\\
&=\frac{r_1^{2m+n}-r_2^{2m+n}+r_1^{m+n}r_2^m-r_1^mr_2^{m+n}}{r_1-r_2}\\
&=\frac{r_1^{2m+n}-r_2^{2m+n}+(r_1r_2)^m\left(r_1^n-r_2^n\right)}{r_1-r_2}\\
&=\frac{r_1^{2m+n}-r_2^{2m+n}}{r_1-r_2}+(r_1r_2)^m\left(\frac{r_1^n-r_2^n}{r_1-r_2}\right)\\
&=F_{p,q,2m+n}+(-q)^mF_{p,q,n}.
\end{aligned}$$

□

Theorem 2. Suppose that p, q, m and n be positive integers. We get

$$F_{p,q,m}L_{p,q,m+n}=F_{p,q,2m+n}-(-q)^mF_{p,q,n}.$$

Proof. Let p, q, m and n be positive integers. We have

$$\begin{aligned}
&F_{p,q,m}L_{p,q,m+n}\\
&=\left(\frac{r_1^m-r_2^m}{r_1-r_2}\right)\left(r_1^{m+n}+r_2^{m+n}\right)\\
&=\frac{r_1^{2m+n}-r_2^{2m+n}-r_1^{m+n}r_2^m+r_1^mr_2^{m+n}}{r_1-r_2}\\
&=\frac{r_1^{2m+n}-r_2^{2m+n}-(r_1r_2)^m\left(r_1^n-r_2^n\right)}{r_1-r_2}\\
&=\frac{r_1^{2m+n}-r_2^{2m+n}}{r_1-r_2}-(r_1r_2)^m\left(\frac{r_1^n-r_2^n}{r_1-r_2}\right)\\
&=F_{p,q,2m+n}-(-q)^mF_{p,q,n}.
\end{aligned}$$

□

Theorem 3. Suppose that p, q, m and n be positive integers where $m>n$. We get

$$F_{p,q,m-n}L_{p,q,m+n}=F_{p,q,2m}-(-q)^{m-n}F_{p,q,2n}.$$

Proof. Let p, q, m and n be positive integers where $m>n$. We have

$$\begin{aligned}
&F_{p,q,m-n}L_{p,q,m+n}\\
&=\left(\frac{r_1^{m-n}-r_2^{m-n}}{r_1-r_2}\right)\left(r_1^{m+n}+r_2^{m+n}\right)
\end{aligned}$$

$$= \frac{r_1^{2m} - r_2^{2m} - r_1^{m+n} r_2^{m-n} + r_1^{m-n} r_2^{m+n}}{r_1 - r_2}$$

$$= \frac{r_1^{2m} - r_2^{2m} - (r_1 r_2)^{m-n} (r_1^{2n} - r_2^{2n})}{r_1 - r_2}$$

$$= \frac{r_1^{2m} - r_2^{2m}}{r_1 - r_2} - (r_1 r_2)^{m-n} \left(\frac{r_1^{2n} - r_2^{2n}}{r_1 - r_2} \right)$$

$$= F_{p,q,2m} - (-q)^{m-n} F_{p,q,2n} .$$

□

Theorem 4. Suppose that p, q, m and n be positive integers where $m > n$. We get

$$F_{p,q,m+n} L_{p,q,m-n} = F_{p,q,2m} + (-q)^{m-n} F_{p,q,2n} .$$

Proof. Let p, q, m and n be positive integers where $m > n$. We have

$$F_{p,q,m+n} L_{p,q,m-n}$$

$$= \left(\frac{r_1^{m+n} - r_2^{m+n}}{r_1 - r_2} \right) \left(r_1^{m-n} + r_2^{m-n} \right)$$

$$= \frac{r_1^{2m} - r_2^{2m} + r_1^{m+n} r_2^{m-n} - r_1^{m-n} r_2^{m+n}}{r_1 - r_2}$$

$$= \frac{r_1^{2m} - r_2^{2m} + (r_1 r_2)^{m-n} (r_1^{2n} - r_2^{2n})}{r_1 - r_2}$$

$$= \frac{r_1^{2m} - r_2^{2m}}{r_1 - r_2} + (r_1 r_2)^{m-n} \left(\frac{r_1^{2n} - r_2^{2n}}{r_1 - r_2} \right)$$

$$= F_{p,q,2m} + (-q)^{m-n} F_{p,q,2n} .$$

□

Theorem 5. Suppose that p, q, m and n be positive integers where $n > k$. We get

$$F_{p,q,m+n} L_{p,q,m+k} = F_{p,q,2m+n+k} + (-q)^{m+k} F_{p,q,n-k} .$$

Proof. Let p, q, m and n be positive integers where $n > k$. We have

$$F_{p,q,m+n} L_{p,q,m+k}$$

$$= \left(\frac{r_1^{m+n} - r_2^{m+n}}{r_1 - r_2} \right) \left(r_1^{m+k} + r_2^{m+k} \right)$$

$$= \frac{r_1^{2m+n+k} - r_2^{2m+n+k} + r_1^{m+n} r_2^{m+k} - r_1^{m+k} r_2^{m+n}}{r_1 - r_2}$$

$$= \frac{r_1^{2m+n+k} - r_2^{2m+n+k} + (r_1 r_2)^{m+k} (r_1^{n-k} - r_2^{n-k})}{r_1 - r_2}$$

$$= \frac{r_1^{2m+n+k} - r_2^{2m+n+k}}{r_1 - r_2} + (r_1 r_2)^{m+k} \left(\frac{r_1^{n-k} - r_2^{n-k}}{r_1 - r_2} \right)$$

$$= F_{p,q,2m+n+k} + (-q)^{m+k} F_{p,q,n-k} .$$

□

Theorem 6. Suppose that p, q, m and n be positive integers where $n < k$. We get

$$F_{p,q,m+n} L_{p,q,m+k} = F_{p,q,2m+n+k} - (-q)^{m+n} F_{p,q,k-n} .$$

Proof. Let p, q, m and n be positive integers where $n < k$. We have

$$F_{p,q,m+n} L_{p,q,m+k}$$

$$= \left(\frac{r_1^{m+n} - r_2^{m+n}}{r_1 - r_2} \right) \left(r_1^{m+k} + r_2^{m+k} \right)$$

$$= \frac{r_1^{2m+n+k} - r_2^{2m+n+k} + r_1^{m+n} r_2^{m+k} - r_1^{m+k} r_2^{m+n}}{r_1 - r_2}$$

$$= \frac{r_1^{2m+n+k} - r_2^{2m+n+k} + (r_1 r_2)^{m+n} (r_1^{k-n} - r_2^{k-n})}{r_1 - r_2}$$

$$= \frac{r_1^{2m+n+k} - r_2^{2m+n+k}}{r_1 - r_2} + (r_1 r_2)^{m+n} \left(\frac{r_1^{k-n} - r_2^{k-n}}{r_1 - r_2} \right)$$

$$= F_{p,q,2m+n+k} - (-q)^{m+n} F_{p,q,k-n} .$$

□

CONCLUSION

In this paper, we consider the (p,q) – Fibonacci sequence and the (p,q) – Lucas sequence. We used the Binet's formulas to show that some properties of the product of the (p,q) – Fibonacci number and the (p,q) – Lucas number. We get some generalized properties on the product of the (p,q) – Fibonacci number and the (p,q) – Lucas number.

ACKNOWLEDGEMENTS

This research is the part of the project 'Solutions of Diophantine Equations' which was supported the foundation (In 2016) by the Faculty of Sciences and Technology, Rajammangala University of Technology Thanyaburi, Thailand.

REFERENCES

[1] C. Bolat, A. Ipeck and H. Kose, On the Sequence Related to Lucas Numbers and Its Properties, Mathematica Aeterna, Vol. 2, No. 1, 2012, pp. 63-75.

[2] S. Falcon and A. Plaza, On the Fibonacci k-Numbers, Chaos, Solitons and Fractals, Vol. 32, No. 5, 2007, pp. 1615-1624.

[3] S. Falcon and A. Plaza, The k-Fibonacci Sequence and the Pascal 2-Triangle, Chaos, Solitons and Fractals, Vol. 33, No. 1, 2007, pp. 38-49.

[4] S. Falcon and A. Plaza, On the 3-Dimensional k-Fibonacci Spiral, Chaos, Solitons and Fractals, Vol. 38, No. 4, 2008, pp. 993-1003.

[5] S. Falcon, On the k-Lucas Numbers, International Journal of Contemporary Mathematical Sciences, Vol. 6, No. 21, 2011, pp. 1039-1050.

[6] T. Koshy, Fibonacci and Lucas Numbers with Applications, Wiley-Interscience, New York, NY, USA, 2001.

[7] B. Singh, K. Sisodiya and F. Ahmad, On the Product of k-Fibonacci Numbers and k-Lucas Numbers, Chaos, Solitons and Fractals, Vol. 33, No. 1, 2007, pp. 38-49.

[8] M. Thongmoon, Identities for the Common Factors of Fibonacci and Lucas Numbers, International Mathematical Forum, Vol. 4, No. 7, 2009, pp. 303-308.

[9] M. Thongmoon, New Identities for the Even and Odd Fibonacci and Lucas Numbers, International Journal of Contemporary Mathematical Sciences, Vol. 4, No. 14, 2009, pp. 671-676.

[10] S. Vajda, Fibonacci and Lucas Numbers and the Golden Section, Ellis Horwood, Chichester, UK, 1989.

[11] A. Suvarnamani and M. Tatong, Some Properties of (p; q) – Fibonacci Numbers, Science and Technology RMUTT Journal, Vol. 5, No. 2, 2015, pp. 17-21.

[12] A. Suvarnamani, Some Properties of (p; q) – Lucas Number, Kyungpook Mathematical. Journal, Vol. 56, 2016, pp. 367-370.

[13] R. K. Raina and H. M. Srivastava, A class of numbers associated with the Lucas numbers, Math. Comput. Modelling,, Vol. 25, No. 7, 1997, pp. 15-22.

[14] G. B. Djordjevic'c and H. M. Srivastava, Some generalizations of certain sequences associated with the Fibonacci numbers, Journal Indonesian Mathematical. Society, Vol 12, 2006, pp. 99-112.

Second International Conference on Science, Engineering & Environment,
Osaka City, Japan, Nov.21-23, 2016, ISBN: 978-4-9905958-7-6 C3051

ANTIOXIDANT PROPERTIES AND INHIBITORY EFFECTS OF TRIGONA HONEY AGAINST *STAPHYLOCOCCUS AUREUS* PLANKTONIC AND BIOFILM CULTURES

Wen Jie, Ng[1,2,*], Yek Jia, Chan[1], Zhi Khoon, Lau[1], Ping Ying, Lye[1], and Kah Yaw, Ee[1,2]
[1]Faculty of Science, Universiti Tunku Abdul Rahman, Malaysia; [2]Centre for Biodiversity Research, University Tunku Abdul Rahman, Malaysia

ABSTRACT

Trigona honey was analyzed for bactericidal and antibiofilm potencies using plate count and spectrophotometry methods, respectively, against different *Staphylococcus aureus* isolates, including ATCC 25923 strain, ATCC 33591 methicillin resistant strain (MRSA), and two clinical isolates from wounds. Besides, the relationship between anti-staphylococcal effects and antioxidant capacity of Trigona honey was discussed. All *S. aureus* isolates were highly susceptible to the antibacterial action of Trigona honey. Lysis of the planktonic bacterial cells was observed using scanning electron microscopy. Despite moderate levels of phenolic content (106.62 mg GAE/kg), DPPH free radical scavenging activity (40.94% RSA), and FRAP value (419.50 μM Fe (II)/100g), Trigona honey exhibited potent inhibitory effect (75-90%) on biofilm formation, especially in 20% (v/v) honey. Additionally, the effects of functional phytochemicals and acidity (pH 2.31) in 20% (v/v) honey were suggested to contribute up to 70% reduction on established biofilm. In short, Trigona honey exhibited high antibacterial and antibiofilm activities, suggesting a potential therapeutic agent in staphylococcal wound infection.

Keywords: Stingless bee honey, Antioxidant, Antibacterial, Antibiofilm

INTRODUCTION

Antibiotics have been used extensively to ward off bacteria in modern medical treatments. Although the efficiency of antibiotics is highly significant, excessive usage or exploitation of antibiotics could lead to the emergence of antibiotic-resistant bacteria. Generally, the multidrug-resistant bacteria are not easily eliminated due to evolvement in adaption model and surviving pattern against antibiotics [1]. Their extended survival within a patient could lead to persistent infection by forming bacterial biofilm [2]. Biofilm is a type of self-produced extracellular matrix which embedded by the bacteria to provide a protective environment for them to grow. The biofilm supplies nutrient to the bacteria and protects them from eradicated by the drugs [2]. Wound is one of the common sites for biofilm formation. The infected wounds are always associated with Gram-positive bacteria, especially *Staphylococcus aureus* [3].

Honey, a natural product derived from the nectar of flowers, has been used widely in different aspects, such as culinary, nutritional supplement, as well as a medicine. Also, it has been used as a traditional therapeutic agent to treat a wide range of microbial diseases and wounds [4]. The availability of hydrogen peroxide in honey as well as its hyperosmolarity and acidic properties, honey possesses significant inhibitory activity on the proliferation of bacteria [5]. In addition, the therapeutic value of honey is also credited to its antioxidant properties which are mainly due to the substantial amount of phenolic compounds [6], [7]. However, the potency of antioxidant properties of honey could be varied with different geographical origins and the floral sources.

Stingless bee farming has been gaining attention in tropical countries recently. In Malaysia, *Trigona* spp., a native stingless bee is commonly cultivated in farming areas as major pollinators and also for honey production [7]. Trigona honey has been recognized to have economic potential due to its growing availability and its higher effectiveness in antibacterial activity with a wider spectrum compared to honeybee honey [7]. To date, however, no scientific study has been done on the potential antibiofilm effects of Trigona honey. Hence, this study was carried out to investigate the inhibitory activities of Trigona honey against *Staphylococcus aureus* planktonic and biofilm clinical cultures, as well as to study its antioxidant capacity and physicochemical properties.

MATERIALS AND METHOD

Honey Samples and Chemicals

Trigona honey sample was obtained from authorized bee farmers in Malaysia. The sample was

kept in the dark at room temperature. All chemicals used were of analytical grade, unless stated otherwise.

Bacterial Sample Collection and Identification

Clinical wound samples were collected from a local hospital and were cultured on agar plates. Single colonies formed were further identified with mannitol fermenting test, Gram staining, catalase and coagulase tests, API® Staph identification system, and Kirby-Bauer antibiotic susceptibility test. Standard strains of *S. aureus* (ATCC 25923 and ATCC 33591) were also tested and adopted as the reference for the identification of clinical isolates.

Antibacterial Assessments

Plate count method

The anti-staphylococcal activity of Trigona honey was evaluated via plate count method. A 20 µL of 0.5 McFarland bacterial suspensions was mixed with 1980 µL of honey in a tube. After that, 20 µL of the mixture was added into 180 µL of normal saline (NaCl, 0.85% w/v) in another tube. Then, 10 µL of the mixture was evenly spread onto mannitol salt agar (MSA) followed by incubation at 37°C for 24 h together with the tube. A second set of spread plate was performed after 24 h of incubation using the same dilution method. The number of colonies formed on the MSA at 0-hour and 24-hour were recorded. The assay was triplicated and the mean value was obtained.

Scanning electron microscopic examination

Bacterial cultures were centrifuged (3500 rpm, 10 min) after 24-h incubation with Trigona honey at 37°C and the pellets were fixed with glutaraldehdye, 2.5% (v/v) overnight. The cultures were then washed with PBS and underwent serial dehydration with ascending concentrations of ethanol and subjected to critical point drying. The sample was then subsequently coated with platinum, placed onto the copper stage holder and examined by scanning electron microscope (JEOL JSM-7610F FEG).

Antibiofilm Evaluation

Effect of Trigona honey on established biofilm

According to the modified procedure of [3], 200 µL of 0.5 MacFarland bacterial cell suspensions was pipetted into corresponding wells of a 96-well, flat-bottomed microtitre plate and incubated at 37°C for 24 h without shaking. After incubation, planktonic cells were carefully removed without touching the side and the bottom of the wells. After that, 200 µL of honey sample with a concentration range of 20-100% (v/v) was added into respective wells and was incubated overnight. Bacterial suspension in the well without honey was served as positive control. After incubation, honey samples were removed and the wells were washed with 200 µL of 0.01 M PBS. The biofilm was then fixed with 200 µl of 2.5% (v/v) glutaraldehyde for 10 min and then washed again with 200 µL of PBS. The fixed biofilm was then stained with 200 µL of 0.25% (v/v) crystal violet for 10 min followed by washing with 200 µL PBS for five times. The microtiter plate was then kept at room temperature overnight. The dried stained biofilm was reconstituted with 200 µL acetone-ethanol solvent (1:1 ratio) and kept for 10 min. A 20 µL of resulting solution was diluted into 200 µL final volume with acetone-ethanol solvent (1:1 ratio) prior recording the absorbance (*A*) reading at 570 nm using microtiter plate reader. The assay was triplicated and the average value was obtained. The biofilm biomass reduction (%) was calculated with Eq. (1).

$$\frac{\textbf{positive control } (\boldsymbol{A}) - \textbf{sample } (\boldsymbol{A})}{\textbf{positive control } (\boldsymbol{A})} \times \mathbf{100}\% \quad (\mathbf{1})$$

Inhibition of biofilm formation

According to the procedure of [3] with modification, 1 mL of 0.5 McFarland bacterial cell suspensions was mixed with 1 mL of honey sample with a concentration range of 20-100% (v/v). Then, 200 µL of the mixture was pipetted into corresponding wells of a 96-well, flat-bottomed microtitre plate and was incubated at 37°C for 24 h without shaking. Bacterial suspension in the wells without honey was served as positive control. After incubation, the mixture of honey sample and planktonic bacteria was removed. The formed biofilm was fixed with 200 µL of 2.5% (v/v) glutaraldehyde for 10 min and then washed with 200 µL of PBS. Next, the biofilm was stained with 200 µL of 0.25% (v/v) crystal violet for 10 min followed by washing with 200 µL PBS for five times. The microtiter plate was then kept at room temperature overnight. The dried stained biofilm was reconstituted with 200 µL acetone-ethanol solvent (1:1 ratio) and kept for 10 min. A 20 µL of resulting solution was diluted into 200 µL final volume with acetone-ethanol solvent (1:1 ratio) prior recording the absorbance (*A*) reading at 570 nm using microtiter plate reader, and the reduction extent (%) of biofilm biomass was calculated with Eq. (1) .

Physicochemical Analyses

Total phenolic content

Folin-Ciocalteu procedure was adopted as described by [8], [9] with modification. Briefly, 0.5 mL of Folin-Ciocalteu's phenol reagent was mixed with 0.5 mL of honey sample and was allowed to stand for 3 min. After that, 0.5 mL of 10% (w/v) Na_2CO_3 solution was added, followed by distilled water to the final volume of 5 mL. After incubation in the dark for 90 min, the absorbance of the mixture at 725 nm was measured using a spectrophotometer. This assay was standardized against a calibration curve of gallic acid (20-100 µg/mL) in distilled water. This assay was triplicated and the results were expressed as milligrams of gallic acid equivalents (GAE) per kilogram of honey accordance to Eq. (2).

$$\frac{\textbf{Gallic acid}\ \left(\frac{\textbf{mg}}{\textbf{mL}}\right) \times \textbf{honey}\ (\textbf{mL})}{\textbf{honey}\ (\textbf{kg})} \qquad (\mathbf{2})$$

DPPH free radical scavenging activity (RSA)

In this assay [8], 1.5 mL of DPPH methanol solution (0.09 mg/mL) was mixed with 0.75 mL of honey sample (0.1 g/mL). The negative control was prepared by mixing 1.5 mL of DPPH methanol solution (0.09 mg/mL) with 0.75 mL of distilled water. The mixture was shaken vigorously and incubated at room temperature in the dark for 30 min prior to the measurement of absorbance (*A*) at 517 nm using a spectrophotometer. This assay was triplicated and the average value was obtained and expressed as % RSA by using Eq. (3).

$$\frac{\textbf{1} - \textbf{negative control}\ (\boldsymbol{A})}{\textbf{sample}\ (\boldsymbol{A})} \times \mathbf{100}\% \qquad (\mathbf{3})$$

Ferric reducing antioxidant power (FRAP)

According to the procedure of [10] with modification, FRAP reagent was prepared by mixing 50 mL of acetate buffer (0.3 M, pH 3.6) with 5 mL of 2,4,6-tri[2-pyridyl]-s-triazine (TPTZ) solution (10 mM in 40 mM HCl solution) and 5 mL of $FeCl_3 \cdot 6H_2O$ solution (20 mM). Prior to the assay, FRAP reagent was warmed at 37°C for 30 min. After that, 1.5 mL of FRAP reagent was mixed with 200 µL of ferrous sulfate standard solution (100-1000 µM) and 200 µL of honey sample (0.1 g/mL) individually. The mixtures were then incubated at 37°C for 4 min prior to the measurement of absorbance at 593 nm. The assay was triplicated and the average FRAP value was reported as µM Fe (II) equivalent per 100 g of honey accordance to Eq. (4).

$$\frac{\textbf{Ferrous sulfate}\ \left(\frac{\mu\textbf{M}}{\textbf{mL}}\right) \times \textbf{honey}\ (\textbf{mL})}{\textbf{honey}\ (\textbf{g})} \times \mathbf{100} \qquad (\mathbf{4})$$

pH measurement

The pH value of the Trigona honey was measured using a calibrated pH meter (Sartorius, Germany). Triplicate measurements were performed and the mean value was obtained.

RESULTS AND DISCUSSION

Identification of Clinical Isolate

Both reference strains (ATCC 25923 and ATCC 33591) and two clinical isolates (Isolate 1 and Isolate 2) were found to be Gram-positive, appeared as cocci in cluster, tested positive for mannitol fermentation, catalase and coagulase activities; with *S. aureus* identification percentage of 97.8%, 97.8%, 97.7% and 97.8%, respectively. According to the interpretation guideline [11], ATCC 25923 was confirmed to be the only antibiotic sensitive *S. aureus* strain, whereas ATCC 33591, Isolate 1 and Isolate 2 were resistant to more than one antibiotic including methicillin, ampicillin, penicillin, chloramphenicol, tetracycline and trimethoprim.

Antibacterial Effects

Table 1 shows bactericidal rate (%) of Trigona honey using plate count method. No bacterial colony was observed on agar plate after 24-h incubation, suggesting the antibacterial action of Trigona honey. The bacteria also experienced significant morphological changes as shown in Fig. 1B, in which the lysed cells started to clump together as compared to typical spherical morphology of *S. aureus* as shown in Fig. 1A.

Results demonstrated that Malaysian Trigona honey possessed antibacterial activity against both antibiotic-sensitive and antibiotic-resistant *S. aureus*. One hundred percent bactericidal rate was observed after the bacteria were incubated with Trigona honey for 24 hours.

Table 1 Bactericidal rate (%) of Trigona honey after 24-hour incubation with *S. aureus* culture at 37°C

S. aureus	Number of colony		Bactericidal
	0-h	24-h	rate (%)
ATCC 25923	13	0	100
ATCC 33591	16	0	100
Isolate 1	5	0	100
Isolate 2	11	0	100

(A)

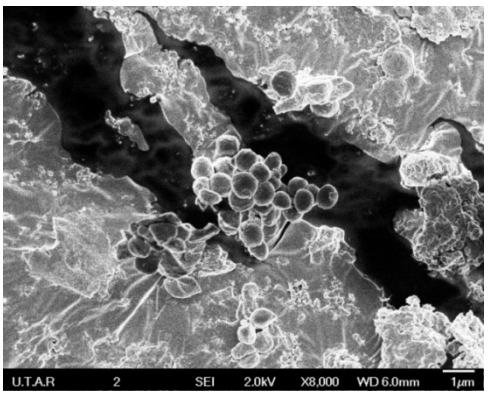

(B)

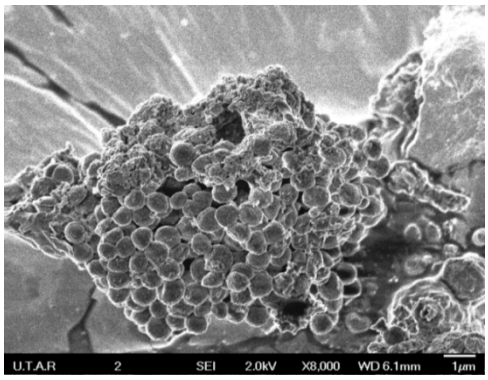

Fig. 1 The morphology (8000 × magnification) of *S. aureus* before (A) and after (B) treated with Trigona honey.

A similar study reported that the viability of *S. aureus* was significantly reduced after treated with Thailand stingless bee honeys [12]. Furthermore, the morphological changes of honey-treated *S. epidermidis* and *P. aeruginosa* exemplified by the swelling and lyses of the bacterial cells upon exposure to honey were also demonstrated in another similar study [13].

Honey has several well-known characteristics that are generally accepted as the contributing factors to its total antimicrobial activity. These factors include hydrogen peroxide production, phytochemical compounds, osmotic effect and low pH [14]. Although the antimicrobial activity of some honey is attributed predominantly to hydrogen peroxide activity, but certain honey, such as Manuka honey, remains bactericidal active after catalase treatment. This suggested that the antibacterial activity was not due to hydrogen peroxide activity but mostly attributable to the presence of unique phytochemicals in honey [14].

Antibiofilm Properties

Figure 2 shows the reducing effect of Trigona honey on established biofilm of four *S. aureus* isolates. In general, the higher the concentration of honey (% v/v), the lower the reducing effect of Trigona honey on biofilm. For each isolate, the greatest reduction of biofilm was found to be 51.84% for ATCC 33591 in 20% (v/v) honey; 27.14% for ATCC 25923 in 20% (v/v) honey; 74.69% for Isolate 1 in 40% (v/v) honey; and 44.99% for Isolate 2 in 60% (v/v) honey. The lowest biofilm reduction was found in 100% (v/v) honey for all isolates, where the lowest reduction (9.34%) was observed in ATCC 25923.

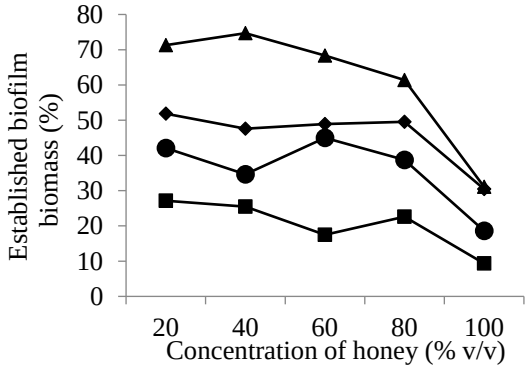

Fig. 2 Reducing effect of Trigona honey on established biofilm of ATCC 33591 (♦), ATCC 25923 (■), Isolate 1 (▲), and Isolate 2 (●).

Figure 3 shows the inhibitory effect of Trigona honey on biofilm formation of four *S. aureus* isolates. Results exhibited a steady rise of the inhibition on biofilm formation from 20% (v/v) until it reached the apex at about 40% (v/v) and steady afterward.

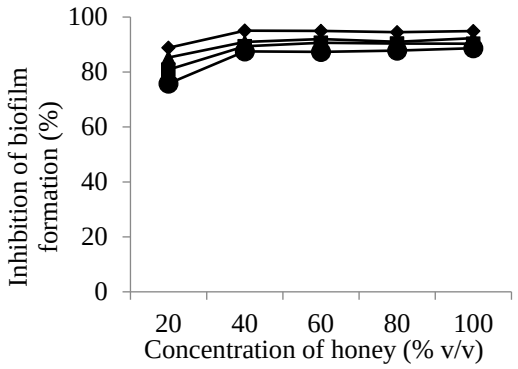

Fig. 3 Inhibitory effect of Trigona honey on biofilm formation of ATCC 33591 (♦), ATCC 25923 (■), Isolate 1 (▲), and Isolate 2 (●).

The presence of water in honey is crucial for glucose oxidase to covert glucose into gluconic acid

and hydrogen peroxide [15]. Trigona honey exhibited two to three times the reducing effect on biofilm at 20% (v/v) concentration than the undiluted sample. Results suggested that dilution of Trigona honey, especially 20% (v/v), led to the hydrolysis of glucose due to the activation of glucose oxidase to produce hydrogen peroxide. Low reduction effect on established biofilm was believed due to low moisture content in the undiluted honey.

Dilution slightly reduced inhibitory activity of Trigona honey on biofilm formation, but the inhibition remained at high level (75%-95%), suggested the synergism of other factors, such as phenolic compounds, acidity, and hyperosmorality, contributing the minimal inhibitory effect of biofilm formation. In addition, quorum sensing, which the bacterial cells communicate to each other and grow together, is one of the important steps for biofilm formation. It has been reported that honey was able to suppress a quorum sensing gene, AL-2, to prevent the formation of biofilm [1].

Antioxidant Capacity and Acidity

Trigona honey contains lower phenolic compounds (Table 2) than other stingless bee honeys that have been reported, such as stingless bee honey from Brazil (17-66 mg GAE/g of extract) [16] and from Australia (557.4 mg GAE/kg) [17], as well as other Malaysian honeybee honey, including Melaleuca honey (513.8 mg GAE/kg) [6], Acacia honey (186.70 mg GAE/kg), Pineapple honey (226.29 mg GAE/kg), Borneo honey (206.33 mg GAE/kg), and Tualang honey (352.73 mg GAE/kg) [18].

Table 2 Total phenolic content, antioxidant properties and pH value of Trigona honey

Assay	Value
Total phenolic content	106.62 mg GAE/kg honey
DPPH free radical scavenging activity	40.94% RSA
Ferric reducing antioxidant power	419.50 μM Fe (Π) equivalent/100g honey
pH	2.31

Note: GAE, gallic acid equivalents; RSA, radical scavenging activity.

Phenolic compounds that are generally found in honey include caffeic, chlorogenic, ellagic, ferulic, gallic, and *p*-coumaric acids, as well as kaempferol, chrysin, herperetin, luteolin, myricetin, and quercetin [19], [20]. In addition, a study [20] showed that the presence of phenolic acids, such as benzoic, caffeic, cinnamic, ferulic and gallic acids in honey, contributed the antibacterial activities against *S. aureus*, including MSSA and MRSA. The type and proportion of phenolic compounds in honey, however, vary depending on its botanical source since phenolic compounds are generally derived from plants [16].

Furthermore, DPPH free radical scavenging activity and ferric reducing antioxidant power were shown to be positively correlated with the antibacterial effect of honey [6]. The presence of proton donor from antioxidant compounds causes the release of more protons which creates an acidic environment. The hyperacidification of bacterial plasma membrane occurs due to the acidification of intracellular cytosolic and proton donation, resulting in the disruption of bacterial cell. In addition, the acidic environment can also further inhibit the production of ATP by blocking H^+-ATPase enzyme [21]. However, Trigona honey (Table 2) exhibited relatively low radical scavenging activity (40.94%) and antioxidant power (419.50 μM Fe (Π) equivalent/100 g honey) than other Malaysian honey [6], [18]. This could be mainly attributed to low quantity of phenolic content in Trigona honey.

The pH of Trigona honey (pH 2.31) was lower than the reported average pH value of stingless bee honey (2.9–3.7) [16]. Due to the presence of gluconic acid, the acidity of honey is able to eradicate bacteria and prevent the development of biofilm [22]. Under experimental conditions, in particular with strongly diluted honey, the culture medium used tends to neutralize the acidity of the honey, thereby reducing or eliminating the inhibitory action; however, when honey is applied directly on a wound or ulcer, the bacteria can come into contact with the honey and thus acidity could be an important factor to eradicate bacteria [5].

CONCLUSION

Despite of moderate level of phenolic content and antioxidant capacity, acidic Trigona honey exhibited high level of inhibitory activity against *Staphylococcus aureus*, regardless planktonic or biofilm culture. Further studies could be directed towards the identification of bioactive components, *in vivo* bioactive properties and allergenecity tests, to discover the remedy using Trigona honey in *S. aureus* wound infection.

ACKNOWLEDGMENTS

The authors thank Faculty of Science, UTAR, for financial support.

REFERENCES

[1] Lee, J.H., Park, J.H., Kim, J.A., Ganesh, P.N., Moo, H.C., Lee, C.S., Lee, J., "Low concentration of honey reduce biofilm formation, quorum sensing, and virulence in

Escherichia coli 0157:H7", Biofouling, Vol. 27(10), 2011, pp. 1095-1104.

[2] Costerton, J.W., Stewart, P.S. and Greenberg, E.P., "Bacterial biofilm: a common cause of persistent infections", Science, Vol. 284(5418), 1999, pp. 1318-1322.

[3] Cooper, R., Jenkins, L., Rowlands, R., "Inhibition of biofilms through the use of Manuka honey", Wounds, Vol. 7(1), 2011, pp. 24-32.

[4] Maryann, N., "Honey as medicine has a long history - New Zealand honey is focus of intensive research", HealthFacts, Vol. 25(11), 2000, p. 4.

[5] Molan, P.C., "Honey as a topical antibacterial agent for treatment of infected wounds", 2001, Web. 5 May 2015, http://www.worldwidewounds.com/2001/november/Molan/honey-as-topical-agent.html

[6] Ng, W.J., Lim, M.S., "Anti-staphylococcal activity of Melaleuca honey", Southeast Asian J. Trop. Med. Public Health, Vol. 46(3), 2015, pp. 472-479.

[7] Garedew, A., Schmolz, E., Lamprecht, I., "The antimicrobial activity of honey of the stingless bee *Trigona* spp.", J. Apic. Res., Vol. 47(1), 2003, pp. 37-48.

[8] Khalil, M.I., Mahaneem, M., Jamalullail, S.M.S., Alam, N., Sulaiman, S.A., "Evaluation of radical scavenging activity and color intensity of nine Malaysian honeys of different origin", J. Anal. At. Spectrom., Vol. 3(1), 2011, pp. 4-11.

[9] Ee, K.Y., Agboola, S.O., Rehman, A., Zhao, J., "Characterisation of phenolic components present in raw and roasted wattle (*Acacia victoriae* Bentham) seeds", Food Chem., Vol. 129, 2011, pp. 816-821.

[10] Benzie, I.F.F., Strain, J.J., "Ferric reducing/antioxidant power assay: Direct measure of total antioxidant activity of biological fluids and modified version for simultaneous measurement of total antioxidant power and ascorbic acid concentration", Methods Enzymol., Vol. 299(1), 1999, pp. 15-27.

[11] CLSI. Performance standards for antimicrobial susceptibility testing; Twenty-first informational supplement. CLSI document M100-S21. Wayne, PA: Clinical and Laboratory Standards Institute; 2011.

[12] Boorn, K.L., Khor, Y.Y., Sweetman, E., Tan, F., Heard, T.A., Hammer, K.A., "Antimicrobial activity of honey from the stingless bee *Trigona carbonaria* determined by agar diffusion, agar dilution, broth microdilution and time-kill methodology", J. Appl. Microbiol., Vol. 108(5), 2009, pp. 1534-1543.

[13] Chakraborti, T., Barman, S., Mandal, N.C., Bhattacharya, K., "Evaluation of antibacterial potential of some Indian honey samples against throat and skin infective pathogens", Int. J. of Current Microbiol. Appl. Sci., Vol. 3(1), 2014, pp. 362-369.

[14] Cooper, R.A., Molan, P.C., Harding, K.G., "The sensitivity to honey of Gram-positive cocci of clinical significance isolated from wounds", J. Appl. Microbiol., Vol. 93(5), 2002, pp. 857-863.

[15] Tao, Z., Raffel, R., Souid, A., Goodisman, J., "Kinetic studies on enzyme-catalyzed reactions: oxidation of glucose, decomposition of hydrogen peroxide and their combination", Biophys. J., Vol. 96(7), 2009, pp. 2977-2988.

[16] Silva, I.A.A., Silva, T.M.S., Camara, C.A., Quieroz, N., Magnani, M., Novaise, J.S., Soledade, L.E.B., Olivaira Lima, E., Souza, A.L., Souza, A.G., "Phenolic profile, antioxidant activity and palynological analysis of stingless bee honey from Amazonas", Northern Brazil, Food Chem., Vol. 141(4), 2013, pp. 3552-3558.

[17] Oddo, L. P., Heard, T.A., Rodríguez-Malaver, A., Pérez, R.A., Fernández-Muiño, M., Sancho, M.T., Sesta, G., Lusco, L., Vit, P., "Composition and antioxidant activity of *Trigona carbonaria* honey from Australia", J. Med. Food, Vol. 11(4), 2008, pp. 789-794.

[18] Moniruzzaman, M., Sulaiman, S.A., Khalil, M.I., Gan, S.H., "Physicochemical and antioxidant properties of Malaysian honeys produced by *Apis cerana*, *Apis dorsata* and *Apis mellifera*", BMC Complement. Altern. Med., Vol. 13(43), 2013, pp. 1-12.

[19] Kassim, M., Yusoff, K.M., Achoui, M., Mustafa, M.R., Mohd, M.A., "Ellagic acid, phenolic acids and flavonoids in Malaysian honey extracts demonstrate *in vitro* anti-inflammatory activity", Nutr. Res., Vol. 30(9), 2010, pp. 650-659.

[20] Aljadi, A.M., Kamaruddin, M.Y., "Isolation and identification of phenolic acids in Malaysian honey with antibacterial properties", Turk. J. Med. Sci., Vol. 33, 2002, pp. 229-236.

[21] Kwon, Y.I., Apostolidis, E., Labbe, R.G., Shetty, K., "Inhibition of *Staphylococcus aureus* by phenolic phytochemicals of selected clonal herbs species of Lamiaceae family and likely mode of action through proline oxidation", Food Biotechnol., Vol. 21(1), 2007, pp. 71-89.

[22] Chanchao, C., "Antimicrobial activity by *Trigona laeviceps* (stingless bee) honey from Thailand", PaK. J. Med. Sci., Vol. 25(3), 2009, pp. 364-369.

Second International Conference on Science, Engineering & Environment,
Osaka City, Japan, Nov.21-23, 2016, ISBN: 978-4-9905958-7-6 C3051

THE POTENTIAL OF INDIGENOUS BACTERIA TO INCREASE POROSITY AND PERMEABILITY OF RESERVOIR ROCK: PRELIMINARY STUDY FOR MICROBIAL ENHANCED OIL RECOVERY (MEOR)

Astri Rinanti
Environmental Engineering Department, Trisakti University, Jakarta, Indonesia

ABSTRACT: Oil content extraction from the rock pores can be very complicated due to the high viscosity of petroleum oil and low degree of reservoir rock porosity as well as its permeability. A research had been carried out with the use of mix populations of indigenous bacteria isolated from formation water, well-site sludge and well mud. Limestones was used as samples. This cores were soaked for 2 (two) weeks in temperature of 55^0C in a media contained of 1% molasse dissolved in sterillized formation water and 20% crude oil as covering. During the research, there was a change in the pH environment from neutral to acid. Acid production from the reaction result with carbonate in the solution will lower pH of the water that was produced. Changing value of porosity (%) that was injected by bacteria from formation water, well site sludge, and wel mud, increases respectively 23.22, 68.29, 14.89, and changing value of permeability (%) respectively 56.28, 137.83, 35.77. Even though on average there were an increase in value of porosity and permeability, there were also a decrease in the value of porosity and permeability of a few of the limestones samples, caused by suspended of carbonate matrix and suspended from material in the formation water. Inoculum bacteria from the pollution around the oil well are much more adaptive and give more carbonate dissolving reaction than the other actions. This group of bacteria are a better plugging comparing to the other groups of microbes from the formation and well mud. This plugging mechanism can be developed as a MEOR technique known as microbial selective plugging. MEOR is really dependent on the growth of the microbes in site, and the development of the secondary metabolit products that can change the porosity and permeability of the reservoir limestones

Keywords: Indigenous bacteria, Limestones, Oil recovery, Porosity, Permeability.

INTRODUCTION

Needs of petroleum fuel has greatly risen in recent decades, while new oil reserves are increasingly difficult to obtain. Given the important role and nature of petroleum oil that can not be renewed, the efforts to optimize oil extraction continues to be improved. Exploitation of petroleum oil in early stage (primary recovery) generally relies on the driving force derived from reservoir pressure. When this phase ends, in line with the reduced driving force, further extraction techniques are then applied to the reservoir, including thermal injection, chemical injection, solvent injection (solvent flooding), as well as mixed injection (miscible process). The main purpose of all these techniques is to mobilize the remaining oil to the surface. Current exploitation techniques are capable to lift only about 30% of remaining oil to the surface. The rest remains in the pores of reservoir rock [1]. Oil content extraction from the rock pores can be very complicated due to the high viscosity of petroleum oil and low degree of reservoir rock porosity as well as its permeability.

MEOR (microbial enhanced oil recovery) is one of the techniques used to exploit petroleum oil, developed since 1950s. It represents advanced oil recovery attempt by utilizing the ability of bacteria to produce secondary metabolites such as fatty acids, gases, surfactants, and biopolymers. MEOR technique begins by injecting bacteria into the reservoir, followed by pursuing formations of bacterial growth. Principally, MEOR is highly dependent on the growth of in situ bacteria and the production of secondary metabolites. Metabolic process basically results in the organism growth and development. However, not all of its products are consumable for growth and development. Residuals of metabolism in the form of secondary metabolites are excreted from the cell to the surrounding environment. Direct utilization of these secondary metabolites can alter the porosity and permeability of reservoir rock, potentially enhancing oil recovery process from the rock pores.

Basically, every type of rock can act as a reservoir rock as long as it has the ability to hold and to release petroleum oil. Thus, reservoir rock has to have porosity as the retention capability and also permeability as the discharging capability of petroleum oil. Porosity determines the amount of

liquid contained, whereas permeability determines the amount of liquid yielded [2]. A permeable rock will be considered porous with interconnected pores. Contrarily, a porous rock is not necessarily permeable because of the disconnected pores. Porosity does not depend on the particle size, while permeability is a direct function of the grain size.

This research aims to exploit the potential of indigenous bacteria isolated from the reservoir environment to increase the porosity and permeability of carbonate formation in reservoir rock.

MATERIALS AND METHODS

Preparation of Indigenous Bacteria and Bacterial Penetration into the Reservoir

Indigenous bacteria were isolated from three materials consisting of formation water, waste around oil wells, and used drilling sludge. Bacterial isolates were injected into the sample carbonate rock reservoir containing pure carbonate (100% limestone) according to Vance diagram (1950)[3], [4] . The rocks were formed into a cylinder with a diameter of 2.5 cm and a length of 3 cm, then were cleaned and its initial porosity and permeability were measured. The crude oil used in this study was classified as paraffin or low-density oil category. Sampling were performed at the beginning and the end of the treatment for 14 days to count the number of bacteria, porosity value, and permeability value of the rock sample. Rock samples that have been cleaned were wrapped in alumunium foil and were sterilized in an oven at 100°C for an hour to measure the initial porosity and permeability. After cooling down, the rock samples were aseptically inserted using large tweezers into erlenmeyers containing treatment media before the inoculation. Each erlenmeyer containing rock sample was stored in an incubator at 55°C for 14 days. Agitation was carried out using a shaker incubator at 120 rpm for 30 minutes, everyday during the experiment. Dilution plate method was choosen for bacterial count.

Porosity Measurement

Porosity is the ratio of pore volume (total medium/rock volume minus matrix volume/grain volume) to the total volume of rock. Porosity is usually expressed in percent (%), calculated as follows [4]

$$\phi = \frac{(\textbf{total volume} - \textbf{volume of grains})}{\textbf{Total volume}} \text{ x } 100\%$$

An instrument called Helse Gauge Porosimeter was used to measure porosity of the rock samples. The working principle is based on Boyle's law: at constant temperature, the product of pressure and volume of an object will be constant as well. This device was connected to a computer software called autoporosimeter. Helium gas was used to fill the pores of rock samples, considering that helium molecules are tiny enough to penetrate the smallest pore, helium atomic mass is low (high diffusion rate), and helium adsorption rate at the rock surface is also low and insignificant.

After 48 hours in the oven, the length and diameter of the samples were then measured. Turn on the autoporosimeter, then insert a disc of the same size with the sample diameter into the Helse tube and seal the tube. The computer will record the data of the correction disc. Remove the disc and replace it with a sample. Keep the space left inside the Helse tube to be minimum by adding the correction disc. Type the number and dry weight data of the sample, together with the number of the inserted correction disc into the computer. The computation result will then display GV (grain volume) and CD (core density) data. These are needed to calculate BV (bulk volume) = A x l; PV (pore volume) = BV – GV; Porosity is then determined by the equation below:

$$\varphi = (PV/BV) \text{ X } 100\%$$

Permeability measurement

Permeability is a property of reservoir rock to be able to convey liquid matter through the interconnected pores without damaging the rock structure or particles. Based on Darcy's law, permeability can be formulated as follows [5]

$$q = - (k\ A\ dp) / (\mu f\ dl)$$

According to the API code 27, a porous medium has a value of permeability (k) of 1 Darcy if a single-phase liquid with a viscosity (μ f) equals to 1 centiPoise flows at a velocity (q) of 1 cm per second through a cross-section (A) covering an area of 1 cm^2 with a hydraulic gradient (dp/dl) of 1 atm (76.0 cm Hg) per cm^2 and if the liquid entirely occupies the medium. Negative sign in the equation above shows an opposite flow to the hydraulic gradient. Unit of permeability is often expressed in miliDarcy (mD) due to its common value of only between 5–1000 mD (1 mD = 0.001 D).

Permeability of rock samples were measured using an instrument called gas permeameter. Its principle is also based on Darcy's law, stating that the fluid rate in porous media is directly proportional to the pressure force driving the fluid and rock permeability, but inversely proportional to fluid viscosity. Data obtained from this device are orifice flowrate value (Or = orifice), height of water column (W = ortifice water), and C value whose magnitude depends on the type of applied pressure. The pressure value can be read at the center water manometer which needs to be corrected later due to

the friction loss. This number is then converted to C value using Water to Water permeability C chart. Samples of limestone were estimated to have low permeability that require measurement at high pressure. In this case, C value was constant at 4. Permeability (Ka) can be calculated by using orifice flowrate data (Or), height of water column (W), C value, the average length (L), and total area of the cross-section (A), based on following equation:

$$Ka = \frac{\mathbf{Or \times W \times C \times L}}{\mathbf{200 \times A}} \text{ x correction factor to temperatur}$$

RESULTS AND DISCUSSION

The use of bacteria in carbonate formations is highly dependent on the presence of carbonate and acid production of fermented carbohydrates that will react with the carbonate. The influence of gas production is considered very small and insignificant to the acquisition of oil residue. The reaction occurs between acid of fermented carbohydrates and the rock matrix in the form of carbonate can be written as follows: $H^+ + CaCO_3 \rightarrow HCO_3^- + Ca^{2+}$

Results from porosity and permeability measurement of limestone samples can be seen in Figure 1. Outcomes of the three treatments generally indicate an increase in the porosity and permeability value.

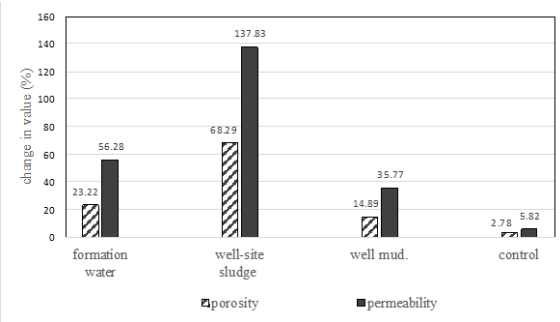

Fig 1. The test results of the porosity and permeability of the limestone samples

During the first treatment using formation water inoculum, porosity raised between 1.35%–52.15% with an average of 23.22% and permeability increased between 21.8%–94.50% with an average of 56.28%. The second treatment using bacterial inoculum taken from waste around the oil wells shows an increased porosity of 13.71%–94.10% with an average of 68.29% and increased permeability of 89.35%–188.68% with an average of 137.83%. The third treatment by drilling mud inoculum increased the porosity value between 0.60%–26.67% with an average of 14.39% and permeability between 5.91%–98.21% with an average of 35.77%. Acid production is the basic mechanism for MEOR technique and is also a specific target for the implementation of the carbonate-based reservoir. The reaction expected to occur between the products of carbohydrate fermentation by bacteria and the rock matrix can be written as follows: $H^+ + CaCO_3 \rightarrow HCO_3^- + Ca^{2+}$

Acidic compounds yielded from this reaction will lower the pH of the produced water. Acid production is expected to disperse in the reservoir on a broad scale, then dissolute and shed the rock matrix so that it can increase the porosity and permeability of the rock.

For the control samples, porosity value changed irregularly between -5.31% (down) to 4.95% (up) with an average of 2.78%, whereas permeability entirely decreased between 2.15%–8.55% with an average of 5.82%. These controls were not injected with bacteria. Irregular porosity change were mostly caused by the agitation process on shaker incubator (it cracked the samples and sank most of the matrix). Several injected samples also experienced this irregular change, but it was mostly caused by bacterial activity. The difference can be seen in the declining permeability value of controls which were caused by the presence of carbonate matrix sediment and also sediment of other substances contained in formation water that blocked the cleft off.

Bacterial count from the first day (day 0) to day 14 decreased immensely. It may be caused by the shifting of environmental pH from neutral to acidic condition. Acid production induced by carbonate reaction in the solution will lower the pH of produced water. In this study, environmental pH in all treatments dropped from neutral point (7.0) to acidic range (5.2 ± 0.5). This sharp decline in pH can interfere with bacterial metabolism. According to [6], at 5.0–5.5 pH range, metabolic process of certain type of bacteria may be interrupted.

The increase in porosity and permeability obtained in this study were not significant due to the very small permeability value of the rock samples, whereas an effective bacterial EOR typically comes in an average permeability of 150 mD. Nevertheless, considering that the permeability have risen indeed, bacterial penetration into the rock samples may have been taken place, enabling carbonate dissolution by acidic compounds generated from bacterial fermentation. The results show that the treatment using bacterial inoculum from waste around the oil wells has better ability to increase porosity and permeability compared to the other two.

Bacterial population monitoring portrays a decrease of bacterial count in each treatment. For the treatment using waste inoculum, the population tended to approach a constant growth. Taking into account of the bacteria properties to clog and to reduce porosity and permeability, it can be seen that the decrease of porosity value by this treatment was much larger than the other two. It can be concluded that in this study, indigenous bacteria played a decent role in reducing the porosity and permeability.

Presence of red bacterial colonies (due to the colour of safranin) is depicted in the photograph of the rock structure after the treatment. There were no sign of it in the control samples, bringing clear pictures of the rock-forming material in the form of cavities/pores between grains, filled by oil. On the other hand, it can be seen in the treated samples that visible colonies of bacteria were able to penetrate into the rock pores, either forming a thin layer attached to the grains or even lumps that clogged the pores.

In the water injection technique, these blockages can be exploited to clog high permeability formations so that the water flow can be redirected and focused to sweep out the remaining oil trapped in the low permeability formations. This way, sweeping efficiency can be optimized. In this technique (known as selected/targeted cloggings), the condition of bacteria greatly affects its ability to penetrate. The bacteria that are in a state of hunger has a smaller size than normal bacteria in the vegetative state, so it can penetrate deeper into the reservoir rock formations [7]. The bacteria growth and reproduction itself will subsequently serve as the agent of the formations clogging. The effectiveness of this technique is highly dependent on the accuracy of the bacteria placement/seeding in the specified high permeability formations and the impact inflicted by the cloggings established later.

Reference [8] estimated that the vertical movement of water in the aquifer affects the ability of bacterial penetration. Although the penetration of bacteria from the surface takes many years, but as long as the flow of water in the aquifer contains organic carbons (particularly of rocks passed by), the penetration of the slow-developed colonies can keep going. Based upon the properties of its permeability, Jaranyl in [1] recommends that the use of microorganism in EOR should only be introduced to rock formations having permeability value of larger than 60 MD. MEOR technique, according to [1], will be effective on moderate (150–300 MD) to high permeability rocks (400–700 MD). However, strains studied by Myers and McCready apparently were able to penetrate 'Mississippian limestone' and 'late Mesozoic sandstone' formations with permeability value of less than 0.1 MD.

CONCLUSION

Bacterial isolates that have been collected from formation water, well-site sludge, and well mud, then have been injected into the reservoir carbonate rock, were able to improve rock porosity (%) to 23.22, 68.29, and 14.89 respectively, also rock permeability (%) to 56.28, 137.83, and 35.77 respectively, due to the dissolution of carbonate rock matrix by acidic substances generated from bacterial metabolism. Bacterial inoculum derived from the well-site sludge was more adaptive and gave a greater carbonate dissolution effect compared to the formation water and mud well bacteria. Bacterial isolates collected from the well-site sludge was also found to be a better clogging agent.

REFERENCES

[1] Shibulal, B., Al-Bahry SN, Al-Wahaibi YM, Abdulkader E. Elshafie, Ali S. Al-Bemani, and Sanket J. Joshi, “Microbial Enhanced Heavy Oil Recovery by the Aid of Inhabitant Spore-Forming Bacteria: An Insight Review”, Hindawi Publishing Corporation, The Scientific World Journal, Vol. 2014, 2014, pp. 1-13

[2] K. Fujiwara, Y. Sugai, N. Yazawa, K. Ohno, C. X. Hong, and H. Enomoto, “Biotechnological approach for development of microbial enhanced oil recovery technique”, Studies in Surface Science and Catalysis, Vol. 151, 2004, pp. 405–445,

[3] Vandecasteele JP, “Petroleum Microbiology: Concepts, Environmental Implications, Industrial Applications”, Translated by Jones, T. France : Editions Technic, 2008.

[4] Amiyx, J.W., D.M. Base, Jr., & R.L.Whitting, “Petroleum Reservoir Engineering: Physical Properties”, New York : McGraw-Hill, 1982.

[5] Monicard, R.P, “Properties of Reservoir Rocks : Core Analysis”, Houston: Gulf Publ. Co., 1980.

[6] Latha, R. and R. Kalaivani, Bacterial, “Degradation of Crude Oil by Gravimetric Analysis”, Advances in Applied Science Research, Vol. 3, 2012, pp.2789-2795.

[7] R. Al-Hattali, H. Al-Sulaimani, Y. Al-Wahaibi, “Microbial biomass for improving sweep eficiency in fractured carbonate reservoir using date molasses as renewable feed substrate”, Proceedings of the SPE Annual Technical Conference and Exhibition, San Antonio, Tex, USA, 2012.

[8] H. Suthar, K. Hingurao, A. Desai, and A. Nerurkar, “Evaluation of bioemulsier mediated microbial enhanced oil recovery using sand pack column”, Journal of Microbiological Methods. Vol. 75(2), 2008, pp. 225–230.

[9] Ollivier, B, “Petroleum Microbiology”, New York: American Society of Microbiology Press, 2005.

Second International Conference on Science, Engineering & Environment,
Osaka City, Japan, Nov.21-23, 2016, ISBN: 978-4-9905958-7-6 C3051

ASSESSMENTS OF GROWTH, VOLUME AND ABOVE GROUND BIOMASS OF FOUR FOREST PLANTATION SPECIES IN SARAWAK, MALAYSIA

Irawani Abdul Rahman[1] and Mohd Nazip Suratman[1,2]
[1]Faculty of Applied Sciences and [2]Centre for Biodiversity and Sustainable Development
Universiti Teknologi MARA (UiTM), Malaysia

ABSTRACT

Timber industry is one of major economy contributors to the Malaysian economy. In view of declining trends of supply of logs from natural forests, the role of forest plantations in supplementing the industry's need for logs is becoming increasingly crucial. In addition, forest plantation has received much attention because it is one of carbon reservoirs and offers potential for carbon sequestration. This study was aimed at assessing the growth, stand volume and above ground biomass (AGB) of forest plantations in Sarawak, Malaysia. A field data collection was conducted to measure the diameter at breast height (DBH) and total tree height of four plantation species i.e, *Acacia mangium* × *A. auriculiformis* (Acacia hydbrid), *A. mangium* (Acacia superbulk), *Eucalyptus pellita* (Red mahogany) and *Neolamarckia cadamba* (Kelempayan) in the study sites. All species were planted at 3 × 3 m spacing and approximately four years of age at the time of measurements in 2015. Published allometric functions were used to compute the stand volume and AGB of all species. From the study, it was found that there were significant differences in the mean DBH, total tree height, basal area (BA) and volume between the plantation species ($p \leq 0.05$). All variables measured were significantly higher for *A. mangium* ($p \leq 0.05$) than other species, whereas *N. cadamba* was being the least. The highest stand AGB was recorded for *A. mangium* (247.5 t/ha) followed by *E. pellita* (195.3 t/ha), *A. mangium* × *A. auriculiformis* (80.0 t/ha) and *N. cadamba* (69.0 t/ha). This study provides the baseline data needed not only to improve the country's forestry planning and plantation sectors, but also for meaningful participation in the national REDD+ process.

Keywords: Acacia mangium × *A. auriculiformis* (Acacia hydbrid), *A. mangium* (Acacia superbulk), *Eucalyptus pellita* (Red mahogany) and *Neolamarckia cadamba* (Kelempayan)

INTRODUCTION

In the coming decades and beyond, wood-based industries in Malaysia will face many challenges especially in the availability of raw materials from natural forests. It is envisaged that by 2020, the production of logs from these areas will decline greatly due to reduced state land forests and alienated lands for development. As a result, the processing capacity for wood-based industries is expected to be reduced. Therefore, in order to compensate for the reduction of supply of raw materials, the forest plantation programme implemented by the government is expected to fill the vacuum.

The Malaysian government has long recognized the roles of forest plantations as an essential part of the strategic development plan for forest resources in the country. The implementation of the Compensatory Forest Plantation Programme (CFPP) in 1983 has marked the important milestone for this strategy in which three exotic plantations species were introduced *Acacia mangium*, *Paraserianthes falcataria*, *Gmelina arborea* for the plantation programme in a total area of 188.200 ha throughout the country [1].

In the state of Sarawak, despite the large tracts of natural productive forests, there has been some concerns regarding the large areas of forest land that have become degraded due to shifting cultivation. To address these issues, some experimental trials were initiated by planting species that had agroforestry potential [2]. In the mid-1960s, pines were introduced for restoration purposes and in 1970s, the growing performance of some fast-growing exotic trees were studied [3].

Besides their potential as sources for wood production for national and international wood-based industries, forest plantations also provide ecosystem functions in accumulating biomass and sequestrating carbon for climate change mitigation, given the high growth rate of the species. The information may be required by government agencies in developing policies on issues relating to reducing emissions from deforestation and degradation (REDD++) mechanism.

In general, estimation of carbon stocks in trees is conducted on the above ground biomass (AGB). The carbon stocks in the above are derived from AGB by assuming the 50% of the biomass is made up of carbon [4]. Therefore, this study aimed at assessing the growth performance, stand basal area (BA),

stand volume and stand AGB of four plantation species, i.e., *Acacia mangium* × *A. auriculiformis* (Acacia hybrid), *A. mangium* (Acacia superbulk), *Eucalyptus pellita* (Red mahogany) and *Neolamarckia cadamba* (Kelempayan) in Sarawak, Malaysia.

MATERIALS AND METHODS

The study was conducted in the forest plantations at Sabal, Sarawak, Malaysia. The study sites were located around Simunjan district about 104 km west from the capital state of Kuching (1° 03' 44.4" N; 110° 53' 14.3" E) (Fig.1). The study area is about 54 m above sea level with the mean temperature of 26°C and humidity of 93%. Four plantation species selected were *A. mangium* × *A. auriculiformis*, *A. mangium*, *E. pellita* and *N. cadamba*. All plantations were established in 2011 (Table 1) and are jointly managed by the Forestry Department of Sarawak and the Malaysian Timber Industry Board (MTIB). All trees were planted at spacings of 3 m × 3 m. A total of 30 trees were randomly selected for each species within the stands in each plantation. The diameter of breast height (DBH – 1.3 meters from the ground level) of all sampled trees was measured using a DBH tape. The total tree height was measured using a Suunto clinometer.

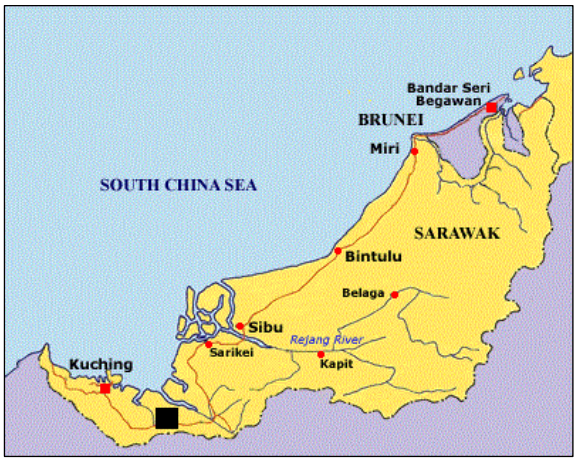

Fig. 1 Map of a study location (■) at Sabal, Sarawak, Malaysia.

Table 1 Field information of the plantation species

Species	Area (ha)	Date planted
A. auriculiformis × *A. mangium*	9.81	18.04.2011
A. mangium	16.17	18.04.2011
E. pellita	17.77	19.05.2011
N. cadamba	8.57	10.06.2011

Basal Area

The BA which represents the cross-sectional area of a tree trunk measured at breast height over bark was calculated using Eq. (1) [5]:

(1)

Where: *BA*= Basal area (m^2)
DBH=Diameter at breast height (cm)

Tree Volume

The tree volume for each species was calculated using published allometric functions as listed in Table 2.

Table 2 List of published volume allometric functions

Species	Allometric functions	Ref.
A.auriculiformis × *A. mangium*	$V= 0.748\times D^2H^{0.764} \times 10^{-4}$	[6]
A. mangium	$V= 0.00006 \times (D^2H)^{0.934}$	[7]
E. pellita	$V= 0.02997+0.0039 \times D^2H/100+ 0.00000018\times (D^2H/100)^2$	[8]
N. cadamba	$V= 0.00002663 \times D^2H - 0.0252$	[9]

Notes: V=volume (m^3), D=DBH (cm), H=Total tree height (m), Ref.=References

Above Ground Biomass

The AGB was calculated in accordance to generalized allometric functions as given in Eq. (2) [10]:

(2)

Where:
AGB= Above ground biomass (kg)
D=DBH (cm)

One-way analysis of variance (ANOVA) was used to determine significant differences in the means of all measured variables. If significant difference was detected, a post-hoc test (i.e., Fisher's LSD) was used to determine the means that are significant from each other. All analyses were performed using Statistical Analysis System (SAS) version 9.3 [11].

RESULTS AND DISCUSSIONS

Tree Diameter at Breast Height

Results from ANOVA indicated that the

differences in the mean DBH between the four species were statistically significant ($p \leq 0.05$). Of all species, *A. mangium* recorded significantly greater DBH at 18.0 cm. A post hoc test indicated the mean DBH for *A. mangium* was significantly greater than *A. mangium* × *A. auriculiformis* and *N. cadamba* (Fig. 2). However, no significant differences were found in the mean DBH between *A. mangium* vs. *E. pellita* and *A. mangium* × *A. auriculiformis* vs. *N. cadamba*.

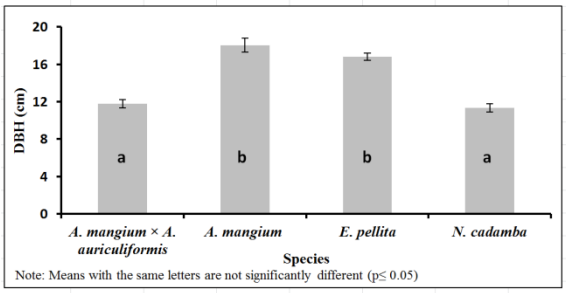

Fig. 2 Trends of the mean DBH (cm) for four plantation species.

In a study of growth characteristics of forest plantations in Bintulu, Sarawak, Nur Syazni *et al.* [12] found the mean DBH of a four-year old *A. mangium* stand was 22.8 cm which was greater than what was obtained for this species in this study (i.e., 18.0 cm). From their study, the DBH size has increased after two years to 26.6 cm during the subsequent measurement which translated into 4 cm DBH increment.

In North Queensland, Australia, Bristow [9] studied the effects of mixed planting of *E. pellita* and *A. peregrine* in various proportions and found that volume growth of the former trees were positively affected by the presence of the latter up to 10 years of age. She mentioned that it was possible the increased in total Nitrogen under the Acacias may have facilitated the growth of *E. pellita.*

In a study conducted by Krisnawati *et al.* [13] in a small farm in South Kalimantan, Indonesia, they found that a five-year old stand of *N. cadamba* recorded the mean DBH of 25.3 cm. This was more than two-fold from what has been recorded by the same species in this study (i.e., the mean of 11.3 cm; minimum of 7.1 cm and maximum of 15.7 cm). In constrast, a slightly lower DBH was reported by Lachica-Lustica [14], where the mean of a four-year old *E. pellita* plantation in Capiz, Philippines, was 10.4 cm. Meanwhile, Ahmad Zuhaidi and Hashim [15] found that the means DBH of a four-year old *N. cadamba* at four different locations in Malaysia i.e, Sandakan, Kanowit, Setul and Bukit Lagong.were 22.4, 19.0, 11.1 and 11.9 cm, respectively which is within the range with the findings from the present study.

In this study, *N. cadamba* recorded the lowest DBH could be attributed to the edaphic characteristics which are less suitable for this species. According to Krisnawati *et al.* [13], *N. cadamba* grows best the moist and alluvial sites along riverbanks or between the swampy permanently and periodically flooded areas.

Other factors of differences in the DBH growth between or within species could be due to the variations in site quality between different regions. Components such as soil drainage, soil physical and chemical compositions, soil moisture availability and general climate of the area can influence the growth and productivity of plantation forests.

Total Tree Height

Results from ANOVA indicate that the difference in the mean of total tree height between species was statistically significant ($p \leq 0.05$). The mean height of *A. mangium* was significantly greater than other species ($p \leq 0.05$) (Fig. 3). However, no significant different was detected in the means height between *A. mangium* × *A. auriculiformis* and *E. pellita*. *N. cadamba* recorded significantly lower height as compared to the other three species ($p \leq 0.05$).

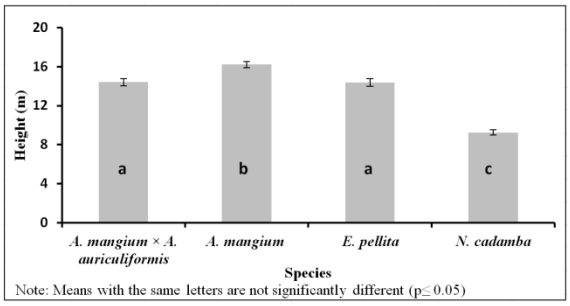

Fig. 3 Trends of the mean total tree height (m) of four plantation species.

A much lower tree height was attained for *E. grandis* plantation in four sites of forest plantations in Sabah, Malaysia (i.e., Sipitang, Mendulong and Basio, Ketanon) as measured by the co-author of this paper and his team recently. The mean heights for four, five, six and seven years old *E. grandis* stands were 11.7, 14.9, 15.3 and 16.5 m, respectively. Meanwhile, a study conducted by Wack *et al.* [16] at Monte do Prado, Portugal found that the 12-year old *Eucalyptus* stands reached a total height of 20 m which were ready to be harvested. This value is lower as compared to the total height of a ten-year old *E. pellita* stands (i.e., 23.9 m) established in North Queensland, Australia as reported by Bistow et al. [9]. The *Eucalyptus* stands in Ketanon, Sabah, established for pulp-wood production, reach harvestable size within eight years of age with the mean total height of 12.7 m.

Basal Area

Results from ANOVA indicated that there was a significant difference in the mean BA per tree between the four plantation species ($p \leq 0.05$). As shown in Table 3, the BA per tree calculated for *A. mangium* (i.e., 2.7 m^2) was significantly higher than *E. pellita* (i.e, 2.3 m^2) and *A. mangium* × *A. auriculiformis* and *N. cadamba* (i.e, 1.1 m^2, respectively). BA per tree for *E. pellita* was significantly higher than *A. mangium* × *A. auriculiformis* and *N. cadamba*. However, no significant difference was observed in the mean BA per tree between *A. mangium* × *A. auriculiformis* and *N. cadamba*.

Table 3 Descriptive statistics of mean BA per tree (m^2) (n=30)

Species	Mean	SD	Min	Max.
A. auriculiformis × *A. mangium*	1.1c	0.4	0.4	2.2
A. mangium	2.7a	1.2	1.0	5.7
E. pellita	2.3b	0.6	1.2	3.6
N. cadamba	1.1c	0.4	0.4	1.9

Note: Means with the same letters are not significantly different ($p \leq 0.05$)

The stand BA was obtained by totaling the individual values of for each species and converting the results into per ha using the area factor (1:area of plot). Figure 4 shows the stand BA for each species that indicates *A. mangium* produced higher stand BA (45.7 m^2/ha) followed by *E. pellita* (37.7 m^2/ha), *A. mangium* × *A. auriculiformis* (18.0 m^2/ha) and *N. cadamba* (17.5 m^2/ha).

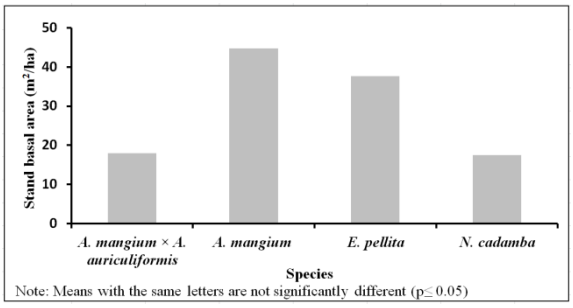

Fig. 4 Trends of stand BA (m^2/ha) of four plantation species.

In this study, BA was measured to determine the average amount of an area occupied by each tree trees in the plantations. The BA of each tree was calculated and summed for all trees in the study plots in hectare to measure size-density relationship in a stand. Previous studies have used BA many purposes for instances, to predict biomass of trees and identify the ratio of biomass and basal area.

Ahmad Zuhaidi and Hashim [15] studied the field performance of trial plantings of *N. cadamba* and *Octomeles sumatrana* (Binuang) in four locations in Malaysia. All stands were four years old with the proposed rotation period is 15 years. The results indicated that the variation existed in the stand BA of *E. cadamba* between locations. The highest BA was recorded for planted stands in Bukit Lagong, Selangor at 16.6 m^2/ha which was slightly lower than value recorded in the present study of 17.5 m^2/ha for the species. This was followed by Kanowit, Sarawak (13.2 m^2/ha), Sandakan, Sabah (13.1 m^2/ha) and Setul, Negeri Sembilan (6.8 m^2/ha). According to the authors, there were reduction in the productivity in the planted stands of *N. cadamba*. They also concluded that the mean annual volume increment decreases as the elevation and distance from water source increases.

Tree Volume

Estimates of volume for different plantation species of stands are essential for effective forest production management as they assist in the determination of potential species to be selected for forest plantation projects. In addition, the estimates also are useful for estimating the amount of biomass and carbon stocks.

From ANOVA, there was a significant difference in the mean volume per tree between the four plantation species ($p \leq 0.05$). The mean volume per tree for *A. mangium* was significantly higher than the other species (Table 4). *E. pellita*, *A. mangium* × *A. auriculiformis* and *N. cadamba* recorded a similar mean volume per tree at 0.08 m^3.

Table 4 Descriptive statistics of mean volume per tree (m^3) (n=30)

Species	Mean	SD	Min	Max
A. auriculiformis × *A. mangium*	0.08a	0.03	0.02	0.17
A.mangium	0.19b	0.09	0.06	0.41
E. pellita	0.08a	0.04	0.02	0.19
N. cadamba	0.08a	0.02	0.04	0.13

Note: Means with the same letters are not significantly different ($p \leq 0.05$)

Figure 5 shows the stand volume (m^3/ha) for four plantation species. As expected, results from stand volume show a similar trend to stand BA. *A. mangium* recorded highest stand volume at 320.7 m^3/ha as compared to other species. There was not much variation observed in the stand volume between *E. pellita* (147.0 m^3/ha), *A. mangium* × *A. auriculiformis* (138.8 m^3/ha) and *N. cadamba* (134.6 m^3/ha).

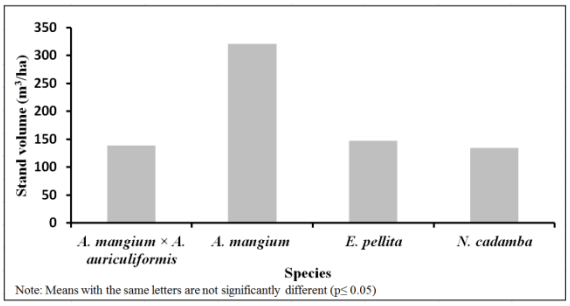

Fig. 5 Trends of stand volume (m^3/ha) of four plantation species.

Surprisingly, a case study on tropical forest plantation in Malaysia reported that the mean timber volume for 15 years old *A. mangium* plantation was 229.0 m^3/ha [17]. This is only about 72% as compared to value for the same species obtained in the present study (i.e., 320.7 m^3/ha).

The stand volume of *N. cadamba* recorded from this study is higher than what had been reported by Ahmad Zuhaidi and Hashim [15] for the similar species and age in four locations in Malaysia. They found that the means of stand volume for *N. cadamba* in Sandakan, Bukit Lagong, Kanowit and Setul were 119.3, 108.8, 87.0 and 33.8 m^3/ha, respectively.

A much lower stand volume was reported by Jusoff [18] in his study on the estimations of the timber standing volume of *A. mangium* using airborne hyperspectral imaging system in 0.8 ha Universiti Putra Malaysia's (UPM) campus field. In this study, the species recorded stand volume only 20.7 m^3/ha. This low stand volume was due the fact that the *A. mangium* plantation in UPM campus field was not well managed which was evidenced from the occurrences of many pioneer species such as *Macaranga* spp. and *Mallotus macrostachyus* found within the plantation area.

The variation in the stand volume in present study and other studies elsewhere could be due the differences in silvicultural systems practiced in different sites. Furthermore, environmental factors including such as soil types, topographical position and precipitation may have also been contributed to the differences. In addition, during plantation establishment, site preparation and stand density may also result in the variation in the growth of yield of the plantation.

Stand Above Ground Biomass

As shown in Figure 6, the highest accumulation of stand AGB was recorded for *A. mangium* (247.5 t/ha) followed by *E. pellita* (195.3 t/ha), *A. mangium* × *A. auriculiformis* (80.0 t/ha) and *N. cadamba* (69.0 t/ha). The range of AGB between 69.0 to 247.5 t/ha obtained in the present study was higher than the earlier reported ranges of 12 t/ha to 194 t/ha estimated for Sabah Softwood plantations, Malaysia by Morel *et al.* [19].

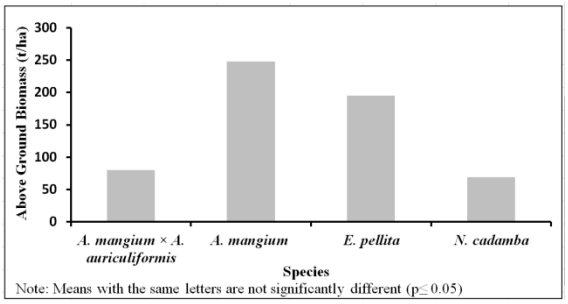

Fig. 6 Trends of AGB (t/ha) for four plantation species.

In a study to determine the AGB in smallholder *A. mangium* plantation in Misamis Oriental, Philippines, Palma [20] found that the AGB of *A. mangium* at ages 3, 10 and 17 years were 3.3, 33.1 and 73.1 t/ha, respectively. When site quality was incorporated in the ABG mean annual increment study, the AGB increases at the early age and increases at a declining rate as the trees approach maturity. The increase in AGB and consequently carbon stocks as the stand age increases was reported by several authors [21, 22].

In a study on AGB accumulation of selected provenances of *A. mangium* and *A. aulacocarpa* in Kuala Lipis, Pahang, Malaysia, Mat *et al.* [23] found the range of AGB was 25.3 t/ha to 380.8 t/ha. They mentioned that there were significant differences in the biomass production between species and sites.

The amount of AGB accumulated by *A. mangium* from this study is higher to that of the species in Pantabangan-Caranglan Watershed, Philippines. In that study, Lasco *et al*. [24] found that the AGB was 54.3 t/ha. In another study in West Java, Indonesia, Hediyanti and Sulistyawati [21] reported that the AGB of a three-year old *A. mangium* plantation was 75.5 t/ha.

Many studies on carbon sequestration have been focusing on the sequestration in terms of biomass and carbon stocks. Therefore, estimation of AGB is considered to the most important aspect in carbon sequestration studies. The potential of forest plantations to enhance carbon sequestration can be assessed either through the amount of carbon stocks or estimating the annual carbon sequestration rate.

CONCLUSION

Establishment of forest plantation has traditionally been geared towards maximizing wood production. However, in recent years, a wider appreciation and awareness of the need to balance economic goals with ecosystem functions such as carbon sequestration. Stand volume and AGB are

among important indicators that provide measures of the capacity of forest plantation to sequester carbon dioxide.

Observations made on *A. mangium* × *A. auriculiformis*, *A. mangium*, *E. pellita* and *N. cadamba* indicated that *A. mangium* has shown to be the most promising fast-growing tree species for plantation and the best in production of biomass. The species has consistently recorded significantly greater DBH, total height, stand volume, stand BA and AGB as compared to other species.

This study could shed important information that shows the variability and capability of forest plantation species in terms of wood production and carbon sequestration potential. Furthermore, findings from the study can be an essential aid to the related agencies in developing policies and guidelines pertaining to the species selection in relation to timber production and environmental services.

ACKNOWLEDGEMENTS

The author wish to thank the Ministry of Education Malaysia for providing the Fundamental Research Grant Scheme (FRGS) 600-RMI/FRGS 5/3 (38/2014). We thank the Institute of Research Management and Innovation (IRMI), Universiti Teknologi MARA, Malaysia for administering the grants, and the Forestry Department of Sarawak for providing logistic assistance to the study locations.

REFERENCES

[1] Chin T, "A preliminary review of compensatory forest plantation in peninsular Malaysia" Electronic these and dissertation, 1992, paper 17.
[2] Fahlman R, "Project S.4 – Species trials", Research Report No. S.R.7, 1975.
[3] Kendawang JJ, "Forest plantation in Sarawak", Forestry Department, Sarawak, 1996.
[4] Basuki TM, *et al.*, "Allometric equations for estimating the above-ground biomass in tropical lowland Dipterocarp forests", For. Ecol. and Manage., 257, 2009, pp. 1684–1694.
[5] Hovind HJ, and Rieck CE, "Basal area and point-sampling, interpretation and application" Technical Bulletin Number 23, Wisconsin, 1970.
[6] FIPI, "Manual in forest inventory and planning", Agricultural Publishing House, Hanoi, 1996.
[7] Chongrak W *et al.*, "Effect of thinning on growth and yield of *Acacia mangium Dipterocarpus alatus* mixed plantation", Kasetsart University, Thailand, 2005.
[8] Pinard MA, "Carbon retention by reduced-impact logging', PhD Thesis, 1995, University of Florida, USA.
[9] Bristow M, "Growth of *Eucalyptus pellita* in mixed species and monoculture plantations', Southern Cross University, NSW, 2008.
[10] Brown S, "Estimating biomass and biomass change of tropical forests: a primer", FAO Forestry Papers 134, 55 pp., 1995.
[11] SAS Inst., "Language reference: Concepts" third edition, Cary, North Carolina, 2014.
[12] Nur Syazni A, Ismail J, and Nur Diyana I, "Growth characteristics of *Acacia mangium* plantation in Sarawak", UNIMAS, 2009.
[13] Lachica-Lustica A, "Trial planting of introduced reforestation species in Dumarao, Capiz", In Dev. in Agroforestry Research, No. 160, 1997.
[14] Ahmad Zuhaidi Y, and Hashim MN, "*Neolamarckia cadamba* vs *Octomeles sumatrana*: is it promising forest plantation species?" in Proc. of IPPM Conf., 2012, 10 pp.
[15] Krisnawati H, Kalio M, and Kanninen M, "*Anthocephalus cadamba* Miq: ecology, silviculture and productivity, CIFOR, 2011.
[16] Wack R, *et al*., "Forest inventory for Eucalyptus plantations based on airborne laserscanner data" Proc. of the Int. Soc. for Photo. and Remote Sensing Comm. III, WG3, 2003, pp. 293-296.
[17] Krishnapillay DB, "Case study of the tropical forest plantations of Malaysia", Forest Plantations Working Papers (FP/23), FAO, 48 pp., 2002.
[18] Jusoff K, "Eestimating *Acacia mangium* plantation's standing timber volume using an airborne hyperspectral imaging system", Open Forest Sc. Jour., 1(1), Sept. 2008, pp. 61-67 ·
[19] Morel AC, Fisher JB, and Malhi Y, "Evaluating the potential to monitor aboveground biomass in forest and oil palm in Sabah, Malaysia, for 2000–2008 with Landsat ETM+ and ALOS-PALSAR", Int. Jour. of Remote Sensing, 33:11, 2009, pp. 3614-3639.
[20] Palma RA, Catacutan DC, Pailagao CT, "Yield prediction model for mangium (*Acacia mangium*) in Cleveria, Misamis Oriental. Claveria, Misamis Oriental, MOSCAT, 2006.
[21] Hediyanti I, and Sulistyawati E, "Carbon stocks in *Acacia mangium* Willd. stands at different ages", Jour. of Tropical Forest Sc., 23(3), 2010, pp. 318–327.
[22] Peichl M, and Arain MA, "Above-and belowground ecosystem biomass and carbon pools in an age-sequence of temperate pine plantation forests", Jour. of Agric. and For. Meteo., 140, (1-4), 2006, pp. 51-63.
[23] Mat S. *et al.*, "Aboveground biomass of selected provenances of *Acacia aangium* and *Acacia aulacocarpa* multiple-leadered trees", Jour. of Agric. Sc. Dec. 2009, (2):1, pp. 74-82.
[24] Lasco RD, *et al.*, "Carbon budgets of terrestrial ecosystems in the Pantabangan-Carranglan watershed", Working Paper No. 10, 2005.

Second International Conference on Science, Engineering & Environment,
Osaka City, Japan, Nov.21-23, 2016, ISBN: 978-4-9905958-7-6 C3051

ASSESSMENTS OF ABOVE GROUND BIOMASS (AGB) AND CARBON STOCKS OF EUCALYPTUS PLANTATIONS IN SABAH, MALAYSIA

Ahmad Farid Mohsin, Mohd Nazip Suratman and Shaikh Abdul Karim Yamani Zakaria
Faculty of Applied Sciences and Centre for Biodiversity and Sustainable Development
Universiti Teknologi MARA, Malaysia

ABSTRACT: Timber resources from natural forest in Malaysia are becoming scarce and scarce. Therefore, forest plantations are established to provide renewable resource base to meet the raw material requirements for the country. Eucalyptus is one of forest plantation species extensively established and managed for pulp wood production. However, despite providing raw material for wood-based industries, their critical ecosystem roles in sequestering carbon are often overlooked. Therefore, this study was conducted to provide estimates of the above ground biomass (AGB) and carbon stocks of Eucalyptus plantations in Sabah, Malaysia. For this purpose, forest plantation field inventory and data analysis were conducted to provide inventory data for *Eucalyptus grandis* and *E. pellita* in Sipitang, Mendulong and Basio, Sabah. A 30 m ×30 m quadrat plots were established based on random start. Within each plot, diameter at breast height (DBH in cm), total height (m), crown width (cm) and crown closure (%) were recorded. Several published allometric functions developed for these species were used and evaluated to analyse the accuracy of estimations and predictions. Generally there were significant differences in the means of DBH, basal area (BA) and volume between the ages of plantations ($p \leq 0.05$). The highest stand AGB was recorded for seven years stand (i.e. 247.5 t/ha) with the total stand carbon stocks was estimated to be 67.8 tC/ha**.** This analysis is expected to provide crucial insights into the ecosystem roles of forest plantation in mitigating climate change.

Keywords: Eucalyptus, Above Ground Biomass, Carbon Stocks

INTRODUCTION

Awareness of environmental issues has increased on an unprecedented scale. Deforestation, loss of biodiversity, global warming and climate change are some of the environmental issues linked directly to terrestrial ecosystems, both natural and human-managed. The natural resources are crucial in the industry as raw materials. However, timber resources from natural forest in Malaysia are becoming scarce and scare. In addition, a more sustainable way such as forest plantation practices shall be taken and studied specifically on its ability to supply timbers and also the potential on sequestering carbon.

Nowadays, forest plantation enhances the creation of resources to meet high demand for wood and wood product, development to produce innovative products for internal and external market. Forest plantations are important inreducing emissions from deforestation and degradation mechanism (REDD+) strategies for increasing carbon sequestration while enhancing local livelihoods.

Malaysia, through the National Timber Industry Policy (NATIP) provides the strategic thrusts and policy directions in addressing the challenges to ensure that the industry remains sustainable and competitive. Therefore, many fast growing species have been established such as *Acacia mangium*, *Gmelina arborea*, *Tectona grandis*, *Eucalyptus* spp. and few more species [1].

Eucalyptus is commonly used for woody crops due to their fast growth and high productivity. Furthermore, they adapt well to various sites and their management is simple compared with other common forest species. Consequently, *Eucalyptus* spp. is one of the most important commercial species in Australia, Brazil, South Africa, Sri Lanka and Indonesia for its principal use in pulpwood productions**.** In Sabah, Malaysia, the industry utilizes this species for timber and paper productions. Sabah has established some 226,000 ha of forest plantations, of which about 55 % are cultivated with high-value commercial species with Sabah Forest Industries Sdn. Bhd. (SFI), took the lead with total plantation areas covering more than 45,400 ha [2].

While this important role of *Eucalyptus* spp. forest plantations in strengthening the socio-economic has been established, their roles in ecosystem functions are not fully understood and well documented in Malaysia. Quick responses are essential to face the emerging challenges of the forest plantation industry

This study was conducted to provide estimates of above ground biomass (AGB) with respect to different plantation ages of plantations for *E.*

grandis and *E. pellita* in Sipitang, Mendulong, Ketanon and Basio, Sabah. Considering the fact that biomass represent the role of tree as a key indicator of carbon source and sink, the information from this study is expected to provide the carbon stock estimates of the *Eucalyptus* spp. plantations.

MATERIALS AND METHOD

Study Site and Field Data Collection

This study was conducted to provide estimates of AGB and carbon stocks of *Eucalyptus* spp. plantation. The selected study areas for field data collection were in managed forest plantations owned by SFI in Sipitang, Sabah, Malaysia (Fig.1). Sipitang is a town, district and also a parliamentary constituency located in the interior division of Sabah, east Malaysia on the island of Borneo. It spans an area of approximately 273,249.69 ha. This district is located at the southwest portion of the state of Sabah located between latitude 4°7' and 5°10' North and between longitude 115°25' and 115°37' East with elevation 45 to 1200 meter above sea level.

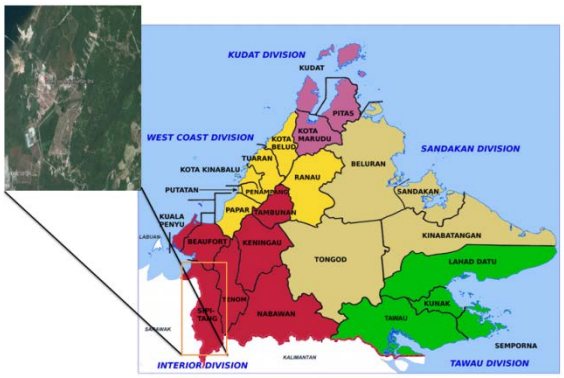

Fig. 1 Map of the study area

Data from field plots were collected from various age groups during March to April 2016 from a total of 65 plots. Each quadrat plot was 30 m × 30 m in size and the plots were established based on random start using random number table. Age groups of plantations were 2 and 3 years for *E. pellita* and 4, 5, 6, 7 and 8 years for *E. grandis*. Data on plantation age were obtained from the SFI management. Within each plot, diameter at breast height (DBH in cm), total height (m), crown width (cm) and crown closure (%) were recorded. The DBH – 1.3 m from the ground level of all sampled trees was measured using a DBH tape. Total tree height was measured using a hypsometer. The global positioning system (GPS) readings were taken at the corners of each plot using a GPS receiver and recorded.

Measurement and Estimation of Field Variables

Basal area

Basal area (BA) is the common term used to describe the average amount of an area occupied by tree stems. It is defined as the total cross-sectional area of all stems in a stand measured at breast height, and expressed as per unit of land area as follows [3].

$$\mathbf{BA} = \frac{\boldsymbol{\pi} \times \mathbf{D^2}}{\mathbf{4} \times \mathbf{10000}} \qquad (\mathbf{1})$$

Where BA is basal area in m² and D is DBH in cm. The calculated BA was then divided by the plot area in ha.

Stand volume

The volume equation developed by Meskimen [4] for *E. grandis* was used to calculate tree volume. The stand volume was calculated from the total plot volumes. Calculated volume was converted to metric units for further analysis.

$$\mathbf{V} = \mathbf{D^2}(\mathbf{0.001818H} + \mathbf{0.0136}) \qquad (2)$$

Where, V is volume in ft³, D is DBH in in (outside bark) and H is total height in ft.

Aboveground biomass

Several published allometric functions developed for these species are used and evaluated to analyze the accuracy of estimations and predictions.Table 1 provides a list of the equations to calculate aboveground biomass.

Table 1 List of allometric functions

No.	Equations	Ref.
1.	$\boldsymbol{W = 21.297 - 6.953 \times +0.740 \times D^2}$	[5]
2.	$\boldsymbol{W = 0.0678 D^{2.5794}}$	[6]
3.	$\boldsymbol{W = 0.0509 \times \rho D^2 H}$	[7]
4.	$\boldsymbol{B = -0.14 + 0.02 \times D}$	[8]
5.	$\boldsymbol{Bi = e^{(-2.81+1.92lnC)}}$	[9]

Where, *W* is AGB in t/ha, *D* is DBH in cm, *H* is total height in m, *B* is total biomass in ton and *Bi* is total biomass in kg.

Carbon stocks

According to Onrizal [6] the average of carbon content of *E. grandis* tree part was 44.92% of biomass with varying from 36.72 to 54.01% of biomass. The equation used for calculating carbon stocks for all the *Eucalyptus* spp. in this study is as below.

$$C = 0.0266D^{2.6470} \quad (3)$$

Where, *C* is carbon stocks in tC/ha and *D* is DBH in cm.

Statistical Analysis

All analyse of data procedures were performed using Statistical Analysis Software (SAS v. 9.4). Tests of significance for the means of DBH, BA, stand volume, AGB and carbon among the various ages was undertaken using one-way analysis of variance (ANOVA). When the statistical significant in the means of parameters were obtained, multiple comparison test (i.e. Duncan test) was used to compare the means of variables.

RESULTS AND DISCUSSION

Diameter at Breast Height

A descriptive statistics for the means of DBH for the seven different ages of plantation is shown in Table 2. As seen from the table, the means of measured DBH for seven ages range from 6.7 cm to 16.9 cm.

Table 2 Descriptive statistics of the means of DBH (cm)

Age	n	Mean	SD	Min.	Max.
2	1861	6.7	3.5	0.2	16.8
3	2134	8.7	3.5	0.5	20.0
4	507	11.3	5.2	1.5	28.0
5	510	14.8	7.7	2.5	146.0
6	879	15.5	5.3	3.1	29.0
7	837	16.9	5.6	2.8	32.8
8	211	11.9	4.5	3.3	24.3

Figure 2 shows the trends of DBH in relation to plantation ages. The DBH increases as the ages increases from 2-7 years old after which it reduces at the age of eight years old. Result from ANOVA indicated that there were significant differences in the mean DBH between tree ages ($p \leq 0.05$). The mean DBH at age 7 was significantly greater than ages 8, 6, 5, 4, 3 and 2 years. This suggests that the age of *Eucalyptus* spp. is significantly affected size of tree.

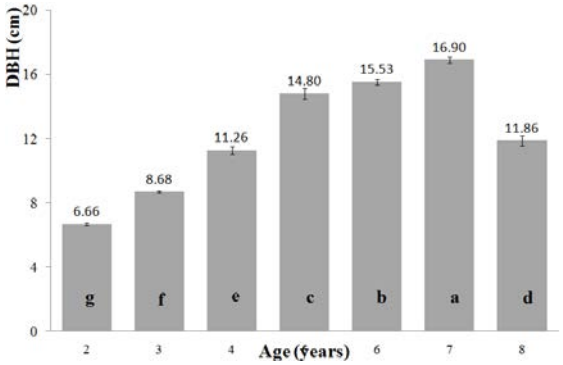

Notes: Means with the same letter are not significantly different ($P \leq 0.05$).

Fig. 2 Age of *Eucalyptus* spp. versus DBH

The DBH size decreases at 8 years might be due to lack of sample size for this age stand. In addition, it also may due to the condition of the samples that were stunted due to poor site condition (soil type, elevation), a poor site management and competition with other pioneer species (e.g. *A. mangium*) which affects the growth.This is based on the previous studies stated that, different sites support the tree growth in different manner, even for the same species [10]. Furthermore, a study reported diameter growth in stands of *E. grandis* plantation is very rapid during early years and then the rate of increase becomes slower, as is characteristic of most species and after competition-induced mortality makes additional growing space available, the rate of diameter growth increases again [11].

In a study conducted for *E. pellita* in a commercial plantation in Mexico by Maria *et al*. [8], they found that the age of two and a half years plantation recorded the means of DBH at 14.4 cm. This is due to selection of sample was measured for 12 to 18 cm. The result was more than the range of age in this study with means of DBH of 6.7 cm and 8.7 cm for 3 years age plantation with minimum 0.5 cm, and maximum 20 cm. Meanwhile, it was found that the mean DBH for 2, 3, 6 and 8 years were 8.8 cm, 11.1 cm, 11.9 cm and 14.2 cm for planted *E. grandis* forest in North Sumatera [6] which is comparable with the present study.

Several of factors between different regions may influence the variation in the DBH growth and productivity of forest plantation. It might due to site index, elevation, soil condition, rainfall and general climate of the area.

Basal Area

Table 3 shows the descriptive statistics of mean of BA per tree in relation to plantation ages. Result from ANOVA indicates that there was significant difference in the means of BA per tree between different ages of stand ($p \leq 0.05$). From a post-hoc

test, the mean BA for age 7 was significantly higher than the rest of ages. Mean BA per tree for age 4 was lower than the others.

Table 3 Descriptive statistics of mean BA per tree (m^2)

Age	Mean	SD	Min.	Max.
2	0.0045d	0.004	0.000003	0.02
3	0.0069d	0.005	0.000001	0.03
4	0.0121c	0.01	0.0002	0.06
5	0.0218b	0.07	0.0005	1.7
6	0.0212b	0.01	0.0008	0.07
7	0.0249a	0.02	0.0006	0.08
8	0.0126c	0.009	0.0009	0.05

Note: Means with the same letters are not significantly different ($p \leq 0.05$)

Analysis of stand BA indicates that the was highest at the age of 7 years (29 m²/ha), followed by 5 years (24.7 m²/ha), 6 years (23 m²/ha), 8 years (14.8 m²/ha), 4 years (m²/ha), 3 years (8.6 m²/ha) and 2years (5.9 m²/ha), respectively. From the results, the stand BA increases as the ages increases, depicting a similar increasing trend as the previous findings.

Onrizal [6] studied the allometric functions of biomass and carbon stocks of planted *E. grandis* in Toba Plateau, North Sumatra, Indonesia. Different stand ages (1-, 2-, 3-, 6-, 8-, and 9-years) using destructive method. The results indicated the variation existed in the stand BA of *E. grandis* between ages. The highest stand BA for 9 years plantation age was 66.9 m²/ha as for 8 years plantation was 43.78 m²/ha which is higher than what was recorded in the present study. However, only at age 6 years plantation with stand BA of 19.46 m²/ha was slightly lower than the findings in this study.

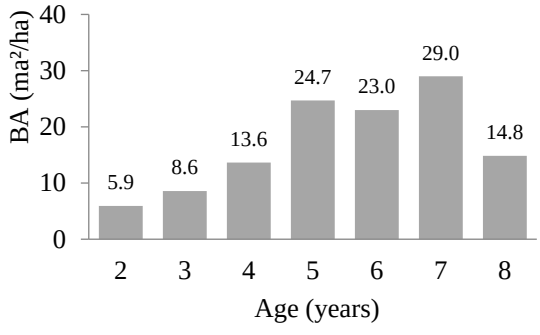

Fig. 3 Age versus basal area (m²/ha) of *Eucalyptus* spp. plantations

A study in Swaziland for *E. grandis* recorded the mean stand BA at 38.7 m²/ha for age 6.75 years [12] which is also higher than what was obtained in the present study with the range ages of 6 to 7 years.

Stand Volume

Table 4 presents the descriptive statistics of mean of volume per tree in relation to plantation age. Result from ANOVA indicates that there were significant differences in the mean of volume per tree between different ages of stand ($p \leq 0.05$). From a post-hoc test, the mean volume for age 7 was significantly higher than the rest of ages. Mean volume for age 2 years was the lowest.

Table 4Descriptive statistics of mean volume per tree (m^3)

Age	Mean	SD	Min.	Max.
2	0.0191d	0.02	0.000003	0.1
3	0.0319d	0.03	0.000005	0.3
4	0.0680c	0.08	0.0003	0.5
5	0.1396b	0.4	0.001	10.0
6	0.1429b	0.1	0.001	0.6
7	0.1782a	0.2	0.001	4.1
8	0.0768c	0.1	0.002	0.4

Note: Means with the same letters are not significantly different ($p \leq 0.05$)

Fig. 4 presents the result of the mean stand volume between different ages of plantations which shows a similar trend to the previous finding. Seven years plantation recorded the highest mean which is 207.2 m³/ha. Age of 5 years plantation recorded the second with 158.2 m³/ha and the lowest is age of 2 years plantation with only 23.2 m³/ha. Stand volume value correlates with BA since stand volume equation basically derived from BA value. Even though there was a large difference in the mean volume between ages, it is insufficient to detect a statistical difference among several ages that might be due to large variation in individual volume measurement in the study area.

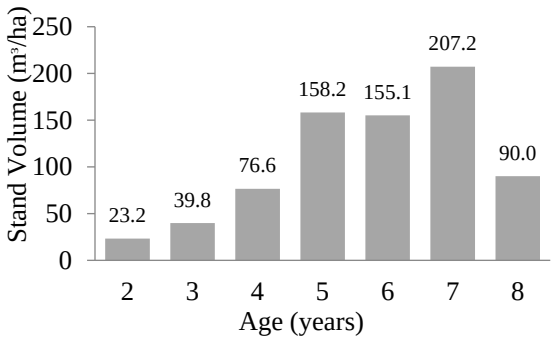

Fig. 4 Age versus Stand volume (m³/ha) versus of *Eucalyptus* spp. plantations

The stand volume in the present study appears to be lower than volume yields measured for spacing trials in Hawaii 214 m³/ha [13]. Sample plots used

for comparison from the Hawaii study were for *E. saligna* species, unthinned at a stocking of 1,100 trees per hectare. *E. saligna*, *E. pellita* and *E. grandis* are closely related species with comparable characteristics. The differences between these species should not result in dramatic differences of volume yields [14].

The variation in the stand volume in present study and other studies elsewhere could be due the differences environmental factors including soil types, topographical position and precipitation. Furthermore, silvicultural systems practiced in different sites may have also been contributed to the differences. Moreover, during plantation establishment, site preparation and stand density may also result in the variation in the growth of yield of the plantation.

Above Ground Biomass

Figure 5 shows a comparison of stand AGB estimates computed from five different allometric functions listed in Table 1. In general, all equation produce a similar trends of estimates from age 2 to 8 years. As can be observed, the highest AGB was calculated from allometric function [8] while allometric function [6] produced the lowest. Based on these trends, AGB of allometric function [6] is selected since the multiple coefficient of determination reported from the study was the highest (i.e. R^2=98.8%) compared to the rest.

Table 5 shows the descriptive statistics of stand AGB based on [6]. The result indicates that the highest mean of AGB was recorded at five years plantation (i.e 134.5 t/ha) while lowest was at 2 years (14.3 t/ha).

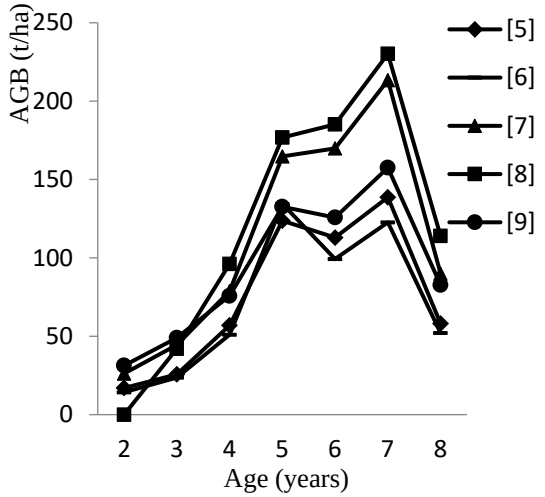

Fig. 5 Age versus AGB (t/ha) versus of *Eucalyptus* spp. plantations

Table 5 Descriptive statistics of Onrizal [6] AGB equation

Age	Mean	SD	Min.	Max.
2	14.3	16.4	0.001	98.1
3	23.7	20.6	0.01	153.9
4	51.0	60.1	0.2	366.5
5	134.5	1146.93	0.7	25939.5
6	99.3	76.9	1.25	401.2
7	122.7	104.0	0.97	551.2
8	52.1	47.6	1.5	254.3

The AGB values recorded in this study are comparable with several studies as in North Sumatera. AGB of 129.5 t/ha was recorded for *E. grandis* of stand age of 9 years [6] which is much lower than recorded in this study. In addition, a case study on *A. mangium* plantations in West Java reported to be only 69.7 t/ha for 10 years plantation age [15]. However, studies of *A. mangium* in Papua New Guinea and in Vietnam produced stand AGB of 121.10 t/ha and 121.30 t/ha respectively [16][17]. A study on stand AGB of *A. Mangium* plantation in Claveria was at the ranges between 2.05 to 54.13 t/ha which are also comparable with the present study [18].

Carbon Stocks

Based on the selected allometric carbon stocks equation [6], the total of aboveground carbon stocks of planted *Eucalyptus* spp. at different ages were estimated (Fig. 6).The highest carbon stocks was produced for age 5 at 67.8 tC/ha. This is followed by 59.1 tC/ha at age 7 years. The 2-years old plantation recorded the lowest stand carbon stocks at 6.6 tC/ha.

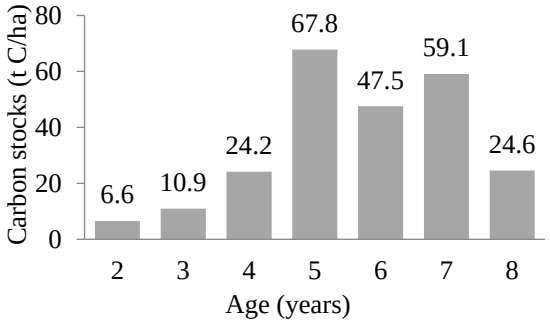

Fig. 6 Age versus carbon stocks (t C/ha) versus of *Eucalyptus* spp. plantations

When compared to the previous studies, the amount of carbon stocks obtained in this study are comparable with their findings. For example, in a study of planted *E. grandis* Onrizal *et al*. [6] found the amounts of 62.84 t C/ha and 39.43 t C/ha were recorded for 9- and 8-year-old stand. In addition, The carbon stocks of Eucalypt forests in South Eastern Australia were 52 tC/ha [19]and 63.7 tC/ha in Southeast Brazil [20] which were lower than what is recorded in the present study comparing to 5 years plantation age. Previous findings indicate that the

most important environmental variables associated with carbon stocks irrespective of stand type were edaphic variables, most commonly total and available soil nitrogen [19]. Tree carbon was the only component stocks more strongly associated with climatic and spatial than edaphic variables.

CONCLUSION

The AGB and carbon stocks were estimated using non-destructive method. In general, there were significant differences in the means of DBH and for basal area (BA) and volume between the age of plantations ($p \leq 0.05$). The highest stand AGB was recorded for seven years stand (i.e., 247.5 t/ha) with the total stand carbon stocks was estimated to be 67.8 tC/ha. The carbon content was comparable to other studies. However, the variation of results could be due to differences related to the site and species/clones. Therefore, further studies of carbon content in the laboratory should be conducted to allow more reliable comparisons.

ACKNOWLEDGEMENT

The authors would like to express their deepest gratitude to Ministry of Education, Malaysia for providing research grants through the Fundamental Research Grant Scheme (FRGS) (600-RMI/FRGS 5/3 (38/2014)), Universiti Teknologi MARA (UiTM) and Sabah Forest Industries (SFI) for providing logistic related services and data field collection.

REFERENCES

[1] National Timber Industry Policy 2009-2010. Supply of raw materials. Min. of Plantation Industries & Commodities Malaysia. 2009.

[2] Jack Wong (2012, July20). The Star: Business news"Sabah has 226000ha of forest plantations"

[3] Hovind HJ and Rieck CE, "Basal area and point-sampling interpretation & application" Tech. Bulletin Number 23, Wisconson, 1970.

[4] Meskimen G, and Franklin EC,"Spacing *E. grandis* in southern Florida- a question of merchantable versus total volume" Southern J. of applied forestry. 1978,2(1);3-5.

[5] Brown S, *et al*."Biomass estimation methods for tropical forests with applications to forest inventory data. For Sci1989, 35:881–902.

[6] Onrizal, CK, *et al*., "Allometric biomass & carbon stock equations of planted *E. grandis* in North Sumatra" Proceeding Int. Seminar Research on Plantation Forest Management, 2010. pp 1-6

[7] Chave, et al. "Tree allometry & improved estimation of carbon stocks & balance in tropical forests" Ecosystem Ecology, 2005.

[8] Maria RS, *et al*., "Biomass assessment, volume equations & crown architecture of *E. pellita* F. Muell in a commercial plantation in Mexico"Revista Forestal Mesoamericana Kurú Vol. 12, No. 29, Julio, 2015.

[9] Burrows, WH., *et al*., "Allometric relationships & community biomass estimates for some dominant eucalypts in Central Queensland woodlands. Australian J. of Botany 2000, 48:707–714.

[10] S.M.C.U.P. S, "Modelling Total Height of *E.grandis* Hill ex Maiden",J. of Tropical Forestry & Environment Vol. 4. No 02 (2014) 31-44.

[11] Brian VB, "Diameter Growth of *E. grandis* under Conditions of Extreme Suppression", New Zealand J. of Forestry Science 1990, 20(2): 162-7.

[12] M dP and Kotze H, "Growth and yield models for *E.grandis*grown in Swaziland"Southern Forests 2011, 73(2): 81–89.

[13] Walters G,"Saligna eucalyptus growth in a 15-year-old spacing study in Hawaii", Pacific Southwest Forest & Range Exp. Stn., Forest Serv., 1980, Paper PSW-151:6.

[14] Brook FA, "Vol. Yields of Smallholder *E. grandis* W. Hill Ex Maiden Stands in Eastern Paraguay", Dissertations, 2014

[15] Heriansyah, I, *et al*., "Estimating carbon fixaxion potential of plantation forests: case study on *A. mangium* plantations", Forest Research. Bulletin,2003, 634: 1-14

[16] Yamada, M., *et al.,* "Carbon stock in fast-growing tree species *A. mangium* man made forest in Papua New Guinea", Tropical Forestry 2002, 49: 20-33

[17] Yamada M, *et al*.,"Carbon stock in fast-growing tree species *A. mangium, A. auriculiformis*, and *E. camaldulensis*man made forest in Sonbe, Vietnam". Tropical Forestry 2000, 47: 33-39

[18] Richmund AP,"Determination of Aboveground Carbon Density of Mangium (*A. mangium* Willd.) using Biomass Expansion Factor", Mindanao Journal of Science and Technology Vol. 12 (2014) 39-50.

[19] Melissa F,*et al.*, "Carbon stocks in temperate forests of south-eastern Australia reflect large tree distribution and edaphic conditions", Forest Ecology and Management 334 (2014) 129–143.

[20] Sabina CR, *et al*, "Aboveground & Belowground Biomass & Carbon Estimates for Clonal Eucalyptus Trees in Southeast Brazil", Revista Árvore, Viçosa, v.39, 2015 p.353-363.

Second International Conference on Science, Engineering & Environment,
Osaka City, Japan, Nov.21-23, 2016, ISBN: 978-4-9905958-7-6 C3051

STAND STRUCTURE AND FLORISTIC COMPOSITION OF FRAGMENTED FRESHWATER SWAMP FORESTS IN MALAYSIA

Siti Maisarah Che Abdullah[1, 2], Mohd Nazip Suratman[1, 2] and Judith Gisip[1]
[1]Faculty of Applied Sciences, Universiti Teknologi MARA (UiTM), Malaysia
[2]Centre for Biodiversity and Sustainable Development, Universiti Teknologi MARA (UiTM), Malaysia

ABSTRACT

Freshwater swamp forests in Malaysia are getting scarce from time to time due to land use and land cover changes, which turns their populations to become vulnerable to extinction. A study was conducted to determine the stand structure and tree species composition in the remnants of freshwater swamp forests located in Parit Forest Reserve, Perak, Malaysia. For this purpose, transect lines with random start method were established in two sites (i.e., wet condition [WC] and dry condition [DC]). The width of transect lines was 20 m and the length was ranged from 40-200 m. Distance between transect lines was 50 m apart. Transect lines were gridded into subplots (20 m × 20 m). All trees (DBH> 10 cm) were measured and identified at species level. From the study, the diameter distribution of trees displays the characteristic of inverse J distribution, indicating the presence of regeneration in both study sites. In terms of floristic composition, a total of 1,263 trees, representing 179 species in 109 genera from 41 families were enumerated in the study area. Two dominant families in the study locations are Euphorbiaceae and Sapotaceae. Tree species such as *Artocarpus scortechinii* and *Nephelium lappaceum* are among the important part of the floristic composition in the study areas. The Shannon-Weiner diversity index (*H'*) is uniform for both study sites, (i.e., 2.39), which is within the range of other studies in freshwater forests. The results from this study are useful in providing a valuable reference for conservation of biodiversity for the freshwater swamp forests.

Keywords: Floristic Composition, Freshwater Swamp Forest, Stand Structure, Endangered Species

INTRODUCTION

Malaysia is endowed with richness in biodiversity of the tropical rain forests [1][2] The major types of forest in Malaysia are peat swamp forest, mangrove forest, lowland dipterocarp forest, hill dipterocarp forest and montane forest. However, there are only about 3.3 million ha of forested wetlands and freshwater swamps forests occupying about 2.5% of the areas in the country as compared to others forest types [3].

In Malaysia, freshwater swamp forest has received scant attention due to the less economic values. In addition, deforestation and urban expansion lead to the reduction of the habitat [4], which turn freshwater swamp forest into critically threatened habitats. This forest is very peculiar and unique because it gives rise to a habitat from the surrounding lowland dipterocarp forests [5]. Thus, the reduction of this forest gives an impact to endemic tree species that need specific habitat requirements.

Dipterocarpaceae is listed as one of the most threatened tree families in Malaysia [6]. *Shorea* is the genus of this family that has the highest number of taxa and unfortunately one species of this genus was assessed as extinct (i.e., *Shorea kuantanensis*). A few more species from the genera *Dipteracarpus, Hopea, Shorea, Vatica* and *Parashorea* are categorised as critically endangered [7]. Among all these species, few species are restricted to freshwater swamp forests. *D. semivestitus* or locally known as Keruing padi is restricted to freshwater swamp forest in Parit Forest Reserve, Malaysia.

Information on density, species composition, diversity of tree species and species-rich communities are of primary importance in the planning and implementation of biodiversity conservation efforts. To conserve the forests from declining, it is essential to examine the current status of species diversity as it will provide useful information for the management of the forest. Therefore, this study was conducted to assess the stand structure of freshwater swamp forests of Parit Forest Reserve and to determine the floristic composition in this area. Information from this study will provide a valuable knowledge in identification of ecologically useful species as well as species of special concerns, thus identify conservation efforts required for sustainability of forest biodiversity.

MATERIALS AND METHODS

Description of Study Area

This study was conducted in freshwater swamp

forest remnants in Parit Forest Reserve, Perak, Malaysia (Fig. 1). The study area lies between the latitude of 4° 21' 21" N and longitude of 100° 57' 14" E with the topography ranges from 20-45 m above sea level. The climate is characterized by permanent high temperatures range from 20-35°C. The weather is dry and warm from January till March with the lowest rainfall occurs in January (60-100 mm of rainfall). The highest rainfall occurs in October to November (i.e., 230-350 mm) [8].

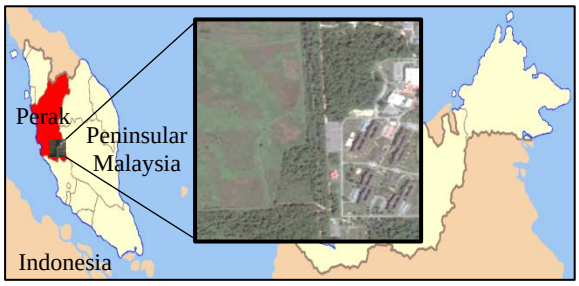

Fig. 1 Location of the study area.

This forest is classified as freshwater swamp forest and the entire forest reserve is surrounded by fragments of secondary forests within the district of Perak Tengah, Perak. Much of the area has been developed into urban sites leaving very small patches of isolated swamps. From the field observation, it is apparent that the area belongs to two conditions of distinct microhabitat (i.e., wet condition (WC) and dry condition (DC)). The total size of area covers an area about 12.39 ha (7.73 ha for WC and 4.66 ha for DC). The two habitats support different tree communities due to a variation in habitat characteristics.

Due to the water logged condition of this forest that causes by rainfall runoff, the trees exhibit different strategies for survival which include growth of buttresses and stilt roots. The hydrophytic trees (i.e., *Ficus* spp., *Macaranga* spp. and *Syzygium* spp.) dominate the vegetation type in the forest. Other than that, *Livistona saribus* palm is frequently occurred in the area. In terms of stratification, the forest comprises irregular canopies that range from 10-25 m height and the emergent trees range between 30-35 m height.

Data Collection

Transect lines with the width of 20 m were established in a systematically using random start. The length of transect lines vary from 40-200 m depending on the length of study sites. Distance between transect lines were 50 m apart. Each transect line was gridded into subplots, 20 m × 20 m in size, as workable units. Each subplot was inventoried by measuring all tree species within a diameter at breast height (DBH) ≥ 10 cm. All trees were identified at the species level. If field identification was not possible, the botanical specimens were taken to the herbarium section of the Forest Research Institute Malaysia (FRIM) for identification and confirmation.

Data Analysis

In this study, the stand structure was described based on the number of individual trees per hectare, basal area and distribution of trees by diameter classes. Therefore, the basal area was calculated based on the equation from Husch *et al.* [9], the data of DBH were classified into diameter classes which gave a frequency of trees then used to draw bar chart graphs.

Data of all tree species were summarized to describe the species composition, abundance and diversity of the tree communities. The abundance data include determination of density, frequency and basal area. In order to determine the most importance species in the communities, the Important Value Index (*IVI*) was calculated by summing up the values of relative density (R_D), relative dominance (R_{Do}) and relative frequency (R_F) of each species or family [10].

Different species richness in terms of indices were calculated using Margalef's diversity index (D_{Mg}) [11] and Menhinick's diversity index (D_{Mn}) [12]. The Shannon-Wiener's Diversity Index (*H'*) [13] and Simpson's Diversity Index (*D*) [14] were used to determine the species diversity in a community. Evenness was used to measure of how similar the abundances of different species were determined using Shannon's equitability (E_H) [15] Community similarity between the two study sites was determined using the Sörensen's Similarity Index (S_s) [15].

Statistical Analysis

For data analysis, an independent t-test was performed to determine any statistical differences between the means of variables of floristic composition between the two conditions of microhabitat in the study area. The analysis of the data was performed using Statistical Analysis System (SAS) software version 9.3.

RESULTS AND DISCUSSIONS

Stand Structure Analysis

Density

From the analysis, study site at DC recorded

higher tree density of 663 individuals ha^{-1} as compared to 484 individuals ha^{-1} in the WC study site. However, both study sites contain low density of trees ha^{-1}. From the t-test, there was a significant difference in mean of tree density between the both study sites ($p \leq 0.05$).

Previous study conducted by Mata *et al.* [16] that determined the floristic composition in three tropical freshwater forested wetlands (i.e., Cienaga, Apompal and Chica) in Mexico, reported the wetland density of 1750, 2889 and 2400 individuals ha^{-1}, respectively. Other study in Malaysia by Khairil *et al.* [17] on tree species composition and community structure in a tropical watershed forest reported that inland forests have higher density with 1472 individuals ha^{-1} followed by riverive forest and seasonal flood forest with density 1277 individuals ha^{-1} and 1132 individuals ha^{-1}, respectively.

When compared to other findings, the result of this study for density in the present study is lower in both study sites. It is apparent that density of trees in freshwater swamp forests shows high variation due on various factors. The effects of natural and anthropogenic disturbances could be the factors that influence tree density. The lower stand density in WC might be due to hydroperiod which may disturb the growth of small trees [17].

Basal area

In terms of stand basal area, WC recorded 23.9 m^2 ha^{-1} and DC was 29.2 m^2 ha^{-1}. However, there was no significant difference in the mean of basal area between both locations ($p \geq 0.05$). *Ficus carica* in DC is the largest tree for both locations, thus, it may contribute to an overall basal area.

Examining the tree species diversity and forest stand structure of Kuala Keniam in Pahang, Suratman *et al*. [23] recorded the basal area ranged from 17.2-34.3 m^2 ha^{-1}, in which within in the range with the present study even they are different types of forest.

Diameter class distribution

As shown in the Figure 2, 39.5 % of trees fell within the 10-14.9 cm, 22.7% fell within 15-19.9 cm, 12.8% fell within 20-24.9 cm, 8.5% fell within 25-29.9 cm and 5.3% fell within 30-34.9 cm in WC study site. In addition, it shows a less or an absent number of stems in diameter classes from 70-79.9 cm onwards. When compared to DC study site, has higher portion of smaller trees with percentage of 10-14.9 cm is 45.2%. However, trees in diameter classes from 60-64.9 cm until 85-89.9 cm appear to be absent (Fig. 3).

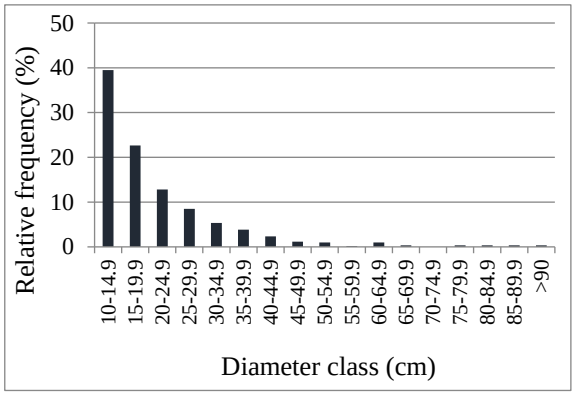

Fig. 2 Diameter class distribution of WC study site.

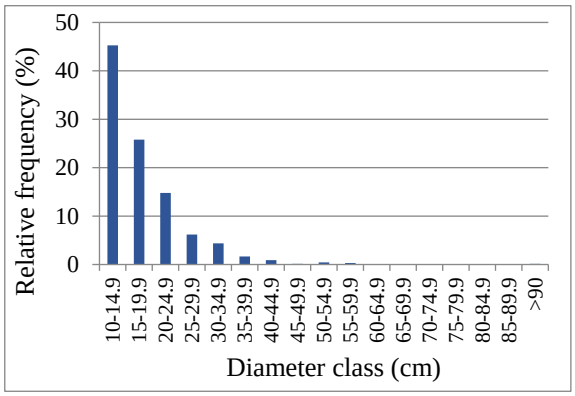

Fig. 3 Diameter class distribution of DC study site.

The presence of growth of the forest in both study sites are indicated by the movement of trees in various diameter classes. The findings show DC has higher regeneration due to high percentage of small trees compared to WC. Moreover, it may suggest higher mortality due to less number of larger trees that could be due to the natural causes. However, the stand structure shows both study sites confirm to the characteristic of De iocourt's factor procedure (inverse J-distribution) where stems frequencies decreasing with increase in DBH for all trees. Thus, the stands in both study sites are developing and regeneration in the forest is present.

Floristic Composition Analysis

A total of 1263 trees representing 179 species in 109 genera from 41 families were enumerated from both study sites. As shown in Table 1, the total number of 600 trees in WC study site belong to 38 families, 88 genera and 130 species, whilst the DC consist of a total of 663 trees that belong to of 36 families, 79 genera and 100 species.

Table 1 Summary of floristic composition in two

study sites.

Study site	No. of families	No. of genera	No. of species
WC	38	88	130
DC	36	79	100

Different size of study sites may have affected the number of taxa present. The larger area of study site WC tends to have higher number of families, genera and species as compared to DC that only half of WC site.

Species diversity

A summary the analysis for five indices of diversity, richness and evenness for the two study sites is presented in Table 2.

Table 2 Summary of species diversity for two study sites.

Variables	Study sites	
	WC	DC
Shannon-Weiner index (*H'*)	2.39a	2.39a
Simpson's diversity (*D*)	0.95a	0.91b
Margalef's diversity index (D_{Mg})	4.22a	4.05a
Menhinick's diversity index (D_{Mn})	3.07a	2.77a
Shannon's equitability (E_H)	0.93a	0.92a

Note: Means with the same letters are not significantly different ($p \leq 0.05$)

As shown in the table, the *H'* value for both study sites recorded a similar value of 2.39. The *D* values for sites WC and DC was 0.95 and 0.91, respectively. Results from t-test indicated that the *D* was significantly difference between both study sites ($p \leq 0.05$). Generally, the finding suggest that both study sites are uniform as there no significant differences in means of most of the indices.

Other study by Mata *et al.* [16] recorded the *H'* value for tropical freshwater forested wetlands in Veracruz, Mexico, ranged from 2.25-3.37. Based on Rosenzweig and Waide *et al.* [18][19], the area and environmental heterogeneity have strong effects on species diversity. These may suggest that the different of environment factors within study locations have influenced the species diversity in a community.

Similar patterns were found for species richness which was computed using D_{Mg} and D_{Mn}. The D_{Mg} was 4.22 and 4.05 where the D_{Mn} was 3.07 and 2.77 in WC and DC, respectively. Both indices show that the WC had higher species richness as compared to DC. There was no significant difference in means of species richness between both study sites ($p \geq 0.05$). Rajkumar and Parthasarathy [20] reported that lower species richness can be related to small size of study sites.

For evenness, the E_H value was 0.93 in site WC and 0.92 in site DC. There was no significant difference in the means of evenness between both study sites ($p \geq 0.05$). Evenness is a measure of the relative abundance of the different species making up the richness of an area. A community dominated by several different species that have a similar abundance is considered to be more diverse, thus as species richness and evenness increase, so diversity increases.

From a similarity analysis (*Ss*) on the species composition of both sites revealed that the similarity between the sites was low with a value of 31.4% (table not shown). This could be due to WC site which contains higher species richness as compared to DC, and majority of species occurred only at the DC.

Family-wise distribution

Data for tree families were pooled for both study sites. A total of 41 tree families were encountered in the study sites. The maximum number of tree species belongs to the family of Euphorbiaceae which accounts for 11.7% of the total individuals encountered in the study sites. This is followed by Sapotaceae, Guttiferae and Myrtaceae which account for 8.9%, 7.8% and 5.6% of the total individual encountered in the study sites, respectively. A few families have lowest percentages of the total individual encountered in the study sites with 0.6 % (i.e., Anisophylleaceae, Aquifoliaceae, Celastraceae, Icacinaceae, Lecythidaceae, Olacaceae, Opiliaceae, Passifloraceae, Polygalaceae, Rosaceae, Sterculiaceae and Verbenaceae) (Fig. 4).

A study in Cambodia on the evergreen swamp forest by Theilade *et al.* [21] also reported Euphorbiaceae as the dominant family with the highest number of species in that area, followed by Dipterocarpaceae, and Meliaceae. In other study on floristic composition at freshwater swamp forest in south eastern Brazil by Magalhaes and Maimoni-Rodella [22] reported that Orchidaceae, Rubiaceae and Myrtaceae are the three dominance families in that area.

In Malaysia, a study on tree species diversity and forest stand structure of Kuala Keniam by Suratman *et al.* [23] at Pahang National Park, Malaysia reported that Euphorbiaceae was the dominant family with 23.9 % of the total individuals were encountered in the study area. In addition, Khairil *et al.* [17] who studied the tropical watershed forest in Peninsular Malaysia also found that Euphorbiaceae as a dominant family in the study sites.

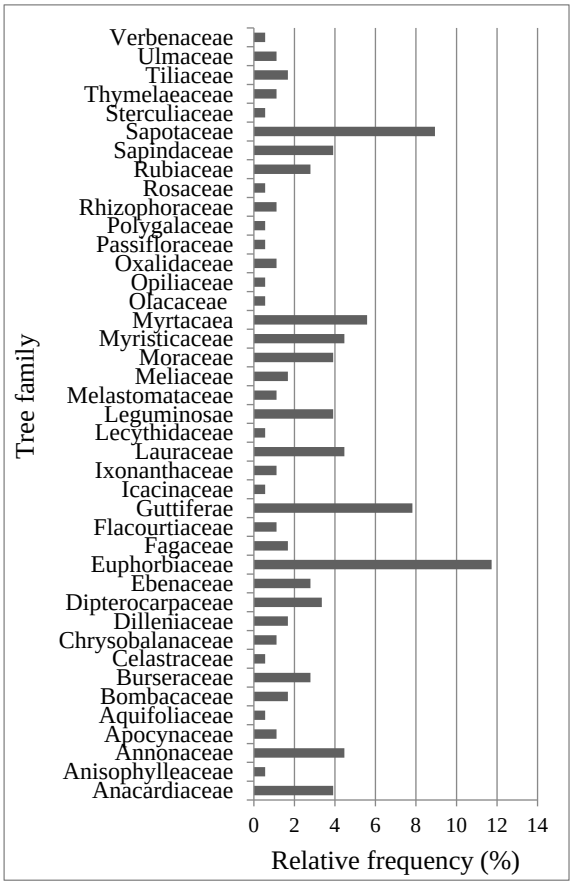

Fig. 4 Family-wise distribution of trees in the study sites.

The study area presented high family richness as commonly found in swamp forest [24]. In total, 53.7 % of tree families in this area is similar to the previous studies conducted at evergreen swamp forest in Cambodia by Theilade *et al.* [21] and at freshwater swamp forest in south eastern Brazil by Magalhaes and Maimoni-Rodella [22]. Based on the present and previous study, freshwater swamp forests consist of common families such as Euphorbiaceae, Guttiferae, Myrtacaea, Lauraceae and Moraceae.

Important Value Index (IVI)

Table 3 shows that *Artocarpus scortechinii* was dominant species with the highest value of *IVI* (i.e., 28.44), followed by *Nephelium lappaceum* as co-dominant species (i.e., 26.99). In DC, the five most dominance species contributed 37.0% *IVI*. *Macaranga* spp. was the dominant species in WC site with an *IVI* of 24.73%. The co-dominant species in DC is *Ficus carica* with an *IVI* of 19.61 (Table 3).

Table 3 Species importance value (*IVI*) for the five most dominance species in both locations

Species	Family	*IVI*
WC		
Artocarpus scortechinii	Moraceae	28.44
Nephelium lappaceum	Sapindaceae	26.99
Syzygium papillosum	Myrtacaea	20.15
Palaquium spp.	Sapotaceae	12.57
Shorea macrantha	Dipterocarpaceae	11.85
Total (& % for top five species)		100.00 (27.3%)
DC		
Macaranga spp.	Euphorbiaceae	24.73
Ficus carica	Moraceae	19.61
Syzygium spp.	Myrtacaea	16.40
Artocarpus integer	Moraceae	14.95
Nephelium lappaceum	Sapindaceae	10.69
Total (& % for top five species)		86.38 (37.0%)

Others studies was Theilade *et al.* [21] recorded *Macaranga triloba* being dominant in swamp forest of Cambodia and Mata *et al.* [16] found that *Pachira aquatic* was the dominance species in Chira forested wetland, Mexico.

Tree species of special interest

From the field observation, some of critically endangered species were encountered in the study sites. Based on the IUCN Red List data list, six species of Dipterocarpaceae (i.e., *D. semivestitus, H. apiculata, S. hemsleyana, S. macrantha, S. platycarpa and V. flavid*a) are listed in the category [25]. All these species are restricted to freshwater swamp forest in Peninsular Malaysia except for *H. apiculata* that can be found in lowland to hill dipterocarp forests up to 610 m altitude.

CONCLUSION

The freshwater swamp forest of Parit Forest Reserve comprises of natural vegetation and is dictated by microhabitat conditions. The findings show that DC has higher regeneration and mortality compared to WC. However, both study sites confirm to the characteristic of De iocourt's factor procedure (inverse J-distribution) that indicate stands are developing and regeneration in the forest is present. The similar value of *H*' (2. 39) suggests that both study sites are uniform in terms of species diversity. The most dominance families in the study area are Euphorbiaceae, Sapotaceae, Guttiferae and Myrtaceae. The sites are represented by different combinations of the dominant and co-dominant species where *Artocarpus scortechinii* was dominant species followed by *Nephelium lappaceum* as co-dominant in WC, whilst in DC the dominant and co-dominant species are *Macaranga* spp and *Ficus*

carica, respectively. More comprehensive information are required to identify conservation efforts towards the protection of freshwater swamp forests.

ACKNOWLEDGEMENTS

The authors would like to thank to the Ministry of Education (MoE), Malaysia for providing research grants through the Fundamental Research Grant Scheme (FRGS) 600-RMI/FRGS 5/3 (41/2014) and Universiti Teknologi MARA (UiTM) for providing support and logistic related services.

REFERENCES

[1] Woodruff DS, "Neogene marine transgressions, paleogeography and biogeographic transitions on the Thai–Malay Peninsula", Journal Biogeography No. 30, 2003, pp. 551-567.
[2] Mittermeier RA *et al*., "Hotspots revisited: earth's biologically richest and most terrestrial ecoregions", Conservation International, Washington, 2005.
[3] Department of Agriculture M, "Vegetation Cover of Peninsular Malaysia", Kuala Lumpur: Department of Agriculture Malaysia, 2006.
[4] Pfaff A, Amacher GS, & Sills E, "Realistic REDD: improving the forest impacts of domestic policies in different settings", Rev. Environ. Econ. Policy 7 (1), 2013, pp. 114–135.
[5] Suratman MN, Noh NA, & Nawi L, "Spatial Distribution and Demographic Structure of the Critically Endangered Dipterocarpaceae in Fragmented Habitat in Malaysia", 2014
[6] Suhaida M & Chua LS, (2012). "Conservation status of threatened dipterocarps in Peninsular Malaysia", International Union of Forest Research Organizations, Vienna, Austria: IUFRO Headquarters, 2012, pp. 62.
[7] IUCN, "The IUCN Red List of Threatened Species", Retrieved from http://www.iucnredlist.org, 9 March, 2015.
[8] Department Meteorology Malaysia, "Annual Rainfall Statistic of Perak", Retrieved from http://www.met.gov.my/index.php?option=com_weathertimeseries&purpose=humidity&Itemid=907, 2 May, 2016.
[9] Husch B, Beers TW & Kershaw JA, Forest Mensuration, fourth edition. New York: John Wiley and Sons Publishing, 1982.
[10] Brower CA, Zar JH, & Ende CN. Field and Laboratory Methods for General Ecology. Boston: McGraw Hill, 1997.
[11] Margalef FR, "Evolution and measurements of species diversity", Taxon. Vol. 21, 1972, pp. 213-251.
[12] Menhinick EF, "A comparison of some species individual diversity indices applied to samples of field insects", Ecology 45, 1964, pp. 839-861.
[13] Shannon CE & Weaver W, The Mathematical Theory of Communication. Urbana: University of Illinois Press, 1949
[14] Simpson EH, "Measurement of diversity", Nature 163, 1949, pp. 688.
[15] Kent M & Coker P, Vegetation description and analysis: a practical approach. London: Belhaven Press, 1992.
[16] Mata Di *et al*., " Floristic composition and soil characteristics of tropical freshwater forested wetlands of Veracruz on the coastal plain of the Gulf of Mexico", Forest Ecology and Management 262, 2011, pp. 1514-1531.
[17] Khairil M, Wan Juliana WA, & Nizam MS, " Edaphic influences on tree species composition and community structure in a tropical watershed forest in Peninsular Malaysia", Journal of Tropical Forest Science 26(2), 2014, pp. 284-294.
[18] Rosenzweig ML, Species Diversity in Space and Time. Cambridge University Press, 1995.
[19] Waide *et al.* RB, "The relationship between productivity and species richness", Annu. Rev. Ecol. Systematics, vol. 30, 1999, pp. 257-300.
[20] Rajkumar M, & Parthasarathy N, "Tree diversity and structure of Andaman Giant Evergreen Forests, India", Taiwani 53 (4), 2008, pp. 356-368.
[21] Theilade I *et al*., "Evergreen swamp forest in Cambodia: floristic composition, ecological characteristics, and conservation status", Nordic Journal of Botany 29, 2011, pp. 71-80.
[22] Magalhaes JHR, & Maimoni-Rodella RCS, "Floristic composition of freshwater swamp forest remnant in southeastern Brazil", Journal of species lists and distribution, 2012, pp. 833-838.
[23] Suratman MN *et al*., Beyond Biodiversity Conservation. Shah Alam: UiTM Press, 2014, pp. 1-17.
[24] Marques MC, Silva S, & Salino A, "Florística e estrutura do componente arbustivo-arbóreo de uma floresta higrófila da bacia do Rio Jacaré-Pepira", Acta Botanica Brasilica 17(4), 2003, pp. 495-506.
[25] Saw LG *et al*., "Conservation of some rare and endangered plants from Peninsular Malaysia", Kew Bulletin Volume 65, 2010, pp. 681-689.

Second International Conference on Science, Engineering & Environment,
Osaka City, Japan, Nov.21-23, 2016, ISBN: 978-4-9905958-7-6 C3051

ASSESSING TSUNAMI VULNERABILITY AREAS USING SATELLITE IMAGERY AND WEIGTHED CELL-BASED ANALYSIS

Abu Bakar Sambah[12], Guntur[1], Fusanori Miura[3], Fuad[1], and Defrian Marza Arisandi[1]
[1]Faculty of Fisheries and Marine Science, Brawijaya University, Indonesia; [2]Marine Resources Exploration and Management Research Group, Brawijaya University, Indonesia; [3]Graduate School of Science and Engineering, Yamaguchi University, Japan

ABSTRACT

The application of multi-criteria analysis followed by weighted cell-based processing is one of the methods for tsunami vulnerability mapping. In this study, vulnerability due to tsunami disaster in coastal area of East Java Province Indonesia was carried out. Appropriate input criteria were derived from Digital Elevation Model data, satellite remote sensing and survey data. The criteria applied were elevation, slope, coastal distance, river proximity, coastal type, and land use. Five classes of vulnerability were defined from low to high vulnerability. Analytical hierarchy process described that elevation was the highest weight. The area that identified as slightly high and high class of tsunami vulnerability spread in the coastal area which has a lower elevation and predict as inundated area. Most of the area was developed areas with low vegetation density. The high vulnerability areas were mostly found in the coastal area with the sloping coast type. The result presented here can aid as a basic data for city planning related to disaster mitigation and for the evacuation process and management strategy during a disaster.

Keywords: Tsunami Vulnerability, Weighted Cell-based, Geo-spatial Data

INTRODUCTION

Assessing tsunami vulnerability areas can provide basic information that is important for tsunami disaster risk management plans and mitigation. Tsunami vulnerability assessment is essential to disaster management planning. This includes pre-planning appropriate response activities in order to minimize the impact of disaster and all possibilities that will happen. This also plays an important role in preparing and mitigating for the future events [1].

Geologically, the south coast of Java Island is in the confluence of two major plates meet each other, Eurasian and Indo-Australian, where the movement of tectonic plates in this area will cause an earthquake that could trigger a tsunami. Based on the historical data of the earthquake event that followed by a potential destructive tsunami in the period of 1991 to 2006, recorded a tectonic earthquake in the Indian Ocean which triggered the tsunami on the southern coast of East Java, namely on June 3, 1994. A magnitude of 7.8 Mw, earthquake triggered a tsunami that affect southern coastal areas of Banyuwangi, East Java with estimated death toll reached 215 people [2]. The same events have the possibility to occur again in the same area in near future.

The development of geo-spatial analysis in the concept of a multi-criteria analysis for disaster management study provides an important integrated contribution in conducting a tsunami vulnerability assessment. A multi-criteria approach will be integrated into geo-spatial analysis. The study aims are to assess the vulnerability areas due to tsunami disaster and to analyze vulnerability area to different land use type. The use of multi-criteria and weighted cell-based analysis to assess the tsunami vulnerability areas was introduced in this study, in which this approach has not been applied before.

METHODS

Study Area

The study area includes coastal area of Jember District, East Java Province, Indonesia (Fig. 1).

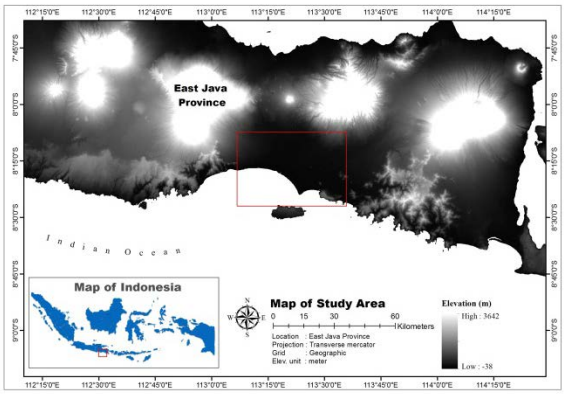

Fig. 1 Study area.

This area is one of the important areas for marine fisheries resources along southern part of Java Island, Indonesia. This area also affected by 1994 tsunami event along coastal area of East Java.

Dataset

ALOS satellite imagery with the instrument of panchromatic (PRISM) in the spatial resolution of 2.5 m and the Advanced Visible and Near Infrared Radiometer type 2 (AVNIR-2) with the spatial resolution of 10 m was analyzed for land use observation. The elevation data was obtained from The ASTER Global Digital Elevation Model (ASTER GDEM) version 2. The Advanced Space-borne Thermal Emission and Reflection Radiometer (ASTER) GDEM is a joint product developed and made available to the public by the Ministry of Economy, Trade, and Industry (METI) of Japan and the United States National Aeronautics and Space Administration (NASA) [3]. In addition to prepare coastal morphology data, digital vector map of the study are was applied.

CRITERIA AND GEO-SPATIAL DATA PROCESSING

Criteria Construction

Vulnerability mapping has been carried out using the parameters elevation, slope, coastal distance, river proximity, coastal type, and land use. The steps of analysis are data collection, surface analysis of DEM data, vector map extraction, land use mapping, and multi criteria processing using pair-wise comparison analysis (see Fig. 2 and Fig. 3).

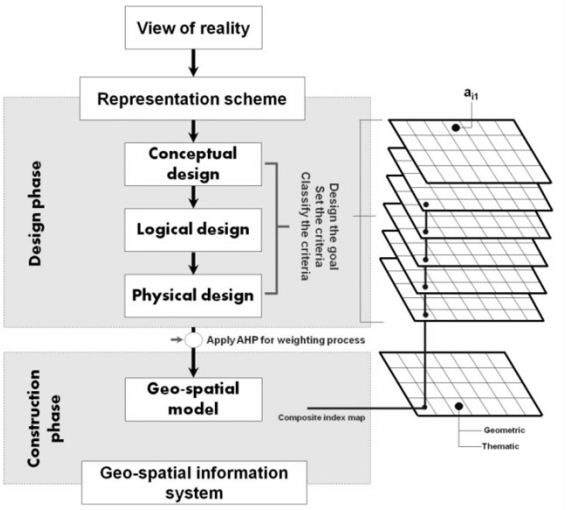

Fig. 2 General methodology adopted in this study.

The two steps of this concept are the design and construction phases. The design phase includes the selection of criteria which is used for the vulnerability assessment, while the construction phase describes the process of geo-spatial data. Each of those criteria weighted based on analytical hierarchy process due to lack of knowledge regarding the impact level of each criteria.

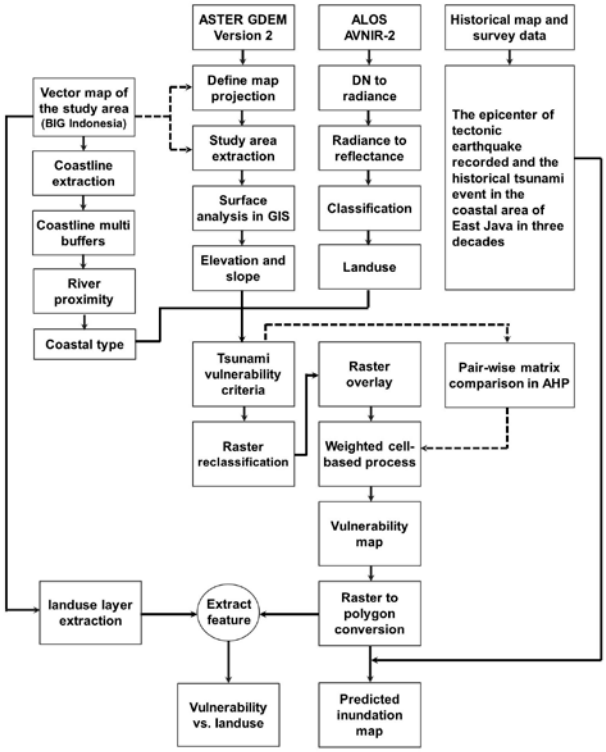

Fig. 3 Flow diagram of data processing.

Geo-spatial Data Processing

A set of criteria that describe the physical vulnerability are ; (1) elevation, that generated using ASTER GDEM version 2 data (downloaded from http://gdem.ersdac.jspacesystems.or.jp/; (2) slope, which is generated from elevation data; (3) coastal distance, which is calculated the distance from coastline to the land using multi-buffering and was set based on the possibility range of the tsunami to reach the land; (4) river proximity; (5) coastal type; and (6) land use, as the result of ALOS AVNIR-2 image classification.

Slope was generated using Eq. (1). The rates of change (delta) of the surface in the horizontal (dz/dx) and vertical (dz/dy) directions from the center cell determine the slope. At a given point on a surface z=f (x,y), S is defined as a function of gradients at X and Y (i.e., West-East and North-South) directions.

$$\mathbf{S} = \sqrt{\left(\frac{\delta z}{\delta x}\right)^2 + \left(\frac{\delta z}{\delta y}\right)^2} \quad (1)$$

Coastal distance generated using vector map provided by Indonesia Geo-spatial Authority, and created using Eq. (2).

$$\boldsymbol{log X_{max} = log 1400 + {}^{4}/_{3}\, log\left({}^{Y_0}/_{10}\right)} \qquad (2)$$

X_{max} is the maximum reach of the tsunami over land, and Y_0 is the height of the tsunami at the coast.

Land use map generated from supervised classification process of ALOS image. Land use class was divided into five classes. We select representative samples for each land use class in the reflectance value of digital image. The classification of land use was based on the spectral signature defined in the training set. Maximum likelihood classification was applied in the supervised process.

Criteria was calculated using its vulnerability value range as shown in Table 1 and Table 2, while map of tsunami vulnerability based on the criteria described in Fig. 4, Fig. 5, Fig. 6, Fig. 7, Fig. 8, and Fig. 9.

Table 1 Tsunami vulnerability value range (a)

Vulnerability class	Elevation (m)[1]	Slope (%)[2]	Landuse[3]
High	<5	0-2	Urban
Slightly high	5-10	2-6	Agriculture
Moderate	10-15	6-13	Bare soil
Slightly low	15-20	13-20	Water
Low	>20	>20	Forest

[1][4]
[2][5]
[3][6]

Table 2 Tsunami vulnerability value range (b)

Vulnerability class	Coastal distance (m)[4]	River proximity (m)[5]	Coastal type[5]
High	<293	0-100	V bay
Slightly high	293-514	100-200	U bay
Moderate	514-762	200-300	Cape
Slightly low	762-1032	300-500	Straight
Low	>1032	>500	Neutral

[4] Based on Eq. 2 calculations
[5] [7]

Tsunami vulnerability maps based on elevation and slope (in Fig. 4 and Fig. 5) show vulnerability classes of slightly high and high were found to the western side of coastal areas. This area identified as an urban and agricultural, with the slope range between 0-13% and elevation of 0-15m. The highest elevation (1185m) was found to the eastern side of the study area and is classed as a low vulnerability to tsunami area.

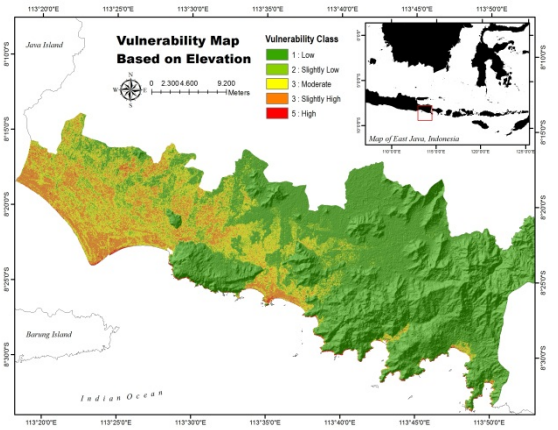

Fig. 4 Tsunami vulnerability map based on elevation.

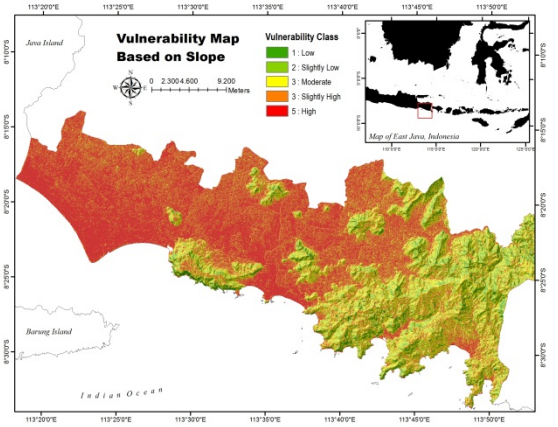

Fig. 5 Tsunami vulnerability map based on slope.

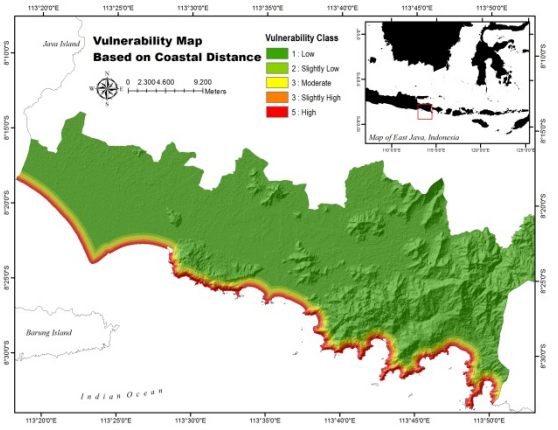

Fig. 6 Tsunami vulnerability map based on coastal distance.

The tsunami vulnerability map based on coastal distance (in Fig. 6) was calculated based on the historical data collected during previous tsunami events by USGS. Minimum run up recorded in the study area was 3.1m. The calculation of Eq.2 describes that 3.1m of run up will reach 293m of the proximity from coastline to land, while in the proximity range of 1032m will have 11.2m of run up.

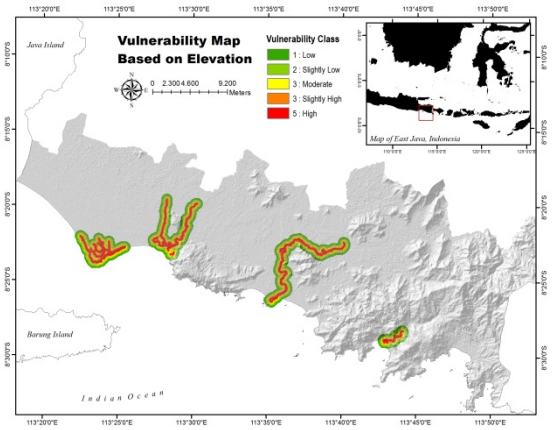

Fig. 7 Tsunami vulnerability map based on river proximity.

As shown in Fig 7, rivers were identified in four different areas. Rivers can play an important role in expanding the impact of the damage during tsunami event. The run-up of the tsunami reaches the hinterland not only through the low elevation of the area, but also through rivers. Rivers also act as flooding strips transporting inundation [8].

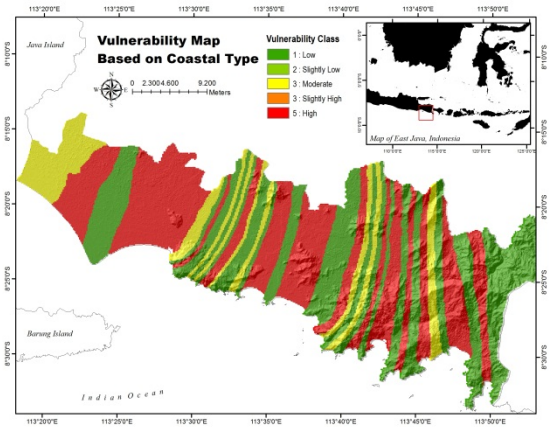

Fig. 8 Tsunami vulnerability map based on coastal type.

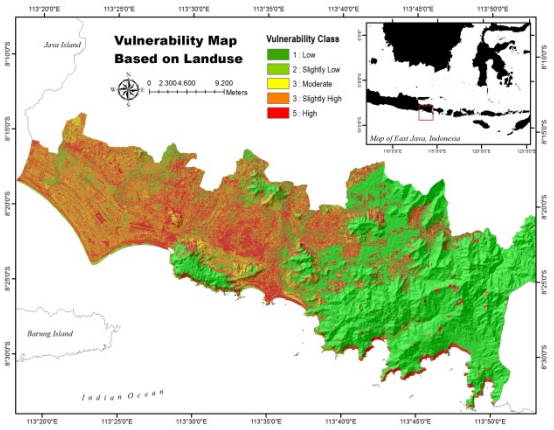

Fig. 9 Tsunami vulnerability map based on land use.

In the classification of tsunami vulnerability based on land use (Fig. 9), urban area represents a high class of tsunami vulnerability. Low density urban area was classified as bare soil and forested areas as the area with the lowest vulnerability to tsunami damage. High density of vegetation can have a significant effect on protecting the land from tsunami [9].

VULNERABILITY ASSESSMENT

Weighted Cell-based

Weighted overlay is a technique for applying a common measurement scale of values to diverse and dissimilar inputs to create an integrated analysis. Weighted overlay also is a type of suitability analysis that helps in analysing site conditions based on multiple criteria. By identifying and rating areas based on criteria, weighted overlay analysis allows the user to combine weight and rank several different types of information and visualize it, so multiple factors can be evaluated at once [10].

All parameters are displayed in grid cells within this paper. Cells are then classified based on its value to five classes of vulnerabilities; represent low, slightly low, medium, slightly high and high vulnerability. Grouping cells in this raster data followed zonal function operation. Each cell is encoded based on the criteria that make up a zone.

Weighted linear combination is very straightforward in a raster GIS and factors are combined by applying a weight value to each followed by a summation of the results to create a vulnerability map using Eq. (3) [11].

$$\sum (W_i \cdot X_i) \qquad (3)$$

Where, Wi is the weight values of the parameter i, and Xi is the potential rating of the factor.

Tsunami Vulnerability Mapping

In order to create the vulnerability map, each raster cell of the criteria was calculated to its weight. The weight of each criterion was calculated using pair-wise comparison matrix and normalized matrix processing until 6th iteration (see Table 3).

Table 3 Pair-wise comparison matrix

					Normalized principal eigenvector (6th iteration)		
	c.1	c.2	c.3	c.4	c.5	c.6	%
c.1	0.28	0.29	0.353	0.288	0.184	0.273	28
c.2	0.187	0.194	0.176	0.231	0.184	0.182	19
c.3	0.14	0.194	0.176	0.231	0.245	0.136	18
c.4	0.112	0.097	0.088	0.115	0.184	0.182	12
c.5	0.187	0.129	0.088	0.077	0.122	0.136	13
c.6	0.093	0.097	0.118	0.058	0.082	0.091	9

CI = 0.032, CR = 2.6%

c.1 : elevation; c.2 : slope; c.3 : coastal distance; c.4 : river proximity; c.5 coastal type; c.6 : land use

The comparison matrix of each parameter (c.1

until c.6) as shown in Table 3 was calculated using Saaty scale of AHP (1 to 9 scales) [12]. Fig. 10 shows the output map as a result of weighted cell-based analysis. In the comparison matrix, elevation has the highest score out of other criteria, and is considered to be more important than slope, coastal distance, river proximity, and land use. In term of coastal distance, even if the area is close to coastline, a higher elevation will have low vulnerability. The elevation parameter is considered the only reliable parameter of the tsunami magnitude to vulnerability functions on buildings that can be observed or measured following all tsunami events, while water depth during a tsunami will differ according to the ground elevation [13]-[1].

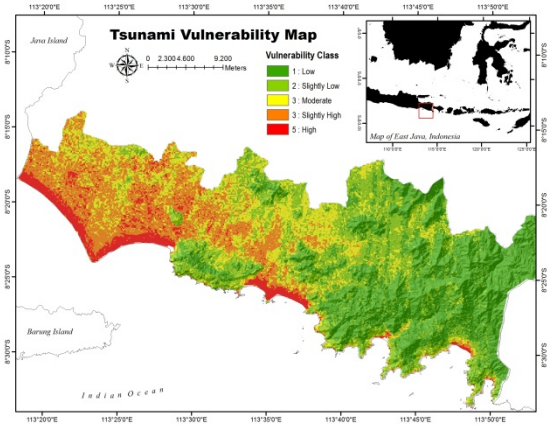

Fig. 10 Tsunami vulnerability map.

DISCUSSION

Vulnerability is the characteristics of a person or group and their situation that influences their capacity to anticipate, manage, resist, and recover from the impact of a hazard. It also represents the susceptibility of a given population to damaging effects from exposure to hazardous events [14][15]. Class of vulnerability could be based on physical criteria, such as elevation, slope, coastline proximity, and land use. Some research [1][7][8] also put the criteria of coastal geomorphology, coastal ecosystem resources, direction of tsunami wave, and distance from river.

Coastal ecosystem including mangrove areas and reefs can be a barrier zone to reduce the effect of tsunami wave, as well as the islands with steep-sided fringing is only at moderate risk from tsunamis. Tsunami waves may undergo extensive refraction and create a process that may converge their energy to particular areas on the coastal areas and increase the heights. This is depending on the water depth, the coastal geomorphology, and the direction of tsunami wave. Moreover, rivers can be a tsunami flooding strips and brings the tsunami wave to the hinterland.

During the 2011 Tōhoku's tsunami [16], some of the most dramatic flooding occurred close to the river, where flood water washed across large tracts of farmland and urban area. Research conducted by scientists at Tōhoku University suggests that waves from the tsunami travelled nearly 50 kilometres upstream from the coastal area (mouth of the Kitakami River) [16].

The use of pair-wise comparison matrix helps in the analysis of spatial multi criteria where all of the parameters used in this study were calculated based on its weight factor to create vulnerability map. Research conducted in coastal area of Miyagi Prefecture, Japan [8] also describes the application of pair-wise comparison matrix in weight calculation for each parameter. The result of this research shows a similar pattern of high class of tsunami vulnerability area to the real tsunami inundation area during the 2011 Tōhoku's tsunami [8]. The calculation of weight as a result of pair-wise comparison matrix was created from expert judgment. Expert knowledge about the weight scale of each parameter is a necessity, so that every parameter was weighted not equally since the individual importance of each parameter. Other research on tsunami vulnerability in Alexandria was applied all parameter in equal weight due to the limitation of knowledge regarding to the study area [17].

The high vulnerability areas were mostly found in the coastal area with the sloping coast type. Elevation and slope play an important role in governing the stability of a terrain [18]. Tsunami vulnerability research in Bali, Indonesia shows the distribution of vulnerability is not uniform and physically it is highly influenced by coastal proximity, elevation, and slope [19].

The historical data of run up height in study area was used to assess tsunami inundated areas. Spatial analysis through grid overlay between historical run up height and tsunami vulnerability classes shows the inundated area may spread along the high class of vulnerability where the elevation was less than 20m (Fig. 12 and Fig. 13). Inundated area mapping is important for preparing the evacuation route and evacuation building. Elevation more than 20m indicates the area may select as evacuation area.

In the process of weighted overlay, elevation is the parameter that has the highest weight (28% of six parameters). Most of the area that identified as slightly high and high class of tsunami vulnerability is developed areas (urban areas) with low vegetation density. Previous research [20] stated different ways in which coastal vegetation may reduce the impact of tsunami. Vegetation will stops driftwood and other flotsam, reduces water flow velocity and inundation depth, provides a life-saving snare for people swept off land by a tsunami run-down, and amasses wind-blown sand and create dunes, which

act as a natural barriers against tsunamis [20]. However, in the case of a huge tsunami event, narrow belts of coastal vegetation may be ineffective in providing protection, and in some cases may create more damage because of uprooted trees flowing inland [21].

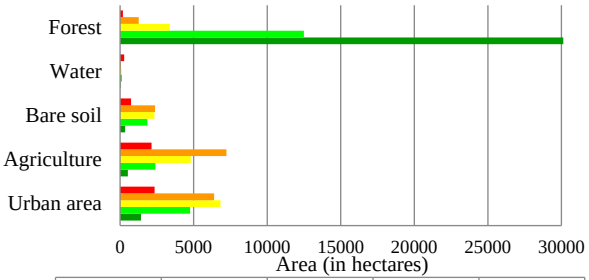

	Urban area	Agriculture	Bare soil	Water	Forest
5	2344.00	2139.00	742.00	282.00	191.00
4	6388.27	7229.85	2379.87	53.51	1262.98
3	6825.22	4801.37	2333.54	108.81	3379.93
2	4761.21	2404.74	1854.33	125.12	12495.11
1	1420.97	528.22	348.55	41.41	33422.98

1 : low; 2 : slightly low; 3 : moderate; 4 : slightly high; 5 : high

Fig. 11 Overlay graph of tsunami vulnerability class and land use (in hectares).

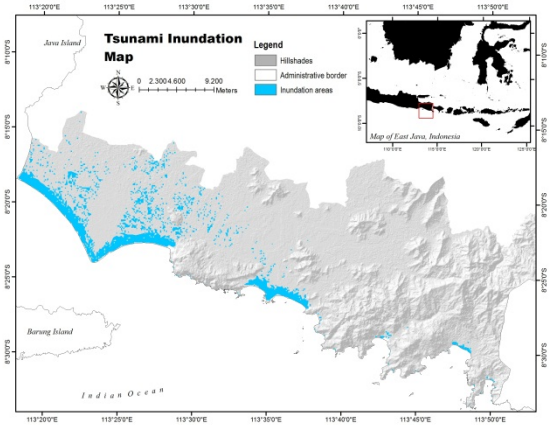

Fig. 12 Tsunami inundation assessment.

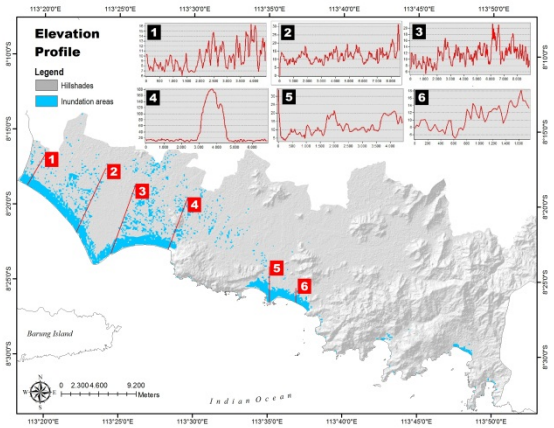

Fig. 13 Elevation profile along inundation areas.

CONCLUSIONS

The application of multi criteria analysis followed by weighted cell-based processing is useful for tsunami vulnerability mapping. It can be used for the evacuation and reconstruction plan due to tsunami disaster. The combination of raster weighted overlay in the geo-spatial data analysis indicated the vulnerability area due to tsunami and described the possibility area that could be affected by tsunami wave. The weight of each parameter was calculated by pair-wise comparison matrix of expert judgment, in which every parameter was weighted not equally. Parameter of elevation was 28% of weight, while land use has the lowest weight (9%). Tsunami inundated area was indicated in the high class of vulnerability with the elevation less than 20m. The spatial overlay result of tsunami vulnerability to land use classes describe that high class of tsunami vulnerability mostly in the class of urban area, while forest area was indicated in the low class. The more parameters that are applied, the more detailed is the assessment that can be displayed. Several parameters can be applied, such as land cover, geological structures, coastal type, and tsunami wave direction. In addition, the social and economic parameters also can be added, such as population density, type of building, household income, and business centre.

ACKNOWLEDGEMENTS

Authors are thankful to METI and NASA for the Aster GDEM version 2 products, Japan Aerospace Exploration Agency (JAXA) for the ALOS images and BIG Indonesia for providing the basic map of the study area. We also thank to Laboratory of Disaster Prevention System, Yamaguchi University, Japan.

REFERENCES

[1] Papathoma M, Dominey-Howes D, “Tsunami vulnerability assessment and its implications for coastal hazard analysis and disaster management planning, Gulf of Corinth, Greece”, Natural Hazards and Earth System Sciences, Vol. 3, 2003, pp. 733–747.

[2] Synolakis C, F. Imamura, Y. Tsuji, H. Matsutomi, S. Tinti, B. Cook, Y. P. Chandra, and M. Usman, Damage, “Conditions of East Java Tsunami of 1994 Analyzed”, Eos, Transaction, American Geophysical Union, Vol. 76, No. 26, June 27, 1995, p. 257, 261-262.

[3] Bollin C, Cardenas C, Hahn H, Vatsa KS, “Natural Disaster Network; Disaster Risk Management by Communities and Local

Governments", Washington, D.C., Inter-American Development Bank, 2012.

[4] Iida K., "Magnitude, energy and generation mechanisms of tsunamis and a catalogue of earthquakes associated with tsunamis", Proceeding of Tsunami Meeting at the 10th Pacific Science Congress, 1963, pp. 7-18.

[5] Van Zuidam RA, "Guide to Geomorphologic - Aerial Photographic Interpretation and Mapping", International Institute for Geo-Information Science and Earth Observation, Enschede, 1983, The Netherlands.

[6] Sambah AB and F. Miura, "Spatial Data Analysis and Remote Sensing for Observing Tsunami-Inundated Areas", International Journal of Remote Sensing. 2016, Vol. 37, Issue 9, pp. 2047-2065.

[7] Sengaji E and B. Nababa, "Tsunami Risk Level Mapping in Sikka, East Nusa Tenggara", Journal of Tropical Marine Science and Technology, June 2009, Vo. 1 No. 1, pp 48-61, (Indonesia edition).

[8] Sambah AB and F. Miura, "Remote Sensing and Spatial Multi-Criteria Analysis for Tsunami Vulnerability Assessment", Disaster Prevention and Management, 2014, Vol. 23 (3), pp. 271–295.

[9] Tanaka N, "Effectiveness and Limitations of Vegetation Bioshield in Coast for Tsunami Disaster Mitigation", The Tsunami Threat - Research and Technology, Nils-Axel MÃrner (Ed.), ISBN: 978-953-307-552-5, 2011. InTech.

[10] ESRI, "Environmental Systems Research Institute, Inc. Analyze Site Conditions Using Weighted Overlay", 2015, ESRI.

[11] Eastman JR, Jin W, Kyem PAK, Toledano J, "Raster procedures for multi-criteria/multi-objective decisions", Photogrammetric Engineering & Remote Sensing, American Society for Photogrammetry and Remote Sensing, 1995, Vol. 61(5), pp. 539–547.

[12] Saaty T.L., "Decision Making for Leaders; The Analytical Hierarchy Process for Decisions in a Complex World", 1982, RWS Publication, Pittsburgh, PA.

[13] Atillah A, El Hadani D, Moudni H, Lesne O, Renou C, Mangin A, and Rouffi F, "Tsunami vulnerability and damage assessment in the coastal area of Rabat and Sal´e, Morocco", Nat. Hazards Earth Syst. Sci., 2011, Vol. 11, pp. 3397–3414.

[14] Blaikie P, Cannon T, Davis I, and Wisner B. "At risk: Natural Hazards, People's Vulnerability, and Disasters", London: Routledge, 2004.

[15] Du Y, Yibo D, Zixiong L, and Guangwen C, "The role of hazard vulnerability assessments in disaster preparedness and prevention in China", Mil Med Res, 2015, 2:27.

[16] Mori N, T. Takahashi, T. Yasuda, and H. Yanagisawa, "Survey of 2011 Tohoku Earthquake Tsunami Inundation and Run-Up", Geophysical Research Letters, 2011, Vol. 38, Issue 7.

[17] Eckert, S., Jelinek, R., Zeug, G. and Krausmann, E. (2012), "Remote sensing-based assessment of tsunami vulnerability and risk in Alexandria, Egypt", Applied Geography, Vol. 32 No. 2, pp. 714-723.

[18] Yashon O. Ouma, and R. Tateishi, "Urban Flood Vulnerability and Risk Mapping Using Integrated Multi-Parametric AHP and GIS: Methodological Overview and Case Study Assessment", Water 2014, Vol. 6, pp. 1515-1545.

[19] Eddy, "GIS in Disaster Management: a Case Study of Tsunami Risk Mapping in Bali, Indonesia", Masters (Research) Thesis, 2006, Jamas Cook University, Australia.

[20] Shuto, N, "The Effectiveness and Limit of Tsunami Control Forest", Coastal Engineering in Japan, 1987, 30 (1): 143–153.

[21] Latief H and S. Hadi, "The Role of Forests and Trees In Protecting Coastal Areas Against Tsunamis', Coastal protection in the aftermath of the Indian Ocean tsunami: What Role for Forests and Trees?, Proceedings of the Regional Technical Workshop, Khao Lak, Thailand, 28–31 August 2006, Food and Agriculture Organization of The United Nations Regional Office for Asia and The Pacific Bangkok.

Second International Conference on Science, Engineering & Environment,
Osaka City, Japan, Nov.21-23, 2016, ISBN: 978-4-9905958-7-6 C3051

APPLICATION OF GAUSSIAN PROCESS TO SEABED LOGGING MODELS TO STUDY THE EFFECT OF FREQUENCY VARIATIONS TO HYDROCARBON EXPLORATION

Siti Mariam Mukhtar[1], Hanita Daud[2] and Sarat Chandra Dass[3]

[1, 2, 3]Universiti Teknologi PETRONAS, Department of Fundamental and Applied Sciences, 32610 Bandar Seri Iskandar, Perak, Malaysia

ABSTRACT

Hydrocarbon exploration is the process of finding hydrocarbon (HC) deposits beneath the Earth's surface by petroleum geologists or oil and gas companies. Seabed Logging (SBL) is a technique that uses controlled electromagnetic (EM) waves for finding potential HC reservoirs in deep water environments. Nowadays, the computer experiments in lieu of physical experiment for conducting the empirical research have been conducted in many fields. This paper investigates the correlation between variations frequencies of the transmitter to the depth of HC for SBL data. Computer Simulation Technology (CST) software was used to generate synthetic data that mitigated the real environment of SBL in a deep water environment. Parameters such as frequency, HC thickness and depth are the important physical inputs that determine the successful HC identification. The frequencies used in this work were 0.5Hz, 0.25Hz, 0.125Hz, and 0.0625Hz. The initial location of the HC was 1,000 m below the seabed and was incremented by 250 m until 3,000 m. By varying the frequency at each depth, the magnitudes of the E-field were recorded and they were processed using an algorithm of Gaussian process using MATLAB software. It was found that Gaussian Process is able to identify the presence of HC up to 2750m under the seabed at the lowest frequency (0.0625Hz) compared to only 2250m at the highest frequency (0.5Hz). This finding shall help geophysicists to decide on what frequency to use at optimum cost to obtain good results on HC exploration

Keywords: Seabed Logging, Gaussian Processes, Frequencies and Electromagnetic Wave.

INTRODUCTION

Hydrocarbon exploration is the process of finding hydrocarbon (HC) deposits beneath the Earth. Since 1970, a seismic method is a major technique in HC exploration because it can identify structures that might be expected to contain HC, but it is practically blind to the fluid contained in the formation [1]. This is because sound waves generated will only be reflected if there are rock layers beneath the seafloor. Therefore, a new technique called Seabed Logging (SBL) method was introduced and could overcome the ambiguity encountered in the seismic method.

SBL is an application of the marine Controlled Source Electromagnetic (CSEM) technique that is endeavoring to detect and depict HC bearing reservoirs in deep water exploration. The central principle of SBL which makes it as a revolutionizing tool in the exploration performance is the guiding electromagnetic (EM) wave in resistive layers between HC traps and sediments [2]. SBL is the approach that utilizes the use of a mobile horizontal electric dipole (HED) source and an array of seafloor electric field receivers by emitting a low-frequency electromagnetic signal both into the overlying water column and downwards from the transmitter close to the seabed [3]. In practice, SBL can examine the presence of high resistivity but it is difficult to dictate the exact geometry of the resistivity structure using SBL data alone due to low resolution [4]. Normally, in practice the seismic method will be used first to detect the presence of liquid underneath the seabed followed by SBL to confirm whether the liquid is water or HC traps. Indeed, both seismic interpretations and SBL data analysis play complementary roles.

In this research, forward modeling was developed by using a Gaussian process function which is a famous and good type of machine learning process. The standard GP modeling framework has been applied in various prediction problems. The data set was generated by using simulations software named Computer Simulation Technology (CST) software that replicates the real SBL environment. It is also used to generate synthetics data for various parameter variations.

To date, numerous applications are applying using Gaussian Process (GP) method to solve their problems. However, no literature on Gaussian

Process (GP) for SBL application has been found. GP is a collection of random variables, any finite number of which has consistent joint Gaussian distributions. A Gaussian process is fully parameterized by its mean function $m(x)$ and covariance function $k(x, x')$ on which the Gaussian distribution has mean and covariance in the form of vector and matrix respectively [5]. GP is a probabilistic, non-parametric model based on a principle of Bayesian probability. It differs from most of the other black-box identification approaches as it does not try to approximate the modeled system by fitting the parameters of the selected basis function, but more of searching for the relationship among the measured data. The output of the GP model is a normal distribution, expressed in terms of the mean and variance. The mean value represents the most likely output and the variance can be interpreted as a measure of its confidence level. Based on these properties, GP models are suitable for modeling uncertain processes or modeling unreliable data, data with noise and incomplete or missing data.

SIMULATION SETUP

In this research, as mentioned earlier CST software was used to simulate the SBL models. In the preliminary step, all constants or material properties that were used in the SBL models had been defined. We established a layered model where it replicated the actual SBL applications as showed in Table 1.

Table 1 The material properties for SBL models

Layer	Thermal permittivity, F/m	Electrical conductivity, (S/m)	Thermal conductivity, W/K/m
Air	1.000	1.0E-11	0.024
Sea water	80.000	1.63	0.593
Sediment	30.000	1.000	2.000
Hydrocarbon	4.000	0.002	0.492

Generating data

The base model for this study is the rectangular cuboid reservoir as shown in Fig. 1(a) and 1(b), for model with HC and without HC respectively. The model area was assigned as 10 Km x 10 Km x 5 Km that was considered previously in [6]. There were 5 main layers; air layer (300 m), seawater layer (1000 m), overburden layer (starts from 1000 m and increased by 250 m), hydrocarbon layer (200 m), and under burden layer (starts with 2500 m and decreased by 250 m) as shown in Table 2. As continuation from the previous paper in [6], depth of the overburden were varied from 1000 m (initial location) to 3000 m at increment of 250 m for each model. Frequencies of the transmitter were also varied at 0.0625 Hz, 0.125 Hz, 0.25 Hz, and 0.5 Hz respectively. In the simulations, a fixed HED-source was placed at 35 meters above the seabed at each operating frequency. The transmitter used was 270 m long with 1250A while the receiver was represented by a straight line parallel to the transmitter and placed at the seabed.

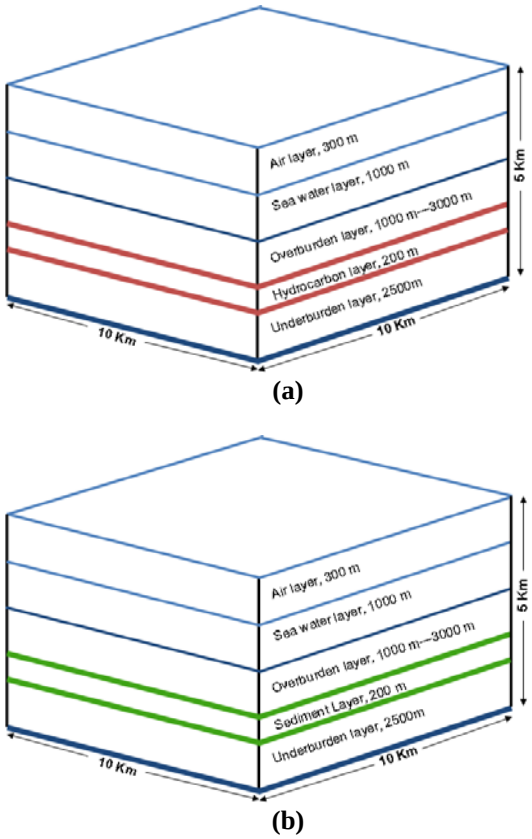

Fig. 1 Snapshot of SBL models with (a) presence of hydrocarbon and (b) absence of hydrocarbon.

Table 2 The stratified layered-media model for SBL models

Layer	Medium	Thickness, (m)	Variables
Layer 1	Air	300	Fixed
Layer 2	Sea water	1000	Fixed
Layer 3	Overburden	1000 -3000	Increased by 250 m for each model
Layer 4	Hydrocarbon	200	Fixed
Layer 5	Underburden	2250	Decreased 250 m for each model

THEORETICAL BACKGROUND

Gaussian Process Regression (GPR)

A GPR is a flexible and probabilistic regression method that also gives an uncertainty estimate [7]. Its uses and properties for modeling are reviewed in [8]. In this section, we derive the framework to train GP models under uncertain input data. For a given data set, a training set with *n* output data points is considered. Let x_i denote the offset where $y_i, i = 1,2,3...,n$ denotes as a new predicted E-field. Assuming there exist a relationship as in Eq. (1) between input *x* and output *y*.

$$y = f(x) \tag{1}$$

A Gaussian process is completely parameterized by its mean function and covariance function and are defined as in Eq. (2) and (3) below

$$m(x) = \mathrm{E}\left[f(x)\right] \tag{2}$$

$$k(x, x') = \mathrm{E}\left[(f(x) - m(x))(f(x') - m(x'))\right] \tag{3}$$

Then, will write the GP as

$$f(x) \sim GP(m(x), k(x, x')) \tag{4}$$

Available *n* training data, n_* test data, and $k(x, x')$ shall be used to represent the $n \times n_*$ matrix of covariances evaluated at all pairs of training and test points. A kernel $K(x_i, x_j)$ satisfies the property that it is an inner product in the feature space F as in Eq.(5).

$$\left\langle \phi(x_i), \phi(x_j) \right\rangle = k(x_i, x_j) \tag{5}$$

There are several types of covariance functions available, but squared exponential (SE) covariance (eq. 6) is the most commonly used kernel in machine learning.

$$k(x, x') = \sigma_f^2 \exp\left(\frac{(x - x')^2}{2\ell^2}\right) + \sigma_n^2 \delta_{ii'} \tag{6}$$

Where $\theta = \{a, b, \sigma_f, \sigma_n, \ell\}$ are called the free parameters. In general, it considered as hyperparameters. The signal variance σ_f^2 defined as the maximum allowable covariance and it is should be high for functions which cover a wide range on the y axis. In other to make it the function to look smooth, the neighbor must be alike. It means $f(x)$ is perfectly correlated with $f(x')$. If *x* is far away from the *x'*, these two pints cannot reach each other, therefore it will affect the interpolation at new x values. How much effect this separation has will depend on the length parameter ℓ, so there is much flexibility built into Eq. (6). Give the covariance between output points corresponding to input x_p and x_q respectively. Thus, the mean $\mu(x)$ and the covariance function $C(x_p, x_q)$ fully specify the GP. In GP regression, for every input *x* there is an associated random variable $f(x)$, which is the value of the stochastic function *f* at that location.

In order to make inferences about all of the hyperparameters in the light of the data, the probability of the datasets given the hyperparameters are computed. The marginal likelihood can be computed by integration over function *f*.

$$p(y \mid x) = \int p(y \mid f, \sigma^2)\, p(f \mid x, \theta)\, df \tag{7}$$

Assumed the distribution of the data is Gaussian, then from Eq. (7) the log marginal likelihood is obtained as in Eq. (8),

$$\begin{aligned} L &= \log p(y \mid x, \theta) \\ &= -\frac{1}{2}\log|\Sigma| - \frac{1}{2}(y - \mu)^T \Sigma^{-1}(y - \mu) - \frac{n}{2}\log(2\pi) \end{aligned} \tag{8}$$

The unknown hyperparameters can then be estimated from Eq. (8) by using a gradient-based algorithm [9]. The predictive distribution of any new test data x_* can then be evaluated. It can be shown that its mean and variance are given by Eq. (9) and (10).

$$m(x_*) = \Theta(x_*)^T \mu = k_*^T (K + \sigma^2 I)^{-1} \tag{9}$$

$$\begin{aligned} v^2(x_*) &= \Theta(x_*)^T \Sigma \Theta(x_*) \\ &= k_{**} - k_*^T (K + \sigma^2 I)^{-1} K \end{aligned} \tag{10}$$

RESULTS AND DISCUSSION

Training of a GP model typically took less than 10 s on a laptop (Lenovo) equipped with Intel Core-i7 CPU. Then, the implementation of the GPR process was realized using a MATLAB toolbox (GPML Toolbox) [10] . The commands used to define, minimize and predict the new test points x_* were formulated from the appropriate equations in

GPR section. All the models for SBL have been developed using CST software by varying the following parameter; depth of hydrocarbon and frequency of the transmitter. It is to observe the differences in E-field magnitude by changing both parameters.

Variations of frequency of the transmitter

In this work, the focused is on the magnitude of the hydrocarbon by varying the frequency of the transmitter. At each depth, 4 different frequencies had been run and the magnitudes of the E-field were recorded as in Fig. 2.

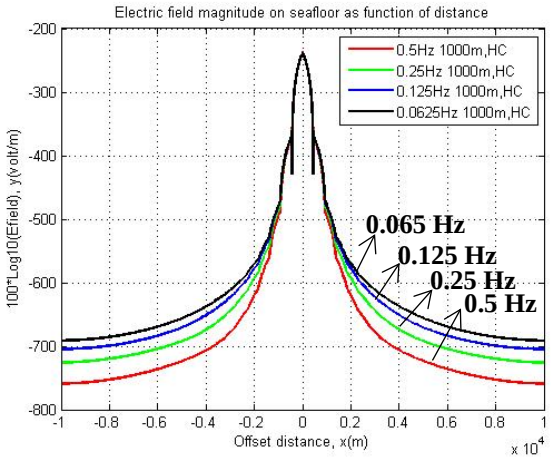

(a)

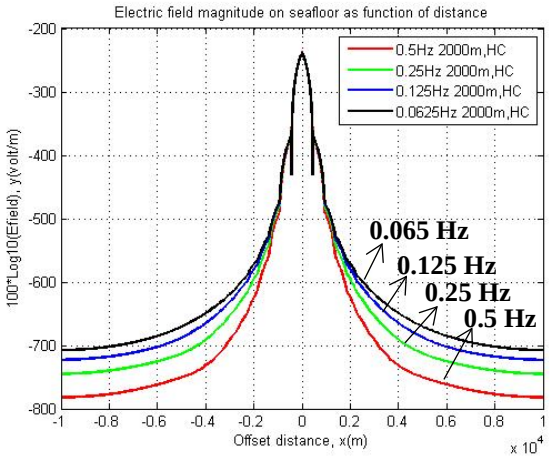

(b)

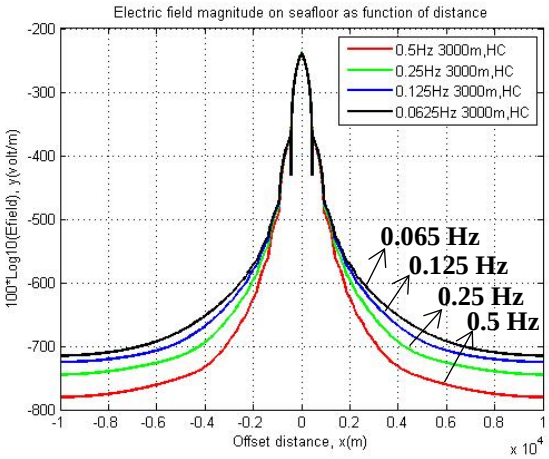

(c)

Fig. 2 Magnitude of E-field at Depth 3000 m for frequencies 0.5Hz, 0.25Hz, 0.125Hz, and 0.0625Hz at depth (a) 1,000 m, (b) 2,000 m and (c) 3,000 m

The magnitude of E-field at four different frequencies at depth 1,000 m, 2,000 m and 3,000 m are shown in Fig. 2(a), 2(b) and 2(c) respectively. Other depths are not shown due to space limitation of this paper.

It can be seen that, as the depth going deeper, the magnitude of E-field is getting smaller for all frequencies. Frequency of 0.0625Hz has the highest magnitude followed by 0.125Hz, 0.25Hz and 0.5Hz respectively. Therefore, from Fig. 2, it can be seen that lower frequency has bigger wavelength and higher wavelength lead to the higher magnitude of E-field due to large penetration rate. Then, based on the application of the Gaussian process, effects of the different frequencies with two scenarios (with and without hydrocarbon) at 1000 m and 3000 m will be discussed in the next section. These two depths were chosen because the contrasts in E-field magnitudes are clearly seen.

Implementation of Gaussian process for SBL using MATLAB

The aim of the simulation is to generate synthetic data for SBL models. Then, the data was extracted from CST and make them the training and predictions data for presence of HC using a MATLAB scripts. For this work, datasets with 60 points were used as the training data and 300 points were used as the test point. Since the transmitter was located at the center (zero offsets), the right and left of the SBL models give the same magnitude of E-field. Therefore, one side of the graph is only used as depicted by Fig. 3 and 4. Figures below also shows the 2 standard deviation error bars for the predictions obtained using the values of the hyperparameters. In this paper, only two depths with

two different frequencies are discussed due to space limitation. Frequency of 0.25Hz is demonstrated instead of 0.5Hz (as mentioned in abstract) due to low E-field magnitude obtained at depth of 2,250 m and below. Therefore, presence and absence of HC cannot be distinguished.

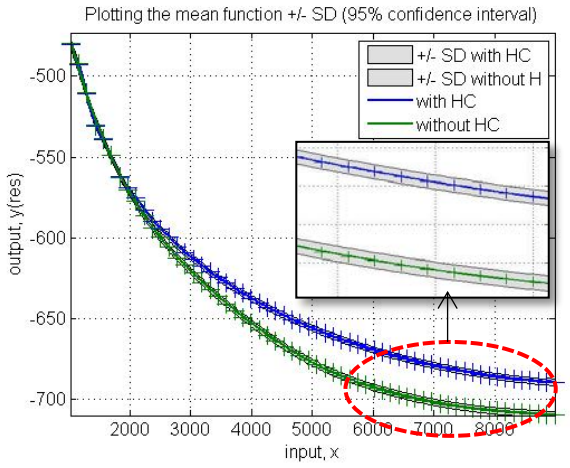

(a)

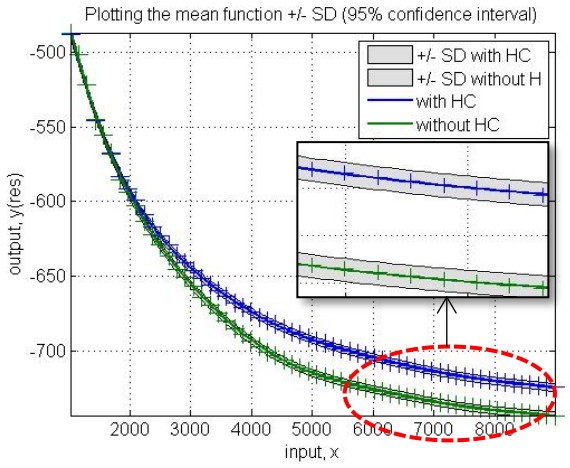

(b)

Fig. 3 Using Gaussian process prediction with the hyperparameters we obtain 95% confidence region for the underlying function *f* for (a) 0.125 Hz m and (b) 0.25 Hz at 1000 m.

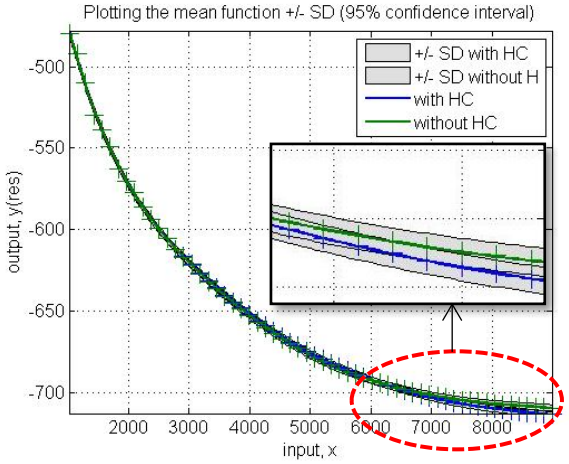

(a)

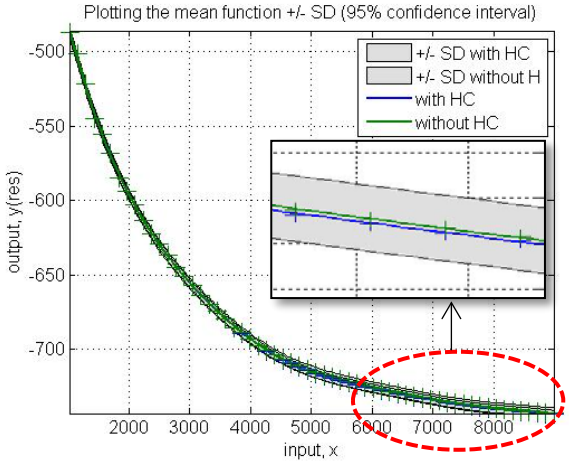

(b)

Fig. 4 Gaussian process prediction with the hyperparameters at 95% confidence region for the underlying function *f* for (a) 0.125 Hz and (b) 0.25 Hz at 3000 m

From Fig. 3 and 4, the predicted values for the test datasets shown that as the magnitude of E-field is reducing, the depth of the hydrocarbon is getting deeper. At depth 1000 m, presences of hydrocarbon are at both frequencies clearly seen. However, at depth of 3000 m, the magnitude of E-field with and without hydrocarbon is almost equal and not distinguishable for both frequencies.

CONCLUSION

Gaussian process has shown that, it shows that as the depth going deeper, the magnitude of E-field is getting smaller for all the frequencies. These finding are in line with all the findings as discussed in [1] - [4] .

In conclusion, kernel-based machine learning algorithm, GPR, is well implemented to perform hydrocarbon prediction. Results have shown that as

the frequencies increase the skin depth decrease accordingly thus this will affect the magnitude of EM waves received. Given a set of training data, GP provides a flexible Bayesian framework for identifying the nonlinear relationship between input *x* and output *y*.

Acknowledgements

The authors would like to express their gratitude to those who have contributed to the success of this paper directly or indirectly. We also would like to express our gratitude to The Ministry of Higher Education Malaysia for the financial support and University Technology PETRONAS for guidance, assistants and support throughout the research.

References

[1] A. Kumar and J. E. Lie, "Sea Bed Logging – Direct Hydrocarbon Detection Technique in Offshore Exploration," 2002.

[2] L. O. Løseth, H. M. H. M. Pedersen, T. Schaug-Pettersen, S. Ellingsrud, T. Eidesmo, L. Loseth, and T. Schaugpettersen, "A scaled experiment for the verification of the SeaBed Logging method," *J. Appl. Geophys.*, vol. 64, no. 3–4, pp. 47–55, 2008.

[3] T. Eidesmo, S. Ellingsrud, L. M. MacGregor, S. Constable, M. C. Sinha, S. Johansen, F. N. Kong, and H. Westerdahl, "Sea Bed Logging (SBL), a new method for remote and direct identification of hydrocarbon filled layers in deepwater areas," *First Break*, vol. 20, no. 3, pp. 144–152, 2002.

[4] A. Bhuiyan, T. Wicklund, and S. Johansen, "High-resistivity anomalies at Modgunn arch in the Norwegian Sea," *First Break*, vol. 24, no. January, pp. 39–44, 2006.

[5] C. Rasmussen, "Gaussian processes for machine learning," *Inst. Biol. Cybernatics. 70276 Tubingen, Ger.*, pp. 68–75, 2012.

[6] S. Mariam, H. Daud, and S. Chandra, "Prediction of Hydrocarbon using Gaussian Process for Seabed Logging Application," in *Procedia Computer Science*, 2015, vol. 72C, pp. 225–232.

[7] D. Petelin, A. Grancharova, and J. Kocijan, "Evolving Gaussian process models for prediction of ozone concentration in the air," *Simul. Model. Pract. Theory*, vol. 33, pp. 68–80, 2013.

[8] C. E. Rasmussen, *Gaussian processes for machine learning.*, vol. 14, no. 2. 2006.

[9] A. Y. Sun, D. Wang, and X. Xu, "Monthly streamflow forecasting using Gaussian process regression," *J. Hydrol.*, vol. 511, pp. 72–81, 2014.

[10] C. E. Rasmussen and H. Nickisch, "Gaussian Processes for Machine Learning (GPML) Toolbox," *J. Mach. Learn. Res.*, vol. 11, pp. 3011–3015, 2010.

QUANTUM PARTICLE SWARM OPTIMIZATION FOR ECONOMIC DISPATCH PROBLEM USING CUBIC FUNCTION CONSIDERING POWER LOSS CONSTRAINT

Fahad Parvez Mahdi[1], Pandian Vasant[1], Vish Kallimani[2], Patrick Yeoh Siew Fai[2] and M. Abdullah-Al-Wadud[3], Junzo Watada[2]
[1]Department of Fundamental and Applied Sciences, [2]Department of Computer & Information Sciences, Universiti Teknologi PETRONAS, Malaysia; [3]Department of Software Engineering, College of Computer and Information Sciences, King Saud University, Riyadh, KSA

ABSTRACT

In this paper, quantum integrated particle swarm optimization (QPSO) algorithm is utilized to solve economic dispatch (ED) problem. Here, authors use cubic fuel cost function, instead of the traditional quadratic cost function, to make the system robust against nonlinearities of actual power generators. Power loss and generator limit constraints are considered in this paper. To show the efficiency and robustness of the proposed method, authors have compared the obtained results with other algorithms used for ED on 3-unit and 5-unit generator systems using cubic fuel cost function, and obtained comparatively better results with less computational time in most of the cases.

Keywords: Economic dispatch, Quantum particle swarm optimization, Cubic function, Power loss, Optimization, Quantum computing.

INTRODUCTION

Economic dispatch (ED) is one of the most crucial problems of power generation system. It has the objective to find an optimal combination of power generation in order to minimize the total production cost satisfying all other constraints [1]. Many assumptions have been made in order to optimize ED in power systems and these assumptions are sometimes impractical to real systems and can no longer be ignored. These assumptions are later included by different researchers as constraints such as emissions, uncertainties, reactive power dispatch, ramp rates, valve points and integration of Renewable Energy (RE) generators [2]-[4]. In this work, for simplicity, authors consider only transmission loss and generator limit constraint.

A significant amount of research have been done to get the minimum solution for economic dispatch problem in power generation system. Various classical methods like lambda iteration [17], gradient approach [18] etc. have been used to solve ED problems. But, these conventional methods cannot optimize ED problems efficiently if fuel-cost curves of the generating units are not piece-wise linear and monotonically increasing [19]. Generally, ED problems are formulated using quadratic function. But quadratic function couldn't represent the actual power response of generating unit accurately [20]. Thus, higher order polynomial function is preferred to counter this problem. To avoid the complexities of higher order polynomial function, authors have used cubic function to represent ED problems here in this paper. Khoa et al. [3] proposed a new Mean-Variance Mapping Optimization ($MVMO^S$) method to solve ED problems using cubic function and showed that it performs better than PSO, Genetic algorithm (GA), Firefly algorithm (FA) etc.

The methods used previously in economic dispatch problem have evolved from traditional methods to heuristic methods, and finally to hybrid methods in solving optimization issues [15], [16]. Adhinarayanan and Sydulu [21] proposed PSO in to solve economic problem using cubic function, and showed that it improves the effectiveness of particle swarm optimization (PSO) in solving ED problems. PSO is considered as one of the modern swarm based heuristic algorithms for optimization problems in power systems [5],[6]. It is a population-based technique which is an alternative tool to genetic algorithms and this behavioral interaction technique gained popularity in control system applications [7]. It is computationally efficient and easier to implement compared to other evolutionary algorithms proposed in recent studies [8]-[12].

One key edge is this algorithm is the capability to allocate memory for storage. Each particle stores the best solution and the solution is compared to that of the group's best solution to tackle optimization issues. PSO works best when there is no need to differentiate conditional variables and the constraints are visible throughout the process. In practical applications, however, PSO has defects such as premature convergence [10]. The disparities of PSO are prone to optimization issues and the quantum

particle swarm optimization algorithm (QPSO) improves such shortcomings.

Quantum particle swarm algorithm is a new intelligent optimization algorithm which can be easily implemented into the control system optimization issues. The algorithm introduces quantum computing into the particle swarm algorithm with the manipulation that the particles in the space have quantum behavior. The algorithm succeeds in dealing with the non-linearity while sustaining the advantages of particle swarm algorithm [13], which will result in positive outcomes.

The principle of quantum mechanics claims that the PSO algorithm is applied to quantum space as an approach within physics and quantum mechanics [14].

Latest progress in solving ED problems in a large number of units has been struck by the high computational time and growing nonlinearities of power generating systems. To reduce the computational efficiency, Meng et al. [22] proposed Quantum PSO using quadratic function to solve this cost problem. QPSO proved better for its stronger search ability and quicker convergence speed than other algorithms like GA and PSO. In this research, we have added dimension to the previous research by exploiting quantum computing technique in cubic cost function with the help of QPSO to solve ED problems.

Next section of this paper presents the QPSO methodology, describing QPSO and its operation with flowchart and algorithm. After that, problem statement section briefly discusses about the economic dispatch and the constraints that have been considered in this paper. Finally, result and analysis section shows the obtained result and analysis in each part with tables and figures. The paper is concluded with discussion and conclusion sections, where the contribution, short-comings of this research, future direction are described to make further improvement in solving economic dispatch problem.

THE QPSO METHODOLOGY

Quantum PSO is a new and efficient version of PSO which is basically the integration of quantum computing into PSO. Due to the introduction of quantum bit and quantum rotation gate along with implementation of self-adaptive probability selection and chaotic sequences mutation, QPSO demonstrates stronger search ability and quicker convergence speed. QPSO uses quantum bit and angle to depict the state of a particle rather than position and velocity used in the classical PSO. The performance and capabilities of the QPSO has gone beyond that of the classical methods, e.g. PSO, in terms of convergence speed and cost function [23].

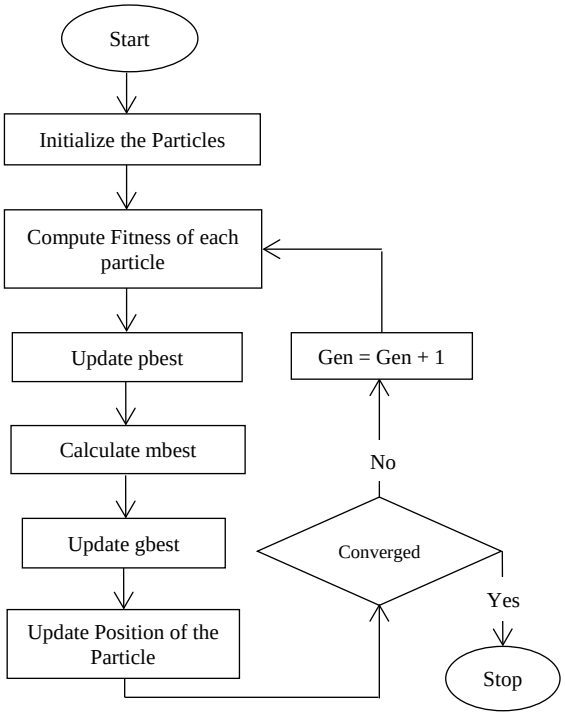

Fig. 1 Flowchart of standard Quantum PSO

QPSO uses qubit to denote particles. The basic difference between qubit and classical bit used in PSO is that qubit can simultaneously stay in the superposition of two different quantum states,

$$|\psi\rangle = \alpha|0\rangle + \beta|1\rangle \quad (1)$$

where α and β are complex numbers that satisfy the following equation,

$$|\alpha|^2 + |\beta|^2 = 1 \quad (2)$$

|0> represents spin up state and |1 > represents the spin down state. From Eq.1, we can see one qubit is representing two state of information (|0> and |1>) simultaneously. This superposition state can also be expressed as,

$$|\psi\rangle = \sin\theta|0\rangle + \cos\theta|1\rangle \quad (3)$$

where θ represents the phase of the qubit. The relation among θ, α and β can be defined as,

$$\theta = \arctan\frac{\beta}{\alpha} \quad (4)$$

The structure of QPSO is depicted in fig. 1. Some of the main steps of QPSO are initialization of qubit encoding for particles, evaluation and changing particle forms, updating particles and decoding particles. Detail description of these steps are out of the scope of this paper. However,

interested readers may check [26] for details.

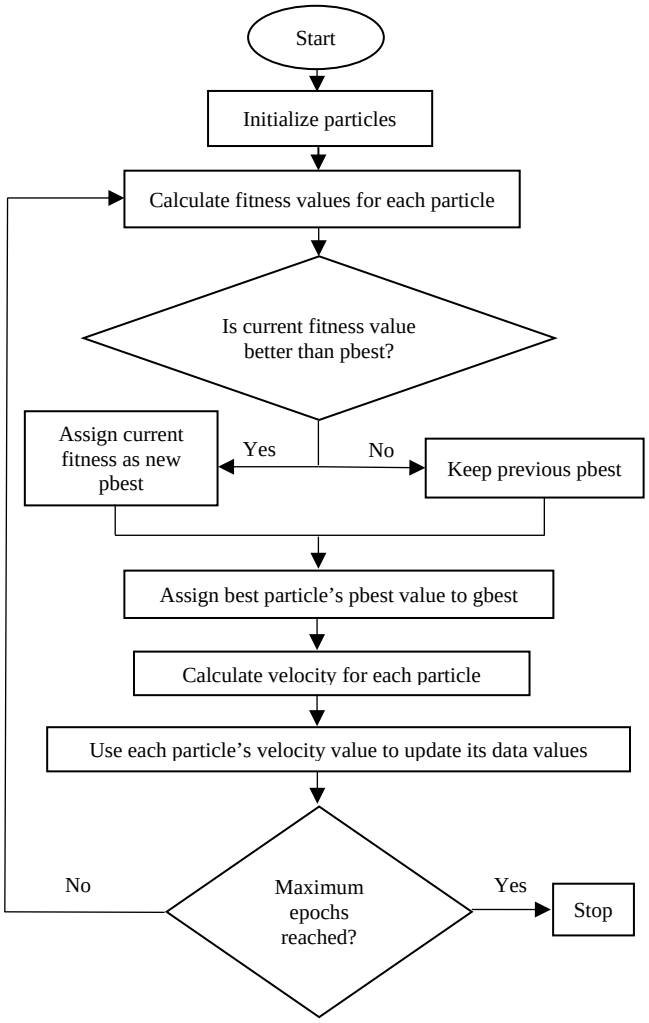

Fig. 2 Detail flowchart of Quantum PSO used in this research to solve economic dispatch problem

The procedure for implementing the QPSO algorithm is given below as Algorithm 1.

Algorithm 1. The QPSO algorithm.

Initialize the population size (M), the positions and the dimensions of the particles;
For t = 1 to Maximum Iteration T
Compute the mean best position C;
$\alpha = (\alpha_1 - \alpha_0) \bullet (T - t)/T + \alpha 0;$
For i = 1 to population size M
If $f(X_i) < f(P_i)$ *then* $P_i = X_i$;
Endif
$G = argmin\ (f(P_i))$;
For j = 1 to D
$\omega = rand(0,1)$;
$u = rand(0,1)$;
$P_{ij} = \omega \bullet P_{ij} + (1 - \omega) G_j$;

If (rand (0,1) > 0.5)
$X_{ij} = P_{ij} + \alpha \bullet abs(C_j - X_{ij}) \bullet log(1/u)$;
Else
$X_{ij} = P_{ij} - \alpha \bullet abs(C_j - X_{ij}) \bullet log(1/u)$;
Endif
Endfor
Endfor
Endfor

Positions of all particles in the population, M, are initialized randomly. The fitness value for all particles are then calculated and evaluated according to the problem at hand. The personal best (pbest) position of every particle is updated if the current fitness value is found to be better. The best pbest among the particles is then assigned to global best (gbest) in the next step.

After the gbest is assigned, the velocity for all particles is determined. The calculated velocities are then updated to its data values and these values are compared to each other in iterations to get the best fitness value (target value). The best fitness value is considered as the criterion in the algorithm.

If the criterion is not satisfied, the fitness value of the particle is calculated again and the steps are repeated until there is no further update of best fitness value.

PROBLEM STATEMENT

The main objective of economic dispatch is to find an optimal combination of generated power in order to minimize the total generation cost while satisfying all other constraints. Economic dispatch using cubic function can be written as:

$$F_i(P_{gi}) = a_i P_{gi}^{\ 3} + b_i P_{gi}^{\ 2} + c_i P_{gi} + d_i \quad \text{RM/h} \qquad (3)$$

where, F_i is the fuel cost calculated in Malaysian Ringgit per hour (RM/h) of generating unit *i*. a_i, b_i, c_i and d_i are fuel cost coefficients of generating unit *i*. Additionally, P_{gi} and *n* are the real power generation of the *i*th unit (in MW) and the total number of generation units, respectively. Our goal is to minimize total fuel cost, which can be defined as:

$$Minimize, F_T = \sum_{i=1}^{n} F_i(P_{gi}) \qquad (4)$$

In this research, two constraints are considered to solve economic dispatch that can be formulated as below:

Power Balance Constraint: The total output power should be equal to the total power demand plus transmission losses:

$$P = \sum_{i=1}^{n} P_i = P_D + P_L \quad (5)$$

where P, P_D and P_L are total output power generated (in MW), total power demand (in MW) and transmission loss (in MW) respectively.

Generator Limit Constraint: The output power generation of each power generating unit has its minimum and maximum value. The power generation should be between its maximum and minimum value. This inequality can be formulated as below:

$$P_{i,min} \leq P_i \leq P_{i,max} \quad (6)$$

RESULT AND ANALYSIS

Quantum particle swarm optimization (QPSO) technique has been applied here to solve economic dispatch problem for 3-unit and 5-unit systems [19], [25] using cubic function where the total load demand is 2500 MW and 1800 MW respectively. Authors have implemented this proposed algorithm in MATLAB R2015a and executed with Intel® Core™ i5-3470 CPU @ 3.20 GHz (4 CPUs), ~3.2GHz and 4GB RAM personal computer. Tables 1 and 4 are showing the cost coefficient values, minimum and maximum limit of each power generating unit without considering power loss for 3-unit and 5-unit system respectively.

Table 1 Settings of parameters for PSO

Parameters	Values
Population Size	100000
Maximum Position	100
Maximum Velocity , v_{max}	1
Minimum Velocity, v_{min}	1.05
Maximum Iteration	20
Number of Runs	50

Table 1 shows the parameter settings of QPSO. 50 number of runs have been considered as a fair test of robustness. Larger population size has been taken to get better result which ultimately slows down the computational efficiency.

Table 2 Cubic cost function coefficients for 3 units system without considering power loss

Unit	1	2	3
a_i	749.55	1285	1531
b_i	6.95	7.05	6.531
c_i	0.000968	0.000738	0.00104
d_i	$\mathbf{1.27 \times 10^{-7}}$	$\mathbf{6.45 \times 10^{-8}}$	$\mathbf{9.98 \times 10^{-8}}$
P_{imin}	320	300	275
P_{imax}	800	1200	1100

Tables 2 and 5 are showing comparison of simulation results among GA, PSO and QPSO. From Table 3, it can be seen that QPSO performs better result than GA and PSO for 3-unit system where PSO performs better than QPSO for 5-unit system.

Table 3 Comparison of results (total cost) for 3 units system without considering power loss

Unit	GA	PSO	QPSO
1	725.02	724.99	733.29
2	910.19	910.15	914.1
3	864.88	864.85	852.64
Total Power, P (MW)	2500	2500	2500
Total Cost, F_T (RM)	22730.14	22729.35	22729.07

Table 4 Test system data for 3 units system considering power loss

Unit	1	2	3	P (MW)	F_T (RM)
QPSO	714.22	891.53	898.3	2504.05	22766.66

Our proposed method used for economic dispatch considering power loss shows straight line for both 3-unit and 5-unit (Figs. 3 and 5) i.e. with the increase of iteration the result is found to be same. This interesting behavior can be explained as fast convergence to the best value.

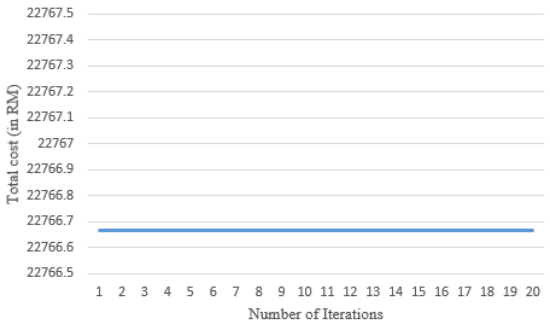

Fig. 3 Convergence curve of the QPSO for economic dispatch of 3-unit system considering power loss

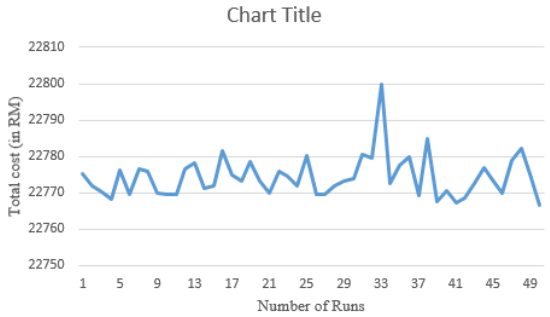

Fig. 4 Total cost (in RM) vs number of runs curve for economic dispatch considering 3-unit system with power loss constraint using QPSO.

Table 5 Cubic cost function coefficients for 5 units system without considering power loss

Unit	1	2	3	4	5
a_i	749.6	1285	1531	749.6	1285
b_i	6.95	7.05	6.531	6.95	7.05
c_i	$\mathbf{9.68 \times 10^{-4}}$	$\mathbf{7.38 \times 10^{-4}}$	0.0010 4	$\mathbf{9.68 \times 10^{-4}}$	$\mathbf{7.38 \times 10^{-4}}$
d_i	$\mathbf{1.27 \times 10^{-7}}$	$\mathbf{6.45 \times 10^{-8}}$	$\mathbf{9.98 \times 10^{-8}}$	$\mathbf{1.27 \times 10^{-7}}$	$\mathbf{6.45 \times 10^{-8}}$
P_{imin}	320	300	275	320	300
P_{imax}	800	1200	1100	800	1200

Tables 3 and 6 represents the best result obtained by QPSO for economic dispatch using cubic function considering power loss constraint. When power loss is considered, the total cost becomes higher than the cost without considering power loss.

Table 6 Comparison of results (in Malaysian Ringgit) for 5 units system without considering power loss

Unit	GA	PSO	QPSO
1	320.00	320.00	325.05
2	343.74	343.70	360.44
3	472.60	472.60	486.24
4	320.00	320.00	302.49
5	343.74	343.70	325.76
P (MW)	1800	1800	1800
F_T (RM)	18611.07	18610.4	18613

Table 7 Test system data using QPSO for 5 units system considering power loss

Unit	QPSO
1	341.86
2	309.48
3	471.46
4	325.28
5	355.90
Total Power, P (MW)	1803.98
Total Cost, F_T (RM)	18648.17

Total 50 number of runs have been conducted to test the reliability and robustness of the proposed method. Authors have found that for 3-unit system QPSO is more stable, reliable and robust as the deviation is not high (Fig 4). But for the 5-unit system the deviation has been found higher (Fig. 6).

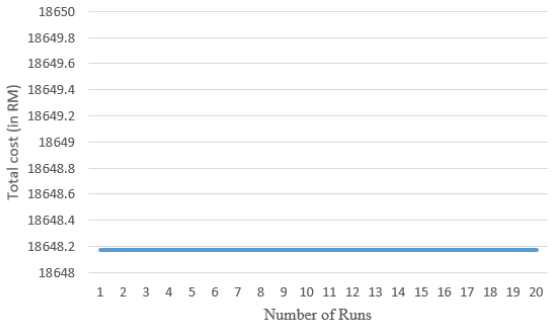

Fig. 5 Convergence curve of the QPSO for economic dispatch of 5-unit system considering power loss

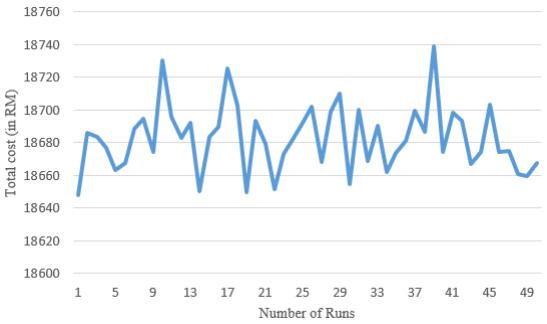

Fig. 6 Total cost (in RM) vs number of runs curve for economic dispatch considering 5-unit system with power loss constraint using QPSO.

DISCUSSION

This paper has considered 3-unit and 5-unit system in this research to compare the obtained results with other methods like Genetic algorithm (GA) and PSO. For comparison purpose, authors have taken the same coefficients value and have not considered power loss. Simulation results show QPSO performs better to predict minimum total cost function for 3-unit system than other methods like GA and PSO. But for 5-unit system, PSO and GA predict slightly better results than QPSO. This proposed method is computationally powerful as it takes less time for each run than PSO. But sometimes it needs larger population size to find the global optimal value and for this reason it sometimes need more computational time to achieve the global value. Authors have also shown the results for 3-unit and 5-unit system considering power loss. What is your comment regarding power loss???

CONCLUSION

In this paper, quantum PSO (QPSO) technique is presented to solve the economic dispatch problem using cubic function. QPSO technique is successfully implemented into ED problems considering 3-unit and 5-unit systems with power loss and generator limit constraints. Simulation results show its effectiveness in solving economic dispatch problems by demonstrating better and stable results. The obtained results are compared with PSO and GA. For 3-unit system, QPSO gives better result but for 5-unit system, PSO gives better result. To reduce the nonlinearities of power generating systems, cubic function of economic dispatch works well. In this paper, total 50 number of runs have been considered as a fair test of robustness of the proposed method. Obtained results for the test systems confirm that this proposed method gives better global solution, is more robust and computationally powerful in solving the economic dispatch problems. To the best of the authors' knowledge, this is the first work on single objective economic dispatch problem with cubic function considering power loss using QPSO. Authors' next work is to include emission dispatch as another objective i.e. it will be a multiobjective problem, where the authors shall consider Quantum Cuckoo Search (QCS), Quantum Bat (QBAT) and Quantum Teaching and Learning Based Optimization (QTLBO) techniques.

ACKNOWLEDGEMENTS

The authors would like to thank Universiti Teknologi PETRONAS (www.utp.edu.my) for supporting the research under Graduate Assistance Scheme. This research paper is financially sponsored by the Centre of Graduate study with the support of the Department of Fundamental & Applied Sciences, Universiti Teknologi PETRONAS.

NOMENCLATURE

F_i – Fuel cost (RM/h) of generating unit *i.*
a_i, b_i, c_i, d_i – Fuel cost coefficients of generating unit *i*
Pi – Real power generation of the *i*th unit
n – Total number of generation units
P – Total output power generated (in MW)
P_D – Total power demand (in MW)
P_L – Transmission loss (in MW)
ED – Economic Dispatch
FA – Firefly Algorithm
GA – Genetic Algorithm
$MVMO^S$ – Mean-Variance Mapping Optimization
PSO – Particle Swarm Optimization
QPSO – Quantum Particle Swarm Optimization
QBAT – Quantum Bat Algorithm
QCS – Quantum Cuckoo Search
QTLBO – Quantum Teaching and Learning Based Optimization

REFERENCES

[1] Thanushkodi SMVPK, Apragash RSD, Jothikumar M, Sriramnivas S, and Vinodh K, "An Efficient Particle Swarm Optimization for Economic Dispatch Problems With Non-smooth cost functions," The WSEAS Transaction on Power Systems, vol. 3, 2008, pp. 257-266.

[2] Pazheri FR, Othman MF, Malik NH, and Al-Ammar EA, "Pollution Emission Reduction with Minimum Transmission Loss in Power Dispatch Including Renewable Energy and Energy Storage," International Review of Electrical Engineering-Iree, vol. 7, Sep-Oct 2012, pp. 5769-5778.

[3] Khoa T, Vasant P, Singh BSM, and Dieu V, "Swarm based mean-variance mapping optimization ($MVMO^s$) for economic dispatch problem with valve—Point effects," in Industrial Engineering and Engineering Management (IEEM), 2014 IEEE International Conference on, 2014, pp. 59-63.

[4] Osorio GJ, Lujano-Rojas JM, Matias JCO, and Catalao JPS, "A probabilistic approach to solve the economic dispatch problem with intermittent renewable energy sources," Energy, vol. 82, Mar 2015, pp. 949-959.

[5] Zhao B, Guo C, Bai B, and Cao Y, "An improved particle swarm optimization algorithm for unit commitment," International Journal of Electrical Power & Energy Systems, vol. 28, 2006, pp. 482-490.

[6] Eberhart RC and Shi Y, "Particle swarm optimization: developments, applications and resources," in evolutionary computation, 2001. Proceedings of the 2001 Congress on, 2001, pp. 81-86.

[7] Lee TY and Chen CL, "Unit commitment with probabilistic reserve: An IPSO approach," Energy conversion and Management, vol. 48, 2007, pp. 486-493.

[8] Hassan R, Cohanim B, Weck OD, and Venter G, "A comparison of particle swarm optimization and the genetic algorithm," in Proceedings of the 1st AIAA multidisciplinary design optimization specialist conference, 2005, pp. 18-21.

[9] Ganesan T, Elamvazuthi I, Shaari K, and Vasant P, "Multiobjective optimization of bioethanol production via hydrolysis using hopfield-enhanced differential evolution," Contemporary advancements in information technology development in dynamic environments, 2014, pp. 340-359.

[10] Rahman I, Vasant P, Singh BSM, and Abdullah-Al-Wadud M, "On the performance of accelerated particle swarm optimization for charging plug-in hybrid electric vehicles," Alexandria Engineering Journal, vol. 55, 2016, pp. 419-426.

[11] Rahman I. Vasant P, Singh BSM, and Abdullah-Al-Wadud M, "Hybrid Particle Swarm and Gravitational Search Optimization Techniques for Charging Plug-In Hybrid Electric Vehicles," in Handbook of Research on Modern Optimization Algorithms and Applications in Engineering and Economics, V. Pandian, W. Gerhard-Wilhelm, and D. Vo Ngoc, Eds., ed Hershey, PA, USA: IGI Global, 2016, pp. 471-504.

[12] Vasant P and Nikolai V, Eds., Sustaining Power Resources through Energy Optimization and Engineering. Hershey, PA, USA: IGI Global, 2016.

[13] Yumin D and Li Y, "Quantum behaved particle swarm optimization algorithm based on artificial fish swarm," Mathematical Problems in Engineering, 2014, Article ID 592682.

[14] Mikki SM and Kishk AA, "Physical theory for particle swarm optimization," Progress In Electromagnetics Research, vol. 75, 2007, pp. 171-207.

[15] Rathinam A and Phukan R, "Solution to Economic Load Dispatch Problem Based on FIREFLY Algorithm and Its Comparison with BFO,CBFO-S and CBFO-Hybrid," in Swarm, Evolutionary, and Memetic Computing. vol. 7677, B. K. Panigrahi, S. Das, P. N. Suganthan, and P. K. Nanda, Eds., ed, 2012, pp. 57-65.

[16] Chen SD and Chen JF, "A direct Newton–Raphson economic emission dispatch," International Journal of Electrical Power & Energy Systems, vol. 25, 2003, pp. 411-417.

[17] Singhal PK, Naresh R, Sharma V, and Kumar NG, "Enhanced lambda iteration algorithm for the solution of large scale economic dispatch problem," in Recent Advances and Innovations in Engineering (ICRAIE), 2014, 2014, pp. 1-6.

[18] Chen CL and Wang SC, "Branch-and-bound scheduling for thermal generating units," Energy Conversion, IEEE Transactions on, vol. 8, 1993, pp. 184-189.

[19] Wood AJ and Wollenberg BF, Power generation, operation, and control: John Wiley & Sons, 2012.

[20] Ganesan S and Subramanian S, "Non‐convex economic thermal power management with transmission loss and environmental factors: Exploration from direct search method," International Journal of Energy Sector Management, vol. 6, 2012, pp. 228-238.

[21] Adhinarayanan T and Sydulu M, "Particle swarm optimisation for economic dispatch with cubic fuel cost function," in TENCON 2006. 2006 IEEE Region 10 Conference, 2006, pp. 1-4.

[22] Meng K, Wang HG, Dong Z, and Wong KP, "Quantum-Inspired Particle Swarm Optimization for Valve-Point Economic Load Dispatch," IEEE Transactions on Power Systems, vol. 25, 2010, pp. 215-222.

[23] Mikki SM and A. A. Kishk, "Quantum particle swarm optimization for electromagnetics," Antennas and Propagation, IEEE Transactions on, vol. 54, 2006, pp. 2764-2775.

[24] Sun J, Wu X, Palade V, Fang W, Lai CH, and Xu W, "Convergence analysis and improvements of quantum-behaved particle swarm optimization," Information Sciences, vol. 193, 2012, pp. 81-103.

[25] Kumaran G and Mouly V, "Using evolutionary computation to solve the economic load dispatch problem," in Evolutionary Computation, 2001. Proceedings of the 2001 Congress on, 2001, pp. 296-301.

[26] Zhisheng Z, "Quantum-behaved particle swarm optimization algorithm for economic load dispatch of power system," Expert Systems with Applications, vol. 37, 2010, pp. 1800-1803.

Second International Conference on Science, Engineering & Environment,
Osaka City, Japan, Nov.21-23, 2016, ISBN: 978-4-9905958-7-6 C3051

CONCEPT OF PLASTICITY INDEX TO INFLUENCE MECHANICAL BIFURCATION OF SOILS AND SOFT-SEDIMENT DEFORMATION

Naoto Kaneko[1], Jun Muto[1] and Hiroyuki Nagahama[1]
[1]Department of Earth Science, Graduate School of Science, Tohoku University, Japan

ABSTRACT: A triaxial compression test is one of the laboratory soil tests in the field of soil mechanics. Yielded specimens have various deformation patterns depending on loading stages and stress ratios in spite of the same ground materials. Failure patterns of ground materials bifurcationally change to diamond, bulge and a pair of oblique shear patterns. Symmetry of deformation patterns (e.g. shear band patterns) has been illuminated by bifurcation analysis by governing equation based on Cam-clay model. On the other hand, plasticity index tested by Casagrande liquid limit device and plastic limit instruments is known to describe mechanical characteristics (e.g. compressibility) of soils. Relationship between plasticity index and mechanical bifurcation controls the evolution of deformation patterns. Here, from the view point of concept of plastic potential, we show that plasticity index theoretically determines deformation patterns of soils based on Cam-clay model on the basis of Shibi and Kamei (2002)'s bifurcation analysis. Furthermore, because deformation facies of rocks are described by mean ductility of rocks similar to the concept of plasticity index, we point out that mean ductility controls mechanical bifurcation of the geologic materials such as soft-sediments.

Keywords: Plasticity index, Cam-clay model, Bifurcation

1. INTRODUCTION

1.1 Theoretical and Experimental preface

When deformation phenomena of geologic materials such as soils, rocks, soft-sediments, and even tectonic plates are described, we generally use Mohr's circle or simulations based on Cam-clay model. However, it is difficult to explain a soil parameter about deformation phenomena from a unified fields of geology and soil mechanics. The reason for the difficulty is that physical properties controlling on deformations of soils and rocks are hardly known, and their specified mechanical parameters as stress σ, strain ε and so on cannot be determined uniquely. For example, Paterson [1] used cylindrical marbles under various confining pressures up to 1000 kg/cm^2 by triaxial compression test. Significantly, the developed shear zones differently displays three different patterns in spite of same starting materials. With respect to these fracture developments, Shibi and Kamei [2] and Ikeda *et al*. [3] pointed out that the surface fractures of cylindrical specimens of geomaterials bifurcationally changes to diamond pattern, bulge pattern and a pair of oblique shear patterns. Plasticity index I_P is an extremely important parameter in Shibi and Kamei [2]'s analysis, so we theoretically introduce that the concept of I_P can be unifiedly related to mechanical formulae and Cam-clay model based on elastoplasticity.

Plasticity index I_P has been a conventional and simple experimental parameter to evaluate mechanical properties of soils. Voight [4] and Kanji [5] mentioned direct correlations between internal friction angle φ and I_P. Slope stability is related to I_P which can be also related to compressibility by water content. On the other hand, the relationship between I_P and mechanical parameters (such as mean and deviatoric stress) and the theoretical relationships between soil strength φ and I_P have been derived [4]–[7]. Interestingly, Uemura [8] proposed that classification of folding can be expressed by mean ductility of rocks similar to the concept of I_P.

1.2 Concept of plastic potential

Cam-clay model can be derived from flow rule and some constitutive laws [2]. Flow rule used by plastic potential f is given by [9];

$$d\dot{\varepsilon}^p = h\frac{\partial f}{\partial \sigma'_{ij}}, \quad h > 0, \tag{1}$$

where $d\dot{\varepsilon}^p$ is incremental tensor of plastic strain rate, σ'_{ij} is effective stress tensor, and h is plastic multiplier. Increment of plastic strain tensor is partial differential of the potential due to effective stress in q–p'–v space, where q is the deviatoric stress, v is the specific volume and p' is the mean effective stress. In q–p'–v space, the condition of soil and rock under triaxial compression is expressed by critical state line. When stress state of soil reached to the critical state, the state of soil yields and behaves fluidity. Regarding plastic potential on q–p' plane, it causes plastic expansion on the upper side of the critical state line and causes plastic compression on the lower side of the line. Therefore, the critical state line can be understood as condition boundary line. Then, the slope of critical state line by M_c is defined by;

$$q = M p'. \tag{2}$$

The work increment at shear process is assumed to equal the energy dissipation at the critical state [10], [11]. Moreover, Eq. (2) is displayed as follows,

$$p'd\varepsilon_v + qd\varepsilon_d = M_c p'd\varepsilon_d, \tag{3}$$

where M is constant, ε_v is volumetric strain and ε_d is deviatoric strain. From Eq. (3), we can obtain,

$$\frac{q}{p'} = M_c - \left(\frac{d\varepsilon_v}{d\varepsilon_d}\right). \tag{4}$$

This is the relationship between stress ratio and stain increment ratio in Cam-clay model [10], [11], which is similar to Eq. (2). Moreover, Rowe [12] microscopically studied Eq. (4) from the view point of deformation of granular materials and obtained a similar relation as,

$$\frac{\sigma_1}{\sigma_3} = K\left(\frac{-d\varepsilon_3}{d\varepsilon_1}\right) = -\frac{2\dot{\varepsilon}_3}{\dot{\varepsilon}_1}\tan^2\left(\frac{\pi}{4}+\frac{\varphi}{2}\right), \tag{5}$$

where σ_1 is major principal stress, σ_3 is minor principal stress, ε_1 is axial strain, and ε_3 is lateral strain. This is an expression for the relationship between principal stress ratio (= σ_1/σ_3) and principal strain incremental ratio during the shear of granular materials (= $-d\varepsilon_3/d\varepsilon_1$). This is usually called stress-dilatancy relation. Moreover, K is internal energy ratio of soil. Besides, we can regard Eq. (2) or Eq. (4) as Eq. (5). Then, the outward plastic strain increment vector components ($d\varepsilon_v^p$ and $d\varepsilon_d^p$) orthogonally intersects as shown by Eq. (1). At this point, normal vector of plastic potential plane is equivalent to the yield function of $\dot{\varepsilon}^p$ on q–p' plane. Then, we obtain

$$\frac{d\varepsilon_v^p}{d\varepsilon_d^p} = -\frac{dq}{dp'}. \tag{6}$$

From Eqs. (4) and (6), we can get

$$\frac{q}{p'} - \frac{dq}{dp'} = M_c. \tag{7}$$

Then, setting from the case ($p' = p_y$, $q = 0$; p_y is a hardening parameter) and integrating Eq. (7), we get

$$f = \frac{q}{M_c p'} + \ln\left(\frac{p'}{p'_0}\right) - \ln\left(\frac{p_y}{p'_0}\right), \tag{8}$$

where f is the yield function of Cam-clay model. As shown in the present study, Cam-clay model can be derived from flow rule and some constitutive laws. By using p_y, the plastic void ratio e^p is given by,

$$de^p = -(\lambda - \kappa)\frac{dp_y}{p_y}, \tag{9}$$

where κ is swelling index, and λ is compression index at the critical state line [11]. On the other hand, the relationship between plastic volumetric strain ε_v^p and plastic volume ratio v^p is given by,

$$d\varepsilon_v^p = \frac{dv^p}{v} = -\frac{de^p}{1+e}, \tag{10}$$

where v is expressed by void ratio e ($v = 1 + e$). Projecting Eq. (2) onto a v–p' plane, we obtained

$$v = \Gamma - \lambda \ln p', \tag{11}$$

where Γ is constant. Moreover, the normal consolidation line is given by

$$v = N - \lambda \ln p', \tag{12}$$

where N is constant. This line runs parallel to Eq. (11). Eqs. (11) and (12) are related to e determined by Eq. (10).

1.3 Experimental definition of plasticity index

For more consideration about consolidation phenomenon, we need to confirm that I_P essentially connects v. These directly link to the compressibility of soil. Compression index C_c representing the compressibility of soil can be obtained by

$$e = e_0 - C_c \log p', \tag{13}$$

where e_0 is initial void ratio. C_c is expressed by

$$C_c = \frac{I_P}{74}, \tag{14}$$

where I_P is defined by non-dimensional units as follows;

$$I_p = w_L - w_P, \tag{15}$$

where w_L means liquid limit [%]: the water content at which the soil ceases to be liquid, and w_P means plastic limit [%]: the water content at which the soil ceases to be plastic [13], [14]. Plasticity index I_P is an empirical parameter to characterize the range of water contents where the soil exhibits plastic property, and is known to describe mechanical characteristics (e.g. compressibility) of soils.

On the other hand, there is a theoretical relationship between I_P and mechanical bifurcation controlling the evolution of deformation patterns [2].

From Eq. (14), that is to say, the more consistency of soils increases, the more compressibility increases substantially than several tens to hundred times. Moreover, I_P links to the parameters of Cam-clay model widely used for simulation of consolidation and shearing of clay.

1.4 Bifurcationally deformation in Cam-clay model: I_P and mechanical parameters

From previous researches [2], [3], bifurcation analysis can be applied to failure patterns of ground materials. Under the condition of mechanical parameter, deformation patterns behave characteristically.

Shibi *et al.* [15] analyzed that the specimen was introduced by initial imperfection based on a coaxial Cam-clay model. Then, the function of coaxial Cam-clay model f_c is given by

$$f_c = \frac{\lambda - \kappa}{1+e}\ln\frac{p'}{p'_0} + \tilde{D}\frac{q}{p'} - \varepsilon_v^p, \quad (16)$$

where $\tilde{D}$ is coefficient of dilatancy, and v_0 is initial specific volume. The ratio of q to p' is called stress ratio η (= q/p') and is expressed in dimensionless unit. Peculiarly, when deformation patterns bifurcate, the stress ratio is defined as bifurcation load η_y [2]. That is to say, Eq. (16) describes that deformation of all rock and soils are controlled in q–p'–v space. Based on Cam-clay model [2, 16], bifurcation behavior of the soil with the lower I_P occurred at larger η and smaller ε_1 than those with higher I_P. I_P related to C_c can be theoretically expressed by λ (Eq. 11). Moreover, some soil parameters (λ, κ, M) in Cam-clay model (Eq. 16) can be linked to I_P. Significantly, I_P closely affects critical state theory from specific volume v (= 1 + e).

In addition, various soil parameters can be determined simply by using I_P because of linear correlations among them as shown in Table 1.

Table 1 Soil parameters and plasticity index

$\lambda = 0.02 + 0.0045I_P$
$\kappa = 0.00084\ (I_P - 4.6)$
$N = 1.517 + 0.019I_P$
$M = 1.65$
$\tilde{D} = 0.00082I_P + 0.0159$

Nakase *et al.*, [17] and Kamei [18] tested the reconstituted twelve soils which ranges of I_P from 10 to 55.

1.5 Bifurcation analysis based on Cam-clay model

By means of the bifurcation analysis based on a coaxial Cam-clay model, Shibi *et al.* [15], [19] reveals deformation patterns of specimen by simulation. Shibi and Kamei [2] derived a governing equation from flow rule including plastic potential and constitutive law.

The velocity v_i, in the coordinate system on (x_i) = $(x_1, x_2) \equiv (x, y)$, and i = 1, 2, is defined by the stream function ψ as

$$v_1 = \psi_{,2},\ v_2 = -\psi_{,1}, \quad (17)$$

By using the stream function in Eq. (17), the governing equation of ψ can be given by

$$a\psi_{,1111} + b\psi_{,1122} + c\psi_{,2222} = 0, \quad (18)$$

where the constitutive parameters of a, b and c are determined by virtue of I_P through various parameters shown in Table 1 [2]. Moreover, the results of Shibi and Kamei [2] indicates the influence of soil parameters on bifurcation behavior of normally consolidated cohesive soils under plane strain undrained compression loadings, and they applied to the prediction of slip surface. Then ψ can be expressed by

$$\psi = V(x_1)\cos(k_m x_2),\ k_m = \frac{m\pi}{2H}, \quad (19)$$

where $V(x_1)$ is the general solution at x_1 coordinate, k_m is the function of deformation mode m, and H is height of specimen. By Eq. (19), Eq. (18) can be written by

$$(aD^4 + 2bk_m{}^2D^2 + ck_m{}^4)V(x_1) = 0, \quad (20)$$

where D is differential [2]. Then, a governing equation is expressed by

$$a\rho^4 + 2b\rho^2 + c = 0, \quad (21)$$

where ρ is bifurcation solution [18].

2. SAMPLES AND METHODS

In this study, the physical properties of geologic materials are measured. Firstly, Futaba-fault gouge (Fukushima prefecture, Japan) is used to investigate mechanical properties of active fault gouge. Moreover, we also measure the physical property of volcanic ashes (Mt. Aso, Kyusyu, Japan) which may cause disastrous lahars with fluidity by rain. The ashes are picked at Mt. Aso (Kyusyu, Japan). On the other hand, the landslide surface is potentially formed by the trigger of porcelain clay consisting of fine-granited soil consists of fine grains and is deposited in the Chubu region (central Japan). We used two porcelain clays (Gaerome and Kibushi clay). Two types of clay minerals (halloysite and montmorillonite) are also investigated in this study.

Secondly, we measured physical parameters of soils through experiments, and noticed especially the consistency signifying the physical state of soils. The soil tests are followed by Japanese Industrial

Standards (JIS). Samples are well-mixed for adjusting the grain size and uniformity property. According to the JIS A 1202, the density of particles of soil ρ_s can be determined by the particles density test with a pycnometer. For estimating plastic index I_P, two tests are used to determine the liquid limit w_L and plastic limit w_P according to JIS A 1205. In the liquid limit test, samples with various water contents are placed in a brass cup. Then a number of blows is counted until the two separated parts of the soil sample on the cup come into contact. From the relationship between numbers of brows and water content for various samples, the water content at 25 blows is determined to be a liquid limit. For the plastic limit, the sample is rolled on a glass plate using the palm of hand until crack formation occurs at 3 mm diameter. Then the water content of the sample at the crack formation is calculated to be the plastic limit of the soil. The liquid limit and plastic limit of sandy and silty soil cannot be determined and hence the soil consistency is called non-plastic; NP [20], [21]. The w_P and w_L express the physical states of soil. Moreover, we conducted the ignition loss L_i test for measuring the content of organic matter of the soil according to JIS A 1226.

3. RESULTS

The results of soil tests are as listed in Table 2. In comparison with density and consistency, Mino kibushi porcelain clay has similar to the parameters to those of halloysite except their ignition losses L_i. The difference in density between Mino kibushi porcelain clay and halloysite are only 0.02 g/cm^3, also the difference of consistency is under 2%. Then, the parameter of L_i of Seto kibushi porcelain clay is similar to the parameter of halloysite except its ρ_s and consistency. Moreover, montmorillonite has high I_P because of structural feature (layer structure of the mineral). From this result, the permeability of montmorillonite is expected to be extremely low. Based on these findings, the consistency of various geomaterials differs from sedimentary/formation environments, constituent mineral types, and weathering. The reason why the plasticity indices of Aso volcanic ashes show "NP" is because these aches are not weathered well, and behave as dry sand to the touch when it contains water. Therefore, it is difficult to measure its liquid/plastic limit, and these ashes are not strong enough with increasing its water content. On the other hand, the ignition loss for volcanic ashes has negative value. The ignition loss represents the content of organic matter in the soil, consequently, two ashes does not have organic matter. It is thought that the mass is increased by oxidized metals in the soil under high temperature during the test (temperature of kiln; 750 ± 50 degrees Celsius).

4. DISCUSSIONS

4.1 Bifurcation determined by the concept of I_P

Based on above discussion, we consider physical meaning of I_P theoretically. When the Mohr-Coulomb's failure criterion is reviewed, void ratio e of the soil is not included. And the lateral pressure corresponding to p' in triaxial compression test relates to φ obtained by the test. The φ is given by Eq. (5). Strains ε_1 and ε_3 can be differentiated by time. Hence, Eq. (5) shows that energy ratio can be a new factor for frictional instability such as deformation of fault gouge [22]. Moreover, the empirical relationship between I_P and φ is approximately given by

$$\varphi = \alpha I_P^{-\beta}, \tag{22}$$

where α and β are specific values on soil types (e.g. α = 46.6 and β = -0.446; [5]).

Based on Eq. (5), we can obtain

$$\varphi = -\frac{\pi}{2} + 2\tan^{-1}\left(\sqrt{\frac{\sigma_1\dot{\varepsilon}_1}{2\sigma_3\dot{\varepsilon}_3}}\right). \tag{23}$$

Table 2 Results of soil tests for geologic materials

	Density ρ_s (g/cm^3)	Liquid limit w_L (%)	Plastic limit w_P (%)	Plasticity index I_P	Ignition loss L_i (%)	Estimated φ (°)
Halloysite	2.63	44.93	26.23	18.71	12.30	12.5
Montmorillonite	2.81	1042.13	80.94	961.19	4.99	2.1
Mt. Aso volcanic ash （Mt. Naka）	2.75	NP	NP	NP	-0.27	–
Mt. Aso volcanic ash （Hino Pass.）	2.74	NP	NP	NP	-0.30	–
Futaba-fault gouge	2.72	40.64	7.80	32.84	6.24	9.8
Mino gaerome porcelain clay	2.65	42.44	22.50	19.96	3.80	12.2
Mino kibushi porcelain clay	2.61	46.51	28.60	17.91	9.94	12.8
Seto gaerome porcelain clay	2.62	52.43	22.10	30.31	7.69	10.1
Seto kibushi porcelain clay	2.55	59.90	28.10	31.80	12.62	9.9
Shigaraki gaerome porcelain clay	2.64	40.10	20.40	19.70	4.13	12.3
Shigaraki kibushi porcelain clay	2.66	37.75	21.10	16.67	4.47	13.2

From Eqs. (22) and (23), we can get

$$I_{\mathrm{P}} = \left(\frac{\alpha}{2\tan^{-1}(\sqrt{K}) - \pi/2} \right)^{\frac{1}{\beta}}. \quad (24)$$

In this way, I_{P} is linked to Eq. (24) through Rowe's energy ration of granular material. On the other hand, deformation mode can be analyzed. Significantly, it is remarked that parameters *a*, *b* and *c* in Eqs. (18), (20) and (21) relate to I_{P}. Eventually, deformation mode analysis by the governing equation derived from flow rule based on plastic potential is determined by I_{P}. In this paper, we detected the procedure of dealing with the view point of I_{P} in regard to deformation patterns. From the above, we evaluate that I_{P} theoretically determines the bifurcationally deformed patterns of soils.

The internal friction angle φ can be approximately estimated (by I_{P} based on Eq. 22). From the viewpoint of φ, the landslide is predicted to happen in condition that φ is around 10° or less [23]. Interestingly, the φ of each porcelain clay and Futaba-fault gouges are also low. Kuwahara and Hirama [24] indicated fault gouges behave as a water barrier sheet partially to surrounding jointed bedrocks because the permeability of faults was low. Hence, application of liquid/plastic limit tests to geologic materials is able to assess the basic mechanical data of materials such as φ and/or cohesion evaluating a physically weak zone in ground and geology conditions.

4.2 Deformation implication materials of soils and rocks

Finally, we discuss deformation patterns of geomaterials (soils and rocks) through the concept of I_{P}. We can discuss the relationship between the concept of I_{P} and "Deformation facies diagram". The deformation facies proposed by [8] are represented by means of their series and grades on the coordinate axes. Uemura [8] said, "*The former allows the discrimination of the deformation series in definite environment, and the latter is expressed by the deformation grade for a definite material. Ductility contrast and mean ductility are available as indices to qualify such series and grades, respectively [25]. Taking into account that most rocks are not homogeneous in lithology but have some internal structures or they consist of multilayered strata, the ductility as a whole should be expressed by the average of constituent portions and layers. This is mean ductility. On the other hand, internal movement of rocks, which results in the deformation fabric, is expected to be largely dependent on the relative difference of ductility between adjacent constituents, namely it is the second index ductility contrast"*. By the Uemura [8]'s proposal, deformation facies diagram shows that stratum including rocks is that fluidly deformed when its character change more ductile. The Uemura [8]'s concept versatilely represents the various deformation patterns of various rocks. However, its problem is that the indices of mean ductility and ductility contrast are qualitative ones and hence difficult to argue the development of deformation patterns quantitatively, as discussed in the present study. In deformation facies diagram, the vertical axis defines mean ductility and illustrated interestingly deformation patterns of specimens. On this vertical axis, mean ductility controls the deformation patterns: a pair of oblique shear pattern-diamond pattern-bulge pattern from low to high mean ductility. In other words, the concept of I_{P} is important to determine patterns of folds and tectonics besides mechanical parameters (e.g. stress and strain). It should be noted that I_{P} is an index characterizing the state of soils, especially clay. However, we point out the possibility on that we can mesoscopically discuss the evolution of deformation patterns of the geologic materials such as soft-sediment deformation in virtue of I_{P}. For example, geological observation of soft sediments in subduction zones [26] reveals that the mode of sediment deformation are complex and incompletely understood as an interaction of porosity, pore pressure, and state of accreting sediments. As shown in the present paper, it has been already understood theoretically that the porosity of soft sediments corresponds to plasticity index of soil. We found the concept of the void ratio of soils can be related to porosity of rocks. Moreover, from this previous study, the deformation of strata is closely controlled by brittlely (mudstone) and ductilely (sandstone). This is, namely, ductility contrast can be explained by composition of the ratio of mud and sand. In conclusion, the geological deformation phenomena (including folds, tectonics and landslides) are not constantly controlled by physical parameter such as stress or strain. The concept of plasticity index I_{P} determines deformation patterns.

5. CONCLUSION

Firstly, we showed that I_{P} theoretically determines deformation patterns of soils by Cam-clay model. Moreover we prove that the index closely affects the bifurcation formulas by [2] and mention that this concept of plasticity index can reflect a mechanical bifurcation of rocks (e.g. variety of folds or soft-sediments). Explicating the hidden meaning Eq. (22), we might discuss about landslides with lower φ from the view point of the physical mean of I_{P}.

Based on mathematical conversion [27], Yamaguchi et al. [28] related L_{i} to C_{c} by Eq. (13). Therefore, by Eq. (14), I_{P} can be linked to L_{i}. So, in

the future, we need to study why organic matter is a parameter of Cam-clay model.

REFERENCES

[1] Paterson MS, "Experimental deformation and faulting in Wombeyan marble", Geol. Soc. America Bull., Vol. 69, no. 4, 1958, pp. 465-476.

[2] Shibi T and Kamei T, "Effect of plasticity indices on bifurcation analytical results of normally consolidated cohesive soils", Proc. Jpn. Soc. Civ. Eng., Vol. 715, 2002, pp. 297-309. (Japanese with English abstract)

[3] Ikeda K, Ichimura T, Takamura H, Sudo Y, and Tsutsumi S, "Image processing of deformation behavior of plane strain compression specimens based on bifurcation mechanism", Proc. Jpn. Soc. Civ. Eng., Vol. 757, 2004, pp. 167-176. (Japanese with English abstract)

[4] Voight B, "Correlation between atterberg plasticity limits and residual shear strength of manual soils", Géotechnique, Vol. 23, no. 2, 1973, pp. 265-267.

[5] Kanji MA, "The relationship between drained friction angles and atterberg limits of natural soils", Géotechnique, Vol. 24, 1974, pp. 671-674.

[6] Kenny TC, "Discussion", J. Soil Mech. Found. Div., ASCE, Vol. 85, no. SM 2, 1959, pp. 67-79.

[7] Mandar MD and Huzjak RJ, "Drained residual shear strength of some claystones from Front Range", Colorado, J. Geotech. Geoenviron. Eng., Vol. 131, no. 12, 2005, pp.1543-1551.

[8] Uemura T, "Deformation facies, series and grades", Jour. Geol. Soc. Japan, Vol. 87, no.5, 1981, pp. 297-305.

[9] Mises R von., "Mechanik der plastischen Formänderung von Kristallen", Z. angew., Math. Mech. Vol. 8, no.3, 1928, pp. 161-185.

[10] Roscoe KH, Schofield AN, and Wroth CP, "On the yielding of soils", Géotechnique, Vol. 8, no. 1, 1958, pp. 22-53.

[11] Roscoe KH, Schofield AN, and Thurairajah A., "Yielding of clays in state wetter than critical", Géotechnique, Vol. 13, no. 3, 1963, pp. 211-240.

[12] Rowe PW, "The stress-dilatancy relation for static equilibrium of an assembly of particles in contact", Proc. Roy. Soc., Vol. 269, no. 1339, 1962, pp. 500-527.

[13] Kulhawy FH and Mayne PW, "Manual on estimating soil properties for foundation design", Electric Power Research Inst., Palo Alto, CA (USA); Cornell Univ., Ithaca, NY (USA). Geotechnical Engineering Group, no. EPRI-EL-6800, 1990.

[14] Casagrande A, "Research on the Atterberg limits of soils", Public roads Vol. 13, no. 8, 1932, pp. 121-136.

[15] Shibi T, Kamei T, and Nagayoshi T, "The transition of localized strain for undrained plane strain compresion loading of normally consolidated clay", Ground Engineering, Vol. 18, no. 1, 2000, pp. 41-46. (in Japanese)

[16] Yatomi C, Yashima A, Iizuka A, and Sano I, "General theory of shear bands formation by a non-coaxial cam-clay model", Soils Found., Vol. 29, no. 3, 1989, pp. 41-53.

[17] Nakase A, Kamei T, and Kusakabe O, "Constitutive parameters estimated by plasticity index", J. Geotech Engrg., Vol. 114, no. 7, 1988, pp. 844-858.

[18] Kamei T, "Dilatancy characteristics of normally consolidated cohesive soils", Soils Found., Vol. 29, no. 1, 1989, pp. 165-172.

[19] Shibi T, Yatomi C, and Kamei T, "Influences of aspect ratio on the bifurcation analysis for a normally consolidated clay under the plane strain undrained compression loading", Proc. Jpn. Soc. Civ. Eng., Vol. 666, 2000, pp. 181-192. (Japanese with English abstract)

[20] Mitchell JK and Soga K, Fundamentals of Soil Behavior, 3rd ed. New York: John Wiley & Sons, Inc., 1976, ch. 10.

[21] Sakai T, Katsuyama K, Md. Zakaria H, and Laura, J. P. N., Soil Mechanics (1) - Fundamental Properties-, Tokyo: CORONA PUBLISHING CO., LTD, 2010.

[22] Hirata M, Muto J, and Nagahama H, "Experimental Analysis on Rowe's Stress-Dilatancy Relation and Frictional Instability of Fault Gouges", Episodes, Vol. 37, no. 4, 2014, pp. 303-307.

[23] Sassa K and Lee J, "Measurement of apparent friction angle during motion by the high-speed ring shear apparatus", Landslides, Vol. 30, no. 1, 1993, pp. 1-10. (Japanese with English abstract)

[24] Kuwahara T and Hirama K, "Study on engineering material evalution of fault and sheared zone", Rep. Eng, Res. Lab., Obayashi-gumi, Ltd., Vol. 43, 1991, pp. 99-106. (Japanese with English abstract)

[25] Donath FA and Parker RB, "Folds and folding", Geol. Soc. America Bull., Vol. 75, no. 1, 1964, pp. 45-62.

[26] Lash GG, "Accretion-related deformation of an ancient (early Paleozoic) trench-fill deposit, central Appalachian orogeny", Geol. Soc. America Bull., Vol. 96, no. 9, 1985, pp. 1167-1178.

[27] Yamagichi H, Ohira Y, and Kogure K, "Volume change characteristics of undisturbed fibrous peat", Soils Found., Vol. 25 no. 2, 1985, pp. 119-134.

[28] Ohira Y, Kotani A, and Harada S, "Some investigations of the relationship between consolidation pressure and void ratio on the poor soil", Mem. Def. Acad., Vol. 9, no. 1, 1969, pp. 311-317.

Second International Conference on Science, Engineering & Environment,
Osaka City, Japan, Nov.21-23, 2016, ISBN: 978-4-9905958-7-6 C3051

NORMAL RATIO IN MULTIPLE IMPUTATION BASED ON BOOTSTRAPPED SAMPLE FOR RAINFALL DATA WITH MISSINGNESS

Siti Nur Zahrah Amin Burhanuddin[1], Sayang Mohd Deni[2] and Norazan Mohamed Ramli[3]
[1,2,3] Center for Statistics and Decision Science Studies, Faculty of Computer and Mathematical Sciences,
Universiti Teknologi MARA, 40450 Shah Alam, Selangor, Malaysia

ABSTRACT

The existence of missing values in rainfall data series is inevitably affects the quality of the data. This problem will influence the results of analysis and subsequently provide imprecise information to the hydrological and meteorological management. A practical and reliable approach is needed in developing estimation methods to impute the missing values. Single imputation is the most commonly used approach for missing values, but, it encounters with the limitation of not considering the uncertainty and natural variability in missing data imputation. Thus, this study has proposed multiple imputation approach based on bootstrap samples in order to overcome the limitation of single imputation approach. Three normal ratio estimation methods are implemented using the proposed approach. The performances of the estimation methods are evaluated at six different levels of missingness. Complete 40 years daily rainfall data from four meteorology stations were considered for the analysis purpose with Johor Bahru station was selected as the target station. The results of the proposed approach were compared to the results obtained from single imputation approach and the widely known built in software for multiple imputation, Amelia II package, in assessing the performance of proposed approach. The results showed that all estimation methods that implemented using proposed approach provided the most accurate estimation results at all percentages of missingness. This proves the advantage of adaption of variability and uncertainty element in the proposed approach in estimating the missing rainfall data at the area of the current study.

Keywords: Missing Rainfall Data, Single Imputation, Multiple Imputation, Bootstrap, Normal Ratio

INTRODUCTION

Complete rainfall dataset is highly necessary to the effective hydrological and meteorological analyses. However, the presence of missing data in the rainfall dataset is inevitable [1]. This is due to several factors such as relocation of stations and faulty instruments. This problem will influence the accuracy of the analysis results and subsequently provide inaccurate information to the management and development of hydrology and meteorology.

Concerning this situation, various estimation methods have been explored in treating the missing values in rainfall time series, i.e. normal ratio, inverse distance weighting, multiple linear regression, and kriging. However, normal ratio (NR) has appeared to be the most commonly used method in estimating missing rainfall values as stated in literature [2]–[4] due to its simplicity and efficiency.

Reference [7] introduced the application of NR method in estimating missing rainfall records. The NR method was then modified by [8] and [9] through the adaption of correlation coefficients and the effect of distance in the original version of NR method to improve its performance. The development of the NR method is continually being explored and is recently being studied by [4], [5], and [6]. Reference [5] and [6] compared NR method to their more sophisticated proposed methods to estimate the missing values in monthly meteorological data. They have discovered that the proposed method produced more accurate results compared to the old NR method.

Due to its simplicity, NR method is considered as an evergreen method in imputing missing rainfall data. However, the limitations of the NR method are disclosed from its applications in missing data imputation. The implementation of NR method in the previous studies is only through the single imputation (SI) approach. This approach is commonly known with the limitation of not accurately represents the variability of missing data and the uncertainty of imputed values [10]. Therefore, in order to overcome the limitation of SI approach, multiple imputation approach is introduced by [11]. Multiple imputation (MI) is one of the advanced approaches in imputing the missing rainfall data.

MI is an approach that handles missing data in a way to produce a valid statistical inference instead of estimate the missing values as close as possible to the observed ones [12]. The approach has proven to be a powerful tool in studies conducted by [13] and [5]. [5] were successful in developing such

estimation methods based on MI approach called EM-MCMC. Although the method is computationally inefficient, it has produced more robust results compared to the SI based methods. Reference [13] applied four stages of imputation approach (based on MI approach) in estimating the missing rainfall values at Paya Kangsar, Malaysia, and proved that the MI performed better than the SI.

Recently, various built-in packages are created for implementing the MI, hence, Amelia II package is the one that commonly used in estimating the missing rainfall data. The package is a bootstrapping-based algorithm that estimates the statistics by applying the expectation maximization method. The method imputes each missing value *m* times (*m*=5 is the program default), that created five completed datasets. The datasets can be straightly used for analysis purpose. General bootstrap used in this package is not suitable to be used for time series data since it does not preserve the original time series structure. Therefore, moving block bootstrapping (MBB) is considered in this study to improve the accuracy of bootstrap for time series data. MBB divides the data into several blocks and samples the whole blocks before concatenate them. The dependency structure of the time series was preserved within each block [14]

Accordingly, this study is aimed to propose multiple imputation approach onto the NR method, which will result in more accurate estimations of missing rainfall values by considering the variability and uncertainty of imputation at the same time. This effort is of the consideration in providing a good quality dataset to be used for public domain.

The remaining of this paper are organized as follows: Materials and Methods part describes the data preparation and the proposed multiple imputation approach with the performance criteria used in evaluating the performance of the estimation methods. Results and Discussions part presents the results of the study with a comparative evaluation of the method's performance followed by the conclusions.

MATERIALS AND METHODS

Data Preparation

This study was performed for the south region of Peninsular Malaysia. For the purpose of estimation method evaluation, four rainfall measuring stations were selected throughout this region. The name of the stations with their respective geographical coordinates and spatial and descriptive information are listed in Table 1.

Johor Bahru station is considered as the target station (station in bold). In estimating the missing values of the target stations, rainfall data from their surrounding stations are also necessary. Data from stations that are closer to the target station tend to share similar characteristics with the target station, which are definitely valuable in providing more accurate estimation results [4]. Thus, the stations within the radius of 100 km to the target stations were all considered as neighboring stations (see Table 1).

Table 1 List of the selected stations with their geographical coordinates and spatial and descriptive information

Name of Station	Latitude	Longitude	Euclidean Distance (km)	Mean	Standard Deviation	Max Value
Johor Bahru	**103.75**	**1.47**	**0.00 (0)**	**6.635**	**10.43**	**285.4**
Sek. Men. Bkt. Besar	103.72	1.76	0.29 (32)	5.369	8.806	298
Kuala Sedili	103.97	1.85	0.44 (49)	7.067	10.369	397.5
Jln. Kluang/Mersing	103.74	2.26	0.79 (88)	6.431	10.265	305

The complete daily rainfall records from these stations were obtained from the Malaysian Drainage and Irrigation Department (DID) for the analysis of this study. The data consists of the daily rainfall amounts for the period of 40 years from January 1, 1975 to December 31, 2014.

Estimation Methods for Missing Rainfall Values

Three normal ratio methods, i.e. old normal ratio (ONR), normal ratio based on trimmed mean (NRTR), and normal ratio based on geometric median (NRGMED) are considered to be implemented using the multiple imputation (MI) approach proposed in this study. The application of these methods through the MI approach is rarely found in the previous studies. Generally, the NR methods are implemented using SI approach by most of studies, for example, [4], [5], and [6].

The old normal ratio (ONR) method was firstly introduced by [7] in estimating rainfall missing values. It is based on the mean ratio of data between the target station and the neighboring stations. The NR method is further expressed as follows:

$$\hat{Y} = \frac{1}{N}\sum_{\substack{i=1 \\ i\neq t}}^{N}\left(\frac{\mu_t}{\mu_i}\right)Y_i \quad (1)$$

where; μ_t is the arithmetic mean of the available data at target station *t*; μ_i is the arithmetic mean of the available data at i^{th} neighboring station; $\hat{Y}$ is the estimated missing data at target station *t*; Y_i is the concurrently observed data at the i^{th} neighboring station; and N is the number of neighboring stations.

Normal ratio based on trimmed mean (NRTR) method is the modified version of ONR which considering the trimmed mean as the weighting factor. Trimmed mean reduced the effect of outliers on the calculated average. Several levels of trimming (1%, 5%, and 10%) considered to assess the consistency of the estimation results. The application of the trimmed mean in the estimation methods can produce more accurate estimation results. The NRTR method is defined as follows:

$$\hat{Y} = \frac{1}{N}\sum_{\substack{i=1 \\ i\neq t}}^{N}\left(\frac{\mu_{trim_t}}{\mu_{trim_i}}\right)Y_i \quad (2)$$

where; μ_{trim_t} is the trimmed mean of the available data at target station *t*; μ_{trim_i} is the trimmed mean of the available data at i^{th} neighboring station.

The last method is normal ratio based on geometric median (NRGMED). Geometric median (Gmed) is a robust estimator of centrality in Euclidean spaces [15]. Gmed of a dataset is the data minimizing the sum of distances to the sample dataset. It is defined as a robust version of geometric mean that is more stable in the presence of outliers [15]. The method is expressed as follows:

$$\hat{Y} = \frac{1}{N}\sum_{\substack{i=1 \\ i\neq t}}^{N}\left(\frac{Gmed_t}{Gmed_i}\right)Y_i \quad (3)$$

Gmed is defined as: $Gmed_i = e^{(\text{median}(\ln(y_i)))}$

where; $Gmed_t$ is the geometric median of the available data at target station *t*; $Gmed_i$ is the geometric median of the available data at i^{th} neighboring station.

Proposed Multiple Imputation using Bootstrapped Samples

Multiple imputation approach is proposed for the implementation of the estimation methods explained in the previous. Generally, MI consists of three consecutive phases; (1) imputation phase, (2) analysis phase, and (3) pooling phase [12]. Imputation phase is the most complicated phase which involves the process of estimating the missing values as in the SI approach. However, in MI, the imputation process is simulated *m* times ([11] suggested 3 to 5 times) producing *m* estimated values for each individual missing values, consequently resulting in *m* different imputed datasets. The imputed datasets are then going through the process of analysis, which is the second phase. Several sets of parameter estimates and standard errors are produced before being pooled into single results through the last phase

The implementation of MI approach proposed in this study is quite different from the other studies. The execution has adapted the concept used in Amelia II package which involves bootstrapping. Moving block bootstrapping (MBB) is applied to rainfall time series in preserving the original time series structure. This effort is expected to produce more accurate missing values estimation results due to the variability and uncertainty inherent in the proposed approach algorithm. Figure 2 shows the diagram of the proposed MI approach.

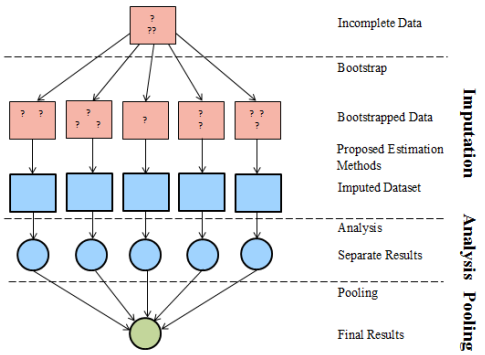

Fig. 2 A Schematic of Proposed Approach to MI

Five bootstrapped samples are created to produce five sets of estimated values for each missing dataset. The bootstrapped sample are generated based on the procedure of MBB proposed in this study. The procedure of MBB in this study is a bit different from other studies. Rainfall time series of the target station are divided into several parts according to the characteristics of rainfall data, such as the seasonal pattern and the rainfall amounts before going through the MBB process. The MBB is applied separately on each part of the data. The procedure is as follows:

i. Divide rainfall time series into four parts (blocks) according to monsoon seasons, i.e. (1) the month of May to August, (2) March to April, (3) November to February, and (4) September to October.

Block 1	Block 2	Block 3	Block 4
(Mar - Apr)	(May - Aug)	(Sep - Oct)	(Nov - Feb)

ii. Resample each block of rainfall time series obtained in (i) for 100 times (the size of bootstrap sample is the sample size of the original data). Then merge the blocks of bootstrapped data to produce a year daily rainfall time series.

Block 1	Block 2	Block 3	Block 4
x_i	x_j	x_k	x_l
$i = 1, \ldots, 61$	$j = 1, \ldots, 123$	$k = 1, \ldots, 61$	$l = 1, \ldots, 120$

iii. Repeat step (i) and (ii) for all 40 years daily rainfall data and merge them to generate a set of bootstrapped sample representing the new sample for a period of 40 years and equal to 14610 daily data.

New Sample
x_n
$n = 1, 2, 3, \ldots, 14610$

iv. Repeat step (i) to (iii) for 5 times to produce 5 new samples

The new samples produced are used in the proposed MI approach (NRMI-boot). The NRMI-boot is implemented based on the following procedures:

a) The same procedures of introducing missing data in the target station used in the SI approach are applied in NRMI-boot.

b) The ratio means of each new sample of the target station and the data of its nearby stations are considered as the weighting factor for the estimation methods (an example of ONR method - refer to Eq. (1)).

$$w_{L_i} = \frac{\mu_{L_i}}{\mu_i}, \quad L = \mathbf{1}, \mathbf{2}, \ldots, \mathbf{5} \tag{4}$$

where, w_{L_i} is the weight of the i^{th} neighboring station for bootstrapped sample L; μ_{L_i} and μ_i the sample mean of the available data for bootstrapped sample L and i^{th} neighboring station respectively.

c) Five weighting factors are produced to yield five different estimated values for each individual missing value.

d) Each estimated values is then used to impute the missing values in the original rainfall dataset, in which producing five complete datasets with different imputed values and the same observed values.

e) The complete imputed datasets are analyzed and the results of analysis are pooled to produce a single result of analysis.

The results obtained from the proposed NRMI-boot were compared to the results of SI approach and the results obtained from Amelia II package. The performance of the considered NR methods is evaluated based on the implementation of these three approaches. Two error measurements are considered in evaluating the performance of the estimation methods, namely root mean square error (RMSE) and similarity index (SIndex). They are defined as follows:

$$\text{RMSE} = \sqrt{\frac{1}{n}\sum_{i=1}^{n}\left(\hat{Y}_i - Y_i\right)^2} \qquad \text{SIndex} = \frac{\sum_{i=1}^{n}\left(\hat{Y}_i - Y_i\right)^2}{\sum_{i=1}^{n}\left(\left|\hat{Y}_i - \bar{Y}\right| + \left|Y_i - \bar{Y}\right|\right)^2}$$

where; $\hat{Y}_i$ is the estimated value; Y_i is the actual value of the observation; $\bar{Y}$ is the mean of actual values; n is the number of observations.

RESULTS AND DISCUSSIONS

Six levels of missingness ranges from 5% to 30% are used in assessing the performance consistency of estimation methods. The performance of estimation methods is investigated through their implementation using SI and MI approaches. The results of the NRMI-boot are compared to the SI at various level of missingness and displayed in Table 3. The results of estimation methods using NRMI-boot produced slight improvements compared to the SI approach based on the least RMSE and the highest SIndex (see the values in bold). It also produced better estimation results than SI at varying percentages of missingness. This shows that the variability and uncertainty accounts in the NRMI-boot produced more accurate results of estimation.

Of the five estimation methods, ONR appears as the best method in estimating the missing rainfall values, whereas NRGMED is the worst. The NRTR method was divided into three based on different levels of trimming, i.e. NRTR1 (1% trimming), NRTR5 (5% trimming), NRTR10 (10% trimming), in order to investigate the effects of the trimming levels of the mean on the accuracy of the estimation results. The accuracy of the estimation results using NRTR decrease with the increase of the trimming percentage.

Table 3 Performance of NR methods through single imputation (SI) and proposed NRMI-boot approaches at various level of missingness

Level of Missingness	Estimation Method	RMSE		SIndex	
		SI	NRMI-boot	SI	NRMI-boot
5%	ONR	14.869	**13.952**	0.648	**0.688**
	NRTR1	15.093	**14.174**	0.642	**0.682**
	NRTR5	15.340	**14.421**	0.635	**0.675**
	NRTR10	15.442	**14.540**	0.632	**0.672**
	NRGMED	15.633	**14.871**	0.627	**0.662**
10%	ONR	14.744	**13.672**	0.643	**0.682**
	NRTR1	14.985	**13.860**	0.637	**0.676**
	NRTR5	15.224	**14.060**	0.630	**0.671**
	NRTR10	15.322	**14.154**	0.627	**0.668**
	NRGMED	15.441	**14.400**	0.624	**0.661**
15%	ONR	14.182	**13.553**	0.646	**0.669**
	NRTR1	14.417	**13.752**	0.639	**0.664**
	NRTR5	14.642	**13.959**	0.632	**0.657**
	NRTR10	14.729	**14.053**	0.630	**0.655**
	NRGMED	14.870	**14.247**	0.626	**0.649**
20%	ONR	14.319	**14.296**	0.662	**0.656**
	NRTR1	14.538	**14.515**	0.656	**0.650**
	NRTR5	14.730	**14.732**	0.650	**0.644**
	NRTR10	14.806	**14.831**	0.648	**0.641**
	NRGMED	14.884	**15.051**	0.646	**0.635**
25%	ONR	14.610	**14.391**	0.660	**0.655**
	NRTR1	14.849	**14.621**	0.654	**0.648**
	NRTR5	15.055	**14.829**	0.649	**0.643**
	NRTR10	15.135	**14.920**	0.646	**0.640**
	NRGMED	15.333	**15.106**	0.641	**0.634**
30%	ONR	14.584	**14.157**	0.667	**0.664**
	NRTR1	14.821	**14.381**	0.660	**0.658**
	NRTR5	14.984	**14.571**	0.656	**0.652**
	NRTR10	15.044	**14.652**	0.654	**0.650**
	NRGMED	15.223	**14.892**	0.649	**0.643**

The next comparison involved the results of the best estimation method using the proposed NRMI-boot, i.e. ONR method with the results obtained from the Amelia II package. Table 4 presents the results comparison of these MI approaches. The method in bold represented the most appropriate method in estimating the missing values. Based on the comparison, it can be seen that the results obtained from NRMI-boot gives more accurate results compared to the Amelia results. This may due to the moving block bootstrapping adapted in the NRMI-boot, in which it preserved the original time series structure in imputing the missing rainfall values.

Table 4 Performance of NR methods through the NRMI-boot and the Amelia II package results at various level of missingness.

Error Measures	Level of Missingness	Amelia	NRMI-boot
RMSE	5%	22.360	**13.952**
	10%	141.935	**13.672**
	15%	209.194	**13.553**
	20%	196.579	**14.296**
	25%	139.747	**14.391**
	30%	66.473	**14.157**
SIndex	5%	0.475	**0.688**
	10%	0.134	**0.682**
	15%	0.197	**0.669**
	20%	0.031	**0.656**
	25%	0.163	**0.655**
	30%	0.244	**0.664**

Although the computation of the proposed approach is quite intensive compared to the SI approach, it is recommended to be applied in any studies related to missing values since it provided a robust approach and more accurate estimation results. For future research, the degree of suitability of the proposed MI approach (NRMI-boot) towards other climatic variables (e.g. temperature and wind speed) and time scales (e.g. monthly and yearly) needs to be investigated. Other suggestions are to consider other estimation methods such as inverse distance weighting and geographical coordinate methods in estimating the missing values by using the proposed approach.

CONCLUSIONS

The implementation of estimation methods through the NRMI-boot produced the most accurate results among the SI approach and Amelia II package in estimating the missing rainfall values. This shows the advantage of the proposed approach that considering the variability in creating the missing values and uncertainty in estimating the imputed values. The involvement of these two elements has successfully improved the estimation results' accuracy for the area of the current study. Furthermore, the adaption of MBB gives advantage to the NRMI-boot and is more suitable when dealing with the time series data compare to the general bootstrapping adapted in Amelia II package.

ACKNOWLEDGEMENTS

The authors are indebted and thankful to the staff of Malaysian Meteorological Department, and Drainage and Irrigation Department for providing the daily rainfall data used in this study. This research would not have been possible without the sponsorships from Ministry of Higher Education and also Universiti Teknologi MARA, Malaysia. This research is funded by the Malaysian Fundamental Research Grant, 600-RMI/FRGS 5/3 (58/2014).

REFERENCES

[1] Firat M, Dikbas F, Koc AC, and Gungor M, "Missing data analysis and homogeneity test for Turkish", Sadhana, Vol. 35, 2010, pp. 707–720.

[2] De Silva RP, Dayawansa NDK, and Ratnasiri MD, "A Comparison of methods used in estimating missing rainfall data", J. Agric. Sci., Vol. 3, 2007, pp. 101–108.

[3] Khorsandi Z, Mahdavi M, Salajeghe A, and Eslamian S, "Neural network application for monthly precipitation data reconstruction", J. Environ. Hydrol., Vol. 19, 2011, pp. 1–12.

[4] Suhaila J, Deni SM, and Jemain AA, "Revised spatial weighting methods for estimation of missing rainfall data", Asia-Pacific J. Atmos. Sc, Vol. 44, 2008, pp. 93–104.

[5] Yozgatligil C, Aslan S, Iyigun C, and Batmaz I, "Comparison of missing value imputation methods in time series: the case of Turkish meteorological data", Theor. Appl. Climatol., Vol. 112, Jul. 2013, pp. 143–167.

[6] Khosravi G, Nafarzadegan AR, Nohegar A, Fathizadeh H, and Malekian A, "A modified distance-weighted approach for filling annual precipitation gaps: application to different climates of Iran", Theor. Appl. Climatol., Jan. 2014, pp. 1–10.

[7] Paulhus JLH and Kohler MH, "Interpolation of missing precipitation records", Mon. Wea. Rev, Vol. 80, 1952, pp. 129–133.

[8] Young KC, "A three-way model for interpolating for monthly precipitation values", Mon. Weather Rev., Vol. 120, 1992, pp. 2561–2569.

[9] Tang WY, Kassim AHM, and Abubakar SH, "Comparative studies of various missing data treatment methods -Malaysian experience", Atmos. Res., Vol. 42, 1996, pp. 247–262.

[10] Donders ART, Van Der Heijden GJMG, Stijnen R, and Moons KGM, "Review: a gentle introduction to imputation of missing values", J. Clin. Epidemiol., Vol. 59, Oct. 2006, pp. 1087–91.

[11] Rubin DB, "Multiple Imputation After 18 + Years", J. Am. Stat. Assoc., Vol. 91, 1996, pp. 473–489.

[12] Enders CK, Applied Missing Data Analysis. New York: The Guilford Press, 2010.

[13] Yendra R and Jemain AA, "Methods on handling missing rainfall data with Neyman-Scott rectangular pulse modeling", Proc. 2nd Natl. Symp. on Math. Sci., vol. 1213, 2013, pp.1213-1220.

[14] Li J, "The block bootstrap test of Hausman", Econ. Lett., Vol. 91, 2006, pp. 76–82.

[15] Das KR and Imon AHMR, "Geometric median and its application in the identification of multiple outliers", J. Appl. Stat., Vol. 41, 2014, pp. 817–831.

Second International Conference on Science, Engineering & Environment,
Osaka City, Japan, Nov.21-23, 2016, ISBN: 978-4-9905958-7-6 C3051

REAGENT PREPARATION FOR TEST KIT ANALYSIS OF HARDNESS

Somporn Pleanjai[1]
[1]Faculty of Science and Technology, Rajamangala University of Technology Thanyaburi, Thailand

ABSTRACT

Every household and every factory uses water, and none of it is pure. One of impurity that is of special interest is “hardness”. Hardness is defined as calcium and magnesium ion content. These “hardness ions” cause two major kinds of problems. First, the metal cations (Ca^{2+} and Mg^{2+}) react with soaps, causing precipitation of the soap scum. More seriously, the calcium and magnesium carbonates tend to precipitate out as adherent solids on the surfaces pipes and especially on the hot heat exchanger surfaces of boilers. The resulting scale buildup can impede water flow in pipes. Hard water also contributes to inefficient and costly operation of water-using appliance. Water hardness can be readily determined by titration with the chelating agent ethylenediaminetetra acetic acid (EDTA). Most water testing laboratories offer hardness test for fee. Also, many companies that sell water treatment equipment offer hardness tests. An approximate estimate of water hardness can be obtained without the aid of testing facilities or testing kits or strips. Consequently, this study aimed to prepare a chemical solution a portable kit (Test kit) for water hardness analysis. In this experiment the chemical solution will be standardized by titration against a known solution made from calcium carbonate, $CaCO_3$. The titration is carried out at a pH10. Eriochrome black T and Calmagite were used on comparison indicator in the analysis process. Then use the same titration techniques to measure the hardness of four unknown water samples. The results found that both indicators can use for hardness determination. In addition, our chemical reagent preparation are available that can be alternative water hardness testing kits for purchase through water testing supply companies. The significance of test results will be discussion.

Keywords: Calcium, Hardness, Reagent preparation, Test kit, Water analysis

INTRODUCTION

Every household and every factory uses water, and none of it is pure. One of impurity that is of special interest is “hardness”. Hard water contains multiply charged ions such as calcium, magnesium, and heavy metal ions, which replace sodium and potassium ion in soaps and detergents to form precipitates. These precipitates interfere with cleansing action and leave unsightly bathtub rings and scum. High levels of hard water ions such as Ca^{2+} and Mg^{2+} can cause scaly deposits in plumbing, appliances, and boilers. Hard water does not present a health risk, as long as the minerals are not heavy metal salts [1]. Water hardness is usually express as the milligrams of $CaCO_3$ equivalent to the total amount of Ca^{2+} and Mg^{2+} present in one liter of water. Water hardness has usually been determined by titration with ethylenediaminetetraacetic acid (EDTA) and Eriochrome Black T or Calmagite [2], employing a manual procedure. Magnesium and calcium will be determined together. Eriochrome Black T and Calmagite are often used in water hardness determination [3]. In order to hard water contributes to inefficient and costly operation of water-using appliance especially for industries and company limited and so on. Therefore, practicing and mastering quantitative analysis relating to water quality, total hardness, and making accurate dependent calculations. The titration method is still widely used for the determination of water hardness [4]. However, only a few studies encompass the greener alternatives in formulation of chemical reagent. In addition, in the past there are only a few researches studying data deviation for environmental impacts, assessment, especially chemical reagent products data by using life cycle assessment (LCA) in Thailand.

Therefore, in this study, the primary objective was to analyze and compare water hardness of using commercial reagent (Test kit) and chemical prepared reagent (Test kit). The results were used to determine the options that would minimize the cost of the chemical reagents utilization and provide recommendation environmental data before T R Water Engineering Company Limited that acts in the design and installation of water treatment systems to produce clean water for industrial companies and government, etc. which industry was selected before they consider substituting from commercial reagent to a chemical prepared reagent.

EXPERIMENTAL

EDTA Titrimetric Method

Hardness, which reads the concentration of calcium and magnesium ions, was determined as indicated in literature [2]. Accordingly, 50 mL sample was transferred to conical flask. 2 mL buffer solution (will be sufficient to give a pH of 10.0 to 10.1) was added followed by about 0.4 g of solid indicator or 1 or 2 drop indicator solution. Add standard titrant slowly, with continuous stirring, until the last reddish tinge disappears and blue color was observed. Reagent blank used for comparison was titrated in a similar way as for the sample. Finally, Ethylenediaminetetraacetic acid (EDTA) titrant was standardized against Calcium standard (a known solution made from calcium carbonate, $CaCO_3$). Eriochrome Black T as indicator was used in chemical prepared reagent for test kit. Calmagite as indicator was used in commercial reagent for test kit. Record the titrant volumes for the Data and Calculations sheet. The result shows in Table 1 and Table 2. Finally, comparing cost performance and other parameter of water hardness analysis between using chemical prepared reagent and commercial reagent for test kit. The result shows in Table 3.

Calculation:

Hardness (EDTA) as mg $CaCO_3$/L

= (A x B x 1000)/mL sample

Where:

A= mL titration for sample and,

B= mg $CaCO_3$ equivalent to 1.00 mL EDTA titrant.

Reagents and Solutions

Hard water samples

A hard water sample that mimics very hard water with approximately 0.015M $CaCO_3$ may be prepared by creating slurry of 0.3750 g of anhydrous $CaCO_3$ with 3-4 mL of deionized water. Add 6 M HCl, a few drops at a time, until the $CaCO_3$ has dissolved. Dilute to 250 mL with deionized water.

pH 10 buffer

Solution I: Dissolve 1.1790 g of disodium salt dehydrate of EDTA and 0.7800 g of Magnesium sulfate heptahydrate ($MgSO_4 \cdot 7H_2O$) in 50 mL distilled water.

Solution II: Dissolve 16.90 g of Ammonium chloride (NH_4Cl) 143.00 mL of conc. Ammonium hydroxide (conc.NH_4OH)

Add solution I into solution II and dilute to 250 mL with distilled water.

Eriochrome Black T Indicator

A mixture of 0.50 g of Eriochrome Black T and100.00g of Sodiumchloride(NaCl) was employed.

EDTA titrant

A solution of approximately 0.015 M of EDTA prepared by weighing 5.5836 g of disodium salt dehydrate of EDTA and dilute to 1.00 L with distilled water. The solution of EDTA will be standardized by titration against 0.015 M $CaCO_3$ (three replicate samples).

HI 3812 Hardness Testing Kit

The HI 3812 test kit tests the hardness level as mg/L (ppm) calcium carbonate, via an EDTA titration. HI 3812 Hardness Test Kit which there are 2 ranges. They are high range-0 to 300 mg/L $CaCO_3$ and low range-0.0 to 30.0 mg/L $CaCO_3$.The Order Information: HI 3812test kit comes with 30mL *hardness* buffer, 10mL calmagite indicator, 120mL EDTA solution, 20mL plastic beaker with cap, 50 mL plastic beaker with cap and 1mL syringe with tip[5]. The testing kit tests were obtained from T R Water Engineering Company Limited.

RESULTS AND DISCUSSION

Hardness by EDTA Trimetric Method

Hardness, as mg$CaCO_3$/L or $CaCO_3$ ppm by using EDTA-titration method, the result shows in Table1.

Table 1 Comparing of EDTA-titration and test kit method with standard value

Standard Solution $CaCO_3$ (ppm)	Titration				Test Kit	
	Eriochrome Black T		Calmagite		Eriochrome Black T	
	(ppm)*	SD	(ppm)*	SD	(ppm)*	SD
6.00	6.09	0.12	6.09	0.12	6.47	0.06
9.00	9.18	0.26	9.18	0.26	9.81	0.48
12.00	12.17	0.23	12.17	0.23	12.98	0.36
15.00	15.23	0.32	14.97	0.15	15.66	0.64
18.00	18.04	0.07	18.16	0.18	19.33	0.15
60.00	60.33	0.31	60.33	0.31	63.72	1.44
90.00	90.20	0.35	90.20	0.35	91.79	1.80
120.00	120.27	0.46	120.27	0.46	122.07	3.64
150.00	149.93	0.13	149.93	0.13	153.31	1.50
180.00	180.19	0.32	180.19	0.32	184.35	4.76

Note : * Arithemic mean from three replicate samples

SD = Standard Deviation

From Table1, the result was found that difference of standard deviation values is 0.06-4.76 for both methods. The percentage of error found 0 to 9. Based on the evaluations from Table 1, our achievement focused not only on analytical chemistry knowledge in designing experiment in

laboratory, but also on field. It was found that 0% to 3% error in Table2. Thus, it can use both the indicators in chemical prepared reagent for EDTA-titration method and test kit which according to both of indicator was used in conventional titration [3].

Table 2 Hardness in different types of water using EDTA-titration as a reference method

Sample No.	Titration Eriochrome Black T Hardness(mg/L)	Test Kit* Calmagite (mg/L)	%Error	Test Kit** Eriochrome Black T (mg/L)	%Error
1.Natural Water (Prathumetane Province)	140.06	141.00	0.67	134.10	0.45
2. Tap Water (Prathumetane Province)	107.28	108.00	0.67	110.26	2.78
3.Tap Water (Ayutthaya Province)	89.40	87.00	2.68	89.40	0.00
4.Water Drinking (Saraburi Province)	2.98	3.00	0.67	2.98	0.00

*Commercial reagent solution **Chemical prepared reagent solution

Table 3 Comparing between commercial reagent solution and chemical prepared reagent solution for test kit

Parameter	Unit	Commercial reagent	Chemical prepared
1.Quantity of using (per set)	time	100	125
2.Accuracy (compared with titration method)	% error	0-9	0-9
3.Indicator	type	Calmagite (solution)	Eriochrome Black T (solid)
4.Price (per set)	Baht*	1,500.00	589.00

Note:* 1 USD = 35.2004 Baht[6]
"Bank of Thailand", Last update: April 12, 2016, available on line:https://www.bot.or.th

An acceptable design chemical prepared reagent for hardness water analysis by test kit method that must have a process that is capable to yield a profit or more reduce the cost of water testing laboratories. An estimation of the investment is required and the cost of production is needed before profitability of a project is evaluated. In this section, the equipment cost and chemical reagent cost are discussed. The chemical reagents cost has been estimated to be 5,600 Baht [7, 8]. The equipments (titration apparatus set, reagent bottle, volumetric flask etc., excluded equilibrium balance) cost has been estimated to be 6,677 Baht [9- 12]. Table 3 shows the chemical reagent's price that was calculated per set from price in the year 2016 [7, 8]. To further value from Table3, cost of saving has been calculated to be 913.35 Baht per set. Assuming that company which sell water treatment equipment offer hardness test 300 samples per year if using chemical prepared reagent will be saved money 2,740.05 Baht (2,740.05 = (3 set x 1,500/set) - (3 set x 586.65/set)) than using commercial reagent. Therefore, a reduction cost of hardness water analysis can be achieve by reducing the cost Hardness Test Kit set (using chemical prepared reagent alternative to commercial reagent).

Opportunities for greener alternatives in chemical formulation

Due to EDTA is mainly used in above the process. It should be considered. In addition to EDTA is used as a complexing agent in many industrial branches. During the use as complexing agent, the major amount of the applied EDTA is emitted into the wastewater. EDTA and its metal complexes are highly soluble in water. Because of the ionic properties, volatilization from aqueous solution will not occur [13]. Furthermore, the other reagents such as in most ammonia plants, CO_2 is separated from hydrogen at an early stage, generally use solvent adsorption. Energy savings can be achieved by using new solvents, with a potential of up to 1.4 GJ/t. Much of the CO_2 separated is used to produce urea, a popular type of nitrogen fertilizer. It takes 0.88 tonnes of CO_2 to produce a tonne of urea [14]. These mean can minimize global warming potentials which depending on their method of manufacture. Due to their manner of use, many of these materials end up in the sewer system or directly dispersed into the environment. Therefore greener replacements are actively sought. Fortunately, this study based on the result that using of chemical prepared reagent was effective more than using commercial reagent, especial saving cost per set.

CONCLUSION

As a conclusion of this study, the chemical prepared reagent can use for total hardness determination by test kit method as well as commercial reagent use in accuracy. Its price are not expensive per set so that they can identify the effective for promoting chemical prepared reagent utilization in companies and industries which solve a water quality problem realize and reducing cost for operation in the future.

ACKNOWLEDGEMENTS

The author is grateful for financial support of Rajamangala University of Technology Thanyaburi. The author also would like to thank analyst who provided helpful comments the analysis.

REFERENCES

[1] WHO, "Hardness in drinking-water", in Background Document for Development of WHO Guideline from Drinking-water Quality, WHO/SDE/WSH/03.04/06, WHO, Geneva, 1996.
[2] Standard Methods for the Examination of Water and Wastewater, American Public Health Association, 18th ed., 1992, pp. 2-36, Method 2340C.
[3] Yappert, M.C. and DuPré, D.B. Complexometric Titrations: Competition of Complexing Agents in the Determination of Water Hardness with EDTA. Journal of Chemical Education, Vol. 74, No. 12, Dec.1997, pp. 1422-1423.
[4] Skoog, D. A., West, D. M., Holler, F. J. and Crouch, S. R. Fundamental Analytical Chemistry, 8th ed., 2004, 870 pp. USA: Thomson Brooks/Cole.
[5] Instruction Manual, "HI 3812 Hardness Test Kit", available on line: http://shop.hannasingapore.com/media/pdf/manHI_3812.pdf
[6] "Bank of Thailand", Last update: April 12, 2016, available on line : https://www.bot.or.th
[7] Last update: April 14, 2016, available online: https://www.vittayapun.com
[8] Last update: April 14, 2016, available online: npchemsupply.weloveshopping.com/store/product/MERCK-2030774-th.html
[9] Last update: April 14, 2016, available online: https://gammco.com
[10] Last update: April 14, 2016, available online: https://www.globalgilson.com/volumetric-flasks
[11] Last update: April 14, 2016, available online: http://www.pelletlab.com/reagent.bottles
[12] "Business Finance Online", Last update: April 16, 2016, available online: http://www.zenwealth.com/businessfinanceonline/CB/PaybackPeriod.html
[13] Summary Risk Assessment Report, "Tetrasodium Ethylenediamineacetate (NA_4EDTA), CAS No: 64-02-8, EINECS No:200-573-9, Institute for Health and Consumer Protection European Chemicals Bureau I-21020 Ispra(VA), Italy, 2004.
[14] IFA for type and production of feedstock, 2006.

Second International Conference on Science, Engineering & Environment,
Osaka City, Japan, Nov.21-23, 2016, ISBN: 978-4-9905958-7-6 C3051

VIRTUAL SCREENING OF COMMERCIAL CYCLIC PEPTIDES AS β -OG POCKET BINDER INHIBITOR IN DENGUE VIRUS SEROTYPE 2

Usman Sumo Friend Tambunan[1*], Arli Aditya Parikesit[1], Vincentia Cheryl Adam[1], Mochammad Arfin Fardiansyah Nasution[1], Ratih Dyah Puspitasari[1], Djati Kerami[2]

[1]Bioinformatics Research Group, Faculty of Mathematics and Natural Science, Universitas Indonesia, Indonesia.
[2]Mathematics Computational Group, Faculty of Mathematics and Natural Science, Universitas Indonesia, Indonesia.

ABSTRACT

Dengue virus (DENV) has caused infectious disease which puts roughly 40% of world population at risk. An antiviral drug against DENV infection remains unavailable up until now. This research aims to find a drug candidate, which can inhibit β-OG binding site by a screening of 308 commercial cyclic peptides virtually. Through molecular docking and molecular dynamics simulation, it is discovered that Cyclo (-D-Trp-Tyr) ligand has good affinity with β-OG binding pocket. Ligand forms a stable complex with envelope protein in 310 K and 312 K. Cyclo(-D-Trp-Tyr) ligand is revealed to be a potential inhibitor of β-OG binding pocket. Thus, it is feasible for further development as an antiviral drug against DENV infection.

Keywords: Dengue, β-OG pocket binder, Fusion inhibitor, Cyclic peptide, Docking

INTRODUCTION

Dengue virus (DENV) still becomes a major health problem worldwide. According to the World Health Organization (WHO), the exposure to DENV increases in a recent decade. Approximately more than 2.5 billion people or 40% of the world's population is at risk of DENV. Before the 1970s, only 9 countries were experiencing the dengue epidemic, but now more than 100 countries in Africa, Americas, Eastern Mediterranean, Southeast Asia and the Western Pacific are exposed to this deadly disease [1].

The efforts from the researchers and scientists are being made to prevent the transmission of DENV. One of them is focused on the eradication of Aedes sp. as DENV vector [2]. Nowadays, the research is concentrated on finding an antiviral drug candidate that able to inhibit the DENV pathways, such as replication path, the path of synthesis of RNA, viral maturation pathway, and lane fusion with host cells [3].

The peptide is an amino acid based molecule which able to inhibit the enzyme's activity with good specificity. Furthermore, it is also has a tendency of non-accumulate in the body [4]. However, the peptide can also be easily degraded in our body. To prevent the peptide degradation by protease enzymes, the peptide molecules need to be cyclized into cyclic peptide[5]. Several previous studies were conducted in an effort to inhibit β-OG pocket binders: Kampmann et al., (2009) have obtained five molecules (namely A1-A5) out of 135,000 small molecules selected. However, A1-A5 molecules need further analysis and biological assay. The results showed that A5 can inhibit the fusion process of DENV [3]. Li et al., (2008) have obtained the thiazoles-modified compounds for inhibiting the DENV envelope protein in the β-OG binding site [6]. Wang et al., (2009) have screened 586.829 compounds by using in silico approach into 111 compounds to be tested further in order to obtain six compounds that can inhibit the DENV effectively based on immunofluorescence study [7]. Finally, Zhou et al., (2008) have screened compounds of the National Cancer Institute (NCI) library and obtained the compounds that can inhibit the viral reproduction at μmol concentrations, and NMR spectroscopy proves PO_2 compound bound to the virus and may compete with the β-OG natural ligand in its binding site with greater affinity [8].

This research aims to screen commercial cyclic peptides to be used as an inhibitor of β-OG pocket binder on DENV serotype 2 based on molecular docking and dynamics simulations to obtain the novel antiviral drug. We also deployed computational ADMET test, such as health effect and toxicity prediction, in order to eliminate the remaining compounds from molecular docking simulation to be selected into molecular dynamics simulation.

RESEARCH METHODOLOGY

A. Tools and Material

This research used some online and offline softwares such as Accelrys Discovery Studio 2.5, Accelrys Discovery Studio 4.1 Visualizer [9], GROMACS

4.6.5 [10], ChemDraw Ultra 12.0, OSIRIS Property Explorer [11], ACD-iLabs [12], VegaZZ 2.4.0 and Toxtree 3.5.0 softwares [13]. DENV envelope protein sequence database could be obtained from the National Center for Biotechnology Information (NCBI) (http://www.ncbi.nlm.nih.gov/), and for the three-dimensional structure could be searched by using SWISS-MODEL then downloaded from the Research Collaboratory for Structural Bioinformatics Protein Data Bank (RCSB-PDB) (http://www.rcsb.org/pdb/home/home.do) database in .pdb format. The structure of commercial cyclic peptide ligands can be obtained from these following chemical company databases: BaChem, Mimotopes, PolyPeptide Group, AnaSpec and the American Peptide.

B. Preparation of Cyclic Peptide Ligands

The cyclic peptide sequences were drawn manually by using the ChemBioDraw Ultra 14.0 with .mol file format. All ligands that have been drawn then converted into a 3D structure with VegaZZ 2.4.0 software, then imported into Accelrys Discovery Studio 2.5 software for ligand optimization in .sd format, CHARMm forcefield and the addition of partial charge MMFF94 ligands were conducted as well.

C. Preparation of Envelope Protein

DENV envelope protein sequence data was obtained from NCBI (National Center for Biotechnology Information) database in FASTA format, which was accessible on http://www.ncbi.nlm.nih.gov/. DENV envelope protein structure prediction was performed by homology modeling. Homology modeling step was accessed online using SWISS-MODEL server (http://swissmodel.expasy.org/).

The homology modeling results were used to obtain the 3D structure of DENV envelope protein as a template. The 3D structure of proteins could be downloaded from the PDB database by RCSB-PDB database and was stored in .pdb format. Then validated the 3D structure of proteins using RAMPAGE server for generating the Ramachandran plot (http://mordred.bioc.cam.ac.uk/~rapper/rampage.php)[14].

Furthermore, the DENV envelope protein was prepared and optimized by eliminating the unnecessary ligand and water molecules in the protein sequence. Then, the CHARMm Force Field was applied, along with the energy minimization.

D. Molecular docking simulations

The whole docking process was done by using Accelrys Discovery Studio 2.5 software, with LibDock module applied in binding free energy calculation. First, we set the parameters to determine the amount of Docking 'Hotspot' and 'Tolerance', other parameters were set according to the default of Accelrys Discovery Studio 2.5 software. The results of the molecular docking simulation process were identified by the 'Calculate Binding Energy' module in Accelrys Discovery Studio 2.5 software. Finally, 2D visualization and molecular interaction of the best ligand-receptor complex from molecular docking simulation could be seen by using Accelrys Discovery Studio 4.1 Visualizer software.

E. Computational ADMET test

In this study, we deployed two kinds of ADMET test by using OSIRIS Property Explorer, Toxtree 3.5.0 and ACD-iLabs softwares to determine the ligand's drug-likeness, mutagenicity/carcinogenicity prediction, and the health effect prediction, respectively. These tests were conducted to eliminate the remaining ligands from the previous simulation, in order to get the best ligand, based on its pharmacological properties and drug-likeness, to be selected for molecular dynamics simulation.

F. Molecular dynamics simulation

Molecular dynamics simulation was utilized to look at the protein-ligand complexes stability based on the RMSD (Root Mean Square Deviation) graph. The preparation of protein-ligand complexes, such as geometry optimization and energy minimization, was required before performing molecular dynamics simulation. The molecular dynamics simulation was performed using GROMACS 4.6.5 software. The GROMOS43a1 force field and TIP3P explicit solvent models parameters were utilized while the rest of the parameters were set by default.

The molecular dynamics simulation process was performed on the best cyclic peptide ligands which have the lowest $\Delta G_{binding}$ value, the best affinity, and interaction with the target cavity, as well as having the best pharmacological properties, based on computational ADMET test. Molecular dynamics simulations were performed in 20.000 ps (20ns) twice, at 310K and 312K, respectively. The result of molecular dynamics simulation could be seen in GROMACS viewer. Protein-ligand interactions between molecular dynamics during the process could be viewed by using Accelrys Discovery Studio 4.1 Visualizer.

RESULTS AND DISCUSSIONS

Geometry optimization and energy minimization of DENV envelope protein

In this study, we used PDB file 1OKE as the 3D structure of DENV envelope protein [15]. This 3D structure was opened by using Accelrys Discovery Studio 2.5 software. Furthermore, this PDB contains β-OG, the natural ligand of DENV envelope protein, and it appears in dimer form. First, we prepared the structure by eliminating one envelope protein chain, removing water, unnecessary molecules, and

protonating the structure. After that, the minimization of the structure was conducted by using CHARMm forcefield. Finally, we determined the binding cavity of the DENV envelope protein by using 'Find Receptor Sites Cavity' feature in Accelrys Discovery Studio 2.5. In this study, we selected the residues that bind β-OG. The residues around the cavity are: His27, Leu45, Ile46, Lys47, Thr48, Glu49, Ala50, Lys51, Gln52, Pro53, Val130, Leu135, Glu136, Tyr137, Phe193, Leu198, Leu199, Gln200, Met201, Lys202, Asp203, Lys204, Ala205, Trp206, Leu207, Thr268, Glu269, Ile270, Gln271, Met272, Ser273, Ser274, Gly275, Asn276, Leu277, Leu278, Phe279, Thr280, and Gly281.

Molecular docking simulation

The molecular docking simulation was done by using LibDock module in Accelrys Discovery Studio 2.5. LibDock module offers a rapid process of docking with the precision of the docking's position [16]. The suitable interaction, that can be expected to inhibit the DENV envelope protein, can be achieved if the ligands capable of binding to a target receptor of the β-OG binding site. The purpose of this study is to deploy 308 commercial cyclic peptide ligands that went into molecular docking simulation. In the end, 4129 poses of the ligands were obtained. Furthermore, we selected 487 poses, that have better binding value than the others, and proceed into 'Calculate Binding Free Energy' process. The free binding energy value ($\Delta G_{binding}$) of the commercial cyclic peptide was expected to have a negative value and lower than the standard ligands (the β-OG compound, Yennamalli R1, and Kampmann A5). Free binding energy is associated with the binding affinity between ligand and receptor and can be determined the stability of ligand-protein complexes. To find a ligand that able to inhibit β-OG pocket binder, this ligand must have a better interaction with the binding site of β-OG pocket, in terms of binding energy and molecular interaction. So, this ligand can be utilized as a novel compound to inhibit the DENV envelope protein.

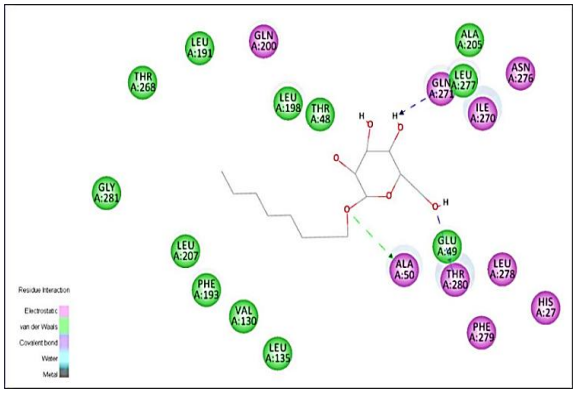

Fig. 1 Visualization of Interaction between β-OG with Envelope Protein

From the molecular docking simulations results, it showed that β-OG ligand can interact with 3 residues (Ala50, Gln271, and Thr280) in the β-OG pocket binder. It can be concluded that the three residues are the main residues of the β-OG binding site, the visualization of the β-OG ligand with its binding sites can be seen in Figure 1. The interaction can be shown by using Accelrys Discovery Studio 4.1 Visualizer. The virtual screening of 308 commercial cyclic peptide ligands yields ten best ligands that have a better interaction and binding affinity than the standard ligands. The results of the $\Delta G_{binding}$ calculations and the inhibition constant of the ligands can be seen in Table 1.

Table 1. The Results of Binding Free Energy Calculation and Inhibition Constants

Ligands	**ΔG binding (Kcal/mol)**	**Inhibition Constant (Psi)**
Acetyl-(N1e4, Asp5, D-2Na17, Lys10-cyclo-αMSH (4-10) amide	-29.7963	21.7062
Cyclo(-Arg-Gly-Asp-D-Phe-Val)	-27.0986	19.7409
Acetyl(n1e4, Asp5, Dtyr7, Lys10)-cyclo-α-MSH (4-10) amide	-26.8260	19.5423
(D-Cys6, Asn7, D-Ala11, Cys14)-Bombesin (6-14	-26.2073	19.0916
(Arg8)-Deamino Vasopressin Desglycinamide	-24.4771	17.8312
Cyclo(-D-Trp-Tyr)	-23.7543	17.3046
Cyclo(-Arg-Gly-Asp-D-Phe-Lys)	-23.0906	16.8212
Cyclo(-Gly-Tyr(PO3H2)-Val-Pro-Met-Leu	-19.3360	14.0860
Bremelanotide	-19.1494	13.9500
Felypressin	-17.7451	12.9270
β-OG	-14.2837	10.4055
Kampmann	-7.8441	5.7143
Yennamalli R1	-2.6863	1.9569

*Note: **Bold** ligand indicates standard ligand

In silico prediction of pharmacological and toxicity properties of ligands

This study aims to find new drug candidates, so it is very important to know whether ligands that have passed the screening has good pharmacological properties. This can be reached by obeying into Lipinski's Rules of Five. This rule specifically evaluates the oral drug administered into the body [17]. The virtual prediction of pharmacological properties can be done either by offline or online softwares. One of the software that is frequently used in this field is Osiris Property Explorer, which can be accessible online at http://www.organic-chemistry.org/prog/peo/. The results of these tests can be seen in Table 2.

Cyclo(-Gly-Tyr(PO3H2)-Val-Pro-Met-Leu) and Felypressin ligands cannot be tested by the Osiris Property Explorer software because it cannot read the ligand structure perfectly. Based on the results in Table 2, only Cyclo(D-Trp-Tyr) that has drug score above 0.70, while the rest of commercial cyclic peptide ligands and standard ligands have a drug score below 0.70. Besides, the molecular weight of the cyclic peptides tends to be above 500 Da and relatively have a large size, except for Cyclo (-D-Trp-Tyr), which led to poor drug score results based on the molecular weight indicators and Total Polar Surface Area (TPSA).

Table 2. Pharmacological property prediction by using OSIRIS Property Explorer

Ligand	LogP	Solubility	MW	TPSA	Drug-likeness	Drug score
Acetyl-(Nle4, Asp5, D-2-Nal7, Lys10)-cyclo-α-MSH (4-10) amide	-0.56	-6.88	1073	382.20	-3.99	0.09
Cyclo(-Arg-Gly-Asp-D-Phe-Val)	-2.30	-1.94	574	244.70	7.09	0.63
Acetyl-(Nle4, Asp5, DTyr7, Lys10)-cyclo-α-MSH (4-10) amide	-2.99	-4.81	1039	402.40	-2.60	0.12
(D-Cys6, Asn7, D-Ala11, Cys14)-Bombesin (6-14)	-3.97	-5.08	1012	440.00	5.78	0.37
(Arg8)-Deamino Vasopressin Desglycinamide	-2.59	-4.25	1012	451.10	-0.70	0.28
Cyclo(-D-Trp-Tyr)	1.53	-3.32	349	94.22	6.98	0.84
Cyclo(-Arg-Gly-Asp-D-Phe-Lys)	-4.66	-1.89	603	270.70	4.86	0.60
Cyclo(-Gly-Tyr(PO3H2)-Val-Pro-Met-Leu)	ND					
Bremelanotide	-0.95	-5.20	1024	376.40	-3.69	0.19
Felypressin	ND					
β-OG	1.28	-2.07	306	99.38	-23.03	0.46
Kampmann A5	7.97	-7.58	468	87.64	1.80	0.12
Yennamalli R1	5.03	-6.25	414	72.95	5.58	0.32

*Note: ND = not determined, MW = molecular weight, **Bold** ligand indicates standard ligand

In addition to the pharmacological properties, it is very important to know the toxicity properties of the ligand, such as mutagenic and carcinogenic properties. In drug design and development, mutagenic and carcinogenic properties should be avoided because it will give bad side-effects of the drugs. One of the approaches that can be taken in the toxicity test is QSAR (Quantitative Structure-Activity Relationship). In this study, we determined the ligand's toxicity properties by using two kinds of software, which were Osiris Property Explorer and Toxtree. The former one, besides from predicting the drug-likeness properties, can be also deployed to determine the toxicity properties of the ligand such as tumorigenic, mutagenic, irritant and reproduction effect. The prediction results of this test can be seen in Table 3. Based on the results, we observed that Acetyl-(Nle4, Asp5, D-2-Nal7, Lys10)-cyclo-α-MSH (4-10) amide ligand has a tumorigenic risk while Acetyl-(Nle4, Asp5, DTyr7, Lys10)-cyclo-α-MSH (4-10) amide ligand has a risk to be an irritant. It can be seen also that the Kampmann A5 ligand has a tumorigenic risk, and Yennamalli R1 ligand tends to be irritants. Furthermore, the rest of the ligands, including the β-OG ligand, have good pharmacological properties due to lack of tumorigenic, mutagenic, irritant and reproduction effect properties.

Toxicity properties of these ligands can be searched further by using Toxtree v.2.6.6 software, this toxicity test is based on Benigni-Bossa rule, which stated that the ligand may potentially mutagen or carcinogen if this ligand has the fragments that can cause mutagenic or carcinogenic, such as acyl halides, haloalkane, epoxides, aldehyde, hydrazine, alkyl/aromatic nitro, isocyanates and polyaromatic hydrocarbons. Furthermore, there are two

carcinogenic parameters that can be used, they are genotoxic and non-genotoxic carcinogenicity. While the former one is based on the potential of the compound to induce cancer by using the irreversible mechanism in the genetic material, the latter one is based on the potential of the compound to induce cancer by using a different mechanism other than the genotoxic carcinogenicity. Along with the carcinogenicity test, mutagenicity test was also conducted, using the *Salmonella typhimurium* bacteria as the indicator [18]. The result of this test can be seen in Table 4.

Table 3. Toxicity prediction by using OSIRIS Property Explorer.

Ligand	**Toxicity Risk**			
	Mutagenic	**Tumorigenic**	**Irritant**	**Reproductive Effect**
Acetyl-(Nle4, Asp5, D-2-Nal7, Lys10)-cyclo-α-MSH (4-10) amide	No	High Risk	No	No
Cyclo(-Arg-Gly-Asp-D-Phe-Val)	No	No	No	No
Acetyl-(Nle4, Asp5, DTyr7, Lys10)-cyclo-α-MSH (4-10) amide	No	No	High Risk	No
(D-Cys6, Asn7, D-Ala11, Cys14)-Bombesin (6-14)	No	No	No	No
(Arg8)-Deamino Vasopressin Desglycinamide	No	No	No	No
Cyclo(-D-Trp-Tyr)	No	No	No	No
Cyclo(-Arg-Gly-Asp-D-Phe-Lys)	No	No	No	No
Cyclo(-Gly-Tyr(PO3H2)-Val-Pro-Met-Leu)	ND			
Bremelanotide	No	No	No	No
Felypressin	ND			
β-OG	No	No	No	No
Kampmann A5	No	High Risk	No	No
Yennamalli R1	No	No	Low Risk	No

*Note: ND = not determined, **Bold** ligand indicates standard ligand

From this test, we can see that all ligands, including the standard ligands, are not mutagenic, whereas four out of ten ligands are predicted to be a carcinogen. The reason why Acetyl-(Nle4, Asp5, D-2-Nal7, Lys10)- cyclo-α-MSH (4-10) amide, Acetyl-(Nle4, Asp5, DTyr7, Lys10)-cyclo-α-MSH (4-10) amide, (D-Cys6, Asn7, D-Ala11, Cys14)-Bombesin (6-14), and bremelanotide ligands are predicted so because they have imidazole or benzimidazole fragments in their chemical structure. In addition, Acetyl-(Nle4, Asp5, DTyr7, Lys10)-cyclo-α-MSH (4-10) amide ligand also predicted as a genotoxic carcinogen. This is due to the aldehyde functional group in the structure of Acetyl-(Nle4, Asp5, DTyr7, Lys10)-cyclo-α-MSH (4-10) amide ligand.

Finally, the ADMETox test was conducted to determine the oral bioavailability, health effect, maximum passive adsorption and Central Nervous System (CNS) activity of the ligand. This test was performed by using ACD/I-Lab software. We selected four ligands ((Arg8)-Deamino Vasopressin Desglycinamide, Cyclo(-D-Trp-Tyr), Cyclo(-Gly-Tyr(PO_3H_2)-Val-Pro-Met-Leu), and Felypressin) that have better results than the rest of the ligands from our previous tests. The results of this test can be seen in Table 5.

Oral bioavailability can be defined as the rate and extent of a compound/substance that is absorbed by our body through oral delivery [19,20]. In this test, the Cyclo(-D-Trp-Tyr) ligand has the highest oral

bioavailability (between 30% and 70%) while the rest of the ligands have a low oral bioavailability (lower than 30%). The similar results were occurred as well in the health effect prediction, other than Cyclo(-D-Trp-Tyr) ligand, the other three ligands have a high probability to affected our internal organs. Hence, these ligands may have an undesirable side effect to our body when it is consumed.

The active transport prediction can be also done in this test, based on the chance of the ligand can be carried by peptide transporter 1 (PepT 1) and apical sodium-dependent bile acid transporter (ASBT) protein. These proteins are the carrier protein that has an important role in the active transport process. From the result of this test, we discovered that there is no ligand that can be carried by these proteins. In addition to active transport, there is also another way for the drug to be absorbed into our body by passing through cell membranes, such as passive adsorption. Passive adsorption is a diffusion movement through a semi-permeable membrane from the high concentration gradient into a low one. Unlike the active transport, which requires energy or a carrier protein, the passive adsorption does not require energy nor carrier to be able to penetrate the cell membrane [21]. In this test, we can also see that the Cyclo(-D-Trp-Tyr) ligand have a good passive adsorption while the rest were completely unable to passively adsorbed into out body. Finally, based on this test, all the ligands cannot penetrate the blood-brain barrier, thus, they cannot interfere with the CNS.

Based on all tests that we were conducted in this phase, we discovered that the Cyclo(-D-Trp-Tyr) ligand has the best results among all. Thus, this ligand will enter the final step of this study; molecular dynamics simulation.

Table 4. Mutagenicity and Carcinogenicity Prediction by Toxtree software

Ligand	QSAR-based Carcinogenicity	Genotoxic Carcinogenicity	Non-Genotoxic Carcinogenicity	Potential Mutagenicity (on *S.typhimurium*)
Acetyl-(Nle4, Asp5, D-2-Nal7, Lys10)-cyclo-α-MSH (4-10) amide	No	Negative	Positive	No
Cyclo(-Arg-Gly-Asp-D-Phe-Val)	No	Negative	Negative	No
Acetyl-(Nle4, Asp5, DTyr7, Lys10)-cyclo-α-MSH (4-10) amide	No	Positive	Positive	No
(D-Cys6, Asn7, D-Ala11, Cys14)-Bombesin (6-14)	No	Negative	Positive	No
(Arg8)-Deamino Vasopressin Desglycinamide	No	Negative	Negative	No
Cyclo(-D-Trp-Tyr)	No	Negative	Negative	No
Cyclo(-Arg-Gly-Asp-D-Phe-Lys)	No	Negative	Negative	No
Cyclo(-Gly-Tyr(PO3H2)-Val-Pro-Met-Leu)	No	Negative	Negative	No
Bremelanotide	No	Negative	Positive	No
Felypressin	No	Negative	Negative	No
β-OG	No	Negative	Negative	No
Kampmann A5	No	Negative	Negative	No
Yennamalli R1	No	Negative	Positive	No

*Note: **Bold** ligand indicates standard ligand

Table 5. The result of the ADMETox test by ACD/I-Labs software

Parameters/ Ligands	(Arg8)-Deamino Vasopressin Desglycinamide	Cyclo(-D-Trp-Tyr)	Cyclo(-Gly-Tyr(PO3H2)-Val-Pro-Met-Leu)	Felypressin	**β-OG**	**Kampmann A5**	**Yennamalli R1**
Oral Bioavailability	<30%	30%-70%	<30%	<30%	30%-70%	30%-70%	30%-70%
Blood	100%	56%	98%	100%	36%	47%	31%
Cardiovascular System	0%	84%	94%	0%	36%	86%	70%
Gastrointestinal System	68%	84%	60%	89%	1%	97%	84%
Kidneys	100%	87%	92%	99%	10%	57%	52%
Liver	100%	89%	100%	99%	7%	15%	62%
Lung	16%	40%	93%	63%	8%	94%	47%
Active Transport	No	No	No	No	No	No	No
Passive Adsorption (Maximum)	0%	100%	0%	0%	100%	100%	100%
CNS *Active*	Inactive	Inactive	Inactive	Inactive	Active	Active	Inactive

*Note: **Bold** ligand indicates standard ligand

Molecular Dynamics Simulation

In general, molecular dynamics simulation consist of three phases: initialization, equilibration, and production [22]. In the initialization phase, the solute-solute interaction is simulated to determine the coordinate system of the complex, then, we proceed into the equilibration phase, which is influenced by the temperature (this step may be included with the heating process). Finally, the production phase is performed to see the stability and molecular interaction of the ligand-protein complexes under the influence of solvent and temperature at the desirable intervals, at this phase, the RMSD graph will be obtained, this graph is necessary needed to observe the stability of ligand-protein complexes. Furthermore, the molecular interaction from the docking and dynamics simulation can be compared each other to determine their stability without and under the influence of temperature, solvent, and time, respectively.

In Figure 2, it can be observed that the interaction of hydrogen bonds from Cyclo(-D-Trp-Tyr) ligand and DENV envelope protein were formed at two different temperatures, at the normal body temperature (310 K) and at the fever body temperature (312 K), respectively. Furthermore, the Cyclo(-D-Trp-Tyr) ligand still able to maintain the hydrogen bonds at the binding site residues (Gln271 and Gly275) in the both temperature. The intervention of explicit solvent and temperature can change the overall interaction of the ligand-protein complex, including the hydrogen bonds. As we can see in Table 6. The Cyclo(-D-Trp-Tyr) ligand was able to maintain its hydrogen bonds with Gln271 and Gly275 at both temperatures on molecular dynamics simulation. However, it can be also seen at molecular docking simulation that Cyclo(-D-Trp-Tyr) ligand interacts with the Ala50, Gln200 and Lys202 residues of DENV envelope protein. Although that was slightly different, this indicates that the Cyclo(-D-Trp-Tyr) ligand was able to inhibit binding sites of DENV envelope protein at either normal or fever body temperature.

Table 6. Comparison of hydrogen bonding between the Cyclo(-D-Trp-Tyr) ligand with DENV envelope protein in molecular docking and molecular dynamics simulation

Docking simulations	Dynamics simulation (310K)	Dynamics simulations (312K)
Ala 50	**Gln271**	**Gln271**
Gln 200	**Gly275**	**Gly275**
Lys 202		

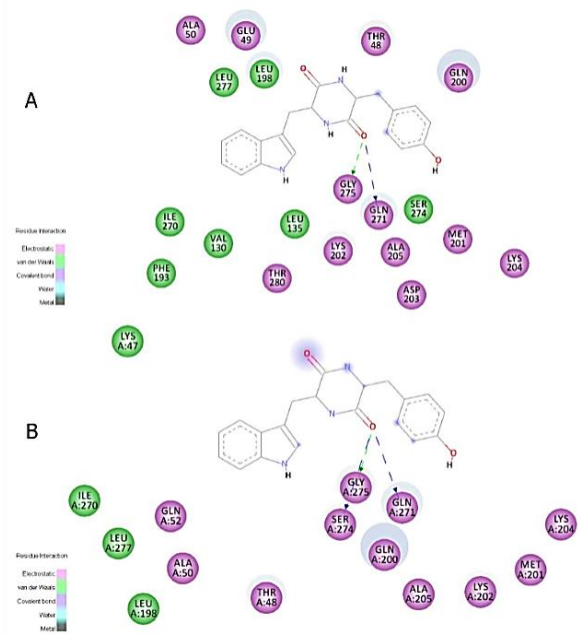

Figure 2. 2D visualization of molecular interaction between Cyclo(-D-Trp-Tyr) ligand with DENV envelope protein in 310 K (A) and 312 K (B)

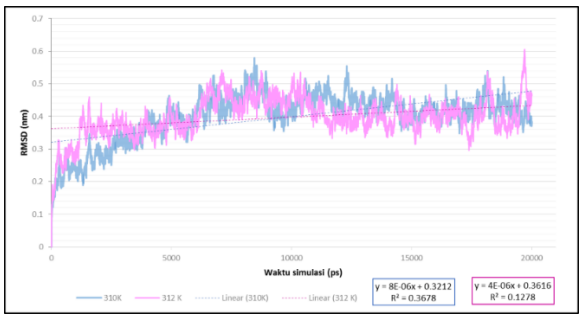

Figure 3. RMSD graph of Cyclo(-D-Trp-Tyr) ligand with DENV envelope protein

In the molecular dynamics simulation, the interaction between the protein and ligand can occur in a solvent, then they can move dynamically. This may lead to the changes in the complex conformation. These changes can be observed from the RMSD graph. From the Figure 3, we can see that there are no significant difference between the two complex conformation in the both temperature (310 K and 312 K), although the protein-ligand complex tends to be more linear or stable at 310 K. This means that the Cyclo(-D-Trp-Tyr) ligand is more likely to form a ligand-protein complex in the normal body temperature, but it can still able to maintain its interactions in the fever body temperature (due to slight RMSD difference between the two temperatures). Additionally, the absence of significant RMSD change between the two temperatures indicates that the conformation of the DENV envelope protein does not change dramatically, so that the Cyclo(-D-Trp-Tyr) ligand may disrupt the conformational change in the DENV envelope protein that holds the key factor to the fusion process and DENV attachment to the host cells.

CONCLUSIONS

The virtual screening of commercial cyclic peptide compounds was made by in silico method to find a novel inhibitor of β-OG pocket binder in DENV-2 envelope protein. This research has screened 308 commercial cyclic peptide ligands through molecular docking, computational ADMET test, and molecular dynamics simulation. From the first phase, we discovered that ten out of 308 ligands have good binding affinity on the β-OG pocket binder residues, such as Ala50, Gln271, and Thr280. Moreover, the computational ADMET test uncovered that Cyclo(-D-Trp-Tyr) ligand is the best ligand, owed to its pharmacological properties and low toxicity prediction. This ligand was further analyzed for its interaction with DENV envelope protein through 20 ns molecular dynamics simulation. The results are the Cyclo(-D-Trp-Tyr) ligand formed a stable complex with DENV envelope protein at normal (310 K) and fever body temperature (312 K), and able to maintain its interaction with the binding site of the β-OG pocket binder residues. Therefore, we conclude that the Cyclo(-D-Trp-Tyr) ligand is the best ligand among all the commercial cyclic peptides to inhibit DENV envelope protein. Thus, it can be viable to be developed into a novel antiviral drug candidate through in-vitro and in-vivo experiment.

ACKNOWLEDGMENT

The authors would like to thanks Hibah Penelitian Unggulan Perguruan Tinggi (PUPT) Dikti 2016 No: 1713/UN2.R12/HKP.05.00/2016. We also would like to thank Directorate of Research and Community Engagement-University of Indonesia (DRPM-UI) for the Riset Unggulan 2016. Usman Sumo Friend Tambunan and Arli Aditya Parikesit supervised this research. Vincentia Cheryl Adam and Ratih Dyah Puspitasari worked on the technical details. Mochammad Arfin Fardiansyah Nasution was writing the manuscript and added more relevant data in “Result and Discussion” section. Djati Kerami

gave important suggestion to improve our pipeline.

REFERENCES

[1] W.H.O, Dengue and Severe Dengue, (2015).

[2] S. Bhatt, P.W. Gething, O.J. Brady, J.P. Messina, A.W. Farlow, C.L. Moyes, J.M. Drake, J.S. Brownstein, A.G. Hoen, O. Sankoh, M.F. Myers, D.B. George, T. Jaenisch, G.R.W. Wint, C.P. Simmons, T.W. Scott, J.J. Farrar, S.I. Hay, The global distribution and burden of dengue., Nature. 496 (2013) 504–7. doi:10.1038/nature12060.

[3] T. Kampmann, R. Yennamalli, P. Campbell, M.J. Stoermer, D.P. Fairlie, B. Kobe, P.R. Young, In silico screening of small molecule libraries using the dengue virus envelope E protein has identified compounds with antiviral activity against multiple flaviviruses., Antiviral Res. 84 (2009) 234–41. doi:10.1016/j.antiviral.2009.09.007.

[4] A. Sehgal, Peptides 2006 New Applications in Discovery, Manufacturing, and Therapeutics, 2006.

[5] S.D. Jois, U.S. Tambunan, S. Chakrabarti, T.J. Siahaan, Solution structure of a cyclic RGD peptide that inhibits platelet aggregation., J. Biomol. Struct. Dyn. 14 (1996) 1–11. doi:10.1080/07391102.1996.10508923.

[6] Z. Li, M. Khaliq, Z. Zhou, C.B. Post, R.J. Kuhn, M. Cushman, Design, synthesis, and biological evaluation of antiviral agents targeting flavivirus envelope proteins, J. Med. Chem. 51 (2008) 4660–4671. doi:10.1021/jm800412d.

[7] Q.-Y. Wang, S.J. Patel, E. Vangrevelinghe, H.Y. Xu, R. Rao, D. Jaber, W. Schul, F. Gu, O. Heudi, N.L. Ma, M.K. Poh, W.Y. Phong, T.H. Keller, E. Jacoby, S.G. Vasudevan, A small-molecule dengue virus entry inhibitor., Antimicrob. Agents Chemother. 53 (2009) 1823–31. doi:10.1128/AAC.01148-08.

[8] Z. Zhou, M. Khaliq, J.E. Suk, C. Patkar, L. Li, R.J. Kuhn, C.B. Post, Antiviral compounds discovered by virtual screening of small-molecule libraries against dengue virus E protein, ACS Chem. Biol. 3 (2008) 765–775. doi:10.1021/cb800176t.

[9] Discovery Studio Visualizer, (2014). http://accelrys.com/products/discovery-studio/.

[10] D. Van Der Spoel, E. Lindahl, B. Hess, G. Groenhof, A.E. Mark, H.J.C. Berendsen, GROMACS: Fast, flexible, and free, J. Comput. Chem. 26 (2005) 1701–1718. doi:10.1002/jcc.20291.

[11] T. Sander, J. Freyss, M. von Korff, J.R. Reich, C. Rufener, OSIRIS, an entirely in-house developed drug discovery informatics system., J. Chem. Inf. Model. 49 (2009) 232–46. doi:10.1021/ci800305f.

[12] ACD/I-Lab 2.0, (n.d.). https://ilab.acdlabs.com/iLab2/index.php# (accessed May 26, 2015).

[13] Toxtree - Toxic Hazard Estimation by decision tree approach, (n.d.). http://toxtree.sourceforge.net/ (accessed May 26, 2015).

[14] S.C. Lovell, I.W. Davis, W.B. Arendall, P.I.W. De Bakker, J.M. Word, M.G. Prisant, J.S. Richardson, D.C. Richardson, Structure validation by Cα geometry: φ,ψ and Cβ deviation, Proteins Struct. Funct. Genet. 50 (2003) 437–450. doi:10.1002/prot.10286.

[15] Y. Modis, S. Ogata, D. Clements, S.C. Harrison, A ligand-binding pocket in the dengue virus envelope glycoprotein., Proc. Natl. Acad. Sci. U. S. A. 100 (2003) 6986–6991. doi:10.1073/pnas.0832193100.

[16] S.N. Rao, M.S. Head, A. Kulkarni, J.M. LaLonde, Validation studies of the site-directed docking program LibDock., J. Chem. Inf. Model. 47 (2007) 2159–71. doi:10.1021/ci6004299.

[17] C. a. Lipinski, Drug-like properties and the causes of poor solubility and poor permeability, J. Pharmacol. Toxicol. Methods. 44 (2000) 235–249. doi:10.1016/S1056-8719(00)00107-6.

[18] R. Benigni, C. Bossa, N. Jeliazkova, T. Netzeva, A. Worth, The Benigni / Bossa rulebase for mutagenicity and carcinogenicity – a module of Toxtree, Heal. San Fr. (2008).

[19] D.F. Veber, S.R. Johnson, H. Cheng, B.R. Smith, K.W. Ward, K.D. Kopple, Molecular Properties That Influence the Oral Bioavailability of Drug Candidates, J. Med. Chem. 45 (2002) 2615–2623. doi:10.1021/jm020017n.

[20] A.M. Hillery, A.W. Lloyd, J. Swarbrick, Drug delivery and targeting: for pharmacists and pharmaceutical scientists, CRC Press, 2002.

[21] D.L. Nelson, M.M. Cox, Lehninger Principles of Biochemistry 6th ed., 2013. doi:10.1016/j.jse.2011.03.016.

[22] A.A. Parikesit, K. Kinanty, U.S.F. Tambunan, Screening of Commercial Cyclic Peptides as Inhibitor Envelope Protein Dengue Virus (DENV) Through Molecular Docking and Molecular Dynamics, Pakistan J. Biol. Sci. 16 (2013) 1836–1848.

Second International Conference on Science, Engineering & Environment,
Osaka City, Japan, Nov.21-23, 2016, ISBN: 978-4-9905958-7-6 C3051

THE RELATION BETWEEN PREVALENCE OF APPLIED THAI MASSAGE AND CAUSE OF DISEASE: CASE STUDY WITH THAI TRADITIONL MEDCINE

Nittaya Putthumrugsa[1], Benchawan Sopha[2] and Kamolruth Na Nongkai[3]
[1,2,3]Thai Traditional Medicine College, Rajamangala University of Technology, Thailand.

ABSTRACT

To find out the relationship between the prevalence of disease cure for the applied Thai massage and bio-social factors, through the cause and behaviors of disease and to be under the principles of Thai traditional medicine. This project use Cross-sectional method by prospective studies from a sample of patients at the Clinic of Applied Thai Traditional Medicine College. The random sampling was used on 1552 patients of Applied Thai Traditional Medicine College in 2007-2008 year,(every other group) at a confidence level of 99.7% according to the Yamane theory. The 776 random patients were distributed to 3 groups(as per 3 illness seasons : Summer, Winter and Rainy).All patients were interviewed and the general data was analyzed under the relationship between the prevalence of applied massage and bio-social factors. By using Chi-square statistical analysis technic.

Result : Found the most of serviced patients got problems on backaches 42.4 % and neck shoulder pains 39.3%, that both pains were impacted from the prevalence of gender, occupation, the four traditional elements (Earth, Air, Fire & Water), age group, weather, period of day and causes of 5 diseases, work characteristics, overwork, sadness, anger, and surroundings with a significance of ≤ 0.05.

Reccommentation : People should understand and take action in personal health care by correctly especially meal and human practice in each people, in case knowledge require, they should learn from public health care staff that is based on the principles of Thai traditional medicine.

Keywords: Cause of disease, Applied Thai massage, io-social factors.

INTRODUCTION

A survey of National Statistical Office[7] in 2005, Thais got problem of Diseases of the musculoskeletal system and connective tissue such as Osteoarthritis, Gouty arthropathy, myofascial pain syndrome, soft tissue disorders etc., and Thailand imported drugs to cure the patients of Muscle aches ,Tendon and orthopedic surgery cost 1,706.020 Million baht (Bureau of drug control, 2547)[3].Also doctors from Bangkok Orthopedic Center[1] said there were many cause of Orthopedic surgery such as inborn, infection ,accident the deterioration of the body and behavior etc. The National economic and social development Plan no. 10 "Green and Happiness Socity".So we request to study The Relation between Prevalence of Applied Massage and Cause of Disease by Case Study at Applied Thai Traditional Medicine Clinic Rajamangala University of Technology Thanyaburi. The analysis by symptom of Applied Massage compare age, sex, occupation, cause of disease and behaviors of disease according to the principles of Thai traditional medicine. This result is used to development of the health services, prevent disease and rehabilitation.

MATERIALS AND METHODS

Study Design

To be cross-sectional by prospective studies from sampling of 1552 patients at the Clinic of Applied Thai Traditional Medicine.

Study population

The population were 776 patients of Clinic of Applied Thai Traditional Medicine, Rajamangala University of Technology, Thanyaburi. They were treated with Thai traditional massage, They were classified to 3 groups as per their illness season (Summer, Winter, Rainy season). And then; They

The 776 patients were interviewed and their data were analyzed on relationship between the prevalence of applied massage and bio-social factors with Chi-square statistical analysis.

Tool :

The Interview form content include : Demographic characteristic, Cause of illness, Behavior, and Meal was used.This interview used form is consulted and validated by specialist.

Analysis

Our Statistical data significance was set at probability level less than 0.05 ($p \leq 0.05$)**,**By these data were normal distributed, and the statistical were used as followed:

1. Descriptive statistics explain demographic characteristic in Percentage
2. Inferential statistics in Chi-square. That include Tathu, Season, Age, Time, Source, and cause of the disease.

RESULTS

Demographics characteristics

All of 776 patients were :

- Sex : 64.7 % female, 35.3% male.
- Occupation : 36.7% Public servant,17.5% trader, 14.7%worker, 14.0% monk 10.4% housewife, 4.8% student, and 1.8% farmer respectively.
- Tathu Genesis : 36 %Fire, 23.3% Air, 23.1% Earth and 17.7% Water.
- Age cause : 87.8% Final period of life(over 32 years old), 12.0%Middle-aged(16–32 years old) and 0.3%Childhood(infant–16 years old).
- Seson : 43.4% Summer, 35.7% Rainy and 20.9% Winter.
-Born:79% CentralRegion,8.5%North, 7.1% Northeast and 5.4% South.
- Habitation while illness : 99.2%Central Region, 0.4%North, 0.3%Northeast and 0.1 %South.
- Illness duration : 36.7% at 02.00 – 06.00 PM. and 02.00 – 06.00AM., 34.0% at 06.00 – 10.00AM. and 06.00 – 10.00PM., and 29.3% at 10.00 AM. - 14.00PM. and 10.00 PM – 02.00 AM
-Manner : 69.3% take Starchy foods, 53.5% Normal life style, 48.1.% eat three meals ~~3~~ on time, 40.5% food tasteless , 33.1%sit at long time.
-Illness : 42.4 % Backpain, 39.3% Neck pain and Upper back pain, 8.1% Knee ache, 3.2% Ankle pain, 1.9% Paralysis, frozen shoulder and trigger finger were equal 1.8%, and got 1.4% pains and aches.
-The patients got 57.5% 1 Tathu abnormality, 40.9% 2 Tathu, abnormality and 1.7% 3 Tathu abnormality.

Summarize of The Relation between Prevalence of Applied Massage and Cause of Disease study data :

Table Patients characteristic

characteristics	Pearson Chi-Square	P - Value
1. Sex	17.329	0.015*
2. occupation	131.513	0.000*

* P - Value ≤ .05

Table Cause relation of illness

Cause of illness	Pearson Chi-Square	P - Value
1. Tathu Genesis	54.849	0.000*
2. Age	33.818	0.002*
3. Season	28.988	0.010*
4. Birthplace	27.476	0.156
5. Current address	13.663	0.884
6. Illness place	16.828	0.721
7. Time	30.211	0.007*

* P - Value ≤ .05

Table Beha ior

Beha ior	**Pearson Chi-S uare**	**P - Value**
1. Job description	78.077	0.000*
2. Drinking water	16.290	0.269
3. Drinking alcohol	14.344	0.424
4. Drink tea or coffee	21.044	0.101
5.Rest	53.959	0.000*
6. Work overload	37.091	0.001*
7.Sad	42.848	0.000*
8.Angry	37.215	0.016*
9.Temperature	47.475	0.001*
10. Exercise	55.794	0.001*
11. Defecate	7.099	0.419
12. Restrain feces	47.567	0.000*
13. Urine	21.327	0.094
14. Restrain urine	18.952	0.167
15. Abnormal of Tathu	526.085	*0.000

* P - Value ≤ .05

Table Meal

Meal	**Pearson Chi-S uare**	**P - Value**
1. Mealtime	21.566	0.088
2. taste of food	92.057	0.000*
3. carbohydrate	24.777	0.037*
4.protein	36.618	0.001*
5. Fried foods	60.417	0.000*
6. Meal bitter	62.323	0.000*
7. Meal sour	23.947	0.046*

* P - Value ≤ .05

DISCUSSION

Most patients have 64.7% Tathu genesis and season of illness were Fire element , 87.0% age of illness, 36.7% time of illness and 99.3% Country of illness were Air element.Then Tathu 4 was related in prevalence of applied Thai massage and cause of disease and shown statistically significant difference ($P \leq .05$),that the Fire element related to issue catalysis in body. It was Shiranudkee. Shiranudkee was degenerative catalyst.For Air element was Angkamangkanusarevata that it effect with blood circulation system.

CONCLUSION

42.4 % Backaches and 39.3% Neck and Shoulder pains patients. They got abnormal on 1 tathu from 42 tathu. And also related with tathu genesis and season of diseases causes, age , time, weather, behavior of 8 diseases causes (such as: carbohydrates, meat, bitter food, sour food, relaxation, work characteristics, overwork, sadness, anger, body temperature, exercise, suppression of bowel movements and abnormalities in body systems) with a significance of 0.05. The samples of serviced patients have good behaviors about health care. The results of this study suggest an alternative for health care for public health care staff that is based on the principles of Thai traditional medicine.

Health personnel should promote the provision of advice to the public in health care. Tathu, Season, Age Time,Clime and Appropriate behavior.

FUTURE STUDY

The study primary health care compare with Thai traditional medicine theory.

REFERENCES

[1] Prat Boonyawongvirote,MD.2006 . Rheumatology International. Web site: http://www.dtam.moph.go.th/alternative/news/ 8 October 2006

[2] Ayurved Thamrong School . Thai Traditional Medicine in the Faculty of Medicine Siriraj Hospital. Supavanich Press, 767/3 Arunamarin Road. Bangkok

[3] Bureau of drug control.2006 cost of annual imports medicine 2004. by Pharmacological http://drug.fda.moph.go.th/zone_bioequivalence /be.asp, 13 September 2006.

[4] Department for Development of Thai Traditional and Alternative Medicine.2003. The5th Conventional of Thai Traditional Medicine and Nationl herb.The Institute Of Traditional Medicine Ministry of Public Health. Nonthaburi.

[5] Green, L.W. and M.W. Kreuter. (1991). Health Promotion Planning; An Education and Environment Approach. Mayfield Publishing Company, Toronto.

[6] Mehlum,Kjuus,Veiersted,&Wergeland(2006).Self reported work related health problems from the Oslo health study.Occupational Medicine.

[7] National Statistical Office. (2005).Health statistics.Statistics patients in primary health care. 2001 -2005. Web site: http://www.service.nso.go.th/nso/G_data23/data 23_4.html. 13 September 2006.

[8] Pender, N.J. (1987). Health promotion in nursing praetice. 2nd ed. Appleton century-crofts,East Norwalk.

[9] Somporn Putiyanan&Khesorn Nantachit. 2002. Food Consumption Behavior and Traditional Thai Medicine. Faculty of Pharmacy Chiang Mai University, Chiang Mai.

Second International Conference on Science, Engineering & Environment,
Osaka City, Japan, Nov.21-23, 2016, ISBN: 978-4-9905958-7-6 C3051

ETHICS ON SOCIAL NETWORKING: A PRELIMINARY SURVEY IN THAILAND

Lachana Ramingwong and Sakgasit Ramingwong
Department of Computer Engineering, Faculty of Engineering, Chiang Mai University, Thailand

ABSTRACT

The rapid growth of social networks and their users has been phenomenon. This brings numerous changes in everyday life, both positively and negatively. Ethics have become a major growing challenge in this area. Sensitive issues such as privacy, impersonation and cyberbullying are increasingly causing more damage to the community. This research reviews ethical issues on social networks. It also reports results from a survey on the most anticipated ethical concerns from the viewpoints of undergraduate students from Chiang Mai University, Thailand. Lost of privacy, misinformation and impersonation are anticipated as the worst ethical misconducted.

Keywords: Social networking, Ethics, Risks, Survey

INTRODUCTION

It is estimated that there are approximately 2.2 billion social network users worldwide in 2016 [1]. Compared to the past decades, this technology has brought numerous changes to global community [2], along with the rapid growth of smartphone users. Although social networking brings numerous benefits, it also represent an increasing number of inevitable risks [3].

There were more than 44.6 million Internet users In Thailand in 2014 [3]. This was roughly 65.7% of the total population of 67.9 million. The most popular social networking platform is Facebook with the total of 30 million active users. YouTube, twitter and Instagram are also well-known amongst the Thais with the total users of 26.2, 4.5 and 1.7 million, respectively. This high number of users are related to a number of undesirable ethical incidents which can also happen in other countries.

This research focuses on ethical risks which arise from the use of social networking. It identifies 15 sensitive issues, i.e. loss of privacy, identity theft, phishing, misinformation, malicious software, cyberbullying, hacking, piracy, plagiarism, spamming, trolling, clickbait, inappropriate contents, witch hunting and disagreement lacking dialectic. It discusses the characteristics and impacts of these risks based on cases from the use of social networks in Thailand, a developing Southeast Asian country. It also report results of a survey on the perceptions towards them from undergraduate students from Chiang Mai University.

The second section of this paper discuss ethical issues in social networking can cases in Thailand. The survey methodology and results are represented in the third section. Then, the fourth section discuss the results. Finally, the fifth section concludes the paper.

ETHICAL ISSUES ON SOCIAL NETWORKING

It is undeniable that there are risks from the use of social networking. This research mainly focuses on ethical risks which have impacts on individual level.

A. Loss of Privacy

Loss of privacy is arguably the most anticipated risks during the recent years. This can surface from various situations, such as leakage of personal information from the providers, either intentionally or deliberately. Emerging technologies such as the use of geolocation also adds the vulnerability to the users [4]. As a result, the social network users are left vulnerable from unsolicited acts. Advertisement is one of the most common form of unwelcome approach from loss of privacy [5]. Yet, it mostly provides minor disturbances. On the other hand, loss of privacy could lead to other more serious problems such as identity theft or social engineering which could lead to major loss of social status, money or life-threatening cases.

Thai Netizen Network reported that several privacy issues recently took place in Thailand [6]. For example, in 2013, an online payment system accidentally leaked the email list of its customers. In addition, there were cases that some companies disclosed their customer's information to their partners, resulting in involuntary activities. Leaked information from unprotected online databases or systems were also reported [6].

B. Impersonation

Impersonation or identity theft is an online mimicry of a person for indecent reason. Actually, this can be easily and very quickly done without gaining authentic information from the real users. Indeed, with appropriate information, identity theft can be even more convincing. Being a victim of identity theft leads to loss of money or compromised security [7].

There are a number of impersonation cases in Thailand. The objectives of this misbehavior vary from comedic to criminal. A wide range of impersonate identity is also found [8]. There have been cases which criminals fake identities of celebrities, businesspersons or government offers for a mass fraud. For example, there are more than 50 fake Facebook pages for a businessperson who is famous in lucky draw activities. Some of them edit their profile pictures so they are looked like a verified identity. Interestingly, some of them have more than 150,000 followers. These fake pages usually make the people believe that they somehow won a lucky draw and need to transfer a small amount of money to certain accounts to verify themselves [9].

C. Scamming and Phishing

Scamming and phishing involve online mimicry similar to impersonation. However, instead of an impersonation, this case escalates to the level of a business entity. In general, scamming and phishing can be seen in the form of a fake website or business contact which is directly copied from the authentic source. The offered appearance and feeling of the fake and the real services are indifferent. The only noticeable inconsistency is usually the URLs of the phishing sites which would slightly deterred from the genuine ones.

Online banking is one of the main target for scamming and phishing in Thailand. There have been reports on phishing sites which is visually a duplication of the authentic ones [10].

D. Misinformation

News and information circulate and penetrate extremely quickly in modern social networks. Misinformation denotes news and information which is incorrect, either intentionally or unintentionally. It is literally an upgraded version of traditional hoax with additional bad intentions. Spreading of misinformation lead to misconception towards knowledge, individuals, or perceptions. Social network users are vulnerable to misinformation since sharing them can be done very easily. Without careful considerations, misinformation from friends, networks or well-known sources can be quickly perceived as authentic. This deteriorates public knowledge as a whole. Unfortunately, spreading of corrective information seems to be slower.

In Thailand, despite there is a law against spreading of false information, misinformation is commonly circulated in social networks. Basic hoaxes like ‘using something to cure some disease’ or ‘something cannot be eaten along with something’ cases are there. The more serious misinformation is used for political intentions and this leads to major breakdown in general community.

E. Malicious Software

Viruses, worms, spywares and other forms of malicious software can cause damage to computer systems. Preventing selves from this unethical act can be complicated since new malicious software are released endlessly. More than 400 million malicious software elements were discovered in 2015 [11]. Amongst these malicious software, the latest form of attack is arguably the “ransomware” and it has recently become a major problem to the community [12].

There have not been reports on major malware cases in Thailand. However, attacks on individual level are found everywhere.

F. Cyberbullying

Cyberbullying is the abuse of social network to humiliate, harass or threaten another person [13]. Generally, this happens to younger persons and usually results in the victims’ deteriorated psychology. Serious cases of cyberbullying can lead to violence or even suicidal acts. Related misbehaviors, such as racism and sexism, may also be considered as cyberbullying in a broader context.

A report indicated that 35% of Thai youths involve in cyberbullying, either the actors or the victims [14]. Fortunately, no serious cases on cyberbullying have been yet reported. Nevertheless, this figure shows an alarming potential of this risk

and highlights how quickly it should be mitigated.

G. Hacking

Hacking and other forms of technical attacks can cause major damage to computer systems. It could happen to anyone or any organizations. A number of hacking tools is distributed around the Internet so basic hacking, such as dictionary attack, can be performed rather easily without real technical knowledge. Serious incidents such as the hacking of major networks have been reported during the recent years [15]. These led to many related ethical risks.

Major hacking incidents also periodically affected Thailand. Recently, a group of Internet users showed dissident against a government policy by attacking several legislative websites [16]. The attack was, in fact, performed by the most basic action, i.e. normal but repeatedly refreshing of the websites. However, when this is done with voluminous users, it became a major distributed denial of service (DDoS) attack which ultimately crashed the systems. This shows the vulnerability of the systems and databases run by the government.

H. Piracy

The nature of sharing on the Internet usually cause violation in intellectual property rights. Certain download services, peer-to-peer protocols such as BitTorent are major threats to the copyrights owners.

It has been reported that software piracy is still common [17]. The use of unauthorized contents does nothing but damages to innovation industries.

Rates of illegal software installation in Thailand is gradually declining [17]. Yet, the rate of 69% illegal installation is still unacceptable. There are also a widespread of unauthorized content sharing amongst social networks and other online services which periodically leads to arguments on the society.

I. Plagiarism

Plagiarism is the act of taking certain contents and use them as own idea without a proper citation. It has been considered as one of the worst misconducts in academic society. With the current Internet technology and the enormous resources of knowledge, it is increasingly convenient to commit a plagiarism.

In Thailand, it is reported that the seriousness of plagiarism is well aware in the academia. However, due to certain excuses, such as language proficiency or imminent deadline, it is still conducted by a number of people [18]. Detection systems has been implemented in many higher study institutions with an intention to reduce this problem [19].

J. Spamming

Generally, the main objective of spamming is advertising. Apart from spam email which has been rather common since the beginning of the Internet, spamming on social network is increasingly committed. Unlike other ethical misconducts, spamming does not directly result in serious consequences. Most of the time, it is considered as an online nuisance. However, spamming can sometimes involve malicious software which further cause problems to the users.

There has been no reports on serious case from spamming on social network in Thailand. Yet, arguably the most impactful scenario is the spamming of chain marketing network which result in loss of money, time and opportunity.

K. Trolling

Trolling is an act of ignorance users who intend to incite the online community. Usually this is committed just for a pleasure. However, it is possible that the agitated conversation can lead to broader level of arguments and resulting in disharmony amongst the related users. It is reported that trolling can be found more easily on social networks which do not require real identity, such as Twitter [20].

Trolling is common in popular Thai websites. Many times, it caused commotions in the community. General successful trolling subjects in Thailand involve political views, academic institutes, sports, and celebrities.

L. Clickbait

Clickbait has recently been a technique to lure users to visit certain websites. It usually appears as a link with a very intriguing but incomplete name. After the user clicked the link, he or she will find a number of advertisement with the shallow or, many of the time, plagiarized contents. It is highly possible that clickbait may be associated with malicious

software and consequently harm the users.

Clickbait has become an increasingly popular marketing technique in Thailand. It is astonishing to find that a clickbait website successfully became the second most visited websites of Thailand during the early of 2015 [21].

M. Inappropriate Contents

Inappropriate contents involve pornography, vandalism, violence, gambling and etc. which are deemed unsuitable to certain group of users or cultures. Obviously, these contents are spreading around the Internet and social networking sites. Installing certain mechanisms can partly help preventing such access. However, tools such as virtual private network can still allow users to retrieve inappropriate contents.

The Royal Thai Government has installed a national firewall which protect users against browsing to certain websites [22]. Yet, its effectiveness is still doubtful since a large number of inappropriate websites are still accessible.

N. Witch hunting

Online witch hunting is a social trial on certain entity. It is similar to cyberbullying but with a larger group of accuser and virtually stronger consequence. Witch hunting is usually based on bias, agitation, speculation, or misinformation. Innocent persons can be wrongfully condemned from this unethical activity. Recent cases of witch hunting led to major false allegation on impeccable victims [23].

In Thailand, there have been cases on online witch hunting which involve personal behaviors, accidents, crimes and different political views [24]. Some of them lead to social sanction to certain persons or organization while some of them later judged not guilty by the court of laws.

O. Disagreement Lacking Dialectic

Disagreement lacking dialectic is an intensified version of online arguments. Unlike witch hunting or cyberbullying, this ethical issue involves a dispute of at least two parties who have completely different perceptions on the same subject and they are not listening to each other's opinion.

Disagreement lacking dialectic is commonly found in Thailand's major social network websites. Recently, the main debate revolves around political parties, celebrities, religions and spirits, and trendy events. It is unfortunate that most disagreement lacking dialectic do not end well with mutual agreements but rather loose ending arguments.

PERCEPTIONS ON ETHICAL ISSUES FROM UNDERGRADUATE STUDENTS, CHIANG MAI UNIVERSITY

To study the perceptions towards the ethical issues, a survey was conducted in Chiang Mai University. Three hundred and eighty seven undergraduate students who enrolled in the "Internet and Online Community" elective course participated in the study. The students were from various faculties and various study years. All of them were familiar to social networking and major online services.

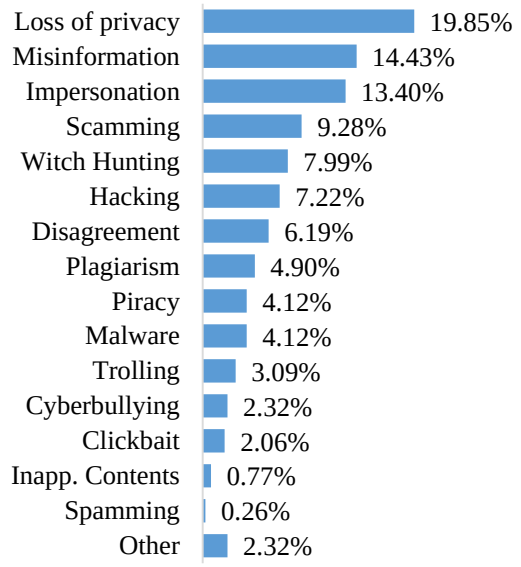

Fig. 1 Percentage of worst ethical misconduct perceived by undergraduate students from Chiang Mai University, Thailand.

Prior to the survey, the students joined a lecture on online ethics. All fifteen ethical issues in the previous section were discusses along with their case studies. After the session, the students were asked to identify their perceived worst ethical misconduct and reasons. Fig. 1 lists the ranked percentage summary of the answers. It is important to note that seven of the feedbacks contains more than one ethical issues therefore each item is counted as one separated feedback, resulting in a total of 397 feedbacks.

It can be seen from Fig. 1 that the worst perceived ethical misconduct is, not surprisingly, the loss of privacy. The participated students reveal that

they fear that, especially according to case studies, the leak of their personal information can lead to several misfortunes. One of the major concern on this issue is the risk may not be caused by the users' careless but from the involuntary change in the providers' policy. Some of them also indicated that they were surprised to learn that normal social activities, such as posting status or photos with geolocation information, can unfortunately be used to initiate serious crimes.

Misinformation is ranked as the second worst ethical issues in social networking. This unexpected finding reflects the growing concern on abusing of social networks in Thailand. Two major scenarios in misinformation are specially denoted from the feedback. Firstly, the fault information on daily activities, especially on foods or medicines, such as the use of Formaldehyde for food preservation without evidence, may lead to major misconception. This, most of the time, can affect related businesses. A serious cases of this, such as a fault advertisement on weight-loss drugs, could lead to life threatening scenarios. The second misinformation case is related to politics. This exposes the current major unstable politics in Thailand where misinformation become an efficient tool to condemn the oppositions. More importantly, this case can be very detrimental because they are mostly created deliberately. The students were especially concern that social networks help spreading these cases of misinformation very quickly and widely.

The third and the fourth misconducts are related and may be even considered as the same issue from some perspective. If being counted together, impersonation and scamming will be ranked the most concerned ethical issue instead of loss of privacy. Yet, in this research, they are separated based on their practices. Impersonation, as a mimicry of a person, is perceived by the students as the third most serious misbehavior. Students commented that due to the ease of acting as another person on the social network, this risk is extremely apprehensive. The fact that it takes only minutes to almost perfectly duplicate an account makes them realize this imminent threat. On the other hand, scamming and phishing take considerable more efforts to make themselves credible. Students also indicated that it seems to be slightly easier to notice the unauthentic elements of these fraud. This includes suspicious URLs, emails, phone numbers or other means of contact.

Witch hunting is ranked fifth on the list. The participants denoted that the judging on other people by community bias is unacceptable. Some of them added that the result of witch hunting can be enormous to the victim, therefore, it is best to refrain from such actions. If inevitable, the students insisted that they will need information from various stakeholders before making the decision.

The sixth ethical issue, hacking, is a top concern for more than 7% of the participated students. Many of them reported that they fear of hacking because they feel this threat is out of their control. Yet, some of the students learnt that one of the easiest but effective basic mitigation towards hacking is the strength of their password and how easy the dictionary words can be hacked.

Disagreement lacking dialectic has been a common source of online arguments in Thailand. It is ranked ninth in this research. The students agreed that bias from different backgrounds or different perspectives can exacerbate the disagreement. This ultimately leads to disruption in the community. Few students suggested that such threat is best mitigated by disregarding the entire scenario. On the other hand, some other students argued that they would try to learn from all perspectives and support the most rational side of the argument.

Plagiarism is the tenth ranked ethical concern in this research. Several students admitted that they just realized the impact of plagiarism and why it is deemed unacceptable in the international level from the lecture. As a result, they promised not to commit this action and will help spreading the appropriate action against this case to their networks.

Other ethical issues were considered the worst misconduct by comparatively less students than the aforementioned items. Yet, it is undeniable that all of them can bring serious consequences and should all be mitigated. Apart from the previously discussed items, the students also proposed that some other issues, such as dishonesty and lack of moral judgment, could lead to undesirable outcomes.

DISCUSSION

The results of the survey depict how a group of Thai students perceived risks that came with the use of social networks and how significant those issues are to them. Loss of privacy, misinformation and impersonation, scamming and phishing are ranked on the top. The case studies on these issues can be found more often from news media including social media. When it became viral or spreads out on social networks, people feel its presence, and start to realize that these types of threats exist. Once the similar cases are speared on their social network feeds, they start to perceive its seriousness and significance of the problems. Because the negative effects of these issues to other individuals involved are usually made public on social networks, people can relate those effects to what may have happened to themselves if they come across such the cases. That makes them feel more vulnerable to those

threats and lead to them relate to those issues more than the others.

On the contrary, witch hunting, hacking, disagreement lacking dialectic, plagiarism, piracy, malware, trolling and cyberbullying are the issues that mostly effects on particular groups of people such as political support group, sport fan group and users of the website. People who are not a part of such groups are unlikely to be affected. Therefore, the chance for them to realize the trouble of these issues are less than the issues listed on top. Moreover, the participants who took this survey are students whom may not have experience with witch hunting, hacking or disagreement lacking dialectic.

Clickbait, inappropriate contents and spamming are not considered the worse issues because the effects of the issues are not as serious as the others. Some people does not realize what appears on their social page as a spam or inappropriate. They rather get used to it or does not feel the appropriateness. Clickbait is not much of a big problem similar to spamming when a person does not feel it is a problem. Those who click through did because they were interested in what they see or read. So they are likely to accept the consequence.

CONCLUSION

The survey result reveals that the participated undergraduate students believed that loss of privacy, misinformation and impersonation are as the top most serious ethical issue in social networking. Issues ranked from the fourth place down to the floor include scamming and phishing, witch hunting, hacking, disagreement lacking dialectic, plagiarism, piracy, malware, trolling, cyberbullying, clickbait, inappropriate contents, spamming, respectively. It is interesting to repeat this survey in a boarder population and diverse culture, which will reflect the perceptions of the more general social network users.

REFERENCES

[1] Statista, “Number of Worldwide Social Network Users 2010-2019,” Statista, 2016. [Online]. Available: http://www.statista.com/statistics/278414/number-of-worldwide-social-network-users/. [Accessed: 07-Jun-2016].

[2] Mao J and Shen Y, “Cultural Identity Change in Expatriates: A Social Network Perspective,” Hum. Relations, vol. 68, no. 10, pp. 1533–1556, 2015.

[3] Digital Advertisting Association of Thailand, “Thailand Social Media Landscape,” Digital Advertisting Association of Thailand, 2014. [Online]. Available: http://syndacast.com/wp-content/uploads/2015/01/Thailand-Social-Media-Landscape.pdf. [Accessed: 07-Jun-2016].

[4] Armerding T, “RSA: Geolocation Shows Just How Dead Privacy Is,” CSO, 2016. [Online]. Available: http://www.csoonline.com/article/3040374/security/rsa-geolocation-shows-just-how-dead-privacy-is.html. [Accessed: 13-Jun-2016].

[5] Tucker CE, “Social Networks, Personalized Advertising, and Privacy Controls,” J. Mark. Res., vol. 51, no. 5, pp. 546–562, 2014.

[6] Thai Netizen Network, “Online Privacy Violation in Thai Community,” 2014.

[7] S. Hinde, “Identity Theft: Theft, Loss and Giveaways,” Comput. Fraud Secur., vol. 2005, no. 5, pp. 18–20, 2005.

[8] Thairath Online, “Impersonation: It Can be Easily Done Online. Is This True?,” Thairath Online, 06-Aug-2014.

[9] Komchadluek Online, “Warning on 21 Fake ‘Ichitan’ Facebook Pages,” Komchadluek Online, 31-Mar-2016.

[10] Siam Commercial Bank, “Beware of Phishing,” Siam Commercial Bank, 2016. [Online]. Available: http://www.scb.co.th/en/about-scb/phishing-mail. [Accessed: 13-Jun-2016].

[11] Symantec, “2016 Internet Security Threat Report,” 2016.

[12] Trend Micro, “Ransomeware One of the Biggest Threats in 2016,” Trend Micro, 2016. [Online]. Available: http://blog.trendmicro.com/ransomware-one-of-the-biggest-threats-in-2016/. [Accessed: 14-Jun-2016].

[13] Bastiaensens S, et. al., “Cyberbullying on Social Network Sites: An Experimental Study into Bystanders’ Behavioural Intentions to Help the Victim or Reinforce the Bully,” Comput. Human Behav., vol. 31, pp. 259–271, 2014.

[14] DTAC Insight, “The Spreading of Cyberbullying: An Online Threat,” Brand Buffet, 2016. [Online]. Available: http://www.brandbuffet.in.th/2016/02/cyberbullying-dtac-internet-behavior/. [Accessed: 14-Jun-2016].

[15] Broder JM, “Hacking Inquiry Closes With Mystery Unsolved,” The New York Times, 18-Jul-2012.

[16] BBC News, “Thai Government Websites Hit by Denial-of-Service Attack,” BBC, 01-Oct-2015.

[17] Business Software Alliance, “Seizing Opportunities Through License Compliance: BSA Global Software Survey,” 2016.

[18] Charubusp S, “Plagiarism in the Perception of Thai Students and Teachers,” Asian EFL J. Prof. Teach. Artic., no. 87, pp. 61–81, 2015.

[19] Nagi K, “Plagiarism in Education and What We Can Do About It,” Nation Multimedia, 2012.

[20] Edwards J, “One Statistic Shows that Twitter Has a Fundamental Problem Facebook Solved Years Ago,” Business Insider UK, 17-Apr-2015.

[21] Truehits.net, "Truehits Statistics," Truehits.net, 2015. [Online]. Available: http://truehits.net/. [Accessed: 14-Jun-2016].
[22] Technology Crime Suppression Division, "TSCD: Technology Crime Suppression Division," Technology Crime Suppression Division, 2016. [Online]. Available: http://www.tcsd.in.th/. [Accessed: 14-Jun-2016].
[23] BBC News, "Reddit Apologises for Online Boston 'Witch Hunt,'" BBC, 23-Apr-2013.

Second International Conference on Science, Engineering & Environment,
Osaka City, Japan, Nov.21-23, 2016, ISBN: 978-4-9905958-7-6 C3051

RUTHENIUM BIS-BIPYRIDINE COMPLEXES WITH *N*-BENZOYL-*N*'-(1,10-PHENANTHROLIN-5-YL)THIOUREA AS AN OPTICAL pH SENSOR

Siew San Tan[1], Norhashimah Bt. Ramli[2] and Mohammad B. Kassim [1,3]

[1]School of Chemical Sciences and Food Technology, Faculty of Science and Technology, Universiti Kebangsaan Malaysia, 43600 Bangi, Selangor, Malaysia.
[2]Center for Research and Instrumentation Management, Universiti Kebangsaan Malaysia, 43600 Bangi, Selangor, Malaysia.
[3]Fuel Cell Institute, Universiti Kebangsaan Malaysia, 43600 Bangi, Selangor, Malaysia

ABSTRACT: pH is a measurement that eventually relates to environmental, biological, chemical and industrial activities. The optical pH sensing technique based on the absorption and luminescence activities offers a better thermal performance and faster response time. Ruthenium based optically active complexes are suitable for optical pH devices, due to their long-lived metal-to-ligand charge transfer excited states and strong luminescence at ambient temperature. A $[Ru(bpy)_2(phen)$-*n*BT$)](PF_6)_2$ {bpy= 2,2'-bipyridine, (phen)-*n*BT= *N*-benzoyl-*N*'-(1,10-phenanthrolin-5-ly)thiourea was synthesized and characterized by elemental analyses, mass spectrometry, infrared, ultraviolet-visible, and nuclear magnetic resonance spectroscopy. The absorption and luminescence spectra of the complex vary with pH changes. We observed a bathochromic shift in the absorption and emission bands as the pH increases. Higher luminescence intensity and lifetimes were exhibited for acidic solutions, while there is a red shift in the absorption and luminescence bands in basic medium. This was attributed to a decrease in the energy of the ligand based π^* orbital, which stabilizes the MLCT states. This complex exhibits a linear absorption and luminescence intensity response between pH 1 to pH 11. The absorption and emission results for optical pH sensing offer greater sensitivity and selectivity and hence, can be applied to optical devices to monitor environmental pollutions from various chemical and industrial activities.

Keywords: optical pH sensing, ruthenium polypyridyl, thiourea, luminescence, environmental

1. INTRODUCTION

pH plays a far greater role in our lives than we realized, that affects and enables chemistry throughout our daily lives. pH is significantly essential in pharmaceutical processing, food and beverage processing, seawater analysis, powerplant cooling water as well as determines the rate of many industrial processes. Accurate measurement of pH allows us to monitor and fine-tune chemical processes, protect the environment and the living things within it. There are several methods exist for pH sensing. The simplest and most inexpensive is pH paper, in which paper is infused with various indicator compounds that change colour in response to pH. They are convenient but lack of accuracy and no high throughput analysis [1]. Electrodes are the most common pH sensor, using a milli-voltmeter with very high input impedance to measure the potential difference between hydronium-sensitive electrode and reference electrode. However, they are often salinity dependent and not compatible with all the chemical environments. Optical pH sensor is one of the most promising method that use the interaction of light with pH sensitive molecules, for instance, ruthenium(II) polypryidyl complexes to determine the pH. Although they lack of convenience and handy detection, they offers many advantages, such as small probe size, high sensitivity and accuracy. They are based on the varying of physical behaviour such as calorimetric absorbance and fluorescence, all of which use an optical detector [2]. The development of optical pH sensors has improved the response time as well as the range of chemical compatibility compared to pH paper and electrodes [3]. Ruthenium(II) polypyridyl complexes which have bipyridine or phenanthroline moieties especially [4], have been used extensively for optical pH sensors due to their high photochemical stability, high molar absorptivity and long luminescence time-resolved [5]-[6].

Herein, we report on the synthesis, characterization as well as the effect of pH on the emission and absorption spectra of the ruthenium bis-bipyridine complexes with *N*-benzoyl-*N*'-(1,10-phenanthrolin-5-yl)thiourea.

2. EXPERIMENTAL

2.1 Materials and chemicals

All the chemicals used in this study were

analytical-reagent grade and were used as received without further purification. $RuCl_3.3H_2O$ and lithium chloride were purchased from Merck. 1,10-phenanthroline-5-amine and benzoyl chloride were obtained from Fluka (Malaysia) and 2,2'-bipyridine (bpy) was obtained from Aldrich Chemical Co. *Cis*-$Ru(bpy)_2Cl_2.2H_2O$ was prepared using published procedures [7].

2.2 Spectroscopic Analyses

The infrared spectra were recorded on a Agilent Cary 630 spectrophotomer in the range of 4000-400 cm^{-1} in the ATR Diamond mode. The microanalyses (C, H, N and S) were obtained with a Leco 932 elemental analyzer. The ^1H and ^{13}C NMR spectra were collected in deuterated dimethyl sulfoxide using Bruker Ascend 400 spectrophotometer. The chemical shift values were scaled to parts per million (ppm) with reference to TMS. Mass spectrum was recorded on a DIMS 2010 Shimadzu mass spectrometer. Magnetic susceptibility measurements were determined on a Sherwood Scientific MSB-AUTO, at room temperature (25.5 ºC) using $HgCo(SCN)_4$ as calibrating agent and the diamagnetic susceptibility correction was calculated from Pascal's constants.

2.2.1 Absorption and luminescence spectra

Electronic absorption spectra were measured on a Perkin-Elmer Lambda 35 spectrophotometer in the range of 900-200 nm. Steady state emission spectra were recorded on a Edinburgh FLS920 time resolved fluorescence spectrometer at 298 K in CH_3CN, using 1 cm path length quartz cell. Time-correlated single-photon-counting (TCSPC) measurements were used for the luminescence decay of the ruthenium complex in different pH. For TCSPC measurement, the photoexcitation was made at 472.4 nm using a picosecond diode laser (EPL-375). The lifetimes of the receptor were obtained as a function of different anions and the emission was monitored as a function of time. The luminescence quantum yields were calculated by Eq. 1, [8]-[9] using $[Ru(bpy)_3(PF_6)_2]$ as the standard.

$$\boldsymbol{\varphi_r} = \boldsymbol{\varphi_{std}} \frac{\boldsymbol{A_{std}}}{\boldsymbol{A_r}} \frac{\boldsymbol{I_r}}{\boldsymbol{I_{std}}} \frac{\eta_r^2}{\eta^2_{\boldsymbol{std}}} \quad (1)$$

where $\boldsymbol{\varphi_r}$ and $\boldsymbol{\varphi_{std}}$ are the quantum yield of the ruthenium complex and standard sample $[Ru(bpy)_3(PF_6)_2]$, $\boldsymbol{\varphi_{std}}$ is 0.042. A_r and A_{std} (< 0.1) are the solution absorbance at the excitation wavelength (λ_{ex} = 450 nm). $\boldsymbol{I_r}$ and $\boldsymbol{I_{std}}$ are the integrated emission intensities, and η_r and $\eta_{\boldsymbol{std}}$ are the refractive indices of the solvent. Radiative lifetimes, $\tau_{\boldsymbol{m}}$ was obtained by dividing the measured lifetime (τ_r) with the quantum yield. Radiative (k_r) and nonradiative (k_{nr}) rate constants were calculated using the Eq. 2 and Eq. 3 [10].

$$\boldsymbol{k_r} = \frac{\boldsymbol{\varphi_r}}{\tau_{\boldsymbol{m}}} \quad (2)$$

$$\boldsymbol{k_{nr}} = \frac{\mathbf{1}}{\tau_{\boldsymbol{m}}} - \frac{\mathbf{1}}{\tau_r} \quad (3)$$

For the investigation on the effect of pH to absorbance and emission intensities, 0.6 mg of the $[Ru(bpy)_2(phen\text{-}n\text{BT})(PF_6)_2$ was dissolved in 100 mL of deionized water. Five solutions with various pH value (pH= 1, 3, 5, 9, 11) were prepared by adding drops of 0.1 M NaOH or 0.1 M HCl. The UV-vis spectra of the samples were recorded in the range of 180-600 nm. The emission spectra were then recorded in the range of 500-800 nm, with excitation being performed at absorption maximum for the metal-to-ligand charge transfer (MLCT) transition.

2.3 Synthesis

2.3.1 Synthesis of the ruthenium(II) bipyridyl with phenanthroline, cis-$Ru(bpy)_2(5\text{-}NH_2phen).2PF_6$

Cis-$Ru(bpy)_2(5\text{-}NH_2phen).2PF_6$ was synthesized according to previously reported literature methods [11], with some modifications. The apparatus were thoroughly degassed and performed under a gentle stream of argon by standard Schlenk techniques. A *cis*-$Ru(bpy)_2Cl_2).2H_2O$ (0.50g, 0.96 mmol) was dissolved in 50 mL of hot distilled water, followed by addition of 1,10-phenanthroline-5-amine (0.21 g, 1.08 mmol) which was dissolved in 100 mL of hot ethanol. The mixture solution was brought to reflux (100°C) for 3 hours. Three quarter of the ethanol was then removed by rotary evaporation and a cold aqueous solution of NH_4PF_6 (0.98g, 4.8 mmol) was added to produce orangish precipitate. The precipitate was collected by filtration, washed with 25 mL of cold distilled water followed by 25 mL of cold diethyl ether to give a pure solid product. Yield, 0.834 g (97 %). FTIR (cm^{-1}): $\upsilon(NH_2)$ 3409, $\upsilon(C\text{-}N_{heterocyclic})$ 1445, $\upsilon(C{=}C)$ 1638, υ(uncoordinated PF_6) 829. λ_{max}, nm (CH_3CN), $\varepsilon(Lmol^{-1}cm^{-1})$: 245 (35,402), 286 (63,595), 362 (11,893), 457 (15,597). ^1H NMR (400 MHz, DMSO-d^6), δ: 8.92 (dd, 1H), 8.90-8.80 (m, 4H), 8.32 (dd, 1H), 8.20 (tdd, 2H), 8.11 (td, 2H), 8.06 (dd, 2H), 7.87-7.80 (m, 3H), 7.64-7.53 (m, 2H), 7.44-7.35 (m, 2H), 7.09 (s, 1H), 6.93 (d, 2H). ^{13}C NMR (400 MHz, DMSO-d^6) δ: 157.26, 157.06, 152.22, 151.91, 146.69, 145.78, 140.92, 138.27, 138.77, 132.38, 128.27, 126.46, 125.31, 124.88, 123.78.

2.3.2 Synthesis of the ruthenium(II) bipyridyl N-benzoyl-N'-(1,10-phenanthrolin-5-yl)-thiourea [Ru(bpy)$_2$(phen-nBT](PF$_6$)$_2$

There are two methods of synthesizing the complex and one of the method has been reported [12]. The reaction was performed in dark condition and under inert argon gas in latter method. To a solution of benzoyl chloride (0.012 mL, 0.1 M) in acetonitrile was added ammonium thiocyanate (8.0 mg, 0.1 mmol) and the mixture was stirring for 20 minutes to give benzoyl isothiocyanate. Then, Ru(bpy)$_2$(5-NH$_2$phen).2PF$_6$ (9.0 mg, 0.1 mmol) in acetonitrile was added into it and stirred for 8 hours. The solvent was removed under reduced pressure, wherein an orange sticky solid was obtained. The solid was then dissolved in a minimal volume of cold ethanol to give a bright orange precipitate, filtered, washed with cold water (25 mL) and followed by cold diethyl ether (25 mL). Yield, 53 mg (50 %). Anal. Calc: C, 45.25; H, 2.85; N, 10.55, S, 3.02. Found: C, 44.42, H, 3.35, N, 9.87, S, 2.18. FTIR (cm^{-1}): υ(NH) 3408, υ(C-N $_{heterocyclic}$) 1446, υ(C=C) 1587-1484, υ(C=O) 1670, υ(C=S) 1243, υ(uncoordinated PF$_6$) 829. λ_{max}, nm (CH$_3$CN), ε (Lmol^{-1}cm^{-1}): 236 (91,588), 284 (104,022), 451 (20,545). Luminescence, wavelength, nm (CH$_3$CN): 617 nm. ^{1}H NMR (400 MHz, DMSO-d^6), δ: 12.88 (s, 1H), 12.05 (s, 1H), 8.92-8.81 (m, 4H), 8.76 (d, 1H), 8.70 (s, 1H), 8.23 (t, 2H), 8.20-8.10 (m, 4H), 8.11-8.05 (m, 2H), 7.97-7.88 (m, 2H), 7.85 (d, 2H), 7.75-7.65 (m, 2H), 7.64-7.58 (m, 4H), 7.57-7.47 (m, 2H), 7.45-7.37 (m, 2H). ^{13}C NMR (400 MHz, DMSO-d^6), δ: 182.40, 168.99, 157.29, 157.09, 153.16, 147.59, 146.35, 138.48, 135.48, 133.88, 133.28, 132.49, 130.13, 129.35, 129.02, 128.52, 127.17, 125.73, 125.00. Mass spectrum (*m/z*): 917.05 (917.10 theory), [Ru(bpy)$_2$(phen)-*n*BT)(PF$_6$)]$^+$, 771.09 (771.10 theory), [Ru(bpy)$_2$(phen)-*n*BT + H]$^+$.

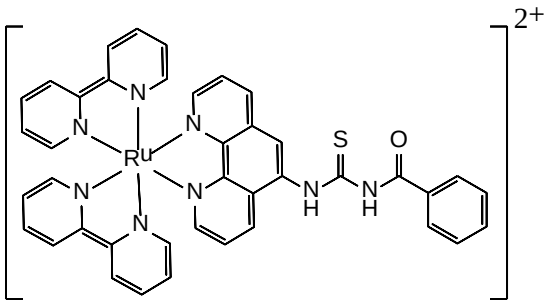

Fig. 1 Structural formula of the examined complex

3. RESULT AND DISCUSSION

3.1 General

The [Ru(bpy)$_2$(phen-*n*BT](PF$_6$)$_2$ complex (Fig. 1) was obtained by in-situ reaction of *cis*-Ru(bpy)$_2$(5-NH$_2$phen).2PF$_6$ with benzoyl isothiocyanate. The structure of the complex was elucidated based on elemental analysis and IR, UV-Vis, mass spectrometry, ^{1}H and ^{13}C NMR spectroscopic measurements. The analyses results were consistent and in good agreement with reported data [12]. The ruthenium complex exhibited the expected magnetic susceptibility value of 0 suggesting the Ru(II) metal centre adopts a diamagnetic d^6 configuration. This observation was in agreement with previously reported magnetic properties of similar [Ru(bpy)$_2$(thio-based imine)](ClO$_4$)$_2$ complex [13].

3.2 Absorption and luminescece spectroscopy

The Ru(II) complex displayed strong absorption bands in the ultra-violent region with absorption maxima at 236 nm (ε= 91,588 L mol^{-1}cm^{-1}) and 284 nm (ε= 104,022 L mol^{-1}cm^{-1}) that can be attributed to the π→π* ligand-centered (LC) transitions. This transitions basically denoted the excitation of electrons from filled π to vacant π* orbitals of the bpy, phen or benzoylthiourea moieties [14]. The complex also exhibited an absorption band in the visible region, 451 nm (ε= 20,545 L mol^{-1}cm^{-1}) that was attributed to spin-allowed Ru^{II}(dπ)^6→bipy(π*) and Ru^{II}(dπ)^6→phen(π*) MLCT transitions [15]-[16]. Excitation of the complex at their metal-to-ligand charged transfer (MLCT) wavelength typically leads to visible light emission that shows an asymmetric band at 617 nm. This emission band was assigned to a radiative transitions from Ru^{II}(dπ)^6→ π* (ligand) transition [15]. Typically, the emission energy of the Ru(II) complex will be smaller than the energy of the first absorption peak, as the emission of ruthenium complex is expected to stem from its low-energy triplet state which is phosphorescence, rather than the excited singlet state [17].

3.2.1 The pH influence on spectroscopy

Protonation and deprotonation equilibrium in the complex will undergo changes in their emission and/or absorption spectra, in particular of whether the pH affects the ground state or the excited state. If the excited state of the complex is affected by the pH changes, the emission spectra will be notably change with pH, and vice versa [18]. It is important to note that the complex exhibited a greater sensitiviy and selectivity in emission [6] and also absorption based sensing. Fig 2 and Fig. 3 depict the absorption and luminescence spectra of the ruthenium complex in

different pH values, respectively.

The absorption spectrum of the Ru(II) complex in acetonitrile exhibits a maximum at 451 nm and undergo 4 nm bathochromic shift in acid and basic medium. In line with the absorption spectral behaviour, the emission band of the complex is also red-shifted in protonation and deprotonation equilibrium. Both cases are experience the bathochromic effect, albeit to a small extent, probably due to the lowest unoccupied molecular orbital (LUMO) of its ground state and excited state are stabilized in protonated/deprotonated complexes.

The UV-Vis spectral data of the complex in acetonitrile over the pH range of 1-11 is cataloged in Table 1. The maxima absorption with the variation of pH displayed an isosbestic point at 455 nm and decreases relatively with the pH (Fig. 2). There is a bathochromic shift in the absorption bands when the pH increases due to decrease in the energy of π* orbital of the ligands and stabilized the MLCT levels.

Table 1 Absorption data for Ru(II) complexes in acetonitrile solution at different pH value

$[Ru(bpy)_2(phen)$-nBT$)]^{2+}$	Absorption, λ_{max} = 455 nm
	ε (L mol^{-1} cm^{-1})
pH 1	7738
pH 3	5292
pH 5	4508
pH 9	3392
pH 11	2887

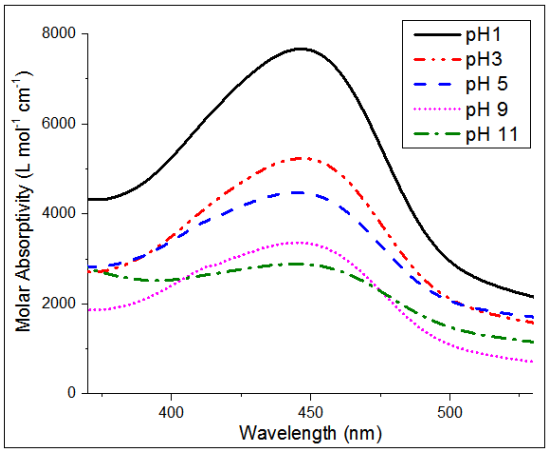

Fig. 2 The effect of pH on the absorption spectra of $[Ru(bpy)_2(phen)$-nBT$)](PF_6)_2$ in acetonitrile

The plot of the emission intensity of the ruthenium complex versus pH shows a sigmoidal relationship (Fig. 3). This result complementary agreed with previous report [6]. The sigmoidal shape of the curve suggests the existence of just one process of protonation/deprotonation of the complex in excited state [19].

The maximum peak of the emission intensity is centered at 620 nm and decreases significantly with pH in the range of 1-11. In line with the effect of pH to absorption spectral, a higher luminescence intensity and lifetimes are also observed in acidic solutions, while a bathochromic shift occured in basic media. The red shift of the band upon protonation/deprotonation can be interpreted in terms of the stabilization of the MLCT levels caused by the energy decrease in the π* orbital of the ligands. The higher the pH value, the more red-shifted of the band, resulting in an overall broadening and flattening of the curve.

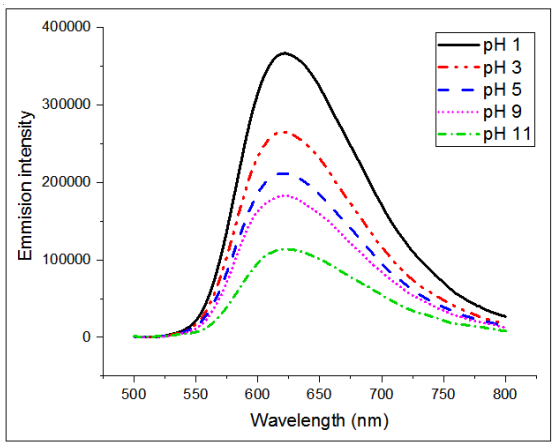

Fig. 3 The effect of pH on the emission spectra of $[Ru(bpy)_2(phen)$-nBT$)](PF_6)_2$ with excitation at 455 nm in acetonitrile

The complex exhibits a longer lifetime in lower pH solution, most likely due to the thermally activated decay of the lowest MLCT state to the short-lived metal center states is slowed down, consequence of the stabilization of the MLCT and the destabilization of the metal-centered (MC) level [20]. The radiative and nonradiative decay rate constants, k_r and k_{nr} respectively were also calculated for the complex, as shown in Table 2. The decrease of the emission quantum yield is owing to the increase of k_{nr} and decrease of k_r. In general, a greater k_{nr} value contributes to a lower emission quantum yield and shorter lifetime of the complex. Noteworthy is the lower energy excited state in the complex decays more efficiently to the ground state via a non-radiative pathway [10].

Table 2 Luminescence data for Ru(II) complexes in acetonitrile solution at different pH value

	Luminescence, 620 nm				
	φ_{em}	τ_m	τ_r	k_r	k_{nr}

		(ns)	(μs)	(μs^{-1})	(μs^{-1})
pH 1	0.044	501	11.39	0.088	1.908
pH 3	0.041	446	10.88	0.092	2.150
pH 5	0.039	419	10.74	0.093	2.294
pH 9	0.038	391	10.29	0.097	2.460
pH 11	0.032	339	10.59	0.094	2.855

4. CONCLUSION

The optical response of the Ru((II) complex was good for the pH range of 1-11. The ruthenium(II) complex with polypyridyl ligand shows an excellent absorption and luminescent pH sensitivity and selectivity and hence, is a promising agent for an optical pH sensor.

5. ACKNOWLEDGEMENTS

The author would like to acknowledge Universiti Kebangsaaan Malaysia for sponsoring the project under FRGS/1/2016/ST01/UKM/02/2.

6. REFERENCES

[1] H. X. Chen, X. D. Wang, X. H. Song, T. Y. Zhou, Y. Q. Jiang, and X. Chen, "Colorimetric optical pH sensor production using a dual-color system", Sensors Actuators, B: Chemical, Vol. 146, No. 1, 2010. pp. 278–282.

[2]H. Nam, M. Jeong, O. J. Sohn, J. Il Rhee, J. Oh, Y. Kim, and S. Lee, "Synthesis of phenanthroline derivative by Suzuki coupling reaction and the use of its ruthenium complex as an optical pH sensor", Inorganic Chemistry Communication, Vol. 10, No. 2, 2007. pp. 195–198.

[3] C. M. Chan, W. Lo, and K. Y. Wong, "Application of a luminescence-based pH optrode to monitoring of fermentation by *Klebsiella pneumoniae*", Biosensors Bioelectronics, Vol. 15, No. 1–2, 2000. pp. 7–11.

[4] M. Jeong, H. Nam, O. J. Sohn, J. I. Rhee, H. J. Kim, C. W. Cho, and S. Lee. "Synthesis of phenanthroline derivatives by Sonogashira reaction and the use of their ruthenium complexes as optical sensors", Inorganic Chemistry Communication, Vol. 11, No. 1, 2008, pp. 97–100.

[5] H. J. Kim, Y. C. Jeong, J. Heo, J. Il Rhee, and K. Hwang, "A wide-range luminescent pH sensor based on ruthenium (II) complex", Vol. 30, No. 3, 2009, pp. 539–540.

[6] E. C. Constable, C. E. Housecroft, A. C. Thompson, P. Passaniti, S. Silvi, M. Maestri, and A. Credi, "pH-sensitive Ru(II) and Os(II) bis(2,2':6',2"-terpyridine) complexes: A photophysical investigation", Inorganica Chim. Acta, Vol. 360, No. 3, 2007, pp. 1102–1110.

[7] C. Viala and C. Coudret. "An expeditious route to *cis*-$Ru(bpy)_2C1_2$ (bpy=2,2'-bipyridine) using carbohydrates as reducers", Inorganica Chim. Acta, Vol. 359, No. 3, 2006, pp. 984–989.

[8] S. Baitalik, U. Flo, K. Nag, "Mononuclear and binuclear ruthenium (II) complexes containing 2,2'-bipyridine or 1,10-phenanthroline and pyrazole-3,4-bis(benzimidazole). Sythesis, structure, isomerism, spectroscopy and proton-coupled redox activity", Vol. 38, No. 14, 1999, pp. 3296–3308.

[9] S. Dutta, S. Baitalik, M. Ghosh, U. Flörke, and K. Nag. "Structural, photophysical and electrochemical studies of $[RuN_6]^{2+}$ complexes having polypyridine and azole mixed-donor sites", Inorganica Chim. Acta, Vol. 372, No. 1, 2011, pp. 227–236.

[10] K. Nakamaru. "Synthesis, luminescence quantum yields, and lifetimes of trischelated ruthenium(II) mixed-ligand complexes including 3,3′-dimethyl-2,2′-bipyridyl", Bulletin of the Chemical Society of Japan, Vol. 55. pp. 2697–2705, 1982.

[11] C. D. Ellis, L. D. Margerum, R. W. Murray, and T.J. Meyer, "Oxidative Electropolymerization of Polypyridyl Complexes of Ruthenium", Inorg. Chem., Vol. 22, No. 192, 1983, pp. 1283–1291.

[12] S. S. Tan and M. B. Kassim, "Structure and spectroscopic properties of ruthenium(II) bipyridyl *N*-benzoyl-*N*'-(1,10-phenanthrolin-5-yl)-thiourea", 2015, p. 050010.

[13] D. Bhattacharyya, S. Chakraborty, P. Munshi, and G. K. Lahiri, "Ruthenium (II/III) bipyridine complexes incorporating thiol-based imine functions. Synthesis, spectroscopic and redox properties", Vol. 18, 1999, pp. 2951–2959.

[14] C. Dragonetti, L. Falciola, and P. Mussini. "The role of substituents on functionalized 1, 10-phenanthroline in controlling the emission properties of cationic iridium (III) complexes of interest for electroluminescent devices", Inorganic Chemistry, Vol. 46, No. 21, 2007, pp. 8533–8547.

[15] D. Saha, S. Das, S. Mardanya, and S. Baitalik, "Structural characterization and spectroelectrochemical, anion sensing and solvent dependence photophysical studies of a bimetallic Ru(II) complex derived from 1,3-di(1H-imidazo[4,5-f][1,10]phenanthroline-2-yl)benzene", Dalton Trans., Vol. 41, No. 29, 2012, pp. 8886–98.

[16] N. a F. Al-Rawashdeh, S. Chatterjee, J. a. Krause, and W. B. Connick, "Ruthenium bis-

diimine complexes with a chelating thioether ligand: Delineating 1,10-phenanthrolinyl and 2,2′-bipyridyl ligand substituent effects", Inorganic Chemistry, Vol. 53, No. 1, 2014, pp. 294–307.

[17] E. Badaeva, V. V Albert, S. Kilina, A. Koposov, M. Sykora, and S. Tretiak, "Effect of deprotonation on absorption and emission spectra of Ru(II)-bpy complexes functionalized with carboxyl groups", Physical Chemistry Chemical Physics, Vol. 12, No. 31, 2011, pp. 8902–13.

[18] J. C. Ellerbrock, S. M. McLoughlin, and A. I. Baba, "The effect of pH on the emission and absorption spectra of a ruthenium complex", Inorganic Chemistry Communication, Vol. 5, No. 8, 2002, pp. 555–559.

[19] S. Pizarro, M. Gallardo, C. Leyton, E. Castro, F. Gajardo, and A. Delgadillo, "Effect of pH in the photoluminescence of a ruthenium complex featuring a derivative of the ligand pyrazine[2,3-f][1,10]-phenanthroline", Spectrochimica Acta Part A: Molecular and Biomolecular Spectroscopy, Vol. 146, pp. 61–65, 2015.

[20] L. Troian-Gautier and C. Moucheron, "Ruthenium (II) complexes bearing fused polycyclic ligands: From fundamental aspects to potential applications", Molecules, Vol. 19, No. 4, 2014, pp. 5028–5087.

Second International Conference on Science, Engineering & Environment,
Osaka City, Japan, Nov.21-23, 2016, ISBN: 978-4-9905958-7-6 C3051

THE STUDIES ON TINTED GLASS USAGE FACTORS AMONG VEHICLE USERS IN MALAYSIA

Mustaffa, A. A., Ahmad, H. N., Rohani, M., Basil, D. and Khairul Nizar, M.Y.
Smart Driving Research Centre (SDRC),
Faculty of Civil and Environmental Engineering, Universiti Tun Hussein Onn Johor, Malaysia.

ABSTRACT

Malaysia is located on a equator line with minimum and maximum temperature of 23.1°C and 35.7°C, respectively. The stated temperature is around in Peninsular Malaysia, and the recorded temperatures are according to the Malaysian Meteorological Department (MetMalaysia). Due to invariable recorded temperatures, the road and highway users forced to install and used a layer or cover of the inner of their vehicles so that their journey will be smooth and comfortable till the destination. Therefore, the tinted glass is the alternative to that inner layer of cover. However, tinted glass issue is often dealt with at present. There are various advantages and disadvantages of the uses of tinted glass. This study aimed to identify the probability numerical factor of tinted glass usage. This paper provides quantitatively study of a questionnaire feedback, and involvement of the respondents from private vehicle users in Malaysia, especially multi-purpose vehicle (MPV) and sport utility vehicle (SUV). This questionnaire is in form handout, where it is includes listed of constructed of 33 questions, and consists of four sections, namely (i) demography respondents;(ii) questions related factors of use of tinted glass; (iii) questions related to the rules of use of tinted glass and views; and finally the (iv) comments and suggestions from respondents about the use of tinted glass. The Statistical Packages for Social Sciences (SPSS) was applied to analyze and obtained the some part of a statistical and probability results. The Cronbach's Alpha reliability coefficient of factors of tinted glass usage and the rule of tinted glass usage are greater than 0.7, where this is resulted from the climatic factor and safety factors. In addition, the analysis of Spearman's Rank Order (SRO) is conducted to identify the strength of the relationship of questions related factors of use of tinted glass; and questions related to the rules of use of tinted glass. Yet, the visible light transmission (VLT) specifications provide and enhancing the authority's effort in monitoring the purchasing by users of tinted glass and also the entry of imported vehicles in Malaysia. Nevertheless, the correlation in this study found that the tinted glass usage makes it difficult to see the vehicle from the driver's seat and rear mirror, and in order to enhance the usage of the tinted glass among of all the vehicle users, the education and information regarding the use of tinted glass should be acknowledged. This being is an expected as to support the authorities in improving the regulation of tinted glass usage in Malaysia.

Keywords: Tint, Questionnaire Studies, Statistical and Probability Approach, Passenger Vehicle Users

INTRODUCTION

Every year, total vehicle production in the world is increasing. Malaysia also contributes the increasing of the vehicle production in line with the socio-economic development in Malaysia. Furthermore, sales of passenger vehicles such as cars, multi-purpose vehicle (MPV) and sport utility vehicle (SUV) increased in 2015 were 591,298 units, compared to 588,341 units in 2014. The sales of commercial vehicles decreased from 78,124 to 75,736 units [1]. This shows that passenger vehicles become the preferred vehicle in Malaysia compared to commercial vehicles. Moreover, the enforcement of offenses tinted glass held from time to time, whether on the local vehicles and imported vehicles. For vehicle user who have the vehicles that are not in accordance with specifications of tinted glass having committed offenses under the Rules of Motor Vehicles (Prohibition of Certain Types of Glass) 1991. Statistics of enforcement of tinted glass which is detected by the Road Transport Department (JPJ) in 2011 was 15,336 cases. Meanwhile, in 2012 a total of 51,431 cases and up to June 2013 a total of 22,663 cases. This shows an increase in the fault of tinted glass usage in Malaysia.

In general, there are some well known factor in the used of tinted glass, such as the weather factor, safety factor and health factors. In addition, the Rules of Motor Vehicles (Prohibition of Certain Types of Glass) Act 1991 also provides for the exclusion of tinted glass usage in vehicles based on safety and health issues. Therefore, this study attempts to look at the factors against the use of tinted glass in the passenger vehicle users, altogether with some research questions that can be raised, namely (i) Item A: What the causes of tinted glass usage on their vehicles; and (ii) Item B: Do vehicle users understand the rules which allowed the use of tinted glass in Malaysia.

FACTORS AFFECTING THE TINTED GLASS

There are various factors that led to the use of tinted glass. Among them are the weather factors, the factors of safety, health factors, a reduction in vehicle cabin temperature, the privacy of vehicle users and the aesthetic of the vehicles.

Night driving vision is the fundamental safety issue regarding light transmittance of windows. The visual detection of an object depends on its brightness contrast with the background. The contrast sensitivity of the human eye depends on the overall brightness of the scene. In daylight, a low contrast target on a dark road surface can be seen, but at dusk, it cannot be seen because the contrast sensitivity of the eye at dusk or twilight is insufficient to detect a target of its contrast [2].

In our countries, the Rule 5(1) and 5(3) of the Motor Vehicles (Prohibition of Certain Types of Glass), 1991 allows windscreen of a vehicle to be tinted but must permit transmission of at least seventy percent (70%) visible light. Whereas for other side windows, including rear glass must permit fifty percent (50%) light transmission [3].

However, the issue of regulation of tinted glass is said to be less relevant to current practice. Therefore, a discussion was held to review the use of tinted glass, including existing regulations, enforcement, security and usability. The result of amending regulation of tinted glass has been determined during the discussion, where the glass must permit visible light transmission (VLT) 70% for the windscreen and 50% for driver side mirror. While, the level of VLT in the passenger side mirror and the other mirrors reduced from 50% to 30%. Figs. 1 (a) and 1 (b) show the previous and current tint rules of visible light transmission (VLT) accordance to Malaysia's Road Transport Dept. (JPJ). The new or current tint rules were commenced after the 1st May 2015 [4].

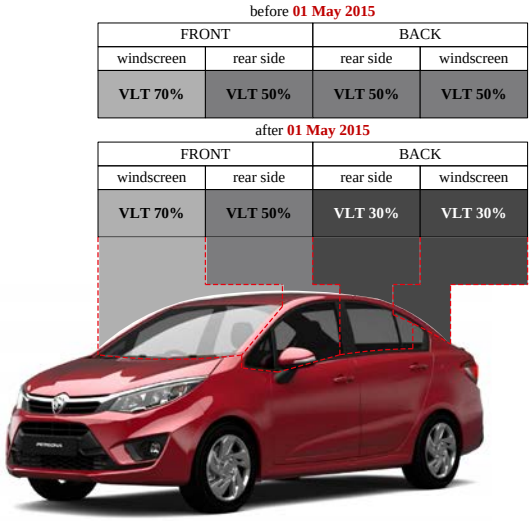

Fig. 1(a) The isometric view of VLT's used

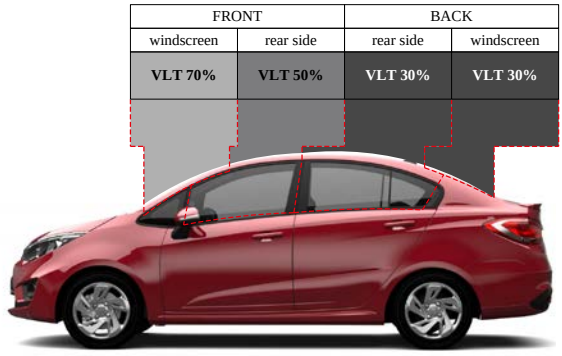

Fig. 1(b) The rear side view of VLT's used

Fig. 1 The previous and current tint rules of visible light transmission (VLT) accordance to JPJ [4].

In these three presented papers, such as A Study on Automotive Tint Glazing in Malaysiain 2015 page 6 [5]; Front Side Window Tinting Visual Light Transmittance Requirements in 2004 page 3 [6]; and External Viewing of Vehicle Contents under Varying Window Tinting and Illumination Conditions in 1995 pages 2 to 4 [7]; they are all agrees with Proffitt's view, where Mohd Hafzi et al. pointed out, and Figs. 2(a) and 2(b), are associated with the text below.

Fig. 2(a) Clearvision: No 35% VLT tinted glass

Fig. 2(b) Blurry vision: with 35% VLT tinted glass

Fig. 2 The Clear and blurry vision with and without 35% VLT usage (remodified from [5]).

"In certain circumstances in traffic environment, there exist needs for other road users, such as pedestrians and cyclists, to look through vehicle windows for vital traffic cues.

In other words these users exploit the see-through windows, for information beyond the ordinary mechanism of unobstructed visual confrontation, where the VLT 35% of front side windows could substantially reduce the external viewers' traffic cues to check the presence of pedestrians, cyclists or other road users.

In brief, similar principle applies situation where when two cars are facing in opposite directions, waiting to turn at traffic islands in the middle of a main road or at the intersections or when cars lined up.

Furthermore, such situation is foreseen to become worse during low ambient lighting."

In 1994, Griffiths and Jones reported in their studies regarding the window tinting and road safety, is also associated with the above statements, where drivers turning into an intersecting road need to look through their front side windows to detect the presence of pedestrians or cyclists. The analysis claims that visibility through side windows is not a problem because the driver always has the benefit of being able to see the headlights or signals of other cars but this will not help in the recognition of the presence of pedestrians or of many cyclists [8].

Besides, health factor also one of factors of tinted glass usage in Malaysia. Previous research has proven that skin exposed to the sun shining through window glass, even in the office, can over time lead to significant skin damage [9]. The UV exposure we receive driving a car, especially adds up. In a US study, the researchers found asymmetric photo-damage (sun induced skin damage) on the face, with more brown pigment (color) and deeper wrinkles on the left. The more time subjects spent driving a vehicle, the more severe their photo-damage on the left side. Reinforcing this research, in countries where the driver's side is the right side, people tend to develop more sun damage and skin pre-cancers on the right. Certain pre-cancers can turn into squamous cell carcinoma, the second most common form of skin cancer [10].

The tinting industry has argued that tinting has a positive effect on cooling vehicles, reducing the load on air conditioning systems. The past researchers found mobile air conditioning can reduce fuel consumption and vehicle emissions [11]. Studies have shown temperature reductions of only around one degree in a moving vehicle as a result of having tinting and that the corresponding reduction in air conditioner load was almost insignificant[12].Some drivers believe tinting will give the vehicle occupants greater privacy, since people cannot see inside the vehicle's tinted windows as clearly as with non-tinted windows. The Police oppose this because they are less able to see if the occupants are behaving appropriately, such as wearing seatbelts and driver using phone or other device during driving [7]. Some people believe tinting improves the appearance of their vehicle. This should not over-ride safety requirements [13].

THE METHODOLOGY

The study consists of three phases. First, the topic was selected and analyzed to identify the scope and the problems of study. Next, the research and data were collected through literature review and a questionnaire. The questionnaire was given to private vehicle user, such as cars, vans, MPV and SUV as respondents. The method of questionnaire studies was almost similar were carried out by Malaysian Institute of Road Safety Research in 2014 [10]. In fact, it also includes either local vehicle users or imported vehicle users. Overall, the study used a descriptive approach to look at the frequency and percentage of respondent demographics. The questionnaire is divided into four parts; A (demographic -16 items); B (the factors of tinted glass usage –17 items); C (the rules of tinted glass usage – 4 items); D (suggestions). Questionnaires were distributed through on-line, through car clubs on the social networking. Data obtained from questionnaires were analyzed using SPSS version 22.

The study population consisted of vehicle users in Malaysia. 396 vehicle users from various states are chosen as respondents. Data collected and analyzed using descriptive analysis and pilot study was conducted to test the questionnaire that has been prepared. The objectives of pilot survey were conducted to test reliability and validity of the instruments. After analyzed, some questions were modified to improve the questionnaire. Table 1 shows the result for the coefficient of reliability for each of the two variables.

Table 1 Analysis of reliability - Cronbach's Alpha

Variable	Cronbach's Alpha	Item
Factors of tinted glass usage	0.806	12
Rule of tinted glass usage	0.704	4

The reliability for the factor of tinted glass usage is 0.806 and the rule of tinted glass usage is 0.704. The value of both these variables exceeds 0.70. Therefore, the items of the questionnaire are reliable and applicable. Lastly, recommendations and conclusions have been made after analysis of data.

RESULT AND DISCUSSION

The evaluation and analysis of data were carried out using the SPSS Version 22 as a tool to obtain the required parameter, such as the percentages of each factor division, the chi-squared, the p-value, the mean, the standard deviation, and other required that is discussed in the following matters.

Demographic Analysis

The results of the analysis showed that the majority of respondents were males of the 345 respondents (87.1%) than female respondents. In addition, the Malays are the majority of respondents in this study, a total of 373 respondents (94.2%) compared to other races like the Chinese, Indians and others. This shows that the Malays male respondents are more interested in the study of the use of tinted glass. Besides, the study found that more than half of the respondents aged between 20 to 30 years, a total of 216 respondents (54.6%).

The study found that respondents who live in Selangor state more like to modify their vehicle glass and have been sued for tinted glass usage compared to other states (Fig.3). This can be proven by statistics on the number of summons due to tinted glass usage issued by the Road Transport Department of Malaysia (JPJ).

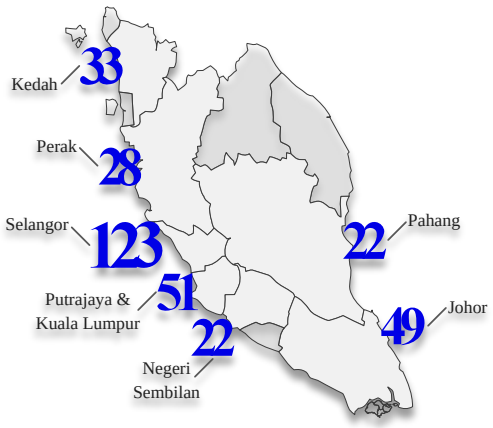

Fig. 3 Total number of respondents based on state in Peninsular Malaysia

Status of tinted glass users

Table 2 shows the analysis of Cross tabulation of modified tinted glass user and Malaysia's vehicle inspection specialist (PUSPAKOM). The Chi-Square test was 2.823 and p-value less than 0.05. When the p-value less than 0.05, it means there is a significant relationship between users who modify tinted glass and PUSPAKOM inspection. The study said that, the modified tinted glass user has a strong relationship with PUSPAKOM inspection of 82.3%. Conduct the PUSPAKOM inspection is important. In terms of frequency and percentage of users who modify tinted glass and went to PUSPAKOM inspection only a total of 18 (4.5%), while that modified tinted glass user and never go PUSPAKOM inspection is 200 people or 50.5%. However, there are also those who did not modify the glass, but also want an assurance from the PUSPAKOM are 24 people or 6.1%. This analysis clearly shows that the attitude of users to request permission from the PUSPAKOM tinted glass is still deficient.

Table 2Cross tabulation of modified tinted glass used corresponded to PUSPAKOM inspection

			PUSPAKOM inspection		Total
			Yes	No	
Modified Users	Yes	F	18	200	218
		%	4.5%	50.5%	55.1%
	No	F	24	154	178
		%	6.1%	38.9%	44.9%
Total		F	42	354	396
		%	10.6%	89.4%	100.0%
Chi-Square			2.823		
p- value			0.019*		

F: frequency;χ^2: chi-squared; *: significant p_{value}<0.05.

Perception of users toward tinted glass usage

Fig.4 shows the vehicle users in Malaysia are using tinted glass due to weather factors (344 respondents, 86.9%). Users prefer to use tinted glass to suit the hot weather in the Malaysia. The second factor is due to safety factors (265 respondents, 66.9%), where users worry about crimes such as car break-ins and robberies. The third factor is due to health factors (119 respondents, 30.1%). Less confirming the use of tinted glass is due to the type of vehicle (SUV, MPV and imported vehicles).

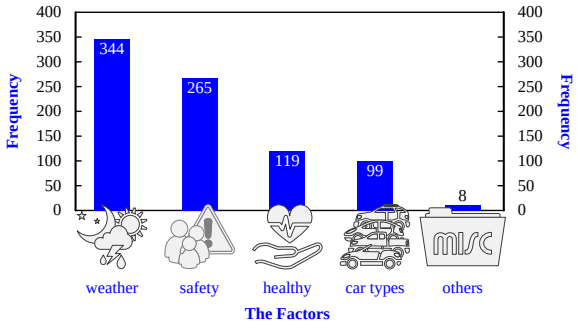

Fig. 4 Factors of tinted glass used

Based on the Table 3, the highest mean score was 4.53, the respondents strongly agreed that the use of tinted glass can reduce glare to the driver.

Meanwhile, the lowest mean score was 1.72, which respondents disagreed that the use of tinted glass can increase the accident rate. In addition, the respondents agreed with the statement that the tinted glass is a necessity for all types of vehicles, the use of tinted glass helps to reduce the use of air conditioning, use of tinted glass can reduce robberies of vehicles and the use of tinted glass helps to reduce the crime rate with mean scores in the range of 3.51 to 4.50. Whereas, for the other statement, mean scores indicate that respondents disagreed with the statement submitted.

Table 3 Mean and standard deviation of factor of tinted glass used

Item A	N	Mean	Std. Deviation
17. The tinted glass is a need for all vehicles.	396	4.47	0.764
18. The tinted glass usage will affect the driving.	396	1.77	0.922
19. The tinted glass usage can reduce glare to the driver.	396	4.53	0.771
20. The tinted glass usage will affect the vision of driver during night.	396	2.28	1.160
21. The tinted glass usage will affect the vision of driver during heavy rains.	396	2.08	1.047
22. The tinted glass usage can reduce the use of air conditioning.	396	4.27	0.974
23. The tinted glass usage can reduce vehicle robbery case.	396	4.44	0.952
24. The tinted glass usage can reduce the crime rate.	396	4.11	1.124
25. The tinted glass usage can increase the accident rate.	396	1.72	0.947
26. The tinted glass usage makes it difficult to see the driver of the vehicle from the forward direction.	396	1.82	1.095
27. The tinted glass usage makes it difficult to see the vehicle from the driver's side.	396	1.97	1.091
28. The tinted glass usage makes it difficult to see the driver of the vehicle from the rear mirror	396	1.90	1.065

Table **4** Mean and standard deviation of rule of tinted glass used

Item B	N	Mean	Std. Deviation
29. You understand the meaning of visible light transmission (VLT) allowed in the vehicle.	396	4.05	1.005
30. You know how much the level of visible light transmission (VLT) allowed in the vehicle.	396	4.03	1.023
31. The existing regulations on the tinted glass usage in accordance with the requirements of the vehicle users.	396	2.25	1.335
32. The latest regulations on the tinted glass usage in accordance with the requirements of the vehicle users.	396	2.76	1.504

Table 4 shows the mean and standard deviation of user perception of the rules of tinted glass usage. The study found that respondents agree that they understand the meaning of visible light transmission, and how much the level of transparency that allowed light vehicles, based on the mean score in respectively, by 4.05 and 4.03. In addition, based on the mean score 2.25, respondents did not agree that the existing rules on the use of tinted glass in accordance with the requirements of the user. However, respondents agree that new regulations on the use of tinted glass in accordance with the requirements of users with a mean score of 2.76.

Based on the analysis of output Spearman's Rho correlation. The number of data, N is 396, while the significant (two - tailed) is 0.00, which is less than 0.05. The greatest value of the correlation coefficient is 0.803. Level measurements show a perfect correlation between items A27; the tinted glass usage makes it difficult to see the vehicle from the driver's side and item A28; the tinted glass usage makes it difficult to see the driver of the vehicle from the rear mirror.

In addition, the lowest correlation coefficient is 0.184. This indicates that almost no correlation between the item A22; the tinted glass usage can reduce the use of air conditioning and A26; the tinted glass usage makes it difficult to see the driver of the vehicle from the forward direction. Based on Table 5, we can conclude that there is a relationship between each variable based on the value of the correlation coefficient.

CONCLUSION

This paper investigates the questionnaire studies on tinted glass usage factors among vehicle users in Malaysia, where the present study was designed to determine the questionnaire study results through the mean and the standard deviation of factor of tinted glass usage, and also the based rule of tinted glass usage. The findings can be summarized as follows:

(i) The respondents are showed that roughly 87% of male gender, 94% of Malays as in races context, and 55% of ranging ages between 20 and 30 years.

(ii) Selangor state with total of 123 is recorded as the highest number of respondents, while Negeri Sembilan and Pahang state, recorded with the lowest number of respondents of 22.

(iii) Approximately 55% of users had modified their vehicles without carrying out the inspection at PUSPAKOM, while 45% of users did not perform any modification and carrying out the inspection.

(iv) The factors of tinted glass usage as in the highest frequency to the lowest frequency is in sequence of the weather > the safety > the healthy > the car types > others.

(v) Items A and B as associated with the research questions, with values of 4.53 and 4.05, resulting as the tinted glass usage can reduce glare to the driver, and the users understand the meaning of VLT allowed in the vehicle, respectively, as the highest mean. In addition, values of 1.77 and 2.25, recorded the lowest mean with the tinted glass usage will affect the driving, and the existing regulations on the tinted glass usage in accordance with the requirements of the vehicle users, respectively.

(vi) The most correlation uses of tinted is difficult to see the vehicle from driver's side (0.803) and the lowest correlation (0.184) is tinted can reduce mobile air conditioning. The analysis results showed that many respondents are not sure whether the tinted glass of their vehicles according to specifications allowed.

Therefore, the conclusion was made based on the objective that has been set. Finally, it is hoped that this study will be used and exploited in the future and could intensify studies on the use of tinted glass in Malaysia.

ACKNOWLEDGEMENTS

The author would like to express gratitude to the Ministry of Higher Education Malaysia, and Universiti Tun Hussein Onn Malaysia for their support with grant RSGS Vot U101.

REFERENCES

[1] Malaysia Automotive Association (MAA). "Malaysia Automotive Info Summary of Sales and Production Data", 2015, Retrieved from http://www.maa.org.my/info_summary.htm

[2] Boyd, P., "Report to Congress on Tinting of Motor Vehicle Windows". Washington, D.C. U.S Department of Transportation National Highway Traffic Safety Administration. 1991.

[3] Road Transport Department Malaysia (2010) "In The Dark Over Tinted Glass Ruling"., 2010, Retrieved from, http://www.jpj.gov.my/en/

[4] Road Transport Department Malaysia, "Modification of Private Vehicles", 2015 Retrieved from, 2016, http://www.jpj.gov.my.

[5] Mohd Hafzi MI, Maslina M., Mohd Khairudin R., Aqbal Hafeez A., Azhar H., Syazwan S., Nor Fadilah S., Rabihah I., and Wong S. V. "A Study on Automotive Tint Glazing in Malaysia, Research Report, Malaysian Institute of Road Safety Research (MIROS), MRR 159, 2015.

[6] Baldock MRJ, McLean AJ, and Kloeden CN, "Front Side Windows Tinting Visual Light Transmittance Requirements", Australia Centre for Automotive Safety Research, 2004.

[7] Proffitt DR,, Joseph JE, Bhalla M., Durgin, FH, Bertamini M., Lynn C. & Jernigan JD, "External Viewing of Vehicle Contents Under Varying Window Tinting and Illumination Conditions", Final Report No. VTRC 95-R3, Virginia Transportation Research Council, 1995.

[8] Griffiths MJ, & Jones CJ, "Window Tinting And Road Safety" Proceedings of A Symposium held in Sydney, Australia 10 May 1994 (pp 21-26). New South Wales: Roads and Traffic Authority.

[9] Susan TM, "Sun Hazards in Your Cars, Watch out for Skin Cancers and Photo aging on the Left Side of Your Body". The Skin Cancer Foundations Journal. Vol. XXIX, 2011, pp 36-37

[10] Singer R, Hamilton T, Voorhees J, Griffiths C., "Association of asymmetrical facial photodamage with automobile driving" Arch Derm 1994, Vol.130, 1994, pp 121-123.

[11] Nazenin G., and Mustafa Y., "Alternative Way to Reduce Vehicle Emission in Summer With the Help of Car Windows Filming and Car Window Filming's Economics Benefits Over WA, NY, NC, U.S.A, and Istanbul, Turkey". Proceeding of 12th Annual CMAS Conference, 2013.

[12] Rugh JP, Hendricks TJ, and Koram K., "Effect of Solar Reflective Glazing on Ford Explorer Climate Control, Fuel Economy, and Emissions", International Body Engineering Conference and Exposition, 2001.

[13] Institute of Transportation Engineers Australia and New Zealand (ITEANZ), "Motor Vehicle Window Tinting". ITEANZ, 2013.

Engineering

Second International Conference on Science, Engineering & Environment,
Osaka City, Japan, Nov.21-23, 2016, ISBN: 978-4-9905958-7-6 C3051

PUNCHING SHEAR STRENGTH OF BUBBLEDECKS UNDER ECCENTRIC LOADS

Nazar K. Oukaili [1], Luma F. Husain [2]
[1] Professor, College of Engineering, University of Baghdad, Iraq; [2] Lecturer, College of Engineering – University of Al- Mustansiriyah, Iraq

ABSTRACT

The new prefabricated construction technology using BubbleDeck is recently applied in many industrial projects in the world. BubbleDeck uses hollow plastic spheres and therefor it is an innovate method of virtually eliminating the concrete part in the middle of conventional slab which does not contribute to the structural performance. Hence, this part significantly reduces the structural self-weight. So, this study aims to investigate the effect of plastic bubbles on punching shear resistance of flat slabs. Six specimens of dimensions (1500×1500 mm) with total thickness of (100 mm) without shear reinforcement were casted and tested in order to study the difference between solid deck and BubbleDeck in ultimate load capacity, deflection of the slab at three points, strain in flexural reinforcement and in concrete, crack width, area and perimeter of the failure zone and the value of the failure angle. Self-compacting concrete with compressive strength of (30 MPa) is used for casting the specimens, the main variables used are the effect of eccentric loads, subjected at 100 mm from the center of the column, on the behavior of the tested slabs and the position of bubbles with respect to the critical section, (inside or outside the critical section), where the critical section is considered to be at (2d) from the face of the column according to Euro-Code.

Keywords: Punching Shear Strength, BubbleDeck, Self- Compacting Concrete, Solid Decks, Eccentric Loads.

INTRODUCTION

The punching shear or two-way shear phenomenon is a localized failure. It occurs when the column, punches through the slab, and it can be characterized by the truncated or pyramid failure surface. This type of failure is extremely dangerous and should be prevented, since it may lead to brittle, with little or no warning, and progressive collapse of floors [1]. One of the most popular solutions to avoid this failure is increasing the slab thickness, thereby increasing the weight of the structure by requiring the use of large amounts of concrete [2].

A new solution to reduce the weight of concrete structures and increase the spans of two-way reinforced concrete slab systems is referred to BubbleDeck system which was developed in the 1990s in Europe and is gaining popularity and acceptance worldwide [2].

BubbleDeck slab is the slab in which some amount of the concrete is replaced by the plastic bubbles or ellipsoid which are made by the waste plastic material, which reduces the self-weight of the structure [3]. The main components of BubbleDeck are reinforcing mesh at top and bottom, between them there are air bubbles, (hollow ball), made of recycled plastic. While, lattice girder made of steel is used between the bubbles. Usually, any grade of concrete can be used. Generally grade 20 or 30 is used [4, 5].

In this study, the bubbles are tighten with the bottom reinforcing mesh by using tighten wires without using top reinforcing mesh or lattice girder.

EXPERIMENTAL PROGRAMME

The experimental work of this study consists of a series of tests carried out on six half-scale two-way slab specimens of dimensions (1500×1500 mm) with total depth of (100 mm) which were casted and tested in order to evaluate the effect of several variables on punching shear strength of solid and bubbled flat plates.

All the specimens are reinforced with bottom mesh steel reinforcement of (6 mm) diameter at (50 mm) c/c. The steel yield strength is 627 MPa. The magnitude of the cover is (20 mm) and the diameter of the bubble is (60 mm) while the distance between bubbles is (15 mm). The bubbles are tighten with the flexural reinforcement by using tighten wires.

Table 1 and Plate 1 show the details of the specimens. While Plate 2 shows the details of the reinforcement of column and corbel, where all the dimensions are indicated in mm:

Table 1 Details of the specimens

Slab No.	Slab Type	Loading Type	Position of bubbles*
SD1	Solid	Concentric	-
SD2	Solid	Eccentric	-
BD1	Bubbled	Concentric	2d
BD2	Bubbled	Eccentric	2d
BD5	Bubbled	Concentric	D
BD6	Bubbled	Eccentric	D

Note: The position of bubbles measured with respect to the face of the column

(a)

(b)

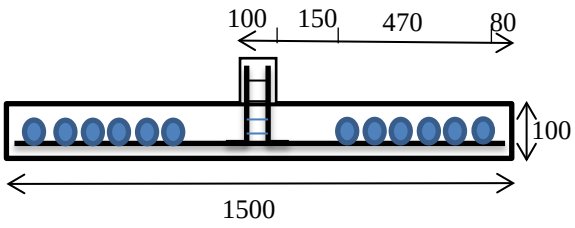

(c)

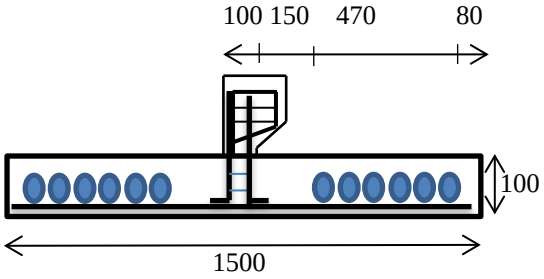

(d)

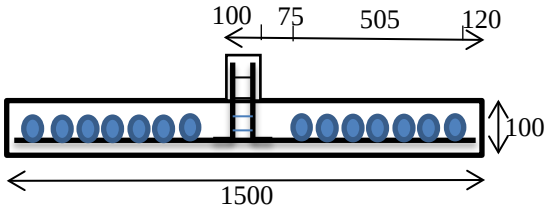

(e)

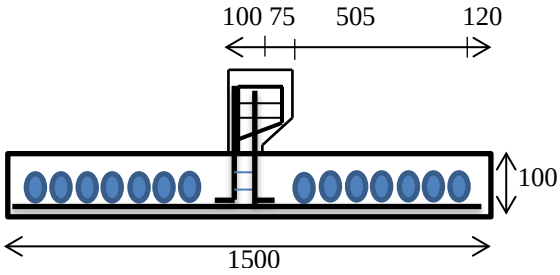

(f)

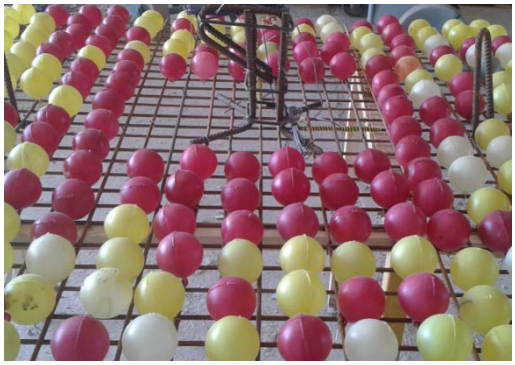

(g)

Plate 1 Details of slab specimens (a) SD1 (b) SD2 (c) BD1 (d) BD2 (e) BD5 (f) BD6 (g) a specimen with tighten bubbles.

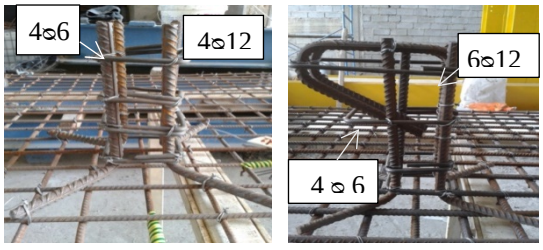

Plate 2 Details of column reinforcement

TESTING SETUP AND TESTING RESULTS

All slabs are simply supported along the four edges. The test was done by subjecting a universal load on the column as shown in Plate 3. The vertical deflection was measured at the center and at one third the span at each direction using dial gages of sensitivity of 0.01mm. The strain of concrete at compression face and of flexural steel reinforcement is measured at each load stage using strain gages.

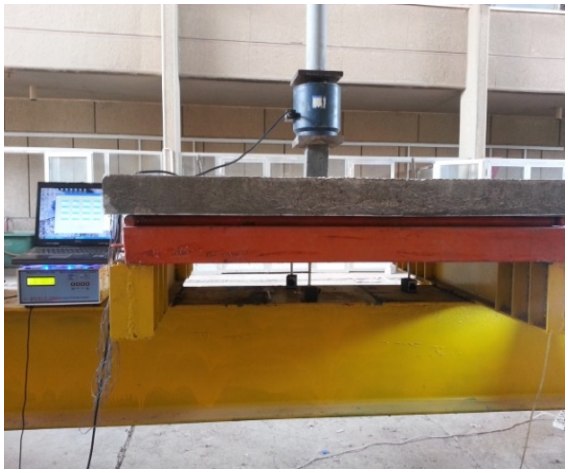

Plate 3 Testing setup

Four strain gages are located at (d and 2d) from the face of the column on two orthogonal directions on the flexural reinforcement. While six strain gages are located at (d and 2d) from the face of the column at the compression face of slab in diagonal and orthogonal directions.

When the load is applied on the slab, the initial cracking of all tested slabs was first observed in the tension zone of the slab near one or more of the corners of the column. With further loading, cracks increased in number from the center towards the four edges of the slab. In general, the first flexural crack load initiated at (27-36%) of the ultimate load, as shown in Table 2. While the ultimate capacity of BubbleDecks is lower than that of solid decks by about (20-31%). Also, the test results show that the eccentricity of the loading decreased the ultimate load and that caused by the increasing of unbalanced moment.

During the tests, it was observed that the punching crack tends to be at one side of slabs subjected to eccentric load due to presence of unbalanced bending moment, while the crack pattern in slabs subjected to concentric load seems to be as circle. Also, on the compression face there were no flexural cracks noticed, only the crack from the column penetration inside the slab.

The width of the cracks is measured at each stage of loading. The cracks are usually increased in number but the width is constant and its magnitude is about 0.05 mm. As the load increased and particularly at stages of loading near ultimate load, the crack width increased and reaches about 1mm. After that sudden failure occurred.

Table 2 Ultimate values of load and deflection

Slab No.	Pcr, (ton)	Pu, (ton)	Δcr, (mm)	Δu, (mm)	Pcr/Pu	Pu(BD)/ Pu(SD)
SD1	5.5	17.5	3.15	19.45	0.314	-
SD2	4.0	15	2.25	16.70	0.266	-
BD1	5.0	14	2.54	17.1	0.357	0.8
BD2	4.0	12	2.35	14.5	0.333	0.8
BD5	4.0	12	2.73	12.7	0.333	0.69
BD6	2.5	11	2.1	11.6	0.227	0.73

The magnitude of area and perimeter of failure zone as well as the failure angle is measured for each slab as shown in Table 3.

Table 3 Area, perimeter and failure angle

Slab No.	Area, (m^2)	Perimeter, (m)	Failure Angle, (Ø°)
SD1	0.58	2.7	9.02
SD2	0.223	2.7	14.74
BD1	0.497	2.5	9.95
BD2	0.214	2.0	15.5
BD5	0.637	2.83	9.46
BD6	0.234	2.9	14.04

From Table 3, it is noticed that the eccentric loading increases the failure angle in the direction near the load and cause a collapse at one side only. Also, the perimeter and area of failure zone in slabs subjected to eccentric load is lower than that slabs subjected to concentric load, this is due to semi-punching failure.

Plate 4 shows the crack pattern of all the tested specimens.

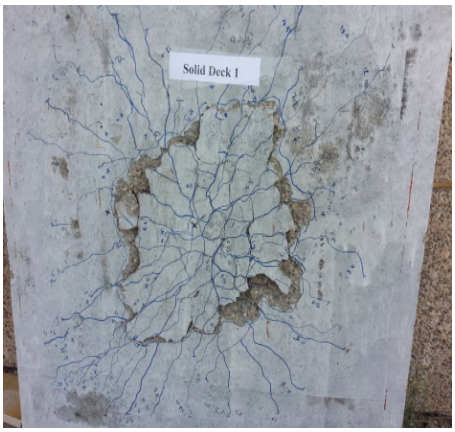

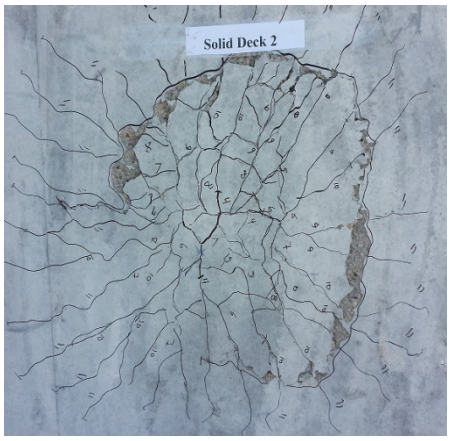

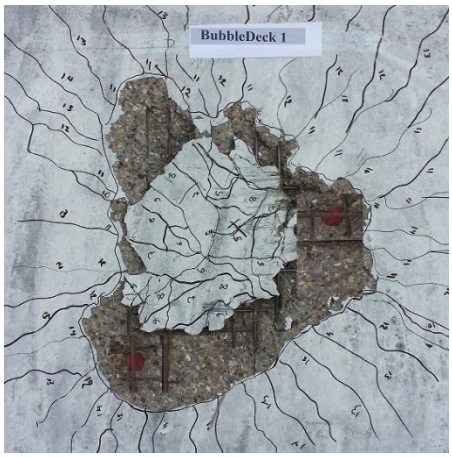

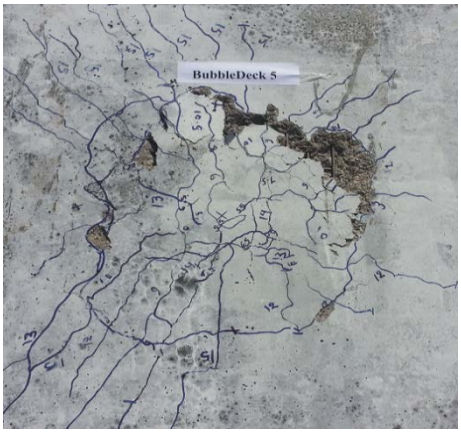

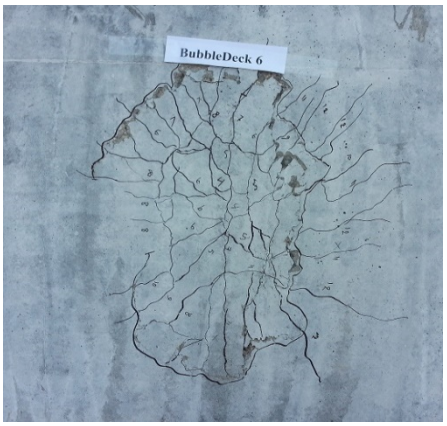

Plate 4 Crack pattern of tested specimens

Figure 1 shows the load- central deflection relationship.

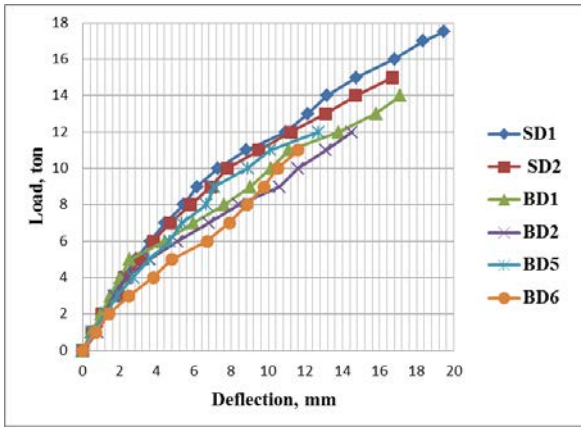

Fig. 1 Load-central deflection relationships

As shown in Fig. 1, all the slabs have a small value of deflection before appearing of the first crack, and these values increased with the increment of loading. However, the presence of bubbles in the specimens (BD1, BD2, BD5 and BD6) increases the deflection at the same stage of loading in comparison with reference solid slab specimens (SD1 and SD2). This is may be due to a reduction in the overall stiffness of BubbleDecks compared with the solid slabs.

During the test, the strain in flexural reinforcement and in concrete is measured with each loading step. Figure 2 shows the position of the strain gages in flexural reinforcement and in concrete.

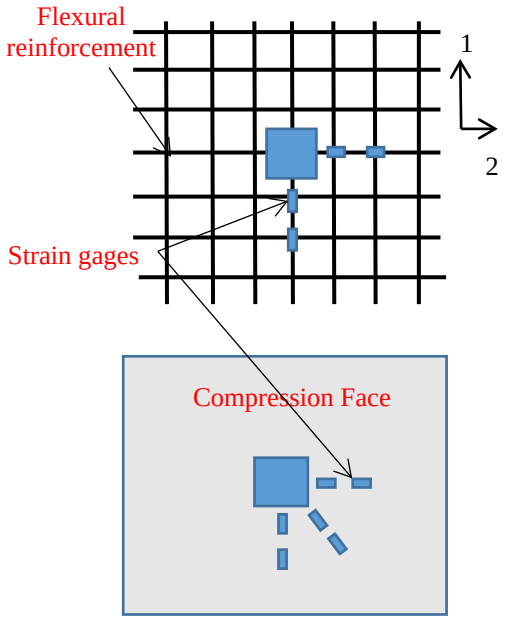

Fig. 2 Position of strain gages

The load-stain relationships are shown in Figs. 3 and 4 which represent the strain results of one direction only (direction 2) in order to show the effect of eccentric load on strain results. In each direction, there is two strain gages located at (d and 2d) from the face of the column.

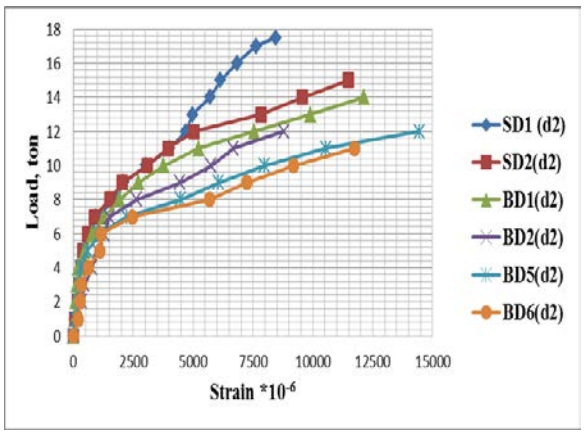

(a)

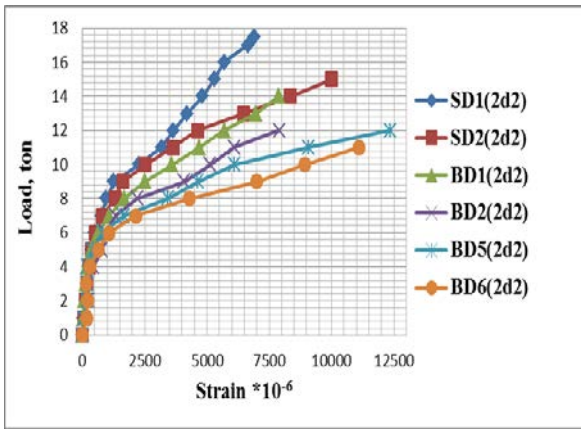

(b)

Fig. 3 Load-strain relationship for steel reinforcement (a) at d; (b) at 2d

As shown in Fig. 3, the magnitude of strain in steel reinforcement at (d and 2d) from the face of the column is influenced by the presence of the bubbles. Ultimate strain in flexural reinforcement at (d) from the face of the column in BD1 and BD5 is higher than that of SD1 by about (202 and 206%), respectively at the same loading stage. While this increment is about (63 and 220%), respectively at (2d) from the face of the column. This may be due to the reduction in stiffness in BubbleDecks. Besides the values of strain in SD2, BD2 and BD6 is higher than that of SD1, BD1 and BD5, this is due to the effect of eccentric load.

The same act of strain in flexural strength mentioned above is noticed in the strain of concrete as shown in Fig. 4.

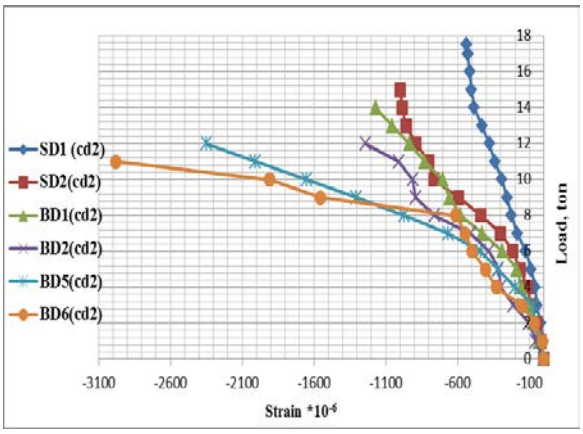

(a)

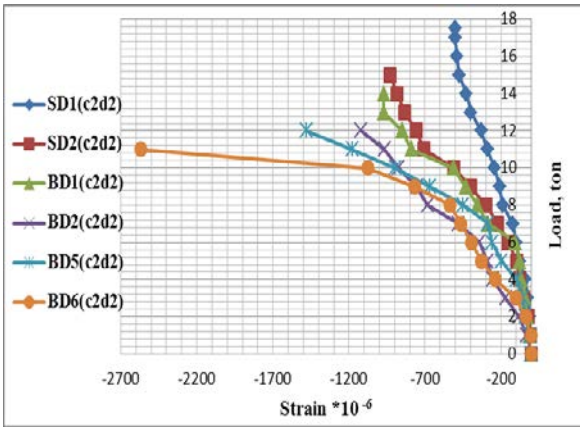

(b)

Fig. 4 Load-strain relationship for concrete (a) at d; (b) at 2d

CONCLUSIONS

The following conclusion can be drawn:

1. The first flexural crack load initiated at (27-36%) of the ultimate load.
2. The ultimate capacity of BubbleDecks is lower than that of solid decks by about (20-31%).
3. The eccentricity of the loading decreased the ultimate load and that caused by the increasing of unbalanced moment.
4. Punching crack tends to be at one side of slabs subjected to eccentric load due to presence of unbalanced bending moment, while the crack pattern in slabs subjected to concentric load seems to be as circle.
5. The eccentric loading increases the failure angle in the direction near the load and causes a collapse at one side only.
6. The perimeter and area of failure zone in slabs subjected to eccentric load is lower than that slabs subjected to concentric load.
7. The presence of bubbles in the specimens increases the deflection at the same stage of loading in comparison with reference solid slab specimens.
8. Ultimate strain in flexural reinforcement and in concrete at (d and 2d) from the face of the column in BubbleDecks is higher than that of Solid decks at the same loading stage.

REFERENCES

[1] Fariborz Moeinaddini, “Concentric Punching Shear Strength of Reinforced Concrete Flat Plates”, M.Sc. Thesis, Swinburne University of Technology, Melbourne, Australia, 2012.

[2] Corey, J., Midkiff, " Plastic Voided Slab Systems: Applications and Design", M.Sc. Thesis, Kansas State University, Manhattan, Kansas, 2013.

[3] Churakov A, "Biaxial Hollow Slab With Innovative Types of Voids", Строительство уникальных зданий и сооружений. ISSN 2304-6295. 6 (21). 2014, pp.70-88.

[4] Mihai Bindea, Raul Zagon, Zoltan Kiss, "Flat Slabs With Spherical Voids. Part II: Experimental Tests Concerning Shear Strength", Acta Technica Napocensis: Civil Engineering and Architecture, Vol. 56, No. 1, 2013.

[5] Lai T., "Structural Behavior of Bubbledeck Slabs And Their Application To Lightweight Bridge Decks”, Msc Thesis in Civil Engineering, Massachusetts Institute of Technology, 2009.

Second International Conference on Science, Engineering & Environment,
Osaka City, Japan, Nov.21-23, 2016, ISBN: 978-4-9905958-7-6 C3051

BEHAVIORAL ANALYSIS OF CONTINUOUS CONCRETE BEAMS REINFORCED BY PRESTRESSED CONCRETE PRISMS

Nazar K. Oukaili [1], Qusai Kh. Hameed [2]
[1] Professor, College of Engineering, University of Baghdad, Iraq; [2] Lecturer, College of Engineering – University of Al- Mustansiriyah, Iraq

ABSTRACT

The paper describes a numerical analysis, using ANSYS finite element program, of the structural behavior at serviceability and ultimate stages of two spans continuous concrete beams reinforced with prestressed concrete prisms (PCP). Six rectangular (310x200 mm) continuous concrete beams with, (4550 mm) length, were modeled. These beams are reinforced with mild steel bars and prestressed concrete prism, of (70x70mm) dimensions concentrically prestressed with (12.7mm) diameter seven wire steel strand, (composite concrete beams). The parametric studies of this work were the concrete compressive strength of prestressed concrete prisms (PCP), the effective prestressing force and the location of the prestressed concrete prisms. Nonlinear materials behavior of all types of reinforcement and concretes were simulated using appropriate constitutive models. Numerical load deflection response, strain in mild steel bars, prestressed strands and concrete, crack pattern and crack width at different loading stages and ultimate loading capacity were determined and compared with experimental results of the six tested continuous concrete beams. The comparison showed good agreement between experimental data and numerical analysis using finite element method and the numerical analysis can considered satisfactorily predict the structural behavior of such composite concrete beams.

Keywords: Finite Element, Prestressed Concrete Prism, Continuous Beam, Deflection, Composite

INTRODUCTION

The main approaches to understand concrete member behavior under loading to assists its application efficiency are, experimental, numerical and theoretical. The main numerical method to accurately simulate the behavior of concrete member is Finite Element Analysis (FEA) by dividing the member to many simple elements in which it's mechanical and physical properties have to be defined accurately [1, 2]. This paper presents an analytical investigation of the nonlinear behavior of reinforced, partially prestressed and composite continuous concrete beams under various loading stages using finite element software package ANSYS 16.1 and comparing the results with the behavior of experimentally tested concrete beams.

EXPERIMANTAL TEST PROGRAM

Prestressed Concrete Prisms (PCP) and Continuous Concrete Beams

Ten prestressed concrete prisms, with 70x70 mm cross sectional dimensions, were casted using two different concrete types. High strength concrete (HSC) with compressive strength of 60 MPa was used in beams B4 & B5. Ultra-high strength concrete (UHSC), which prepared using reactive powder concrete (RPC) with 13 mm length steel fibers of 1.5% of the mix volume, with compressive strength of 90 MPa was used in beams B6, B7, B8 & B9. Prisms were subjected concentrically to two prestressing levels 55% or 70% of the steel yield strength, respectively, using single 12.7 mm seven - wire strand of 1860 MPa ultimate tensile strength.

Six continuous concrete beams, of 4550 mm length and 200x310 mm cross sectional dimensions, tested under two point loads. Four beams reinforced with mild steel and one PCP only. Two beams reinforced with mild steel and three PCP's, at tension zones of middle supports and mid-spans, (see Fig. 1 and Fig. 2). For shear, all beams reinforced with 10 mm diameter stirrups at 100 mm c/c for the entire beam length. Table 1 shows the reinforcement details of these beams. The concrete design compressive strength of the beams was 35 MPa at 28 days age.

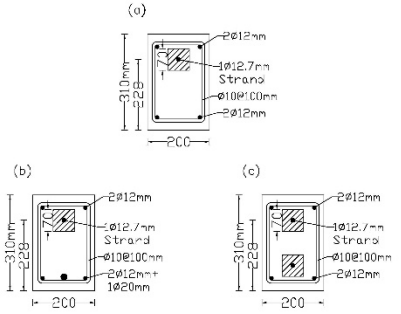

Fig. 1 Cross section of beams: (a) at middle support of beams B4 to B9, (b) at load point of beams B4 to B7; (c) at load point of

beams B8 and B9

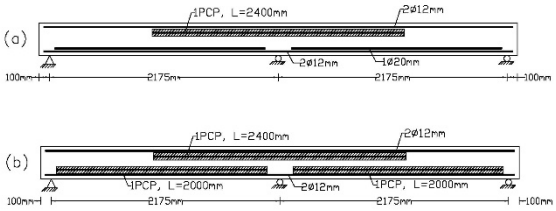

Fig. 2 Beams reinforcement details: (a) B4, B5, B6 & B7; (b) B8 & B9

Table 1 Reinforcement details of tested beams

Beams	Steel at mid support			Steel at midspan		
	A_s, mm²	No of PCP	A_s', mm²	A_s, mm²	No. of PCP	A_s', mm²
B4	228	1	228	542	0	228
B5						
B6						
B7						
B8				228	1	228
B9						

FINITE ELEMENT MODEL

Modeling of Concrete

The three dimensional 8- node brick element (solid65 reinforced concrete solids) is used as a model of concrete of the main continuous beams and PCP. The element has eight corner nodes; each node has three degrees of freedom, translation in the x, y, and z directions. This element is capable of plastic deformation, cracking in three orthogonal directions and crushing (see Fig. 3).

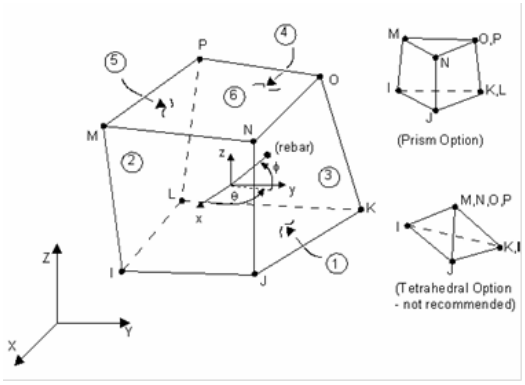

Fig. 3 Brick element with 8 nodes (SOLID65)

Modeling of Steel Reinforcement

To model steel reinforcement such as stirrups, main longitudinal reinforcement and PCP strand in finite element, the discrete model LINK 180 was used in this study (see Fig. 4). LINK 180 is a spar (or truss) element which can be used to model trusses, sagging cables, links, springs, etc. The 3-D spar element is a uniaxial tension-compression element with three degrees of freedom at each node: translations of the nodes in x, y, and z-directions. No bending of the element was considered.

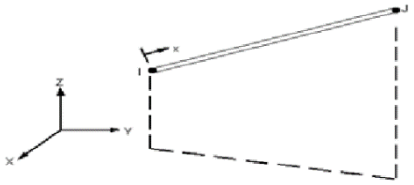

Fig. 4 3D spar element with 2 nodes (LINK180)

Modeling of Steel Plates and Supports

Loading and supports steel plates were modeled using SOLID186 which is a higher order 3-D 20-node solid element that exhibits quadratic displacement behavior. The element is defined by 20 nodes having three degrees of freedom per node; translations in the nodal x, y, and z directions. The element supports plasticity, hyper elasticity, creep, stress stiffening, large deflection, and large strain capabilities (see Fig. 5).

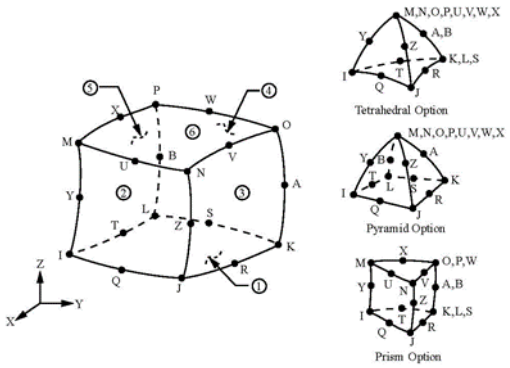

Fig. 5 Brick element with 20 nodes (SOLID186)

Material Properties

Concrete material properties

The concrete is assumed to be homogeneous and initially isotropic. The compressive uniaxial stress strain relationship for the concrete model is obtained by using the following equations to compute the multi-linear isotropic concrete stress-strain curve, [3].

$$f_c = \varepsilon . E_c \qquad \text{for } 0 \le \varepsilon \le \varepsilon_1 \qquad (1)$$

$$f_c = \frac{\varepsilon.E_c}{1+\left(\frac{\varepsilon}{\varepsilon_o}\right)^2} \quad \text{for } \varepsilon_1 \le \varepsilon \le \varepsilon_o \qquad (2)$$

$$f_c = f_c' \quad \text{for } \varepsilon_o \le \varepsilon \le \varepsilon_{cu} \qquad (3)$$

$$\varepsilon_o = \frac{2.f_c'}{E_C} \qquad (4)$$

where:
f_c = stress at any strain ε, MPa,
ε_o = strain at the ultimate compressive strength f_c',
ε_{cu} = ultimate compressive strain,
ε_1 = strain corresponding to (0.3 f_c').

Concrete compressive and tensile strength used for all types of concrete elements were obtained from experimental test results. In PCP reinforced beams, the analysis required that the main continuous beams will be not intuit the initial strain subjected by steel strand on the PCP before applying of external load, this will be required include contact elements to solve this issue. In order to simplify finite element analysis, initial compressive stress on each PCP converted to additional tensile strength to the PCP itself and assuming full bonding between the PCP and the surrounding concrete, where the cracking capacity of each PCP is the summation of PCP tensile strength and the decompressive stress came from initial strain which convert to PCP tensile strength. Table 2 shows material properties of all types of concrete used in this study, stress-strain relationship tabulated for only beam B6 and its PCP.

Steel material properties

Moduli of elasticity for all types of mild steel were 200000 MPa and for prestressing strands were 197500 MPa, poisons ratio were 0.3. In steel strand, no initial strains were input for all PCP reinforced beams, where strand effective prestressed were convert to PCP tensile strength, yielding strength of steel strand for each PCP were measured by multiplying the ultimate tensile strength by 0.9 then subtract the effective prestress, steel strand were modeled as bilinear isotropic with tangent modulus of 3% of initial modulus of elasticity [4]. Table 3 shows the properties of all types of steel reinforcement.

Table 2 Concrete material properties

Beam No.		Linear isotropic		Concrete			
		EX, MPa	PRXY	ShrCf-Op	ShrCf-Cl	UnTensSt, MPa	UnCompSt, MPa
B4	Beam	28213	0.2	0	0.8	3.86	37.5
	PCP	34146		0	0.8	26.5	63.2
B5	Beam	26355		0	0.8	3.82	383
	PCP	33008		0	0.8	21.9	63.2
B6	Beam	29423		0	0.8	4.41	39.4
	PCP	39324		0	0.9	33.6	95.3
B7	Beam	27176		0	0.8	3.95	38.2
	PCP	38753		0	0.9	28.9	93.7
B8	Beam	29423		0	0.8	4.41	39.4
	PCP	39324		0	0.9	34.4	95.3
B9	Beam	27176		0	0.8	3.95	38.2
	PCP	38753		0	0.9	29.1	93.7
Multi-linear isotropic							
B6	f_c	11.82	25.82	33.59	37.78	39.4	
	ε	0.000402	0.001	0.0015	0.002	0.003	
B6 PCP	f_c	28.59	38.28	55.58	70.92	94.30	
	ε	0.000732	0.001	0.0015	0.002	0.003	

Table 3 Steel material properties

Mild steel properties			
Bar diameter, mm	Area, mm^2	Yield strength, MPa	Tangent modulus, MPa
10	78	392	0
12	113	661	
16	201	641	
20	314	551	

Prestressing strand properties				
Strand diameter, mm	Strand existence	Area, mm^2	Yield strength, MPa	Tangent modulus, MPa
12.7	$B4_{PCP}$	99.6	754	5925
	$B5_{PCP}$		982	
	$B6_{PCP}$		784	
	$B7_{PCP}$		968	
	$B8_{PCP}$		744	
	$B9_{PCP}$		959	

Meshing Modeling

Meshing was conducted for lines and volumes after dividing overall volume at the location of steel stirrups and the PCP (Fig. 6). Fig. 7 and Fig. 8 show the wireframe view for continuous concrete beams.

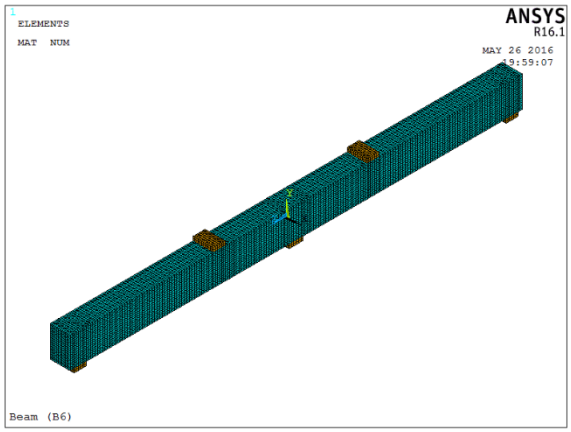

Fig. 6 Continuous concrete beam meshing.

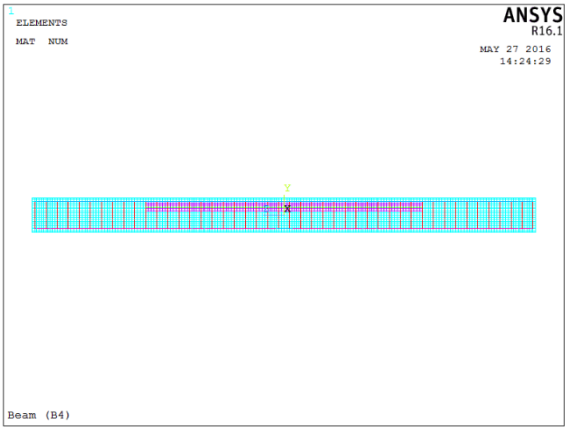

Fig. 7 Continuous concrete beam with one PCP.

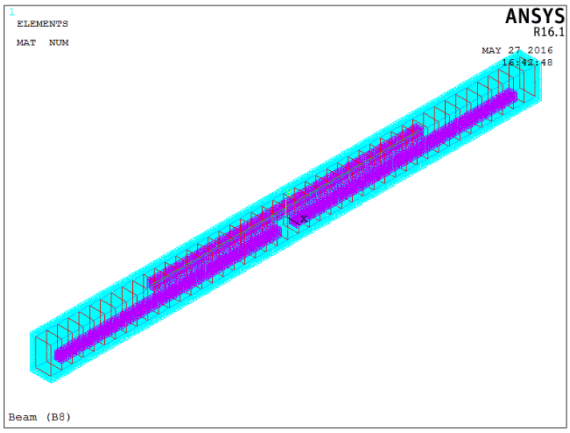

Fig. 8 Continuous beam with three PCP's.

RESULTS AND DISSCUSSIONS

Load Deflection Response

Deflections were experimentally and analytically measured at mid-spans and under load points (see Fig. 9 and Fig. 10). Both figures show the effect of increasing of PCP tensile strength, resulted from different prestressing levels and different concrete compressive strength, on PCP cracking load and increasing beams flexural stiffness at serviceability stage. These figures show approximately linear relationship and good agreement between experimentally and analytically measured deflection at service load until the cracking of prestressed concrete prisms, after cracking of PCP's, the beam stiffness was reduced and the linear load –deflection behavior ended when the tension steel reinforcement starts to yield, the difference becomes slightly larger at ultimate failure of continuous concrete beams.

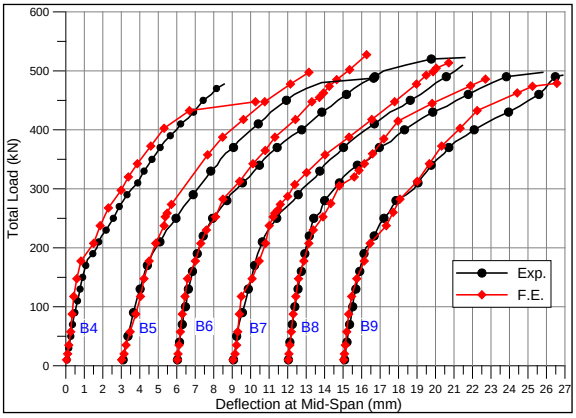

Fig. 9 Deflection at mid-span of continuous beams.

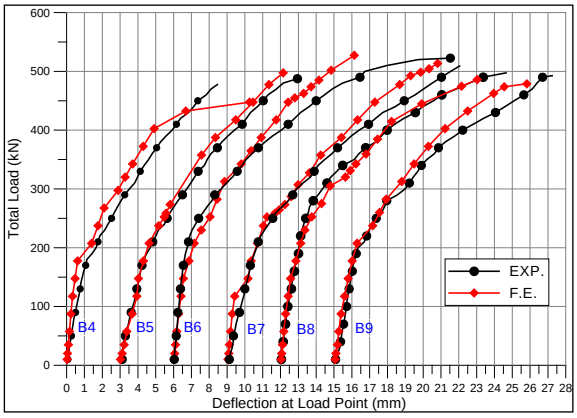

Fig. 10 Deflection at load point of continuous beams.

Deflected shape in Y-direction at ultimate load obtained from finite element analysis of beams (B6) and (B8) are shown in Fig. 11 and Fig. 12, respectively. It has to be mentioned that the maximum deflection were occurred at location rather than mid-span or at load point.

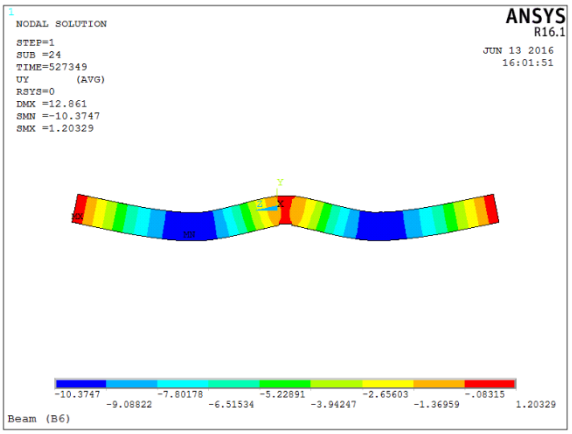

Fig. 11 Deflected shape of beam (B6).

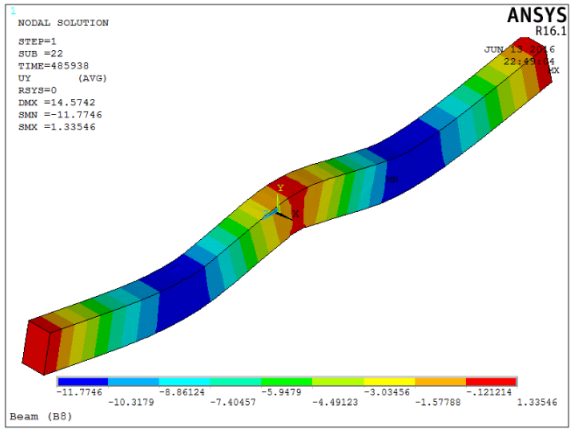

Fig. 12 Deflected shape of beam (B8).

Load Strain Response

Steel reinforcement strain

Load strain relations in mild steel at load point and strain increment relations in prestressing strand at middle support are shown in Fig. 13 and Fig. 14, respectively. Both figures show good agreement between experimental and analytical strain until cracking of PCP. Difference between both strains is more obvious due its sensitivity to PCP cracking.

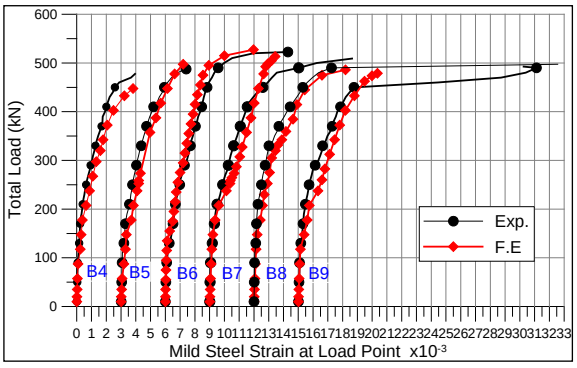

Fig. 13 Load-strain relations in mild steel.

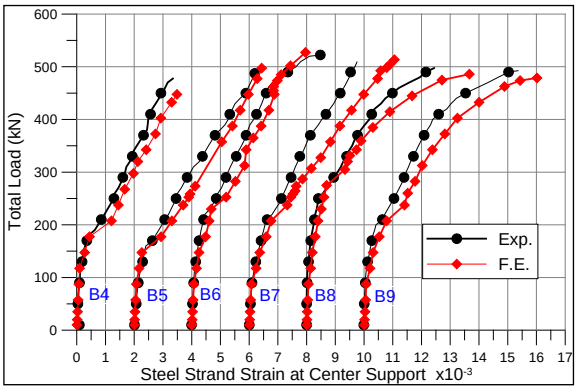

Fig. 14 Load-strain relations in prestressing strand.

Surface concrete strain

Load strain relations in concrete surface at compression zone under load point of beams (B6) to (B9) are shown in Fig. 15. It shows also good correlation between experimentally measured and finite element analysis results at the entire loading stages. Fig. 15 shows also less effect of PCP cracking on concrete strain under load point. In both measurements, concrete strain didn't reach ultimate concrete strain tabulated in different cods, where the location of strain gauges far away by (41mm) from the extreme compression fiber.

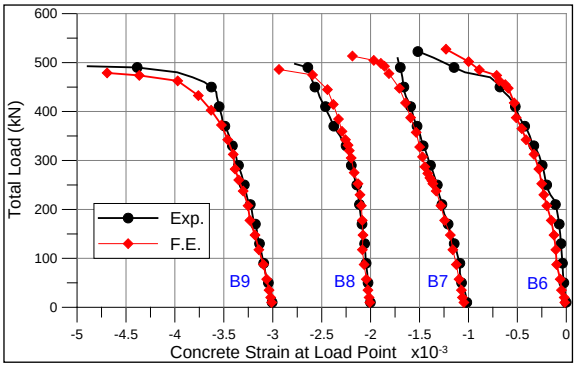

Fig. 15 Concrete load-strain relations.

Crack patterns and ultimate load carrying capacities

Crack patterns in experimentally tested beams are shown in Fig. 16, while crack patterns obtained from finite element analysis using crack/crashing plot option in ANSYS program are shown in Fig. 17 for beams (B7) and (B9). Crack initiated at the middle support section due to the high elastic bending moment then followed by cracks at mid-span and load point sections. It can be observed that,

all beams having approximately similar crack patterns at mid-span and load point and were mostly flexural, flexure-shear cracks were appeared at higher loading stages. Crack pattern and failure mode of FE models show good agreement with experimentally tested beams.

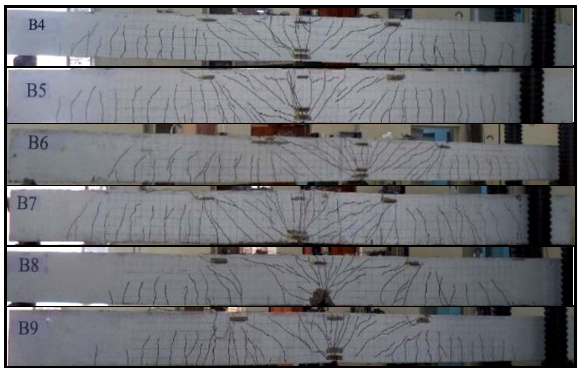

Fig. 16 Crack pattern of tested beams.

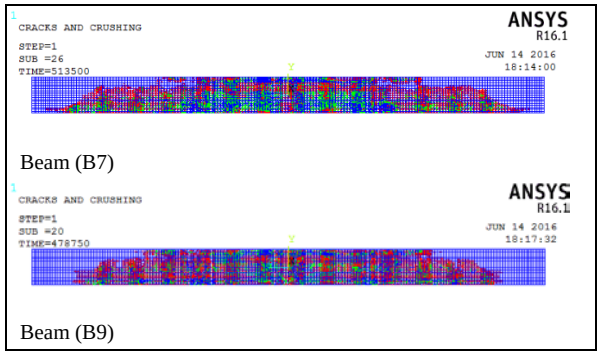

Fig. 17 FE crack pattern of beams (B7) and (B9).

Table (4) shows beam cracking load, PCP cracking load and ultimate failure load for both experimentally tested beams and FE models. Beam cracking load and PCP cracking load in FE models were measured at loading steps once cracking initiated on concrete beams or cracking passing the PCP level, respectively. Table (4) shows good agreement between experimentally and FE cracking loads, while it show excellent agreement between experimentally failure and FE load for all beams, this lead to a conclusion that strain compatibility method is valid and conservative in analysis of PCP reinforced beams. Obviously, that increasing PCP tensile strength didn't affected neither beam cover cracking load nor beams ultimate failure loads.

Table 4 Beams cracking and ultimate loads

Beams	Beam cracking load, (kN)			PCP cracking load, (kN)			Ultimate Load, (kN)		
	Exp.	F.E	Exp. /F.E	Exp.	F.E	Exp. /F.E	Exp.	F.E	Exp. /F.E
B4	62	57	1.08	185	207	0.89	477	477	1.0
B5	71	87	0.81	165	177	0.93	487	497	0.98
B6	83	87	0.95	225	252	0.89	522	527	0.99
B7	71	87	0.82	215	237	0.91	509	513	0.99
B8	82	87	0.94	255	305	0.84	497	486	1.02
B9	77	87	0.88	205	237	0.86	492	479	1.03

CONCLUSIONS

The following conclusions can be drawn:

1. The general behavior of experimentally tested beams and FE models shows good agreements in deflection, steel and concrete strain curves at entire loading stages, however, FE deflection curves show more stiffness after cracking of PCP while steel strand curves show more strain in FE models.
2. Crack patterns at ultimate load in FE models are well agreed with experimentally tested beams.
3. Ultimate failure load for both FE models and experimentally tested beams show that the strain compatibility method is valid and conservative in analysis of PCP reinforced beams.

REFERANCES

[1] Al-Hadithy, L., and Abdal-Kareem, H., "Behavior of Reinforced Concrete Composite Beams with Embedded Prestressed Concrete Prisms Using Nonlinear Finite Element Analysis", The 1st Regional Conference of Eng. Sci. NUCEJ Spatial ISSUE vol.11, No.1, 2008 pp202-215.

[2] Kote P. B., et al, "Finite element Analysis of Prestressed Beams", International Journal of Advance Foundation and Research in Science & Engineering (IJAFRSE), Vol.1, Issue 3, August 2014.

[3] Wolanski A. J., "Flexural Behavior of Reinforced and Prestressed Concrete Beams using Finite Element Analysis", M.Sc. Thesis, University of Marquette, May 2004.work but accepted", accepted, Year.

[4] Desayi P., and Krishnan, S., "Equation for the Stress-Strain Curve of Concrete", Journal of the American Concrete Institute, Vol. 61, March 1964, pp. 345- 350.

Second International Conference on Science, Engineering & Environment,
Osaka City, Japan, Nov.21-23, 2016, ISBN: 978-4-9905958-7-6 C3051

IMPACT RESPONSE OF REINFORCED CONCRETE T-BEAMS WITH MUILTIPLE WEB OPENINGS AND ITS THEORETICAL SIMULATION

Nazar K. Oukaili[1] and Abeer H. Al-Shammari[2]
[1]College of Engineering, University of Baghdad, Iraq.[2]College of Engineering, University of Mustansiriya, Iraq.

ABSTRACT

The purpose of this study is to experimentally examine the response of reinforced concrete (RC) T-beams with multiple web circular openings to repeated impact loading and to make a theoretical simulation to represent their impact response. Seven simply supported RC T-beams were tested first under repeated impact loading at mid-span by a dropping mass of 24.5 kg from pre-determined height until the width of shear crack reached the limiting of the ACI318M-14 [1] (0.3 mm for exterior exposure). Subsequently, a static test was conducted under one point load to find out the residual load carrying capacity of the RC beams after impact loading. Three design parameters were considered including number of web openings (four or six), the method which was used to strengthen the member at openings (either using internal deformed steel bars or using carbon fiber reinforced polymer (CFRP) fabric) and the height of drop (100, 250, 400, 750, 1000, 1500 and 2000) mm. The experimental results indicated that the beam with four openings does not show remarkable increase in the maximum mid-span deflection as compared with the solid one while that with six openings shows increase in the maximum mid-span deflections clearly by about 75% greater than the maximum mid-span deflection of the solid one, strengthening of specimens can overcome the increase in deflections. It is also found that the number of drops required to cause shear crack of 0.3 mm width decreases where four and six openings were created while the number of drops increases for strengthen specimens. ANSYS 12.1 3-D transient finite element analysis program was used for this study, comparisons between finite element predictions and experimental results in terms of mid span deflection-time histories were presented and showed good agreements.

Keywords: Concrete Beams, Web Openings, Impact.

INTRODUCTION

In some cases, it is necessary to create multiple openings in the web of the beam to permit a systematic layout of utility duct and pipes which resulted in a significant reduction in the story height and major saving in material and construction cost especially in multistory buildings. Creating openings in the web of the beam reduces the cross sectional area and therefore decreases the shear capacity and deformation ability. If the openings are planned before casting the beam, internal deformed steel bars can be fabricated around the openings while if the openings will be created in the existing beam, strengthening by external steel plates or fiber reinforced polymer (FRP) materials can be used to restore the original capacity. The combination of low weight and high strength to weight ratio of fiber reinforced polymer (FRP) material are advantageous for this type of material. Moreover, FRP materials having high resistance to corrosion, hence they are satisfactory in terms of durability requirement.

According to [2], a circular opening may be considered as large when its diameter exceeds 0.25 times the depth of the web because introduction of such openings reduces the strength of the beam. As in [3], Mansur *et al.* carried out an experimental investigation on eight reinforced concrete continuous beams, each containing a large transverse opening. This study showed that an increase in the depth of opening from 140 mm to 220 mm led to a reduction in collapse load from 240 KN to 180 KN.

Impact loading is an extremely severe loading condition characterized by its application of a force of great intensity within a short duration. Impact loads may result from the crushing of comparatively rigid heavy objects such as falling rocks in mountain areas and falling heavy loads dealt with in factories and warehouses due to accidents. To the researcher's knowledge, there are no researcher studies the behavior of RC beams with multiple web openings under impact loading.

In this paper, the experimental program addresses the behavior of reinforced concrete T-beams under impact load when four or six circular openings in shear region are created, the efficiency of using internal deformed steel bars or external CFRP fabric around the openings to restore the original characteristics of the RC beams due to creating web openings. The results in terms of

impact force-time history, mid span deflection-time history, number of drops required to cause shear cracks of width 0.3 mm and the residual strength of the impact tested beams are presented. For validation, a three dimensional finite element program, ANSYS 12.1 Release, was used to simulate the tested beams.

EXPERIMENTAL PROGRAM

In the experimental program, a total of seven reinforced concrete T-beams were fabricated and tested as simply supported beams under repeated impact load at mid span. The design parameters are the number of web openings (four or six), the method used to strengthen beams at openings (using internal deformed steel bars or CFRP fabric) to re-gain the loss in the original characteristics due to creating web openings.

TEST SPECIMENS

Designation of test specimens and their details are listed in Table 1. One of these beams was the solid control beam without openings, two of them were with unstrengthened openings and the remaining four beams were with strengthened openings.

Table 1 Details of specimens

Beam symbol	Number of openings	Type of strengthening at opening regions
BIW	Without openings	---
BIO4	4	No strengthening
BIO6	6	No strengthening
BIO4S	4	Internal steel bars
BIO6S	6	Internal steel bars
BIO4F	4	CFRP fabric
BIO6F	6	CFRP fabric

All openings were of circular shape with diameter equal to 110mm. The ratio of the opening diameter to the web depth was 0.48 which was enough to cause a sizeable reduction in shear capacity (web containing a circular opening of three-eighths the web depth dose not reduce the strength of the specimen [4]). This made it possible to evaluate the efficiency of different strengthening techniques. The distance between the support and the beginning of the first opening was 130 mm which equals about half the effective depth. Specimens with multiple web openings fail in the post (element between two openings when these openings are placed closed to each other) when the width of the post is smaller than 3/8 the web depth [4]. In this research, the width of the post was about 5/8 the web depth.

In order to investigate the shear behavior of the test specimens, the solid control beams were designed to fail in shear (the flexural capacity was designed to exceed the shear capacity of the control beams) according to [1]. A schematic diagram of the test specimens showing the dimensions and reinforcement details is depicted in Fig. 1a. The length of the test specimen was 2000 mm with an effective span of 1800 mm, the effective depth (d) was 256 mm. identical T-shape cross-section was used for all specimens. The tension steel reinforcement consists of two ϕ 20 mm, the compression reinforcement consists of four ϕ 6 mm. Stirrups consist of ϕ 4 mm at 130 mm center to center. This reinforcement was used for control beams, beams with unstrengthened openings and beams with CFRP fabric strengthened openings as shown in Figs. 1b-1d. The rest beams were strengthened with pre-fabricated internal steel bars consisting of three ϕ 8 mm as diagonal bars around the openings, two ϕ 8 mm horizontal bars below and above the openings and concentrated stirrups ϕ 4 mm above, below and beside the openings, see Fig. 1e.

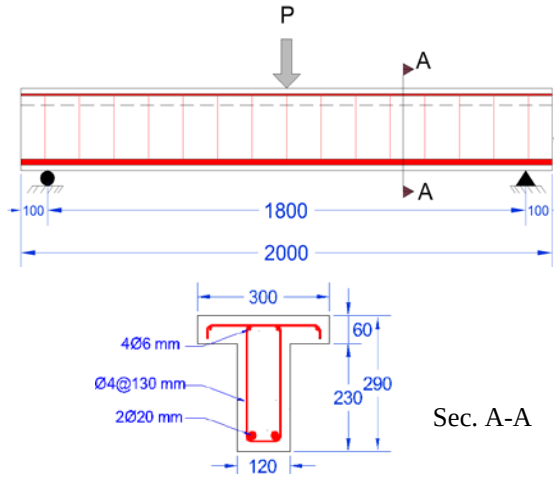

(a) Dimension of beams and reinforcement details.

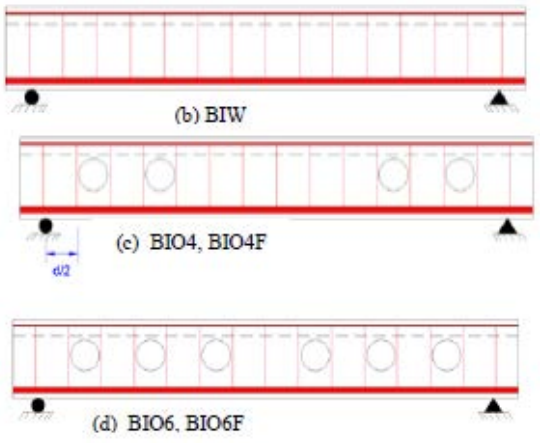

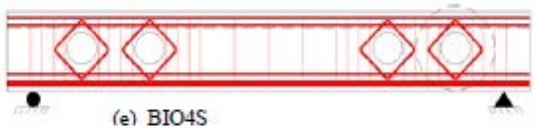

Fig. 1 Details of beam specimens (unit: mm).

CFRP STRENGTHENING LAYING

Beams BIO4F and BIO6F were strengthened with CFRP fabric having uni-directional fibers (SikaWrap-230C type) which cut into segments and placed around the openings in two layers, the first layer was of horizontal and vertical segments of CFRP fabric placed around openings while the second layer was of diagonal segments of CFRP fabric placed beside openings with an angle of inclination of 45°, see Fig. 2.

Fig. 2 Alignment of CFRP fabric.

In general, the concrete surface beneath the CFRP fabric was roughed and then cleaned prior to the adhesive application using epoxy resin (Sikadur-330 type) with average thickness of 1 mm.

MATERIAL PROPERTIES

Properties of concrete, steel reinforcement and fiber reinforced polymer used in this study are given in Table 2.

Table 2 Material properties

Material	Diameter, mm Thickness, mm	Yield strength, MPa	Compressive strength, MPa	Tensile strength, MPa	Modulus of elasticity, GPa
Concrete	---		27	3.2	23
Steel	20	600	---	747	200
	6	420	---	570	
	4	400	---	553	
	8	450	---	602	
CFRP fabric	0.131	---	---	4300	238
Epoxy resin	---	---	---	30 @ 7 days	4.5 @ 7 days

IMPACT LOADING TEST

A drop mass impact loading frame was used for impact loading tests as shown in Fig. 3. Each beam subjected to a drop mass of 24.5 kg which was dropped freely onto the top surface of the RC beam at mid-span from seven different heights: 100, 250, 400, 750, 1000, 1500 and 2000 mm then the impact load was repeated from height of drop of 1000 mm until the width of shear crack reached the serviceability limit state (0.3 mm in width for exterior exposure [1]). The drop mass system consists of three parts: the steel cylindrical shaft, the dynamic load cell (MLC213 model) and the impactor of stainless steel with curved tip. The RC beam was supported over a span of 1800 mm with specially design devices allowing it to freely rotate while preventing it from moving out of displacement.

The contact force developed between the mass and the RC beam was measured using the dynamic load cell, which was rigidly connected to the drop mass system between the steel shaft and the impactor. The mid-span deflection response of the RC beam was measured using the LVDT (linear variable differential transformer). Strains at different locations were measured using electrical strain gages. Signals from load cell, strain gages and LVDT were amplified and then recorded using storage type oscilloscopes having band width of 100 MHz.

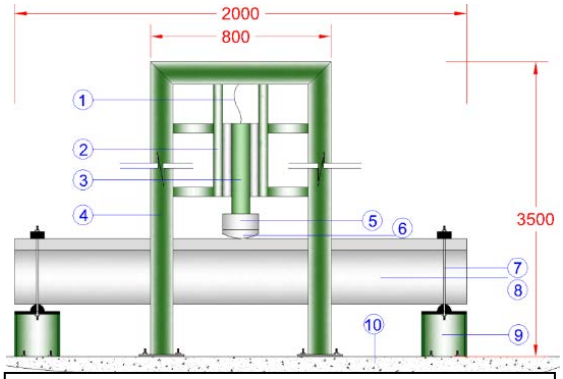

1. Rope. 2. Guide frame. 3. Falling mass.4. Main frame. 5. Load cell. 6. Impactor. 7. Mechanism. 8. Concrete beam. 9. Support. 10.

Fig. 3 Schematic diagram of the impact test setup (units: mm).

RESIDUAL LOAD CARRYING CAPACITY TEST

The residual load carrying capacity of the RC beam after impact loading was examined using static loading tests, in these tests each RC beam was simply supported over a span of 1800 mm and concentratedly loaded at mid-span until failure, the

ultimate loads were recorded and compared with the ultimate loads of the pure static RC beams which were tested by the authors [5].

EXPARIMENTAL RESULTS

Cracking, Failure Mode and Number of Drops

The first visible crack was a vertical crack which appeared under the point of impact loading on the flange of all beams then a flexural crack started from the soffit of the beam and propagated upward. Shear cracks then appeared after successive drops of height 1000 mm, these cracks started near mid height of the beam and propagated diagonally with an angle of inclination of about 40˚- 60˚. All beams showed this behavior except two beams: BIO6 which did not show web flexural crack and BIO6F which did not show web crack since CFRP covered almost whole web surface area.

For all beams, the impact test was stopped when the width of shear crack reached 0.3 mm. a crack detection microscope was used for this purpose. Number of drops required to reach the serviceability limit state were recorded and presented in Fig. 4. As compared with the solid beam (BIW), it is concluded that the number of drops required to form shear cracks of width 0.3 mm decreased when four and six openings were created, specimens BIO4 and BIO6, by about 30% and 86%, respectively. Also, when opening regions were strengthened with additional reinforcement, specimens BIO4S and BIO6S, the number of drops required to form shear cracks of width 0.3 mm increased by about 33% and 97%, respectively. And, when opening regions were strengthened with CFRP fabric, specimens BIO4F and BIO6F, the number of drops required to form shear cracks of width 0.3 mm increased significantly by about 85% and 125%, respectively.

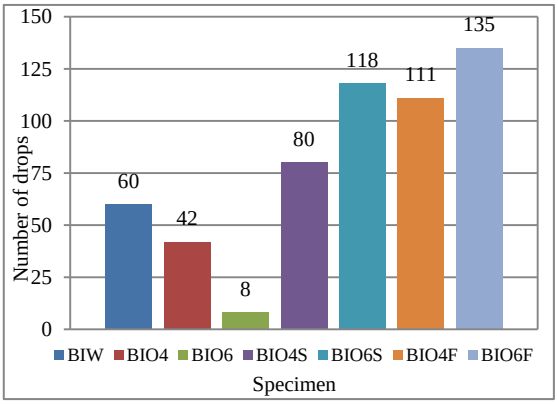

Fig. 4 Number of blows required to reach the serviceability limit state for tested beams.

IMPACT RESPONSE

Impact load-time histories were recorded for each beam for heights of drop of (100, 250 and 400) mm and the deflection-time histories were recorded for each beam for the seven heights of drop. Accordingly, typical impact force response for BIW specimen is presented in Fig. 5. From the impact load-time history, it can be noticed that the measured impact loads are characterized by two parts: the first part is the impact force directly induced by dropping mass, this part represents the incidental wave with comparatively high amplitude, and the second part is the inertia force produced by the vibration of the beam, this part with comparatively low amplitude as presented in many previous researches [6].

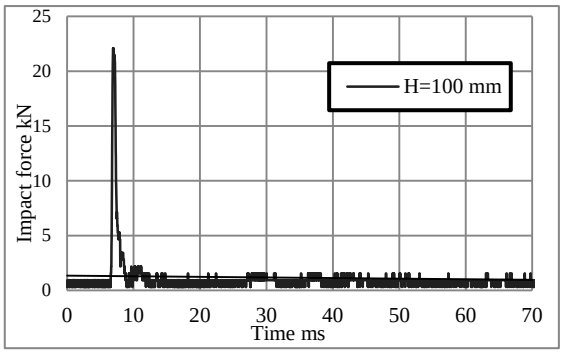

Fig. 5 Impact force response for BIW specimen, drop height = 100 mm.

Figure 6 shows comparisons of the maximum impact force for specimens BIW, BIO4 and BIO6, the maximum impact force values of specimen BIW are slightly larger than those of specimens BIO4 and BIO6. This indicates that the impact and inertia forces depend on the structural stiffness; the higher the stiffness, the larger the impact and inertia forces.

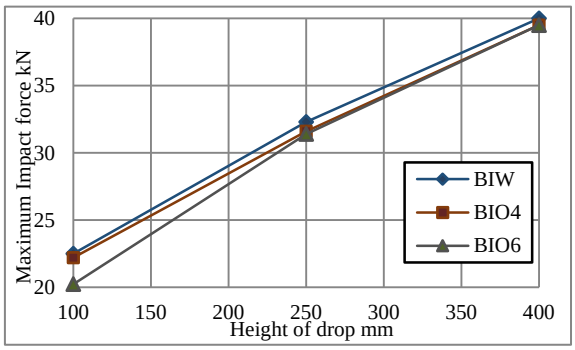

Fig. 6 Comparisons of the maximum impact force of specimens for different heights of drop.

Figures 7 and 8 show comparisons of the maximum transient mid span deflections for the seven impact tested beams. From these figures it is concluded that the maximum mid span deflections increase as the height of drop is increased (the increase is almost linearly for the first three heights of drop). From these figures it is also noticed that the beam with four openings does not show obvious increase in the maximum mid span deflections while the beam with six openings shows increase in the maximum mid span deflections clearly by about 75% greater than those of the solid beam, strengthening of specimens around openings either by additional reinforcement or by CFRP fabric can overcome this increase in the deflections, also the strengthening improves the deflection behavior of specimen with four openings.

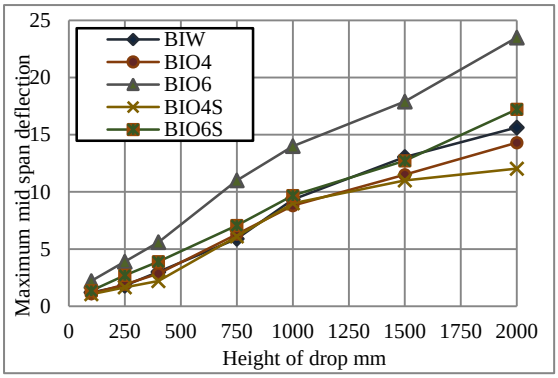

Fig.7 Comparisons of the maximum mid span deflections of specimens for different heights of drop.

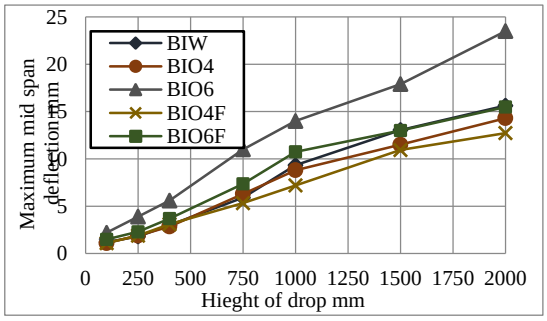

Fig.8 Comparisons of the maximum mid span deflections of specimens for different heights of drop.

RESIDUAL STATIC STRENGTH OF IMPACTED BEAMS

The residual static strengths for impacted beams were obtained through static tests and compared with strengths of pure static tested beams, test results in Table 3 show that the percentage of the residual static strength decreases with the increase in the number of drops which the beam subjected to. Also it can be noticed that the maximum difference between the percentages of the residual static strength of impacted beams does not exceed 15%, this may belong to the failure limit that considered for all beams to end the repeated impact load (when width of shear crack reaches 0.3 mm).

Table 3 Residual static strengths of impacted beams

Impacted beam symbols	Strengths of Pure static tested beams. kN	No. of drops on exerted impact tested beams	Static strengths of impacted beams, kN	Residual static strengths, %
BIW	160	60	125	78
BIO4	112	42	92.5	82.5
BIO6	95	8	81.5	85.5
BIO4S	142.5	80	108.5	76
BIO6S	137.5	118	102	74
BIO4F	147.5	111	110.5	75
BIO6F	182.5	135	130	71

FINITE ELEMENT MODELING AND ANALYSES

A simulation is done by using ANSYS finite element software for the investigated experimental study. The FEM and experimental results are compared and the level of consistency between them is investigated.

Transient dynamic analysis (sometimes called time-history analysis) is a technique in used to determine the dynamic response of a structure under the action of any general time-dependent loads. This type of analysis can be used to determine the time-varying displacements, strains, stresses, and forces. Three methods are available in ANSYS program to do a transient dynamic analysis: full, mode superposition, and reduced. ANSYS analysis was done using the reduced method; this method condenses the problem size by using master degrees of freedom and reduced matrices. After the displacements at the master DOF have been calculated, ANSYS expands the solution to the original full DOF set.

Beams were modeled with the solid65 element (has eight nodes and three degrees of freedom at each node) which was used to represent concrete, the link8 element (three dimensional spar element and it has two nodes with three degrees of freedom at each node) which was used to represent steel reinforcement, and the solid185 layered structural element (has eight nodes and three degrees of freedom at each node) which was used to represent CFRP fabric. Perfect bond was assumed between different materials and the self-weight of the beams

was considered. Beams were modeled as volumes. Taking advantages of the symmetry, only quarter of the beam was modeled. Rollers were used to show the symmetry condition at internal faces whereas the nodes at the support were restrained against vertical displacement. Multiple load steps are usually required to specify the load history in a transient analysis. The first load step is used to establish initial conditions, and second and subsequent load steps are used for the transient loading. Figure 9 shows FE mesh, load step and boundary conditions.

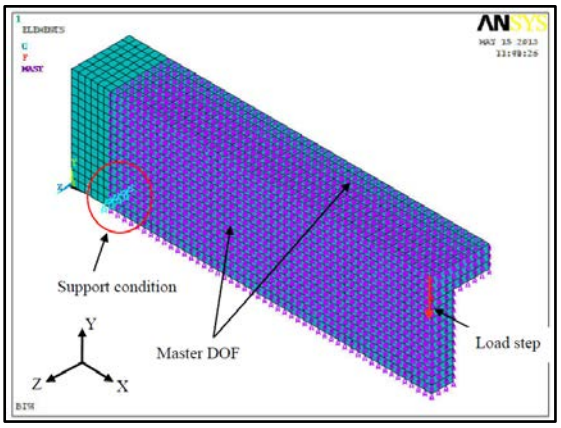

Fig. 9 FE mesh, load step and boundary conditions.

FINITE ELEMENT ANALYSIS RESULTS

Transient analyses were made for height of drop of 250 mm for each impact tested beam. Finite element result in terms of mid span deflection-time histories for specimen BIW is shown in Fig. 10. In general, the agreement is good and the plots have similar trends.

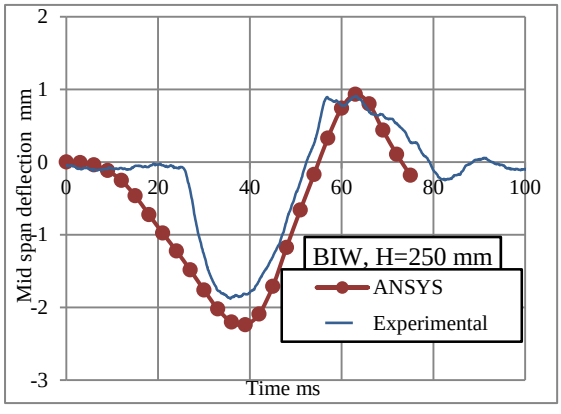

Fig. 10 Comparison of predicted results to test results for mid span deflection-time history.

CONCLUSIONS

1. The number of drops required to form shear cracks of width 0.3 mm (the serviceability limit state) decreased when four and six openings were created by about 30% and 86% respectively as compared with the solid reference one. This number of drops increases when opening region was strengthened either by additional reinforcement or by CFRP fabric.
2. The maximum impact force values of the solid beam are slightly larger than those of beams with four and six openings. This indicates that the impact and inertia forces depend on the structural stiffness; the higher the stiffness, the larger the impact and inertia forces.
3. The impact force and mid span deflections of the reinforced concrete beams increase proportionally with increases in drop height.
4. The beam with four openings does not show obvious increase in the maximum mid span deflections while the beam with six openings shows increase in the maximum mid span deflections clearly by about 75% greater than those of the solid beam, strengthening of specimens around openings either by additional reinforcement or by CFRP fabric can overcome this increase in the deflections, also the strengthening improves the deflection behavior of specimen with four openings.
5. Numerical models using finite element analysis ANSYS program were developed to determine the maximum mid span deflection which is an important index for evaluating damage levels of the reinforced concrete beams subjected to impact loading. The numerical models were shown to be in good agreement and the plots have similar trends to the experimental results. However, the predicted peak deflections were overestimated.

REFERENCES

[1] ACI 318M-14 Building code requirements for structural concrete and commentary. (2014). Farmington Hills, Michigan, American Concrete Institute.
[2] Somes, N.F. and Corley, W.G., "Circular openings in webs of continuous beams", American Concrete Institute, Detroit, MI, 1974, pp. 359-398.
[3] Mansur, M.A., Lee, Y.F., Tan, K.H. and Lee, S.L., "Test on RC continuous beams with openings", Journal of Structural Engineering, Vol. 117, No. 6, 1991, pp.1593-1605.
[4] ACI-ASCE Committee 426, "Shear Strength of Reinforced Concrete Members (ACI 426R-74) (Reapproved 1980)", Proceeding, ASCE, Vol.99, No.ST6, June 1973, pp. 1148-1157.
[5] Oukaili, N. K., and Al-Shammari, A. H. , "Response of reinforced Concrete Beams with Multiple Web Openings to Static Load", APFIS

Conference, Melbourne, Australia, December 2013.

[6] Fujikake, K., Li, B., and Soeun, S., "Impact Response of Reinforced Concrete Beam and Its Analytical Evaluation." Journal of Structural Engineering, Vol.135, No.8, 2009, pp. 938-950.

Second International Conference on Science, Engineering & Environment,
Osaka City, Japan, Nov.21-23, 2016, ISBN: 978-4-9905958-7-6 C3051

TRACTOR DRIVING TECHNICAL LEARNING OF AGRICULTURAL STUDENT IN AGRICULTURAL MACHINERY SUBJECT

Dowroong Watcharinrat[1]
[1]Faculty of Agricultural Technology, Rajamangala University of Technology Thanyaburi, Thailand

ABSTRACT

Ability for driving a tractor is one of objective in Agricultural Machinery subject. Student also would learn about part of tractor and their function. Learning was easier than learn how to drive a tractor. Comfortable condition was one of student need. This research compare about technical driving tractor between a lecturer and staff who able to drive tractor. There were forty five students divided into two group. First group (Group 1) teached by a staff and second group (Group 2) teached by lecturer. This research used questionnaire to know student ability in ride transportation before driving practice. After driving teaching a mount, students got questionnaire about their satisfied in tractor driving teaching. Mean, standard deviation, frequency, percent, and t-test were statistical that used in this research. The result show in mean that after a mount, the group 1 was 3.60 better in driving tractor than the second group 2 was 3.50. Male students in mean were 3.61 better than female students were 3.51. But, there were no significant difference in statistical t-test between group 1 and group 2 were 1.57 at level α 0.5 also t-test between male student and female students were 1.65 at level α 0.5. The result between male and female student also group 1 and group 2 were no different ability in driving tractor after a mount. Students ability in drive a tractor after teaching by staff and lecturer were same between group 1 and group 2 also between male students and female students.

Keywords: Tractor Driving, Farm Tractor, Agricultural Machinery

INTRODUCTION

Agricultural machinery subject is important to development student role in agricultural. Agricultural machinery subject explain all about machinery in farm or agriculture side. It start from part of machine, how to use machine, how to maintenane a machine and how to safety when we use the mechine. Their knowledge of agricultural machinery will apply in farm directly. From this course also student explore about tractor exactly. Students need to understand more about tractor , part of tractor and safety in tractor. Because tractor was basic machine that used by farmer.

Student need to know about drive a tractor and able to ride it. But, learning how to drive a tractor as well as teaching student how to drive new transportation. It need more courage in order they believe and safety. It is also need some comfortable condition that make student feel nice and fun learning. From the above mention the research need to find the suitable method for improve technical driving for a tractor.

The objectives of this research to find teaching methodology on tractor driving in agricultural machinery subject. Because, more lecturer is better than a lecturer to teach tractor driving. It should find a solution to solve and make student able to ride a tractor well.

METHODOLOGY

The population of this research was second year student of agriculture machinery subject of Crop Production major Agricultural Technology Faculty Rajamangala University of Technology Thanyaburi Thailand academic year 2/2014. This research was on February 16, 2015 – March 14, 2015. There were forty five students divided into two group. Group 1 there were taught by staff who able in drive tractor and Group 2 taught by lecturer. Group 1 was nineteen students and group 2 was twenty six students.

All students got questionnaire before driving teaching to know about their ability in ride kind of transportation. That questionnaire also include about driving experience, driving license and maintenance machine. They got driving teaching once every week and three hours each practice, but different day between two groups depend on their free time. After a month, student got questionnaire to know their ability and satisfied. That questionnaire ask about their satisfied and ability in machine checking before driving, start engine, increase and decrease speed, hydraulic control, safety in tractor driving and student satisfied with the trainer between lecturer and staff. The statistical of this research was mean, standard deviation, frequency, percentage, and t-test.

RESULTS AND DISCUSSION

This result showed about questionnaire score of all students. This questionnaire there were nine items. They will get score 1 in need improvement ability/satisfied each item, 2 in fair ability/satisfied each item, 3 in good ability/satisfied each item and 4 in very good ability/satisfied each item. It would compared questionnaire score between Group 1 and Group 2 also between male and female student in mean. It also compared questionnaire score between Group 1 and Group 2 also between male and female student in t-test statistical and probability in level 0.05.

Table 1 Questionnaire score after a month driving tractor practice of Group 1

No	Gender	Check	Start	Begin	Gear	h-i	Hydro	Safety	Trainer	Lesson	Total
1	M	3	3	4	3	4	4	4	4	4	3.67
2	M	4	4	3	4	4	4	3	4	4	3.78
3	M	3	3	3	3	4	4	4	3	3	3.33
4	F	4	4	3	3	3	4	4	4	4	3.67
5	M	3	3	3	3	3	4	4	4	3	3.33
6	F	3	4	3	4	3	4	3	4	4	3.56
7	M	4	4	3	3	3	4	4	4	4	3.67
8	M	4	4	4	4	3	4	4	4	4	3.89
9	F	4	4	4	4	3	4	4	4	4	3.89
10	F	4	4	3	3	3	4	4	4	4	3.67
11	F	3	4	3	3	3	4	4	3	3	3.33
12	F	3	4	3	3	3	4	4	4	4	3.56
13	F	4	3	3	3	3	4	4	4	4	3.56
14	F	3	4	4	3	3	4	4	4	3	3.56
15	F	3	4	3	3	4	4	3	4	4	3.56
16	F	4	4	3	3	4	3	4	4	3	3.56
17	F	3	4	3	4	4	4	3	3	4	3.56
18	F	4	3	3	3	3	4	4	4	4	3.56
19	F	4	3	3	3	4	4	4	4	4	3.67
$\overline{X}$		3.53	3.68	3.21	3.26	3.37	3.95	3.79	3.84	3.74	3.60
S.D.		0.51	0.48	0.42	0.45	0.50	0.23	0.42	0.37	0.45	0.16

There were six male students and thirteen students in group 1. Students of group 1 got good score in all items. Most of the student were expert in hydraulic control, that showed by $\overline{X} = 3.95$. Group 1 has $\overline{X} = 3.60$ in total and standard deviation 0.16 in total.

Table 2 Questionnaire score after a month driving tractor practice of Group 2

No	Gender	Check	Start	Begin	Gear	h-i	Hydro	Safety	Trainer	Lesson	Total
1	M	4	3	3	3	3	3	4	3	3	3.22
2	F	4	3	3	3	3	4	3	4	4	3.44
3	F	3	3	3	3	3	4	3	3	3	3.11
4	M	4	3	3	4	4	4	4	4	4	3.78
5	F	4	4	3	3	3	4	4	4	4	3.67
6	F	3	4	4	3	3	3	4	4	4	3.56
7	F	3	4	4	4	4	4	4	3	3	3.67
8	F	3	3	4	3	3	3	3	3	3	3.11
9	F	4	3	3	3	4	4	4	4	4	3.67
10	M	4	4	3	3	4	4	4	4	4	3.78
11	F	3	3	3	4	4	3	3	4	4	3.44
12	M	4	3	3	4	4	4	4	4	4	3.78
13	M	3	4	3	3	3	4	4	4	4	3.56
14	F	3	3	3	3	4	3	4	3	3	3.22
15	F	4	3	4	4	3	3	4	4	4	3.67

Table 2 Continue

16	F	4	3	4	3	3	4	3	3	3	3.33
17	M	3	4	3	3	3	3	4	4	4	3.44
18	F	4	3	4	4	4	4	4	4	4	3.89
19	M	4	3	4	4	4	4	4	4	4	3.89
20	M	4	3	3	3	4	3	4	4	4	3.56
21	M	4	4	4	4	3	3	3	3	3	3.44
22	M	3	3	4	4	4	3	4	4	4	3.67
23	F	3	3	3	3	3	4	3	3	3	3.11
24	F	3	3	3	4	4	4	3	4	3	3.44
25	F	3	3	3	3	3	4	4	3	4	3.33
26	F	3	3	3	3	3	3	4	4	4	3.33
$\overline{X}$		3.50	3.27	3.35	3.38	3.46	3.58	3.69	3.65	3.65	3.50
S.D.		0.51	0.45	0.49	0.50	0.51	0.50	0.47	0.49	0.49	0.24

Ten male students and twenty six female students were in group 2. Most of them expert in safety in driving tractor that showed by $\overline{X}$ = 3.69. Mean of all item was 3.50 and standard deviation 0.24

Table 3 Questionnaire score after a month driving tractor practice of male student

No	**Gender**	**Check**	**Start**	**Begin**	**Gear**	**h-i**	**Hydro**	**Safety**	**Trainer**	**Lesson**	**Total**
1	M	3	3	4	3	4	4	4	4	4	3.67
2	M	4	4	3	4	4	4	3	4	4	3.78
3	M	3	3	3	3	4	4	4	3	3	3.33
4	M	3	3	3	3	3	4	4	4	3	3.33
5	M	4	4	3	3	3	4	4	4	4	3.67
6	M	4	4	4	4	3	4	4	4	4	3.89
7	M	4	3	3	3	3	3	4	3	3	3.22
8	M	4	3	3	4	4	4	4	4	4	3.78
9	M	4	4	3	3	4	4	4	4	4	3.78
10	M	4	3	3	4	4	4	4	4	4	3.78
11	M	3	4	3	3	3	4	4	4	4	3.56
12	M	3	4	3	3	3	3	4	4	4	3.44
13	M	4	3	4	4	4	4	4	4	4	3.89
14	M	4	3	3	3	4	3	4	4	4	3.56
15	M	4	4	4	4	3	3	3	3	3	3.44
16	M	3	3	4	4	4	3	4	4	4	3.67
$\overline{X}$		3.63	3.44	3.31	3.44	3.56	3.69	3.88	3.81	3.75	3.61
S.D.		0.50	0.51	0.48	0.51	0.51	0.48	0.34	0.40	0.45	0.21

Sixteen male students was high ability in safety in driving tractor that showed by $\overline{X}$ = 3.88. Mean of all items was 3.61 and standard deviation 0.21.

Table 4 Questionnaire score after a month driving tractor practice of female student

No	Gender	Check	Start	Begin	Gear	h-i	Hydro	Safety	Trainer	Lesson	Total
1	F	4	4	3	3	3	4	4	4	4	3.67
2	F	3	4	3	4	3	4	3	4	4	3.56
3	F	4	4	4	4	3	4	4	4	4	3.89
4	F	4	4	3	3	3	4	4	4	4	3.67
5	F	3	4	3	3	3	4	4	3	3	3.33
6	F	3	4	3	3	3	4	4	4	4	3.56
7	F	4	3	3	3	3	4	4	4	4	3.56
8	F	3	4	4	3	3	4	4	4	3	3.56
9	F	3	4	3	3	4	4	3	4	4	3.56
10	F	4	4	3	3	4	3	4	4	3	3.56
11	F	3	4	3	4	4	4	3	3	4	3.56
12	F	4	3	3	3	3	4	4	4	4	3.56
13	F	4	3	3	3	4	4	4	4	4	3.67
14	F	4	3	3	3	3	4	3	4	4	3.44
15	F	3	3	3	3	3	4	3	3	3	3.11
16	F	4	4	3	3	3	4	4	4	4	3.67
17	F	3	4	4	3	3	3	4	4	4	3.56
18	F	3	4	4	4	4	4	4	3	3	3.67
19	F	3	3	4	3	3	3	3	3	3	3.11
20	F	4	3	3	3	4	4	4	4	4	3.67
21	F	3	3	3	4	4	3	3	4	4	3.44
22	F	3	3	3	3	4	3	4	3	3	3.22
23	F	4	3	4	4	3	3	4	4	4	3.67
24	F	4	3	4	3	3	4	3	3	3	3.33
25	F	4	3	4	4	4	4	4	4	4	3.89
26	F	3	3	3	3	3	4	3	3	3	3.11
27	F	3	3	3	4	4	4	3	4	3	3.44
28	F	3	3	3	3	3	4	4	3	4	3.33
29	F	3	3	3	3	3	3	4	4	4	3.33
$\overline{X}$		3.45	3.45	3.28	3.28	3.34	3.76	3.66	3.69	3.66	3.51
S.D.		0.51	0.51	0.45	0.45	0.48	0.44	0.48	0.47	0.48	0.20

Twenty nine female students was high satisfaction in trainer in driving tractor that showed by $\overline{X}$ = 3.69. Mean of all item was 3.51 and standard deviation 0.20.

Table 5 Compared of questionnaire score after a month driving tractor practice of Groups by using independent samples t-test

Group	$\overline{X}$	S.D.	t-value	Probability
Group 1	3.60	.16	1.57	1.24
Group 2	3.50	.24		

Note: significant at 0.05.

Students got questionnaire about their satisfied in driving tractor teaching.The result showed in mean that after a mount, the group 1 was 3.60 better in driving tractor than the second group 2 was 3.50. But, there were no significant difference in statistical t-test between group 1 and group 2 were 1.57 with probability 1.24 at level α 0.5. The result between group 1 and group 2 were no different ability in driving tractor after a mount. Students ability in driving tractor after teaching by staff and lecturer were same.

Table 6 Compared of questionnaire score after a month driving tractor practice between male and female student by using independent samples t-test

Group	$\overline{X}$	S.D.	t-value	Probability
Male	3.61	.21	1.65	.107
Female	3.51	.20		

Note: significant at 0.05.

After driving teaching a month, students got questionnaire about their satisfied in driving tractor teaching. Mean, standard deviation, frequency, percentage, and t-test were statistical that used in this research. The result show in mean that after a month,male students in mean were 3.61 better than female students were 3.51. But, there were no significant difference in statistical t-test between male students and female students were 1.65 with probability .107 at level α 0.5. The result between male and female student were no different ability in driving tractor after a mount. Students ability/ satisfaction in driving tractor after teaching by staff and lecturer were same.

CONCLUSION

There were sixteen male and twenty nine female in forty five students. There were six students can drive a car. There were two female and four male. One of them can drive a tractor. That information known by questionnaire before driving tractor practice. Fourty five students divided into two group. Group 1 there were nineteen students teached by staff and group 2 teached by lecturer as researcher for twenty six students. Students did not knoew about this research. They divided into two group based on they free time to practice. Because, researcher and staff teached student in different day but same time.

The first practice week, most of students were afraid. Because, tractor was big and it's engine was noise. They tried to start the engine and check tractor components before driving on the second practice week. But, they did not step the clutch and break together that make them afraid because the engine stop directly. They tried to apply the gear for increase or decrease the speed also for high and low speed on the third practice week. On the last week, they tried enjoy high speed with safety way.

Researcher experience showed that male was better than female to drive a tractor. But from this research, there was no different ability between them to drive a tractor, also they was no different satisfaction between practiced by staff and lecturer. Because, they have experience to observation drive a car with the family. They also have lecture in this subject. They also observed their friend how to drive a tractor**.**

ACKNOWLEDGEMENTS

The authors would like to express their sincere thanks for the participated of Faculty of Agricultural Technology, Rajamangala University of Technology Thanyaburi and other. We would also say thanks for who could not be mentioned here for their kindness and encouragement.

REFERENCES

[1] Watcharinrat D, Agricultural Machinery (Handout Theory). 2013. Rajamangala University of Technology Thanyaburi, Faculty of Agricultural Technology. Pathumtani Province, Thailand.

[2] Watcharinrat D, Agricultural Machinery (Handout Labratory). Rajamangala University of Technology Thanyaburi, Faculty of Agricultural Technology. Pathumtani Province, Thailand, 2013.

[3] Goering CE, Engine and Tractor Power. University of Illinois, United States of America, 1986.

[4] Hunt D, Farm Power and Machinery Management. Iowa State University Press, Ames, Iowa, 1973.
[5] Deere J, Fundamentals of Machine Operation, Tillage. John Deere Service Training Dept. F., Moline , Illinois, 1976.
[6] Deere J, Fundamentals of Machine Operation, Agricultural Machinery Safety. John Deere Service Training Dept. F., Moline, Illinois. 1974.
[7] Intarawichai P, Farm Machinery Part 2. Agricultural Engineering Training Center. Pathumthani Province, Thailand, 1992.
[8] Policy and Planning Division, Policy of RMUTT. Rajamangala University of Technology Thanyaburi, Pathumtani Province, Thailand, 2014.
[9] Smith HP & Wilkes LH, Farm Machinery and Equipment. McGraw-Hill Book Company, Thailand.

Second International Conference on Science, Engineering & Environment,
Osaka City, Japan, Nov.21-23, 2016, ISBN: 978-4-9905958-7-6 C3051

A STUDY OF NATURAL COLOR IN FIBRE ENRICHED FRUIT MILK POWDER

Suzihaque, M.U.H[1], Raja Maizatulakmal Raja Abdullah and Ummi Kalthum Ibrahim[3]
[1,2,3]Faculty of Chemical Engineering, Universiti Teknologi MARA, Malaysia

ABSTRACT

Five different sources of natural color were selected in order to study the stability of the natural colors which were blended with milk prior to spray drying process. Five different colors of fruit milk powder were produced: dragonfruit milk (magenta color), carrot milk (orange color), pandan milk (green color), orange milk (yellow color) and strawberry milk (light pink color). Different types of color produced were contributed from different color pigments incorporated in the fruit naturally. Each of the milk sample were run through the spray drying at three different inlet temperatures, 110, 130 and 150℃. By using Sphere Spectrohotometer, the color was visualized in which the color space ; L*, a* and b* values of each sample were obtained. The total color changes after the drying process were also calculated. From the results, the total colour changes of carrot milk powder after drying process were the highest followed by orange, pandan, dragonfruits and strawberry. After one week of storage, the color changes was measured again. The results showed that different color had different color stability. By using UV/Vis spectrophotometer, the solubility of the powder in water was measured after the drying process and after 1 week of storage period. The solubility of the powder which remains in the water signified the concentration of the color pigment that were not degraded during the drying process. Different color pigment were measured at different wavelength relative to their maximum absorbance wavelength. From the results obtained, all five type of milk showed that after drying, the highest absorbance values were recorded at 110℃ followed by 130 and 150 ℃. The surface topography of the powder was viewed at 500x and 1500 magnification by using Scanning Electron Microscope (SEM). From the image obtained, higher temperature of drying resulted to a smaller size of molecules which also signified the level of degradation at three different temperatures.

Keywords:Milk, Fruit, Natural colour, Pigment, Spray drying

INTRODUCTION

Nowadays, children are drinking less milk and dislike eating healthy food such as vegetables and fruits. For them, the taste and sensory properties are becoming important factor in choosing food [1] and this behavior will lead them to consume unhealthy diet which is lack in calcium and fiber and other more having nutrient deficiency which is very important for their growth. Different approaches has been analyzed in order to make sure that children can consume those foods which is combining fruit flavor with the milk . Instead of liquid product, the fruit flavored milk is suggested to be commercialized in powder form for longer storage stability and more attractive appearance with different types of color based on the natural color of fruits.

In the recent studies, it is found that the consumption of milk especially among children becoming lower and this had grow the concern of many parents since drinking milk is very crucial for growth development and intake of other nutrients that needed to maintain our body health[2]. Furthermore, children nowadays are very picky and they are more prefer to drink flavored milk rather than plain milk. Therefore, it is highly believe that flavored milk will be a good approach to attract children, adolescent and adults to consume milk in their daily diet

Color is one of the most important quality attributes affecting consumer's acceptance of food since it gives the first impression of food quality. Moreover, the food industries nowadays are more focused on the demand for natural colorant instead of synthetic dyes highly due to safety issues. However, the practice of natural pigment compels knowledge especially on their stability in order to adapt them to the condition of use during processing, packaging and distribution.

It was reported that natural pigment from biological sources came into consideration especially pigment extracted from plant fungi, bacteria, algae and insect. Soma major categories of plant pigment include betalain, anthocyanins, carotenoids and chlorophylls. Among thse categories, anthocyanin earned the most attention due to its colour and antioxidant properties [3]. Besides that, natural colorant sources such as pandan leaves are widely used in food industries as pandan contains various bioactive compound especially natural green colorants [4]. Betalain pigment that can be obtained

from dragonfruit have also been one of the widely used colorants in food industries. However, the research done about these color pigment was not fully conducted. There are several major factors that affect the color produced and the pigment stability such as pH, temperature, oxygen, ascorbic acid, light, enzyme[5] etc. Generally, the major plant pigment and their colors can be divided intocategories as shown in Table 1a below:

Table 1a Major plant pigment and their concurrency [6]

Pigment	Common type	Colors
Chlorophylls	Chlorophyll	Green
Carotenoids	Carotenes and xanthophylls	Orange, reds, yellow
Flavonoids	Anthocyanins, aurones, flavonols	Yellow, red, blue, purple
Betalains	Betacyanins	Red to violet, also yellow to orange

In this study, four types of fruits and one types of vegetable were extracted and incorporated with milk and the effect of spray-drying procedure on the color changes of the pigments, concentrations and solubility of the pigments under three different temperatures were determined. The effects of the temperatures on the spray-dried product were monitored right after the drying process and one week storage.

METHODOLOGY

A. Preparation of 5 Types of Fruit Milks

Seventy gram fresh pandan leaves, 68gripe dragon fruit, 162g carrots, 413g oranges and 350g Strawberries were prepared. Each of them were then blended with 600 mL of Dutch Lady Full Cream Milk. Then each of the blended mixture was filtered using filter cloth to remove any insoluble solids and other impurities.Each of the mixture was added with 3g of maltodextrins to obtain homogenous mixture.

B. Spray Drying Process

The equipment used was a spray dryer model SD-Basic. Initially, the inlet temperature of dryer was set to 110°C and the pump of the equipment was adjusted at desired rotation speed in the range of 3 rpm. When the process ended, the nozzle was left to cool down for a few minutes and then the powder was collected. This step were repeated for inlet temperature of 130 and 150 for each of the fruit milk sample which gives 3 samples for each types of fruits milk.

C. Storage of the Samples

All the samples powder were sealed and stored in dark place at room temperature, 25℃ .

D. Determination of Color Parameters and Total Color Changes by Colorimetric Analysis

The color of the product can be visualized using the colorimetric analysis by measuring the color space which the color values were expressed as L*, a* and b*. The color was measured using Lovibond RT400 Sphere Spectrophotometers. The instrument was initially calibrated. Then, the measurement was taken by placing the head of the spectrophotometer vertically above the sample and then the head of the spectrophotometer was pushed slightly and was kept on hold until a light appeared and a click sound was heard which signify the measurement was finished. From the results obtained, The color changes for each type of fruit milk from liquid into powder for each temperature is calculated by using formula below[2]:-

$$\Delta E^* = \sqrt{(\Delta L^* + \Delta a^* + \Delta b^*)}$$

ΔE^*= total color changes
L* = lightness which range from 100 for perfect white to zero for black
a* = redness when positive ,grey when zero, greenness when negative
b* = yellowness when positive, grey when zero and blueness when negative

The reading of color measurement were taken in triplicate for each sample with the mean values reported. The colorimetric analysis was done by calculating the color changes between the original forms which is in liquid mixture with the powder form and the changes of the color after one weekof storage.

E. Spectrophotometric Analysis

0.04 gram of each powder samples were diluted with 10 mL of distilled water. After the powder solubilized completely, the samples were then centrifuged at 12,000 rpm for 10 minutes. The absorbance reading of each powder sample were taken at different wavelength depending on the type of the color pigment as shown in Table 2 below:

Table 2 Type of Fruits with their relative Color Pigment and Wavelength

Types Fruit	Color pigment	Wavelength (nm)
Dragon fruit	Betalain	482
Carrot	Beta carotene	470
Pandan	Chlorophyll	645
Orange	Flavonoids	352
Strawberry	Anthocyanin	510

F.Surface Topography and Composition Analysis by Using Scanning Electron Microscope (SEM)

Scanning electron microscope (Hitachi TM3000 Tabletop Microscope) was used to examine the morphology and surface appearance of microencapsulated powder. The samples were attached with a two sided adhesive tape to the specimen stubs and then coated with gold in Sputter Coater (Quarom SC7620). The coated samples then examined at 50x, 500x and 1500x magnifications.

RESULTS AND DISCUSSION

A. The Effect of Spray Drying on Color Fruit Milk

Fig. 1 Dragon-fruit milk powder, Strawberry milk powder, Carrot milk powder, Orange milk powder and Pandan milk powder.

As shown in Fig.3.1, there were five different colorpowders with respect to different types of fruit milk used in this study. From left, magenta colors was produced from dragonfruits milk, followed by light pink color for strawberry milk, orange color for carrot milk, light yellow for orange milk and lastly green for pandan milk.

Table 3.1 Color space reading for Dragonfruit milk

	Average values			ΔL^*	Δa^*	Δb^*	ΔE
	L*	a*	b*				
Liquid	35.16	20.07	-4.97				
T=110℃	73.23	22.73	-9.97	7.65	18.37	11.91	23.19
T=130℃	71.58	21.80	-9.42	6.00	17.44	11.36	21.66
T=150℃	71.19	20.95	-8.82	5.61	16.59	10.76	20.55

Table 3.2 Color space reading for carrot milk

	Average values			ΔL^*	Δa^*	Δb^*	ΔE
	L*	a*	b*				
Liquid	46.69	9.03	14.29				
T=110℃	84.03	9.44	30.24	18.45	5.08	28.30	34.16
T=130℃	83.37	8.73	32.83	17.79	4.37	30.89	35.91
T=150℃	83.93	7.01	33.62	18.35	2.65	31.68	36.71

Table 3.3 Color space reading for Pandan milk

	Average values			ΔL^*	Δa^*	Δb^*	ΔE
	L*	a*	b*				
Liquid	69.73	-17.24	18.27				
T=110℃	84.03	-15.89	18.05	15.63	20.25	16.11	30.23
T=130℃	83.37	-16.03	18.52	14.66	20.39	16.58	30.09
T=150℃	83.93	-16.69	19.63	14.69	21.05	17.69	31.18

Table 3.4 Color space reading for Orange milk

	Average values			ΔL^*	Δa^*	Δb^*	ΔE
	L*	a*	b*				
Liquid	75.09	0.08	24.28				
T=110℃	84.03	0.69	26.19	23.52	-3.67	24.25	33.98
T=130℃	83.37	0.72	25.90	21.97	-3.64	23.96	32.72
T=150℃	83.93	0.61	26.72	22.18	-3.75	24.78	33.47

Table 3.5 Color space reading for Strawberry milk

	Average values			ΔL^*	Δa^*	Δb^*	ΔE
	L*	a*	b*				
Liquid	70.26	3.41	6.37				
T=110℃	79.98	7.92	4.86	14.40	3.56	2.92	15.12
T=130℃	79.42	9.12	4.58	13.84	4.76	2.64	14.87
T=150℃	78.25	9.26	4.99	12.67	4.90	3.05	

Generally, based on Table 3.1, 3.2, 3.3, 3.4 and 3.5, all the samples powder which has been produced appeared to have higher lightness (higher L*) compared to liquid form. The lighter color which results in spray drying was due to addition of maltodextrin carrier which was necessary to reduce the stickiness of the fruits and milks to enhance the drying process [7]. From table 3.1, the a* (redness) values of dragon fruit milk powder were significantly higher than b* (blueness) values and this is highly due to presence of dominant betalain pigment in dragon-fruits which gives off red violet colour[3]. As the temperature increase, the a* values becomes decreased as result from the thermal effect, the betanin pigment were degraded by isomerization, decarboxylation or cleavage which lead to gradual

reduction of red color as the temperature increased[8].

In Table 3.2,the values of b* (yellowness) for carrot milk powder was higher than a* (redness) values. Both yellow and red color were contributed by the carotenoids pigment [9]. However, the values of b* (yellowness) were higher than a* (redness) was observed highly due to the domination of yellow color in the pigment. As the temperature increase, the b* values decreased which was expected, because the higher the drying temperature, the higher the color degradation [10]. In contrast with b* the a* values were decreased as the temperature increased. The study has also found that the values of a* were decreased while b* were increased for spray drying effect of apricot which is also dominated by carotenoids pigment color.

For pandan milk, the values of a* values are different from carrot and dragon fruit milk thatthe a* values are in negative values which signify greenness of the sample color as shown in Table 3.3. So, obviously, the main factor of the color differences is because the presence of the chlorophyll which contributed the green color of pandan[4]. From the results, compared with b* (yellowness) values, the values of b* did not differ significantly with the a* values. This results are supported by Muhammad (2010) which also found that not only chlorophyll, but carotenoids is also present in the pandan leaves which gives contribution to the color [11]. As the temperature increase, the greenness of the color also increased which results from the heat that forces the gas surrounding the plant cells to expand and escape hence allow the light reveals the bright green chloroplasts within the cell.

From Table 3.4, as results from the drying process, the a* and b* values were increased. Compared to a* values, the b* values were significantly higher as the flavonoids pigment was the main contributor to the yellowness of the color in orange fruits[6] The increase of the redness which may seen as brown color which contributed by the degradation of the color pigment[12].

As seen in Table 3.5, the a* values which signify the redness are much more higher than the b* values as the red strawberry are donated by 2 types of anthocyanin pigment, which are pelargonidin and cyanin [13]. During heat treatment, the athocyanins was degraded due to theirsensitivity toheat. This has lead to browning effect to the color of the pigment [13]. This may be the reason why the color of the powder becomes more red as the temperature increase.

B. The Effect of Storage on Colour Stability

From the Fig 3(a) and (b), the values of a* and b* of the carrot were decrease slightly after 1 week of storage. The same finding was found in study of orange powder by Pitchiah (2004) in which after 2 weeks of storage, the chroma values which indicate the a* and b* intensity were decrease[14]. This is highly due auto-oxidative reaction which result to discoloration of the Beta-carotene in low moisture model system [15]. From the same study, it was assumed that the dried powder of carrots is assumed to undergo the same reaction[15]

From Figure 4(a) and (b), it was clearly showed that after 1 week of storage, the a* (yellowness) values and b* (greenness) values decreased for all the three sample. It was found that the chlorophyll will be oxidized and green color will significantly reduced under room temperature condition. The oxidation of chlorophyll will change the color from green to grey [16].

Contrary to other fruit milk powder, for Dragonfruit milk powder, the a* and b* values are increase slightly after 1 week of storage for the three samples as in Figure 2(a) and (b). According to Woo et al (2010), under 85 degree Celsius, the heating treatment will cause degradation of colour up to 30% at the initial stage of the storage and besides after3 weeks storage, the samples which was kept in 25 degree will experience about 70-90% of color loss [3]. Different from the results obtained in this experiment, the causes may highly due to presence of ascorbic acid in the milk powder where even 1% of ascorbic acid are proved to preserve the red hue of the color [17].

The stability of anthocyanin in strawberry depends highly on the surrounding effect as it can react with other compound to promote colored or discolorifing effect. The main reasons for color changes during storage is the enzymatic browning [13].However several studies have shown that a short processing at temperatures above 70 and 90 degree Celsius is enough to inactivate the enzyme completely. On the other hand, a reducing agent such as ascorbic acid from the milk [18] with presence of oxygen can oxidize the anthocyanin to become colorless compound [13] . Hence, this is the main reason the a* were decrease slightly after a week storage especially after a higher temperature of drying as seen in Figure 5 (a) and (b).

After 1 week storage, the a* and b* values were increased for the three samples as shown in Figure 6(a) and 6(b). Similar to the effect of heat treatment, the browning effect was also increase during the storage period. Besides degradation of the pigment, other cause such as non-enzymatic reactions could be the sources to the rise of the color. As mentioned before, the presence of high ascorbic acid in milk and also in the orange fruit[19] will contribute to the browning effect [12].

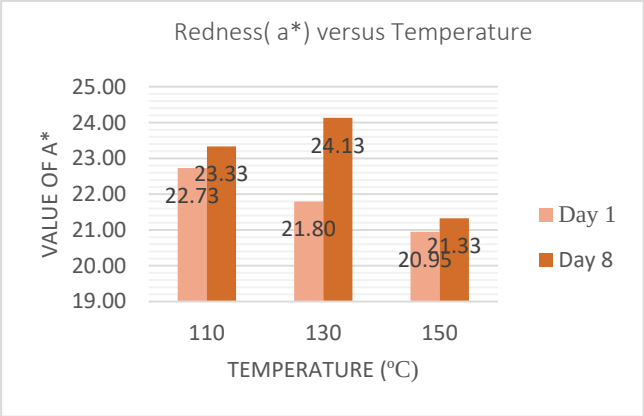

2(a)

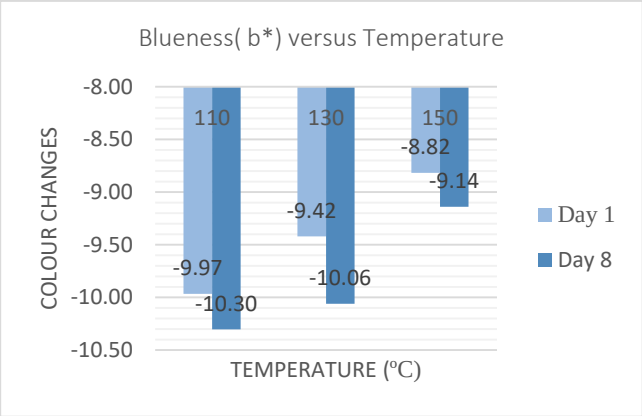

2(b)

Figure 2(a) and 2(b) shows the Changes in a* and b* values of Dragon fruit Milk after 1 weeks

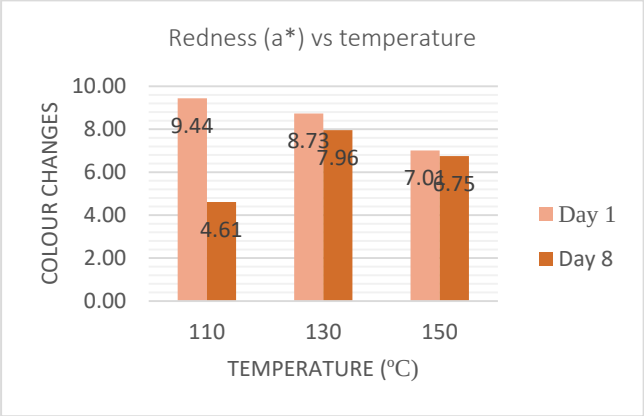

3(a)

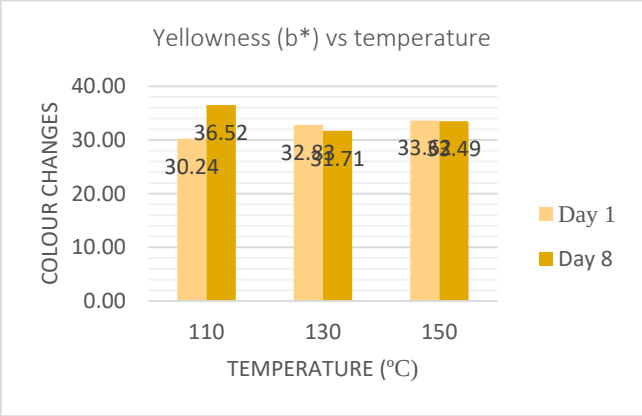

3(b)

Figure 3(a) and b(b) shows the Changes in a* and b* values of Carrot Milk after 1 weeks

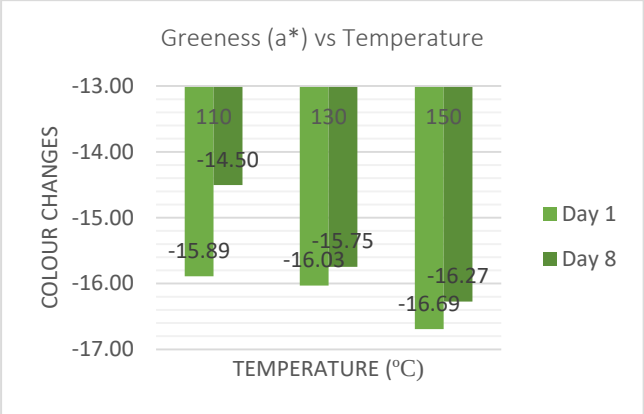

4(a)

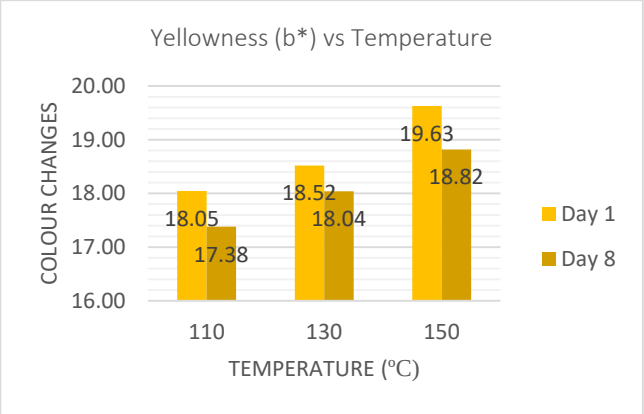

4(b)

Figure 4(a) and 4(b) shows the Changes in a* and b* values of Pandan Milk after 1 weeks

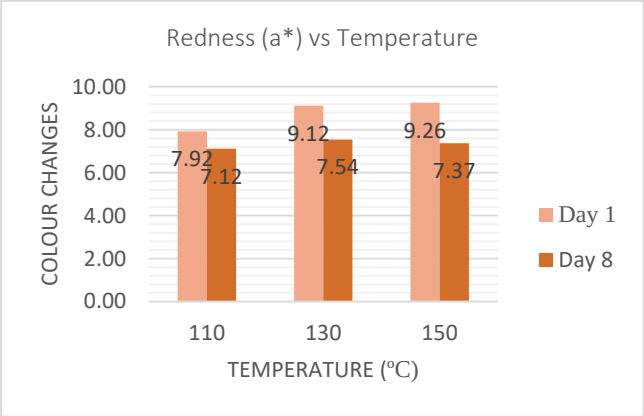

5(a)

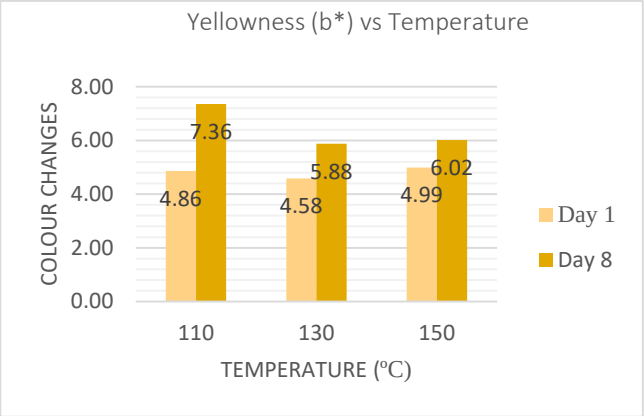

5(b)

Figure 5(a) and 5(b) shows the Changes in a* and b* values of Strawberry Milk after 1 weeks

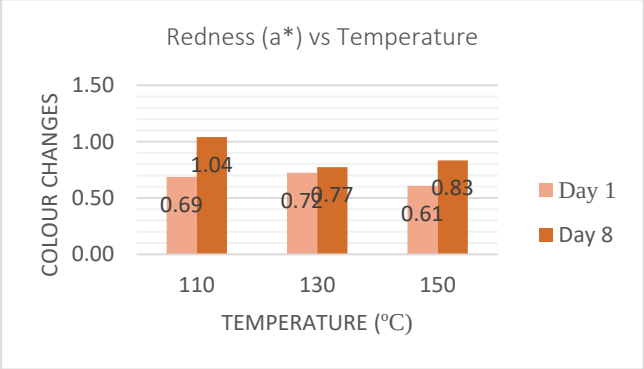

6(a)

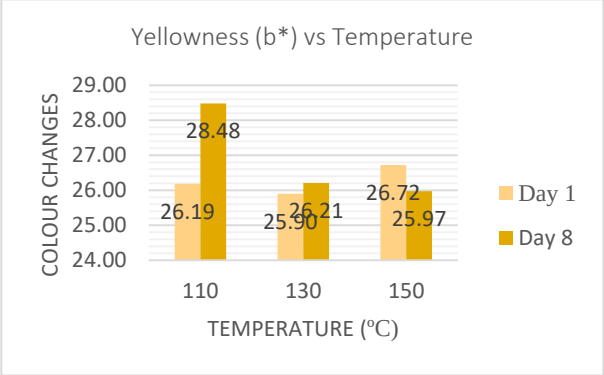

6(b)

Figure 6(a) and 6(b) shows the Changes in a* and b* values of Orange Milk after 1 weeks

Table 3.6: The Absorbance Reading

	Dragon fruit		Carrot		Pandan		Orange		Strawberry	
	Day 1	Day 8	Day 1	Day 8	Day 1	Day 8	Day 1	Day 8	Day 1	Day 8
110	2.107	1.109	1.613	0.762	1.439	1.223	2.956	2.832	1.205	0.345
130	2.091	0.936	1.238	1.028	1.295	1.103	2.942	2.954	1.127	0.368
150	2.086	1.636	0.827	0.818	1.278	1.029	2.882	2.938	0.883	0.482

C. Spectrophotometry analysis

Table 3.6 showed that difference type of color pigment which have different wavelength is required to read their absorbance reading using spectrophotometer. Based on results in Table 3.7 above, it was observed that the reading of the absorbance values on Day 1 for all the five fruit milk powder gives the same results, where the highest absorbance values was observed at 110℃followed by 130 and 150℃. Higher absorbance values reading indicates higher concentration of the color pigment which remain soluble in the water.After the powder samples were diluted with distilled water and centrifuged at 10,000 rpm. With increase of temperature, the denaturation of protein and other molecule such as the pigment were increased which results to higher amount of insoluble proteins and pigment. These insoluble molecules were then removed as sediment during centrifugation. Thus, the soluble protein and pigment molecules left in the supernatant was expected to decreased[20]. After 1 week of storage, the absorbance reading were decreased for all the samples at all the three different temperatures. Although all the values observed were decreased, the behaviors at three different temperatures are different for all five fruit milk.

In this study, as each of the fruit color were contributed by different types of color pigment, so

the stability of color pigment are differ especially after 1 weeks compared to the reading on the day of the experiment. So it is highly suggested that a color stabilizer is added for further research and future benefits of natural color study.

D. Scanning Electron Microscope (SEM)

Fig. 3.2, Fig 3.3 and Fig 3.4 showed the microstructure of the powder particle size of orange milk powder at three different temperatures which are 110, 130 and 150 ℃ respectively. The photographs were viewed usingtwo different magnification, 50x and 1500x magnification. Based on the observation, as the temperature increased, the size of the particles becomes much smaller where the highest shrinkage were shown at 150 degree Celsius. The molecule size were also smaller with numerous presence of crumbled small molecules as results from high thermal degradation[21]. Compare to sample at 110℃, the size of the molecules are bigger, with less amount of round shaped molecules around the bulk.

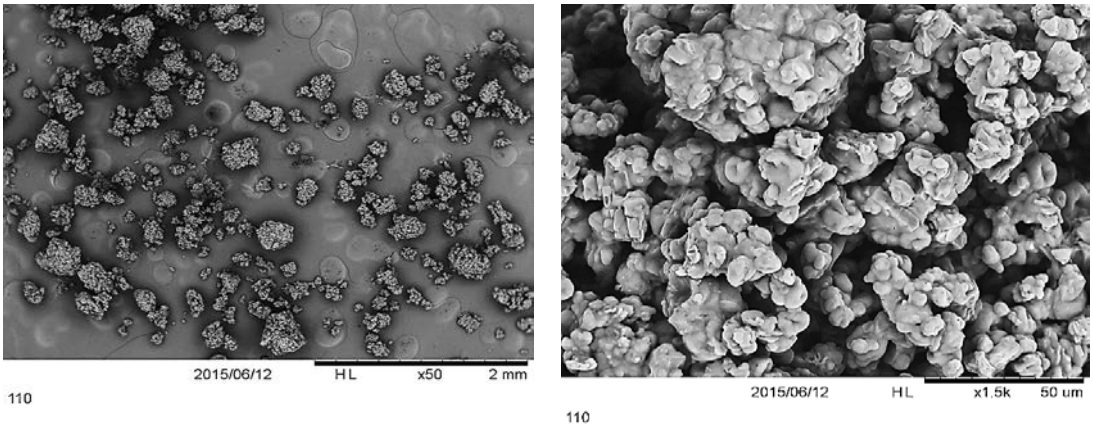

(a) (b)

Figure 3.2 SEM image of particles at 110℃ (a) 500x magnification (b) 1500x magnification

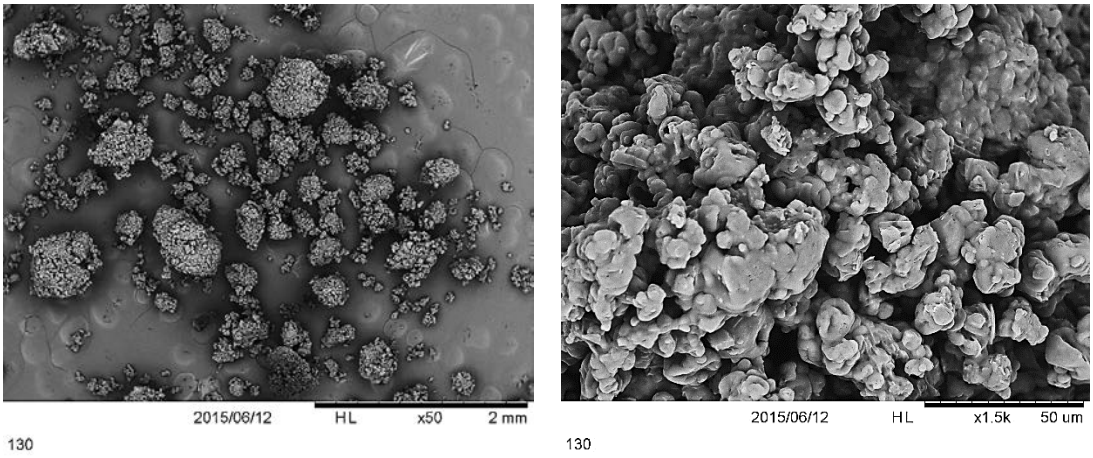

(a) (b)

Figure 3.3 SEM image of particles at 130℃ (a) 500x magnification (b) 1500x magnification

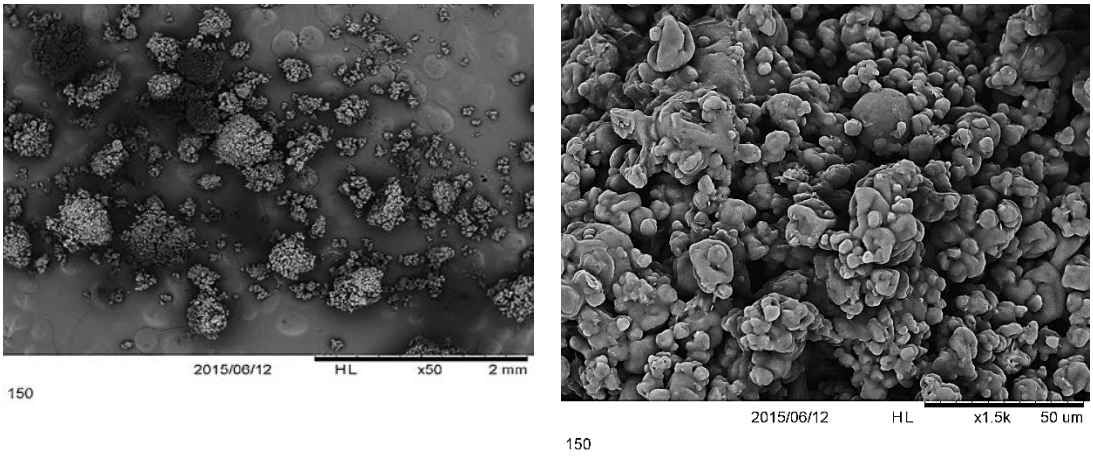

(a) (b)

Figure 3.4 SEM image of particles at 150℃ (a) 500x magnification (b) 1500x magnification

CONCLUSIONS

This study proved that there were a lot of factors need to be considered in order to achieve stability and preserve the natural color intensity incorporated in the milk powder especially after the heat treatment process. Different color was contributed by different natural color pigment that signified different stability level, sensitiveness or even oxidation effect. All these aspects can be influenced by the presence of the milk itself which contained active compounds that aresusceptible to any possible chemical reaction which can affect the color changes especially after the heat treatment and storage period. Other important factors necessary to maintain the color stability are the environment factors such as presence of air, light and the packaging of the product. Besides that, it was also proved that natural color have the potential to be commercialized and applied in the bigger scale especially in food color industries during the processing, packaging, storage and distributions. Thestabilities of the colors can be enhanced and controlled with sufficient chemical knowledge structure and reactions of the molecules that can be analyzed anddiscovered throughout the current and future research.

ACKNOWLEDGMENT

Support for this research was provided by a grant(RAGS/1/2014/TK05/UITM//4) from the Ministry of Higher Education of Malaysia. Thank you to Universiti Teknologi MARA and to all who may contribute directly or indirectly towards making this research successful.

REFERENCES

1. De Pelsmaeker, S., J. Schouteten, and X. Gellynck, *The consumption of flavored milk among a children population. The influence of beliefs and the association of brands with emotions.* Appetite, 2013. 71(0): p. 279-286.
2. Fayet, F., et al., *Australian children who drink milk (plain or flavored) have higher milk and micronutrient intakes but similar body mass index to those who do not drink milk.* Nutrition Research, 2013. 33(2): p. 95-102.
3. Woo, K.K., et al., *Stability of the Spray-Dried Pigment of Red Dragon Fruit [Hylocereus polyrhizus (Weber) Britton and Rose] as a Function of Organic Acid Additives and Storage Conditions.* The Philippine Agricultural Scientist, 2011. 94(3).
4. Porrarud, S. and A. Pranee, *Microencapsulation of Zn-chlorophyll pigment from Pandan Lea by spray drying and its characteristics.* International Food Research Journal 2010. 17: p. 1031-1042.
5. Kne, E. *Maintaining Color Stability*. 2006 [cited 2015; Available from: http://www.foodproductdesign.com/articles/2006/08/maintaining-color-stability.aspx.
6. Douma, M. *Cause of Color*. 2008; Available from: http://www.webexhibits.org/causesofcolor/7H.html.
7. Abonyi, B.I., et al., *Quality Retention in Strawberry and Carrot Purees Dried with Refractance Window.* Journal of Food Science, 2002. 67(2).
8. Nollet, L.M.L. and F. Toldra, *Food Analysis by HPLC*. 3rd ed. 2012: CRC Press.
9. Wagner, L.A. and J.J. Warthesen, *Stability of Spray Dried Encapsulated Carrot Carotene.* Journal of Food Science, 1995. 60(5): p. 1048-1053.
10. Ihns, R., et al., *Effect of Temperature on Drying Characteristics, Colour, Antioxidant and Beta*

carotene Content of Two Apricot Varieties. International Journal of Food Science & Technology, 2011. 46: p. 275-283.
11. Muhammad, D.B.S., *Extraction of Green Pigment From Pandanus Odorus*, in *Faculty of Chemical and Natural Resources Engineering*2010, Universiti Malaysia Pahang.
12. Wibowo, S., et al., *Colour and carotenoid changes of pasteurised orange juice during storage.* Food Chemistry, 2015. 171(0): p. 330-340.
13. Avasoo, M. and L. Johansson, *Evaluation of Thermal Processing Technologies fior Strawberry Jam*, in *Department of Food Technology, Engineering and Nutrition*2011, Lund University, Sweden.
14. Pitchiah, S., *Development and Evaluation of Carrot Powder As a Food Ingredient*, in *Department of Education, Nutrition, Restaurant, Hotel and Institutional Management* 2004, Texas Tech University.
15. Inazu, T. and Y. Makino, *Modelling of Discoloration of Dried Powder of Carrots.* Agriculture 1998. 69: p. 294-254.
16. Coles, R. and M.J. Kirwan, *Food and Beverage Packaging Technology*. 2nd Edition ed. 2011: John Wiley and Sons.
17. Reynoso, R., et al., *Stability of Betalai Pigments from Cactacea Fruit.* Journal of Agricultural and Food Chemistry, 1997. 45(8): p. 2884-2889.
18. Mosure, J., *Vitamin C (Ascorbic Acid)*, 2004, The Ohio State University.
19. Maltejan, G., *The World's Healthiest Food*. 2nd ed. 2001: George Maltejan Foundation.
20. Fang, Y., et al., *Functionality of milk protein concentrate: Effect of spray drying temperature.* Biochemical Engineering Journal, 2012. 62(0): p. 101-105.
21. Bahnasawy, A.H., A.E. Okasha, and Gonbeej, *Performance Evaluation of A Laboratory Scale Spray Dryer*. 2010.

Second International Conference on Science, Engineering & Environment,
Osaka City, Japan, Nov.21-23, 2016, ISBN: 978-4-9905958-7-6 C3051

NUMERICAL SIMULATION OF DESICCATION CRACKING PROCESS BY WEAK COUPLING OF DESICCATION AND FRACTURE

Sayako Hirobe[1] and Kenji Oguni[2]
[1,2] Department of System Design Engineering, Keio University, Japan

ABSTRACT

The prediction of the possibilities for the desiccation cracking is important for the building construction because they could cause damages to the foundation structures. While the experimental and numerical researches were performed with the various materials and conditions, the mechanism of the desiccation cracking is still not clear. In this research, the desiccation cracking is modeled by the coupling of the desiccation governed by the diffusion equation, the deformation, and the fracture. We perform the weak coupling analysis of finite element analysis for the desiccation and the analysis of Particle Discretization Scheme Finite Element Method (PDS-FEM) for the deformation and the fracture. The simulation is carried out with the different thickness of the desiccation layer under various boundary conditions. The simulation results show the satisfactory agreement with the experimental observation in terms of the crack pattern with net-like structure, pattern formation process, and the change in size of the cells framed by the cracks depending on the thickness of the desiccation layer. This agreement between the simulation results and the experimental observations indicates that the coupling of desiccation, deformation, and fracture is a fundamental mechanism of the desiccation cracking.

Keywords: Desiccation Cracks, Pattern formation, Coupled Problem, PDS-FEM

INTRODUCTION

The prediction of the possibilities for the desiccation cracking is important for the building construction because they could cause damages to the foundation structures. While the experimental and numerical researches were performed with the various materials and conditions, the mechanism of the desiccation cracking is still not clear.

The results of the previous experimental researches show that the desiccation cracking has geometric features conserved in various materials and conditions [1]-[4]. For instance, the desiccation cracking has a net-like structure and form polygonal cells framed by the cracks and the size and the shape of the cells change depending on the constraint conditions and the thickness of the specimen.

In previous numerical approaches, some models and numerical methods are proposed to reproduce these geometric features of the desiccation cracking [5]-[7]. While these models and methods can reproduce the net-like crack patterns, they cannot reproduce the increase of the cell sizes depending on the thickness of the specimen or the change in crack pattern depending on the constraint conditions.

In this paper, the desiccation cracking is modeled by the coupling of the desiccation governed by the diffusion equation, the deformation, and the fracture. This model can reflect the inhomogeneous water distribution due to desiccation on the problem of deformation and fracture. We perform the weak coupling analysis of finite element analysis for the desiccation and the analysis of Particle Discretization Scheme Finite Element Method (PDS-FEM) [8] for the deformation and the fracture. The results of the simulation are compared with the experimental results qualitatively.

MATHEMATICAL MODEL OF DESICCATIO CRACKING

The desiccation process in the mixture of the powder and the water is described by the diffusion equation in terms of the volumetric water content θ when the moisture diffusion coefficient D is assumed as constant and the gravitational effect is neglected. Consider a permeable and linearly elastic body Ω with external boundary Γ^1. When the water evaporated from the boundary Γ^1, the water distribution in Ω is given by the next initial boundary value problem:

$$\frac{\partial \theta}{\partial t} = D\nabla^2\theta \qquad \boldsymbol{x} \in \Omega \tag{1a}$$

$$D\frac{\partial \theta}{\partial \boldsymbol{n}} = -Q^1(\theta) \qquad \boldsymbol{x} \text{ on } \Gamma^1 \tag{1b}$$

$$\theta(\boldsymbol{x},0) = \bar{\theta} \qquad \boldsymbol{x} \in \Omega \tag{1c}$$

where $Q^1(\theta)$ is a water flux due to the evaporation from the boundary Γ^1 and θ is a function of position $\boldsymbol{x}$ and time t. Here, only the liquid water movement is considered.

For the coupling of the desiccation and fracture, the effect of the cracks should be embedded in the desiccation problem. In this research, the crack surface Γ^2 is considered as a newly created evaporation surfaces and a shield for the permeable flow. The evaporation from the crack surface Γ^2 can be introduced as additional Neumann boundary condition of the initial boundary value problem for the desiccation process Eq. (1):

$$D\frac{\partial\theta}{\partial\boldsymbol{n}} = -Q^2(\theta) \qquad \boldsymbol{x} \text{ on } \Gamma^2 \tag{2}$$

where $Q^2(\theta)$ is a water flux from the crack surface Γ^2 due to evaporation.

The shield for the permeable flow can be expressed as the elimination of the water flux normal to the crack surface Γ^2. The Darcy's low in orthonormal coordinate system $\{\boldsymbol{e}_i\}$ is

$$\boldsymbol{J} = -D\nabla\theta \tag{3}$$

where $\boldsymbol{J}$ is a water flux vector in the coordinate system $\{\boldsymbol{e}_i\}$. We define the orthonormal coordinate system $\{\boldsymbol{e}_i'\}$ with $\boldsymbol{e}_3'$ in the normal direction of the crack surface Γ^2. The projection of $\boldsymbol{J}$ on Γ^2 (denoted as $\boldsymbol{J}^c$) in the coordinate system $\{\boldsymbol{e}_i\}$ is expressed as

$$J_i^c = T_{ji}P_{jk}T_{kl}J_l \tag{4}$$

where the coordinate transform matrix T_{ij} and the projection matrix which eliminates the water flux normal to Γ^2 are

$$T_{ij} = \boldsymbol{e}_i' \cdot \boldsymbol{e}_j \tag{5}$$

$$P_{ij} = \begin{cases} 1 & \text{if } i = j = 1, 2 \\ 0 & \text{otherwize.} \end{cases} \tag{6}$$

The introduction of $\boldsymbol{J}^c$ in the place of the $\boldsymbol{J}$ corresponds to the introduction of anisotropic moisture diffusion coefficient in the initial boundary value problem Eq. (1) and the Neumann boundary condition Eq. (2) on the crack surfaces. We solve this initial boundary value problem for the water movement Eq. (1) with the Neumann boundary condition Eq. (2) on the crack surfaces by the ordinary FEM with linear tetrahedral elements.

For the coupling of desiccation and deformation, the volume shrinkage corresponding to the change in the volumetric water content θ should be embedded in the deformation problem. The relationship between the change in volumetric water content and the volumetric drying shrinkage strain ε^v is

$$\varepsilon^v(\boldsymbol{x},t) = \frac{1}{\alpha}\frac{\rho_w}{\rho_d}\{\theta(\boldsymbol{x},0) - \theta(\boldsymbol{x},t)\} \tag{7}$$

where α is a moisture shrinkage coefficient of the powder, ρ_w is the mass density of the water, and ρ_d is a dry bulk density of the powder. When Ω is homogeneous and isotropic, the drying shrinkage strain ε_{ij}^s is

$$\varepsilon_{ij}^s = \begin{cases} \dfrac{1}{3}\varepsilon^v & \text{if } i = j \\ 0 & \text{if } i \neq j. \end{cases} \tag{8}$$

In the case of the desiccation crack phenomenon, the total strain ε_{ij} can be divided into the elastic strain ε_{ij}^e and the drying shrinkage strain ε_{ij}^s. The shrinkage strain ε_{ij}^e does not contribute to the generation of the stress and the strain energy. Therefore, the stress strain relationship and the strain energy I for the desiccation induced deformation problem become

$$\sigma_{ij} = c_{ijkl}(\varepsilon_{kl} - \varepsilon_{kl}^s) \tag{9}$$

$$\mathrm{I} = \int_\Omega \frac{1}{2}\left(\varepsilon_{ij} - \varepsilon_{ij}^s\right)c_{ijkl}\left(\varepsilon_{kl} - \varepsilon_{kl}^s\right)dV \tag{10}$$

where σ_{ij} is a stress tensor and c_{ijkl} is an elastic tensor.

In this paper, the analysis of deformation and fracture are performed by PDS-FEM. For the evaluation of the functional I in Eq. (10), PDS-FEM applies the particle discretization for the variables with a pair of the conjugate geometries; Voronoi tessellations $\{\Phi^\alpha\}$ and Delaunay tessellations $\{\Psi^\beta\}$. The Delaunay block is a tetrahedron on the three-dimensional problem. The detail discretization scheme is shown in Oguni *et al.* [8]. Then, the discretized strain energy I is

$$\hat{\mathrm{I}} = \sum_{\beta=1}^{M}\frac{1}{2}\left(\varepsilon_{ij}^\beta - \varepsilon_{ij}^{s\beta}\right)c_{ijkl}^\beta\left(\varepsilon_{kl}^\beta - \varepsilon_{kl}^{s\beta}\right)\Psi^\beta \tag{11}$$

where M is the number of Delaunay blocks and Ψ^β is the volume of the β-th Delaunay blocks. The displacement u_i^α minimizing the discretized strain energy Eq. (11) is satisfying the next equation of the force equilibrium:

$$\sum_{\gamma=1}^{N} K_{ik}^{\alpha\gamma}u_k^\gamma = f_i^\alpha \tag{12}$$

where

$$K_{ik}^{\alpha\gamma} = \sum_{\beta=1}^{M} B_j^{\beta\alpha} c_{ijkl}^{\beta} B_l^{\beta\gamma} \Psi^{\beta} \quad (13)$$

$$\varepsilon_{ij}^{\beta} = \sum_{\alpha=1}^{N} \frac{1}{2} (B_j^{\beta\alpha} u_i^{\alpha} + B_i^{\beta\alpha} u_j^{\alpha}) \quad (14)$$

$$f_k^{\alpha} = \sum_{\beta=1}^{M} \varepsilon_{ij}^{s\beta} \left(c_{ijkl}^{\beta} B_l^{\beta\alpha} \right) \Psi^{\beta}. \quad (15)$$

Here, N is the number of Volonoi blocks. Once the traction on the boundary of Voronoi blocks reach to the tensile strength, the interaction between the Voronoi blocks is lost. This loss of the interaction is introduced by changing a $B_i^{\beta\alpha}$ (and thus stiffness matrix $K_{ij}^{\beta\gamma}$).

NUMERICAL ANALYSIS OF DESICCATION CRACKING

We perform the weak coupling analysis of finite element analysis for the desiccation and the analysis of PDS-FEM for the deformation and the fracture. The FEM analysis for the desiccation process is carried out with a constant time step Δt=0.1 hour. Then, the analysis for the deformation and the fracture is performed by PDS-FEM at each time step. When the maximum traction among all elements reached to the 97% of the tensile strength, the time step us reduced to Δt=0.01 hour to capture the effect of the fracture surfaces on the desiccation and deformation promptly.

One-dimensional Crack Pattern

In the case of desiccation test on bars in Peron *et al.* [4], the mixture of water and clayey silt is shaped in a thin rectangular bar and the bar is dried on the plate. The bottom surface of the bar is constrained in the long side direction only by the notches on the plate. In this test, the cracks formed on the top surface are parallel to each other and normal to the long side.

In this paper, we perform the simulation to reproduce this experimental result. The model size and the parameters for the simulations are determined from the experiments of Peron *et al.* [4]; see Table 1. The water evaporates from the top surface and the sides of the model. The initial volumetric water content is 72.1% (constant) and the desiccation proceeds until the averaged volumetric water content reached to the 32.4% (the averaged volumetric water content at which the crack propagation terminated in the desiccation test of Peron *et al.* [4]). The nodal displacement of the bottom surface of the model is constrained in the long side direction and the vertical direction. We prepared the finite element model with the unstructured mesh (the number of the elements is 56,597 and the number of nodes is 11,822).

Table 1 The model size and the parameters for the simulation of one-dimensional crack pattern.

Model size	300 × 50 × 12 mm
Soil dry density ρ_d	2.77×10^3 kg/m^2 hour
Evaporation speed on Γ^1	2.0×10^{-4} m/hour
Evaporation speed on Γ^2	1.0×10^{-4} m/hour
Moisture shrinkage coefficient α	0.64
Moisture diffusion coefficient D	3.6×10^{-6} m^2/hour
Poisson's ratio	0.3
Young's modulus	5.0 MPa
Tensile strength	0.45 MPa

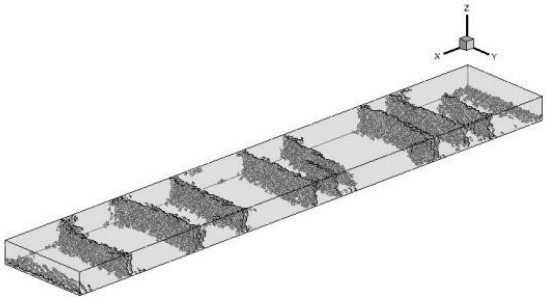

Fig. 1 Simulation results of the one-dimensional crack pattern.

The simulation result (Fig. 1) shows that the final crack pattern formed by the simulation. The all cracks are parallel to each other and normal to the long side. These geometric features of the cracks and the number of cracks formed on the top surface are coincide with the experimental observation of Peron *et al.* [4].

Two-dimensional Crack Pattern

The drying tests for the comparison with simulation results of two-dimensional crack pattern

We perform the drying tests of calcium carbonate slurry to observe the crack patterns corresponding to the thickness of the specimen and measure the parameters for the simulation of two-dimensional crack pattern. The calcium carbonate slurry was prepared at volumetric water content 72%. The slurry was poured into the rectangular acrylic container (100×100×50 mm). The thickness of the specimen was set as 5 mm, 10 mm, 20 mm, and 30 mm. The slurry was dried in the air (20 °C temperature and at 50 % relative humidity) until the

specimen dried out completely.

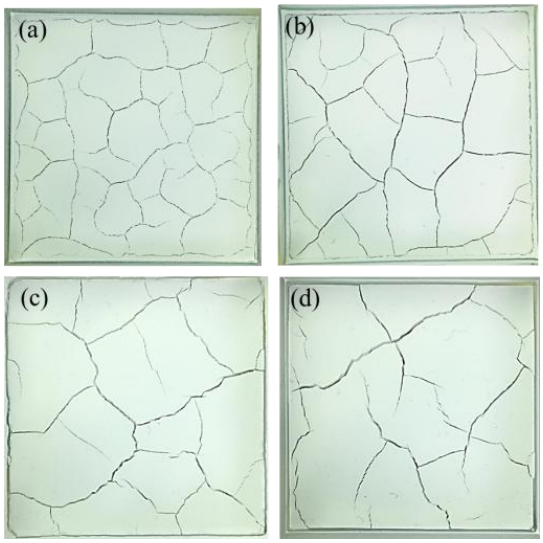

Fig. 2 Final crack pattern on the top surface of the specimen formed in drying test. (a) 5 mm, (b) 10 mm, (c) 20 mm, and (d) 30 mm.

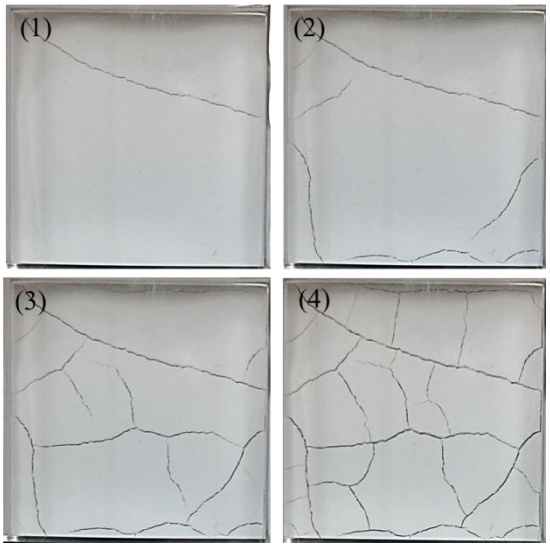

Fig. 3 Crack propagation process of the drying test in the case of 10 mm thickness.

The excessive water layer disappeared at the volumetric water content 56.0% and the crack initiated at the volumetric water content 22.4%. The crack propagation terminated at the volumetric water content 20.4%. Figure2 shows the final crack patterns on the top surface of the specimen with different thickness. The cracks with net-like structure form the polygonal cells framed by the cracks and the averaged size of the cells increase with the increase of the specimen thickness. As shown in Fig. 3, in the crack pattern formation process, some long cracks initiates on the edge of the specimen and traverse the specimen on the initial stage of the desiccation cracking. Then, relatively short cracks appear to tessellate the lager cells. These cracks often branch and terminate when they meet the existing cracks.

The simulation of two-dimensional crack pattern

We perform the simulation to reproduce the two-dimensional crack pattern observed in the drying test of calcium carbonate slurry. The width and height of the model is set as 100 mm and the depth was set as 5 mm, 10 mm, 20 mm, and 30 mm. The parameters for the simulation of two-dimensional crack pattern are shown in Table 2. The water evaporates from the top surface of the model and the nodal displacement on the sides and bottom surface of the model is constrained. The initial volumetric water content is 56.0% (constant) and the desiccation proceeds until the averaged volumetric water content reached to the 20.4%. We prepared the finite element model with the unstructured mesh; the mesh sizes are shown in Table 3.

The final crack pattern on the top surface model with different thickness is shown in Fig.3. The cracks have a net-like structure and form polygonal cells. The cell sizes are almost constant on each thickness and the averaged cell size increases with the increase of the thickness. These geometric features of the crack patterns and the increase tendency of the averaged cell size qualitatively coincide with the observation of the drying experiments of calcium carbonate slurry shown in Fig.2. In the crack pattern formation process, some long cracks extend traversing the top surface. Then, relatively short cracks propagate to tessellate the lager cells. This hierarchical sequence of the cell formation can be also observed in the drying tests of calcium carbonate slurry.

Table 2 The parameters for the simulation of two-dimensional crack pattern.

Soil dry density ρ_d	800 kg/m^2 hour
Evaporation speed on Γ^1	8.8×10^{-5} m/hour
Evaporation speed on Γ^2	1.0×10^{-5} m/hour
Moisture shrinkage coefficient α	0.69
Moisture diffusion coefficient D	3.6×10^{-6} m^2/hour
Poisson's ratio	0.3
Young's modulus	5.0 MPa
Tensile strength	1.6 MPa

Table 3 The mesh sizes for the simulation of two-dimensional crack pattern.

model size [mm]	number of nodes	number of elements
100×100×5	253,930	50,355
100×100×10	278,337	51,726
100×100×20	309,509	55,304
100×100×30	347,551	61,146

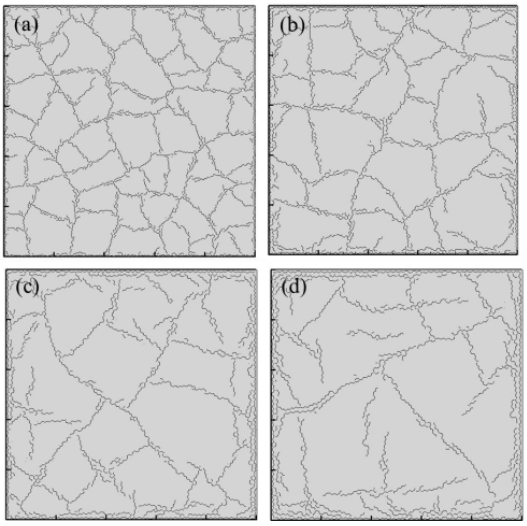

Fig. 4 The final crack pattern on the top surface of the specimen formed in the simulation. (a) 5mm, (b) 10mm, (c) 20mm, and (d) 30mm.

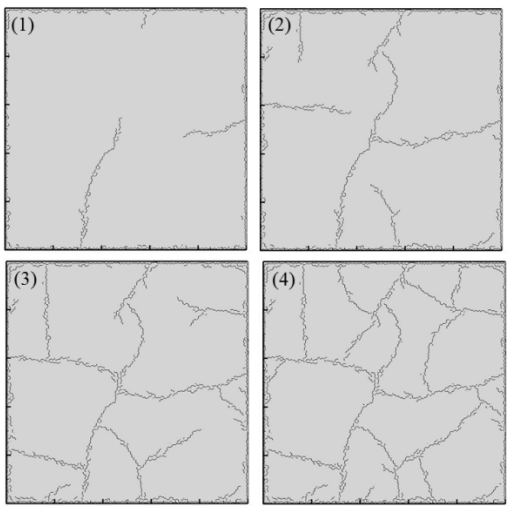

Fig. 5 The crack propagation process of the drying test in the case of 10 mm thickness.

CONCLUSION

In this paper, the coupling model of desiccation, deformation, and fracture is proposed. The simulation for the one-dimensional crack pattern and two-dimensional crack pattern is performed based on this model and the results of the simulation of the two-dimensional crack pattern are compared with the results of the drying test of calcium carbonate slurry. The simulation results show the satisfactory agreement with the experimental observation in terms of the crack pattern with net-like structure, pattern formation process, and the change in size of the cells framed by the cracks depending on the thickness of the desiccation layer. This agreement between the simulation results and the experimental observations indicates that the coupling of desiccation, deformation, and fracture is a fundamental mechanism of the desiccation cracking.

REFERENCES

[1] A. Groisman and E. Kaplan, “An experimental study of cracking induced by desiccation”, Europhysics. Letters. Vol. 25, 2006, pp. 415-420.

[2] H. Nahlawi and J.K. Kodikara, “Laboratory experiments on desiccation cracking of thin soil layers”, Geotechnical and Geological Engineering. Vol. 24, 2006, pp. 1641-1664.

[3] H.J. Vogel, H. Hoffmann, A. Leopold and K. Roth, “Studies of crack dynamics in clay soil II. a physically based model for crack formation”, Geoderma. Vol.125, 2005, pp. 213-223.

[4] H. Peron, T. Hueckel, L. Laloui and L.B. Hu, “Fundamentals of desiccation cracking of fine-grained soils: experimental characterization and mechanisms identification”, Canadian Geotechnical Journal. Vol. 46, 2009, pp. 1177-1201.

[5] G. Musielak and T. Śliwa, “Fracturing of clay during drying: modelling and numerical simulation”, Transp Porous Med. Vol. 95, 2012, pp. 465-481.

[6] J.Sima, M. Jiang and C. Zhou, “Numerical simulation of desiccation cracking in thin clayey layer using 3D discrete element modelling”, Computers and Geotechnics. Vol. 56, 2014, pp. 168-180.

[7] R. Rodríguez, M. Sánchez, A. Ledesman and A.L loret, “Experimental and numerical analysis of desiccation of mining waste”, Canadian Geotechnical Journal. Vol. 44, 2007, pp. 644-658.

[8] H. Peron, J.Y. Delenne, L. Laloui and M.S. El Youssoufi, "Discrete element modelling of drying shrinkage and cracking of soils", Computers and Geotechnics. Vol. 36, 2008, pp. 61-69.

[9] M. L. L. Wijerathne and K. Oguni and M. Hori, "Numerical analysis of growing crack problems using particle discretization scheme", International Journal for Numerical Methods in Engineering, Vol. 80, 2009, pp. 46-73.

[10] K. Oguni, M.L.L. Wijerathne, T. Okinaka and M. Hori, "Crack propagation analysis using PDS-FEM and comparison with fracture experiment", Mechanics of Materials. Vol. 41, 2009, pp. 1242-1252.

Second International Conference on Science, Engineering & Environment,
Osaka City, Japan, Nov.21-23, 2016, ISBN: 978-4-9905958-7-6 C3051

DEVELOPMENT OF A DYNAMIC NETWORK DEA MODEL TO MEASURE PRODUCTION LINE'S PERFORMANCE: A CONCEPTUAL PAPER

N.A.M.A.Zainal[1], M.A.Mansor[1] and S.N.M.Saffe[1]
[1]Faculty of Engineering Technology, Universiti Malaysia Pahang,
Lebuhraya Tun Razak, 26300 Gambang, Kuantan,
Pahang, Malaysia;

ABSTRACT

Production line in manufacturing industry usually is made up of several processes and must go through performance measurement to determine whether they are efficient or inefficient. The extended Data Envelopment Analysis (DEA) which is the Network Data Envelopment Analysis (NDEA) is developed to look inside the production line and find the source of inefficiency of each sub process. However, the model can only measure the efficiency of the production line for current time periods only without considering the past time periods and detect any changes of performances that might occur during the time periods. In this paper, we proposed a Dynamic Network DEA model that can be used to measure the performance of the same production line by taking into account any changes according to time. We treat these changes as a Decision Making Units (DMUs) which is the entity that are going to be measured. This dynamic network model only considered the data inputs from different time periods. Our goals of developing the DNDEA model on the production line are to identify the inputs and outputs required and to consider the relationship and connection between each of the processes in the production line and thus measure the performance of the entire production line. The expected outcome of this paper is to propose a conceptual model that can be used for performance measurement in manufacturing production line dynamically.

Keywords: Dynamic Network DEA, Performance Measurement, Manufacturing System

INTRODUCTION

In the manufacturing industry, a production line is quite an efficient setup for manufacturing and assembling large quantities of products. For example, in the automotive industry, a car is composed of thousands of components and still hundreds of cars are being produced on the production line every single day. If each car was to be assembled individually rather than on a production line, it could take months to produce just one car. Other than quantity, the quality of the product as well as the performance of production line must also be taken into consideration during the products manufacturing. There are many tools that appear great for performance measurement, which one of them is called Data Envelopment Analysis (DEA).

DEA deal with measurements of decision making units (DMU) to find the relative efficiency based on multiple inputs and outputs. The traditional DEA treats the DMU mainly as a black box, within which inputs are supplied to produce outputs and measuring the efficiency of a DMU as a whole unit without taking into account the sub DMUs inside the structure. It also usually neglects carry-over activities between two consecutive terms and only focus on the separate time period independently aiming local optimization in a single period, even if these models can consider the time change effect [1].

Our approach, however, used the combination of dynamic and network DEA model that can overcome the limitation above by measuring the whole DMU, considering the inside of the DMU as well. Thus, in this paper, we proposed a conceptual dynamic network DEA (DNDEA) model that can be implemented for performance measurement of the network structured production line for different time scales in details. By using this model, each of the processes in the production will be measured to find the efficiencies and thus measuring the whole performance of the production line from one period to one another.

LITERATURE REVIEW

Data Envelopment Analysis (DEA)

Data Envelopment Analysis (DEA), first introduced by Charnes et al. (1978), has been proved to be a useful tool in evaluating relative performance of homogeneous decision-making units (DMU) in a multiple-input multiple-output setting [2]. A few of the characteristics that make it powerful is that it can handle multiple input and multiple output models

and doesn't require an assumption of a functional form relating inputs to outputs. It also estimates the efficiency index by calculating the ratio of weighted outputs to weighted inputs, and the input and output weights are decided according to the best interests of the DMU being evaluated.

- DEA can handle multiple input and multiple output models.
- It doesn't require an assumption of a functional form relating inputs to outputs.
- DMUs are directly compared against a peer or combination of peers.
- Inputs and outputs can have very different units. For example, X1 could be in units of lives saved and X2 could be in units of dollars without requiring an a priori tradeoff between the two.

Previous Models of Dynamic Network Data Envelopment Analysis (DNDEA)

Fare and Grosskopf (1996) introduced the dynamic network DEA model which used the formulation of storable inputs to allow a synchronism between the appearance of inputs and the use of inputs in the dynamic production model [2]. These network DEA models allow the researcher to study the "inside" of the usual black box technology both in static and dynamic ways.. They achieve this by providing a very general framework for specifying the inner workings of the black box. The basic idea of the network model is thus to "connect" processes, providing a single model framework for multi-stage production (with intermediate products, for example) or multi-period production. This situation has typically been handled in the DEA literature as a rather ad hoc series of DEA problems, or through the use of multiple stages [3].

Apart from that, Tone and Tsutsui (2014) has developed a dynamic model with network structures within the slack-based measures. Divisions are connected by links and consecutive periods are connected by carry-overs. In the dynamic situation, carry-overs appear in many enterprises. For example, in financial institutions, non-performing loans and profit earned forward are respectively undesirable and desirable carry-overs [3]. Also in medical institutions, numbers of bed and hospital bond are non-discretionary and undesirable ones. Meanwhile, in the electric power industry, the representative carry-overs are generation capacity, transmission line length and distribution transformer [2]. They apply the DNSBM model to a data set consists of 21 U.S. electric utilities over five years and compare the results with those given by the dynamic SBM (DSBM) model. This example deals with the production side of relevant enterprises but not financial side, as shown in Fig.1.

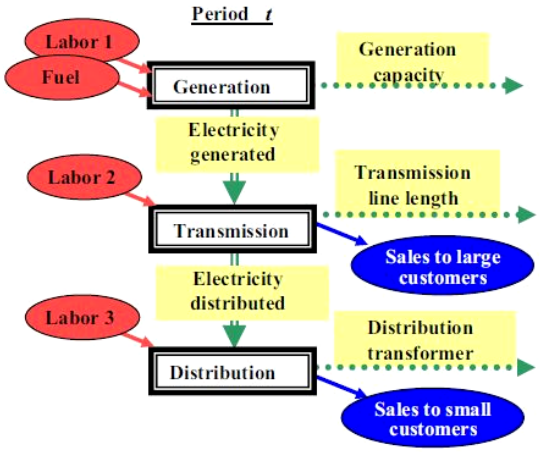

Fig.1 Vertically integrated electric power company

Bogetoft, Färe et al. (2009) introduced the dynamic technology which is their basic model for estimation of optimal private and public investment. The dynamics of our technology are modeled as the choice of consuming total output in the period of production or instead diverting some current production toward adding to the next period capital stock [4]. To provide some intuition for their model, assume that we have three time periods $t-1; t; t+1$ and that there is a technology P^{τ}, $\tau = t-1; t; t+1$. In addition at each τ there are some exogenous inputs x^{τ} and final outputs fy^{τ}. The final output is that part of total production y^{τ} that is not allocated to private iy^{τ} or public gy^{τ} investments, i.e.,

$$y^{\tau} = \boldsymbol{f}\boldsymbol{y}^{\tau} + \boldsymbol{i}\boldsymbol{y}^{\tau} + \boldsymbol{g}\boldsymbol{y}^{\tau} \quad (1)$$

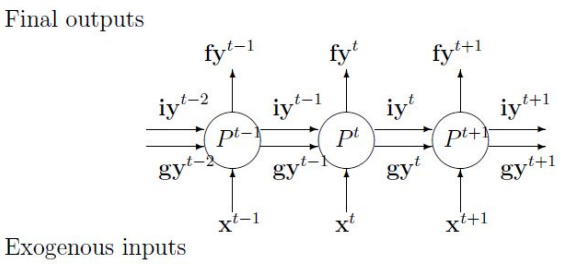

Fig.2 The dynamic technology.

The bottom vertical arrows indicate the exogenous inputs into the respective technologies P^{τ}. The top vertical arrows indicate the final output from each technology. They define the objective function over these final outputs, just as in the Ramsey model. The two horizontal arrows entering each technology represent the private and public investment from the previous period. Thus, decisions concerning consumption versus

investment in one period have consequences in the ensuing periods. One attractive feature of the dynamic model illustrated in Fig 2 is that it can be implemented as a dynamic activity analysis or DEA model. Given that we have k = 1,…, K observations of m = 1,…, M outputs (y_1,…, y_M) and n = 1,…, N inputs (x_1,…, x_N) in each period t, the model may be written for the three period case as;

$$\boldsymbol{P}(\boldsymbol{x}^{t-1}, \boldsymbol{x}^{t}, \boldsymbol{x}^{t+1}, \boldsymbol{iy}^{t-2}, \boldsymbol{gy}^{t-2} = \{\big(\boldsymbol{fy}^{t\text{-}1}, \boldsymbol{fy}^{t}, (\boldsymbol{fy}^{t+1} + \boldsymbol{iy}^{t+1} + \boldsymbol{av}^{t+1} \big)\big) \tag{2}$$

$$\boldsymbol{fy}_{\boldsymbol{m}}^{\boldsymbol{t-1}} + \boldsymbol{iy}_{\boldsymbol{m}}^{\boldsymbol{t-1}} + \boldsymbol{gy}_{\boldsymbol{m}}^{\boldsymbol{t-1}} \leqq \sum_{\boldsymbol{k=1}}^{\boldsymbol{K}} \boldsymbol{z}_{\boldsymbol{k}}^{\boldsymbol{t-1}} \big(\boldsymbol{fy}_{\boldsymbol{km}}^{\boldsymbol{t-1}} + \boldsymbol{iy}_{\boldsymbol{km}}^{\boldsymbol{t-1}} + \boldsymbol{gy}_{\boldsymbol{km}}^{\boldsymbol{t-1}} \big), \forall \boldsymbol{m}, \tag{3}$$

$$\leqq \sum_{\boldsymbol{k=1}}^{\boldsymbol{K}} \boldsymbol{z}_{\boldsymbol{k}}^{\boldsymbol{t-1}}\ \boldsymbol{x}_{\boldsymbol{kn}}^{\boldsymbol{t-1}} \leqq \boldsymbol{x}_{\boldsymbol{n}}^{\boldsymbol{t-1}}, \boldsymbol{n} = \boldsymbol{1}, \dots, \boldsymbol{N}, \tag{4}$$

$$\leqq \sum_{\boldsymbol{k=1}}^{\boldsymbol{K}} \boldsymbol{z}_{\boldsymbol{k}}^{\boldsymbol{t-1}}\ \boldsymbol{iy}_{\boldsymbol{km}}^{\boldsymbol{t-2}} \leqq \boldsymbol{iy}_{\boldsymbol{m}}^{\boldsymbol{t-2}}, \boldsymbol{m} = \boldsymbol{1}, \dots, \boldsymbol{M} \tag{5}$$

$$\leqq \sum_{\boldsymbol{k=1}}^{\boldsymbol{K}} \boldsymbol{z}_{\boldsymbol{k}}^{\boldsymbol{t-1}}\ \boldsymbol{gy}_{\boldsymbol{km}}^{\boldsymbol{t-2}} \leqq \boldsymbol{gy}_{\boldsymbol{m}}^{\boldsymbol{t-2}}, \boldsymbol{m} = \boldsymbol{1}, \dots, \boldsymbol{M} \tag{6}$$

$$\boldsymbol{z}_{\boldsymbol{k}}^{\boldsymbol{t-1}} \geqq \boldsymbol{0}, \boldsymbol{k} = \boldsymbol{1}, \dots, \boldsymbol{K}, \tag{7}$$

$$\boldsymbol{fy}_{\boldsymbol{m}}^{\boldsymbol{t}} + \boldsymbol{iy}_{\boldsymbol{m}}^{\boldsymbol{t}} + \boldsymbol{gy}_{\boldsymbol{m}}^{\boldsymbol{t}} \leqq \sum_{\boldsymbol{k=1}}^{\boldsymbol{K}} \boldsymbol{z}_{\boldsymbol{k}}^{\boldsymbol{t}} \big(\boldsymbol{fy}_{\boldsymbol{km}}^{\boldsymbol{t}} + \boldsymbol{iy}_{\boldsymbol{km}}^{\boldsymbol{t}} + \boldsymbol{gy}_{\boldsymbol{km}}^{\boldsymbol{t}} \big), \forall \boldsymbol{m}, \tag{8}$$

$$\leqq \sum_{\boldsymbol{k=1}}^{\boldsymbol{K}} \boldsymbol{z}_{\boldsymbol{k}}^{\boldsymbol{t}}\ \boldsymbol{x}_{\boldsymbol{kn}}^{\boldsymbol{t}} \leqq \boldsymbol{x}_{\boldsymbol{n}}^{\boldsymbol{t}}, \boldsymbol{n} = \boldsymbol{1}, \dots, \boldsymbol{N}, \tag{9}$$

$$\leqq \sum_{\boldsymbol{k=1}}^{\boldsymbol{K}} \boldsymbol{z}_{\boldsymbol{k}}^{\boldsymbol{t}}\ \boldsymbol{iy}_{\boldsymbol{km}}^{\boldsymbol{t-1}} \leqq \boldsymbol{iy}_{\boldsymbol{m}}^{\boldsymbol{t-1}}, \boldsymbol{m} = \boldsymbol{1}, \dots, \boldsymbol{M}, \tag{10}$$

$$\leqq \sum_{\boldsymbol{k=1}}^{\boldsymbol{K}} \boldsymbol{z}_{\boldsymbol{k}}^{\boldsymbol{t}}\ \boldsymbol{gy}_{\boldsymbol{km}}^{\boldsymbol{t-1}} \leqq \boldsymbol{gy}_{\boldsymbol{m}}^{\boldsymbol{t-1}}, \boldsymbol{m} = \boldsymbol{1}, \dots, \boldsymbol{M}, \tag{11}$$

$$\boldsymbol{z}_{\boldsymbol{k}}^{\boldsymbol{t}} \geqq \boldsymbol{0}, \boldsymbol{k} = \boldsymbol{1}, \dots, \boldsymbol{K}, \tag{12}$$

(13)

$$\leqq \sum_{\boldsymbol{k=1}}^{\boldsymbol{K}} \boldsymbol{z}_{\boldsymbol{k}}^{\boldsymbol{t+1}}\ \boldsymbol{x}_{\boldsymbol{kn}}^{\boldsymbol{t+1}} \leqq \boldsymbol{x}_{\boldsymbol{n}}^{\boldsymbol{t+1}}, \boldsymbol{n} = \boldsymbol{1}, \dots, \boldsymbol{N}, \tag{14}$$

$$\leqq \sum_{\boldsymbol{k=1}}^{\boldsymbol{K}} \boldsymbol{z}_{\boldsymbol{k}}^{\boldsymbol{t+1}}\ \boldsymbol{iy}_{\boldsymbol{km}}^{\boldsymbol{t}} \leqq \boldsymbol{iy}_{\boldsymbol{m}}^{\boldsymbol{t}}, \boldsymbol{m} \tag{15}$$

$$\leqq \sum_{\boldsymbol{k=1}}^{\boldsymbol{K}} \boldsymbol{z}_{\boldsymbol{k}}^{\boldsymbol{t+1}}\ \boldsymbol{gy}_{\boldsymbol{km}}^{\boldsymbol{t}} \leqq \boldsymbol{gy}_{\boldsymbol{m}}^{\boldsymbol{t}}, \boldsymbol{m} = \boldsymbol{1}, \dots, \boldsymbol{M} \tag{16}$$

$$\boldsymbol{z}_{\boldsymbol{k}}^{\boldsymbol{t+1}} \geqq \boldsymbol{0}, \boldsymbol{k} = \boldsymbol{1}, \dots, \boldsymbol{K}, \tag{17}$$

where the $\boldsymbol{z}_{\boldsymbol{k}}^{\boldsymbol{t+1}}$ are intensity variables for k = 1,…, K, $\tau = t-1,\dots, t+1$ in our example. The P technology for period t–1 is modeled by the (3)-(7), where (3) is the output constraint, (4) is the input constraint, (5)-(6) is the intertemporal investment constraints and (7) is the constraint on the intensity variables. Similarly, the period t technology is modeled by (8)-(12) and the t + 1 technology by (13)-(17). Note that each period's technology has its own intensity variables $\boldsymbol{z}_{\boldsymbol{k}}^{\boldsymbol{t+1}}$; $\tau = t–1; t; t + 1; k$ = 1,…, K. Fare and Grosskopf (1996) have shown that the dynamic technology inherits its properties from the single period sub technologies, so in this case the dynamic technology exhibits constant returns to scale and strong disposability of inputs and outputs [4].

Hashimoto et al. (2013) then developed a weighted dynamic network model (WDNM) by adopting a slacks based similar to Tone and Tsutsui (2010, 2012) that focuses on the following matters.

- WDNM does not include slacks of divisions or sub processes in the objective function of the optimization problem.
- WDNM allows for joint outputs produced by more than one division.
- WDNM incorporates ;aged variables in each period.

As an illustration in Fig 3, they assess the dynamic efficiency or productivity performance of Japanese prefectures. Their framework specifies that a prefecture's production process is expressed as a two parallel network system that allows resources to be reallocated between periods so that larger final outputs can be achieved through intertemporal optimization [5].

$$\boldsymbol{fy}_{\boldsymbol{m}}^{\boldsymbol{t+1}} + \boldsymbol{iy}_{\boldsymbol{m}}^{\boldsymbol{t+1}} + \boldsymbol{gy}_{\boldsymbol{m}}^{\boldsymbol{t+1}} \leqq \sum_{\boldsymbol{k=1}}^{\boldsymbol{K}} \boldsymbol{z}_{\boldsymbol{k}}^{\boldsymbol{t+1}} \big(\boldsymbol{fy}_{\boldsymbol{km}}^{\boldsymbol{t+1}} + \boldsymbol{iy}_{\boldsymbol{km}}^{\boldsymbol{t+1}} + \boldsymbol{gy}_{\boldsymbol{km}}^{\boldsymbol{t+1}} \big), \forall \boldsymbol{m},$$

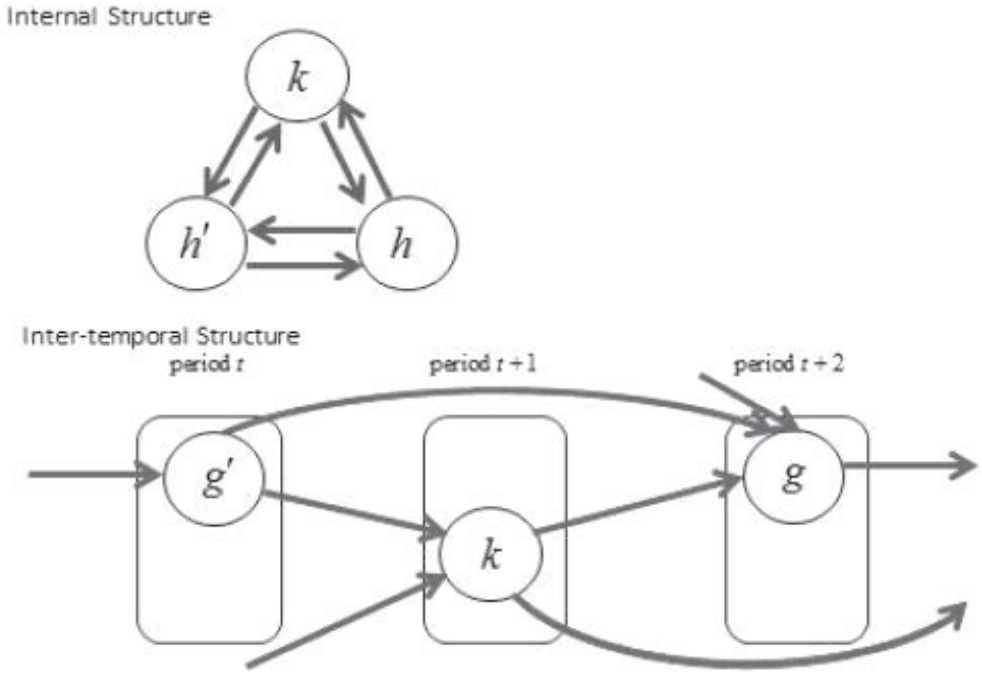

Fig.3 Dynamic Network Structure

Another research done by You and Jie (2016) applied the dynamic network slacks-based measurement model with free links and fixed links to evaluate the operational performance of 31 electric power supply companies in China from 2010 to 2012. Their approach allows for the consideration of the group heterogeneity of electric power transmission and also considers the new structural reform in the power grid of China in the near future, i.e., the separation of the transmission division and the distribution division [6].

RESEARCH APPROACH

In this paper, we implemented the DNDEA model to a manufacturing production line in one of a company in Malaysia. In this model, we treated the production line as the DMU, which is the entity that will be measured to find the efficiency, while the processes in the production line is treated as the sub DMUs. This model enables us to study the relationship between each of the processes in the production line, thus measuring the whole production line in a different time scale.

This research begins by gathering the data set required considering the past and current time periods, which consist of the inputs consumed and the outputs produced by the DMU and sub DMUs. Unlike the previous dynamic models developed by other researchers, our proposed model does not consider any carry-overs because there are no stocks or products kept at the end of the process. The production line should not have stocks or products, causing the production line to be inefficient that will put the company in big losses. All of the stocks and products are produced based on customer's demand and delivered straight away to the customers. Therefore, there will be no links between the production line in a certain period. Theoretically, there are four inputs that literally used in the manufacturing production line, which are the 4M; Manpower, Money, Machine and Method [7]. However, we are going to neglect the Method because it is not a numeric value and thus, it cannot be measured.

There are also other possible inputs that need to be considered in the production line which is the 2T; Time and Training [8]. Time is an index to show how long it takes to complete a certain task where the shorter time consumed is preferred than longer time while training is an activity that can improve the workers' skill that lead to better performance of productivity compared to the workers with less skills [7]. During this research, we might consider other inputs and outputs consumed in the manufacturing industry other than the 4M2T and account the relationship between each of the production line's processes.

Prior to conceptualizing the model, the processes in the production line were studied for better understanding in presenting the structures of the model. At the end of this research, we will compare

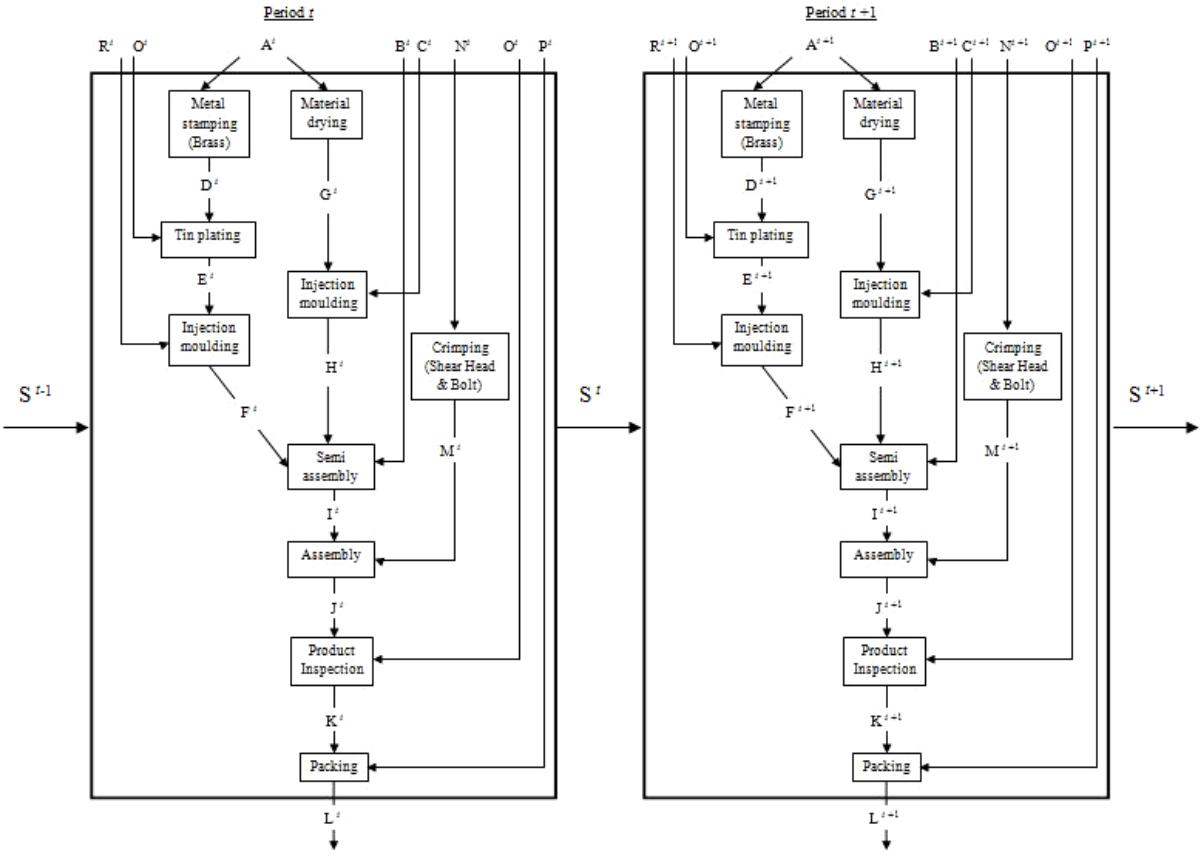

Fig.4 The DMU model for manufacturing production line.

between the DMUs from different periods to observe the efficiencies measured.

CONCEPTUAL MODEL FOR POWER DISTRIBUTION PRODUCTION LINE

As a case study, the DNDEA model was implemented on one of the manufacturing production line that produced electrical parts for power distribution. This production line does describe a network structured model with a combination of a series and parallel structure to form a complex structured model, which enable us to find the source of efficiencies in details. As illustrated in Fig 4, there are 10 processes consist of direct and indirect processes that are denoted as the sub DMUs inside the two production lines, which denoted as the DMUs from two different time scales. Since this model does not consider any carry overs, we illustrated this model to measure the efficiency of the production line, which denoted as S, from period to period and obtain the results, whether they affect each other in terms of the performance and compare which of the production line are efficient or inefficient.

In this model, some of the sub DMUs are linked to the other sub DMUs based on the inputs they consumed and the outputs they produced.

Table 1 Inputs and outputs determined.

Items	Inputs/Outputs
A	Material, Money, Machine, Manpower, Time
B	Machine, Manpower, Time
C	Machine, Time
D	Time, Number of Parts Produced
E	Time, Number of Parts Produced
F	Time, Number of Parts V
G	Time, Number Of First Piece Sample
H	Time, Number of Parts W
I	Time, Number of Semi Finished Product X
J	Time, Number of Semi Finished Product X
K	Time, Number of Finished Product Z, Number of Rejected Parts
L	Time, Number of Finished Product Z
M	Time, Number of Parts Y
N	Material, Money, Manpower, Time
O	Machine, Manpower
P	Machine, Manpower
Q	Machine, Manpower
R	Machine, Manpower

The numbers and types of inputs and outputs

used may vary according to the sub DMUs determined, refer to Table 1.

CONCLUSION

We proposed the Dynamic Network DEA model to look inside the DMU, allowing greater insight as for measuring the efficiency of the production line. In this research, the model proposed is a combination of both series and parallel structures to form a complex structure. This model applies to the DMUs that consist of several sub DMUs, some of which consume the outputs produced by other sub DMUs and some of which produce the inputs consumed by another sub DMUs. The relationship between the sub DMUs will also be considered during the performance measurement of the production line. Our Dynamic Network DEA model allows for either an input orientation or an output orientation, and it's the only also can used to measure the network structures of the DMU for a different time scale. The model proposed is based on a case study of manufacturing production line that produced electrical parts power distribution and might differ from other production line, especially the relationship between the processes.

To complete the research, this model will be applied as a benchmark for different time scales. Then the results will be computed as to acknowledge which time scale of the production is more efficient and assist the company to appraise the production line's performance.

ACKNOWLEDGEMENTS

The research for this paper was financially supported by the Ministry of Higher Education (MOHE) of Malaysia under the project amount RDU151310 of the Research Acculturation Collaborative Effort (RACE) research grant.

REFERENCES

[1] Tone, K. and M. Tsutsui (2010). "Dynamic DEA: A slacks-based measure approach." Omega 38(3–4): 145-156.

[2] Chen, C.-M. (2009). "A network-DEA model with new efficiency measures to incorporate the dynamic effect in production networks." European Journal of Operational Research 194(3): 687-699.

[3] Tone, K. and M. Tsutsui (2014). "Dynamic DEA with network structure: A slacks-based measure approach." Omega 42(1): 124-131.

[4] Bogetoft, P., Färe, R., Grosskopf, S., Hayes, K., & Taylor, L. (2009). Dynamic network DEA: An illustration. Journal of the Operations Research Society of Japan, 52, 147–162.

[5] Hashimoto, A., Fukuyama, H., & Tone, K (2013). "Dynamic Network DEA and An application to Japanese Prefectures."

[6] You, Y. Q. and T. Jie (2016). "A study of the operation efficiency and cost performance indices of power-supply companies in China based on a dynamic network slacks-based measure model." Omega **60**: 85-97.

[7] N.A.M.A.Zainal, M.A.Mansor & S.N.M.Saffe (2016). "Development of A Network DEA Model To Measure Production Line's Performance: A Conceptual Paper." Manuscript accepted for International Journal of Applied Engineering Research (IJAER) online special issue.

[8] M.A.Mansor, L.H.Shah, & H.Che Hussain (2012). "Maintenance performance of Malaysia's automotive sector: A case study." ICoCSIM vol. 1 (2012) 271-275

Second International Conference on Science, Engineering & Environment,
Osaka City, Japan, Nov.21-23, 2016, ISBN: 978-4-9905958-7-6 C3051

INVESTIGATING THE RELATIONSHIP BETWEEN RAINFALL INTENSITY, CATCHMENT VEGETATION AND DEBRIS MOBILITY

Rick Jaeger[1] and Terry Lucke[1]
[1]Stormwater Research Group, University of the Sunshine Coast, Australia

ABSTRACT

Urbanisation creates the need for engineered hydraulic structures in catchments, floodplains and watercourses. These include piped and open-channel drainage networks, flood control systems and waterway crossings such as culverts and bridges. During larger storm events, debris and other material located higher in the catchment can be mobilised and transported towards these hydraulic structures creating the potential for blockages. This debris is often trapped by the hydraulic structures, causing partial or full blockage which can reduce the flow capacity of the structure. This may cause upstream flooding during high intensity rainfall events. This study investigated the debris transport behaviour in a natural channel. A model of an existing catchment and culvert system in Australia was build based on Froude similitude scaling. Different sized twigs were used to replicate natural debris of various sizes. The experimental results demonstrated that the mobility of debris during rainfall events was dependent on a range of factors including stream depth and width, the size and availability of debris, and on the condition of the riparian vegetation within the catchment. This could have significant implications for culvert design and maintenance procedures.

Keywords: Culvert design, catchment vegetation, flooding, debris transport, stormwater.

INTRODUCTION

The increase in impervious surface areas accompanying urban development has increased both the total volume of stormwater runoff, and the speed at which concentrated stormwater flows reach downstream receiving waters [1, 2]. Consequently, the management of stormwater in urban areas has become a significant issue for those responsible for planning and construction of new developments, and the maintenance of existing stormwater infrastructure [3].

The installation of culverts is a traditional approach to managing stormwater flows caused by the runoff from storm events and they have been shown to be a reliable method of managing flood risk in urban areas [4]. Culverts are generally placed within the channel of both natural and artificial waterways and this can often result in flow constrictions within the channel. These constrictions can be the limiting factor during high intensity rainfall events which might lead to flooding. Culverts are also prone to blockage by a range of different flow conditions which can further increase the risk of flooding. Culvert blockages can also result in higher flood levels, changes to stream flow patterns, changes to stream bed and bank erosion, changes in sediment deposition patterns in channels, as well as physical damage to the culvert and surrounding structure caused by debris [5, 6].

Several main factors have been identified that influence the blockage of culverts by debris. These include:

- Debris (variety, size, amount, type)
- Debris availability (permanent, infrequent)
- Mobility (capability of debris to be moved)
- Interactions of debris with the structure itself.

The type, size and amount of debris, and its influence on blockage have been classified previously in a report by Engineers Australia [7]. However, many of the assumptions underpinning the classifications in this report remain untested. There is still much uncertainty regarding debris movement in natural channels where a variety of factors can influence the debris mobility. To further investigate these uncertainties and to address this knowledge gap, a series of laboratory experiments was undertaken in this study. The hydraulic performance of an existing culvert and channel in Nambour, Australia, was modelled in the laboratory in order to improve understanding of debris movement within the channel, as well as the main factors influencing this movement.

PREVIOUS RESEARCH

A scaled laboratory model was used to investigate the debris mobility of the existing Nambour culvert. Froude similitude scaling was used to achieve realistic flows in the model [5]. Froude similitude scaling is one of the most traditional methods used to scale laboratory experiments [5, 8-10]. The Froude number is a dimensionless ratio between the flow velocity and gravitational forces together with the characteristic length [11]. This method focuses on sub- and super-critical flow conditions, as well as on the flow velocities within the stream, rather than relying on turbulence differences described by the Reynolds number [9]. While there are limitations to this method, it has been found to be an acceptable method of analysing open-channel flows with low Reynold numbers in the area of interest [12].

Blockage of hydraulic structures remain unpredictable in most cases as the process is based on a number of highly-variable factors. The first unknown factor is blockage of the culvert itself. While much research has been done in this area, a precise tool to predict blockage has yet to be developed [13]. The likelihood of a blockage is highly dependent on the dimension and geometry of the culvert, as well as the debris shape, size and availability. Whereas culvert geometry can be determined precisely, the debris availability is highly dependent on the upstream riparian fauna and on its mobility [7, 14]. Riparian vegetation is not as easy to assess as culvert properties and its composition is also likely to change over time. However, it is possible to obtain a general assessment of upstream conditions through local inspections or low-level aerial photography [15]. Knowledge regarding the condition of the upstream vegetation is an important factor in predicting the shape and size of the debris. However, an element of uncertainty still remains [15].

Debris availability in Australia is generally classified into high, medium and low availabilities [6]. A high availability of debris can be found in dense forests with thick vegetation, as well as in urban areas where a variety of loose materials are available. Areas with an irregular distribution of rainfall with high rainfall intensities are also known for their high debris availability [6]. Low debris availability areas on the other hand are characterized by rural lands, uniform annual rainfall and stable banks with flat or moderate slopes. The medium debris availability covers everything in between the first two categories [7].

If debris is available, it is often mobilized by wind or by flooding. Branches, and even whole trees, can break off or fall down during strong winds and these can end up in the channel and be washed downstream. During flooding, more area is covered by water and debris deposited on higher ground might be mobilized by the expanded channel flow [16]. Once the debris is entrained in a stream, it generally travels a random distance depending on the length and size of the debris, the width and depth of the streambed, flow velocities and the number of obstacles, as well as the distance between them [10, 17].

A number of previous studies have investigated the entrainment and transportability of debris. van Sickle and Gregory [18] developed a general probabilistic model for the provision of large woody debris (LWD) from falling trees. Their model could predict LWD's volume and orientation in the stream fairly well, but lacked the ability to accurately predict the length of the LWD. This was due to a missing function to allow for the breakage of falling trees [18].

In an experiment by Braudrick and Grant [19], the transport and deposition of LWD was investigated using a flume model. They concluded that there is a relationship between the LWD's length, the average channel width and the maximum radius of the channel's curvature. They found that in cases where a large portion of the channel area was less than the buoyant depth of the debris, once they were entrained within the flow, the smaller LWDs would not travel as far along the channel as larger LWDs because of their lack of momentum [19].

Whether or not a LWD is entrained by a stream depends on two main factors: The LWD's orientation and the existence of root balls. LWDs with root balls achieve more stable flow compared to the ones without root balls [8]. The root ball creates an unsymmetrical LWD shape and this tends to result in a bias towards one flow orientation which is more stable than others [8]. At the same time, root balls often result in a greater overall draft, which could result in the LWD getting stuck in shallow depth.

Bocchiola et al. [10, 20] performed a series of laboratory flume experiments to collate information on the jamming behaviour of LWDs. They found that the travelling distance of a LWD depends on its

length, the spacing between any obstacles in the flow, and the force exerted by the current [10]. Their results demonstrated that the likelihood of trapping increases with the LWD's length and decreases with an increasing Froude number, as well as with a greater distance between one obstacle to the next [10].

In cases where the debris reaches the culvert inlet two possibilities may occur: 1) the debris flows through the culvert without causing a reduction in the hydraulic performance; or 2) it gets stuck at the culvert inlet, which can reduce the flow capacity of the culvert and cause upstream flooding. The likelihood for the first case was investigated in experiments as well as in a transient 1D flow model which was able to reproduce the experimental measurements [21].

A review of previous literature has shown that the factors affecting debris mobility in channels and culvert blockage by debris are not well understood. This paper attempts to address this knowledge gap by investigating the mobility behaviour of debris in natural channels both with and without riparian vegetation.

APPROACH

To increase the knowledge on LWD transport behaviour during high intensity rainfall events this study investigated debris movability of an existing culvert by undertaking a modelling study on a scaled laboratory testing rig. The first step involved undertaking a detailed topographic survey of an existing field site located in Nambour, Queensland, Australia (Figure 1). Contour levels of the 15 ha site were established, mapped, and then overlayed into AutoCAD to provide a detailed 3D digital elevation model (DEM). The DEM was then used to construct a 1:25 scale laboratory model of the site to be used in the study.

a)

b)

c)

Figure 1: Study site; a) Existing culvert; b) Upstream catchment characteristics; c) Study area

To scale the model and the flowrates, a Froude similitude approach was chosen. To describe high intensity rain events, the Average Recurrence Interval (ARI) was used, which gives a likelihood on how often certain rainfall events happen statistically [22]. The estimated flowrates for ARI events from 2 to 100 years were modelled with a hydrological analysis using the Watershed Bounded Network Model (WBNM) [23]. The flowrates used in the study were calculated using a Froude similitude scaling approach using Equation 1 [24].

$$\frac{Q_m}{Q} = L^{5/2} = \left(\frac{1}{25}\right)^{5/2} \quad (1)$$

where:

Q_m = Model Discharge (m^3/s)

Q = Real Discharge (m^3/s)

L = Linear Scale Ratio

The flowrates calculated using Equation 1 and tested in the study are listed in Table 1.

Table 1: ARI Flowrates using Froude similitude

ARI (Years)	**Real Flow** (m^3 / s)	**Model Flow** (L / s)
2	14.8	4.74
5	22.0	7.04
10	26.8	8.56
20	33.0	10.5
50	37.7	12.1
100*	43.8*	14.0*

**100 year flows were observed to overtop the model culvert are not included in the paper results*

To model the site topography, a custom-made culvert test rig (Figure 2), comprised of structural steel frame supporting a sealed plywood surface was constructed for the study. The test rig has a capacity to create slopes of up to 15% and had a surface area of approximately 20 m^2. A submersible pump placed in an underground concrete tank (maximum flow rate of 35 L/s) was used to supply any pre-defined storm event for testing.

The site survey DEM was used to produce a 1:25 scaled model test rig. Overlain by a non-woven geotextile and topped with washed river sand, a precisely contoured layer of washed gravel (up to 25 mm diameter) was placed on the culvert test rig to produce the scale model of the upstream characteristics of the field study culvert (Figure 2).

Twigs and other natural materials were placed along the sides of the channel model up to 2 m upstream (50 m in real stream) to replicate existing vegetation. No vegetation was replicated along the channel sides between 2 m and 4 m (Figure 2) in order to evaluate the effects of having no vegetation.

Purpose built, transparent scale models of the existing Nambour culverts were positioned two-thirds of the way along the test rig to simulate (as far as practicable) a scale model of the existing site conditions (Figure 2).

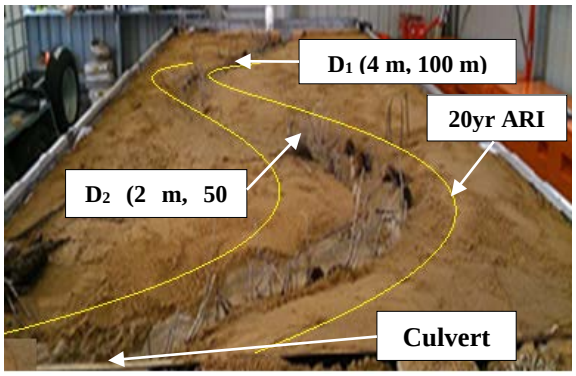

Figure 2: Laboratory Model Used in Study (looking upstream); 20yr ARI flowlines highlighted

The existing Nambour culverts were designed to withstand a 1% average exceedance probability (AEP) flood event [22] and the range of flows in Table 1, calculated by Froude similitude were tested in the study. It was found that the model overtopped at the 100 years ARI rainfall intensity of 43.8m^3/s (14.0 L/s on model) so these results were not included in the study findings.

DEBRIS – TRANSPORT

For the debris mobility testing, scaled twigs were used to model LWD movement within the stream. Smaller diameter, shorter twigs were used to model smaller LWDs and larger diameter, longer twigs were used to model large LWDs (Table 2).

Table 2: Debris dimensions and scaling at 1:25

Debris		**S**	**M**	**L**
Length	Real (m)	L < 1.5	1.5 >L < 2.9	3 > L < 4.5
	Real (mm)	L < 60	60 > L < 116	120 > L < 180
Diameter	Real (m)	50 - 100	125 - 150	175 - 200
	Real (mm)	2 - 4	5 - 6	7 - 8
Channel width	Real		3 m	
	Model		120 mm	

To compare the mobility between different release areas and the influence of the vegetation, two different LWD drop-in locations were chosen (D_1 and D_2). D_1 was approximately 4 m upstream (100 m in real channel) of the model culvert inlet and was directly within the first curve of the stream. D_2 was approximately 2 m upstream (50 m in real channel) of the model culvert inlet and was in the second curve. Vegetation was installed along the sides of the model channel up to location D_2 to replicate the real vegetation (Figures 3 & 4).

A set amount of various sized debris was dropped at these locations and then monitored. Each flowrate was tested with all three different debris sizes. After stable flow conditions were established for each ARI, 10 twigs of each debris size were released at points D_1 and D_2. After 10 minutes, the flow was switched off and the number of twigs stuck in the stream bed were counted as well as the number that went through the culvert. Each test was repeated five times.

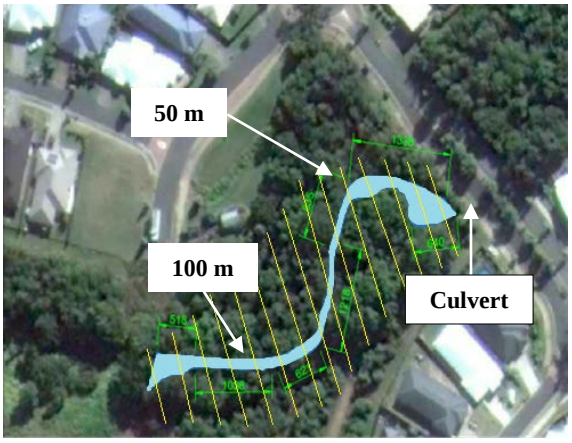

Figure 3: Real stream debris release distances (scaled in model); streambed and 50yr ARI flow area highlighted (hatched yellow)

The vegetation installed along the sides of the second curve would become submerged incrementally as higher flowrates were tested. As vegetation was only modelled in the curve (Section B-B in Figure 4) and stream closer to the culvert, its influence on the debris trapping could be analysed and compared to the debris mobility upstream in Section A-A (Figure 4) as both curves had similar shapes and profiles. Only the directions of the curves were different.

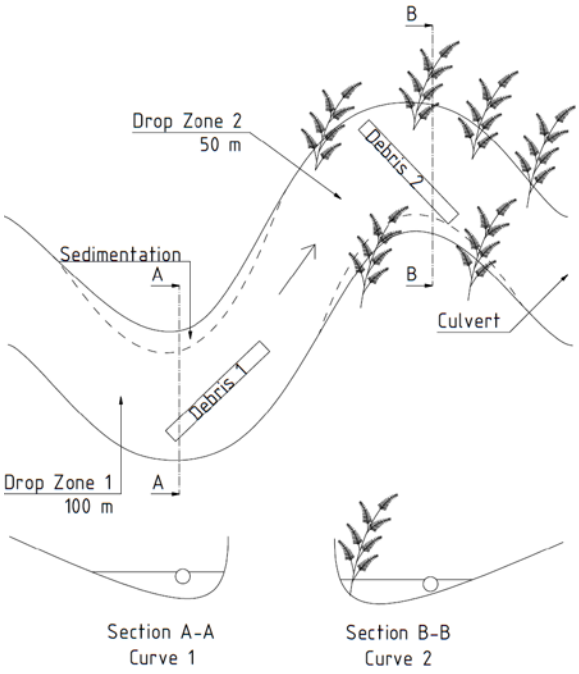

Figure 4: Debris flow in the channel (not scaled)

DEBRIS – TRANSPORT – PRELIMINARY RESULTS

The debris mobility testing identified different trends depending on the distance the debris travelled. When the twigs were deposited into the stream at location D_1 (100 m), the maximum amount of debris reaching the culvert was found to occur during the simulated 10 year or 20 year ARI flows for all three debris types (Fig. 5). The amount of debris reaching the culvert was generally less for lower, or higher simulated ARI flow conditions. Interestingly, the percentage of debris reaching the culvert during the 50 year ARI flow was similar to that observed during the 2 year ARI flow. It was observed that the debris gained mobility with increasing depth and width of the channel.

Between the 20 year and the 50 year simulated ARI flows, the behaviour of the channel flow changed significantly. The main flow remained in the channel up to the 20 year ARI. However, as the flow approached the 50 year ARI flowrate, the flow tended to overtop the sides of the channel and spread out over a greater area (Fig. 2). This resulted in a variety of new, shallower flow paths being established. A significant amount of the debris was found to become trapped in these newly flooded areas due to the shallower water depths, despite having no vegetation.

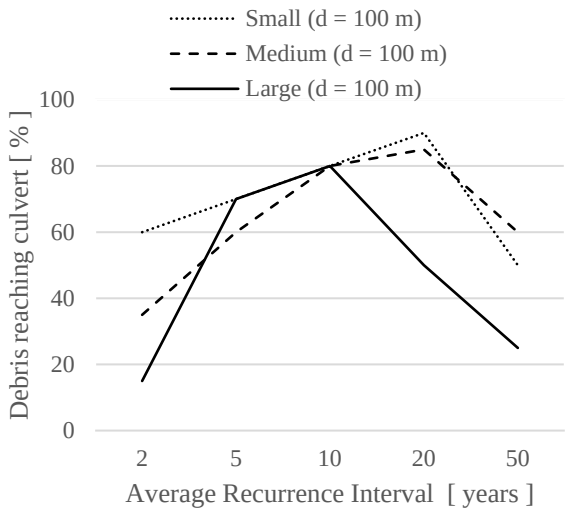

Figure 5: Percentage of debris reaching the culvert when dropped in at location D_1 (100 m)

When the debris was dropped into the stream at location D_2 (50 m from the culvert), the results demonstrate very different mobility behaviour (Figure 6). Initially, the amount of debris reaching the culvert reduced as the channel flowrate increased. The minimum amount reaching the culvert was observed to occur between the simulated 10 year and 20 year ARI flows for all three debris types. At

flows of 20 years and above, the amount of debris reaching the culvert started increasing again (Figure 6).

It was observed that the simulated vegetation next to the streambed became more submerged as the water levels increased with the higher ARI flowrates. This resulted in more debris becoming stuck within the riparian vegetation zones while trying to establish a stable position within the flow. The minimum amount of debris reached the culvert during the simulated 10 year ARI flow event for the small and medium sized debris. However, the minimum amount of large debris was observed during the 20 year ARI event. With higher flowrates during the 20 and 50 year ARI the flow velocities increased, which lead to higher dragging forces that tended to move the debris further downstream.

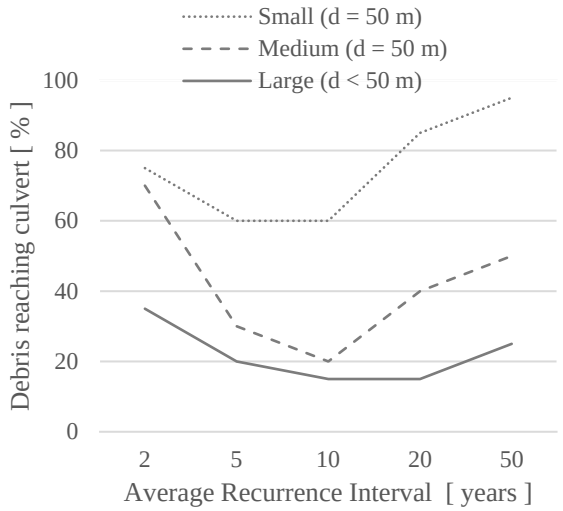

Figure 6: Percentage of debris reaching the culvert when dropped in at location D_2 (50 m)

DISCUSSION

During the drop-in location D_1 experiments, it was found that most of the debris would try to align itself with the stream flow and then travel downstream to reach the culvert. As there was no vegetation next to the stream between locations D_1 and D_2, the debris had more time to align itself with the flow in the stream without being hindered by riparian vegetation. It was observed that once the debris found a stable position within the flow, it tended to maintain this position and travel all the way to the culvert entrance.

However, for the 2 year and 50 year ARI flowrates, a higher amount of the debris became lodged in the channel due to lower water depth and smaller channel width. During the 50 year ARI flow, the water levels were relatively high and some debris left the former streambed which led to debris being trapped in these flooded area due to low water depths.

The results of the experiments using drop-in location D_2 with simulated vegetation along the channel sides were very different. At flows above the 2 year ARI, when the debris started to flow in between the simulated channel vegetation at location D_2, a high proportion of the debris became trapped within the vegetation. It was observed that the minimum amount of debris was trapped during the simulated 10 year and 20 year ARI flows (Figure 6).

With further increasing flowrates, a higher percentage of debris reached the culvert. This appeared to be due to higher flow velocities, and therefore higher drag forces being exerted on the debris. The flooded terrain had no significant influence on the debris when it was released closer to the culvert at location D_2. The most direct route to the culvert was still within the existing channel and this led to most debris remaining in the channel and reaching the culvert.

In order to visualise the general differences between debris dropped in to the flow at locations D_1 and D_2, the average of the two sets of results were calculated. These results are shown on Figure 7.

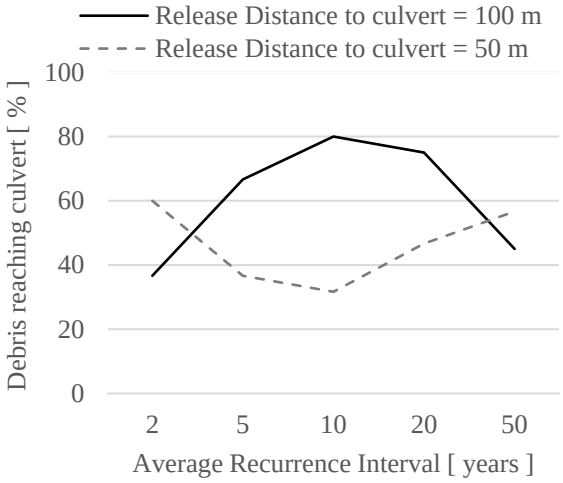

Figure 7: Average amount of debris reaching the culvert from both locations (50 m and 100 m)

Figure 7 shows that the maximum amount of debris reached the culvert during the 10 year ARI flowrate in non-vegetated channels. Conversely, Figure 7 shows that the 10 year ARI flowrate also resulted in the minimum amount of debris reaching the culvert in vegetated channels.

These results suggest that the potential for culvert blockage could be highly dependent on the condition of the riparian vegetation in the catchment. This could have significant implications for culvert design and maintenance procedures. However, further research would be required to investigate this in more detail.

CONCLUSION

This study investigated debris mobility in natural channels during high intensity rainfall events. The Although the study was undertaken on a 1:25 scaled laboratory model. Due to the extremely variable characteristics of natural (and simulated) rainfall events [25], and the associated risk of flooding, results observed during testing of the culvert rig were also found to be highly variable. The study findings have resulted in a better understanding of the factors that affect debris transportability and mobility in natural streams and channels. The main findings of the study were:

- Smaller debris is more likely to move downstream - the ratio between debris length and shape to channel width was found to be an important predictor of debris mobility.
- Low water depth can hinder debris mobility - greater water depth and a greater channel width promote debris transportability.
- Obstacles within the stream increase the likelihood of debris becoming trapped.
- Higher flow velocities were generally found to reduce debris trapping within the main channel due to increased drag forces.

The variable nature of the results of this study suggest that further research is required to develop an accurate model to predict debris transport. The experiments showed that the debris transportability is not only highly dependent on the flowrate and the size of the debris, but also on the point of entrance into the stream and on any obstacles along the stream bed.

The results of this study may have implications for culvert cleaning and maintenance schedules. They also suggest that it may be important for designers to take the amount and size of existing, and future, upstream catchment vegetation, as well as the local site environmental conditions into account during the culvert design stage.

The study results suggest that the increased stream depth and width (and the rate of this change) that occur during rainfall events, as well as the size and availability of debris, may be the main drivers that influence culvert blockage and potential flooding. However, more research is needed to verify this.

REFERENCES

[1] T. Lucke and S. Beecham, “Field investigation of clogging in a permeable pavement system,” *Building Research and Information*, vol. 39, no. 6, pp. 603–615, 2011.

[2] M. E. Dietz, “Low impact development practices: A review of current research and recommendations for future directions,” *Water, Air, and Soil Pollution*, vol. 186, no. 1-4, pp. 351–363, 2007.

[3] P. W. Nichols, R. White, and T. Lucke, “Do sediment type and test durations affect results of laboratory-based, accelerated testing studies of permeable pavement clogging?” *Science of The Total Environment*, vol. 511, pp. 786–791, 2015.

[4] E. J. Plate, “Flood risk and flood management,” *Journal of Hydrology*, vol. 267, no. 1-2, pp. 2–11, 2002.

[5] J. Blanc, N. P. Wallerstein, G. B. Wright, and S. Arthur, “Analysis of the performance of debris screens at culverts,” *Proceedings of the Institution of Civil Engineers: Water Management*, vol. 167, no. 4, pp. 219–229, 2014.

[6] W. Weeks, G. Witheridge, E. Rigby, A. Barthelmess, and G. O'Loughlin, “Australien Rainfall & Runoff - Project 11: Blockage of Hydraulic Structures: Stage 1 Report,” Engineers Australia, Barton ACT 2600, Australia, 2009. Accessed on: May 10 2016.

[7] W. Weeks, G. Witheridge, E. Rigby, A. Barthelmess, and G. O'Loughlin, “Australien Rainfall & Runoff - Project 11: Blockage of Hydraulic Structures: Stage 2 Report,” Engineers Australia, Barton ACT 2600, Australia, Feb. 2013. Accessed on: Apr. 07 2016.

[8] C. A. Braudrick and G. E. Grant, “When do logs move in rivers?,” (en), *Water Resources Research*, vol. 36, no. 2, pp. 571–583, http://onlinelibrary.wiley.com/doi/10.1029/1999WR900290/pdf, 2000.

[9] N. P. Wallerstein, C. V. Alonso, S. J. Bennett, and C. R. Thorne, “Distorted Froude-scaled flume analysis of large woody debris,” (en),

Earth Surface Processes and Landforms, vol. 26, no. 12, pp. 1265–1283, 2001.

[10] D. Bocchiola, M. C. Rulli, and R. Rosso, "Transport of large woody debris in the presence of obstacles," *Geomorphology*, vol. 76, no. 1-2, pp. 166–178, 2006.

[11] H. Chanson, *The Hydraulics of Open Channel Flow: An Introduction; Basic Principles, Sediment Motion, Hydraulic Modelling, Design of Hydraulic Structures*. Amsterdam: Butterworth-Heinemann, 2004.

[12] H. Chanson, "Turbulent air–water flows in hydraulic structures: Dynamic similarity and scale effects," *Environ Fluid Mech*, vol. 9, no. 2, pp. 125–142, 2009.

[13] J. B. Bradley, D. L. Richards, and C. C. Bahner, *Debris control structures: Evaluation and countermeasures*, 3rd ed. [Washington, D.C.]: U.S. Dept. of Transportation, Federal Highway Administration, 2005.

[14] A. M. Gurnell, H. Piegay, F. J. Swanson, and S. V. Gregory, "Large wood and fluvial processes," *Freshwater Biol*, vol. 47, no. 4, pp. 601–619, 2002.

[15] C. J. Gippel, B. L. Finlayson, and I. C. O'Neill, "Distribution and hydraulic significance of large woody debris in a lowland Australian river," (en), *Hydrobiologia*, vol. 318, no. 3, pp. 179–194, http://link.springer.com/content/pdf/10.1007%2FBF00016679.pdf, 1996.

[16] A. A. Webb and W. D. Erskine, "Distribution, recruitment, and geomorphic significance of large woody debris in an alluvial forest stream: Tonghi Creek, southeastern Australia," *Interactions between Wood and Channel Forms and Processes*, vol. 51, no. 1–3, pp. 109–126, 2003.

[17] J. C. Curran, "Mobility of large woody debris (LWD) jams in a low gradient channel," *Geomorphology*, vol. 116, no. 3-4, pp. 320–329, 2010.

[18] J. van Sickle and S. V. Gregory, "Modeling inputs of large woody debris to streams from falling trees," *Can. J. For. Res*, vol. 20, no. 10, pp. 1593–1601, 1990.

[19] C. A. Braudrick and G. E. Grant, "Transport and deposition of large woody debris in streams: A flume experiment," *Geomorphology*, vol. 41, no. 4, pp. 263–283, 2001.

[20] D. Bocchiola, M. C. Rulli, and R. Rosso, "A flume experiment on the formation of wood jams in rivers," *Water Resources Research*, vol. 44, no. 2, 2008.

[21] J. Paik and S.D. Park, *Numerical simulation of flood and debris flows through drainage culvert*, Italian J. Eng. Geol. Environ. vol. 11, pp. 487-493

[22] D. H. Pilgrim and R. P. Canterford, *Australian rainfall and runoff: A guide to flood estimation*, 3rd ed, 1987.

[23] M. J. Boyd, E. H. Rigby, and R. VanDrie, "WBNM — a computer software package for flood hydrograph studies," *Environmental Software*, vol. 11, no. 1-3, pp. 167–172, 1996.

[24] F. M. Henderson, *Open channel flow*. Upper Saddle River, NJ: Prentice Hall, 1966.

[25] D. A. Lyn, T. Cooper, Y.-K. Yi, R. Sinha, and A. R. Rao, "Debris Accumulation at Bridge Crossings: Laboratory and Field Studies," FHWA, Purdue University, Oct. 2003.

Second International Conference on Science, Engineering & Environment,
Osaka City, Japan, Nov.21-23, 2016, ISBN: 978-4-9905958-7-6 C3051

MECHANICAL PROPERTIES OF FIBER REINFORCED CONCRETE USING PINEAPPLE LEAF FIBER TREATED IN SODIUM HYDROXIDE (NaOH)

Joseph Berlin P. Juanzon[1], James Emerson de Leon[2], Patrick Robert Divina[2] and Mark Fernan Tividad[2]
[1]Faculty, Malayan Colleges Laguna; [2] Civil Engineering Department, Malayan Colleges Laguna Philippines

ABSTRACT

The objective of this study is to evaluate the mechanical properties of Fiber Reinforced Concrete (FRC) utilizing Pineapple leaf fiber (PALF) treated in sodium hydroxide and an untreated PALF. Four types of concrete mixes are made with varying percentages of the treated and the untreated PLF. Concrete specimens with PALF of varying volume percentages of 0%, 2%, 4%, and 6% were tested according to ASTM standards on compressive, flexural and split-tensile strength analysis. Six samples of each type of mix and control mix of 0% were tested. The test results is analyze using Two-Way Analysis of Variance (ANOVA) with a 5% level of confidence. Test results show a decrease in compressive and split-tensile strength for all test specimens. However, for the flexural strength, the 2% volume replacement of PALF treated in sodium hydroxide exhibited the largest amount of flexural strength of 5.87MPa as compared to the control mix of 4.27MPa, these signifies an increase in flexural strength by 37.47%. It is therefore concluded that PLF treated in sodium hydroxide has significantly increased the flexural strength of concrete which will eventually reduce the volume of concrete in structures.

.

Keywords: Fiber Reinforced Concrete, Leaf Fiber, Flexural, Compressive, Direct Tensile

INTRODUCTION

Fiber reinforced concrete is a concrete composite with strands of fibers from plants, animals, or even synthetic materials. These fibers can minimize cracking and shrinkage, increase the toughness and reduce the permeability of concrete [1]. Fibers are often considered mainly as replacement for reinforcement for concrete because it is organic, a natural fiber. The quantity of replacement of fibers in a concrete mix is acquired by considering a percentage of the total volume of the specimen, called the volume fraction. These fibers are usually cut into 2-inch size (51 millimeters) and added to the mix evenly.

Although natural fibers are good substitute as reinforcement for composites, its exposure to the alkali environment of the cement tends to deteriorate the fibers, thus rendering it useless. That is why treatments, commonly chemical, are introduced to improve the properties of fibers for better reinforcement in the composites [2].

The main objective of the study was to be able to evaluate the effect of untreated and treated pineapple leaf fiber (PALF) with 2%, 4% and 6% volume fraction to the mechanical properties (compressive, flexural and split tensile strength) of plain concrete.

The scope of this study focused on testing the mechanical properties of PALF-reinforced concrete with volume fraction of 2%, 4% and 6%. The PALF that was used in this experiment was obtained from Lumil, Purok 1, Silang Cavite. The study made used of plain concrete and concrete with PALF that was cut into 40-millimeters as additional reinforcement for the concrete cylinders and beams. The mechanical properties that were determined in the study includes the compressive, flexural and split tensile strength of the plain and PALF-reinforced concrete. Mainly, comparison of the strengths between PALF-reinforced and plain concrete cylinders and beams was included through a graphical analysis in 28th day strength basis. The Analysis of Variance (ANOVA) was used in this study to compare the relationship of the properties of the plain and PALF-reinforced concrete with varying percentages of volume fraction. Lastly, cost analysis was neglected in this study since this was for experimentation purposes only.

LITERATURE REVIEW

Natural fibers are renewable resources, where the production of these fibers require little energy, plus the fact that it is ecological, although some of the disadvantages of natural (plant) fibers is their non-uniformity, variety of dimensions, and their mechanical properties (even between individual natural (plant) fibers in the same cultivation. For this reason, high performances of natural reinforcing

fibers are developed in order to gain its acceptance of use [3].

Natural fibers are classified hair-like material that are perpetual filaments or are in discrete elongated pieces, similar to pieces of thread. These fibers can be kindred to pieces of thread, or it can be spun into filaments, either thread or rope [4].

Also, these fibers can be used as a component of composite materials. These fibers can also be matted into sheets to make products such as paper or felt. Fibers are of two types: natural fiber and man-made fiber or synthetic fiber.

Treated Natural Fibers

Although natural fibers are renewable resource and inexpensive [5], the biodegradable characteristic of the natural fibers can present problems in its durability, this can cause reduction in its strength and toughness if these fibers were not treated [6].

Chemical treatments have been introduced to prevent or resist chemical attacks in fibers present in cementitious composites. These treatment methods improve the adhesion between fiber surfaces and cement matrix, hence improving the surface roughness for better anchorage or interlocking between matrix and fiber, tensile strength, and reduce its moisture absorption [7].

Various chemical treatments have been presented in a study by [8] with regards to natural fibers as reinforcements for composites. Treatments such as alkali, silane, acetylation, benzoylation, acrylation, maleated coupling agents, isocyanates, permanganate, and others are discussed.

Alkaline treatment, or mercerization, is one of the most common methods of treating fibers chemically. This treatment is typically used when fibers are used as reinforcements for thermoplastics and thermosets. Addition of aqueous sodium hydroxide (NaOH) to fibers stimulates the ionization of the hydroxyl group to the alkoxide [9]. In alkaline treatment, fibers are immersed in a sodium hydroxide (NaOH) solution for a brief period of time.

The treatment that yielded the highest tensile strength with the required roughness was obtained by treating the fibers for duration of twenty-four (24) hours in a solution of 4% sodium hydroxide. Using higher concentrations and longer treatment durations only caused the fiber to deteriorate, thus reducing the tensile strength of the fibers itself [2].

History of Pineapple Fibers

Pineapple, also known as *Ananas comosus*, is a natural plant from the family of Bromeliaceae Family. It is the leading edible member of its kin with a multicellular lignocellulose material. The denomination was derived from its conical shape akin to a pine tree. The plant grows to a height of one meter and the first crop is ready for harvesting approximately 18 months after planting. Its fruit is commercially manufactured for food and drug industry and is widely known to be processed for beverage or refreshment. The flesh and juice are used in cuisines around the world. The leaves, on the other hand, are used in making textile by extracting its fibers. Pineapple comes in different varieties like Red Spanish, Hilo, Smooth Cayene, St. Michael, Kona Sugarloaf, Natal Queen of Formosa, and Pernambuco [3].

According to Food and Agriculture Organization of the United Nations, Costa Rica is the leading producer of pineapple with 2,685,131 metric tons. The Philippines on the other hand, ranked third with a quantity of 2,458,420 metric tons of pineapple annually. Other leading producers are Brazil, Thailand, and Indonesia. Table 1 shows the tabulated leading global producers of pineapple in the world.

Table 1 Leading Global producers of Pineapple

Country	Quantity(metric tons)
Costa Rica	2,685,131
Brazil	2,483,831
Philippines	2,458,420
Thailand	2,209,351
Indonesia	1,837,155

Piña, *Ananas comosus (Linn)*, also known as the Pineapple Leaf Fiber (PALF), comes from strong flowery leaves that are commonly used in the Philippines. Usually mixed with polyester or silk to create a textile fabric, it is used to make the traditional formal wear of the Filipinos, the Barong Tagalog. Other applications of which are hand woven bags, linens, and mats, which are of export quality and it is being shipped to China, South Korea, Japan, Middle East, Qatar, Canada, Russia, Germany, Guam, New Zealand, and Hong Kong.

Fiber Reinforced Concrete

Fiber reinforced concrete (FRC) is cementing concrete reinforced mixture with more or less randomly distributed small fibers. In the FRC, a number of small fibers are dispersed and distributed randomly in the concrete at the time of mixing, and thus improve concrete properties in all directions [10]. These fibers contributed in the improvement of flexural-tensile strength, resistance to spitting, impact resistance, excellent permeability and frost resistance [11]. It also increases the toughness, shock resistance and resistance to plastic shrinkage

of the mortar. Existing studies of these fibers include steel, glass, polymer, natural fiber and synthetic fibers [10].

In a study conducted by [1] with regards to fibers as a construction material, it has been stated that the maximum length of the fiber and the optimum volume fraction of the composite is 4 centimeters in length and 3% in volume fraction as replacement for the whole quantity of the composite or partial quantity of cement or aggregates.

METHODOLOGY

This study analyzed the compressive and split tensile strength of the concrete cylinders and the flexural strength of concrete beams all reinforced with chemically treated and untreated PALF. Standard cylindrical steel and rectangular molds that conform to ASTM specifications for testing purposes were used. A total of forty-two (42) concrete specimens comprising twenty-eight (28) concrete cylinders and fourteen (14) concrete cubes were to be made with 0%, 2%, 4% and 6% percentage replacement of fiber by volume.

Preparation of Pineapple Leaf Fibers (PALF)

Figure 1 shows the pineapple leaves that were obtained from the pineapple farm in Lumil, Purok 1, Silang Cavite. The leaves were cut from the stalk of the plant as shown.

Fig. 1 Freshly collected PALF samples

In the sampling process, 8 kg of pineapple leaf were collected for the extraction of its fibers using a ceramic plate. Samples of the extracted fibers are presented in Figure 2. The extracted fibers were then cut into 40 millimeters segments/pieces.

Fig 2 Samples of extracted PALF

Chemical Treatment of PALF

A solution of water and sodium hydroxide at 4% concentration was prepared in a water basin with a room temperature. The pineapple leaf fibers were soaked in the solution for 24 hours. After that, the fibers were immersed in a distilled water bath for one hour to remove residual sodium hydroxide. Finally, the fibers were air-dried (Fig. 3) and stored in a sealed plastic bag to prevent any exposure to moisture.

Fig 3 Air dried treated PALF

Batching and Designing of Concrete Mix

The concrete mix used in this experiment was patterned according to ACI specifications. An ASTM standard mold for concrete cylinders and concrete cubes was used in pouring the concrete mix. Four batches were prepared sequentially, a batch for the concrete with 0% fiber, another with 2%, 4% and 6% fiber content of volume by mass. The PALF has a density of 1001.3 kilogram per cubic meter [12]. Multiplying the density of the pineapple leaf fiber to the volume of the concrete per batch gives the volume replacement of fiber by weight in the concrete specimens.

Two sub-batches were prepared for each batch, one sub-batch for the untreated fibers and the other for the concrete mix with treated fibers. Cement, sand and fibers were first prepared.

Materials Testing

The equipment used for the different tests was the Universal Testing Machine (UTM), which is capable of conducting the Compressive, Flexural and Split Tensile Tests. Two (2) specimens each were prepared for the plain concrete, for the concrete composite with 2%,4% and 6% volume of fiber by mass of the concrete specimen.

Compression Test. The test for compressive strength of the concrete specimens was patterned according to ASTM C39 "Standard Test Method for Compressive Strength of Concrete Specimens" where a concrete cylinder with dimensions of one hundred (100) millimeter by diameter and two hundred (200) millimeter by height was placed in the UTM in a vertical position. The compressive strength of concrete cylinders was computed using the equation:

$$\sigma = \frac{P}{A} \quad (1)$$

Flexural Test. The test for the flexural strength of the concrete specimens was patterned according to ASTM C78. The flexural strength of a concrete beams was computed using the equation:

$$R = \frac{3PL}{2bd^2} \quad (2)$$

Split Tensile Test. The Split Tensile Strength for the concrete specimens was patterned according to ASTM C496. The split tensile strength of concrete cylinders was computed by the equation:

$$\mathrm{T} = \frac{2\mathrm{P}}{\pi \mathrm{dL}} \quad (3)$$

Data Analysis

Two specimens each for the compressive, flexural and splitting tensile strength for twenty-eight (28) day strength were tested and the results were averaged. Two parameters, namely the volume fraction and the chemically treated and untreated fiber, were considered and the significant interactions between the two parameters were determined.

RESULTS AND DISCUSSIONS

The unit weight of the course and fine aggregates adhered to the required specifications presented by ASTM C29, which ranges from 1,450 kg/m^3 to 1,750 kg/m^3. The specific gravity of the course and fine aggregates also conformed to the ASTM C127 and ASTM C128 specifications.

Prior to the design of concrete mix as per ASTM standards, information for the experimentation of construction materials were gathered and are shown in Table 3.

Table 3 Summary of Concrete-Mix Parameters from Material Testing

Kinds of Materials	Unit Weight (kg/m^3)	Specific Gravity (SSD)	Absorption (%)	Fine Modulus
Cement	-	3.10	-	-
3/4" Coarse Aggregates	1,696.72 (Bulk)	2.75	8.5	-
Fine Aggregates	1,696.72 (Bulk)	2.5	3.54	2.6
Water	9,810	1	-	-

Design of Concrete Mix

Based on the "Class A" mixture (1:2:3) with design strength of 3000 Psi. The mass of the fibers was added based on its density, multiplied to the total volume of the batch, and then multiplied to the percent volume to be replaced. The equivalent mass of the PALF were added to the concrete mix with 2%, 4% and 6% volume replacement.

In accordance with the total volume obtained from the concrete specimens, a total of 4 concrete mixes was prepared. The first mix was prepared for the control sample, plain concrete without fibers. The second, third and fourth concrete mix was prepared with 2%, 4% and 6% volume replacement of treated and untreated fibers. The summary of the quantity of cement, sand, gravel, water, and PALF for each mix is shown in Table 4.

Table 4. Quantity of Cement, Sand, Gravel and Water by Weight for Concrete with PALF Replacement

Percent Replacement	Cement (kg)	Sand (kg)	Gravel (kg)	Water (kg)	PALF (kg)
0%	8.52	17.31	25.79	4.26	0
2%	8.35	16.96	25.27	4.17	0.4005
4%	8.18	16.62	24.76	4.09	0.801
6%	8.02	16.29	24.26	4.01	1.202

Compressive Strength Test

A tabulated summary of the compressive strength of the plain concrete, treated and untreated PALF-reinforced concrete with varying percentage of total replacement by volume of fibers is shown in Table 5.

Table 5. Summary of Compressive Strength of Concrete Cylinders

Percent Replacement of	Untreated Pineapple Leaf	Treated Pineapple Leaf

Fiber (%)	Fiber	Fiber
	Mean Strength at 28th day (MPa)	
0	22.35	22.35
2	14.76	22.17
4	7.58	13.18
6	8.62	14.06

As shown in Figure 5, the compressive strength of the concrete cylinders decreases as the volume percentage replacement of fibers, treated or untreated, increases. For the concrete specimens with untreated PALF, a decrease from 22.35 MPa to 14.76 MPa, with a percentage decrease of 33.96%, was observed when the concrete cylinder with 2% volume fraction was compared to the control specimen. A decrease from 22.35 MPa to 7.58 MPa and 8.62 MPa, with 66.09% and 61.43% decrease in percentage, were also observed when the control specimen was compared to the concrete specimens with 4% and 6% volume fraction of untreated PALF, respectively.

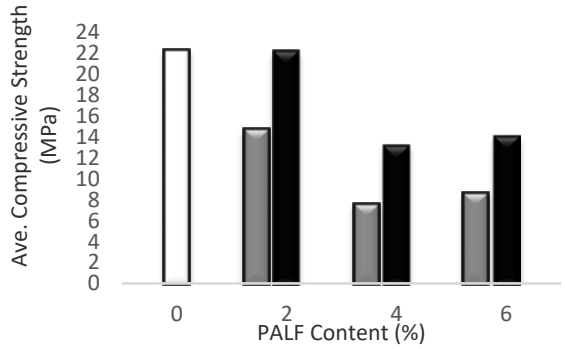

Fig. 5. Compressive strength comparison of different volume percentage of PALF

The results from the compressive strength of concrete cylinders validate the study of [13] that adding fibers to the concrete specimens decrease the value of its compressive strength.

PALF provides an increase in the compressive strength of the concrete cylinders. When comparing the concrete cylinders with 2% volume fraction of untreated to the treated PALF, there was an increase from 14.76 MPa to 22.17 MPa. Also, an increase of 73.88% and 63.11% was observed when comparing the specimens with 4% and 6%.

Flexural Strength Test

Table 6 shows the results of the flexural strength of the plain concrete, treated and untreated PALF-reinforced concrete with varying percentage of total replacement.

Table 6. Summary of Flexural Strength of Concrete Beams

Percent Replacement of Fiber (%)	Untreated Pineapple Leaf Fiber	Treated Pineapple Leaf Fiber
	Mean Strength at 28th day (MPa)	
0	4.27	4.27
2	3.49	5.87
4	3.34	5.21
6	3.05	4.99

Figure 6 shows that the flexural strength of the concrete cylinders with the untreated PALF decreases as the volume percentage replacement of fibers increase. The largest strength documented was 3.49 MPa, which was still smaller as compared to the control mix. A decrease of 18.27% in its flexural strength is recorded and it continues to decrease as the volume fraction of the concrete specimen increases. A decrease of 21.78% and 28.57% were also recorded when the concrete specimens with 4% and 6% volume fraction of untreated PALF was compared to the control mix, respectively.

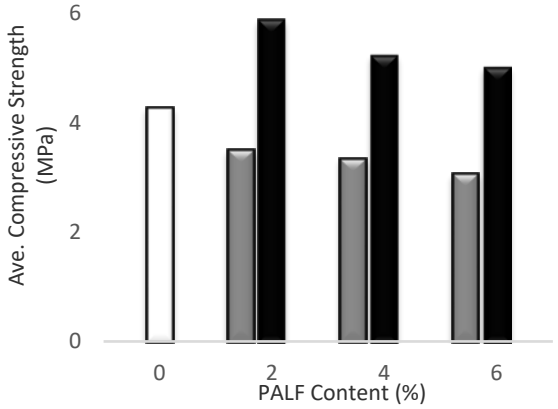

Fig. 6 Flexural strength comparison of different volume percentage of PALF

The flexural strength of the concrete specimens with PALF treated in sodium hydroxide decreased as the volume fraction increases. However, the specimens with treated fiber exhibited an increase when compared to the control specimen. An increase from 4.27 MPa to 5.87 MPa, with a percentage increase of 37.47% was observed when the concrete specimen with 2% volume fraction of treated PALF was compared to the control specimen, the same trend continues as it was compared to 4% and 6% volume fraction with an increased strength of 22.01% and 16.86% respectively.

Direct Tensile Strength Test

A tabulated summary of the direct tensile strength of the plain concrete, concrete with treated fibers and concrete with untreated fibers with

varying percentage of total replacement by volume of fibers is shown in Table 7.

Table 7. Summary of Direct Tensile Strength of Concrete Samples

Percent Replacement of Fiber	Untreated Pineapple Leaf Fiber	Treated Pineapple Leaf Fiber
	Mean Strength at 28th day (MPa)	
0%	1.94	1.94
2%	1.87	1.89
4%	1.44	1.60
6%	1.24	1.65

As shown in Fig. 7, the direct tensile strength of the concrete cylinder decreases as the volume percentage replacement of fibers, treated or untreated, increases. For the concrete specimens with untreated PALF, a decrease from 1.94 MPa to 1.87 MPa, with a percentage decrease of 3.61%, was observed when the concrete cylinder with 2% volume fraction is compared to the control specimen.

A decrease from 1.94 MPa to 1.44 MPa and 1.24 MPa, with 25.77% and 36.08% decrease in percentage, were also observed when the control specimen was compared to the concrete specimens with 4% and 6% volume fraction of untreated PALF, respectively.

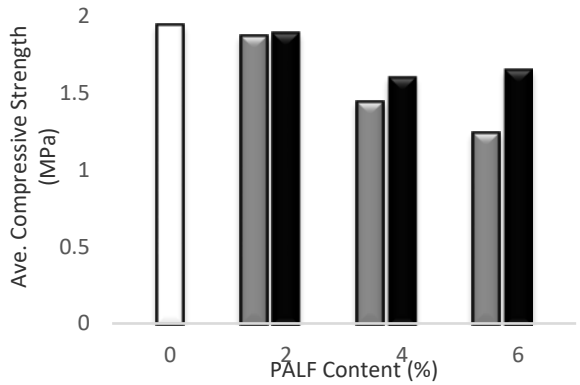

Fig. 7. Direct tensile strength comparison of different volume percentage of PALF

CONCLUSION

Based on the results of the test and the statistical treatment comparing the effect of treated and untreated fibers reinforcement, the PALF treated with sodium hydroxide gave a greater strength (22.17 MPa) compared to the untreated pineapple leaf fibers (14.76 MPa) when subjected to compression test. Similarly, the treated PALF subjected to flexural test presented a higher value of 5.87 MPa compared to the untreated PALF with only 3.49 MPa. Also, the strength of the control mix tested in flexure increased by 37.47% when the 2% of treated PALF were added. Furthermore, in split tensile test, the treated PALF enhanced the concrete with a strength of 1.89 MPa compared to the untreated PALF with a strength of 1.87 MPa. However, the split tensile strength of control mix which is 1.94 MPa did not improve when treated or untreated pineapple leaf fibers were mixed.

..

ACKNOWLEDGEMENTS

The authors would like to express its gratitude to Malayan Colleges Laguna for the support given in using its facilities and equipment. To the Divine Almighty, who gave us the strength, courage, and wisdom to fulfil this achievement, this work is humbly offered to HIM.

REFERENCES

[1] Ali, M. (2012) Natural Fibers as Construction Materials. Journal of Civil Engineering and Construction Technology, 80-89.

[2] Machaka, M., Basha, H., Chakra, H., & Elkordi, A. (2014). Alkali Treatment of Fan Palm Natural Fibers For Use in Fiber Reinforced Concrete. European Scientific Journal.

[3] Asim, M., Abdan, K., Jawald, M., Nasir, M., Dashtizadeh, Z., Ishal, M.R., Hoque, M.E. (2015). A Review on Pineapple Leaves Fibre and Its Composites.

[4] Chandramohan, D., & Marimithu, K. (2011). A Review on Natural Fibers. IJRRAS, 196-198.

[5] Oladele, I., Omotoyinbo & Adewara, J. (2010). Investigating the Effect of Chemical Treatment on the Constituents and Tensile Properties of Sisal Fiber. Journal of Minerals and Materials Characterization & Engineering, 569–582.

[6] Filho, R.D, Ghavami, K., England, G. & Scrivener, K. (2003). Development of Vegetable Fibre–Mortar Composites of Improved Durability. Cement & Concrete Composites.

[7] Hashim, M, Amin, M.R.A., Zaidi, A., & Ariffin, S. (2012). Mercerization Treatment Parameter Effect on Natural Fiber Reinforced Polymer Matrix Composite: A Brief Review.

[8] Li, X., Tabil, L. G., & , S. (2007). Chemical Treatments of Natural Fiber for Use in Natural Fiber Reinforced Composites. J Polym Environ, 25-33.

[9] Agrawal R, Saxena NS, Sharma KB, Thomas S, Sreekala MS (2000). Material Science Engineering: A 277:77.

[10] Amit, R., & Joshi, Y. (2014). Applications and Properties of Fibre Reinforced Concrete.Journal of Engineering Research and Applications, 121-131.

[11] Uzomaka, O.J. (1976). Characteristics of Akwara as a Reinforcing Fibre. Magazine of Concrete Research, 28(96), 162-167.
[12] De Aro, E., Fajardo, B. H., & Perez, M. (2012). Properties of Pineapple Leaf Fiber Reinforced Concrete Beams.
[13] Elsaid, A., Dawood, M., Seracino, R., Bobko, C. (2010). Mechanical Properties of Kenaf Fiber Reinforced Concrete.

Second International Conference on Science, Engineering & Environment,
Osaka City, Japan, Nov.21-23, 2016, ISBN: 978-4-9905958-7-6 C3051

STEEL FIBRE REINFORCED CONCRETE: FROM X-RAY IMAGING OBSERVATION TO MODELLING

Trevor NS Htut[1], Tian Sing Ng[1] and Stephen J Foster[2]
[1]Department of Civil Engineering, Curtin University, Australia;
[2] School of Civil & Environmental Engineering, University of New South Wales, Australia

ABSTRACT

In developing the constitutive model for steel fibre reinforced concrete, insight of fibre behaviour in tension is vital. The steel fibres in the concrete are randomly distributed and orientated. Not all fibres are aligned in the direction of the applied load; instead, fibres lie at various angles to the loading direction. This paper reports on the observation of the behavior of steel fibre reinforced concrete in tension using X-ray imaging. It is observed that crack paths find ways of minimum resistance; (i) through a section with poor fibre dispersion and/or (ii) divert around fibre ends, where possible. The results of digital imaging analysis are reviewed and statistical models for fibre dispersion are presented. A model is also proposed to determine the limiting maximum fibre volume percentage for which, beyond the limit, additional fibre content does not further improve the tensile performance due to the weaker cementitious matrix and crack paths are likely to divert around fibre ends.

Keywords: Steel Fibre, Tension, Dispersion, Distribution, X-Ray, Fibre-Matrix Interaction

INTRODUCTION

In the early 1960's, Romualdi and Batson [1] demonstrated that the tensile strength and crack resistance of concrete can be improved by providing suitably arranged, closely spaced, wire reinforcement. By adding fibres to a concrete mix the objective is to bridge discrete cracks providing for some control to the fracture process and increase the fracture energy. To-date, after more than 50 years of research in the development and placement of steel fibre reinforced concrete (SFRC), the concept has matured to the stage where it is finding increasing use in practice.

Insight of fibre behaviour during pullout is vital for developing a constitutive model for fibre reinforced concrete. However, there is no easy method to determine the fibre-matrix interfacial mechanics and fibre pullout micromechanics other than undertaking experimental discrete fibre pullout test. Discrete fibre pullout tests allow observation and understanding of all stages of pullout process starting from the initial elastic deformation of the fibre been pulled-out or fractured. Space in this paper prohibits an extensive review of the literature on the discrete fibre behaviour during pullout but more information on the topic can be found in studies by the authors [2], including the study using X-ray imaging technique [3], and by other researchers such as [4-12].

Based on the discrete fibre pullout data, the authors developed the Unified Variable Engagement Model (UVEM) [13-15] that is capable of predicting the stress versus crack opening response of steel fibre reinforced concrete composites. The model is developed by assuming that (i) the matrix remains intact during the fibre pull-out in the SFRC composite, and (ii) fibres are uniformly dispersed in the SFRC. However, in reality, a weak cementitious matrix is prone to spalling and local damage due to localised stress concentrations. This can be particularly apparent for fibres where a high degree of mechanical anchorage is generated within the matrix and without fracturing. In addition, based on the observations from studies by the authors [13, 15] and others [16, 17], the tensile fracture of SFRC do not always occur at the narrowest part of the dog bone shaped specimens. This is believed to be caused by the variability of dispersion and distribution of fibres within the matrix and may be due to the methods of mixing, placing and compaction.

In this study, X-ray imaging was used to view the internal mechanism that evolves in the randomly distributed SFRC in tension. The results of digital imaging analysis are reviewed and statistical models for fibre dispersion are presented. Finally, a limiting maximum fibre volume percentage model is introduced for which, beyond the limit, additional fibre content does not further improve the tensile performance due to the loss of efficiency in bond between fibres and the matrix, where the matrix spalls and cracks before the fibres are engaged.

EXPERIMENTAL PROGRAM

Eleven 30 mm thick dog-bone shaped specimens were cast with 40 MPa cement mortar reinforced

with end hooked, cold drawn, 25 mm long, 0.5 mm diameter, 2300 MPa high strength fibre and volume percentages of between 0.5% and 2%.

Fig. 1 shows the specimen size and test setup details adopted in this study. All the specimens were X-ray imaged prior to the uniaxial tension testing. The displacements were measured using two linear variable differential transducers (LVDTs), one placed on each side of the specimen to allow for the X-ray film to be attached. The displacement plotted is taken as the average of the LVDT readings. Loading was conducted using displacement control at a rate of 0.12 mm per minute up to the crack opening displacement of 2 mm and then increased to a minimum of 0.1 mm per minute. Of the eleven specimens, seven were loaded and tested under X-ray observations.

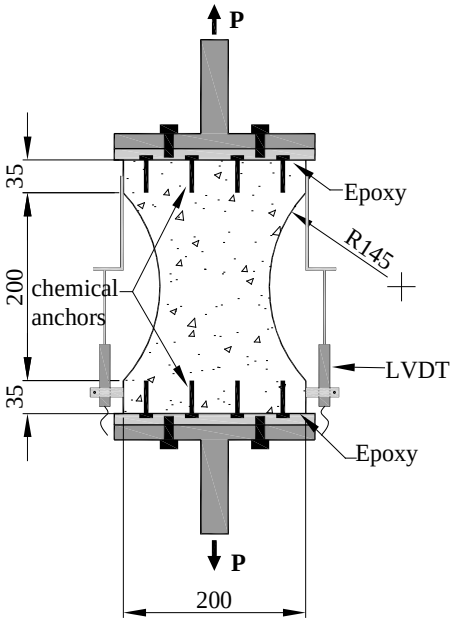

Fig. 1 Test arrangement for uniaxial tension test

TEST RESULTS & ANALYSIS

The average load versus displacement results are presented in Fig. 2 and it shows that for the 25 mm long high yield strength fibres used in this study, there was no improvement in the post cracking behaviour from a 0.5% fibre volume to a 2.0% fibre volume.

The X-ray images taken prior to testing were analysed for fibre concentration over various regions (Fig. 3); to avoid the wall effect in the analyses, the region near the side walls was excluded.

The digital image analysis was undertaken using IMAQ™ Vision Builder software. Each sample image was filtered to distinguish the fibres from the background image (Fig. 4). An image analysis was then undertaken to determine the area of fibres in the image (white area in Fig. 4b) with the fibre dispersion factor (F_{fd}) defined as the ratio of white area to the total sample area. The sampling sizes of 25 mm × 25 mm and 12.5 mm × 12.5 mm were compared and only a limited improvement (approximately 2%) was observed when the sampling size was reduced much below the length of the fibres. The dispersion results are presented in Fig 5.

For a sample of statistical significance, the median value of F_{fd} for samples taken within one dog-bone specimen represents the average fibre volume fraction, ρ_f. This data is plotted in Fig. 6 for the dog-bone shaped specimens for the different, known, fibre volumetric ratios (ρ_f from 0.5% to 2.0%). With the relationship F_{fd} and ρ_f established, for the given fibre type and specimen thickness, (Fig. 6), the volume fraction as a function of F_{fd} is determined as:

$$\rho_f = F_{fd}/(126 - 136F_{fd}) \quad (1)$$

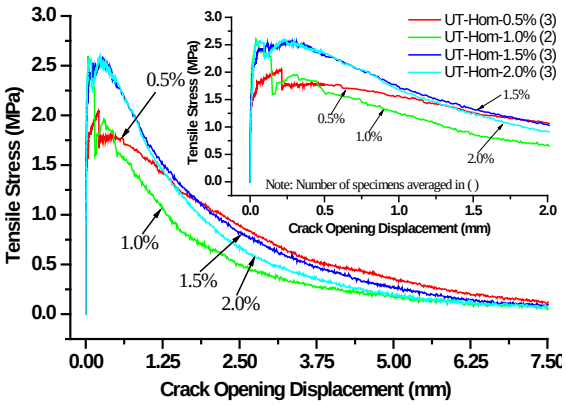

Fig 2 Plot of average tensile stress versus crack opening response for unixial tension test.

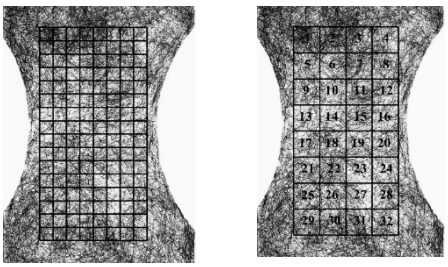

Fig. 3 Sampling locations and grids for fibre dispersion analysis: 12.5 mm × 12.5 mm and 25 mm × 25 mm.

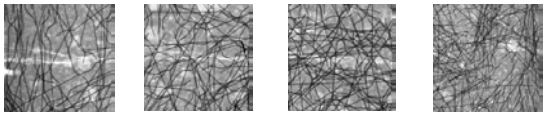

(a)

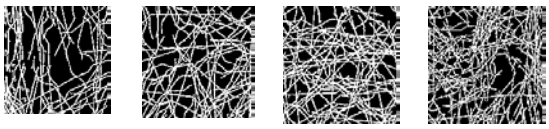

(b)

Fig 4 Digital X-ray image along the crack path: (a) before; and (b) after, the image analysis

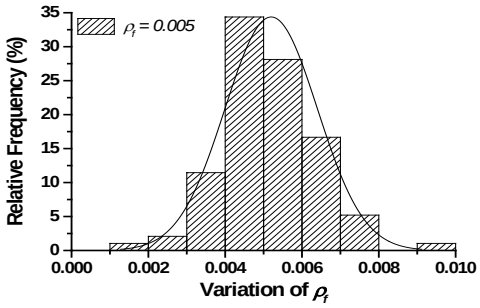

(a)

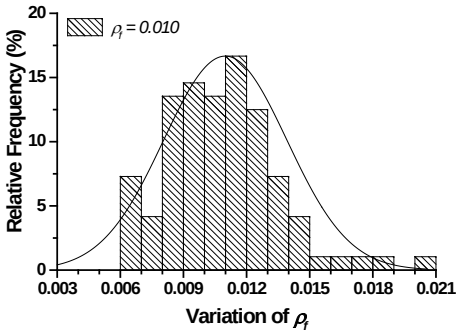

(b)

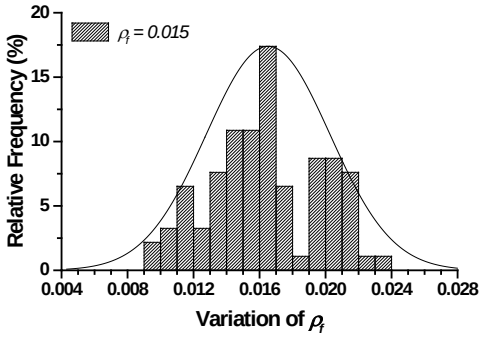

(c)

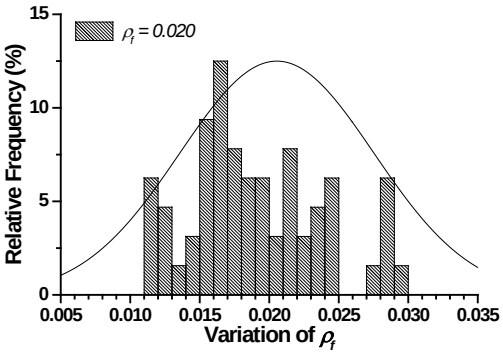

(d)

Figure 5: Distribution of fibres for fibre volume percentage (ρ_f) of 0.5, 1, 1.5 and 2.

With the fitting Eq. (1) established, variations in the fibre volume fraction within one specimen can then be determined.

From the fibre dispersion data, the standard deviation for the test series was $\sigma = 0.27\rho_f$, and, considering the fibres to be normally distributed, the 75th and 90th percentiles are $\rho'_{75} = 0.82\rho_f$ and $\rho'_{90} = 0.65\rho_f$, respectively.

It is important to note that, in this study, the specimen thickness was 30 mm or 100 times the diameter of a single fibre. Fibres are more likely to overlap one another in the digital image analysis as the specimen thickness increases. Consequently, in the digital image analysis, specimen thickness is a significant component in determining of the fibre dispersion factor. For the hypothetical case of a fibre diameter thick specimen, there is no possibility of fibre being overlapped and the fibre dispersion factor is linearly proportional to the fibre volume concentration. Probability of fibre overlapping is a function of the specimen thickness, and, consequently, a nonlinear relationship is observed.

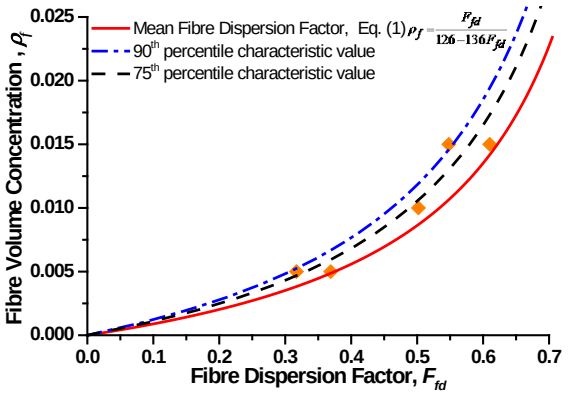

Figure 6: Fibre volume concentration ratio versus average fibre dispersion along the crack path.

Influence of Fibre Dispersion

It was observed that the crack initiation is likely to commence at the location at which least number of fibres are located; that is, cracks initiate from areas with poor fibre dispersion rather than at the narrowest part of the dog-bone specimen. Thus, fibre dispersion plays a significant role in crack initiation and, consequently, on the tensile strength.

The digitised X-ray images taken during the tension test of the dog-bone specimens show the importance of fibre dispersion on the crack formation/initiation and propagation processes. To validate the findings presented above, further digital image analysis was undertaken to determine the fibre dispersion along the crack path of the specimens containing fibre volume concentrations of 0.5%, 1.0% and 1.5%. A typical X-ray image around

the crack path is shown in Fig 4a. Digital image analysis was undertaken on a sample size of 12.5 mm square (Fig. 4b) and the fibre volume ratio versus fibre dispersion ratio is plotted in Fig 6.

The results show that the cracks are likely to form or propagate along the path of least resistance. The fibre volume concentration along the crack path was found to average through the 75th percentile characteristic value (Fig 6). This confirms the conclusion that fibre dispersion contributes significantly to the fracture process in uniaxial tension and this observation needs to be taken into consideration during the development of behavioural models. In the context of this study and Amin [16], the proposed statistical fibre dispersion factor, K_{fd}, can be taken as 0.8.

Influence of Fibre and Matrix Relationship on fracture process

It is a common assumption that the improvement in tensile performance of a fibre composite can be achieved by incorporating a high fibre volume content, especially in the case of steel fibres [18].

In this study, however, it was noted that increases in fibre volume percentage can have an adverse effect on the tensile performance. In addition to the dominant crack forms where the local fibre concentration is at its lowest across a section, in this study and Markovic et al. [17], it was also observed that the crack path follows the easiest propagation route and is often near the end of fibres or around them (Fig. 7). Consequently, many of the end-hooked fibres fail to engage and do not deform during the fracture process.

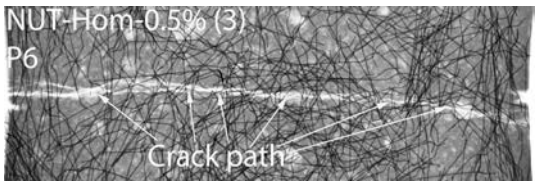

Fig. 7 Crack propagation during a uniaxial tension test

Fig. 8 shows the fracture (or failure) plane of the dog-bone shaped specimens with various fibre volume percentages. Based on visual observation, a higher proportion of the end hooked fibres were deformed (i.e. straightened) in the case of specimens with fibre volume of 0.5%. Increase in fibre volume percentages, however, leads to a decreased in proportion of end-hooked fibres being straightened through the end-hook (Fig. 8). Rather, failure of the matrix surrounding the hook significantly influenced the behaviour. Similarly, it is observed that the shape and contour of the failure plane is dependent on the fibre volume percentages. Fig. 8(a) shows that relatively flat and even fracture plane was observed in the case of specimen with 0.5% fibre volume. Increase in fibre volume percentages also results in in- and/or out- of plane rotations of the fracture planes (Figs. 8(b), 8(c) & 8(d)).

In order to investigate this phenomena, the end-hooked fibres across the fracture planes were counted after the tests were conducted and the numbers of fibres that had, and had not, straightened through the end hook were noted. A total of eight dog-bone shaped specimens were studied and the results are presented in Fig. 9. The results support the observation that the proportion of straightened end-hooked fibres is inversely proportional to the fibre volume percentages.

Fig. 9 shows that for the specimen containing 0.5% of fibre volume percentages, approximately 45% of fibres were deformed during the uniaxial tension tests, which is in agreement with the findings of Markovic et al. [17]. As the fibre volume percentage increases, more energy is required to fully deform the end-hooks sufficiently to pull through the fibre tunnel. It was observed that due to the higher energy required to fully deform the end-hooked fibres, cracks propagate around or near the end of the end-hooked fibres, which results in an uneven crack surface (Figs. 8(b) to 8(c)). The additional energy in the matrix cracks going around the fibre ends is more than offset by the loss of efficiency of the fibres being pulled through the fibre tunnel.

The importance of the inter-relationship between the mechanical properties of fibres and the mechanical properties of the matrix can be used to optimize the performance of SFRC.

(a)

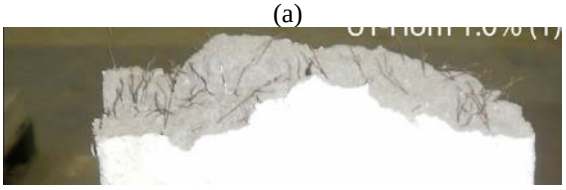

(b)

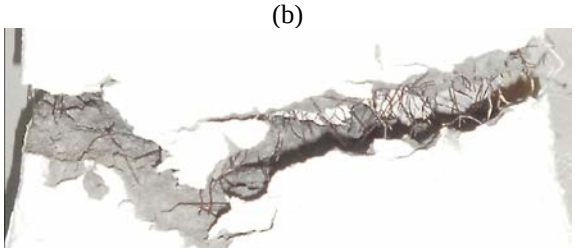

(c)

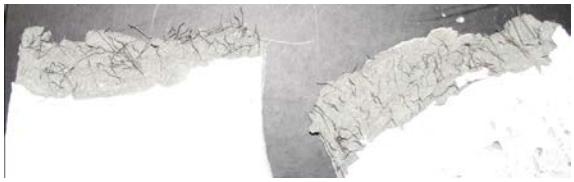

(d)

Fig. 8 Fracture plane of dog-boned shaped specimens for fibre volume percentages of (a) 0.5%, (b) 1.0%, (c) 1.5% and (d) 2.0%

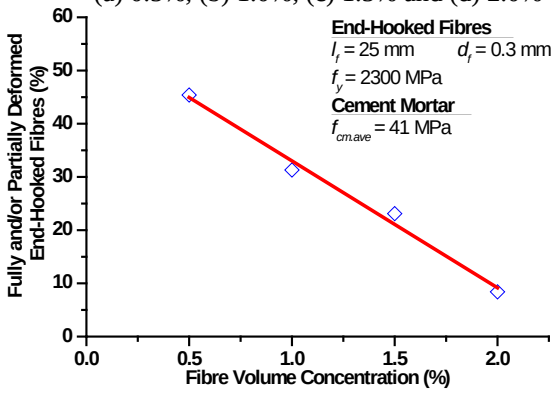

Figure 9: Plot of fibre volume concentration versus surveyed fully and/or partially deformed end-hooked fibres after the tests

The pullout load, P_f, of an individual fibre can be determined from

$$P_f = \tau_b \, l_a \, \pi \, d_f \tag{2}$$

For multi-fibres composite like SFRC, the strength assuming failure is by fibre pullout is

$$P = \tau_b \, \pi \, d_f \sum_{i=1}^{N} l_a \tag{3}$$

where N is the number of fibres crossing the cracking plane, τ_b is the average fibre bond stress, l_a is initial fibre embedment length and d_f is fibre diameter.

On the other hand, the matrix tensile capacity may be calculated as

$$P_c = k_0 \, f_{ct} \, bD \tag{4}$$

where k_0 is a factor to account for the energy required to deflect the crack around the fibre ends, bD is the cross-sectional area of a crack plane, and f_{ct} is tensile strength of matrix. For argument we shall conservatively assume k_0 as unity.

It is hypothesised that fibre pullout will occur when the matrix strength, P_c is greater than the fibre pullout load, P_f. If the tensile resistance provided by the fibre is greater than that provided in a path through the concrete, failure will occur through the concrete, which is undesirable. Based on this hypothesis, fibres will pull out from the matrix without cracks being propagating around the ends of fibres provided that:

$$\tau_b \, \pi \, d_f \sum_{i=1}^{N} l_a \le k_0 \, f_{ct} \, Db \tag{5}$$

The average length of initial embedment across a crack is given by Marti et al. [19] as

$$l_{a.ave} = \frac{l_f}{4} \tag{6}$$

Aveston and Kelly [20] showed that for a crack plane with a cross-sectional area of A_c, the total number of randomly distributed fibres in the three-dimensional space crossing the plane is:

$$N = \frac{A_c}{2} \sum_{i=1}^{n} \frac{\rho_{fi}}{A_{fi}} = \frac{\rho_f \, A_c}{2 \, A_f} \tag{7}$$

Substituting Eqs. (6) and (7) into Eq. (5) gives the minimum tensile strength of the matrix, f_{ct}, to ensure fibre pullout action as

$$f_{ct} \ge \frac{\tau_b \, \alpha_f \, \rho_f}{2k_0} \tag{8}$$

and, similarly, an upper limit of fibre volume (or optimum fibre volume) to ensure that a failure plane passes through the fibres, and not around the fibre ends can be determined as

$$\rho_{f.optimum} \le \frac{2k_0 \, f_{ct}}{\tau_b \, \alpha_f} \tag{9}$$

where ρ_f is the fibre volume friction and α_f is the fibre aspect ratio (l_f / d_f).

The average bond stress (τ_b) is calculated from discrete fibre pullout tests as

$$\tau_b = \frac{P_{f.max}}{\pi \, d_f \, l_a} \tag{10}$$

where $P_{f.max}$ is the maximum force in the fibre and l_a is the embedded length of the fibre at the point of engagement. In the development of the UVEM model [13-15], the point of engagement is taken as the crack (or separation plane) opening displacement corresponding to a force in the fibre of $0.5P_{f.max}$. Thus, in Eq. (10), $l_a = l_f/2\text{-}w_e$, where w_e is the separation plane displacement at the point of engagement. While the model has also been

developed based on the observation from this study, no test data is yet available to test its performance in this regard.

CONCLUSION

While the tensile and fracture behaviour of SFRC have been researched for more than five decades, their use in structures has been limited by a lack of design models and standardization. With design rules for SFRC introduced in some national concrete structures standards, it could be expected that more use will be made of this higher performance material in building and bridge structures for the carrying of tensile stresses. Ideally, design models should be based on a physical understanding of fracture processes and physical-mechanical models adopted as the model basis, rather than empirically based modelling approaches.

Through X-ray imaging of tensile tests, pre-loading and under load, the effect of fibre distribution, dispersion and influence of fibre-matrix relationship on the fracture processes is quantified. Based on this X-ray observation in this study, the proposed statistical fibre dispersion factor, K_{fd}, can be taken as 0.8.

A weak cementitious matrix is prone to spalling and local damage due to localised stress concentrations. Crack path follows the easiest propagation route and is often near the end of fibres or around them. A limiting maximum fibre volume percentage model is introduced for which, beyond the limit, additional fibre content does not further improve the tensile performance due to the loss of efficiency in bond between fibres and the matrix, where the matrix spalls and cracks before the fibre is engaged.

REFERENCES

[1] Romualdi JP and Batson GB, “Behaviour of reinforced concrete beams with closely spaced reinforcement”, ACI Journal, Vol. 60, June 1963, pp. 775-789.

[2] Ng TS, Htut TNS and Foster SJ, "Mode I and II Fracture Behaviour of Steel Fibre Reinforced High Strength Geopolymer Concrete: An Experimental Investigation", in Proc. of the 7th Int. Fracture Mechanics of Concrete and Concrete, May 2010.

[3] Htut TNS and Foster SJ, “X-Ray Imaging for the Observation of Mode I Fracture in Fibre Reinforced Concrete”, in Proc. of the 5th Australasian Congress on Applied Mechanics, December 2007.

[4] Gray RJ, “Analysis of effect of embedded fibre length on fibre debonding and pull-out from an elastic matrix. Part 2 - application to steel fibre-cementitious matrix composite system”, Journal of Materials Science, Vol. 19, May 1984, pp. 1680-1691.

[5] Gopalaratnam VS and Shah SP, “Tensile failure of steel fibre-reinforced mortar”, Journal of Engineering Mechanics, Vol. 113, Jan. 1987, pp. 635-652.

[6] Mandel JA, Wei S and Said S, “Studies of the properties of the fibre-matrix interfaced in steel fibre reinforced mortar”, ACI Materials Journal, Vol. 84, Mar. 1987, pp. 101-109.

[7] Namur GG and Naaman AE, “A bond stress model for fiber reinforced concrete based on bond stress slip relationship”, ACI Materials Journal, Vol. 86, Jan. 1989, pp. 45-57.

[8] Wang Y, Li CV and Backer S, “Experimental determination of tensile behavior of fiber reinforced concrete”, ACI Materials Journal, Vol. 87, Sep. 1990, pp. 461-468.

[9] Banthia N and Trottier JF, “Deformed steel fiber-cementitious matrix bond under impact”, Cement and Concrete Research, Vol. 21, Jan. 1991, pp. 158-168.

[10] Banthia N and Trottier JF, “Effects of curing temperature and early freezing on the pullout behaviour of steel fibres”, Cement and Concrete Research, Vol. 19, May 1989, pp. 400-410.

[11] Gray RJ and Johnston CD, “Effect of matrix composition on fibre/matrix interfacial bond shear strength in fibre-reinforced mortar”, Cement and Concrete Research, Vol. 14, Mar. 1984, pp. 285-296.

[12] Guerrero P and Namman AE, “Effect of mortar fineness and adhesive agents on pullout response of steel fibres”, ACI Materials Journal, Vol. 97, Jan. 2000, pp. 12-20.

[13] Htut TNS, “Fracture Processes in Steel Fibre Reinforced Concrete”, PhD Thesis, School of Civil & Environmental Engineering, the University of New South Wales, 2010, pp. 389.

[14] Ng TS, Htut TNS and Foster SJ, “Fracture of Steel Fibre Reinforced Concrete – The Unified Variable Engagement Model”, Report No. UNICIV R-460, School of Civil & Environmental Engineering, the University of New South Wales, 2012.

[15] Ng TS, “An Investigation into the Development of High Performance Geopolymer Concrete”, PhD Thesis, School of Civil & Environmental Engineering, the University of New South Wales, 2011, pp. 579.

[16] Amin A, “Post Cracking Behaviour of Steel Fibre Reinforced Concrete: From Material to Structure”, PhD Thesis, School of Civil & Environmental Engineering, the University of New South Wales, 2015, pp. 400.

[17] Markovic I, Walraven JC and Van Mier JGM, “Tensile Behaviour of High Performance Hybrid Fibre Concrete”, in Proc. of the 5th International

Conference on Fracture Mechanic of Concrete & Concrete Structure, 2004, pp 1113-1120.

[18] Li Z, Li F, Chang TYP and Mai YW, "Uniaxial tensile behaviour of concrete reinforced with randomly distributed short fibres", ACI Materials Journal, Vol. 95, Sep. 1998, pp. 564-574.

[19] Marti P, Pfyl T, Sigrist V and Vlaga T, “Harmonized test procedures for steel fibre-reinforced concrete”, ACI Materials Journal, Vol. 96, Nov. 1999, pp. 676-685.

[20] Aveston J and Kelly A, "Theory of multiple fracture of fibrous composites", Journal of Materials Science, Vol. 8**,** Mar. 1973, pp. 352-362.

Second International Conference on Science, Engineering & Environment,
Osaka City, Japan, Nov.21-23, 2016, ISBN: 978-4-9905958-7-6 C3051

PERFORMANCE OF BAMBUSA BLUEMANA LAMINATED BAMBOO BOARDS (LBB) IN TERMS OF MECHANICAL AND PHYSICAL PROPERTIES UTILIZING POLYVINYL ACETATE GLUE AS ADHESIVE

Hermie M. del Pilar[1], Azel Ronn L. Barera[1], Dylan C. Gavino[1], Juvy Lee D. Gomez,[1]
[1]Department of Civil Engineering Malayan Colleges Laguna
Pulo-Diezmo Road, Cabuyao City, 4025 Laguna, Philippines

ABSTRACT

Utilization of Bambusa Bluemana as alternative material for hardwood products was explored in this study. Three types of Laminated Bamboo Boards (LBBs) with different configurations: parallel, perpendicular and alternate type were produced. Treated bamboo culms of *bambusa blumeana* were fabricated, measuring 200mm x 20mm x 5mm, double-laminated by Polyvinyl Acetate (PVA) glue under 200 psi cold-pressed to produce 200mm x 200mm x 10mm board. The Water Absorption (WA), Thickness Swelling (TS) and Delamination Test (DT) evaluated the physical properties of the boards, while Modulus of Rupture (MOR) and Hardness Test (HT) had shown their mechanical properties. Each test subjected 12 specimens both for the physical and mechanical performance of the product. Physical tests showed no significant difference on means of all specimens, while the MOR of alternate type LBB demonstrated highest mean value at 150.99 MPa significantly higher than the perpendicular type at 53.66 MPa. Hardness Test showed highest mean on perpendicular type at 5.22 kN, significantly higher than the parallel and alternate type LBBs with 2.83 kN and 2.74 kN, respectively. Based on these results, the perpendicular type LBB exhibited highly satisfactory performance on hardness, while the alternate type provides high flexural strength. The flexural strengths of the alternate and parallel type are better than those of previous studies, which has an MOR value ranging from 68-128 MPa, and are comparable to that of a commercial laminated wood with mean MOR of 140.6 MPa. Bambusa Bluemeana glued with PVA, produces a high quality flooring or tile construction material.

Keywords: *Laminated Bamboo Board, Bambusa Blumeana, Bamboo Culms, Laminae,*

INTRODUCTION

With the rapid growth of the global economy and constant upsurge in population, the overall demand for wood and wood-based composites is rising while the sources of wood from natural forest continue to decrease due to the biomass demands for green energy generation (Chaowana, 2013). Deforestation of wood causes serious local environmental problem and possibly relates to the climate change in the world (Verma and Chariar, 2012). Consequently, to meet the future demand, a sustainable, cost-effective, ecologically responsible and fast-growing material that offers alternatives to traditional wood products must be considered. A suitable raw material should have comparable strength and physical properties to that of the wood and should also be compatible with the existing processing technologies (Chaowana, 2013). Bamboo could be such this alternative raw material.

Worldwide, there is a growing interest in bamboo as an environmentally acceptable building material for construction projects because of its superior properties like high strength-to-weight ratio, high tensile strength and other factors like low cost, easy availability, sustainability and environmental friendliness (Nguyen et al., 2010; Li et al., 2013). Attempts have been made to study the mechanical strength of bamboo in order to explore its capability, in lieu of wood, as a construction and structural material (Verma et al., 2014).

The Forest Products Research and Development Institute (FPRDI) based at Los Baños, Laguna, is at the center of the country's bamboo-processing technology. Increasing research demonstrates a growing industry and demand for sustainable building products. As detailed by Bello and Espiloy (1995), many bamboo-based products have been manufactured in the country, such as bamboo mat, boards, bamboo slivers laminated boards, bamboo strip ply boards, fiberboards, cement-bonded particleboards and resin-bonded particleboards. Laminated bamboo boards (LBBs), similar to glue-laminated timber products, are of particular interest due to the standardization of shape and the relatively low variability in material properties (Sharma et al., 2015). Test results and comparisons from early studies clearly show that LBBs can be used as alternative for wood-based composites for building construction.

The fabrication of LBBs requires the bamboo culms to be disassembled into thin flat laminae. These

laminae are then laminated together with prevailing binding material such as adhesives. The adhesive is not only a significant cost factor in wood composite production but also the key factor for some of the product properties (Chaowana, 2013). The Polyvinyl Acetate (PVA) glue was selected as adhesive in this study which is in liquid form and ready to use. In this study, three types of laminated bamboo board specimens with three different lamina configurations were fabricated utilizing PVA as adhesive.

The mechanical and physical properties of the LBBs were thoroughly investigated to determine which lamina configuration will maximize its strength and durability.

METHODOLOGY

Materials and Equipment

Bamboo culms and the Polyvinyl Acetate (PVA) glue are the main materials used in this paper.

HEADINGS

Use at most three levels of headings that correspond to chapters, sections and subsections. The first level headings for chapter titles should be in 10pt, bold, justified, and upper case font. Leave one-blank line before and after the first level headings, respectively.

The Second Level Headings

The second level headings should be in 10pt, bold, justified, and First Characters of Each Word are in Capital font. Leave one blank line both before and after the heading, respectively.

Bambusa Bluemana Bamboo Culms

Treated and dried bamboo culms of *bambusa bluemana* or the *kawayan tinik* specie are purchased from a bamboo dealer located at Brgy. Dita,, Santa Rosa City, Laguna. The culms were cut at a length suitable for the production of the laminae in which, 1m is said to be the minimum. Culms in the best condition and with the thickest internodes were chosen to maximize the specifications of the product.

Polyvinyl Acetate(PVA) glue

In this study, Polyvinyl Acetate glue with brand Rakoll was used. The glue enhances the boards property due to its water resisting quality. The PVA glue was purchased at Maquiling Hardware Lumber and Construction Supply Inc. located at Brgy. Batong Malake, Los Baños, Laguna. The liquid PVA can be applied directly or pressed at room temperature using machine press. The glue has a white, tan or yellow color, but when applied for bonding, it possesses a colorless bond line. The high dry strength of PVA and its low resistance to moisture make it workable for laminated composites (Forest Products Laboratory, 1999).

Auxiliary materials for the board such as nails, sand paper, and brushes are purchased from the local home depot and hardware stores.

Bamboo Laminae Production

Treated and dried bamboo culms prepared for the production of the bamboo laminae are sliced longitudinally producing six pieces of slender bamboo slats. Depending on the diameter of the culms, some may produce a total of eight slats, still enough to be shaped into the desired dimensions. The outer skins of the slats are carefully removed with minimal reduction to the overall thickness of the slats.

Bamboo slats will undergo three phases of machine process, shaping them into bamboo laminae.

Trimming

Trimming the thickness of the bamboo slats is the first of the three phases in producing the bamboo laminae. The thickness planer is used to flatten the slats for consistency of the dimension. Two people are necessary to operate the machine: one insert slats on one side and the other receives the trimmed slats. Before using the planer, the slats must be examined and rid of the outer skin and hard nodal parts since they may cause damage to the machine. Slats are repeatedly inserted until a thickness of 5mm is achieved.

Cutting

The next phase involves cutting the length of the slats using the table saw. Like the thickness planer machine, the table saw requires two operators, one inserting and the other receiving. Each slender bamboo slat can be cut into three pieces with a length of 200mm with small allowance.

Calibrating

The third phase of shaping them into laminae is calibrating the width and length of each slat to 20mm and 200mm respectively, using the table saw. Each bamboo slats should have the final dimension 200mm x 20mm x 5mm and can now be justifiably classified as lamina.

Double Lamination

The laminae were glued together using double lamination. This process involves the first lamination which is applying glue on the side of each lamina (side pressing), and the second lamination which is applying glue on the face of each board (cold pressing) produced on the first lamination. In the first lamination process, the laminae are oriented in a way that the inner part of the bamboo is on the top. Glue is applied on the side of each lamina and are pressed using the bar clamp.

Taking into account the lamina configuration shown in Figure 1, each layer of the parallel and perpendicular type are the same with the first layer of the alternate type. However, the second layer of the alternate type has one lamina sliced length-wise at the center and placed at the opposite ends of the board.

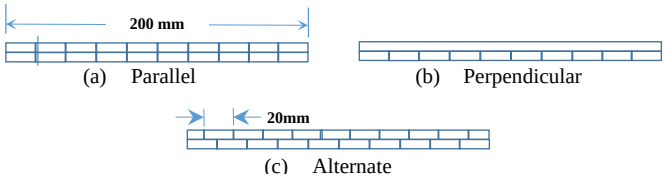

Fig.1 Lamina Configuration

Bamboo boards with dimension 200mm x 200mm x 5mm were produced, stored and cured for at least 10mins.

Inter-face bonding between boards which is classified as the second lamination uses the hydraulic pressing machine at a constant pressure of 200psi (1.38MPa) in room temperature. Adequate amount of glue is evenly spread on the face of each bamboo boards with the correct orientation of the laminae as joined together. Boards are stacked according to their lamina configuration. After pressing, the boards are left for 24 hours to cure. The final laminated bamboo board products possess the final dimension 200mm x 200mm x 10mm and are sand-grinded to achieve smooth surface.

Fig. 2: The finished LBB product in (a) parallel, (b) perpendicular, and (c) alternate type lamina configuration.

Testing

Laminated bamboo boards are tested for its performance in terms of physical properties including the water absorption, thickness swelling and delamination test, and mechanical properties including hardness, and modulus of rupture test.

Water Absorption (WA) and Thickness Swelling (TS)

Twelve 50mm x 50mm samples were cut, 4 from each configuration for the physical performance test. Initially, the weight and thickness of each sample were measured and recorded using digital balance and caliper respectively. The samples were soaked in tap water for 24 hours. The final weight and thickness were re-measured to determine the absorbed water and the apparent increase in thickness. Equations 1 & 2 determine the water absorption and thickness swelling respectively:

$$\mathrm{WA}(\%) = \frac{\text{Wet Weight} - \text{Dry Weight}}{\text{Dry Weight}} \text{ x } 100\% \quad (1)$$

$$\mathrm{TS}\ (\%) = \frac{\text{Final Thickness} - \text{Initial Thickness}}{\text{Initial Thickness}} \text{ x } 100\% \quad (2)$$

Delamination Test (DT)

Another twelve samples, 4 from each configuration with dimensions 127.5mm x 50mm were tested for delamination test in accordance with PNS 196:2000, the standard test for delamination using hot and cold soaking test. The specimens were soaked in water for 6 hours and oven-dried for another 6 hours, under a temperature of 49°C. This cycle has been repeated for three consecutive times during the process of Delamination Test. The delamination ratio formula is given by equation 3.

$$Delamination\ ratio = \frac{sum\ of\ delaminated\ length\ of\ cross-section}{sum\ of\ gluing\ length\ of\ cross-section}\ x\ 100\% \quad (3)$$

Hardness Test (HT)

Hardness of the laminated bamboo boards were tested in accordance with ASTM D143-94 Standard method of testing for small clear specimens of timber. Twelve 100mm x 100 mm were subjected to the Janka Hardness Test to determine the resistance to indentation, where the force required to embed an 11.28 mm steel ball to half of its diameter was measured.

Modulus of Rupture (MOR)

Modulus of Rupture (MOR) test was done using the three-point bending test in accordance with the ASTM D3043-87 Standard for Methods of Testing Structural Panels in Flexure. Four pieces of

200mm x 50mm were cut in each LBBs for the MOR mechanical test. MOR was calculated using equation 4 as:

$$MOR = \frac{3PL}{2bd^2} \qquad (4)$$

Cutting Pattern

Figure 3 shows the cutting pattern for the physical and mechanical property tests.

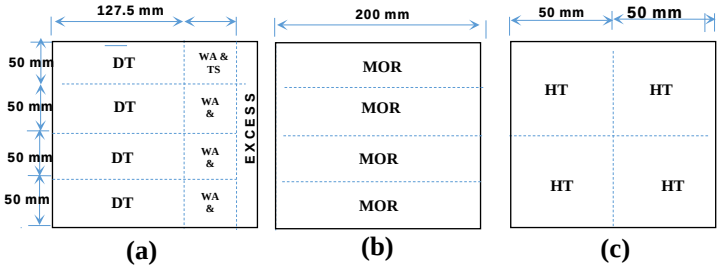

Fig.3 Cutting pattern for delamination, modulus of rupture,hardness test, water absorption and thickness sweelling

Statistical Tool

Utilizing the Analysis of variance (ANOVA), differences in means on the properties of the laminated bamboo boards with different lamina configuration were determined at $\alpha = 0.05$. The simple user interface Stat-plus was used for the analysis. Tukey's Honestly Significant Difference (HSD Test is used for post-hoc analysis to determine which means are different to the level of significance. A post-hoc analysis is performed only if the ANOVA test shows a p-value less than the significance level.

RESULTS AND DISCUSSION

Water Absorption and Thickness Swelling

Based on the results shown in Table 1, the LBBs, regardless of the lamina configuration, exhibit slight changes on their weight and thickness. Using one-way Analysis of Variance (ANOVA) with 5% significance level for the three lamina configurations of the LBBs, it shows that there was *no significant difference between the means of the boards in Water Absorption and Thickness Swelling tests.*

Delamination Test

Based on the results shown in Table 1, 0% delamination is observed for all three lamina configurations. The laminated bamboo boards, regardless of the lamina configuration, exhibit high adhesive bond performance and were able to resist delamination during accelerated exposure to water and heat.

Modulus of Rupture

The MOR means as shown in Table 2 shows that the LBBs which yield the highest and lowest MOR were the alternate type and the perpendicular, respectively. The one-way Analysis of Variance (ANOVA) with 5% significance level records a p-value less than 0.05 thus implying a *significant difference between the means of the MOR* derived from the three-point bending (flexural) test.

Further analysis using Tukey's HSD test shows that the MOR of the LBB with perpendicular lamina configuration is significantly lower than that of the parallel and alternate type. Since p-values are lower than 0.05, the MOR of the other two lamina configurations far exceeds that of the perpendicular type LBB. This test also shows that there is no significant difference between the means of the MOR of the parallel and alternate type laminated bamboo boards.

Hardness Test

From each type of boards, four pieces of 100mm x 100mm were tested using ASTM D143-94 Standard method of testing small clear specimen of timber. Test results in Table 2 show that perpendicular type LBB yields the highest mean of 5.22 kN, while alternate type LBB yields the lowest mean of 2.74 kN. The difference on the means for hardness of the LBBs produced is significant according to the one-way ANOVA test.

The Tukey's HSD test shows that, while the means of the parallel and alternate type displays no significant difference, the mean of the perpendicular-type LBB far exceeds that of the other two bamboo boards for the hardness test. The results from hardness test shows that the perpendicular type has good resistance to plastic deformation caused by penetration.

Table 1
Summarized test results for physical properties of LBBs with different lamina configuration

Board Type	Qty.	Water Absorbed (g)	Thickness Swelling (mm)	Delaminated Board	
				Cycle 1	Cycle 2
Parallel	Mean	7.60	0.72	0	0
	SD	0.92	0.19	0	0
Perpendicular	Mean	8.90	0.90	0	0
	SD	1.09	0.14	0	0
Alternate	Mean	7.83	0.89	0	0
	SD	0.15	0.16	0	0

Table 2

Summarized test results for mechanical properties of LBBs with different lamina configuration

Board Type	Qty.	MOR (MPa)	HT (KNf)
Parallel	Mean	**149.02**	**2.83**
	SD	12.58	0.35
Perpendicular	Mean	**53.66**	**5.22**
	SD	4.89	0.42
Alternate	Mean	**150.99**	**2.74**
	SD	18.75	0.54
Commercial Board	Mean	**140.60**	**5.74**
	SD	14.23	0.38

Figure 4 shows theMOR of the 3 LBBs and the commercial board. The graph shows that the perpendicular configuration is the weakest at 53.6 MPa in terms of bending, which is obvious due to the useless effect of one layer. The alternate configuration exceeds the commercial laminated board.

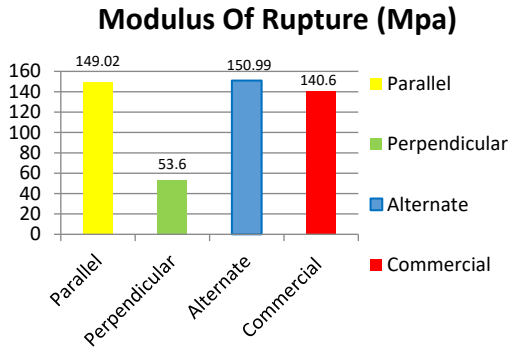

Fig.4 MOR values of the 3LBBs and the commercial board

The hardness test shows that the commercial board has the highest value, while the parallel configuration demonstrates lowest in terms of hardness.

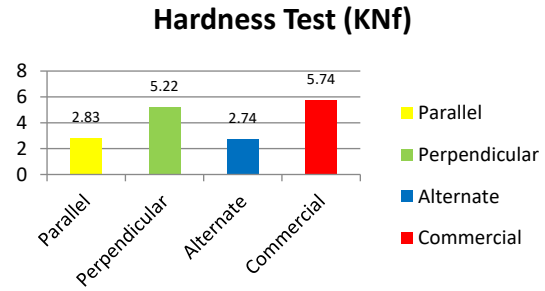

Fig.5 Hardness of the 3LLBs and the commercial board

Statistical Analysis

Table 3 shows the summary on the test for significance in means of the 3 LBBs for the different properties

Table 3
Summary for the test for significance on means of the 3LBBs

Property	**P value**	**Significance**
WA	0.46>0.05	NS[a]
TS	0.06>0.05	NS
MOR	0.00<0.05	S[b]
HT	0.00<0.05	S

[a]NS – Not Significant(all means are equal); [b]S – Significant (not all means are equal)

Table 4 shows the summary of the of the Turkey's HSD Test for the Modulus of Rupture and the Hardness of the LBB specimens

Table 4
Turkey's HSD test results on MOR and HT

PAIR	**MOR**	**Hardness Test**
Parallel vs Perpendicular	S[a]	S
Parallel vs. Alternate	NS[b]	NS
Perpendicular vs. Alternate	S	S

[a]S-Significant (not all means are equal) [b]NS – Not Significant (all means are equal)

Results, shown in Table 4, depicted that, since p-values were lower than 0.05, the MOR of the alternate and parallel type LBBs far exceeded that of the perpendicular type LBB. The hardness test shows that the mean of the perpendicular type LBB was significantly higher than that of the other two bamboo boards. The Tukey's HSD test also shows that the means of the parallel and alternate type LBBs were statistically the same for both the MOR and hardness test.

CONCLUSION

Based on the results on Physical and Mechanical properties of the Laminated Bamboo Boards, the following conclusions were drawn:

1. All laminated bamboo specimens demonstrated slight change in weight and thickness, but not significantly, on WA and TS tests. Regardless of the lamina configuration, all LBBs had shown excellent quality against delamination during accelerated exposure to water and heat.
2. The mechanical test of the LBBs with parallel and alternate type lamina configuration exhibit good performance in resisting bending or flexure (149 MPa and 150 MPa), far exceeding that of the perpendicular type LBB with 53 MPa. Their flexural strength are even better than that of the laminated bamboo composite

from a previous study (68-128 MPa), and are comparable to the flexural strength of a normal laminated wood (140.6MPa). Hence, these two types of LBBs have good potential for engineering applications.

3. The perpendicular type LBB yielded the highest load of 5.22 kN in the Hardness test. This is nearly 50% greater than that of the parallel and alternate type (2.83 kN and 2.74 kN). Thus, perpendicular type LBB is the best laminate to be used for flooring in terms of hardness.
4. The mechanical properties of the parallel and alternate type LBBs, both for MOR and Hardness, had shown no significant difference.

REFERENCES

Bello, E.D. & Espiloy, Z.B. (1995). New products and applications of bamboo. Paper presented at the 'National Symposium on the Sustainability of the Bamboo Industry, College, Laguna, 20–21 December 1995'. Ecosystems Research and Development Bureau: College, Laguna.

Chaowana, P. (2013). Bamboo: an alternative raw material for wood and wood-based composites. Journal of Materials Science Research, 2(2), 90-102.

Forest Products Laboratory. (1999). Wood handbook—Wood as an engineering material. Gen. Tech. Rep. FPL–GTR–113. Madison, WI: U.S. Department of Agriculture, Forest Service, Forest Products Laboratory. 463.

Li, H.-t., Zhang, Q.-s., Huang, D.-s. & Deeks, A.J. (2013). Compressive performance of laminated bamboo. Composites Part B Engineering, 54, 319-328.

Nguyen, T.H., Shehab T. & Nowroozi, A. (2010). Use of bamboo composites as structural members in building construction. Challenges, Opportunities and Solutions in Structural Engineering and Construction – Ghafoori (ed.), 605-608.

Sharma, B., Gatóo, A., Bock, M. & Ramage, M. (2015). Engineered bamboo for structural applications. Construction and Building Materials, 81, 66–73.

Tesoro, F. O., & Espiloy, Z. B. (1990). Bamboos Current Research. In I. V. Ramanuja Rao, R. Gnanaharan, & C. Sastry (Eds.), Bamboo Research in the Philippines (pp. 15–21). Canada: International Development Research Centre.

Verma, C.S. & Chariar, V.M. (2012). Development of layered laminate bamboo composite and their mechanical properties. Composites Part B Engineering, 43, 1063-1069.

Verma, C. S., Sharma, N. K., Chariar, V. M., Maheshwari, S., & Hada, M. K. (2014). Comparative study of mechanical properties of bamboo laminae and their laminates with woods and wood based composites. Composites Part B Engineering, 60, 523–530.

Virtucio, F.D. (2009). Silvicultural management of bamboo in the Philippines and Australia for shoots and timber: General overview of bamboo in the Philippines. Proceedings of a workshop held in Los Baños, the Philippines, 22–23 November 2006. ACIAR Proceedings No. 129 – Midmore (ed.), 18-23.

Second International Conference on Science, Engineering & Environment,
Osaka City, Japan, Nov.21-23, 2016, ISBN: 978-4-9905958-7-6 C3051

A COMPARISON OF PARALLEL BRANCH AND BOUND ALGORITHMS FOR LOCATION-TRANSPORTATION PROBLEMS IN HUMANITARIAN RELIEF

Chansiri Singhtaun[1] and Suriya Natsupakpong[2]
[1]Department of Industrial Engineering, Faculty of Engineering, Kasetsart University, Bangkok, Thailand
[2]Institute of Field Robotics, King Mongkut's University of Technology Thonburi, Bangkok, Thailand

ABSTRACT

This paper studies the effect of branching rules (BR) and heuristic algorithms (HA) to find feasible solutions for a branch and bound (BB) algorithm used to solve sub-problems in a parallel two-phase branch and bound (PTBB) approach. The nine PTBB algorithms, which are developed by varying 3^2 combinations of BR and HA strategies, are tested on the facility location-transportation problem for disaster response (FLTDR). The mathematical model for the problem determines the number and location of distribution centers in a relief network, the amount of relief supplies to be stocked at each distribution center and the vehicles to take the supplies in order to maximize the percentage of needs coverage of disaster victims under capacity restriction, transportation and budgetary constraints. To examine the performance of the algorithms, computational experiments are conducted on the various sizes of generated problems. Three strategies of BR and HA provided in the "intlinprog" function of MATLAB were applied for these problems. The objective function values and the computational times of all algorithms were collected and analyzed. The results showed that all PTBB algorithms can solve problem sizes of four candidate locations with fifteen demand points without premature termination by time. The PTBB algorithm using "maxfun" branching rules and "rss" heuristic to find a feasible solution is recommended for FLTDR because of the least computational time usage.

Keywords: Disaster Response, Facility Location, Transportation, Humanitarian Relief

INTRODUCTION

Disaster operations management has been a popular issue for decades because of the increase in the number and severity of natural disasters. During 2007-2011, natural disasters killed 23.64% more people and there was a 59.21% increase in economic damage when compared with 2002-2006 [1]. The life cycle of disaster operations management comprises four phases, which are the mitigation phase, the preparedness phase, the response phase, and the recovery phase [2]. The first two phases are pre-positioning phases that need to be performed prior to the onset of a disaster. The other two are post-disaster phases. The period of time of each phase depends on the type of disaster (a quick-onset or a slow-onset disaster). The disaster response is a crucial phase. The objective of disaster response in the humanitarian relief chain is to rapidly provide relief (emergency food, water, medicine, shelter, and supplies) to areas affected by large-scale emergencies, so as to minimize human suffering and death. Relief logistics play an important role in this phase. The scope of relief logistics relates to ten subsystems, which are planning, inventory distribution, transportation, procurement, maintenance, control, human resources, information and communication, and administration subsystems [3]. The first three subsystems have been intensively studied under the following topics: facility location problems, inventory problems, transportation/routing problems and scheduling problems. Both individual analyses and the integration of these four problems have been researched. Moreover, most research topics have emphasized designing a disaster management framework, such as the study appearing in [4]. Few research papers have focused on constructing a disaster response operation framework and application, which aims to determine a solution based on numerical data by using a mathematical method.

The facility location-transportation problem for disaster response (FLTDR) relates to solving both location and transportation problems simultaneously. The location problem requires determining the number, the position and the mission of a humanitarian aid distribution centre within the disaster region. The transportation problem deals with the distribution of humanitarian aid from the distribution centre to demand points [5]. Most of the mathematical models for FLTDR are Mixed Integer linear Programming (MIP) problems with complex constraint structures [6]. The traditional Branch and Bound (BB) algorithm is currently the only general tool available for finding optimal solutions to these difficult formulations [7]. However, finding an optimal solution for a complex and large size FLTDR using a BB takes excessive computing time.

Parallel computing is one of the most efficient alternatives that has been used since the beginning of the twenty-first century. The use of parallelism to speed up the execution of a typical (sequential) BB algorithm is widely known as a Parallel Branch and Bound (PBB) algorithm. There are three main approaches of PBB algorithms according to the degree of parallelism of the search tree. Parallelism of type 1 introduces parallelism when performing the operations on generated sub-problems (e.g., bounding computations). In the type 2 approach, the search tree is built in parallel by performing operations on several sub-problems simultaneously. In the parallelism of type 3, several trees are explored concurrently [8]. Both the selection of computer architectures and PBB approaches for a particular MIP problem affect the computational performance. Much of the research in the PBB approach area has emphasized developing new or improving the existing computer architectures such as [9, 10, 11]. Little research has focused on developing new or improving PBB approaches such as [12]. However, the various strategies of the BB algorithm, which are used in sub-problem solving in the PBB algorithm and affect the branching sequence of the PBB algorithm, have not been studied. Therefore, this research intends to determine the impact of these strategies, which are BR and HA, on computational time and quality of solutions (in the case of premature termination). The goal of this research is to determine the best strategy for the PBB algorithms.

RESEARCH METHODOLOGY

Problem Description

The FLTDR in this study focuses on calculating the number of distribution centres to be constructed; determining the locations of distribution centres (y_l); identifying the quantity of relief items to be stored (p_{jl}) and determining the assignment of vehicles (X_{ilhkv}) and quantities of the humanitarian aid (Q_{ilhkv}) to serve demand points in order to maximize the relief item coverage under the following assumptions. Each particular house or building within the affected area could require humanitarian aid and is thus a potential demand point. The demand quantities are estimated by a homeland security organisation or experts. The demand quantities can only be satisfied by the distribution centre, which is assumed to stock and distribute multiple types of relief item. The relief items are divided with respect to their response time criticalities and target response time intervals.

The amount of stock to be held at the distribution centre depends on the number and location of distribution centres in the network as well as the assignment of demand locations to the distribution centres, while distribution centre location and assignment decisions are affected by the quantity of relief items to be stocked at each distribution centre. Each distribution candidate site has a global and a per product capacity that fixes the maximum quantity to be stored within the site. The location candidates and the capacity of distribution centres are considered in the pre-disaster phase based on the demand locations and quantities. Both location and stock decisions are limited by pre-disaster budgetary restrictions.

The vehicles available at candidate sites are of various types and there are different numbers of available vehicles. The different docking times of each vehicle type at each site and the time needed for loading and unloading one unit of each product for each vehicle type are considered. The traveling time from a distribution centre to a demand location is determined corresponding to distance and vehicle type. There are also some restrictions on the total weight and the total volume of vehicles. A maximum daily work time for each vehicle type is imposed. A given vehicle can perform as many trips as needed during a day as long as the corresponding work time limit is respected. Each vehicle trip is assumed to visit only one demand point at a time. One demand point may be visited many times. However, because of the maximum daily work time, the number of trips to a specific delivery point by a particular vehicle will be limited to a maximum value, which is set at two. Finally, shipping costs from distribution centres to demand points are restricted by post-disaster budgetary restrictions. The mathematical model formulation of this problem refers to [12].

Parallel Branch and Bound Algorithms

In order to analyse the effect of BR and HA on the performance of the PTBB1 algorithm, which is an PBB approach that was proposed in [12], for various sizes of FLTDR, a 3^4 full factorial design with single replication is used to carry out the numerical experiments. Two following hypotheses are tested. The first hypothesis is to test whether treatments, which are the parameter of the problem (the number of demand points n and the number of candidate locations of distribution centres u) and the options of the BB algorithm (BR and HA), affect the responses. The other hypothesis is to test whether a treatment interaction affects the responses. Three generated problems are tested in each combination of treatments. The response is the average computational time. Each treatment is composed of three levels, which are shown in Table 1. The levels of BR and HA are options of BB that are provided in the “intlinprog” function in MATLAB. For BR, the rules that choose the fractional component with a maximal corresponding component in the absolute

value of the objective function (maxfun); the fractional component with maximum pseudocost (maxpscost); and the component whose fractional part is closest to 0.5 (mostfractional) to be branched are carried out. Three levels of HA are used to enhance bound tightening as follows. For the first level or strategy (none), there is no search for a feasible point. Any feasible point that is encountered in the BB search is taken. The second strategy takes the linear programming (LP) solution to the relaxed problem at a node. It rounds the integer components in a way that attempts to maintain feasibility. The last strategy applies a hybrid procedure that combines searching the neighbourhood of the current best integer feasible solution point (if available) and local branching to find a new and better solution. Therefore, the nine PTBB algorithms are developed by applying 3^2 combinations of BR and HA strategies for the PTBB1 algorithm. These algorithms are tested on nine problem cases.

Table 1 The Levels of all Treatments

Treatment	n	u	Branching rules	Heuristic for finding feasible solutions
Low level	5	1	maxfun	none
Intermediate level	10	2	maxpscost	rss
High level	15	3	mostfractional	round

The PTBB1 proposed in [12] is composed of 10 steps as follows. Parallel computing is applied in steps 2 to 10 using the "*parfor*" function in MATLAB. The nine strategies of the BB algorithm are implemented in step 6.

Step 1: Calculate the upper bound of the number of distribution centers to be located (ub_{NumDC}) using the budgetary constraint. Let the set of current solutions (y_l, $X_{ilhkv,}$ p_{jl} and Q_{ilhkv}) be an empty set and the current objective function (Z_{cur}) is zero.

Step 2: Set the current number of distribution centers to be located ($NumDC_{cur}$) at 1.

Step 3: Find all possible patterns of selecting $NumDC_{cur}$ locations out of u candidate locations. Now all possible sets of decision variables y_l corresponding to $NumDC_{cur}$ are created. Let the number of all possible patterns corresponding to $NumDC_{cur}$ be $NumPat_{cur}$.

Step 4: Set the current pattern (Pat_{cur}) at 1.

Step 5: Select the set of decision variables y_l relating to $NumDC_{cur}$ and Pat_{cur} .

Step 6: Solve a transportation sub-problem relating to y_l using a BB algorithm. At this step the solutions for variables X_{ilhkv}, Q_{ilhkv}, and p_{jl} are found and the objective function *(Z)* corresponding to y_l is known.

Step 7: Update the set of current solutions and Z_{cur} by employing a new solution and a new Z obtained from step 6 if the Z is better (more) than Z_{cur}. Otherwise, go to step 8.

Step 8: Set $Pat_{cur} = Pat_{cur}+1$. If $Pat_{cur} \leq NumPat_{cur}$ go to step 9. Otherwise, go to step 10.

Step 9: Select the set of decision variables y_l relating to a new Pat_{cur}. Solve the LP relaxation problem of the transportation sub-problem using an interior point algorithm. If $Z > Z_{cur}$, go to step 6. Otherwise, go to step 8.

Step 10: Set $NumDC_{cur} = NumDC_{cur}+1$. If $NumDC_{cur} \leq ub_{NumDC}$ go to step 3. Otherwise, stop the iterative process.

All PTBB algorithms are coded with MATLAB. The numerical experiments are implemented on an asynchronous shared memory system, which is constructed from a workstation with a CPU Intel Core i7-5820K 3.30 GHz 6-core processor with 16 GB RAM. The data sets of nine problem cases with the specific n and u in [12] are used. All algorithms are set to be prematurely terminated at 28,800 sec or 8 h in order to limit the computational time for large-size problems. The percentage of weight demand coverage, computational time and the solutions of the decision variables are recorded. The results of the experiments are statistically analysed by using analysis of variance (ANOVA) at a level of significance $\alpha = 0.10$ with MINITAB.

RESULTS

Since there is no premature termination by time; only the average computational time of all combinations or algorithms is shown in Table 2. All nine strategies of BR and HA give the optimum solution. To statistically analyse the effect of four factors (n, u, BR, and HA) on the average computational time, ANOVA is carried out using MINITAB. Four-factor interaction effects are ignored. The ANOVA table is shown in Table 3. Before drawing any conclusions from the ANOVA table, the assumption of experimental or residual error, which is normally and independently distributed, should be examined by analysing the residual plots illustrated in Fig. 1. From Fig. 1, the Normal Probability Plot shows that the residuals are in linear form. It can be concluded that the data distribution is a normal distribution. Likewise, the Histogram shape also shows that the data distribution is normal. The other two graphs show

that the residual is independently distributed because the plotted data is distributed randomly. Thus, it can be concluded that the residual is normal and independently distributed.

Table 2 Average computational time of all treatment combinations

n		u = 1			u = 2			u = 4		
		none	rss	round	none	rss	round	none	rss	round
5	maxfun	2.75	2.74	2.74	2195.40	2166.10	2156.70	23110.90	13099.10	13098.70
	maxpscost	905.52	883.69	878.36	3723.50	3733.80	3733.40	12415.10	12991.80	12975.10
	mostfractional	1.42	1.42	1.41	3322.20	3346.60	3332.20	15800.35	15817.50	15849.50
10	maxfun	902.78	906.63	1962.30	5097.00	3159.50	3148.20	5450.40	5431.50	5410.50
	maxpscost	3689.56	3875.15	4138.40	5396.70	5394.90	5371.10	11921.00	13998.00	12092.00
	mostfractional	2879.67	2987.35	3170.60	5201.04	5178.25	5124.90	8970.87	8991.50	8931.00
15	maxfun	5190.74	5720.61	4840.17	7319.20	7008.91	7201.00	26730.17	24711.03	23548.00
	maxpscost	3050.82	2080.04	2610.83	3456.10	2437.20	2640.70	27192.78	24920.10	28801.68
	mostfractional	3410.38	3060.36	3100.21	8001.49	7013.41	7201.00	27610.90	23450.00	25548.00

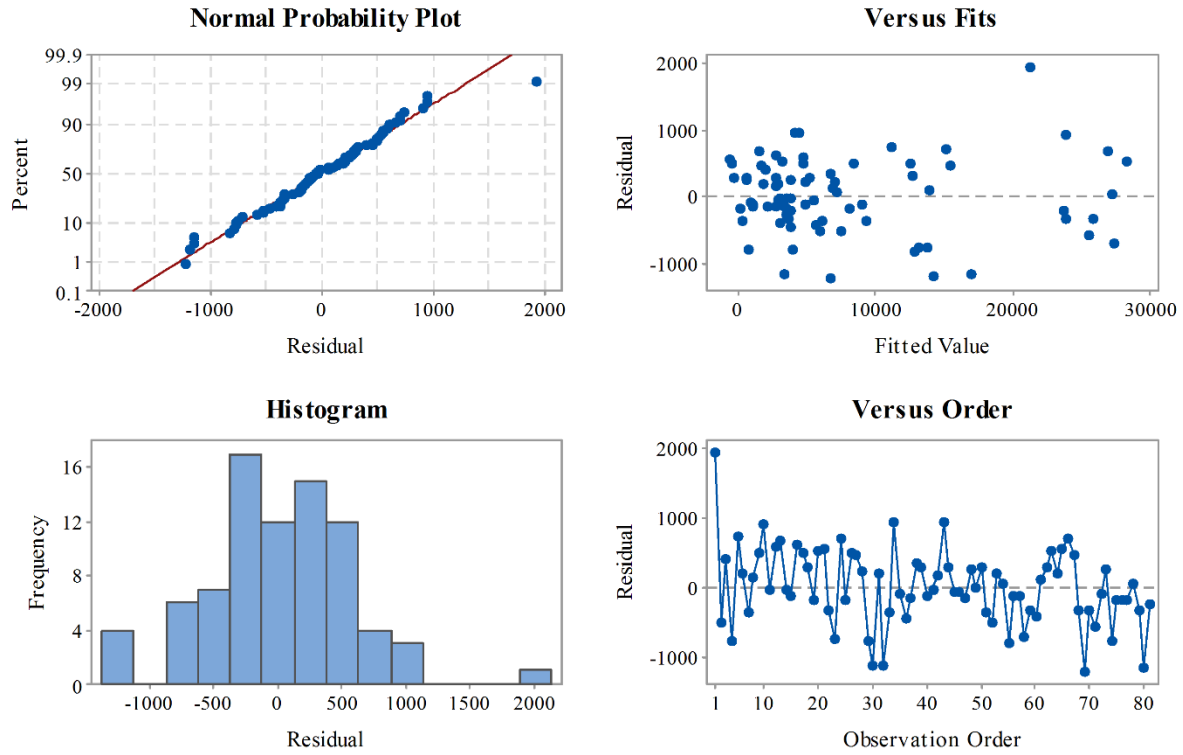

Fig. 1 Residual plots for computational time data

From Table 3, the factors n, u, HA, the n*u interaction and n*BR interaction, the u*BR interaction, and the n*u*BR interaction significantly affect the response because the p-values are less than the level of significance α = 0.10. According to Table 3, factor u has a greater effect on the computational time than n because it has a higher F-value. Moreover, the combination of these two factors, which leads the numerous decision variables and problem size, shows a nonlinear impact on the computational time. Because the n*u*BR interaction has a significant effect, only the three-factor interaction plots of n, u and BR (shown in Fig. 2) are used and the main effect plots of n, u and BR are ignored to interpret the results and to set the levels of these factors. To set the appropriate HA strategy, the main effect plot of HA (shown in Fig. 2) is considered. According to the main effect plot of HA, the efficient option of HA is the "rss" option because it gives the least computational time. The top-left graph of the interaction plots indicate that BR should be set at the "maxfun" option. The bottom-left graph and the bottom-right graph of the interaction plots show that the least values of n and u (the smallest size problem) use the least computational time.

Table 3 ANOVA for the computational time data

Source of Variation	Degrees of Freedom	Adjusted Sum of Squares	Adjusted Mean Square	F-Value	P-Value
n	2	643906702	321953351	213.80	0.000
u	2	3230007029	1615003515	1072.47	0.000
BR	2	6889907	3444954	2.29	0.134
HA	2	9088131	4544065	3.02	0.077
n*u	4	753671742	188417935	125.12	0.000
n*BR	4	74963016	18740754	12.45	0.000
n*HA	4	5580682	1395170	0.93	0.473
u*BR	4	18863426	4715856	3.13	0.044
u*HA	4	8259167	2064792	1.37	0.288
BR*HA	4	8213325	2053331	1.36	0.290
n*u*BR	8	77731263	9716408	6.45	0.001
n*u*HA	8	12449772	1556222	1.03	0.452
n*BR*HA	8	13052877	1631610	1.08	0.422
u*BR*HA	8	16062604	2007825	1.33	0.296
Error	16	24093874	1505867		
Total	80	4902833518			

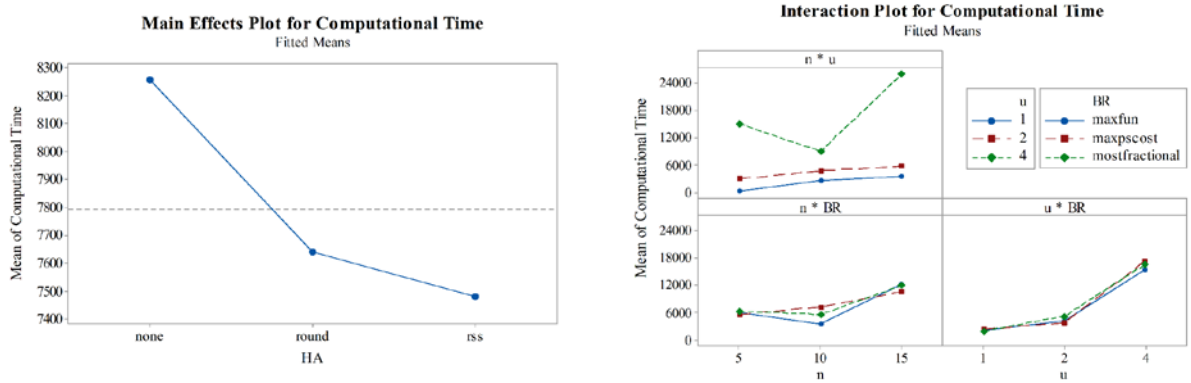

(a) (b)

Fig. 2 Main effect plot of HA (a) and three-factor interactions of n, u and BR for computational time (b)

CONCLUSION AND RECOMMENDATIONS

Both BR and HA impact the computational time of PTBB algorithms. The selection of BR options affect the computational time of PTBB1 in a nonlinear relation corresponding to n and u. The most efficient BR and HA for the PTBB algorithms to solve the generated FLTDR are the "maxfun" and "rss" options, respectively. This is because the "maxfun" option just looks for and picks up the fractional component with the maximal corresponding component in the absolute value of the objective function without much calculation. Unlike the "maxfun" option, the "maxpscost" option takes time to calculate the pseudocost in selecting the component to be branched while the "mostfractional function" option needs to search and compare the values of all possible pairs of variables. These two options may help to reduce the number of branches to be visited, but this advantage cannot be observed in this study. The "rss" option, which uses a hybrid procedure to find a new and better solution, is more efficient than the "round" option, which just rounds the integer components in a way that attempts to maintain feasibility. This result shows that it is worthwhile to take time to find the best quality feasible solution and tightening bound. This is because it can help PTBB algorithms to fathom a number of inferior branches to be visited. Therefore, the PTBB algorithm using "maxfun" branching rules and "rss" heuristic to find a feasible solution is recommended for FLTDR because it can deliver the optimum solution with the least computational time. For future research, other strategies of BR and HA or other factors such as node selection rules should be investigated. Moreover, to extend the

performance of the PTBB algorithms and computer architecture to develop a parallel computing machine should also be considered.

ACKNOWLEDGEMENTS

This study was supported by Kasetsart University Research and Development of Thailand under Grant No. 36.51.

REFERENCES

[1] UNISDR. (January 2012). The Economic and Human Impact of Disasters in the last 12 years. United Nations Office for Disaster Risk Reduction. Available: http://www.unisdr.org /files/ 25831_20120318disaster20002011v3.pdf

[2] Altay N and Green WG, "OR/MS research in disaster operations management", European Journal of Operational Research, Vol. 175, No. 1, 2006, pp. 475–493.

[3] Balcik B and Beamon BM, "Facility location in humanitarian relief", International Journal of Logistics Research and Applications, Vol. 11, No. 2, 2008, pp. 101–112.

[4] Aslanzadeh M, Rostami EA, and Kardar L, "Logistics Management and SCM in Disasters", Supply Chain and Logistics in National, International and Governmental Environment, Farahani RZ, Asgari N and Davarzani H, Ed. Physica-Verlag, Heidelberg, New York: Springer-Verlag, 2009, ch.10, pp. 221-252.

[5] Abounacer R, Rekik M, and Renaud J, "An exact solution approach for multi-objective location-transportation problem for disaster response", Comput. Operations Res., Vol. 41, 2014, pp. 83-93.

[6] Minoux M, "Networks synthesis and optimum network design problems: Models, solution methods and applications", Networks, Vol.19, 1989, pp. 313-360.

[7] Bourbeau B, Crainic TG, and Gendron B, "Branch and bound parallelization strategies applied to a depot location and container fleet management problem", Parallel Computing, Vol. 26, 2000, pp. 27-46.

[8] Gendron B and Crainic TG, "Parallel Branch-and-Branch Algorithms: Survey and Synthesis," Operations Res., Vol. 42, 1994, pp. 1042-1066.

[9] Barreto L and Bauer M, "Parallel Branch and Bound Algorithm-A comparison between serial, OpenMP and MPI implementations", Journal of Physics: Conference Series, Vol.256, No.1, 2010, pp. 1-14.

[10] Otten L and Dechter R, "Load Balancing for Parallel Branch and Bound", in Proc. of the 10th International Workshop on Preferences and Soft Constraints, 2010, pp. 51–65.

[11] Leroy R, Mezmaz M, Melab N and Tuyttens D, "Work stealing strategies for multi-core parallel branch-and-bound algorithm using factorial number system", in Proc. of the Programming Models and Applications on Multicores and Manycores, 2014, pp. 111-119.

[12] Singhtaun C and Natsupakpong S, "Applications of Parallel Computing for Facility Location-Transportation Problems for Disaster Response", Journal of Computer Science, Vol.11, No.4, 2015, pp. 612-620.

Second International Conference on Science, Engineering & Environment,
Osaka City, Japan, Nov.21-23, 2016, ISBN: 978-4-9905958-7-6 C3051

FLOW CONTROL THROUGH VORTEX SHEDDING INTERACTION OF ONE CYLINDER DOWNSTREAM OF ANOTHER

Jonathan Payton and Sam M Dakka
Department of Engineering and Mathematics, Sheffield Hallam University, United Kingdom

ABSTRACT

This study investigates the vortices produced between two 2d cylinders, and the relationship between the structures of the vortices produced at both cylinders when one is placed in the wake flow of another. CFD simulations using ANSYS Fluent were used to determine the coefficients of lift and drag, as well as the frequency of vortex shedding and size of vortices at three separate Reynolds numbers of 16000, 32000 and 65000 in different arrangements. Each arrangement of cylinders was compared against controls, which consisted of a single cylinder to determine the alteration of forces produced. Two trip wires at 7 different angles of 40, 45, 50, 55, 60, 65, and 70 degrees were then investigated at a Reynolds number of 65000 which was compared to the smooth cylinder control forces and frequency of vortex shedding. The most optimum angle of trip wires was then combined with linear cylinder arrangements also at a Reynolds number of 65000 for comparison with only the upstream cylinder utilizing the trip wires.

Keywords: Vortex, Shedding, Flow, Control, Strouhal

INTRODUCTION

Vortex shedding is a phenomenon that occurs with non-aerodynamic bodies at specific Reynolds numbers. The vortex shedding of the air in this periodic system can occur because the air flow sticks to the surface of the cylinder due to the Coanda effect [1], whereby the entrainment, the transportation of a fluid between two separate bodies of fluid by a shear induced turbulent imbalance [2], is reduced, due to the restriction caused by the interference by the surface of the cylinder. A pressure difference occurs between the surface and the fluid jet or flow, from the uneven distribution of momentum, and the change in acceleration that results from it to reach equilibrium [1]. This pressure change deflects the fluid jet towards the surface, causing the air to attach to, and follow the curvature of the surface. The separation of the boundary layer causes a large pressure difference forming the wake flow of the cylinder, and forms vortices generated by this pressure difference.

A vortex or Eddy is a circulating flow of air around an axis. The acceleration of this air increases with the reduction in diameter closer to the central axis in irrotational vortices. Using Helmholtz's vortex theorems relating to inviscid flows, negating any influence from shear stresses, the theoretical behavior of these vortices can be explained, whereby the strength of a vortex remains equal along its entire length, the vortex lines of the path traveled by the air in the vortex remains on that same line and is constant; and irrotational vortices remain irrotational providing there are no rotational forces external to the vortex [3]. In Karman vortex streets, the rotation direction about these axes of the vortices alternates with each successive vortex produced, because each one is being generated by the air flow from either side of the bluff body.

The flow instability is caused by the Kelvin–Helmholtz instability [4], which is formed when two flows of different velocities interact, Fig. 2. The turbulence experienced in both of these separate flows over both sides of the cylinder causes varying velocities, which generates the formation of this instability when these velocities interact in the wake flow [4].

The trip wires, control rods, or some form of a roughness element body can be used to reduce the vortex shedding produced by the cylinders [5]. The angle at which the rods are placed in front of the cylinder influences the airflow around the cylinder. A trip wire reduces the drag by accelerating the transition of the boundary layer separation from the laminar stage to the turbulent **[**6]. This allows for the air to reattach to the surface of the bluff body at an earlier stage across the bluff body, because the kinetic energy is increased. This effect of reducing the drag only occurs at certain Reynolds numbers that are above subcritical. Subcritical flow means the transition from laminar to turbulent occurs in the wake of the cylinder [7].

NUMERICAL METHOD

ANSYS Fluent software was used for simulations with an incompressible flow regime implemented. A no slip condition was placed on the cylinder walls. Walls of the domain parallel to the flow were set as symmetry to ensure no influence of the wake flow was introduced. A pressure outlet was generated to accommodate the returning flow of the Von Karman Streets into the computational domain.

The model used to simulate the vortices was the Detached Eddy Simulation SST k-Omega with double precision to accurately model the flow in a transient state with hybrid initialization. One two dimensional, theoretically infinite cylinder of diameter 0.0127m was generated, and separate Reynolds numbers were simulated at 16000, 32000 and 65000. Higher Reynolds numbers required lower time steps, with 16000 being simulated at time steps of 0.0005, 32000 being simulated at 0.0001, and 65000 being simulated at 0.00005 time step intervals. Monitors were placed on each cylinder, a coefficient of drag monitor parallel to the flow of the fluid and a coefficient of lift perpendicular to the flow direction. Arrangements of the two cylinders used can be seen in Fig 1.

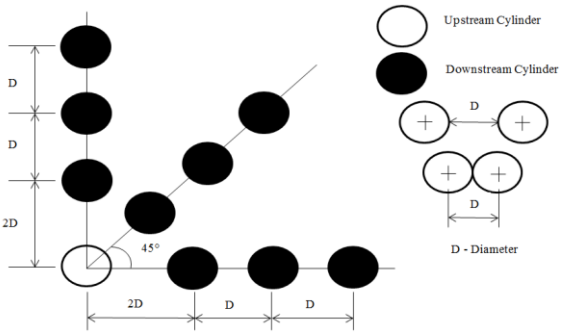

Fig. 1 Smooth cylinder arrangements.

For each Reynolds number, the boundary layer thickness was determined using the following Equations; Eq. 2 was used due to the boundary layer becoming turbulent as the rolling motion of the boundary layer occurs across the cylinder with 10 inflation layers used at inflation sizing 0.0002.

$$\ell = (0.491 * d) / \sqrt{\mathrm{Re}} \quad (1)$$

$$\ell^* = (0.382 * d) / \mathrm{Re}^{0.2} \quad (2)$$

Table 1 Boundary Layer Thickness

Reynolds Number	Laminar Boundary Layer Thickness (m)	Turbulent Boundary Layer Thickness (m)
16000	0.00049	0.0007
32000	0.00035	0.00061
65000	0.00025	0.00053

The inlet velocity was calculated based on equation 3, Re- Reynolds number, p- density, μ - dynamic viscosity. This can be seen in Table 2.

$$\mathrm{Re} = (p * d * U) / \mu \quad (3)$$

Table 2 Inlet Velocity Relating to Reynolds Number

Re. No. 10^3	Density (kg/ m^3)	Dynamic Viscosity (kg/m/s) 10^{-5}	Diameter (m)	Inlet Vel. (m/s)
16	1.225	1.7894	0.0127	18.4
32	1.225	1.7894	0.0127	36.806
65	1.225	1.7894	0.0127	74.76

Equation 4: St- Strouhal number, w- vortex frequency, i- vortex length.

$$St = (w * i) / U \quad (4)$$

Simulations were run for a minimum of five coefficients of lift oscillations, to be able to record the average value when calculating the frequency for the Strouhal number. Each graph was magnified to reduce the margin of error with the pixel ruler being used for each measurement taken. A mean average was taken of the coefficient of lift oscillations to ensure that any minor variations that could generate errors were reduced. These were taken by the distances between crests, and between troughs. The frequency was scaled - dependent to the time step used - to 1 second, to meet the metric standard constraints to calculate the Strouhal number, and divided by the average distance between oscillations. A similar method was also used finding the average maximum coefficient of lift with a zero origin line on the y axis to be able to calculate this distance vertically to the y axis scale.

The size of the control rods used was one tenth the size of the diameter of the cylinder. For this specific cylinder the diameter of the control rods were 1.27mm. In order to prevent the mesh becoming highly skewed from tangent circles and influencing the simulation, fillets were placed between the tangent contact points, which were equal to the radius of the control rods (Fig. 2). Reference values for total circumference in fluent was calculated accordingly.

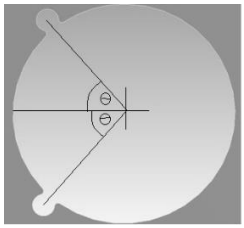

Fig. 2 Example of a dual control rod arrangement

RESULTS

Averaged results were obtained and plotted to identify trends.

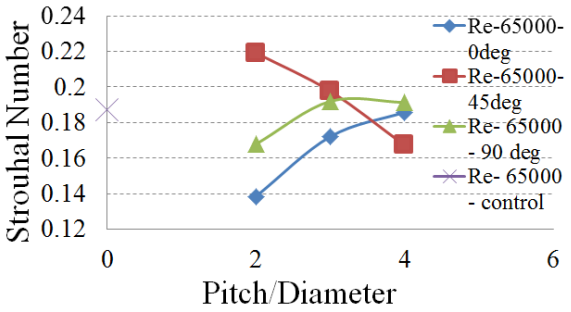

Fig. 3 Strouhal number Reynolds number 65000 in each arrangement

The same frequencies of shedding was experienced on the upstream cylinder and the downstream cylinder. The length of the vortices produced had little change with each arrangement.

Table 3 Strouhal Number Comparison Linear Arrangement

Re. No.	Pitch/ Diam Ratio	Strouhal Number [5]	Strouhal Number Simulated	% Diff.
16000	0	0.197	0.177	10.15
16000	2	0.17	0.159	6.47
16000	3	0.156	0.161	3.21
16000	4	0.19	0.166	12.63
32000	0	0.198	0.168	15.15
32000	2	0.158	0.164	3.80
32000	3	0.149	0.143	4.03
32000	4	0.195	0.161	17.40
65000	0	0.195	0.187	3.50
65000	2	0.149	0.139	6.71
65000	3	0.141	0.160	13.48
65000	4	0.187	0.186	0.53

The Strouhal number relative to each arrangement was close to that expected (Table 3). To obtain a more accurate result with the simulated graphs, the time step could be reduced to an even smaller iteration to allow for a graph that contains wider oscillations for more accurate measurements since will reduce the error obtained from pixel variations from the measurements taken with more definitive crests and troughs. The longer the simulations were left to run, the more compressed the graphs became, making the margin of error larger.

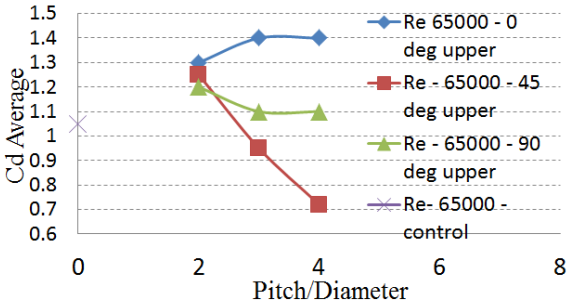

Fig. 4 Coefficient of Drag of the upstream cylinder in each arrangement

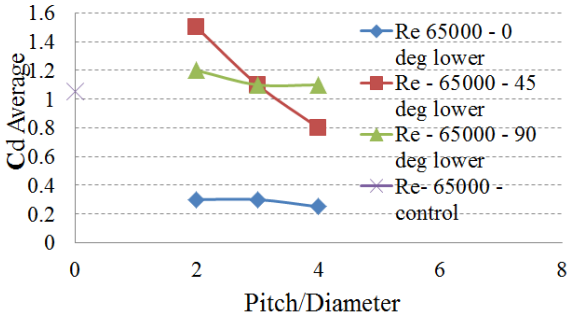

Fig. 5 Coefficient of Drag of the downstream cylinder in each arrangement

The drag force exerted by the cylinders, vary with the arrangement. The formation at a 90 degree angle results in a lower coefficient of drag with an increasing pitch to diameter ratio (Fig. 4, 5).

When compared to the downstream cylinder (Fig. 4, 5), the linear formation shows a significant drop in coefficient of drag compared to the upstream cylinder, which is caused by the cylinder located directly in the wake flow of the upstream cylinder. Since the arrangement of the downstream cylinder at 45 and 90 degrees is not directly in the wake flow at any pitch to diameter ratio, the coefficient of drag of the downstream cylinder in this arrangement is higher than the linear formation downstream cylinder.

The coefficient of drag generally decreases with an increasing pitch to diameter ratio, which is the same relationship for the coefficient of drag at 90 degrees for the downstream cylinder. At 90 degrees, both the upstream and downstream cylinder share the same coefficient of drag due to the arrangement being perpendicular to the flow, meaning the downstream cylinder is not influenced by the wake flow of the upstream cylinder (Fig. 4, 5).

When Fig. 6 and 7 are compared, a slight asymmetry exists between the 90 arrangement that was not experienced at Reynolds numbers 16,000 and 32,000 which could mean that the issue is mesh based in that it is potentially too coarse locally**.** Both

increase with an increasing pitch to diameter ratio, but in a linear formation the downstream cylinder experiences the same maximum coefficient of lift at all three ratios at 2.25 (Fig. 7) and an increasing coefficient in the upstream cylinder with increasing pitch to diameter ratios (Fig. 6).

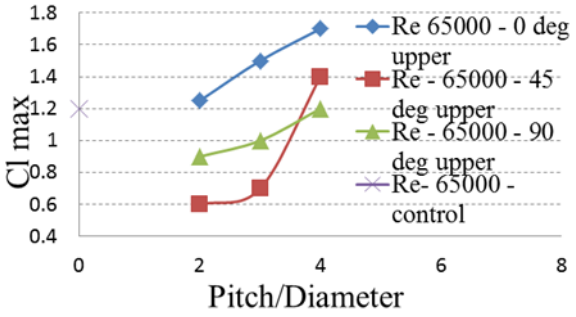

Fig. 6 Maximum Coefficient of lift reached – upstream cylinder

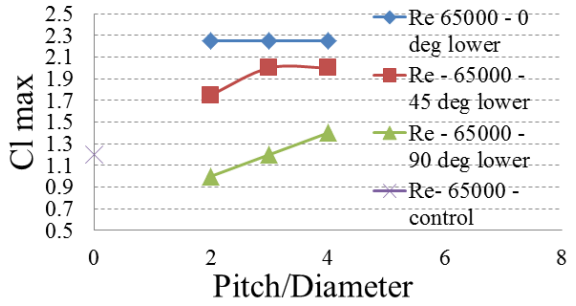

Fig. 7 Maximum Coefficient of Lift reached – downstream cylinder

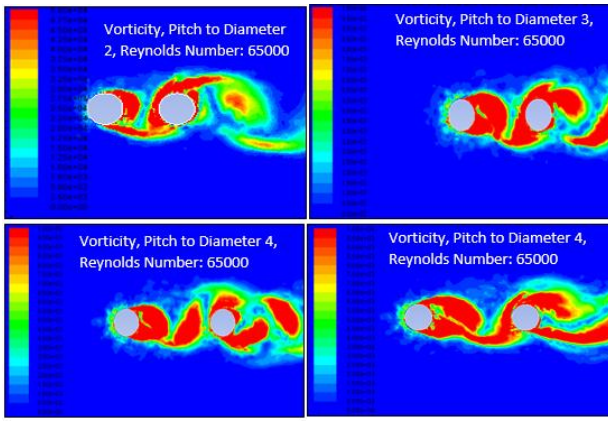

Fig. 8 Vorticity cut plot at different pitch to diameter ratios with two shown at a ratio of 4

The 45 degree arrangement results in a shedding that is interrupted towards the downstream cylinder at lower ratios of pitch to diameter (Fig. 6) and some reduction in low pitch to diameter ratios of the downstream cylinder (Fig. 7).

The structure of the flow in the linear formation parallel to the freestream velocity, changed with changing pitch to diameter ratios. The flow structure seen in Fig. 8 is similar to that documented by Alam MM. At a pitch to diameter ratio of 2, front side reattachment of the flow is visible at a Reynolds number 65000, which fits in Alam's flow structure range at a pitch to diameter of 1.5 to 2.2. At a pitch to diameter ratio of 3, the same type of flow is seen as before, which matches the flow structure described by Alam's in the range of a pitch to diameter ratio of 2.7 to 3.9. At a pitch to diameter ratio of 4 both the forms of the bi-stable flow was seen at Reynolds number 65000 (Fig. 8).

Table 4 shows a reduction in the sum of the upstream and downstream cylinders coefficient of drag, averaged across the three angles simulated. The drag reduces with an increased pitch to diameter ratio, and also with an increase of the three Reynolds numbers simulated.

Table 4 Cumulative Mean Average Coefficient of Drag Comparison that includes all 3 Angles of Arrangements

Re. No.	Pitch/ Diam. Ratio of 2	Pitch/ Diam. Ratio of 3	Pitch/ Diam. Ratio of 4
16000	2.46	2.43	2.42
32000	2.43	2.08	1.98
65000	2.21	1.93	1.79

The frequency of shedding increased when compared to a cylinder without control rods present for control rod arrangements simulated at angles 40, 45 and 70 degrees (Fig. 10). It is expected the Strouhal number would increase further after 70 degrees. The Strouhal number decreased significantly up to an angle of control rod arrangement of 55 degrees.

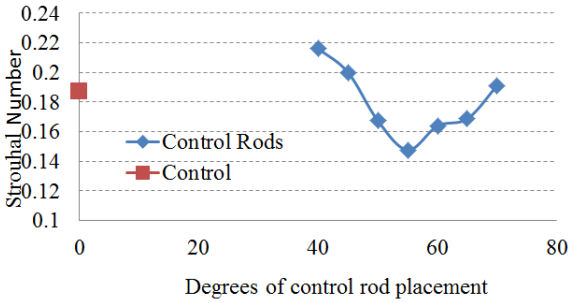

Fig. 10 Strouhal number of Trip wire angles compared to smooth cylinder – Reynolds number 65000

The control rods reduce the overall coefficient of drag produced by the cylinder, with all coefficients of drag lower than that of the control (Fig. 11). With an increasing angle of the arrangement of the control rods, the coefficient of drag increases. It is expected that the coefficient of drag will increase until a 90 degree formation, since this will generate the highest profile drag.

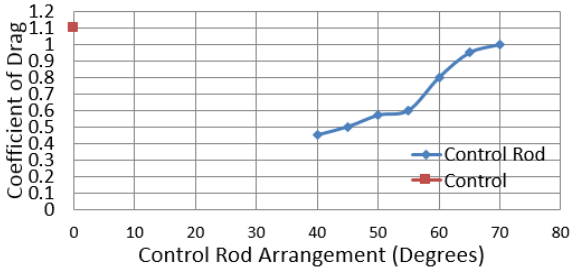

Fig. 11 Coefficient of Drag of Trip wire angles compared to smooth cylinder control – Reynolds number 65000

Similar to the coefficient of drag, the maximum coefficient of lift (Fig. 12) generally increases with an increasing angle arrangement. The maximum coefficient of lift produced (Fig. 12) is lower than the coefficient of lift produced by the control. The coefficient of drag is lowest at an angle of 40 degrees (Fig. 11) - and is expected to be even lower at lower angles since it separates the boundary layer at an earlier stage of the cylinder.

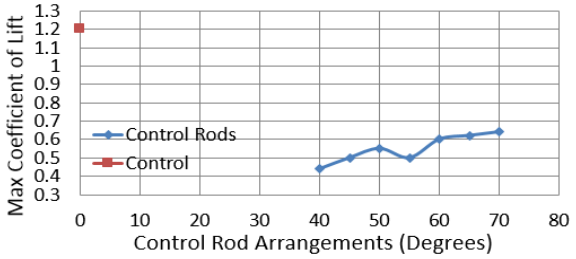

Fig. 12 Coefficient of Lift of Trip wire angles compared to smooth cylinder control Reynolds number 65000

Figure 12 shows the reduction of the coefficient of lift when control rods are introduced. The coefficient gradually increases with an increase in angle of trip wire placement.

The vorticity cut plot comparison (Fig. 13) shows the decreased frequency of the vortex shedding when control rods are used at a 55 degree angle placement. The vorticity of the vortices produced later in the wake of the cylinder when the control rods are used are consequently less than that of the control cylinder. The frequency of the shedding per second is close to 1100 with the control, to close to 870 when the trip wires are introduced at a 55 degree angle.

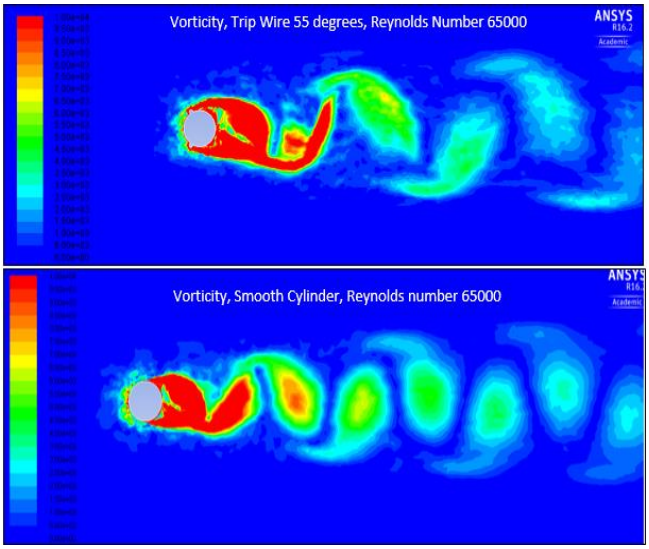

Fig. 13 Vorticity cut plot of Trip wire 55 degrees compared to smooth cylinder

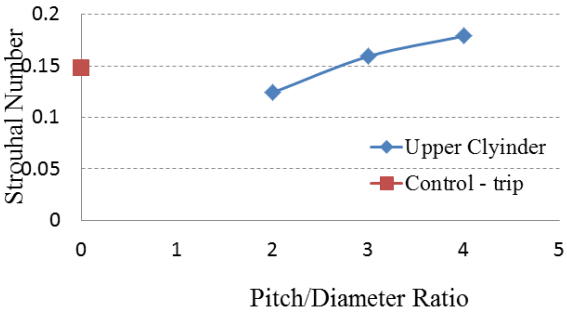

Fig. 14 Strouhal number of Trip wire 55 degrees within arrangement –Reynolds number 65000

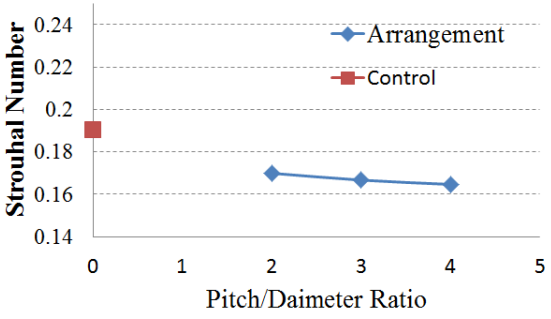

Fig. 15 Strouhal number of the downstream smooth cylinder within the trip arrangement against the Strouhal of a control smooth cylinder – Reynolds number 65000

When Fig. 14, 15 are compared, different Strouhal numbers are experienced on each cylinder theoretically unlike dual smooth cylinders. The vortices experienced in a linear arrangement aft of the arrangement is that of the downstream cylinder, since this bluff body interrupts the upstream vortex production.

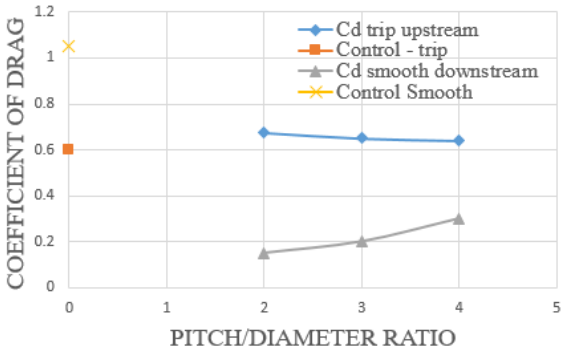

Fig. 16 Comparison between the trip upstream cylinder and the smooth downstream cylinder average coefficient of drag against each of the original control values

The results of the downstream cylinder linear arrangement with changing pitch to diameter ratios increasing, with the most optimum control rod angle placement of 55 degrees on the upstream cylinder showed an increase in the coefficient of drag greater than the trip control, a similar relationship to Fig. 4, . This increase from the control in Fig. 16 is reduced in comparison to Fig. 4. The coefficient of drag decreases towards the value of the control with an increasing pitch to diameter ratio (Fig 14). The downstream cylinder showed a mirrored relationship whereby the coefficient of drag increased with an increase in pitch to diameter ratio (Fig. 16). When Fig 4, 5 and Fig. 16 are compared, the reduction between the cumulative coefficients of drag with the linear arrangement is 0.775 at a pitch to diameter ratio of 2, 0.85 at a pitch to diameter ratio of 3 and 0.68 at a pitch to diameter ratio of 4.

CONCLUSIONS

To reduce the frequency of the shedding, and also to reduce the overall drag produced if multiple cylinders in close proximity are used, a linear arrangement with a pitch to diameter ratio of 2 would be used with no trip. More investigation is needed into pitch to diameter ratios lower than this point in order to find the most optimum performance for shedding frequency. It would be expected that reverse flow reattachment would be seen in the structure of the flow, with an even lower coefficient of drag from the downstream cylinder. The highest drag produced by the downstream cylinder is in the 90 degree formation since little interaction occurs between the cylinders. Due to the increased difference of drag at increasing Reynold numbers, the importance of the arrangement is high.

The trip wire arrangement showed a reduced coefficient of drag at a Reynolds number of 65000; and a reduced maximum coefficient of lift which gradually increased with an increasing angle of control rod placement. The most optimum angle for flow control was 55 degrees.

The arrangement with the presence of a trip on the upstream cylinder resulted in a reduced coefficient of lift on both the upstream and downstream cylinder when compared to the same non-trip arrangement. The coefficient of drag of the downstream cylinder arrangement with a trip is also lower than the non-trip arranged downstream cylinder. The upstream cylinder also has a reduced coefficient of drag, making it the lowest overall coefficient of drag with two cylinders.

ACKNOWLEDGEMENT

The work is part of dissertation submitted by Jonathan Payton in partial fulfillment of Bachelor Degree in engineering at Engineering and Math Department, Sheffield Hallam University, UK

REFERENCES

[1] S. &. C. Thermofluids, "Coanda Effect," 2014. [Online].Available: http://www.thermofluids.co.uk/effect.php

[2] Turner J S, Buoyancy Effects in Fuids, Cambridge University Press,1973.

[3] Yang J, "Vorticity Theorems," 2012.

[4] Laroussi M et al. "Triggering vortex shedding for flow past circular cylinder by acting on initial conditions: A numerical study," Computers & Fluids, Vol. 10, 2014, pp. 194–207.

[5] Alam MM, "Suppression of fluid forces on two staggered cylinders," Procedia Engineering, Vol. 56, 2013, pp. 173-178.

[6] S. Behara, "Transition of the boundary layer on a circular cylinder in the presence of a trip," Journal of Fluids and Structure, Vol. 27(5), 2011, pp.702-715.

[7] Doolan CJ, "Large eddy simulation of the near wake of a circular cylinder at sub-critical Reynolds number", Enginnering applications of fluid mechanis, Vol. 4 (4), 2010, pp. 496-510.

[8] [Online]. Available: http://www.thermofluids.co.uk/effect.php.

Second International Conference on Science, Engineering & Environment,
Osaka City, Japan, Nov.21-23, 2016, ISBN: 978-4-9905958-7-6 C3051

CHALLENGES OF HACCP IMPLEMENTATION IN AGRICULTURAL FOOD PRODUCTS IN THAILAND

Kanokwan Kingphadung and Woraruthai Choothian
Faculty of Engineering and Industrial Technology, Silpakorn University, Thailand

ABSTRACT

Agricultural food industry in Thailand could generate incomes about 10.5% gross domestic product (GDP) of the country in 2015. The demands of trend of agricultural food products around the world has been increased. However, agricultural food products from Thailand could not be exported as many as the market growth. Analysis and Critical Control Points (HACCP) is a minimal requirement for companies to export food products. Not all companies in agricultural food industry have HACCP certificates. There might be some challenges that have been obstructed the implementation of HACCP in food industry in Thailand. This objective of this research is identify challenges faced by companies in Thailand when implementing HACCP plans. An online survey was conducted to collect data from companies in food industry. Twenty companies completed the survey. identify challenges which obstructed the HACCP implementation in agricultural food industry in Thailand. All twelve challenges proposed in the research survey were experienced by participating companies during the HACCP implementation. The challenges, identified as barriers to implementing HACCP, were a lack of employee engagement in HACCP implementation, a lack of employees who understand the HACCP system, and a lack of advanced statistical knowledge. The results suggest companies to developing effective plans for communications and trainings to handle those challenges faced in the HACCP implementation.

Keywords: a ard Analysis and Critical Control oints, ACC , Challenges, ood Safety Management, Agricultural ood roducts

INTRODUCTION

The food industry is one of the most important industries influencing the economy of Thailand. Agricultural food products are one of the main types of exported products. In 2015, the agricultural food industry in Thailand generated a revenue of about 10.5% of Thai gross domestic product (GDP). The demand for exported agricultural food products has increased. However, agricultural food products from Thailand could not be exported as many as the market growth. Exporting food products to other countries requires food safety certification, such as Hazard Analysis and Critical Control Points (HACCP) and ISO 22000, to ensure that food products do not contain any hazards and are safe to consume, especially in Europe or North America.

HACCP is a food safety management system that is accepted by many countries and can be implemented in companies of all sizes. The implementation of HACCP can result in better product quality and the opportunity to penetrate the new market, especially exporting markets [1]. Complying with HACCP could be a minimal requirement for exporting food companies to be certified. Although food is the main industry in Thailand, not all companies that produce food products have food safety certificates. Meanwhile, many companies tried to implement HACCP but did not succeed. Companies might face common challenges during the implementation of HACCP. Knowing these challenges could allow companies to create plans to respond with challenges, and allow government sectors, such as universities or food agents, to assist companies in achieving HACCP implementation, especially small and medium-sized companies that do not have a lot of resources to invest for the purpose of establishing a food safety management system. This research aimed to identify the challenges that companies face in implementing HACCP in Thailand.

LITERATURE REVIEW

Ha ard Analysis and Critical Control Points (HACCP)

HACCP is a system that is used to identify, evaluate, and control food safety. HACCP can be compatible with other quality management systems, such as ISO 9000, that focus on the quality of products. The application of HACCP is considered for promoting food safety, which is considered one of the aspects of food quality [2]. It is a systematic approach to the identification, evaluation, and control of food safety hazards based on the seven principles presented [2, 3]:

Principle 1: Conduct a hazard analysis.
Principle 2: Determine the critical control points (CCPs).
Principle 3: Establish critical limits.
Principle 4: Establish monitoring procedures.
Principle 4: Establish monitoring procedures.
Principle 5: Establish corrective actions.
Principle 6: Establish verification procedures.
Principle 7: Establish record-keeping and documentation procedures.

To approach these seven principles, the following 12 steps are recommended [2, 3]:

(1) Set up an HACCP team to develop plans that contain tasks, activities, and responsible persons.
(2) Describe products, including all food safety information, such as packaging, containers, storage conditions, durability, and distribution methods.
(3) Identify how the user consumes or uses products.
(4) Construct flow diagrams of all of the operations in food production processes.
(5) Confirm the flow diagrams created in the previous step via onsite checking against the actual production processes.
(6) List all potential hazards associated with each step, conduct a hazard analysis, and consider any measures for controlling the identified hazards.
(7) Determine the CCPs used as a control measure for food safety.
(8) Establish critical limits for each CCP.
(9) Establish a monitoring system for each CCP.
(10) Establish corrective actions.
(11) Establish verification procedures.
(12) Establish documentation and record keeping.

The Challenges of HACCP

Many changes take place during the transition to the HACCP system. Some companies can endure this transformation, while other companies were unable to successfully implement HACCP. Successful HACCP implementation requires the involvement of all levels in the companies, from top management to work-floor employees. Much new knowledge is necessary to comply with HACCP principles. A few studies on the challenges of HACCP implementations were published. Previous studies on both HACCP and other food safety management systems were used to investigated what makes food safety management systems difficult. Five aspects were considered to be challenges.

) Top Management Support

Top management agreement is needed to ensure that the HACCP implementation will have strong support since it requires an investment, human resources, and policy supports [1]. Top management can be key in the implementation process because they can ask all employees to be involved and concerned with HACCP. Authorizations on any investments on equipment, tools, and trainings can be done by the top management. Top management can help the HACCP team in develop company policy. All departments or functions will voluntarily cooperate with the HACCP team. Without top management support, the implementation of HACCP might not be achieved [4].

) Consultants and Auditing of ACC

Companies mostly hire consultants who have a rich knowledge of HACCP and expertise in the food industry field to help in planning and establishing HACCP knowledge for companies [5]. For many countries that have just started using the HACCP system for mandatory food safety certification purposes, it might be difficult to find consultants who have expertise with HACCP. Companies might invite consultants from overseas. In addition to consultants, companies have to connect with auditors or HACCP certification companies to certify their HACCP systems. Unfortunately, it can take a long time to proceed with HACCP auditing when a limited number of auditors exist.

) Employee Engagement

Companies have to control all productions and operations to meet HACCP requirements. In addition, all employees who operate in those processes have to pay attention to all standards and procedures [6]. Employees who work in technical areas specifically should have sufficient knowledge to test or run experiments on detecting hazards and controlling food safety. Thus, the HACCP implementation requires collaborations and involvements from all employees. Many employees might perceive that the HACCP system make more workloads and complicated on their job. This leads to negative attitudes on the HACCP system. Employees might not be motivated to contribute in the HACCP implementation [7]. Without employee engagement, it might be challenging to successfully implement HACCP [4].

) Insufficient Knowledge

In production processes, companies must set up the control measures for critical control points (CCPs) in the HACCP system. The control measures might require new techniques or knowledge for testing food safety and monitoring systems or processes [8, 9]. Specific knowledge might be required, such as risk assessments and advanced statistical knowledge, to identify and assess the risks that might occur in the system and to control processes under CCPs [3, 7]. If employees do not have sufficient knowledge, it could challenge companies during HACCP implementation [6].

) Suppliers

The HACCP system concerns all processes related to products, from the time they are with suppliers until their delivery to customers. Suppliers should have adequate knowledge about food safety [3]. Companies must develop systems for controlling suppliers in following the standards. If companies do not have collaborations with or involvement from suppliers, the implementation of HACCP might not be successful.

) acilities and E uipment

All processes have to be under control. Facilities are required to be adjusted or added when needed. If companies have appropriate building structures and facilities, they might not need adjusting. When structures and facilities need to be rebuilt or changed, this might be difficult to accomplish due to limitations, such as the size of an area and the current building structure [10].

When all CCPs are defined, control measures are designed to test and find hazards or risks associated with each CCP. New tools and equipment might be needed [8]. Some equipment is expensive, however, or needs to be imported. Employees who use new tools and equipment also require training to operate them. This can result in more interment costs and in taking a longer time to receive the equipment needed for implementing HACCP.

RESEARCH METHODOLOGY

An online survey was conducted to identify the challenges that companies faced during the implementation of HACCP. The survey link was posted on websites, blogs, and webpages related to the food industry. The survey developed for this research included two sections.

The first section asked for participant and company information, such as participant position, company size, and products. The second section included a list of 12 potential challenges that organizations face when implementing HACCP. The list of challenges included on the survey was based on a review of the literature and on experts in the food industry. Participants were asked to rate the extent to which a challenge was a barrier to HACCP implementation. A five-point Likert scale, with responses ranging from 1 (not at all) to 5 (to a very large extent), was used.

RESULTS AND DISCUSSIONS

Participants and Companies

Targeted companies for this research study were companies that produced agricultural food products in Thailand. Twenty companies completed the survey. Of the 20 responding companies, 17 companies had implemented HACCP. The targeted participants for completing the survey included business owners, managers, supervisors, and staffs who worked in the targeted organizations.

Participant positions and company sizes are summarized in Table 1 and Fig. 1, respectively. Participants' positions included production supervisors, general managers, research and development (R&D) staffs, quality assurance (QA) staffs, owners, QA managers, production managers, and others. This enabled the researchers to see the wide range of view on HACCP systems. The highest number of participants identified themselves as supervisors and managers.

Table 1 Participant position

Position	No. of Participants
Production Supervisors	7
General Managers	3
R&D Staffs	2
QA Staffs	2
Owners	2
QA Managers	1
Production Managers	1
Others	1
R&D Managers	1
Total	20

According to the Ministry of Industry Thailand, company sizes are defined by capital investments into three groups. The first group includes small businesses with less than 50 million baht in capital. The second group includes medium-sized business with between 50 and 200 million baht in capital. The third group includes large business with more than 200 million baht in capital. Most participating companies were large businesses. The sizes of the participating companies are summarized in Fig. 1.

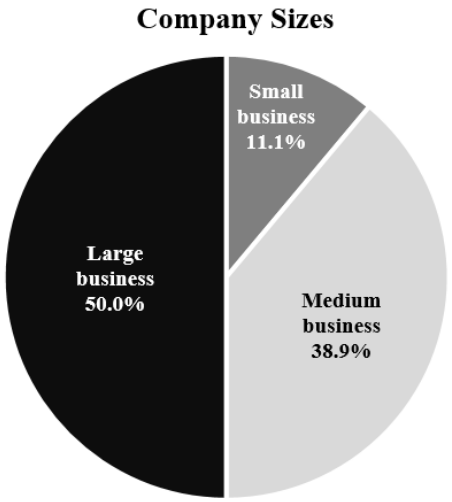

Fig. 1 Company sizes

HACCP Implementation in Thailand

Eighty percent of the participants thought that HACCP is very important to the agricultural food industry of Thailand. Participating companies had implemented HACCP for a range of three years to more than 10 years. Fifty percent of the responding companies had implemented HACCP for more than 10 years. Thus, the majority of the responses were from companies that had experienced the implementation of HACCP for more than 10 years, while the shortest time of implementation reported was three years. On average, companies would take about a year for preparation until getting the HACCP certification.

Challenges in Implementing HACCP in Thailand

All twelve challenges proposed in the survey were experienced by participating companies during the HACCP implementation. Eight of 12 proposed challenges were rated as the moderate extent to which challenge was a barrier to HACCP implementation. Hierarchical cluster analysis was used to divide challenges into groups, based on perceived barriers while implementing HACCP. The results of hierarchical cluster analysis are shown in the agglomeration schedule in Table 2 and in the dendrogram in Fig. 2. The difference between the coefficients in the agglomeration schedule and in the distances of linkage points in the dendrogram suggest that there are two clusters of challenges, based on perceived as barriers in the HACCP implementation**.** Cluster 1 included challenges that were more often perceived as HACCP barriers**.** Cluster 2 included challenges that were less often perceived as HACCP barriers**.** A summary of the clusters of challenges is shown in Table 3.

Table 2 Agglomeration schedule

Stage	Cluster Combined		Coefficients	Stage Cluster First Appears		Next Stage
	Cluster 1	Cluster 2		Cluster 1	Cluster 2	
1	6	7	.000	0	0	3
2	2	12	1.500	0	0	8
3	6	11	3.500	1	0	4
4	5	6	6.250	0	3	7
5	1	10	9.250	0	0	7
6	4	8	12.250	0	0	9
7	1	5	17.333	5	4	9
8	2	3	22.500	2	0	11
9	1	4	30.292	7	6	10
10	1	9	45.333	9	0	11
11	1	2	68.667	10	8	0

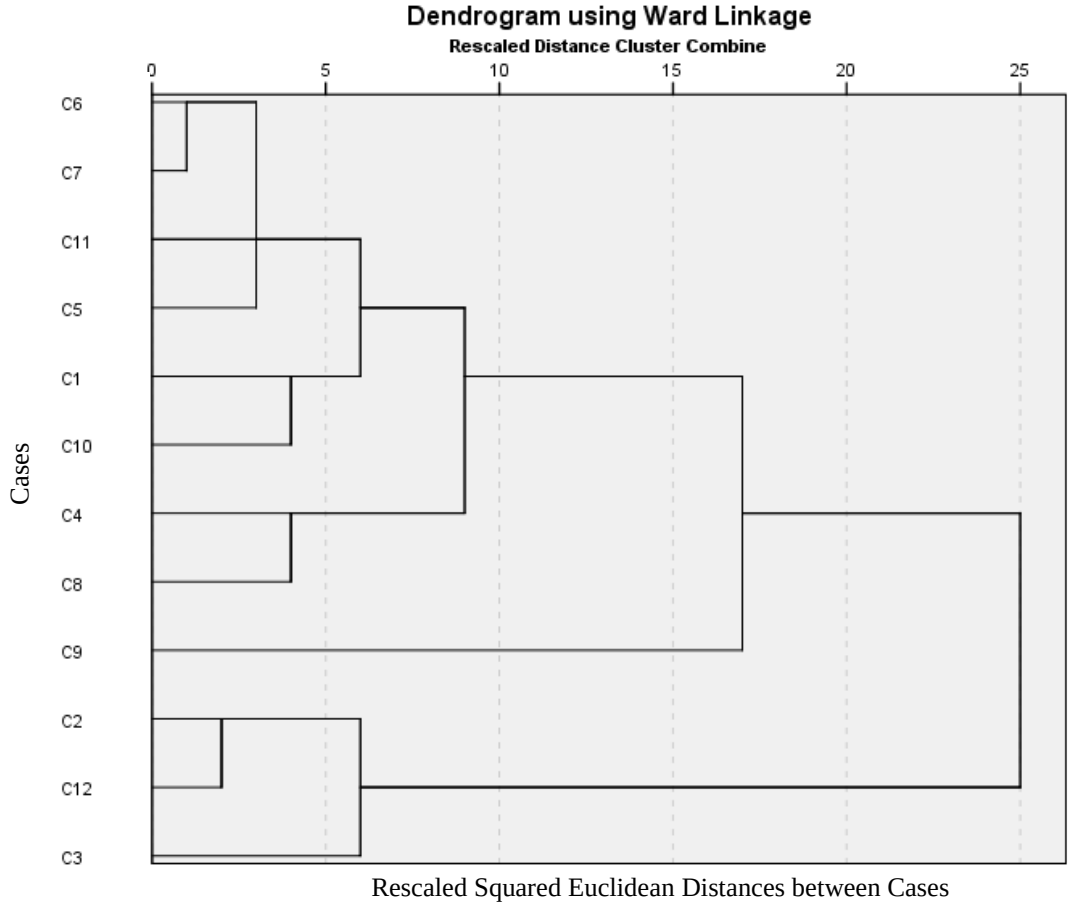

Fig 2 Dendrogram of perceived barriers

Table 3 Clusters of challenges based on perceived barriers during HACCP implementation

Code	Items	Mean	S.D.	Cluster
C3	Lack of employee engagement on the HACCP implementation	3.43	1.60	
C2	Lack of employees who understand the HACCP system	3.36	1.15	1
C12	Lack of advanced statistical knowledge	3.29	0.91	
C5	The need for building modification and facility adjustment to suit HACCP requirements	2.93	1.49	
C10	Difficulties of suppliers or vendors with proceeding under HACCP standards	2.86	0.86	
C11	Lack of knowledge about risk assessment in food production processes	2.86	1.10	
C6	The need to acquire new equipment and tools for testing food hazards	2.79	1.25	
C7	Lack of knowledge or techniques for testing food hazards to meet HACCP requirements	2.79	1.25	2
C1	The complication of HACCP certifying processes	2.43	1.02	
C8	Insufficient number of HACCP consultants in Thailand	2.43	1.34	
C4	Lack of management support	2.29	1.49	
C9	The limitation of auditing companies or auditors who can audit and certify HACCP in Thailand	1.71	0.73	

Cluster 1 which are challenges that were perceived more often as a barrier includes a lack of employee engagement in HACCP implementation, a lack of employees who understand the HACCP system, and a lack of advanced statistical knowledge.

Lack of employee engagement is the most concerned as barrier in the HACCP implementation of agricultural food companies in Thailand. According to HAPPC requirements, companies must develop guidelines and work standards for all processes. The developed guidelines might change the way that employees used to work before, or might add more tasks on their jobs, such as, record and report data. Inflexible work and additional tasks could result in the resistance of employees on the HACCP implementation and the negative attitude on HACCP system [6, 7]. This finding is important because it emphasizes how important it is for companies to develop effective plans for the HACCP implementation including communication plans and implementing plan. Companies should communicate the goals and plans of implementing HACCP to employees at all levels. Sufficient information related to the changes of work tasks, the supports by companies, and the trainings should be well transferred to employees. When employees know the benefit of the HACCP implementation and the supports by companies during the HACCP implementation, they might be motivated and cooperate with the company.

Lack of employees who understand the HACCP system and lack of advanced statistical knowledge were also perceived as a large barrier. This result implies that employees might not have insufficient knowledge to work in the HACCP system. Without fully understanding in HACCP and required knowledge, it is difficult to successfully implement Although employees put efforts on the HACCP implementation. Although most technical employees in food companies have back grounds in food science or food technology, they might need additional specific knowledge that can help in analysis data, such as statistics. This finding suggests that companies should create effective training plans to ensure that employees have sufficient knowledge to work on their jobs in the HACCP system.

It is interesting that the limitation of auditing companies and auditors was perceived as a small barrier. This finding suggests that companies easily access to auditing companies and auditors although the HACCP system has been well-known for a decade. The trend of implementing HACCP in Thai companies was increased because of the government policy in agricultural food product exports, the food safety control regulations, and the competition in the market. Thus, the numbers of auditing companies and auditors, supported by both government or private sectors, are also increased to meet the demands.

In addition, the cost of the HACCP implementation is a main challenge faced by companies in many countries [8]. Many participants also agree that the implementation of HACCP are vast investments which is a challenge that can be barriers in the HACCP implementation. Most companies spend much money on consultants, equipment, and modifying facilities [8]. Thus, companies should have a good financial plan when implementing HACCP as well.

CONCLUSION

There are many changes and adaptations required in implementing HACCP. Many companies were unable to successfully navigate this transformation. Knowing challenges that companies might face during the HACCP implementation could assist companies in developing plans to handle challenges. The challenges found in this research are similar to the previous research HACCP barrier in other countries and in other products [1, 8].

Challenges that were perceived often as barriers in Thailand were a lack of employee engagement in HACCP implementation, a lack of employees who understand the HACCP system, and a lack of advanced statistical knowledge. Effective communications can help in engaging employees involve in the HACCP implementation. Technical trainings and working with universities and researchers can fulfill in the lacking knowledge and the HACCP implementation. In addition to three challenges mentioned above, companies should also consider other nine challenges. Many companies experienced these nine challenges during the HACCP implementation. This implies that these challenges could occur and obstruct the HACCP implementation.

The limitation of this research was the number of participants. It is difficult to see significant differences in challenges based on perceived barriers. A larger number of companies could provide additional understanding into potential differences in challenges.

REFERENCES

[1] Macheka, L., et al., "Barriers, benefits and motivation factors for the implementation of food safety management system in the food sector in Harare Province, Zimbabwe," Food Control, vol. 34, 2013, pp. 126-131.

[2] Commission, C.A. (1997, 6/1/2015). Basic texts on food hygiene. Available: http://www.fao.org/docrep/005/Y1579E/y1579e03.htm

[3] Dahiya, S., Khar, R.K., and Chikara, A., "Opportunities, challenges and benefits of using HACCP as a quality risk management tool in the pharmaceutical industry," The Quality

Assurance Journal, vol. 12, 2009, pp. 95-104.
[4] Ramírez Vela, A. and Martín Fernández, J., "Barriers for the developing and implementation of HACCP plans: Results from a Spanish regional survey," Food Control, vol. 14, 2003, pp. 333-337.
[5] Kokkinakis, E., et al., "HACCP implementation in local food industry: A survey in Crete, Greece," Procedia Food Science, vol. 1, 2011, pp. 1079-1083.
[6] Toropilová, J. and Bystrický, P., "Why HACCP might sometimes become weak or even fail," Procedia Food Science, vol. 5, 2015, pp. 296-299.
[7] Azanza, M.P.V. and Zamora-Luna, M.B.V., "Barriers of HACCP team members to guideline adherence," Food Control, vol. 16, 2005, pp. 15-22.
[8] Maldonado-Siman, E., et al., "Comparison of implementing HACCP systems of exporter Mexican and Chinese meat enterprises," Food Control, vol. 38, 2014, pp. 109-115.
[9] Lu, J., et al., "The implementation of HACCP management system in a chocolate ice cream plant," Journal of Food and Drug Analysis, vol. 22, 2014, pp. 391-398.
[10] Hasnan, N.Z.N., et al., "Food factory design: Reality and challenges faced by Malaysian SMEs," Agriculture and Agricultural Science Procedia, vol. 2, 2014, pp. 328-336.

Second International Conference on Science, Engineering & Environment,
Osaka City, Japan, Nov.21-23, 2016, ISBN: 978-4-9905958-7-6 C3051

TREATMENT EFFICIENCY AND COMPRESSIBILITY BEHAVIOR OF SOIL MODIFIED WITH POWDERED ACTIVATED CARBON

Mohd Yuhyi Mohd Tadza[1], and Fauzi Baharudin[2]
[1]Faculty of Civil Engineering and Earth Resources, Universiti Malaysia Pahang, Malaysia [2]Faculty of Civil Engineering, Universiti Teknologi MARA, Malaysia

ABSTRACT

Riverbank filtration (RBF) systems are often used to treat surface water near rivers. The effectiveness of such systems depends heavily on the properties of the riverbank material that is used for filtering and treating the water. To improve the system's treatment efficiency, modifications may be conducted to the riverbank soil. Altering the properties of the soil might, however, affect the stability of the riverbank. In this study, soil and water samples near Lake Chini were collected and characterized. Filtration test was conducted to evaluate the efficiency of the soil in treating the water. The soil was modified by mixing it with powdered activated carbon (PAC) at varying percentage of 5 and 10%. In addition, compressibility test was carried out using a standard oedometer. Test results indicated that the soil alone was insufficient to treat the water to drinking water quality standards. Modification with activated carbon improved the water quality from Class II to Class I. However, compressibility test revealed that there were some changes to the pressure - void ratio relationship, indicating that the alteration of soil properties with the addition of activated carbon filters might affect the stability of the riverbank.

Keywords: Riverbank Filtration, Water Treatment, Compressibility, Actived Carbon, Oedometer, Lake Chini

1.0 INTRODUCTION

Lake Chini is the second largest natural riverine lake in Peninsular Malaysia [1]. The area with its diverse flora and fauna has been declared as Man and Biosphere Reserve by UNESCO in 2008 [2]. Despite being isolated, the lake is also home to the indigenous Jakun tribe [3]. For decades, the sustainability of the tribe is highly dependent on Chini's ecosystems for economic activities such as fishing, hunting and herb gathering. The Lake also provides fresh water for the tribe. In recent years however, Lake Chini has been developed for agricultural and tourism purposes, which have led to the deterioration of the lake [2][4]. High concentrations of contaminants from development activities resulted in the decrease in biodiversity as well as increased sedimentation in the lake [1]. Furthermore, chemical influx from the use of pesticides and fertilizers from nearby agricultural activities increased the chemical concentration in both water and sediment [5][6]. The construction of a small barrage downstream of Chini River to form a recreational lake has caused the water to become stagnant, resulting in higher pollution [1].

Studies have revealed that limited movement in a lake would severely affect its water quality [7]. Although the water quality of the lake has deteriorated over the years, communities of the Jakun tribe still rely on it as their sole source of fresh water. Due to the isolated nature of the lake, the construction of a water treatment plant would be challenging. Riverbank filtration (RBF) has been used successfully in treating surface water nearby rivers [8][9]. The system utilizes riverbanks as filtration media for the removal of contaminants and suspended solids in order to improve the quality of surface water [10][11]. Thus, RBF would be a viable alternative solution for supplying sustainable fresh water within the vicinity. However, the efficiency of the RBF system depends on the type, as well as the filtration and absorption capacity of the riverbank material [12]. In some cases, modification of the riverbank with other filtration material (i.e. sand, activated carbon, zeolite) or the construction of artificial barriers may be required to increase the riverbank's treatment efficiency to produce water of drinking water standards [13][14].

Both granular activated carbon (GAC) and powdered activated carbon (PAC) have been extensively and successfully used in water treatment applications [15][16][17]. They have been proven to be effective adsorbing agents for the removal of a wide range of organic and inorganic pollutants from water bodies. They are also capable of removing taste and odor from wastewater [18]. Modification of the riverbank with activated carbon filters however, may affect the stability of the riverbank. Malusis *et al*., [19] reported that soil modified with activated carbon up to 10% by weight would result in decreased permeability and increased compressibility. Thus, in constructing a RBF, the balance between water treatment efficiency and the compressibility should be taken into consideration.

To tackle the aforementioned issues, this study

investigated the treatment efficiency of natural soil from Lake Chini as well as soil that has been modified with PAC in laboratory column tests. The compressibility behaviors (pressure-void ratio relationships) of both natural and modified soils were also evaluated using the double oedometer technique.

2.0 MATERIAL AND METHODS

2.1 Sampling

Soil sampling was carried out at selected sites at Kuala Brang around the Lake Chini area. Using a hand auger, undisturbed soil samples were collected to a depth of 1 meter below the ground surface. The samples were placed in sealed bags prior to being tested in the laboratory. Water samples were also collected from the lake. The samples were stored in plastic containers and chilled at 4 ± 1°C.

2.2 Determination of Soil Geotechnical Properties and Water Quality Parameters

The geotechnical properties namely, specific gravity, particle size distribution, liquid and plastic limits and organic content of both unmodified and PAC-modified soils were determined according to BS1377 standard laboratory procedures. The six main water quality parameters namely dissolved oxygen (DO), biological oxygen demand (BOD), chemical oxygen demand (COD), ammonia nitrogen (AN), suspended solids (SS) and pH were determined in accordance with AHPA standard method procedures [20]. The water quality parameters were then used to calculate the Malaysian water quality index (WQI) as described by Norhayati *et al*. [21] using the following equation:

$$WQI = 0.22(SI\ DO) + 0.19(SI\ BOD) + 0.16(SI\ COD) + 015(SI\ AN) + 0.16(SI\ SS) + 0.12(SI\ pH) \quad (1)$$

where SI is the sub-index function of each given parameter. The water quality was later classified according to the Interim Water Quality Standards (INWQS). The apparent water quality, namely turbidity, was also measured. Each test was conducted in triplicates to ensure the reliability of the readings.

2.3 Adsorption and Filtration Tests

A simple adsorption test was conducted before the column filtration test was carried out. The adsorption tests were carried out at varying intervals of 5, 15, 30, 60 and 120 minutes on soil specimens which were slowly agitated (i.e. 100 rpm) in 500 ml conical flasks on an orbital shaker. Similar tests were carried out on soil specimens that have been mixed with PAC (Sigma-Aldrich) (at 5 and 10% by weight). . The PAC used in this study has a particle distribution finer than 142 μm and a specific surface area of about 900 m^2/g. Turbidity improvement was the only parameter evaluated in this test. The above tests were conducted to determine (i) the optimum hydraulic retention time (HRT) and (ii) the optimum mixture of soil and activated carbon. Once the optimum conditions have been determined, column filtration was carried out using a standard falling head apparatus. The water samples were retained in the column in accordance with the optimum HRT that has been determined in the adsorption tests.

2.4 Compressibility Behavior

The volume change behaviors of both unmodified and PAC-modified soils were carried out simultaneously using the standard oedometer method [19]. It is anticipated that changes in the pore fluid ionic concentrations would affect the engineering behavior of soils [22][23][24]. Estabragh *et al*. [25] noted that the magnitude of soil deformation is affected by the water quality. In order to replicate the on-site interaction between water from the lake and the soil in terms of volume change behavior, the distilled water in the standard oedometer method was replaced with the water samples obtained from Lake Chini. Soil specimens were initially prepared by thoroughly mixing with water samples from the lake to slightly greater than liquid limit before being carefully placed inside the oedometer rings. A total of 8 specimens of each soil were tested at varying pressures of 0.125, 0.25, 0.50, 1.02, 2.03, 4.06, 8.13 and 16.26 MPa. Duplicate specimens were prepared at different applied vertical pressures.

3.0 RESULTS AND DISCUSSION

3.1 Soil Geotechnical Properties and Water Quality Parameters

The geotechnical properties and mean initial water quality parameters are presented in Table 1. It was found out that the soil contained a high amount of fine-grained fractions. The soil was also found to have low plasticity characteristics with a plasticity index of 12.46. Under the INWQS, the water was classified as Class II, which is suitable for recreational activities and direct contact with the human body. Based on this classification, the water in the lake is not suitable for direct consumption and hence, some treatment would be required to improve the water quality to Class I (i.e. drinkable level).

Table 1 Geotechnical properties and mean initial water quality parameters

Geotechnical properties	
Specific gravity, G*s*	2.67
Liquid limit, *wl* (%)	39.38
Plastic limit, *wp* (%)	26.92
Particle size distribution % Passing (< 2 mm)	63
Mean initial water quality parameters*	
BOD (mg/l)	8.04
COD (mg/l)	16.43
DO (mg/l)	5.20
AN (mg/l)	0.08
SS (mg/l)	12.74
pH	6.57
Turbidity (NTU)	181.1

*INWQS – Class I => 92.7 (no treatment required); Class II = 76.5-92.7 (conventional treatment required), Class III = 51.9-76.5 (extensive treatment required); Class IV = 31.0-51.9 (suitable for irrigation only); Class V =< 31.0 (heavily contaminated - not suitable for daily use).

3.2 Adsorption and Filtration Test Results

Figure 1 shows the changes in turbidity with elapsed time for unmodified soil and soil mixed with PAC. Adsorption test results indicated that, the turbidity of the water decreased with increasing agitation time. A period of approximately 30 minutes was found to be sufficient for the turbidity readings to be equilibrated. Figure 1 also shows that, the turbidity decreased as the percentage of PAC increased.

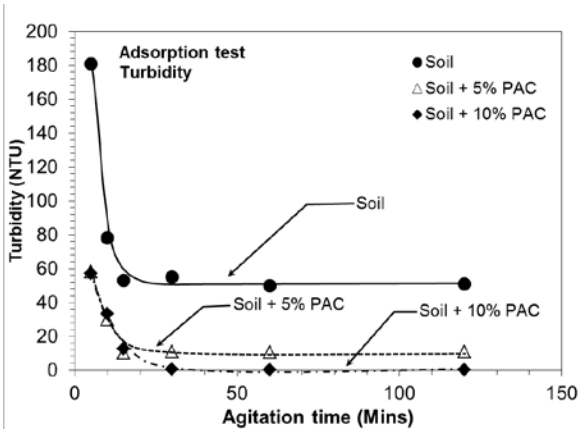

Fig. 1 Changes in turbidity with agitation time

Soil mixed with 10% PAC was found to have the highest reduction in turbidity as compared to unmodified soil and soil mixed with 5% PAC. Interestingly, in the absence of PAC, the soil alone was found to be ineffective in reducing the turbidity to Class I (i.e. NTU <50). Thus, constructing RBF in the area would require some modifications to the existing riverbank.

Based on the adsorption test results (see Fig. 1), the filtration test was subsequently conducted only on the unmodified soil and soil mixed with 10% PAC. The filtration test results are presented in Table. 2. Some improvements on the water quality (i.e. water quality improved to Class I) were observed after the filtration test for both soils with and without the presence of PAC. However, no reduction in BOD, COD and DO concentrations were obtained following the filtration tests (i.e. water remained as Class II). In other words, no treatment is required for the water filtered using soil and 10% PAC mixture. Slight increase in the pH was observed due to the presence of PAC. Similar findings were also reported i.e. increased in pH with the presence of activated carbon [26][27].

Table 2 Improvement in water quality after filtration test

Water quality parameters*	Soil	Soil + 10% PAC
BOD (mg/l)	7.98	6.57
COD (mg/l)	16.45	16.1
DO (mg/l)	5.31	6.83
AN (mg/l)	0.03	ND*
SS (mg/l)	10.59	0.06
pH	6.57	7.14
Turbidity (NTU)	55	0.18

*ND – non detected

3.2 Compressibility behavior – pressure-void ratio relationships

The effect of PAC on the geotechnical properties of the soil is shown in Table 3. Test results showed that the addition of PAC caused the specific gravity of the soil mixture to go down. However, the larger specific surface area resulted in increases in the liquid limit and plastic limit for the soil mixture.

Table 3 Effect of 10% PAC on the geotechnical properties of the soil studied

Geotechnical properties	
Specific gravity, G*s*	2.64
Liquid limit, *wl* (%)	42.13
Plastic limit, *wp* (%)	27.56

The compression results from the oedometer tests are plotted in terms of void ratio, *e* and applied vertical pressures, *P* as shown in Fig. 2. A decrease in the void ratios was noted with an increase in the

applied vertical pressures. Test results revealed that at the same applied pressures, there were differences in the void ratios between the unmodified soil and the soil with 10% PAC. Addition of PAC would result in some decrease in the void ratio, irrespective of the

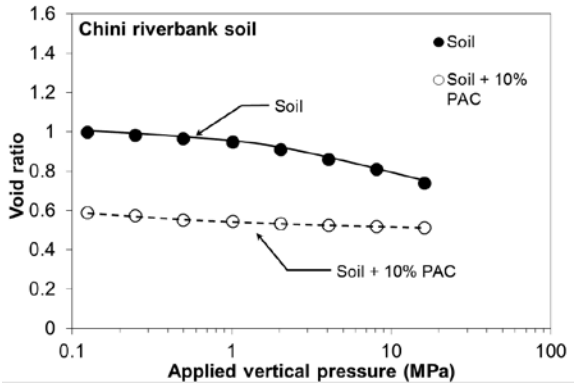

Fig. 2. Pressure – void ratio relationships

applied pressure. Similar observation on the behavior of soil modified with GAC and PAC was reported by Malusis *et al.* [19]. Calculation of the compression index was carried out using Eq. 1 following Herrero [28].

$$C_C = 0.185\left[G_S\left(\frac{\gamma_w}{\gamma_d}\right)^2\right] - 0.144 \qquad (1)$$

where *Cc* is the compression index, *Gs* is the specific gravity of soil solids, γ_w is unit weight of water in kN/m^3 and γ_d is dry unit weight of soil in kN/m^3. The Cc values calculated were found to be 0.24 and 0.27 for unmodified soil and soil-PAC mixture, respectively. Addition of PAC is expected to cause slight reduction in the microstructural rigidity of the soil skeleton [19]. Furthermore, since the compressive strength of PAC is lower than soil, rearrangement in the microstructure is expected to occur.

These results also suggest that, the stability of a riverbank may be affected when modified with PAC, even though some improvements in the water quality were obtained (see Tables 1 and 2). The results also suggest that determination of appropriate percentage of PAC is crucial in maintaining the stability of the riverbank without jeopardizing the water quality. Construction of artificial barriers could therefore be considered as an alternative option to RBF in areas where instability and volume change issues could arise with riverbanks that are modified for RBF purposes.

5.0 CONCLUSION

The aboriginal Jakun community living around Lake Chini deserves a supply of clean water. The Lake has also grown to be a popular tourist destination. The need for water treatment to improve its water quality is becoming more imperative. The viability of modifying the Lake Chini riverbank material with PAC was investigated and evaluated in terms of treatment efficiency and compressibility behavior. Results of this study showed that the existing riverbank material was ineffective in improving the water from Class II to Class I. Modification of the riverbank material is therefore necessary. The addition of PAC improved several water quality parameters except BOD, COD and DO, from Class II to Class I. However, the addition of PAC up to 10% resulted in the reduction of the void ratios which might lead to instability of the banks. An alternative option to RBF would be the construction of artificial barriers on Lake Chini riverbanks to improve its water quality so as to be fit for drinking and other consumption purposes.

ACKNOWLEDGEMENTS

The authors would like to express their gratitude to Universiti Malaysia Pahang for providing financial support under RDU 130384.

REFERENCES

[1] Shuhaimi-Othman, M., Ahmad, A., Mushrifah, I and Lim E.C. "Seasonal influence on water quality and heavy metals concentration in Tasik Chini, Peninsular Malaysia." Proceedings of Taal2007: The 12th World Lake Conference. 2007. pp. 300-303.

[2] Khairil, M., Wan Juliana, W.A., Nizam, M.S. and Razi Idris, W.M. "Soil properties and variation between three forest types in tropical watershed forest of Chini Lake, Peninsular Malaysia." Sains Malaysiana Vol. 43, No. 11. 2014. pp. 1635-1643.

[3] Habibah, A., Hamzah, J. and Mushrifah, I. "Sustainable livelihood of the community in Tasik Chini biosphere reserve: the local practices." Journal of Sustainable Development. Vol.3, No. 3. 2010. pp. 184.

[4] Latif, M.T., Ngah, S.A., Dominick, D., Razak, I.S., Guo, X., Srithawirat, T. and Mushrifah, I. "Composition and source apportionment of dust fall around a natural lake". Journal of Environmental Sciences. Vol. 33. 2015 pp.143-155.

[5] Ebrahimpour, M., and Mushrifah, I. "Heavy metal concentrations in water and sediments in Tasik Chini, a freshwater lake, Malaysia". Environmental monitoring and assessment, Vol. 141, No.1-3. 2008. pp. 297-307.

[6] Sujaul, I. M., Ismail, B. S., Tayeb, M. A., Muhammad Barzani, G., and Sahibin, A. R. “Morphological and physico-chemical characteristics of soils in the tasik chini catchment in Pahang, Malaysia”. Pertanika Journal of Science and Technology, Vol. 24, No.1. 2016. pp. 71-87.

[7] Dudgeon, D., Angela H. A., Mark O. G., Zen-Ichiro K., Duncan J. K., Christian L., Robert J. N. "Freshwater biodiversity: importance, threats, status and conservation challenges." Biological reviews. Vol. 81, No. 2. 2006. pp. 163-182.

[8] Kuehn, W., and Uwe M. "Riverbank filtration: an overview." American Water Works Association Journal. Vol. 92, No. 12. 2000. pp. 60.

[9] Schubert, J. "Hydraulic aspects of riverbank filtration—field studies." Journal of Hydrology. Vol. 266, No. 3. 2002a. pp. 145-161.

[10] Schubert, J. "Water-quality improvements with riverbank filtration at Düsseldorf waterworks in Germany." Riverbank Filtration. Springer Netherlands, 2002b. pp. 267-277.

[11] Hoppe-Jones, C., Oldham, G., & Drewes, J. E. Attenuation of total organic carbon and unregulated trace organic chemicals in US riverbank filtration systems. Water research. Vol. 44, No. 15. 2010. pp. 4643-4659.

[12] Schijven, J., Berger, P., & Miettinen, I. Removal of pathogens, surrogates, indicators, and toxins using riverbank filtration. Riverbank Filtration. Springer Netherlands. 2002. pp. 73-116.

[13] Rashid, N. A. A., Roslan, M. H., Rahim, N. A., Abustan, I., and Adlan, M. N. “Artificial barrier for riverbank filtration as improvement of soil permeability and water quality”. Jurnal Teknologi, Vol. 74, No. 11. 2015.

[14] Rashid, A., Aziemah, N., Abd Rahim, N., Abustan, I., Munawar, R. F., Awalludin, A., and Atiqah, N. “The potential and benefits of artificial barrier application at RBF. Applied Mechanics and Materials. Vol. 802. Trans Tech Publications. 2015. pp. 611-616.

[15] Brasquet, C., and P. Le Cloirec. "Adsorption onto activated carbon fibers: Application to water and air treatments." Carbon Vol. 35, No. 9 1997. pp. 1307-1313.

[16] Konieczny, K., and Grzegorz, K. "Using activated carbon to improve natural water treatment by porous membranes." Desalination Vol. 147, No. 1. 2002. pp. 109-116.

[17] Rivera-Utrilla, J., Sánchez-Polo, M., Gómez-Serrano, V., Alvarez, P.M., Alvim-Ferraz, M.C.M and Dias, J.M. "Activated carbon modifications to enhance its water treatment applications. An overview." Journal of Hazardous Materials. Vol. 187, No. 1. 2011. pp. 1-23.

[18] Suffet, I. H., and Wable, O. "Removal of taste-and-odor compounds by activated carbon." Advances in Taste-and-Odor: Treatment and Control. American Klater Works Assoc. Res. Foundation, Denver, 1995. pp. 157-208.

[19] Malusis, M. A., Barben, E. J., and Evans, J. C. “Hydraulic conductivity and compressibility of soil-bentonite backfill amended with activated carbon”. Journal of Geotechnical and Geoenvironmental Engineering, Vol. 135, No.5. 2009. pp. 664-672.

[20] Federation, Water Environmental, and American Public Health Association. "Standard methods for the examination of water and wastewater." American Public Health Association (APHA), Washington, DC, USA 2005.

[21] Norhayati, M.T., Goh, S.H., Tong, S.L., Wang, C.W. Abdul Halim, S. “Water quality studies for the classification of Sungai Bernam and Sungai Selangor. J. Ensearch. Vol. 10. 1997. pp. 27-36.

[22] Mitchell, J. K. Fundamentals of Soil Behavior. Wiley. Third Edition. 1993.

[23] Mathew, P.K. and Rao, S.N. “Influence of cations on compressibility behavior of a marine clay”. Journal of Geotechnical and Geoenvironmental Engineering, Vol. 123, No. 11. 1997. pp.1071-1073.

[24] Tripathy S., M. Tadza M.Y. and Thomas H.R, “Soil-water characteristic curves of clays”, J. of Canadian Geotechnical Journal, Vol. 51, No. 8, 2014, pp. 869-883.

[25] Estabragh, A. R., Moghadas, M., and Javadi, A. A. “hydrochemical effect of different quality of water on the behaviour of an expansive soil during wetting and drying cycles. Irrig. and Drain. 2016.

[26] Farmer, R.W. Dussert, B.W. and Kovacic, S.L. “Improved granular activated carbon for the stabilization of wastewater pH”. Div. Fuel Chem., Vol. 41. 1996. pp. 24–28.

[27] Streubel, J.D., Collins, H.P., Tarara, J.M. and Cochran, R.L. “Biochar produced from anaerobically digested fiber reduces phosphorus in dairy lagoons”. Journal of environmental quality, Vol. 41, No. 4. 2012. pp.1166-1174.

[28] Herrero, O.R., “Universal compression index equation: closure”. Journal of the Geotechnical Engineering Division, ASCE, 109(5), 1983. pp. 755-761.

Second International Conference on Science, Engineering & Environment,
Osaka City, Japan, Nov.21-23, 2016, ISBN: 978-4-9905958-7-6 C3051

STRENGTH OF SOFT CLAY REINFORCED WITH SQUARE AND TRIANGULAR PATTERN ENCAPSULATED BOTTOM ASH COLUMNS

Muzamir Hasan[1,2], Nurul Aina Husaini[2] and Norhayani Pangee[2]
[1]Centre for Earth Resources Research & Management, Universiti Malaysia Pahang, Malaysia;
[2] Faculty of Civil Engineering & Earth Resources, Universiti Malaysia Pahang, Malaysia

ABSTRACT

Soft clay is known as problematic soil that consists of low shear strength, low permeability and high compressibility where the existing soil on the given site is unable to carry the load of proposed structure by itself, so the use of ground improvement is necessary. The stone columns are increasingly being used as ground improvement technique for supporting a wide variety of structures including buildings and flexible structures. In practice, the bearing capacity on soft clay can be improved by a layer of compacted sand or gravel. Bottom ash as by product of coal burning that has similar properties to granular material can be applied as one of the stabilizing method to the existing soil. Hence, by using bottom ash as substitute, the cost of construction can be reduced and make great progress of a growing awareness of the environmental consideration. This research discusses the results of the improvement in the shear strength of soft clay after being reinforced with a group of square and triangular encapsulated bottom ash columns. The physical and mechanical properties of the materials used such as kaolin and bottom ash were determined first. The results show that kaolin can be classified ad clayey soil and bottom ash has similarities of characteristic with granular material. A total of 52 unconfined compression tests had been conducted on kaolin specimens to determine the shear strength. The diameter for specimen is 50 mm and 100 mm in height. The diameter of bottom ash columns are 10 mm and 16 mm respectively and the height of the column are 60 mm, 80 mm and 100 mm. The group columns have been arranged in square and triangular pattern. It can be concluded that the shear strength parameters were improved based on the different diameter and the height of the column.

Keywords: Soft clay, Encapsulated, Bottom Ash, Columns

INTRODUCTION

The stone column technique, also known as vibro-replacement or vibro-displacement, is a ground improvement process where vertical columns of compacted aggregate are formed through the soils to be improved. Pivarc [1] stated that the stone column technique has adopted in European countries in the early 1960s. The stone columns technique is one of the most used techniques for ground improvement processes all over the world among various methods of soft soil improvement. In practice, the bearing capacity on soft clay can be improved by a layer of compacted sand or gravel.

Many researchers have developed theoretical solutions for estimating the bearing capacity and settlement of foundations reinforced with stone columns. On the research done by Hughes [2], it is found that bulging is the one of the mode to show the characteristic of stone column. The experimental and numerical analysis on singles and group stone column were conducted by Ambily and Gandhi [3], Black et al. [4] and Hasan et al. [5].

Ground improvement techniques continue to make great progress of a growing awareness of the environmental and economic consideration. The significant aspect is to protect environment since more solid waste are produced from day to day. The selection of the correct ground improvement technique can have significant effect on foundation choice and can often lead to more economical solutions when compared to traditional approaches. It is noted that by nature, the existing soil on the given site unable to carry the load of proposed structure by itself, so the use of ground improvement is necessary. Considering for instance soft clay with relatively low shear strength, two kinds of column reinforcement techniques might be envisaged. One of the techniques is stone column technique which consists in introducing within the soft clay a vibro-compacted stone or ballast material.

The soil improvement directly depends on the stress distribution between soil and column. Stone columns act mainly as rigid inclusions with a higher stiffness, shear strength and permeability than the natural soil and the effects or improvements caused by these three properties were independently studied by different solutions (Castro et al. [6]).The soil types need to be enhanced in order to allow building and other heavy construction, so it is necessary to create stiff reinforcing elements in the soil mass (Zahmatkesh and Choobbasti [7]). The stone column

consists of granular material such as crushed aggregates or sand.

Coal is being one of the main sources of energy in our country fuelling about 40% of the total. Two kinds of coal waste products consist of fly ash and bottom ash. Based on the findings by Singh and Siddique [8], bottom ash forms up to 25% of the total ash and fly ash forms the remaining 75%. Muhardi et al. [9] has reported that the Tanjung Bin power station is one of the four coal power plant in Malaysia, producing 180 tons/day of bottom ash and 1620 tons/day of fly ash from 18000 tons/day of coal burning As well known, coal bottom ash is formed in coal furnaces. Bottom ash by product of coal burning as stone column can be apply as one of the stabilizing method to the existing soft soil before construction to reduce the unacceptable settlement and improve the load bearing capacity of the foundations.

Soft clay is known as a problematic soil and the design of foundation on soft clay has been the concern of engineers since the beginning of soil engineering. Soft soil foundations can cause excessive settlement, initiating undrained failure of the infrastructure if proper ground improvement is not carried out (Indraratna et al. [10]). The substitution of granular material such as coal bottom ash could lead to significant effect on soft clay improvement. According to Marto et al. [11]), coal is one of natural resources that existed due to the chemical and geological alteration of materials formed by plants over tens or hundreds of millions of year in the past.

The utilization of waste material is one of the best techniques to achieved sustainable development (Hasan et al. [5]). Most of the waste disposals are being dumped near the factory. Hence, it will increase the expenses as there need to obtain large areas of dump yard. In construction industry, the utilization of coal ash which needs large quantity of material shows the problem of coal ash disposal. Other than that, the power industry need to take responsibility of disposal unused coal ash and finally places a concern to the electricity consumer. It has been reported that the Tanjung Bin power plant needs about 18,000 tons/day of coal to generate electricity (Marto et al., [11]).

However, the large quantity disposal of coal ash in landfills will be considerable concern to an environmental issues and creating to the increase requirement for disposal space. The disposal of coal ash becomes an environmental issues due to coal bottom ash is simply disposed of on open land. Environment concerns are increasing day by day because the disposal of bottom ash is risk to human health and the environment. The method of burning the residues create the fuss of environmental problem which it generates air pollution.

Previously, stated that there is strongly possibility of coal bottom ash being as substitute as granular material for ground improvement technique. The using of bottom ash as an alternative to replace the natural sand in produced concrete. Bottom ash use in concrete is important to show the fact that sources of natural sand are getting depleted gradually. The methods of burning the residues often become environmental issues which generates air pollution. But, if in the positive side, it is an alternative method that has provided to optimize the usage of waste as product in construction industry.

METHODS

Preparation of Samples

The soft clay was prepared using customized compaction method and bottom ash columns (BAC) had been installed in the soft clay using the replacement method. Every kaolin specimen was created with 50 mm in diameter and 100 mm in height. The kaolin was air dried and then mixed with 20% of water which is the optimum moisture content of the kaolin. After uniform mixing of kaolin and distilled water, the 341 g of wet kaolin was required to fill into the customized mould to create one test specimen. The kaolin was poured into the customized mould in 3 layers. Every layer was compacted with 5 free fall blows by customized steel extruder. The customized mould was designed so that the amount of clay using inside it will be compressed into a 50 mm diameter and 100 mm high of specimen. By this uniformity, the dimension and volume of each specimen could be maintained since the mass and volume of the mould were almost same.

Installation of Bottom Ash Column

One batch of kaolin specimen had 52 samples with 50 mm in diameter and 100 mm in height. Each batch of kaolin specimen contains the same penetration ratio which is 0, 0.6, 0.8 and 1.0, but different size diameter of columns and area replacement ratio. The sample without any reinforcement of bottom ash which is 0 penetration ratio was used as the ‘controlled sample’ to determine the shear strength of unreinforced sample. Unconfined compression test was applied to test every same penetration ratio for four times to obtain an average value. For installation of bottom ash, the holes were drilled in square and triangular for different sizes with 10 mm and 16 mm in different height of 60 mm, 80 mm and 100 mm. The raining method was used through the process of installation and densification of bottom ash. The, the non-woven geotextile with 6 different holes has been

encased for each sample.

There were four different batches of specimens installed with geotextile tested as tabulated in Table 1. The replacement method was selected to remove clay and created holes for the bottom ash column to be installed. Fig. 1 and 2 show the detailed arrangement of the columns with different area replacement ratio.

Table 1 Sample with Variables of Bottom Ash Installation

Sample	No. of Columns	Diameter of Columns (mm)	Area Ratio, A_c/A_s (%)	Height of Penetration Ratio (H_c/H_s)
A	3	10	12.0	0, 0.6, 0.8 , 1.0
B	3	16	30.72	0, 0.6, 0.8 , 1.0
C	4	10	16	0, 0.6, 0.8 , 1.0
D	4	16	40.96	0, 0.6, 0.8 , 1.0

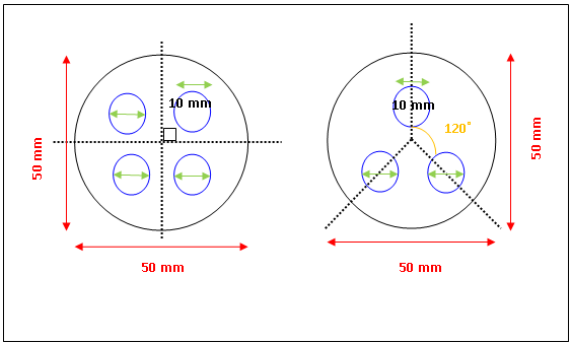

Fig. 1 Detailed Columns Arrangement for 12% and 16% Area Replacement Ratio

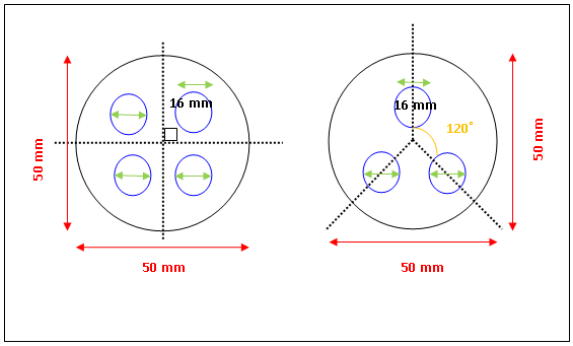

Fig. 2 Detailed Columns Arrangement for 30.72% and 40.96% Area Replacement Ratio

RESULTS

Summary of Main Materials

Table 2 and 3 show the summary of the properties of kaolin clay and bottom ash. A summary of non-woven geotextile was tabulated in Table 4. Based on the tests done kaolin clay, it can be observed that kaolin clay had the similarity characteristic with the soft clay. Meanwhile, bottom ash was proven that are relatively similar to the granular material such as sand and fine gravel. Therefore, bottom ash has the potential to be used as substitute for granular column.

Table 2 Summary of kaolin clay properties

Properties	Result
Liquid Limit	41.3%
Plastic Limit	31.25%
Plasticity Index	10.05%
Specific Gravity	2.62
Falling Head Permeability	1.124 x 10^{-9} m/sec
Standard Compaction Characteristic:	
-Maximum dry density, $\rho_{d\,max}$	1.58 kg/m^3
-Optimum moisture content , w_{opt}	20%
Soil Classification	
-(AASHTO)	A-7-6[b]
-USCS (Plasticity Chart)	ML

Table 3 Summary of bottom ash properties

Properties	Result
Particle Size Range	2 mm to 0.6 mm
Relative Density Test	98%
Specific Gravity	2.33
Constant Head Permeability	1.57 x 10^{-3} m/sec
Standard Compaction Characteristic:	
-Maximum dry density, $\rho_{d\,max}$	1.34kg/m^3
- Optimum moisture content , w_{opt}	21.75%
Shear Strength (Direct Shear Test)	
- Cohesion	89.71 kPa
- Friction Angle	23.93°

Table 4 Summary of Polyster Non-woven Geotextile Needle punched properties (MTS 130)

Properties (Typical)	Unit	MTS 130
Material		Polyster
Unit Weight, ɣ	g/m^2	130

Thickness	mm	1.08
Mechanical Properties	Unit	MTS 130
Max. Tensile Strength, MD	kN/m	10.0
Max. Tensile Strength, MD	kN/m	9.3
Elongation at Max. Tensile Strength, MD	%	56.0
Elongation at Max. Tensile Strength, CD	%	84.0
CBR puncture strength	kN/m	2.2
Trapezoid Tearing Strength, MD	N	350
Trapezoid Tearing Strength, CD	N	280
Index puncture Strength, MD	N	310.3
Apparent opening size	µm	140
Vertical permeability	cm/s	0.27
Grab Tensile Strength, MD	N	620.2
Grab Tensile Strength, MD	N	668..0

Unconfined Compression Test

Stress-Strain Behaviour under Axial Load

A total of 52 unconfined compression test (UCT) had been conducted on kaolin specimens to determine the shear strength of soft clay reinforced with bottom ash column. Each batch of kaolin specimen contains the same penetration ratio, which is 0, 0.6, 0.8, and 1.0, but different size diameter of columns and area replacement ratio. Unconfined compression test was applied to test every same penetration ratio for four times to obtain an average value. The sample without any reinforcement of bottom ash, which is of 0 penetration ratio, was used as the 'controlled sample' to determine the shear strength of unreinforced sample. The non-woven geotextile with 6 different sizes as same as the drifted holes has been encased for each samples.

The values of average stress and average axial strain for 'controlled sample' and specimens reinforced with triangular and square pattern of bottom ash columns had been tested under Unconfined Compression Test were tabulate in the Table 5. The stress-strain responses of 12% and 30.72% area replacement ratio at different penetration ratio (0, 0.6, 0.8 and 1.0) were plotted in Fig. 3 and Fig. 4, respectively. From the graph, the shear strength and axial stiffness of the specimens increase after being reinforced by triangular bottom ash column. Similar behavior was obtained in 16% and 40.96% area replacement ratio with different penetration ratio (0, 0.6, 0.8 and 1.0) and the graph were plotted as shown in Fig. 5 and 6 respectively. Both triangular and square pattern of bottom ash columns reinforcement increase the stiffness of the specimens.

Table 5 Average stress and average axial strain at different replacement ratio and different penetration ratio

Area replacement ratio, A_c/A_s (%)	Height of penetration ratio, H_c/H_s	Average Stress (kPa)	Average Axial Strain (%)
0	0	18.88	1.79
12%	0.6	19.45	1.37
	0.8	28.23	1.82
	1.0	22.11	1.35
16%	0.6	24.12	1.86
	0.8	27.54	1.93
	1.0	25.25	1.78
30.72%	0.6	22.12	1.3
	0.8	19.62	1.23
	1.0	19.07	1.43
40.96%	0.6	21.48	2.26
	0.8	19.68	1.55
	1.0	20.82	1.45

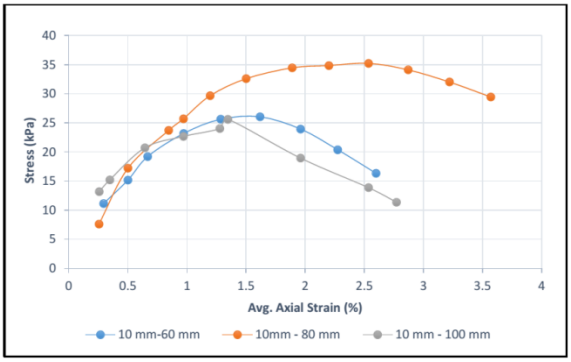

Fig. 3 Average Stress versus Axial Strain for 12% area replacement ratio

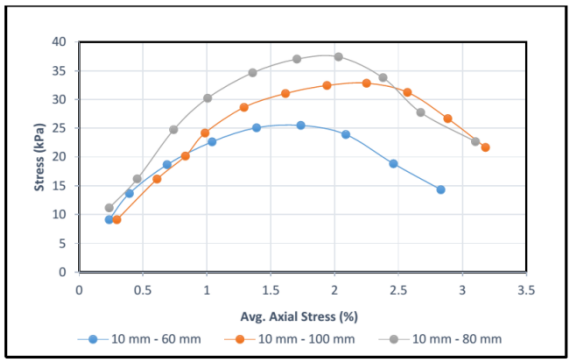

Fig. 4 Average Stress versus Axial Strain for 30.72% area replacement ratio

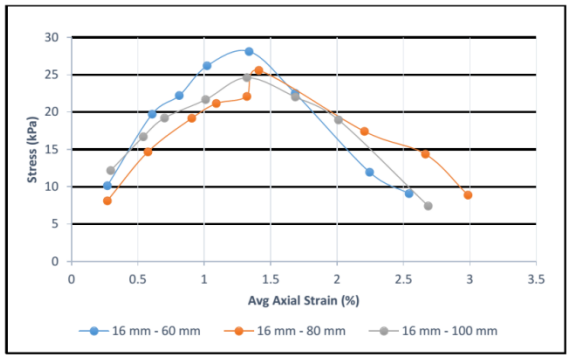

Fig. 5: Average Stress versus Axial Strain for 16% area replacement ratio

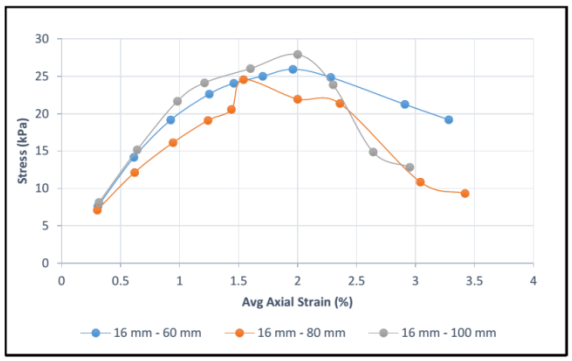

Fig. 6 Average Stress versus Axial Strain for 40.96% area replacement ratio

Effect of Bottom Ash Columns on Shear Strength

Table 6 shows the result of shear strength for 'controlled sample' and samples reinforced with different diameters for both triangular and square pattern of bottom ash at different column penetration under Unconfined Compression Test (UCT).

For triangular bottom ash column reinforcement with 12% area replacement ratio, the increase in improvement shear strength are 3.05%, 49.54% and 17.09% at sample penetration ratio, Hc/Hs of 0.6,0.8 and 1.0 respectively. As for 30.72% area replacement ratio, the improvement shear strengths are 17.16%, 3.9% and 1.03% for 0.6, 0.8 and 1.0 of sample penetration ratio respectively.

Meanwhile, for square bottom ash column reinforcement with 16% area replacement ratio, the increase in improvement shear strength are 27.74%,45.88% and 33.75% at sample penetration ratio, Hc/Hs of 0.6,0.8 and 1.0 respectively. While for 40.96% area replacement ratio, the increasing of improvement shear strength are 13.78%, 4.24% and 10.25% at 0.6, 0.8 and 1.0 sample penetration ratio respectively. The shear strength of triangular and square pattern reinforced with bottom ash column was increased significantly compared to the samples without reinforcement.

Table 6 Result of Unconfined Compression Test

Sample	No of Columns	Column Diameter (mm)	Area Ratio, A_c/A_s (%)	Column Height (mm)	Column Height Penetration Ratio, H_c/H_s	Shear Strength (kPa)	Improvement Shear Strength (%)
			Controlled Sample				
C	0	0	0	0	0	18.88	0
			Triangular Column (10 mm)				
	3	10		60	0.6	19.46	3.05
Batch 1	3	10	12	80	0.8	28.23	49.54
	3	10		100	1.0	22.11	17.09
			Triangular Column (16 mm)				
	3	16		60	0.6	22.12	17.16
Batch 2	3	16	30.72	80	0.8	19.62	3.9
	3	16		100	1.0	19.07	1.03
			Square Column (10 mm)				
	4	10		60	0.6	24.12	27.74
Batch 3	4	10	16	80	0.8	27.54	45.88
	4	10		100	1.0	25.25	33.75
			Square Column (10 mm)				
	4	16		60	0.6	21.48	13.78
Batch 4	4	16	40.96	80	0.8	19.68	4.24
	4	16		100	1.0	20.82	10.25

Effect of Bottom Ash Columns on Shear Strength

Improvement shear strength versus area replacement ratio is shown in Fig. 7, Ac/As of triangular and square pattern for area 12%, 30.72%, 16% and 40.96% with sample penetration ratio at 0.6, 0.8 and 1.0 respectively. For triangular encapsulated bottom ash column, the performance of 12% area replacement ratio contribute the greater increment in improvement shear strength compare to 30.72% area replacement ratio. While, the square encapsulated bottom ash column with area replacement of 16% has the greater value in improvement shear strength compare to area 40.96%. This is due to the area replacement of column is too big. As reported by Malarvizhi and Ilamparuthi [12], when the encased stone column is subjected to vertical load, the column material tends to dilate and induces lateral pressure.

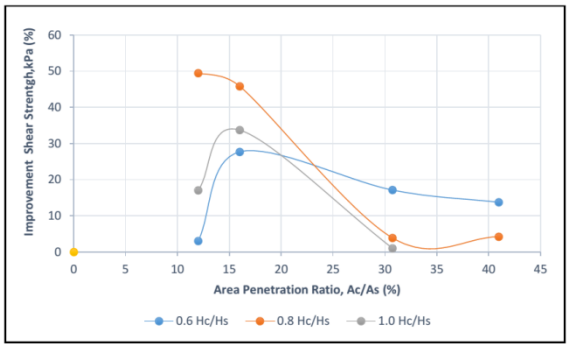

Fig. 7 Improvement Shear Strength versus Area Replacement Ratio

The results show that as the shear strength decrease as the diameter of the bottom ash columns increase. The results are in contradicted with the results done by Maakaroun et al. [13]. They explained that as the reinforcement area ratio increased, both the stiffness and shear strength of the specimens increased.

Effect of Height Penetration Ratio

Fig. 8 shows the increment of improvement shear strength at different height penetration ratio (0.6, 0.8 and 1.0) for triangular and square pattern encapsulated bottom ash column respectively. The percentage of improvement shear strength increased as the column penetration of bottom ash is increased. This is due to where the amounts of soil replaced by stiffer material which is bottom ash that help increase the strength improvement of the specimens. The result is in line with the previous research which done by Hasan et al. [5], who explained the shear strength of soft clay was increased as the height of the column increased. The improvement of shear strength for group column is in line with the increase of height of the bottom ash column.

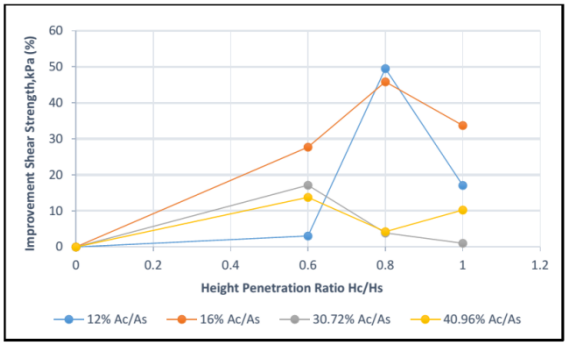

Fig. 8 Improvement Shear Strength versus Height Penetration Ratio

Based on figure above, it shows that the samples triangular partially reinforced with bottom ash column at 0.8 penetration ratio with area penetration 12%, the improvement shear strength is much higher compared to partially at 0.6 and fully-reinforced at 1.0 with area 30.72%. Similar to triangular column, the square partially penetrating column at 0.8 with area penetration ratio of 16% gives high increment in improvement shear strength compared to partially

at 0.6 and fully-reinforced at 1.0 with area 40.96%. It proves that the improvement shear strength does not depend on area penetration only, but the height penetration ratio of bottom ash column as well.

The result from this study is in line with the 'critical column length' idea proposed by McKelvey et al. [14], Maakaroun et al. [13] and Hasan et al. [5] where there is no improvement in shear strength beyond the 'critical column length'. Results of the experimental investigations indicate that 'critical column length' occurred particularly in the top 4 to 5 diameter of the column. The column length greater than five diameters may no longer participate in increasing the load carrying capacity of soft cohesive clays attributed to the brittleness of bottom ash; the risk of the column to fail is higher beyond this critical length.

CONCLUSIONS

The improvement of shear strength for group triangular and square column is in line with the increase of the height of the bottom ash column. It proves that the improvement shear strength does not depend on area penetration only, but the height penetration ratio of bottom ash column as well. The samples triangular partially reinforced with bottom ash column at 0.8 penetration ratio with area penetration 12%, the improvement shear strength is much higher compared to partially at 0.6 and fully-reinforced at 1.0 with area 30.72%. Similar to triangular column, the square partially penetrating column at 0.8 with area penetration ratio of 16% gives high increment in improvement shear strength compared to partially at 0.6 and fully-reinforced at 1.0 with area 40.96%.

The results proved there is no improvement in shear strength beyond the 'critical column length'. The column length greater than five diameters may no longer participate in increasing the load carrying capacity of soft cohesive clays due to the brittleness of bottom ash, the risk of the column to fail is higher beyond the critical length. The results show that in the area ratio of 12%, shows more significant improvement at penetration 0.8 of bottom ash column. Hence, it can be concluded that both area replacement ratio and height penetration ratio possessed an important role in improving the shear strength of the sample.

ACKNOWLEDGEMENTS

The authors would like to acknowledge the Universiti Malaysia Pahang (UMP) and Ministry of Higher Education Malaysia for financing this research through the UMP Short Term Grant RDU 140373 and Fundamental Research Grant RDU150112, respectively. The cooperation given by all parties involved in this research is greatly acknowledged.

REFERENCES

[1] Pivarc J, "Stone Columns-Determination of the Soil Improvement Factor", Slovak Journal of Civil Engineering. Vol. XIX, No. 3, 2011, pp. 17-21.

[2] Hughes JM, "Reinforcing of soft cohesive soil with stone columns", Ground Engineering. 7 (3), 1974, pp. 42-49.

[3] Ambily AP & Gandhi SR "Behavior of Stone Columns Based on Experimental and FEM Analysis", Journal of Geotechnical and Geoenvironmental Engineering, American Society of Civil Engineers (ASCE), 2007.

[4] Black J, Sivakumar V & McKinley JD, "Performance of Clay Samples Reinforced with Vertical Granular Columns", Canadian Geotechnical Journal", 44, 2007, pp. 89-95.

[5] Hasan M, Marto A, Hyodo M. & Makhtar AM, "The Strength of Soft Clay Reinforced with Singular and Group Bottom Ash Columns", Electronic Journal of Geotechnical Engineering. Vol. 16 (M), 2011, pp. 1215-1227.

[6] Castro J, Cimentada A, Costa AD, Canizal J, & Sagaseta C, "Consolidation and Deformation around Stone Columns: Comparison of Theoretical and Laboratory Results", Computers and Geotechnics. Vol. 68, 2012, pp. 326-337.

[7] Zahmatkesh A, & Choobasti AJ, "Settlement Evaluation of Soft Clay Reinforced By Stone Columns", Department of Civil Engineering, Babol University of Technology, Babol, Iran, 2010.

[8] Singh M & Siddique R, "Compressive Strength, Drying Shrinkage and Chemical Resistance of Concrete Incorporating Coal Bottom Ash as Partial or Total Replacement of Sand", Construction and Building Material, Vol. 68, 2014, pp. 39-48.

[9] Muhardi, Marto A, Kassim KA, Makhtar AM, Wei LF, & Lim YS, "Engineering Characteristic of Tanjung Bin Coal Ash", Electronic Journal of Geotechnical Engineering, (EJGE), 2010.

[10] Indraratna B, Rujikiatkamjorn C, & Sloan SW, "Coupled Discrete Element-Finite Difference Method for Analyzing the Load-Deformation Behavior of a Single Stone Column in Soft Soil", Computers and Geotechnics. Vol. 63, 2015, pp. 267-278.

[11] Marto A, Hasan M, Makhtar AM, & Othman BA "Shear Strength Improvement of Soft Clay Mixed with Tanjung Bin Coal Ash", APCBEE Procedia, 2013, pp. 116-122.

[12] Malarvizhi & Ilamparuthi, “Comparative Study on the Behavior of Encased Stone Column and Conventional Stone Column”, Soils and Foundations, Japanese Geotechnical Society, Vol.47, No. 5, 2007, pp. 873-885.

[13] Maakaroun T, Najjar SS, & Sadek S, “Effect of Sand Columns on the Load Response of Soft Clays”, International Foundation Congress and Equipment Expo, American Society of Civil Engineers (ASCE), 2009, pp. 217-214.

[14] McKelvey D, Sivakumar V, Bell A, & Graham J, “Modelling Vibrated Stone Columns in Soft Clay”, Geotechnical Engineering, 127, 2004, pp. 137-149.

Second International Conference on Science, Engineering & Environment,
Osaka City, Japan, Nov.21-23, 2016, ISBN: 978-4-9905958-7-6 C3051

MODEL TEST AND NUMERICAL ANALYSIS ON THE EFFECT OF THE LENGTH AND INTERVAL OF THE FACE BOLT IN SANDY TUNNEL

Yoshifumi Taguchi [1]

[1]Department of Comprehensive Engineering, Urban Environment Course, Kindai University Technical College, Japan

ABSTRACT

In the tunnel excavating unconsolidated sand layer of urban areas, it is important to stabilize the tunnel cutting face and to prevent the surface settlement. Therefore, the long face bolts are used by this purpose. As the effect of the face bolts for the cutting face stability and the surface settlement control, it is thought that reinforcing effects are different according to length and the interval. In this study, we changed the length and the interval of the face bolts by the two-dimensional model test used Toyoura-sand and examined the influence level on the effect of the face stability and the surface settlement. As a result, when the length of the face bolt is longer than 0.3H（H: cutting face height）, the reinforcing effect of the cutting face becomes higher. It is small in length 0.2H. For the surface settlement, when the length of the face bolt is longer than 0.5H, the reinforcing effect becomes higher. Moreover the face stabilizing effect is higher better installation interval of the face bolt is small. In bolt's installation interval 0.2H, face stabilizing effect and surface settlement control effect is high, but bolt's installation interval 0.5H is small. In addition, we examined the reinforcing effect and the mechanism of the face bolts by a numerical analysis using the finite element method.

Keywords: Tunnel, Face bolt, Numerical analysis, Model test, Unconsolidated sandy soil

INTRODUCTION

In the tunnel excavating unconsolidated sandy layer in NATM as shown in Fig.1, it is important to stabilize the tunnel cutting face and to prevent the surface settlement. Therefore, the various auxiliary methods of tunnel construction are used by this purpose, and it becomes the effective method to drive the long face bolts recently [1]-[2]. As the effect of the face bolts for the cutting face stability and the surface settlement control, it is thought that reinforcing effects are different according to length and the interval [3]-[8].

In this study, we changed the length and the interval of the face bolts by the two-dimensional model test used Toyoura-sand and examined the influence level on the effect of the face stability and the surface settlement[9]-[11]. In addition, we evaluated the reinforcing effect and the reinforcement mechanism of the face bolts by a numerical analysis using the finite element method.

OUTLINE OF MODEL TEST

Model Test Equipment

A model test equipment shown in Fig. 2. The size of the soil tank is 65cm in height, 80cm in width, and 15cm in depth. As shown in Fig. 3, Tunnel part of the model is the two-dimensional cross section of the longitudinal direction taken along the center of the actual tunnel cross section, a rectangular cross-section of the cutting face model is 15cm in height and 15cm in width. In this test, a cutting face bolt modeled with a thin Kent paper thicknesses 0.12mm of a flat plate shape, was placed at a predetermined interval in cutting face, as shown in Fig. 3.

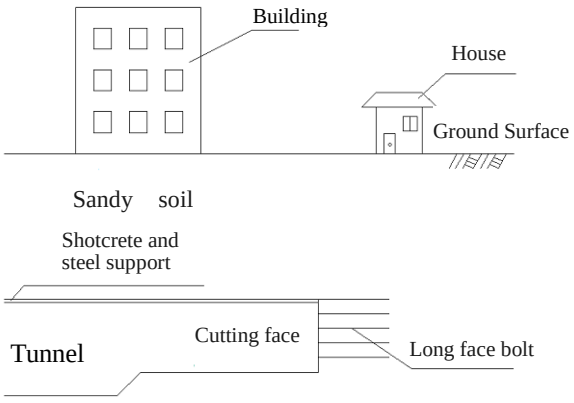

Fig.1 MATM tunnel in unconsolidated ground (face bolt combination)

The model test reproduced the excavation by pulling out the tunnel cutting face model by a screw jack. Upon reaching a predetermined pull-out amount was measured the load acting on the tunnel cutting face and the surface settlement. The load acting on the tunnel cutting face sets the load-cell on the back side of the tunnel cutting face, was measured change of the load in accordance with the pull-out.

Fig.2 (a) Model test equipment (Photo)

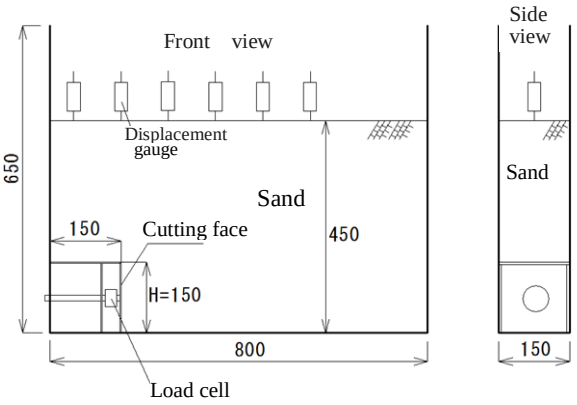

Fig.2 (b) Model test equipment (unit mm)

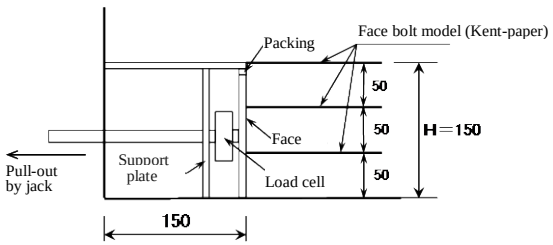

Fig.3 Cutting face part enlarged view (unit mm)

Table 1 shows the case of the model test. The length of the face bolt model (Kent paper) was changed 15cm (1.0H, H: cutting face height of model tunnel), 7.5cm (0.5H) and 3cm (0.2H). Further, the installation interval was changed 7.5cm (1-stage), 5cm (3-stage) and 3cm (5 -stage), it was examined the influence.

Table 1 Case of model test

Test case	length (ℓ)	Installation interval
1	Non-reinforced	
2	15.0cm (1.0H)	1,3,5-stage
3	7.5cm (0.5H)	1,3,5-stage
4	3.0cm (0.2H)	5-stage

Model ground was used Toyoura-sand of the air-dried state. The model sand was free-fall from the outlet of a fixed size at the position of the height 60cm, and the model ground was introduced to overburden thickness 30cm (2.0H). The density of the sand is 1.54g/cm^3.

The pull out of the tunnel, one by 0.2mm up to 0 ～2mm, one by 0.5mm up to 2～10mm, one by 1mm up to 10 ～ 15mm was carried out. The measurement of the surface settlement used a displacement gauge. It was placed in five locations in the 10cm interval.

Overview of the Model Test Results

Surface settlement (non-face bolt)

Figure 4 shows the change in surface settlement due to tunnel cutting face pull-out when there is no face bolt. The measurement point just above the face, and front 10cm, 20cm, 30cm and 40cm from the cutting face just above. It is the point of the rear 10cm from the cutting face just above. The surface settlement of the point of the cutting face immediately above and the front 10cm is large. With the pull-out amount of the cutting face increases, the surface settlement is increasing linearly.

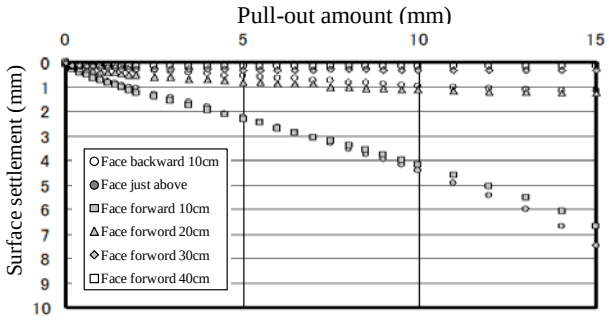

Fig.4 Surface settlement due to the pull-out (non-reinforced)

The reason for this surface settlement has increased because its position is within the range of the sliding surface of the ground. The surface settlement amount at the position of the cutting face behind 10cm and face forward 20cm~40cm is small and the surface settlement is not significantly increased even if the pull-out amount of the cutting face is increased. The reason is because the surface settlement is not significantly increased in order to that position the outside than the range of the sliding surface.

Surface settlement (using face bolts)

Figure 5 shows the change in surface settlement due to cutting face pull-out in the case of the face bolt installed 5-stage at the installation interval 3cm and length 15cm. The settlement measurement points are the same as described above the non-face bolt case. The surface settlement amount of point of the face above and face the front 10cm is slightly larger. The maximum surface settlement at the time of pull-out 15mm of tunnel face is about 2 mm, the surface settlement than non-face bolt is considerably suppressed.

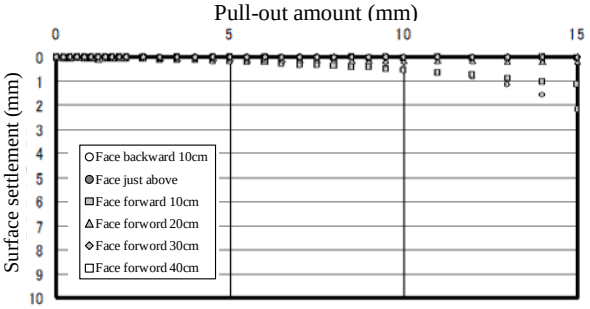

Fig.5 Surface settlement due to pull-out
(Bolt length 15cm, 5- stage)

Surface settlement of the tunnel longitudinal direction

Figure 6 shows the surface settlement of the tunnel longitudinal direction of the case changing the installation interval in the case of face bolt length 7.5cm (0.5H). It shows the surface settlement when pulled out 15mm (0.1H) of the cutting face. In the case of non-reinforcement are about 6 ～ 7mm settlement at the point of the face front 10cm. On the other hand, in the installation interval 5-stage and 3-stage is a settlement of about 2mm, a settlement of about 3mm in the 1- stage.

Similarly, Fig.7 show the surface settlement of tunnel longitudinal direction of the case changing

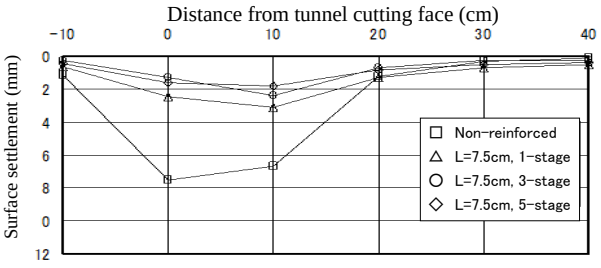

Fig.6 Surface settlement curve
(Longitudinal direction, on 15mm pull-out)

the face bolt length 15cm (1.0H), 7.5cm (0.5H) and 3cm (0.2H) in installation interval 5-stages.It shows the surface settlement when pulled out 15mm (0.1H) the cutting face. In the case of non-reinforcement are about 7～8mm settlement at the point of the face front 10cm. Although the settlement amounts of the same degree in the face bolt length 15cm and length 7.5cm are about 2mm settlement, the control effect of settlement is high. On the other hand, in the face bolt length 3cm (0.2H), settlement amount has been increased to about 4mm just above tunnel face, the control effect of the settlement is small.

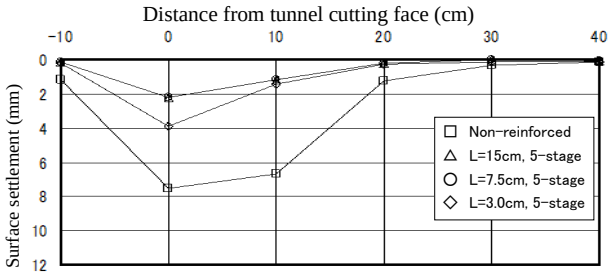

Fig.7 Surface settlement curve
(Longitudinal direction, on 15mm pull-out)

Among the model test results, Table 2 shows a comparison of the surface settlement of each case. The comparison position of the surface settlement is the value of the position of the front 10cm from the cutting face just above. It is shown in detail in reference [4].

Table 2 Experimental results
(Comparison of surface settlement)

№	Test case	Surface settlement (mm)		
		Pull-out 1.5mm	Pull-out 4.5mm	Pull-out 15mm
1	Non-reinforced	0.7	2.0	6.6
2	length15cm, 5stage	0.1	0.2	1.1
3	length15cm, 3stage	0.1	0.2	2.0
4	Length7.5cm, 3stage	0.3	0.8	2.4

NUMERICAL ANALYSIS

Analysis Method and Model

The analysis used the two-dimensional plane strain elastic analysis by the finite element method. The analysis model is shown in Fig.8. Although the analysis of the tunnel face portion is inherently three-dimensional, used a two-dimensional cross-section in order to correspond to the model tests described above.

The materials properties used in the analysis are shown in Table 3. The model ground used a quadrilateral element of the 4-node, the face bolt used a beam element. The bending rigidity of the beam element was a small value that can not be resistance to bending due to the use of Kent paper model test.

In accordance with the above-mentioned model test, the tunnel excavation was simulated in a way that extracting the elements of the shaded portion of Fig.8. The stress release ratio as 100% was carried out excavation analysis of the tunnel. For boundary conditions, the soil tank's bottom is a fixed both vertical and horizontal directions, tunnel crown was fixed condition in accordance with the model test.

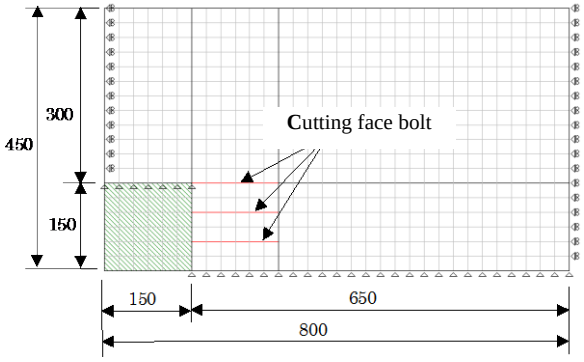

Fig.8 Analysis model and boundary conditions

Table 3 Material properties

	Deformation Modulus	Poisson's ratio	moment of inertia of area
Ground	1.0M P a	0.3	—
Face bolt	1.0×10^{4}MPa	—	1.0×10^{-7}cm^4

Analysis Results

Analysis was varied with the length of the face bolts 15cm (1.0H, H: face height) and 7.5cm (0.5H) in correspondence with model test case of Table 2. Moreover, was changed the face bolt's installation interval in the 3-stages and 5-stages.

Non-face bolts

The displacement mode diagram and contour diagram of the horizontal displacement of the analysis results are shown in Fig. 9 to 10. Figure 9 is deformation diagram in the case where there is no face bolt, and Fig.10 is a contour diagram of the horizontal displacement.

From the figure, the cutting face has swelled large, if ground strength is low, is expected to lead to face collapse. In addition, from the contour diagram of the horizontal displacement, it has spread a large area of the horizontal displacement toward the surface in the direction of the obliquely upward 45 °.

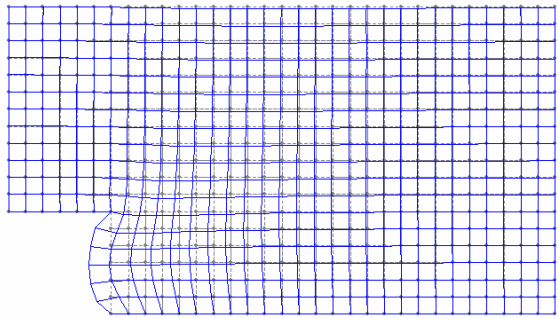

Fig.9 Deformation mode diagram (non-face bolt)

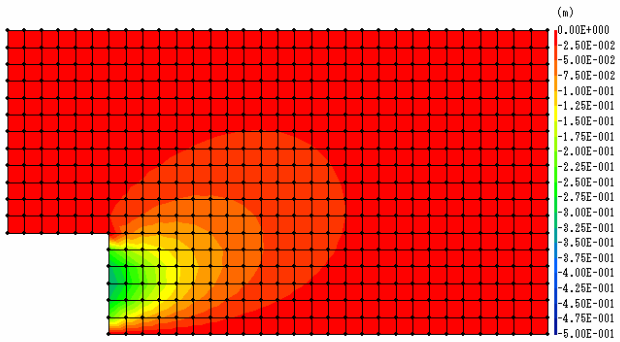

Fig.10 Contour diagram of the horizontal displacement (non-face bolt)

Using face bolts

Figure 11 is a displacement mode diagram of the face bolt's length 15cm (1.0H) in installation interval 3-stages. Figure 12 is a contour diagram of the horizontal displacement. From this figure, in the face bolt installation position have been suppressed swelling of the cutting face, the amount of horizontal displacement is smaller. Moreover, the contour diagram, a large area of deformation does not extend toward the ground surface, the cutting face is stable, it is expected that the surface settlement is reduced.

Figure 13 shows the axial force diagram of the

face bolt. From the axial force distribution, the axial force is the largest is near the center of the face bolt, the face bolts are functioning well as the role of the ground anchor. The face bolt does not function as a ground anchor, if the face bolt is pulled out, the axial force distribution dose not become indicating a maximum near the center as shown in the figure, the distribution shape becomes the largest near the cutting face.

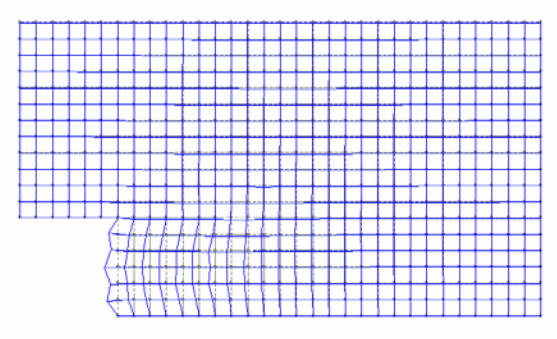

Fig.11 Deformation mode diagram
(Bolt's length 1.0H, installation interval 3-stage)

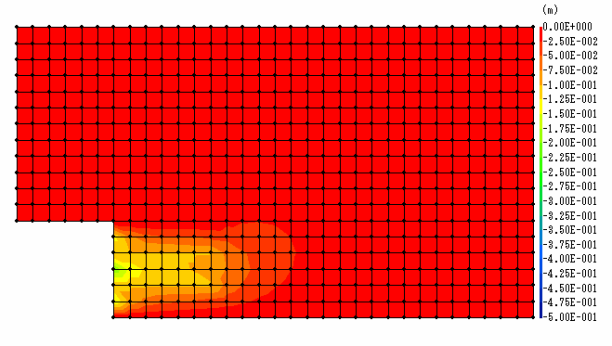

Fig.12 Contour diagram of horizontal displacement
(Bolt's length 1.0H, installation interval 3-stage)

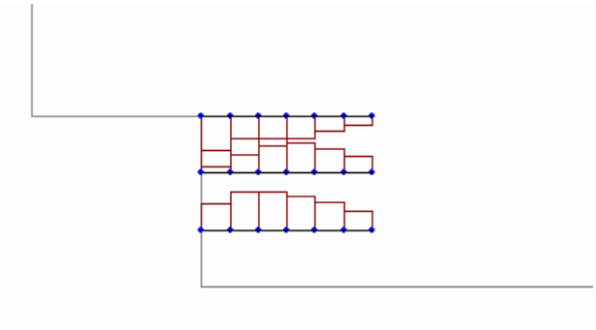

Fig.13 Axial force mode of face bolts
(Bolt's length 1.0H, installation interval 3-stage)

Comparison of the Model Test

Table 4 is a comparison of the surface settlement and the cutting face's swelling amount to the model test and numerical analysis results. Comparing the position of the surface settlement is the position of the face front 0cm ~ 15cm, was using the maximum value. In the table is also shown the ratio of the case of no face bolt in parentheses. Because it is elastic analysis the amount of deformation of the ground is proportional to the deformation modulus E. Therefore, hereafter we described using the ratio of the no face bolt's case.

From this table, when inserting the face bolts and the tunnel pull-out amount is small in 1.5mm or 4.5mm, which is an elastic state, the analysis result of the settlement become larger. The poll-out amount becomes large as 15 mm, the ground is expected to become a plastic state, as compared to the model test, the degree of deformation is well reproducible.

Paying attention to the swelling amount of the cutting face, in the case that the length of the face bolt is short and installation interval is large, it is larger than the trend of surface settlement. However, the tendency of the reinforcing effect of the length and spacing of the face bolt is able to reproduce. From these results, the numerical analysis of the face bolt using the elastic analysis can obtain an analysis result of the safety side with respect to the reinforcing effect of the cutting face bolt.

CONCLUSION

The two-dimensional longitudinal direction of the model tests using Toyoura -sand, was examined influence of the surface settlement by changing the installation interval and the length of the cutting face bolts. Moreover, we examine the reinforcing effect and the reinforcement mechanism of the cutting face bolt using a numerical analysis method by the finite element method. As a result, it was found that the following.

Table4 Comparison of numerical analysis and model test results

№	Test case	Surface settlement of model test (mm)			Result of numerical analysis	
		Pull-out 1.5mm	Pull-out 4.5mm	Pull-out 15mm	Settlement	Swelling of face
1	Non-reinforced	0.7(1.0)	2.0(1.0)	6.6(1.0)	2.8(1.0)	3.3(1.0)
2	length15cm, 5stage	0.1(0.1)	0.2(0.1)	1.1(0.2)	0.8(0.3)	1.1(0.3)
3	length15cm, 3stage	0.1(0.1)	0.2(0.1)	2.0(0.3)	1.2(0.4)	2.0(0.6)
4	Length7.5cm, 3stage	0.3(0.4)	0.8(0.4)	2.4(0.4)	1.9(0.7)	2.6(0.8)

Compared to the model test results, in the region where the tunnel pull-out amount is small and the natural ground seems to be within the elastic range, an elastic analysis result has a bigger ratio of the settlement. When the pull-out amount of the cutting face is as large as 15mm, and the ground becomes the plastic state, the elastic analysis results show the same tendency as the model test results. For the elastic analysis, the swelling amount of the cutting face is larger in the case that the length of the face bolt is short and installation interval is large. However, the tendency of the surface settlement control effect is consistent. The numerical analysis of the face bolt using the elastic analysis can obtained of the safety side analysis results with respect to reinforcing effect of the natural ground deformation by the cutting face bolt.

REFERENCES

[1] The Japan Geotechnical Society**, "**To construction from the design of the mountain tunnel construction method", 2007, pp.140-141. (in Japanese)

[2] Japan Society of Civil Engineers,"Practice of model experiments and numerical analysis in the mountain tunnel", 2006,pp.22-59. (in Japanese)

[3]Fukusima S, Mochizuki Y,Kagawa K, Yokoyama A, "Model test on pre-reinforcement of shallow tunnel in sandy ground", Japan Society of Civil Engineers, No.406, Ⅲ-11, JUN.1989,pp.79-86.(in Japanese)

[4] Taguchi Y, Kagawa K, Sagara M, Yoshikawa K, "Reinforcing effects of thin flexible pre-lining", Japan Society of Civil Engineers, No. 645,Ⅲ-50,Mar.2000, pp.125-135. (in Japanese)

[5]Mitarasi Y, Matsuo T,Tezuka T,Okamoto T,Nisimura S,Matsui T,"Evaluation of effect of long face reinforcement method in tunneling", Japan Society of Civil Engineers, No.743,Ⅲ-64, SEP.2003,pp.213-222.(in Japanese)

[6]Miyanomae S,Morita A,Sakai T,Matsui M,Nasimoto Y,Okubo S, "A proposal of the simplified model to evaluate the effect of long bolting", Journal of Japan Society of Civil Engineers, Ser. F,vol.62,No. 2,APR.2006,pp258-267(in Japanese)

[7]Domon T, Seo K, Nishimura K, "Simplified design method for face bolting based on the reinforcing effect", Journal of Japan Society of Civil Engineers, Ser. F1,Tunnel Engineering, vol. 66, No. 1,NOV.2010,pp.29-39.(in Japanese)

[8]Yokota Y,Yamamoto T,Date K, "Evaluation of reinforcing effects on new face bolts using steal checker pipes by centrifuge model tests and 3D-numerical analysis", Journal of Japan Society of Civil Engineers, Ser. F1,Tunnel Engineering, vol. 67, No. 3,2011 ,pp.67-79.(in Japanese)

[9] Tanaka T, Taguchi Y, " Model Test on reinforcing effect of the long face bolt in unconsolidated sand", Chubu branch Japan Society of Civil Engineering,Mar.2010, pp 297-298. (in Japanese)

[10] Taguchi Y, Tanaka T," Model test on the effect of reinforcing the face bolt in unconsolidated sand tunnel", Kindai University Technical College Research Reports, vol.4, JAN.2011, pp.79-84. (in Japanese)

[11] Taguchi Y, Tabira T, "Model test on tunnel face stabilizing effect of the face bolt", Kindai University Technical College Research Reports, vol.6, MAR.2013,pp.71-76.(in Japanese)

Second International Conference on Science, Engineering & Environment,
Osaka City, Japan, Nov.21-23, 2016, ISBN: 978-4-9905958-7-6 C3051

INTEGRAL FRAMEWORK FOR SUSTAINABILITY MANAGEMENT IN CIVIL ENGINEERING WORK

Vanissorn Vimonsatit[1], Chandana Kulasuriya[1], Priyan Dias[2]
[1]Department of Civil Engineering, Curtin University, Perth, Western Australia
[2]Department of Civil Engineering, University of Moratuwa, Sri Lanka

ABSTRACT

With the need to maintain global sustainability, achievements in a civil engineering project are not just to meet the typical triple goals (time, cost, and quality), but also other sustainability goals and requirements. This paper presents an overview of an integral framework created to achieve sustainability objectives in civil engineering related works. This research focusses on devising an innovative tool by incorporating the context of quality management system according to ISO9001 requirements. The tool is based on the Integral Sustainability Framework, called All Octants All Levels (AOAL) Framework, which has been expanded from the eminent Ken Wilber's All Quadrants All Levels (AQAL) Framework. The developed tool provides a generic framework for assessing sustainability quadrants, which are 'objective', 'inter-objective', 'subjective', and 'inter-subjective' entities, as well as the expanded octants which highlight the need to consider the certainty and uncertainty aspects of the assessments. An example is provided to demonstrate how to use the tool to consider integral sustainability of a civil engineering project. The results show that sustainability management can be facilitated by using the tool to reduce the risks and to meet the targeted outcomes.

Keywords: integral theory, civil engineering, integral sustainability, ISO 9001, sustainability management

INTRODUCTION

It is commonly accepted that the three spheres - economics, environment and society - are to be considered when managing sustainability. However, the term sustainability itself is still unclear despite much research that has been conducted to address all these three aspects of sustainability [1], [2]. In a commercial world, sustainability would be taken more seriously towards the economic performance. In construction projects, the environmental matters are accounted for in the pre-construction phase whereby an environmental impact assessment is to be conducted and approved prior to construction. Then, any procedures required to meet the environmental sustainability requirements are to be implemented. With the existing sustainability indicators, design and construction using renewable energy are also encouraged if not compulsory. Hence, the two aspects of the sustainability (economics and environment) are reasonably dealt with, but the third aspect, the social consideration, is usually taken lightly, except for the matters directly relevant to the stakeholders of a particular project.

In that background, the concept of 'integral sustainability' has emerged as a critique to conventional concept of sustainability, highlighting the non-integration of all the aspects related to sustainability. It implies the necessity of a critical debate with society, regarding shared meanings and values related to the concept of sustainability. In other words, a research of this nature demands a critical paradigm, which uses a reflective dialogic method [3].

The integral theory introduced by an eminent philosopher, Ken Wilber, in the late 1990s is considered one of the major philosophical paradigm shifts in the post-post-modern era. The theory integrates four types of realities, namely, subjective, inter-subjective, objective and inter-objective realities. De Kay [4] applied integral theory for sustainable design of architecture by considering the four realities in a form of All Quadrants All Levels (AQAL). However, not until the work by Kulasuriya and Vimonsatit [5] had the integral theory been adopted for sustainability in Civil Engineering. Further, Kulasuriya et al [6], [7] has extended the AQAL framework to distinguish the certainty and uncertainty aspects when investigating the four realities.

This paper presents an integrated framework for managing sustainability in civil engineering work. An integrated framework is created to incorporate the quality management system framework outlined in ISO9001-2015 [8]. Then, based on recent research into an Integral Sustainability Framework for Alkali Pozzolan Cement, the developed Octa-octant framework [7] is adopted to create an integrated sustainability management framework. The new framework is outlined generically for a construction project, which is typical of civil engineering work. An example is also provided to

demonstrate how to use the framework for managing sustainability in a construction project.

A BRIEF REVIEW OF SUSTAINABILITY FRAMEWORK IN CONSTRUCTION

There are several theoretical frameworks for determining the relationship of the performance between the three aspects of sustainability. A comprehensive review on the business case for corporate sustainability can be found in Salzmann, Ionescu-Somers and Steger [9]. They pointed out how a sustainability culture has been developed over the past few decades.

In construction, Rodríguez and Fernández [10] pointed out that the new goals and requirements for integrated project management are not just to achieve the time, cost and quality of construction projects, but also to achieve sustainability objectives and requirements. Several techniques and tools have been developed for sustainability assessment in the building sector but these tools are mainly in the form of a rating system, by providing an indicator to give rank, or certification, to the project. These systems may not represent the variability of engineering projects therefore classification of opportunities in term of the project outcomes, promoter requirements, and sustainability requirements is needed [10].

A conceptual framework has been developed for sustainable design principles and strategies [11]. Methods for the framework were distinguished into three domains of sustainable development, namely, resource management, life cycle design and design for human. Culture resources such as historical buildings and urban context were considered in the design for human. It was highlighted that an integrated and holistic process for creating environmentally conscious and healthy spaces that provide human contact to the natural environment, while supporting the local economy and culture [11].

An example of a highway construction project designed under a framework for developing construction sustainability items was reported [12]. Sixty sustainability items were indicated, however, they could only be considered as objective and inter-objective aspects according to the definitions in integral theory. Therefore, there is still a lack in considering subjective aspects if one is to adopt integral theory approach for sustainability management.

PDCA CYCLE FOR INTEGRATED SUSTAINABILITY MANAGEMENT

A process-based approach is defined in ISO9001-2015 as an approach that involves "systematic definition and management of processes and their interactions, so as to achieve the intended results." The PDCA (Plan-Do-Check-Act) cycle can be applied to all processes and to the quality management system. Adopting the PDCA cycle and the process based approach; an integral framework for sustainability management can be formulated generically as shown in Figure 1. This system is similar to a Corporate Sustainability Management System proposed by Azapagic [13], who suggested the system to consist of five stages, policy development, planning, implementation, communication, and review and corrective action. The proposed system shown in Figure 1 is however divided into four stages, as provided in ISO9001-2015.

The sustainability aims and requirements can be described based on the requirements, needs and expectations of the client and stakeholders of the project. Then, through the organisation policy, the project organisation and its context, and the sustainability policy and regulation, planning can be made accordingly. Therefore the main task is to identify those requirements, needs and expectations of the client and stakeholders. The client usually has a definitive set of specifications and requirements, but the stakeholders' needs and expectations are not easily identified and collated. It is therefore proposed to use an integral theory framework [4], [5] whereby all realities, both objective and subjective, can be assessed within the framework of the sustainability aims and requirements. Figure 2 demonstrates the integral theory framework which will be adopted to create an integrated framework for sustainability management.

The front four octants, subjective (S), inter-subjective (IS), objective (O)and inter-objective (IO) are known as the AQAL framework [4], and has been extended to account for certainty and uncertainty by introducing additional four octants [7] as shown in Figure 2.

AN EXAMPLE OF SUSTAINABILITY MANAGEMENT OF A CONSTRUCTION PROJECT

This example is provided to demonstrate how the PDCA cycle (Fig. 1) and the integral theory octant framework (Fig. 2) can be used for sustainability management of a construction project. The process is divided into four steps as follows:

Step 1: The sustainability aims and requirements are to be defined. In this example, the aims and requirements are set generically as: time, cost, quality and energy.

Step 2: Each aim/requirement shall be analysed based on Integral Theory Octant Framework to account for the subjective and objective aspects of the aim/requirement from the individuals and collective individuals. To further demonstrate this

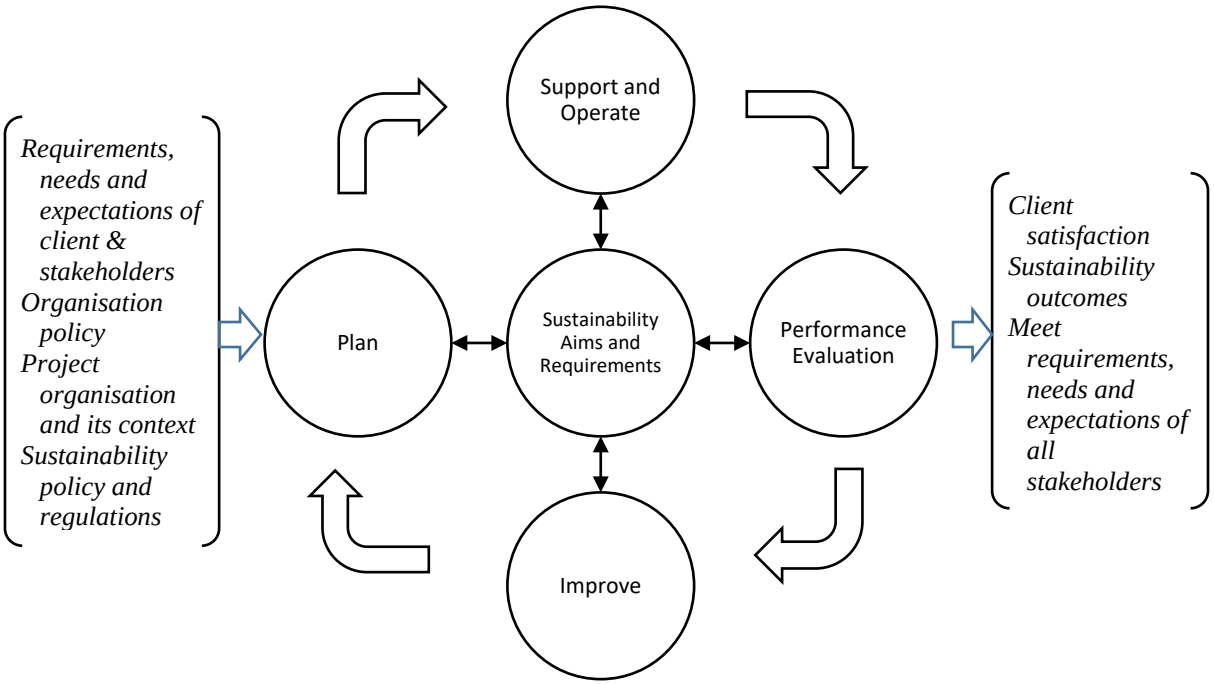

Figure 1 PDCA Cycle for Sustainability Management (adapted after ISO9001-2015)

such as, the cultural beliefs, values and practices.

Similarly, the analysis of cost, quality, and energy can be carried out in the same manner. The details of the analysis are not presented in this paper as they are in the scope of an on-going research.

With the analysis based on this framework, it can be seen that the project is not necessarily a success if the shortest time for completion is achieved. Other factors such as inter-objective requirements, also need to be considered. Also, just because a project is delayed, it needs not be considered a failure, if the inter-subjective value on time is low. Similarly, the subjective attitude regarding time of various stakeholders could guide the actual allocation of the contract time.

Step 3: The outcome of the analysis in Step 2 will be collated to provide an overview of what need to be considered to achieve a particular aim, or to fulfil a particular requirement. In this step, the PDCA cycle for sustainability management as shown in Fig. 1 can be used.

Step 4: The key to the project management is to identify and manage uncertainties which will result in the deviation from the aim of the project. For example, the uncertainties that could affect the time aim are such as materials delivery problem, machine breakdown, poor weather condition, personal illness, accident, etc. These uncertainties can be considered as risks to the project success, thus, the project management team will need to make plans to eliminate these risks which may cause any delay to the project. This aspect is reflected by the certainty and uncertainty domains in the Octant Framework as shown in Fig. 2. An example of an integration of certainty and uncertainty of subjective, inter-subjective, objective and inter-objective aspects of realities for a building material can be found in [7].

In civil engineering work such as a construction project, it is not deniable that there are uncertainty elements in every activity. As mentioned

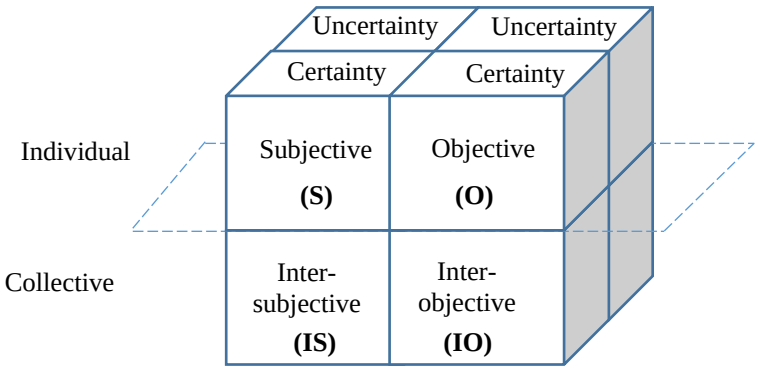

Figure 2 Integral Theory Octant Framework

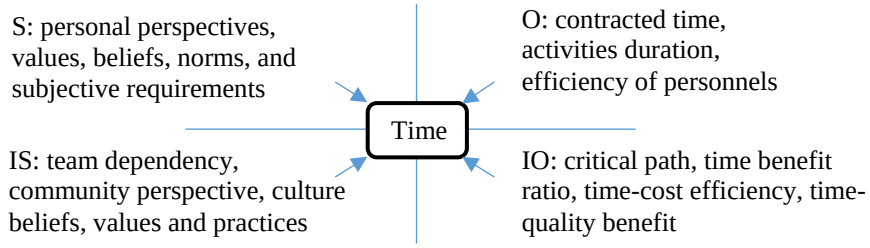

Figure 3 Integral theory framework for considering all aspects of Time

previously, the benefit of the Octa/Octant framework is to identify the certainty and uncertainty elements. Certainty elements can be managed without much attention by the project management team as they are without risks, for example, quality assurance of materials and equipment used. On the other hand, the uncertainty elements need much more attention. For example, the critical path in the project scheduling needs to be managed very carefully as any uncertainties affecting one activity will affect the dependent activities and result in a delay of the whole project. If the project timeline is planned with more independent (parallel) activities or with time lapse (float), i.e., the following activity is not critically dependent of the precedent activity, any uncertainties causing a delay in one activity will not be critical to the project timeline. In this case, the uncertainty in these activities will not need much attention by the management.

INTEGRAL FRAMEWORK FOR SUSTAINABILITY MANAGEMENT

Incorporating the PDCA framework and the integral theory framework, the integral framework for sustainability management of this project can be illustrated as seen in Fig. 4. The outcome of Step 1 is shown at the centre of the diagram, Step 2 is depicted by the AQAL, which is represented by the S, O, IS, IO arrows on the diagram. Step 3 is the PDCA cycle, and Step 4 is depicted by the identification of certainty and uncertainty in AQAL. It can be seen that there is interplay between Octa/Octant and PDCA at every stage. The two-head arrows indicate that the outcome of Steps 1 and 2 contributes directly to all PDCA stages, starting from Plan; then to be managed in Support and Operate; checked in Performance Evaluation; and to take action for any improvement in the Improve stage. Effectively, the integral sustainability framework shows that all aspects of realities from the four quadrants (AQAL) and the certainty and uncertainty domains are to be considered in the PDCA cycle. The performance evaluation can be benchmarked against the set target, which should be detailed in the plan.

With the proposed framework, any sustainability assessment systems such as those cited in [10] can also be used to measure the outcomes. It should be emphasised though that the goal here is not just to achieve a high score in a sustainability index system, but to achieve the sustainability goal whereby all aspects of realities according to the integral theory are evidently considered.

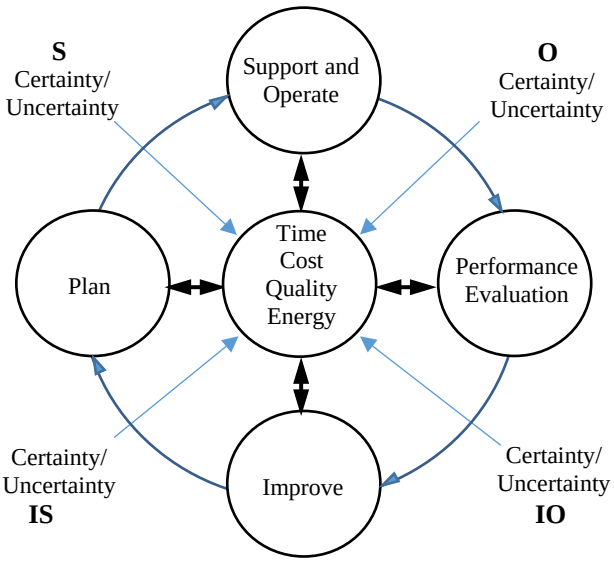

Figure 4 Integral framework for sustainability management of a construction project

A classic example is seen in Le Corbusier's Chandigarh in 1950s for the design attributes to the surrounding nature, neighbourhood grids, and hierarchical circulation pattern [14]. The city setting is so functional, designed with an extensive control of the built environment, and recognised as a perfect city of the world in terms of architecture, cultural growth and modernisation [14]. However, the perception, need and expectation of individuals and of the local community on the design were not mentioned and it was not clear whether these aspects were considered and assessed. Using the integrated framework presented in Figure 4 will enable a designer to incorporate these aspects to optimise the requirements relating to subjectivity of individuals and society.

CONCLUSION

This paper presents a new integrated framework for sustainability management in civil engineering work based on the PDCA cycle and the integral theory framework. An example is provided to demonstrate how to use the new developed framework for sustainability management of a construction project. The main idea is to ensure all aspects of realities are considered, and by identifying all these aspects, sustainability outcomes can be achieved.

The developed framework can also be used to implement with existing sustainability assessment systems by recognising the objective, inter-objective, subjective and inter-subjective aspects of the systems.

REFERENCES

[1] Oscar Ortiz, Francesc Castells, Guido Sonnemann, Sustainability in the construction industry: A review of recent developments based on LCA, Construction and Building Materials 23, 2009, 28–39.

[2] Gonzalo Fernández-Sánchez, Fernando Rodríguez-López, A methodology to identify sustainability indicators in construction project management—Application to infrastructure projects in Spain, Ecological Indicators 10, 2010, 1193–1201

[3] Chandana Kulasuriya, Alkali Pozzolan Cement for Integral Sustainability, Thesis submitted to fulfil a Doctor of Philosophy at Curtin University, Bentley, Western Australia, 2016.

[4] DeKay M, Integral Sustainable Design, Transformative Perspectives, London: Earthscan, 2011.

[5] Kulasuriya, Chandana and Vanissorn Vimonsatit, Integral Research Framework for Sustainable Structures for Future, Proceedings of Australian Structural Engineering Conference 2012. Perth, Australia, 2012, 740-747, at http://search.informit.com.au/documentSummary;dn=003971378892872;res=IELENG

[6] Kulasuriya, Chandana, Priyan Dias, Vimonsatit, Vanissorn, Developing an Approach to Assess 'Integral Sustainability' of Alkali Pozzolan Cement, Proceedings of the 3rd Biennial Integral Theory Conference, California, USA, 2013, available at https://foundation.metaintegral.org/sites/default/files/Kulasuriya_ITC2013.pdf

[7] Kulasuriya, Chandana, Priyan Dias, and Vanissorn Vimonsatit, "Integral Sustainability of Alkali Pozzolan Cement." Journal of Integral Theory & Practice 9(1), 2014, 74-87.

[8] ISO 9001:2015, Quality management systems – Requirements, accessed via SAI Global, Australia.

[9] Oliver Salzmann, Aileen Ionescu-Somers, Ulrich Steger, The Business Case for Corporate Sustainability: Literature Review and Research Options European Management Journal Vol. 23, No. 1, 2015, 27–36.

[10] Fernando Rodríguez, Gonzalo Fernández, Sustainable engineering: new objectives for construction projects, Revista Ingeniería de Construcción Vol. 25 No2, 147-160, Agosto de 2010 www.ing.puc.cl/ric, accessed on 8 March 2016.

[11] Aysin Sev, How Can the Construction Industry Contribute to Sustainable Development? A Conceptual Framework, Sustainable Development, Sust. Dev. 17, 2009, 161–173

[12] Calista Y. Tsai, Andrew S. Chang, Framework for developing construction sustainability items: the example of highway design, Journal of Cleaner Production 20, 2012, 127 - 136

[13] A. Azapagic, Systems Approach To Corporate Sustainability A General Management Framework Trans IChemE, Vol 81, Part B, September 2003, 303-316.

[14] Chandigarh, "BBC Names Chandigarh as a perfect city of the world" by Ajay Deep, "Is this the perfect city?", www.bbc.com, cited in https://en.wikipedia.org/wiki/Chandigarh, accessed on 3 May 2016.

Second International Conference on Science, Engineering & Environment,
Osaka City, Japan, Nov.21-23, 2016, ISBN: 978-4-9905958-7-6 C3051

DEEP BASEMENT EXCAVATION IN SOFT BANGKOK CLAY CLOSED TO PALACES

Wanchai Teparaksa
Department of Civil Engineering, Chulalongkorn University, Thailand

ABSTRACT

The Bank of Thailand (BOT) head office is a large building constructed in the inner Ratanakosin Island of Bangkok along Chao Phraya River, a main river of Bangkok, where high-rise building construction with more than three stories is not permitted. The BOT building consists of five basements with excavation depth of 15.8 meters and only three stories of super structure. The soil condition consists of 15 m. thick soft to medium clay followed by stiff silty clay and sand layer. The basement construction was constructed only five meters away from Tewavej Palace and ten meters away from Bangkhunphrom Palace. The damage assessment by means of Finite Element Method (FEM) with simulation of basement construction method was carried out to predict the influence on both palaces. Finally, the top-down construction method was selected for basement construction with one meter thick and 20 meters long of diaphragm wall which was designed together with the 50 meters long bored pile to support the whole building. The full set of instrumentation was installed at the palaces, diaphragm wall and ground surface for monitoring the field performances and effect to the palaces during and after basement construction. The field measurement and FEM prediction is compared and the time dependent of lateral wall movement is discussed. The construction was completed without any damage or effect to both palace.

Keywords: Deep Basement; FEM Analysis; Deep Excavation; Historical Building; Palace

INTRODUCTION

The demand for deep underground basement construction is increasing in Bangkok city especially in the inner zone due to the optimized land use for underground car park and retail of the department store. The design and construction of deep basement in the large city have to take the impact of the nearby structure as well as public utilities into account. Even though there are a large number of theoretical methods that studied the stability of braced excavation [1-3] and ground movement induced from excavations [4-6], the study on an actual construction work is still slight. The designs of the deep basement in Bangkok subsoil done by the author are the Bai Yok II tower with 12 m. deep (Teparaksa [7]), Library of Thammasat University with 14 m. deep (Teparaksa, [8]), Central World with 9 - 14 m. deep (Teparaksa, [9]), Millennium Sukhumvit hotel next to Bangkok Mass Rapid Transit (MRT) Tunnel with 14 m. deep (Teparaksa [10]), the impact assessments of deep basement construction in the MRT Protection Zone (Teparaksa et al. [11]), the deep basement construction in Soft Bangkok clay next to British Embassy (Teparaksa [12]), and the deep excavation in safety zone of subway (Teparaksa [13-14]).

The head office, Bank of Thailand (BOT) is located in the inner Ratanakosin Island where high-rise building construction more than three stories is not allowed. The location of the new head office of BOT is planned along Chao Phraya riverbank and closed to two historical palaces; Tewavej Palace and Bangkhunphrom Palace as shown in Fig. 1.

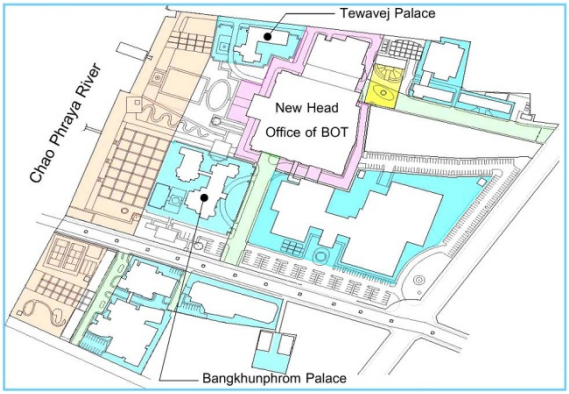

Fig. 1 The location of new head office, Bank of Thailand (BOT) and the surrounding palaces

The design and construction of the deep basement for head office of the BOT consists of five basements for underground car park with 15.8 m deep excavation and three floors of head office above ground surface.

The analysis and the diaphragm wall design as well as the impacted assessment of two palaces were carried out by Finite Element Method (FEM) analysis by simulating the full method of excavation and construction in the model. The instrumentation

was installed in both diaphragm wall and at the palaces to monitor the safety and stability of the palaces. The behavior of diaphragm wall movement is also discussed and compared with FEM prediction.

SOIL CONDITIONS

The soil conditions at BOT site based on nine boreholes soil investigation consists of 12.5 m. thick soft dark grey clay and followed by medium stiff clay and stiff to hard clay until reached the first dense sand layer at about 28.5 m. deep. The second very dense sand where the pile tip of the building is seated is found at about 46 m. deep below ground surface. Table 1 presents the soil condition and the engineering properties.

Table 1 Summary of soil conditions and properties

Depth (m.)	Soil Description	γt	Su	N	Eu	E'
0 - 12.5	Soft Clay	16	15	-	8,750	-
12.5 - 15.0	Medium Stiff Clay	16.5	40	-	18,000	-
15.0 - 20.0	Stiff to Very Stiff Silty Clay	19	-	12	85,000	-
20.0 - 28.5	Hard Clay	20	-	35	300,000	-
28.5 – 39.0	Dense Silty Sand	20	-	40		80,000
39.0 – 46.0	Hard Silty Clay	20	-	45	-	-
46.0 – 65.0	Very Dense Silty Sand	20	-	>50	-	-

Note: γt = Total Unit Weight (kN/m^3)
Su = Undrained Shear Strength (kN/m^2)
N = SPT N-Value (Blows/ft)
Eu, E' = Undrained and Drained Young's Modulus (kN/m^2)

PROJECT DESCRIPTION

The basement design and construction of the new head office of bank of Thailand aims to solve the problem of car park from both staff as well as visitors. The surface area of excavation is approximately 10790 m^2 with 5 m. and 10 m. away from Tewavej Palace and Bangkhumphrom Palace accordingly as shown in Fig 2. The Tewavej Palace and Bangkhunphrom Palace is the historical palace constructed by brick and bearing wall seated on shallow foundation. In order to minimize the influence on these two palaces, the basement of BOT was designed to be constructed by top-down construction method which has been used only in Bangkok city restricted area such as the subway station of MRT project.

The diaphragm wall (D-Wall) of 1.0 m. thick and 20 m. deep was designed as the temporary wall for 15.8 m. deep excavation and used as permanent wall at the final stage. Five basement floors consist of F1 ,P1 ,P2 ,P3 and P4 floor at -1.20 m., -4.70 m., -7.70 m., -10.70 m., and -13.70 m. deep respectively as illustrated in Fig 3.

The top-down construction method was started by casting the first basement F1 at -1.20 m. then moving to third basement floor (P2) at -7.70 m. and constructing the fifth basement floor and mat foundation at -13.70 m. deep as shown in Fig 3. Loading of the permanent basement floor during construction was transferred through the stanchion at the centerline of the column which was installed into the bored pile during construction of the bored pile.

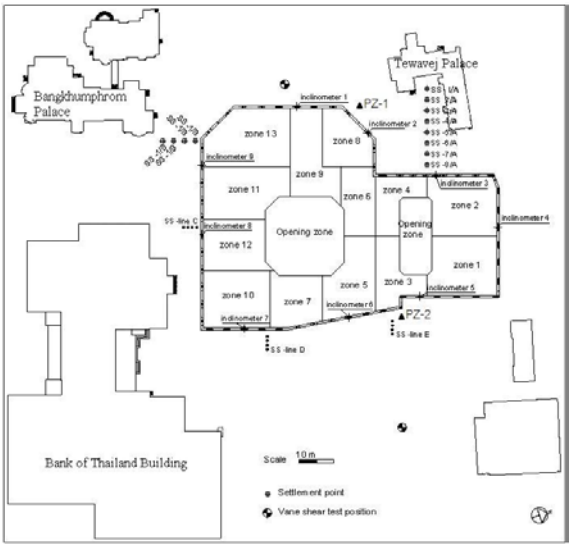

Fig. 2 The BOT project plan view

INSTRUMENTATION

The head office of BOT was constructed in the large area of more than 10790 m^2; therefore, the excavation area for top-down construction was divided into 13 zones as presented in Fig 2. Two large opening zones were provided for excavation work. The excavation at the deeper basement required to excavate step by step from far corner to the opening zone where the excavated soil was moved out of the project area. For safety reason and to monitor basement wall behavior, the full scheme of instrumentation was installed at the palaces on the ground surface and in the diaphragm wall as shown in Fig 2 and Table 2.

ANALYSIS AND DESIGN OF DIAPHRAGM

WALL

The analysis and design of the diaphragm wall was carried out by means of the FEM [16]. The construction sequence was simulated in the FEM analysis. The sequence of basement construction consists of 8 steps as follows:

1. Excavating to -1.75 m. deep and casting lean concrete.
2. Casting the first permanent basement floor at -1.20 m. (thickness 0.45 m.)
3. Excavating to the third basement floor at -8.10 m. deep and casting lean concrete.
4. Casting the third permanent basement floor at -7.70 m. (thickness 0.30 m.)
5. Excavating to the fifth basement floor (base slab) at -15.60 m. deep and casting lean concrete.
6. Casting the fifth basement floor (base slab) at -13.70 m. (thickness 1.30 m.)
7. Casting the permanent fourth basement floor at -10.70 m. (thickness 0.30 m.)
8. Casting the permanent second basement floor at -4.70 m. (thickness 0.30 m.)

The detail of construction sequence is presented in Fig. 4.

The analysis and design of the diaphragm wall for 15.6 m. deep excavation were carried out by FEM. As the basement constructed in soft clay layer, the undrained concept based on bi-linear Mohr-Coulomb failure theory was used for FEM analysis. The Young's modulus (Eu) was used in terms of an undrained shear strength (Su) of Eu/Su = 500 and 1000 for soft clay and stiff clay respectively (Teparaksa [10]). The value of Young's modulus is also presented in Table 1.

The Young's modulus or shear modulus (G) of clay depends on the shear strain of the system as proposed by Mair [15] as shown in Fig. 5. The relationship of the Eu/Su and strain level presented in Fig. 6 is the modulus of soft and stiff Bangkok clay based on the results of self-boring pressuremeter test during construction of MRT Subway Blue Line in Bangkok city. Fig. 7 presents deformed mesh of the FEM analysis at the final stage of excavation at 15.6 m deep.

The result of FEM analysis presents the envelope of lateral movement of D-wall at final stage of excavation in the order of 28.2 mm. and maximum ground surface settlement of 23.7 mm. This maximum ground surface settlement behind the D-wall and lateral movement of the D-wall was set as the trigger level to control the method of excavation as well as the stability of Tewavej Palace.

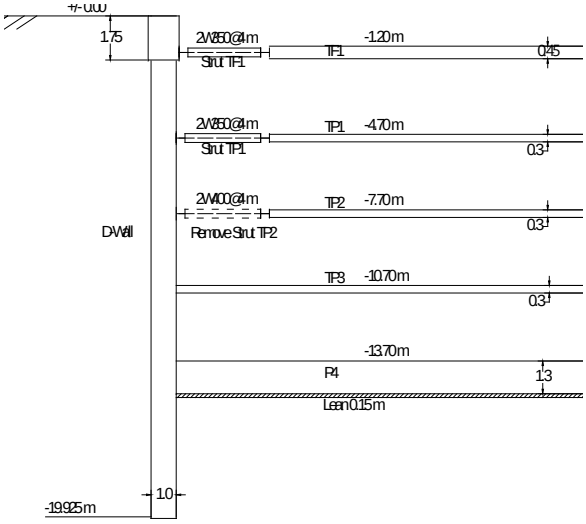

Fig. 3 Typical section of underground basement

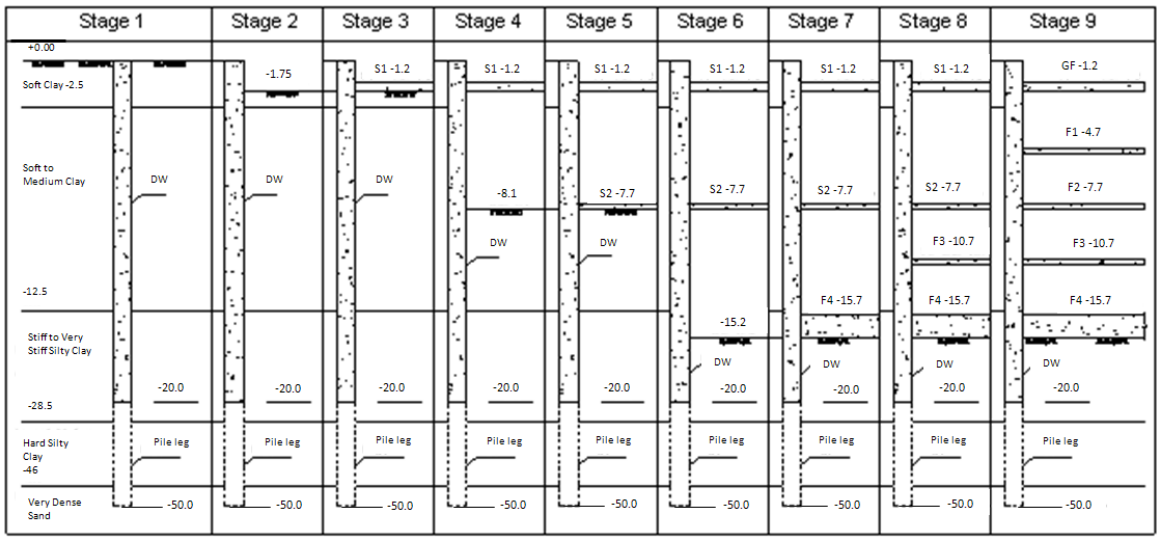

Fig. 4 Detail of construction sequences

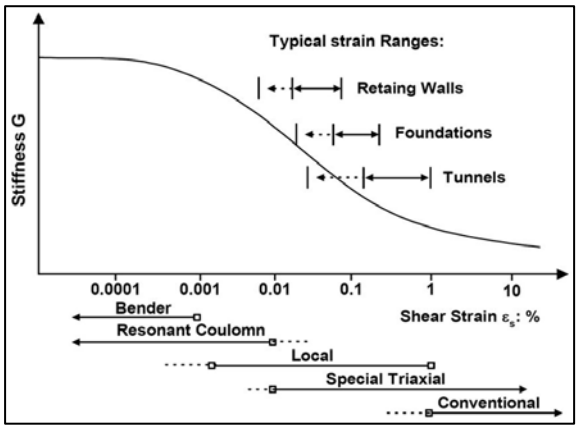

Fig. 5 The relationship between modulus and shear strain level (Mair [15])

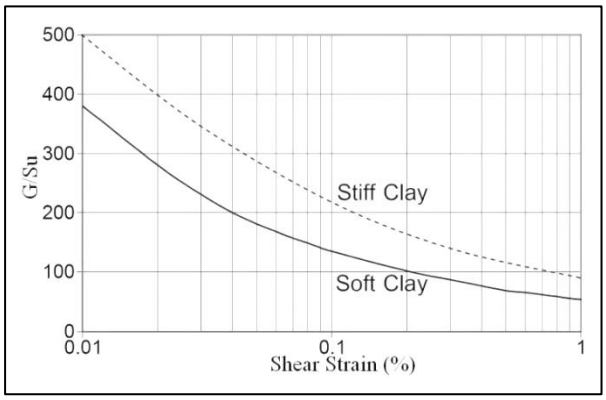

Fig. 6 The relationship between modulus and shear strain level of soft and stiff Bangkok clay (Teparaksa [10])

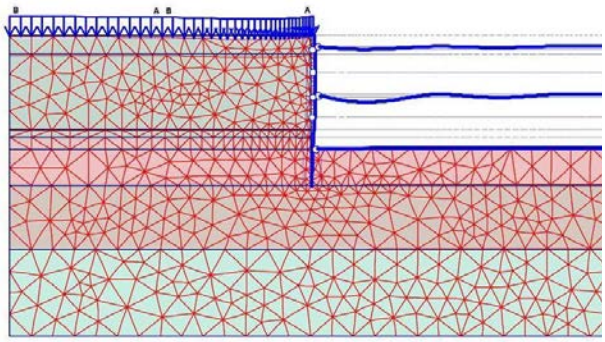

Fig. 7 Deformed mesh of FEM analysis at the final stage excavation at -15.6m.

INSTRUMENTATION AND PERFORMANCE OF DIAPHRAGM WALL

The full set of the instrumentation was proposed to monitor the behavior of the diaphragm wall and surrounding palaces as presented in Table 2 and Fig. 2. The results of the piezometer monitoring by pneumatic type in soft clay was constant with hydrostatic pore water pressure of ground surface water at 1.00 m. below ground surface.

Table 2 Instrumentation at the Palaces and Diaphragm Wall

Instrumentation	Location	Purpose
Vibration Sensor	At Tewavej Palace and Bangkhunphrom Palace	Vibration at the palace
Tiltmeter	At Tewavej Palace and Bangkhunphrom Palace	Tilt of the palaces
Ground Surface Settlement point	Ground Surface	Ground Surface Settlement
Inclinometer	In the Diaphragm Wall	Lateral D-Wall movement
Piezometer	Outside the D-Wall	Ground water level

The measurement of the lateral diaphragm wall movement at all steps of excavation and basement floor casting at inclinometer no. I-3 next to Tewavej Palace is shown in Fig. 8 together with the predicted maximum envelope of diaphragm wall movement estimated by FEM.

It can be seen that the predicted wall movement by FEM agrees well with field performance. The tiltmeter measured at the Tewavej Palace is also less than the trigger level. Figs. 9 and 10 present the photograph during excavation closed to Tewavej Palace. The basement construction of the new head office of Bank of Thailand was completed without any disturbance to both Bangkhunphrom Palace and Tewavej Palace.

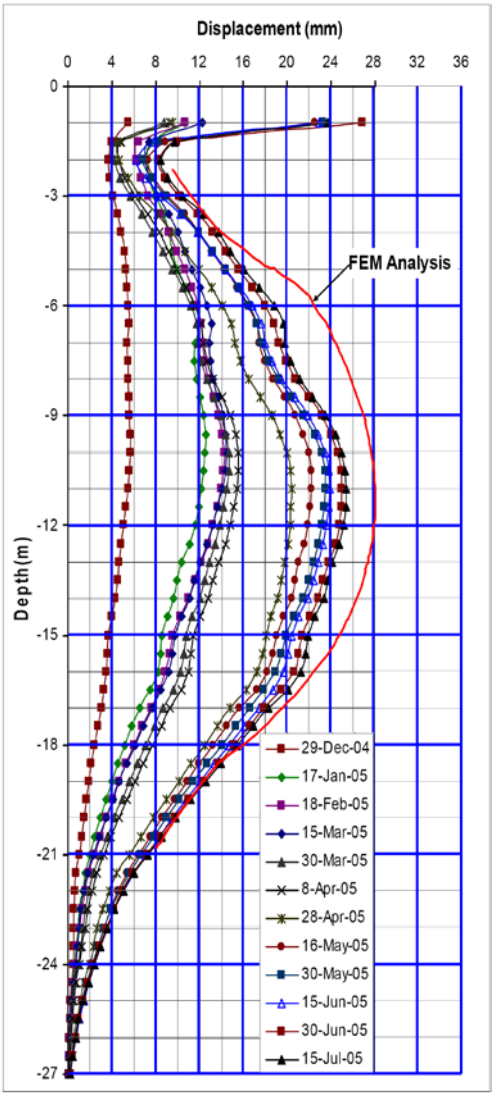

Fig. 8 The inclinometer I-3 monitoring results with the predicted maximum movement by FEM analysis.

Fig. 9 Photograph during excavation closed to Tewavej Palace

Fig. 10 Basement construction during excavation to the final depth

CONCLUSIONS

This paper presents the cause of uplift at the The basement of 15.6 m. deep excavation was constructed at the new head office of Bank of Thailand. The deep basement consists of 5 basement floors at -1.20 m., -4.70 m., -7.70 m., -10.70 m. and -13.70 m. depth. The basement constructed area is closed to two palaces; Bangkhunphrom Palace and Tewavej Palace, which are the historical buildings and also located close to the Chao Phraya river bank. The top down construction method was used for basement construction. The prediction of diaphragm wall movement and its effect to the palaces were carried out by FEM analysis. The instrumentation was installed in D-wall, ground surface and the palaces in order to measure the wall behavior and their effect. The lateral movement of D-wall by means of inclinometer at all stages of construction is compared with FEM prediction. The FEM prediction agrees well with measured values. The deep basement was completed without any disturbance to both palaces.

REFERENCES

[1] Bjerrum L., and Eide O., “Stability of strutted excavations in clay”, Geotechnique, Vol. 6, pp. 115–128, 1956.

[2] Ukritchon B., Whittle A.J., and Sloan S.W., “Undrained stability of braced excavation in clay”, ASCE J. Geotech. Geoenviron. Eng. Vol. 129, No. 8, pp. 738-755, 2003.

[3] Khatri V.N. and Kumar J., “Stability of an unsupported vertical circular excavation in clays under undrained condition”, Comput. Geotech. Vol. 37, pp.419–424, 2010.

[4] Terzaghi K., Theoretical soil mechanics. Wiley, New York, USA, 1943.

[5] Eide O., Aas G., and Josang T., "Special application of cast-in-place walls for tunnels in soft clay", Proceeding of 5th European Conference on Soil Mechanics and Foundation Engineering, Madrid, Spain, pp. 485–498, 1972.

[6] O'Rourke T.D., "Base stability and ground movement prediction for excavations in soft clay", Retaining structures, Thomas Telford, London, pp. 131–139, 1993.

[7] Teparaksa W., "Deep basement construction in Bangkok soft clay by sheet pile braced cut system", Journal of Engineering of Thailand, 1992. (in Thai)

[8] Teparaksa W., Thassananipan N. and Tanseng P. "Analysis of lateral movement for deep braced excavation in Bangkok subsoil", Civil and Environmental Engineering Conference-New Frontier & Challengers, AIT, Bangkok, 1999.

[9] Teparaksa W., "Principal and application of instrument for the first MRTA Subway Project in Bangkok", The 5th Int. Symposium on Field Measurement in Geomechanics. Singapore, 1999.

[10] Teparaksa W., "Deformation of subway tunnel induced by deep basement excavation in MRT Protection Zone, Bangkok", Theme Speaker. 13th Asian Regional Conference in Soil Mechanics and Geotechnical Engineering, Decrmber, Kalkate, India, 2007.

[11] Teparaksa W., Sontiprasart P., Prachayaset N., and Keawsawasvong S, "Impact Assessments of the Deep Basement Construction in the MRT Protection Zone", The 28th KKHTCNN Symposium. Civil Engineering, Bangkok, Thailand, 2015.

[12] Teparaksa W., "Recent Development on Deep Basement Construction in Soft Bangkok Clay next to British Embassy", Proc. of the 15th Asian Regional Conference on Soil Mechanics and Geotechnical Engineering, Fukuoka, Japan, 2015.

[13] Teparaksa W., "Deformation of Subway Tunnel Induced by Deep Excavation in MRT Protection Zone", the 6th Regional Symposium on Infrastructure Development (RSID), Bangkok., 2008.

[14] Teparaksa W., "Diaphragm Wall for Deep Excavation in Safety Zone of Subway", the 21st KKCNN Symposium in Civil Engineering, October, Singapore, 2008.

[15] Mair R.J., "Unwin Memorial Lecture 1992 Developments in geotechnical engineering research: application to tunnels and deep excavations", Proceeding of the Institution of Civil Engineers. Civil Engineering. Vol. 97, No. 1, pp. 1993, 27-41.

[16] Brinkgreve, R.B.J., PLAXIS 2D Version 8 Manual, A.A. Balkema Publishers, 2002.

Second International Conference on Science, Engineering & Environment,
Osaka City, Japan, Nov.21-23, 2016, ISBN: 978-4-9905958-7-6 C3051

A NEW QUEUING TECHNIQUE IN ADAPTIVE MULTIPATH ROUTING FOR CONGESTION CONTROL WITH PACKET PRIORITY IN WIRED DATA NETWORKS

N.Krishna Chaitanya[1], S.Varadarajan[2]
[1]Research Scholar, ECE Department, JNT University College of Engineering, Kakinada, INDIA;
[2]Professor, ECE Department, S V University College of Engineering, Tirupati, INDIA

ABSTRACT

This paper proposes an Adaptive Multi-Path routing based on packet priority. Simultaneous Multi-Path routing is used to improve the data performance over a congested network. The traditional method of transmitting the data is done by using Simultaneous Multi Path Communication (SMPC). Two types of SMPCs are proposed, in which SMPC-I, which uses multiple paths independently and SMPC-P, which uses path priority control algorithm in conjunction with SMPC. SMPC-I and SMPC-P maintains throughput regardless of path length and priority control. In addition to available SMPC methods, proposed method provides better solution to improve the performance of communication network. A theoretical approach of AMPC-PP proposed here based on packet priority for important data over normal data on a congestion network with route adaptability.
Keywords: Multi-path communication, Path priority, Independent paths, Packet priority.

INTRODUCTION

A Network comprises a number of nodes and links for processing of data from source to destination. The process of transmitting the data from source to destination is called routing and it is done by making use of the best path through the network. Data packet can be routed either by using single or multipath routing techniques [1]. Single path routing is the traditional method of transmitting the data through the network. But, the major problems here with this scenario are: less network bandwidth utilization, more delay; if any node or link fails entire data will be lost, less throughput and leads to scope for congestion. These problems can be minimized by using multipath routing. Here in this method, a number of hosts are connected by using a number of nodes and links. All node and link capacities differ in the network. Data packets are transmitted from source to destination through a number of paths. Best paths are selected based on shortest path and it is computed in the network based on traffic. Paths are selected by the type of service requested by the user in the network. For different applications, multiple paths may be used to meet their requirements [2].

Multipath transmission is realized in source and hop-by-hop routing, multi-topology routing, Software-Defined Networks, Multi-Protocol Label Switching, Flow-Aware Multi-Topology Adaptive Routing that interconnects a number of links in network virtualization, and Multipath TCP [2]. The major advantage of choosing multi-path routing is reduced delay.

LITERATURE REVIEW

Although, multi-path routing is used to reduce congestion by splitting the data over several potential paths without knowing the path capacity. This problem can be minimized by using load balancing technique. In load balancing, load over a path is decided by available resources and traffic in that particular path [1]. A number of multipath routing techniques have been proposed. The basic technique is Simultaneous Multi-Path Communication (SMPC) [3]. First method in SMPC is SMPC-I based on independent paths. This method is based on bandwidth control. Second method is SMPC-P, which is based on path priority. These techniques does not support for packet priority. The major drawbacks in these methods are greater delay and reduced network performance [4].

A method proposed by Peter Key et al. [5] for avoiding congestion in multi path routing using load balancing, but this method is unable to route the data packets if there are more link failures.

There after a number of multi path routing techniques proposed with load balancing [1], [6-9], but these methods requires more control messages, does not support for route recovery, as well as supports only for single link failures.

Paganini proposed Multi Protocol Label Switching (MPLS). This method provides better routing and capable of interfacing to existing routing protocols, but it requires additional layer between data link and network layer and also router requires knowledge about MPLS [10].

ADAPTIVE MULTIPATH ROUTING FOR CONGESTION WITH PACKET PRIORITY:

Major disadvantage in multipath routing is that, if any link or router fails, source chooses alternate path based on the available routing table information. This process takes more delay, there by increases the data transmission delay, reduces the network performance. This drawback can be eliminated by using adaptive multipath routing. If a link fail or router fails, then the nearest router sends a request to another neighbouring router. If any one of the router responds then the data packets will be forwarded to that router. By using this technique the source routing can be avoided, thereby reducing the delay and improves the network performance.

In addition with adaptive multi path routing, importance is also given for urgent data packets by indicating the packet priority. Here we have tested the performance by using only two packet priorities. The priority will be verified at the router based on the following technique.

- If there is any congestion at a router or any other important data is being transmitting through the router, a check point is created at the router to identify whether the data packet is having a priority or not.
- If the data packet is not having highest priority then it is passed to the queue.
- If the data is having highest priority, then it is directly transmitted to output side without passing through the queue.

The packet priority is verified at the router using additional block called packet priority verifier. It will verify the packet with highest priority, if the condition satisfies, then the packet will be directly forwarded to routing decision and switch allocator unit. This method will eliminate the unnecessary queuing delay. This will reduce the overall delay in the network, thereby increasing the system performance.

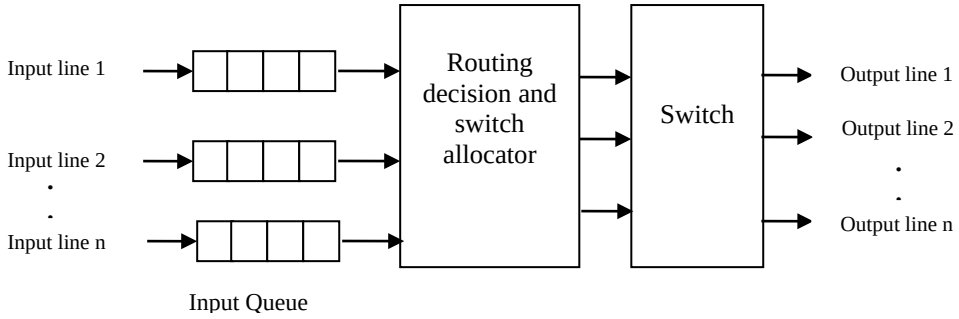

Fig.1: Traditional router functionality

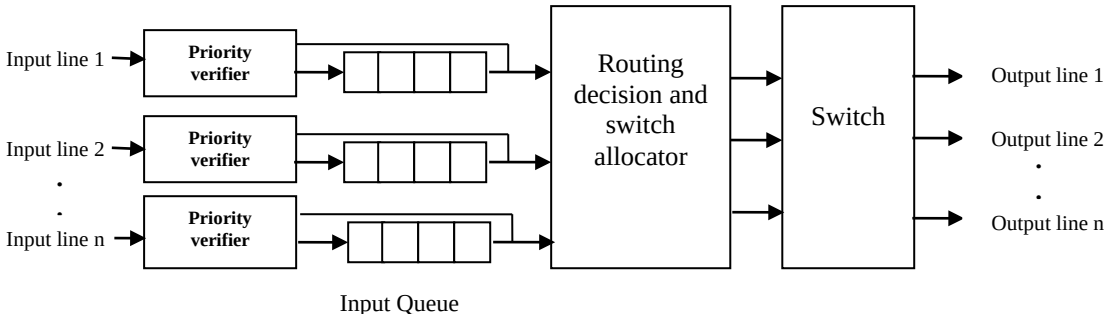

Fig.2: Proposed packet priority based router functionality

The simplest and most popularly used queuing technique in the internet is tail drop or drop tail. In this queuing technique, each packet is treated as same without concerning the packet priority. This queuing technique is based on FIFO (First In First Out), means whichever packet comes first into the queue will be transmitted first to output. If the queue length reached to its maximum capacity, then newly arrived packets are dropped until there is a space in the buffer.

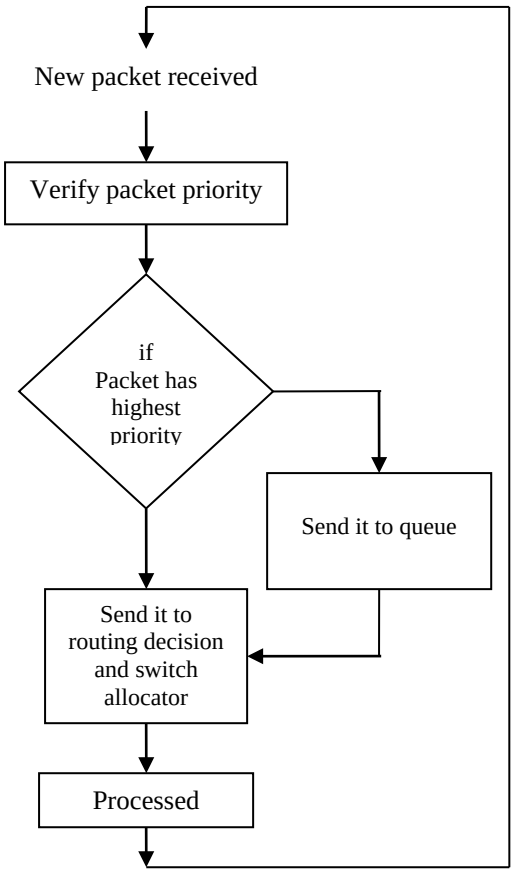

Fig.3: Flow diagram for proposed technique

Fig.1 shows the basic functionality of a router, where the packets are received at the input line of the router. Then the packets enter into queue, there after the packet is passed through routing decision unit. In routing decision unit, the packet output line is decided based on source address and destination address and then the packet is switched through a switch by switch allocator. It takes more amount of time for processing the packets by the router. The amount of time taken at the router depends upon the number of input lines and the maximum queue length. In conventional method all the packets are processed without considering any packet priority. This drawback is eliminated by using our proposed method at the router. The diagram for packet priority based router functionality is shown in Fig.2.

Fig.3 shows the flow diagram for the proposed method. It is very much clear that, prioritised packets transmitted first and the priority is based on their importance or type of service.

SIMULATION RESULTS AND DISCUSSIONS:

The results are tested by using Network Simulator-2 for data transmission through wired data networks. Simulation results are tested for various scenarios such as single path routing, multipath routing and adaptive multipath routing with and without packet priority.

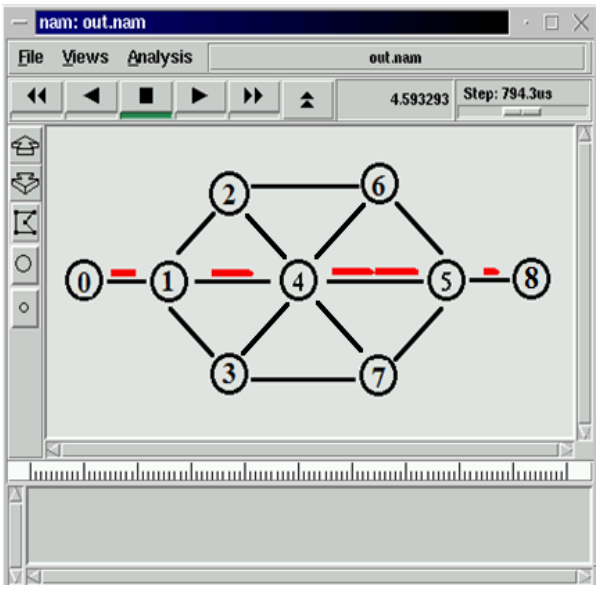

Fig.4: Single path routing

For the entire routing simulation a simple network environment is considered in which, it consists of 7 routers and two stations. “0” is designated as sender and “8” is designated as destination.

In Fig.4, single path routing is simulated and verified the end-to-end delay for with and without priority. The same procedure was repeated for multipath routing as well as adaptive multipath routing techniques. Multipath routing simulation result is shown in Fig.5. Fig.6 shows the adaptive multipath routing which provides an alternate path whenever a link failure occurs in the network.

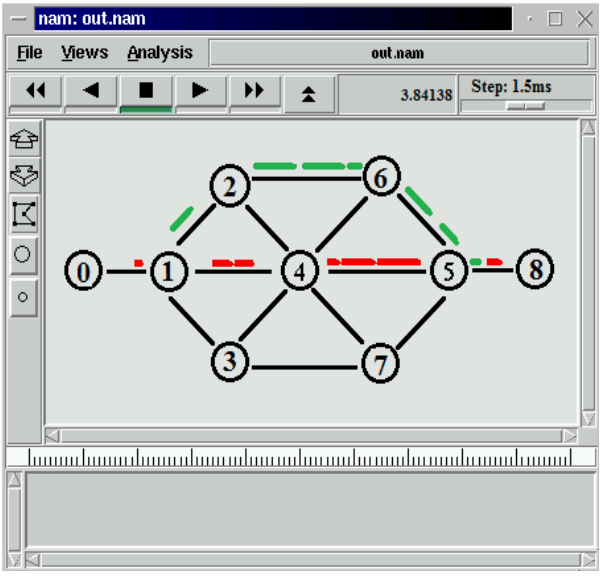

Fig.5: Multipath routing

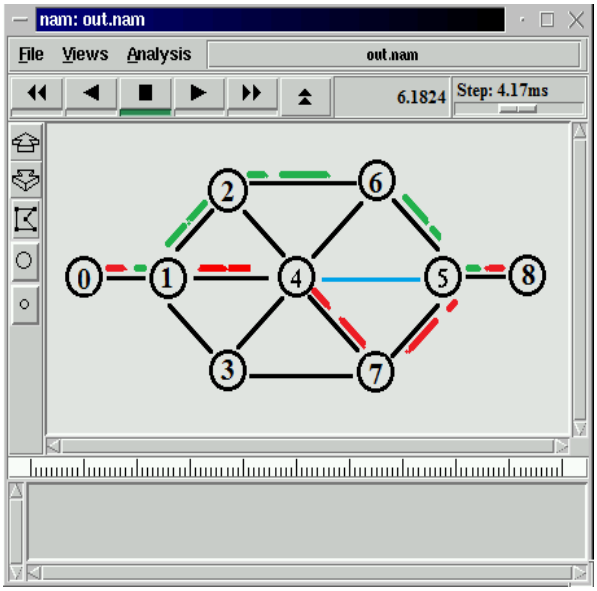

Fig.6: Adaptive Multipath routing

From Fig.6, it is evident that, link between 4 and 5 is failed; in traditional methods alternate path is chosen from source router. But here router4 sends a request to adjacent router and re-routes the data packets to destination. The end-to-end delay for single path, multipath and adaptive multipath routing with and without packet priority is shown in Fig.7, Fig.8 and Fig.9. Fig.10 shows packet delivery ratio by using packet priority for transmitting a video stream, which we have tested our method for various link capacities.

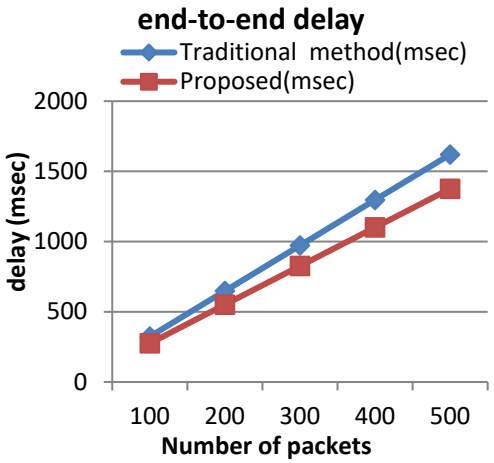

Fig.7: End-to end delay in single path routing with and without packet priority

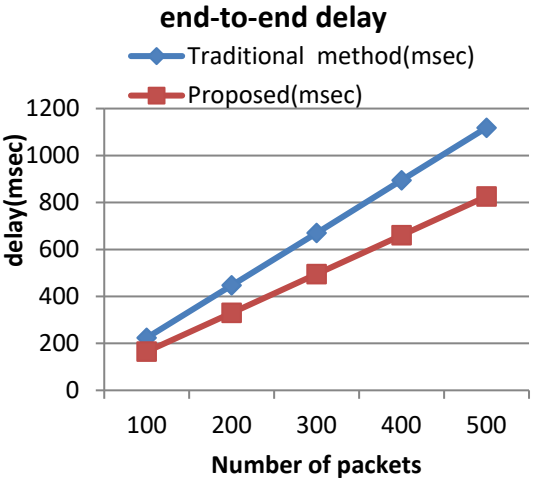

Fig.8: End-to end delay in multi path routing with and without packet priority

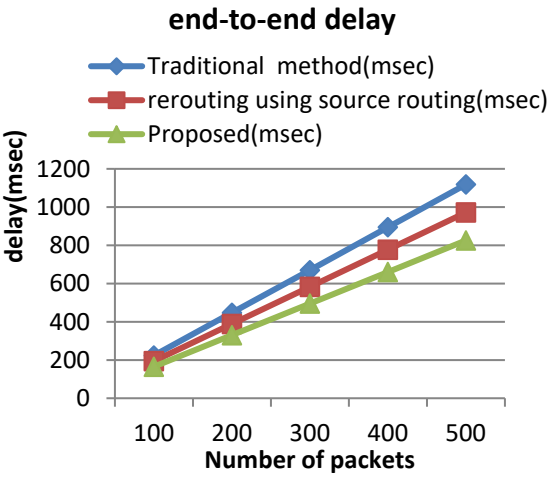

Fig.9: End-to end delay in adaptive multi path routing with and without packet priority

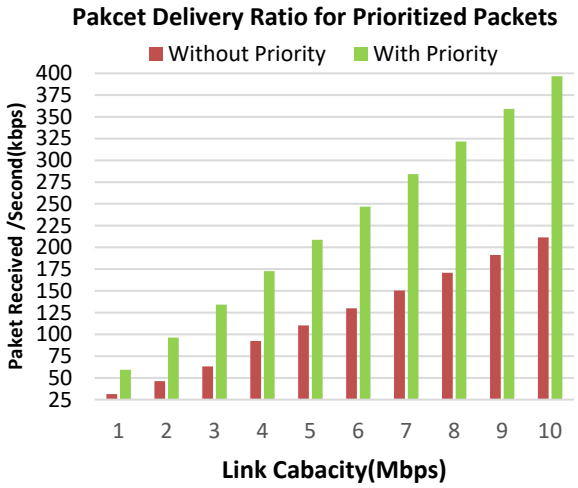

Fig.10: Packet delivery ratio with and without packet priority for various link capacities

CONCLUSIONS:

Here in this paper, we have shown adaptive multipath routing technique in addition with packet priority at router. Simulation results are carried out by using NS-2. It is evident that, proposed method has less end-to-end delay for packet transmission in the network. Simulation results will alter if we change link capacities, queue length and packet length. Here we considered link capacity of 1024Kbps, packet size of 1000 bits, queue length of 1000 packets. If any change in parameters, delay also changes. Now in the current internet research, routing plays a vital role especially in wired data networks. There are a number of multipath routing techniques available, but the proposed method gives a better performance compared to existing methods. Whenever there is a link failure or congestion, there is a necessity for traffic rerouting. This method not only provides adaptability in multipath routing it also provides the priority for important data to be sent without passing the data packets through queue.

REFERENCES

[1]. Chaitanya, N. Krishna, and S. Varadarajan. "Load Distribution using Multipath-Routing In Data Networks: A Comparative Study." *Perspectives in Science* (2016).

[2]. Domżał, Jerzy, et al. "A survey on methods to provide multipath transmission in wired packet networks." *Computer Networks* 77 (2015): 18-41.

[3]. Tanaka, Akiji. "Effects of length and number of paths on simultaneous multi-path communication." *Applications and the Internet (SAINT), 2011 IEEE/IPSJ 11th International Symposium on*. IEEE, 2011.

[4]. Chaitanya, N. Krishna, and S. Varadarajan. "An Implementation of Adaptive Multipath Routing Algorithm for congestion control." *International Journal of Computer Science and Network Security (IJCSNS)*, volume no.16, issue no.2, 2016, pp.6-9.

[5]. Peter Key, Laurent Massoulie, Don Towley, 2007, "Multipath Routing, Congestion Control and Dynamic Load balancing" IEEE Network, Vol.4, pp. 1341-1344.

[6]. He Jiayue, Rexford Jennifer, 2008, Toward Internet-Wide Multipath Routing, IEEE Network, Vol.22,pp. 16-21

[7]. Palomar D. P., Mung Chiang, 2007, Alternative Distributed Algorithms for Network Utility Maximization: Framework and Applications, IEEE Transactions on Automatic Control, Vol.52, pp.2254-2269.

[8]. Theodore Elhourani, Srinivasan Ramasubramanian, Amund Kvalbein, 2011, "Enhancing Shortest Path Routing for Resilience and Load Balancing" IEEE Communication, pp. 1-6.

[9]. Sumet Prabhavat, Hiroki Nishiyama, Nirwan Ansari, Nei Kato, 2011, "On Load Distributionover Multipath Networks", IEEE Communications, Vol.99, pp 1-19.

[10]. Paganini F. Congestion control with adaptive multipath routing based on optimization, In Information Sciences and Systems, 2006 40th Annual Conference on 2006 Mar 22 (pp. 333-338). IEEE.

Second International Conference on Science, Engineering & Environment,
Osaka City, Japan, Nov.21-23, 2016, ISBN: 978-4-9905958-7-6 C3051

EFFECT OF PARTICLE SHAPE ON THE PACKING AND FLOW BEHAVIOUR OF GRANULAR MATERIALS

Jieqing Gan, Sida Liu, Aibing Yu, and **Zongyan Zhou**
Laboratory for Simulation and Modeling of Particulate Systems, Department of Chemical Engineering, Monash University, VIC 3800, Australia
Zongyan.zhou@monash.edu

ABSTRACT

Particle shape is one of the most important properties of particles, and it affects the packing and flow structures that are critical to transport properties such as permeability related to pore connection and thermal conductivity related to particle connection. Particle shape can be regular or irregular. To be more quantitative, recent studies are focused on particles of well-defined shapes. In particular, ellipsoids attract a lot of attention in recent years as it can represent a large number of shapes, e.g. from platy to elongated. In this paper, we give a brief review of studies of ellipsoidal particles on the basis of discrete element method, and examine the effects of particle shapes in some typical particulate systems, including: (1) particle packing, focusing on how aspect ratio affects packing density and structure for coarse and fine ellipsoids; (2) hopper flow, demonstrating the dependence of discharging rate of hopper flow on particle shapes; (3) sandpile formation, focusing on how aspect ratio affects the angle of repose and stress dip distribution; and (4) fluidization, illustrating how particle shape affects the bed permeability, orientation, and bed flow/force structures. The results show that discrete element method for ellipsoids provides a useful approach to investigate shape effect on the behavior of granular materials.

Keywords: DEM, ellipsoids, particle packing, hopper flow, sandpile, fluidization

INTRODUCTION

Particulate science and technology is a rapidly developing interdisciplinary research area with its core being the understanding of the relationships between micro- and macro-scopic properties of particulate matter. In particular, discrete particle simulation (e.g., typically DEM or coupled with different fluid flow modelling approach such as CFD, DNS, LBM) has been widely used to tackle fundamental problems in particle research [1, 2]. However, so far, most of the simulation studies deal with spherical particles. The resulting findings are useful, but may have limitation in addressing practical problems. In reality, most particles are non-spherical, of either regular or irregular shapes.

Particle shape is identified as one of the most important particle properties, and significantly affects the packing/flow structures of particles which are critical to transport properties such as permeability related to pore connection and thermal conductivity related to particle connection. For example, studies on how particle shape affects porosity have been done by some researchers [3, 4]. Correspondingly, this will affect the bed permeability significantly, as reflected by the well-known Ergun equation. However, because of the difficulty in representing irregular shapes and heavy computational requirement, relatively few studies are concerned with non-spherical particles, with majority limited to simple regular shapes and not systematic. In recent years, efforts have also been made to develop the DEM approach further to study the packing and flow dynamics of ellipsoidal particles [5-9].

In this paper, we give a brief review of our recent studies of ellipsoidal particles on the basis of discrete element method, and examine the effects of particle shapes in some typical particulate systems, including particle packing, hopper flow, sandpile formation, and fluidization. The results show that discrete element method for ellipsoids provides a useful approach to investigate shape effect on the behavior of granular materials in particulate systems.

MODEL DESCRIPTIONS

A particle can have two types of motions: translational and rotational. Such motions obey Newton's second law of motion. DEM for ellipsoids has been reported in the literature [5-9]. Comparing with spheres, the key features for ellipsoids are summarized below:

- The normal force can generate a toque to make the particle rotate when the normal force does not pass through the particle centre;
- Equations used to calculate the interaction forces and torques for spheres are applied to ellipsoids;

- Calculation of radius R^* to determine the contact forces where R^* is closely related to radii of the curvature at a contact point;
- Geometric potential algorithm used to detect the contacts between ellipsoids, the most time-consuming part for DEM simulation of non-spherical particles;
- Particle orientation is described by three Euler angles (ϕ, θ, ψ) based on quaternion method;
- Fluid drag force for spheres needs to be modified to consider the effect of particle shape; and
- Aspect ratio is less than 1.0 for oblate spheroids, equal to 1.0 for spherical, and larger than 1.0 for prolate spheroids.

RESULTS AND DISCUSSION

Particle Packing [5]

Particle packing is the simplest particulate system, where all particles involved are static and in their stable positions. Proper description of packing of particles is fundamental to many industrial processes ranging from raw material preparation to advanced material manufacturing in many industries. It has been an important research topic in engineering and physics fields for many years. One significant research area is the effect of particle shape on packing properties. For example, the highest densities obtained are 0.70 for spherocylinders with aspect ratio about 0.4 [10] and 0.74 for ellipsoids with aspect ratio around 1.25 [3]. Furthermore, local alignment was found in packing of ellipsoids bean [5], nail and cylinder shaped particles [11]. In our work, we have addressed how particle shape (ellipsoids here) affect porosity and some microscopic structures [5]. A packing of ellipsoids is formed by the so-called poured packing method. Figure 1 shows the packings for three different aspect ratios of spheroids.

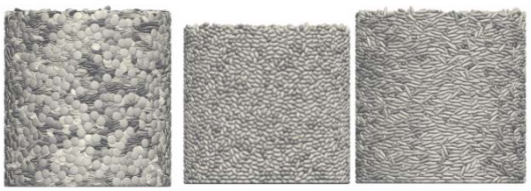

(a) (b) (c)

Fig. 1 Final packings of 25,000 ellipsoids with aspect ratio of: (a), 0.2; (b), 2.0; and (c), 4.0. *Reprinted from [5] with permission from ACS.*

The relationship of packing fraction vs aspect ratio is shown in Fig. 2, and compared with those of Donev et al. [3]. It can be observed that they are qualitatively comparable. The relationship between packing fraction and aspect ratio gives an M-shaped curve. Ellipsoidal particles can pack more densely than spheres in a certain range of aspect ratios, e.g. from ~0.25 to ~4.0. If particles are too platy or elongated, the packing becomes looser than spheres.

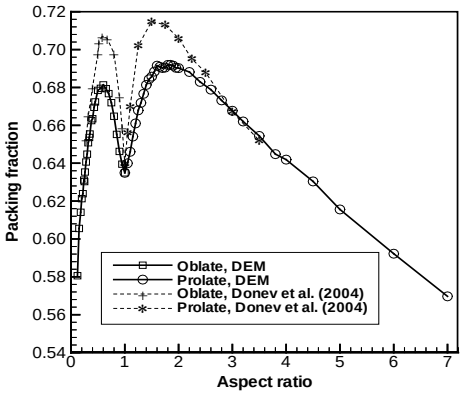

Fig. 2 Variation of packing fraction with aspect ratio under poured packing conditions. *Reprinted from [5] with permission from ACS.*

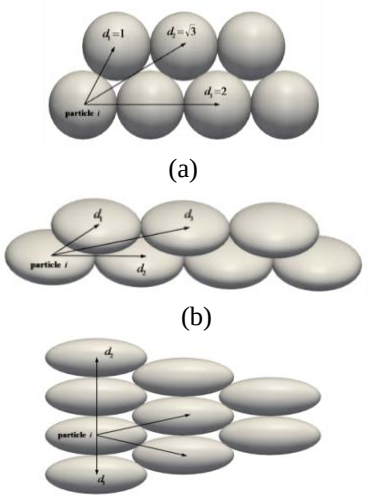

(a) (b) (c)

Fig. 3 Ordered packing structures for (a), spheres; (b), oblate spheroids when aspect ratio=0.4; and (c), prolate spheroids when aspect ratio=3.0. *Reprinted from [5] with permission from ACS.*

Radial distribution function (RDF) is often used to describe the structure of a packing, and is defined as the probability of finding one particle centre at a given distance from the centre of a given particle. The results illustrated that the typical features for spheres can be observed, with a split second peak (the first peak at $\sqrt{3}d$ and the second one at $2d$). This is correspond to the well-established structures in the literature, e.g., edge-sharing in-plane equilateral triangles and three spheres along a line (Fig. 3(a)). For platy particles, the split second peak cannot be observed, and also the first peak decreases significantly. The possible structures are shown in Fig. 3(b). For elongated particles, the first peak exists at the distance of 1.0, which means that

particles prefer contacting at the equator plane (shown by d_1 in Fig. 3(c)). The RDFs illustrated that ellipsoids have preferred orientation, which should be fully investigated further in the future.

Hopper flow [6]

Hoppers are widely used in many industries such as mining, metallurgy, and food industries. As summarized by Zhu et al. [2], the studies of hopper flow by DEM mainly include wall stress/pressure, discharge rate and internal properties. Many attempts have been made to examine the effect of particle shape on the discharge rate using DEM. For example, Cleary [12] indicated a linear decrease in mass flow rate with increasing particle elongation, while Langston et al. [13] found that elliptical particles of aspect ratio 5 are discharged 40% faster than circles. There are also controversies on whether inter-particle friction has little effect on the flow rate for non-spherical particles [14. 15]. In this work, steady-state granular flow in a cylindrical hopper with a flat bottom is investigated by DEM. Four typical flow zones are identified, consisting of plug flow zone where particles descend relatively uniformly at the top part, converging flow zone where particles move toward outlet with high velocities, stagnant zone where particles stay motionless at hopper corners, and transition flow zone between plug flow zone and converging flow zone. Such general flow characteristics can be observed for ellipsoids with different aspect ratios, as shown in Fig. 4. The effect of aspect ratio on these flow zones is summarized as follows: (i) *Mixed region near the side wall*. For spheres, the wall effect is relatively significant, causing large mixed region extending up to 6 particles diameter from side wall into the bulk flow. Interestingly, such near-wall mixed regions are not observed for ellipsoids. (ii) *Shapes of particle layers*. As in Figures 4(a) and (b), oblate particles form a V-shaped layer as spheres (Fig. 4(c)) at the upper part, while layers of prolate particles remain relatively flat. (iii) *The size of the stagnant zone*. The stagnant zone for ellipsoids is significantly enlarged compared with spheres, with a "rat-hole" formed with high particle velocities in the central core (Figs. 4(a) and (e)).

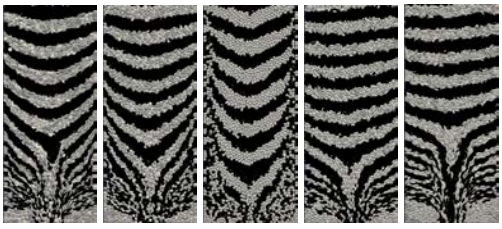

(a) (b) (c) (d) (e)

Fig. 4 Snapshots for different aspect ratios at the steady state: (a) 0.3, (b) 0.5, (c) 1.0, (d) 2.0, and (e) 3.0. *Reprinted from [6] with permission from Elsevier.*

One particular aspect for the stress distribution is the wall stress, a major concern in plant applications of hoppers. Figure 5 shows the wall stress distribution with hopper height for various shapes. For spheres, wall stress increases significantly firstly with the distance increasing from the top till the height of 0.4 m, then the increase slows down. For ellipsoids excluding the case of aspect ratio 3.0, wall stress reaches the first peak at height 0.3 m, then decrease significantly. Further, wall stress increases again sharply, then may reach the second peak. Moreover, spheres experience the largest wall stress.

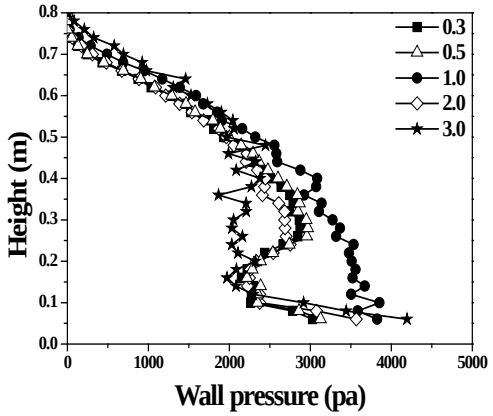

Fig. 5 Variation of wall pressure with hopper height from DEM for different aspect ratios. *Reprinted from [6] with permission from Elsevier.*

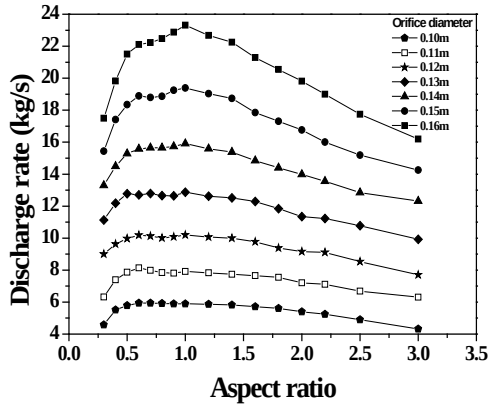

Fig. 6: Hopper discharge rate for different aspect ratios and orifice diameters. *Reprinted from [6] with permission from Elsevier.*

The prediction of discharge rate from storage hoppers is of primary importance in industrial processes which involve bulk solids handling and transportation. One of the most popular prediction correlations of discharge rate is the Beverloo

equation [16]. However, it is required to modify for the prediction of the flow rate of non-spherical particles, e.g., ellipsoids. Figure 6 shows the discharge rate of ellipsoids with various aspect ratios and different orifice sizes. Clearly, there is no significant change of discharge rate at aspect ratio close to 1. Spherical particles obtain the highest discharge rate at large orifices. An interesting trend observed here is that under the simulated conditions, the discharge rate of oblate particles varies little from spheres when the orifice is relatively small; but when the orifice size exceeds a certain value (e.g., 0.13 m), spheres exhibit noticeably higher discharge rates. Based on this, the Beverloo equation [16] is modified for ellipsoids.

Sandpile Formation [7]

A sandpile is one of the most typical particulate systems which are widely encountered in nature and many industries. It has two important properties, angle of repose and stress distribution, which have been investigated extensively and stimulated granular research significantly. It has been well documented that these two important properties are closely related to particle shape. For example, the angle of repose increases with sphericity decreasing [17, 18]. As to the stress distribution, Matuttis et al. [18] used polygons to study the effect of particle shape and found that the more eccentric the polygons are, the more pronounced the dip is observed in the vertical stress under the apex of the sandpile. DEM has been used to study the effect of aspect ratios on these two important properties of sandpiles. A comparison has been made between the measured and DEM simulated results of sandpiles, as shown in Fig. 7. It can be observed that the obtained profiles of sandpiles are quite comparable, confirming that the proposed DEM model can produce reliable results.

(a) (b)

Fig. 7 Comparison of the observed (top) and simulated (bottom) sandpiles. *Reprinted from [7] with permission from Springer.*

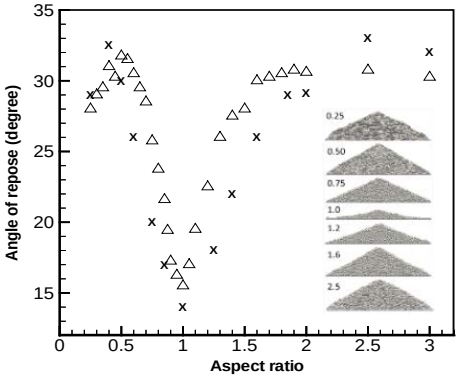

Fig. 8 Angle of repose for different aspect ratios. *Reprinted from [7] with permission from Springer.*

Figure 8 shows the variation of angle of repose with aspect ratio, revealing that spheres have the lowest angle of repose. For oblate spheroids, the angle of repose increases first with aspect ratio, then reaches a maximum at aspect ratio 0.5, finally decreases. For prolate spheroids, the angle of repose increases, then maintains a constant value after aspect ratio 1.8. Thus, prolate and oblate particles follow different variation trends of angle of repose with aspect ratio. A prediction equation for angle of repose is established, and given in [7].

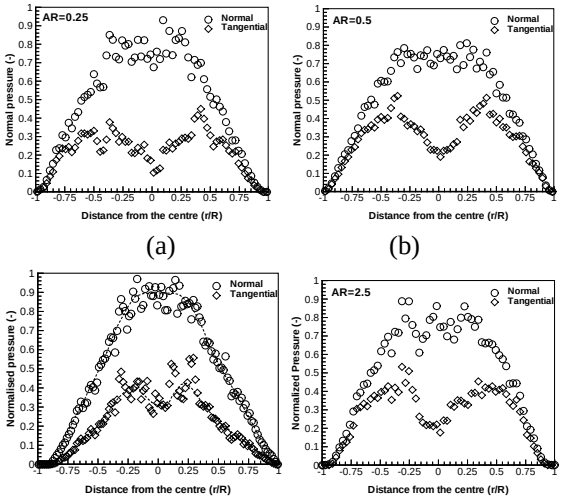

(a) (b)

(c) (d)

Fig. 9 Pressure underneath sandpiles with aspect ratios: (a) 0.25; (b) 0.5; (c) 1.0; and (d) 2.5. *Reprinted from [7] with permission from Springer.*

A stress dip is often observed underneath a sandpile, which is affected by various factors. Here, to illustrate the stress dip distribution, the non-dimensional vertical and horizontal pressure are used. Figure 9 shows the normal and shear pressure distributions for various aspect ratios. For spheres (Fig. 9(c)), clearly, there is a normal pressure dip in the middle, which is generally consistent with that reported in the literature [16]. But the pressure dip

predicted in our simulation is not so significant. The key feature is that the normal pressure in the central region distributes more evenly or relatively uniform. The stress dip in the centre is not obvious. For ellipsoids, the pressure dip region still exists, and the feature is similar to spheres. For oblate particles, with aspect ratio of 0.25 or 0.5, the stress dip region becomes wider, suggesting an enhancement in the normal pressure dip.

Gas fluidization [8, 9]

Fluidization is widely used in industries and as a typical gas-solid two-phase flow system, has been extensively studied both experimentally and theoretically in the past. Gan et al. [9] and Liu et al. [20] showed that non-spherical particles give poor fluidizing quality as compared to spherical particles in terms of pressure drop, minimum fluidization velocity, etc. Hilton et al. [21] also demonstrated that particle shape has a significant effect on the dynamics of the fluidized bed, including increased pressure gradients within the bed and lower fluidization velocities when compared to beds of spherical particles. Various correlations have been proposed to determine the fluid drag coefficient in CFD-DEM. As the correlation of Holzer and Sommerfeld [22] considers the effects of both shape and orientation, and is hence more preferable for the simulations.

Figure 10 shows the relationship between pressure drop and gas superficial velocity, illustrating the consistent results with the Ergun equation for spheres. For oblate particles with aspect ratios varying from 0.25 to 0.75, the bed with spheres has the lowest pressure drop, indicating the highest bed permeability. In fluidized beds, the pressure drops for all cases are similar, fluctuating around the bed weight. Figure 11(b) shows cases for prolate particles. One interesting finding is that the relationships are similar when aspect ratios are larger than 1.5. They have the similar bed permeability, but much less than spherical particles.

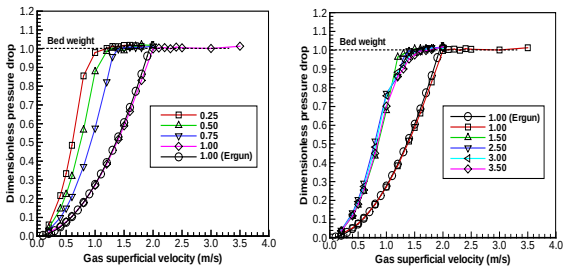

(a) (b)

Fig. 10 The relationship between pressure drop and gas velocities: (a) oblate; and (b) prolate spheroids. *Reprinted from [8] with permission from Elsevier.*

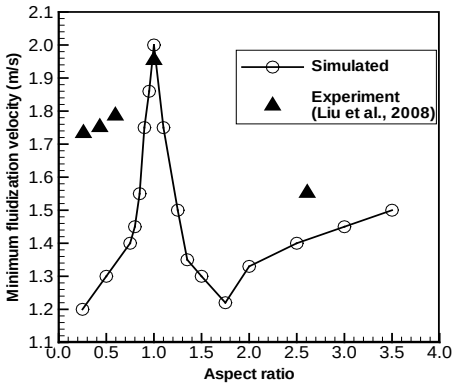

Fig. 11 Effect of aspect ratio on the minimum fluidization velocity. *Reprinted from [8] with permission from Elsevier.*

Figure 11 shows the effect of aspect ratio on the minimum fluidization velocity. Clearly, with aspect ratio decreasing from 1.0, the minimum fluidization velocity decreases. This is qualitatively consistent with the reported in the literature. With aspect ratio increasing from 1.0, the minimum fluidization velocity deceases first and then increases. The lowest minimum fluidization velocity occurs at around 1.75, which indicates the highest bed permeability.

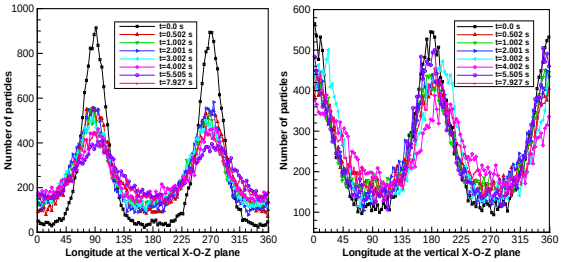

(a) (b)

Fig. 12 Distributions of particle orientations for (a) aspect ratio of 0.25; and (b) aspect ratio of 3.5. *Reprinted from [8] with permission from Elsevier.*

Orientation is one most important property for non-spherical particles. For example, one vector **OA** of ellipsoids can indicate particle orientation (more details can be seen in [8]). Figure 12 shows such information of orientation. It indicates oblate particles in fixed beds prefer facing upward or downward, forming an ordered structure to some degree (Fig. 12 (a)). This is consistent with the general understanding that such a structure is stable for platy particles, with a minimum potential energy of the system. But in fluidized beds, the degree of non-uniformity is reduced. This is because of strong particle-particle collisions which will affect the particle orientation. Similarly, prolate particles prefer oriented horizontally (Fig. 12 (b)). This is because prolate particles at high aspect ratios, e.g. 3.5, can obtain the stable structure for such an

orientation. This is particularly true for particles which are not fluidized.

CONCLUSIONS

DEM and CFD-DEM are used to study the packing, hopper flow, and sandpile formation, fluidization of ellipsoids. The effect of particle shape can be summarized as follows:

- *Particle packing*: The relationship between packing fraction and aspect ratio shows an M-shaped curve. RDF indicates that ellipsoids tend to have local ordered structures.
- *Hopper flow*: The four flow zones, such as plug flow, converging flow, stagnant and transition flow zone, exist for both spheres and ellipsoids. However, quantitatively flow characteristics and wall stress vary with aspect ratio. The Beverloo equation is modified for ellipsoids.
- *Sandpile formation*: The relationship between angle of repose and aspect ratio shows an M-shaped curve. Two equations are formulated between the angle of repose and aspect ratio. Non-spherical particles have a more pronounced stress dip than spherical particles.
- *Fluidization*: The bed permeability becomes worse for oblate particles, but is not affected much for prolate particles. The minimum fluidization velocity decreases with aspect ratio decreasing from 1.0, but for prolate particles, it decreases first then increases. The orientation analysis shows that oblate particles prefer facing upward/ downward while prolate particles prefer horizontal orientation.

ACKNOWLEDGEMENTS

The authors are grateful to the Australian Research Council (ARC) and BlueScope Steel Research for the financial support of this work, and NCI (National Computational Infrastructure) in Computation.

REFERENCES

[1] Zhu, H.P., Zhou, Z.Y. Yang, R.Y. and Yu, A.B. "Discrete particle simulation of particulate systems: Theoretical developments". Chem. Eng. Sci. Vol. 62, 2007, pp. 3378-3396.

[2] Zhu, H.P., Zhou, Z.Y. Yang, R.Y., and Yu, A.B. "Discrete particle simulation of particulate systems: a review of major applications and findings". Chem. Eng. Sci. Vol. 63, 2008 5728-5770

[3] Donev, A., Cisse, I., Sachs, D., Variano, E., Stillinger, F.H., Connelly, R., Torquato, S., Chaikin, P.M. "Improving the density of jammed disordered packings using ellipsoids". Science. Vol. 303, 2004, pp. 990-993.

[4] Zou, R.P. and Yu, A.B., "Evaluation of the packing characteristics of mono-sized non-spherical particles". Powder Technology. Vol. 88, 1996, pp. 71-79.

[5] Zhou, Z.Y. Zou, R.P. Pinson, D. and Yu, A.B., "Dynamic simulation of packing of ellipsoidal particles", Ind. Eng. Chem. Res. Vol. 50, 2011, pp. 9787-9798.

[6] Liu, S.D., Zhou, Z.Y., Pinson D. and Yu, A.B. "Flow characteristics and discharge rate of ellipsoidal particles in a flat bottom hopper". Powder Technology. Vol. 253, 2014, pp. 70-79.

[7] Zhou, Z.Y., Zou, R.P., Pinson, D. and Yu, A.B. "Angle of repose and stress distribution of sandpiles formed with ellipsoidal particles". Granular Matter. Vol. 16, 2014, pp. 695-709.

[8] Zhou, Z.Y., Pinson, D., Zou, R.P. and Yu, A.B. "Discrete particle simulation of gas fluidization of ellipsoidal particles". Chem. Eng. Sci. Vol. 66, 2011, pp. 6128-6145.

[9] Gan, J.Q., Z.Y. Zhou, and A.B. Yu, "CFD–DEM modeling of gas fluidization of fine ellipsoidal particles". AIChE J. Vol. 62, 2016, pp. 62-77.

[10] Williams, S.R., and Philipse, A.P., "Random packings of spheres and spherocylinders simulated by mechanical contraction". Physical Review E. Vol. 67, 2003, pp. 051301-051309.

[11] Nolan, G.T., and Kavanagh, P.E., "Random packing of nonspherical particles". Powder Technology. Vol. 84, 1995, pp.199-205.

[12] Cleary, P.W. and Sawley, M.L. "DEM Modelling of Industrial Granular Flows: 3D Case Studies and the Effect of Particle Shape on Hopper Discharge", Applied Mathematical Modelling. Vol. 26, 2002, pp. 89-111.

[13] Langston, P.A. Al-Awamleh, M.A. Fraige, F.Y. and Asmar, B.N. "Distinct Element Modelling of Non-spherical Frictionless Particle Flow", Chem. Eng. Sci. Vol. 59, 2004, pp. 425-435.

[14] Li, J.T. Langston, P.A. Webba, C. Dyakowskia, D. "Flow of Sphero-disc Particles in Rectangular Hoppers—a DEM and Experimental Comparison in 3D", Chem. Eng. Sci. Vol. 59, 2004, pp. 5917-5929.

[15] Campbell C.S., "Elastic Flows of Ellipsoidal Particles", in: M. Nakagawa, S. Luding (Eds.) Powders and Grains 2009. 2009, pp. 591-594.

[16] Beverloo, W.A., H.A. Leniger, and J. van de Velde, "The flow of granular solids through orifices". Chem. Eng. Sci. Vol. 15, 1961, pp. 260-269.

[17] Yong, R.W. and Warkentin, B.P. "Soil properties and behavior". Elsevier Scientific. New York. 1975.

[18] Matuttis, H.G. Luding, S. and Herrmann, H.J. "Discrete element simulations of dense packings and heaps made of spherical and non-

spherical particles", Powder Technology. Vol 109, 2000, pp. 278-292.

[19] Zuriguel, I., T. Mullin, and J.M. Rotter, "Effect of particle shape on stress dip under a sandpile". Phys. Rev. Lett. Vol. 98, 2007, pp. 028001.

[20] Liu B, Zhang X, Wang L, Hong H. "Fluidization of non-spherical particles: Sphericity, Zingg factor and other fluidization parameters". Particuology. Vol 6, 2008, pp. 125-129.

[21] Hilton J.E, Mason L.R, and Cleary P.W. "Dynamics of gas–solid fluidised beds with non-spherical particle geometry". Chem. Eng. Sci. Vol 65, 2010, pp. 1584-1596.

[22] Hölzer, A. and M. Sommerfeld, "New simple correlation formula for the drag coefficient of non-spherical particles". Powder Technology. Vol. 184, 2008, pp. 361-36

Second International Conference on Science, Engineering & Environment,
Osaka City, Japan, Nov.21-23, 2016, ISBN: 978-4-9905958-7-6 C3051

EFFECTS OF BEND-TWIST COUPLING DEFORMATION ON THE AERODYNAMIC PERFORMANCE OF A WIND TURBINE BLADE

Nawapon Sompong and Pongtorn Prombut*
Department of Mechanical Engineering, Faculty of Engineering, Kasetsart University, Thailand
*pongtorn.p@ku.ac.th

ABSTRACT

Comprehensive research exists on passive pitch control of wind turbines using bend-twist coupling property of composite materials. Blades with bend-twist coupling deformation can increase energy capture, improve dynamic stability, or reduce aerodynamic loads.

The objectives of this work are to apply bend-twist coupling into an existing blade design and to investigate the resulting aerodynamic performance. The 41.25-meter blade was based on GE 1.5 GLX wind turbine. Aerodynamic loads were calculated using Blade Element Momentum (BEM) theory and Computational Fluid Dynamics (CFD) simulation. The resultant thrust and torque from both methods agree well. However, only the CFD can provide details of pressure distribution over the complex blade surface.

Three levels of bend-twist coupling were designed for the Glass/Epoxy blade skins i.e. no coupling, low coupling, and high coupling. From Finite Element Analysis, the deflections of the three blades were slightly different while the twist angles were considerably different. The deformed geometries of the blades were then used to produce new three dimensional (3D) models for the prediction of the power coefficient (C_P) by CFD. The results show that the proper bend-twist coupling laminate can improve the performance of the blade. At low wind speed, the C_P is higher than the baseline blade. At wind speed greater than rated speed, the C_P decreases together with the wind load. Simulation of 3D blade models can help in the design of a bend-twist coupling level suitable to the blade shape and wind speed. Since this is an aeroelastic problem, deformed geometries should be used to calculate the blade performance.

Keywords: Wind Turbine, Bend-Twist Coupling, Composite Materials, Simulation

INTRODUCTION

Wind turbines operate in uncertain wind conditions both in terms of speed and direction. Yawing mechanism is used to maintain the rotor plane normal to the wind direction. Pitch adjustment is used to achieve optimum angle of attack of the blade in varying wind speed. Comprehensive research exists on passive pitch control of wind turbines using bend-twist coupling property of composite materials. Blades with bend-twist coupling deformation can increase energy capture, improve dynamic stability, or reduce aerodynamic loads. Lobitz et al. [1] found that, for a blade that twists 2 degrees toward stall, the annual energy production can increase by 10-15%. The twist behavior was created as a function and was prescribed into the blade geometry. An investigation of bend-twist coupling in composite box-beams showed that induced twist can be produced by tip-loading on the beams [2]. Full blade Finite Element Analysis (FEA) with bend-twist coupling produced from the off-axis carbon spar cabs has been studied [3]. Twisting deformation was obtained when concentrated loads were applied at 4 stations along the blade span. However, the effects of the twist on the aerodynamic performance have not been addressed. Aerodynamic-structure interaction simulation using Blade Element Momentum theory for power prediction and Finite Element (FE)-based code for blade deformation has been studied [4]. The FE part modeled a wind turbine blade as a beam made by orthotropic materials and optimized it with Genetic Algorithm-based tools to achieve optimum power production. Mirror layups of the blade shells produced an induced twist toward stall and improved in the energy capture by 15.5%. Another Fluid-Structure Interaction approach used BEM to calculate the aerodynamic loads and used 3D FEA to predict the deformation of the blade [5]. This iterative analysis showed that the deflection of the blade reduces the power output. However, blade twist was not considered.

Passive pitch control by bend-twist coupling of wind turbine blades involves aerodynamic analysis, structural analysis, and composite structural design. Limited work has been done in all three aspects, especially on 3D blade geometries. The present work aims to produce bend-twist coupling deformation in an existing blade geometry. Full 3D blade models are used for CFD and FEA analyses. The coupling properties of composite materials

produce twisting deformation as the blades bend under wind loads. The deformed geometries from FEA are assumed to be the blade shapes in operation. The second round of CFD simulation is performed to predict and compare the power coefficient of the blades with different level of bend-twist coupling.

BEND-TWIST COUPLING OF COMPOSITES

The relationship between stresses and strains in composite laminates can be described by the classical lamination theory [6]

$$\begin{Bmatrix} N_x \\ N_y \\ N_{xy} \\ M_x \\ M_y \\ M_{xy} \end{Bmatrix} = \begin{bmatrix} A_{11} & A_{12} & A_{16} & B_{11} & B_{12} & B_{16} \\ A_{12} & A_{22} & A_{26} & B_{12} & B_{22} & B_{26} \\ A_{16} & A_{26} & A_{66} & B_{16} & B_{26} & B_{66} \\ B_{11} & B_{12} & B_{16} & D_{11} & D_{12} & D_{16} \\ B_{12} & B_{22} & B_{26} & D_{12} & D_{22} & D_{26} \\ B_{16} & B_{26} & B_{66} & D_{16} & D_{26} & D_{66} \end{bmatrix} \begin{Bmatrix} \varepsilon_x^0 \\ \varepsilon_y^0 \\ \gamma_{xy}^0 \\ \kappa_x \\ \kappa_y \\ \kappa_{xy} \end{Bmatrix} \quad (1)$$

[A]: Extensional stiffness matrix
[B]: Bending-extension coupling stiffness matrix
[D]: Bending stiffness matrix

The bend-twist coupling occurs when D_{16} and D_{26} are non-zero. These parameters relate bending moments (M_x, M_y) to twisting deformation (κ_{xy}) and twisting moment (M_{xy}) to bending deformations (κ_x, κ_y). The dimensionless parameter used to indicate the level of coupling is [7]

$$B_t = \left| \frac{D_{16}}{D_{11}} \right| \quad (2)$$

BLADE GEOMETRY

Geometry used for the construction of blade model is based on the technical specifications of GE 1.5 XLE wind turbine. This 41.25 m blade produces 1.5 MW in the wind speed of 10 m/s. Three airfoils are used in 20 blade stations [8] as shown in Table 1.

Table 1 Distribution of chord, twist, and shape

Station	Span (m)	Chord (m)	Twist (deg.)	Airfoil
1	3.09375	2.5328	42.00	S818
2	5.15625	2.8157	32.00	
3	7.21875	3.0740	23.00	
4	9.28125	3.2101	15.00	
5	11.34375	3.1115	11.50	
6	13.40625	2.9651	8.20	
7	15.46875	2.8182	7.00	
8	17.53125	2.6726	6.00	
9	19.59375	2.5270	5.00	S825
10	21.65625	2.3805	4.00	
11	23.71875	2.2337	4.15	
12	25.78125	2.0881	3.85	
13	27.84375	1.9146	3.25	
14	29.90625	1.7985	2.75	
15	31.96875	1.6599	1.25	
16	34.03125	1.5279	0.75	
17	36.09375	1.3963	0.85	S826
18	38.15625	1.2647	0.55	
19	40.21875	1.3331	0.05	
20	41.25000	1.0000	0.00	

The airfoils are created at the specified span as shown in Fig. 1.

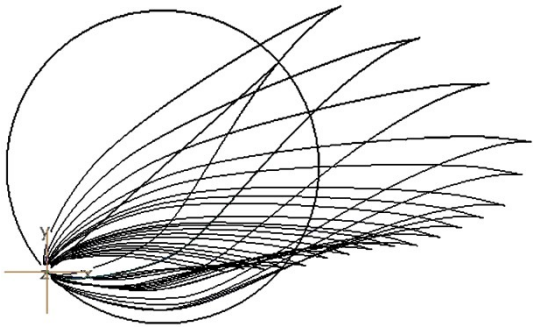

Fig. 1 Airfoils distribution along the blade span.

The blade geometry is then created using 3D surface features in a CAD program to produce the blade surfaces between the airfoils (Fig. 2).

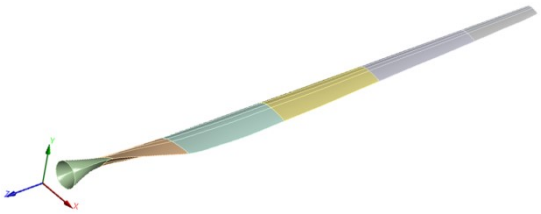

Fig. 2 Blade geometry.

AERODYNAMICS ANALYSIS

Determination of aerodynamic forces acting on the blade is carried out using two methods. An analytical method uses Blade Element Momentum theory and a numerical method use Computational Fluid Dynamics simulation.

Blade Element Momentum (BEM) Theory

The BEM theory consists of Momentum theory

and Blade Element theory. For the Momentum theory, energy conservation of air stream passing through the wind turbine yields an equation for the normal force (thrust, F_x) and conservation of angular momentum yields an equation for the torque (T) of an annular element of airstream [9].

$$dF_x = 4a(1-a)\rho V_1^2 \pi r dr \quad (3)$$

$$dT = 4a'(1-a)\rho V_1 \Omega \pi r^3 dr \quad (4)$$

The Blade Element theory uses force equilibrium in each blade section to produce equations for the thrust and torque.

$$dF_x = \sigma' \pi \rho \left[\frac{V_0(1-a)}{sin\phi}\right]^2 (C_L cos\phi + C_D sin\phi) r dr \quad (5)$$

$$dT = \sigma' \pi \rho \left[\frac{V_0(1-a)}{sin\phi}\right]\left[\frac{\Omega r(1+a')}{cos\phi}\right](C_L sin\phi + C_D cos\phi) r^2 dr \quad (6)$$

The thrust and torque equations from Momentum theory and Blade Element theory can be matched to produce equations for the axial induction factor (a) and angular induction factor (a').

$$\frac{a}{1-a} = \frac{\sigma'}{4sin^2\phi}(C_L cos\phi + C_D sin\phi) \quad (7)$$

$$\frac{a'}{1-a'} = \frac{\sigma'}{4sin\phi cos\phi}(C_L sin\phi + C_D cos\phi) \quad (8)$$

Equation (7) and (8) can be solved iteratively for a and a'. The lift and drag coefficients (C_L and C_D) are from JavaFoil [10].

The aerodynamic thrust force and torque can then be obtained by integrating Eq. (5) and (6) respectively. Additionally, the power coefficient (C_P) of the blade can be calculated with the following equation [9].

$$C_P = \frac{8}{\lambda^2}\int_{\lambda_h}^{\lambda} {\lambda_r}^3 a'(1-a) d\lambda_r \quad (9)$$

Computational Fluid Dynamics (CFD)

The CFD simulation is performed on the full blade model shown in Fig. 2. To reduce the computing resource, only one blade in a 120° domain section is modeled as shown in Fig. 3. Periodic boundary condition is used to keep the simulation equivalent to three blades in a circular-section domain. The inlet radius is 3 times the blade length and 2.5 times upstream from the blade. The outlet radius is 6 times the blade length and the distance is 4.5 times downstream from the blade. The simulation is performed using SST k-ω turbulence model. The mesh contains about 970,000 tetrahedron elements which give the non-dimensional parameter Y+ equals 220 or the wall distance 0.01 m.

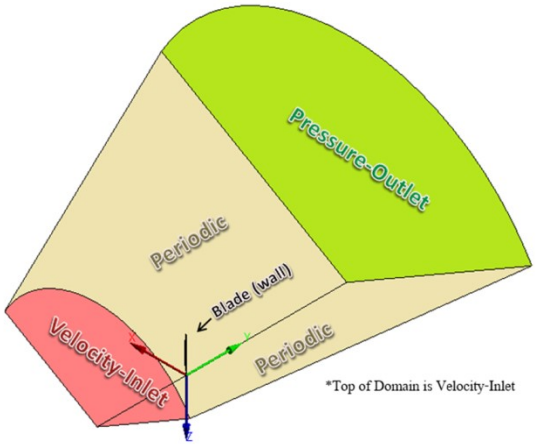

Fig. 3 CFD Model of blade, domain, and boundary.

The aerodynamic loads on the undeformed blade under the wind speed of 10 m/s are presented in Table 2. The results from the BEM and CFD methods agree well. Hence, both methods can be used with confidence.

Table 2 Thrust and torque on rigid blade at 10 m/s

Aero. Load	BEM	CFD	Diff (%)
Thrust (N)	104,805	115,624	10.32
Torque (kN-m)	2,574	2,614	1.55

BLADE STRUCTURAL ANALYSIS

Blade Internal Structure

A blade section has a shape of an airfoil. The blade skin is divided by the chord line into upper and lower shells. A spar is used to provide bending resistance which reduces the blade deflection. The present work adopts the blade construction from Zuteck [11]. The spar caps cover from 15% to 45% of the chord. The spar web is placed at 30% of the chord as shown in Fig. 4.

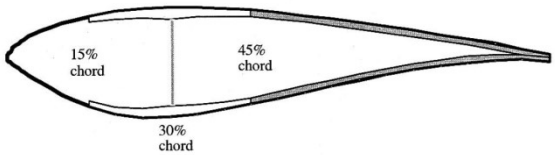

Fig. 4 Internal structure of a wind turbine blade [11].

The blade skin is modeled with E-Glass/Epoxy unidirectional (UD) composite while Carbon/Epoxy is used for the spar caps. The spar web is modeled with steel to simplify the model construction. Table 2 shows properties of the composites [12].

Table 3 Properties of UD laminae ($V_f = 60\%$)

Material	E_1 (GPa)	E_2 (GPa)	G_{12} (GPa)	ν_{12}
E-Glass/Epoxy	40	8	4	0.25
Carbon/Epoxy	135	10	5	0.30

Three sets of layups are used for the blade skin. Layup B1 is for $[0/90/0/90/0]_X$, B2 for $[20/-70/-70/-70/20]_X$, and B3 for $[20_5]_X$, where X is the number of sets needed to attain a desired thickness. The layups are selected to produce different level of coupling. From existing literature, layup B1 does not have coupling property, layup B2 produces high extension-twist coupling [13], while layup B3 yields better bend-twist coupling [3], [4]. Using Eq. (1) and (2) with the properties of E-Glass/Epoxy, the bend-twist coupling parameter B_t for the layups B1, B2, and B3 are 0.0000, 0.2274, and 0.2587 respectively. The layups are expected to cause different twisting deformation, thus different power production efficiency.

Figure 5 shows the thickness variation of the blade skin. The blade length is divided into 5 sections with the thickness of 30 mm, 26 mm, 22 mm, 18 mm, and 14 mm from root to tip. The E-Glass/Epoxy has the thickness of 0.2 mm/ply, therefore the Section 1 can be produced with the layup $[20/-70/-70/-70/20]_{30}$, for example. The spar cap is made from Carbon/Epoxy with the layup of $[0/0/0/90/90/90/90/0/0/0]_3$. Its thickness is 6 mm throughout the blade length. An example of the laminate in the Section 1 using layup B2 is shown in Fig. 6.

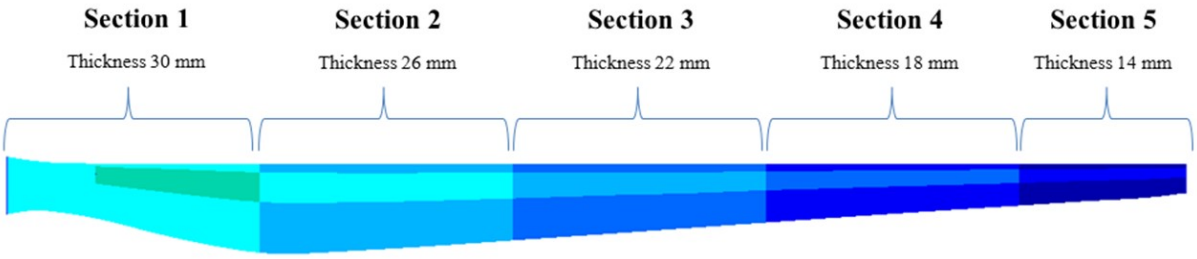

Fig. 5 Blade skin thickness along the span.

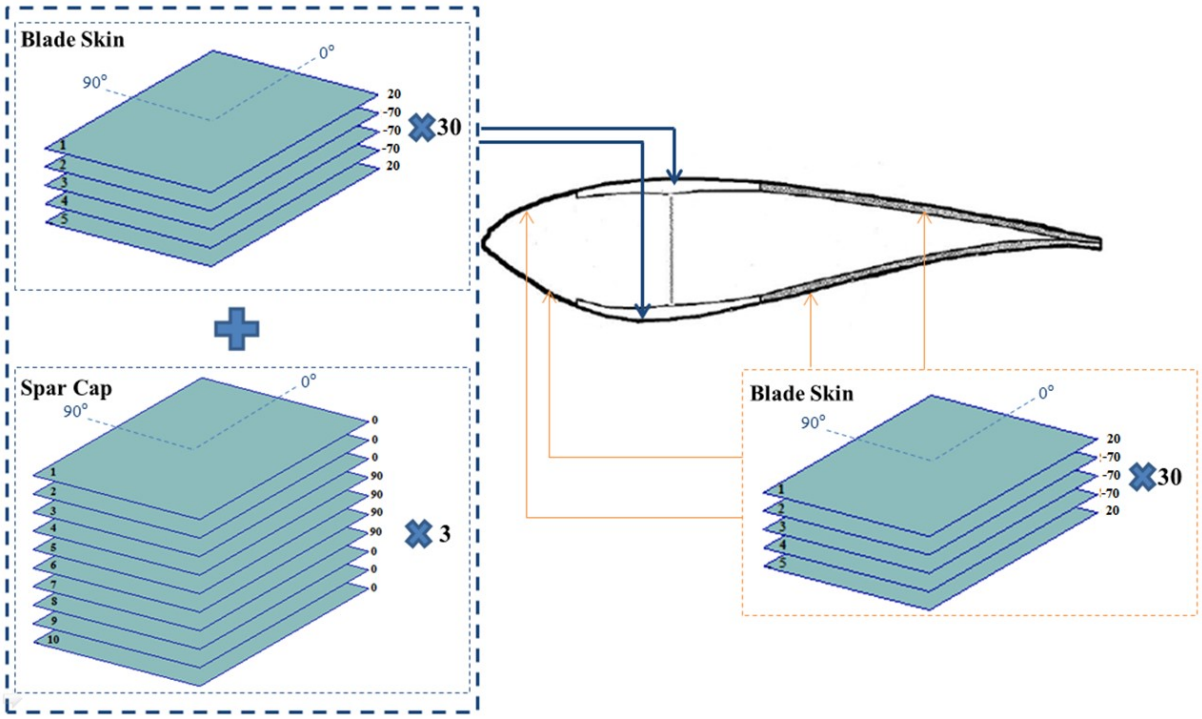

Fig. 6 Layup B2 and spar caps of blade section 1.

Finite Element Analysis (FEA)

The finite element model uses the blade geometry and construction details of the preceding sections and represents the blade with 120,000 quadrilateral elements. The aerodynamic load, taken from the CFD analysis, is applied as pressure on the elements. The present work is focused on the deformation of the blade. Bending and twisting results are used to create deformed blade geometries. These new geometries assume that there is no deformation of the airfoils, the blade deflection can be represented by the displacement of the leading edge, and the twist can be represented by the rotation about the leading edge. A deformed blade geometries is shown in Fig. 7. The aerodynamic loads at the wind speed of 3.5, 8, 12.5, and 16 m/s were obtained from the CFD simulation.

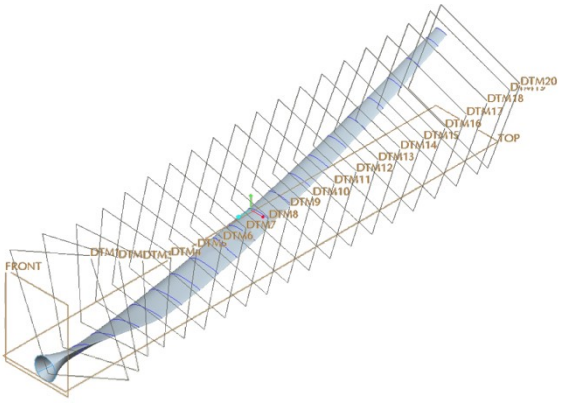

Fig. 7 Deformed blade geometry.

The tip deflection of the blades with 3 types of skin layups is presented in Fig. 8. The deflections resulting from layups B2 and B3 closely match each other. The maximum different of 5.68% occurs at the wind speed of 16 m/s. The blade with layup B1 is more rigid because it contains higher proportion of 0° layers.

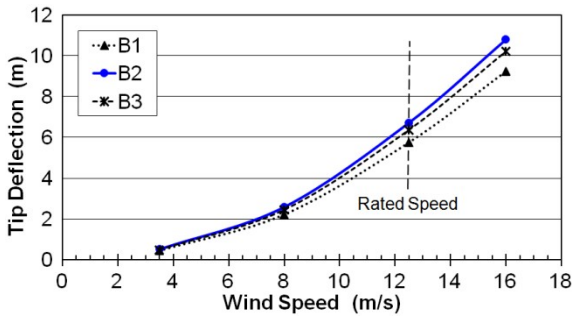

Fig. 8 Blade tip deflection.

The twist angle of the blade tip at various wind velocities is shown in Fig. 9. The blade with layup B1 does not have bent-twist coupling. The twist results are probably due to external forces and moments acting on the blade. The blade with layup B3 twists more than the blade B2, which can be expected from the values of parameter B_t. The average twist angle of the blade B3 at all wind velocities is 1.77 times that of the blade B2.

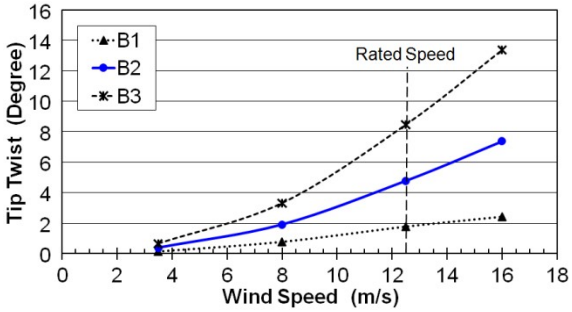

Fig. 9 Blade tip twist.

BLADE EFFICIENCY

Deformed blade geometries are reproduced for each layup type at each wind speed. In total, 12 blade geometries are obtained from the FEA results. New CFD simulations are then performed on these blades to determine the power coefficients. The deformed geometries should resemble the real blade shapes in operation and thus should be used for efficiency evaluation. The original blade geometry is also retained for power coefficient evaluation. It is treated as a rigid blade that does not deform in any wind speed. The results serve as a baseline for other blades.

Figure 10 presents the power coefficient of the 4 blades. At wind speed 3.5 m/s, the C_P of all blades are comparable. The deformable blades still have very small difference at 8 m/s but their C_P values are noticeably higher than that of the baseline. The blades perform differently at wind speed 12.5 m/s. The C_P of blade B1 does not change much. The C_P of the blade B2 keeps increasing while that of the blade B3 decreases considerably. Since the blades twist toward stall, small twist angles can increase the lift force and efficiency. However, the twist angle of the blade B3 could become too large thus induce flow separation which spoils the lift force and decreases efficiency. At wind speed 16 m/s, the blade B1 does not twist much further and the C_P is practically the same as that of lower speeds. The blades B2 and B3 become noticeably less efficient, likely because of too large twist angles.

From the efficiency standpoint, the blade with layup B2 is suitable for the designed wind speeds. The twist angles are 1.91° at 8 m/s and 4.79° at 12.5 m/s. However, other structural design constraints such as maximum tip deflection, allowable stresses and strains, weight etc must be considered before the blade configuration can be serviceable.

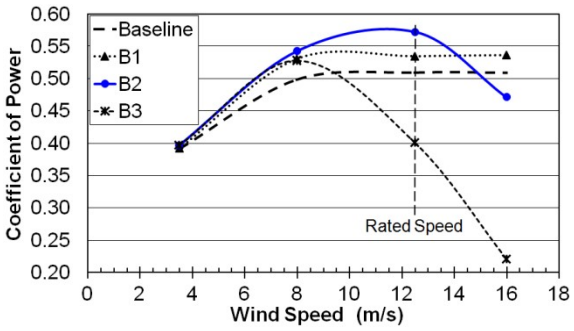

Fig. 10 Coefficient of Power (C_P).

CONCLUSION

Coupling deformation is a particular property of composite laminates. Three levels of bend-twist coupling were implemented into a 41.25-meter blade geometry based on GE 1.5 GLX wind turbine. The coupling was produced from the E-Glass/Epoxy blade skins to twist toward stall under bending loads. Aerodynamic loads were obtained from CFD simulation and cross-checked with the analytical BEM theory. The blade structural configuration and the aerodynamic loads were then modeled for finite element analysis. Finally, the deformed geometries of the blades were used to produce new 3D models for the prediction of the coefficient of power (C_P) by CFD.

The blades made from 3 types of layups have similar deflection, vastly different twist, and notably different efficiency. The results show that the deflection has little influence on the power coefficient. On the other hand, the blade twist has strong influence on the power coefficient. Small twist toward stall helps increasing efficiency while too large twist produces flow separation and decrease efficiency.

Simulation of 3D blade models can help designing for a bend-twist coupling suitable to the blade shape and wind speed. Since this is an aeroelastic problem, deformed geometries are assumed to be the blade shapes in operation and should be used to calculate the blade performance. Other structural design constraints must be considered before the blade configuration can be serviceable.

REFERENCES

[1] Lobitz DW, Veers PS, Eisler GR, Laino DJ, Migliore PG, and Bir G, "The use of twist-coupled blades to enhance the performance of horizontal axis wind turbines", Sandia National Laboratory, SAND2001-1303, 2001, 84 p.

[2] de Goeij WC, van Tooren MJL, and Beukers A, "Implementation of bending-torsion coupling in the design of a wind-turbine rotor-blade", Applied Energy, Vol. 63, 1999, pp. 191-207.

[3] Locke J and Valencia U, "Design studies for twist-coupled wind turbine blades", Wichita State University, SAND2004-0522, 2004, 127 p.

[4] Maheri A, Noroozi S, and Vinney J, "Application of combined analytical/FEA coupled aero-structure simulation in design of wind turbine adaptive blades", Renewable Energy, Vol. 32, 2007 , pp. 2011–2018.

[5] Rafiee R, Tahani M, and Moradi M, "Simulation of aeroelastic behavior in a composite wind turbine blade", Journal of Wind Engineering and Industrial Aerodynamics, Vol. 151, 2016, pp.60-69.

[6] Jones RM, “Mechanics of composite materials”. Pennsylvania, USA: Taylor & Francis, Inc., 1999, 519 p.

[7] Sun CT and Zheng S, "Delamination characteristics of double-cantilever beam and end-notched flexure composite specimens", Composites Science and Technology, Vol. 56, 1996, pp. 451-459.

[8] Phelps C and Singleton J, "Wind turbine blade design", Cornell University, M.Eng. Report, 2011, 35 p.

[9] Ingram G, "Wind Turbine Blade Analysis using the Blade Element Momentum Method", Durham University, Note, 2011, 21 p.

[10] Hepperle M, “Java Foil”, www.mh-aerotools.de/airfoils/javafoil.htm, accessed on 17/6/2015.

[11] Zuteck M, "Adaptive Blade Concept Assessment: Curved Planform Induced Twist Investigation", Sandia National Laboratory, SAND2002-2996, 2002, 24 p.

[12] Performance Composite Ltd., "Mechanical Properties of Carbon Fibre Composite Materials, Fibre / Epoxy resin (120°C Cure)", www.performance-composites.org, accessed on 17/6/2015.

[13] Yeo H, Truong KV, and Ormiston RA, "Assessment of 1-D Versus 3-D Methods for Modeling Rotor Blade Structural Dynamics", in Proc. 51st Structures, Structural Dynamics, and Materials Conf, AIAA/ASME/ASCE/AHS/ ASC, 2010, 19 p.

Second International Conference on Science, Engineering & Environment,
Osaka City, Japan, Nov.21-23, 2016, ISBN: 978-4-9905958-7-6 C3051

NUMERICAL INVESTIGATION FOR THE ENHANCEMENT OF THE AERODYNAMIC CHARACTERISTICS OF NACA 0012 AEROFOIL BY USING A GURNEY FLAP

Julanda Al-Mawali and Sam M Dakka
Department of Engineering and Mathematics, Sheffield Hallam University, United Kingdom

ABSTRACT

Numerical investigation was carried out to determine the effect of a Gurney Flap on NACA 0012 aerofoil performance with emphasis on Unmanned Air Vehicles applications. The study examined different configurations of Gurney Flaps at high Reynolds number of $Re = 3.6 \times 10^5$ in order to determine the optimal configuration. The Gurney flap was tested at different heights, locations and mounting angles. Compared to the clean aerofoil, the study found that adding the Gurney Flap increased the maximum lift coefficient by19%, 22%, 28%, 40% and 45% for the Gurney Flap height of 1%C, 1.5%C, 2%C, 3%C and 4%C respectively, C represents the chord of the aerofoil. However, it was also found that increasing the height of the gurney beyond 2%C leads to a decrease in the overall performance of the aerofoil due to the significant increase in drag penalty. Thus, the optimal height of the Gurney flap for the NACA 0012 aerofoil was found to be 2%C as it improves the overall performance of the aerofoil by 21%. As for the location, it was found that the lifting-enhanced effect of the gurney flap decreases as it is shifted towards the leading edge. Thus the optimal location of the Gurney Flap mounting was found to be at the trailing edge or at distances smaller than 10%C. The Gurney flap was also tested at different mounting angles of -45, 90 and +45 degrees and it was found that the Gurney flap at +45 mounting angle leads to the optimal performance of the aerofoil.

Keywords: Gurney flap, Aerodynamic simulation, NACA0012 Airofoil, FLUENT

INTRODUCTION

High lift devices have a significant effect on the performance of the aircraft. Having an effective and efficient high lift system enables the aircraft to take-off and land at lower speed and it also allows the aircraft to have higher payload capacity and higher range. All high lift devices are designed to keep the drag at lowest during take-off phase in order for the aircraft to reach its cruising speed faster and to increase the drag at approaching phase so it can land at lower speed and shorter runway.

All the advantages resulting from the high lift system improve the performance of the aircraft and make the aircraft more fuel-efficient. However, high lift systems such as flaps and slats are considered to be complex devices and this is due to the behaviour of the flow around the surface of the flap where several types of flow travel over the flap's surfaces such as, the wake resulting from the wing, boundary layer as well as the flow travelling through the flaps slot and all these flows generate a circulating boundary layer over the flap's surface. This unstable flow around high lift device makes the design of the flap very difficult and also increases the cost of manufacturing and maintenance. Therefore, a simple mechanical device is required to reduce the cost of manufacturing as well as to make the aircraft more profitable.

Gurney flap is a very simple mechanical device that is able to increase the lift coefficient with low drag penalty. Gurney flap can be simply defined as a flat plate fitted vertically to the trailing edge of the wing. This kind of flap is used to change the lifting characteristics of the aerofoil.

Many researchers conducted different studies on the effect of the Gurney flap on aerofoil performance. These studies cover a wide range of applications. The outcome [1] of a comprehensive literature review indicated, optimal size of the Gurney flap is equal or slightly bigger than the thickness of the boundary layer at the trailing edge. The boundary layer thickness at the trailing edge depends mainly on the Reynolds number; however the typical thickness at the trailing edge is between 1% to 2% of the chord length. At this length, the gurney flap increased the lift generation with a slight increase in the drag penalty. This review also found that adding the Gurney Flap at the trailing edge does delay the flow separation on the suction surface of the aerofoil.

The first study on the gurney flap was carried out experimentally in 1978 [2] aimed to find to what extent the gurney flap affects the aerofoil performance. The study used a symmetric Newman aerofoil with a Gurney flap of 1.25% of chord length. The data obtained from the experiment showed that adding 1.25%c gurney flap resulted in an increase in the lift coefficient and a slight decrease in both aerofoil drag as well as the zero lift angle-of-attack. The study also tested a Newman aerofoil with larger gurney flap and it was found that Gurney flap with

2%c or larger resulted in a significant increase in the lift coefficient with a noticeable increase in the drag penalty. Another study was carried out by Wadcock [3] on NACA 4412 aerofoil tested at Reynolds number 1.64 x 10^6 in the wind tunnel. The findings of the study showed an effective increase in the total lift generated by the aerofoil with the gurney flap, moving the lift curve up by a magnitude of 0.3 for NACA 4412 with Gurney flap of 1.25%c. The addition of this Gurney flap to the trailing edge did not cause any significant increase in the drag penalty.

An experimental investigation was made on a racing car wing with Gurney flap by Katz and Largman [4]. The Gurney flap was installed at the trailing edge; the results showed that adding Gurney flap of 5% of chord length caused a high increase in the lift coefficient of about 50% compared to a clean baseline wing. However, this size of Gurney flap also caused a very significant drag penalty which in turns, decreased the lift-to-drag coefficient.

A numerical investigation [5] carried out on different sizes of Gurney flaps ranging from 0.5% to 3% chord length. These different flaps were tested on NACA 23018 aerofoil. The study concluded that increase in the size of the Gurney flap leads to an increase in the lift coefficient for the sizes tested, also, it was noticed from the obtained data that the relationship between flap size and lift-curve shift does not seem to be linear. As an example, the increase in the lift coefficient between 0% and 0.5% chord length of the Gurney flap is higher than the increase in the lift coefficient due to changing the size of the Gurney flap from 1.5% and 2% chord length [6]. Adding a Gurney flap to the trailing edge of the wing not only increase the lift, but it also has a positive effect on delaying the separation on the suction surface. Some studies concentrated on the effect of delay separation of the upper surface at certain values of angle of attack, utilising of a Gurney flap in order to control flow separation at low Reynolds number. The results showed that adding such flap has effectively eliminated the separation region. Thus, confirming the benefit of the delayed separation by a Gurney flap [7].

The Gurney flap was also found to have some effects on the boundary layer. A study was conducted [8] aimed to find a scaling for the optimal size of the Gurney flap that would result in the maximum Lift-to-Drag ratio. LA203A Aerofoil was utilized in this study at Reynolds number of $2.5\times10^{5.}$ The findings of this study indicated that the optimal size of the Gurney flap is the same as the thickness of the boundary layer at the trailing edge. Overall, for most aerofoils, the studies revealed that Gurney flap with sizes ranging between 1% to 2% of the chord length had generated the optimal lift-to-drag performance.

Increasing the Gurney flap size beyond the thickness of the boundary layer will result in a dramatic increase in the drag penalty. This was corroborated [9] by investigation Gurney flap of 5%C on NACA0012 at low Reynolds number of 2×10^5. The effect of wing seep on Gurney flap performance was investigated experimentally; the results showed sweep attenuates the Gurney flap lift enhancement [10]. Another study was focused on reduction of the drag penalty associated with Gurney flap deployment based on adjoint shape optimization of aerofoils [11].

AIM AND OBJECTIVES

The goal of this study is to conduct a thorough investigation in order to enhance the aerodynamic characteristics of a thin symmetric aerofoil NACA 0012 at low Reynolds number. This investigation includes testing this aerofoil with different configurations of the Gurney Flap. These configurations are: Different heights of the Gurney flap, different locations of the Gurney flap from the leading edge. Different deflection angles of the Gurney flap and T-strip configuration.

NUMERICAL APPROACH

The study used a Numerical method to analyse the effect of addition of Gurney flap on the behaviour of the airflow around the aerofoil. An overview of the numerical simulation will be introduced followed by mesh generation and implementation.

The aim of the study is to determine the optimal configuration for a thin symmetric NACA 0012 aerofoil. Four different configurations of the Gurney flap were tested for this investigation. These configurations are related to the height, location, mounting angle and T-strip of the Gurney Flap. These tested configurations can be seen from the table below.

Table 1 GF-Gurney Flap Configuration Tested

No	Configuration	Tested Values
1	GF Height	0%C,1%C,2%C,3%C and 4%C
2	GF Location	S=0%C,5%C,10%C and 20%C
3	GF T-strip	1%C T-strip and 2%C T-strip
4	GF Mount Angle	-45, +90 and +45 degrees

The followed procedure for the selection of the optimal configuration started with testing different heights of the Gurney flap and then analysing these data in order to select the optimal height. After

selecting the optimal height, this Gurney Flap then was tested as T-strip in order to determine whether it would be more efficient than the normal configuration. The optimal Gurney height then was tested at different locations from the trailing edge to determine the optimal location for this device. After determining the optimal location, the gurney flap was then tested at different mounting angle in order to select the best angle by which the flap will improve the overall performance of the NACA0012.

Computational Fluid Dynamics (CFD) used for solving set of equations in order to model the flow-field. FLUENT 15 was utilized in order to solve set of equations called Reynolds-averaged Navier-Stokes equations (RANS). RANS equations are based on the basic physics of energy, mass and momentum conservation [12]. Two of the turbulence models were used to determine which one would give better results in modelling the flow of interest. These two models are K-ω SST and K-ε Realizable, the latter was used for the testing as it has the capability to enhance the wall treatment. The second order was also selected for the upwind discretization to solve all equations. As for the pressure-velocity coupling, the SIMPLE scheme was selected.

Enhanced wall functions with K-ε were used for the wall boundary conditions. These were applied for the aerofoil surface as well as the two walls of the wind tunnel. Inlet velocity was applied for the 'velocity-inlet' condition with the speed of 29 m/s. A 'pressure-outlet' condition was applied for the outlet pressure surface. As for the turbulence of the inflow, the turbulent intensity and turbulent viscosity ratio were specified as 5% and 10% respectively.

After creating the geometry (aerofoil), a flow domain was created around the aerofoil. C-mesh technique was used in this test, as it is a very popular technique when it comes to generating a mesh around the aerofoil. Therefore, the number of mesh elements increases as the elements goes towards the edges of the aerofoil. The triangles mesh method was used for this study as it creates a better mesh quality and more refined compared to the Quadrilateral method. Sphere of influence was also used during the mesh process as it allows us to control the size of the mesh around the aerofoil wall. Y+ value was also considered and the distance between the aerofoil wall and the first node was calculated to be 1.1 mm. this value was then used in the Inflation as the first layer thickness. As for the mesh quality, the maximum skewness of the mesh was found to be 0.54 which means that the generated mesh is high quality according to ANSYS measurements.

RESULTS AND DISCUSSION

CFD results were compared to the experimental results for the clean aerofoil The Reynolds number that was used in the computational test ($Re=3\times10^5$) which is based on the chord length (152mm) and this can be seen from Fig. 1.

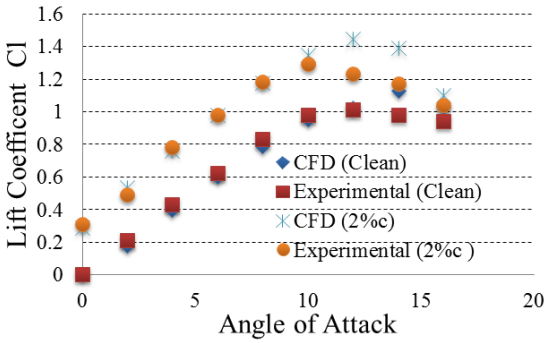

Fig.1 Computational versus experimental [13] results, for clean airofoil and 2%c Gurney Flap.

It can be seen that the CFD results agree well with the measured results up to α = 12°. It appears that beyond the stall angle of attack, the CFD data slightly over predicted the experimental data. This shows a very slight difference between the experimental and the numerical result for high angle of attack which indicates the highly refined and a good mesh method used for the numerical test. This comparison between the CFD results and the Experimental results was made to prove that the method used in the computation was satisfactory.

Figure 2 shows the lift coefficient for NACA0012 aerofoil equipped with 0%,1%,2% and 4%C at angles of attack from 0° to 16°. It can be clearly seen from the same Fig. 2 that Gurney flap effect is to increase the lift coefficient of the aerofoil. Comparison of the maximum lift coefficient of the clean NACA0012 illustrates that the maximum lift coefficient of the Gurney Flap of 1%c,2%c and 4%c is increased about 19%,28% and 45%, respectively. Adding a Gurney flap does not only have an effect on the lift coefficient but it also has a significant effect on the stall angle of the aerofoil. It can be seen from the Fig. 2 that the stall angle decreased from 14° for the clean aerofoil to 12° for the aerofoil with a Gurney flap. It also can be noticed from the Fig. 2 that the zero lift angle of attack becomes more negative as the size of the Gurney flap increases.

Therefore, increasing the size of the Gurney flap was found to increase the lift generated by the aerofoil. This significant increase in lift is mainly due to the increase in the effective camber of the aerofoil. In summary, the lift coefficient curves of Gurney flaps were shifted upwards and to the left.

However, the slope of the curves seems to remain constant. These results demonstrate that the effect of the Gurney flap is mainly to increase the effective camber of the aerofoil.

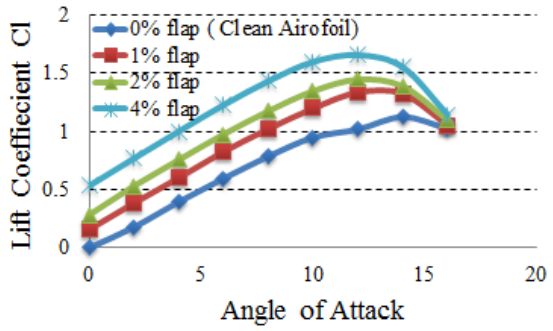

Fig. 2 Lift coefficients for different GF heights.

The effect of the Gurney flap on the drag coefficient can be seen from Fig. 3, the drag coefficient of the aerofoil increases as the height of The Gurney flap increases. As for 1%c and 2%c, compared to the clean aerofoil, the increase in the drag penalty was noticed to be very small at angle of attacks between 0° to 8° and as the angle of attack increases beyond 8° the drag penalty started to increase significantly. However, for a gurney flap above 2%, the drag penalty was noticed to be high compared to the clean aerofoil.

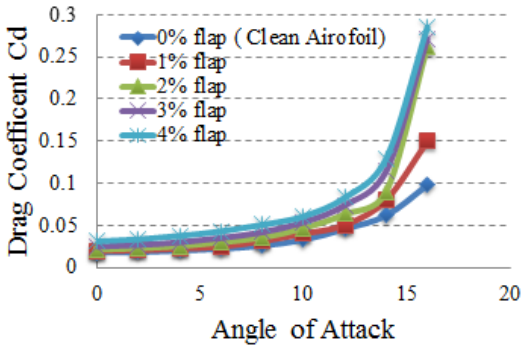

Fig. 3 Lift coefficients for different GF heights.

Figure 4 shows the lift-to-drag ratio as a function of angle of attack α. The L/D ratio increases with the increase of the angle of attack. However, this increase is not linear. As for the Gurney flap with the size of 1%C and 2%C, the lift-to-drag ratio increased up to the stall angle 14°.

It also can be noticed that the aerofoil with a Gurney flap higher than 2%c generates higher lift-to drag ratio than the clean aerofoil for the angle of attack between 0° to 6°. Beyond this angle of attack, these flaps generate less lift-to-drag ratio due to the high generation of drag. Compared to the clean aerofoil performance, the aerofoil with 1%c and 2%c seems to improve the overall performance of the aerofoil. However, the latter was selected as the optimum size as it was found to improve the performance of the NACA 0012 aerofoil by 21% which is considered to be high for the small size of the flap.

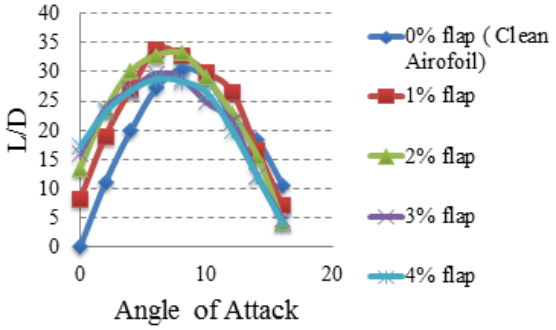

Fig. 4 Lift to Drag ratio for different GF heights.

Gurney flaps with different sizes were tested and the optimal flap that enhances the overall performance of the aerofoil was found to be 2%C. This specific aerofoil was also tested to determine whether the deflection of the gurney flap about the chord line would affect the performance of the aerofoil. The aerofoil was already tested earlier at 90 degrees and then it was tested at +45 and -45 degrees at the same boundary conditions. They were all tested at different angles of attack from 0 to 16 degrees. Fig. 5 and 6 shows the lift and drag coefficient as a function of angle of attack respectively.

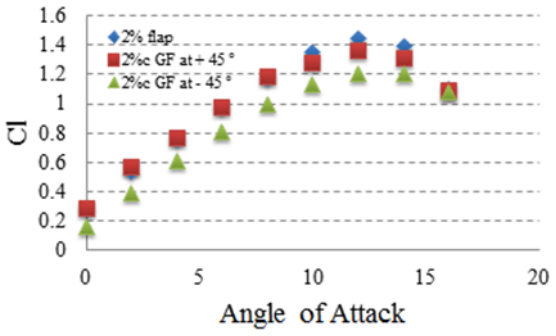

Fig. 5 Lift coefficient vs angle of attack for different deflection angle 90, +45 and -45 degrees of the Gurney flap.

From the lift coefficient plot it can be clearly seen that the Gurney flap with +45 degrees deflection generates the same lift as the flap with 90 degrees for the low to moderate angle of attacks

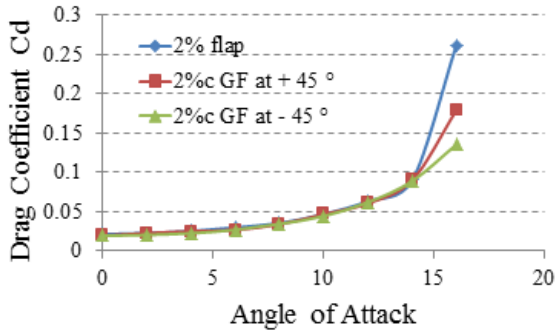

Fig. 6 Drag coefficient vs angle of attack for different deflection angle 90, +45 and -45 degrees of the Gurney flap.

As the angle of attack increases beyond 8 degrees, the former flap started to generate higher lift than the latter. As for the gurney flap with the deflection of -45, there was a significant decrease in the lift coefficient at all tested angles of attack.

As for the drag coefficient, it was noticed from Fig. 6 that deflecting the flap does not affects the drag generated by the aerofoil before the stall angle of attack. After the stall angle of attack, the flap with 90 degrees deflection generated higher drag coefficient where the aerofoil with -45 deflections generated the least drag coefficient.

The lift-to-drag ratio plot of the aerofoil with gurney flap with different deflection angles is shown in the Fig. 7 as a function of angle of attack.

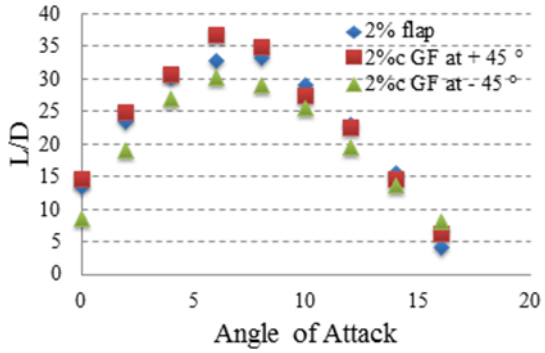

Fig. 7 Lift to Drag ratio vs angle of attack for different deflection angle 90, +45 and -45 degrees of the Gurney flap.

It can be seen that deflecting the aerofoil with -45 degrees generates the least lift-to-drag ratio. However, compared to the flap with 90 degrees deflection, the gurney flap with +45 deflections seems to enhance the performance of the aerofoil at low to moderate angle of attack. Thus, the optimum size of the aerofoil is 2%c with the deflection angle of +45.

The effect of the T-strip flap on the performance of the clean aerofoil can be seen from the Fig. 8 and 9. It can be seen that the T-strip increases the maximum lift coefficient by 8% compared to the clean aerofoil. However, it produces 6% less of maximum lift coefficient as that of normal gurney flap with the same size. It was also noticed that the T-strip flap does not produce any lift at zero angle of attack due to the flow field around the aerofoil being symmetric as the lower half of the T-strip cancels the effect of the upper half effect resulting in zero effect at zero angle of attack. From Fig. 8 the T-strip seems to produce more drag compared to clean aerofoil with normal gurney flap which in turns, makes the T-strip less efficient as it produces lower lift-to-drag ratio compared to the normal gurney flap with the same size. Thus, the T-strip does not produce better performance compared to the gurney flap with the same size for the NACA 0012 aerofoil.

The lift-to-drag ratio plot can be seen from Fig 10. It can be seen that as the location of the gurney flap shifted forward toward the leading edge, lift-to-drag ratio curve also shifted down due to the significant increase in the drag coefficient. It was also found that mounting the gurney flap between 0%c to 10%c improve the aerofoil performance beyond 10% and the lift-enhancement effects drops significantly. Overall, mounting the gurney flap at the trailing edge provides the optimum performance of the aerofoil.

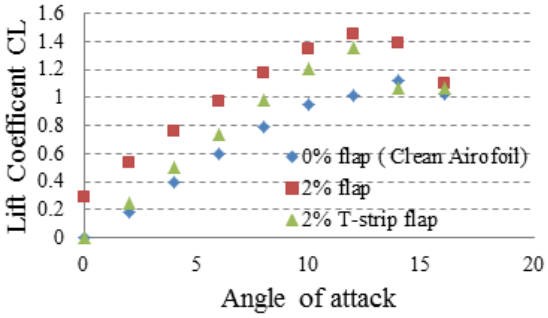

Fig. 8 Lift coefficient vs angle of attack T-strip Gurney flap shape.

CONCLUSION

Adding the Gurney flap resulted in a significant increase in the maximum lift coefficient. Compared to clean aerofoil, the maximum lift coefficient increased by 19%, 28% and 45% for the Gurney flap height of 1%c, 2%c and 4%c respectively. Optimum height for the Gurney flap was found to be 2%c. This height increased the maximum lift coefficient with small drag penalty.

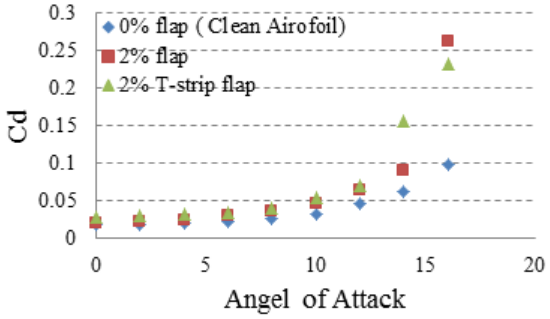

Fig. 9 Drag coefficient vs angle of attack T-strip Gurney flap shape

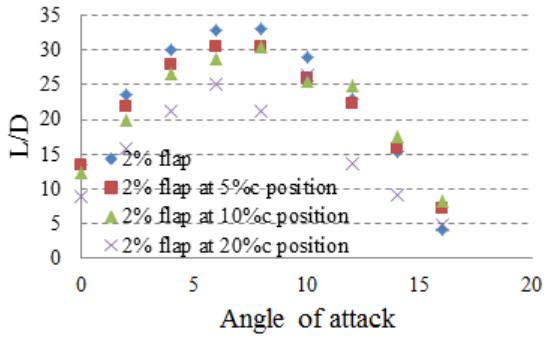

Fig. 10 Lift to drag ratio with Gurney flap mounted at different position as a percentage of the chord.

Overall, this specific height enhanced the overall performance (lift-to-drag ratio) of the clean aerofoil NACA0012 by 21%. Adding a T-strip Gurney flap of 2%c increased the drag coefficient and reduced the lift coefficient compared to the 2%c Gurney flap. As for the location of the Gurney flap, as the gurney flap shifted towards the leading edge, the lifting-enhancement effect of the flap decreased. The optimum location for the gurney flap was found to be exactly at the trailing edge. However, the performance of the gurney flap was not reduced when it is placed within 10%c distance from the trailing edge. The flap deflection of +45 degrees enhanced the overall performance of the aerofoil compared to the normal 2%c Gurney flap. Future work will be focused on innovative ways incorporating this technology into unmanned air vehicles.

ACKNOWLEGMENTS

This work is part of dissertation submitted by Julanda Al-Mawali in partial fulfillment of the degree of Bachelor of Engineering

REFRENCES

[1] Cavanaugh MA, Robertson P. and Mason WH, “Wind tunnel tests of Gurney flaps and T-strips on an NACA 23012 wing”, 2007, accessed online: http://www.dept.aoe.vt.edu/~mason/Mason_f/AIAA2007-4175.pdf

[2] Liebeck R H. "Design of subsonic airfoils for high lift". Journal of Aircraft, Vol.15, 1978 pp.547-561.

[3] Wadcock AJ, (1987) " Investigation of low-speed turbulent separated flow around airfoils" NASA-CR-177450

[4] Largman R, Katz J, " Effect of 90 degrees flap on the aerodynamic of a two element airfoil". J. Fluids Engineering, Vol. 111**,** 1989, pp.93-94

[5] Nouri M, Sayehvand H and Mekanik A, "Numerical investigation of aerodynamic characteristics of NACA 23018 airfoil with a Gurney flap", International Journal of Mechanical Engineering and Robotics Research Vol. 1 (3), Oct. 2012**,** pp.341-349.

[6] Altmann, GF, “An investigation study of Gurney flaps on a NACA0036 airfoil”. Ph.D. Thesis, Cal poly Uni. , 2011, accessed online http://digitalcommons.calpoly.edu/cgi/viewcontent.cgi?article=1554&context=theses

[7] Salcedo S, Monge F, Palacios F, Gandia F, Rodrigues A and Barcala M, “Gurney flaps and trailing edge devices for wind turbines” in Poceedings of European wind energy conference, EWEC 2006, Athens, Greece.

[8] Giguere P, Dumas G and Lemay J, “Gurney flap Scaling for Optimum Lift-to-Drag ratio” AIAA Journal, Vol. 35, 1997, pp.1888-1890.

[9] Gai SL, Palfrey R “Influence of Trailing-Edge Flow Control on Airfoil Performance” Journal of Aircraft , Vol 40(2), 2003, pp.332-337

[10] Traub L and Chandrachekar SM, “ experimental study on the effect of wing sweep on Gurney flap performance” Aero Sci & Tech, 55, 2016, pp. 57-63

[11] Amini Y, Emdad H and Farid H, “Adjoint shape optimization of airfoils with attached gurney flap”, Aero Sci & Tech 41, 2015, pp. 216-228

[12] Temam P, NAVIER-STOKES EQUATIONS. accessed online: http://math.univ-lille1.fr/~calgaro/ENS/biblio-m2ma/T.pdf

[13] Windi IS, Faris MA and Kareem H, "Experimental and numerical investigation of the improvement of aerodynamic characteristic of NACA 0012 airfoil”, IJMMME, Vol.2, 2014, pp. 11-15

Second International Conference on Science, Engineering & Environment,
Osaka City, Japan, Nov.21-23, 2016, ISBN: 978-4-9905958-7-6 C3051

ORGANIC SOLVENT-RESISTANT PROPERTIES OF PROTEINS ADSORBED ONTO BIOMASS CHARCOAL POWDER

Hidetaka Noritomi[1], Jumpei Nishigami[1], Nobuyuki Endo[2], Satoru Kato[1] and Katsumi Uchiyama[1]
[1]Department of Applied Chemistry, Tokyo Metropolitan University, Japan; [2]EEN Co., Ltd., Japan

ABSTRACT

We have found out that biomass charcoal powder (BCP), which is prepared from plant biomass wastes by pyrolysis at low temperatures under nitrogen atmosphere, imparts organic solvent resistance to proteins by using BCP as a protein carrier. α-Chymotrypsin (α-CT), which was used as a model protein, was sufficiently adsorbed onto the surface of BCP. When free α-CT and BCP-adsorbed α-CT were immersed in acetonitrile containing 5%(v/v) water, they catalyzed the transesterification of *N*-acetyl-L-tyrosine ethyl ester (*N*-Ac-Tyr-OEt) with *n*-butanol (BuOH) to produce *N*-acetyl-L-tyrosine butyl ester (*N*-Ac-Tyr-OBu), which did not proceed in an aqueous solution, where α-CT worked as a hydrolase. The initial rate of transesterification catalyzed by BCP-adsorbed α-CT was strongly dependent upon the kind of BCP, and was about fifty times higher than that catalyzed by free α-CT when bamboo charcoal powder was used as a carrier.

Keywords: Biomass Charcoal Powder, Protein, Adsorption, Organic Solvent Resistance, α-Chymotrypsin

INTRODUCTION

There has been a growing interest in using biomass as energies and functional materials to establish a recycling society [1]-[4]. However, enormous amount of plant biomass wastes, which are exhausted in the world, have hardly been taken advantage of, although they are renewable resources and carbon neutral. Consequently, the development in the higher value-added function of plant biomass wastes has been promoted all over the world to provide the multiple effective utilization system of plant biomass wastes.

On the other hand, the application of proteins to environmentally benign processes such as biotransformation, biosensor, biofuel cell, and so on in aqueous and non-aqueous media has recently attracted much attention, since proteins exhibit their outstanding biological activities and specificities under mild conditions [5]-[7]. Especially, the biotransformation catalyzed by an enzyme, which is a kind of proteins, in non-aqueous media has been applied to numerous synthetic processes because of the following benefits [8]: 1. The solubility of non-polar reactants and products is improved. 2. Synthetic reactions can take place by use of a conventional hydrolase without an expensive energy substance such as adenosine triphosphate (ATP). 3. The stereoselectivity of enzymes is markedly altered. 4. The thermal stability of enzymes is highly improved. 5. Enzymes are easily recycled by recovering them with the filtration or the centrifugation. 6. The product is easily recovered with the evaporation when using the volatile organic solvent as a reaction medium. 7. The contamination due to the growth of microorganisms is inhibited by organic solvents. However, the enzyme tends to show the low activity in organic solvents, compared with that in water, since an organic solvent in general works as a denaturant of proteins [9]. In order to improve the performance of enzymes in organic solvents, there have been some modes of enzyme preparation such as entrapped enzymes, lyophilized enzyme powders, lipid-coated enzymes, cross-linked enzyme crystals, and so on [10]-[15]. However, those preparation modes need expensive reagents, fine techniques, or a special apparatus. On the other hand, the adsorption of proteins onto various carriers has been widely used from the laboratory scale to the industrial scale because of the simplest and most economical method of stabilizing proteins [16], [17]. The physical and chemical surface properties of carriers strongly affect the performances of adsorbed proteins such as activity, specificity, and stability. Accordingly, it is possible that the suitable selection of carriers makes enzymes exhibit their desired performances in organic solvents. However, there have been few reports regarding the performances of adsorbed enzymes in organic solvents.

In order to investigate the high value-added function of biomass charcoal powder (BCP) derived from plant biomass wastes by pyrolysis at low temperatures, we have so far examined the usefulness of BCP as a protein carrier in an aqueous solution. We have found out that proteins are effectively adsorbed onto BCP [18],[19], and BCP-adsorbed proteins exhibit the enhanced storage stability and the high heat stress resistance in an aqueous solution, compared to free proteins [20]-[23].

In our present work, we have assessed

whether BCP can effectively enhance the organic solvent resistance of proteins by using BCP as a carrier of proteins to improve the activity of proteins in an organic solvent. We have employed bovine pancreas α-chymotrypsin as a model protein, since it is well investigated regarding its structure, functions, and properties [24].

2. MATERIALS AND METHODS

2.1. Materials

α-Chymotrypsin (EC 3.4.21.1 from bovine pancreas)(type II, 52 units/mg solid)(α-CT) was purchased from Sigma-Aldrich Co. (St. Louis, USA). *N*-Acetyl-L-tyrosine ethyl ester (*N*-Ac-Tyr-OEt) and *N*-acetyl-L-tyrosine (*N*-Ac-Tyr-OH) were also from Sigma-Aldrich Co. (St. Louis, USA). All solvents used were of guaranteed grade, commercially available, and were used without further purification. Before acetonitrile was used as a reaction solvent, it was dried by storing it over dry 0.3 nm molecular sieves (Wako Chemical Co.) for at least 24 h.

2.2. Preparation of Biomass Charcoal Powder (BCP)

Under nitrogen atmosphere, dumped bamboos were dried at 180 ℃ for 2 hr, were pyrolyzed at 450 ℃ for 2 hr, were carbonized at 350 ℃ for 3 hr, and then were cooled at 100 ℃ for 1 hr by pyrolyzer (EE21 Pyrolyzer, EEN Co. Ltd., Japan). Bamboo charcoal powder was obtained by grinding the resultant bamboo charcoal with jet mill (100AS, Fuji Sangyo Co. Ltd., Japan). Adzuki bean charcoal powder and wood charcoal powder were prepared by the same method.

2.3. Characterization of Biomass Charcoal Powder

The SEM micrograph was obtained using a scanning electron microscope (JSM-7500FA, JEOL, Japan) operating at 15 kV. The sample for SEM was prepared on a carbon tape without vapor deposition.

All samples were outgassed at 300ºC for 8 h prior to the nitrogen adsorption measurements. The specific surface area of BCP was calculated with the use of the Brunauer-Emmett-Teller (BET) method using a micropore system (BELSORP-mini II, BEL JAPAN, INC.).

The surface of BCP was analyzed by X-ray photoelectron spectroscopy (XPS) (Quantum-2000, ULVAC-PHI Co. Ltd.) operating at an x-ray beam size of 100 μm.

2.3. Adsorption of α-Chymotrypsin onto Biomass Charcoal Powder

As a typical procedure, 5 mL of 0.01 M phosphate buffer solution at pH 7 containing 300 μM α-CT and 3 g/L BCP was placed in a 10-mL test tube with a screw cup, and was incubated at 25 ℃ and 120 rpm for 24 h. After adsorption, the mixture was filtrated with a membrane filter (pore size: 0.1 μm, Millipore Co. Ltd.). The amount of α-CT adsorbed onto BCP was calculated by subtracting the amount of α-CT included in the supernatant liquid after adsorption from the amount of α-CT in the aqueous solution before adsorption. The amount of α-CT was measured at 280 nm by UV/vis spectrophotometer (UV-1800, Shimadzu Co. Ltd.).

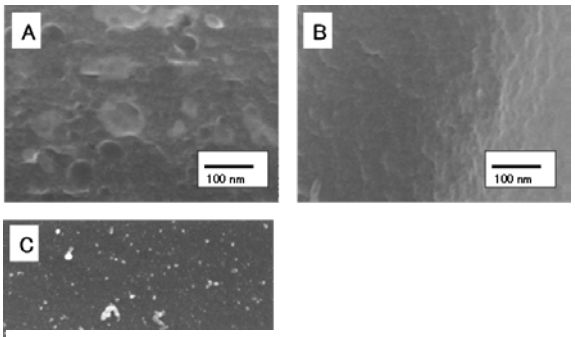

Fig. 1 SEM images of (A) adzuki bean charcoal, (B) bamboo charcoal, and (C) wood charcoal.

2.4. Measurement of Activity of Free and BCP-Adsorbed α-Chymotrypsin

The standard reaction for transesterification was carried out as follows: Three milliliter of acetonitrile containing 5%(v/v) water, 10 mM *N*-Ac-Tyr-OEt, 1000 mM *n*-butanol, 1 mM acetanilide, and free or BCP-adsorbed α-CT (30 μM) was placed in a 4 mL screw-cap vial, and was incubated at 120 rpm and 25 ºC. The amounts of the reaction components were periodically determined with HPLC (Shimadzu LC-10A) (Shimadzu Co., Kyoto, Japan) using a TSK-GEL ODS-80TM column (Tosoh Co., Tokyo, Japan) eluted with water-acetonitrile (6:4 by volume) at 0.5 mL/min with detection at 270 nm. Acetanilide was used as an internal standard.

2.5. Measurement of Fourier Transform Infrared Spectroscopy (FTIR)

FTIR measurements of free and BCP-adsorbed α-CT were carried out using a Jasco FT/IR spectrometer model FT/IR-4100. A KBr pellet containing 0.5 mg of free or BCP-adsorbed α-CT powder per 100 mg of KBr was prepared, and the measurements were performed using 512 scans under 4.0 cm^{-1} resolution.

3. RESULTS AND DISCUSSION

Table 1 Specific surface area of BCP and adsorption property of α-CT onto BCP.

Sample	Specific surface area (m^2/g)	Amount adsorbed (μmol/g)	Coating rate (%) end-on	Coating rate (%) side-on
Adzuki bean charcoal	204	17	63	80
Bamboo charcoal	294	9.8	25	32
Wood charcoal	117	21	135	172

3.1 Characterization of Biomass Charcoal Powder

We have pyrolyzed plant biomass wastes at low temperatures under nitrogen atmosphere to produce functional groups on the surface of biomass charcoals and to make use of the resultant functional groups as a binding site for the adsorption of proteins. In order to observe the surface of BCP, we have examined SEM images. As seen in Fig. 1, the morphology of BCP was strongly dependent upon the kind of materials. The roughness of BCP was remarkably low, and any pores were not observed at the magnification measured in the present work. The surface of bamboo charcoal was smoother than that of any other charcoal.

Table 1 shows the specific surface area of BCP obtained from low-temperature (-196 ℃) nitrogen adsorption isotherms, the amount of α-CT adsorbed onto BCP, and the coating rate, which is the ratio of the total in the cross-sectional area of α-CT molecules adsorbed on the surface of BCP to the surface area of BCP. The shape of α-CT molecule is a spheroid, the size of which is 5.1 x 4.0 x 4.0 nm [24]. In Table 1, the end-on means that the major axis direction of α-CT molecules contacts with the surface of BCP perpendicularly, while the side-on means that the minor axis direction of α-CT molecules contacts with the surface of BCP perpendicularly. α-CT molecules were sufficiently adsorbed onto the surface of BCP. The coating rate indicates that α-CT molecules are adsorbed onto adzuki bean charcoal and bamboo charcoal at monolayer, since their coating rates are less than 100%, and α-CT molecules are adsorbed onto wood charcoal at multilayer, since its coating rate is more than 100%.

In order to assess the chemical property of the surface of BCP, the measurement on X-ray photoelectron spectroscopy (XPS) was carried out. Figure 2 shows the elemental ratio of the surface of BCP detected by XPS. The main element was carbon atom, and oxygen and nitrogen atoms were also located on the surface of BCP to some extent. The ratios of oxygen and nitrogen atoms in adzuki bean charcoal were greater than those in any other charcoal. From narrow scan spectra of XPS, the chemical states of carbon were mainly C-C and C-H, while as chemical states of carbon with oxygen and nitrogen, C-O, O-C-O, C=O, COOH, and C-N were detected, as shown in Fig.3. Many radical species due to functional groups containing oxygen atoms,

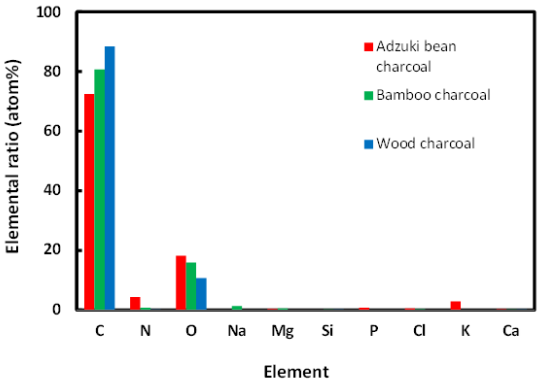

Fig. 2 The elemental ratio of the surface of BCP detected by XPS.

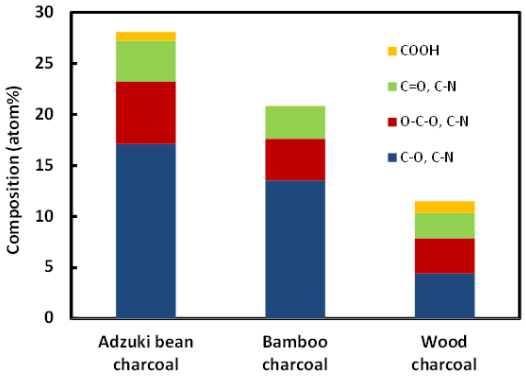

Fig. 3 The chemical bond ratio of BCP obtained from narrow scan spectra of XPS.

which are formed by thermal decomposition of cellulose and hemicelluloses, are detected in charcoals carbonized at 500°C by the measurement of electron spin resonance, and functional groups decrease with increasing carbonization temperature [25],[26]. On the other hand, the ζ-potential of BCP was negative at pH 7 while that of α-CT was positive due to the isoelectric point of α-CT (9.1) [18],[24]. Consequently, it is suggested that α-CT molecules are adsorbed onto the surface of BCP mainly through the electrostatic force which tends to strengthen the adsorption due to the low dielectric constant in acetonitrile, compared to that in water [27].

3.2. Activity of BCP-Adsorbed α-Chymotrypsin

In an aqueous solution, a synthase and an expensive energy substance such as adenosine triphosphate (ATP) are needed to carry out the enzymatic synthetic reaction. On the other hand, in an organic solvent, hydrolases such as lipase, protease, and so on can function as a synthase without energy substances [8]. In the present work,

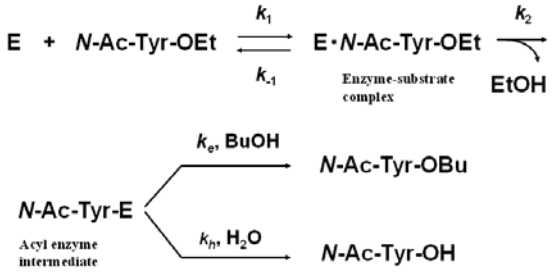

Fig. 4 α-CT-catalyzed transesterification of *N*-acetyl-L-tyrosine ethyl ester (*N*-Ac-Tyr-OEt) with *n*-butanol (BuOH) to *N*-acetyl-L-tyrosine butyl ester (*N*-Ac-Tyr-OBu) and competing hydrolysis (*N*-Ac-Tyr-OH).

α-CT-catalyzed transesterification was examined as shown in Fig. 4. When *N*-acetyl-L-tyrosine ethyl ester (*N*-Ac-Tyr-OEt) is used as a substrate, the transesterification is a kinetically controlled reaction process. This process involves the competitive distribution of the rapidly formed acyl enzyme intermediate (*N*-Ac-Tyr-E) between water (hydrolysis) and *n*-butanol (BuOH) as another nucleophilic reagent (transesterification). Since the nucleophilic reaction is rate-determining step, and k_1, k_{-1}, and k_2 are much greater than k_e and k_h [28], the initial rates are shown as

$$\boldsymbol{V_e = k_e[N-Ac-Tyr-E][BuOH]} \quad (1)$$
$$\boldsymbol{V_h = k_h[N-Ac-Tyr-E][H_2O]} \quad (2)$$

where V_e is the initial rate of transesterification, V_h the initial rate of hydrolysis, k_e the rate constant of transesterification, and k_h the rate constant of hydrolysis. From Eqs. (1) and (2), the selectivity (k_e/k_h) is derivated as the following equation.

$$\boldsymbol{\frac{k_e}{k_h} = \frac{V_e[H_2O]}{V_h[BuOH]}} \quad (3)$$

Table 2 Ratio of the absorbance at 1650 cm^{-1} to the absorbance at 1630 cm^{-1} (ABS_{1650}/ABS_{1630}) of α- CT provided by the FTIR measurement.

Sample	ABS_{1650}/ABS_{1630} (-)
Free α-CT	1.1
Adzuki bean charcoal-adsorbed α-CT	1.5
Bamboo charcoal-adsorbed α-CT	1.5
Wood charcoal-adsorbed α-CT	1.3

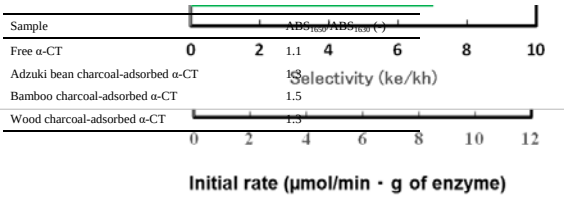

Fig. 5 Dependence of kind of BCP on BCP-adsorbed α-CT-catalyzed transesterification. Free or BCP-adsorbed α-CT was placed in acetonitrile containing 5% (v/v) water, 10 mM *N*-Ac-Tyr-OEt, 1000 mM BuOH, and 1 mM acetanilide, and the resulting mixture was shaken at 120 rpm and 25 °C.

In an aqueous solution, the activity, specificity, and stability of enzymes adsorbed onto the surface of carriers markedly depend upon the chemical and physical properties in the surface of carriers [16], [17]. In order to evaluate the effect of the surface properties of carriers on the activity of adsorbed enzymes in an organic solvent, we have examined the transesterification catalyzed by α-CT adsorbed onto the different kind of BCP in acetonitrile containing 5%(v/v) water. Figure 5 shows the initial rates of *N*-acetyl-L-tyrosine butyl ester (*N*-Ac-Tyr-OBu) and *N*-acetyl-L-tyrosine (*N*-Ac-Tyr-OH) catalyzed by free and BCP-adsorbed α-CT in acetonitrile containing 5%(v/v) water. Both initial rates of *N*-Ac-Tyr-OBu and *N*-Ac-Tyr-OH catalyzed by BCP-adsorbed α-CT were much higher than those catalyzed by free α-CT. α-CT adsorbed onto bamboo charcoal powder was the most effective of all, with respect to the enhancement in the initial rates of *N*-Ac-Tyr-OBu and *N*-Ac-Tyr-OH. With regard to the transesterification catalyzed by hydrolase, which is characteristic of the non-aqueous enzymology, the initial rate of *N*-Ac-Tyr-OBu catalyzed by α-CT adsorbed onto bamboo charcoal powder was about fifty times higher than that catalyzed by free one. Enzymes are aggregated in an organic solvent, and most of them can not directly come in contact with the bulk organic phase containing substrates, although they are soluble in an aqueous solution. On the other hand, most of the enzymes adsorbed onto BCP are directly in contact with the bulk organic phase, since they are located on the surface of BCP. Accordingly, BCP-adsorbed enzymes can effectively proceed the reaction, compared to free enzymes, since mass transfer of substrates and products is rapidly facilitated [29].

Fig. 6 Dependence of kind of BCP on the selectivity of BCP-adsorbed α-CT-catalyzed transesterification. Free or BCP-adsorbed α-CT was placed in acetonitrile containing 5% (v/v) water, 10 mM *N*-Ac-Tyr-OEt, 1000 mM BuOH, and 1 mM acetanilide, and the resulting mixture was shaken at 120 rpm and 25 °C.

Figure 6 shows the selectivity of the reaction catalyzed by free and BCP-adsorbed α-CT in acetonitrile containing 5%(v/v) water. The selectivity corresponds to the transesterification preference. The selectivity of BCP-adsorbed α-CT was superior to that of free one. A hydrophilic organic solvent such as acetonitrile is a good solvent for an amino acid derivative, which is an important intermediate in fine chemistry, but tends to denature proteins strongly [8],[10]. It appears that the structure and microenvironment of the active site in BCP-adsorbed α-CT is suitable for the transesterification, compared to that in free one.

3.3. Secondary Structure of BCP-Adsorbed α-Chymotrypsin

In order to elucidate the influence of adsorption on the secondary structure of α-CT, we have measured the FTIR spectra of free and BCP-adsorbed α-CT. The most sensitive spectral region to protein secondary structural components is amide I (1700 – 1600 cm^{-1}), which is due to the C=O stretching vibrations of the peptide linkages [30]. Table 2 shows the ratio of the absorbance at 1650 cm^{-1} to the absorbance at 1630 cm^{-1} (ABS_{1650}/ABS_{1630}) of free α-CT and α-CT adsorbed onto BCP. The band located at ca. 1650 cm^{-1} is assignable to α-helix, and the band located at ca. 1630 cm^{-1} is assignable to intramolecular β-sheet. The order of the ABS_{1650}/ABS_{1630} ratio was bamboo charcoal-adsorbed α-CT > adzuki bean charcoal-adsorbed α-CT = wood charcoal-adsorbed α-CT > free α-CT. The order of the ABS_{1650}/ABS_{1630} ratio was similar to that of the initial rate of transesterification. The α-helical structure of α-CT molecule is more changeable than β-sheet, since the β-sheet structure is the main backbone of α-CT molecule [24]. Thus, the results indicate that at the higher initial rate the transesterification is catalyzed by α-CT molecules having the secondary structure kept more highly.

4. CONCLUSION

We have demonstrated that the adsorption of α-CT onto BCP sufficiently improves the organic solvent resistance of α-CT. Both initial rates of transesterification and hydrolysis catalyzed by BCP-adsorbed α-CT were much superior to those catalyzed by free α-CT. Bamboo charcoal improved the more effective organic solvent resistance of α-CT than any other charcoal. BCP-adsorbed α-CT exhibited an excellent transesterification preference, compared to free α-CT. The higher the ratio of α-helix to β-sheet in α-CT, the higher the initial rate of transesterification catalyzed by α-CT was shown. The enhancement in the initial rate of transesterification catalyzed by BCP-adsorbed α-CT results not only from the facilitation in the mass transfer of substrates and products due to the inhibition of aggregation of α-CT molecules but also from the high secondary structure of α-CT molecules adsorbed onto BCP.

5. REFERENCES

[1] Ho YC, Show KY, “A perspective in renewable energy production from biomass pyrolysis-challenges and prospects”, Current Organic Chem., Vol. 19, 2015, pp. 423-436.

[2] Straathof AJ, “Transformation of biomass into commodity chemicals using enzymes or cells”, Chem. Rev., Vol. 114, 2014, pp. 1871-1908.

[3] Peterson SC, Jackson MA, Appell M, “Biochar: Sustainable and versatile”, ACS Symposium Series, Vol. 1143, 2013, pp. 193-205.

[4] Manya JJ, “Pyrolysis for biochar purposes: A review to establish current knowledge gaps and research needs”, Environmental Sci. Technol., Vol. 46, 2012, pp. 7939-7954.

[5] Buchholz K, Kasche V, Bornscheuer UT, Biocatalyst and Enzyme Technology 2nd ed. Wiley-Blackwell, 2012.

[6] Silwana B, Horst CVD, Iwuoha E, “Amperometric determination of cadmium, lead, and mercury metal ions using a novel polymer immobilized horseradish peroxidase biosensor system”, J. Environmental Sci. Health Part A, Vol. 49, 2014, pp.1501-1511.

[7] Leech D, Kavanagh P, Schuhmann W, “Enzymatic fuel cells: Recent progress”, Electrochimica Acta, Vol. 84, 2012, pp. 223-234.

[8] Klibanov AM, “Improving enzymes by using them in organic solvents”, Nature, Vol. 409, 2001, pp. 241-246.

[9] Lehninger AL, Nelson DL, Cox MM, Principles of Biochemistry 2nd ed. Worth, 1993, p. 180.

[10] Kise H, Hayakawa A, Noritomi H, “Protease-catalyzed synthetic reactions and immobilization-activation of the enzymes in hydrophilic organic solvents”, J. Biotechnol., Vol. 14, 1990, pp. 239-254.

[11] Noritomi H, Almarsson O, Barletta GL, Klibanov AM, “The influence of the mode of enzyme preparation on enzymatic enantioselectivity in organic solvents and its temperature dependence”, Biotechnol. Bioeng., Vol. 51, 1996, pp. 95-99.

[12] Kamiya N, Kasagi H, Inoue M, Kusunoki K, Goto M, “Enantioselective recognition mechanism of secondary alcohol by surfactant-coated lipases in nonaqueous media”, Biotechnol. Bioeng., Vol. 65, 1999, pp. 227-232.

[13] St. Clair NL, Navia MA, “Cross-linked enzyme crystals as robust biocatalysts”, J. Am. Chem. Soc., Vol. 114, 1992, pp. 7314-16.

[14] Wescott CR, Noritomi H, Klibanov AM, “Rational control of enzymatic enantioselectivity through solvation thermodynamics”, J. Am. Chem. Soc., Vol. 118, 1996, pp. 10365-10370.

[15] Noritomi H, Sasanuma A., Kato S, Nagahama K, “Catalytic properties of , Biotechnol. Tech. 12 (1998), 467-469.cross-linked enzyme crystals in organic media”, Vol. 33, 2007, pp. 228-231.

[16] Elnashar MMM, "Review article: Immobilized molecules using biomaterials and nanobiotechnology", J. Biomaterials Nanobiotechnol., Vol. 1, 2010, pp. 61-77.
[17] Mateo C, Palomo JM, Fernandez-Lorente G, Guisan JM, Fernandez-Lorente R, "Improvement of enzyme activity, stability and selectivity via immobilization techniques", Enzyme Microbial Technol., Vol. 40, 2007, pp. 1451-1463.
[18] Noritomi H, Iwai D, Kai R, Tanaka M, Kato S, "Adsorption of lysozyme on biomass charcoal powder prepared from plant biomass wastes", J. Chem. Eng. Jpn., Vol.v46, 2013, pp. 196-200.
[19] Noritomi H, Hishinuma K, Kurihara S, Nishigami J, Takemoto T, Endo N, Kato S, "Adsorption of α-chymotrypsin on plant biomass charcoal", J. Surface Eng. Materials Adv. Technol., Vol. 3, 2013, pp. 269-274.
[20] Noritomi H, Kai R, Iwai D, Tanaka H, Kamiya R, Tanaka M, Muneki K, Kato S, "Increase in thermal stability of proteins adsorbed on biomass charcoal powder prepared from plant biomass wastes", J. Biomedical Sci. Eng., Vol. 4, 2011, pp. 692-698.
[21] Noritomi H, Ishiyama R, Kai R, Iwai D, Tanaka M, Kato S, "Immobilization of lysozyme on biomass charcoal powder derived from plant biomass wastes", J. Biomaterials Nanobiotechnol., Vol 3, 2012, pp. 446-451.
[22] Noritomi H, Kurihara S, Endo N, Kato S, "Heat-resistant properties of α-chymotrypsin adsorbed onto biomass charcoal powder", J. Biomaterials Nanobiotechnol., Vol. 5, 2014, pp. 179-185.
[23] Noritomi H, Kurihara S, Endo N, Kato S, Uchiyama K, "Effect of adsorption condition on thermal stability of proteins adsorbed onto biomass charcoal powder", International J. GEOMATE, Vol. 11, 2016, pp. 2123-2128.
[24] Kumar A, Venkatesu P, "Overview of the stability of α-chymotrypsin in different solvent media", Chemical Reviews, Vol. 112, 2012, pp. 4283-4307.
[25] Asada T, Ishihara S, Yamane T, Toba A, Yamada A, Oikawa K, "Science of bamboo charcoal: study on carbonizing temperature of bamboo charcoal and removal capability of harmful gases," Journal of Health Science, Vol. 48, 2002, pp. 473-479.
[26] Nishimiya K, Hata T, Imamura Y, Ishihara S, "Analysis of chemical structure of wood charcoal by X-ray photoelectron spectroscopy," Journal of Wood Science, Vol. 44, 1998, pp. 56-61.
[27] Reichardt C, Solvents and Solvent Effects in Organic Chemistry 2nd ed. Wiley-VCH, 1988, p. 408.
[28] Fersht A, Structure and Mechanism in Protein Science: A Guide to Enzyme Catalysis and Protein Folding, W. H. Freeman and Company, 1999, pp. 216-244.
[29] Fogler HS, Elements of Chemical Reaction Engineering 2nd ed. Prentice Hall PTR, 1992, pp. 607-628.
[30] Surewicz WK, Mantsch HH, "New insight into protein secondary structure from resolution-enhanced infrared spectra", Biochim. Biophys. Acta, Vol. 952, 1988, pp. 115-130.

Second International Conference on Science, Engineering & Environment,
Osaka City, Japan, Nov.21-23, 2016, ISBN: 978-4-9905958-7-6 C3051

DC AND RF CHARACTERISTICS FLUCTUATION OF INALAS/INGAAS HEMTS ACCORDING TO THE OPERATING TEMPERATURE VARIATION

Kenta Otsuki[1], Yuta Kainuma[1], Ryuichi Miyashita[1], Kimihiro Yamanaka[1] and Hirohisa Taguchi[1]

[1] Department of Electrical and Electronic Engineering, School of Engineering, Chukyo University 101-2 Yagoto Honmachi, Shouwa-Ku, Nagoya City, Aichi, Japan,

ABSTRACT

InAlAs/InGaAs high electron mobility transistors (HEMTs) are a type of field effect transistor that can achieve extremely high high-frequency gain owing to quantum effects operating in the channel layer. HEMTs are important components for devices that involve millimeter waves and high-speed optical transmission systems. However, InAlAs/InGaAs HEMTs have a frequency dispersion that depends on carrier recombination within the device. This is an InGaAs-specific phenomenon, which degrades the device's high-frequency gain performance. In this study, we investigated the direct current (DC) and radio frequency (RF) characteristics of InAlAs/InGaAs HEMTs by varying the operating temperature from liquid nitrogen temperature to 125 °C. The DC characteristics showed an increase of the device transconductance (*Gm*) at low temperature. Reducing the operating temperature from 125 °C to liquid nitrogen temperature increased G_m to 60 mS. High-frequency gain was also confirmed in the RF characteristics. The current gain cutoff frequency was 50.2 GHz at room temperature, and 66.8 GHz at liquid nitrogen temperature, representing an increase of 33.1%. Analyzing the high-frequency characteristics showed that the high-frequency gain increase at low temperature was related to the temperature dependence of the parasitic capacitance.

Keywords: HEMT, Current gain cutoff frequency, parasitic capacitance, Liquid nitrogen temperature

INTRODUCTION

Since their release, the communication speed of mobile communication devices has continued to increase. Nippon Telegraph and Telephone Company first realized the car phone for mobile communications in 1979. The maximum reception speed at this point was 0.3 kbps [1]. The advanced mobile phone system, later developed in North America, improved the maximum reception speed to 10 kbps. Mobile communications technology has continued to evolve, achieving even greater maximum reception speeds. In March 2016, a proposal for an LTE-Advanced Pro network was announced, representing a new general-purpose wireless technology that offers ultra-high-speed mobile communication of more than 10 Gbps. In only 37 years, the maximum reception speed has increased from kbps to Gbps [2]. However, further increases in communication speed are still in demand. For these purposes, it is necessary to understand the physical phenomena inside electronic devices used for high-speed communications.

We have been studying the physical properties of a phenomenon expressed in high electron mobility transistors (HEMTs) of the kind used in ultra-high-speed field effect transistors (FETs) [3-5]. Our previous research on inhibitors of carrier transport led us to propose fusing a high-speed device with a photo-responsive device [6].

However, the active layers of many semiconductor devices reach temperatures in excess of 100 °C when operating. This heat is generated when carriers pass through the active layer and collide with the crystal lattice. Lattice vibrations reduce the transport properties of carriers passing through the active layer. These thermal characteristics can be considered in terms of the electronic circuit performance, i.e., the temperature change can be considered from the response characteristics of the device. Previous studies have revealed changes in the performance of electronic devices at low temperature; however, there are no reported cases investigating the performance under cryogenic temperatures.

In this paper, we investigated how changing the device operating temperature affected the electronic properties of InAlAs/InGaAs HEMTs. The operating temperature was varied from liquid nitrogen temperature (−196 °C) to 125 °C. We confirmed changes in the radio frequency (RF) characteristics of the HEMTs operating over this temperature range. The direct current (DC) characteristics showed that the transconductance (*Gm*) increased with decreasing temperature. When the operating temperature was reduced from 125 °C to liquid nitrogen temperature, *Gm* almost doubled to 60 mS. The current gain cutoff frequency (*Ft*) was measured to be 50.2 GHz at room temperature; however, it increased to 66.8 GHz at

liquid nitrogen temperature, indicating an improvement of 33.1%. By analyzing the high-frequency characteristics of the devices, we showed that the increase in the high-frequency gain at low temperatures was related to the temperature dependence of the parasitic capacitance.

EXPERIMENTAL METHOD

Target Device and Experimental Setup

A schematic of the HEMT device structure used for these experiments is shown in Fig. 1.1. The carrier supplying InAlAs layer was silicon δ-doped to provide a high transconductance and a high degree of threshold-voltage uniformity. The epitaxial layers used in the experiment were grown on an Fe-doped semi-insulating InP substrate using metal-organic chemical vapor deposition. These layers comprised of an undoped InAlAs layer, an undoped InGaAs channel layer, an Si δ-doped layer, and an undoped InAlAs insulator layer. Heavily doped n-InAlAs/InGaAs capping layers were grown to lower the source and drain contact resistances. The electrode metals for the gate, source, and drain were non-alloyed.

A semiconductor parameter analyzer was used to measure the DC characteristics and a network analyzer with a frequency range of 1–20 GHz was used to measure the S parameters (HP8510B). The temperature of the sample device was controlled between −40 and 125 °C using a device holder with a Peltier element (VICS ITH-700). The operating temperature of the sample devices was monitored using a thermocouple placed directly under the device. Sample devices were placed directly in a liquid nitrogen environment for experiments conducted at liquid nitrogen temperatures (−196 °C). The temperature of the sample device was confirmed to be −196 °C using the thermocouple, and the DC and RF characteristics were measured. All the measuring systems were performed within a microwave system.

EXPERIMENTAL RESULTS

Figure 2.1 shows typical drain current and voltage characteristics (I–V characteristics) of an HEMT at room temperature. The HEMT used in this experiment showed a high *Gm* of up to 30 mS at V_{gs} = −0.6–0 V and V_{ds} = 1.5 V. The temperature dependence of the *Gm* maxima are shown in Figure 2.2. Although the *Gm* values were low at high temperature, *Gm* gradually increased at lower temperatures. This phenomenon can be attributed to suppressed phonon scattering by the lattice vibrations of the crystal at lower temperatures.

The frequency dependence of the current gain is shown in Figure 2.3. Frequency measurements were performed in the range of 1–20 GHz. Representative examples of the frequency characteristics at 125 °C,

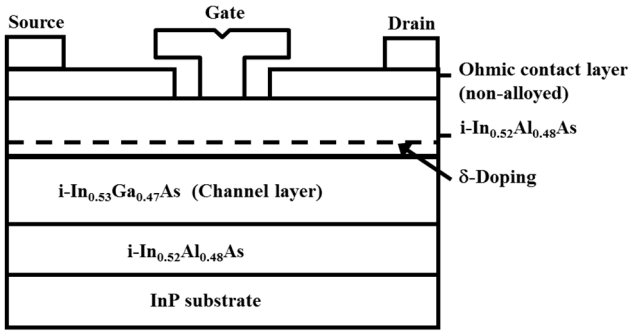

Figure 1.1 Schematic cross section of the HEMTs

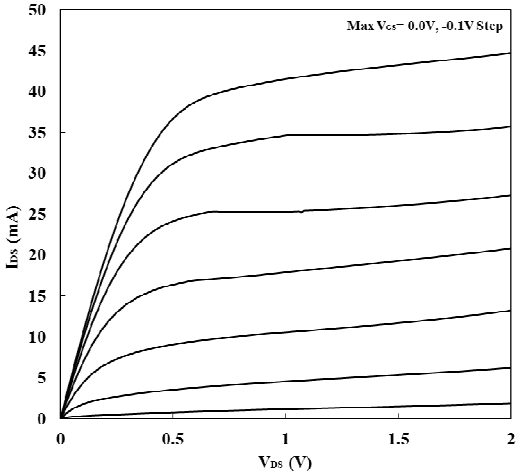

Figure 2.1 Typical drain current and voltage characteristics of HEMT.

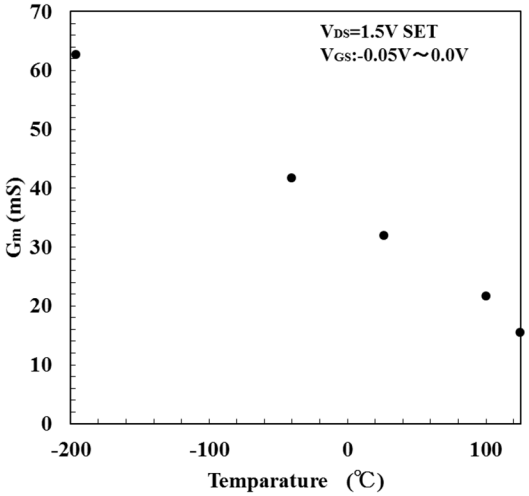

Figure 2.2 Temperature dependence of the transconductance (G_m) maximum values

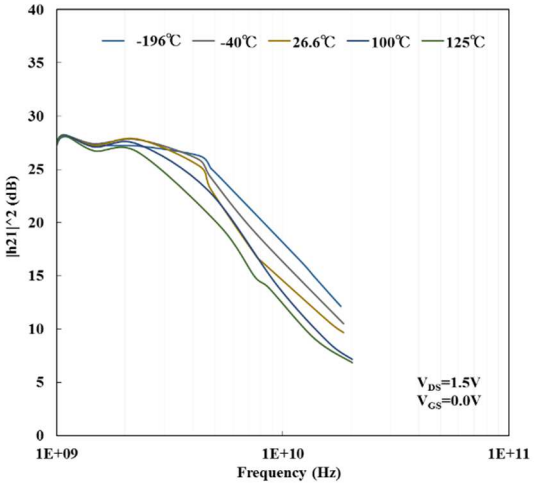

Figure 2.3 Frequency dependence of the current gain.

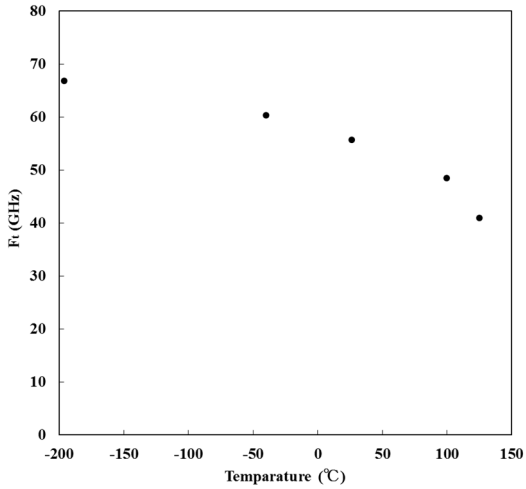

Figure 2.4 Temperature dependence of the current gain cutoff frequency f_t.

room temperature, −40 °C, and −196 ° C are shown in Fig. 2.3. Up to 10 GHz, the devices showed a stable gain of approximately 17 dBm at all temperatures; however, the gain dropped to −20 dB/decade above 10 GHz. Figure 2.4 shows the temperature dependence of the current gain cutoff frequency, f_t. At room temperature and −196 °C, the values of f_t were 50.2 and 66.8 GHz, respectively. This represents a 33.1% improvement in the cutoff frequency at low temperature.

DISCUSSION

As shown in Figures 2.2 and 2.4, the DC and RF characteristics improved at low temperature. In particular, the bandwidth increase contributed strongly to the high-frequency gain improvement. Considering that f_t is proportional to G_m in the theoretical formula for the current gain cutoff frequency [7], we may expect G_m to also increase at low temperature. This HEMT may be treated using the small-signal circuit model. Based on this model, G_m is strongly dependent on parasitic components [8]. High-frequency gain was calculated from the S parameter measured using the network analyzer. It is possible to convert S parameters to Y parameters, which allows calculation of the frequency response characteristics of the gate–source capacitance C_{gd} and gate–source capacitance C_{gs}. Figures 3.1 and 3.2 show the frequency response characteristics of C_{gs} and C_{gd}, respectively. The parasitic capacitance component showed large fluctuations with frequency for both C_{gs} and C_{gd}. This fluctuation may be attributed to small changes of the S parameters; however, here we consider only changes with temperature. At −196 °C, C_{gs} decreased considerably, and C_{gs} showed a slight reduction. However, C_{gd} was unchanged even at low temperature. Considering the factors that affect the parasitic capacitance of a FET, C_{gs} is most strongly affected by charging time and dominates the time constant of the carriers passing through the channel layer. However, C_{gd} represents the capacitance when carriers move rapidly through the gate, and does not strongly depend on temperature.

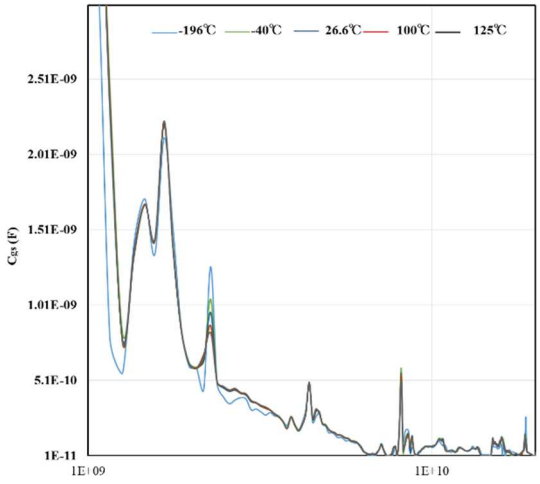

Figure 3.1 Frequency response characteristics of the gate–source capacitance C_{gs} values.

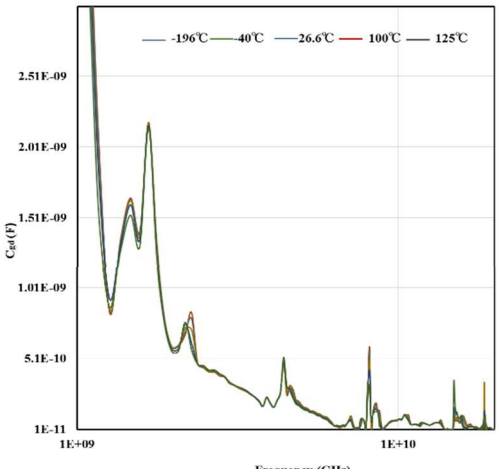

Figure 3.2 Frequency response characteristics of gate–drain capacitance C_{gd} values.

The temperature dependence of C_{gs} is caused by phonon energy reduction within the crystal layer itself. Thus, the improvement in high-frequency gain can be attributed to the shorter time constant.

CONCLUSION

We investigated the effects of operating temperature on the electronic properties of InAlAs/InGaAs HEMTs. The operating temperature was changed from liquid nitrogen temperature to 125 °C. We confirmed that the frequency characteristics of HEMTs varied with operating temperature. The DC characteristics showed an increase in *Gm* at low temperature. When the operating temperature was reduced from 125 °C to liquid nitrogen temperature, G_m increased to 60 mS. The values of F_t were 50.2 and 66.8 GHz at room and liquid nitrogen temperatures, respectively. This represents a 33.1% improvement at low temperature. Analyzing the high-frequency characteristics revealed that the cause of the high-frequency gain was related to the temperature dependence of the parasitic capacitance.

ACKNOWLEDGEMENTS

The authors are grateful to the Chukyo University Research Found for financial assistance with this research.

REFERENCES

[1] A. Takahashi, et. J. Mag. Soc. Jpn., vol. 22, No. S2, 1998.
[2] Wang Hai, International Conference on Intelligence Science and Information Engineering (ISIE), pp.167-170, 2011.
[3] H.Taguchi, et.al., Physica status solidi (c) Vol. 5, No. 9, pp.2791-2796, 2008
[4] H.Taguchi, et.al., *Phisica stetus solidi (c)* Vol. 6, No. 6, PP.1386-1389, 2009.
[5] H.Taguchi, et.al. JAPANESE JOURNAL OF APPLIED PHYSICS, Vol. 49, No. 4, PP. 04DF03-07, 2010.
[6] H.Taguchi, et.al., Physica Status Solidi (c), Vol. 9, No. 2, pp.357-360, 2012.
[7] S. M. Sze,Smiconductor Device, John Welly & Sons, INC, 2nd Edition, pp-264
[8] H. Fukuda, et. Al., Solid State Electron, vol. 41, No. 10, pp-1599-1604, 199

Second International Conference on Science, Engineering & Environment,
Osaka City, Japan, Nov.21-23, 2016, ISBN: 978-4-9905958-7-6 C3051

IMPROVEMENT OF THE TRANSFER PATH USING A MOVING FLOW SEPARATION SYSTEM AND A TRANSPORTATION VULNERABLE ESCALATOR SYSTEM

Minjung Shin[1], Jinho Hur[2], Minju Sung[3], Youngsam Moon[4], Jinho Kim[5] and Heekyu Kim[6]*
[1,2,3,4,6] MORE Engineering & Architecture Co.,Ltd., Korea;
[5] Korea Railroad Research Institute, Korea

ABSTRACT

Traffic demands have increased rapidly, and traffic congestion has been raised due to the urbanization in Seoul. Most of the metro stations of commuting time have a moving speed and a density corresponding to the E or F grade in LOS(Level of Service). In particular, Jongno-sam-ga Station has a geometric structure because it is the transfer station of the 3 lines located in the center of Seoul. So the long transfer distances and the complex transfer system of Jongno-sam-ga Station induce an increment in transfer time and a decrement in public transportation demands. Therefore, this research was investigated the present conditions of the movement and transfer path on Jongno-sam-ga Station through a site inspection, and it presented the improvement plan through the analysis on the movement and transfer path for the general public, the disabled and the elderly. Based on the results, the improvements of the transfer paths by separating the moving flow and the transfer paths and applying the transportation vulnerable escalator system are suggested.

Keywords: Transfer Path, Traffic Congestion, Moving Speed and Density, Moving Flow Separation System, Transportation Vulnerable Escalator System

CONSIDERATION OF TRANSFER SYSTEM

Domestic public transportation transfer system

It is estimated that usage time on public transportation is average 48.0 minutes and transfer time is 9.9 minutes in table 1 by the survey on public transportation status research [3]. It means 21.6% of usage time is needed by moving and waiting for transfer. This is because the existing transfer facilities are installed for the operators, not users.

As age increases, the utilization rate decreases because of the inconvenience for walking up and down the stairs in the case of more than age 65 in table 2 [6].

The select rate of urban railway is 10.4% as transportation method for the disabled. On the other hand, the select rate of bus is 35.8% in table 3 [5]. It is investigated this gap is due to the lack of amenities.

Table 1 Transfer time

Division	Metropolitan area	Busan, Ulsan	Daegu	Gwangju	Daejeon	Total
The number of cases	7,120	2,350	1,780	1,250	1,880	14,380
Transfer time (min.)	10.5	10.2	8.1	9.1	9.7.	9.9
Boarding time (min.)	42.8	53.2	20.7	33.3	35.0	38.1
Total time (min.)	35.3	45.5	23.3	42.4	44.7	48.0
Transfer rate (%)	39.9	37.9	22.3	22.3	22.1	21.6

Note: Transfer rate (%) = Transfer time/Total time, Infrastructure and Transport, “The Survey on public transportation”, 2009.

Table 2 Transportation methods of the elderly

Division	Total	Age 65 ~ 69	Age 70 ~ 74	Age 75 ~ 79	Age 80 ~ 84	Age over 85
None	0.5	0.2	0.3	0.5	0.9	1.6
Bus	48.9	47.6	50.9	53.2	46.0	34.0
Metro	***19.3***	***21.3***	***22.3***	***16***	***17.4***	***9.9***
Taxi	6.7	3.5	4.3	8.9	12.2	16.4
Car	18.4	21.5	14.7	14.9	18.3	35.2
Bicycle	2.0	2.1	2.3	1.9	1.9	1.0
Motorcycle	3.1	2.8	4.1	3.2	2.1	0.7
Electric Wheelchair	0.4	0.3	0.3	0.5	0.3	0.7
Cultivator	0.2	0.1	0.1	0.3	0.1	0.0
etc.	0.6	0.6	0.6	0.6	0.8	0.5
Sum (People)	100.0 (10,543)	100.0 (3,150)	100.0 (3,229)	100.0 (2,389)	100.0 (1,163)	100.0 (614)

Note: Ministry of Health and Welfare, “The Survey on the elderly conditions”, 2011.

Table 3 Main transportation methods of the disabled

Division	Physical disability	Brain lesions	Visual impairment	Hearing impairment	Speech impairment	Low intelligence	Autism.	Mental disorder
Bus	35.9	22.7	38	41.2	51.2	33.9	23	47.4
Taxi	7.0	13.3	6.8	5.3	5.2	2.6	2.7	3.1
Metro	***8.0***	***9.2***	***15.8***	***15.3***	***14.4***	***7.9***	***6.2***	***16.4***
Minicab	0.2	1.8	0.4	0.0	0.0	0.0	0.2	0.0
Center Bus	0.2	1.3	0.7	0.0	0.3	1.4	1.3	0.3
Car	37.1	34.3	26.7	24.3	16.6	22.6	43.2	9.1
Shuttle Bus	0.0	0.7	0.2	0.0	0.2	3.0	2.5	0.0
Electric Wheelchair	1.0	3.5	0.0	0.2	0.0	0.0	0.0	0.0
Motorcycle	0.9	2.9	0.8	0.2	0.0	0.0	0.0	0.0
Walk	3.7	3.3	5.3	5	6.6	10.2	6.0	9.7
etc.	6.0	6.9	5.4	8.4	5.5	18.3	14.8	14.0
Sum	100.0	100.0	100.0	100.0	100.0	100.0	100.0	100.0

Note: Ministry of Health and Welfare, “The Survey on the disabled”, 2008.

Table 3 Main transportation methods of the disabled –cont'd

Division	Kidney disorder	Heart disorder	Respiratory disorder	Hepatopathy	Facial disorders	Urinary fistula	Epilepsy	Total
Bus	30.7	34.1	31.8	20.9	28.8	40	52.2	35.8
Taxi	10.8	7.4	11.4	6.0	2.5	6.3	4.4	6.9
Metro	***14.4***	***14.7***	***11.3***	***18.3***	***11.8***	***20.6***	***16.8***	***10.4***
Minicab	0.7	2.8	0.0	0.4	0.0	0.0	0.0	0.3
Center Bus	0.1	0.0	0.0	0.0	0.0	0.0	0.3	0.4
Car	33.9	30.1	35.7	43.8	42.9	24.2	14.9	32.2
Shuttle Bus	0.9	0.1	0.0	0.0	0.0	0.2	0.0	0.3
Electric Wheelchair	0.0	0.3	0.5	0.5	0.0	0.0	0.0	0.9
Motorcycle	0.1	0.9	0.2	0.6	0.0	0.0	0.0	0.8
Walk	2.3	4.7	2.4	6.1	5.3	4.0	5.7	4.6
etc.	6.3	5.0	6.8	3.4	8.8	4.6	5.6	7.4
Sum	100.0	100.0	100.0	100.0	100.0	100.0	100.0	100.0

Note: Ministry of Health and Welfare, "The Survey on the disabled", 2008.

Transfer System for the disabled

The more layer to transfer and moving system, the much times and inconvenient for the disabled. It especially takes over 7 minutes to move by wheelchair lift, which means it takes too much time for transfer. As the results on the comparison of the transfer time from Gwanghwamun station to Hyehwa station for the disabled and the general public, there are many differences.

In case of the disabled, it needs to use a wheelchair lift in 4 times and an elevator from Gwanghwamun station to Hyehwa station.

And it takes 12 minutes 36 seconds from Gwanghwamun square to Gwanghwamun station platform. On the contrary, it takes only 2 minutes 30 seconds for the general public to go same route by walking or using escalator. At Dongdaemun History & Culture Park Station which is the transfer station, it takes only 3 minutes 30 seconds for the general public by stairs and escalator. However, it takes 19minutes for the disabled to transfer from Line 5 to Line 4. Because it needs to use a wheelchair lift twice and also the disabled needs to wait for former user to finish using it. It takes 3 minutes for both cases from Hyehwa station to exit by using an

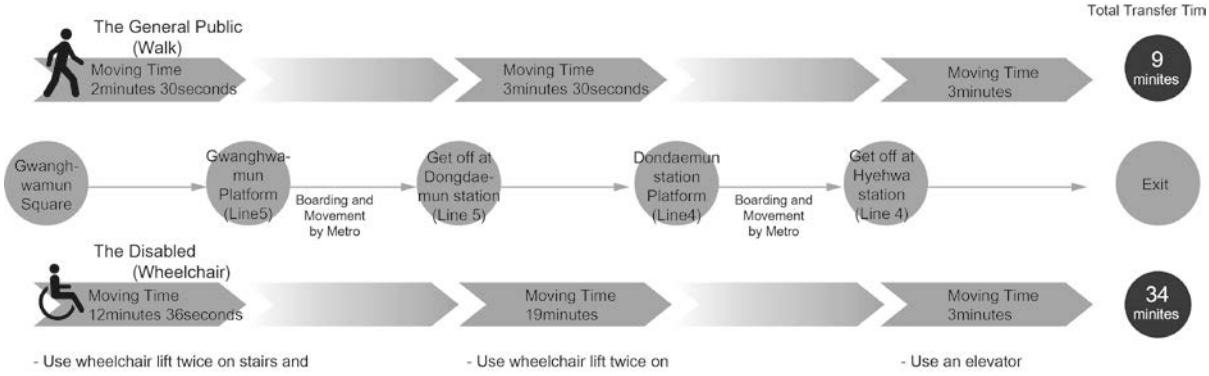

Fig. 1 Comparison to transfer time of the general public and the disabled

elevator. Consequently, total transfer time takes 9 minutes for the general public; on the other hand, it takes 34 minutes for the disabled. Hence, it is necessary to secure moving convenience for the disabled.

TRANSFER MOVING FLOW IN JONGNO-SAM-GA STATION AND IMPROVEMENT SUGGESTION

Present Conditions of Transfer Moving flow in Jongno-sam-ga Station

Jongno-sam-ga Station is the transfer station of Line 1 (the 2nd basement), Line 3 (the 4th basement), and Line 5 (the 5th basement). It is used for 55,193 public, 34,084 the disabled and 230,258 transfer passenger per day by a Study on the Survey of the Transportation Transfer Facilities and the Level of Service Analysis [4]. Jongno-sam-ga Station has a geometric and layered structure because it is the transfer station of the 3 lines located in the center of Seoul. Transfer time is about 4.07 minutes and transfer distance is about 273m for the general public. And transfer time is about 39.26 minutes and transfer distance is about 415m for the disabled.

There are 5 transfer moving flows for the general public as shown in figure 2. But it is difficult to find the direction guide in Line 1 and it is crowded because of the narrow width of stairs. It is necessary to suggest the directions for the improvement of the moving flows to the transfer passage which has width 4m and length 80m. It is necessary to separate moving flows because of the superposition between the transfer flows and exit flows. And it takes long time to pass the transfer passage because moving walkway is installed in the center of the transfer passage.

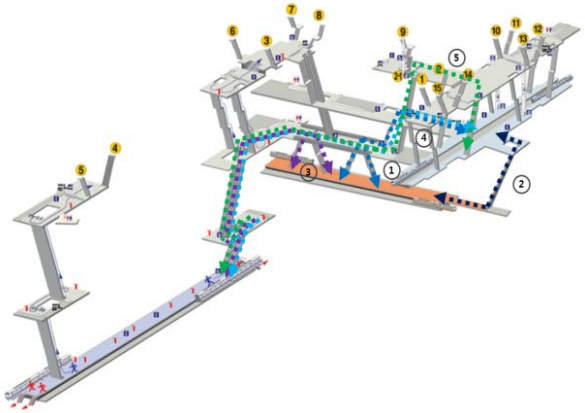

Fig. 2 Transfer flows of the general public in Jongno-sam-ga Station

Fig. 3 Transfer flow status of the general public in Jongno-sam-ga Station

There are 6 transfer moving flows for the disabled as shown in figure 4. There is the only way for wheelchair users. But it is difficult to move because of many users and narrow width of passage. It is also difficult to transfer because there is no elevator for the disabled. Since there is the elevator on the exit flow in Line 1, it is convenient to transfer. And also there is the new plan to install elevators in Line 3 and Line 5.

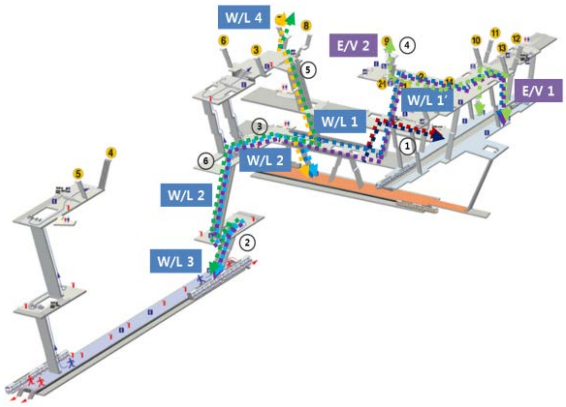

Fig. 4 Transfer flows of the disabled in Jongno-sam-ga Station

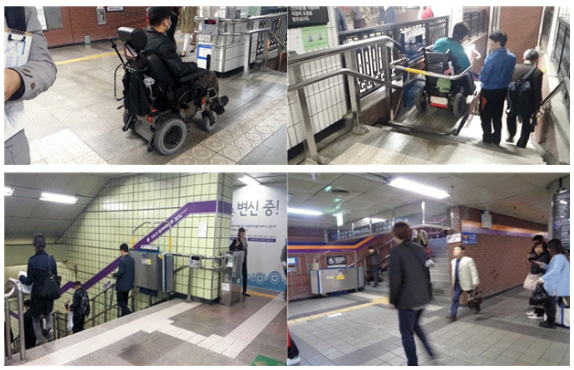

Fig. 5 Transfer flow status of the disabled in Jongno-sam-ga Station

Improvement of the Moving Flow for the General Public

It is possible to improve the traffic congestions by separating the moving flow and the transfer paths. Among the parts that flows are congested in figure 6, it is possible to improve LOS grade when the system is applied [1], [2]. It is required to separate the flows because of the superposition of the moving flows and the transfer flows and narrow width of stairs. And also, it is possible to improve the flow by utilizing the unused area in waiting room in Line 3

Improvement of the Moving Flow for the Disabled

If the escalator that can accommodate both the general public and the disabled at the same time is installed, it can reduce the risk of an existing wheelchair lift and connect the place where it cannot be installed on the elevator.

If the system for both the general public and the disabled is applied, it is possible to shorten the transfer distance and time.

In case of being installed between the waiting room and platform in Line 5(the 4th basement), it shows the improvement rate on approximately 23%. However it is difficult to install because of the location of the beam and insufficient front space. When the wheelchair lift in platform of Line 3 is replaced, it shows the improvement rate on approximately 27%. However it is difficult to install because of the location of the beam and the column.

Lastly, in case of being installed between platform in Line 5(the 1st basement) and platform in Line 3, it is possible to improvement rate on approximately 68%.

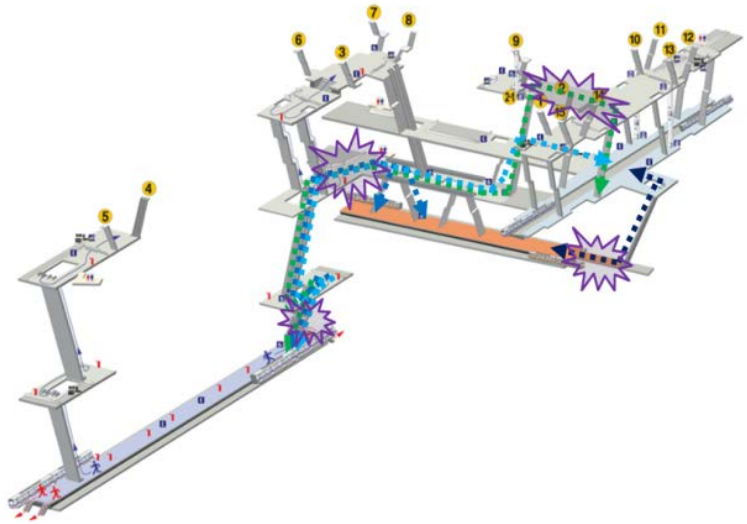

Fig. 6 Improvement of the moving flows for the general public in Jongno-sam-ga Station

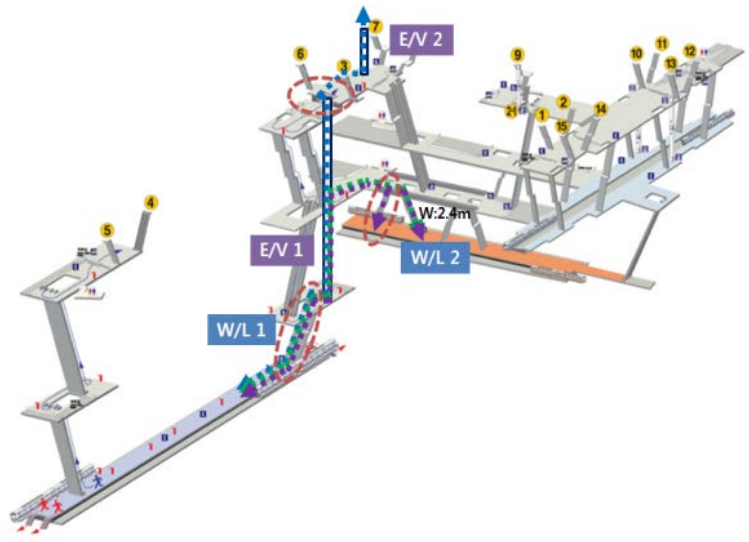

Fig. 7 Improvement of the moving flows for the disabled in Jongno-sam-ga Station

The Analysis of the Space and Structure Interface

In order to judge whether it is possible to install the system, it was carried out the analysis of the interface. It is the stairs with the width 8.2m, height 2.56m from the waiting room of Line 3(the 1st basement) to the waiting room of Line 5(the 1st basement).

There are 3 places for the new elevator plans. One is the place from waiting room of Line 5(the 4th basement) to waiting room of Line 3(the 1st basement). Two is the place from platform of Line 3 to waiting room of the 3rd basement. And the last is the place from waiting room of the 3rd basement to exit 8.

Through these plans, it is possible to connect all flows between platform, exit and transfer passage in Line 1 and Line 3. But it is necessary to connect the flows in Line 5, so it is needed to install the system. The width of stairs is length 8.2m by the analysis on the interface. So it can be installed and the general public is also available at the same time. It is necessary to secure more than height 2.3m for installation of the system. The height of stairs is 2.56m. In addition stairs floor height is also satisfied by depth 1.65m. In case of the bottom space, it is possible to secure ceiling 400mm, ceiling height 4,000m. Besides it is possible to install sprinklers, CCTV, fluorescent lights.

Fig. 8 Inspection of structure interface status in situ

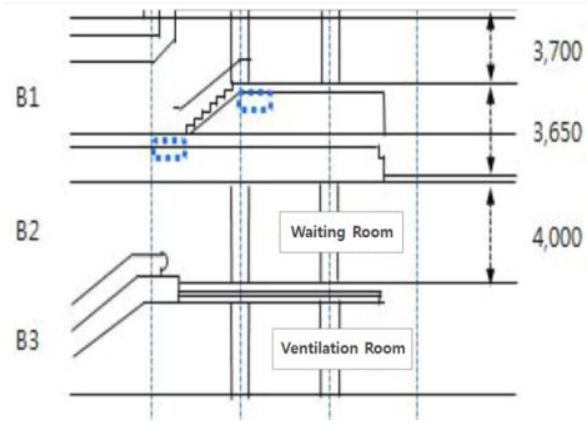

Fig. 9 Structural interfaces in situ

CONCLUSIONS

This research was investigated the present conditions of the movement and transfer path on Jongno-sam-ga Station through a site inspection, and it presented the improvement plan through the analysis on the movement and transfer path for the general public and the disabled.

Conclusions of this research are as follows:

1) It is necessary to suggest the directions for the improvement of the moving flow by reflecting the behavioral characteristics of the general public and the disabled.

2) In case of the transportation vulnerable escalator system, it was estimated 68% of improvement rate compared with the transfer time of an existent wheelchair lift by connecting the new elevators and waiting room.

3) It was confirmed to be expressively reduced the traffic congestions by separating the moving flow and the transfer paths and changing the positions of the obstructions as well.

ACKNOWLEDGEMENT

This research is supported by the grant from “Development of convenience improvement technology for passengers in the metro station (16RTRP-B067918-04)" funded by for Ministry of Land, Infrastructure and Transport of Korean government.

REFERENCES

[1] Fruin, J. J., “Pedestrian Planning and Design”, Metropolitan Association of Urban Designers and Environmental Planners, 1971.
[2] Infrastructure and Transport, “Metro station and transfer Facilities complementary design guidelines”, 2013.
[3] Infrastructure and Transport, “The Survey on public transportation”, 2009.
[4] Korea Transportation Safety Authority, “A Study on the Survey of the Transportation Transfer Facilities and the Level of Service Analysis”, 2014.
[5] Ministry of Health and Welfare, “The Survey on the disabled”, 2008.
[6] Ministry of Health and Welfare, “The Survey on the elderly conditions”, 2011.

Second International Conference on Science, Engineering & Environment,
Osaka City, Japan, Nov.21-23, 2016, ISBN: 978-4-9905958-7-6 C3051

SOME ASPECTS OF THE BEFAVIOR OF UNSATURATED SOILS IN RELATION TO MOISTURE CONTENT

Gabriela B. Cazacu[1] , Cornel Ciurea[2]
[1,2] University Ovidius, of Constanta, Romania

ABSTRACT

The study of soil adhesion on the surface of other bodies to which they are brought into contact is interesting for earthwork construction, foundations etc. The article describes some preliminary laboratory tests carried out in order to establish the variation of soil properties depending on moisture content and on consistency index.

Keywords: geotechnical parameters, oedometers test

1. Introduction

The problems that may arise in time regarding the stability of a construction could be due to: the wrong sizing of the foundations or the instability of the foundation soil.

It was found that the lands with water influenced stability are the loess soil (collapsible) and the loamy soils which can have bumps and big contractions.

This article presents some of the characteristics of loess soils.

Figure 1 shows a map of the loess distribution around the world, made by J.A. Catt.

Usually, the thickness of the loess layer varies from 3 m to 60 m in Romania, the maximum being reached in China, on the Yellow River, where it can be 400 m thick.

2. Geotechnical properties

The medium characteristics of the geotechnical parameters of loess soil in Romania are: from a granulometrical point of view, they are made of 25% clay, (0,005 mm) , dust 65, sand 10 %; the highest limit of plasticity 18%; the porosities are very diverse (depending on the depth and moisture), between 45 and 52 %.

The parameter that decides the loess soils behaviour is their sensitivity to humidity, a characteristic that requires a special design regulatory. NP 125 -2010- Design Norm for foundations on moisture sensitive soils (loess soils).

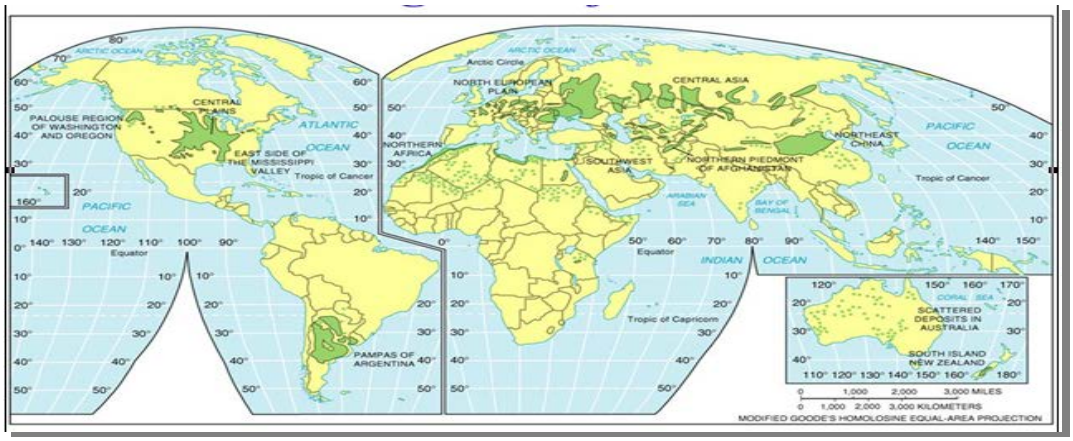

Figure 1.World distribution of loess deposits

3. Modifications of the geotechnical parameters depending on moisture

Various double oedometric tests were carried in order to find out how the soils react to moisture variations (both on naturally moistened samples and on saturated samples).

Double oedometer collapse test: two identical samples are placed in oedometers; one tested at *in situ* natural moisture content and the other is fully saturated before the test begins and then subjected to identical loading.

We are going to present the results obtained for a soil that has almost the same 48 porosity and different degrees of moisture.

Sample 1 has 13% humidity and results are presented in table 1 and sample 2 has 26% humidity and results are presented in table 2.

The increment of vertical strain Δε for each loading increment is given by:

$$\varepsilon = \frac{\Delta h}{h_0} \times 100$$

where Δh is the final settlement for the loading increment (i.e. the change in sample height) and h_o is the initial sample height.

The coefficient of volume compressibility E_{oed} is defined as the ratio of volumetric strain over change in effective stress: $E_{oed} = \frac{\Delta \sigma`}{\frac{1}{100}\Delta\varepsilon}$ (KPa).

The specific compaction when moistened index (i_{mp}) is:

$$i_{mp} = \left(\frac{\Delta h_i}{h_0} - \frac{\Delta h}{h_0} \right) \times 100 = \varepsilon_{sat.} - \varepsilon_{in}$$

This is the reason why it is very important to know how the land reacts to moisture variations.

In figure 2 we have the following results :

- sample 1 – 1st series – natural humidity, 2nd series – satured soil

-sample 2 – 3rd series – natural humidity, 4th series – satured soil

s (KPa)	In situ		Saturated		E_{oed} (KPa)		i_{mp} (cm/m)
	Dh	e	Dh	e			
25	0,06	0,30	0,08	0,40	8333,33	6250,00	0,10
50	0,18	0,90	0,2	1,00	4166,67	4166,67	0,10
100	0,42	2,10	0,48	2,40	4166,67	3571,43	0,30
200	1,1	5,50	1,2	6,00	2941,18	2777,78	0,50
300	1,67	8,35	1,9	9,50	3508,77	2857,14	1,15

TABLE 1 OEDOMETER TEST –SAMPLE 1

s (KPa)	In situ		Saturated		E_{oed} (KPa)		i_{mp} (cm/m)
	Dh	e	Dh	e	In situ	saturated	
25	0,03	0,15	0,2	1,00	16666,67	2500,00	0,85
50	0,15	0,75	0,34	1,70	4166,67	3571,43	0,95
100	0,33	1,65	0,69	3,45	5555,56	2857,14	1,80
200	0,56	2,80	1,49	7,45	8695,65	2500,00	4,65
300	0,9	4,50	2,5	12,50	5882,35	1980,20	8,00

TABLE 2 OEDOMETER TEST – SAMPLE 2

By analysing the graphs, we can ascertain the influence of humidity on the loess soils that are sensitive to moisture.

The value of geotechnical parameters are showing in table 3.

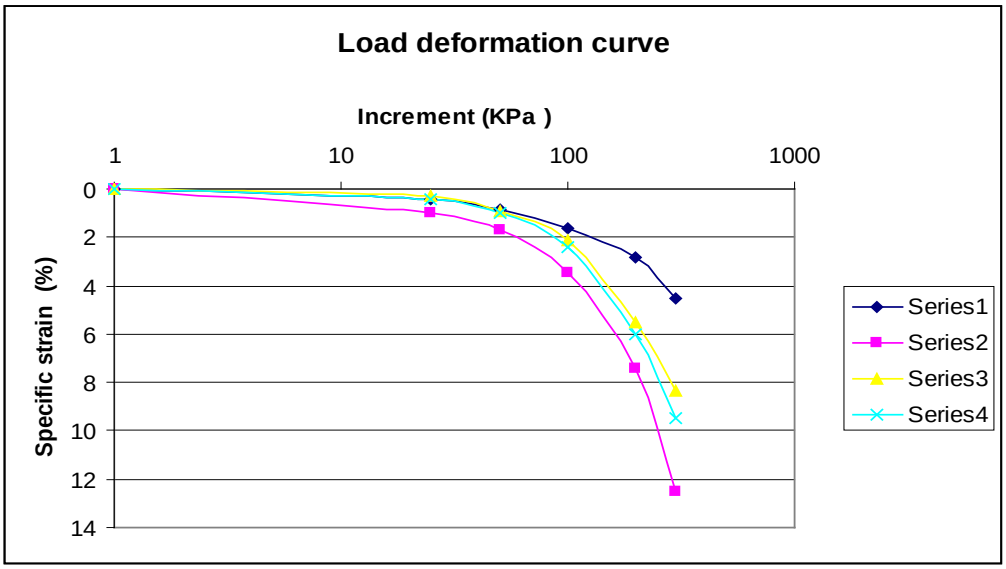

Figure 2. Load deformation curve

Oedometric modulus Eoed 3 nat (KPa)	Oedometric modulus Eoed 3 u (KPa)	Specific strain under load ε 2nat (%)	Specific strain under load ε 2i (%)	im3 (%)
5900	2000	2,8	7,45	8
3500	2900	5,5	6	1,15

Table 3.Geotechnical parameters

Abelev (1948) used stress level of 300 kPa and defined the collapse potential (i m ^{3}).

It is possible to quantification of volume change occurs when soil undergoes collapse is obtained from oedometer test.

Observe collapse earth character whose porosity is high and humidity is low, im^3 value obtained is 8 cm / m.

In Roumania if im^3 is biger than 2 , the soil is sensibile to humidity there's a possibility to collapse.

Moreover it can be estimated coefficient of volume compressibility values Eoed to variations in pressure.

4. Variations of supplementary compaction when moistened, depending on moisture

One of the main conditions for keeping the stability in time of a building founded on loess is that the values of supplementary compaction when moistened must be little.

Supplementary compaction when moistened due to the weight of the layer (I_{mg}) or only under the action of compression loads transmitted by the foundations (I_{mp}).

$$I_{mg} = \sum_{1}^{n} \times i_{mg} \times h_i \times m$$

$$I_{mp} = \sum_{1Df}^{n`} \times i_{mp} \times h_i \times m$$

where I_{mp} is supplementary compaction when moistened index, h = the thickness of the layer, n = the number of layers, df = the foundation depth. The moisture sensitive soils are classified in:

- group A: soils that when moistened, under their own weight (the geological load) present Img supplementary compactions, smaller than 5 cm;
- group B: soils that when moistened, under their own weight (the geological load) present supplementary compactions, larger or equal to 5 cm;

The specific compaction when moistened index (I_{mp}) is the specific compaction difference, at a σ pressure on the pressure – compaction scale, obtained for the naturally moistened sample (ε_n) and previously flooded (ε_i), during oedometer tests.

Because a soil is considered to be sensitive to moisture if the i_m3 value is bigger than 2 cm/m, the 300 KPa pressure was the pressure at which the results were analysed.

The results obtained for the compaction when moistened index (I_m3) in double oedometres, for the same type of soil, loess, have been centralized, mathematically processed in order to eliminate extreme values that could have introduced errors.

It was attempted to make a graphical representation of the im3 values, equal to 1cm/m, 2 cm/m, 4 cm/m, 6 cm/m, depending on the moisture and porosity of the soil. The results obtained are shown in figure 5.

There is a clear dependency of the specific compactions value when moistened, depending on porosity and moisture.

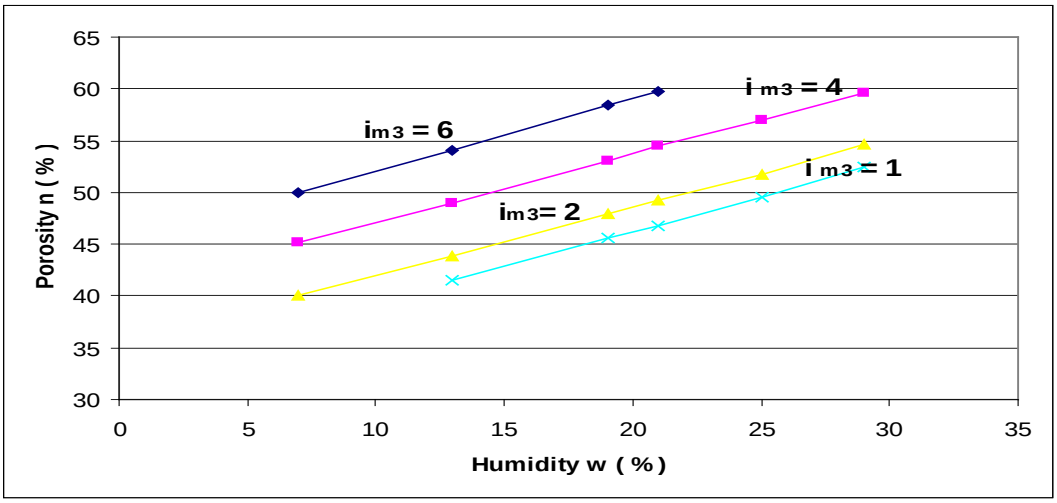

Figure 5. Lines with the same values of im^3

With the help of the data presented in the graph we can forecast the changes of the soil when the moisture varies.

We can observe a parallelism between the lines of equal specific wetting index of subsidence at 300 kPa pressure.

5. Conclusions

The way in which the soils react when moistened depends on the porosity and humidity of the soil.

Correlations between the geotechnical parameters that will have a double role can be made.

- to verify the obtained results;
- to forecast the changes of the soil when the moisture varies.

REFERENCES

1. Andrei S. and Manea – Systematization and re – use of geotechnical data Individual papers Committes and Working Groups,Xx th World Road Congres PIARC ,Montreal 1995 (386- 389);
2. Andrei S. et. al. – The systematiyation and storing methods af information concerning the geotechnical parameters, XIII Danube European Conference on Geotechnical Engineering , Ljubljana 2006;
3. Cazacu G.B. – Doctoral Thesis Contributions concerning the methods of establishing of geotechnical parameters of soils moisture sensitivity";
4. J.A. Catt, Soils and Quaternary geology. A Handbook for Field Scientist, Oxford Sciences Publications, Clarendon Press, Oxford, 1986

Second International Conference on Science, Engineering & Environment,
Osaka City, Japan, Nov.21-23, 2016, ISBN: 978-4-9905958-7-6 C3051

PREDICTION OF LOCAL SCOUR DEPTH AROUND WIDE BRIDGE PIERS UNDER CLEAR-WATER CONDITIONS

Nordila A.[1], Thamer A. M.[2] and Zuliziana S.[3]
[1,3]Faculty of Engineering, National Defense University of Malaysia, Malaysia; [2] Faculty of Engineering, Universiti Putra Malaysia, Malaysia

ABSTRACT

Local scour is the removal of sediment from around bridge piers due to flowing of water. A large amount of local scour is dangerous to the bridge piers and causes the structure tend to collapse and loss of life without any warning. Many researchers have already investigated the phenomenon of local scour around bridge piers. The literature search revealed that there is very little information on predictive equations or data on scour around wide piers. Most of the predictive equations in the literature are intended to apply equally well to large and small piers. Hence, this leads to a situation in which design is prioritised over prediction, which thus proves costly and economically inefficient. This study attempted to fill this gap where new experimental data from a physical model of scouring around a cylindrical and rectangular wide pier embedded in two types of uniform sediment beds are presented. The effects of sediment sizes and various pier widths on equilibrium scour depth of wide bridge piers are described. New empirical relation for the estimation of non-dimensional maximum scour depth for a wide pier were proposed as functions of the sediment coarseness. The experimental data obtained in this study and data available from the literature are used to validate the predictions of existing methods and the accuracy of the proposed method. The proposed method gives reasonable scour depth predictions and was verified with statistical methods where the root mean square error was reduced from 71% to 26%. The new empirical relation agrees satisfactorily with the experimental data.

Keywords: Local Scour, Wide Piers, Equilibrium Scour, Existing Equations, Scour Prediction

INTRODUCTION

Failure of bridges due to local scour has motivated many investigators to explore the causes of scouring and to predict the maximum scour depth around piers. Numerous studies have been conducted with the purpose of predicting scour and various equations have been developed [1], [2], [3], [4], [5], [6], [7], [8], [9], [11] and [22]. In addition, the equations and methodologies have been developed as well for estimating design scour depths around wide and long skewed piers. Bridge scour is the meaning of removal of soil, sand and rocks from around a bridge supports or piers as shown in Fig.1.

Fig. 1 Local scour at bridge pier

MATERIALS AND METHODS

The scour experiments were performed in a flume that was 2.0 m deep, 1.5 m wide, and 50 m long which is in the hydraulic laboratory of the National Hydraulic Research Institute of Malaysia (NAHRIM). A test section that was 10 m long and 0.4 m deep was filled with uniform sediment. The depth of flow was maintained at 0.25 m for all of the experiments. The velocity of both sediments was 0.27 m/s (d_{50}=0.23mm) and 0.36 m/s (d_{50}=0.80mm). An area velocity module (AVM) was used to measure the velocity of flow. In order to measure the depth of scour, a vertical point gauge on the vernier scale was applied. The critical shear velocity, U*c, and critical flow velocity, Uc, for entrainment of sediment, were calculated from the equations given in [13]. The experiments were performed under clear-water conditions at threshold flow intensity U/Uc ≈ 0.95. A single pier model was fixed at the centre of the flume width. Two pier shapes– cylindrical and rectangular –were used to perform the experiment on wide piers. Each pier shape had the same pier width, b, which was tested at 60, 76, 102, 140, and 165 mm; two sizes of cohesionless uniform sediments with median particle size, d_{50} = 0.23 mm and d_{50} = 0.80 mm were also tested. Therefore, there were a total of 20 experiments conducted on wide piers. The experiments were

conducted in two sizes of cohesionless uniform sediments with d_{50} = 0.23 mm and d_{50} = 0.80 mm, thus giving a total of 20 experiments.

To achieve flow transition in smooth condition in the flume, ramps with a 1:5 (vertical: horizontal) slope were constructed at opposite ends of the mobile bed. Fig. 2 shows the schematic drawing for the experimental set up. Uniform sand was used in this experiment to eliminate any possibility of local scour depth reduction expected to occur in non-uniform sand. This is because in non-uniform sand, the armouring effect allowed the downflow to penetrate through the voids between the particles and then reduced the spiral action effect by dissipating some of the flow energy. The degree of uniformity of the particle size distribution of a sediment sample is defined by the value of geometric standard deviation, σ_g, which is less than 1.3 for uniform sediments [13]. The sediments used were well rounded and had a shape factor = 1.0. The Shield's function was used in the calculation of the critical shear velocity on the approach flow bed, u_{*c}, for the mean particle size, d_{50}, of each sediment. The method proposed by [13] was used to determine the critical shear velocity, u_{*c}.

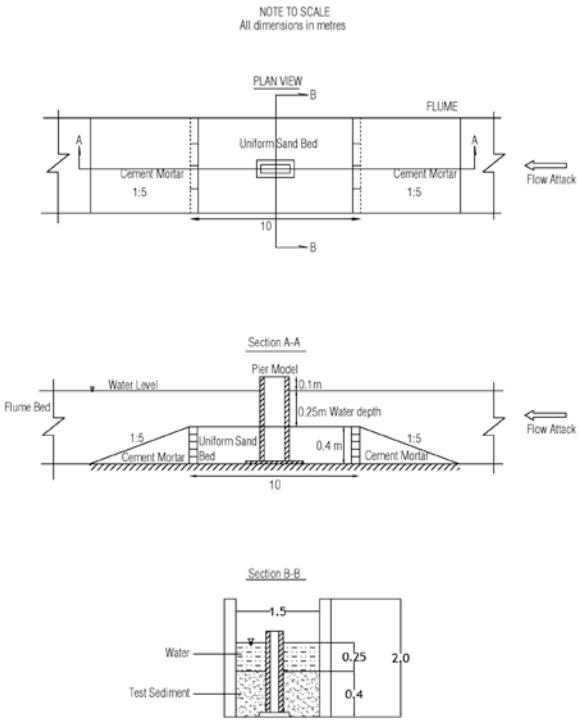

Fig. 2 Schematic drawing for the experimental setup with plan view and side view

RESULTS AND ANALYSES

Twenty experiments were carried out. All of them were run for a single cylindrical and rectangular wide pier with various diameters. To show the relationship of dimensionless d_s/b on b/d_{50}, all of the twenty data sets were shown in Figure 3. It was found that d_s/b reduced as b/d_{50} increased and thereafter d_s/b became constant. From the curves, it is indicate that a high value of equilibrium scour depth was achieved at b/d_{50} = 330 with b = 76 mm in fine sediment with d_{50} = 0.23 mm. The values of d_s/b for the pier sizes of 102, 140, and 165 mm show a smaller peak value compared with that observed for the smaller pier sizes at d_{50}=0.23 mm. The smaller maximum equilibrium scour depths recorded for the larger pier sizes can be attributed to greater localised scour of the bed surface around the rim of the scour hole at each of these piers compared with that occurred for the smaller pier sizes. As in [14] also noted that the reductions of scour depth for larger pier sizes were influenced by the adjustment of bed level at the upstream rim of the scour hole.

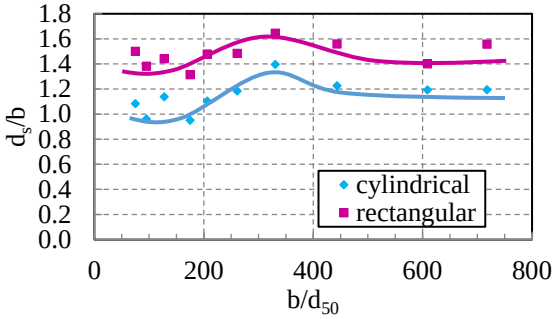

Fig 3 Equilibrium-normalised scour depth versus b/d_{50}

To show more specific patterns and a wider range of applicability for the relationship between d_s/b and b/d_{50}, laboratory data in the present study were merged with the data from the researchers as listed in Figure 4 [15], [14], [16], [17], [18] and [19]. The range of the data up to 4,000. The equilibrium scour depth versus b/d_{50} for large ranges of sediment coarseness (b/d_{50}) was plotted and is shown in Figure 4. These plots evidently demonstrate that d_s/b values were reduced as values of b/d_{50} increased. A least-squares regression analysis using a fitting criterion of mean square error was applied to all data and found the optimum coefficients which minimised the mean square error between the experimental and predicted values. The best fit relationship between d_s/b and b/d_{50} is described by Equation (1).

$$\frac{d_s}{b} = 3.4 - \frac{30}{\left(\frac{b}{d_{50}}\right)} exp\left[0.088\left(ln\left(\frac{b}{d_{50}}\right)\right)^2\right] \quad (1)$$

Assessment of existing equations for estimating the depth of maximum local scour at wide piers

In this section, the laboratory data sets from the present study and literature were used to validate the predicted maximum scour depth at wide piers using equations proposed by [5], [20] and [21]. Statistical

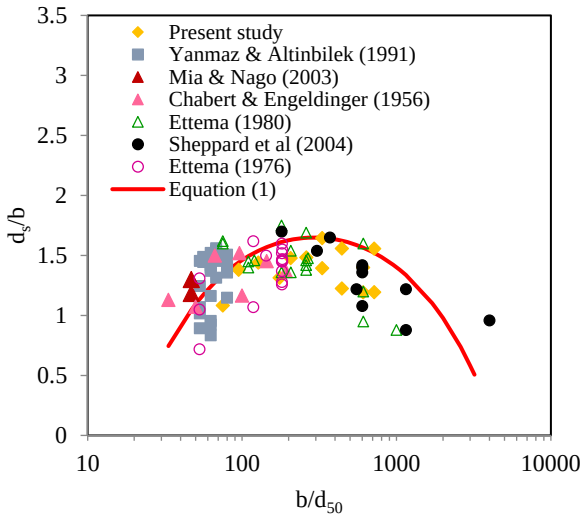

Fig 4. Effect of b/d_{50} on the equilibrium local scour depth around piers

analysis was carried out to assess the performance of each predictive equation. The discrepancy ratio (r), the standard deviation of the discrepancy ratio (σ_r), and the root mean square error (RMSE) were determined. The formulae for the statistical analysis are described below:

$$\boldsymbol{RMSE} = \sqrt{\frac{\sum_{i=1}^{N}\left(d_s/b_{predicted,i} - d_s/b_{measured,i}\right)^2}{N-1}} \quad (2)$$

$$\boldsymbol{r} = \frac{(d_s/b)_{predicted}}{(d_s/b)_{measured}} \quad (3)$$

$$\boldsymbol{\sigma_r} = \sqrt{\frac{1}{N-1}\sum_{i=1}^{N}(r_i - \bar{r})^2} \quad (4)$$

Where $\bar{r}$ is the average of the discrepancy ratio. A value of unity for $\bar{r}$ shows perfect agreement between the dimensionless scour depths of the predicted and measured values. σ_r represents an evaluation of the scatter in the predictions relative to the average value.

The results of the statistical analysis for each predictive equation are given in Table 1. By using the laboratory data sets, the average values of the discrepancy ratio, $\bar{r}$, showed that the [5], [20] and [21] equations over-predict the d_s/b values by19% to 47%, while Equation (1) gave an average value of a 4% over-prediction. Next, the smallest standard deviation of the discrepancy ratio, σ_r, was obtained by applying Equation (1) where the average value was found to be±1.06 and the RMSE value was ±0.26.

Visual comparison (scattergrams) is another method that can be used to evaluate the predictive equations using the predicted and measured scour depths at wide piers. Figures 5 demonstrate the dimensionless scour depth for laboratory and field data sets. The plots indicate how much the predicted values of normalised scour depth deviate from the line of perfect agreement.

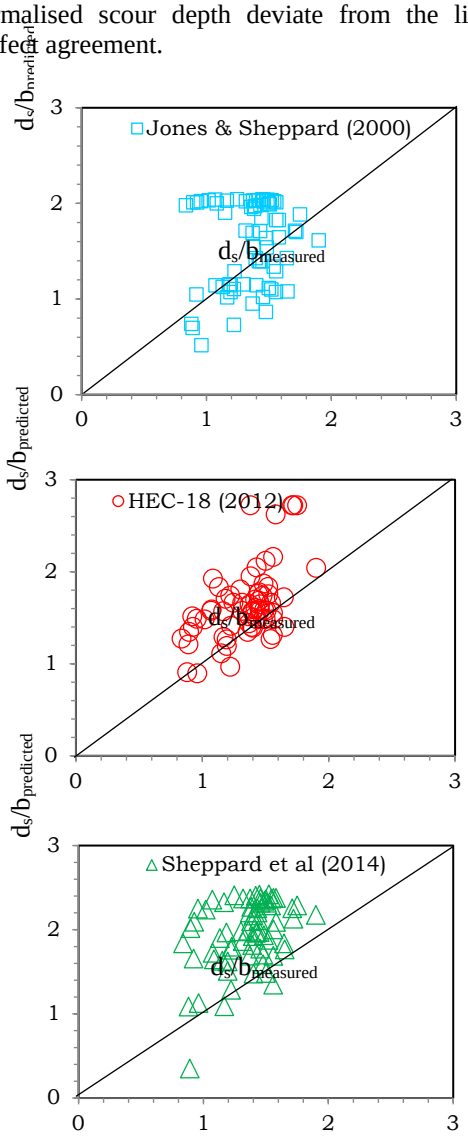

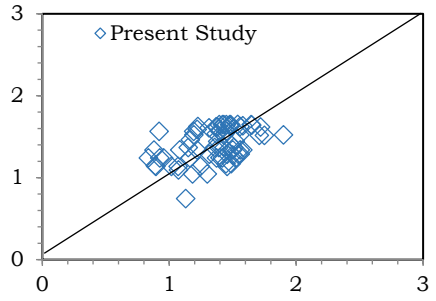

Fig. 5 Comparison of the predicted and measured normalised scour depths from laboratory experiments including Chabert and Engeldinger (1956), Ettema (1980), Yanmaz and Altinbilek (1991), Mia and Nago (2003), and Sheppard et al. (2004) data with selected existing scour depth predictive equations

Table 1. Summary of the discrepancy ratio, r, and root mean square error, RMSE, for each predictive equation

	Laboratory data		
	r		
	$\bar{r}$[1]	σ_r^2	RMSE[3]
Jones and Sheppard (2000)	1.19	1.27	0.52
HEC-18 (2012)	1.26	1.30	0.53
Sheppard et al. (2014)	1.47	1.47	0.71
Present study	1.04	1.06	0.26

$\bar{r}$ [1]= average discrepancy ratio, σ_r^2 = standard deviation of discrepancy ratio, RMSE[3] = root mean square error

From the observation, the selected scour prediction equations over-predict the scour depth if the laboratory data sets are used, while the results obtained from applying Equation (1) are found to be in agreement with the results obtained from applying the selected equations when field data sets are used. As a factor of safety, 25% can be added to the value obtained from Equation (1) in order to consider the value of the maximum scour depth for all data sets used. Meanwhile, it needs to be stressed that the applicability of Equation (1) is limited to values of b/d_{50} from 50 – 4200, to skewed piers with angle of attack, $\alpha < 45°$, to piers in shallow flows and to graded sediments with σ_g less than 7.

$d_s/b_{predicted}$

$d_s/b_{measured}$

ACKNOWLEDGEMENTS

The financial support from the Research University Grant Scheme (RUGS) given by University Putra Malaysia (Grant No. 05-01-10-0904RU) for this project is acknowledged. The experiments were conducted in the Hydraulic Laboratory in the National Hydraulic Research Institute of Malaysia (NAHRIM**).**

REFERENCES

[1] Ansari, S. A., and Qadar, A. (1994). "Ultimate depth of scour around bridge piers." In: *Proc. ASCE National Hydraulics Conference*, Buffalo,

[2] Breusers, H. N. C., and Raudkivi, A. J. (1991). "Scouring." In: *Hydraulic Structures Design Manual*, International Association of Hydraulic

[3] Chiew, Y. M. (1984). "Local scour at bridge piers." *Report No 355*, Department of Civil Engineering, University of Auckland, New Zealand.

[4] Johnson, P.A., 1999. Scour at wide piers relative to flow depth,stream stability and scour at highway bridges, in: Richardson, E.V., Lagasse, P. F. (Eds.),*Compendium of ASCE Conference Papers*,pp. 280–287.

[5] Jones, J. Sheppard, D. 2000, Scour at wide bridge pier. *Building Partnerships*, pp. 1–10.

[6] Lee, S.O., Sturm, T.W., 2009. Effect of sediment size scaling on physical modeling of bridge pier scour.*J. Hydraul. Eng*

[7] 10.1061/(ASCE)HY.1943-7900.0000091, 793–802.

[8] Melville, B. W. (1997). "Pier and abutment scour: Integrated approach." *Journal of Hydraulic Engineering–ASCE*, 123(2), 125–136.

[9] Richardson, E. V., and Davis, S. R. (2001). "Evaluating scour at bridges." Fourth Edition. Hydraulic Engineering Circular No. 18 (HEC-18), Federal Highway Administration, Washington, D.C.

[10] Sheppard, D. M, Huseyin, D. Melville. B. W. (2011). Scour at wide piers and long skewed piers. Report (National Cooperative Highway Research Program) ;682. Washington, D.C.: Transportation Research Board, 2011

[11] Sheppard, D.M., Miller, W., 2006. Live-bed local pier scour experiments.*Journal of Hydraulic Engineering*, ASCE,132(7), 635–642

[12] Melville, B. W., and Sutherland, A. J. (1988). "Design method for local scour at bridge piers." *Journal of Hydraulic Engineering–ASCE*, 114(10), 1210–1226.

[13] Melville, B.W., Coleman, S.E., 2000. *Bridge Scour*. Water Resources Publications,LLC, Colorado, U.S.A., 550 p.

[14] Ettema, R., 1980. Scour around bridge piers.Report No. 216, University of Auckland, Auckland, New Zealand.

[15] Chabert, J., and Engeldinger, P. (1956). "Étude des affouillements autour des piles de ponts."

Laboratoire National d'Hydraulique, Chatou, France (in French).

[16] Yanmaz, A. M., and Altinbilek, H. D. (1991). "Study of time-dependent local scour around bridge." *Journal of Hydraulic Engineering–ASCE*, 117(10), 1247–1268.

[17] Ettema, R. (1976). "Influence of bed material gradation on local scour,"M.S. thesis, University of Auckland, New Zealand.

[18] Mia, F., and Nago, H. (2003). "Design method of time-dependent local scour at circular bridge pier." *Journal of Hydraulic Engineering–ASCE*, 129(6), 420–427.

[19] Sheppard, D. M. (2004). "Overlooked local sediment scour mechanism." *Transportation Research Record: Journal of the Transportation Research Board*, 1890, 107–111.

[20] Arneson, L. A., Zevenbergen, L. W., Lagasse, P. F., and Clopper, P. E. (2012). Evaluating scour at bridges, 4th Ed. Hydraulic Engineering Circular No. 18 (HEC-18), Federal Highway Administration, Washington, DC

[21] Sheppard, D. M, Huseyin, D. Melville. B. W. (2014). Evaluation of Existing Equations for Local Scour at Bridge Piers. *Journal of Hydraulic Engineering–ASCE*, 140(1), 14–23

[22] Ibrahimy M. I. and S. M. A. Motakabber. Bridge Scour Monitoring by Coupling Factor Between Reader and Tag Antennas of RIFD System. *International Journal of GEOMATE*, 8(2), 1328-1332

SUSPENDED SEDIMENT DYNAMICS CHANGES IN MEKONG RIVER BASIN: POSSIBLE IMPACTS OF DAMS AND CLIMATE CHANGE

Zuliziana Suif[1], Chihiro Yoshimura[2], Oliver Saavedra[2], Nordila Ahmad[1] and Seingheng Hul[3]
[1]Department of Civil Engineering, Faculty of Engineering, Universiti Pertahanan Nasional Malaysia, Sungai Besi Camp, Kuala Lumpur; [2] Department of Civil Engineering, Tokyo Institute of Technology, Tokyo, Japan; [3]Institute of Technology of Cambodia, Phnom Penh, Cambodia.

ABSTRACT

This paper evaluates the potential impact of climate change and dams on suspended sediment (SS) dynamics in the Mekong River Basin (MRB). To this end, a distributed process-based sediment transport model was used to examine the potential impact of future climate and dams on suspended sediment dynamics changes in the MRB. Climate scenarios from two GCMs outputs together with effects of 3 existing, 5 under construction and 11 planned dams were considered in the scenario analysis. The simulation results show that the reductions in annual suspended sediment load (SSL) are likely to range from a 20 to 33%, 41 to 62%, and 71 to 81% for existing, under construction, and planned dams respectively in case of no climate change for baseline scenario (1991-2000). Moreover, the reductions on sediment concentration (SSC) are even greater (23% to 78%) due to the potential impact of dams. In contrast, the SSL and SSC shows 40% to 92% increase in the near future (2041-2050) and 28% to 90% in the far future (2090-2099). As the projected climate change impact of sediment varies remarkably between the different climate models, the uncertainty should be taken into account in sediment management. Overall, the changes in SSL and SSC can have a great implication for planned reservoirs and related sediment management.

Keywords: Climate change, Dam, Suspended sediment dynamics, Mekong River Basin

INTRODUCTION

The sediment dynamics of a river are sensitive to both a wide range of human activities and climate change within its drainage basin. These factors could influence sediment mobilization and transfer through action like clearing land, agricultural development, mineral extraction, urbanization, dam and reservoir construction and soil conservation and sediment control programs [1]. Accelerated erosion due to human-induced environmental alterations at the global scale is causing an increase in geomorphic process activity and sediment fluxes in many basins in the world [2], [3]. It is also becoming increasingly obvious that sediment loads in the world's river, particularly in large rivers have been impacted by human activities.

A recent study of 145 major rivers with longer-term records of annual sediment loads and runoff showed that around 50% of river records demonstrated a statistically significant upward or downward trend [4]. The majority of these rivers demonstrated declining sediment loads due to dams and other river control structures trapping sediment. The variables such as climate, soil type, land cover, topography and anthropogenic activities influences soil erosion and sediment transport in the watershed [5], [6], [7].

The main objective of this study is to evaluate the potential impact of anticipated future climate and dam constructions on the suspended sediment (SS) dynamics under near future (2041-2050) and far future (2091-2099) scenarios. The magnitude of the change is demonstrated with different scenarios. In this work, the past suspended sediment load (SSL) and suspended sediment concentration (SSC) in the MRB were simulated to the conservations from 1991 to 2000. Using the calibrated model parameters, the sediment dynamics processes were then projected for the 2040s and 2090s, considering the expected changes in two factors; climate and dams (existing, under construction and planned).

METHODOLOGY

Target River Basin

The present study focused on the MRB, which covers an area of approximately 795,000 km^2 (Fig. 1). The most dominant land use in the basin consists of approximately is forest with 33%. Among major rivers of the world, the Mekong ranks 12th in length (4880 km), and 22nd in catchment area. The wet

season lasts from May to October when the average rainfall around 80-90% of the annual total. The dry season period starts from November and lasts until April. The minimum annual rainfall is 1000 mm/year (NE of Thailand) and the maximum is 4000 mm/year (West of Vietnam).

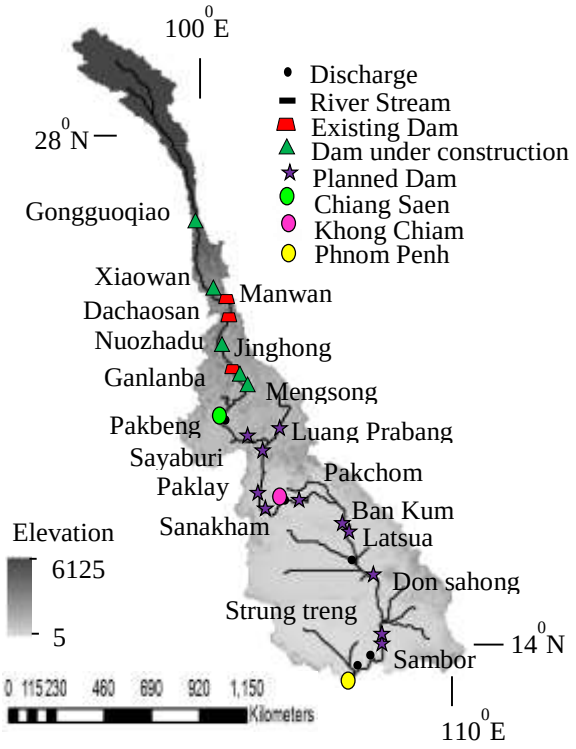

Fig.1 Map of the Mekong River Basin with existing, under construction and planned dams.

The MRB is populated with approximately 60 million people and is considered to be one of the most culturally diverse regions of the world. Agriculture, fishing and forestry provide employment for approximately 85% of the basin's residents. In this basin, acrisols were found the dominant soil type (59%), which are tropical soils that have a high clay accumulation in a horizon and are extremely weathered and leached. Their characteristics include low fertility and high susceptibility to erosion if used for arable cultivation [8]. The rest of the areas are mixtures of deciduous and evergreen covers as well as woodland and shrubland with some undisturbed forest land.

Distributed Sediment Model

The important processes of sediment dynamics were modelled and integrated with a process-based distributed hydrological model (DHM) [9]. It solves the continuity, momentum and energy equations using two modules; hillslope and river routing. The integrated distributed model uses a basin subdivision scheme, a sub grid parameterization scheme, a physically based hillslope hydrological simulation and kinematic wave flow routing in river network [10]. In sediment model, sediment dynamics on hillslope and rivers was separately modelled and systematically linked each other. Hydrological and sediment processes are calculated on daily time-step. Further details can be described by [9] for hydrological model and for sediment model in [11]. Furthermore, the parameters distributed sediment model were calibrated for baseline scenario in previous study.

Dam Scenarios

The location of reservoirs [12] in the mainstream of the MRB are presented in Fig. 1. Four different scenarios were used for investigating the effects of the dam which are D1: baseline (without dam), D2: three existing dams, D3: scenario D2 and 5 construction dams and D4: scenario D3 and 11 planned dams, Table 1.

Eleven dams are proposed (nine in Lao PDR and two in Cambodia) in the Lower Mekong Basin (LMB) and five dams are under construction or designed in Upper Mekong Basin (UMB) in addition to the three existing ones (Xiaowan, Manwan and Dachaosan). The cumulative storage of all the existing and planned reservoirs was obtained from Mekong River Commission [12] and by [13]. The dam release at each dam (existing, construction and planned) was assumed equal with inflow, assumed no water withdrawal. Additionally, the trap efficiency (TE) equations by [14] were used to approximate individual reservoir sedimentation.

Table 1 Scenarios to examine dams on suspended sediment dynamics in the Mekong River Basin. CPO used the observed precipitation in the past, while CPM used the model output from GCMs for precipitation.

Dam Scenario (D)		Past Observation (CPO)	Past Model (CPM)
Baseline (no dam)	D1	D1-CPO	D1-CPM
3 dams (existing)	D2	D2-CPO	-
8 dams (D2 + under construction)	D3	D3-CPO	-
19 dams (D3 + planned)	D4	D4-CPO	D4-CPM

Climate Change Scenario

For the climate impact assessment, the distributed sediment model was driven with outputs of two biases corrected datasets. The first Inter-Sectoral Impact Model Intercomparison Project (ISI-MIP), RCP 2.6 and RCP 8.5. ISI-MIP is designed to synthesize impact projections in the agriculture, water, biome, health, and infrastructure sectors at different levels of global warming. The ISI-MIP datasets comprises bias-corrected daily. The GCMs data were archived from MIROC-ESM-CHEM and HadGEM2-ES. Later the following abbreviations were used by for scenarios produces by these models: MIROC and HadGEM2. Moreover, these two GCMs were selected on the basis of their performance in the simulation of precipitation in the 20th century in the Southeast Asia region [15], [16]. These two models were selected based on the availability of daily data and all the representative concentration pathway (RCP) scenarios.

The RCPs scenarios are based on four greenhouse gas concentration (not emissions) trajectories adopted by the IPCC in its fifth Assessment Report (AR5). The four RCPs are named after a possible range of radiative forcing values in the year 2100 (+2.6, +4.5, +6.0 and +8.5 W/m^2 respectively). The different pathways are coded according to their radiative forcing at the end of the 21st century as RCP2.6, RCP4.5, RCP6.0, to RCP8.5. Climate scenarios were downscaled to a grid resolution of 0.5 degrees and bias-corrected by the ISI-MIP project using a trend-preserving bias-correction method with the WATCH reanalysis data [17].

Table 2 Scenarios to examine climate change on suspended sediment dynamics in the Mekong River Basin

Dam Scenario	(D)	Near Future Climate (CN) RCP 2.6	Near Future Climate (CN) RCP 8.5	Far Future Climate (CF) RCP 2.6	Far Future Climate (CF) RCP 8.5
Baseline (no dam)	D1	D1-CN 2.6	D1-CN 8.5	D1-CF 2.6	D1-CF 8.5
19 dams (D3 + planned)	D4	D4-CN 2.6	D4-CN 8.5	D4-CF 2.6	D4-CF 8.5

In this study, climate scenarios were divided into three decades which are past climate observation 1990-2000 (CPO) and past climate measured from GCMs model (CPM), near future climate 2041-2050 (CN) and far future climate 2090-2099 (CF). Two GCM model output was selected (MIROC and HadGem) and two RCPs (RCP2.6 and 8.5) were used for each model output. These climate scenarios were combined with dam scenario (Table 2).

RESULT AND DISCUSSION

Impact of dams on river discharge, SSL and SSC

The average annual river discharge remains same in each dam scenario because no water withdrawal was assumed in each scenario (Fig. 2a). The average annual SSL shows changes with dam scenario at three observation station, Chiang Sean, Khong Chiam and Phnom Penh (Fig. 2b). It shows decreasing trends in scenario D2 to D3 and D4. However, the SSL at each station shows a slight change from scenario D2.

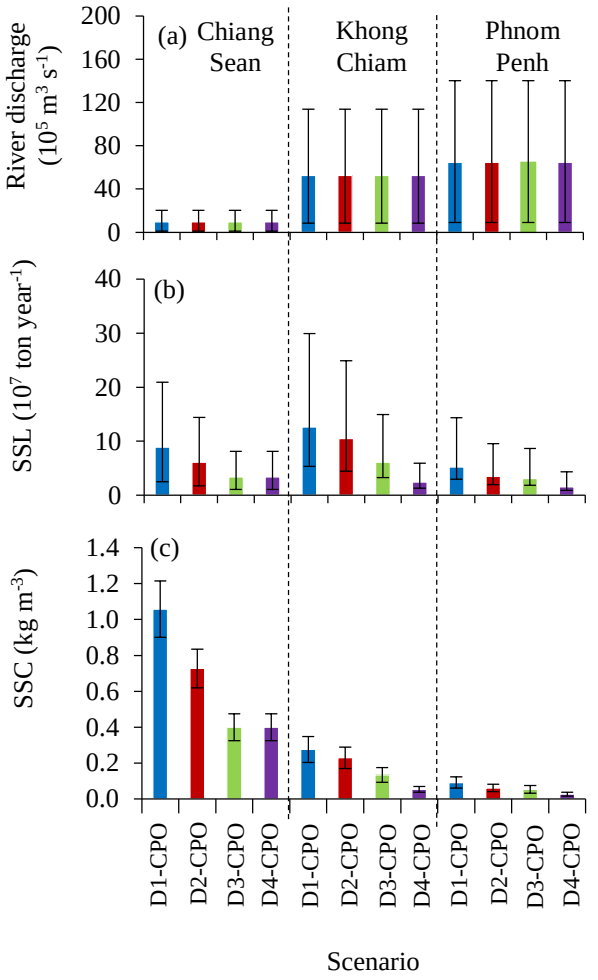

Fig. 2 Average annual (a) river discharge, (b) suspended sediment load, and (c) suspended sediment concentration at Chiang Sean, Khong Chiam and Phnom Penh stations for dam scenario. Error bars show the minimum and maximum value of an average annual river discharge (a) and SSL (b) and standard deviation of average annual SSC (c). Note: See Table 1 for scenario code

The result shows that the existing dam in the upper part of MRB does not show much effect to the downstream SSL. But, obviously, the increasing number of dams affected the amount of SSL (scenario D3 and D4). The reduction in SSL is large in upstream dams and becomes small as it moves downstream, which may be due to variations in the rate of change of rainfall and soil loss from sub basin to sub basin.

Figure 2c shows the average annual SSC with similar trend with SSL which are decreasing from D1 to D4. This implies that the impact of dams on the SSC is same as SSL because of the deposition losses, reducing the SSL as it transported downstream, these will also contribute to the reduction in SSC. In addition, the SSC profile shows the decreasing trend from upstream to the downstream.

Overall, an increasing number of dams are linearly decreased with SSL and SSC. Changes in SSL and SSC in the future can have implications for planned reservoirs and related sediment management. For instance, decreasing SSL will frequently bring obvious benefits in terms of reduced sedimentation and siltation. It is important to recognize that there can also be a negative impacts associated with reduced nutrient inputs to lakes, wetlands, floodplains, delta and coastal areas, resulting in major ecosystem disturbances [18], [19].

Impact of climate change on river discharge, SSL and SSC

The simulated discharge driven by bias-corrected climate model outputs in the period 1991-2000 (D1-CPM) was compared with the observed one. The simulated and observed discharge agrees well for both driving climate models due to the bias-correction of climate model outputs.

Figure 3a and 4a shows the average annual river discharge using output models MIROC and HadGem2 respectively. In general, river discharge on far future (2090-2099) is higher than near future (2041-2050) due to increasing precipitation. However, both model outputs show the same increasing trend from the past in term of river discharge.

The average SSL shows a decreased trend with increasing number of dams (from D1 to D4) for all climate scenarios (Fig. 3b and 4b). The average annual SSL changes ranges from 44% increased at Phnom Penh respectively from near future climate (2041-2050) to far future (2090-2099) for scenario without a dam. The variation in simulated SSL between the climates models used in this study is significant, as it indicates a high degree of uncertainty in the direction of hydrological change due to climate change. As [20] indicate that the changes of sediment yield and discharge in response to climate change do not always happen in the same direction in the Song Cau watershed in Northern Vietnam. Error bars in Fig. 3a, b and 4a, b shows value of maximum and minimum average annual river discharge and SSL.

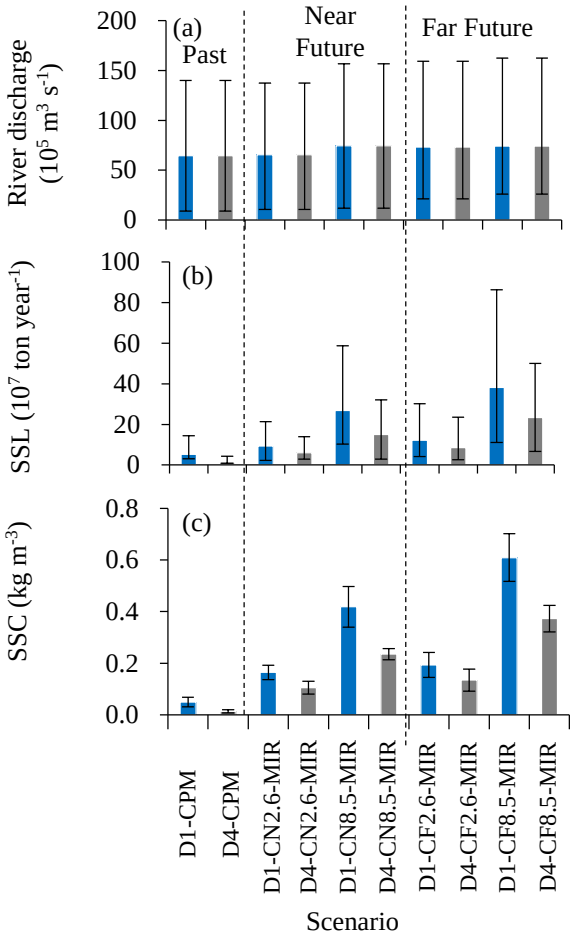

Fig. 3. Average annual of (a) river discharge, (b) suspended sediment load, and (c) suspended sediment concentration at Phnom Penh station using MIROC output. Error bars show the minimum and maximum value of an average annual river discharge (a) and SSL (b) and standard deviation of average annual SSC (c). Note: See Table 2 for scenario code.

Figure 3c and 4c show the average of simulated annual SSC in near future and far future under various MIROC and HadGEM2, climate models. A significant change in average annual SSC Phnom Penh (Fig. 3c and 4c) was confirmed. A reduction in SSC is predicted to occur from 1% to 50%, depending on the scenarios and locations. Moreover, the results show that MIROC estimated higher SSL and SSC in the future than HadGEM2. This is mainly due to higher precipitation projections by MIROC than

HadGEM2. However, both model outputs showed the same trends on SSL and SSC.

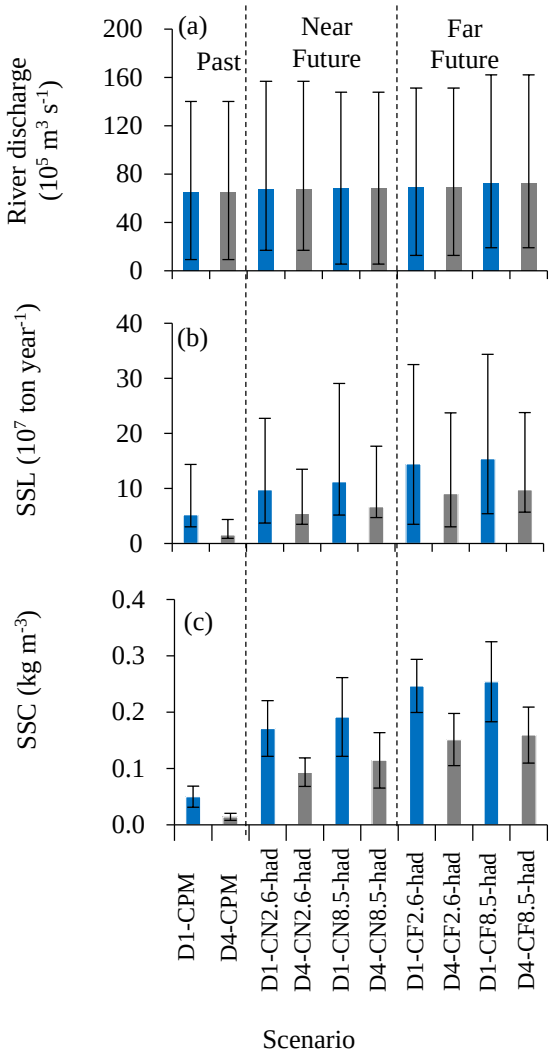

Fig. 4. Average annual of (a) river discharge, (b) suspended sediment load, and (c) suspended sediment concentration at Phnom Penh station using HadGEM2 output. Error bars show the minimum and maximum value of an average annual river discharge (a) and SSL (b) and standard deviation of average annual SSC (c). Note: See Table 2 for scenario code.

CONCLUSIONS

This study assessed the impact of dams and climate change on SSL and SSC in the MRB. In this work, scenarios considering climate change and dam construction were applied for the examination on their potential effects on SSL and SSC. A distributed process-based model is used to simulate the present situation and future changes in sediment load and concentration in the target basin. Distributed models' parameters of river discharge and sediment were calibrated and applied to simulate future changes in river discharge, SSL and SSC.

In general, SSL and SSC values decreased from upstream to downstream due to increasing number of dams. Higher river discharge and SSL are expected when the heavy rainfall takes place. The climate change showed higher impact on sediment than on river discharge, and those changes do not necessary happen in the same direction. The results indicate that large uncertainties exist in all projected future hydrological variables (i.e., rainfall, discharge and sediment) due to differences in the climate model projections.

The outcomes of this study may be helpful to development planners, decision makers and other stakeholders when planning and implementing appropriate basin-wide sediment management strategies. Moreover, the results may support relevant sectors to reassess the design, operation and sedimentation of dams.

ACKNOWLEDGMENTS

This research was funded by Asian Core Program of Japan Society for the Promotion of Science (JSPS). The part of the modeling work was also supported by Core-to-Core Program (B. Asia-Africa Science Platforms) of Japan Society for the Promotion of Science (JSPS) and Collaborative Research Program (CRA) of AUN/SEED-Net.

REFERENCES

[1] Walling DE, "The changing sediment load of the Mekong River", Ambio, Vol. 37, 2008, pp 150-157.

[2] Turner BL, Clark WC, Kates RW, Richards JF, Matthews JT and Meyer WB, The earth as transformed by human action. Cambridge Univ. Press, Cambridge, 1990.

[3] IGBP-BAHC (International Geosphere–Biosphere Programme), Modeling the transport and transformation of terrestrial materials to freshwater and coastal ecosystems, IGBP Report, vol. 39, IGBP,1997, Stockholm, Sweden.

[4] Walling DE and Fang D, "Recent trends in the suspended sediment loads of the world's rivers", Global Planetary Change, Vol. 39, 2003, pp 111-126.

[5] Jain MK and Kothyari, UC, "Estimation of soil erosion and sediment yield using GIS", Hydrology Sciences Journal, Vol. 45, 2000, pp 771-786.

[6] Lee S, "Soil erosion assessment and its verification using the Universal Soil Loss Equation and Geographic Information System: A Case Study at Boun, Korea", Environmental Geology, Vol. 45, 2004, pp 457-465.

[7] Jain MK, Kothyari UC and Rangaraju, KG, "Geographic Information System Based Distributed Model for soil erosion and rate of

sediment outflow from catchments", Journal of Hydraulic Engineering-ASCE, Vol. 131, 2005, pp 755-769.

[8] Mohamdreza H, Mehran N R, and Akbar B, "Dispersive clay stabilized by alum and lime", International Journal of GEOMATE, vol. 12, no. 12, pp. 156-162, 2015.

[9] Yang D, Herath S, Oki T and Musiake K, "Application of distributed hydrological model in the Asian monsoon tropic region with a perspective of coupling with atmospheric models", Journal of the Meteorology Society of Japan, Vol. 79, 1B, 2001, pp 373-38.

[10] Yang D, Herath S, Oki T and Musiake K, "A geomorphology-based hydrological model and its applications, In: V.P. Singh, and D.K. Frevert, eds: Mathematical Models of Small Watershed Hydrology and Applications, Water Resources Publications, Littleton, Colorado, USA, Chapter. 9, 2000, pp. 259-300.

[11] Zuliziana S, Tanuma K, Yoshimura C and Saavedra O, Submitted to Hydrology and Earth System Sciences, 2015.

[12] MRC, "Existing, under construction and planned/proposed hydropower projects in the Lower Mekong Basin", 2008.

[13] Kummu M, Lu XX, Wang JJ and Varis O, "Basin-wide sediment trapping efficiency of emerging reservoirs along the Mekong", Geomorphology, Vol. 119, 2010, pp 181-197.

[14] Brune GM, "Trap efficiency of reservoirs", Transactions of the American Geophysical Union, Vol. 34, 1953, pp 407-418.

[15] Easthan J, Mpelasoka F, Mainuddin M, Ticehurst C, Dyce P, Hodgson G, Ali R. and Kirby M, "Mekong River Basin water resources assessments: impacts of climate change, CSIRO: water for a Healthy Country National Research Flagship, CSIRO, 2008, Australia.

[16] Cai X, Wang D, Zhu T and Ringler C, "Assessing the regional variability of GCM simulations", Geophysical Research Letters, 36, 2009.

[17] Hempel S, Frieler K, Warszawski L, Schewe J and Piontek F, "A trend-preserving bias correction - the ISI-MIP approach. Earth System Dynamics, Vol. 4, 2013, pp 219-236.

[18] Kummu M and Varis O, "Sediment-related impatcs due to upstream reservoir trapping, the Lower Mekong River", Geomorphology, Vol. 85, 2007, pp 275-293.

[19] Kummu M, Keskinen M and Varis O, "Modern myths of the Mekong. A critical review of water and development concepts, principles and policies", Water & Development Publicatons – Helsinki University of Technology, 2008, pp 206.

[20] Phan DB, Wu CC and Hsieh SC, "Impact of climate change on stream discharge and sediment yield in Northern Viet Nam", Water Research, Vol. 38, 2011, pp 827-836.

Second International Conference on Science, Engineering & Environment,
Osaka City, Japan, Nov.21-23, 2016, ISBN: 978-4-9905958-7-6 C3051

SYNERGISTIC EFFECT OF OZONATION AND BIOLOGICAL PROCESSES ON THE TREATMENT OF POLYMER-LENS WASTEWATER

Liza Bautista-Patacsil[1]
[1]Department of Chemical Engineering - MITL, Malayan Colleges Laguna, Philippines

ABSTRACT

The wastewater generated from the cleaning of polymerized lenses was found to contribute to the high BOD and COD level of the composite wastes generated by a polymer-lens manufacturing plant, hence resists biodegradation. Biological degradation and a combination of both biological and ozonation processes were investigated for the treatment of such wastewater. Aerobic degradation was conducted and was measured in terms of removal in COD and BOD of the substrate. The effect of different initial COD concentration of the wastewater on % COD removal by the developed inoculum was studied. Results revealed that the rate of COD removal was highly affected by the initial COD concentration of the substrate. The lower the COD concentration the faster the initial rate of COD removal. The 30% v/v ratio of inoculum/volume of substrate was found to give the highest percent of COD reduction. Results obtained also confirmed that biodegradation was the dominant process as compared to possible chemical oxidation and facultative degradation. The application of ozonation prior to aerobic degradation of the wastewater enhanced its % COD and % BOD removal. The combined ozonation – biological treatment gave 80.1% COD removal and 93.7% BOD removal whereas only 38% COD removal and 91.3% BOD removal was achieved when the sole treatment used was biological. The results showed that ozonated substrate, as compared to raw substrate, exhibits higher biodegradability.

Keywords: Biodegradation, Ozonation, Polymer-lens Wastewater, COD and BOD Reduction

INTRODUCTION

Polymers have greatly affected and modified human lives for almost a century now as it found applications not just in the medical field but also in various industrial fields such as pharmaceuticals, rubber, plastics, etc. In the early eighties, polymers were not yet thought of as a dangerous chemical that can pose serious problems when released in the environment. Lemaire et al. [1] cited that they were still considered as macro-pollutants with low toxicity and side effects until 1985. With the rapid development of polymeric materials in the packaging industry and to a huge increase in untreated plastic wastes, the status of polymers as pollutants in the environment has drastically changed in the late eighties.

Nowadays, campaign for the use of biodegradable plastics is extensive but environmentalist was too focused on the minimization of polymeric solid wastes that they failed to recognize that the wastewater associated with the mass production of such polymeric materials can posed equally alarming harmful effects to the environment.

Many studies have been conducted on the degradation of wastes and wastewater containing toxic and recalcitrant organic matter. Several processes have evolved focusing on the treatment of more complex industrial wastewater with the primary aim of reducing its biochemical oxygen demand (BOD), its chemical oxygen demand (COD) as well as its total solids content. Despite the many studies conducted on the treatment of different kinds of wastewater, none had been found to treat wastewater from soft plastic lenses. According to Hamilton et al. [2], such wastes posed a threat to the aquatic ecosystem because of their persistence and toxicity and some other risks associated with the fate of such wastes in bodies of water. Plastics contains halogenated organics and halogenation is often implicated as a reason for its persistence [3], which may result to considerable environmental pollution and human health problems, thus treatment is needed prior to disposal.

Ozonation had already been used in wastewater treatment as a pre-treatment in order to enhance another process [4]. Such processes involve ozonation-coagulation, ozonation-activated carbon adsorption and sometimes used to transform initially non-biodegradable compounds into biodegradable molecules before a biological process [5].

This study focused only on the treatability study of wastewater generated from the cleaning of the polymerized lenses since preliminary studies revealed that such wastewater contributes to the high BOD and COD concentration of the composite wastewater. Aerobic biological treatment was

employed in order to address the problems that are being experienced by the Polymer-lens Manufacturing Plant with their existing wastewater treatment facility (WWTF). The effect of ozonation process on the enhancement of the biodegradability of such wastewater was also studied. Treatability studies were based only on the reduction of Biochemical Oxygen Demand (BOD) and Chemical Oxygen Demand (COD).

METHODOLOGY

Acclimatization of the Developed Inoculum

Acclimatization of the developed culture of microorganism with the wastewater was done in 2-L shake flasks. A phosphate ammonium salts (PAS) medium was used as the dilution water. Acclimatization was done starting with 1000 mg/L COD of wastewater. It was inoculated with 30% v/v of inoculum and placed in a shaker until visible growth of microorganisms was already observed. A negative control was run containing PAS medium with the wastewater but without inoculum. The acclimatization continued for four subsequent transfers of 30% v/v inoculum to a freshly prepared culture medium using 2–1L Erlenmeyer flasks with 300 ml total working volume and subjected to five days shaking. For each transfer, one flask was kept in a refrigerator at 4 ºC while the other was used as the inoculum for the next transfer.

After the fourth transfer, the COD concentration of the wastewater was increased to 2000 mg/L and same procedure as above was followed and then the crude inoculum was further acclimatized to 3000 and 5000 mg/L COD of wastewater. These acclimatized microorganisms were used as the inoculum for the aerobic treatability study.

Aerobic Treatability Study

Effect of Different Initial COD Concentrations

Four different initial COD concentrations of wastewater was prepared using the PAS medium as the dilution water. A 30% volume of inoculum per volume of pre-treated substrate was added to a 4-L bottle reactor having a 3-L working volume. The samples were aerated at 1L/min using a porous stone diffuser. Aeration was extended to 72 hrs. Sampling was done every 24 hrs for COD analyses. Each run was done in duplicate.

Test to Confirm Biodegradation VS Chemical Oxidation and Facultative Degradation

Foaming has been a problem in the previous run, so this study was conducted in a fabricated laboratory-scale reactor made of 3.175 mm thick flexi glass with a working volume of 3L (Fig. 1). Each unit had a porous stone diffuser at the bottom to supply air and agitate the mixture. Air was supplied at the rate of 2L/min.

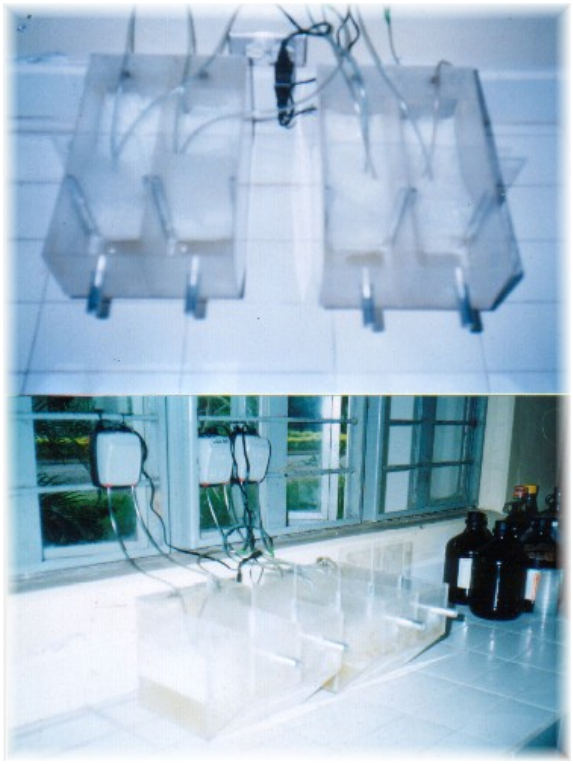

Fig. 1 Biological treatability study set-up for the polymer-lens wastewater.

To confirm if the developed inoculum has the capacity to biodegrade the wastewater, the PAS medium containing 5000 mg/L initial COD of wastewater was subjected to three different treatments. To test for possible chemical oxidation, no inoculum was added but the medium was aerated for 144h. To test for possible facultative degradation, 30% v/v inoculum was added but with no aeration and was allowed to stand for 144h. For biodegradation, 30% v/v inoculum was added and aerated at 2L/min. In all runs, samples were withdrawn at 24h interval for COD analysis.

Effect of Ozonation on COD and BOD Removal

A fresh batch of wastewater sample was first subjected to pre-treatment with concentrated sulfuric acid to neutralize its pH and was further diluted to 10% v/v with distilled water. The initial COD and BOD concentrations was analyzed before it was divided into two. One substrate was subjected to a maximum ozone dose of 390.1 mg/h, while the other substrate was aerated at 2L/min. This experiment was conducted in duplicate. After 24h of separate aeration and ozonation, samples were taken from

each treated wastewater for BOD and COD analyses. The two treated substrates were then dispensed to the biological treatment reactor at equal volume and approximately the same BOD and COD concentrations. A 30%v/v inoculum was then added to each biological unit and started the biological treatment maintaining the pH in all tank neutral and aeration rate of 2L/min. Samples were taken every 24h for BOD and COD analyses.

Analytical Methods

A Hach Model DR/1A portable colorimeter (1990) was used to characterize the wastewater in terms of its color and turbidity. The pH of the sample was measured using Orion pH electrode meter model EA 940, Orion Co., Germany.

The characteristics of the wastewater was determined using the standard procedures for the analysis of water and wastewater [6] in terms of BOD, COD, Total Suspended Solids (TSS), Phosphate-P, TKN, and chloride.

The BOD of the sample was measured by the 5-day BOD test using Azide Modification Test. The Dichromate Open Reflux method was used for COD analyses.

TSS was determined by drying at 103-105ºC after suction filtration.

For phosphate-P analysis, 50-ml of sample were evaporated to dryness then ignited in a furnace for 3h; the ash was then dissolved in 1:1 (v/v) HCl which was then neutralized with NaOH and diluted to 50 ml. Phosphorus content was determined using the ascorbic acid method [6]. All analyses were done in duplicate.

RESULTS AND DISCUSSION

Characteristics of the Wastewater

The Polymer-lens manufacturing plant combines wastewater coming from all point sources of wastewater generated from the manufacturing processes in one equalization basin prior to biological treatment. This made the composite wastewater complex, hence resists degradation. In order to identify the main contributor to the complexity of the composite wastes, the characteristics of all point sources of wastewater generated by the plant were analyzed. The results revealed that the wastewater generated from the cleaning of the polymerized lenses was the one contributing to the high BOD and COD concentrations of the composite wastewater. It was then recommended to separate such wastewater and this was used as substrate for treatability studies.

The results of the analysis of the characteristics of the batch sample of the identified wastewater are presented in Table 1.

Table 1 Characteristics of the wastewater

Parameter	Concentrations
COD (mg/L)	54, 000.0
BOD (mg/L)	12, 300.0
TSS (mg/L)	9, 185.0
TKN (mg/L)	240.0
Phosphate-P (mg/L)	412.7
CL^- (mg/L)	411.4
Color (TCU)	1, 133.0
DO (mg/L)	7.2
pH	13.8

With the COD value of 54, 000 mg/L, this type of wastes can be considered as high strength because it is far above the requirements set by DAO 35 which is 150 and 250 mg/L for class “C” and “D” waters, respectively. The BOD value, 12, 300 mg/L, is only about 23 % of the total COD. COD values are actually higher than BOD because more compounds can be chemically oxidized than can be biologically oxidized. A BOD_5/COD ratio of 0.23 only indicates that the wastewater may contain only a small fraction that can be biologically degraded although its COD value suggests that it contains a high organic load.

The TKN value of 240 mg/L indicates that the wastewater has insufficient nutrients to efficiently support the microbial growth and somehow aid in the removal of BOD, thus addition of other nutrients is necessary. The high phosphate content, 412.7 mg/L, could not be accounted from the general flow diagram of the manufacturing process alone. The company was not giving any other information that can support for the high phosphate content. However, its presence in the wastewater is beneficial since it is also one of the nutrients necessary to support growth of microorganisms that may be used to reduce the BOD content.

The high chloride content, 411.4 mg/L, could be accounted to the presence of unreacted monomer since chloride is one of the raw materials of the monomer.

The high pH, 13.8, is due to the presence of NaOH that was being used for washing the polymerized lenses. Microorganisms will not survive at this pH so neutralization of the wastewater prior to any treatability study was done.

Aerobic Treatability Study

Effect of Different Initial COD Concentrations

In the preparation of substrate, a synthetic media (PAS) was used to prepare the desired initial COD of the wastewater. The nutrients present in the

culture medium was already sufficient to satisfy the nutrient mass ratio of 100:5:1 (BOD_5:N:P) required for efficient microbial growth and BOD removal. The acclimatized inoculum was added at 30% v/v.

Actual concentrations of the four initial COD of substrates that were used in the study were 2332 mg/L, 2972 mg/L, 4409 mg/L, and 5505 mg/L. The results are presented in Fig. 2. It shows that the %COD removal is affected by the initial COD concentrations of the substrate. The Duncan's grouping for the results of the experiment are shown in Table 2.

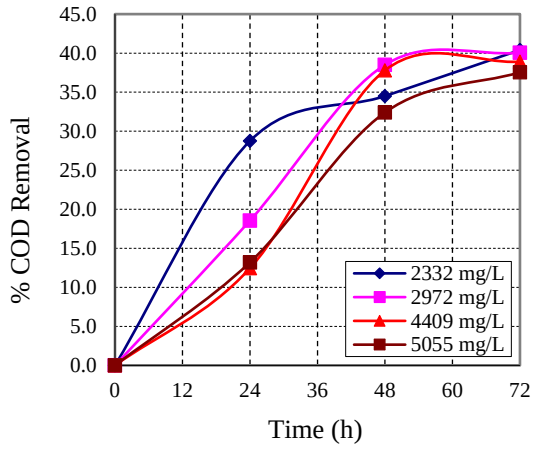

Fig. 2 Effect of different initial COD concentrations vs time of treatment on %COD reduction.

Table 2 Duncan's Multiple Range Test (DMRT) Summary for the four different initial concentrations

Original Order			Ranked Order		
Initial COD	Means	Duncan's Grouping	Initial COD	Means	Duncan's Grouping
2332	25.91	A	2332	25.91	A
2972	24.27	B	2972	24.27	B
4409	22.29	C	4409	22.29	C
5055	20.79	D	5055	20.79	D

LSD Value = 0.9391; s/x = 0.3132 at alpha = 0.050
* Means with the same letter are not significantly different.

It can be seen from Fig. 2 that the substrate with the lowest COD loading gave the highest COD removal for the first 24h, which was closely followed by the substrate with 2972 mg/L COD. From the result of the DMRT test, it shows that the %COD removal is affected by the initial COD concentration of the substrate at 5% level of significance. The substrate with the lowest initial COD was given the highest rank in terms of the rate of COD removal while the substrate with the highest initial COD obtained the lowest rank. Such behavior can be explained by the fact that with the same ratio of inoculum used per unit volume of wastewater treated, the microorganisms can easily use up the available biodegradable substrate at a faster rate but as the substrate diminishes the rate of removal also decreases due to limitation of substrate.

In the case of the substrate with the highest COD, 5505 mg/L, the initial rate of COD removal was observed to be slow, which could be explained by the fact that there are no enough microorganisms to process the substrate. But as they start to multiply the rate of removal increases, as shown in Fig. 2, after the 36th h. However, on the 72nd h, noticed that all the four substrate gave an average rate of removal of only 38%.

Biodegradation VS Chemical Oxidation VS Facultative Degradation

The 38% removal in COD is still quite low and does not conforms to the standards set by DAO 35, hence additional process would be necessary. But before looking for non-biological process to retrofit the existing WWTF of the plant, tests were made to confirm if the developed inoculum has the capacity to degrade the polymer-lens wastewater. The results are shown in Fig. 3. Noticed that biodegradation is still the dominant process as compared to possible chemical oxidation and facultative degradation.

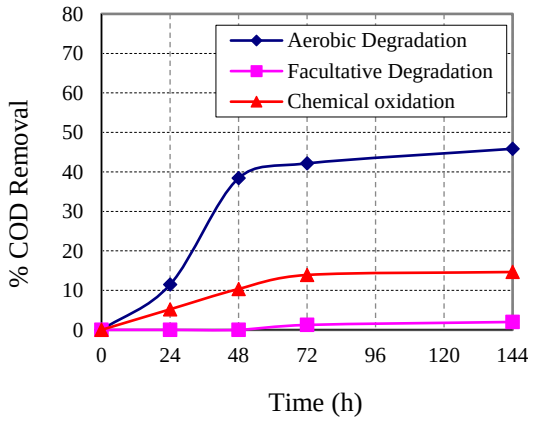

Fig. 3 Comparison of aerobic degradation with facultative degradation and chemical oxidation on %COD removal against time of treatment.

The possible degradation by facultative microorganism is easily eliminated because the result shows that the developed inoculum cannot degrade the wastewater without enough aeration. No significant decrease in COD was observed when air was removed from the system, which only proves that the developed inoculum can only function under aerobic condition. On the other hand, possible degradation by chemical oxidation also did not give

a significant results in terms of reduction in COD. This means that the naturally occurring microorganism in the wastewater cannot process the waste and oxidation by air only gives minimal reduction in COD. With the combined aeration and the developed inoculum, a 42% reduction in COD was achieved after 72h. This proves that the developed microorganism was already capable of degrading the wastewater though such removal is not yet sufficient to conform to the set standards for COD based on DAO 35. Thus, it is now necessary to look for an additional treatment to somehow increase the biodegradability of the wastewater.

Effect of Ozonation on COD and BOD Removal

Since the polymer-lens wastewater was found to be recalcitrant, the effectiveness of ozone as an oxidizing agent for the enhancement of its biodegradability was studied. Batch treatability studies for the raw substrate and ozonated substrate were conducted simultaneously using the same treatment parameters as well as the initial COD concentrations to provide valid data for comparison.

It was found out that at the highest ozone dose of 390.1 mg/h, a maximum COD reduction equal to 30.1% was achieved after 24h of treatment. This ozonated substrate was used for the aerobic biological treatment. The % COD removal for raw and ozonated substrate with time is shown in Fig. 4 while Fig. 5 shows the variation of % BOD removal with time for raw and ozonated substrates.

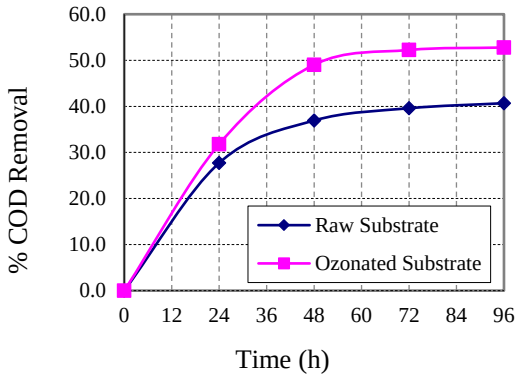

Fig. 4 Comparison of using ozonated vs raw substrate on % COD removal with time of treatment.

In Fig. 4, it can be seen that a 50% COD removal was again achieved after 48h of treatment for the ozonated substrate while only 38% of COD was removed in the raw substrate. After 48h, no further reduction in COD was observed, which means that all the biodegradable component of the wastewater can be exhausted by the microorganism within 48 hrs. This was supported by the BOD data plotted in Fig. 5.

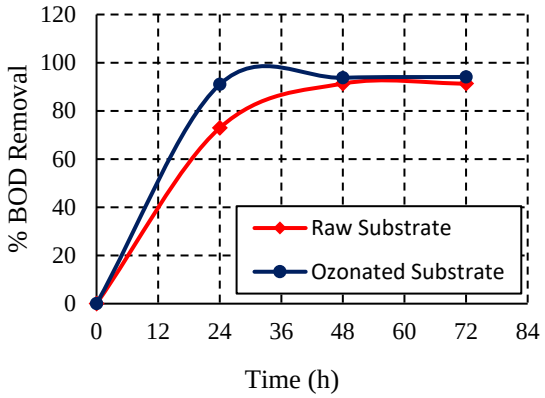

Fig. 5 Comparison of using ozonated vs raw substrate on % BOD removal with time of treatment.

It was evident that the microorganisms in the developed inoculum are efficient in removing the BOD of the wastewater (Fig. 5). At 24h, 91% of BOD was already removed from the ozonated substrate while 72.9% BOD removal was effected when raw substrate was used. A 91% BOD removal was only achieved from the raw substrate on the 48th hr. It can now be concluded that ozonation can really enhance the biodegradability of the wastewater as well as increase the rates of BOD and COD removal.

At 5 % level of significance, the COD and BOD removal for ozonated substrate is highly significant as compared to the untreated substrate. This was supported by the results of the DMRT test on the obtained data as presented in Tables 3 and 4.

The summary of the COD and BOD removal for ozonated and raw substrate are presented in Table 5. For combined ozonation and biological treatment, 80.1 % COD reduction and 93.7 % BOD reduction were achieved, respectively after 48h, whereas only 38% COD reduction was attained when the sole treatment is biological.

Table 3 Duncan's Multiple Range Test Summary Results on the % COD removal of Raw and Ozonated Substrate.

Original Order			Ranked Order		
Substrate	Means	Duncan's Grouping	Substrate	Means	Duncan's Grouping
Raw	29.000	B	Ozonated	37.180	A
Ozonated	37.180	A	Raw	29.000	B

LSD Value = 1.436; s/x = 0.4556 at alpha = 0.050
* Means with the same letter are not significantly different.

Table 4 Duncan's Multiple Range Test Summary Results on the % BOD removal of Raw and Ozonated Substrate.

Original Order			Ranked Order		
Substrate	Means	Duncan's Grouping	Substrate	Means	Duncan's Grouping
Raw	69.390	B	Ozonated	74.560	A
Ozonated	74.560	A	Raw	69.390	B

LSD Value = 2.032; s/x = 0.6448 at alpha = 0.050
* Means with the same letter are not significantly different.

Table 5 clearly shows the synergistic effect of ozonation and biological processes in enhancing the degradability of polymer-lens wastewater. The ozone may have caused fragmentation of the polymer present in the wastewater, which makes it more susceptible to degradation by the microorganisms. The presence of C = C functional groups that are found in the diallyl diglycol carbonate monomer was confirmed under IR analysis. But after ozonation, this functional group has disappeared, which supports the assumption that fragmentation of the monomer have occurred, thus increasing the biodegradability of the recalcitrant wastewater.

Table 5. Summary of % BOD and COD removal for ozonated and raw substrate.

Method of Treatment	Raw Substrate		Ozonated Substrate	
	% COD Removal	% BOD Removal	% COD Removal	% BOD Removal
Ozonation			30.1	
Biological Treatment (after 48h)	38	91.3	50.0	93.7
Total % Removal	38	91.3	80.1	93.7

CONCLUSION

This study focused on the treatability of polymer-lens wastewater. The wastewater generated from cleaning the finished lenses immediately after it had undergone polymerization process was found to be the main contributor to the high COD and BOD concentrations of the composite wastewater of the manufacturing plant. These wastes consist of a small portion of polymerized monomer and NaOH concentration, which was used as cleaner.

The characterization of the polymer-lens wastewater indicates a high concentration of organics in terms of COD. The calculated BOD_5/COD ratio of 0.23 is an indication that only a small fraction of the organic load is biodegradable.

The developed enriched inoculum had successfully grown on the wastewater even at 5000 mg/L COD. It was observed that initial COD concentrations highly affect the performance of the microorganism in terms of the % reduction in COD. The lower the initial COD concentration of the substrate the highest the % conversion attained and the higher the initial rate of COD removal.

Results of ozonation process confirmed that it was able to increase the degradability of the wastewater and was able to convert some non-degradable components to degradable ones as proven by the disappearance of some functional groups in the monomer as a result of the IR spectral analysis.

The combined process of ozonation and aerobic treatment gave a total of 80.1% reduction in COD and 93.7% BOD removal after 48 hrs. With aerobic treatment alone, only 38% COD and 91.3% BOD was removed after 48 hrs. We can now conclude that ozonation is an effective pre-treatment process for it was able to increase the biodegradability of the wastewater.

ACKNOWLEDGEMENTS

This study was conducted at BIOTECH, University of the Philippines Los Baños. Special acknowledgement is given to the author's reposed mentor, Dr. Sixto A. Valencia.

REFERENCES

[1] Lemaire, J, Davin, P and Arnaud, R, "Mechanisms of Abiotic Degradation of Synthetic Polymers," in Proceedings of the 2nd Int. Sci. Workshop on Biodegradable Polymers and Plastics, Montpellier, France, 1992.

[2] Hamilton, JDK, Reinert, H and Freeman, MB, "Aquatic Risk Assessment of Polymers", Env. Sci. Tech. 28 (4), 1994, 187A – 192A.

[3] Chaudhry, GR and Chapalamadugu, S, "Biodegradation of halogenated organic compounds", Microbio. Rev. Vol 55 No. 1, 1991.

[4] Derco, J, Gulyasova, A and Horoak, M, "Influence of Ozonation on Biodegradability of Refractory Organics in a Landfill Leachate", Chem. Pap. 56(1), 2002, pp. 41-44.

[5] Oloibiri, V, Ufomba, I, Chys, M, Audenaert, WTM , Demeestere, K, and Van Hulle, SWH, "A comparative study on the efficiency of ozonation and coagulation–flocculation as pretreatment to activated carbon adsorption of biologically stabilized landfill leachate", Waste Mgt., Vol 43, September 2015 , pp. 335-342.

[6] APHA. 1998. Standard Methods for the Examination of Water and Wastewater. 20th edition. American Public Work Association. Washington, DC.

Second International Conference on Science, Engineering & Environment,
Osaka City, Japan, Nov.21-23, 2016, ISBN: 978-4-9905958-7-6 C3051

UTILIZATION OF BENTONITE MATERIALS FOR IMPROVING THE BEARING CAPACITY OF LOOSE SANDY SOILS

Tark, M.F.[1], Bahr, M.A.[1], El-Mashad, M.A.[2] and EL-Hanafy, A.M.[3]

[1] Faculty of Engineering, AL-Azhar University, Egypt.

[2, 3] Construction Research Institute, National Water Research Center, Egypt.

ABSTRACT

Construction of irrigation utilities above weak soils such as “Loose sandy soils” with extendable depths requires high precautions and improvement before using as bearing layer. In the current research, improvement of loose sandy soil was conducted using blends of bentonite with different mixing proportions. Enhancing the bearing capacity along with reduction of the expected settlement is the main measures for the improvement efficiency. The aim of using bentonite is to utilize a cheap locally available material to interact with the weak sandy soil changing it from non-plastic material with loose behavior to almost a plastic material with limited volumetric change. The aim of this paper is to investigate the improvement of bearing capacity for loose sandy soil by mixing with different bentonite ratio. Experimental work was conducted for this purpose using a laboratory physical model. In addition, laboratory tests such as compaction, direct shear, and consolidation tests were performed to measure the mechanical characteristics of the stabilized materials. Specimens of loose sand were prepared using mixing ratio of 3, 6, and 9% of bentonite by weight. The preparation of tested specimens in the model was done in a controlled manner with special attention to the effect of optimum moisture content and maximum dry density. The prepared soil mix was tested using strip a footing model and the load – settlement curves were plotted and compared with that of pure loose sand in its natural and compaction states. The results showed that the substantial improvements in a bearing capacity by about 22% with 3% of bentonite gives an optimum results which becomes more suitable and enough light to medium loading criteria for the foundations of irrigation utilities.

***Keywords**: Bentonite, Bearing Capacity, Loose Sandy Soil, Model Test, Settlement.*

INTRODUCTION

To make use of loose sandy soil as base course for foundation structures, it must be improved with some suitable admixtures. The bentonite material is widely used for many purposes in relation to civil engineering works improvement materials and stabilization for weak soil, filler of voids to improve the permeability, strength, density and filler materials for slurry cutoff walls. Bentonite is an effective material in enhancing the plasticity properties of soil. it increases the liquid limit, plastic limit, the maximum dry density and the Optimum Moisture Content (OMC). [1] Concluded that the consistency limits, liquid limit, plasticity index and linear shrinkage increased linearly with bentonite content in lateritic soil mixed with bentonite. Also, the results showed that the geotechnical performance of compacted loose sandy soil - bentonite mixtures proposed as liner material in waste landfills showed that bentonite addition resulted in an increase in plasticity index, optimum moisture content and a reduction in dry unit weight. Expectedly, the hydraulic conductivity and unconfined compression strength of compacted mixtures decreased non-linearly while the volumetric shrinkage increased with increase in bentonite content. [2] Investigate the use of bentonite and lime in stabilizing dune sands for possible uses in geotechnical engineering. The bentonite added to the mix was helping in making cohesive bond in the mix. The results showed substantial improvements in unconfined compression strength with addition of 15% bentonite and 3% lime. Further addition of bentonite and lime in dune sand causes compaction difficulties as the mix becomes sticky. The minimum values of unconfined compressive strength were found in the mixture 5% bentonite and 1% lime. [3],[4] Concluded that the bentonite is the effective material for plasticity properties, where it increases the liquid limit, plastic limit, the OMC increase, but the maximum dry density and, the CBR ratio decrease. Bentonite should have been used in small amount to keep plasticity, CBR, and economy, and hence 5% or less was recommended through the experiments. [5] Concluded that the bentonites should be used 6% to keep enough plasticity and reduce the cost of grouting. Compacted bentonite is used as engineered barrier mainly for limiting migration of leachate from the wastes which may contain elements that are

detrimental to the quality of groundwater for their designated uses. The use of compacted natural clayey soils due to very low hydraulic conductivity, self healing quality and a marked capacity to adsorb and retain contaminants for this purpose is well established by [6], [7].

SCOPE OF RESEARCH

The objective of this paper is to investigate the improvement of bearing capacity for loose sandy soil by mixing with different bentonite ratio, to change its properties from non plastic material to plastic material. Physical model tests were done by adopting a strip footing supported on loose sandy soil mixed with different bentonite ratio (3, 6, and 9) %.

MATERIALS

Loose Sand

In the current research, air-dried clean siliceous yellow sand was used. The used sand was obtained from El-menia Governorate, West Desert Road, Maty, Egypt. Where soil layer in this area consist of loose sandy soil. Grain size analysis was performed on several-mixed samples of the tested sand according to ASTM D421 [8]. Fig. 1 shows the grain size distribution of used sample. The plot shows that a medium to fine sand was selected. The tested sand was classified as poorly graded sand (SP) according to the unified soil classification system [USCS]. Physical properties of the sand were determined as shown in Table 1.

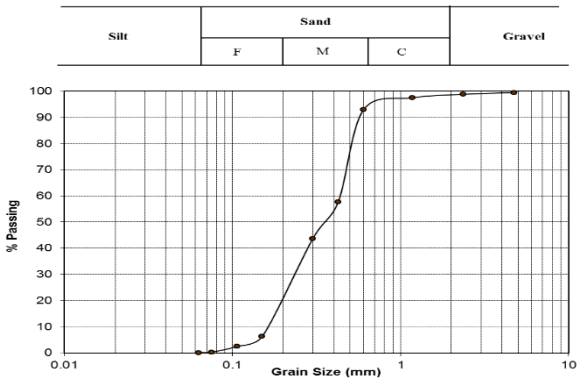

Fig.1 Grain Size Distribution of Used Sand.

Table 1 Summary of the Physical Properties of the Used Sand.

Property	Value	Property	Value
Specific gravity (Gs)	2.64	Maximum dry unit weight (γ_{dmax})(kN/m^3)	16.80
Void ratio (e)	0.70	Minimum dry unit weight (γ_{dmin})(kN/m^3)	13.90
% of Clay	0.00	Maximum void ratio (e_{max})	0.907
% of Silt	0.09	Minimum void ratio (e_{min})	0.52
% of fine Sand	3.94	Relative Density (D_r) (%)	53.49
% of medium Sand	88.84	Angel of internal friction ϕ°	30.0
% of coarse Sand	3.52	Effective diameter (D_{10}) mm	0.161
% of fine Gravel	3.61	Coefficient of uniformity(C_u)	2.703
Unit weight (γ_b)(kN/m^3)	16.41	Coefficient of gradation(C_c)	0.776

Bentonite

Calcium bentonite produced in Egypt was used in this research. Physical and chemical analysis was done. The Atterberg limits of bentonite were 576.8% (LL), 46.1% (PL), 30% (SL) and 530.7 % (PI). The clay content was about 82% with Activity 4.88 and Free Swelling 380 %. The total dissolved salts (TDS ppm) was 3328, and composed mainly of Calcium (CL ppm) 568, (SO3 ppm) 40, with PH equal 7.3.

EXPERIMENTAL PROGRAMME

Laboratory Testing

Compaction Test

Standard compaction tests were performed in accordance to the modified Proctor method (ASTM D1557, ASTM 2000a), [9] using suitable moisture–density points. The results of the tests for the four Groups were drawn in Fig.2 revealed the maximum dry unit weight and optimum moisture contents. Also, the values of the results were listed in table 2. Comparison was made between loose sand, and loose sand with different bentonite ratios.

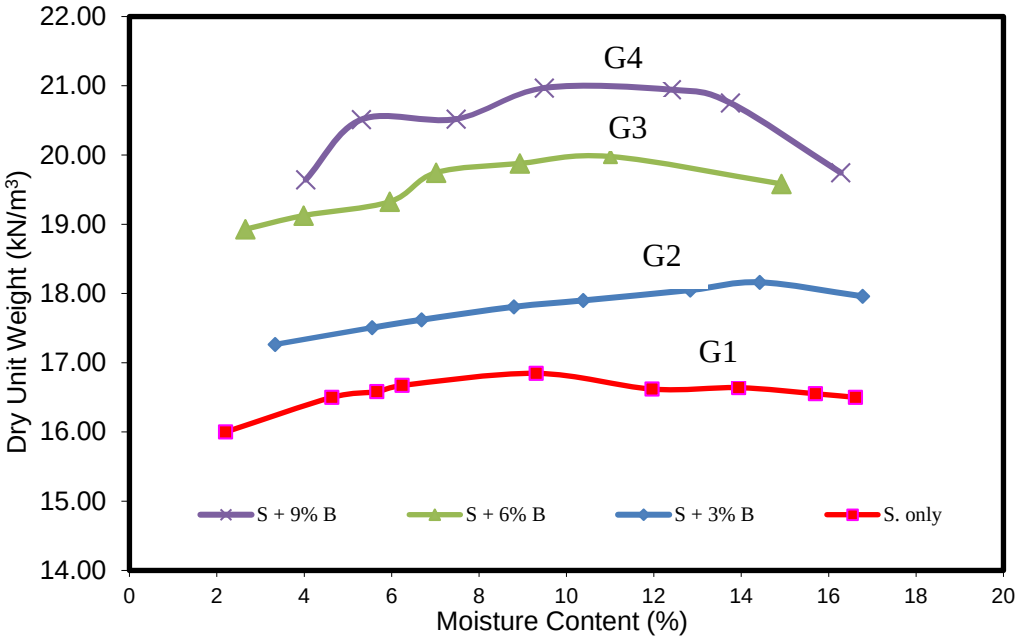

S: Sandy soil, B: Bentonite

Fig. 2 Dry unit Weight Vs. Moisture Content for Different Mixes.

Table 2 Summary of Maximum Dry Unit Weight and the Corresponding O.M.C.

Group No.	Group	Maximum dry unit weight ($\gamma_{d\ max}$)(kN/m^3)	Corresponding O.M.C % Value	Relative Density (D_r) (%)
G1	Loose Sand	16.85	9.31	53.49
G2	Loose Sand+ 3% Bentonite	18.16	14.42	56.18
G3	Loose Sand+ 6% Bentonite	19.98	11.01	59.46
G4	Loose Sand+ 9% Bentonite	20.96	9.49	61.08

In the present research, it was observed that the maximum dry density of the Mix. from 1 to 4 varied from 16.85 kN/m^3 to 20.96 kN/m^3. It was observed that the increase in the bentonite ratio lead to increase in dry unit weight. The optimum moisture content of the mixture varied from 9.31% to 14.42%. It was observed that the increase in the bentonite ratio up to 3 % lead to increase in O.M.C%, but the increase in the bentonite ratio over 3 % lead to decrease in O.M.C%. This concluded that the optimum mix ratio for bentonite ratio was found 3% and the compaction characteristics of loose sand with bentonite mixture were found to be in good agreement with the results reported in literature.

Direct Shear Test

Due to using dry sand in the model, the apparent cohesion was almost equal to zero in original case for loose sand. The angle of internal friction of used loose sand was determined by means of direct shear apparatus according to (ASTM D3080) [10]. Fig. 3-a, b show the relation between cohesion (kN/m^3) and angle of internal friction (ϕ) with Bentonite content respectively, from Direct Shear test.

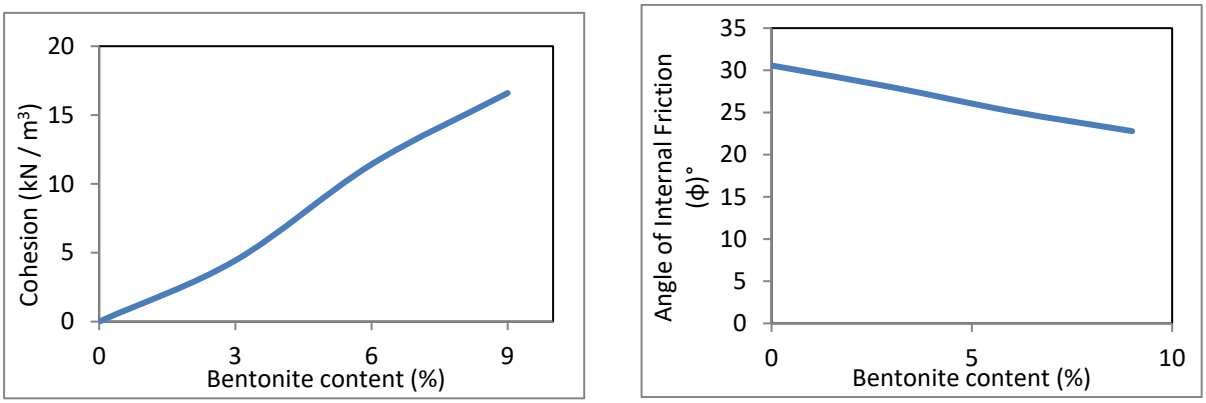

(a) (b)

Fig. 3: a) Relation between Cohesion and b) Angle of Internal Friction (ϕ) ° with Bentonite Content.

From Fig. 3 it can be seen that the increase in bentonite mixture with loose sand lead to increase in cohesion and decrease angle of internal friction for loose sand.

Oedometer Test

The coefficients of consolidation (Cv), (mv) and (av) for sandy soil with bentonite mixtures were evaluated using oedometer test according to Egyptian code for soil mechanics and design and executing the foundations, 2009, part 2, section 2-13-2 [11]. The results from oedometer test for case of no bentonite mix shows that the void ratio equal 0.907 %. Fig. 4 shows the relation between (e- log p) for loose sandy soil with 3, 6 and 9 % bentonite mix.

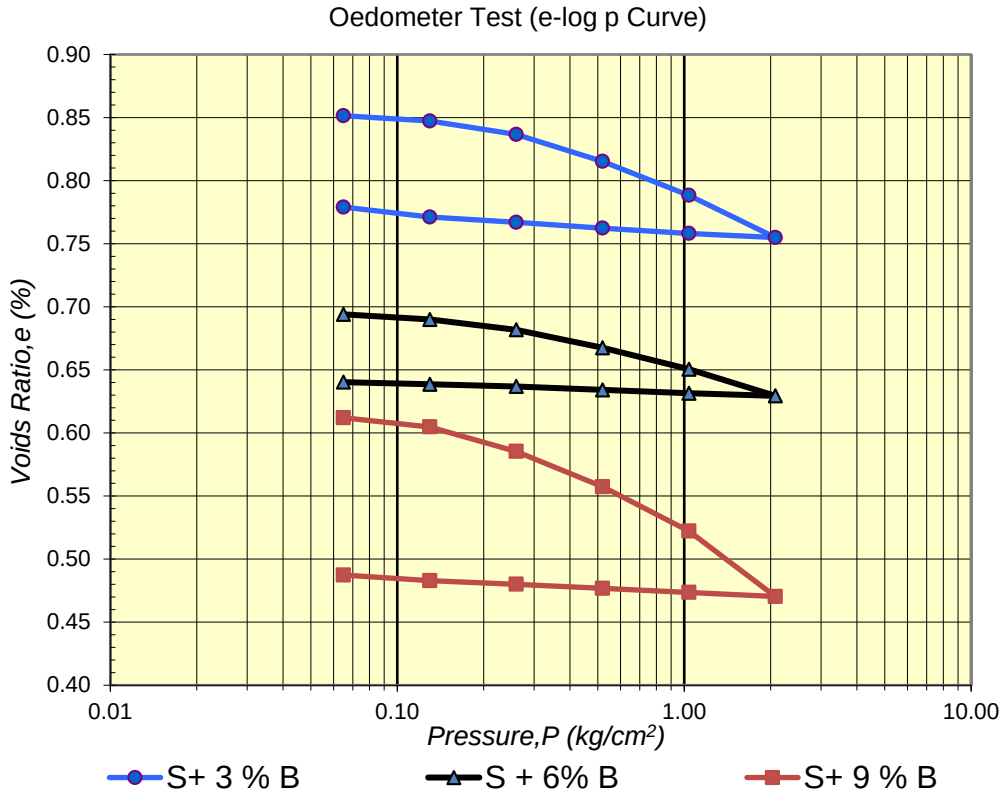

S: Sandy soil, B: Bentonite

Fig. 4 Relation between (e- log p) for Loose Sandy Soil with 3, 6 and 9 % Bentonite.

From Fig. 4 it can be noticed that the voids ratio decrease with increase the bentonite ratio from 3 to 9 % with increase the applied pressure. This decrease in voids ratio due to that the bentonite make interlocking with sand and fill the voids between sand particles.

Lap Physical Model

Physical model was used to investigate the behavior of loose sandy soil with different mix ratio of bentonite. The tests in this research were conducted by the steel structures model facility at the Construction Research Institute (CRI). In Egypt, it is a large model with Perspex box with internal dimension (1760 x 850 x 1000) mm as shown in Fig. 5 the box of this model which filled with soil has four Perspex sides, and the top is open to allow the application of vertical pressure. Vertical pressure is applied by 3 hydraulic cylinders (Pistons) with a maximum capacity 5 ton for each piston controlled by digital close loop controller by hydraulic system arranged in one row. These pistons connected with one I-beam which are attached to the box by steel pins as shown in section elevation in Fig. 6 for physical model. In this research, the box was filled with soil using moving steel hopper to level of bentonite mix without compaction then the soil in the layer mixed with bentonite was compacted using manual compacting on layers of 100 mm thickness. Compaction was subsequently conducted using steel hammer with circular base of 270 mm in diameter and weight of 17.5 Kg, dropped from a height of 300 mm until reaching the target unit weight. The maximum, minimum density and moisture content were measured actually from soil in the box.

Fig. 5 Physical Model Configuration.

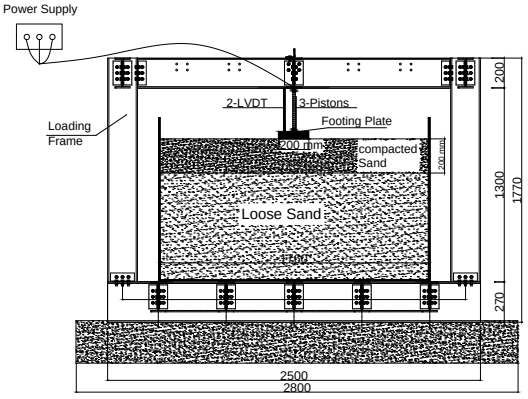

Fig. 6 Section Elevation of Physical Model.

The vertical displacement of the footing was measured by a linear variable differential transducer (LVDT) which was calibrated before beginning the testes. At the conclusion of the test, the cables of load cell and LVDT were connected to the data logger which recorded of the data then it was connected to the computer to input the recorded data and draw the load verses settlement. The test was stopped when a failure in soil was occurred. Then, series of tests were done for loose sandy soil. Fig. 7 (a,b) show the test setup and measuring devices.

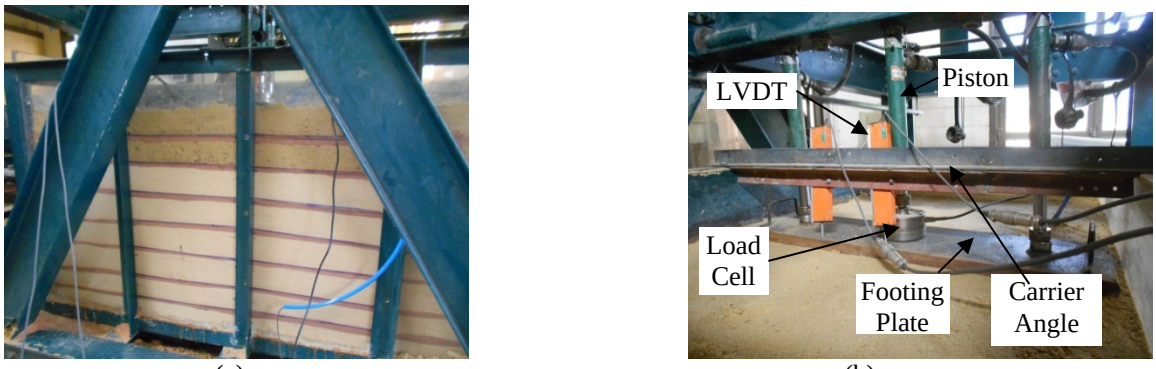

(a) (b)

Fig. 7 (a,b) Test Setup Showing Measuring Devices.

RESULTS AND DISCUSSIONS

Bearing Capacity Behavior

Four tests were performed on strip footing (200 x 840 x 20) mm. to show the effect of bentonite ratio on the bearing capacity, settlement of the footing and failure stress for loose sand. In this study a treated layer of depth (B) equal to the short dimension of the footing was mixed with different bentonite ratio and compacted to the same depth under the footing. Fig.8 shows section elevation for test configuration. The cumulative curve for these groups results were presented in Fig. 9.

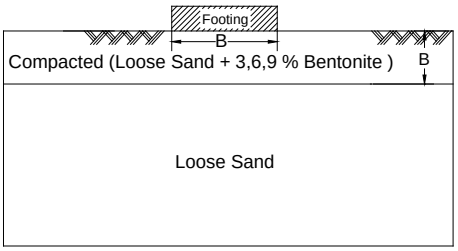

Fig. 8 Section Elevation of Test Configuration.

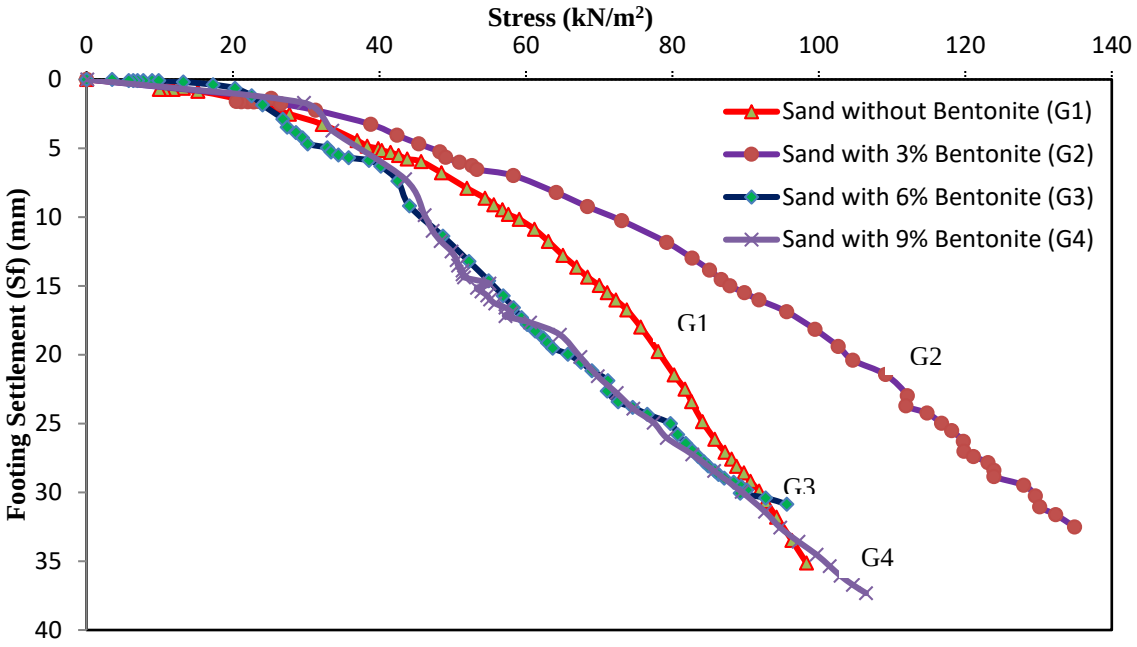

Fig. 9 Ultimate Stress - Settlement Curve for Examined Soil with Different Bentonite Ratio.

In order to estimate the improvement of the soil produced by the inclusion of bentonit, the bearing capacity ratio B.C.R was calculated for all testes. The B.C.R was defined as the ratio of the bearing load capacity of improved soil by bentonite divided by bearing load capacity of unimproved soil. The ratio was performed for vertical failure stress between improved and unimproved tests. This value was calculated for each group and is defined as:

$$(B.C.R) = (q)\ I\ /\ (q)\ U \qquad (1)$$

Where q(I) and q(U) are the bearing load capacity values for improved and unimproved foundations, respectively. Table 3 shows the failure stress, corresponding settlement and B.C.R (%) for each test.

Table 3 Ultimate Stress at Failure Load and Rate of Increase in B.C.R (%).

Group No.	*Group*	*Failure Stress (kN / m²)*	*(B.C.R) %*	*Corresponding Settlement (mm)*
G1	Loose Sand without Bentonite	65.03	1.0	12.78
G2	Loose Sand with 3 % Bentonite	79.23	1.22	11.84
G3	Loose Sand with 6 % Bentonite	52.22	0.80	11.22
G4	Loose Sand with 9 % Bentonite	50.74	0.78	13.52

From Fig. 9 and table 3, it can be seen that the improvement ratio in bearing capacity for loose sand occurred when mixed with 3 % bentonite by 22 % compared with case of without using bentonite ratio. But when using 6, 9 % bentonite ratio, the bearing capacity decreased by 20, 22 % respectively, compared with case of without using bentonite. The maximum improvement ratio in bearing capacity occured at 3 % bentonite ratio compared with case of without bentonite as shown in Fig 10. The maximum vertical settlement occurred at 9 % bentonite ratio compared with case of without bentonite, 3 and 6 %. Extensive settlement with a wedge shaped soil zone in elastic equilibrium beneath the foundation. Vertical shear occurs around the edges of foundation. After reaching failure, stress - settlement curve continuous mostly linear.

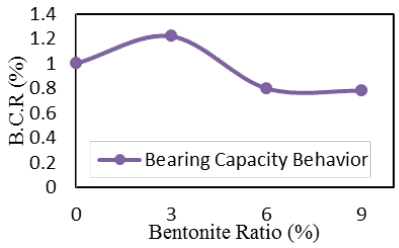

Fig. 10 Bearing Capacity Behavior for Sandy Soil Mixed with Various Bentonite Ratios.

Vertical Deformation

The vertical settlement of soil mass was measured for loose sandy soil without bentonite as shown in Fig. 11 at the middle distance in long direction of tank.

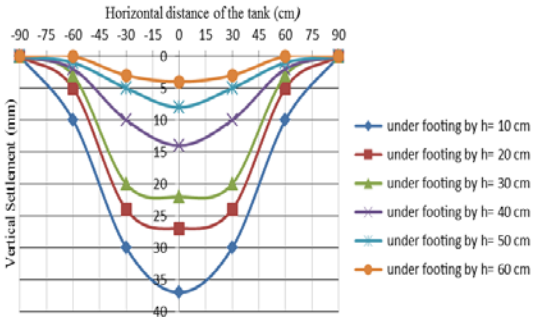

Fig. 11 Vertical Settlement (mm) on Face of Side Tank for Sandy Soil without Bentonite.

Also, it was presented for each test with mix of bentonite ratio as shown in Fig. 12, 13, 14 to observe the influence of various bentonite ratios in improvement the bearing capacity of loose sand. The values of vertical deformation on the layers were measured from the upper horizontal layer to the bottom layer of the tank. Vertical deformation measurements were taken every 10 centimeters along the axis shown at the middle tank.

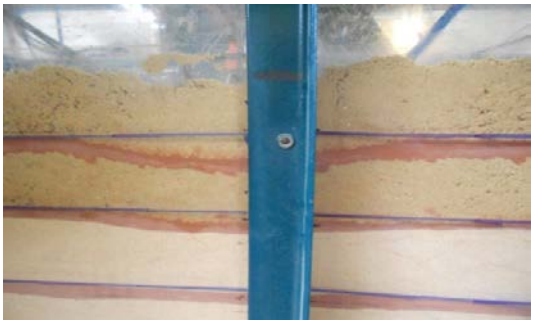

(a)

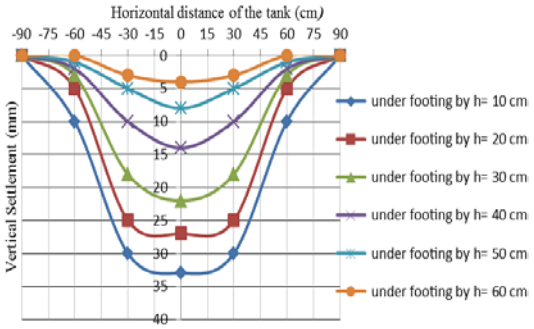

(b)

Fig. 12 Vertical Settlement (mm) on Face of Side Tank for Sandy Soil with 3 % Bentonite. A)Experimentally, and b) Measured.

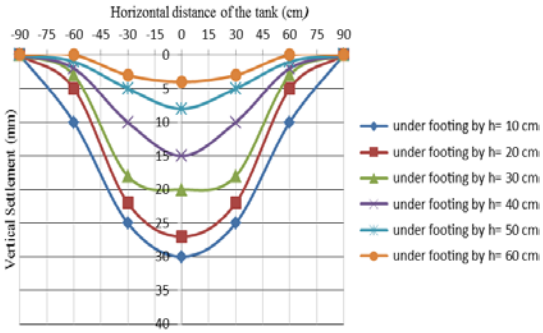

Fig. 13 Vertical Settlement (mm) on Face of Side Tank for Sandy Soil with 6 % Bentonite.

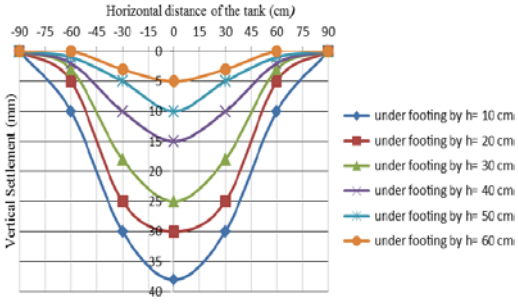

Fig. 14 Vertical Settlement (mm) on Face of Side Tank for Sandy Soil with 9 % Bentonite.

From Fig. 12, 13 and 14, it can be seen that the vertical settlement for loose sand decreased when mixed with 3, 6 % bentonite ratio, but when mix 9 % bentonite ratio with loose sand, the vertical settlement for mixture was increase.

CONCLUSIONS

The current research was carried out to clarify the effect of mixing loose sandy soil with 3, 6 and 9 % bentonite ratio. The following conclusions were drawn:-

1- The bearing capacity for loose sand increased when mixed with 3 % bentonite by 22 %. But when using 6, 9 % bentonite, it was decreased by 20, 22 % respectively, from the original bearing capacity. Thus, the maximum improvement ratio occurred at 3 % bentonite compared with the case of no bentonite ratio.
2- To improve the bearing capacity by bentonite mixing, it should be used a small enough and economy ratio, hence 3% is recommended through the experiments
3- The increase in bentonite ratio mixed with loose sand lead to increase the maximum dry density. But increase in bentonite ratio lead to increase the optimum moisture content (OMC) till 3% ratio, then the optimum moisture content decreased with increase the bentonite ratio more than 3%.
4- Bentonite is an effective material for plasticity properties, where it increases the liquid limit, and plastic limit was increased.
5- Bentonite is an effective material for decreasing voids ratio with increasing the applied pressure, for mix of bentonite ratio 3, 6 and 9 %.
6- The bentonite ratio of 3 % is recommended for enhancing the bearing capacity for loose sandy soil mixed with bentonite in field application.

REFERENCES

[1] Agapitus, and Kolawole “Evaluation of the Performance of Compacted Lateritic Soil - Bentonite Mixtures as Landfill Liner Material” 14th International Conference on Structural and Geotechnical Engineering, Ain Shams University, Cairo, Egypt, December, 20 - 22, 2015, pp.146 - 147.

[2] Wayal A.S., Ameta N.K and D.G.M. Purohit “Dune Sand Stabilization Using Bentonite and Lime” Journal of Engineering Research and Studies (JERS),Vol. III, Issue I, January-March, 2012, pp.58 - 60

[3] El.Mashad M. and Tetsuya H. “ Slag as Cementing Mixtures Used for Tunneling Tail Grouting”, 2nd Ain Shams University International Conference on Environmental Engineering, volume 3, Cairo, Egypt, April 10 -12, 2007, pp.16 - 31.

[4] El.Mashad Mohie Eldin, Tetsuya Hanamura “ Use of dune sand with fly ash, bentonite, and slag powder for road construction”, international conference on solid waste management International Conference on, for a Better Tomorrow: Sustainable Solid Waste Management in Developing Countries, Kathmandu, Nepal, January 8 - 13, 2006.

[5] Tetsuya H. and El.Mashad M. E. “Development of Dune Sands for Road Construction with Fly ash, Slag Powder and Bentonite”, 1st Ain Shams University International Conference on Environmental Engineering Cairo, Egypt, April 9 -11, 2005, pp.1189 - 1200.

[6] Rowe, R. K.; Quigley, R. M. and Booker, J. R., “Clayey Barrier Systems for Waste Disposal Facilities”, E & FN Spon, London, UK, 1995.

[7] Gleason, M. H., Daniel, D. E., and Eykholt, G. R., “Calcium and Sodium Bentonite for Hydraulic containment Applications”, J. Geotech and Geoenviron. Engrg, ASCE, 1997, Vol. 123, No. 5, pp. 438 – 445.

[8] American Society for Testing and Materials (ASTM - D421) “Standard Practice for Dry Preparation of Soil Samples for Particle-Size Analysis and Determination of Soil Constants” ASTM Book of Standards, Published in September, 2007.

[9] American Society for Testing and Materials (ASTM D1557- 09) “Standard Test Methods for Laboratory Compaction Characteristics of Soil Using Modified Effort (56,000 ft-lbf/ft^3 (2,700 kN-m/m3))” ASTM Book of Standards, Published in October, 2009.

[10] American Society for Testing and Materials (ASTM D3080-04) “Standard Test Method for Direct Shear Test of Soils Under Consolidated Drained Conditions” ASTM Book of Standards, Published in December, 2004.

[11] Egyptian code for soil mechanics and design and executing the foundations, 2009, part 2.

[12] José L.M. Clemente and Mounir Bouassida “Soil property improvement and environmental contamination” session in 6th International Conference on Case Histories in Geotechnical Engineering, Arlington, VA, August, 11 - 16, 2008.

Second International Conference on Science, Engineering & Environment,
Osaka City, Japan, Nov.21-23, 2016, ISBN: 978-4-9905958-7-6 C3051

A PRELIMINARY STUDY OF SOUND ABSORPTION COEFFICIENT FOR NATURAL FIBRES

N.H. Zunaidi[1], Wei-Hong Tan[2], M.S. Abdul Majid[3], EA Lim[4]
[1,2,3]Mechanical Engineering Programme, School of Mechatronic Engineering, Universiti Malaysia Perlis (UniMAP), Pauh Putra Campus, 02600 Arau, Perlis, Malaysia;
[4]Institute of Engineering Mathematics, Universiti Malaysia Perlis (UniMAP), Pauh Putra Campus, 02600 Arau, Perlis, Malaysia.

ABSTRACT

Malaysia is a country that has many types of natural fibre from the agriculture by-products. There are a lot of initiatives had been taken by the government and non-government sector to make use the agriculture waste and might generate on extra income for the farmers. One of the agriculture wastes is natural fibre which can be extracted from stems, leaves, roots, fruits and seeds of plants. In this study, natural fibres will be taken as the sound absorbent materials for the noise absorption purposes. There are two common natural fibres in Malaysia market was proposed for the sound absorption performance investigation, which include kenaf fibre and coir fibre. Sound absorption coefficients of the natural fibres were measured using the impedance tube according to ISO 10534-2. It can be observed that as the mass of natural fibre increase, the sound absorption coefficient also will increase relatively. Some of the others feature which affect the sound absorption coefficient of natural fibres also will be studied. As a conclusion the sound absorption coefficient investigation on the natural fibres was successfully conducted and it is a promising sound absorbent materials.

Keywords: Natural Fibre, Kenaf Fibre, Coir Fibre, Sound Absorption Coefficient and Impedance Tube

INTRODUCTION

As the development of industry is rapidly growth, there are a lot of noises produced which may cause the sound pollution for surrounding community. Sound pollution may contribute hearing loss to human [1]. In our surrounding, the average noise frequency produced is less than 2 kHz. The mechanisms for noise treatment include isolation, absorption and reflection [2]. Typically, the noise can be absorbed using the acoustic materials such as foam and stone wool which normally are synthetics porous material. Synthetic porous material is made from minerals which may cause health problem to human. Natural fibre is seems the good alternative absorbent material which is not only able to reduce the noise level and also environment friendly [3].

Natural fibre is the by-products of agriculture. In Malaysia, there are many type of agricultural activities. Those agricultural products have contributed to the economy growth. Apparently, majority of the plants have the fibre. The fibre of plants normally is extracted from the stem, leaf and pulp to produce the acoustic absorbent material. The advantages of natural fibre are cheaper, renewable, abundance and bio-degradable. Recent study has shown that natural fibres are capable as the effective acoustic materials [4]. However, natural fibre also has the limitations such as humidity, fungus and flammable [5]-[7]. There are many studies have been conducted to minimize the limitation of the natural fibre such as composite fibre with resin, chemically treated fibre and many more.

Based on the literature study, it is founded that natural fibre is considered as a good sound absorption acoustic material. It has been experimentally tested by using the industrial tea fibre waste. It showed a good sound absorption of 0.5 for the frequency range of 1500-6300Hz [8]. Besides that, there is another study on oil palm fruit where the fibre is extracted from the fruit. The result shows that the average sound absorption coefficient is 0.75 for the frequency 2500Hz and above [9]. Moreover, rice straw fibre also gives the good performance in sound absorption. From the experiment, it shows that the good sound absorption performance for the frequency 2000Hz and above [10].

In this study, two types of natural fibre will be investigated for the sound absorption coefficient. The frequency range to be considered is 60-1800Hz using fabricated impedance tube. The sound absorption performances of the natural fibres will be determined and analysed.

METHODOLOGY

Experiment setup

The experiment of sound absorption coefficient

measurement is conducted using impedance tube. The impedance tube is fabricated according to the ISO Standard 10534-2 Transfer Function Method. It is suitable for the sample in small size. Sound wave direction in the impedance tube is normal incidence. It means that the direction of sound wave is considered in one direction only. The frequency limit of the impedance tube is 60-1800Hz. The normal incidence sound absorption coefficient of the sample can be determined using the impedance tube. The sound absorption coefficient value range is from 0 to 1. The highest value of sound absorption coefficient is 1 with the meaning of all the sound wave energy is fully absorbed by the material. Figure 1 shows the experiment setup for sound absorption coefficient measurement.

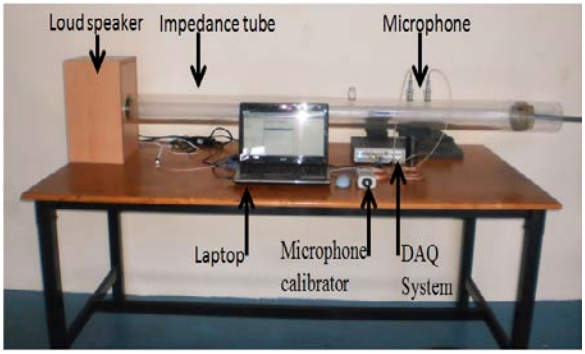

Fig. 1 Experiment setup for sound absorption coefficient measurement.

The fabricated impedance tube is used for the experiment. The impedance tube had been validated and ready to be used for the measurement. Every time before conducting the sound absorption coefficient measurement, the impedance tube is calibrated together with the microphones. The sample is fitted into one end of the impedance tube. Distance between both microphones is 70 mm. Meanwhile, the distance between first microphone and sound source is 1130 mm.

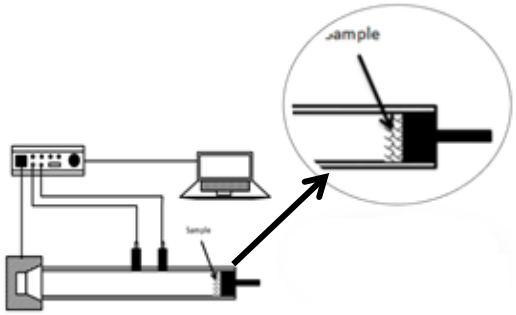

Fig. 2 Placement of sample at one end of impedance tube.

The distance between sample and nearest microphone is 350 mm. The loud speaker is allowed to warm up about 10 minutes before first measurement. This is to ensure the impedance tube is ready for measurement. Figure 2 is the placement of the sample in one end of the impedance tube.

Sample preparation

Two types of natural fibre are used in these experiments which are kenaf fibre and coir fibre. Cocos nucifera L. and Hibiscus cannabinus L. are the scientific names for coir fibre and kenaf fibre respectively. The coir fibre is bought in the market and kenaf fibre is obtained from Lembaga Kenaf dan Tembakau Perlis, Malaysia. The coir fibre and kenaf fibre in the form of loose as shown in Fig. 3.

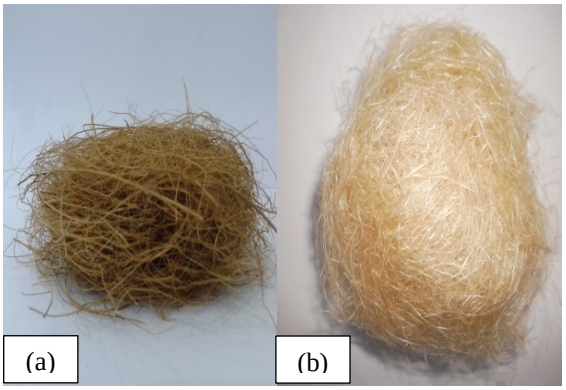

Fig. 3 (a) coir fibre and (b) kenaf fibre in the form of loose before compression.

The fibres are weighted in 5g, 10g and 15g. The fibres are cut into 1 inch long and fitted into a mild steel mould. The inner diameter of the mould is 99.5 mm which is 0.5mm smaller than the inner diameter of impedance tube [11]. Figure 4 is the mould and Shimazu Universal Testing Machine used to prepare the sample. By using the Universal Testing Machine, the natural fibre is compressed with an average force of $45 kg/cm^2$ [12]. Figure 5 shows the samples of compressed fibre.

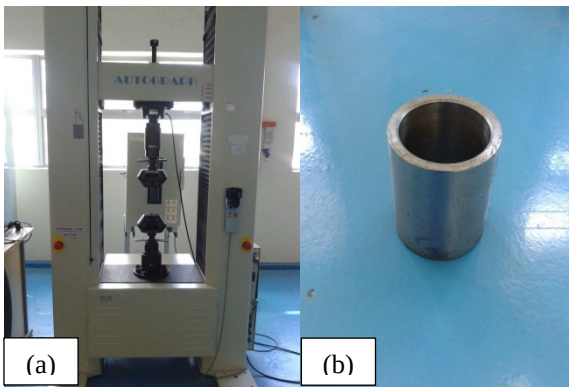

Fig. 4 (a) Shimazu Universal Testing Machine and (b) mould used for the sample preparation.

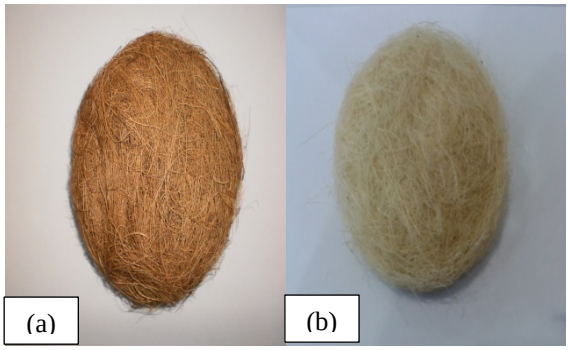

Fig. 5 The samples of compresses fibre, (a) coir fibre and (b) kenaf fibre.

RESULT AND DISCUSSION

Based on the sound absorption measurement, it is founded that coir fibre and kenaf fibre are able to absorb sound energy wave. Figure 6 shows the sound absorption coefficient of 5g coir fibre and kenaf fibre for the frequency up to 1800Hz. The maximum sound absorption coefficient for kenaf fibre and coir fibre are 0.15 and 0.2 respectively. Kenaf fibre has a higher sound absorption coefficient compared to coir fibre. Same phenomena happened as the mass of fibre increased, both also have increased in sound absorption coefficient [4],[13].

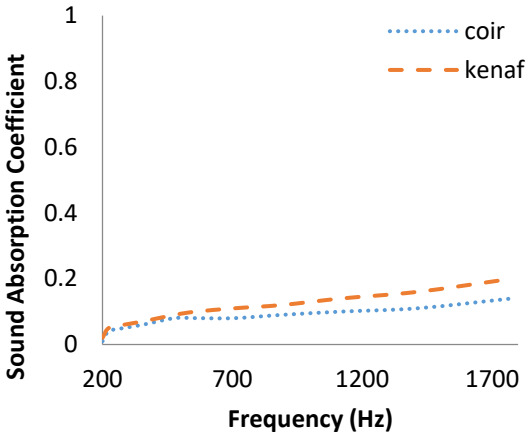

Fig. 6 Comparison of sound absorption coefficient of 5 g sample of coir fibre and kenaf fibre.

As the mass of fibre increases, it will enhance the sound absorption coefficient at low frequency. It can be seen clearly throughout the graph plotted in Fig. 6, Fig. 7 and Fig. 8. It is because, when the mass of fibre increases, sample becomes more porous and induces more sound energy waves will be absorbed by the sample [10].

According to the experiment conducted by Jailani et al., it shows that as the sample is compressed, it will cause the sample has many small pores. As the number of small pores increase, there are large frictional forces that will increase the sound absorption coefficient. Compressed fibre has a significant effect on the sound absorption. The compressed fibre is able to improve sound absorption and the increment of sound absorption coefficient is shifted to lower frequency range [14],[15].

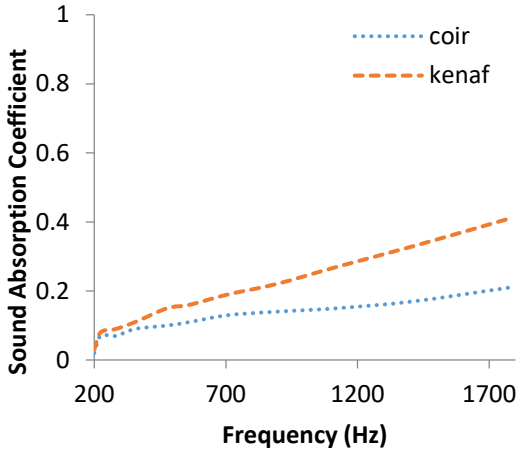

Fig. 7 Comparison of sound absorption coefficient of 10 g sample of coir fibre and kenaf fibre.

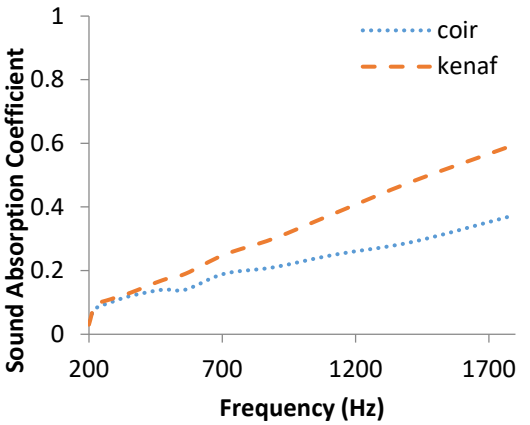

Fig. 8 Comparison of sound absorption coefficient of 15 g sample of coir fibre and kenaf fibre.

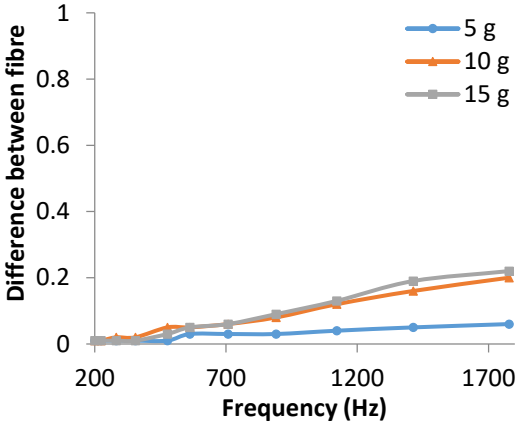

Fig. 9 Differences of sound absorption coefficient for coir fibre and kenaf fibre of 5g, 10g and 15g respectively

When compared with the diameter size of coir fibre and kenaf fibre, kenaf fibre diameter is found smaller than coir fibre. This will result a significant effect on the sound absorption performance and enhancing the sound absorption coefficient at low frequency [16]. Figure 6, Fig. 7 and Fig. 8 show that kenaf fibre sound absorption coefficient is relatively higher than coir fibre. It is because when the diameter of fibre is small and it will produce much more pores when compressed into the shape.

In Fig. 6, the difference of sound absorption coefficient between coir fibre and kenaf fibre is very small. This is because the mass of sample is low. When the sound wave energy strikes on the sample, most of the sound wave energy has been converted into heat energy and dissipated in the surrounding. This explains sample with lower 5g of natural fibre is unable to absorb much sound waves energy.

Figure 7 and Fig. 8 show a big different of sound absorption coefficient between of coir fibre and kenaf fibre. This is because 10g and 15g of fibre have much pores and it will absorb as much as possible the sound waves energy which strike on it. Therefore, as the mass increases, the sound absorption coefficient will also increase. By referring to the Eq. 1 with the constant velocity of sound when the frequency increases, the wave length will decrease. The relationship between the frequency and velocity of sound is inversely proportional. This is the reason, to explain the high frequency range has a higher sound absorption coefficient compared with low frequency range in this study.

$$v = f\lambda \tag{1}$$

where v is sound wave velocity, f is frequency and λ is wave length.

The difference of sound absorption coefficient of coir fibre and kenaf fibre is shown in Fig. 9. Based on the graphs of sound absorption coefficient in the Fig. 7 and Fig. 8, there are a small difference between 10g natural fibre and 15g natural fibre. It shows a slightly increase in sound absorption coefficient of 15g natural fibre compared with 10g natural fibre. However, sound absorption coefficient shows much difference as compared with 10g natural fibre and 15g natural fibre. Thus, this phenomenon is observed due to 5g of natural fibre unable to absorb expected sound energy wave.

CONCLUSIONS

In this study, there are two types of natural fibre – kenaf fibre and coir fibre are investigated. The sound absorption coefficient of two types natural fibres are determined and measured successfully using impedance tube for the frequency range of 60-1800Hz. As a conclusion, both natural fibres are able to absorb sound wave energy effectively. At the same time, it is also observed that as the mass of natural fibre increases, the sound absorption coefficient also increases relatively.

ACKNOWLEDGEMENTS

Authors would like to acknowledge the Ministry of Higher Education of Malaysia (MOHE) for supporting this research through the FRGS Grant (9003-00435) and the Lembaga Kenaf dan Tembakau Negeri Perlis, Malaysia for supplying the kenaf fibre.

REFERENCES

[1] L. Peng, B. Song, J. Wang, and D. Wang, “Mechanic and acoustic properties of the sound-absorbing material made from natural fiber and polyester,” *Adv. Mater. Sci. Eng.*, vol. 2015, Article ID 274913, 5 pages, 2015. doi: 10.1155/2015/274913.

[2] E. Jayamani, S. Hamdan, and N. B. Suid, “Experimental Determination of Sound Absorption Coefficients of Four Types of Malaysian Wood,” *Appl. Mech. Mater.*, vol. 315, pp. 577–581, 2013.

[3] I. F. Conference, C. Energy, and T. Cet, “Kenaf Arenga Pinnata,” *Investig. Nat. Waste Fibers from Dried Paddy Straw as a Sustain. Acoust. Absorber*, pp. 311–314, 2011.

[4] M. Nor, N. Jamaludin, and F. Tamiri, “A preliminary study of sound absorption using multi-layer coconut coir fibers,” *Elect. J. Tech. Acoust.*, vol. 3, 8 pages, 2004.

[5] M. Hosseini Fouladi, M. Ayub, and M. Jailani Mohd Nor, “Analysis of coir fiber acoustical characteristics,” *Appl. Acoust.*, vol. 72, no. 1, pp. 35–42, 2011.

[6] S. Fatima and a. R. Mohanty, “Acoustical and fire-retardant properties of jute composite materials,” *Appl. Acoust.*, vol. 72, no. 2–3, pp. 108–114, 2011.

[7] S. Y. Peng, S. Y. Wen, P. Z. Xin, S. Jegachandra, M. H. Fouladi, M. M. Shamel, C. C. Hwa, S. N. Namasivayam, M. Ghassem, and M. J. M. Nor, “Improvement of Fire Retardant Property of Natural Fiber,” *Appl. Mech. Mater.*, vol. 471, no. March 2016, pp. 261–266, 2013.

[8] S. Ersoy and H. Küçük, “Investigation of industrial tea-leaf-fibre waste material for its sound absorption properties,” *Appl. Acoust.*, vol. 70, no. 1, pp. 215–220, 2009.

[9] K. H. Or, a Putra, and M. Z. Selamat, “Oil palm empty fruit bunch fibers as sustainable

acoustic material," no. March, pp. 1–2, 2015.

[10] A. Putra, Y. Abdullah, H. Efendy, W. M. F. W. Mohamad, and N. L. Salleh, "Biomass from paddy waste fibers as sustainable acoustic material," *Adv. Acoust. Vib.*, vol. 2013, Article ID 605932, 7 pages, 2013. doi: 10.1155/2013/605932.

[11] N. Kino and T. Ueno, "Investigation of sample size effects in impedance tube measurements," *Appl. Acoust.*, vol. 68, no. 11–12, pp. 1485–1493, 2007.

[12] M. H. Fouladi and M. H. Nassir, "Utilizing Malaysian Natural Fibers as Sound Absorber," pp. 161–170, 2013.

[13] H. M. Akil, M. F. Omar, A. A. M. Mazuki, S. Safiee, Z. A. M. Ishak, and A. Abu Bakar, "Kenaf fiber reinforced composites: A review," *Mater. Des.*, vol. 32, no. 8–9, pp. 4107–4121, Sep. 2011.

[14] N. Amin, M. H. Fouladi, and S. Jaya, "Effect of Compression on the Acoustic Absorption of Coir Fiber Mohd Jailani Mohd Nor , 1 Md . Ayub , 1 Rozli Zulkifli , Department of Mechanical and Materials Engineering , Department of Electrical , Electronic and System Engineering , Faculty of Engineer," vol. 7, no. 9, pp. 1285–1290, 2010.

[15] C. N. Wang, Y. M. Kuo, and S. K. Chen, "Effects of compression on the sound absorption of porous materials with an elastic frame," *Appl. Acoust.*, vol. 69, no. 1, pp. 31–39, 2008.

[16] M. Nor, M. Ayub, Rozli Zulkifli, Nowshad Amin and M. H. Fouladi, "Effects of different factors on the acoustic absorption of coir fibre, " *Appl. Sci.*, vol. 10, no. 22, pp 2887-2892, 2010.

Second International Conference on Science, Engineering & Environment,
Osaka City, Japan, Nov.21-23, 2016, ISBN: 978-4-9905958-7-6 C3051

THE WORKLOAD ANALYSIS OF HIGHLY STRESSED CRITICAL APPLICATION

Rich Lee[13], Ing-Yi Chen [2]
[12]Computer Science, National Taipei University of Technology, Taiwan
[3]Systems Department, IBM, Taiwan

ABSTRACT

The intensity and variability of workload may attribute to most system failures or the sluggish performance. It is simply owing to the design strength not being able to respond the imposed stress from the stimulus. The successive impacts are severe especially when a critical application fails. Usually such kind of the workflow flooding toward the system may have distribution patterns across the time. Understanding these patterns of workload will disclose the insights of the imposed stress to the system and imply the root causes of the failure or the poor performance. This paper presents a novel analytic framework, designing the performance data collection scheme, analyzing the gathered data, identifying the likely-patterns, to disclose these insights by applying various statistical procedures against the workload. The empirical case was to improve the performance of their most critical and highly stressed trading application from a global financial security service firm; the sluggish performance will result huge monetary loss and wreck the business as well. The paper also discusses such a highly stressed critical application design issues about the efficiency improvement and the resource optimization, including the system and the software architecture to meet the performance requirement, the response time must be within microseconds.

Keywords: Software Engineering, Performance Analysis, System Reliability, Business Analytics

INTRODUCTION

The system's reliability is not just about the failures. If a system cannot meet the business requirements to give enough support against the competition of rivals, it is still a failed system. The security warrant bidding system is a speed race among the rivals; the winner usually takes major market share. In this competition, it is not enough just to improve the hardware equipment such as the computing resources and the bandwidth of the network because this is the easiest effort that every participants of the game will invest on. The system performance improvement requires the mature software design [1] and the problem analytic capability which always plays the decisive role in winning the competition.

The mature software design in this application is about knowing: (1) the multitasking programming, (2) how operating system works, (3) the consideration of choosing the proper inter-process-communication, and (4) the business essentials and the domain knowledge. Besides offering the solid solution about the modern bidding system, this paper presents an effective approach to elaborate the essence of the mature software design; it begins from the identifying the problem frame; giving the reasoning of potential resolution; to the real implementation.

THE PROBLEM FRAME

The Trading Exchange Center propagates the stock quotes every few seconds using the UDP communication scheme shown in **Fig. 1**. The security warrant firms receive all the stock quotes in a batch periodically. Every firm may have different concerned stocks than others based on their investors' interests. First, the firm's bidding system needs to decode the received data packets from UDP and then store them into a data structure that will facilitate the following process.

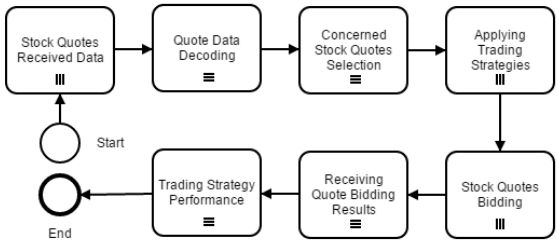

Fig. 1 The Stock Quotes Bidding Process

The system will drop those quotes that are not concerning to the investors. Each coming quote needs to look up a table to see if the stock is on the concerned list or not; if the coming quote is on the list, the system will apply a number of trading strategies based on the predefined criterion, sell high or buy low. Once the qualified criterions are met, the system will submit these bidding quotes to the Stock

Exchange Center. If the system executes the bidding quote strategies fast enough, for instance, after few cycle terms of propagation, the performance of the system will satisfy the investors' expectations, otherwise, the investors might switch to a better trading performance firm; consequently, the original one will lose the business competition.

The performance challenges of such as a system are: (1) the bandwidth of network and the associated equipment must be sufficient and efficient enough to receive the propagated data without any loss; (2) the propagation is similar to the streaming behavior—a random combination of stocks' data floods into the system in which time complexity is subject to the number of the quotes; (3) the efficiency of decoding the received packets and storing them into the desired data structure will determines the effectiveness of the following quote bidding; (4) the system must look up the concerned stock list—the process time complexity will be the multiplication of the number of received quotes and the number of the list—efficient for each received quote to decide whether to apply the strategies or not; (5) there are random number of investors' strategies—the process time complexity will be subject to the number of associated strategies—await the system to merit the received associated listed quote; and (6) the investors may require the trading performance proof—a comprehensive report based on the analytics of the trading logs—to convince themselves to continue their financial activities with the firm. Therefore, how to minimize the total consumed time,Time_{total}, is formulated in **Eq. 1**, will be the goal of the bidding system improvement.

$$\begin{aligned}\text{Time}_{total} = \text{Time}_{receving} + \text{Time}_{decoding} \\ + \text{Time}_{selection} \\ + \text{Time}_{strategies} \\ + \text{Time}_{bidding} \\ + \text{Time}_{result}\end{aligned} \quad (1)$$

Apparently, observing from the equations of **Eq.2**, **Eq. 5**, and **Eq. 6**, these time factors are either determined by the network equipment or the volatility of the stock market that impact to all firms; thus it can be treated as the constant functions. As long as the computing resources are sufficient, the equations of **Eq.3** and **Eq.4** actually determine the overall bidding performance and worth to look into the associated algorithms where can be further improved.

$$\begin{aligned}&\text{Time}_{decoding} \\ &= f3(\text{Quote}_{number}, \text{Algorithm}_{efficiency})\end{aligned} \quad (3)$$

$$\begin{aligned}&\text{Time}_{selection} \\ &= f4(\text{Quote}_{number}, \text{List}_{number}, \\ &\qquad \text{Algorithm}_{efficiency})\end{aligned} \quad (4)$$

$$\begin{aligned}&\text{Time}_{receving} \\ &= k2(\text{Quote}_{number}, \text{Network}_{efficiency})\end{aligned} \quad (2)$$

$$\begin{aligned}&\text{Time}_{bidding} \\ &= k5(\text{Quote}_{number}, \text{Network}_{efficiency})\end{aligned} \quad (5)$$

$$\text{Time}_{result} = k \quad (6)$$

THE COMMON APPROACH

The common approach of a bidding system, an abstract code, using the representation of the *Python* computer language listed in **Fig. 2**, basically is a loop process whenever the system receives a quote. The *ReadStockQuote*() shown in the line 2 is a function that receives the data stored in the *receivedPacket* variable from the UDP communication channel. The function of *TransformPacket*() shown in the line 3 transforms the *receivedPacket* into a desirable map data structure—a key-value pair—stored in the *incomingQuote* variable. If the *incomingQuote* is not on the concerned stock list through the function of *CheckStockList*(), the process drops that *incomingQuote* and return to the beginning of the loop and awaits the next *receivedPacket*.

```
1  while True:
2      receivedPacket = ReadStockQuote()
3      incomingQuote = TransformPacket(receivedPacket)
4
5      if not CheckStockList(incomingQuote['ID']):
6          continue
7
8      strategyList = GetStrategies(incomingQuote)
9      successCount = 0
10     failCount = 0
11
12     for strategy in strategyList:
13         if strategy['OBJECTIVE'] == 'SELL':
14             if incomingQuote['PRICE'] >= \
15                     strategy['PRICE']:
16                 if SubmitBid(
17                         incomingQuote['ID'],
18                         incomingQuote['PRICE']):
19                     successCount += 1
20                 else:
21                     failCount += 1
22         elif strategy['OBJECTIVE'] == 'BUY':
23             if incomingQuote['PRICE'] <= \
24                     strategy['PRICE']:
25                 if SubmitBid(
26                         incomingQuote['ID'],
27                         incomingQuote['PRICE']):
28                     successCount += 1
29                 else:
30                     failCount += 1
```

Fig. 2 The Common Approach of the Bidding System

The function of *GetStrategies*() shown in the line 8 loads all the stock associated trading strategies that predefined by the investors into the array of a map data stored in the *strategyList* variable. Every *strategy* shown in the line 12—in a map data structure—of the *strategyList* must be enumerated and checked to see if it meets the criterion or not.

The function *SubmitBid*() shown in the line 16 and 25 proposes a new quote of the strategy to the Stock Exchange Center; it returns the status of the proposal, success or fail. The system logs the stock, the quote, the new quote, and the status for latter bidding performance analysis.

The sub-process from the line 8 to the end will be more efficiently by using the threading scheme. The *SubmitBid*() associated blocks from the line 16 to 21 and from the line 25 to 30 can also be design in the threading approach, however, the log mechanism might require additional time in dealing with the locks to maintain the consistency of the values of the variables such as the *successCount* and the *failCount*.

THE SMARTER APPROACH

The aforementioned common approach does not consider the following factors: (1) the quotes might not have the equal probability of the occurrence flooding into the system; (2) the system might have not completed all the trading strategies before the next new quote comes in; (3) the overhead of marginal threading requests—the operating system asks for more RAM and CPU time to initiate a new thread—might cause more time consumption [2]; (4) more software threads might not be efficient due to the limitation of the kernel threads and the computing resources overhead when threads perform the context switches [3]—the operating system scheduling process that puts the active threads or processes into the hibernate state and resumes them back into the running state for better resource management; and (5) the total process time against a reasonable number of quotes in batch might be more efficient than dealing with the quotes separately by applying the proper algorithms.

The smart approach is to take advantage of GPU and to use big chunks of RAM to reduce the impacts of aforementioned factors. Since the trading strategies have been defined before the stock market opens, thus these strategies can be preloaded onto the RAM to save the time of on-demanded data loading. Secondly, using the super performance in mathematical computation of GPU to reduce the time in threading process might be a solution of better performance against the criterion searches. Lastly, if the time of the quotes flooding into the system is in a different and random way, then the smart approach can analyze the trading volatility of stocks based on the transactions of previous days. The idea is to find a better optimized workload execution plan according to the volatility behaviors of stocks, so that the deploying the systems onto additional servers will be helpful in consuming the coming quotes.

This approach is based on two assumptions: (1) the system processes the requests in batch would have better performance than in the individual; and (2) such a batch process would complete the trading strategies before next quotes flood in. Thus the conclusive factor is that the quotes must have some sort of patterns so that the smart approach can apply the divide-and-conquer tactics against different groups of stocks with various degrees of volatility.

THE RESEARCH PROCESS

As earlier mentioned, the first challenge of the smart approach is to affirmative that the quotes do have some patterns over a period of time. The research process illustrated as **Fig. 3** starts with gathering the received quotes including the following fields: (1) the stock identifier, (2) the time elapsed in seconds since the market opened, and (3) the quoted price. The velocity of a quote shown in **Eq. 7** is defined as the time difference between two consecutive quotes; and the acceleration of a quote shown in **Eq. 8** is defined as the velocity changed between two consecutive periods.

$$v(x, t_i) = time_i(x) - time_{i-1}(x), \quad i > 1, x \text{ is the quote identifier} \tag{7}$$

$$a(x, t_i) = v(x, t_i) - v(x, t_{i-1}), \quad i > 2, x \text{ is the quote identifier} \tag{8}$$

The next step is to transform the received quotes into a big two-dimensional matrix to hold all the quotes; the quotes may have different number of occurrences: $m \neq$ n; and $t_{i-1}(x_i) < t_i(x_i)$. The set of all stock identifiers $\{x_i \quad \cdots \quad x_k\}$ is fixed before the market opens.

$$\begin{bmatrix} x_i & t_1(x_i) & t_2(x_i) \cdots & t_m(x_i) \\ \vdots & \vdots & \vdots \quad \vdots & \vdots \\ x_k & t_1(x_k) & t_2(x_k) \cdots & t_n(x_k) \end{bmatrix} \tag{9}$$

Deriving from the **Eq. 9** to form the velocity shown in **Eq. 10** and the acceleration shown in **Eq. 13** matrices are shown as follows. These two derived matrices are important for pattern determination.

$$\begin{bmatrix} x_i & v_1(x_i) & v_2(x_i) \cdots & v_m(x_i) \\ \vdots & \vdots & \vdots \quad \vdots & \vdots \\ x_k & v_1(x_k) & v_2(x_k) \cdots & v_n(x_k) \end{bmatrix} \tag{10}$$

$$Mean_v(x_i) = \sum_{\varepsilon=1}^{m} v_\varepsilon(x_i) \,/\, m \tag{11}$$

$$Stdev_v(x_i) = \sqrt{\left\{\sum_{\varepsilon=1}^{m} [v_\varepsilon(x_i) - Mean_v(x_i)]^2\right\} / m} \tag{12}$$

The **Eq. 11** represents the mean velocity value of the stock $\boldsymbol{x_i}$; the smaller mean value implies that the stock trades in a more volatile manner. The **Eq. 12**

represents the standard deviation of the stock; the smaller value means the velocities are steadier than others.

$$\begin{bmatrix} x_i & a_1(x_i) & a_2(x_i) \cdots & a_m(x_i) \\ \vdots & \vdots & \vdots \quad \vdots & \vdots \\ x_k & a_1(x_k) & a_2(x_k) \cdots & a_n(x_k) \end{bmatrix} \quad (13)$$

In the similar way, deriving from the **Eq. 13** to form the acceleration shown in **Eq. 14** and the acceleration shown in **Eq. 15** matrices are shown as follows. These two derived matrices are also important for pattern determination.

$$Mean_a(x_i) = \sum_{\varepsilon=1}^{m} a_\varepsilon(x_i) \,/\, m \quad (14)$$

$$Stdev_a(x_i) = \sqrt{\left\{\sum_{\varepsilon=1}^{m} [a_\varepsilon(x_i) - Mean_a(x_i)]^2\right\} / m} \quad (15)$$

The **Eq. 14** represents the mean acceleration value of the stock $\boldsymbol{x_i}$; the smaller mean value implies that the stock velocity changes in a steadier manner. The **Eq. 15** represents the standard deviation of the stock velocity change; the smaller value means the velocity changes are more promising than others.

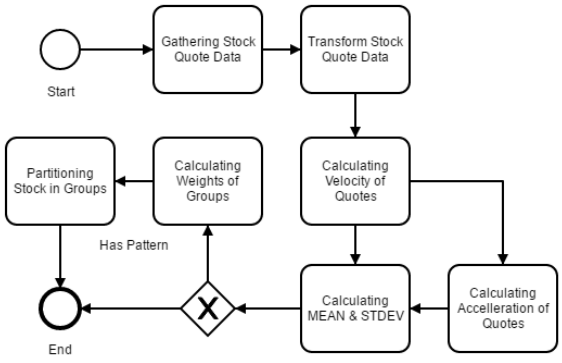

Fig. 3 The Research Process

THE RECEIVED QUOTE DATA OBSERVATION

This paper collected the received quote data from *2016-04-25* to *2016-06-01*, total 14 days. The Stock Exchange Center starts propagating the quotes from 09:00 for every trading day. There are about 400 stocks everyday; each stock may have different number of quotes than others according to its market volatility. The maximal time frames for a trading day are $(60_{sec}/5_{sec}) * 60_{min} * 4.5_{hr} = 3{,}240_{frame}$ if using 5 seconds as the time length of a frame. So the total volume of the received data is $400_{stcoks} * 3{,}240_{frame} = 1{,}296{,}000_{packet}$; each packet data length is a constant. Suppose that the firm has 1,000 clients, each client has 40 stocks ($400_{stcoks} * (1/10)$, one tenth of the total stocks) on-hand, each client sets two trading strategies (Buy-Low and Sell-High) for each on-hand stock. It means the system requires matching up total 4,000 strategies for each received quote; therefore, the total occurrence of the matchup is $400_{stcoks} * 4{,}000_{strategy} = 1{,}600{,}000_{times}$. If the system wishes to complete these matchup tasks within 5 seconds; each strategy only has 3.125μ seconds to match up.

It is worth noting that the length of time frame, the number of clients, and the number of on-hand strategies for a stock are conservative estimates. The actual time length for a strategy to match up will be more challenging and less than 3.125μ seconds.

The **Fig. 4** shows the most velocities (the time difference between two consecutive quotes) fall into 5 to 10 seconds for the sample stock (id:0050). The **Fig. 5** shows the average velocity is 5.620 and the average standard deviation is 1.783. The **Fig. 6** shows the average and the standard deviation of the acceleration are almost "stable" (mean: -0.001, stdev:2.447) if exclude the first two days. This information implies that the system must put this sample stock on the highest priority to complete the matchup. Because in the 5-second time frame scenario, the stock quotes flood into the system every time frame during the observed 14-day period.

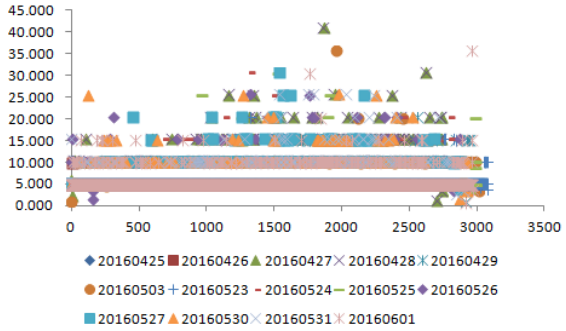

Fig. 4 The Sample Velocity Scatter Plot

The **Fig. 7** using the same scenario, examines the quotes of *2016-05-28*, calculating the probabilities of the quotes' falling into the time frames, shows there is general positive nonlinear pattern ($\boldsymbol{R^2 = 0.711}$) of $\boldsymbol{y = ax^2 + bx + c}$ **[4]**. This implies when the system will be busy and the resources peaks. From the aforementioned received quotes analysis, this paper concludes that the critical assumption—the received quotes flooding into the system has some sort of pattern—of the smart approach is affirmative. These findings are also confirmed by the international financial service firm, the research subject.

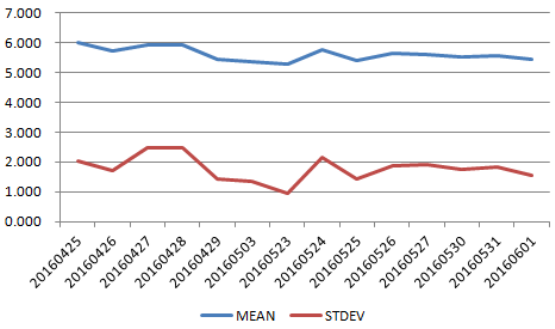

Fig. 5 The Sample Velocity MEAN/STDEV Plot

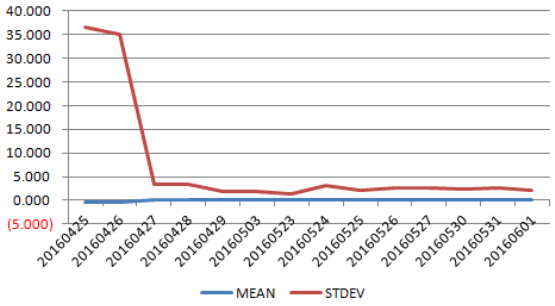

Fig. 6 The Sample Acceleration MEAN/STDEV Plot

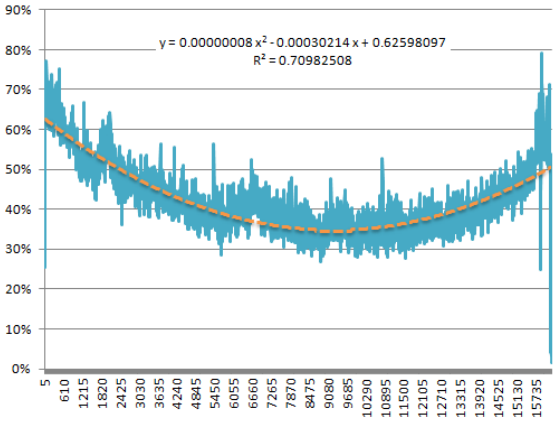

Fig. 7 The Sample Probability/Frame Plot for a Day

THE ALGORITHM

To reduce the repetitive strategy matchup time for every coming quote, this paper proposes a novel way to deal with the selection and the matchup time efficiently by using the matrix arithmetic operations and taking advantage of the use of big memory chunks. Since the number stocks and the strategies are fixed before the market opens, the system can preload these information onto the RAM illustrated in **Fig. 8**. The first two columns are the received quote information namely the stock identifier and the price in a particular time frame; the zero-priced stocks are not received at this time frame. Each trading strategies contains two columns, the prices of buy and sell; the zero-priced stocks are none concerned by the clients. This may be a big scare matrix with zeros.

$$\boldsymbol{Q_m} = [\boldsymbol{q_1}, \boldsymbol{q_2}, \cdots \boldsymbol{q_m}], \quad (16)$$
$$\boldsymbol{q_m}\ \textbf{is the quote of}\ \boldsymbol{stock_m}$$

$$\boldsymbol{S_{m,i}} = [\boldsymbol{s_{m,1}}, \boldsymbol{s_{m,2}}, \cdots \boldsymbol{s_{m,n}}], \quad (17)$$
$$\boldsymbol{s_{m,n}}\ \textbf{is the strategy}\ _{\boldsymbol{n}}\textbf{of}\ \boldsymbol{stock_m}$$

$$\boldsymbol{R_{m,i}} = [\boldsymbol{r_{m,1}}, \boldsymbol{r_{m,2}}, \cdots \boldsymbol{r_{m,n}}], \quad (18)$$
$$\boldsymbol{r_{m,n}}\ \textbf{is the strategy}\ _{\boldsymbol{n}}\ \textbf{result of}\ \boldsymbol{stock_m}$$

Received		Strategy 1		Strategy 2		Strategy 3		Strategy 4	
Stock	Quote	Buy	Sell	Buy	Sell	Buy	Sell	Buy	Sell
0050	63.900	63.000	66.000	62.000	65.000	65.000	63.000	62.000	60.000
0051	24.230	25.000	29.000	21.000	20.000	30.000	30.000	21.000	22.000
0052	0.000	37.000	39.000	31.000	38.000	39.000	37.000	38.000	31.000
0053	27.190	24.000	28.000	29.000	25.000	22.000	27.000	20.000	21.000
0054	20.220	23.000	27.000	22.000	30.000	23.000	24.000	24.000	24.000
0055	12.710	16.000	62.000	18.000	70.000	20.000	61.000	13.000	69.000
0056	22.050	21.000	30.000	29.000	25.000	24.000	30.000	21.000	23.000
0057	0.000	32.000	33.000	33.000	38.000	36.000	32.000	34.000	37.000
0058	0.000	37.000	35.000	31.000	38.000	30.000	36.000	39.000	31.000
0059	29.930	30.000	21.000	20.000	27.000	25.000	26.000	30.000	30.000
6203	29.830	27.000	24.000	28.000	26.000	25.000	23.000	22.000	24.000
6204	42.340	45.000	44.000	50.000	40.000	43.000	46.000	50.000	48.000
6205	27.200	20.000	27.000	22.000	22.000	26.000	21.000	27.000	26.000
6206	25.980	25.000	21.000	26.000	29.000	22.000	24.000	20.000	20.000
6207	20.510	30.000	24.000	24.000	28.000	27.000	23.000	21.000	27.000
6208	0.000	38.000	38.000	37.000	30.000	30.000	30.000	36.000	35.000
00631L	19.610	15.000	16.000	15.000	15.000	19.000	20.000	19.000	18.000

Fig. 8 The Sample Matrix of Quotes and Strategies

Received		Strategy 1		Strategy 2		Strategy 3		Strategy 4	
Stock	Quote	Buy	Sell	Buy	Sell	Buy	Sell	Buy	Sell
0050	63.900	0.000	0.000	0.000	63.000	0.000	0.000	61.000	0.000
0051	24.230	0.000	24.000	0.000	0.000	23.000	0.000	0.000	0.000
0052	0.000	0.000	0.000	0.000	0.000	0.000	0.000	0.000	0.000
0053	27.190	23.000	0.000	0.000	27.000	0.000	0.000	0.000	21.000
0054	20.220	0.000	0.000	0.000	0.000	20.000	0.000	0.000	0.000
0055	12.710	0.000	0.000	0.000	0.000	0.000	0.000	0.000	0.000
0056	22.050	0.000	20.000	20.000	0.000	0.000	0.000	22.000	21.000
0057	0.000	0.000	0.000	0.000	0.000	0.000	0.000	0.000	0.000
0058	0.000	0.000	0.000	0.000	0.000	0.000	0.000	0.000	0.000
0059	29.930	0.000	27.000	22.000	24.000	27.000	23.000	26.000	27.000
6203	29.830	0.000	24.000	22.000	24.000	20.000	28.000	0.000	23.000
6204	42.340	0.000	40.000	42.000	0.000	0.000	0.000	40.000	41.000
6205	27.200	24.000	0.000	23.000	27.000	24.000	0.000	0.000	26.000
6206	25.980	0.000	25.000	23.000	0.000	25.000	25.000	0.000	25.000
6207	20.510	0.000	0.000	0.000	0.000	0.000	0.000	0.000	20.000
6208	0.000	0.000	0.000	0.000	0.000	0.000	0.000	0.000	0.000
00631L	19.610	15.000	16.000	19.000	17.000	17.000	19.000	18.000	0.000

Fig. 9 The Sample Result Matrix of Strategies

The **Eq. 16** represents **Fig. 9** the second column, a scalar vector containing the received quotes', $\boldsymbol{Q_m}$. The **Eq. 17** represents a tuple vector, each $\boldsymbol{S_{m,i}}$ has two elements—the prices of buy and sell, containing the associated trading strategy. The $\boldsymbol{R_{m,i}}$ is the matchup result of the represented strategy.

$$\boldsymbol{R_{m,i}(Buy)} = \boldsymbol{IF}(\boldsymbol{AND}(\boldsymbol{q_m}, \boldsymbol{s_{m,n}}, \boldsymbol{q_m} \geq \boldsymbol{s_{m,n}}), \boldsymbol{s_{m,n}}, \boldsymbol{0}) \quad (19)$$

$$\boldsymbol{R_{m,i}(Sell)} = \boldsymbol{IF}(\boldsymbol{AND}(\boldsymbol{q_m}, \boldsymbol{s_{m,n}}, \boldsymbol{q_m} \leq \boldsymbol{s_{m,n}}), \boldsymbol{s_{m,n}}, \boldsymbol{0}) \quad (20)$$

The **Eq. 19** represents the result of the buy-strategy, $\boldsymbol{AND}()$ is the and-logic operator, $\boldsymbol{IF}()$ returns the second parameter if the criteria is met, otherwise it returns the third parameter. The **Eq. 20** is similar to **Eq. 19**; the only difference is the criteria. The **Fig. 9** illustrates the results of the above

mentioned equations (**Eq. 19** and **20**); the results of zeros mean the associated strategies were not met.

THE IMPLEMENTATION

This paper proposes a new daily operation for better management in using the techniques addressed in the smart approach. First, the bidding system will be deployed onto several different servers based on the selected stock groups by their market volatility. The deployed server only manages the concerned stocks and the associated strategies to reduce the matchup cost instead of searching a full concerned list for each received quote. The *Stock Volatility Analysis* in the **Fig. 10** consists of the aforementioned calculations of the velocity and the acceleration. Sort the acceleration's standard deviations and the mean values to pick the most "stable" stocks; then sort the velocity mean values based on the stable stock list. Partition the stable stock list into groups according to the number of the available servers equipped with GPU and huge RAM.

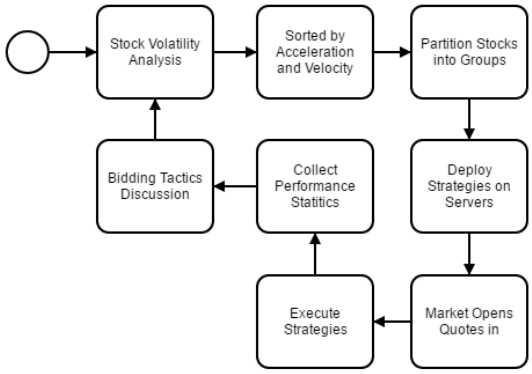

Fig. 10 The Proposed Daily Operation

The proposed new bidding system will collect the performance statistics during the trading hours. After the market closed, the business team holds a daily discussion meeting to evaluate the performance of the tactics defined by the previous trading date; the topics should cover the quote volatility behaviors, the priority list, and the adjustments suggested by the trading analysts.

DISCUSSION AND CONCLUSION

From the promising performance result of the empirical implementation, it demonstrates the orchestration of CPU and GPU **[5]** to resolve a heavy computational problem; let CPU manage the main program and the I/O, and push the complicated redundant calculations to GPU which was the purpose of design. The major pitfall is the time consumption of moving from the CPU-managed memory to the GPU's **[6]** through the PCIe bus. There is a technology of "*Coherent Accelerator Processor Interface*" **[7]** which let CPU and GPU share the memory module to reduce the time in moving the data back and forth between the processors.

Apparently, the business team emphasizes the trading impact from the financial perspective as well as the competition of rivals. The stocks with higher prices are more important to the firm because of the significance of the investment. The proposed smart approach is fully capable of reliving this concern. It seemly slightly improves the sorting formula as: $\boldsymbol{F = Quote_i * a_i \ or \ MV = Quote_i * v_i}$, borrowed from the *Newton's* 2nd *Law* by using the price of the quote as the mass, to reflect the importance of higher price stocks.

Nowadays, the software design requires the multidisciplinary skills and knowledge to resolve the real world problem. The proposed smart approach leverages the GPU's high performance calculation capability, the capability of identifying the problem frame; and most importantly, applying the mathematical and the statistical techniques to improve or giving the supporting rationale to the resilience of design.

REFERENCES

[1] V. M. G. M. A. &. R. S. Bendinskas, "Towards Mature Software Process," *Information Technology And Control,* vol. 34, no. 2, 2015.

[2] A. Silberschatz, Operating System Concepts, 9th Edition, Wiley, 2012.

[3] Illinois Institute of Technology, "User and Kernel Level Threads," 2016. [Online]. Available: http://www.cs.iit.edu/~cs561/cs450/ChilkuriDineshThreads/dinesh's%20files/User%20and%20Kernel%20Level%20Threads.html.

[4] F. Yao and H.-G. Müller, "Functional Quadratic Regression," *Biometrika,* vol. 97, no. 1, pp. 49-64, 2010.

[5] J. D. Owens, M. Houston, D. Luebke, S. Green, J. E. Stone and J. C. Phillips, "GPU Computing," *Proceedings of the IEEE,* vol. 96, no. 5, pp. 879-899, 2008.

[6] B. Jang, D. Schaa, P. Mistry and D. Kaeli, "Exploiting Memory Access Patterns to Improve Memory Performance in Data-Parallel Architectures," *IEEE Transactions on Parallel and Distributed Systems,* vol. 22, no. 1, pp. 105-118, 2010.

[7] IBM, "POWER8 Coherent Accelerator Processor Interface (CAPI)," 2016. [Online]. Available: http://www-304.ibm.com/support/customercare/sas/f/capi/home.html.

Second International Conference on Science, Engineering & Environment,
Osaka City, Japan, Nov.21-23, 2016, ISBN: 978-4-9905958-7-6 C3051

VERTICAL HANDOVER DECISION BASED ON LEARNING VECTOR QUANTIZATION NEURAL NETWORKS WITH MULTI-CRITERIA FOR UBIQUITOUS WIRELESS NETWORKS

Sunisa Kunarak
Department of Electrical Engineering, Srinakharinwirot University, Nakhonnayok, Thailand 26120
Email: sunisaku@g.swu.ac.th

ABSTRACT

Vertical handover decision management is an essential to keep the seamless ubiquitous heterogeneous wireless networks since each access network has different operations in the next generation. In this paper, WCDMA, LTE and WLAN are cooperated in the architecture of mobile IP regional registration (MIP-RR). We propose the Learning Vector Quantization Neural Networks (LVQNNs) approach in order to maintain uninterrupted communication that depends on received signal strength indicator, data rate requirement, monetary cost of service and mobile terminal device speed metrics are considered as multi-criteria to initial handover. Furthermore, the multi-criteria are dynamic to influence for real-time and non-real time services in different networks and the users select the optimal target network which is the highest handover factor score in order to balance against the network condition and user preference. To ensure the Always Best Connected (ABC) demands, the simulation results illustrate that our proposed algorithm provided outperform the performance in term of unnecessary handover, the call dropping probability, data packet delay and network utilization compared with conventional method as fuzzy logic and neural network based machine learning.

Keywords: Always Best Connected, Heterogeneous Wireless Networks, Learning Vector Quantization Neural Networks, Mobile IP Regional Registration, Vertical Handover

INTRODUCTION

The growing demand of the mobile users for accessing diverse services anywhere and anytime in order that react the trouble so the mobile and wireless systems introduce to cooperate the integration of different mobile users and wireless access technologies that is called next generation wireless networks. Next generation wireless networks as multimedia services are to be offered with various quality of service (QoS) settings. Thus, sophisticated handover method are to be developed to cope with such diverse QoS requirements. Handover is the procedure of changing the mobile connection between different base stations or access points. In heterogeneous wireless networks separated into horizontal handover and vertical handover. The horizontal handover is a traditional handover that occurs in the same link layer technology. Contrast to horizontal handover, the vertical handover happens between access networks with different link layer technologies and the decision process not only requires as received signal strength indicator (RSSI), but also requires the dynamic factors are mainly dependent on mobile terminals such as speed and battery status, and network conditions as bit error rate (BER), Signal Interference Ratio (SIR) and so on.

In general the vertical handover process involves three main phases as following 1) system discovery i.e. the mobile terminals equipped with multiple interfaces have to determine the available candidate networks and the available services; 2) handover decision i.e. the mobile device has to decide whether the connections should continue using current network or be switched to another network so this phase is a crucial procedure in the wireless communication; and 3) handover execution as the connections need to be rerouted from the current network and the transfer of context information.

Therefore, many researchers have been done on vertical handover decision algorithm. Reference [1] is considered the RSSI that is only main criterion for the vertical handover procedure so this algorithm is not practical. The hysteresis-based and dwelling time-based are evaluated the vertical handover approach [2] but these method rely on sampling and averaging RSS points, which introduces increased handover delay. Analytic Hierarchy Process (AHP) was proposed by [3-4]; the network with the highest performance score is selected on target network but this method ignores the wireless environment. Finally, Multiple Attribute Decision Making (MADM) approach is the combination of methods and uses the many parameters at the same time (e.g. neural networks, fuzzy logic, neuro-fuzzy, etc.) however this algorithm neglects the wireless surrounding, which may cause handover delay and increase the dropped call [5-9]. To defeat these

problems, the received signal strength indicator, bandwidth (BW), mobile speed (MS) and monetary cost (MC) metrics are used the multi-criteria parameters for Learning Vector Quantization Neural Networks process in our proposed. In addition, the wireless surrounding as receiving signal strength indicator is considered the log-linear path loss with shadow fading model.

The remainder of the paper is organized as follow. Learning Vector Quantization Neural Networks (LVQNNs) approach is explained in section II. Section III, vertical handover decision based on LVQNN with multi-criteria is presented. Finally, simulation results and conclusion are discussed in section IV and V, respectively.

LEARNING VECTOR QUANTIZATION NEURAL NETWORKS

The learning vector quantization (LVQ) is presented by Kohonen as a classification approach. LVQ architecture composes a first competitive layer and a second linear layer as shown in Fig. 1. The competitive layer learns to classify input vectors in much the same way as the competitive layer of cluster with Self-Organizing Map (SOM) neural network that is a similar method for unsupervised learning. Moreover, the linear layer transforms the competitive layer's classes into target classifications defined by the user. The classes learned by the competitive layer are referred to as subclasses and the classes of the linear layer as target classes. This algorithm is much more efficient, since the number of vectors that should be stored and compared with is significantly reduced [11], [12].

Learning Vector Quantization

The learning vector quantization process and type of learning as distance learning are following [13]. The training data set is assigned as $\mathbf{X} = \left\{ \left(\mathbf{x}_i, y_i \right) \subset \Re^D \times \left\{ 1,...,C \right\} \middle| i = 1,...,N \right\}$ where $\mathbf{x} = \left(x_1,..., x_D \right) \in \Re^D$ are input samples with $D-$ dimensional and have cardinality $\left| \mathbf{X} \right| = N$. Also, the sample labels are $y_i \in \left\{ 1,...,C \right\}$; $i = 1,..., N$ form, and C is the number of classes. The neural network includes a number of training patters, that are characterized by vectors $\mathbf{w}_i \in \Re^D$, for $i = 1,..., M$ and their class labels $c\left(\mathbf{w}_i \right) \in \left\{ 1,...C \right\}$ with output sets as $\mathbf{Y} = \left\{ c\left(\mathbf{w}_j \right) \in \left\{ 1,...,C \right\} \middle| j = 1,...,M \right\}$. The winner-takes-all strategy is brought to the classification scheme also known as the best matching unit (BMU). The $\mathbf{w}_i$ is defined as the receptive field of training patterns as following:

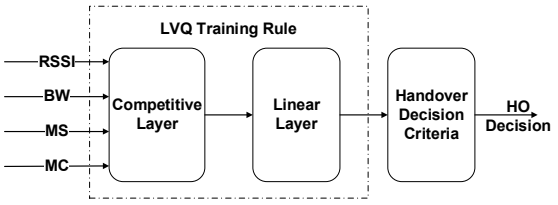

Fig. 1 Learning vector quantization process.

$$R^i = \left\{ \mathbf{x} \in \mathbf{X} \middle| \forall \mathbf{w}_j \left(j \neq i \right) \rightarrow d\left(\mathbf{w}_i, \mathbf{x} \right) \leq d\left(\mathbf{w}_j, \mathbf{x} \right) \right\} \quad (1)$$

where $d\left(\mathbf{w}, \mathbf{x} \right)$ is a distance measure. The objective of learning process is to determine the weight vectors, so that the training data samples are mapped to their corresponding class label.

Distance Learning

The LVQ approach is based on the Euclidean distance. We use the received signal strength indicator, bandwidth, mobile speed and monetary cost metrics as the heterogeneous datasets. Nevertheless, there can be different scaling and correlations of the dimensions, thus the estimate errors accumulate can confuse the classification. The distance measure is adaptive during training also known as a generalized distance metric is proposed as

$$d^{\Lambda}\left(\mathbf{w}, \mathbf{x} \right) = \left(\mathbf{x} - \mathbf{w} \right)^T \Lambda \left(\mathbf{x} - \mathbf{w} \right) \quad (2)$$

where Λ is a full $D \times D$ matrix size. To get a valid metric, Λ must be positive definite. So, this is achieved by substituting $\Lambda = \Omega^T \Omega$ which yield $\mathbf{u}^T \Lambda \mathbf{u} = \mathbf{u}^T \Omega^T \Omega \mathbf{u} = \left(\Omega^T \mathbf{u} \right)^2 \geq 0$ for all $\mathbf{u}$, where $\Omega \in \Re^{D \times D}$. The receptive field of training patterns $\mathbf{w}_i$ becomes

$$R_{\Lambda}^i = \left\{ \mathbf{x} \in \mathbf{X} \middle| \forall \mathbf{w}_j \left(j \neq i \right) \rightarrow d^{\Lambda}\left(\mathbf{w}_i, \mathbf{x} \right) \leq d^{\Lambda}\left(\mathbf{w}_j, \mathbf{x} \right) \right\} \quad (3)$$

If Λ is ignored to being diagonal matrix, then arbitrary Euclidean distance in Eq. (2) is reduced to

$$d^{\lambda}\left(\mathbf{w}, \mathbf{x} \right) = \left\| \mathbf{x} - \mathbf{w} \right\|_{\lambda}^2 = \sum_{j=1}^{D} \lambda_j \left(x_j - w_j \right)^2. \quad (4)$$

VERTICAL HANDOVER DECISION BASED ON LVQNN WITH MULTI-CRITERIA

The heterogeneous networks join with Wide-band Code Division Multiple Access (WCDMA), Long Term Evolution (LTE) and Wireless Local Area Network (WLAN). There are two types for

combinations as tightly and loosely coupled interworks. In tightly coupled type, WLAN and LTE are connected to WCDMA core network via radio access network. In loose coupling type, WLAN and LTE can access an IP network without connecting to WCDMA as illustrated in Fig. 2. So, the loosely coupled type is used in our proposed algorithm since its coupling provides a flexible and independent environment due that this scheme is based on mobile IP (MIP) [14]. Additionally, the management of mobile nodes to move between two sub-networks within one domain is referred to as the micro-mobility. In the micro-mobility management using hierarchical Mobile IP Regional Registration (MIP-RR), a visited domain consists of two hierarchy levels of foreign agents (FA) and Gateway FA (GFA). GFA is an entity located at the top of hierarchy whereas one or more FAs are organized under a GFA. The benefit of the MIP-RR is to reduce the packet loss and signaling delay by only regional registering to the GFA transparent to the home agent (HA).

The handover decision criteria in our proposed algorithm is different depending on the user preferences and network characteristics. For example, the real time applications (e.g. video conference), handover should be performed as rapid as possible in order to minimize the delay. On the contrary, non-real time services (e.g. e-mail) the amount of data transmission is more important than the delay. Therefore, the handover criteria for non-real time service is to attempt to connect WLAN/LTE as long as possible due to higher data rate provided as shown in Table 1 and Table 2, respectively. Table 1 is illustrated the some multi-criteria cases for WCDMA whereas the user is in WLAN/LTE thus our algorithm use instead Table 2.

Our proposed approach as vertical handover decision based on LVQNN with multi-criteria is shown in Fig. 3. The procedure correct the handover metrics such as RSSI, BW, MS and MC from users and the information leads to LVQNN process based on multi-criteria. If the handover factor is greater than 0.6 so the handover is established. Otherwise, the handover call is dropped.

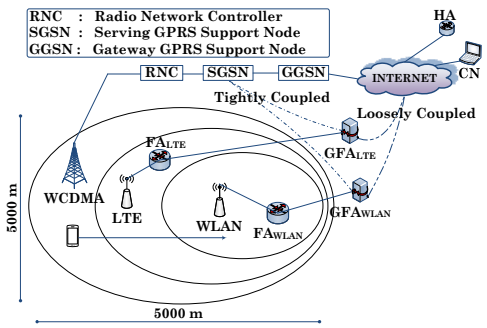

Fig. 2 Heterogeneous wireless networks topology.

Table 1 Handover decision criteria for WCDMA

RSSI	BW	MS	MC	HO Decision
L	M	L	L	HO
L	H	L	L	HO
M	L	L	L	NOHO
H	L	L	L	NOHO
M	M	L	L	HO
M	M	M	L	HO
M	M	H	L	NOHO
H	M	L	M	NOHO
H	M	L	H	NOHO

Table 2 Handover decision criteria for WLAN/LTE

RSSI	BW	MS	MC	HO Decision
L	M	L	L	HO
L	H	L	L	NOHO
M	L	L	L	NOHO
H	L	L	L	NOHO
M	M	L	L	NOHO
M	M	M	L	NOHO
M	M	H	L	HO
H	M	L	M	NOHO
H	M	L	H	NOHO

Note that: L = Low, M = Medium, H = High, HO = Handover, NOHO = No Handover

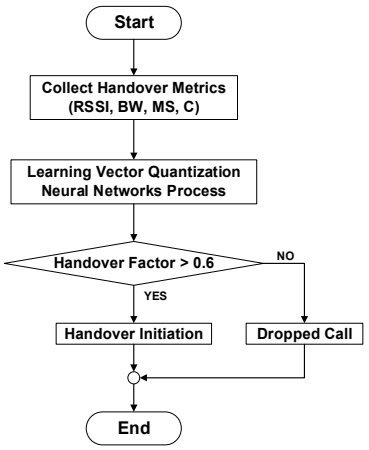

Fig. 3 Vertical handover decision based on LVQNN with multi-criteria.

SIMULATION RESULTS

In our simulation, the handover decision is performed by a mobile terminal (MT). We adopt the mobile-controlled handover (MCHO) strategy. Also, we utilize the simulation parameters of WCDMA, LTE and WLAN as depicted in Table 3.

Table 3 Simulation parameters

Parameters	WCDMA	LTE	WLAN
Frequency (GHz)	2.1	2.6	2.4
Coverage area (m)	5000	1000	100
Transmission power (w)	1.0	0.5	0.1
Bit rate (Mbps)	0.384	35	54
Latency (ms)	35	25	3
Mobile speed (m/s)	80	130	5
Bit error rate (per 10^8)	50	100	200
Monetary cost rate	0.8	0.7	0.4

Received Signal Strength Indicator

The channel propagation model of the RSS received by a mobile terminal is different in various types of networks. We use a log-linear path loss channel propagation with shadow fading model in WLAN as following

$$RSS(d) = P_T - L - 10\beta \log_{10}(d) + \varepsilon \quad (5)$$

where P_T is the transmitted power, L is a constant power loss, β is the path loss exponent, d is the distance between mobile user and base station or access point, ε is a zero-mean Gaussian random variable with standard deviation.

In LTE, the path loss at distance is formulated as

$$PL(d)_{\mathrm{dB}} = 20\log\left(\frac{4\pi d_0}{\lambda}\right) + 10n\log\left(\frac{d}{d_0}\right) + \chi_\sigma \quad (6)$$

where the first term represents the free space path loss at the reference distance d_0, λ is the wavelength.

Finally, the path loss of WCDMA at distance is created as

$$PL(d)_{\mathrm{dB}} = S + 10n\log(d) + \chi_\sigma \quad (7)$$

where S denotes the path loss constant, n denotes the path loss exponent and χ_σ represents the shadow effects which is a zero-mean Gaussian distributed random variable with standard deviation σ (dB).

Learning Vector Quantization Neural Network Interval Analysis

The received signal strength, bandwidth, mobile speed and monetary cost as the input are introduced into LVQNN process and these parameters are separated into 3 intervals such as low, medium and high as shown in Table 4-7, respectively. Note that, each parameter is designed that is covered by all network characteristics.

Table 4 Received signal strength interval

Networks	Low (dBm)	Medium (dBm)	High (dBm)
WLAN	[-87, -85]	(-85, -83]	(-83, -81]
LTE	[-135, -133]	(-133, -131]	(-131, -129]
WCDMA	[-147, -145]	(-145, -143]	(-143, -141]

Table 5 Bandwidth interval

Networks	Low (MHz)	Medium (MHz)	High (MHz)
WLAN	[0, 1]	(1, 20]	(20, 40]
LTE	[0, 1]	(1, 10]	(10, 20]
WCDMA	[0, 1]	(1, 5]	(5, 10]

Table 6 Mobile speed interval

Networks	Low (m/s)	Medium (m/s)	High (m/s)
WLAN	[0, 2]	(2, 4]	(4, 6]
LTE	[0, 20]	(20, 40]	(40, 60]
WCDMA	[0, 47]	(47, 93]	(93, 130]

Table 7 Monetary cost rate interval

Networks	Low	Medium	High
WLAN	[0, 0.1]	(0.1, 0.2]	(0.2, 0.3]
LTE	[0, 0.2]	(0.2, 0.4]	(0.4, 0.6]
WCDMA	[0, 0.3]	(0.3, 0.6]	(0.6, 0.9]

Performance Investigation

We estimate the performance of our proposed algorithm under different mean arrival times ranging from 5-30 sec. The average arrival rate of new calls is fixed at 10 calls/sec and average call holding time is 180 sec. The user's speed is a uniform distribution as equal to 1-30 m/s and user movement is modeled as the random waypoint mobility in 5000 (m) x 5000 (m) topology size for each speed. To test more accurately, each point was run 10 times, and then we take their average based on OPNET simulator and is linked with MATLAB. Correspond to an actual situation for the simulating process, the correspondent node (CN) generates constant bit rate (CBR) multimedia traffic using a 64-byte packet size and is sent every 1 ms and user datagram protocol (UDP) is the transport protocol applied between the networks that includes the detection of the new networks and the allocation of new IP address. These tasks are often handled by Dynamic Host Configuration Protocol (DHCP). Figure 4 shows the number of handover for proposed method as Learning Vector Quantization Neural Network: LVQNN has less than Compositional Rule of Inference Fuzzy Logic: CRIFL [8], Neural Network Based Handover Management Scheme: NNBHMS [9] and Algorithmic Vertical Handoff

Decision and Merit Network Selection: VHODM [15] since LVQ method is suitable the non-linear data communication and can learns by itself for new information. Correspondingly, the call dropping probability refers to unsuccessful handover procedure causes the user to be disconnected and is the fewest by using LVQNN as demonstrated in Fig. 5. In additional, Figs. 6-8 illustrate the data packet delay in WCDMA, LTE and WLAN of proposed method that yields the lowest value for all networks compared with conventional method. The data packet delay means the time delay between client send data to end user which correctly receives of the last packet data. On the contrary, LVQNN has the highest network utilization that represents the all resources are useful at all time to connect.

CONCLUSION

The received signal strength indicator, bandwidth requirements, mobile speed and monetary cost are the multi-criteria factors that are introduced a learning vector quantization neural networks in order to vertical handover decision. The simulation results indicate the proposed approach outperforms the other algorithms as reducing the unnecessary handover, call dropping probability and data packet delay, respectively. On the other hand, our proposed method can increase the network utilization compared with previous algorithms.

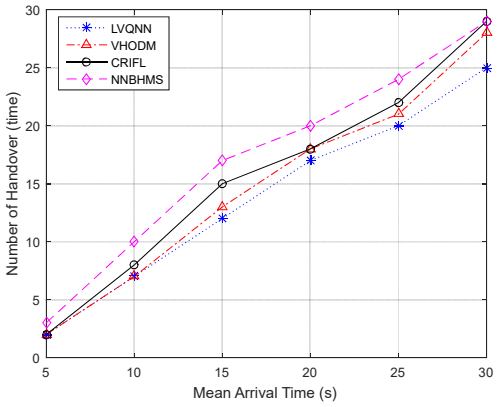

Fig. 4 Number of handover versus mean arrival time.

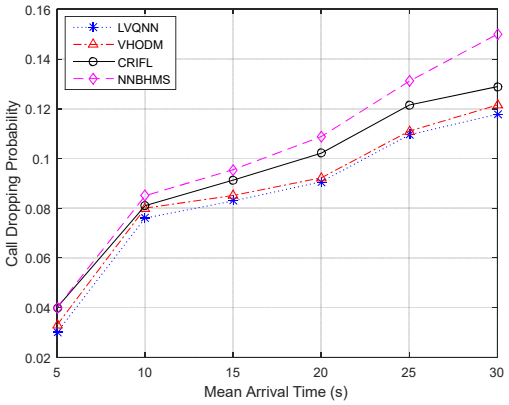

Fig. 5 Call dropping probability versus mean arrival time.

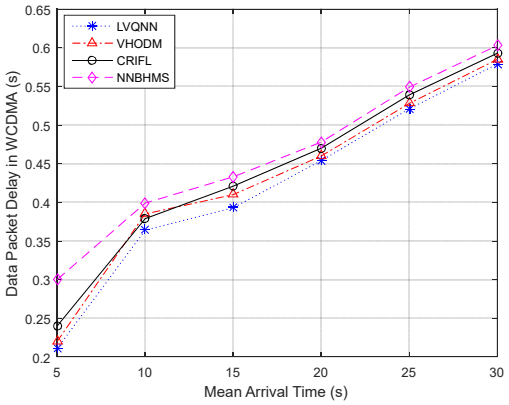

Fig. 6 Data packet delay in WCDMA versus mean arrival time.

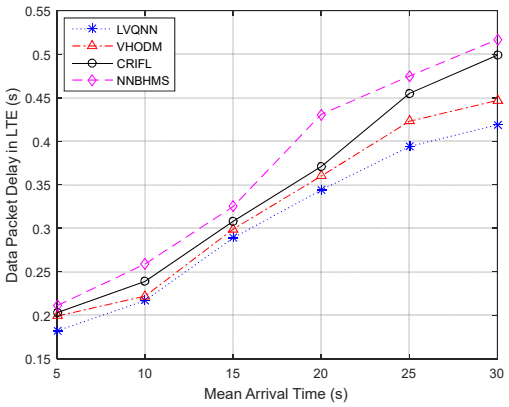

Fig. 7 Data packet delay in LTE versus mean arrival time.

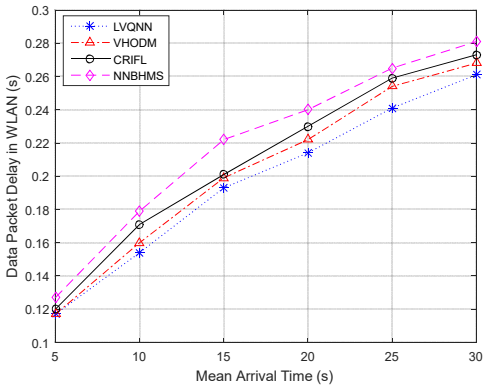

Fig. 8 Data packet delay in WLAN versus mean arrival time.

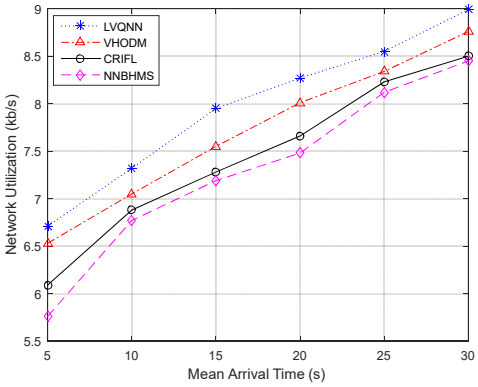

Fig. 9 Network utilization versus mean arrival time.

ACKNOWLEDGEMENTS

This research was supported by the research grant (No. 792/2558) from Srinakharinwirot University revenue 2558, for the 2558 fiscal year.

REFERENCES

[1] L. Xia, J. Ling-ge, H. Chen and L. Hong-wei, "An Intelligent Vertical Handoff Algorithm in Heterogeneous Wireless Networks", International Conference on Neural Networks and Signal Processing, 2008, pp. 550-555.

[2] M. Liu, Z. Li, X. Guo and E. Dutkiewicz, "Performance Analysis and Optimization of Handoff Algorithms in Heterogeneous Wireless Networks", IEEE Transaction on Mobile Computing, Vol. 7, July 2008, pp. 846-857.

[3] Y. Sun, C. Liu, P. Yang and X. Wen, "A Smart Vertical Handoff Decision Algorithm Based on Queuing Theory," Advanced Communication Technology, 2014, pp. 1217-1222.

[4] Y. Zhang and J. Wang, "Multi-Criteria Pre-Selection in Heterogeneous Wireless Networks," Third International Conference on Information Science and Technology, 2013, pp. 798-801.

[5] R. Chai, J. Cheng, X. Pu and Q. Chen, "Neural Network Based Vertical Handoff Performance Enhancement in Heterogeneous Wireless Networks," 7th International Conference on Wireless Communications, Networking and Mobile Computing, 2011, pp. 1-4.

[6] P. Haoliang, S. Wenxiao, L. Shuxiang and X. Chuanjun, "A GA-FNN Based Vertical Handoff Algorithm for Heterogeneous Wireless Networks," 2012 IEEE International Conference on Computer Science and Automation Engineering, 2012, pp.37-40.

[7] I. Kustiawan and K. H. Chi, "Handoff Decision Using a Kalman Filter and Fuzzy Logic in Heterogeneous Wireless Networks," IEEE Communications Letters, Vol. 19, December 2015, pp. 2258-2261.

[8] M. Hu, W. Yang, K. Liu and S. Cong, "An CRI Based Vertical Handoff Algorithm in Heterogeneous Networks," 2014 IEEE International Conference on Computer and Information Technology, 2014, pp. 258-262.

[9] N. M. Alotaibi and S. S. Alwakeel, "A Neural Network Based Handover Management Strategy for Heterogeneous Networks," IEEE 14th International Conference on Machine Learning and Applications, 2015, pp. 1210-1214.

[10] L. Nithyanandan and I. Parthiban, "Seamless Vertical Handoff in Heterogeneous Networks Using IMS Technology," IEEE International Conference on Communications and Signal Processing, 2012, pp. 32-35.

[11] J. C. Ortiz-Bayliss, H. Terashima-Marin and S. E. Conant-Pablos, "Learning Vector Quantization for Variable Ordering in Constraint Satisfaction Problems," Pattern Recognition Letters, Vol. 34, March 2013, pp. 423-432.

[12] W. A. Yang, "Monitoring and Diagnosing of Mean Shifts in Multivariate Manufacturing Processes Using Two-Level Selective Ensemble of Learning Vector Quantization Neural Networks," Journal of Intelligent Manufacturing, Vol. 26, August 2015, pp. 769-783.

[13] D. Nova and P. A. Estévez, "A Review of Learning Vector Quantization Classifiers," Neural Computing and Applications, Vol. 25, September 2014, pp. 511-524.

[14] L. Nithyanandan and I. Parthiban, "Seamless Vertical Handoff in Heterogeneous Networks Using IMS Technology," IEEE International Conference on Communications and Signal Processing, 2012, pp. 32-35.

[15] S. Kunarak, and R. Suleesathira, "Algorithmic Vertical Handoff Decision and Merit Network Selection Across Heterogeneous Wireless Networks", WSEAS Trans on Communications, Vol. 12, January 2013, pp. 1-13.

Second International Conference on Science, Engineering & Environment,
Osaka City, Japan, Nov.21-23, 2016, ISBN: 978-4-9905958-7-6 C3051

OBTAINING COMPLETE MIXING USING HYDRODYNAMIC ANALYSIS ON BATCH REACTOR

Rositayanti Hadisoebroto[1], Suprihanto Notodarmojo[2], Idris Maxdoni Kamil[2], Yazid Bindar[3] and Rangga Santosa[2]
[1]Environmental Engineering Department, Faculty of Landscape Architecture and Environmental Engineering, Trisakti University, Indonesia; [2]Environmental Engineering Program, Faculty of Civil and Environmental Engineering, Institut Teknologi Bandung, Indonesia, [3]Chemical Engineering Program, Faculty of Industrial Technology, Institut Teknologi Bandung, Indonesia

ABSTRACT

This research is aims to find the best possible mixing conditions in a multi-phase reactor consist of wastewater, activated sludge and aeration. This has been done by analyzing flow profiles in the system using experimental and computational work. Hydrodynamic characteristics, such as influent flow rate, aerator configuration, baffle installment, play important role for waste water treatment process. Determination of influent flow rate and the reactor configuration have done by analyzing flow profile in laboratory scale single-phase reactor with the dimension of 16 L. Velocity profile was developed from tracer study. There were 2 influent flow rate variations of 0,0095 L/s and 0,02 L/s, in 3 variations of reactor configuration. The first configuration was without any configuration (control), the second was baffled reactor and the third was porous reactor. From the experimental work, it was obtained that the influent flow rate of 0,0095 L/s gave longer Residence Time Detention (RTD) and longer time to reach the outlet than flow rate of 0,02 L/s. The baffled configuration gave longer RTD and longer time to reach the outlet as well than other configurations. This two results was reasonable since the first influent flow rate and the baffled reactor have higher volume effective than other variations. In multi-phase system, experimental work was done in batch system to observe the contact between air-bubble and sludge in reactor, which then calibrated using CFD (Computational Fluid Dynamic) model. The result showed that the model of mixture in k-ε equation was considerable to use in future simulation work.

Keywords:Hydrodynamic, CFD Model, Single-phase and Multi-phase System, Batch Reactor

INTRODUCTION

Chemical reactor is an important part of wastewater and water treatment. Inside the reactor, it occurs chemical process that could change the substance of various chemical compounds. Reactor effectiveness is an integral part of every wastewater and water treatment industry. This affect materials used in processing, energy required, to reliability of the process.

Chemical reactor is divided into two types, the stirred tank reactor and a plug flow reactor. When viewed from the kinetic parameters and chemical reactions under isothermal conditions, a plug flow reactor is more efficient than stirred tank reactor. However, a plug flow reactor usually works in adiabatic conditions or non-isothermal (Minsker et al., 1999) [1].

In a plug flow reactor, one of the factors that make process inside ineffective is the nature of the flow. When the flow in the reactor is not ideal, reactants and reaction products flow at a different speed across the cross section of the pipe. It can be caused by the hydraulic factors of the reactor is being overlooked or disregarded.

Based on above, hydraulic simulation on a laboratory-sized plug flow reactor will be conducted with discharge variation to analyze its effect to flow patterns. Moreover, effects from it to residence time distribution (RTD) will be analyzed with tracer test. Tracer Test technique is an effective method to identify efficiency of a purification process that occurs in a wastewater treatment, both in design optimization and process performance (IAEA, 2011)[2]. Thus, this study was conducted to obtain the most optimum pollutant removal efficiency in a plug flow reactor with physical modification such as discharge variation.

The use of tracer and dye are very helpful to determine the ideal conditions to make the reactor design. Determination of the ideal conditions can be done by finding the resident time distribution curve (RTD) to determine the hydraulic character of a reactor. To find the RTD curve, tracer test must be conducted.

One of the characters that must be owned by a tracer substance is the tracer substance should not interfere with the flow (Denbigh and Turner,

1965)**[3]**. Therefore the usual tracer substance is one that has the same density with water. There are lots of tracer substances that do not interfere with the flow of water in the reactor. Tracer substance that will be used is an organic compound, rhodamine B, which has been widely used in several hydrological studies. As with other fluorescent dye, rhodamine B is a tracer that easily detected by the on-site use of high frequency (0.1 Hz) to facilitate observation and concentration fluctuations can generate a good estimate of the RTD. In addition, rhodamine B is relatively inexpensive and safe, both for operators, system processing, and receiving environment (Giraldi et al., 2009)**[4]**.

Beside doing the experimental works, research focus as well to the hydrodynamics simulation in computational works using Computational Fluid Dynamics software. Reference [5] Le Moullec et. al. (2008) indicates that CFD simulation shows the good work on analyzing Residence Time Distribution and flow field.

MATERIALS AND METHODS

The research was started from preparation of batch reactor, preparation of tracer substance and media, reactor trial, building and meshing geometry on computational works and then data sampling in experimental works, doing simulation, and analysis.

Batch Reactor

In this study, a batch reactor is used to perform tracer test. Dimensions of the reactor can be seen in Table 1, while the scheme of the device can be seen in Figure 1.

Tabel 1.Dimension of Batch Reactor

Dimention	Magnitude (cm)
Length	40
Width	20
Height	20
Ø inlet	0.9

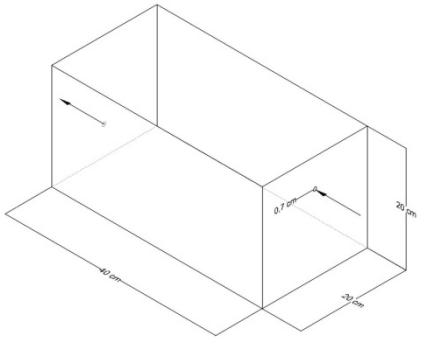

Figure 1.Batch Reactor sketch

The reactor is made of block-shaped acrylic with open surface. Therefore, 25 mL of tracer substance is being injected into the reactor. The reactor is shown in Figure 2.

Figure 2.Batch reactor

Experimental Works on Batch Reactor

Tracer substance that used is a mixture of textile dye brand "WANTEX" with "MERAH DELIMA 34" series. It is used because in the textile dye contains Rhodamine B, which is a compound that is often used for tracer test.

The independent variable in the study is the discharge of water at the inlet and the concentration of the tracer fluid at minute 0 operation. The dependent variable is the concentration of tracer fluid in the water at any time of the test. While the control variable is the water in the reactor and test time. This research was conducted by using the independent variables mentioned above, the flow of water into the reactor. Thus, it can be seen spread the concentration of tracer in each discharge.

Water is flowed into the reactor and will flows thoroughly along the reactor. After a steady flow occurs, tracer substance is injected into the reactor using pulse technique, which is injected entirely. After that, tracer substance concentration is measured from the outgoing water flow based on time. That procedure is conducted to discover water movement inside the reactor.

Measurement of Tracer Substance Concentration

Water at the outlet analyzed directly without going through the process of preservation in advance. Concentration of the tracer substance in the reactor outlet is measured. Measurements were performed by using the spectrophotometric method, which is a water sample is measured inside the spectrophotometer and fired with light at specific wavelengths in order to know the concentration of the tracer in the sample fluid. Before performing this method, the wavelength that will be used for

measurement by spectrophotometer have to be. After the wavelength that will be used is known, absorbance curve is made for a standard to determine the concentration of tracer substance.

Geometry and Mesh Building of Batch Reactor

Building geometry and meshing is done using Gambit Processor. Geometry is based on batch reactor dimension, while meshing is using Tet/Hybrid elements in map and sub-map scheme type.

Computational Works of Hydrodynamic Simulation

The computational works starts from define the model and parameter. In this study, simulation is done based on unsteady, turbulent, eulerian model. The model is run in 3 dimensional in multi-phase system.

RESULTS AND DISCUSSIONS

Two discharge variations is being used on this preliminary study. The first discharge variation s 0.0263 L/second while the second discharge is 0.0277 L/second. The measurement results can be seen in Figure 3.

As can be seen in Figure 3 that in Variation 1, the peak concentration is in 25 seconds. While in the second variation, the peak concentration is occured in 30 to 70 seconds.

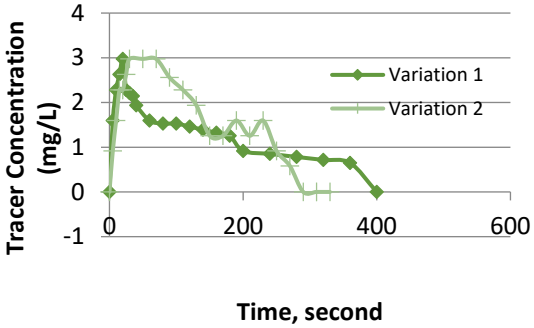

Figure 3. Tracer concentration in various discharge variations

Based on the results obtained, the average detention time is calculated by using equation (1) (Metcalf and Eddy, 2003) :

$$\bar{t}_c = \frac{\int_0^\infty tC(t)dt}{\int_0^\infty C(t)dt} \qquad (1)$$

Where $\bar{t}_c$ is detention time, t is the time (s) and C (t) is the concentration of tracer at time t (ML^{-3}). From equation (1), detention time for Variation 1 is 82.789 seconds and 90.593 seconds for Variation 2.

After that, the theoretical detention time is calculated using discharge data and water height in the reactor. Therefore, theoretical detention time for variation 1 is 350 seconds and 288 seconds for Variation 2.

There is a significant difference detention time in the both variation. It can be caused by the water discharge that flows into the reactor is unstable, causing errors in the calculation. In addition, there may be a short flow in the reactor, which can cause a dead zone. In this zone, the flow is stagnant so fluid does not mix well. If the inlet and outlet are not placed properly, fluids will be flows straight from the inlet to the outlet, without being mixed with the fluid in the reactor (Hayes, 2012).

To standardize the measure result for tracer concentration at the outlet versus time curve with pulse injection method, tracer substance in the outlet usually normalized first. Normalized curve is called RTD Curve (residence time distribution curve). RTD curve function can be calculated using equation (2) :

$$E(t) = \frac{C(t)}{\int_0^\infty C(t)dt} \qquad (2)$$

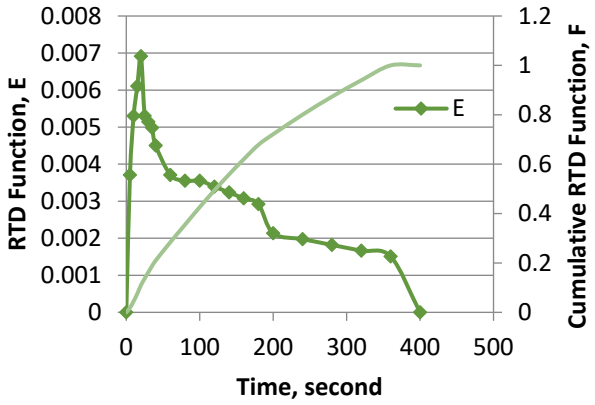

Figure 4.RTD curve in discharge variation 1

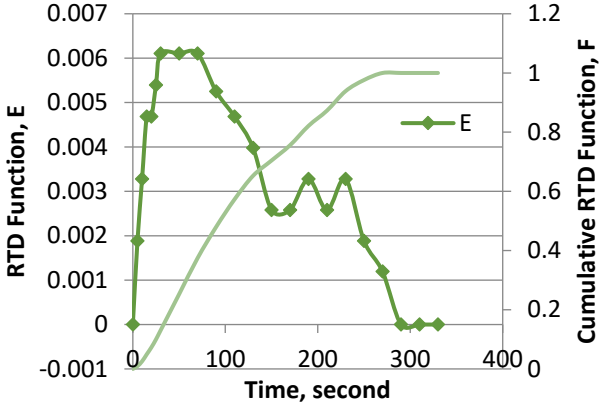

Figure 5.RTD curve in Variation discharge 2.

Based on the equation (2), RTD curve function calculated and transformed into graph as shown in Figure 4 and Figure 5 :

Based on the image above, obtained a time when the majority of the tracer substance spends time in the reactor. At discharge variation 1, approximately 50% of the tracer substance takes between 0 to 100 seconds to get to the outlet. While in the discharge variation 2, the time required approximately 50% tracer substance to come out through the outlet is 0 to 110 seconds.

The simulation result is shown that the mixing condition is almost completely mixed, as can be seen in Figure 6. In batch reactor, mixing is occurred because of air flow from the diffuser located 10 cm from edge and submerged, with the air flow velocity is 0,2 L/min.

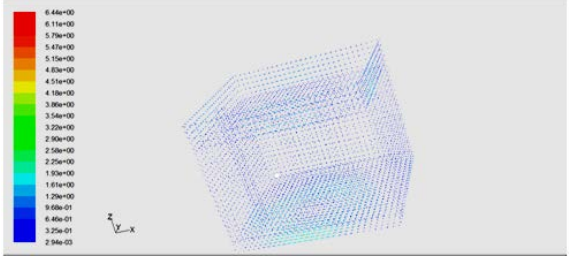

Figure 6. Water flow pattern in batch reactor

It can be seen that in batch reactor, there are some dead zone in the edge and corner. The effective area of the reactor is about 50%, according the existence of zero velocity is about 50%. It can be concluded that even the reactor equipped by diffuser, the dead zone is still exist. The modification in hydrodynamic aspect, like inlet position, number of diffuser and air flow velocity, as well as other type of aerator need to be simulated in future works.

CONCLUSION

Conclusions obtained in this preliminary study is the in first discharge variation, the theoretical detention time is 350 seconds and experimental detention time is 82.788 seconds. In the second variation, the theoretical detention time is 288 seconds and experimental detention time is 90.59 seconds.

In addition, the results obtained in the form of 50% tracer substance takes between 0 to 100 seconds to get to the outlet on the variation of 1 and 0 to 110 seconds in the second discharge variation. That happened because of a dead zone occurs in the reactor that caused by short circuit flow.

The simulation result shows that the eulerian multiphase system could relied to get the great picture of water flow pattern inside the reactor. It is concluded that the mixing condition with diffuser aeration still generate some dead zone which mean not so effective volume inside reactor. In future works, other hydrodynamics aspect variations are needed to be simulated.

KNOWLEDGEMENT

The authors would like to thank Directorate of Intellectual Property Management, Directorate General of Research and Development Strengthening, Ministry of Research, Technology and Higher Education, Program of Decentralization 2015 for funding part of this research through Doctoral Dissertation Scheme.

REFERENCES

Denbigh, K. 1966. Chemical reactor theory an introduction. Cambridge [England]: C.U.P.

Giraldi, D., Vitturi, M., Zaramella, M., Marion, A., danIannelli, R. 2009.*Hydrodynamics of Vertical Subsurface Flow Constructed Wetlands: Tracer Tests with Rhodamine WT and Numerical Modelling. Ecological Engineering* Vol. 35: 265–273.

Hayes, R., &Mmbaga, J. 2012. Introduction to chemical reactor analysis (Second ed.). CRC Press.

International Atomic Energy Agency (IAEA). 2011. Radiotracer Applications in Wastewater Treatment Plants. Vienna

Metcalf dan Eddy. 1991. Wastewater Engineering Treatment, Disposal, Reuse. 3rd ed. McGraw-Hill Inc.

Second International Conference on Science, Engineering & Environment,
Osaka City, Japan, Nov.21-23, 2016, ISBN: 978-4-9905958-7-6 C3051

WASTE MINIMIZATION OF CHEESE-MAKING BY-PRODUCT DISPOSAL THROUGH ETHANOL FERMENTATION AND THE UTILIZATION OF DISTILLERY WASTES FOR FERTILIZER

Gemilang Lara Utama[1,2], Tb. Benito A. Kurnani[3], Sunardi[4], Roostita L. Balia[3]
[1]Doctorate Program on Environmental Science, Universitas Padjadjaran, West Java, Indonesia
[2]Faculty of Agro-Industrial Technology, Universitas Padjadjaran, West Java, Indonesia
[3]Faculty of Animal Husbandry, Universitas Padjadjaran, West Java, Indonesia
[4]Faculty of Sciences, Universitas Padjadjaran, West Java, Indonesia

ABSTRACT

Whey as cheese-making by-product has become a threat toward the sustainability of production process at small medium enterprises (SMEs) cheese producer. High organic contents lead high pollution load to the environment, because until now the producer still dispose the waste to the stream or land. Whey utilization through simple ethanol fermentation could reduce high organic content and highly implementable in SMEs level because its easiness. The research aimed to determine waste minimization through ethanol fermentation and the utilization of distillery wastes for fertilizer. Research was done experimentally with substrate variation (whey and napa cabbage) with and without 10% molases addition that fermented by indigenous yeasts consortium (*Candida lambica* and *Prototheca zopfii*) on various temperature (24-27°C and 17-21°C) for 96 hours. The ethanol contents measured by using dichromate oxidation methods. After fermentation finished substrates distilled two stages, the first stage distillery wastes were analyzed for the contents of N (Kjeldahl), P_2O_5 (Bray I) and Potassium (AAS). Results showed that the combination of whey and napa cabbage (1:1) with 10% molasses addition that fermented by *Candida lambica* and *Prototheca zopfii* on 17-21°C resulted in 11.06% of bioethanol contents in 72 hours fermentation. After two stages distillation, 11.2% substrates can converted into ethanol and 37.9% of water resulted from second stage distillation that can disposed to the environment. Meanwhile, 50.9% of first stage distillery wastes has 0.56% N, 0.83% P and 0.35 K which suitable with the Indonesian Agriculture Ministerial Decree No.28/2009 of minimum technical requirement for organic fertilizer. Ethanol fermentation from cheese whey with napa cabbage wastes and 10% molasses addition that fermented by *Candida lambica* and *Prototheca zopfii* consortium and the utilization of its distillery wastes for fertilizer could minimize wastes up to 62.1%.

Keywords: cheese whey, napa cabbage, ethanol, fertilizer, wastes minimization

INTRODUCTION

Cheese making by-products which was known as whey increasingly to the attention of cheese producers especially in Small Medium Enterprises (SMEs) scale. Cheese whey often discharged directly to the environment and supposed to be one of the causes of pollution. Cheese whey has low acidity (pH) so that can cause problems, especially if disposed into stream that have low water discharge. The organic matter left behind on cheese whey was potential to cause eutrophication if discharged directly into water bodies. Meanwhile, organic materials owned allow cheese whey to be processed into commodities.

Organic materials with the largest number owned by cheese whey is lactose. Lactose is a specific carbohydrate owned by dairy products and its content up to 5% [1]. As carbon source for microorganisms, lactose widely used in bioprocess medium for the growth of lactic microorganisms. Lactic microorganisms synthesized lactose into glucose and galactose, then metabolized through the glycolytic pathway to generate energy, organic acids and ethanol [2][3].

Several indigenous yeasts and yeast-like microorganisms have good ability in ethanol fermentation from wastes. *Candida lambica* isolated from mozzarella whey to ferment ethanol up to 0.15% within 48 hours at room temperature and have a sugar content and resistance to high ethanol [4]. *Prototheca zopfii* was yeast-like organism that capable in fermenting ethanol in extreme conditions, this type was found in some milk-based and cellulose-based wastes [5][6].

The addition of sugar complex based substrates such as cellulose is one way that can be done to increase the ethanol contents resulting from cheese whey fermentation. Napa cabbage waste was a potential cellulose-based substrate for ethanol fermentation [7]. The addition of other cellulose-based substrate such as molasses in cheese whey fermentation resulting in 2.06% ethanol with 92.71% sugar conversion [8].

Fermented substrates were purified by

distillation. Distillation at temperature of 78º-100°C resulted in ethanol evaporation, and through the condensing unit ethanol with desired purity will be released.

The distillation also resulted distillery waste that potentially polluting the environment because it's contains high organic materials. Undilluted organic load on distillery wastes could results toxic effect on aquatic organisms and the color could also block out sunlight thus hamper photosynthesis inside the waters [9]. Distillery wastes have low pH of 3.8-4.4, BOD of 45000-60000 ppm and COD of 70000-98000 ppm with suspended solids of 2000-14000 ppm [10].

The distillery wastes with the organic materials contained could applied as organic liquid fertilizer [11]. Common characteristic of distillery wastes showed the contents of 0.10-0.12% N, 0.05-0.15% P and 0.5-1.2% K [10]. Meanwhile, distillery wastes generated from the residue of neufchatel whey fermentation contains 0.1% N, 0.07% P and 0.14% K [12].

Cheese whey utilization through ethanol fermentation with the utilization of distillery wastes for fertilizer aimed to minimize wastes disposal into environment. Aside from being able to decrease organic material load through reduction of BOD and COD, the amount of wastes to be released can be reduced. Therefore, the research was conducted to determine waste minimization through ethanol fermentation and the utilization of distillery wastes for fertilizer.

MATERIALS AND METHODS

Materials

Cheese whey taken from Koperasi Peternak Bandung Selatan (KPBS), napa cabbage (*Brassica rapa subsp. pekinensis*) wastes and molasses from Pangalengan traditional market, Bandung District.

Methods

Yeasts isolates prepartion

Candida lambica isolated from cheese whey and *Prototheca zopfii* isolated from broccoli leaves. The yeasts isolates grown in Nutrient Broth/NB with the addition of 3% yeast extract (Kraft Foods Inc.) and 10 ppm amoxycilline (PT. Kimia Farma), then incubated for 36 hours at room temperature (26-28°C) [4].

Ethanol production

Cheese whey and napa cabbage wastes (1:1) mixed then set into two replications treatments i.e. : with and without 10% molasses addition, incubation temperature of low temperature (17-20°C) and room temperature (24-27°C) for 96 hours fermentation. Ethanol contents measured with dichromate oxidation methods every 24 hours [13]. Data analyzed with multivariate regression analysis (SPSS 18).

Distillery wastes characterization

Fermented substrates distilled two stages at 78-100°C. Residue of first stage distillation measured on the contents of Nitrogen/N (Kejldahl), Phospate/ (P_2O_5)/P (Bray I), and Potassium/K (*Atomic Absorbtion Spectrophotometer*/AAS) then compared with the ministerial decree No.8/2009 for minimum technical requirement for organic fertilizer. Volume of distillery wastes measured as basis for waste minimization calculation.

RESULTS AND DISCUSSIONS

Results of ethanol fermentation (Fig.1) shown increased until 72 hours and decreased at 96 hours. Highest ethanol contents (11.06%) resulted by treatment of 10% molasses addition that incubated at low temperature for 72 hours. Analysis of multivariate regressions showed that the variables of molasses addition, temperature and incubation time significantly affected the ethanol contents with R^2=0.945 and the multivariate regression equation of Y = 15,12 – 6,11X1 – 0,06X2 + 0,33X3 with X1 for molasses addition, X2 for temperature and X3 for incubation time.

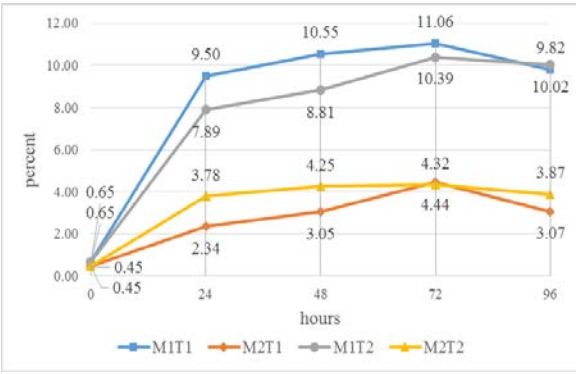

Note :
M1T1 : 10% Molasses addition, low temperature
M2T1 : 0% Molasses addition, low temperature
M1T2 : 10% Molasses addition, room temperature
M2T2 : 0% Molasses addition, room temperature

Fig. 1 Ethanol production

The addition of 10% molasses could produce 11.06% ethanol contents. Molasses contains 50% sugars that can be fermented and enhanced ethanol productivity [14][15]. The mixture of cheese whey and molasses as much as 10% was an effective and efficient treatment for ethanol fermentation [8].

Ethanol contents declined at 96 hours incubation. At this stage, yeasts has been through stationary phase and lead to death phase. The optimum incubation time for ethanol fermentation from cheese whey with the addition of cellulose-based

substrates was 72 hours. Incubation until 96 hours will reduce the ethanol levels because it's converted to other compounds such as esters [16].

Low temperature (17-21°C) produced the best ethanol contents on 72 hours of fermentation. At low temperatures, yeasts sensitivity to the toxicity of ethanol to be lower so that the fermentation continues, meanwhile at warmer temperatures (> 20°C) loss of viability of yeasts happens faster [17].

After the fermentation done, fermented substrates was distilled 2 stages and the distillery wastes were characterized then compared to the Indonesian Agriculture Ministerial Decree No.28/2009 of minimum technical requirement for organic fertilizer (Table 1). The results showed that the distillery wastes characteristics was suitable with the requirements.

Table 1 Distillery wastes characteristics

Items	%	Decree No.28/2009
Nitrogen (N)	0.56	< 2
P_2O_5 (P)	0.83	< 2
Potassium (K)	0.35	< 2

The potential of distillery wastes as organic fertilizer can be characterized from the raw materials. Cheeses whey still contain 0.06% N, 0.38% P, and 0.12% K, while the molasses had 0.20% N, 0.27% P, and 0.11% K [8]. In addition, there were 1.3% N and various minerals including P and K in napa cabbage [18].

Aside from cheese whey, napa cabbage and molasses, the number of N, P and K on the distillery wastes could derived from yeast cells that assimilate and utilize the elements. Yeasts were able to utilize methionine, histidine and lysine that available in cheese whey as the primary nitrogen source for growth and keep it inside the cell up to 10% of the dry weight of yeast cells [19][20]. Phosphorus contained in cheese whey were essential nutrients required for the growth of yeasts then stored inside the cell in the form of orthophosphate (H2PO4) [21][22]. Meanwhile potassium were macro minerals needed by yeasts as cofactor of various enzymes involved in oxidative phosphorylation, biosynthesis of protein and carbohydrate metabolism [19].

Volume of distillate and the residue of 2 stages distillation were measured and shown at Table 2. Fermentation of cheese whey with napa cabbage and molasses addition, for ethanol and the utilization of distillery wastes as organic fertilizer could minimize wastes disposal significantly.

Table 2 Distillation results volume

Items	ml	%	
Fermented substrates	2000	100	
Residue stage 1	1018	50.9	Fertilizer
Distillate 1	982	49.1	
Residue stage 2	224	11.2	Ethanol
Distillate 2	758	37.9	Water

First stage distillation was resulted 50.9% of total substrates volume that can used as fertilizer. The second stage distillation was resulted average 11.2% of total substrates volume of ethanol and 37.9% residue in the form of distilled water which can be released to the environment. The results showed that the utilization made an impact on waste minimization up to 61.2% and leaving distilled water residue that can disposed to the environment.

CONCLUSION

The fermentation of whey and napa cabbage (1:1) with 10% molasses addition by *Candida lambica* and *Prototheca zopfii* at the temperature of 17-21°C for 72 hours resulted in bes ethanol contents of 11.06%. Two stages distillation resulting in 37.9% distilled water, 11.2% ethanol, and 50.9% distillery waste. The distillery wastes has suited the Indonesian Agriculture Ministerial Decree No.28/2009 of minimum technical requirement for organic fertilizer with N of 0.56%, P of 0.83% and K of 0.35. Ethanol fermentation and utilization of distillery wastes for fertilizer could minimize wastes up to 62.1%.

ACKNOWLEDGEMENTS

Author would like to thanked Beasiswa Unggulan, Bureau of Planning and International Cooperation of Indonesian Ministry of Education for the Doctorate Program Scholarship. Also the Government of West Java Province for the Research Grant.

REFERENCES

[1] Ghaly, A.E., Ramkumar, D.R., Sadaka, S.S., Rochon, J.D. "Effect of reseeding and pH control on the performance of a two stage mesophilic anaerobic digester operating on acid cheese whey", Can. Agric. Eng., Vol. 42, 2000, pp. 173–183.

[2] Ghaly, A.E. and E.A. Echiegu. "Kinetic of a continuous flow no-mix anaerobic reactor", Energy Sources, Vol. 15 (3), 1993, pp. 1-17.

[3] Maullu, C., Lampis, G., Basile, T., Ingianni, A., Rossolini, G.M., Pompei, R. "Production of lysozyme enriched biomass from cheese

industry by-products", Journal of Applied Microbiology, Vol. 86, 1999, pp. 182-186.

[4] Utama, G.L., Kurnani, T.B.A., Sunardi and Balia, R.L. "The isolation and identification of stress tolerance ethanol-fermenting yeasts from mozzarella cheese whey", International Journal of Advanced Science, Engineering and Information Technology, Vol. 6 (2), 2016, pp. 252-257.

[5] Ueno, R., Urano, N., Suzuki, M. and Kimura, S. "Isolation, characterization, and fermentative pattern of a novel thermotolerant *Prototheca zopfii var. hydrocarbonea* strain producing ethanol and CO2 from glucose at 40°C". Arch. Microbiol., Vol. 177, 2002, pp. 244-250.

[6] Cuc, C., Catoi, C., Fit, N., Rapuntean, S., Nadas, S., Bolfa, P., Taulescu, M., Gal, A., Tabaran, F., Nagy, A., Borza, G., Moussa, R. "The inhibitory effect of some natural essential oils upon *Prototheca* algae in vitro growth". Bulletin USAMV, Veterinary Medicine, Vol 67 (1), 2010, 34-38.

[7] Thenmozhi, R. and Victoria, J. "Optimization and improvement of ethanol production by the incorporation of organic wastes". Advances in Applied Science Research, Vol. 4 (5), 2013, pp. 119-123.

[8] Sadik, M. W. And Halema, A.A. "Production of ethanol from molasses and whey permeate using yeasts and bacterial strains". International Journal of Current Microbiology and Applied Sciences, Vol. 3 (3), 2014, pp. 804-818.

[9] Tripathi, K. N., Ahmad, M. I. And Jamal, M. Y. "Comparative study of 'BOD', 'DO' and pH od distillery treated and untreated waste water". International Journal of Scientific and Research Publications, Vol. 5 (9), 2015, pp. 1-7.

[10] Ali, N., Ayub, S. and Ahmad J. "A study on economic treatment of distillery effluent". International Journal of Current Reseatch and Review, Vol. 7 (11), 2015, pp. 8-12.

[11] Utama, G. L., Roostita L. B., Kurnani T. B. A. and Sunardi. "Cost Benefit Analysis of bioconversion neufchatel whey into rectified ethanol and organic liquid fertilizer in semi pilot scale". AgroLife Scientific Journal, Vol. 4 (1), 2015, pp. 192-196.

[12] Utama, G. L., Roostita T. B., Kurnani T. B. A., Sunardi and Setiawan, I. "Fermentations of various whey types with using Kluyveromyces lactis in the production of bioethanol and organic liquid fertilizer". Lucrari Stiintifice, Medicina Veterinara Partea 2 Editura "Ion Ionescu De La Brad" Iasi, Vol. 54 (12), 2011, pp. 214-219.

[13] Fakruddin, Md., Islam, Md. A., Ahmed, M. M., Chowdury, N. "Process optimization of bioethanol production by stress tolerant yeasts isolated from agro-industrial waste". International Journal of Renewable and Sustainable Energy, Vol. 2 (4), 2013, pp. 133 – 139.

[14] Schweinitzer, T. and Josenhans, C. "Bacterial energy taxis: a global strategy?". Arch. Microbiol. J. Bacteriol. Vol. 170, 2010, pp. 5507 5511.

[15] Khoja, A. H., Ali, E., Zafar, K., Ansari, A. A., Nawar, A. And Qayyum, M. "Comparative study of bioethanol production from sugarcane molasses by using *Zymomonas mobilis* and *Saccharomyces cereviseae*". African Journal of Biotechnology, Vol. 14 (31), 2015, pp. 2455-2462.

[16] Azizah, N., Al-Baari, N. and Mulyani, S. "Pengaruh lama fermentasi terhadap kadar alkohol, pH dan produksi gas pada proses fermentasi bioetanol dari whey dengan substitusi kulit nanas". Jurnal Aplikasi dan Teknologi Pangan, Vol. 1 (2), 2012, pp. 72 – 77.

[17] Sener, A. Canbas, A. and Unal, M. U. "The effect of fermentation temperature on the growth kinetics of wine yeast species". Turk. J. Agric. For. Vol. 31, 2007, pp. 349-354.

[18] Kallabis-Rippel, K. "Studies on pak choi: cultivation and characterization". Ph.D. Thesis, Technische Universität München, Germany. . 2000.

[19] Walker, G.M., Yeast Physiology and Biotechnology. John Wiley and Sons Ltd., 1998.

[20] Messenguy, F., Andre, B. and Dubois, E. "Diversity of nitrogen metabolism among yeast species : regulatory and evolutionary aspects". The Yeasts Handbook : Biodiversity and Ecophysiology of Yeasts. Springer-Verlag Berlin Heidelberg. 2006, pp. 123-153.

[21] Theobald, U., Mohns, J. And Rizzi, M. "Determination of in vivo cytoplasmic orthophosphate concentration in yeast". Biotechnology Techniques, Vol. 10 (2), 1996, pp. 297-302.

[22] Parrondo, J., Garcia, L. A. and Diaz, M. "Nutrient balance and metabolic analysis in a Kluyveromyces marxianus fermentation with lactose-added whey". Brazilian J. Of Chem. Eng. Vol. 26 (03), 2009, pp. 445-456.

Second International Conference on Science, Engineering & Environment,
Osaka City, Japan, Nov.21-23, 2016, ISBN: 978-4-9905958-7-6 C3051

Determining Peak Discharge Factor Using Synthetic Unit Hydrograph Modelling (Case Study: Upper Komering South Sumatera, Indonesia)

Rosmalinda Permatasari [a], Dantje Kardana Natakusumah [b], Arwin Sabar[c]
[a] Doctoral Candidate, Environmental Department, ITB and Civil Department, Faculty of Civil Engineering, Tridinanti University, Palembang, Indonesia
rosmalinda_mt@yahoo.com
[b] Civil Department, Faculty of Civil and Environmental Engineering, ITB, Bandung, Indonesia
dknpri@gmail.com
[c] Civil Department, Faculty of Civil and Environmental Engineering, ITB, Bandung, Indonesia

ABSTRACT

Synthetic unit hydrograph methods are popular and play an important role in many water resources design especially in the analysis of flood discharge of ungagged watersheds. These methods are simple, requiring only watershed characteristics such as area and river length and in some cases it may also include land use characteristics. Therefore, these methods serve as useful tools to simulate runoff from ungagged watersheds and watersheds undergoing land use change. To develop a synthetic unit hydrograph, several techniques are available. Several most popular unit hydrographs methods such as Nakayasu, Snyder-Alexeyev, SCS, and GAMA-1 are popular and commonly used in Indonesia for computing both peak discharge rate and the shape of flood hydrograph. This paper presents a simple approach for determining a consistent dimensionless unit hydrograph based on mass conservation principles. The results for peak discharge in several hydrographs methods are Nakayasu 607.32 m^3/sec, SCS 668.62 m^3/sec, ITB-1 675.42 m^3/sec, ITB-2 642.805 m^3/sec in periode time return 2 years.

Key Words: Synthetic Unit Hydrograph (SUH), Flood Hydrograph, Hydrology, Rainfall, Runoff.

INTRODUCTION

Unit Hydrograph (UH) is the most popular and widely used method for analyzing and deriving flood hydrograph resulting from a known storm in a basin area. The term 'Synthetic' in synthetic unit hydrograph (SUH) denotes the unit hydrograph (UH) derived from watershed characteristics rather than from rainfall-runoff data [1].

The determination of the pick discharge value and the runoff volume of a watershed are crucial in managing natural disasters and designing and constructing water structures. Therefore different methods have been developed. Dimensionless unit hydrograph developed by United States soil conservation service (SCS) provides a shape to the unit hydrograph and therefore leads to more reproducible results than the Snyder method [2]-[3].

The plotting positions of the SCS dimensionless unit hydrograph are expressed as the ratios t/t_p and Q/Q_p. tp is the time to peak Q_p is the peak discharge. S-curve hydrograph may be defined as the hydrograph of direct runoff resulting from a continuous effective rainfall of uniform intensity 1/D cm/h [4].

Human activities have always been accompanied by changes in land structure, the destruction of natural resources and urban developments. Cosmopolitan developments on the surface of the watershed will be included in the increase in peak discharge and runoff volume of the watershed [2]-[3]. Upper Komering basin is part of Musi River support operational at South Sumatera and it is located in equatorial region with the average annual rainfall is 2000 mm [5]. Estimating the maximum flood discharge is necessary for predicting watershed hydrological behavior. Major problems concerning hydrological predictions include a lack or low accuracy of rain data, high cost, lack of information about catchments and the length of time required to obtain study results [2].

The production and behavior of runoff are functions of land use types and changes. The hydrological response of a river basin is based on the relationship between basin geomorphology (catchments area, shape of basin, topography, channel slope, stream density and channel storage) and its hydrology. Many studies have been carried out on the efficiency of artificial unit hydrographs in Indonesia such as study at Citarum Basin and Upper Ciliwung [6]-[7].

STUDY AREA

The Upper Komering watershed an area of about 4260 km^2. The temperate humid climate $28.4^0 – 32.2^0$ C, humidity 80% and ratio sunshine 29%. An average annual rainfall 2602.08 mm, wet season during October-May and dry season during June-September [8]. The area's climate is equatorial region and it's present at Figure 1.

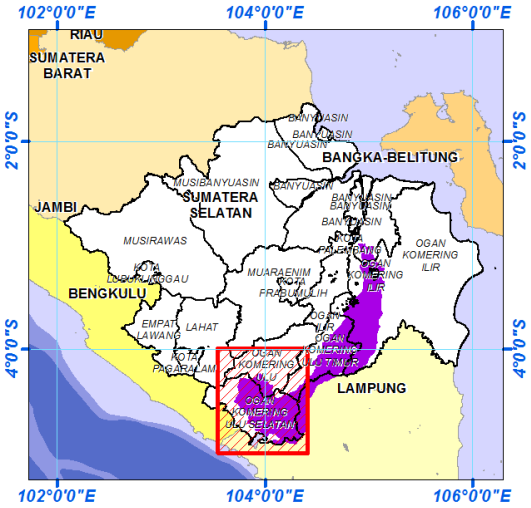

Fig. 1 The location of study area

MATERIALS AND METHOD

The study was intended to use methods and models to simulate rainfall-runoff processes in unit hydrograph. In addition, this study attempted to determine the shape and dimensions of outlet runoff hydrographs in a 4260 km^2 area in the Upper Komering Basin, which is located in the South Sumatera Province of Indonesia.

Model Description

SCS Model

The SCS (1957) method computes the runoff volume (V) and peak discharge (q_p) of a triangular hydrograph, respectively, as follows :

$$V = \frac{1}{2} q_p t_a - \frac{1}{2} q_p (t_p + t_e) \quad (1)$$

$$q_p = \frac{3}{4} V/t_p \quad (2)$$

where q_p is peak discharge in mm/h/mm, t_e is the time from peak to the tail end of the hydrograph ($1.67t_p$), and t_p is in hours (=1/2T + tL). To determine the SUH shape from the non-dimensional q/q_p versus the t/t_p hydrograph, the time to peak (tp) and peak discharge (q_p) are computed as follows :

$$t_p = D/2 + t_L \quad (3)$$

$$q_p = 484A/t_p \quad (4)$$

where D is the duration of rainfall (h), q_p is in cfs A is the area in square miles, t_p is in h (base time = $3/8t_p$), and t_L is the lag time from centroid of rainfall to peak discharge (q_p) (h). The t_L can be estimated from watershed characteristics using curve number CN, watershed length, and slope. With known q_p, t_p, and the specified dimensionless UH, an SUH can be derived [1]-[2]-[9]-[10].

Snyder's Model

Snyder (1938) used three parameters, i.e., lag to peak t_L, peak discharge Q_p, and base time t_B, to describe the hydrograph, and these are expressed as :

$$t_L = C_T(L.L_{CA})^{0.03} \quad (5)$$

$$Qp = 640.Cp.A/t_L \quad (6)$$

$$t_B = 3 + 3.(t_L/24) \quad (7)$$

where L is the length of the main stream from the outlet to the catchment boundary in miles, LCA is the distance from the outlet to a point on the stream nearest to the centroid of the catchment in miles, CT is a non-dimensional coefficient, A is the area of the catchment in square miles, C_p is another non-dimensional coefficient, t_L, Q_p, and t_B are in h, ft^3/s (or cfs), and days. The formula hold for rainfall-excess duration $T_D = t_L/5.5$. For varying duration, the lag time is adjusted as: $t_{LR} = t_L + (T - T_D)/4$, where t_{LR} is revised lag time (h) and T is actual T_D. Snyder's method is applicable to fairly large catchments only, e.g., 100– 500 km^2 [1]-[2]-[9]-[10].

SUH ITB Model

SUH ITB model have two basic method SUH ITB-1 and SUH ITB-2 to describe curve hydrograph and these expressed as: SUH ITB -1 has curve equation is computed as :

$$q(t) = \{t^*\exp(1-t)\}^{\alpha Cp} \quad \alpha=3.7 \quad (8)$$

The formula given by (8) is express Incompletee Gamma Function, which is the curve also used by NRCS to defined NRCS SUH curve forms. SUH ITB-2 are computed as follows :

Rising curve ($0 \leq t < 1$):

$$q(t) = t^{\alpha} \quad \alpha=2.40 \quad (9)$$

Declining curve ($1 \leq t < \infty$) :

$$q(t) = \{t^*\exp(1-t)\}^{\beta Cp} \quad \beta= 0.86 \quad (10)$$

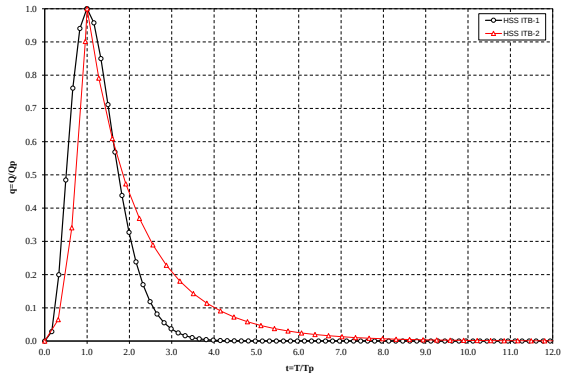

Fig. 2 SUH ITB-1 and ITB -2 dimensionless

Figure 2 describe the horizontal axis is $t = T/T_p$ and the vertical axis $q = Q/Q_p$. Base on SUH definition and mass conversion principle, it can be inferred the effective rainfall volume in watershed,

SUH volume should equal with peak time (T_p) so the computation peak discharge derived ITB formula [11]-[12]-[13]. The formula respectively as :

$$Qp = \frac{Kp.R.Aw}{Tp} \ m^3/s \qquad (11)$$

Qp = Peak discharge unit hydrograph m^3/s
Kp = $1/(3.6 \ . \ A_{SUH})$ = peak rate factor $m^3/s/km^2/mm$
R = Rainfall unit in 1.00 mm
Tp = peak time in hour
Aw = Watershed area km^2
A_{SUH}= Dimensionless unit hydrograph area

Nakayasu Model

The Nakayasu method was developed by applying a dimensionless unit hydrograph based on the Horner and Flynt method for estimating design floods in several small urban watersheds of Japan [9]-[14]-[15]-[16]-[17]-[18]-[19].

RESULTS AND DISCUSSIONS

Komering river in upper has a catchment area 4260 km^2, effective lenght 180 km. In this study the rainfall datas undertaken from three rainfall station Banding Agung, Muara Dua and Martapura, then peak discharge data undertaken from Perjaya headwork. Table 1 describes of characteristics study area undertaken. Simulated hydrographs were used to observed hydrographs.

The model results for peak discharge (q_p) and the time to peak (t_p). From listed in Table 1, were calculated by applying a SUH models and it present in Table 2. Table 3 shows the values of peak discharge. It were computed from rainfall distribution and the values of base flow from dimension unit hydrograph at the first hour 0.034. The peak discharge were computed and the values is 5,131.036 m^3/s. In addition, similarities were observed for the outlet runoff volume parameter in SCS, Snyder, ITB-1 and ITB-2. Triangular and comparisons have proven the difference among UH not significant and it presents in Table 4.

Table 1 Characteristics of Upper Komering area

Name	Remarks
Basin	Upper Komering
Catchment area	A = 4260 km^2
Lenght	L = 180 km
Height unit Rainfall	R = 1.00 mm
Duration	Tr = 1.00 hour
Time coeff.	Ct = 1.00
Time lag	Tl = 18.32 hours
Peak time	Tp = 17.73 hours
Base time	Tb = 177.3 hours
Peak coeff.	1.00
Alpha	2.00
SUH area	1.3161
Qp	50.7 m^3/s
Rainfall volume	4,260,000 m^3

Table 4 Peak discharge values in all method

Time return (year)	QT (m^3/s) Nakayasu	SCS	ITB-1	ITB-2
2	607,315	668,617	675,420	642,805
5	844,157	977,715	978,548	913,429
10	1045,578	1218,335	1220,946	1128,841
20	1267,438	1481,886	1486,444	1481,886

Table 4 defines the hydrograph dimensions in the study basin using the Snyder, SCS and ITB methods. The results demonstrate that a comparable level of performance was achieved for all methods and it describes in Figure 3. Peak discharge hydrographs were similar and showed negligible errors, but the hydrographs differed more noticeably for peak discharge.

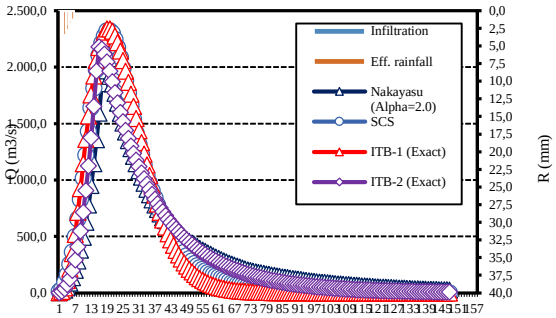

Fig. 3 The hydrograph in the study area

CONCLUSION

This study has determined that, compared to other models, to defined the model which is the most efficient model to use in determining peak discharge. The results demonstrate peak discharge hydrographs were similar. The proposed parameter estimations methods are simple to use, and gives accurate results of the actual as verified using simulation and field data.

ACKNOWLEDGEMENTS

This paper is part of dissertation research in The Research Division of The Environmental Technology Management-Bandung Institute of Technology (ITB). I wish to thank to The Head of Research Division Prof. Dr. Ir. Arwin Sabar, MS and Dr. Ir. Dantje Kardana Natakusumah as research promotor.

Table 2. Dimensionless and dimension unit hydrograph of Upper Komering River

i	T (hours)	Dimensionless unit hydrograph			Dimension unit hydrograph	
		t = T/Tp	q = Q/Qp	A	Q (m^3/s)	V (m^3)
	(1)	(2)	(3)	(4)	(5)	(6)
0	0.00	0.0000	0.0000	0.0000	0.0000	0.0000
1	1.00	0.0564	0.0007	0.0000	0.0335	60.3146
2	2.00	0.1128	0.0074	0.0002	0.3743	734.0876
3	3.00	0.1692	0.0277	0.0010	1.4054	3203.5774
4	4.00	0.2256	0.0666	0.0027	3.3769	8608.2457
5	5.00	0.2819	0.1253	0.0054	6.3533	17514.2962
6	6.00	0.3383	0.2020	0.0092	10.2395	29867.0299
7	7.00	0.3947	0.2925	0.0139	14.8319	45128.5658
8	8.00	0.4511	0.3919	0.0193	19.8689	62461.3640
9	9.00	0.5075	0.4946	0.0250	25.0743	80897.7093
10	10.00	0.5639	0.5954	0.0307	30.1882	99472.4853
11	11.00	0.6203	0.6901	0.0362	34.9867	117314.7935
15	15.00	0.8458	0.9510	0.0524	48.2126	169516.7717
89	89.00	5.0185	0.0001	0.0000	0.0056	21.9193
90	90.00	5.0749	0.0001	0.0000	0.0047	18.4722
			A_{SUH}	1.3161		

Table 3. The values of peak discharge

T	UH	Rainfall distribution						(BF)	Qb
Hours	m^3/s	59.84 mm	15.55 mm	10.91 mm	8.69 mm	7.34 mm	0.00 mm	mm	m^3/s
0.00	0.000	0.000						0.034	0.034
1.00	0.034	2.005	0.000					0.034	2.039
2.00	0.374	22.399	0.521	0.000				0.034	22.953
3.00	1.405	84.101	5.822	0.366	0.000			0.034	90.321
4.00	3.377	202.071	21.859	4.084	0.291	0.000		0.034	228.338
5.00	6.353	380.172	52.521	15.333	3.251	0.246	0.000	0.034	451.557
6.00	10.240	612.724	98.812	36.842	12.208	2.746	0.000	0.034	763.365
7.00	14.832	887.525	159.256	69.314	29.332	10.309	0.000	0.034	1155.769
8.00	19.869	1188.934	230.680	111.713	55.184	24.770	0.000	0.034	1611.315
9.00	25.074	1500.421	309.021	161.816	88.941	46.601	0.000	0.034	2106.833
10.00	30.188	1806.431	389.981	216.769	128.830	75.107	0.000	0.034	2617.152
11.00	34.987	2093.569	469.517	273.561	172.581	108.792	0.000	0.034	3118.053
12.00	39.292	2351.220	544.148	329.353	217.795	145.738	0.000	0.034	3588.288
13.00	42.978	2571.752	611.115	381.705	262.215	183.920	0.000	0.034	4010.741
15.00	48.213	2884.992	714.869	468.888	341.294	256.627	0.000	0.034	4666.705
89.00	0.006	0.333	0.103	0.085	0.081	0.081	0.000	0.034	0.716
90.00	0.005	0.281	0.087	0.072	0.068	0.068	0.000	0.034	0.609
						Peak discharge = 5,131.036 m^3/s			

REFERENCES

[1] Bhunya, P.K., Berndtsson, R., Ojha, Mishra. (2007). Suitability of Gamma, Chi-square, Weibull, and Beta distributions as synthetic unit hydrographs. *Journal Hydrology - Elsevier*.

[2] Khaleghi,M.R.,Gholami, V., Ghodusi, Hosseini. (2011). Efficiency of the geomorphologic instantaneous unit hydrograph method in flood. *Journal of Hydrology*.

[3] Jena, S.K., Tiwari, K.N. (2006). Modeling synthetic unit hydrograph parameters with geomorphologic parameters of watersheds. *Journal of Hydrology*.

[4] Chow, V. (1964). *Handbook of Applied Hydrology*. New York: McGraw-Hill, NY, USA.

[5] Tjasyono, B. (2004). *Klimatologi.* Bandung: Penerbit ITB.

[6] Harlan, D. d. (2009). Penentuan Debit Harian Menggunakan Pemodelan Rainfall Runoff GR4J untuk Analisa Unit Hidrograf pada DAS Citarum Hulu. *Jurnal Teknik Sipil, Jurnal Teoretis dan Terapan Bidang Rekayasa Sipil, ITB.*

[7] Nugroho, S. (2001). Analisis Hidrograf Satuan Sintetik Metode Snyder, Clark dan SCS dengan Menggunakan Model HEC-1 di DAS Ciliwung Hulu. *Jurnal Sains dan Teknologi Modifikasi Cuaca*.

[8] Rusman, A. (2004). *Simulasi Alokasi Air pada Daerah Aliran Sungai Komering Bagian Hulu dalam Pemenuhan Kebutuhan Air Tahun 2020.* Bandung: FTSL-ITB.

[9] Kang, M.S., et.al. (2013). Estimating design floods based on the critical storm duration for small watersheds. *Journal of Hydro-Enviroment*.

[10] Karmaker,T., Dutta, S. (2010). Generation of synthetic seasonal hydrographs for a large river basin. *Journal Hydrology-Elsevier*.

[11] Natakusumah D.K., Hatmoko W., and Harlan D. (2011). Prosedure Umum Perhitungan Hidrograf Satuan Sintetis (HSS) dan Contoh Penerapannya Dalam Pengembangan HSS ITB-1 dan HSS ITB-2. *Journal Teknik Sipil ITB, Vol. 18 No. 3* .

[12] Natakusumah, D. (2009). Prosedure Umum Penentuan Hidrograf Satuan Sintetis Untuk Perhitungan Hidrograf Banjir Rencana. *Seminar Nasional Sumber Daya Air.* Bandung.

[13] Natakusumah, D. (2014). *Cara Menghitung Debit Banjir Dengan Metoda Hidrograf Satuan Sintetis* . Bandung: ITB.

[14] Junia, N., dkk. (2015). Kesesuaian Model Hidrograf Satuan Sintetik Studi Kasus Sub Daerah Aliran Sungai Siak Bagian Hulu. *Jom FTEKNIK* .

[15] Sihotang, R., dkk. (2011). Analisis Banjir Rancangan dengan Metode HSS Nakayasu pada Bendung Gintung. *Universitas Gunadarma* . Depok: Proceeding PESAT (Psikologi, Ekonomi, Sastra, Arsitektur dan Sipil, Vol.4 , ISSN:1858-255.

[16] Hadisusanto, N. (2011). *Aplikasi Hidrologi.* Yogyakarta: Media Utama.

[17] Indarto. (2010). *Dasar Teori dan Contoh Aplikasi Model Hidrologi.* Jakarta: Bumi Aksara.

[18] Kamiana, I. (2012). *Teknik Perhitungan Debit Rencana Bangunan Air*. Yogyakarta: Graha Ilmu.

[19] Limantara, L. (2010). *Hidrologi Praktis.* Bandung: Lubuk Agung.

Second International Conference on Science, Engineering & Environment,
Osaka City, Japan, Nov.21-23, 2016, ISBN: 978-4-9905958-7-6 C3051

IMPROVING BIOSORPTION OF CU(II)-ION ON ARTIFICIAL WASTEWATER BY IMMOBILIZED BIOSORBENT OF TROPICAL MICROALGAE

Astri Rinanti, Melati Ferianita Fachrul, Rositayanti Hadisoebroto, Mawar Silalahi
Environmental Engineering Department, Trisakti University, Jakarta, Indonesia

ABSTRACT

This research purposes to study the role of microalgae in tropical environment – isolated from Wastewater Treatment Plant (WWTP) Setiabudi, Jakarta, Indonesia – on biosorption of Cu(II) ion in heavy metal wastewater. The effects of pH and contact time on the rate of metallic biosorption were examined to reach the greatest biosorption efficiency. Microalgae diversity analysis through phenotypic approaches showed that the microalgae community was comprised of 3 species of Chloropyceae i.e *Ankistrodesmus braunii*, *Chlorella* sp., and *Scenedesmus quadricauda var quadrispina*. Immobilized biosorbent from microalgae was prepared by oven-drying, grinding, and entrapping the microalgae biomass into polymeric matrix of alginate. The sorption properties of biosorbent was characterized by using infrared spectroscopy and SEM micrograph analysis. The optimization of sorption parameters was conducted in batch systems using Cu(II)-artificial wastewater of 300 ppm with pH arrangement of 2-7 and the contact time arrangement of 60, 90, 120, 180, 240 minutes. During the experiment, the Chlorophyceae free and Na-alginat immobilized biomass were added. The research showed that either free and immobilized biomass could adsorb Cu(II) metal ion and reduce its concentration into 25-50 ppm. A maximum biosorption by the alginate-immobilized biosorbent obtained at pH 3,0 and contact time of 180 minutes with 43% absorption efficiency. Sorption properties of microalgae biomasses were indicated by various functional groups presence on biosorbent that could bind heavy metals compared to others. The research proved that the alginate-immobilized biosorbent was highly effective for the treatment of Cu(II)-artificial wastewater and that tolerant cholorophyceae could act as an effective biosorbent in further optimization.

Keywords: Biosorption, Immobilized biosorbent, Cu(II), Microalgae diversity, Tropical environment

INTRODUCTION

The increasing of industrial development leads to heavy metal pollution in aquatic environment. Heavy metals are certainly needed by organisms to support the enzymatic process. However, in excessive amount, they can interfere the growth of the organisms. Copper or Cu is a heavy metal found in natural waters and is an essential matter to microalgae. Copper acts as a constituent of 13 plastocyanin, functioning in electron transport in photosynthesis [1]. Copper is encountered in the center of cytochrome c oxidase that makes up the superoxide dismutase enzyme and carries oxygen in hemocyanin pigments. Many kinds of enzymes contain copper [2]. Copper is considered to be toxic to plants at concentration above 0.1 ppm. Copper level in potable water should be not more than 1 ppm and is toxic to sheeps at concentration above 20 ppm. The presence of copper in wastewater ordinarily appears in the form of bivalent ion of Cu(II) as a hydrolytic product. Copper often found in wastewater of dyeing, paper, oil, and coating industry.

Conventional removal techniques for Cu(II) i.e precipitation, electrochemical, ion exchange, and membrane filtration, have their own limitations such as involving high installation cost, causing secondary pollution due to the chemicals use, and yielding toxic sludge [3], [4]. In addition, these processing techniques are also not able to meet the existing quality standards [5], [6]. Therefore, it is necessary to develop an alternative method of heavy metal removal to tackle the shortcoming mentioned above, among them is biosorption technology.

Biosorption is an absorption process utilizing the ability of biological materials (either macro or micromatters; either living or dead materials) to accumulate heavy metals from a solution metabolically or physicochemically [7]. Advantages gained from the use of microorganisms as biosorbent are low operational cost, high efficiency and high metal binding capacity, minimum sludge product leading to minimum environmental impact, having a possibility of metal recovery as a result of desorption mechanism, having a regeneration mechanism (can be reused as biosorbent), as well as easily obtained, abundant raw materials [5].

Metal biosorption may occur due to the complexity of the positively charged metal ions with negatively charged active centers on the surface of the cell wall or on the extracellular polymers, such as proteins and polysaccharides as a source of functional groups playing important role in binding metal ions. This absorption process takes place rapidly in living cells as well as dead cells [7]

This absorption process does not depend on the metabolism, primarily because it occurs on the surface of the cell wall. Absorption by microorganisms is divided into two, namely metabolically independent absorption occuring on the surface of dead cells and metabolically dependent absorption taking place on the surface of living cells, that is slow and depends a lot on the nutrient availability and environmental conditions, e.g. solution pH and temperature [8]. Many factors can affect metal biosorption, among them are the type of biosorbent [5], pre-treatment of the biosorbent [6], solution pH [8], [9], [10], initial concentration of the adsorbate [11], also the influence of other ions in the solution [4].

The application of microalgae as a biosorbent is more favorable considering that small size of the cells provides larger specific surface that implicates on the higher absorption capacity. Moreover, high sorption ability is led by the presence of functional groups on the microalgae cell wall that are able to bind metal ions, particularly carboxyl, hydroxyl, amine, sulfhydryl, imidazole, sulfate and sulfonate chains [7]. As the raw material of biosorbent, microalgae is handily found, plenteously available, and does not need additional nutrients so that the operational cost can be cheaper [8].

On the other hand, the small size of the particles has disadvantages such as low mechanical strength, causing column plugging and clogging [8], the difficulty of biosorbent regeneration [12], also the requirement of complicated solid-liquid separation process [13]. To overcome these problems, immobilization of the tropical microalgae biomass in a biopolymeric matrix was applied in this study.

Immobilization can be defined as physical entrapment or localization of microalgae cell in such a way to limit the freely migration of microbes [14], while [15] explain that the biomass immobilization is a technique in which the target cell will be coated by porous polymeric layer that allows subtrate diffusion process into the cell. Several synthetic materials e.g. silica, polysulfone, polyurethane, polyvinyl alcohol, and acrylic polymers as well as natural polymers such as alginate, gelatin, agar, and cellulose derivatives can be used for the immobilization of microalgae biomass [16].

The objective of this study was to obtain the highest removal efficiency of heavy metal Cu(II) by utilizing immobilized tropical microalgae biomass in order to optimize the pH and contact time of biosorption.

MATERIAL AND METHODS

Isolation and Identification of Tropical Microalgae

Isolation and sampling 3 species of Chloropyceae i.e *Chlorella* sp., *Ankistrodesmus braunii*, and *Scenedesmus quadricauda var quadri-spina* derived from algal-blooming took place in stabilization pond of Wastewater Treatment Plant (WWTP) Setiabudi, Jakarta, to be used as biosorbent. The method employed in identification of microalgae was phenotype approach, based on microscopical morphology analysis.

Preparation of Biosorbent

Washed microalgae biomass were activated chemically using acidic and alkali solution. Biomass rinsed with distilled water were used as the controls. Some biomass were suspended and soaked for 3 hours in a solution of 0,1 N HCl; 0,1 N NaOH, and distilled water (dH_2O) with a biomass to solution weight ratio of 1:3. Activated biomass then dried in an oven at 70°C for 20 hours, grinded using mortar, and screened using sieve size of 50-mesh (0,3 mm). Biomass powder sized ≤ 0,3 mm were used as biosorbent. This research was conducted in a batch reactor.

Immobilization of Biosorbent

Immobilization of biosorbent was carried out using entrapment method [17]. Some biomass powder were suspended in 100 mL solution of sodium alginate 2% (w/v). The suspension was dripped into a 500 mL solution of $CaCl_2$ 4%. When in contact with $CaCl_2$ solution, biomass suspension of sodium alginate were then polymerizing into bead forms—Na-alginate entrapped the biomass in its structure.

Preparation of Artificial Wastewater

Artificial wastewater containing Cu(II) (1,000 mgL^{-1}) was made by weighing a certain amount of copper sulphate ($CuSO_4 \cdot 5H_2O$) pro analysis and dissolving it in a deionized distilled water to make a stock solution. To obtain different concentration of Cu(II), the stock solution was diluted in accordance to the necessary concentration. The value of pH was adjusted using HCl solution of 0,1 N and NaOH 0,1 N.

Optimization of pH

A total of 10 g immobilized biosorbent was contacted with 50 mL solution of Cu^{2+} 50 mg/L in an Erlenmeyer flask of 150 mL capacity. The value of pH was set in a range of 2, 3, 4, 5, 6, 7, 8. Furthermore, Selanjutnya, Erlenmeyer containing the mixture was stirred using a shaker with a speed of 180 rpm at optimum contact time and temperature. The metal (Cu^{2+}) remained in the solution was analyzed using AAS (Atomic Absorption Spectroscopy).

Optimization of Contact Time

A total of 10 g immobilized biosorbent was contacted with 50 mL solution of Cu^{2+} 20 mg/L in an Erlenmeyer of 150 mL volume. The Erlenmeyer then stirred using a shaker at 180 rpm. The metal Cu^{2+} remained in the solution at contact time of 60, 90, 180, and 240 minutes were then analyzed using AAS spectrophotometer.

Removal Efficiency of Cu(II)

Absorption efficiency of metal Cu(II) by the immobilized biomass of tropical microalgae was calculated using following formula:

$$\% \text{ Cu(II) removal} = [(Co - Ce) / Co] \times 100\% \quad (1)$$

Co = initial concentration of Cu (II) solution (mg/L)
Ce = equilibrium concentration (mg/L)

RESULTS AND DISCUSSION

Effect of the Biosorbent Immobilization

The effects of both immobilized and mobile (free) biosorbent are depicted in Fig.1.

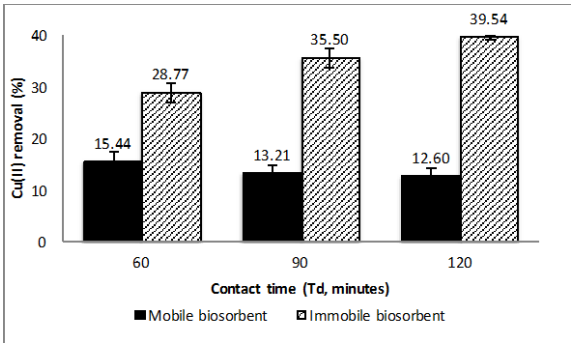

Fig. 1 Removal efficiency of heavy metal Cu(II) by mobile and immobilized tropical microalgae, at temperature 28 °C ± 2 and pH 3

The results show that both free and immobilized biosorbent have the ability to absorb heavy metal Cu(II) and reduce its concentration in the artificial wastewater. However, immobilized biosorbent delivered a better Cu(II) removal efficiency which is 2-3 times higher than mobile biosorbent efficiency.

Chlorella homospaera immobilized in alginate brought favorable system to lower the level of copper, cadmium, zinc, and gold in a contaminated water [1], meanwhile [17] stated that immobilized *Chlorella emersoni* cells was better in accumulating copper than mobile cells. Researcher [14] stated that adsorption capacity of *Spirulina* sp. microalgae biomass can reach 213 mg/g. This ability is considered to be exceptional because according to [5], the adsorption capacity of biomass has to exceed 150 mg/g to be able to compete with other technologies.

Optimization of pH

The effects of pH and contact time towards the rate of metal biosorption were examined to determine the highest biosorption efficiency. The value of pH is one of the crucial physicochemical parameters in biosorption process [8], [9], [10]. The effect of pH on the sorption of Cu(II) by the immobilized biosorbent of tropical microalgae can be seen in Fig. 2.

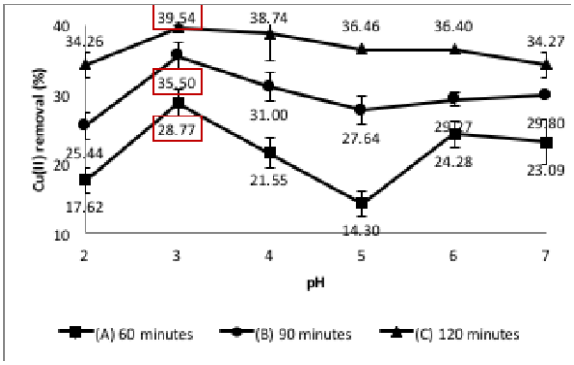

Fig. 2 The effect of pH towards Cu(II) biosorption by microalgae biosorbent, at temperature 28 °C ± 2 and contact time (Td) 60, 90, 120 minutes

Among the physicochemical factors affecting biosorption, apparently pH value is the key factor that was most responsible. The pH value of the solution affects metal speciation [5] and the ionization of biosorbent's functional chains [5], [18]. Most studies of metal biosorption by microalgae showed the dependence relationship to pH value (pH-dependent). At low pH, competition between protons and metal cations such as Cu occured to the active sites of biosorbent. As a result, the cation removal efficiency decreased at low pH. On the contrary, in the biosorption of metal anion such as SO_4^{2-}, the anion metal removal efficiency increased at low pH [18].

Figure 1 reflects that pH value greatly affect the biosorption process of Cu(II) by the biosorbent. The value of pH affects not only the charge of biosorbent functional groups, but also the metal ion speciation [19]. At pH value of 3, the biosorbent

with all variation of contact time (60, 90, 120 minutes) removed Cu(II) of 28-40% more than the removal at higher pH. At low pH, the biosorbent surface becomes positively charged so that it can enhance the sorption of metal anion. Researcher [19] also proved that the highest removal of Cu(II) was at pH value of 1.5. The highest Cu(II) removal reached at a very acidic pH condition (≤ 2) was also reported by other researchers [10], [18], [20].

Optimizing the Contact Time

The effect of contact time towards the sorption of Cu(II) by phytoplankton biomass is shown in Fig 3 below. Figure 3 represents that in such condition, more than 25% of metal removal was obtained during the first 60 minutes in this study. This fast metal removal kinetics could be triggered by the stirring treatment that minimizes the mass transfer constraints. In addition, the rapid sorption kinetics could also indicate that the adsorption occured physically to the pores of the biosorbent.

The optimum percentage of Cu(II) removal was obtained after 180 minutes of contact time, whereas longer than that, the removal percentage proned to be stable with a slight decline (Figure 3). It shows that the sorption process began to reach equilibrium state between sorption rate and desorption rate. Based on that, the optimization of physicochemical parameter in the future studies will be carried out with a contact time of 180 minutes.

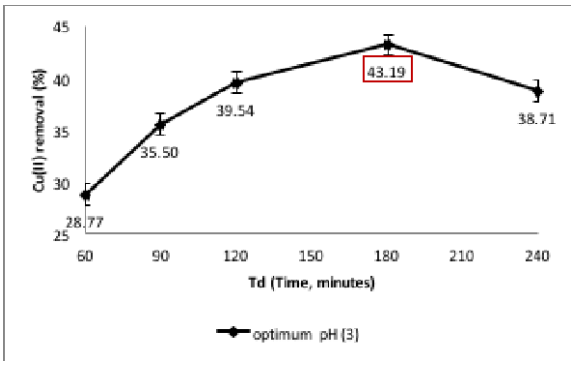

Fig. 3 The effect of contact time on the sorption of Cu(II) by microalgae biosorbent, at temperature 28°C ± 2 and pH 3

The optimum contact time generated in this study is longer compared to the research done by [20], which stated that initial Cu and Zn concentration of 20-27 ppm could be reduced by 99% within 60 minutes contact time and 90% decreased after 30 minutes. Presumably, the type of biosorbent affects its ability to restrain the adsorbate for different kind of biosorbents have different adsorption properties indeed. Such difference may be caused by variation of dominant functional groups, surface area, as well as size and pore volume, which in turn affects the ability to interact with the adsorbate.

CONCLUSION

Based on the results obtained in this study, it can be concluded that the biomass of microalgae consortium in tropical environments have a character as a biosorbent that potentially act as a binder of heavy metal Cu(II). Immobilized biosorbent of tropical microalgae consisting of *Ankistrodesmus braunii, Scenedesmus quadricauda var quadrispina,* and *Chlorella* sp., are considered to be promising biomaterial for it was able to set aside Cu(II) at pH value of 3 and optimum contact time of 180 minutes. Thus, immobilized biosorbent of microalgae was proven to increase sorption process compared to the free (mobile) biosorbent. It is necessary to conduct further research on the variations of temperature and initial concentration of biosorbent.

ACKNOWLEDGEMENTS

The authors would like to thank Directorate for Research and Community Services as well as Directorate General for Strengthening Research and Development at the Ministry of Research, Technology, and Higher Education Indonesia for funding this study through Universities Prime Research Grant Program (Penelitian Unggulan Perguruan Tinggi-PUPT) 2016.

REFERENCES

[1] Reynold C, Ecology of Phytoplankton. New York: Cambridge University Press, 2006
[2] Banfalvi G. Cellular Effects of Heavy Metals. London: Springer, 2011, pp. 364 http://dx.doi.org/10.1007/978-94-007-0428-2
[3] Velásquez L, Dussan J, "Biosorption and Bioaccumulation of Heavy Metals on Dead and Living Biomass of *Bacillus sphaericus*", *J. Hazard. Mater*, Vol. 167, 2009, pp. 713-716.
[4] Oboh I, Aluyor E, Udu T, "Biosorption of Heavy Metal Ions from Aqueous Solutions Using a Biomaterial", *Leonardo J. Sci*, Vol. 14, 2009, pp. 58-65, ISSN 1583-0233.
[5] Gadd GM, "Biosorption : Critical Review of Scientific Rationale, Environmental Importance and Significance for Pollution Treatment", J. Chem. Technol. Biotechnol, Vol. 84, 2009, pp. 13-28.
[6] Eccles H, "Treatment of Metal-Contaminated Wastes: Why Select a Biological Process?", Trends Biotechnol, Vol. 17, 1999, pp. 462-465.
[7] Volesky B, Naja G, "Biosorption : Application Strategies", Department of Chemical

Engineering, Montreal, Quebec, 3610 University Street, Canada: McGill University, 2003, H3A 2B2.

[8] Wang C, Chen J, "Biosorption for Heavy Metals Removal and Their Future", Biotechnol.Adv., Vol. 27, 2009, pp. 195-226.

[9] Gokhale SV, KK Jyoti, SS Lele, "Modelling of Chromium (VI) Biosorpion by immobilized S. platensis in Packed Column", J. Hazard. Mater., Vol. 170, 2009, pp. 735-743.

[10] Chojnacka K, Chojnacki A, Gorecka H, "Biosorption of Cr^{3+}, Cd^{2+}, and Cu^{2+} ions by Blue-Green Algae *Spirulina* sp.: Kinetics, Equilibrium and the Mechanism of the Process", Chemosphere, 59, 2005, pp. 75-84.

[11] Pagnanelli F, Esposito A, Toro L, Veglio F, "Metal Speciation and pH Effect on Pb, Cu, Zn, and Cd Biosorption onto *Sphaerotilus natans*: Langmuir-type Empirical Model", Water Res, Vol. 37, 2003, pp. 627–633.

[12] Ivánová D, Horváthová H, Kaduková J, Kavuličová J, "Stability of Immobilized Biosorbents and Its Influence on Biosorption of Copper", Nova Biotechnologica, Vol. 10 (1), 2010, pp. 45-51.

[13] Atkinson BW, Bux F, Kasan HC, "Considerations for Application of Biosorption Technology to Remediate Metal-Contaminated Industrial Effluents", Water SA, Vol. 24, 1998, pp. 129-136.

[14] Covizzi LG, Giese EC, Gomes E, Dekker RFH, Silva R, "Immobilization of Microbial Cells and Their Biotechnological Applications", Seminar: Ciências Exatas e Tecnológicas. Vol. 28, 2007, pp. 143-160.

[15] Horvathova, "Biosorption of Cu^{2+} and Zn^{2+} by Immobilized Algae Biomass of *Chlorella kessleri"*, Acta Metallurgica Slovaca, Vol. 15, 2009.

[16] Akar T, Kaynak Z, Ulusoy S, Yuvaci D, Ozsari G, Tunali-Akar S, "Enhanced Biosorption of Nickel(II) Ions by Silica-gel Immobilized Waste Biomass: Biosorption Characteristics in Batch and Dynamic Flow Mode", J. Hazard Mater, Vol. 163, 2009, pp. 1134–1141.

[17] Rosevear A, "Immobilised Biocatalysts: A Critical Review", J. Chem. Technol. Biotechnol., Vol. 34B, 1984, pp. 127-150.

[18] Krishnani KK, Meng X, Christodoulatos C, Boddu VM, "Biosorption Mechanism of Nine Different Heavy Metals onto Biomatrix from Rice Husk", J. Hazard. Mater, Vol.153(3), 2008, 1222–34.

[19] Rangsayatorn N, Upatham ES, Kruatrachue M, Pokethitiyook P, Lanza, GR, "Phytoremediation Potential of *Spirulina (Arthospira) platensis*: Biosorption and Toxicity Studies of Cadmium", Environ. Pollut., Vol. 119, 2002, pp. 45-53.

[20] Hernandez E, Olguin EJ, "Biosorption of Heavy Metals Influenced by The Chemical Composition of *Spirulina* sp. (*Arthrospira*) Biomass", Environ. Technol., Vol. 23, 2002, pp. 1369-1377.

Second International Conference on Science, Engineering & Environment,
Osaka City, Japan, Nov.21-23, 2016, ISBN: 978-4-9905958-7-6 C3051

SELF-ORGANIZING MAP BASED SURROGATE MODELS FOR UNKNOWN CONTAMINANT SOURCE IDENTIFICATION UNDER UNCERTAIN HYDRAULIC CONDUCTIVITY

Shahrbanoo Hazrati Y.[1] and Bithin Datta[1, 2]
[1]Discipline of Civil Engineering, College of Science and Engineering
James Cook University, Townsville QLD 4811, Australia
[2] CRC for Contamination Assessment and Remediation of the Environment, CRC CARE, University of Newcastle, Callaghan NSW 2308, Australia

ABSTRACT

Identification of unknown groundwater contaminant sources is a complex problem. The complexities arise mainly due to the uncertainties related to the hydrogeologic information, sparsity of measurement data and unavoidable concentration measurement errors. The process of contaminant source identification with sparse and limited concentration measurement data especially when the hydrogeologic parameters are uncertain requires an efficient procedure. The existing methodologies to tackle this problem in real world cases usually require huge computational time and the solutions may be non-unique. The goal of this study is to evaluate a developed methodology to characterize the groundwater contamination sources in a heterogeneous, multi layered aquifer. This developed methodology utilizes the Self Organizing Maps (SOM) algorithm to design the surrogate models for source characterization. The most important advantage is that in this methodology, the trained SOM based surrogate models is directly utilized for groundwater contaminant source characterization without the necessity of using a separate linked simulation optimization model. The performance of the developed methodology is evaluated by using deterministic hydraulic conductivity values, and uncertain hydraulic conductivity values. These results indicate that the developed methodology could efficiently approximate groundwater flow and transport simulation models, and also characterize unknown groundwater contaminant sources in terms of location, magnitude and release history.

Key words: Self-Organizing Maps, Surrogate Models, Source Identification, Uncertainty.

INTRODUCTION

Widespread human activities and improper management practices have caused widespread deterioration of groundwater quality worldwide, and have seriously threatened its beneficial use in recent decades. However, usually when groundwater contamination is detected after a long time, often there is not enough information regarding the characteristics of groundwater contamination sources as well as the hydrogeologic parameters of the system. On the other hand, the efficiency and reliability of contaminant source identification depends on the availability, adequacy and accuracy of hydrogeologic information and contaminant concentration measurements data. For instance, the crux of previous approaches is highly vulnerable to the accuracy and adequacy of contaminant concentration measurements and hydrogeologic data. A significant number of previously proposed approaches considered that all the hydrogeological parameter values are known. These approaches include: embedded optimization method [1], [2] and linked simulation optimization method which is the most effective approach to contaminant source identification. In linked simulation optimization approach different optimization algorithms were utilized such as Genetic Algorithm (GA) [3], [4], Simulated Annealing (SA) [5] and Adaptive Simulated Annealing (ASA) [4], [6]. Only a few of previously developed methodologies such as [4], [6] were evaluated under uncertain hydrogeological parameter conditions.

In this study, to characterize the unknown characteristics of contaminant sources a new approach is developed and evaluated for potential applicability in practical scenarios. In this new methodology, a trained Self Organizing Map (SOM) based surrogate model for source characterization approximates the flow and transport simulation models as well as an optimization algorithm. In other words, this model independently provides a procedure to characterize unknown groundwater contaminant sources in terms of location, magnitude and duration of source activity, without the necessity of using a linked

simulation optimization model. However, in this methodology and other methods the accurate analysis of the process of groundwater flow and transport requires accurate and adequate information of hydrogeologic parameters and contaminant concentration values. On the other hand, the simulation of groundwater flow and solute transport involves intrinsic uncertainties due to the sparsity or lack of enough hydrogeologic information of the porous medium. For example, hydraulic conductivity plays a main role in the process of groundwater flow and transport and this parameter may be the most uncertain parameter in the groundwater flow and transport models. It is not possible to measure this parameter in every location or discretization nodes, where the ground water flow and transport simulation model needs hydraulic conductivity values. Generally, in real world cases limited numbers of measured hydraulic conductivity are available and the values of this parameter for other locations are subject to uncertainty and these values need to be estimated.

Therefore, utilizing a proper method to estimate the unknown hydrogeologic parameters based on limited available data is essential in any contaminant source identification strategy. If these estimations do not approximate the hydrogeologic parameters accurately, it will result in the propagation of more errors and uncertainty in the groundwater flow and transport simulation models. Thus, the specific, main objective of this study is to develop an efficient methodology to characterize unknown contaminant sources. Also, this developed methodology is evaluated especially where contaminant concentration measurement data are missing for long time intervals, and hydraulic conductivity is only known at limited sample points. These evaluation results demonstrate the potential applicability of this methodology to contaminant source identification in real world cases.

METHODOLOGY

Surrogate Models

Surrogate models or Response Surface Models (RSM) are compact analytical models. These compact models are based on limited numbers of input and output sets obtained from computationally extensive simulation models. If these models are precisely constructed, surrogate models are able to approximate the behavior of complex system at reduced computational time [11]. Surrogate Model Based on Optimization (SMBO) is one of the most practical types of surrogate models which are utilized to solve the nonlinear complex problems. The main steps of constructing a SMBO are: sampling plan, implementing numerical simulation models, construction of surrogate models, model evaluation and finalizing model by utilizing termination criteria [12]. These steps are broadly explained in the section on construction of SMBO.

Simulation Models

To solve the flow equation, numerical simulation model MODFLOW is used. MODFLOW was developed by the United States Geological Survey (USGS). The three-dimensional equation of groundwater flow through porous media is utilized by MODFLOW which is a partial-differential equation that represents the groundwater flow in non-equilibrium, anisotropic and heterogeneous conditions [7].

In addition, a Modular Three-Dimensional Multi species Transport Model (MT3DMS) is used in this study. This model is used for the groundwater system in order to simulate the advection, dispersion, and chemical reactions process of contaminants to calculate the contamination concentration values. The governing equation is a partial differential equation and considers the fate and transport of contaminants of species in a 3-D transient groundwater flow system[8].

Self-Organizing Maps

The Self-Organizing Maps (SOM) algorithm transforms complex non-linear statistical multidimensional data problems in to simple geometric relationships [9]. The SOM abstracts the main information and their topologic relationships on a visual display. Therefore, reducing the dimensions and visualizing of data are the two main characteristics of SOM that enable SOM to be practically utilized in different complex fields of sciences [9]. In this study, due to the SOM's ability to abstract the nonlinear relationships of high-dimensional complex system; SOM is utilized as the tool to construct the surrogate model. The main steps of SOM algorithm are initialization, competition, cooperation and adaptation which are described below:

a. Initialization: all the units in the output domain connect with the input units with an initial network weights value.

b. Competition: for each input pattern, the output neurons compete to declare the winner neuron for each input vector. The winner neuron or Best Matching Unit (BMU) is that one which has the most similarity with the input vector.

c. Cooperation: The winning neuron calculates the spatial distance of exited neighborhood neurons to cooperate with them and update all weights of the winning neuron.

d. Adaptation: For this step, the process repeats steps b to d until the desired iteration is reached, or the changes in the map for two consecutive iterations are less than a specified target value.

In this study, the software "SOM Toolbox for Matlab 5" is used to construct the SOM based surrogate models [10].

Definition of a Generic Objective Function

The implicit objective function of source identification problem can be defined as by Eq. (1) which minimizes the difference between the estimated and the observed concentration values at specific monitoring locations at specific time [13], [4].

$$\text{Minimize E} = \sum_{k=1}^{nk} \sum_{iob=1}^{nob} \left(\text{Cest}_{iob}^{k} - \text{Cobs}_{iob}^{k}\right)^2 . w_{iob}^{k} \qquad (1)$$

Where Cest_{iob}^{k} and Cobs_{iob}^{k} are estimated concentration values and observed concentration values at observation well location iob and at the end of time period k, respectively. nk and nob are total number of concentration observations time and total number of observation wells, respectively. It is also possible to normalize the objective function using weights w_{iob}^{k}, where is weight corresponding to observation location iob at the end of time period k, this parameter can be defined as:

$$w_{iob}^{k} = \frac{1}{\left(Cobs_{iob}^{k} + \eta\right)^2} \qquad (2)$$

Where η is a constant and should be sufficiently large to prevent the denominator become near zero at very low concentration [1]. The main constraints of the optimization model are

$$Cest_{iob}^{k} = f(x, y, z, v_x, q_s, C_s, t) \qquad (3)$$

Where $f(x, y, z, v_x, q_s, C_s, t)$ represents the simulation models or SOM based surrogate model at time step t. x, y, z is Cartesian coordinates of the monitoring locations, v_x is groundwater velocity along the x coordinate axis, q_s is volumetric flux of water per unit volume of aquifer (T^{-1}), C_s is concentration of the sources or sinks (ML^{-3}) and $q_s C_s$ is contaminant source fluxes ($ML^{-3}T^{-1}$). This approach is the linked simulation optimization approach as proposed by [3], [5].

However, in this new approach using the SOM based surrogate model, the surrogate model is utilized in an inverse mode to characterize the unknown sources of contamination from concentration measurement data. The SOM based surrogate model is first trained and tested to approximate the flow and transport processes in the aquifer study area. Once the training and testing processes are complete, the surrogate model represents the approximate simulation model.

In the traditional approach, the surrogate model once developed can be linked to the optimization model represented by objective functions and constraints (1)-(3). In the developed methodology in this study, the optimization model is not solved, and the source characterization based on concentration measurement data is accomplished by running the SOM based surrogate model in inverse mode. The SOM based surrogate model is used to estimate the contaminant source characteristics as the output, while the concertation measurements resulting from the unknown contaminant sources are used as inputs. Therefore, the optimization for an objective similar to the defined objective (1) is actually implicitly carried out by using the developed SOM based surrogate model in inverse mode. The limited performance evaluation results presented here for an illustrative contaminated aquifer study area, utilizing synthetic hydrogeologic data, and simulated concentration measurements establish the potential applicability of this approach.

Performance Evaluation

The performance of the developed methodology is evaluated for an illustrative contaminated aquifer study area (Fig. 1), with simulated concentrations measurements. The performance evaluation is carried out for two different scenarios based on two different assumptions as stated below.

1. All the hydrogeologic parameters of the model are precisely known; and
2. Uncertainties are associated with the hydraulic conductivity of the study area; and these parameter values are known only at limited sparse locations.

As for the first assumption, the study area considered is heterogeneous and the actual hydraulic conductivity values are assumed to be a random variable. Therefore, in order to generate hydraulic conductivity throughout the entire study area the values of hydraulic conductivity (K) are assumed to follow the Lognormal distribution [14]. Thus, it is possible to define a new parameter such as Y = log K which is normally distributed. Also, the Latin Hypercube Sampling (LHS) method is utilized to randomly generate the hydraulic conductivity field throughout the study area following the method used in [15].

The second assumption implies that the hydraulic conductivity measurements are available only at limited locations, while the simulation models need this parameter values at all its nodes. Therefore, hydraulic conductivity should be estimated at other nodes. According to [16] the Inverse Distance Weighting (IDW) methodology could be the most suitable method to generate hydraulic conductivity

because of its simplicity, and thus, associated computational ease. This study also demonstrated that the more complicated interpolation methods such as Kriging or fractal-based methods perform little better compared to simplified method such as the IDW. Also, with very sparse measurement data these two methods are not suitable. Therefore, in this study IDW is utilized to generate hydraulic conductivity values at locations where these values are unknown. Moreover; to quantify the performance evaluation of the developed procedure, Normalized Absolute Error of Estimation (NAEE) is used as a criterion in this study. This parameter calculates a normalized error of estimation. Equation (4) represents NAEE [4]:

$$NAEE(\%) = \frac{\sum_{i=1}^{S}\sum_{j=1}^{N}\left|\left(q_i^j\right)_{est} - \left(q_i^j\right)_{act}\right|}{\sum_{i=1}^{S}\sum_{j=1}^{N}\left(q_i^j\right)_{act}} \times 100 \qquad (4)$$

Where S is number of pollution source(s); N is number of transport stress periods; $\left(q_i^j\right)_{act}$ is actual source flux at potential source number i in stress period j; and $\left(q_i^j\right)_{est}$ is estimated source flux at source number i in stress period j.

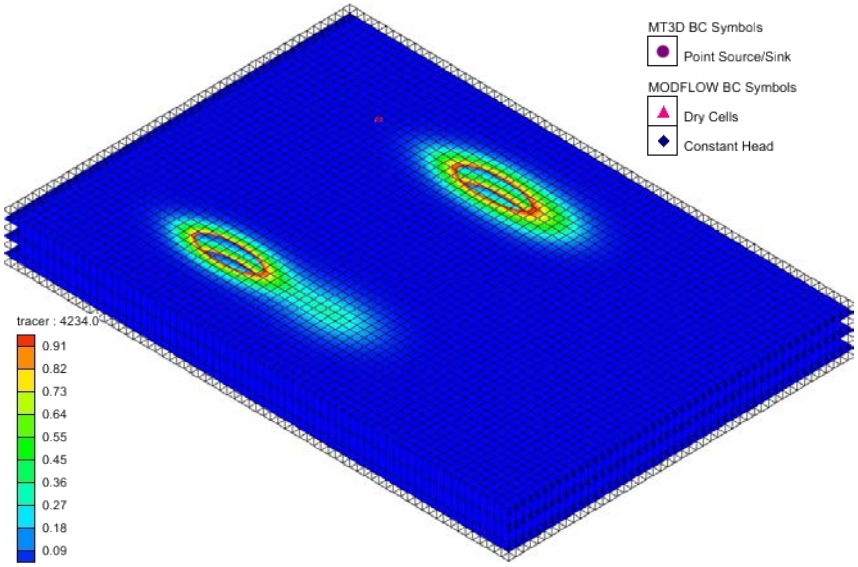

Fig. 1 Illustrative study area representing typical concentration plumes 4234 days after start of first source activity (concentration values g/l)

Construction of SMBO

In order to solve the source identification problem and evaluate the performance of the SOM based surrogate model a type of SMBO, the following steps are followed.

1. Scenarios for sampling plan: LHS is utilized to produce three groups of 250, 500, and 1000 initial sample sets with 2 potential contaminant sources with contaminant fluxes in the range of 0-10 g/s.
2. Implementing simulation models: groundwater flow and transport simulation models MODFLOW and MT3DMS (within GMS 7) are solved for three randomly generated groups of source fluxes. The simulation results provide the contaminant concentration values at five specified monitoring locations resulting from these two contaminated sources as specified.
3. Construction of the surrogate models: SOM algorithm is applied to create surrogate models representing the relationship between the aquifer stresses in the form of contaminant injection and the resulting impacts in terms of the concentration values at specified monitoring locations and times. The randomly generated potential source fluxes and their corresponding contaminant concentration magnitudes at specified monitoring locations at specified time are used as the inputs for training of the SOM based surrogate models. Then, to find the unknown characteristics (magnitude, location and duration) of potential contaminant sources, the BMU of SOM algorithm that satisfies similar criterion as the implicit objective function (1) of this problem is utilized. Therefore, this capability of SOM based surrogate models eliminates the necessity of using any complex and explicit optimization model.
4. Validation of the model: A group of 100 randomly generated sample sets of potential contaminant source fluxes and corresponding simulated measured

concentrations are utilized to test the performance of the developed model once it has been adequately trained. In this step, the performance of the trained SOM models for different scenarios representing different numbers of initial sample sizes and SOM map units are evaluated in terms of NAEE defined by Eq. (4).

5. Finally, based on the validation results obtained in the previous step, the best candidate SOM based surrogate model is selected. Once the best candidate SOM model is validated and chosen, it is used for further performance evaluation.

RESULTS AND DISCUSSION

The illustrative study area utilized for the performance evaluation of the proposed methodology is a heterogeneous aquifer which consists of three unconfined layers. This study area is shown in Fig. 1. Table 1 shows the aquifer characteristic values and dimensions of this study area. In this study area, the north and south boundaries are considered as no-flow boundaries. Whereas, the east and west boundaries are considered as specified head boundaries. Only a conservative contaminant and two potential contaminant source locations (S1 and S2) are considered. Table 2 shows the locations and flux magnitudes of the actual contaminant sources. There are five monitoring wells; their locations are presented in Table 3. The total time of simulation is divided into 5 different stress periods (SP1 to SP5). The first four stress periods are each of two years duration and the last stress period is of 12 years duration. Potential contaminant sources are assumed to be active only in the first four stress periods. It is specified that the contamination is detected just two years after the contaminant sources had stopped their activity. It is also specified that the five monitoring locations are monitored over the last 10 years at an interval of 73 days.

Table 1 Hydrogeologic characteristics of the study area

Parameter	Unit	Value
Maximum length of study area	m	2100
Maximum width of study area	m	1500
Saturated thickness, b	m	30
Grid spacing in X and Y-directions	m	30
Grid spacing in Z-direction	m	10
Vertical anisotropy		5
Hydraulic gradient		0.00238
Porosity		0.3
Longitudinal Dispersivity	m	15
Transvere Dispersivity	m	3
Initial Contaminant Flux	g/s	0-10

Table 2 Locations and flux magnitudes of actual contaminant sources

Potential contaminant source location (row, column, layer)	Contaminant fluxes (g/s)				
	SP 1	SP 2	SP 3	SP 4	SP 5
S1 (12, 15, 1)	6.3	4.6	9.0	5.6	0.0
S2 (38, 9, 2)	6.7	9.3	6.1	7.3	0.0

Table 3 Locations of monitoring wells

Monitoring Location	Row	Column	Layer
1	12	21	1
2	12	35	1
3	26	28	1
4	38	16	1
5	38	29	1

In this study, different surrogate models using different numbers of initial sample sets i.e., 250, 500, 1000, 1500 and 1750 are constructed. The randomly generated source fluxes at two potential contaminant sources and corresponding concentration measurement data at 5 selected monitoring locations at an interval of 73 days over the last 10 years of simulation are used to construct these surrogate models. In these scenarios, the numbers of SOM map units are maintained constant (100×100 units). The average NAEE percentages of these constructed SOM based surrogate models for 100 sample sets varied from 24.1 to 38.8. The best results among these SOM based surrogate models are obtained by using 1500 initial sample sets.

Also, different SOM based surrogate models representing different numbers of SOM map units are constructed. The different SOM map units considered are 50×50, 75×75, 100×100, 120×120, 130×130 and 140×140 units. In these scenarios, the number of initial sample sets is maintained constant at 1500. The average NAEE of these constructed SOM based surrogate models for 100 sample sets varied from 24.1 to 38.8.The best solution result for source identification is obtained by utilizing 100×100 map units. An important constraint in these evaluations of different scenarios is the required CPU time, which significantly increases when the numbers of SOM map units are more than 120×120 (Fig.2).

When utilizing the first assumption, the hydraulic conductivity field for the whole study area is generated by assuming that the mean of hydraulic conductivity in each of the three layers

(layer 1, 2 and 3) are 20, 17, and 21 m/day and the standard deviation are 0.1, 0.08, and 0.12, respectively. In the second assumption, it is assumed that the hydraulic conductivity measurements are available only at 20 locations. The distances between any two locations along the maximum length and minimum length of the study area are 300 and 450 meters, respectively. Therefore, to generate hydraulic conductivity values at other locations; the IWD method is utilized as the interpolation method, due to its efficiency and simplicity [16]. Figure 3 represents the generated hydraulic conductivity field for layer 1 using IWD interpolation method.

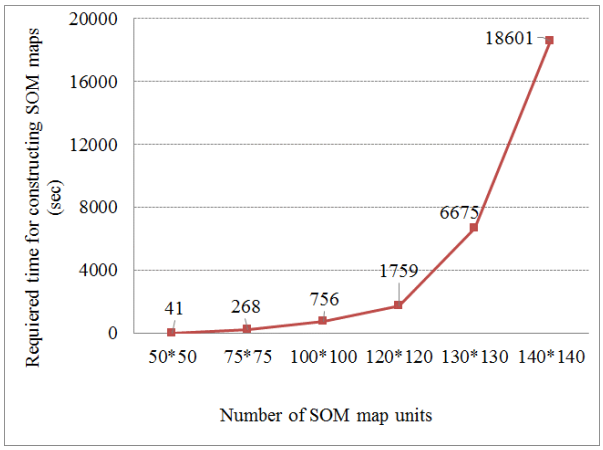

Fig. 2 Computational times for constructing different SOM based surrogate models representing different numbers of SOM map units

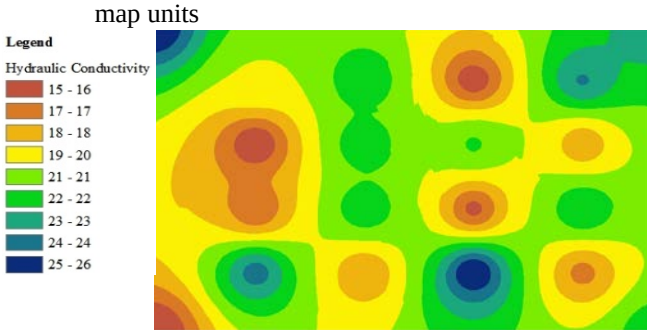

Fig. 3 Generated hydraulic conductivity for layer 1

The obtained NAEE values for source identification are based on the first and second assumptions are equal to 14 and 16 percent, respectively. These results are obtained by applying the best SOM based surrogate model among the constructed models for this study area. These NAEE values are averaged over the 5 stress periods (SP1, SP2, SP3, SP4 and SP5) for two actual contaminant sources (S1 and S2). Figure 4 represents the results of source identification for both the assumptions. This figure compares the estimated source flux values with the actual source flux values.

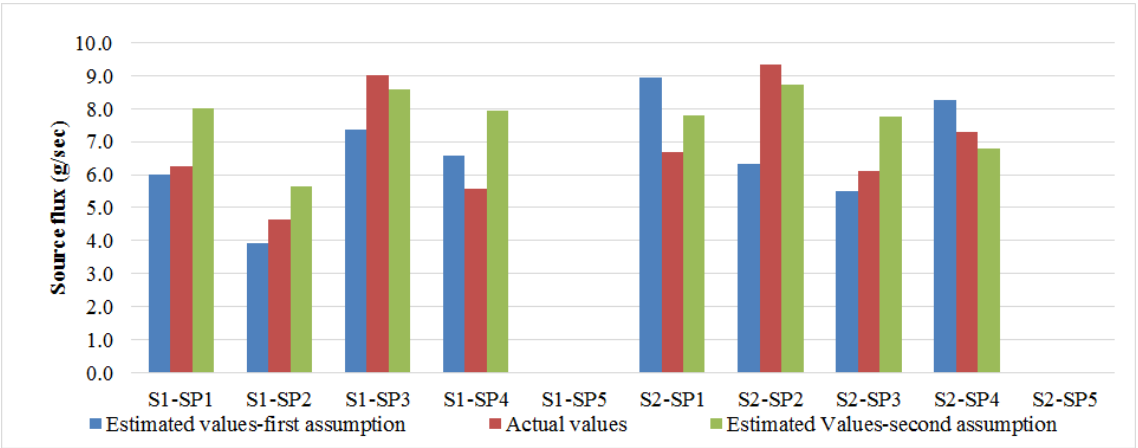

Fig.4 Source identification results

CONCLUSION

In this study, in order to develop a SOM based surrogate model, different scenarios representing different numbers of initial sample sizes and SOM map units are considered. Also, the performance of the developed methodology is evaluated by considering two scenarios representing two assumptions: first, the hydrogeologic parameters, i.e., hydraulic conductivity are assumed to be known. Second: hydraulic conductivity values are uncertain and it is assumed that measurement values are known only at 20 locations. Main conclusions that can be obtained from these limited performance evaluation results are:

1. The SOM based surrogate model could approximate groundwater flow and transport simulation models adequately. Also, this developed methodology provides an alternative methodology to identify unknown characteristics of

unknown contaminant source in terms of location, magnitude and duration of source activity, without explicitly using a linked simulation-optimization approach.

2. The initial sample size used for training has crucial role on the efficiency of the SOM based surrogate models. This size should be sufficient to properly cover the whole range of potential contaminant source fluxes and corresponding contaminant concentration values. However, very larger number of initial sample sizes may also sometimes decrease the accuracy of the solution results. For example in this study the best result is achieved by utilizing 1500 initial sample sets, and not 1750 sample sets.
3. The optimal numbers of SOM map units are important. This parameter relates to the memory of the PC used and initial sample sizes (Fig.2).
4. The most important conclusion is that the SOM based surrogate models independently provide a procedure for contaminant source identification, without the necessity of using a linked simulation optimization model.
5. The performance evaluation results are based on very limited scenarios and therefore restricted in scope. Further performance evaluations are required to fully establish the applicability of the proposed methodology.

ACKNOLOGMENTS

The second author thanks CRC-CARE, Australia for providing financial support for this research through Project No. 5.6.0.3.09/10(2.6.03), CRC-CARE-Bithin Datta which partially funded the Ph.D. scholarship of the first author.

REFRENCES

[1] Mahar, P.S. and B. Datta, *Optimal monitoring network and ground-water-pollution sources identification.* Journal of Water Resource Planning and Management, 1997. **123 (4)**: p. 199-207.

[2] Mahar, P.S. and B. Datta, *Identification of pollution sources in transient groundwater systems.* Water Resources Management, 2000. **14**(3): p. 209-227.

[3] Singh, R.M. and B. Datta, *Identification of groundwater pollution sources using GA-based linked simulation optimization model.* Journal of Hydrologic Engineering, 2006. **11**(2): p. 101-109.

[4] Jha, M. and B. Datta, *Three-Dimensional Groundwater Contamination Source Identification Using Adaptive Simulated Annealing.* Journal of Hydrologic Engineering, 2013. **18**(3): p. 307-317.

[5] Prakash, O. and B. Datta, *Optimal characterization of pollutant sources in contaminated aquifers by integrating sequential-monitoring-network design and source identification: methodology and an application in Australia.* Hydrogeology Journal, 2015. **23**(6): p. 1089-1107.

[6] Amirabdollahian, M. and B. Datta, *Reliability Evaluation of Groundwater Contamination Source Characterization under Uncertain Flow Field.* International Journal of Environmental Science and Development, 2015. **6**(7): p. 512-518.

[7] Harbaugh, A.W., *MODFLOW-2005, The U.S. Geological Survey Modular Ground-Water Model-the Ground-Water Flow Process*. 2005: U.S. Geological Survey Techniques and Methods 6–A16.

[8] Zheng, C. and P.P. Wang, *MT3DMS: A Modular Three-Dimensional Multispecies Transport Model for Simulation of Advection, Dispersion, and Chemical Reactions of Contaminants in Groundwater Systems; Documentation and User's Guide*. 1999: US Army Corps of Engineers-Engineer Research and Development Center, Contract Report SERDP-99-1. p. 220.

[9] Kohenon, T., et al., *Engineering Applications of the Self-Organizing Map.* IEEE, 1996. **84(10)**: p. 1358-1384.

[10] Vesanto, J., et al., *Self-Organizing Map in Matlab: the SOM toolbox*. 2000.

[11] Gorissen, D., et al., *A Surrogate Modeling and Adaptive Sampling Toolbox for Computer Based Design.* Journal of Machine Learning Research, 2010. **11**: p. 2051-2055.

[12] Forrester, A.I.J. and A.J. Keane, *Recent advances in surrogate-based optimization.* Progress in Aerospace Sciences, 2009. **45**(1-3): p. 50-79.

[13] Mahar, P.S. and B. Datta, *Optimal identification of ground-water pollution sources and parameter estimation.* Journal of Water Resources Planning and Management-Asce, 2001. **127**(1): p. 20-29.

[14] Freeze, R.A., *A Stochastic-Conceptual Analysis of One-Dimensional Groundwater Flow in Nonuniform Homogeneous Media.* Water Resources Research, 1975. **11**: p. 17.

[15] Dokou, Z. and G.F. Pinder, *Optimal search strategy for the definition of a*

DNAPL source. Journal of Hydrology, 2009. **376**(3-4): p. 542-556.

[16] Borman, G.K., F.J. Molz, and O. Guven, *An Evaluation of Interpolation Methodologies for Generating Three-Dimensional Hydraulic Property Distribution from Measured Data*. 1995. **33**: p. 12.

Second International Conference on Science, Engineering & Environment,
Osaka City, Japan, Nov.21-23, 2016, ISBN: 978-4-9905958-7-6 C3051

MECHANICAL PROPERTIES OF BIO-COMPOSITE CONCRETE PANEL UTILIZING COCO COIR DUST AND LOW DENSITY POLYETHYLENE

Neslyn E. Lopez[1] and Joseph Berlin P. Juanzon[2]
[1,2]Faculty, Malayan Colleges Laguna, Philippines

ABSTRACT

Incorporation of waste has proven its potential by many studies to develop an alternative construction material. Bio-composite boards made from agricultural waste and plastic have been investigated by many researchers. Coco coir dust and low density polyethylene (LDPE) are abundant due to the high demand in the agricultural and industrial waste, respectively. These were used to produce a bio-composite board that can be substitute for commercial boards. This study extended the application of bio-composite board to produce a concrete panel by utilizing it as permanent formwork. The produced bio-composite concrete panel (BCCP) was compared to concrete block with the same dimensions of 200 mm x 100 mm x 50 mm. The thickness of the boards on each face of the concrete core was 5 mm and 12 mm. Results showed the potential of the BCCP to be a lighter material compared to concrete panel with a density of 1640 kg/m^3 for BCCP with 12 mm boards. Considerably, BCCP had a good architectural finish compared to concrete block without finishes yet. Furthermore, BCCP had a significant mechanical performance as non-load bearing wall construction with a mechanical and flexural strength of 7.53 MPa and 2.78 MPa, respectively, for BCCP with 12 mm boards.

Keywords: Bio-composite concrete panel, Mechanical performance, Bio-composite board, Coco coir dust

INTRODUCTION

The incorporation of waste as alternative construction materials is some of the focuses of the researches in order to give solution for environmental issues the world's facing today. Agro-waste such as sugarcane bagasse, rice hull and coco coir performed excellently as construction building materials regarding its strength, durability and especially to thermal conductivity [1].

The Philippines is an agricultural country which comprises the 47% of the total land area. According to Zafar [2], the country has the largest number of coconut trees in the world. In this regard, the contribution of the coconut wastes includes the coconut shell, coconut husk and coconut coir dust. Approximately 500 million coconut trees produce remarkable amounts of biomass as husks (4.1 million tonnes), shells (1.8 million tonnes), and fronds (4.5 million tonnes) annually.

Coir dust also known as coco peat is the by-product in the processing of husk to coco fiber which appears as short spongy fibers and dust. The application of coco coir in the fiberboard performs acceptable results in the mechanical properties which can be an alternative construction material such as formworks [3]. Moreover, A study conducted by Brasileiro et al. [4] about the use of coco coir pith particles in composites with Portland cement which performed good compressive strength as a lightweight material. According to Rodríguez et al. [5], on the other hand, the heat wave intensity with the help of coconut fiber as barrier has significantly reduced regardless of fiber orientation as an insulation material to slab.

Furthermore, plastic waste is also abundant. The production of plastics has increased due to wide usage in the food industry, automobiles and construction. Low density polyethylene (LDPE) is one of the widely used thermoplastic polymers which have a significant mechanical and physical strength. It has the following properties: soft, flexible, waxy surface, translucent and softens at 70°C [6]. It is one of the highest demand plastics because of its uses such as plastic film for food products; agricultural protective cloth/tarp; bags; the lining of milk packaging; electric cable coverings; and gas and water pipes [7]. Consequently, it may lead to higher solid waste sources since plastics are non-biodegradable. Due to the rapid industrialization and economic development, it affects the natural resources and became a major problem in solid waste [8].

Many researches have shown the potential of plastics to produce composite boards. A study conducted by Youssef et al. [9] used recycled LDPE as a binder to corn husk fiber which improved the tensile strength at 90/10 binder to material ratio. Same results were derived on using coconut coir and wax instead of corn husk at 90/5/5 ratio (LDPE/coconut coir/wax ratio) [10]. Likewise, from the study of Del Pilar et al. [11] about the

combination of coco coir as base material and PVC pellets as binder to form a composite board has a high significant result in its mechanical properties. It also possesses good water resistance and better texture. Thus, using finer coco coir helped to obtain smooth finish on the board. In line with this, the composite board can be developed into alternative construction materials. However, PVC is considered a hazardous plastic. The replacement of LDPE which is low hazardous plastic may provide solution for health risk issues [12]. Fortunately, a study conducted by Atuanya et al. [13] about incorporation of wood saw dust and recycled LDPE also showed good mechanical performance. This is also recommended for alternative building materials to paneling, partitioning and ceiling.

Above all, it showed the potential of the composite boards made from waste agricultural fibers and plastics which can alter the wood fibers (as base material) and either Urea formaldehyde or Phenol formaldehyde (as binder), respectively. A bio-composite board made from coco coir and LDPE pellets are utilized as a permanent formwork of concrete to produce a bio-composite concrete panel (BCCP). This extends the application of the produced composite boards as sandwich concrete panel. In this study, the bio-composite boards were used as facings; and concrete was the core material for sandwich panel. The requirement of flexure and compressive strength as composite material were determined since it is subjected to both bending and compressing for wall construction.

The main objective of the study is to determine the potential of a bio-composite board made from coco coir dust and LDPE pellets with varying thickness of 5 mm and12 mm as a permanent formwork for concrete to produce BCCP with a total thickness of 50 mm.

METHODOLOGY

Materials and Equipment

Coco coir dust and LDPE pellets were collected from the Soriano Multi-Purpose Fiber Corporation in San Pablo City and Transworld Trading Co. Inc., respectively. Portland cement (Type I), sand and ¾" gravel are purchased at a local market

For the production of bio-composite board, the two-roll mill machine and heat press machine were found in the Industrial Technology Development Institute (ITDI) DOST Compound, Gen. Santos Ave., Bicutan, Taguig City, Philippines.

Universal Testing Machine (UTM) was used to determine the maximum load and breaking load for the computation of compressive and flexural strength (three-point bending test), respectively.

Production of bio-composite board

The desired density of the bio-composite board was in the range of from 800 kg/m^3 to 1000 kg/m^3 which were classified as high density board. For this study, the initial density of 950 kg/m^3 was used. The weights of the LDPE pellets and coco coir dust were determined with the ratio of 70:30, respectively, in order to fill the 200 mm x 200 mm mold on a different thickness of 5 mm and 12 mm.

The two roll mill machine was used for mixing the LDPE binder and coco coir dust. It rotated with temperature set at 130°C which is about the same as the melting point of LDPE. The LDPE pellets were poured between the two roll mills until melted. Then the coco coir dust is mixed with the melted LDPE while repeatedly kneaded by the rotating roll mill to mix the compositions thoroughly. After mixing, the mixture was placed on a 200 mm x 200 mm mold at different thickness of 5 mm and 12 mm.

The mold was placed between two parallel plates of the heat press machine on a set temperature of approximately 180 °C that was subjected to a pressure of around 3000 KPa for 5 minutes. Then the boards will be cooled for 5 minutes. Produced boards were cut into half with the dimensions of 100 mm x 200 mm. Good architectural finish and texture of produced composite boards were required.

Production of BCCP

Gypsum screws with 38 mm length were placed on the bio-composite boards at 100 mm spacing on both ways to provide connections between the concrete and boards.

The cement, sand and gravel were mixed together with the mixture ratio of 1:2:3. For binder, water-cement ratio of 0.5 was used.

Bio-composite board was set as the formwork upon concrete pouring. Assemble the formworks in each side of the panel with the total thickness of 50 mm. For the controlled samples, composed of concrete blocks with dimensions of 200 mm x 100 mm x 50 mm, is placed onto ordinary formworks (usually made of plywood).

The concrete was poured into the mold to produce a panel. Then the concrete was dried for 1 day before removing from the forms.

The produced BCCP and concrete block (with the same dimensions of 200 mm x 100 mm x 50 mm) was cured for 28 days at room temperature before testing.

Mechanical test

Compressive strength test

The compressive strength of the composite panels was obtained by determination of the

maximum load using the UTM. The dimensions of the samples were 100 mm x 200 mm subjected to compressive force downward. The compressive strength was calculated as:

$$\sigma = \frac{P}{bL} \quad (1)$$

Flexural strength test

The flexural strength was determined by using the three-point bending test of UTM which is in accordance to ASTM C393 - 00 (Standard Test Method for Flexural Properties of Sandwich Constructions) with the same dimensions of 100 mm x 200 mm x 50 mm BCCP and concrete block [14]. The sample was subjected to load at the midspan considering a simple support which is separated by 150 mm. The flexural strength was calculated as:

$$f = \frac{3PL}{2bd^2} \quad (2)$$

Statistical Tool

Analysis of Variance (ANOVA) of single factor was used to determine if there was a significant difference on the means among concrete block, BCCP with 5 mm bio-composite boards and BCCP with 12 mm bio-composite boards on the compressive strength and flexural strength. The degrees of freedom, α, equal to 0.5 were used in the study.

Post hoc analysis was also performed to evaluate further the differences between combinations of pair samples using least significant difference (LSD), HSD and Scheffe's test. The computed values at each combination should attain greater than the values of post hoc analysis.

RESULTS AND DISCUSSION

The coco peat collected had passed sieve numbers 6, 8, 12 and 18. Coco coir dust used for production of bio-composite boards was passed on sieve number 12 with the moisture content less than 5%. The produced board with 80:20 ratios by mass of coco coir dust and LDPE resulted to undesirable architectural finish. In this regard, the ratio of the produced bio-composite board made from coco coir dust and LDPE was 70:30 by mass which produced better quality. On the other hand, the produced bio-composite boards as shown in Fig.1 with thickness of 5 mm and 12 mm had densities of 925 kg/m^3 and 923 kg/m^3, respectively. This is classified as high density boards according to standards.

Fig. 1 Bio-composite board made from coco coir dust and LDPE pellets

As shown in Fig.2 is the produced BCCP. Densities of the concrete block, BCCP with 5 mm boards and BCCP with 12 mm boards was 2,370 kg/m^3, 2168 kg/m^3 and 1640 kg/m^3, respectively. The lightest among the samples was BCCP with 12 mm boards which had lowered the densities compared to concrete block and BCCP with 5 mm boards by 30.80% and 24.35%, respectively. Likewise, utilizing bio-composite boards as sandwich faces, increasing the thickness correspond to lighter weight. Since the produced composite boards has a lighter density compared to concrete in which decreasing the volume of the concrete and increasing the thickness of composite boards made the material lighter. This showed the potential of BCCP to become a lightweight material for building construction.

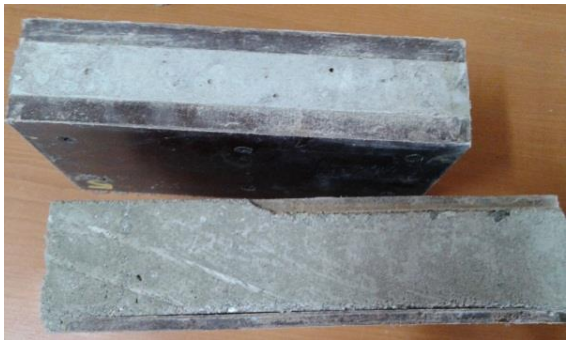

Fig. 2 Produced BCCP cross-sectional area

Compressive strength

Concrete block obtained the highest average compressive strength of 18.04 MPa among the three samples as shown on Table 1. It was followed by BCCP with 5 mm boards with compressive strength of 9.52 MPa. And, the lowest compressive strength was obtained by BCCP with 12 mm boards of 7.53 MPa.

Table 1 Compressive strengths

Sample	Compressive strength (MPa)
Concrete block	18.04
BCCP with 5 mm boards	9.52
BCCP with 12 mm boards	7.53

As shown in Fig.3, concrete block had enormous difference compared to BCCP. It is 89% and 140% higher compressive strength than of the BCCP with 5 mm boards and 12 mm boards, respectively. Nevertheless, BCCP with 5 mm boards was 27% higher than BCCP with 12 mm boards. The graph showed that by decreasing the concrete thickness from 50 mm thick BCCP reduced its compressive strength.

Based from single factor analysis of variance as statistical tool for comparing the means of compressive strengths of the samples, the calculated p-value was 0.002 that was less than the degree of freedom of 0.05. These showed that there were significant differences between the means of the samples. On the other hand, using post hoc analysis of variance further statistical analysis was performed to determine among which average compressive strengths were statistically different from each other. The results showed that all combination of samples were significantly different except from BCCP with 5 mm to 12 mm board. A value of 1.990333333 was computed which was less than all values of LSD, HSD and Scheffe. This signified that increasing the thickness of bio-composite boards to BCCP had no significant increase in the compressive strength.

Flexural strength

Based from three- point bending test, concrete block yielded the highest flexural strength of 4.30 MPa among the three samples as shown on Table 2. It was followed by BCCP with 12 mm boards with flexural strength of 2.28 MPa. And, the lowest among the three samples to withstand flexural stress was BCCP with 5 mm boards with flexural strength of 2.78 MPa.

Table 2 Flexural strengths

Sample	Flexural strength (MPa)
Concrete block	4.30
BCCP with 5 mm boards	2.28
BCCP with 12 mm boards	2.78

As shown in Fig.3, concrete block had 89% and 55% higher flexural strength than of the BCCP with 5 mm boards and 12 mm boards, respectively. The graph trend somehow showed that the bio-composite board contributed to increase the strength by 22% from 5 mm thickness board to 12 mm thickness board.

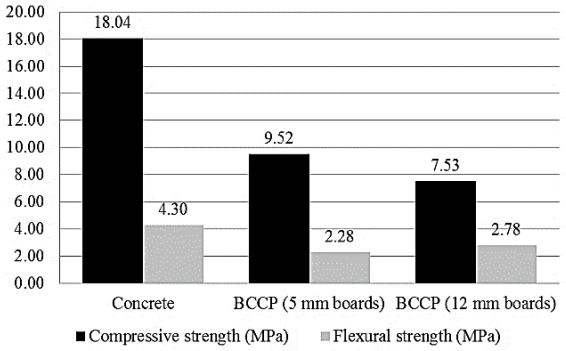

Fig. 3 Compressive and flexural strengths of concrete block and BCCP

Using single factor analysis of variance as statistical tool for comparing the means of flexural strengths of the samples, the calculated p-value was 0.037 that was less than the degree of freedom of 0.05. These showed that there was significant difference between the means of the samples. Based from post hoc analysis of variance, further observation was shown that all combination of samples were significantly different to each other except from BCCP with 5 mm to 12 mm board. It had a value of 0.492855 which was less than all values of LSD, HSD and Scheffe values. This also indicated that increasing the thickness of bio-composite boards to BCCP had no significant increase in the flexural strength. Also, the concrete block was significantly higher to BCCP for flexural strength.

Cost analysis

The cost of the following samples was calculated as shown on Table 4. Among the samples, concrete block without finishes (dimensions as the same of BCCP) was estimated to have the material cost of USD 0.50 per block excluded of labor cost and indirect cost. It was followed by BCCP with 12 mm boards with material cost of USD 0.97. And, the most expensive among the samples with total material cost of USD 1.15 for BCCP with 5 mm boards.

Table 3 Material cost

Sample	Cost
Concrete block	USD 0.50
BCCP (5 mm boards)	USD 1.15
BCCP (12 mm boards)	USD 0.97

The values showed drastic increase on the cost of BCCP with 5 mm boards and 12 mm boards from concrete with 127.97% and 91.69%, respectively. However, the produced BCCP had good architectural finish, thus finishing cost could be eliminated. On the other hand, increasing the thickness of bio-composite boards (from 5 mm to 12 mm) decreased the volume of concrete showed reduction on the cost by 15.91%.

CONCLUSION

The produced bio-composite boards had a good architectural finishes and classified as high density board with a density of 925 kg/m^3. Moreover, the bio-composite board utilizing LDPE as a binder is considered as less hazardous compared to PVC can be used as alteration since it also achieved good architectural finish. The used of bio-composite board to produce concrete panel had decreased the density compared to concrete block for about 30% with a density of 1640 kg/m^3 for BCCP with 12 mm boards. This showed the potential of BCCP as lightweight material which were less than 1,840 kg/m^3 as stated at ASTM C330.

The results showed that the concrete block without bio-composite boards were the toughest compared to BCCP considering both mechanical properties. Assessing the effect of bio-composite boards on the BCCP, increasing the thickness of the boards had lowered the compressive strength by 27%. This showed that the compressive stress was mainly carried by the concrete. On the other hand, increasing the thickness of the boards had increased the flexure strength by 22%. This showed that the bio-composite boards contributed to the flexure properties of sandwich panel. Based from statistical methods, there was no significant difference between BCCP with 5 mm and 12 mm boards for both compressive strength and flexure strength through post hoc analysis. Thus, increasing the thickness of the bio-composite boards does not improve the mechanical properties of BCCP.

According to cost analysis, the concrete block has the lowest material cost of USD 0.50 for dimensions of 100 mm x 200 mm x 50 mm. The cost of BCCP with 5 mm and 12 mm are higher than concrete block of 127.97% and 91.69%, respectively.

It may not be favorable to the BCCP of having lower mechanical properties and less economical compared to concrete block. The incorporation of bio-composite boards as the faces of sandwich panel did not improve the overall strength since the volume of the concrete was lessened. However, the strength obtained by BCCP can be considered as non-structural wall and lightweight material according to the code strength requirement. Thus, it can alter other non-load bearing wall such as sandwich panels, bricks and concrete hollow blocks.

ACKNOWLEDGEMENTS

The authors would like to express her gratitude to Malayan Colleges Laguna for rendering their facilities from preparation of materials, preliminary tests and specimen testing. Special thanks to all of the staffs and personnel under the Industrial Technology Development Institute (ITDI) of the Department of Science and Technology (DOST) Compound located at Gen. Santos Ave., Bicutan, Taguig City for their assistance for board production.

REFERENCES

[1] Madurwar, M., Ralegaonkar, R., & Mandavgane, S., "Application of agro-waste for sustainable construction materials: A review. Construction and Building Materials", 38, 2013, 872–878

[2] Zafar, S, "Agricultural Wastes in the Philippines", Southeast Asia: BioEnergy Consult, 2014.

[3] Mahzan, S., Ahmad Zaidi, A., Ghazali, M., Arsat, N., Hatta, M., & Rasool Mohideen, S., "Mechanical Properties of Medium Density Fibreboard Composites. Mechanical", Materials and Manufacturing Engineering, 2013, pp. 21-27.

[4] Brasileiro, G., Vieira, J., & Barreto, L., "Use of coir pith particles in composites with Portland cement", Journal of Environmental Management, 131, 2013, 228 - 238.

[5] Rodríguez, N., Yáñez-Limón, M., Gutiérrez-Miceli, F., Gomez-Guzman, O., Matadamas-Ortiz, T., Lagunez-Riverad, L., & Vazquez Feijoo, J., "Assessment of coconut fibre insulation characteristics and its use to modulate temperatures in concrete slabs with the aid of a finite element methodology", Energy and Buildings, 43, 2011, 1264–1272.

[6] UNEP, "Valuing Plastics: The Business Case for Measuring, Managing and Disclosing Plastic Use", Japan: United Nations Environment Programme, 2014.

[7] Klar, M., Gunnarsson, D., Prevodnik, A., Hedfors, C., & Dahl , U., "Everything you (don't) want to know about plastics", Europe: Swedish International Development Cooperation Agency, 2014.

[8] UNEP, "Convering waste plastic into a resource", Japan: United Nations Environment Programme, 2009.

[9] Youssef, A. M., El-Gendy, A., & Kamel, S., "Evaluation of corn husk fibers reinforced recycled low density polyethylene composites",

Materials Chemistry and Physics, 152, 2015, 26-33.

[10] Kannan, R., Mohd, A. C., Mohd, Y. Y., & Haeryip , S., "Effect on Mechanical Properties of Hybrid Blended Coconut Coir/Paraffin Wax/LDPE", International Journal of Integrated Engineering,, 3(2), 2011, 63-67.

[11] Del Pilar, H. M., Antonio, M. Z., Ilagan, M. A., & Seva, J. E., "Wood-tile quality composite board from coco coir dust and unplasticized polyvinyl chloride waste materials", International Journal of GEOMATE, 8(2), 2015, pp. 1250-1256.

[12] Hansen, E., Nilsson, N. H., Lithner, D., & Lassen, C., "Hazardous substances in plastic", Vejle, Denmark: COWI, 2013.

[13] Atuanya, C., Ibhadode, A., & Igboanugo , A., "Potential of using recycled low-density polyethylene", African Journal of Environmental Science and Technology, Vol. 5(5), 2011, pp. 389-396.

[14] American Society for Testing and Materials, "ASTM C330 / C330M-14, Standard Specification for Lightweight Aggregates for Structural Concrete", STM International, West Conshohocken, PA, 2014.

Second International Conference on Science, Engineering & Environment,
Osaka City, Japan, Nov.21-23, 2016, ISBN: 978-4-9905958-7-6 C3051

GENERATION OF LIGHT EMISSION FABRIC USING PMMA/PS BASED CLAD-STRIPPED PLASTIC OPTICAL FIBER

Sun Hee Moon and InHwan Sul*
Dept. of Materials Design Engineering, Kumoh National Institute of Technology, Rep. of Korea

ABSTRACT

Plastic optical fibers (POF) have several advantages over the conventional glass optical fibers (GOF), such as flexibility and transfer of visible lights. For information delivery, various IT devices can be interconnected into or onto the fabric. For aesthetic value, fabric can be active light emission device using optical fiber. In this work, we propose a light emission fabric which contains optical fiber structure with the external clad layer removed using mechanical or chemical method.

Keywords: Wearable Computer, Light-Emission Fabric, Clad-Removed Optical Fiber, Plastic Optical Fiber

INTRODUCTION

6T technologies and their fusions are gaining more interest to make a new market. Among various products, wearable computer is the typical example of textile-IT fusion. Wearable computer can deliver both information and aesthetic value through fabric structure. For information delivery, various IT devices can be interconnected into or onto the fabric. For aesthetic value, fabric can be active light emission device using optical fiber. Such light-emission fabric is already commercialized such as Lumitex® and so on. When the visible light is used, the optical fiber based fabric can be fashionable products. Otherwise UV can be delivered through optical fiber, in which can the fabric can be used for medical uses. Previous works delivered light using fiber Bragg grating (FBG) [1,2] or light-scattering materials. In this work, we propose a light emission fabric with optical fiber structure whose external clad layer has been removed using mechanical or chemical method especially. The clad-removed optical fiber was observed at its cross-section and its light-delivering property was measured. Theoretical waveguide prediction of plastic optical fiber(POF) [3] will be provided also.

The aim this paper is to develop efficient light emission POF structure that is based on cladding stripped for wearable computer. There are a few methodologies for fiber cladding stripping; h such as mechanical, chemical and thermal treatment [4,5,6]. Among them, a mechanical-emission based techniques was adopted in this work. The role of cladding is to protect total internal reflection of light inside the optical fiber waveguide. Once the cladding is removed in the middle of the fiber, the lights can be scattered out of the fiber core and this scattering can be more vigorous when the fiber is under global bending. This behavior is not favored in the communication purpose, but can be applied for other purposes also. Typical example based of emission of fiber optic sensors include sensors for liquid level measurement [7,8]. UV light, especially useful for anti-microbial treatment [9,10], as well as visible light can be used for the input light source. The goal of this paper is to provide an efficient clad removal mechanism and optimal POF based textile structure which can emit UV or visible light to the width-wise direction of the fabric.

EXPERIMENT

Plastic optical fiber

PRG-FB250 (a step index POF, Toray Industries) was used. It is composed of poly methyl methacrylate / fluorinated polymer as core and cladding, respectively . Refractive index was a 1.49 /1.41, and diameter was a 240 ㎛ /250 ㎛ . A small jig structure with heat (not shown here for patent filing) was used for the removal of cladding layer. Figure 1 shows the microscopic image of the original structure of the POF when visible light was injected. Figure 2 is the result of the clad-removed one.

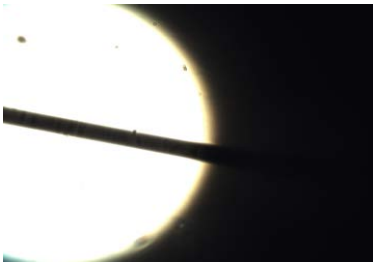

Fig. 1 the optical image of the original result of the POF with visible light LED.

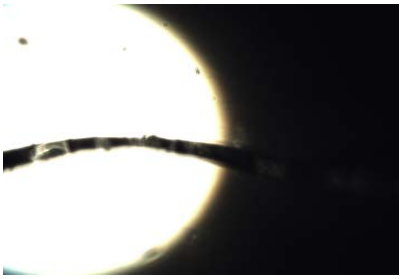

Fig. 2 the optical image of the clad-removed result of the POF with visible light LED.

Light source and spectroscopy device

The light transfer efficiency was measured using a spectroscopy HL-2000 (Ocean Optics corp.) with measurement range of 190-1100 nm, 0.1 nm resolution (Figure 1). An ultraviolet radiation LED light source LLA-225 (Ocean Optics corp.) with a 6 W power was used as a light source (Figure 2). The 255 nm as chosen as the range is close to the optical sterilization spectrum, which is known to be 250nm [11,12].

Fig. 3 Spectroscopy device (HL-2000).

Fig. 4 Ultraviolet radiation LED light source (LLA-225, 255nm)

Testing of light emission of POF under textile crimp structure

The final purpose of our work is to generate a light-emitting textile weave structure using clad-removed POF's (Figure 5). The fibers in the fabric weave structure are given global bending, which is called as "crimp structure" [13,14]. The crimp gives more bended structure to the POF and the light emission becomes more efficient.

Fig. 5 Example of the proposed clad-removed POF based weave structure (plain weave)

3D printed artificial weave structure for POF light emission testing

As the fabric is very flexible in its width-direction because of low bending rigidity, light emission testing is not feasible. As an alternative method to test the light emission quantitatively, a rigid plastic structure was devised which simulates a real fabric crimp structure. As a first step, a straight fiber path was designed using Google Sketch Up Make 2016 (Figure 6). The dimension of each part is 30 (width) x 50 (length) x 20 (height) mm.

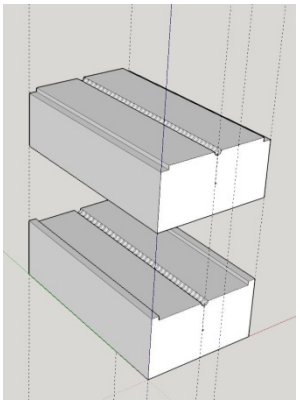

(a) perspective view

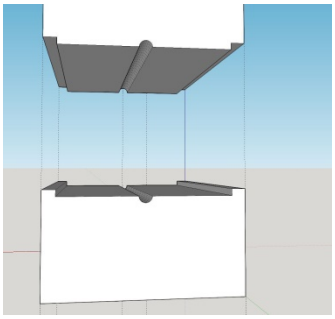

(b) side view

Fig. 6 Straight fiber path structure design

A commercial 3D printer (Cube Pro Tri by 3D systems) was used for the prototyping generation. ABS resin filament was used with blue and red colors (each correspond to bottom and upper parts of Figure 6).

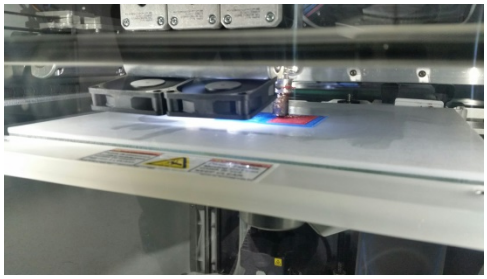

Fig.7 3D printing process of the fiber path structure

Figure 8 shows the final printing result of straight fiber path structure. The rough surface from the support structure was smoothed using an acetone steam treatment for an hour in a fume hood. The POF is inserted amidst of the two parts. Note that the upper part contains a small hall to insert the spectroscopy sensor stylus.

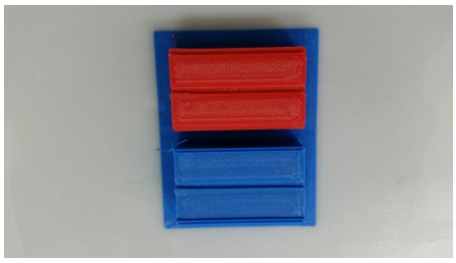

(a) 3D printing result

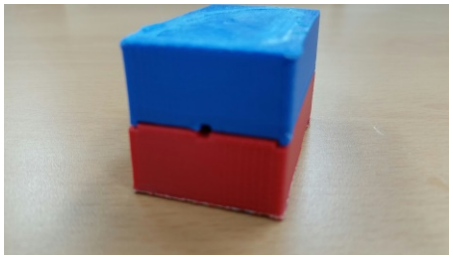

(b) combined result

Fig.8 3D printing result of the straight fiber path structure

Figure 9 is the example of the spectroscopic measurement graph using the proposed POF textile structure.

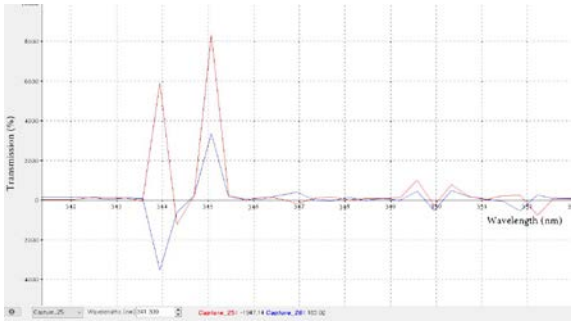

(a) magnified view near the 344nm

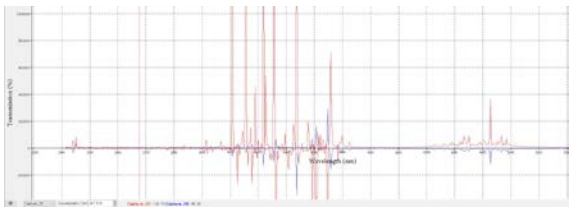

(b) overall visible light range signal

Fig. 9 Example of spectroscopic measurement of the proposed clad-removed POF structure (red : stripped the cladding POF signal, blue : original(unharmed) POF signal)

RESULT AND DISCUSSION

Figure 3, 4 shows the optical image of the original and clad-removed result of the plastic optical fiber. Note that the fibers are given visible light LED input at the one end, respectively. The original fiber (Figure 3) does not show any light emission at the entire fiber surface, because total internal reflection occurs due to the existence of the clad. Meanwhile, the clad-removed fiber shows decreased diameter at the center and some light is shown as a white spot (Figure 4), which shows the clad was successfully removed. The refractive index measurement of the fibers, theoretical prediction of

the light transfer and results from other clad removing mechanism is on-going.

The artificial weave structure was devised to simulate the complex textile crimp structure. As a first step, the straight fiber path structure was designed and 3D printed. The structure gave a stable and reproducible experiment environment for POF light emission as shown in Figure 8 and 9. The second step will be more general crimps, such as plain, twill and satin weave structure.

CONCLUSION

Thermal and mechanical force based clad removal mechanism was used for the cladding removal of plastic optical fiber. And the fiber was inserted in the fabric weave structure. The side-emission of POF fabric structure was observed quantitatively using a novel 3D printed artificial crimp structure. The 3D printed provided an efficient environment for POF light emission measurement. Only a straight fiber path was tested in this work. More general crimps from various textile weave structures will be reported in the next work with theoretical modeling.

ACKNOWLEDGEMENTS

This work was supported by the National Research Foundation of Korea (NRF) grant funded by the Korea government (MSIP) (No. NRF-2014R1A1A1002463).

REFERENCES

[1] Hill, K. O. ; Malo, B. ; Bilodeau, F. ; Johnson, D. C., “Bragg gratings fabricated in monomode photosensitive optical fiber by UV exposure through a phase mask”, Appl. Phys. Lett., 62,1993, pp. 1035-1037.

[2] G. D. Peng, Z. Xiong, and P. L. Chu, "Photosensitivity and Gratings in Dye-Doped Polymer Optical Fibers", Optical Fiber Technology, vol. 5, 1999, pp. 242-251.

[3] S. Louvros, Athanassios C. Iossifides, “Impulse response analysis of graded index polymer optical fiber”, Optical Fiber Technology, vol. 12, 2006, pp. 262-264.

[4] D.F Merchanta, , P.J Scullya, N.F Schmittb, “Chemical tapering of polymer optical fibre”, Sensors and Actuators A: Physical, Volume 76, Issues 1–3, 30 August 1999, Pages 365–371

[5] A.J.C. Grellier, N.K. Zayer, C.N. Pannell, “Heat transfer modelling in CO laser processing of optical fibres”, Optics Communications, 152 (4–6) (1998), pp. 324–328

[6] C.R. Zamarreño, , S. Lopez, M. Hernaez, I. Del Villar, I.R. Matias, F.J. Arregui, “Resonance-based refractometric response of cladding-removed optical fibers with sputtered indium tin oxide coatings”, Sensors and Actuators B: Chemical, Volume 175, December 2012, Pages 106–110

[7] H. Golnabi, M. Bahar, M. Razani, M. Abrishami, A. Asadpour, “Design and operation of an evanescent optical fiber sensor”, Optics and Lasers in Engineering, vol. 45, 2007, pp. 12-18.

[8] E. Udd, "Fiber optic smart structures," in Proceedings of the IEEE, vol. 84, no. 6, Jun 1996, pp. 884-894.

[9] Lodovico Parmegiani, B.Sc.a, , , Antonio Accorsi, B.Sc.b, Graciela Estela Cognigni, M.D.a, Silvia, “Sterilization of liquid nitrogen with ultraviolet irradiation for safe vitrification of human oocytes or embryos”, Fertility and Sterility, Volume 94, Issue 4, September 2010, Pages 1525–1528

[10] Bingshe Xua, b, , , Mei Niua, b, c, Liqiao Weia, b, Wensheng Houa, b, Xuguang Liua, d, “The structural analysis of biomacromolecule wool fiber with Ag-loading SiO2 nano-antibacterial agent by UV radiation”, Journal of Photochemistry and Photobiology A: Chemistry, Volume 188, Issue 1, 30 April 2007, Pages 98–105

[11] Laurent Urbana, Florence Charlesa, Maria Raquel Alcântara de Mirandab, Jawad Aarroufa, “ Understanding the physiological effects of UV-C light and exploiting its agronomic potential before and after harvest”, Plant Physiology and Biochemistry, Volume 105, August 2016, Pages 1–11

[12] T. Bintsis, E. Litopoulou-Tzanetaki, R.K. Robinson, “Existing and potential applications of ultraviolet light in the food industry – a critical review”, J. Sci. Food Agric., 80 (2000), pp. 637–645

[13] R. H. Brand and Stanley Backer, “Mechanical Principles of Natural Crimp of Fiber”, Textile Research Journal January 1962 vol. 32 no. 1 39-49

[14] A.S. Abhiraman, “Mechanics of Crimp Formation in a Bicomponent Fiber Model”, Textile Research Journal April 1974 vol. 44 no. 4 319-323

Second International Conference on Science, Engineering & Environment,
Osaka City, Japan, Nov.21-23, 2016, ISBN: 978-4-9905958-7-6 C3051

EVALUATION OF SMED CONTRIBUTION USING SHAPLEY VALUE: A CONCEPTUAL PAPER

M.A.Mansor[1], S.S.Sulaiman[1], S.N.M.Shaffe[1] and A.R.Ismail[2]
[1]Faculty of Technology Engineering, University Malaysia Pahang,
Lebuhraya Tun Razak, 26300 Gambang, Malaysia
[2]Faculty Of Creative Technology and Heritage, University Malaysia Kelantan,
Beg Berkunci No.1, 16300 Bachok, Kelantan

ABSTRACT

Single Minutes of Exchange Die (SMED) is one of the most popular approaches to reduce machine set-up time and provide quick equipment changeover and rapid die exchange. This approach allows manufacturers to produce products in small batches with short lead time by rapidly change one product to another. There are four important stages in SMED and these activities are working together to achieve the goal, which is to shorten machine set-up time. Therefore, we need to know how important one activity compared to another or how an activity contributes to achieve the goal. In this paper, we apply a method called Shapley Value to investigate the fairest allocation of the contributions obtained between the activities in every production line. Each activity in SMED are considered as the contributors while each production line will be considered as the players. The combinations of the contributors and players will create a number of permutations. From these permutations, the marginal contribution of each player to coalition can be evaluated. We also determined an index called "Scale of Balance" (SoB) where the SoB gives the position of each player against the best-performing player. A conceptual model to evaluate the fairest allocation of the contributions of each SMED activity in production lines will be proposed during this study. We believe that by knowing the importantness of certain activity, more effort can be put to improve the activity in proper balance.

Keywords: Shapley Value, Single Minutes of Exchange Die (SMED), Performance Measurement

INTRODUCTION

In addition to the excellent functions, customers are also looking for more attractive design of the product. This can be seen when manufacturers often release their new models in a short cycle time. This phenomenon also makes the competition between manufacturers to attract customers has become intense.

The use of mold or die is one of the methods for producing an attractive design and to fulfill the rapid changing of the product. However, the mold or die should always be changed depending on the type of the model need to be produced. Usually, the process to change the mold or die will take time and during the changeover time, the production line had to be stopped. This will result in a loss for the company if the changeover time is long.

To overcome this problem, many companies implement the SMED approach to reduce the changeover time mold or die. SMED is one of the most popular approaches to reduce machine set-up time and provide quick equipment changeover and rapid die exchange. This approach allows manufacturers to produce products in small batches with short lead time by rapidly change one product to another [1].

There are four conceptual stages in SMED; preliminary stage, separating internal and external setup stage, converting internal to external setup stage, and finally streamlining all aspects of the setup operation stage [2]. These activities are working together to achieve the goal, which is to shorten machine set-up time. Therefore, we need to know how important one activity compared to another or how an activity contributes to achieve the goal.

In this paper, we apply a method called Shapley Value to investigate the fairest allocation of the contributions obtained between the activities in every production line. Each activity in SMED is considered as the players while each production line will be considered as the contributors. The combinations of the contributors and players will create a number of permutations. From these permutations, the marginal contribution of each player to coalition can be evaluated. We also determined an index called "Scale of Balance" (SoB) where the SoB gives the position of each player against the best-performing player [3].

LITERATURE REVIEW

Single Minutes Of Exchange Die (SMED)

SMED, introduced by Shingo in the early 1950s is a theory and a set of techniques that aims to reduce the setup time, that is, the time elapsed between producing the last good product of the first lot and the time of producing the first good product of the next lot [4]. The objective of SMED is to make it possible to perform equipment setup (changeover) operations in single minutes, which is less than 10 minutes.

According to Shigeo (1989), setup operations consists of two fundamentally different types: Internal setup and External setup. Internal setup is a process that can be performed only when a machine is stopped such as mounting or removing dies while External setup is a process that can be conducted while a machine is in operation such as such as transporting old dies to storage or conveying new dies to the machine [5].

Shigeo (1989) [5] stated that setup time is comprised of following four functions;

- Preparation of material, dies, jigs, and fixtures that take 30 percent of setup time,
- Clamping and removing dies and tools that take 5 percent,
- Centering and determining the dimensions of tooling that takes 15 percent, and finally,
- Trial and adjustment that takes 50 percent from the overall setup time.

Stage one in SMED is the preliminary stage, where the goal of this phase is to have an overall image for all setup activities included in the changeover process. At this stage, data about current setup procedures will be collected. This can be done through the interviews with the person in-charge of machines, followed by time and motion study to determine the standard time for each operation. A Standard operation setup check sheet need to be used to list all setup operations and their correspondence required resources.

Stage two is to identify which set-up operation must be performed while the machine is shut down (internal setup) and which can be performed when the machine is running (external setup). This stage is the most crucial stage in the implementation of SMED because we only can reduce setup time if most of the necessary tasks in exchanging the die are performed while machine is running.

In stage three, the current setup operation to determine whether any of the activities conducted as internal setup can be converted to external setup will be analyzed. If more internal set-up time to can be converted to external set-up time, the setup time will be shorter. Finally, stage four is the stage where we examine both internal and external setup operations for additional opportunities for improvement.

As SMED had been developed 60 years ago, many researchers attempt to make improvements to the SMED. For example, Almomani et al (2013) incorporates Multiple Criteria Decision-Making Techniques (MCDM) techniques to SMED's stage three. The MCDM techniques used in this work are Analytical Hierarchal Process (AHP), Technique for Order Preference by Similarity to Ideal Solution (TOPSIS) and Preference Selection Index (PSI). In addition to the reduction in the setup time, the proposed approach takes into consideration various factors, that govern the setup selection technology; including: cost, energy, facility layout, safety, life, quality and maintenance [4].

Karasu et al (2014) incorporated Taguchi design of experiment into SMED methodology to achieve the parameter set that provides the quality product with fewer trials to start the mass production [3]. Moxham and Greatbanks (2001) suggested that the effective implementation of SMED necessitates a number of fundamental requirements. Therefore, the authors proposed prerequisite requirements for successful SMED application, defined as SMED-ZERO. According to Moxham and Greatbanks, the SMED-ZERO attributes must be in place before the traditional SMED techniques can be applied successfully [4].

SMED can give the benefits such as; machine operating rates will be increased by shortening setup times, small lot production significantly reduces finished goods inventories and the buildup of stocks between processes, increased production flexibility to respond to rapidly changes in model and delivery time requirements, and finally, eliminate time spent in waiting for processing of one lot to be completed before another lot can be processed [5].

Shapley Value

The Shapley Value [6], proposed by Lloyd Shapley in 1953 is a Game Theory concept to determine the fair distribution to each player of the profit obtained by collaboration among players. Its also can be used to determine the importantness of each player in a coalition game to achieve the goal.

A coalition game is where groups of players (coalitions) may enforce cooperative behavior between their members. For example, in a soccer game, eleven players are working together as a team to win the game. Each player contributes their skills

to the team and the team with the higher value of a combination of skills will win the game. Hence, the game is a competition between coalitions of players, rather than between individuals.

In this paper, we define a subject that contributes to the whole activity as the player and the elements that players contribute to the whole activity as the contributor. A player's Shapley Value reflects how much that player contributes to a coalition—that is, how much value the contributor adds to the coalition. A contributor that never adds much has a small Shapley Value, while the contributor that always makes a significant contribution has a high Shapley Value.

Assume that there are n players with m contributor and let w be the weight to the contributor. Any subset S of the player set N=(1,…, n) is called a coalition. The record for the coalition S is defined by

$$\boldsymbol{x_i(S) = \sum_{j \in S} x_{ij} \qquad (i = 1, \ldots, m)} \qquad (1)$$

where:

x_{ij} is the record of player j to the contributor i.

This coalition aims at obtaining the maximal outcome c(S):

$$\boldsymbol{c(S) = \sum_{i=1}^{m} w_i\, x_i(S)} \qquad (2)$$

subject to: $c(S) = \max \sum_{i=1}^{m} w_i x_i(S)$

$$\boldsymbol{\sum_{i=1}^{m} w_i = 1 \qquad w_i \geq 0 (\forall_i)}$$

The $c(S)$, with $c(\varnothing)$=0, defines a characteristic function of the coalition S. Thus, we have a game in coalition form with transferable utility, as represented by (N,c).

The Shapley Value of the game (N,c) for the player k is the average of its marginal contribution topossible coalitions:

$$\boldsymbol{\varphi_k(c) = \sum_{all\, S} \gamma_n(S)[c(S) - c(S - \{k\})]} \qquad (3)$$

with weights of probability to enter into a coalition S defined as following:

$$\boldsymbol{\gamma_n(S) = \frac{(s-1)!\,(n-s)!}{n!}} \qquad (4)$$

In (3) and (4), n is the total number of all the participants, s is the number of members in the S^{th} coalition, and $c(\times)$ is the characteristic function used for estimation of utility for each coalition. If a subset $S(\subset N)$includes player k, k's marginal contribution is obtained as $c(S)$-$c(S$-$\{k\})$. [7][8]

ILLUSTRATIVE EXAMPLE

Assume that there are 4 metal stamping machines in a production line, namely M_1, M_2, M_3, and M_4. All machines have been through 3 SMED activities, namely A_1, A_2, and A_3 to reduce its die changeover time. Table 1 shows the example to illustrate the concept of this paper. The time consumed for each activity is denoted by t_{mn}. J_m is the total times spent by each contributor or activity.For example, J_1 is the total time spent to identify the overall image of all setup activities for each machine.

Table 1: Illustrative example

Player / Contr-ibutor	M_1	M_2	M_3	M_4	Sum
A_1	t_{11}	t_{12}	t_{13}	t_{14}	J_1
A_2	t_{21}	t_{22}	t_{23}	t_{24}	J_2
A_3	t_{31}	t_{32}	t_{33}	t_{34}	J_3

From Table 1, we normalized the sum to 1 as exhibited in Table 2.

Table 2: Normalized values

Player / Contr-ibutor	M_1	M_2	M_3	M_4	Sum
A_1	$\frac{t_{11}}{J_1}$	$\frac{t_{12}}{J_1}$	$\frac{t_{13}}{J_1}$	$\frac{t_{14}}{J_1}$	$\frac{J_1}{J_1}$
A_2	$\frac{t_{21}}{J_2}$	$\frac{t_{22}}{J_2}$	$\frac{t_{23}}{J_2}$	$\frac{t_{24}}{J_2}$	$\frac{J_2}{J_2}$
A_3	$\frac{t_{31}}{J_3}$	$\frac{t_{32}}{J_3}$	$\frac{t_{33}}{J_3}$	$\frac{t_{34}}{J_3}$	$\frac{J_3}{J_3}$

From equation (2), maximum outcome of c(M_1) is given by;

c(M_1)=max $t_1w_1+ t_2w_2 + t_3w_3$

subject to:

$w_1 + w_2 + w_3 = 1$,

$w_1, w_2, w_3 \geq 0$

where w is the weight of the contributor. The optimal solution, c(M_1) can be obtained when w_1=1, w_2 =0, and w_3=0.

From Table 2, all coalition's values for each contributor will be enumerated. For example, the value of coalition {M_1,M_2} for contributor A_1 is given as $\frac{t_{11}}{J_1} + \frac{t_{12}}{J_1}$.

Coalition {M_1,M_3} and {M_2,M_3} are calculated by $\frac{t_{11}}{J_1} + \frac{t_{13}}{J_1}$, $\frac{t_{12}}{J_1} + \frac{t_{13}}{J_1}$, respectively.

The combination of Player M_1, M_2, M_3 and M_4 created 24 permutations. In permutation $M_1M_2M_3M_4$, player M_1 is the first comer to the coalition, follows by player M_2, M_3 and finally player M_4, Thus, the marginal contribution of each player to coalition can be evaluated as below;

M_4's marginal contribution is;
c({M_1,M_2,M_3,M_4 }) - c({M_1,M_2,M_3})

M_3's marginal contribution is;
c({M_1,M_2,M_3}) - c({M_1,M_2})

M_2's marginal contribution is;
c({M_1,M_2}) - c({M_1})

Lastly, M_1's marginal contribution can be derived from;
c({M_1}) - c({∅})

The same calculation then was repeated for every permutation. The average of the marginal contribution of the player was respectively taken and this average is described as the Shapley Value. Furthermore, each player's Shapley Value was divided by the highest value of the Shapley Value to obtain a score for each player.

SoB = Shapley Value for each player /(the best Shapley Value among the players)

We refer to this score as the "Scale of Balance"(SoB) [5]. The SoB was proposed by Mansor and Ohsato (2010) to give the position of each player against the best-performing player. They defined SoB=1 when a high contribution with a good combination balance from the contributor will lead to higher allocation for the player.

Assume that the result of above exercise is as shown in Figure 1. From the figure, the value of contribution for each player can be observed. M_1 contributed most to achieve the goal the while the M_4 is the worst player among all machines. At the same time , from the form of graphs, its shows that the activities were imbalanced because the gaps between the contribution of M_1 and M_4 are quite large.

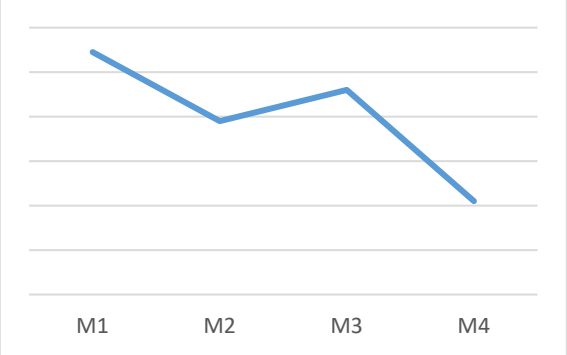

Figure 1. The SoB for each player

Data and results shown above are only for a single point of time. If the data can be collected and this exercise can be done every particular time, for example every 3 months or every 6 months, the trends in the value of the contribution for each machine can be observed. Figure 2 illustrates the example of how the contributions for each machines have changed over time.

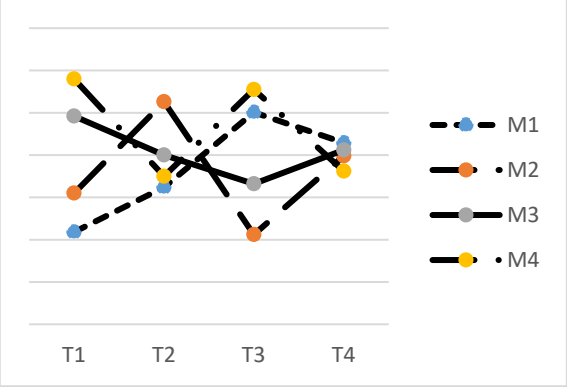

Figure 2. Example of the changes over time.

Assume that T_1 to T_4 in Figure 2 are the period where the data is collected and analyzed. The form of graphs shows that the activity was carried out disproportionately. It is important for us to ensure that the activities performed are in good balanced so

that resources that be consumed in the activity such as in SMED are being used properly.

CONCLUSION

The concept proposed in this paper is suitable to be practiced by the company that will start the SMED activity or the company that has been implementing SMED and have complete data since SMED been implemented in their production lines. The most crucial element in this exercise is the data. Data should be collected accurately and periodically. Incorrect data will lead to a wrong decision and this decision could give a bad impact to the company.

Although SMED is known for more than sixty years, a number of companies have failed on implementation. Some companies put too much emphasis on transferring changeover internal tasks to external, missing the importance of minimizing or streamlining internal and external activities by design improvements[9].Therefore, it is important to carry out the activities in proper balance to ensure that such activities will not fail.

FUTURE WORKS

The basic idea presented in this paper had been implemented to find out the contribution of measurable elements in Overall Equipment Effectiveness. However, the implementation of this exercise to find the value of the contributions and the balance of activities in SMED has not been practiced yet. Therefore, as our future works, we would like to validate this idea using the real data from the company that will start their SMED activity or the company that has been implementing SMED and recorded all the data properly. We also would like to observe the contribution from various points of view by using other tools such as "Moving Coalition Analysis" or "Transpose Moving Coalition Analysis"[10].

ACKNOWLEDGEMENTS

This research was fully supported by the Ministry of Higher Education (MOHE) of Malaysia under the project no. RDU130128 of Fundamental Research Grant Scheme (FRGS).

REFERENCES

[1] Almomani et al, "A proposed approach for setup time reduction through integrating conventional SMED method with multiple criteria decision-making techniques", Computers & Industrial Engineering 66, 2013,pp.461–469

[2] Shigeo Shingo, translated by Andrew P.Dillon, A Study of the Toyota Production System From an Indusrial Engineering Viewpoint., Productivity Press, 1989, USA.

[3] Karasu et al, Improvement of changeover times via Taguchi empowered SMED/case study on injection molding production, *Measurement 47*, 2014, pp.741–748.

[4] C. Moxham and R. Greatbanks, 2001,Prerequisites for the implementation of the SMED methodology:A study in a textile processing environment, *International Journal of Quality & Reliability Management,Vol. 18 No. 4*, pp. 404-414.

[5] M.A. Mansor, A. Ohsato, "Evaluation of the contributors of overall equipment effectiveness using shapley value", International Journal Of Research And Reviews In Applied Sciences, Volume 2, Issue 3, 2010, pp.257-263.

[6] Roth,E.A., ,The Shapley Value,Cambridge University Press, 1988, New York, USA.

[7] K.Nakabayashi, K.Tone, "Egoist's dilemma: a DEA game" ,Omega 34, 2006,pp.135-148

[8] M.Conklin, K.Powaga, S.Lipovetsky, "Customer satisfaction analysis: Identification of key drivers", European Journal of Operational Research 154,2004,pp:819-827

[9] Ferradás, P. G., & Salonitis, K. (2013). Improving changeover time: A tailored SMED approach for welding cells. *Procedia CIRP*, *7*, 598–603.

[10] Mansor, M. A., & Ohsato, A., The Concept of Moving Coalition Analysis and its Transpose, European Journal of Scientific Research, Vol.39 No.4, 2010, pp.548–557.

Second International Conference on Science, Engineering & Environment,
Osaka City, Japan, Nov.21-23, 2016, ISBN: 978-4-9905958-7-6 C3051

DAMAGES CAUSED TO INFRASTRUCTURE DUE TO GEOTECHNICAL FAILURES BY THE TC WINSTON IN FIJI

Ravikant R Singh[1], Faijal Ali[1], Darga N Kumar[2], Sanjay Prasad[3], Atinesh V Prasad[3] and Ravindra Chand[3]
[1]Lecturer, [2] Professor, [3] Graduate Student, College of Engineering Science and Technology, Fiji National University, Fiji Islands.

ABSTRACT

On 20th of February 2016, Fiji had experienced earth's second strongest cyclone of category 5 with wind speed up to 185 mph. Geotechnical failures were observed in the western part of Viti Levu and the northern part of Fiji islands like Koro, Vanabalavu, Taveuni etc., which mostly falls on the cyclone path. This paper presents the detailed inspection carried out on geotechnical failures of infrastructure such as highways, electric poles, foundations of buildings and bridge abutments in the western part of Viti Levu especially the provinces like Rakiraki, Tavua and Ba. A team from Fiji National University had inspected the damaged infrastructure and assessed the damages in terms of engineered structural connections, foundation soil strengths and associated environmental factors around the area. This paper presents the inspection carried out along with the relevant geotechnical analysis explaining the reasons of failures and also recommendations for building a cyclone resistant infrastructure.

Keywords: TC Winston, Geotechnical Failures, Soil Grain Size, Sinkhole.

INTRODUCTION

Fiji *is* located in the Pacific Ocean and covers a total area about 194,000 square kilometres. Fiji is the hub of the *South* West Pacific, midway between Vanuatu and Tonga. Fiji consists of 332 islands in the southwest *Pacific Ocean* about 1,960 mi (3,152 km) from Sydney, Australia. About 110 of these islands are inhabited. The two largest islands are *Viti Levu* (10,642 sq km) and *Vanua Levu* (5,807 sq. km). The population of Fiji was estimated to be 902 964 people as of January 2016 census. Due to its location in the Pacific Ocean Fiji has been facing seasonal cyclones from November to April every year. This year it has experienced earth's second strongest cyclone of category 5 with wind speed up to 185 mph.

Even though records don't date too far back for Fiji's tropical weather, meteorologists know it's fairly rare for a tropical cyclone to hit the country's capital city. The western part of Viti Levu and the northern part experienced a lot of disturbance including islands like Koro, Vanabalavu, Taveuni etc, which mostly falls on the cyclone path. It is indeed a great concern and challenge for the Engineers of Fiji. This paper presents the report on geotechnical failures caused due to TC Winston.

As per [1] a proper design of foundation system requires the following (i) purpose of engineering structures, probable service life loadings, types of framing, soil profile, construction methods, construction costs, and client/owner's needs, (ii) design without affecting environment and enough margin of safety with respect to unforeseen events and uncertainty in determination of engineering properties of soil and acceptable tolerable risk level to all the parties, i.e., public at large, the owner, and the engineer. The geotechnical or structural "failure is an unacceptable difference between expected and observed performance". The failure of a structure may be due to poor design, faulty construction, excessive loads and soil related failure. The soil failure leads to foundation failure and in turn overall failure of whole structure, loss of life as well as economical loss. There are several factors contributing to the failure of foundation, if overlooked or addressed improperly, such as, construction error, improper soil investigation, fluctuation of ground water table, seismic loads, etc [2]. Commonly one can find two types of construction errors such as temporary protection measures and actual foundation work itself [3]. As per [4]-[5] the soil type is very important in terms of offering resistance to the landslide. Also, the slope geometry can be another responsible parameter to cause slope failure. In the recent past there were many preventive and remedial measures came up into the real practice which includes modifying the geometry of the slope, controlling the groundwater; constructing tie backs, spreading rock nets, providing proper drainage system, provision of retaining walls, etc. Most of the

places on the earth, the sinkholes are observed commonly. As per [6], it can be suggested three types of sinkholes such as solution sinkholes, cover collapse sinkholes and cover subsidence sinkholes. The occurrence of sinkholes within the subsurface can be attributed to the redirection of surface water flow, leaking drainage, water and sewage systems and in many cases, heavy traffic in their vicinities [8]. The destructive effects of soil liquefaction, sudden drawdown, ground water flow can cause sometimes sudden or excessive settlements in the ground. These sudden settlements can cause sinking of structures or pavements in the order of 0.5m to even 2m from the original ground level. In the recent past impressive progress has been made in understanding the various ground failures associated with environmental factors and developing the technology for mitigating ground related hazards such as liquefaction, sudden drawdown, sinkhole formations is very essential [7].

The over consolidation ratio of clay soil is an essential geotechnical parameter to understand the consolidation behavior and associated settlements of structures founded on these clay soils. As per [9] the clay response to construction is not truly undrained. A significant consolidation develops initially in the over consolidated natural clay, which becomes normally consolidated during construction. An undrained behavior develops only in the normally consolidated clay during the initial stages of the construction.

Soft clay soils are prone to excessive settlements and almost the structures found on these soils can punch through in the order of 3m to 4m depending upon the state of consistency of clay in-situ. These soils are required to be treated before construction of any infrastructure such as highway pavement or high rise buildings etc. As per [10] reliability analysis is a necessary component of design for embankments supported on columns installed by the deep mixing method. The strength of deep mixed materials is quite variable, and reliability analyses permit this variability to be rationally incorporated in the design process. Furthermore, these systems are complex, and typical variations in clay strength, if not accounted for, could induce abrupt bending failure in isolated columns. Consequently, the ordinary values of factor of safety that geotechnical engineers use to develop reliable designs for other embankment systems are not applicable to embankments supported on columns installed by the deep mixing method.

METHODOLOGY AND SOIL SAMPLES

The team consisting of academic's and students of Fiji National University of Fiji Islands visited the sites which were most affected by the TC Winston in Viti Levu, Fiji immediately after the Cyclone. Figure 1 shows the map of Viti Levu in Fiji highlighting the Kings road in red colour. Extensive damages to the infrastructure were observed along the Kings road. The team carried out the forensic studies by visiting the sites where the structures suffered due to geotechnical failures.

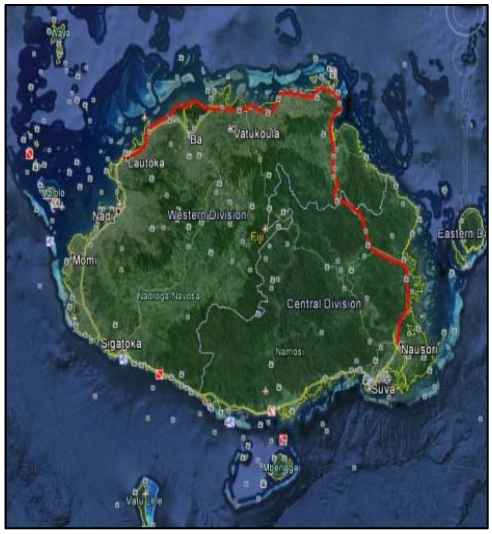

Fig 1 Google map of Viti Levu showing Kings Road in red color.

The post cyclone investigation was carried out in the form of in-situ geotechnical testing such as field vane shear, core cutter and visual inspection. Also the soil samples were collected at the respective sites and were tested in the laboratory for index properties such as grain size analysis and consistency limits. The data relevant to soil properties is presented in Tables 1 and 2.

The symbols presented in the Tables 1 and 2 are as follows: G = Gravel, CS = Course Sand, MS = Medium Sand, FS = Fine Sand, SC = Silt and Clay, LL = Liquid Limit, PL = Plastic Limit. PI = Plasticity Index, γ_d = Dry Unit Weight. The samples location is presented from A to I. A is Tailevu road failure, B1 is Korovou road failure, B2 is Korovou road failure, C is the site of electric post failure, D is landslide site at Ra, E is landslide site at the Bucalevu, Church, F is bridge failure at Bucalevu, G is sinkhole site near to Nabulini village, H is the steel structure failure site near to Navitilevu alongside Kings road, I is the road failure site near Naria Rakiraki Kings road.

Along with the visual inspection notes, some of the pictures were taken for analysis of various geotechnical failures that took place during TC Winston. In the next section, the failures are explained with the respective pictures.

Table 1 Grain size analysis of soil samples

Sample Location	Grain Size Distribution (%)				
	G	CS	MS	FS	SC
A	0	0	1	3	96
B1	0	0	0	1	99
B2	0	0	7	8	84
C	0	0	7	9	84
D	10	15	30	23	22
E	0	0	10	10	80
F	3	5	10	15	67
G	20	27	16	17	20
H	0	0	10	10	80
I	10	11	28	23	28

Table 2. Consistency limits and dry unit weight

Sample Location	Consistency Limits			γ_d
	LL	PL	PI	(kN/m^3)
A	48	30	18	14.5
B1	50	30	20	14.7
B2	50	31	19	14.6
C	50	31	19	14.7
D	-	-	-	16.3
E	45	38	7	15
F	-	-	-	14.9
G	-	-	-	16.4
H	58	32	26	14.6
I	-	-	-	16.3

GEOTECHNICAL OBSERVATIONS AND FAILURE ANALYSIS

In this section the discussion is presented about the failures that have had occurred during TC Winston. Discussion is made based on the visual inspection, pictures and soil samples, data obtained from the laboratory testing. Figure 2 shows the typical soil conditions alongside the King's road highway in Viti Levu, Fiji. The soil subgrade is brownish to reddish in color of lateritic formation having silt and clay portion about 96% with plasticity index 18 (Table 1). This soil has slope height ranging from 6m to 20m at different locations. It is very common to notice small to medium size soil slides alongside the highway due to increase of pore water pressure during cyclone and rainy season. The vane shear strength of these soils is varying from 30 kPa to 60 kPa comprising soft to medium consistency. Soil has slippery behavior and when heavily loaded vehicles passes over the road, the subgrade soil was unable to resist the shearing and in turn moves down towards valley side, causing sinking of road in the order of 0.5m to 2m. These soils are problematic and are to be required to analyze sustainability of infrastructure built on these soils.

Figure 3 shows picture taken at the Korovou road failure site where vane shear test was conducted. The average in-situ vane shear strength of soil at the site is recorded as 35 kPa and field dry unit weight of soil from the core cutter method was found to be 14.6 kN/m^3.

Fig.2 Soil conditions at site A

Fig.3 Filed vane shear test at site B

Alongside the Kings highway, it was observed that many precast electric poles were fallen horizontally on the ground due to lack of soil support. As most of the electric poles were embedded alongside the highway drain, due to the drain the soil was eroded leaving loss of support to the poles. Figure 4 presents the damaged electric pole. It is observed that all the electric poles were embedded to a same depth of 1.8m standard irrespective of subsurface soil conditions. It can be suggested that, there is a need to carryout subsurface investigation and also lateral load analysis of embedded poles and consideration of high intensity cyclone characteristics. Some of the locations alongside the highway there are steep vertical limestone cuts of weathered and disintegrated nature. The height of these cuts ranging from 50 to 70m with slope angle varying from 75 to 85 degree to the horizontal ground (Fig.5). As the slope is steep and predominantly with weathered and

disintegrated limestone formations, landslides were observed due to the internal seepage of storm water (Fig.6). It can be suggested that there is a need to stabilize these slopes with the rock anchors so as to avoid future landslides and blockage of highway.

Fig.4 Electric post failure at site C

Fig.5 The slope of the cut at site D

Figure 7 presents the picture taken at the landslide site E, where the soil formations are having field vane shear undrained strength in the range of 25 to 40 kPa the height of the slope is varying from 10 to 15m just behind the residential area. On the day of TC Winston due to storm water, the surficial soil got wet and became soft which intended moved down causing damage to the nearest house. It can be recommended that the slope can be made into benches of width 1 to 1.5m for every 3m height especially at the residential area and also can be suggested a retaining wall to be constructed to avoid building damages due to landslides.

Fig.6 Landslide at site D

Fig.7 Damage of building due to landslide at site E

Figure 8 presents the road failure near the bridge abutment at Rakiraki site F. From this figure, it can be clearly seen that there is a downward movement of soil due to storm water. The gabion wall was placed as a protection for the bank near the abutment of the bridge. As the gabion wall was not properly anchored at the foundation level, the entire wall is moved down into the river and collapsed due to scouring effect at the foundation level. Consequently the soil beneath the highway pavement lost its support and moved down due to the storm water leaving wider gap formation beneath the road and behind the abutment. It can be suggested that there is a need to consider appropriate foundation soil stability concerns, sufficient geotechnical characterization and stability analysis to avoid these types of failures.

Figure 9 presents the picture taken at the sinkhole at site G. which was observed alongside the highway, where the water creek is flowing across the road bridge. Beneath the bridge there exists a 2.5m radius semicircular steel culvert. On top of downstream side there was a gap observed between the bottom of the bridge and the culvert. Loose to medium dense silty sand mixed with little portion of gravel of dry unit weight 16.5 kN/m^3 is identified. The collapse potential of soil was fund to be 5% as shown in figure.10 after the samples were analyzed in the Lab.

Fig.8 Erosion of soil under the road near the bridge abutment at site F

Fig.9 Sinkhole formation alongside the road over the creek at site G.

Sufficient soil compaction were not achieved to avoid the internal erosion associated with storm water flow. The sinkhole formation at this location is mainly attributed due to internal seepage of storm water flow that caused loss of soil underneath where sinking of soil took place to reach the soil stable state.

It is very interesting to observe the total collapse of roofed steel structure built for sugar processing near to Navitilevu village alongside the Kings road. Figure 12 presents the location and collapsed steel structure due to the unexpected uplift wind forces. As the structure was not having walls and was directly exposed to wind forces to act internally, it suffered from uplift forces and experienced overall collapse from the foundation level. The causes of overall failure of the structure are mainly observed due to the following points: i. uplifting wind force actions, ii. Lack of sufficient connectivity between the members and iii. Lack of sufficient anchorage for the foundations in terms of embedment depth and also connectivity (Fig.12).

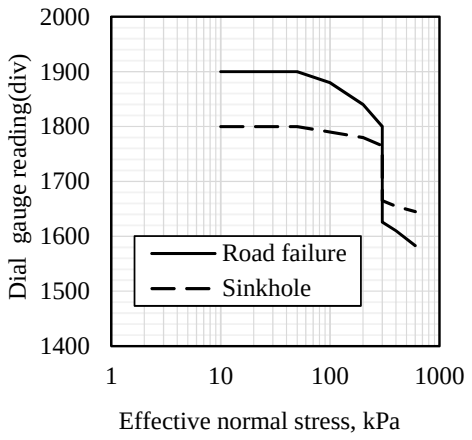

Fig.10 Collapse potential of soil at site G and site I.

Fig.11 Failure of steel structure at site H

Fig.12 Foundation failure at site H

Figure 13 presents the picture taken at the site I, where typical road failure is observed. This is the main highway which connects to industrial towns in the western part of Viti Levu and it is a very busy highway. This highway is alongside the ocean and farming land. The mean sea level is 20 m below the road formation level. As the road is laid on silty sand with little gravel portion with a steep slope with an angle of 65 degree towards the sea, the road sank to a depth of 0.2 m to 1m along the failure cure towards the sea. The overall length of the curve of failure is recorded as around 50m. Also there were multiple ground fractures that were observed at different depths towards down side of the slope. The reasons of failure of the road at the site can be attributed due to cross drainage beneath the road through the porous soil layer lying below the road surface and also due to heavy vehicular movement. It can be suggested to have thorough subsurface investigations and also proposing appropriate geotechnical site improvement schemes such as stone columns, lime piles, dynamic compaction etc. to mitigate this type of failures. The collapse potential of soil is evaluated from the consolidation

test in the laboratory was 8.7% (Fig. 10). It indicates that the soil is prone for collapse, when subjected to saturation.

Fig.13 Road failure at site I

CONCLUSION

From the above-mentioned discussion, some important points are observed towards the damages to the infrastructure due to geotechnical failures. Most of the geotechnical failures that were noticed are associated to compaction of soils, subsurface investigations, storm water flow through porous media. The failures were observed due to unexpected TC Winston of category 5. The foundations and other geotechnical structures were designed to sustain category 3 cyclone as per the standards of Fiji. The failure of electric poles was observed mainly due to scouring of soil and in turn it caused loss of soil support to resist the lateral forces caused by TC Winston. It is highly recommended to consider geotechnical investigations, geotechnical design and suitable ground improvement schemes such as lime piles, dynamic compaction, stone columns etc., to avoid the geotechnical failures and in turn damages to the infrastructures.

ACKNOWLEDGEMENTS

We are thankful to Mr. Salabogi L. Mavoa the Acting Dean, College of Engineering Science and Technology, Fiji National University for having provided us an opportunity to work on assessment of infrastructure damages due to TC Winston. Also we are thankful to the university officials and the staff who directly or indirectly supported us to complete the project.

REFERENCES

[1] Bowles, JE, “Foundation Analysis and Design”, McGraw – Hill Publications, 1996.
[2] Leonards, GA, “Investigation of failures”, Journal of Geotechnical Engineering, ASCE, 108, No. GT-2, 1982, pp.187-246.
[3] Campbell, P, “Learning from construction failures”, Applied forensic engineering, John Wiley and Sons, 2001.
[4] Popescu, ME, “A Suggested Method for Reporting Landslide Remedial Measures”, IAEG Bulletin, 60, No. 1, 2001, pp.69-74.
[5] Glade, T, Anderson MG and Crozier MJ, “Landslide Hazard and Risk” John Wiley, 2006.
[6] Tony Waltham, Fred Bell and Martin Culshaw, “Sinkholes and Subsidence”, Praxis Publishing Ltd., Chichester, UK, 2005.
[7] Xanthakos PP, Abramson LW and Bruce DA, “Ground control and improvement”. Wiley-IEEE, 1994.
[8] Marcus, Robert B, “Florida-A Geographical Approach”, Dubuque, Iowa: Kendall/Hunt Publishing Co, 1975, pp. 64.
[9] Bujang BK Huat, “Behaviour of Soft Clay Foundation beneath an Embankment”, Pertanika J. Sci. & Technol. 2(2): 1994, pp.215-235, ISSN: 0128-7680 © Universiti Pertanian Malaysia Press.
[10] Michael P Navin, “Stability of Embankments Founded on Soft Soil Improved with Deep-Mixing-Method Columns”, Ph.D Thesis, Faculty of the Virginia Polytechnic Institute and State University.

Second International Conference on Science, Engineering & Environment,
Osaka City, Japan, Nov.21-23, 2016, ISBN: 978-4-9905958-7-6 C3051

STRUCTURAL DAMAGES CAUSED BY CYCLONE WINSTON TO BUILDINGS IN FIJI

Faijal Ali[1], Ravikant R Singh[1], Darga N Kumar[2], Ravindra Chand[3], Atinesh V Prasad[3] and Sanjay Prasad[3]
[1]Lecturer, [2] Professor, [3] Graduate Student
College of Engineering Science and Technology, Fiji National University

ABSTRACT

This paper presents the detailed inspection carried out on building damages in the western part of Viti Levu especially the provinces of Rakiraki, Tavua and Ba. A data sheet containing information about various structural connections, type of materials and on-site information from the owners of the buildings was used to understand the structural damages. Structural strength of reinforced concrete beams and walls was measured in-situ by conducting rebound hammer test. During the inspection the thickness of roof cladding was measured mainly to understand the variations in the thickness used. From the observations and tests carried out, it is noticed that most of the buildings had suffered in terms of roof cladding failure, which are noticed mainly due to large spacing of rafters and purlins and also due to variation in BMT ranging from 0.38mm to 0.6 mm of roof cladding. The shape of the roof also contributed for the entire roof failure. The strength of the walls is ranging from 7 to 15 MPa. The failure of beams and columns in some of the buildings is noticed mainly due to use of natural mix of river gravel which consisted dominantly silt, sand and gravel. About 70% of the buildings had experienced complete roof failures and 15% undergone structural failures like wall, beam-column and combination failures. Remaining 15% of the buildings had total damage starting from foundation level.

Keywords: TC Winston, Roof Cladding, BMT, River Gravel, RCC Beams.

INTRODUCTION

Fiji is located in the Melanesia, Oceania and covers a total area about 194,000 square kilometres of which around 10% is land. Fiji is the hub of the South West Pacific, midway between Vanuatu and Tonga. Fiji consists of 332 islands in the southwest Pacific Ocean about 1,960 miles (3,152 km) from Sydney, Australia. About 110 of these islands are inhabited. The two largest islands are Viti Levu (10,642 sq km) and Vanua Levu (5,807 sq. km). The population of Fiji was estimated to be 902 964 people as of January 2016 census. Due to its location in the Pacific Ocean, Fiji has been facing seasonal cyclones from November to April every year. This year it had experienced earth's second strongest cyclone of category 5 with wind speed up to 185 mph.

Temperature gradient of the atmosphere due to variable solar heating of the earth's surface generates wind. Large-scale air flows are so-called global atmospheric circulations, and generation of strong winds is closely related to these circulations, and also to smaller scale temperature differences. Tropical cyclones are intense cyclonic storms that occur over tropical oceans, mainly in summer and early autumn [1]. The objective of any design codes and standards is to protect public safety and property by preventing structural collapse or failure during rare events such as earthquakes, cyclones etc. in a building's lifetime. While this objective has largely been achieved for buildings in the US subjected to hurricane windstorms, economic losses and social disruption related to hurricane events are still unacceptable. This has led to current trends toward performance-based design in which the structural system is designed to meet specific performance criteria under different hazard levels [2]. The climatological conditions under which tropical cyclones occur have been well established over decades of research. These include a requirement for warm sea surface temperatures, low vertical wind shear and high values of large scale relative vorticity in the lower layers of the troposphere [3-4]. Some of the issues in the current codes and standards that need to be clarified, and one of them is the recurrence periods of design wind loads for structural frames and for cladding/components [5]. If the window panes and claddings of a tall building are damaged, property inside the building can be seriously damaged and lose its value, and this property loss can be very significant, especially if only the main structural frames remain. The miserable situation of a building with damaged window panes is often reported after extreme wind attacks in urban areas [6].

Very high wind speed records exceeding 90m/s as a peak gust is measured by seven sonic-anemometers and nine vane-anemometers set at heights of around 15m - 16m in an experimental site for power transmission cables in Miyakojima Island in Okinawa Prefecture, Japan, during a very strong

typhoon, Maemi, in 2003 [7]. Damage caused to the houses during tropical cyclones in Australia introduced awareness for wind resistance in house design [8]. Style of construction can affect the wind loads and structural damages. Also the age of the structure influence the failure pattern. Overall the age of the structure and the style of construction decide the vulnerability during cyclone [9].

Although records don't date too far back for Fiji's tropical weather, meteorologists know it's fairly rare for a tropical cyclone to hit the country's capital city. The western part of Viti levu and the northern part experienced a lot of disturbance including islands like Koro, Vanabalavu, Taveuni etc, which mostly falls on the cyclone path. It is indeed a great concern and challenge for the Engineers of Fiji. The report presents the various technical aspects of failures and recommendations.

METHODOLOGY ADOPTED

The post cyclone studies are carried out for the buildings which are damaged due to the TC Winston. The investigation is carried out based on the visual inspection at the site, pictures, questionnaire or structural data sheet and sample analysis. The data sheet consists of 38 structural related technical questions which are related building failure from foundation level to roof cladding. A part of typical data sheet is presented in Table. 1.

Table. 1 Typical data sheet

No	Item	Remarks
1	Terrain Category: Hilly area/Slope/Valley/Plain ground	
2	Surrounding: Trees/Vegetation/Farm/Buildings/Mountains/Wetland/Dry land	
3	Ground Type: Clay soil/soapstone/Sand/Sheet Rock	
4	Type of Roof (Gable/Lean to /Flat Roof/Pitched Roof /Butterfly Roof/Hip Roof, concrete roof etc.)	
5	C/C Spacing of Rafters and Rafter Size	
6	C/C Spacing of Purlins and Purlin Size	
7	Type of wood used for rafter	
8	Type of wood used for purlin	
9	Rafter to Purlin Connection (Galvanized Strapping/No.8 wire/ Nails/No Strapping)	

The BMT was measured in the laboratory by using micrometer. The rebound hammer test was conducted on site to know the strength of walls and beams. The aggregate mix used in the walls and beams was tested in the laboratory by using the sieve analysis. The mix typically consisted of fine aggregate with more than 8% silt. Silt and sand together was varied from 60 to 70% and gravel fraction of size varying from 4.75mm to 80mm was 30 to 40%.

DISCUSSION OF TC WINSTON DAMAGES

Roof Cladding Failure

Figures 1 to 4 present the failures relevant to roof structure and roof cladding due to TC Winston. Figure1. presents the cladding failure which is the result of falling Mango tree onto the roof. The Mango tree was standing in between the School and Tanoa Hotel which had a life of more than 50 years and about 15m in height. Due to the action of cyclic wind pressure, the tree could not resist the force and consequently fallen on nearby Tanoa Hotel roof in Rakiraki town. It not only damaged the Tanoa Hotel but the school as well. As such, the mitigation for such scenarios would be to cut down or trim any large trees that exist nearby any infrastructure during cyclone season. Most of the building suffered roof cladding failures and the BMT of roof cladding ranges from 0.38mm to 0.6mm. Poor connections of purlin to rafter are noticed in most of the timber structures. The purlins are fastened with no. 8 binding wires and galvanized strappings. Purlins used in roof truss construction had knots and cracks. This may be due to use of low grade timber.

Figure1. Damage of roof due to fallen tree

Figure 2. Complete damage of roof of the stadium

Figure 2 shows the complete destruction of roof

structure at Govind Park Ba Stadium. Due to use of 1300mm span of treated pine timber with size of 250mm x 25mm purlins, the roof did not sustain the cyclonic wind speed of 185mph, thus the timber purlin sheared from weak points and knots. It is further noticed that there are no traces of bridging end purlin connectivity. Even though the cyclone screws were used for roof fixing, it did not sustain the uplift force caused by the wind. The cyclone screws came out together with the roof cladding from the purlins.

Figure 3 shows that despite proper roof fixing been used, the roof cladding ripped off at the roof to purlins connections. The roof gauge was measured as 0.38mm. Also noticed that rafter to top plate connection is found to be poor. There are no traces of tie down rods.

Figure 4 presents that the maintenance for the roofing is done recently before the TC Winston, but the internal members of the truss were not upgraded or maintained. Top plate to rafter connections is fastened with no. 8 wires also subjected to rusting and lost its strength over the years. The members of the truss are not assembled properly and also noticed that the fasteners are not provided as required. Top chord and bottom chord splices are also not placed as per the requirements [10-11].

Figure 3. Failure of roof cladding

Figure 4. Failure of roof and roof truss

Roof and Structural Failure

Figure 5 presents the details that the timber used as rafter is of low grade (boxing timber) and also further noticed that the timber used in the construction is not treated as required (Figure 6), consequently it resulted in total failure of the roof structure (Figure 5). Even though two M12 bolts are used as fasteners, yet the timber broke at the connection point due to use of poor quality timber. It is also noted that the angle irons embedded into the concrete to a length of 300mm is structurally not suggestible. In some places it is also noticed that the entire roof structure is not designed appropriately and structural members of the truss are found to be missing. Starting from the type of timber, size of timber, roof pitch, connections, rafter and purlins spacing of treated pine timber used for roof framing has contributed to the failure and collapse of the entire roof structure of buildings.

Figure 7 shows the structural failure due to lack of proper reinforcement connectivity between column and beam. Therefore the failure can be attributed to lack of reinforcement connectivity and which resulted in uplift of beam from the column and overall it resulted in entire roof structural failure starting from terrace. Also observed that the coarse and fine aggregate used in the mix for beams and columns is not as per the design mix [11]. The materials used are mainly from river, wherein the required gradation is not fulfilling.

Figure 5. Roof members made with boxing timber

Figure 6. Typical boxing timber failure

Figure 7. Column beam joint failure

Figure 8 shows that the entire steel structure failure starting from foundation level. It is clearly noticed that the structure has no side walls thus the cyclonic wind resulted in uplift of the entire roof with the foundation and took the horizontal position. There are certain points clearly noticed that the foundation is made as concrete block anchor without proper pad, and the depth of anchor block, is not designed appropriately as per the soil conditions existing at the site. The connection from the anchor foundation block to the gusset plate and to the steel I section is not properly aligned and the quality and size of the bolts used are not sufficient to take the uplift forces.

Figure 8. Collapse of steel structure

Figure 9. Masonry wall failure

Figure 9 presents the picture taken at one of the hotels in Rakiraki. It is clearly seen from the picture that there is a crack in the wall extending from the window level to down. Also this crack is exactly noticed at the interface between wall and the plinth beam. It can be attributed that the masonry wall has not provided proper tie connections with the plinth beam and the lateral wind pressure of continued action in nature for about three hours, caused the wall to undergo fatigue and finally crack. Also it is attributed to lack of proper mix design consideration for the masonry wall.

Further at one of the school buildings the wall damage is noticed as shown in Figure 10. From this figure, it can be clearly seen that the masonry wall blocks are not provided with sufficient reinforcement to connect each other in an aligned way to bear the compressive loads and lateral forces due to the cyclone. Also the cavities of the blocks are not filled with the appropriate mortar and instead some of these hollow portions of wall are filled with locally available aggregate without any bonding material. It can be attributed to the poor workmanship and lack of site supervision.

Figure 10. Wall failure due to poor workmanship

Figure 11 shows the total structural failure of the building due to poor workmanship and cavities of masonry are not filled with design mortar and proper anchorage. Also noticed that round mild bars are used for starter bars instead deformed bars. It is also noticed that there is no bond beam. The compressive strength of block walls tested using rebound hammer ranges from 7 to 8 MPa. From this figure it can be further noticed that separation and tilting of two block walls which are at 90 degrees to each other is due to the absence of corner blocks and proper reinforcement binding.

Figure 11. Failure of wall due to lack of Corner block and reinforcement binding

Another wall failure is noticed in one of the school buildings as shown in Figure 12. The failure is attributed due to use of river gravel in place of appropriate builders mix. As per the design mix ratio,

the aggregate with more than 8% silt and clay should not be used for making concrete [11]. It is noticed that the content of silt and clay more than 8% (Figure 12).

Figure.12 Failure of wall due to use of river gravel

Figure 13. Beam with insufficient cover and poor quality materials

Table 2 Roof cladding BMT

No	Site Name	BMT (mm)
1.	Tavua Muslim Primary School	0.60
2.	Rakiraki Public High School	0.54
3	Rakiraki High School	0.48
4.	Naria Primary School	0.38
5.	Waimaro Police Post	0.38

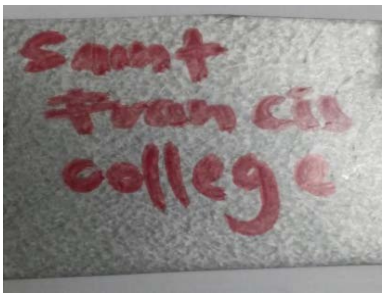

Figure 14. Typical roof cladding sample

Table 2 presents the typical bear metal thickness (BMT) of roof cladding. From the table it can be noticed that the thickness is varying from building to building ranging from 0.38 mm to 0.6 mm. Those roofs whose thickness is less than 0.48mm were suffered extensive damages. Figure 14 presents the typical picture of the roof cladding. The Table 3 presents the typical summary of failure noticed during the investigation of damaged buildings. From this table it can be seen that the roof structure and cladding suffered severely from the top beam up wards and some wall collapse was also noticed.

Table 3. Summary of data sheet

No.	Name of Building	Damaged Sustained
1	Turaqarua Primary School, Turaqarua	Newly constructed classroom totally destroyed.
2	Nabau District School, Nabua	Whole roof blown away.
3	Dobuilevu Muslim Primary School, Dobuilevu	Roof blown away with concrete terrace beam.
4	Ra High School, Ra	Building completely blown away. Concrete Wall cracked.
5	Barotu Primary School, Barotu	Roof Badly damaged. Truss failure.
6	Saint Francis College, Ra	Roof damage, weak rafter and purlin damage.
7	Steel portal framed structure, Rakiraki	Whole structure uplifted from foundation and tilted to one side.

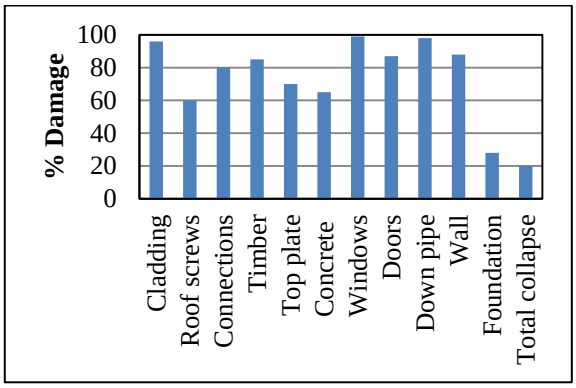

Figure 15. % Damage of components of buildings inspected

Figure 15 presents the % damage of various components of buildings inspected. From this chart it can be seen that all buildings suffered roof cladding failure. The total collapse is noticed in 20% of the buildings inspected. Rafter and purlin failures are noticed around 80% of the buildings inspected.

CONCLUSION

From the discussion some of the conclusions are made. Fiji has been experiencing tropical cyclones every year from November to April. The recent cyclone is the world second strongest cyclone with wind speed of 185 mile per hour (category 5). The buildings in Fiji are designed to resist up to category 3 cyclone. As per the statistics of cyclone history in Fiji, the intensity of cyclone and flooding of low lying areas are increasing every year. About 70% of the buildings have experienced complete roof failures and 15% have undergone structural failures like wall, beam, column and combination failures. Remaining 15% of the buildings are totally damaged starting from foundation level. The TC Winston not only caused damages to the buildings but also other infrastructure such as electric poles, foundations of structures, road and bridge failures, landslides and forestry are badly damaged. This cyclone lasted for about 4 hours. Some of the reasons of failures of roofs are due to usage of thin roof cladding of minimum thickness 0.38mm-0.6mm, which cannot withstand the category 5 cyclones. Also noticed at some places that the timber materials used for rafters, studs, walls, purlins, and bearers are not up to the standard [11].

The timber used for rafters and purlins is not seasoned properly before been used as structural members. Clear indication of glue and shrinkage of timber materials is noticed. In some of the buildings, the timber materials used consist of multiple knots and cracks. Also the beams and columns are designed as reinforced concrete members, but the aggregate used is not as per the design mix in fact readily available river gravel of unspecified gradation is used. The reinforcement used is not as per the design standard and also most of the masonry walls are suffered due to not filling the cavities with the specified bonding mortar [11].

Based on the above observations some of the interesting suggestions are made. The building supervision and maintenance to be appropriately carried out. Materials quality should be ensured through proper testing. All houses should be ensured with cyclone shutters of opening size of timber or steel gothic mesh should not be more than 25mm. All the opening should be properly fixed or maintained before the cyclone season so as to avoid further damages of the building as it may result to failure of roofing structure. The beams and columns of single storey building should have at least 20 to 25 MPa of compressive strength and that of two storey building should not be less than 30 MPa.

ACKNOWLEDGEMENT

We are thankful to Mr. Salabogi L. Mavoa the Acting Dean, College of Engineering Science and Technology, Fiji National University for providing us the opportunity to work on assessment of infrastructure damages due to TC Winston. Also we are thankful to university officials and staffs who directly or indirectly have given their support.

REFERENCES

[1] Yukio Tamura, “Wind -induced damage to buildings and disaster risk reduction”, The Seventh Asia-Pacific Conference on Wind Engineering, Keynote Lecture, November 8-12, 2009, Taipei, Taiwan.

[2] Ellingwood BR, Rosowsky DV, Li Y, Kim JH. “Fragility assessment of light-frame construction subjected to wind and earthquake hazards”, ASCE; 130(12): 2004 pp.1921–30.

[3] Gray WM, “Tropical cyclone genesis”, Dept. of Atmospheric Science, Paper No. 234, Colorado State University, Fort Collins, CO, 1975 , pp.121.

[4] McBride JL, Tropical Cyclone Formation. Global perspectives on tropical cyclones, WMO/TD-No. 693, 1995, pp.289.

[5] Tamura, Y, “Wind and tall buildings”, Keynote Lecture, The 5th European and African Regional Conference on Wind Engineering (EACWE 5), Florence, Italy, 19-23 July, 2009.

[6] Brewick P, Divel L, Butler K, Bashor R, Kareem A, “Consequences of urban aerodynamics and debris impact in extreme wind events”, Proceedings of the 11th Americas Conference on Wind Engineering, June 22-29, 2009, San Juan, Puerto Rico.

[7] Cao S, Tamura Y, Kikuchi N, Saito M, Nakayama I, and Matsuzaki Y, “Wind characteristics of strong typhoon”, Proceedings of the 12th International Conference on Wind Engineering, Cairns, Australia, July 2007, pp.719-726.

[8] Walker, GR, "Report on Cyclone Tracy – Effect on buildings”, Dec 1974, Australian Dept. of Housing and Construction.

[9] Henderson DJ, Ginger J, Leitch C, Boughton G, and Falck D, "Tropical Cyclone Larry – Damage to buildings in the Innisfail area" TR51, James Cook University, Townsville, 2006.

[10] AS/NZ 1170.2, “Australian/New Zealand Standard, Structural design actions, Part 2: wind actions, Standards Australia & Standards New Zealand”, 2002.

[11] Home Building Manual Fiji, Printed by Davui Printery Ltd, Fiji, 1990.

Second International Conference on Science, Engineering & Environment,
Osaka City, Japan, Nov.21-23, 2016, ISBN: 978-4-9905958-7-6 C3051

EFFICIENCY OF POLYSTYRENE INSULATED CEMENT BLOCKS IN ARID REGIONS

Muawia A Dafalla[1] and Mohammed I. Al Shuraim[2]

[1]A. Professor and Geotechnical Consultant, Civil Engineering, King Saud University, Riyadh 11421, E-mail: mdafalla@ksu.edu.sa

[2]Student, Mechanical Engineering, King Saud University. Riyadh 11421, Saudi Arabia.

ABSTRACT

Polystyrene insulated cement blocks emerged recently as an energy saving building material in construction practice. Expanded polystyrene of 5cm thickness or more is introduced as a middle fill layer within the cement block in order to improve the thermal properties of walls. This study is made to investigate the efficiency of insulation provided by this type of insulation. Two chambers were constructed in an open area where the walls are subjected to variable weather conditions ranging from moderate to hot weather for a period of three months. The arid region selected was Riyadh, Saudi Arabia. Temperature was found to vary between day and night through this period from as low as 9 ºC to as high as 48 ºC. Each chamber is built in the form of four block walls 20 cm in thickness, one meter wide and one meter high. The chambers were founded on grade slabs with a wood board used as a roof. The two chambers are identical except for the type of blocks; one is built using polystyrene insulated blocks and the other without insulation. Construction was carried out the same way as used in local practice. Thin mortar layer is used for bonding blocks. 5TE sensors and a data logger were used to record ambient temperature and temperature inside each chamber. Hourly records throughout the testing period were used to evaluate and compare the insulated and non-insulated blocks. It was found that the improvement provided by the polystyrene cement blocks is less efficient in hot temperature than in moderate temperature. The insulation provided by the blocks as constructed is very poor and heat transfer is enabled through mortar filled gaps and joints. The temperature gradient has influence on the polystyrene insulation material.

Keywords: Polystyrene, cement-block, Temperature, Insulation, Weather.

INTRODUCTION

This work is aimed at investigating issues related to polystyrene insulated cement blocks introduced to masonry industry in recent decades. The thermal conductivity is a term commonly used to define the ability of the material to transfer heat from a warmer part to a less warm part per unit time for unit area over a given temperature gradient. The unit of thermal conductivity is W m^{-1} K^{-1}. Materials of good thermal properties include mineral wool, EPS, XPS, polyurethane and others. Expanded polystyrene ranks second in use as insulation material in Europe and many other countries [1]. However, the flow of heat through any material is influenced by several factors and is not correctly predicted without considering all significant parameters. The flow of heat through materials, is affected by moisture, humidity and air content as prime factors. Reference [2] stated that heat conduction is influenced by the soil composition, structure, density, porosity, and grain geometry and pore or opening size. The same factors can be reflected to cement sand building materials. Moisture absorption, density and air components of EPS can cause thermal properties to change. In addition to material related properties the overall settings of the insulation system may also have its influence. Energy Efficiency and Renewable Energy (EERE) of the United States quoted that filling the block cavities or special block designs can improve a block wall's thermal characteristics, but doesn't reduce heat movement very much when compared to insulation installed over the surface of the blocks either on the exterior or interior of walls [3]. The present practices involve mortar between brick layers and some block designs include web of concrete that can transfer heat. Figure 1 presents two typical designs used in construction. It is becoming a routine to examine thermal properties of newly introduced construction material [4] and [5]. This study follows a similar approach in order to highlight the efficiency of polystyrene insulated cement blocks.

a-V-groove polystyerene filled.

b- Cuboid filled cavity

Fig 1. Two typical designs used in construction.

MATERIALS AND TESTING PROGRAM

Commercial cement blocks of dimensions 200mmx250mmx400mm with and without polystyrene insulation were obtained for the purpose of constructing two chambers in an open yard of college of civil engineering in King Saud University. The chambers are 1m by 1m rooms of 1m height covered with a plywood board. The construction was performed in a similar way as practiced in wall construction. Mortar prepared with 1:2 water cement ratio and 1:2 cement sand ratio was used. Thin mortar was applied in between layers. No plastering was made as the goal of the study was to compare the types of cement blocks with regard to heat transfer and energy savings. Figure 2 presents the two chambers as constructed. Arrangements were made to have equipment for recording temperature inside each chamber and also ambient temperature.

Variations in volumetric water content, temperature and electrical conductivity were recorded using 5TE Decagon sensors connected to Em50 data logger. The sensors were set to take records every one hour intervals. In order to reduce heat losses, 1cm thick pvc tube was used to guide wires through the walls in order to place the sensors right in the middle and mid-height of the chambers.

The expanded polystyrene material used in cement blocks insulation is white in colour and sandwiched between two parts of the cement block. The polystyrene is shaped with a V groove to interlock with the block concrete. The expanded polystyrene density is in the range of 25/29 Kg/m3. As marked by the manufacturer, the insulation brick has many advantages, such as heat preservation (coefficient of thermal conductivity is 0.045 ~ 0.065 W / (m k., sound proofing and better fire prevention. This typical cement block insulation is widely used in Southeast Asia, India, Middle East and other countries.[6].

TEST RESULTS AND GENERAL DISCUSSION

Temperature was found to vary between day and night through the investigation time from as low as 9 ºC to as high as 48 ºC. Two periods were considered for comparing the cement blocks. The first period is the February month, referred to as moderately hot, with temperature range during the day in the order of 10 ºC to 35 ºC degrees and the second period is end of May which is referred to as hot period where temperature range within the day is 25 ºC to 48 ºC degrees.

It can be seen that from Fig. 3 that both types of block provide a heat shield and reduce the maximum daily temperature from 35 ºC degrees to an average of 24 ºC and also elevate the minimum temperature from 10 ºC to an average of 16 ºC. The improvement of heat insulation indicated 1 ºC or less than 2 ºC degrees difference. The improvement is also reflected as time delay or shift. The improvement during the hot period is less compared to the moderately hot period. Difference in peaks is hardly observed but shift of graph reflect the delay due to the lower conductivity of the insulated cement blocks.

The improvement could have been much better if the mortar between the bricks is not used. Dry stacking will require other structural bonds like steel bars or joining mechanism. Other better alternatives include overall external or internal shielding with polystyrene board.

The present block laying method is not efficient. If mortar can be limited to the concrete portions of the bricks and the polystyrene is protruding by a centimeter or so to fix with other polystyrene face then the heat transfer through mortar can be eliminated.

The time shift associated with polystyrene insulated blocks can be clearly observed in Fig. 4. This is clearer in Fig. 5 which shows a 24 hour temperature profile during the hot period. Fig. 6 presents the ambient temperature site records over three months.

The insulation provided by the blocks as constructed is very poor and heat transfer is enabled through mortar filled gaps and joints. The temperature gradient has some influence on the polystyrene insulation material.

Measurement carried out by Yucel et al 2003 [1] showed that thermal conductivity coefficient is indirectly proportional to the density. The thermal conductivity is between 0,036 and 0,046 W/mk, for densities of expanded polystyrene between 10 and 30 kg/m3. Water absorption was measured as 3.5% for 30 kg/m3 and 5.5% for 15 Kg.

Fig.2 View of the two chambers constructed.

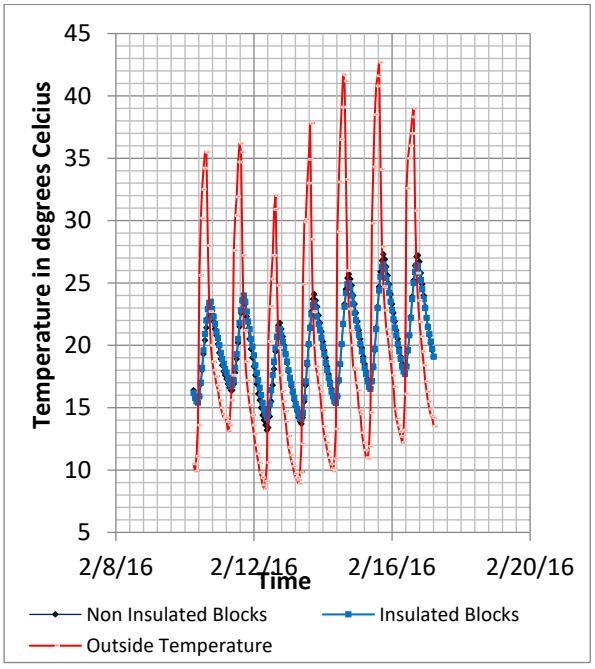

Fig 3. Temperature of insulated and non-insulated blocks compared to outside temperature.

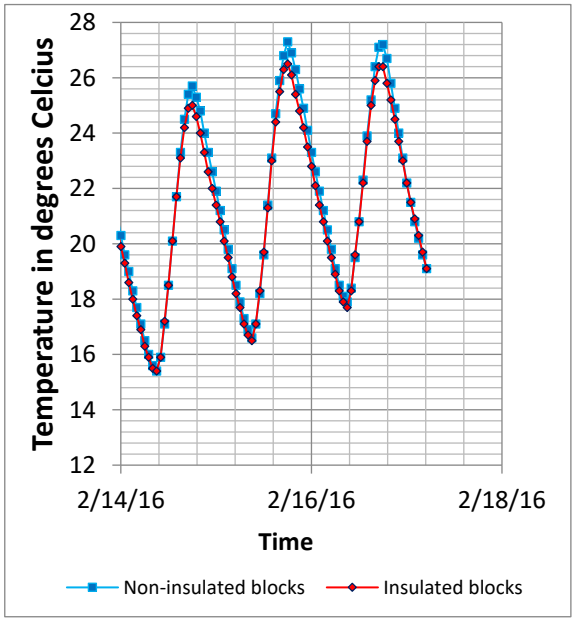

Fig 4. Comparing Insulated and non-insulated blocks temperature profile over three days in moderately hot period (February).

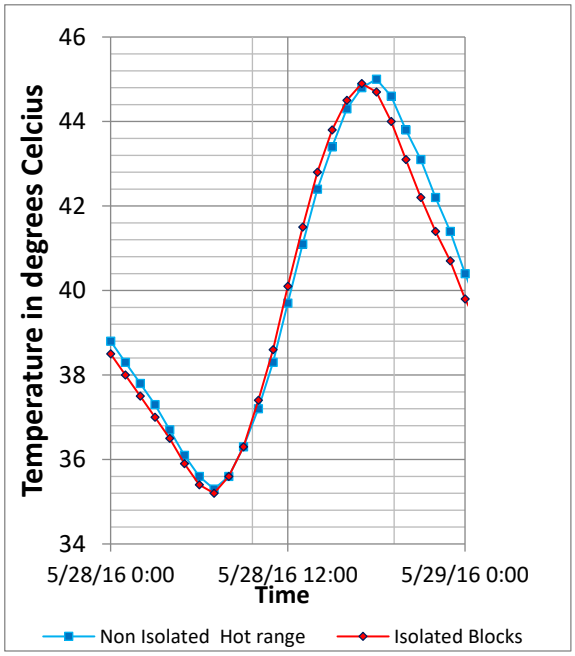

Fig 5. Comparing Insulated and non-insulated blocks temperature profile over 24 hours during hot period (End of May).

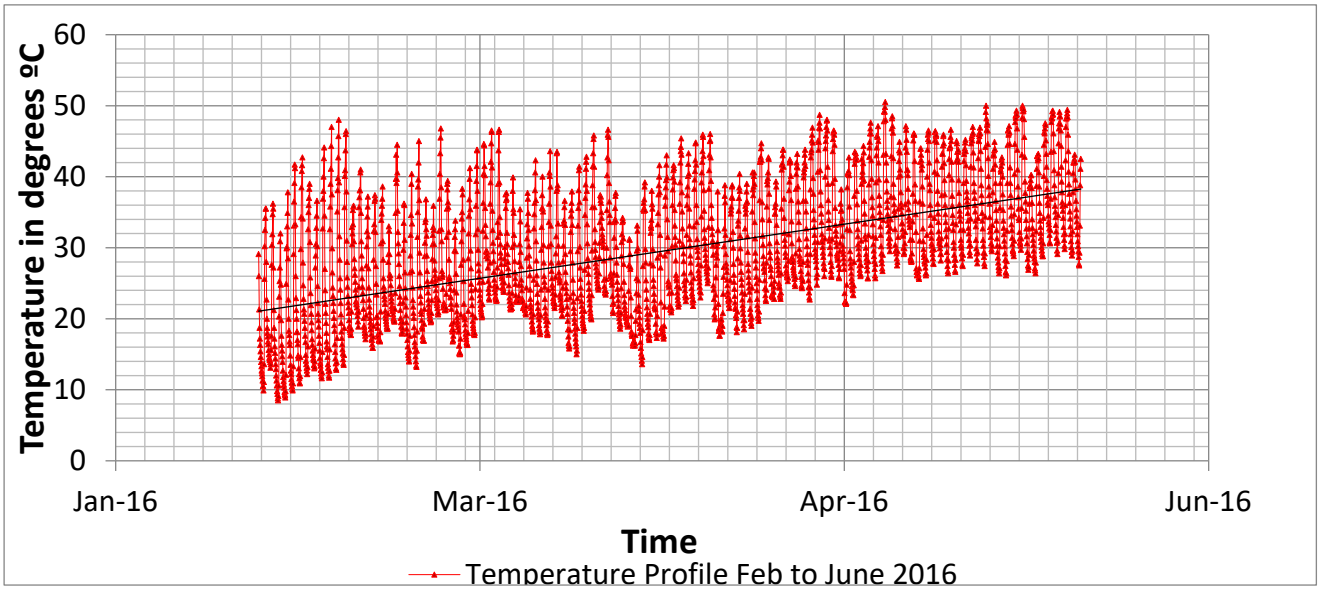

Fig. 6 Temperature site records over three months

CONCLUSION

The polystyrene insulated cement blocks behave differently for different temperature gradients and different levels of heat. The insulation provided by the blocks as constructed is very poor and heat transfer is enabled through mortar filled gaps and joints. The temperature gradient has influence on the polystyrene insulation material.

Reliable insulation can be achieved if use of mortar is limited to fix the concrete parts alone. External and internal heat insulation using polystyrene boards can be more efficient but may not stand strong to weather or impact conditions. Designers can use this nature as required to provide extended hours of comfortable times. In winter times insulated walls will retain the heat for several hours and provide relatively warm conditions. In summer times, the insulated cement blocks will shield the rooms during the day.

ACKNOWLEDGEMENT

The authors extend their appreciation to the Deanship of Scientific Research at King Saud University for funding this work through undergraduate students research support program project on (USRSP).

REFERENCES

[1] K. T. Yucel, C. Basyigit and C. Ozel, (2003). Thermal insulation properties of expanded polystyrene as construction and insulating materials. 15th Proceeding of Symposium on Thermophysical Properties, in Boulder, Colorado, NIST/ASME, pp.54-66.

[2] Farouki, O.T., 1986. “Thermal properties of soils.”, series on rocks and soil mechanics, Vol.11, Trans Tech Publications, Germany.

[3] The U.S. Department of Energy’s Office of Energy Efficiency and Renewable Energy (EERE). http://energy.gov/energysaver/energy-saver.

[4] Edremit, A., 1997. Performing Economical Analyses of Insulation Materials by Determining Physical Properties; Master Thesis, Yıldız Technical University of Istanbul, p. 114.

[5] Dafalla, M. A. and Samman, A. (2016).Soil and backfill material of environmental friendly thermal properties. International Journal of Geomate, Vol 10, Issue 22, 2083-2087.

[6] Gotop high-tech co.,ltd .China Polystyrene Injection molded Thermo block Insert Thermo Block Insert manufacturer)

Second International Conference on Science, Engineering & Environment,
Osaka City, Japan, Nov.21-23, 2016, ISBN: 978-4-9905958-7-6 C3051

PHYSICAL PROPERTIES OF MEA-BASED HYBRID SOLUTION AS A SOLVENT FOR HIGH CONCENTRATION CO_2 CAPTURE

L.S. Tan[1,2], A.M. Shariff[2], K.K. Lau[3] and G. Murshid[4]
[1]Department of Chemical and Petroleum Engineering, UCSI University, Malaysia, [2,3]Research Centre for CO_2 Capture, Universiti Teknologi PETRONAS, Malaysia, [4]Department of Petroleum and Chemical Engineering, Sultan Qaboos University, Oman.

ABSTRACT

Alkanolamines such as monoethanolamine (MEA) and diethanolamine (DEA) are commonly used for carbon dioxide (CO_2) absorption due to its high reactivity and fast absorption rate, which allows absorption to take place in a shorter column. However, it has disadvantage mainly due to the limitation on CO_2 loading capacity. As such, the development of an improvised and more efficient absorbent is important especially for the absorption of high CO_2 concentration in natural gas for potential offshore application. In this work, the physical properties of a MEA hybrid solution, i.e. density and viscosity were measured. The hybrid solution consisted of 20 wt% of MEA, 40 wt% water and 40 wt% n-methyl-2-pyrrolidone (NMP). These properties were measured at different temperatures from (303.15 to 333.15) K. The analysis from the experimental results showed that the density and viscosity of the hybrid solution decreased with increasing temperature. The data were crucial in order to understand the physical characteristics of the MEA hybrid solution and as input for modeling of MEA hybrid solution since the data were not available in the literature.

Keywords: Density; Viscosity; Hybrid solvent; CO_2 capture

INTRODUCTION

Carbon dioxide (CO_2) removal is essential process in sweetening of natural gas from underground reservoir. Natural gas generally contains a large quantity of methane (CH_4) along with heavier hydrocarbons such as ethane, propane, isobutene, normal butane and considerable amount of CO_2. CO_2 must be removed from natural gas because CO_2 is highly corrosive and rapidly destroys pipelines and equipment. It also reduces the heating value of a natural gas stream and wastes pipeline capacity [1].

There are many treating processes available for removal of CO_2. These processes include chemical absorption [2, 3], physical absorption [4], adsorption process [5], membrane separation [6] and cryogenic fractionation [7]. Currently, chemical absorption system has been widely used to treat high CO_2 concentration gases for synthesis-gas production and natural gas processing. Amine based chemical absorption system is considered as the most suitable current process to capture CO_2 because of its successful commercial implications, flexibility to low CO_2 partial-pressure gas streams and higher purity of CO_2 product [6].

Monoethanolamine (MEA) is the most popular and widely used solvent in industrial process for capturing CO_2 due to its high reactivity with CO_2 and low solvent cost [8-10]. However, the maximum CO_2 loading capacity for MEA is limited by stoichiometry to 0.5 mol of CO_2/mol of amine [10-12]. As such, the development of an improvised and more efficient absorbent is important especially for the absorption of high CO_2 concentration in natural gas for potential offshore application.

In this work, the physical properties of a MEA hybrid solution, i.e. density and viscosity were measured experimentally. The hybrid solution consisted of 20 wt% of MEA, 40 wt% water and 40 wt% n-methyl-2-pyrrolidone (NMP). This formulation of MEA hybrid solution was observed to provide fine cleanup using absorption column for inlet gas with high concentration of CO_2 and at high pressure condition [13]. The physical properties data of this hybrid solution is crucial in order to understand the physical characteristics of the MEA hybrid solution and as input for modeling and simulation of the MEA hybrid solution since the data were not available in the literature.

MATERIALS AND METHOD

Materials

MEA (99%) and NMP (99%) used in this study were purchased from Acros Organics. The chemicals were used without further purification. Double distilled water was used to prepare the hybrid solvent for this work.

Density Measurement

The density of MEA hybrid solution was measured using DMA 4500 M density meter (Anton Paar). It can measure density with an accuracy of ±0.00005 g/cm3. The density meter consists of an oscillating U-tube made of borosilicate glass as a measuring cell in a thermostatic jacket. It was equipped with a built-in platinum resistance thermometer which could measure the temperature with an accuracy of ±0.03 K.

Viscosity Measurement

The viscosity of MEA hybrid solution was measured using viscometer Lovis 2000 M (Anton Paar). It has viscosity measurement accuracy up to ±0.5 % and temperature accuracy of ±0.02 K. The capillary used for this study was of 1.59mm size. It is calibrated at regular interval using standard mineral oil produced by CANNON Instrument.

The equipment operates based on the rolling/falling ball principle according to DIN 53015 and ISO 12058 'Hoeppler principle'. The capillary block rotates to a defined inclination with a golden plated ball rolling inside. The dynamic viscosity was calculated by the viscometer based on the following equation:

$$\mu = K(\rho_b - \rho_s)\Delta t \quad (1)$$

where μ is the dynamic viscosity (mPa.s), K is the constant of proportionality (preset in the viscometer by the manufacturer), ρ_b is the ball density (g/cm^3), ρ_s is the sample density (g/cm^3) and Δt is the rolling time. Since the value of ρ_s was required as input into the equipment before the start of viscosity measurement, density measurement of the sample was a prerequisite before viscosity measurement could be conducted.

RESULTS AND DISCUSSION

Before measurement for MEA hybrid solution was conducted, validation of the experimental methods and results were carried out in order to ensure the validity of the experimental data. For this purpose, experimental measurement of density, viscosity and surface tension were carried out at temperatures (T) ranging from 303.15 K to 333.15 K for water, pure NMP and 20wt% MEA aqueous solution. The results obtained were compared in with literature data and summarized in Table 1 for density values, Table 2 for viscosity values and Table 3 for surface tension values. The validity of the measured data was evaluated based on the percent average absolute deviation between experimentally measured values with literature values published for relevant work. The percent average absolute deviation (% AAD) was calculated using Eq. 2 [14]:

$$\%AAD = \frac{1}{n}\sum \left|\frac{X_{exp}-Y_{lit}}{Y_{lit}}\right| 100 \quad (2)$$

where n is the number of experimental data points, X_{exp} and Y_{lit} are experimental and literature values, respectively.

Table 1 Comparison between the measured density (g/cm^3) data from this work with literature values.

Solution	T (K)	This work	Published work	%AAD
Water	303.15	0.9956	0.9956 [15]	0.026
	313.15	0.9922	0.9922 [15]	
	323.15	0.9880	0.9880 [15]	
	333.15	0.9823	0.9832 [15]	
NMP	303.15	1.0239	1.0247 [16]	0.072
	313.15	1.0150	1.0157 [16]	
	323.15	1.0061	1.0068 [16]	
20wt% MEA aqueous	313.15	0.9994	0.9991 [17]	0.025
	323.15	0.9945	0.9943 [17]	

Table 2 Comparison between the measured viscosity (mPa.s) data from this work with literature values.

Solution	T (K)	This work	Published work	%AAD
Water	303.15	0.8005	0.8020 [15]	0.323
	313.15	0.6588	0.6560 [15]	
	323.15	0.5555	0.5550 [15]	
	333.15	0.4788	0.4760 [15]	
NMP	303.15	1.578	1.592 [16]	1.161
	313.15	1.338	1.353 [16]	
	323.15	1.152	1.170 [16]	
20wt% MEA aqueous	313.15	1.169	1.18 [17]	0.870
	323.15	0.942	0.95 [17]	

Based on the analysed results in Table 1 and Table 2, the maximum %AAD between the experimental data and literature values are well below 5% for all the properties measured. The deviation between experimental and literature values could be due to the difference in purities of chemicals used, the different suppliers of chemicals, as well as the different measurement apparatus. The minimal deviation values indicated fairly good agreement between the experimental results and literature data.

With that, the physical properties of MEA hybrid solution were measured. The properties were measured from the temperature of 303.15 K to 333.15 K. The results of the measured properties are summarized in Table 3. All properties were observed to decrease with the increase of temperature.

At a glance, the higher viscosity value of MEA hybrid solvent compared to NMP and MEA aqueous solution was thought to be an error. However, a cross-check with data from literature [18, 19] indicated that the viscosity of pure MEA was actually quite high at approximately 15 mPa.s. Although the mass fraction of MEA in both hybrid and aqueous solution was the same, it is deduced that the partial replacement of water percentage with organic solvent, NMP, could possibly reduce the dilution dominance by water properties significantly. The interaction of molecules in MEA hybrid solution could also vary from MEA aqueous solution, hence, the viscous behaviour contributed from the pure MEA was more pronounced.

Table 3 Physical properties of MEA hybrid solution at different temperature condition.

Properties	T (K)	Value
Density (g/cm^3)	303.15	1.0325
	313.15	1.0244
	323.15	1.0162
	333.15	1.0077
Viscosity (mPa.s)	303.15	4.365
	313.15	3.050
	323.15	2.244
	333.15	1.707
Surface tension (mN/m)	303.15	49.75
	313.15	48.60
	323.15	47.76
	333.15	47.01

The measured data were transformed into graphical form as shown in Fig. 1 and Fig. 2 for density and viscosity respectively. The data were then fitted using Curve Fitting function in Matlab R2013a software and the correlations with respect to temperature were generated accordingly.

From the graphs, it was observed that the best fit for density and surface tension was linear function while the best fit for viscosity was exponential function. The following equations were used to fit the physical properties data.

Density:

$$\rho = A_0 + A_1 T \tag{3}$$

Viscosity:

$$\eta = A_0 \exp(A_1 T) \tag{4}$$

where ρ is density (g/cm^3), η is the viscosity (mPa.s), A_0 and A_1 are the fitting parameters while T is the temperature (K).

The fitting equation parameters are listed in Table 4 with standard deviations (SD) calculated using Eq. 5:

$$SD = \left[\frac{\sum_i^n (X_{exp} - X_{calc})^2}{n}\right]^{0.5} \tag{5}$$

where n is the number of experimental data points, X_{exp} and X_{calc} are experimental and calculated values, respectively.

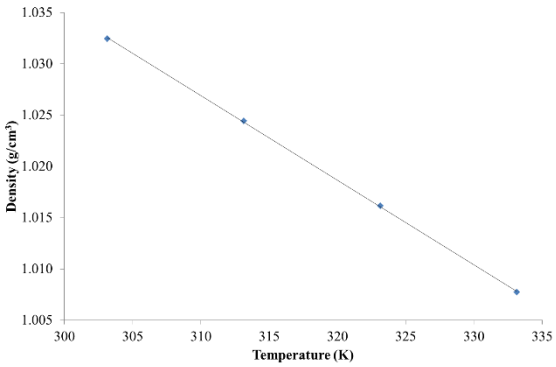

Fig. 1 Plot of density versus temperature for MEA hybrid solution.

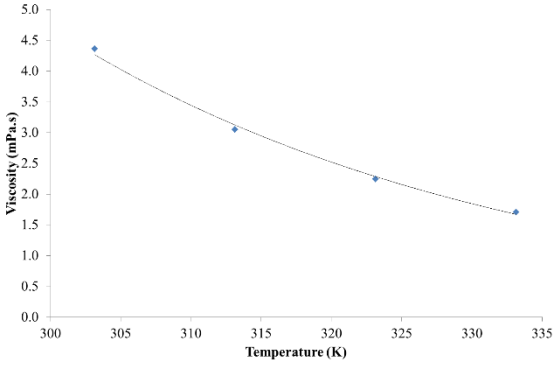

Fig. 2 Plot of viscosity versus temperature for MEA hybrid solution.

Table 4 Fitting parameters and standard deviation for physical properties of MEA hybrid solution.

Properties	A_0	A_1	R^2	SD
Density	1.283	-0.00083	0.9999	1.16 x 10^{-8}
Viscosity	78390	-0.0323	0.9968	5.08 x 10^{-3}

Figure 3 and Fig. 4 show the comparison of experimental and predicted density and viscosity values respectively. Based on Table 4, the coefficient of determination, R^2, of the fitted data was approximately 0.99 for both properties. This indicated that the predicted data are in good relation with the measured data. Therefore, the fitted equations can be used for prediction of the physical properties for the MEA hybrid solution.

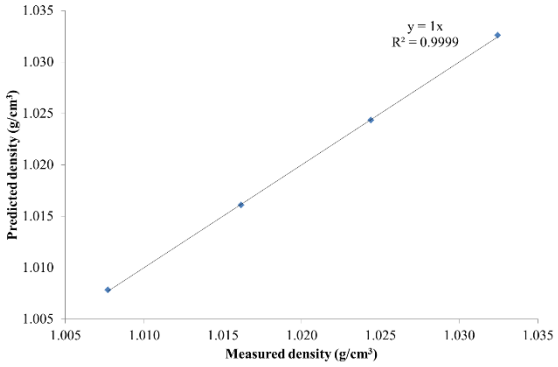

Fig. 3 Comparison between experimental values versus predicted values of density for MEA hybrid solution.

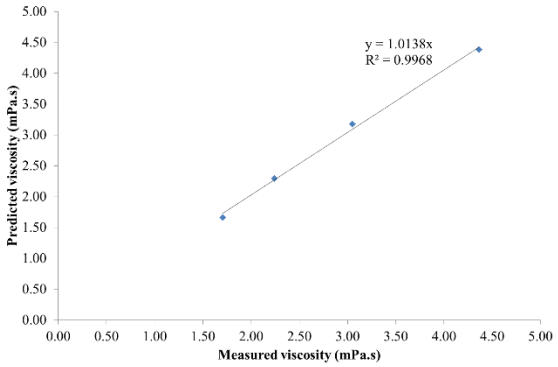

Fig. 4 Comparison between experimental values versus predicted values of viscosity for MEA hybrid solution.

CONCLUSION

The physical properties (i.e. density, viscosity and surface tension) of an MEA-based hybrid solution were measured at a range of temperatures from (303.15 to 333.15) K. The measured properties were observed to decrease with the increase of temperature. The measured density, viscosity and surface tension data were correlated by mathematical fitting equations of least-squares in order to calculate the predicted data. Minimal deviation was obtained between measured and predicted data. Therefore, the developed correlations could be used for prediction of physical properties for the MEA hybrid solution.

REFERENCES

[1] Safari M, Ghanizadeh A, and Montazer-Rahmati MM, "Optimization of membrane-based CO_2-removal from natural gas using simple models considering both pressure and temperature effects," Int. J. Greenh. Gas Control, Vol. 3, 2009, pp. 3-10.

[2] Aroonwilas A, Veawab A, and Tontiwachwuthikul P, "Behavior of the Mass-Transfer Coefficient of Structured Packings in CO_2 Absorbers with Chemical Reactions," Ind. Eng. Chem. Res., Vol. 38, 1999, pp. 2044-2050.

[3] Notz R, Asprion N, Clausen I, and Hasse H, "Selection and pilot plant test of new absorbents for post-combustion carbon dioxide capture," Trans IChemE, Part A, Chem. Eng. Res. Des., Vol. 85, 2007, pp. 510-515.

[4] Kohl AL and Nielsen RB, Gas Purification, 5th ed. Texas: Gulf Publishing Company, 1997.

[5] Siriwardane RV, Shen MS, Fisher EP, and Poston JA, "Adsorption of CO_2 on Molecular Sieves and Activated Carbon," Ener. & Fuels, Vol. 15, 2001, pp. 279-284.

[6] Yan S, Fang M, Zhang W, Zhong W, Luo Z, and Cen K, "Comparative analysis of CO_2 separation from flue gas by membrane gas absorption technology and chemical absorption technology in China," Ener. Convers. Manage., 2008, Vol. 49, pp. 3188-3197.

[7] IEA, CO_2 Capture and Storage: A key carbon abatement option. France: OECD/IEA, 2008.

[8] Aroonwilas A and Tontiwachwuthikul P, "High-efficiency structured packing for CO_2 separation using 2-amino-2-methyl-1-propanol (AMP)," Sep. Puri. Tech., Vol. 12, 1997, pp. 67-79.

[9] Dave N, Do T, Puxty G, Rowland R, Feron PHM, and M. I. Attalla, "CO_2 capture by aqueous amines and aqueous ammonia-A Comparison," Ener. Proc., Vol. 1, 2009, pp. 949-954.

[10] Dawodu OF and Meisen A, "Solubility of carbon dioxide in aqueous mixture of

alkanolamines," J. Chem. Eng. Data, Vol. 39, 1994, pp. 548-552.

[11] Shen KP and Li MH, "Solubility of carbon dioxide in aqueous mixtures of MEA with MDEA," J. Chem. Eng. Data, Vol. 37, 1992, pp. 96-100.

[12] Sartori G and Savage DW, "Sterically hindered amines for carbon dioxide removal from gases," Ind. Eng. Chem. Funda., Vol. 22, 1983, pp. 239-249.

[13] Tan LS, Shariff AM, Lau KK, and Bustam MA, "Impact of High Pressure on High Concentration Carbon Dioxide Capture from Natural Gas by Monoethanolamine/N-Methyl-2-Pyrrolidone Solvent in Absorption Packed Column," Int. J. Greenh. Gas Control, Vol. 34, 2015, pp. 25-30.

[14] Shaikh MS, Shariff AM, Bustam MA, and Murshid G, "Physicochemical Properties of Aqueous Solutions of Sodium l-Prolinate as an Absorbent for CO_2 Removal," J. Chem. Eng. Data, Vol. 59, 2014, pp. 362-368.

[15] Al-Ghawas HA, Hagewiesche DP, Ruiz-Ibanez G, and Sandall OC, "Physicochemical properties important for carbon dioxide absorption in aqueous methyldiethanolamine," J. Chem. Eng. Data, Vol. 34, 1989, pp. 385-391.

[16] García-Abuín A, Gómez-Díaz D, La Rubia MD, López AB, and Navaza JM, "Density, Speed of Sound, Refractive Index, Viscosity, Surface Tension, and Excess Volume of N-Methyl-2-pyrrolidone + 1-Amino-2-propanol {or Bis(2-hydroxypropyl)amine} from T = (293.15 to 323.15) K," J. Chem. Eng. Data, Vol. 56, 2011, pp. 2904-2908.

[17] Amundsen TG, Qi LE, and Eimer DA, "Density and Viscosity of Monoethanolamine + Water + Carbon Dioxide from (25 to 80) °C," J. Chem. Eng. Data, Vol. 54, 2009, pp. 3096-3100.

[18] DiGuilio RM, Lee RJ, Schaeffer ST, Brasher LL, and Teja AS, "Densities and viscosities of the ethanolamines," J. Chem. Eng. Data, Vol. 37, 1992, pp. 239-242.

[19] Maham Y, Liew CN, and Mather AE, "Viscosities and Excess Properties of Aqueous Solutions of Ethanolamines from 25 to 80°C," J. Sol. Chem., Vol. 31, 2002, pp. 743-756.

Second International Conference on Science, Engineering & Environment,
Osaka City, Japan, Nov.21-23, 2016, ISBN: 978-4-9905958-7-6 C3051

ANTITUMORAL PROPERTIES OF XANTHONES FROM MANGOSTEEN *GARCINIA MANGOSTANA* L HULL

Cheok, C.Y[1, 2] and Chin, N.L[3]

[1] Department of Chemical and Petroleum Engineering,
Faculty of Engineering, Technology & Built Environment (FETBE),
UCSI University, Lot 12734, Jalan Choo Lip Kung,
Taman Tayton View Cheras,
56000 Kuala Lumpur, Malaysia.

[2] Process System Engineering Center,
Faculty of Engineering, Technology & Built Environment (FETBE),
UCSI University, 56000 Kuala Lumpur, Malaysia

[3] Department of Process and Food Engineering,
Faculty of Engineering,
Universiti Putra Malaysia, 43400 UPM Serdang, Selangor, Malaysia.

ABSTRACT

Mangosteen is known as "the queen of fruits" in Malaysia, and the fruit is usually available during seasons from June to August yearly. This fruit comprises substantial amount of hull which disposes off as waste. However, it is the hull that has been discovered having various pharmaceutical properties such as antioxidant, anti-inflammatory, and antitumoral. The sudden surge of antitumoral properties studies of mangosteen hull in recent years is due to the rising of cancer which is the leading cause of death worldwide. This review highlights the recent discoveries of antitumoral properties of mangosteen hull. The major xanthones isolated from mangosteen hull which attribute to antitumoral properties are α-mangostin and γ-mangostin. They have been majorly discovered against cancers of colon, breast, and leukemia, followed by skin, bone, lung, brain, pancreatic, prostate, and head and neck.

Keywords: Mangosteen hull Antitumoral properties α-mangostin; γ-mangostin

INTRODUCTION

Mangosteen (*Garcinia mangostana* L.), is a large tropical evergreen tree from the *Guttiferae* family with a straight trunk, and it takes almost 6 to 7 years to cultivate before it fruits [1]. The fruit comprises of 25-29% of edible flesh, 60-65% of hull, and 6-10% of seed [2]. Its sweet and mild sour delicious pulp are the contributing factors for its popularity among the tropical fruits. Mangosteen has become an economically important species in recent decades since it is popular to Western Europe and United States most probably because of its pharmaceutical properties discovery, especially antitumoral [30, 33]. As reported by World Health Organization, cancer is the leading cause of death worldwide and accounted for 7.6 million deaths (around 13% of all deaths) in 2008 [35]. Mangosteen is the local seasonal fruit of Malaysia, which the delicious pulp is a target by local but the deep reddish purple hull (exocarp) is disposed as waste. The hull which contains bioactive compounds of xanthones has been widely discovered having various pharmaceutical properties. Among the xanthones, α-mangostin is the most extensively discovered having inhibition capabilities against various cancer cells. This paper discusses the recent discoveries and research trend of antitumoral properties of α-mangostin on various cancer cells. The γ-mangostin and other xanthones which have been proven as potential anticancer agents are also highlighted.

THE α-MANGOSTIN

The most abundant xanthone found in mangosteen hull is the α-mangostin [26-27]. α-mangostin is one of the earliest naturally occurring xanthone isolated from mangosteen hull using gas chromatography [28]. Numerous studies have revealed that the α-mangostin not only possesses properties of antioxidant, anticancer, anti-inflammatory, anti-allergy, antimicrobial, and

antiparasitic, it also has potential for anti-obesity and treatment of Alzheimer's disease [33]. Within the many pharmaceutical properties, its antitumor capabilities against various cancer cells have been extensively researched in recent decades. Figure 1 illustrates recent scientific findings of antitumoral properties of α-mangostin against various cancer cells. Approximately 25% of previous studies have proven the inhibition capabilities of α-mangostin against colon cancer cells. Its inhibition effects on other cancer cells such as breast cancer, leukemia, skin cancer, prostate, bone, lung, brain, pancreatic, head and neck have also been investigated and discovered (Fig. 1).

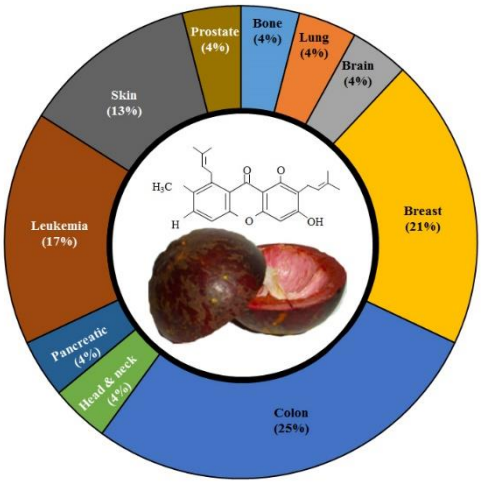

Fig. 1 Recent discoveries of antitumoral properties of α-mangostin on various cancers

Figure 2 demonstrates the trend of antitumoral properties discovery of α-mangostin from 2000 to 2014. The earliest finding on antitumoral properties of α-mangostin were on leukemia [20] and colon [12] cell lines in 2003 and 2005, respectively. For the period from 2006 to 2010, α-mangostin's inhibition effects against breast cancer [5, 8], prostate [25], and lung [32] was reported. Most recently from year 2011 to 2014, the finding of α-mangostin's inhibition for cancer cells have extended to bone [3], brain [4], skin [22-24], pancreatic [17], head and neck [16].

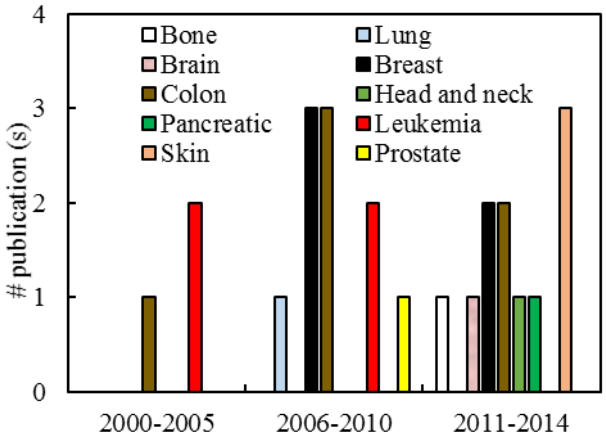

Fig. 2 Research trend of antitumoral properties of α-mangostin derived from mangosteen hull

THE γ-MANGOSTIN AND OTHER XANTHONES

The γ-mangostin is another xanthone derived from mangosteen hull and is another widely studied pharmaceutical property. It appears as a pale yellow powder after isolation with a thin layer chromatography [29]. The γ-mangostin isolated from mangosteen hull has been discovered to have antitumoral property against leukemia [19-20], breast cancer [5], skin [22], and colon cancer [15].

Further to this, the 1,3,6,7-tetrahydroxy-2,8-(3-methyl-2-butenyl) xanthone and epicatechin that were studied and tested *in vitro* also showed good cytotoxicities against human breast and colon cancer cells [11]. Both have been suggested as a potential anticancer agent [11]. Other two newly identified xanthones, the tetrahydroxanthone and garcimangosxanthone were revealed to exhibit *in vitro* cytotoxicity against human lung cancer, pulmonary carcinoma, and hepatoma [34]. More recently, xanthone of 8-deoxygartanin derived from mangosteen pericarp has been discovered having cytotoxicity against skin cancer [22].

CONCLUSION

Cancer, as the leading cause of death worldwide in recent decades, has triggered the quest of plant materials which containpotential antitumoral properties to combat the disease. The α-mangostin derived from mangosteen has natural occurring bioactive compounds which is anti-cancer. The recent research trend on the discovery of this compound provides an insight for scientists or researchers to further explore its inhibition capabilities against more cancer cell lines.

REFERENCES

[1] Osman M, Milan AR. Taxonomy. In: *Mangosteen garcinia mangostana L*., ed. J.T. Williams et al., Southampton Centre for Underutilised Crops, 2006, pp. 1–16.

[2] Chen Y, Huang B, Huang M, Cai B. On the preparation and characterization of activated carbon from mangosteen shell. J. Taiwan Inst. Chem. Engineer, Vol. 42, 2011, pp. 837–842.

[3] Krajarng A, Nakamura Y, Suksamrarn S, Watanapokasin R. α-mangostin induces apoptosis in human chondrosarcoma cells through downregulation of ERK/JNK and Akt signaling pathway. J. Agric. Food Chem. Vol. 59, 2011, pp. 5746–5754.

[4] Chao AC, Hsu YL, Liu CK, Kuo PL. α-mangostin, a dietary xanthone, induces autophagic cell death by activating the AMP-activated protein kinase pathway in glioblastoma cells. J. Agric. Food Chem. Vol. 59, 2011, pp. 2086–2096.

[5] Balunas MJ, Su B, Brueggemeier RW, Kinghorn AD. 2008. Xanthones from the botanical dietary supplement mangosteen (*Garcinia mangostana*) with aromatase inhibitory activity. J. Nat. Product. Vol. 71, 2008, pp. 1161–1166.

[6] Lee YB, Ko KC, Shi MD, Liao YC, Chiang TA, Wu PF, Shih YX, Shih YW. *α*-Mangostin, a novel dietary xanthone, suppresses TPA-mediated MMP-2 and MMP-9 expressions through the ERK signaling pathway in MCF-7 human breast adenocarcinoma cells. J. Food Sci. Vol. 75, 2010, pp. H13-H23.

[7] Shibata MA, Matoba Y, Tosa H, Iinuma M. Effects of mangosteen pericarp extracts against mammary cancer. Alternative Integrative Medic. Vol. 2, 2013, pp. 139. Doi:10.4172/2327.5162.1000139.

[8] Suksamrarn S, Komutiban O, Ratananukul P, Chimnoi N, Lartpornmatulee N, Suksamrarn A. Cytotoxic prenylated xanthones from the young fruit of *Garcinia mangostana*. Chemical and Pharmaceutical Bulletin. Vol. 54, 2006, pp. 301–305.

[9] Won YS, Lee JH, Kwon SJ, Kim JY, Park KH, Lee MK, Seo KI. α-Mangostin-induced apoptosis is mediated by estrogen receptor α in human breast cancer cells. Food Chem. Toxic. Vol. 66, 2014, pp. 158-165.

[10] Abdalrahim FAA, Khalid MAS, Mohammad JS, Zhari I, Amin Malik SAM. In vitro and in vivo anti-colon cancer effects of Garcinia mangostana xanthones extract. BMC Complementary Alternative Medic. Vol. 12, 2012, pp. 104. DOI: 10.1186/1472-6882-12-104.

[11] Yu L, Zhao M, Yang B, Bai W. Immunomodulatory and anticancer activities of phenolics from *Garcinia mangostana* fruit pericarp. Food Chem. Vol. 116, 2009, pp. 969–973.

[12] Matsumoto K, Akao Y, Ohguchi K, Ito T, Tanaka T, Iinuma M, Nozawa Y. Xanthones induce cell-cycle arrest and apoptosis in human colon cancer DLD-1cells. Bioorganic Medic. Chem. Vol. 13, 2005, pp. 6064–6069.

[13] Nabandith V, Suzui M, Morioka T, Kaneshiro T, Kinjo T, Matsumoto K, Akao Y, Iinuma M, Yoshimi N. Inhibitory effects of crude α-mangostin, a xanthone derivative, on two different categories of colon preneoplastic lesions induced by 1, 2-dimethylhydrazine in the rat. Asian Pacific J. Cancer Prevent. Vol. 5, 2004, pp. 433–438.

[14] Nakagawa Y, Iinuma M, Naoe T, Nozawa Y, Akao, Y. Characterized mechanism of a-mangostin-induced cell death: Caspase-independent apoptosis with release of endonuclease-G from mitochondria and increased miR-143 expression in human colorectal cancer DLD-1 cells. Bioorganic Medic. Chem. Vol. 15, 2007, pp. 5620–5628.

[15] Watanapokasin R, Jarinthanan F, Jerusalmi A, Suksamrarn S, Nakamura Y, Sukseree S, Uthaisang-Tanethpongtamb W, Ratananukul P, Sano T. Potential of xanthones from tropical fruit mangosteen as anti-cancer agents: Caspase-dependent apoptosis induction *in vitro* and in mice. Applied Biochem. Biotech. Vol. 162, 2010, pp. 1080–1094.

[16] Kaomongkolgit R, Chaisomboon N, Pavasant P. Apoptotic effect of alpha-mangostin on head and neck squamous carcinoma cells. Arch. Oral Bio. Vol. 56, 2011, pp. 4 83 – 490.

[17] Hafeez B, Mustafa A, Fischer JW, Singh A, Zhong W, Shekhani MO, Meske L, Havighurst T, Kim KM, Verma AK. α-Mangostin: A dietary antioxidant derived from the pericarp of *Garcinia mangostana* L. inhibits pancreatic tumor growth in xenograft mouse model. Antioxidant. Redox Signal. 2014, DOI:10.1089/ars.2013.5212.

[18] Ee GCL, Daud S, Izzadin SA, Rahmani M. *Garcinia mangostana*: a source of potential anti-cancer lead compounds against CEM-SS cell line. J. Asian Nat. Product. Research. Vol. 10, 2008, pp. 475–479.

[19] Itoh T, Ohguchi K, Iinuma M, Nozawa Y, Akao Y. Inhibitory effect of xanthones isolated from the pericarp of Garcinia mangostana L. on rat basophilic leukemia RBL-2H3 cell degranulation. Bioorganic Medic. Chem. Vol. 16, 2008, pp. 4500–4508.

[20] Matsumoto K, Akao Y, Kobayashi E, Ohguchi K, Ito T, Tanaka T, Iinuma M, Nozawa Y. Induction of apoptosis by xanthones from mangosteen in human leukemia cell lines. J. Nat. Product. Vol. 66, 2003, pp. 1124–1127.

[21] Matsumoto K, Akao Y, Yi H, Ohguchi K, Ito T, Tanaka T, Kobayashi E, Iinuma M, Nozawa Y. Preferential target is mitochondria in α-mangostin-induced apoptosis in human leukemia HL60 cells. Bioorganic Medic. Chem. Vol. 12, 2004, pp. 5799–5806.

[22] Wang JJ, Sanderson BJS, Zhang W. Cytotoxic effect of xanthones from pericarp of the tropical fruit mangosteen (*Garcinia mangostana* Linn.) on human melanoma cells. Food Chem. Toxic. Vol. 49, 2011, pp. 2385–2391.

[23] Wang JJ, Sanderson BJS, Zhang W. Significant anti-invasive activities of alpha-mangostin from the mangosteen pericarp on two human skin cancer cell lines. Anticancer Research. Vol. 32, 2012, pp. 3805-3816.

[24] Wang JJ, Shi QH, Zhang W, Sanderson BJS. Anti-skin cancer properties of phenolic-rich extract from the pericarp of mangosteen (*Garcinia mangostana* Linn.). Food Chem. Toxic. Vol. 50, 2012, pp. 3004-3013.

[25] Hung SH, Shen KH, Wu CH, Liu CL, Shih YW. α-mangostin suppresses PC-3 human prostate carcinoma cell metastasis by inhibiting matrix metalloproteinase-2/9 and urokinase-plasminogen expression through the JNK signaling pathway. J. Agric. Food Chem. Vol. 57, 2009, pp. 1291–1298.

[26] Chaivisuthangkura A, Malaikaew Y, Chaovanalikit A, Jaratrungtawee A, Panseeta P, Ratananukul P, Suksamrarn S. Prenylated xanthone composition of *Garcinia mangostana* (mangosteen) fruit hull. Chromatographia. Vol. 69, 2008, pp. 315–318.

[27] Wittenauer J, Falk S, Schweiggert-Weisz U, Carle R. Characterisation and quantification of xanthones from the aril and pericarp of mangosteens (*Garcinia mangostana* L.) and a mangosteen containing functional beverage by HPLC–DAD–MS^n. Food Chem. 2012, Doi:10.1016/j.foodchem.2012.02.094.

[28] Jefferson A, Stacey CI. 1971. Gas-liquid chromatography of naturally occuring xanthones and related derivatives. J. Chromatography. Vol. 57, 1971, pp. 247–254.

[29] Sen AK, Sarkar KK, Mazumder PC, Banerji N, Uusvuori R, Hase TA. The structures of garcinones a, b and c: Three new xanthones from *Garcinia mangostana*. Phytochem. Vol. 21, 1982, 1747–1750.

[30] Pedraza-Chaverri J, Cárdenas-Rodríguez N, Orozco-Ibarra M, Pérez-Rojas JM. Medicinal properties of mangosteen (*Garcinia mangostana*). Food Chem. Toxic. Vol. 46, 2008, pp. 3227–3239.

[31] Yoo JH, Kang K, Jho EH, Chin YW, Kim J, Nho CW. 2011. α- and γ-mangostin inhibits the proliferation of colon cancer cells via β-catenin gene regulation in Wnt/c GMP signaling. Food Chem. Vol. 129, 2011, pp. 1559-1566.

[32] Shih YW, Chien ST, Chen PS, Lee JH, Wu SH, Yin LT. α-Mangostin suppresses phorbol 12-myristate 13-acetateinduced MMP-2/MMP-9 expressions via avb3 integrin/FAK/ERK and NF-kB signalling pathway in human lung adenocarcinoma A549 cells. Cell Biochem. Biophys. Vol. 58, 2010, pp. 31-44.

[33] Ibrahim MY, Hashim NM, Mariod AA, Mohan S, Abdulla MA, Abdelwahab SI, Arbab IA. α-mangostin from Garcinia mangostana Linn: An updated review of its pharmaceutical properties. Arabian J. Chem. 2014, http://dx.doi.org/10.1016/j.arabjc.2014.02.011.

[34] Zhang Y, Song Z, Hao J, Qiu S, Xu Z. Two new prenylated xanthones and a new prenylated tetrahydroxanthone from the pericarp of *Garcinia mangostana*. Fitoterapia. Vol. 81, 2010, pp. 595–599.

[35] Cancer. World Health Organization. Retrieved on 1 June 2016. http://www.who.int/mediacentre/factsheets/fs297/en/

Second International Conference on Science, Engineering & Environment,
Osaka City, Japan, Nov.21-23, 2016, ISBN: 978-4-9905958-7-6 C3051

INFLUENCE OF RAILINGS STIFFNESS ON WHEEL LOAD DISTRIBUTION IN ONE- AND TWO-LANE CONCRETE SLAB BRIDGES

Mohammad Abou Nouh[1], Ghassan Fawaz[2], Mounir Mabsout[3], and Kassim Tarhini[4]
[1]Former Grad. Stud., Dept. of Civil and Envir. Engineering, Amer. Univ. of Beirut, Lebanon.
Email: mha70@mail.aub.edu
[2]Instructor, Dept. of Civil and Envir. Engineering, Amer. Univ. of Beirut, Lebanon.
Email: gmf02@mail.aub.edu
[3]Professor, Dept. of Civil and Envir. Engineering, Amer. Univ. of Beirut, Lebanon.
Email: mounir@aub.edu.lb
[4]Professor, Dept. of Civil Engineering, U.S. Coast Guard Academy, New London, CT 06320, USA.
Email: Kassim.M.Tarhini@uscga.edu

ABSTRACT

The American Association of State Highway and Transportation Official (AASHTO) and Load and Resistance Factor Design (AASHTO LRFD) do not account for the presence of railings as integral parts of highway bridges. This paper presents the parametric investigation of the influence of railings stiffness on the wheel load distribution in simply-supported, one-span, one- and two-lane reinforced concrete slab bridges using the finite-element analysis (FEA). A total of 80 bridge cases are modeled and bridge parameters such as span lengths and slab widths were varied within practical ranges. Various railings built integrally with the bridge deck are placed on both edges of the concrete slabs. The FEA wheel load distribution and bending moments are compared with reference bridge slabs without railings as well as to the AASHTO design procedures. According to the FEA results, the presence of railings reduces the longitudinal bending moment in slabs by 25% to 60% depending on the stiffness of the railings. The results of this investigation will assist structural and bridge engineers in better designing or evaluating concrete slab bridges in the presence of railings. This can also be considered to be a possible alternative for strengthening existing concrete slab bridges.

Keywords: Concrete Slab Bridges, Railings Stiffness, Finite-Element Analysis, AASHTO Procedures, Load-Carrying Capacity.

INTRODUCTION

A significant number of highway bridges are short-span reinforced concrete slabs that are owned and maintained by local and state governments. The main advantage of concrete slab bridges is the ease of construction and the ability to field adjustment of the roadway profile during construction. The design of highway bridges in the United States conforms American Association of State Highway and Transportation Official (AASHTO) [1] or Load and Resistance Factor Design (LRFD) Bridge Design Specifications (2012) [2]. The current AASHTO procedures do not consider the effect of railings that are built integrally with bridge deck in the evaluation of the load-carrying capacity of bridges. Therefore, this study investigates the effect of railings in resisting highway loading and increasing the load-carrying capacity of reinforced concrete slab bridges.

A parametric study investigated straight, single-span, simply-supported reinforced concrete slab bridges using finite-element analysis (FEA) [9]. Results indicated that AASHTO Specs moments overestimate the FEA moments for short spans, one lane bridges and agreed with FEA moments for short spans in combination of two or more lanes. Also, AASHTO Specs underestimates the FEA moments for longer spans. As for AASHTO LRFD procedure, it overestimates FEA moments for all bridge cases. Several studies were conducted to investigate the influence of sidewalks and railings on wheel load distribution in steel and prestressed girder bridges which was shown to increase the stiffness of the superstructure and improve the load-carrying capacity of these bridges [3]–[4]–[5]–[6]–[8].

Recently, a parametric investigation studying the influence of one standard railings size on straight concrete slab bridges was performed [7]. The results indicated that placing two railings on straight bridges, AASHTO Standard Specifications procedures overestimated the FEA moments by 100% for one-lane bridges, and by 20% for bridges with two lanes. AASHTO LRFD overestimated the FEA moments in all bridge cases by 150% for one-lane, and 70% for two-lanes when placing two

railings on slab bridges. It is worth mentioning noting that the AASHTO Procedures which overestimated the FEA results above do not consider the effect of side railings.

This paper presents the results of a parametric study investigating the influence of railings stiffness on the increase in load carrying capacity in reinforced concrete slab bridges.

AASHTO BENDING MOMENTS AND SLAB THICKNESS

For simply-supported concrete slab bridges, AASHTO Standard Specifications (2002) suggest three approaches in determining the live-load bending moment but only one procedure is used in this study that was compared with the finite-element analysis results.

$$M = 13{,}500S \ \ for\ S \le 15m \quad (1)$$

$$M = 1{,}000(19.5S - 90) \ \ for S > 15m \quad (2)$$

Where:
S = span length in m
M = longitudinal bending moment per unit width in N-m/m

AASHTO LRFD Section 4.6.2.3 (2012) provides an equivalent strip width procedure to design reinforced concrete slab bridges that is comparable to procedures specified in the Standard Specifications. However, the AASHTO LRFD Section 3.6.1.2 requires the use of HL93 (addition of HS20 Truck plus lane loading) live loading. This approach is to divide the total bending moment by an equivalent width to obtain a statically design moment per unit width. The equivalent width "E" of longitudinal strips per lane for both shear and moment is determined using the following formulas:

Width for one lane loaded is:

$$E = 250 + 0.42\sqrt{L1 \times W1} \quad (3)$$

Width for multi-lanes loaded is:

$$E = 2{,}100 + 0.12\sqrt{L1 \times W1} \quad (4)$$

Where:
E = equivalent width of longitudinal strips per lane, "mm"
L1 = span length in "mm", the lesser of the actual span or 18,000 mm
W1 = edge-to-edge width of bridge in "mm" taken to be the lesser of the actual width or 18,000 mm for multi-lane loading, or 9,000 mm for single-lane loading.

AASHTO Specs and AASHTO LRFD do not take in to account the influence of side railings on concrete slab bridges.

DESCRIPTION OF BRIDGE CASES

Typical simply-supported one-span, one-lane, and two-lane reinforced concrete slab bridge cases were analyzed in this investigation. Four single span lengths were considered in this parametric study: 7.2, 10.8, 13.8, and 16.2 m (24, 36, 46, and 54 ft) with corresponding slab thicknesses of 450, 525, 600, and 675 mm (18, 21, 24, and 27 inches), respectively. The concrete slab thicknesses were calculated using the AASHTO equations reported in earlier sections. The overall slab widths were assumed to be: 4.2 m (14 ft) for one lane, and 7.2 m (24 ft) for two lanes.

The base case for the standard railings size adopted from previous research was 200 mm (8 in) wide and 760 mm (30 in) high above slab [7]. Another parameter considered in this study was varying the railings stiffness, which is represented by the moment of inertia of the railing (I) computed at the bottom of the railing section.

$$I_{(bottom)} = I_{(center)} + Ad^2 = \frac{bh^3}{12} + bh(\frac{h}{2})^2 = \frac{bh^3}{3}$$

$$\therefore I_{(bottom)} = 4I_{(center)}$$

Five stiffness factors are considered including X0,
X1, X2, X3, X4, and X0.5, along with X0 case with no railings).
(reference
Where:
X0 No Railings, Reference case = 0
X0.5 Half the base case moment of inertia = 2Ic
X1 Moment of inertia of base case = 4Ic
X2 Twice the base case moment of inertia = 8Ic
X3 Triple the base case moment of inertia = 12Ic
X4 Four times the base case moment of inertia = 16Ic

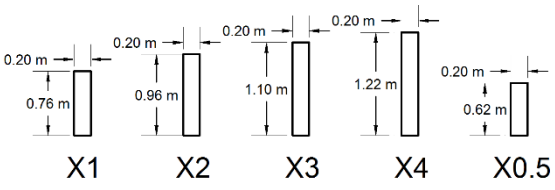

Fig. 1 Various railing sizes (X0, X1, X2, X3, X4, X0.5).

Various railings sizes are shown in Fig.1. Figure 2 shows a typical cross-section and plan-view of two-lane bridge cases with/without railings (base case, X1), with HS20 trucks placed transversely

close to one edge of the slab deck with minimum spacing between trucks (Edge loading condition).

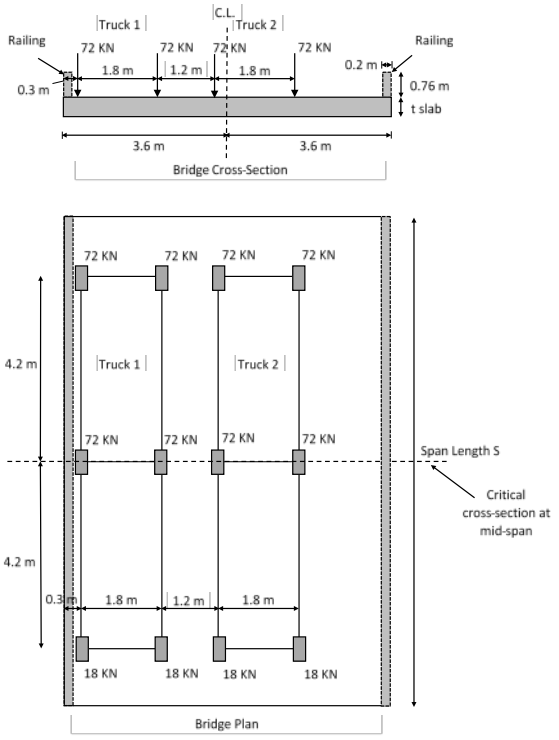

Fig. 2 Typical cross-section and layout for a two-lane bridge subject to Edge loading condition with base case railings (X1).

BRIDGE LOADING

The bridge cases considered in this study were subjected to AASHTO HS20 design trucks assuming to be traveling in the same direction when considering multiple lanes. AASHTO HS20 design trucks were placed longitudinally and transversely to produce maximum bending moments. The results of a previous study indicated that the Edge loading condition is more critical than the Centered loading condition [7]. Therefore, only the Edge loading condition was adopted in this study. Figure 2 shows the Edge loading condition for the two-lane bridge case where the first design truck was placed close to one edge of the slab, such that the center of the left wheel of the left most truck is positioned at 0.3 m (1 ft) from the left edge of the slab, and the other trucks were placed side-by-side with a distance 1.2 m (4 ft) between the adjacent trucks in order to produce the worst live loading condition on the bridge.

FINITE ELEMENT MODELING

A total of 80 slab bridge cases were investigated using the FEA. The computer program SAP2000 (version 17) was used to discretize the bridge into a convenient number of square four-node shell elements with six degrees of freedom at each node [10]. A previous study which investigated the influence of railings, showed that railings modeled as beam elements placed “eccentrically” along the slab edges with the second moment of area calculated about its base, gave similar results for longitudinal moments for models where railings were modeled as shell elements placed orthogonally on top and along the edges of each slab which represent a realistic geometric model [7]. Therefore, the simpler eccentric beam element was adopted to model the railings in this study. Figure 3 illustrates a typical finite-element model with the corresponding longitudinal bending moment contours for a 10.8 m (36 ft) span, two-lane bridge, in the presence of two railings, and subject to HS20 Edge loading condition.

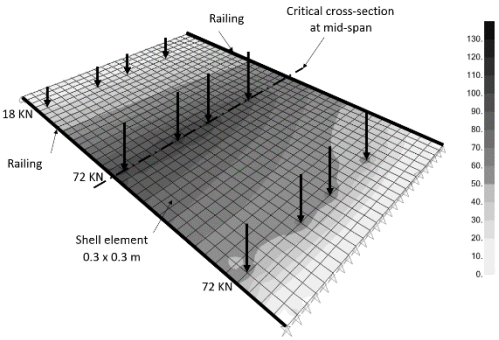

Fig. 3 FEA longitudinal bending moments (KN-m/m) in a 10.8 m (36 ft) span, two-lane bridge, with base case railings (X1) subject to Edge loading condition.

FINITE-ELEMENT ANALYSIS RESULTS

The FEA results are reported in terms of the maximum longitudinal bending moments at critical locations in the concrete slab bridges. The FEA results for bridges with railings of different stiffness factors were compared with reference bridge cases without railings as well as with AASHTO Standard Specifications and LRFD procedures.

FEA Results vs. AASHTO

Figure 4 shows sample plots of the FEA longitudinal bending moment at the critical sections for all the two-lane bridge cases in combination with the four span lengths (S) with base case railings (X1). Figure 5 shows the bending moment plots for all the two-lane bridges with 10.8 m (36 ft) span length, with different railing configurations (X0, X0.5, X1, X2, X3, X4), along with the AASHTO moments. The maximum FEA longitudinal moments in Fig. 5 for the concrete slabs was defined as the first peak value occurring after the maximum value at the leftmost edge which is assumed to be resisted by the edge beam.

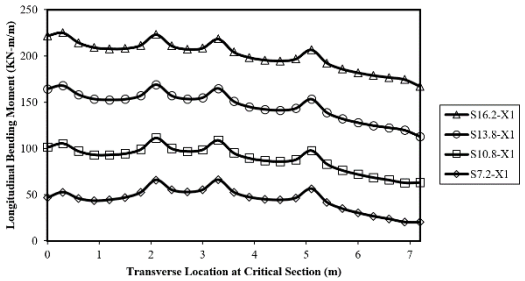

Fig. 4 FEA longitudinal bending moments for two-lane bridges for all spans (S), with base case railings (X1).

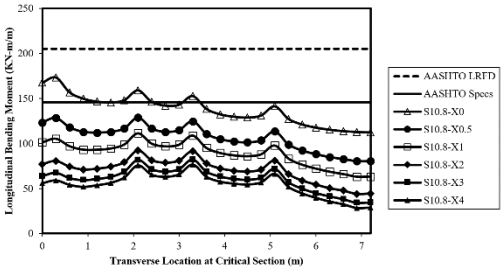

Fig. 5 FEA longitudinal bending moments for a 10.8 m (36 ft) span, two-lane bridge, with various railings sizes (X0, X0.5, X1, X2, X3, X4), with AASHTO Specs and LRFD.

Table 1 summarizes the increase or decrease in predicting bending moments in the concrete slabs when comparing the maximum FEA with the AASHTO Specs moments for all the bridge cases.

Table 1 Comparison of FEA Maximum Slab Longitudinal Bending Moments and AASHTO Specs Moments

Number of Lanes	Span Length (m)	FEA Maximum Longitudinal Moments (KN-m/m) and Percent Difference with AASHTO Specs						AASHTO Specs Moments (KN-m/m)
		Stiffness Factor						
		X0		X1		X2		
1	7.2	74.5	30%	44.8	117%	39.0	149%	97.2
	10.8	131.0	11%	75.9	92%	59.6	145%	145.8
	13.8	188.8	-1%	119.0	57%	91.8	103%	186.3
	16.2	235.1	-4%	162.8	39%	128.1	76%	225.9
2	7.2	92.3	5%	65.9	47%	60.5	61%	97.2
	10.8	159.0	-8%	111.3	31%	92.4	58%	145.8
	13.8	226.6	-18%	168.8	10%	139.4	34%	186.3
	16.2	280.6	-19%	222.9	1%	188.3	20%	225.9
		X3		X4		X0.5		
1	7.2	36.5	166%	35.2	176%	52.2	86%	97.2
	10.8	51.8	181%	47.3	209%	93.1	57%	145.8
	13.8	77.3	141%	68.2	173%	144.1	29%	186.3
	16.2	107.8	110%	94.4	139%	191.2	18%	225.9
2	7.2	58.0	68%	56.5	72%	73.4	33%	97.2
	10.8	82.2	77%	76.4	91%	128.6	13%	145.8
	13.8	121.4	53%	109.3	70%	192.0	-3%	186.3
	16.2	165.2	37%	148.5	52%	247.6	-9%	225.9

Using Table 1, it can be observed that, for bridge cases with no railings (X0), AASHTO Standard Specifications generally tends to give similar results to the FEA slab moments, with the exception of one-lane with spans less than 12 m (40 ft) where the AASHTO overestimates FEA moments by about 20%. This is more pronounced with more lanes and longer spans, where AASHTO underestimates FEA moments reaching up to 20% for two lanes with spans greater than 12 m (40 ft). When base case railings (X1) are present in a concrete slab, the FEA slab moments decrease significantly and AASHTO overestimates or gives similar moments in almost all cases, reaching 100% for the one-lane bridges with spans less than 12 m (40 ft), and gives similar moments for two-lane bridges with spans longer than 12 m (40 ft). Also, as the stiffness factor of railings increases as the FEA moments decrease and a more significant AASHTO overestimation is observed. This overestimation reaches 170% for one-lane bridges and is around 70% for two-lane bridges with (X4) railings stiffness factor.

Table 2 Comparison of FEA Maximum Slab Longitudinal Bending Moments and AASHTO LRFD Moments

Number of Lanes	Span Length (m)	FEA Maximum Longitudinal Moments (KN-m/m) and Percent Difference with AASHTO LRFD						AASHTO LRFD Moments (KN-m/m)
		Stiffness Factor						
		X0		X1		X2		
1	7.2	74.5	70%	44.8	182%	39.0	224%	126.5
	10.8	131.0	62%	75.9	180%	59.6	256%	212.4
	13.8	188.8	50%	119.0	138%	91.8	208%	283.1
	16.2	235.1	44%	162.8	108%	128.1	164%	338.9
2	7.2	92.3	18%	65.9	65%	60.5	79%	108.5
	10.8	159.0	29%	111.3	84%	92.4	122%	205.2
	13.8	226.6	30%	168.8	74%	139.4	111%	293.9
	16.2	280.6	31%	222.9	65%	188.3	95%	367.7
		X3		X4		X0.5		
1	7.2	36.5	246%	35.2	259%	52.2	142%	126.5
	10.8	51.8	310%	47.3	350%	93.1	128%	212.4
	13.8	77.3	266%	68.2	315%	144.1	96%	283.1
	16.2	107.8	214%	94.4	259%	191.2	77%	338.9
2	7.2	58.0	87%	56.5	92%	73.4	48%	108.5
	10.8	82.2	150%	76.4	169%	128.6	60%	205.2
	13.8	121.4	142%	109.3	169%	192.0	53%	293.9
	16.2	165.2	123%	148.5	148%	247.6	48%	367.7

With reference to Table 2, AASHTO LRFD overestimates the FEA slab moments in almost all bridge cases with or without railings. AASHTO LRFD overestimates the FEA slab moments by about 50% for one-lane bridges and about 30% for two-lane bridges. This overestimation decreases with the increase in span length. When base case railings (X1) are present, the AASHTO LRFD overestimation of the FEA slab moments becomes more significant reaching an average high of 150% in one-lane bridges or 70% in two-lane bridges. This overestimation is further increased as the railings stiffness factor increases where it reaches 250% for one-lane bridges and around 150% for two-lane bridges with (X4) railings stiffness factor.

FEA Results with Railings vs. No Railing

The maximum slab bending moments are summarized in Table 3 for all bridge cases in terms of ratios of FEA results for cases with various

railings stiffness factors to the corresponding cases without railings (reference case, X0). Table 3 shows that the presence of railings reduces the maximum longitudinal slab moment and this increase is more pronounced as the railings stiffness factor increases. For one-lane bridges, maximum longitudinal moment reduces by 40% when adding railing with stiffness factor (X1) and it reduces by 60% with (X4) railing stiffness factor. As for two-lane-bridges, the slab moment reduces by 25% with X1 railing stiffness factor and by about 50% with X4 railing stiffness factor. Worth mentioning that the rate of the increase of the reduction decreases as the railing stiffness factor increases.

Table 3. Comparison of FEA Results with Railings to Reference Case without Railings

Number of Lanes	Span Length (m)	Ratio of FEA Maximum Longitudinal Moment with Railings to Reference Case without Railings						Reference Moment X0
		Stiffness Factor						
		X0		X1		X2		
1	7.2	74.5	1.00	44.8	0.60	39.0	0.52	74.5
	10.8	131.0	1.00	75.9	0.58	59.6	0.46	131.0
	13.8	188.8	1.00	119.0	0.63	91.8	0.49	188.8
	16.2	235.1	1.00	162.8	0.69	128.1	0.54	235.1
2	7.2	92.3	1.00	65.9	0.71	60.5	0.66	92.3
	10.8	159.0	1.00	111.3	0.70	92.4	0.58	159.0
	13.8	226.6	1.00	168.8	0.74	139.4	0.62	226.6
	16.2	280.6	1.00	222.9	0.79	188.3	0.67	280.6
		X3		X4		X0.5		
1	7.2	36.5	0.49	35.2	0.47	52.2	0.70	74.5
	10.8	51.8	0.40	47.3	0.36	93.1	0.71	131.0
	13.8	77.3	0.41	68.2	0.36	144.1	0.76	188.8
	16.2	107.8	0.46	94.4	0.40	191.2	0.81	235.1
2	7.2	58.0	0.63	56.5	0.61	73.4	0.80	92.3
	10.8	82.2	0.52	76.4	0.48	128.6	0.81	159.0
	13.8	121.4	0.54	109.3	0.48	192.0	0.85	226.6
	16.2	165.2	0.59	148.5	0.53	247.6	0.88	280.6

SUMMARY AND CONCLUSIONS

AASHTO Standard Specifications and AASHTO LRFD empirical equations do not account for the presence of railings as integral parts of a bridge slab, and these elements are neglected during the design stage. Based on the finite-element analysis, it is clearly evident that these elements increase the capacity of the bridges if they are modeled as integral parts of the slab. It was found that the maximum slab moment was reduced due to the presence of two railings. This reduction in the slab moment decreases with the increase in the number of lanes, and increases with the increases in the railing stiffness. These railings can be used as one alternative strengthening technique to upgrade existing bridges that require rehabilitation or to allow permit vehicles on the bridge.

ACKNOWLEDGMENT

This research was supported by a grant from the University Research Board (URB) at the American University of Beirut to whom the authors are indebted and thankful.

REFERENCES

[1] AASHTO (2002). *Standard specifications for highway bridges*, 17th Ed., American Association of State Highway and Transportation Officials (AASHTO), Washington, D.C.

[2] AASHTO (2012). *LRFD bridge design specifications*, 5th Ed., American Association of State Highway and Transportation Officials (AASHTO), Washington, D.C.

[3] Akinci, N.O., Liu, J., and Bowman, M.D. (2008). "Parapet strength and contribution to live load response for super load passages." *J. Bridge Eng.*, 13(1), 55-63.

[4] Chung, W., Liu, J., and Sotelino, E.D. (2006). "Influence of secondary elements and deck cracking on the lateral load distribution of steel girder bridges." *J. Bridge Eng.*, 11(2), 178-187.

[5] Conner, S., and Huo, X.S. (2006). "Influence of parapets and aspect ratio on live-load distribution." *J. Bridge Eng.*, 11(2), 188-196.

[6] Eamon, C., and Nowak, A. (2002). "Effects of edge-stiffening elements and diaphragms on bridge resistance and load distribution." *J. Bridge Eng.*, 7(5), 258-266.

[7] Fawaz, G., Waked, M., Mabsout, M., and Tarhini, K. (2016). "Influence of railings on load carrying capacity of one- and two-lane concrete slab bridges." Sixth Annual International Conference in Civil Engineering, Athens, Greece.

[8] Mabsout, M., Tarhini, K., Frederick, G., and Kobrosly M. (1997). "Influence of sidewalks and railings on wheel load distribution in steel girder highway bridges." *J. Bridge Eng.*, 2(3), 88-96.

[9] Mabsout, M., Tarhini, K., Jabakhanji, R., and Awwad, E. (2004). "Wheel load distribution in simply supported concrete slab bridges." *J. Bridge Eng.*, 9(2), 147-155.

[10] SAP2000 (version 17). Computers and Structures Inc., Berkeley, California.

Second International Conference on Science, Engineering & Environment,
Osaka City, Japan, Nov.21-23, 2016, ISBN: 978-4-9905958-7-6 C3051

A SIMULATION OF RISK MANAGEMENT IN INFORMATION SYSTEM PROJECTS FOR INDUSTRIAL ENGINEERING POSTGRADUATES

Sakgasit Ramingwong[1,2] and Lachana Ramingwong[2]
[1]Excellence Center in Logistics and Supply Chain Management, Chiang Mai University, Thailand;
[2]Department of Computer Engineering, Faculty of Engineering, Chiang Mai University, Thailand

ABSTRACT

Risks management is an essential element which can help increasing success rate in engineering projects. Undeniably, efficient implementation of this process requires not only knowledge but also real experience in the project context. In information system projects, which are widely known for its challenging and unique nature, the importance of risk management increase substantially. It is significant that all stakeholders, either at technical, management or other levels, need to realize the potentials of major risks. This research reports a result from an implementation of a simulation on risk management in information system projects based on a simulation called ARMI: A Risk Management Incorporation for industrial engineering postgraduate students. The results show that the simulation can be effectively implemented for participants with non-technical background.

Keywords: Information system development, Risk management, Simulation, Case study

INTRODUCTION

Information system is arguably one of the most important foundation of modern business. An efficient information system can provide a sharp competitive edge for organizations [1], [2]. However, interestingly, it has been reported that the success rate of information system development is rather unsatisfactory. The report by Standish Group shows that the overall success rate of software projects was only 19% in 2015 which is inferior to the years before [3], [4]. The numbers reveals that, although with current technologies, approaches, attempts and advanced development processes, this mediocre rate of success shows no significant improvement.

It is obvious that risks, although usually undesired, inhibit in most engineering projects [5]. Different type of projects involve in different types and effects of risks [6]. Management of risks in an unfamiliar project context could be more than challenging. Such difficulties could escalate in projects which is highly intangible such as information system projects [7]. Indeed, increase in knowledge towards the project nature could help increasing the chance of success [8]. Additionally, since these projects usually involve a number of stakeholders, e.g. executives, managers, consultants, users, engineers, sponsors and vendors, it is important that all of them realize the potential risks so they can contribute their efforts towards appropriate mitigation strategies [9].

ARMI: A Risk Management Incorporation is a simulation based on risk management and information system development processes [10]. Originally, it was developed as a tool for teaching risk management in project management course for undergraduate computer engineering student. The results of past simulations show that this simulation can help moderating the participants' perception towards risks. After completing the activity, the participants learn the process of risk management, information system development as well as potential risks and impact on the project.

This research implements ARMI in a different domain. Instead of computer engineers, industrial engineering students are the participants on this research. Thus, the results from this research is likely to reflect the viewpoints from the management side in an information system project than the usual technical counterpart. Statistical analyses reveal several interesting findings which are later discussed in this paper.

The second section of this paper reviews ARMI, the main simulation, and its past implementation. Then, the research methodology and background of the participants are described in section three. The fourth section discusses the results and findings. Finally, the fifth section concludes this paper.

INFORMATION SYSTEM DEVELOPMENT AND ASSOCIATED RISKS

The development of an information system is challenging. Reports reveal that their success rate is far from acceptable [3], [4]. Indeed, unlike other forms of engineering project, the development of

information systems heavily relies on several intangible components, especially software [11]. This leads to unique risks and mitigation strategies. To improve the survival rate of the project, it is critical that all stakeholders need to realize the importance and nature of these challenges.

The phases of information system development are indifferent from general engineering projects. It involves collecting of requirements, translate the requirements into design, develop the system from the design and finally test for the product's quality [12]. Typical information systems consists of three major components, e.g. hardware, software and networking [13]. Indeed, the most mysterious part of the system is the software. Due to its intangibility, tracking progress of software can be complicated [14]. Moreover, although the hardware and networking seems be mainly related on physical equipment, they inevitably involve abstract processes such as configuration. This, too, could also lead to major drawbacks in the projects.

Both researchers and practitioners have been proposing major risks in information system development [6], [15]–[17]. From the technical point of view, continuously expanding of requirements or "Scope creep" has been perceived as the more, if not the most, important risk [18]. This is because many stakeholders do not realize that even minor changes can cause major impact to the structure of the information systems, which could further lead to other problems such as defects, delay and inefficiency of the products. This problem is not likely to happen often in other engineering scenarios which almost every critical elements can be physically seen.

Inexperienced staff is another risk which highlight the uniqueness of information system development [19]. When developing an information system, every attempt which translates the inputs to the output in each phase is design. Requirement engineering, system analysis and designing, coding and testing all involve design of certain products. As such, unskilled labors are mostly irrelevant in information system project. Positioning staffs with inappropriate experiences could also cause damage to the project.

As aforementioned, realizing of potential risks could greatly moderate the perspectives of stakeholders in information system projects. A simulation could be an effective tool to bridge the gap between these perceptions. This not only improve the success but also the efficiency of the entire development.

ARMI: A RISK MANAGEMENT INCORPORATION

ARMI is developed to serve as an activity which coaches computer engineering students on risk management of software project [10]. All six phases of risk management, i.e. identification, analysis, planning, tracking, control and learning, are represented and repeated. On the technical side, ARMI simulates an entire cycle of an information system development project. This development cycle follows the classic Waterfall Model for its simplicity. As a result, the stages of system development defined in this simulation involve requirement, design, implementation, testing, and maintenance. ARMI is designed to be ideally played by three teams of participants. Each team consists of 2-8 persons. An equal amount of risk management fund is distributed amongst them. The team which completes the simulation with the most remaining fund wins.

ARMI follows each stage of system development in sequence. This results in 5 turns of simulation. In each turn, the participants brainstorm and identify potential risks which may surface during that development stage from a list of 25 risks which are recognized as top threats in information system development project. The followings designate potential risks which could be materialized in ARMI:

- Inexperienced staff
- Delay of schedule
- Lacks of executive involvement
- Lacks of user involvement
- Lacks of user IT skills
- Scope creep
- Inadequate development facilities
- Inadequate staffing
- Staff turnover
- Inefficient management
- Missing of payment from clients
- Unable to fulfill customer's objectives
- Cost escalation
- Low software performance
- High number of defects
- User resistance
- Incompatibility to the legacy system

- Unable to integrate modules
- Increased number of users
- Inappropriate system design
- Inaccurate requirement analysis
- Conflicts between internal staffs
- Conflicts between stakeholders
- Low stability of new technology
- Lack of external communication

The participants are expected to analyze for potential impacts and probabilities of occurrence of the identified risks. In order to save the valuable resources, less important and irrelevant risks are expected to be ignored. Expert's opinions are given as a guideline to assist them in this process. They are notified that the expert's opinions could be wrong and misleading sometimes. After that, the teams prioritize the risks and choose the most appropriate mitigation strategies for each of them. There are four mitigation strategies to be chosen in ARMI. Firstly, Method A, this strategy costs most but can prevent any upcoming penalty if the risk actually surfaced. Secondly, Method B, this strategy costs less but can mitigate only 50% of the consequence. For instance, if the team choose this practice and the related risk is materialized, they are required to pay half of the damage caused by this risk. Thirdly, Method C costs even less but only cover 20% of the penalty. Finally, the teams can also choose to not pay for any protections and suffer the full impact of the risks.

After the mitigation bill is concluded, a representative from each team draws a number which indicates the number of materialized risks. Then, the representatives draw risk cards from the deck of risk. Although this seems random, the number of risks in the deck is actually controlled. Subsequently, the moderator announce the materialization of the risks. At this phase, the team can argue if they feel that certain risk is not relevant to that development stage. If they win the argument, the risk is considered void so they do not need to pay for penalties. Otherwise, the teams then pay for each impacts of the risks which they fail to mitigate. The participants learn the risk management process and nature of risk in information system development along with the repetition of these activities in each turn.

A pretest and a posttest revealed noticeable changes of the participants' risk pre- and post-analyses. Their perceptions towards risks seemed to be moderated by the ratio of risks in the deck. This suggests that ARMI may influence the players' risk perceptions therefore it could be an effective tool to help shaping stakeholders' perception towards risks in information system development projects.

RESEARCH METHODOLOGY

This research attempts to study the effectiveness of ARMI when being applied to less-technical groups of stakeholders. Seventeen postgraduate students on a master degree on logistics and supply chain management participated in the experiment, using the standard rules. Only one of them had some real experience in information system development, as a web developer. Others know about technologies and general knowledge on information systems but not from the development perspective. Prior to the simulation, the students were asked to anonymously rate each risk, on a scale of 1 to 5, for their overall probabilities and impacts on information system development project. Their perceived risk exposures were recorded and ranked. After the simulation, the students were asked to retake the survey. Some additional questions on their opinion towards the simulation was also inquired. Then, the results were comparatively analyzed and interpreted.

RESULTS AND DISCUSSION

Table 1 and Fig. 1 summarize risk exposures of the selected risks from the pre and post survey as well as their ranks.

Table 1 Risk exposures of the selected risks from the pre and post survey

Risk	Pretest		Posttest	
	RE	#	RE	#
Scope creep	15.1	1	23.1	1
Delay of schedule	14.5	2	21.4	2
Cost escalation	13.2	4	20.3	3
Lack of ex. commun.	13.3	3	17.2	4
Conflict b/w staffs	10.8	20	15.9	5
High number of defects	12.9	6	15.8	6
Low stability of tech.	11.9	11	14.8	7
Missing of payment	13.1	5	14.7	8
Conflict b/w stakehold.	11.9	12	14.7	9
Inaccurate req. analysis	11.2	16	14.7	10
Staff turnover	9.2	24	14.4	11
Inappropriate design	12.6	9	14.2	12
Inexperienced staff	11.8	13	14.1	13
Lacks of user involve.	12.8	7	13.8	14
Incompat. to the legacy	11.5	14	13.8	15
Unable to fulfill obj.	10.9	17	13.6	16
Unable to integrate	11.5	15	13.5	17

Inefficient management	12.8	8	13.3	18
Low soft. performance	10.8	19	13.2	19
Inadequate facilities	10.5	21	13.2	20
Lacks of exec. Involve.	10.4	22	12.6	21
Lacks of user IT skills	12.3	10	11.9	22
User resistance	10.9	18	11.1	23
Inadequate staffing	9.7	23	10.6	24
Increased users	8.4	25	8.6	25

Note: RE = Risk Exposure; # = Risk Rank

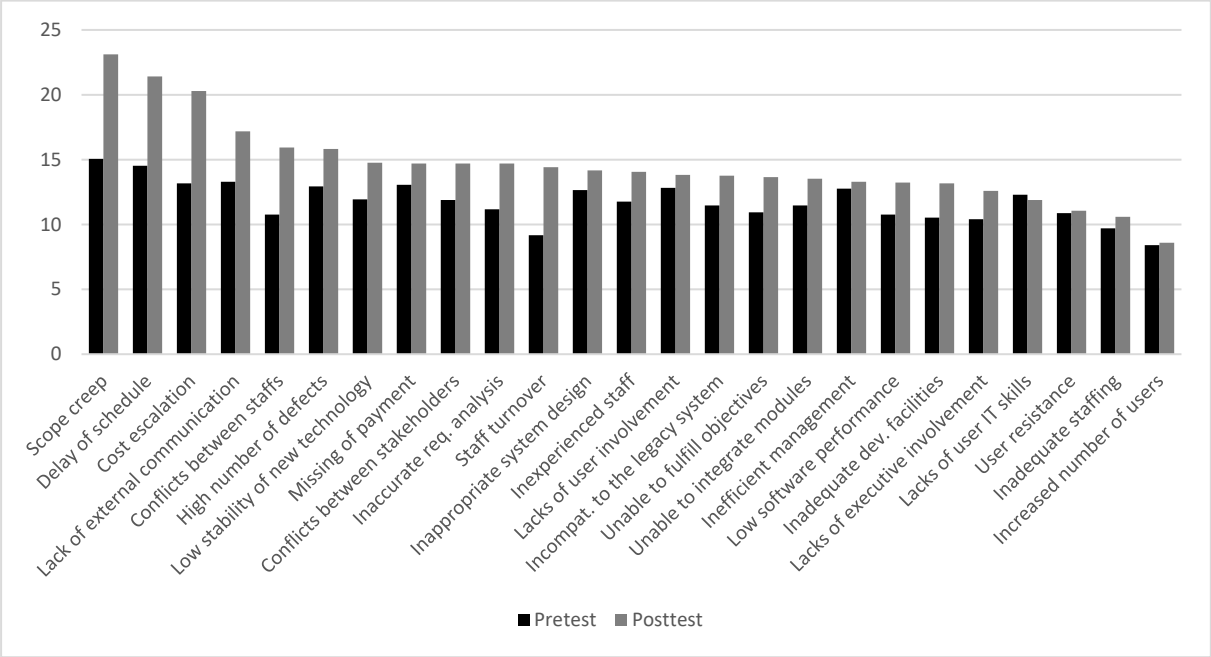

Fig. 1 Risk exposures of the selected risks from the pre and post survey.

It can be seen from Table 1 that, although the order of the top four perceived risks remains almost the same, several changes can be found in the lower ranked risks. Some of these changes are significant. Few notable mentions include the plunge in ranking of incompatibility to the legacy system (from 7th to 14th), user resistance (from 8th to 18th) and lacks of executive involvement (from 10th to 22nd). On the other hand, sharp rises in rankings are found in missing of payment from clients (from 20th to 5th), lacks of user involvement (from 11th to 7th) and lacks of user IT skills (from 16th to 10th). As previously denoted, all of these changes reflects the materialized risks during the simulation. Since the risks were randomly drawn during the simulation, some of them unexpectedly materialized while other of them did not. Likewise, some of them had more impact than the participants' anticipation while other of them did not cause much problems to the project. As a result, the more often the risk occurs, the higher scores they earn at the posttest. Among these, the missing of payment from clients is exceptional. Although it only occurred once during the entire simulation, this risk brought the highest loss on the project. One of the team almost went bankrupt from this single risk because they failed to mitigate. This scenario alone proves that the simulation can effectively moderate the perception of the participants. Further customization to specific environment can help bridging the perception of the project stakeholders.

Another major difference between the pretest and posttest is the degree of risk exposures. Figure 1 reveals that the exposures of most risks are significantly higher in the posttest. This suggests that the participants become more aware on each risk than before the simulation. Certain risks which were frequently materialized in the workshop, such as scope creep, delay of schedule and cost escalation, become major concerns for the students.

Table 2 further investigates the differences between pretest and posttest's perceptions. One-way ANOVA is used to compare the means of each risk exposure. Five significances are found between the means of pretest and posttest's risk exposures. This further fortifies that although the ranks of the top risks remain approximately the same after the simulation, participants became much more concern with them. At a p level of 0.05, it can be seen that means of scope creep, delay of schedule, cost escalation, conflicts between internal staffs and staff turnover between the pretest and the posttest are significant. This is a direct result from the quantity of risk cards drawn during the simulation.

Anonymous feedbacks from the participants suggested several benefits from the simulation. The players indicated that the simulation is not only educating but also stimulating. They found that the activities encourage communication, team working and exchanging of ideas. However, the participants criticized that although the probabilities of the risks are partly controlled, the materialized item could still be too random. They also suggested that an introducing of some beneficial risks could even improve the depth and strategic facet of the simulation.

Table 2 Comparison on perceptions toward risks from pre and post survey

Posttest Rank	Pretest Rank	Risks	F	Sig.
1 (-)	1	Scope creep	25.428	.000*
2 (-)	2	Delay of schedule	12.553	.001*
3 (↑)	4	Lack of external communication	3.405	.074
4 (↓)	3	Cost escalation	14.354	.001*
5 (↑)	20	Missing of payment from clients	.605	.443
6 (-)	6	High number of defects	1.682	.204
7 (↑)	11	Lacks of user involvement	.209	.650
8 (↓)	5	Inefficient management	.073	.789
9 (↑)	12	Inappropriate system design	.411	.526
10 (↑)	16	Lacks of user IT skills	.050	.824
11 (↑)	24	Low stability of new technology	2.130	.154
12 (↓)	9	Conflicts between stakeholders	1.617	.213
13 (-)	13	Inexperienced staff	2.169	.151
14 (↓)	7	Incompatibility to the legacy system	1.277	.267
15 (↓)	14	Unable to integrate modules	.937	.340
16 (↑)	17	Inaccurate requirement analysis	3.355	.076
17 (↓)	15	Unable to fulfill customer's objectives	2.450	.127
18 (↓)	8	User resistance	.008	.927
19 (-)	19	Low software performance	1.512	.228
20 (↑)	21	Conflicts between internal staffs	6.382	.017*
21 (↑)	22	Inadequate development facilities	2.272	.142
22 (↓)	10	Lacks of executive involvement	1.032	.317
23 (↓)	18	Inadequate staffing	.348	.559
24 (↓)	23	Staff turnover	7.003	.013*
25 (-)	25	Increased number of users	.010	.922

Note :* = Statistically significant at p=0.05, (-) = Unchanged in ranking, (↑) = Increased in ranking, (↓) = Decreased in ranking

When being asked whether they gain new knowledge on information system development from the simulation, the participants denoted that they gain insights on the phases of development, importance and impact of risks, and importance of communication. They also admitted that some of the critical risks were previously unforeseen and they realized that such risks can occur in every phase of the project.

The participants further stated that in the view of risk management, they learned the importance of each activity. Moreover, they acknowledged that appropriate management of risk could yield more benefits and losses. In addition, they realized that "learning" is the most important phase in risk management.

CONCLUSION

One major challenge of information system development is the gap between technical and management stakeholders. This is due to different perspectives and lack of knowledge on the nature of the project. Bridging this gap could be an efficient strategy to increase the success rate.

This research attempts to implement a risk management simulation which was originally for technical staff on the management counterpart. This includes seventeen postgraduate students on logistics and supply chain management from Chiang Mai University, Thailand. Most of them have little to none experience on actual software development. The results are analyzed from their pretest, posttest

risk analysis as well as an anonymous questionnaire at the end of the session.

Statistical analyses reveal several interesting findings from the simulation. Firstly, the risk exposures from the posttest are generally higher than those from the pretest. This indicates the growing caution on the participants' perceptions. Some of these changes are statistically significant. Further analysis reveals that there are many changes in ranking of the risks between the pretest and posttest. This reflects the effectiveness of the controlled elements in the simulation.

The participants denote in the questionnaire that they experience several key learning points from the simulation. This includes the nature of information system development, its risks, as well as the importance of each risk management processes. These results suggest that implementing the simulation could be a strategic step to bridge the gap between stakeholders and thus lead to improving rate of success in information system development projects.

REFERENCES

[1] Rainer RK, Prince B, and Cegielski CG, Introduction to Information Systems: Supporting and Transforming Business. 2013.

[2] Ives B and Learmonth GP, "The Information System as a Competitive Weapon," Commun. ACM, vol. 27, no. 12, pp. 1193–1201, 1984.

[3] The Standish Group International, "CHAOS Report 2015," 2015.

[4] Project Smart, "The Standish Group Report CHAOS," 2014.

[5] Lessard DR and Miller R, "Understanding and Managing Risks in Large Engineering Projects," Int. J. Proj. Manag., vol. 19, no. 8, pp. 437–443, 2001.

[6] Sonchan P and Ramingwong S, "Top Twenty Risks in Software Projects: A Content Analysis and Delphi Study," in 2014 11th International Conference on Electrical Engineering/Electronics, Computer, Telecommunications and Information Technology, ECTI-CON 2014, 2014.

[7] Gibson D, Managing Risk In Information Systems. 2010.

[8] Bowers J and Khorakian A, "Integrating Risk Management in the Innovation Project," Eur. J. Innov. Manag., vol. 17, no. 1, pp. 25–40, 2014.

[9] Gualandris J, Klassen RD, Vachon S, and Kalchschmidt M, "Sustainable Evaluation and Verification in Supply Chains: Aligning and Leveraging Accountability to Stakeholders," J. Oper. Manag., vol. 38, pp. 1–13, 2015.

[10] Ramingwong S and Ramingwong L, "ARMI: A Risk Management Incorporation," in 2014 11th International Conference on Electrical Engineering/Electronics, Computer, Telecommunications and Information Technology, ECTI-CON 2014, 2014.

[11] Khatavakhotan AS and Ow SH, "Development of a Software Risk Management Model using Unique Features of a Proposed Audit Component," Malaysian J. Comput. Sci., vol. 28, no. 2, 2015.

[12] Sommerville I, Software Engineering, 10th ed. Pearson, 2015.

[13] Vermaat ME, Sebok SL, Freund SM, Campbell JT, and Frydenberg M, Discovering Computers. Cengage Learning, 2016.

[14] Cantor MR, Klinger EDT, Stanley MJrS, and Tarr PL, "Method and System for Estimating the Progress and Completion of a Project Based on a Bayesian Network," 20160004982, 2016.

[15] Kemerer CF and Sosa GL, "Systems Development Risks in Strategic Information Systems," Inf. Softw. Technol., vol. 33, no. 3, pp. 212–223, 1991.

[16] Addison T, "E-commerce Project Development Risks: Evidence from a Delphi Survey," Int. J. Inf. Manage., vol. 23, no. 1, pp. 25–40, 2003.

[17] Latif R, Abbas H, Assar S, and Ali Q, "Cloud Computing Risk Assessment: A Systematic Literature Review," Lect. Notes Electr. Eng., vol. 276, pp. 285–295, 2014.

[18] Qassim AA, "Why Information Systems Projects Fail: Guidelines for Successful Projects," 2008.

[19] Han WM and Huang SJ, "An Empirical Analysis of Risk Components and Performance on Software Projects," J. Syst. Softw., vol. 80, no. 1, pp. 42–50, 2007.

Second International Conference on Science, Engineering & Environment,
Osaka City, Japan, Nov.21-23, 2016, ISBN: 978-4-9905958-7-6 C3051

ENHANCED PHOTOCATALYTIC DEGRADATION OF PHENOL BY NEODYMIUM-DOPED ZINC OXIDE HIERARCHICAL MICRO/NANOSPHERES UNDER FLUORESCENT LIGHT IRRADIATION

Jin-Chung Sin[1], Sze-Mun Lam[2] and Abdul Rahman Mohamed[3]
[1]Department of Petrochemical Engineering, Faculty of Engineering and Green Technology, Universiti Tunku Abdul Rahman, Perak, Malaysia.
[2]Department of Environmental Engineering, Faculty of Engineering and Green Technology, Universiti Tunku Abdul Rahman, Perak, Malaysia.
[3]School of Chemical Engineering, Universiti Sains Malaysia, Pulau Pinang, Malaysia.

ABSTRACT

There are growing concerns about the increasing trends of emerging phenols in the environment due to their potential negative impacts on natural ecosystems and humans. The photocatalytic degradation of phenol was studied in aqueous solution using neodymium-doped ZnO hierarchical micro/nanospheres (Nd/ZnO). The catalysts were prepared using a facile and surfactant-free chemical precipitation method with zinc nitrate hexahydrate and neodymium nitrate hexahydrate as precursors. The products were characterized by X-ray diffraction, field-emission scanning electron microscopy, energy-dispersive X-ray spectroscopy, transmission electron microscopy, high-resolution transmission electron microscopy, UV–visible diffuse reflectance spectroscopy, nitrogen adsorption-desorption and photoluminescence spectroscopy. The results showed that the as-prepared products were well-crystalline and accumulated by large amount of interleaving nanosheets. It was also observed that the Nd doping improved the light absorption ability of the catalysts and increased the separation efficiency of electron-hole pairs. The photocatalytic studies revealed that the Nd/ZnO exhibited excellent photocatalytic degradation of phenol compared with the pure ZnO, ZnO nanorods (ZNRs) and commercial TiO_2 under fluorescent light irradiation. The photocatalytic enhancement of Nd/ZnO products was attributed to the high charge separation efficiency and hydroxyl radical generation ability as evidenced by the photoluminescence spectra. By using several radical scavengers, hydroxyl radical was determined to play pivotal role for the phenol degradation. In addition, the photocatalytic studies also showed that the effects of initial phenol concentration, solution pH and light sources exerted their individual influence on the phenol degradation.

Keywords: ZnO, Neodymium, Phenol, Hierarchical, Photocatalysis

INTRODUCTION

Water pollution is a serious problem experienced by nations throughout the developed and developing countries. In the last few decades, the contamination of water bodies due to organic pollutants including phenols, dyes and pesticides has considerably increased in view of global industrialization and increasing human population. Phenol is an endocrine disrupting chemical which is produced worldwide in millions of tons each year and widely used in manufacturing of resins, insulation panels, pesticides, paints and lubricants. Widespread occurrences of phenol in surface waters have been reported at concentrations up to 7.8 μg/L [1]. Numerous studies have demonstrated positive results on the increased chromosome aberrations in spermatogonia and primary spermatocytes of mice treated with phenol solution [2]. The semiconductor-mediated photocatalysis reaction has become a desirable method to convert the organic pollutants into harmless compounds to eliminate the environmental pollution. ZnO is a promising semiconductor because of its wide band gap, catalytic and photochemical properties along with its low cost [3]. In particular, three-dimensional ZnO hierarchical micro/nanostructures have become a class of attractive materials owing to their peculiar structure and unique properties [3,4]. For example, flower-like ZnO hierarchical microarchitectures have been synthesized with an economical citrate-mediated hydrothermal method and showed excellent ability to remove dye pollutants compared with the other nanostructured ZnO powders of nanoparticles, nanorods and nanosheets [4]. Previous work revealed that the unique hierarchical porous structure of ZnO hierarchical micro/nanospheres offered greater opportunity for the diffusion and mass transportation of organic molecules and reactive radicals in the photodegradation [3]. However, the low quantum yields and the lack of visible light utilization limited its wide applications.

To address this lapse, much efforts have been made to improve the photocatalytic efficiency of ZnO including doping with metal or non-metal ions and coupling with semiconductors [5,6,7]. Recently, some studies have reported that ZnO doping with rare earth ions can produce impurity energy levels within the band gap and expanded its visible light response [5]. Moreover, rare earth doping can produce traps for photogenerated charge carriers and reduced the electron–hole ($e_{cb}^{-}-h_{vb}^{+}$) pairs recombination rate [5,7]. Hitherto, the scientific reports regarding the application of rare earth-doped ZnO hierarchical structure are still lacking and insufficient.

On the basis of the above consideration, this work reports on the synthesis of Nd-doped ZnO hierarchical micro/nanospheres (Nd/ZnO) by a simple chemical solution route without any organic solvent or surfactant. The as-synthesized ZnO products were characterized by different techniques and used for the photocatalytic degradation of phenol under fluorescent light irradiation. The effects of initial phenol concentration, solution pH and light sources on the photocatalytic activities of Nd/ZnO were investigated. The mechanisms of influence on the photocatalytic activity of the Nd/ZnO were also discussed.

EXPERIMENTAL

In the experiment, 5.0 mmol zinc nitrate hexahydrate ($Zn(NO_3)_2{\cdot}6H_2O$) and 0.1 mmol neodymium (III) nitrate hexahydrate ($Nd(NO_3)_3{\cdot}6H_2O$) were dissolved in 80 mL of deionized water. Then 30 mmol NaOH was added into the above solution and stirred continuously for 3 h at room temperature. After stirring, the as-formed precipitates were filtrated, washed with deionized water for several times, dried at 60ºC in air for 12 h and finally calcined at 450ºC in air for 2 h. Pure ZnO was also prepared by the same procedure without the addition of $Nd(NO_3)_3{\cdot}6H_2O$.

The obtained products were characterized by X-ray diffraction (XRD, Philips PW1820 diffractometer), field-emission scanning electron microscopy with energy dispersion X-ray (FESEM-EDX, Quanta FEG 450), transmission electron microscopy (TEM, Philips CM 12), high-resolution transmission electron microscopy (HRTEM, Tecnai 20), UV-vis diffuse reflectance spectroscopy (UV-vis DRS, Perkin Elmer Lambda 35), N_2 adsorption–desorption (Micromeritics ASAP 2020) and photoluminescence spectroscopy (PL, Perkin Elmer Lambda S55).

The photocatalytic experiments were performed as follows: 100 mL of 20 mg/L phenol in the presence of catalysts (100 mg) was exposed to the 55 W compact fluorescent lamp positioned 12 cm away from the vessel after the mixture was magnetically stirred for 1 h in the dark to get the adsorption-desorption equilibrium. The concentration of phenols was determined using a HPLC (Perkin Elmer Series 200) at given time intervals after the ZnO products were centrifuged. Meanwhile, the comparison studies with commercial TiO_2 (100% anatase) and ZnO nanorods (ZNRs) prepared by the solvothermal method [5] were also conducted.

The roles of photogenerated positive charged hole (h_{vb}^{+}), hydroxyl radical (•OH) and superoxide anion radical ($O_2^{\bullet-}$) in the photocatalytic reactions were evaluated by adding 0.2 mM of different scavengers in a manner similar to the above photocatalytic experiment. In a separate experiment, terephthalic acid photoluminescence (TA-PL) probing technique was also used in the detection of •OH. The detailed TA-PL experiment was similar to [6].

RESULTS AND DISCUSSION

Characterization Of The As-synthesized Products

Fig. 1 is the XRD patterns of as-synthesized products. The diffraction peaks in the XRD spectra indicated that the synthesized products had typical hexagonal wurtzite structures and no peaks were detected from any other impurities. The sharp and narrow peaks also showed that the products obtained to be well in a crystallized form. In addition, the XRD pattern of Nd/ZnO showed the shifting of diffraction peaks slightly toward the lower angles, indicating the substitution of Nd partly in the crystalloid of ZnO. Since the ionic radii of Nd^{3+} (0.098 nm) was larger than that of Zn^{2+} (0.074 nm), doping of Nd ion into the ZnO can cause the expansion of ZnO lattice and thus, led to a shift of ZnO peaks to lower angles as also observed by other researchers [7,8].

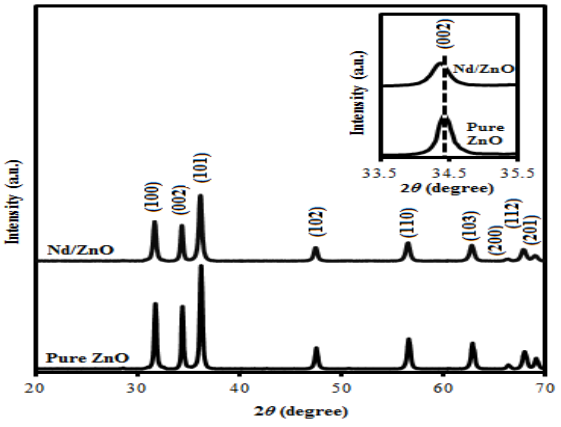

Fig. 1 XRD patterns of pure ZnO and Nd/ZnO. Inset is the magnified region of (002) peak.

The specific surface area of catalysts was determined from nitrogen adsorption-desorption. The specific surface area of the synthesized Nd/ZnO was measured to be 21.0 m^2/g, which was larger than those of the pure ZnO (17.4 m^2/g), ZNRs (7.3 m^2/g) and other reported nanostructured ZnO [6,9].

Figs. 2a and b show the FESEM images of the as-synthesized products. It was clear that the synthesized products were spherical shape and had sizes in the range of several hundred nanometers to several micrometers. It can also be seen that the microspheres had hierarchical structure accumulated by lots of interleaving nanosheets with average thickness of ~17 nm. The nanosheets intersected with each other, which resulted in a net-like morphology with porous structure. Furthermore, doping of the ZnO hierarchical micro/nanospheres with Nd did not show any significant effect on the overall morphology. The formation of the hierarchical micro/nanospheres was achieved via a two-stage nucleation-growth process, the details of which could be found in [10]. Further evidence of the formation of Nd/ZnO came from the EDX analysis. The Zn, O and Nd peaks can be easily observed (Fig. 2c). The weak C peak was originated from the supporting carbon tape.

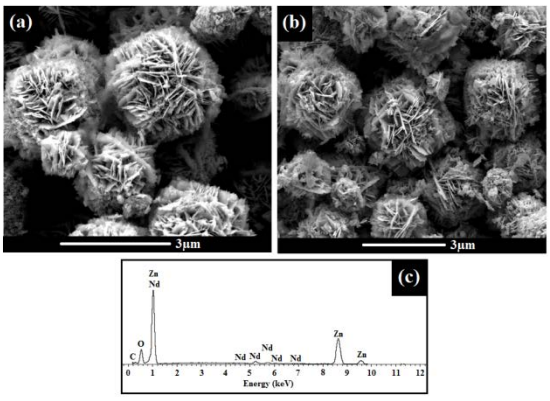

Fig. 2 (a) FESEM image of pure ZnO, (b) FESEM image of Nd/ZnO and (c) EDX spectrum of Nd/ZnO.

Fig. 3a shows the typical TEM image of the synthesized Nd/ZnO. The TEM examination of the as-synthesized products further confirmed the FESEM observations. It was clear from the examined TEM image that the microstructure of the product was consisted of a large number of nanosheets. The HRTEM image in Fig. 3b showed that the ZnO products had very clear lattice fringes with interplanar spacing of 0.26 nm. Moreover, pores were found in the nanosheets, which could be the result of loss of volatile gases during the heat treatment [11]. From the TEM and HRTEM images, it can be confirmed that the synthesized ZnO products have highly crystalline structure, which is essential for excellent photocatalytic materials.

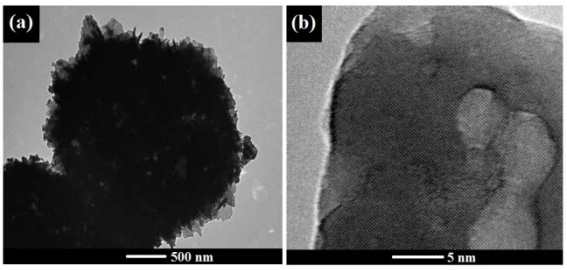

Fig. 3 (a) TEM and (b) HRTEM images of Nd/ZnO.

Fig. 4a shows the UV–vis DRS spectra of the as-synthesized products. It was noticeable that the Nd doping led to red shift in the absorption band and improved the visible light absorption ability of the catalysts. Furthermore, the Nd/ZnO (at 473, 527 and 581 nm) has much absorption bands in agreement with the visible-light absorbability. These peaks were attributed to the Nd characteristic of 4f electron transitions [12]. The optical band gap energies of as-synthesized ZnO products were calculated according to the equation Eg (eV) = $hc/\lambda = 1240/\lambda$ (nm), where Eg is the band gap energy (eV), h is the Planck's constant (4.135667 x 10^{-15} eVs), c is the velocity of light (3 x 10^8 m/s) and λ is the wavelength (nm) of absorption onset [6]. Using the equation, the measured band gap energies of the pure ZnO and Nd/ZnO were 3.26 and 3.18 eV, respectively. The observed narrower band gap of Nd/ZnO was originated from the charge transfer between the ZnO valance band and the Nd ion 4f level [12]. From Fig. 4b, it can be seen that the Nd/ZnO gave lower PL intensity as compared to pure ZnO. A lower PL intensity implied a lower photogenerated $e_{cb}^- - h_{vb}^+$ recombination rate, revealing more photogenerated e_{cb}^- and h_{vb}^+ can participate in the oxidation and reduction reactions. Therefore, the observed PL spectra showed that the radiative recombination was lowered by doping with Nd, leading to weak recombination of photogenerated charge carriers, which will benefit the photocatalytic reaction.

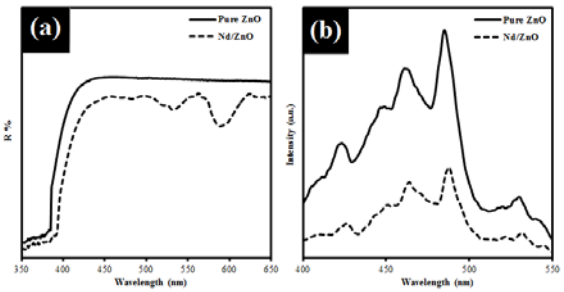

Fig. 4 (a) UV-vis DRS and (b) PL spectra of pure ZnO and Nd/ZnO.

Photocatalytic Activity

Fig. 5 shows the photocatalytic activities of the as-synthesized ZnO products towards phenol degradation. The blank tests revealed that the removal of phenol under dark adsorption and phenol photolysis were extremely slow. However, in the presence of photocatalysts and light irradiation, 61.8% of phenol degraded by pure ZnO within 300 min irradiation, whereas only 48.8% and 39.7% degradation were obtained for ZNRs and commercially available TiO_2, respectively at the same duration. The high photocatalytic activity of the synthesized ZnO hierarchical micro/nanospheres can be attributed to the unique hierarchical porous surface and large surface area, thus increasing the surface activation sites available to participate in the photocatalytic degradation of phenol. When the Nd/ZnO was used under the same conditions, 90.6% degradation occurred. This demonstrated the promoting effect of Nd modification that was beneficial to charge separation and agreed well with the results of PL spectra. The mechanism for the photocatalytic enhancement of Nd/ZnO will also be discussed in detail below.

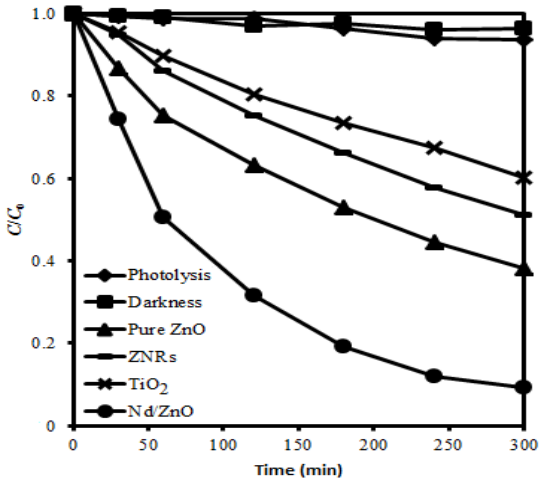

Fig. 5 Photocatalytic degradation of phenol using different catalysts under fluorescent light ([Phenol] = 20 mg/L; catalyst amount =100 mg; pH 5.6).

The effect of initial substrate concentration for the degradation of phenol on Nd/ZnO was studied over a range of 20 mg/L to 80 mg/L. Fig. 6a shows that the degradation efficiency decreased with an increase in the concentration of phenol. The degradation efficiency related to the active species formation on catalyst surface and probability of active species reacting with phenol molecules. The increase of phenol concentration can occupy a greater number of active sites of photocatalysts, which then suppressed the generation of the active species and resulted in lower degradation efficiency. Furthermore, the increase in phenol concentration also decreased the path length of photon entering into the phenol solution and this can essentially reduce the degradation efficiency of phenol when high concentrated phenol was used [5].

The effect of solution pH on photocatalytic degradation of phenol was studied in the pH range of 3.0 to 10.0 (Fig. 6b). The range covered the pH at point of zero charge (pzc) of Nd/ZnO measured by zeta potential (Fig. 6c) and pKa of phenol which were 8.7 and 7.9, respectively. Here, pH 5.6 was the pH value of phenol solution in deionized water without using any pH adjustor. The pH of the suspension was adjusted by adding small amount of equimolar H_2SO_4 or NaOH before irradiation and it was not controlled during the course of the reaction. It was observed that the unadjusted phenol solution was the best pH for the degradation process using the Nd/ZnO. The interpretation of pH effects on the efficiency of the photocatalytic process is an intricate task since it has multiple roles. First, dissociation ions from pH adjustors could create competition with the phenol molecules on the surface of catalyst. It was noted that in acidic condition, SO_4^{2-} ions from H_2SO_4 might have been adsorbed on the surface of catalyst and decreased the phenol degradation [13]. On the other hand, in alkaline condition, the competitive adsorption of the ions from NaOH salt might also result in lower photocatalytic activity [5]. In addition, both photocatalyst and phenol at higher pH were negatively charged, developing repulsive forces between them and opposed the degradation of phenol. For pH 5.6, the electrostatic attraction between positively charged synthesized photocatalysts with molecular form of phenol molecules led to a maximum degradation efficiency of phenol.

Plot of photocatalytic degradation of phenol under fluorescent light and natural sunlight irradiation as a function of time is presented in Fig. 6d. The photocatalytic degradation efficiency of phenol was higher under natural sunlight than under fluorescent light. At 30 min of reaction time using Nd/ZnO, maximum degradation of phenol under sunlight and fluorescent light were found to be 100% and 25.6%, respectively. However, with pure ZnO, 62.7% and 13.2% degradation was obtained under sunlight and fluorescent light, respectively at the same duration. Above results revealed that the Nd/ZnO synthesized by this facile method was promising for practical applications in environmental cleanup and solar energy conversion.

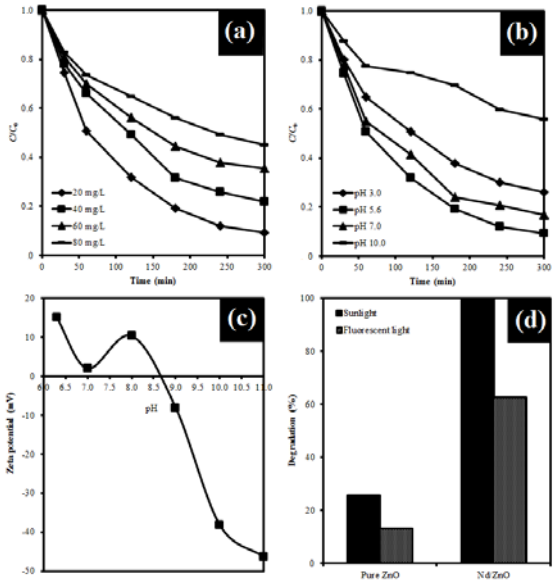

Fig. 6 (a) Effect of initial substrate concentration on photocatalytic degradation of phenol over Nd/ZnO (catalyst amount = 100 mg; solution pH = 5.6). (b) Effect of solution pH on photocatalytic degradation of phenol over Nd/ZnO ([Phenol] = 20 mg/L; catalyst amount = 100 mg). (c) Zeta potential analysis of Nd/ZnO as a function of pH. (d) Effect of variation of light source on photocatalytic degradation of phenol over Nd/ZnO ([Phenol] = 20 mg/L; catalyst amount =100 mg; solution pH = 5.6).

Possible Mechanism Of Phenol Degradation Over Nd/ZnO

In general, photogenerated active species including h_{vb}^+, •OH and $O_2^{\bullet-}$ were involved in the photocatalytic process. Therefore, the effects of different scavengers on the degradation of phenol were investigated in an attempt to elucidate the photocatalytic mechanism. In this study, sodium iodide (NaI), ethanol and *p*-benzoquinone (BQ), were adopted as the scavengers of h_{vb}^+, •OH and $O_2^{\bullet-}$, respectively [10]. As a consequence of quenching, the photocatalytic reaction of phenol degradation will be suppressed. The extent of decrease in the phenol degradation efficiency induced by the scavenger indicated the importance of the corresponding active species. Fig. 7a shows that the photocatalytic degradation of phenol was significantly suppressed when ethanol was added into the reaction system. The degradation of phenol was also suppressed by the addition of NaI and BQ, but it was not as significant as that with ethanol added. Therefore, •OH was the main active species responsible for phenol degradation.

The formation of •OH on the as-synthesized ZnO products was further confirmed by the TA-PL technique. The PL emission spectra of pure ZnO and Nd/ZnO products excited at 315 nm from terephthalic acid solution were measured after 180 min fluorescent light irradiation. The result showed that an obvious PL signal at about 425 nm was observed, revealing that •OH radicals were formed during the photocatalytic reactions, which was consistent with the results in Fig. 7a. The peak intensity of pure ZnO and Nd/ZnO is shown in Fig. 7b. It was clear that the formation rate of •OH on the Nd/ZnO was higher than the pure ZnO. This implied that the former has higher photocatalytic activity than the latter, which also agreed well with the results of PL emission spectra in Fig. 4b. The observed TA-PL result also suggested that the doping of Nd on ZnO was a good route to accelerate the interfacial charge transfer and inhibited the recombination of $e_{cb}^- - h_{vb}^+$ pairs, which resulted in the increase of •OH formation.

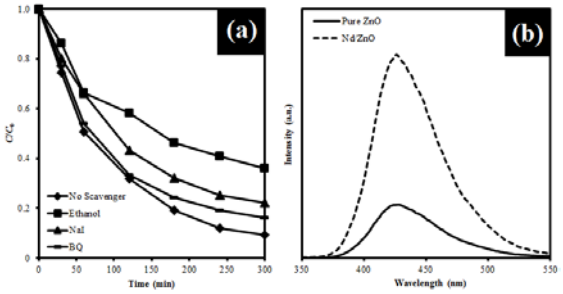

Fig. 7 (a) Effects of different scavengers on degradation of phenol in the presence of Nd/ZnO ([Phenol] = 20 mg/L; catalyst amount =100 mg; pH 5.6) and (b) PL spectra of the aqueous basic solution of terephthalic acid with an excitation at 315 nm for 180 min irradiation under fluorescent light.

Combining our experiment results with the related literatures [5,7,12], a possible mechanism for the enhanced photocatalysis of Nd/ZnO could be proposed in Fig. 8. Under the irradiation, the e_{cb}^- are excited from the valence band to the conduction band of ZnO leaving behind h_{vb}^+. Nd^{3+} doping in ZnO being strong Lewis acid, apparently are superior to the O_2 molecules in the capability of trapping e_{cb}^-. This suggested that the Nd dopant can act as effective electron scavenger to trap the e_{cb}^- and inhibit the recombination with h_{vb}^+. The e_{cb}^- can transfer to the adsorbed O_2 promoting the $O_2^{\bullet-}$ formation and then converted to active •OH. At the same time, the photogenerated h_{vb}^+ can trap on the catalyst surface undergoing charge transfer with adsorbed water molecules or with surface bound hydroxide species to generate active •OH. The •OH radicals have been formed by many semiconductors like TiO_2, ZnO, etc. via effective separation of $e_{cb}^- - h_{vb}^+$ pairs under irradiation [6,12], which can act as strong oxidizing agents to degrade the phenol molecules. Thus, the separation of the charge carriers was attributed to such trapping by Nd

dopant in ZnO. Subsequently, enhanced the yield of •OH quantities in the degradation of phenol, which further improved the photocatalytic activity of Nd/ZnO.

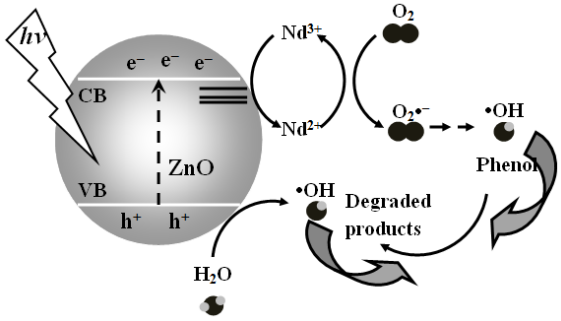

Fig. 8 Possible photocatalytic mechanism of Nd/ZnO.

CONCLUSION

In the absence of any surfactants, neodymium-doped ZnO hierarchical micro/nanospheres (Nd/ZnO) were successfully obtained by a facile chemical precipitation method and confirmed by XRD, FESEM, EDX, TEM, HRTEM, UV-vis DRS, N_2 adsorption-desorption and PL measurements. The investigation of photocatalytic ability showed that the Nd/ZnO exhibited excellent photocatalytic degradation of phenol compared with the pure ZnO, ZNRs and commercial TiO_2 under fluorescent light irradiation. The photocatalytic enhancement of Nd/ZnO was attributed to the high charge separation efficiency and •OH generation ability as evidenced by the PL spectra. Furthermore, the photocatalysis worked best at low pollutant concentration and the optimum solution pH for phenol degradation was found to be 5.6. The Nd/ZnO also exhibited high degradation ability of phenol under sunlight, showing great potential for practical applications in sunlight photocatalysis.

ACKNOWLEDGEMENTS

This work was supported by Universiti Tunku Abdul Rahman (UTARRF/2015-C1/L02 and UTARRF/2015-C1/S04) and Ministry of Higher Education of Malaysia (FRGS/1/2015/TK02/UTAR/02/2).

REFERENCES

[1] Schmidt-Bäumler K, Heberer Th, Stan HJ, "Occurrence and Distribution of Organic Contaminants in the Aquatic System in Berlin.Part II: Substituted Phenols in Berlin Surface Water", Acta Hydrochim. Hydrobiol., Vol. 27, 1999, pp. 143–149.

[2] Fawell JK, Hunt S, Environmental Toxicology: Organic Pollutants. Chichester: Ellis Horwood Limited, 1988.

[3] Sin JC, Lam SM, Lee KT, Mohamed AR, "Self-assembly fabrication of ZnO hierarchical micro/ nanospheres for enhanced photocatalytic degradation of endocrine-disrupting chemicals", Mater. Sci. Semicond. Process., Vol. 16, 2013, pp. 1542–1550.

[4] Lu HB, Wang SM, Zhao L, Li JC, Dong BH, Xu ZX, "Hierarchical ZnO microarchitectures assembled by ultrathin nanosheets: hydrothermal synthesis and enhanced photocatalytic activity", J. Mater. Chem., Vol. 21, 2011, pp. 4228–4234.

[5] Sin JC, Lam SM, Lee KT, Mohamed AR, "Preparation and photocatalytic properties of visible light-driven samarium-doped ZnO nanorods", Ceram. Int., Vol. 39, 2013, pp. 5833–5843.

[6] Lam SM, Sin JC, Abdullah AZ, Mohamed AR, "Transition metal oxide loaded ZnO nanorods: preparation, characterization and their UV–vis photocatalytic activities", Sep. Purif. Technol., Vol. 132, 2014, pp. 378–387.

[7] Yayapao O, Thongtem T, Phuruangrat A, Thongtem S, "Ultrasonic-assisted synthesis of Nd-doped ZnO for photocatalysis", Mater. Lett., Vol. 90, 2013, pp. 83–86.

[8] Yayapao O, Thongtem T, Phuruangrat A, Thongtem S, "Sonochemical synthesis of Dy-doped ZnO nanostructures and their photocatalytic properties", J. Alloy. Compd., Vol. 576, 2013, pp. 72–79.

[9] Gu CP, Huang JR, Wu YJ, Zhai MH, Sun YF, Liu JH, "Preparation of porous flower-like ZnO nanostructures and their gas-sensing property", J. Alloy. Compd., Vol. 509, 2011, pp. 4499–4504.

[10] Sin JC, Lam SM, Lee KT, Mohamed AR, "Preparation of cerium-doped ZnO hierarchical micro/nanospheres with enhanced photocatalytic performance for phenol degradation under visible light", J. Mol. Catal. A: Chem., Vol. 409, 2015, pp. 1–10.

[11] Liu SW, Li C, Yu JG, Xiang QJ, "Improved visible-light photocatalytic activity of porous carbon self-doped ZnO nanosheet-assembled flowers", CrystEngComm, Vol. 13, 2011, pp. 2533–2541.

[12] Štengl V, Bakardjieva S, Murafa N, "Preparation and photocatalytic activity of rare earth doped TiO_2 nanoparticles", Mater. Chem. Phys., Vol. 114, 2009, pp. 217–226.

[13] Liang HC, Li XZ, Yang YH, Sze KH, "Effects of dissolved oxygen, pH, and anions on the 2,3-dichlorophenol degradation by photocatalytic reaction with anodic TiO_2 nanotube films", Chemosphere, Vol. 73, 2008, pp. 805–812.

Second International Conference on Science, Engineering & Environment,
Osaka City, Japan, Nov.21-23, 2016, ISBN: 978-4-9905958-7-6 C3051

TRANSITION METAL OXIDE (WO_3, CuO, Nb_2O_5)-LOADED ON ZnO NANORODS WITH ENHANCED VISIBLE-LIGHT CATALYTIC ACTIVITY IN ERASURING PHENOL

Sze-Mun Lam[1], Jin-Chung Sin[2], Abdul Rahman Mohamed[3]
[1] Department of Environmental Engineering, Faculty of Engineering and Green Technology, Universiti Tunku Abdul Rahman, Jalan Universiti, Bandar Barat, 31900 Kampar, Perak, Malaysia.
[2] Department of Petrochemical Engineering, Faculty of Engineering and Green Technology, Universiti Tunku Abdul Rahman, Jalan Universiti, Bandar Barat, 31900 Kampar, Perak, Malaysia.
[3] School of Chemical Engineering, Universiti Sains Malaysia, Engineering Campus, 14300 Nibong Tebal, Pulau Pinang, Malaysia.

ABSTRACT

Over the years, the surge of industrial activities that inevitably resulted in an increasing flux of pollutants in the environment still remains an intricate challenge for nations. Heterogeneous photocatalysis, particularly on transitional metal oxide loaded on one dimensional (1D) ZnO nanorods (ZNRs) as promising heterostructured photocatalysts were employed to treat a recalcitrant pollutant, namely phenol. In this study, ZNRs have been prepared using a hydrothermal method and different transition metal oxides (WO_3, CuO and Nb_2O_5) were loaded on the photocatalysts using a co-precipitation method. The samples were characterized by X-ray diffraction, transmission electron micrograph, high resolution transmission electron micrograph, energy dispersive X-ray analyzer, UV-vis diffuse reflectance spectra, surface analytical method and photoluminescence spectra. The results showed that the crystallized transition metal oxide-loaded ZNRs had a hexagonal phase with the respective transition metal oxides being attached on ZNRs. The photoabsorption of the transition metal oxide-loaded ZNRs were responsive to visible light. The photocatalytic activity of transition metal oxide-loaded ZNRs towards phenol degradation under visible light irradiation were investigated and compared with pure ZNRs. The reactivity was in the order of WO_3 > Nb_2O_5 > CuO. The different photoreactivities were ascribed to the combine effects of relative energy band position of metal oxides and predominant oxidation species generated in the photocatalysis. It was worth nothing that the cooperative photocatalytic mechanism of the transition metal oxides-loaded ZNRs was also discussed.

Keywords: Transition metal oxide, ZnO Nanorod, Photocatalysis, Phenol

INTRODUCTION

Phenol is widely used as a monomer for the manufacture of disinfectants, fertilizers, explosives, lubricants, rubbers, textiles and plastic plasticizers [1]. During product manufacturing and wasteland filling, the phenol chemicals easily migrate and make their way into the surface water bodies, groundwater and soils. In Malaysia, the main sources of phenol pollution has been identified as effluents from rubber processing factories, timber sawmills, motor and battery workshops, engineering workshops and pig farms areas (0.8–53.6 μg/L) [2]. For example in the Seremban municipality, the level of phenols in the Linggi River exceeded the recommended Malaysian standard of 2.0 μg/L for raw water [2]. Since phenol is termed recalcitrant pollutant, one relevant challenge for science concerns to the study and the development of pollution-degradation strategies is indispensable.

In recent years, heterogeneous photocatalysis has been emerged as a potential technology because it presents 'green' treatment approach since toxic organic pollutants are converted into carbon dioxide and water using light energy. Zinc oxide (ZnO) as one of the most extensively investigated photocatalysts has been shown relatively high catalytic efficiency, low cost, non-toxicity and environmental stability [3]. Nevertheless, owing to its large band gap (~3.3 eV), ZnO is mostly responsive to UV irradiation, which greatly impedes its practical applications. Additionally, the lack of effective surface area and low transfer rate of charge carriers also limit the photocatalyst developments.

The photocatalytic activity of ZnO has been improved by various techniques such as modification of ZnO by structural morphology, non-metal doping, addition of transition metals as well as use of coupled semiconductors [3–5]. To date, various ZnO has been synthesized with variety of well-defined nanostructures with various morphologies including nanorods, nanowires, nanosheets, nanobelts and nanotubes [3]. Our previous reports have also demonstrated that the

morphologies of the ZnO nanostructures can greatly affect their effective surface areas, their interaction with organic molecules, their photodegradation capability of organic molecules and consequently the whole photocatalytic activities [6,7]. However, structural morphology modification is still not satisfactory, which can be attributed to short e^-–h^+ pair lifetime. To further improve its photocatalytic activity, semiconductor coupled with ZnO photocatalysts has been proposed. The coupled semiconductor materials have two different energy-level systems which play an important role in achieving charge carrier separation. Coupling of different transition metal oxides could reduce the band gap, extending the absorbance range to visible light region and thus, leading to e^-–h^+ pair separation under irradiation [8,9].

In the present study, three different transition metal oxides (WO_3, CuO and Nb_2O_5)-loaded ZNRs photocatalysts were prepared via a hydrothermal-precipitation method and their photocatalytic performance was tested by phenol degradation under visible light irradiation. The relationship between the photocatalytic activities and the structural features of the prepared catalysts were investigated through various systematic characterization analyses. The cooperative photocatalytic mechanism by which transition metal oxides enhanced photocatalytic activities was also discussed.

EXPERIMENTAL

In a typical procedure, 2.0 g of ZnO powder (Acros Organics) was weighted into Teflon-lined stainless steel autoclave of 200 mL capacity. Then, 150 mL of 30 vol % H_2O_2 solution was added in with stirring. The autoclave was sealed and maintained at a temperature of 180 °C for 24 h and then allowed to cool to room temperature naturally. The as-formed precipitates were filtrated, washed with deionized water (DI) and ethanol for several times and finally dried in air. 1.0 g of prepared ZNRs was dispersed in 50 mL DI and the suspension was ultrasonicated for 30 min. Subsequently, 0.24 mmol of $(NH_4)_6{\cdot}(H_2W_{12}O_{40}){\cdot}nH_2O$ or $Cu(NO_3)_2{\cdot}6H_2O$ or $NbCl_5$ in 0.9 mL of NH_4OH (25 wt.% NH_3) was added to the ZnO suspension and stirred for 12 h. The precipitates were collected by centrifugation, washed with DI and ethanol, dried in air and finally calcined at 400ºC for 2 h.

The obtained product was characterized by X-ray diffraction (XRD, Philips PW1820 diffractometer), transmission electron microscopy (TEM, Philips CM-12), high resolution transmission electron microscopy (HRTEM, Fei Tecnai 20) energy dispersion X-ray spectrum (EDX, Quanta FEG 450) analysis, UV-vis diffuse reflectance spectroscopy (UV–vis DRS, Perkin Elmer Lambda 35) and photoluminescence (PL, Perkin Elmer Lambda 35).

In a typical experiment, 1.0 g L^{-1} of the sample was dispersed in 100 mL of 20 mg L^{-1} phenol solution in a 150 mL beaker. During all experiments, air was bubbled through the solution at a fixed flow rate of 6 mL min^{-1} using an air pump. The suspensions were continuously stirred with the aid of a magnetic stirrer. The heterogeneous mixture was equilibrated for 1 h in the dark. Subsequently, the solution was irradiated under a 55 W compact fluorescent lamp (World Lighting, Germany). The average light intensity striking the surface of the reaction solution was about 14,500 lux as measured by a digital luxmeter. This light was fixed about 12 cm above the reaction solution. At specific time intervals, 2 mL of the sample was withdrawn from the system, centrifuged and then the concentrations of the phenol and products were monitored by HPLC. The detailed photocatalytic process was similar to our previous report [1]. The analysis of hydroxyl radicals (•OH) formation on the sample under visible light irradiation was performed using terephthalic acid with photoluminescence (TA–PL) techniques. Experimental procedures were similar to the measurement of photocatalytic activity except that phenol solution was replaced by the 5×10^{-4} M TA aqueous solution with a concentration of 2×10^{-3} M NaOH solution.

RESULTS AND DISCUSSION

The crystal structure of pure ZNRs and transition metal oxide-loaded ZNRs was examined by XRD as shown in Fig. 1. The XRD pattern revealed sharp peaks, indicating the high degree of crystallinity. The XRD pattern of all samples matched closely with their characteristic peaks according to the data base of the Joint Committee on Powder Diffraction Standards (JCPDS). Hexagonal ZnO (JCPDS 36-1451) [8], monoclinic WO_3 (JCPDS 72-1465) [5], monoclinic CuO (JCPDS 5-0661) [9] and monoclinic Nb_2O_5 (JCPDS 37-1468) [10] were the major phases detected on the XRD patterns. The signals assigned to the respective transition metal oxides were extremely weak and probably due to their amount present too low and dispersed. Moreover, the XRD peaks belonging to ZnO in all the catalysts do not shift compared with the pure ZNRs, implying that the transition metal oxides did not substitute into the ZnO lattices for the Zn.

TEM and HRTEM images of pure ZNRs and transition metal oxide-loaded ZNRs are shown in Fig. 2. As shown in Fig. 2a, pure ZNRs indicated rod-like structures with width ranging from 23–111 nm and their length from several hundred

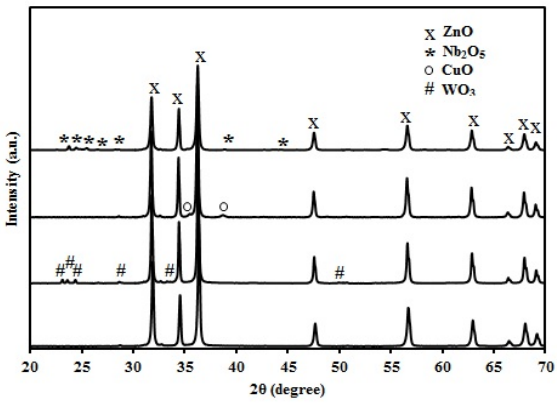

Fig. 1 XRD patterns of the (a) pure ZNRs, (b) 2.0% WO_3/ZNRs, (c, 2.0% CuO/ZNRs and (d) 2.0% Nb_2O_5/ZNRs.

nanometers to micrometers. The HRTEM image in the Fig. 2b shows that the ZNRs have lattice spacing of 0.26 nm, which elongated along the direction of [0001] plane. For loaded ZNRs, it was observed that morphology of ZNRs did not have significant changes after the modification with the studied coupled metal oxides. In addition, spherical-shaped nanoparticles of the coupled metal oxides were observed to be randomly deposited on the surface of the ZNRs. The TEM image of 2.0% CuO/ZNRs shown in Fig. 2c revealed that the CuO nanoparticles were in the particle diameter range of 20–80 nm. The HRTEM image in the Fig. 2d indicated that the individual CuO nanoparticles had clear lattice spacing of 0.27 nm corresponded to the (110) plane of CuO in a monoclinic crystal system. For the 2.0% WO_3/ZNRs (Fig. 2e), the WO_3 nanoparticles had the particle diameter of 27–93 nm. The lattice fringes of 0.37 nm can be attributed to the (020) plane of WO_3 monoclinic phase as shown in the Fig. 2f. On the other hand, the Nb_2O_5 particle diameter in the 2.0% Nb_2O_5/ZNRs (Fig. 2g) was in the range of 40–120 nm. Fig. 4f shows HRTEM image indicated that the lattice spacing of 0.25 nm and can be assigned to (007) plane of Nb_2O_5 monoclinic phase. The clear lattice spacing obtained from the HRTEM image also suggested that the transition metal oxide-loaded ZNRs had highly crystalline structure, which was essential for excellent photocatalytic materials.

The transition metal oxide-loaded ZNRs were also confirmed by energy dispersive X-ray spectroscopy (EDX) (data not shown). The transition metal oxide-loaded ZNRs were composed of the Zn, O and a small amount of transition metal (W, Cu and Nb) elements. These results showed that each considered metal oxides were indeed present in the catalysts.

The specific surface areas of catalysts were determined and the data are presented in Table 1. When the surface area data of pure ZNRs and

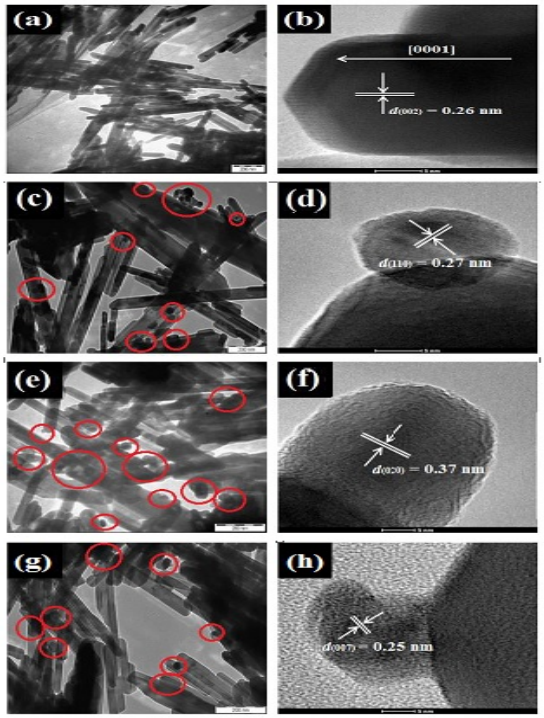

Fig. 2 TEM and HRTEM images of (a–b) pure ZNRs, (c–d) 2.0% CuO/ZNRs, (e–f) 2.0% WO_3/ZNRs and (g–h) 2.0% Nb_2O_5/ZNRs, respectively (recorded from red circle was metal oxide nanoparticles).

transition metal oxide-loaded ZNRs were compared, pure ZNRs was observed to have smaller surface area than the metal oxide loaded catalysts. This was attributed to the presence of metal oxide could produce diminution in the crystallize sizes of ZnO catalysts to a certain degree and consequently increased the surface area of the transition metal oxide-loaded ZNR catalysts. The larger surface area was found for CuO-loaded ZNR catalysts when compared to WO_3- and Nb_2O_5-loaded ZNR catalysts. This implied that finer CuO particles would have been synthesized on the surface of ZNRs.

Fig. 3 shows the UV–vis DRS spectra as a function of wavelength for loaded and pure ZNRs. Compared to pure ZNRs, the transition metal oxide-loaded ZNRs led to a more apparent red-shift with the trailing edges in the region of 385–403 nm. The absorption edges of the transition metal oxide loaded ZNRs showed a red-shift in the order of CuO/ZNRs > WO_3/ZNRs > Nb_2O_5/ZNRs. This red-shift can be attributed to the fact that the different band gap energies of metal oxides involved in the coupling of the ZNRs. Similar findings were also reported in the literatures when different band gap metal oxides were used to couple with ZnO and other photocatalysts [8,9,11]. From the spectra, the band gap values for all the catalysts were calculated using the Plank's formula:

$$E_g = hc/\lambda = 1243.1/\lambda \quad (1)$$

Table 1 BET surface area and band gap for the

synthesized catalysts.

Sample	Bet surface area (m^2/g)	Band gap (nm)
Pure ZNRs	8.53	3.24
CuO/ZNRs	19.69	3.07
WO_3/ZNRs	17.65	3.17
Nb_2O_5/ZNRs	11.45	3.22

where E_g is the band gap energy (eV), h is the Planck's constant (4.135667×10^{-15} eV s), c is the velocity of light (3×10^8 m s^{-1}) and λ is the wavelength (nm) of absorption onset. The results are listed in Table 1. Loading with metal oxides can decrease the band gap of ZNRs. These results implied that the photocatalytic activity of loaded photocatalysts would be better than that of the pure ZNRs with respect to the visible light irradiation.

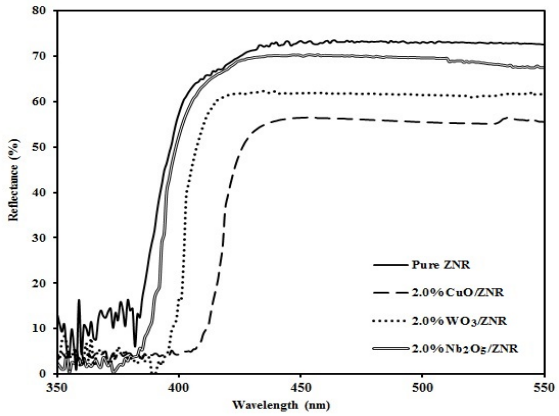

Fig. 3 UV–vis DRS spectra of (a) pure ZNRs, (b) 2.0% WO_3/ZnO, (c) 2.0% CuO/ZNRs and (d) 2.0% Nb_2O_5/ZNRs.

Fig. 4 demonstrates the PL spectra of pure ZNRs and loaded samples. PL spectra patterns of metal oxide-loaded samples indicated the dramatic decrease in emission yield compared to pure ZNRs. The PL emission mainly resulted from the recombination of photogenerated e^-–h^+, thus the lower PL intensity indicated the lower recombination rate of e^-–h^+. Based on the PL results, the order of the photogenerated e^-–h^+ recombination which was as follows: WO_3/ZNRs < Nb_2O_5/ZNRs < CuO/ZNRs < pure ZNRs. Such, it might be deduced that the order of photocatalytic activities of samples was WO_3/ZNRs > Nb_2O_5/ZNRs > CuO/ZNRs > pure ZNRs.

The photocatalytic activities of the all the synthesized WO_3, CuO and Nb_2O_5 loaded ZNRs were examined towards the degradation of phenol and the results are shown in Fig. 5. It can be observed that the degradation of phenol without photocatalysts was only 7.3% after 5 h of irradiation.

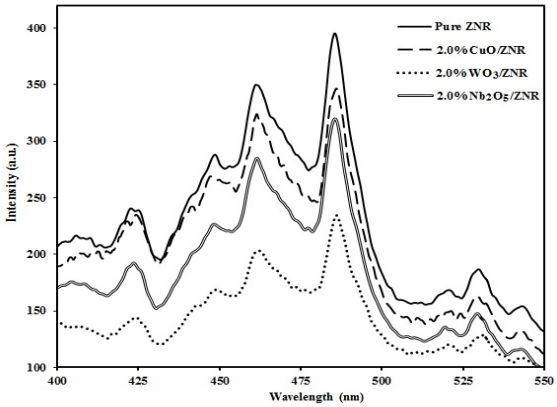

Fig. 4 PL spectra of (a) pure ZNRs, (b) 2.0% WO_3/ZnO, (c) 2.0% CuO/ZNRs and (d) and 2.0% Nb_2O_5/ZNRs.

The degradation of phenol decreased drastically after turning on the fluorescent light. For commercial TiO_2 and pure ZNRs, the degradation percentages reached 50.6% and 57.2%, respectively. Among the transition metal oxide loaded photocatalysts, WO_3/ZNR photocatalysts had the best degradation performance (100%) in 5 h, which was 1.75 times higher than of the pure ZNRs. Nb_2O_5/ZNRs photocatalysts also achieved a high degradation percentage of about 94.3%. For the CuO/ZnO photocatalysts, the percentage was about 88.0%, about 30.8% higher than that of pure ZNRs. The obtained degradation efficiencies were also higher than the previously reported values based on ZnO coupled photocatalysts [5,9]. For example, the degradation efficiency was about 70% within 300 min in Ref. [9] and about 31.5% within 180 min in Ref. [5].

From the results in the photocatalytic activities of transition metal oxide-loaded ZNRs, it was obvious that the relative energy band position between the coupled metal oxides and ZnO was an important factor. For an ideal coupled photocatalysts, Vinu and Madras [4] reported that the redox potential of VB h^+ for both two semiconductors must be sufficiently positive to generate •OH radicals and that of the CB e^- must be sufficiently negative to generate $O_2^{\bullet -}$ radicals. Illustration of the heterojunction structures formed by transition metal oxide-loaded ZNRs based on the estimated CB and VB positions is shown in Fig. 6.

In the WO_3/ZNR heterojunction (Fig. 6a), the CB of the WO_3 (+0.50 V) was positioned more positive side than that of the ZnO (–0.50 V vs. NHE) [5]. With visible light irradiation to this system, both ZnO and WO_3 were excited. The e^- in the CB of ZnO was then transported to the CB of WO_3 because the CB position of WO_3 was lower than that of ZnO. The e^- at both side of ZnO and WO_3 can then induce various reduction reactions to form the $O_2^{\bullet -}$, $HO_2^{\bullet}$ and H_2O_2 as shown in Eqs. (2)–(4) [1,8].

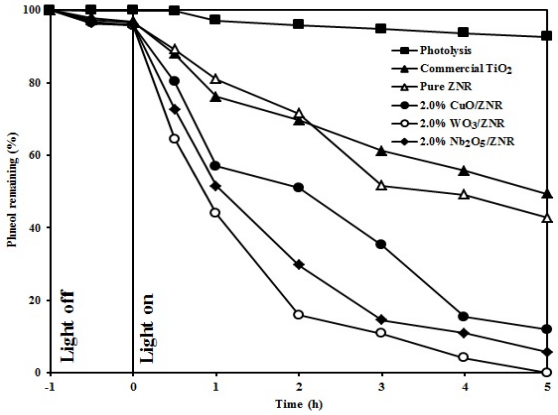

Fig. 5 Time course of the visible light degradation of phenol under different experimental conditions ([phenol] = 20 mg L^{-1}; [catalyst] = 1 g L^{-1}).

$$O_2 + e^- \rightarrow O_2^{\bullet -},\ E_o = -0.33\ V \quad (2)$$

$$O_2 + H^+ + e^- \rightarrow HO_2^{\bullet},\ E_o = -0.046\ V \quad (3)$$

$$O_2 + 2H^+ + 2e^- \rightarrow H_2O_2,\ E_o = +0.682\ V \quad (4)$$

Considering that the CB position of WO_3 was lower than the standard redox potential $E_o(O_2/O_2^{\bullet -})$(–0.33 V vs. NHE) and $E_o(O_2/HO_2^{\bullet})$(–0.046 V vs. NHE), direct *e*– transfer to molecular O_2 to form the $O_2^{\bullet -}$ and $HO_2^{\bullet}$ radicals will be difficult. Thus, the e^- in the CB of WO_3 would be transported to O_2 species via the reactions described in the Eq. (4). The resulted H_2O_2 could then undergo several reactions to produce active •OH radicals to some extent. At the same time, the generated h^+ in the WO_3 VB will be transported to that of ZnO. The h^+ at the VBs of ZnO (2.80 V vs. NHE) and WO_3 (3.30 V vs. NHE) would further produce •OH radicals via the Eqs. (5) and (6) that induced the degradation the phenol molecules [8,11].

$$OH^- + h^+ \rightarrow {}^{\bullet}OH,\ E_o = +1.99\ V \quad (5)$$

$$H_2O + h^+ \rightarrow H^+ + {}^{\bullet}OH,\ E_o = +2.72\ V \quad (6)$$

For the case of CuO/ZNR heterojunction (Fig. 6b), the CB (+0.46 V) and VB (+2.16 V) of the CuO were located between the band gap of ZnO [9]. Under visible light irradiation, both e^- in the ZnO and CuO were excited to their CBs and the e^- in the CB of ZnO transported to the CB of CuO. Here again, the e^- in CuO can only reduce the molecular O_2 to H_2O_2 because the CB level of CuO was positioned with more positive than the standard potential of $E_o(O_2/H_2O_2)$(0.682 V vs. NHE). On the other hand, the h^+ in VB of the ZnO will be transferred to the VB of CuO. The h^+ in the VB of CuO can then oxidize the OH^- groups because of its VB was positioned more negative than the standard redox potential of $E_o(h^+/OH^-)$(+1.99 V vs. NHE). The phenomenon as described in CuO/ZNRs also led to the belief that favoured the increase of charge carriers on the CuO [12].

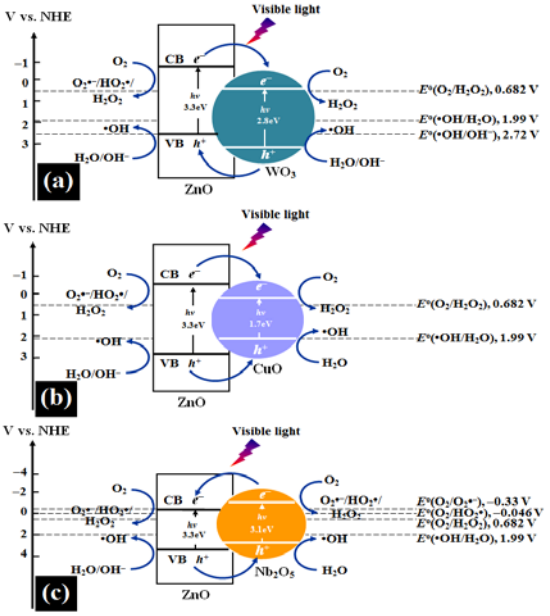

Fig. 6 The schematic profile depicting the energy band structure and occurrence of e^- and h^+ transfer in (a) WO_3/ZNRs, (b) CuO/ZNRs and (c) Nb_2O_5/ZNRs.

In the Nb_2O_5/ZNR heterojunction system (Fig. 6c), the VB of the Nb_2O_5 (–0.60 V) [1] was positioned at a more negative side than that of ZnO VB. With irradiation of visible light to this coupled system, both the ZnO and Nb_2O_5 were excited. In this case, the e^- in the CB of Nb_2O_5 transferred to the CB of ZnO. Meanwhile, the generated h^+ in the ZnO VB will be transported to that of Nb_2O_5 VB. Both the e^- and h^+ then underwent all the reactions shown in Eqs. (2)–(6) (except Eq. (6) for Nb_2O_5) due to the insufficient potential of h^+ at the VB of Nb_2O_5 to oxidize surface adsorbed H_2O to •OH radicals $E_o(h^+/H_2O)$ (2.72 V vs. NHE). It is well known that the oxidation of h^+ with OH^- and H_2O to form •OH radicals was a single-step reaction, whereas the $O_2^{\bullet -}$, $HO_2^{\bullet}$ and H_2O_2 reacted with e^- to produce •OH radicals involved multi-step conversions [3,4]. Thus, this mechanism can describe higher •OH radicals generation for WO_3/ZNR than those of Nb_2O_5/ZNR and CuO/ZNR photocatalysts.

To support the charge carrier transfer at the loaded ZNRs heterostructure interface (as shown in Fig. 6), TA–PL analysis was performed to detect •OH radicals formed on the catalysts. The PL spectra changes observed during the visible light irradiation of the transition metal oxide-loaded ZNRs in the aqueous solution of TA are shown in Fig. 7. Typically, PL intensity at about 425 nm was proportional to the amount of produced •OH radicals [11]. It can be easily seen that all the transition metal oxide-loaded ZNRs showed higher PL intensity than pure ZNRs, suggesting that loading of metal oxide on the surface of ZNRs was a good way to photogenerated charge carriers, which led to the of

accelerate the separation and transfer of the increase •OH radicals formation. Additionally, the amount of •OH radicals produced by the WO_3/ZNRs was larger than that of other transition metal oxide-loaded ZNRs. This result implied that the former has higher photocatalytic activity than the latter, which was also consonant with the results of the PL emission spectra.

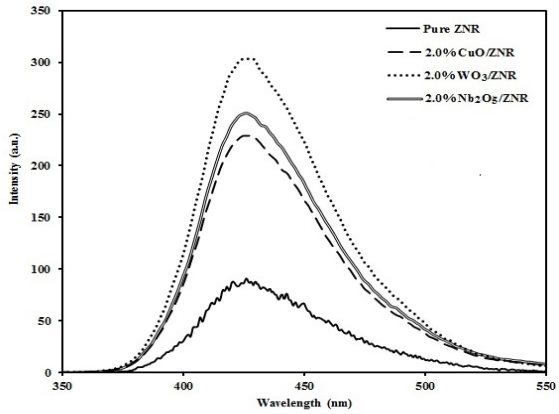

Fig. 7 PL spectra of the TA solution with an excitation at 315 nm under pure ZNRs and transition metal oxide-loaded ZNRs.

CONCLUSION

Tungsten, copper and niobium oxides loaded ZNR catalysts were synthesized successfully by a hydrothermal-precipitation method. XRD, TEM, HRTEM and EDX measurements confirmed the existence of transition metal oxides over ZnO semiconductor surface. It was found that the band gap energies of ZNRs were narrowed by loading with studied metal oxide as estimated using UV–vis DRS spectra. All ZnO samples loaded with transition metal oxides displayed excellent photocatalytic activities toward the degradation of phenol under visible light irradiation. Among the loaded ZNRs, WO_3/ZNRs exhibited the best photocatalytic performance. The enhancement of the photocatalytic activity was mainly brought by the inter-semiconductor e^- and h^+ transfer due to the heterojunction structural as evidenced using PL and PL–TA measurements.

ACKNOWLEDGEMENTS

This work was supported by the UTARRF schemes (UTARRF/2015–C1/L02 and UTARRF/2015–C1/S04) and Fundamental Research Grant Scheme (FRGS/1/2015/TK02/UTAR/02/2).

REFERENCES

[1] Lam SM, Sin JC, Satoshi I, Abdullah AZ, Mohamed AR. "Enhanced sunlight photocatalytic performance over Nb_2O_5/ZnO nanorod composites and the mechanism study", Appl. Catal. A: Gen. Vol. 471, 2014, pp. 126-135.

[2] Abdullah MDP, Nainggolan H. "Phenolic water pollutants in a Malaysian river basin", Environ. Monit. Assess. Vol. 19, 1990, pp. 423-431.

[3] Lam SM, Sin JC, Abdullah AZ, Mohamed AR. "Degradation of wastewaters containing organic dyes photocatalysed by zinc oxide: a review", Desalin. Water Treat. Vol. 41, 2012, pp. 131-169.

[4] Vinu R, Madras G. "Environmental remediation by photocatalysis", Journal of Indian Inst. Sci. Vol. 90, 2010, pp. 189-231.

[5] Chen LC, Tu YJ, Wang YS, Kan RS, Huang CM. "Characterization and photoreactivity of N-, S- and C-doped ZnO under UV and visible light illumination", J. Photochem. Photobiol. A: Chem. Vol. 199, 2008, pp. 170-178.

[6] Lam SM, Sin JC, Abdullah AZ, Mohamed AR. "Green hydrothermal synthesis of ZnO nanotubes for photocatalytic degradation of methylparaben", Mater. Lett. Vol. 93, 2013, pp. 423-426.

[7] Sin JC, Lam SM, Satoshi I, Lee KT, Mohamed AR. "Sunlight photocatalytic activity enhancement and mechanism of novel europium-doped ZnO hierarchical micro/nanospheres for degradation of phenol", Appl. Catal. B: Environ. Vol. 148-149, 2014, pp. 258-268.

[8] Liu W, Wang ML, Xu CX, Chen SF, Fu XL. "Ag_3PO_4/ZnO: An efficient visible-light-sensitized composite with its application in photocatalytic degradation of Rhodamine B", Mater. Res. Bull. Vol.48, 2013, pp. 106–113

[9] Paz DS, Folletto EL, Bertuol DA, John SL, Collazzo GC, Silva SSD, Filho CO. Nascimento CAOD. "CuO/ZnO coupled oxide films obtained by the electrodeposition technique and their photocatalytic activity in phenol degradation under solar irradiation", Water Sci. Technol. Vol. 68, 2013, pp. 1031–1036.

[10] Graca MPF, Meireles A, Nico C, Valente MA, "Nb_2O_5 nanosize powders prepared by sol–gel – Structure, morphology and dielectric properties", J. Alloy Compd. Vol. 553, 2013, pp. 177–182.

[11] Liu W, Wang ML, Xu CX, Chen SF. "Facile synthesis of g-C_3N_4/ZnO composite with enhanced visible light photooxidation and photoreduction properties", Chem. Eng. J. Vol. 209, 2009, pp. 386–393.

[12] Bessekhouad Y, Robert D. Weber JV. "Photocatalytic activity of Cu_2O/TiO_2, Bi_2O_3/TiO_2 and $ZnMn_2O_4/TiO_2$ heterojunctions", Catalysis Today, Vol. 101, 2005, pp. 315–321.

Second International Conference on Science, Engineering & Environment,
Osaka City, Japan, Nov.21-23, 2016, ISBN: 978-4-9905958-7-6 C3051

RELIABILITY ANALYSIS OF REINFORCED CONCRETE SLAB BRIDGES

Ali Mahmoud[1], Shadi Najjar[2], Mounir Mabsout [3] and Kassim Tarhini[4]
[1]Master's candidate, American University of Beirut, Lebanon
Email: aam70@mail.aub.edu
[2]Associate Professor, Dept. of Civil and Envir. Engineering, Amer. Univ. of Beirut, Lebanon.
Email: sn06@aub.edu.lb
[3]Professor, Dept. of Civil and Envir. Engineering, Amer. Univ. of Beirut, Lebanon.
Email: mounir@aub.edu.lb
[4]Professor, Dept. of Civil Engineering, U.S. Coast Guard Academy, New London, CT 06320, USA.
Email: Kassim.M.Tarhini@uscga.edu

ABSTRACT

Empirical expressions for estimating the wheel load distribution and live-load bending moment are typically specified in highway bridge codes such as the AASHTO procedures. The objective of this paper is to assess the reliability levels that are inherent in concrete slab bridges that are designed based on the simplified empirical live load equations in the AASHTO LRFD procedures. To achieve this objective, typical one and two-lane straight bridges with different span lengths were modeled using finite-element analysis (FEA) subjected to HS20 truck loading, tandem loading, and standard lane loading per AASHTO LRFD procedures. The FEA results were compared with the AASHTO LRFD moments in order to quantify the biases that might result from the simplifying assumptions adopted in AASHTO. A reliability analysis was conducted to quantify the reliability index for bridges designed using AASHTO procedures. To reach a consistent level of safety for one lane and two lane bridges, the live load factor in the design equation proposed by AASHTO LRFD needs to be revised by increasing the live load factor to 2.07 for one lane and 1.8 for two lanes. The results will provide structural engineers with more consistent provisions to design concrete slab bridges or evaluate the load-carrying capacity of existing bridges.

Keywords: Concrete Slab Bridges, Finite-Element Analysis, Load-Carrying Capacity, Reliability Analysis.

INTRODUCTION

The design of highway bridges in the United States conforms to the American Association of State Highway and Transportation Officials (AASHTO) Standard Specifications for Highway Bridges (Specs) or AASHTO Load and Resistance Factor Design (LRFD) Bridge Design Specifications [1]-[2]. The analysis and design of any highway bridge must consider live loads such as HS20 (truck or lane) or HL93 (combination of truck or tandem, and lane loading). To analyze and design reinforced concrete slab bridges, AASHTO specifies a distribution width for live loading that simplifies the two-way bending problem into a beam or one-way bending problem. Empirical expressions for estimating the wheel load distribution and live-load bending moment are typically specified in highway bridge codes such as the AASHTO standards. These equations do not take into account the many factors that govern the actual live load such as the transverse position of a truck or tandem on a specific lane, leading to either over-estimation or under-estimation of the live-load bending moment. The objective of this paper is to assess the AASHTO LRFD code provisions used for calculating the bending moment due to live loads. AASHTO provisions tend to either over-estimate or under-estimate the bending moment due to live loads when compared with the resulting maximum bending moment obtained using finite element analysis. In addition, finite element analyses show that by alternating the position of the truck loads transversely, the resulting bending moments tend to increase as the applied live loads come closer to the transverse edge of a bridge (Mabsout et al., 1997; Mabsout et al., 2004) [3]-[4].

Reliability analysis has been proven to be an effective tool for developing and assessing new and existing design codes. AASHTO LRFD code was calibrated to create new load and resistance factors to reach a pre-selected safety target based on a reliability analysis using the basic design Eq. (1) (Nowak,1999) [5]:

$$\sum \gamma_i X_i < \phi R_n \qquad (1)$$

Where γ_i represents a set of load factors that are greater than one and that are applied to the different load effects X_i, while ϕ represents a resistance factor

that is generally less than one and that is multiplied by the nominal resistance R_n.

In the first step in the analysis conducted in this paper, a finite element analysis was performed to evaluate numerically the maximum bending moments of single span, one and two lane bridges, with different span lengths and various slab thicknesses subjected to AASHTO LRFD live loads. Next, the bending moments were calculated using the simplified AASHTO LRFD provisions. The ratio of the FEA moments to the LRFD moments (α_{LL}) was then quantified for the different bridge cases analyzed.

The second step involved defining the statistical characteristics of the different load effects and resistance as per Nowak (1995) [6]. This was followed by a reliability analysis that is aimed at quantifying the reliability levels that are inherent in the traditional LRFD design methodology as per the load and resistance factors that are recommended by AASHTO LRFD. The quantification of the reliability level was accomplished using Monte Carlo simulations whereby the reliability index of the bridge design was evaluated for the different bridges analyzed. The reliability analysis was then repeated while correcting the nominal LRFD live load moments to account for the more representative moments that were obtained from the finite element analysis.

The final step involves proposing modifications to the live load factors of the AASHTO LRFD equation to achieve a target reliability index of 3.5 for all the concrete slab bridges analyzed in this study.

FINITE ELEMENT ANALYSIS

The finite element method was used to investigate the effects of live loads on concrete slab bridges. The bridges are modeled as simply supported slabs divided into shell elements. The size of each shell element is taken to be 1 ft. x 1 ft. The spans length chosen in this study for each bridge are 24, 36, 46, and 52 ft. Lane widths are taken to be 14 ft for a single lane bridge (this takes into account a 1 ft offset on each side) and 24 ft for two-lane bridges. Slab thicknesses are calculated to take into account the deflections.

Live loads are simulated in this analysis as either a combination of HS20 trucks and lane loads, or tandems with lane loads. HS20 loads are taken to be 4 kip point load per tire for the front axles while the middle and rear axles are taken to be 16 kips point load per tire for each axle. The maximum moment developed by the HS20 truck or tandem loads are calculated based on several truck positions. The truck positions are assumed as either centered in each lane or located close to the edge of a lane with a 1 ft of separation distance between the edge of the bridge and the first truck while the separation distance for two side by side trucks are taken to be 4 ft. Figure 1 shows a typical arrangement for HS20 trucks for centered and edge cases, respectively.

Tandem loads were assumed as 4 point loads with a transverse separation distance of 6 ft. and a longitudinal separation distance of 4 ft. Tandem load positions were assumed to be either centered on each lane, or near the edge of a lane with the same separation distances as the HS20 truck load case. Figure 2 shows a typical setup for a tandem load for the centered and edge cases, respectively. Lane loads were assumed to be uniform loads centered in each lane with a magnitude of 640 pounds-ft/ft.

Results from the finite element analysis are presented in Table 1 for all the bridge cases analyzed. Results indicate that the maximum moment based on a combination of tandem loads and lane loads governs in short spans (24 and 36 ft) while the maximum moment found from the combined effect of the HS20 truck loads and lane loads governs in the longer spans. Results also show that the moments that were calculated for the edge loading case are generally larger than the moments calculated for a center loading case. This is applicable for the cases of shorter and longer spans, respectively.

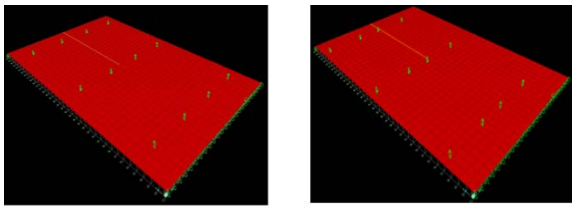

(a) Centered Truck Loading (b) Edge Truck Loading

Fig. 1 Typical Concrete Slab Bridge with Truck Loading.

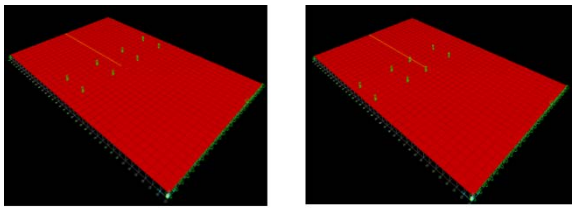

(a) Centered Tandem Loading (b) Edge Tandem Loading

Fig. 2 Typical Two Lane Concrete Slab Bridge with Tandem Loading.

Table 1. FEA Maximum Longitudinal Moment vs AASHTO LRFD Moment

Span length (ft)	Lane	FEA center Kip-ft/ft	FEA edge Kip-ft/ft	LRFD Kip-ft/ft	α_{LL} (FEA/LRFD)
24	One	23.65	24.21	34.95	0.69
36		38.45	39.1	49.44	0.79
46		54.49	56.91	60.68	0.94
54		69.35	72.91	69.84	1.04
24	Two	27.29	29.34	29.97	0.98
36		44.72	47.07	47.85	0.98
46		63.26	67.86	63.19	1.07
54		80.63	86.52	75.82	1.14

To allow for a one to one comparison between the FEA bending moments and the bending moments calculated from the simplified AASHTO LRFD method, the maximum bending moments that were obtained from the simplified method were divided by the equivalent width (E) for each span. The equivalent width could be determined from Eq. (2) and Eq. (3) such that:

$$E = \frac{10 + 5\sqrt{L_1 W_1}}{12} \quad (2)$$

$$E = \frac{84 + 1.44\sqrt{L_1 W_1}}{12} \quad (3)$$

Where:
L_1= span length in ft, the lesser of the actual span or 60 ft and W_1 = edge-to-edge width of bridge in ft taken to be the lesser of the actual width or 60 ft for multi-lane loading, or 30 ft for single-lane loading

In this study and for the purpose of comparison, it was assumed that the largest value of the maximum longitudinal moment governs the span. The maximum bending moments that were calculated using the simplified AASHTO LRFD procedures are presented in Table 1. These results indicate that for a single lane, the moments calculated using the simplified LRFD procedure for shorter spans deviate from the FEA moments for both the centered and edge loading cases. For the case of one lane, the ratio between the FEA moments and the AASHTO moments (α_{LL}) ranges from 0.67 to 1.04. In the case of two lanes, the two moments tend to be closer to each other with α_{LL} range of 0.98 to 1.14.

DESIGN USING AASHTO LRFD

The design of the bridge slab using Eq. (1) (LRFD) requires knowledge about the nominal values of the bending moments due to dead load, live load, and impact load. The nominal bending moment due to dead loads includes the effects of the dead load coming from the slab's own weight (DC) and the weight of the wearing surface above it (DW). To determine the stress due to the own weight of the slab, the thickness of the slab was multiplied by the unit weight of concrete (0.145 kcf as per AASHTO LRFD, table 3.5.1-1). Similarly, the stress due to the wearing surface was calculated as the product of the thickness (0.25 ft) and the unit weight of 0.14 kcf. The nominal bending moment due to the components of the dead load was then determined based on the simply supported moment equation. Table 2 shows a summary of the bending moments determined based on the different dead load components.

The total nominal maximum live load moment (M_{LL+IL}) was calculated as the summation of the static live load moment (M_{LL}) and the dynamic/impact live load (M_{IL}). AASHTO LRFD defines the ratio of the dynamic load allowance as 33% of the static moment of the truck or tandem components of the static live load (M_{LL}) only. To calculate the impact load, the contribution of the truck/tandem load to the static live load was isolated and multiplied by a factor of 0.33. Table 3 shows the values of the static, impact, and total nominal live load moments.

Given the nominal dead load and live load moments, the AASHTO LRFD design Eq. (1) can be applied to calculate the nominal moment resistance (R_n) for each bridge such that:

$$R_n = \frac{(1.25M_{DC} + 1.5M_{DW} + 1.75(M_{LL} + M_{IL})}{0.9} \quad (4)$$

Table 2. Dead Load Moments due to Concrete (DC) and Wearing (WC)

Span length (ft)	Lane	Slab thickness (ft)	Moment DC (kip-ft/ft)	Wearing surface thickness(ft)	Moment DW (kip-ft/ft)
24	One lane	1.5	15.66	0.25	2.52
36		1.75	41.11	0.25	5.67
46		2	76.71	0.25	9.26
54		2.25	118.92	0.25	12.76
24	Two lanes	1.5	15.66	0.25	2.52
36		1.75	41.11	0.25	5.67
46		2	76.71	0.25	9.26
54		2.25	118.92	0.25	12.76

Table 3. Static (M_{LL}) and Dynamic (M_{IL}) Nominal Live Load Moments

Span length (ft)	Lane	Width (ft)	Governing M_{LL} source	M_{LL} (kip-ft/ft)	M_{IL} (kip-ft/ft)	$M_{(LL+IL)}$ (kip-ft/ft)
24	One lane	14	Tandem	34.95	9.84	44.79
36		14	Tandem	49.44	13.13	62.57
46		14	Truck	60.68	18.93	79.61
54		14	Truck	69.84	18.77	88.61
24	Two lanes	24	Tandem	29.97	7.69	37.66
36		24	Tandem	47.85	10.23	58.08
46		24	Truck	63.19	14.71	77.90
54		24	Truck	75.82	14.57	90.39

RELIABILITY ANALYSIS

Monte Carlo simulations were utilized to conduct a reliability analysis for concrete slab bridges that are designed based on the AASHTO LRFD design equation. Failure was defined using the performance function shown in Eq. (5).

$$g = R - DC + DW + (LL + IL) \quad (5)$$

Where R, DC, DW, and (LL+IL) were assumed to be random variables. The probability of failure (P_f) was determined from the Monte Carlo simulations by counting the realizations with ($g < 0$) and dividing them by the total number of simulations (1,000,000 simulations). The reliability

index β, which is a measure of structural safety, was then calculated as:

$$\beta = \phi^{-1}(P_f) \quad (6)$$

Where Φ^{-1} constitutes the inverse of the standard normal cumulative distribution function. The probabilistic models and the statistical parameters (mean and standard deviation) describing the uncertainty in the different design variables are discussed in the following sections.

Statistical Load and Capacity Models

The statistical parameters (bias λ and coefficient of variation V) for the bending moments due to slab weight and wearing surface were adopted from (Nowak, 1995) as λ_{DC} = 1.05 and V_{DC} = 0.1 and λ_{DW} = 1.0 and V_{DW} = 0.25, respectively. The bias factor is defined as the ratio of the mean of a given parameter to the nominal value of that parameter. As a result, the mean values for DC and DW for all bridges considered can be defined from λ_{DC} and λ_{DW} together with the nominal values shown in Table 2.

The bias factors λ_{LL} of the static live load moments (M_{LL}) were presented by Nowak (1995) [6] and are dependent on the number of lanes and span lengths, while the coefficient of variation of (M_{LL}) has been found to be constant with a value of 0.12. Table 4 shows the bias factor of the live load moment for each span and the corresponding mean values of the total live load.

Table 4. Live Load Statistical Parameters

No. of lanes	Span (ft)	λ_{LL}	$V(M_{LL})$	Mean of $M_{(LL+IL)}$	Standard Deviation $M_{(LL+IL)}$	V $M_{(LL+IL)}$
1	24	1.38	0.12	61.80	9.77	0.158
	36	1.39	0.12	86.97	13.36	0.154
	46	1.37	0.12	109.01	18.14	0.166
	54	1.36	0.12	120.5	18.85	0.156
2	24	1.16	0.12	43.68	7.43	0.170
	36	1.19	0.12	69.11	10.66	0.154
	46	1.19	0.12	92.70	14.83	0.160
	54	1.18	0.12	106.65	15.85	0.149

The mean and standard deviation of the total live load $M_{(LL+IL)}$ are determined according to Equations (7) and (8) (Kulicki et al., 2007) by combining the statistics of the static live load and the impact load. In Eq. (8), the values of 0.12 and 0.8 represent the coefficients of variation of the static live load and the dynamic impact load, respectively. The resulting means and standard deviations of the total live load for the cases analyzed in this study are presented in Table 4 together with the corresponding estimates of the coefficient of variation of the $M_{(LL+IL)}$ [7].

$$\text{Mean of } M_{(LL+IL)} = \lambda_{LL} * M_{(LL+IL)_{\text{nominal}}} \quad (7)$$

$$\text{St. Dev. } M_{(LL+IL)} = \sqrt{(0.12\lambda_{LL}M_{LL})^2 + (0.8M_{IL})^2} \quad (8)$$

Finally the statistical parameters for the moment capacity for reinforced concrete slab bridges were adopted from Kulicki et al. (2007) [7] based on a bias factor λ_R of 1.14 and a V_R of 0.13.

In the reliability analysis, the moments due to slab weight, wearing surface, and total live load were assumed to be normally distributed as per the recommendations of Kulicki et al. (2007) [7]. Along the same lines, the moment capacity was taken to be lognormally distributed.

Results of the Reliability Analysis

The first set of reliability analyses were conducted to assess the reliability levels that are inherent in concrete slab bridges that are designed in accordance with the current LRFD design equation which is based on a live load factor of 1.75. The results of this set of analyses are presented in Fig. 3a and indicate that the reliability index β ranges from 2.6 to 3.0 for the cases involving single lane bridges and is slightly below 3.5 for the cases involving two-lane slab bridges. The results of the single lane concrete bridges reflect reliability levels that fall short of the target reliability index of 3.5 that was set by AASHTO LRFD, Nowak (1995) [6]. On the other hand, the results of the two-lane bridges are closer to the target reliability level.

Results on Fig. 3b point to the need for revising the AASHTO LRFD live load factors if a reliability index as high as 3.5 is to be targeted. This is particularly important for the case involving single lane bridges. As a result, the reliability analysis was repeated assuming different live load factors in an attempt to identify the factors that would ensure the desired level of reliability in the design. Results indicated that for single lane bridges, a live load factor that is as high as 2.07 is required to ensure that bridges with all span lengths would achieve a target reliability index of 3.5. For the two lane loading case, the LRFD load factor needs to be increased slightly from 1.75 to 1.8 to achieve the target reliability level. The revised LRFD design equations for the single and double lane scenarios are presented in Eq. (9) and Eq. (10), respectively. The resulting reliability levels for the revised cases are presented in Fig. 3b.

For single lane bridges:

$$\phi R_n = 1.25M_{DC} + 1.5M_{DW} + 2.07(M_{LL} + M_{IL}) \quad (9)$$

For two lane bridges:

$$\phi R_n = 1.25M_{DC} + 1.5M_{DW} + 1.8(M_{LL} + M_{IL}) \quad (10)$$

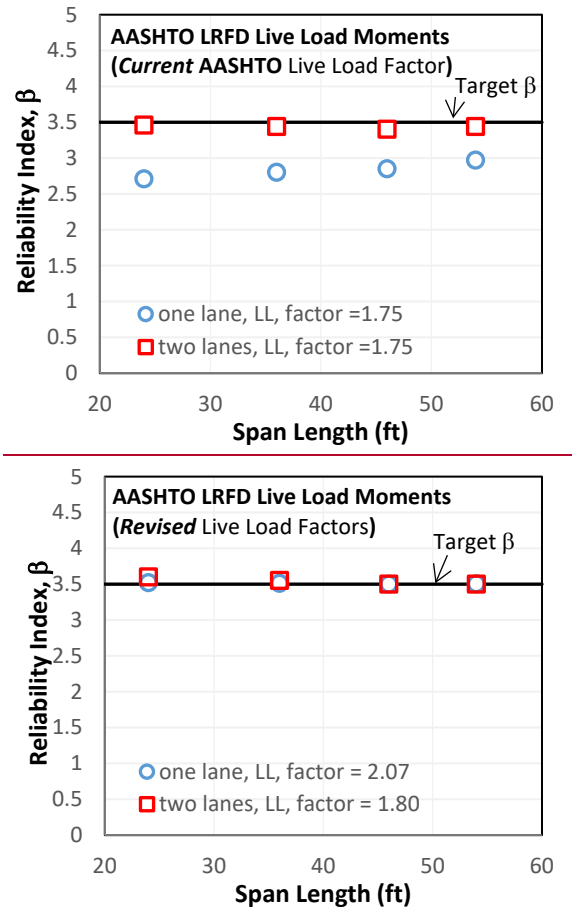

Fig. 3 Reliability Indices for Concrete Slab Bridges per Simplified AASHTO LRFD Moments for (a) AASHTO Live Load Factors and (b) Revised Live Load Factors.

The results presented in Fig. 3 pertain to bridge designs that are based on the live load moments M_{LL} that are calculated using the simplified procedure recommended by AASHTO LRFD. Results presented in Table 1 indicate that these M_{LL} values could deviate from the more representative finite element values, particularly for cases involving single lane bridges with relatively shorter spans (24ft and 36ft). To account for this discrepancy in the value of M_{LL}, the reliability analyses were repeated such that the simplified AASHTO live load moments were corrected by multiplying these moments by the ratio α_{LL} (see Table 1). For the cases involving single-lane bridges with shorter spans (24, 36 ft) where the tandem/lane combination governed, an α_{LL} value of 0.74 (average of the two α_{LL} values for the two span lengths) was adopted. For a single lane with longer spans (46, 54 ft) where the HS-20 truck/lane combination governed, an α_{LL} value of 0.99 was adopted. For the two lane bridge cases, the α_{LL} ratios of 0.98 and 1.11 were adopted for the shorter and longer spans, respectively. To incorporate the ratio α_{LL} in the reliability analysis, the static live load moment that is based on the simplified AASHTO LRFD procedure was multiplied by α_{LL} as reflected in the modified performance function shown in Eq. (11):

$$g = R - (DC + DW + \alpha_{LL}(LL) + IL) \qquad (11)$$

The results of the reliability analysis that was conducted using the revised performance function that is presented in Eq. (11) are shown in Fig. 4. Results pertain to the conventional live load factor of 1.75 that is recommended by AASHTO LRFD. As expected, the calculated reliability indices for the single lane bridges with the shorter span lengths of 24 and 36 ft increased significantly compared with the earlier results (Fig. 3a). This increase in the reliability index (up to values of 3.8) is directly correlated to the smaller α_{LL} ratio (average of 0.74) which indicates that the simplified AASHTO LRFD procedure overestimated the maximum live load moments on the bridge. For the single lane bridges with the longer spans, the reliability indices were found to be still less than the target reliability index since the α_{LL} ratio for these cases was close to 1.0.

For the two lane bridges, results in Fig. 4a indicate that the target reliability index was achieved for the shorter spans, but fell short of achieving a target reliability index of 3.5 for the longer spans for the case where the conventional AASHTO LRFD load factor of 1.75 was adopted.

To ensure a target reliability index of 3.5 for the longer spans, the LRFD live load factors need to be revised for the single lane and the two-lane bridge cases. Results from the reliability analysis indicated that for the one-lane case with longer spans, the live load factor has to be increased from 1.75 to 2.07, even if the live load moments are corrected based on the FEA results. As for the two lane bridge cases, the target reliability levels for the longer spans cases could be ensured with a revised live load factor of 1.95 as shown in Fig. 4b. Thus, it is recommended that Eq. (12) and Eq. (13) in the design of single and two lane reinforced concrete bridges with longer spans, respectively.

For single lane bridges:

$$\phi R_n = 1.25M_{DC} + 1.5M_{DW} + 2.07(M_{LL} + M_{IL}) \qquad (12)$$

For two lane bridges:

$$\phi R_n = 1.25M_{DC} + 1.5M_{DW} + 1.95(M_{LL} + M_{IL}) \qquad (13)$$

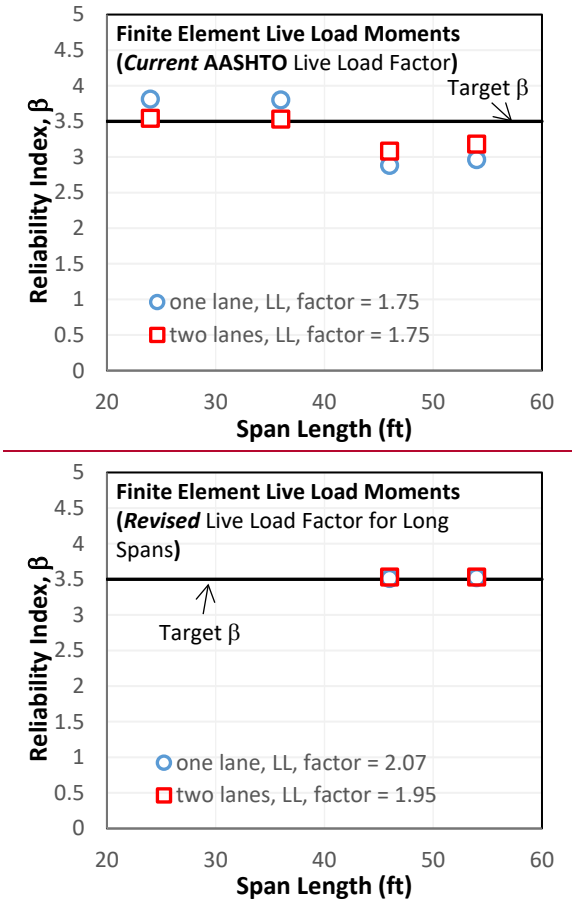

Fig. 4 Reliability Indices for Concrete Slab Bridges where the AASHTO LRFD Live Load Moments are Corrected using the FEA Results for (a) AASHTO Live Load Factors and (b) Revised Live Load Factors.

SUMMARY AND CONCLUSIONS

The method used to calculate the bending moment in AASHTO LRFD tends to overestimate the live load moments for shorter spans in one and two lane bridges when compared to the moment obtained from the finite element analysis. For longer spans, the bending moment obtained from AASHTO LRFD provisions tends to slightly underestimate the moment when compared with the FEA moment for one and two lane reinforced concrete bridges.

The reliability analysis performed in this study is used to check the level of safety for the reinforced concrete bridges that are designed with the AASHTO LRFD provisions. The results of the reliability analysis showed that the reliability index is slightly lower than the target reliability index for two lane bridges. The reliability indices for one lane reinforced concrete bridges were considerably lower than the target reliability index. To reach a consistent level of safety for one lane and two lane bridges, the live load factor in the design equation proposed by AASHTO LRFD needs to be revised by increasing the live load factor to 2.07 for one lane and 1.8 for two lanes.

When the difference between the moments obtained from AASHTO LRFD and FEA is incorporated in the reliability analysis, the results showed acceptable target reliability levels for shorter span bridges and relatively inferior reliability indices for longer spans. To achieve the target reliability levels for these cases, the load factors in the AASHTO LRFD provisions needed to be increased to 2.07 for a single lane with longer spans and to 1.95 for two lanes with longer spans.

REFERENCES

[1] AASHTO (2002). *Standard Specifications for Highway Bridges*, 17th Ed., American Association of State Highway and Transportation Officials (AASHTO), Washington, D.C.

[2] AASHTO (2012). *LRFD Bridge Design Specifications*, 5th Ed., American Association of State Highway and Transportation Officials (AASHTO), Washington, D.C.

[3] Mabsout, M., Tarhini, K., Frederick, G., and Tayar C. (1997). "Finite element analysis of steel girder highway bridges." *J. Bridge Eng.*, ASCE, 2(3), 83-87.

[4] Mabsout, M., Tarhini, K., Jabakhanji, R., and Awwad, E. (2004). "Wheel load distribution in simply supported concrete slab bridges." *J. Bridge Eng.*, ASCE, 9(2), 147-155.

[5] Nowak A. (1999). "Calibration of LRFD Bridge Design Code". *NCHRP Report 368*, Washington, D.C.

[6] Nowak A. (1995). "Calibration of LRFD bridge code." *J. of Struct. Eng.*, 121(8), 1245-1251.

[7] Kulicki J., Prucz Z., Clancy C., Mertz D., and Nowak A. (2007). "Updating the Calibration Report for AASHTO LRFD Code." *NCHRP Report 20-7/186*, Washington, D.C.

[8] SAP2000 (version 17). Computers and Structures Inc., Berkeley, California.

Second International Conference on Science, Engineering & Environment,
Osaka City, Japan, Nov.21-23, 2016, ISBN: 978-4-9905958-7-6 C3051

VENDOR MANAGED INVENTORY MODEL FOR SINGLE-SUPPLIER MULTI-BUYERS SUPPLY CHAINS

Chaowalit Hamontree
Department of Industrial Engineering, Faculty of Engineering
King Mongkut's Institute of Technology Ladkrabang, Thailand

ABSTRACT

Vendor managed inventory (VMI) is a supply chain coordination mechanism that has been gaining a lot of attention. This paper develops model for a single supplier and multiple buyers with VMI policy that model is derived from financial perspective called Net Present Value (NPV) under deterministic condition. Under the proposed strategy, the supplier specified common replenishment periods and requires all buyers to replenish only at those time periods. In order to reduce costs through coordination in the supply chain, the technique of common replenishment epochs model (CRE) or periods is utilized by the supplier. The supplier is able to combine several replenishment orders from the buyers, and save on order processing and delivery costs. The proposed model will be compared with classic model to find the optimal solution including of optimal lot-size, cycle replenishment time, and total cost. The numerical results are conducted to show the utility of the proposed model.

Keywords: Vendor managed inventory, Supply chain coordination, Financial perspective, Replenishment policy

INTRODUCTION

Vendor Managed Inventory (VMI) is a collaborative buyer-supplier partnership whereby the supplier is authorised to manage the buyer's inventory. In VMI, the buyer instead provides the supplier with Point of Sale (POS) and inventory status data on a real time basis. The supplier will use this information to coordinate its own replenishment actions with the replenishment service provided to the buyer. The supplier takes responsibility for the operational management of the inventory within a mutually agreed framework of performance targets, which are constantly monitored and updated to create an environment of continuous improvement [4]. In a VMI system, the operations of the buyer and supplier can be integrated through information sharing by using the technologies such as Electronic Data Interchange (EDI) or internet-based protocols. The supplier can use this information to plan production, schedule deliveries, and manage inventory levels at the buyer.

As a consequence, system cost can likely be reduced while capacity utilization will be increased. These benefits of VMI have been widely recognized in different industries, especially in the retail industry. The popularity of VMI has led to the claim that it is a vital policy for the future and that this concept will revolutionize the tactical decisions in the distribution channel. For further discussion of the VMI system, we refer the reader to [3], [5], [7], and [8].

Under VMI concept, the supplier makes replenishment decisions on behalf of the buyer, and pays for the cost of replenishment decision-making. The agreement also provides the supplier with data on the final customer demand. When there are multiple buyers, the supplier may choose to implement VMI with n buyers to reduce production and holding costs at his warehouse. Furthermore, the supplier may wish to deliver large quantities to achieve economies of scale in production cost.

In financial perspective analysis, the Net Present Value (NPV) framework is broadly accepted as an alternative valid framework for studying production and inventory systems. In NPV technique, all cash flows are applied that related to activities are valued by their time of occurrence using discount rate, which represents the opportunity cost of the next best alternative for the firm. NPV is presented [6] that the capital costs of inventories in the various stages of a supply chain can then be retrieved from the linearized NPV or Annuity Stream (AS) of this cash-flow function. NPV has been used in this manner in quite a number of studies, see also [2], and [6].

ASSUMPTIONS AND NOTATIONS

The system studied consists of a single supplier with multiple buyers. In order to reduce costs through coordination in the supply chain, the technique of or periods is utilized by the supplier. The supplier is able to combine several

replenishment orders from the buyers, and save on order processing and delivery costs.

It is assumed that the buyers have constant demand rates, and buyer's demand parameters are known to the supplier. The other assumptions are: both parties have perfect information about the other player's characteristics and the transportation charges paid out to a third party 3PL; shortages are not allowed; lead-time is zero; the supplier produces at (in) finite production rate; there are no capacity constraints. The replenishment interval for each retailer should be an integer multiple of the common replenishment period T, that minimise the total average costs.

The following notational scheme is made ($\boldsymbol{i} = \boldsymbol{b}$ for buyer, $\boldsymbol{j} = \boldsymbol{s}$ for supplier):

$\boldsymbol{d_i}$: The demand rate for buyer $\boldsymbol{i} \in \boldsymbol{N}$;
$\boldsymbol{D}$: Total demand rate $\boldsymbol{D} = \sum_{i=1}^{N} \boldsymbol{d_i}$;
$\boldsymbol{R}$: The supplier's production rate ($\boldsymbol{R} > \boldsymbol{D}$);
$\boldsymbol{N}$: The set of buyers $\{\boldsymbol{1}, \ldots, \boldsymbol{n}\}$;
$\boldsymbol{c}$: The supplier's variable cost per product for buyer $\boldsymbol{i} \in \boldsymbol{N}$;
$\boldsymbol{s_i}$: The fixed order processing cost for buyer $\boldsymbol{i} \in \boldsymbol{N}$;
$\boldsymbol{h_i}$: The holding cost per product per year for buyer $\boldsymbol{i} \in \boldsymbol{N}$;
$\boldsymbol{\alpha_i}$: The buyer's internal annual holding cost rate;
$\boldsymbol{t_i}$: The variable transport cost per product for buyer $\boldsymbol{i} \in \boldsymbol{N}$;
$\boldsymbol{Q_i}$: The lot-size between supplier and buyer;
$\boldsymbol{Q}$: The total number of items dispatched from supplier to all buyers $\boldsymbol{Q} = \sum_{i=1}^{N} \boldsymbol{Q_i}$;
$\boldsymbol{Q_s}$: The supplier's optimal lot-size;
$\boldsymbol{s_s}$: The fixed order (set-up) processing cost per supplier's acquiring order;
$\boldsymbol{s_p}$: The supplier's fixed order processing cost per buyer's order;
$\boldsymbol{h_s}$: The supplier's holding cost per product per year;
$\boldsymbol{\alpha_s}$: The supplier's internal annual holding cost rate;
$\boldsymbol{Q_s}$: The supplier's lot-size;
$\boldsymbol{T}$: The ordering cycle time of buyer $\boldsymbol{j} \in \boldsymbol{N}$.
$\boldsymbol{m}$: The integer multiplication ($\boldsymbol{Q_s} = \boldsymbol{mQ_b}, \boldsymbol{m} \geq \boldsymbol{1}$);

In the models, the annuity stream for the buyer is denoted as AS_b and the annuity stream for supplier AS_s. These approximations are obtained by Maclaurin expansion of the exponential terms in α_i, where $k \in \{1, D/R, m\}$, and then linearization of the expansion in $\alpha_i (i \in \{b, s\})$

THE CLASSIC INVENTORY MODEL

Assume there are n buyers and under the independent policy model, each buyer would determine his own optimal policy. The buyer's average cost per unit time incurred by the i^{th} buyer can be expressed in Eq. (1):
The buyer's average cost:

$$\boldsymbol{AC_b} = \boldsymbol{s_i}\frac{\boldsymbol{d_i}}{\boldsymbol{Q_i}} - \boldsymbol{h_i}\frac{\boldsymbol{Q_i}}{\boldsymbol{2}} \tag{1}$$

The holding costs of buyer and supplier is $\boldsymbol{h_i} = \boldsymbol{\alpha}(\boldsymbol{w_i} + \boldsymbol{t_i})$ and $\boldsymbol{h_s} = \boldsymbol{\alpha c}$.

Where the first term in Eq.(1) represents the set-up costs, the second the holding costs. The holding cost for the buyer is valued at w and t where the money is invested for keeping product at inventory stock.

$$\boldsymbol{Q_i^*} = \sqrt{\frac{\boldsymbol{2S_i d_i}}{\boldsymbol{\alpha_b(w_i + t_i)}}} \tag{2}$$

$$\boldsymbol{T^*} = \frac{\boldsymbol{Q_i^*}}{\boldsymbol{d_i}}\sqrt{\frac{\boldsymbol{2S_i}}{\boldsymbol{d_i \alpha_b(w_i + t_i)}}} \tag{3}$$

The supplier's average cost:

In the perspective of supplier, the supplier faces a demand rate of $D = d_1 + d_2 + \cdots d_n$ and need to satisfy the delivery of Q_i unit of stock to the i^{th} units of time. The largest possible amount of ordering face by the supplier is that all the buyers replenish at the same time in the total of ordering of $\sum_{i=1}^{n} Q_i$ unit of stock. The supplier average cost can be expressed as:

$$\boldsymbol{AC_s} = (\frac{\boldsymbol{S_s}}{\boldsymbol{m}} + \boldsymbol{S_p})\frac{\boldsymbol{D}}{\boldsymbol{Q_i}} - \boldsymbol{h_s}[(\boldsymbol{m} - \boldsymbol{1}) \tag{4}$$

The first term in Eq.(4) represents the set-up costs, and the other two terms in $Q_i/2$ are the inventory holding costs.

The supplier accepted the optimal lot-size Q_i^* from each buyer and then determines the optimal value of m where is the number of shipments from supplier to buyer during the supplier's production cycle based on his own profit function.

The supplier's optimal m^* is thus:

$$\boldsymbol{m_i^*} = \boldsymbol{max}\left(\sqrt{\frac{\boldsymbol{2S_s}\left(\boldsymbol{1} + \boldsymbol{\alpha}\frac{\boldsymbol{D}}{\boldsymbol{R}}\right)}{(\boldsymbol{S_b} + \boldsymbol{S_p})(\frac{\boldsymbol{R}}{\boldsymbol{D}} - \boldsymbol{1})}}, \boldsymbol{1}\right) \tag{5}$$

The index $\boldsymbol{i}$ denotes that it is derived from the classic

framework.

Where m^*, as always, should be again rounded up to 1 if it is smaller, and otherwise rounded to the nearest higher or lower integer, whichever gives the highest profit function value.

THE FINANCE MODEL WITH NPV

Following [6], the NPV of an activity for firm j is generally the Laplace transform of a cash-flow function $a_j(t)$ where the Laplace frequency is the continuous capital rate α_j of the firm:

$$\boldsymbol{NPV_j = \int_0^t a_j(t) e^{-\alpha_j t} dt} \tag{6}$$

The cash-flow function represents all the costs and revenues, and their exact timing that will be incurred in relation to the executing of the activities of the firm in the context of the supply and delivery of these products. The annuity stream function AS_j, for an infinite horizon model, is then defined as $AS_j = \alpha_j NPV_j$. The Maclaurin expansion of the exponential terms in the decision variables leads to more tractable analytical models. In particular, the linear approximation in α_j is often leading to models of comparable complexity as those arrived at from the classical inventory modelling principles which it can be written as:

$$\boldsymbol{AS = \alpha \int_0^\infty a(t) e^{-\alpha t} dt} \tag{7}$$

This aim is to derive functions for buyer and supplier to evaluate their profit when they would act independently, and a profit function for their joint supply chain. These functions are defined as annuity streams and thus represent a continuous stream of cash-flows with the same NPV as the real set of cash flows encountered. Linearization of these functions in the discount rate can be directly compared with average profit models. The inventory model for supplier and buyer with NPV is shown in Fig. 1 and cash flow diagram for both supplier and buyer is shown in Fig. 2.

The buyer average cost is:

$$\boldsymbol{AS_b = pD - (s_b + wDT)\left(\sum_{i=0}^{\infty} \alpha_b e^{-i\alpha_b T}\right)} \tag{8}$$

This can be rewritten as:

$$\boldsymbol{AS_b = (s_b + wDT)\left(\frac{\alpha_b}{1 - e^{-\alpha_b T}}\right)} \tag{9}$$

The Maclaurin expansion of the exponential term with respect to $\boldsymbol{\alpha_b T}$ gives:

$$\boldsymbol{AS_b = (s_b + wDT)\left(\frac{1}{T} + \frac{\alpha_b}{2} + O\left(\alpha_b^2 \frac{T}{12}\right)\right)} \tag{10}$$

Giving the following linearization in $\boldsymbol{\alpha_b}$ of the annuity stream:

$$\boldsymbol{\overline{AS_b} = s_b \frac{D}{Q_b} - \alpha_b w \frac{Q_b}{2} - \alpha_b \frac{s_b}{2}} \tag{11}$$

The buyer's optimal lot-size is thus:

$$\boldsymbol{Q_b^* = \sqrt{\frac{2S_b D}{\alpha w}}} \tag{12}$$

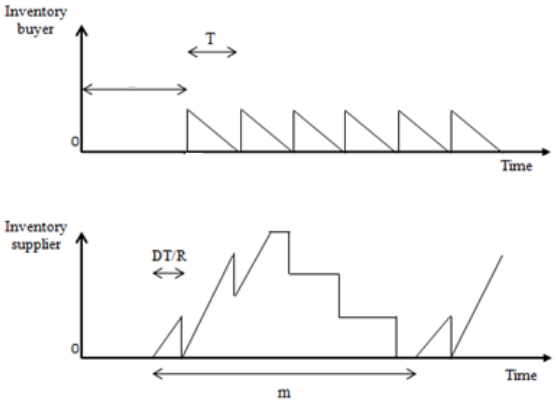

Fig. 1 Inventory model for supplier and buyer

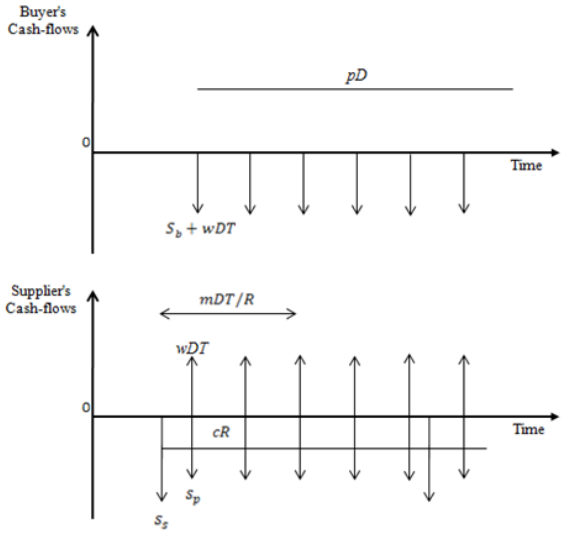

Fig. 2 Supplier and buyer cash-flow over time

The average cost function where $h_b = \alpha_b w$ is equal to the first four terms of the annuity stream approximation. The last term $-\alpha_b s_b/2$ measures the average interest costs related to set-up payments. It is well known that such terms appear in annuity streams with set-up costs. Since it is a constant term, it is of lesser importance.

The supplier average cost can be expressed as:

$$\boldsymbol{AS_s = (-s_p + wDT)\left(\sum_{i-0}^{\infty} \alpha_s e^{-i\alpha_s T}\right) - (S_s + cDmT)\left(\sum_{i-0}^{\infty} \alpha_s e^{-i\alpha_s mT}\right) - (m-2)\frac{D}{R}]} \quad (13)$$

$$\boldsymbol{AS_s = (-s_p + wDT)\left(\frac{\alpha_s}{1-e^{-\alpha_s T}}\right) - (S_s + cDmT)\left(\frac{\alpha_s}{1-e^{-\alpha_s mT}}\right)} \quad (14)$$

The Maclaurin expansion of the exponential term with respect to $\boldsymbol{\alpha_b T}$ gives:

$$-\left(\boldsymbol{S_s + cmT}\right)\left(\frac{1}{mT} + \frac{\alpha_2}{2} + O\left(\alpha_s^2\left(\frac{mT}{12}\right)\right)\right) \quad (15)$$

$$\boldsymbol{AS_s = (-s_p + wDT)\left(\frac{1}{T} + \frac{\alpha_s}{2} + O\left(\alpha_s^2\left(\frac{T}{12}\right)\right)\right)} \quad (16)$$

Giving the following linearization in $\boldsymbol{\alpha_b}$ of the annuity stream:

$$\boldsymbol{\overline{AS_s} = (w-c)D - \left(S_p + \frac{S_s}{m}\right)\frac{D}{Q_b}\alpha_s c(m-1)\frac{Q_b}{2}} \quad (17)$$

THE COMMON CYCLE REPLENISHMENT

The common model is proposed by [1]. Under this model, all buyers replenish cycle time T_b and the supplier's production cycle is an integer multiplier m.

The buyer average cost is:

$$\boldsymbol{AC_i^t = \frac{s_i}{T} - \frac{h_i d_i T}{2}} \quad (18)$$

The supplier average cost can be expressed as:

$$\boldsymbol{AC_s^t = \frac{1}{T}\left(\frac{S_s}{m} + \sum_{i=1}^{n} S_j\right) - \frac{h_s DT}{2}[(m-1)} \quad (19)$$

The supply chain average cost is:

$$\boldsymbol{AC_{sc} = \frac{1}{T}\left(\frac{S_s}{m} + \sum_{i=1}^{n}(S_b + S_p)\right) - \frac{h_s DT}{2}[(m-1) - (m-2)\frac{D}{R}] + \sum_{i=1}^{n} h_s \frac{DT}{2}]} \quad (20)$$

The optimal common cycle time is:

$$\boldsymbol{T^* = \sqrt{\frac{2\left(\frac{S_s}{m} + \sum_{i=1}^{n}(S_b + S_p)\right)}{h_s D[(m-1) - (m-2)\frac{D}{R} + \sum_{i=1}^{n} h_s d_i}}} \quad (21)$$

The optimal integer multiplier $\boldsymbol{m = m^*}$ satisfies

$$\boldsymbol{m^*(m^*-1) \le \frac{S_s\left(\frac{1}{Dh_s}h_i d_i + 2\frac{D}{R} - 1\right)}{\left(1-\frac{D}{R}\right)\left[\sum_{i=1}^{n}(S_b + S_p)\right]} \le m^*(m^*+1)} \quad (22)$$

Under the common cycle approach, all the buyers are forced to order every T_b^* unit of time. According to [1], since the deliveries to all the buyers can be made at the same time, the order processing and delivery cost can be reduced. This leads to a lower system cost.

THE PROPOSED WITH VMI MODEL

The buyer's annuity stream for average cost is:

$$\boldsymbol{AC_b = [(s_i + t_i DT)\sum_{i=0}^{\infty} \alpha_b e^{-\alpha_b T}]e^{-\alpha_b L}} \quad (23)$$

This can be rewritten as:

$$\boldsymbol{AC_b = [(s_i + t_i DT)\left(\frac{\alpha_b}{1-e^{-\alpha_b T}}\right)]e^{-\alpha_b L}} \quad (24)$$

Maclaurin expansion of the exponential term with respect to $\boldsymbol{\alpha_b T}$ gives:

$$\boldsymbol{AC_b = \left[(s_i + t_i DT)\left(\frac{1}{T} + \frac{\alpha_b}{2} + O\left(\alpha_b^2\frac{T}{12}\right)\right)\right]} \quad (25)$$

The linear approximation can be written as:

$$\boldsymbol{\overline{AC_b} = \left[\frac{s_i}{T^*} - \alpha_b\frac{s_i}{2} - \alpha_b(t_i)\frac{d_i T^*}{2}\right]e^{-\alpha L}} \quad (26)$$

The first term in Eq.(26) represents the ordering costs, the second is the average interest cost of set-

up payments, and the third is the transportation costs. In this case, the buyer's holding cost is paid by supplier.

The supplier's annuity stream for average cost is:

$$AC_s = \begin{bmatrix} (DT - s_p)\dfrac{\alpha_s}{1-e^{-\alpha_s T}} \\ -s_s \dfrac{\alpha_s e^{\alpha_s \frac{DT}{R}}}{1-e^{-\alpha_s mT}} \\ -cR\dfrac{1-e^{-\alpha_s \frac{mDT}{R}}}{1-e^{-\alpha_s mT}} e^{\alpha_s \frac{DT}{R}} \end{bmatrix} e^{-\alpha_s L} \quad (27)$$

The Maclaurin expansion of the exponential term with respect to $\alpha_s T$ gives:

$$AC_s = \begin{bmatrix} (DT - s_p)\left(\dfrac{1}{T} + \dfrac{\alpha_s}{2}\right) \\ -s_s\left(1 + \dfrac{\alpha_s DT}{R}\right)\left(\dfrac{1}{mT} + \dfrac{\alpha_s}{2}\right) \\ -cR\left(\dfrac{mDT}{mRT} + \alpha_s \dfrac{mDT}{2R} - \alpha_s \dfrac{m^2D^2T^2}{2R^2 mT}\right) \end{bmatrix} e^{-\alpha_s L} \quad (28)$$

Giving the following linearization in α_b of the annuity stream:

$$\overline{AC_s} = \begin{bmatrix} \dfrac{1}{T^*}\left(s_p + \dfrac{s_s}{m}\left(1 + \alpha_s \dfrac{D}{R}\right)\right) \\ -\alpha_s \dfrac{s_j + s_s}{2} - \alpha_s c(m-1)\dfrac{d_i T^*}{2} \\ +\alpha_s c(m-2)\dfrac{D}{R}\dfrac{d_i T^*}{2} + \alpha_s(c)\dfrac{d_i T^*}{2} \end{bmatrix} e^{-\alpha_s L} \quad (29)$$

The supplier's average cost in VMI is composed of the set-up costs in the first term. The second term is the average interest costs of set-up payments, and the other three terms composed of the inventory holding costs. Assuming from this policy supplier will thus aim to determine the optimal lot-size based on his own profit function obtained by the following equations:

The optimal order quantity in the **VMI** policy is:

$$Q_s^* = \sqrt{\frac{2\left(S_p + \dfrac{s_s}{m}\left(1 + \alpha_s \dfrac{D}{R}\right)\right)D}{\alpha_s c(m-1) - \alpha_s c(m-2)\dfrac{D}{R} + \alpha_s(c)}} \quad (30)$$

$$T^* = \sqrt{\frac{2\left(\dfrac{s_s}{m}\left(1 + \alpha_s \dfrac{D}{R}\right) + \sum_{i=1}^{n}(S_b + S_p)\right)}{\alpha c D\left[(m-1) + \alpha_s c(m-2)\dfrac{D}{R}\right] + \sum_{i=1}^{n}\alpha_b(c)d_i}} \quad (31)$$

NUMERICAL RESULT

We present the set of data to study a single supplier multiple buyers from for numerical results. The problem instance is used from [1] for single supplier and 5 buyers.

Table 1 Problem instance characteristics

Instances	d_i	s_b	w_i	c	s_p	s_s
1	8	20	0.04	0.025	40	250
2	15	15	0.045	0.025	40	250
3	10	6	0.05	0.025	40	250
4	5	10	0.05	0.025	40	250
5	20	18	0.035	0.025	40	250

For each instance: $\alpha_b = \alpha_s = 0.2$, $h_s = \alpha_s c$; $h_b = \alpha_b w$.

Table 2 Independent strategies and optimal policies from Classic framework

No. Buyers	Classic model					
	Q_b^*	m^*	T^*	AC_b	AC_s	AC_{sc}
1	200	3	158.11	1.6	4.76	6.36
2	224	2	32.68	2.0	9.65	13.26
3	110	2	35.11	1.1	14.36	19.07
4	100	2	35.31	1.0	16.83	22.53
5	321	2	31.80	2.24	20.94	28.90

Table 3 Independent strategies and optimal policies from Classic with NPV framework

No. Buyers	Classic with (NPV) model					
	Q_b^*	m^*	T^*	AC_b	AC_s	AC_{sc}
1	200	3	50.62	1.6	4.25	5.85
2	224	2	37.14	2.0	8.01	11.6
3	110	2	41.63	1.1	10.7	15.4
4	100	2	42.05	1.0	12.9	18.6
5	321	2	36.86	2.24	19.1	27.0

Table 4 Coordinated strategies and optimal policies from Classic framework

No. of Buyers	Classic model					
	Q_s^*	m^*	T^*	AC_b	AC_s	AC_{sc}
2	2145	3	32.68	1.66	4.75	6.41
	2145	3	32.68	2.66	7.82	12.14
3	2569	2	35.11	1.69	5.40	7.09
	2569	2	35.11	2.80	7.86	12.35
	2569	2	35.11	1.93	9.87	16.29
4	2757	2	35.31	1.70	5.38	7.08
	2757	2	35.31	2.81	7.84	12.34
	2757	2	35.31	1.94	9.85	16.29
	2757	2	35.31	1.17	11.43	19.03
5	3406	2	31.80	1.65	5.82	7.47
	3406	2	31.80	2.62	8.27	12.54
	3406	2	31.80	1.78	10.33	16.37
	3406	2	31.80	1.11	11.98	19.14
	3406	2	31.80	2.79	14.83	24.78

Table 5 Coordinated strategies and optimal policies from Classic with NPV framework

No. of Buyers	Classic with (NPV) model					
	Q_s^*	m^*	T^*	AC_b	AC_s	AC_{sc}
2	870	3	37.14	1.73	3.99	5.72
	870	3	37.14	2.91	5.89	10.53
3	1476	2	41.63	1.81	4.30	6.11
	1476	2	41.63	3.17	5.40	10.39
	1476	2	41.63	2.23	5.88	13.09
4	1584	2	42.05	1.82	4.26	6.08
	1584	2	42.05	3.20	5.36	10.37
	1584	2	42.05	2.25	5.83	13.09
	1584	2	42.05	1.29	6.78	15.33
5	1957	2	36.86	1.72	4.77	6.49
	1957	2	36.86	2.89	5.99	10.60
	1957	2	36.86	2.01	6.65	13.27
	1957	2	36.86	1.19	7.73	15.55
	1957	2	36.86	3.07	12.02	22.91

Table 6 VMI strategies and optimal policies

No. of Buyers	Classic with (NPV) model					
	Q_s^*	m^*	T^*	AC_b	AC_s	AC_{sc}
2	870	3	37.14	0.54	5.18	5.72
	870	3	37.14	0.40	9.74	10.68
3	1476	2	41.63	0.48	5.63	6.11
	1476	2	41.63	0.36	9.71	10.55
	1476	2	41.63	0.14	12.75	13.74
4	1584	2	42.05	0.48	5.61	6.08
	1584	2	42.05	0.36	9.71	10.54
	1584	2	42.05	0.14	12.76	13.74
	1584	2	42.05	0.24	14.77	15.98
5	1957	2	36.86	0.54	5.95	6.49
	1957	2	36.86	0.41	9.80	10.75
	1957	2	36.86	0.16	12.73	13.84
	1957	2	36.86	0.27	14.74	16.12
	1957	2	36.86	0.49	19.51	21.38

From table 3 and 4, the numerical results show that the optimal cost function constructed from the classic and NPV approaches. In independent case, the classic framework presents the buyer's optimal lot-size Q_b and m^* and also cost functions are equal to obtain in the NPV framework, but it is different in supplier's and supply chain's cost functions as the NPV framework gives minimum costs less than a classical framework.

From table 4-6, the proposed policy from VMI can achieved minimizes supply chain's cost that better than other frameworks. In this policy, the buyers are gained benefit from all logistics and inventory costs that transferred to respond by the supplier, but meanwhile supplier is facing increasing costs at the same time. The buyer can earn lower cost because he only pays for purchasing price to the supplier when the products have been sold to the final customer. Meanwhile, the supplier faced increasing cost from this policy because he need pay in the financial holding cost to the buyer at the buyer's warehouse.

CONCLUSIONS

This paper proposed VMI model derived from financial perspective with NPV and common replenishment epochs or time periods (CREs) for a single-supplier multi-buyers in supply chain. In general problem, the supplier requires all buyers to place replenishment orders at CRE to reduce a total inventory cost. Deriving cost function from NPV approach, the mathematical modeling has been developed from cash-flows in order to derive the optimal lot-size for buyer Q_b and supplier Q_s and minimize cost for supply chain system as the performance measure. An extensive numerical study was conducted to understand the influence of VMI derived from NPV and CRE strategy lead to achieve the optimal lot-size and also give the minimum supply chain cost that better than classic model.

REFERENCES

[1] Banerjee, A., Burton, J., 1994. Coordinated vs. independent inventory replenishment policies for a vendor and multiple buyers. Int. J. of Production Economics, 35, pp. 215-222.

[2] Beullens, P., Janssens G.K., 2011. Holding costs under push or pull conditions – The impact of the Anchor Point. European Journal of Operational Research 215, pp. 115-125.

[3] Darwish, M. A., Odah O.M., 2010. Vendor managed inventory model for single-vendor multi retailer supply chains. European Journal of Operational Research, 3(1), 473-484

[4] Dong, Y, Xu, K., 2002, "A supply chain model for a vendor managed in inventory system", Transportation Research and Logistics, Vol. 38, No. 2, pp. 75-95.

[5] Goyal, S.K., 1995. "A One-Vendor Multi-Buyer Integrated Inventory Model: A comment." European Journal of Operational Research. 82(1), pp. 209-210.

[6] Grubbström, R.W., 1980. A principle for determining the correct capital costs of work-in-progress and inventory. *Int. J. of Production Research*, 18(2). pp. 259–271.

[7] Gumus, M. Elizabeth, M., 2008. Impact of consignment inventory and vendor-managed inventory for a two-party supply chain. International Journal of Production Research 113, pp. 502-517.

[8] Yao, M.J., C.C. Chiou., 2004. On a replenishment coordination model in an integrated supply chain with one vendor and multiple buyers. *European Journal of* Operational Research, 159, pp. 406-419.

Second International Conference on Science, Engineering & Environment,
Osaka City, Japan, Nov.21-23, 2016, ISBN: 978-4-9905958-7-6 C3051

FLOW CHARACTERISTICS FOR LOW PRESSURE SOLAR PARABOLIC TROUGH COLLECTOR

Ahmad Hammad[1], Wael Al-Kouz[1], Aiman Alshare[1], Suhil Kiwan[2], and Ammar Alkhalidi[3]
[1]School of Applied Technical Science, German Jordanian University, Jordan;
[2]Mechanical Engineering Department, University of Science and Technology, Jordan;
[3]Energy Engineering Department, German Jordanian University, Jordan.

ABSTRACT

A finite volume code is used to solve for the steady-state two-dimensional laminar gaseous low pressure flows in the annulus region between two concentric horizontal cylinders with an attached solid fin to the inner cylinder. Such flows can be found in the receivers of the solar Parabolic Trough Collectors (PTCs). It is found that local heat transfer coefficient depends inversely on Knudsen number. In addition, it is found that attaching a fin will enhance the heat transfer for such flows. Other flow characteristics also depend on Knudsen Number, dimensionless vertical velocity decreases as Knudsen number increases for a certain limit of dimensionless radial distance, then it increases with Knudsen number. Moreover, when Knudsen number increases, the temperature jump at outer cylinder surface will increase.

Keywords: Low ressure, Rarefaction, Concentric Cylinders, arabolic Tough.

INTRODUCTION

Rarefied flows had been studied in the past two decades due to its wide industrial applications. It can be classified based on Knudsen number (Kn) into four regimes [1]; (I) continuum flows in which Knudsen number is equal to zero, (II) slip flow in which Knudsen number is greater than 0.01 and less than 0.1, (III) transitional flow in which Knudsen number is greater than 0.1 and less than 10, and (IV) free molecular in which Knudsen number is greater than 10.

One of the applications of the flow in the region between two horizontally oriented concentric cylinders is the parabolic trough collectors. The effects of Rayleigh number and radius ratio on the characteristics of the flow in the annuli of two infinite concentric cylinders using numerical techniques were studied by El-Sherbiny [2]. Rayleigh number was varied between 102 to 106, and the radius ratio was taking the values between 1.25 and 10.

The effect of fin conductivity ratio, Darcy number and Rayleigh number on the average Nusselt number for porous fins attached to the inner cylinder of the annulus between two concentric cylinders were investigated by Kiwan et al. [3]. They found that the heat transfer is enhanced for the case of a porous fin, also it was found that for porous fin, unlike the solid fins, the heat transfer decreases by increasing the inclination angle of the fin. The heat transfer of this application was analyzed by Padilla et al. [4]. Based on their model they presented correlations for the heat transfer in the parabolic trough solar receiver. Al-Kouz et al [5] investigated the low-pressure flows in the annulus region between two concentric cylinders, they studied the effect of rarefaction on the flow and heat characteristics of such flows. In addition, a correlation for the conductivity ratio was proposed for such flows.

In this work, Fluent16 is used to obtain the solution for the flow characteristics between two concentric horizontal cylinders. The inner cylinder is attached to a solid fin and is subjected to a constant high temperature while the outer cylinder is held at constant lower temperature. Effects of Knudsen number (*Kn*) on the flow and heat transfer characteristics are investigated.

MATHEMATICAL MODEL

In this study, a steady-state, two dimensional, and laminar flow is investigated. Boussinesq approximation is utilized to account for the buoyancy force and all fluid properties are considered constant. Figure (1) shows one of the most relevant applications to our study; namely, the receiver of the parabolic trough collectors. Figure (2) illustrates the geometry of the flow in the annulus region between the two concentric cylinders in which the inner cylinder is attached to a solid fin. In this study, the slip and temperature jump boundary conditions were imposed at the boundaries and the slip flow regime is investigated.

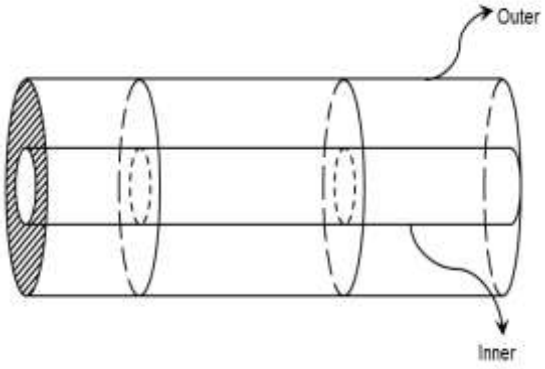

Fig. 1 Receiver of the parabolic trough collectors.

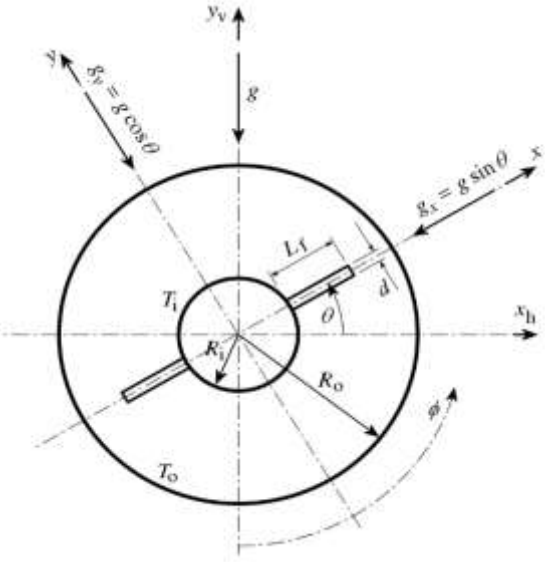

Fig. 2 The geometry of the annulus region between the two concentric cylinders.

The governing equations that describe the problem under investigation are summarized as follow; conservation of mass:

$$\frac{\partial u}{\partial x}+\frac{\partial v}{\partial y}=0 \tag{1}$$

where u and v are the velocities in x direction and y direction respectively. The x-momentum:

$$\rho u\frac{\partial u}{\partial x}+\rho v\frac{\partial u}{\partial y}=-\frac{\partial}{\partial x}+\mu\left[\frac{\partial^2 u}{\partial x^2}+\frac{\partial^2 u}{\partial y^2}\right] \tag{2}$$

where ρ is the density of air given by ideal gas equation, is the pressure, and μ is the dynamic viscosity. Note that the x component of the gravity is not equal to zero since there is a rotation for the solid fin that is attached to the inner cylinder of the annulus. y-momentum:

$$\rho u\frac{\partial v}{\partial x}+\rho v\frac{\partial v}{\partial y}=-\frac{\partial}{\partial y}-\rho g_y+\mu\left[\frac{\partial^2 v}{\partial x^2}+\frac{\partial^2 v}{\partial y^2}\right] \tag{3}$$

Energy:

$$\rho C_p u\frac{\partial T}{\partial x}+\rho C_p v\frac{\partial T}{\partial y}=\left[\frac{\partial^2 T}{\partial x^2}+\frac{\partial^2 T}{\partial y^2}\right] \tag{4}$$

where C_p is the specific heat, T is the temperature in kelvin, and is thermal conductivity.

The boundary conditions applied are the slip and temperature jump at the inner and outer walls of the annulus as reported by Karniadakis et al. [1]. The corresponding Knudsen number (Kn) is defined as follows:

$$Kn=\frac{\lambda}{L_g} \tag{5}$$

where λ is the molecular mean free path, and L_g is the gap spacing between the inner and outer cylinders. Thermal boundary conditions are imposed at inner and outer annulus radii such that:

$$\text{at } r=r_i, T=T_i \tag{6}$$

$$\text{at } r=r_o, T=T_o \tag{7}$$

where r_i and r_o are the inner and outer annulus radius respectively, and T_i is the hot surface temperature measured at inner annulus surface and T_o is the cold surface temperature measured at outer annulus surface.

The average heat transfer coefficient along the wall of the inner cylinder is calculated from

$$\bar{h}_i=\frac{}{(T_i-T_\circ)A_i} \tag{8}$$

where $\bar{h}_i$ is the average heat transfer coefficient, is heat transfer per unit length, and A_i is the area of the inner annulus surface.

CODE VERIFICATION

The mathematical model solved numerically using finite volume technique. Figure 3 shows a sample of the mesh of the domain of the problem. It consists of a simple two-dimensional mesh. To verify the numerical code, results of the current code are tested and compared with the results obtained by Kuehn and Goldstein [6] as was documented in AL-Kouz et

al.[5] with an acceptable error. Figure 4 illustrates the comparison between $_r = \frac{eff}{}$ obtained by the current code and that obtained by Kuehn and Goldstein [6]. The results show a matching of more than 93%.

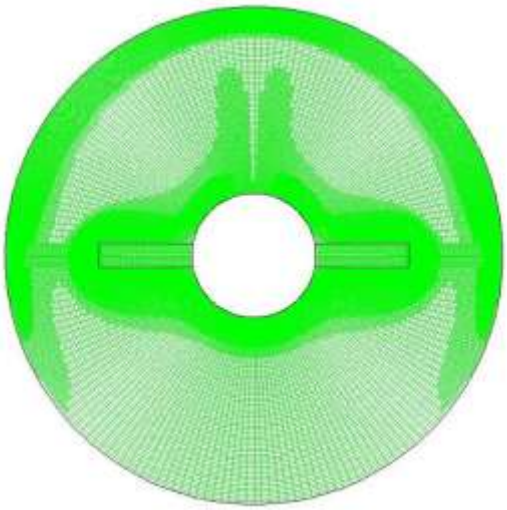

Fig. 3 The adaptive grid system used in calculation.

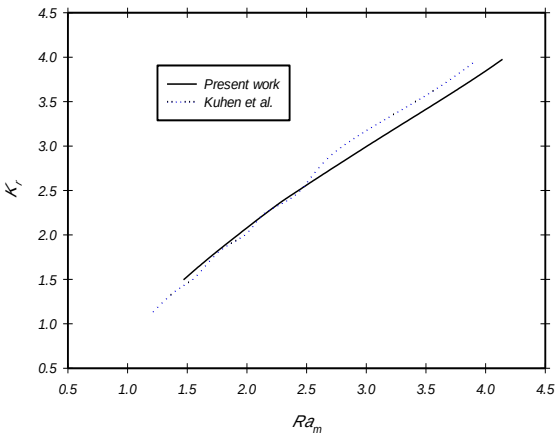

Fig. 4 Comparison between current data and Kuhen et al. data.

RESULTS AND DISCUSSION

Figure 5 illustrates the variation of the local heat transfer coefficient along with the angle phi. The figure shows that as phi increases then the local heat transfer coefficient increases. Also, the figure shows that as Knudsen number increases then the heat transfer represented by the local heat transfer coefficient will decrease. In addition, the graph shows that there is no effect for the angle phi on the local heat transfer coefficient for angles less than 30 degrees. The graph also shows that attaching a fin to the inner cylinder will enhance the local heat transfer coefficient.

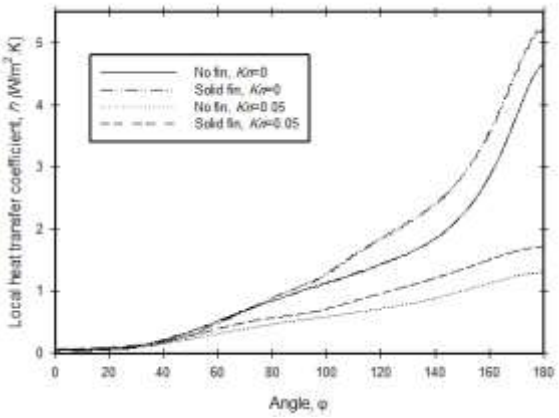

Fig. 5 Variation of the local heat transfer coefficient along with the angle.

Figure 6 shows the dimensionless vertical velocity V_y variations with the dimensionless radial distance r for different values of Knudsen numbers. It is obvious from the graph that the higher the Knudsen number, the lower dimensionless vertical velocity for cases where r is less than one. The opposite will occur for the cases where r is higher than unity, the higher Knudsen number will result in lower dimensionless vertical velocity.

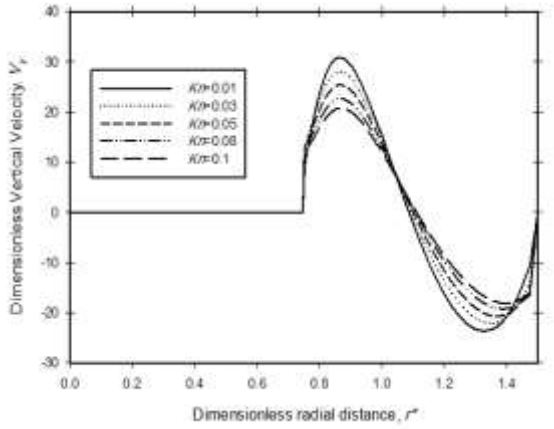

Fig. 6 Variation of the dimensionless vertical velocity V_y with the dimensionless radial distance r for different values of Knudsen numbers.

In Fig. 7, the dimensionless temperature distribution T is plotted against the dimensionless radial distance r . The graph shows that as Knudsen number increases then the temperature jump at the outer cylinder surface will increase.

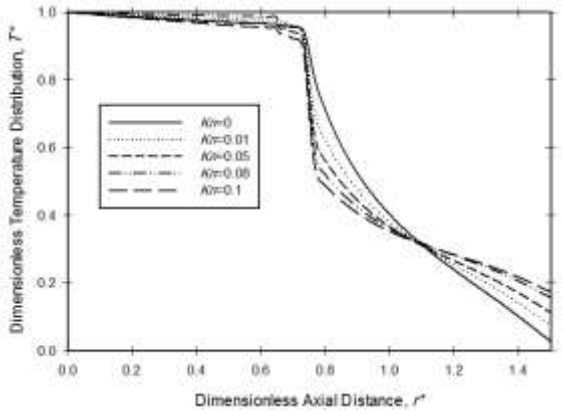

Fig. 7 Variation of the dimensionless temperature distribution T with the dimensionless radial distance r for different values of Knudsen numbers.

CONCLUSIONS

A flow analysis for low pressure solar parabolic through collector in which the inner surface is attached to a solid fin is carried out using fluent16. The flow could be modeled as a steady, two-dimensional low-pressure laminar flow between two concentric cylinders. It is found that as Knudsen number increases then the heat transfer represented by the local heat transfer coefficient will decrease. Also, attaching a fin to the inner cylinder will enhance the local heat transfer coefficient.

Moreover, it is concluded that flow characteristics also depend on Knudsen Number; dimensionless vertical velocity decreases as Knudsen number increases for a certain limit of dimensionless radial distance, then it increases with Knudsen number. Also, when Knudsen number increases, the temperature jump at outer cylinder surface will increase.

REFERENCES

[1] G. Karniadakis, A. Beskok, and N. Aluru, 2005, Microflows and Nanoflows, Springer.

[2] A. El-Sherbiny, Natural convection in air layers between horizontal concentric isothermal cylinders, Alexandria Engineering Journal., 43 (3) (2004), 297-311

[3] S. Kiwan, O. Zeitoun, Natural convection in a horizontal cylindrical annulus using porous fins, International Journal of Numerical Methods for Heat & Fluid flow, 18 (2008), 618-634.

[4] R. Padilla, G. Demirkaya, D. Goswami, E. Stefankos, Heat transfer analysis of parabolic trough solar receiver, Applied Energy, 88(2011), 5079-5110.

[5] Al-Kouz W, Alshare A, Alkhalidi A, and Kiwan S, 2016, Two dimensional analysis of low pressure flows in the annulus region between two concentric cylinders, Springerplus (2016) 5:529.

[6] T. H. Kuehn and R. J. Goldstein., Correlating equations for natural convection heat transfer between horizontal circular cylinders, Int J. Heat and Mass Transfer., 19 (1976), 1127-1134.

Second International Conference on Science, Engineering & Environment,
Osaka City, Japan, Nov.21-23, 2016, ISBN: 978-4-9905958-7-6 C3051

ENSEMBLE MLP NETWORKS FOR VOICES COMMAND CLASSIFICATION TO CONTROL MODEL CAR VIA PIFACE INTERFACE OF RASPBERRY PI

Narissara Eiamkanitchat[1, 2], Nontapat Kuntekul[1] and Phasit Panyaphruek[1]
[1]Department of Computer Engineering, Faculty of Engineering;
[2] Social Research Institute;
Chiang Mai University, Thailand

ABSTRACT

This research, exploration displays the aftereffects of utilizing the blend of the multi-layer perceptron network system to classify Thai speech. The parameters of the training process are used in the mobile application to using Thai voice commands to control the model car. The PiFace interface of the Raspberry Pi is attached to the model car for receiving the command from mobile and control the model car. The 1,000 Thai voice commands of both men and ladies are used as the training set in the experiment. The preliminary experiments have been done to find the best possible structure of the classification model, and the appropriate proportion of classes in the training set. From the experiment results using 1 network for one voice command, the average accuracy of the classification results in the environment without noise is higher than 80%, which considered favorable in the speech recognition field of study.

Keywords: Thai voices command, ML neural networ , Speech recognition, Classification.

INTRODUCTION

There are many researches using voice command to control electronic devices [1]-[5]. One of the useful application, is use voice command to control wheelchair for some handicap person who not able to use hand to control the wheelchair. Usually, user needs to ware headphone and speak their command in the headphone. In this research, we try to utilize the mobile phone those most people already have one, to use as the input device. Anyway, most voice commands are using the English language, and still have problem for Thai people who cannot speak English fluently. The Thai voice command is used in this research, in order to facilities Thai handicap people.

Table 1 Thai word use to control the model car.

Thai word	Pron.	English meaning	Activity of model car
ซ้าย	Ŝāy	Left	Turn left 90 degrees then move forward
ขวา	K̄hwā	Right	Turn right 90 degrees then move forward
หน้า	H̄n̂ā	Front	Move forward
หลัง	H̄lạng	Back	Turn right 180 degrees then move forward
หยุด	H̄yud	Stop	Stop moving

The Mel-Frequency Cepstral Coefficients (MFCC) for speech recognition in many researches [6]-[8] is used as the features extraction in this research. Short 5 Thai words are used as the input to control the model car. The commands are displayed in table 1.

Each word have 200 voices of both men and women, with various pronunciations. The details of the preparatory analysis are described in the following section including and the normalization method and subtle elements of the MLP structure. The consequences of the preparatory tests are lead to the general basic configuration of the framework, describe in overall structure section. Section experimental results demonstrate the Thai voice command classification results in various circumstances. The final section is the conclusion of the propose structure and suggestion for future work.

THE PRELIMINARY EXPERIMENT

The feature extraction process in speech recognition is techniques for converting an analog signal to the digital signal. In processing for converting MFCC algorithm has a quality point, with a particular deciding objective to work properly to the human sound. The MFCC is a procedure to convert an ordinary frequency to the Mel frequency. The frequency of human discourse has a lower frequency by utilizing the Mel scale can increase the low frequency scale range meanwhile decrease the range of high frequency. The processing of MFCC is shown in Fig. 1. The process begins from the sampling signal process for converting an analog signal to the computerized signal. Next stride the data is partitioned to form a frame where every frame is changed over by Fast Fourier Transform (FFT) to transform data to time domain, frequency spectrum. The information from FFT is sampled by using triangular overlapping windows converted from hertz unit to Mel-scale unit. The Mel-scale value calculated

the power and take logarithm. Finally, data is reconverted by the Discrete Cosine Transform (DCT) and results the MFCC feature vector, in this progression the quantity of DCT can be assigned.

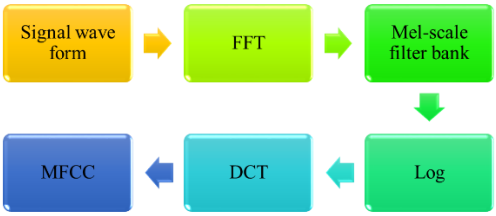

Fig. 1 The feature extraction process using MFCC.

The number of DCT utilizing as a part of this research is 21, which mean 21 of MFCC feature vectors. Subsequent to dissecting the estimation of all features, 6 features need to normalize the quality. The normalization by decimal scaling is applied in these features. The new value is figured by

$$f' = \frac{f}{10} \quad (1),$$

where f is the original value of feature,

is the minimal value that makes $|v'| < 1$.

The MLP is popular algorithm to use as the classification model for the voice command [9]-[12] and other applications [13-15]. The first experiment is to locate the appropriate structure of the MLP. The principle objective is to find the superior structure with less complexity, so the number of hidden layers is not more than 2 layers. The Thai voice command to use in the experiment is the word "Ħńā", which mean front. The first MLP structure has 3 layers including, input layer number of nodes equivalent to the number of input features. The hidden layer has 3 nodes and the output layer has 1 node. The second MLP structure has 4 layers including, input layer, 2 hidden layers and output layer. The nodes of input layer equivalent to number of input features. The following layers has 3 nodes, 2 nodes and 1 node respectively. Three experiments have been done, each experiment using 10 fold cross validation to check the precision. The experimental results appear in figure 2.

Clearly seen from every experiment displayed in figure 2 that, the MLP with 2 hidden layers have favored execution over MLP with 1 hidden layer. Notification of the parameters results of every experiments the weight estimation of input feature 1 is converted to small value almost equivalent 0. The experiment that eliminates the first input feature is done and the outcomes is approximately the same, so the 1 feature is considered not imperative for the classification and deleted.

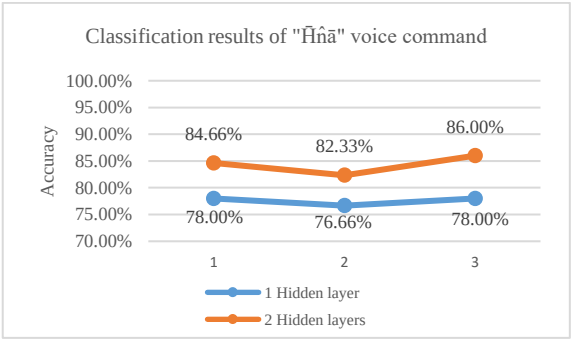

Fig. 2 The comparison of the classification results of 2 MLP structures.

Since the objective of this research is to apply the voice command classification to use with model car via the PiFace interface of Raspberry Pi, the programming language must be considered. The typical procedure of classification, including learning phase and testing phase. The learning phase using a training dataset to modify the parameters. The testing phase is receiving the value of parameters from learning process and use to classify unseen data. The consequences of using programming language as a part of learning and testing process are shown in table 2.

Table 2 The results of using different programming language in learning and testing process.

Expt. No.	Learning	Testing	Accuracy
1	Matlab	Matlab	85.33%
2	Matlab	Python	27.80%
3	Python	Python	84.67%
4	Java	Java	84.67%

The results in table 2 demonstrated that using Matlab as a part of both phase is the most astounding classification result. Nonetheless, in experimental 2, clearly seen that using training parameters from Matlab cannot classify voice command when implement by Python. This research is utilizes the Python in both learning and testing phase. The reason is a Raspberry Pi can use Python [16], [17] to implement and using Python results the same high accuracy as using Java, as found in experiment 3 and 4.

The objective of the next preliminary experiment is to locate the portion of classes in the training data set. The preparation of the training data set in this research is for the specific purpose, to classify 5 Thai voice command. Normally perception, the desire class need to have the highest portion. The ratio using in the experiments is 80:20 of the desire class versus other classes, and 20:80 of the desire class versus other classes. Totally 3 experiments are done to each

voice. The average of 5 fold cross validation is used to verify the classification accuracy. The 80:20 ratio results are displayed in figure 3, and results of 20:80 are displayed in figure 4 separately.

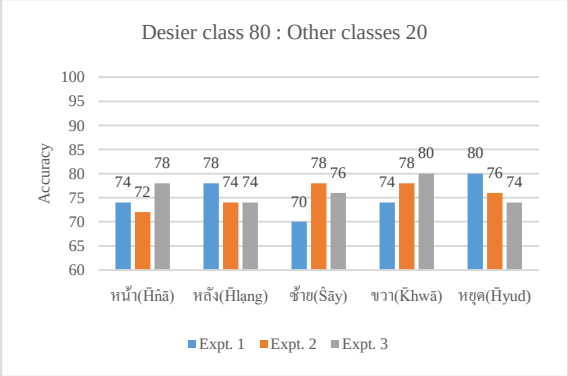

Fig. 3 The training dataset ratio 80: 20.

Figure 3 shown the average accuracy from 5 fold cross validation of training dataset ratio 80:20 of desire class and other classes. The most noteworthy accuracy form 3 experiments of ratio 80:20 of each voice are 74.60%, 75.30%, 74.60%, 77.30% and 76.60%. The average accuracy from all voices of this type of ratio is 75.68%.

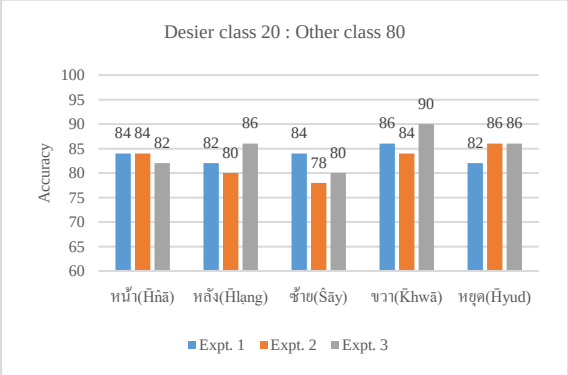

Fig. 4 The training dataset ratio 80: 20.

Figure 4 shown the average accuracy from 5 fold cross validation of training dataset ratio 20:80 of desire class and other classes. The highest accuracy form 3 experiments of ratio 20:80 of each voice are 83.30%, 82.60%, 80.60%, 86.60% and 84.60%.

The average accuracy from all voices of this type of ratio is 83.54%. The results unmistakably demonstrated that the ratio of desire class 20: other classes 80, results better accuracy in every experiment. The reason is the portion 80:20, to create a training data set for voices "H̄nâ", the 200 voices of "H̄nâ" are added in the training data set. The voices of other classes, including, H̄lạng, Ŝāy, K̄hwā, and H̄yud are added in the training dataset totally 50 voices. The neural network has just a few sample of other classes, result to higher miss classification. On the other hand, the portion 20:80 with the same example the 50 voices of "H̄nâ" are added in the training data set. The voices of other classes, including, H̄lạng, Ŝāy, K̄hwā, and H̄yud are added in the training dataset totally 200 voices. The neural network has enough sample of other classes to learn, result to higher accuracy of classification.

THE OVERALL STRUCTURE

As the prior mansions, the objective of the Thai voice command development is aimed to be able to apply to utilizing mobile and the PiFace interface of Raspberry Pi. The overall structure is appeared in figure 5.

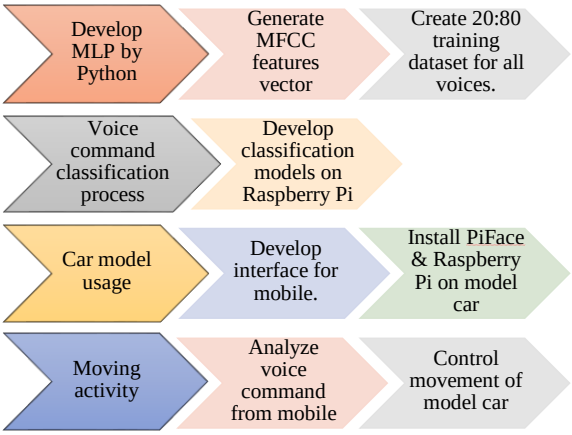

Fig. 5 The overall structure of the Thai voice command application system.

The structure in figure 5 comprises of 4 main processes. The first process is to discover the parameters to classify the Thai voice command using MLP. The second process is to implement the voice command classification models using the parameters from the training process to install in Raspberry Pi. The third process is the mobile application implementation and the car model execution. The last process is the moving activity process, the voice command from mobile is send to classify the order by Raspberry Pi and control the movement of the car by PiFace.

The multi-layer perceptron neural network is used as the classification model in this research. Each network can have numerous layers, and each layer can have multiple perceptron or neural. The structure of 1 perceptron is consists of the input values, weights between perceptron, bias of each perceptron and 2 computation functions. The first function will consolidate the value of all inputs those already

adjusted by weights. The second function is called activation function or transfer function that will transfer value from the first function to the output value. The sigmoid is utilized as a transfer function in this research, the output results from sigmoid is displayed in figure 6.

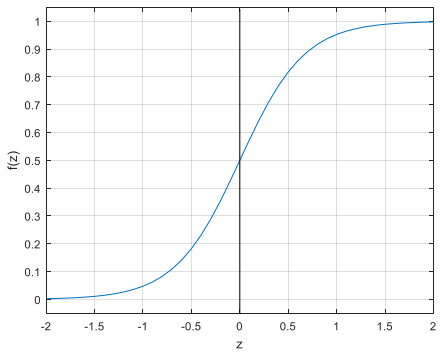

Fig. 6 The output from sigmoid function.

Firstly, all input features to each node are adjust by multiply to weight it connected, and summarize including with the bias of each node as

$$= \sum_{i=1}^{n} w_i x_i + bias \quad (2),$$

x_i represent the value of input feature, and w_i is the weight connected to each input feature.

The value of is fed to the sigmoid activation function to calculate the output as

$$f(\ ) = \frac{1}{(1+e^{-}\ )} \quad (3).$$

In the machine learning literature, the adaptive learning is the most important function. The learning process of MLP, delta rule is applied in the backpropagation algorithm. The parameters of each node, including the weights and bias connected to it. The small values call delta of weight (Δw) and delta of bias $(\Delta bias)$ are calculated from miss classification error and use for the parameter modification. After the feed forward process, the errors from output are calculated by

$$e_n = t_n - y_n \quad (4).$$

The output calculated from the feed forward process is represented by y_n, the target value is represented by t_n. The error is used to calculate Δw as Eq. (5).

$$\Delta w(n) = \eta \delta(n) x(n) \quad (5),$$

where η is learning rate , the local gradient is represented by $\delta(n)$, which can be separate into 2 cases. The gradient for output layer calculate from Eq. (6) and for hidden layer calculate from Eq. (7).

$$\delta(n) = e(n)\varphi'(\ (n)) \quad (6),$$

where $\varphi'(\ (n))$ is the first derivative of the activation function. For hidden layer

$$\delta(n) = \varphi'(\ (n)) \sum_{i=1}^{n} \delta_i(n) w_i(n) \quad (7),$$

where $\sum_{i=1}^{n} \delta_i(n)$ is the summation gradient of the adjacent layer. The weights of the next iteration is updated by

$$w(n+1) = w(n) + \Delta w \quad (8).$$

The bias value of each neuron are updated similarly to the weights as displayed in Eq. (5) to Eq. (6). The initial parameters of learning rate is 0.1, the maximum iteration of the training process is 10,000 rounds. The sigmoid is utilized as the activation function for every node. As the experimental results shown earlier, the structure of MLP with 2 hidden layers result preferable execution over 1 hidden layer.

EXPERIMENTAL RESULTS

The primary experiment is to find the best neural network structure for 5 voices command classification. Three analyses have been done to compare whether using 1 model to classify 5 voices or 5 models for 5 voices. The experimental results are appeared in table 3.

Table 3. The average accuracy results of using 1 model comparing with using 5 models.

Expt. No.	5 fold cross validation of all voices command	
	1 network	5 networks
1	78.80%	84.00%
2	78.00%	85.60%
3	79.20%	83.20%

The structure of 1 network has 4 layers, including input layer with 20 nodes, first hidden layer with 15 nodes, second hidden layer with 8 nodes and lastly an output layer with 3 nodes. The other structure is the

combination of 5 networks. The nodes of input layer are equivalent to input features. The first hidden layer has 3 nodes, the second input layer has 2 nodes and output layer has 1 node for 1 voice command. Agreeing from table 3, the outcomes from using 5 networks for classification are higher than using only 1 network in all experiments. Furthermore, the learning time of using 1 network, is longer than using 5 networks in 1 structure. Along these lines, the final structure of this research are as demonstrated in figure 7.

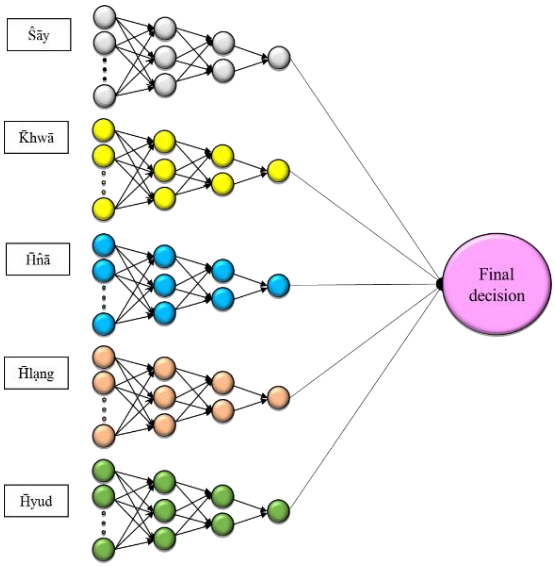

Fig.7 The overall structure of voices commands classification model.

Next experiment using the structure in figure 7 to actualize in PiFace and Raspberry Pi to control the model car and separated experiments into 4 sections. The first experiment, using men voices in both training and testing process. The second experiment, using women's voices in both training and testing process. The third and fourth experiments utilizing both men's voices and women's voices in the training process and using men's voices and women's voices in testing processing separately. The average of 5 fold cross validation, experimental results are shown in table 4.

Table 4 The experimental results based on gender.

Expt. No.	Training	Testing	Avg. Acc.
1	Male	Male	85.33%
2	Female	Female	80.67%
3	Male & Female	Male	76.00%
4	Male & Female	Female	74.67%

The results in table 4 demonstrated that using men's voice as a part of both training and testing process result the most astounding precision. Utilizing blend gender voices in the training process and test with female voices result the lowest accuracy compared to all experiments.

.

CONCLUSION

From aggregate analyses in this research the best proportion for creating a training data set is 20% of desire class and 80% of all other classes. The structure of neural networks is using 2 hidden layers and using 1 network for classifying 1 voice command. Obviously seen from experiment that using the same gender voices as a part of training and testing process results better than using blend gender voices in the training process. The proposed research results demonstrated that the propose methodology is appropriate to apply to utilizing Thai voice command to control the model car. Furthermore, can be used as a prototype model to implement for using Thai voice commands to control a wheelchair or other electronic appliances later on.

REFERENCES

[1] Ansari, J.A., Sathyamurthy, A., Balasubramanyam, R., "An Open Voice Command Interface Kit", IEEE Transactions on Human-Machine Systems, Vol. 46, pp. 467- 473.

[2] Bartišiūtė, G., Ratkevičius, K., Paškauskaitė, G., "Hybrid recognition technology for isolated voice commands", Advances in Intelligent Systems and Computing, Vol.432, 2016, pp.207-216.

[3] Srijiranon, K., Eiamkanitchat, N., "Application of neuro-fuzzy approaches to recognition and classification of infant cry", IEEE Region 10 Annual International Conference, Proceedings/ TENCON, 2015.

[4] Srijiranon, K., Eiamkanitchat, N., "Thai speech recognition using Neuro-fuzzy system", ECTI-CON 2015 - 2015 12th International Conference on electrical engineering / Electronics, computer, Telecommunications and Information Technology, 2015.

[5] Xiao, X. , Zhao, S. , Ha Nguyen, D.H. , Zhong, X. , Jones, D.L. , Chng, E.S., Li, H., "Speech dereverberation for enhancement and recognition using dynamic features constrained deep neural networks and feature adaptation", Eurasip Journal on Advances in Signal Processing, Vol. 2016, December 2016, pp.1-18.

[6] Mannepalli, K., Sastry, P.N., Suman, M., "MFCC-GMM based accent recognition system for Telugu speech signals", International Journal of Speech Technology, Vol.19, March 2016, pp.87-93.

[7] Ali, S.M., Karule, P.T., "MFCC, LPCC, formants and pitch proven to be best features in diagnosis of speech disorder using neural

networks and SVM", Vol. 11, March 2016, pp. 897-903.

[8] Borde, P., Varpe, A., Manza, R., Yannawar, P., "Recognition of isolated words using Zernike and MFCC features for audio visual speech recognition", International Journal of Speech Technology, Vol. 18, June 2015, pp.167-175.

[9] Zarrouk, E., Ben Ayed, Y., Gargouri, F., "Hybrid continuous speech recognition systems by HMM, MLP and SVM: A comparative study", International Journal of Speech Technology, Vol. 17, September 2014, pp.223-233.

[10] Ben Nasr, M., Saoud, S., Cherif, A., Optimization of MLP using genetic algorithms applied to Arabic speech recognition, International Review on Computers and Software, Vol.8, February 2013, pp. 653-659.

[11] Park, J., Diehl, F., Gales, M.J.F., Tomalin, M., Woodland, P.C., "The efficient incorporation of MLP features into automatic speech recognition systems", Computer Speech and Language, Vol. 25, July 2011, pp. 519-534.

[12] Pujol, P., Pol, S., Nadeu, C., Hagen, A., Bourlard, H., "Comparison and combination of features in a hybrid HMM/MLP and a HMM/GMM speech recognition system", IEEE Transactions on Speech and Audio Processing, Vol. 13, January 2005, pp. 14-22.

[13] Kazuhiro O., Minsun L., Shotaro K., "Spatial Interpolation of consolidation properties of Holocene clays at Kobe Airport using an artificial neural network", International Journal of GEOMATE, Vol. 4, April 2015, pp 423-428.

[14] Sakthivel P.B., Ravichandran A., Alagumurthi. N., "MODELING AND PREDICTION OF FLEXURAL STRENGTH OF HYBRID MESH AND FIBER REINFORCED CEMENT-BASED COMPOSITES USING ARTIFICIAL NEURAL NETWORK (ANN)", International Journal of GEOMATE, Vol. 10, October 2015, pp 1623-1635.

[15] Hafez Dahlia H., Mahgoub A.G., Abu Kiefa. Mostafa A., "GENERAL REGRESSION NEURAL NETWORK MODELING OF SOIL CHARACTERISTICS FROM FIELD TESTS", International Journal of GEOMATE, Vol. 12, June 2016, pp 132-139.

[16] Guerra, H., Cardoso, A., Sousa, V., Leitao, J., Graveto, V., Gomes, L.M., "Demonstration of programming in Python using a remote lab with Raspberry Pi", exp.at 2015 - 3rd Experiment International Conference: Online Experimentation, 29 April 2016, pp. 101-102.

[17] Weychan, R., Marciniak, T., Dabrowski, A., "Implementation aspects of speaker recognition using Python language and Raspberry Pi platform", Signal Processing - Algorithms, Architectures, Arrangements, and Applications Conference Proceedings, SPA, December 2015, pp. 162-167.

Second International Conference on Science, Engineering & Environment,
Osaka City, Japan, Nov.21-23, 2016, ISBN: 978-4-9905958-7-6 C3051

DOMESTIC RECHARGE WELLS FOR RAINWATER-HARVESTING IN DENPASAR CITY, BALI - INDONESIA

Lilik Sudiajeng[1], I Wayan Wiraga[2], I Gusti Lanang Parwita [3], and Gede Santosa[4]

[1]Civil Engineering Department, Politeknik Negeri Bali, Indonesia; [2]Civil Engineering Department, Politeknik Negeri Bali, Indonesia[3]Civil Engineering Department, Politeknik Negeri Bali, Indonesia, [4]Mecanical Engineering Department, Politeknik Negeri Bali, Indonesia

ABSTRACT

This research is to create the design of shallow recharge wells for harvesting rainwater in Denpasar City, Bali-Indonesia. The growth of the tourism industry is increasing rapidly. It has been able to accelerate the economic growth, but also followed by some negative effects, including rapid growth of population, changes in land use, reduced the catchment area and groundwater exploitation for tourism infrastructure development. The result showed that in several strategic locations have shown an indicator of water crisis, especially in North and East Denpasar. Based on the permeability analyses, the recharge area was in the north and a little part of west Denpasar. The rainfall was between 1500 - 1750 mm/year with 4 wet months a year. The shallow groundwater level reaches 16.10 m below ground surface in the North, while in the West was 18.2 m with the maximum infiltration rate was 0.00000054 mm/sec. Based on those data, it has been designed the appropriate shallow recharge wells for rainwater harvesting to offset the domestic water usage. The analyses showed that if all 220.150 households make at least one shallow recharge wells, it can harvest rainwater about 222.40 l/sec, and is able to return about 63.87% of water which should be recharge to the ground. In conclusion, making one-recharge wells for each household has not been able to recover the domestic water usage. It is recommended to create another innovation for water conservation program such as building the recharge wells along the drainage tunnel.

Keywords: Recharge wells, Rainwater harvesting, Denpasar City-Indonesia.

INTRODUCTION

In a few decades, Bali with a unique culture has changed from an agricultural area became very famous tourist areas. The growth of the tourism industry are increasing rapidly been able to accelerate economic growth, but also followed by some negative impacts, including the rapid increasing of population growth, changes in land use, reduces catchment areas, and the exploitation of natural resources with less consideration to preserve environment, including the exploitation of groundwater usage.

Strategic environmental assessment in 2010 at the province of Bali has produced a map that shows the high level of groundwater usage and there were 13 points area experienced seawater intrusion [1]. Following up the assessment in 2010, Denpasar government, in cooperation with Politeknik Negeri Bali (Bali State Polytechnic) has built research collaboration on Groundwater in Denpasar City (2013-2014). As the result, it was identified that there were indicators of water crisis in some strategic area, especially in Panjer, Peguyangan village (North Denpasar), and Penatih Village (East Denpasar). The pumping test of 15 deep wells showed that 5 wells (33%) indicated in a good design and well developed (well loss value <0.5), 13% suffered minor damage (well loss value between 0.5 - 1), 33% suffered severe damage with some blockage (well loss value between 1-4), and the rest was experienced heavy damage and difficult to be restored (well loss values > 4). This is consistent with the statement of the Bouwer [3] that the main cause of the global water crisis is partly due to increased water demand, global climate change, and lack of catchment areas. Wang et al. [4] reported that the exploitation of groundwater during the years 1985 to 2010 led to a decrease in the depth of groundwater in Linze County. Meanwhile, Adham at all [5] reported that the numerical simulation showed the effect of climatic change on the decreasing of groundwater quality. Liu et al. [6] reported that the land conversion in China Alagan the period 1980-2000 has led to changes in flow and groundwater levels. Meanwhile,

Water is essential for life. Abundant water resources with good quality will lead all living beings to a better life as well. Therefore all efforts for the conservation of water resources must be fully

supported. Changes in land use must be done carefully so the deterioration in the green land area can be avoided. Deforestation must be avoided so that the sustainable rainwater harvesting is naturally guaranteed as well as the sustainability of other living creatures. For example, the research done by Ma, Le [7] has demonstrated that woodland has potential positive effects on *Margaritifera margaritifera*. Therefore, the protection of riparian woodland is important for the conservation and management of freshwater pearl mussels.

Ground water is renewable natural resource, but un controlled exploitation with lack awareness to preserve it will lead to the water crisis as well as the decreasing of the quality of life. Therefore it is important to undertake a program of conservation of groundwater and building awareness of society, especially in urban areas such as Denpasar City. There are some ways for ground water conservation; one simple program that can be done is harvesting rainwater through recharge wells.

MATERIAL AND METHOD

Time and Location

The research was started on 2013 and now is still ongoing. It was conducted in Denpasar City, one of the strategic tourism destinations in Bali Fig. 1).

Fig.1 The map of Denpasar City

Denpasar city is located between 08 ° 35 "31'-08 ° 44 '49' south latitude and 115 ° 10" 23'-115 ° 16 "27 'east longitude. Denpasar City area is 12 778 ha, 2.18% of the total land area of Bali province. It is divided into four sub-districts, North, East, South, and West Denpasar. The largest of sub-districts is South Denpasar, followed successively by the Northern, West and East Denpasar. The land use is consisting of wetland covering 2,717 ha. and dry land 10 051 ha. Dry land consists of 7,831 ha. yard land, dry land 396 ha, pond/pool 10 ha, not cultivated 81 ha., 613 ha. of forest, 35 ha. of plantation and others is 1,162 Ha. The topography of the city of Denpasar is generally skewed towards the south with a height ranging from 0-75m above sea level. Morphology ramps with a slope of land mostly range between 0-5% however on cut slope can reach 15% [8]

Research Approach

This paper reported part of the research with focused on the innovation design of recharge wells for harvesting rainwater for domestic usage through ergo-hydrogeology approach. One of the factors contributed on the changing of the groundwater condition is the human activity. Therefore, in designing the conservation program should put a man with all the activities, behavior and socio-cultural background as a primary consideration in accordance with the basic principles of ergonomics SHIP approach as shown in Fig. 2.

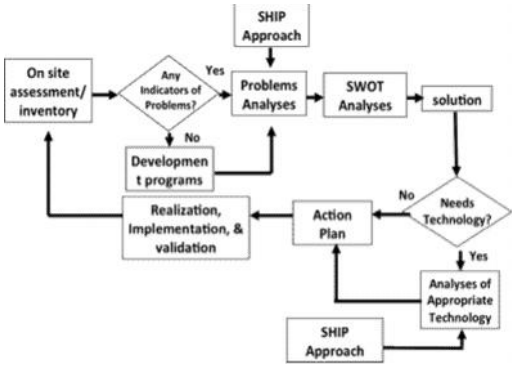

Fig. 2 The Model of Ergonomics SHIP Approach [9]

The design process was involved all parties through Focus Group Discussion (FGD) which has been held on July 31, 2015. The FGD brought together all participants from local governments, state companies, the private sector, and local communities. The FGD participants were divided into four groups - each consisting of representatives of every stakeholder. The result of FGD presented lists of prioritized issues related to the existing water resources management, expectations of the future, as well as challenges and constraints in meeting those expectations.

The hydrological approach was done to analyze the capacity of the recharge wells based on the basic formula of rainfall (R), permeability (K), infiltration rate (I), and water discharge (Q).

Data collecting

General data on groundwater obtained from the Public Works Department of Denpasar City, included data of geography, hydrology, topography, hydrogeology, and the list of licensed deep bore wells.

The primary quantitative data was collected through assessments, included data of permeability (K) and infiltration rate (I), while the subjective data was collected through questionnaire.

The technical data analyses were conducted by using the basic formula of hydrology.

Data Analyses

Descriptive Analyses

The results of questionnaire analysis, which is reinforced by the results of FGD show some strategic issues as follows:

1. Prioritized of strategic issues on technical aspects:
   a. Excessive exploitation of ground water by industry
   b. Decreased groundwater quality and resources
   c. Increased seawater intrusion
   d. Lack of monitoring wells
   e. Many buildings on the watershed
   f. Decreased green spaces

2. Prioritized of strategic issues on Management aspect
   a. Ground water drilling permits are easy to obtain, but many groundwater drilling unlicensed
   b. Monitoring system for groundwater exploitation and quality is still weak
   c. The data series on groundwater characteristics are not yet available
   d. Taxes groundwater utilization is too low
   e. There are no regional regulations governing the use of groundwater
   f. Efforts to control the destructive force of groundwater resources is still weak
   g. Ground water conservation programs that have been implemented less on target
   h. There are many overlaps in the tasks and functions related agencies in the conservation of water resources
   i. There are no clear SOPs for ground water conservation activities
   j. Less of public awareness

3. Expectations on Technical Aspect
   a. Engineering effort required to overcome the problem of groundwater
   b. Drilling groundwater should be accompanied by building a recharge well
   c. Recharge shallow wells need to be made in every yard
   d. Need to build reservoirs / artificial lake to accommodate / rainwater harvesting
   e. Need to develop green areas

4. Expectations on Managements Aspect
   a. Necessary organizational restructuring related efforts to conserve water resources
   b. Required Groundwater Management Model that able to synergize all sustainable water resource conservation programs
   c. Required a clear vision and mission related to the preservation of water resources
   d. Monitoring and control the utilization of ground water must be carried out periodically and continuously
   e. Need strict sanctions for those who violate the rule of water resources
   f. Need to build an IT data base systems
   g. Need to improve the quality of human resources
   h. Keep in groundwater conservation efforts
   i. Need enacted progressive tariff system, the more water utilization, higher tariffs
   j. Need to be coordination between the relevant agencies in the implementation of groundwater conservation program
   k. The role of communities in groundwater conservation needs to be improved
   l. Need to be controlling and regulating the use of groundwater

Quantitative Analyses

Characteristic of Shallow wells

Analyses was done for identified the characteristics of shallow wells spread over four districts in the city of Denpasar as presented in Table 1. From Table 1 it can be seen that the maximum depth of the water table wells in North Denpasar achieved 16.10 m below the ground level (bgl); East Denpasar 11.55 m bgl, South Denpasar 4.50 m bgl; and West Denpasar 18.20 m bgl. Data depth of water table wells will be used as a basis for determining the depth of recharge wells.

Table 1. Characteristic of Shallow Wells

Sub-District		Groundwater table (m-bgs)	Debt of wells (m-bgs)
North Denpasar	Span	0.80 – 16.10	2.60 – 24.10
	Average	5.63	10.24
East Denpasar	Span	0.40 – 11.55	1.90 – 20.55
	Average	4.06	7.22
South Denpasar	Span	0.45 – 4.50	2.00 – 6.40
	Average	1.53	3.54
West Denpasar	Span	2.40 – 18.20	8.90 – 21.20
	Average	7.41	12.41

Recharge Area

The results of the analysis and mapping of soil permeability indicate that the recharge area is located in the north of Denpasar area with a maximum permeability (K) of 0.0434 m / day (Fig. 3)

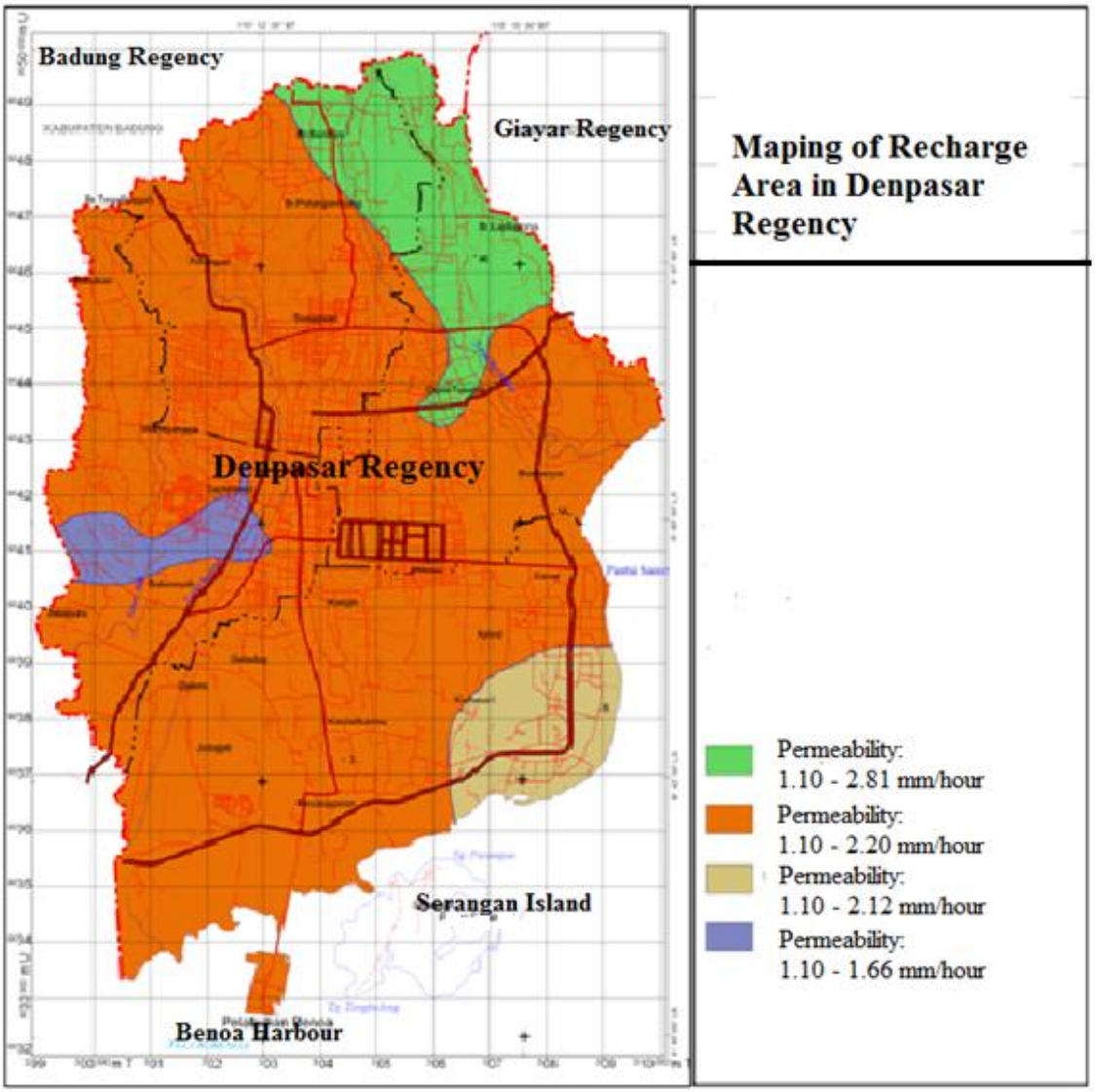

Fig. 3. Map of Recharge Area in Denpasar Regency

Based on the recommended recharge area, then the design of recharge wells was based on the characteristics of the groundwater in the area of North Denpasar.

Rain Water Harvesting Analyses

1. Effective Rainfall (R (Ef))
   Rainfall (R)
   R = 1500 mm/year
   = 375 mm/month
   = 0.0001447 mm/sec

   Wet months (Wm)
   = 4 month/year
   = 10.368.000 second

   Effective rainfall :
   R (Ef) = R/Wm
   = 375 mm/month
   = 0.0001447 mm/second
   = 0,00000015 m/second

2. Rainwater Harvesting (Q1)
   Rainwater harvesting was analyzed for 100 m2 of catchment area (estimation of covered land/household)

   Q1 = A * R(Ef)
   = 100 * 0,00000015

= 0.000015 m3/sec.
= 1,296 m3/day

Statistic data of Denpasar City showed that there are 220,150 households with 4 person average in each household.

If each household harvest at least 20% of rainwater, it means that the effective rainwater harvesting = 0.20 * 1,296 m3/day
= 259.2 m3/day/household

3. Domestic ground water usage

The water needs of each person (N)

N = 165 l/person/day

Water needs = 165 * 4 l/day/household
= 660 l/day/household
= 0.66 m3/day/household
Total water needs = 0.66 * 220.150
= 145.299 m3/day

The analyses of effective rainwater harvesting and total water needs/household showed that Denpasar will never meets the water crisis, but the fact showed in contrary. Therefore, the water conservation program is still needed.

Recharge Wells Design

Based on the results of technical analysis that includes data characteristic of shallow groundwater, soil permeability, infiltration rates, and the result of FGD, produced designs of recharge wells (Fig. 4) with technical specification as followed:

1. It made from concrete pipes with 1 m diameter
2. The debt is at least 1 m above the groundwater table, in this research, it was assigned 9 m
3. The filtration pond was constructed around the top of wells to ensure the quality of incoming water to the wells meet eligibility standards
4. To facilitate operations and maintenance, as well as the safety and health considerations, recharge wells equipped with a ladder made of galvanized pipe diameter of 1 ".
5. From the socio-cultural aspects of Bali, the wells designed and positioned to blend with the surrounding beauty and fulfilling aspects of asta-Kosala-Kosali, ie the spatial arrangement based on the culture of Bali.
6. The charging process are as follows:
   - Rainwater that falls directly on the filtration pond will be filtered and fed into the well through pipes that installed in the bottom of the pond
   - Rainwater that fell in the courtyard flows through the intake tunnel into the sedimentation pond, the mud will be settled to the bottom of the pond, the water flows to the filtration pond, filtered and fed into the recharge wells

The Capacity of rechrge wells

Data :
Diameter (d) = 1 m
Debt of recharge wells (L) = 9 m
The water volume in the recharge wells (V)

$V = 1/4\ \pi\ d^2 * 9\ m$

$= ¼\ \pi * 1\ m^2 * 9\ m$

$= 7{,}07\ m^3$

Rainwater harvesting (Q1) = 1,296 m3/day

The estimate effective that will fulfill the recharge wells is 70%

The period needs to fulfill the recharge wells (T1)

T1 = 70% * V / Q1 = 7.79 days

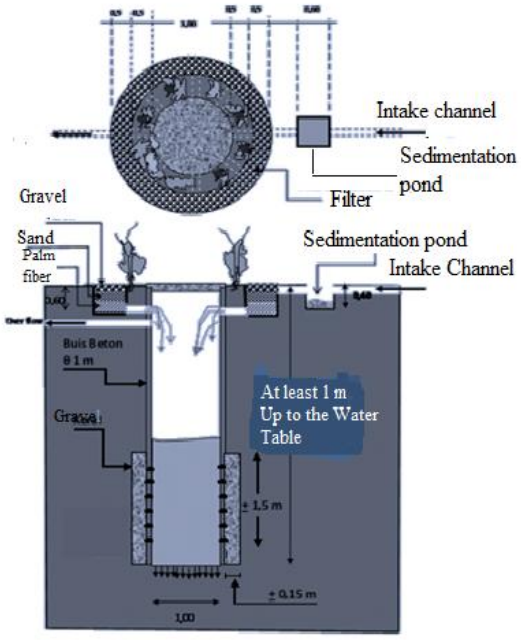

Fig. 4 Concrete Recharge Wells

Analyses showed that the average infiltration rate in the region of North Denpasar is:

If = 0.00000054 mm/sec.
= 0.001944 m/hour

The water infiltration volume (Q2)

Q2 = ¼ π x 1 * 1 * 0.001944
= 0.0110322 m3/hour
= 0.2647728 m3/day ~ 0,265 m3/day

Thus, the time required absorbing water until all the water in the recharge wells entirely permeated (T2)

T2 = 7,07/0.265 = 26,68 day ~ 27 day

If each household makes 1-recharge wells, the total volume of water infiltration (Q3) during wet month (4 months = 120 days)

Q3 = Total household*Wm/T2*V
= 220.150 * 4/27) * 7.07
= 6.917.602 m3/year
= 18.952,33 m3/day = 222,40 l / sec

Deficit of recharge water

The average of daily needs in Denpasar City is 165 l/day/person.

The wet months (Wm) is 4 months/year

Total water needs

Q4 = Total household*Wm*Dn
= 220.150 x 4 x 165
= 150.552.600 l/day = 1.742 l/sec

The daily needs that supplied by local government company is 478 l/sec. Thus, the ground water usage (Q5)

Q5 = 1.742 l/sec - 478 l/sec
= 1.264 l/sec

The obligation to restore ground water is at least 20% of usage (Qr) = 0.2 * 1.264 l/sec = 252,8 l/sec

Rainwater harvesting Q3 = 222,40 lt/dt (87.975% Qr)

Then the groundwater deficit that has not been recovered is:

Q6 = 252 l/sec - 222,40 l/sec
= 30.4 l/sec
= 12.025% Qr.

DISCUSSION

Groundwater comes from rainwater infiltration through pores or cracks in rock formations as well as of the flow of surface water such as rivers, lakes, and reservoirs that seep through the soil into the lane saturated through hydrological processes [10]. Arimitsu at all [11] found out that hydraulic gradients between 100 cm depth and the soil-bedrock interface were indicating that subsurface water flowed from the upper area to the lower end of the slope at all times. These results indicate that the saturation occurred after very small amounts of rainfall, regardless of soil moisture conditions. Under ideal conditions, the hydrological cycle will naturally maintain a balance between inputs, savings and output, but the development of the industry as well as changes in activity/human behavior disturbing the balance so that there arises the issue of global water crisis. The main cause of the global water crisis is partly due to increased water demand, global climate change, the lack of catchment areas or the lack of surface water storage [3] [4] [5]. The main problem in the management of groundwater, especially in developing countries is the limited supply of water from surface water sources due to land conversion, exploitation of groundwater due to industrial development, the behavior of people who are less concerned about the preservation of the environment which ultimately led to the decline of groundwater, sea water intrusion, groundwater pollution, and land subsidence. This is similar to the results of research by Tirtomihardjo and Setiawan [12]. It was reported that the changing in land use in Bali have led to a decline in groundwater levels up to 60-73 m below ground surface (bgs). Meanwhile, Sudiajeng et all. [13] reported that the exploitation of groundwater through deep bore wells by the hotel and supporting industries in Denpasar reached depths between 70-200 m bgs and caused the critical potencies of groundwater resources. Exploitation of groundwater on a large scale through the deep bore wells can cause the seawater intrusion and degrade groundwater quality. Sudiajeng [2] reported that in the whole area of Denpasar has been experienced of seawater intrusion. Based on the 134 wells tested, 89.06% had Electrical Conductivity (EC) <1000 µ mhos/cm and 10.94% between 1000-2079 µ mhos/cm (Figure 2. & Figure 3.). Moreover, Sukaarsana et al. (2015) [14] reported that in the region of North Kuta - Badung Bali, an EC of 60 samples had reached 1,677 µ mhos/cm. those data showed that the EC in most of area in Bali, including Denpasar regency had already in the upper limit, even exceeding the threshold limit (EC <2000 µ mhos/cm). One of the simple programs to increase the water level as well as the quality of groundwater is by building domestic recharge wells.

Building the domestic recharge wells is simple and easy, but one of the obstacles is the lack of awareness of people. This could happen because

people did not know how important is the water conservation program and they were not directly involve both in the identification of problems, building plan and implementation for solutions. Therefore, this research used the ergonomics approach that puts all stakeholders to participate in the planning process as well as the implementation programs so the sustainable implementation of the domestic recharge wells for harvesting rainwater can be assured. All the stakeholders contributed their opinion in the FGD through Systemic, **H**olistic, **I**nterdisciplinary, and **P**articipatory (**SHIP**) approach. Systemic means that the plan should be analyze through a system; Holistic means that each teamwork should interrelate with other team works; Interdisciplinary means that the analyses should be utilized by all related discipline; and Participatory means that all relevant stakeholders should be involved. The main goal of ergonomics SHIP approach is to attain the humane and sustainable work system [15][16]. By synergizing the principle of ergonomics approach with the science of hydrology, is expected to have a domestic recharge wells in which emphasizes the advantages, limitations, and the permissibility of human as a subject in each phase of the design and implementation. As the result, it can be designed an appropriate technology which is humane, fit with the local socio-culture, friendly to environment, and preserve energy. Through the ergonomic SHIP approach, this research has changed the mind-set that the wells are not always there in the back yard with slum condition, but it can be placed in the front yard, together with the beauty of the house. With this mind-set, people will have self-motivation to build the domestic recharge well in their yard and finally increasing the awareness to the environment.

The application of ergonomics in various aspects began to grow rapidly. This is emphasized by some implementation of ergonomics in the working system that has been shown the increasing awareness of stakeholders on the sustainable development programs [7][17][18].

Hydrogeological analyses showed that the domestic recharge wells could harvest the rainwater about 1,296 m3/day or recovered about 87.975% of the obligation of recharge water for domestic usage with assumption that each household build about 100 m2 of the house. It is expected to increase the groundwater level as well as the water quality. Refers to the Stiefel and Melles [19], rainwater harvesting was improve the water quality through the dilution of chemical constituents in groundwater. In addition, the rainwater harvesting is still safe to drink and can be a potential alternative source of water supply [20].

Currently, in the ongoing research is being built two prototype domestic recharge wells and will be measured empirically about its effectiveness in recharging water into the ground. It is expected that rainwater harvesting through the domestic recharge wells will reduces the effect of seawater intrusion as well as increases the groundwater level in Denpasar Regency. The previous research showed that all area in Denpasar regency experienced of seawater intrusion, although some of area were still under threshold limit, but some others were already in the upper limit, even out of the limit, especially in South Denpasar, which is directly adjacent to the sea.

Water is life. Groundwater is a renewable resource, but it is not infinite. If the sustainability of groundwater resource is threatened, our lives will be in danger. Therefore, groundwater conservation programs are very important ranging from the simplest things such as domestic recharge wells to injection wells in high technology.

CONCLUSSION

1. Ergonomic SHIP approach has changed the mind-set that the wells are not always there in the back yard with slum condition, but it can be placed in the front yard, together with the beauty of the house.
2. Hydrogeological analyses showed that the domestic recharge wells could harvest the rainwater about 1,296 m3/day or recovered about 87.975% of the obligation of recharge water for domestic usage.

RECOMMENDATION

1. Law-reinforcement is needed to build awareness of people on the conservation program.
2. People that build more than 100 m2 should build more than one recharge wells or bigger dimension of recharge wells.
3. It is needed water conservation to meet the groundwater exploitation by industry, especially tourism industry.
4. Socialization about “saving water” should be done started from the early age.

ACKNOLEDGMENT

This research paper is made possible through the help and support from everyone, especially the Public Work Department of Denpasar City and the Directorate General of Research and Development – Ministry of Research, Technology, and Higher Education.

REFERENCES

[1]. Bali Province. 2010. Report of Strategic environmental assessment in the province of Bali.

[2]. Sudiajeng, Lilik.; Parwita, I Gusti Lanang Made; Wiraga, I Wayan.; Andayani, Kt. Wiwin. 2014. Analyses of Recharging Area for Ground Water Conservation in Denpasar Regency. Proceeding of the 2nd National Conference on Vocational Civil Engineering. Bali – Indonesia, 18 – 19 September 2014 (written in Indonesia).

[3]. Bouwer, Herman. 2001. Artificial recharge of groundwater: hydrogeology and engineering, Hydrogeolosy Journal (2001) Vol. 10. Page : 121-142.

[4]. Wang, Jinfeng; Gao, Yanchun; Wang, Sheng. 2015. Land Use/Cover Change impacts on Water Table Change over 25 Years in a Desert-Oasis Transition Zone of the Heihe River Basin, China. Water 2016, 8, 11; doi:10.3390/w8010011.

[5]. Adham, A.K.M.; Kobayashi, Akira; Murakami, Akira. 2011. Effect of Climatic Change on Groundwater Quality Around the Subsurface Dam. International Journal of Geomate, Oct. 2011, Vol. 1, No.1 (Sl. No. 1), pp. 25-31

[6]. Liu, Hai-Long; Bao, An-Ming; Pan, Xiang-Liang; & Chen, Xi. 2013. Effect of Land-Use Change and Artificial Recharge on the Groundwater in an Arid Inland River Basin. Water Resour Manage (2013) 27:3775–3790. DOI 10.1007/s11269-013-0380-6

[7]. Ma, Le. 2016. The Links Between Land Use and Water Quality for Freshwater Pearl Mussel, Margaritifera, in the River South Esk, Scotland. International Journal of Geomate, July, 2016, Vol. 11, Issue 23, pp. 2222-2227.

[8]. Denpasar Regency. Available at www.denpasarkota.go.id

[9]. Sudiajeng, Lilik; Sumetri, Wayan; Rumini, Inten; and Paramita, Patricia. 2007. Total Ergonomics Approach in Developing Sustainable Mangrove Forest Action Project in Bali. Proceeding of Agriculture Ergonomics Development Conference. Malaysia, 26-29 November 2017.

[10] Toth, J. 1990. Introduction to Hydrogeology. Geology Department, Faculty of Science, University of Alberta, Edmonton, Canada.

[11]. Arimitsu, Yuuki; Fujimoto, Masamitsu; Hiraoka, Nobutaka; Danjo, Toru; Ishida, Yuko; and Ryoichi Fukagawa. 2016. Characteristics of Rain Infiltration in Soil Layers on the Hillslope Behind Important Cultural Asset. International Journal of Geomate, June, 2016, Vol. 10, Issue 22, pp.2109-2115

[12]. Tirtomihardjo, H. and Setiawan, T. 2011. Simulation of Denpasar-Tabanan Groundwater Basin Flow, Bali Province. Indonesian. Journal of Geology, Vol. 6, No. 3, September 2011. Page. : 145-163 (written in Indonesia).

[13]. Sudiajeng, Lilik. 2015. The Study on Ground Water Conservation in Bali Province. Keynote paper in the National Seminar of Indonesian Geologists Association (IAGI), Denpasar, April 25, 2015 (written in Indonesia).

[14] Sukaarsana, I Made; Dharma, I Gusti Bagus Sila; and Nuarsa, I Wayan. 2015. The Study on the Sewater Intrussion in Coastal Area North Kuta Sub-Regency, Badung Regency. *Ecotropic :* journal of Environmental Science, Vol. 9, No. 2 (2015), 72-78; 22 September 2015. University of Udayana Press. (Written in Indonesia).

[15] Manuaba, A. 2007. Total Ergonomics Approach on Product and Development to attain Humane, competitive, and Sustainable Work System and Product. National Seminar on Ergonomics 2007. Ergonomics Integration on Product Development. Bandung – Indonesia. July 26-28, 2007.

[16] Zink, Klaus. 2007. Ergonomics in the Past and the Future: from a German Perspective to an International One. Ergonomics, Vol. 23. Taylor & Francis. London.

[17] Sudiajeng, Lilik. 2010. Ergonomics SHIP Approach for Sustainable Development of Woodworking Workshop. Proceeding of International Conference on APCHI-Ergofuture 2010, Bali – Indonesia, 2 – 5 August 2010.

[18] Sudiajeng, Lilik; Adiputra, N.; Lebbrandt, R. 2012. Ergonomics Work Station Decreases the Health Impairment and Save Electrical Energy at the Woodworking Workshop in Bali, Indonesia. Journal of Human Ergology, Vol. 41, No. 1,2, 2012. Japan.

[19] Stiefel, John M. and Melesse, Assefa M. 2009. Effect of rainwater-harvesting-induced artificial recharge on the groundwater of wells in Rajasthan, India. Hydrology Journal (2019), 17:2061-2073.

[20] Payus, Carolyn and Meng, Kui Jun. Consumption of Rainwater Harvesting in Term of Water Quality. International Journal of Geomate, Dec., 2015, Vol. 9, No. 2 (Sl. No. 18), pp. 1515-1522.

Second International Conference on Science, Engineering & Environment,
Osaka City, Japan, Nov.21-23, 2016, ISBN: 978-4-9905958-7-6 C3051

ESTABLISHMENT OF JET INDEX J_i FOR SOIL ERODIBILITY COEFFICIENTS USING JET EROSION DEVICE (JEd)

Saerahany L. Ibrahim[1], Jazuri Abdullah[1], Khairulafinawati Hashim[2] and Junaidah Ariffin[1]
[1]Faculty of Civil Engineering, Universiti Teknologi MARA, Shah Alam, Malaysia, [2]Faculty of Civil Engineering, Universiti Teknologi MARA, Pulau Pinang, Malaysia

ABSTRACT

Soil erodibility has been identified as one of the major factors that govern threshold of resistance to erosion. Accurate measurement of soil erodibility in the field is indeed important for the determination of critical shear stresses. Critical shear stress is the stress that initiates particle movement that promotes shifting of the bankline. An attempt to establish soil erodibility parameters was successfully carried out using a newly fabricated Jet Erosion Device (JEd) based on soil properties. Soil erodibility coefficients are introduced to represent the erodibility of the soils under study. Statistical test is used to confirm the validity and accuracy of the proposed technique. Field data measurements were carried out on 3 rivers. Empirical models were developed using data from Selangor river and validated using data from Bernam and Lui rivers and other secondary river data. Analyses have shown high correlations and the parameters were further examined and analysed for the development of a predictive relationship for Ji. The most accurate model was selected based on the adjusted R^2, standard error of the estimate and discrepancy ratio to illustrate its significance. Selection of the predictive variables was based on their ability to explain the variation of J_i. The models established could significantly reduce the cost, time and usage of water supply for field data collection using JEd.

Keywords: Jet index, soil erodibility coefficients, Jet Erosion Device (JEd), statistical analysis

INTRODUCTION

Increased in river bank erosion and lateral migration rates are conceivably due to the increasing of hydraulic shear or increasing of bank erodibility [1]. The evaluation of critical shear stress and erodibility is of main importance for modelling river bank erosion problems.

Most relationship for soil erodibility is shown either through equations or lists of parameters. The variables reviewed indicated that the most repetitively mentioned variables for soil erodibility are critical shear stress, bulk density, shear strength and particle size distribution (percentages of clay, silt and sand). The three latter values can be obtained directly through laboratory experiments. Critical shear stress, τc determination requires indirect measurement and calculations. Besides the mentioned variables, erodibility coefficient, K or k_d is also used as a representation of soil erodibility which consists of various different variables. However, it is found that established relation of erodibility coefficient, k_d are mostly for surface erosion. (e.g. [2]). Most fluvial erosion studies were focused on critical shear stress relationship to soil properties. Some researchers had linked τc to k_d (e.g. [3]-[6]). Soil properties such as water content and densities tests were also identified in the determination of erodibility [7].

There are a number of measurement techniques to identify the soil erodibility. One of the methods which can be employed both in the laboratory and in the field is the Jet Erosion Test (JET). This study particularly utilized the newly developed equipment fabricated from the aforementioned JET namely Jet Erosion Device (JEd) as shown in Fig. 1 which was introduced briefly by [8] and explained comprehensively by [9] on the method procedures, calibration and verification of the fabricated equipment and appropriate analysis chosen. This paper involves the relationship of soil erodibility parameters established from the Jet Erosion Device (JEd) to the soil properties obtained through the laboratory and in situ tests. Statistical regression analysis were performed on these parameters against the erodibility coefficients to assess whether basic soil properties results could be used to represent the erodibility of a particular river as an extension of the JEd results.

STUDY AREA

Three different rivers located in the state of Selangor, Malaysia were chosen for this study. Each river was reported to experienced series of flood events that causes riverbank erosion and bank

failures. JEd tests were conducted on different points of locations and soil samples were taken at each point.

Fig. 1. JEd test at field location

JEd Testing and Soil Properties Determination

Riverbanks at each site of Selangor River, Bernam River and Lui River were tested in situ using the Jet Erosion Device (JEd) to obtain the soil erodibility parameters of Jet Index (J_i) and erodibility coefficient (k_d). Undisturbed or disturbed soil samples at each location were either tested in situ or were collected and tested in the laboratory to obtain the soil properties values. Disturbed soil samples were extracted from each location of selected sites using a hand auger at locations where Jet Erosion Device (JEd) tests were conducted (Fig. 2). In total, 30 samples were collected from each site and taken to the laboratory for further testing prior to the required basic soil parameters.

Fig. 2. Post JEd test soil condition

The soil samples laboratory analysis using ASTM standards were conducted to identify the basic soil properties such as the moisture content (WC(%)), soil classification (%Sand, %Silt, %Clay), Atterberg limits consisting of plastic limit (PL), liquid limit (LL) and plasticity index (PI), specific gravity (SG), bulk density (ρ_b) and dry densities (ρ_d). In situ tests for the undrained soil shear strength (S_u) were also conducted at each test points using a pocket penetrometer.

Some of these physical properties influence the cohesive soils erosion [10]. Some riverbank erosion studies incorporate soil properties characteristics to enhance the analysis results such as the effect of seepage behavior due to water fluctuations on riverbank stability [11]. There are substantial differences between the effects of soil parameters towards erodibility of cohesive and noncohesive soils [12] where the erodibility of cohesive soils are influenced by grain size distribution, bulk density, clay type and clay content, organic matter content, and pore and water chemistry [11]. Reference [13] stated that the soil properties shown to be most important in noncohesive soils erosion, which is controlled primarily by gravitational forces, grain size distribution, grain shape, and particle density. The selection of variables for the soil properties to be tested is based upon the works of previous researches on channel erosion such as [14], [15], [10], [16], [17], [18] and [12]. More recent relationship established are from [19], [20] and [21].

DATA ANALYSIS

Jet Erosion Device (JEd) Test Analysis

Data from the JEd tests were evaluated to determine soil erodibility coefficients, k_d, following the procedures of [22] and [23]. Initially jet indices were obtained from the plotted graph of D_s/t versus $U_o\ (t)^{-0.931}$ where D_s is the maximum depth of scour for each time interval (cm) and U_o is the velocity of the jet at the nozzle (m/s) and t is time in seconds. The equation $k_d=0.003e^{385J_i}$ introduced by [24] where k_d is the erodibility coefficient (cm3/N-s) and J_i is the jet index were used to assess the category of the JEd results. The physical soil properties results were also compared. The results indicated the categories of resistance to erosion from moderate resistance to high resistance based on the Jet Index values. Selangor River and Bernam River seem to have a mixture of moderate and high resistance categories while Lui River was dominated by the high resistance category.

Graphs in Fig. 3(a) and 3(b) depicts the boxplots of Jet Index, J_i and erodibility coefficient, k_d data range for all three rivers. The vast difference in k_d variability between Bernam River, Selangor River and Lui River can be observed in both figures. The jet index and erodibility coefficient values of Bernam River are wider in range as compared to Selangor River and Lui River. This most probably caused by the variability of the soil condition of the locations selected in performing the JEd tests. The large variability of both values measured in the field suggest that changes in streambank surface soils due to subaerial processes play a significant role in determining the minimum shear stress required to

initiate sediment movement for cohesive soils. The variability of these results could be caused by variety of variables such as the presence of gravel or roots at the JEd site, differences in moisture content, or soil heterogeneity. Subaerial processes and soil heterogeneity are the most possible variability occurrence mentioned by previous studies ([4] and [19]).

Statistical Analysis of Overall Data Set

The field data were analyzed using statistical analysis to observe the correlation between parameters by using the Pearson's correlation coefficient calculation which include Pearson's r for the entire data set of erodibility coefficient, k_d with the corresponding p-value. For clarity, only those coefficients greater than 0.3 with p-values less than 0.05 are considered. Results from this analysis indicated k_d was negatively correlated to percentage of water content (%WC; r = -0.336, p = 0.045), void ratio (e; r = -0.442, p = 0.007) and porosity (n; r = -0.46, p = 0.005). Soil k_d is positively related to the bulk density (ρ_b; r = 0.516, p = 0.001) and dry density (ρ_d; r = 0.452 , p = 0.006).

Having over 50% of the variance in each erosion parameter, bulk density appeared to have the greatest influence and positively related to k_d. This finding endorses the observations made during jet erosion test field data collection that density of soils influences the scour depths of each tests. It was found that little scour occurred on high density soils during jet tests [19]. However, the Pearson correlation indicated the other significant soil parameters were strongly correlated to soil water content though the contradicting results do not affect the development of the erodibility parameters relationship to soil properties. Attempts were made to establish the relationship of J_i to the observed soil properties as published in the past ([12], [25] and [21]).

Model Regression and Validation

The statistical analysis was utilized to assess the goodness fit and the goodness prediction of a regression model in order to choose the best model. In the linear multiple regression models considered for J_i, the predictors selected are soil water content (%), bulk density (Mg/m^3), dry density (Mg/m^3), void ratio, particle size distribution (% clay, silt and sand), plasticity index (PI) and activity which is the PI divided by the clay percentage of the soil. The selection of these variables is based on the reported Pearson correlation analysis.

The Selangor River data were regressed using simple linear regression backward method. The models developed with the coefficient of determination, R^2, significance of F value and p-value are summarized in Table 1. The coefficients produced from the analysis were then verified using a total of 45 combined data sets obtained from Jet Erosion Device (JEd) field measurement for Lui River and Bernam River with additional secondary data from [12] to vary the data hence giving a more reliable relationship. Based on this step, the accuracy of the equation is measured using discrepancy ratio (DR) distribution of 0.5 – 2.0 limit. The developed models showed the DR value ranging from 67.4% to 72.1% for the combined data sets for the accuracy evaluation of the equations. The equations and details statistical outputs for the models are shown in Table 2.

Out of the all eight models, Model 2, Model 4 and Model 7 gave highest DR values of 72.1%. However, the lowest significance of p-value is shown for Model 7 which is 0.06. The rule of thumb of statistical evaluation specified that p-value greater than 0.05 will give a poor fit for the linear curve. Therefore, Model 7 is considered the best-fit linear equation model for this relationship although its p-value slightly higher than 0.05 and low R^2. However, other models could also be considered due to DR values higher than 50% and depending on the availability of soil properties information provided for each specific site locations. Graphs of the predicted erodibility coefficient to observed erodibility coefficient for each linear equation are given in Fig. 4. The plotted graphs show that the range of observed and predicted data falls within the DR distribution limits.

CONCLUSION

Erodibility parameters using Jet Erosion Device (JEd) can be measured directly through a designated analysis of ASTM-D5852 standard or by [22] and [26]. However, the method requires the availability of the specialized equipment and also the results are site specific. Therefore, an attempt was made to allow for results of in situ and laboratory testing of soil materials to be used to quantify the erodibility parameters. The establishment of this relationship would significantly limits the cost and time spent for field data collection studies. Additionally, it would also allow for the extension of the erodibility parameters throughout the upstream to downstream of a studied river assuming that the site geology and measurable soil material consists of homogeneous properties.

ACKNOWLEDGEMENT

This research was financially supported by the project: "Soil Erodibility Assessment for Stream Bank Erosion and Stability. (600-RMI/RAGS 5/3 (172/2014))" funded by the Ministry of Higher Education, Malaysia.

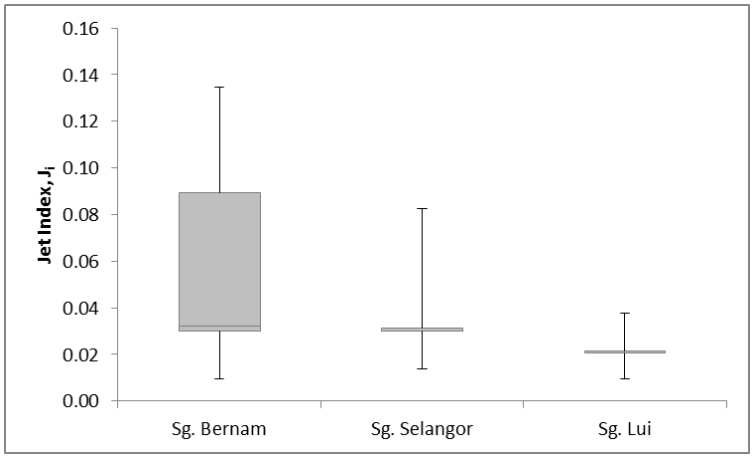

(a)

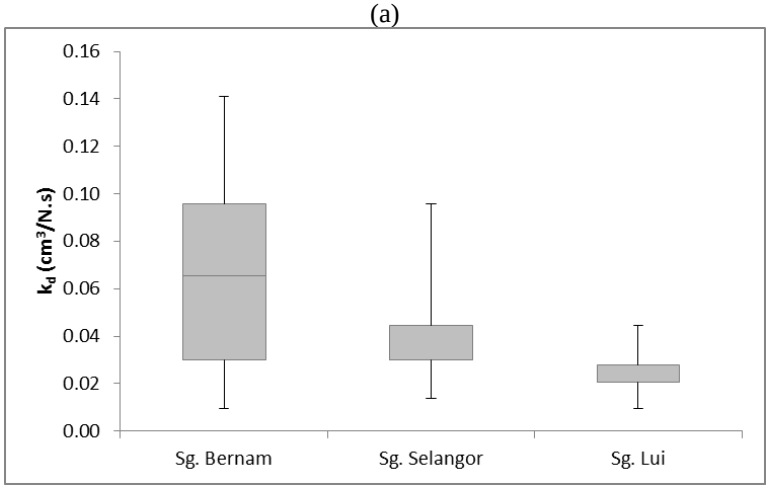

(b)

Fig. 3. Boxplot of Jet Index, Ji (a) and soil erodibility, kd (b) measurements for Bernam River, Selangor River and Lui River

Table 1 Model equations and verification statistical output details

No.	Model	R^2	F	p-value	Discrepancy Ratio, DR
1	$J_i = 0.02 + 0.0004w\% - 0.022\rho_b + 0.022\rho_d - 0.015e + 1.44\times10^{-5}\%clay - 4.01\times10^{-5}\%silt - 8\times10^{-5}\%sand - 0.0001PI + 0.0015Act$	0.418	0.879	0.57	67.4
2	$J_i = 0.021 + 0.0004w\% - 0.021\rho_b + 0.02\rho_d - 0.015e - 5.06\times10^{-5}\%silt - 8.60\times10^{-5}\%sand - 9.17\times10^{-5}PI + 0.0013Act$	0.418	1.076	0.44	72.1
3	$J_i = 0.0087 + 0.0002w\% + 0.028\rho_b - 0.0092e - 4.56\times10^{-5}\%silt - 8.11\times10^{-5}\%sand - 6.59\times10^{-5}PI + 0.0013Act$	0.408	1.279	0.33	69.8
4	$J_i = 0.014 + 0.0002w\% - 0.106e - 4.60\times10^{-5}\%silt - 8.01\times10^{-5}\%sand - 6.21\times10^{-5}PI + 0.0012Act$	0.407	1.599	0.22	67.4
5	$J_i = 0.013 + 0.0002w\% - 0.012e - 3.96\times10^{-5}\%silt - 5.62\times10^{-5}\%sand + 0.0007Act$	0.392	1.933	0.15	72.1
6	$J_i = 0.012 + 0.0002w\% - 0.011e - 2.2\times10^{-5}\%silt - 3.45\times10^{-5}\%sand$	0.377	2.418	0.09	67.4
7	$J_i = 0.011 + 0.0002w\% - 0.011e - 2.47\times10^{-5}\%sand$	0.351	3.061	0.06	72.1
8	$J_i = 0.08 + 0.0002w\% - 0.009e$	0.300	3.856	0.04	67.4

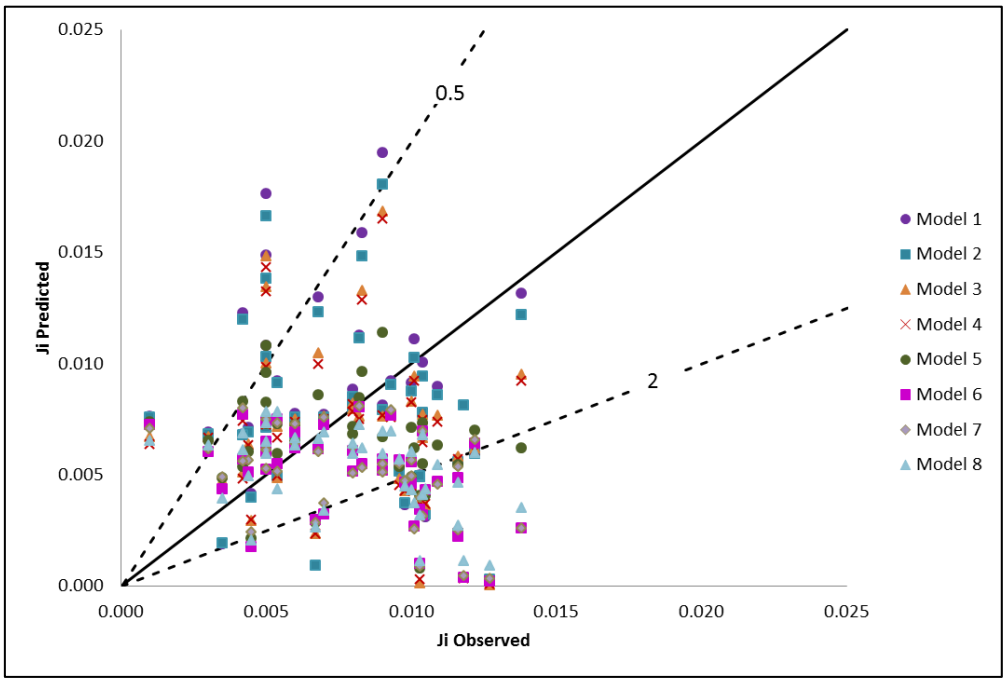

Fig. 4. Predicted J_i versus Observed J_i

REFERENCES

[1] Howard AD, "Simulation model of meandering", In: C.M. Elliott (Editor), River Meandering. Am. Soc. Civ. Eng., New York, N.Y., 1984, pp. 952-963.

[2] Grabowski RC, "The erodibility of fine sediment deposits in lowland chalk streams", PhD Thesis submitted In Geography: Queen Mary, University of London. 2010.

[3] Osman AM and Thorne CR, "Riverbank stability analysis I: Theory", The Journal of Hydraulic Engineering, V. 114, 1988, pp. 134-150.

[4] Hanson GJ and Simon A, " Erodibility of cohesive streambeds in the loess area of the Midwestern USA", Hydrol. Proc. 15(1), 2001, pp. 23-38.

[5] Wynn TM, "The effects of vegetation on stream bank erosion." Doctor of Philosophy, Biological Systems Engineering, Virginia Polytechnic Institute and State University, Blacksburg, Virginia, 2004.

[6] Karmaker T and Dutta S, "Erodibility of fine soil from the composite river bank of Brahmaputra in India", Hydrological Processes, vol. 25, no. 1, 2011, pp. 104–111.

[7] Hanson GJ, "Field and laboratory jet test testing method for determining cohesive material erodibility", Proc. Of Federal Interagency Sedimentation Conference, Reno, Nevada, 2001.

[8] Ariffin J and Ibrahim SL, "Jet Erosion Device For Bank Erodibility Measurement", International Conference on Advances in Civil and Environmental Engineering (ACEE 2015) Conference Proceedings, 28th – 30th July 2015, pp. D-128-D-133

[9] Ibrahim SL, Ariffin J, Abdullah, J, and Muhamad NS, "Jet Erosion Device (JED) - Measurement of Soil Erodibility Coefficients", Jurnal Teknologi (Sciences & Engineering) 78:5–5, 2016, pp. 63–67

[10] Grissinger EH, "Bank erosion of cohesive materials", In: Hey, R. D., J. C. Bathurst, and C. R. Thorne, eds.: Gravel-bed Rivers, John Wiley & Sons: Chichester, UK, 1982, pp. 273-287.

[11] Oya1 A, Bui HH, Hiraoka N, Fujimoto M and R. Fukagawa, "Seepage Flow-Stability Analysis of The Riverbank of Saigon River Due To River Water Level Fluctuation", Int. J. of GEOMATE, Vol. 8, No. 1 (Sl. No. 15), March, 2015, pp. 1212-1217.

[12] Allen PM, Arnold J, and Jakubowski E, "Prediction of stream channel erosion potential", Environmental and Engineering Geoscience, v. 3, 1999, pp. 339-351.

[13] Graf WH, "Hydraulics of Sediment Transport", McGraw Hill, New York, 1971, pp. 513.

[14] Lyle WM and Smerdon ET, "Relation of compaction and other soil properties to the erosion resistance of soils", Transactions of the ASCE, v. 8, n. 3, 1965, pp. 419-422.

[15] Thorne CR, "Processes and mechanisms of river bank erosion." Gravel- bed rivers, R. D. Hey, J. C. Bathurst, and C. R. Thorne, eds., John Wiley and Sons, United Kingdom, 1982.

[16] Partheniades E, "Erosion and deposition of

cohesive soils" Journal of the Hydraulics Division, ASCE, 91(HY1), 1965, pp.105–139.
[17] Samad MA, Baird DC, Vermeyen TB, and Mefford BW, "Erosion Characteristics of Cohesive Sediments", Water Resources Engineering: Proceedings of the First International Conference, ASCE, 1995, pp.425-429.
[18] Roberts J., Jepsen R., Gotthard D., and Lick W. 1998, Effects of particle size and bulk density on erosion of quartz particles. Journal of Hydraulic Engineering, Vol. 124, No. 12, pp. 1261–1268.
[19] Wynn TM, Henderson MB, and Vaughan DH, "Changes in streambank erodibility and critical shear stress due to subaeriel processes along a headwater stream, southwest Virginia, USA",Geomorphology, 97(1), 2008, pp.69-82.
[20] Thoman RW, and Niezgoda SL, "Determining erodibility, critical shear stress and allowable discharge estimates for cohesive channels: Case study in the Powder River basin of Wyoming." Journal of Hydraulic Engineering, 34(12), 2008, pp.1677-1687.
[21] Egwuonwu CC and Okereke NAA, "Characterization of erodibility using soil strength ans stress-strain indices for soils in some selected sites in Imo State", Research Journal of Environmental and Earth Sciences, 4(7), 2012, pp.688-696.
[22] Hanson GJ, "Development of a jet index to characterize erosion resistance of soils in earthen spillways", Transactions of the ASCE, v. 34, n. 5, 1991, pp.2015-2020.
[23] ASTM, Annual Book of ASTM Standards, Section 4: Construction. West Conshohocken, Pa, 2006.
[24] Hanson GJ, "Surface erodibility of earthen channels at high stresses: I. Open channels testing", Trans. ASAE, 33(1), 1990, pp.127-131.
[25] Potter KN, de Velázquez-Garcia J, Torbert HA, "Use of a submerged jet device to determine channel erodibility coefficients of selected soils of Mexico", Journal of Soil and Water Conservation 57 (5), 2002, pp.272–276.
[26] Hanson G, Cook K, "Development of excess shear stress parameters for circular jet testing" ASAE Paper 972227, 1997.

Second International Conference on Science, Engineering & Environment,
Osaka City, Japan, Nov.21-23, 2016, ISBN: 978-4-9905958-7-6 C3051

ESTIMATING FLEXURAL RELIABILITY OF CARBONATED RC BRIDGE BEAMS USING PARTICLE FILTER

Jonathan Sanchez[1], Samantha Louise Jarder[2], Nestor de Ocampo[3],
Allen Cyro Teruel[4] and Lessandro Estelito O Garciano[5]
[1]Undergraduate student, De La Salle University;[1-4] Associate Professor, De La Salle University;[5]

ABSTRACT

Many of our reinforced concrete structures today are ageing at the same time subjected to carbonation. It occurs when atmospheric carbon dioxide reacts with the components of the hydrated cement. In this regard, the authors estimated the probability of flexural failure of a deteriorated reinforced concrete (RC) beams subjected to carbonation. In the reliability analysis, the resistance degrades over time due to a change in the concrete compressive strength caused by carbonation. The load was modeled as a uniformly distributed on a simply supported beam. The results of the Monte Carlo simulation of an example bridge showed a decrease in the compressive strength due to carbonation. To estimate the present state of the RC beams, particle filter was used in conjunction with observation data from rebound hammer tests on the bridge.

Keywords: Carbonation, Monte Carlo, reinforced concrete, reliability analysis

INTRODUCTION

Several studies have shown that carbonation can affect the durability of concrete (Chi, J. M. Huang, R. and Yang, C. C., 2002, Saetta, A.V., and Vitaliani, R. V., 2004) as well as its service life (Liang, M., Qu, W., and Liang, C., 2002, Liang, M., Huang, R., and Fang, S., 2013). Carbonation occurs when atmospheric carbon dioxide (CO_2) reacts with the compounds of hydrated cement such as calcium hydroxide, di-calcium silicate, and tri-calcium silicate (Claisse, P. A., Elsayad, H. I., and Shaaban, I. B., 1999). As carbonation progresses to the concrete layer surrounding the reinforcing steel, the pH of this high alkaline layer drops initiating corrosion. Over time the surrounding concrete spalls or crack leading to a higher probability of serviceability failure or service life reduction.

The rate carbonation is affected by the temperature, relative humidity, water-cement ratio, aggregate-cement ratio and CO_2 concentration. Carbonation also shrinks the volume of concrete due to the change in the morphology of the C-S-H gel from fibrous to dense. This causes the coarse pores to change into much finer pores. Water also initiates carbonation process and occurs mostly on submerged foundation and underwater reinforced concrete (RC) columns. In this case the amount of carbonates in water is far less so the rate of carbonation is significantly lower (Gode, K. and Paeglitis, A., 2009). Reliability assessment on the effects of carbonation depth to the performance of RC structures have also been studied (Hagino, T., Akiyama, M., and Frangopol, D, 2014, Akiyama, M., Frangopol, D. M., and Yoshida, I, 2010; Na, U.J., Kwon, S-J, Chaudhuri, S. M., and Shinozuka, M, 2011). However studies on how the probability of flexural failure (P_f) degrades over time due to carbonation-induced change in the compressive strength of concrete is lacking.

Consider a time variant reliability problem shown in Fig. 1 where M_S and $M_R(t)$ are the random load and resistance, respectively. Due to the deteriorating nature of $M_R(t)$, the probability of failure (p_f) increases over time. If the mathematical models (and the parameters) for $M_R(t)$ and M_S are prescribed, simulation techniques such as Monte Carlo simulation will suffice to determine p_f.

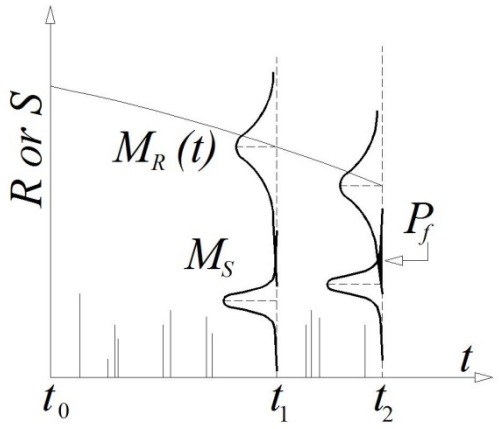

Fig.1Time dependent reliability problem

In this paper, the authors estimate the p_f of a simply supported RC bridge using Monte Carlo simulation subjected to a random moment load and a carbonation-induced deteriorating moment

resistance. In Figure 1 the resistance is deteriorating while the load varies randomly. At a specific time t_1 the p_f is low but at t_2 it increases. The above results (at a specific time T) can be updated using particle filter when data related to carbonation such as compressive concrete strength and relative humidity are observed as shown in Figure 2.

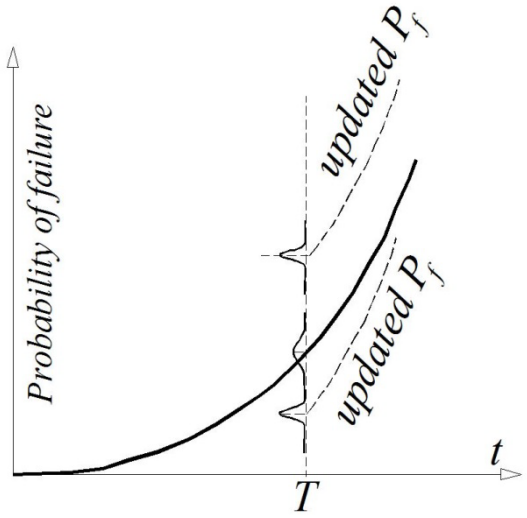

Fig. 2 Updated P_f conditioned on the observation

Depending on the severity of the observed data, the previously estimated p_f can either be under or over estimated. Thus with this new information and the carbonation-induced deteriorating RC beam model an updated curve can be obtained. This paper is organized as follows: (*a*) the general filtering problem and its usage in the present problem of carbonation, (*b*) reliability analysis of a RC beam (*c*) analysis and results of the research and finally (*d*) some recommendations.

RELIABILITY ANALYSIS

Limit state function

Consider a limit state function of the form

$$g(t) = M_R(t) - M_S, \tag{11}$$

with the probability of failure as

$$p_f = p(g(t) < 0). \tag{12}$$

If the distribution and parameters of $M_R(t)$ and M_S are known then Monte Carlo simulation will suffice to determine p_f(or the reliability index). If n_s is the total number of sample realizations of G while n_o is the sample realizations where $G< 0$, then the p_f is obtain using Eq. 13 below.

$$p_f \approx \frac{z_o}{z} \tag{13}$$

Furthermore if inspection data related to any of the random variables of $M_R(t)$ can be obtained, then p_f can be updated using Bayesian updating technique such as particle filter (Garciano and Yoshida, 2011).

Resistance of RC beam

Moment Resistance of beam

The moment resistance $M_R(t)$ of a RC rectangular section can be described as

$$M_R(t) = 0.85 f_c(t)(b)(a)\left(d - a/2\right) \tag{14}$$

where a is the depth of the stress block, effective d of the reinforcement, b is the width of the RC section and $fc(t)$ is the compressive strength of concrete at time t. In the research, three bridges were considered, but in this paper only one will be shown. The design parameters of the chosen bridge are as follows:

Dungon Bridge

This bridge runs through a small river and the columns are under water. The beams were also classified under both exposure class 1 and 3 with a mean RH of 53%. It has been in service for 33 years and is still being used for vehicular traffic.

Table 1 Bridge Characteristics

Variables	Value
service life (years)	33
length in (m)	27
w (kN/m)	11
span (m)	13.5
base (mm)	400
height (mm)	550
concrete cover (mm)	75
depth (mm)	475
no. of steel reinforcements	4
reinforcement diameter (mm)	28
f_y (MPa)	276
relative humidity (mean)	53%
exposure class classification	RH < 70, e_{c1} / e_{c3}

For the exposure class (e_c), four classes for carbonated-induced corrosion were used (Silva 1984):

e_{c1} – permanently dry / wet concrete,
e_{c2} – concrete with long periods in contact with water,
e_{c3} – concrete in open air structures sheltered from rain,
e_{c4} – concrete in open air structures not sheltered from rain.
The value of e_c depends on the distance of the structure from the shoreline or any other large body of water.

Carbonation rate

The relationship between carbonation depth and the compressive strength of concrete can be modeled as follows (Breccolotti M., Bonfigli, M. F. and Materazzi, A. L., 2013 and AIJ, 1983):

$$f_c(t) = \frac{f_c}{1 + a_{11} y^{a_{12}}} \quad (15)$$

where: $a_{11} < 0$ and $a_{12} > 0$ are constants (shown in Tables 2 and 3), y is the carbonation depth and f_c is the 28th day compressive strength of concrete.

Table 2 a_{11} values

Age (days)	a
less than 28	1.0
28-182	0.9 – 1.0 (varies linearly)
greater than 182	0.9

(Tanigawa, Baba and Mori, 1984)

Table 3 Proposed a_{12} by AIJ

Age (days)	a_{12}
28	1.0
50	0.87
70	0.84
100	0.78
200	0.72
500	0.67
1000	0.65
3000	0.63

(AIJ, 1983)

The depth of carbonation y can be determined as follows:

$$y = k\sqrt{t} \quad (16)$$

where k is the carbonation coefficient (mm/year $^{0.5}$). The carbonation rate (when $RH \leq 70\%$) is estimated using the following equation (Silva, 2014):

$$k = 0.556c - 3.602e_c - 0.148 f_c + 18.734 \quad (17)$$

Where c is the carbon dioxide content in perecent. However if $RH > 70\%$ Eq. 18 is used.

$$k = 3.355c - 0.019C - 0.042 f_c + 10.83 \quad (18)$$

where C is the clinker content (kg/m^3).

Load

The maximum moment of a simply supported beam subjected to a uniform load is given as:

$$\boldsymbol{S = M_s = wl^2/8} \quad (19)$$

where w is the deterministic uniformly distributed load and l is the length of the beam

Observation Equation

The relationship between the rebound number and the compressive strength can be represented by the equation (Shang 2012) below

$$f_c(t) = 0.032509R^{1.94172} \times 10^{-0.00789y(t)} \quad (20)$$

where R is the rebound number and $y(t)$ is the carbonation depth at time t.

ANALYSIS AND RESULTS

Time updating process

To evaluate the resistance, a total of 1000 sample realizations for every random variable were generated for each time step until t = 100 years. The parameters used in the Monte Carlo simulation are provided in the table below.

Table 4.Statistics of the random variables

Variable	Distribution Type	mean	std. dev.
c	Normal	0.80%	0.3
C	Normal	281.7	0.3
fc	Normal	21	0.3

The results of the simulation show a logarithmic relationship between time and carbonation depth (Fig. 3). Attention is directed to the upper right of the graph with e_{c1} and RH < 70% which shows the highest carbonation depth from 122.9 mm to 131 mm at t = 100 years. The bottom right of the graph

with RH < 70% and e_{c4} had the lowest results of carbonation depth of 58.9 mm. This is due to the wet and dry cycles that tend to vary the amount of CO_2 that penetrated into the structure.

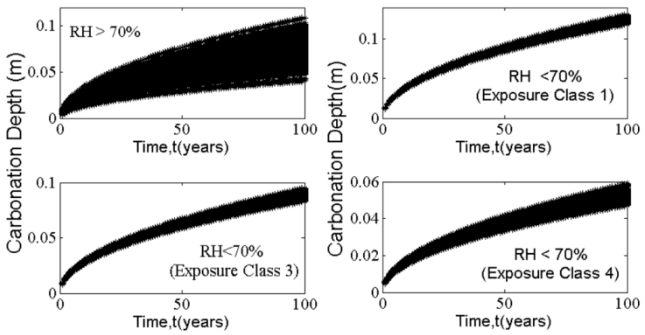

Fig.3 Carbonation growth over time

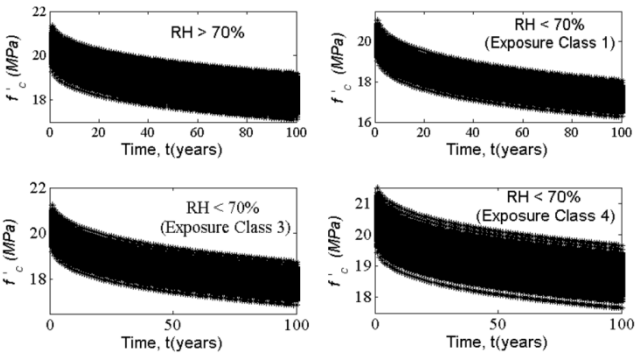

Fig.4 Compressive strength over time

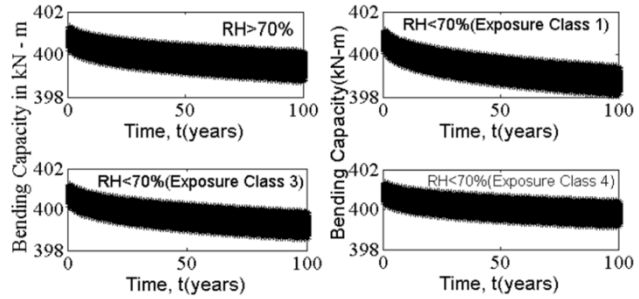

Fig.5 Bridge beam bending capacity over time

The compressive strengths of concrete as time progresses were estimated considering an increasing carbonation depth as simulated earlier (see Fig. 4). These results correspond to a reduction in the bending capacity of the beam. Since all the variables in Eq. 14 have been calculated, the bending capacity of the RC beam is calculated as shown in Fig. 5. Exposure class 1 produces the lowest bending capacity of 398.08 kN-m, followed by exposure class 3 with a bending capacity of 398.58 kN - m. Case 1 with a bending capacity of 398.74 kN - m, and finally exposure class 4 with a bending capacity of 399.1 kN - m. Having a mean bending strength of 401.11 kN - m computed from the simulation, the RC beam lost 0.75% of its bending capacity solely due to carbonation. Figure 6 shows the plot between the resistance and the load at t = 25 years. The 45 degree line of each sub-graph is the limit state (R = S) for each exposure class and RH value.

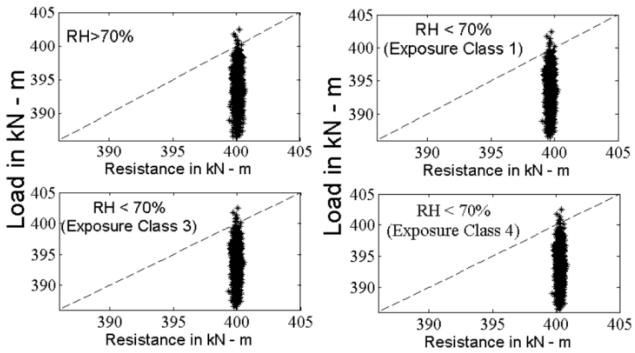

Fig.6 ***R*** vs. ***S*** (t = 25 years)

In Figure 7 the different probabilities of failure for all four cases under a uniformly distributed load of 14.175 kN/m are shown. As can be seen from this figure, exposure class 1 had the highest P_f in 100 years, at 0.032. This is followed by exposure class 3 with P_f = 0.007, followed by RH > 70% with P_f = 0.004 and finally exposure class 4 had the lowest P_f = 0.001.

These flexural probabilities of failure were based on the carbonation equations coupled with Monte Carlo simulations and the severe case (exposure class) will be the case considered in the particle filter. The next step is to estimate the present state of the bridge RC beams conditioned on observations obtained from the rebound hammer tests. The succeeding section updates the P_f using observation data from rebound hammer tests and particle filter.

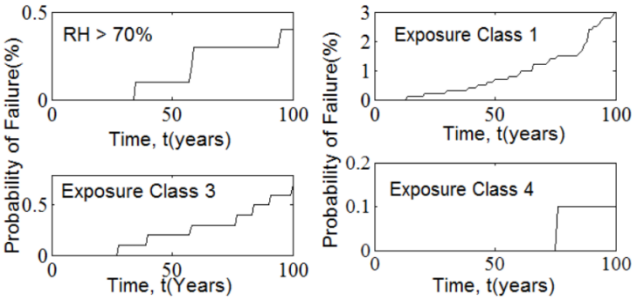

Fig.7 Failure Probabilities over time

Observation updating process

In the observation updating process, on-site rebound hammer tests on the underside of the RC beams of Dungon bridge. A total of 150 rebound hammer tests were conducted. The results are shown in Figure 8 which has a mean is 54.84 with variance of 46.55. These statistics are then used in particle filter.

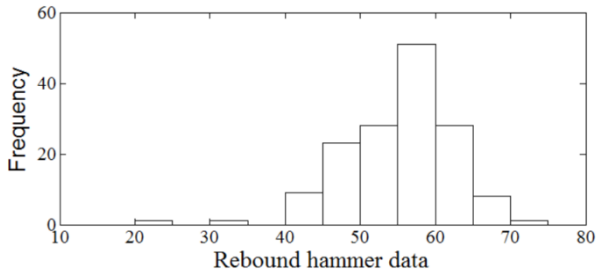

Figure 8.Dungon Bridge rebound hammer data

With data available from hammer tests (for t = 33 years) the p_f is then updated. Figure 9 shows the result before updating and after updating. The model predicted a p_f equal to 0.003 but site observations show that this is under-estimated by around 0.001.

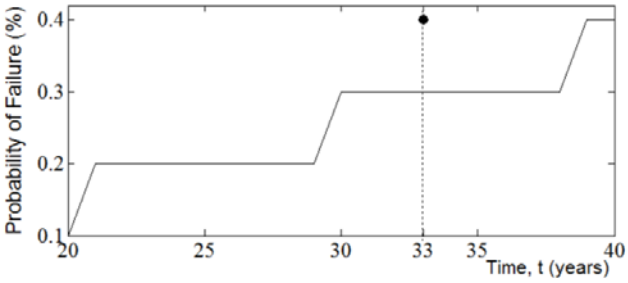

Figure 9. Updated p_f of Dungon Bridge

CONCLUSION

Carbonation is one of several environmental factors that contribute to the deterioration of RC beams. This paper emphasizes the estimation of the flexural reliability of RC bridge beams subjected to carbonation using Monte Carlo simulation and particle filter. In general, the results show that the time-variant probability of flexure failure of RC beams due to carbonation can be estimated using an appropriate state equation model. The present state therefore, in terms of the probability of failure, P_f , is 003. However the predicted probability of failure at any given time t can under-estimate or over-estimate the present state of the RC beam. Using an appropriate observation equation, particle filter and the results from rebound hammer tests the predicted probability of failure can be updated. In this case at t = 33 years, p_f = 0.004.

ACKNOWLEDGEMENTS

The authors would like to acknowledge the assistance of Mr. Dyland Moises and Engr. Bryan Peroy during the site inspections. We also acknowledge the help extended by the Department of Public Works and Highways (DPWH) office of Iloilo City during the bridge inspection.

REFERENCES

[1] Architectural Institute of Japan (1983). AIJ manual of nondestructive test methods for the evaluation of concrete strength.

[2] Akiyama, M., Frangopol, D. M., and Yoshida, I. (2010). “Time-dependent reliability analysis of existing RC structures in a marine environment using hazard associated with airborne chlorides," *Engineering Structures*, *32*(*11*), 3768 - 3779.

[3] Breccolotti, M., Bonfigli, M. F., and Materazzi, A. L. (2013). Influence of Carbonation Depth on Concrete Strength Evaluation Carried Out Using the SonReb Method. *NDT&E International*, *59*, pp. 96 - 104.

[4] Chi, J. M., Huang, R., and Yang, C. C. (2002). “Effects of Carbonation on Mechanical Properties and Durability of Concrete Using Accelerated Testing Method," *Journal of Marine Science and Technology*, *10*(*1*), 14 - 20.

[5] Claisse P. A., Elsayad H. I., Shaaban I. G. (1999). Permeability and Pore Volume of Carbonated Concrete, *Materials Journal*. *96*(*3*), 378 – 381.

[6] Garciano, L. E. and Yoshida, I. (2011): Reliability Analysis of a Brittle Facture due to Crack Instability using Sequential Monte Carlo Simulation. In Faber, M. H., Jochen, K., and Nishijima, K. (eds.), Proceedings of the 11th Int’l Conference on the Application of Statistics and Probability in Civil Engineering (ICASP11) pp. 2949 - 2956. Zurich, Switzerland. CRC Press LLC.

[7] Gode K., and Paeglitis A. (2009). Investigation of Environmental Influence on Carbonation and Chloride Ingress in Concrete Bridge Structures. Proceedings of the International Baltic Road Conference. pp. 1- 5. Riga, Latvia.

[8] Hagino, T., Akiyama, M., and Frangopol, D. (2014).Reliability Assessment of RC Structures Subjected to Carbonation by Incorporating Spatial Variations, Proceedings of the International Conference on Sustainable Development of Critical Infrastructure. ASCE.

pp. 115 – 122, Shanghai, China.

[9] Liang, M., Qu, W., and Liang, C. (2013). Mathematical Modeling and Prediction Method of Concrete Carbonation and its Applications. *Journal of Marine Science and Technology*, *10*(2), 128-135.

[10] Liang, M., Huan, R., and Fang, S. (2013). Carbonation Service Life Prediction of Existing Concrete Viaduct / Bridge Using Time-dependent Reliability Analysis. *Journal of Marine Science and Technology*, *21*(*1*), 94-104.

[11] Na, U. J., Kwon, S-J., Chaudhuri, S. M. and Shinozuka, M. (2011). Stochastic model for service life prediction of RC structures exposed to carbonation using random field simulation. *KSCE Journal of Civil Engineering*, *16*(*1*), 133-143.

[12] Saetta A. V. and Vitaliani R. V. (2004). Experimental Investigation and Numerical Modeling of Carbonation Process in Reinforced Concrete Structures Part I: Theoretical Formulation, *Cement and Concrete Research* (*34*), 571 – 579.

[13] Shang, H.S., Yi, T. H. and Yang, L. S. (2012). Experimental Study on the Compressive Strength of Big Mobility Concrete with Nondestructive Testing Method. *Advances in Materials Science and Engineering*. (2012): 6 pages.

[14] Silva A., Neves, R., and de Brito J. (2014). Statistical modeling of carbonation in reinforced concrete, *Cement & Concrete Composites*. (50): pp. 73 – 81.

[15] Tanigawa, Y., Baba, K., and Mori, H. (1984). Estimation of concrete strength by combined nondestructive testing method, *American Concrete Institute*. (82): pp. 57 – 76.

Second International Conference on Science, Engineering & Environment,
Osaka City, Japan, Nov.21-23, 2016, ISBN: 978-4-9905958-7-6 C3051

ENHANCED OIL RECOVERY USING BIOTRANSFORMATION TECHNIQUE ON HEAVY CRUDE OIL

Abdullah Al-Sayegh[1], Dr. Yahya Al-Wahaibi[1], Prof. Saif Al-Bahry[2], Prof. Abdulkadir Elshafie[2], Dr. Ali Al-Bemani[1], Dr. Sanket Joshi[3]

[1]Department of Petroleum and Chemical Engineering, Sultan Qaboos University, Oman
[2]Department of Biology, Sultan Qaboos University, Oman
[3]Central Analytical and Applied Research Unit, Sultan Qaboos University, Oman

ABSTRACT

Abundance of heavy crude oil resources and costly enhanced oil recovery (EOR) techniques necessitate development of inexpensive heavy oil recovery methods. Microbial EOR (MEOR) techniques are environmentally friendly and need little input of energy to produce MEOR agents. One potential application of MEOR is in the biotransformation of heavy oil where bacteria break heavier fractions of heavy crude oil to lighter compounds; thus, improving oil recovery. In this study, two spore forming bacteria: *Bacillus subtilis* AS2 and *Bacillus licheniformis* AS5, which were isolated from heavy oil (13.3 °API) contaminated soil samples from a heavy oil field, Oman, were tested for their biotransformation abilities. Bacterial growth was analyzed by optical density measurements and heavy crude oil recovery was determined by core flooding experiments. At aerobic biodegradation flask experiments, M2 medium spiked with glucose had the highest bacteria growth and crude oil biodegradation in comparison with: (1) M2 medium with no added chemicals and (2) M2 medium spiked with sodium thiosulfate. At anaerobic *in situ* conditions Berea sandstone core flooding experiments, additional 2.9% and 3.1% of residual oil saturation was recovered by *B. subtilis* AS2 and *B. licheniformis* AS5 respectively after one week of incubation. By increasing the incubation time and inoculation percentage for isolate AS5, the oil recovery increased to 5.0%. When glucose was added to M2 medium, AS5 oil recovery increased to 16.4%.The results showed that locally isolated bacterial strains have the potential for biotransformation of heavy oil and enhanced oil recovery.

Keywords: Enhanced oil recovery, Heavy oil, Biotransformation, B. subtilis, B. licheniformis

INTRODUCTION

Low quality heavy crude oil resources are estimated at seven times that of conventional crude oils [1] and are hard and costly to produce since expensive enhanced oil recovery (EOR) techniques are needed to extract the viscous crude oil to surface. In comparison to other EOR techniques, microbial EOR (MEOR) needs little input of energy to produce oil recovering agents, i.e. the microorganisms and their metabolic products at such technique. Also, they do not directly depend on the global crude oil price [2]. MEOR is environmentally friendly compared to conventional EOR [3]-[4]. Biotechnological applications at the petroleum industry include a very wide range of applications such as biotransformation, biosulfurization, biodenitrogenation and biocatalysis [5].

Microbial biotransformation of crude oil include all activities that make it easier to produce and transport, as well as the chemical changes that increase the value of the oil [6]. Crude oil biotransformation involves utilization of crude oil as a substrate for introduced microbiological population [7] and alteration of physical properties through bioproducts [4]. Molds, yeasts, algae and protozoa are not suitable for *in situ* reservoir conditions because of their size or inability; only bacteria are applicable at such conditions [5]. There are more than 175 genera of bacteria that are able to grow using hydrocarbons as sole or major carbon source [8]. Crude oils are essentially complex mixtures of hydrocarbons and other organic and inorganic compounds. Carbon is the main constituent of crude oils representing 85% to 90% of the crude, followed by hydrogen (10% to 14%) and non-hydrocarbon elements such as nitrogen, sulfur and oxygen and organo-metallic compounds [9-12]. Heavy crude oil contains substantial quantities of complex hydrocarbons, heteroatoms and metal contents, which are costly to process. [13, 12].

Soil contamination with crude oil drastically changes the soil's physical and chemical properties to the extent that it jeopardizes the safety of constructions on contaminated soil [14]. It also causes microbial (archaea, bacteria and fungi)

community shifts [15] in favor of microbes which could feed on or at least adapt to the type of crude oil contaminant. Thus, oil contaminated soils are rich sources for biotransformation bacteria.

At an earlier study, 15 spore forming Bacillus species bacteria were isolated from contaminated soil samples at an Omani heavy oil field and identified [16]. Soil samples were heated at 80°C at 100 ml of distilled water at 250 ml flasks in order to eliminate all bacteria that cannot withstand the heat and retain only the spore forming bacteria since these could survive the harsh *in situ* reservoir conditions. All bacteria growth media did not contain carbon, which is an essential element for the growth of living organisms. The only carbon source was is the heavy crude oil; thus, obliging bacteria to utilize the heavy crude oil and biodegrade it. M2 medium was proven the most suitable medium and biotransformation results were encouraging.

Many strains of *Bacillus subtilis* and *Bacillus licheniformis* species were reported as effective crude oil biodegraders. *Bacillus subtilis* DM-04 strain that was isolated from North-East India was used effectively for in situ bioremediation [17]. Also, a bacterial consortium of five strains including a *Bacillus licheniformis* strain achieved 48% biodegradation of asphaltene [18]. Asphaltene is the most difficult crude oil compound to biodegrade. Generally, biodegradability of crude oil components decreases in the following order: n-alkanes, branched-chain alkanes, branched alkenes, low molecular weight n-alkyl aromatics, monoaromatics, cyclic alkanes, polycyclic aromatic hydrocarbons (PAHs) and asphaltenes [19].

For biodegradation to occur, bacteria should gain direct cell contact with the substrate which could be facilitated by producing biosurfactant in order to increase substrate bio-availability [20]. Bacillus species could produce biosurfactants that aid degradation process by increasing oil emulsification and its accessibility [21-23] if suitable nutrients and growth conditions are present.

In this study, *Bacillus subtilis* AS2 and *Bacillus licheniformis* AS5 bacteria were tested for their biotransformation abilities at aerobic flask conditions (which could be used for bioremediation purposes if properly optimized at later stages) considering the M2 medium spiked with different chemicals. The bacteria were also tested at anaerobic conditions using Berea sandstone core flooding experiments to test the pursued *in situ* MEOR biotransformation objective.

MATERIALS AND METHODS

Minimum Salt Medium and Crude Oil

The composition of the used minimum salt medium (MSM) M2 was (g/l): KH_2PO_4, 1.0; K_2HPO_4, 1.0; KNO_3, 0.5; $MgSO_4 \cdot 7H_2O$, 0.5; yeast extract, 0.5. The concentrations of trace elements of M2 were (g/l): $ZnSO_4 \cdot 7H_2O$, 2.32; $MnSO_4 \cdot 4H_2O$, 1.78; H_3BO_3, 0.56; $CuSO_4 \cdot 5H_2O$, 1.00; $Na_2MoO_4 \cdot 2H_2O$, 0.39; $CoCl_2 \cdot 6H_2O$, 0.42; EDTA, 1.00; $NiCl_2 \cdot 6H_2O$, 0.004 and KI, 0.66. The viscosity and density of the sampled heavy crude oil were 968 cP and 0.961 g/cc, at 40 °C respectively. The crude oil had 13.3 °API and 5.5% asphaltene content. Oil contaminated soil samples were collected from heavy crude oil field oil-sludge pits (Fig. 1).

Aerobic Flask Experiments

The experiments were conducted in order to evaluate bacterial growth of each bacteria at M2 medium when other compounds are added. 3% glucose was added to M2 medium as a supplementary source of carbon since M2 does not contain a carbon source to kick start bacterial growth and biotransformation. At another set, 3% of sodium thiosulfate was added to M2 medium to oxidize the PAH present at the crude oil into a more bioavailable form [24]. 2 ml of bacteria in Luria Bertani (LB) seed medium were inoculated in 250 ml flasks containing 100 ml of M2 medium and 1 g of the heavy crude oil. M2 flasks were incubated at 40°C in shaker set at 160 rpm. 1 ml samples were taken daily from each flask to measure optical density at 660 nm (OD_{660}).

Anaerobic Core Flooding Experiments

Core flooding experiments were run to evaluate the ability of the isolated bacteria to biotransform heavy crude oil at *in situ* anaerobic conditions using Berea sandstone cores. Enhancement in oil recovery was quantified from the residual oil production.

The cores were cleaned by using the soxhlet extraction method with methanol and dried at 65 °C for 24 hours before usage. The cores were saturated with filtered reservoir water (i.e. formation brine) using vacuum desiccators and pore volume (PV) was determined using the dry and wet weights of the cores. The cores were flooded with oil at 0.4 cm^3/min until no more water was produced. The oil initially in place (OIIP) which was determined by measuring the displaced volume of water. The core was subjected to water flood (WF) at 0.4 cm^3/min. The residual oil was calculated by measuring the amount of oil produced from the water flood. Bacteria were inoculated from LB seed medium to M2 production medium and then the mixture of bacteria and nutrients were injected into the cores (i.e. bacteria and nutrients flooding; BNF). The tertiary recovery of extra oil was calculated by measuring oil that was produced by water flooding

the core after incubation of bacteria (i.e. WF after BNF). Core floods were conducted at 40°C.

RESULTS

Minimum Salt Medium and Crude Oil

The MSM M2 performed as expected showing rapid bacterial growth of small circular colonies in less than 3 days. Other media were tested however resulted in slow growing rhizoidal colonies that needed at least a week to grow and had low biodegradation level. Figure 2 shows samples of observed bacterial cultures at M2 medium (circular colonies) and M4 medium petri dishes (rhizoidal colonies).

Fig. 1: The oil-sludge pit where the soil samples were collected.

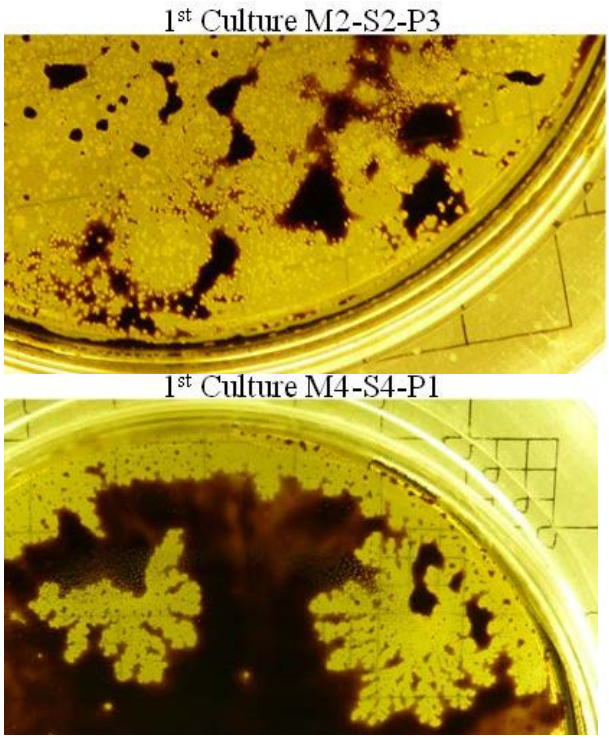

Fig. 2: Samples of observed bacterial cultures of M2 medium (top) and M4 medium (bottom) at petri dishes.

Aerobic Flask Experiments

AS2 and AS5 growth curves are shown at Fig. 3. M2 medium spiked with 3% glucose had the highest bacteria growth and crude oil biodegradation in comparison with M2 medium with no added chemicals and M2 medium spiked with 3% sodium thiosulfate.

The sodium thiosulfate that was supposed to enhance biodegradation, inhibited bacterial growth in comparison to the M2 medium bacterial growth where no chemicals were added.

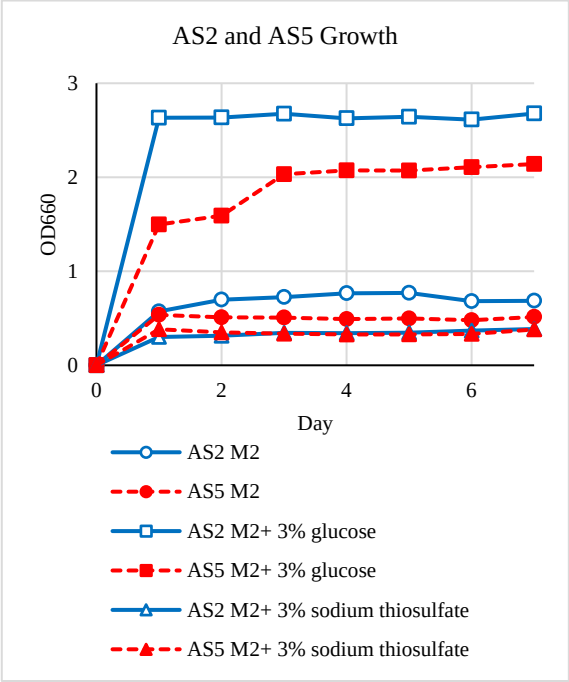

Fig. 3: AS2 and AS5 growth curves.

Anaerobic Core Flooding Experiments

At anaerobic *in situ* conditions Berea sandstone core flooding experiments, additional 2.9% and 3.1% of residual oil saturation was recovered by *B. subtilis* AS2 and *B. licheniformis* AS5 respectively after one week of incubation at the core and 5% inoculation from LB seed medium as shown at Fig. 4 and Fig. 5 respectively. Since it had a higher percentage of oil recovery, further experiments focused on the AS5 bacteria.

By increasing the incubation time of AS5 bacteria from 1 week to 2 weeks and increasing inoculation percentage from 5% to 20%, oil recovery increased to 5.0% as shown at Fig. 6. When glucose was added to M2 medium, AS5 oil recovery increased to 16.4% after 2 weeks of incubation and to 18.3% after 6 weeks of incubation (Fig. 7).

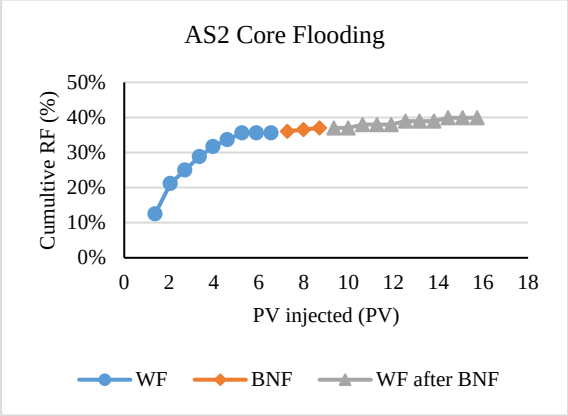

Fig. 4: AS2 core flooding (1-week incubation; 5% inoculation).

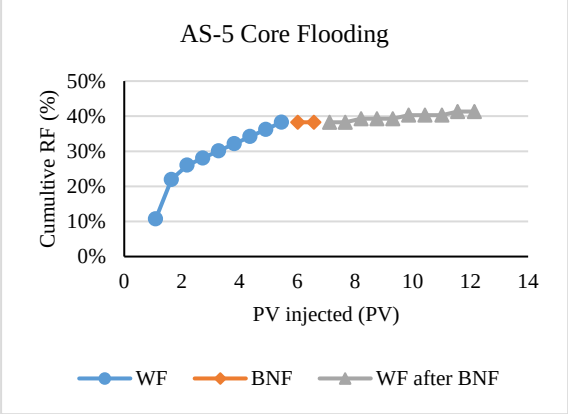

Fig. 5: AS5 core flooding (1-week incubation; 5% inoculation).

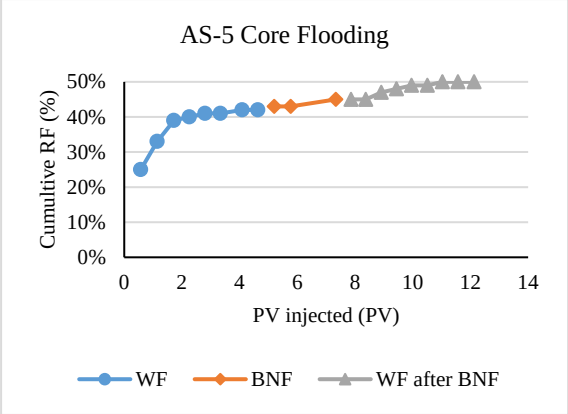

Fig. 6: AS5 core flooding (2-weeks incubation; 20% inoculation).

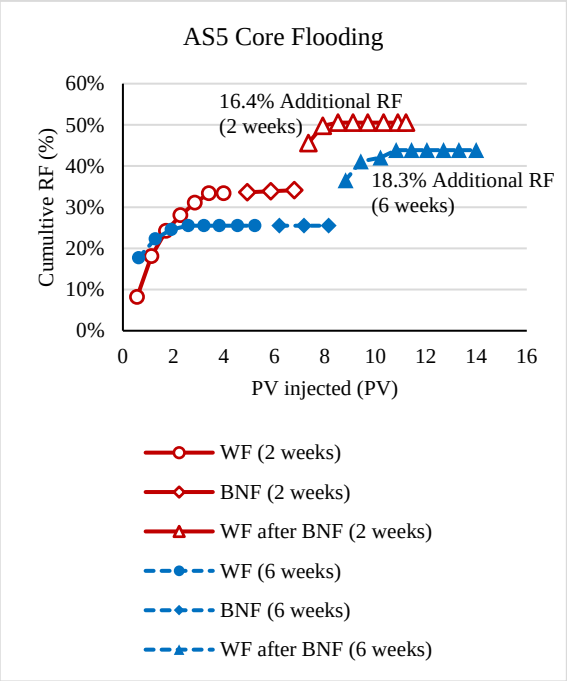

Fig. 7: AS5 core flooding (20% inoculation and glucose was added).

CONCLUSION

B. subtilis AS2 and *B. licheniformis* AS5 bacteria isolated from soils contaminated with heavy crude oil were successfully able to biotransform heavy crude oil at both aerobic and anaerobic conditions.

Addition of glucose at aerobic conditions was found beneficial to the bacterial growth as AS2 and AS5 bacterial growth increased by 3.9 and 4.1 folds respectively. However, addition of sodium thiosulfate was detrimental as AS2 and AS5 bacterial growth decreased by 40% and 37% respectively in comparison to the base M2 growth.

The anaerobic *in situ* core flooding results confirmed the effectiveness of the glucose addition as oil recovery by the AS5 bacteria increased more than 3 folds in comparison to the base M2 recovery. Increase of incubation time increased recovery; however, the increase was limited to below 3% recovery at all cases.

The results confirm that environmentally friendly and reasonably priced biotransformation process is an effective method for utilizing heavy crude oil resources if suitable medium and optimum growth conditions are taken into account.

REFERENCES

[1] Ramérez-Corredores MM, Abhijeet PB. Chapter 3 Emerging biocatalytic processes. Studies in Surface Science and Catalysis. Elsevier; 2007. p. 65-226.

[2] Sen R. Biotechnology in petroleum recovery: The microbial EOR. Progress in Energy and Combustion Science. 2008;34(6):714-24. doi:http://dx.doi.org/10.1016/j.pecs.2008.05.001.

[3] Lazar I, Petrisor IG, Yen TF. Microbial Enhanced Oil Recovery (MEOR). Petroleum Science and Technology. 2007;25(11):1353-66. doi:http://dx.doi.org/10.1080/10916460701287714.

[4] Bachmann RT, Johnson AC, Edyvean RGJ. Biotechnology in the petroleum industry: An overview. International Biodeterioration & Biodegradation. 2014;86, Part C(0):225-37. doi:http://dx.doi.org/10.1016/j.ibiod.2013.09.011.

[5] Singh A, Singh B, Ward O. Potential applications of bioprocess technology in petroleum industry. Biodegradation. 2012;23(6):865-80. doi:10.1007/s10532-012-9577-2.

[6] Leon V, Kumar M. Biological upgrading of heavy crude oil. Biotechnology and Bioprocess Engineering. 2005;10(6):471-81. doi:10.1007/bf02932281.

[7] Bubela B. Geobiology and Microbiologically Enhanced Oil Recovery. In: Donaldson EC, Chilingarian GV, Yen TF, editors. Microbial Enhanced Oil Recovery. vol Developments in Petroleum Science. April 1989: Elsevier Science Ltd 1989. p. 75-97.

[8] Prince RC, Gramain A, McGenity TJ. Prokaryotic Hydrocarbon Degraders. In: Timmis K, editor. Handbook of Hydrocarbon and Lipid Microbiology. Springer Berlin Heidelberg; 2010. p. 1669-92.

[9] Donaldson EC, Knapp RM, Yen TF, Chilingarjan GV. The Subsurface Environment. In: Donaldson EC, Chilingarian GV, Yen TF, editors. Microbial Enhanced Oil Recovery. vol Developments in Petroleum Science. April 1989: Elsevier Science Ltd 1989. p. 15-36.

[10] Mansoori GA. A unified perspective on the phase behaviour of petroleum fluids. International Journal of Oil, Gas and Coal Technology. 2009;2(2):141. doi:10.1504/ijogct.2009.024884.

[11] Moustafa YM, Morsi RE. Biomarkers. In: Dhanarasu DS, editor. Chromatography and Its Applications: InTech; 2012.

[12] Chaudhuri UR. Crude Petroleum Oil (Chapter 1). Fundamentals of Petroleum and Petrochemical Engineering. Chemical Industries: CRC Press; 2010. p. 1-23.

[13] Akmaz S, Iscan O, Gurkaynak MA, Yasar M. The Structural Characterization of Saturate, Aromatic, Resin, and Asphaltene Fractions of Batiraman Crude Oil. Petroleum Science and Technology. 2011;29(2):160-71. doi:10.1080/10916460903330361.

[14] Abousnina RM, Manalo A, Shiau J, Lokuge W. An Overview on Oil Contaminated Sand and Its Engineering Applications. International Journal of GEOMATE. 2016;10(19):1615-22.

[15] Morais D, Pylro V, Clark IM, Hirsch PR, Totola MR. Responses of microbial community from tropical pristine coastal soil to crude oil contamination. PeerJ. 2016;4:e1733. doi:10.7717/peerj.1733.

[16] Al-Sayegh A, Al-Wahaibi Y, Al-Bahry S, Elshafie A, Al-Bemani A, Joshi S. Microbial enhanced heavy crude oil recovery through biodegradation using bacterial isolates from an Omani oil field. Microbial Cell Factories. 2015;14(1):1-11. doi:10.1186/s12934-015-0330-5.

[17] Das K, Mukherjee AK. Crude petroleum-oil biodegradation efficiency of Bacillus subtilis and Pseudomonas aeruginosa strains isolated from a petroleum-oil contaminated soil from North-East India. Bioresource Technology. 2007;98(7):1339-45. doi:http://dx.doi.org/10.1016/j.biortech.2006.05.032.

[18] Tavassoli T, Mousavi SM, Shojaosadati SA, Salehizadeh H. Asphaltene biodegradation using microorganisms isolated from oil samples. Fuel. 2012;93(0):142-8. doi:http://dx.doi.org/10.1016/j.fuel.2011.10.021.

[19] Tyagi M, da Fonseca MMR, Carvalho CCCR. Bioaugmentation and biostimulation strategies to improve the effectiveness of bioremediation processes. Biodegradation. 2010;22(2):231-41. doi:10.1007/s10532-010-9394-4.

[20] Wentzel A, Ellingsen T, Kotlar H-K, Zotchev S, Throne-Holst M. Bacterial metabolism of long-chain n-alkanes. Applied Microbiology and Biotechnology. 2007;76(6):1209-21. doi:10.1007/s00253-007-1119-1.

[21] Joshi S, Bharucha C, Jha S, Yadav S, Nerurkar A, Desai AJ. Biosurfactant production using molasses and whey under thermophilic conditions. Bioresource Technology. 2008;99(1):195-9.

[22] Al-Sulaimani H, Al-Wahaibi Y, Al-Bahry S, Elshafie A, Al-Bemani A, Joshi S et al. Optimization and Partial Characterization of Biosurfactants Produced by Bacillus Species and Their Potential for Ex-Situ Enhanced Oil Recovery. SPE Journal. 2011;16(3):672-82.

[23] Chandankere R, Yao J, Choi MMF, Masakorala K, Chan Y. An efficient biosurfactant-producing and crude-oil emulsifying bacterium Bacillus methylotrophicus USTBa isolated from petroleum reservoir. Biochemical Engineering Journal. 2013;74:46-53. doi:http://dx.doi.org/10.1016/j.bej.2013.02.018.

[24] Dhamodharan D, Jayapriya J. Integrated Approach for Polycyclic Aromatic Hydrocarbon Solubilization from the Soil Matrix to Enhance Bioremediation. Bioremediation Journal. 2015;19(4):287-95. doi:10.1080/10889868.2015.1066303.

Second International Conference on Science, Engineering & Environment,
Osaka City, Japan, Nov.21-23, 2016, ISBN: 978-4-9905958-7-6 C3051

SIMULATION–OPTIMIZATION TRUCK DISPATCH PROBLEM USING LOOK – AHEAD ALGORITHM IN OPEN PIT MINES

Achmad Yusaq Faiz Fadin[1], Komarudin[2] and Armand Omar Moeis[3]
Systems Engineering, Modeling, and Simulation Laboratory, Department of Industrial Engineering
[1,2,3]Industrial Engineering, Universitas Indonesia, Indonesia

ABSTRACT

Material transportation in open-pit mines area contributes to 50% of the operating costs. Therefore, efficiency on the material transportation, specifically in truck dispatching problem needs to be done in order to get the best dispatching rules for the allocation of trucks and loaders. This research uses look-ahead algorithm approach as a new method to solve truck dispatch problem in open-pit mines area. The proposed approach was developed by simulation and optimization model in solving the truck dispatch problem using real data-situation. The dispatching result aims to answer the question where and when should a truck go so that could maximize the number of production and provide significant operating cost savings to the mining industry. This study uses a discrete event simulation to test several scenarios methods of truck dispatch, including LP-Gap, the percentage of LP-Gap, multi-stage algorithm and look-ahead algorithm. The results of the research shows that the look-ahead algorithm scenario gives the highest result with the number of production, productivity of loaders, productivity of trucks with block and without block; 43,533 ton, 64.44%, 80.53% and 63.47%.

Keywords: Discrete Event Simulation, Look-Ahead Algorithm, Simulation and Optimization, Truck Dispatch Problem

INTRODUCTION

Indonesia became one of the richest countries in energy and mineral resources. With an area of 1,910,931 km^2, Indonesia has abundant resources such as petroleum, natural gas, nickel, coal and others. Based on Mineral Resources and Energy Ministry [1] in 2011 the availability of coal resources Indonesia reached 120,338 million tons and reserves of 28,017 million tons. This amount is spread in several parts of Indonesia, both South Sumatra and East Kalimantan was the two regions that have the resources and the largest coal reserves compared to other areas. In addition, Indonesia also has one of the largest coal producers in the world as much as 281.7 million tons have been successfully produced in 2014 as the third world rankings after China (1844.6 million tons) and the United States (507.8 million tons) [2].

As one of the highest coal producing countries, Indonesia has a reliance on the use of coal as a power plant, it can be seen from the General Plan of Power-Owned National Electricity Company in 2013-2022 states that the total capacity of power plants in Indonesia reached 47 GW in 2015 with 25 GW of which are coal-fired power plants. Proven by a report from Indonesia Energy Outlook [3] there was a significant increase to the growth of new coal-fired plants of 2014 amounted to 0.76 thousand MW by 2016 of 1.86 thousand MW and forecast to 2020 by 7.16 thousand MW.

Moreover, the energy mix of coal has increased the portion of the year 2013 by 24% to 2025 by 31% [3]. It shows that the coal in Indonesia has a very important role for national energy security, as a revenue generator for the Indonesian economy. However, since the year 2011 to 2016 there has been decreasing of the coal price index by 63.4% from the highest price in 2011 (139.05 USD) [4]. Decreasing of coal prices led to the coal company declining in profits. Therefore, it needs to improve efficiency in order to make profit.

One of the efficiencies that can be done through efficiency on the operational side. As mentioned by Alarie & Gamache [5] and Ercelebi & Bascetin [6] the material transportation represents 50 per cent of the operating costs for an open pit mine. Therefore, one of the efficiencies that can be done and has a substantial impact through efficient on truck dispatching problem in the mine area. Zhang and Xia [7] stated that truck dispatch system, where the transport of material from the mine site to the dump area for further processing, plays an essential role on the issue of open-pit mining.

Therefore, one of the steps of efficiency for the company to survive by increasing operational performance on truck dispatch problems in coal mine area through optimization and simulation approach.

METHODS

Truck dispatch problem occur in some circumstances practical in the real world, both in the mining industry or any industry outside of it, especially in industries that require their settings fleet use, as quoted from Subtil, Silva, and Alves [8] as an example of the shipping industry and delivery of goods [5], oil and gas product delivery [9], transportation of raw materials [10] and etc.

Transportation and material movements by truck and loader particularly in coal represent 50-60% of operating costs in the mining industry [6]-[7].

Based on Alarie and Gamache [5] said that the truck dispatch problem in mining industry is trying to answer the question of "Where should this truck when it go and leave this place?" Therefore, become important thing to decide where the best destination to send a truck and when, in order to meet the requirements of production targets and minimize operating costs.

In addition, a lot of the mining industry still applies one strategy assignment truck called Fixed Truck Assignment (FTA) approach as a best practice to Truck Dispatching Policy in the area of mining operations [7],[11]. FTA approach is truck assigned to a fix route between the loaders and dump point during operational shift work [12]. FTA caused very long queues in the area of loaders for their randomness of equipment breakdown and the stochastic nature of the haulage process [12].

In answer to these challenges, there was a research done by He et al [13] with optimization of the number of trucks in the mine area by using Genetic Algorithm. Different to other researcher, Subtil, Silva & Alves [8] discussed about maximize the amount of mine production by using Multistage Algorithm (Allocation Planning & Dynamic Allocation). Another issue Zhang and Xia [7] have already done by minimize operating costs truck using Integer Programming - Lower Stage (Truck Assignment for Shovel).

Completion by using the above methods have been carried out and the impact is quite effective to the objectives to be achieved. However, solving the above problem has not been able to predict the future of the optimal routes for truck toward loader in real-time and optimal to meet production target. Therefore, look-ahead algorithm method becomes one of method which could apply to the truck dispatch problem in open pit mine area. This method has been widely used for utilization of container relocation problem by Jin, Zhu, & Lim [14] and Zhu & Lim [15]. Look-ahead method aims to take into account and react to changes in real-time systems [16]. Hence through this method two to five trucks behind the queue before it reaches the point for dispatching, the trucks have to know in advance the loader point which will be addressed based on the needs of each shovel to transport and based on a production target that has been set.

Look-ahead procedure is an approach used in solving the problems to dispatch the truck to look ahead what will happen near future in a system based on previous information gathered, as a reference to decide the scheduling for entities that exist in back of the queue [17]. A look-ahead can save a lot of information about the system status, such as information about what is scheduled in the near future with great accuracy, which can be used to control manufacturing operations.

Look-ahead could predict two or more of the truck's destination. In general, it can be narrowed down to two steps as can be seen in Fig. 1, i.e. Look-ahead procedure and level of evaluation function [14].

Look ahead dispatching procedure apply limited tree search in giving alternatives or suggestions in order to make the combination of assignment to an entity that will be assigned. The size of the look-ahead tree would increase exponentially as the search depth increases, so it is impossible to explore the whole search space [14]. To overcome this drawback, we impose limitation both on the depth of the tree search and on the number of children generated for each branch node. So there are only a limited few combinations to be inspected on the look-ahead tree, to be able to build a search tree consisting of branches that are very promising in the hope of leading to a high-quality solution [14].

Evaluation function in the look-ahead algorithm has to evaluate the function of each node resulting from the previous procedure on the look-ahead tree. Possible future system conditions further assessed based on the stages of evaluation function [17]. So at this stage of the evaluation function, as can be seen in Fig. 1 has a function as a determinant of decision rules in determining the combinations of existing nodes in accordance with the desired or expected criteria of the modeler.

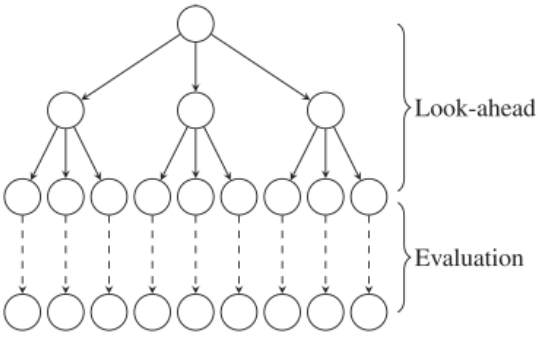

Fig. 1 Look-Ahead algorithm structure.

In addition, this study will compare the results of the use of multi-stage method to methods that have been developed by a company called LP-Gap

method and the percentage of LP-Gap. LP-Gap method is the development of a model to optimize the dispatch of the truck to loader based on the difference of the truck needs (LP-Truck) in each shovel compared to the number of trucks being and heading to shovel point. The percentage of LP-Gap method is to calculate the percentage of LP-Gap at each loader by dividing the number of LP-Gap at each loader with number of LP-Truck in each loader.

The objective of this study aims to obtain best assignment rules for the allocation of the truck and loader used in the mining industry through the optimization and simulations are conducted to increase production targets and reduce operating costs.

MODEL CONSTRUCTION

In the logistic business, trucks are important vehicle type used for transporting of goods [18]. Defining the speed limits based on the concept of optimal speed of road transport systems has a significant part in the speed management of vehicles [18]. Based on research which has been conducted by Outapa, Kondho & Thepanondh [18] stated that speed of truck which gave the best optimal result in terms of logistic business was 40 km/hr. But the behavior of a system built on the model in accordance with the real situation where the speeds of truck vary widely due to the standard deviation of the traveling time is very high in each of the routes.

First step of model construction is gathering data and collecting data. The data area mentioned as follows i.e. truck cycle time, travelling time truck, hauling time truck, the quantity of load, loader maneuver time, loader loading time and loader spotting time.

Referring to the behavior of a system that has been described, this research conducts a conceptual model that describes the characteristics of the model building process. The conceptual model consists of input, process and output in running models. The output variables generated are the number of production, loader productivity, truck productivity with blocks and truck productivity without block. The input variables used are the number of trucks used, the amount of the existing loader, truck cycle times, and service time loader. The objective of this model is to get the best dispatch rules for the allocation of truck and loader to be able to increase the amount of production. This model consists of one dumping point, one intersection point and three point loader which has 3 different routes. In the conceptual model, there are four methods of scenario as a strategy to solve the problems in the area of the mine truck assignment among which LP-Gap, Percentage LP-Gap, Multi-Stage Algorithm, and Look-Ahead Algorithm.

LP-Gap Method

In the scenario method LP-Gap, in the early stages will be calculated on the LP-Truck or the truck needs at each loader by using a comparison between the cycle time in each the truck loader divided by spotting and loading time of each loader. LP-Gap itself is the result of the calculation of the difference between the number of trucks on the needs of each loader with the number of trucks that were to and heading in each loader. This method can be calculated both in dumping point and intersection point. It was called Reassignment Calling Point (RCP). This method would dispatch the truck loader which has the biggest LP-Gap.

$$\text{LP-Truck} = \text{——————————} \quad (1)$$

i = Route option

$$\text{LP-Gap} = \alpha - \beta \quad (2)$$

α = Amount of LP-Truck i
β = Trucks heading to and being in the loader i

Percentage of LP-Gap Method

In the scenario method percentage LP-Gap generally have the same stage with LP-Gap method. In the next stage is to calculate the percentage of LP-Gap in respective loader by dividing the number of LP-Gap at each loader with the number of LP-Trucks in each loader. This method has been used; due to a loader could be less utilization. Then, it was done because there are others loader who have a greater LP-Gap. This method can be calculated both in dumping point and in intersection point. It was called Reassignment Calling Point (RCP). This method would dispatch the truck loader which has the largest percentage of LP Gap.

$$\text{Percentage of LP-Gap} = \text{——————} \quad (3)$$

i = Route option

Multi-Stage Algorithm

In the scenario method Multi-Stage algorithm based on Subtil, Silva, & Alves [8] there were two stages to be conducted. In the initial phase, find a maximum production capacity of the mine area and determine the optimal number of the truck required to achieve production targets. In the second phase, dynamic allocation, the allocation algorithm is looking for the best schedule to request assignment to comply with the allocation plan, using heuristic dynamic delivery using multi-criteria and discrete simulation.

Stage 1 is called with the allocation planning. Allocation planning is to determine the needs of

each truck loader by calculating hourly load rate shovel.

$$HLRS = \frac{\quad}{\quad} \qquad (4)$$

HLRS = Hourly load rate shovel
i = Route option

Next, calculate the difference between the requirement hourly load rate shovel with the number of trucks that have been dispatched to each loader. Loader which has the biggest difference will be assigned to its loader's route. Moreover, there are two other constraints are considered to determine the decision in dispatching a truck on this method, i.e. considering the loader idle status and the number of queues at each loader.

In this method will be recalculated at the point of intersection. Therefore by doing these calculations could be information which has been received from the system will be much more accurate. It can increase productivity in the field. Stage 2 is dynamic allocation. This phase runs every time the truck asking for allocation i.e. when one finishes dumping, when a truck starts to work, and when the loader has been idle. It aims to find an allocation for the trucks that best meets the allocation planning, i.e., finds the allocation to meet the following goals are: to improve truck productivity, to minimize queuing time at the loader, and to minimize the loader idle time; all of these goals are treated considering all the operational constraints at the mine [8].

Look-Ahead Algorithm

Look-Ahead algorithm implement tree search limited in providing an alternative to create a combination order of assignment to an entity that will be assigned. In this study is limited to 5 trucks backward will be calculated. This study has three route options, the combination of route options that will be generated as many as 243 combinations of routes option.

After created 243 a combination of route options, the next step is determining the choice of the route to be selected based on the criteria of evaluation function. Evaluation function in the look-ahead algorithm tasked to evaluate each node resulting from the previous procedure on the look-ahead tree. Furthermore, the possibility of future conditions in the system assessed based on the stage of evaluation function.

The evaluation function used in this study is taking into account productivity each loader and loader queue. The formula of productivity loader calculation could be seen in the below.

$$\text{Loader Productivity} = \frac{\quad}{\quad} \qquad (5)$$

PLW = Prediction duration trucks and shovel work
i = Combination route option

Look Ahead method also considers the number of queues resulting from each of route option combination. The combination of route option previously is generated on the limited tree search that has been built on the model algorithm. Therefore the route option obtained is a combination of routes options which have high loader productivity and minimize the number of queues. Through this method, the algorithm will be tested at the dumping point and also at the intersection point.

This algorithm tries to predict what will happen next and keep updating for real time condition. Therefore, the information on this system will be constantly updated to make it more accurate and able to predict events that will happen next.

RESULTS AND DISCUSSION

The model was being verified by debugging on the simulation model and examining the conformity of the model with the model formulation to show that the model is appropriate to the model conceptualization and ensure that it works correctly. Then the model was also being validated by comparing the model configuration to the factual data. The configurations which are compared are amount of coal production, loader productivity, truck productivity with block and without block. All methods used have been developed using discrete event simulation by using software ProModel 7.5. Simulations have been run for 11 hours / 660 minutes / 39600 seconds with a precision clocked 0.001 seconds and replicated 30 times.

Figure 3 shows boxplot chart of the overall scenario methods that have been done on the simulation and optimization models. It is calculated based on the amount of daily production with replicated 30 times. Through the boxplot, it can be conclude that look-ahead algorithm method is able to give the best results compared to other scenarios method. It can be seen from the median production quantities are in the range of 43,000 to 44,000. While the amount of production in other scenarios method (LP-Gap and Percentage LP-Gap) lie in the range of 38,000 to 42,000. In addition, from the boxplot could be seen that each algorithm which is done recalculation at the intersection point (RCP) or the calculation only at the intersection point showed better results than the calculation which is done at the dumping point only. The condition is caused due to the information obtained by the algorithm in real time condition will be more accurate if the calculation at the intersection point.

Table 2 shows the results of output indicators of the whole scenario methods that have been done.

From the table, it can be seen that scenarios look-ahead algorithm method is better than other methods. This can be demonstrated on the average loader productivity produced by 64.44%. The condition is caused due to look-ahead algorithm try to resolve the truck dispatch problem by looking forward (look-ahead) what will happen on near future. It is done based on the information previously collected as a reference to decide the scheduling for entities that are behind the queue. Look-ahead algorithm is also able to predict every five trucks to carry out the assignment to the loader in need.

Moreover, Look-ahead algorithm not only focuses on productivity loader as the evaluation function of the basis for decision making but also focuses on the number of queues generated on each loader. Both look-ahead algorithm and multi-stage algorithm has been simulated to eliminate the aspect of 'myopic' or short sited decision making as defined by the Alarie and Gamache [5], where the dispatch of the current truck strongly considers its effect on the next requests.

Percentage of Productivity is generated in scenario methods which do the calculations at the intersection point have a greater value than the scenario method performed calculations on the dumping point only. It can be conclude that if the calculation carried out on the intersection point will give the greater and more accurate result.

CONCLUSIONS

This research proposes the use of look-ahead algorithm method as the new method to obtain best assignment rules for the allocation of the truck and loader used in the mining industry through the optimization and simulations.

Based on the analysis from simulation-optimization models truck dispatch problems in the open pit area mining, it can be concluded that look-ahead algorithm provides the best result compared to the other scenarios method. It showed that coal production generated at 43,532.50 tons per day with productivity of loader on average by 64.44% and the productivity of the truck without a block by 80.53% and with the block by 63.47%

Multi-stage algorithm also showed better results than the method LP-Gap and percentage LP-Gap, because the method is not only based on the needs of truck in each loader every hour but also strongly considers status of utilization loader (idle or no idle status) and also consider to the number of queues in each loader.

Each algorithm method of scenario calculations performed recalculation at the intersection point or the calculation only at the intersection point showed better results than the calculation is only done at the dumping point.

On top of these results, the use of the look-ahead algorithm for truck dispatch problem has shed new light on the solving the material transportation specifically on truck dispatch problem in open pit mine. The model was able to generate the best output indicators result that presents the improvement of production targets and reduce operating costs.

ACKNOWLEDGEMENTS

The authors greatly appreciate the support with technical support from the Systems Engineering, Modeling and Simulation Laboratory Universitas Indonesia (SEMS UI). Financial support of this research was granted by Directorate of Research and Community Service Universitas Indonesia.

Table 1 Simulation results all scenario method of truck dispatch problem

Indicator	Scenario Method						
	LP-Gap RCP	% LP - Gap RCP	LP-Gap	% LP-Gap	Multi-Stage Algorithm	Look-Ahead Algorithm Dumping	Look-Ahead Algorithm Intersection
Coal Production	39,587	41,519	37,847	39,565	42,968	42,879	43,533
Loader 1	11,139	13,091	9,642	12,775	15,786	16,164	16,537
Loader 2	11,215	12,408	9,642	11,519	14,471	14,668	15,057
Loader 3	17,928	16,708	18,677	15,772	13,306	12,703	12,606
Loader Productivity	55.93%	58.98%	49.26%	53.14%	63.90%	63.21%	64.44%
Loader 1	59.36%	66.93%	48.93%	59.91%	79.68%	80.38%	82.85%
Loader 2	59.90%	65.37%	48.27%	54.31%	74.24%	74.19%	75.21%
Loader 3	48.52%	44.64%	50.59%	45.20%	37.77%	35.07%	35.25%
DT Productivity without block	84.28%	84.36%	82.97%	83.73%	81.26%	81.23%	80.53%
DT Productivity with block	61.44%	62.89%	58.27%	60.03%	63.59%	63.39%	63.47%

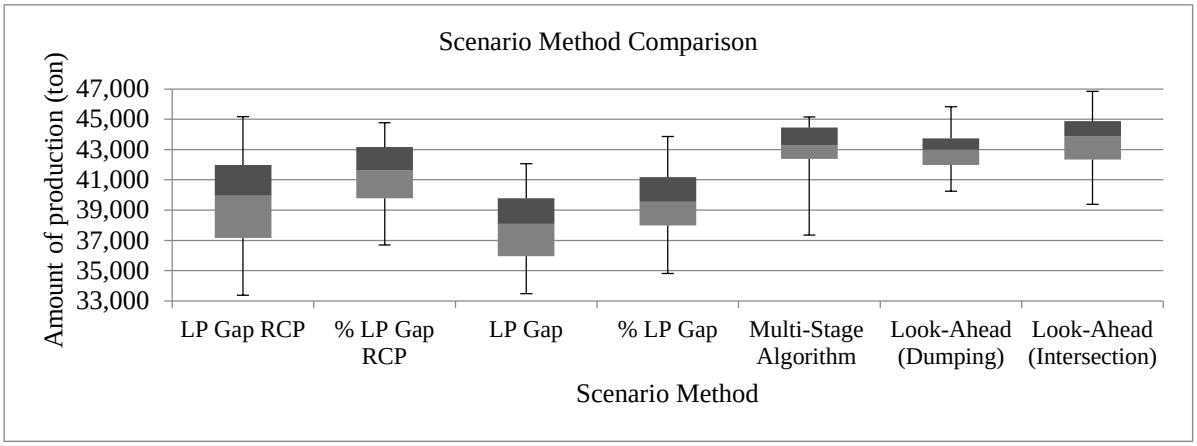

Fig. 2 Boxplot chart comparison to the scenario method.

REFERENCES

[1] ESDM, Kajian Supply Demand Energy, Kementrian Energi dan Sumber Daya Mineral. 2012

[2] British Petroleum. BP Statistical Review of World Energy June 2015. US Securities and Exchange Commission. 2015

[3] BPPT. Indonesia Energy Outlook 2014. Badan Pengkajian dan Penerapan Teknologi. 2014

[4] Trading Economics. Trading Economics | 3000 Indicators From 196 Countries | Coal 2009-2016. Available from : http://www.tradingeconomics.com/commodity/coal [Accessed 21 February 2016]

[5] Alarie S, Gamache M, "Overview of Solution Strategies Used in Truck Dispatching Systems for Open Pit Mines", Int. J. of Surface Mining, Reclamation, and Environment, Vol. 16, Mar. 2002, pp. 59-76.

[6] Ercelebi S, Bascetin A, "Optimization of shovel-truck system for surface mining", J. of the Southern African Institute of Mining and Metallurgy, Vol. 109, Jul. 2009, pp. 433-439.

[7] Zhang L, Xia X, "An Integer Programming Approach for Truck-Shovel Dispatching Problem", Energy Procedia, Vol. 75, Aug. 2015, pp. 1779-1784.

[8] Subtil RF, Silva DM, Alves JC, "A Practical Approach to Truck Dispatch for Open Pit Mines" 35TH Apcom Symposium, Sept. 2011, pp. 765-777.

[9] Gendreau M, Guertin F, Potvin JY, Seguin R, "Neighborhood search heuristics for a dynamic vehicle dispatching problem with pick-ups and deliveries", Transportation Research Part C: Emerging Technologies, Vol. 14, Jun. 2006, pp. 157-174.

[10] Rego C, Roucairol C, "Using tabu search for solving a dynamic multi-terminal truck dispatching problem", European J. of Operational Research, Vol. 83, Jun 1995, pp. 411-429.

[11] Arelovich A, Masson F, Agamennoni O, Worrall S, Nebot E, "Heuristic rule for truck dispatching in open-pit mines with local information-based decisions", in Proc. 13th International IEEE Conference on Intelligent Transportation Systems, Sep. 2010, pp. 1408-1414.

[12] Munirathinam M, Yingling JC, "A review of computer-based truck dispatching strategies for surface mining operations", Int. J. of Surface Mining, Reclamation and Environment, Vol. 8, Jan 1994, pp. 1–15.

[13] He MX, Wei JC, Lu XM, Huang BX, **"**The genetic algorithm for truck dispatching problems in surface mine", Information Technology Journal, Vol. 9, Apr. 2010, pp. 710–714.

[14] Jin B, Zhu W, Lim A, "Solving the container relocation problem by an improved greedy look-ahead heuristic", European J. of Operational Research, Vol. 240, Feb 2015, pp. 837–847.

[15] Zhu W, Lim A, "A new iterative-doubling Greedy–Lookahead algorithm for the single container loading problem", European J. of Operational Research, Vol. 222, Nov. 2012, pp. 408–417.

[16] Song L, Eldin NN, "Adaptive real-time tracking and simulation of heavy construction operations for look-ahead scheduling", Automation in Construction, Vol. 27, Nov. 2012, pp. 32–39.

[17] Jang J, Suh J, Park N, Liu R, "A Look-Ahead Routing Procedure for Machine Selection in a Highly Informative Manufacturing System", The Int. J. of Flexible Manufacturing System, Vol. 13, 2001, pp. 287–308.

[18] Outapa P, Kondo A, Thepanondh, "Effect of speed on emissions on air pollutants in urban environment: case study of truck emissions", Int. J. of Geomate, Vol. 11, Jul. 2016, pp. 2200-2207.

Second International Conference on Science, Engineering & Environment,
Osaka City, Japan, Nov.21-23, 2016, ISBN: 978-4-9905958-7-6 C3051

DESIGNING LINER SHIPPING NETWORK IN INDONESIA WITH DEMAND UNCERTAINTY

Komarudin[1], Ayudya Triastika[2], Irvanu Rahman[3]
[1,2,3] System Engineering, Modeling, and Simulation Laboratory, Department of Industrial Engineering
Faculty of Engineering, University of Indonesia, Indonesia

ABSTRACT

The problem of maritime logistics in Indonesia lies on the unbalanced trade flow between west and east region of Indonesia. Since the east region does not have many comodity to be transported, to accommodate the demand on the east region liner shipping companies have to face the increasing amount of operational costs which makes the company failed to achieve the optimal profit. According to that situation, liner shipping companies needs a service network design which accomodate demand on each ports and give maximum profit. This research uses stochastic modeling to best portray the real condition of maritime logistics by taking demand uncertainty into consideration. The algorithm used in this research aims to determine the ship routes, ship types, and the cargo allocation that yields higher profits. The result was presented as a comparison between deterministic and stochastic modeling. The result shows that companies can yield higher profit if they use stochastic modeling approach from the initial decision making stage. The proposed solution method was designed to optimize Indonesian liner shipping services.

Keywords: Liner Shipping, Demand Uncertainty, Container Shipment, Stochastic Model

INTRODUCTION

Indonesia's logistics costs are quite high, which is 27% of its GDP, if compared to other countries (Meeuws, Sandee, & Bahagia, 2013). Even though there is fluctuation over the years, in average the transportation cost component gives the biggest contribution (State of Logistics Indonesia, 2013). One of the factors influencing the high logistics costs in Indonesia is the unbalanced trade flow between the west and the east region.

The trading activities take place in the western part of Indonesia, mostly in Java and Sumatera, while there are not much trading activities going on in the eastern part of Indonesia (BAPPENAS, 2011). The commodities for Eastern Indonesia are actually shipped from the western regions. This might due to lacks of industrial development in Eastern regions. In a frequent basis, ships sailing to the Eastern regions have to sail back with empty containers because there is no commodity to pick up. As a result, shipping companies must spend a high amount of operational costs. This leads to the elevation of prices in the market.

This issue emphasizes the importance of designing a better liner shipping network that is potent to solve the problem above. However, the uncertainty of demand becomes the main challenge in solving maritime logistics problems. Moreover, Wang and Meng (2010) point out that cargo demand has a quite high level of uncertainties and makes container shipment is hardly done in precise way (Wang, 2013). This issue has not been well-addressed in the growing research concern in maritime logistics studies. This paper aims to generate a model that optimizes liner shipping network in Indonesia by including cargo demand uncertainty in order to maximize the profit of liner shipping company.

LITERATURE REVIEW

There are three types of service in the shipping market: industrial shipping, tramp shipping, and liner shipping (Lawrence, 1972). In liner shipping, the company determines which demand to fulfill by which ships schedule. Liner shipping is widely used since it is carries containers. Liner shipping aims to determine which port that will be visited and in what order (Wang, Meng, Niu, & Tan, 2013). In liner shipping there are three levels of decision making: strategic level, tactical level, and operational level (Pesenti, 1995). Since the decisions made on each level are strongly related to each other, it is important to solve the problem simultaneously. This research are made based on Mulder and Dekker's research on 2014 which offered a formulation to solve the problems on each decision making level simultaneously.

In this research we develop deterministic model and stochastic model. Deterministic model is a model which predict the output of an event by using known parameter, while stochastic model predicts several possible output based on the event's characteristics (the characteristics are usually described as

probabilityin stochastic model is a series of stochastic events along with the probability of the event's realization (Bisschop, 2016).

RESEARCH METHOD

This research uses stochastic modeling because it includes the uncertainty of container demand.

Problem Formulation

The stochastic model used in this research is developed based on the liner shipping network problem formulation made by Mulder and Dekker (2014).

Sets

h ∈ H,	Set of ports;
t ∈ T ⊆ H,	Set of transhipment ports;
s ∈ S,	Set of ship routes;
j ∈ J,	Indicator set denoting whether a ship passed both ports $h_1 \in H$ and $h_2 \in H$ on ship route s ∈ S, where j = (h_1,h_2,s);
k ∈ K,	Indicator set denoting whether port $h_2 \in H$ is directly visited after port $h_1 \in H$ on ship route s ∈ S, where k = (h_1,h_2,s);

Parameters

$r_{h_1,h_2,s}$	Revenue of transporting one TEU from port $h_1 \in H$ to $h_2 \in H$
c_t^t	Cost of transhipping one TEU in transhipment port $t \in T$
c_h^h	Cost of (un)loading one TEU in origin or destination port $h \in H$
d_{h_1,h_2}	Demand with origin port $h_1 \in H$ and destination port $h_2 \in H$
b_s	Capacity on ship route $s \in S$
$I^{path}_{h_1,h_2,h_3,h_4,s}$	(0/1) parameter that takes the value 1 if a ship passes consecutive ports $h_3 \in H$ and $h_4 \in H$ when sailing from port $h_1 \in H$ to port $h_2 \in H$ on ship route s ∈ S
f_s	Fixed cost of using route s ∈ S
$dist_{h_1,h_2}$	Distance from sailing from port $h_1 \in H$ to port $h_2 \in H$
f_s^f	Fuel price of ship s ∈ S per nautical miles

Decision Variables

$x_{h_1,h_2,s}$	Cargo flow on ship route s ∈ S between consecutive ports $h_1 \in H$ and $h_2 \in H$;
y_s	Integer variable that denotes the number of times the route is used;
$x^{od}_{h_1,h_2,s}$	Direct cargo flow on ship route s ∈ S between ports $h_1 \in H$ and $h_2 \in H$;
$x^{ot}_{h_1,t,h_{2,}s}$	Transhipment flow on ship route s ∈ S between port $h_1 \in H$ and transhipment port t ∈ T with destination port $h_1 \in H$;
$x^{td}_{t_1,t_2,h_2,s_1,s_2}$	Transhipment flow on ship route $s_2 \in S$ between transhipment port t ∈ T and destionation port h ∈ H, where the flow to transhipment port t ∈ T was transported on ship route $s_1 \in S$;
$x^{tt}_{t_1,t_2,h_2,s_1,s_2}$	Transhipment flow on ship route $s_2 \in S$ between transhipment port $t_1 \in T$ and transhipment port $t_2 \in T$ with destination port h ∈ H, where the flow to transhipment port $t_1 \in T$ was transported on route $s_1 \in S$;
$x^{tot}_{h_1,h_2,s}$	Total cargo flow on ship route $s_1 \in S$ between ports $h_1 \in H$ and $h_2 \in H$.

Linear programming formulation

$$\boldsymbol{max} \sum_{h_1\in H}\sum_{h_2\in H}\sum_{s\in S} r_{h_1,h_2}\left(x^{od}_{h_1,h_2,s} + \sum_{t\in T} x^{ot}_{h_1,t,h_2,s}\right) - \sum_{h_1\in H} c^h_{h_1}\left(\sum_{t\in T}\sum_{h_2\in H}\sum_{s\in S}\left[x^{ot}_{h_1,t,h_2,s} + x^{ot}_{h_2,t,h_1,s}\right] + \sum_{h_2\in H}\left[x^{od}_{h_1,h_2,s} + x^{od}_{h_2,h_1,s}\right]\right) - \sum_{t_1\in T} c^t_{t_1}\left(\sum_{t_2\in T}\sum_{h_2\in H}\sum_{s_1\in S}\sum_{s_2\in S} x^{tt}_{t_1,t_2,h_2,s_1,s_2} + \sum_{h_2\in H}\sum_{s_1\in S}\sum_{s_2\in S} x^{td}_{t_1,h_2,s_1,s_2}\right) - \sum_{s\in S} f_s y_s - \sum_{s\in S}\sum_{k\in K} dist_{h_1,h_2} y_s f^f_s \quad (1)$$

s.t.:

$$\sum_{t\in T}\sum_{s\in S} x^{ot}_{h_1,h_2,s} + \sum_{s\in S} x^{od}_{h_1,h_2,s} \le d_{h_1,h_2},\ h_1 \in H,\ h_2 \in H \quad (2)$$

$$x_{h_1,h_2,s} \le b_s y_s \quad (h_1,h_2,s) \in K \quad (3)$$

$$\sum_{h_1\in H} x^{ot}_{h_1,t_1,h_2,s_1} + \sum_{t_2\in T}\sum_{s_2\in S} x^{tt}_{t_2,t_1,h_2,s_2,s_1} - \sum_{s_2\in S} x^{td}_{t_1,h_2,s_1,s_2} - \sum_{t_2\in T}\sum_{s_2\in S} x^{tt}_{t_1,t_2,h_2,s_1,s_2} = 0 \quad (h_1,h_2,s) \in K \quad (4)$$

$$x_{h_1,h_2,s} - \sum_{h_3\in H}\sum_{h_4\in H} x^{tot}_{h_3,h_4,s} I^{path}_{h_3,h_4,h_1,h_2,s} = 0 \quad (h_1,h_2,s) \in K \quad (5)$$

$$x^{tot}_{h_1,h_2,s_1} - x^{od}_{h_1,h_2,s_1} - \sum_{h_3\in H} x^{ot}_{h_1,h_2,h_3,s_1} - \sum_{s_2\in S} x^{td}_{h_1,h_2,s_2,s_1} - \sum_{h_3\in H}\sum_{s_2\in S} x^{tt}_{h_1,h_2,h_3,s_2,s_1} = 0 \quad h_1 \in H,\ h_2 \in H,\ s_1 \in S \quad (6)$$

$$x_{h_1,h_2,s} \ge 0 \quad (h_1,h_2,s) \in K \quad (7)$$

$$x^{od}_{h_1,h_2,s} \ge 0 \quad h_1 \in H\ h_2 \in H,\ s \in S \quad (8)$$

$$x^{tt}_{t_1,t_2,h,s_1,s_2} \geq 0 \quad h \in H \; s_1 \in S, \; (t_1,t_2,s_2) \in J \quad (9)$$

$$x^{td}_{t,h,s_1,s_2} \geq 0 \quad s_1 \in S \; (t,h,s_2) \in J \quad (10)$$

$$x^{ot}_{h_1,t,h_2,s} \geq 0 \quad h_2 \in H \; (h_1,t,s) \in J \quad (11)$$

The objective function (1) maximizes the profit, which is equal to the revenue minus all costs; fuel costs, transhipment costs, handling costs and fixed costs. Constraints (2) make sure that the cargo shipped between every combination of ports doesn not exceed the demand for those combinations. Constraints (3) make sure that the amount of cargo transported on each leg does not exceed the capacity of the ship sailing this route. Constraints (4) ensure that all containers which have to be transhipped will also be loaded on another route. Constraints (5) define the amount of flow between two consecutive ports. Constraints (6) define the total flow between each two ports in the same cycle. Constraints (7) – (11) all make sure that cargo flow is nonnegative.

Algorithm Used to Design Liner Shipping Service Network with Demand Uncertainty

The above-mentioned linear programing formulation was translated into a mathematical programming on Netbeans IDE 8.1 using Java programming language optimized by using Gurobi Optimizer 6.5.0. The following passage would explain how we create a liner shipping service network design in Indonesia under demand uncertainty:

1. Generate combinations of back and forth route between 6 ports and 5 types of ships. There will be 75 routes combination as a result.
2. For each route, calculate the optimal speed by setting the route duration such that the route duration is an integer number of weeks or as close as possible. The sailing speed has to be set between the maximum and minimum speed.
3. Determine the number og ships needed for each route by assuming that the number of ships needed is equal to the rote duration in weeks (rounded above).
4. Calculate the total fuel costs by calculating the sailing costs and idle costs.
5. Calculate fixed costs of each route.
6. Use the calculation result from step 4 and 5 as an input in deterministic model.
7. Generate scenario of stochastic container demand from the data.
8. Include the scenario inside the model in order to get the stochastic model as a result.
9. Check the profit yielded from deterministic and stochastic models.

Verification

Netbeans IDE 8.1 facilitates its users to check whether there is a code error inside a model or not. It shows if there is an error by showing the line number and describing what kind of error on that line. The first verification step, debugging, is done by using the embedded function within the program.

The verification process is later done by evaluating the process which the model performs. It is done by checking whether the desired process inside the models are running as planned in the concept or not.

The verification process were done for each stage of decision. There are two stages of decision making in a stochastic model. In this research, the first stage decision is to decide which route and type of ships to use. After running the model we can see that it is successfully generate the first stage decision; route and ships type to use.

In this research, the second stage decision is to decide the amount of container shipped based on the scenario. The container shipment has worked well both for direct shipping and transhipment. The containers are sent to its destination ports. The model also showed that it does the loading and unloading process based on the container destination. All of those process were successfully built inside the model. Table 1 shows the result of the verification process.

Table 1 Model verification

No.	Process	Result
1.	Container shipment using direct shipping	Successful
2.	Container shipment from origin port to transhipment port	Successful
3.	Container shipment from transhipment port to destination port.	Successful
4.	Revenue calculation	Successful
5.	Handling costs calculation	Successful
6.	Transhipment costs calculation	Successful
7.	Fuel costs calculation	Successful
8.	Fixed cost calculation	Successful
9.	Profit calculation	Successful
10.	Determining which route to use	Successful

Validation

The model was validated by comparing its result to Meijer's result (2015). Meijer's research was also about designing liner shipping network design in Indonesia by using the same 6 ports mentioned in this research. The comparison between model's result and Meijer's result can be seen at Table 2.

There are 4 components that was validated, revenue, handling costs, transhipment costs, and weekly profit. The main idea of validation process is

to the error percentage between model and Meijer's result. The error was calculated by subtracting the result of both mentioned models. As shown in Table 2, the model are able to produce the same result as Meijer. Revenue, handling costs, and transhipment costs are showing exactly the same output as Meijer's produce in his research. However, there is a slightly difference on the weekly profit. The error is 1% which means the model is validated because the normal limit of error is 5%. Therefore, we can consider that the model is quite representative to portray Indonesian maritime logistics.

Table 2 Result from model and result from Meijer (2015) in comparison

	Result from Model	Meijer's Result (2015)	% error
Revenue	$12,062,360	$12,062,360	0%
Handling cost	$3,815,072	$3,815,072	0%
Transhipment cost	$68,510	$68.510	0%
Weekly profit	$6,094,145	$6,184,309	1%

RESULT AND DISCUSSION

The analysis of the result simulation is divided into three parts. The first part compares the result of deterministic model with the result of predetermined-route stochastic model. The second part compares the result of predetermined-route stochastic model with the result of stochastic model. The third part discusses the analysis of sensitivity, which compares three different stochastic models distinguished by a variety number of scenario and level of standard deviation.

Comparison of Results of Deterministic Model and Stochastic Model

As shown in Figure 1, deterministic model tends to yield higher profit than stochastic model. Compared to stochastic model with 100 scenarios (N=100), deterministic model yields profit USD 151,374.55 higher, or, 2.5% higher. Compared to stochastic model with 50 scenarios (N=50), deterministic model yields profit USD 162,853.76 higher, or, 2.7% higher. At last, compared to stochastic model with 10 scenarios (N=10), deterministic model yields profit USD 207,675.10 higher, or, 3.5% higher.

The result shown in Figure 1 is common to be found when comparing deterministic and stochastic model. Deterministic model uses average demand as the model input which shows the same number every week, while stochastic model uses probability and uncertainty on the container demand. Stochastic model shows different conditions through its scenarios, that is why the demand is different on each scenario. The extreme condition appearing in the scenarios makes the model yield lower profit. However, it is important to note that the profit resulted by stochastic model is more realistic. A liner shipping company has to make a plan based on reality. The use of stochastic model helps company have a more precise estimation of container demand, thus, it helps the company to make a realistic decision.

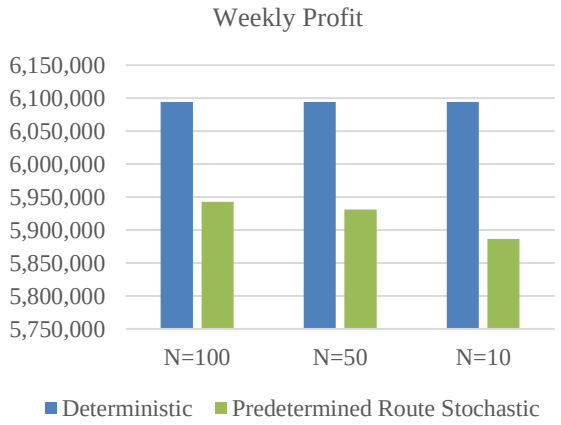

Fig. 1 Comparing profit of deterministic model and stochastic model (in USD)

Comparison of Results of Stochastic Model and Predetermined-Route Stochastic Model

Predetermined route stochastic model uses route and type of ships that is generated from the deterministic model, while stochastic model has no predetermined route. Those two types of stochastic models are created to analyze what happens if a shipping company uses stochastic model from the beginning of planning period. The results of those two different stochastic models are shown in Figure 2.

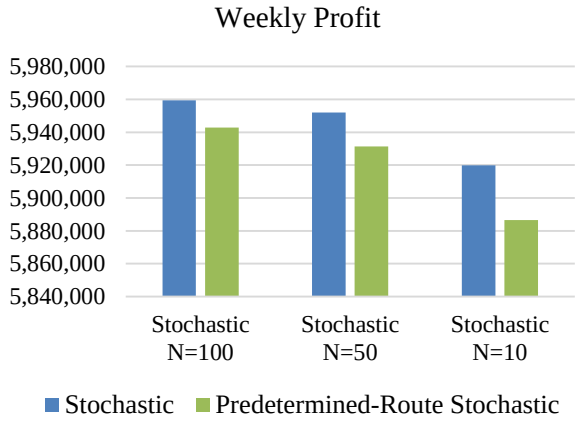

Fig. 2 Comparing profit of stochastic Model and predetermined route stochastic model

Figure 2 shows that, with the same number of scenarios, the average profit of stochastic model is higher than the average profit of predetermined route stochastic model. Not only differs in generating the amount of profit, the models are also differs in generating the routes.

In the result, stochastic model suggested to use route [69], unlike the predetermined route stochastic model that uses route [56]. Again, as stochastic model uses scenarios, it generates the routes based on various conditions of container demand. It is logical to say that the routes being used in stochastic model is better because it could tackle various conditions of container demand and yet yields higher profit than the predetermined route stochastic model. It gives a strong proof that using stochastic model from the beginning would be more beneficial for liner shipping company. The different routes being used in both models are shown in Figure 3 and Figure 4.

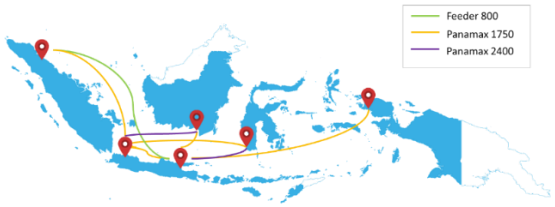

Fig. 3 Routes generated by deterministic model is used in predetermined route stochastic model

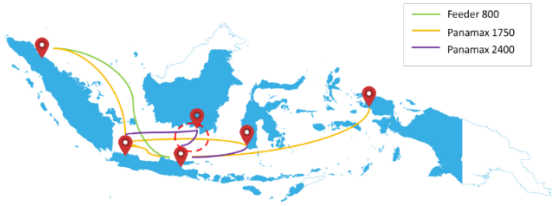

Fig. 4 Routes generated by stochastic model

The difference lies on the route between Tanjung Perak and Banjarmasin. Stochastic model shows that it is better to use bigger ship on that route (Panamax 2400). This result further confirmed that it is more beneficial for liner shipping companies to use stochastic model from the beginning as it generates better routes and higher profit.

Sensitivity Analysis of the Number of Scenario Used in Stochastic Model

The stochastic models uses 10, 50, and 100 scenarios inside the model, N={10,50,100} which was formulated by using sample average approximation method. Table 3 shows the gap on each number of scenario. The result gathered by running the model using Gurobi Optimizer 6.5.0. Based on the table, we can see that the more number of scenario used the lesser the gap between best bound and best objective. The less gap shows that the method is effective.

Table 3 Statistics of various scenarios in stochastic model

N	Best objective	Best bound	Gap
10	5,919,764.74	5,924,893.06	0.09%
50	5,952,043.96	5,952,043.96	0.00%
100	5,959,340.97	5,959,340.97	0.00%

Not only takes effect on the gap between best objectie and best bound, using different number of scenario also takes effect on computation time. The more scenarios used in the model, the ore time needed for the software to generate solution. There is trade-off between optimal solution and computation time. That is why in creating stochastic model researchers have to use sufficient number of scenarios and it is not allowed to exceed the computer's ability to process the model.

This research used a personal computer with Intel (R) Core (TM) i7-4930K CPU 3.40 GHz 3.70 GHz with 16.0 GB RAM under Windows 7. The comparison between computation time on different number of scenarios is shown in Table 4 below.

Table 4 Comparing computation time among different number of scenario

N	Computation Time
10	20 sec
50	2 min 55 sec
100	10 min 8 sec

The effect of using different number of scenario on company's profit can be observed on Figure 5. The graphic shows that models with more scenarios generate higher profit. Take a look back at the gap of each series, stochastic model with more scenario also generates lesser gap which means the high profit generated by more scenario is acceptable.

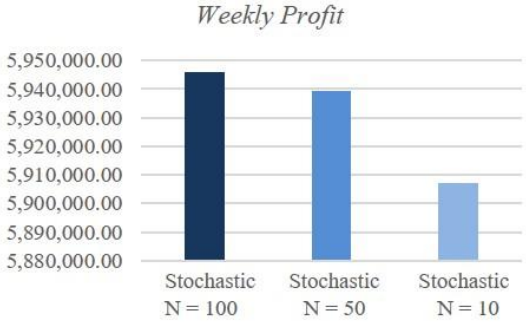

Fig. 5 Effects of using different number of scenario to profit of stochastic model

Analyzing Stochastic Model with Various Level of Standard Deviation

Figure 6 shows comparison between profit on deterministic model and profit on stochastic model with different level of standard deviation. The average profit generated by stochastic model decreases as the level of variance in container demand increase. It confirmed that the information related to container demand is significant for liner shipping company. The less the standard of deviation, the less variance on container deman, which means the container demand data is accurate. By usign the precise estimation of container demand, liner shipping company can make a decision based on reality and gain more benefits.

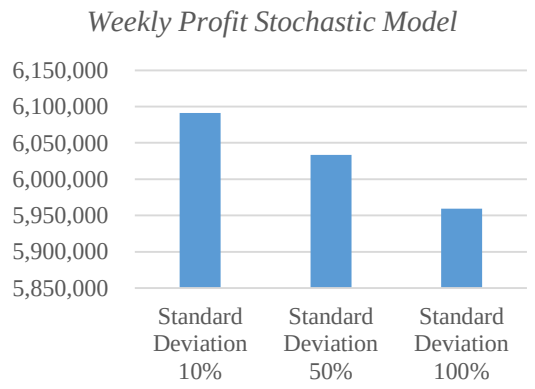

Fig. 6 Comparing profits in stochastic models with Different Level of Standard Deviation

CONCLUSION

Based on the analysis explained beforehand, we can see that compared to deterministic model, stochastic model yields lower profit. However, it is better for liner shipping company to rely on stochastic model as it is uses scenario that portray the variance and extreme condition of container demand. Stochastic model shows result which is closer to reality.

Using stochastic model from the beginning of planning period yields higher profit than predetermined stochastic model that used the route generated by deterministic model. It confirms that using stochastic model from the beginning is considered more beneficial for liner shipping companies.

The number of scenario influences the effectivity of solution generated by the model. The more scenario being used, the less gap appears which means the solution is nearly optimum. However, using more scenario needs more computation time. That is why researchers have to carefully choose between optimal solution and effectie computation time.

Variability on container demand scenario has significant effect on the solution. Increasing standard deviation resulting on decreased profit. Thus, we can also conclude that information about container demand is very important for liner shipping company.

According to the coclusions, the suggestions given for the future reearch is to create a stochastic model for liner shipping network design by taking other ports into considerations. Future research can also use route combinations other than back and forth or to create a multi-period stochastic model for maritime logistics in Indonesia.

REFERENCES

[1] Meeuws R, Sandee H, & Bahagia N, “State of Logistics Indonesia 2013”, 2013.

[2] BAPPENAS, “Infrastructure Development Strategy in Indonesia”, Jakarta, 2011.

[3] Wang S, & Meng Q, “Liner shipping fleet deployment with cargo transshipment and demand uncertainty”, in 1st International Conference on Logistics and Maritime Systems Korea, 2010.

[4] Wang T, Meng Q, Niu B, & Tan Z, “Hub-and-spoke liner shipping network design with demand uncertainty”, in International Forum on Shipping, Ports and Airports (IFSPA) 2013: Trade, Supply Chain Activities and Transport: Contemporary Logistics and Maritime Issues, 2013, pp. 1–13.

[5] Lawrence S, International Sea Transport: The Years Ahead. Lexington: Lexington Books, 1972

[6] Pesenti R, “Hierarchical resource planning for shipping companies”. European Journal of Operational Research, Vol. 86(1), pp. 91–102.

[7] Mulder J, & Dekker R, “Methods for strategic liner shipping network design”. European Journal of Operational Research, Vol. 235(2), 2014, pp. 367–377.

[8] Bisschop J, AIMMS Optimization Modeling. Bellevue: AIMMS B.V., 2016.

Second International Conference on Science, Engineering & Environment,
Osaka City, Japan, Nov.21-23, 2016, ISBN: 978-4-9905958-7-6 C3051

MULTI-PERIOD MARITIME LOGISTICS NETWORK OPTIMIZATION USING MIXED INTEGER PROGRAMMING

Komarudin[1], Mellianna Fiannita C. Purba[2], Irvanu Rahman[3]
[1,2,3]Faculty of Engineering, Universitas Indonesia, Indonesia

ABSTRACT

Indonesia, as an archipelago country, is dependent to maritime logistics on transporting goods and transportation. However, its performance is still poor, indicated by high cost of logistics. Designing maritime logistics network is crucial for shipping company on developing their business. The objective of this research is to design a liner shipping logistics network on multi-period planning horizon using mixed integer programming with maximizing profit as objective function. Three given scenarios (fixed route and fleet size, fixed route but fleet size may increase, and random route and fleet size) are analyzed for ten years within three different conditions of demand (demand equals to forecasted demand, demand equals to forecasted demand certain period, and demand is constant). The result shows that the second scenario give the most satisfying result of objective function in profit and fleet allocation variables. The third scenario gives the highest profit on every condition and first scenario has the lowest number of vessels. The profit margin between the third and second scenario on each conditition are 2.99%, 1.32%, and 0.004 % and fleet allocation gap between the first and second scenario are 1 ship, 1 ship, 0 ship respectively.

Keywords: Maritime Logistics, Liner Shipping, Multi-Period, Mixed Integer Programming.

INTRODUCTION

According to Meeuws and Bahagia (2012), Indonesia as an archipelago country is dependent to maritime-based logistics for transporting goods and transportation. However, its performance are still poor. According to Logistics Performance Index 2014 from World Bank, the score of Indonesia's logistics performance is 3.08. The indicators are: customs, infrastructure, international shipments, logistics competence, tracking and tracing, timeliness. The score puts Indonesia in 53rd place worldwide and 5th place in ASEAN. Furthermore, logistics cost in Indonesia is relatively high. According to State of Logistics 2013 from World Bank, Indonesia logistics cost until 2011 made up 24.64 percent of Indonesia GDP.

The growth of Indonesia is centralized in the western part, especially in Java Island. This cause the imbalance trade activities on both parts of Indonesia. Moreover, often times the ships from the east have to go back empty loaded. That is why the cost of logistics in Indonesia become high. Hence, it leads to the disparity of commodity price in the western and eastern part of Indonesia.

Liner shipping is the fastest growing sector among shipping services. Liner shipping company usually operates on various fleet or various size of vessels on many routes that creates shipping networks on regular basis, to transport containers between ports. Liner shipping company is seeking for optimization technology for an effective cost planning in operating and enhancing their fleets. This plan is intended to match the capacity of the fleets with container demand effectively. However, in a multi-period planning, the container demand between ports may vary from one period to another. To cope with container demand pattern from one period to another, liner shipping company has to adjust their fleet planning, including fleet size, mix and allocation of vessels periodically.

BASIC THEORY

Maritime logistics networks are the main channels for transporting goods with large volume on long distance. Three distinctions are made in the shipping market: tramp shipping, industrial shipping and liner shipping (Lawrence, 1972). The cargo owners on industrial shipping are also the owners of the ships who strive to minimize the cost of transporting container between ports. On tramp shipping, vessels are sent to ports according to the availability of container demand. Goods carried in tramp shipping are bulk cargo. Liner shipping is the common container shipping type where there are fixed routes on regular schedules. The focus of this research is on liner shipping.

Operation of liner shipping is based on characteristics associated with routing and scheduling of transporting containers and cargo. Liner shipper is a company that owns or operates

fleets of container ships. Liner shipping usually operates on close routes, loading and unloading cargo at any ports of destination.

The purpose of liner shipping services is to design network services that can provide a stable and regular service schedule and also operations that generate profit (Carranza, 2008). The decision making in the liner shipping consists of three different time-horizon level by Pesenti (1995): strategic level (3-5 years), tactical level (4-12 months) and operational level (1-4 weeks). Strategic level has the longest time-horizon. On a strategic level optimal fleet size is determined. Planning on a tactical level is done in several months and it involves determining the routes used. While on the operating level that has the shortest span of time, planning the allocation of cargo must be done.

Liner shipping company usually operates on various fleets or various size of vessels on many routes that creates shipping networks on regular basis, to transport containers between ports. Liner shipping company is seeking for optimization technology for an effective cost planning in operating and enhancing their fleets. This plan is intended to match the capacity of the fleets with container demand effectively. However, in a multi-period planning, the container demand between ports may vary from one period to another. To cope with container demand pattern from one period to another, liner shipping company has to adjust their fleet planning, including fleet size, mix and allocation of vessels periodically.

Traditional multi-period liner ship fleet planning begins with a forecasted or estimated container shipment demand pattern for each single period using some demand forecasting techniques such as regression and time series models. However, a forecasted container shipment demand pattern as a necessary input of the multi-period liner ship fleet planning problem can never be forecasted with complete confidence. It is almost impossible to precisely match estimated demand with the one realized. In reality, the container shipment demand at one period has effect on the future demand, which indicates that the container shipment demand is dependent on the demand in previous periods (Meng and Wang, 2015).

There have been many studies on multi-period fleet planning problems over the last few decades. Cho and Perakis (1996) developed an integer linear programming model for a long-term liner ship fleet planning to determine the optimal fleet size, mix and route allocation. However, the model is a period-independent model. Xinlian et al. (2000) thus reformulated the model as a dynamic programming model. They divided the multi-period planning horizon into single periods. Integer linear programming was used for each period to determine the optimal fleet size, mix, and routes allocation in order to minimize cost. However, the annual operating cost and capacity of each vessel on each route were assumed constant. This assumption is unrealistic because the costs are voyage-dependent. Recently, Meng and Wang (2011) formulated multi-period liner shipping fleet planning problem as a scenario-based dynamic programming model. However, the study did not consider container transshipment into account.

METHODS

On the strategic level, the composition of the fleet has to be determined, we call it fleet-design problem. In this research, it is assumed that the company has no fleet in the beginning and the company is the sole container shipment provider to fulfill all of demand.

Constructing the network design is the main problem on the tactical planning level. It consists of two problems: the construction of the shipping routes and the assignment of the different types of ships to the routes. For the construction of routes, several types of routing are possible. One can make use of a feeder network, port-to-port routes and butterfly routes. In this research, the route that is used is port-to-port.

In the case of intra Indonesian shipping, it might be a good decision to select hub ports as the ports with the largest throughput. The ports used in this research are Belawan, Tanjung Priok, Tanjung Perak, Banjarmasin, Makassar, and Sorong. Aggregation of ports are based on throughput and geographical position of each ports.

Hence, there are 15 combinations of ship routes. There are 5 types of vessels that are used on this research, therefore the total of routes become 75 combinations.

The main problem on the operational planning level is the assignment of cargo to the ships sailing to the determined routes. This problem is called the cargo-routing problem and can be formulated as a linear programming model.

Mathematical model that is used in this research was made by Mulder and Dekker (2014) with modification of objective function and few constraints by Meijer (2015). By rewriting the objective funtion and some of the constraints the model changes to a mixed integer programming problem and can be used to determine the optimal fleet, routes and cargo-allocation.

Sets, parameters, decision variables, and equation that are used in this research, are listed in the following.

Sets:

$h \in H$,	Set of ports
$t \in T \subseteq H$,	Set of transhipment ports
$s \in S$,	Set of ship routes
$j \in J$,	Indicator set denoting whether ship passes both ports $h_1 \in H$ and $h_2 \in H$ on ship route $s \in S$, where $j = (h_1, h_2, s)$
$k \in K$,	Indicator set denoting whether port $h_2 \in H$ is directly visited after port $h_1 \in H$ on ship route $s \in S$, where $k = (h_1, h_2, s)$

Parameters:

$r_{h_1,h_2,s}$	Revenue of transporting one TEU from port $h_1 \in H$ to $h_2 \in H$
c_t^t	Cost of transhipping one TEU in transhipment port $t \in T$
c_h^h	Cost of (un)loading one TEU in origin or destination port $h \in H$
d_{h_1,h_2}	Demand with origin port $h_1 \in H$ and destination port $h_2 \in H$
b_s	Capacity on ship route $s \in S$
$I^{path}_{h_1,h_2,h_3,h_4,s}$	(0/1) parameter that takes the value 1 if a ship passes consecutive ports $h_3 \in H$ and $h_4 \in H$ when sailing from port $h_1 \in H$ to port $h_2 \in H$ on ship route $s \in S$
f_s	Fixed cost of using route $s \in S$
$dist_{h_1,h_2}$	Distance from sailing from port $h_1 \in H$ to port $h_2 \in H$
f_s^f	Fuel price of ship $s \in S$ per nautical miles

Variables:

$x_{h_1,h_2,s}$	Cargo flow on ship route $s \in S$ between consectutive ports $h_1 \in H$ and $h_2 \in H$
y_s	Integer variable that denotes the number of times the route $s \in S$ is used
$x^{od}_{h1,h2,s}$	Direct cargo flow between ports $h_1 \in H$ and $h_2 \in H$ on ship route $s \in S$
$x^{ot}_{h1,t,h2,s}$	Transhipment flow between port $h_1 \in H$ and transhipment port $t \in T$ on ship route $s \in S$
$x^{td}_{t_1,h_2,s_1,s_2}$	Transhipment flow on ship route $s_2 \in S$ between transhipment port $t \in T$ and destination port $h_2 \in H$ where the flow to transhipment port $t \in T$ was transported on ship route $s_1 \in S$
$x^{tt}_{t_1,t_2,h_2,s_1,s_2}$	Transhipment flow on ship route $s_2 \in S$ between transhipment port $t_1 \in T$ and transhipment port $t_2 \in T$ with destination port $h_2 \in H$, where the flow to transhipment port $t_1 \in T$ was transported on route $s_1 \in S$

The objective function (1) maximizes the profit, which is equal to the revenue minus all costs; fuel costs, transshipment costs, handling costs and fixed costs. Constraint (2) makes sure that the cargo shipped between every combination of ports does not exceed the demand for those combinations. Constraint (3) makes sure that the amount of cargo transported on each leg, does not exceed the capacity of the ship sailing this route. Constraint (4) ensures that all containers which have to be transhipped, will also be loaded on another route. Constraint (5) defines the amount of flow between two consecutive ports. Constraint (6) defines the total flow between each two ports in the same cycle. Constraints (7) - (11) all make sure that cargo flow is nonnegative.

The model was runned using Gurobi and Netbeans software. CPU used in running the optimization model is Intel Core i3 U 380 1.33 GHz.

Model simulation are based on three conditions: (1) demand equals to forecasted demand, (2) demand equals to forecasted demand until certain period then constant, and (3) demand is constant. Each conditions also have three scenario: (1) fixed route and fleet size, (2) fixed route but fleet size may increase, (3) random route and fleet size.

Objective Function:

$$\max \sum_{h_1 \in H}\sum_{h_2 \in H}\sum_{s \in S} r_{h_1,h_2}\left(x^{od}_{h_1,h_2,s} + \sum_{t \in T} x^{ot}_{h_1,t,h_2,s}\right) - \sum_{h_1 \in H} c^h_{h_1}\left(\sum_{t \in T}\sum_{h_2 \in H}\sum_{s \in S}\left[x^{ot}_{h_1,t,h_2,s} + x^{ot}_{h_2,t,h_1,s}\right] + \sum_{h_2 \in H}\left[x^{od}_{h_1,h_2,s} + x^{od}_{h_2,h_1,s}\right]\right)$$

$$- \sum_{t_1 \in T} c^t_{t_1}\left(\sum_{t_2 \in T}\sum_{h_2 \in H}\sum_{s_1 \in S}\sum_{s_2 \in S} x^{tt}_{t_1,t_2,h_2,s_1,s_2} + \sum_{h_2 \in H}\sum_{s_1 \in S}\sum_{s_2 \in S} x^{td}_{t_1,h_2,s_1,s_2}\right) - \sum_{s \in S} f_s y_s - \sum_{s \in S}\sum_{k \in K} dist_{h_1,h_2} y_s f^f_s \quad (1)$$

Subject to:

$$\sum_{t\in T}\sum_{s\in S} x^{ot}_{h_1,h_2,s} + \sum_{s\in S} x^{od}_{h_1,h_2,s} \le d_{h_1,h_2} \quad h_1 \in H,\ h_2 \in H \tag{2}$$

$$x_{h_1,h_2,s} \le b_s y_s \quad (h_1,h_2,s) \in K \tag{3}$$

$$\sum_{h_1\in H} x^{ot}_{h_1,t_1,h_2,s_1} + \sum_{t_2\in T}\sum_{s_2\in S} x^{tt}_{t_2,t_1,h_2,s_2,s_1} - \sum_{s_2\in S} x^{td}_{t_1,h_2,s_1,s_2} - \sum_{t_2\in T}\sum_{s_2\in S} x^{tt}_{t_1,t_2,h_2,s_1,s_2} = 0 \quad (h_1,h_2,s) \in K \tag{4}$$

$$x_{h_1,h_2,s} - \sum_{h_3\in H}\sum_{h_4\in H} x^{tot}_{h_3,h_4,s} I^{path}_{h_3,h_4,h_1,h_2,s} = 0 \quad (h_1,h_2,s) \in K \tag{5}$$

$$x^{tot}_{h_1,h_2,s_1} - x^{od}_{h_1,h_2,s_1} - \sum_{h_3\in H} x^{ot}_{h_1,h_2,h_3,s_1} - \sum_{s_2\in S} x^{td}_{h_1,h_2,s_2,s_1} - \sum_{h_3\in H}\sum_{s_2\in S} x^{tt}_{h_1,h_2,h_3,s_2,s_1} = 0 \quad h_1\in H,\ h_2\in H,\ s_1\in S \tag{6}$$

$$x_{h_1,h_2,s} \ge 0 \quad (h_1,h_2,s) \in K \tag{7}$$

$$x^{od}_{h_1,h_2,s} \ge 0 \quad h_1\in H \ \ h_2 \in H,\ s \in S \tag{8}$$

$$x^{tt}_{t_1,t_2,h,s_1,s_2} \ge 0 \quad h \in H \ \ s_1 \in S,\ \ (t_1,t_2,s_2) \in J \tag{9}$$

$$x^{td}_{t,h,s_1,s_2} \ge 0 \quad s_1\in S \ \ (t,h,s_2) \in J \tag{10}$$

$$x^{ot}_{h_1,t,h_2,s} \ge 0 \quad h_2\in H \ \ (h_1,t,s) \in J \tag{11}$$

RESULT AND ANALYSIS

The purpose of this study is to obtain maximum profit for liner shipping company. Thus, the intial step is analyzing profit generated in each scenarios. Based on the results of the model, we can see that third scenario generate the highest profit, compared to first scenario and second scenario, for each condition. Comparison of profit results is shown in Figure 1.

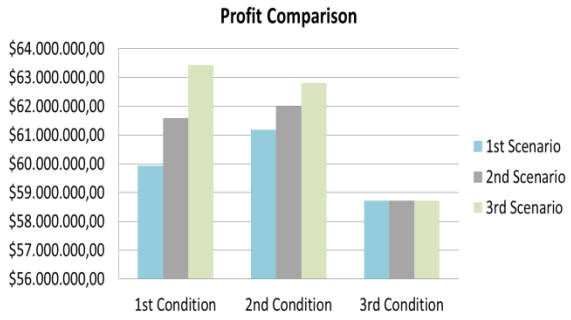

Fig. 1 Profit comparison.

Third scenario has the highest profit because it can adjust its route and the allocation of the fleet at each period based on demand and costs so as to provide maximum profit compared to first scenario, which routes and fleet size are fixed, and second scenario, which has a fixed route but allows the addition of vessels on each period.

Thus, the next step is to conduct an analysis of fleet allocation for each scenario on each condition. Table 1 shows the comparison of fleet size at the beginning of period.

Table 1 Comparison of fleet size at the beginning of period

	1st condition	2nd condition	3rd condition
1st scenario	17	17	16
2nd scenario	13	15	16
3rd scenario	16	16	16

At the beginning of period, first scenario has the highest number of fleet size and second scenario has the least. First scenario has the highest number of fleet size because the optimal fleet size has to be determined at the beginning of period and will have the same number on each period. Whereas second scenario has the least number because the number of fleet size is adjusted in accordance to demand on each period. Because on the second scenario, the number of fleet size can be fixed or increased as time goes by, based on demand and costs. Comparison of fleet size at the end of period is shown in Table 2.

Table 2 Comparison of fleet size at the end of period

	1st condition	2nd condition	3rd condition
1st scenario	17	17	16
2nd scenario	18	18	16
3rd scenario	23	21	18

From the table above, we can see that third scenario has the highest number of fleet size in comparison to first and second scenario. Third scenario has the highest number of fleet because it can determine routes and allocate the fleet freely. Thus, enabling fleet allocation randomly changes in each period. This leads to the allocation of the fleet in third scenario has greater number compared to first scenario, which has been determined at the beginning of the period and will remain until the end of the period, and also compared to second scenario, which already has the fixed composition of the fleet for each period but allows to increase the number of fleet.

The addition of vessels is certainly a cost for the company. On the composition of the fleet in third scenario it can be seen that each year, the number of ships needed are unstable. In addition, it tends to increase the number of ships from one period to another. The changing of demand makes third scenario are likely to change and replace the fleet composition, in order to achieve maximum profit.

First scenario has fixed routes and fleet size for each period. In multi-period planning horizon where demand will certainly change, the addition of ships is necessary for shipping company. But first scenario can not fulfill this condition.

Based on the results, it can be seen that the profit margin of second scenario and third scenario is relatively small. The profit margin between the third and second scenario on each conditition are 2.99%, 1.32%, and 0.004 % fleet allocation gap between the first and second scenario are 1 ship, 1 ship, 0 ship respectively. The result shows that the second scenario give the most satisfying result of objective function in profit and fleet allocation variables.

CONCLUSION

Planning a multi-period maritime logistics network services plays an important role in the businesss development of shipping company. A long-term planning is useful for liner shipping company for decision support such as routes used, fleet-design, fleet size, cargo allocation, vessels purchase,etc. Scenarios help to give comparison for company to be considered in decision-making. Based on results, the scenario that is suitable for maritime logistics multi-period planning on liner shipping services in Indonesia is the second scenario.

REFERENCES

[1] Bahagia N & Meeuws R, “Logistics Costs Indonesia”, Jakarta: NEA in collaboration with ITB, STC, and ALI, 2012.

[2] Logistics Performance Index [Internet]. Lpi.worldbank.org. 2014 [cited 14 February 2016]. Available from: http://lpi.worldbank.org/

[3] Lawrence S, “International sea transport: the years ahead”, Lexington, Mass.: Lexington Books, 1972.

[4] McLean Carranza A, “Discrete-event simulation approach for the analysis of liner shipping services of containerized cargo”, Louisville: ProQuest Dissertations and Theses database, 2008. (UMI No. 3308353).

[5] Pesenti R, “Hierarchical resource planning for shipping companies, European Journal of Operational Research, 1995, pp. 86(1) , 91-102.

[6] Meng Q, Wang T, Wang S, “Multi-period liner ship fleet planning with dependent uncertain container shipment demand”, Maritime Policy & Management, 2013, pp. 42(1):43-67.

[7] Cho S, Perakis A, “Optimal liner fleet routeing strategies”, Maritime Policy & Management, 1996, pp. 23(3):249-259.

[8] Xinlian X, Tengfei W, Daisong C, “A dynamic model and algorithm for fleet planning”, Maritime Policy & Management, 2000, pp. 27(1):53-63.

[9] Meng Q, Wang T, “A scenario-based dynamic programming model for multi-period liner ship fleet planning”, Transportation Research Part E: Logistics and Transportation Review, 2011, pp. 47(4):401-413.

[10] Mulder J & Dekker R, “Methods for strategic liner shipping network design”, European Journal of Operational Research, 2014, pp. 235(2):367-377.

[11] Meijer J, “Creating A Liner Shipping Network Design (Bachelor Thesis)”, Rotterdam: Erasmus University Rotterdam, 2015.

DEVELOPMENT OF FAN LAWS SYSTEM TRAINER FOR LYCEUM OF THE PHILIPPINES UNIVERSITY – CAVITE MECHANICAL ENGINEERING LABORATORY

Ramon C. Maniago ME, Ariston M. Alimo-ot, Glenmour Bocar, Jim Rodger T. Navarro, and Engr. Eduardo M. Manzano

College of Engineering, Computer Studies, and Architecture, Lyceum of the Philippines University – Cavite

Abstract. The **purpose** of this research is to design and construct a Fan Laws System trainer that can be used by Mechanical students in Lyceum of the Philippines University Cavite. The speed and discharge varies on the system. Manometer was used by the researchers for the measurements that can be used for evaluation. Third Fan Law equation was used to evaluate the system which is $H2/H_1 = (N_2/N_1)^2$. The **results** show that in terms of computation, the actual value which was measured is almost equal to computed value. There are some discrepancies on the measurements since the Manometer was not calibrated. Hence, it can be **concluded** that the trainer for Fan Laws is possible to design and construct with proper parameters. It was justified by the evaluation conducted. It is also concluded that the variation on speed will have a huge contribution on these laws. Added to that, there are many options to be considered in order to increase the efficiency of fan laws system. It is **recommended** to use other parameters by trying other variations that can be achieved by studying more about Fan Laws in order to develop the system more efficiently. It is also recommended to use other measuring equipment such as Pitot tube, or other kind of Manometers like Differential Manometer and Inclined Manometer, since the researchers have already used a U-tube manometer that is the most basic type of manometer, in order to have a precise and accurate measurements. It is also recommended to have a different designs for the pipe in order to have a different measurements and to show more accurate Fan Laws. Design a more presentable table and put key way on the step-pulley in order to lessen the vibration. Try to improve the way of changing the belt in order to lessen the time it takes. Lastly, make the change in speed automatic since these system is in manual operation.

Keywords: Fan Laws, LPU Cavite, Manometer, and System Trainer

INTRODUCTION

Fan Laws are rules governing fan performance such as flow rate of fluid, head (pressure), and power. It can help in determining the alternate performance criteria or development of a fan. According to da Cunha, Strack, and Stricker (2008), Fans that are oversized for their service requirements do not operate at their best efficiency points.

Studying these laws are difficult to understand without experimenting the actual process happening in a fan system. Thus, theories and formulas may not be enough to fully understand the subject matter. With this problem, the researchers thought of having a system trainer of these laws that can be easily use by students. It will not only help the students, but also the instructors.

The general scope of the study is to develop a system trainer for affinity laws of fans. Step-pulley is used to connect the motor and blower. Manometer is used for the measurements. It will also covers the creation of laboratory manual for operation and evaluation of the system.

However, this study will not cover the internal circuit design of the motor and blower and other parameters that are not mentioned in the scope of the study.

LITERATURE REVIEW

Use of the fan laws is based on a fixed system and a non-modified fan. Adding or deleting system components such as dampers, or incurring density changes, will create completely new system curves. Changing fan accessories such as inlet boxes, evases, or inlet dampers will alter the fan's performance curve from standard. These variables must be considered before the fan laws can be applied.

During the process of system design, the fan laws can be helpful in determining alternate performance criteria or in developing a minimum/maximum range. If safety factors are applied to system calculations, it should be recognized that a 10% factor on volume will result in an increase in horsepower of 33% according to the third fan law. An evaluation should be made weighing the necessity of the safety factor versus the cost penalty incurred.

A manometer may be any device that measures pressure. However, unless otherwise qualified, the term "manometer" most often refers specifically to a U-shaped tube filled with fluid. This type of manometer can be easily built as part of a laboratory experiment to demonstrate the effect of pressure on a liquid column.

1. Construction

A simple manometer can be built by partially filling a clear plastic tube with a colored liquid to allow the fluid level to be easily observed. The tube is then bent into a U-shape and fixed in an upright position. The levels of the fluid in the two vertical columns should be equal at this point, as they are currently exposed to the same pressure. This level is therefore marked and identified as the zero point of the manometer.

2. Measurement

The manometer is placed against a measured scale to allow any difference in the height of the two columns. This height differential can be used directly to make relative comparisons between different test pressures. This type of manometer can also be used to calculate the absolute pressure when the density of the liquid in the manometer is known.

3. Use

One end of the tube is connected with a gas-tight seal to a test pressure source. The other end of the tube is left open to the atmosphere and will therefore be subjected to a pressure of approximately 1 atmosphere (atm). If the test pressure is greater than the reference pressure of 1 atm, the liquid in the test column is forced down the column. This causes the fluid in the reference column to rise by an equal amount.

METHODOLOGY

Research Design

This study requires gathering of relevant data from the specified documents and compiling databases in order to analyze the material and to arrive to deeper understanding of Fan Laws. The researchers produced a trainer for fan laws that can be used to fully understand it.

Time and Place of the Study

The duration of the study is from the first semester to second semester of the Academic year 2015-2016. The study was done mainly in Lyceum of the Philippines University – Cavite and in some parts of Cavite.

Data Gathering Procedure

Gathering of data is a very important factor on creating the system in order to determine the efficiency and evaluation of the system. In this study, the researchers gathered data by manual measurement through manometer since it is the first trainer to be developed with the Fan Laws System. After measuring, the data collected were tabulated and used the available formulas related to Fan Laws such as Fan Speed Variation formula and pressure head in order to evaluate the system.

Project System Development

The system trainer for fan laws has six components. These six components will worked together in order to show the rules in fan laws. In order to have a high efficiency of the system, proper connections of the components must be considered.

1. Designing of the Trainer. This study includes the designing of components to be used such as connection of motor and blower in order to work, diameter of step-pulley, and size of belt.
2. Working Principle. The motor and blower are connected by the used of step-pulley. The blower is connected a ducting/piping system with manometer installed. The manometer is responsible for the measurements.
3. Operation and Testing Procedures. After the construction of the system, it is important to test whether the components of the system are in good condition before its installation, maintenance, adjustment, or repair. The connections must be checked whether it is properly installed and in good working condition

Evaluation Procedure

The system is evaluated with the use of the Fan Speed Variations since the speed is varied, constant fan size, and constant density. The methodology of fan performance assessment will be used in order to assess the efficiency of fan. But before fan efficiency be calculated, the researchers measured different parameters including air velocity, pressure head, temperature of air stream on fan side and electric motor kW. In order to obtain correct operating figures it should be ensured that the Fan and its components are operating properly at its rated speed and operations are at stable conditions.

RESULTS AND DISCUSSION

Presentation of Project

a. Designing of Components

The motor to be used by the researchers was acquired on an available catalogue for motors.

Specifications of Motor:

- Mindong Electric Capacitor Start Motor Type YC90L-4
- 220V, 1100W, 60Hz, 1.5 HP, 10.8A, 1740 rpm.

Specifications of Belt:

- Mitsuboshi Automotive Belt B – 40

Figure 4. Fabrication of Step-pulley and Blower

The blower and step-pulley were fabricated. As mentioned by the fabricator, Mr. Junar, the step-pulley's diameters are, 2,3,4,5 in. The blower was fabricated by introducing a shaft at center since most of the blowers are already connected with motor.

For the size of Pipe, the researchers are going to use the Equal-Friction method. This

method is very useful in computing the pipe specifications.

Material: Sheet Metal Circular Pipe
Assign the following:

a. Length of Duct 0.25 m
b. Temperature of Air 20°C

Step 1. Find the Pressure Drop

Velocity, V = 13.88 m/s
Viscosity and Density

Look for Table 6-2 in Refrigeration (Stoecker, 1983) for Viscosity and Density of Dry Air at Standard Atmospheric Pressure. At 20°C,

Viscosity μ = 18.178 μPa
Density = 1.2041 kg/m^3

Reynold's Number

Re = VDp/μ
Re = [(13.88 m/s) x (0.0762 m) x (1.2041 kg/m^3)]/18.178 μPa
Re = 140, 500

Look for Table 6-1 in Refrigeration (Stoecker, 1983) for Absolute Roughness of Some Surfaces. Roughness of Sheet metal = 0.00015 m so, Relative Roughness Ɛ/D = 0.0005 m. From Moody Chart Fig. 6-1, look for the friction factor. Friction factor = 0.0195
Pressure Drop = f (L/D) (V^2/2) p

Pressure Drop = (0.0195) x (1m/0.0762m) x (13.88^{2}m/s/2) x (1.2041kg/m^3)
Pressure Drop = 59.36 Pa/m

Step 2. Compute for equivalent length of all runs

Since the design is just a straight duct, the equivalent length is equal to 0.25m.

Step 3. Divide the available pressure drop by the equivalent length

59.36m/0.25 m = 237.45

Step 4. Size of Pipe

For the size of Pipe, use Fig. 6-2 in Refrigeration (Stoecker, 1983). In the design, the dimension of the Pipe to be used is 3 in diameter.

Steps of Fan Performance Assessment:

1. Gas Density = 273x1.293/273+21.3 = 1.199
2. Average Velocity = 0.85 x√2x9.81x322.59x1.2041/1.2041 = 61.63 m/s
3. Volumetric Flow = 61.63 m/s x π(0/0.0762)^2/4 = 0.28 m^3/s
4. Fan Mechanical Efficiency = (0.28x 322.59/102x1.1)x 100 = 80.50%

TABLE 1. *Methodology of Fan Performance Assessment*

Fan Speed Ratio	Air Velocity m/s	Pressure Head (in of waterx249.1)	T_{air} Fan side °C	Motor kW
4350	17.36	3.25 = 809.58	21.3	1.1
2320	9.26	0.95 = 236.65	21.3	1.1
1305	5.21	0.4 = 99.64	21.3	1.1
696	2.78	0.58 = 144.48	21.3	1.1

TABLE 2. *Efficiency of Various Fans*

Type of fan	Peak Efficiency Range
Centrifugal Fan	
Airfoil, backward curved/inclined	79-83
Modified radial	72-79
Radial	69-75
Pressure blower	58-68
Forward curved	60-65
Axial fan	
Vanaxial	78-85
Tubeaxial	67-72
Propeller	45-50

Based on the table provided by BEE India 2004, for the efficiency of fan, the researchers fan used is on the peak efficiency range since the researchers used Backward Curved centrifugal fan. It means that the used is efficient enough for the system.

Evaluation of the System

The researchers used the formula to evaluate the system since the speed varies, and have constant fan size and density.

TABLE 3. *Values computed to be used for evaluation*

Speed	$(N_2/N_1)^2$
4350 vs 2320	0.284
2320 vs 1305	0.316
1305 vs 696	0.284

TABLE 4. *Data gathered from testing. 4350 vs 2320*

4350 vs 2320	Mano meter	Head		H_2/H_1	$(N_2/N_1)^2$
		H_1	H_2		
Fully – Open (3)	1	3.5	1	0.286	0.284
	2	3	0.9	0.3	0.284
2.25	1	5.2	1.5	0.288	0.284
	2	5	1.4	0.28	0.284
1.5	1	5.7	1.6	0.28	0.284
	2	5.5	1.5	0.28	0.284
0.75	1	5.8	1.6	0.276	0.284
	2	5.6	1.6	0.286	0.284
Fully - Closed	1	6	1.7	0.283	0.284
	2	6	1.7	0.283	0.284

Table 3 shows the value to be considered in order to evaluate the system that came from the formula. The formula states that the Head 2 over Head 1 should be equal to the square of Speed 2 over Speed 1.

TABLE 5. *Data gathered from testing 2320 vs 1305*

2320 vs 1305	Mano meter	Head		H_2/H_1	$(N_2/N_1)^2$
		H_1	H_2		
Fully – Open (3)	1	1	0.3	0.3	0.316
	2	0.9	0.3	0.3	0.316
2.25	1	1.5	0.5	0.3	0.316
	2	1.4	0.45	0.32	0.316
1.5	1	1.6	0.5	0.313	0.316
	2	1.5	0.5	0.3	0.316
0.75	1	1.6	0.5	0.313	0.316
	2	1.6	0.5	0.313	0.316
Fully - Closed	1	1.7	0.55	0.32	0.316
	2	1.7	0.55	0.32	0.316

TABLE 6. *Data gathered from testing 1305 vs 696*

1305 vs 696	Manometer	Head		H_2/H_1	$(N_2/N_1)^2$
		H_1	H_2		
Fully – Open (3)	1	0.3	0.08	0.27	0.284
	2	0.3	0.08	0.27	0.284
2.25	1	0.5	0.14	0.28	0.284
	2	0.45	0.13	0.29	0.284
1.5	1	0.5	0.14	0.28	0.284
	2	0.5	0.14	0.28	0.284
0.75	1	0.5	0.14	0.28	0.284
	2	0.5	0.14	0.28	0.284
Fully - Closed	1	0.55	0.15	0.27	0.284
	2	0.55	0.15	0.27	0.284

Table 4, 5, and 6 show that the head gathered and computed were almost equal to the square of the speed. There are some discrepancies, it is because of how manometers were installed and how the researchers gathered the measurements. Calibration is really an important factor for the system to be more accurate. Therefore, the values gathered were a great evidence that it is possible to develop the system since the values were near to the actual value.

CONCLUSION

The fans operate under a predictable set of laws concerning speed, power and pressure. A change in speed of any fan will predictably change the pressure rise and power necessary to operate it at the new speed.

The researchers able to design and construct a system that will incorporate Fan Laws and it was justified by the evaluation conducted. The evaluation was done with the use of the Third Fan Law Equation which is $H_2/H_1 = (N_2/N_1)^2$

Based on the evaluation, the system developed was efficient enough because the measured value is almost equal to the computed value as stated on the equation given. It is also concluded that the variation on speed will have a huge contribution on these laws. Added to that, there are many options to be considered in order to increase the efficiency of fan laws system.

RECOMMENDATION

The researchers recommend to use other parameters by trying other variations that can be achieved by studying more about Fan Laws in order to develop the system more efficiently. It is also recommended to use other measuring equipment such as Pitot tube, or other kind of Manometers like Differential Manometer and Inclined Manometer, since the researchers have already used a U-tube manometer that is the most basic type of manometer, in order to have a precise and accurate measurements. It is also recommended to have a different designs for the pipe in order to have a different measurements and to show more accurate Fan Laws.

Design a more presentable table that can lessen the vibration. Put key way on the step-pulley in order to lessen the vibration. Try to improve the way of changing the belt in order to lessen the time it takes. Lastly, make the change in speed automatic since these system is in manual operation.

REFERENCES

BOOKS

Bureau of Energy Efficiency (BEE), Government of India.
Energy Efficiency Guide Book, chapter 5, p 93-112. 2004
Department of Energy, Mines, and Resources. *Fans and Blowers.* Ontario, Canada.
Fantech. (2008). *Fan Laws.*
McPherson M,J. (n.d). *Fans.*
Miller, R. W. 1996. *Flow Measurement Engineering Handbook*.3rd Ed. McGraw-Hill Book Co., New York, N.Y.
Pruftechnik LTD. (2002). *A Practical Guide to Pulley Alignment*. 4th Ed. Ludeca Inc. Florida, USA.

JOURNALS

Daly W., (1992). *Practical Guide to Fan Engineering*. Woods of Colchester.
Ellison G. (1995, October). *Fan cooled Enclosure Analysis Using First Order Method*, Electronics Cooling.
Turner M., (1996, May). *All you need to know about Fans.* Electronics Cooling.

MANUALS

da Cunha I., Strack, T., Stricker, S. (2008). CEATI International Corp. *Fans and Blowers: Energy Efficiency Reference Guide.* Ontario, Canada.
Dwyer Instruments Inc. (2010). *Inclined and Vertical Stationary Manometers*. Michigan City, USA.
USBR. 1996. *Flow Measurement Manual*. Water Resources Publications, LLC. Highlands Ranch Co.

INTERNET

Canadian Blower. *Industrial Fans and Blowers,* Retrieved from www.canadianblower.com/blowers/index.html
FanAir Company, *Product Presentation*. Retrieved from www.fanair.com/products.pdf
Ganasean, Indian Institute of Technology. *Fans, Pumps and Compressors*
Northern Industrial Supply Company (NISCO), *Products – Fans and Blowers, New York Blowers.* Retrieved from www.nisco.net/nyb.html

Second International Conference on Science, Engineering & Environment,
Osaka City, Japan, Nov.21-23, 2016, ISBN: 978-4-9905958-7-6 C3051

RESOURCE USAGE PREDICTION BASED ON ARIMA-ARCH MODEL FOR VIRTUALIZED SERVER SYSTEM

Biju R Mohan[1], and G Ram Mohana Reddy[2]
[1,2] Department of Information Technology,
National Institute of Technology Karnataka.Mangalore,Karnataka 575025, India

ABSTRACT

Performance degradation is unavoidable in server systems and this is because of factors such as shrinkage of system resources, data corruption, and numerical error accumulation. The resource shrinkage leads to the system failure due to the error propagation. Thus the resource prediction is useful to the administrator of the system so that an accidental outage can be avoided. It has been observed in past that most of the failures occur due to the exhaustion of free physical memory, so here free physical memory of a server consolidation setup is observed. It is also found that most of the studies in this direction were using the measurement-based approach with time series models for prediction. This paper reviews the effectiveness of such models and it examines whether volatility is present in the data or not. It checks whether Gauss-Markov assumptions about homoscedasticity holds good for the ordinary least square estimators of such models or not. This paper applies a combination of AutoRegressive Integrated Moving Average - AutoRegressive Conditional Heteroskedastic (ARIMA-ARCH) model to predict resource usage. Experimental results demonstrate that the goodness of fit of the ARIMA-ARCH Model has improved when compared to the linear ARIMA model.

Keywords: Cloud Computing; Performance Degradation; Resource Exhaustion; Server Consolidation; ARIMA-ARCH Model

1. INTRODUCTION

Resource usage prediction is essential in a server virtualized system because Virtual Machines (VMs) use resources on demand. The other reason why resource prediction is important because of the progressive performance degradation of long running server systems. Performance degradation is due to operating system's resource shrinkage [4] .The most common causes for performance degradation include memory resource leakages, file descriptors which are not released and errors which occur during numerical approximation. From [1,2,3] , it is found that memory exhaustion contributes majorly to the system failure due to resource shortage. This is the reason why the free available memory has been chosen in the proposed work for the detailed analysis of resource prediction.

Here a virtualized server system is used to collect the free available memory. The reason for selecting server virtualized system is due to the increased popularity of cloud computing, and the resource allocation in such system is dynamic in nature. The dynamic nature of allocating resources in server virtualized system makes resource prediction more challenging. There are two types of server virtualization which are most commonly used, the first one is the full virtualization and the second one is the paravirtualization. The full virtualization is popular among both because it offers better isolation and security for VMs, and simplifies migration and portability. Another advantage is that full virtualization avoids the extra layer of abstraction as in the case of paravirtualisation.

It is common to use time series models to predict the dynamic behavior of the resource usage. The leading choices are linear models like AutoRegressive (AR) models, Moving Average (MA) models, AutoRegressive Moving Average (ARMA) and AutoRegressive Integrated Moving Average (ARIMA) models. These models are successful in places where resource usage do not show nonlinear dynamic patterns like asymmetry, frequency amplitude dependence and volatility clustering. In this paper, resource usage data shows volatility clustering both at the beginning and at the

beginning and at the end of system's lifetime. This dynamic nature of the data prompted us to use volatility model for resource prediction.

The major contribution of the paper lies in the fact that it is the first work on using AutoRegressive Integrated Moving Average - AutoRegressive Conditional Heteroskedastic (ARIMA-ARCH) model to analyze the resource usage data of any system. Most of the previous work in this area using the time series model never considered the heteroscedastic nature of data or the clustered volatility of the data which is prevalent. Another worth point to be noted is that no such study has happened before on the server consolidated system. The proposed model has reduced prediction error 55 times when compared to ARIMA model.

2. RELATED WORK

Next paragraphs discusses the merits and demerits of the previous work in this area. It is clear that none of the works in this area studied about the volatility and structural change of the data. Moreover, the Gauss-Markov assumptions about Ordinary Least Square (OLS) estimators have violated in many cases.

Lei Li et al. [5] used time-series analysis methods for identifying software performance deterioration. Apache web server system, a Linux system status monitoring tool, and a web server workload generator were used in the Experiment. Linear Regression and Sen's slope estimation methods were used to detect an aging trend. An autoregressive exogenous (ARX) model was used to estimate the usage of system resources and the result is compared with a linear regression model's estimation. The non-linear nature of the data was not taken into consideration. The goodness of fit of the ARX model was not discussed in this paper.

Hoffmann et al. [6] integrated the best practices from the experiences of two different studies; the first study was on how the selection of variables contributes more to model quality than selecting a particular modeling technique. In the second study, they compared five linear and non-linear models and found that the superiority of non-linear model was not always significant while comparing the model complexity. They proposed a coherent approach by integrating the goodness of the above studies. The main lacuna in this paper is that it stands as a guideline rather than as an effective methodology. The results for call availability prediction of an industrial telecommunication system were presented at the end of the paper. The paper did not discuss the adequateness of the model for the results presented.

Yongquan Yan et al.[7] proposed a hybrid model that combines autoregressive integrated moving average (ARIMA) and artificial neural network (ANN) to improve the prediction accuracy of resource consumption of an IIS web server which suffered from software aging problems. Their assumption was that the error term was nonlinear in nature and they used the ANN to model it. This paper did not discuss the goodness of the fit for the linear component using ARIMA model and further authors did not throw light on the residual analysis.

Araujo et al. [8] proposed a method which depends on multiple thresholds for ensuring a safe scheduling of rejuvenation actions. This method ensured that there will be minimal interference on system's performance due to time series computation. The experiments were conducted using the Eucalyptus cloud computing framework and thus they proved the efficacy of the method. The time series trend analysis was done and compared actual virtual memory utilization with the predicted results. But their study did not consider the non-linearity in the data.

Simeonov and Avresky [9] presented a framework, which is used for identifying anomalies that lead servers to crash. Further authors theoretically justified their proposed framework. The experimental validation did not consider the model adequacy. Matias [10] presented a full factorial design of experiment to predict the factors which were most influential on apache web servers aging. They found that page type and page size are the primary causes for the memory size variation in *httpd* processes. Further, no specific model was been discussed by the authors.

It is clear from the related work that the most popular model among the researchers studying the resource exhaustion is time series models. The reason is quite obvious because the resource utilization is collected against the time which forms a time series. It is surprising that

none of the authors considered the clustered volatility generally prevalent in such data.

3. PROPOSED METHODOLOGY

The major problem identified during the literature survey is that none of the previous works try to address the volatility in the system resource data. This study focuses on modeling volatility in the time series data. The structure of the volatility model can be described as

$$x_t = \mu_t(\theta) + \varepsilon_t \quad (1)$$

$$\varepsilon_t = \sigma_t z_t \quad (2)$$

Where

$$\mu_t(\theta) = E[x_t \mid F_{t-1}],$$

$$\sigma_t^2(\theta) = E\left[\left(x_t - \mu_t(\theta)\right)^2 \mid F_{t-1}\right],$$

$$z_t \sim N(0,1).$$

In Eq. (1), the time series x_t is decomposed into a conditional mean $\mu_t(\theta)$ and a residual term ε_t. The conditional mean $\mu_t(\theta)$ may be an *ARIMA(p,d,q)* where p is the order of the autoregressive terms, d is the order of differencing and q is the order of moving average terms. F_t is the set of information available at time *t*. It may include the current and past values of x_t, current and past values of the residuals or any other variable known at time *t*. According to Eq. (2) , the residual term ε_t has a volatility conditional on the information available at time *t-1* denoted by σ_t. θ is a vector of unknown parameters. The variable z_t follows normal distribution with mean *zero* and variance *one*. The overall structure of the proposed methodology is shown in Fig. 1.

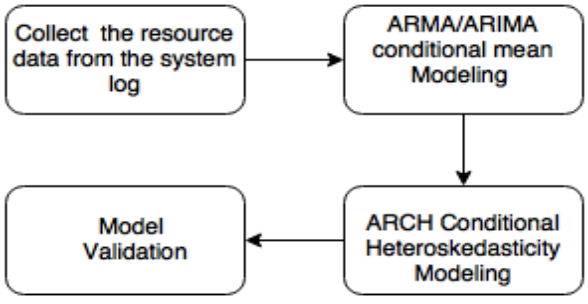

Fig. 1. Overall structure of Proposed Methodology

3.1 ARIMA Modeling

ARIMA(p,q,d) (Autoregressive Integrated Moving Average with orders *p,d,q*) is used as the mean process. *The ARIMA(p,q,d)* can be represented as in Eq. (3)

$$\left(1 - \sum_{k=1}^{p} \propto_k B^k\right)(1-B)^d X_t = \left(1 + \sum_{k=1}^{q} \beta_k B^k\right)\varepsilon_t \quad (3)$$

Where X_t is the time series, $\propto$ and β are the parameters/coefficients of autoregressive and moving average terms with order p and q respectively. ε_t are error terms generally assumed to be independent, identically distributed variables sampled from a normal distribution with zero mean. B is the difference operator defined as follows by Eq. (4). Where d is the order of the difference operator.

$$\Delta X_t = X_t - X_{t-1} = (1-B)X_t \quad (4)$$

The overview of the statistical analysis is given by the flowchart as shown in Fig 2.

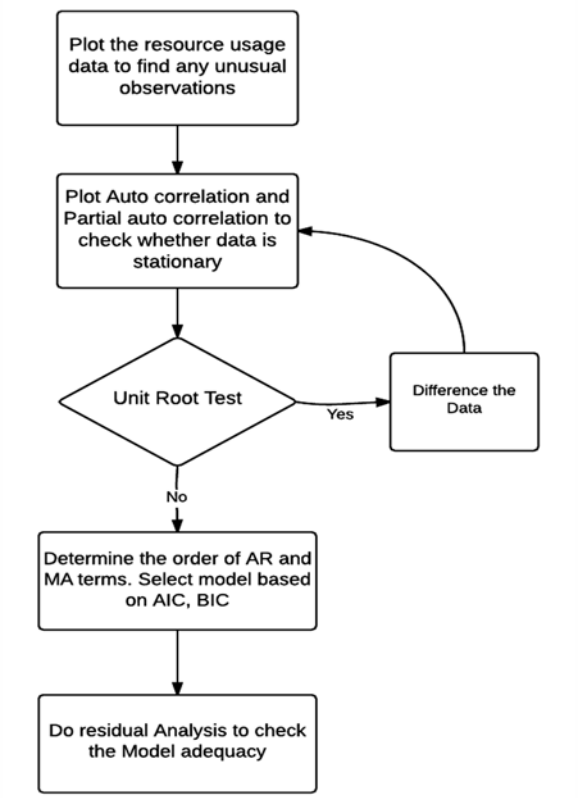

Fig. 2. The flowchart for ARIMA Conditional Mean Modeling .

In order to find the series is stationary or not, the autocorrelation of the series has to be found out. Autocorrelation, also known as serial correlation, is the cross-correlation of a signal with itself. Informally, it is the similarity between observations as a function of the time lag between them. It is a mathematical tool for finding repeating patterns, such as the presence of a periodic signal obscured by noise, or identifying the missing fundamental frequency in a signal implied by its harmonic frequencies. It is often used in signal processing for analyzing functions or series of values, such as time domain signals.

The autocorrelation between time X_t and $X_{t+\tau}$ is given by the Eq. (5). Where X_t and $X_{t+\tau}$ are the time series with lag τ . μ is the mean of the population. $\sigma_{X_t}, \sigma_{X_{t+\tau}}$ are standard deviations at the time t and $t+\tau$. ρ_k is the autocorrelation at lag k

$$\rho_k = \frac{E[(X_t - \mu)(X_{t+\tau} - \mu)]}{\sigma_{X_t}\sigma_{X_{t+\tau}}} \quad (5).$$

The sample estimate r_k of the same is given by Eq. (6). $\bar{X}$ s the sample mean and N is the number samples

$$r_k = \frac{\frac{1}{N}\sum_{t=1}^{n-k}(X_t - \bar{X})(X_{t-\tau} - \bar{X})}{\frac{1}{N-1}\sum_{t=1}^{n}(X_t - \bar{X})^2} \quad (6)$$

From Fig. 2. it is clear that the first step is to plot the resource variable against time, this is to find any unusual observations. The next step in the flowchart is to plot the autocorrelation function and partial autocorrelation function of the resource usage data. This is to check whether the resource usage data is stationary or not. If the plot shows that data is non-stationary, the non stationarity of the data has to be confirmed. This is done by doing a unit root test. Here augmented dickey fuller test[11] has been used as unit root test. Once the series is proved to be non-stationary then the series is differenced. By looking at the autocorrelation function (ACF) and partial autocorrelation (PACF) plots of the differenced series, one can tentatively identify the numbers of AR and/or MA terms that are needed. Once the number of autoregressive terms, the number of differencing and moving average terms are decided, parameters of the model have to be estimated. The maximum likelihood or least square estimators are commonly used to estimate the parameters.

For Model selection, three measures of goodness are used Akaike information criterion (AIC), Akaike information criterion corrected(AICc), Bayesian information criterion (BIC) [12]. The Akaike information criterion (AIC) deals with the trade-off between the goodness of fit of the model and the complexity of the model. It offers a relative estimate of the information lost when a given model is used to represent the process that generates the data. AIC does not provide a test of a model in the sense of testing a null hypothesis; i.e. AIC can tell nothing about the quality of the model in an absolute sense. Given a set of candidate models for the data, the preferred model is the one with the minimum AIC value. The Eq. (7) gives the AIC measure.

$$AIC = 2k - 2\ln(L) \quad (7).$$

Where k is the number of parameters and L is the maximum value of the likely hood function. Given a set of candidate models for the data, the preferred model is the one with the minimum AIC value.

AICc is AIC with a correction for finite sample sizes given by the Eq. (8) where n is the sample size.

$$AIC_c = AIC + \frac{2k(k+1)}{n-k-1} \quad (8).$$

Bayesian information criterion (BIC) or Schwarz criterion (also SBC, SBIC) is a criterion for model selection among a finite set of models. It is based likelihood function and it is closely related to the Akaike information criterion (AIC). Both BIC and AIC resolve this problem by introducing a penalty term for the number of parameters in the model; the penalty term is larger in BIC than in AIC. BIC is given by the Eq. (9).

$$BIC = -2.\ln(\mathrm{L}) + k.\ln(n) \quad (9).$$

3.2 ARCH Modeling

(ARCH) Autoregressive conditional heteroskedasticity models are used to characterize and model time series. ARCH models assume the variance of the current error term or innovation to be a function of the actual sizes of the previous time periods' error terms: often the variance is related to the squares of

the previous innovations. So an $ARCH\ (p)$ assumes that the conditional variance $\sigma_t^2(\theta)$ is a linear function of the past *p* squared innovations where θ is a vector of unknown parameters which could be estimated by maximum likelihood estimators. $ARCH\ (p)$ is given by Eq. (10).

$$\boldsymbol{\sigma_t^2(\theta) = \omega + \alpha_1 \varepsilon_{t-1}^2 + \cdots + \alpha_p \varepsilon_{t-p}^2 = \omega + \sum_{i=1}^{p} \alpha_i \varepsilon_{t-i}^2} \quad (10).$$

According to Eq. 10., the conditional volatility is assumed as moving average of squared innovations $\boldsymbol{\varepsilon_t^2}$. For the model to be well defined and the conditional variance to be positive, the parameters must satisfy the following constraints: $\boldsymbol{\omega > 0}$, and $\boldsymbol{\alpha_i \geq 0}$, $\boldsymbol{i = 1, \cdots, p}$. The unconditional variance of innovation, denoted by $\boldsymbol{\sigma^2}$, is the unconditional expectation of $\boldsymbol{\sigma_t^2}$: $\boldsymbol{\sigma^2 = E\left[\varepsilon_t^2\right]_{\omega} = E\left[\sigma_t^2\right]}$. It can be easily shown that $\boldsymbol{\sigma^2 = \frac{\omega}{1-\sum_{i=1}^{p} \alpha_i}}$.

This shows that the process $\boldsymbol{\varepsilon_t}$ is covariance stationary only when sum of the autoregressive terms less than one, i.e., $\boldsymbol{\sum_{i=1}^{p} \alpha_i < 1}$.

4. RESULT ANALYSIS

The resource usage data collected from the experimental setup discussed below is analyzed here. The free physical memory and swap read and write rates are the main focus because these resources are major indicators of performance degradation.

4.1 Experimental Setup and Data Collection

Experiments were done on an HP ProLaint ML350 G6 machine, it has two processors with 6 cores in each processor. It has 24 logical processors (when hyper threading enabled). This Intel Xeon architecture processors work at the speed of 2.40 GHz. 1 TB hard disk and 16 GB physical memory capacity are available for the machine. The machine has 2 NIC cards to effectively manage the network traffic.

VMware ESXi 5.0.0 is used as the hypervisor/Virtual Machine Monitor (VMM) in this experimental setup. This VMM belongs to type 1 VMM or this is a bare metal Hypervisor. 25 virtual machines have loaded on top of the hypervisor. Virtual machines (VMs) use Ubuntu 14.10 as the operating system. Each VM is configured with 4 vCPUs, 1 GB physical memory space, and 10 GB Hard disk space.

The *esxtop* command has been used to collect the information about CPU usage, swap in and swap out rate, interrupts, context switches, network statistics and power usage. In this experiment, the memory statistics alone has been used for further analysis. In this experiment, *httpref* tool is used in order to generate requests with constant time intervals between two requests. Each request accesses one specified file of size 5kb from the server. httpref is used not only as a workload generator but also used as a performance measuring tool.

The memory reclamation techniques[13] in VMware ESXi 5.0.0 like Transparent page sharing (TPS), Ballooning, Hypervisor swapping, and Memory compression has been enabled to increase the dynamicity of the resource allocation, thus making resource prediction more challenging. Transparent page sharing reclaims memory by removing redundant pages with identical content while ballooning reclaims memory by artificially increasing the memory pressure inside the guest. With memory compression, ESXi stores pages, which would otherwise be swapped out to disk through host swapping, in a compression cache located in the main memory. Memory compression outperforms host swapping because the next access to the compressed page only causes a page decompression, which can be an order of magnitude faster than the disk access. In the cases where ballooning, transparent page sharing, and memory compression are not sufficient to reclaim memory, ESXi employs hypervisor swapping to reclaim memory. Hypervisor swapping is a guaranteed technique to reclaim a specific amount of memory within a specific amount of time. However, hypervisor swapping is used as a last resort to reclaim memory from the virtual machine due to limitations on performance.

4.2 Analysis of Resource Utilization

Fig. 3. shows the time series plot of free physical memory over a period of time. The data is collected over a period of 10 days with the time interval of 30 minutes.

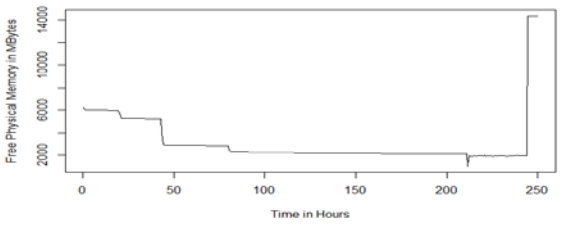

Fig. 3. Free Physical memory collected over a period of 250 hours.

The memory over commitment during this period is kept as 4.11. The Memory Overcommitment during this period is shown as in Fig. 4. The memory overcommit is given by the Eq. (11). Where N is the number of VMs switched on and $EsxMemory$ is the total host *VMware Esxi* memory.

$$memoryovercommit = \frac{\sum_{i=1}^{N} memsize}{EsxMemory}. (11)$$

It is clear from the Fig. 3. that at the 245th hour the Free Memory has increased from 1900 Mbytes to 14000 Mbytes. From Fig. 4., there is a clear indication that the Memory Overcommitment (15 Minutes Average) has decreased from 4.11 to zero, which clearly shows that some VMs or all VMs has been switched off and swapped into the secondary memory. It clearly gives an indication of thrashing. For further investigation swap read and write rates are plotted against time.

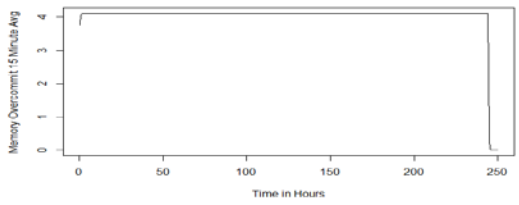

Fig. 4. Memory Overcommit (15 Minutes Average) plotted against time

Fig. 5. and Fig. 6. gives swap read and write per second respectively.

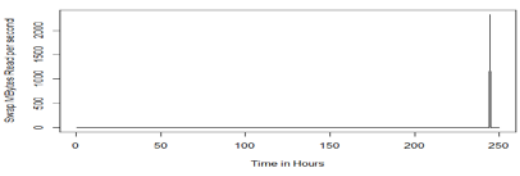

Fig. 5. Swap Mbytes Read per Second against time

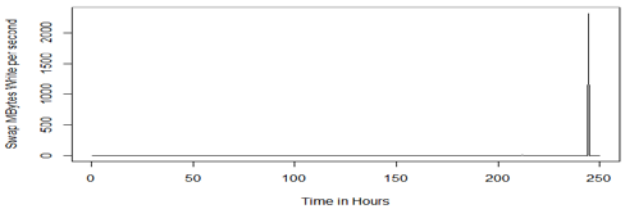

Fig. 6. Swap Mbytes Writes per Second against Time

The huge swap read and write rates at 245th hour shows the free physical memory has shrunk to a level, where the virtualized server system has forced one or more VMs to virtual space of the hypervisor. This forced the system to fail, so this point is considered as the failure point of the setup.

4.3. ARIMA Mean Modelling

The resource which is most vulnerable in terms of the crash is free physical memory because the system mainly crashes/hangs due to the memory leakage. So here the variable chosen for time series analysis is free physical memory. In order to find the series is stationary or not, the autocorrelation of the series has to be found out. Fig. 7. shows the Autocorrelogram plot of Free Physical Memory against Lag.

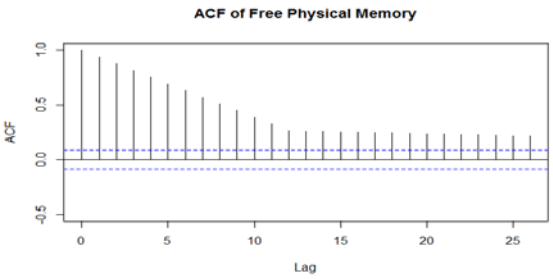

Fig. 7. Autocorrelogram of Free Physical Memory

It is clear from the Fig. 7. that all the values up to 25 lags are significant or above the significant band. This indicates a possibility of nonstationarity in the series which has been confirmed by the augmented dickey fuller test. The augmented dickey fuller test confirms there is no statistical evidence that series is stationary. That means the series is nonstationary.

Before differencing the series, the partial autocorrelation function has to be obtained. In time series analysis, the partial autocorrelation

function (PACF) plays an important role in identifying the extent of the lag in an autoregressive model. The use of this function was introduced as part of the Box–Jenkins approach to time series modeling, whereby plotting the partial autocorrelative functions one could determine the appropriate lags p in an *AR (p)* model or in an extended *ARIMA (p,d,q)* model. Fig. 8. shows PACF of Free Physical memory.

ACF and PACF slowly die down which gives a clear indication of non-stationarity, So the time series has to be differenced once. The ACF and PACF of the differenced series show no clues of non-stationarity. The Augmented dickey fuller test was conducted again on the differenced series, to know whether the series is non-stationary or not. There is no statistical evidence of non-stationarity in the time series.

From the ACF and PACF, *ARIMA (0,1,1), ARIMA(2,1,0), ARIMA(1,1,0), ARIMA(1,1,1), ARIMA(1,0,0)* are to be verified. These models are arbitrarily selected because the ACF and PACF gives a clue that the series is random as there are no significant terms in both ACF and PACF.

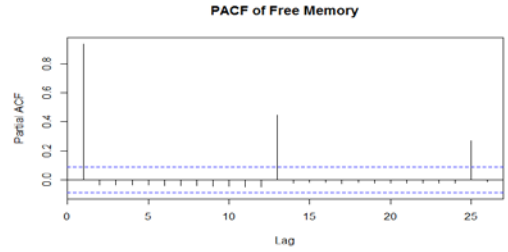

Fig. 8 Partial autocorrelation function of free physical memory

To analyze the goodness of fit, three measures of goodness are used Akaike information criterion (AIC), Akaike information criterion corrected (AICc), Bayesian information criterion (BIC). The values of this measures are given as below in Table 1. It is clear from Table 1, that none of the models fit the data well so the residuals of the best available model i.e.; *ARIMA (1,1,0)* has to be analysed.

Table 1. The Goodness of Fit Measures ARIMA Models.

Model	AIC	BIC	AICc
ARIMA(0,1,1)	7740.269	7741	7752
ARIMA(2,1,0)	7742.27	7643	7543
ARIMA(1,1,0)	7739.27	7132.1	7564.1
ARIMA(1,1,1)	7742.27	7432.1	7432
ARIMA(1,0,0)	7732.76	7432	7679
ARIMA(0,0,1)	8598	8432.1	8564

4.4 ARCH Modelling

Analysis of residuals from the fitted model gives a clue for modification. Here one model with less AIC values is selected for the analysis. *ARIMA(1,1,0)* which is the best among the analyzed models is selected for residual analysis. Standardized residuals of this model are plotted as shown in Fig. 9.

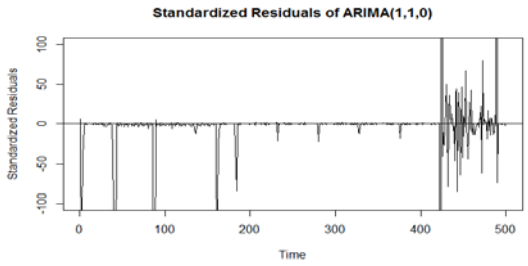

Fig. 9 Standardized Residual of ARIMA(1,1,0)

Fig. 9. shows that there is a huge variation in residuals, which is the indication of heteroskedasticity. In order to test the normality of the residual quantile-quantile plot is plotted from the residuals of *ARIMA(1,1,0)* model. Fig. 10. shows the quantile-quantile plot of the residuals of *ARIMA(1,1,0)* model.

Fig. 10 clearly shows that the residual series is not normal. It is clear from the Model diagnostics that the time series is heteroskedastic in nature.

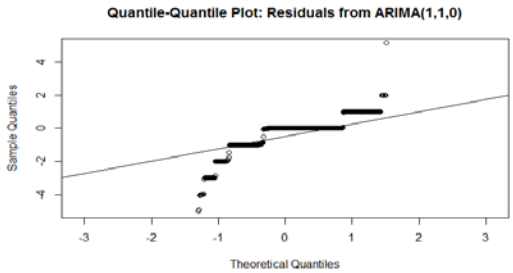

Fig. 10 The Q-Q Plot of Residuals from ARIMA(1,1,0)

The ARCH model has to be applied to the residuals after fitting with a linear mean model. In this case ARIMA(1,1,0) has been used as the

mean model. The next step is to obtain the order of ARCH model. ARCH(p) model from p = 1 to 6 are considered to fit residual data, and the AIC and BIC values of these models are listed in the Table 2.

Table 2. The goodness of Fit Measures ARCH Models.

Model	AIC	BIC	AICc
ARCH(1)	5.0833	5.1382	5.0833
ARCH(2)	5.0875	5.1518	5.0875
ARCH(3)	5.4833	5.2382	5.4833
ARCH(4)	5.567	5.512	5.567
ARCH(5)	5.5872	5.5231	5.5872
ARCH(6)	5.5987	5.6385	5.5987

It is clear from the Table 2 that the *ARCH(1*) has the best goodness of fit value. The goodness of measure has improved 1548 fold roughly when compared to the *ARIMA(1,1,0)* model. In order to check the accuracy of prediction, Root Mean Square Error (RMSE) and Mean Absolute Error (MAE) of *ARIMA(1,1,0)* and *ARCH(1)* Models are compared as shown in the Table 3.

Table 3. Comparison of ARIMA and ARCH Models.

Model	RMSE	MAE
ARIMA(1,1,0)	2051.62	1427.41
ARCH(1)	37.69	37.02

ARCH(1) model has reduced the error by 55 times roughly when RMSE measure is taken into consideration.

CONCLUSION

The primary objective of the paper was to analyze prediction models of the resource usage in the server virtualized systems. Resource prediction is essential in order to predict the Time to Exhaustion (TTE) in any system so that the administrator of the system could avoid an accidental outage. It is also found that most of the studies in this direction were using the measurement-based approach with time series models for prediction. This paper reviewed the effectiveness of ARIMA model and it examined whether Gauss-Markov assumptions about homoscedasticity holds good for the Ordinary Least Square estimators of such models. It is clear from the model diagnostics that the time series is heteroscedastic in nature. ARIMA models are not suitable for predicting the resource usage and to predict time to exhaustion of the system. AutoRegressive Conditional Heteroscedastic model has been used to model the residuals of ARIMA mean process. Results show that the goodness of fit has improved roughly 1500 times. The clustered volatility at the end and beginning of the time series shows that a regime switching model is much apt for predicting resources.

REFERENCES

1. Matias Rivalino, Pedro Alberto Barbetta, and Kishor S. Trivedi. "Accelerated degradation tests applied to software aging experiments." Reliability, IEEE Transactions on 59.1 (2010): 102-114.
2. Matias Rivalino, Kishor S. Trivedi, and Paulo Romero Martins Maciel. "Using accelerated life tests to estimate time to software aging failure." Software Reliability Engineering (ISSRE), 2010 IEEE 21st International Symposium on. IEEE,2010.
3. Zhao, Jing, et al. "Injecting memory leaks to accelerate software failures." Software Reliability Engineering (ISSRE), 2011 IEEE 22nd International Symposium on. IEEE, 2011.
4. Y. Huang, C. Kintala, N. Kolettis and N.D. Fulton, “Software Rejuvenation: Analysis, Module and Applications,” Proc. of FTCS-25, Pasadena, CA, Jun. 1995.
5. Lei Li; Vaidyanathan, K.; Trivedi, K.S., "An approach for estimation of software aging in a Web server," in Empirical Software Engineering, 2002. Proceedings. 2002 International Symposium, vol., no., pp.91-100, 2002
6. Hoffmann, G.A.; Trivedi, K.S.; Malek, M., "A Best Practice Guide to Resource Forecasting for Computing Systems," in Reliability, IEEE Transactions on, vol.56, no.4, pp.615-628, Dec. 2007
7. Yongquan Yan; Ping Guo; Lifeng Liu, "A Novel Hybridization of Artificial Neural Networks and ARIMA Models for Forecasting Resource Consumption in an IIS Web Server," in Software Reliability Engineering Workshops (ISSREW), 2014 IEEE International Symposium on, vol., no., pp.437-442, 3-6 Nov. 2014
8. Araujo, J.; Matos, R.; Maciel, P.; Vieira, F.; Matias, R.; Trivedi, K.S., "Software Rejuvenation in Eucalyptus Cloud

Computing Infrastructure: A Method Based on Time Series Forecasting and Multiple Thresholds," in Software Aging and Rejuvenation (WoSAR), 2011 IEEE Third International Workshop on , vol., no., pp.38-43, Nov. 29 2011-Dec. 2 2011

9. D. Simeonov and D.R. Avresky. “Proactive Software Rejuvenation Based on Machine Learning Techniques,” Institute for Computer Sciences, Social Informatics and Telecommunications Engineering, vol. 34, pp. 186-200, 2010.
10. Matias, R.; Filho, P.J.F., "An Experimental Study on Software Aging and Rejuvenation in Web Servers," in Computer Software and Applications Conference, 2006. COMPSAC '06. 30th Annual International, vol.1, no., pp.189-196, 17-21 Sept. 2006
11. Elliott, G.; Rothenberg, T. J.; Stock, J. H. (1996). "Efficient Tests for an Autoregressive Unit Root". Econometrica 64 (4): 813–836. JSTOR 2171846.
12. Aho, K.; Derryberry, D.; Peterson, T. (2014), "Model selection for ecologists: the worldviews of AIC and BIC", Ecology 95: 631–636, doi:10.1890/13-1452.1
13. Understanding Memory Resource Management in VMware ESX Server https://www.vmware.com/files/pdf/perf-vsphere-memory_management.pdf

Second International Conference on Science, Engineering & Environment,
Osaka City, Japan, Nov.21-23, 2016, ISBN: 978-4-9905958-7-6 C3051

LIFE DATA ANALYSIS OF SERVER VIRTUALIZED SYSTEM

Biju R Mohan[1], and G Ram Mohana Reddy[2]
[1,2] Department of Information Technology,
National Institute of Technology Karnataka.Mangalore,Karnataka 575025, India

ABSTRACT

The use of reliability metrics and life data analysis has received considerable attention recently in the software engineering literature. Life data analysis under the actual operational profile can, however, be expensive, time consuming or even infeasible. In this paper, a systematic approach has been adopted in order to reduce the experimentation time for estimating time to failure of a server virtualized system. The study of time to failure (TTF) is very essential in server virtualized system, because it is the crux of the cloud computing infrastructure. In order to meet service-level agreements (SLAs) like availability, reliability and response time, prediction of reliability metrics like mean time to failure (MTTF), life distribution etc are indispensable. The most important contributions of this paper are the reduction of experimental time, and the life data analysis of the server virtualized systems which were not addressed so far. Experimental results demonstrate that there is only four percentage deviation from the observed results from the Normalized Root Mean Square Error and resulting in 96% accuracy of predicting MTTF.

Keywords: Accelerated testing; Software reliability; Cloud computing; Server virtualised system; Life data Analysis;

1. INTRODUCTION

Life data analysis involves analyzing times-to-failure (TTF) data obtained under the normal operating conditions in order to quantify the life characteristics of a product, system or component. For many reasons, obtaining such life data (or times-to-failure data) may be very difficult or impossible. The reasons for this difficulty can include the long life times of today's products, the small time period for testing products. In order to overcome this difficulty, reliability practitioners have attempted to devise methods to force these products to fail more quickly than they would under normal operational/use conditions. In other words, they have attempted to accelerate their failures. Over the years, the phrase accelerated life testing has been used to describe all such practices. Accelerated life testing involves the acceleration of failures with the purpose of quantifying the life characteristics of the product at normal operational/use conditions. Accelerated life testing can be classified as: qualitative accelerated testing and quantitative accelerated life testing. Qualitative accelerated testing focuses on identifying failures and failure modes while quantitative accelerated life testing concentrates on predicting the life of the product at normal operational/use conditions. This paper concentrates on quantitative accelerated life testing of server virtualized system. To the best of our knowledge, this is the first work on life data analysis of server consolidated systems.

In order to accelerate the failure time generally two methods of acceleration are employed: usage rate acceleration and overstress acceleration methods. Usage rate acceleration is employed for the product that does not operate continuously; one can accelerate the time it takes to induce failures by continuously testing these products, this is called usage rate acceleration. For products for which the usage rate acceleration is impractical, one can apply stress at levels which exceed the levels that a product will encounter under normal use conditions; this is called overstress acceleration. The time-to-failure data obtained in this manner is used to extrapolate the times-to-failure at operational/use conditions. Server consolidation systems are built to run for a longer period of time so overstress acceleration is used in this case

In life data analysis, life distribution of the system under test (SUT) has to be determined from the failure data. Once this probability density function has been obtained, all other desired reliability results can be easily determined. However, we face the challenge of determining the use level probability density function from accelerated failure data, rather than from failure data obtained under use conditions. To accomplish this there should be mechanism that allows us to extrapolate from data collected at accelerated conditions to arrive at an estimation of use level characteristics. In order to extrapolate the data life stress models are used.

Life data analysis has been done on many platforms like Web Server, Operating Systems and Embedded Systems. Recently, virtualized platforms are getting more popular due to cloud computing applications. Virtualization [10] can be viewed as part of an overall trend in enterprise information technology that refers to the act of creating a virtual (rather than actual) version of something, including virtual computer hardware platforms, operating systems, storage devices, and computer network resources. The main goal of virtualization is to centralize administrative tasks while improving the scalability [3]. Server virtualization is a technique by which multiple servers are hosted on one physical machine. There are many advantages for server virtualization as this technique increases the resource utilization, makes the system highly available, easy to administer, reduces the power usage, reduces the man power and it also reduces the spending on physical infrastructure.

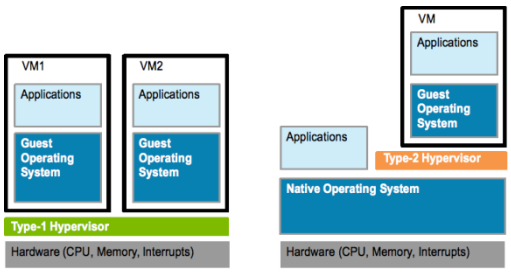

Fig.1 (a) Fig.1 (b)

Fig. 1(a),(b) Different types VMM ; Fig. 1 (a) Type 1 Hypervisor ; Fig.1(b) Type 2 Hypervisor

Server virtualization is developed on the software architecture known as virtual machine. Virtual machine is concept by which underlying physical architecture is hidden from upper layers by a layer of abstraction. In server virtualization system a hypervisor or virtual machine monitor (VMM) will be used to hide the underlying physical architecture from upper layers. The hypervisor is of two types, Type 1 and Type 2. Type 1 (Bare Metal) VMM runs directly on the physical machine to control the hardware and to manage guest operating systems. In Type 2 (hosted) VMM runs within a host operating system. Fig. 1(a),(b) shows different types of VMMs.

The life data analysis is very essential as it helps in making predictions about product life by “fitting” a statistical distribution to life data from a representative sample. This distribution can then be used to estimate important life characteristics of your product such as reliability or probability of failure at a specific time, the mean life for the product and failure rate. This kind of study is very essential in server consolidated systems which helps the system administrators to avoid the unnecessary outages. Due to the long operational life of the server consolidated such a study is difficult, hence in this paper, an accelerated life testing has been adopted to reduce the experimentation time. This is the first time such an approach has been adopted in server consolidation or server virtualized system. The prediction of reliability metric like mean time to failure helps the system administrator in turn to predict the time to rejuvenate and time for migrating the virtual machines in the server consolidated system.

The rest of the paper is organized as follows. Section 2 of this paper deals with the related work, here similar works in the related domains are compared. Section 3 discusses about how the acceleration in stress can be applied, what are the appropriate distributions for life data analysis and it discuss about the different life stress relationships. The experimental setup, the results of goodness of fit of different distributions and prediction of the mean time to failure at different stress levels are topics of discussion in Section 4. Finally we conclude the paper in Section 5.

2. RELATED WORK

Pengcheng Yin et al. [1] used support vector machine (SVM) to predict the life of an electric motor. Ten motors are chosen to perform accelerated life testing at three different temperature levels. A practical model is proposed in this paper to predict the life of the items in accelerated life testing based on support vector machine. Authors claimed that reliability can be predicted accurately for small size of sample data, without using life stress models and the specific life distribution types. This method is easy to use and it has no prior assumptions of distributions are major advantages; but it can be used only for small sample size.

Shuzhen Li et al. [2] adopted accelerated degradation testing (ADT) to verify the reliability and life of high-reliable, long-life product. In this paper, a new degradation prediction method based on Support Vector Machine (SVM) is proposed and developed to predict time-to-failure of product. This prediction method is also compared with Back Propagation Artificial Neural Networks (BPANN) and regression methods to validate its effectiveness. The paper concludes that, SVM gives better result compare to BPANN. This paper compared three models and suggested that SVM is better for given

data set. This paper never discusses about the scalability of the results in comparison with observed results.

Matias et al. [3] applied accelerated degradation test (ADT) on apache web server. The memory consumed by *httpd* process has been assumed as performance degradation factor. Design of Experiment (DOE) factors used was page size, page type and request rate. Page type signifies whether it is static page or dynamic page. They considered regular and high load factor for each parameters. According to analysis, Page size and page type influenced degradation, not the request rate. Experiments are based on accelerated degradation tests (ADT), which do not look for failure times; instead degradation measure of a product's performance has taken over time. Tests containing dynamic requests forced the amount of memory used by *httpd* processes to reach the limit of the total main memory available. It forced the Linux kernel to thrashing. The main advantage is the reduction of the experimental time, but the results are not compared with observed ones.Further Matias et al [4] proposed and evaluated the use of quantitative accelerated life tests (QALT) to reduce the time to obtain the lifetime distribution of systems that fail due to software aging. This approach has experimentally estimated the lifetime distribution of a real web server system. The accuracy of the estimated distribution is evaluated by comparing its reliability estimates with a sample of failure times observed from the real system under test. Major advantages of this method are the reduction of experimental time and the selection of the stress variable based on the aging related failures. The lacuna of this method lies in the lack of lucidity in the explanation of estimating pseudo failure time.

Jing Zhao et. al. [5] created a test bed of a web server, a database server, and a set of clients. The experiments were conducted on Tomcat web container, and all *html* pages were dynamically generated by the server. TPC-W standard bench mark has been used. The web traffic is generated by a Remote Browser Emulator, which emulates users of the website. Memory leaks are injected artificially to accelerate degradation. Inverse Power Law-Lognormal distribution is used to calculate Life characteristic relationship. Major advantages of their approach are the reduction of experimental time and the use of semi-Markov process, to optimize the software rejuvenation trigger interval. The tests are conducted at application level so the readings used for estimation may not be accurate.

Tingting Huang et. al. [6] presented an optimum design of constant stress accelerated life testing based on proportional hazards-proportional odds using penalized local D-optimality. It established the objective function as the product of the Fisher information matrix as defined in proportional hazards-proportional odds model and penalty functions which describe the closeness of the probability density functions of two specified stress levels. This optimum method avoids obtaining limit stress levels of test planning using D-optimality for some cases. The comparison of the optimization results by D-optimality and penalized local D-optimality shows that optimization results using penalized local D-optimality is more reasonable. It is non parametric method, hence it does not require the prior knowledge about the data. Proportional hazards-proportional odds model assumes data follow weibull or lognormal distribution and this assumptions may lead to erroneous results in some cases.

Javier Alonso et. al. [7] proposed a framework that monitors the system level metrics and predicts the time until the system crashes. The authors evaluated two different families of Machine learning algorithms: Linear Regression and Decision Trees. They have considered M5P and REPTree algorithms for Decision Trees. They have captured the system snapshot and evaluated the variation of resource consumption rate. The metrics used are: Throughput, Response time, workload, System load, disc usage, swap used, number of processes, number of threads, free system memory, memory occupied by the running application, number of http connections received, and number of connections to the data base. M5P algorithm gives comparatively better result. The authors did not assume the distributions of the data. The reasons for selecting the metrics for prediction is not explained and the models failed to predict the crashes accurately.

Tao Yuan et. al. [8] developed a method for planning optimal step-stress accelerated life testing. Most of the studies in this area used Maximum Likelihood Estimators for the reliability metrics of interest; Authors used Bayesian method for parameter estimation. Maximum Likelihood Estimation requires precise data and it cannot be applied if there is uncertainty. This study applied the method to design a simple step-stress accelerated life test with Type-I censoring and the Weibull life distribution. The Bayesian optimal plans are compared with the plan obtained by maximum likelihood method. Influence of sample size and prior distribution on the optimal plan is also investigated. Results indicate that the Bayesian

approach has promising potential in the planning of reliability life testing when there is uncertainty in the precise values of the model parameters. This model can be applied even there are uncertainties exist in the data. The disadvantage of this method is that it requires prior knowledge about the product life characteristics.

Table 1. shows the merits and demerits of different existing approaches.

Table 1. Merits and Demerits of Existing Works

Paper	Merits	Demerits
Pengcheng Yin et al. [1]	Easy to use and it has no prior assumptions about the probability distributions	Tested only for small sample sets
Matias et al. [3]	Reduction of the experimental time	Results are never compared with observed ones
Matias et al [4]	The selection of the stress variable based aging related failures	Lack of clarity in the estimation of pseudo failure time
Jing Zhao et. al. [5]	Use of semi-Markov process for the optimization of rejuvenation interval	Application level metrics reading are prone to errors
Tingting Huang et. al. [6]	Does not require prior knowledge about the data	Proportional hazards-proportional odds assumes data follows weibull or lognormal distribution
Shuzhen Li et al. [2]	Proposed new degradation prediction model based on SVM	Silent about the scalability of the results
Tao Yuan et. al. [8]	Model can be applied even when data is not certain.	Require prior knowledge about the product

It is clear that none of these studies are focused on life data analysis of server virtualized system. Most of these studies concentrated on the hardware systems where the stresses are temperature, vibration, humidity, voltage, and thermal cycling. In [3],[4] the system under test was web server. In this paper the system under test is server virtualized system which consists of a Hypervisor/Virtual Machine Monitor and a set of Virtual Machines. The motivation behind taking server virtualized system as our system under test is that it forms the crux of any datacenter. It is important to study the life data analysis of server virtualized setup because it avoids unnecessary outages which help the system administrator of any server virtualized system to migrate the Virtual Machines to a fresh Hypervisor to reduce the down time. That in turn helps the enterprise to meet its service level agreements.

3. PROPOSED METHODOLOGY

Figure 2 shows the overall architecture of the proposed methodology of accelerated life testing on server virtualized or server consolidated system.

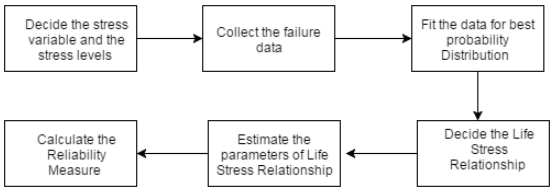

Fig 2. The Overall Architecture of the Proposed Methodology

As shown in Figure 2, the primary step in the test planning is the definition of accelerating stress variable and its levels of utilization (load). Commonly used accelerating stresses are temperature, vibration, humidity, voltage, and thermal cycling [9]. These stresses are appropriate for many engineering applications, where tests are applied to physical or chemical components that are governed by well-known physical laws. However, for software components, we cannot adopt the above mentioned accelerating stresses. From [3],[4],[5], it is clear that memory exhaustion is the main reason for system failure, so memory usage has been used as the stress variable.

The failure data at the selected stress levels were collected, the collected failure times has to be fitted for the best probability distribution. Log-normal, Weibull and exponential distributions have been used quite effectively in analyzing positively skewed data, which play important roles in the reliability analysis. In order to find the best fit for the failure data three goodness-of-fit tests are conducted: *Kolmogorov–Smirnov test (K-S Test), Akaike information criterion (AIC) and Bayesian information criterion (BIC).*

The collected failure times are for System Under Test (SUT) operating under stress, not under its normal operational/use condition. Hence a model is

required, that relates the failure times observed at the tested stress levels to the underlying lifetime distribution of the SUT operating in its normal use condition. This model is called life-stress relationship [9], [10]. Several life-stress relationship models have been developed for different engineering fields. Examples of such well-known models are Arrhenius, Eyiring, Coffin-Manson, Peck, and Zhurkov [9], [10], [11]. Based on the SUT's physical/chemical properties, the underlying theories used to build these models assume specific stress types. For this reason, traditional models applied to physical systems cannot justifiably be employed to build life-stress relationship models for software systems. An exception is the Inverse Power Law (IPL) relationship model, the IPL is applicable to any type of positive stress, unlike the above mentioned models that are used for specific types of stress variables. The Algorithm 1 shows overall steps involved in the life data analysis of server consolidated systems.

Algorithm 1 Overall steps involved in the Life Data Analysis of Server Virtualized System

Algorithm 1
Step1 : Decide the stress variables and the stress levels
Step 2: Collect the failure data
Step 3: Find the best fit for the failure data from the positively skewed distributions
Step 4: Decide the Life stress relationships
Step 5: Estimate the parameters of Life Stress Relationship
Step 6: Calculate the reliability Measures

The IPL life-stress relationship can be expressed in Eq.(1) , Where *L* represents a quantifiable life measure. *V* represents stress levels, *K* and *n* represents model parameters to be determined from the life distribution. Based on the life distribution, the following are the Life stress probability distribution function.

$$L = 1/(KV)^n \quad (1)$$

The life stress probability distribution function of IPL-Exponential is given by Eq. (2)

$$\boldsymbol{f(t,V) = KV^n e^{-KV^n t}} \quad (\mathbf{2})$$

where *t* is the time in hours, *K*, *n* is model parameters to determined and *V* is the stress level.

The life stress probability distribution function of IPL-Weibull is given by Eq. (3)

$$\boldsymbol{f(t,V) = \beta KV^n (KV^n t)^{\beta-1} e^{-(KV^n t)^{\beta}}} \quad (\mathbf{3})$$

where *t* is time in hours, β is shape parameter, *K and n* are model parameters to be determined and *V* is the stress level.

The life stress probability distribution function of IPL-Log-Normal is given by Eq. (4)

$$\boldsymbol{f(T,V) = \frac{1}{T\sigma_{T'}\sqrt{2\pi}} e^{-\frac{1}{2}\left(\frac{T' + \ln(K) + n\ln(V)}{\sigma_{T'}}\right)^2}} \quad (\mathbf{4})$$

where $\boldsymbol{\sigma_{T'}}$ is the standard deviation of the natural logarithms of the Time to Failure, *K*, *n* are the model parameters to determined and *V* is the stress level.

Once an underlying life distribution and the life-stress relationship model to fit the accelerated data have been decided, the next step is to decide the parameter estimation method. Here Maximum Likelihood Estimation method is employed as it is more robust than probability plotting and least square estimators. The required reliability information is Mean Time to Failure (MTTF). MTTF give the rejuvenation time of the Virtual Machines. MTTF for IPL- Exponential life stress probability distribution is given by Eq.(5)

$$\boldsymbol{\overline{T} = \frac{1}{KV^n}} \quad (\mathbf{5})$$

where *K*, *n* are the model parameters to determined, and *V* is the stress level. MTTF for IPL- Weibull life stress probability distribution is given by Eq.(6)

$$\boldsymbol{\overline{T} = \frac{1}{KV^n} . \Gamma\left(\frac{1}{\beta} + 1\right)} \quad (\mathbf{6})$$

Where *K*, *n* are the model parameters to determined, and *V* is the stress level. And $\boldsymbol{\Gamma\left(\frac{1}{\beta} + 1\right)}$ is the gamma function to be evaluated at $\boldsymbol{\left(\frac{1}{\beta} + 1\right)}$, where β is the shape factor of the Weibull distribution. MTTF for IPL-Lognormal life stress probability distribution is given by Eq.(7)

$$\boldsymbol{\overline{T} = e^{-\ln(K) - n\ln(V) + \frac{1}{2}\sigma_{T'}^2}} \quad (\mathbf{7})$$

Where $\boldsymbol{\sigma_{T'}}$ is the standard deviation of the natural logarithms of the Time to Failure, *K*, *n* are the model parameters to determined, and *V* is the stress level.

4. RESULTS ANALYSIS

The system under test used in this experiment is VMWare ESXi 5.5 on LENOVO 5498-PR1, 4 Cores, 500GB hard disk, 2.93 GHz processor with Hyperthreading enabled and 8GB RAM. 8 Virtual Machines (VMs) were created on this machine and installed Ubuntu 14.04 operating system on all of them. Apache 2.0 and PHP 5.0 were installed on these VMs. In these setup 8 VMs are acting as servers. In the same virtualised environment, a client VM is created with Ubuntu 14.04 operating system

and *httpref* [12] installed on it. Shell program is written to call the *test.php* page using *httperf* continuously with the rate of 500 requests per second. Server VMs used 1vCPU, 4GB RAM and 100GB hard disk with thin provisioning. The Client VM used 1GB RAM, 1 vCPU, 16GB of Hard disk. 8VMs using 4GB RAM results in 32GB of logical RAM plus client VM is using 1 GB, but physically only 8 GB RAM is present. Hence main memory is over-committed to approximately four times.

The basic assumption behind the workload is that a memory leak is injected randomly after "N"clients requests. This number is taken as the stress factor in this experiment. In this paper three stress values N=5, 10, 20 are considered and it means that a memory leak is deliberately injected within that number of client requests. To make it clear let us suppose N=5, then a memory leak is injected between 0 to 5 client requests. So N=5 is the overstressed condition among the three stress levels used. The flowchart for the memory leak injection is shown as in the Figure 3.

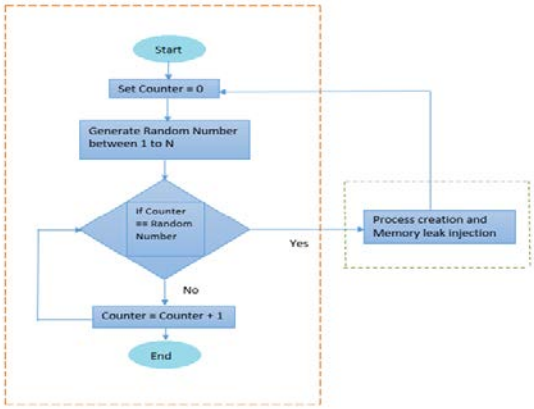

Fig 3. Flowchart of the memory injection algorithm

After collecting the failure times, the best probability distribution has to identified from the failure data of Virtual Machines at each stress levels N=5, N=10 and N=20. For each stress level, three sets of failure data has been collected. Since there are 8 Virtual Machines 24 failure data has been collected for each stress level.

The twenty four times failure data were collected at each stress level is shown as below. For the first stress i.e. at N=5, 24 failure data are collected as shown below in Table 2.

Table 2. Failure times of the Virtual Machines collected for the first stress level at N = 5

Virtual Machine	Experiment 1	Experiment 2	Experiment 3
1	37	33	37
2	23.5	24	39
3	14	27.5	15.5
4	37	37	34
5	28.5	23.5	41
6	37	28	40
7	32.5	30	38.5
8	25.5	37.5	26

For the second stress i.e. at N=10; twenty four failure data are collected as shown below in Table 3.

Table 3. Failure times of the Virtual Machines collected for the second stress level at N = 10

Virtual Machine	Experiment 1	Experiment 2	Experiment 3
1	40.5	38.5	34.5
2	40.5	32.5	43
3	40	32.5	33.5
4	45.5	15	39.5
5	45.5	39	37
6	21.5	36.5	35
7	21	18	35.5
8	67.5	35.5	35.5

For the second stress i.e. at N=20; twenty four failure data are collected as shown below in Table 4.

Table 4. Failure times of the Virtual Machines collected for the third stress level at N = 20

Virtual Machine	Experiment 1	Experiment 2	Experiment 3
1	48.5	71	38
2	60.5	54.5	47.5
3	70	67	40
4	62.5	72.5	44
5	47.5	41	45
6	50	53	52.5
7	48.5	54.5	39.5
8	50.5	58	40.5

The failure data at the selected stress levels were collected, the collected failure times has to be fitted for the best probability distribution. Three distribution were chosen Log-normal, Weibull and exponential distributions because they have been used quite effectively in analyzing positively skewed data, which play important roles in the reliability analysis. In order to find the best fit for the failure data three goodness-of-fit tests are conducted. The Kolmogorov–Smirnov test (K-S Test), Akaike information criterion (AIC), Bayesian information criterion (BIC) were used to find the best fit among the three probability distributions chosen. For the

stress level N=5, N=10, N=20 the results are shown as below. Table 5 gives the goodness-of-fit scores of the first data set ; i.e. The experiment conducted at stress level N=5.

Table 5. Goodness-of-fit scores of failure data for the first stress level at N = 5

Distributions	Kolmogorov–Smirnov test (K-S Test)	Akaike information criterion (AIC)	Bayesian information criterion(BIC)
Weibull	0.535	166.1789	168.535
Log Normal	0.3557	174.0621	176.4182
Exponential	0.5385	175.777	178.1331

Table 6. gives the goodness-of-fit scores of experiments conducted at stress level N=10. Table 7 gives the goodness-of-fit scores of experiments conducted at stress level N=20.

Table 6. Goodness-of-fit scores of failure data for the second stress level at N = 10

Distributions	Kolmogorov–Smirnov test (K-S Test)	Akaike information criterion (AIC)	Bayesian information criterion(BIC)
Weibull	0.2033	185.3682	187.4354
Log Normal	0.07237	186.3865	188.7426
Exponential	7.11E-15	586.8487	589.2048

Table 7. Goodness-of-fit scores of failure data for the second stress level at N = 20

Distributions	Kolmogorov–Smirnov test (K-S Test)	Akaike information criterion (AIC)	Bayesian information criterion(BIC)
Weibull	0.995	178.3682	182.7243
Log Normal	0.9888	181.5825	183.9386
Exponential	0.9676	180.986	183.3421

The goodness-of-fit scores shows two-parameter Weibull fits the data well. So the IPL-Weibull stress relationship has been used to identify the MTTF of the Server Virtualized system. The parameters are estimated using Maximum Likelihood Estimation. The shape parameter, β = 4.462529, the model parameters K = 0.054748 and n = -0.367017.

Table 8 gives the details of the observed failure time and calculated mean time to failure.

Table 8. Comparison of the observed failure time and calculated mean time to failure

Stress level	Calculated using MTTF IPL-Weibull	Observed Failure Time
100	91.3	110
200	130.4	124
500	182.6	167
1000	228.5	211
2000	304.3	310
4000	456.5	467

The MTTF has been calculated for six different stress levels and it is compared with the observed ones. The root mean square error (RMSE) is calculated from the observed and predicted values. The RMSE is given Eq.(8)

$$RMSE = \sqrt{\frac{1}{n}\sum_{i=1}^{n}(y_i - \hat{y}_i)^2} \quad (8)$$

The root mean square is 13.43, which is reasonably good for the values. The normalized root mean square error shows only 4% deviation from the observed results. i.e. 96% accuracy in terms of MTTF.

5. CONCLUSION

The approach considerably reduced the experimental time to predict the mean time to failure. It has introduced a new approach to predict the rejuvenation time. Another contribution worth mentioning here is that to the best of our knowledge this is first time this kind of experiment strategy has performed on the server virtualized systems. This approach may be effectively utilized for predicting the migration time of a Virtual Machine. The results obtained are reasonably good at the experimented level and it could be tested at lower stress levels. The experimental results presented above confirm that the tested experimental plan is a good starting point for future efforts. The life stress relationship IPL-Weibull model showed very good accuracy for predicting the failures which helps system administrators to avoid unnecessary outages. It may motivate other researchers to apply it to similar software systems.

The paper could be extended by comparing the existing technique with some machine learning techniques or Regression models. This model could be used to predict the rejuvenation time in physical routers/networking devices or embedded systems when there are signs of performance degradation.

REFERENCES

[1] Yin, Pengcheng, and ChengdongWang. "Life-prediction of accelerated life testing based on support vector machine." Quality, Reliability, Risk, Maintenance, and Safety Engineering (ICQR2MSE), 2011 International Conference on. IEEE, 2011.

[2] Shuzhen Li; Xiaoyang Li; Tongmin Jiang, "Life and reliability forecasting of the CSADT using Support Vector Machines,"

Reliability and Maintainability Symposium (RAMS), 2010 Proceedings - Annual , vol., no., pp.1,6, 25-28 Jan. 2010.

[3] Matias Rivalino, Pedro Alberto Barbetta, and Kishor S. Trivedi. "Accelerated degradation tests applied to software aging experiments." Reliability, IEEE Transactions on 59.1 (2010): 102-114.

[4] Matias Rivalino, Kishor S. Trivedi, and Paulo Romero Martins Maciel. "Using accelerated life tests to estimate time to software aging failure." Software Reliability Engineering (ISSRE), 2010 IEEE 21st International Symposium on. IEEE,2010.

[5] Zhao, Jing, et al. "Injecting memory leaks to accelerate software failures." Software Reliability Engineering (ISSRE), 2011 IEEE 22nd International Symposium on. IEEE, 2011.

[6] Huang, Tingting, and Tongmin Jiang. "Design of accelerated life testing using proportional hazards-proportional odds." Reliability and Maintainability Symposium (RAMS), 2010 Proceedings-Annual. IEEE, 2010.

[7] Alonso, Javier, Jordi Torres, and Ricard Gavalda. "Predicting web server crashes: A case study in comparing prediction algorithms." Autonomic and Autonomous Systems, 2009. ICAS'09. Fifth International Conference on. IEEE, 2009.

[8] Yuan, Tao, and Xi Liu. "Bayesian planning of optimal step-stress accelerated life test." Reliability and Maintainability Symposium (RAMS), 2011 Proceedings Annual. IEEE, 2011.

[9] B. N. Nelson, Accelerated testing: statistical method, test plans, and data analysis, New Jersey: Wiley, 2004.

[10] A. Mettas, “Understanding Accelerated Life Testing Analysis,” In Proc. of International Reliability Symposium, 1-16, 2003.

[11] W. Q. Meeker, and L. A. Escobar, Statistical Methods for Reliability Data. New York: Wiley, 1998.

[12] http://www.hpl.hp.com/research/linux/httperf/

Environment

Second International Conference on Science, Engineering & Environment,
Osaka City, Japan, Nov.21-23, 2016, ISBN: 978-4-9905958-7-6 C3051

INOCULANTS FUNGAL *Trichoderma, Mucor* AND *Bacillus* FOR COMMUNITY DEVELOPMENT BASED ON SUFFICIENCY ECONOMY PHILOSOPHY

Sukhan Rattanaloeadnusorn[1]
[1]Faculty of Science and Technology,
Rajamangala University of Technology Thanyaburi, Thailand
e-mail: sukhan@mail.rmutt.ac.th or sukhanratt@hotmail.co.th

ABSTRACT

His Majesty King Bhumibol Adulyadej of Thailand has conceived and developed a new philosophy to improve the lives of the Thai people and bring them a genuine and lasting happiness. This new philosophy is called "sufficiency economy" or "sufficiency economy philosophy". This research has the objective to create and develop new innovation bio-fertilizer for development communities by inoculants *Trichoderma, Mucor* and *Bacillus* based on sufficiency economy philosophy. Khok-kham community in Samut Sakhon province and Khanom community in Nakhon Si Thammarat province were selected for studying the efficiency of new innovation bio-fertilizer. For nutrient analysis of new innovation bio-fertilizer, we found high macronutrients: Nitrogen, Potassium and Phosphorus with the average value 84.33 percent. In addition, when we used for planting mangrove tree, it can help to remove heavy metals such as Lead (Pb), Cadmium (Cd) and Copper (Cu) in soil with the average value 98.6 percent. Moreover, it can help for inducing growth rate of mangrove tree up to 4 folds when compared with the control case. This result can be applied for recovering mangrove forest area in the condition of limits of times. For planting organic rice by new innovation bio-fertilizer, it can help to increasing productivity, reducing costs 5-6 folds and improving soils acid. In summary, new innovative bio-fertilizer is very useful to planting mangrove and organic rice, also restoring mangrove forest area for developing community based on sufficiency economy philosophy.

Keywords: Inoculants fungal and bacteria, Innovative bio-fertilizer, Sufficiency economic, Mangrove forest

INTRODUCTION

In recent years, mangrove forest areas at Khok-kham community in Samut Sakhon and Khanom community in Nakhon Si Thammarat were decreased significantly. There are many causes led to decreasing of mangrove forest areas. For example, the effect of coastal erosion, increasing shrimp farming and salt farming, microbial diseases, waste pollutants from industry, soil acid pH 3-4 etc. [1] and the survival rate of tree less than 30% when plants are grown without bio-fertilizer plant by inoculants *Trichoderma Mucor* and *Bacillus.* [8] Thus, both public and private sectors including the community should be integrated planning and working together for restoring mangrove forest areas and developing community. For sustainable developing community, His Majesty King Bhumibol Adulyadej of Thailand has conceived and developed a new philosophy to improve the lives of the Thai people and bring them a genuine and lasting happiness. This new philosophy is called "sufficiency economy" or "sufficiency economy philosophy". Moreover, His Majesty King Bhumibol had explained a meaning of "sufficiency" in which has three components: moderation, reasonableness, and self-immunity, with two accompanying conditions: appropriate knowledge and ethics & virtues [10]. The sufficiency economy philosophy of His Majesty King Bhumibol as shown in Figure 1. By applying science and technology knowledge based on sufficiency economy of His Majesty King Bhumibol, a process of developing by new innovative bio-fertilizer with inoculants *Trichoderma, Mucor* and *Bacillus* from the wastes in community for the sustainable community lead to environmental social economy and culture is presented as Figure 2. [5][6][7][8]

This research has the objective to research and developing new innovation for developing soils acid in communities. The new innovative bio-fertilizer with inoculants *Trichoderma, Mucor* and *Bacillus* [5] from the wastes in community such as hyaline salt (Kigdadnakluea) from salt farming or Straw and rice husk from investment on paddy for planting mangrove tree *Rhizophora mucronata* in Khok-kham community, Samut Sakhon province and Khanom community in Nakhon Si Thammarat province and organic rice verities RD. 47 in

Nongsoae community, Phathum Thani province, replacement of traditional mangrove tree *Rhizophora mucronata* and organic rice verities RD 47. Which leads to acid soil conservation and development of the communities with inoculants *Trichoderma, Mucor* and *Bacillus* following the philosophy of sufficiency economy. Figure 3

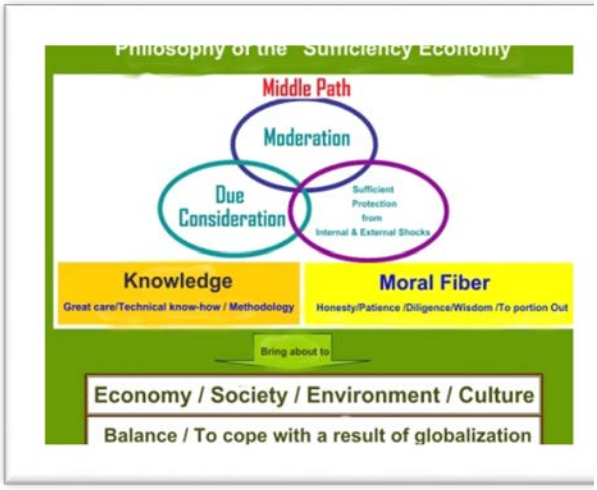

Figure 1 Sufficiency economy philosophy of His Majesty King Bhumibol Adulyadej. (source:http://www.thaiembassy.ca/en/about-embassy/news/the-royal-initiative-of-the-philosophy-of-sufficiency-economy)

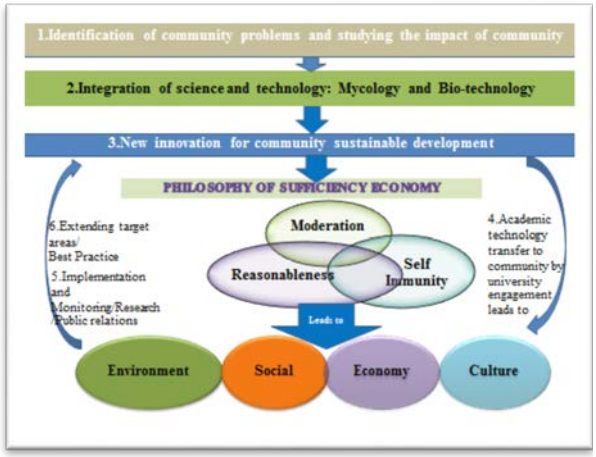

Figure 2 Process of community developing by new innovative bio-fertilizer with inoculants *Trichoderma, Mucor* and *Bacillus* based on sufficiency economy philosophy of King Bhumibol Adulyadej.

RESEARCH METHODOLOGY

STUSDY AREA

Khok-kham community, Samut Sakhon province (a) and Khanom community in Nakhon Si Thammarat province(b) and Nongsoae community, Phathum Thani province.(c)

Figure 3 Study areas, (a) Samut Sakhon province and (b)Nakhon Si Thammarat province and (C)Phathum Thani province.Thailand.

METHODOLOGY

Research driven community development engagements by explored problems and of the community. First integrate bio- technology to solutions and eliminate waste and garbage of community by new innovations bio-fertilizer with inoculants *Trichoderma, Mucor* and *Bacillus* from biodiversity of antagonistic fungal and bacteria. Make bio- fertilizer with inoculants *Trichoderma, Mucor* and *Bacillus* from the wastes of communities for use in seeding and mangrove planting in soil acid, Samut Sakhon province and Nakhon Si Thammarat province and organic rice and vegetables developments in soil acid, Phathum Thani province Thailand. Following steps of driven community research or process of corporate social responsibility (CSR) were 5 steps as Figure 4

1) Community problem and impact surveyed in area Khokkham, Samut Sakorn province and Khanom, Nakhorn Si Thammarat Thailand.

2) Wastes and garbage of the community were rhizo-degraded with new innovation by antagonistic *Trichoderma*, *Mucor* and *Bacillus* in semisolid's tanks in during time 28-30 days.

3) Quality control the bio fertilizer products follow Standard bio-fertilizer products.[8]

4) Utilization and analysis data after the bio fertilizer products with inoculants *Trichoderma, Mucor* and *Bacillus*, it using mangrove restoration and organic planting development compared with non-using the bio fertilizer products in soils acid. It is analysis about increase percent of growth rate tree *Rhizophora mucronata* and percent productivity yields and reducing costs to restored at shrimp abandoned area and organic rice agriculture developments by new innovation with inoculants *Trichoderma, Mucor* and *Bacillus* in soils acid. Figure 4

5) Bio-technology transfer for the development of community based on sufficiency economic philosophy in to sustainable restore the nature balance and organic rice developments.

RESULTS

Based on sufficiency economic philosophy, a researcher transferred bio-technology into the community to sustainable nature balance, increase mangrove forest area and organic rice and vegetables. The communities can produce new innovative bio-fertilizer by inoculants *Trichoderma, Mucor* and *Bacillus* from the wastes in community. Figure 5-6 We found new innovative bio-fertilizer have macronutrient and micronutrient higher than the standard bio-fertilizer up to 84.33 percent. Moreover, it also can removal of heavy metals, such as cadmium (Cd) and copper (Cu) in soils up to 98.6 percent. While when the inoculants only *Trichoderma* has detected major nutrient 66 percent, inoculants *Bacillus* has detected major nutrient 59 percent. Reduced the amount of heavy metals is 93.6 and 93.1 percent respectively.

Figure 4 Process of research driven community development engagement through by new innovation with inoculants *Trichoderma, Mucor* and *Bacillus*.[5]

Found that the community has higher productivity yields at when they use the bio-fertilizer *Trichoderma, Mucor* and *Bacillus* instead of bio- fertilizer *Trichoderma* and bio-fertilizer *Bacillus* bacteria for restoration in abandoned shrimp farms to natural balance within 5 years. Normal restoration of shrimp abandoned without new Innovative bio-fertilizer with inoculants *Trichoderma, Mucor* and *Bacillus* rehabilitation time required for 10-15 years. [1] [2] The growth rate of mangrove tree *Rhizophora mucronata* increasing up to 4 folds, and the survival rate of more than 95% when the plants are grown by bio-fertilizer with inoculants *Trichoderma Mucor* and *Bacillus*.[8] as shown in Table 1 and Figure 7 Moreover, when bio-fertilizer with *Trichoderma, Mucor* and *Bacillus* for develop organic rice and vegetable cultivation in acid soils, Pathum Thani, Thailand found that many farmers have increased productivity yields and reduced costs 5-6 folds (7,000 baths to 1,800 baths)[7] as much neutral soil

condition(pH6-7), increased survival rate, reduced the amount of heavy metals in soil, biodiversity antagonistic fungi increased, Control of Pathogens.[3][4][7] Table 1 and Figure 8 Due to antagonistic microorganism in new inoculants with *Trichoderma*, *Mucor* and *Bacillus* products produced extra-enzyme such as hemicellulase, peroxidase, phosphatase laccase etc. to accelerated degradation of the organic and inorganic to the macronutrients and micronutrients will been uptake through the root system, removal of heavy metal, pretreatment soil pH. The plants grow better than grown without the use of innovative inoculants *Trichoderma*, *Mucor* and *Bacillus*. [3] [4] [6] [7] [8]

Figure 5 Khok-kham bio- fertilizer with inoculants *Trichoderma*, *Mucor* and *Bacillus* from the wastes in community.

Figure 6 Transfer bio technologies to community developments for produing bio- fertilizer with inoculants *Trichoderma*, *Mucor* and *Bacillus* from the wastes in community.

Figure 7 Restored mangrove forest by new innovative Khok-kham bio- fertilizer with inoculants *Trichoderma*, *Mucor* and *Bacillus*

- **A.** Seeding and root of *R. mucronata* seeding by Khok-kham bio- fertilizer with inoculants *Trichoderma*, *Mucor Bacillus* and inoculants only *Trichoderma* and inoculants *Bacillus*.
- **B.** Inducing growth *R. mucronata* 4 folds (B,C) compare without bio-fertilizer(D)at abandoned shrimp farms in 1and 2 year.

Figure 8 Organic rice and vegetable developments by new bio-fertilizer with inoculants *Trichoderma*, *Mucor* and *Bacillus* for increase the productivity yields, reducing costs 5-6 folds instead of bio-fertilizer with inoculant only *Trichoderma* or bio-fertilizer with inoculant *Bacillus.*

Table 1 Comparison percent increasing nutrients, heavy metal, increasing productivity yields and reducing costs of innovative(folds).

Lists	Percent efficiency of Innovative (%)		
	inoculants *Trichoderma Mucor* and *Bacillus*	inoculant *Trichoderma*	inoculant *Bacillus*
Nitrogen(N)	80	50	43
Potassium(K)	93	74	74
Phosphorus(P)	80	75	60
%mean	84.33	66	59
Pb(Lead)	100	95	85
Cd(Cadmium)	100	100	100
Cu(Copper)	96	98	97
%mean	98.6	97.6	93.1
increasing productivity yields, reducing costs of rice	5-6 folds	2-3 folds	1.5 folds
increasing growth rate of *R. mucronata*	4 folds	2 folds	1 folds

CONCLUSIONS

Community development by new innovation inoculants *Trichoderma, Mucor* and *Bacillus* as bio-fertilizer products from the wastes in community those are better than the usual standard bio- fertilizer products. This bio- fertilizer were using for development of mangrove reforestation and development of organic agriculture. To answer problems and impact of the community and environmental, social economic development base on the philosophy of sufficiency economy sustainability. [4] [5] [6] [7] [8]

So new innovative bio-fertilizer with inoculants *Trichoderma, Mucor* and *Bacillus* [5] were been used in the development of bio- fertilizer from the wastes in community. It found that the volume of macronutrient and the micronutrient in bio- fertilizer higher than the standard 84.33 percent. Moreover, the removal of heavy metals such as cadmium (Cd) and copper (Cu) contamination in soil are at high rate of 98.6 percent.

When we lead new bio-fertilizer with inoculants *Trichoderm*a, *Mucor* and *Bacillus* development to planting *R. mucronata* in acid soils. The rate of growth 4 folds higher than growing traditional, survive rate more than 95%.[6] [7] [8] and the farmers have higher productivity yields and lower costs at 5-6 folds when they use this new bio- fertilizer with inoculants *Trichoderm*a, *Mucor* and *Bacillus* instead of bio-fertilizer with inoculants only *Trichoderm*a 2-3 folds or bio- fertilizer with inoculants *Bacillus* 1.5 folds in soils acid. Due to antagonistic microorganism in inoculants *Trichoderma*, *Mucor* and *Bacillus* products produced extra-enzyme such as cellulase, peroxidase, phosphatase etc. to accelerated degradation of the organic and inorganic to the macronutrients and micronutrients will been uptake through the root system, removal of heavy metal, pretreatment soil pH. The plants grow better than grown without the use of innovative inoculants *Trichoderma*, *Mucor* and *Bacillus*. [3] [4] [6] [7]
From the results of the implementation of community development projects by new innovation bio-fertiizer with inoculants *Trichoderma, Mucor* and *Bacillus* is consistent with studies of Rattanaloeadnusorn *et. al.* 2014 for restoring mangrove forest and organic rice development inrecent years. [4] [6] [7] [8]

ACKNOWLEDGMENT

This research was supported by research grants from the NSTDA, Ministry of Science and Technology, and thanks to RMUTT engagement, community Moo 3 Tambon Khok Kham, Samut Sakorn, and Nakornsri Thamarat and Nongsoae community, Phathum Thani province Thailand to cooperate in this research

REFERENCES

[1] Aksomkoae, S. and Khemnark C., 1994. Nutrient cycling in mangrove forest of Thailand Proc. As. In Symp. Mangrov-Res & Manag, p13.
[2] Kucey,R.M.N..,H.H. Janzen and M.E. Leggett.1989.Microbially mediated increases in plant available phosphorus. Advances in Agronomy.42:199-227.
[3] Lacambra, C., Friess, D., Spencer, T., & Moller I., 2013. Bioshields: mangrove Ecosystems as resilient natural coastal defenses. In F. Renaud, K. Sudmeier-Rieux, &M. Estrella (Eds.), The role of ecosystems.
[4] Liu,Q.,P.Loganathan and M.J.Hedley.2005. Influence of ectomycorrhizal hyphae on phosphate fractions and dissolution of phosphate rock in rhizosphere soils of *Pinus radiate*. Journal of Plant Nutrition. 28:1525-1540.
[5] Rattanaloeadnusorn Sukhan, 2013. Fungal Pellets Patents
[6] Rattanaloeadnusorn Sukhan, Thitaya Sronkwan, Sujaya Ritthisor and Sirikhae pongswat. 2012. Biofertilizer from Stock Fungus and Natural Material for Sufficiency Economy Philosophy Community Development, *st International Symposium on Local Wisdom and Improving Quality of Life*, in 8-11 August 2012 Chai mai, Thailand. P. 49-56
[7] Rattanaloeadnusorn Sukhan, 2012. Mangrove Restoration and Vegetable Growth with Biological Technique, Naresuan University Journal 2012; 20(1)
[8] Rattanaloeadnusorn Sukhan, Pongswat Sirikhae and Rattanaloeadnusorn Atchanut. 2014. Antagonistic Fungal Pellets for Community Development based Sufficiency Economy Philosophy. The 2 nd Asia Engage Regional Conference 2014: Innovation and Creativity: collaboration with communities to tackle problems across ASEAN, Asia and Beyond, 17 – 20 November 2014 at Hotel Grand Nikko, Nusa Dua Bali Indonesia.
[9] Intana, W., Chamswang. C., Intanoo, W., Hongprayoo, C and Sivasithamparam, K. 2003. Use of mutantstrain for improved efficacy of *Trichodrema* for controlling cucumber damping-off. Thai Journal of Agricultural Science.36 (3): 45-50.
[10] http://www.thaiembassy.ca/en/about-embassy/news/the-royal-initiative-of-the-philosophy-of-sufficiency-economy)

Second International Conference on Science, Engineering & Environment,
Osaka City, Japan, Nov.21-23, 2016, ISBN: 978-4-9905958-7-6 C3051

HORIZONTAL TRANSFER OF PLASMID DNA BETWEEN DIFFERENT BACTERIA SPECIES UNDER MICROBIAL INTERACTIONS

Kazuhito Murakami[1] and Akiko Inoue-Kohama[2]
[1]Department of Life Science, Chiba Institute of Technology, Japan; [2] Department of Environment and Energy, Tohoku Institute of Technology, Japan

ABSTRACT

Horizontal transfer of plasmid DNA was investigated under phytoplankton metabolites / zooplankton predation exposure condition, to obtain some basic information about the prosperity and decay of GMO (genetically modified microorganisms) in filed release was investigated in this study. *Escherichia coli* HB101, *E.coli* C600, *E.coli* S17-1, *Pseudomonas aeruginosa* PAO1 (gram-negative) and *Bacillus cereus* MC (gram-positive) as recipient strain of plasmid DNA, *E.coli* HB101/pBR325, *E.coli* C600/RP4 and *E.coli* S17-1/pSUP104 as donor of plasmid DNA, were supplied. As phytoplankton,*Microcystis aeruginosa* (cyanophyceae), *Melosira varians* (bacillariophyceae) and *Scenedesmus quadricauda* (chlorophyceae) collected from Lake Tega as donor of metabolites, were supplied. As zooplankton,*Tetrahymena pyriformis* (cilliata) and *Philodina erythrophthalma* (rotifer) collected from Lake Tega as predator were supplied. The results can be concluded as follows; 1) Phytoplankton metabolites leads acceleration of horizontal transfer between not only same strains but also different strain in spite of whether transmissible or not, 2) Zooplankton predation leads decrease of bacterial individual number and horizontal transfer of plasmid DNA, and 3) Horizontal plasmid DNA transfer is influenced greatly, because the natural ecosystem includes phytoplankton as producer and zooplankton as consumer in the same time.

Keywords: plasmid DNA, horizontal transfer, phytoplankton, zooplankton, eutrophicated lake, bioremediation

INTRODUCTION

The practical utilization of GMO (genetically modified microorganism) has been in real, and some GMO is released in market in fact, such as microbial pesticides and so on. The environmental effect of GMO has been much discussed in these 30 years, such as the prosperity and decay, *i.e.*, fate of GMO in a case of the field release [1][2]. However, how not only the genetically modified microorganisms but also the modified gene behave in the environment, how the impact to the environment is given, is not still made clear [3][4][5][6][7][8].

Horizontal transfer of plasmid DNA between different bacterial species was investigated in this study, under phytoplankton metabolites and zooplankton predation exposure condition, to obtain some basic information about the prosperity and decay of GMO in filed release such as bioremediation technology.

MATERIALS AND METHODS

Bacterial Strains

Escherichia coli HB101, *E.coli* C600, *E.coli* S17-1, *Pseudomonas aeruginosa* PAO1 (gram-negative) and *Bacillus cereus* MC (gram-positive) as recipient strain of plasmid DNA, *E.coli* HB101/pBR325, *E.coli* C600/RP4 and *E.coli* S17-1/pSUP104 as donor of plasmid DNA, were supplied. The appearance of these banteria is shown in Photo 1. Plasmid DNA pBR325 (Cm^r, Tc^r, Ap^r) is non-transmissible, RP4 (Ap^r, Tc^r, Km^r) is transmissible, and pSUP104 (Cm^r, Tc^r) is mobilized transmissible, respectively [1].

Phytoplankton Strains

Microcystis aeruginosa (cyanophyceae), *Melosira varians* (bacillariophyceae) and *Scenedesmus quadricauda* (chlorophyceae) as donor of metabolites, were supplied. The appearance of these phytoplankton were shown in Photo 2. These phytoplankton were collected from Lake Tega which is well known as one of the most eutrophicated lakes in Japan, and the occurrence of water bloom (Aoko) is observed in summer. *M.aeruginosa* is one of the dominant species in summer, *M.varians* is in autumn and winter, and *S.quadricauda* is in spring [9][10].

Zooplankton Strains

Tetrahymena pyriformis (cilliata) and *Philodina erythrophthalma* (rotifer) as predator were supplied. The appearance of these zooplankton were shown in

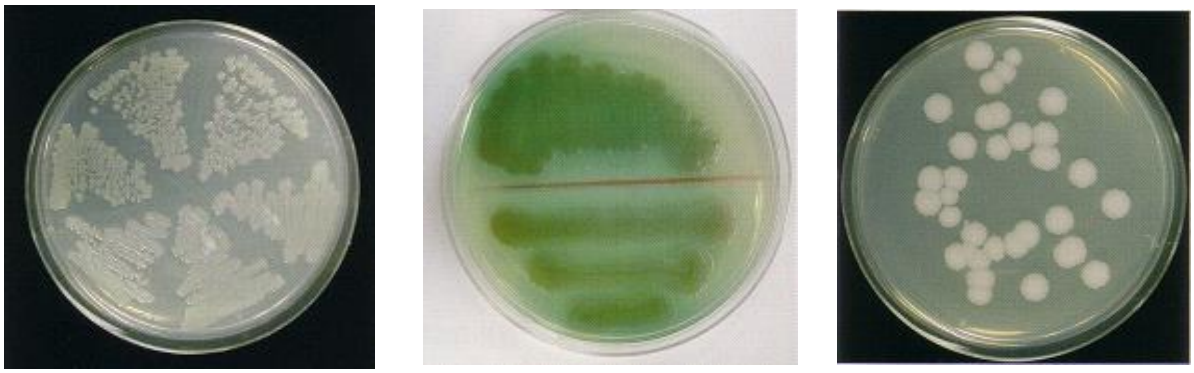

a) *Escherichia coli* (gram negative)

b) *Pseudomonas aeruginosa* (gram negative)

c) *Bacillus cereus* (gram positive)

Photo 1 Bacterial strains supplied in this study (colony on agar plate)

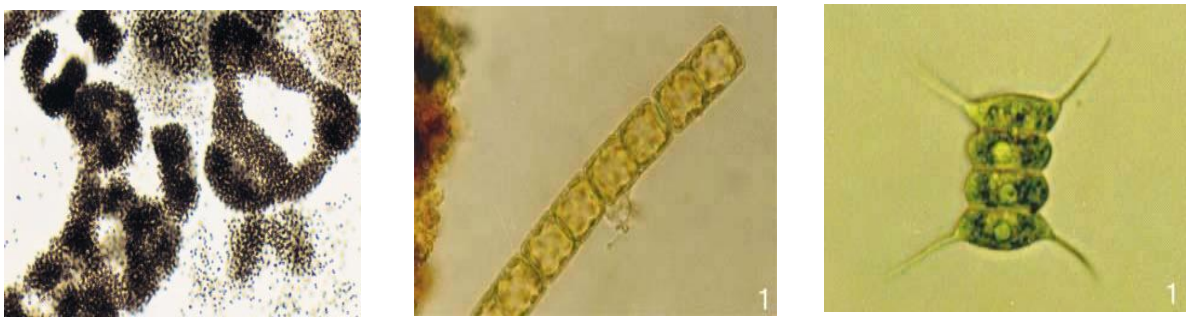

a) *Microcystis aeruginosa* (cyanophyceae)

b) *Melosira varians* (bacillariophyceae)

c) *Scenedesmus quadricauda* (chlorophyceae)

Photo 2 Phytoplankton strains supplied in this study

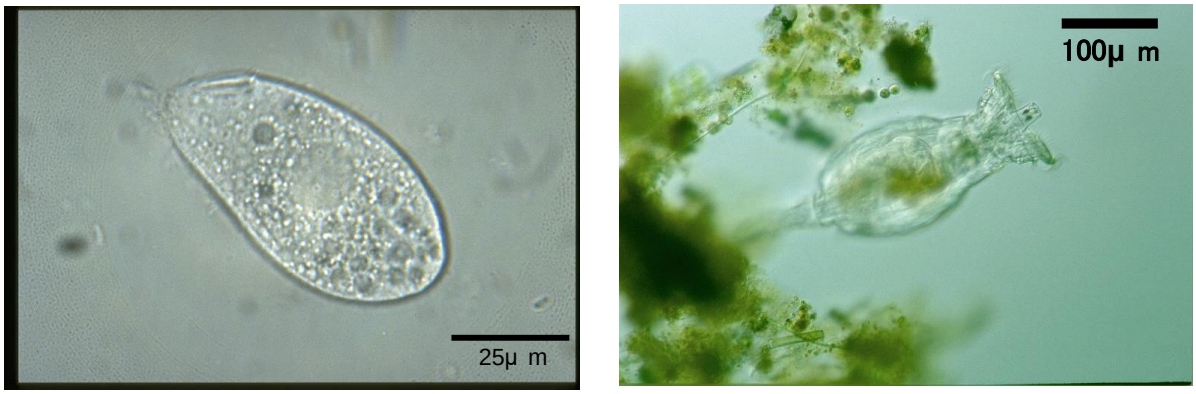

a) *Tetrahymena pyriformis* (ciliata)

b) *Philodina erythrophthalma* (rotifer)

Photo 3 Zooplankton strains supplied in this study

Photo 3. These zooplankton were collected from Lake Tega which is well known as one of the most eutrophicated lakes in Japan. *T.pyriformis* and *P.erythrophthalm*a are ordinary observed in not only Lake Tega but also Japanese lakes and marshes through a year [11][12].

Experimental Procedure

Each bacterial strain was pre-cultured in liquid culture medium under dark, 30℃ and shaking condition for 12hr. with and/or without antibiotics, and the log-phased bacteria was collected by centrifugation. Each phytoplankton strains was pre-cultured under light (20,000lux), 30℃ and non-shaking condition for 2 weeks in modified M11 basic medium. Each zooplankton strains was pre-cultured under dark condition and 20℃ for 5 days and/or 2 weeks.

Pre-cultured each bacterial strain was supplied in combination of experimental series to liquid culture medium containing each phytoplankton metabolite adjusted to phased concentration (dilution rate; ×1, ×2, ×10) and/or polypeptone to investigate the effect of phytoplankton metabolite on plasmid DNA transfer, and containing each zooplankton species (initial individual number; 100 N・ml^{-1} in *T.pyriformis*, 10 N・ml^{-1} in *P.erythrophthalma*) to investigate the effect of zooplankton predation on plasmid DNA transfer.

Plasmid transfer culturing was conducted under dark, 30℃ and shaking condition, considering with the maximum growth rate of bacteria. Colony forming units (CFU) was counted by selection medium plate containing each antibiotic, and transfer rate was calculated to estimate the phytoplankton/zooplankton effect on plasmid DNA transfer.

RESULTS AND DISCUSSION

Effect of Phytoplankton Species on Plasmid DNA Transfer

As results, about the effect of phytoplankton species, in the case of same bacterial strain, that is, the combination of i) *E.coli* HB101 + *E.coli* HB101/pBR325, ii) *E.coli* C600 + *E.coli* C600/RP4, iii) *E.coli* S17-1 + *E.coli* S17-1/pSUP104, the effect of acceleration of horizontal plasmid DNA transfer was higher in *M.aeruginosa* and lower in *S.quadricauda*, which shows the influence is different in different phytoplankton species. In the case of different bacterial strain, that is, the combination of iv) *E.coli* HB101/pBR325 + *P.aeruginosa* PAO1, v) *E.coli* HB101/pBR325 + *B.cereus* MC, vi) *E.coli* C600/RP4 + *P.aeruginosa* PAO1, vii) *E.coli* C600/RP4 + *B.cereus* MC, viii) *E.coli* S17-1/pSUP104 + *P.aeruginosa* PAO1, ix) *E.coli* S17-1/pSUP104 + *B.cereus* MC, the effect of acceleration of horizontal plasmid DNA transfer was higher in *M.aeruginosa* and lower in *M.varians* and *S.quadricauda*, which shows the influence is also different in different phytoplankton species to different bacterial strains. The plasmid DNA transfer rate (%) in each combination of donor and recipient bacteria were shown in Table 1.

The horizontal transferring mechanism between different bacterial species such as gram-negative and gram-positive is not made clear. However, the possibility of outer releasing of plasmid DNA from donor bacterial body after its death and/or body solution, and intaking into recipient bacterial body during its growth, were considered. Form these outcomes, it was made clear that phytoplankton metabolites leads acceleration of horizontal transfer between not only same strains but also different strain in spite of whether transmissible or not.

Effect of Metabolite Concentration on Plasmid DNA Transfer

The effect of metabolite concentration was also investigated. In the case of same bacterial strain, the horizontal plasmid DNA transfer was accelerated under the highest concentration exposure of *M.aeruginosa* metabolite. The other hand, polypeptone, instead of phytoplankton metabolite, did not show any influence on the transfer rate. This indicates that horizontal plasmid DNA transfer is most frequent in summer season when water bloom, that is, Aoko is occurred. The plasmid DNA transfer rate (%) in each metabolite concentration were shown in Table 2.

The horizontal plasmid DNA transfer was also accelerated under the highest concentration exposure of *M.aeruginosa* metabolite between different bacterial strains. Polypeptone did not show any influence in this case. This indicates that not only the quantity but also the quality of phytoplankton metabolite influences much to horizontal transfer of plasmid DNA. In addition, the possibility that GMO which holds artificially modified DNA, survive with changing the host strain in eutrophicated lake where water bloom such as *M.aeruginosa* occurs in summer season, was suggested.

Effect of Zooplankton Species on Plasmid DNA Transfer

As results, about the effect of zooplankton species, in the case of same bacterial strain, that is, the combination of i) *E.coli* HB101 + *E.coli* HB101/pBR325, ii) *E.coli* C600 + *E.coli* C600/RP4, iii) *E.coli* S17-1 + *E.coli* S17-1/pSUP104, *T.pyriformis* and *P.erythrophthalma* grew rapidly in all cases. All bacteria decreased in their individual

Table 1 Effect of phytoplankton metabolite on plasmid DNA transferring rate

	M.aeruginosa	*M.varians*	*S.quadricauda*	polypeptone
E.coli HB101/pBR325 + *E.coli* HB101	13.4	11.8	5.7	3.0
E.coli C600/RP4 + *E.coli* C600	98.3	92.7	89.1	90.0
E.coli S17-1/pSUP104 + *E.coli* S17-1	85.7	69.1	60.1	67.4
E.coli HB101/pBR325 + *P.aeruginosa* PAO1	14.2	9.3	6.7	1.2
E.coli HB101/pBR325 + *B.cereus* MC	6.4	3.4	1.6	1.1
E.coli C600/RP4 + *P.aeruginosa* PAO1	72.2	54.8	42.6	45.2
E.coli C600/RP4 + *B.cereus* MC	8.8	6.1	2.6	2.1
E.coli S17-1/pSUP104 + *P.aeruginosa* PAO1	80.1	67.1	67.0	68.4
E.coli S17-1/pSUP104 + *B.cereus* MC	9.1	7.2	2.9	2.2

(unit : %)

Table 2 Effect of metabolite concentrations on Plasmid DNA transferring rate

	×1	×2	×10	polypeptone
E.coli HB101/pBR325 + *E.coli* HB101	13.4	4.1	2.1	3.0
E.coli C600/RP4 + *E.coli* C600	98.3	93.2	90.5	90.0
E.coli S17-1/pSUP104 + *E.coli* S17-1	85.7	68.8	65.1	67.4
E.coli HB101/pBR325 + *P.aeruginosa* PAO1	14.2	6.8	1.4	1.2
E.coli HB101/pBR325 + *B.cereus* MC	6.4	2.1	1.1	1.1
E.coli C600/RP4 + *P.aeruginosa* PAO1	72.2	65.1	45.9	45.2
E.coli C600/RP4 + *B.cereus* MC	8.8	7.1	4.6	2.1
E.coli S17-1/pSUP104 + *P.aeruginosa* PAO1	80.1	69.2	68.7	68.4
E.coli S17-1/pSUP104 + *B.cereus* MC	9.1	3.2	3.1	1.7

(unit : %)

Table 3 Effect of zooplankton predation on Plasmid DNA transferring rate

	Tetrahymena pyriformis			*Philodina erythrophthalma*		
	μ max	Nmax	transfer rate	μ max	Nmax	transfer rate
E.coli HB101/pBR325 + *E.coli* HB101	4.0	51,000	1.5	0.36	3,100	1.7
E.coli C600/RP4 + *E.coli* C600	4.1	50,000	67.1	0.35	3,100	76.2
E.coli S17-1/pSUP104 + *E.coli* S17-1	4.0	50,000	55.7	0.31	3,000	61.8
E.coli HB101/pBR325 + *P.aeruginosa* PAO1	4.0	48,000	1.7	0.32	3,100	1.8
E.coli HB101/pBR325 + *B.cereus* MC	3.8	46,000	1.9	0.28	2,800	1.8
E.coli C600/RP4 + *P.aeruginosa* PAO1	4.0	48,000	54.2	0.33	3,000	55.9
E.coli C600/RP4 + *B.cereus* MC	3.8	46,000	10.5	0.28	2,800	9.8
E.coli S17-1/pSUP104 + *P.aeruginosa* PAO1	3.9	46,000	49.2	0.30	2,900	46.3
E.coli S17-1/pSUP104 + *B.cereus* MC	3.7	47,000	11.6	0.30	2,600	10.2
	(unit : day^{-1})	(unit : N/ml)	(unit : %)	(unit : day^{-1})	(unit : N/ml)	(unit : %)

number as food source for *T.pyriformis* and *P.erythrophthalma.* In the case of different bacterial strain, that is, the combination of iv) *E.coli* HB101/pBR325 + *P.aeruginosa* PAO1, v) *E.coli* HB101/pBR325 + *B.cereus* MC, vi) *E.coli* C600/RP4 + *P.aeruginosa* PAO1, vii) *E.coli* C600/RP4 + *B.cereus* MC, viii) *E.coli* S17-1/pSUP104 + *P.aeruginosa* PAO1, ix) *E.coli* S17-1/pSUP104 + *B.cereus* MC, the predator *T.pyriformis* and *P.erythrophthalma* grew rapidly in all cases. All bacteria decreased in their individual number as food source for *T.pyriformis* and *P.erythrophthalma*. The specific growth rate (μ) and the maximum individual number (Nmax) of each zooplankton as predator and the plasmid DNA transfer rate (%) in each combination of donor and recipient bacteria were shown in Table 3.

As described above, all bacterial strains were good food source for *T.pyriformis* and *P.erythrophthalma*, in any culture combination.

Effect of Predation on Plasmid DNA Transfer

As results, about the effect of zooplankton species, in the case of same bacterial strain, that is, the combination of i) *E.coli* HB101 + *E.coli* HB101/pBR325, ii) *E.coli* C600 + *E.coli* C600/RP4, iii) *E.coli* S17-1 + *E.coli* S17-1/pSUP104, *T.pyriformis* and *P.erythrophthalma* grew rapidly in all cases. All bacteria decreased in their individual number as food source for *T.pyriformis* and *P.erythrophthalma*. In the case of different bacterial strain, that is, the combination of iv) *E.coli* HB101/pBR325 + *P.aeruginosa* PAO1, v) *E.coli* HB101/pBR325 + *B.cereus* MC, vi) *E.coli* C600/RP4 + *P.aeruginosa* PAO1, vii) *E.coli* C600/RP4 + *B.cereus* MC, viii) *E.coli* S17-1/pSUP104 + *P.aeruginosa* PAO1, ix) *E.coli* S17-1/pSUP104 + *B.cereus* MC, *T.pyriformis* and *P.erythrophthalma* grew rapidly in all cases. All bacteria decreased in their individual number as food source for *T.pyriformis* and *P.erythrophthalma*.

As described above, all bacterial strains were good food source for *T.pyriformis* and *P.erythrophthalma*, in any culture combination. Same results were obtained in the case of one bacterial strain containing different kind of plasmid DNA, and the case of some different kind of host bacterial strain containing one same plasmid DNA as food source for ciliate *T.pyriformis* and *Colpidium campylum*, rotifer *P.eruthrophthalma* and oligochaeta *Aeolosoma hemprichi* as predator [1]. This result suggests that the apitude for food source of micro animals is dependent on the kind of host bacterial strain not on the kind of DNA information coding on plasmid. From these outcomes, it was made clear that zooplankton predation leads decrease of bacterial individual number and horizontal transfer of plasmid DNA. On the other hand, ciliates rapidly enhance the frequency of conjugation between *E. coli* strains through bacterial accumulation in vesicles is reportrd [6][8]. More information should be obtained to discuss the prosperity and decay of GMO in natural ecosystem.

CONCLUSIONS

This study was conducted to investigate horizontal transfer of plasmid DNA under phytoplankton metabolites and zooplankton predation exposure condition, to obtain some basic information about the prosperity and decay of GMO in filed release. The results can be concluded as follows;

1) Phytoplankton metabolites leads acceleration of horizontal transfer between not only same strains but also different strain in spite of whether transmissible or not.

2) Zooplankton predation leads decrease of bacterial individual number and horizontal transfer of plasmid DNA.

3) Plasmid DNA transferring between different bacterial strains is influenced greatly by biological interaction, because the natural ecosystem includes phytoplankton as producer and zooplankton as consumer in the same time.

4) Monitoring of the prosperity and decay of not only the genetically engineered microorganisms but also the modified gene itself is necessary for wise use of bioremediation technology.

REFERENCES

[1] Sudo R, Inamori Y, Murakami K, Okada M, Ohtake H, “Effect of Micro Animals on Prosperity and Decay of Plasmid DNA Transconjugant”, Preprint of Poster Papers on Water Pollution Research and Control, Kyoto, Vol.1, 1990, pp.331-334.

[2] InamoriY, Murakami K, Sudo R, Kurihara Y, Tanaka N, “Environmental Assessment Method for Field Release of Genetically Engineered Microorganisms using Microcosm Systems”, Water Science and Technology, Vol.26, No.9-11, 1992, pp.2161-2164.

[3] Murakami K, “Effect of Biological Interactions on Plasmid DNA Transferring in Bioremediation Technology”, Annual Journal of Civil Engineering in the Ocean, JSCE, Vol.25, 2009, pp.485-490. (in Japanese)

[4] Matsui K, “Horizontal gene transfer in microbial ecosystem”, Jpn.J.Protozool., Vol.48, No.1,2, 2015, pp.31-43.

[5] Maruyama F, Tani K, Nasu M, “Dynamics and contributions to Horizontal gene transfer of extracellular DNA in natural ecosystem”, J.of Environmental Biotechnology, Vol.4, No.2, 2005, pp.131-137.

[6] Matsuo J, Oguri S, Nakamura S, Hanawa T, Fukumoto T, Hayashi Y, Kawaguchi K, Mizutani Y, Yao T, Akizawa K, "Ciliates rapidly enhance the frequency of conjugation between *Escherichia coli* strains through bacterial accumulation in vesicles", res. Microbiol., Vol.161, 2010, pp.711-719.

[7] Matsui K, Ishii N, Kawabata Z, "Release of extracellular transformable plasmid DNA from Escherichia coli cosultivated with algae", Appl. Environ. Microbiol., Vol.69, 2003, pp.2399-2404.

[8] Kawabata Z, Ishii N, Nasu M, Min MG, "Dissolved DNA produced through a prey-predator relationship in a species-defined aquatic microcosm", hydrobiolgia, Vol.385, 1998, pp.71-76.

[9] Murakami K, Taki K, Matsushima H, "Sucession Mechanism on Dominant Phytoplankton in Eutrophicated Lakes", Papers on Environmental Information Science, Vol.17, 2003, pp.331-334. (in Japanese)

[10] Murakami K, "Plasmid DNA Transfer between Different Bacterial Strains with Phytoplankton in Eutrophicated Lake", in Proc. of IWA 14th International Symposium on Health-Related Water Microbiology (WaterMicro2007), 2007.

[11] Inamori Y, Kuniyasu Y, Hayashi N, Ohtake H. Sudo R, "Monoxenic and Mixed Culture of the Small Metazoa *Philodina erythrophthalma* and *Aeolosoma hemprichi* isolated from a Waste-water Treatment Process", Applied Microbiology and Biotechnology, Vol.34, 1990, pp.404-407.

[12] Murakami K, Matsushima H, Tanaka K, Ishii T, Taki K, "Inspection of Magnesium Treatment Effect on Nutrient Elution from Eutrophicated Lake Sediment", in Proc. of 1st World Water Congress of the International Water Association (Paris 2000), 2000.

Second International Conference on Science, Engineering & Environment,
Osaka City, Japan, Nov.21-23, 2016, ISBN: 978-4-9905958-7-6 C3051

ADSORPTIVE BEHAVIOR OF LOW-COST MODIFIED NATURAL CLAY ADSORBENTS FOR ARSENATE REMOVAL FROM WATER

Borano Te[1,2], Chatpet Yossapol[1] and Boonchai Wichitsathian[1]
[1]School of Environmental Engineering, Suranaree University of Technology, Thailand; [2]Department of Civil Engineering, Preah Kossomak Polytechnic Institute, Cambodia

ABSTRACT

Millions of people in more than 70 countries are at risk of developing arsenicosis and other health issues due to consuming elevated arsenic contaminated water. The present study aimed to use natural clays to heat at high temperature and treat with ferrous and ferric solutions through a simple coating technique enhanced by heating at a moderate temperature for arsenate uptake from water. BET, XRF, XRD and SEM methods were applied for the adsorbent characterization. Adsorption experiments were conducted in a series of batch systems in terms of contact time, solution pH, initial concentration and the presence of coexisting anions. The adsorption kinetics was better described by the pseudo-second order rate model for all adsorbents. All adsorbents exhibited higher arsenate uptake efficiency in the acidic pH value. Langmuir model provided the maximum arsenate adsorption capacity of 250µg/g, 429.74µg/g and 747.38µg/g for calcined clay (MC), ferric calcined clay (MC-FeIII) and ferrous calcined clay (MC-FeII), respectively. Among added coexisting anions, phosphate (PO_4^{3-}) significantly decreased the arsenate adsorption capacity of all adsorbents. Overall, regarded to a wide availability of raw materials, simplicity of the modification and improvement of arsenate adsorption capacity, modified natural clay adsorbents, especially MC-FeII, could be considered to be effective and low-cost to remove arsenate from water.

Keywords: adsorption, calcined clay, ferrous calcined clay, ferric calcined clay, isotherm, kinetics

INTRODUCTION

Arsenic is a toxic and carcinogenic element polluting water sources. This element enters into the environment through natural factors such as weathering reactions, biological activities, geochemical reactions and volcanic emissions, as well as anthropogenic activities such as mining activities, combustion of fossil fuels, use of arsenic pesticides and arsenic additives to livestock [1]. Health issues related to a long term exposure to arsenic include conjunctivitis, hyperkeratosis, hyper pigmentation, cardiovascular diseases, disorder of central nervous systems, skin cancer and gangrene of the limbs [2]. More than 100 million people in over 70 countries are at risk of having the diseases [3]. The World Health Organization (WHO) has lowered the maximum contaminant level of arsenic in drinking water from 50µg/L to 10µg/L [4].

Elevated arsenic concentration found in natural water is ranged from <100µg/L to 5000µg/L, i.e., an average of 552µg/L in groundwater in Cambodia, a country with widespread contaminated sites [5], [6]. The major arsenic forms in natural water are arsenate and arsenite. Arsenite favors and predominates in reducing environments like groundwater, whereas arsenate predominates in oxygen-rich environments like surface water [7]. Practically, arsenite has been oxidized to arsenate before the treatment. Among several arsenic remediation methods, adsorption has gained a considerable attention due to its simple operation and maintenance, high removal efficiency and low-cost [8]. Adsorption is based on either natural or synthetic materials possibly providing high affinity for dissolved arsenic. Several low cost materials such as natural materials, agricultural wastes, and industrial wastes have increasingly gained interest to be used as adsorbents for arsenic removal from water [9]. Local available clay has been interestingly used as adsorbents to uptake various pollutants due to its widely availability and low cost [10].

However, clays or clay minerals appeared as adsorbents in the form of powder occur to be difficult to separate after adsorption and limit further potential applications like in a dynamic flow system. From a preliminary observation, natural clays with bigger size tends to break down when mixing with water, while clays heated at high temperature appear to be stable in the particle size. Furthermore, the arsenic adsorption capacity of natural adsorbents seems to be lower than that of synthetic or modified adsorbents with metal oxides known for having high affinity toward arsenic. Thus, modification of natural clay to produce a more effective adsorbent is needed. Among many modification methods, iron coating or impregnation seems to be simple, cost-effective, pollutant removal efficiency-improved and gaining more popularity to be applied for developing and efficient adsorbent for pollutant removal.

The objective of this study was to use natural clays calcined at high temperature and treated with ferrous and ferric solutions through a simple coating technique enhanced by heating at a moderate temperature to conduct arsenate adsorption from water in term of effect of contact time, initial concentration, solution pH and coexisting anions.

MATERIALS AND METHODS

Chemical Reagents

All experiments were conducted with chemicals of analytical grade without further purification. Arsenate stock solution (100 mg/L) was prepared by dissolving $Na_2HAsO_4 \cdot 7H_2O$ (Sigma Aldrich, USA) in deionized water. $FeSO_4 \cdot 7H_2O$ and $FeCl_3 \cdot 6H_2O$ were used for ferrous and ferric solutions, respectively. NaOH and HCl were used for pH adjustment. NaCl, $NaNO_3$, $NaHCO_3$, Na_2CO_3, Na_2SO_4, and Na_3PO_4 were used for developing coexisting anion solutions. To prevent chemical interferences, all needed glassware and apparatus were washed with DI water and exposed to a 5% nitric acid solution overnight prior to being used in the experiments.

Preparation and Characterization of Adsorbents

Natural clay (collected from Dan Kwian District, Nakhonratchasima 30000, Thailand) was manually cleaned and ground for the particle size of 0.45-0.85 mm. The natural clay was then calcined at 550˚C for 4 to 5h in a muffle furnace. The calcined clay was labeled as MC. The modification process was conducted with ferrous or ferric solutions. Twenty gram (20g) of MC was added to 100 mL of 0.25M $FeCl_3 \cdot 6H_2O$ or 0.25M $FeSO_4 \cdot 7H_2O$. The mixture was magnetically stirred on a hot plate with temperature of 60˚C under agitation speed of 250 rpm for 24h. The suspension was dried at 105˚C for 24h and then further heated at 350˚C for 3h to ensure higher effective affinity of iron. The product was washed with deionized water and labeled as MC-FeII and MC-FeIII, respectively.

The chemical composition was determined by the Energy Dispersive XRF (HORIBA Ltd., Japan). The mineralogical phases were analyzed by the X-ray diffraction method with the Bruker XRD (D2-PHASER). The surface morphology were examined by a scanning electron microscope (SEM, JSM-6010LV, JEOL, Japan). The surface area, pore volume, and average pore diameter were obtained from the Brunauer-Emmett-Teller (BET) methods using the BET analyzer (BELSORP Mini II, BEL Inc., Japan). The point of zero charge (pH_{pzc}) was evaluated by plotting the initial pH versus the equilibrium pH (using 0.01M NaCl as background electrolyte with the equilibrium time of 72h) [11].

Adsorption Experiments

Adsorption experiments were conducted in a series of batch at room temperature (25±1˚C). The mixtures between adsorbents and adsorbate were agitated at 200 rpm on a horizontal mechanical shaker. The supernatant was filtered through 0.22 µm syringe filter and the filtrates were acidified with concentrated nitric acid and stored at 4˚C until arsenate measurement within 24h. Arsenate concentration was measured by ICP-OES (Optima 8000, PerkinElmer, USA) using a wavelength of 193.7nm. The contact time was conducted by mixing 10g/L of the adsorbents with 25mL of the 500µg/L arsenate solution (pH=7 ± 0.1) from 0 to 72h. The effect of solution pH was investigated in the pH range of 3 to 11. Isotherm study was carried out by varying arsenate concentrations from 100 to 10000µg/L. The effect of coexisiting anions was investigated by adding a certain amount of anions to 500µg/L arsenate solution. Each experiment was conducted in duplicate and the average was reported. The arsenate adsorption efficiency and capacity were calculated with the following equations:

$$P = \frac{(C_o - C_t)}{C_o} \times 100 \quad (1)$$

$$q_e = \frac{(C_o - C_e) \times V}{M} \quad (2)$$

where P is the adsorption efficiency (%); q_e is the adsorption capacity at equilibrium (µg/g); C_o and C_e are the initial and equilibrium arsenate concentration (µg/L), respectively; V is the adsorbate volume (L); and M is the mass of adsorbents (g).

RESULTS AND DISCUSSION

Characterization of Adsorbents

The characteristic analysis of the physico-chemical properties of the adsorbents is illustrated in Table 1. The results indicated that the main chemical constituents of all the adsorbents were silicate, alumina and iron oxide. After a long time exposure to ferrous solution (pH=3.08) and ferric solution (pH=1.28), the percentage of silica and alumina of MC-FeII and MC-FeIII were observed to be lower than those of MC. This could be explained by the occurrence of corrosion due to the acidic behavior of iron solutions. However, an increase of iron oxide was observed for modified adsorbents compared to that of MC (roughly 1.5 and 2 times for MC-FeII and MC-FeIII, respectively). This indicated that applied iron coating technique in this study successfully improved iron content.

Table 1 The physico-chemical properties of MC, MC-FeII, and MC-FeIII

Properties	MC	MC-FeII	MC-FeIII
SiO_2	71.25	68.34	68.63
Al_2O_3	20.51	20.07	16.55
Fe_2O_3	5.585	8.361	11.77
K_2O	1.039	1.008	0.893
CaO	0.435	0.314	0.264
MnO_2	0.067	0.063	0.078
S_{BET} (m^2/g)	41.69	55.41	55.99
a_T (cm^3/g)	0.059	0.067	0.068
a_0 (nm)	5.712	4.807	4.799
pH_{pzc}	6.3	5.9	5.1

Note: S_{BET} = Surface area; a_T = Total pore volume; a_0 = Mean pore diameter

The surface area of MC, MC-FeII and MC-FeIII were 41.69m^2/g, 55.41m^2/g and 55.99m^2/g, respectively. The improvement of surface area after the treatment was due to the open space by acidic corrosion. It was consistent with the increase of total pore volume. All adsorbents exhibited the mean pore size within 2 to 50 nm, indicating that the materials are relatively mesoporous according to the pore classification recommendation of the International Union of Pure and Applied Chemistry [12].

XRD pattern analysis of the adsorbents is presented in Fig. 1. The pattern of all adsorbents was almost identical. However, the intensity to develop peaks for the modified adsorbents increased and the development of new peaks was observed for MC-FeIII. This may be contributed to the increase in the amount of iron oxide on the surface. The main composting minerals for the adsorbents include quartz, illite-montmorillonite, kaolinite and hematite.

Figure 2 shows the surface morphological feature of MC, MC-FeII and MC-FeIII analyzed by SEM.

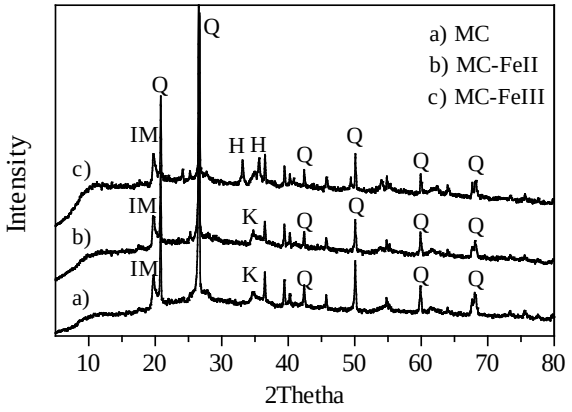

Fig. 1 XRD patterns of the adsorbents: Q (Quartz), K (Kaolinite), IM (Illite-montmorillonite), and H (Hematite).

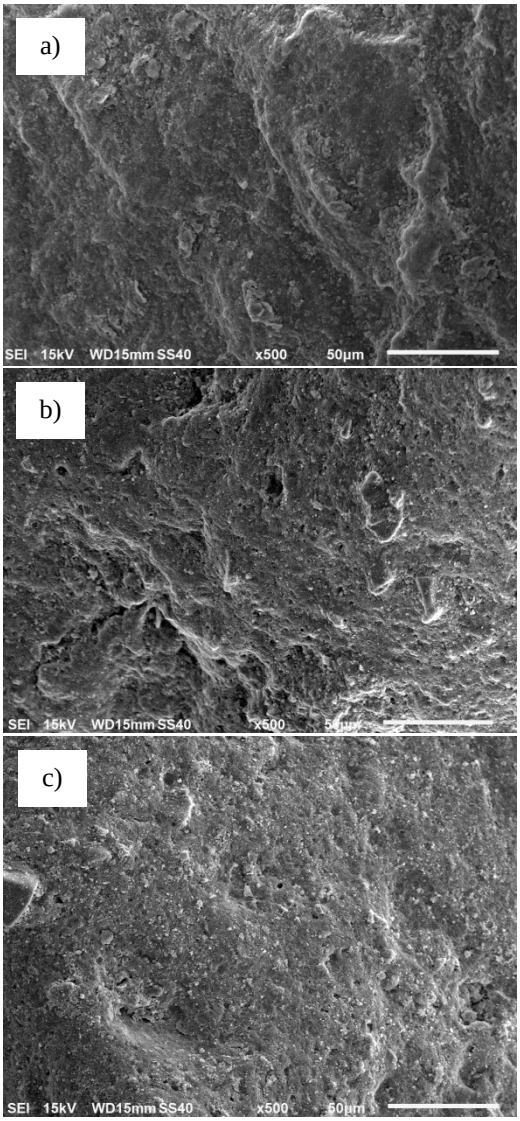

Fig. 2 SEM analysis of (a) MC, (b) MC-FeII, and (c) MC-FeIII.

A pretty smooth with few rough particle attachments was observed on the surface of MC, that could be a result of exposure of silica to high temperature. Surface features of MC-FeII and MC-FeIII were similar with the occurrence of several concave shapes and many small pores. This was strongly supportive to the corrosion effect of iron solutions.

Kinetic Studies

Figure 3 shows the effect of time dependent for arsenate adsorption onto the adsorbents. Within the first 18h, all adsorbents expressed fast adsorption toward arsenate in the aqueous solution. Later, the uptake rate was insignificantly improved and reached the equilibrium with 72h. This was due to having more active sites initially and later filled up.

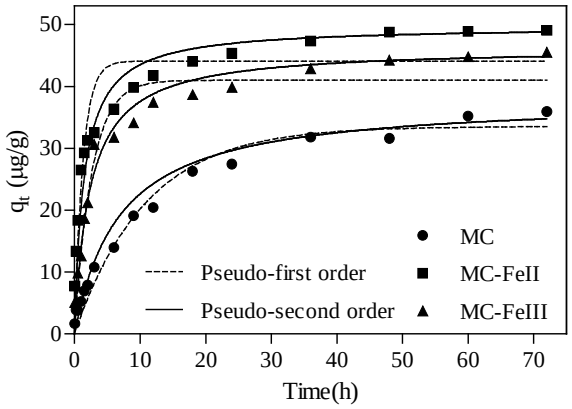

Fig. 3 Effect of contact time and its fitting model for arsenate adsorption efficiency by the adsorbents.

Pseudo-first order and pseudo-second order models were applied to predict the kinetic data. Their non-linearized equations can be expressed as follow:

Pseudo-1st order: $$q_t = q_e(1-e^{-k_1 t}) \quad (3)$$

Pseudo-2nd order: $$q_t = \frac{q_e^2 k_2 t}{1+q_e k_2 t} \quad (4)$$

where q_t (µg/g) is the adsorption capacity at time *t* (h), and k_1 (h^{-1}) and k_2 ($g \cdot \mu g^{-1} \cdot h^{-1}$) are pseudo-first order and pseudo-second order rate constant, respectively. Kinetic parameters obtained from the kinetic models are presented in Table 2. For all adsorbents, the correlation coefficients (R^2) of pseudo-second order model were higher than those of pseudo-first order model.

Table 2 Kinetic parameters for arsenate adsorption onto the adsorbents

Models	MC	MC-FeII	MC-FeIII
$q_{e,exp.}$ (µg/g)	36.00	49.05	45.51
Pseudo-1st order model			
$q_{e,cal.}$ (µg/g)	33.54	44.08	41.00
k_1 (h^{-1})	0.092	0.763	0.378
R^2	0.972	0.883	0.945
Pseudo-2nd order model			
$q_{e.,cal.}$ (µg/g)	38.09	49.77	46.34
k_2 ($g.\mu g^{-1}.h^{-1}$)	0.004	0.014	0.009
R^2	0.986	0.999	0.998

Plus, the arsenate adsorption capacity obtained from pseudo-second order model ($q_{e,cal.}$) was comparable to the arsenate adsorption capacity from the experiment ($q_{e,exp.}$). Thus, kinetic data were well described by pseudo-second order model. This suggests that the adsorbate and adsorbents exchange or share electron and the surface properties of adsorbents and adsorbate concentration play significant roles in controlling the uptake rate [13].

Isotherm Studies

Langmuir and Freundlich models were applied to fit the isotherm data. Their non-linearized equations are represented as follow:

Langmuir: $$q_e = \frac{q_m K_L C_e}{1+K_L C_e} \quad (5)$$

Freundlich: $$q_e = K_F C_e^{1/n} \quad (6)$$

where q_m(µg/g) is the maximum adsorption capacity based on Langmuir equation; K_L (L/µg) is Langmuir constant; K_F and *n* are the adsorption coefficient from Freundlich equation. Figure 4 shows the plots of the models for obtaining the isotherm parameters.

The calculated isotherm parameters including the maximum arsenate adsorption capacity are summarized in Table 3. The results indicated that MC-FeII and MC-FeIII were better fitted to Langmuir model due to the higher values of correlation coefficient (R^2). However, MC was well described by Freundlich model. This implied that MC possessed a heterogeneous surface with multi layers adsorption for arsenate. The improvement of iron contents of MC-FeII and MC-FeIII seems to overpass the uptake capacity of other parallel existing minerals and possibly provided a monolayer arsenate adsorption on the their homogeneous surface without having any interaction between adsorbed adsorbate [14]. The maximum arsenate adsorption capacity from Langmuir models were 250µg/g, 747.38µg/g and 429.74µg/g for MC, MC-FeII and MC-FeIII, respectively.

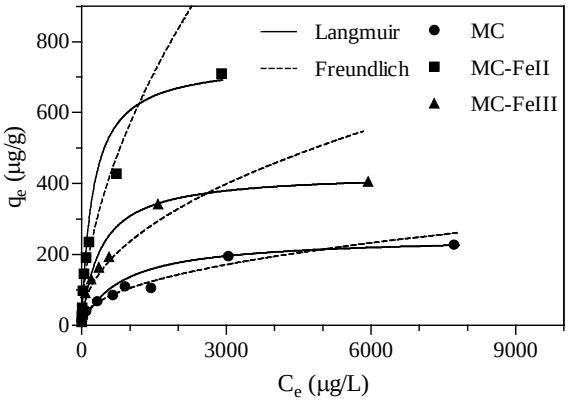

Fig. 4 Isotherm models for arsenate adsorption by the adsorbent.

A separation factor constant, $R_L = 1/(1 + K_L C_o)$ where C_o (µg/L) is the initial arsenate concentration,

and Freundlich constant (1/n) were used to category the type of isotherm of the adsorbents. The adsorption process is irreversible if R_L=0, favorable if 0<R_L<1, linear if R_L=1 and unfavorable if R_L>1 and the adsorption is favorable when 0<1/*n*<1, irreversible when 1/*n*=1 and unfavorable when 1/*n*>1 [15]. For all adsorbents, 1/n values were within 0-1. With the studied arsenate range, R_L were 0.07-0.89, 0.02-0.67 and 0.04-0.79 for MC, MC-FeII and MC-FeIII, respectively. This implied adsorbents expressed favorably adsorption toward arsenate.

Table 3 Isotherm parameters for arsenate adsorption by the adsorbents

Models	MC	MC-FeII	MC-FeIII
Langmuir			
q_m	250.00	747.38	429.74
K_L	0.0012	0.0043	0.0025
R^2	0.9556	0.9801	0.9883
Freundlich			
1/n	0.4427	0.5584	0.4765
K_F	4.9413	11.989	8.7845
R^2	0.9887	0.9619	0.9438

Effect of pH

The effect of solution pH on the arsenate adsorption onto MC, MC-FeII and MC-FeIII is presented in Fig. 5. All the adsorbents shared a similar pattern of the adsorption efficiency over the studied pH range. The arsenate adsorption efficiency gradually decreased for pH from 3 to 7. When pH was beyond 7, the decrease was significantly improved and the dramatically decline was observed for pH 11.

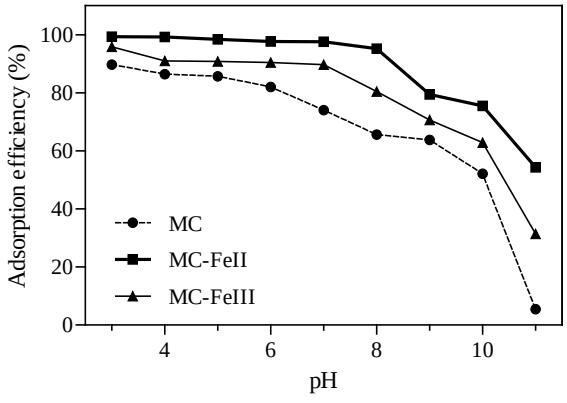

Fig. 5 Effect of initial arsenate solution pH on the adsorption of the adsorbents.

The results could be reasoned by the surface properties of the adsorbents and arsenate speciation with various pH values. The surface of the adsorbent was more positively charged for pH < pH_{pzc} and predominated the negative charge for pH > pH_{pzc} [16]. Arsenate mainly exists in water as H_3AsO_4 at pH less than 2.2, $H_2AsO_4^-$ at pH between 2.2 and 6.98, $HAsO_4^{2-}$ at pH between 6.98 and 11.5, and AsO_4^{3-} at pH above 11.5 [1]. The point of zero charge (pH_{pzc}) for MC, MC-FeII and MC-FeIII were 6.3, 5.9 and 5.1, respectively (Table 1). Apparently, the repulsive force between the adsorbents and the adsorbate is most probably responsible for the decrease of arsenate uptake from the solution at higher pH values.

Effect of coexisting anions

The effect of coexisting anions on the arsenate adsorption by the adsorbents were conducted by separately adding 0.1mM of univalent anions (Cl^-, NO_3^-, HCO_3^-), bivalent anions (CO_3^{2-}, SO_4^{2-}) and trivalent anion (PO_4^{3-}) to 500µg/L of arsenate solution. The arsenate adsorption efficiency in the presence of each individual anion is shown in Fig. 6.

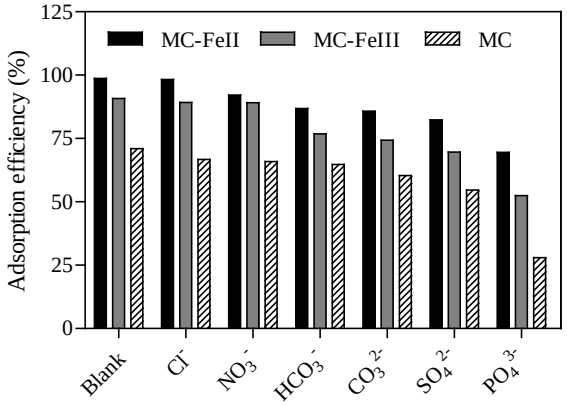

Fig. 6 Effect of co-existing anions on the arsenate removal using the adsorbents.

The results showed that a similar trend of influence on the arsenate efficiency was observed for all adsorbents. The presence of univalent anions showed less reduction in arsenate adsorption efficiency. The increasing reduction of adsorption efficiency was observed when bivalent anions were added. Trivalent anion (PO_4^{3-}) significantly influenced on decreasing the arsenate adsorption efficiency. The competition for active sites on the surface of the adsorbents could be a reason for remarkably reduction of arsenate adsorption efficiency in case of PO_4^{3-}. Phosphate shares similar chemical properties to arsenic and easily attaches to iron hydroxide to form an inner-sphere complex compared to arsenic [17], [18].

CONCLUSION

Natural clay could be stabilized the particle size by calcination. Iron impregnation on MC improved the iron oxide content for MC-FeII and MC-FeIII, as

well as their adsorption efficiency. Pseudo-second order model was more suitable for fitting the kinetic data for all adsorbents. Both applied isotherm models were suitable to describe the isotherm data for MC adsorbent. Langmuir was better in case of iron modified adsorbents. All adsorbents exhibited high arsenate adsorption efficiency at lower initial solution pH and significant reduction occurred at high pH value. The introduced coexisting anions influenced on the arsenate adsorption efficiency of all adsorbents in the following order: trivalent> bivalent> univalent anions. Modified adsorbents, particularly MC-FeII and MC-FeIII, were easily and economically produced that could be effective and low-cost adsorbents to remove arsenate from water.

ACKNOWLEDGEMENTS

The authors gracefully thank School of Environmental Engineering, Suranaree University of Technology, Nakhon Ratchasima 30000, Thailand.

REFERENCES

[1] Mohan D and Pittman Jr. CU, “Arsenic removal from water/wastewater using adsorbents—a critical review”, J Hazard Matter, vol. 142, 2007, pp.1-53.

[2] Goswami A, Raul PK, and Purkait MK, “Arsenic adsorption using copper (II) oxide nanoparticles”, Chemical Engineering Research and Design, vol. 90, 2012, pp. 1387-1396.

[3] Brammer H and Ravenscroft P, “Arsenic in groundwater: a threat to sustainable agriculture in South and South-east Asia”, Environment International, vol. 35, 2009, pp. 647-654.

[4] Glocheux Y, Pasarín MM, Albadarin AB, Allen SJ, and Walker GM, “Removal of arsenic from groundwater by adsorption onto an acidified laterite by-product”, Chemical Engineering Journal, vol. 228, 2013, pp. 565-574.

[5] WHO, “Environmental Health Criteria 224: Arsenic and Arsenic Compounds”, Geneva, 2001, pp. 28.

[6] Luu TTG, Sthiannopkao S, and Kim KW, “Arsenic and other trace elements contamination in groundwater and a risk assessment study for the residents in the Kandal Province of Cambodia”, Environmental International, vol. 35, 2009, pp. 455-460.

[7] Genç-Fuhrman H, Bregnhøj H, and McConchie D, “Arsenate removal from water using sand–red mud columns”, Water Research, vol. 39, 2005, pp. 2944-2954.

[8] Mahmood T, Din SU, Naeem A, Mustafa S, Waseem M, and Hamayun M, “Adsorption of arsenate from aqueous solution on binary mixed oxide of iron and silicon”, Chemical Engineering Journal, vol. 192, 2012, pp. 90-98.

[9] Baig SA, Sheng T, Hu Y, Xu J, and Xu X, “Arsenic removal from natural water using low cost granulated adsorbents: a review”, CLEAN–Soil, Air, Water, vol. 43, 2015, pp. 13-26.

[10] Srinivasan R, “Advances in application of natural clay and its composites in removal of biological, organic, and inorganic contaminants from drinking water”, Advances in Materials Sci and Eng, vol. 2011, 2011, pp. 1-17.

[11] Su J, Huang HG, Jin XY, Lu XQ, and Chen ZL, “Synthesis, characterization and kinetic of a surfactant-modified bentonite used to remove As(III) and As(V) from aqueous solution”, J Hazard Matter, vol. 185 2011, pp. 63-70.

[12] Kuila U, and Prasad M, “Specific surface area and pore size distribution in clays and shales”, Geophysical Prospecting, vol. 61, 2013, pp. 341-362.

[13] Li Y, Cai X, Guo J, Zhou S, and Na P, “Fe/Ti co-pillared clay for enhanced arsenite removal and photo oxidation under UV irradiation”, Applied Surface Science, vol. 324, 2015, pp. 179-187.

[14] Ouadjenia-Marouf F, Marouf R, Schott J, and Yahiaoui A, “Removal of Cu (II), Cd (II) and Cr (III) ions from aqueous solution by dam silt”, Arabian Journal of Chemistry, vol. 6, 2013, pp. 401-406.

[15] Fufa F, Alemayehu E, and Lennartz B, “Sorptive removal of arsenate using termite mound”, J Environ Manage, vol. 132, 2014, pp. 188-196.

[16] Chang Q, Lin W, and Ying WC, “Preparation of iron-impregnated granular activated carbon for arsenic removal from drinking water”, J Hazard Matter, vol. 184, 2010, pp. 515-522.

[17] Maliyekkal SM, Philip L, and Pradeep T, “As (III) removal from drinking water using manganese oxide-coated-alumina: performance evaluation and mechanistic details of surface binding”, Chemical Engineering Journal, vol. 153, 2009, pp. 101-107.

[18] Hsu JC, Lin CJ, Liao CH, and Chen ST, “Evaluation of the multiple-ion competition in the adsorption of As (V) onto reclaimed iron-oxide coated sands by fractional factorial design”, Chemosphere, vol. 72, 2008,pp.1049-1055.

Second International Conference on Science, Engineering & Environment,
Osaka City, Japan, Nov.21-23, 2016, ISBN: 978-4-9905958-7-6 C3051

ESTIMATION OF POTENTIAL CONTAMINATED AREA FROM EROSION FOR A REMOTED CONTMIANTED WATERSHED: A CASE STUDY OF THE MAE TAO BASIN, THAILAND

Somprasong K.[1] Chawiwatworakul P[2]

[1]International Postgraduate Program in Environmental Management, Graduate School, Chulalongkorn University, Bangkok, Thailand

[2] Department of Environmental Engineering, King Mongkut's University of Technology Thonburi, Bangkok 10140, Thailand.

ABSTRACT

The Mae Tao Basin locates in Mae Sot district, Thailand. This area has been contaminated by cadmium, where the dominant transporter is sediment leached into the water resources by surface runoff. The Revised Universal Soil Loss Equation (RUSLE) incorporated with remote sensing and geographic information system software was applied, in order to estimate the potential erosion that can occur in the Mae Tao Basin. The erosion potential was combined with the cadmium concentration profile, obtained using secondary data from both government and private sectors, to calculate the potential cadmium flux due to erosion. The results indicate that maximum value of potential cadmium flux due to erosion occurred in the mining production area of the Mae Tao Basin which is concordant with some of the real field observation results from the real monitoring stations.

Keywords: Remote sensing, Land use, Contamination, GIS, RUSLE

INTRODUCTION

Cadmium, a hazardous heavy metal, has been concerned in terms of its toxicity affecting to the environment. It is a main by-product of zinc treatment processes. Cadmium can be transported though environmental phases by trapping with sediments and bound back into water system, and their accumulation are dominated by physical-chemical properties of the sediment. Its solubility are depended on water chemical properties such as pH, chelating agents, redox conditions and, salinity ([2], [3], [4])

The Mae Tao Basin, Thailand's largest zinc deposit is located in Mae Sot district, Tak province. As a byproduct in zinc industries, cadmium contamination can be occurred in the mining production area and spread to the environmental phases as can be seen in Table1. [5]

Erosion due to rainfall upstream of the Mae Tao Creek, the main water resources of the area, was found to be one of the major mechanics that make cadmium available for transport to the downstream. However, mining procedures and the mine area management have also been blamed for contributing to the problem [1].

Overland sediments from surface runoff have a possibility to be the transmission intermediate that reinforces the spread of hazardous substances leaching into area soil. Consequently, the potential erosion rate of the basin can be estimated to determine its cadmium contribution potential in the study area attaching with overland erosion.

The Revised Universal Soil Loss Equation (RUSLE) is greatly accepted as a simple and accommodating equation for soil surface erosion estimations. It necessitates less data and entails a short period of time to run, compared to other models that calculate soil erosion.

Table 1 Summary of the cadmium contamination status in the Mae Tao Basin

Sample	Cadmium concentration	Standard for Thailand
Water	0.0001-0.1 mg/L	≤ 0.05 mg/L [1]
Soil	0.1-1,458 mg/kg	≤ 37 mg/kg [1]
Sediment	<1-1,350 mg/kg	≤ 3.5 mg/kg [6]
Rice	0.02-7.75 mg/kg	≤ 0.2 kg/kg [7]

RUSLE is familiar in both scientific work and land development. A combination of geographic information system (GIS) technology and this erosion models has been proven to be effective at estimating the magnitude and distribution of erosion ([8], [9],[10])

The application based of RUSLE in this study was mainly focused on presenting the remote-estimation of the soil erosion in the study areas which is surrounded by deciduous forest. The estimation results were evaluated with the real field observation data of soil erosions in a reachable area of the Mae

Tao Basin especially, the mining production area. In this study, contamination concentration data is integrated with RUSLE to utilize this equation in a contamination assessment.

METHODOLOGY

Figure 1 illustrates the framework of the study, and the steps of each study procedure are described as follows.

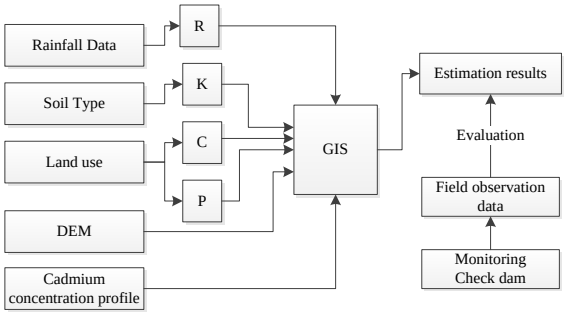

Fig.1 Methodology frame work of the estimation method

This study applies a combination between remote sensing, secondary data interpolation, and GIS technology to estimate the leaching potential of cadmium contamination sources. It aims to estimate the potential erosion of the Mae Tao Basin in relation to its potential cadmium contributors based on the Revised Universal Soil Loss Equation (RUSLE).

The study began with data acquisition. For the boundary of the study area, the Mae Tao Basin, covers 59.61 km^2.The basin contains mining production areas, crop fields, and residential areas.

Daily precipitation data from 2010 to 2014 were gathered from the Thai Meteorological Department (TMD), while soil type and land use maps of the Mae Tao Basin were acquired from the Land Development Department of Thailand (LDD). Furthermore, a digital elevation map [11] of the study area was afforded by the Royal Thai Survey Department (RTSD).

Each set of data was analyzed individually to obtain the values of the required RUSLE parameters. The values were operated by GIS software and combined with the cadmium concentration profile of the Mae Tao Basin from the Thai Pollution Control Department [1].

The results from the GIS estimation were evaluated with the field observation data from ten monitoring check dams to compare the value between real erosion and the estimated one.

POTENTIAL EROSION ESTIMATION

Revised Universal Soil Loss Equation (RUSLE)

Soil loss or soil erosion refers to the amount of soil moved from one particular area to another in the form of sediment yield. This phenomenon depends on the relationship between raindrops, runoff and the erodibility of a certain area. RUSLE have a capability in estimating of the relentlessness of erosion in the form of quantifiable results by extending the terms of cover management and support practices into the equation.

Since cadmium adsorbed from overland sediment as residue from surface runoff, applying RUSLE to quantify the erosion sediment from the Mae Tao Basin can be used to estimate the potential amount of cadmium that is spreading through the creeks. The Revised Universal Soil Loss Equation is presented in Eq. (1).

$$A = R \times K \times C \times P \times LS \qquad (1)$$

The R factor refers to the erosivity by rainfall runoff at a particular location. The K factor represents the specific value of the inherent erodibility of the soil surface material at a particular site. The LS is the effects of topography, specifically a hill's slope, length, and steepness, on the rates of soil loss at a site.

The C factor expresses the effects of surface cover and roughness, soil biomass, and soil-disturbing activities on the rate of soil loss at a particular site, while the P factor is the effects of soil conservation practices at a particular site, such as contouring and buffer strips for cover vegetation.

Parameter determination

R factor

The R factor in this study was calculated based on the study of [12]. These set of equations (Eq. (2) to Eq. (4) are appropriate or calculating the R value of a small area for short monitoring period. They were also used in R-factor calculations in Laos, which shares a similar climate with Thailand and can also yield the advantages of reducing the chances of data insufficiency.

$$Fi_x = \frac{M_x^2}{P_y} \qquad (2)$$

$$Ei_{30,x} = kFi_x^{0.584} \qquad (3)$$

$$R = \frac{1}{n}\sum_{x=1}^{n} Ei_{30,x} \qquad (4)$$

Fi_X refers to the Fourier index of rainfall in month x (mm). M_x is the rainfall precipitation during month x (mm), while P_y stands for the

amount of yearly precipitation (mm). Parameter k is a constant value, 227 (MJ ha^{-1} h^{-1}), and $Ei_{30,x}$ is the maximum intensity rainfall energy of month x (MJ mm ha^{-1} h^{-1}).

The monthly rainfall data, have been recorded by TMD since 2010, were applied to calculate the R value of the study area. From the calculation, R factor value use in this study was equal to 319.75 mm/ha/y.

C and P factor

Since some parts of the Mae Tao Basin are inaccessible area, direct field observation was merely impossible. To avoid this limitation, secondary data collection (e.g., land use observation data from the LDD) was applied to gain the required values as can be seen in Table 2.

K factor

The data on land use and soil properties (including soil type identification) of the Mae Tao Basin are provided by LDD and the study of [13]. These sets of data were compared and matched with soil taxonomy to retrieve the K factor value. The soil type and the K-factor applied in this study are mentioned in Table 3.

Table 2 C and P factor for specific land use of the Mae Tao Basin

Land use type	Parameter value	
	C	P
Abandoned farm house	0	0.4
Abandoned crop field	0.85	0.45
Active crop field	0.28-0.40	0.10-0.71
Corn field	0.52	0.92
Dense deciduous forest	0.003	1
Disturbed deciduous forest	0.048	1
Mine/Landfill /Waste dump site	1	1
Mixed orchard	0.15- 0.31	0.2-0.4

Table 3 K factor value based on soil type

No	Soil Type (Thai)	Soil Characteristic	K factor value
1	31	Fine, mixed, Isohyperthermic-very fine, Kaolinitic, Isohyperthermic	0.25
2	33	Finesilty,Mixed,Isohyperthermic	0.37
3	55	Fine,Mixed,Isohyperthermic	0.24
4	60	Well drained	0.29
5	62	Slope complex	0.25

LS factor

LS-factor calculation methods have been developed for both direct field observation techniques and digital analysis techniques [14]. As a remote estimation study, GIS application was assigned in the calculation of LS factor for the surface area of The Mae Tao Basin based on the study of [15] as presented in Eq.(5).

$$LS = \left(\frac{Flowacc \times resolution}{22.13}\right)^{m} (0.065 + 0.045s + 0.0065s^{2}) \quad (5)$$

The GIS calculation procedure for LS factor is illustrated in Fig.2.

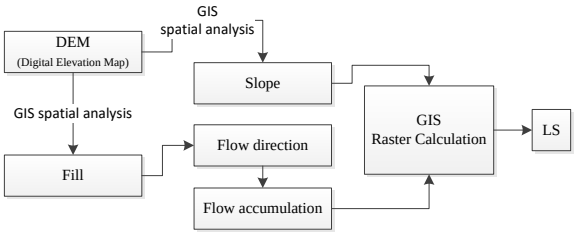

Fig.2 LS factor determination method in GIS application

Potential erosion estimation

The calculation for potential erosion of the Mae Tao Basin was operated under the spatial analysis for raster calculation in GIS application, based on Eq. (1).

POTENTIAL CADMIUM FLUX FROM EROSION ESTIMATION

Cadmium concentration profile interpolation

Since the Mae Tao Basin is a large remote area, the direct field observation for contamination status cannot be continuously arranged and disseminated. The interpolation based on Kriging method based on GIS application was applied. In this interpolation, 40 stations from the existing studies of the cadmium contaminated level of soil surface are integrated and interpolated in to raster calculation layer as can be seen in Fig.3.

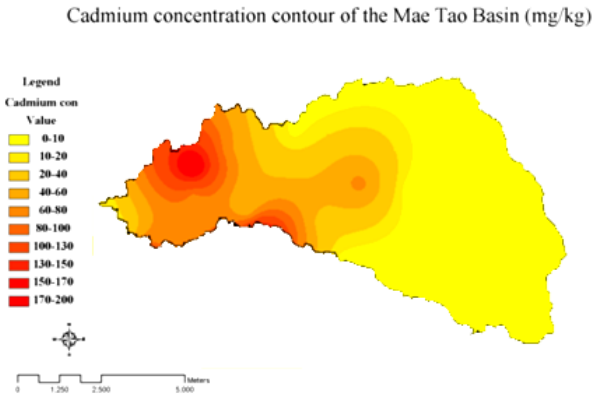

Fig.3 Cadmium concentration profile interpolated by Kriging's method

Potential cadmium flux from erosion estimation

Bear a resemblance to the raster calculation of RUSLE estimation, the concentration profile of cadmium in the Mae Tao Basin was interpolated into an attribute table and transformed into a raster layer for calculation. The following equation was applied in the raster calculation to estimate the potential cadmium flux from erosion of the Mae Tao Basin area.

$$Cd_{erosion} = cA \times 10^{6} \qquad (6)$$

Where

$Cd_{erosion}$ = Potential cadmium flux from erosion (t/ha/y)

C = Cadmium concentration (mg/kg)

A = Soil erosion from RUSLE (t/ha/y)

EVALUATION OF POTENTIAL CADMIUM FLUX FROM EROSION ESTIMATION

Monitoring check dam

In order to evaluate the efficiency of the estimation results, ten monitoring check dams were installed during July to October 2014 at the significant location representing the differences land utilization of the Mae Tao Basin. At each station, the sediments from rainfall erosion were collect and analyzed for both cadmium concentration and mass of the eroded sediment. Table 4 demonstrates a location of the monitoring check dams.

Table 4 the locations of monitoring check dam

Station	UTM		Location
	Easting	Northing	
SED_OB1	459400	1843330	Downstream (MT02)
SED_OB2	463430	1842304	Heavy Equipment plant
SED_OB3	464087	1847923	Active Mining zone
SED_OB4	465266	1842053	Bench (Overburden Dump site 3)
SED_OB5	464285	1841898	Green Mining zone
SED_OB6	464667	1841792	Water Management HQ office
SED_OB7	465259	1842050	Overburden Dump Site
SED_OB8	464279	1841892	Bench (Overburden Dump site 1)
SED_OB9	465642	1841200	Sediment Pawn (E1)
SED_OB10	466937	1842750	Upstream (MT07)

Estimation evaluation

The mass of the collected sediment from the monitoring check dam were converted into potential erosion based on Eq. (7).

$$E_{Observation} = \left(\frac{m_E \times Cd_{erosion}}{AT} \right) \qquad (7)$$

Where

$E_{Observation}$ = Potential cadmium flux from erosion of observation station (t/ha/y)

M_E = Mass of sediment sample (kg)

A = Area of monitoring check dam (m^2)

T = Monitoring time (year)

The potential cadmium flux from erosion of the monitoring check dams were compared to the estimated result from RUSLE estimation to evaluated the effective of the estimation in form of error from the real value of the erosion.

RESULT AND DISCUSSION

Potential erosion estimation

According to the estimation result from RUSLE, the potential erosion of the Mae Tao Basin area can be ranged from 0.00 to 4.10 x 10^5 t/ha/y. The highest values of erosion can be detected at the junction point of the creeks and in the mining production area while low potential erosion can be found in the forest area and the upstream of the basin due to the cover practice and topography respectively. Figure 4 illustrates the potential erosion of the Mae Tao Basin.

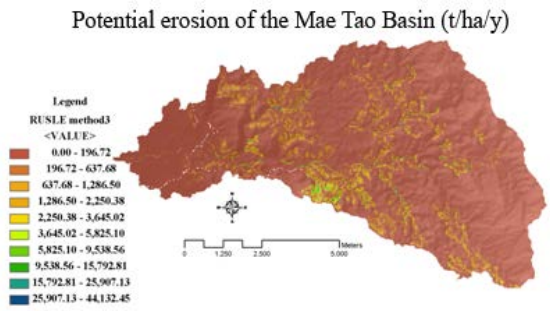

Fig.4 The result of potential erosion estimation

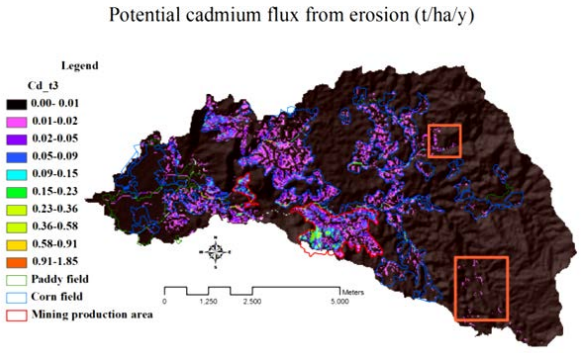

Fig. 5 Potential cadmium fluxes from erosion

Potential cadmium flux from erosion estimation

Figure 5 and Table 5 illustrates the potential flux of erosion of the Mae Tao Basin. Consistent with Eq.6, the potential cadmium flux from erosion can be illustrated in form of raster map. The map designates the scattered distribution of cadmium contamination from erosion in many parts of the basin.

A high potential flux value is located in the mining production area, while moderate values of potential flux are found scattered in the corn field area of the Mae Tao Basin. There is an evidence of contamination in the left branch of the Mae Tao creeks, especially the area that passes through an active mine. The results from also designate some other areas with high contamination potential due to being natural sources and having high soil erosion capabilities.

The highest value of potential cadmium flux from erosion was found in the mining production areas at 1.854 ± 0.088 t/ha/y. Similar to the mining production area, corn fields, abundantly detected in the middle of the basin, have the potential in releasing high levels of cadmium. The highest value of cadmium flux due to erosion in corn field area was 1.324 ± 0.049 t/ha/y.

Even though the highest values of potential flux were detected in the mining production areas and corn fields, cadmium contamination from erosion can be found in other areas of the Mae Tao Basin. In some paddy fields downstream, the potential cadmium flux due to erosion was discovered to be 0.451 ± 0.012 t/ha/y. The existence of a cadmium contamination potential signals the risk of utilizing the soil and water in areas that have accumulated cadmium from an upstream part of the basin.

Moreover, the deciduous forest area, located in an undisturbed upstream area of the basin, had a potential flux of 0.517 ± 0.002 t/ha/y. This can be one of the evidences that some part of the basin can be naturally contaminated due to the geological characteristic of the area that contains zinc-cadmium mineral deposition.

Table 5 Potential erosion estimation of the Mae Tao basin

Land use type	All area	Mining production	Corn field	Rice paddy field	Forest area
Area(km^2)	5961.87	262.53	616.22	174.33	3352.64
Area contribution (%)	100	4.4	10.34	2.92	56.23
Maximum $Cd_{erosion}$ (t/h/y)	1.854	1.854	1.324	0.451	0.517
mean (t/h/y)	0.005	0.044	0.013	0.002	0.002
SD	0.032	0.088	0.049	0.012	0.011
RSD (%)	587	201	375	595	712
Potential cadmium erosion in one year (t)	32.195	11.527	8.03	0.36	5.24

Evaluation of potential flux from erosion estimation

Table 6 demonstrates the estimation evaluation between real field observation's result and the estimation from RUSLE. The result of total cadmium indicates the highest value of cadmium concentration at SED_OB 6 which is located mining production area at 303.49±155.59 mg/kg.

According to the natural properties of zinc mineral vein, cadmium can occur in association with zinc so that the high significant level of cadmium is ordinary. For the upstream and the downstream area of the Mae Tao Basin, the total overland sediment transport is compiled with PCD's standard (37mg/kg).

In keeping with the observation result, the potential cadmium flux from erosion in the area, where uncomplicated land utilization located, can give a close value to the empirical estimation based on RUSLE.

The potential cadmium flux from erosion at the mining production area, including station SED_OB2 to SED_OB9, is equal to 1.75 t/ha/y while the estimation result from RUSLE is equal to 1.854t/ha/y which contains 5.94% error compare to the real erosion.

The complexity in land utilization can cause the effect to the precision of the estimation. This was evidenced by the comparison between station SED_OB1 and SED_OB10. Station SED_OB1 at the downstream in which contains complex land utilization activity in one area grid, the value of potential cadmium fluxes from erosion between the field observation and empirical estimation are larger than SED_OB10 located in the deciduous forest area.

The estimated potential cadmium flux from erosion of the corn field at station SED_OB1 is 56 times higher than the real field erosion at 0.003 t/ha/y, while in deciduous forest, the estimated value contains only 2 times higher than the real field observation at 0.01 t/ha/y due to the low complexity of the real land utilization.

Table 6 Evaluation between estimated values and real field observation

Station	Sediment (kg)	[Cd] (mg/kg)	$Cd_{erosion}$ (Field) (t/ha/y)	$Cd_{erosion}$ (RUSLE) (t/ha/y)	Error (%)
SED_OB1	62.80	2.37	0.00	0.17	-5566.67
SED_OB2	21.90	15.43	0.01	1.44	-20514.29
SED_OB3	3580.00	260.87	19.43	1.67	91.38
SED_OB4	8.00	18.75	0.01	0.62	-6140.00
SED_OB5	2500.00	58.15	3.02	1.65	45.30
SED_OB6	10.35	303.49	0.07	0.13	-106.15
SED_OB7	1000.00	84.12	1.75	1.85	-5.94
SED_OB8	34.00	32.79	1.02	1.41	-38.12
SED_OB9	970.00	3.03	0.06	1.21	-1888.52
SED_OB10	60.92	7.75	0.01	0.03	-200.00

DISCUSSION AND RECOMMENDATION

The estimation based on integrated RUSLE, remote sensing and GIS technique is effective. The results can designate the potential contributor of cadmium contaminant. From the estimation map, explicit evidences of contamination can be detected along the left branch of the Mae Tao creeks, especially the area that passes through an active mine. Even though a high potential of cadmium from erosion was distinguished, practices to diminish the outflow from the mine were found to be in place. To enhance the efficiency with which the mine manages its outflow, a study on the relationship between the quantity of outflow from the mine and the capacity of the tailing dam should be performed.

In proportion to the result, the dense corn fields, located in an area of natural zinc reservoirs, also leach cadmium downstream. The combination between the effects of low erosion resistance and being situated in a mountainous area with mining activities results in the area's high cadmium erosion potential. This is evidently exposed by the cadmium concentrations detected in the upstream area of the Mae Tao creeks.

Although rice paddies, located on hill slopes, contains low cadmium contamination potentials, higher levels of potential at 0.45 t/ha/y were found in the rice paddies located in the flat area downstream as a consequence of the local public irrigation system and daily household water consumption from the Mae Tao creeks.

The deciduous forest released a small proportion of cadmium because of its high resistance to erosion. However, parts of the deciduous forest undisturbed by human activity did have some cadmium contamination. This can inferred that natural deposits contribute to the cadmium contamination in the area.

As a recommendation, developments in vegetation planning like strip cropping must be promoted. However, in areas that are already contaminated, subsidizing of existed vegetation to other crops can reduce the risk of the contamination of cadmium into human.

CONCLUSION

Empirical estimation based on RUSLE can illustrate the significant potential area which have a capability in releasing cadmium attaching in form of the residue in the rainfall runoff In the area, in which uncomplicated cover practice area are defined, RUSLE can effectively applied to use as a primary tool to estimate the potential contaminated area effected by rainfall erosion.

Moreover, this integrated method using RUSLE, GIS and remote sensing can effectively map out the potential sources of contamination in an area. The results of the study designate the cadmium contamination behavior of each land use type and also identify the areas where cadmium contamination is most likely to occur. Even remote areas such as thick forests or unreachable valleys can be evaluated, as this study has shown the capability of customizing this integrated method to characterize a remote heavy metal contaminated area.

Although the result from the estimation based on RUSLE is desirable, the error in some complicate land use area can be determined with high value of error. The further study and development in utilizing more precise parameter for soil erosion estimation will enhance the estimation efficiency of this

integrate method and can be applied to another similar contaminated site.

ACKNOWLEDGMENT

The Center of Excellence for Environmental and Hazardous Waste Management (EHWM), Chulalongkorn University provided partial funding for this work in addition to a full academic scholarship and full use of its facilities. The study was also funded by the Ratchadaphiseksomphot Endowment Fund in honor of the 90th anniversary of Chulalongkorn University.

REFERENCES

[1]. Pollution Control Department (PCD). Thai Environment Regulations. . 2009; Available from: http://www.pcd.go.th/info_serv/en_regulation.html
[2]. Arnason J. G. and Fletcher B. A., 40+ year record of Cd, Hg, Pb, and U deposition in sediments of Patroon Reservoir, Albany County, NY, USA. Environmental Pollution, 2003. 123: p. 383-391.
[3]. Jain C.K., Metal fractionation study on bed sediments of River Yamuna,. India Water Research., 2014. 38: p. 569-578.
[4]. Yunus K., Heavy Metal Concentration in the Surface Sediment of Tanjung Lumpur Mangrove Forest, Kuantan, Malaysia. Sains Malaysiana, 2011. **40**(2): p. 89-92.
[5]. Unhalekhaka U. and Kositanont C., Distribution of cadmium in soil around zinc mining area. . Thai Journal Toxicology, 2008. 23: p. 170-174.
[6]. Simmons R.W., et al., Analysis of field-moist Cd contaminated paddy soils during rice grain fill allows reliable prediction of grain Cd levels. Plant Soil. 2008: Bangkok, Thailand. p. 125-128.
[7]. Codex Alimentarius Commission Report of the 34th Session of the Codex Committee on Food Additives and Contaminants (CCFAC). 2002: Rotterdam.
[8]. Mitasova H., et al., Modeling topographic potential for erosion and deposition using GIS. International Journal of Geographical Information Systems, 1996. **10**(5): p. 629-641.
[9]. Molnar D.K. and Julien P.Y., Estimation of upland erosion using GIS. Computers and Geosciences, 1998. 24(2): p. 183-193.
[10]. Millward AA and Mersey JE, Adapting the RUSLE to model soil erosion potential in a mountainous tropical watershed. Catena, 1999. **38**(2): p. 109-129.
[11]. Demattê* J.A.M., Fioriob P.R., and Ben-Dorc E. , Estimation of Soil Properties by Orbital and Laboratory Reflectance Means and its Relation with Soil Classification The Open Remote Sensing Journal,, 2009. 2: p. 12-23.
[12]. Shamshad A., et al., Development of an appropriate procedure for estimation of RUSLE EI30index and preparation of erosivity maps for Pulau Penang in Peninsular Malaysia. Catena, 2008. 72: p. 423-433.
[13]. Supakij N. and Burin C., Internet GIS, Based on USLE Modeling, for Assessment of Soil Erosion in Songkhram Watershed, Northeastern of Thailand. Kasetsart J. (Nat. Sci.), 2012. 46: p. 272-282.
[14]. José L G.R. and Martín C. GS., Historical review of topographical factor, LS, of water erosion models. Aqua-LAC, 2010. 2(2): p. 56-61.
[15]. Bizuwerk A. , Taddese G. , and Getahun Y. , Application of GIS for modeling soil loss rate in a wash basin, Ethiopia. 2008, International Livestock Research Institute (ILRI).

Second International Conference on Science, Engineering & Environment,
Osaka City, Japan, Nov.21-23, 2016, ISBN: 978-4-9905958-7-6 C3051

EVALUATION OF THE EFFECTIVENESS AND APPROPRIATENESS OF BANGKOK ACTION PLANS ON GLOBAL WARMING MITIGATIONS

Anna Kiewchaum[1,2], Sarawut Thepanondh[1,2], Duanpen Sirithian[1,2],
Kamoltip Mahavong[1,2], and Pantitcha Outapa[1,3]
[1] Department of Sanitary Engineering, Faculty of Public Health, Mahidol University Thailand
[2] Center of Excellence on Environmental Health and Toxicology (EHT), Bangkok, Thailand [3]Faculty of Public Health, Thammasat University, Lampang, Thailand

ABSTRACT

Bangkok Metropolitan Administration (BMA) action plans consist of 10 action plans aimed to reduce at least 15% of the total greenhouse gases emissions anticipated in the year 2012 under business as usual projection. In this study, the Multi Criteria Attribute (MCA) analysis was carried out to determine the most appropriate greenhouse gas mitigation measures for implementation in Bangkok, Thailand. Five criteria were used in this analysis included 1) mitigation potential, 2) total costs, 3) feasibility, 4) owner of benefits and 5) environmental benefits. Although, the action plan which focused on improving electricity consumption of the building and promoting electricity conservation campaign for Bangkok resident was expected to the highest reduction of greenhouse gases (2.7 million tons of CO_2 reduction). However, effort on expanding of the park area was evaluated as the most appropriate initiative when consider both of its effectiveness in reducing emissions, and its implementation cost. These predicted results were coincided with actual outcomes evaluated from the implementation of each policy in the metropolitan area. Methodology of this study can be applied for further use in analysis and selection of appropriate measures for policy maker in other cities as well as in the national level.

Keywords: Bangkok, action plan, greenhouse gas, mitigation, MCA

INTRODUCTION

Climate change is recognized as a global issue concerned the international community. In Asia, the rapid increases in industrialization and urbanization over the past several decades enhance increasing of the emission of greenhouse gases and the impacts of climate change are starting to occur and are predicted to be more severe particularly in some areas of the region. Thus, they are worthy of increased study and vigorous remedial action. Thailand has long been actively participating in the global efforts to prevent or at least ameliorate the effects of climate change. Now its capital city, Bangkok, is starting to participate in these efforts since it is a significant source of greenhouse gases emitted into the atmosphere, and as the nation's economic hub it has a lot to lose [1].

One of the indexes used to evaluate the extent of effect from climate change is changing of ambient temperature. In Bangkok the average maximum temperatures has an increasingly warming trend over the period 1961-2007 (Fig. 1). The same pattern of warming is also observed in the average minimum temperatures measured in Bangkok, as illustrated in Fig. 2. The number of days having the maximum air temperature exceeding 35°C also has an increasing tendency as presented in Fig. 3. The impacts of climate change on Bangkok have thus become increasingly visible and have been the subject of serious concern among residents since 1967, as they experience increasingly hotter weather [2].

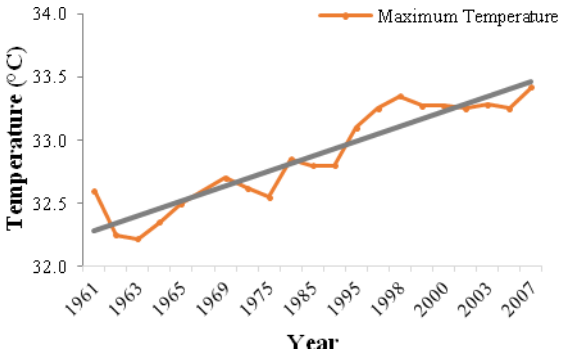

Fig. 1 Average maximum temperature in Bangkok, 1961-2007.

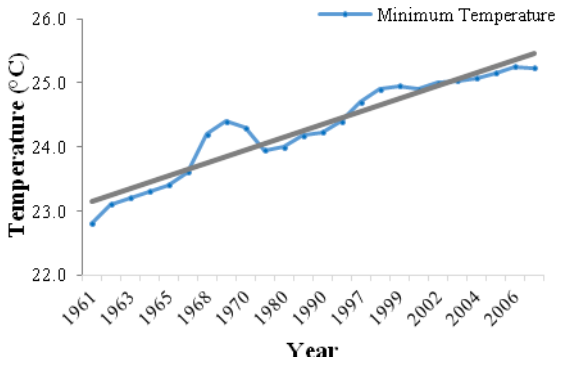

Fig. 2 Average minimum temperatures in Bangkok, 1961-2007.

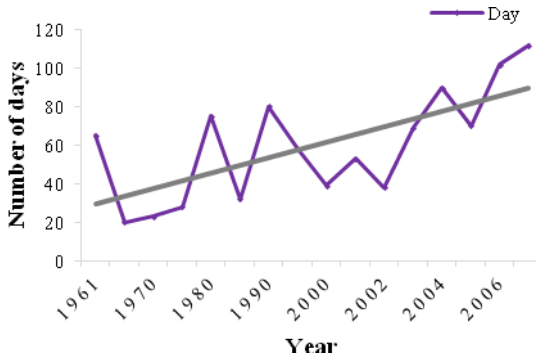

Fig. 3 Number of days exceeding 35˚C in Bangkok, 1961-2007.

In 2007, total greenhouse gas emission in Thailand was estimated as 61.23 million tons CO_2e. It was estimated that 43 million tons CO_2e (about 70%) of the country's emission was contributed from Bangkok. Although, these emissions were much greater amount than that of Toronto (24 million tons), they were about the same as those of London (44 million tons). The greenhouse gas emissions from Bangkok were reported to be lower than those emissions of New York City (58 million tons) [1]. However, results from the calculation of greenhouse gas emissions per capita reveals that the residents of Bangkok were responsible for producing 7.1 tons of CO_2e per annum which is, the same level of emissions as produced by New Yorkers (7.1 tons per capita). This level was significantly higher than the annual emissions of Londoners (5.9 tons per capita) but lower than the levels produced by residents of Toronto (9.6 tons per capita). Results are as summarized in Table 1.

Table 1 Greenhouse gas emissions of Bangkok and selected cities

City	Total emission (million tons of CO_2e)	Tons per capita of CO_2e emissions
Bangkok	43	7.1
Toronto	24	9.6
New York	58	7.1
London	44	5.9

Bangkok Metropolitan Administration (BMA), being aware of the global warming crisis and the necessity to take initial action to be part of the global effort in mitigating the problem. Bangkok Action Plan on Global Warming Mitigation was designated covering the period from the year 2007-2012. The action plan was aimed to reduce at least 15% of the total greenhouse gases (GHG) emissions by using emission amount under business as usual activities of the year 2012 as benchmarking. This action plan comprised of 5 initiatives: 1) Expand the mass transit rail system within Bangkok metropolitan area; 2) Promote the use of renewable energy; 3) Improve building electricity consumption efficiency; 4) Improve solid waste management and wastewater treatment efficiency; and 5) Expand park area. Each initiative consisted of several implementation plans to reach its goal. For the long term management, basic dimensions of sustainability consisted of environmentally, technically, economically, and socially sustainable alternatives should be reliable, adequate, and affordable [3]. Therefore, in order to select and evaluate alternatives, this work proposes the use of the multi-criteria attribute (MCA) which anticipates the three dimensions: environmental, technical, and economic needs. The purpose of this study was to analyze the appropriateness and effectiveness of each mitigation measure in order to prioritize actions under the plan for further implementation of the policy. In addition, the results from MCA analysis was compared with actual outcomes after implementing mitigation actions to validate all criteria of MCA for proposing appropriate mitigation action on greenhouse gases mitigation.

BMA ACTION PLAN

The BMA Action Plan on Global Warming Mitigation was used to serve the Thai policy in reducing emissions of greenhouse gases in Bangkok. Five initiatives have been set under this plan. They were 1) expanding the mass transit rail system within Bangkok Metropolitan area; 2) promoting the use of renewable energy; 3) improving building electricity consumption efficiency; 4) improving solid waste management and wastewater treatment efficiency; and 5) expanding park area.

MULTI-CRITERIA ATTRIBUTE (MCA)

Multi-criteria attribute (MCA) is generally understood as an assessment method that does not try to monetize everything, but to supply an unrefined view on the many different dimensions of the multiple effects of a certain policy or project or investment options. Nevertheless, the MCA can integrate monetary values like investment costs as one of the many dimensions it takes into account. In addition, it is a tool to calculate overall scores and rankings based on the scores given for each criterion for each individual option. Key elements of the MCA are the performance matrix, the weighting and the ranking process. Normally, the scoring of each criterion is from zero (worst) to five (best). And, each criterion weighted across all criteria are 100 [4]. In order to compare alternative options scoring on different criteria scales in different directions (trade-offs), it is necessary to put weights representing the relative importance associated with the respective criteria on the scoring results. Then, the MCA shows the effects of baseline developments and management scenarios on the multiple dimensions of the ecological, economic and social systems. The advantages of MCA, it has ability to deal with complex and unstructured decision problems in the sphere of environmental and natural resources managements, which involve a number of conflicting ecological, environmental, societal and economic objectives, multiple interests groups and different languages of valuation [5]. MCA methods have been used to prioritize urgent and immediate adaptation options during the formulation of National Adaptation Programs of Action (NAPAs) that Least Developed Countries (LDCs) developed under the United Nations Framework Convention on Climate Change (UNFCCC) [6]. Moreover, the use of MCA in the context of agricultural organic food production is sparse, and the relatively few studies that have been published are quite wide-ranging – from 'narrow' applications focusing on specific products [7] and it also used for the identification of spatial land-use conflicts in the Bucharest Metropolitan Area [8]. In addition, MCA is a popular tool in Dutch environmental impact assessment [9]. It also can be used for selecting an optimal configuration for an Air Quality Model as well [10].

For each dimension, the criteria was set taking into consideration impact of implementing activities under each action plan which can be explained as follows:

– The environmental aspect: The amount of greenhouse gas reduction is used to evaluate the extent of environmental benefit in implementing each activity. Reduction of greenhouse gas is expressed as CO_2e/5 years. The environmental benefit also determines by considering whether the project can provide other beneficial beside reduction of greenhouse gases. Examples of these in-direct benefits include potential in reducing water pollution, waste minimization, local air and noise pollution control, etc.

– Economic and social systems: The criteria used to evaluate this aspect included the operation and implementation cost as well as the possessor of benefit occurred from each activity. For example, the energy saving policy will give direct benefit to the implementing agency while forest plantation will provide the benefit to the public, etc.

– Technical and operational feasibility: This item is analyzed by considering the involving of technology involved in implementing measures under each action plan. The complicated technology will require much technical and operational knowledge and efforts. Therefore, higher score is given to the activities which can be implemented base on local or simple technology.

CRITERIA

To evaluate achievement of the appropriate action plan to mitigate greenhouse gases emissions in Bangkok, five criteria were set. Two major criteria are mitigation potential and implementation cost. Weighting of these two criteria are 30% each. Meanwhile, environmental benefits is a sensitive criterion which weighted 20%. And, the others criteria were feasibility (both in technical and operational feasibility) and the owner of benefits. Weighting of these criteria were 10% each. Indicators of each criterion were set for appropriated rating system. Summarized of criteria, indicators and score weighting are presented in Table 2.

RESULTS AND DISCUSSION

Results from MCA evaluation indicated that the most effective initiative was the 3rd initiative which was improving building electricity consumption efficiency. This initiative focused on management of energy consumption by improving energy efficiency and promoting electricity conservation campaign in Bangkok. It could mitigate greenhouse gases in the middle level but it was feasible, less investment cost and good for community and environment. Under the energy efficiency program, there are some countries in Asia proposing the mitigation action under Nationally Appropriate Mitigation Actions (NAMA). For instance, China expressed the intension submitted to the UNFCCC to increase the share of non-fossil fuels in primary consumption to around 15% by 2020. Meanwhile, Indonesia proposed to reduce emission 26% by 2020 which would reduce deforestation rate and promote energy efficiency. And, Singapore would begin

implementing the mitigation and energy efficiency measures announced under the sustainable Singapore blueprint [11]. As well as, Thailand would reduce emission 7% by 2020 and 20% by 2030 particularly in energy sector.

Table2 Criteria, indicators and score of criteria for BMA action plan

Criteria	Indicators	Score
Mitigation Potential (potential to reduce GHG)	0-1 million tons CO_2e	1
	1-2million tons CO_2e	2
	2-3million tons CO_2e	3
	3-4million tons CO_2e	4
	More than 4 million tons CO_2	5
Total Costs[1] (implementation cost)	0-2,000 Million Baht	1
	2,001-4,000Million Baht	2
	4,001-6,000Million Baht	3
	6,001-8,000Million Baht	4
	More than 8,000 Million Baht	5
Feasibility (technical and operational feasibility)	Not Good	1
	Bad	2
	Fair	3
	Good	4
	Very Good	5
Owner of Benefits	To implementing authority	1
	To public	5
Environmental Benefits[2]	having1 potential benefit	1
	having 2 potential benefits	2
	having 3 potential benefits	3
	having 4 potential benefits	4
	having 5 potential benefit	5

Note: [1] ref. [12], [13], [14], [15], [16], [17], [18]
[2] selected from 1) Potential for reducing air pollution, 2) Potential for reducing water pollution, 3) Potential for reducing noise pollution, 4) Potential for reducing solid waste, and 5) Potential for increasing visualization

The second rank of initiatives was the expanding park area, the 5th initiative, which includes planting trees in Bangkok Metropolitan area and the neighboring provinces around Bangkok. Even though, the potential of greenhouse gases mitigation was low but the other benefits were high, such as community benefits, environmental benefits, feasible implementation, and lower implementing cost. Moreover, urban trees also influence air temperatures, use of energy in the building energy, and consequently alter carbon emissions from numerous urban sources (e.g., power plants) [19]. Numerous benefits of urban forests studied in China indicated that urban forests are integral components of urban ecosystems, which could generate significant ecosystem services, such as offsetting carbon emission, removing air pollutants, regulating the microclimate, and recreation [20]. The last three initiatives were expanding mass transit and improving traffic system (the 1st initiative), promoting the use of renewable energy (the 2nd initiative), and improving solid waste management and wastewater treatment efficiency (the 4th initiative), respectively. Total score of each criterion ranking from the lowest to the highest were 66, 61, 57.3, 52, and 48 in improving building electricity consumption efficiency, expanding park area, expanding the mass transit rail system within Bangkok Metropolitan area, promoting the use of renewable energy, and improving solid waste management and wastewater treatment efficiency, respectively (Table 3).

Table 3 Scoring of each initiative for GHG reduction mitigation in BMA and other benefit

Criteria	Criteria weight	Initiative				
		1th	2nd	3rd	4th	5th
Mitigation Potential	30	30	6	18	6	6
Total Costs	30	6	30	24	18	24
Feasibility	10	6	10	10	4	9
Owner of Benefits	10	10	2	6	6	10
Environmental Benefits	20	5.3	4	8	14	12
Total	100	57.3	52	66	48	61
Ranking	-	3	4	1	5	2

Note: the 1st Initiative: expanding the mass transit rail system within Bangkok Metropolitan area;
the 2nd Initiative: promoting the use of renewable energy;
the 3rd Initiative: improving building electricity consumption efficiency;
the 4th Initiative: improving solid waste management and wastewater treatment efficiency; and
the 5th Initiative 5 expanding park area.

The result was compared with an analyzing of each measure conducted by BMA [21]. Results of mitigation measures of BMA action plan in 2007-2012 indicated that the most effective action was the improvement of building electricity consumption efficient. It could achieve reduction target which reduce emission 2.70 million tons CO_2. Likewise, the result of MCA analysis, energy efficiency in the building was the most appropriate measure to implement. Subsequently, expanding park area was another appropriate mitigation measure both from MCA and BMA results which could remove GHG 1.69 million tons CO_2. The other three initiatives were expanding mass transit and improving traffic system, promoting use of renewable energy, and improving solid waste management and wastewater

treatment efficiency which reduced GHG 1.01, 0.88, and 0.70 million tons CO_2, respectively. Table 4 shows the result of BMA and MCA analysis.

Table 4 Result of greenhouse gas emission reduction after implementing BMA action plan and prioritize action using MCA analysis

Initiative	BMA*			MCA
	CO_2 emission reduction	Compare to target	Ranking	Ranking
1st	1.01	under	3	3
2nd	0.88	over	4	4
3rd	2.70	over	1	1
4th	0.70	over	5	5
5th	1.69	over	2	2

Note: the 1st Initiative: expanding the mass transit rail system within Bangkok Metropolitan area;
the 2nd Initiative: promoting the use of renewable energy;
the 3rd Initiative: improving building electricity consumption efficiency;
the 4th Initiative: improving solid waste management and wastewater treatment efficiency; and
the 5th Initiative 5 expanding park area.
* [21]

Meanwhile, mitigation of each action was higher than their targets, which had been set up when proposed the action plan, except the 1st initiative. Even if it had the potential to reduce emission, it was still costly nor minor contributed to the environment benefits. Besides, it was inadequate opportunity to develop as well.

CONCLUSIONS

The consideration of action plan and initiatives for GHG reduction mitigation in Bangkok Metropolitan Administration (BMA) by using five criteria including mitigation potential, total costs, feasibility, community benefits and environmental benefits indicated that the appropriate action plan was the 3rd initiative (Improve Building Electricity Consumption Efficiency). The example activities are a campaign for efficient use of electrical appliance, a campaign for reduced use of air-conditioning, supporting energy efficiency labeling, and proper maintenance schemes for electrical appliance, promoting the use of energy-saving appliances, and promoting the use of energy-saving light bulbs. In contrast, promoting the use of biofuels of the 2nd initiative included promoting the use of gasohol and bio-diesel was the lowest score which is less appropriate than the others. The result from actual implementation showed the same direction to the result from MCA of this study. Hence, it could imply that this methodology can be applied to preliminary assess greenhouse gases mitigation measures to reduce for policy making decision.

ACKNOWLEDGEMENTS

This research work is partially supported by the China Medical Board (CMB) and Center of Excellence on Environmental Health and Toxicology (EHT), Faculty of Public Health, Mahidol University, Thailand.

REFERENCES

[1] Bangkok Metropolitan Administration, 2009 Bangkok assessment report on climate change 2009.
[2] Thai Meteorological Department, 2008. http:www.tmd.go.th/.
[3] Garrido-Baserba M., Reif R., Molinos-Senante M., Larrea L., Castillo A., Verdaguer M., Poch M., 2016. Application of a multi-criteria decision model to select of design choices for WWTPs. Clean Technologies and Environmental Policy 18: 1097–1109.
[4] Nowak D.J., 1993. Atmospheric carbon reduction by urban trees. Journal of Environmental Management 37 (3): 207–217.
[5] The Forest of Broceliande, 2014. Social Multi-Criteria Assessment: Multi-Criteria Assessment. https://proxy.reeds.uvsq.fr/galleries/broceliande 7/social-multi-criteriaassessment, Available on: 30 June 2014.
[6] United States Agency for International Development, 2013. Analyzing climate change Adaptation options using Multi-criteria analysis. African and Latin American Resilience to Climate Change (ARCC) Arlington, VA.
[7] Christensen T., Olsen S.B., Dubgaard A., Kærgård N., 2012. Organic farming and multi-criteria decisions: An economic survey. Institute of Food and Resource Economics, University of Copenhagen, Denmark.
[8] Ioja C.I., Nit M.R., Vân˘au G.O., Onose, D.A. Gavrilidis A.A., 2014. Using multi-criteria analysis for the identification of spatial land-use conflicts in the Bucharest Metropolitan Area. Ecological Indicators 42: 112–121.
[9] Janssen R., 2001. On the Use of Multi-Criteria Analysis in Environmental Impact Assessment in the Netherlands. J. Multi-Crit.Decis. Anal. 10: 101–109.
[10] Almanza V.H., Batyrshin I. Sosa G., 2014. Multi-criteria selection of an Air Quality Model configuration based on quantitative and linguistic evaluations. Expert Systems with Applications 41: 869–876.

[11] Energy Efficiency related NAMAs and Policy and Program Actions in Non-Annex I countries, 2014. http://prod-http-80-800498448.us-east1.elb.amazonaws.com/w/images/d/d6/List_of_EE_NAMAs_and_Actions.pdf. Available on: 23 June 2014.
[12] Bangkok Mass Transit Authority, 2012. Annual Report 2012.
[13] Bangkok Metropolitan Administration, 2012. BMA Action Plan 2013.
[14] Energy Conservation Promotion Fund, 2010. http://www.eppo.go.th/nepc/ako/ako-022.htm#1). Available on: 20 June 2014.
[15] Energy Policy and Planning Office (EPPO), 2011. 20-Year Energy Efficiency Action Plan (2011-2030). Ministry of Energy.
[16] Energy Policy and Planning Office, 2014. Annual Report 2012.Ministry of Energy.
[17] Mass Rapid Transit Authority of Thailand, 2009. Annual Report 2009.
[18] Ministry of Energy, 2011. Annual Report 2013.
[19] Stockholm Environment Institute, 2012. Greenhouse Gas Mitigation Screening Exercise for LEAP and Excel.
[20] Jim C.Y., Chen W.Y., 2009. Ecosystem services and valuation of urban forests in China. Cities 26: 187–194.
[21] Bangkok Metropolitan Administration, 2015. http://www.rfcc2015.ait.asia/Contents/Downloads/plenary_sessions/PanelDiscussion/PanelDiscussionClimateAndCities/Climate%20Change%20AIT1July2015_2.pdf.

Second International Conference on Science, Engineering & Environment,
Osaka City, Japan, Nov.21-23, 2016, ISBN: 978-4-9905958-7-6 C3051

RESULTS OF FIELD EXPERIMENTS OF RESERVOIRS' SILTATION FOR HARMONIOUS REALIZATION OF HYDROPOWER AND COASTLINE PROBLEMS

Lia Matchavariani[1], Giorgi Metreveli[1], Merab Alaverdashvili[1], Lamzira Lagidze[1],
Davit Svanadze[1], Zaza Gulashvili[1], Giorgi Bregvadze[1], Nino Paichadze[1]
[1]Faculty of Exact & Natural Sciences, Ivane Javakhishvili Tbilisi State University, Georgia

ABSTRACT

Georgia, as a seaside mountain country, faces three opposing issues: hydropower development, coastal protection, and flooding risks for riparian settlements and infrastructure. Present climate change will even more strengthen processes of beach abrasions. For study of silting prisms formation process and forecasting of the equilibrium channel on it, field natural experiment has been carried out on the small mountain rivers. The experiment showed that approximately for a year silting prism on some rivers closely reached its limited size and the equilibrium channel was formed. The silting prism in the tributaries, forms the sediment train that extended till the boundary of the top water level in the river. Length of train (L) is a function of the maximum flow discharge (QM), the deposit of runoff (R), diameter of bottom sediment (d) and initial inclination of riverbed (I). With the purpose of harmonious decision of all problems, eroded beaches periodically should be artificially filled by the river sediment, accumulated in the reservoirs. It's necessary to organize a system of the quarries in reservoirs.

Keywords: Accumulated Deposits, Equilibrium Channel, Mountain Reservoirs, Prism Train, Georgia's Seashore

INTRODUCTION

High values of mountain reservoirs condition the construction of these facilities worldwide. However, at the selection of their location is ignored the threat possible catastrophic floods of the settlements. High values of mountain reservoirs condition the construction of these facilities worldwide. However, at the selection of their location is ignored the threat possible catastrophic floods of the settlements. In addition, in coastal zone causes heavy deficit along the beachmaker sediments.

Mentioned negative aspects are the result of the lack of corresponding knowledge. During designing, the project developers don't take into account rising of riverbeds.

Current climate change has strengthened processes of sea shore abrasions and mountain reservoir sedimentation. According to the National Communications of Georgia to the UNFCCC [1], [2] the trend of change in the mean annual air temperature, precipitation and the moistening regime were estimated between the times: 1955-1970, 1990-2005 and 1986-2010. The increment of temperature and precipitation in West Georgia appeared to vary in the range of 0.2-0.4°C and 8-13%, respectively, while in East Georgia the relative values were found to be 0.6°C and 6.0%.

Research on reservoirs worldwide was dedicated to study of sedimentation, monitoring [3], balancing [4], ecology, sustainability [5], comparative analysis [6] and assessment [7]-[11], methodology [12], management [13] and modeling [14], [15] of reservoirs, dynamic of silting prism [16], [17], avoiding the effect on the Environment and catastrophic water floods [18], [19], Dam-Breach Hydraulic Analyses [20, 21], as well as hydro-regime of Caucasus reservoirs [22], etc.

In scientific literature, currently the emphasis is placed on silting processes taking place in headrace of water reservoirs, since this issue was not examined before. Particular interest is focused on interest in accumulative processes running in the headrace is caused by the fact that without study of these processes is impossible to identify settlements and infrastructure caught in the zone of catastrophic water floods and assess appropriate risks. Another important reason is that mentioned negatives appear in the middle phase of operation, while dramatic and sometimes tragic nature they take only after expiration of reservoirs' lifetime.

Because of the fact that the study of silting prism i.e. sediments accumulated in reservoirs and equilibrium channel formation processes and their parameters for acting water reservoirs is complicated, expensive and longstanding process, expected negatives are completely ignored during the selection of location for reservoirs. This problem is not highlighted in sufficient volumes, neither in Georgian, nor in foreign scientific-technical literature. Respectively, interests and safety of population domiciled aren't taken into account when selecting their location. Herewith doesn't occur determination of volumes and fractional composition of accumulated

sediments and assessment of risks of seacoast degradation, caused by lack of sediments. Due to the same reason are not elaborated the methods of avoiding or adaptation of these negatives.

Natural experiments are the highly effective means for assessment of solid material accumulation and variations of bed processes in mountain reservoirs and tributaries and for filling the lack of knowledge. For these purposes must be created artificial reservoirs, where will be possible to carry out an integrated study of silting prism and equilibrium channel formation processes for less than two years, to determine functional relations between their parameters and hydrological hydraulic characteristics of the river. Obtained results allow us to elaborate recommendations on avoidance and adaptation of mentioned negatives.

STUDY AREA AND RESEARCH METHODS

Research area covers Georgia's mountain reservoirs and sea coastal zone (fig.1). The studies were conducted in the following directions:

- Method of Natural experiment on small artificial reservoirs;
- Field method for a long-operated reservoirs (operating for several decades);
- Methods of Mathematical statistics.

For spatial-temporal study of silting prism and equilibrium channel formation process, the method of Natural experiments was used. We have selected three small rivers: Ru and Ruchula from the southern slope of the Great Caucasus Range – tributaries of the Rioni river (Racha region) and Vere from the northern slope of the Small Caucasus Range – tributary of the Kura river (near Tbilisi city). On these rivers were constructed one meter height dams. A flooded sections of the rivers were covered by the network for stationary observation on the riverbed deformation. This network covers part of the reservoir and mouth of tributaries. Measurement of silting prism and its train (continuation of silting prisms above the normal level) was made taking into account the frequency of floods and freshet of tributaries.

Fig. 1 Location of Study Area

Field studies were carried out on long operated reservoirs: Gumati (constructed at the Rioni River in 1953, West Georgia), Sioni (at the Iori River, 1963, East Georgia), Jinvali (at the Aragvi River, 1986, East Georgia), using a GPS-receiver Leica GS08. This apparatus is connected to a network of the National Agency of Public Registry and provides a high precision of geodetic measurements throughout the country.

For analysis of obtained results were used the methods of mathematical statistics (least square method) and differential calculus. Approbation of calculation results were implemented at Gumati, Sioni and Jinvali reservoirs.

RESULTS AND DISCUSSION

At this time the most part r(≥70%) of river deposits and solid materials formed due to reservoir's coast deformation. This accelerates the sedimentation of reservoirs. Herewith, prism formation occurs simultaneously, but with different rate in reservoir and riverbed.The phases of silting prism and train formation of the experimental rivers are shown in the table 1.

Table 1 Silting prism and train formation phases

Length of reservoir, m	Length of experimental part of riverbed, m	Inclination, ‰	Average annual water discharge, m^3/sec.	Measurement date	Silting prism length, m
River Ru					
1.45	4.5	34.5	0.002	07.07.15 18.11.15 05.04.16 29.05.16	0.0 2.1 2.4 4.4
River Ruchua					
2.5	6.0	17.4	0.6	20.08.15 25.08.15 28.08.15 05.03.16	0.0 3.0 3.0 4.5
River Vere					
7.5	45.0	5.3	1.45	07.08.15 17.09.15 24.09.15 27.11.15 09.03.16	0.0 11.0 13.0 15.0 20.0

By the results of natural experiments on the river Ru, the silting prism and its train has evolved so fast that it has become twice more than the reservoir's volume, as well as the length, compared to its initial state (fig.2).

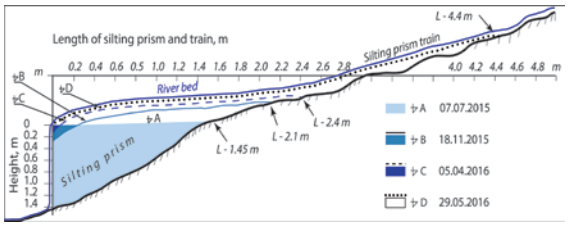

Fig. 2 Silting prism and train formation phases on the river Ru (by the natural experiment).

Sediment fractions (clay – fine sand), the hydraulic size of which in turbulent medium U≤1.0 m/sec, is transported by streams in the initial phase of operation through the whole reservoir and one part of them forms the layer with size corresponding to reservoir regulation type. The remaining part of such fractions (≥30%) not involved in prism formation, since it is transported by outlet water to the tailrace. Transportation of detritus (coarse sediments) in this phase to the tailrace occurs sporadically, during emergency water outlets.

In following phases the share and diameter of sediments transported from the reservoir gradually increase and reaches its maximum in the third phase of the operation. At the end of this phase silting prism reaches limit values of development and is formed as accumulation terrace, on which equilibrium channel is developed by tributaries.

Development of silting prism and train becomes especially active, when coarse-fraction sediment (d≥10 mm), which is precipitated in the zone of flood curve, forms crests. This accumulative formation has the form of beach ridge (falls), which slope exposed towards dam is sharper than the bench – slope formed in tributaries. Such crest gradually increases in height, comes close to the dam and when reaches it, silting prism volume and equilibrium channel length will become equal to their limit values.

The experiment showed that the sediment discharge (R kg/sec.) is divided into two components: coarse fraction (r_s kg/sec.), which is silted in the reservoir and the small fraction (r_u kg/sec.), which is taken out from the reservoir by the flow into the downstream.

$$R = r_s + r_u \quad (1)$$

The rate of silting prism growth is diminishing – average annual volume (r_s) of materials precipitated in reservoir and tributaries is the biggest in the initial phase of operation, afterwards it decreases in time in second and third phase and finally becomes equal to zero, when silting prism reaches its limit value.

$$\lim_{n\to T} r_s = 0 \quad (2)$$

Time distribution (r_u) of sediment transported from the reservoir is opposite to this process, it gradually increases and at the end of reservoir operation, i.e. after T time (in years) will become equal to the average annual volume (R) of sediments (r_u=R) and this sediment along with letting out water completely moves to tailrace:

$$\lim_{n\to T} r_s = R \quad (3)$$

Here, r_s and r_u are average annual volumes (m^3/year) of debris precipitated in reservoir and tributaries and sediments transported by the stream to tailrace, correspondingly, R is annual volume (m^3/year) of sediments brought by tributaries to the water reservoir, T – duration of reservoir operation time (years), while n=1, 2,…,T-1,T.

Equilibrium channel starts above the initial riverbed, at the height (h) of dam outlet. It follows silting prism surface and ends at the imaginary cross section, above which the river permanently keeps its natural ability of sediment transportation. Equilibrium channel length (L) and slope (I ‰) determine the value of the silting prism surface area (F km^2) and by means of this parameter is possible to calculate F value in any phase of equilibrium channel development. The process of equilibrium channel forming occurred under the Erie low, which is very important for mountainous rivers.

$$d^3\gamma = Av^6 \quad (4)$$

Here, $d^3\gamma$ is the weight of the deposit, v – stream velocity (m/sec.), A – proportional coefficient.

Processes of silting prism and equilibrium channel formation proceeded with the rate corresponding to the ratio (W/V) of their useful capacity (W) and annual amount of sediments (V).

Silting prism consists of two growing part. First of them is a part formed right in the reservoir, and the second part is an accumulated in tributary channels, called as train. Growth of the latter causes rising of the riverbed that lasts until the silting prism its maximum limit, i.e. the volume after which accumulative processes in the headrace completely cease. In these conditions river has already a developed equilibrium channel on the surface of the silting prism, the parameters of which (length L and slope I) are so big that river is able to completely move deposits to the convey as transit.

Silting prism surface area (F) in limit state is represented by the plain inclined towards the dam, which begins from dam outlet. Its area significantly (sometimes f≥60%) exceeds the reservoir surface. It is extended in tributaries up to the cross section, to which reservoir's water flood curve reaches during floods and freshets. Silting prism bench sizes basically are depended on hydrological and hydraulic characteristics of tributaries [19]: bench length (L),

dam outlet height (h), sediment diameter (d), maximum discharge of water and sediment (Q_m, R_m) and inclination of the bed located above the reservoir (I ‰):

$$L= f (h, Q_m, R_m, d, I-1) \quad (5)$$

At the same time equilibrium channel length is inversely proportional to the inclination of that river section (I‰), which is located above the reservoir. This fact means that the more riverbed is inclined, the shorter is equilibrium channel. According to experimental results, a length of the latter (L) doesn't exceed a double length of the reservoir (2l).

$$L \leq 2l \quad (6)$$

The experiment showed that the silting prism is a combination of two bodies, the first of which is formed in the reservoir (Wr), and the second one – above it and in tributary channels (Wt). Herewith, water flood risks for the population and infrastructure located above reservoir increase proportionally to the height of silting prism and its train. The more place is occupied by a train in the riverbed, the more higher is a probability of the river flowage.

Consequently, the limiting volume of silting prism (Wp) is equal to the sum of the volumes of both bodies. The first of them is the reservoir's volume at the normal level; the second one is the volume of the body (Wt), which based on the surface of the limited prism (ABK). Height (h_1) of the body is a distance between the equilibrium channel and the initial position of the riverbed at the end (E) of the reservoir.

$$Wt = 0.33\, h_1\, F_{ABK}, \quad h_1 = EF \quad (7)$$

Thus,

$$Wp = Wr + 0.33\, h_1\, F_{ABK} \quad (8)$$

A straight line is the simplest approximated form of equilibrium channel. When the river crosses a tectonic fault line its form comes closer to convex or concave curve. In this case it may be described by coordinates of the parabola, which begins from dam outlet and lasts up to above mentioned imaginary cross section.

Forecast based on calculations, made according to results of natural experiments in the near future (2025-2030 years) silting prisms and riverbed parameters will change by another 15-20% that creates a real risk of disaster for neighboring settlements. As a consequence the probability of catastrophic floods and related risks are so high that floods, which usually are repeated once in two decades (P≥5-10%), become a serious threat for population and environment

Results of natural experiments are tested on Gumati (constructed in 1953), Sioni (constructed in 1963) and Jinvali (constructed in 1986) reservoirs, since silting prism and equilibrium channel are nearest to limited values (fig. 3).

Sediments accumulated during many decades in Gumati reservoir and in riverbed located above, much exceeds than the volume of the reservoir (40 million m^3) and reaches about 65-70 million m^3. These sediments have raised the Rioni riverbed level so much that it every year overflows its banks and submerges adjacent settlements and infrastructure. Territory adjacent to Sioni reservoir is in a more dangerous situation, since sediments precipitated above the reservoir (45-50 mln. m^3) already have raised riverbed by 3-5 meters.

Fig. 3 Silting prism fragments (Jinvali reservoir)

Due to this fact Iori River several times overflows protective structures and heavily damaged riverine area, while it would seem that settlements are reliably protected by the dam. Almost 98% of

Gumati reservoir is occupied by sediments (fig.4), while Sioni reservoir already lost approximately 75% of volume. Both reservoirs are located in the active tectonic zone. As of 2015, the silting prism has changed riverbed parameters in these reservoirs (by 5-6 meters at Gumati and 2-3 meters at Sioni). Because of this, during the floods, rivers every year overflow their banks and do damage to the settlements, infrastructure and environment.

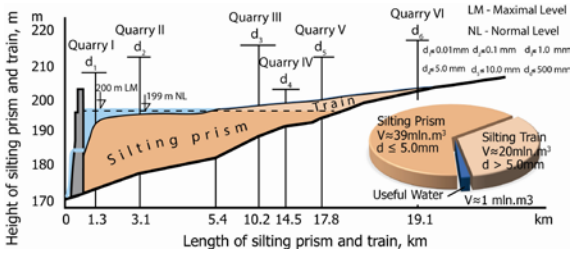

Fig. 4 Longitudinal section of Gumati Reservoir after 60 year exploitation

Silting prism and train of Gumati reservoir contain about 60 million m^3 beach-forming materials. Among them, about 60% are technically easily accessible and can be used to recharge of degrading coasts. Transporting of this material from Gumati to the seashore has been recommended by railway (Kutaisi-Poti), and after that by special courts along the coastline (fig. 5).

Fig. 5 Trajectory of sediments' transportation from Gumati reservoir to seashore

According to recent calculations, the annual volume of sediment, needed to prevent coastal erosion along the seashore of Georgia, is about 0.4-0.45 million m^3 of beach-maker material (d≥1 mm). Even the stock of solid material, accumulated only in Gumati reservoir, is sufficient to maintain Georgia's coast for at least 80-85 years.

Among the many ways to fill degraded beaches, using of silting material, removed from the reservoirs, is the most beneficial from the environmental and economic point of view.

In addition, as a result of periodic cleaning of the reservoirs, the useful volume of water in them will increase, that will contribute to efficient hydropower.

As a user of the proposed approach can be any mountainous country, with a high hydro power potential, where the rivers, flowing into the sea, are blocked by the reservoirs, for the reason of which coastal beaches are exposed to a sharp deficit of sediments.

CONCLUSION

Annual volume of material participating in the formation of silting prism and its train, wanes in time. Respectively, this is the most intense in the initial phase of reservoir operation and is negligible, when silting prism and equilibrium channel increases to the limit values.

Silting prism with limit value of volume completely covers reservoir and a part of a valley above it up to the imaginary cross-section. Its value is a sum of a reservoir's and train's volume.

Silting prism surface represents an inclined plane, which starts from dam outlet and lasts up to the beginning of the equilibrium channel.

The limit amount of silting prism more than 60% higher than the initial volume of reservoir. Therefore, the reservoir holds significantly more sediment than its volume is.

The most effective way to save the operating parameters of the reservoir and prevent deficiency of beach-forming material on the coast, is the creation of a quarry system in the reservoirs and the transportation of deposit to the seashore. This allows the solution of coastal protection and hydropower issues without the ecological damage and with some significant economic profit.

ACKNOWLEDGEMENTS

This study is funded by Shota Rustaveli National Science Foundation of Georgia within the scope of grant "Modern Methods of the Joint Problem Realization for Shore Protection and Hydropower" (AR/220/9-120/14).

REFERENCES

[1] Georgia's Second National Communication to the United Nations Framework Convention on Climate Change. National Climate Research Centre, Tbilisi, 2009

[2] Georgia's Third National Communication to the United Nations Framework Convention on Climate Change. National Climate Research Centre, Tbilisi, 2015

[3] Amitrano D., Di Martino G., Iodice A., Riccio D., Ruello G.,Papa M.N., Ciervo F., Koussoube Y. (2013). High resolution SAR for monitoring of reservoirs sedimentation and soil erosion in semi-arid regions. Geosciences and Remote

Sensing Symposium (IGARSS), 2013 IEEE International, 911-914

[4] Yasir S.A., Crosato A., Mohamed Y.A., Abdalla S.H., Wright N.G. (2014). Sediment balances in the Blue Nile River basin. International Journal of Sediment Research, 29(3), 316-328

[5] Detering M., Schuettrumpf H. (2014). Reservoir Siltationand Ecological Life Span of Dams. Wasser Wirtschaft, Springer,104 (1-2), 30-33

[6] Hajji O., Abidi S., Habaieb H., Mahjoub M. R. (2014). Regionalization and contribution to the study of reservoir sedimentary: Lakes of Cape Bon and the Tunisia Central. 11th International Conference on Hydroscience & Engineering "Hydro-Engineering for Environmental Challenges", Germany, Proceeding 2014, 575-582

[7] Bennett S.J., Dunbar J. A., Rhoton F.E., Allen P.M., Bigham J.M., Davidson G.R., Wren D.G. (2013). Assessing sedimentation issues within aging flood-control reservoirs. Reviews in Engineering Geology, 21, 25-44

[8] Garg V., Jothiprakash V. (2013). Evaluation of reservoir sedimentation using data driven techniques. Applied Soft Computing, Elsevier, 13(8), 3567-3581

[9] Wisser D., Frolking S., Hagen S., Bierkens M.F. (2013). Beyond peak reservoir storage? A global estimate of declining water storage capacity in large reservoirs. Water Resources Research, 49(9), 5732-5739

[10] Andredaki M., Georgoulas A., Hrissanthou V., Kotsovinos N.(2014). Assessment of reservoir sedimentation effect on coastal erosion in the case of Nestos River, Greece. International Journal of Sediment Research, 29(1), 34-48

[11] Gopinath G., Ashitha M. K., Jayakumar K.V. (2014). Sedimentation assessment in a multipurpose reservoir in Central Kerala, India. Environmental Earth Sciences, 72(11), 4441-4449

[12] Hosseinjanzadeh H., Hosseini K., Kaveh K., Mousavi S.F. (2015). New proposed method for prediction of reservoir sedimentation distribution. International Journal of Sediment Research, 30(3), 235-240

[13] Dewals B., Rulot F., Erpicum S., Archambeau P., Pirotton M. (2012). Long-term sediment management for sustainable hydropower. Comprehensive Renewable Energy. Vol. 6, 355-376

[14] Caputo M., & Carcione J. M. (2013). A memory model of sedimentation in water reservoirs. Journal of Hydrology, Elsevier, 476, 426-432

[15] Mattheus C.R., & Norton M.S. (2013). Comparison of pond-sedimentation data with a GIS-based USLE model of sediment yield for a small forested urban watershed.Anthropocene, Elsevier, 2, 89-101

[16] Metreveli G.S., Kereselidze D.N. Rehviashvili Sh.D. (2004). The dynamic of SP of mountain reservoirs.dynamics and thermic of rivers, reservoirs and sea coastal zone. Proceedings of the VI Conference,. IWP RAS, Moscow,70-73 (in Russian)

[17] Mansikkamaki H. (2013). Monthly sedimentation in some reservoirs of hydroelectric stations in Finland. Fennia – International Journal of Geography, 143 (1)

[18] Ran L., Lu X. X., Xin Z., & Yang X. (2013). Cumulative sediment trapping by reservoirs in large river basins: A case study of the Yellow River basin. Global and Planetary Change, 100, 308-319

[19] Metreveli G., Matchavariani L. Research Method of Silting the Mountain Reservoirs Under the Current Climate Change. Journal of Water Resources and Ocean Science. Science Publishing Group, vol. 5, #2, 2016, 22-27

[20] Galen K. Hoogestraat. Flood Hydrology and Dam-Breach Hydraulic Analyses of Four Resrvoirs in the Black Hills, South Dakota. US Geological Survey, Virginia, 2011, 37

[21] Michael R. Stevens and Galen K. Hoogestraat. Flood Hydrology and Dam-Breach Hydraulic Analyses of Five Reservoirs in Colorado. US Geological Survey, Virginia, 2013, 24.

[22] Metreveli G. Reservoirs of South Caucasus. Gidrometeoizdat, Leningrad, 1985, 165

Second International Conference on Science, Engineering & Environment,
Osaka City, Japan, Nov.21-23, 2016, ISBN: 978-4-9905958-7-6 C3051

THE VALUE OF GREEN BELTS IN URBAN SPRAWL: A CASE STUDY OD TAICHUNG CITY, TAIWAN

Chih-Hao Chen, Walter Den
Department of Environmental Science and Engineering, Tunghai University, Taiwan

ABSTRACT

The role of green belts is not only to provide the recreation for human activities but also to improve environmental quality and to provide refuges for wildlife under intensified urban development. After the new demarcation of administrative areas, the influx and construction of industrial zones and commercial buildings has caused a major change of the original landscape in the Dadu hill area in Taichung City, Taiwan. The aims of this study are to provide recommendations pertaining the design of ecological corridors to improve the connectivity of the remaining green places, and the assessment of the health of habitat for the developed urban area. We compared the biodiversity (birds, mammals, plantation) and carbon flux in three different suburban areas including a campus, a metropolitan park and an undeveloped woodland in regular disturbance by human and fire. According to the results of habitat similarity, the metropolitan park and campus were grouped with the higher diversity of birds, but the woodland had the higher diversity of plantation and mammals. Seasonal change is the main factor which affects the carbon flux and vegetation growth situation, and the disturbance by human activities and canopy and coverage by plantation are the causes of fluctuations. The habitat assessment which integrated the biodiversity and carbon flux provided another angle to evaluate the greenbelt design comprehensively. However, the quantification of the whole ecosystem service value is a further direction of environment management, especially in green place conserving under the urban sprawl.

Keywords: Carbon flux, Urban Sprawl, Environmental Index

INTRODUCTION

With the industrial development and the transformation in Taiwan, urban renewal , re-zoning had changed the patterns of land using , as the agriculture and coastal area had reclaimed to industrial zones. However, the changing land using pattern had caused the direct impact to the original inhabit of human life, but also lead to the result about the habitat losing of wildlife.

The measurement and assessment are the basic work of the carrying capacity for an ideal sustainable and friendly urban environment. Despite the social and economic values, as the clean air, water, noise, and traffic, the ecosystem service value of the consideration of natural resource would make up for a complete environmental value[1, 2].

When the high-density population gathered in the urban, the accompanying high-intensity human activities and resource requirements, including the land development, had caused high pressure for itself, but also to force the surrounding resource supply and even further afield .

In recent year, the night calls of the Nightjars (Caprimulgus affinis) in Taiwan is a case of wildlife invasion in the urban because of the habitat losing by urban sprawl. Due to the urban expansion, the wildlife could not migrate to another suitable habitat , the nearby and similar habitat type would because their only selection..

The coexistence of wildlife and human could be the best solution at the present, but not the best treatment for both. When the construction could cause the direct environmental impact, as the habitat losing and fragment, the mitigation, and restoration[3] as the in-situ, ex-situ conservation, the design of the corridors between the small habitat[4, 5] , could provide the refuges for the wildlife and maintain the biodiversity. The habitats with linkability and buffer, play the essential role in the urban ecosystem for the vegetation, birds, mammals, amphibians, even the material flows, and also provide an excellent field of environmental education and observation[6-8].

This aim of this paper is to provide a design direction of the ecological corridors to save the green places under the pressure of construction and habitat fragment by integrating the biodiversity and carbon flux survey.

METHODS

Quadrat Setting and Species Census

The study area located on the Dadu hill area in Mid-Taiwan was classified by NDVI (Normalized Difference Vegetation Index) for habitat

classification, and divided into three main quadrats (13 sampling plots)(Fig1), Tunghai University campus, the southern of the Dadu hill, and the Northern part, including the Taichung Metropolitan Park, by vegetation condition, canopy(natural and human-made), landscape coverage, human disturbance and water area. The census of birds, small mammals and vegetation and the monitoring of carbon flux were carried out from March 2013 to November 2014.

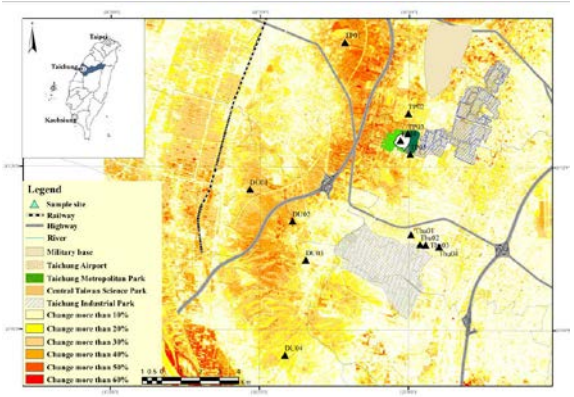

Fig 1 The satellite map of the study area by NDVI index.

The small mammal was trapped for species identification and released to original habitat after maker for population estimation. The line transect and point count method were used for bird census by binoculars and voice identification. In vegetation, 10 m x 10 m square sample area was settled in each plot for the investigation of woody plant and the herb. An Infrared gas analyzer (IRGA, LI-820, LI-COR Inc.))for carbon dioxide were used for carbon flux, and the light intensity was recorded at the same time by Li-Core 1400.

Habitat Similarity and Statistic Analysis

The difference of the community structure and species composition are quantified by Euclidean Distance Method. All data was handled by MS Office Excel 2011, StatPlus （AnalystSoft, StatPlus:mac - statistical analysis program for Mac OS. Version 5.）and the figures were performed using GraphPad Prism version 6.00 for Mac, GraphPad Software, La Jolla California USA, www.graphpad.com

RESULTS

Biological Census

Nine species of small mammals(Table1), 73 species of birds(Table2) and 188 species of flora(Table3) were detected and trapped on 13 plots where we conducted between March 2013 and November 2014. The distribution of the small mammal in Southern is better than other quadrats, and the percentage of conservation and endemic species of the birds in 3 quadrats are higher, especially in Tunghai University Campus. In the part of the flora, the species in the Northern, and the diversity and coverage in the Southern are higher.

Season effect and Carbon Flux

The carbon flux in Tunghai University Campus(371.60 ± 217.04 mg/m^2/s) is higher than the Southern (250.02 ± 94.98 mg/m^2/s)and Nothern(327.39 ± 215.15 mg/m^2/s)during the monitoring, and the difference between each plot are significantly($p<0.05$). The vegetation growth and the organic carbon would be affected by season, but also for the carbon flux(Fig2). The human disturbance, as the tread, traffic, even agriculture, would cause the significant difference(Fig3), the plot with lower disturbance would have higher flux($p<0.05$). In high vegetation coverage, the carbon flux would be higher than low ones significantly($p<0.05$), but the fluctuation in the different season is not significantly($p=0.053$)(Fig4).In this study, the definition of the canopy is not only the aboveground portion of the crop but also including the human buildings. The difference is not significant in the higher canopy(>25%), and the carbon flux is higher under the lower canopy(Fig 5). The season factor didn't affect the flux in the different canopy($p=0.053$).

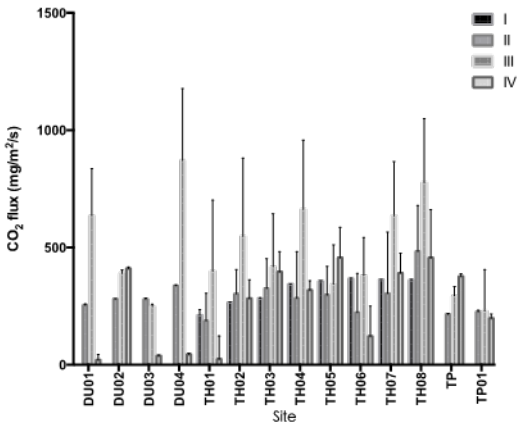

Fig 2 The carbon flux of each plot in different season

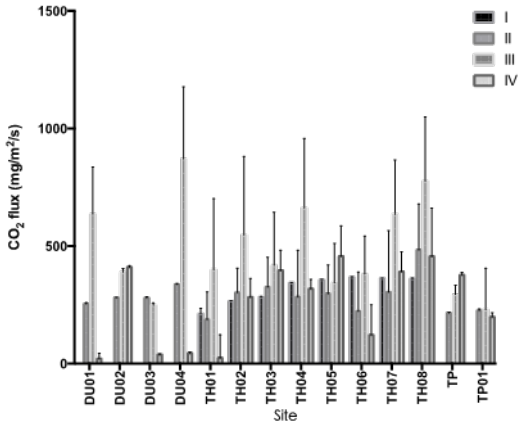

Fig3 The carbon flux in different disturbance degree

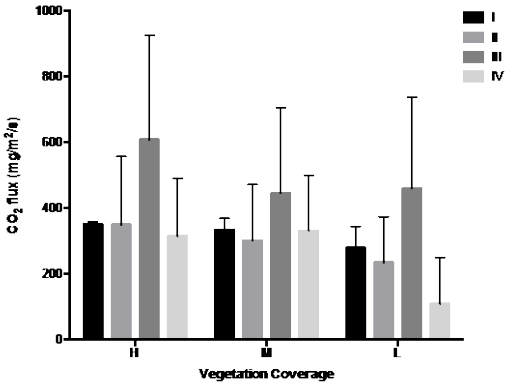

Fig 4 The carbon flux in different land coverage

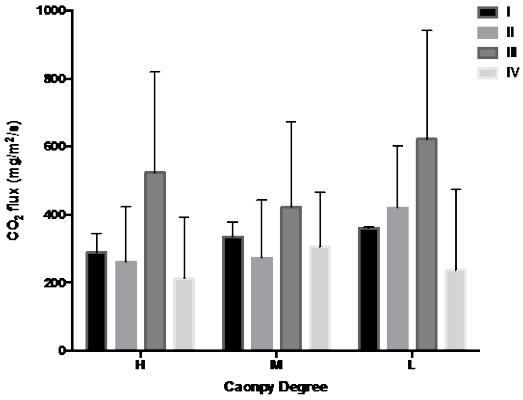

Fig5 The carbon flux in different canopy percentage

Note1: I : Jan-Mar ; II : Apr-Jun ; III : Jul-Sep ; IV : Oct-Dec

Note2: H: High degree; M: Medium degree; L: Low Degree

The relationship between the carbon flux and biological index

Table 4 shows the correlation about the mammals and plants in spring and winter are opposite, the season is the main factor. Otherwise, the correlation about the birds only exists in the winter as the migratory species, and lack of the food would result in the gathering situation.

CONCLUSION

Disturbance and Invasion species

Since the fire and construction had to be happened in the Dadu hill area usually, the Guinea Grass(*Panicum maximum*) from Africa had been the one of the dominant species and completed the habitat with the native species, Eulalia grass(*Miscanthus sinensis*). However, the grassland with the Guinea grass had become the main habitat type after the repeated fire and human disturbance. The similar situation had happened in Western American, the cheatgrass(*Bromus tectorum*) from Asia had completed with the native species, Sagebrush (*Artmesia tridentata*) and Sandberg bluegrass (*Poa ampla*), because of the high fire frequency and overgrazing. The invasion species not only change the habitat type but also result in the carbon sink to carbon source, the carbon emission had been 8 ±3 Tg C in Great Basin area[9].

In addition to the invasive species, due to the horticulture, agriculture and other needs of the cultivation in the metropolitan area and suburban area, the domestic species are cultivated widely, especially in the park, school or private gardens and other green places. It would not only affect the carbon flux, but also biodiversity.

Twenty(10%) domestic and 53(26%) naturalized species are found during the survey, and there are not significantly different between native species or not in carbon flux($p=0.2098$), but the naturalize and native species in the winter($p=0.0104<0.05$).

Therefore, although the non-native species did not significantly affect the circulation of carbon flux, however, the native species should have priority for plantation in the particular area, as a park, campus, and garden, to avoid and reduce the dispersal of invasionspecies[9, 10].

The planning of ecological corridors and area

According to the habitat similarity (Fig6,7,8,9), the habitat types of Tunghai University Campus and the Northern part are similar, and these two areas are under stable succession with better human management. In the southern part, the regular succession environment due to the repeated fire and agriculture, the influence of carbon flux by season was significantly than others.

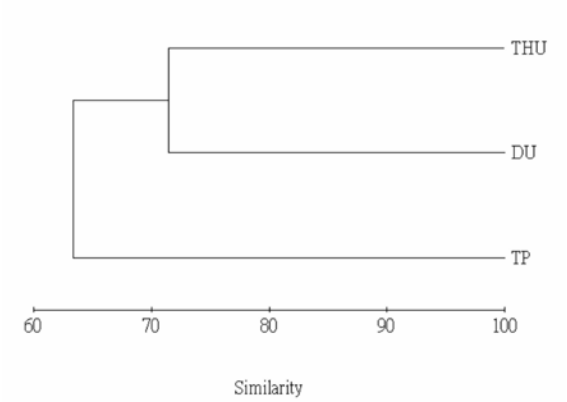

Fig 6 The similarity of small mammal in three quadrat

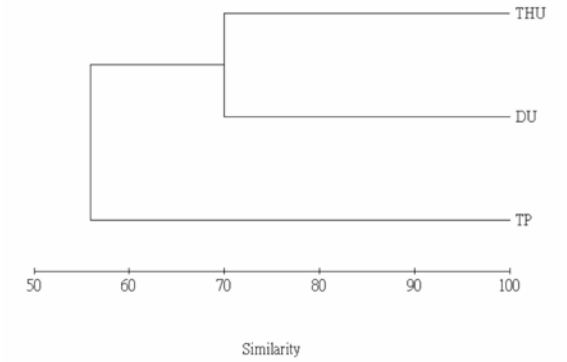

Fig 7 The similarity of birds in three quadrat

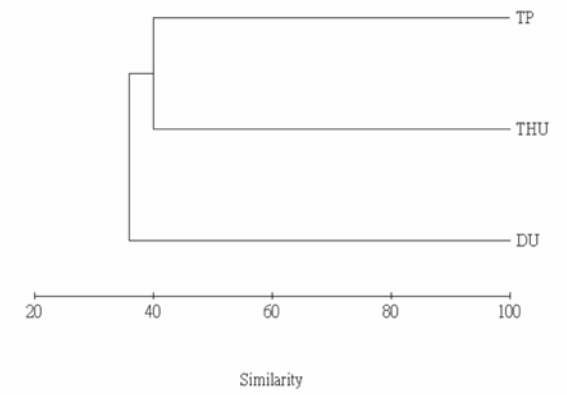

Fig 8 The similarity of plant in three quadrat

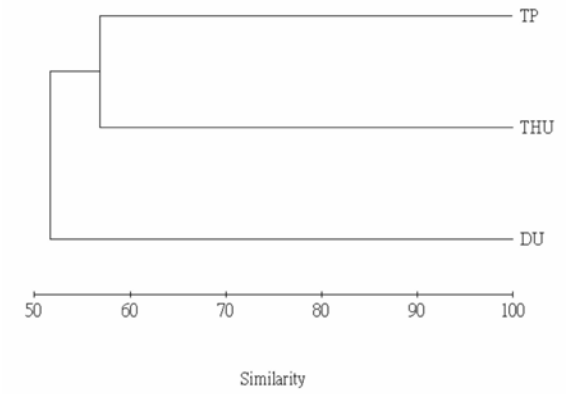

Fig 9 The similarity of habitat integrated indics in three quadrat

The whole area could be divided into two blocks for considerations, one is the Northern part and the campus, and anther one is the Southern part, as a wildlife refuge. An industrial park and a business area are located on the connection between this two area, and could be suspended or cut off the possibility of species exchange. The human-made green belt, as the small park, and the replanting of the vegetation could improve the connectivity of the patches.

In conclusion, the season is the major impact factor on the carbon flux and biological distribution and dispersal. However, the influence of disturbance is greater than canopy and vegetation coverage. No matter for biodiversity conservation, human recreation, or improve the environmental quality, the green places in the urban and suburban area could seem as the refuge for wildlife and human. The monitoring of carbon flux could be an auxiliary tool for the traditional biological census to assess the habitat heterogeneity in Landscape ecology, and to reinforce the consideration in urban environment assessment.

REFERENCES

[1] D. Argüeso, J. P. Evans, A. J. Pitman, and A. Di Luca, "Effects of City Expansion on Heat Stress under Climate Change Conditions.," in *PLoS ONE* vol. 10, ed, 2015, p. e0117066.

[2] R. S. de Groot, R. Alkemade, L. Braat, L. Hein, and L. Willemen, "Challenges in integrating the concept of ecosystem services and values in landscape planning, management and decision making," *Ecological Complexity*, vol. 7, pp. 260-272, 2010.

[3] C. Clauzel, C. Bannwarth, and J.-C. Foltete, "Integrating regional-scale connectivity in habitat restoration: An application for amphibian conservation in eastern France," *Journal for Nature Conservation*, vol. 23, pp. 98-107, 2// 2015.

[4] C. S. Zhao, S. T. Yang, C. M. Liu, T. W. Dou, Z. L. Yang, Z. Y. Yang, *et al.*, "Linking hydrologic, physical and chemical habitat environments for the potential assessment of fish community rehabilitation in a developing city," *Journal of Hydrology*, vol. 523, pp. 384-397, 4// 2015.

[5] B. Xun, D. Yu, Y. Liu, R. Hao, and Y. Sun, "Quantifying isolation effect of urban growth on key ecological areas,"

Ecological Engineering, vol. 69, pp. 46-54, 8// 2014.

[6] R. Lal and B. Augustin, *Carbon sequestration in urban ecosystems*: Springer, 2012.

[7] S. B. Lerman, K. H. Nislow, D. J. Nowak, S. DeStefano, D. I. King, and D. T. Jones-Farrand, "Using urban forest assessment tools to model bird habitat potential," *Landscape and Urban Planning*, vol. 122, pp. 29-40, 2// 2014.

[8] S. T. A. Pickett, B. McGrath, and M. L. Cadenasso, "The Ecology of the Metacity: Shaping the Dynamic, Patchy, Networked, and Adaptive Cities of the Future," in *Resilience in ecology and urban design: Linking theory and practice for sustainable cities*. vol. 3, ed Dordrecht: Springer Netherlands, 2012, pp. 463-489.

[9] Y. Paker, Y. Yom-Tov, T. Alon-Mozes, and A. Barnea, "The effect of plant richness and urban garden structure on bird species richness, diversity and community structure," *Landscape and Urban Planning*, vol. 122, pp. 186-195, 2014.

[10] N. H. N. Mohamad, S. Idilfitri, and S. K. S. O. Thani, "Biodiversity by Design: The attributes of ornamental plants in urban forest parks," *Procedia - Social and Behavioral Sciences*, vol. 105, pp. 823-839, 12/3/ 2013.

Table 1 The diversity and biological indices of the small mammal

	Southern				THU Campus				Northern				
	DU01	DU02	DU03	DU04	Thu01	Thu02	Thu03	Thu04	TP01	TP02	TP03	TP04	TP05
Species	2	5	6	4	2	5	2	2	0	2	2	1	1
Population	2	35	22	11	4	9	7	19	0	8	12	2	6
Richness	1.44	1.13	1.62	1.25	0.72	1.82	0.51	0.34	NA	0.48	0.40	0.00	0.00
Evenness	1.00	0.83	0.81	0.81	0.81	0.89	0.59	0.83	NA	0.54	0.41	NA	NA
Shannon-Weaver Index	0.69	1.33	1.45	1.12	0.56	1.43	0.41	0.58	0.00	0.38	0.29	0.00	0.00
% of Alien spceis	0%	0%	0%	0%	0%	0%	0%	0%	0%	0%	0%	0%	0%
% of Conservation spceies	0%	0%	0%	0%	0%	0%	0%	0%	0%	0%	0%	0%	0%
Integrated Index	5.13	5.00	5.65	4.85	3.59	5.50	2.80	3.16	0.00	2.65	2.27	1.00	1.00

Table 2 The diversity and biological indices of the birds

	Southern				THU Campus				Northern
	DU01	DU02	DU03	DU04	Thu01	Thu02	Thu03	Thu04	TP01	TP
Species	13	14	13	15	13	33	26	20	20	67
Population	200	116	116	257	212	745	833	534	224	2928
Richness	2.26	2.73	2.52	2.52	2.24	4.84	3.72	3.03	3.51	8.27
Evenness	0.79	0.78	0.89	0.69	0.74	0.73	0.71	0.74	0.74	0.77
Shannon-Weaver Index	2.04	2.06	2.29	1.87	1.90	2.56	2.32	2.22	2.22	3.23
% of Alien spceis	0%	4%	3%	1%	0%	1%	0%	5%	2%	4%
% of Conservation spceies	1%	3%	2%	1%	1%	1%	2%	1%	0%	7%
Integrated Index	6.32	6.80	7.11	6.27	6.02	9.36	7.93	6.98	7.54	13.76

Table 3The diversity and biological indices of the vegetation

		Southern				THU Campus				Northern				
		DU01	DU02	DU03	DU04	Thu01	Thu02	Thu03	Thu04	TP01	TP02	TP03	TP04	TP05
Woody	Species	5	2	4	3	4	5	4	2	1	1	1	1	3
	Shannon-Weaver Index	1.56	0.50	1.33	0.94	1.28	1.48	1.39	0.69	0.00	0.00	0.00	0.00	1.01
Herb	Species	2	8	3	4	6	2	7	2	2	3	4	6	8
	Shannon-Weaver Index	0.36	0.60	0.58	1.17	1.43	0.13	1.55	0.63	0.42	0.25	0.18	0.86	1.89
	% of Coverage	97.50	91.00	93.00	5.50	40.50	103.00	21.00	125.00	107.00	101.00	96.50	112.00	8.50
	Integrated Index	5.44	4.55	5.33	4.60	5.32	5.10	5.35	5.51	3.89	3.59	3.45	4.08	5.29

Table 4. The correlation between the carbon flux and biological index in spring and winter

Season	Group	Index	Pearson correlation coefficient	p-value
Winter	Mammals	Richness	-0.654	0.078
	Birds	Shannon-Weaver Index	0.802	0.017
	Plant	Shannon-Weaver Index	-0.768	0.026
Spring	Mammals	Richness	0.536	0.089
	Plant	Shannon-Weaver Index	0.505	0.087

Second International Conference on Science, Engineering & Environment,
Osaka City, Japan, Nov.21-23, 2016, ISBN: 978-4-9905958-7-6 C3051

THE CHANGES OF PRECIPITATION IN SAMTSKHE-JAVAKHETI REGION (GEORGIA) AGAINST THE BACKGROUND OF CLIMATE CHANGE

Lamzira Lagidze[1], Dali Nikolaishvili[1], Lia Matchavariani[1] and Nino Paichadze[1]
[1]Faculty of Exact and Natural Sciences, Ivane Javakhishvili Tbilisi State University,Georgia

ABSTRACT

Georgia with its complex physical-geographical conditions (the altitude of the country above sea level is 0-5068 m), is considered as classical example of a mountainous country with diversified climatic conditions. In this respect, Samtskhe-Javakheti, is outstanding region of Georgia. On the background of global warming, the change of the regional climate has special peculiarities, which are important in the regions, located in a warming or cooling border area. The boundary between these opposite processes (warming, cooling), must be found on the territory of Georgia. The main cause of regional climate change, besides of Global climate change, is due to the region's climate and orographic distinctiveness.

For evaluation of the climate change of this region, the research was conducted about the changes in precipitation amounts (monthly and annual). Studies were carried out on the bases of data, fixed by the local meteorological stations during the 40 year period for the following geographical points: Akhalkalaki and Paravani, the observation period was between 1967-2006 years, for Akhaltsikhe it was done between 1971-2010 years. Statistical, climatological and graphical analyses of specified periods multi-year meteorological data was used for research. Research results present the ability to make the following conclusions: due to climate changes of the region the sharp changes in monthly and annual precipitation amounts occur: During the period of 1967-2006 years, in Akhalkalakhi an increment of annual precipitation till 895 mm was found. In Paravani Precipitation is decreased till 1808 mm. In Akhaltsikhe, during the observation period of 1971-2010 years, the annual amount of precipitation was increased till 167 mm.

Key words: Samtskhe-Javakheti, Orography, Circulation Processes, Climate Change, Precipitation

INTRODUCTION

According to data of the International Panel on Climate Change (IPCC), in the course of 100 years (1906-2005) average air temperature has increased by 0,74°C [1], while in 1961-2005 average global temperature has raised by 0,44°C [2], [3].

The problem of mankind's impact on the environment from the viewpoint of effect on climate formation, is the most important at the modern stage. In the future it may become the reason of further progress or degradation [4]. Georgia with its complex physical-geographical conditions (the altitude of the country above sea level is 0-5068 m), is considered a classical example of a mountainous country with diversified climatic conditions. In this respect, Samtskhe-Javakheti, one of the most important regions of Georgia, is outstanding and characterized by the diversified climatic conditions (fig. 1). It is located to the southward of the country and climate here is sharply distinguished from climate conditions of other regions of Georgia (that is caused by effect of local factors).

Absolute altitude of Samtskhe-Javakheti varies in the 900-3300 m range. It is surrounded by high ridges. Meridian disposition of mentioned ridges weakens the impact of large-scale atmospheric circulation processes developed in the territory of the Transcaucasus and significantly strengthens the influence of local complex orographic factors (tablelands, plateaus, basins) that has considerable effect on the cloud regime [5].

Fig. 1 Location of study area (Samtskhe-Javakheti region), Georgia

Both climate and natural conditions markedly differ from each other according to regions of Samtskhe-Javakheti. Even climate and natural conditions of Samtskhe and Javakheti are different. Javakheti is characterized by a very continental climate, according to the nature of hypsometric

development and vegetative cover. The situation is comparatively different in settlements located in gorges and on Akhalkalaki plateau, where due to terrace system are developed different sectors of economy and agriculture [6].

Agriculture is the leading branch of the regional economy. As is known the climate is one of the most important natural components of agriculture, that's why an assessment of precipitation amount in the region is of special significance in order to rationally use climate conditions of the region [7], [8].

Region of Samtskhe-Javakheti is also distinguished from the recreational viewpoint. Different kinds of resorts are located there: mountain ski resort (Bakuriani), health-related (Likani), mineral waters (Borjomi). That's why the study of this region against the background of climate changes is especially important for sustainable development of economy, power engineering, agriculture, etc.

Crucial role in the formation of a climate of Samtskhe-Javakheti is assigned to atmospheric precipitation.

Basic Circulation Processes – Conditioning Factors of Precipitation

Western processes, which cause cloudy and rainy weather in the western part of the region, play a significant role in weather formation in Samtskhe-Javakheti, that's why the major part of the fallout down throughout a year is related to these processes [9].

The role of air masses intrusion from the East in the formation of weather and climate of Samtskhe-Javakheti is relatively lesser. Its impact is important in Akhaltsikhe hollow and Akhalkalaki plateau.

Eastern processes are more intense in spring, since during these processes takes place increase of instability of air masses and temperature of underlayer surface that promotes the development of convectional processes [10].

Peculiar synoptic processes and characteristic weather conditions are developed due to wave perturbations formed southward of the South Caucasus, which are mainly bilateral or develop after completion of air masses intrusion from the west. Among total atmospheric precipitation falling out throughout a year up to 150 mm of precipitation falls on southern processes. Sometimes they are distinguished by high intensity and continue for several days. Process duration depends on the intensity of air masses intrusion [5].

Climate peculiarities of Samtskhe-Javakheti, especially its moisture regime (humidity conditions), are mainly conditioned by convectional processes (due to south location of the region), which have great influence on the total amount of precipitation and their annual distribution. Abundant precipitation for a short time and of local character are characteristic for mentioned processes. Usually they don't cover large territories, but about 30-40% of precipitation falling out in summer fall on these processes.

As it turned out from analysis of atmospheric circulation processes, their action and intensity in the region varies according to seasons that causes seasonal peculiarities of climate conditions here.

Orographic barriers also are significant precondition of climate peculiarities of the area. The Greater Caucasus mountains are important for the formation of regional climate, since they impede intrusion of cold air masses from the north to the Southern Caucasus and, in particular, to the territory of Samtskhe-Javakheti. Arsiani and Adjara-Imereti ridges, which impede diffusion of humid air masses coming from the west, also represent an important orographic barrier for Samtskhe-Javakheti. That's why their windward slopes are characterized by abundant precipitation, while leeward slopes, adjacent gorges and basins are distinguished by less precipitation. All this creates very important climate contrast here [10].

Observation data from meteorological stations, in particular basic characteristics of precipitation, their monthly and annual amounts, were used for establishment of atmospheric precipitation dynamics in Samtskhe-Javakheti (fig. 2).

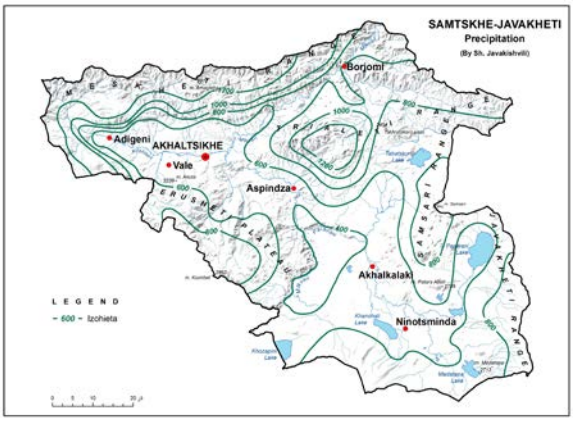

Fig. 2 Total precipitation in Samtskhe-Javakheti region, Georgia (1903-1967)

INITIAL MATERIAL

Data of observation over atmospheric precipitation obtained from the following (formerly existing and currently acting in Samtskhe-Javakheti) meteorological stations and weather shelters are used for the study, namely: Akhalkalaki (1967-2006), Akhaltsikhe (1971-2010) and Paravani (1967-2006). Statistical, climatological and graphical analyses of multi-year meteorological data is used for research.

RESULTS

The dynamics of the total amount of precipitation according to seasons and 10-year periods is determined for 40-year period with the use of the basic characteristics of precipitation – their monthly and annual amounts. Materials of observations over the annual precipitation amount according to periods are represented in the form of diagrams (Fig. 3-11).

Akhalkalaki – for determination of precipitation changes we used 1967-2006 observation materials, which were divided into four 10-year periods: 1967-1976, 1977-1986, 1987-1996, 1997-2006.

Study analysis shows, that under the influence of global climate changes in Akhalkalaki, from 1967 to 2006 (40-year period) total amount of precipitation (according to 10-year periods) experiences the following changes: during the period precipitation amount varies from 190 to 1004 (Fig. 3).

In period I (during 1967-1976), total amount of precipitation changes from 245 mm to 1004 mm. In winter – from 245 mm to 274 mm, in spring – from 275 mm to 859 mm, in summer – from 516 mm to 1004 mm, in autumn period – from 349 mm to 419 mm. The total amount of precipitation of the mentioned period equals to 5633 mm.

In period II (1977-1986), in the course of nine years, the total amount of precipitation changes from 190 mm to 865 mm. The minimum is registered in January, while the maximum – in May. In the winter period, total amount of precipitation changes from 190 mm to 274 mm, in spring – from 301 mm to 865 mm, in summer – from 501 mm to 846 mm, in autumn – from 315 mm to 429 mm. Annual precipitation amounts of this period equals to 5360 mm.

In period III (1987-1996), the total amount of precipitation varies from 265 mm to 920 mm. The maximum is registered in June, while the minimum – in March. In the winter period, annual precipitation amount changes from 303 mm to 371 mm, in spring – from 265 mm to 689 mm, in summer – from 441 mm to 920 mm, and in autumn – from 326 mm to 428 mm. Precipitation amount of this period (1987-1996) equals to 5421 mm.

In period IV (1997-2006), the annual precipitation amount varies from 310 mm to 901 mm. The maximum is registered in May, while the minimum – in November. In the winter period, annual precipitation amount changes from 354 mm to 388 mm, in spring – from 555 mm to 901 mm, in summer – from 541 mm to 845 mm, and amount of the IV period is 6528 mm.

Comparison of 10-year periods in Akhalkalaki (1967-2006) has shown that during winter period, minimum precipitation amount is observed in the II period – 190 mm, while the maximum is in the IV period – 388 mm (fig. 3). In spring, we have a minimum annual precipitation amount in the III period – 265 mm, while the maximum – in the IV period – 901 mm. Minimum value in summer is registered in the III period – 441 mm, while the maximum is registered in the I period – 1004 mm. Minimum value in autumn is observed in the IV period – 310 mm, and the maximum is in the IV period – 512 mm.

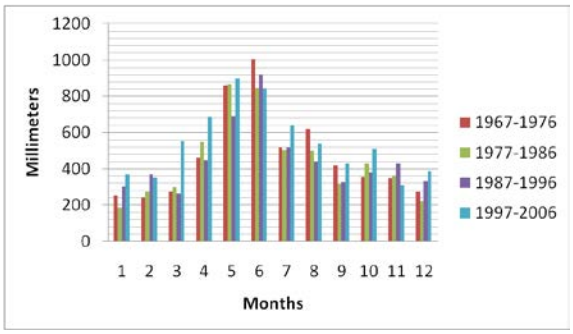

Fig. 3 Precipitation change according to months in 10-year periods – 1967-2006 (Akhalkalaki)

In the mentioned period, according to data on precipitation (1967-2006) during four 10-year periods is observed the change of precipitation amount according to periods (from I to IV period). During periods I and II, the total amount of precipitation decreased by 273 mm, from II to III period, it increased by 61 mm, also from III to IV period precipitation amount increased by 1107 mm. So, during 40 years, the increase in precipitation is registered equal to 895 mm (Fig. 4).

Materials of observations over the annual precipitation amount in the course of years (1967-2006) are presented in Fig. 5, where clearly shows the rapid change of total precipitation during last period.

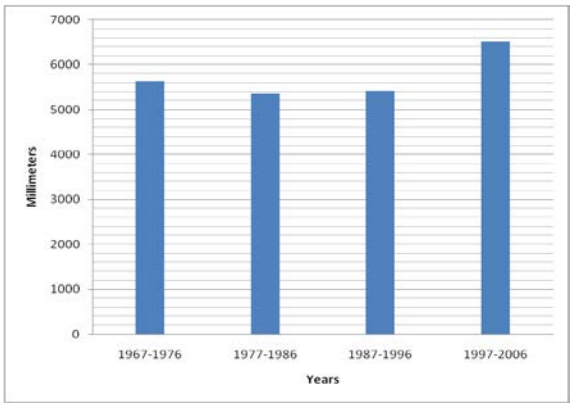

Fig. 4 Total precipitation change in 10-year periods – 1967-2006 (Akhalkalaki)

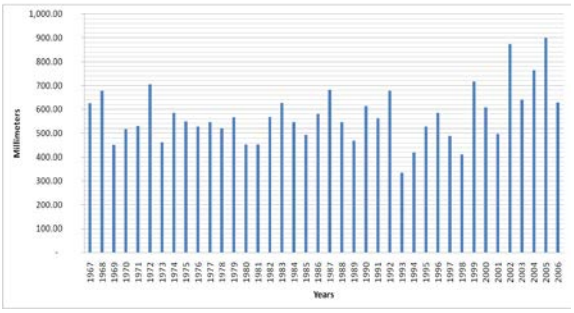

Fig. 5 Annual variations of total precipitation in 1967-2006 (Akhalkalaki)

Akhaltsikhe – for determination of precipitation changes we used 1971-2010 observation materials, which were divided into four 10-year periods: 1971-1980, 1981-1990, 1991-2000, 2001-2010.

Materials of observations over the annual precipitation amount according to periods are represented in the form of diagrams (Fig. 6-7).

Study analysis shows that under the influence of global climate changes in Akhaltsikhe, from 1971 to 2010 (40-year period) total amount of precipitation (according to 10-year periods) experiences the following changes: during the period total precipitation vary from 183 mm to 880 mm (December-June) (fig. 6).

In period I (1971-1980) in the course of years, the total amount of precipitation changes from 187 mm to 810 mm (January-May), in winter – from 187 mm to 360 mm, in spring – from 325 mm to 810 mm, in summer – from 436 mm to 794 mm, in autumn period from 318 mm to 367 mm. The total amount of precipitation of mentioned period is 5273 mm.

In period II (1981-1990) in the course of the years, the total amount of precipitation changes from 259 mm to 880 mm, minimum is in December, the maximum – in June. In the winter period, the total amount of precipitation changes from 259 mm to 291 mm, in spring amount changes from 277 mm to 742 mm, in summer – from 475 mm to 880 mm, in autumn from 274 mm to 376 mm. The total amount of precipitation of this period is 5389 mm.

In period III (1991-2000), the total annual precipitation amount changes from 207 mm to 758 mm, maximum precipitation is registered in June, minimum – in February. In winter period precipitation change from 207 mm to 326 mm, in spring - from 363 mm to 636 mm, in summer – from 434 mm to 758 mm, in autumn from 323 mm to 350 mm. The total amount of precipitation of this period (1991-2000) is 4867 mm.

In period IV (2001-2010), the total amount of precipitation, changes from 183 mm to 726 mm, maximum is registered in June, minimum – in December. In the winter period, precipitation amount changes from 183 mm to 292 mm, in spring – 435-660 mm, in summer –372-726 mm, in autumn – from 293 mm to 480 mm. The total amount of precipitation of the IV period equals to 5440 mm.

Comparison of a 10-year periods in Akhaltsikhe (1971-2010) shows that during a winter period minimum precipitation amount is observed in the IV period – 183 mm, while the maximum is in I period – 360 mm. In spring we have a minimum amount in the II period – 277 mm, while the maximum – in the IV period – 810 mm (fig. 5). Minimum value in summer is registered in the III period – 434 mm, while the maximum is registered in the II period – 880 mm. Minimum value in autumn is observed in the II period – 274 mm, and the maximum is in the IV period – 480 mm.

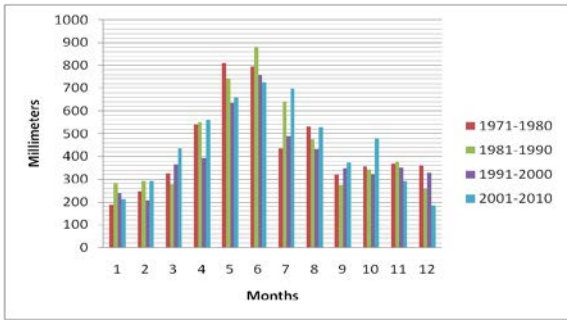

Fig. 6 Precipitation change according to months in 10-year periods – 1971-2010 (Akhaltsikhe)

In the mentioned period, according to data on precipitation (1971-2010) during four 10-year periods is observed the change of precipitation amount according to periods (I-IV periods). During 40 years, is registered the increase in precipitation, which equals to 167 mm/40 years (Fig. 7).

Materials of observations over the annual precipitation amount in the course of years (1971-2010) are represented in figure 8, where have observed the changes (decrease-increase) of total annual precipitation during last period.

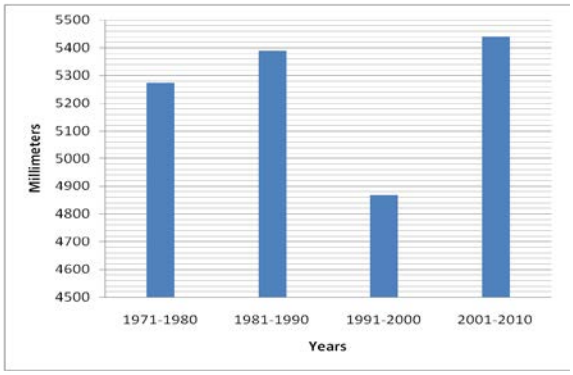

Fig. 7 Total precipitation change in 10-year periods – 1971-2010 (Akhaltsikhe)

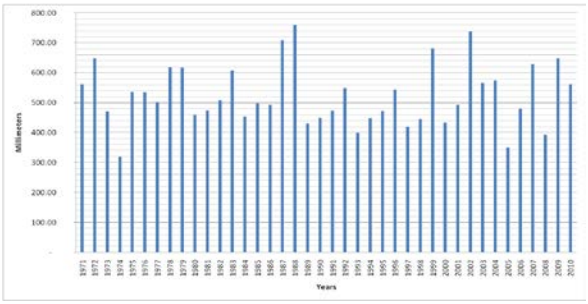

Fig. 8 Annual variations of total precipitation in 1971-2010 (Akhaltsikhe)

Paravani. 1967-2006 observation materials were used for determination of Paravani precipitation change. They were divided into 4 periods: 1967-1976, 1977-1986, 1987-1996, 1997-2006.

Materials of observation over the total amount of precipitation according to periods are represented in the form of table and diagrams (fig. 9-11).

Study analysis shows that under influence of global climate changes in Paravani, from 1967 to 2006 (40-year period) total amount of precipitation (according to 10-year periods) experiences the following changes: throughout a year total precipitation vary from 198 mm to 996 mm (January-May) (fig. 9).

In the I period (during 1967-1976) total amount of precipitation changes from 360 mm to 996 mm, in winter – from 425 mm to 570 mm, in spring – from 541 mm to 996 mm, in summer – from 497 mm to 929 mm, in autumn period – from 360 mm to 482 mm. The total amount of precipitation of this period equals to 6936 mm.

In the II period (1977-1986) total amount of precipitation in the course of years varies from 369 mm to 977 mm, it is minimal in November, while is maximal in May. In winter period, the total amount of precipitation changes from 387 mm to 455 mm, in spring – from 406 mm to 977 mm, in summer – from 487 mm to 935 mm, in autumn - from 369 mm to 453 mm. The total amount of precipitation of this period equals to 6490 mm.

In the III period (1987-1996) total amount of precipitation varies from 224 mm to 876 mm. The maximum amount is registered in June, the minimum – in September. In the winter period, total amount of precipitation changes from 281 mm to 380 mm, in spring – from 255 mm to 628 mm, in summer – from 355 mm to 876 mm, in autumn – from 224 mm to 389 mm. The total amount of precipitation of this period (1987-1996) equals to 4810 mm.

The total amount of precipitation of the IV period (1997-2006) varies from 198 mm to 706 mm, a maximum amount is registered in June, minimum – in January. In the winter period, total amount of precipitation changes from 198 mm to 330 mm, in spring – from 316 mm to 693 mm, in summer – from 469 mm to 706 mm, in autumn – from 255 mm to 416 mm. The total amount of precipitation of the IV period is 5128 mm.

Comparison of 10-year periods in Paravani (1967-2006) shows that during a winter period minimum precipitation amount is observed in the IV period – 198 mm, while the maximum is in the I period – 996 mm (fig. 9). In winter the minimum amount is in the IV period – 198 mm, while the maximum – in the I period – 570 mm. In spring we have a minimum precipitation amount in the III period – 255 mm, while the maximum is in the I period – 996 mm. Minimum value in summer is in the III period – 355 mm, while the maximum is registered in the II period – 935 mm. Minimum value in autumn is observed in the III period – 224 mm, and the maximum is in the I period – 482 mm.

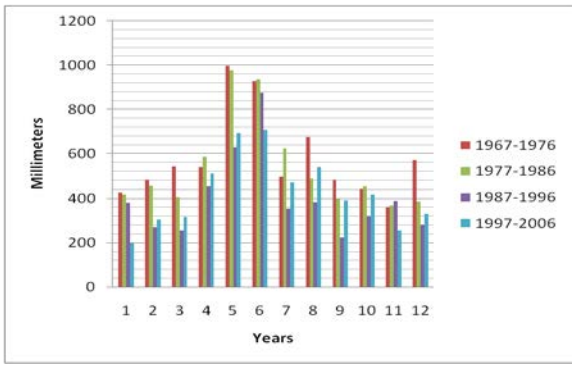

Fig. 9 Total precipitation change according to months in 10-year periods – 1967-2006 (Paravani)

In the mentioned period, according to data on precipitation (1967-2006) during four 10-year is observed the change of the total amount of precipitation according to periods (from I to IV period) (fig. 10). During I and II periods, the total amount of precipitation decreased by 446 mm, from II to III period, it decreased by 1680 mm, and from III to IV period precipitation amount increased by 318 mm. So, during 40 years, is registered the decrease in precipitation.

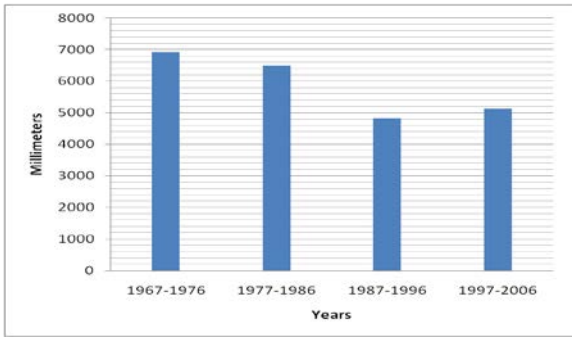

Fig. 10 Total precipitation change in 10-year periods – 1967-2006 (Paravani)

Material of observations over annual precipitation amount is represented in figure 11, where is observed the rapid changes of precipitation amount during mentioned years.

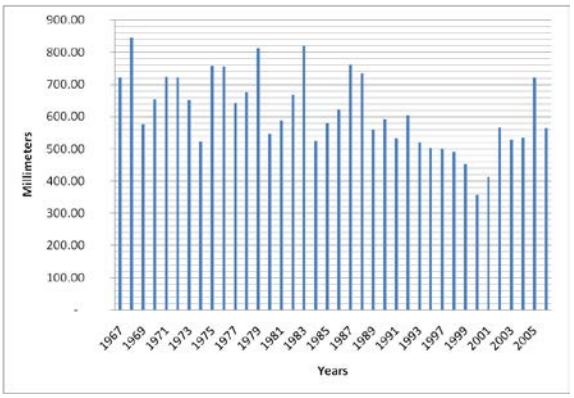

Fig. 11 Annual variations of total precipitation in 1967-2006 (Paravani)

DISCUSSION

As seen from analysis of studies carried out for assessment of global climate change, in Samtskhe-Javakheti, the diverse picture of precipitation changes was observed. These was based on a 10-year period of meteorological observation data available at each meteorological station but in some cases a study was carried out in different years (due to unavailability of materials). As a result of analysis on 10-year average values of precipitation amounts (40-year periods) we obtained the following results:

- in Akhalkalaki during I-IV periods (1967-2006) total amount of precipitation increased by 895 mm. In I-II periods was registered the decrease by 273 mm, in II-III periods, it increased by 61 mm, while in III-IV periods it was increased again by 1107 mm.
- in Akhaltsikhe during I-IV periods (1971-2010) total amount of precipitation in the whole time range increased by 167 mm. From here in I-II periods, it increased by 116 mm, in II-III periods were registered a decrease by 522 mm, while in III-IV periods it was increased again by 573 mm.
- in Paravani during I-IV periods (1967-2006) total amount of precipitation in the whole time range decreased by 1808 mm. From here in I-II periods, it decreased by 446 mm, in II-III periods were registered a decrease by 1680 mm, while in III-IV periods it was increased by 318 mm.

CONCLUSION

On the background of global warming, the change of the regional climate in Samtskhe-Javakheti has special peculiarities, which are important in the regions, located in a warming or cooling border area. The boundary between these opposite processes must be found on the territory of Georgia. The main cause of regional climate change, besides of Global climate change, is due to the region's climate and orographic distinctiveness.

Results of study of meteorological observation materials in Samtskhe-Javakheti allow us to make the conclusion that against the background of climate changes takes place rapid variation of total precipitation: in 1967-2006 in Akhalkalaki was observed increase in annual total precipitation by 895 mm, and in Paravani – decrease by 1808 mm. In Akhaltsikhe (1971-2010) total amount of precipitation was increased by 167 mm.

REFERENCES

[1] Kordzakhia M, Climate of Georgia, Tb., Publishing house of Academy of Sciences, 1961, 247 p.
[2] Georgia's Second National Communication to the United Nations Framework Convention on Climate Change. National Climate Research Centre, Tbilisi, 2009
[3] Georgia's Third National Communication to the United Nations Framework Convention on Climate Change. National Climate Research Centre, Tbilisi, 2015 Geography of Georgia. Tbilisi, "Metsniereba", 2005, 316 p.
[4] Javakhishvili Sh, Atmospheric precipitation on territory of Georgia, TB., TSU, 1981, 289 p.
[5] Javakhishvili Sh, Climate of Meskhet-Javakheti. Tb., TSU, 1990, 32 p.
[6] Javakhishvili Sh, Climatology of Georgian SSR. TB., TSU, 1977,236 p.
[7] Climate Change 2007, The physical science basis, IPCC, 2007.
[8] Washington R, Hodson A, Isaksson E, Macdonald O, Northern hemisphere teleconnection indices and the mass balance of Svalbard glaciers. International Journal of Climatology, 2000, vol. 20, pp. 473-487.
[9] Bates B., Kundzewiz Z., Shaohong Wu. (2008). Climate Change and Water: Intergovernmental Panel on Climate Change.
[10] Karamouz M, Nazif S, Galahi M, Hydrology and Hydroclimatology: CRC Press, Taylor & Francis Group, Boca Baton London New York, 2013.

Second International Conference on Science, Engineering & Environment,
Osaka City, Japan, Nov.21-23, 2016, ISBN: 978-4-9905958-7-6 C3051

HYGROSCOPIC SALTS AND ANTIMICROBIAL PROPERTIES

John V Smith
School of Engineering, RMIT University, Australia

ABSTRACT

The ability of some salts to absorb moisture and enhance the desiccation process has potential antimicrobial applications. These properties have not been studied in detail. A range of inorganic and organic salts were selected for testing in conditions of drying on a textile substrate. Microbial contaminants of *Escherichia coli* and *Staphylococcus epidermidis* were investigated. The hygroscopicity of the various salts has been measured by use of reference humectants. The salts were found to have an antimicrobial effect when compared to the control samples. The relationship between the salts and relative humidity was tested to infer how the salts and microbes interact. Scanning electron images showed the nanoscale formation of salt crystals on the substrate. Even salts which are not inhibitory of microbial growth in the petri dish were found to reduce microbial growth after drying – compared to a control sample dried without salts present. This implies the observed antimicrobial effect is physical rather than chemical in nature. Enhanced desiccation by hygroscopic salts is a new type of antimicrobial factor requiring further investigation. A range of environmental and human health applications are discussed.

Keywords: Salt, Hygroscopic, Antimicrobial, Desiccation, Bacteria

INTRODUCTION

It has been recently demonstrated that drying of a textile in the presence of precipitating soluble salts can have a measurable antimicrobial effect [1]. That study outlined the effectiveness of four salts on one strain of bacteria *Staphylococcus Epidermidis*. It was proposed in [1] that it is the hygroscopic character of the selected salts that enhances desiccation of microbes during drying to produce the antimicrobial effect. It has long been known that bacteria are very sensitive to conditions of temperature and humidity and that one of the most effective methods of sterilization of surfaces is the application of dry heat [2-3]. Naturally occurring minerals and salts have also been investigated for their antimicrobial properties [5-7]. In this paper the effectiveness of the same four salts as [1] on another bacterial strain, *Escherichia coli*, is reported. In addition, measurements of the hygroscopic characteristics of the four salts are reported to investigate the hypothesis that it is the hygroscopic behavior of these salts that provides the antimicrobial effects.

ANTIMICROBIAL TEST METHODOLOGY

The testing reported in [1] for *S epidermidis* and reported here for *E. coli* involved the following procedure (Fig. 1). Circular discs of plain cotton textile were wet with 1M salt solution and subsequently dried. The textile discs were then placed in sample vials (Fig. 2). A preparation of 100 µL of bacterial culture was poured over the textile discs. Three different concentrations of bacteria were used. The sample vials were incubated at 37 °C for 24 hrs. The vials were allowed to dry gradually during this period. The dried textile discs then received 1 ml of media, poured to each vial and put on a shaker for an hour at 37 °C before plating. Plates were kept in an incubator 37 °C for 24 to 48 hrs and bacterial colonies were counted manually.

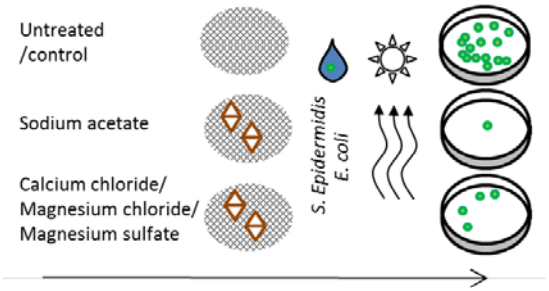

Fig. 1 Schematic summary of the experimental procedure explained in the text

ANTIMICROBIAL RESULTS

The results with *Staphylococcus epidermidis* have been reported previously [1] and will be briefly summarized here. Drying for 24 hours in the presence of sodium acetate reduced viable bacteria (*Staphylococcus epidermidis*) to 1.5% or less of the total bacterial count in the control. For calcium chloride, magnesium chloride and magnesium sulfate, the count of viable cells after drying was more variable and ranged from 0.3% to 44% relative to the count in the control sample (Fig. 3).

For *E. coli* no growth or insignificant growth was observed in the control and all of the salt-treated

samples. Therefore the experimental procedure was unable to detect any difference between drying with and without the salts for *E. coli.*

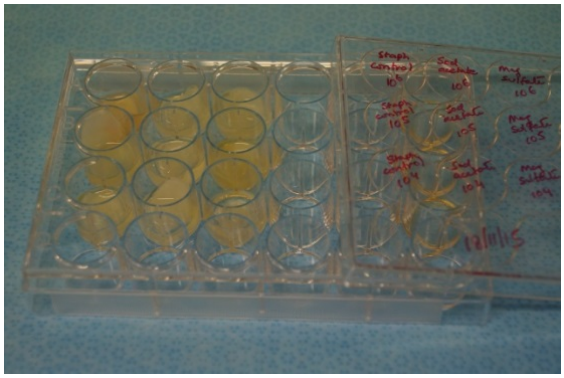

Fig. 2 Example of sample vials used in the experimental procedure

ANTIMICROBIAL MECHANISM

Staphylococcus epidermidis which is a Gram positive bacteria, with thick cell wall along and spore formation capacity, resisted drying conditions and was able to survive after the treatment in control in all tests. The survival of this bacteria is consistent with it being commonly found on human skin [8].

In contrast *Escherichia coli*, as a Gram negative bacteria with relatively thin cell walls was not able to survive the drying regime in either the control or salt-enhanced experiments. Since *E coli* has been shown to survive some desiccation conditions [9] it is expected that the experiment can be modified to test the relative influence of salts by finding drying conditions that a control sample of *E coli* can survive.

The effectiveness of drying with salts in suppressing the viability of *Staphylococcus epidermidis* was proposed to be due to the hygroscopic behavior of the salts [1]. The hypothesis stated that microbes within the microclimate between fibres may remain sufficiently hydrated to survive normal drying conditions. In contrast if hygroscopic salts were also precipitating, the microscopic salt crystals would be present on the surface of the fibres and would make the drying process more effective within the micro-environment of the fibres.

A scanning electron microscope (FEI Quanta 200 ESEM at RMIT University) was used to observe the distribution of the precipitated salts. Samples of textile were gold coated and observed at a voltage 30 kV under low pressure (0.5 Torr). Scanning electron microscopy of the control and treated textile showed that salt crystals are distributed over the fibre surfaces (Fig. 4).

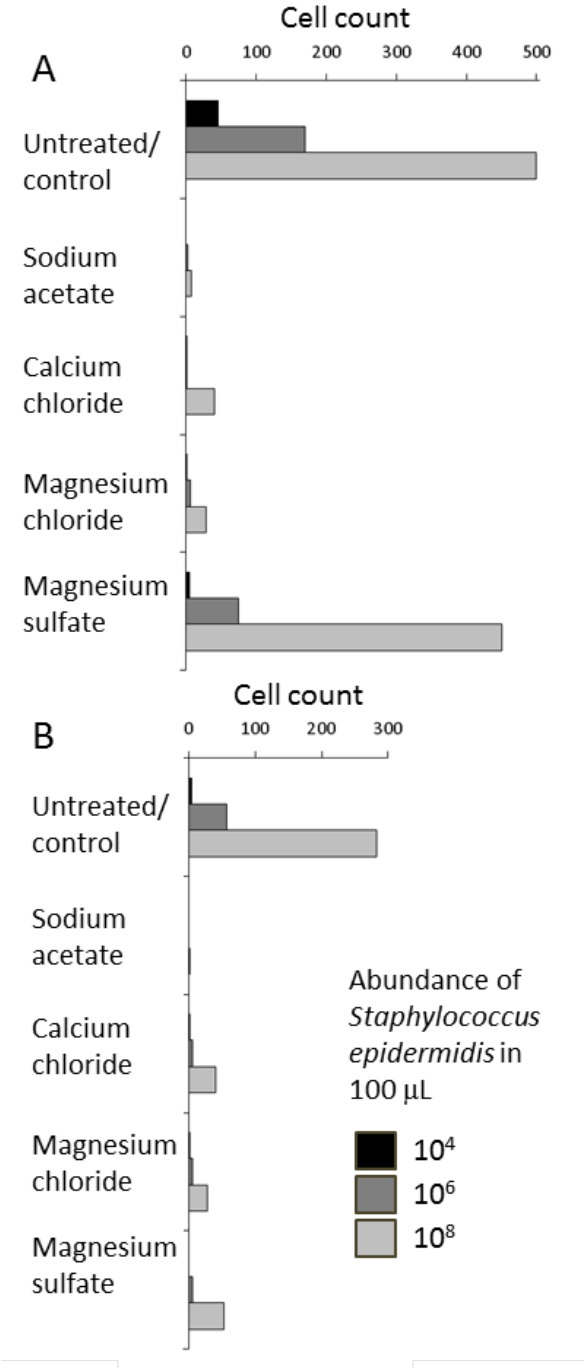

Fig. 3 (A and B) Results (average of duplicates) of experiments (repeated) on effects of drying with hygroscopic salts on *Staphylococcus epidermidis* counts reported in reference [1]

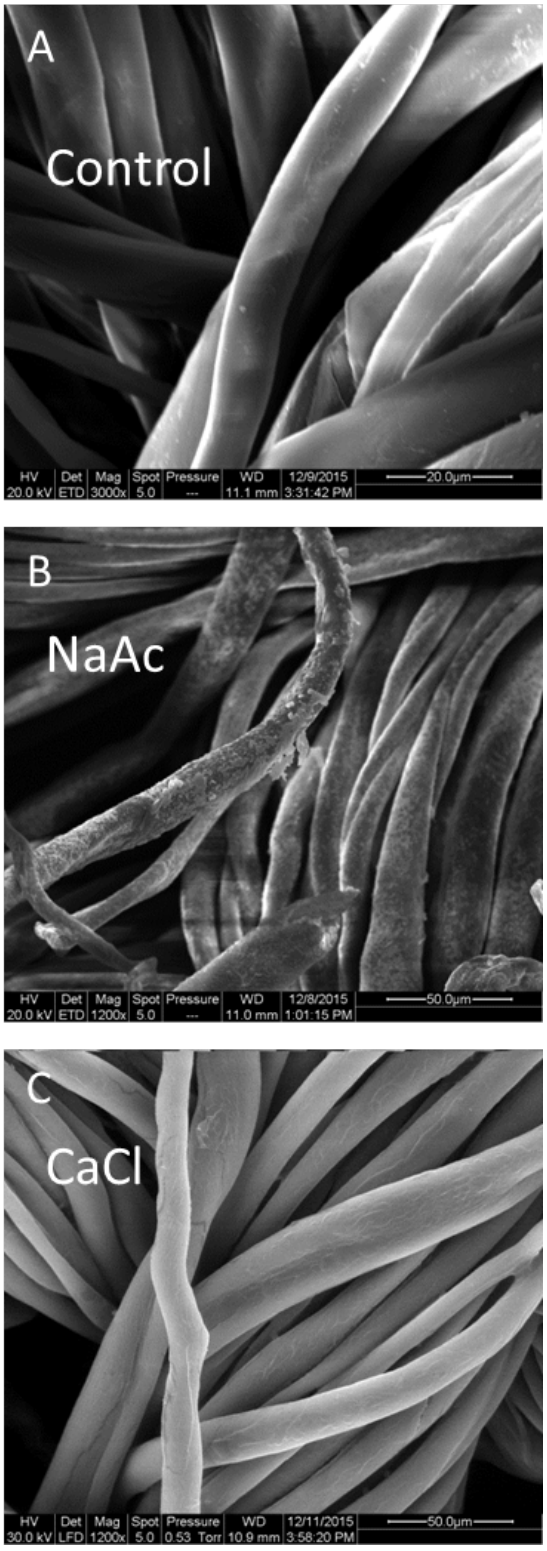

Fig. 4 Scanning electron microscope images (FEI Quanta 200 ESEM at RMIT University) of cotton textiles with examples of dried salt compounds. Individual fibres are approximately 10 μm across

HYGROSCOPICITY

Hygroscopic compounds change water content in response to changes in relative humidity of the surrounding atmosphere. The conventional method of classifying compounds according to hygroscopicity is to measure their change in moisture content after equilibrating in a controlled-humidity environment. A simple way to control the humidity is by having a sealed environment in the presence of compounds with a known hygroscopic behavior. These reference compounds will release moisture if the humidity fall below the reference level and absorb moisture if humidity rises. The most commonly used [10-11] reference compounds and their stable humidity at 25ºC are: lithium chloride (11%), potassium carbonate (43%), sodium chloride (75%) and potassium nitrate (93%).

Determining the equilibrium moisture content (EMC) at these and/or other reference humidity levels allows the degree of hygroscopic behavior to be classified. Early approaches to classifying hygroscopicity attempted to define specific ranges of relative humidity under which particular compounds could be handled without detrimental effects (Fig. 5A) [10]. The pharmaceutical industry, in particular, has required more sophisticated classifications to cover the many compounds that are used in the preparation of tablets and powders. A study of approximately 30 commonly used inactive pharmaceutical compounds led to the classification according to typical trends shown in Fig. 5B [10]. A more recent study of a similar set of 30 inactive pharmaceutical compounds classified compounds using overlapping ranges as shown in Fig. 5C [11]. The definition of the terms used is given in Table 1.

The sample material used in the antimicrobial experiments described here was tested in this study for its hygroscopic behavior using the same reference compounds described above and used in the reference [11]. The measurements were conducted in triplicate in humidity-controlled desiccation jars (Fig. 6). All four compounds showed the commonly observed behavior of increasing equilibrium moisture content with increasing relative humidity (Fig. 7).

For sodium acetate, one test had an EMC near zero but the other tests ranged between EMC 2% and 11%. For calcium chloride the EMC ranged from 3% to 9%. The EMC values were anomalously low for the 93% test. For magnesium chloride the EMC ranged from 4% to 12%. For magnesium sulfate the EMC ranged from 3% to 7%. When compared to the ranges of hygroscopicity classification of reference [11] the following classifications can be applied. Sodium acetate, calcium chloride and magnesium chloride were found to be moderately to slightly hygroscopic. Magnesium sulfate was found to be slightly

hygroscopic.

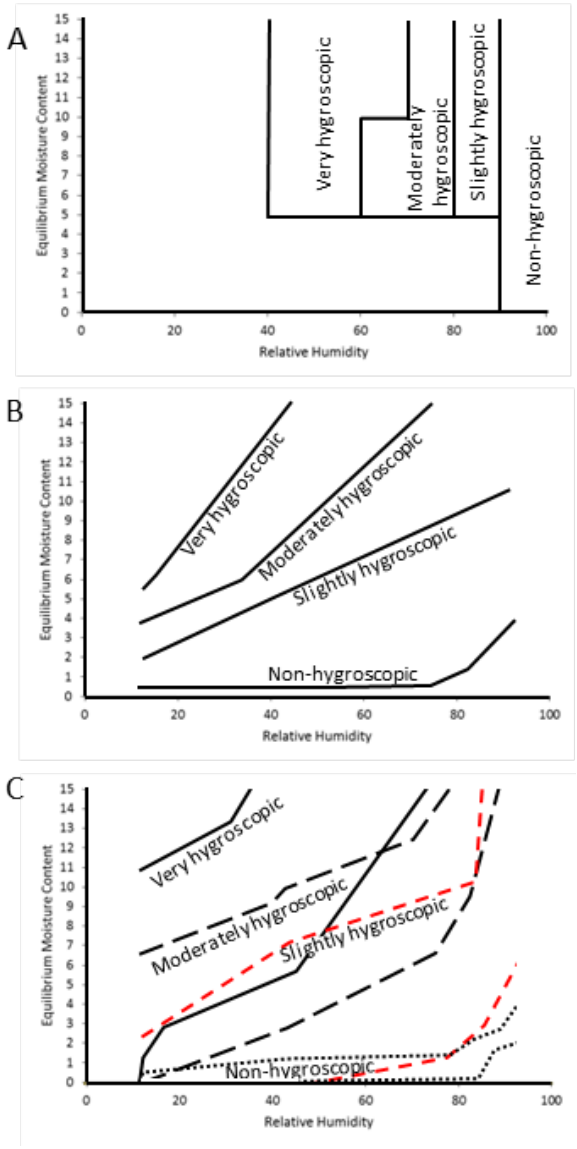

Fig. 5 A) Simple classification of hygroscopicity expressed as equilibrium moisture content (EMC) at specific ranges of relative humidity. B) Classification of the main trend lines of hygroscopic behavior of compounds used in pharmaceutical preparations [10]. C) Classification of hygroscopic behavior ranges of compounds used in pharmaceutical preparations [11]. Labels are placed at the upper bound of the range. Very hygroscopic = solid line, Moderately hygroscopic = long dash line, Slightly hygroscopic = short dash line, Non-hygroscopic = dotted line

Table 1 Conventional classification of hygroscopicity

Classification	Criteria
Non-hygroscopic	Essentially no moisture increase below 90% RH; less than 20% (w/w) increase in moisture content above 90% RH in 1 week
Slightly hygroscopic	Essentially no moisture increase below 80% RH; less than 40% (w/w) increase in moisture content above 80% RH in 1 week
Moderately hygroscopic	Moisture content does not increase >5% (w/w) below 60% RH; less than 50% (w/w) increase in moisture content above 80% RH in 1 week
Very hygroscopic	Moisture content will increase as low as 40–50% RH; greater than 20% (w/w) increase in moisture content above 90% RH in 1 week

Fig. 6 Desiccation jar measurement of triplicate salt samples with humidity controlled by reference salts placed in base of jar

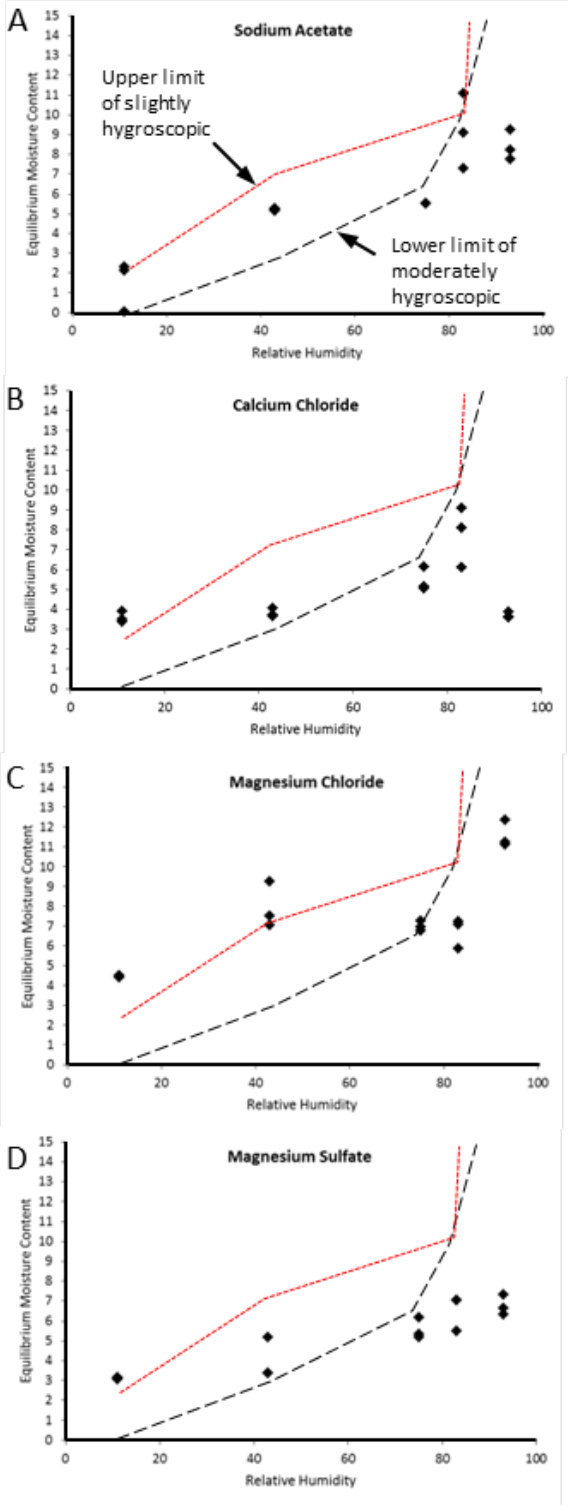

Fig. 7 Measurements (triplicate) of equilibrium moisture content (EMC) at five relative humidity levels for the four salts in this study. Part of the ranges of slightly and moderately hygroscopic as defined in reference [11] are shown to aid classification

CONCLUSION

The four salts investigated in this study: sodium acetate, calcium chloride, magnesium chloride and magnesium sulfate, were found to have similar hygroscopicity profiles. The equilibrium moisture content at five relative humidity levels between 11% and 93% corresponded to the moderately to slightly hygroscopic classification for sodium acetate, calcium chloride and magnesium chloride. Magnesium sulfate was found to be classified as slightly hygroscopic. The hygroscopic behavior of sodium acetate was slightly less than calcium chloride and magnesium chloride. This finding indicates that the greater antimicrobial properties observed for sodium acetate compared to calcium chloride and magnesium chloride cannot be directly attributed to the degree of hygroscopic behaviour.

While it has been established antimicrobial effects during drying of these salt compounds on the common human skin bacteria *Staphylococcus epidermidis*, the same experimental conditions did not allow differentiation between experiment and control for the common human intestinal bacteria *Escherichia coli*. Further experimental testing with modified conditions is required to establish the general occurrence of this novel antimicrobial phenomenon.

ACKNOWLEDGEMENTS

Dr Muthu Pannirselvam (Rheology and Materials Characterisation laboratory) assisted with planning of the study. Laboratory work was conducted by Dr Vinita Chaudhary with supervision by Dr Zahra Homan.

REFERENCES

[1] Smith JV, Antimicrobial effect of sodium acetate and other hygroscopic salts. International Journal of GEOMATE. 2016 Oct;11 (26):2671-8.

[2] Webb SJ, Factors affecting the viability of air-borne bacteria: I. Bacteria aerosolized from distilled water, Canadian Journal of Microbiology, 5(6), 1959, 649-669.

[3] Rutala WA and Weber DJ, Guideline for disinfection and sterilization in healthcare facilities CDC. 2008, pp. 158.

[4] Williams LB and Haydel SE, Evaluation of the medicinal use of clay minerals as antibacterial agents, International Geology Review, 52(7-8), 2010, 745-770.

[5] Morrison KD, Underwood JC, Metge DW, Eberl DD and Williams LB, Mineralogical variables that control the antibacterial effectiveness of a natural clay deposit,

Environmental Geochemistry and Health, 36(4), 2014, 613-631.

[6] van Tubergen A and van der Linden S, A brief history of spa therapy, Annals of the Rheumatic Diseases, 61(3), 2002 273.

[7] Halevy S, Giryes H, Friger M and Sukenik S, Dead Sea bath salt for the treatment of psoriasis vulgaris: a double-blind controlled study, Journal of the European Academy of Dermatology and Venereology, 9(3), 1997, pp.237-242.

[8] Vuong C and Otto M, Staphylococcus epidermidis infections, Microbes and Infection, 4(4), 2002, 481-489.

[9] Billi D, Wright DJ, Helm RF, Prickett T, Potts M and Crowe JH, Engineering desiccation tolerance in Escherichia coli, Applied and Environmental Microbiology, 66(4), 2000, 1680-1684.

[10] Callahan JC, Cleary GW, Elefant M, Kaplan G, Kensler T, Nash RA, Equilibrium moisture content of pharmaceutical excipients. Drug Development and Industrial Pharmacy. 1982 Jan 1;8(3):355-69.

[11] Murikipudi V, Gupta P, Sihorkar V, Efficient throughput method for hygroscopicity classification of active and inactive pharmaceutical ingredients by water vapor sorption analysis. Pharmaceutical development and technology. 2013 Apr 1;18(2):348-58.

Second International Conference on Science, Engineering & Environment,
Osaka City, Japan, Nov.21-23, 2016, ISBN: 978-4-9905958-7-6 C3051

FEASIBILITY STUDY OF BIODIESEL PRODUCTION FROM RESIDUAL OIL OF PALM OIL MILL EFFLUENT

Monthatip Klabsong [1], Nipapun Kungskulniti[1,2], Chanakan Puemchalad[3]
Naowarut Charoenca[1,2], and Vittaya Punsuvon[4]
[1]Department of Sanitary Engineering, Faculty of Public Health, Mahidol University, Thailand
[2]Center of Excellence on Environmental Health and Toxicology, Thailand
[3]Energy Technology Department, Thailand Institute of Scientific and Technological Research
[4]Department of Chemistry, Faculty of Science, Kasetsart University, Thailand
(Corresponding Author: Nipapun Kungskulniti; Email: nipapun.kun@mahidol.ac.th)

ABSTRACT

Pollution from residual oil contaminating wastewater is a serious environmental problem. The rapid development and growth of palm oil industries in Thailand have generated large volumes of palm oil mill effluent (POME) which contains residual oil. Instead of becoming a pollutant in the environment, residual oil from POME can be used as raw material for producing biodiesel. Biodiesel has recently become more attractive as an alternative energy source due to its environmental friendly properties generated from renewable resources. This study investigated the characteristics of residual oil and found: a free fatty acid content of 22.034 % wt, fatty acid methyl ester (FAME) of 3.767 % wt, acid value of 49.29 mg KOH/g, water content of 1.01 % mg/Kg, and Total Glycerines as Monoglycerides, Diglycerides, and Triglyceride at 1.15 % m/m, 11.88 % m/m, and 87.54 % m/m respectively. Optimal conditions to separate water from oil contents are also determined. Separation of residual oil from POME is carried out using the solvent extraction process.

Keywords: Residual oil, Palm oil mill effluent (POME), Biodiesel, Fatty acid methyl ester (FAME)

INTRODUCTION

The palm oil industry is one of the most important industries in Thailand. Increasing palm oil industry capacity also increases its effluent output [1]. The number of registered palm oil mill extraction operations nationwide numbered approximately 80 plants having a capacity of around 2,801 tons of fresh fruit bunch per hour with the volume of crude palm oil extracted at approximately 1,832,151tons / year [2]. There are a lot of factories and palm oil production which results in high energy consumption and effluent resulting during palm oil production.

The disposal of effluent is therefore a serious problem that must be solved. Although no chemicals are used during oil extraction, the effluent still must satisfy threshold values set by the Department of Industrial Works [3]. This palm oil or residual palm oil floats on the surface of wastewater in wastewater treatment ponds and covers the surface of wastewater [4].

Biofuel is inherently renewable as it is derived from biomass or waste matter. There are different types of biofuel such as biodiesel biogas and bioalcohol [5]. Biodiesel or fatty acid methyl ester (FAME) is a renewable, economically viable alternative to petroleum-derived diesel and has received much attention as the world seeks to prevent the future oil crisis and the unpredictable consequences of climate change [6]. It is generally produced from the oils of palm, soybeans, canola, and jatropha [7].

The reaction for synthesis of biodiesel is transesterification. Transesterification is the most widely used process to reduce the viscosity of oil. Transesterification occurs due to the reaction between fat or oil and alcohol to form methyl esters or biodiesel as a product and glycerol as a by-product [8].

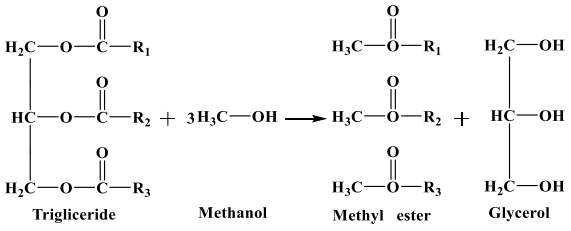

Fig. 1 Transesterification reaction

In this case, the water of residual oil was extracted using solvent extraction due to the ease of removing the solvent to separate water from oil. The objective of this study is to characterize the properties of residual oil from Palm oil mill effluent (POME) for biodiesel production carried out under a subcritical methanol condition.

MATERIALS AND METHODS

Materials

Samples of residual oil from POME were collected from a palm oil mill plant in Eastern part of Thailand. The chemicals for this research are analytical grade hexane and methanol.

Oil-Water Separation

Experiments were conducted to evaluate the performance of the organic solvent n-hexane in extracting residual oil from POME. POME was transferred into a conical flask and mixed with n-hexane as the solvent for the extraction process [1]. The ratios of solvent to POME were 6:1, 9:1 and 12:1 by volume at 60 ^{o}C with a 15 min mixing rate of 200 rpm. Then the mixture product was filtrated on filter paper under vacuum filtration immediately to separate the solid particles from the mixture product. The n-hexane solution in filtrate was evaporated by using a rotary evaporator.

Transesterification Reaction

The reactions were carried out in the system shown in Fig 2. It is a cylindrical reactor of 250 mL located in a vessel of stainless steel and equipped with magnetic stirring, heating system, sampling outlet, pressure gauge and temperature controller. The pressure and temperature were monitored in real time up to a maximum value of 300 bars and 430 ^{o}C, respectively. Then, the reactor was heat with an external electrical furnace to the desired temperature while the liquid solution was stirred at a constant speed of 500 rpm. The operational temperature (180-230 ^{o}C) of the reactor was measured with a thermocouple and automatically controlled at ± 5 ^{o}C for a set time with pressure at 30-35 bars. After the transesterification was complete, the sample was recovered by simple decantation. The reaction mixture was evaporated with a rotary evaporator at 60 ^{o}C for 60 min to remove methanol.

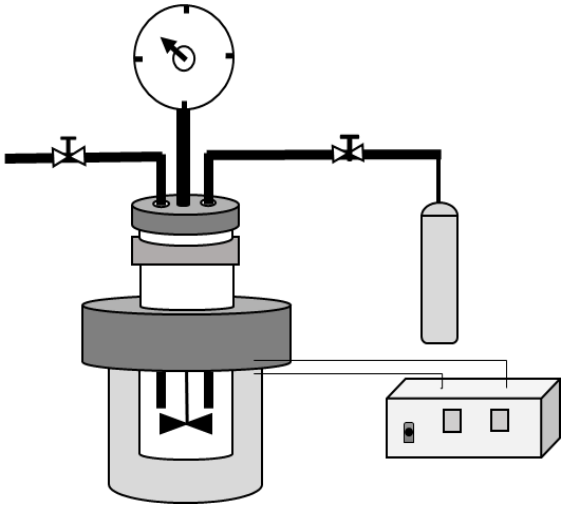

Fig. 2 Parr reactor model 4848 for transesterification.

Methods of Analysis

Biodiesel samples were analyzed by gas chromatography (GC Agilent 6890, FID). The GC was equipped with a DB-5HP capillary column with dimensions of 30.0 m x 0.1 μm x 250 μm. Gas chromatography was used to analyze the composition and to determine the amount of FAMEs, mono-, di-, triglycerides, free glycerol and methanol in the samples. A split injector was used with a split ratio of 20 and temperature of 370 ^{o}C. Total run time of this method was 52 min. The calibration curve of peak area and the quantity of biodiesel was linear.

The analytical method used to determine the characteristics of the biodiesel according to the European Standard EN 14214 [9].

RESULTS AND DISCUSSION

The operational variables employed were molar ratios methanol to oil, temperature, and retention time that were fixed as common parameters in all experiments. Table 1 shows the composition of the fatty acid of the residual oil used as raw material in this study.

Table 1 Characterization of residual palm oil

Fatty acid composition (% by weight)	
Palmitic acid (C16:0)	45.458
Oleic acid (C18:1)	50.850
Linoleic acid (C18:2)	11.364
Linolenic acid (C18:3)	0.414
Molecular weight ($g \cdot mol^{-1}$)	849.52
Water content	1.01
Free fatty acid (%wt)	22.034
Acid value (mg KOH/g)	49.29

Effect of Solvent Ratio on Percent of Water Content

Experiments were conducted at solvent ratios of 6:1, 9:1 and 12:1. The extraction time and mixing rate were 15 minutes and 200 rpm. The optimum solvent extraction was found using organic solvents at a ratio of solvent to POME of 9:1, mixing rate of 200 rpm for 15 min. Figure 3 shows the optimal ratio of solvent (n-hexane) to oil at 9:1 which can reduce the water content in the sample of POME down to 0.02 %. Its relatively low molecular weight and saturation made n-hexane completely miscible with oil [10].

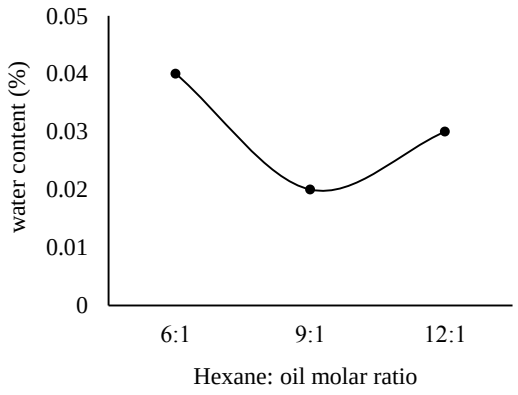

Fig. 3 Separation of residual oil from POME with different solvent ratios.

Effect of Methanol: Oil Molar Ratio

Effects of the most important variables in the transesterification of residual palm oil under subcritical methanol conditions were studied. These variables were molar ratio of methanol to oil, reaction temperature and reaction time. The condition of the runs carried out are shown in Table 2.

Table 2 Reaction condition of different methods for biodiesel

MeOH:oil	Temperature (°C)	Time (hour)	Pressure (bar)
24:1	220	1	30
24:1	220	3	30
42:1	220	4	30
24:1	220	4	30
24:1	230	4	30
36:1	220	4	30
24:1	220	5	30
24:1	210	4	30

Experimental results are shown in Fig 4. Reactions were carried out at a fixed temperature of 220 °C with a fixed reaction time of 4 hours under different molar ratios of methanol: oil as 24:1 36:1 and 42:1. When the molar ratio of methanol to oil increased from 24:1 to 36:1 and 42:1, the methyl ester was 61.51 to 61.19 and 68.23%, respectively. Furthermore, increasing alcohol in the optimal ratio increases the yield, but also increases cost for alcohol recovery [11].

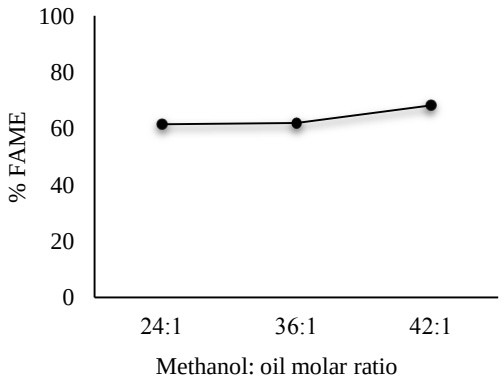

Fig. 4 Effect of methanol to oil molar ratio on biodiesel production (conditions of 220 °C reaction temperature, 4 hour reaction time).

Effect of Reaction Temperature

The non-catalytic transesterification reactions with subcritical methanol were carried out at a fixed molar ratio of methanol to oil of 24:1 and fixed reaction time of 4 hours under different temperatures, 210-230 °C. The critical temperature of methanol is 240 °C. Figure 5 presents the variations of the methyl ester yield with different reaction temperatures.

Experimental results show that the temperature used affect reaction rate slightly due to short term temperature increases. The methyl ester yields were 59.61, 61.51, and 66.65 % as temperature rose, 210 to 220 and 230 ºC. This indicates that at high temperatures, the conversion rate of FAME increases. One of the most important factors of biodiesel production is temperature. Optimizing temperature is required for the reaction and suboptimal temperature can slow the reaction and reduce the yield of biodiesel.

.

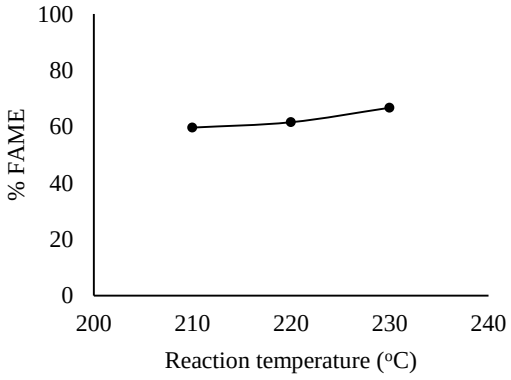

Fig. 5 Effect of reaction temperature on biodiesel production (conditions 24:1 molar ratio of MeOH: oil, 4 hour reaction time).

Effect of Reaction Time

Figure 6 shows the effect of reaction time on the biodiesel production conversion at various times: 1, 3, 4, and 5 hours, respectively. Reactions were carried out at a fixed temperatures of 220 ºC and a fixed molar ratio of methanol to oil of 24:1. At 1 hour, the methyl ester conversions was 42.19 %. When the reaction time increased from 1 to 3 and then 5 hours, FAME increased from 42.19 to 60.67 and 77.64 %, respectively. At 4 hours, methyl ester only slightly increased compared with that at 3 hours. However, it is possible to obtain a high conversion with a molar ratio of methanol: oil at 24:1 by increasing the reaction time to 7 hours.

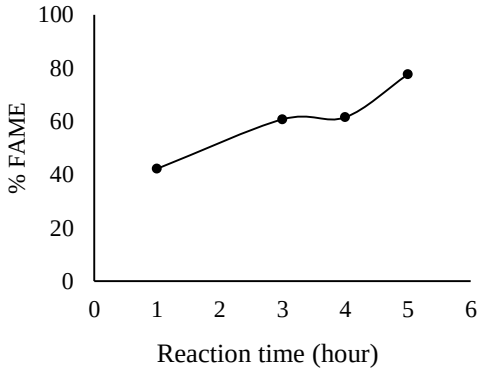

Fig. 6 Effect of reaction time on biodiesel production (conditions 24:1 molar ratio of MeOH: oil, 220 ºC reaction temperature).

CONCLUSION

In this work, the transesterification of residual oil under subcritical conditions was carried out. Results of solvent extraction using of organic solvents at a ratio of solvent to POME of 9:1 are produced. The effect of the main variables were evaluated under different conditions molar ratio of methanol: oil (24:1, 36:1, and 42:1), reaction temperatures (210, 220 and 230 ºC) and reaction times (1, 3, 4 and 5 hours). The highest methyl ester yield of 77.64 % was at a reaction temperature of 220 ºC, reaction time of 5 hours and a molar ratio of methanol to oil at 24:1. However, even higher temperatures can enhance the biodiesel content, although small improvements would require high energy expenses.

ACKNOWLEDGEMENTS

The authors sincerely thank the Faculty of Public Health, Mahidol University, Thailand. This study received support of facilities at the laboratories of the Energy Technology Department, Thailand Institute of Scientific and Technological Research.

REFERENCES

[1] Rizki, S., Primandari, P., Yaakob, Z., Mohammad, M., Mohamad, A.B. Characteristics of Residual Oil Extracted from Palm Oil Mill Effluent (POME). World Applied Science Journal, 2013, pp. 1482-1484.

[2] Tanakorn, T., Research and Development in Steamless Nut-Separated Palm Oil Extraction Technology [Online], Available: http: //www.nstda.or.th/nac2013/download/presentati

on/NAC2013_Set2/CO-11303/Tanakorn.pdf. [14 April 2016]

[3] Ahmad, A.L., Sumathi S. and Hameed, B.H. Adsorption of residue oil from palm oil mill effluent using powder and flake chitosan: Equilibrium and kinetic studies. Water Research, 2005, pp. 2483-2494.

[4] Timyamprasert, A., Punsuvon, V., and Chunkao K. Use of Waste Palm Oil in Wastewater Pond to Prepare Community Biodiesel. Journal of Burapha Sci, 2013, pp. 215-221.

[5] Ghanshyam P, Saurabh P, Kumar N. Biofuel as green energy source: a review. Int J. Eng Tech Res (LJETR), 2014, pp. 124–6.

[6] Rasoul-Amini S, Montazeri-Najafubady N, Mobasher, MA, Hoseini-Alhushemi, S., Ghasemi Y, Chlorellasp. A new strain with highly saturated fatty acids for biodiesel production in bubble-column photobioreactor. Appl Energy, Vol. 88, 2011, pp. 3354–3356.

[7] Hoekman, SK., Broch A., Robbins, C., Ceniceros EJ, Natarajan, M. Review of biodiesel composition, properties, and specification. Renew Sust Energy Rev, Vol. 16, 2012, pp. 143–69.

[8] J. Van Gerpen, G. Knothe. Basics of the Transesterification Reaction. 2nd ed. Gerhard Knothe, Jürgen Krahl, Jon Van Gerpen , Ed. Publisher's Elsevier. 2010, pp. 31–65, 67–96

[9] UNE-EN 14214, Automotive fuels-Fatty acid methyl esters (FAME)-for diesel engines. Requirements and test methods, European Committee for Standardization, 2008.

[10] Ahmad, A.L., I, Suzylawati., I, Norliza., and B, Subhash. Removal of suspended solids and residual oil from palm oil mill effluent. Journal of Chemical Technology and Biotechnology, Vol. 78, 2003, pp. 971-987.

[11] Encinar, J. M., Pardal, A., and Martínez, G., "Transesterification of rapeseed oil in subcritical methanol conditions," Fuel Processing Technology, Vol. 94, 2012, pp. 40-46.

Second International Conference on Science, Engineering & Environment,
Osaka City, Japan, Nov.21-23, 2016, ISBN: 978-4-9905958-7-6 C3051

SURFACE CHLOROPHYLL-A BLOOM ALONG THE SOUTHERN COAST OF JAVA DURING 2015 INDIAN OCEAN DIPOLE EVENT

Iskhaq Iskandar[1,3,4], Qurnia Wulan Sari[2], Eko Siswanto[3] and Dedi Setiabudidaya[1]
[1]Department of Physics, Faculty of Mathematics and Natural Sciences, University of Sriwijaya, South Sumatra, Indonesia;
[2]Graduate School of Environmental Science, University of Sriwijaya, South Sumatra, Indonesia
[3]Japan Agency for Marine-Earth Science and Technology, Yokohama, Japan
[4]Center for Geo-hazard and Climate Change Study, Faculty of Mathematics and Natural Sciences, University of Sriwijaya, South Sumatra, Indonesia

E-mail: iskhaq@mipa.unsri.ac.id

ABSTRACT

Surface chlorophyll-a images from a Moderate Resolution Imaging Spectroradiometer (MODIS) on board of Terra/Aqua satellites along with other observational data were used to evaluate the oceanic response to a climate mode anomaly in the tropical Indian Ocean during 2015, so-called the positive Indian Ocean Dipole (IOD) event. The positive IOD event is associated with anomalously strong southeasterly winds along the southern coast of Java that caused strong upwelling event. During 2015, the positive IOD event developed in August, rapidly matured in September – October, and terminated in November. Anomalous sea surface temperature (SST) along the southern coast of Java, however, only shows negative anomaly in September. Meanwhile, the peak of surface chlorophyll-a bloom was observed in September – October coincident with anomalous strong offshore Ekman transport induced by the southeasterly winds.

Keywords: Chlorophyll-a, Indian Ocean Dipole, MODIS, Sea Surface Temperature, Upwelling.

INTRODUCTION

Spatio-temporal surface chlorophyll-a variability in the Southern Java coastal waters has been subject to various studies during the last few decades [1,2,3,4]. The studies have shown that on seasonal time-scale, the chlorophyll-a variability is mostly driven by the seasonal monsoonal wind. In addition, the Southern Java coastal waters also experience interannual variation associated with the Indian Ocean Dipole (IOD) [5,6] and the El Niño-Southern Oscillation (ENSO) [7]. In particular, during positive IOD and/or El Niño events, anomalously strong southeasterly winds along the southern coasts of Sumatra and Java enhance strong upwelling leading to surface chlorophyll-a bloom [2,3].

During boreal summer-fall 2015, the positive IOD event took place in the tropical Indian Ocean. Therefore, it is hypothesized that strong upwelling occurred along the southern coast of Java. In this study, we investigated how the physical process (e.g. strong upwelling) influences surface chlorophyll-a distribution in the Southern Java coastal waters. A combined remote sensing and reanalysis data were utilized to elucidate the dynamics of chlorophyll-a bloom.

DATA

The datasets used include monthly surface chlorophyll-a data from the Moderate Resolution Imaging Spectroradiometer (MODIS), monthly Optimum Interpolation Sea Surface Temperature (OI-SST) based on Advanced Very High-Resolution Radiometer (AVHRR), National Oceanic and Atmospheric Administration (NOAA), and monthly surface winds from National Centers for Environmental Prediction (NCEP)/National Centers for Atmospheric Research (NCAR) Reanalysis. The MODIS has horizontal resolution of 9 km. While the OI-SST has resolution of $0.25^o \times 0.25^o$, the surface winds has horizontal resolution of $2.5^o \times 2.5^o$. In addition, monthly near-surface currents from the Ocean Surface Current Analysis-Realtime (OSCAR) at $1^o \times 1^o$ resolution were also used in this study [8]. All of the data cover a period of January 2004 – December 2015, in which the mean climatology fields were calculated from. The anomaly fields, then, were defined as deviations from the mean monthly climatology.

RESULTS

Evolution of the 2015 positive Indian Ocean Dipole (pIOD) event

Evolution of the 2015 pIOD event was evaluated based on the Dipole Mode Index (DMI) as shown in

Fig. 1. It is shown that the evolution of 2015 pIOD started in late summer (August), peaked in autumn (September – October) and diminished in early winter (November – December). It is noticed that there were short-weakening intensities of the pIOD occurring in late-September and late-October.

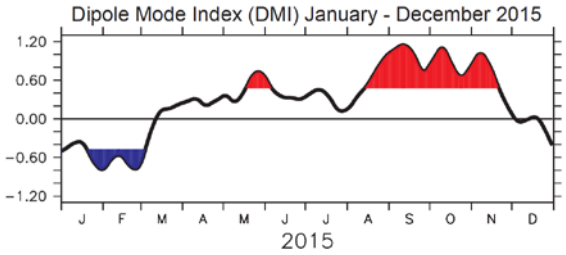

Fig. 1. Time series of Dipole Mode Index (DMI) during January – December 2015. The DMI is defined as the difference in SST anomaly between western region (50°E - 70°E, 10°S - 10°N) and eastern region (90°E -110°E, 10°S - Equator).

In order to have a spatial view of the 2015 pIOD event, spatial evolution of the Sea Surface Temperature (SST) and surface wind stress are presented in Fig. 2. It is shown that the pIOD evolution was started in August as the surface wind stress anomalously southeasterly along the southern coast of Java and Sumatra (Fig. 2a). These southeasterly winds drive upwelling along the coast as indicated by anomalous negative SST off south Java (Fig. 2a).

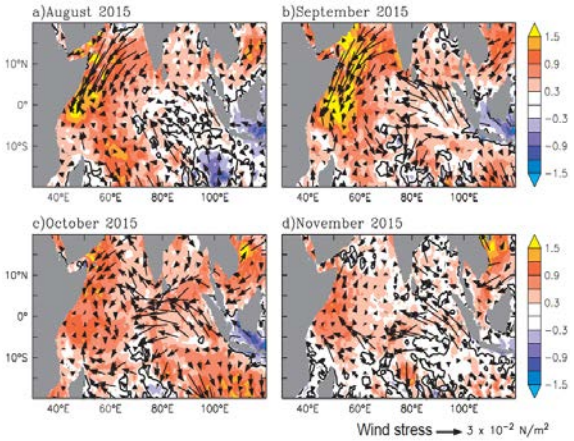

Fig. 2. Anomalous SST (ºC; shaded) and surface wind stress (N/m^2; vector) during August – November 2015.

The anomalous easterly winds in the eastern equatorial Indian Ocean were strengthened in September and October (Figs. 2b-c). However, there were no significant changes in the SST, except in the area near the southern coast of Java. This indicates an important role of air-sea flux in maintaining warm SST there. We noted that anomalously strong northeasterly winds were observed off eastern coast of Africa, indicating a weak summer monsoon (Figs. 2a-c). These anomalous northeasterly winds play important role in warming SST in the western pole of the pIOD. In November, the anomalous easterly winds in the eastern equatorial Indian Ocean and anomalous northeasterly winds along the eastern coast of Africa were weakened (Fig. 2d). As a result, the SST gradient between the western an eastern tropical Indian Ocean reduced significantly and the pIOD were terminated (Fig. 1 and Fig 2d).

The spatial evolution of the 2015 pIOD was also shown by the spatio-temporal variation of sea surface height (SSH) and surface currents (Fig. 3). In contrast with the SST patterns (fig. 2), the SSH pattern clearly showed a typical dipole pattern: anomalous negative (positive) SSH in the eastern (western) tropical Indian Ocean during August – November 2015 (Figs. 3a-d). The strong negative SSH along the southern coast of Java and Sumatra indicates an anomalously strong upwelling event was occurred there. We also noted that the pattern of surface currents was following the pattern of surface wind stress. In September, anomalous westward currents were observed in the eastern equatorial Indian Ocean (Fig. 3b). The anomalous westward currents strengthened in October (Fig. 3c) as the anomalous easterly winds also strengthened (Fig. 2c). In November, there were anomalous westward currents along the equator (Fig. 3d) as the surface winds were still observed in the eastern equatorial Indian Ocean (Fig. 2d).

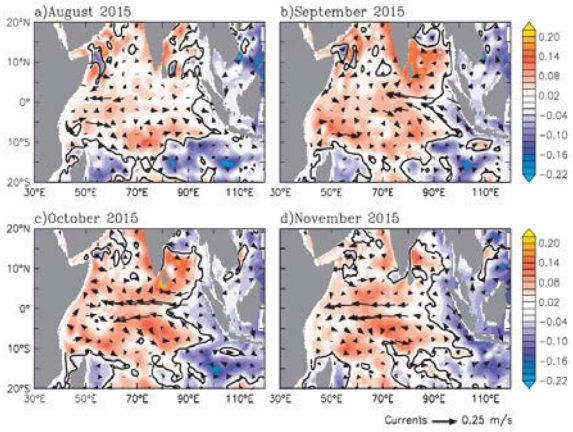

Fig. 3. As in Fig. 2 except for SSH (cm; shaded) and surface currents (m/s; vector) during August – November 2015.

Surface chlorophyll-a bloom during 2015

As shown in Figs. 2 and 3, anomalous strong upwelling occurred along the southern coast of Java and Sumatra during August – October 2015. Therefore, we hypothesized that these strong upwelling could lead to surface chlorophyll-a bloom there. In order to evaluate the impact of strong

upwelling during the evolution of 2015 pIOD, satellite observed surface chlorophyll-a from MODIS were used here.

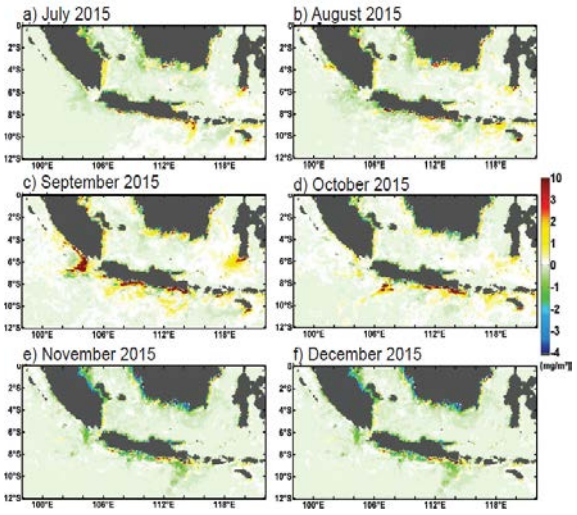

Fig. 4. Monthly anomalies of the surface chlorophyll-a (mg/m^3) from MODIS for a period of July – December 2015.

The surface chlorophyll-a anomalies in the southeastern tropical Indian Ocean are presented in Fig. 4. Positive anomalies of the chlorophyll-a concentration (≥ 1mg/m^3) were first observed in the eastern region off south East Nusa Tenggara Island chain, Sumbawa Island and Bali Island in July 2015 (Fig. 4a). The positive chlorophyll-a anomalies seem to move westward in August as the pIOD started to develop (Fig. 4b). During this period, we found that positive anomalies (≥ 1mg/m^3) were observed off south Java and off south West Nusa Tenggara Island chain. As shown in previous study, the abundance of surface chlorophyll-a concentration in early summer is driven by southeasterly winds during the southeast monsoon [9].

As the pIOD came to its peak phase in September, the positive anomalies of chlorophyll-a concentration were intensified and expanded westward and seaward (Fig. 4c). These positive anomalies can be observed along the coast from west Sumatra (approximately 4ºS) to southern Nusa Tenggara Island chain. We noted that very high positive anomalies were observed off South Sumatra near the Sunda Strait and off south Central-Java and West-Java. It is also shown that there was offshore chlorophyll-a bloom about 200 km off south Java. Previous studies have indicated that this offshore chlorophyll-a bloom is associated with an intensification of cyclonic eddy during pIOD event [2,3,4].

As indicated in previous section, the termination period of the pIOD event was occurring in November when the southeasterly winds were weakened along the southern coast of Sumatra. Weakening of the southeasterly winds resulted in weakening of the upwelling and thus termination of the surface chlorophyll-a bloom (Figs. 4e-f). We also noted that high positive anomalies of the surface chlorophyll-a were still observed off southern coast of the east Java in October – November 2016.

CONCLUSION

Surface chlorophyll-a bloom in the southeastern tropical Indian Ocean off south Java was evaluated using monthly images from the MODIS data combined with the oceanic (SST, SSH, surface current) and atmospheric (surface wind stress) data. The analysis was focusing on the boreal summer – fall 2015 when the pIOD event took place. The analysis shows that surface chlorophyll-a bloom started in the late boreal summer (July – August), peaked in the boreal fall (September – October) and terminated in the early boreal winter (November). We noted that the time evolution of the surface chlorophyll-a bloom was co-incidence with the evolution of the 2015 pIOD event. Very high surface chlorophyll-a concentration was observed in September when the pIOD event reached its peak phase. Anomalously strong southeasterly winds along the southern coast of Java and Sumatra promoted nutrient flux into the euphotic zone leading to a surface chlorophyll-a bloom.

ACKNOWLEDGEMENTS

The first author was supported the Ministry of research, Technology and Higher Education, Republic of Indonesia through grand-in-aid of "Hibah Kompetensi" 2016. Part of this study was supported by a grant from the Asia-Pacific Network for Global Change Research (CAF2015-RR11-NMY-SISWANTO).

REFERENCES

[1] Asanuma I, Matsumoto K, Okano H, Kawano T, Hendiarti N, Sachoemar S. I., "Spatial distribution of phytoplankton along the Sunda Islands: the monsoon anomaly in 1998". 2003, J Geophys Res., 108:3202. doi:10.1029/ 1999JC000139.

[2] Iskandar, I., Rao, S.A., and Tozuka, T., Chloropyhll-*a* bloom along the southern coasts of Java and Sumatra during 2006, 2009, Int. Journal of Rem. Sen., 30, 663-671.

[3] Iskandar, I., Sasaki. H., Sasai, Y., Masumoto, Y. and Mizuno, K., "A numerical investigation of eddy-induced chlorophyll bloom in the southeastern tropical Indian Ocean during Indian Ocean Dipole – 2006", 2010, *Ocean*

Dyn., 60: 731-742, doi: 10.1007/s10236-010-0290-6.

[4] Susanto, R. D., and Marra, J., "Effect of the 1997/98 El Niño on chlorophyll *a* variability along the southern coast of Java and Sumatra". 2005. *Oceanography*, 18, 124-127.

[5] Saji, N. H., Goswami, B. N., Vinayachandran, P. N., and Yamagata, T., "A dipole mode in the tropical Indian Ocean", 1999. *Nature*, 410, 360 – 363.

[6] Webster, P. J., Moore, A. W., Loschnigg, J. P. and Leben, R. R., "Coupled ocean-atmosphere dynamics in the Indian Ocean during 1997-98", 1999. *Nature*, 401, 356 – 360.

[7] Susanto, R. D., Gordon, A. L. Zheng, Q., "Upwelling along the coasts of Java and Sumatra and its relation to ENSO", 2001. *Geophy. Res. Lett.*, 28, 8, 1599-1602.

[8] Bonjean, F., and G. S. E. Lagerloef, Diagnostic model and analysis of the surface currents in the tropical Pacific Ocean, 2002. *J. Phys. Oceanogr.*, **32**, 2938–2954.

[9] Susanto, R. D., T. Moore II and J. Marra, "An ocean color variability in the Indonesian Seas during the SeaWifs era, 2006. *Geochem., Geophys., Geosys.*, **7,** 5, doi:10.1029/2005GC001009, 1-16.

Second International Conference on Science, Engineering & Environment,
Osaka City, Japan, Nov.21-23, 2016, ISBN: 978-4-9905958-7-6 C3051

ANALYSIS OF TIME-DEPENDENT MERCURY FLOWS THROUGH THE USE OF THERMOMETERS AND SPHYGMOMANOMETERS IN THAILAND

Manaporn Wongsoonthornchai[1], Ruth Scheidegger[2], Suphaphat Kwonpongsagoon[1*] and Hans-Peter Bader[2]
[1]Department of Sanitary Engineering, Faculty of Public Health, Mahidol University, Bangkok, Thailand;
Center of Excellence on Environmental Health and Toxicology (EHT), Bangkok, Thailand;
[2]Swiss Federal Institute of Aquatic Science and Technology, Dubendorf, Switzerland

ABSTRACT

Thermometers and sphygmomanometers pose a potentially large source of mercury emissions to the environment due to their high elemental mercury content. Many countries, e.g. most European countries, US have banned their uses already and many more strictly limited their use. However, in Thailand these mercury-based devices are still used, accumulating large stocks in the use phase as well as in landfills. To understand the development of mercury stocks and flows from thermometers and sphygmomanometers, a time-dependent mathematical material flow model is used in this study. The flows of mercury through these two products were calculated based on data between the years of 1962 and 2013. The simulation showed that the stock of mercury in thermometers is about 20 times smaller than the stock in sphygmomanometers. However the sum of waste flows and emissions to air and water from thermometers is 3 times larger than from sphygmomanometers. The reason is the lifetime of thermometers which is about 70 times shorter than the lifetime of sphygmomanometers. The calculated emission to air from mercury thermometers in hospitals can explain the higher mercury level measured in urine of health care staff. In order to reduce the mercury flows to the environment mercury thermometers should be replaced by alternative products as soon as possible.

Keywords: Mathematical Material Flow Analysis (MMFA), Mercury, Thermometer, Time-dependent, Sphygmomanometer

INTRODUCTION

Mercury (Hg) has been known as highly toxic for both environment and human health since 1956 when the so called Minamata disease was first discovered near the city of Minamata, Japan. It became widely known in 1968 when the company responsible for it stopped the production [1], [2]. Mercury affects the nervous, digestive, respiratory, immune system, kidneys, and lungs [3]. Several studies indicate that mercury emission is one of the most global concerns for hazardous air pollutants because once released into the air Hg may stay in the atmosphere for long periods, and can be transported across borders before being deposited and accumulated in the environment and living organisms [4], [5]. According to Health Care Without Harm (HCWH) report [6], the health care sector is a significant source of mercury demand and emission in the world. Mercury has been extensively used in health care products such as thermometers, sphygmomanometers (blood pressure measuring devices), dental amalgam, as disinfectant, as preservative in vaccines and eye drops, and in some traditional medicine for health care purposes [7]. The World Health Organization (WHO) is most concerned with thermometers and sphygmomanometers since both of them contain elementary mercury [8]. Sphygmomanometers in particular, build up a large stock since each of them contains up to 100 grams of metal mercury [8]. As long as they are used and mercury is not spilled from them, this is of minor concern, but as soon as they are either broken or become obsolete, they cause large waste flows of mercury. Waste containing mercury is hazardous waste and should never be mixed with municipal solid waste. It has to be treated separately, but unfortunately Thailand still lacks such treatment processes.

Pastore et al. [9] claim that the breakage of mercury-containing devices causes mercury spills to the environment, leading to mercury exposure of health care staff and patients. This is mainly due to unprofessional cleanup of mercury spills caused by broken thermometers which lead to mercury vapors slowly saturating the indoor air. Around 80% of inhaled mercury vapors from elementary mercury are absorbed in the blood through the lungs and cause harmful effects to human health [10]. So far, nothing indicates that mercury is a main cause of morbidity in Thailand [11] even though several studies show that health care staffs in Thailand always have high mercury level in their urine [12], [13]. These studies indicate that the mercury

problem in the health care sector should be of concern in Thailand.

To prevent health effects from mercury exposure, WHO and United Nations Environmental Program (UNEP) have issued guidelines for mercury free health care in 2011 and 2013 [8], [14], aiming to phase out both Hg-thermometers and Hg-sphygmomanometers. In 2010, WHO in cooperation with Health Care Without Harm (HCWH) set to phase out 70% of Hg-thermometers and Hg-sphygmomanometers used in health sector by 2017 [15].The "Minamata Convention on Mercury" by UNEP decided to phase out both devices by 2020 [14].Currently, United State and European Union (EU) already banned mercury-based devices in their countries, while other countries such as Philippine, Argentina, and India are attempting to implement mercury-free health care in their countries [15], [16]. However, Thailand, which is promoted as a hub of health services in Asia, has neither signed the Minamata Convention on Mercury nor implemented mercury-free health care so far. Therefore, the understanding of mercury flows and stocks could be the first step to manage mercury in health care in Thailand.

Mathematical Material Flow Analysis (MMFA) is an approach to study stocks and flows of goods and substances in anthropogenic systems. MMFA can be applied to (quasi) stationary as well as time-dependent models. The difference is that (quasi) stationary models cover a fixed time period, typically a one year period, for any kind of goods, in order to understand the system considered. Time-dependent model are used to investigate the development of the system including stocks and flows of goods over longer time spans in order to understand the development of stocks and flows over time and is often used for environmental management. Time-dependent models have been applied for different products and different scales such as country level for metals [17], [20], [21] and housing [18], on city level for durable goods [19], and on farm level for resources [22].

This study applies a time-dependent model to understand the mercury flows through the two health care products of concern, thermometers and sphygmomanometers in Thailand over time. The question below will be answered by this study:

1. How large is the demand, stock, and emissions of mercury through thermometers and sphygmomanometers used in health care facilities?
2. What are feasible scenarios to manage mercury from the health care sector in Thailand?

METHODOLOGY

Mathematical material flow analysis (MMFA) approach was used for this study. MMFA is the combination of conventional material flow analysis (MFA) with modeling concept developed by Baccini and Bader [23]. MMFA has been applied in many studies fields for environmental management: Zeltner et a. [17]; Binder et al. [19]; Sörme and Lagerkvist [20]; Bader et al. [24]; Huang et al. [25]; Kwonpongsagoon et al. [26]; Schaffner et al. [27]; Bader et al. [28]; Wongsoonthornchai et al. [29].

The procedure of MMFA consists of

1. System analysis: define both temporal and spatial boundaries; identify the products and processes related to mercury;
2. Time-dependent mathematical model: formulate time-dependent equations to describe the system and process in mathematical term;
3. Data acquisition and calibration: collect the input data set for the model;
4. Simulation: the model is used for simulating the past and current state and to investigate scenarios

The MMFA model for mercury flows in Thailand has been solved using the SIMBOX simulation program [30].

System Analysis

The geographic border of this study is Thailand and the time period selected is from 1960 to 2050. The system consists of the healthcare sector and includes only the products of thermometers and sphygmomanometers (blood pressure devices).

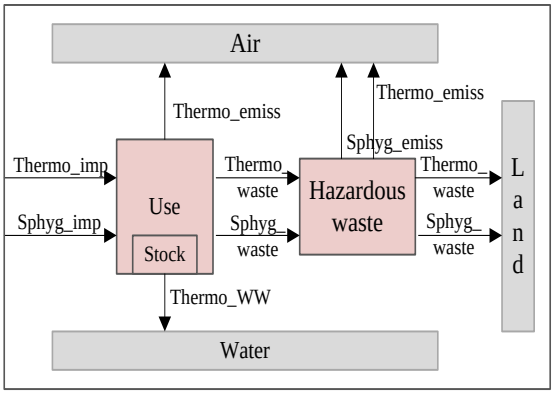

Fig. 1 System analysis for mercury flows through thermometers and sphygmomanometers in the healthcare system in Thailand

Figure 1 shows the system analysis for mercury flows through thermometers and sphygmo-manometers in the health care system in Thailand. Thailand has no production plants for thermometers

and sphygmomanometers and therefore they are imported directly to the use process. Accordingly only mercury flows from import are considered and no domestic production processes are included. Mercury emissions were considered during the use phase of thermometers through breakage and wrong (or no) treatment of the waste afterwards and after use in the hazardous waste treatment. Sphygmomanometers were assumed to cause no or only little emissions during the use phase. Therefore no emissions in use phase were taken into account.

Model Approach

A time-dependent model is important because it allows understanding how stocks and flows evolve over time. The model used here is an adaption and generalization of the model developed for the simulation of the production, use and disposal including all emissions of flame retardants [31]. The approach is so called "stock-driven", which means that the stocks in use in function of time are given together with the residence time distribution [31]. The emissions during the use phase are proportional by emission factors to a fraction of the stock. For a detailed description of the model see [32].

The 25 input parameters for each subsystem were needed for the simulation of the mercury flows though thermometers and sphygmomanometers in Thailand.

Data Acquisition and Calibration

Different types of data were collected for the estimation of mercury flows though thermometers and sphygmomanometers in Thailand between the year of 1962 and 2013. The data was retrieved from data sources such as the government sectors, surveys, interviews, company reports, and literatures.

Unfortunately no time series data were available for the number of thermometers and sphygmo-manometers in Thailand.

Instead, such data were estimated as follows:

$$Thermo = (B * TB) + (D * TD) \qquad (1)$$

Where:

Thermo = Number of thermometers in use [pieces]
B = Number of bed [beds]
TB = Number of thermometers per bed [pieces/bed]
D = Number of doctors in Thailand [persons]
TD = Number of thermometers per doctor [pieces/doctor]

$$Sphygmo = [(B / BW) * BP] + (D * BD) \qquad (2)$$

Where:

Sphygmo = Number of sphygmomanometers in use [pieces]
BW = Number of bed per ward [beds/ward]
BP = Number of sphygmomanometers perward [piece/ward]
BD = Number of sphygmomanometers perdoctor [pieces/doctor]

The basic assumption for equation (1) and (2) is that both thermometers and sphygmomanometers are assigned to beds in hospitals and to the doctors since only hospitals and doctors own such equipment.

Figure 2 shows the estimated time series extrapolated from 2015 to 2050 assuming a linear growth of hospital beds and number of doctors due to population growth and improvement of health care.

Estimation of average lifetime:

The results for lifetime gained through interviews with nurses and doctors are about 1.5 month for thermometers and about 9 years for sphygmomanometers. Therefore we assumed as lifetimes 1.5±0.7 month and 9±5 years for thermometers and sphygmomanometers, respectively.

Ratio of mercury thermometers to mercury free thermometers:

This ratio is 1 up to 2001 since Thailand used only mercury thermometers before then. From 2001 to 2050 it is assumed that the ratio decreases exponentially, stabilizing at 0.3 in 2030. This assumption is very conservative, but faster phasing out of mercury thermometers are discussed in the scenario section. A similar assumption was made for sphygmomanometers.

Emission factors:

For thermometers it is assumed that they are broken after their lifetime and 50% of mercury is emitted to air, 40% to the water phase and the rest to soil.

It was assumed that no emissions occurred during the use phase of sphygmomanometers because they are well covered and the staff handles them carefully during use.

Calibration:

Using this data set and the model the flows in Fig. 1, except the emissions from the hazardous waste were calculated. Figure 2 shows the results for the stocks, and inputs for thermometers and sphygmomanometers, as well as the statistical data

for import of mercury thermometers. A recalibration of the lifetime for thermometers was necessary since the number of calculated imported thermometers between 1960 and 2000 was too high. Therefore the lifetime for this time period was assumed to be 4.5 month since 1950, decreasing gradually to 1.5 month in 2000. This assumption can be justified by the fact, that the equipment was handled more carefully in the past.

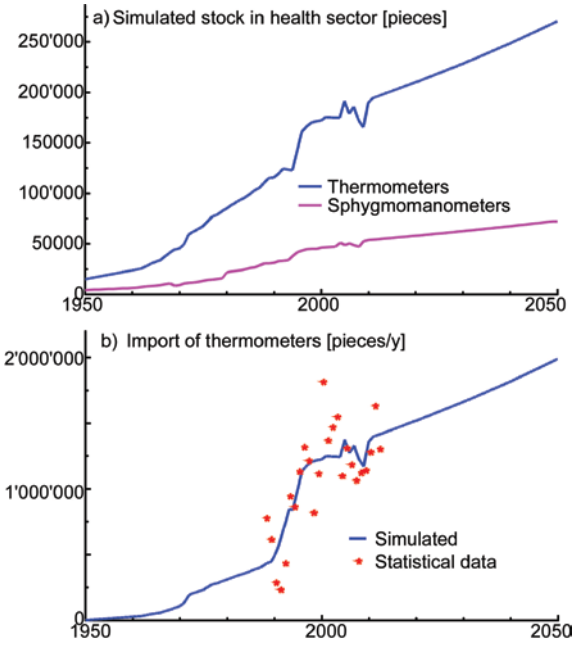

Fig. 2 a) Stock of thermometers and sphygmomanometers in Thailand between 1950 and 2050, b) Import of thermometers between 1950 and 2050

RESULTS AND DISCUSSION

Stock of Mercury

Figure 3 shows the stock of mercury in thermometers and sphygmomanometers in use. The double peak of the joint stock is roughly 3700 kg and occurs around 2000-2010. Compared to the amalgam stock in dental fillings which is about 10,080 kg according to [29], this is roughly 37% of that stock. The assumption that mercury free thermometers and sphygmomanometers replace continually the mercury containing equipment in the 21st century leads to the decrease of the mercury stock after 2010 shown in Fig. 3.

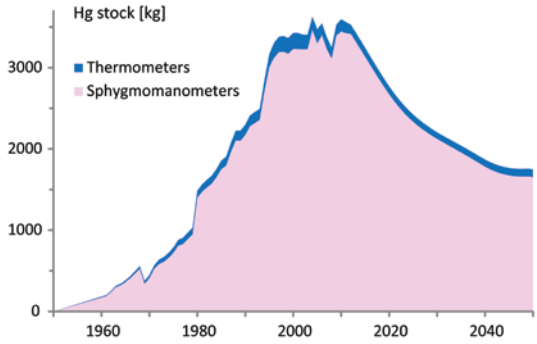

Fig. 3 Mercury stock in Thailand through thermometers and sphygmomanometers

Mercury Emissions and Flow to Hazardous Waste

The short lifetime of thermometers of about 1.5 month is due to breakage during use. About 70% of mercury from broken thermometers is collected as hazardous waste, 23% is emitted to air and 7% to water. Figure 4 shows the mercury flows of import, hazardous waste and emissions to air and water for thermometers.

The flows in Fig. 4 in function of time show a similar behavior as the stocks in Fig. 3. The reason is the same as for the stocks.

The peak values of the residual flows are about 1,000 kg, 250 kg and 51 kg to hazardous waste, air and water, respectively. A comparison with Wongsoonthornchai et al. [29] shows that the residual flows from the thermometers are about 20%, 14% and 5% of the flows from intentional use to waste, air and water, respectively.

The maximum of emissions to air is about 250 kg/y in the year 2001. According to the number of beds in hospitals of 136,000 in 2001 this gives an emission of 1.84 g Hg per bed and year. The maximum tolerable workplace exposure limit of mercury is 0.05 mg Hg / m^3 [33]. To be below the limit the emission per bed would have to be diluted in more than 36,700 m^3 air per bed and year. Assuming a space column of about 15 m^3 per bed, this means that the air would have to be exchanged completely almost 7 times per day in each hospital room in order to be below the limit. This could explain the high mercury level in urine of health care staff.

From the simulations follows that until 2010, about 24,000 kg of mercury from thermometers ended in hazardous waste, 5,400 kg and 1,100 kg were emitted to air and water, respectively.

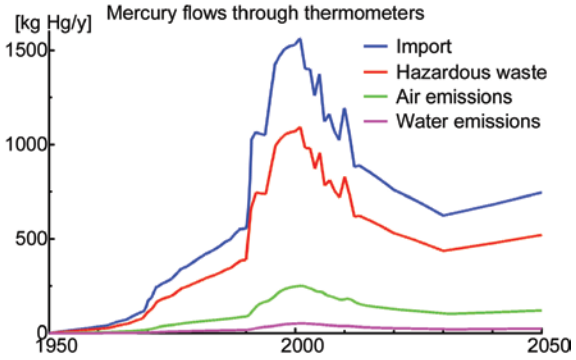

Fig. 4 Mercury through thermometers in flows from import, to hazardous waste, emissions to air and water

Scenario Analysis

As suggested by WHO and HCWH [15], thermometers and sphygmomanometers are interesting health products to reduce mercury on the global scale. Therefore, the following scenario is considered to reduce mercury emission in Thailand.

Scenario: Replace all Hg-thermometers and Hg-sphygmomanometers with alternative products by 2020

Since the lifetimes of thermometers are very short, the residual flows to hazardous waste, and the emissions to air and water would be zero after 2020. The simulation shows that the reduction would be in average 540 kg/y, 122 kg/y and 25kg/y for the flows to hazardous waste, emissions to air and water after 2020. For sphygmomanometers, because of their lifetime of about 9 years the flows to hazardous waste would be reduced to zero in about 2030.

In total this scenario would reduce the residual flows by 25,730 kg between 2020 and 2050. This is quite a large amount, even compared with the already deposited and emitted amount of 38,900 kg up to 2010.

CONCLUSION

This paper analyzed the time-dependence of mercury flow and stock through thermometers and sphygmomanometers using MMFA approach. The simulation showed that the stock of mercury in thermometers is only about 5% of the stock of mercury in sphygmomanometers. However with thermometers 3 times more mercury is imported than in sphygmomanometers. The reason is the short lifetime of thermometers of about 1.5 month, which is about 70 times shorter than for sphygmo-manometers. Therefore also the residual flows of mercury from thermometers to hazardous waste, air and water are about 3 times larger than those for sphygmomanometers.

The calculated emission to air from mercury thermometers in hospitals can explain the higher level mercury measured in urine of health care staff.

To reduce the emissions to air and water mercury thermometers should be replaced as soon as possible by alternative products.

ACKNOWLEDGEMENTS

This research work is supported in part by the grant from Center of Excellence on Environmental Health and Toxicology, Science & Technology Postgraduate Education and Research Development Office (PERDO), Ministry of Education. Moreover, this study was supported for publication by the China Medical Board (CMB), Faculty of Public Health, Mahidol University, Bangkok, Thailand.

REFERENCES

[1] Harada Y, “Congenital (or Fetal) Minamata Disease”, In: Study Group of Minamata Disease, (M. Katsuna, editor). Minamata Disease. Kumamoto: Kumamoto University, 1968, pp. 93–117.

[2] Harada M, “Minamata disease: Methylmercury poisoning in Japan caused by environmental pollution”, Crit. Rev. Toxicol, Vol.25 (1), 1995,pp.1-24

[3] Jeanne, MS, “Metals: Chemical properties and toxicity”, Encyclopaedia of Occupational Health and Safety: Chemical, industries and safety, 4th ed. Vol. 3, Geneva: International Labor office (ILO), 1988, pp. 63.28-63.29.

[4] UNEP, “Global mercury assessment”, Geneva: UNEP Chemicals, 2002, pp. 1-118.

[5] Driscoll CT, Mason RP, Chan MH, Jacob DJ, and Pirrone N, “Mercury as a Global Pollutant: Sources, Pathways, and Effects”, Environ Sci Technol. Vol. 47, May. 2013, pp. 4967–4983.

[6] Karliner J, Harvie J. “The global movement for mercury-free health care”, Health Care Without Harm Publication; 2007. Available at: https://noharm-global.org/sites/default/files/documents-files/746/Global_Mvmt_Mercury-Free.pdf.

[7] UNEP, “Module 4: Mercuryuse in healthcare settings and dentistry”, Geneva: UNEP, 2008, pp. 1-8.

[8] WHO, “Replacement of mercury thermometer and sphygmomanometer in health care: technical guidance”, Geneva: WHO, 2011, pp. 1-50.

[9] Pastore P, Singh R, and Jain N, “Mercury in healthcare”, Mercury in Hospital Indoor Air: Staff and Patients at Risk, New Delhi: Toxics Link, January, 2007, pp. 12-13.

[10] WHO, “Mercury”, Air quality guideline, 2nd Ed. Copenhagen: WHO Regional Office for Europe, 2000, pp. 4.
[11] National Statistical Office, “Number of in – patients by 75 cause groups according from health service units”, Ministry of public health, whole kingdom: 2003–2012, Available at: http://service.nso.go.th.
[12] Sangsirinavin C, “Mercury levels in urine and head hair of dental personnel”, Journal of the Dental Association of Thailand, 38(4), 1988, pp. 170-178.
[13] Chatngoen J, “Urinary mercury level in dental personnel in Chonburi province”, Master Thesis, Burapha University, Chonburi,2002, pp 47-73.
[14] UNEP “Minamata convention on mercury”Geneva: UNEP, 2013, pp. 1-62.
[15] WHO and HCWH, “The Global Initiative for Mercury-Free Health Care”, WHO-HCWH global initiative to substitute mercury-based medical devices in health care: a two year report, 2010, pp. 4-6.
[16] US.EPA, “Eliminating Mercury in Hospitals”, Environmental Best Practices for Health Care Facilities, November, 2002, pp. 1-12.
[17] Zeltner C, Bader H-P, Scheidegger R, Baccini P “Sustainable metal management exemplified by copper in the USA”, Reg Environ Changes 1, 1999, pp. 31–46
[18] Johnstone IM, “Energy and mass flow of housing: a model and example”, Build Environ 36, 2001, pp. 27–41
[19] Binder C, Bader H-P, Scheidegger R, and Baccini P, “Dynamic models for managing durables using a stratified approach: the case of Tunja, Colombia”, Ecological Economics, 38(2), 2001, pp. 191-207.
[20] Sörme L, and Lagervist R, “Sources of heavy metals in urban wastewater in Stockholm”, Sci Total Environ, 298(1-3), 2002, pp. 131-145.
[21] Hedbrant J,“Structuring empirical knowledge on environmental issues”, Dissertation, Linkoping Studies in Arts and Science, 2003, no.283
[22] Pfister F, Bader H-P, Scheidegger R, and Baccini P, “Dynamic modelling of resource management for farming systems”, Agricultural System, 86(1), 2005, pp. 1- 28.
[23] Baccini P and Bader H-P, “Regionaler Stoffhaushalt,Erfassung, Bewertung und Steuerung”, Heidelberg: Spektrum Akademischer Verlag, 2007, pp. 221-294 .
[24] Bader H-P, Scheidegger R, and Real M, “Global renewable energies: a dynamic study of implementation time, greenhouse gas emissions and financial needs”, Clean Technologies and Environmental Policy, 8(3), 2006, pp. 159-173.
[25] Huang DB, Bader H-P, Scheidegger R, Schertenleib R, and Gujer W, “Confronting limitations: new solutions required for urban water management in Kunming City”, Journal of Environmental Management, 84, 2007, pp. 49-61.
[26] Kwonpongsagoon S, Bader H-P, and Scheidegger R, “Modelling cadmium flows in Australia on the basis of a substance flow analysis”, Clean Technol. Environ. Policy, 9 (4), 2007, pp. 313-323.
[27] Schaffner M, Bader H-P, and Scheidegger R, “Modeling the contribution of pig farming to pollution of the Thachin River”, Clean Technologies and Environmental Policy, 12, 2010, pp. 407-425.
[28] Bader H-P, Scheidegger R, Wittmer D, and Lichtensteiger T, “Copper flows in buildings, infrastructure and mobiles: a dynamic model and its application to Switzerland”, Clean Techn. Environ. Policy, 13, 2011, 87-101.
[29] Wongsoonthornchai M, Kwonpongsagoon S, and Scheidegger R, “Modeling Mercury Flows in Thailand on the Basis of Mathematical Material Flow Analysis”, CLEAN - Soil, Air, Water, 44(1), 2016, pp. 16-24.
[30] Bader, H.P. and Scheidegger, R., “MMFA Framework”, Report from Eawag. Swiss Federal Institute of Aquatic Science and Technology, Duebendorf, Switzerland. 2012.
[31] Morf L, Buser A, Taverna R, Bader H-P and Scheidegger R, “Dynamic substance flow analysis as a valuable risk evaluation tool - A case study for brominated flame retardants as an example of potential endocrine disrupters”,Chimia, 62(5), 2008,pp. 424-431.
[32] Kwonpongsagoon S, Scheidegger R, Wongsoonthornchai M, and Bader H-P, “Mercury flows in fluorescent lamps, a dynamic model for the flows through Thailand”, in preparation.
[33] SUVA Arbeitsmedizin, 2013, Available at:http://www.suva.ch/factsheet-quecksilber.pdf

Second International Conference on Science, Engineering & Environment,
Osaka City, Japan, Nov.21-23, 2016, ISBN: 978-4-9905958-7-6 C3051

MERCURY CONTAMINATION IN ENVIRONMENT SURROUNDING COAL-FIRED POWER PLANT

Kamolthip Mahavong, Poranee Pattaranawat and Sopa Chinwetkitvanich
Department of Sanitary Engineering, Faculty of Public Health, Mahidol University, Bangkok, Thailand

ABSTRACT

Fossil fuels combustion has been widely known of their emission containing various heavy metals and gaseous substances. This study is to investigate the distribution of mercury (Hg) in environmental media surrounding the lignite coal-fired power plant in Lampang province, Thailand. Samples of surface soil and waters were collected within the vicinity of the power plant in order to analyze mercury contamination. Also, Hazard Quotient (HQ) will be determined to estimate environmental potential risks in this area of concern. Mercury contents in surface soil samples were observed in the range of 65.01 – 1337.64 µg/kg. The results also revealed that the distribution of mercury contamination in surface soils did not completely correlate with monsoon domination or distance from the power plant. Some samples of surface water and ground water in this area contained mercury concentration in the range of 0.1 µg/l – 0.2 µg/l. These mercury contents were further considered for environmental potential risks by HQ calculation. The environmental potential risks of mercury content in surface soil samples were classified as 'no hazard exist' while those in water samples were classified as 'hazard is low'.

Keywords: Mercury, Lignite, Coal-Fired Power Plant, Environmental Potential Risks, Health Risks Assessment

INTRODUCTION

The coal-fired power plant has been widely known for an important source of air pollution due to its emission from fossil fuel burning contains several pollutants, i.e., gases, particulate matters, heavy metals, or some substances such as dioxin, radiation, etc. These pollutants can affect respiratory, circulatory, neural, hormonal and reproductive systems, as well as, can stimulate some diseases and carcinogenic effect in human organs. Especially, approximately ninety percent of accumulated mercury in human body is organic mercury (methyl mercury), which is highly toxic and stable for quite long period. Pregnant women and young children are the most sensitive groups, as well as, the accumulated mercury can be passed on from mother to daughter [1].

At present, Thailand's economic and industrial sector has expanded greatly in recent years, resulting in increasing of electricity demand. Currently, natural gas accounts for 70 percent of fuel used in electricity production due to its high efficiency, low pollutants emission and local supply. Coal was responsible for the second amount of fuel used in power plant (about 20 percent). In contrast with Thailand's fuels utilization for thermal power plant, the global fuels consumption was mainly coal combustion, which accounted for about 40 percent, while natural gas combustion was only about 20 percent [2]. However, the natural gas reserve in Thailand is predicted to be adequate for only next ten years from now while the demand of natural gas in other industries also continues to rise. Therefore, the alternatives to replace natural gas in power plant such as coal, petroleum, biomass, nuclear energy, etc., are considered [3]. Lignite coal is the majority of coal reserves in Thailand, which is considered as low quality coal due to its low heat and high humidity, high ash and sometimes high sulfur content. The largest source of lignite in Thailand is located in Mea Moh district, Lampang province. Besides lignite, the higher quality coals found in Thailand is sub-bituminous and bituminous. Anthracite is also found, but with a very small amount, in Loei province area. Although a variety of coal species is found in Thailand, most of them are low quality coal (lignite and sub-bituminous) [4].

The Mae Moh Coal-fired Power Plant in Lampang province is the largest one in Southeast Asia using coal-lignite as fuel. This power plant consists of ten generating units with a total capacity of 2,400 MW, representing about 20% of the capacity of Thailand. This power plant distributed electricity to the North, the Central and the Northeast of Thailand with using coal as the fuel of about 16 million tons per year [5]. Several studies have been reported about toxic elements contaminated in emission from coal-fired power plant [6-9]. The Mae Moh power plant was also reported of high concentrations of As, Pb and Hg in its fly ash samples [10]. Although, this power plant installed flue gas desulfurization (FGD) to reduce air pollutants from their flue gas, the contamination of

heavy metals in their ashes and particulates were still observed [11]. Mercury contamination in environmental media and some plants in the surrounding area of Mae Moh power plant were reported elsewhere [12], but not clear enough to indicate the source of contaminated mercury.

However, there is quite a few of information about the distribution and environmental risk of mercury emitted from the coal-fired power plant in this area. The aim of this study is to investigate the contaminant concentrations of mercury from the coal-fired power plant in surface soil and water as well as the potential environmental risks and food safety in vicinity area surrounding the coal-fired power plant.

MATERIALS AND METHODS

The study area is designated to be within the 30-km radius surrounding of the Mae Moh coal-fired power plant with 2400 MW capacity. This study area covers several districts of Lampang Province including Maung Lampang, Mae Moh, Mae Tha and Long District of Prae Province. This area named as Mae Moh basin is one of important basins in Thailand due to large coal reserve has been found here[13]. This Mae Moh basin has a pan shape (syncline) with average ground level of 320 meters above mean sea level. The northern part of Mae Moh basin is mostly covered with mountain and forest (about 80 percent of the districts) while the others of approximately 4,000 hectares are lowlands for cultivation. Soil characteristics are generally classified as sandy soil. The climate is quite roasting in the summer, cold in the winter and a little chance of rain about 60-80 days/year [14] due to the rain shadow. The predominant wind direction in this area is usually blowing along the SW/NE and the wind speed is in the range of 0.5 - 3.6 m/s.

The site of coal-fired power plant is mostly flat in the valley surrounded by mountains easily causing high air pressure and temperature inversion [15]. According to several studies [11-12], the atmosphere in this area was sometimes difficult for dispersion of air pollution. The major pollution released by the coal-fired power plant is mostly from fuel combustion for steam generation. Besides gaseous pollutions emitted from fossil fuel burning, some metals as components in the fuel also escape along and disperse into the atmosphere. These emitted metals eventually deposit and can be accumulated on surface soil and water in the surrounding area.

Sampling sites in this study were located in different directions and distances within the radius of 30 km from the coal fired power plant as shown in Fig. 1 equipped with the representative wind rose of this area. Fourteen sampling stations for surface soil (twelve for contaminated sites and two for background sites) and three sampling stations for surface water and ground water were designated. Samples collection for this study were conducted during August 8 – 11th, 2015.

Sampling Methods

Surface soil samples (0-15 cm depth) were collected from the rice field by applying the 'random sampling' procedure [16] with using clean disposable gloves, a stainless steel spade and a plastic scoop. Each soil sample weighted not less than 1 kg, was packed in plastic bag and kept in ice box at 4 ºC. For each station, representative soil sample were mixed and homogenized from three subsamples grabbed from three different points with approximately 3 m. distance from each other. Samples were air dried under shade and hot air oven at 103 – 105ºC. They were further crushed and sieved to obtain not larger than 2 mm size of soil particles. Then, they were analyzed on the basis of dry weight (dw).

The deposition of air pollution may contaminate aquatic compartment such as reservoir and streams nearby the coal-fired power plant, as well as, indirectly contaminate groundwater. Three sites of water samples were selected in the vicinity of the power plant. High density bottles and a Kemmerer water sampler were used to collect water sample from reservoir, streams and wells (that in use for household consumption). All water samples for mercury analysis must be preserved with conc. HNO_3 acid (pH < 2) and kept in ice box at 4ºC during transportation to the laboratory and before analysis.

Sample Analysis and Quality Control

Analysis of THg content was performed by Cold Vapor Atomic Absorption Spectrometry (CVAAS) with detection limit of 0.001 µg/L. Samples were digested according to the procedure of the Wetland Biochemistry Institute, Lousiana State University [17], [18]. About 0.5-2 g of dried samples were weighed and digested with concentrated 5 ml H_2SO_4 + 5 ml HNO_3. Then, the digested solutions were washed and made up to be 100 ml with deionized water (DI), and 10 ml $SnCl_2$ solution were added prior CVAAS analysis. Mercury concentrations were determined against a set of Hg standard solutions. Quality assurance was maintained by inserting a blank at the beginning of each sample run.

The accuracy of analytical procedure was calibrated by using three replicate samples of standard reference materials (SRM 1646a for sediment) from U.S. Department of Commerce, National Institute of Standard and Technology (NIST) and 4 samples of blank. The Method Detection Limit (MDL) was calculated (by 3.143 multiplies the standard deviation of the seven

reagent blank samples in the sample batch) and used as a tool for verification of all Hg analysis.

Evaluation of the potential environmental risks was estimated numerically using the Hazard Quotient (HQ) as presented by equation (1). The equation (1) is the ratio of the estimated exposure to the effect concentration representing a safe environmental concentration or screening benchmark [19].

HQ = EEC / Screening Benchmark (1)

EEC = estimated (maximum) environmental contaminant concentration in the samples at site. (e.g. mg contaminant/kg soil).

Screening Benchmark = maximum allowable of mercury concentration; if the contamination concentration is below this level, the contaminant is not likely to cause harmful effects.

If HQ < 0.1, no hazard exists
If HQ = 0.1-1.0, hazard is low
If HQ = 1.1-10, hazard is moderate
If HQ > 10, hazard is high.

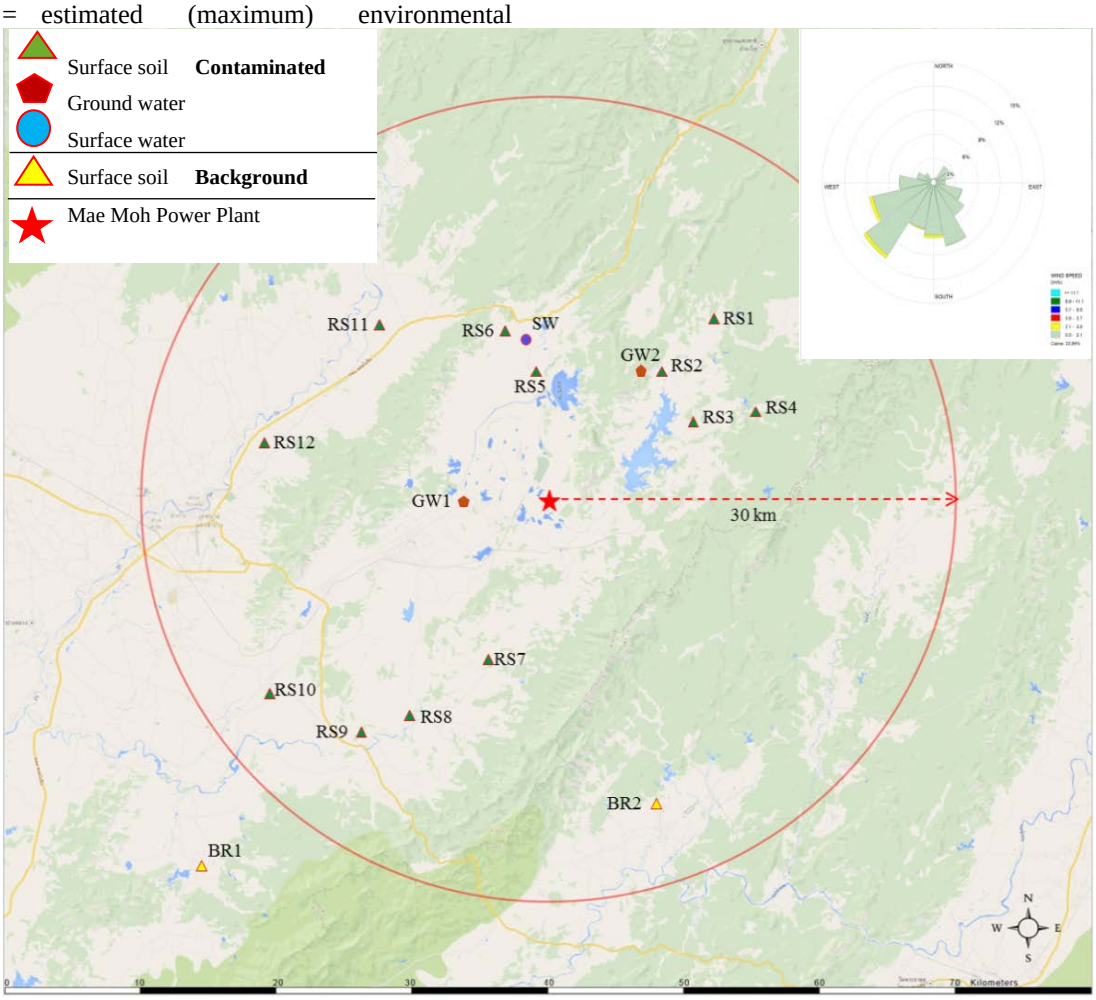

Fig. 1 The sampling locations within the radius of 30 km from the Mae Moh Power Plant.

RESULTS AND DISCUSSION

Mercury Concentrations in Surface Soil

Total mercury (THg) concentrations in surface soil samples of paddy fields around the coal-fired power plant are shown in Table 1. The results show that THg concentrations in samples taken from this study area during August 8 – 11th, 2015 did not exceed the critical value for Hg content in soil of 23,000 µg/kg announced by the Thai Soil Quality Standards for Residential and Agriculture. Soil characteristics of these samples were analyzed, but not shown here. The highest THg level in surface soil of 1,338 µg/kg was found in station RS9, which 23 km. distance from the power plant in Southwest direction. The second high THg level of 1,050 µg/kg was found in stations RS4 located at 18 km. in Northeast direction of the power plant. The other high THg levels of 261 and 248 µg/kg were found at stations BR1 and RS12, respectively. Surprisingly, station BR1 was initially expected to be a representative of background site due to its long distance (39 km.) from the power plant. However,

there were some activities, especially, maintenance of nearby highway that might possibly affect the result. Also, station RS12 was not expected of this high THg level due to it was not in the predominant Southwest-Northeast (SW-NE) wind direction of this area. Anyway, there is a small crematory placed nearby but not in operation during the sampling period. Moreover, the other THg levels of surface soil were in the range of 65 to 99 µg/kg. These THg levels indicate some contamination of mercury in surface soil of this area and some THg levels were higher than Hg concentrations in soils around a coal-fired power plant in China (606 µg/kg) [20] and Serbia (100 µg/kg) [21], where their amounts were already higher than the average content of Hg in world soil.

Mercury Concentrations in Water

Table 2 shows the THg concentrations found in water samples, two of which were sampling from groundwater wells while another was sampling from surface water. Groundwater sample from station GW1, the nearest station to the power plant, contained THg concentration of 0.2 µg/l while another groundwater sample (GW2) contained lower THg concentration of 0.1 µg/l. Only one sample of surface water (SW) had THg concentration of 0.2 µg/l. The THg results in all water samples did not exceed the critical level of 1 µg Hg/l of Thai Ground water quality Standards and the critical level of 2 µg Hg/l of Thai Surface Water Quality Standard.

Table 1 Concentrations of THg in surface soil.

Station	Location	Distance from coal-fired power plant (km)	Total Mercury (THg) (µg/kg dw)
Contaminated sites			
RS1	Ban Na Chae	18	70
RS2*	Ban Sob Chang	13	-
RS3	Ban Na Sak	12.5	78
RS4	Ban Pong Thaen	17	1050
RS5	Ban Dong	10	77
RS6	Ban Hua Fai	13	66
RS7	Ban Pha Maew	14	99
RS8	Ban Hau Sua	18	70
RS9	Ban Pong Papao	23	1338
RS10	Mae Tha Luang	24.5	65
RS11	Ban Sadet	18	68
RS12	Pichai	22	248
Background sites			
BR1	Mae Tha	39	261
BR2	Ban Na Phai Lom	24	94

* Surface soil was disturbed because of plant seedlings during the time of sampling.

Table 2 Concentrations of THg in water samples and their Hazard Quotient (HQ) levels.

Station	Location	Type of Sample	Distance from coal-fired power plant (km)	Total Mercury (THg) (µg/l)
GW1	Ban Huy King	Ground water	6	0.2
GW2	Ban Sob Jang	Ground water	13	0.1
SW	Ban Hua Fai	Surface water	12	0.2

Mercury is the most volatile element during the coal combustion process [22]. Its emission and speciation depended on the Hg concentration in the fuels, type of coals, and flue gas temperature and composition [23]. Mercury emitted from coal combustion is transported through the atmosphere and deposited onto the ground as wet or dry precipitation. The Hg in the environment may be transformed by microorganisms into methylmercury, a highly toxic form [24]. However, mercury content in coal-lignite or other coals used in this power plant have been not clarified.

Environmental Risks Assessment

The potential environmental risks assessment calculated by using Hazard Quotient (HQ) equation. In this study, HQ calculation of surface soil used the screening benchmark (23,000 µg/kg) based on Thai Soil Quality Standards for Residential and Agriculture notified by Pollution Control Department [25], and their results were illustrated in Fig. 2. The potential environmental risks evaluation in surface soil of fourteen sampling stations were found in the range of 0.003 – 0.058. These results illustrated that all sampling stations in this study were classified as no hazard exists (HQ < 0.1).

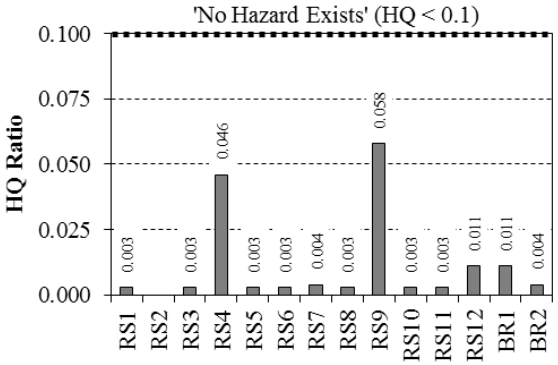

Fig. 2 Concentrations of THg (µg/kg dw) and HQ levels in surface soil.

For water sample, the screening benchmarks based on Thai Groundwater quality Standards [26] and Thai Surface Water Quality Standard [27] announced by Pollution Control Department was used to calculate HQ values as shown in Fig. 3. In case of groundwater, the potential environmental risk evaluations were 0.24 and 0.11 for station GW1 and GW2, respectively, which were classified as hazard is low (HQ = 0.1 – 1.0). In addition, the potential environmental risk evaluation of surface water was 0.11, which were classified as hazard is low similar to groundwater.

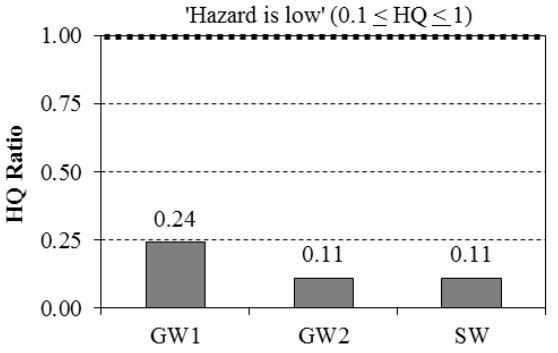

Fig. 3 Concentrations of THg (µg/l) and HQ levels in water samples.

CONCLUSION

Although the concentrations of THg in surface soil of paddy fields around the coal-fired power plant in this study did not exceed the critical Hg value of Thai Soil Quality Standards for Residential and Agriculture (23,000 µg/kg), these results illustrated some level of mercury content in this area (65.01 -1337.64 µg/kg). The spatial distribution of THg in surface soil tends to consistent to the predominant SW-NE wind direction. That is, sampling stations located in northeast direction (RS4) and southwest direction (RS9) from the power plant seemed to found higher level of mercury in surface soil (1049.85 and 1337.64 µg/kg, respectively). Nevertheless, the potential environmental risks evaluations in surface soil were classified only as 'no hazard exists' (HQ < 0.1). Similarly, THg concentrations in water samples (0.11 - 0.24 µg/l) did not exceed the critical values both of groundwater and surface water standards (1 and 2 µg/l, respectively). However, the potential environmental risks evaluation in water sample were classified as 'hazard is low' (HQ = 0.1 – 1.0), which should be concerned. Anyway, this sampling was only one time sampling, the further sampling and monitoring in this area was planned and scheduled.

ACKNOWLEDGEMENTS

This research was financially supported by National Research Council of Thailand (NRCT) and Mahidol University. The authors would like to thanks the Department of Sanitary Engineering, Faculty of Public Health, Mahidol University for laboratory assistance.

REFERENCES

[1] Health Impact Assessment Co-ordinating Unit, 2014, Pollution from coal-fired plant. Retrieved August 9, 2014, from Health Impact Assessment Co-ordinating Unit, http://www.thia.in.th/welcome/article_read/69.
[2] Department of Primary Industries and mines, Consumption of Coal in Thailand. Department of Primary Industries and mines, 2011, Bangkok.
[3] Sirianuntapiboon S, Trakarnjindanont N, Menasveta P, "Coal and Electricity Generation in Thailand", J. of the Royal Institute of Thailand, Vol. 37(4), 2012, pp. 22-40.
[4] Department of Primary Industries and mines, Mineral Statistics of Thailand 2009-2014, Department of Primary Industries and mines, 2014, Bangkok.
[5] Electricity Generating Authority of Thailand (EGAT), 2014, The Mae Moh coal-fired power plant, Retrieved August 9, 2014, from

Electricity Generating Authority of Thailand, http://maemoh.egat.com/index_maemoh.

[6] Goodarzi F, Huggins F, Sanei H, "Assessment of elements, speciation of As, Cr, Ni and emitted Hg for a Canadian power plant burning bituminous coal", J. of Coal Geology, Vol. 74(1), 2008, pp. 1-12.

[7] Shah P, Strezov V, Prince K, Nelson P, "Speciation of As, Cr, Se and Hg under coal fired power station conditions", J. of Fuel, Vol. 87(10-11), 2008, pp. 1859-1869.

[8] Yungang W, Jiaoyan H, Philip K, Oliver V, David C, Mark J, Thomas M, "Effect of the shutdown of a large coal-fired power plant on ambient mercury species", J. of Chemosphere, Vol. 92, 2013, pp. 360-367.

[9] Pham T, Junpen A, Garivait S, "An Investigation of Atmospheric Mercury from Power Sector in Thailand", J. of Atmosphere, Vol. 6, 2015, pp. 490-502.

[10] Brigden K, Santillo D, Stringer R, Hazardous emissions from Thai coal-fired power plants:Toxic and potentially toxic elements in fly ashes collected from the Mae Moh and Thai Petrochemical Industry coal-fired power plants in Thailand, Greenpeace Research Laboratories, Department of Biological Sciences,University of Exeter, 2002, Exeter, UK.

[11] Greenpeace, Case studies of toxic contaminants in the water near the lignite-fired power, Mae Moh district, Lampang, Greenpeace Thailand, 2008, Bangkok.

[12] Meemuk M, Distribution of Mercury Emitted from The Coal- Fired Power Plant Activities: Case Study in Lampang Province, 2011, (Environmental Technology) Faculty of Graduate Studies Mahidol University.

[13] Department of Mineral Resources, Geology of Thailand. Department of Mineral Resources, Ministry of Industry, 2001, Bangkok.

[14] Community Development District Mae Moh, 2014, Information of Lampang. Retrieved August 9, 2014, from Community Development Mae Moh, https://cddmaemo.wordpress.com.

[15] Dacha A, 2004, The Mae Moh power plant issue. Retrieved August 9, 2014, from Prachatai, http://www.prachatai.com/journal/2004/10/894.

[16] IAEA (International Atomic Energy Agency), Soil Sampling for Environmental Contaminants, IAEA-TECDOC-1415, IAEA, 2004, Vienna.

[17] Gambrell R, Metal (Hg), analysis procedures, U.S.A.: Wetland Biogeochemistry Institute, 1991, Louisiana State University.

[18] Pataranawat P, Parkpian P, Polprasert C, Delaune R, Jugsujinda A, "Mercury emission and distribution: Potential environmental risks at a small-scale gold mining operation, Phichit Province, Thailand", J. of Environmental Science and Health Part A, Vol. 42, 2007, pp. 1081-1093.

[19] United States Environmental Protection Agency (US EPA), Ecological Risk Assessment Guidance for Superfund Step 2: Screening-level Exposure Estimate and Risk Calculation, 2006, USA: Environmental Protection Agency.

[20] Yang X, Wang L, "Spatial analysis and hazard assessment of mercury in soil around the coal-fired power plant: a case study from the city of Baoji, China", J. of Environmental Geology, Vol. 53, 2008, pp. 1381–1388.

[21] Snežana D, Mirjana Ć, Latinka S, Boško G, Branislav B, Milan K, Antonije O, "Trace element distribution in surface soils from a coal burning power production area: A case study from the largest power plant site in Serbia", J. of Catena, Vol. 104, 2013, pp. 288-296.

[22] Bunt J, Waanders F, "Trace element behaviour in the Sasol-Lurgi MK IV FBDB gasifier. Part 1 — the volatile elements: Hg, As, Se, Cd and Pb", J. of Fuel, Vol. 87, 2008, pp. 2374–2387.

[23] Park K, Seo Y, Lee S, Lee J, "Emission and speciation of mercury from various combustion sources", J. of Powder Technology, Vol. 180, 2008, pp. 151–156.

[24] Liugen Z, Guijian L, Chen-Lin C, "The distribution, occurrence and environmental effect of mercury in Chinese coals", J. of Science of the Total Environment, Vol. 384, 2007, pp. 374–383.

[25] Pollution Control Department (PCD), Thai Soil Quality Standards for residential and agriculture, Pollution Control Department, 2004, Government Gazette on 2004 Oct 20, Bangkok.

[26] Pollution Control Department (PCD), Thai Groundwater quality Standards, 2000, Gazette on 2000 Sep 15, Bangkok.

[27] Pollution Control Department (PCD), Thai Surface Water Quality Standard, Pollution Control Department, 1994, Gazette on 1994 Feb 24, Bangkok.

Second International Conference on Science, Engineering & Environment,
Osaka City, Japan, Nov.21-23, 2016, ISBN: 978-4-9905958-7-6 C3051

ADSORPTION OF Cd AND Pb USING BIOMASS OF MICROALGAE *Spirulina platensis*

Lily Surayya Eka Putri[1*], Putri Sintya Dewi[1], and Dasumiati[1]

[1*]Department of Biology, Faculty of Science and Technology, State Islamic University Syarif Hidayatullah Jakarta

ABSTRACT

Microalgae are one of the biomass sources commonly used for heavy metals uptake from wastewater. *Spirulina platensis* is one of blue green algae type of Indonesia abundantly found in Indonesia water and has the ability to adsorp heavy metals, but it is very little used to metals adsorption. As cost effectiveness approach, *S. platensis* was chosen in this research which aimed to determine the effectiveness of Cd and Pb uptake by *S. platensis* for 10 days of experiments, using Dutatonik solution as growth media of microalgae. The method used was a complete random sampling with 3 varied treatments of concentration and 3 repetitions on each metal. The variation of concentration for Cd were 0.1, 1, 5 mg/L, and 1, 2, 4 mg/L for Pb, then the optimum concentration of adsorption was tested by spectrophotometer. Density and size of cells were also measured to understand the physiological impact of Cd and Pb exposures to *S. platensis*. The results showed that Cd was more effectively adsorbed by *S. platensis* than Pb which was reached 91.8 % (day 5) at concentration of 1 mg/L Cd and 84.3 % (day 5) at concentration of 1 mg/L Pb. Cell density and cell size (length and width) of *S. platensis* were not affected by the variety of Cd concentration (p>0,05), while Pb was significantly at 5% level of significance (p<0,05). It can be assumed that Pb was more toxic than Cd for *S. platensis* as cell density decreased within increasing concentration of Pb.

Keywords: Biosorbent, Cadmium, Lead, Microalgae Spirulina platensis

INTRODUCTION

Industrial wastewater without pre-treatment has resulted in many heavy metals pollution problems especially in aquatic ecosystems [1] ,[2]. This is the major issue in Indonesia was reported the serious effects to organisms [3], [4]. Heavy metals like cadmium and lead are very toxic even at low concentrations [5], [6]. Due to the toxic effects to organisms, cadmium and lead need to be removed before they accumulate in the environment and finally will pass into the human food chain which could be resulted in health problems.

Biological agent, such as algae had been studied extensively as biosorbent due to their ubiquitous occurrence in nature [7]-[11] and high efficiency in removing metals through an ion-exchange mechanism [12]-[14]. *Spirulina platensis* is one of microalgae belonging to *Cyanobacteria* has high adaptive ability because it is not affected by fluctuating environmental changes in physical and chemical parameters [15]. Many studies had been carried out using *S. platensis* on heavy metal removal [5], [16], [17]-[19]. However, none of them observed the effects of heavy metals to density and cell size of microalgae biomass. Moreover, dead cells of *S. platensis* were mostly used in many studies [16], [17], [19], but less studies used living cells.

The study using local strain of *S. platensis* for heavy metal adsorption is also limited. Therefore, this study used living cells of *S. platensis* from local strain-INK to observe the adsorption ability of Cd and Pb in aqueous solution. The efficiency of Cd and Pb ions removal were also analyzed associated with density and size of cells.

MATERIALS AND METHODS

The algae species used in this study was *Spirulina plantesis* obtained from the Laboratory of Limnology, Cibinong LIPI Bogor. The microalgae culture was maintained for mass multiplication in modified commercial leaf fertilizer (Dutatonik H-16) and incubated at 25^{o}C in a growth chamber for 8h-16h and 3000-3500 lux light using fluorescent tube lamps.

Stock solutions of the heavy metals Cd and Pb were prepared, from which concentrations 0 (control), 0.1, 1, 5 mg/L, and 0 (control),1, 2, 4 mg/L were used in case of algae tolerance experiments, respectively. A density 500,000 cells/ml of *S. platensis* was inoculated and exposed by Cd and Pb, with each

concentration then incubated for 5 and 10 days, in triplicate. Physical measurement was also observed including temperature, light intensity, humidity and pH of the media.

Each incubation period, day 5 and day 10, 25 ml of solution was stirred at 4000 rpm for 10 minutes, then the supernatant was measured using Atomic Absorption Spectrophotometer Perkin Elmer Analyst 700 to obtain the metal concentration in each solution treatments. The bioremoval efficiency of metals by *S. platensis* algae was calculated by the formula adapted from Clesceri et al. [20]:

$$S = \frac{(Ci-Ce)}{Ci}\ x\ 100\% \quad (1)$$

where, S: biosorption efficiency (biosorption efficiency) (%); C_i: initial metal concentrations in aqueous solution (mg/L); C_e: equilibrium metal concentrations in aqueous solution (mg/L).

To understand the effect of Cd and Pb on *S. platensis* cells, density and size of cell were observed. Weight of biomass was counted every day for 10 days observation from 3 ml of solution. The solution was filtered using filter paper and dried in the oven 105°C for two hours. The cell density is the difference between the weight of filter paper with dried sample on it and the weight of filter paper. The cell size consists of length and width of cells which were counted using SEM (*Scanning Electron Microscopy*) with magnification of 10x40. All the data were analyzed using Minitab version 16 to obtain the significance of correlation at each variable, including adsorption of Cd and Pb ions, cell density, and cell size.

RESULTS AND DISCUSSION

In this study the biosorption of Cd and Pb from aqueous solution was examined using the local algal strain-NKI of Indonesia *Spirulina platensis* at different variation of initial concentration. The biosorption of Cd and Pb after 5 and 10 days of incubation period with *S. platensis* is given in Fig. 1 and Fig. 2.

Figure 1 shows that the highest Cd adsorption by *S. platensis* was 91.8% at concentration 1 mg/L of Cd, in day 5 of incubation (H5). It was supported with decreasing equilibrium concentration at each initial concentration. This rapid Cd adsorption for *S. platensis* was due to the abundant availability of active binding sites on microalgae such as – COOH, –OH and $–NH_2$ [21]. After day 5, cadmium adsorption tended to decline as saturation had already occurred.

The highest adsorption of Pb by *S. platensis* reached 84.3% higher than Cd which also occurred in

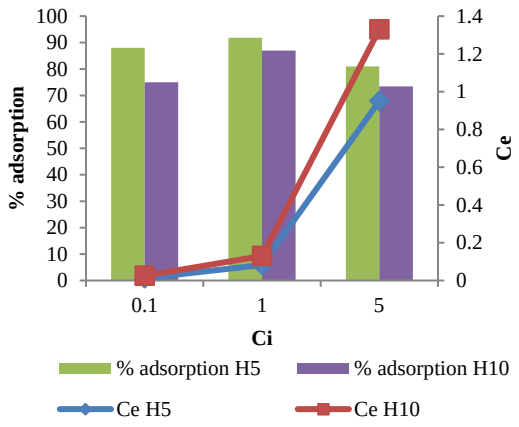

Fig. 1 Percentage of adsorption and equilibrium concentration of Cd

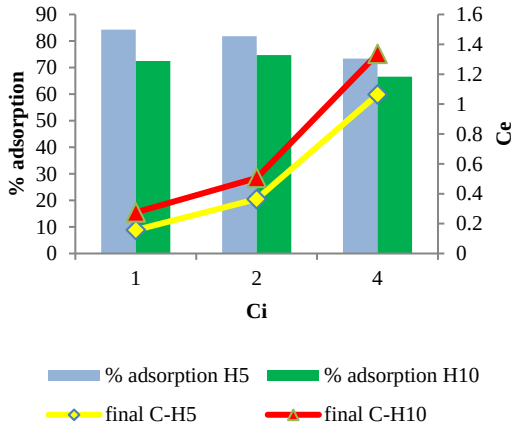

Fig. 2 Percentage of adsorption and the equilibrium concentration of Pb

day 5 of incubation. This confirms that Cd ions bond more selective to *S. platensis* than Pb ions. This is related to the mechanism for intracellular metal detoxification in living organisms which is the formation of metal-binding peptides or proteins such as metallothioneins [22], [23]. Since *S. platensis* was exposed to Cd ions, they secrete proteins from intracellular or extracellular spaces to bind the toxic metals, so toxic effect is inhibited [22]. Although increasing Pb concentration, algae are not all died, in opposite some of algae cells are still alive and can still adsorp more ions. Whereas decreasing adsorption ability of metals at day 10 was due to toxicity effect of metals in biomass of *S. platensis*. It also could be caused by the large surface area and the presence of various active sites in the cell walls which is dependent on a number of parameters: pH [24], heavy

metal type [24], algae type [25], [26] and concentration of biomassa [24].

The adsorption of metals are also related to cell density which provides more availability of active sites for binding of ions and this was proved by Huang and Lin [27], Putri et al. [28] and Soeprobowati & Hariyati [5]. The studies showed decreasing cell density at the longer incubation time, after rapid growth at first period of incubation. Figure 3 and 4 exhibit the trend of cell density in variety of incubation time. It shows that density of cells increased until day 5 and 6, then decreased slightly with longer incubation time. The increasing initial concentration of metals also affected declining cell density which occurred in Pb exposure on *S. platensis* but not in Cd exposure. Statistically, exposure of Pb on *S. platensis* was significantly correlated to cell density ($p<0.05$) while for Cd was not ($p>0.05$). This is related to toxic effect of metals

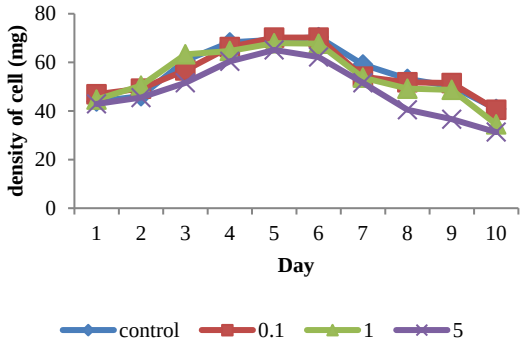

Fig. 3 Cell density of *S. platensis* exposed by Cd

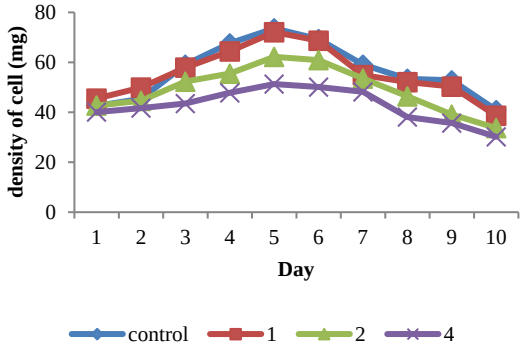

Fig. 4 Cell density of *S. platensis* exposed by Pb

[28]. It can be assumed that Pb ions were more toxic for *S. platensis* than Cd ions. However, the toxicity of metals could be different for other microalgae depending on the presence of various active sites in the cell walls [21].

Cells density of *S. platensis* followed the exponential pattern which showed growth phase of cell including phase of lag, exponential, stationary and death [29]. The lag phase occurred at day 1 followed by exponential phase at day 2 to 5 when cells grew increasingly and density of cells increased. After day 5 to 7, cells were in stationary phase marked by maximum density of cells. Death phase occurred from day 8 to 10 and cells decreased slightly.

The highest cell density reached 70.2 mg at 0.1 mg/L of Cd concentration on day 5, whereas 72.1 mg of cells was obtained on day 5 at 1 mg/l of Pb concentration. It proves that cell density can also used to analyze metals adsorption by living cells such as microalgae. The living cells can adapt well on the treatment medium since availability of nutrients in medium was maintained. Nutrients [30] and rapid growth ability of living cells are the main advantage of biosorption technology.

On day 10, cell density decreased both in Cd and Pb exposures which also occurred in higher concentration of metal ions. This showed that the higher concentration of metal ion, the more toxic metal ions which further caused cell dead and poisoned. Only surviving cells were able to form colonies and continue in cell division.

Biosorption ability of *S. platensis* to adsorb metal ions was also supported by pH. During the 10 days of observation, pH of observed culture medium was fluctuated. The highest adsorption of Cd and Pb were in pH 8.8 and 8.79 respectively. Increasing pH value on observed medium was caused by the breakdown of proteins and other nitrogen compounds which was ammonium (NH_4^+) as a form of organic compounds which proceed decomposition [31]. This compound will accumulate and settle in the the bottom of culture medium which in further will poison cells and cells died. It also interferres the adsorption of dissolved oxygen and nutrients which is conducted by the cells are still alive [32].

However, alkaline pH is not suitable for the adsorption of Pb due to precipitation of ions. This was supported by Al-Homaidan et al. [18] which reached up to 91% lead adsorption at acidic pH 3, while less adsorption of lead obtained in this study, only 84.3% at pH 8.79.

For Cd adsorption, it showed higher adsorption at alkaline pH 8.8. This result was the same as reported by Al-Homaidan et al. [17]. The control of pH in culture medium is very important to maintain the balance of cell growth of *S. platensis*. Temperature and light is able to accelerate the metabolism of *S. platensis* in absorbing metal ions, [33]. In this study, the physical condition of culture room demonstrated suitable conditions for growth of *S. Platensis*. The temperature was at 26.6°-27.9°C,

the humidity ranged 71-79%, and the light intensity of the culture was around 3008-3014 Lux.

Other parameter used in this study was cell size to analyze the adsorption effects of Cd and Pb on *S. platensis* biomass. The cell size was differed from length and width of cells given in Fig. 5 and 6.

The length and width of *S. platensis* had similar trend both in Cd and Pb exposures which increased slightly at day 5 of incubation, then decreased at day 10. It exhibited the same pattern as growth of *S. platensis* biomass which was exponential pattern.

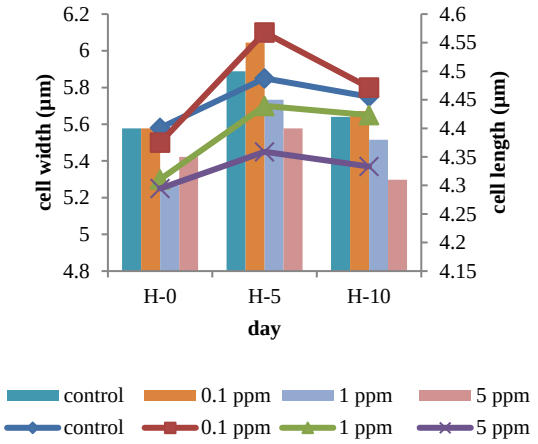

Fig. 5 Cell size of *S. platensis* exposed by Cd

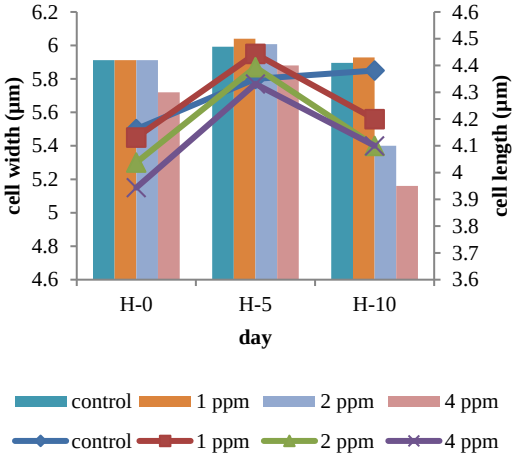

Fig. 6 Cell size of *S. platensis* exposed by Pb

Based on statistical analysis, cell size of *S. platensis* had significant correlation with cell density ($p<0.05$), however it was not correlated significantly with initial concentration of metal ions ($p>0.05$).

Higher concentration of Cd and Pb were resulted in shorter length and width of cell and lower cell density. This is presumably due to the excessive concentration of metals which can damage the chloroplast, since the chloroplast is the most sensitive part of cell to heavy metals [29]. Destruction of chloroplast implies loss of pigment and will disturb photosynthetic activity which occurred in thylakoid membranes [34]. Broken chloroplast will inhibit respiration process in cells so that the ability of cells to proliferate is reduced. This led to the increase in number of cells to be blocked. If protein in *S. platensis* cells is damaged then nutrient transport into the cells was inhibited, so that most of the *S. platensis* cells die [35].

CONCLUSION

Spirulina platensis, the local algae strain-INK was proved effectively remove Cd and Pb ions from aqueous solution and indicated a very good candidate as biosorption agent of heavy metals. The highest biosorption of Cd and Pb were 91.8% and 84.3% both at 1 mg/L of initial concentration on day 5, respectively. Only density cells can also be considered as adsorption parameter of heavy metals removal in water or wastewater, since in this study cell density showed significant correlation with metal ions adsorption ($p<0.05$).

ACKNOWLEDGEMENT

Authors would like to thank Indonesian Institute of Sciences (LIPI) which had given stock culture of *Spirulina platensis*. Authors also thank to laboratory staff of Biology Department, Faculty of Science and Technology, State Islamic University Syarif Hidayatullah Jakarta who had helped in preparation of the experiments.

REFERENCES

[1] Inthorn D, Nagase H, Isaji Y, Hirata K and Miyamoto K, "Removal of cadmium from aqueous solution by the filamentous cyanobacterium *Tolypothrix tenuis"*, J. Ferment Bioeng, 82, 1996, pp. 580-584.

[2] Rai LC, Gaur JP and Kumar HD, "Phycology and heavy-metal pollution", Biol Rev, 56, 1981, pp. 99-103.

[3] Putri LSE, Prasetyo AD and Arifin Z, "Green mussel and bioindicator of heavy metals pollution at Kamal Estuary, Jakarta Bay, Indonesia", J. Environmental Research and Development, Vol 6, No. 3, Jan-March 2012, pp. 1-8.

[4] Govind P and Mudhori S, "Heavy metals causing toxicity in animals and fishes",

Research J. of Animal, Veterinary and Fishery Sciences, Vol. 2, No. 2, February 2014, pp. 17-23.

[5] Soeprobowati TR and Hariyati R, "Phycoremediation Pb^{2+}, Cd^{2+}, Cu^{2+}, and Cr^{3+} by *Sprirulina platensis* (Gomont) Geitler", American J. of Bioscience, Vol. 2, No. 4, 2014, pp. 165-170.

[6] Vimala R and Das N, "Biosorption cadmium (II) and lead (II) from aqueous solutions using mushrooms: A comparative study", J. Hazard. Mater., 168, 2009, pp. 376-382.

[7] Wilde EW and Benemann JR, "Bioremoval of heavy metals by the use of microalgae", Biotechnol. Adv. Vol. 11, 1993, pp. 781–812.

[8] Wong KH, Chan KY and Ng SL, "Cadmium uptake by the unicellular green alga *Chlorella salina* CU-1 from culture media with high salinity", Chemospheres Nos, Vol. 11/12, 1979, pp. 887-891.

[9] Sakaguchi T, Tsuji T, Nakajima A and Horikos T, "Accumulation of cadmium by green microalgae", Eur J Appl Microbiol Biotechnol, Vol. 8, 1979, pp. 207-15.

[10] Hans JG and Urbach W, "Sorption of cadmium by the green microalgae *Chlorella vulgaris*", *Ankistrodesmus braunii* and *Eremosphaera viridis*. Z Pflanzenphysiol, Vol. 109, 1983, pp. 127-241.

[11] Inthorn D, Incharoensakdi A and Sidtitoon N, "Removal of mercury, cadmium and lead in aqueous solution by microalgae", Asian Journal of Microbiology Biotechnology and Environmental Sciences (AJMBES), Vol. 3, 2001, pp. 109-116.

[12] Crist DR, Crist RH, Martin R and Watson JR, "Ion exchange system in proton-metal reactions with algal cell walls FEMS", Microbiol. Rev, Vol. 14, 1994, pp. 309-314.

[13] Schiewer S and Volesky B, "Modelling multi metal ion exchange in absorption", Environ. Sci. Technol., Vol. 30, 1996, pp. 2921-2927.

[14] Kratochvil D and Volesky B, "Advances in biosorption of heavy metals", Tib. Tech., Vol. 16, 1998, pp. 291-300.

[15] Kabinawa INK, *Spirulina* as healer for diseases. Jakarta: PT. Agromedia Pustaka, 2006.

[16] Monika B, Alka S, Srivastava JK and Palsania J, "Biosorption of heavy metals from wastewater by using microalgae", International J. of Chemical and Physical Sciences, Vol. 3, No. 6, Nov-Dec 2014, pp. 67-81.

[17] Al-Homaidan AA, Al-Alabdullatif JA, Al-Hazzani AA, Al-Ghanayem AA and Alabbad AF, "Adsorptive removal of cadmium ions by *Spirulina platensis* dry biomass"', Saudi J. of Biological Sciences, Vol. 22, issue 6, November 2015, pp. 795-800.

[18] Al-Homaidan AA, Alabbad AF, Al-Hazzani AA, Al-Ghanayem AA, and Al-Alabdullatif JA, "Lead removal by *Spirulina platensis* biomass", International J. of Phytoremediation, Vol. 18, No. 2, 2016, pp. 184-189.

[19] Zinicovzcaia I, "Removal of chromium from wastewater by activated carbon and *Spirulina platensis*: a comparative study", J. of Science and Art, No. 2(32), 2015, pp. 239-248.

[20] Clesceri L, Arnold E, Greenberg E, Eaton AD, Standard Methods for Examination of Water and Wastewater, 20 ed. American Public Health Association, American Water Work Association, Water Environment Federation, 1999.

[21] Wang J dan Chen C, "Biosorbents for Heavy Metals Removal and Their Future", Biotechnol Advanced., Vol. 27, 2009, pp. 195-226.

[22] Perales-Vela HV, Pena-Castro JM and Canizares-Villanueva RO, "Heavy metal detoxification in eukaryotic microalgae", Chemosphere, Vol. 64, 2006, pp. 1–10.

[23] Arunakumara KKIU and Zhang X, "Heavy metal bioaccumulation and toxicity with special reference to microalgae", J. Ocean Univ. Chin., Vol. 7, 2008, pp. 60-64.

[24] Naja G and Volesky B, "The mechanism of metal cation and anion biosorption", Microbial Biosorption of Metals, P. Kotrba, M. Mackova & T. Macek, Ed.. Springer, Dordrecht, 2011, pp. 19–58.

[25] Kaplan D, Christiaen D and Arad (Malis) S, "Chelating properties of extracellular polysaccharides from *Chlorella* spp", Appl. Environ. Microbiol., Vol. 53, 1987, pp. 2953–2956.

[26] De Philippis R, Paperi R and Sili C, "Heavy metal sorption by released polysaccharides and whole cultures of two exopolysaccharide producing cyanobacteria", Biodegradation, Vol. 18, 2007, pp. 181–187.

[27] Huang S and Lin G, "Biosorption of Hg(II) and Cu(II) by biomass of dried *Sargassum fusiforme* in aquatic Solution", J. Environ. Health Sci. Eng., Vol. 13, No. 21, 2015, pp. 1-8.

[28] Putri LSE, Fauziah and Dasumiati, "Biosorption ability of *Scenedesmus dimorphus* for Cr (VI) and Cd in aqueous solution", Advance Science Letter, Vol 21, 2015, pp. 196-198.

[29] Becker EW, Microalgae Biotechnology and Microbiology. London: Cambridge University Press., 1994.

[30] Hala Y, Suryati E and Taba P, "Biosorption of Pb^{2+} and Zn^{2+} by *Chaetoceros calcitrans*" (thesis). Makassar, Indonesia: Chemistry Department, Faculty of Math and Life Science, University of Hassanudin, 2012.

[31] Prihantini NBP, Putri DB and Yuniati R, "Growth of *Chlorella* spp in MET medium with intial pH variation", accepted by University of Indonesia, 2005.

[32] Suantika G and Pingkan S, "Effect of initial density to quality of *Chaetoceros gracilis* (Schuut) culture in batch system (thesis). Bandung, Indonesia: Bandung Institute of Technology, 2009.

[33] Fachrullah MR, "Growth rate of biofuel produced microalgae *Chlorella* sp. and *Nannochloropsis* sp. cultivated in tin mining wastewater at Bangka Island" (thesis). Bogor: Marine and Fishery Faculty, Bogor Agriculture Institute, 2011.

[34] Olivares E, "The Effect of Lead on Phyto Chemistry of Tithonia Exposed to Roadside Automotive Pollution or Grown in Pots of Pb Suplemented Soil", *Braz J Plant.*, Vol. 15, No. 3, 2003, pp. 149-158.

[35] Perales HV, González S, Montes C and Canizares RO, "Growth, Photosynthetic and Respiratory Responses to Sub-lethal Copper Concentrations in *Spirulina* (*Chlorophyceae*)", Journal of Algae, Vol. 67, 2007, pp. 2274-2281.

Second International Conference on Science, Engineering & Environment,
Osaka City, Japan, Nov.21-23, 2016, ISBN: 978-4-9905958-7-6 C3051

ENVIRONMENTAL IMPACTS OF RECYCLED NONMETALLIC FRACTION FROM WASTE PRINTED CIRCUIT BOARD

Suphaphat Kwonpongsagoon[1*], Sawanya Jareemit[1], and Premrudee Kanchanapiya[2]
[1] Department of Sanitary Engineering, Faculty of Public Health, Mahidol University, Bangkok, Thailand;
Center of Excellence on Environmental Health and Toxicology (EHT), Bangkok, Thailand
[2] National Metal and Materials Technology Center, National Science and Technology Development Agency,
Ministry of Science and Technology, Pathumthani, Thailand

ABSTRACT

Recently in Thailand, the recycling process of waste printed circuit board (WPCB) has retained a large volume of nonmetallic fraction (NMF), which has entered the industrial waste stream and awaits an appropriate treatment to be suggested. The aim of this paper was to assess environmental impacts of the recycled nonmetallic fraction from waste printed circuit board in Thailand, using the ReCiPe midpoint assessment method of life cycle assessment approach. For this purpose, one of the glass fiber reinforced plastic (GFRP) manufacturers in Thailand was selected to obtain data for NMF waste and the production of two new recycled NMF products. The environmental impacts of two new recycled NMF products compared with traditional GFRP product, and two recycled NMF products compared with conventional waste disposal methods by means of landfilling and incineration were considered. The result showed that the potential environmental impacts were in the damage categories of climate change, human toxicity, marine ecotoxicity, and fossil depletion. For overall comparison, the recycled NMF as a modified GFRP product (recycled product 1) showed the worst impacts to human toxicity, marine ecotoxicity, and fossil depletion categories compared with other methods because of the complex production technique and the chemical-based process. Moreover, the recycling of NMF as a new product (recycled product 2) is likely to be the most suitable waste management option in Thailand.

Keywords: Nonmetallic Fraction, Waste Printed Circuit Board, Recycling, Waste Management, Life Cycle Assessment

INTRODUCTION

E-waste, or Waste from Electrical and Electronic Equipment (WEEE), is an emerging and fast-growing waste stream with complex characteristics in both developed and developing countries. According to the global e-waste report in 2014, although the average highest per capita e-waste quantity (15.6 kg/cap.) was estimated in Europe, Asia is the largest e-waste generation source, around 16Mt [1]. In Thailand without related regulation in force, e-waste generation was estimated at 6.4 kg per capita in 2014 and has increased steadily around 10 to 20% every year [2], [3]. Therefore, the handling and treatment of these wastes have become a topic of worldwide concern.

Printed Circuit Board or PCB is a basic component in all electrical and electronic devices ranging from large to small items such as fridges, washing machines, computers, TVs, CD/DVD players, radios, mobile phones, and shavers. Although overall, the PCB proportion is only about 3% to 6% by WEEE total weight, the complex array of toxic substances present in PCBs are very specific and need to be treated carefully [4]. In general, PCB contains approximately 28 to 30% metals and 70 to 72% nonmetals [5], [6]. The typical metals in PCB consist of copper (20%), iron (8%), tin (4%), nickel (2%), lead (2%), zinc (1%), silver (0.2%), gold (0.1%), and palladium (0.005%) [7]. The value of the metallic fractions (MF) of PCB is a major economic driving force to recycle Waste Printed Circuit Board (WPCB). In Thailand, the commercial recycling process of the WPCB industry currently focuses only on the recovery of copper. After the recycling process of WPCB, a large volume of nonmetallic fraction (NMF) mainly consisting of resin and glass fiber, has entered the industrial waste stream and awaits appropriate treatment. This waste can be usually treated by conventional waste disposal methods, like incineration or secured landfilling. The incineration of NMF will cause the formation of highly toxic substances such as polybrominated dibenzodioxins and dibenzofurans (PBDD/Fs) while landfilling of the NMF will lead to secondary pollution caused by heavy metals and brominated flame retardants (BFRs) leaching to the groundwater [8], [9]. In addition, NMF disposal by incineration and landfilling can cause the loss of resource use because of the resin and glass fiber contained in NMF. In view of sustainable waste management and urban mining concepts, not only valuable metals such as copper, silver and gold in PCB can be recovered but also NMF should be

exploited as a resource in other related industrial processes. In our previous studies [10], [11], NMF could be recycled as a filler in fiber-reinforced polymer to make products, e.g., artificial wall tile. Other studies also found that possible applications of NMF include construction materials, composite boards, sewer gates, heavy metal absorbers, activated carbon and sound absorbers [12]-[14].

The highlighted questions below have arisen and will be answered in this study.

1) What is the environmental impact(s) of these new fiber-reinforced plastic (FRP) products containing NMF compared with traditional Glass Fiber Reinforced Plastic (GFRP) products?

2) In terms of the environment, which method is the most appropriate waste management option for NMF in Thailand? Four different waste management methods including landfilling, incineration, recycling as a modified GFRP product, and recycling as a new product were considered in this study.

To answer these questions, the Life Cycle Assessment (LCA) method, a technique to assess the potential environmental impacts associated with a product, process, or service was applied in this study. The method could be undertaken by compiling an inventory of relevant energy and material inputs and environmental releases, evaluating the potential environmental impacts associated with identified inputs and releases and interpreting the results to help us make a decision. The four basic stages in conducting the LCA include goal and scope definition, inventory analysis, impact assessment and interpretation [15]. The method has been widely applied in many research studies, e.g., [16]-[18].

MATERIALS AND METHODS

Materials and Recycled Products

The waste material NMF was obtained from one of the WPCB recycling plants located in Samut Sakhon Province, Thailand. The physical and chemical characteristics of NMF from WPCB were thoroughly analyzed and can be found in our previous investigations [10], [11]. The NMF collected was then used as a resource (a secondary raw material) in the glass fiber reinforced plastic (GFRP) manufacturing process at the F.R.P. Industry Co., Ltd. In general, the compositions of fiber reinforced plastic (FRP) consist of resin mixed with a monomer, accelerator, hardener and filler. Because NMF material mainly consists of resin and glass fiber, it can be used to substitute for primary raw materials, i.e., resin and filler, of the FRP production process. The two types of furniture products (table top) listed below, containing NMF material, were finally selected as recycled products for this study.

1. Modified GFRP table top (or recycled product 1): using traditional production method by hand lay-up technique, together with NMF composite material to replace plywood (which is used to increase the thickness of the product), and to replace glass fiber.

2. New table top (or recycled product 2): a casting process transforming NMF waste to make a new composite product.

To make the NMF composite (we introduced this new composite to the GFRP factory) for both recycled products mentioned above, the type of chemicals used and ratio of chemical composition of each type of table top product in accordance with our Thai petty patent No. 8341 were used and summarized in Table 1. All details of raw materials including equipment used, manufacturing process, production techniques, processing time and properties tested are all found in Jareemit [19].

Table 1 Raw materials used for the 1x1 m^2 table top product with 1 cm thickness

Ingredients	Content (kg)		
	Traditional product	Modified product	New product
Polyester resin	2.90	10.81	8.56
Glass fiber	0.9	0.9	-
Methyl ethyl ketone peroxide	0.045	0.167	0.122
Plywood	12	-	-
NMF from WPCB	-	10.2	10.2
Styrene monomer	-	2.04	2.04
Acetone	1	1	1
Water	1	1	1
Total weight	17.845	26.117	22.922

Life Cycle Assessment (LCA)

As can be seen in Fig. 1, the system boundary of the study that defines what is included in the assessment starts by collecting of NMF from a waste generator in the Samut Sakhon area, transportation, waste treatment alternatives (recycling, incineration and landfilling), and manufacturing of FRP furniture products. The functional unit of the LCA study is based on 1x1 m^2 table top with 1 cm thickness. In this study, the waste treatment options detailed below are modeled so that we can compare their environmental impacts.

Option 1: NMF waste landfilling and traditional GFRP table top production. In this option, all NMF waste is transported to a hazardous waste landfill site located in Saraburi Province, about 140 km northeast of Samut Sakhon. The cement-based solidification/stabilization is usually applied to immobilize toxic substances before depositing the waste in a secured landfill. The traditional GFRP

table top with no NMF used as a resource is normally manufactured in Samut Sakhon.

Option 2: NMF waste incineration and traditional GFRP table top production. All NMF waste is treated at an incineration plant in Samut Prakan Province, located 65 km east of the waste generating plant. Similar to option 1, the traditional GFRP table top with no NMF used as a resource is normally manufactured in Samut Sakhon.

Option 3: NMF waste recycling as a modified GFRP table top (or recycled product 1). This option explores the potential environmental impacts of recycled product 1 as described above. The waste is used as a secondary material for the FRP production process at F.R.P. Industry Company, only 10 km away from the waste generator.

Option 4: NMF waste recycling as a new table top product (or recycled product 2). Similar to option 3, the NMF is used as a secondary material at the F.R.P. Industry Company, but to produce a new table top product.

The data used for life cycle inventory was primarily gathered from the F.R.P. Industry Co., Ltd. (e.g. raw materials in Table 1), previous researches [17]-[19], relevant reports, literature, and databases provided in SimaPro Version 7.3. The World ReCiPe Midpoint impact assessment method was chosen to estimate the environmental impacts in this study. The environmental impacts of NMF waste for all impact categories were assumed to be zero. In life cycle impact assessment, all emissions of the inventory were sorted into classes according to the effect on the environment. These emissions were then multiplied by the characterization factors of each substance within each impact category as presented in Eq. (1).

$$CI = \sum_s EL \times CF \quad (1)$$

Where subscript "s" mean substance; CI is category indicator; EI is emission load; and CF is characterization factor.

All collected data in relation to the four waste management models mentioned above was used as input data in SimaPro LCA software version 7.3 to calculate all environmental impact categories in this study (see more details of method in SimaPro Database Manual for the impact category indicators [20]).

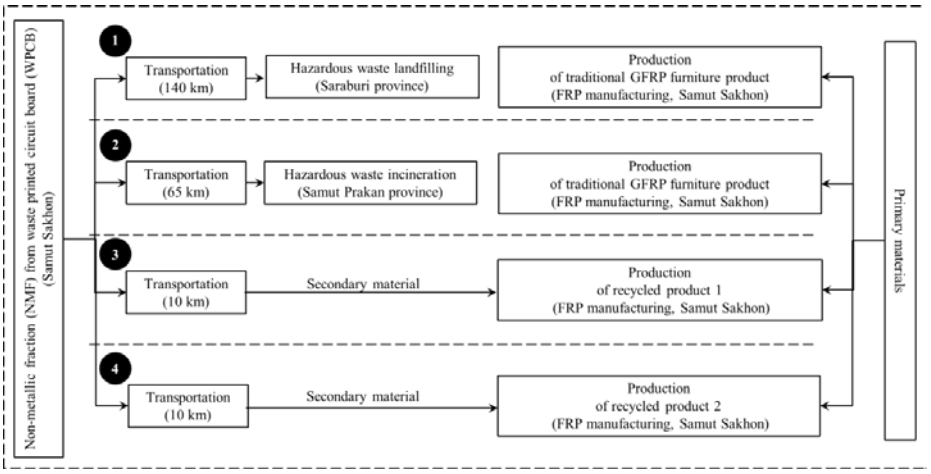

Fig. 1 System boundary of LCA study for NMF from WPCB (option 1 – 4)

RESULTS AND DISCUSSION

In the case of NMF recycling, the weight percentage of raw materials used for the two products (recycled products 1 and 2) compared with traditional GFRP products are shown in Fig. 2. It can be seen that among those primary chemicals used to produce products, the highest amount of polyester resin is present in recycled product 1 (modified GFRP table top), followed by recycled product 2 (new table top product) and traditional product. The NMF from WPCB can be used to replace primary raw materials, like the plywood sheet, and glass fiber of the traditional GFRP product. However, the newly made NMF composite required another chemical (styrene monomer) to reduce the viscosity of the NMF mixture during the casting process [19]. Thus, the styrene monomer was additionally applied to make both recycled products about 8 to 9% as shown in Fig. 2 (calculated from data inventory of Table 1).

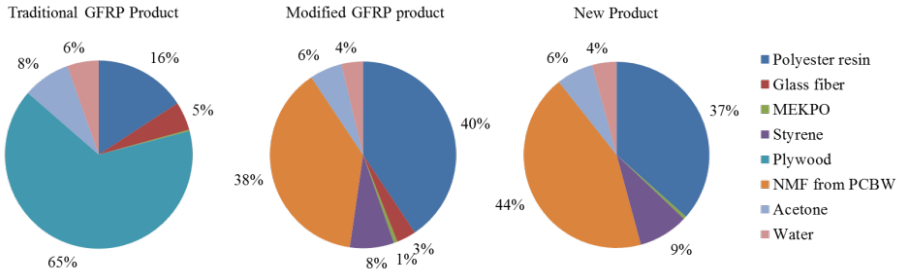

Fig. 2 Weight percentage of different raw materials used for traditional GFRP, modified GFRP and new product

From the calculation results of SimaPro program, Fig. 3 shows the environmental impacts of two new products containing NMF composite compared with the traditional GFRP product. They relate to raw materials used for a 1x1 m^2 table top with 1 cm thickness. Four damage categories, consisting of climate change, human toxicity, marine ecotoxicity and fossil depletion, are present for all three products. Only traditional GFRP product contributes agricultural land occupation impact because of the use of plywood sheet (see Fig.3). In the light of those four impact categories, except agricultural land occupation, overall the highest impact values resulted from the modified GFRP product (recycle product 1), followed by the new product (recycled product 2) and the traditional GFRP product. It became obvious that almost 100% of environmental impacts in all categories of the two recycled products resulted from polyester resin, a major raw material required in the production process (assuming zero impact for NMF waste). This is because these recycled NMF products depend highly on chemical use (see also Fig.2)

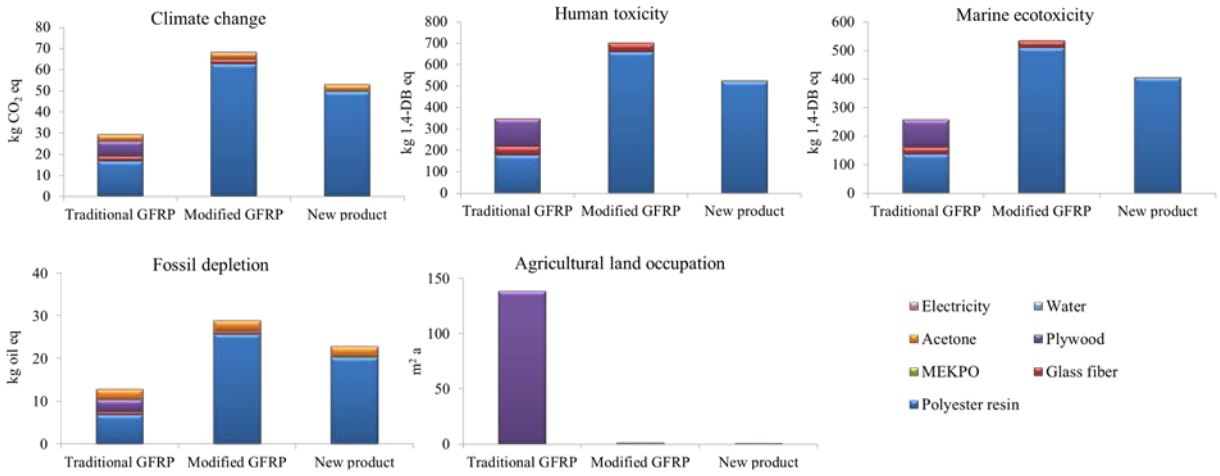

Fig. 3 Environmental impacts of traditional GFRP, modified GFRP and new product related to raw materials used for a 1x1 m^2 table top with 1 cm thickness

According to material selection guidelines for eco-compatible products [21], one recommendation here is to change most used chemicals to more environmentally friendly ones. In this case, based on the same production technique of GFRP manufacturing, two types of resin can be used in the process, namely, polyester resin and epoxy resin. When comparing the environmental impacts between polyester and epoxy resins, we found that epoxy resin has a much lower impact to human toxicity and marine ecotoxicity, around 80% while not differing much regarding climate change and fossil depletion impacts (see Fig. 4). However, after discussion with several manufacturers and suppliers in Thailand, polyester resin is still preferred over epoxy resin. Although epoxy resin has less toxicity, and can give a better property of products in terms of product strength, it costs more around twice compared with polyester resin. In addition, those manufacturers claimed that the properties of polyester resin were adequate for their customers' needs to produce GFRP products in terms of product strength and durability.

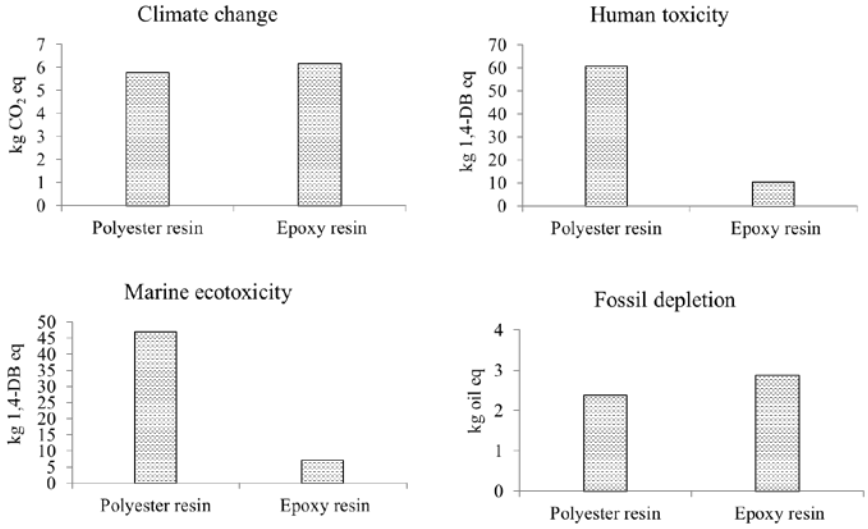

Fig. 4 Environmental impacts of 1 kilogram polyester resin compared with1 kilogram epoxy resin

Finally, comparative environmental impacts of two recycled NMF products and conventional waste disposal methods by means of landfilling and incineration were conducted. As can be seen in Fig. 5, all options contribute to the five damage categories including climate change, human toxicity, marine ecotoxicity, fossil depletion and agricultural land occupation. Since plywood was not used as a raw material in the recycled products, no impact to the agricultural land occupation category was caused by the recycling options 3 and 4.

Looking at the climate change damage category, option 1 caused the worst impact when compared with other options. This could have resulted from the disposal process of landfilling, followed by the FRP production and the transportation between the waste generator and disposal site. In other words, landfilling is the most inappropriate method for this case in terms of climate change impact. Recycling option 3 shows the worst impact to human toxicity, marine ecotoxicity, and fossil depletion categories compared with other options (see Fig. 5). This is because recycled product 1 (option 3) required a more complicated production process by applying both traditional production method (hand lay-up technique) and casting NMF composite. Comparing between two recycling products (options 3 and 4), the new product option 4 had less impact on all damage categories.

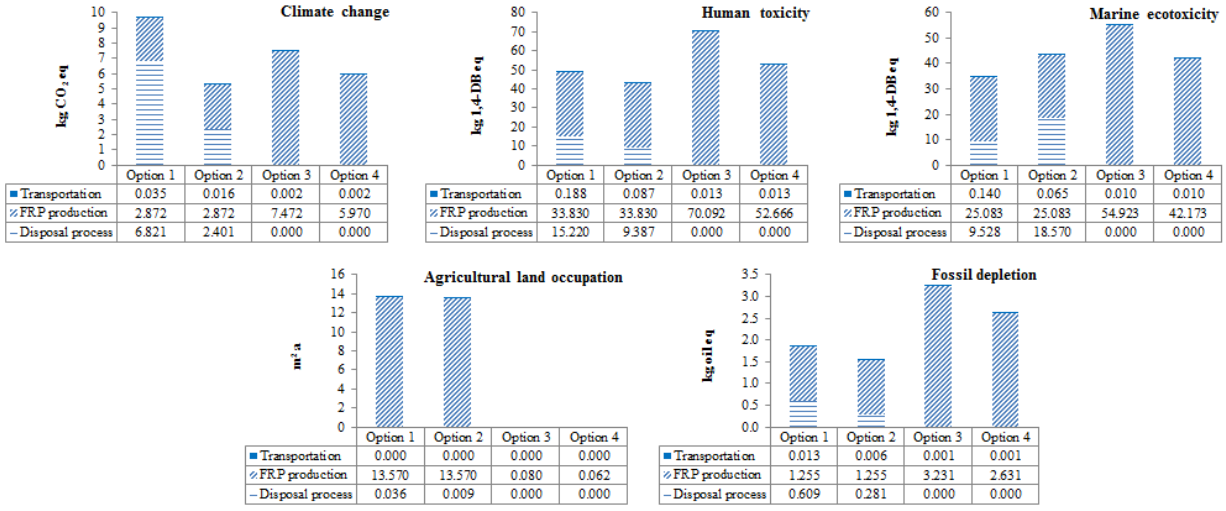

Climate change	Option 1	Option 2	Option 3	Option 4
Transportation	0.035	0.016	0.002	0.002
FRP production	2.872	2.872	7.472	5.970
Disposal process	6.821	2.401	0.000	0.000

Human toxicity	Option 1	Option 2	Option 3	Option 4
Transportation	0.188	0.087	0.013	0.013
FRP production	33.830	33.830	70.092	52.666
Disposal process	15.220	9.387	0.000	0.000

Marine ecotoxicity	Option 1	Option 2	Option 3	Option 4
Transportation	0.140	0.065	0.010	0.010
FRP production	25.083	25.083	54.923	42.173
Disposal process	9.528	18.570	0.000	0.000

Agricultural land occupation	Option 1	Option 2	Option 3	Option 4
Transportation	0.000	0.000	0.000	0.000
FRP production	13.570	13.570	0.080	0.062
Disposal process	0.036	0.009	0.000	0.000

Fossil depletion	Option 1	Option 2	Option 3	Option 4
Transportation	0.013	0.006	0.001	0.001
FRP production	1.255	1.255	3.231	2.631
Disposal process	0.609	0.281	0.000	0.000

Fig.5 Environmental impacts of four waste management options for NMF from WPCB

CONCLUSION

After comparing our two recycled NMF products with the traditional GFRP product, it can be concluded that the highest impact values resulted from modified GFRP product (recycle product 1), followed by new product (recycled product 2) and traditional GFRP product. Although the recycling of NMF waste as new products shows higher environmental impacts than the traditional products, the traditional product contributes more damage categories than our recycled products. Among waste management options, it can be concluded that the potential environmental impacts were the damage categories of climate change, human toxicity, marine ecotoxicity and fossil depletion. For the overall comparison, because of a more complicated production technique and a chemical-based process, the recycled NMF as a modified GFRP product showed the worst impacts in human toxicity, marine ecotoxicity and fossil depletion categories compared with other methods. However, the manufacturers can help to reduce the toxicity of products by changing the raw material from polyester to epoxy resin. Thus, the recycling of NMF as a new product (recycled product 2) is likely to be the most suitable waste management option in Thailand.

ACKNOWLEDGEMENTS

This research work was supported in part by a grant from the Center of Excellence on Environmental Health and Toxicology, Science & Technology Postgraduate Education and Research Development Office (PERDO), Ministry of Education. Moreover, this study was supported for publication by the China Medical Board (CMB), Faculty of Public Health, Mahidol University, Bangkok, Thailand.

REFERENCES

[1] Baldé CP, Wang F, Kuehr R, and Huisman J, " The global e-waste monitor – 2014", United Nations University, IAS – SCYCLE, Bonn, Germany, 2015.

[2] Bureau of Policy and Strategy, "Electronic waste", J. of Health Fact sheet, Vol. 8, 2015, unpaged.

[3] Kanchanapiya P, "E-waste: technology of printed circuit board management", Bangkok: Thai effect studio, 2011.

[4] Hadi P, Barford J, and Mckay G, "Novel application of the nonmetallic fraction of the recycled printed circuit boards as a toxic heavy metal adsorbent", J. of Hazardous Materials, Vol. 252–253, 2013b, pp. 166-170.

[5] Pinyo W, Nusom Y, Saeheng P, Karnchanapiya P, and Annanon K, "Resource recovery process from industrial waste", in Proc. 4th International Workshop and Conference on Earth Resources Technology, 2010.

[6] Jianzhi L, Shrivastava P, Zong G, and Hong-Chao Z, "Printed circuit board recycling: a state-of-the-art survey", Electronics Packaging Manufacturing, IEEE Transactions on, Vol. 27(1), 2004, pp. 33-42.

[7] Huang K, Guo J, and Xu Z, "Recycling of waste printed circuit boards: a review of current technologies and treatment status in China", J. of Hazardous Materials, Vol. 164(2–3), 2009, pp. 399-408.

[8] Tesanan S, Kwonpongsagoon S, and Kanchanapiya P,"Solidification/stabilization of nonvaluableresidue from waste printed circuit board assembly", Int. J. of GEOMATE, Vol. 11(24), 2016, pp. 2307-13.

[9] Duan H, Li J, Liu Y, Yamazaki N, and Jiang W, "Characterization and inventory of PCDD/Fs and PBDD/Fs emissions from theincineration of waste printed circuit board", Environmental Science & Technology, Vol. 45(15), 2011, pp. 6322-6328.

[10] Kanchanapiya P, Pinyo W, Jareemit S, and Kwonpongsagoon S, "The recycling of non-metallic powder from printed circuit board waste as filler material in fiber reinforced polymer", Environmental Protection Engineering, Vol.41(4), 2015, pp.151-166.

[11] Jareemit S, Kanchanapiya P, Saeheng P, Pinyo W, and Kwonpongsagoon S, "The recycling of non-metallic fraction from printed circuit board waste as reinforcing material in the artificial wall tile", in Proc. 3rd International Conference on Green and Sustainable Innovation, 2012.

[12] Sun Z, Shen Z, Ma S, and Zhang X, "Sound absorption application of fiberglass recycled from waste printed circuit boards", Materials and Structures, Vol. 48(1-2), 2015, pp. 387-392.

[13] Wang X, Guo Y, Liu J, Qiao Q and Liang J, "PVC-based composite material containing recycled non-metallic printed circuit board (PCB) powders", J. of Environmental Management, Vol. 91(12), 2010, pp. 2505-2510.

[14] Zheng Y, Shen Z, Ma S, Cai C, Zhao X, and Xing Y, "A novel approach to recycling of glass fibers from nonmetal materials of waste printed circuit boards", J. of Hazardous Materials, Vol. 170(2–3), 2009b, pp. 978-982.

[15] International Organisation for Standardisation, "ISO 14040 (2006): environmental management - life cycle assessment - principles and framework", 2006.

[16] Rigamonti L, Grosso M, Møller J, Martinez Sanchez V, Magnani S, and Christensen TH, "Environmental evaluation of plastic waste management scenarios", Resources, Conservationand Recycling, Vol. 85(0), 2014, pp. 42-53.

[17] Song YS, Youn JR, and Gutowski TG, "Life cycle energy analysis of fiber-reinforced composites", Composites Part A: Applied Scienceand Manufacturing, Vol. 40(8), 2009, pp. 1257-1265.
[18] Merrild H, Damgaard A, and Christensen TH, "Life cycle assessment of waste paper management: the importance of technology data and system boundaries in assessing recycling and incineration", Resources, Conservation and Recycling, Vol. 52(12), 2008, pp. 1391-1398.
[19] Jareemit S, "The recycling of non-metallic fractions from printed circuit boards wastes as a FRP (Fibers Reinforced Plastic) furniture product", Master's thesis, Mahidol University, 2015.
[20] PRé Consultant, "SimaPro database manual – methods", 2016.
[21] Allione C, De Giorgi C, Lerma B, and Petruccelli L, "From eco-design products guidelines to materials guidelines for a sustainable product. qualitative and quantitative multicriteria environmental profile of a material", J. of Energy, Vol 39, 2012, pp 90-99.

Second International Conference on Science, Engineering & Environment,
Osaka City, Japan, Nov.21-23, 2016, ISBN: 978-4-9905958-7-6 C3051

THE ANAEROBIC BAFFLED REACTOR (ABR) : PERFORMANCE AND MICROBIAL POPULATION AT VARIOUS COD LOADING RATES

Sopa Chinwetkitvanich[1*] and Apaporn Ruchirased[1]
[1]Department of Sanitary Engineering, Faculty of Public Health, Mahidol University, Bangkok, Thailand

ABSTRACT

Anaerobic Baffled Reactor (ABR) is one type of high-rate anaerobic reactor equipped with a series of baffles. This baffles plays an important role of biomass retaining, consequently, sludge retention time (SRT) could be operated separately from hydraulic retention time (HRT) without needs of filter or media packing. Three 10-liter laboratory scale ABRs with different compartment numbers (3, 6 and 8 compartments) were operated with constant HRT of 24 hrs. Synthetic carbohydrate-protein wastewater was fed to these reactors with COD loading rate of 4 g COD/l-d. The results evidently showed that the compartmentalized structure of ABR helped retard sludge washout rate. The more compartments, the lower of sludge washout rate was. The ratios of SRT/HRT were found as 35, 73 and 134 d/d in the reactors with three, six and eight compartments, respectively. In addition, COD removal efficiencies were observed with percentages of 74, 78 and 83, respectively. Moreover, studying of the microbial populations by FISH technique proved the existence of microbial phase (methanogens and acidogens) separation in ABR system with six and eight compartments, but not clearly distinguishable in three-compartment ABR.

Keywords: Anaerobic Baffled Reactor, FISH Technique, Methanogens, Acidogens, COD Loading Rates

INTRODUCTION

Anaerobic process usually has a problem of maintaining biomass within reactor. A conventional digester has usually been operated with solid retention time (SRT) equal to hydraulic retention time (HRT). Therefore, in order to keep the biomass within the reactor as long as possible, high volume of reactor is necessary. Subsequently, several modifications to solve this problem were attempted, such as returning the biomass into the reactor, using a filter for trapping the biomass or even packing some media in the reactor. However, the cost of filter and packing material becomes the disadvantage.

An anaerobic baffled reactor (ABR) is a high-rate anaerobic reactor using a series of vertical baffles to direct the flow upward and downward from inlet to outlet. ABR has a higher resistance of both hydraulic and organic shock loads than some anaerobic processes. ABR can be designed to improve biomass retention in reactor, resulting in a longer SRT [1], [2] without need of packing media or a solid-settling chamber or sludge granulation. The compartmentalized structure in ABR is an important key of retaining biomass within the reactor. The more compartments in a reactor, the better biomass retention is. Also, this structure is helpful in separating acidogenic and methanogenic phases, which will enhance stability and higher organic loading rate (OLR) of the anaerobic process, as well as, increase the overall removal efficiency with shorter HRT [3]. Several studies have found that the ABR could be operated with HRT less than 1 day [4], [5]. The successful operation of ABR in treating of domestic, industrial and agricultural wastewater with the removal efficiency higher than 90% were reported [6]-[10].

Although ABR has been developed for over twenty years, the knowledge in designing such a reactor has still not been much clarified. The most advantage of ABR is its SRT and HRT can be operated separately. Therefore, SRT can be increased over HRT several times. This will benefit in a smaller size of reactor while still achieving high biomass concentration and consequently high performance. The SRT/HRT ratio is an important parameter to compare the effectiveness of ABR technically and economically. The aim of this study is to study effect of compartment numbers on SRT/HRT ratios and appropriate OLR for treating carbohydrate-protein wastewater.

MATERIALS AND METHODS

Laboratory Scale Reactors

A schematic diagram of experimental setup was shown in Fig. 1. Three laboratory-scale ABRs were made of clear acrylic with the detail and dimension of reactors as shown in Fig. 2. All three reactors were having ten liters effective volume and most of

the components are similar. The difference was the number of compartment consisted in each reactor, which three, six, and eight compartments were applied for this study. Each compartment had a vertical baffle that directs the liquid flow alternately downward and upward. The ratio of down-flow and up-flow width in each compartment was 1:3 as suggested by Dama et al. [9]. Also, the 45-degree slanting baffle was recommended to reduce the region of dead space and direct the flow to the center of the up-flow region [9]. The wastewater flows from one compartment to the next through window cut on the acrylic partition. The gas outlets are on the upper part of the reactor and sampling ports are at the side.

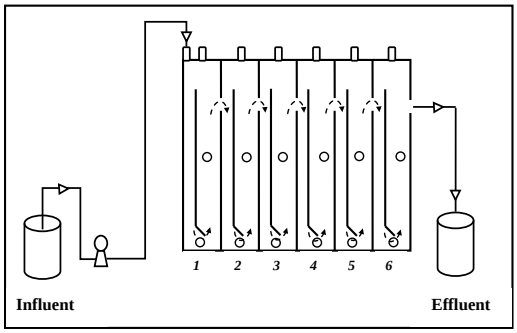

Fig. 1 A schematic diagram of experimental setup (6-compartments).

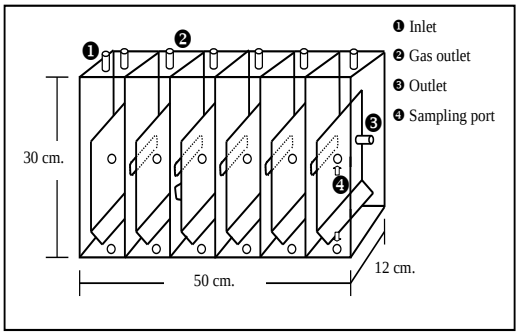

Fig. 2 Details and dimension of experimental reactor (6-compartments).

Seeding and Acclimatization

The systems were inoculated with anaerobic sludge from ABR treating swine wastewater for approximately three months. Each reactor was seeded with initial MLSS of about 28 g/l, then; they were allowed to settle for about two days. For acclimatization, synthetic carbohydrate-protein wastewater containing a designate strength was fed with an operating HRT of 80 hrs, which was suggested for high stability and COD removal [11]. Then, it was gradually decreased to the designated HRT of 24 hrs. All reactors were operated until a steady state was reached.

Experimental Design

This experiment was divided into two parts; the first part was conducted with three reactors equipped with three, six and eight compartments, named as 3C-OLR4, 6C-OLR4, and 8C-OLR4, respectively. They were all operated with OLR of 4 g COD/l-d and HRT of 24 hrs. The second part was operated with three more different OLRs of 8, 12 and 16 g COD/l-d using reactors with a certain compartment number. According to the results from the first part, the eight-compartment reactor showed the most appropriate reactor for overall performance. Hence, six experiments were conducted with operating conditions as detailed in Table 1.

Table 1 The operating conditions in this study.

Exp. names	No. of compartments	COD (mg/l)	HRT (hrs)	OLR (g COD/ l-d)
Part I: Effects of compartment numbers				
3C-OLR4	3	4,000	24	4
6C-OLR4	6	4,000	24	4
8C-OLR4	8	4,000	24	4
Part II: Optimum organic loading rate.				
8C-OLR8	8	8,000	24	8
8C-OLR12	8	12,000	24	12
8C-OLR16	8	16,000	24	16

Analytical Methods

Samples were regularly collected by grab sampling method. Influent and effluent sample were collected from storage container. Supernatant of each compartment was collected from sampling ports as shown in Figure 2. The parameters of total COD (tCOD), soluble COD (sCOD), Alkalinity, TSS, VSS, pH, and ORP were performed in accordance with Standard Methods for the Examination of Water and Wastewater [12]. Biogas was collected and counted by gas meters using water displacement method. Bacterial community was determined by FISH technique.

RESULTS AND DISCUSSION

Part I: Effects of Compartment Numbers

Performance in COD removal

Average influent COD levels fed into 3C-OLR4, 6C-OLR4, and 8C-OLR4 experiments were 4,050, 4,230, and 4,230 mg/l, respectively. The pH values of the feeds were 8.2, 8.1, and 8.1 with prepared alkalinity of 2,220, 2,040, and 2,040 mg/l as $CaCO_3$, respectively. Figure 3 illustrated that COD removal

efficiencies during high HRT of 80 hrs were quite high (>80% removed) in all ABRs. The lower HRT, the lower COD removal appeared, due to low HRT might induce channeling occurrence, resulting in less contact between sludge and substrate, as well as higher sludge washout.

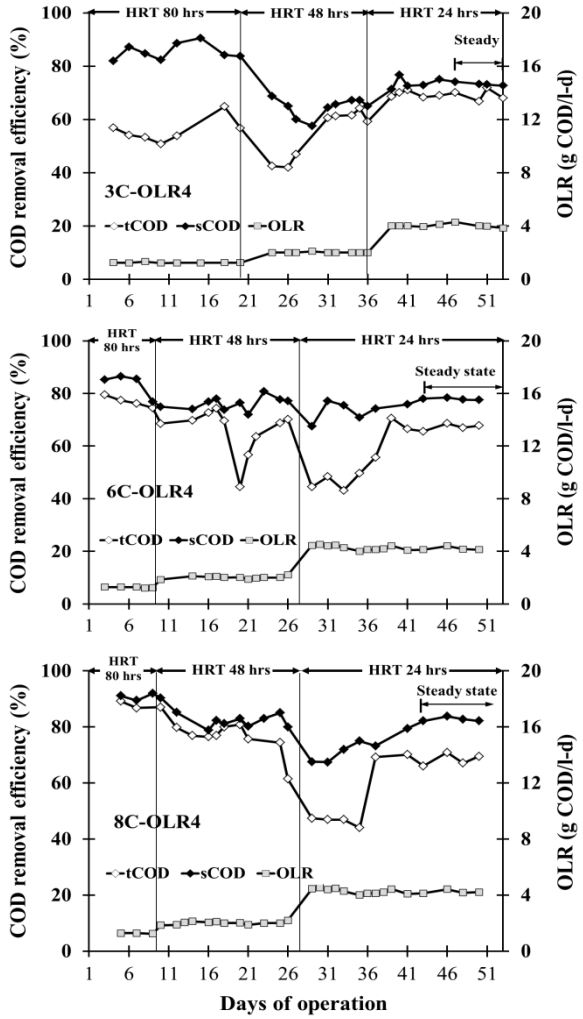

Fig. 3 COD removal efficiencies and OLRs of the Part I experiments.

Average COD removal efficiencies during a steady state of 74, 78 and 83% were found in 3C-OLR4, 6C-OLR4 and 8C-OLR4 experiments, respectively. In addition, COD utilization rates were averagely 29.8, 32.8, and 35.0 g/d, respectively. This could be said that more compartments could enhance COD utilization rate. Moreover, HRT adjusting during acclimatization (especially decreasing HRT or increasing OLR) affected COD removal efficiency more dramatically in less compartment number reactor. The ABR with more compartment numbers exhibited higher tolerability to hydraulic change.

In addition, a profile of soluble COD values in every compartment of each reactor (data not shown here) illustrated that COD was mostly removed in the first compartment (40 – 58%), then, slightly decreased throughout the reactor.

pH values and microbial phase separation

Lengthwise increasing pH was observed throughout the reactors, which microbial phase separation in ABR could be implied. The front of reactor acts like an acidogenic phase, and the latter performs as methanogenic phase. However, a phase separation was not obvious in the 3C-OLR4 experiment where little different pH values occurred among its three compartments (6.8, 6.9, and 7.1, respectively). Anyway, phase separation was more evident in other two experiments (6C-OLR4 and 8C-OLR4), especially in consideration of pH values. That is, pH values in the first and the last compartments of a 6C-OLR4 experiment were 6.8 and 7.5, while those of 8C-OLR4 experiment were 6.5 and 7.7. It appears that more compartments in a reactor could induce the proper environment for two- phase anaerobic operation.

Sludge mass balance

Figure 4 shows a component of sludge mass balance in Part I experiments based on initial sludge concentration of around 28 g TSS/l inoculated into 10-litre reactors. Initial sludge mass in reactors 3C-OLR4, 6C-OLR4, and 8C-OLR4 were calculated at 288, 273 and 276 g TSS, respectively. Effluent suspended solids (SS) were regularly analyzed and used for total sludge washout calculation. Total mass of sludge washout were 269, 205 and 110 g TSS, while final sludge mass of 99, 159 and 257 g TSS resided at the end of experiments, respectively. According to mass balance, produced sludge mass were calculated at 79, 90 and 91 g TSS, respectively. Observed yield in all reactors were obtained at 0.04 g VSS/g COD.

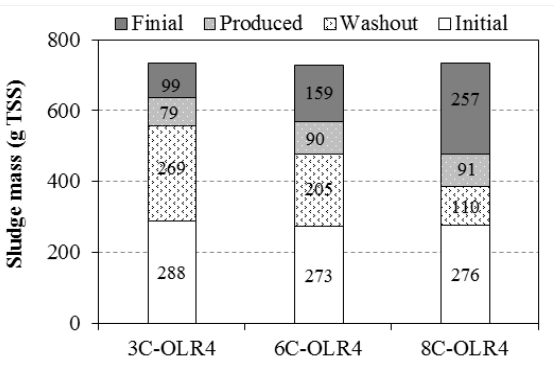

Fig. 4 Sludge component in consideration of different compartment numbers (Part I).

Sludge produced in the reactor 3C-OLR4 was significantly lower than the other two (6C-OLR4

and 8C-OLR4). It could be due to larger compartment in a three-compartment reactor than six- and eight-compartment reactors. Though the recommended ratio of up-flow and down-flow width of 1:3 was installed in all reactors, more dead-space still occurred in a three-compartment reactor, and could reduce contact opportunity between sludge and substrate. Also, the mixing in six- and eight-compartment reactors was visually better.

As mention above, one may conclude that the number of compartment affects on maintainability of sludge within ABRs, the more compartment numbers, the lower sludge washout rate is and the higher sludge resides in the reactor. Also, higher SRT and SRT/HRT ratio were observed in reactors equipped with more compartment numbers as shown in Fig. 5.

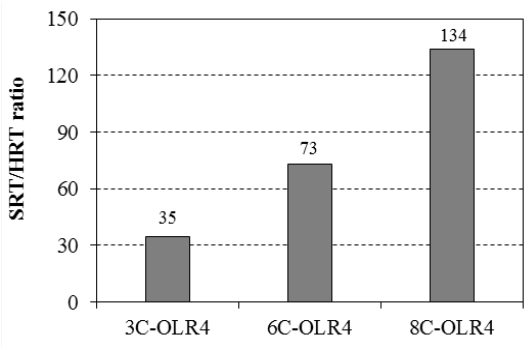

Fig. 5 SRT/HRT ratios in consideration of different compartment numbers (Part I).

The SRT/HRT ratios achieved in this study evidently showed that SRT and HRT could be separately controlled under ABR configuration. These SRT/HRT ratios (Figure 5) were similar to those of ABRs reported elsewhere [4], but still could not compete with that found in UASB configuration reactors [13]. However, the complexity of UASB reactor design and its operation might cause grave concern. Nonetheless, lower SRT/HRT ratios in ABRs were sometimes reported, especially when treating high solid content associated with low biodegradability wastewater [14].

Part II: Optimum Organic Loading Rate (OLR)

Performance and microbial phase separation

According to the results from previous experiments (Part I), eight-compartment ABRs were selected for this experimental part (Part II). COD content in synthetic wastewater were adjusted to obtain designated OLRs. Average influent COD concentrations in the experiments of 8C-OLR8, 8C-OLR12, and 8C-OLR16 were at 8,300, 12,463 and 16,301 mg/l, respectively. Averages of influent pH were 8.3, 8.3, and 8.5, as well as, of alkalinity were 2,148, 1,963, and 2,606 mg/l as $CaCO_3$, respectively.

Average COD removal efficiencies achieved during a steady state of the experiments 8C-OLR8 and 8C-OLR12 were 96 and 88%, respectively, which were similar to one of 8C-OLR4 experiment (83%) mentioned in the previous part. For the experiment of OLR at 16 g COD/l-d (8C-OLR16), resided sludge from the experiment with OLR of 8 g COD/l-d was inoculated. During the acclimatization, this reactor with the OLR of 8 g COD/l-d showed COD removal efficiencies near 90% level. After final adjustment of the OLR up to 16 g COD/l-d, COD removal efficiency rapidly decreased to 34% level within a week and failure eventually appeared.

More acidic pH values of 5.4 and 5.7 were observed in the first compartments of the 8C-OLR8 and 8C-OLR12 while neutral pH of 7.8 and 7.3 were still maintained in the last compartment. It is possibly believed that microbial phase separation was more obvious when operating OLR increased.

Sludge mass balance

Similarly, initial sludge concentration of around 28 g TSS/l was inoculated into every reactor. After reaching a steady state, sludge component of every experiment with eight-compartment was analyzed and exhibited in Fig. 6 (Note: result of the 8C-OLR4 was referred from previous part). Total sludge washout and final sludge mass of the 8C-OLR4, 8C-OLR8, 8C-OLR12 and 8C-OLR16 experiments were 110, 144, 168 and 206 g TSS, as well as 257, 256, 321 and 378 g TSS, respectively. In addition, produced sludge mass were calculated at 91, 122, 201 and 308 g TSS, respectively.

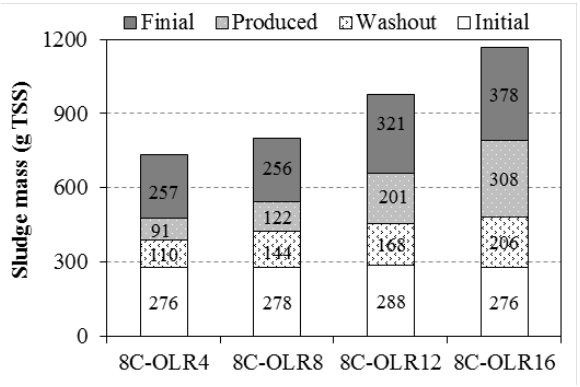

Fig. 6 Sludge component in consideration of different OLRs (Part II).

Although these ABRs were equipped with the same number of compartment, the SRT and SRT/HRT ratios were not similar. It can be seen that the different OLRs affected on the SRT/HRT ratios, higher OLR resulted in lower SRT/HRT ratio as shown in Fig. 7. The explanation should be that higher OLRs resulted in more biogas production,

consequently, rising biogas enhanced turbulence in sludge bed. Therefore, total sludge washout mass (g TSS) accordingly increased when OLRs were raised. However, sludge mass and a SRT/HRT ratio of the 8C-OLR16 must be remarked that they were calculated from only 34 days of operation before failure.

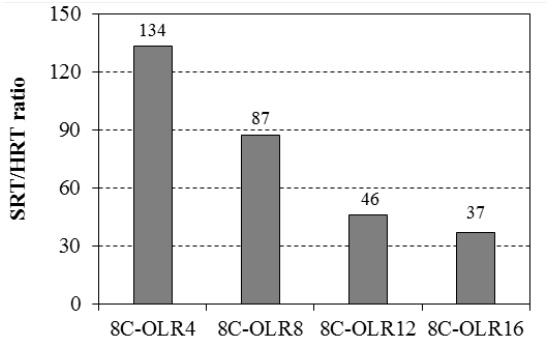

Fig. 7 SRT/HRT ratios in consideration of different OLRs (Part II).

Fluorescence In Situ Hybridization (FISH)

The microbial populations were studied by FISH technique using probe EUB338 labeled with FITC (green) for domain Eubacteria, which acidogens belong to this bacterial group. Also, probe ARC915 labeled with CY3 (red) was used for domain Archaea, which methanogens were categorized into this group. DAPI (blue) staining was applied to determine total cell bacteria. Figure 8 shows FISH images of the 3C-OLR4 experiment.

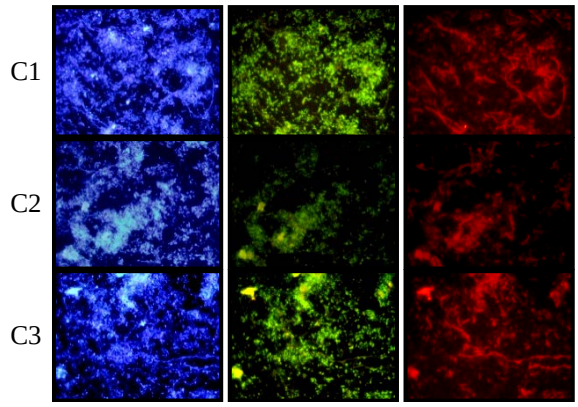

Fig. 8 DAPI-staining/epifluorescence micrographs of microbial cells **3C-OLR4** experiment; Left: DAPI staining, Middle: Bacterial cells hybridized with FITC-labeled EUB338, and Right: Archaeal cells hybridized with Cy3-labeled ARC915.

The ratio of acidogens (EUB338 probed; green color) to total bacteria cell (DAPI stained; blue color) were quite similar to the ratio of methanogens (ARC915 probed; red color) to total bacteria cell (DAPI stained; blue color) in every compartment (C1, C2 and C3). This could be stated that the populations of methanogens and acidogens were almost identical throughout the ABR. Three compartments could not stimulate microbial phase separation in this case. This was consistent to the mentioned pH values of 6.8, 6.9 and 7.1 in C1, C2 and C3, respectively. It was obvious that three compartments could not promote the microbial phase separation.

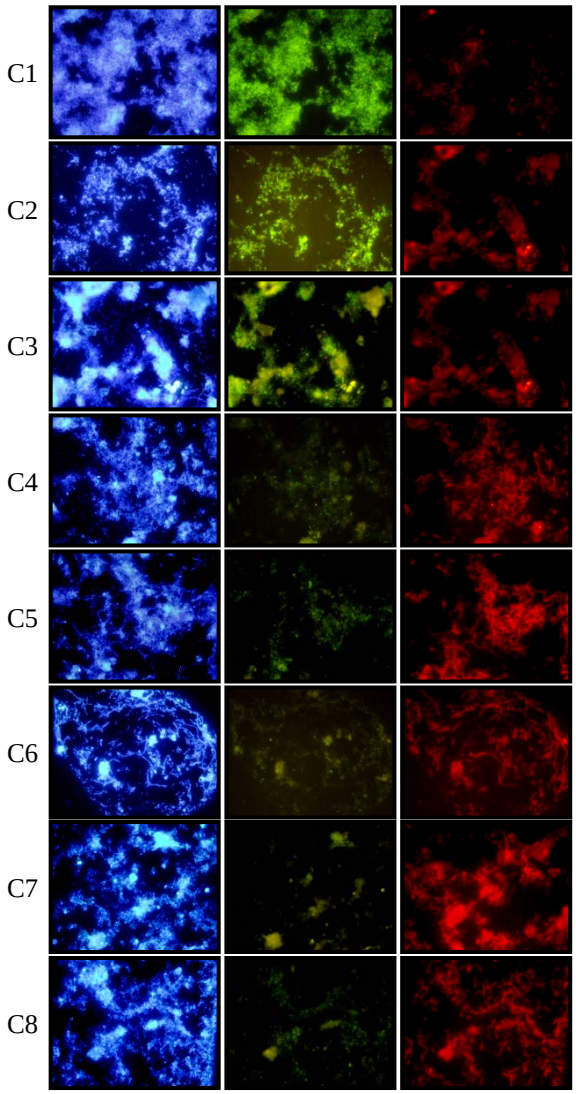

Fig. 9 DAPI-staining/epifluorescence micrographs of microbial cells **8C-OLR8** experiment; Left: DAPI staining, Middle: Bacterial cells hybridized with FITC-labeled EUB338, and Right: Archaeal cells hybridized with Cy3-labeled ARC915.

In case of eight compartments, lengthwise difference of microbial population in the ABR was revealed in Fig. 9. The ratio of acidogens and methanogens in each compartment of the 8C-OLR8 experiment was visually estimated at 90:10 in the

first compartment. Since the second compartment, acidogens were relatively lower than methanogens, especially in the last two compartments (C7 and C8) that acidogens were greatly less than methanogens. Similarly, FISH results of the experiments 8C-OLR12, and 8C-OLR16 (data not shown here) also illustrated compartmentalized change of microbial population. Increased OLRs (up to 16 g COD/l-d) did not affect microbial phase separation in this study.

Acidogens (EUB338 probed; green) was a prominent group in the front compartment while methanogens (ARC915 probed; red) was in the rear compartments. Thus, it is interesting to note that acidogenic phase was evident in the first three compartments where low pH values between of 5.4-6.7 occurred. Whereas methanogenic phase was manifested in the last four to five compartments (pH values were about 7.0-7.8). In addition, the visual observation of sludge in different compartments exhibited that sludge in the first three compartments was more whitish, while those in the latter compartments were more blackish. This was similar to a study [15] mentioning about blackish color of methanogenic phase.

CONCLUSION

The compartmentalizing configuration is an important factor affecting on SRT/HRT ratio. More compartments help retarding sludge washout, resulting in higher SRT with smaller HRT. Consequently, high COD removal efficiency was obtained by using eight-compartment ABR. Though microbial phase separation was not obvious in three-compartment ABR, fair COD removal efficiency (over 70%) was still achieved. Eight-compartment ABR could handle operating OLRs up to 12 g COD/l-d and still provided COD removal efficiency higher than 80%, especially for ABR treating low solid content wastewater.

ACKNOWLEDGEMENTS

The authors gratefully acknowledge assistance for FISH technique from Dr. Somkiet Techkarnjanaruk, National Center for Genetic Engineering and Biotechnology of Pilot Plant Development and Training Institute, KMUTT.

REFERENCES

[1] Nachaiyasit S, Stuckey DC, “The effect of shock loads on the performance of an anaerobic baffled reactor (ABR): 1, step changes in feed concentration at constant retention time” Water Research, Vol 31(11), 1997, pp. 2737-2746.

[2] Nachaiyasit S, Stuckey DC, “The effect of shock loads on the performance of an anaerobic baffled reactor (ABR): 2, step and transient hydraulic shocks at constant feed strength” Water Research, Vol 31(11), 1997, pp. 2747-2754.

[3] Demirer GN, Chen S, “Two-phase anaerobic digestion of unscreened dairy manure” Process Biochemistry, Vol 40(11), 2005, pp. 3542-3549.

[4] Grobicki A, Stuckey DC, “Performance of the anaerobic baffled reactor under steady-state and shock loading condition” Biotechnology and Bioengineering, Vol 37, 1991, pp. 344-355.

[5] Bell J, Buckley CA, “Treatment of a textile dye in the anaerobic baffled reactor” Water SA, Vol 29(2), 2003, pp.129-134.

[6] Ahamed A, Chen CL, Rajagopal R, Wu D, Mao Y, Ho IJR, Lim JW, Wang JY, “Multi-phased anaerobic baffled reactor treating food waste” Bioresource Technology, Vol 182, 2015, pp. 239-244.

[7] Pirsaheb M, Rostamifar M, Mansouri AM, Zinatizadeh AAL, Sharafi K, “Performance of an anaerobic baffled reactor (ABR) treating high strength baker’s yeast manufacturing wastewater” J. of the Taiwan Institute of Chemical Engineers, Vol 47, 2015, pp.137–148.

[8] Zhu GF, Li JZ, Wu P, Jin HZ, Wang Z, “The performance and phase separated characteristics of an anaerobic baffled reactor treating soybean protein processing wastewater” Bioresource Technology, Vol 99, 2008, pp. 8027–8033.

[9] Dama P, Bell J, Foxon KM, Brouckaert CJ, Huang T, Buckley CA, Naidoo V, Stuckey D, “Pilot-scale study of an anaerobic baffled reactor for the treatment of domestic wastewater” Water Science and Technology, Vol 46(9), 2002, pp. 263-270.

[10] Bell J, Plumb JJ, Buckley CA, Stuckey DC. “Treatment and decolorization of dyes in an anaerobic baffled reactor” J. of Environmental Engineering, 2002, 1026-1032.

[11] Barber WP, Stuckey DC, “The influence of start-up strategies on the performance of an anaerobic baffled reactor” Environmental Technology, Vol 19, 1998, pp. 489-501.

[12] APHA; AWWA; WEF, “Standard Methods for the Examination of Water and Wastewater, 22nd Ed.; Rice EW, Baird RB, Eaton AD, Clesceri LS, Eds.; American Public Health Association; Washington D.C., USA, 2012.

[13] Singh KS, Viraraghavan T, “Impact of temperature on performance, microbiological, and hydrodynamic aspects of UASB reactor treating municipal wastewater” Water Science and Technology, Vol 48(6), 2003, pp. 211-217.

[14] Boopathy R, “Biological treatment of swine waste using anaerobic baffled reactors” Bioresource Technology, Vol 64, 1998, pp.1-6.

[15] Demirel B, Yenigun O, "Two-phase anaerobic digestion processes: a review" J. of Chemical Technology and Biotechnology, Vol 77(7), 2002, pp. 743-755.

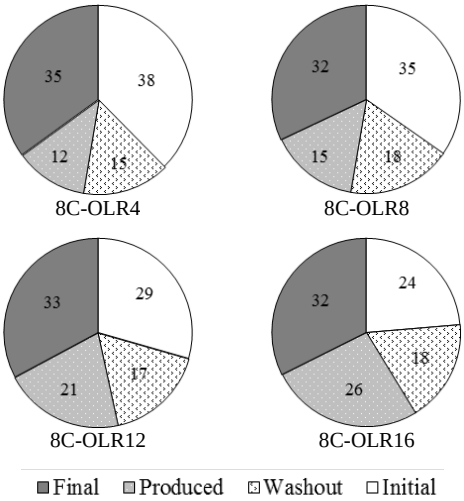

Fig. 8 Percentage of sludge mass balance in consideration of different OLRs (Part II)

Second International Conference on Science, Engineering & Environment,
Osaka City, Japan, Nov.21-23, 2016, ISBN: 978-4-9905958-7-6 C3051

INTRODUCING SUSTAINABILITY TO FIRST-YEAR CIVIL ENGINEERING STUDENTS USING DROUGHT AS A CASE STUDY

Gregg L. Fiegel[1], Tom R. Trice[2], and Ryan C. Alaniz[3]
[1]Civil Engineering, [2]History, and [3]Sociology Faculty, Cal Poly, San Luis Obispo, USA

ABSTRACT

Recently we introduced sustainability to first-year civil engineering students using drought as a case study. In this article we discuss sustainability-related activities incorporated into an introductory civil engineering course taken by 160-180 undergraduate students annually. Objectives of the course include introducing the profession, outlining steps for success as an undergraduate, motivating on-campus involvement, improving study habits, and introducing engineering design. Sustainability and drought, as instructional topics, provide interesting and engaging opportunities for addressing the course objectives. In the course, we address sustainability and drought through two activities. During the first activity, students research drought and monitor their own water usage. We discuss this personal reflection assignment in more detail in the paper. In addition, we comment on student submissions and assessment results. The second activity is a group project where students work in 4-person teams to research a drought-related topic. We discuss this assignment in the paper. In addition, we discuss challenges associated with implementing the above activities. We also discuss course improvements based on student and instructor feedback. We comment on the value of interdisciplinary collaboration and the approach taken in teaching sustainability; the authors teach in engineering, history, and sociology.

Keywords: Sustainability, Drought, Teaching, Education, Resilience

INTRODUCTION

At California Polytechnic State University (Cal Poly), San Luis Obispo, the topic of sustainability has received increased attention over the past decade. In 2007, Cal Poly adopted seven University Learning Objectives (ULOs) to define the institution's expectations for student learning. One of these objectives states that students should, by the time they graduate, be able to "make reasoned decisions based on an understanding of ethics, a respect for diversity, and an awareness of issues related to sustainability."

Following the adoption of the ULOs, Cal Poly defined sustainability as the ability of natural and social systems to survive and thrive together to meet current and future needs. Further, the Cal Poly Academic Senate passed a resolution adopting four additional "sustainability learning objectives" [1]. The university developed the additional objectives given the complexity surrounding the original ULO. At Cal Poly, an Academic Senate sustainability committee informs and supports the activities of other committees whose scopes encompass environmental responsibility. In addition, the committee makes recommendations, as appropriate, regarding the provisions of the Talloires Declaration and sustainability policies under the California State University system [2].

The topic of sustainability has received even greater attention and scrutiny in recent years as Cal Poly and its stakeholders have coped with persistent drought conditions. As mandated by the California Governor in 2015, potable urban water use throughout the state has been reduced by 25-percent. Cal Poly accommodated this water restriction with the installation of low-flow bathroom and kitchen fixtures, improved irrigation practices, and turf removal, among other remedies. Evidence of drought is clearly visible for incoming Cal Poly students. In addition, many students arrive on campus with personal stories of how drought has affected them, their families, and their home communities. Approximately 10- to 15-percent of students come from more rural and agricultural communities significantly impacted by recent water shortages and intense conservation efforts.

Instructors at Cal Poly consider the ULO focused on ethics, diversity, and sustainability to be one of the more challenging to address in program curricula. However, drought as a case study provides opportunities for student learning and discovery in these areas. The topic is thought-provoking. Furthermore, Cal Poly graduates will likely face drought-related challenges for many years to come. For these reasons and others, we chose drought as a case study in addressing sustainability concepts with first-year students. Our experience includes teaching courses for the Civil Engineering Program and the Cal Poly Honors Program.

In the following paper we describe a recent effort to introduce sustainability to first-year civil

engineering students using the California drought as a case study. We include background information on the course, a discussion of the individual and group instructional activities, a summary of student work, and an assessment of the results. We conclude the paper with a discussion of lessons learned and plans for improving instruction in the future.

BACKGROUND

Course Format and Enrollment

We incorporated sustainability-related activities and instruction into the introductory civil engineering course (CE 111) taught at Cal Poly. Students must declare a major prior to admission to the university. First-year civil engineering students are then required to take the subject course during their first quarter on campus. The academic year at Cal Poly is divided into four quarters, each eleven weeks long. Course instruction takes place over a ten-week period with examinations scheduled during the eleventh week. The subject course is a 1-unit lecture course, which means it meets in a classroom for one hour each week. The course is graded credit/no-credit and is included in the required Bachelor of Science degree curriculum for civil engineering majors. The course is currently taught once each year in a large lecture hall with a typical enrollment of 160 to 180 students.

Course Design

Primary course objectives include introducing the civil engineering profession, outlining steps for success as an undergraduate, motivating on-campus involvement, improving study habits, and introducing engineering design. In support of these objectives, the course instructor and guest speakers deliver presentations on curricular issues and advising, co-curricular learning opportunities, keys to success in engineering study, engineering design, professional skill development, and contemporary issues. To receive credit for the course, the students must regularly attend class, attend at least two student organization meetings or events, write two individual reflection essays, complete a team research project, and complete a team design project. Assessments of student performance during the past ten years show that greater than 95 percent of enrolled civil engineering students receive credit for the course. The students generally consider the course assignments challenging and the workload representative of a 1-unit undergraduate course.

Previous Experience Teaching Sustainability

Prior to teaching the civil engineering course, we worked together in developing course content and activities for an introductory Honors course. This course serves first-year, first-quarter students and focuses on sustainability. In fact, the primary emphasis is the previously described ULO on ethics, diversity, and sustainability. The Honors Program at Cal Poly represents a campus-wide program serving students from the university's six colleges and nearly 60 different majors. Diversity and sustainability themes link well with the program and the introductory course, as addressing issues and challenges in these areas requires collaboration and sharing of knowledge among multiple disciplines.

To receive credit in the introductory Honors course, students must attend class regularly, complete at least five hours of service with a local community partner organization, complete six written reflection exercises, and complete a group response project. Students work in teams comprised of students from different disciplines/majors. In-class discussions take place in these groups and are led by the instructor as well as continuing Honors students trained as teaching assistants. The small group discussions are designed to be representative of future learning experiences available to students enrolled in the Honors Program.

We support student learning in the Honors course through readings, in-class group discussions, written reflection exercises, and group project work. Papers, articles, and reports focus the in-class discussions and reflection while providing introductions to sustainability [3], systems thinking, resilience thinking and "livelihood resilience" [4], stakeholder theory [5], social justice [6], economics, public policy, and environmental justice [7]. The collection of class readings is not meant to represent a comprehensive bibliography. Rather, the course references provide background information related to the course learning objectives. We expect the students to investigate important topics and stimulate their own critical thinking though independent research. Recent group projects have included needs assessment and project research for local non-profit organizations, research into the California drought, and an analysis of how sustainability issues figure in current political debates and elections.

In teaching the Honors course, we have learned that first-year students often experience significant challenges when working in groups; need to improve their information literacy skills; require regular and constructive feedback; find the subject of sustainability interesting, relevant, and challenging; relate well to the subject matter when it is linked with contemporary issues; require support and direction when asked to self-direct their learning; and appreciate hands-on demonstrations and project-based learning. We reflected on these observations when developing a learning module on sustainability for the introductory civil engineering course. In the

following sections we summarize our experiences in developing and teaching this learning module.

COURSE ASSIGNMENTS AND ACTIVITIES

For the introductory civil engineering course, we prepared several activities and assignments to inform and support a course learning module on sustainability. These activities and assignments required both individual and group work and were developed based on set of working student learning outcomes. The learning outcomes were:

1) Explain how sustainability concepts are linked with the environment and civil engineering;
2) Define resilience in the context of sustainability and human livelihoods;
3) Analyze individual water usage and the effectiveness of different conservation measures;
4) Compare and contrast different ways Californians and their communities may address the issue of drought - beyond conservation; and
5) Discover, review, evaluate, analyze, and summarize published information (including data and images) related to sustainability.

We describe the course activities and assignments in some detail in the following sections.

Individual Work

We required all of the students in the class to complete a short reflection paper on the California drought and livelihood resilience. Prior to preparing their papers, the students reviewed two required references [4], [8]. In addition, each student perused the internet and local media for additional articles, essays, news videos, and photos essays on the drought and its effects on the local community. Through individual research, we asked the students to develop their own understanding of the concepts of sustainability and livelihood resilience. In addition, we expected the students to become more aware of the local community and the impact of the ongoing drought on the Central Coast of California.

As part of this assignment, the students were also tasked with investigating their own water use. During a weeklong period, the students selected two days to conduct their investigation. On the first day, they estimated their daily water use (in gallons) while engaged in normal activities. On the second day, they restricted their water use to a minimal but comfortable level and re-estimated their water use. After completion of their investigations, the students prepared a 2- to 3-page reflection essay discussing daily water use and topics relevant to their own research and experience. We designed this hands-on learning activity while keeping in mind Cal Poly's motto: learn by doing.

We reviewed each student essay to record their water use and to review their thoughts on the California drought, water conservation, and livelihood resilience. Table 1 summarizes reported water use and conservation efforts for the 168 students enrolled in the course. The table shows the high, low, and average values reported for both days of the study.

Table 1 Summary of water use as evaluated during individual student investigations

Value	Day 1: Normal Water Use (gallons)	Day 2: Conserved Water Use (gallons)
High	195	100
Low	16	11
Ave	57	37

Note: Data collected from 168 students.

The students employed various conservation efforts and reduced their water use, on average, by about 35 percent. By and large, the students attributed their water use to tangible everyday activities such as drinking, doing the dishes, brushing their teeth, showering, and flushing the toilet. Within their writing, about 30 percent of the students demonstrated a more comprehensive view of their water use, recognizing they were using water in other ways not easily measured (e.g. the water used by campus dining and other university departments to support student success, the amount of water used to grow the food in their diet, etc.). Only about 14 percent of the students researched average water use by typical California residents, comparing this water use with their own. Those that performed this research often reflected that their water use estimates seemed somewhat low, which was most likely due to their campus living arrangements.

Group Work

We required all of the students in the class to complete a research project on the California drought. The students worked on their research projects in teams of four. We assigned students to their project teams simply by grouping students together by their last names. Once in their groups, we presented the students with the following prompt: "You will work in your group to research a specific topic related to the California drought. There are many different issues, challenges, stories, and themes you could investigate when examining this very broad subject. You and your teammates have the freedom to select the topic for your presentation. However, this topic must be approved by the CE 111 course instructor prior to you beginning your research."

We formed 42 research teams from the class of 168 students. We asked each team to summarize their research findings and conclusions in a research poster. Students prepared their posters in MS PowerPoint according to guidelines and format requirements presented on the course website. Some students had never prepared a research poster before, so more detailed instructions, examples, and templates were provided. We expected each team to prepare a research poster that provided a detailed, well-written, properly referenced, and engaging summary of their findings, conclusions, opinions, and/or recommendations. We gave each team the freedom to discuss and agree on the content included in their poster presentation. However, we required that all posters include the following: (1) At least two photographs (taken by members of the group) illustrating the impact of the California drought; (2) At least one quote from someone working outside of the university describing an impact of the drought (e.g. the students needed to interview someone); and (3) A description of at least one creative way Californians and their communities can address the issue of drought beyond conservation.

The students selected a number of different drought-related topics for their research investigations. Table 2 lists the most popular topics researched by this class.

Table 2 Listing of the five most popular drought research topics

Drought Research Topic	Number of Teams
Desalination	7
Cattle and Dairy Farming	5
Water Reservoirs and Storage	4
Groundwater	3
Vineyards and Viticulture	3

Note: Research completed by 42 teams.

We reviewed the 42 research topics and posters and grouped the topics into five different theme or subject areas, namely: engineering, agriculture, science, public policy, and business and economics. We summarize the breakdown of the team research projects by subject area in Figure 1. The wide variety of selected topics helped to illustrate to the students the broad impacts of the drought as well as the reach of sustainability-related issues, problems, and solutions. Interestingly, the number of agriculture-focused research studies outnumbered those focused on engineering. A possible reason for student interest in agriculture is the impact that farming and ranching has on many communities throughout California. Furthermore, the subject of agricultural water use and its possible regulation figured prominently in the news during the time this course was offered. Additionally, our first-year students were less likely to know and understand contemporary issues related to civil engineering at this point in their academic careers.

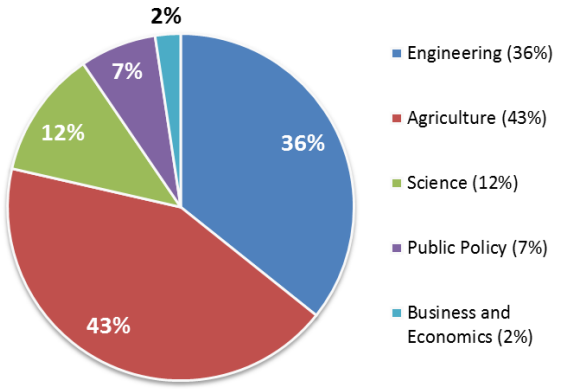

Fig. 1 Breakdown of the team research topics by theme areas.

Additional Reflection Questions

In addition to the individual reflection paper and the group research project, each student answered additional reflection questions related to sustainability and the California drought. As part of a required assignment administered during the final week of the term, the students answered a number of questions related to the course and their experiences as a new student at Cal Poly. Several of the questions focused on sustainability and drought:

- In your own words, provide a one-sentence definition for the term "sustainability."
- Provide a one-word definition for the term "sustainability."
- In 2020, what will we wish we had done in 2015 to mitigate the consequences of the California drought? What will we potentially look back on and regret, not realizing it was necessary to take action now?

Most of the students provided well-thought-out answers to the first two questions on sustainability, often incorporating elements of the readings as well as issues they had studied as part of the team research project. Figure 2 illustrates a word cloud generated from student answers to the request to provide a one-word definition for sustainability. Such illustrations can serve as useful tools for student reflection and classroom assessment. As suggested by the students, the most common terms associated with sustainability included renewable, maintainable, supportable, endurance, continuity, and everlasting.

Fig. 2 One-word definitions for sustainability as articulated by the students (word cloud generated using tagxedo.com, copyright 2016).

We received a variety of responses to the third question in the above list. We reviewed the responses and grouped them into six categories: continued and improved conservation measures; research, development, and implementation of desalination technology; improvements in agricultural practices; changing of personal attitudes toward water use, scarcity, and conservation; implementation of new policies and regulations for water use and distribution; and improvements to infrastructure as related to water storage, water recycling, groundwater management, etc. Figure 3 shows the distribution of responses by the students.

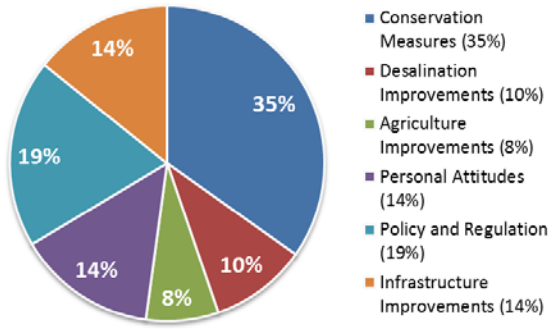

Fig. 3 Student response to the following question: "In 2020, what will we wish we had done in 2015 to mitigate the consequences of the California drought?"

In May 2016, approximately 6 months after the completion of the course, we asked the students to again reflect on their experiences in CE 111 and on the ongoing California drought. Student responses were voluntary. The students answered the following question as part of this follow-up assignment:

- During Fall 2015, we discussed the California drought and you investigated your own water use. As a follow-up, please provide an honest self-assessment of your water use since that time. Specifically, what best describes your individual daily water use between the months of January and June of this year as compared to when you first arrived at Cal Poly: (a) much less; ((b) less; (c) about the same; (d) more; (e) much more.

We continue to collect student responses to this question. However, to date, about 60% of those responding continue to use less or much less water. No students described their water use as more or much more than when they first arrived at Cal Poly.

In addition to the above question, the students indicated their level of agreement with the following three statements. We used a five-point Likert scale in collecting student feedback (i.e. possible student responses included strongly agree, agree, neutral, disagree, or strongly disagree).

- Between January and June 2016, coursework and/or curricular experiences at Cal Poly provided me with regular opportunities to learn about connections between sustainability and civil/environmental engineering;
- Living sustainably is an issue I am personally concerned about; and
- Upon graduation, working on projects and solving problems related to sustainable development will represent a significant portion of my duties as a professional engineer.

We tallied the number of "agree" and "strongly agree" responses to these three statements with the following results: 50%, 77%, and 77%, respectively. Approximately 23% of the students "disagreed" or "strongly disagreed" when asked if they continued to be provided with opportunities to learn about connections between sustainability and engineering. This result is somewhat surprising given the importance of the topic and the recent emphasis by the university on the subject of sustainability.

COURSE ASSESSMENT

We reviewed student work and activities in relation to the five previously defined student learning outcomes. Our comments follow.

Explain how sustainability concepts are linked with the environment and civil engineering: Each

student defined sustainability in their own words and demonstrated improved understanding through research. We used the California drought to link the concept of sustainability with the environment. Approximately 50% of the students linked sustainability with topics in science and engineering when conducting their research. Surprisingly, over 40% of the students linked sustainability with topics in agriculture. In the future, we will ask students to reflect on sustainability in an engineering context, as engineering is the focus of this course.

Define resilience in the context of sustainability and human livelihoods: The students addressed the concept of resilience as part of their individual paper assignment. In support of this assignment, we asked each student to read and reflect on an article addressing this subject [4]. After a review of their papers, we concluded approximately 40% of the students demonstrated a basic understanding of livelihood resilience. We intend to improve student understanding of this challenging topic in the future through more in-class discussions and questioning.

Analyze individual water usage and the effectiveness of different conservation measures: Based on our observations and a review of the individual reflection papers, most students completed their water use investigations with interest and enthusiasm. Many authors assert that demonstrations or hands-on learning methods such as this are essential in engineering [9]. Most students attributed their water use to tangible everyday activities without considering or realizing potential hidden uses. Few students assessed the reasonableness of their observations and calculations by reviewing published information on typical and/or average water use for California residents.

Compare and contrast different ways Californians and their communities may address the issue of drought beyond conservation: All of the student groups researched and presented at least one idea for addressing the drought beyond conservation. Many students recommended solutions beyond engineering, recognizing the importance of policy, regulation, and personal attitudes. We intend to provide more opportunities for students to share their findings and recommendations in the future as these opportunities were limited during this course.

Discover, review, evaluate, analyze, and summarize published information (including data and images) related to sustainability: Our assessments of individual and group work revealed that first-year students need information literacy skills training. The students should not be expected to learn these skills on their own. In the future, we intend to collaborate with library staff to improve student performance in this area.

CONCLUSIONS

In this article we discussed the incorporation of sustainability-related activities, discussions, and learning outcomes into a course for first-year civil engineering students. We used the California drought as a case study for introducing and teaching important sustainability concepts. The case study motivated student interest in the subject and the course assignments. Based on our success, we encourage other educators to consider similar learning outcomes and hands-on activities in their own courses. In collaborating to develop the course materials and assignments, we relied on our varied experiences in teaching sustainability, solving problems, and working with diverse student populations. Focusing on historical, social, and environmental elements of sustainability provided the students with a broad perspective of the drought challenge and the potential impacts to people and communities. We believe aspiring engineers must appreciate broader perspectives and value collaboration if they are to be successful.

REFERENCES

[1] Cal Poly Academic Senate, "Resolution on sustainability learning objectives", No. AS-688-09, 2009.
[2] Cal Poly Academic Senate, "Resolution on the creation of a standing sustainability committee", No. AS-622-04, 2004.
[3] Prugh, T and Assadourian E, "What is sustainability anyway?" World Watch, Sep./Oct. 2003, pp. 10-21.
[4] Thomas, T, et al., "Livelihood Resilience in the Face of Climate Change", Nature Climate Change, Jan. 2015, pp. 23-26.
[5] Maak, T and Pless, NM, "Responsible leadership in a stakeholder society", J. of Business Ethics, Vol. 66, No. 1, Jun. 2006, pp. 99-115.
[6] Oram, D, "Designing for sustainability: negotiating ethical implications", IEE Technology and Society Magazine, Fall 2010, pp. 31-36
[7] Agyeman, J, "Where justice and sustainability meet", Environment: Science and Policy for Sustainable Development, Vol. 47, No. 6, Aug. 2010, pp. 10-23.
[8] Nagourney, A, "As California drought enters 4th year, conservation efforts and worries increase", The New York Times, Mar. 17, 2015.
[9] Lowman, J, Mastering the techniques of teaching, Jossey-Bass, San Francisco, 1995.

Second International Conference on Science, Engineering & Environment,
Osaka City, Japan, Nov.21-23, 2016, ISBN: 978-4-9905958-7-6 C3051

INCIDENTS INDUCED BY ELECTROMAGNETIC WAVES EMITTED BY CELL PHONES

Yoshiro Fujii
Shin Kobe Dental Clinic, Hyogo, Japan

ABSTRACT

Cell phone (smart phone) use has increased considerably in recent years. These devices have facilitated communication on a global scale. However, there have been a number of reports of health problems related to the electromagnetic waves emitted by such electronic devices. A long list of both general and severe symptoms, including headaches, fatigue, tinnitus, dizziness, memory loss, irregular heartbeat, and whole-body skin lesions, have been reported. These are reportedly associated with the condition known as electromagnetic hypersensitivity (EHS). In Japan, since cell phones use has increased considerably in recent years, accidents involving people falling from a platform at a train station onto the tracks also seems to be increasing. When the electromagnetic waves emitted by a cell phone were irradiated to the subject, the subject's sense of balance was obstructed, and a subject's body also was destabilized by even a little external force. The author attributes the cause of accidents of this nature to instability caused by the electromagnetic waves emitted by cell phones. It is necessary to consider regulating the use of cell phones on train platforms to prevent these accidents. The underlying mechanism behind such accidents has not been decisively proven. However, decreased blood flow within the brain has been proposed. The regulation of using electronic devices should be considered to prevent severe accidents.

Keywords: Cell phone, Personal computer, Electromagnetic waves, Electromagnetic hypersensitivity, Involuntary body movement

INTRODUCTION

With the development of a technology-based society, the use electronic devices, such as cell phones and personal computers, has become increasingly widespread and has enabled communication on a global scale [1, 2]. However, there have been many reports pertaining to health problems related to the electromagnetic waves emitted by such electronic devices [3-10]. Physically unpleasant symptoms including headache, fatigue, tinnitus, dizziness, memory loss, irregular heartbeat, and whole-body skin lesions caused by exposure to electromagnetic waves are recognized as electromagnetic hypersensitivity (EHS) [11-15]. The author has reported that scoliosis could be caused by exposure to electromagnetic waves [16]. Additionally, the author has reported how a subject's involuntary movements, caused by electromagnetic waves, were treated using a gold alloy dental inlay [17]. In current report, the author hypothesizes that falling-related train accidents are due to electromagnetic waves emitted by active cell phones (smart phones).

METHOD

One standing subject, a man in his 40s, kept his legs spread about shoulder width apart in order to resist force exerted by the author. (Fig. 1). Next, an active smart phone was placed about 4m away from the subject. The phone was turned on, and irradiating electromagnetic waves toward the subject. The author then pushed the subject from the side. Next, the subject held the cell phone to his ear and the author pushed from his side again.

Fig.1: The subject spreading his legs shoulder-width apart in order to resist outer force.

RESULT

When the active smart phone was located about 4m away and the author pushed him from his side, the subject became unstable (Fig.2). When the subject held the active smart phone and the author pushed from his side, the subject was even more unstable (Fig.3).

Fig.2: When the active smart phone was located about 4m away from the subject (the phone is not shown in this figure) and the author pushed his side, the subject became unstable.

Fig.3: When the subject held the active smart phone to his ear and the author pushed his side, the subject moved very easily.

DISCUSSION

Fall accidents from a platform of the station seem to be increasing in Japan. Time seems to be parallel with the spread of electronic devices like cell phones for increase of these accidents. The author thinks the reason why such accidents increase is due to electromagnetic waves emitted by cell phones. In order to confirm this hypothesis the author made the experiment which checks a relation between the electromagnetic waves emitted by cell phone and the body balance. The result indicated that the electromagnetic waves emitted by cell phone may interfere the normal balance condition of human.

The underlying mechanism behind this phenomenon remains unclear, but decreased blood flow within the brain has been proposed [4]. The results of this study show that the distance between the smart phone and the subject is correlated to physical instability i.e. the shorter the distance between them the bigger the effectiveness of electromagnetic waves. The author has conducted similar experiments. The author has tried same experiment, and 48 out of 50 subjects showed the same result. The author suggests the two subjects who did not show this effect have the objects on their person which neutralized harmful electromagnetic waves emitted by the smart phone [17]. However, confidence over such ratios is a little debatable because the cell phones used in those experiments varied. Thus, the electromagnetic waves emitted by the cell phones also varied; the strength and quality of the radio waves depends on the phone model. The effects shown in this study may occur in front of personal computers [18][19] or other electronic devices. Although, there are a lot of indefinite factors for this field, the mechanisms behind this phenomenon should be researched immediately, and the regulation of cell phones (smart phones) must be considered to prevent severe accidents e.g. falling from train platform. Recently, smart phone spread widely and the person who operates smart phone became a lot while walking (Fig 4). Such act also leads to a similar accident [20].

Fig.4: Many people are walking while operating smart phone.
This photo is cited from
http://www.askadamskutner.com/pedestrian-accident/dangers-of-texting-while-walking/

CONCLUSION

The electromagnetic waves emitted by cell phones may interfere the balance function of the body. They may be one of the critical causes of falling-related accidents from a platform of the station. It may become serious accidents. However, the underlining mechanism has not clarified yet. More research is required. The regulation of electronic devices should be considered as a countermeasure to this accident.

REFERENCES

[1] Geser, H. Towards a Sociological Theory of the Mobile Phone, Release 3.0, University of Zurich, 2004,(http://socio.ch/mobile/t_geser1.htm/).

[2] Van Dijk, J. and Hacker, K. The Digital Divide as a Complex and Dynamic Phenomenon, The Information Society, 19, 2003, pp. 315-326.

[3]http://www.holisticdentistry.net/blog/2013/07/entry_242/ (last accessed, 2 May 2014).

[4] Aalto, S., Haarala, C., Brück, A., Sipilä, H., Hämäläinen, H. and Rinne, J.O. Mobile Phone Affects Cerebral Blood Flow in Humans. J Cereb Blood Flow Metab, 26, 2006, pp. 885-900.

[5] Feychting, M., Jonsson, F., Pedersen, N.L. and Ahlbom, A. Occupational Magnetic Field Exposure and Neurodegenerative Disease. Epidemiology, 14, 2003, pp. 413-419.

[6] Håkansson, N., Gustavsson, P., Johansen, C. and Floderus, B. Neurodegenerative Diseases in Welders and Other Workers Exposed to High Levels of Magnetic Fields. Epidemiology, 14, 2003, pp. 420-426.

[7] Ahlbom, A. Neurodegenerative Diseases, Suicide and Depressive Symptoms in Relation to EMF. Bioelectromagnetics, Suppl 5, 2001, pp.132-143.

[8] Linet, M.S., Hatch, E.E., Kleinerman, R.A., Robison, L.L., Kaune, W.T., Friedman, D.R., Severson, R.K., Haines, C.M., Hartsock, C.T., Niwa, S., Wacholder, S. and Tarone, R.E. Residential Exposure to Magnetic Fields and Acute Lymphoblastic Leukemia in Children. N Engl J Med, 337, 1997, pp. 1-7.

[9] Röösli, M., Moser, M., Baldinini, Y., Meier, M. and Braun-Fahrländer, C. Symptoms of ill health ascribed to electromagnetic field exposure--a questionnaire survey. Int J Hyg Environ Health, 207, 2007, pp. 141-150.

[10] Edelstyn, N. and Oldershaw, A. The acute effects of exposure to the electromagnetic field emitted by mobile phones on human attention. Neuroreport, 13, 2002, pp. 119-121.

[11] Rea, W., Pan, Y., Yenyves, E., Sujisawa, I., Suyama, H., Samadi, N. and Ross, G. Electromagnetic Field Sensitivity. J Bioelectricity,10,

[12] Rubin, G.J., Das Munshi, J. and Wessely, S. Electromagnetic Hypersensitivity: A Systematic Review of Provocation Studies. Psychosom Med, 67, 2

[13] Rubin, G.J., Das Munshi, J. and Wessely, S. A Systematic Review of Treatments for Electromagnetic Hypersensitivity. Psychother Psychosom, 75, 2006, 12-18.

[14] Norbert, L. Electromagnetic Hypersensitivity. Advances in Electromagnetic Fields in Living Systems, 5, 2009, pp. 167-197.

[15] Kimata, H. Microwave Radiation from Cellular Phones Increases Allergen-specific IgE Production. Allergy, 60, 2005, pp. 838-839.

[16] Fujii, Y. Do dental implants cause scoliosis?: A case report. Personalized Medicine Universe, 1, 2012, pp. 79-80.

[17] Fujii, Y. Gold alloy dental inlay for preventing involuntary body movements caused by electromagnetic waves emitted by a cell phone. OJAPr, 2, 2014,pp.37-43.

[18]Fujii Y. Dental Treatment for Dizziness and Joint Mobility Disorder Caused by Harmful Electromagnetic Waves. OJAPr 2015, pp.3:1-7.

[19]Fujii Y. Sensation of Balance Dysregulation Caused/Aggravated by a Collection of Electromagnetic Waves in a Dental Implant. OJAPr, 2, 2014, pp29-35.

[20] http://www.askadamskutner.com/pedestrian-accident/dangers-of-texting-while-walking/

Second International Conference on Science, Engineering & Environment,
Osaka City, Japan, Nov.21-23, 2016, ISBN: 978-4-9905958-7-6 C3051

EVALUATION OF CU CONTAMINATION FOR RIVER USING BRYOPHYTE IN THE KINOKAWA RIVER CATCHMENT

Takuma Kubohara[1] and Hiroyuki Ii[2]

[1] Graduate School of Systems Engineering, Wakayama University, Japan; [2] Faculty of Systems Engineering, Wakayama University, Japan

ABSTRACT

Cu concentrations of bryophyte sampled downstream of the closed Cu mine were 120 to 26,000 mg/kg-dry, higher than background Cu concentrations of bryophyte, 2 to 96 mg/kg-dry. The closed Cu mine composed of massive ore deposit produced a lot of Cu and Fe sulfide ore and then waste water was low pH and contained high concentration of sulfate with metal. Therefore, it was thought that high Cu concentrations of bryophyte sampled downstream of the Cu mine were affected by the closed Cu mines. A kind of copper bryophyte similar *Scopelophila cataractae* was often found around the Cu mine. Its Cu concentration was high, 1,100 to 26,000 mg/kg-dry. Therefore, a kind of copper bryophyte similar *Scopelophila cataractae* was thought to be a Cu contamination index. Cu concentrations of another copper bryophyte similar *Scopelophila cataractae* had high and a wide range of Cu concentrations (2 to 5,900 mg/kg-dry). Therefore, another copper bryophyte similar *Scopelophila cataractae* was useful species for an index of Cu contamination in the catchment. The closed Cu mines affected Cu concentrations of bryophyte at about 2 to 20 km downstream.

Keywords: Bryophyte, Metal Contamination Evaluation, Cu, River

INTRODUCTION

Metal concentration of river water is not always high nor stable. Therefore, metal concentration of river water is not always useful for evaluating metal contamination in a catchment. On the other hand, in the past study, it was reported that bryophyte was useful species for an index of metal contamination for river among river plants [1]. It is known that *Scopelophila cataractae* that lives in high copper concentration environment like under the copper roof in a temple, soil around a metal mine including a large amount of copper [2]. And then, the tolerance ability of *Scopelophila cataractae* for copper is high [3]. Moreover, it is known that bryophyte has been used to the index of atmospheric pollution [4], [5], [6]. However, river metal contamination has not been evaluated using the metal concentration of bryophyte. Then, we measured metal concentrations of bryophyte in the Kinokawa River catchment and studied the evaluation of river metal contamination using the metal concentration of bryophyte.

STUDY AREA

Figs.1 and 2 show location of study area and the Kinokawa River catchment. The Kinokawa River is located in the center of Kinki district and flows into the Kii Channel through the Kii plain. The Kinokawa River is classified into A river based on the Ministry of Land, Infrastructure, Transport and Tourism of Japan. The length and total area of the Kinokawa River are 136 km and 1,750 km^2 [7]. The Izumi Group composed of sedimentary rocks, sandstone, mudstone and conglomerate is distributed in the northwest part of the catchment. The Sanbagawa Belt composed of metamorphic rocks, serpentinite and crystalline schist is distributed in the southwest part and the northeast part of the catchment. The Hidakagawa Group composed of sedimentary rocks, sandstone and shale is distributed from the southern part to the northeast part of the catchment. The Chichibu Belt composed of sedimentary rocks, sandstone, mudstone, limestone and chert is distributed in the eastern part of the catchment [8]. The Ryoke Complex composed of plutonic rocks, granite and gneiss is distributed in the northeast part of the catchment.

Fig.1 Study area

In the Kinokawa River catchment, there are serpentinite and the closed Cu mines. The chemistry of serpentinite is quite different from the other rocks

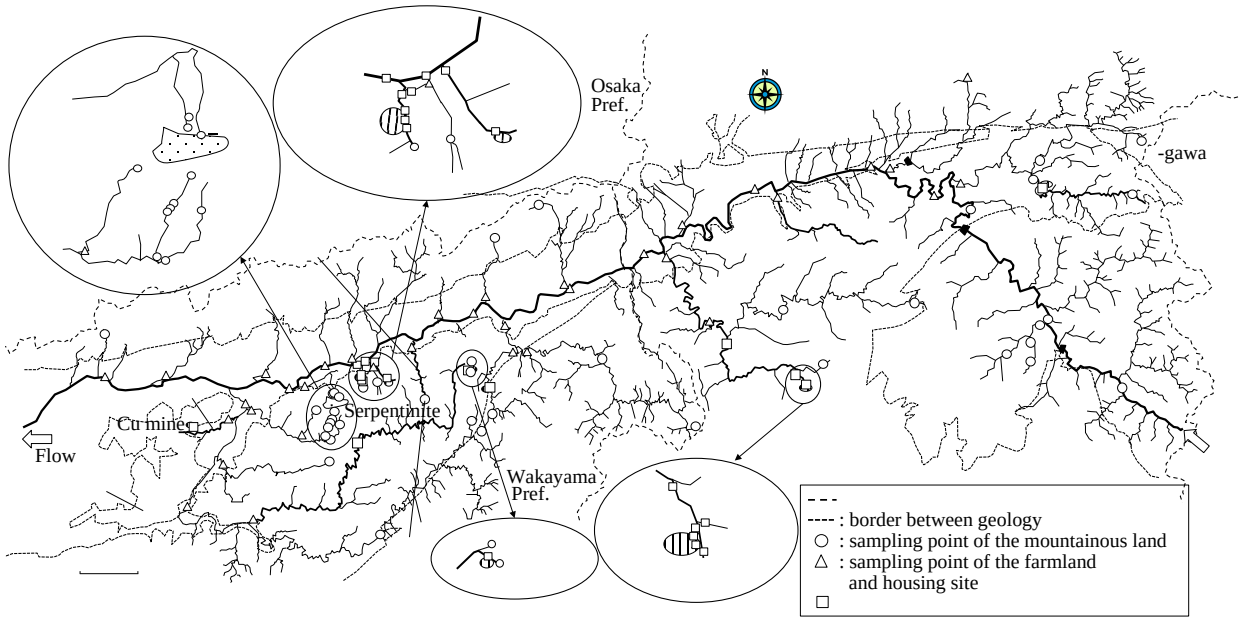

Fig.2 Distribution of Cu concentrations of bryophyte in the catchment

and in particular Mg and Ni concentrations of serpentinite are high. The closed Cu mine produced a lot of Cu and Fe sulfide ore and waste water was low pH and high concentration of sulfate with metal.

STUDY METHOD

Bryophytes were sampled in the Kinokawa River catchment. Sampling points were shown in Fig.2. The number of sampling point and sample were 97 points and 148 samples, respectively. The sampled bryophyte species were 12 species. Investigation period is April 2014 to April 2016. Cu concentrations of bryophyte were measured. The sampled bryophytes were desiccated by dryer at first. After drying, they were dissolved with concentrated nitric acid and it was filtered with the membrane filter with 0.45 micrometer of pore size before analysis. Cu concentrations of bryophyte were measured by ICP-AES. The actual detection limit of ICP-AES is 0.01ppm for Cu.

RESULTS AND DISCUSSION

Distribution of Cu concentrations of bryophyte in the catchment

Fig.2 shows the distribution of Cu concentrations of bryophyte in the Kinokawa River catchment. Underlined value indicates Cu concentration of bryophyte under the detection limit of concentration for sample solution. The point that indicates plural Cu concentrations of bryophyte means sampling plural species of bryophyte.

Cu concentrations of bryophyte in the catchment were 2 to 26,000 mg/kg-dry. In the past study, Cu concentrations of bryophyte in the normal area in the Kinokawa River catchment were 9 to 87 mg/kg-dry [1]. Then, it was thought that Cu concentrations of bryophyte in the non-contaminated area were up to about 90 mg/kg-dry.

Cu concentrations of bryophyte in the lower stream of main stream, branch A, B, C, D, E, F, G and H were over 90 mg/kg-dry. Some of Cu concentrations of bryophyte in the lower stream of main stream, the lower stream of branch A located in the eastern part of the catchment, the upper stream of branch B located in the center part of the catchment, branch C located in the western part of the catchment, the middle and lower stream of branch D located in the western part of the catchment, the upper and middle stream of branch E located in the southwest part of the catchment, the upper stream of branch F located in the western part of the catchment, the lower stream of branch G located in the eastern part of the catchment and the upper stream of branch H located in the western part of the catchment were 120 to 160, 1,600, 160 to 26,000, 280 to 1,100, 350 to 3,000, 180 to 22,000, 5,900 to 21,000, 180 and 450 to 630 mg/kg-dry, respectively. The closed Cu mines were located in the lower stream of branch A, the upper stream of branch B, the upper stream of branch C, the middle stream of branch D, the upper stream of branch E and the upper stream of branch F. The closed Cu mine composed of massive ore deposit produced a lot of Cu and Fe sulfide ore and then waste water was low pH and contained high concentration of sulfate with metal. Moreover, it is known that the closed Cu mine in the Kinokawa River catchment contains Cu and Co [9]. Therefore, it was thought that high Cu concentrations of bryophyte in the lower stream of main stream, branch A, B, C, D, E and F were caused by waste water and Cu sulfide

ore from the closed Cu mines.

On the other hand, the closed Cu mines were not located in branch G and H. Then, it was thought that high Cu concentrations of bryophyte were caused by other factors excluding the closed Cu mines.

Cu concentrations of bryophyte excluding the high Cu concentration points were 2 to 96 mg/kg-dry. Then, it was thought that the concentrations were background concentration.

The relationship between bryophyte species and Cu concentrations of bryophyte

From Fig.2, variation for Cu concentrations of bryophyte sampled at one point in the branch A to F was large. For example, in the upper stream of branch B, Cu concentrations of two kinds of bryophyte were 300 and 12000 mg/kg-dry and variation of their concentrations was 40 times. On the other hand, Cu concentrations of same kind of bryophyte in the upper stream of branch D were 47 to 50 mg/kg-dry and variation of concentrations for same kind of bryophyte was small. Then, the large Cu concentration variation depended on difference of species but Cu concentration variation for same species at the same point was small.

Fig.3 shows Cu concentrations of bryophyte for each species. And then, those concentrations were classified in three groups, mountainous land, the farmland and housing site and the around the Cu mine on land use.

Most of Cu concentrations of a kind of copper bryophyte similar *Scopelophila cataractae*, the species 1 in the around the Cu mine were high, 1,100 to 26,000 mg/kg-dry. Then, it was found that a kind of copper bryophyte similar *Scopelophila cataractae*, the species 1 lived in the around the Cu mine and had high accumulation ability. It is known that copper bryophyte lives in high copper concentration environment like under the copper roof in a temple, soil around a metal mine including a large amount of copper [2]. Moreover, it is reported that copper bryophyte have high Cu accumulation ability at the past study [10]. Therefore, a kind of copper bryophyte similar *Scopelophila cataractae*, the species 1 was thought to be a Cu contamination index. However, it could not accurately identify the species 1. Cu concentrations of species 2, 3, 4, 5, 6, 7, 8, 9, 10, 11 and 12 were 2 to 5,900, 48 to 1,900, 42 to 1,700, 5 to 350, 64 to 120, 10 to 1,500, 40 to 96, 23 to 60, 6 to 450, 10 to 39 and 24 to 31 mg/kg-dry, respectively. The species 2 to 5 were sampled in three groups. The species 6 was sampled in the farmland and housing site and the around the Cu mine. The species 7 was sampled in the mountainous land and the around the Cu mine. The species 8 was sampled in the farmland and housing site. The species 9 was sampled in the mountainous land and the farmland

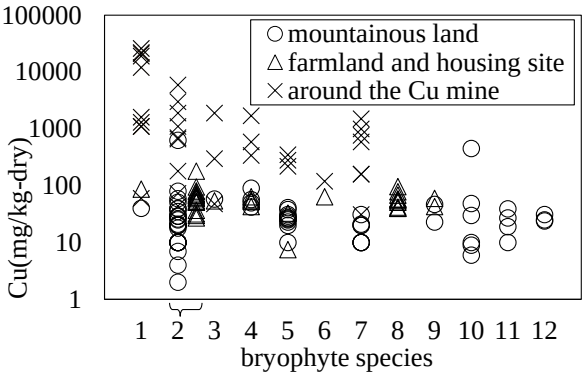

Fig.3 Cu concentrations of bryophyte species

and housing site. The species 10 to 12 were sampled in the mountainous land. Most of Cu concentrations of species 2 to 7 in the around the Cu mine were more than 90 mg/kg-dry and were high. Then, the species 2 had the highest and a wide range of Cu concentrations among species 2 to 12. Moreover, maximum Cu concentration of species 2 was high next to species 1. And then, the species 2 can be sampled in every land use in the catchment. Therefore, the species 2 was useful species for an index of Cu contamination in the catchment. Moreover, it was thought that the species 2 was another copper bryophyte similar *Scopelophila cataractae*. However, it could not accurately identify the species 2.

Influence of the closed Cu mine for Cu concentrations and species of bryophyte

Fig.4 shows the relationship between Cu concentrations of bryophyte and the distance from the Cu mine in branch A to F. Branch A to F were picked up in order to investigate the effect of the Cu mine.

In branch A, Cu concentrations of bryophyte at 0 and 1.20 km from the mine were 48 to 1,600 and 20 to 42 mg/kg-dry, respectively. In branch F, Cu concentrations of bryophyte at 0 and 4.38 km from the mine were 5,900 to 21,000 and 68 mg/kg-dry, respectively. Then, Cu concentrations of bryophyte in branch A and F decreased with flowing down. Moreover, Cu concentrations of bryophyte below 0 km were not high in branch A and F. In branch B, Cu concentrations of bryophyte at 0, 0.03, 0.08, 0.11, 1.46, 12.30 and 16.40 km from the mine were 160 to 1,100, 770 to 26,000, 590 to 19,000, 300 to 12,000, 1,300 to 1,700, 340 and 64 mg/kg-dry, respectively. In branch D and the main stream below branch D, Cu concentrations of bryophyte at 0, 0.10, 0.44, 0.98, 2.24 and 3.74 km from the mine were 350 to 700, 660, 1,900, 1,500 to 3,000, 120 and 40 to 43 mg/kg-dry, respectively. Then, Cu concentrations of bryophyte with flowing down in branch B and D were increased first, but were decreased afterwards. In branch C and the main stream below branch C,

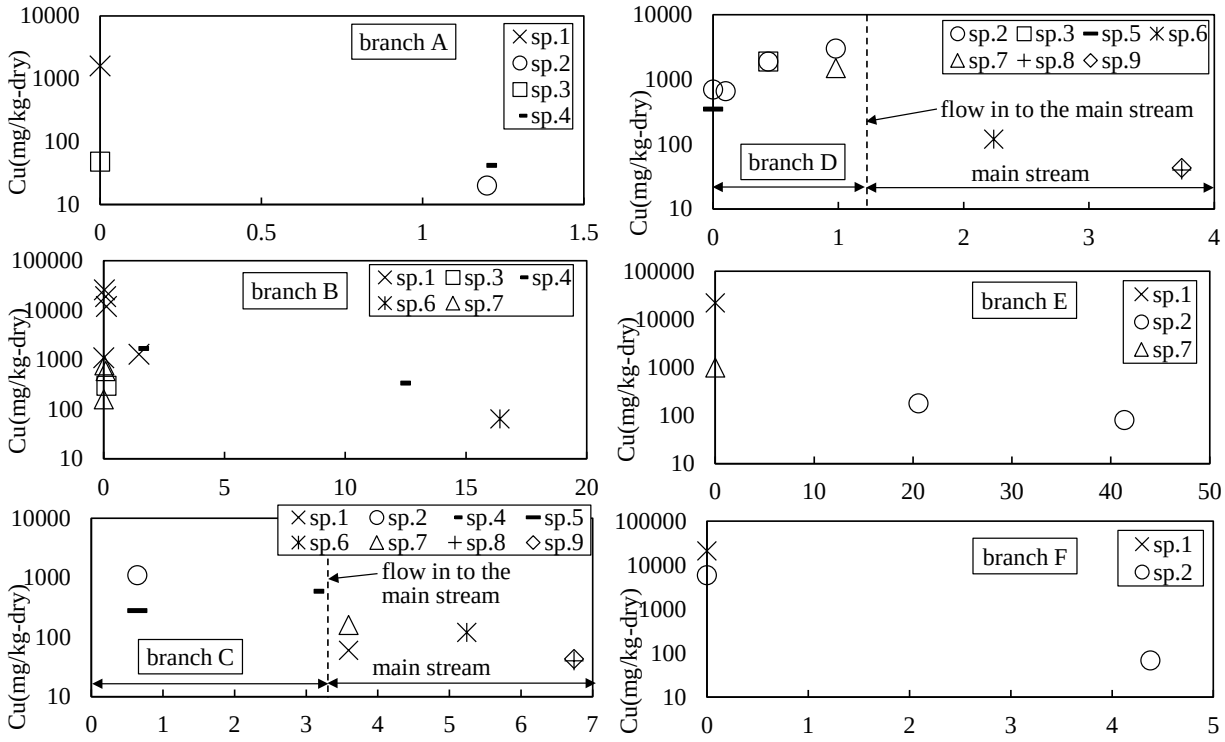

Fig.4 Relationship between Cu concentrations of bryophyte and the distance from the Cu mine in branch A to F.

Cu concentrations of bryophyte at 0.64, 3.11, 3.59, 5.24 and 6.74 km from the mine were 280 to 1,100, 590, 60 to 160, 120 and 40 to 43 mg/kg-dry, respectively. In branch E, Cu concentrations of bryophyte at 0, 20.54 and 41.36 km from the mine were 1,000 to 22,000, 180 and 81 mg/kg-dry, respectively. Then, Cu concentrations of bryophyte in branch C and E decreased with flowing down. Moreover, Cu concentrations of bryophyte were high not only at 0 km but also below 0 km in branch B, C, D and E. From the above results, the ranges of high Cu concentrations of bryophyte in branch B, branch C and the main stream below branch C, branch D and the main stream below branch D and branch E were 0 to 12.3, 0.64 to 5.24, 0 to 2.24 and 0 to 20.54 km, respectively. Then, it was thought that the closed Cu mines affect Cu concentrations of bryophyte at about 2 to 20 km downstream. In the past study, it is reported that the mining sewage affect the stream organisms at about 5 to 11 km downstream [11]. Therefore, the result of this study was about the same as the past study.

And now, in branch A, bryophyte species at 0 and 1.20 km from the mine were species 1 and 3 and species 2 and 4, respectively. In branch B, bryophyte species at 0, 0.03, 0.08, 0.11, 1.46, 12.30 and 16.40 km from the mine were species 1 and 7, species 1 and 7, species 1 and 7, species 1 and 3, species 1 and 4, species 4 and species 6, respectively. In the branch C and main stream below branch C, bryophyte species at 0.64, 3.11, 3.59, 5.24 and 6.74 km from the mine were species 2 and 5, species 4, species 1 and 7, species 6 and species 8 and 9, respectively. In the branch D and main stream below branch D, bryophyte species at 0, 0.10, 0.44, 0.98, 2.24 and 3.74 km from the mine were species 2 and 5, species 2, species 2 and 3, species 2 and 7, species 6 and species 8 and 9, respectively. In branch E, bryophyte species at 0, 20.54 and 41.36 km from the mine were species 1 and 7, species 2 and species 2, respectively. In branch F, bryophyte species at 0 and 4.38 km from the mine were species 1 and 2 and species 2, respectively. Then, bryophyte species were varied with flowing down in branch A to F. However, species 1 was existed at 0 to 1 km from the mine in branch A, B, E and F. Moreover, Cu concentrations of species 1 at 0 to 1 km from the mine in branch A, B, E and F were 1,100 to 26,000 mg/kg-dry. Then, species 1 had high accumulation ability. It is known that copper bryophyte lives in high copper concentration environment like under the copper roof in a temple, soil around a metal mine including a large amount of copper [2]. Moreover, it is reported that copper bryophyte have high Cu accumulation ability at the past study [10]. Therefore, the species 1 was thought to be a Cu contamination index.

CONCLUSION

In this study, Cu concentration of bryophyte in the Kinokawa River catchment was investigated in order to evaluate river metal contamination. High Cu concentration of bryophyte with over 90 mg/kg-dry was found because normal value in the area was 9 to 87 mg/kg-dry at the past study.

High Cu concentrations of bryophyte in the lower stream of the closed Cu mines were 120 to 26,000 mg/kg-dry. The closed Cu mine composed of massive ore deposit produced a lot of Cu and Fe sulfide ore and then waste water was low pH and contained high concentration of sulfate with metal. Therefore, high Cu concentrations of bryophyte in the lower stream of closed mines were thought to be caused by waste water and Cu sulfide ore from the closed Cu mines. Background Cu concentrations of bryophyte sampled at the non-mine area were 2 to 96 mg/kg-dry.

A kind of copper bryophyte similar *Scopelophila cataractae* were often sampled in the around the Cu mine. And then, their Cu concentrations were high, 1,100 to 26,000 mg/kg-dry. Therefore, a kind of copper bryophyte similar *Scopelophila cataractae* was thought to be a Cu contamination index however was not able to be identified into in detail species name. Another copper bryophyte similar *Scopelophila cataractae* was sampled in all group of land use and was unidentified in detail name and its concentration was 2 to 5,900 mg/kg-dry. Therefore, it was useful species for an index of Cu contamination in the catchment because of its wide concentration depending on land use and wide distribution for land use.

High Cu concentration bryophyte with over 90 mg/kg-dry was found till 20.54 km downstream of the Cu closed mine. Therefore, it was thought that the closed Cu mines affected Cu concentrations of bryophyte till 20 km downstream. Bryophyte species were varied with flowing down and then species of bryophyte was thought to indicate river environment.

REFERENCES

[1] Kubohara T and H. Ii, “Cu, Co and Ni contamination index for river using river insects and river plants”, International Journal of GEOMATE, Vol. 11, Issue 26, Oct., 2016, pp. 2651-2658.

[2] Satake K, “A “copper bryophyte” *Scopelophila cataractae* and copper (1) - Distribution of *Scopelophila cataractae* in the world”, Proceedings of the Bryological Society of Japan, Vol.5, No.4, April, 1990, pp.49-53.

[3] Nomura T and Hasezawa S, “Regulation of gemma formation in the copper moss *Scopelophila cataractae* by environmental copper concentrations”, Journal of Plant Research, Vol.124, Issue 5, Sep.2011, pp.631-638.

[4] Hamada N, “Lichens as a Bioindicator of Air Pollution - Theory and Practice of Surveying -”, Seikatsu Eisei, Vol.42, No.2, 1998, pp.43-51.

[5] Isibasi R, Sugi Y and Kito T, “Heavy metal determination of epiphytic bryophytees as an attempt to indicate industrial pollution of environment”, J. Japan Soc. Air Pollut., Vol.17, No.1, 1982, pp.63-69.

[6] Tsuji Y, Morishita T and et al., “Elements in epiphytic bryophyte as indicators of atomospheric environment in Wakayama Prefecture”, Bulletin of the Wakayama Research Center of Agriculture, Forestry and Fisheries, No.5, 2003, pp.15-23.

[7] River Bureau Kinki Regional Development Bureau Ministry of Land, Infrastructure, Transport and Tourism, Kinokawa Basin, http://www.kkr.mlit.go.jp/river/kasen/kinokawa.html

[8] Wakayama City Children’s Science Museum, “Wakayama no ishi”, Dec.2002, 20pp.

[9] Kubohara T and Ii H, “Cu, Co, Cr and Ni of river water, river insect and water plant in the Kinokawa river catchment”, Int. J. of Geomate, Vol.10, No.1, Feb.2016, pp.1600-1606.

[10] Satake K, Shibata K and et al., “Copper accumulation and location in the moss *Scopelophila cataractae*”, Journal of Bryology, Vol.15, Issue 2, 1988, pp.353-376.

[11] Gose K, “On the influence of mine-effluents of the Tateri mine, Kawamata mine (Nara prefecture) and Imori mine (Wakayama prefecture) on stream organisms”, Japanese Journala of Ecology, Vol.10, No.1, Feb.1960, pp.38-45.

Second International Conference on Science, Engineering & Environment,
Osaka City, Japan, Nov.21-23, 2016, ISBN: 978-4-9905958-7-6 C3051

SUNLIGHT SURFACE ANALYSIS ON EARLY MODERN APARTMENT FRONT FACADES IN KUALA LUMPUR, MALAYSIA

Ahmad Sanusi Hassan[1] and Yasser Arab[2]
Professor[1] & Ph.D Research Fellow[2]
School of Housing, Building & Planning
Universiti Sains Malaysia
11800 USM, Penang, Malaysia

ABSTRACT

This study analyzes sunlight performance on front facades of high-rise apartments in Malaysia built with early modern style. Early modern style apartments were popularly built from the 1950s to 1970s using mass produced and fast construction techniques with standardized design by the government to elicit housing shortage problem due to population increase in the city. The apartments are built with open corridor system as the image of the frontages and functioned as the main access to entrance doors of the apartment units. The results from the study will provide information on awareness of passive facade design. The government recently introduces Green Building Index (GBI) as an awareness strategy in architectural building design. By having this awareness, it is expected the building design in the future will able to help reducing electricity consumption. Three early modern apartments are selected in the case studies located in Kuala Lumpur. The survey will measure the percentage of the apartments' front façades shaded from direct sunlight. Its simulation uses SunTool software at a position when the sun path is at perpendicular to the apartment facades. The sunlight surface data indicates that all the facades have slightly above 75% under the excellent category of the shading performances. The wide corridor plays the most important role as a sun shading device to all three apartments' recessed wall facade. The open corridor system has more emphasis on horizontal sun shading device. Less emphasis is on vertical sun shading device limited to the brick railing fence and parapet walls of the corridor roof on each floor. The sun shading devices are only able to give shades to the apartment façades slightly above 50% from evening sunlight.

Keywords: High rise Apartments, Early Modern, Shading, Facades, Kuala Lumpur

INTRODUCTION

The purpose of this study is to evaluate shading performances on early modern style apartment façades designed with. The style was popularly designed by architects from 1950s to 1980s in Malaysia. At that time Kuala Lumpur had experienced population booming due to a trend of rural to urban migration by the rural population to find better jobs in the city. The early modern style is an early form of modern architecture after the end of the popularity of art deco style in the1940s. The construction applied to mass produced system and fast construction technique which is necessary to meet the demands of house units by the city population.

This study embarks on apartment buildings because not until recently apartments are becoming the most popular house type in this country. This study is very important to understand a level of emphasis and awareness on the apartment design to shading elements. Design with excellent shades on the building façade is important to provide optimum indoor thermal comfort to the occupants. Bakhlah and Hassan [1] affirmed that excellent shading elements are necessary to shade building facades from intense sunlight in a tropical region. Apartment facades exposed to direct sunlight causes heat gains on its façade surface which becomes one of the factors causing urban heat island.

Urban heat island occurs in most cities because it reradiates heats from the built up areas with buildings, open spaces and roads constructed with sensible heat materials which absorb heats when exposed to direct sunlight. As a result, the cities have comparatively warmer temperature than their greenery surrounding rural areas.

Poor design on apartment façades causes solar radiations inside the building. The reason for poor façade design is because it is unable to give optimum shade on its vertical surface area. The outer wall surface will reradiate the heat to the indoor area [2], [3]. It induces more heats inside the house creating warmer temperature than 28oC above the comfort zone. Thus, self-awareness to the importance of shading devices during the design stage by the architects is crucial.

This study imparts research findings from the analysis of building simulation using SunTool software. With the findings, this study is able to

promulgate significant contributions to the research study with recommendations for excellent facade design as important self-awareness by the architects.

SELECTED CASE STUDIES

Three apartments are selected for the case studies. Their façade design exemplifies a typical early modern architectural style which connotes 'Less is more' concept with simple geometrical form and unornamented design. The primary construction uses reinforced concrete space-frame structures, brick walls and cement render finishes. Location of all the apartments is in Kuala Lumpur. Sulaiman Courts is the first high-rise apartment in Kuala Lumpur as well as in Malaysia about a year before the country independence in 1957. A few years after that the government built the second apartment, Pekeliling Flats in 1964.

Early modern architecture had signified a popular style from the 1950s to 1970s in Malaysia (Figure 1). Some apartments with this style were continuously constructed until the early 1980s. During this period, the government actively built low-cost apartments to house low-income families who lived in squatter area under relocation program towards 'Zero Squatter' policy in Kuala Lumpur [4]. During that time, the word 'flat' was popularly used to indicate apartment building.

Today, this word is barely used replaced with the name 'apartment'. Early modern style applied mass-produced construction technique, a design with modular and the standard size of the apartment units. This technique had speed up the construction time to cater a problem of housing shortage in Kuala Lumpur [5]. High rise apartments were a solution to provide house units to low-income people as their basic shelter [6].

Fig. 1 Sri Perak Flat in Sentul, Kuala Lumpur.

The style was compatible with mass produced and quick construction concept using technological advancement. The design had a simple composition with reference to basic geometric shapes like square, rectangle and circle to draw standardized modular house units in design and production process of working drawing for submission to the local authority's approval. The design simplicity speed up the progress [7], [8], [9].

Apartments with open corridor system at the front facade were a typical design during the early modern period. The corridor functions as accessibility route for the pedestrians and residents to the entrance door. The design was introduced during British Administration slightly before the country's independence which later nurtured the development of the apartments' style.

It was an influence from architects during Industrial Revolution in Europe like Le Corbusier, Mies Van der Rohe and Walter Gropius in building high rise flats for labor workers, with the use of elevator in building design [10], [11], [12]. Open corridor system became the popular design for the apartments such as Flat Isokon built in 1932 in Hampstead, London [13]. Reinforced concrete structures with brick walls, wooden frame for doors and glass louver windows were the archetypal construction materials. Most apartments had either flat or nearly flat roof.

The federal government projects prefer to build high-rise apartments in Kuala Lumpur due to the scarcity of available land. According to data from Department of Statistics Malaysia [14], apartment units have the largest percentage of the total house types with 73% in Putrajaya, the new administrative city for the federal government of Malaysia. The number of apartment units has superseded the number of terrace house type. The government favors building high-rise apartments, able to supply hundreds of house units per hectare to cater the high demand due to the population booming. By the year 2000, slightly more that 2 million people live in high rise apartments in Malaysia [14].

The selected apartments namely Melati, Sri Selangor and Sri Sarawak were selected for the case studies. They were located in Pudu area, Kuala Lumpur. They were amongst the earliest apartments built in this city like Sulaiman Court apartment. The first apartment construction in Pudu area was completed in 1958, and the last completed in 1965. Figure 2 illustrates the apartments varies from 15 to 18 stories in Loke Yew Road. The location of the apartments in this survey is as follows:

1. Melati Apartment (Figure 1) at Loke Yew Road, also known as Loke Yew Apartment
2. Sri Selangor Apartment (Figure 2) at Gelugor Road
3. Sri Sarawak Apartment (Figure 3) at Kenanga Road

Fig. 2 Melati flats at Loke Yew Road in Pudu area.

The study only focuses on analyzing the shading performance. Three drawings (Figure 3-5) which illustrate foundation to roof detail of the front apartment facades are drawn at the initial stage before they will be utilized in the building simulation. The details were drawn at a sectional cut of the corridor and recessed wall with window location. All buildings have a similar design with open corridor system. They have a slight variation of dimensions of the length, width and height.

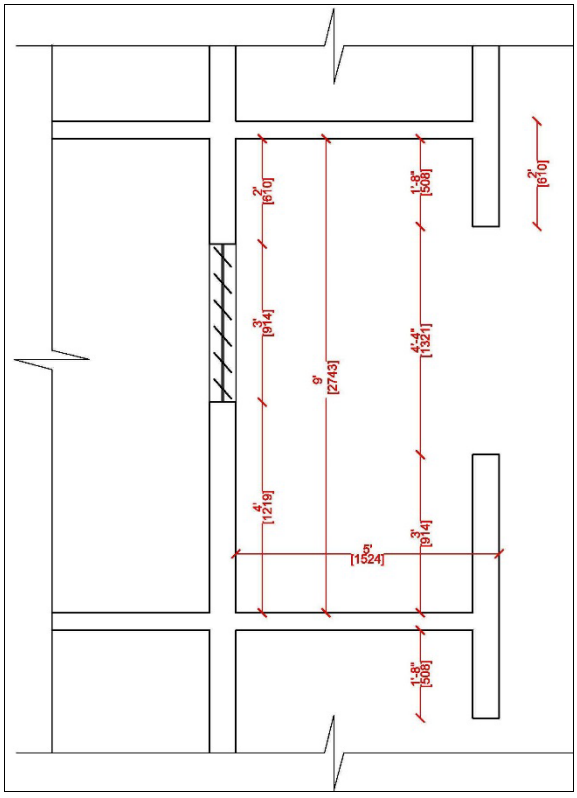

Fig. 3 Foundation to roof detail of Melati Apartment.

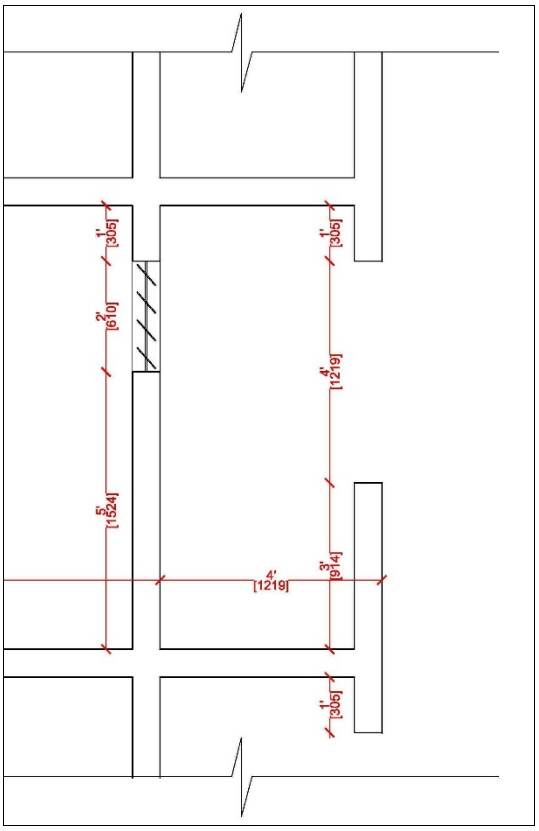

Fig. 4 Foundation to roof detail of Sri Selangor Apartment.

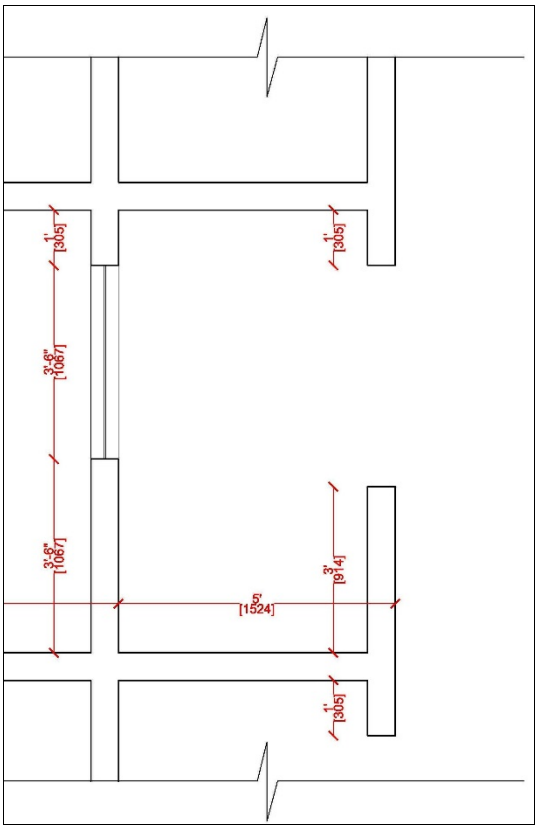

Fig. 5 Foundation to roof detail of Sri Sarawak Apartment.

RESEARCH METHODOLOGY

The survey will use SunTool software to generate shading simulation on the apartment front facades. This software will provide a series of calculations of the amount of shading area cast on the façade surface. The facades will be simulated only at positions when they were perpendicularly exposed to the sunlight. The simulation will measure the shading performance during morning and evening sunlight simulation when it has the facades perpendicularly facing direct sunlight during morning and evening time. The reason is the apartments selected in the case studies are mass produced buildings with the standardized design built at various building orientations with a lack of reference to the sun path direction.

The SunTool software will help to determine the annual sun path position perpendicular (90°) to the façade's surface, both at the east and west direction. However, there is a limitation in positioning the perpendicular sun path. The limitation is that there is no sun path (the sun's angle direction) which intersects at all times perpendicular to the facade in any single day times.

The other limitation is not all the sun paths have exactly perpendicular to the facades in a case of a location at Kuala Lumpur. Thus, the azimuth with closest to 90° will be applied during the simulation. The angle of the sun path slightly varies from time to time during the day time. Table 1 shows the annual times and dates deduced by SunTool software when azimuth of the sun path perpendicular to the apartment façades at Kuala Lumpur's latitude (N 3.1°) and longitude (E 101.7°) [15], [16].

Table 1 Times and dates when azimuth perpendicular to the apartment façades in Kuala Lumpur.

Orientation	Time	Date	Azimuth
East 90°	7 am	23 March	90°
	8 am	25 March	90°
	9 am	27 March	89.8°
	10 am	28 March	90.1°
	11 am	29 March	90°
	12 pm	29 March	92.2°
West 270°	1 pm	16 September	90.5°
	2 pm	29 March	89.8°
	3 pm	18 September	89.8°
	4 pm	26 March	89.9°
	5 pm	24 March	89.9°
	6 pm	22 March	89.9°

With an aid of the SunTool program, it is possible in this survey to pinpoint the effectiveness of the apartment design by measuring the amount of shades cast on the facade surface. Figure 6 illustrates briefly how the amount of shade and exposed area to the direct sunlight measured with reference to a foundation to the roof section of the façade.

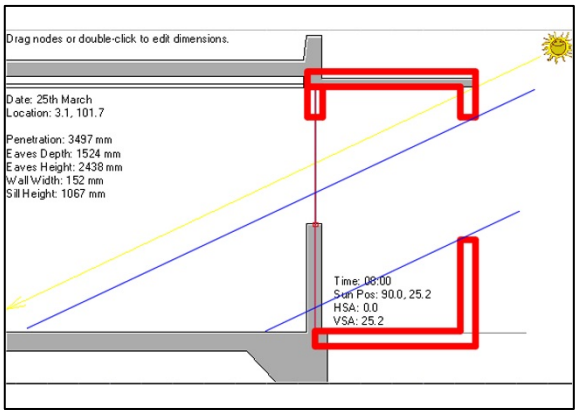

Figure 6 Example of the simulation using SunTool program.

ANALYSES AND FINDINGS

The analysis found that 'open corridor system' is a common design concept in early modern style apartments [17]. Corridors become the main circulation system for the residents to get access to the entrance door of their apartment unit on each floor. The corridors signify the frontage of the apartment façade. The apartments constructed from the 1950s to 1980s were to house low-income people and their family who had moved from their village to Kuala Lumpur as their new workplace.

They were also known as 'the worker's house' [17], [18] and at that time these buildings were called 'flats'. Dimensions of these low-cost apartments are very basic and minimal to meet the standard of the living requirement by the Municipal Council. In the case studies, these apartments have their corridor's width varies from 4 to 5 feet which create a recessed wall of the apartment units with a height varied from 8½ to 9½ feet. The corridors have 3 feet height brick railing fence wall functioned as a railing. The extended parapet wall below the brick railing fence at Melati Apartment is 1 feet 8 inches while Sri Selangor and Sarawak Apartment are only 1 feet.

In this country, the standard brick wall has ½ feet or 6 inches wide. Each apartment unit has 20 feet wide façade front wall with a series of glass louver window and one entrance door. Frontage wall at Melati Apartment has 4 feet high window sill and 3 feet high window, Sri Selangor has 5 feet high window sill and 2 feet high window, and Sri Sarawak has 3½ feet high window sill and window.

Table 2 and Figure 7 shows the result of shading area cast at the recessed wall surface of the

apartment unit's frontage in all the case studies. This analysis counts 0-25% as poor, 25-50% as fair, 50-75% as good and 75-100% as excellent shading performance. The results are as follows:

Table 2 Percentage of shading area from the building simulation.

Time	Shading Area (%)		
	Melati/Loke Yew	Sri Selangor	Sri Sarawak
8:00 am	53%	51%	51%
9:00 am	54%	53%	53%
10:00 am	67%	58%	68%
11:00 am	100%	89%	100%
12:00 pm	100%	100%	100%
1:00 pm	100%	100%	100%
2:00 pm	100%	100%	100%
3:00 pm	100%	100%	100%
4:00 pm	87%	75%	90%
5:00 pm	58%	54%	58%
6:00 pm	54%	52%	52%
7:00 pm	53%	51%	51%
Average (%)	**77%**	**74%**	**77%**

- All the case studies have their shading performances with above 50% shade (good category) on the façade surfaces.
- All the case studies have excellent shading performance with 77% except Sri Selangor with 74% slightly below 75% mark to be included under an excellent category.
- Melati Apartment has the best result of the overall shading performance, followed by Sri Sarawak and Sri Selangor Apartment. This apartment has the widest corridor and longest extended parapet wall below the brick corridor.
- Sri Selangor Apartment has the lowest performance result in the case studies. It has the narrowest corridor's width and shorter extended parapet wall below the brick railing fence with only 1 feet 2 inches compared to that of Melati Apartment with 2 feet long.
- All apartments have the same height of brick railing wall with 3 feet high which are the standard height in the corridor design in this country.
- The time from 8 to 10 am has a cool morning sunlight which does not affect solar radiation and heat gain to the indoor area of the apartment. The focus of this result's analysis is in the evening sunlight which induces intense heat to the apartment facades and causes solar radiation.
- All apartment façades have 100% shades from 11 am to 3 pm except Sri Selangor façade at 11 am with 89%.
- At 4 pm, all the case studies have excellent shading performance.
- At 5 pm, all the apartment facades have shades fall under the good category. Nearly half of the surfaces in each apartment are exposed to direct sunlight. The same condition occurs on the apartment facades at 6 pm.
- From 6 to 7 pm, the discussion on the result of this analysis is not really necessary. The sun does not create harsh sunlight during this time.

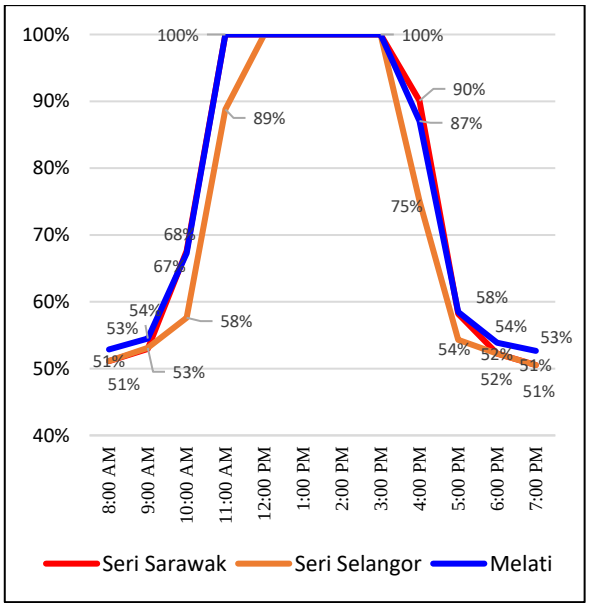

Fig. 7 Line chart graph which shows the percentage of shading area from the building simulation.

CONCLUSIONS

This study concludes all the apartments in the case studies designed with early modern style are under the excellent category of the shading performance with an average sunshade of 76%. The open corridor system as a part of the apartments' frontage design elements is very effective sun shading devices which give shade to the recessed wall facades. The findings of this study recommend, as one of the design solution, apartment with open corridor system as a part of awareness strategy to meet the requirement in Green Building Index (GBI). From 11 to 3 pm, the recessed facades are fully under shade. It is necessary to have the building facades under full shade from intense sunray during this time to prevent solar radiation. The open corridor system also gives excellent shade to the apartment façades at 4 pm.

The only necessary evening time that apartment facades do not have excellent shading performance is from 5 to 6 pm. Only slightly above 50% of the facades are under shade. The study finds that the open corridor system has more emphasis on blocking high angle (elevation/altitude) compared to

low angle sunlight. The design has an emphasis on horizontal rather than vertical sun shading devices. The wide corridor plays the most important element as horizontal sun shading device besides functions as circulation access to entrance doors of the apartment units. This horizontal design creates the recessed wall apartment façade. The vertical sun shading elements used in the design is corridor brick railing fence and parapet wall of the corridor roof.

The vertical sun shading devices become more important sun shades when the evening sunlight descends at a lower angle (elevation/altitude). From 5 to 6 pm, the sun shading elements are only able to block the apartment façade slightly above 50% from direct sunlight. The analysis shows that additional vertical sunlight to block sunlight at low elevation should be additionally integrated. The morning low sunlight at low elevation till 10 am is not intense sunlight. During this time, it is good to have continuous human skin exposure to direct sunlight which provides ultraviolet B from the sun ray for skin cells to generate vitamin D without having the skin with sunburn problem.

ACKNOWLEDGEMENT

The authors would like to express appreciation for the financial support under Fundamental Research Grant Scheme by Universiti Sains Malaysia under Ministry of Higher Education.

REFERENCES

[1] Bakhlah MSO and Hassan AS, "The study of air temperature when the sun path direction to Kaabah: with a case study of Al-Malik Khalid Mosque, Malaysia", International Transaction Journal of Engineering, Management, & Applied Sciences & Technologies, Vol. 3(2), 2012, pp. 185-202.

[2] Hassan AS and Ramli M, "Natural ventilation of indoor air temperature: A case study of the Traditional Malay House in Penang", American Journal of Engineering and Applied Sciences, Vol. 3(3), 2010, pp. 521 - 528.

[3] Feriadi H and Nyuk HW, "Thermal comfort for naturally ventilated apartments in Indonesia", Energy and Building, Vol. 36, 2004, pp. 614-626.

[4] Sufian A and Mohamad NA, "Squatters and Affordable Houses in Urban Areas: Law and Policy in Malaysia", Theoretical and Empirical Researches in Urban Management, Vol. 4 (13), 2009, pp. 108-124.

[5] Hassan AS, Konsep Rekabentuk Bandar di Semenanjung Malaysia: Kuala Lumpur dan Bandar-Bandar di Sekitarnya *(Urban Design Concepts in Peninsular Malaysia: Kuala Lumpur and Its Su rrounding Towns*), Penang: Universiti Sains Malaysia Press, 2005.

[6] Labin AMJE, Che-Ani AI and Kamaruzzaman SN, "Affordable Housing Performance Indicators for Landed Houses in the Central Region of Malaysia", Modern Applied Science, Vol. 8(6), 2014, pp. 70-86.

[7] Cheung CK, Fuller RJ, and Luther M, "Energy-efficient envelop design for high-rise apartments", Energy and Buildings, Vol 37, 2005, pp. 37-48.

[8] Curtis WJR, Modern Architecture Since 1900, 3rd ed. 1996.

[9] Badir FY, Kadir MRA, and Hashim AH, "Industrialized Building Systems Construction in Malaysia". J. Archit. Eng., Vol. 8(1), 2002, pp. 19-23.

[10] Hassan AS, Issues in Sustainable Development of Architecture in Malaysia, Penang: Universiti Sains Malaysia Press, 2004.

[11] Ching FDK, Jarzombek M and Prakash V, A Global History of Architecture, 2nd ed. New Jersey: John Wiley & Sons, 2011.

[12] Cruickshank D and Fletcher B, Sir Banister Fletcher's A History of Architecture. 20th ed. Oxford: Architectural Press, 1996.

[13] Kostof S, A History of Architecture: Settings and Rituals, New York: Oxford University Press, 1995.

[14] Department of Statistics Malaysia, General Report of the Housing Census, Putrajaya: Department of Statistics Malaysia Press, 2010.

[15] Hassan AS and Arab Y, "The Extent of Sunlight Penetration Performance on Traditional Style's Apartment Façade in Putrajaya, Malaysia", Modern Applied Science Vol. 8(5), 2014, pp. 132-142.

[16] Arab Y and Hassan AS, "Daylighting Analysis of Pedentive Dome's Mosque Design during Summer Solstice with Case Studies in Istanbul, Turkey', International Transaction Journal of Engineering, Management, & Applied Sciences & Technologies, Vol. 3(2), 2012, pp. 167-183.

[17] Kosman KA et al., 50 Tahun Perumahan Awam di Kuala Lumpur (*50 Years Public Housing in Kuala Lumpur*), Bangi: Institut Alam dan Tamadun Melayu (ATMA), 2008.

[18] Mohamad Rasdi MT, Housing Crisis, Skudai: Universiti Teknologi Malaysia Press, 2007.

Second International Conference on Science, Engineering & Environment,
Osaka City, Japan, Nov.21-23, 2016, ISBN: 978-4-9905958-7-6 C3051

A COMPARATIVE ANALYSIS OF LEGAL SYSTEM OF RIGHT EXCHANGE FOR URBAN DEVELOPMENT PROJECTS -LAND READJUSTMENT SYSTEM IN DEVELOPING COUNTRIES IN ASIA AND SOUTH AMERICA-

Norihiko YANASE[1], Takeo OCHI[2] and Shigeo OKABE[3]

[1]Faculity of Engineering, Ashikaga Institute of Technology, Japan, [2]Japan International Corporation Agency, Japan, [3]Faculity of Urban management, Fukuyama City University, Japan

The aim of this study is to indicate some basic points regarding legal system of Land Readjustment (LR) through comparative analysis of Japan and some developing countries in South America and Asia. Especially, there is a big difference between countries such as Japan where it is based on the public law system and countries such as Brazil where it is based on the private law system. Land ownership in some developing countries is controlled for social purpose, for example in Brazil, squattersô occupancy is approved in public and private land for resettlement policy. Thinking from an international view point, the LR system in Japan stands on a unique land and administrative system. Therefore for the technology transfer, the Japanese system must be modified to account for such countriesô system. This paper proposes some important points for technology and system transfer of LR.

Keywords: Land Readjustment, Right Exchange, Urban Development, Legal System, Comparative Analysis

INTRODUCTION

Land readjustment system in Japan

Normally all the land within a development area is bought up to carry out development. On the other hand, there is also a development method in which the form of all the asset rights is changed in accordance with the landuse plan prior to development, without purchasing the land. The latter is referred to as the rights conversion method, in contrast to the former land purchasing method. The rights conversion method is normally referred to as land readjustment (hereafter, LR).

More than 1/3 of the urban land of Japan is developed by LR, and the large scale earthquake restoration projects in 1995 and 2011 also used LR[1)]. From 1980 the Japanese Government promoted the transfer of the LR method and techniques to developing countries of South-east Asia [2),3),4)]and South America[5)], etc., and in 2004 a Land Readjustment Act was adopted in Thailand[6)].

Position of this research

The basis of the LR method is conversion of land rights based on administrative disposition[(1)], and is referred to as Replotting Disposition. German law was introduced into administrative law within the Japanese legal system, which is similar to Umlegungsverfarhen in German law. However, in countries with legal systems where there is no concept of public law and it is assumed that titles are exchanged by private law, as in British and American law, sufficient legal study is necessary in order to transfer the system of LR, but research into the systems has not been sufficient compared with research into the transfer.

The objective of this research was to carry out a comparative analysis of the systems in the countries that have introduced the system and technique of Japanese LR, to obtain knowledge for transfer of systems and techniques in the future.

The documents analyzed included reports by Japan International Cooperation Agency (JICA) on Technical cooperation projects currently being implemented in Brazil and Colombia[7)] and other open literature papers, etc.

COMPARATIVE ANALYSIS OF LR SYSTEMS

Features of LR

The origin of LR was in the consolidation of farm land in order to improve productivity. Referred to as land consolidation (hereafter, LC), there are examples of it all over the world. In 1899 Japan introduced LC into the legal system, with reference to the German system[8)]. In 1919 legal measures were adopted to enable LC to be used as a tool for urban planning, and as a result LR was born[9)]. Thereafter it was used for housing development in the outskirts of cities, and earthquake and war restoration projects, and in 1954 the independent Land Readjustment Act was adopted as the culmination of the system to date.

LR is a means to realize land use plans within urban planning, but it is a method that enables the title relationships prior to development to be maintained after development, in other words, it enables communities to be maintained.

Normally, real estate development produces a large development profit for the landowners, and with LR the development profit and cost burden can be fairly and transparently allocated. The mechanism is to objectively evaluate the land before and after development, and to proportionally allocate the development profit to the individual owners[10]. These features promote consensus formation of residents for development. In addition it includes a self-contained mechanism for converting a part of the development profit for sale, and appropriation of the sale profit to costs[11]. This beneficiary liability mechanism enables infrastructure development with a small financial burden.

From the above, it was recognized that LR is effective as a measure for slum improvement or suburban sprawls in developing countries, and designs and techniques of land evaluation with the above features were introduced. One issue is a system to avoid disputes associated with title exchange. In other words, a mechanism is constructed to incorporate rights compartments in accordance with a plan against a minority that does not agree with title conversion.

Comparison of the title exchange method and the registration method

Mechanism in Japan

Explained in legal terms, LR in Japan defines new rights by the ñtentative validity (kouteiryoku)ò of administrative disposition. In addition, there is a mechanism that enables registration of new rights by ñcommissioned registrationò by the developer instead of the right holder.

Mechanisms in Asian countries

The mechanism for determining new rights areas is a procedure[12] referred to as land pooling (hereafter, LP), that is the basis of LR in Thailand[13], Nepal[14], Bhutan[15], etc. With LP all the land of owners that agree to a project is pooled, and subsequently divided in accordance with a land use plan. However the land of those opposed is excluded. This exclusion has the possibility of obstructing the realization of a rational land use plan in urban planning.

A new use plan is determined through discussions between the developer and the owners, but ultimately it is possible to avoid a breakdown of consensus formation as a result of the land of a small number of opponents being the target of expropriation. It is said that in practice choices not involving expropriation can be taken through tough negotiations.

In Thai law, a special measure for examination of registration of deeds is provided in law for new land by LR, and a new certificate of title is issued upon application by the developer[13].

Mechanisms in South America

A title exchange method that differs from Japanese or Asian type LP has been developed in Colombia, and at present legislation is in progress in Curitiba City in the Federative Republic of Brazil. The mechanism in Colombia is an exchange of title by a private law contract. Colombiaôs Urban Act, which uses the provisions of the existing private law such as civil law, commercial law, trust law, etc., does not have provisions for title exchange for land. Also title exchange is not limited to land, but also applies to floor space of buildings. The procedure is the landowner transfers the land owned in trust to a trustee organization such as a local government, a trust bank, a developer, etc., and after completion of the project the trustee returns it to the original owner.

The validity of the title exchange is guaranteed by the power of the contract based on civil law or trust law, etc., and ultimately the Land Expropriation Act could be applied in accordance with the strength of the public nature of the project.

Application for registration is carried out by the right holder[16),17),18)].

In Brazil the ñTransferencia do Potencial Construtivo: TPCò of the City Statute §35 corresponds to the transferable Development Right in the USA or the ñrental building design systemò or ñarea of special application of floor area ratioò in the Building Standard Act of Japan. Curitiba City has much experience in development by TPC, and the system has been designed with reference to the method in Colombia[19,20),21)].

Relationship between urban planning and LR

The case of Japan and other Asian countries

LR projects in Japan and various countries in Asia are realized by positioning wide area facilities in urban planning, and district facilities in the project plan.

The case of South America

The urban planning system in Colombia has a 3-layer structure: the ñPlan de Ordenamiento Territorial: POTò which corresponds to a master plan in urban planning, a ñPlan Parcial: PPò which

Table 1 Comparison of title exchange methods in LR development projects

	Japan	Thailand	Columbia
Relationship to urban planning	District facilities are determined by a project plan	District facilities are determined by a project plan	Part plans positioned in ñPlan Parcialò
Title exchange Procedure	Administrative disposition	Land pooling Special provision for	Private law contract Right holder
Relationship to registration system	Commissioned registration	examination and application by the right holder	application
Mechanism for avoiding disputes	Administrative disposition	Expropriation law	Expropriation law

is a local detailed plan, and a ñUnidades de Actuacio Urbanistica: UAUò which is an implementation plan positioned in the PP. It is a requirement for implementation of LR to be positioned in the PP. Besides the UAU, the PP includes a public spaces development plan, and measures to realize fair benefits and liabilities among the land rights owners. With UAU the unit of implementation of urban development projects is the block, and 3 types of project are included: Reajustte de Terrenos, Intergracion Immobiliaria, and Cooperracion entre particpes[22].

Curitiba City has designed a system that is close to that of Colombia.

The above outline is summarized in Table 1.

SUMMARY OF THE RESEARCH: CHARACTERRISTIC CONCEPTS OF JAPANESE LR

For a long period of time Japan has transferred the techniques of LR using its characteristic concepts and terminology such as replot, contribution, and reserve land. This research has compared the Japanese LR system which is behind these techniques with the systems in Asia and South America. It is considered that this research will facilitate the understanding and introduction of LR among people of various other countries based on the infrastructure of systems in their own countries.

Note that the Japanese category 1 urban redevelopment project has the mechanism of right exchange from original lots and houses to new building flowers. It superficially resembles the South American LR system, but their bases are completely different in that the mechanisms of right exchange are public law.

Category 2 urban redevelopment does not come within the scope of right exchange. The mechanism is to purchase original property from many owners who agree to the redevelopment project. After the project, they are distributed property right of new building flowers. Some land owners who didnôt agree to the project, withdraw from the project with compensation money. This mechanism is based on expropriation law.

Notes)

(1) Administrative disposition is recognized as having ñtentative validityò as a ñspecial validityò that is not normally seen in legal actions. Administrative disposition is considered as valid until established by lawsuit[23].

ACKNOWLEDGEMENTS

This paper owns a lot to òThe Project on Capacity Development for Land readjustment in Curitiba ò by JICA, of which the team leader was Dr. Kobayashi, an honorary professor of Hokkaido University. In particular analysis of legal system we are indebted to Mr. Yohji Kinoshita who has researched city planning law system in Colombia and Brazil as a JICA expert.

Reference

[1]Nakayama H, òCommunity development for Disaster prevention by popular sovereignty-to study Hanshin-Awaji great earthquake and to provide for Nankai Trough earthquakes, Minerva Shobo, 2015

[2]Nakano M,ò International contribution by land readjustment, City planning review Vol.42/No.1,pp.52-61,1993

[3]Yanase N,òA hundred yearsô Journey of land Readjustment-From Germany to Japan, and Asian countriesò, JSCE Magazine,Vol.86/No.6, pp. 74-78, 2001

[4] Ministry of Land, Infrastructure, Transport and Tourism & Infrastructure Development Institute, ñResearch report of formulate guidelines for technology transfer: land readjustment, 2002

[5]Tanaka H, "Overseas technical support by collaboration of Obihiro city and JICA, Shintoshi magazine, vol.65/No.10, pp.46-48, Urban planning association, 2011

[6]Hino Y, Seta F, Kishita M, Kishii T,ò A study on the transfer of Land Readjustment institutional system: A case study on the transfer of Land Readjustment from Japan to Thailand, Journal of the City planning Institute of Japan, Vol.41, pp.553-558, 2006

[7] Miura J, Ochi T, òIn the future of international development of land readjustmentò, LR forum 2014, pp.188-191,2014

[8] Yanase N, ñA historical view on modern legal system for land readjustment, Journal of JSCE, D3, Vol.70/No.5, pp.403-475, 2014

[9]Mitsui Y, òA Study on Tsukuba Academic New townò, pp.35-54, Kajima publishing co. 2015

[10]Yanase N,ò A study of benefit-allocation model in land readjustment project, Proceedings of JSCE, No.401/Ⅳ-10, pp.89-98, 1989-1

[11]Yanase N, A study on historical process of financial and subsidy for land readjustment project by landownersô corporativeò, Journal of the city planning institute of Japan, No.36, pp.493-498,2001

[12] Yanase N, Hayashi K,òA study on the system of converting land title in land readjustment projectò, Journal of the city planning institute of Japan, Vol.29, pp.631-636, 1994

[13] Hino Y, ñA practical study on technology transfer of land readjustment to Thailandò, Ph. D. dissertations (Technology), pp.177-202 , Nihon University, faculty of science, 2010

[14]Ochi T, òCircumstance of urban development and international corporation in Nepalò, Kuaku-Seiri magazine, vol.44/No2, pp.100-106, 2001

[15] The Department of Urban Development and Engineering Services, òBhutan: Urban Infrastructure Development Projectò, 2006, http://indrrg/wp-content/uploads/2014/01/437-Urban-Infrastructure-Development-Project-in-Bhutan-Draft-Resettlement-Framework-June-2006.

[16]Kinoshita Y, òCity planning and land readjustment in Andean countriesò, Kukaku-Seiri magazine, vol.50/No.4, pp.59-65, 2007

[17]Kinoshita Y, "Possibility of Japanese style land readjustment in South America", City Planning Review vol.50/No.5, pp.127, 2008

[18] Kinoshita Y, òInternational range of Japanese land readjustment systemò, Chiiki-Kaihatsu, magazine, vol.585, pp29-33, 2013

[19] Hattori K,ò A Japanese who developed an environment city in Brazilò, p.119,Mirai-sha, 2014

[20]JICA Urban Focused on Land Readjustment BAZIL, Final Report , JICA Urban Development Course 2008

[21]Ana Ristina Ramalho Teixerira Gomes , "Land Readjustment Sprawl Prevention Typeò, Interim Report, JICA Urban Development Course, 2009

[22]Okabe S,ò Colombian-adapted Version of Land Readjustmentò, Summaries of technical papers of annual meeting Architectural Institute of Japan, pp.879-880, 2013

[23]Sakurai K, ñEssence of the administrative lawò, pp. 92-107, Gakuyoshobo, 2007

Second International Conference on Science, Engineering & Environment,
Osaka City, Japan, Nov.21-23, 2016, ISBN: 978-4-9905958-7-6 C3051

GEOTHERMAL AND HOT SPRING WATER ORIGIN DETERMINATION USING OXYGEN AND HYDROGEN STABLE ISOTOPE IN THE TOYOHIRAKAWA CATCHMENT, HOKKAIDO, JAPAN

Hiroyuki Ii[1], Hiroshi Kanbara[2], and Yohei Kawabata[2]
[1]Faculty of Systems Engineering, Wakayama University, Japan;
[2]JX Nippon Mining & Metals Corporation, Japan

ABSTRACT

Jyozankei Hot Spring, located near Sapporo City in Hokkaido, is visited by as many as 2.4 million people annually. Ground temperatures of 220 °C were reached in the Toyoha Mine10 km west of Jyozankei Hot Spring where several boreholes less than 2000 m in depth for investigating geothermal water were drilled. Subsequently, a hydrological investigation to clarify the influence of geothermal development on Jyozankei Hot Spring was performed. Snow, river, well, spring, hot spring and the geothermal borehole waters in the Toyohirakawa catchment including Jyozankei Hot Spring were sampled and oxygen and hydrogen stable isotopes of water were analyzed to determine water origin for hot spring and geothermal water. As a result, Jyozankei Hot Spring and the borehole waters were thought to arise from mixed waters of magmatic and surface waters. Borehole water, from less than 2000 m in depth, was 10 to 30 % of the magmatic water and Jyozankei Hot Spring water was less than 10 % of the magmatic water. Surface water was recharged at the upstream of the Toyohirakawa catchment, with snow from the upper stream of the northwest catchment being an important resource of surface water for both Jyozankei Hot Spring water and geothermal water from the boreholes.

Keywords: Geothermal, recharge, oxygen isotope, hydrogen isotope, hot spring

INTRODUCTION

Jyozankei Hot Spring, located near Sapporo City in Hokkaido, is visited by as many as 2.4 million people annually. There are 56 hot spring sources in the Jyozankei district, from which 8,600 liters of hot water with temperatures ranging from 60 to 80 °C surface each minute [1]. The active area of ground temperature in the Toyoha Mine area was 220°C 10 km to the west of Jyozankei, and geothermal water sampled from bore holes at the -300 m level tunnel in the Toyoha Mine was 30 to 100 l/min [2], [3]. Although metal ore production in the Toyoha Mine ceased, waste water treatment from the Mine area was still active. The mining company responsible planned to obtain revenue from geothermal power to compensate for the treatment of waste water.

Geothermal power stations require large amounts of geothermal water. It is necessary to evaluate the influence of pumping up geothermal water on hot spring temperature and quantity around geothermal boreholes [4]. In particular, hydrogen and oxygen isotopic ratios were very useful in determining recharge or water sources of hot spring and geothermal water [4], [5], [6]. As a result, a hydrological investigation was performed to clarify the influence of geothermal development on Jyozankei Hot Spring. Snow, river, well, spring, hot spring and the borehole waters in the Toyohirakawa catchment including Jyozankei Hot Spring were

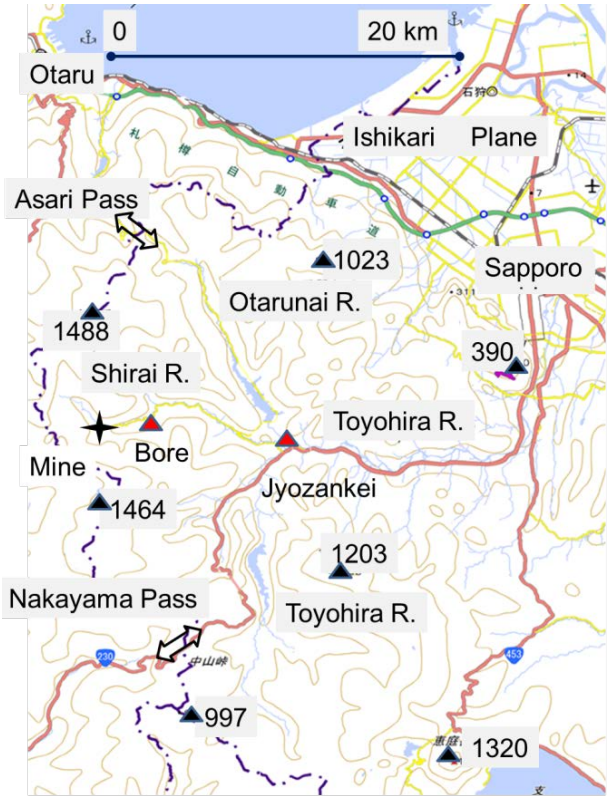

Fig. 1 Study area at the west of Sapporo

sampled and their respective oxygen and hydrogen stable isotopes were analyzed to determine water origin for both the hot spring and the geothermal waters.

STUDY AREA AND METHODS

Volcanic and sedimentary rocks from the Miocene to the Quaternary are found in the Toyohirakawa catchment. Basalt, andesite and rhyolite make up the volcanic rocks. Sapporodake and Eniwadake, located 10 and 20 km south of Jyozankei Hot Spring, erupted one million and several tens of thousands of years ago respectively. The Toyoha Mine was located 10 km to the west of Jyozankei Hot Spring and its high ground temperature was found south-east of the Toyoha Mine[2], [3]. Deep boreholes less than 2000 m in depth were drilled south-east of the Toyoha Mine for researching geothermal water. The catchment at the upstream of Jyozankei is composed of three rivers, the Otarunai, Shirai and Toyohira river as shown in Fig.1. The catchment was covered with heavy snow in winter.

Water sampling was performed using snow, river, hot spring and the geothermal water obtained from bore holes. Geothermal waters over 250 °C were sampled from deep boreholes in June 2012 and March 2013. Hot spring waters around Jyozankei were sampled in 2013. To determine the recharge area, a small branch river was selected for sampling. Branch river waters in the catchment were sampled in October 2012, June 2013 and August 2013. In particular, Takami and Migioe creeks at the upstream of the Toyoha Mine, were sampled every day from April 2013 to April 2014 and again from June 2013 to April 2014. Snow was sampled in March 2014 beside roads and ski slopes. Measurement of δD and $\delta^{18}O$ for sampled water was carried out using an isotopic ratio measurement system (Sercon Geo Wet System). δD and $\delta^{18}O$ are presented in per mil (‰) of the standard average seawater (SMOW: Standard Mean Ocean Water). The formulas are shown in equation (1) and (2). δD and $\delta^{18}O$ of SMOW are denoted as (D/H) SMOW, ($^{18}O/^{16}O$) SMOW and δD and $\delta^{18}O$ of sample are denoted as (D/H) Sample, ($^{18}O/^{16}O$) Sample. Measurement error of δD is ±1.0 ‰ and measurement error of $\delta^{18}O$ is ±0.1 ‰.

$$\delta D = [(D/H)\ Sample/\ (D/H)\ SMOW-1] \times 1000: \quad (1)$$

$$\delta^{18}O = [(^{18}O/^{16}O)\ Sample/\ (^{18}O/^{16}O)\ SMOW-1] \times 1000: \quad (2)$$

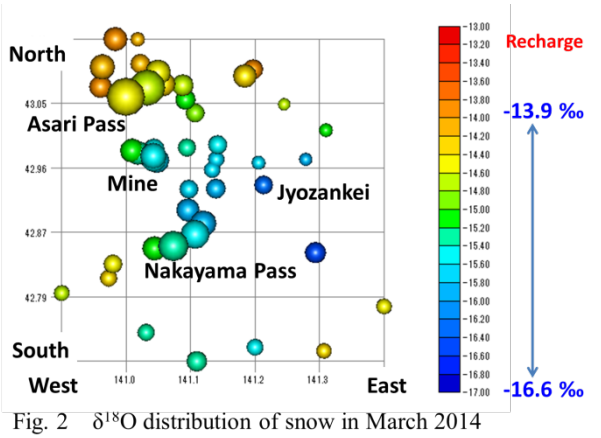

Fig. 2 $\delta^{18}O$ distribution of snow in March 2014 color and circle size show $\delta^{18}O$ value and altitude

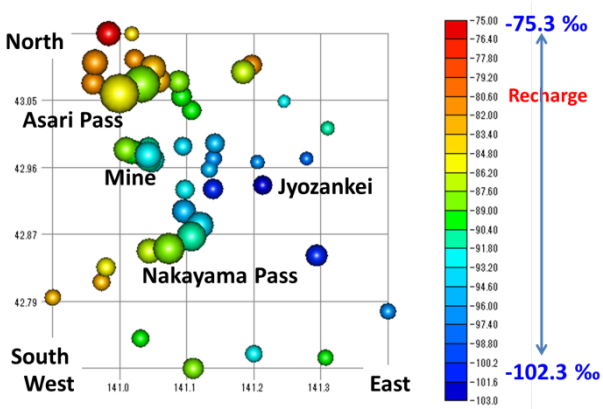

Fig. 3 δD distribution of snow in March 2014 color and circle size show δD value and altitude

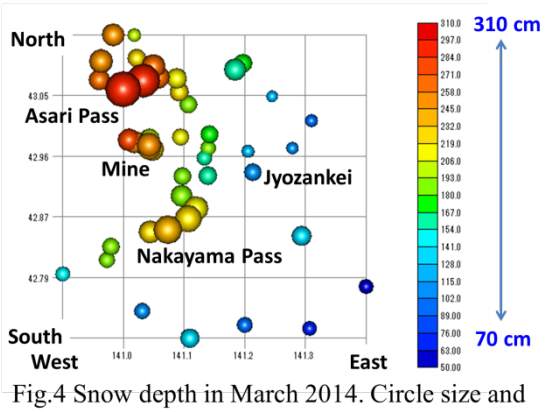

Fig.4 Snow depth in March 2014. Circle size and color show altitude and snow depth (cm)

RESULTS

Fig.2 and Fig.3 show oxygen and hydrogen isotopic ratios for snow sampled in March 2014. Oxygen and hydrogen isotopic ratios for snow varied from -16.6 to -13.9 ‰ and -102.3 to -75.3 ‰ respectively. Both values were lowest around the Jyozankei Hot Spring area and highest around Asari Pass in the north-west of Toyohirakawa catchment. Both values were medium around Nakayama Pass and low in the south area. Fig.4 shows snow depth in March 2014. Snow depth was found to increase with both oxygen and hydrogen isotopic ratios. Snow

depth was found to increase with altitude and decrease from north-west to south-east. Therefore, oxygen and hydrogen isotopic ratios for snow increased with precipitation owing to precipitation effect for isotope [6]. In winter, precipitation depended on cloud from the Japan Sea so isotopic ratios were thought to increase from north-west to south-east.

Fig.5 and Fig.6 show oxygen and hydrogen isotopic ratios for river water sampled in October 2012. These ratios varied from -12.9 to -10.7 ‰ and -82.3 to -64.1 ‰ respectively. Both values were higher than those for snow and their variations were smaller than those for snow. Both values were highest around Jyozankei Hot Spring area and lowest north of the Toyohirakawa catchment. Both values increased from south to north and decreased with altitude. The pattern of both isotope values in October 2012 was reverse to those for snow in March 2014. Excluding winter, cloud passes through the south of Jyozankei from the Pacific side. Thus the pattern was thought to be due to an inner effect from the Pacific side and an altitude effect for isotope [7].

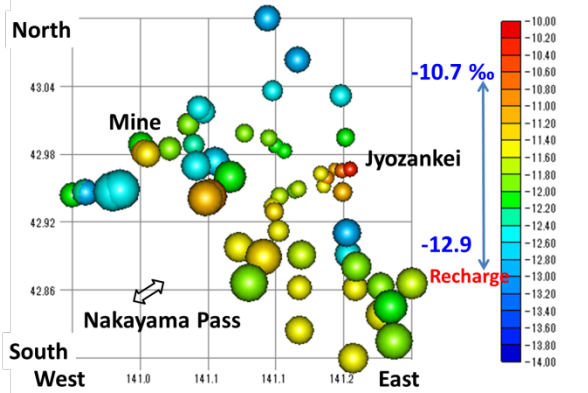

Fig. 5 $\delta^{18}O$ distribution of river water in October 2012 color and circle size show $\delta^{18}O$ value and altitude

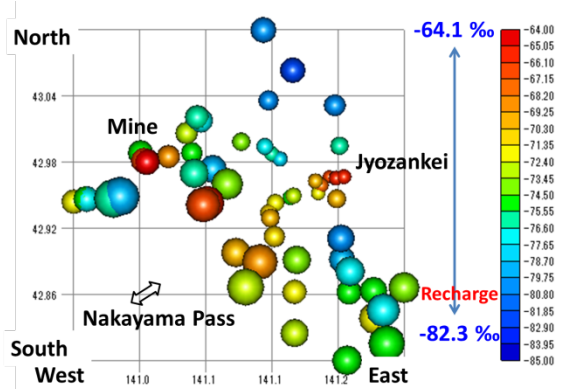

Fig. 6 δD distribution of river water in October 2012 color and circle size show δD value and altitude

Fig.7 and Fig.8 show oxygen and hydrogen isotopic ratios for river water sampled in June 2013. These ratios for river water varied from -13.6 to -11.9 ‰ and -82.6 to -72.7 ‰ respectively. Both values were higher than those for snow and

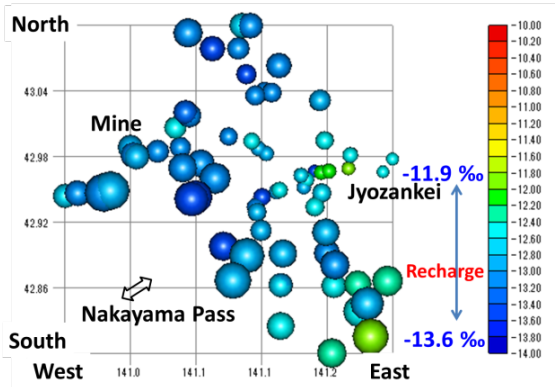

Fig. 7 $\delta^{18}O$ distribution of river water in June 2013 color and circle size show $\delta^{18}O$ value and altitude

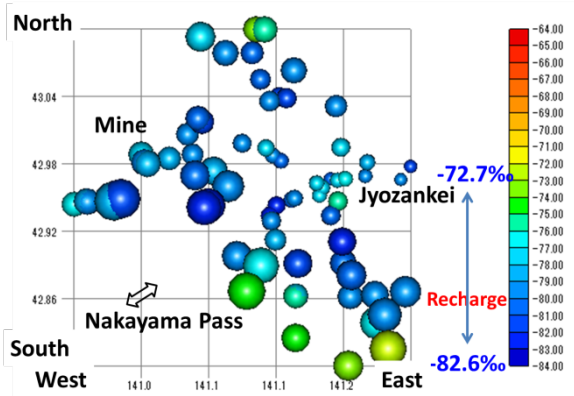

Fig. 8 δD distribution of river water in June 2013 color and circle size show δD value and altitude

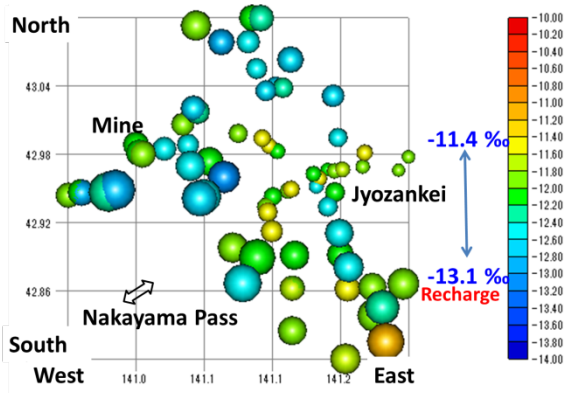

Fig. 9 $\delta^{18}O$ distribution of river water in August 2013 color and circle size show $\delta^{18}O$ value and altitude

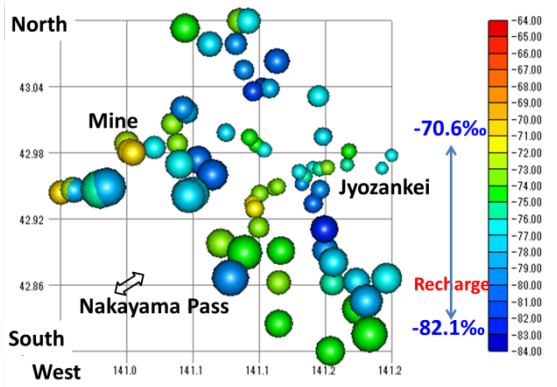

Fig. 10 δD distribution of river water in August 2013 color and circle size show δD value and altitude

marginally smaller than those of October 2012 and their variations were smaller than those for snow. Both values were high around Jyozankei Hot Spring area and in the south of catchment and lowest in the west of the Toyohirakawa catchment. The pattern for both isotope values was not clear.

Fig.9 and Fig.10 show oxygen and hydrogen isotopic ratios for river water sampled in August 2013. These ratios for river water varied from -13.1 to -11.4 ‰ and -82.1 to -70.6 ‰ respectively. Both values were higher than those for snow and marginally smaller than those of October 2012 and their variations were smaller than those for snow. The pattern for both isotope values was not clear. The pattern for both isotope values in August 2013 was thought to be somewhere between those in October 2012 and those in June 2013.

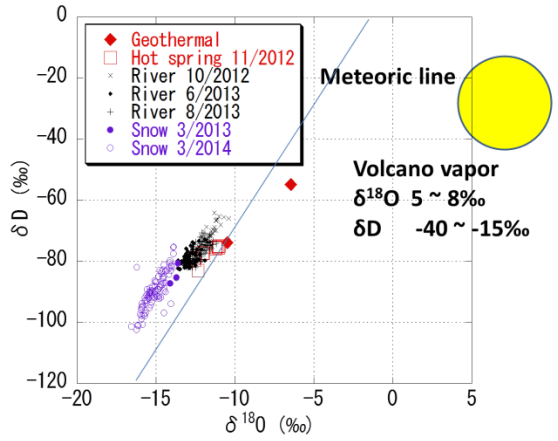

Fig. 11 δD and $\delta^{18}O$ values for water in Toyohira catchment and volcanic vapor

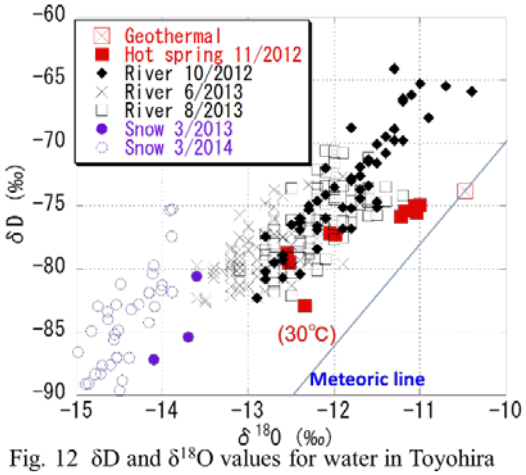

Fig. 12 δD and $\delta^{18}O$ values for water in Toyohira catchment

DISCUSSION

The pattern of oxygen and hydrogen isotopic ratios for snow and river water seemed to change seasonally. Both values for all waters were plotted as shown in Fig.11 and 12. Geothermal water and hot

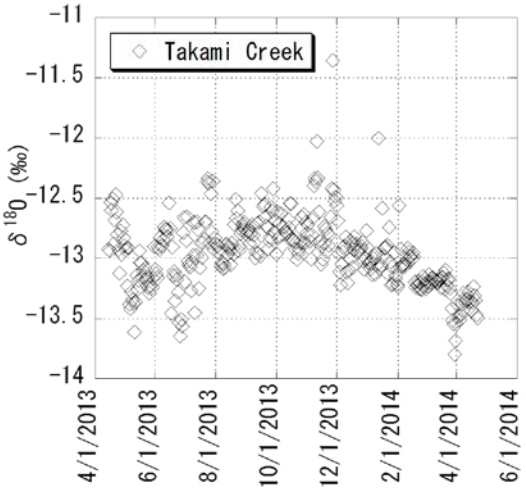

Fig. 13 Time series of $\delta^{18}O$ of Takami creek

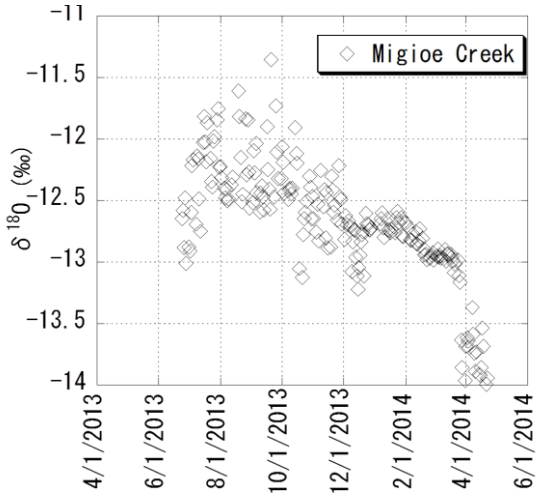

Fig. 14 Time series of $\delta^{18}O$ of Migioe creek

spring water was not on the Meteoric line. Oxygen and hydrogen isotopic ratios for volcanic vapor were 5 to 8 ‰ and -40 to -15 ‰ [8] and oxygen and hydrogen isotopic ratios for volcanic vapor, the geothermal water and hot spring water could all be on one line which then crossed the river water isotopic value at the point where the oxygen isotopic ratio was -13 ‰ and the hydrogen isotopic ratio was -80 ‰.

Subsequently, estimated oxygen and hydrogen isotopic ratios for recharge water from the surface were thought to be -13 and -80 ‰. Therefore, geothermal and hot spring waters were thought to be a mix of volcanic vapor with recharge water. The difference between hot spring and geothermal water was the mixing ratios for volcanic vapor and recharge water. Volcanic vapor ratios for geothermal water were high, 1/10 to 1/3, however volcanic vapor ratios for hot spring water was very low, less than 1/10. This lead to the conclusion that the main water origin for hot spring water was recharge water.

Oxygen and hydrogen isotopic ratios for the estimated recharge water were -13 and -80 ‰. Although most oxygen and hydrogen isotopic ratios for snow were lower than that for recharge water, these isotopic ratios around Asari Pass and north areas were close to that for the recharge area. In contrast, although most oxygen and hydrogen isotopic ratios for river water sampled in October 2012 were higher than that for the estimated recharge water, these isotopic ratios around the north area were close to those for the estimated recharge water as shown in Fig.5 and 6. Oxygen and hydrogen isotopic ratios for western and mountainous river water sampled in June 2013 were the same as those for estimated recharge water as shown in Fig.7 and 8. Similarly, some oxygen and hydrogen isotopic ratios for river water sampled in August 2013 were the same as those for recharge water as shown in Fig.9 and 10. Then, from Fig.12, isotopic ratios for snow and river water in October 2012 were the lowest and the highest among snow and three-season river waters. Isotopic ratios for river water in June and August 2013 were midway between ratios for snow and river water from October 2012. As isotope values for river water decreased from October to June and then increased from June to August, and the isotope value for snow was lowest, melting snow was thought to cause the decrease isotope values in June.

Fig.13 and 14 show the time series of $\delta^{18}O$ for Takami and Migioe creeks at the upstream of the Toyoha Mine. Isotope values for both creeks reached their minimum value in snow melting seasons and then gradually increased till autumn. They decreased from winter to spring. Average values for both creeks were about -13.0 to -12.5 ‰. As oxygen isotopic ratios for snow in the catchment were markedly lower than those for river water, snow melt water was thought to decrease river water isotopic ratios. And low isotope values in winter were also thought to be brought out by snow or rain in winter. Therefore, two types of precipitation based on isotope values and cloud origin were determined. One precipitation is derived from the Japan Sea in winter and the other is derived from the Pacific Ocean excluding winter. Consequently, isotope values for river water was influenced by two types of precipitation and were lowest in snow melting season and the highest before winter. Then the average isotopic ratio for the catchment was thought to be values for river water in August. As the estimated oxygen and hydrogen isotopic ratios for the recharge area were -13 and -80 ‰, the recharge area was, from isotope values for river water sampled in August, estimated to be the northern and western mountain areas as shown in Fig. 9 and 10. The western and northern mountainous areas in the catchment were also heavy snow areas

Fig. 15 Snow sampling at Asari Pass

with snow reaching depths of over 200 cm as shown in Fig.15. Therefore, snow was important for recharge water.

As oxygen and hydrogen isotopic ratios for volcanic vapor, geothermal and Jyozankei Hot Spring waters were on the one line and that line intersected with river water values at the point where the oxygen isotopic ratio was -13 ‰ and the hydrogen isotopic ratio was -80 ‰, river water with an oxygen isotopic ratio of -13 ‰ and a hydrogen isotopic ratio of -80 ‰ was thought to be recharge water. Therefore, as the recharge water for the geothermal and Jyozankei Hot Spring waters was thought to be the same.

CONCLUSION

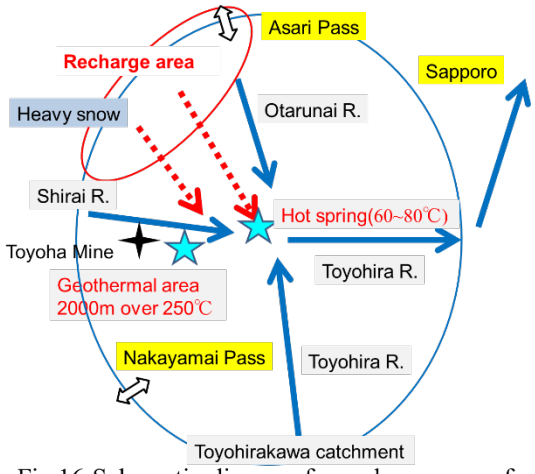

Fig.16 Schematic diagram for recharge area of hot spring and geothermal water

Geothermal power stations require large amounts of geothermal water. It is necessary to evaluate the influence of pumping up geothermal water on hot spring temperature and quantity around geothermal boreholes. Jyozankei Hot Spring is an important hot spring in Hokkaido and many people visit the hot spring annually. 10 km upstream of Jyozankei Hot Spring, is a geothermal area. Investigative bore holes less than 2000 m in length were drilled and 250 °C

geothermal water was sampled. To determine the water source of Jyozankei Hot Spring and geothermal waters, river water and snow in the Toyohirakawa catchment which includes Jyozankei Hot Spring and geothermal area was sampled and isotope values were studied. As a result, Jyozankei Hot Spring and borehole waters were thought to be a mixture of water between magmatic water and surface water. Borehole water from 2000m in depth was composed of 10 to 30 % magmatic water and Jyozankei Hot Spring water was less than 10% magmatic water. The surface water was recharged at the upstream of the Toyohirakawa catchment and in particular snow at the upper stream of the northwest catchment was an important source of surface water for both Jyozankei Hot Spring water and geothermal water from the boreholes.

As oxygen and hydrogen isotopic ratios for volcanic vapor, geothermal and Jyozankei Hot Spring waters were on the one line and the line intersected with river water values at the point where the oxygen isotopic ratio was -13 ‰ and the hydrogen isotopic ratio was -80 ‰, river water with the oxygen isotopic ratio -13 ‰ and hydrogen isotopic ratio -80 ‰ was thought to be recharge water. Therefore, as recharge water for the geothermal and Jyozankei Hot Spring waters was thought to be the same.

ACKNOWLEDGEMENTS

The authors of this study are sincerely grateful for the year-long water sampling of Takami and Migioe creeks performed by Mr. Yosuke Ono from the Toyoha Mines Co. Ltd

REFERENCES

[1] http://www.welcome.city.sapporo.jp/find/recreational/jozankei_onsen/?lang=en

[2] Sanga T., Kanbara H., Shoji T. And Takeyama T. “Characteristics feature of the later stage mineralization and its vein system at the Toyoha polymetallic vein deposits, Hokkaido, Japan”, Journal of the Society of Resource Geology, Vol. 42(2), 1992, pp.85-100.

[3] Kanbara H., Sanga T., Oura T. and Kumita K. “Mineralization of Shinano vein in the Toyoha polymetallic vein-type deposits, Hokkaido, Japan”, Journal of the Society of Resource Geology, Vol. 39(2), 1989, pp. 107-122.

[4] Sasaki K., Ueda A., Zhang J., Kageyama S., Koseki T. and Muraoka H. “Geochemical study of hot springs associated with new geothermal exploration in the eastern part of Toyama, Prefecture, Japan”, Procedia Earth and Planetary Science,Vol.7, 2013, pp. 766-769.

[5] Chandrajith R., Barth J., Subasinghe N.D., Merten D., and Dissanayake C. B. “Geochemical and isotope characterization of geothermal spring waters in Sri Lanka” Journal of Hydrology, Vol. 476, 2013, pp. 360-369.

[6] Yaguchi M., Muramatsu Y., Chiba H., Okumura F., Ohba T., and Yamamuro M. “Hydrochemistry and isotopic characteristics of non-volcanic hot springs around the Miocene Kofu granitic complex surrounding the Kofu Basin in the South Fossa Magna region, central Honshu, Japan”, Geochemical Journal, Vol.48, 2014, pp. 345-356.

[7] Liu, Z., Bowen G.J., and Welker J.M., “Atmospheric circulation is reflected in precipitation isotope gradients over the conterminous United States”, Journal of geophysical research, Vol.115, 2010, D22120.

[8] Giggenbach, W. F. “Isotopic composition of geothermal water and steam discharges”, In D’Amore, F. (editor), Application of Geochemistry in Geothermal Reservoir Development. UNITAR/UNDP publication, Rome, 1991, pp. 253 – 273.

Second International Conference on Science, Engineering & Environment,
Osaka City, Japan, Nov.21-23, 2016, ISBN: 978-4-9905958-7-6 C3051

EFFECT OF TEMPERATURE ON REMOVAL OF COD AND TSS FROM ARTIFICIAL RIVER WATER BY MUDBALLS MADE FROM EM4, RICE BRAN AND CLAY SOIL

Fadjari Lucia Nugroho, Deni Rusmaya, Yonik Meilawati Yustiani, Fajar Ibnil Hafiz and Runie Besty Teta Putri
Department of Environmental Engineering, Pasundan University, Indonesia;

ABSTRACT

In Indonesia surface water is often polluted by domestic waste causing degradation of river water quality. The use of activated Effective Microorganism Solution (EMS) mixed with rice bran or wheat bran, as well as soil and shaped into mudballs has in recent years shown promise as a direct method to improve quality of polluted river water. This study examined the effect of temperature on removal of COD and TSS by mudballs made from activated EM4 solution, rice bran and clay soil. Batch experiments treating artificial river water by the mudballs were conducted at temperatures 25ºC and 30ºC with the artificial river water having initial levels of 120 mg/L COD and 100 mg/L TSS. Efficiency removals of COD by 2.5 cm ϕ mudballs at 25ºC and 30°C were 66.7% and 59.4%, whereas that of TSS were 100% and 99.7% respectively. TSS sorption by the mudballs appears to better fit the Langmuir than the Freundlich isotherm models. At 25ºC and 30°C, maximum sorption (Q_m) of TSS is 6.89 mg/g and 7.52 mg/g; Langmuir constant (K_L) is 0.0196 L/mg and 0.0168 L/mg, while equilibrium parameter (R_L) is 0.338 and 0.373 respectively. Statistical hypothesis testing of the experimental data suggests that at α=0.05, temperature affects removal efficiency of COD but not that of TSS.

Keywords: Adsorption Isotherm, Effective Microorganisms, Mudballs, River Water

INTRODUCTION

Urban rivers are major assets to communities as they provide numerous benefits, including fresh water, recreation, landscape amenity, habitat provision and flood control [1]. In Indonesia surface water such as rivers is often polluted by both domestic as well as industrial waste, thus causing degradation of river water quality and making it aesthetically displeasing. For example, the average COD and TSS levels of Cikapundung River, Bandung City, West Java, Indonesia in 2013 were 120 mg/L and 100 mg/L respectively; with maximum levels of COD and TSS at times reaching as high as 400 mg/L and 350 mg/L respectively. Although conventional physical-biological treatment methods can be applied to treat polluted river water, they are often costly and not eco friendly [2]. Hence, in recent years the use of Effective Microorganisms (EM) has shown promise as a direct method for improving or restoring polluted river water quality. EM itself is a mixed culture of naturally occurring effective, beneficial, nonpathogenic microorganisms capable of purifying and reviving nature [3]. The concept of EM was first developed by Professor Dr. Teruo Higa of the University of Ryukus, Okinawa Japan [4]. EM has been used in water and sewage purification, improvement of recycled water and solving sanitary problems. As such, EM is also used in the preparation of "Mudballs" or "Bokashi-balls", made from activated EM solution mixed with either rice or wheat bran as well as ordinary dry clay soil and then shaped into balls called "Mudballs" that are left to ferment for about a week. Thereafter, the "Mudballs" are thrown into rivers with the aim of improving river water quality [3]. This technique has been tried out in countries such as Malaysia, Singapore and South Africa. Theoretically, the "Mudballs" act as a sorbent to remove turbidity, while the community of EM heterotrophic microorganisms degrade organic pollutants. Thus, the Mudballs assist in reducing suspended solids, turbidity as well as COD, and improving DO levels of the river water. Rusmaya et al. [5] reported that mudballs made from EM4 mixed with rice bran and clay soil were capable of reducing the TSS and COD concentrations of artificial river water solution. The mixed culture of microorganisms in the EM4 consisted of both Gram negative and Gram positive rod shaped bacteria, some of which were spore-forming, as well as *Mucor sp.* and *Penicillium sp.* fungi and actinomycetes.

The objective of this present study was to examine the effect of different temperatures on the removal of COD and TSS in artificial river water by mudballs made from EM4, rice bran and clay soil, thus determining whether mudballs can be used to improve river water quality under fluctuating temperatures. Given that TSS removal is believed to be achieved by adsorption, the equilibrium data of

the TSS removal was also analysed using the Langmuir and Freundlich adsorption isotherm models in order to determine the adsorption capacity for TSS by the mudballs.

METHODS

All experiments were conducted as batch experiments. COD was measured by closed reflux titrimetry, whereas TSS was measured by gravimetry methods.

Materials

The EM4 used in the experiments was manufactured by Songgo Langit Persada and was bought locally in Bandung, Indonesia. As EM4 is sold in a dormant state, activation of the latter followed the procedure established by Rusmaya et al. [5], this being by diluting 5% EM4 solution with distilled water and left to ferment for a day at room temperature.

The mudballs were prepared by mixing 20% rice bran and 80% dry clay soil with 40% activated EM4 solution (v/w), which was then left to ferment in covered baskets for 7 days at room temperature.

Based on the procedure established by Rusmaya et al. [5], the artificial river water was prepared by adding glucose and 60 mesh sieved kaolin powder into tap water and adjusting the pH of the solution to 4. The initial COD value of the artificial river water was 120 mg/L; whilst initial TSS value was 100 mg/L.

Experiments

Batch experiments for COD and TSS removal

The batch experiments on COD and TSS removal were carried out in 250 mL Erlenmeyer flasks under 2 different temperatures, this being 25°C and 30°C. For this, 2.5 cm ϕ mudballs were added into flasks containing 200 ml artificial river water. The experimental flasks were then placed in a shaker water bath which was adjusted to either 25°C or 30°C. The COD and TSS concentrations of the artificial river water were measured daily until no further reduction of COD and TSS occurred.

TSS adsorption experiments

The TSS adsorption experiments were carried out in 250 ml Erlenmeyer flasks containing 200 ml tap water mixed with kaolin powder producing a TSS concentration of 100 mg/L. Varying quantities of mudballs (1 - 10 g) were then added into the TSS solution and the flasks placed in a shaker water bath adjusted to either 25°C or 30°C. The TSS was measured after 3 days of shaking.

Calculation of adsorption isotherms.

Adsorption isotherms describe the equilibrium relationships between adsorbent and adsorbate [6]. The isotherm equations used to determine the TSS adsorption model were the Freundlich and Langmuir isotherm equations. The Freundlich isotherm is an exponential equation that assumes that as the adsorbate concentration increases so too does the concentration of the adsorbate on the adsorbent surface [7]. This isotherm can be used for non-ideal sorption that involves heterogeneous surface energy systems.The mathematical expression of the Freundlich isotherm is as follows:

$$\frac{X}{M} = K_F C_e^{\frac{1}{n}} \quad (1)$$

where $\frac{X}{M}$ is the amount of adsorbate adsorbed by the adsorbent, K_F is a rough indicator of the adsorption capacity (mg/g), *1/n* is the adsorption intensity and C_e is the equilibrium liquid-phase concentration of the adsorbate (mg/L).

The Langmuir isotherm equation is based on the assumption of monolayer coverage of adsorbate over a homogenous adsorbent and that when equilibrium is attained no further adsorption can take place. Adsorption is assumed to take place at specific homogenous sites in the adsorbent and the adsorption of each molecule has equal adsorption energy [8]. The theoretical Langmuir isotherm equation is as follows:

$$\frac{X}{M} = \frac{Q_m K_L C_e}{1+K_L C_e} \quad (2)$$

where Q_m is the maximum amount of adsorption corresponding to complete monolayer coverage on the surface (mg/g); and K_L is the Langmuir constant related to the energy of adsorption (L/mg).

RESULTS AND DISCUSSIONS

Effect of Temperature on COD and TSS Efficiency Removal

Table 1 shows the effect of temperature on COD and TSS efficiency removal by the mudballs. As shown in Table 1 maximum COD removal was attained within 5 days; whereas all TSS was removed after 3 days.

Table 1 COD and TSS efficiency removal at 25° and 30°C

Day	% COD removal		% TSS removal	
	25°C	30°C	25°C	30°C
0	0	0	0	0

1	39.2	31.2	56.7	48.7
2	44.2	48.9	73.3	82.7
3	47.5	44.8	100	99.7
4	62.5	53.1	100	99.7
5	67.5	59.4		
6	67.5	59.4		

The results also show that although after 5 days the COD levels at both 25°C and 30°C decreased, slightly better COD removal was attained at 25°C. COD efficiency removal at 25°C was 67.5%, whereas COD removal efficiency at 30°C was 59.4%. COD removal is attributed to biosorption followed with degradation of the organic matter by the EM4 microorganisms in the mudballs. As reported in an earlier paper, the EM4 solution consisted of a mixed culture of Gram negative and Gram positive rod shaped bacteria, some of which were spore-forming, as well as *Mucor sp.* and *Penicillium sp.* fungi and actinomycetes [5]. These are heterotrophic, mesophilic microorganisms. Mesophiles grow best at moderate temperatures, typically between 20° and 45°C. Each microorganism have their own optimum temperature for growth and metabolism. In this regard, the consortia of microbes in the EM4 solution appear to grow and carry out metabolism slightly better at 25°C than 30°C. To further confirm this assumption, statistical hypothesis testing of the experimental data was carried out. The results are summarised in Table 2, indicating that at $\alpha = 0.05$, temperature affects removal efficiency of COD, with better COD removal obtained at 25°C.

Table 2 Statistical hypothesis testing of experimental data

	% COD removal	% TSS removal
α	0.05	0.05
Hypothesis	$H_0: \mu_{25°C}=\mu_{30°C}$ $H_1: \mu_{25°C}>\mu_{30°C}$	$H_0: \mu_{25°C}=\mu_{30°C}$ $H_1: \mu_{25°C}>\mu_{30°C}$
Results of t testing	$t_{calculated}>t_{table}$	$t_{calculated}<t_{table}$
Conclusion	% COD removal at 25°C > % COD removal at 30°C	% TSS removal at 25°C = % TSS removal at 30°C

Figure 1 below shows the comparison in COD removal when only rice bran (RB) mixed with clay soil (CS) were used as sorbent to remove COD, versus mudballs (MB) made from EM4, rice bran and clay soil. As shown in Fig.1 at both temparatures of 25°C and 30°C greater removal of COD was obtained with mudballs in comparison to that obtained with RB + CS. Accordingly, given these results COD removal can therefore be attributed to both physical (sorption) as well as biological process (biodegradation). In fact, the mixed RB+CS can even add to the COD content of the solution (Fig. 1), as RB is organic in nature and can dissolve into the solution. It appears that the presence of fungal mycelia in the mudballs prevent the mudballs from quickly dissipating into the solution, which could increase the COD of the solution.

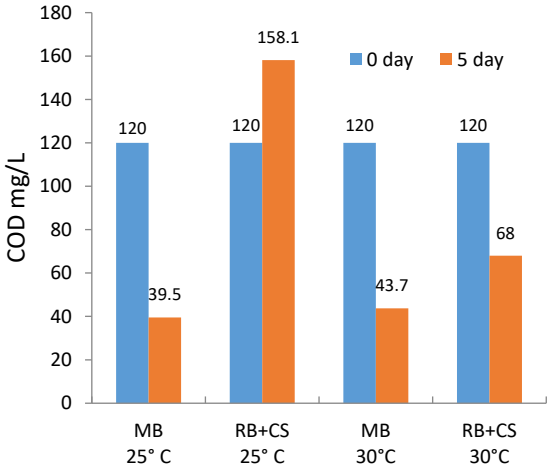

Figure 1 COD removal by MB (Mudballs) versus RB (rice bran) + CS (clay soil) at 25°C and 30°C, C_0 of COD=120 mg/L

With regard to TSS removal, 100 % removal by the mudballs was achieved within 3 days (Table 1). Given that in this study the TSS was derived from kaolin, TSS removal is therefore attributed to physico-chemical process, this being by adsorption. Accordingly, TSS removal by 2.5 cm ϕ mudballs was more rapid and efficient than COD removal as the latter is attributed to physico-biological activity which is slower than physico-chemical reactions. Differing from COD, statistical testing of the experimental data indicates that there is no difference in TSS removal efficiency at 25°C and 30°C (Table 2).

Adsorption of TSS

Figures 2 and 3 depict the TSS adsorption ($\frac{X}{M}$ mg/g) and TSS removal efficiency (%) by different quantity of mudballs under different temperatures (i.e 25°C and 30°C).

As shown in Fig. 2, under both temperatures adsorption of TSS is higher at lower amounts of mudballs. Three consecutive mass transport steps are involved in the adsorption of adsorbate from solution by a porous adsorbent. First, the adsorbate migrates through the solution to the exterior surface of the adsorbent particles by film diffusion, followed by solute movement from the particle surface into the interior site by pore diffusion and finally the

adsorbate is adsorbed into the active sites at the interior of the adsorbent particle [9]. Hence, smaller quantity of mudball allows tbe adsorbate to move more easily from the surface into the interior as the interior of the adsorbent is less compacted in comparison to the more dense, heavier and thicker mudballs. As such, under such conditions, more adsorbate can be adsorbed with smaller sized mudballs.

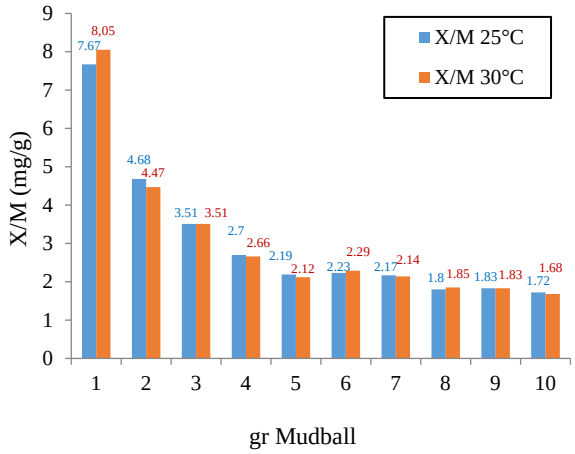

Figure 2 Adsorption of TSS (mg/g) by different quantities of EM4 mudballs at 25°C and 30°C, C_0=100 mg/L

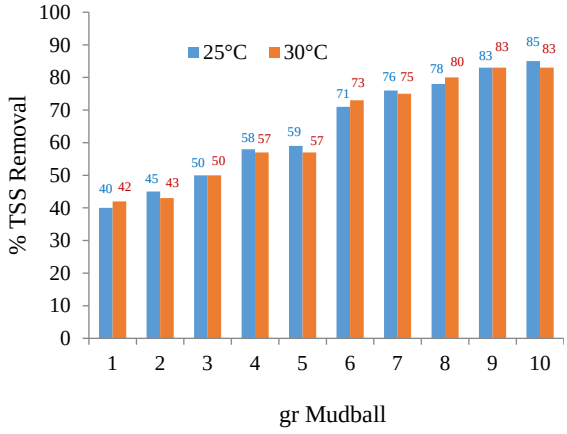

Figure 3 Removal efficiency of TSS by different quantities of EM4 mudball at 25°C and 30°C, TSS C_0=100 mg/L

With regard to TSS removal efficiency, Fig. 3 shows that at both temperatures, increasing amounts of mudballs produce better TSS removal efficiency. Increasing the quantity of the mudballs resulted in larger diameter mudballs, which in turn provided more surface areas for adsorption of the TSS. Hence, removal efficiency is greater with larger sized mudballs, given that adsorption is a surface phenomena.

The experimental data were plotted against the Freundlich and Langmuir isotherm models in order to determine which of these two models better describe TSS adsorption by the mudballs. Table 3 presents the results obtained from this exercise.

The regression coefficients (R^2) shown in Table 3 suggest that TSS adsorption by the mudballs at temperatures 25°C and 30°C can better be described by the Langmuir isotherm model. As such, at 25ºC and 30°C temperatures, maximum adsorption (Q_m) of TSS by the mudballs is 6.89 mg/g and 7,52 mg/g respectively; while the Langmuir constant (K_L) is 0.0196 L/mg and 0.0168 L/mg respectively.

Table 3 Calculated isotherm parameters and regression coefficients for TSS adsorption by mudballs

	Langmuir			Freundlich		
	Q_m	K_L	R^2	n	K_F	R^2
	mg/g				mg/g	
25°C	6.89	0.0196	0.737	1.212	0.155	0.721
30°C	7.52	0.0168	0.743	1.212	0.153	0.679

According to Hall, *et al*. [10] the essential features of the Langmuir adsorption isotherm is expressed by a dimensionless constant known as the separation factor or equilibrium parameter *(R_L)*, which is defined as follows:

$$\boldsymbol{R_L} = \frac{1}{1+K_L C_0} \quad (3)$$

The $\boldsymbol{R_L}$ indicates the shape of the isotherm to be either irreversible ($R_L=0$), favourable ($0<R_L<1$), linear ($R_L=1$), or unfavourable ($R_L>1$). The R_L of this study is given in Table 4.

Table 4 R_L of TSS adsorption by mudballs

	25°C	30°C
R_L	0.338	0.373

The results given in Table 4 show that adsorption of TSS by mudballs at both temperatures are indeed favourable to the Langmuir isotherm. A lower R_L value reflects the adsorption nature to be more favourable [11].

CONCLUSION

Removal of COD and TSS from artificial river water was achieved in batch experiments by mixing artificial river solution having initial COD of 120 mg/L and TSS of 100 mg/L with mudballs made from activated EM4 solution mixed into rice bran, as well as clay soil and shaking the experimental flasks

in a water bath adjusted to 25°C and 30°C. Statistical hypothetical testing shows that the lower temperature produced better COD removal, but that differences in temperature did not affect TSS removal. COD removal by the mudballs is attributed to adsorption followed by biodegradation, whilst TSS removal is by physical process only. Although COD removal was obtained at both 25°C and 30°C, the mesophilic EM4 microorganisms appear to carry out metabolism slightly better at 25°C. Smaller quantity of mudball increased adsorption of TSS, however more TSS removal efficiency was achieved with increasing quantity of mudball, which resulted in larger diameter mudballs. The adsorption mechanism of TSS is better described by the Langmuir isotherm model. At 25°C and 30°C the Langmuir parameters of Q_m are 6.89 mg/g and 7.52 mg/g, and K_L is 0.0196 L/mg and 0.0168 L/mg respectively. K_L represents binding energy, hence the energy of adsorption appears to be slightly larger at 25°C. The equilibrium parameter (R_L) obtained at 25°C and 30°C, i.e. 0.338 and 0.373 respectively, indicates that the adsorption is favourable to the Languir isotherm model. The results of this study also suggest that diameter of the mudballs will affect TSS removal efficiency.

ACKNOWLEDGEMENTS

The works were financially supported by the Indonesian Ministry of Technological Research and Higher Education.

REFERENCES

[1] Covarrubia JC, Rayburg S, Neave M, “The influence of local land use on the water quality of urban rivers”, International Journal of GEOMATE, July 2016, Vol. 11, Issue 23, pp. 2155-2161.

[2] Dhote S, Dixit S, "Water quality improvements through macrophytes - a review", Environmental Monitoring and Assessment, 152, 2009, pp. 149-153.

[3] Zakaria Z, Gairola S, Shariff N, "Effective microorganisms (EM) technology for water quality restoration and potential for sustainable water resources and management", in Proc. International Congress on Environmental Modelling and Software Modelling for Environment's Sake, Fifth Biennial Meeting, Ottawa, Canada, 2010, p. S.0.04.

[4] Higa T, Parr JF, "Beneficial and effective microorganisms for a sustainable agriculture and environment", International Nature Farming Research Center, Atami Japan, 1994, p. 4

[5] Rusmaya D, Nugroho FL, Yustiani YM, Hafiz FI, Putri RBT, "Improving artificial river water quality using mudballs made from EM4, rice bran and clay soil" in Proc. 5th Environmental and Management Conf on Green Technology Towards Sustainable Environment, 2015, pp. OP/AE/002-1 - OP/AE/002-8.

[6] Hossain MA, Ngo HH, Guo WS, Nguyen TV, “Removal copper from water by adsorption onto banana peel as bioadsorbent”, Int. J. of GEOMATE, June, 2012, Vol. 2, No. 2, (SI. No. 4), pp. 227-234.

[7] Freundlich H, "Adsorption in solution", Chemie, 57, 1906, pp. 384-410.

[8] Langmuir I, "Adsorption of gases on plane surfaces of glass, mica and platinum”, J. Am. Chem. Soc. 40, 1918, pp. 1361-1403.

[9] Malik PK, "Dye removal from wastewater using activated carbon developed from sawdust: adsorption equilibrium and kinetics", Journal of Hazardous Material. B113, 2004, pp. 81-88.

[10] Hall KR, Eagleton LC, Acrivos A, Vermeulen T, "Pore and solid diffusion kinetics in fixed bed adsorption under constant pattern conditions", Ind. Eng. Chem. Fundamentals, Vol. 5, No. 2, May 1966, pp. 212-223.

[11] Foo KY, Hameed BH, "Insights into the modelling of adsorption isotherm systems", Chem. Eng. J. 156, 2010, pp. 2-10.

Second International Conference on Science, Engineering & Environment,
Osaka City, Japan, Nov.21-23, 2016, ISBN: 978-4-9905958-7-6 C3051

EVALUATION OF RESUSPENSION OF ROAD DUST IN A CEMENT INDUSTRIAL COMPLEX AREA

Tipawan Phetrawech[1,2] and Sarawut Thepanondh[1,2]

[1]Faculty of Public Health, Mahidol University, Bangkok, Thailand,
[2]Center of Excellence on Environmental Health and Toxicology (EHT), Bangkok, Thailand.

ABSTRACT

Re-suspended road dust is an important contributor to ambient particulate matter (PM) particularly in an area where fugitive dust is significant emission source. This study evaluate PM-10 and PM-2.5 emissions as fugitive re-suspended dust from the road network in the Thai's Pollution Control Zone. Emissions of road dust are determined by using the analysis of silt loading and physical characteristics of the roads located in the study domain. Diurnal profile of vehicles travelling on each roads were used to calculate temporal variation of the emission data. Diurnal pattern of PM-10 ambient concentration measured from curbside station in the study area was used to reveal the contribution of road dust emissions to particulate concentration in the air. Results indicated that road dust greatly influenced the temporal profile of PM-10 concentrations in this area. Therefore, the effort to control particulate emissions in this Pollution Control Zone should also give a priority not just only to the industrial sources but also to mobile source emissions particularly from those re-suspended road dust.

Keywords: Road dust, PM-10, PM-2.5, AERMOD, Emission rate

INTRODUCTION

Non-exhaust traffic induced particle emissions are known to contribute significantly to the total concentrations of inhalable airborne particulate matter in the size range <10 mm (PM-10) [1]. The evidence on airborne particulate matter (PM) and its public health impact is consistent in showing adverse health effects at exposures that are currently experienced by urban populations in both developed and developing countries [2]. Particulate matter, is a complex mixture of extremely small particles and liquid droplets. The size of particles is directly linked to their potential for causing health problems. Once inhaled, these particles can affect the heart and lungs and cause serious health effects [3].

In Thailand, PM-10 concentrations monitored in several places had been higher than both of its 24-hour and annual standards (> 120 and > 50 µg/m^3, respectively). Figure 1 presents the status of PM-10 measured nationwide over the decade (from 2003 – 2013). The worst polluted area from PM-10 of the country is at the Na Phra Lan Sub-district, Saraburi Province (Figure 2). This area is located in the central region where it is home to the cement manufacturing complex of the country. Due to the problem of very high concentration of PM-10, this area had been designated as "the Pollution Control Zone" by the Thai government since 2004 with an objective to set up specific action plans as well as budgets to combat with this problem.

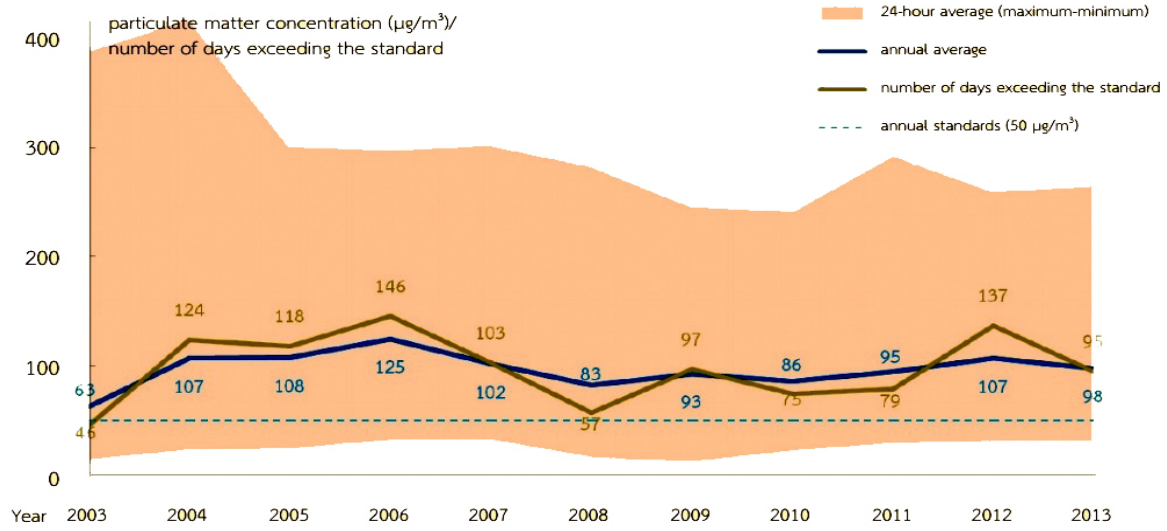

Figure 1 PM-10 concentrations from 2003- 2013 [1].

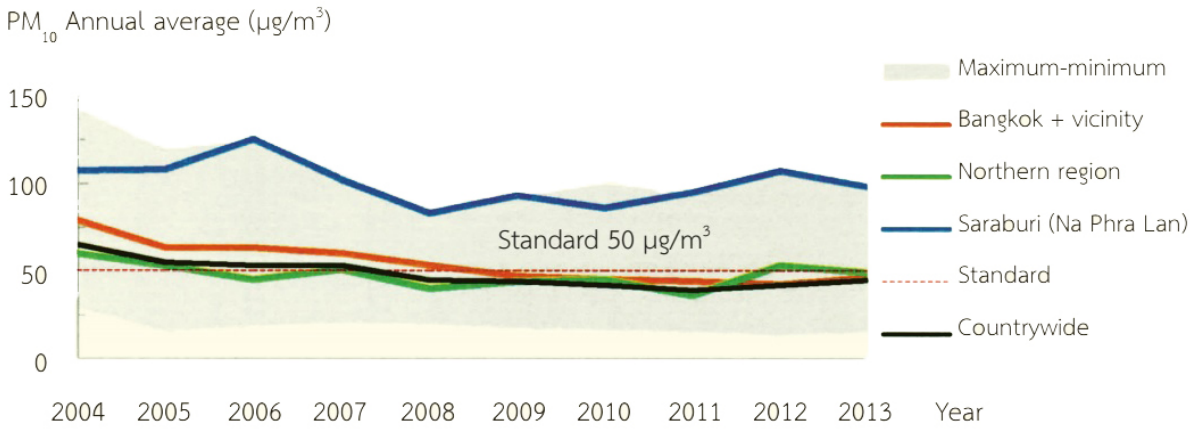

Figure 2 Spatial comparison of PM-10 measured nationwide in Thailand. [1]

High concentrations of ambient PM-10 in this area are contributed from activities related to cement manufacturing processes. However, it is suspected that PM-10 measured in the community area are also contributed by the re-suspended road dust. It is well recognized that traffic and road transport are main sources to ambient PM-10 concentrations especially at hot spots in urban environment [4]. Particulate emissions from road transport include tail exhaust, products of wearing processes and re-suspended road dust [5]. Particulates emitted from exhaust of diesel engine are relevant to speed of the vehicle [6] Field measurements in urban areas or megacities shown elevated levels of PM10 in the vicinity of roads coming from the contribution from re-suspended particles from paved roads [7]. In urban areas fugitive dust emissions due to vehicles travelling on roads is the most important source of rude particles.

Emissions from road transfer climb from both exhaust and non-exhaust sources. The most important sources of non-exhaust PM are wearing of brake and tyre element of machine vehicles and wearing of the road surface itself. An additional non-exhaust source is the suspension or re-suspended of previously placed material from the road surface road dust by vehicle induced confusion, tyre crop and the turbulent achievement of the wind. In addition to direct tailpipe emissions of particulates, mobile sources are also accountable for fugitive dusts such as those re-suspended from road.

This study assessed PM-10 and PM-2.5 emissions of re-suspended dust from the road network in the Na Phra Lan Pollution Control Zone. Emissions of road dust are determined by using the analysis of silt loading and physical characteristics of the unpaved and pave roads located in the study domain. Then emission faction of PM-10 and PM-2.5 re-suspended from road are developed and further be used as input data for interpretation of their ambient concentration using the air pollution dispersion model. This study presents results of the diurnal profile of emissions of PM-10 and PM-2.5. Calculated emission data were compared with ambient PM-10 concentration measured from the curbside of the road. The finding of this study assist in elucidate the contribution of re-suspended road dust to the dust concentration in this pollution control zone.

METHODOLOGY

In this study, amount of PM-10 and PM2.5 emitted from re-suspension of road dust in the Na Phra Lan Pollution Control Zone was estimated. The study domain covered area of 3 x 3 km^2 was centered at the Na Phra Lan ambient air monitoring station of the Pollution Control Department (reference point). There were 5 major roads within the study domain as illustrated in Figure 3.

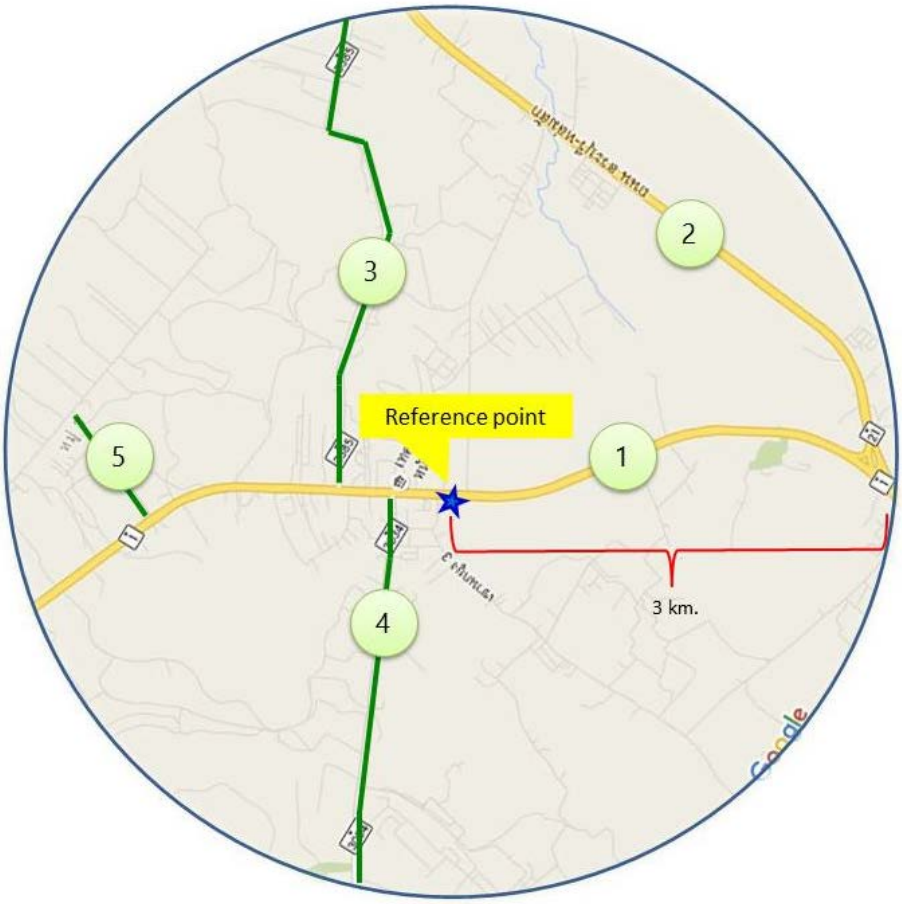

Figure 3 Major roads within the study domain

Sampling locations in each road were designed according to their length and distant between road conjunction/intersection. Criteria of selection of sampling points are presented in Figure 4. Totally, there were 21 dust sampling locations in these roads. The road dusts were collected directly from road pavement by manual sweeping of the dust. The dust sample plot used in this study was patterned after the ASTM-C-136 method. It had been designed with a rectangular-shaped leading edge. The sample plot was made of plastic and had the size of 0.3 x 0.3 m^2 with 0.15 m wing. At least 3-5 plots were sampled at the same sampling location. Collected samples at each sampling locations were then put in the same plastic bag (composite sampling).

In this study, the emission rates of PM-10 and PM-2.5 emitted from re-suspended road dust was calculated following the US.EPA AP-42 (section 13.2.1 and 13.2.2). The data collected on-site included amount of dust in the study plot, and diurnal profile of number and type of vehicles traveling on the roads within the study domain. Details are as followed.

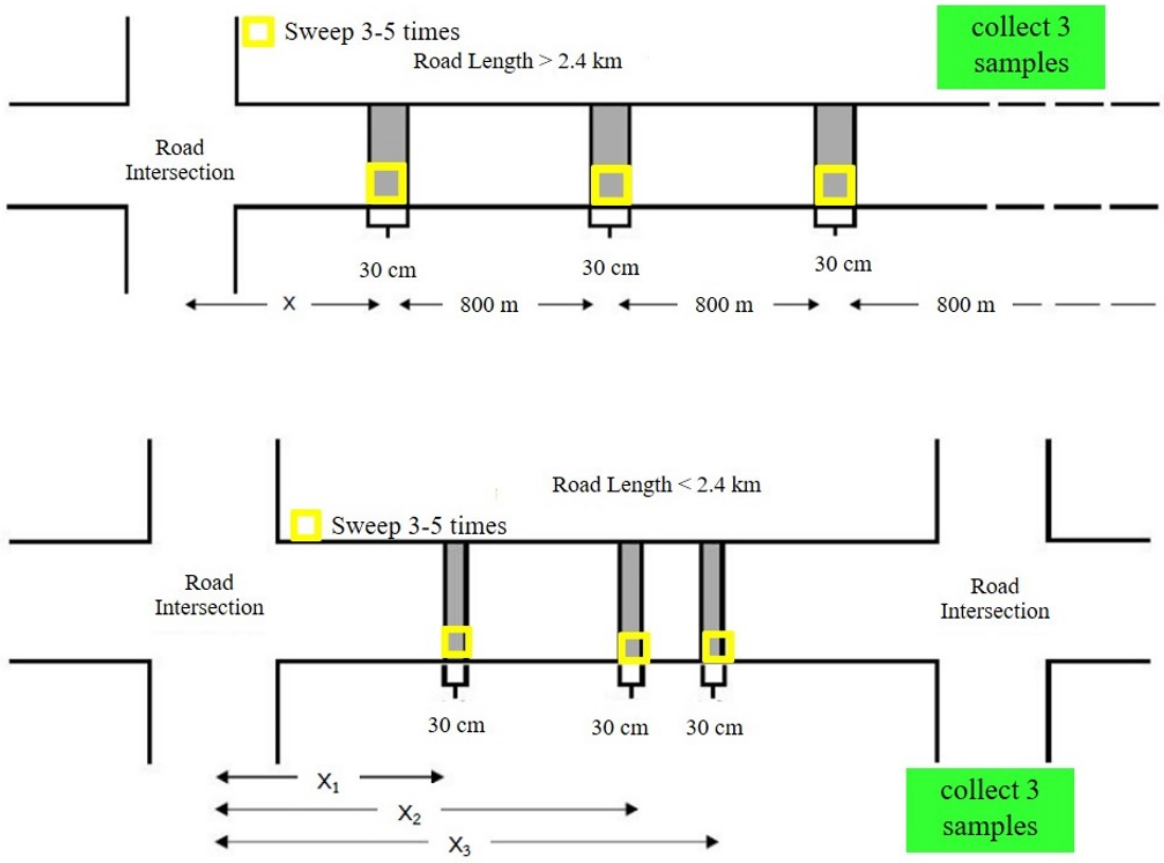

Figure 4 Locations of sampling points [8].

Silt Analysis

Dust emissions from paved and unpaved roads have been found to vary with the "silt loading" present on the road surface as well as the average weight of vehicles traveling the road. The term silt loading refers to the mass of silt-size material (equal to or less than 75 µm in physical diameter) per unit area of the travel surface. The total road surface dust loading consists of loose material that can be collected by broom sweeping and vacuuming of the traveled portion of the road. The silt fraction is determined by measuring the proportion of the loose dry surface dust that passes through a 200-mesh screen using the ASTM-C-136 method. Silt loading is the product of the silt fraction and the total loading.

Several open dust emission factors have been found to be correlated with the silt content (< 200 mesh) of the material being disturbed. The basic procedure for silt content determination is mechanical, dry sieving. For sources other than paved roads, the same sample which was oven-dried to determine moisture content is then mechanically sieved. The broom swept particles are weighed in a container, which was tarred before sample collection. After weighing the sample to calculate total surface dust loading on the traveled lanes, the broom swept particles were combined as a composite sample [8]. The samples were dried in an oven at 130^0C to remove moisture and were equilibrated in the desiccator prior be sieved.

Collected dust were then sieved using mechanical shaker (model: Retsch AS200) through the 200 mesh screen (75 µm) for 10 minutes. The total net weight and net weight of particle < 200 mesh were used to calculate percent of silt using equation (1). Results of percent of silt measured from each road are as presented in Table 1

$$\%\mathbf{Silt} = \frac{\mathbf{Net\ Weight\ <200\ mesh}}{\mathbf{Total\ Net\ Weight}} \times \mathbf{100} \qquad (1)$$

Table 1 Percent of silt on each road

Roads	Silt (g/m^2)	% Silt
Phaholyothin	5.38	2.79
Saraburi-Lomsuk	0.78	1.80
Kung Khao Kaew	38.11	3.49
3385	1.22	1.12
3034	1.33	1.92

PM-10 and PM-2.5 Emissions

The PM-10 and PM-2.5 emitted from re-suspended road dust were calculated by equation 2.

$$\mathbf{EF = k \times sL^{0.91} \times W^{1.02}} \quad (\mathbf{2})$$

where; EF is particulate emission factor (having units matching the units of k), k is particle size multiplier for particle size range and units of interest shown in table 2, sL is road surface silt loading (grams per square meter; g/m^2), and W is average weight (tons) of the vehicles traveling the road.

Table 2 Empirical constants used in the calculation

Size range	Particle Size Multiplier k (g/VKT*)
PM-2.5	0.15
PM-10	0.62

* VKT = vehicle kilometer traveled

RESULT AND DISCUSSION

Diurnal variation of emission rates of PM-10 and PM-2.5 from each roads are presented in Figure 5 and 6. The difference between amounts of dust emitted from these road was mainly caused by number of vehicle travelling on each road. Phaholyothin road emitted the highest amount of re-suspended road dust due to its largest number of total vehicle as well as it was served as the main road for industrial transportation with a large number of truck travelling on this road (Figure 7).

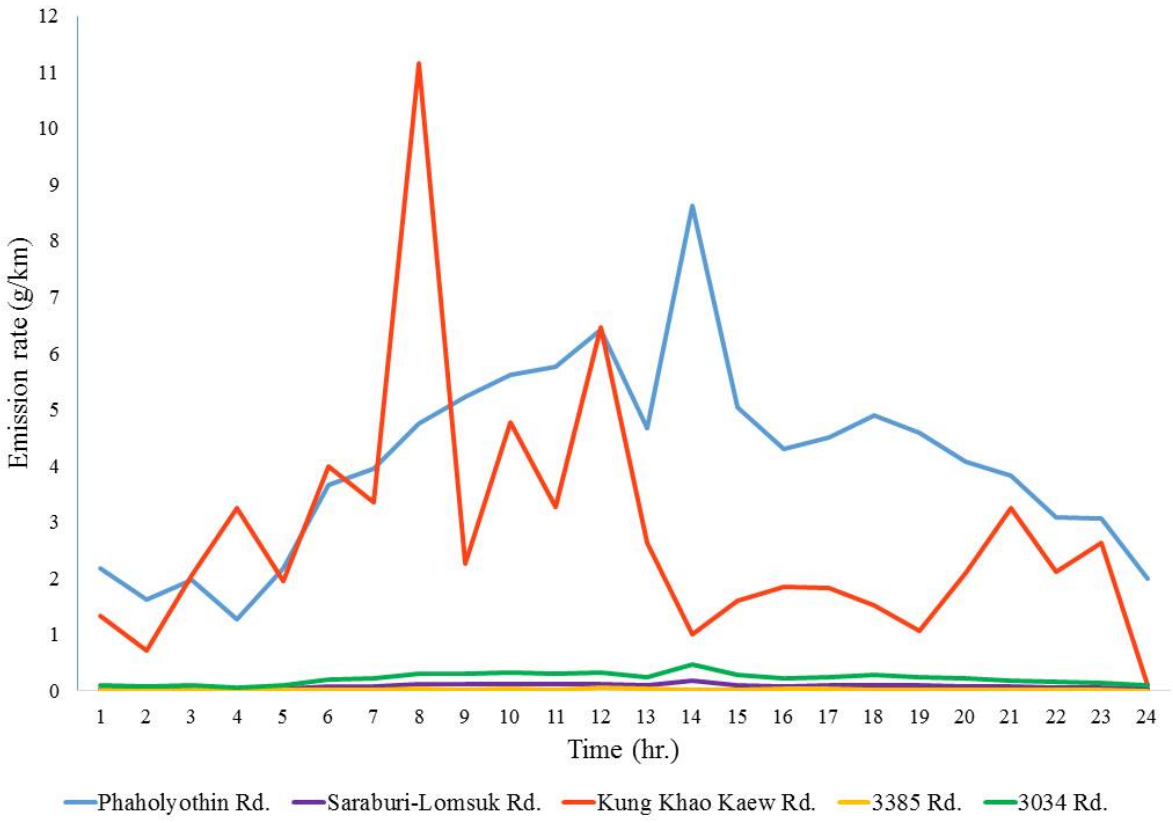

Figure 5 Emission rate of PM-10 from re-suspended road dust

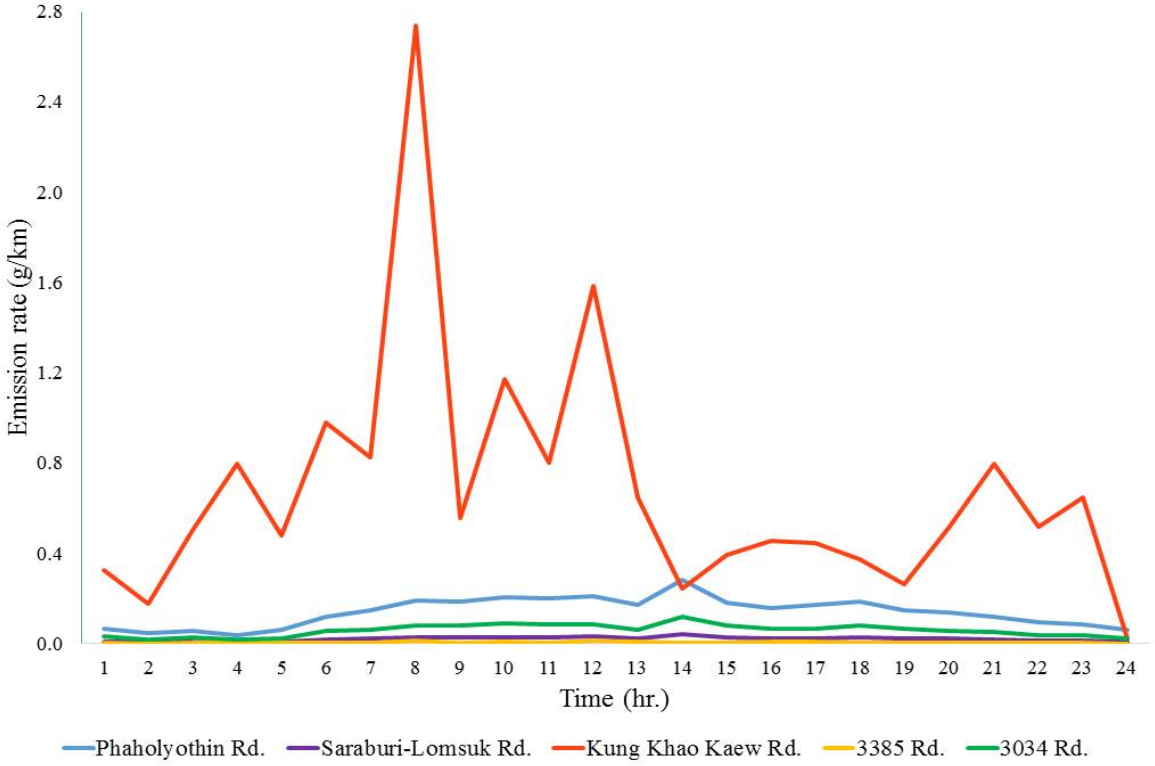

Figure 6 Emission rate of PM-2.5 from re-suspended road dust

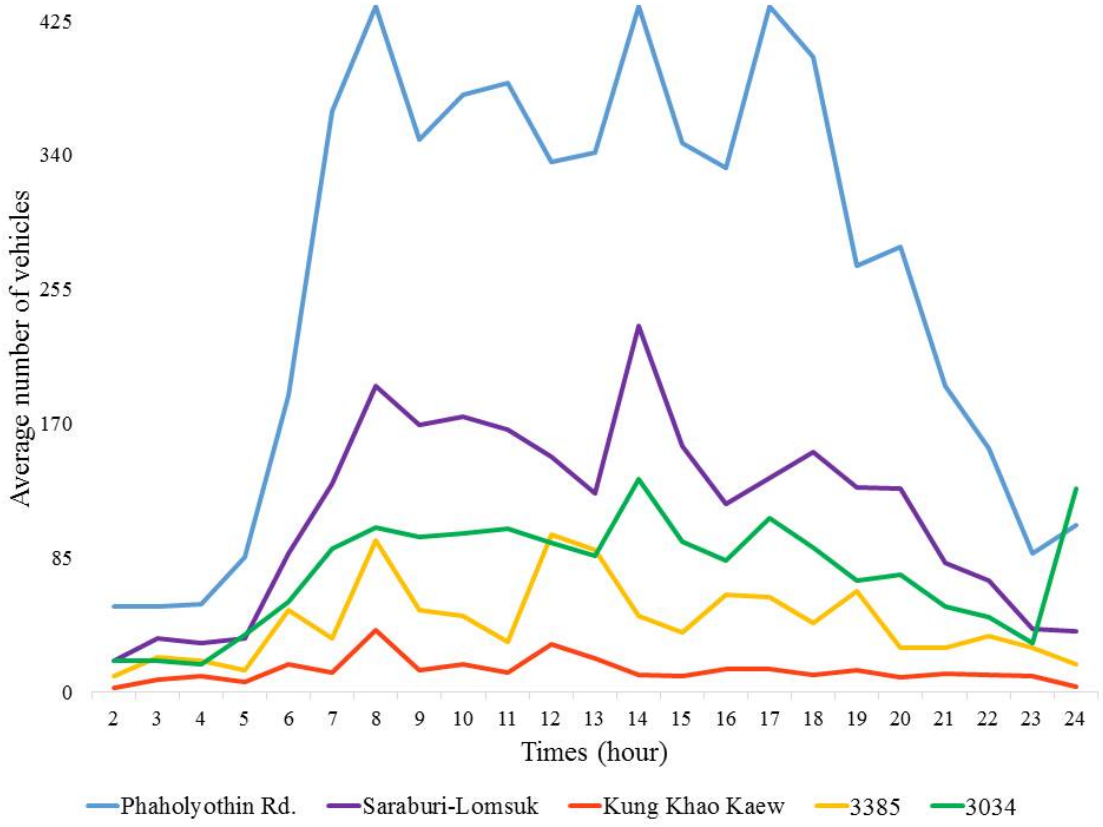

Figure 7 Total number of vehicles travelling on each road

The diurnal profile of PM-10 emission rate estimated as Phaholyothin road was used to evaluate the influence of re-suspended road dust to particulate concentration in the study area. Hourly average of PM-10 concentrations measured from the curbside of this road during the sampling period were compared with its emission profile as presented in Figure 8. It should be noted that there were no activities related to cleaning of the road during the dust sampling period. Results clearly indicated the contribution of re-suspended road dust to the PM-10 concentration. These results suggested that the efforts should be made in controlling not only emissions from industrial sources but also those released as re-suspended road dust in this Pollution Control Zone. For the reduction of daily concentration of PM-10 to meet its legislative ambient air quality standard, the silt loading on the road surface should be removed.

One of the possible mitigation action is scheduling the cleaning period of the road during morning and evening times.

Table 3 Emission rate of worst case

Roads	Worst case emission rate (g/km)	
	PM-10	PM-2.5
Phaholyothin	35155	8002
Saraburi-LomSuk	3782	1165
Kung Khoa Keaw	27784	39017
3385	616	265
3034	6273	3069

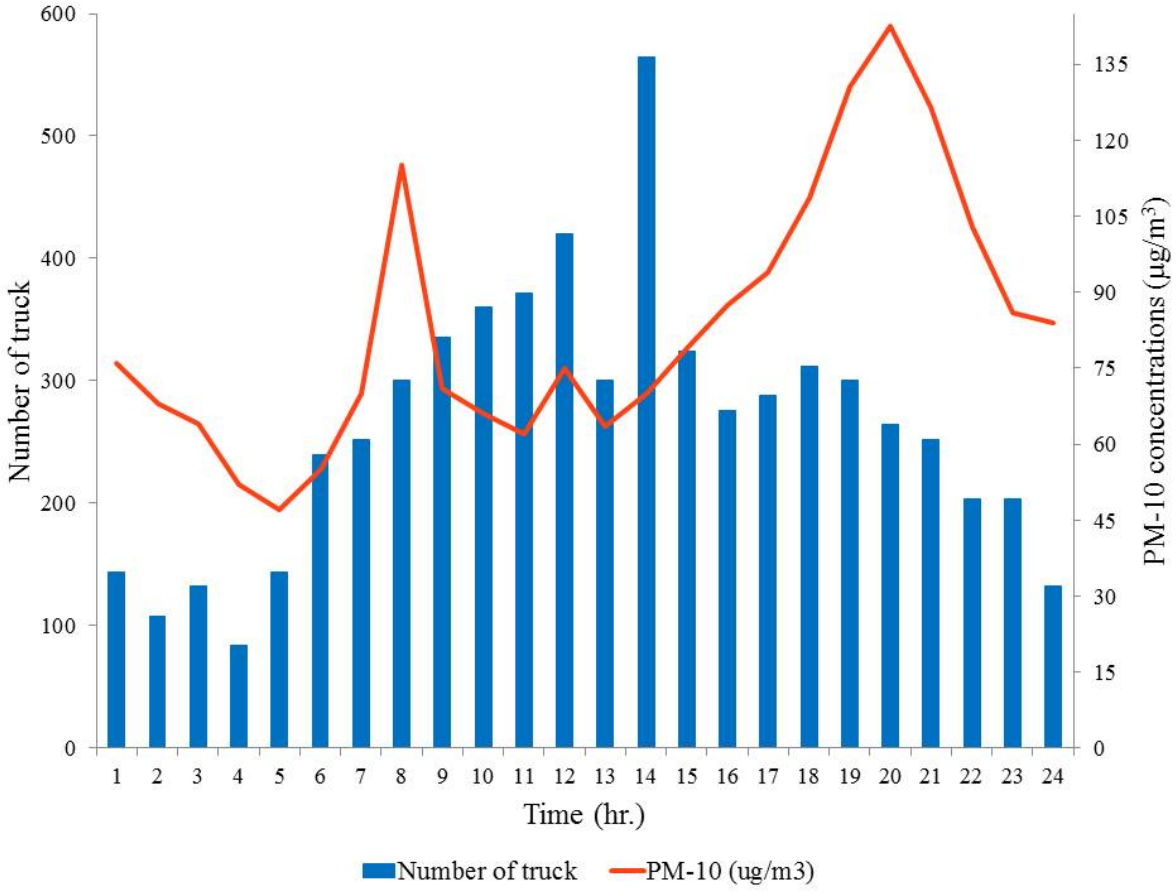

Figure 8 Diurnal variation of PM-10 concentrations and PM-10 emissions from re-suspended road dust

CONCLUSION

Emission rates of PM-10 and PM-2.5 released from re-suspended road dust were evaluated for an area designated as Pollution Control Zone in Thailand. Direct measurement of particle deposition on the road surface was carried out covering entire roads within the zone. These data were evaluated for amount of PM-10 and PM-2.5 emissions following the concept of analysis of the silt content. Results revealed the diurnal profile of amount of particulate emissions with respect to number of total vehicle

and contribution of heavy duty truck travelling in this area. It also provided the information that the PM-10 concentrations measured in this area was associated with amount of re-suspended road dust.

ACKNOWLEDGEMENTS

The authors sincerely thanks the Pollution Control Department, the Siam Cement Public Company Limited, and Na Phra Lan Sub-district Municipality for providing input data used in this study. This study was partially supported for publication by Center of Excellence on Environmental Health and Toxicology (EHT), Faculty of Public Health, Mahidol University, Thailand.

REFERENCES

[1] Modelling road dust emission abatement measures using the NORTRIPmodel: Vehicle speed and studded tyre reduction M. Norman b, I. Sundvor c, B.R. Denby a, , C. Johansson b, d, M. Gustafsson e, G. Blomqvist e, S. Janhall e Atmospheric Environment 134, 2016, pp. 96-108.

[2] World Health Organization, WHO Air quality guidelines for particulate matter, ozone, nitrogen dioxide and sulfur dioxide Global update 2005 Summary of risk assessment, 2006, pp. 9.

[3] Environmental Protection Agency; Particulate matter (PM), 2016. https://www3.epa.gov/pm. Accessed May 25, 2016.

[4] Ketzel M., Omstedt G., Johansson C., Ingo Du¨ RI., Pohjola M., Oettl D., Gidhagen L., Wa˚ HP., Lohmeyer A., Haakana M., and Berkowicz R., Estimation and validation of PM2.5/PM10 exhaust and non-exhaust emission factors for practical street pollution modelling, Atmospheric Environment, 2007, 41, pp. 9370-9385.

[5] Cheng YH., and Li YS., Influences of Traffic Emissions and Meteorological Conditions on Ambient PM-10 and PM-2.5 Levels at a Highway Toll Station, Aerosol and Air Quality Research, 2010, 10, pp. 456-462.

[6] Outapa P., Kondo A., and Thepanondh S., Effect of speed on emissions of air pollutants in urban environment: case study of truck emissions, International Journal of GEOMATE, 2016, 11, pp. 2200-2207.

[7] Pay MT., Guerrero PJ., and Baldasano JM., Implementation of resuspension from paved roads for the improvement of CALIOPE air quality system in Spain, Atmospheric Environment, 2011, 45, pp. 802-807.

[8] Measurement Policy Group Office of Air Quality Planning and Standards U.S. Environmental Protection Agency, Emission Factor Documentation for AP-42, January. 2011.

Second International Conference on Science, Engineering & Environment,
Osaka City, Japan, Nov.21-23, 2016, ISBN: 978-4-9905958-7-6 C3051

PAIN MANAGEMENT KNOWLEDGE AMONG MEDICAL WARD NURSES IN MALAYSIA

Kim Lam Soh[1], Salimah Japar [1], Wan Zaida Wan Md Hanapi[2], Rosna Abdul Raman[1], Swee Leong Ong[3] and Kim Geok Soh[4]

[1]Faculty of Medicine and Health Sciences, Universiti Putra Malaysia, Malaysia, [2] Community Nursing College Pasir Mas, Malaysia, [3]Faculty of Medicine and Health Sciences, Universiti Sultan Zainal Abidin, Malaysia, [4]Faculty of Educational Studies / Sport Academy, Universiti Putra Malaysia, Malaysia

ABSTRACT: Pain, a common symptom for patients in medical wards, can be relieved by effective pain management, with nurses playing a vital role in this regard. A study was undertaken to determine the knowledge of nurses on pain management and to examine the factors that influence their acquisition of such knowledge. A total of 143 medical ward nurses (representing 60% response) in a government referral hospital in Malaysia participated in the study. Data from this study derived from a set of questionnaires were analysed using 2 x 2 contingency tables and the chi squared test with Yate's correction. Approximately two thirds of the nurses were deficit in knowledge regarding pain management, registering a mean knowledge score of 40.5 out of a possible 100 points. There was no significant association between the level of knowledge on pain management and demographic characteristics such as age and work experience. There was also no significant relationship between the level of knowledge on pain management and the pain courses attended. A better understanding of the factors that affect the acquisition of such knowledge could provide useful information that can be incorporated in an improved educational program on pain management for nurses.

Keywords: Pain management, Medical wards, Nurses, Malaysia

INTRODUCTION

Pain is defined as an "unpleasant sensory and emotional experience associated with actual or potential tissue damage or described in terms of such damage" [1]. It is one of the most common reasons for seeking health care. According to definition by McCaffrey "pain is subjective and that the patient's pain is whatever the patient indicates" [2]. Prevalence of pain in the first 24 hours of admission to hospital is reported to be in the range of 48 to 88 percent [3]-[4]. Approximately 30% of hospital patients experience severe pain [3]-[5], which affects their physical, psychological and also their social well-being [6]-[7]. Pain also affects hospitalized patients emotionally and spiritually [8]. Unrelieved pain brings much suffering, slows down the recovery process, and may even contribute to other health problems [9] and might also result in undesirable physiological and psychological consequences [10]. It is the main reason for anxiety and emotional distress. In this regard, nurses play an important role in effective pain management [8]-[11]. Poor pain management due to nurses' lack of experience and knowledge has negative effects on pain management, giving rise to complaints on nurses' performance [12]. Insufficient knowledge of pain management among nurses is a continuing concern in Malaysia. It is important to ensure that ward nurses are able to intervene pharmacologically or non-pharmacologically to ease the pain of their patients.

In the management of pain, the majority of healthcare professionals prefer pharmaceutical procedures, although a significant number are acquainted with established and recommended non-pharmaceutical techniques such as distraction and relaxation which can help to prevent or alleviate pain [13]. In many situations, a combination of non-pharmacological methods along with pharmacological approaches can be beneficial to hospitalized patients. Some nurses are reluctant to believe patients' descriptions of their pain despite acknowledging that good pain assessment is dependent on the individual's description of the nature and intensity of pain. According to Edwards-Nash [14], nurses' poor knowledge of the benefits of opioids may cause them to be unduly concerned with the negative attributes of opioids rather than with patients' benefits such as comfort, mobility, and independence.

Previous studies investigated the association of factors such as age, education, and working experience with patients' level of knowledge on pain management [15]-[16]. In this connection, studies have also provided evidence on an association between years of experience of nurses and effective pain management [17]. Nevertheless, other studies point to the contrary [18]. Furthermore, the effect of formal education on the effectiveness of pain management is still far from conclusive [19]-[20]. Some studies focus on education as the most important tool to improve pain management [21] while others highlight the role of personal

experience and interaction with colleagues [22]. Nurses' knowledge, beliefs, and attitudes are key factors in determining their behavior and approach in pain management [19]. There have been unsubstantiated reports attributing nurses' lack of knowledge for their inadequacy in pain relief. [23]-[24]. The present study was therefore aimed at determining the level of nurses' knowledge on pain management and examining the factors that influenced their knowledge or lack of it.

METHODS

A cross-sectional study design was conducted using a structured self-administered questionnaire at one of the largest government referral hospitals in the Klang Valley in Malaysia.

One hundred and forty three out of 238 registered nurses working in nine (9) medical wards at the government hospital took part in this cross-sectional study after informed consent.

Instrument

A self-administered questionnaire was used to assess nurses' knowledge on pain management, which comprised of three sections; A, B and C. Sections A and C adapted from Smart [25], and section B adapted from McCaffrey and Ferrell [26]. Section A elicited a socio-demographic profile of the participants that included data such as age, level of education, and years of nursing experience. There were seven questions pertaining to information on whether the participant had received instruction in anatomy or physiology and in understanding pain management. Section B focused on knowledge concerning pain and pain management. There were seven questions pertaining to knowledge on pharmacologic interventions and another seven pertaining to non-pharmacologic interventions. Participants had to choose the best answer for each question from among the choices: 'True', 'False', and 'Not Sure'. Section C had nine questions that focused on previous (before working in the medical unit) and recent (after working in the medical unit) exposure to pain management courses.

Before its application in this study, the questionnaire was reviewed by three experts in pain management that included an anaesthesiologist, a ward manager in the Emergency Department, and an Acute Pain Service nurse from a government hospital. The three experts agreed to and accepted the content of the questionnaire. To check for clarity of the questions, pre-testing was conducted on 12 nurses from a medical ward at another government hospital. No alteration was done to the questionnaire after the pre-testing.

Data Collection

The data collection process was from 1st December 2008 till 30th January 2009. The Ward Manager in every ward was informed about the study and had agreed to distribute the questionnaires to all nurses, who were given two weeks to complete it. The participants were asked to put the completed questionnaire into the closed envelope provided in Ward Manager's room. For those who were refused to participate, they were also required to return questionnaire into the closed envelope.

Data Analysis

SPSS (Statistical Package for Social Sciences) Version 21.0 for windows was used for data analysis. A knowledge score was calculated based on 14 questions 'true or false' statements concerning pharmacological and non-pharmacological interventions with a total score of 14. There were 3 response choices: 'True', 'False' and 'Not sure'. The respondents scored zero for 'false" or "not sure" answer. A total score was computed for overall pain knowledge based on the nurses' performance on all the individual items. Descriptive data analysis was performed on the demographic information and questionnaire outcome relating to the level of knowledge in pain management. The chi squared test and Yate's correction was performed to evaluate the association between knowledge level and demographic variables, education level, age, years of nursing experience, and recent exposure to pain management course. The level of statistical significance was set at $p < 0.05$.

Ethical Considerations

Approval was obtained from the University Medical Research Ethics Committee and the Ministry of Health Ethics Committee to perform this study. All respondents were given participation information sheets and they could choose whether or not to participate. The information from participants was kept confidential and used only for the purpose of this study.

RESULTS

Out of a total of 238 participants who received the questionnaires, 143 returned completed questionnaires, giving a response rate of 60%.

Table 1 shows the demographic profile of the participants in this study. The age mean and SD of the participants was 27.85 ± 6.16 years. The average length of the nurses' working experience was 4.44 ± 5.82 years. The majority of the participants 131 (91.6%) had a diploma in nursing

while 9 (6.3%) had completed their baccalaureate-degree in nursing.

The mean knowledge score for pain management was 40.5±9.67. The majority of the participants (n=101, 71%) had pain knowledge scores of 49% and below. Only 29% (n=42) had pain knowledge scores of 50% and above (Figure 1). There was no significant association between knowledge score and age, level of education, or working experience (Table 2).

Table 1 Demographic characteristics

Characteristics (n=143)	n (%)	Mean±SD
Age		27.85±6.15
≤26years	78(54.5)	
≥27years	65(45.5)	
Level of nursing education		
Degree	9(6.3)	
Diploma	131(91.6)	
Certificate	3(2.1)	
Year of nursing experience		4.45±5.83
<3years	73(51.0)	
≥3years	70(49.0)	

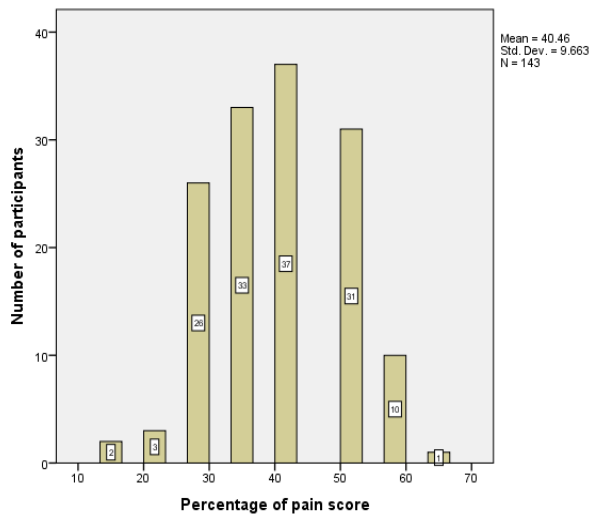

Figure 1 Distribution of pain management knowledge score

Approximately one third of participants (n=59, 41%) reported that they had not previously attended any course on pain management course and 59% of nurses reported had exposure to such courses. The majority of the participants had attended pain management courses recently. Although more than 55% of the participants received in-service training regarding pain management, only six percent of the participants held certificates in pain assessment (Table 3).

Table 2 Relationship between knowledge score and demographic characteristics

Characteristics	Knowledge Score (n=143)				
	≤49 (101;71%)	≥50 (42;29%)			
	n(%)	n(%)	df	$\chi 2$	*P*
Age			1	1.75	.19
≤26years	51(65)	27(35)			
≥27years	50(77)	15(23)			
*Edu level					
Non degree	96(72)	38(28)	1	0.42	.52
Degree	5(56)	4(44)			
**Experience					
<3 years	49(67)	24(33)	1	0.57	.45
≥3 years	52(74)	18(26)			

*Edu level: Nursing education level
**Experience: Nursing Experience

Table 3 participation in pain management courses

Participation in pain-related course (n=143)	Yes n (%)	No n (%)
1. Received in-service education in anatomy/physiology of pain	81(57)	62(43)
2. Received in-service education in pain assessment	99(69)	44(31)
3. Received in-service education in pharmacological intervention	106(74)	37(26)
4. Received in-service education in non-pharmacological intervention	91(64)	52(36)
5. Awarded certificate in pain assessment	9(6)	134(94)
6. Participated in multidisciplinary discussion related to pain assessment/management	56(39)	87(61)
7. Read journal articles or pain literature on the internet related to pain management	64(45)	79(55)
8. Received any education on pain management	84(59)	59(41)
9. Discussed pain management with the acute pain service (APS) team	34(24)	109(76))

There was no significant relationship between recent participation in courses related to pain management and knowledge on pain management (Table 4).

DISCUSSION

This study was undertaken to assess the level of nurses' knowledge on pain management and to examine the factors that influenced their knowledge in this respect. Nurses who lack sufficient knowledge on pain management are not in a position to help alleviate the pain suffered by hospitalized patients [27]. Nurses play an important role in

comforting patients. As such, they should have a good foundation of knowledge regarding pain management as this would allow them to develop a positive perspective towards the patient's discomfort and deliver individualized patient care. The success of any pain management requires the cooperation and participation of patients as previous research has shown that patients' participation in their self-care results in less pain distress, sensation, and analgesic use [28]. Patient involvement in decisions about treatment process is subjective, and only the patients themselves can really describe their pain or discomfort. Pain management programs need to address issues like physiology of pain, myths and misconceptions about pain, precise description of a patient in pain, pharmacological and non-pharmacological techniques for pain management, and ethics in pain management.

This study found that there was a knowledge deficit among nurses in relation to pain management. More than 70% of the participants obtained knowledge scores lower than 50% when questioned about pain management. Such knowledge deficit among nurses may be one of the factors contributing to reports of pain and discomfort experienced by patients seeking healthcare even though healthcare providers are provided with various treatment options and guidelines on the expected standards of care [29-30].

This study found no significant association between the level of pain management knowledge and education level, age, or work experience. The findings of this study are in accordance with two other studies that found no significant difference in pain management knowledge level in relation to age and years of nursing experience [18-31]. On the other hand, Lui-So [8] reported that the nurses who were older and had longer working experience were more knowledgeable and were more likely to apply their knowledge in pain management.

This study did not find any significant association between the level of knowledge and participation in in-service education. A study by Twycross [19] similarly found that attending courses on pain management did not make any difference to the level of knowledge in this area among nurses. On the other hand, Patiraki-Kourbani-Tafas [21] found that attending continuing education programs had a positive impact on knowledge acquisition on pain management. Pud [32] also found that the longer nurses were exposed to correct information regarding pain management, the higher their level of knowledge. Findings in these two studies support the need for continuing education in relation to pain management and underline the importance of knowledge acquisition in this regard. There is also a need to emphasize the implementation of standardized guidelines for pain assessment services [13]. It should be borne in mind that learning happens when the learner acquires knowledge of a topic via processing information through listening, reading, thinking, memorizing, analysing, and application. In other words, learners acquire knowledge not solely from formal educational program or books, but also through hands-on practice [33]

Table 4 Relationship between knowledge scores on pain management and recent participation in courses related to pain management

Recent participation in courses related to pain management (n=143)	Knowledge Score				
	≤49 (n=101; 71%)	≥50 (n=42; 29%)			
	n(%)	n(%)	df	$\chi 2$	*P*
1. Received in-service education in anatomy / physiology of pain			1	3.05	0.08
Yes	52(64)	29(36)			
No	49(79)	13(21)			
2. Received in-service education in pain assessment			1	0.93	0.34
Yes	67(68)	32(32)			
No	34(77)	10(23)			
3. Received in-service education in pharmacological intervention					
Yes	74(70)	32(30)	1	0.24	0.88
No	27(73)	10(27)			
4. Received in-service education in non-pharmacological intervention			1	3.32	0.07
Yes	59(65)	32(35)			
No	42(81)	10(19)			
5. Awarded certificate in pain assessment			1	0.42	0.52
Yes	5(56)	4(44)			
No	96(72)	38(28)			
6. Participated in multidisciplinary discussion related to pain assessment / management			1	0.01	0.98

	Yes	39(70)	17(30)		
	No	62(71)	25(29)		
7.	Read journal article or pain literature on the internet related to pain management			1	0.12	0.91
	Yes	46(72)	18(28)		
	No	55(70)	24(30)		
8.	Received any education on pain management			1	0.47	0.50
	Yes	57(68)	27(32)		
	No	44(75)	15(25)		
9.	Discussed pain management with the acute pain service (APS) team			1	1.15	0.28
	Yes	27(79)	7(21)		
	No	74(68)	35(32)		

As far as practice is concerned, medical units should be committed to effective pain management as an institutional goal by developing standardized guidelines and protocols for pain management for nurses in medical wards. Quality improvement programs should also be instituted with the aim of improving the process of assessing and treating pain by using appropriately pain assessment tools such as a pain scale based on patient's verbal abilities. However, an ideal implementation of this approach would require expertise in applying such knowledge, especially in special care situations. For example, 'looking good' does not always mean that a patient is not suffering from pain. A cycle of treating pain, reassessing results and continuing treatment needs to be established until there is reasonable certainty that the patient feels comfortable. It is also important to be aware of the effects of non-pharmacological methods because a lack of knowledge and uncertainty can render the use of non-drug approaches ineffective [34].

The main limitation of this study is that it was carried out at one government hospital only, and so the findings cannot be generalised to all medical wards in other hospitals in Malaysia. Nevertheless, this study provides an insight into nurses' knowledge on pain management and identifies areas for future improvement.

CONCLUSION

Findings of this study highlight the immediacy of addressing in-service education for all medical wards nurses in the study setting. Introduction of regular in-service training may be necessary to enhance nurses' competency in pain management and to eliminate knowledge deficit. The existing in-service courses may also need to be reviewed with more focus on topics which increase the nurses' interest and awareness of pain endured by patients. An emphasis on new strategies to teach pain management needs to include teaching rounds, case studies and the reading and discussion of relevant papers appearing in medical journals. In this study, learning about pain management did not appear make much difference to knowledge in relation to pain management, However, nurses who had had more years of experience tended to apply their knowledge of pain in their duties; they are likely to be more knowledgeable in this regard. Ultimately, change will not occur until there is public participation and joint efforts to improve pain management.

ACKNOWLEDGEMENT

The authors would like to express special thanks to Director General of Health Malaysia for permission to publish this paper.

REFERENCES

[1] International Association for the Study of Pain. IASP Taxonomy. 2012 [cited 2015 3 May]; Available from: http://www.iasp-pain.org/Taxonomy.

[2] McCaffery, M, Understanding your patient's pain tolerance. Nursing, 1999. 29(12): pp. 17.

[3] Maier, C, et al., The quality of pain management in German hospitals. Deutsches Ärzteblatt International, 2010. 107(36): pp. 607-614.

[4] Sawyer, J, et al., Pain prevalence study in a large Canadian teaching hospital. Round 2: lessons learned? Pain Management Nursing, 2010. 11(1): pp. 45-55.

[5] Lorentzen, V, Hermansen, IL, &Botti, M, A prospective analysis of pain experience, beliefs and attitudes, and pain management of a cohort of Danish surgical patients. European Journal of Pain, 2012. 16(2): pp. 278-288.

[6] Breivik, H, et al., Survey of chronic pain in Europe: prevalence, impact on daily life, and treatment. European Journal of Pain, 2006. 10(4): pp. 287-287.

[7] Joshi, GP &Ogunnaike, BO, Consequences of inadequate postoperative pain relief and chronic persistent postoperative pain. Anesthesiology Clinics of North America, 2005. 23(1): pp. 21-36.

[8] Lui, LYY, So, WKW, &Fong, DYT, Knowledge and attitudes regarding pain management among nurses in Hong Kong medical units. Journal of Clinical Nursing, 2008. 17(15): pp. 2014-2021.

[9] Deng, D, et al., The relationship between cancer pain and quality of life in patients newly admitted to Wuhan Hospice Center of China. American Journal of Hospice and Palliative Medicine, 2011: pp. 1049909111418636.

[10] Saxe, G, et al., Relationship between acute morphine and the course of PTSD in children with burns. Journal of the American Academy of Child & Adolescent Psychiatry, 2001. 40(8): pp. 915-921.

[11] Coulling, S, Nurses' and doctors' knowledge of pain after surgery. Nursing Standard, 2005. 19(34): pp. 41-49.

[12] The Information Centre for Health and Social Care Data on written complaints in the NHS 2006-07. 2007.

[13] Linhares, MBM, et al., Assessment and management of pediatric pain based on the opinions of health professionals. Psychology & Neuroscience, 2014. 7(1): pp. 43-53.

[14] Edwards, HE, et al., Determinants of nurses' intention to administer opioids for pain relief. Nursing & Health Sciences, 2001. 3(3): pp. 149-159.

[15] Terrell, KM, et al., Analgesic prescribing for patients who are discharged from an Emergency Department. Pain Medicine, 2010. 11(7): pp. 1072-1077.

[16] Minick, P, et al., Long-bone fracture pain management in the emergency department. Journal of Emergency Nursing, 2012. 38(3): pp. 211-217.

[17] Hansson, E, Fridlund, B, &Hallström, I, Effects of a quality improvement program in acute care evaluated by patients, nurses, and physicians. Pain Management Nursing, 2006. 7(3): pp. 93-108.

[18] Watt-Watson, J, et al., Relationship between nurses' pain knowledge and pain management outcomes for their postoperative cardiac patients. Journal of Advanced Nursing, 2001. 36(4): pp. 535-545.

[19] Twycross, A, Educating nurses about pain management: the way forward. Journal of Clinical Nursing, 2002. 11(6): pp. 705-714.

[20] Heins, JK, et al., Disparities in analgesia and opioid prescribing practices for patients with musculoskeletal pain in the emergency department. Journal of Emergency Nursing, 2006. 32(3): pp. 219-224.

[21] Patiraki-Kourbani, E, et al., Personal and professional pain experiences and pain management knowledge among Greek nurses. International Journal of Nursing Studies, 2004. 41(4): pp. 345-354.

[22] de Rond, MEJ, et al., A pain monitoring program for nurses: Effects on nurses' pain knowledge and attitude. Journal of Pain and Symptom Management, 2000. 19(6): pp. 457-467.

[23] Gregory, J &Haigh, C, Multi-disciplinary interpretations of pain in older patients on medical units. Nurse Education in Practice, 2008. 8(4): pp. 249-257.

[24] White, PF &Kehlet, H, Improving postoperative pain management: what are the unresolved issues? Anesthesiology, 2010. 112(1): pp. 220-225.

[25] Smart, S, Post-operative pain management knowledge and attitude of paediatric nurses: a New Zealand regional view. 2005, Victoria University of Wellington.

[26] McCaffrey, M &Ferrell, BR, Nurses' knowledge of pain assessment and management: How much progress have we made? Journal of Pain and Symptom Management, 1997. 14(3): pp. 175-188.

[27] Kim, DY, et al., A nationwide survey of knowledge of and compliance with cancer pain management guidelines by korean physicians. Cancer Research and Treatment, 2014. 46(2): pp. 131-140.

[28] Bailey, J, et al., Relationship of nursing education and care management inpatient rehabilitation interventions and patient characteristics to outcomes following spinal cord injury: The SCIRehab project. The Journal of Spinal Cord Medicine, 2012. 35(6): pp. 593-610.

[29] Zoëga, S, et al. Quality pain management in the hospital setting from the patient's perspective. Pain Practice, 2014. DOI: 10.1111/papr.12166.

[30] Tait, RC, Chibnall, JT, &Kalauokalani, D, Provider judgments of patients in pain: seeking symptom certainty. Pain Medicine, 2009. 10(1): pp. 11-34.

[31] Wilson, B, Nurses' knowledge of pain. Journal of Clinical Nursing, 2007. 16(6): pp. 1012-1020.

[32] Pud, D, Personal past experience with opioid consumption affects attitudes and knowledge related to pain management. Pain Management Nursing, 2004. 5(4): pp. 153-159.

[33] Cate, O, et al., Orienting teaching toward the learning process. Academic Medicine, 2004. 79(3): pp. 219-228.

[34] Pölkki, T, Pietilä, AM, &Vehviläinen-Julkunen, K, Hospitalized children's descriptions of their experiences with postsurgical pain relieving methods. International Journal of Nursing Studies, 2003. 40(1): pp. 33-44.

Second International Conference on Science, Engineering & Environment,
Osaka City, Japan, Nov.21-23, 2016, ISBN: 978-4-9905958-7-6 C3051

THE TREND OF ENTERAL FEEDING AMONG CRITICALLY- ILL PATIENTS IN ADULT ICUs IN MALAYSIA

Salimah Japar [1], Kim Lam Soh[1], Hatifah Che Hussin[2], Nor Airini Ibrahim[1], Swee Leong Ong[3] and Kim Geok Soh[4]

[1]Faculty of Medicine and Health Sciences, Universiti Putra Malaysia, Malaysia, [2] Hospital Putrajaya, Malaysia[2] , [3]Faculty of Medicine and Health Sciences, Universiti Sultan Zainal Abidin, Malaysia, [4]Faculty of Educational Studies / Sport Academy, Universiti Putra Malaysia, Malaysia

ABSTRACT

The adequacy of caloric intake is crucial for all critically-ill patients in Intensive Care Units because energy expenditure is higher in these patients compared to normal patients in general wards. Adequate calorie intake will promote positive outcome to the patients while inadequate calorie will lead to malnutrition which will increase the length of stay. The objective of this study was to determine the adequacy of caloric intake received by critically-ill patients in the general ICU in Malaysia. This was a cross sectional study which used a pro forma adapted from ICU protocol. There were 132 participants involved in this study. The descriptive statistic and independent t-test were used for the statistical analysis. The results showed that 75.8% (n=100) received adequate or more than calorie prescribed while 24.2% (n=32) received calorie less than the given prescription. Patients that received early feeding were 72% (n=95) and late feeding were 28% (n=37). The continuous feeding method was most commonly used in early feeding patients from Day 1 to Day 3. There was an association between the adequacy of calorie intake and the length of stay ($p<0.05$). Findings obtained from this study will provide information for the nurses and other health care providers to improve the management of patients so that all patients will receive adequate caloric intake during their stay in ICUs

Key words: Intensive Care Unit (ICU); Enteral feeding; Continuous feeding; Intermittent feeding; Calorie intake

INTRODUCTION

Nutritional support is considered as an essential component in the care of critically-ill patients, either to treat existing malnutrition or to prevent the development of nutritional deficiencies [1]. Despite treatment of patient's disease by using medications, adequate caloric intake has become an important element in patient's management [2]. Malnutrition is very common among ICU patients and frequently it was due to inadequate caloric intake [3, 4]. Evidence shows that malnutrition is associated with poor outcomes among ICU patients as reflected by increased morbidity, mortality, and length of stay [5, 6]. Intensive care patients with adequate caloric requirements are more likely to achieve reduced time on a ventilator support, fewer complications such as low risk of infection and shorter time of hospital stay [7].

Enteral feeding is the most common method used in ICU to provide nutrition support to the critically-ill patients. Enteral feeding is recommended for critically-ill patients who cannot consume oral diet within three days in order to supply the energy to the patients [8] Advantages of enteral feeding include the enhancement of intestinal mucosal integrity and nutrient absorption, improvement of metabolic and immune response, reduction of complications and costs [6].

Early enteral feeding in critically ill patients should commence within 24 hours of admission to the ICU [9]. In order to achieve adequate calories for all patients in ICU, early enteral feeding was recommended as soon as possible after being admitted to ICU. Current recommendations suggest a target calorie intake of 25 kcal/kg/day for patients in ICU [9]. Many studies have been conducted on the adequacy of caloric intake among ICU patients worldwide but there is limited data available in Malaysia especially regarding the adequacy of caloric intake among ICU patients. The objective of this study was to determine the adequacy of caloric intake received by critically-ill patients in the General ICU in Malaysia.

METHODS

Study Design and Participants

This was a cross-sectional study conducted in a General ICU hospital in regional Malaysia from October until December 2008. All participants were above 18 years old. They received intermittent bolus or continuous feeding for more than 24 hours. The study did not include patients who received nutrition support either orally, parenteral, or a combination of

enteral and oral methods during the period of the study. The sample size for this study was 126 patients.

Instrument

Data were collected using a standardized checklist (Proforma) which was developed from ICU management protocol [9]. The proforma was divided into two sections. The first section was focused on patients' demographic characteristics: age, weight, height, diagnosis on admission, ideal body weight (IBW), SOFA (Sequential Organ Failure Assessment) score and SAP II (Simplified Acute Physiology) score followed by admission date to ICU and start date of feeding. The second section included type and formula of enteral feeding. This section also focused on patients' conditions as well as problems encountered from day one until day five. Calculation of calorie intake started from 7 am until 7am (completed for 24 hours) and updated in proforma.

The proforma was reviewed by two Anesthesiologists from a government hospital and one ward manager with critical care background from another government hospital. No alteration was made after the experts reviewed and agreed with the relevancy and adequacy of the proforma that measured the adequacy of calorie intake of critically-ill patients. The proforma was pretested on 10 adult patients with all the listed criteria from the same general ICU in September 2008.

Ethical approval was obtained from University Medical Research Ethics Committee and National Institute of Health Ethics Committee. Patients who fulfilled the inclusion criteria were chosen from the admission book and were selected for this study if they agreed to participate and signed informed consent. The purpose and confidentiality of this study was reported to the Head of Department and ward manager in charge of ICU before data collection. All information gathered during reviews of patients' report was remained confidential.

Data collection

Patients' daily calorie intake was collected in the health information system and the calorie received were calculated and updated in the proforma. Patients' calorie intake was monitored for five days after the initiation of enteral feeding. Data collection lasted for 5 days and each patient was followed up to determine the outcome of either being discharged from ICU or death.

Data Analysis

Data were analyzed by using the Statistical Package for Social Sciences ("SPSS") version 14.0. Descriptive analysis involving percentages, means and frequencies were used to report period of initiation, type of formula, mode of enteral feeding, calorie intake per day and problems encountered. An independent sample t-test was conducted to examine the association between early initiation of enteral feeding and adequacies of calorie intake received by patients with patient's length of stay in ICU.

RESULTS

There were 377 admissions in ICU during the three-month study period. Out of the 377 admissions, 142 admissions were not on enteral feeding, 22 participants did not meet the inclusion criteria and 81 participants had less than 24 hours enteral feeding. The final number of participants in this study was 132. Table 1 shows, participants were mostly of Malay (52%) ethnicity, the majority of them males (71.2%) and mean age was 53.35± SD15.96. The length of stay of the participants ranged from 2 to 61 with majority of the participants stayed in ICU for less than five days 40.2% (n=53).

Table 1 Demographics characteristic of ICU patients

Characteristics		n (%)	Mean± SD
Ethnicity			
	Malays	69 (52)	
	Chinese	26 (19.7)	
	Indians	24 (18.2)	
	Others	13(9.9)	
Sex			
	Male	94 (71.2)	
	Female	38 (28.8)	
Age			53.35± 15.96
ICU LOS (day)			9.12±8.236
	≤5	53(40.2)	
	6-10	48(36.4)	
	11-15	14(10.6)	
	≥16	17(12.9)	

LOS: Length of Stay

The mean SOFA score was 8.65±SD3.969 and mean SAPS II score was 43.11±SD17.75. Meanwhile, the most common disease involved was the respiratory system (35.6%). Severity of illness score of patients' condition are shown in Table 2.

Table 2 Severity of illness

Severity of illness	n (%)	Mean ± SD
SAPS II score		43.11±17.75
SOFA score		8.65±3.969
System		
Respiratory	47(35.6)	
Immune	24(18.2)	
Skeletal	14(10.6)	
Cardiovascular	11(8.3)	
Endocrine	10(7.6)	
Urinary	10(7.6)	
Central Nervous	8(6.1)	
Digestive	8(6.1)	

Table 3 shows the condition of patients in the ICUs. The number of participants with Invasive positive pressure Ventilator (IPPV) decreased from the first day to the fifth day (n=64; 48.5%) and (n=19; 14.4%) respectively. Some participants were discharged from ICU on day two onwards.

Table 3 Number of patients on NIPPV versus IPPV

	Day 1	Day 2	Day 3	Day 4	Day 5
	n(%)	n(%)	n(%)	n(%)	n(%)
Normal	21(15.9)	42(31.8)	67(50.7)	80(60.6)	96(72.7)
NIPPV	47(35.6)	48(36.4)	38(28.8)	28(21.2)	17(31.1)
IPPV	64(48.5)	42(31.8)	27(20.5)	24(18.2)	19(14.4)

Normal: Breathing normally; NIPPV: Non-invasive positive ventilation; IPPV: Invasive positive ventilation

Table 4 shows, the majority of these patients, 53.8% (n=71) were overweight with BMI more than 25kg⁄m². A majority of the participants 72% (n=92) had received early feeding within 48 hours of admission to the ICUs as compared to 30% of the participants who received feeding after 48 hours of admission.

Table 4 Anthropometric characteristic of patients in the ICUs

Anthropometrics(n=132)	n (%)	Mean±(SD)
Height(cm)		159.58±(12.391)
Weight		66.65±(16.626)
BMI(kg⁄m²)		25.9780±(5.39085)
Below 18.5		
18.5-25	4(3.0)	
Over 25	57(43.2)	
Ideal Body Weight	71(53.8)	57.83 (± 6.320)
<50kg	11(8.3)	
50-60kg	70(53)	
>61kg	51(38.7)	
Period of initiation of enteral feeding		
≤ 48 Hours	95 (72.0)	
> 48 Hours	37(28.0)	

Most of the patients used continuous feeding on day one and day two, 68.2% and 60.6% respectively. However, as Table 5 shows, choice of intermittent bolus feeding was increased on third (55.5%) and fourth day (66.7%).

Table 5 Methods of enteral feeding

Methods	Day 1 n=132 n(%)	Day 2 n=127 n(%)	Day 3 n=93 n(%)	Day 4 n=78 n(%)	Day 5 n=58 n(%)
Intermittent	42 (31.8)	50 (39.4)	51 (55.4)	52 (66.7)	38 (65.5)
Continuous	90 (68.2)	77 (60.6)	42 (45.1)	26 (33.3)	20 (34.5)

Table 6 shows the most common feeding formula used on the first day was enercal 43.2 % (n=57) followed by Glucerna 32.5 % (n=43). Only one participant used Isocal on the first day.

Table 6 Types of feeding formula

Formula	Day1 n=(132) %	Day2 n=127 %	Day3 n=93 %	Day4 n=78 %	Day5 n=58 %
Ensure	Nil	0.8	Nil	Nil	Nil
Nephro	13.6	14.2	14.0	12.8	12.1
Enercal	43.2	41.7	28.0	20.5	20.7
Isocal	0.7	Nil	Nil	Nil	Nil
Glucerna	32.5	29.9	39.7	46.1	46.6
Pulmocare	4.5	5.5	7.5	8.9	5.1
Others	5.3	7.9	10.8	11.5	15.5

Patients who received less calorie requirement were decreased from day two onward. Approximately half of the patients received less than their requirement on day one which is 57.6 % (n=76) however, the percentage decreased from day two 45.7% (n=58) onward. The number of patients receiving adequate calories or more than requirement increased from 42.4% (n=56) from day one to 72.4 % (n=42) on day 5 (Table 7).

Table 7 Distribution of caloric intake per day received by patients

Calories intake n(%)	Day 1 n=132 n(%)	Day 2 n=127 n(%)	Day 3 n=93 n(%)	Day 4 n=78 n(%)	Day 5 n=58 n(%)
<25kcal/kg/day 32(24.2)	76 (57.6)	58 (45.7)	39 (41.9)	29 (37.2)	16 (27.6)
≥25kcal/kg/day 100(75.8)	56 (42.4)	69 (54.3)	54 (58.1)	49 (62.8)	42 (72.4)

Table 8 shows the problems encountered during enteral feeding. The majority of the participants had hyperglycemia during five days of enteral feeding. However it decreased at day four and five. There was no problem encountered with vomiting after the third day of feeding. As for gastric fluid, it decreased from day one to day five.

Table 8 Distribution of problem encountered during enteral feeding

Problem Encountered	Day 1 n=132 n(%)	Day 2 n=127 n(%)	Day 3 n=93 n(%)	Day 4 n=78 n(%)	Day 5 n=58 n(%)
Asp >200ml	13 (9.8)	10 (7.8)	6 (6.4)	3 (3.8)	2 (3.4)
Vomit	4 (3.0)	1 (0.7)	nil	nil	nil
Diarrhea	2 (1.5)	5 (3.9)	5 (5.3)	4 (5.1)	nil
Hyperglycemia	46 (34.8)	49 (38.5)	45 (483)	27 (34.6)	26 (44.8)
Omission	11 (8.3)	13 (10.2)	6 (6.4)	1 (1.2)	2 (3.4)

Asp: Aspiration

The results in Table 9 indicates, there was no significant association between patients that received

early feeding more than 48 hours (M=10.16, SD=6.77) and the patients who received early feeding less than 48 hours (M=9.01, SD=8.74, t (130) =0.72, p=0.47 eta score, 0.004). The t-test was also conducted to compare the mean length of stay in ICU for the group receiving adequate calorie requirement and group receiving inadequate calorie requirement. The results of the analysis indicated a significant difference between the group received adequate calorie requirement (M=9.97, SD=8.09) and the group receiving inadequate calorie requirement (M=6.47, SD=4.90; t (97.15) =-2.82 p=0.006, eta squared= 0.06)

Table 9 Association between early initiation of enteral feeding and adequacies of calorie intake received by patients and length of stay (LOS)

	LOS			
	n	mean	SD	P*
Period of initiation				
Less than 48 hours	95	9.01	8.743	0.371
More than 48 hours	37	10.16	6.768	
Calorie received				
Less than requirement	32	6.47	4.90	0.006
Adequate or more than requirement	100	9.97	8.90	

DISCUSSION

Most of the patients (75.8%) received adequate caloric consumption. This is consistent in a study conducted in a ICU at a private tertiary care hospital in Philippines [10]. The authors found that calorie intake was achieved at day three after starting enteral feeding. The majority of the participants in this study were above 50 years of old with the mean age of 53.4 which support the findings of Chittawatanarat et al. [11]. This finding highlights the importance of extra nutritional support for older people when being admitted to hospital due to malnutrition [12].

This study also yielded some information on the ethnicity of the patients which reflects the composition of the population in terms of ethnicity. The majority of patients who received enteral feeding were Malays (52%) followed by Chinese (19.7%), Indians (18.2%) and others races (9.9%) including one aborigine and 12 foreigners. According to Yip et al., [8] Malays, mostly, choose traditional treatment in the early stage and they visit the hospital in critical poor nutrition condition. As a result, more intervention is needed compared to the other ethnic groups. They also reported that 40% of Malay patients went to hospitals only when the diseases such cancer was at the critical stage.

The majority of the patients (72%) had received early feeding within 48 hours of admission to ICU which corresponds with Malaysian Society of Anaesthesiologist [9] guidelines in the initiation of enteral feeding. Clinical stability and poor nutritional status are the factors which interrupt early initiation of enteral feeding [9, 13]. Findings of previous studies also unanimously agree that initiation of enteral feeding within 48 hours after injury or acute illness should be provided for patients requiring intensive care [14].

Provision of early feeding also affects patients' calorie intake as most of the patients achieved their caloric requirements three days after the commencement of their enteral feeding [15]. The findings of previous studies have also provided evidence on the effect of early nutrition support on the duration of patients' intensive care [16]. However, the findings of studies on the effect of early nutritional support on the duration of stay have been far from conclusive because patients who received early feeding had the longer length of stay [17, 18]. It appears that the existence of such variation may be due to different factors that include, but they are not limited to different study populations, types and severity of diseases, and age of patients.

In the context of this study, Enercal (n=57, 43.2 %,) and Glucerna (n=43, 32.5%) which are the polymeric types of formula were commonly used to provide nutritional support to patients with enteral feeding in ICU. Patients' tolerance to formula feeding has an influence on whether they can achieve the caloric requirement in the targeted duration of time. Therefore, enteral feeding should be given based on the guideline while deciding on the appropriate feeding formula for patients to avoid any harm [9]. As a result, establishing guidelines and provision of knowledge on appropriate nutrition are important [19]. However, different studies might yield different results as to appropriate formula for patients in ICUs [20]. In this study patients, who received enteral nutritional support following Nephro formula, were scarce (7.6%) because Nephro formula is suitable for patients with renal diseases since the caloric content is higher than the contents of fluid which is 2kcal/ml [21]. At the same time, it is more concentrated and patients need only half the volume to achieve adequate calories. Still this formula can lead to higher incidences of diarrhea and hyperglycemia.

A majority of the patients used continuous feeding on the first and second days, (68.2%) and (60.6%) respectively, while the choice of intermittent bolus feeding was increased on the third (55.5%) and fourth day (66.7%). Previous studies in the literature have provided support on the use of intermittent feeding on the grounds that patients reach adequacy of calorie intake earlier that continuous feeding [22, 23]. In contrast, continuous feeding is mostly used in acute phases; therefore there may be a delay in receiving adequate calories.

The statement is supported by Chen et al. [22] whereby most of the patients had used continuous feeding during the acute stage to increase intragastric pH that promotes bacteria growth and helps with diarrhea or prevention of dumping in some patients. However, in longer term, continuous feeding will have adverse effect such as aspiration pneumonia especially at night

The majority of patients in this study 75.8 % (n=100) received adequate caloric intake within five days of enteral feeding which support other studies which found that patients with enteral nutrition received caloric requirement after three days of enteral feeding [11, 24, 25]. However, many interruptions including but not limited to high gastric residual, vomiting, and extubation compounded with the severity of the diseases and patients' conditions may interfere with achieving of calorie requirement [26, 27].

Findings of this study also indicated that problems encountered during enteral feeding cause intolerance to enteral nutritional support and as a result affect the adequacy of calorie intake for the patient. High aspiration volume 200ml or more on day one for 9.8% of the patients was the major problem encountered during enteral feeding for this study. However, the aspiration was decreasing to 3.8% volume on day five. Gastrointestinal dysfunction causing intolerance to enteral nutrition is a common reason for not starting, or discontinuing feedings leading to inadequacy of caloric intake [5]. Hyperglycemia was found as another major problem encountered during enteral feeding with 48.3% (n=49) of patients having hyperglycemia during enteral feeding. This finding is in accordance with that hyperglycemia and insulin resistance were common in critically-ill patients with enteral feeding, even if they have no existing diabetes.

The current study found that there was a association between the adequacies of calorie intake received by patients and the patients' length of stay. According to Roberts et al. [16] the adequacy of calorie intake is important to ICU patients because it will reduce the length of stay and infections. In contrast, Higgins et al. [2] found that the adequacy of calorie intake was not associated with the length of stays among critically-ill ICU patients. They had discovered that other factors such as severity of illnesses had an influence on the outcome of the patients. Other studies discovered that the adequacy of calorie intake is important to improve the patients' outcome shortenings the need on IPPV support, to reduce infections, lengths of stay, and health care cost [28].

CONCLUSION

The majority of the critically-ill patients in this general ICU have received adequate calorie intake via enteral feeding but the number of patients received adequate calorie intake was still insufficient. The most common problems occurred during enteral feeding were hyperglycemia and omission of the feeding. Patients who received early enteral feeding and intermittent bolus within 48 hours of admission achieved adequate caloric intake compared to patients who started late and received continuous feeding. The length of stay was not influenced by early initiation of enteral feeding. However, there was an association between patients' length of stay and adequacy of caloric intake. The findings of this study provided invaluable insights to health care providers regarding early time and adequacy of caloric intake among patients in general ICUs. These findings heighten the awareness of health care providers to the importance of maintaining adequate caloric intake for their patients.

ACKNOWLEDGEMENTS

The authors would like to express special thanks to Director General of Health Malaysia for permission to publish this paper.

REFERENCES

[1] Alberda, C., et al., *The relationship between nutritional intake and clinical outcomes in critically ill patients: Results of an international multicenter observational study.* Intensive Care Medicine, 2009. 35(10): p. 1728-1737.

[2] Higgins, P. A., et al., *Assessing nutritional status in chronically critically ill adult patients.* American Journal of Critical Care, 2006. 15(2): p. 166-176.

[3] Abdul Manaf, Z., et al., *Delivery of enteral nutrition for critically ill children.* Nutrition & Dietetics, 2013. 70(2): p. 120-125.

[4] Zamberlan, P., et al., *Nutrition therapy in a pediatric intensive care unit: Indications, monitoring, and complications* Journal of Parenteral and Enteral Nutrition (JPEN), 2011. 35: p. 523-9.

[5] Singer, P., et al., *The truth about nutrition in the ICU.* Intensive Care Medicine, 2014. 40(2): p. 252.

[6] Hoffer, L. J., et al., *Why critically ill patients are protein deprived.* Journal of Parenteral and Enteral Nutrition, 2013: p. 0148607113478192.

[7] Kyle, U. G., et al., *Hospitalized mechanically ventilated patients are at higher risk of enteral underfeeding than non-ventilated patients.* Clinical Nutrition, 2006. 25(5): p. 727-735.

[8] Yip, C., et al., *Review of breast cancer research in Malaysia.* Med J Malaysia, 2014. 69: p. 8-12.

[9] Malaysian Society of Anaesthesiologist *Enteral feeding*. ICU Management Protocol No. 4, 2012.

[10] Umali, M. N., et al., *Recommended and actual calorie intake of intensive care unit patients in a private tertiary care hospital in the Philippines.* Nutrition, 2006. 22(4): p. 345-349.

[11] Chittawatanarat, K., et al., *Enteral feeding in surgical critically ill patients.* Thai Journal of Surgery, 2006. 27(1).

[12] Adams, N. E., et al., *Recognition by medical and nursing professionals of malnutrition and risk of malnutrition in elderly hospitalised patients.* Nutrition & Dietetics, 2008. 65(2): p. 144-150.

[13] Mehta, N. M., *Approach to enteral feeding in the PICU.* Nutr Clin Pract 2009. 24: p. 377-87.

[14] Scurlock, C., et al., *Early nutrition support in the intensive care unit: A US perspective.* Current Opinion in Clinical Nutrition & Metabolic Care, 2008. 11(2): p. 152-155.

[15] Doig, G. S., et al., *Mortality in Intensive Care and the Role of Enteral Nutrition in Trauma Patients.* Diet and Nutrition in Critical Care, 2015: p. 1333-1338.

[16] Roberts, S. R., et al., *Nutrition support in the intensive care unit adequacy, timeliness, and outcomes.* Critical Care Nurse, 2003. 23(6): p. 49-57.

[17] Martin, C. M., et al., *Multicentre, cluster-randomized clinical trial of algorithms for critical-care enteral and parenteral therapy.* Canadian Medical Association Journal, 2004. 170(2): p. 197-204.

[18] Ibrahim, E. H., et al., *Early versus late enteral feeding of mechanically ventilated patients: Results of a clinical trial.* Journal of Parenteral and Enteral nutrition, 2002. 26(3): p. 174-181.

[19] Karim, S. A., et al., *What do healthcare providers know about nutrition support? A survey of the knowledge, attitudes, and practice of pharmacists and doctors toward nutrition support in Malaysia.* Journal of Parenteral and Enteral Nutrition, 2014: p. 1-8.

[20] Tiengou, L.-E., et al., *Semi-elemental formula or polymeric formula: Is there a better choice for enteral nutrition in acute pancreatitis?* Journal of Parenteral and Enteral Nutrition, 2006. 30(1): p. 1-5.

[21] Cano, N., et al., *ESPEN guidelines on enteral nutrition: Adult renal failure.* Clinical Nutrition, 2006. 25(2): p. 295-310.

[22] Chen, Y.-C., et al., *The effect of intermittent nasogastric feeding on preventing aspiration pneumonia in ventilated critically ill patients.* Journal of Nursing Research, 2006. 14(3): p. 167-180.

[23] Hacker, R., et al., *Prospective randomized control trial of intermittent versus continuous gastric feeds for critically ill trauma patients.* Nutrition in Clinical Practice, 2008. 23(5): p. 564-565.

[24] Grau, T., et al., *Liver dysfunction associated with artificial nutrition in critically ill patients.* Critical Care, 2007. 11(1): p. R10.

[25] Binnekade, J., et al., *Daily enteral feeding practice on the ICU: Attainment of goals and interfering factors.* Critical Care, 2005. 9(3): p. R218-25.

[26] O'Meara, D., et al., *Evaluation of delivery of enteral nutrition in critically ill patients receiving mechanical ventilation.* American Journal of Critical Care, 2008. 17(1): p. 53-61.

[27] Nguyen, N. Q., et al., *The impact of admission diagnosis on gastric emptying in critically ill patients.* Critical Care, 2007. 11(1): p. R16.

[28] Reid, C., *Frequency of under-and overfeeding in mechanically ventilated ICU patients: Causes and possible consequences.* Journal of Human Nutrition and Dietetics, 2006. 19(1): p. 13-22.

Second International Conference on Science, Engineering & Environment,
Osaka City, Japan, Nov.21-23, 2016, ISBN: 978-4-9905958-7-6 C3051

ROLE OF PUBLIC PARTICIPAITON IN ENVIRONMENTAL IMPACT ASSESSENT IN THAILAND

Chutarat Chompunth
National Institute of Development Administration, Thailand

ABSTRACT

An integration of public participation in Environmental Impact Assessment (EIA) is significant in terms of its implication for sound decision and a sustainability of development projects. Accordingly, the Thai EIA system provides a public participation process for stakeholders in an assessment and review of the EIA study process. There are a number of different participatory techniques to facilitate public participation. However, in Thailand traditional public participation methods like public hearing is preferred. The public hearing process in the Thai context, stakeholders including the project proponents and the opponents are brought together in a forum to express their view points and recommendations for the proposed projects in order to influence the decision-making process. Frequently, this process leads to violent conflict among stakeholders. This study aimed at trying to close the gap between regulators and civil communities with respect to public participation in the Thai EIA system. A case study approach was applied for this study. The study revealed that appropriate public participation is essential and may lead to enormous benefits for the proponents and stakeholders. Where public participation is ignored and ineffective conducted, environmental conflicts and problems may be created for project implementation and sustainability.

Keywords: Public Participation, Environmental Conflict, EIA, Power Plant, Thailand

INTRODUCTION

Moving from an agricultural base to more industrialization, Thailand is now facing many environmental problems and conflicts. (Chaisomphob *et al*, 2004; Chompunth, 2013). In particular, the impacts from the coal-fired power plant were serious. Either the construction period or the operation period, the communities surrounding the power plant are directly impacted from the pollutants. The cumulative impacts from the power plants were also critical to local communities. In the past, many coal-fired power plant projects had been implemented by the authorities without appropriate public involvement or public participation. In particular, a previous coal-fired power plant, Mae Moa, in the North of Thailand has a bad reputation for its environmental impacts. These rules will rely upon proven and widely available emissions control technologies to level that all power plants follow the same systems (Chesoh, 2011; Chompunth & Chomphan, 2012).

In Thailand, many projects were cancelled or delayed by the local people or the protestors. These projects have faced the problem of public protest due to their impacts and the NIMBY syndrome (Not in My Back Yard) resulting in more expenditures and time delay (Chompunth, 2013). This might because the public participation process has not been taken appropriately in the development of these projects until the conflicts among stakeholders in particular the government/project proponent and the local community occurred (Chompunth, 2013; Creighton, 2005). To solve the problem, the participation in the planning and decision-making process of the project should be carried out in a proper manner. Presently, Thai people demand greater participation in the decision-making processes concerning highly controversial issues of development activities, in particular the sitting of coal-fired power plants. They recognize that public participation should play a substantial role in environmental development projects and the Environmental Impact Assessment (EIA) in order to resolve environmental conflict.

SIGNIFICANCE OF THE STUDY

Immediately, Thailand needs an effective approach to deal with air pollution problem; particularly, air pollutants from coal-fired power plants. However, Thailand has a very limited expert and specialists; this is then still an on-going problem that still needs to be solved. Another problem is that the authorities usually stand by at central government center. Presently, the government recognizes the importance of public participation to play a substantial role in the Environmental Impact Assessment (EIA) of coal-fired power plants in order to prevent their severe impact. Thai citizens also demand greater participation in the decision-making process concerning highly environmental problems (Chompunth, 2013).

To deal with environmental conflict issue, Thai

government encourages the public to involve in preserving and conserving the environment though many mechanisms, in particular legal framework. Thus, public participation in EIA process is expected to be an effective tool to solve these environment impacts and conflicts from the power plants. This study aims to identify the problems of enhancing public participation in solving environmental conflict in EIA process and to investigate strong and weak points of the EIA system in Thailand. A case study of the Khao Hin Son Coal-fired Power Plant Project was studied and analyzed. Finally, recommendations on how to enhance public participation in environmental conflict resolution in the Thai context are presented.

METHODOLOGY

A case study approach Controversy of the Case Study: The Khao Hin Son Coal-fired Power Plant Project

In this study, qualitative approach was applied to examine the current state of EIA of power plant projects and adequacy of public participation in the EIA system. The case study approach is chosen as a key research strategy to explain and conduct an in-depth study of a public participation process in the EIA system in Thailand. The Khao Hin Son Coal-fired power plant project is selected as an example of an inappropriate public participation process.

In-depth interviews and documental reviews were employed to collect data. Stakeholders who or played important roles in the public participation process were identified and interviewed. In this study, key informants were people who have specific knowledge and experience about the studied issue, a public participation process; including, direct impacted people, government organizations, project proponents, NGOs, and academics and experts. The total key informants for this study was 39 participants.

Additionally, snowball sampling was used throughout the data collection process to make interviews with key affected people and stakeholders combined with other tactics as a way to contribute a latent network of interviewees. Initially identified participants were asked to recommend other persons who also played an important role in the participation process of the project and met the selection criteria.

The secondary data were collected from relevant source including publications, substantive document on public participation, government publications, conference proceedings, research, books and journals.

RESULTS AND DISCUSSION

Lesson from the Case Study: The Khao Hin Son Coal-fired Power Plant Project

A coal-fired power plant is mentioned as an important sources to particulate harmful pollutions. The Khao Hin Son coal-fired power plant is one of a large-scale project in Thailand which having significant environmental impacts and conflicts with a high level of controversy among stakeholders. According, the Khao Hin Son coal-fired power plant is appropriate to investigate how, in Thai experience, a public participation program in managing environmental conflict did not succeed. Accordingly, the Khao Hin Son coal-fired power plant is suitable to be examined how public participation process in managing environmental conflicts did not succeed since the project is having conflicts with a high level of controversy among stakeholders.

In this case, the affected villagers claimed that hazardous air pollutions emitted by coal-fired power plant could influence environmental quality and health on local, regional, and continental scales. One local resident claimed that “Their air pollutions blow across state lines into states thousands of miles away”. The protesters said they did not want the power plant in their communities as they feared environmental impacts, particularly air and water pollution. One villager claimed that, “if the coal-fired power plant is built, it may result in the acid rain that will harm crop growing and cause heavy metal pollution in the air and food chains”.

The villagers protesting against the construction of a coal-fired power plant in Chachoengsao called for a revised environmental impact assessment report of the project. They claimed that the existing report was conducted without proper public participation. The authority, the Office of Natural Resource and Environmental Policy and Planning (ONEP), approved the EIA study even though the company had not held public hearings or conducted a health impact assessment study as required by law, Section 67 of the 2007 constitution. One project opponent said that "The project's EIA has been done without appropriate public participation". A coordinator of a network monitoring the impact of the power plant also stated that "This means the EIA study does not cover all well-rounded information”. However, one officer claimed that; “the office had considered the EIA report cautiously and the study complied with all legal requirements”.

The protestors also believed that the power plant would cause massive environmental and social impacts. Importantly, the affected people did not trust the environmental monitoring and mitigation program of the project and still opposed the project.

The local communities did not believe that the project's monitoring programs could control any impacts to the environment from its operation. One villager claimed that; "the government and the project owner were not honestly attempting to solve their problems and did not pay attention to the public's concerns". Thus, the Khao Hin Son power plant project was delayed and conflicts among stakeholders still exist. Similarly finding is found in the study of Tippett et al. (2005). The study found that mistrust has severed impacts to public participation in the EIA process. A lack of trust among stakeholders could hinder effective public participation and lead to conflict among stakeholders.

Public Participation in EIA in Thailand

The EIA process is an essential component of environmental legislation in many countries including Thailand (Harding, 1998). In Thailand, public participation is required to be held in three main stages of the EIA process including screening, scoping, and EIA review. However, public participation as part of the site evaluation and selection processes, which are arguably sub-stages, is not compulsory and this potentially leads to conflict among stakeholders. This might be because project sitting has always been a key issue that created problems for project implementation in Thailand. Indeed, there were several factors that contributed to the conflicts, but the fact that people who lived near the proposed site did not know or have a chance to participate at the beginning stage of the project implementation, in particular the site selection process, is viewed as a key factor that caused the problems (Nuntavarn & Vajanapoom, 2011). Indeed, public participation must be integrated in all steps.

Although the EIA process was established more than 30 years in Thailand, it is still controversial; many developers regard EIA as an undesirable barrier, some seek to avoid the EIA process, and also some government administrators in charge of EIA view the process as a heavy burden. Moreover, political and financial support for EIA study is low in many developing countries, and environmental agencies are practically powerless compared with economic development agencies. Two key reasons for poor quality of EIA reports are lack of qualified environmental experts, and insufficient time and money (Ogunlana et al., 2001), and Thailand is no exclusion in this regard.

Many scholars have commented on ineffective public participation process in Thailand on environmental issues and, particularly in the EIA process (Chompunth, 2013; Ogunlana et al., 2001). The draft EIA does not have to be released to the public, public comments are not asked for, and, critically, the government does not have to officially respond to public concerns. The EIA review is made by the authority in charge of the EIA approval only. Local expert panels and local administrative organization officers are not authorized to take part in the process. Usually after the EIA report is sent to the authority for review, the public could not get access to it. Moreover, the EIA reviewers themselves are not experts in all areas, they work under pressures of time limits.

Clearly, public participation in the EIA process is crucial, particularly in Thailand. Weak public participation and unsatisfied communication produce many limitations, both legally and in practice, and result in limited knowledge and uneven distribution the project information to the local community. Finally, then the local communities distrust the EIA report and violent protests have been happened, like in this case.

Public participation as a conflict management approach

In Thailand, public participation is a key component of the government's administration. The requirements for public participation in Environmental Impact Assessment system have been promoted noticeably by the 2007 Thai Constitution. Public participation is also granted The Official Information Act, and many clauses in the environmental legislation. However, the current status of public participation in environmental impact assessment in Thailand has not been effectively implemented. Thai government prefers a top-down approach to handle environmental conflicts and this lead. There are many limitations to these laws, both legally and in practice. Within these laws and regulations, the public right to information is often subject to the judgment of the government officials in charge. In this case, it was found that public participation of Thai citizens did not comply with a real concept of public participation; direct impacted people in the project did not have an opportunity to be informed and express their views from the very beginning and their concerns were not appropriately influence the decision.

From the case study, it could be seen that the implementation of public participation in Thailand is now reaching an impasse. Many stakeholders, in particular the impacted communities, were reluctant to participate in many participatory forums provided by the government or the developer. Many public hearings or other activities were ignored by affected groups. The protestors did not accept them because they believed that these activities, particularly public hearing should have been processed before the decision-making process was completed. The Khao Hin Son coal-fired power plant is obviously demonstrated for the problem of lack of appropriate public participation in the right stage. Moreover,

many mega development projects in Thailand cause conflict because the location of the proposed project had already been selected. In this case, land was already selected for proposed project without informing local people. There is no alternative for the public. Only the chosen location of the project is introduced and presented to the public during the hearing forum.

Public participation in the EIA process is important. Without the public being participated there is too much of a tendency to hide things, which can eventually lead to corruption and conflict among stakeholders (Persson, 2006). Keeping the EIA study (or related documents) secret completely defeats the purpose of the EIA system. This can especially be a problem where the local communities are adversely impacted. Particularly in this case study, violent protests have been set up. One academic suggested that, "to deal with this issue, the developers should provide effective mechanism such as call centers or hotlines to respond to the public complaints and concerns. Thus, the developer could take prompt action to alleviate the problem".

Although public participation process is possible to express a government's willingness to share all perspective with stakeholders, in many cases in Thailand, public participation has been simply employed to ratify a decision that had already been made (Chompunth & Chomphan, 2012). Furthermore, despite public participation arrangements, to accept these programs does not mean that the final outcomes of participation processes will be accepted and influenced the authority's final decision.

A significant problem is that when opportunities to be involved are distorted and blocked by political structures and processes, affected people may employ direct action to increase their level of participation and power (Thanh & Lefevre, 2001). In Thailand, this direct action is often resulted in direct violence. The foregoing consideration and finding are fully supported by this case study. Similarly, Stampe's (2009) and Vantanen and Marttunen's (2005) studies found that trust was closely related to openness and transparency. If trust is lacking, the public then are difficult to see the decision is transparent and led to protest and antagonism among stakeholders. When the stakeholders did not trust each other, conflict was likely to be more aggressive.

Importantly, in Thailand, the public has a limited role in the monitoring process, including either the constructing or operating stages. Indeed, the project proponents should be provided assurances over the running and maintenance of the power plant in order to increase the public's confidence that the project is of good quality with social, health and environmental soundness. Otherwise, it will be difficult to get support from the public. This is because the participation of local people and NGOs in monitoring the operational impacts of a project can lead to the early identification of environmental and social problems, and can increase public acceptance. One academic recommended that "Most importantly, this participation process must be initiated before any decision has been made. It must be continued throughout the project to prevent failure of the power plant's operation".

CONCLUSION

Enforcement of public participation in the EIA requirements is a compulsion. Public participation is supposed as a sensible strategy for conflict management in a developing country, like Thailand. The public participation process should be started in the earliest stage of project planning to enhance the trust and create good relationship in cooperation between the project owner and local people. Public participation also can prevent argument and conflict between the authority/project proponents and the affected communities and can reach a higher level of support for the decisions during all phases the project's development including planning, construction, and implementation.

Having an appropriate review and approve a project's EIA report could also help reduce the conflicts among stakeholders. However, mitigation of industrial pollutions, particularly from the coal-fired power plant, is not only the responsibility of the developers, but it also involves the diverse stakeholders including the government, experts, local communities and NGOs to participate in brainstorming of finding the desirable and accepted alternatives for pollution abatement. Effective monitoring should be based on constant public participation. The authority and the developer need to get a variety of viewpoints from the affected citizens, particularly different ideas how to improve environmental quality, suggestions and comments. It could be summed that effective public participation can lead to a desirable and acceptable outcome, resolve conflicts, establish cooperation and collaboration among stakeholders, and improve the process and outcome of the environmental decision-making.

It could be seen that the public participation process was not yet appropriately established in the Thai context. Consequently, Thai people demand greater participation in the decision-making processes concerning highly controversial issues. They recognize that public participation should play a significant role in environmental conflict management. Thus, there is an urgent need to create a sound approach and conditions of effective public participation which can assist in resolving environmental problems and conflicts.

REFERENCES

[1] Chaisomphob, T., J. Sanguanmanasak and K. Swangjang. (2004). Role of Public Participation in Planning Power Plant Project in Thailand, Thammasat International 9(1), pp. 67-73.

[2] Chesoh, S. (2011). Environmental Impact Assessment of Power Development Project: Lessons from Thailand Experiences, Asian Social Science, 7(9), pp 119-123.

[3] Chompunth, C. and S. Chomphan. (2012). Evaluating Public Participation Process in Development Projects in Thailand: A Case Study of the Khao Hin Son Power Plant Project, American Journal of Applied Science, 9(3), pp. 865-873.

[4] Chompunth, C. (2013). Public Participation in Environmental Management in Constitutional and Legal Frameworks, American Journal of Applied Science, 10 (1), pp. 73-80.

[5] Creighton, J. L. (2005). The Public Participation Handbook: Making Better Decisions Through Citizen Involvement, San Francisco, Jossey Bass.

[6] Tippett, J., B. Searle, C. Pahl-Wostl and Y. Rees. (2005). Social Learning in Public Participation in River Basin Management: Early Findings from Harmoni COP European Case Studies, Environmental Science and Policy, 8(3), pp. 287-299.

[7] Harding, R. (1998). Environmental Decision-Making: the Role of Scientists, Engineers and the Public: The Role of Scientists Engineers and the Public, New South Wales, Federation Press.

[8] Nuntavarn, V. V. and Vajanapoom, N. (2011). Health Impact from Air Pollution in Thailand: Current and Future Challenges, Environmental Health Perspective, 119(5), pp. 197–198.

[9] Ogunlana, S. O., T. Yotsinsak and S. Yisa. (2001). An Assessment of People's Satisfaction with the Public Hearing on the Yadana Natural Gas Pipeline Project, Environmental Monitoring and Assessment, 72(2), pp. 207-225.

[10] Persson, J. (2006). Theoretical Reflections on the Connection between Environmental Assessment Methods and Conflict, Environmental Impact Assessment Review, 26(7), pp. 605-613.

[11] Thanh, B. D. and Lefevre T.(2001). Assessing Health Benefits of Controlling Air Pollution from Power Generation: the Case of a Lignite-fired Power Plant in Thailand. Environmental Management, 27(2), pp. 303-17.

[12] Stampe, J.W. (2009). Lessons Learned from Environmental Impact Assessments: A Look at Two Widely Different Approaches – The USA and Thailand, The Journal of Transdisciplinary Environmental Studies, 8(1), pp. 1-7.

[13] Vantanen, A. and M. Marttunen. (2005). Public Involvement in Multi-Objective Water Level Regulation Development Projects-Evaluating the Applicability of Public Involvement Methods, Environmental Impact Assessment Review, 25(3), pp. 281-304.

Second International Conference on Science, Engineering & Environment,
Osaka City, Japan, Nov.21-23, 2016, ISBN: 978-4-9905958-7-6 C3051

MOMENT CHARACTERISTICS OF SOLUTE MACRODISPERSION PHENOMENA IN HETEROGENEOUS AQUIFERS

Yasuteru Kobi[1], Kazuya Inoue[1] and Tsutomu Tanaka[1]

[1]Graduate School of Agricultural Science, Kobe University, Japan

ABSTRACT

Solute dispersion is one of the key factors in predicting the subsurface movement and spreading of a contaminant plume. In this study, conservative solute transport simulations were conducted in two-dimensional heterogeneous aquifers to assess the transitional development of moment characteristics up to the fourth order associated with macrodispersion phenomena. The aquifer system investigated here relied on the hydrogeologic data in the southwest of the Netherlands and was modeled as the heterogeneous aquifer. Three types of physical heterogeneities in subsurface materials were represented as randomly correlated hydraulic conductivity fields, which were geostatistically generated under the isotropic assumption. Random walk particle tracking linked with temporal moment approach, which is based on observed breakthrough curves at several predefined control planes, demonstrated asymptotic variations of the second and fourth moments. Results also showed that the degree of the physical heterogeneity affected the degree of the increase of each moment, indicating that this plume behavior reflects the hydraulic conductivity distribution on which the evolution of plume is considerably dependent.

Keywords: Macrodispersion, Moment Characteristics, Random Walk Particle Tracking, Heterogeneous Aquifers

INTRODUCTION

The behavior of groundwater contaminants such as salts and organic compounds is difficult to predict, is described as a complex function of space and time and can be viewed as a spreading of particle crowd [1]. Inherently, the position of the center of particle crowd can be reliably computed because it depends on the mean seepage velocity of groundwater flow, which is observed in a field. On the other hand, the degree of the elongation of the particle crowd around the central position along each orthogonal axis is a more elusive variable due to dispersion processes, especially in heterogeneous aquifers.

In most groundwater aquifers, heterogeneous nature of hydraulic conductivity provides a wide variety of solute pathways at different velocities and governs the fate of solute transport. On a macroscopic scale, spatial distribution of hydraulic conductivity provides enhanced spreading of solute transport, which is a phenomenon referred to as macrodispersion [2]. As for the future prediction of contamination, some remediation or cleanup strategies of contaminated groundwater and the framework of risk assessment associated with human health, hydrogeologic characterization in terms of the degree of the spatial variation in an aquifer is one of key issues [3].

Some of the efforts made to understand better macrodispersion phenomena have been conducted through theoretical, experimental and numerical studies [4]-[8]. Also, several mathematical models for sorbing solute transport in heterogeneous aquifers associated with the retardation factor or the distribution coefficient have been developed. Especially, a negative correlation relation between the hydraulic conductivity and the distribution coefficient is a representative model expressing solute spreading under the sorptive condition [9]-[11]. However, macrodispersion and relevant statistical moments do not provide information about the actual distribution of particle crowd. Ideally, the Gaussian or non-Gaussian features of the growth of spreading should be assessed for a practical use of the findings. This paper attempts to provide additional evidence by performing numerical experiments under controlled conditions.

The objective of this study is to assess the transitional development of moment characteristics up to the fourth order associated with macrodispersion phenomena in conservative solute transport simulations. Random walk particle tracking technique linked with temporal moment approach is conducted in two-dimensional heterogeneous aquifers based on the hydrogeologic data in the Netherlands. Numerical tracer transport experiments are conducted in these aquifers under natural-gradient flow conditions for identifying the four statistical moments in terms of temporal moments of particle arrival times at control planes. Even with hypothetical sources of contamination, the modeling studies shed some light on the complex

pathways contaminates may follow in subsurface systems.

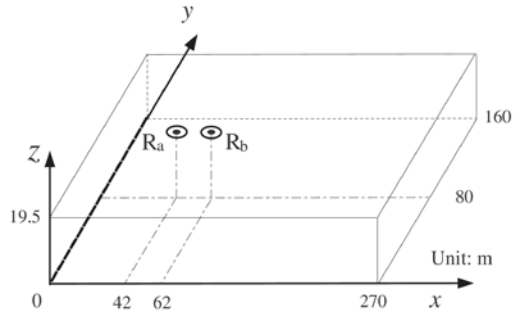

Fig. 1 Model domain used in this study.

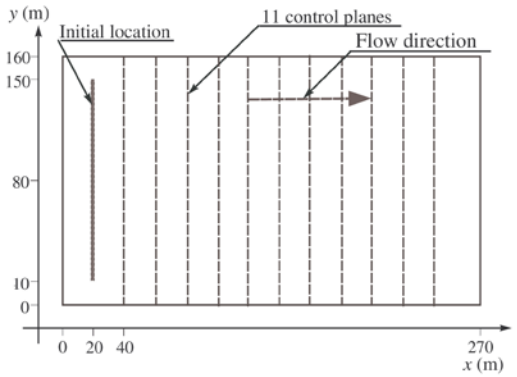

Fig. 2 Sketch of solute transport simulations showing the initial location of particles and the control planes.

DESIGN OF COMPUTATIONAL INVESTIGATIONS

Site Description

The disposal site of concern is located in the dunes near the Hague in the Netherlands. In 1984 a tracer test was conducted to mainly investigate the feasibility of artificial recharge by means of infiltration wells [12]. Solute transport simulations consider a three-dimensional confined aquifer with uniform flow in the *x*-direction driven by a mean hydraulic gradient equal to 0.005. The size of the flow domain extends 270 m in the *x*-direction, 160 m in the *y*-direction and 19.5 m in the *z*-direction as shown Fig. 1. The domain size of interest both in *x* and *y* directions are relatively larger than that in the *z*-direction. Therefore, this study site was treated as a horizontally two-dimensional aquifer as shown Fig. 2.

The hydraulic conductivity data employed in this study are based on the two vertical cores whose locations are shown in Fig.2. Hydraulic conductivity data derived by granular analysis of soil samples are given in Fig. 3 and also the porosity of the aquifer was assumed to be 0.35. In addition, the hydraulic conductivity and the degree of heterogeneity of the

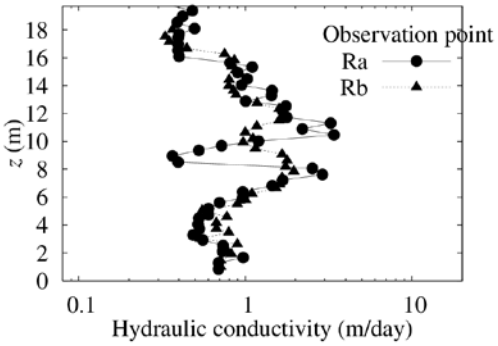

Fig. 3 Variation of hydraulic conductivity derived from granular analysis.

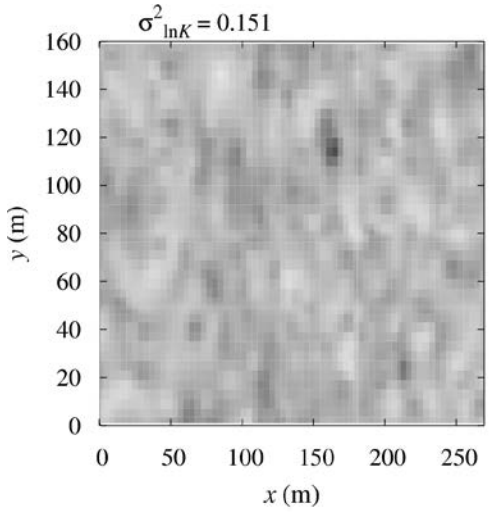

Fig. 4 A representative realization of ln*K* field with the degree of heterogeneity of 0.151.

aquifer are 0.821 m/day and 0.151, respectively.

A two-dimensional, log-conductivity model with an isotropic exponential covariance function was used to generate 30 realizations of the hydraulic conductivity field using the block kriging with the correlation length of 13 m [13]. As a semi-variogram model, exponential model without the anisotropy was utilized. A representative realization showing the physical heterogeneity in terms of the hydraulic conductivity is exhibited in Fig. 4. In addition to the heterogeneity of 0.151, 0.5 and 1.0 of the geometrical variance of hydraulic conductivity were employed as relatively higher heterogeneity and relevant 30 realizations were generated in the same manner.

Flow and Transport Models

For solute transport simulations, a saturated

velocity field within a heterogeneous porous medium must initially be developed [13],[14].

$$\sum_{i=1}^{2}\frac{\partial}{\partial x_i}\left(K_i\frac{\partial h}{\partial x_i}\right)=0 \quad (1)$$

where *h* is the hydraulic head at vector location, K_i is the isotropic hydraulic conductivity and x_i is the coordinate in each direction. Steady fluid flow in this system is described by:

$$v_i=-\sum_{i=1}^{2}\frac{K_i}{n_e}\frac{\partial h}{\partial x_i} \quad (2)$$

where v_i is the pore velocity and n_e is the porosity. The boundary condition of the first type was specified on two sides faces intersecting the plane with x = 0 m and x = 270 m, while other sides were treated as no-flow boundaries. These boundary conditions provided the establishment of the mean hydraulic gradient of 0.005 and are linked with the finite element method for computing spatial distributions of the hydraulic head and seepage velocity.

Random Walk Particle Tracking (RWPT)

Random walk particle tracking (RWPT) simulates solute transport by partitioning the solute mass into a large number of representative particles. The evolution in time of a particle is driven by a drift term that relates to the advective movement and a superposed Brownian motion responsible for dispersion [15], [16].

In RWPT, each particle displacement can be expressed using Ito interpretation of Langevin equation:

$$X_{p,i}(t+\Delta t)=\left(v_i\left(\vec{X}_p(t)\right)+\sum_{j=1}^{2}\frac{\partial D_{ij}}{\partial x_j}\left(\vec{X}_p(t)\right)\right)\Delta t + X_{p,i}(t)+\sum_{j=1}^{2}B_{ij}\left(\vec{X}_p(t)\right)\Xi_j\sqrt{\Delta t},\quad i=1,2 \quad (3)$$

where $X_{p,i}(t)$ is the *i*th component of the particle location at time *t*, Δt is the time increment, Ξ_j is the vector which contains three normally distributed random numbers with zero mean and unit variance. Also D_{ij} is the dispersion coefficient tensor, usually defined as [14]:

$$D_{ij}=\left(\alpha_T|v|+D_d\right)I_{ij}+\left(\alpha_L-\alpha_T\right)\frac{v_i v_j}{|v|},\quad i=1,2 \quad (4)$$

where α_L and α_T is the longitudinal and transverse dispersivity in a microscopic level, respectively, D_d is the molecular diffusion coefficient, and $|v|$ is the magnitude of the velocity vector. In addition, B_{ij} is the displacement matrix and is expressed as:

$$B_{ij}=\begin{pmatrix}\frac{v_1}{|v|}\sqrt{\frac{2(\alpha_L|v|+D_d)}{R}} & -\frac{v_2}{\sqrt{v_1^2+v_2^2}}\sqrt{\frac{2(\alpha_T|v|+D_d)}{R}}\\ \frac{v_2}{|v|}\sqrt{\frac{2(\alpha_L|v|+D_d)}{R}} & \frac{v_1}{\sqrt{v_1^2+v_2^2}}\sqrt{\frac{2(\alpha_T|v|+D_d)}{R}}\end{pmatrix} \quad (5)$$

where *R* is the retardation factor.

Evaluation of Dispersivities from Temporal Moments

Temporal moments associated with observed breakthrough curves (BTCs) at several predefined control planes are able to be computed using a Lagrangian framework in order to statistically characterize the solute transport process. Monitoring the first-passage time of particles passing through control planes allows for the estimation of BTCs and subsequent temporal moments without having to evaluate the actual shape of the BTCs [17]. The *n*th absolute temporal moment can be calculated as the expected value of the arrival time of a particle at the control plane to the *n*th power,

$$M_{n,T}=\frac{1}{N_r}\sum_{r=1}^{N_r}\left(\sum_{k=1}^{NP_s}m_k^p\left(t_k^p(\xi_P)\right)^n\Big/\sum_{k=1}^{NP_s}m_p^k\right) \quad (6)$$

where, $M_{n,T}$ is the *n*th normalized absolute temporal moment, m_p^k is the mass particle assigned to *k*th particle, t_p^k is the first arrival passage time of the *k*th particle, NP_s is the total number of particles arrived at the control plane located at ξ_p in the x direction and N_r is the total number of realizations. Central temporal moments of the averaged BTC can then be calculated using the relationship between absolute and central moments:

Table 1 Parameters used in RWPT

Parameter	Description	
N_P (-)	Number of particles	20000
Δt (day)	Time step	1
α_L (m)	Longitudinal dispersivity	0.02
α_{TH} (m)	Transverse dispersivity	0.005
R (-)	Retardation factor	1.0
n_e (-)	Porosity	0.35
λ (m)	Correlation length	13

$$\Lambda_{n,T} = \sum_{r=0}^{n} \binom{n}{r} M_{n-r,T}(\xi_1)\left(-M_{n,T}(\xi_1)\right)^r \qquad (7)$$

where $\Lambda_{n,T}$ is the *n*th normalized central temporal moment.

The third and the fourth central temporal moments can also be expressed by means of the coefficients of skewness and kurtosis, respectively, which measure the asymmetry and peakedness of the BTCs as compared with a Gaussian distribution [17]

$$C_S = \Lambda_{3,T} / \left[\Lambda_{2,T}\right]^{3/2} \qquad (8)$$

$$C_K = \Lambda_{4,T} / \left[\Lambda_{2,T}\right]^2 - 3 \qquad (9)$$

where C_S is the skewness and C_K is the kurtosis. With the above definitions, a Gaussian BTC leads to zero skewness and kurtosis.

RESULTS AND DISCUSSION

Particle Tracking Implementation

RWPT simulations stated above were repeatedly performed under the prescribed flow conditions while finite element model was the computational framework for expressing the velocity vector at all locations in the model domain. As an initial pulse input, the number of particles used to represent the solute is 20000 with a constant mass of the unit gram per one particle. All particles are applied uniformly distributed at random within the injection line shown in Fig. 2. Additionally, longitudinal dispersivity and transverse dispersivities are chosen to be 0.02 m and 0.005 m, respectively, which are based on the data reported in the literature [12]. To simplify the problem, a particle is assumed to be conservative and not to have the adsorptive nature, leading to 1 of retardation factor. Parameters used in this analysis is listed in Table 1. Representative three results of mass BTCs divided by the total mass at three control planes are exhibited in Fig. 5. A time series mass variation indicates that breakthrough curves exhibit a Gaussian-like shape regardless of the location of a control plane. The first to the fourth moments are assessed to elucidate the moment characteristics in BTCs and the transport property in aquifers.

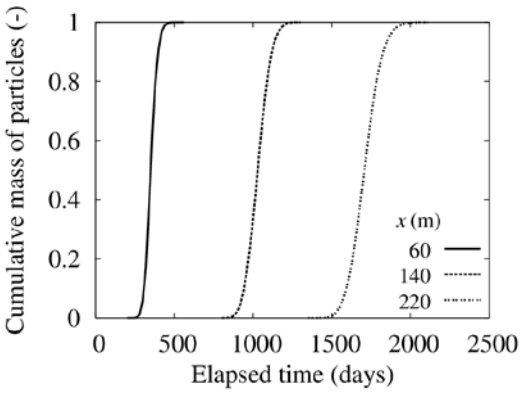

Fig. 5 Illustration of typical measured breakthrough curves.

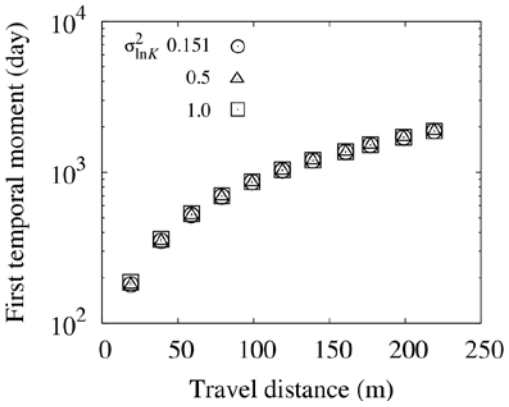

Fig. 6 First temporal moments estimated from BTCs at 11 control planes.

First Temporal Moments

Ensemble of first temporal moments obtained from eq.(6) for all realizations is shown in Fig. 6 as a function of the distance to the control plane from the source for different degrees of heterogeneity. First temporal moment corresponds to the mean arrival time of particles, demonstrating that the degree of heterogeneity little influences on the mean arrival time. In order to visualize this point, the fraction of particle positions along *x*-direction at *t*=100 and 1000 days is depicted in Fig.7 where all distributed particles in the domain were projected onto the *x*-

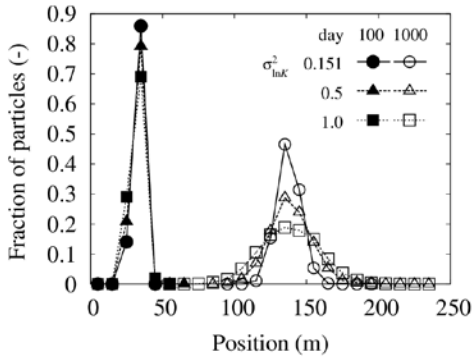

Fig. 7 Fraction of particle positions. Closed symbols are the fraction of particles at day=100 and open symbols are at day=1000.

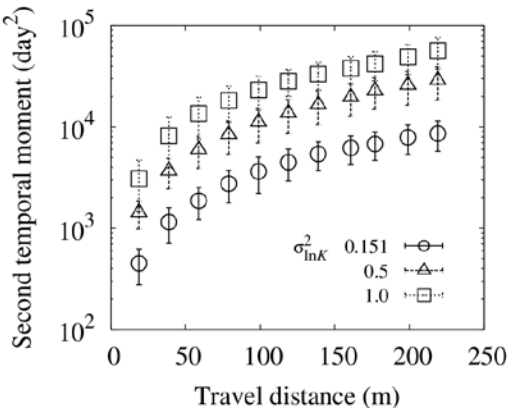

Fig. 8 Second temporal moments estimated from BTCs at 11 control planes.

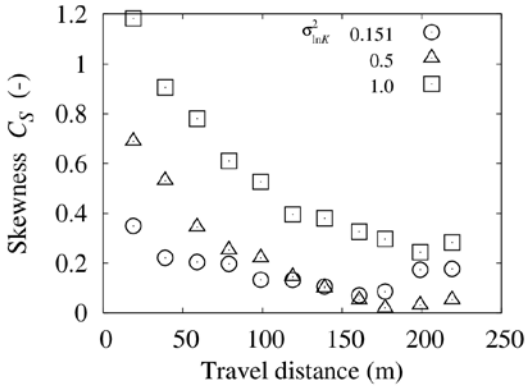

Fig. 9 Skewness ensemble average BTCs as a function of travel distance

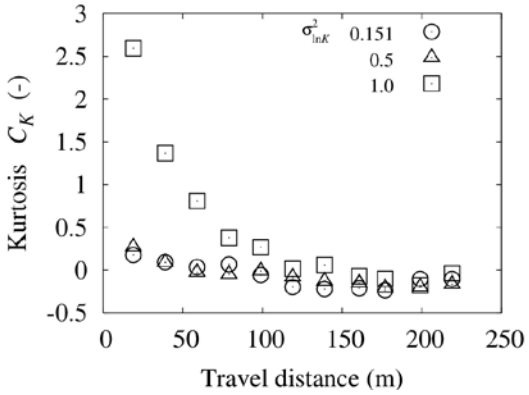

Fig. 10 Kurtosis ensemble average BTCs as a function of travel distance

axis and were counted with the interval of 10 m according to the particle locations. The positions of the peak are almost identical despite of the degree of heterogeneity.

Second Temporal Moments

Figure 8 provides the results of the second temporal moment, which is used to gauge the size of a particle cloud in a given direction and determine the rate of growth with the increase of the displacement. The error bar illustrates the variance of ensemble of all realizations. It can be seen that values of the second temporal moment increase nonlinearly in all heterogeneity. At large travel distance, second temporal moment approaches a constant value whereas an asymptotic value depends on the degree of heterogeneity resulting in larger macrodispersivity [8],[17],[18].

Third Temporal Moments

The study of third and fourth moments of BTCs is a crucial step toward characterizing the shape of the BTC not only Gaussian but non-Gaussian. RWPT can provide accurate estimates of the third and fourth central temporal moments under the influence of heterogeneity of BTCs. Results are expressed by means of the skewness and kurtosis, which measure the asymmetry and peakedness of the BTCs.

Figure 9 shows the results of the skewness estimated from ensemble BTCs as a function of travel distance. The values of the skewness decrease with travel distance and approach the value of zero. This attributes the Wiener process of Eq.(3) in terms of Ito interpretation and Markov process where future movement of a particle depends only on where the particle is, not the history of particle transport pathways. However, non-zero nature of the skewness values under the travel distance of interest and somewhat fluctuation of values at a relatively large distance occur, suggesting the need in terms of a longer transport phenomenon.

Fourth Temporal Moments

Figure 10 presents the variation of the kurtosis as a function of the travel distance from the source estimated from BTCs. Kurtosis expresses the relative peakedness or flatness of a distribution relative to a normal distribution, where positive values indicate a relatively peaked distribution. The kurtosis of the BTCs decrease with time leading to a

Gaussian-like particle distribution. At small distances, the larger decrease appears and gradually dissipates over the course of travel distances. This tendency agrees with earlier work [6], suggesting the reliability of estimates. It is interesting to note that although these deviations in skewness and kurtosis from the values corresponding to a Gaussian distribution increase with the increase of the heterogeneity, the influence of the degree of heterogeneity on the evolution of the kurtosis coefficient gradually dissipates at larger travel distances. This point is similar to the results of the third temporal moments.

CONCLUSIONS

In this study, temporal moment characteristics in heterogeneous two-dimensional aquifers were evaluated using the random walk particle tracking linked with the temporal moment approach. The following findings have been clarified.

1. Non-dependency of the mean arrival times on the degree of heterogeneity was confirmed through the first temporal moments
2. Second temporal moment approaches a constant value according to the degree of heterogeneity.
3. It was observed that skewness and kurtosis decrease with the increase of the travel distance. This point reflects that the shape of the distribution of the particles become Gaussian far away from the source.

REFERENCES

[1] Dagan G, “Solute transport in heterogeneous porous formations”, J. Fluid Mech., 145, 1984, pp.151-177.

[2] Gelhar LW, Welty C, Rehfeldt KW, "A critical review of data on field-scale dispersion in aquifers", Water Resour. Res., 28(7), 1992, pp.1955-1974.

[3] Kitanidis PK, “Prediction by the method of moments in a heterogeneous formation”, J. Hydrol., 102, 1988, pp.453-473.

[4] Dagan G, “Theory of solute transport by groundwater”, J. Fluid Mech., 145, 1984, pp.151-177.

[5] McNeil JD, Oldenborger GA, Schincariol RA, "Quantitative imaging of contaminant distributions in heterogeneous porous media laboratory experiments", J. Contam. Hydrol., 84, 2006, pp.36-54.

[6] Fernàndez-Garcia D, Illangasekare TH, Rajaram H, "Difference in the scale-dependence of dispersivity estimated from temporal and spatial moments in chemically and physically heterogeneous porous media", Water Resour. Res., 28, 2005, pp.745-759.

[7] Beaudoin A, de Dreuzy J-R, "Numerical assessment of 3-D macrodispersion in heterogeneous porous media", Water Resour. Res., 49, 2013, pp.2489-2496.

[8] Inoue K, Fujiwara T, Kurasawa T, Tanaka T, "Quantification of solute macrodispersion phenomena and local heterogeneity using intermediate-scale solute transport experiments in heterogeneous porous formations", J. JSCE A(2), 70(2), 2015, pp.691-702 (in Japanese) .

[9] Chrysikopoulos CV, Kitanidis PK, Roberts PV, "Macrodispersion of sorbing solute in heterogeneous porous formations with spatially periodic retardation factor and velocity field", Water Resour. Res., 28(6), 1992, pp.1517-1529.

[10] Robin MJL, Sudicky EA, Gillham RW Kachanoski RG, "Spatial variability of strontium distribution coefficients and their correlation with hydraulic conductivity in the Canadian forces base Borden aquifer”, Water Resour. Res., 27(10), 1991, pp.2619–2632.

[11] Fernàndez-Garcia D, Illangasekare TH, Rajaram H, "Conservative and sorptive forced-gradient and uniform flow tracer tests in a three-dimensional laboratory test aquifer", Water Resour. Res., 40, 2004, W10103.

[12] Uffink GJM “Analysis of dispersion by the random walk method”, Ph.D. Dissertation, Delft University of Technology, 1990, 150p.

[13] Deutsch, CV, Journel AG, "GSLIB: Geostatistical software library and user’s guide", Oxford University Press, 1992, 340p.

[14] Bear J, "Dynamics of fluids in porous media", Dover Publications, 1972, 764p.

[15] Tompson AFB, Gelhar LW “Numerical simulation of solute transport in three-dimensional, randomly heterogeneous porous media”, Water Resour. Res., 26, 1990, pp.2541-2562.

[16] Salamon P, Fernàndez-Garcia D, Gomez-Hernàndez JJ. “A review and numerical assessment of the random walk particle tracking method”, J. Hydrol., 87(1-4), 2006, pp.277-305.

[17] Fernàndez-Garcia D, Rajaram H, Illangasekare TH. “Assessment of the predictive capabilities of stochastic theories in a three-dimensional laboratory test aquifer: Effective hydraulic conductivity and temporal moments of breakthrough curves”, Water Resour. Res., 41, 2005, W04002.

[18] Inoue K, Kurasawa T, Tanaka T: “Quantification of macrodipsersion in laboratory-scale heterogeneous porous formations**",** Inter. J. GEOMATE, 10, 2016, pp.1854-1961.

Second International Conference on Science, Engineering & Environment,
Osaka City, Japan, Nov.21-23, 2016, ISBN: 978-4-9905958-7-6 C3051

MODELING OF PERMEABILITY OF POROUS MEDIA WITH MIXED WETTABILITIES BASED ON NONCIRCULAR CAPILLARIES

Junichiro Takeuchi, Hidetaka Tsuji and Masayuki Fujihara
Graduate School of Agriculture, Kyoto University, Japan

ABSTRACT

Hydraulic conductivity of hydrophobic porous media becomes greater than that of hydrophilic porous media under the same-saturation condition. One of the reasons for it is considered that the size of pores filled by water in hydrophobic porous media is greater than that in hydrophilic media under unsaturated conditions. The authenticity was ascertained through numerical experiments using pore-network model. But the pore-network model with circular tubes could not account for the phenomena enough. Then, noncircular tubes are employed to take air-water interfaces formed at gaps between grains into account. In one case of hydrophobic grains, water cannot occupy corners, and water flows in a center of capillary tubes. In the other case of hydrophilic grains, water invades corners firstly, and water flows through the corner filaments until water enters the tube fully. In this study, equilateral triangular and cuspate cross-sections are used, and the relation between tube's flow-resistance, which is separated into shape and scale factors, and capillary pressure is investigated. The computed results show that the flow resistance of center flows could become smaller than that of full flow, and that it leads to higher hydraulic conductivity of hydrophobic porous media.

Keywords: Network Flow Problem, Variational Principle, Wettability, Air-water Interface, Hydraulic Conductance

INTRODUCTION

To alter hydraulic properties such as permeability and water retention property of porous media, it is considered that mixing grains with different wettability is one of effective options. Especially, it is known that hydrophobic grains changes hydraulic properties drastically, depending on the mixture proportion [1], [2].

Many works have attempted to model the mechanisms of imbibition and drainage inside porous media in a pore-scale [3], [4]. A pore-network model, which is firstly proposed by Fatt (1956) [5], is a powerful tool to model and understand the mechanisms in a bottom-up manner. In this paper, the pore-network model is employed to reproduce an interesting phenomenon that the permeability of hydrophobic porous media becomes larger than that of hydrophilic media at the same saturation [6]. To deal with this, the hydraulic conductance, which is a physical property assigned to each capillary tube and means an inverse of flow resistance in a capillary tube, needs to be reconsidered. The hydraulic conductance depends on the cross-sectional size and shape of a capillary tube, and is a different property from the hydraulic conductivity that is a macroscopic property of porous media. In this study, air-water interfaces formed between grains are considered by using noncircular capillary tubes, and hydraulic conductance is computed by solving 2-dimensional Poisson equation whose unknown variable is velocity in a cross-section [7]–[9].

So far hydraulic conductance had been defined variously. In some definition, pipe length and/or viscosity are included [7]–[9]. If local losses such as contraction and enlargement in a network flow is not negligible, the pipe length needs to be included in the hydraulic conductance. But these local losses are negligible compared with the friction loss [6]. Hence, it is natural to define the hydraulic conductance without pipe length and viscosity to correspond to the intrinsic permeability of porous media. In addition, a new way to separate the hydraulic conductance into shape and scale factors is proposed, because the effect of cross-sectional shape on the flow resistance is not clear in the conventional way, in which the Manson-Morrow shape factor (defined as area/square of wetted perimeter) is used as a shape factor [6], [7]. But the Darcy-Weisbach friction factor also depends on the cross-sectional shape.

In this study, the shape factor and its effect on the permeability of porous media are inspected through numerical experiments, and it is shown that air-water interfaces in capillary tubes play a large role for the permeability.

NETWORK FLOW IN POROUS MEDIA

Variational Principle in Network Flow

In general, to solve a network flow problem the Hardy-Cross method, in which flow rate in each pipe and potential in each junction are unknown variables and a non-linear simultaneous equation for both of energy loss and mass conservation is formulated [10], is used. In this study, a method based on a variational principle is employed. The variational

principle is a fundamental concept to find a solution of some physical problems. It relies on the idea that many physical phenomena obey a basic principle that the state of the system is determined by minimizing energy consumption. In a pore-network flow problem, a functional ϕ, which would be minimized, is defined as a summation of three terms as follows [11].

$$\phi(\boldsymbol{q}) = \phi^{\mathrm{F}}(\boldsymbol{q}) + \phi^{\mathrm{OUT}}(\boldsymbol{q}) + \phi^{\mathrm{IN}}(\boldsymbol{q}) \qquad (1)$$

where $\boldsymbol{q}$ is the flow rate vector, whose components q_i ($i = 1, ..., N^{\mathrm{tube}}$) are the flow rate in the i th capillary tube, ϕ^{F} is the friction term, and ϕ^{OUT} and ϕ^{IN} are the outflow and inflow terms, respectively. The friction term is represented as follows, based on the Darcy-Weisbach equation.

$$\phi^{\mathrm{F}} = \sum_{i=1}^{N^{\mathrm{tube}}} \frac{1}{3} \kappa_i |q_i| q_i^2 \qquad (2)$$

with

$$\kappa_i = \frac{f_i l_i}{2 g d_i a_i^2}, \qquad d_i = \frac{4 a_i}{p_i} \qquad (3)$$

where N^{tube} is the number of the capillary tubes included in a pore-network; κ_i is a coefficient for the friction loss; f_i is the Darcy-Weisbach friction factor; l_i , a_i , d_i , and p_i are the length, the cross-sectional area, the hydraulic diameter, and the wetted perimeter of the i th capillary tube, respectively; and g is the gravitational acceleration. Here only a friction loss is taken into account, based on the fact that other local losses such as contraction and enlargement are negligible compared with the friction loss [6]. When the flow in capillary tubes is laminar, the friction factor f_i is represented as follows.

$$f_i = \alpha_i / \mathrm{Re}_i \qquad (4)$$

with

$$\mathrm{Re}_i = \frac{d_i |q_i|}{\nu a_i}, \qquad \nu = \frac{\mu}{\rho} \qquad (5)$$

where α_i is a coefficient that depends on the cross-sectional shape and the values for circular, square, and equilateral triangular section are 64, 56.908, and 53.333, respectively [12], Re_i is the Reynolds number, ν is the kinematic viscosity, μ is the viscosity, and ρ is the water density.

The second and third terms in the right hand side of Eq. (1) are represented as follows.

$$\phi^{\mathrm{OUT}} = \sum_{i \in \zeta^{\mathrm{OUT}}} h_i q_i \,, \quad \phi^{\mathrm{IN}} = -\sum_{i \in \zeta^{\mathrm{IN}}} h_i q_i \qquad (6)$$

where ζ^{OUT} and ζ^{IN} are the sets of the capillary tubes connecting to outflow and inflow ports, respectively; and h_i are the piezometric heads at the outflow and inflow ports and these are prescribed variables in this study.

In addition to the functional (1), the following mass balance equations at each junction are added as constraints.

$$\sum_{k \in \zeta_j^{\mathrm{junc}}} q_k = 0 \qquad \left(j = 1, ..., N^{\mathrm{junc}} \right) \qquad (7)$$

where N^{junc} is the number of junctions, ζ_j^{junc} is the set of capillary tubes connecting to the j th junction.

The minimization problem of the functional (1) with the constraints (7) is solved by the Lagrange multiplier method, introducing Lagrange multipliers λ_j ($j = 1, ..., N^{\mathrm{junc}}$). The objective problem is reformulated as a minimization problem with unknown variables $\boldsymbol{q}$ and $\boldsymbol{\lambda}$ by adding the constraints multiplied by λ_j to the functional (1).

$$\Phi(\boldsymbol{q}, \boldsymbol{\lambda}) = \phi(\boldsymbol{q}) + \sum_{j=1}^{N^{\mathrm{junc}}} \lambda_j \left(\sum_{k \in \zeta_j^{\mathrm{junc}}} q_k \right) \qquad (8)$$

where $\boldsymbol{\lambda}$ is a vector whose component is λ_j ($j = 1, ..., N^{\mathrm{junc}}$).

Incidentally, the nonlinear simultaneous equation obtained after partial differentiation of the functional (8) by each unknown variable becomes exactly same with the equations system of an ordinal network flow problem, in which flow rate in each pipe and piezometric head at each junction are unknown variables. For example, the partial differentiation of the functional (8) with respect to an unknown flow rate q_i becomes as follows, if the i th capillary tube connects to neither outflow nor inflow ports.

$$\lambda_{j1} - \lambda_{j0} = \kappa_i |q_i| q_i \qquad (9)$$

where the subscripts $j0$ and $j1$ are the junction indices of both ends of the i th capillary tubes. Equation (9) shows the local head loss by friction, and which means that the Lagrange multiplier λ_j is the piezometric head h_j at each junction. By substituting Eqs. (3) through (5) into Eq. (9), the following equation is induced.

$$q_i = \frac{\Theta_i}{\mu} \frac{\Delta p_i}{l_i} \qquad (10)$$

with

$$\Theta_i = \frac{32 a_i^3}{\alpha_i p_i^2}, \qquad \Delta p_i = \rho g (h_{j1} - h_{j0}) \qquad (11)$$

where Θ_i is the hydraulic conductance, Δp_i is the piezometric potential difference between the junctions $j0$ and $j1$. With regard to the hydraulic conductance Θ_i , the viscosity μ and/or the tube length l_i are excluded in this study, because it is natural to consider that the hydraulic conductance of capillary tubes corresponds to the intrinsic permeability of porous media.

Shape and Scale Factors

The hydraulic conductance Θ in Eq. (10) is considered as an inverse of flow resistance of a capillary tube, and includes shape and scale factors. In some previous works, the Manson-Morrow shape factor G ($= a / p^2$) is introduced and the hydraulic conductance is rearranged as follows [9].

$$\Theta = 32 a^2 G / \alpha \qquad (12)$$

However, the coefficient α also changes depending on the cross-sectional shape. Then, the effective radius r_e and a coefficient β, which satisfy the following relations, are introduced here to separate shape and scale factors completely.

$$a = \pi r_e^2, \quad p = \beta r_e \tag{13}$$

Hence, the hydraulic conductance is represented as follows.

$$\Theta = \pi^2 r_e^4 / \eta \tag{14}$$

with

$$\eta = \frac{\alpha\beta^2}{32\pi} \tag{15}$$

where η is the shape factor, which is flow resistance of capillary tube and depends only on the cross-sectional shape. And the coefficient β ranges from zero to infinity mathematically, and it means the hydraulic conductance also could change from zero to infinity.

Before solving the network flow problem presented by Eq. (8), values of the shape factor η of various cross-sectional shapes needed to be specified. Those are calculated from the flow rate q, based on Eqs. (10), (14) and (15). The flow rate in a constant pipe is calculated from velocity distribution in the cross-section and the velocity is governed by the 2-D Poisson equation, which is a simplified form of the Navier-Stokes equation and the mass conservation equation on the following assumptions: (1) flow is steady, (2) fluid is viscous, (3) inertia is negligible, and (4) velocity components except for the one along the tube axis are negligible [9]. The induced Poisson equation and boundary conditions are described as follows.

$$\nabla^2 v_X = \frac{\rho g}{\mu}\frac{dh}{dX} (= \text{constant}) \tag{16}$$

$$v_X = 0 \quad \text{on the grain-water interface} \tag{17}$$

$$\frac{\partial v_X}{\partial \boldsymbol{n}} = 0 \quad \text{on the air-water interface} \tag{18}$$

where X, Y, and Z are the local Cartesian coordinates and X is in the same direction with the tube axis., ∇^2 ($= \partial^2/\partial Y^2 + \partial^2/\partial Z^2$) is the differential operator, v_X is the velocity component along the X axis, and $\boldsymbol{n}$ is the unit normal vector to the interface (boundary).

When a capillary tube consists of hydrophilic grains, water tends to occupy corners firstly, and hence, water flows along the corner filaments as illustrated in Fig. 1. In contrast, when a tube consists of hydrophobic grains, air, which is wetting fluid in this case, tends to occupy corners, and hence, water flows in a center filament which is contrary to the hydrophilic case. In both cases, the curvature radius of the air-water interface r^{int} is determined from the Young-Laplace equation (19) and the capillary pressure p_c as described in Eq. (20), and the three-phase contact points are determined from grains' contact angles θ_0, θ_1, and θ_2.

$$r^{\text{int}} = \sigma / p_c \tag{19}$$

$$p_c = p_a - p_w \tag{20}$$

where σ is the surface tension of water, and p_a and p_w are the air and water pressures in the vicinity of the air-water interface.

In Fig. 2, some typical examples of velocity distributions obtained by solving the 2-D Poisson equation (16) in corner, center, and full flows through equilateral triangular tube are shown, and Fig. 3 shows changes of shape factors and hydraulic conductances of equilateral triangular and tri-cuspate tubes as the capillary pressure varies. It is assumed that these two types of tube have the same cross-sectional area. Fig. 3 (a) shows that cross-sections with air-water interfaces could have smaller shape factors compared with the circular tube in some range. Nevertheless, it is found from Fig. 3 (b) that corner filaments have much greater flow resistance because its flow cross-sectional areas are very small compared with the whole cross-sectional area of the tube, and that only center flows could have smaller flow resistance.

Hydraulic conductivity

Hydraulic conductivity of a pore-network model is estimated based on the Darcy's law.

$$K = \frac{QL}{A\Delta H} \tag{21}$$

with

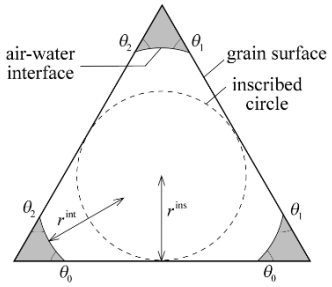

Fig. 1 Schematic of corner filament in triangular capillary tube

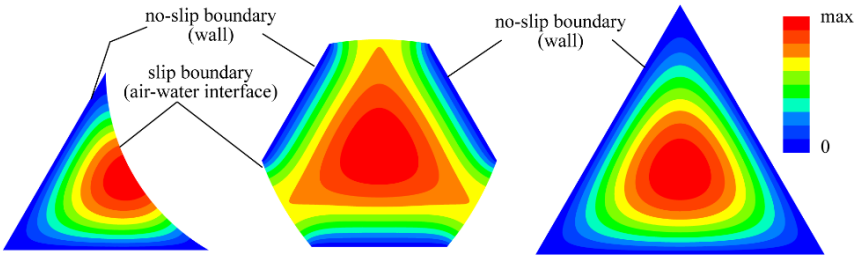

(a) Corner flow (b) Center flow (c) Full flow

Fig. 2 Velocity distributions in triangular capillary tube

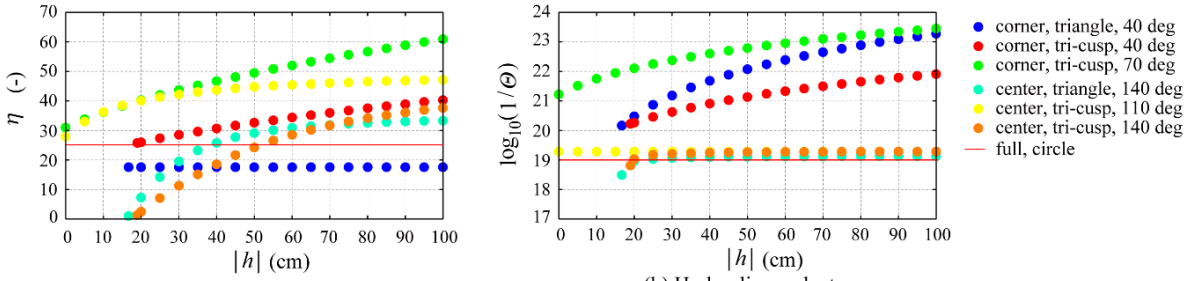

(a) Shape factor (b) Hydraulic conductance

Fig. 3 Flow resistance vs. piezometric head (cross-sectional area of all tube is 1.61×10^{-3} mm^2)

$$Q = \sum_{i=1}^{N^{\mathrm{OUT}}} q_i^{\mathrm{OUT}} = \sum_{i=1}^{N^{\mathrm{IN}}} q_i^{\mathrm{IN}} \qquad (22)$$

where K is the hydraulic conductivity of a variously saturated porous medium, Q is the total flow through the porous medium, A is the cross-sectional area of the porous media, and ΔH is the piezometric head difference between inflow and outflow faces. When the porous medium is fully saturated, the hydraulic conductivity is referred to as the saturated hydraulic conductivity, and represented as K_s. And the relative permeability k_r is defined as

$$k_r = K / K_s . \qquad (23)$$

NUMERICAL EXPERIMENTS

Generation of pore-network

A virtual pore-network is generated from a porous medium model that consists of randomly packed spherical grains with uniform size. The virtual porous medium is computed with the discrete element method by falling grains freely (Fig. 4 (a)), and a pore-network is extracted from the computed porous medium with the modified Delaunay-tessellation method proposed by Al-Raoush et al. [13] (Fig. 4 (b)). The pore-network is composed of pore bodies that are relatively large voids and pore throats that are relatively small voids connecting two pore bodies. In Fig. 4 (b), pore bodies are represented as spheres, and pore throats as tubes. The location and size of all pore bodies and throats are obtained through the generation process as well as those of grains. In this study, the sizes of a pore body and a pore throat are defined as the radius of the maximum inscribed sphere and circle inside the grains void, respectively.

Generation of variously saturated pore-network

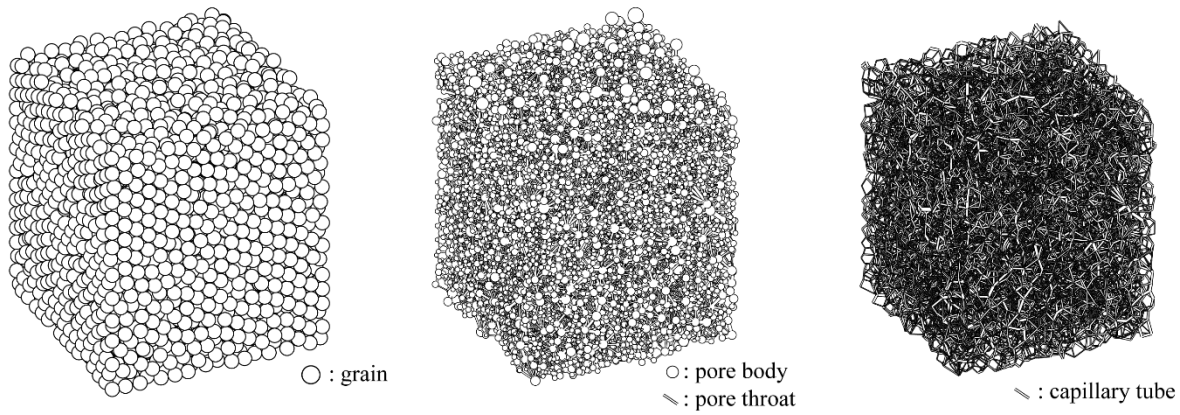

(a) Randomly packed grains (b) Pore network model (pore body and pore throat type) (c) Pore network model (capillary tube type)

Fig. 4 Virtual porous medium and pore-network models

Prior to computation of network flow problems in a porous medium, variously saturated pore-network models are generated in a generalized invasion percolation manner, which is a kind of discrete model to simulate water or air invasion into porous media [14]. The bottom of a dry porous medium, in which any pores are not occupied by water in an initial state, is supposed to be soaked in water.

The bottom and top faces of the pore-network are open-flow boundaries, and water and air pools are connected with the bottom and top faces, respectively. And the four sides are no-flow boundaries, and any fluid cannot pass through these boundaries. Water rises into invadable pores from the bottom, if the following conditions are satisfied: (1) an objective pore is empty, and it connects to the air pool through other empty pores; (2) the objective pore connects with one or more pores that are occupied by water, and at least one of the neighbor pores occupied by water connects to the water pool through other pores occupied by water; and (3) in a case of hydrophilic pores, the objective pore is small enough, or in the other case of hydrophobic pore, the pore is large enough. The conditions (1) and (2) are referred to as a connectivity condition.

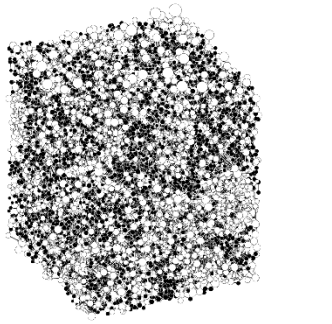

(a) hydrophilic porous medium
(-20 cmH_2O, 0.44)

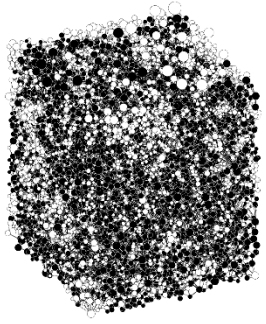

(b) hydrophobic porous medium
(20 cmH_2O, 0.59)

●＼: Water-filled pore ○＼: Air-filled pore

Fig.5 Inundation into hydrophobic and hydrophilic media
(piezometric head posed on bottom, saturation)

By changing the water pressure posed on the bottom of a pore-network, variously saturated pore-networks are obtained. In addition, hydrophobic grains are mixed at specified mixture fraction in this study. In Table 1, grain size, temperature, and the contact angles used for the imbibition process are summarized. The contact angles are fitted ones with measured and computed water retention curves in our previous works [6], [14]. Figure 5 shows some examples of partially inundated hydrophilic and hydrophobic pore-networks. While water can enter hydrophilic media under negative pressure conditions, positive pressure is needed for water to enter into hydrophobic media by the capillary action. Hence, negative and positive pressures are imposed to hydrophilic and hydrophobic media, respectively, to obtain partially saturated pore-networks in Fig. 5. It is found that water invades into smaller pores selectively in the hydrophilic pore-network, and that conversely water invades into larger pores selectively in the hydrophobic pore-network.

Relative permeabilities

For computation of network flows, the pore-network is regarded as the one that consists of volumeless pore bodies and pore throats with constant cross-section, according to our previous work [6]. Hence, appearance of a pore-network model used for network flow problems looks like Fig. 4 (c).

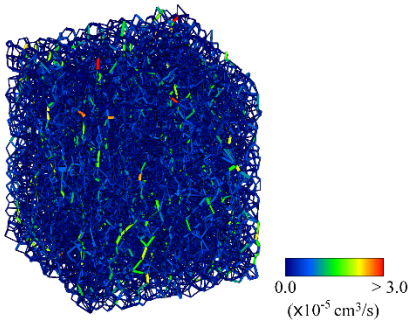

(a) fully saturated porous medium
(0 cmH_2O, 1.00, 2.3×10^{-2} cm/s)

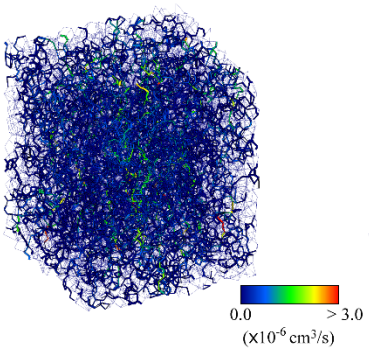

(b) hydrophilic porous medium
(-20 cmH_2O, 0.44, 5.6×10^{-4} cm/s)

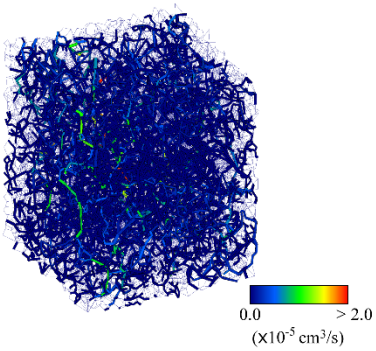

(c) hydrophobic porous medium
(20 cmH_2O, 0.59, 1.7×10^{-2} cm/s)

Fig.6 Flow distributions of variously saturated porous media
(piezometric head posed on bottom, saturation, hydraulic conductivity)

Other conditions for the permeability test such as air and water pressures are given in Table 1. Common water pressure is posed on both the top and bottom of the pore-network, and water flows down by gravity in this numerical test. When the contact

angle is greater than 60° and smaller than 120°, partial invasion such as corner and center filaments will not occur in the equilateral triangular tubes. And tri-cuspate tubes are used here.

In this model, there is one parameter that needs to be fitted. The unknown parameter is the effective radius of capillary tubes, and it is represented as follows here, associated with the inscribed radius r_{ins}.

$$r_{\mathrm{e}} = \gamma r_{\mathrm{ins}} \qquad (24)$$

where γ is the unknown parameter. The value is adjusted by comparing measured and computed hydraulic conductivity in a fully saturated case, where there are no air-water interfaces. In this study, the unknown parameter γ is adjusted so that the saturated conductivity becomes about 2×10^{-2} cm/s. When the value 1.11 was given to γ, the saturated hydraulic conductivity became 2.3×10^{-2} cm/s.

Network flow problems regarding the variously saturated pore-networks are solved, and relative permeability of each pore-network is calculated. In Fig. 6, typical flow distributions of a fully saturated case and partially saturated cases are shown. These figures show that water flows in only some parts of capillary tubes, and that majority of tubes do not contribute to water flow. In Fig. 7, measured and computed relative permeabilities are shown. The measured one was obtained by the constant water-level method with samples variously mixed hydrophilic and hydrophobic grass beads. Samples were variously saturated by sucking air with various suction force after dipping its bottom into water. So, all the hydrophilic samples (0% in Fig. 7 (a)) became high saturation. In the computed result (Fig. 7(c)), full flow was applied in the samples over 0.95 in saturation because it was considered air-water interfaces were not developed well. From the computed result (Fig. 7 (b)), it is found that the relative permeabilities of hydrophobic media (25-100%) are larger than that of hydrophilic one (0%). This is because water enters into larger pores firstly in hydrophobic media as shown in Fig. 5. In addition to this pore size effect, compared with the computed results (Fig. 7 (b) and (c)), relative permeabilities of hydrophobic media with tri-cuspate tube become larger than those with circular tube, which is the effect by the air-water interfaces. Although there is some discrepancy in a low saturation region between measured and computed results, the phenomenon that permeability of hydrophobic porous media is larger than that of hydrophilic media in the same saturation is well reproduced by using tri-cuspate tubes.

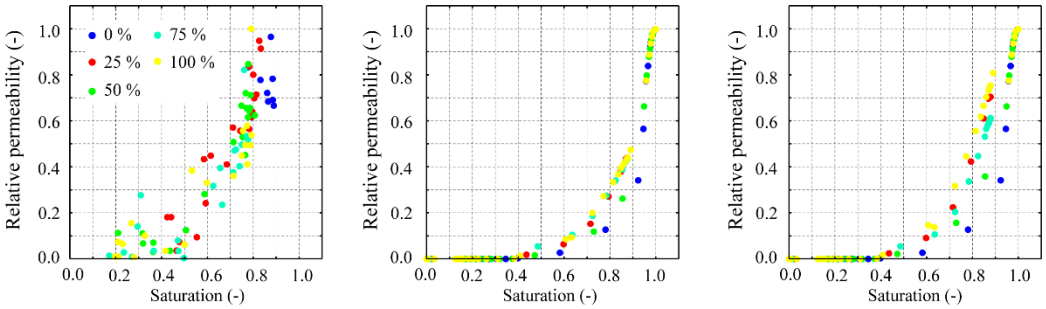

Fig. 7 Measured and computed relative permeability

CONCLUSION

In this study, noncircular tubes were employed in a network flow modeling of porous media to take air-water interfaces formed between grain gaps into consideration. And the network flow problem is formulated with a variational principle. From numerical analysis of hydraulic conductance of tube cross-section, it was shown that the flow resistance of cross-sections with air-water interfaces, which are slip boundary for water flow, could be smaller than that of full flow under a low pressure condition. And through the numerical experiments, it was ascertained that not only the tube size, but also air-water interface contributes to the increase of permeability of unsaturated hydrophobic porous media.

REFERENCES

[1] DeBano LF, “Water repellency in soils: a historical overview”, J. Hydrol., Vol. 231-232, 2000, pp.4-32.

[2] Annaka T, “Wettability indices and water characteristics for sands of mixed wettability”, J. Jpn. Soc. Soil Phys., Vol. 102, 2006, pp. 79-86 (in Japanese).

[3] Ustohal P, Dtauffer F, and Dracos T, “Measurement and modeling of hydraulic characteristics of unsaturated porous media with

Table 1 Conditions for permeability test

grain diameter		0.2 mm
air pressure		1 atm
water pressure		4 cmH_2O
Temperature		20°C
contact angle	mixture rate: 0%	46°
	mixture rate: 25%	92°, 110°
	mixture rate: 50%	98°, 110°
	mixture rate: 75%	98°, 110°
	mixture rate: 100%	110°

mixed wettabilities", J. Contam. Hydrol., Vol.33, 1998, pp. 5-37.
[4] Takeuchi J, Takahashi T., and Fujihara M, "Sub-Darcy scale modeling of non-uniform flow through porous media with mixed wettabilities", Int. J. GEOMATE, Vol. 6, 2014, pp. 840-847.
[5] Fatt I, "The network model of porous media", Trans. AIME, Vol. 207, 1956, pp.144-181.
[6] Takeuchi J, Sumii W, Tsuji H, and Fujihara M, "Estimation of permeability of porous media with mixed wettabilities using pore-network model", Int. J. GEOMATE, Vol. 11, 2016, pp. 2241-2247.
[7] Blunt MJ, Jackson MD, Piri M, and Valvatne PH, "Detailed physics, predictive capabilities and macroscopic consequences for pore-network models of multiphase flow", Adv. Water Resources, Vol. 25, 2002, pp. 1069-1089.
[8] Valvatne PH and Blunt MJ, "Predictive pore-scale modeling of two-phase flow in mixed wet media", Water Resour. Res., Vol.40, 2004, W07406, doi: 10.1029/2003WR002627.
[9] Raoof A and Hassanizadeh SM, "A new formulation for pore-network modeling of two-phase flow", Water Resour. Res., Vol. 48, 2012, W01514, doi: 10.1029/2010WR010180.
[10] Larock BE, Jeppson RW, and Watters GZ, Hydraulics of Pipeline Systems, CRC Press, 2000, p. 537.
[11] Bando O, Flows in pipe network and pump solved with excel, Kogyo Chosakai Publishing, 2008, p. 157 (in Japanese).
[12] Shah RK, "Laminar flow friction and forced convection heat transfer in duct of arbitrary geometry", Int. J. Heat Mass Transfer, Vol. 18, 1975, pp.849-862.
[13] Al-Raoush R, Thompson K, and Willson CS, "Comparison of network generation technique for unconsolidated porous media", Soil Sci. Soc. Am. J., Vol. 67, 2003, pp. 1687-1700.
[14] Takeuchi J, Sumii W, and Fujihara M, "Modeling of fluid intrusion into porous media with mixed wettabilities using pore-network", Int. J. GEOMATE, Vol. 10, 2016, pp. 1971-1977.

Second International Conference on Science, Engineering & Environment,
Osaka City, Japan, Nov.21-23, 2016, ISBN: 978-4-9905958-7-6 C3051

POTENTIAL OF OYSTERS AS AN ENVIRONMENTAL INDEX

Tetsuya Fukano[1] and Hiroyuki Ii[2]
[1]Graduate School of Systems Engineering, Wakayama University, Japan
[2]Faculty of Systems Engineering, Wakayama University, Japan

ABSTRACT

It is difficult to analyze heavy metals in sea water because their concentrations are very low relative to sea salt and not uniform with time and place. Heavy metal concentrations in sludge at the bottom of the sea largely change with sampling places because of large variety of metal concentration for sludge material. So it is difficult to grasp influence of heavy metals contaminations on sea environment by using concentration of sea water and sludge material. Oyster is very popular at coast and lives at the same place for several years, so it has a high potential as an environmental index. To search the potential of oysters as an environmental index, heavy metals concentrations of oysters were measured in wide area of Osaka Bay and in particular more than a year at Takashinohama of Osaka Bay. Then heavy metals concentrations of oysters were largely changed with places. Cu concentrations of the sampled oyster in wide area of Osaka Bay under dry weight condition were from 0.09 ‰ to 7.87 ‰. Even in the small beach at Takashinohama, heavy metals concentrations of oysters changed from 1.21 to 9.59 ‰ with sampling points although its seawater's metal concentrations were almost the same. Then, to confirm Cu concentration of oyster depending on sampling place, exchanged oysters sampled at the high Cu concentration point with oysters sampled at the low Cu concentration point for less than 20 days. As a result, Cu concentration of oyster changed with condition of each point. In this study Cu concentration in Osaka bay was thought to be influenced by anti-fouling paint. Ant –fouling paint was dissolved very slowly and then Cu concentration in sea water was too low to measure. However Cu concentration variation in sea water can be estimated from Cu concentration of oyster. So measuring heavy metal concentration in oysters is useful for grasping heavy metal contamination especially Cu of the sea condition.

Keywords: Oysters, Environmental index, heavy metal concentration, Anti fouling paint

INTRODUCTION

Aquatic organisms absorb heavy metals in sea water. *"Ostrea gigas"* is very popular oyster at coast and lives at the same place for several years, so it has high possibility as heavy metals index. Accumulation of heavy metals in aquatic organisms was reported by Ikuta. [1] Levels and distribution of toxic and essential metals in biological samples collected in Okayama prefecture was reported by Morita and Ogata. [2] Bivalves as a possible sentinel marine organism to monitor metal pollution in coastal water was reported by Takayanagi and Sakami. [3] The purpose of this study is to search the potential of oyster as an environmental index for heavy metal by research at Osaka Bay. Heavy metal concentrations of oyster were measured in wide area of Osaka Bay under the various different conditions. Measured heavy metals were Cu, Zn, Fe, Mn, Pb, Sr, and As. The source of these heavy metals was anthropogenic factor.

SAMPLING OF OYSTERS

Number of sampling points was 21. From Hyogo Prefecture Nishinomiya city to Wakayama Prefecture Kainan City, it covered all west side of Osaka bay. And oyster of Takashinohama was sampled more than a year. Almost oysters fixed at rocks and concrete wall at the wharf however sometimes rolling oysters were found at the beach and the slope of wharf. Oysters were stripped carefully from rocks or concrete wall by spatula and hammer. Table 1 shows detail about sampling points. Sampled oysters were 60 to 70 mm in length.

Table1 Details about sampling points

	Address	Habitat	State
A	Nishinomiya City	Artificial wharf	Stick
B	Osaka City north	Mouth of river	Stick
C	Osaka City south	Artificial wharf	Stick
D	Sakai City	Mouth of river	Stick
E1	Takaishi City	Artificial slope	roll
E3	Takaishi City	Natural beach	roll
F	Izumiohtsu City	Artificial slope	roll
G	Kishiwada City	Mouth of river	Stick
H	Kaizuka City	Mouth of river	Stick
I	Izumisano City	Mouth of river	Stick
J	Izumisano City	Artificial wharf	Stick
K	Sennan City	Mouth of river	Stick
L	Sennan City	Natural beach	roll
M	Hannan City	Artificial wharf	Stick

N	Hannan City	Artificial wharf	Stick
O	Misaki Town	Natural rock	Stick
P	Wakayama City	Artificial wharf	Stick
Q	Wakayama City	Artificial slope	roll
R	Wakayama City	Mouth of river	Stick
S	Wakayama City	Artificial wharf	Stick
T	Kainan City	Natural rock	Stick
U	Kainan City	Artificial wharf	Stick

Note:

Artificial slope was made for ship maintenance. Oysters were rolled by wave with stone on it.

Artificial wharf was made by strong concrete to protect a port against wild waves. Oysters fixed to the concrete.

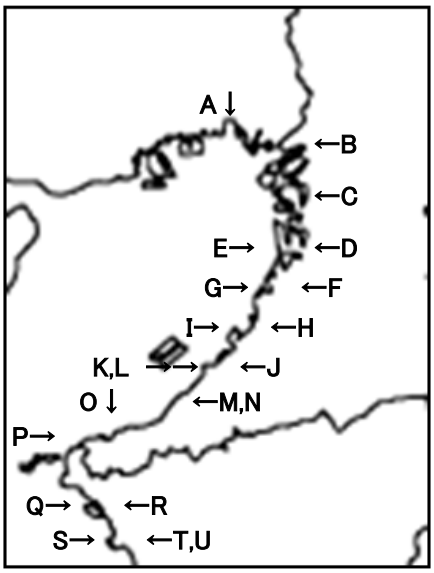

Fig. 1 21 sampling points covered all west side of Osaka bay

METHOD

Sampled oysters were opened shell carefully by stainless steel knife. The soft tissues of the oysters were cut into small pieces and put into pre-weighted laboratory dishes. The soft tissues were dried at 60 degrees for a week. All dried oyster tissues samples were ground manually into fine powder form by a mortar and pestle. Each ground sample was stored separately in airtight polypropylene bag.

Ground oyster tissues were mixed with nitric acid in glass vessel and then kept for a week at room temperature. After oyster powder was dissolved by nitric acid completely, the solution was filtered by 0.45 μm filter and then Cu, Zn, Fe, Mn, Pb, Sr and As concentrations were measured by Inductively Coupled Plasma (ICP).

RESULT

1 Heavy metal concentrations of oysters around Osaka bay.

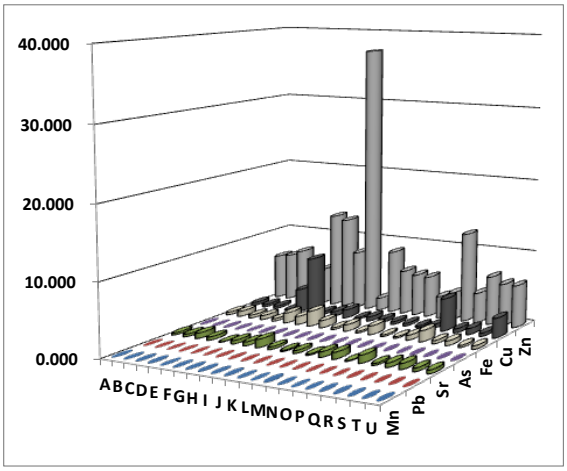

Fig. 2-1 7 kinds of heavy metals were measured at 21sampling points around Osaka bay. The Z axis unit is dry weight ‰.

Concentrations of Mn, Pb, Sr, and As were very low at all sampling points. Concentrations of Cu and Zn were high and their concentrations depended on sampling points. So concentrations of Cu and Zn in oysters are seemed to suitable for an environmental index.

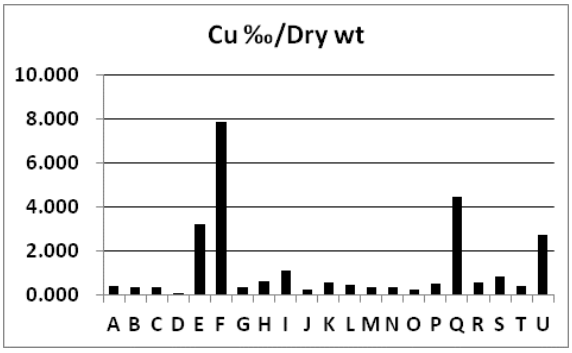

Fig. 2-2 Cu Concentrations measured at 21sampling points

At the sampling points E, F, Q, and U, Cu concentration was high and color of their oyster tissues was green.

The point E, F, and Q were artificial slopes. The point E and Q were fishing ports. The point F was a yacht harbor. The point U was a wharf of the leisure boats. High Cu concentration oyster was found around the fishing port.

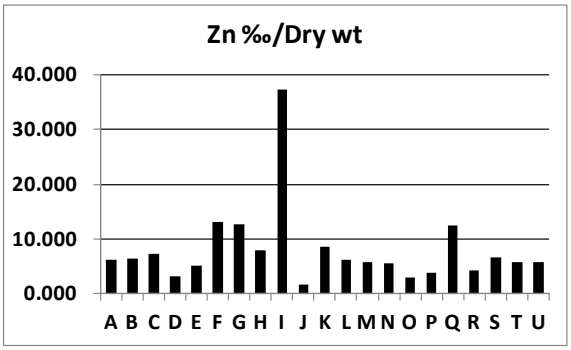

Fig. 2-3 Zn Concentrations measured at 21sampling points.

Most oysters had high concentration of Zn. The highest Zn concentration was the Point I. The Point I located near many food maker's factories.

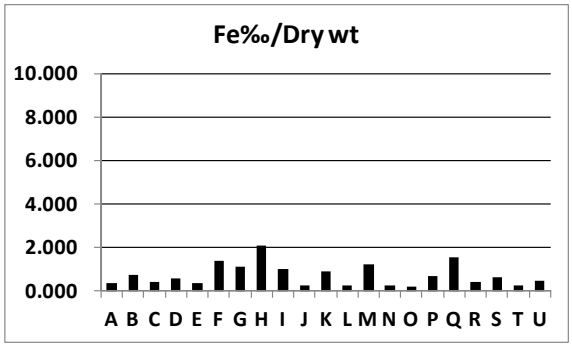

Fig. 2-4 Fe Concentrations measured at 21sampling points

Large difference was not found with concentration of Fe among each sampling points. Point H located near wire rope maker's factories.

Oyster has displayed a high potential as an environmental index by concentration of Cu. Concentration of Zn was influenced by nutrition of sea water, so has a potential for other index.

2 Concentrations of Cu and Zn at sampling point E1..E5

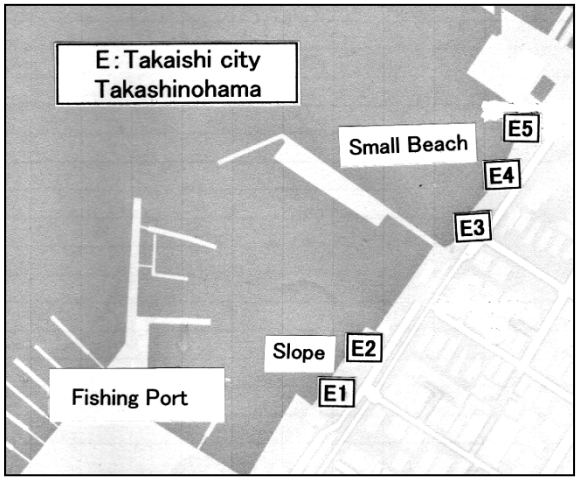

Fig. 3-1 Sampling point E1, E2, E3, E4 and E5

Point E was the small fishing port and small beach. The distance from E1 to E5 was about 200 m. Metal concentrations of sea water at each point were almost the same. Concentrations of Cu, Zn, Fe, Mn, Pb, Sr, and As of sea water were measured by ICP. Cu, Fe, Mn, Pb, Sr, and As concentrations of sea water were about 0ppm. However Zn concentrations were 0.032 ppm at point E1 and 0.043 ppm at the point E3. At the point E1 and E2, oysters were picked at artificial sloop. At the point E3, E4 and E5, oysters were picked at natural beach. Oysters were found under the low tide level. Oysters at the point E1 and E2 had green tissues. They were called "Green oyster".

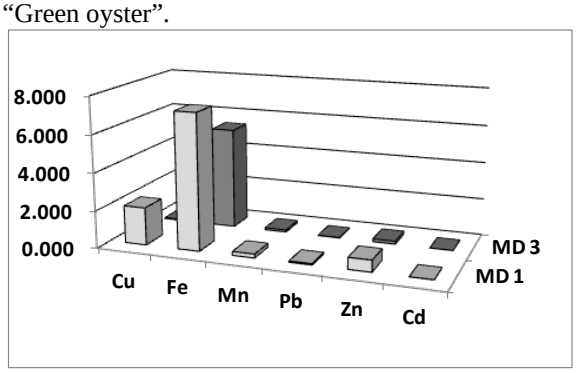

Fig. 3-2 Sludge of E1 (MD1), and E3 (MD3)

Concentration of heavy metals in sludge at the point E1 and E3

Dried sludge 0.02 g and nitric acid 15 mL were mixed in glass vessel and kept for a week at room temperature. After the solutions were filtered by 0.45 μm filter, Cu, Fe, Mn, Pb, Zn and Cd concentrations were measured by ICP.

Concentrations of Fe and Cu were high at the point E1. But at the point E3, concentration of Cu was not high. On the artificial slope of the point E1, many small pieces of red paint were found. The red paint was anti-fouling paint peered off from the bottoms of boats. Anti-fouling paint included Cu_2O as a biocide for biofoulings. [5]

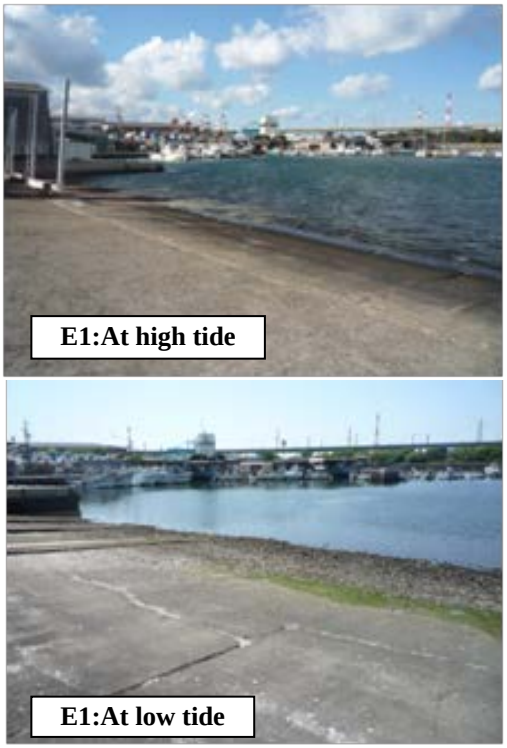

Fig. 3-3 Sampling point E1 is artificial slope of fishing port

Oysters on the artificial slope were found under the low tide level. Oysters were rolled by wave with stone on the slope.

Fig. 3-4 Sampling point E3 is a small natural beach

Width of beach was less than 100 m. Oysters on the natural beach were found under the low tidal level. Oysters were rolled by wave with stone on the beach.

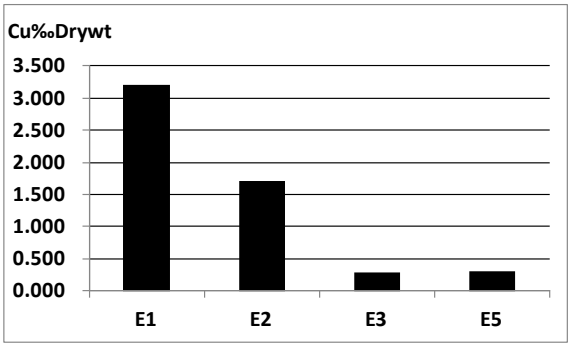

Fig. 3-5 Difference in concentration of Cu between point E1 and point E5

Concentration of Cu was very high at point E1.

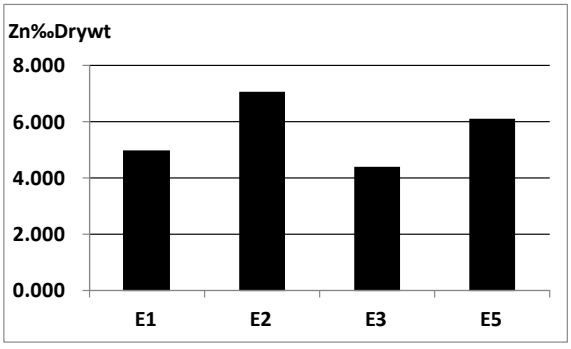

Fig. 3-6 Concentration of Zn at point E1-E5

Concentration of Zn were always high values.

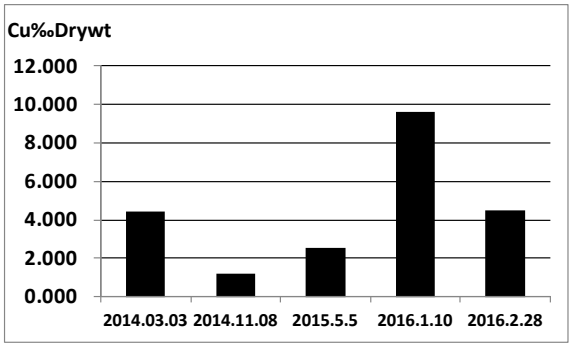

Fig. 3-7 Seasonable change of Cu at point E1

At the E1 point, big increase of Cu concentration for oyster was found in January. In winter fishing boats were pulling up to slope for maintenance. Scrape the old anti-fouling paint off the bottoms of ships and paint newly.

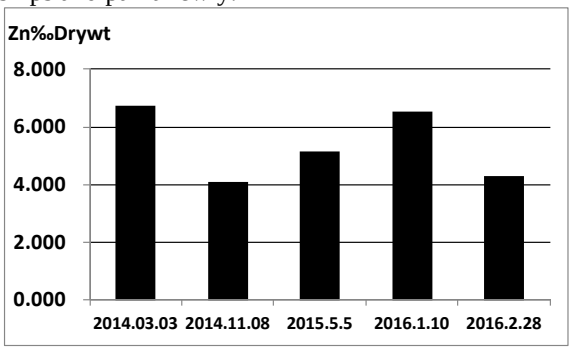

Fig. 3-8 Seasonable change of Zn at the E1 point

Concentrations of Zn were always high values. Seasonable change was not showed clear tendency.

3 Concentration of Cu and Zn in each part of oyster

Fig. 4-1 “Green Oyster” at E1

Oysters at E1, E2 had green tissues.

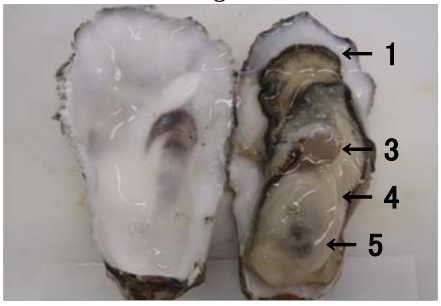

Fig. 4-2 Oyster at E3

Oyster at the point E3-E5 had normal color tissues.

1: Mantle 3: Adductor muscle 4: Others
5: Hepatic gland (liver) [4]

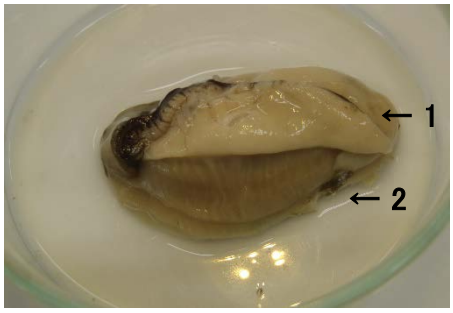

Fig. 4-3 Rolled up mantle1 and appeared gill
1: Mantle 2: Gill

At first, mantle was cut and rolled up then gill was appeared. Second, appeared gill was cut and separated into the adductor muscle. Forth, brownish hepatic gland was cut and each tissue of oyster was picked up separately. Small stainless steel scissors for eyebrow was useful to cut tissues of oyster.

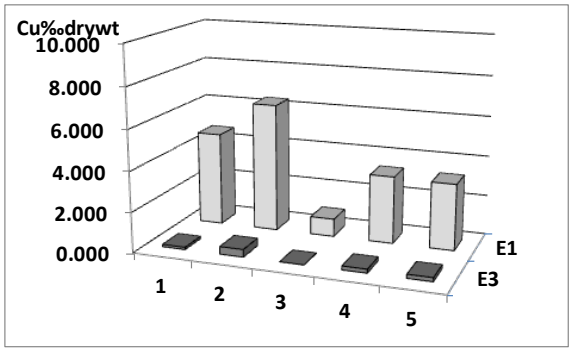

Fig. 4-4 Concentration of Cu in each part of oysters
1: Mantle, 2: Gill, 3: Adductor muscle, 4: Others,
5: Hepatic gland (liver)

At the sampling point E1, Cu concentrations were high values in mantle and gill. But the values in adductor muscle were low. And the values in hepatic gland and others were high values.

At the sampling point E3, Cu concentrations were relative low to the other points at Takasinohama.

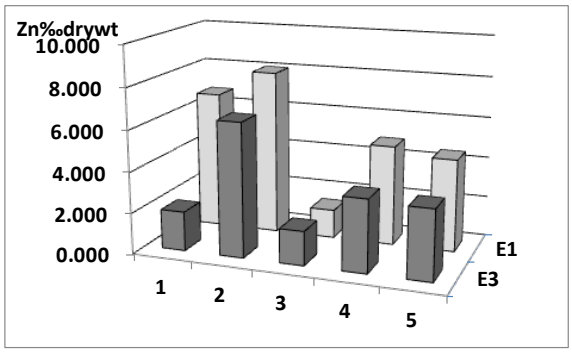

Fig. 4-5 Concentration of Zn in each part of oysters
1: Mantle, 2: Gill, 3: Adductor muscle, 4: Others,
5: Hepatic gland (liver)

At the sampling point E1, Zn concentrations were high values in mantle and gill. But the values in adductor muscle were low. And the values in hepatic gland and others were high values.

But at the sampling point E3, concentration of Zn appeared same tendency with the point E1.

4 Concentrations of Cu and Zn about exchanged oysters

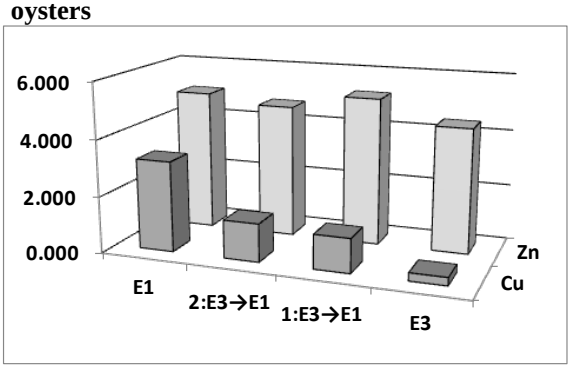

Fig. 5-1 Concentration of Cu and Zn about exchanged oysters among each sampling points

Sampled oyster was returned to another point. “1E3→E1” showed oyster sampled at the point E3 released to the point E1. After 13 days from release, the oyster was resampled at the E1 point.

“2E3→E1” showed oyster sampled at the point E3 released to the point E1. After 17 days from release, the oyster was resampled at the point E1.

Cu concentrations of the exchanged oysters increased with living days at the point E1. But concentrations of Zn were not changed by replacing.

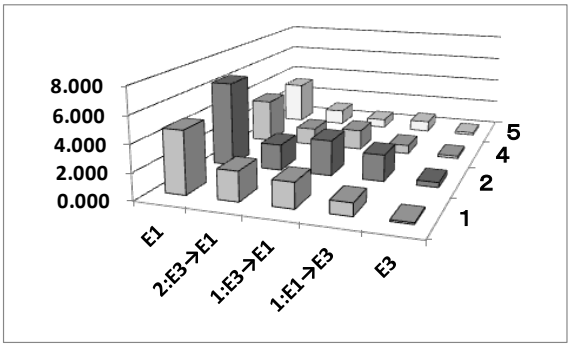

Fig. 5-2 Concentration of Cu in each part of oysters about exchanged oysters
1: Mantle, 2: Gill, 3: Adductor muscle, 4: Others,
5: Hepatic gland (liver)

Similarly sampled oyster was returned to another point. “1E3→E1” showed oyster sampled at the point E3 released to the point E1. After 13 days from release, the oyster was resampled at the E1 point. “1E1→E3” showed oyster sampled at the point E1 released to the point E3. After 13 days from release, the oyster was resampled at the E3 point.

“2E3→E1” showed oyster sampled at the point E3 released to the point E1. After 17 days from release, the oyster was resampled at the E1 point.

Cu concentrations of all part of the exchanged

oysters started to change from replacing. Cu concentrations replacing "E3→E1" increased and Cu concentration replacing "E1→E3" decreased. Cu concentration change in mantle and gill was remarkable.

5 Compare farmed oysters and oysters at Osaka bay

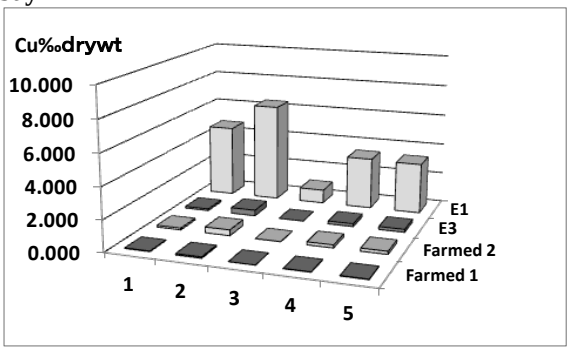

Fig. 6-1 Compare farmed oyster with sampled one 1: Mantle, 2: Gill, 3: Adductor muscle, 4: Others, 5: Hepatic gland (liver)

Farmed 1 is a sold oyster for raw eating produced from Murotsu area in Hyogo prefecture. Farmed 2 is a sold oyster for cook before eating produced from Hiroshima prefecture. Both oyster's concentrations of heavy metals were very low. Especially farmed 1 appeared very low value. Farmed oysters are kept in clear water, and farmed 1 is wash by sterilized water well to eat in law.

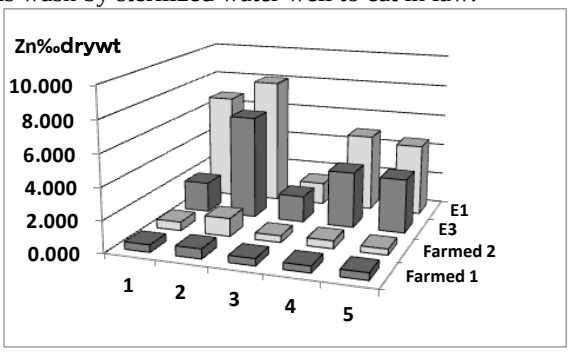

Fig. 6-2 Compare farmed oyster with sampled one 1: Mantle, 2: Gill, 3: Adductor muscle, 4: Others, 5: Hepatic gland (liver)

Zn concentrations in both farmed oyster were lower than natural oysters.

DISCUSION

The first concern was high concentration of Cu in oyster at the ports. Many boats in the ports were thought to increase Cu concentration in oyster. The second concern was high concentration of Cu in oyster at artificial slopes. And red small pieces of anti-fouling paint were found at artificial slopes.

The third concern was high concentration of Cu in oyster in winter season. Winter is maintenance season of boat. In winter, many red small pieces were found on the slope. The red small pieces were anti-fouling paint. The red paint was anti-fouling paint, and the small pieces were peered one from bottoms of the boats. Anti-fouling paint included Cu_2O as a biocide for biofouling.

$$\frac{1}{2}\mathbf{Cu_2O(s)} + \mathbf{H^+} + \mathbf{2Cl^-} \Leftrightarrow \mathbf{CuCl_2^-} + \frac{1}{2}\mathbf{H_2O}$$

$$\mathbf{CuCl_2^-} + \mathbf{Cl^-} \Leftrightarrow \mathbf{CuCl_3^{2-}} \quad [5]$$

Therefore, concentration of Cu in seawater at ports of Osaka was thought to be influenced by anti-fouling paint.

CONCLUSION

In conclusion, Oyster is useful to search changes of Cu concentration in sea water. In this study heavy metals concentrations of oysters measured in wide area of Osaka Bay have been considered. Our results showed Oyster was sensitive to Cu and response with transplantation was found less than 20 days.

This study was an important contribution because Cu concentration in Osaka bay was thought to be influenced by anti-fouling paint. Ant –fouling paint was dissolved very slowly and then Cu concentration in sea water was too low to measure. However Cu concentration variation in sea water can be estimated from Cu concentration of oyster.

REFERENCES

[1] Ikuta K, "Studies on Accumulation of Heavy Metals in Aquatic Organism-1.On the Copper Contents in Oysters", Bulletein of Japanese Society Fisheries, Vol.33, No.5, 1967, pp405_409.

[2] Morita K, Ogata M, "Levels and distribution of toxic and essential metals in biological samples collected in Okayama prefecture", Department of Public Health, Okayama University Medical School, 1983, pp359_376

[3] Takayanagi K, Sakami T, "Bivalves as a possible sentinel marine organism to monitor metal pollution in coastal waters –A review-, Bull. Fish. Res. Agen.,No2.35-46,2002

[4] Hirose H, Suzuki N and Okamoto N, "A New Edition Anatomical Illustration of Aquatic Animals" Seizando Shoten Publishing Co. ,Ltd. 2006, pp. 22_33

[5] Yamaguchi Y, "Copper Speciation and Concentration in Seawater of Japan-Toward the Risk Assessment of Copper Componds for Anti-Fouling Paint-, National Maritime Research Institute ISSN;2186-6598 http://www.nmri.go.jp/main/publications/paper/pdf/21/15/02/PNM21150205-00.pdf

Second International Conference on Science, Engineering & Environment,
Osaka City, Japan, Nov.21-23, 2016, ISBN: 978-4-9905958-7-6 C3051

FISH TOXICITIES OF NOVEL FIRE-FIGHTING FORM FORMULAE ASSAYED IN DIFFERENT WATER CONDITIONS FROM FRESH TO BRACKISH WATERS

Asato Ikemizu[1] and Tomonori Kawano[1],
[1]Graduate School of Environmental Engineering, The University of Kitakyusyu, Japan

ABSTRACT

Toxic impacts of a variety of chemicals to aquatic organisms habitable in fresh water conditions are often assessed in the media made of pure or low laboratory mineral waters. However, such water conditions hardly reflect the actual environments surrounding the organisms including fishes. Therefore, we have proposed the use of natural waters sampled from the natural environments (such as springs, ponds, rivers, lakes, and the ocean) or synthetic water preparations mimicking the natural waters (by supplementation of minerals), in addition to the tests in standard laboratory waters, when examining the toxicity of certain chemicals in aquatic organisms. To date, toxicity of synthetic detergent-based and soap-based formulae of fire-fighting foams (FFFs) against a tiny fish, *Oryzias latipes*, known as medaka fish, have been evaluated in the series of model waters differed in salinity from low mineral fresh water to brackish water, since the model fish species employed is known to be habitable in a wide range of osmotic conditions. In addition, use of a local tap water should be allowed for the evaluation of toxicity if the sources are known, and the mineral compositions were determined since it has been confirmed that river fishes behave more naturally in the river-derived tap waters after de-chlorination, compared to synthetic laboratory water preparations. Here, we have conducted a series of assays for evaluating the toxicity of several soap-based FFFs including a newly developed formula, and the LC_{50} values determined at 48 h after additions of soap-based FFFs were shown to be lowest under the brackish condition and highest in the pure water, suggesting that cationic strength drastically alters the toxicity of the FFFs.
Keywords: Ecotoxicity, Fatty acid salts, Fire-fighting foam, medaka fish, Oryzias latipes

INTRODUCTION

A variety of chemicals including foaming agents are used to aid in the protection of forest resources from the wild land fires (both woodland and grassland fires) [1]. The fire-fighting foams (FFFs) are formulations composed principally of surfactants, and act by increasing the water efficiency [2]. In the last two decades, the use of these formulae have been successfully gaining acceptance as effective and efficient fire-fighting tools in several countries such as USA and Australia [3]. In Japan, local government in Tokyo and Kitakyushu followed by other cities nation-wide, have employed several FFFs in the urban fire controls since 1999 [4].

Compared to the most cases of urban fire controls**,** much greater amounts of fire-fighting chemicals including FFFs might be emitted to the environments in case of wild land fire managements. Since forests and grass lands where wild fires naturally occur are full of wild animals, plants and micro-organisms. In addition, it should be noted that rivers, ponds, and lakes rich in fishes, algae and a variety of aquatic organisms are surrounded by the forests and grasslands. Therefore, both aquatic and terrestrial eco-toxicities of these fire-fighting chemicals should be examined before its applications in the fields as our group has proposed in the last decade [2, 5-12].

In the present study, we focus on the aquatic eco-toxicity of FFFs. As a model fish species habitable in both fresh and brackish water conditions, adult individuals of medaka (*Oryzias. latipes* red-orange variety) were chosen for assessment of FFFs toxicity as previously reported [5, 7, 10, 11], since Japanese medaka, a freshwater teleost, is now popular for laboratory use in the world [13]. In fact, the genus, *Oryzias* consists of more than 14 species including *O. latipes*. Each species within *Oryzias* shows a specific pattern of geo-ecological [14, 15] and seasonal [16] distributions. Interestingly, some are endemic only to freshwater lakes, while other species are widely distributed in the freshwater, brackish water, and seawater in Asia [16-19]. Therefore, the *Oryzias* species may provide a unique model for studying the fish adaptation to changing salinity accompanying the hyper- and/or hypo-osmotic shocks [20]. *O. latipes's* Adaptability to a wide range of water conditions allows us conducting the fish toxicity assays for fire-fighting chemicals which likely alter their toxicity depending on the given water conditions [10, 11]. We have previously shown that the red-orange variety of *O. latipes* known as Himedaka brought up in a local tap water tolerates transferring to severe hypo-osmotic (ultra-pure water) and hyper-osmotic conditions (brackish water and seawater), if the stepwise changes in osmolarity were properly performed [11,16].

Without such adaptation process, fish may die immediately after the shock [13].

Here, we have conducted a series of assays for evaluating the toxicity of several FFFs including a newly developed soap-based formula under both pure water and brackish condition, and the toxicity determined at 48 h after additions of the soap-based FFFs was shown to be lowest under the brackish condition but not in the pure water, suggesting that cationic strength drastically alters the toxicity of the FFFs.

EXPERIMENTAL

Laboratory-sized tests

Adult medaka fish individuals (Red-Orange var., *O. latipes*) brought up in the tap water were purchased from a local animal supplier. Prior to the assays, fishes were kept in a de-chlorinated local tap water.

The de-chlorinated Kitakyushu city local tap water were used as laboratory fresh waters as previously described [5, 7, 10, 11, 16]. Synthetic brackish water was prepared by mixing the artificial sea water and ultra-pure water (equivalent to 25% seawater). Adaptations to various water was step-wisely performed as previously described [10, 11].

Newly developed soap-based FFF and other conventional FFFs were provided by Shabondama Soap Co. Ltd. and Fire and Disaster Management Department of Kitakyushu City.

FFF stock solutions were first dissolved in small amount of de-iononized pure water (≧13MΩ/cm) [9]. Then, various water samples were used for secondary dilutions to the indicated concentrations.

Toxicity of FFFs in medaka fish was tested essentially according to our previously reported protocols [10, 11]. Viability of fish was tested in various waters and the survival rates at 48 h after additions of FFFs were manually monitored and the median lethal concentrations (LC_{50}) for FFFs were worked out. For each test or replication, 5 fishes kept in 1000 ml water were used.

Tests in Aquatic biotopes

Commercially available synthetic FFFs namely, Miracle-foam α+, Forexpan S, and MegaFoam F623-T; and the newly developed soap-based FFF (not yet designated, thus, simply labelled as New soap formula) was used. For comparison, data for conventional soap-based FFF designated as Miracle-foam are referred to when required. Note that similar names were given to a synthetic FFF (Miracle-foam α+) and a soap-based FFF (Miracle-foam). In order to emphasize the difference, additional notes are given to these FFFs as parentheses, *biz*, Miracle-foam α+ (synthetic) and Miracle-foam (soap), when necessary. The mock water or four FFFs (Miracle-foam α+, Forexpan S, MegaFoam F623-T and new soap formula) were jet-sprayed above the compact biotopes in August, 2015, according to the protocol by Kawano et al [7]. Concentrations of above FFF agents in the pre-foaming mixtures were 1 % (w/v), as recommended by the suppliers. Onto each of 0.81 m^2-sized model biotope, 3 L of mock water or a FFF mixture was jet-sprayed after compressing the air in the fire-fighting cylinders (7) (Fig. 2A).

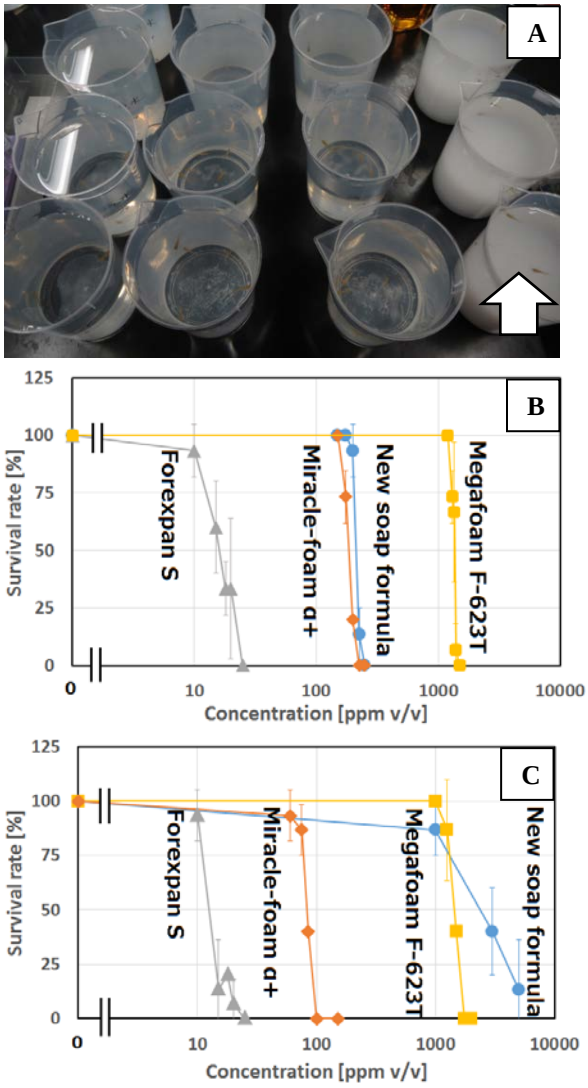

Fig 1. Beaker-size fish toxicity assays forFFFs. (A) Beakers with 1L FFF mixtures each containing 5 medaka individuals. Arrow, formation of insolube white precipitates by soap-based FFF dissolved in breakish water. (B) Toxicity curbs for FFFs obtained in Kitakyushu city tap water. (C) Toxicity assayed in model brackish water (25% sea water).

RESULTS AND DISCUSSION

LC_{50} determined through laboratory tests

Due to the presence of cations such as Mg^{2+} and Ca^{2+}, the soap component (fatty acid salts) forms insoluble complex, therefore, we observed the precipitation of FFF in hard waters (Fig1. A). Using medaka fish as a model fish species, LC_{50} for FFFs was determined through a beaker-sized laboratory tests (Fig1. B, C). In the presence of various concentrations of FFFs, viability of fish at 48 h was assessed in two types of waters, namely, the tap water from Kitakyushu city and a model brackish water prepared with artificial sea salt mixture (25% sea water). We found that toxicity of soap-based FFF is likely scored high in the tap waters with low mineral composition and extremely lowered in the brackish water with high mineral composition (Fig. 1B, C).

The LC_{50} values determined in tap waters at 48 h were around 214 ppm in New soap formula, 186 ppm in Miracle-foam α+ (synthetic), 16 ppm in Forexpan S, 1364 ppm in Megafoam F-623T. The LC_{50} determined in brackish water at 48 h were around 2575 ppm in New soap formula, 83 ppm in Miracle-foam α+ (synthetic), 13 ppm in Forexpan S, and 1446 ppm in Megafoam F-623T (Fig. 1B, C), as summarized in Table 1. (Table 1).

It is likely that the increase in water hardness actively lower the toxicity of New soap formula FFF as previously observed for other soap-based FFFs such as Miracle-foam (soap).

Similarly to our previous demonstration using an aquatic microbe (*Paramecium spp*) exposed to soap components [21-24], alteration of the fish toxicity determined in different water conditions may be due to the cation (Mg^{2+} and Ca^{2+})-dependent detoxification of soap components (formation of metallic soaps) as we observed the precipitation of FFFs in hard waters. It is obvious that soap-based the FFF precipitates in the hard waters are no-longer toxic but edible for medaka fish as performed by Lin et al [11], thus rich in nutriments (fatty acids).

Tests in mini-biotopes

When preliminarily assessing the toxic impacts of FFFs in aquatic biotopes in 2015, mock water or FFF mixtures were jet-sprayed directly onto the surface of water. Therefore, due to mechanical shock which is apparently in excess, major population of fish was severely damaged even in the mock water control. In order to avoid such artifacts, we have repeated the biotope-sized experiments this year (from May 6th) by releasing fish (separately pre-incubated for a week in the tap water) into the water only after the addition of FFFs.

Then, the changes in the viability of fish (started with 50 individuals/treatment) during incubation with and without FFFs were manually monitored (Fig. 2B). Notably, Forexpan S immediately killed out all fish population. Among other FFFs tested, both Miracle-foam α+ and New soap formula showed low toxicity even comparable with the mock water treatment (Fig. 2B). The reason why the fish population in the control mock water treatment gradually decreased could be possibly attributed to over-loading of fish individual, thus the size of fish community was shrunk to the level allowed by environmental capacity predicted by a well-known logistic equation [23].

Table 1. Effect of water condition on LC50 for FFFs determined in medaka fish.

FFFs tested		Tap water	Brackish water
Soap-based foams	New soap formula	214	2575
	Miracle foam	200*	650*
Commercial synthetic foams	Miracle form α +	186	83
	Forexpan S	16	13
	Megaform F-623T	1364	1446

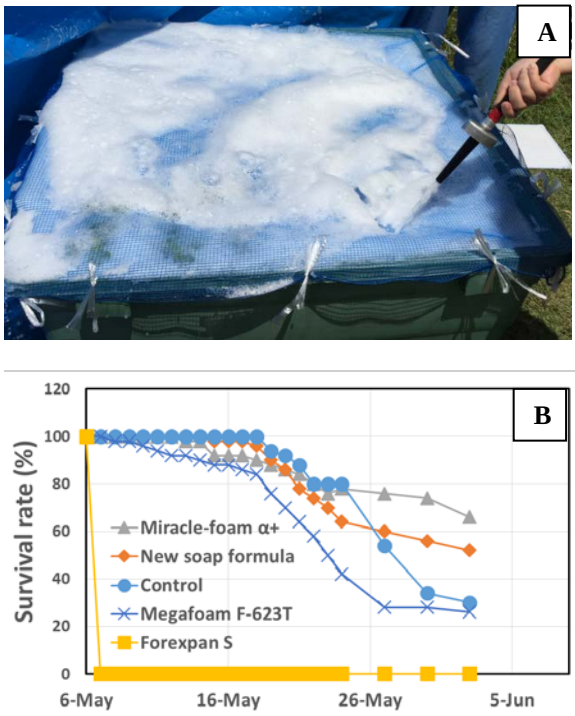

Fig 2. Viability of medaka fish in the presence of FFFs.

ACKNOWLEDGEMENTS

Shabondama Soap Co.Ltd. and Kitakyushu city FDMD are acknowledge for providing FFF samples.

REFERENCES

[1] U.S. Department of Agriculture. (1995). Chemicals used in wildland fire suppression: A risk assessment. USDA Forest Service, Fire and Aviation Management.

[2] Mizuki, H., Uezu, K., Kawano, T., Kadono, T., Kobayashi, M., Hatae, S., Oba, Y., Iwamoto, S., Mitsumune, S., Owari, M., Nagatomo, Y., Umeki, H. and Yamaga, K. (2007) Novel environmental friendly soap-based fire-fighting agent. J. Environ. Eng. Manag. 17: 403-408.

[3] Rawet. D. Smith. R. and Kravainis. G. (1996). A comparison of water additives for mopping-up after forest fires. Int. J. Wildland Fire 6: 37-43.

[4] Kitakyushu City Fire and Disaster Management Department, Research and development of ecologically acceptable fire suppression formula for urban fires (2005) Gekkan Shobo (Monthly Fire Fighting by Tokyo Ho-Rei) 313 : 1-8.(In Japanese)

[5] Goto, K., Takaichi, H. and Kawano, T. (2015) Learning from the eco-toxicology of fire-fighting foams in aquatic organisms: Altered eco-toxicity of sodium alkyl sulfonates in green paramecia and medaka fish maintained in in different waters. J. Disaster. Res. 10: 604-612.

[6] Noriyasu, A., Otsuka, K., Ishizaki, I., Tanaike, Y., Matsuyama, K., Uezu, K. and Kawano, T. (2014) A novel wild-land fire-fighting foam for minimizing the phytotoxicity of wood burning-derived smoke tested in living plant cells. Adv. Mater. Res. 875-877: 725-733.

[7] Kawano, T., Otsuka, K., Kadono, T., Inokuchi, R., Ishizaki, Y., Dewanker, B. and Uezu, K. (2014) Eco-toxicological evaluation of fire-fighting foams in small-sized aquatic and semi-aquatic biotopes. Adv. Mater. Res. 875-877: 699-707.

[8] Mizuki, H., Toyomura, M., Uezu, K., Yasui, H., Kawano, T., Akiba, I., Kawahara, T., Hatae, S., Sakamoto, N., Akiyama, M., Mizota, C., Umeki, H. and Yamaga, K. (2010) Microbial degradation of a soap-based fire-fighting agent in activated sludge. 20: 109-113.

[9] Kawano, T., Kadono, T., Matsuoka, N., Tamura, T. and Uezu, K. (2007) Development of soap-based fire-fighting agents less toxic to germinating rice (*Oryza sativa* L.) seeds. ITE Lett. 8 : 596-600.

[10] Kawano, T., Lin, C., Kadono, T., and Uezu, K. (2007) Ecological risk assessment of fire-fighting chemicals using medaka fish (*Oryzias latipes*) in different water conditions. ITE Lett. 8: 306-311.

[11] Lin, C., Kadono, T., Yoshizuka, K., Uezu, K. and Kawano, T. (2006) Assessing the eco-toxicity of novel soap-based fire-fighting foam using medaka fish (*Oryzias latipes*, Red-orange variety) adopted to river and sea water conditions. ITE Lett. 7: 499-503.

[12] Kawano, T., Kadono, T., Matsuoka, N., Tamura, T. and Uezu, K. (2006) Possible ecological risk assessment of commercial fire-fighting foams using germinating rice (*Oryza sativa* L.) seeds. ITE Lett. 7: 379-382.

[13] Inoue, K., and Y. Takei (2003) Asian medaka fishes offer new models for studying mechanisms of seawater adaptation, Comp. Biochem. Physiol. B. Biochem. Mol. Biol. 136:635-645.

[14] Naruse, K (1996) Classification and phylogeny of fishes of the genus Oryzias and its relatives Fish Biol. J. *Medaka*, 8: 1-8.

[15] Roberts, T.-R. (1998) Systematic observations on tropical Asian medakas or ricefishes of the genus *Oryzias* with descriptions of four new species, Icthyol. Res., 45: 347-354.

[16] Yokawa, K., Kagenishi, T. and Kawano, T. (2009) Effects of water salinity on the cold-induced suspended animation and irreversible damages in Oryzias latipes: Experimental eco-physiology predicting the seasonal changes in limnological fish distribution. J. Environ. Eng. Manag. 19: 195-200.

[17] Naruse, K., A. Shima, M. Matsuda, M. Sakaizumi, T. Iwamatsu, B. Soeroto and H. Uwa, (1993) Description and phylogeny of rice fish and their relatives belonging to the suborder Adrianichthyoidei in Sulawesi, Indonesia. Fish Biol. J. Medaka 8:1-8 (1993).A

[18] Shinomiya, A., H. Otake, K. Togashi, S. Hamaguchi and M. Sakaizumi, (2004)

Field survey of sex-reversals in the medaka, Oryzias latipes: genotypic sexing of wild populations, Zool. Sci. 21:613-619.

[19] Tzeng, C.-S., Y.-S. Lin, S.-M. Lin, T.-Y. Wang and F.-Y. Wang, (2006) The phylogeography and population demographics of selected freshwater fishes in Taiwan, Zool. Stud. 45:285-297 (2006).

[20] Inoue, K. and Y. Takei, (2002) Diverse adaptability in *Oryzias* species to high environmental salinity, Zool. Sci. 19:727-734.

[21] Kadono, T., Uezu, K., Kosaka, T. and Kawano, T. (2006) Altered toxicities of fatty acid salts in green paramecia cultured in different waters. Z. Naturforsc. 61c: 541-547.

[22] Kadono, T., Uezu, K., and Kawano, T. (2006) Confirming the altered toxicities of fatty acid salts in *Paramecium caudatum* cultured in different waters. ITE Lett. 7: 606-609.

[23] Goto, K., Lin, C., Kadono, T., Hirono, M., Uezu, K. and Kawano, T. (2007) Eco-toxicity of a soap component (sodium oleate) and a synthetic detergent cocktail using green paramecia assayed in natural water samples from East Asia. J. Environ. Eng. Manag. 17: 377-383.

[24] Goto, K., Kadono, T. and Kawano T. (2008) Use of natural mineral waters as the sources of diversified natural waters worldwide for testing the eco-toxicity of detergents using green paramecia. ITE-IBA Lett. 1: 184-188.

[25] Takaichi, H. and Kawano, T. (2016+) Expanded and practical use of logistic equations in eco-toxicity evaluation: cases of lethal metal toxicity curves in green paramecia with minimal-sized experiments. J. Adv. Comput. Intell. Intell. Inform. (*in press*)

Second International Conference on Science, Engineering & Environment,
Osaka City, Japan, Nov.21-23, 2016, ISBN: 978-4-9905958-7-6 C3051

HYDROGEN ISOTOPES AND AMOUNT OF PRECIPITATION SAMPLED BETWEEN OSAKA PLAIN AND SOUTH IKOMA MOUNTAIN, JAPAN

Hiroki Nishiwaki[1] and Hiroyuki Ii[2]
1Graduate School of Systems Engineering, Wakayama University, Japan
2Faculty of Systems Engineering, Wakayama University, Japan

ABSTRACT

"The purpose of study is to clarify the precipitation characteristics from plain to mountain. Precipitation samples were gathered every event at between the Osaka Plain and the south Ikoma Mountains. As a result, dew point elevation was clarified to be an important parameter to determine precipitation amount and isotope values. Precipitation amount increased with distance from dew point elevation to ground and hydrogen stable isotope ratios increased with the distance because raindrops was evaporated during rain falling from dew point to ground. Dew point elevation decreased with increase of precipitation amount because humidity increased after rain and then dew point elevation also changed. Then precipitation amount and hydrogen stable isotopic ratios changed with season because precipitation amount changed with season.

Keywords: Precipitation amount, Hydrogen stable isotopic ratio, Dew point elevation, Rainfall evaporate

INTRODUCTION

Precipitation is a uniqueness origin of groundwater and river. About 70 percent area of Japan's land is the mountain. Thus, it is significant to clarify characteristic of precipitation pattern at mountain for efficient use of water. Since heavy rain leads to landslides [1], it is necessary to know how much precipitation amount at each place. However, in particular distribution of precipitation in mountain was not uniform and complicated. Furthermore, the number of precipitation stations in mountain is less than plain therefore precipitation pattern and its characteristics are not clear.

Generally precipitation pattern for short time sampling was variable and precipitation pattern for long term sampling was stable because long term sampling was averaged. Then, from long term sampling, precipitation amount was clarified to increase with elevation [2]. There were two mechanisms for the relation between precipitation amount and elevation. When horizontal wind moves along a mountain, wind goes upward. Air temperature decreases with elevation by adiabatic expansion and then saturated vapor pressure decreases. When air vapor pressure is over the saturated vapor pressure, raindrop occurs and falls. Therefore, mountain makes rain and precipitation amount made by mountain increases with elevation.

On the other hand, Fukano et al (2016) [3] has reported that dew point elevation was clarified to be an important factor determining stable isotope values of precipitation. Evaporation from elevation at dew point to ground during rain falling was thought to change precipitation amount. Distance from elevation at dew point to ground decreases always with elevation and then evaporation rate decreases with elevation. Yabusaki et al (2008) [4] has reported that δD value in raindrop decreased with elevation of sampling points because δD value in raindrop increases with evaporation rate by isotope effect.

Yamada (1984) [5] has reported that precipitation amount increased with strength of slope wind. Yamada et al (1995) [6] has reported that precipitation amount at Mt. Yubari and Mt. Gozaisho in Hokkaido and Mie, Japan (each elevation of mountains: 1667 m, 1210 m) increased with elevation of sampling points.

On the other hand, precipitation amount of Kuki Peninsula (elevation of mountain: 318 m) did not increase with elevation. From two studies, in high elevation mountain, precipitation amount increased with elevation but the relation was not clear for low elevation mountain.

Even for low elevation mountain (elevation 600 m), heavy precipitation with over 100 mm increased with elevation apparently [7]. Then, in certain weather conditions, such as heavy rain, precipitation amount of low elevation mountain was thought to increase with elevation. As mentioned above, the relation between precipitation amount and elevation for low elevation mountain is complicated. Therefore, in this study, the purpose is to clarify the relation between precipitation amount and elevation considering dew point, wind direction and stable hydrogen isotopic ratio changed with evaporation.

METHODE

Sampling and Analysis

Figure 1 shows location of sampling points and enlarged view. Ikoma mountain range is located in the north-south direction on the border of Osaka and Nara in Japan. There were 6 rain gauges points at the east of Osaka, plain, foot, hillside and ridge in west side, top and valley in east side of Ikoma mountains. Rain sampling was performed 36 times by every precipitation for one year from September, 2014. Table 1 shows details of sampling points. Sampler was a 500ml bottle made of polyethylene with wide mouth, 43.6 mm in diameter. It was put on the ground each sampling points. Precipitation amount was measured by the following equation.

(1)

P: Precipitation amount (mm), W : Weight (g), ρ : Density of water (10^{-3} g/mm³), C : Caliber of Sampler (43.6 mm)

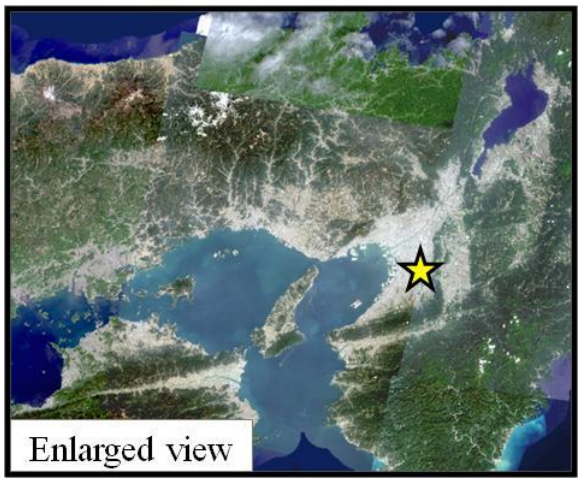

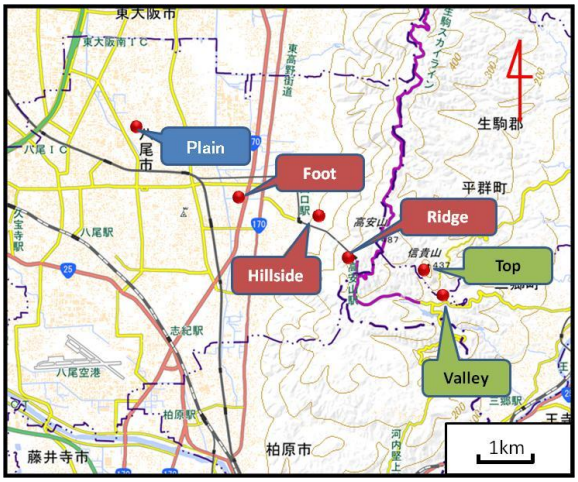

Fig. 1a Enlarged view of sampling area
b Location of sampling points

Using the H_2-H_2O equilibration method with platinum as a catalyst for hydrogen, the isotopic ratios of hydrogen were analyzed by mass spectrometer (Geo Wet System, Sercon Co.). Isotopic ratios are expressed as δ-values ‰ represented by the following equation.

(2)

R : D/H, V-SMOW : Vienna-Standard Mean Ocean Water. The measurement error of hydrogen isotopic ratio (δD) is ±1.0‰.

Estimate of the dew point elevation

Cloud occurs during air rising by adiabatic expansion process when air temperature reaches dew point. Elevation at dew point was the lowest elevation of cloud and dew point elevation determines distance from cloud to ground. Therefore, precipitation pattern was thought to change with dew point elevation. Dew point elevation was estimated by the expression of Henning.

$$H = 125 \qquad (3)$$

H ; elevation at dew point, $\mathbf{T_0}$; Surface temperature, $\boldsymbol{\tau_0}$; Dew point (degree C), and dew point was estimated of Tetens (1930) [8].

(4)

e ; vapor pressure. Surface temperature and vapor pressure are observed by Japan Meteorological Agency at Osaka.

RESULTS AND DISCUSSION

Annual precipitation amount and δD value

Figure 2 shows topographical map and annual precipitation at each sampling point. Annual precipitation amounts sampled at the hillside, ridge

Table 1 Details of sampling points

Point	Elevation(m)	Slope orientation
Plain	0	-
Foot	10	
Hillside	120	West
Ridge	430	
Top	440	-
Valley	280	Southeast

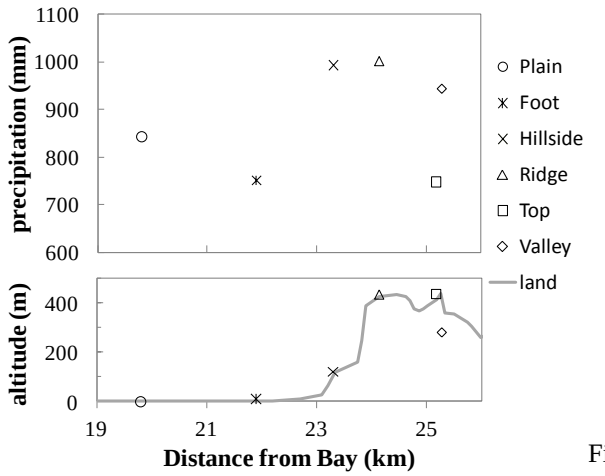

Fig. 2 Topographical map and annual precipitation at each sampling point

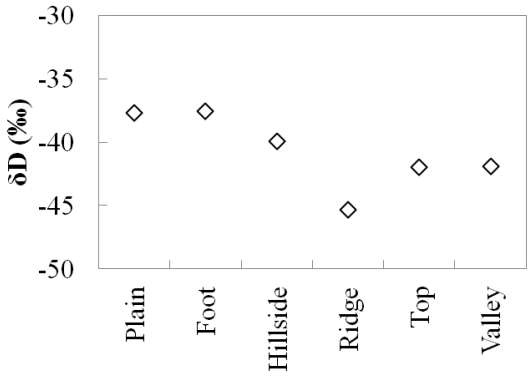

Fig. 3 δD values of each sampling point

and valley were more than those at the plain. Annual precipitation amount sampled at the foot and top of mountain were less than those at the plain. Annual precipitation amount at the ridge was the maximum value however precipitation amount did not always increase with elevation because annual precipitation amount sampled at the top was less than those at the plain. Comparing foot and plain, annual precipitation amount was thought to decrease with distance from sea. Low precipitation at the top was thought to be brought out by effect behind the mountain because generally cloud comes from west by seasonal wind.

Figure 3 shows δD of precipitation at each sampling point. Average δD value of 16 precipitation events sampled from September 2014 to March 2015 decreased from plain to ridge but increased from ridge to valley eastward.

Figure 4 shows relationship between δD value and precipitation amount in each sampling points. Each precipitation amount was average of 16 precipitation events. δD value decreased with precipitation amount. The relation between precipitation amount and δD value of each sampling

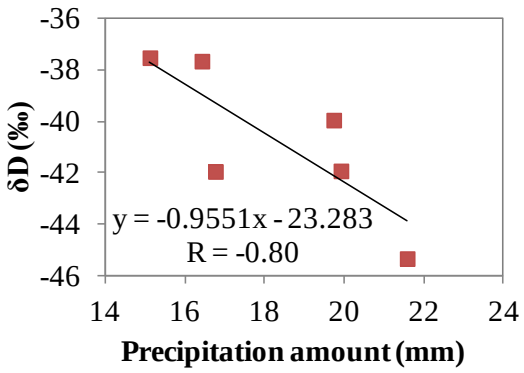

Fig. 4 Relationship between δD value and precipitation amount in each sampling points

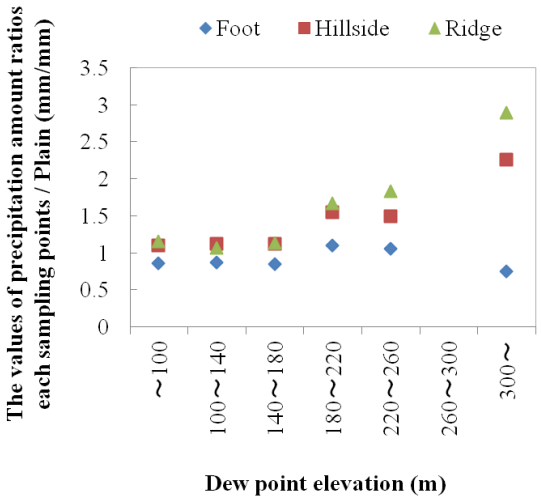

Fig. 5 Relationship between δD value and precipitation amount in each sampling points

point was strong negative correlation with **-0.8**. δD value and precipitation amount in each sampling point was thought to change same mechanism.

Variety of precipitation amount and δD by the dew point elevation

Reason that precipitation amount decreased with increasing δD value was thought to due to raindrop evaporation. Raindrop evaporation is a rain evaporation process during falling from dew point elevation to ground. Under dew point elevation, raindrop evaporates during falling because of unsaturated air. Therefore, precipitation amount decreases with distance from dew point elevation to ground. On the other hand, δD value of raindrop increases with evaporation rate by isotopic fractionation [4]. Then, δD value of raindrop increases with distance from dew point elevation to

ground.

Figure 5 shows relationship between precipitation amount ratio at each point and dew point elevation. Precipitation amount ratio at each point was average precipitation amount at the each point per average precipitation amount at the plain.

The ratios at the foot were about 1 with change of dew point elevation. The ratios of hillside and ridge increased with dew point elevation when dew point elevation was over 180 m. When dew point elevation was under180 m, the ratios of hillside and ridge were about 1. Therefore, when dew point elevation was low less than 180 m, difference of precipitation amount among various elevations was not observed. When dew point elevation was high, difference of precipitation amount was observed.

Figure 6 shows relationship between difference of δD value from plain to ridge and dew point elevation. Difference of δD value was difference between average δD at the plain and average δD at the ridge divided by 100m. Difference of δD increased with dew point elevation. As a result,

Precipitation amount decreased and hydrogen stable isotopic ratios increased with distance from dew point elevation to ground because of raindrop evaporation due to distance from dew point elevation to ground.

Variation factor of dew point elevation

Humidity in air increases after rain because rain evaporates. Then, dew point elevation was thought to decrease after rain and with precipitation amount at each event. Precipitation amount is high in summer and low in winter at the study area. Thus, dew point elevation was thought to be change with season.

Fig.7 shows relationship between precipitation amount and dew point elevation in Yao near the study area. Precipitation amount was average value of the precipitation amount for each precipitation of the Japan Meteorological Agency in Yao. Dew point elevation decreased with precipitation amount.

Seasonal precipitation pattern

Figure 8 shows seasonal dew point elevation and precipitation amount in Yao near the study area. Precipitation amount was average value of the precipitation amount for each precipitation of the Japan Meteorological Agency in Yao. Dew point elevation was average value of each precipitation. Four seasons predetermined that from September to November is autumn, from December to February is winter, from March to May is spring, and from June to August is summer. In autumn and summer, precipitation amount was higher and dew point elevation was lower than those in winter and spring. Then, dew point elevation changed with season in Yao.

Figure 9 shows seasonal precipitation ratio of sampling point in west slope at the study area.

Precipitation ratio was average precipitation amount at the each sampling point in west slope divided by average precipitation amount at the plain.

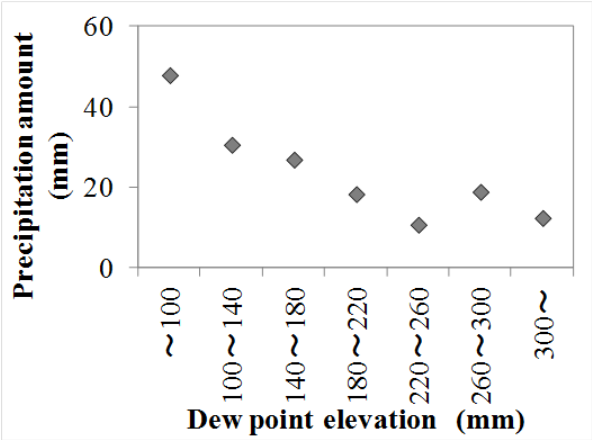

Fig. 7 Relationship between precipitation amount and dew point elevation

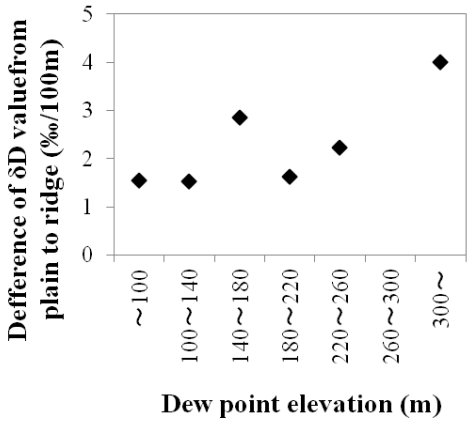

Fig. 6 Relationship between difference of δD value from plain to ridge

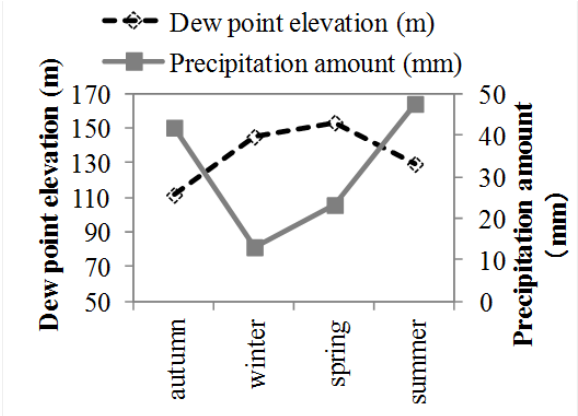

Fig. 8 Seasonal dew point elevation and precipitation amount

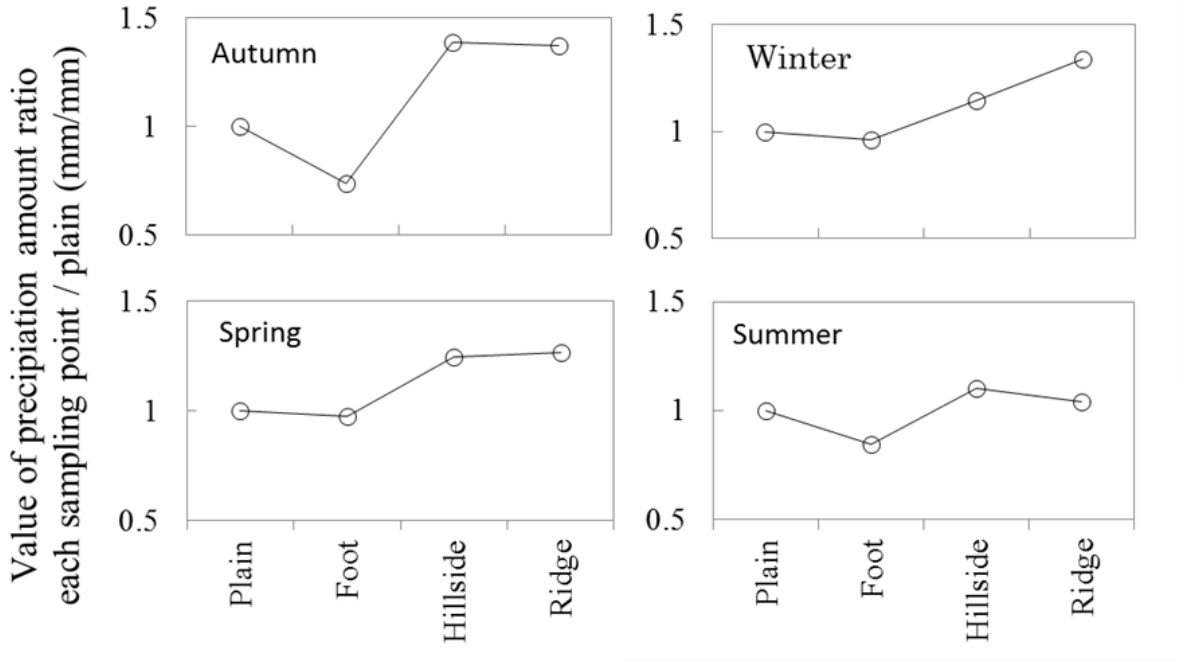

Fig. 9 Seasonal precipitation ratio of sampling point in west slope

Precipitation ratios in winter and spring increased with elevation of sampling point. On the other hand, in summer, precipitation ratio was constant with changes of sampling point elevation. From the above, dew point elevation of each precipitation in sampling area decreases with precipitation amount. As a result, winter precipitation with small amount of precipitation was thought that precipitation amount increased with elevation of sampling point. Precipitation ratio of each sampling point in autumn was variable. Suzuki et al (2010) [7] reported that precipitation amount caused by typhoon increased greatly with elevation. In autumn high precipitation ratio was thought to due to typhoon. Therefore, dew point elevation was thought to determine seasonal change for precipitation.

CONCLUSION

The purpose of study is to clarify precipitation characteristics from plain to mountain. Then, precipitation sampling between the Osaka Plain and the south Ikoma Mountains, Osaka prefecture, Japan was performed for one year.

As the result of sampling and measuring precipitation, annual precipitations sampled at the mountain area were higher than those at the plains. The relation between every precipitation amount and hydrogen stable isotope ratios of each sampling point was strong negative correlation with -0.8.

Hydrogen stable isotopic ratios decreased with annual precipitation amount. Precipitation amount decreased and hydrogen stable isotopic ratios increased with distance from dew point elevation to ground because of raindrop evaporation due to distance from dew point elevation to ground. Humidity in air increases after rain because rain evaporates. Then, dew point elevation decreased after rain and with precipitation amount at each event. Precipitation amount is high in summer and low in winter at the study area. Thus, dew point elevation changed with season and then elevation effect of precipitation amount and isotopic ratio change depended on season with change of dew point elevation. .

REFERENCES

[1] I. M. Patuti, Ahmad R, K. B. Suryolelono, “Mechanism and Characteristics of The Landslides in Bone Bolango Regency, Gorontalo Province, Indonesia”, International Journal of GEOMATE, Vol. 12, Issue 29, pp. 1-8, Jan., 2017.

[2] Nakakita E, Suzuki Y, Ikebuchi S, “Hierarchical Time-Scale Structure in Dependency of Rainfall Distribution on Topography”, Disaster Prevention Research Institute Annals, Bo. 43, B-2, April, 2000.

[3] Fukano T, Hiroyuki I, “Dew Point Elevation and Oxygen and Hydrogen Isotopic Ratios for Precipitation Sampled at Osaka and Matsue, Japan”, International Journal of GEOMATE, Vol. 11, Issue 27, pp. 2712-2716, Nov., 2016.

[4] Yabusaki S, Tase N, Tsujimura M, “Characteristics of Stable Isotopes in Precipitation at South Slope of Mt. Tsukuba”,

Bulletin of the Terrestrial Environment Research Center ,No 9, 2008, pp.15-23.

[5] Yamada K, "Special Distribution of Heavy Rainfall in Mountainous Area", Journal of the Japan Society of Civil Engineers, No.28, 509-513, 1984

[6] Yamada T, Hibino T, Araki T, Nakatsugawa M, "Statistical Characteristics of Rainfall in Mountainous Basins", Journal of the Japan Society of Civil Engineers, No.527, Ⅱ-33, 1-13, 1995.

[7] Suzuki H, Nakakita E, 2010 "Dependence of heavy rainfall on elevation along railroad in mountainous area", Annual Journal of Hydraulic Engineering, Japan Society of Civil Engineers, Vol.54, 2010, pp.337-342.

[8] Tetens O. "Uber einige meteorologische Begriffe", Z. Geophys, 6, pp.297-309.

Second International Conference on Science, Engineering & Environment,
Osaka City, Japan, Nov.21-23, 2016, ISBN: 978-4-9905958-7-6 C3051

THE BEHAVIOR OF STRONTIUM AGAINST THE ADSORBENT IN DIFFERENT SOLUTIONS

Keiichiro Shibata[1], Hidenori Yoshida[2], Naomichi Matsumoto[3] and Yoshihiro Suenaga[4]
[1]Graduate student, Kagawa University, Japan, [2,4]Professor, Kagawa University, Japan, [3]Technical staff, Kagawa University

ABSTRACT

The Tsunami due to the Great East Japan Earthquake on March 11, 2011 indirectly caused a nuclear disaster at the Fukushima Daiichi nuclear energy plant of the Tokyo Electric Power Company. The radioactive strontium dispersed by the accident have spread to the soil, lake, river and marine environments. Alternatively, tainted groundwater continues to be generated by damaged facilities. The increase of collected tainted water makes it difficult to secure the storage facility. In the face of such situation, the decontamination work for the radioactive strontium has not been completed. It is possible that human is exposure by ecological chain and biological concentration when the tainted water including the major quantity of strontium leak to marine. Therefore, the decontamination of strontium is urgent business. In light of these, the experiment which has adsorbed strontium into adsorbent so as to decrease the contamination degree of tainted water had been conducted by the authors in the past. From the results, it was confirmed that the adsorption ability of adsorbent for strontium is varied in different solutions. Therefore, in this study, the adsorption test of adsorbent is conducted to grasp its ability in solution composed of magnesium, potassium or chloride. The hydroxyapatite derived from fish bones is developed and used as the adsorbent. From the result of tests, it is confirmed that the adsorption ability of hydroxyapatite for divalent cation is high level in the various solutions.

Keywords: decontamination, hydroxyapatite, strontium, radiation tainted water

INTRODUCTION

The nuclear disaster at the Fukushima Daiichi nuclear energy plant (F1) of the Tokyo Electric Power Company was indirectly caused by the Great East Japan Earthquake and the Tsunami on March 11, 2011. The amount of radioactive materials discharged from the F1 due to the accident, which contaminated in the surrounding land and ocean. When the marine contamination is occurred by the radioactive materials, the influence on aquatic product is especially needed to be concerned. Figs. 1-4 are recreated on the Report of Radioactivity Surveys by the Hydro-graphic and Oceanographic Department Japan Coast Guard, which are shown as the tainted situations of cesium-137 (^{137}Cs) and strontium-90 (^{90}Sr) as in the references [1]-[5]. The vertical axis in the graphs is the detected value of ^{137}Cs or ^{90}Sr, and the horizontal is the measured year. The survey points of two elements are Off Otaru, Sendai bay, Tokyo bay, Ise bay and Osaka bay. The detected values of ^{90}Sr and ^{137}Cs in the marine water are shown in Fig. 1 and Fig. 2, respectively. The detected values of ^{90}Sr and ^{137}Cs in the marine mud are shown in Fig. 3 and Fig. 4, respectively. The radioactive concentration of strontium in Tokyo bay is almost the same as that in Sendai bay. Whereas, the radioactive concentration of cesium in Tokyo bay is the highest. The spreading of the radioactive materials are evident from the survey results. Alternatively, it is confirmed that a large quantity of cesium and strontium are detected from marine water on 2011 and they are high in the mud after 2012. After that, the detected of strontium does not change. On the other hand, the number of cesium remains on 2014. From these survey results, it is considered that the radioactive contamination in hydrosphere is due to the cesium. Whereas the matter of tainted water in the F1 is needed to be taken notice. The groundwater which is transferred to the nuclear reactor building is contaminated, and the securement of storage facility is a serious problem. Table 1 is recreated base on the results which is obtained from the analysis for groundwater in the F1 by the Tokyo Electric Power Company Holdings as in the reference [6]. The groundwater is collected from the thirty points where flows around seawall of the Units 1-4 of the nuclear reactor building so as to investigate the contaminated situation by ^{137}Cs and beta ray, and the average of detected value of ^{137}Cs and beta ray in groundwater are shown in Table 1. Though the Tokyo Electric Power Company sets out to decrease the inflow of groundwater throw the nuclear reactor building and steps down the contamination degree of tainted water, the sign of solution is not shown. The detected value of beta ray is very high to compare with that of ^{137}Cs. It is considered that the tainted groundwater includes the major quantity of ^{90}Sr, because ^{90}Sr is the representative radioactive material which emits the beta ray. Therefore, the removals of strontium in the tainted water and cesium in marine

mud are respectively demanded, alternatively, the strontium is more dangerous than the cesium. Because it is considered that strontium is more dangerous than cesium due to the following fact. When cesium is taken in the body, it is mainly absorbed into muscle. After that, it is released from the body as sweat or urine. Strontium, on the other hand, is absorbed into bone and is stored in it for long time. When the tainted water including the major quantity of strontium leak to marine, it is possible that human is exposure by ecological chain and biological concentration. Therefore, the decontamination of strontium is urgently needed. The authors have conducted the experiment which strontium is adsorbed to the adsorbent under the marine and tainted water so as to solve this problem in the past (see the reference [7]). It was confirmed that the adsorption ability of adsorbent for strontium is varied
in different solutions. Thus, in this study, the

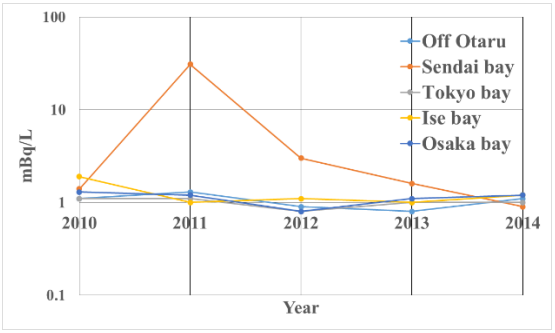

Fig. 1 Secular change of ^{90}Sr in marine water

adsorption ability of adsorbent is examined to

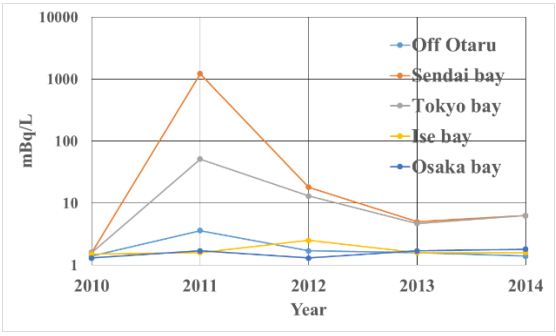

Fig. 2 Secular change of ^{137}Cs in marine water

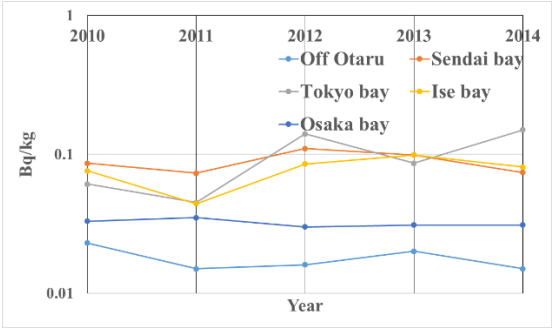

Fig. 3 Secular change of ^{90}Sr in marine mud

maximize the performance of adsorbent for

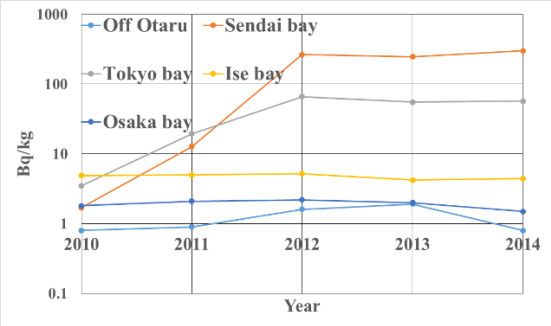

Fig. 4 Secular change of ^{137}Cs in marine mud

strontium under the various environments. In concrete terms, a number of solutions are prepared, and the adsorption tests of the adsorbent for strontium in each solution are conducted. The adsorption ability of adsorbent is grasped throw comparing the test results.

Table 1 Analysis results of tainted water in around F1 (seawall of Unit 1-4)

	^{137}Cs(Bq/L)	Sum of beta ray(Bq/L)
Around seawall of Unit 1	6.75	28.17
2	4797.38	129294.20
3	43.33	1200.00
4	3.43	5478.67

UTILIZED ADSORBENT IN EXPERIMENT

There are two important issues when decontaminating the hydrosphere; the non-proliferation of radioactive materials and volume reduction of radioactive waste. In this study, new adsorption materials, which can adsorb radioactive fallout is developed to solve the issues. To be more precise, the new adsorption material consists of hydroxyapatite (HAp, see Fig. 5). The chemical formula for the HAp is $Ca_{10}(PO_4)_6OH_2$ and is the hydroxyl end member of the complex apatite group. The apatite is the clump of crystalline compound

Fig. 5 Hydroxyapatite

which has the basic structure of $M_{10}(ZO_4)_6X_2$. For example, fluorapatite ($Ca_{10}(PO_4)_6F_2$) is the representative component of phosphate rock, and it is the industrial resource for phosphorus [10]. The HAp receives a lot of attention as the biomaterials for modern tooth and bone implants. The artificial combining is conducted by a lot of methods [9]. The HAp utilized in the study was developed by Suenaga, etc. (application number: 2014-58267, invention name: hydroxyapatite made from fish bones, merely calcined, applicant: national university corporation Kagawa university and Nihon Kogyo CO.LTD, apply date: April 2nd, 2014)

TARGETED MATERIAL FOR EXPERIMENT

A wide variety of radioactive materials were released from the accident at the Fukushima Daiichi nuclear energy plant. For experiments using the HAp, strontium was selected as a target material because it is released vigorously and its half-life is relatively long. Also, the properties of strontium are more or less those of calcium where it is absorbed into the bones after entering the body [8]. The properties of strontium are explained below in detail since it is necessary to grasp their features for the experiment.

Strontium is a fusible alkali-earth metal, which exists as a divalent positive ion in solution. Strontium also has several isotopes. Among those, ^{90}Sr, a by-product of nuclear fission found in the nuclear fallout from the Fukushima Daiichi nuclear power plant, is the removal target. The half-life of ^{90}Sr is about 29 years. ^{90}Sr changes to stable zirconium-90 by twice beta collapse. Radiation exposure is divided into two categories; one is the external exposure, and the other is the internal exposure. The external exposure occurs when an organism receives radiation from outside the body. Once strontium is substituted for calcium in bone, it is rare that the strontium is expelled from the body. This behavior is different from that of cesium, which is absorbed into the muscles in the body.

Knowing the above facts, it can be said that the health threat to humans is caused by strontium and the strontium should be de-contaminated as quickly as possible.

EXPERIMENT AND ANALISYS METHOD

In the experiment, five solutions and pure water are prepared to compare the adsorption ability of the HAp for strontium in different environment. One specimen is prepared in terms of comparison, it is pure water, while the other contains sodium chloride, sodium acetate, potassium chloride, magnesium chloride and sodium nitrate 3%. The reason why the sodium chloride and etc. are 3 % concentration in the each solution is close to that in seawater.

First, 300 ml of each solutions are poured into cylindrical containers, and 5.0 mg of liquid strontium hydroxide is added. After that, the filter bag containing the HAp absorbent is placed on the bottom of cylinders. The filter bag is frequently used as the household kitchen sinks

Secondly, it is immersed for the set period of time (see Fig. 6). After a set immersion time, the HAp is picked up, and the remaining amount of strontium in the solutions is analyzed by inductively coupled plasma atomic emission spectrometry (ICP-AES). In this study, the residual ratio is utilized as the evaluation of experiment result. The residual ratio is defined by the following equation, Eq.(1)

$$R(\%) = \frac{r}{a} \times 100 \quad (1)$$

where "*r*" is the remained amount of strontium, and "*a*" is the additive amount of strontium. An average result is recorded after three times experiments are conducted for each set of 5 solutions and pure water.

Fig. 6 Immersion test

EXPERIMENT AND ANALISYS RESULTS

The residual ratio of strontium in each solution is shown in Figs.7-12. The vertical axis in the figure is the residual ratio of strontium, and the horizontal one is the immersion time. About 10 pieces (6.0~7.0g) of the HAp, one of which has 0.6~0.7g of mass for one piece, are used in each experiment and the immersion times are 24 h, 72 h, 120 h or 168 h.

Solutions containing chloride

The experimental results of three solutions with involvement chloride are shown in Figs. 6-8. It is confirmed that the residual ratio of strontium in three specimens decreases with the passage of time. Especially, when potassium chloride solution or sodium chloride solution is employed as the solution, the residual ratio of strontium is almost zero percent after 168 h, and it is the lowest in the potassium chloride solution after 24 h. It is possible that the

adsorption of HAp for strontium is prompted by the potassium. On the other hand, when magnesium chloride solution is employed, almost thirty percent of strontium remained in the solution. Furthermore, the adsorption ability of HAp for strontium is clearly influenced by divalent cationic magnesium.

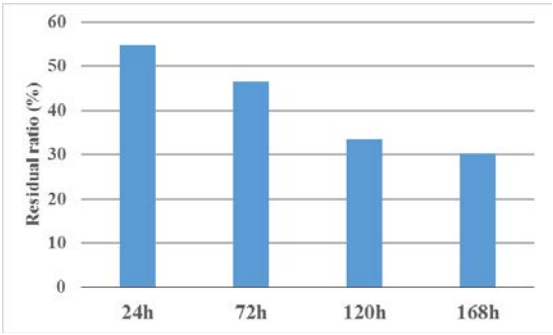

Fig. 7 Residual ratio of strontium in magnesium chloride solution

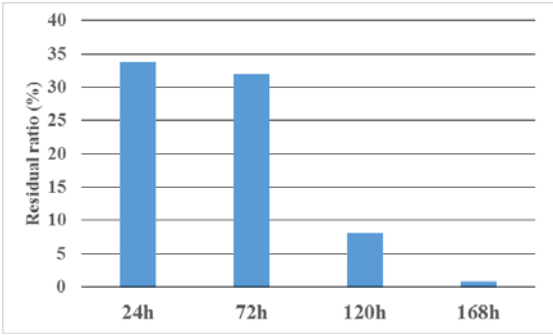

Fig. 8 Residual ratio of strontium in sodium chloride solution

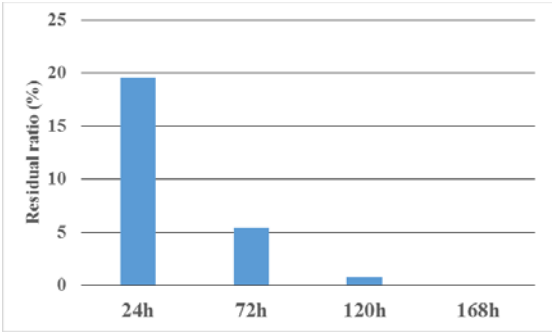

Fig. 9 Residual ratio of strontium in potassium chloride solution

Solutions without chloride

The experiment results of three solutions with non-involvement chloride are shown in Figs. 9-11. It is confirmed that the residual ratio of strontium in three solutions decreases with passage of time. Alternatively, when three solutions are compared in the light of existence or non-existence of sodium, the residual ratio of strontium in solution containing of sodium is relatively high other than the pure water. It is considered that the adsorption ability of the HAp for strontium is slightly influenced by sodium. Nevertheless, more than ninety percent of strontium is adsorbed to the HAp in case of utilizing each solutions.

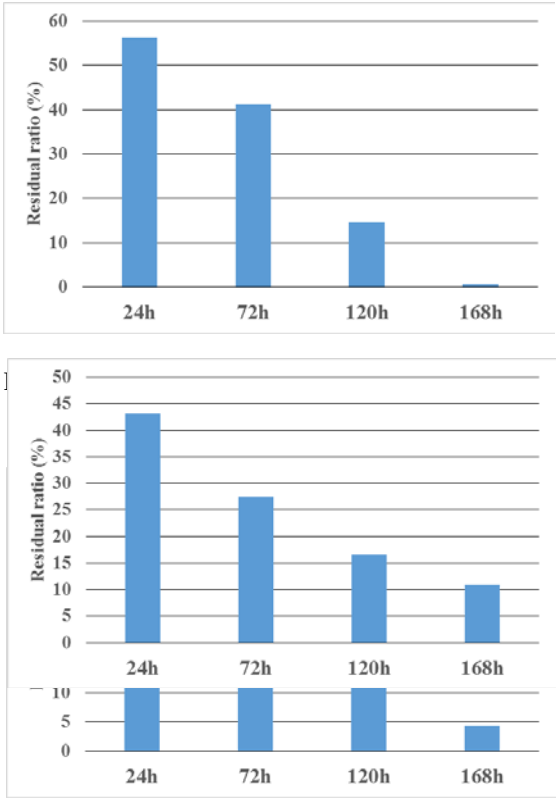

Fig. 12 Residual ratio of strontium in sodium acetate solution

CONCLUSIONS

In this study, adsorption experiments are conducted in various solutions to grasp the adsorption ability of the HAp for strontium. It is confirmed in the results that the adsorption ability of the HAp for strontium has a beneficial effect in every five solution and pure water. The residual ratio of strontium is more or less zero percent in case of using pure water, sodium chloride solution or potassium chloride solution. Especially, the residual ratio of strontium already decrease up to twenty percent after 24 h in the case of potassium chloride solution. It is considered that the ionization tendency of potassium is higher than that of strontium, which makes an effect on the adsorption performance of HAp. The influence on the HAp is examined by

increasing the concentration of potassium in near future. On the other hand, when magnesium chloride solution is utilized, about thirty percent of strontium remained in the solution. It is considered that divalent cationic magnesium blocks strontium adsorption to the HAp. In fact, the seawater and the groundwater include various metal elements. Furthermore, it is necessary to examine the detailed influence on the HAp through conducting the experiment in which the concentrations of potassium, sodium and magnesium are changed.

It is confirmed that the HAp is the effective adsorbent for strontium among various adsorbents, but it is necessary to conduct the laboratory experiment in environment including various environments so as to remove strontium from the seawater which are consisted to include them. Alternatively, the HAp may have a possibility to adsorb a large number of materials other than strontium. The HAp can become the effective device to the cleanup of air and water pollution. A variety of artifice and many experiment are necessary to make use of the HAp in various field. In this study, the adsorption ability of HAp for the alkali metals and the alkaline-earth metal has been examined, but the adsorption ability for the other elements is conducted.

ACKNOWLEDGEMENTS

The authors would like to express cordial gratitude to NIHON KOGYO. CO. LTD for provision of the HAp and the HAp sheet. This work was supported by JSPS KAKENHI Grant Number 24520507.

REFERENCES

[1] Hydrographic and Oceanographic Department Japan Coast Guard, Report of Radioactivity Surveys, Results of Surveys in 2010, ISSN 0910-044X, Mar. 2012, pp. 4-7.

[2] Hydrographic and Oceanographic Department Japan Coast Guard, Report of Radioactivity Surveys, Results of Surveys in 2011, ISSN 0910-044X, Mar. 2013, pp. 5-8.

[3] Hydrographic and Oceanographic Department Japan Coast Guard, Report of Radioactivity Surveys, Results of Surveys in 2012, ISSN 0910-044X, Mar. 2014, pp. 5-14.

[4] Hydrographic and Oceanographic Department Japan Coast Guard, Report of Radioactivity Surveys, Results of Surveys in 2013, ISSN 0910-044X, Nov. 2014, pp. 5-13.

[5] Hydrographic and Oceanographic Department Japan Coast Guard, Report of Radioactivity Surveys, Results of Surveys in 2014, ISSN 0910-044X, Jul. 2015, pp. 5-12.

[6] Tokyo Electric Power Company Holdings, Analysis results of tainted water in around F1 (seawall of Unit 1-4), Jun. 2016.

[7] Shibata K, Yoshida H and Matsumoto N, "Study on removal of cesium and strontium from marine and lake mud", International Journal of GEOMATE, Vol. 11, Aug. 2016, pp. 2259-2256.

[8] Mimura H, Yamagishi I and Akiba K, "Removal of radioactive cesium and strontium by zeolites", The Chemical Society of Japan, vol. 1989, No. 3, Jun. 1988, pp. 621-627.

[9] Tanioka T, Imanishi N and Kawai T, "Apatite for Bioengineering Ceramics, Resources processing", Vol. 37, No. 1, Oct. 1989, pp. 15-22.

[10] Tanioka T, Imanishi N and Kawai T, "Adsorption Characteristic of Hydroxyapatite in aqueous solutions", Resources processing, Vol. 38, No. 3, May. 1991, pp. 121-127.

[11] Nishiyama Y, Hanafusa T, Yamashita J,Yamamoto Y and Ono T, "Adsorption and removal of strontium in aqueous by synthetic hydroxyapatite", Journal of radioanalytical and nuclear chemistry, Vol. 307, Feb. 2016, pp.1279-1285.

Second International Conference on Science, Engineering & Environment,
Osaka City, Japan, Nov.21-23, 2016, ISBN: 978-4-9905958-7-6 C3051

BIODEGRADATION CAPACITY OF URBAN RIVERS IN JAKARTA, INDONESIA

Yonik Meilawati Yustiani[1], Imas Komariah[2]
[1]Department of Environmental Engineering, Engineering Faculty, Pasundan University, Indonesia, [2]Doctoral Student of Faculty of Environmental Engineering, the University of Kitakyushu, Japan

ABSTRACT

Jakarta is a city with dense population and various activities causing the heavy pressure to the environment. Domestic and non-domestic activities are generating pollution to its rivers. The water body actually has itself a self natural purification capability. The characteristic of the river water quality will affect this pollution degradation process. This research is conducted to examine the biodegradation capacity of Jakarta's rivers. Water quality data of 23 rivers were collected for the time period of 2011 to 2015. Biochemical Oxygen Demand (BOD) and Chemical Oxygen Demand (COD) concentrations are then being used to calculate the BOD/COD ratio. The calculation results show that during the period time of 2011-2013 the ratio ranges between 0.36 and 0.63, which indicates that the rivers have average biodegradation capability. However, the 2014 year's data show that almost all of the rivers have ratio less than 0.2, indicating the no-biodegradation capability. Existence of metals can also inhibit the biodegradation process. The water quality data shows significant increase of metals in the year of 2014, especially Copper and Zinc in several rivers. Surfactant was also observed in extremely high concentration. Thus, most of the Jakarta's rivers have relatively low capability in biodegradation capacity and self purification capability. Although the latest year data shows an improvement, yet the BOD/COD ratio is still in the range of slow of biodegradation capacity.

Keywords: BOD/COD ratio, Biodegradation Capacity, self purification

INTRODUCTION

Urban river systems are often heavily degraded, a situation that is not confined to a particular geographic region of the world, but common to all areas subject to urbanization [1]. Urban development imposes enormous changes on the form and function of river systems [2]. Nowhere is the impact of human population growth and land alteration more apparent than in the water quality of urban rivers [3]. River water and sediment quality are affected by storm water and waste water drainage and by point and diffuse inputs of pollutants [2]. Balancing the interactions between natural and constructed systems in urban areas is crucial for the future supply of water for large human settlements [4].

Jakarta, as a capital city of Indonesia, has several rivers crossing across its area. Visually, those rivers water quality apparently suffer with heavy pollution. There are 13 major rivers flowing through the city of Jakarta. These rivers receive pollutants from industrial and household sources in both solid and liquid forms [5].

Naturally, the organic-polluted rivers can purify themselves. Many physical, chemical, and biotic processes are important for the formation of water quality and water purification in aquatic ecosystems. Many of these physical and chemical processes are either controlled or affected to a certain degree by biological factors. For example, the rate of the sorption of pollutants by settling particles of suspensions depends on the concentration of phytoplankton cells; photochemical decomposition of substances is only possible in transparent water, and the transparency is ensured by the filtration activity of hydrobionts. Thus, biotic processes are pivotal for the entire system of water self purification [6]. The removal of pollutants from a water body without any artificial controls is called self-purification, or natural purification. The mechanism of self-purification of water bodies can be divided into three groups: physical processes, chemical processes and biological processes [7].

The characteristic of the river water quality will affect the pollution degradation process. This research is conducted to examine the biodegradation capacity of Jakarta's rivers. Monitoring of biochemical parameter is a routine water quality assessment for river quality where pollution is of concern due to rapid urbanization and industrialization that can post threat to sustainability of river conservation. Thus BOD and COD are two widely used parameters for organic pollution measurements [8]. The BOD/COD ratio is an indicator of biodegradation capacity [9]. The ratio is also affected by the concentration of non-biodegradable material.

BOD/COD ratio is found to be reliable and

useful indicator to relate organic matter content in the river under tropical climate condition. BOD/COD ratio can be used as crucial attribute for characterization of river and critical indicator for pollution measurement in the river water study [8].

A value of >0.5 BOD/COD ratio denotes rapid biodegradation, and a range of 0.2-0.4 indicates biodegradation only in favorable thermal condition [10]. Having the biodegradation capacity will suggest the further treatment and strategy to overcome the polluted urban rivers.

METHODOLOGY

Yearly samples were taken by the River Agency of Ciliwung-Cisadane River Region. The number of sampling stations in the Ciliwung-Cisadane Basin Region is 50; however some of the sampling stations are determined later, started from 2012. In the year of 2011, the sampling stations were lesser that those today. To have a better comparison, this research is only analyzing 34 stations which have complete data since 2011. Figure 1 shows the location of all sampling stations. In the year of 2013, the samples were taken twice a year denoting the rainy and dry seasons.

The biodegradation capacity of river water is determined by using BOD/COD ratio. In most effluents, BOD is less than COD, and elevated BOD5/COD ratio signals a high rate of biodegradation of wastewater [11]. This ratio is generally considered the cut-off point between biodegradable and non-biodegradable waste [12].

Measurement of BOD and COD were carried out using dilution method and dichromate method, respectively, according to the APHA's Standard Method [13].

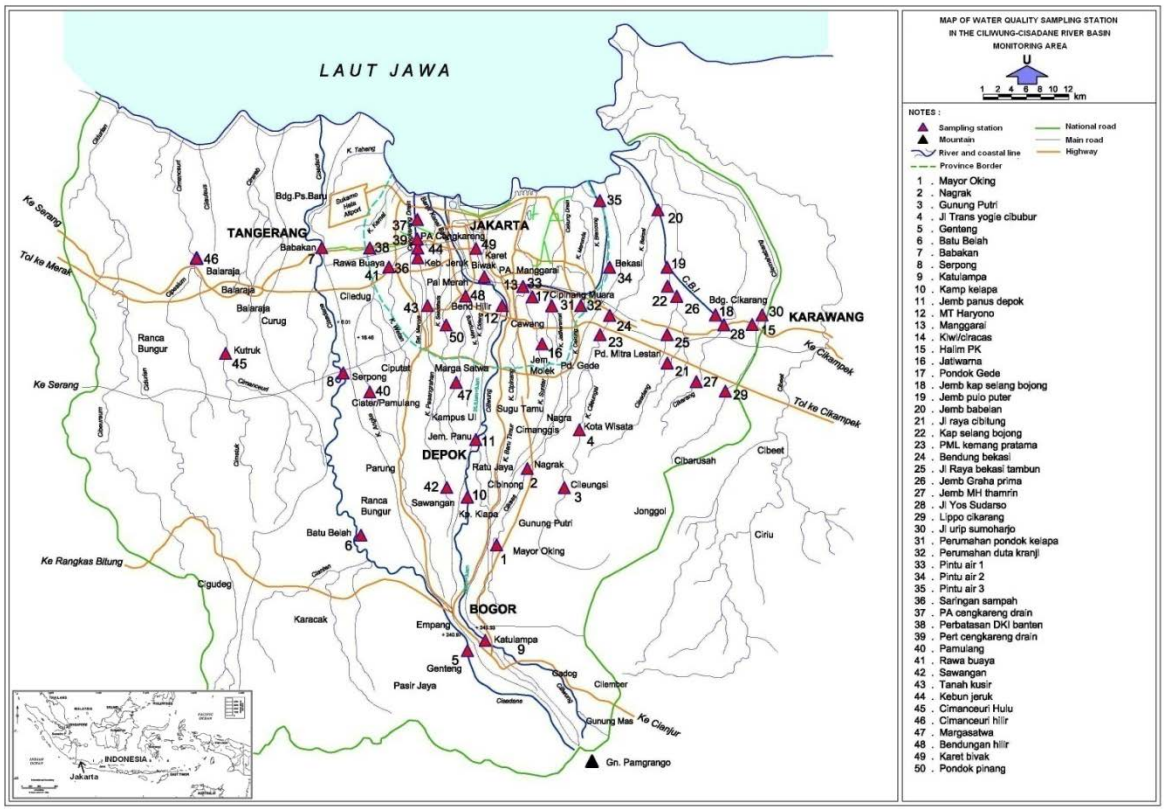

Fig. 1. Map of Ciliwung-Cisadane River Basin and water sampling stations. (BBWS, 2015)

Biodegradation capacity determination can be indicated by observing the inhibitor of self-purification process. Heavy metals and MBAS surfactant were also determined from the water samples to support the result of river water biodegradable capacity results. Measurements of heavy metals were conducted using the spectrometry method [13]. The inhibitory effects of heavy metals on the self-purification process started at much higher concentrations of metals than those typically found in surface water [14].

RESULT AND DISCUSSION

The Figure 2, 3, 4, 5 and 6 depict the BOD/COD ratio of Jakarta's Rivers for the year of 2011, 2012, 2013, 2014 and 2015, respectively. There are two set of data of the year 2013 representing the rainy and dry season. The black shading on the Fig 4 shows the rainy season's data, whereas lighter grey shading on the Fig. 4 shows the dry season's.

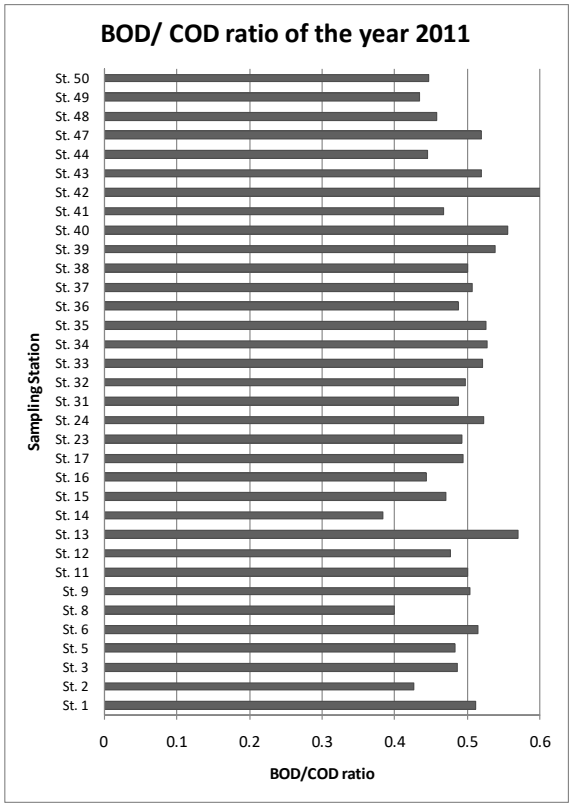

Fig. 2 BOD/COD ratio of the year 2011

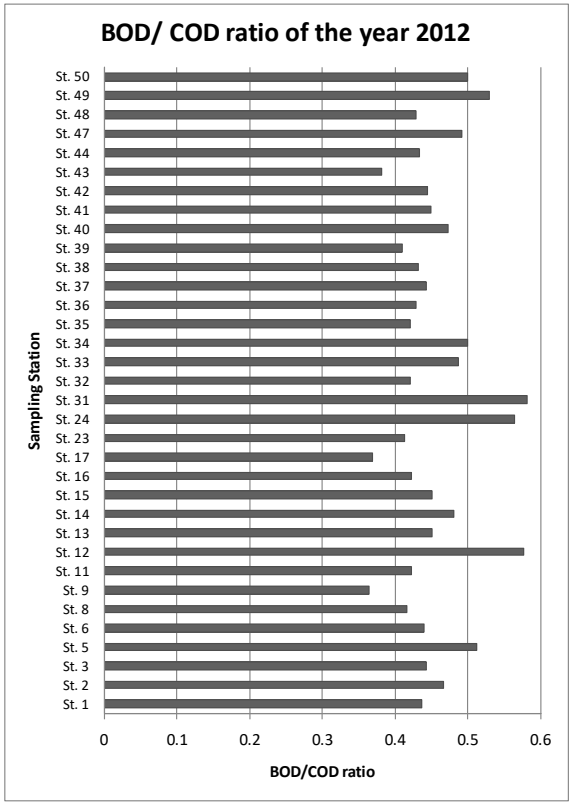

Fig. 3 BOD/COD ratio of the year 2012

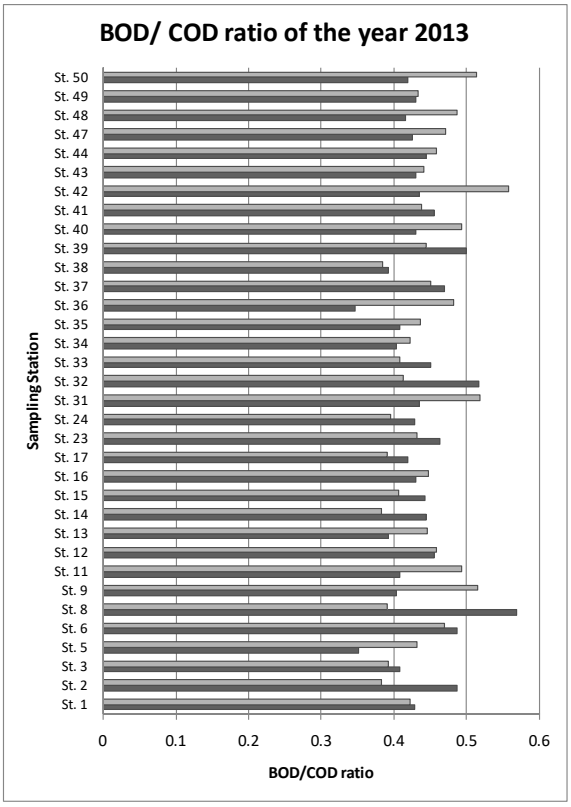

Fig. 4 BOD/COD ratio of the year 2013

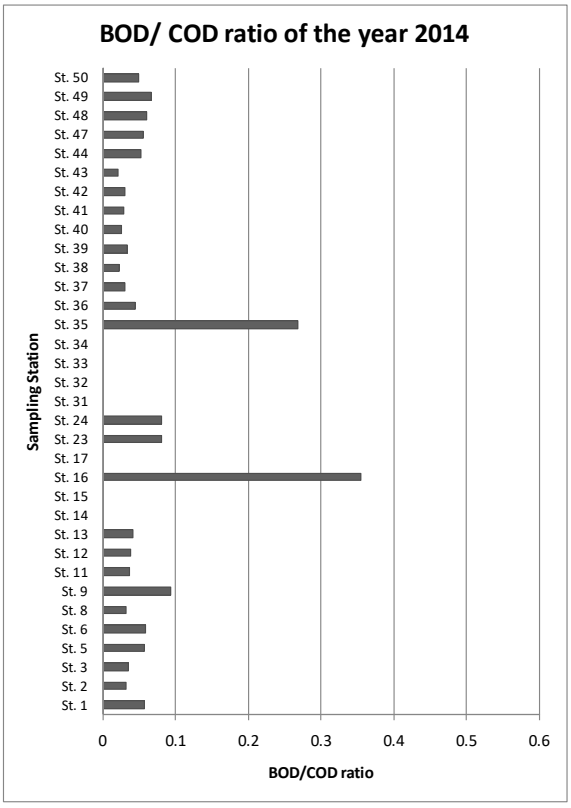

Fig. 5 BOD/COD ratio of the year 2014

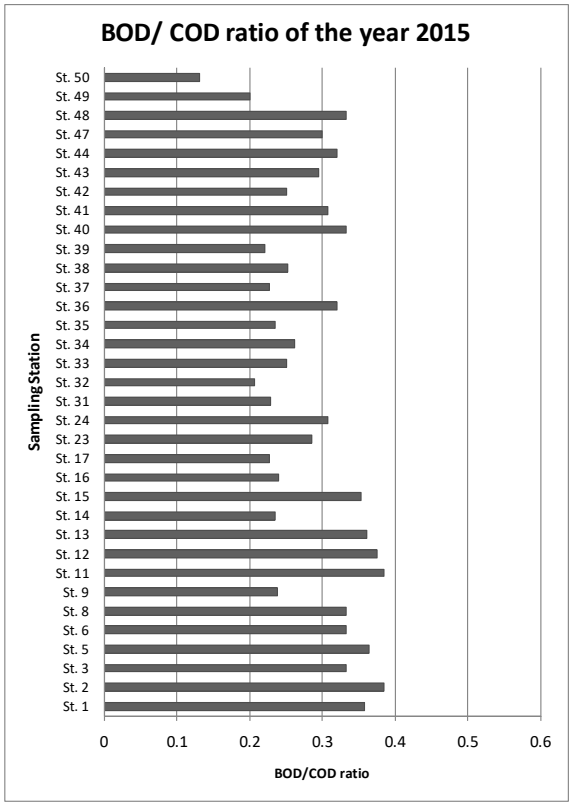

Fig. 6 BOD/COD ratio of the year 2015

The recapitulation of the range and mean value of BOD/COD ratio are displayed in Table 1.

Table 1 The BOD/COD value

Year	min	max	mean value
2011	0.38	0.63	0.49
2012	0.36	0.58	0.46
2013a	0.43	0.56	0.44
2013b	0.38	0.55	0.44
2014	0.02	0.35	0.07
2015	0.13	0.38	0.29

Note: 2013a represents the rainy season, whereas 2013 represents the dry season.

The table and figures show that, the BOD/COD ratio decline from year to year, especially in the year of 2014. It can be seen significantly that the water quality of rivers deteriorated in the year 2014 almost thoroughly. Only two stations showed the value above 0.1. In the year of 2015, the ratios are improved to 0.29 in average. Observing data sets of the year 2013 that are representing the season, it can be seen that there is no significant different between rainy and dry seasons. Low value of BOD/COD ratios can be affected by the increasing of COD concentration. High concentration of COD indicates pollution from non-domestic activities. The results can be used to focus on the industrial wastewater treatment. This measurement might have been conducted to improve the following year's river water quality condition.

The further observation was carried out to investigate the water quality condition of the rivers considering the biodegradable capacity. Table 2 depicts the concentration of Copper, Zinc and MBAS (methylene blue active substances) surfactants to represent the content of heavy metal and detergent. Heavy metals are toxic to the mixed culture of microorganisms responsible for the decomposition of organic compounds in surface waters [14].

Depending on the situation, synthetic surfactants and other pollutants may have different effects on hydrobionts (they can inhibit their growth, change their behavior, and the like), which can affect the water purification processes [15].

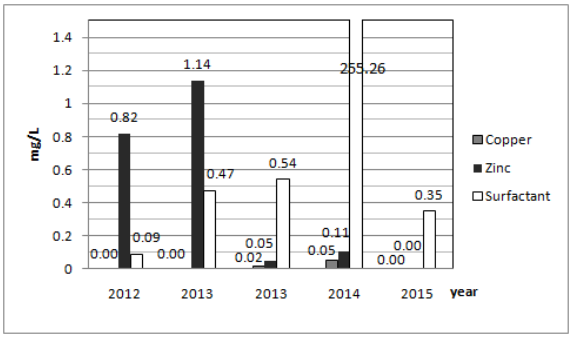

Fig. 7. Concentrations of Copper, Zinc and MBAS Surfactant

Almost all heavy metals concentrations were under the maximum level of the river water quality standard. These metals can be derived from the industrial wastewater. Copper was found slightly high in the year 2013 and 2014, and Zinc was also detected rather high in the year 2012 and 2013. Those metals concentration decrease from year to year. Nevertheless, the MBAS surfactant concentration increase, and reached an extremely high value in the year 2014. This condition worsens the river water considering its capability of self-purification process. Surfactant can be derived from the washing activities in the domestic area. Much of aquatic pollution involves sewage in which organic waste predominate. This waste can increase secondary productivity while altering the character of the aquatic community. Most fishes especially the species desired as food by man are among the sensitive species that disappear with the least intense pollution [16].

The BOD/COD ratios are highly affected by the wastewater discharged into the river. Variation of the ratios in each sampling station shows that every

river segments is influenced by the activity's wastewater located near it.

The conditions of those rivers were improved in the year of 2015. Heavy metals were not detected and the concentration of MBAS surfactant was lowering. This improvement will lead to an enhancement of the biodegradation capacity of the rivers.

CONCLUSION

Jakarta as a capital city of Indonesia has urban rivers affected by its activities. The ratio of BOD/COD decreases from the year of 2011 to 2014, and slightly increases in the latest year. Based on the BOD/COD ratio values, it can be concluded that the Jakarta's rivers generally have slow biodegradation capacity during 2011-2015, except in the year of 2014 that showing the non-degradable condition. Improvement was observed in the latest year which gives slight increment of biodegradation capacity and decrease of self-purification inhibition parameters' concentrations. Although the improvement has been perceived lately, the measurement to manage the domestic and non-domestic wastewater need to be continuously conducted.

ACKNOWLEDGEMENTS

This paper is supported by data set completed by the Ciliwung-Cisadane River Basin Agency.

REFERENCES

[1] Morley SA, Karr JR, "Assessing and restoring the health of urban streams in the Peuget Sound" Basin Conservation Biology, 16(6) 2002 1489-1509.

[2] Gurnell A, Lee M, Souch C, "Urban Rivers: Hydrology, Geomorphology, Ecology and Opportunities of Change", Geography Compass 1/5 (2007): 1118-1137.

[3] [3] Epstein DM, Kelso JE, Baker MA, "Beyond the urban stream syndrome: organic matter budget for diagnostics and restoration of an impaired urban river", Urban Ecosyst, DOI 10.1007/s11252-016-0556-y

[4] [4] Mazari-Hiriart M, Pe´rez-Ortiz G, Orta-Ledesma MT, Armas-Vargas F, Tapia MA, et al. (2014) Final Opportunity to Rehabilitate an Urban River as a Water Source for Mexico City. PLoS ONE 9(7): e102081. doi:10.1371/journal.pone.0102081

[5] Suwandana E, Kawamura K, Sakuno Y, Raharjo P, "Evaluating spatio-seasonal patterns of river- and groundwater quality in the city of Jakarta, Indonesia, using a pollution index", J.JASS, 27(3):91-102, 2011.

[6] Ostroumov SA, "On the Biotic Self-purification of Aquatic Ecosystems: Elements of the Theory", Doklady Biological Sciences, Vol. 396, 2004, pp. 206–211. Translated from Doklady Akademii Nauk, Vol. 396, No. 1, 2004, pp. 136–141.

[7] Thu TCT, Van DL, Duc TT, Xuan SL, "Assessment of Self-Purification Process of Thi Nai lagoon (Binh Dinh Province, Viet Nam)", Environment and Natural Resources Research; Vol. 5, No. 3, 2015, pp. 19-27

[8] Lee AH, Nikraz H, "BOD:COD ratio as an Indicator for River Pollution", International Proceeding of Chemical, Biological and Environmental Engineering Vol. 88 (2015).

[9] Metcalf and Eddy, "Constituents in Wastewater", Wastewater engineering treatment, disposal and reuse, 4th edn. McGraw Hill, New York, 2003, pp. 96-97.

[10] Contreras S, Rodriguez M, Al Momani F, Esplugas S, "Contribution of the ozonation pre-treatment to the biodegradation of aqueous solutions of 2,4 dichlorophenol", Water Research, 2003 37:3164-3171

[11] Pirsaheba M, Ghayebzadeh M, Moradi M, Gharogozlou F, Sharafi K, "Ratio variations of soluble to total organic matters at different units of a full scale wastewater integrated stabilization pond", Journal of Chemical and Pharmaceutical Research, 2015, 7(5):1326-1332.

[12] Turak UG, Fsar HA, "Research of BOD And COD Values of Wastewaters that Contain Certain Organic Materials", A Donor Menderes Univ., 4th AACD congress, Kusadasi – Aydin, Turkey, Proceeding Book , p177, 2004.

[13] American Public Health Association-APHA; American Water Works Association-AWWA; Water Environment Federation-WEF. 2012. Standard methods for the examination of water and wastewater. 22nd edition. Washington.

[14] Mala J, Maly J, "Effect of Heavy Metals on Self-Purification Processes in Rivers", Applied Ecology and Environmental Research 7(4): 333-340.

[15] Ostroumov SA, "The Effect of Syntetic Surfactants on the Hydrobiological Mechanisms of Water Self-Purification" Water Resources September 2004, volume 31, Issue 5, pp 502-510.

[16] Owa FD, "Water Pollution: Sources, Effects, Control and Management", Mediterranean Journal of Social Sciences, Vol. 4 No 8, 2013

Second International Conference on Science, Engineering & Environment,
Osaka City, Japan, Nov.21-23, 2016, ISBN: 978-4-9905958-7-6 C3051

EFFECT OF MODIFIED CASSAVA FLOUR (MOCAF), LENTIL, DATES BISCUIT ON THE BLOOD GLUCOSE LEVEL OF DIABETIC PATIENT

Fatmah[1,2]
[1]Public Health Nutrition Department, Faculty of Public Health, University of Indonesia, Depok City, West Java Province, Indonesia
[2]CAS (Center of Aging Studies) University of Indonesia. Depok City, West Java Province, Indonesia

Problem statement: Management of type 2 diabetes mellitus undertaken through pharmacological and non pharmacological therapies to maintain blood glucose levels (BGL) are still remains within th range of normal values. One of the effort of non pharmacological therapy is eating foods with low GI (glycemic index) value to maintain the value in normal range. **Approach**: The objective of the study was to assess the effect of consumption of biscuits mocaf lentils dates to the change of BGL status of diabetic patients. Randomized Controlled Trial (RCT) pre-post test design was used on 141 subjects who divided in the 4 groups: the treatment group (biscuits mocaf lentils dates) and three control groups (mocaf tempeh dates, tempeh dates, and dates biscuits). Anthropometric data collection; intake of energy, protein, and fat; BGL examination were collected before and 2 hours after eating biscuits at the beginning, middle, and the end of the study. **Results**: Biscuits mocaf lentils dates contains carbohydrates, zinc, and vitamin A is slightly higher than the mocaf tempeh dates; tempeh dates; and dates biscuits. Mocaf lentils dates biscuits has low glycemic index value (less than 50). Increased post-prandial BGL at 2 hours after consumption of biscuits was the lowest (6.4 points) compared with the control group at the end of the study. There were significant differences on the BGL treatment group before and after the study. **Conclusion:** Mocaf lentils dates biscuit can be an alternative choice of nutritious snack foods for diabetics.

Keyword: Type 2 Diabetes, Mocaf Lentils Dates Biscuit, Low GI

INTRODUCTION

The prevalence of diabetes mellitus (DM) is still a nutritional problem in Indonesia as it continues to increase every year. The total prevalence of DM in Indonesia happens to the patients aged over 15 years at 5.7% out of 24 417 citizens in urban areas. It is estimated that in 2030, the prevalence of DM in Indonesia will reach 21.3 million people [1]. International Diabetes Federation (IDF) 2015 estimates that an increasing number of diabetic patients in Indonesia, from 7 million in 2009 predicted to reach 12 million by 2030 [2]. Meanwhile, the WHO estimates that the higher increase is 8 million patients in 2000 to 21 million in 2030. In fact, DM becomes the 2nd cause of death of the elderly in Indonesia [3]. Obesity, smoking habit, eating less fruits and vegetables, often consuming sugary foods and beverages, as well as lack of physical activity such as exercise are risk factors for diabetes mellitus [4]. DM disease often does not cause symptoms, so patients do not know they have suffered from diabetes for a long time. When diagnosed, blood glucose levels are already high unnoticed. Changes in lifestyle modification including diet and physical activity are some preventive actions of type-2 diabetes mellitus. This type occurs in many developing countries especially for patients aged over 45 years old who do not depend on insulin. Diet in patients with DM includes the arrangement of consuming calories, and carbohydrates, fats and proteins that are found in the grouping of seven food classifications. One of some meal arrangements or diet can be made through the correct selection of the amount and type of carbohydrates by using the concept of the Glycemic

Index (GI). Foods which contain high IG increase blood glucose levels faster after food is consumed [5]. Foods which are high in gluten such as wheat flour should also be avoided by diabetics because they can raise blood glucose levels. Managing type-2 diabetes mellitus is done through pharmacological and non-pharmacological therapy to maintain BGL remains within the range of normal values [6]. One of the non-pharmacological therapies is to eat foods with a low GI value so BGL will remain normal. Biscuit made from lentil dates mocaf can be an alternative choice of nutritious snack foods that can lower BGL diabetics. Several studies had proved the third raw material was effective for diabetics in lowering their BGL. Mocaf gluten-free which is safe to be consumed by diabetics can also reduce the absorption of cholesterol, dilute the toxins, and increase the production of short chain fatty acids [7]. Mocaf flour also has a prebiotic effect that helps the growth of microbes in the digestive tract so that the digestive system becomes healthier because it is produced by fermentation. Lentil contains protein and essence that can lower blood sugar, high in antioxidants compared to soybeans [8]. Dates has low GI value so they are safely consumed by diabetics [9].

MATERIALS AND METHODS

Study used a quasi-experimental design of the 172 patients with type-2 diabetes who live in seven selected villages: Rangkapan Jaya Baru, Mekarjaya, Beji, Kukusan, Pangkalan Jati, and Cimanggis. *Ethical Clearance* was obtained from the Research Ethics Committee of Board of Health Research & Development, Ministry of Health of RI. Subjects of the research were chosen if they met the inclusion criteria as follows: male and female, aged between 35-75 years old, suffering from diabetes at least for 12 months, are taking oral diabetic medications, not taking herbal medicines such as sour sop leaves, crown god, rosalia tea, and other foods that can lower blood glucose, not suffering from other chronic diseases such as cancer, coronary heart disease, stroke; diagnosed with type-2 diabetes mellitus by a physician (based on examination of fasting blood glucose > 200 mg / dl and 2 hours after a meal > 126 mg / dl, and having some symptoms of DM patients: polyphagia, polydipsia, and polyuria, and rapid weight loss). A total of 172 subjects who were evenly distributed in four groups participated in this study. The intervention group gets lentil dates mocaf biscuits (Caromma), and three controlled groups get tempeh dates biscuit (Temma), tempeh dates mocaf biscuit (Catemma), and placebo biscuit (Bisma) for 4 weeks. Compliance level of consuming the biscuits made through home visits every two days to record data of daily food consumption and the number of biscuits distributed. In addition, measurements of fasting blood glucose (FBG), random blood glucose, and blood sugar 2 hours after consuming biscuits was conducted at the beginning, in the middle, and at the end of the study. Baseline data collection is done at the beginning of the study (end line) that includes the characteristics of the subjects, history of diabetes mellitus, the health status of the subjects two weeks before the interview, and the last one-day food intake (food recall). Data of weight was analyzed using the standard World Health Organization (WHO) in 2007 by the WHO Anthroplus software version 02 of 2009 based on indicators BB/U. Uni-variate data analysis performed use SPSS version 13. The anthropometric data include weight, height, waist circumference, pelvic circumference, blood pressure, and percentage of body fat was measured by trained field workers.

RESULTS AND DISCUSSION

At the beginning of the study, there were 172 subjects distributed evenly in 4 groups (each consisting of 43 people), but there were 31 subjects who were out of this study, either they resigned themselves or being dropped out by the research team. Their reasons were because they got bored, they did not want to eat the biscuits again, they went hometown without any certainty whether or not they return, and they were hospitalized for a few days that made them stop consuming biscuits. The majority of subjects in all groups were women, the elderly women in the treatment group and the pre-elderly women in three controlled groups. Most subjects in all groups had low education levels and they generally did not work anymore (Table 1). Mean of the highest body weight (BW) in this study was in the controlled group 2 (tempeh dates biscuits), and the lowest is in the treatment group (Table 2). The controlled group of tempeh dates mocaf biscuits has the highest mean of height of all the three other groups. Nutritional status was shown by the indicator of BMI (Body Mass Index) of BB ratio with TB. Average nutritional status of the treatment groups was within normal limits, but all of the controlled groups had better nutritional status (overweight). Mean of waist and pelvis of treatment group was the lowest of all other control groups. Mean of body fat percentage of all subjects in the treatment group and the controlled group were high enough in the range of 30 to 34.9% (Body Fat Monitor, Omron). Mean of

systolic and diastolic blood pressure was already in the category of prehypertension and was at risk of becoming hypertension. High weight, BMI, body fat percentage, mean of waist and pelvis, and hypertension in the study usually found among the type 2 diabetic patients. Most diabetic patients have overweight due to high body fat percentage especially in abdominal area. Body becomes resistant to the effects of insulin. Accumulation of body fat in obese people can improve blood glucose level due to increased insulin resistance [10].Waist circumference and waist hip ratio shows the distribution of fat in abdomen (central obesity) and trigger an increase glucose level [11].Hypertension (high blood pressure) is one of risk factors of diabetes as cause non beta cells to insulin (insulin resistance) [12]. More than three-quarters of the study subjects in the treatment group and the controlled group said that they got the diabetes because of their habit of eating sweet foods and drinks since they were young. The rest subjects said that they get it because of a hereditary (genetic), low physical activity, and obesity. Most subjects have suffered from diabetes since 2-3 years ago. 43.3% of the subjects admitted that his family member is suffering from this disease before. Until now 63.1% of the subjects are still taking drugs such as glibenclamide DM, metmorfin, glimeferid. However, there were also some subjects who consume mahogany fruits, and ginger herbs. BGL changed on the subjects during fasting, and postprandial 2 hours after consuming biscuits can be seen in Table 3. Mean of fasting BGL difference at the beginning and at the end of the study stated that the lowest was in the controlled group of tempeh date biscuits. Most of the subjects in the treatment group, the controlled group of tempeh date mocaf biscuits has a decrease of fasting BGL, except for the group of dates biscuits which had increased by 29.4 points at the end of the study. Mean of the lowest increase in post-prandial BGL 2 hours after consuming biscuits at the end of the study found in the treatment group which was 6.4 points. For the subjects in the controlled group consumed tempeh date mocaf biscuits, the largest increase was in the group of date biscuits which was 67.3 points. Table 4 shows the mean of macro-nutrients intake including energy, carbohydrate, protein, fat, and fiber. The treatment group and two of the controlled groups had a decreased mean of energy intake, except for the controlled group of tempeh date biscuits which had increased 16 calories at the end of the study. The mean of carbohydrate intake in the treatment group showed an increase of 10.6 grams compared to the three controlled groups which had generally decreased of their carbohydrate intake. The treatment group has the most decrease of the mean for protein intake (6.6 grams), the mean of fat intake (8.9 grams), and the mean of fiber intake (1.7 grams) compared to the other controlled groups. The treatment group has the highest rate in consuming biscuits whichwais 850 grams for four weeks of intervention compared to the controlled group. The value of glycemic index (GI) for four types of biscuits can be seen in Table 5. All kinds of dates biscuits have a low glycemic index levels (<50). Tempeh dates biscuits have the lowest GI value and dates biscuits have the highest GI value of the standard glucose and white bread. This study concluded that the nutritional status of the subjects from all groups show the majority of over-nutritious, the waist hip ratio was quite high, prehypertension blood pressure, and percentage level of body fat is quite high. These four indicators show the risk factors of DM. The lowest increase in post-prandial KGD 2 hours after consuming lentil dates mocaf biscuitswais (6.4 points) compared the other controlled groups at the end of the study. There were significant differences of BGL diabetes in the treatment group before and after the study for four weeks. The prolong period of study and the number of subjects need to be done in order to give more significant different results in the treatment group who consume lentil dates mocaf biscuits. In addition, the change of the comparison in BMI value, body fat percentage, waist hip ratio, and blood pressure of the subjects before and after the study are needed to assess the effects of consuming lentil dates mocaf biscuits on all four indicators of the nutritional status.

The Nutrition Facts of the Four Types of Biscuits

Table 6 illustrates the content of macro-nutrients (energy, carbohydrates, protein, fat) and micro-nutrients (Na, Zn, Fe, and vitamin A) of four types of biscuits. Mocaf lentil dates biscuit contains more vitamin A than the other three types of biscuits do. The content of protein in this type of biscuits was equivalent to the content of protein in tempeh date biscuits. Mocaf tempeh date biscuit containd the most

energy and fat. The highest carbohydrates was found in the placebo biscuits.

ACKNOWLEDGEMENT

The study was highly supported by Higher Education - The Indonesian Ministry of Culture and Education. We would like to express our gratitude to all the subjects who participated in the study.

REFERENCES

[1]. Ministry of Health (MOH) 2007. Basic Health Research Year 2007. Jakarta: Board of Health & Research Development.

[2] International Diabeteic Federation (IDF) 2015. www.idf.org

[3] Darmono. 2000. Patophysiology of diabetes vascular complication. Media Medika Indonesiana Faculty of Medicine University of Diponegoro (2).

[4] Kathleen J. Melanson. 2007. Nutrition Review: Diet and Nutrients in the Prevention and Treatment of Type 2 Diabetes. American Journal of Lifestyle Medicine 1 (5): 339-343.

[5] Kelley DE. 2003. Sugars and starch in the nutritional management of diabetes mellitus. Am J Clin Nutr 78 (4): 858S-864S.

[6] Healthy Magazine. 2011.Glychemix index: meaning and its benefit. http://www.majalahkesehatan.com/indeks-glikemik-arti-dan-manfaatnya. Accessed on January 5, 2014.

[7] Nimenibo R, Uadia. 2003. Effect of aqueous extract of *Canavalia ensiformis* seeds on hyperlipidaemia and hyperketonaemia in alloxan-induced diabetic rats. Biokemistri 15 (1): 7-15.

[8] Sinta. 2013. Mocaf as the wheat replacement. http://shintaluki.blogspot.com/2013/11/mocaf-sebagai-pengganti-terigu.html. Accessed on January 5, 2014.

[9] Al-Mamary M, Al-Habori M, Al-Zubairi AS. 2010. The in vitro antioxidant activity of different types of palm dates (*Phoenix dactylifera*) syrups. Arabian Journal of Chemistry. Available online 2 December 2010 .

[10] Wedman William a. et al. Indexing severity of diabetic foot infection with ^{99m}Tc-WBC SPECT/CT Hybrid Imaging. Diabetes Care 35(9): 1826–1831.

[11] Klein Samuel et al. 2007. Waist circumference and cardiometabolic risk: a consensus statement from Shaping America's Health: Association for Weight Management and Obesity Prevention; NAASO, The Obesity Society;the American Society for Nutrition; and the American Diabetes Association. Am J Clin Nutr 85: 1197–202.

[12] Ronnback Matts et al. Complex relationship between blood pressure and mortality in type 2 diabetic patients a follow-up of the Botnia Study. http://hyper.ahajournals.org accessed on July 9, 2016.

Table 1. Profile of sosio-demography

Variable	Type of group							
	Caromma (n=35)		Catemma (n=39)		Temma (n=27)		Bisma (n=40)	
	n	%	n	%	n	%	n	%
Sex								
Man	11	21.8	13	23.6	2	6.5	5	16.1
Woman	24	35.5	26	41.9	25	22.7	35	31.8
Age : < 60 years old	13	17.3	23	30.7	14	18.7	25	33.3
>= 60 years old	22	33.3	16	24.2	13	19.7	15	22.7
Mean ± SD	63.1 ± 10.5		57.8 ± 8.9		57.2 ± 8.8		55,9 ± 7.9	
Educational level								
Low (not graduated from elementary - graduated from junior high school)	19	54.3	28	71.8	15	55.6	32	80.0
Middle (graduated from senior high school – academy/university)	16	45.7	11	28.2	12	44.4	8	20.0
Working status								
No	28	80.0	24	61.5	21	77.8	34	85.0
Yes	7	20.0	15	38.5	6	22.2	6	15.0

Table 2 Subjects' anthropometric profile

Variable	Type of group			
	Caromma (n=35)	Catemma (n=39)	Temma (n=27)	Bisma (n=40)
	Mean ± SD	Mean ± SD	Mean ± SD	Mean ± SD
Weight (kg)	57,. ± 11.2	60.9 ± 11.5	62.2 ± 9.1	58.7 ± 11.5
Height (cm)	151.5 ± 6.5	155.5 ± 8.6	152.6 ± 6.9	152.1 ± 5.9
BMI (kg/m2)	24.7 ± 3.8	25.3 ± 4.7	26.7 ± 3.4	25.3 ± 4.5
Waist (cm)	85.7 ±10.4	88.7 ± 9.2	90.9 ± 8.1	89.8 ± 10.2
Hip (cm)	96.1 ± 8.4	97.4 ± 10.8	99.3 ± 8.5	96.7 ± 8.8
Waist hip ratio	0.9 ± 1.0	0.9 ± 1.1	0.9 ± 1.0	0.9 ± 1.1
Body fat percentage	33,1 ± 4,9	31.5 ± 6.6	34.9 ± 5.1	34.0 ± 6.1
Blood tension (sistolic/diastolic)	134.2 ± 25.0/ 84.3 ± 13.2	136.8 ± 19.7/ 81.1 ± 9.8	132.0 ± 15.5/ 82.1 ± 10.9	186.5 ± 65.1/ 84.6 ± 13.1

Table 3. Mean blood sugar at fasting and at two hours post-prandial after eating biscuit

Variable	Type of group							
	Caromma (n=35)		Catemma (n=39)		Temma (n=27)		Bisma (n=40)	
	Mean ± SD		Mean ± SD		Mean ± SD		Mean ± SD	
	pre	post	pre	post	pre	post	pre	post
Blood sugar shortly	290.3 ± 81.9	346.8± 192.3	212.3 ± 92.8	409. 0 ± 106.5	210.5 ± 69.3	217.0 ± 0.0	209.7 ±76.0	311.6 ± 120.5
Fasting blood sugar	163.3 ± 70.1	152.2 ± 62.3	178.4 ± 83.3	165.1 ± 72.2	126.6 ± 59.9	121.1 ± 43.6	186.5 ± 65.1	215,9 ±73.1
Blood sugar at post-prandial after eating biscuit)	205.8 ± 74.8	212.2 ± 105.8	205.8 ± 83.5	224.6 ± 89.9	149.4 ± 57.0	201.6 ± 63.3	213.3 ± 70.9	280.6 ± 99.8

Table 4. Mean macronutrient intake of subjects

Indicator	Type of biscuit							
	Caromma (n=35)		Catemma (n=39)		Temma (n=27)		Bisma (n=40)	
	Mean ± SD		Mean ± SD		Mean ± SD		Mean ± SD	
	pre	post	pre	post	pre	post	pre	post
Energy (cal)	1339.7± 307.7	1290.5± 409.8	1327.2 ± 369.6	1260.9 ± 435.6	1396.9 ± 293.2	1412.9 ± 249.1	1298.8 ± 310.7	1252.5 ± 370.6
Carbohydrate (gr)	174.5 ± 50.3	185.1 ± 52.2	173.9 ± 57.0	164,6 ± 54.2	202.9 ± 54.1	193.4 ± 53.1	179.8 ± 45.4	168.2 ± 46.
Protein (gr)	43.9 ± 15.2	37.3 ± 15.7	40.6 ± 14.3	36.7 ± 15.9	40.1 ± 14.7	47.3 ± 9.6	39.6 ± 14.5	34.7 ± 15.6
Lemak	54.8 ± 15.7	45.9 ± 22.4	54.9 ± 23.2	53.6 ± 27.5	49.3 ±19.4	52.4 ± 20.8	48.8 ± 20.3	50.2 ± 23.1
Serat	10.2 ± 4.3	8.5 ± 3.9	9.0 ± 3.6	9.0 ± 3.9	8.9 ± 4.6	9.5 ± 3.0	8.6 ± 3.6	8.1 ± 3.7

Table 5. Glycemix Index (GI) of biscuits

Type of biscuit	Reference/standard	
	Glucose	Bread
Caromma	27.2	37.6
Catemma	27.4	37.8
Temma	17.1	23.6
Bisma	32.0	44.1

Source:
Food and Nutrition Center Laboratory UGM Yogyakarta, 2015

Second International Conference on Science, Engineering & Environment,
Osaka City, Japan, Nov.21-23, 2016, ISBN: 978-4-9905958-7-6 C3051

CHARACTERISTICS OF THE SLUDGE PARTICLES IN REMOVAL PROCESS OF RADIOACTIVE CESIUM FROM OCEAN SLUDGE BY DECOMPOSITION SYSTEM WITH CIRCULATION TYPE USING MICRO BUBBLES AND ACTIVATING MICROORGANISMS

Kyoichi OKAMOTO[1], Takeshi TOYAMA[1] and Tomoe KOMORIYA[2]

[1] CST, Nihon University, JAPAN, [2]CIT, Nihon University, JAPAN

ABSTRACT

The Fukushima nuclear accident of March 11, 2011, soil and water had been contaminated by radioactive cesium. Moreover, radioactive cesium was found in the ocean sludge in Tokyo Bay flowing from rivers. Cesium which is adsorbed to the sludge cannot be easily removed. One of the authors developed decomposition and purification system, a circulation-type system by micro bubbles, that is, by creating aerobic state, aerobic bacteria are activated resulting to decomposition and purification of ocean sludge. Based on the hypothesis that radioactive cesium is adsorbed on the surface of the sludge deposition. It is considered cesium can be eluted after decomposing the deposited sludge. Once the cesium is eluted in the water, it can fix to a mineral such as zeolite. Now we need the properties of sludge in removal process by decomposition system with circulation type. In this study, our objects is to check the characteristics of the sludge particle in removal process of radioactive cesium from ocean sludge by decomposition system with circulation type using micro bubbles and activating microorganisms. As the results of this experiments, we had very good purification ratio on total nitrogen and had made 40 times of smaller size on diameter of the particle of sludge.

Keywords: Decontamination, Radioactive Cesium, Ocean Sludge, Micro-bubble, Microorganism, Zeolite

INTRODUCTION

The Fukushima nuclear accident on March 11, 2011, soil and water had been contaminated by radioactive cesium. Moreover, radioactive cesium was found in the ocean sludge in Tokyo Bay flowing from rivers. A report says radioactive cesium is still existing in seashore in Tokyo Bay, 2015 in [1]. Cesium which is adsorbed to the sludge cannot be easily removed.

One of the authors developed decomposition and purification system, a circulation-type system by micro bubbles, that is, by creating aerobic state, aerobic bacteria are activated resulting to decomposition and purification of ocean sludge. Based on the hypothesis that radioactive cesium is adsorbed on the surface of the sludge deposition. It is considered cesium can be eluted after decomposing the deposited sludge.

Once the cesium is eluted in the water, it can fix to a mineral such as zeolite. Now we need the properties of sludge in removal process by decomposition system with circulation type.

In this study, our object is to check the characteristics of the sludge particle in removal process of radioactive cesium from ocean sludge by decomposition system with circulation type using micro bubbles and activating microorganisms.

DECOMPOSITION SYSTEM WITH CIRCULATION TYPE

It is very important to reduce sedimentary sludge in the ocean. Plans to reduce the sludge are usually dreading or sand covering. Dredging is a simple way and aims to cut off the sludge. But after cutting off, treating the dredged sludge takes much more time and, of course, cost. Sand covering, in general, gives a big load to living organisms and the ecological system.

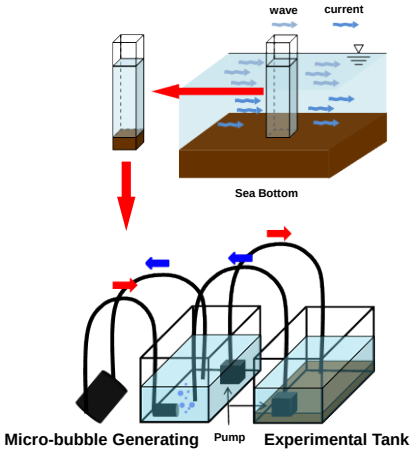

Fig. 1 Purification System of Circulation Type.

So that, a more efficient way is needed to reduce the sludge while not imparting environmental load in the local sea area. Here, attention was paid to micro-bubble technology for application to the purification of the sludge. The important point in this technique is to activate the bacteria existing in the area by micro-bubbles.

Micro-bubbles (that is MB) can change conditions into an aerobic state. If the bubbling stops, the situation changes into anaerobic state, according to recent research. So, we selected a method for decomposing the sludge by microorganisms.

One of the authors had developed the decomposition system for ocean sludge with circulation type by micro-bubbles, shown in Fig.1, which decompose and purification sludge by activating the aerobic bacteria, after creating an aerobic state by micro-bubbles.

MECHANISM ON FIXING OF CESIUM FROM ELUTION

In general, ocean sludge has a negative charge. When cesium with a positive charge flows from river, sludge was adsorbed cesium, shown in Fig 2. So that, sludge adsorbed cesium cannot eliminate by usual way.

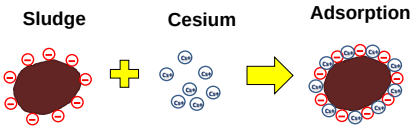

Fig.2 Mechanism on Adsorption of Cesium

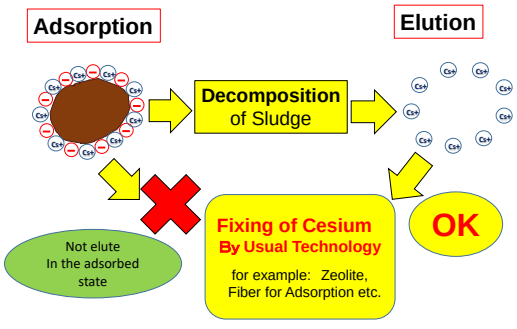

Fig.3 Mechanism on Fixing of Cesium from Elution.

Here, we have a way by using of the decomposition system for ocean sludge with circulation type. After decomposition of the sludge adsorbed cesium by our system, cesium is eluted into water, shown in Fig 3. That is our hypothesis.

ELUTION EXPERIMENTS FOR CESIUM

Procedure of Experiment

The experimental devices consist of two parts, shown in Fig. 4. The water circulates through two tanks. In one tank (Width40xLength28x Hight28cm), micro-bubbles are generated. The micro-bubbles have micro-size diameter and high solubility. This means the water with high concentration of dissolved oxygen circulates through these tanks. The other part is the experimental tank (W60xL29xH35cm). We used sea-water 30(litter) and sludge 1(kg). Here, a micro-bubble generator is based on [4], [5] and the flow rate is 900 (litter/hour). The flow rate of water pumps connected each tanks are 300 (litter/hour).

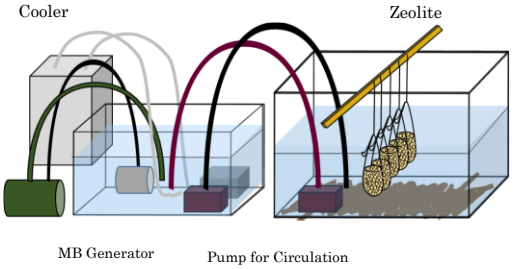

Fig.4 Experimental System for Elution of Cesium.

We had caught the sludge and the sea water at Funabashi Port in Chiba Prefecture in JAPAN, as shown in Fig.5 and 6. Here, we had removed under 10cm of the sludge from seabed before sampling as experimental procedure, because we have to remove the initial value of cesium in the sludge, from [3].

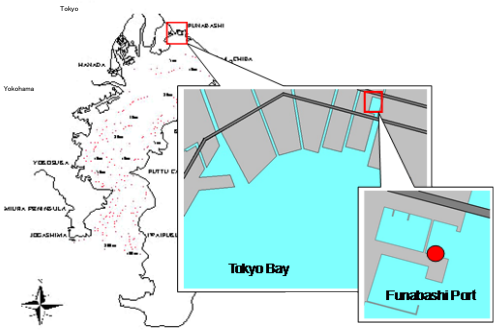

Fig.5 Catching Point of Sludge and Sea Water at Funabashi Port in Tokyo Bay.

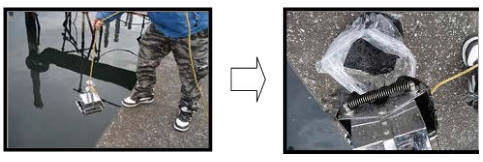

Fig.6 Scene of Catching Sludge.

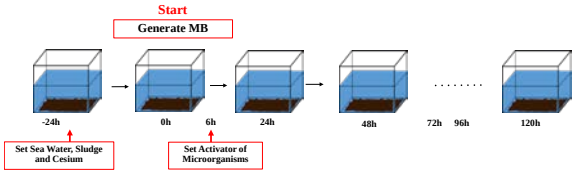

Fig.7 Procedure for Liquid Measurements.

Measurement Procedure for Liquid Phase

We used the cesium chloride before 24 hours of starting time and the concentration of cesium ion is 100 (ppm). A cooler for water tank was set at side of the tank for generating microbubbles, for the purpose of setting water temperature 30 degree centigrade.

After setting the decomposition system with circulation type by micro-bubbles, experiment starts at the same time of generating micro-bubble device and also the zeolites were set in the tank.

After 6 hour, the microorganism activator was put in the experimental tank. Main staff of the activator is Kelp and including nutrients and some enzyme. Our used activator is reported to show effective results in purification for grease trap.

Measurements for liquid phase did each 6 hours until 12 hours, and then every 12 hours to120 hours, shown in Fig.7.

Dissolved oxygen (DO), water temperature and pH are measured by using of multi-parameter water quality meter. Ammonium nitrogen (NH_4-N) and total nitrogen (T-N) are measured by using of digital-water-analyzer by digital “Packtest”, by water filtered after sampling in experimental tank.

Experimental Conditions

Case 1 is to use our purification system with circulation type and Case 2 is not use the system which means do not use the micro bubble and activator of microorganisms.

Case 3 is to do current velocity control in purification system for reducing hydrogen sulfide. As procedure of experiment in case of current velocity control by our purification system with circulation type, setting the water pomp (2400L/h) in a tank is worked from starting time to 24 hours later.

Results and Consideration for Liquid Phase

Results of water temperature, pH and DO as environmental condition

Fig.7-9 show the water temperature, pH and DO (Dissolved Oxygen) as the results of environmental condition of this experiment.

Water temperature was almost constant about 30 degree centigrade after 6 hours, by setting the cooler for water tank in the experimental system. pH was also constant about 8.0 to 9.0. DO in Case 1 and 3 were 7.0 to 8.0 and also saturation state after 24 hours, but DO in Case 2 was about 4.0 and lower oxygen state.

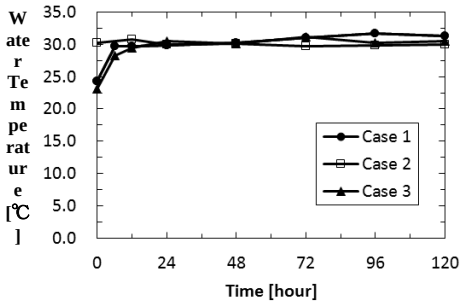

Fig.7 Changes in Water Temperature as Environmental Conditions.

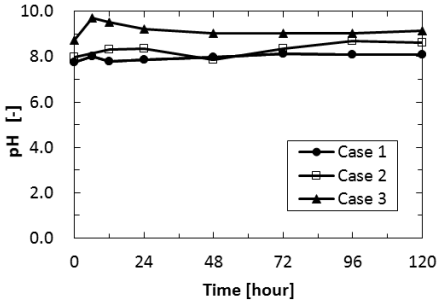

Fig.8 Changes in pH as Environmental Conditions.

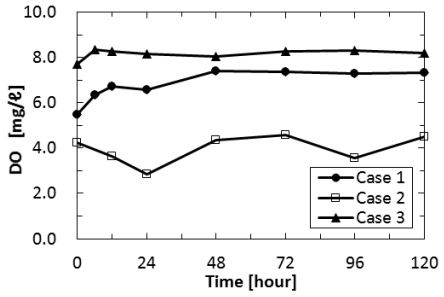

Fig.9 Changes in DO as Environmental Conditions.

Results of H_2S, DIN and T-N

Fig.12-14 are shown in results of H_2S (Hydrogen sulfide), DIN (Total Inorganic Nitrogen) and T-N

(Total Nitrogen).

H2S (Hydrogen sulfide) in Case 1 and 3 decrease rapidly, it seemed by the supply of Oxygen. It decreased more rapidly in Case 3 by flow control and then became N.D. value. Case 2 showed not big change and relatively constant values, because of no supplying oxygen.

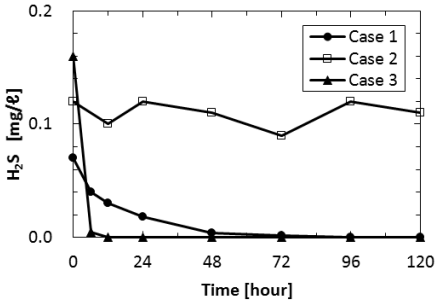

Fig.10 Changes in H2S.

DIN (Total Inorganic Nitrogen = NH4-N+NO2-N+NO3-N), shown in Fig. 11. DIN of Case 1, 3 reduced 100% at 120 hours, it seemed it happen to denitrification by microorganism from [8].

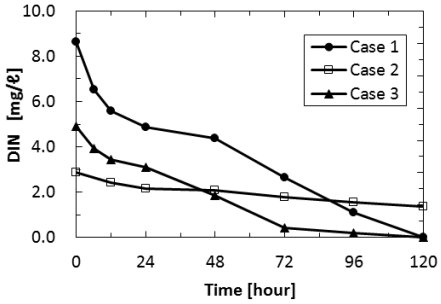

Fig.11 Changes in DIN.

T-N (Total Nitrogen) is expressed in normalization; initial values in Case 1, 2 and 3 were 4.0, 1.5, 4.3, respectively. T-N in Case 1 and 3 reduced 80 and 85 %, respectively. It seems these are activated by microorganisms. A little high values in Case 3 caused rapidly decreasing of H2S by flow control, so that it seems purification efficiency is very good.

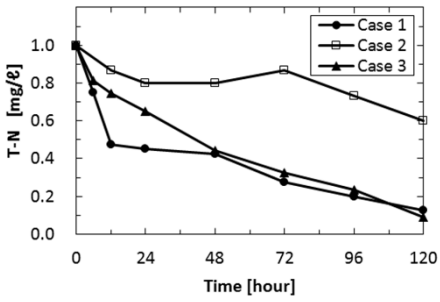

Fig.12 Changes in T-N.

Results and Consideration for Solid Phase

Measurement Procedure for Solid Phase

Measurements for solid phase did every 24 hours to120 hours, shown in Fig.13. There are 6 patterns; 0, 24, 48, 72, 96, 120 hour. When it comes each closing time, the experimental tanks are prepared for measurement of solid phase. The sediment in the tanks are carried out filtration and dry. After filtration and dry, cesium in solid was analyzed by the energy dispersion type X-ray analysis device (EDX).

The characteristics of the sludge particle in removal process are also measured by Scanning Electron Microscope (SEM).

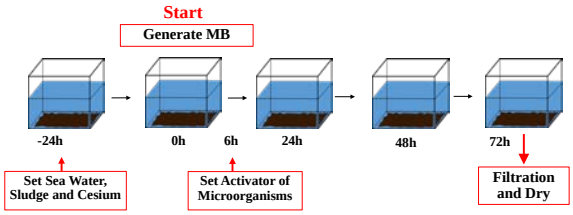

Fig.13 Measurement Procedure for Solid Phase.

Results of Cesium (Solid)

We paid attention to cesium and silica (Si), as there are many chemical elements in sludge. We used the energy dispersion type X-ray analysis device (EDX), because we can measure by the solid state. Weight ratio of cesium and silica (CS/Si) in solid of dry sludge are shown in Fig.14.

Results of cesium in solid phase by EDX in Case 1 reduced 47.1% but in Case of 2 did not reduce. It seems cesium adsorbed on sludge was decomposed and eluted to water by decomposition and purification system of **c**irculation **t**ype.

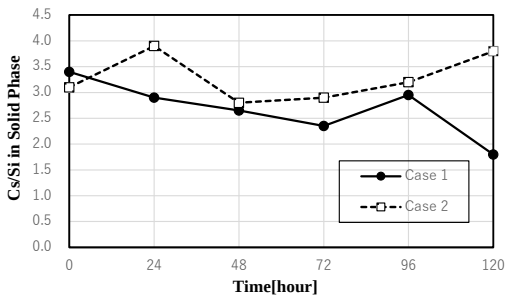

Fig.14 Changes in (Cesium)/(Silica) in Solid Phase.

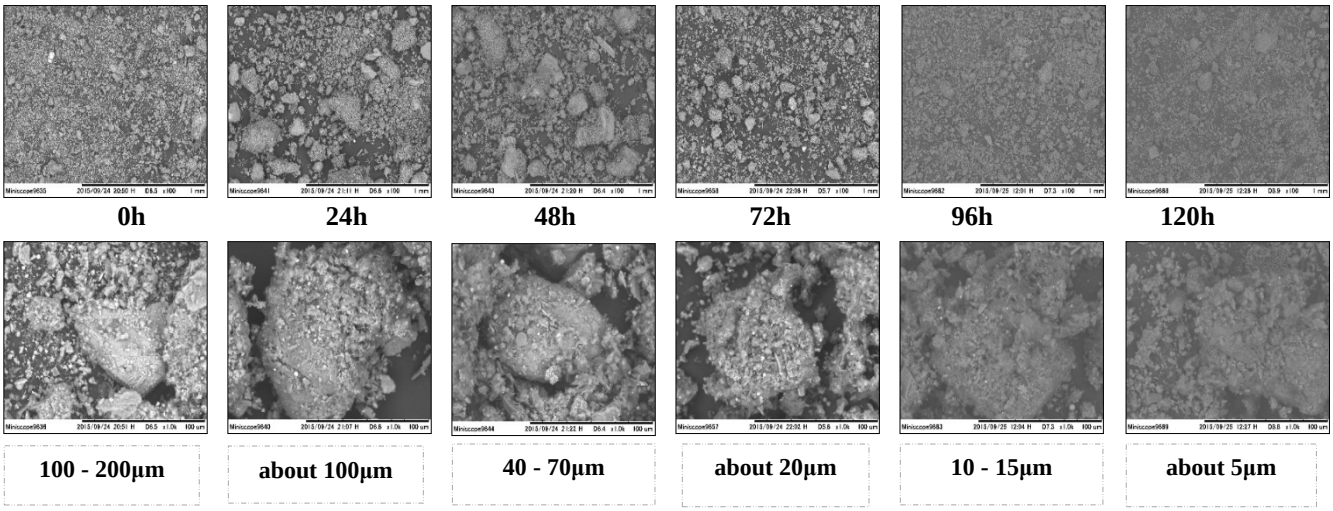

Fig. 15 Photo by SEM (Scanning Electron Microscope) of Case 1 (Upper=100 times / Lower=1000 times)

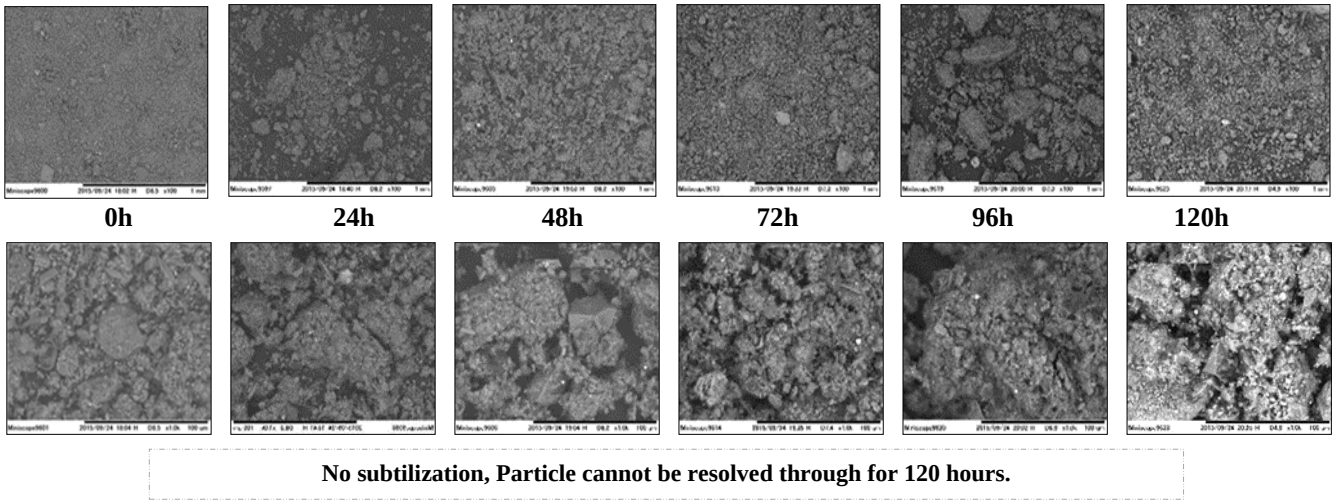

Fig. 16 Photo by SEM (Scanning Electron Microscope) of Case 2 (Upper=100 times / Lower=1000 times)

Characteristics of Sediment by SEM

Results of SEM (Scanning Electron Microscope) are expressed for each 24 hours from 0 to 120 hours, shown in Fig.15 and 16.

Diameter of sludge particle in Case 1 is 100 to 200 (micro meter) when experiment starts, and then it becomes 5 (micro meter) at 120 hours later, so that the size became about 40 times small. That in Case 2 denoted no change. It seems the diameter of sludge particle is decomposed and becomes very small according to the working time of decomposition and purification system of circulation type.

CONCLUSION

We had carried out the elution and fixing cesium by setting zeolite, after decomposing the by using the decomposition system with circulation type, by not using it and by using it adding flow control.

From the results for water qualification,

(1) for T-N, it decreased 80% in case of use the decomposition system and decreased 85% in adding flow control.

From the results for cesium in solid phase,

(2) the eluted performance of absorbed cesium on the sludge is indicated 47.1% by using the decomposition system, compared with no use of microbubble and activator of microorganisms.

(3) Diameter of sludge particle in removal process by using the decomposition system became about 40 times small.

ACKNOWLEDGEMENTS

The authors would like to express sincere thanks for executing the experiments to Takahiro ARAKAWA and Taiyo KOKATSU, Students of Nihon University, in Japan.

This work was supported by KAKENHI (Grant-in-Aid for Scientific Research (C-26420831)).

REFERENCES

[1] Tokyo News Paper, “Radioactivity pollution in the Tokyo Bay, A nuclear power plant, far convergence”, March 10, 2015. http://www.tokyo- np.co.jp/feature/ tohokujisin/archive/fouryears/150310_1.html

[2] Okamoto Kyoichi, Hotta Kenji, Toyama Takeshi and Kohno Hideki, “Purification System of Ocean Sludge by Activating Microorganisms”, International Journal of GEOMATE (Geotec, Const. Mat. & Env.), Vol.6, No.1, pp.791-795, March, 2014.

[3] Okamoto Kyoichi and Toyama Takeshi, “Ocean Decontamination: Removal of Radioactive Cesium from Ocean Sludge by Using Micro bubbles and Activating Microorganisms”, The Japan Society of Naval Architects and Ocean Engineers, May, 2014.

[4] Okamoto Kyoichi and Toyama Takeshi, “Ocean Decontamination: Removal Efficiency of Radioactive Cesium from Ocean Sludge by using Microbubbles and Activating Microorganisms”, International Journal of GEOMATE (Geotec., Const. Mat. & Env.), Vol. 9, No. 1, pp. 1390-1394, May, 2015

[5] Imai, T, Shioshige, K, Ukita, M, Sekine, M, Higuchi, T, Fukagawa, K and Fujisato, T. “Development of Device for Dissolving High Concentration Gas for Purification at bottom layer around enclosed water area like Dam Lake”, Proc. 39th Forum on Environmental Engineering of Civil Engineering Society, 10-12, 2002.

[6] Matsuo, K, Maeda, K, Ohnari, H, Tsunami, Y, and Ohnari, H., “Water Purification of a Dam Lake Using Micro Bubble Technology”, Progress in Multiphase Flow Research I, pp.279-286, 2006.

[7] Okamoto Kyoichi and Toyama Takeshi, “Ocean Decontamination: Removal Performance of Radioactive Cesium from Ocean Sludge by Using Micro bubbles and Activating Microorganisms”, The Japan Society of Naval Architects and Ocean Engineers, May, 2015.

[8] Okamoto Kyoichi and Toyama Takeshi, “Ocean Decontamination: Removal Efficiency of Radioactive Cesium from Ocean Sludge by using Microbubbles and Activating Microorganisms”, International Journal of GEOMATE (Geotec., Const. Mat. & Env), May, 2016, Vol. 10, Issue 21, pp. 1924-1928.

[9] Okamoto Kyoichi and Toyama Takeshi, “Ocean Decontamination: High Efficiency Removal Method of Radioactive Cesium from Ocean Sludge by Using Microbubbles and Activating Microorganisms", The Japan Society of Naval Architects and Ocean Engineers, May, 2016.

Second International Conference on Science, Engineering & Environment,
Osaka City, Japan, Nov.21-23, 2016, ISBN: 978-4-9905958-7-6 C3051

STRATEGY OF TURBIDITY REMOVAL IN CIKAPUNDUNG AND CISANGKUY RIVER AS WATER SOURCES FOR BANDUNG CITY, INDONESIA

Evi Afiatun[1], Hary Pradiko[1] and Hari Prayoga[1]
[1]Department of Environmental Engineering, Pasundan University, Bandung, Indonesia

ABSTRACT

Cikapundung and Cisangkuy river are the sources of raw water used by Bandung City. The special characteristics are the fluctuations of flow and turbidity in the dry season and the rainy season with the highest turbidity > 600 NTU. The turbidity fluctuation is not accompanied significantly by the changes of coagulant dosage. This research was conducted in order to evaluate and strategize the optimal performance of the water treatment plant based on the evaluation of the processed water. The laboratory analysis was carried out to find the dominant parameters, namely turbidity, with the steps such as 1) comparing the coagulation process that has been or has not been through preliminary sedimentation using coagulant polyaluminium Chloride (PAC); 2) observing the stability and efficiency of sedimentation that resulted by coagulation process for the several variation of time; 3) analyzing the efficiency of the preliminary sedimentation and coagulation process. The results of laboratory analysis showed that the optimum time for the deposition process is 35 minutes with a decrease in turbidity of about > 80%. The highest efficiency of sedimentation processes occur at the initial turbidity of 514 NTU in the amount of 85.02%. The optimum coagulant dosage without using the preliminary sedimentation reached at initial turbidity of 147 NTU with an efficiency of 99.76%; while those using the preliminary sedimentation process is achieved at initial turbidity of 514 NTU with an efficiency of 99.46%. Based on these analysis, it is necessary to adjust the operational of preliminary sedimentation process.

Keywords: Coagulant, Strategy, Turbidity, Water resources, Preliminary sedimentation

INTRODUCTION

Cikapundung and Cisangkuy river are the sources of raw water used by Bandung City. Drinking water needs that increasingly higher inversely proportional to the decreasing of raw water availability and quality. The special characteristics are the fluctuations of flow and turbidity in the dry season and the rainy season with the highest turbidity > 600 NTU[1]. Based on observations and data from PDAM (Regional Water Company) Bandung City, raw water sources still meet water quality standards for drinking water even though the turbidity of raw water is often high because of fluctuating every month. Turbidity of water sources is strongly influenced by rainfall fluctuation each month. Rain upriver brings many particles of mud, sand and plant debris and even manure affect turbidity in the river. In the rainy season the turbidity value can reach ± 600 NTU, whereas in the dry season only ± 100NTU. At this time there is a quite important problem in the processing of raw water, the affixing of coagulants do not in line with fluctuations in raw water turbidity value that fluctuates each month[2]. In ideal conditions, a good quality of water sources allocated for drinking water with the aim of improving human health, while the water sources that relatively have low quality can be allocated to the industrial and agricultural need [3] . The aim of this research is to determine the strategy of turbidity removal of Cikapundung River and Cisangkuy River as raw water sources with finding the optimum dosage of coagulant. This research was conducted by comparing the process with and without silt deposition as a pre-sedimentation process illustration to optimize the performance of existing water treatment plants.

MATERIALS AND METHODS

This research was conducted with experimental methods. The experiments were done with determine the optimum dosage of coagulant Polyaluminum Chloride (PAC) through two ways, ie. with and without silt deposition. This research was conducted at the Laboratory of Environmental Engineering Pasundan University, Bandung - Indonesia. The variables which analyzed in this research were the water turbidity (NTU) and the coagulant dose (ppm) which were conducted using jar-test method for each turbidity variation.

The data collection technique started with the preparation phase which includes literature review and field observations. The next stage was the

collection of secondary data to determine turbidity fluctuations and existing coagulant dosage. The next phase was the Jar test method to determine the optimum dosage of coagulant in two ways, with and without silt deposition. The deposition process used Imhoff cone as a pre-sedimentation process approach. The time variation of the deposition conducted to determine the optimum time of silt deposition. It was done by checked the turbidity every 5 to 60 minutes for each turbidity variations, and calculated the stability of turbidity decrease. The best strategy for turbidity removal based on the optimum coagulant dosage and whether or not the pre-sedimentation used. Flow diagram of the research can be seen completely in Fig. 1.

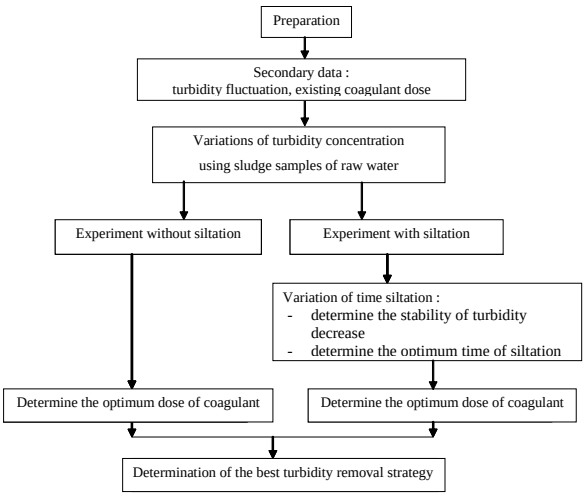

Fig 1. Flowchart of research

RESULTS AND DISCUSSION

Turbidity fluctuation and existing coagulant dosage

Figure 2 and 3 show the turbidity fluctuations in the raw water and coagulant dosage in the existing treatment process from April to August 2014 which represent the dry season and September to December 2014 for rainy season:

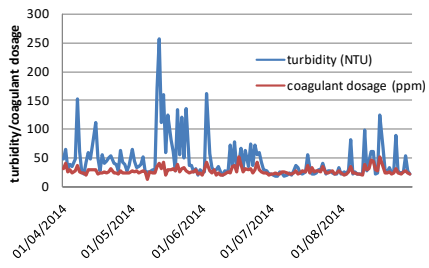

Fig. 2 Turbidity fluctuation and existing coagulant dosage (April – August 2014)[1]

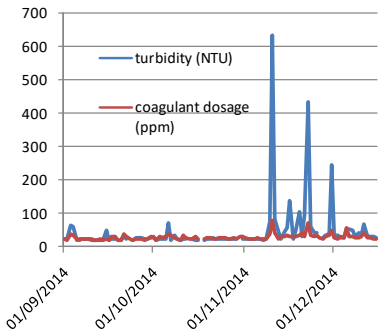

Fig. 3 Turbidity fluctuation and coagulant dosage existing (September – December 2014)[1]

Figures 2 and 3 show that turbidity fluctuation occurs in either the rainy season and dry season. Turbidity fluctuations in the rainy season shows the higher concentrations, which reached > 600 ppm. Based on the above picture can be seen that the turbidity fluctuations do not result in significant changes in the use of coagulants.

Determination of the optimum coagulant dose with and without silt deposition

Comparison of the optimum coagulant dose using the same initial turbidity concentration

The experiments were performed by comparing the optimum dose of coagulant carried out with and without the silt deposition.

Tabel 1. The comparison of the optimum coagulant dosage using the same initial turbidity concentration

Without silt deposition		With silt depositiom		
Initial turbidity (NTU)	Optimum coagulant dose (ppm)	Initial turbidity (NTU)	Turbidity after desposition	Optimum coagulant dose (ppm)
634	98	606	111	40
543	94	514	77	38
435	90	450	70	38
374	40	361	64	30
231	36	223	53	32
147	28	147	47.29	24
99	18	84	36.9	14
25.35	16	28.73	20.98	14

Based on Table 1 it can be seen that the higher of initial turbidity value, need much coagulant dose. Table 1 and Figure 4 shows that the optimum coagulant dosage with and without silt deposition have a considerable margin at the high turbidity (> 400 NTU). The silt deposition process at high turbidity can reduce turbidity significantly, more

than 80%, so the coagulant dosage less than the other.

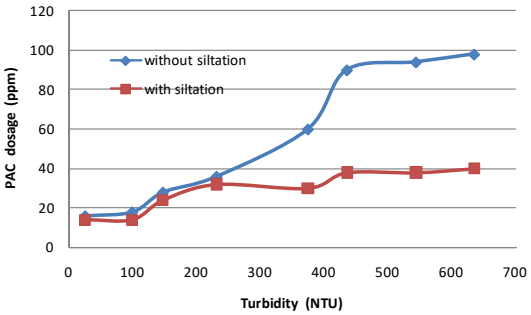

Fig.4 Coagulant dosage with and without siltation process

Comparison of optimum coagulant dose based on turbidity concentration after deposition process

The determination of optimum coagulant dose by comparing the optimum coagulant dose on the initial turbidity concentration after the silt deposition process.

Table 2. The comparison of optimum coagulant dosage using the initial turbidity concentration after silt deposition process

Without silt deposition		With silt depositiom		
Initial turbidity (NTU)	Optimum coagulant dose (ppm)	Initial turbidity (NTU)	Turbidity after desposition	Optimum coagulant dose (ppm)
112	22	606	111	40
79	20	514	77	38
51	20	147	47.29	24
25.35	16	28.73	20.98	14

According to the table 2 the optimum of coagulant dosage without silt deposition is smaller than the turbidity results from the silt deposition. Here is a comparison graphs of determining the optimum coagulant dose for turbidity without silt deposition and turbidity after silt deposition.

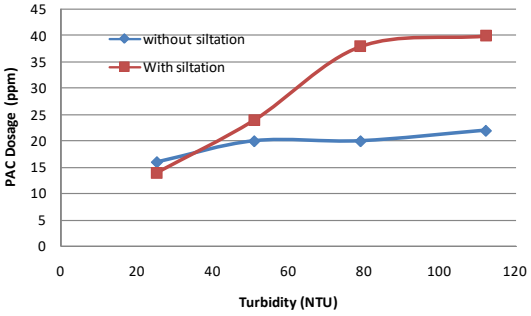

Fig.5 Determination of coagulant dosage using deposition turbidity results

In figure 5 shows that the optimum dose of coagulant in turbidity that has been deposited is greater than the result of the determination of the optimum dosage of coagulant without deposition treatment. This is because the possibility of particles in the sample that helps coagulant to react if the water sample was not deposited in advance.

Variation of Time Precipitation To Prasedimentation Experiment

The following will be displayed settling time efficiency and the percentage of stability reduction in turbidity

Precipitation efficiency

The efficiency of deposition was conducted to determine how many percentage for turbidity removal. The experiment was conducted every 5 minutes within 60 minutes

The results of laboratory experiments that the efficiency of turbidity reduction for 60 minutes for initial turbidity 604 NTU is 89.07%, 559 NTU is 88.73%, and 426 NTU is 85.68%.

The experimental results can be seen in Figure 6.

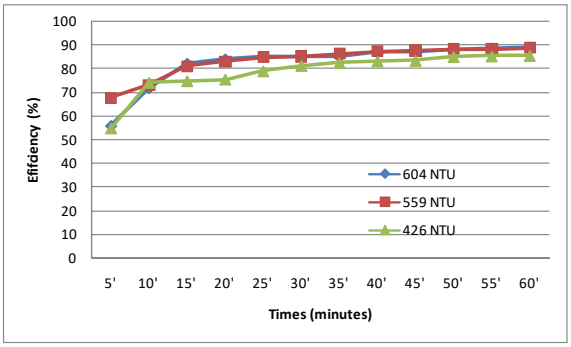

Fig. 6 Efficiency of turbidity reduction without siltation

The stability of Precipitation

The stability of deposition was conducted to determine the time that is considered to be stable, ie two sequential time difference of less than 10% in terms of turbidity before.

Testing is done to achieve a steady state condition, ie with fluctuation of 10% . The results of laboratory experiments that the efficiency of turbidity reduction during the 60 minutes are 89.07% for 604 NTU, 88,73% for 559 NTU, and 88.73% for 426 NTU.

The results of laboratory experiments stated that the stability of the reduction in turbidity is stable if precentage of drop taken at 2 consecutive time less than 10%. Testing is done to achieve steady state, ie

with fluctuation of 10%.

Time deposition taken at the beginning of 604 NTU turbidity is at minute 30 with% reduction in 1.11%, at the beginning of 559 NTU turbidity time taken is in the 35th minute with% decrease 8.43% and at the beginning of 426 NTU turbidity time ie taken at minute 40 with% decrease 4.05%. Here is a chart of stability percentage reduction in turbidity:

Prasedimentation efficiency and coagulant dosage

Efficiency Turbidity Removal With Sludge Doposition (Prasedimentation)

The efficiency of sedimentation was conducted to determine the highest reduction in turbidity performed on sludge deposition process using Imhoff cone. Table 5 below presents data initial turbidity removal efficiency after using Imhoff cone deposited by turbidity variations.

Table 2. Turbidity removal efficiency after using imhoff cone (represent sedimentation process)

Initial Turbidity	Turbidity after deposition (NTU)	Efisiensi (%)
606	111	81.68
514	77	85.02
450	70	84.44
361	64	82.27
223	53	76.23
147	47.29	67.83
84	36.9	56.07
28.73	20.98	26.98

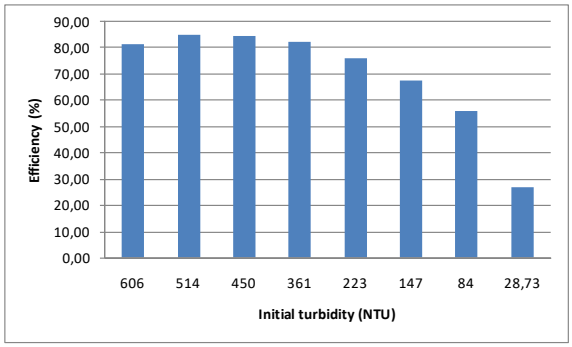

Fig. **7** Turbidity removal efficiency after using omhoff cone (represent sedimentation process)

From the Table 2 and Figure 7 visible turbidity removal efficiency is greatest at the beginning of 514 NTU turbidity of 85.02%. This is due to the high turbidity many contain materials such as mud and sand deposited so many small compared turbidity that contain less material. From the experimental results that turbidity removal efficiency could be devoted to planning prasedimentation on water characteristics of this sample is, if efficiency is > 50% starting from turbidity of 84 NTU.

Coagulation efficiency

Without Slugde Deposition

Table 3. The efficiency of the coagulant dose without sedimentation

Turbidity (NTU)	Optimum dose (ppm)	Turbidity	Efficiency(%)
634	98	4.89	99.23
543	94	4.48	99.17
435	90	2.18	99.50
374	60	4.62	98.76
231	36	4.04	98.25
147	28	0.36	99.76
112	22	3.52	96.86
99	18	2.55	97.42
79	20	2.36	97.01
51	20	4.66	90.86
25.35	16	0.74	97.08

Efficiency of turbidity removal in the experiments is almost the same that is> 90%, with the highest efficiency is on the turbidity of 147 NTU doses achieving 28 ppm final turbidity of 0.36 NTU with an efficiency of 99.75%.

With Slugde Deposition

Table 4. The efficiency of the coagulant dose with sedimentation process

Initial Turbidity (NTU)	Optimum dose (ppm)	Turbidity (ppm)	Efficiency (%)
606	40	3.48	99.43
514	38	2.78	99.46
450	38	4.29	99.05
361	30	3.34	99.07
223	32	2.19	99.02
147	24	4.77	96.76
84	14	2.9	96.55
28.73	14	1.08	96.24

The highest efficiency occurs at the initial turbidity of 514 NTU using optimum coagulant dose achieving 38 ppm final turbidity of 2.78 NTU with an efficiency of 99.46%.

CONCLUSION

There are several conclusions from the research as follows:

1. In the rainy season, fluctuations in raw water turbidity increased significantly in the range of 300-600 NTU.
2. The optimum time of siltation is 35 minutes, with of turbidity removal > 80%.
3. Efisiensi penyisihan kekeruhan tertinggi dengan pemakaian koagulan tanpa pengendapan terjadi pada kekeruhan 147 NTU sebesar 99,76 %
4. The highest turbidity removal efficiency with the use of coagulants without siltation occurs at 147 NTU turbidity of 99.76%

5. The highest efficiency of coagulation without siltation occurs at 514 NTU turbidity of 99.46%

ACKNOWLEDGEMENTS

1. Ministry of Higher Education Republik Indonesia for the cost of research.

REFERENCES

[1] Protokol & Humas PDAM Kota Bandung. 2011. Booklet Informasi PDAM Kota Bandung. Bandung.

[2] Evi Afiatun, Suprihanto Notodarmojo, Styvani Merinda, "The Impact of Water Quality Degradation in Cikapundung River on the Dago Pakar Water Treatment Plant", proceeding The Second International Conference on Sustainable Infrastructure and Built Environment (SIBE-2013), Bandung, Indonesia – November 19th – 20th 2013

[3] Lim, S.R., Suh, S., Kim, J.H., Park, H.S. "Urban Water Infrastructure Optimization to Reduce Environmental Impacts and Costs." Environment Management volume 91 issue 3, 2010: 630-637.

[4] Pemerintah Republik Indonesia (2010) Peraturan Menteri Kesehatan No. 492 Tahun 2010 Tentang Kualitas Air Minum, Jakarta.

[5] Pemerintah Republik Indonesia (2001) Peraturan Pemerintah No. 82 Tahun 2001 Tentang Pengelolaan Kualitas Air Dan Pengendalian Pencemaran Air, Jakarta.

Second International Conference on Science, Engineering & Environment,
Osaka City, Japan, Nov.21-23, 2016, ISBN: 978-4-9905958-7-6 C3051

EFFECTS OF DRYING METHODS ON UTILIZATION OF DIETARY FIBER FROM PINEAPPLE WASTES

Lalita Siriwattananon[1]
[1] Faculty of Agricultural Technology, Rajamangala University of Technology Thanyaburi, Thailand

ABSTRACT

Among the fruits, pineapple is one of the most popular fruits which have high demand all over the world. Recently, Thailand is in the top countries that produce a lot of pineapples and now become the major producers and exporters of pineapple in the world. Due to the high production, there are huge amounts of pineapple wastes remained. To reduce those pineapple wastes is important as it may cause the environmental pollution or affect to the human health. So, research interest has been focused on effective utilization of pineapple wastes; pineapple peels and pineapple cores. These pineapple peels and pineapple cores are expected to be the dietary fiber which can be additional source of fiber in various foods. In the experiment, the drying technique with different drying methods such as sun drying, hot air oven drying and electronic home drying were applied for producing the dietary fiber. After drying process, the amounts of remaining fiber from different methods were analyzed and compared among them. The results of this research showed that the amounts of dietary fiber with hot air oven drying method were higher compared to that with sun drying and electronic home drying. Accordingly, it was concluded that hot air oven drying method was the most effective and to get higher amounts of dietary fiber.

Keywords: Drying, Waste, Dietary fiber, Pineapple

1. INTRODUCTION

Pineapple is one of the most marketable fruit consumed worldwide. Besides the fresh eating, canned fruits are mainly produced [1]. Due to the high consumption and production, there are huge amounts of pineapple wastes remained [2]. There were various studies have been carried out to utilize the possibility of using pineapple wastes, such as [3]-[6] pineapple syrup, bromelain extraction, phenolic antioxidant, organic acids, ethanol, and fiber, etc.

Recently, food manufacturers have embarked on a health criterion in the development of "functional foods", the latter being defined as food products that have an added positive health benefit [7]. High dietary intake of fruits, vegetables and whole grains is strongly associated with reduced risk of developing chronic diseases, such as cancer and cardiovascular diseases, which are the highest causes of death in Europe, United States and in most industrialized countries [8]. It is estimated that one-third of all cancer deaths in industrialized countries could be avoided through appropriate dietary formulations. This suggests that dietary behavioral changes, such as increasing consumption of fruits, vegetables, and whole grains, and related changes in lifestyle, are practical strategies for significant reduction of the incidence of cancer [9]. Now a day, people are concerned more to their consumption quality and food nutrition. Especially, dietary fiber consists of non-digestible carbohydrates and lignin, which is intrinsic and intact in plants that have beneficial physiological effects in humans [10]. Additionally, dietary fiber intake has been linked to the prevention and management of many diseases [11]. There were several researchers have focused on utilizing fibers of pineapple wastes [12]-[14] and have reported that dietary fiber powder prepared from pineapple shell has 70.6% total dietary fiber with better sensory properties than fibers from apple or citrus fruits.

Several processing techniques were applied to produce or preserve dietary fiber from fruits or vegetable for a long use, while one of the most used techniques for preserving is to dehydrate and keep it as a dried products or powder, which are the key ingredients in dairy product, cereals, dietetic foods formulated, etc. In tropical countries dehydration of fruits and vegetables by sun drying method is a popular practice due to its low cost. However, the quality of those products such as color, texture or dying period may resulted in different quality in different dying methods [15-16].

It's inspiring in apply dehydration techniques to produce dietary fiber, while remaining its nutrition value. So, research interest has been focused on effective utilization of pineapple wastes; pineapple peels and pineapple cores. These pineapple peels and pineapple cores are expected to be the dietary fiber which can be additional source of fiber in various foods. Drying technique with different

drying methods of sun drying, hot air oven drying and electronic home drying were applied for producing the dietary fiber. After drying process, the amounts of remaining fiber from different methods were analyzed and compared among them.

2. MATERIALS AND METHODS

2.1 Materials

Pineapple peels and pineapple cores of *Ananas comosus (L.) Merr. cv. Pattavia* were selected for this study as it widely growth and high consumption in Thailand.

2.2 Methods

Cutting pineapple peels and pineapple cores into a size of 10 mm (wide) × 10 mm (long) × 5 mm (high), then boil in hot water of 90°C for 1 hour at ratio of 3:1 (pineapple : water). After that divided into 3 groups, and make dried by the following methods of sun drying, hot air oven drying (at 60°C) and electronic home drying (Fig.1) until the pineapple materials having the moisture content less than 8%. Then dried materials were blended using a moulinex and sieved to get dried pineapple cores and peels powder of 212µm particle, and keep in a locked plastic bag for the chemical and physical analyses.

Fig.1 Electronic home dryer

2.3 Analysis

For a physical property analysis, the color of dried pineapple in both of pineapple peels and pineapple cores were measured and showed as L*, a* and b* using Minolta Color Reader CR.10 [17].

For the chemical analysis, the moisture content, ash and dietary fiber contents were measured according to the AOAC (2000) methods.

2.4 Statistical analysis

Statistical analysis was conducted using SPSS software Ver.20. Significant differences ($p \leq 0.05$) between means were evaluated by one-way ANOVA and Duncan's multiple range tests.

3. RESULTS AND DISCUSSION

3.1 Physical property of dried pineapple

Pineapple cores

Dried pineapple cores using hot air oven dryer (at 60°C) and electronic home dryer (50-60°C) each took 17 hours to decrease the moisture content to become less than 8%, while sun drying method took 40 hours (temperature during drying period was range between 32-55°C). As shown in Table 1 and Figs. 2-4, the color of dried pineapple cores became darker compare to the initial in all drying methods.

Table 1 Colors of dried pineapple cores from different drying methods

Drying methods	L*	a*	b*
Hot air oven	41.66^{c}	1.56^{b}	22.93^{b}
Electronic home dryer	56.56^{a}	0.99^{c}	19.73^{c}
Sun dry	50.90^{b}	3.23^{a}	29.60^{a}

Note: a-c shown significant different ($p \leq 0.05$) in column

According to the experimental results, colors of dried pineapple cores by different drying methods shown significant different ($p \leq 0.05$) and darkness of dried pineapple cores has a direct variation to the increasing of temperature. Drying conditions has effect on the formation of browning in dried food [18].

Fig.2 Dried pineapple cores by hot air over

Fig.3 Dried pineapple cores by sun drying

Fig.4 Dried pineapple cores by electronic home dryer

Pineapple peels

Dried pineapple peels using hot air oven dryer (at 60°C) and electronic home dryer (50-60°C) each took 17 hours to decrease the moisture content to become less than 8%, while sun drying took 36 hours to decrease the moisture (temperature during drying period was range between 32-55°C). However, it was hard to remain certain temperature during the day. As shown in Table 2 and Figs. 5-7, the color of dried pineapple peels became darker compare to the initial in all drying methods. Additionally, color of dried pineapple peels by sun drying showed higher in color of L*, a* and b*, which appeared brighter that other methods. Browning in color is increases with an increase of temperature. Color is one of the quality attributes that influences customers' perceptions of a product, and for fruit, which is preserved by drying, the fruit color also changes due to the drying process. The color of the dried fruit changes due to the formation of browning, which has often been associated with the Maillard reaction [18].

Table 2 Colors of dried pineapple peels from different drying methods

Drying methods	L*	a*	b*
Hot air oven	38.70^{b}	1.14^{c}	14.60^{c}
Electronic home dryer	37.08^{c}	0.63^{b}	20.07^{b}
Sun dry	39.35^{a}	1.68^{a}	29.86^{a}

Note: a-c shown significant different ($p \leq 0.05$) in column

Fig.5 Dried pineapple peels by hot air over

Fig.6 Dried pineapple peels by sun drying

Fig.7 Dried pineapple peels by electronic home dryer

3.2 Chemical properties of dried pineapple

According to the results shown in Tables 3 and 4, different drying methods were not affected to the ash contents in both of dried pineapple cores and peels. So, there were no significant different ($p>0.05$) in ash, however there were significant different ($p\leq0.05$) in moisture contents. Dried pineapple cores using hot air oven dryer (at 60°C) and electronic home dryer (50-60°C) took 17 hours to decrease the moisture content to become less than 8%, while sun drying method took 40 hours (temperature during drying period was range between 32-55°C). Even though, sun drying method took 40 hours but it could not bring the moisture content of dried pineapple cores to below 8%. This is because of the drying temperature of sun drying was lower that other methods of hot air oven drying or electronic home drying. During the day under sun drying process, the temperature was varies up to the time. Even in dried pineapple peels also showed the same tendency of moisture contents by sun drying.

Table 3 Moisture and ash contents in dried pineapple cores from different drying methods

Drying methods	Moisture Content (%)	Ash^{ns} (%)
Hot air oven	6.92^{b}	1.38
Electronic home dryer	6.93^{b}	0.47
Sun dry	9.89^{a}	2.27

Note: a-b shown significant different ($p \leq 0.05$) in column
ns shown no significant different ($p > 0.05$) in column

Table 4 Moisture and ash contents in dried pineapple peels from different drying methods

Drying methods	Moisture Content (%)	Ash^{ns} (%)
Hot air oven	7.40^{b}	2.34
Electronic home dryer	7.13^{c}	2.97
Sun dry	8.90^{a}	2.24

Note: a-c shown significant different ($p \leq 0.05$) in column
ns shown no significant different ($p > 0.05$) in column

As shown in Table 5, dietary fiber contents in dried pineapple cores and peels from hot air oven method showed significantly ($p \leq 0.05$) higher than the other two methods of electronic home dryer and sundry. Additionally, compared the amount of dietary fiber contents between pineapple cores and peels, the results showed that pineapple peels has contain higher dietary fiber than those in pineapple cores in all drying methods.

Table 5 Dietary fiber contents in dried pineapple cores and peels from different drying methods

Drying methods	Dietary fiber content (%)	
	Cores	Peels
Hot air oven	81.56[a]	143.64[a]
Electronic home dryer	65.90[c]	128.43[c]
Sun dry	72.80[b]	137.82[b]

Note: a-c shown significant different ($p \leq 0.05$) in column

Processing methods, especially a process which applying thermal treatments such as boiling, drying or canning, etc. It is well documented that heating can considerably change the texture of plant tissues and that this modification depends on the composition and structure of the fiber components. So, it is crucial to study the effect of thermal treatments on the physic-chemical and physiological properties of the fiber in order to establish the precise amount and bio-availability of the dietary fiber that remains in the final product that gets to the consumer.

In this experimental process, pineapple cores and peels were boiled in hot water in order to breakdown the structure for easier extraction process. This process may results in the inactivation of practically all the enzymes that could negatively affect the organoleptic properties of the final products. Some of the undesirable effects that could happen are excessive softening of the plant tissues, loss of color and flavor. Also, temperature during drying of hot air oven dryer was set at 60°C, electronic home dryer was set in the rang at 50-60°C and the temperature during drying period of sun dry was range between 32-55°C. Those temperatures may affect in the amount of dietary fiber contents. Garau *et al*. (2007)[19] has reported that dehydration promoted important modifications affecting both the physico-chemical properties of dietary fibre and the antioxidant capacity of orange by-products (peel and pulp remaining after juice extraction). The significance of such changes was largely dependent on the air-drying temperature used (from 30°C to 90°C).

4. CONCLUSION

In order to the utilization of pineapple wastes; pineapple peels and pineapple cores as an additional source of fiber in various foods. In this experiment, the drying technique with different drying methods of sun drying, hot air oven drying and electronic home drying were applied for drying pineapple cores and peels in order to compare dietary fiber contents. The results showed that the amounts of dietary fiber with hot air oven drying method were significantly ($p \leq 0.05$) higher compared to that with sun drying and electronic home drying. Therefore, it was concluded that hot air oven drying method was the most effective and to get higher amounts of dietary fiber.

5. ACKNOWLEDGEMENTS

The author gratefully acknowledges use of the services and facilities of the Faculty of Agricultural Technology, Rajamangala University of Technology Thanyaburi (RMUTT), Thailand. Gratefully thanks research funded by the Institute of Environmental Rehabilitation and Conservation (ERECON), Japan.

6. REFERENCES

[1] Tran A. V. “Chemical analysis and pulping study of pineapple crown leaves”, Industrial Crops and Products, 2006, 24: 66-74.

[2] Tanaka K., Hilary Z. D. and Ishizaki A. “Investigation of the utility of pineapple juice and pineapple waste material as low cost substrate for ethanol fermentation by *Zymomonasmobilis*”, J. of Biosci. and Bioeng., 1999, 87: 642-646.

[3] Devakate R. V., Patil V. V., Waje S. S. and Throat B. N. “Purification and drying of bromelain”, Separation and Purification Tech., 2009, 64: 259-264.

[4] Hebbar H. U., Sumana B. and Raghavarao K. S. M. S. “Use of reverse micellar systems for the extraction and purification of bromelain from pineapple wastes”, Bioresource Tech., 2008, 99: 4896-4902.

[5] Beohner H. L. and Mindler A. B. “Ion exchange in waste treatment”, Ind. and Eng. Chem., 1949, 41: 448-452.

[6] Ban-Koffi L. and Han Y. W. “Alcohol production from pineapple waste”, World J. of Micro. and Biotech., 1990, 6: 281-284.

[7] CSPI Reports. “Public Health Boon or 21st Century Quackery International, Functional Foods”, Center for Science in the Public, 1998. Available online http://www.cspinet.org/reports/functional_foods/introduction.html/ (accessed on 22 May 2016).

[8] Liu R.H. “Potential synergy of phytochemicals in cancer prevention: mechanism of action”, J. Nutr. 2004, 134, 3479S-3485S.

[9] Terry P., Giovannucci E., Michels K.B., Bergkvist L., Hansen H., Holmberg L. and Wolk A. “Fruit, vegetables, dietary fiber, and risk of colorectal cancer”, J. Natl. Cancer. Inst. 2001, 93, 525-533.

[10] Institute of Medicine (IOM). “Crossing the Quality Chasm. Crossing the Quality Chasm: A New Health System for the 21st Century”. Washington, D.C: National Academy Press. 2001.

[11] Weinstein J.S., Vogt T.M., and Gerrior S.A. “Healthy eating index scores are associated with blood nutrient concentrations in the third National Health and Nutrition Examination Survey”. Journal of the American Dietetic Association, 2004, 104, pp. 576–584.

[12] Bartolome A. P. and Ruperez P. “Dietary fiber in pineapple fruit”, J. of Clinical Nutr., 1995, 49(S2): 61-S263.

[13] Gorinstein H., Zemser M., Haruenkit R., Chuthakorn R., Grauer F., Martin-Belloso O. and Trakhtenberg S. “Comparative content of total polyphenols and dietary fiber intropical fruits and persimmon”, J. of Nutr. Biochem., 1999, 10: 367-371.

[14] Larrauri J. A., Ruperez P. and Calixto F. S. “Pineapple shell as a source of dietary fiber with associated polyphenols”, J. of Agri. and Food Chem., 1997, 45: 4028-4031.

[15] Derya, A., and Mehmet, M. Ö. “Study the effect of sun, oven and microwave drying on quality of onion slices”. Journal of Food Science and Technology, 2010. 43 (7).

[16] Siriwattananon L. and Maneerate J. “Effect of drying methods on dietary fiber content in dried fruit and vegetable from non-toxic agricultural field”, Int. J. of GEOMATE, 2016, Vol. 11 (28), 2896-2900.

[17] AOAC. “Official Methods of the Association of Official Analytical Chemists. 17thed”. Association Official Analytical Chemists., Washington D.C. 2000.

[18] Maillard, L. “The action of amino acids on sugar: the formation of melanoidin by a methodic route”, Comptes Rendus Hebdomadaires des Seances de l’Academic des Sciences, 1912, 154, 66–68.

[19] Garau M.C., Susana S., Carmen R., Antoni F. “Effect of air-drying temperature on physico-chemical properties of dietary fibre and antioxidant capacity of orange (Citrus aurantium v. Canoneta) by-products”, Food Chemistry, 2007, Vol. 104 (3), 1014–1024.

Second International Conference on Science, Engineering & Environment,
Osaka City, Japan, Nov.21-23, 2016, ISBN: 978-4-9905958-7-6 C3051

SIMULATION OF THE INFLUENCE OF SHADE TREES AND REFLECTIVE PAVEMENTS ON THE MICROCLIMATE IN HOT AND HUMID REGIONS

Julia Md. Tukiran[1], Jamel Ariffin[2] and Abdul Naser Abdul Ghani[3]
[1,2,3]School of Housing, Building and Planning, Universiti Sains Malaysia, Malaysia

ABSTRACT

Shade tree coverage and reflective pavements are useful mitigation strategies to help cool the air and provide shade. It also helps to lower building energy consumption by providing better outdoor boundary conditions. This study presents a simulation approach to evaluate and determine the cooling effect of greening modification developments of a study area on the surrounding environment. This study presents two approaches, including an on-site measurement and a numerical simulation model that uses ENVI-met V 4.0 BETA. Five scenarios with different types of tree coverage and density canopy by adding reflective pavements at ground surface are used. This study was conducted at the RST Complex of Universiti Sains Malaysia. The simulation results showed significantly lower air temperatures in three greening scenarios compared to the current condition scenario with 10% tree coverage. Increasing 20% of tree coverage with less dense and high dense of canopy in the study area led to a maximum air temperature reduction of up to 0.97 °C and 1.15 °C, respectively. Meanwhile, increasing 20% tree coverage with a highly dense canopy and applying reflective pavements on the ground surface contributed to a maximum air temperature reduction of up to 1.16 °C. The outcome of this study could be used to help urban planners and designers to select strategies for designing outdoor spaces to relieve heat stress with the main aim of improving the outdoor living environment.

Keywords: ENVI-met, Microclimate, Cooling effect, Shade tree, Reflective Pavement

INTRODUCTION

Shade trees are actually an ecological solution and one of the strategies that can be used to mitigate heat islands and improve community comfort. It is well-known that plants strategically placed around buildings can bring thermal benefits to the inhabitants. Vegetation not only provides pedestrians with pleasurable visual scenes, but also provides shading, improves air quality and reduces noise levels [1]. The cooling effect of vegetation occurs through the process of shading, evapotranspiration and changing wind patterns [2], [3]. Microclimatic benefits of vegetation have been extensively investigated in previous researches [4], [5].

Pavements (roads, pedestrian walkway, parking area, bicycle path, squares, etc.) are one of the main hardscape contributing to the development of a heat island [6], [7]. Several studies have reported that pavements cover almost 29% to 45% of the urban fabric [8], [9]. Heat islands can also be mitigated by using “cool” materials during the summer period [10]–[12]. Cool materials are characterized by high solar reflectance and high thermal emittance. The two properties could reduce the temperature of the surfaces [13]. Solar reflectance is the ability of a material to reflect solar energy from its surface back into the atmosphere. Many studies report the combined effect of increasing solar reflectance of both roofs and pavements which can reduce summertime urban temperature and improve urban air quality [9], [14], [15].

Many methods have been applied to investigate the effect of vegetation and ground pavements on the microclimate, such as numerical modeling, empirical analysis, on-site measurements and satellite images. However, numerical modeling has become more popular during the recent years because researchers have greater control over modeling in regards to time and resources [16]. The ENVI-met model is normally utilized to simulate urban and landscaped environments in terms of potential air and surface temperature, solar radiation, relative humidity, wind speed, and other variables. The ENVI-met model has also been employed to examine the effect of greenery [17], [18] and paved areas [19], [20] on the thermal environment. Most investigations have focused on either the effect of vegetation and pavements on the environment or the differences between thermal stress in the current state and those in various scenarios. Some studies have investigated the effectiveness of modifying configurations of landscape designs [21], [22] and buildings [23] by comparing the thermal performances of before and after a design is implemented.

This study uses a numerical simulation model

such as ENVI-met to generate microclimate data for the study area and examine the cooling effect of different greening scenarios in an urban thermal environment in Penang. This study produced different scenarios based on the different leaf densities of shading trees and reflective pavement applications on the ground surface.

METHODS

The methods that were used in this study are an on-site measurement program and a simulation model [24], [25], [17]. The on-site measurement program was designed to measure current microclimate conditions in the hostel complex environment at the pedestrian level. These results were used to verify the accuracy of the model. The simulation model was designed to simulate and validate actual conditions and predict the modification effects of the proposed greening scenarios using the ENVI-met V 4.0 BETA.

Study area and climatic condition

The study site is located in a student accommodation area around the Desasiswa Restu, Saujana and Tekun (RST) Complex (5.356042 ° N, 100.292087 ° E), as shown in Fig. 1. The study area is part of the Universiti Sains Malaysia (USM), Penang campus. Penang is situated in the northern part of peninsular Malaysia. Characteristics of the study area climate are hot and humid. In year 2015, the average annual temperature was recorded at 28.1°C with the maximum and minimum average temperatures of 31.6°C and 24.7°C respectively. The site's area measures at 105,650m². The area is dominated by tall buildings of one to ten levels ranging from dormitory buildings, an administrative building, halls and entrepreneur squares.

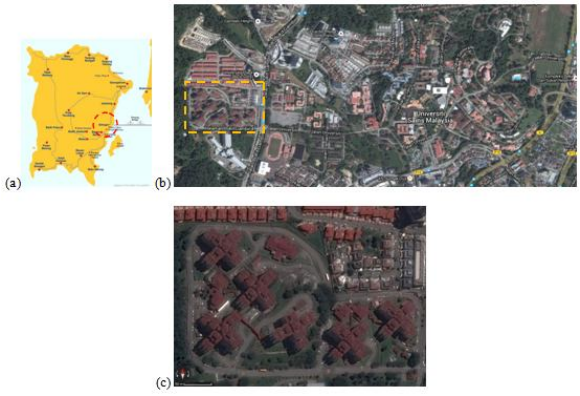

Fig. 1 Plans involved for the study area; (a) key plan, (b) location plan, and (c) site plan

On-site measurement program

On-site field measurements were taken between 10.00 and 14.00 local time on December 30th, 2015. This period was used to collect the variables of climatic data during a clear day. There are a total of 12 observation points in the study site. The observation points were selected as they have various landscape features as shown in Fig. 2.

The first instrument that is involved in this measurement is the (Extech 45160) 3-in-1 Humidity, Temperature and Airflow meter that was placed on a camera tripod at a height of 1.5 m above ground level. This instrument has a sensor to measure air temperature and can record between 0°C to 50°C with an accuracy of ±1.2°C. The sensor for wind speed is capable of measuring outdoor convection air speeds of between 0.4 m/s to 30 m/s with reading speeds from wind ≤ 20 m/s with an accuracy of ± 0.9% m/s, while if the reading speeds winds >20 m/s with an accuracy of ±1.2% m/s. In addition, a relative humidity sensor is used to measure the percentage of humidity of between 10% to 95% with an accuracy of ± 4% between 10% to 70% and ± 5.2%> 70%. The second instrument is the (TES-1333) Solar Power Meter which was also placed on a camera tripod at a height of 1.5 m above ground level. This instrument has a sensor to measure solar radiation with a measurement range of up to 2000 W/m² and an accuracy of ±10 W/m². To consider the thermal effects from the pedestrian level, the two instruments were installed at a height of 1.5 m above the ground level and were calibrated before the on-site operation. The time interval for the measurement of each point of observation is 10 minutes.

ENVI-met model parameterization

For the ENVI-met model geometry settings in this study, the simulated base model domain was built based on satellite images from Google Maps. The number of floors in each building was manually counted. Each level was assumed to be 3 m high. The total maximum building height in the study area was 30 m (10 levels). The main model domain area represented the current conditions in the area of interest and was built within 153 x 109 x 25 grids with input dimensions of dx, dy and dz = 3 m x 3 m x 4 m, as shown in Fig. 2. Only major elements such as trees and ground surfaces were considered in this simulation. Table 1 presents the initial settings of the model.

Table 1 Input configuration data applied in the ENVI-met simulations

Setting data	value
Initial temp. of atmosphere (°C)	28.10
Relative humidity in 2m (%)	70

Wind speed in 10m height (m/s)	2.0
Wind direction (deg)	33:North

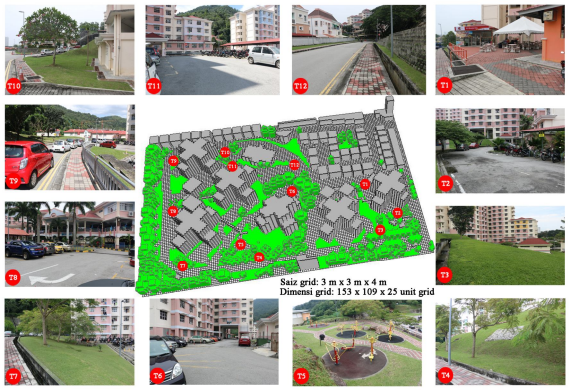

Fig. 2 3-dimensional view of initial model geometry

Systematical calibration process for ENVI-met models of outdoor environment

The aim of the systematical calibrated ENVI-met model for outdoor environment is to predict environmental conditions that agree with the on-site measurements. The initial ENVI-met model was created based on the actual site geometry and the on-site field measurements. The boundary conditions for improving the accuracy of the ENVI-met model in this study were called the Lateral Boundary Conditions (LBC) which include the optimal boundary settings by simulating the initial model domain by adding any grids as nesting areas. For this study, the optimum boundary setting is obtained by adding 18 grids (54m) at the x-axis and 66 grids (198m) at the y-axis. In addition, the simulated air temperature (°C), relative humidity (%), wind velocity (m/s) and solar radiation (W/m2) of the outdoor environment were validated at 12 points with on-site measurements as shown in Fig. 3.

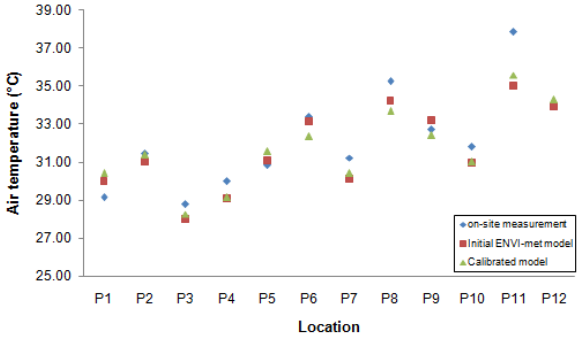

Fig. 3 Comparison of calibration stages for improving the accuracy of the ENVI-met model to obtain a better correlation with measured results for air temperature.

After the calibration process, a paired t-test was used to determine if a significant difference occurred between the average measured values that were made under different conditions which are between the values measured on-site and the simulated values, as shown in Table 2. The paired t-test results from the four validation criteria display the relationships between the paired differences within a 95% confidence interval. The null hypothesis states that there is no significant difference between the means of the twelve on-site measurement points and the simulated results of the four validation criteria. Table 2 and Table 3 indicate that the significance (Sig.) value is greater than 0.05. Therefore, no significant difference occurred and the null hypothesis was accepted. Thus, the calibrated ENVI-met model predictions agreed with all validation criteria and accurately represents the real environment.

Table 2 Paired samples' test for validation criteria which compares the on-site measurements and initial model data from the ENVI-met simulation model

Crite-ria	Paired differences				t	Sig.*
	Mean	StD	95% conf. interval of the difference			
			Lower	Upper		
AT	0.551	0.968	-0.064	1.166	1.970	0.074
RH	1.285	3.420	-0.888	3.458	1.301	0.220
WS	0.333	0.276	-0.142	0.209	0.418	0.684
SR	17.404	28.921	-0.971	35.780	2.085	0.061

Notes: * significant at 0.05 level (2-tailed)

Table 3 Paired samples' test for validation criteria which compares the on-site measurements and calibrated model data from the ENVI-met simulation model

Crite-ria	Paired differences				t	Sig.*
	Mean	StD	95% conf. interval of the difference			
			Lower	Upper		
AT	0.498	0.981	-0.126	1.212	1.756	0.107
RH	2.438	4.583	-0.475	5.350	1.842	0.093
WS	0.058	0.332	-0.152	0.269	0.609	0.555
SR	17.347	28.889	-1.008	35.702	2.080	0.062

Notes: * significant at 0.05 level (2-tailed)

Development of simulation scenarios

To compare and evaluate the cooling potential of greening modifications on 30 December 2015 and

the specific contributions of shade trees and reflective pavements, five different scenarios were simulated, which are (a) case A: current condition, (b) case B: no trees, (c) case C: adding trees with less density, (d) case D: adding trees with high density, and (e) case E: adding trees with high density and reflective pavements. The simulation included three greening development strategies that were proposed to improve the outdoor thermal environment through its implementation.

The differences between cases C and D could indicate the effect of shade trees with different density canopies, while the differences between cases D and E could show the effect of reflective pavements. The tree species that were used in the ENVI-met simulation was *Dalbergia oliveri* to represent low density canopies (LAI = $2m^2/m^2$), and *Swietenia macrophylla* to represent high density canopies (LAI = $5m^2/m^2$). Use of reflective pavements in the ENVI-met scenario simulation focuses on the walkways by using concrete pavement light, while parking lots and driveways use asphalt with red coating.

Table 3 Details of the coverage for different scenarios in the simulation domain

Details	Scenarios				
	Case A	Case B	Case C	Case D	Case E
	Current condition	No trees	Add trees with less dense	Add tree with high dense	Add trees with high dense and reflective pavement
Building coverage	24.30%	24.30%	24.30%	24.30%	24.30%
Tree coverage	10.43%	-	30.04%	30.04%	30.04%
Grass coverage	16.68%	27.11%	14.24%	14.24%	14.24%
Open area	48.59%	48.59%	31.42%	31.42%	15.30%
Reflective pavement	-	-	-	-	16.12%

RESULTS AND DISCUSSSION

The cooling potentials of the current condition

The ENVI-met simulation under the current conditions were done on a summer day with a temperature between 32.58°C and 22.50°C with an average 27.54°C during the peak of the day, as shown in Fig. 4a. Case A was compared with case B, which is the scenario with no trees in the area to produce Fig. 5a. The air temperature has an average difference of 0.22°C when the quantity of current trees was at 10.43%. The air temperature reduction occurred between these scenarios with a maximum average difference of up to 1.12°C. This condition was believed to result from the lack of greenery, the ground pavement material and the greater building density within that area. Thus, the cooling effect of the current conditions was not enough to provide optimum cooling for the entire RST Complex, especially along pedestrian walkways and outdoor spaces where most activities occur during the day.

The cooling potentials of the three greening scenarios

The current conditions were compared with three greening modification strategies. The peak temperature taken at 15:00 of the five different conditions (Fig. 5) were compared at the pedestrian level of 1.5m. This comparison was conducted to understand the impact of these greening modifications on reducing air temperature at the study site, as shown in Fig. 5. The color gradient in Fig. 5 specifies the air temperature range to identify the hot and cool spots in the RST Complex.

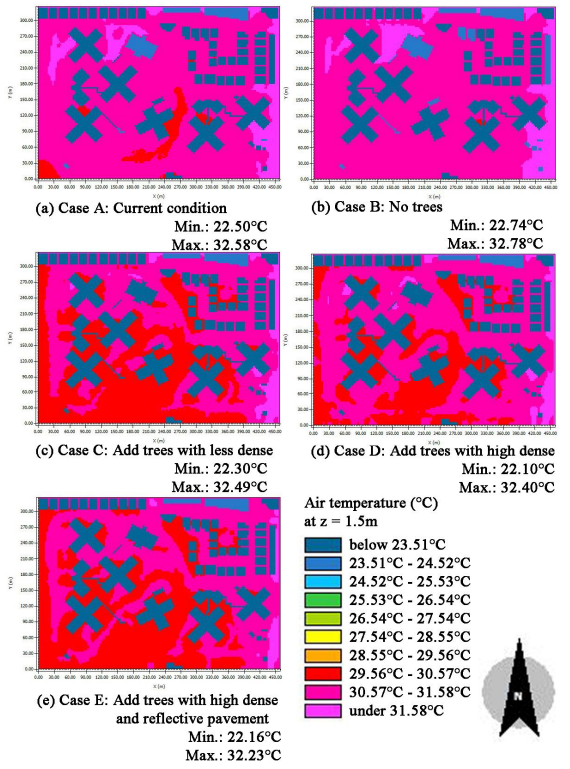

Fig. 4 Air temperature under five different scenarios, taken at 15:00 at the pedestrian level.

Case A was compared with case C, which is after adding trees with low density canopies and the result is shown in Fig. 5b. The air temperature has an average difference of 0.14°C when the quantity of trees with less density was increased by 19.61%. Air temperature reduction occurred between these

scenarios with a maximum average difference of up to 0.97°C. The hot spots which initially occur at the west part of the RST Complex, became much cooler due to the cooling effects of trees with low density canopies.

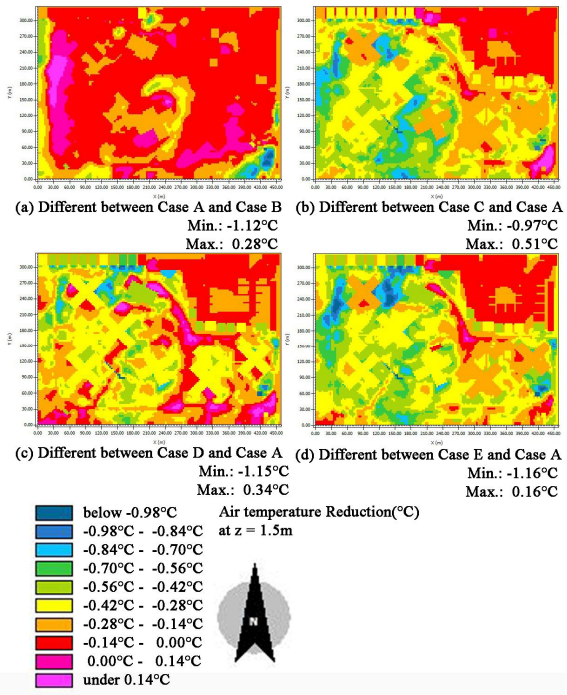

Fig. 5 Comparison of the different air temperature reductions from greening modifications, at 15:00 at the pedestrian level.

Case A was compared with case D which is after adding trees with high density canopies and the result is shown in Fig. 5c. The air temperature has an average difference of 0.29°C. Air temperature reduction occurred between these scenarios with a maximum average difference of up to 1.15°C. These mitigation strategies rely on the density of tree canopies.

Lastly, the combination of both trees with high density canopies and reflective pavement modifications achieved the optimum cooling effects beneath the canopy level as shown in Fig. 5d. Although the results were similar, the yellow color in Fig. 5c becomes greener, while fewer blue spots are shown in Fig. 5d. The air temperature has an average difference of 0.34°C. The largest air temperature reduction occurred between these scenarios with a maximum average difference of up to 1.16°C. The reflective pavements only contributed a small portion of the maximum air temperature reduction by about 0.01°C.

In this study, the modification by adding trees with high density canopies provides a larger cooling potential than adding tree with low density canopies or applying reflective pavements on ground surfaces. The selection or replacement of tree with high density canopies is recommended in open spaces that have no tree to optimize cooling effect on the outdoor thermal environment at the pedestrian level. Therefore, these strategies are recommended in implementation with outdoor landscape designs.

CONCLUSION

The university-in-a-garden concept was conceptualized by Universiti Sains Malaysia (USM), Penang. This study focuses specifically on the RST Complex, USM which is a newly developed area. The study found small quantities of tree coverage in the vicinity. This study developed different scenarios to model the urban thermal impact in order to analyze greening performance following the implementation of feasible green campus policies. The outcome from this study can give solutions and ideas to support the university's planning of improving its thermal environment.

In this study, the ENVI-met computer simulation model was used to understand tree coverage quantities, their canopy densities and reflective pavement on ground surface in an area. These green areas have a pronounced cooling effect and had reduced the ambient outdoor temperature. The calibration and comparison done to improve the accuracy of the ENVI-met model against the initial model, calibrated model and on-site measurements representing the real environment were verified.

Therefore, the use of urban planning and microclimate assessment tools will be useful in assessments of climate which could then feed into decision processes towards providing better living conditions in the future. Designers will be able to assess the impacts of their proposed development on urban climatic conditions.

ACKNOWLEDGEMENTS

Our sincere appreciation goes to our lab assistant Mohd. Faizal Mohd. Nasir and Nurul Huda Zakaria from the Environmental Lab at the School of Housing, Building and Planning, USM for providing instruments and services during the field measurement process. Lastly, special thanks to our families and friends for moral support.

REFERENCES

[1] A. Dimoudi and M. Nikolopoulou, "Vegetation in the urban environment : microclimatic analysis and benefits," *Energy Build.*, vol. 35, no. 1, pp. 69–76, 2003.

[2] Y. J. Huang, H. Akbari, and H. Taha, "The wind-shielding and shading effects of trees on residential heating and cooling requirements," in *Proceedings of the ASHRAE Winter Conference*, 1990, pp. 1403–1411.

[3] R. A. Nasir, S. S. Ahmad, A. Zain-Ahmed, and

N. Ibrahim, “Adapting human comfort in an urban area: The role of tree shades towards urban regeneration,” *Procedia - Soc. Behav. Sci.*, vol. 170, pp. 369–380, 2015.

[4] L. Shashua-bar and M. E. Hoffman, “Vegetation as a climatic component in the design of an urban street An empirical model for predicting the cooling effect of urban green areas with trees,” *Energy Build.*, vol. 31, no. 3, pp. 221–235, 2000.

[5] C. Skelhorn, S. Lindley, and G. Levermore, “The impact of vegetation types on air and surface temperatures in a temperate city: A fine scale assessment in Manchester, UK,” *Landsc. Urban Plan.*, vol. 121, pp. 129–140, 2014.

[6] A. Synnefa, T. Karlessi, N. Gaitani, M. Santamouris, D. N. Assimakopoulos, and C. Papakatsikas, “Experimental testing of cool colored thin layer asphalt and estimation of its potential to improve the urban microclimate,” *Build. Environ.*, vol. 46, no. 1, pp. 38–44, Jan. 2011.

[7] L. Haselbach, M. Boyer, J. T. Kevern, and V. R. Schaefer, “Cyclic Heat Island Impacts on Traditional Versus Pervious Concrete Pavement Systems,” *Transp. Res. Rec. J. Transp. Res. Board*, vol. 2240, no. -1, pp. 107–115, 2011.

[8] L. S. Rose, H. Akbari, and H. Taha, “Characterizing the Fabric of the Urban Environment : A Case Study of Greater Houston , Texas,” Berkeley, Calif., 2003.

[9] H. Akbari, M. Pomerantz, and H. Taha, “Cool surfaces and shade trees to reduce energy use and improve air quality in urban areas,” *Sol. Energy*, vol. 70, no. 3, pp. 295–310, Jan. 2001.

[10] L. Gartland, *Heat Islands: Understanding and Mitigating Heat in Urban Areas*, First. United Kingdom: Earthscan, 2008.

[11] H. Akbari and H. D. Matthews, “Global cooling updates: Reflective roofs and pavements,” *Energy Build.*, vol. 55, pp. 2–6, 2012.

[12] Y. Qin, “Urban canyon albedo and its implication on the use of reflective cool pavements,” *Energy Build.*, vol. 96, pp. 86–94, 2015.

[13] S. Bretz, H. Akbari, and A. Rosenfeld, “Practical issues for using solar-reflective materials to mitigate urban heat islands,” *Atmos. Environ.*, vol. 32, no. 1, pp. 95–101, 1998.

[14] H. Taha, S. Chieh Chang, and H. Akbari, “Meteological and Air Quality Impacts of Heat Island Mitigation Measures in Three U.S. Cities,” Berkeley, Calif., 2000.

[15] H. Taha, H. Hammer, and H. Akbari, “Meteorological and air quality impacts of increased urban albedo and vegetative cover in the greater Toronto Area, Canada,” Berkeley, Calif., 2002.

[16] J. Arnfield, “Two decades of urban climate research: a review of turbulence, exchanges of energy and water, and the urban heat island,” *Int. J. Climatol.*, vol. 23, no. 1, pp. 1–26, Jan. 2003.

[17] M. Srivanit and K. Hokao, “Evaluating the cooling effects of greening for improving the outdoor thermal environment at an institutional campus in the summer,” *Build. Environ.*, vol. 66, pp. 158–172, 2013.

[18] H. Lee, H. Mayer, and L. Chen, “Contribution of trees and grasslands to the mitigation of human heat stress in a residential district of Freiburg, Southwest Germany,” *Landsc. Urban Plan.*, vol. 148, pp. 37–50, 2016.

[19] E. Carnielo and M. Zinzi, “Optical and thermal characterisation of cool asphalts to mitigate urban temperatures and building cooling demand,” *Build. Environ.*, vol. 60, pp. 56–65, 2013.

[20] M. Taleghani, D. J. Sailor, M. Tenpierik, and A. van den Dobbelsteen, “Thermal assessment of heat mitigation strategies: The case of Portland State University, Oregon, USA,” *Build. Environ.*, vol. 73, pp. 138–150, 2014.

[21] Y. Wang and J. Zacharias, “Landscape modification for ambient environmental improvement in central business districts - A case from Beijing,” *Urban For. Urban Green.*, vol. 14, no. 1, pp. 8–18, 2015.

[22] F. O. Minella, E. Kruger, S. Honjo, S. Goyette, and a. Hedjazi, “Daytime microclimatic impacts of the SOVALP project in summer: A case study in Geneva, Switzerland,” *Simulation*, vol. 90, no. 8, pp. 857–873, 2014.

[23] M. Taleghani, L. Kleerekoper, M. Tenpierik, and A. Van Den Dobbelsteen, “Outdoor thermal comfort within five different urban forms in the Netherlands,” *Build. Environ.*, vol. 83, pp. 65–78, 2015.

[24] E. Ng, L. Chen, Y. Wang, and C. Yuan, “A study on the cooling effects of greening in a high-density city: An experience from Hong Kong,” *Build. Environ.*, vol. 47, no. 1, pp. 256–271, 2012.

[25] M. Hajdukiewicz, M. Geron, and M. M. Keane, “Formal calibration methodology for CFD models of naturally ventilated indoor environments,” *Build. Environ.*, vol. 59, pp. 290–302, 2013.

Second International Conference on Science, Engineering & Environment,
Osaka City, Japan, Nov.21-23, 2016, ISBN: 978-4-9905958-7-6 C3051

THE RELATION BETWEEN PRECIPITATION AND THE RIVER RUNOFF IN THE SHINGU RIVER BASIN AT THE TYPHOON NO.12 IN 2011

Masanobu Taniguchi[1] and Hiroyuki Ii[1]
[1]Facultyof System Engineering, Wakayama University, Japan; [1]

ABSTRACT

The water runoff in the river basin was unknown, and therefore the relation between precipitation and the river runoff was analyzed. The residence area had damaged by typhoon No.12 in the Shingu River Basin in 2011. The max of flow rate in the lowest point is estimated 19000m^3/sec, and the value is not confirmed. The value is bigger than the planned river flow. Compared with the rain runoff and the flow rate, the cause of flooding is cleared. As a result, the rainfall intensity is high in the Kitagami River, and however it is estimated that the cause of the flooding is rain runoff in the upper Shingu River. The slope collapse was caused the decrease of river flow rate, the flood was occurred in the upper slope collapse. If the narrow area of flow pass is also exists in one, it is estimate that the place decrease the water sending capacity. Therefore the estimation of flooding is important to grasp of distribution of rainfall runoff.

Keywords: typhoon, runoff, precipitation, river flow rate, flood

INTRODUCTION

The Shingu River Basin has most rain in Japan Main Island. The flood was occurred by typhoon No.12 in 2011 in the Shingu River Basin. The rainfall intensity of the typhoon No.12 was not large, mostly less than 50mm/hour and the average was from 20 mm to 30 mm/hour. However the residence area is big damaged by the typhoon. And the some slope collapse was occurred in the middle of the Shingu River Basin. The rain water was collected, and the amount of water is need to be cleared the cause of flooding. The traveling time is unknown, and the river flow rate become bigger by the traveling time. And finally the flood was occurred at September 4 in the Shingu River Basin. The flow rate is unknown in the time of typhoon, and the station could not recorded the flow rater at the flooding time because water is overflow. The research is clarify to relation between the rainfall runoff and the river runoff, and is clarify the cause of the flooding.

STUDY AREA OVERVIEW

Fig.1 shows study area overview. The flow pass extending of the Shingu River is 183km. The average flow rate is 119m^3/sec. The area of the Shingu River Basin is 2360km. There are 11 dams in the Shingu River Basin. The Odai-ga-hara Plateau has a lot of rain, is the headwaters of three major basin, the Kino River, the Miya River and the Shingu River. The origin of the Shingu River is the Odai-ga-hara Plateau, and the Kitakami and the Shingu River meets at the Miyai, at the lowest point of the Shingu River Basin, and flowing into the Pacific Ocean from Shingu.

In past, The Totsugawa hazard occurred in August 1889 was triggered by heavy rainfall. It was estimated that the maximum daily precipitation was at least about 1000mm. The maximum daily precipitation of typhoon No.12 in 2011 was less than 1000mm. This study is to analyze the cause of the flooding has occurred in a small typhoon than in the past.

Fig. 1 The study area overview

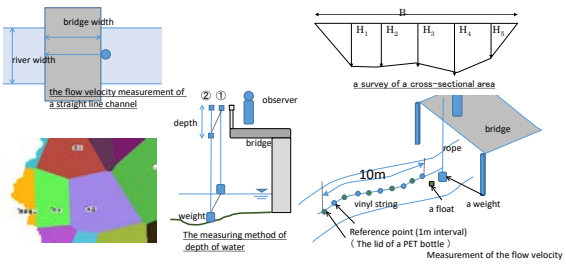

Fig. 2 The creation of analytical data

THE ANALYSIS OF METEOROLOGICAL DATA

The precipitation is water height in situ. To compere river runoff and rainfall runoff, it is necessary to determine the water volume by multiplying the precipitation and area. The area is determined by Thiessen Law method. And the precipitation area is determined by catchment data that the Ministry of Land, Infrastructure and Transport has been published. The precipitation data was the data of the Japan Meteorological Agency and the Ministry of Land, Infrastructure and Transport. The number of observing station of the Japan Meteorological Agency is 27. And the number of observing station of the Ministry of Land, Infrastructure and Transport is 13. The research used data of 25 point.

THE MEASUREMENT OF RIVER CROSS SECTION

The river cross section is important to calculate the river flow rate. The Ouga Station data is important in calculating the flow rate at the time of the flood condition in typhoon No.12 because it is the lowest point in the Shingu River Basin and is point of the flooding. However there was no flow rate data at the Ouga Station in 2011 so it was necessary to estimate the flow rate. Flow rate in 2011 had to be calculated from water level value using relation between water level and flow rate values.

The flow rate at the flood condition is follow formula.

$$v = \frac{1}{n} a^{\frac{1}{2}} H^{\frac{1}{6}} \qquad (1)$$

v:velocity, *n*:Roughness coefficient, *a*:Eigenvalue of observatory, *H*: average water depth

The formula has been proposed by Taniguchi et al. The formula is possible to calculate velocity from water level.

ANALISYS OF THE RAIN RUNOFF

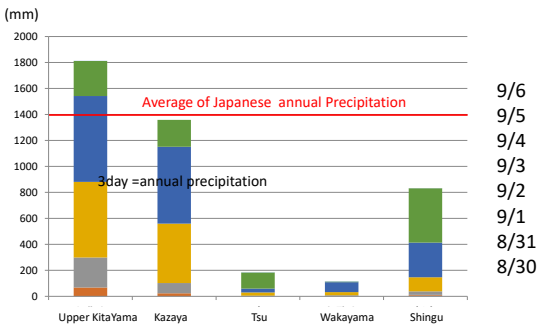

Fig. 3 The amount of precipitation in the typhoon No.12 period (mm/day)

Fig.3 shows the amount of precipitation per day in the typhoon No.12 period. The 3 days of precipitation is same to the annual precipitation at Upper Kitayama and Kazaya. The Upper Kitayama and Kazaya is the observing station of Odai-ga-hara Plateau, most rainfall region in main Island of Japan. The max of precipitation par day is 600mm, and the value is not so big at the region. The Tsu, Wakayama and Shingu station is located in the each City. The precipitation is low value, so residents was not careful to the typhoon. In order to clarify the cause of the flood, it is necessary to clarify the relation between precipitations and rain runoff. And the analysis requires a more detailed rainfall data.

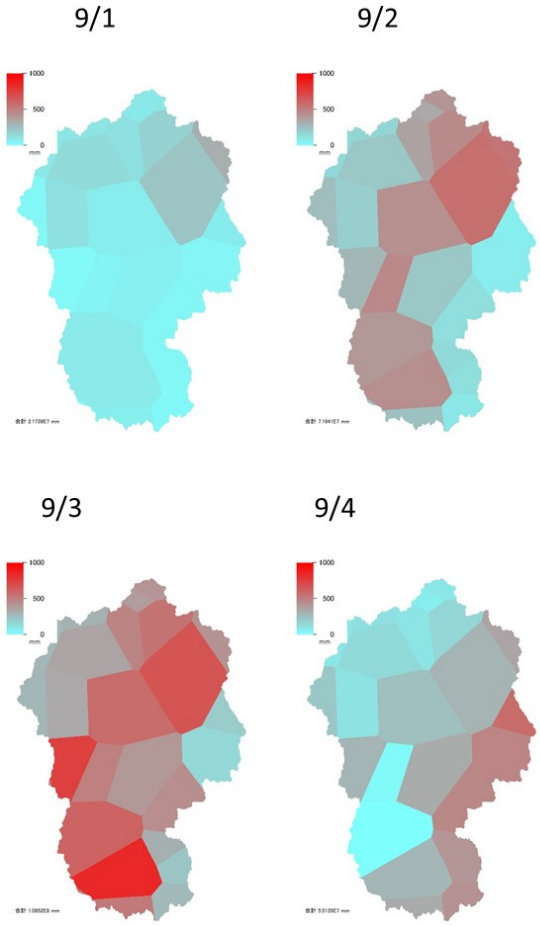

Fig. 4 the distribution of precipitation

Fig.4 shows the distribution of precipitation per each days. The precipitation on September 1 is less in whole basin. The peak of precipitation is September 3, and the value is high in whole basin. The maximum of precipitation of the typhoon period is 1814mm in upper stream of the Kitagami River. And the Kitagami River Basin of precipitation is higher than the main stream of the Shingu River. Moreover lower stream of the Shingu River at Ouga is 1690mm, and the precipitation is tend to always high in the typhoon period. It is estimate that the

high precipitation of Ouga is occurred the slope collapses, and the slope collapse shut off the water, and occurred the flooding in its upper stream. The precipitation in the upper stream of Shingu River is a little rain, the precipitation is more than 500mm in the Kitagami River. The distribution of precipitation is different in a day, so there is no rain in the region, the distribution of precipitation is need for the analysis of the rain runoff.

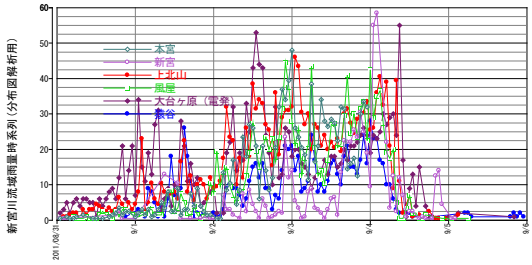

Fig. 5 The time series of precipitation (mm/hour)

The number of precipitation observing station is 25 point. The data of two organizations of the country is different, and we did not know whether the period of the data is present until the analysis of the data. So, the existence of data changes the analysis area, moreover analysis of actually is improved. Therefore the analysis area is determined by existence of measured data. Fig.5 shows the time series of precipitation per hour. The figure shows mainly points of precipitations change. The average value is from 20mm/hour to 30mm/hour, max is 60mm/hour. The characteristic of typhoon is that maximum is not bigger and that long time precipitation is continued. Therefore in order to analyze flooding the rain runoff, it is necessary to grasp the whole Shingu River Basin of rain runoff.

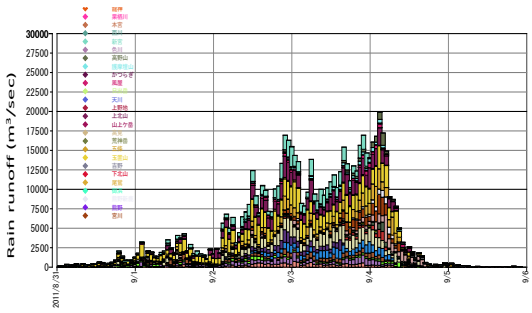

Fig. 6 The time series of rain runoff (m3/sec)

Fig.6 shows the time series of rain runoff in the Shingu River Basin. The rain runoff was calculated from precipitation per hour and sum of precipitation of the whole basin area. The amount of rain runoff exceeds 10000m^3/sec is September 2. The amount of rain runoff had not exceeds 20000m^3/sec. The Shingu River of planed flow rate is 19000m^3/sec, so the rain runoff is almost less than the planed value. It is estimated that the rain water flows late, and that the water had accumulated in the river basin. Therefore it is necessary to compare the rain runoff with the river runoff.

ESTIMATE OF FLOW RATE

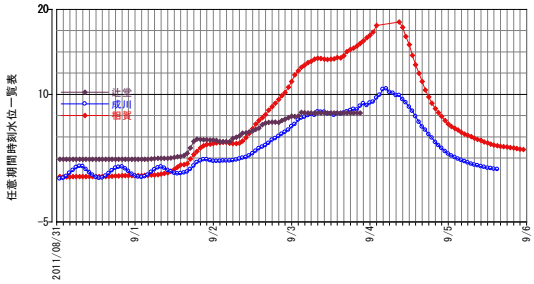

Fig. 7 The time series of river water level

Fig. 7 shows the time series of river water level. The Narukawa is lowest point of the Shingu River, all data is measured in the time of the typhoon. The Ouga is not measured in the flooding peak time. Tujidou is near Sarutani Dam at upper main stream of the Shingu River and is not measured after flooding. Moreover Tujidou and Narukawa did not have flow rate data. Therefore the research used Ouga data for analyze.

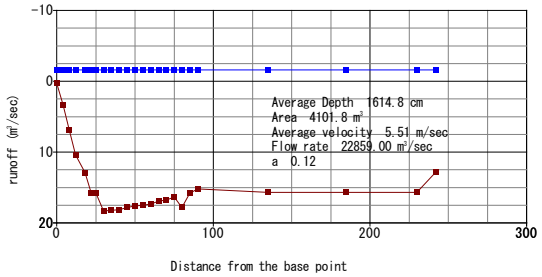

Fig. 8 The measurement of river cross section at Ouga

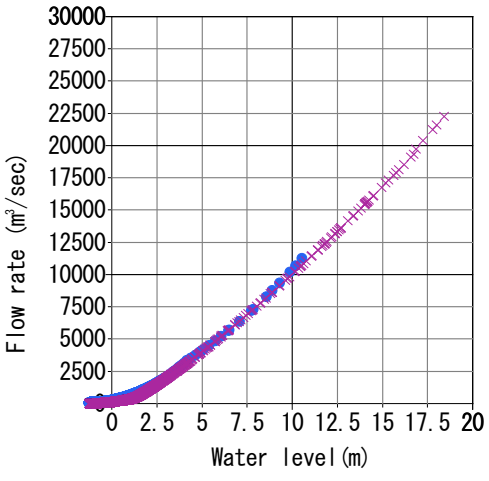

Fig. 9 Relation between water level and flow rate

Fig.8 shows the measurement of river cross section at Ouga. Fig.9 shows relation between water level and flow rate. The circle mark is real data and the cross mark is calculated data. The flow rate in the period of the typhoon was not measured. The observing station was damaged by the flood, so the data was not collected after the typhoon. The flow rate is necessary to estimate from the water level. The flow rate is fitting from the of flow rate data of same year. The parameter a was decided from the real data of slope of relation between water level and flow rate. The velocity is calculated from formula (1), and river cross section area is decided from water level. So, the flow rate is possible to calculate from water level. The parameter a is used by 0.12.

COMPARE THE PRECIPITATION WITH THE RAIN RUNOFF

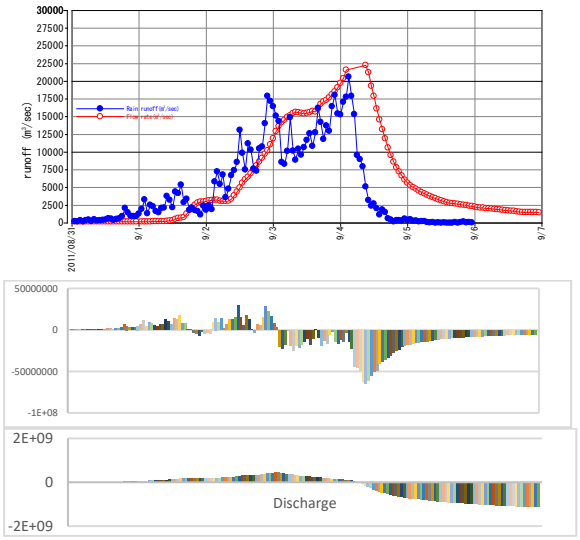

Fig. 10 The time series of rain runoff and river runoff

Fig.10 shows the time series of rain runoff and river runoff. The filled blue circle is rain runoff and red circle of disintermediation is river runoff. The rain runoff is bigger than river runoff before September 3. The bar graph of the above is obtained by subtracting the river runoff from rainfall runoff. The below the bar graph shows the storage amount, integrating the difference in the runoff. The sum of all days of rain runoff is 2,646,764,350m^3, and river runoff is 3,315,617,568 m^3. It is different values, it is estimate that the river runoff is bigger than in fact. The reason has been occurred slope failures before and after September 4, and it is estimated that water did not flow than in fact even if water level is same.

The rain runoff and the river runoff is same value before September 4, the rain runoff is 2,264,114,790m^3 and the river runoff is 2,162,444,796 m^3. Therefore it was estimated that the rain runoff before September 4 is equal to the river runoff and flows out directly. The rain runoff after September 4 is different from the river runoff. it is considered that the reason is either the effect of the delay of the outflow by the dam, or the reduction of river runoff due to slope collapse. In order to conform the reason of the difference of the both runoff, it was necessary to grasp the damage of the condition of the Shingu River Basin.

Table 1 list of storage capacity of dams

River	Dams	Strage capacity(m^3)
Shingu	Kawase	400,000
	Kuo	648,000
	Sarutani	17,300,000
	Seto	12,500,000
	Asahi	12,500,000
	Kazaya	89,000,000
	NItsuno	11,000,000
Kitagami	Sakamoto	68,000,000
	Ikehara	220,100,000
	Nanairo	10,700,000
	Komori	4,700,000
	Sum of volume	446,848,000

It is estimate that the high precipitation of Oauga is occured the slope collapes, and the slope collapse shut off the water, and occurred the flooding in its upper stream. The precipitation in the upper stream of Shingu River is a little rain, the precipitation is more than 500mm in the Kitagami River. The distribution of precipitation is different in a day, so there is no rain in the region, the distribution of precipitation is need for the analysis of the rain runoff.

INFULLUENCE OF DAMS

The Shingu River has 2 big rivers, Shingu main stream and the Kitagami River. The Shingu River has 7 dams, Kawase, Kuo, Sarutani, Asahi, Kazaya nd Nitsuno. The Kitagami River has 4 dams, Sakamoto, Ikehara, Nanairo and Komori. The objective of 8 dams is for electric power, except the Sarutani. The river flow delayed, and it is estimated that the reasons are the long distance of water trip and the reservoir of the dam. The flooding has occurred in this confluence. The dams is usual full of water, so the dams have no flood control function. Table.1 shows list of storage capacity of dams. The sum of volume of all dams in the Shingu River

Basin is 446,848,000m^3, so the rain fall runoff is 2,646,764,350m^3, the value is one fifth of the volume of rain runoff. It is estimate the dams is full at the time of the typhoon No.12 period, and the dams has no water storage capacity. It is estimate that the rain water mostly flow out directly or the effect of dam is little.

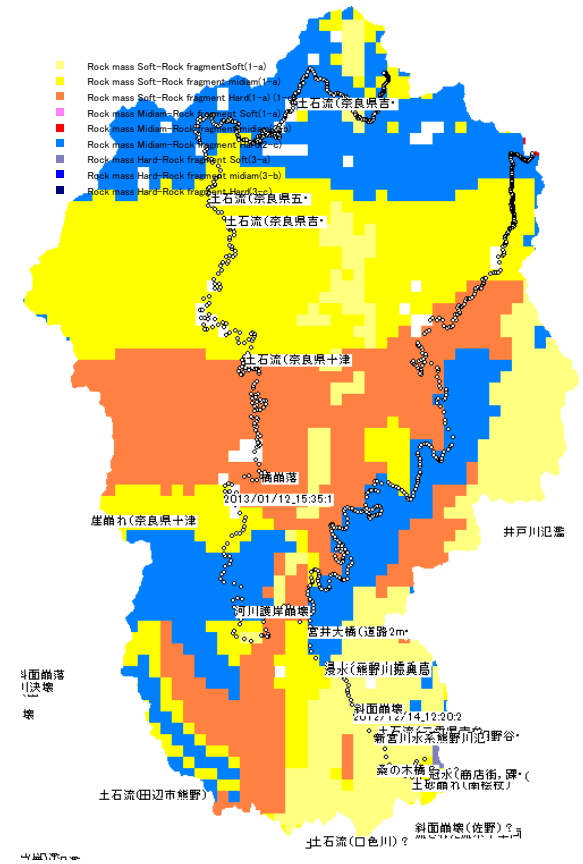

Fig. 11 The location of the disaster and The distribution of geological hardness

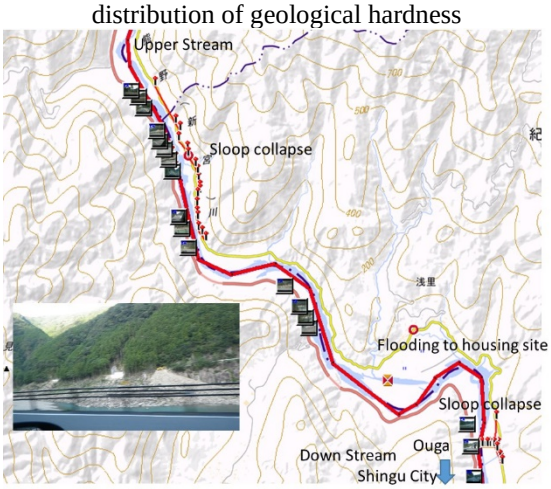

Fig. 12 The location of the disaster and The Field survey by GIS camera

Fig.11 shows the location of the disaster at the time of the typhoon No.11 in 2011 and the distribution of geological hardness. The geological map was created by geological 1km mesh of GIS data and catchment 100m mesh of data that the Ministry of Land, Infrastructure and Transport has been published. The river GPS data is made by tracing a map of the Geographical Survey Institute in Kashmir 3D. The combined map was made using by Taniguchi's GIS software. Yellow is soft rock, blue is hard rock. The disaster tend to be located in the yellow or orange colors. The disaster is not occurred in hard rocks. The map is possible to estimate the location of disasters in future. Particularly, the lowest stream of the Shingu River Basin had many disasters.

Fig.12 shows the location of the disaster and The Field survey by GIS camera. The disaster location data is identified by report of the Ministry of Land, Infrastructure and Transport. The disaster point has no access for the reason that the road is broken. The survey of disaster point was necessary for the grasp of the flow rate. However the no access was impossible to measure both of the distance and volume of the slope collapse and the slope collapse. And so, the slope collapse was estimated by GIS and location data of information of GPS camera. The distance of the slope collapse is total about 2km.

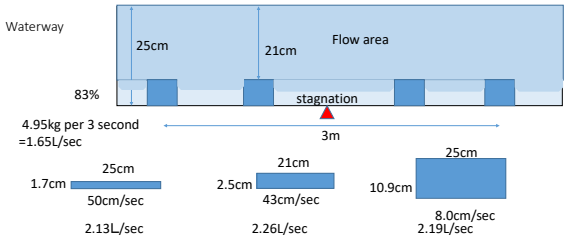

Fig. 13 The waterway experiment

The water flows constantly 1.65L/sec by pump in the flow pass. The experiment was conducted with the next three case, shallow case, deep case, and the case that there is an obstacle. By comparing

the depth water in the presence or absence of an obstacle, the flow rate was verified whether the actual calculated flow rate changes. As the actual flow rate is not changes in the all cases. The velocity of shallow case is 50cm/sec, the water depth is 2cm. The breadth is 25cm, and the flow rate is calculated to be 2.50L/sec.

The velocity of deep case is 8.05cm/sec, the water depth is 10.9cm. The breadth is 25cm, and the flow rate is calculated to be 2.19L/sec. The velocity of the case that there is an obstacle is 43cm/sec, the water depth is 2.5cm. The breadth is 21cm, and the flow rate is calculated to be 2.26L/sec. Therefore the flow coefficient is calculated to be 0.75, the ratio is against for 1.65L/sec. The flow coefficients of three condition is same value, so the obstacles makes the stagnation of water, and it is estimated that the water depth is same condition to the case of constantly waterway of 21cm width. In the Shingu River, the slope collapse was occurred in the typhoon period, and the waterway became narrowly by broken rocks, finally it is estimated that the stagnated water had been occurred the floods.

THE RAIN RUNOFF OF KITAGAMI AND UPPER SHINGU RIVER

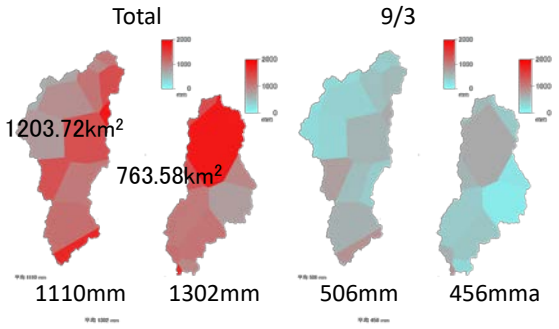

Fig.14 the distribution of precipitation in upper Shingu River Basin
(Left:Upper Shingu River, Right: Kitagami River)

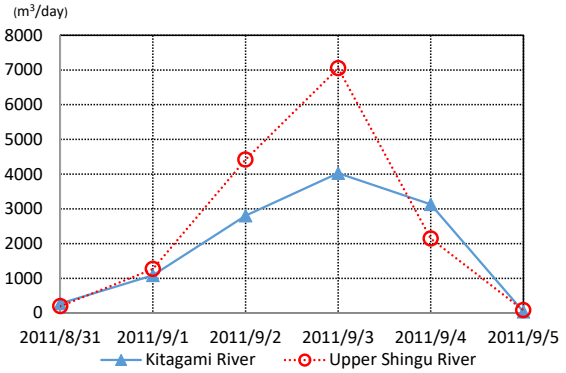

Fig.15 the time series of rain runoff in the upper Shingu River and Kitagami River

Fig.14 shows the distribution of precipitation in upper Shingu River Basin. The total precipitation of the Upper Shingu River is 1110mm per 6 days, and the total precipitation of the Kitagami River is 1302mm per 6 days. The area of the Upper Shingu River is 1203km^2, and the area of the Upper Shingu River is 763km^2. Compared with precipitation of the Kitagami River and Upper Shingu River, the precipitation is much in the Kitagami River Basin. However the precipitation of Upper Shingu River in September 3 is much than the precipitation of Kitagami River. Moreover the area of the Shingu River is larger than the area of the Kitagami River. Therefore it is estimated that the amount of the rain runoff is bigger in the Shingu River.

Fig.15 shows the time series of rain runoff in the upper Shingu River and Kitagami River. The peak of amount of rain runoff is September 3 in the both river basin. The total of the amount of rain runoff in the Shingu River is 1,309,647,360 m^3, the value of Kitagami River is 981,200,300 m^3. The total of the amount of rain runoff in the Shingu River is bigger than the amount of rain runoff in the Kitagami River. Therefore the rainfall intensity is high in the Kitagami River, and however it is estimated that the cause of the flooding is rain runoff in the Shingu River

CONCLUSION

The cause of flood in typhoon No.12 in 2011 was confirmed. The relation between the rain runoff and the flow rate in the Shingu River Basin was analyzed by survey and GIS data and government measured data. The flow rate data is not exist in the typhoon period, therefore the flow data was estimated by the analysis of the flow rate and the water level in the another data in 2011. The calculated flow rate were in good agreement to the sum of rain runoff before the peak of flow rate. However the amount of the flow rate after the peak is bigger compared with the amount of rain runoff. The dam's delay is no longer nothing, the dam capacity of water is full. It is considered that the cause of the different runoff is the sloop collapse in the lowest stream in Ouga, the waterway became narrowly by broken rocks, finally it is estimated that the stagnated water had been occurred the floods. The rainfall intensity is high in the Kitagami River, and however it is estimated that the cause of the flooding is rain runoff in the Shingu River.

REFERENCES

[1] Masanobu Taniguchi, and Hiroyuki Ii ," Distribution characteristics of the Annual nitrogen load in Yamato River Basin in 2011", International Journal of GEOMATE, June, 2016, Vol. 10, Issue 22, pp. 2043-2049 , Japan

[2] Ministry of Land, Infrastructure and Transport, Japan, Water information system, http://www1.river.go.jp/
[3] Digital national land information, http://nlftp.mlit.go.jp/ksj/
[4] Japan Meteorological Agency, http://www.jma.go.jp/jma/index.html
[5] Kashmir 3D, http://www.kashmir3d.com/index-e.h

Second International Conference on Science, Engineering & Environment,
Osaka City, Japan, Nov.21-23, 2016, ISBN: 978-4-9905958-7-6 C3051

IS THE SOUTH CHINA SEA HAS UNDERGONE A SEA LEVEL RISE? A PRELIMINARY STUDY IN TERENGGANU, MALAYSIA

Muhd. Barzani Gasim[1,2] , Hafizan Juahir[1,2] Azizah Endut[1], Azman Azid[1] , Mohd. Khairul Amri Kamarudin and Norsyuhada Hairoma[1]

[1]*East Coast Environmental Research Institute (ESERI), Universiti Sultan Zainal Abidin, Gong Badak Campus, 21300 Kuala Terengganu, Terengganu, Malaysia*

[2]*Faculty of Bio Resources and Food Industries Universiti Sultan Zainal Abidin, Tembila Campus 22200 Besut, Terengganu, Malaysia*

ABSTRACT

The effect of the sea level rise has been detected globally, this study taken more seriously due to the existence of phenomenon such as sea water intrusion, increase of sea waves and coastal erosion. The objective of this study is to determine fluctuation of high and low tides of the South China Sea based on change on water quality trend of Marang and Paka Rivers and from a well monitoring in Terengganu. Sampling was done twice, first in November 2012 and was repeated in November 2015. Selected water quality parameters such as salinity, EC, TDS, DO, pH and turbidity were measured using standard instruments, nine parameters from monitoring well such as Ca, Na, Mg, Fe, Cl, TDS, TSS, EC and pH were carried out from 2006 to 2012. Two-way t-test was used for statistical analysis in this study. There is significant temporal variation in DO and turbidity meanwhile for pH, significant variation is only present during low tide in Marang River. These parameters show an increasing trend from downstream to upstream between 2012 and 2015 due to the increase of land use activities, while other parameters such as EC, salinity, TDS as well as pH were decreased during high tide in Marang River and high and low tides in Paka River. These results were concluded that global change coupled with the enactment of heavy storm and flood phenomenon during 2014 and other external causes was lead to the rising of sea level and salinity dilution of the South China Sea.

Keywords: Marang and Paka Rivers, Northeast and South monsoons, Sea level rise, South China Sea, Water quality parameter

INTRODUCTION

Malaysia received abundance amount of rainfall every year. Peninsular Malaysia received average rainfall approximately 2400mm per year [1]. Some of the water will seep into the ground to become groundwater resources, some will undergo evapotranspiration and the rest will form surface runoff [2, 3]. Some of activities related to the river are fisheries, aquaculture, sand mining, water sport activities, farming activities and many more. Years ago, rivers in Malaysia is commonly very clean and less polluted if it is compared to the present condition, this situation is resulted from the increasing populations living along the riverbank and numerous activities carried out close to river areas [4, 5].

Some of anthropogenic activities, such as settlement, sand quarries, fish farming and the natural phenomenon such as sea level rise and tidal activities are degraded the river water quality [6]. Melting glaciers and thermal expansion of seawater are among the major factors that caused sea level rise [7]. In conjunction to these phenomena, the influx of saltwater into the river through estuary was amplified. As a consequence, there is variation in water quality of surface water. Besides, diurnal variation of sea level which is also known as tidal activities was also affected by this phenomenon. It was shown by the alteration of low and high tides level. Sea level rise interrupts the freshwater characteristics as the projection of salinization towards groundwater and estuaries reservoirs. Thus, disturbance in water quality of freshwater such as rivers by influx of marine water might cause a certain fish in stress condition, as some species especially at juvenile and egg stages which cannot tolerate due to change in quality of water. For example, eggs of trout cod have limited survival rate of 50% when expose to increasing of salinity level of fresh water around 450 mg/L [8].

A study conducted by [9] showed that most of the tidal ranges are usually highest during spring tides and lower during neap tides. In the mixed tides, the diurnal and semidiurnal oscillations are both important factors and the tide is characterized by a large inequality in the high water heights, low water heights, or both. Normally, there are two high and two low waters each day, but occasionally the tide may become diurnal. However, some of the water quality parameters such as calcium, chloride, magnesium, potassium, and sodium are useful chemical analyses to confirm conductivity readings. [10] stated that increase of high tides has influenced the movement of seawater further to the upstream and affected salinity and total dissolve solids concentrations in the river, this is due to the concentration of high dissolved salts mainly consisting of sodium, chloride and magnesium composition in the seawater. Physiochemical parameters such as total dissolve solids (TDS), dissolve oxygen (DO), salinity, electrical conductivity (EC), turbidity and pH are effective in assessing of water quality due to sea level rise [11, 12]. The declination of some water quality parameters are caused by an influx of freshwater into the ocean contributed by rainfall, melted glaciers and ice [13]. Freshwater addition into ocean was lead to salinity dilution [14, 13]. As salinity decreases, electrical conductivity and TDS are also decreases. This is due to linear relationship between salinity, electrical conductivity and TDS, and makes their values varied spatially [15, 16, 17]. The decreased of pH trend toward upstream show that the river water became more acidic when further away from the sea [18]. It has a linear relationship with salinity [18]. As salinity decreases towards upstream and river water became more acidic. Therefore, a water quality assessment with respect to sea level rise impact at Marang and Paka Rivers is carried out in this study to determine water quality trend variations spatially and temporally as well as the potential factors that contributing to this variations. The main objective of the study is to conduct a comparative study on water quality parameters of Marang and Paka Rivers between 2012 to 2015 and 2006 to 2012 wells monitoring assessment which they are can be used and serves as sea level rise indicator.

METHODOLOGY

Sampling stations and Study area

Marang and Paka Rivers were chosen in this study as the two rivers are very affected by high and low tides, located at Marang and Kemaman districts of Terengganu, Malaysia. Water sampling was carried out along these rivers on 13 November 2012 and was repeated on 25 November 2015. Both samplings were conducted during Northeast monsoon period. During this period, the eastern part of Peninsular Malaysia received heavy rainfall and its sea surface temperature declined [19, 6]. A sampling station was selected from upstream to downstream in this water quality assessment, total of nine sampling stations were carried out during second sampling at Marang River and seven sampling stations at Paka River. The first station is located at the estuary where the meeting point between Marang and Paka Rivers and the South China Sea. The last station is located at upstream where this area is less disturb by tidal activities. Each station is 2km apart, the total sampling distance along this study as approximately 18 to 20 km. In this study, tidal activities are considered as one of the factors that influenced river water quality of the river. Sampling is done twice where the first sampling during low tide, the other sampling during high tide. Both samplings were done at the same location according to the coordinate pinpointed by Global Positioning System (GPS). A secondary data of nine water quality parameters from the eleven wells such as Ca, Na, Mg, Fe, Cl, EC, TDS, TSS and pH were provided from the Malaysian Geo Science and Mineral Department for the six years period (2006 to 2012). The selection of these parameters is limited to parameters that related to the activities / reaction with seawater. The location of well is situated along the coastal of the Kuala Terengganu.

Measurement of *in Situ* parameters

Parameters such as DO, EC, TDS, salinity, pH and turbidity were measure using YSI 556 Handheld Multiparameter meter. Turbidity was measured using 2100Q Portable Turbidimeter. To get a more accurate reading, the instruments were calibrated before measurements.

Statistical analysis

Two-way t-test was used to determine the significant difference between two samples [20]. For each parameter, the two-way t-test was performed twice. Firstly, it was performed by using low tide 2012 & 2015 data samples; secondly, it was performed on high tide 2012 & 2015 data samples. The outcome for the two-sample t-test is p-value that will be used to determine either the null hypothesis should be accepted or failed to be accepted. The significance level established for this study is 0.05. Samples with p-value more than significance level (0.05) should accept null hypothesis meanwhile, samples with p-value less than significance level (0.05) has fail to accept null

hypothesis [20, 21]. The first null hypothesis for the first two-sample t-test is stating that there is no mean difference between parameter readings during low tide 2012 & 2015. Meanwhile, the second null hypothesis is stating that there is no mean difference between parameter readings during high tide 2012 & 2015.

RESULTS AND DISCUSSION

Water Quality Analysis

Six physicochemical water quality parameters, such as DO, EC, TDS, salinity, pH and turbidity were analysed to determine their water quality condition of the Marang and Paka Rivers based on temporal and spatial variations. Nine of secondary data water quality well monitoring, such as Na, Ca, Mg, Fe, Cl, TSS, TDS, pH and EC were evaluated for their pattern.

Monitoring Wells

The results of nine water quality parameters from 2006 to 2012 water quality monitoring wells are stated in Table 1. Sampling and analysis of each parameter has been carried twice a year, the sampling time is adjusted based on the monsoon season. Unit of each parameter is ppm or equal to mg/l, except for EC (µS/cm). The result of the analysis shows that each parameter has increased annually or at least has increased in the past 6 years (Table 1).

Table 1 Nine of water quality parameters result based on 2006 to 2012 wells monitoring

Date	Na	Ca	Mg	Fe	Cl	TSS	TDS	pH	EC (µS/cm)
May 2006	56.00	14.00	2.10	1.60	23.00	274.00	216.00	7.20	292.00
Nov 2006	53.00	16.00	1.60	1.40	31.00	266.00	246.00	7.20	305.00
Feb 2007	50.00	15.50	1.10	1.40	30.50	28.00	225.00	5.30	330.00
Feb 2008	43.00	15.00	3.10	2.00	28.00	288.00	158.00	7.30	349.00
June 2008	31.00	16.00	3.40	2.10	18.00	280.00	163.00	7.60	235.00
Mac 2009	41.00	17.00	4.90	4.10	32.00	334.00	328.00	8.80	482.00
Oct 2009	37.00	14.00	3.20	2.10	30.00	266.00	262.00	7.60	359.00
April 2010	48.00	13.00	3.20	2.60	25.00	262.00	202.00	7.80	307.00
Nov 2010	50.00	11.00	3.00	2.20	27.00	254.00	244.00	7.60	323.00
May 2011	53.00	28.00	3.50	2.40	25.00	284.00	268.00	8.20	308.00
June 2012	62.00	16.00	3.70	2.00	36.00	278.00	270.00	7.30	385.00

Water quality of Marang River (M)

Low tide 2012, salinity was ranging from 0.49 to 9.32 ppt with average of 3.26 ppt, during high tide, salinity was ranging from 0.68 to 25.36 ppt with average of 9.37 ppt. Low tide 2015, salinity was ranging from 0.57 to 8.22 ppt with average of 3.26 ppt; during high tide, salinity were ranging from 0.84 to 13.1 ppt with average of 4.13 ppt. Low tide 2012, EC readings were ranging from 1070 to 17541 µS/cm with average of 6407 µS/cm; during high tide EC readings were ranging from 1478 to 44027 µS/cm with average of 16975 µS/cm. Low tide 2015, EC readings were ranging from 1203 to 15432 µS/cm with average of 6309 µS/cm; during high tide, EC readings were ranging from 1755 to 23685 µS/cm with average readings of 8499 µS/cm. Low tide 2012, TDS were ranging from 900 to 10,430 mg/L with average 4,091 mg/L; during high tide, TDS were ranging from 900 to 25,970 mg/L with average 10,046 mg/L. Low tide 2015, TDS were ranging from 745 to 9,276 mg/L with average 3,832 mg/L; during high tide, TDS were ranging from 1,094 – 14,336.8 mg/L with average 5,172 mg/L. Low tide 2012, DO reading were ranging from 4.11 – 4.41 mg/L with average of 4.21 mg/L; during high tide, DO were ranging from 4.01 – 6.02 mg/L with average reading of 4.66 mg/L. Low tide 2015, DO reading were ranging from 2.32 – 2.94 mg/L with average of 2.62 mg/L; during high tide, DO were ranging from 2.45 to 3.26 mg/L with average reading of 3.03 mg/L. In general, distribution trend of DO is increasing from M1 to M9. It has an inversed trend to salinity. Low tide 2012, pH readings were ranging from 5.96 to 7.34 with average of 6.61; during high tide, pH readings were ranging from 6.09 to 8.5 with average of 7.02. High tide 2015, pH were ranging from 5.55 to 8.22 with average of 6.11; during low tide, pH readings were ranging from 5.89 – 7.22 with average of 6.59. During low tide 2012, turbidity were ranging from 10 to 70 NTU with average reading of 35 NTU, during high tide, turbidity were ranging from 4 to 58 NTU with average of 28 NTU. Low tide 2015, turbidity were ranging from 3.7 to 12.87 NTU with average of 8.54 NTU for meanwhile, turbidity were

ranging from 7.18 to 13.2 NTU with average of 9.56 NTU (high tide).

Statistical Analysis of Marang River

Salinity, EC and TDS parameters were showing similar distribution trend which are declining from M1 to M9. The similar trend suggests an association between these parameters. Two-sample t-test ($P < 0.05$) was performed on these three parameters by using low tide 2012 & 2015 as data samples. It revealed that salinity, EC and TDS readings show no significant difference during low tide 2012 & 2015. The p-value for each parameter is 0.552, 0.5182 and 0.4264, respectively. Two-sample t-test ($P < 0.05$) was also performed on high tide 2012 and & 2015 data samples. The results revealed that salinity ($P = 0.0992$), EC ($P = 0.0992$) and TDS ($P = 0.116$) readings during high tide 2012 & 2015 were not significantly different. However, salinity, EC and TDS reading amplitudes for 2012 are greater than 2015 and significantly shown at M1 and M2. These results emphasized a slight declination in salinity, EC and TDS from 2012 to 2015 but it is not significant enough as had been revealed by two-sample t-test. DO in 2012 were rapidly declined from M1 to M3 and then slowly increased until M9. During 2015, DO was slowly increases from M1 to M9. Two-sample t-test ($P < 0.05$) between low tide 2012 & 2015 as well as high tide 2012 & 2015 revealed that the DO readings of low tide and high tide between 2012 and 2015 were significantly different ($P < 0.0001$). The distribution of pH trend was gradually decreasing from M1 to M9 during low and high tides in 2012 and 2015. Two-sample t-test on pH readings during low tide 2012 & 2015 show that there is significant differences ($P = 0.0199$) between the pH reading during 2012 and 2015. However, two-sample t-test ($P < 0.05$) failed to reject that there is no significant difference ($P = 0.1133$) between pH readings during high tide for both years. For turbidity, two-sample t-test ($P < 0.05$) performed on low tide 2012 & 2015 data samples emphasized that the low tide turbidity reading during 2012 and 2015 is significantly difference ($P = 0.008$). Two-sample t-test on high tide data samples is also showing a significant different (0.0119) between the turbidity readings during high tide 2012 & 2015 data samples.

Water quality of Paka River (P)

Low tide 2012, salinity was ranging from 0.01 to 1.67 ppt with average of 0.31 ppt meanwhile during high tide, salinity was ranging from 0.01 to 3.48 ppt with average of 0.77 ppt. Low tide 2015, salinity was ranging from 0.02 to 5.94 ppt with average of 1.25 ppt; during high tide, salinity were ranging from 0.03 – 8.15 ppt with average of 1.34 ppt. Low tide 2012, EC readings were ranging from 33 to 3470 µS/cm with average of 652 µS/cm, meanwhile, during high tide EC readings were ranging from 35 to 6810 µS/cm with average of 1549 µS/cm. Low tide 2015, EC readings were ranging from 56.2 to 13118.7 µS/cm with average of 2712 µS/cm, meanwhile, EC readings were ranging from 68 to 18259 µS/cm with average of 2986 µS/cm during high tide. Low tide 2012, TDS were ranging from 0.022 to 2.1 mg/L with average reading of 0.4 mg/L; meanwhile, TDS were ranging from 0.021 to 4.17 mg/L with average 0.95 mg/L during high tide. Low tide 2015, TDS were ranging from 35.1 to 6905 mg/L with average 150326 mg/L; meanwhile, TDS were ranging from 42.9 – 10244 mg/L with average reading of 1,695.2 mg/L during high tide. Low tide 2012, DO were ranging from 4.9 to 5.65 mg/L with average of 5.25 mg/L, meanwhile, DO were ranging from 4.71 to 5.85 mg/L with average 5.28 mg/L (high tide). Low tide 2015, DO reading were ranging from 2.68 to 3.36 mg/L with average of 3.09 mg/L, meanwhile, DO were ranging from 2.36 to 3.72 mg/L with average reading of 3.27 mg/L (high tide). In general, distribution trend of DO is increasing from P1 to P7. The 2012 pH readings were ranging from 5.19 to 6.43 with average of 5.79 (low tide), meanwhile, pH readings were ranging from 5.54 to 6.8 with average of 6 (high tide). During 2015, pH were ranging from 5.55 – 6.82 with average of 6.05 (low tide), meanwhile, pH readings were ranging from 5.46 to 6.7 with average of 5.95 (high tide). Low tide 2012, turbidity were ranging from 10 to 71 NTU with average reading of 35.57 NTU, meanwhile during high tide, turbidity were ranging from 2 to 61 NTU with average 27.86 NTU. Low tide 2015, turbidity were ranging from 3.96 to 11.9 NTU with average reading of 8.17 NTU for meanwhile, turbidity were ranging from 2.22 to 14.47 NTU with average 9.28 NTU during high tide.

Statistical Analysis of Paka River

The readings trend of salinity, EC and TDS parameters were decreasing from downstream (P1) to upstream (P7) during high and low tides for both years. Two-sample t-test ($P < 0.05$) was performed on low tide and high tide data samples obtained during 2012 and 2015 for salinity, EC, TDS and pH parameters. The tests revealed no significance difference between the readings of low tide 2012 & 2015, where the p-value for salinity, EC, TDS and pH were 0.2862, 0.2888, 0.1374 and 0.3846, respectively. Two-sample t-test also shown that the readings of salinity, EC, TDS and pH during high tide 2012 & 2015 were not significantly different. P-value for salinity, EC, TDS and pH were 0.6597,

0.6100, 0.2595 and 0.8385, respectively. DO shows a steady reading with a small variation between stations, two-sample t-test ($P < 0.05$) determined that there are significant differences between the DO readings for low tide data samples ($P < 0.0001$) and high tide data samples ($P < 0.0001$) during 2012 and 2015. Turbidity readings show an inclining trend from P1 to P7 for both years. Two-way t-test ($P < 0.05$) on turbidity readings revealed a significance difference of turbidity readings between 2012 and 2015 on both low tide ($P = 0.0052$) and high tide (0.0409).

CONCLUSIONS

Basically, high tide 2012 was the highest parameter reading variation between stations, followed by high tide 2015, low tide 2012 and the lowest was low tide 2015 for Marang River while high tide 2015 was the highest for Paka River, followed by low tide 2015, high tide 2012 and the lowest was during low tide 2012. During high tide, sea water level rises and causing saltwater to intrude into river, meanwhile, less of saltwater content in the river during low tide. The readings of salinity, EC and TDS in Marang River were higher during high tide compared to low tide for both in 2012 and 2015. This variation was due to tidal activities. The 2015 reading of TDS, salinity and the EC in Paka River were higher than 2012; pH can be said uneven, but DO and turbidity trend for 2015 show a decreased compared to 2012. The effect of high turbidity and low DO of Paka River is could be the effect of pollution due to anthropogenic activities in the upstream of the river.

Results from the eleven wells water quality data shows that the value of each parameter was increased during dry season and it drops during rainy season, it can be shown that most of the parameters increased during March 2009, it seems as the peak of dry period. Tidal activity, especially during high tide will be move far into the land through the river systems. Due to the above condition, the readings of nine water quality parameters from the eleven wells were increased between 1.4 to 43.2% from May 2006 to June 2012.

The increases of salinity, EC and TDS readings between 2012 and 2015 and the increases of nine water quality parameters from 2006 to 2012 most probably were due to the occurrence of sea level rise. The evidence of global change coupled with the enactment of heavy storm and flood phenomenon during 2014 Northeast monsoon season was lead to the rising of sea level and salinity dilution of the South China Sea. As a consequence, salinity was diluted and resulted in the alteration on water quality of Marang and Paka Rivers.

ACKNOWLEDGMENTS

The authors would like to express an appreciation to the East Coast Environmental Research Institute (ESERI), Universiti Sultan Zainal Abidin (UniSZA) for giving advice, guides, support and for the use of their research facilities.

REFERENCES

[1] Che-Ani, A. I., Shaari, N, Sairi, A, Zain, M F M, & Tahir, M M, "Rainwater Harvesting as an Alternative Water Supply in the Future", European Journal of Scientific Research, 34(1), 2009, pp. 132–140.

[2] Supatimusro, D, Areerachakul, N, & Poomsripanon, J, "The Applied Geographic Information System and the Relation of Mollusk with Water Quality in Ayutthaya Province, Thailand", Energy Procedia, 34, 2013, pp. 99–108.

[3] Taylor, R. G., Scanlon, B., Döll, P., Rodell, M., van Beek, R., Wada, Y., Treidel, H, "Ground water and climate change", Nature Climate Change, 3(4), 2012, pp. 322–329.

[4] Gasim, M B, Zakaria, N, Umar, R & Mustafa, A D, "Analisis Kualiti Air Fiziko-kimia dan Kandungan Mikrob di Hulu Sungai Langat, Selangor", Malaysian Journal of Analytical Sciences 19(5), 2015, pp. 1072–1083.

[5] Azhar, S C, Aris, A Z, Yusoff, M K, Ramli, M F & Juahir, H, "Classification of River Water Quality Using Multivariate Analysis", Procedia Environmental Sciences, 30, 2015, pp. 79–84.

[6] Toriman, M E, Gasim, M B, Ariffin, N H, Muhamad, H & Hairoma, N, "The Influence of Tidal Activities on Hydrologic Variables of Marang River, Terengganu, Malaysia", Malaysian Journal of Analytical Sciences, 19(5), 2015, pp. 1099–1108.

[7] IPCC, Climate Change, Synthesis Report. Contribution of Working Groups I, II and III to the Fifth Assessment Report of the Intergovernmental Panel on Climate Change [Core Writing Team, R K Pachauri and L A Meyer (eds.)]. IPCC, Geneva, Switzerland, 151 pp.Ahmad, S, & Mishra, A, "A Study on

Physico-Chemical Properties of Ground Water Quality of Various Locations of Kanpur City", International Journal of Science and Research, 3(3), 2014, pp. 177–179.

[8] O'Brien, T, "Assessment of the impact of saline drainage on key fish species", In Banens, R J & Lehane, R (Eds.) Riverine Environment Research Forum. Eds. Canberra: Murray-Darling Basin Commission, 1995, pp. 43-46.

[9] Li, L, Barry, D A, Stagnitti, F, Parlange, J Y & Jeng, D S, "Beach water table fluctuations due to spring–neap tides: moving boundary effects", Advances in Water Resources 23(8), 2000, pp. 817-824.

[10] Giménez, E & Morell, I, "Hydrogeochemical analysis of salinization processes in the coastal aquifer of Oropesa (Castellón, Spain)", Environmental Geology 29, 1997, pp. 118-131.

[11] Awang, H, Daud, Z, & Hatta, M Z M, "Hydrology Properties and Water Quality Assessment of the Sembrong Dam, Johor, Malaysia", Procedia - Social and Behavioral Sciences, 195, 2015, pp. 2868–2873.

[12] Gasim, M. B., Khalid, N. A., & Muhamad, H. (2015). The Influence of Tidal Activities onWater Quality of Paka River Terengganu, Malaysia. *Malaysian Journal of Analytical Sciences 19*(5), pp. 979–990.

[13] Werner, A D, Bakker, M, Post, V E A, Vandenbohede, A, Lu, C, Ataie-ashtiani, B, Simmons, C T & Barry, D A, "Seawater intrusion processes, investigation and management : Recent advances and future challenges", Advances in Water Resources, 51, 2013, pp. 3–26.

[14] Sharif, S M, Kusin, F M, Asha'ari, Z H & Aris, A Z, "Characterization of Water Quality Conditions in the Klang River Basin, Malaysia Using Self Organizing Map and K-means Algorithm", Procedia Environmental Sciences, 30, 2015, pp. 73–78.

[15] Iranmanesh, A, Locke II, R A & Wimmer, B. T, "Multivariate Statistical Evaluation of Groundwater Compliance Data from the Illinois Basin – Decatur Project", Energy Procedia, 63, 2014, pp. 3182–3194.

[16] Viswanath, N C, Kumar, P G D & Ammad, K. K, "Statistical Analysis of Quality of Water in Various Watershed for Kozhikode City, Kerala, India. Aquatic Procedia, July 2014, pp. 1078–1085.

[17] Zali, M.A, Retnam, A, & Juahir, H, "Spatial Characterization of Water Quality Using Principal Component Analysis Approach at Juru River Basin, Malaysia", World Applied Sciences Journal, 14, 2011, pp. 55–59.

[18] Dunlop, J, Mcgregor, G, & Horrigan, N, "Potential impacts of salinity and turbidity in riverine ecosystems", 2005, Queensland Department of Natural Resources and Mines.

[19] Curry, R, & Mauritzen, C, "Dilution of the northern North Atlantic Ocean in recent decades", Science, 308(5729), 2006, pp. 1772–1774.

[20] Henneberry, Y, Kraus, T E C, Krabbenhoft, D P & Horwath, W R, "Investigating the Temporal Effects of Metal-Based Coagulants to Remove Mercury from Solution in the Presence of Dissolved Organic Matter", Environmental Management, 57(1), 2016, pp. 220–228.

[21] Ander, E L, Watts, M J, Smedley, P L, Hamilton, E M, Close, R, Crabbe, H, Fletcher, T, Rimell, A, Studden, M & Leonardi, G, "Variability in the chemistry of private drinking water supplies and the impact of domestic treatment systems on water quality", Environmental Geochemistry and Health, 2016, pp. 1–20.

Second International Conference on Science, Engineering & Environment,
Osaka City, Japan, Nov.21-23, 2016, ISBN: 978-4-9905958-7-6 C3051

A SIMPLIFIED METHOD FOR SOIL ANALYSES LABORATORIES

N.CHAOUQI[1, 2], M.EL GHAROUS[2], Z.NACERI[3], M.BOUZZIRI[1]
[1] Laboratory of Applied Chemistry and Environment, Faculty of Sciences and Techniques, University Hassan 1st, Morocco-Settat
[2] INRA, Regional Center for Agricultural Research, Morocco-Settat
[3]Phosphorus-Morocco, Safi-Direction. Quality Control Department (OIS / L / Q)

ABSTRACT

The research goal was to develop a simplified method for estimating the available phosphorus for routine analysis. This study compared the measured Soil-P using the ICP-$NaHCO_3$ with the simplified extraction method (SM-P). The correlation (r=0.99) and the regression(using xlstat-pro) were employed for comparing the data of available phosphorus content in soil samples for a variety of Moroccan soil types, with contrasted physicochemical characteristics: Ali Moumen,, Oued Qibane, Ouled Said, Settat, Dower Lhfaya, and HadGhoualem (are located using ArcGIS 10.1 and fertiMap). SM-P is most suited for soils with pH >= 7 and $CaCO_3$ content above 5%. In this experiment, several parameters are modified, the fineness, the type and degree of mechanical agitation ,the color development solution ((2.5 % $(NH_4)_6Mo_7O_{24}.4H_2O$, in 5 $mol.l^{-1}$ H_2SO_4), 1 %(w/v) ascorbic acid solution), and the adaptation of the reading at 860 nm, are improving the accuracy of P analysis, the high correlation of this method with ICP-$NaHCO_3$ content can be an indication for it. The results of this experiment showed that SM-P can be the best method for predicting the available phosphorus, simple, quick, and easy to execute.

Keywords: Fertilizer Phosphate , Extraction Methods, Available Phosphorus, Moroccan Soils

INTRODUCTION

One of the first problems that arise while studying soil phosphorus is the extraction method to apply in order to determine a fertility scale for the cultivated plant. Several authors highlighted that phosphate-based fertilization of soils should take into account the assimilation of P reserves by the roots [1]-[4]. That is why it is necessary to assess the relationships existing between the fraction of the phosphorus likely to be extracted by cultivation and the phosphorus extracted by the traditional chemical methods. In the field of methods, Dyer (citric acid at 2%) [5]-[6], Bray-1(0.03N NH_4F + 0.025N HCl), Bray-2 (0.03N NH_4F + 0.1N HCl), DA-4 North Caroline (0.05N HCl + 0.025N H_2SO_4), Joret–Hébert (ammonium oxalate)[7],Chang and Jackson (sodium citrate+ sodium hydrosulfite)[8], Olsen modified by Dabin ($NaHCO_3$ + NH_4F)[9],Resin HCO_3^-(DOWEX 2-X8,300-800µm), Mehlich (0.015N NH_4F + 0.012N HCl)[10],Desorption Kinetics (IMPHOS),anion exchange resin, isotopic exchange kinetics$^{32}PO_4^{3-}$ and $^{33}PO_4^{3-}$ [11], Olsen method 0.5N $NaHCO_3$, prevails worldwide over the others[12]-[13].
The information given by Olsen method is the most relevant with the biological results [14]-[15].

The reagents, other than sodium bicarbonate, extracted larger quantities of soil Phosphorus forms or freshly introduced fertilizers, less or non-mobile. Despite the limits observed in the case of acidic soils, these results make one considers that Na HCO_3 is the reagent that reflects the availability of P for the crop in question.

The research goal was to creating a synchronization between the nutritional element demand and offer through a method capable of reproducing the best possible the action of the roots based on extraction by sodium bicarbonate. Accordingly, it is necessary that this method be suitable for all the types of the Moroccan soils. It is also necessary that the implementation of this method be accessible to all Moroccan soil analysis laboratories that are less equipped or have weak means.

MATERIELS AND METHODS

Soil sampling and analysis

This study concerned five types of representative soil with contrasted physicochemical characteristics (The locations of sampling stations on the ground are located using ArcGIS 10.1 and fertiMap). The collected samples have been dried at a temperature of 40°C for 24 hours, ground and sieved (according to AFNOR 11-464), before passing to the other analyses. The soils studied here (iron oxide, vertisol, acidic soil, calcimagnesic soil, isohumic soil) have

been collected from a deepness of 20 cm of thickness from different sites, namely (table 1):

Table 1 Sites of the 1st sampling of soils

Sample N°	X	Y	Soil Type	Zone
1	344632	256690	Iron oxide	Meglou
2	264347	275277		Oulad Abou
3	292803	237400		Oued Qibane
4	274345	255153	Vertisol	Ouled Said
5	285052	258140		Ali Moumen
6	297508	269066		Settat
7	302087	286586	Calcimagnesic	Dower Lhfaya
8	299756	279399		Ben Ahmed
9	306117	285833		
10	269495	251677	Isohumic	Ouled Said
11	265513	260417		
12	272214	247209		
13	284524	258008	Vertisol	Ali Moumen
14	292827	237252	Iron oxide	Oued Qibane
15	265358	260014	Isohumic	Oulad Said
16	272248	246 957		
17	300114	279423	Vertisol	Settat-Dowar Hbatta
18	302158	286592	Calcimagnesic	Settat
19	__	__	Acidic Soil	Had Ghoualem

Table 2 Physicochemical characterization of the seven sites of the five types of the study

	OS_{10}	OS_{11}	S_6	S_7	AL	SA	OQ
pH	7,1	6,9	7,5	7,5	7,6	5,1	7,6
pH (Kcl)	6,24	6,11	7,03	7,37	7,21	5,85	7,6
E.C (mmhos)	0,12	0,14	0,15	0,35	0,14	0,15	0,26
NO_3^- (ppm)	24,4	23,1	28,3	30,9	19,2	17,8	88,5
MO (%)	3,0	3,02	3,78	2,67	2,61	1,02	3,77
N (%)	0,29	0,37	0,39	0,49	0,37	0,41	0,40
C/N	6,01	4,75	5,69	3,19	4,08	1,43	5,41
H (%)	11,74	11,38	7,32	4,29	8,45	0,60	6,70
Ca (%)	1,27	1,23	6,33	5,59	7,01	0,14	6,69
Fe (%)	5	5,01	3,52	1,5	3,77	1,69	4,81
Al (%)	10,2	10,2	6,88	1,33	7,68	2,59	7,76
K (%)	0,25	0,26	0,58	0,129	0,31	0,19	1,42
Cd (ppm)	-1,11	-1,08	-0,74	-0,43	-0,12	-0,50	1,61
Mg (%)	1,018	1,017	1,24	0,43	0,94	0,23	1,98
Na (%)	0,03	0,03	0,036	0,02	0,041	0,02	0,07
S (%)	0,03	0,02	0,107	0,09	0,06	0,041	0,145

After the first analysis of their P content, the representative zones for the evaluation of the bioavailable phosphorus are : Ali Moumen-N°5 (AL_5), Oued Qibane- N°3 (OQ_3), Ouled Said-N°11 (OS_{11}), Ouled Said-N°10 (OS_{10}), Settat- N°6 (S_6), Dower Lhfaya-N°7 (S_7), HadGhoualem-N°19 (SA_{19}). Their main characteristics (These characteristics will help interpret the results after the analysis of the plant that will validate the simplified method), as shown by the physiochemical analyses carried out in the Regional Center for Agricultural Research in Settat (CRRAS) and Phosphorus-Morocco, Safi-Direction (OCP-Safi), are presented in Table 2.

The method used for the comparison of preliminary results

-Inductively Coupled Plasma (ICP) using $NaHCO_3$ as an extracting agent:

weighing 1 g of soil into a 50 mL Erlenmeyer flask, adding 20 mL of extracting solution (0.5M $NaHCO_3$, pH 8.5) to each flask and shaking at 200 epm for 30 minutes at a room temperature at 24 to 27°C,filtering extracts through Whatman N° 42 filter paper.

Analyze for P inductively coupled plasma emission spectroscopy using a blank and standards prepared in the Olsen P extracting solution. [16]

RESULTS AND DISCUSSION

The modified parameters to simplify the available P extraction method

For mineralization phase:

-Fineness

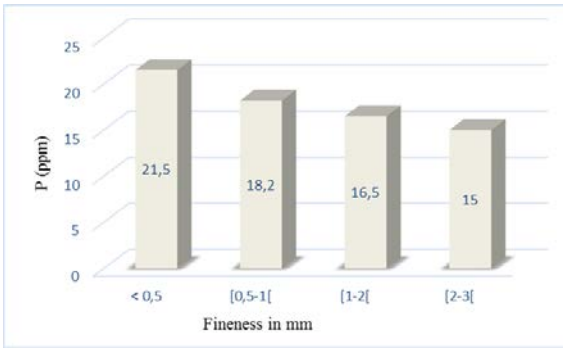

Figure 1 Available P content extracted, based on the fineness of the soil.

-Type and degree of mechanical agitation

Table 3 Available P content extracted based on time and type, of agitation.

Type of agitation	time (min)	P(ppm)
Agitator goes back and forth	30	152
	60	168
Rotating Agitator	30	161

The soil is finely ground in order to increase the specific surface to ensure a good contact and make the reaction as total as possible (Fig 1). The use of a soil with a fineness of 500 µm requires less of $NaHCO_3$ to be attacked (40 ml for 2.5 g).
Rotation speed is fixed at 250 vibrations per minute, this speed is sufficient to allow a good diffusion of reactants.

The necessary duration for the maximum extraction process of P_2O_5 of the soil is determined at 20 min in an attack tank of 250 ml.

For color development phase:

-2.5 % $(NH_4)_6Mo_7O_{24}.4H_2O$, in 5 $mol.l^{-1}$ H_2SO_4
-1 %(w/v) ascorbic acid solution
- 5 min at 99°C
- Wavelength : 860 nm

Describing trial process

-Weigh 2.5 g of 0.5 mm of soil into a 250 ml Erlenmeyer flask Add 40 ml of the extracting solution (0.5M $NaHCO_3$, pH 8.5) to the sample, shake 20 minutes (250 vibrations per minute) in a constant temperature room(22°C).
-At completion of shaking time immediately filter the suspensions through whatman N°42 filter paper. If the filtrates are dark colored add carbon black and filter again to abtain a clear filtrate
-To a 5 ml aliquot of the filtrate add 6 ml of sulfomolybdic solution (2.5 % $(NH_4)_6Mo_7O_{24}.4H_2O$), in 5 $mol.l^{-1}$ (H_2SO_4)) degas by shaking.
-Add 1 ml of 1 %(w/v) ascorbic acid solution.
-Add 14 ml of demineralized water and mix.
-Prepare standards of 0; 0.2 ; 0.4 ; 0.6 ; 1 and 2ppm of P by diluting 0.5 ; 1 ; 1.5 ; 2.5 and 5 ml of the mother solution (Dissolve 0.4393 g of KH_2PO_4 dry at 110°C for 2 hours in 1000 ml of demineralized water) in 250 ml of 0.5M. sodium bicarbonate, pH 8.5(Treat the standards in the same way as the samples).
-Heat all the solutions to be determined for 5 min at 99°C.Immediately cool with running water at 20°C (12 min). Homogenize carefully by turning (1 min).
-Determine P concentration with a spectrophotometer at a wavelength of 860 nm.
Results:
P ($\mu g.g^{-1}$) = (C*V) / S
Where:
C: Micro-grams of phosphorus determined on the calibration curve (µg/ml)
V: Extraction volume in ml
S: Weight of the soil sample in g

Target

Extract the available phosphorus compounds contained in the soil by selective dissolution with the sodium bicarbonate.

Principle

Alkaline solution reduces the concentration of calcium by precipitation in the form of calcium carbonate and that of aluminum and ferric ions by precipitation in the form of hydroxides. Phosphate ions concentration increases accordingly and the phosphorus may be extracted from the soil sample by the solution of sodium hydrogen carbonate and filtration.

Field of application

This method applies to the determination of available phosphorus in the samples of the Moroccan soil for the different types with pH >=7.

Identification of the sources of uncertainties

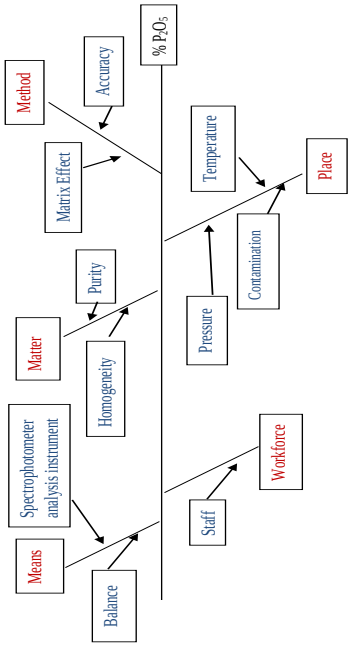

Figure 2 Uncertainties sources/ISHIKAWA Diagram

Several parameters influence the quantity of the extracted available P. A first analysis (Fig 2) for the simplified method allow to exclude certain sources of uncertainties:

Homogeneity and stability

A fineness of 2 mm = 50 %< 500µm + (500µm< 25 %< 1mm) + (1mm< 25 %< 2mm), this fineness does not ensure the granulometric uniformity of the sample, which affects the obtained result. But, sieving with a 500µm ensures homogeneity, and requires less $NaHCO_3$ (40ml).

Temperature

The molecules of the reagents are within the same phase and can therefore easily enter in contact to react. Yet, this is an independent process of temperature so that it will not affect the reaction speed.

Extraction solution (pH)

The pH should be close to the conditions of the soil in place. Yet, the results obtained for the acid soils by the 0.5M $NaHCO_3$, pH 8.5 are far from those obtained by Bray.

Regarding the increase of pH : 8.5/1st day, 8.65/2nd day, 8.77/3rd day and 8.94/4th day, the results were not significant. [21]

*Away from the light, pH remains constant for five days. However, a control is necessary prior to any use.

Spectrophotometer analysis instrument

Color intensity decreases after 45 min. In addition, it is necessary to add the ascorbic acid solution at appropriately adjusted time intervals to ensure that the readings of the molybdenum blue color intensity, related to each sample, are made about 10 min after the addition of this reagent and, in all cases, not more than 15 min.

Method choice justification

ICP method is chosen, in order to compare the results and get an interpretation basis (the statistical analyses were done using xlstat-pro).

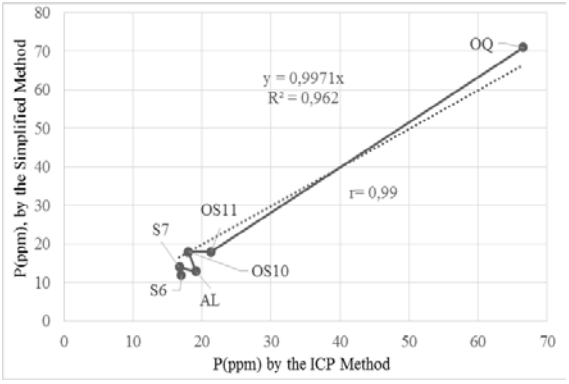

Figure 3 Preliminary comparison between ICP and the simplified method for the available P content (ppm) in relation to the different types of Moroccan soils.

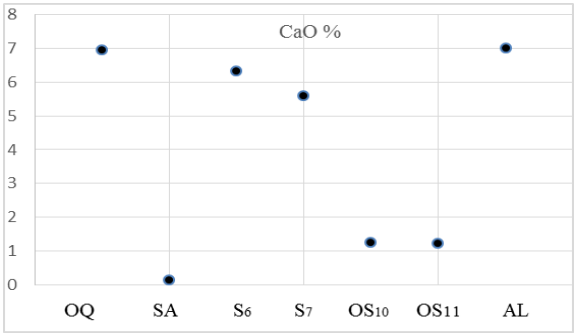

Figure 4 the content of active limestone for the different soils

Chemical methods, in practice, overestimate the availability of phosphorus of the soils which have much free aluminum (table 2), whereas it is not the case for this simplified method which is clearly not affected by aluminum, in contrast to ORSTOM method (a modified version of Olsen method referenced by the AFNOR standard under number NF ISO 11263), which, by the action of the fluoride, reacts more actively with the forms related to aluminum.

Fig (4) shows us that the Moroccan soils contains a dominance of P-Ca, these results confirm the choice of $NaHCO_3$.

Correlations involving the Bray-P method were very low when all soil samples were included in the analyses but improved when calcareous soils were dropped. Concerning the SA_{19} as an acid soil (table 1), the comparison of the extracted content of P, is carried out with Bray, pH 1.5 (104.2ppm).However, It seems that the Bray method extracted a much higher proportion of phosphorus compared to the simplified method (13 ppm) or to the ICP method (33 ppm).

Correlation coefficients (r=0.99) between methods were strongly dependent on the soil pH (Table 2) of the samples included in the analyses. In addition, the slope of linear relationship (y=0.997x) (Fig 3) between the ICP and the Simplified method were similar for the different groups of samples. These results suggest that in many calcareous soils (Fig 4) the simplified method is comparable to the ICP method.

CONCLUSION

The method is not better appropriate to provide criteria for interpreting the phosphoric fertility of the acid soils. The low correlation coefficient between the Bray-P1 and the simplified method was expected

because other research has shown that the Bray-P1 tend to underestimate available P on calcareous soils.

However, it can be recommended for the soils having received large doses of fertilizers (Fig 3), and for the different types of soil with pH >=7.

Taking into account the amount of work that neglected through this SM-P compared to ORSTOM method, as well as the weaknesses of its functioning, namely: Agitation time that takes an hour; Wave length (660 nm), which corresponds at the same time to an interference of soluble organic P; Arsenates that react with the ammonium molybdate to form a blue complex producing an interference on the analysis result; The P extracted comes from the products of the reaction with phosphatic fertilizers and the ammonium fluoride.

Determining available P for the Moroccan laboratories has become unquestionably much more instructive while being much easier to obtain. This simplified method constitute an improvement (r=0.99/ Olsen-ICP) with regard to currently used methods.

PERSPECTIVES

The results obtained by the chemical comparison only are not enough to evaluate the efficiency and the reliability of the chosen method and judge the availability of P. This work is the second part of a study made about the status of phosphorus in the soils of Morocco. Its target is to compare the efficiency of this method of analyzing the available P in order to predict the increase of the yield and sampling of the phosphorus by the plant (chickpea). It also aims at measuring the importance of the chemical and physical characteristics of the studied soils, particularly the content of free iron and aluminum, texture, pH, exchangeable calcium, the form of P dominating the extraction of P, the yield and the sampling of this component by the chickpea.

The plant to be studied is the chickpea because of its important needs of phosphorus and short vegetative cycle. The adopted experimental protocol is a device of complete randomized blocks with three repetitions. The Observations are : Evolution of the dry matter in the growth cycle, yield and amount of the P sampled by the plant.

It is necessary to make sure that, under a given weather, in a given soil, this SM-P provides results that are in correlation with the cultural behavior of the soils and the response to the phosphatic fertilizers.

REFERENCES

[1] Gachon L. & Triboi E. Fiabilité et limites du diagnostic de la fertilité phosphatée des sols établi à partir du phosphore isotopiquement diluable et pouvoir fixateur. C.R Acad. Ag,.ic.Fr. 1979, 13: 981-988.

[2] Admont P.G., Boniface R., Jahiel M. & Morel C. Quelques obeservations sur les méthodes actuelles de dosage du phosphore assimilable des sols. C.R. Acad. Agric.Fr. 1986, 72,69-79.

[3] Bouyadid A. Étude de l'évolution de la solubilité des engrais phosphatés et leurs effets résiduels sur les plantes. Mémoire de 3ème cycle en Agronomie. Institut Agronomique et Vétérinaire Hassan II,Rabat,1989.

[4] Loudyi B. Niveau de carence en phosphore et le phosphore assimilable des sols de la région de Meknès. *Bulletin de l'ENA de Meknès (Maroc)*,1986,23: 23-29.

[5] Olsen S.R.,Cole C.V.,Watabnave F.S. et Dean L.A., Estimation of available phosphorus in soils by extraction with sodium bicarbonate, U.S.D.A., Circular,1954,939,8p.

[6] Dyer B. «On the analytical determination of probably available «mineral» plant-food in soil», I.Chem. Soc., London, 1894, 65,115-129.

[7] Joret G et Hebert J., « Contribution à la détermination du besoin des sols en acide phosphorique »,Ann.Agron., 1955,233-299.

[8] Chang S.C. et Jackson M.L., « Fractionation of soil phosphorus »,Soil Sc., 1957,84,133-144.

[9] Dabin B., « Application des dosages automatiques à l'analyse des sols » 3e partie,Cah. ORSTOM, sér.Pédologie, 1967,vol.3, 257-286.

[10] Mehlich,A. a. Influence of fluoride, sulfate and acidity on extractable phosphorus, calcium, magnesium and potassium.Comm.SoilSci.Plant Anal. 1978, 9:455-476.

[11] Roche P., Griere L., Babre D Calbah et Fallavier P., Le phosphore dans les sols intertropicaux : appréciation des niveaux de carence et des besoins en phosphore, Inst. Mondial du Phosphate, publ.scient.n°2, Prais, 1980.

[12] Oslen S.R. et Sommers C.E., « Phosphorus » in Methods of Soil Analysis, Part 2 Chemical and Microbiological Properties, Sec.édition.Page A.L.,Miller R.H. et Keeny D.R. éd.,Agronomy n°9,Madison,USA,1982, 403-430.

[13] Fardeau J.C., Biodisponibilité du phosphore dans les sols, les déchets et les Sédiments: des approches isotopiques, Com. Séance thématique AFES,6 mars 1997,Paris INA.

[14] Bingham F. T. Chemical tests for available phosphorus. Soil Sci. 1962, 94, 87-95.

[15] Admont P. H., Boniface R., Fardeau J. C., Jahiel M., Morel C., Quelques observations sur les méthodes actuelles du dosage du phosphore assimilable des sols. Applications à l'étude de la valeur fertilisante des phosphates naturels. C.R. Acad. Agri. Fr., 1986, 72, 1, 69-79.

[16] Kuo, S. Phosphorus. *In* D.L. Sparks. (ed.). Methods of Soil Analysis: Part 3- Chemical Methods. SSSA, Madison, WI, 1996, p. 869-919.

[17] Maghanga K.Justin et al., Comparison of soil phosphorus extraction by Olsen and double acid methods in acid soils of western Kenya., East African Journal of Pure and applied Sciences 2012, Vol.2(1):1-5

[18] Fixen, P.E. and J.H. Grove. Testing soils for phosphorus.*In* R.L. Westerman (ed.) Soil Testing and Plant Analysis. SSSA, Madison, WI. 1990. p. 141-180

[19] Kuo, S. Phosphorus.*In* D.L. Sparks. (ed.). Methods of Soil Analysis: Part 3- Chemical Methods. SSSA, Madison, WI. 1996, p. 869-919.

[20] Olsen, S.R., C.V. Cole, F.S. Watanabe, and L.A. Dean. Estimation of available phosphorus in soils by extraction with sodium bicarbonate. USDA Circular 939. U.S. Government Printing Office, Washington D.C. 1954.

[21] M. R. Maghsoodi, A. Reyhanitabar, N. Najafi Development of an alternative to the Olsen test for determining corn plant-available phosphorus in calcareous soils. Iran Iran Agricultural Research, 2015, 34(1) 92-104.

Second International Conference on Science, Engineering & Environment,
Osaka City, Japan, Nov.21-23, 2016, ISBN: 978-4-9905958-7-6 C3051

BIOGEOCHEMICAL FEATURES OF CHEMICAL ELEMENTS ACCUMULATION IN THE ECOSYSTEM OF LAKE ILMENSKOE

Tatyana G. Krupnova, Irina V. Mashkova, Anastasiya M. Kostryukova, Egor V. Artyukov
Chemistry Department, South Ural State University, Russia

ABSTRACT

In the present study Mg, Al, Si, P, S, Cl, K, Ca, Mn, Fe, Zn, Ag, Sr contents were determined by X-ray fluorescence analysis in sediments and organisms of *Contectiana listeri* and *Potamogeton lucens L.* of Lake Ilmenskoe located on the territory of the Ilmen State Reserve (South Ural, Russia). It was shown that microelements-rich sapropels are formed in the Lake Ilmenskoe. The Lake Ilmenskoe is free of anthropogenic impact and may be regarded as models while assessing the lakes under anthropogenic impact. The average element composition of macrophytes, gastropod shells and muscles, sapropel and sandy sediment were compared with the clarkes of elements in the continental crust with a preliminary aluminium rating, aluminium being the least fluent and abiogenic element of the system 'sediment – hydrobiont'. Sapropel was particular rich in microelements in comparison with sandy sediments. Study is shown that most elements are accumulated in aquatic organisms. *Contectiana listeri* and *Potamogeton lucens L.* may be considered as geochemical barriers. They can be used as biomonitors. We found out that low-iron, low-calcium, low-ash sapropel was forming in Lake Ilmenskoe.

Keywords: Sediment, Sapropel, Gastropod, Macrophyte, Bioindication

INTRODUCTION

Sediments and hydrobionts interact with lake water and soluble constituents in such a manner that they give many unique insights into limnological processes. Sediment information use for understanding water quality into lake monitoring and assessment programmes [1], [2].

Environment comprehensively impacts hydrobionts, gastropods in particular. Each region has its own distinctions caused not only by the factors of nature and geography, climate and meteorology, and other similar factors to which hydrobionts adapt, but also by anthropogenic ones that are closely connected with environmental pollution [3], [4]. Due to the natural and anthropogenic factors complex geo-chemical element associations are forming in gastropod shells and muscles. As a result it may change organism functions, and exhaust adaptive resources [5]–[8].

It is well known that gastropods are long-lived mollusks that are sensitive to water- and bed-sediment quality [9]–[11]. Many laboratory studies have documented freshwater gastropods' sensitivity to water and sediment contaminants that include dissolved metals [12]–[15].

Macrophytes are also important as indicators of water quality, water bodies eutrophication and pollution [16]–[18]. Aquatic macrophytes [19], [20] play an important role in the formation of sediments. The results on macro and microelement composition of water plants can be used to assess xenobiotics presence in waterbodies under anthropogenic impact [21]–[23].

The Ilmen State Reserve is situated in the central part of Chelyabinsk region near the town of Miass. There are 30 lakes in its territory. The lakes of the Reserve that are free of anthropogenic impact may be regarded as models while assessing the lakes under anthropogenic impact. For the study we chose the Lake Ilmenskoe, it is located on the territory of the reserve. It has tectonic origin and a small area, which is typical for lakes of the South Urals.

Previous studies of Lake Ilmenskoe are shown that the dominant species of gastropods and macrophytes are *Contectiana listeri* and *Potamogeton lucens L.*, respectively [24]. We also started to study chemical composition of gastropod shells and muscles [25].

The aim of the research is to study chemical composition of sediments and organisms of Contectiana listeri and Potamogeton lucens L. of Lake Ilmenskoe and to investigate their potential use in biomonitoring.

METHODS

Study area

The Ilmen State Reserve is a state nature reserve. In 1920 Ilmen mountains were declared mineralogical reserve. It is one of the first nature reserves created in Russia. Today it is a nature protecting, scientific and researching institution. Specialists protect animals from extinction. There are some rare spices of animals and plants registered

in the Red Book.

Lake Ilmenskoe belongs to the Kars hydrographic basin (Ob basin of the Arctic ocean). It has a flow in a system of rivers Miass – Iset – Tobol – Irtish – Ob. Lake Ilmen runs in the foothills of the South taiga landscapes of the gray forest soils which are covered with pine-birch forests with an admixture of small-leaved breeds such as an aspen, an alder, a linden. Lake Ilmenskoe is of tectonic origin (surface area: 4.56 km², water volume: 14.6 km^3, max. depth: 6.1 m, average depth: 3.0), and is located at an altitude of 331.4 m a.s.l.

The sampling was carried out during the vegetation period in June-July 2015 in 7 stations distributed along the entire Lake Ilmenskoe perimeter (Fig. 1). The coordinates of the sampling stations are: site 1 – 54°59'40.48" N, 60° 9'44.35" E; site 2 – 54°59'45.33" N, 60° 9'49.57" E; site 3 – 55° 0'3.23" N, 60° 9'47.11" E; site 4 – 55° 0'17.20" N, 60° 9'56.03" E; site 5 – 55° 0'51.95" N, 60° 9'9.17" E; site 6 – 55° 1'2.40"N, 60° 8'53.64" E; site 7 – 55° 1'13.31" N, 60° 8'3.24" E.

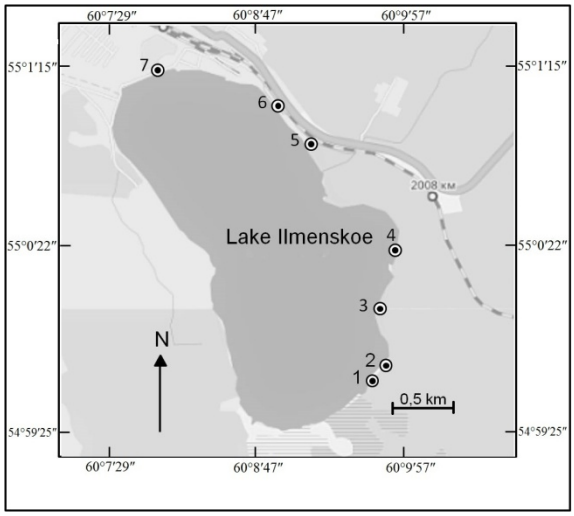

Fig. 1 Map of Lake Ilmenskoe and location of the sampling stations.

Sample collection

In this work, we used the taxonomic system of gastropods developed by Y. I. Starobogatov's school, which is followed by Russian malacologists. *Contectiana listeri* (Forbes et Hanley, 1849) (= *Viviparus contectus auct.*) is a species of a large, freshwater snail with an operculum and a gill, an aquatic gastropod mollusk of *Viviparidae* family. However, it has been found that the waterbodies of South Ural are inhabited by another viviparous species, which has slight, but consistent conchological differences from *Contectiana listeri.* Starobogatov [26]. Vinarski [27] determined it as *Contectiana fennica*, but this suggestion should be confirmed by examining the type material of the species that have been described from Eastern Europe but not accepted by current European malacological taxonomy. So, in this work we determined it as *Contectiana listeri.*

Contectiana listeri was collected using the hydraulic arm. Also manual collection along the lakesides was used. Samples were washed on a 1 mm mesh sieve. Live mature individual gastropods were collected at all sites. Snails ≥20 mm were defined as matures.

Potamogeton lucens L. was hand picked from the freshwater habitat. The plant material was washed thoroughly using water from the sampling sites and was then freed of any adhering material.

Sediment samples were collected from all the sites. Sediment was collected from relatively slow-moving water near physically adequate gastropod habitat consisting of riffle/run complexes with relatively stable gravel sized particles. Each composite sample contained 3 subsamples collected within an approximately 1 m^2 area, from water less than 15 cm deep. Collected subsamples were deposited into a high density polyethylene (HDPE) mixing vessel using a plastic scoop. Approximately 0.5 kg of sediment was collected at each location.

Sample analysis

Samples were collected for verification by X-ray fluorescence (XRF) analytical results.

The gastropods were boiled and separated. The muscles (soft tissue) were removed from each gastropod.

Macrophytes, sediment, shells and muscles were washed and dried. Air-dry samples were ashed at 550°C for five hours. Ashed samples were ground in a mortar. The finely ground rock powder, mixed with a small amount of polyvinyl alcohol dissolved in water, were compressed using a hydraulic press into a pellet.

XRF patterns were registered in the lab of Center for Nanotechnology at South Ural State University. Rigaku SuperMini200 XRF Spectrometer was used for XRF analysis. The relative standard results deviation was not more than 5 %.

Organic matter content was calculated then as the difference in weight between the sample dried at 60ºC and the ash created following ignition at 550ºC within a high temperature muffle furnace

All physico-chemical water parameters were measured in the lab of the Department of Chemistry of South Ural State University according to the standard methods [25].

RESULTS AND DISCUSSION

Lake Ilmenskoe is a freshwater, salinity 114...123 mg/l. The lake belongs to the bicarbonate type, calcium group.

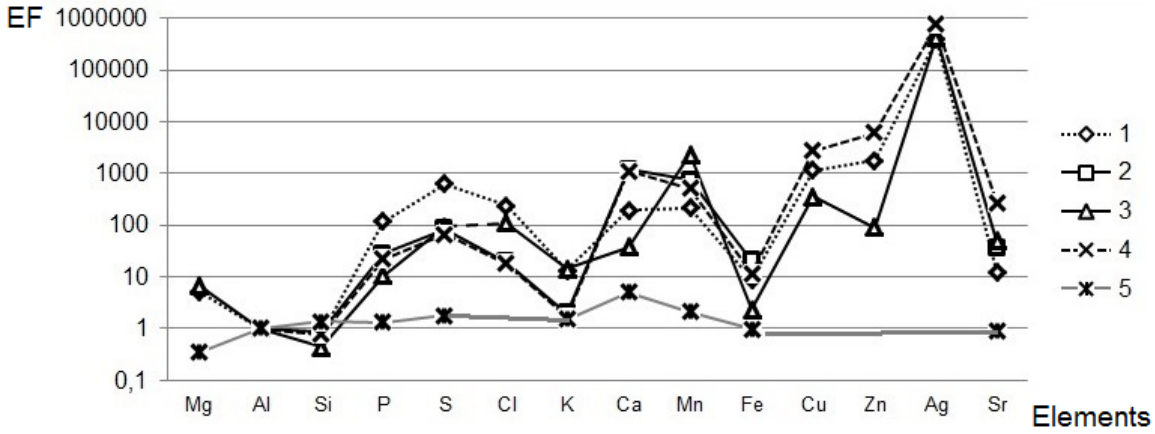

Fig. 2. The abundance coefficients (EF): 1 – gastropod muscles; 2 – gastropod shells; 3 – macrophytes; 4 – sapropels; 5 – sandy sediments of Lake Ilmenskoe. The rating was done with Al and clarkes of the continental crust.

Lake's waters are slightly alkaline with pH of 8.16...8.88. Waters have high levels of oxygen saturation from 76.2 to 98.6 % .

In two stations there were sandy sediments (organic matter content 5.1%, SiO_2 58.5–70.1 %, Al_2O_3 9.9–11.4%). In five stations we found silty sediments (organic matter content – 40.6%, SiO_2 – 0.4–1.8 %, Al_2O_3 – 0.2–0.6 %). According to Korda, silty sediments may be referred to sapropels [28]. Sapropels are organic rich lake sediments formed from aquatic plants, plankton and benthic organisms and transformed under influence of bacteria. Formation of sediments with high organic matter content (over 15%) is typical of freshwater lakes of South Urals [28].

Organic matter content of *Contectiana listeri* shells and muscles was 6.3% and 89.8%, respectively. Potamogeton lucens contained 0.5% of organic matter.

The average element composition of macrophytes, gastropod shells and muscles, sapropel and sandy sediment were compared with the clarkes of elements in the continental crust [29] with a preliminary aluminium rating, aluminium being the least fluent and abiogenic element of the system "sediment – hydrobiont", according to Eq. 1 [30]:

$$EF = \frac{(x_i / x_{Al})_{Sample}}{(x_i / x_{Al})_{ACC}}, \qquad (1)$$

$x_{iSample}$ is the abundance of i-element in the researched object; $x_{AlSample}$ - the abundance of aluminium; x_{iACC} – the abundance of i-element in the continental crust; x_{AlACC} sample – the abundance of aluminium in the continental crust.

Figure 2 illustrates the chemical element abundance coefficients of different researched objects.

Sapropel was particular rich in microelements in comparison with sandy sediments, the abundance coefficient of which is close to 1.

Magnesium is found in gastropod muscles (it is not accumulated in shells) and macrophytes, as it is a part of chlorophyll pigment. Unlike in sandy sediments magnesium abundance in hydrobionts was much higher. There was no magnesium in sapropels. It should be noted that small Mg abundance in sandy sediments may be partly explained by carbonates as they have magnesium (magnesian calcite - $MgCaCO_3$) in their composition.

Cuprum, zink and argentum were found to be extremely abundant in sapropels and gastropods. It is associated with high cuprum and zink concentration in the water. We didn't study the presence of argentum in the lake, but there is a 80-meter-deep well of artesian water rich in Ag. So we may assume that Ag gets into the lake from underground. Hydrobionts are the geochemical reservoirs of these elements. Gastropods actively accumulate Ag, Cu, Zn and it may be connected with their feeding habits. Gastropods are detritophages whose food is primarily silty mass.

The largest cuprum concentration was in sapropels and muscles of *Contectiana listeri*, as Cuprum is a part of respiratory pigments of gastropods. Zink activates ferments in hydrobionts. Cuprum and zink accumulation is associated with physiological processes in living organisms.

Sulfur, phosphorus and chlorine prevailed in gastropod muscles and in sapropels where they have an autochtonous origin, i.e. they are accumulated by plants and with plants withered away they get into the silt.

Mangan abundance coefficient was high, with its most concentration in plants. There is a lode amazonite pegmatite mine on the lakeside. Its distinguishing feature is a great amount of helvine with Mangan concentration of 35 % [31].

Table 1. Oxides in sandy sediments, sapropels, macrophytes, gastropod shells and muscles of Lake Ilmenskoe (average data in all the points, in % in ash)

Oxide	Sandy sediments	Sapropels	Gastropod muscles	Gastropod shells	Macrophytes
MgO	0.58	-	0.87	-	2.59
Al_2O_3	10.68	0.30	1.09	0.29	2.20
SiO_2	64.30	1.0	3.83	1.129	3.73
P_2O_5	1.48	0.70	13.29	0.83	1.95
SO_3	0.32	0.33	11.15	0.40	2.54
Cl	-	0.02	1.13	0.02	1.99
K_2O	3.75	0.12	3.44	0.13	11.79
CaO	15.49	95.56	59.77	94.03	31.30
MnO	0.11	0.72	1.10	0.98	34.55
Fe_2O_3	3.15	1.05	2.90	1.80	2.07
CuO	-	0.12	0.18	-	0.14
ZnO	-	0.82	0.85	0.01	0.13
Ag_2O	-	0.09	0.17	-	0.68
SrO	0.26	0.18	0.27	0.26	0.45

Due to this the water of Lake Ilmenskoe is getting enriched with Mn accumulated by hydrobionts. In addition, there are literature data on the increased content of Mn in the lakes of the South Urals [32].

Calcium was accumulated by gastropod shells, plants and sapropels. Gastropods were rich in Ferrum, when they wither away, Fe is accumulated in sapropels. Kalium was mainly accumulated in plants and gastropod muscles.

Silicon abundance coefficient of all the samples was close to 1. This fact allows us to compare the abundance of different elements not only against Alluminium but also against Silicon as we have done in our previous research [25].

Strontium was particularly worth mentioning, it was accumulated in sapropels, gastropod shells and shining pondweed. Stable strontium is known for its insignificant value for animals and plants but it is always present in them as a constant companion of calcium partially replacing the latter. The Strontium enrichment of the sediment is explained by the fact that this element is included in the composition of carbonates, in particular calcite and aragonite. Strontium is likely to accumulate in hydrobionts of the Ilmen State Reserve from water and silt where its concentration is the highest.

In sandy sediments silicon oxide prevailed – 64.3%, calcium oxide content was slightly higher than 15% (see Table 1). The chemical composition of sapropels (Table 1) was dominated by calcium oxide. Its content was to 95.5% in the organic part of sediment. The content of silicon oxide (terrigenous component) was much lower, around 1%. Thus, sapropels were highly calcareous. It is associated with high phytoplankton production.

Two biological types of sapropels are now known to be forming in small lakes of Ural region. They are plankton-genetic with plankton being the main producer of organic substance; and macrophyte-genetic with macrophytes as the main producer of organic substance of sapropel. Thus, we can assume that sapropel of Lake Ilmenskoe is primarily plankton-genetic, but we can't exclude the sapropel dual character because of the element accumulation both in macrophytes and sapropels.

CONCLUSION

The results of the analysis carried out in this research show that sapropels are formed in Lake Ilmenskoe. The distinguishing geochemical characteristic of the sapropel in the lake is high carbonate content.

It should be conclusions that hydrobionts are natural geochemical reservoirs of metals and may be considered as geochemical barriers. The given research is of an exceptional importance as baseline. The elemental composition data received may be further used in bio-indication study of South Ural lakes.

ACKNOWLEDGEMENTS

The authors wish to thank D. Uchaev (ERC Nanotechnology, SUSU) for XRF quantification measurements.

REFERENCES

[1] Chapman D, Water quality assessments: a guide to the use of biota, sediments, and water in environmental monitoring. London: E&FN Spon, 1996, pp. 1–626.

[2] Vaezi AR, Karbassi AR, Fakhraee M, "Assessing the trace metal pollution in the sediments of Mahshahr Bay, Persian Gulf, via a novel pollution index", Environmental Monitoring and Assessment, Vol. 187, Oct. 2015, pp. 1–12.
[3] Adewunmi CO, Becker W, Kuehnast O, Oluwole F, Dörfler G, "Accumulation of copper, lead and cadmium in freshwater snails in southwestern Nigeria", Science of the Total Environment, Vol. 193 (1), 1996, pp. 69–73.
[4] Sanders BM, "Stress proteins in aquatic organisms: An environmental perspective", Source of the Document Critical Reviews in Toxicology, Vol. 23 (1), 1993, pp. 49–75.
[5] Das S, Khangarot BS, "Bioaccumulation and toxic effects of cadmium on feeding and growth of an Indian pond snail Lymnaea luteola L. under laboratory conditions", Journal of Hazardous Materials, Vol. 182 (1–3), 2010, pp. 763–770.
[6] Gérard C, Carpentier A, Paillisson J-M, "Long-term dynamics and community structure of freshwater gastropods exposed to parasitism and other environmental stressors", Freshwater Biology, Vol. 53 (3), 2008, pp. 470–484.
[7] Noisette F, Richard J, Le Fur I, Peck LS, Davoult D, Martin S, "Metabolic responses to temperature stress under elevated pCO_2 in Crepidula fornicate", Journal of Molluscan Studies, Vol. 81 (2), June 2014, pp. 238–246.
[8] Fenberg PB, Roy K, "Anthropogenic harvesting pressure and changes in life history: Insights from a rocky intertidal limpet", American Naturalist, Vol. 180 (2), 2012, pp. 200–210.
[9] Kontreczky C, Farkas A, Nemcsók J, Salánki J, "Short- and long-term effects of deltamethrin on filtering activity of freshwater mussel (Anodonta cygnea L.)", Ecotoxicology and Environmental Safety, Vol. 38 (3), 1997, pp. 195–199.
[10] Salánki J, Farkas A, Kamardina T, Rózsa KS, "Molluscs in biological monitoring of water quality", Toxicology Letters, Vol. 140–141, 2003, pp. 403–410.
[11] Zipper CE, Donovan PF, Jones JW, Li J, Price JE, Stewart RE, "Spatial and temporal relationships among watershed mining, water quality, and freshwater mussel status in an eastern USA river", Science of the Total Environment, Vol. 541, Jan. 2016, pp. 603–615.
[12] Lau S, Mohamed M, Tan Chi Yen A, Su'Ut S, "Accumulation of heavy metals in freshwater molluscs", Science of the Total Environment. Vol. 214 (1–3), 1998), pp. 113–121.
[13] Warwick RM, "Evidence for the effects of metalcontamination on the intertidal macrobenthic assemblagesof the Fal estuary", Marine Pollution Bulletin, Vol. 42 (2), 2001, pp. 45–148
[14] Mucha AP, Teresa M, Vasconcelos SD, Bordalo AA, "Spatial and seasonal variations of the macro-benthic community and metal contamination in the Douroestuary (Portugal)", Marine Environmental Research, Vol. 60, 2005, pp. 531–550.
[15] Claassens L, Dahms S, Van Vuren JHJ, Greenfield R, "Artificial mussels as indicators of metal pollution in freshwater systems: A field evaluation in the Koekemoer Spruit, South Africa", Ecological Indicators, Vol. 60, 2016, pp. 940–946.
[16] Barko JW, Smart RM, "Sediment-based nutrition of submersed macrophytes", Aquatic Botany, Vol. 10, 1981, pp. 339–352.
[17] Brooks BW, Fulton BA, Hanson ML, "Aquatic toxicology studies with macrophytes and algae should balance experimental pragmatism with environmental realism", Science of the Total Environment, Vol. 536, 2015, pp. 406–407.
[18] Zhang C, Liu H, Gao X, Zhang H, "Modeling nutrients, oxygen and critical phosphorus loading in a shallow reservoir in China with a coupled water quality – Macrophytes model", Ecological Indicators, Vol. 66, 2016, pp. 212–219.
[19] Madsen JD, Bloomfield JA, Sutherland JW, Eichler LW, Boylen CW, "The Aquatic Macrophyte Community of Onondaga Lake: Field Survey and Plant Growth Bioassays of Lake Sediments", Lake and Reservoir Management, Vol. 12 (1), 1996, pp. 73–79.
[20] Murakami K, Inoue-Kohama "Effect of Geological Succession on Macrophyte and Microbiota in Aquifer Ecosystem in Urban Coastal Zone", Int. J. of GEOMATE, Vol. 1, Dec. 2011, No. 2 (Sl. No. 2), pp. 105-110.
[21] , Nichols SJ, Schloesser DW, "Heavy metals in aquatic macrophytes drifting in a large river", Hydrobiologia, Vol. 219 (1), 1991, pp. 333–344.
[22] Markert B, "Multi-element analysis in plant materials. Aanalytical tools and biological questions", Biogeochemistry of Trace, 1992, pp. 402–428.
[23] Baker LF, Ciborowski JJH, MacKinnon MD, "Petroleum coke and soft tailings sediment in constructed wetlands may contribute to the uptake of trace metals by algae and aquatic invertebrates", Source of the Document Science of the Total Environment, Vol. 414, 2012, pp. 177–186.
[24] Samecka-Cymerman A, Kempers AJ, "Aquatic macrophytes as biomonitors of pollution by textile industry", Source of the Document Bulletin of Environmental Contamination and Toxicology, Vol. 69 (1), 2002, pp. 82–96.

[25] Kostryukova AM, Krupnova TG, Mashkova IV, "Composition and structure of gastropods communities in lake Ilmenskoe, Ilmensky Reserve, Russia", in International Multidisciplinary Scientific GeoConference Surveying Geology and Mining Ecology Management, SGEM, Vol. 1, 2014, pp. 175–182.

[26] Krupnova TG, Mashkova IV, Kostryukova AM, Uchaev DA, "Environmental and biological controls on elemental ratios in shells and muscles of freshwater gastropod Contectiana listeri of South Ural" in International Multidisciplinary Scientific GeoConference Surveying Geology and Mining Ecology Management, SGEM, Vol. 1, 2015, pp. 261–268.

[27] Starobogatov YaI, Bogatov VV, Prozorova LA, Saenko EM, Molluscs: Determinant of freshwater invertebrates of Russia and adjacent territories, St. Petersburg: Nauka, 2004, Vol. 6, pp. 9–492.

[28] Vinarski MV, Karimov AV, Grebennikov ME, Lazutkina EA, "Aquatic gastropods of the Ilmeny State Reserve (Southern Urals, Russia)", Tentacle, Vol. 15, 2007, pp. 8–10.

[29] Korde NV, Biostratification and typology of Russian sapropels. Publisher of the USSR Academy of Science, 1960, pp. 1–220.

[30] Wedepohl KH, "The composition of the continental crust", Geochimica et Cosmochimica Acta, Vol. 59 (7), 1995, pp. 1217–1232.

[31] Shotyk W, Cheburkin AK, Appleby PG, Fankhauser A, Kramers YD, "Two thousand years of atmospheric arsenic, antimony and lead deposition in an ombrotrophic bog profile, Jura Mountains, Switzerland", Earth and Planetary Science Letter, Vol. 145, 1996, pp. 1–7.

[32] Rassomahin MA, "Hypergene Mangan mineralization in amazonite pegmatite of Ilmen mountains", Problems and perspectives of modern mineralogy. Yushkin Memorial Seminar, 2014, pp. 141–142.

[33] Valizer PM, Shcherbakova EP, Moroz TN, Nikandrov AS, Nikandrov SN, "About the finds of ferromanganese concretions in the freshwater lakes of the Ilmensky Reserve (South Ural)", Bulletin of the Institute of Geology of Komi NTS Uro ran, Vol. 12 (216), 2012, pp. 17–19.

Second International Conference on Science, Engineering & Environment,
Osaka City, Japan, Nov.21-23, 2016, ISBN: 978-4-9905958-7-6 C3051

ECOLOGICAL RESTORATION OF LAKE UVILDY, RUSSIA: SHORT-TERM BIENNIAL STUDY

Irina V. Mashkova, Tatyana G. Krupnova, Anastasiya M. Kostryukova, Elena E. Shchelkanova
Chemistry Department, South Ural State University, Russia

ABSTRACT

Lake Uvildy is situated in the North of Chelyabinsk region. Lake Uvildy is one of the largest and the most unique of South Ural's lakes. In 1975-1977 the drought occurred and water supplies dried up in South Ural. 234 million cubic meters were moved from the Uvildy lake in Argazi reservoir, which was a source of water supply of the Chelyabinsk city. The lake's water level fell by more than 4 meters. Only in 2008 the water level returned to the previous position, but riparian vegetation was flooded. In July 2014 we carried out an ecological survey of the lake in five sites. We discovered submerged tree and shrub vegetation at 50-70 meters from the bank. Chemical analysis of water revealed the accumulation of organic substances and the transition of nitrogen from nitrate to nitrite and ammonia, of sulfur from sulfate to sulfite and hydrogen sulphide, of carbon to methane. We found blue-green algae (Microcystis, Anabaena, Oscillatoria) in all the sites. It indicates the beginning of water eutrophication. We proposed a new method of ecological restoration of the lake. In August 2014 we cleaned the bottom of the lake in two research points with a special innovative bottom-cleaning machine working both as a pump and a crusher. The research in summer 2015 showed that the water quality had significantly improved and the process of eutrophication had stopped in the points where the bottom was cleaned. Works on the lake trophicity will be continued.

Keywords: Ecological Restoration, Eutrophication, Lake, Water Quality

INTRODUCTION

Lakes are complex ecosystems able to restore and clean themselves. Lake ecosystem is developing very slowly from oligotrophic stage to eutrophic or dystrophic [1]. Nowadays the study of lake evolution to forecast the change in lake trophicity in prospect is of much interest [2]–[4].

Natural eutrophication increases if a lake is subject to human made load. Different characteristics are used to assess the previous and current environmental condition of eutrophic lake under human made impact, e.g. phytoplankton data [5].

There are two basic types of restoration methods relative to eutrophication [6]. The first type is measure which decrease phosphorus availability (increased bottom up control), it is sediment removal, hypolimnetic oxygenation and alum treatment. The second type is measure which increase the zooplankton grazing on phytoplankton (increased top-down control), it is pike stocking and removal zooplankti-benthivorous fish.

The method of lake biomanipulation is now widespread in Europe. The sustainability of the positive effects of biomanipulation has been considered over a decade. But there are cases of failures [6].

The aim of this research was to study the environmental condition of lake Uvildy and to test the device for mechanical cleaning of the lake bottom at the coast.

METHODS

Study Area

Lake Uvildy is a typically tectonic lake in a deep piedmont fault. Its catchment area and water surface are 209 and 69 m^2 respectively [2]. Its length is 13.5 km, its maximum width is 9 km. The average depth of the lake is 15.6 m. The maximum depth measured by echometer is 37 m. The volume of the lake is near 1 km^3. The coasts are considerably fringed by peninsulas and bays. The coastline of the lake is 117 km.

In the forests around the lake there are many small boggy brooks, springs, bogs, especially in the North-West of the lake catchment area where two rivers Cheremshanka and Kosaya flow from low-mountain foothills and vanish in the bogs near lake Uvildy. Water catchment area is in the borderline between two natural zones.

Sample collection

The sampling was carried out during the vegetation period in July 2014 in 5 sites in the North-West and North-East of lake Uvildy (Fig. 1).

Fig. 1 Lake Uvildy and sampling sites.

The coordinates of the sampling sites: site 1 – 55°32'9.13" N, 60°25'34.05" E, site 2 – 55°31'47.91" N, 60°26'50.46" E, site 3 – 55°31'41.29" N, 60°29'58.96" E, site 4 – 55°31'47.42" N, 60°33'38.89" E, site 5 – 55°32'55.95" N, 60°31'54.10" E.

Lake Uvildy is one of the largest lakes of South Ural. In 1974–1978 South Ural was experiencing a severe drought. To tackle a water shortage problem, there was built a channel, through which more than one third of the lake water volume was carried over to Argazinskoye Reservoir. The water level of the lake fell by 4 meters eventually, and most of the coastal areas became outcropped [7]. The water level started to rise only 20 years later, in 1999, and it resulted in a significant transformation of coast geosystem. Birch forest grown in the drainage zones became flooded together with developing soil. It led to eutrophication in the coastal areas [7]. In 2014 five sites with the highest degree of eutrophication were selected, and their physicochemical and microbiological characteristics were studied. After that in 2015 the lake was cleaned in two sites and the water of these sites was probed.

At each site the samples of a known volume subsurface (5–40 cm) water were taken with a 10 L bucket and then filtered through a plankton net (mesh size: 100 µm). The retained organisms were transferred into glass containers. The collected material was preserved in 5 % formalin.

Water Quality Analysis

The following instream parameters including pH, dissolved oxygen (DO), and water temperature (WT) were measured in situ by a Portable Meter (Multitest IPL-513, Semico Ltd, Russia, Novosibirsk). Conductivity (COND) and salinity (SALIN) were measured in situ by a Portable Meter (Multitest KSL-111, Semico Ltd, Russia, Novosibirsk) Air temperature was determined with a mercury thermometer. Oxygen saturation (P, %) was calculated.

At each site, water samples were also collected for further laboratory analysis including redox potential (Eh), nitrate–nitrogen (NO_3^-), nitrite–nitrogen (NO_2^-), ammonium–nitrogen (NH_4^+), orthophosphate-phosphorus (PO_4^{3-}), sulfate–sulfur (SO_4^{2-}), hydrogen sulfide–sulfur (H_2S), chlorides (Cl^-), sodium (Na^+), potassium (K^+), total hardness (H), calcium hardness (Ca^{2+}), bicarbonates (HCO_3^-), carbon dioxide (CO_2), permanganate oxidability ([O]), total iron (Fe). All these parameters were measured in the lab of the Department of Chemistry of South Ural State University according to the standard methods [8]. For spectrophotometric analysis the Spectrophotometer KFK-3 was used. Dissolved CO_2 concentrations were determined by calculating from pH and alkalinity, measured by titration with 0.1 N HCl to an end point pH of 3.5.

Phyto and zooplankton analysis

Non-diatom algae were analyzed using a 0.1 mL counting chamberat a magnification of 600× (Altami BIO 2T microscope, Altami Ltd, Russia, St. Petersburg.). Permanent diatom slides were prepared after oxidizing the organic material (by nitric acid and sulfuric acid) and a minimum of 300 valves were counted for each sample using a Altami BIO 2T microscope at 1000× under oil immersion.

Species were identified using the handbooks by Yarushina et al [9]. Eco-geographical characteristics of species were made using the handbooks by Barinova [10].

RESULTS AND DISCUSSION

Submerged trees and shrubs at 50-70 m from the coast were visually determined (Fig. 2). Organic pollutants in water were formed due to the trees and shrubs decay. There was a significant reduction of dissolved oxygen (DO) concentration and higher values of oxidation ([O]).

Fig. 2 Submerged trees and shrubs.

Table 1 shows the results of physicochemical analysis of water in the sampling sites.

Table 1 Physico-chemical parameters

Chemical parame-ters	Site 1	Site 2	Site 3	Site 4	Site 5
TW, °C	20	18.4	19	20	20
DO, mgO/l	3.12	4.55	3.9	3.4	2.95
P, %	34.6	48.8	42.3	37.7	32.7
pH	8.712	8.751	8.860	8.896	8.950
Eh, mV	259.1	251.1	257.5	256.0	238.2
COND, mS/m	36.1	36.59	34.86	35.94	35.71
SALIN, mg/l	192.3	194.9	185.5	191.4	190.1
NH_4^+, mg/l	0.54	0.70	0.96	0.95	0.75
NO_3^-, mg/l	0.24	0.28	0.51	0.51	0.34
NO_2^-, mg/l	0.005	0.006	0.008	0.006	0.005
SO_4^{2-}, mg/l	32.8	25.6	25.2	28.4	33.1
H_2S, mg/l	0.05	0.05	0.08	0.06	0.09
PO_4^{3-}, mg/l	0.002	0.002	0.04	0.10	0.300
CO_2, mg/l	3.5	3.8	4.2	4.2	4.5
Cl^-, mg/l	32	32	37	32	32
Na^+, mg/l	13.87	12.08	12.08	12.08	13.9
K^+, mg/l	0.80	0.70	0.80	0.695	0.80
HCO_3^-, mmol/l	3.6	3.4	3.6	3.3	3.3
H, mmol/l	4.8	4.8	5	5	4.9
Ca^{2+}, mmol/l	1.9	1.8	1.8	1.9	1.8
Mg^{2+}, mmol/l	2.9	3	3.2	3.1	3.1
Fe, mg/l	0.02	0.05	0.06	0.03	0.07
[O]	8	8.0	15	10.5	11.0

The proportion of different forms of Nitrogen showed the transition of nitrate form into ammonium. Dissolving of organic matters in water results in the accumulation of carbon dioxide and transformation of sulfates into hydrogen sulphide. According to different criteria water pollution at these sites varies from polluted to dirty.

The study of phytoplankton of the waterbody in 2005–2006 revealed [11] diatoms (*Bacillariophyta*, 42 %) as a dominant algal group, green algae (*Chlorophyta*, 31 %) as the second in species diversity, and blue-green algae (*Cyanophyta*) accounted only for 10 %. But new species of *Cyanophyta* were identified, and that became an unfavourable sign for interannual dynamics of species diversity.

The study of phytoplankton species diversity of 2014 showed that diatoms had kept their dominant position. They accounted for 42 % of the total number of species. Blue-green algae became second in species diversity, which corresponds to 39 % of the total number of species [12]. It may be explained by the presence of phosphorous and nitrogen compounds in water [13]. The blue-greens were mainly represented by *Anabaena lemmermannii*, *Microcystis aeruginosa* and *Anabaena flos-aquae*. The most abundant diatoms were the most numerous representatives of *Fragilaria crotonensis* and *Asterionella formosa*. Blue-green algae species (*Microcystis, Anabaena, Oscillatoria*) evolved on the surface of the lake. The waterbody trophic state was characterized as mesotrophic.

The decay of lots of submerged organic matter and the following die-away of water plants rapidly growing on that soil during the first years of flooding led to bogging of the lake coast (Fig. 3). At these sites trophic status develops into eutrophic.

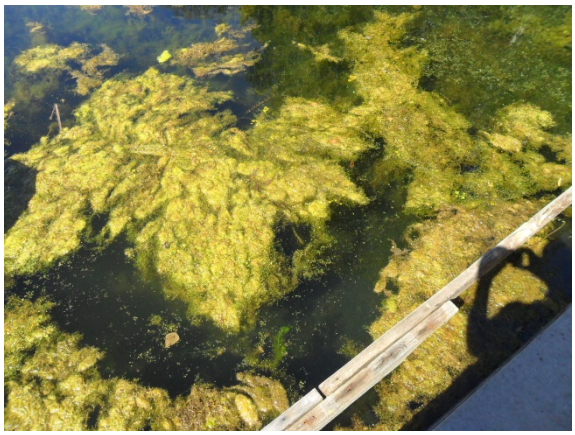

Fig. 3 Boggy site.

In August 2014 at sites 1 and 2 the bottom was mechanically cleaned from the sediments containing thick roots of trees and shrubs remains. A special device was used in cleaning [14].

In July 2015 physico-chemical parameters of water at these sites were analyzed (Table 2).

The analysis results prove water pollution decrease after the use of the device. The oxidation of the lake self-purification is getting more intense, as the analysis showed. Organic pollutants and biogenic elements concentration has substantially

declined. Dissolved oxygen concentration has increased. According to different criteria water condition at these sites varies from clean to moderately polluted.

Table 2 Physico-chemical parameters

Codes of chemical parameters	Site 2	Site 2
TW, °C	20	20
DO, mgO/l	7.36	7.52
P, %	81.6	83.4
pH	8.031	8.074
Eh, mV	259.1	251.1
COND, mS/m	36.1	36.59
SALIN, mg/l	192.3	194.9
NH_4^+, mg/l	0.15	0.17
NO_3^-, mg/l	0.78	2.15
NO_2^-, mg/l	0.006	0.006
SO_4^{2-}, mg/l	5.26	5.87
H_2S, mg/l	0	0
PO_4^{3-}, mg/l	0.002	0.002
CO_2, mg/l	2.2	1.9
Cl^-, mg/l	32	32
Na^+, mg/l	13.87	12.08
K^+, mg/l	0.80	0.70
HCO_3^-, mmol/l	3.1	3.0
H, mmol/l	4.8	4.9
Ca^{2+}, mmol/l	1.9	1.9
Mg^{2+}, mmol/l	2.9	3.0
Fe, mg/l	0.013	0.024
[O]	6	6.8

CONCLUSION

Water eco-system abuse as a result of human-made impact and inefficient water management is one of the most crucial problems today.

The paper considers aggravation of Lake Uvildy trophic status after one third of the lake water volume was carried over, and water level increased later and flooded birch forest that had grown in the drainage zone.

The use of the device for mechanical cleaning of coasts from trees and shrubs remains gave positive results. We suggest using the device for further cleaning of the lake**.**

ACKNOWLEDGEMENTS

The authors thank Genadiy Sidorov for his assistance in the field.

REFERENCES

[1] Björk S, The Evolution of Lakes and Wetlands, Restoration of lakes, streams, floodplains, and bogs in Europe. Principles and case studies, Part 2, Eiseltova, Ed. London New York: Springer, 2010. pp. 25–35.

[2] Izmest'eva LR, Moore MV, Hampton SE, Ferwerda CJ, Gray DK, Woo KH, Pislegina HV, Krashchuk LS, Shimaraeva SV, Silow EA, "Lake-wide physical and biological trends associated with warming in Lake Baikal", Journal of Great Lakes Research, Vol. 48, 2016, pp. 6–17.

[3] Mitraki C, Crisman TL, Zalidis G, "Lake Koronia, Greece: Shift from autotrophy to heterotrophy with cultural eutrophication and progressive water-level reduction", Limnologica – Ecology and Management of Inland Waters, Vol. 34, 2004, pp. 110–116.

[4] Chen X, Yang X, Dong X, Liu E, "Environmental changes in Chaohu Lake (southeast, China) since the mid 20th century: The interactive impacts of nutrients, hydrology and climate", Limnologica – Ecology and Management of Inland Waters, Vol. 43, 2013, pp. 10–17.

[5] Allinger LE, Reavie ED, "The ecological history of Lake Erie as recorded by the phytoplankton community", Journal of Great Lakes Research, Vol. 39, 2013, pp. 365–382.

[6] Søndergaard M, Jeppesen E, Lauridsen TL, Skov C, Van Nes EH, Roijackers R, Lammens E, Portielje RE, "Lake restoration: Successes, failures and long-term effects", Journal of Applied Ecology, Vol. 44, 2007, pp. 1095–1105.

[7] Deryagin VV, Belov SA, "Geoecological features differentiating the coastal landscape and recreational areas of Lake Uvildy", Bulletin of the Tomsk State University, Vol. 333, 2010, pp. 172–176.

[8] Mashkova IV, Krupnova TG, Kostryukova AM, "Water quality and aquatic macrophytes interrelationships for selected reserved lakes of South Ural", in Proc. 15th Int. GeoConf. SGEM 2015, 2015, Book 3, Vol. 1, pp. 763-770.

[9] Yarushina MI, Tanaeva GV, Eremkina TV, Algae flora of water bodies of the Chelyabinsk region. Ekaterinburg: INSS Ural branch of Russian Academy of Sciences, 2004, pp. 50–290.

[10] Barinova SS, Medvedeva LA, Anisimova OV, Biodiversity of algae – indicators of the environment. Tel Aviv, Pilies Studio, 2006, ch. 2.

[11] Snitko LV, Snitko VP, "Water EPNT: A Comparison of the state of phytoplankton Uvildy and Turgoyak lakes at the end of the modern high-water hydrological cycle in the South Urals", Bulletin of the Chelyabinsk State University, Vol. 5, 2011, pp. 105–109.

[12] Kostryukova AM, Krupnova TG, Mashkova IV, "Phytoplankton taxonomic structure as indicator of the trophic status and ecological state of

Uvildi lake", in Proc. 15th Int. GeoConf. SGEM 2015, 2015, Book 3, Vol. 1, pp. 501-508.

[13] Kane DD, Conroy JD, Richards RP, Baker DB, Culver DA, "Re-eutrophication of Lake Erie: Correlations between tributary nutrient loads and phytoplankton biomass", Journal of Great Lakes Research, Vol. 40, 2014, pp. 496–501.

[14] Sidorov GF, Valeev RK, "Apparatus for cleaning the bottom of the reservoir", Patent, 135331, issued date December 10, 2013.

Second International Conference on Science, Engineering & Environment,
Osaka City, Japan, Nov.21-23, 2016, ISBN: 978-4-9905958-7-6 C3051

SOCIO-ENVIRONMENTAL MEASUREMENT FOR TOURIST SERVICE EXPERIENCE

Boo Ho Voon[1], Jamil Hamali[2], Patricia Melvin Jussem[3], Ai Kiat Teo[4], and Agnes Kanyan[5]

[1, 2, 5] Faculty of Business Management, Universiti Teknologi MARA, Malaysia;
[3] Faculty of Tourism and Hospitality, Universiti Teknologi MARA, Malaysia;
[4] Sekolah Menengah Kerajaan DPHA Gapor, Kuching, Malaysia.

ABSTRACT

Culture, adventure and nature (CAN) have been recognized as the critical components of eco-tourism products for tourism-friendly nations like Malaysia. Many tourists have enjoyed the social and environmental aspects of the various tourist destinations and there are also tourists who are not very happy with certain aspects of their experiences. This research investigated the tourists' experiences with the homestay programmes using qualitative and quantitative techniques, namely the focus groups and questionnaire survey to discover their experiences and thereafter developed a multi-item measurement. Responses of 330 sampled respondents were analyzed. A total of nine dimensions were found and the measurement fit indices of these socio-environmental measurement was satisfactory. The socio-environmental issues included culture, guiding, accommodation, services, food and beverages, journey, natural environment, access and cleanliness. The homestay service environment indeed must be holistic and sustainable to create the memorable and delightful tourist experience. Implications and future research were also discussed for continuous improvement of the environment-driven performance measurement and management process.

Keywords: Socio-environmental, Measurement, Homestay, Experience.

INTRODUCTION

The social and natural aspects of the tourist destinations are essential to attract and maintain the critical mass of tourists for sustainable eco-tourism development for handsome socio-economic benefits for the multiple stakeholders. As such, tourism products such as homestays, tend to capitalise on these aspects to create memorable tourist experience. Undoubtedly, the contribution of tourism involves community, well-being of people, creating job, distributing income and sustaining regional development [1]. Specifically, the eco-tourism and cultural-tourism are well-manifested in the homestay programmes and these programmes are potential income generators for the local communities (e.g. Malays, Ibans, Bidayuhs, Kadazans, etc.). The effectiveness and competitiveness of homestay programmes if appropriately and systematically gauged, managed and thereafter enhanced will bring much social and economic benefits to the participating individuals, families and communities. This research explored and thereafter measured the tourist service experience for homestay tourism in the multi-cultural Malaysia which is rich in biodiversity, for sustainable development. The qualitative (i.e., Focus Groups) and quantitative process (Structural Equation Modeling with AMOS) of developing the measurement cum management tool were scientifically done to develop the marketing construct (e.g. [2], [3], [4], [5]).

LITERATURE REVIEW

The consistent and continual offerings of new and beneficial services are critical in all service industries. In fact, creating the desired authenticity [6] is crucial for customer delight. The public and private service organizations have to keep on improving their service products and customer service to gain very high levels of customer satisfaction in order to create and sustain customer loyalty for optimum profitability. Superior service is commonly linked to increase profitability, and it is seen as providing an important competitive advantage by generating repeat sales, positive word-of-mouth, constructive feedbacks, customer loyalty and service differentiation. Services are the products offered to the targeted customers and/or stakeholders and have their unique nature as compared to goods [7]. It is normally characterized by intangibility, inseparability, heterogeneity or variability, and perishability. Most services are intangible as they are performances. The functionality and technical aspects of the service also need to be understood [8] as the more contextual specific domains are necessary to be managed to satisfy the technical needs of the customers (e.g. facility, homestay packages, food and beverages).

Qin and Prybutok (2008) [9] suggested that customers were influenced by the physical environment, reliability of the service and attitude of the employees such as showing empathy to customer

needs, being responsive, courteous, knowledgeable and trustworthy.

Tourist Experience for Sustainable Homestays

Customer experience plays an important role in the service sector, especially in the hedonic setting such as the cultural- and people-driven tourism sector. The very satisfied personal experiences of the tourists will most probably lead to repeat purchases from the same vendor (e.g. [10]). In fact, experience in hospitality services has been regarded as a competitive tool as well as a way to gain superior service performance (e.g. [11], [12], [13], [14], [4]). However, there should be greater emphasis on empirical research of investigating the social and environmental aspects of customer experience for the priority service sector such as homestay tourism.

The natural and engineered environments of the tourist destinations as well as the acts of service from the multiple stakeholders are instrumental to create favourable encounters and experiences. The service experience concerns the emotional feelings of the tourists during the service encounters. Generally, the service encounters are tangible series of interactions between the tourists and the service environment. Emotions are inevitably contagious in social situations [15] and social science researchers tend to agree that the favourable service experience can effectively satisfy the customers and make them more loyal to the services (e.g. [12], [9], [5], [14]).

METHODOLOGY

This measurement-based fundamental research aimed to identify the key dimensions for tourist experience in homestay tourism. The research employed both qualitative and quantitative techniques. The qualitative phrase which involved focus group interviews helped to capture the very satisfied and very dissatisfied experiences of the individual tourists. The main target population of the study was the tourists who had visited the homestay establishments (e.g. villages, longhouses, homes) for the past six months in Malaysia. The research started with a relevant literature review on services marketing and management, hospitality management, and service quality theories and measurements in order to identify the tentative critical dimensions for the customer and service experiences (Figure 1). This was followed by the focus groups and personal interviews. Four focus group interviews were conducted in different locations in Malaysia to discuss the service and living experiences for excellent homestay service delivery and management. Each focus group interview consisted of 8-12 participants representing the various selected groups of customers (by age groups, gender and race). All the group discussions were audio-taped and analyzed accordingly to generate the required dimensions and their respective items for constructing the survey instrument (i.e., structured questionnaire).

The duly designed questionnaire was validated by a few experts in the field of services marketing and hospitality management and service management. The refined questionnaire was used and the printed sets of questionnaires were distributed to the respective respondents, selected through quota sampling technique (controlled characteristics include gender, age and types of tourist - local/foreign), who participated in the survey voluntarily. The tourists returned the duly answered questionnaires to the trained enumerator concerned at the respective homestay destinations. This was an anonymous survey where the respondents' answers would not be personally identified, to enhance the reliability and validity of the data. The collected questionnaires were checked and usable questionnaires were then analyzed. Reliability and Exploratory Factor Analysis (EFA) were done (e.g. [16], [17, [5]) on the survey data to identify the dimensions of the tourist experience. Structural equation model was developed to investigate the impact on tourist satisfaction. The numerous goodness of fit indices (e.g. CFI, GFI, RMSEA) were used to confirm the goodness of the model [18].

FINDINGS AND DISCUSSIONS

The survey research obtained 330 usable questionnaires for quantitative analysis. The characteristics of the respondents are shown in Table 1. There were more female (53%) respondents who participated in the survey and most of the respondents were aged 21-30 years old. The foreigners accounted for 7% and about 54% of the respondents had bachelor degree holders. But, they were from different walks of life (i.e., Students – 48%, Government servants – 18.2%, Private sector – 19.1%, Self-employed – 10.3% and Unemployed 4.5%). About 81% of the respondents earned RM3000 or less per month.

The results of EFA as shown in Table 1 suggested that there were nine dimensions of tourist experience for the homestays that they recently visited. The 9 dimensions could explain 64.1% of the total variance and the main dimension was Culture which contributed 36.7% of the total variance explained. The other 8 dimensions and their respective variance explained were: Guiding (6.8%), Accommodation (4.8%), Services (3.3%), Food and Beverages (2.9%), Journey (2.7%), Natural Environment (2.5%), Accessibility (2.3%) and Cleanliness (2.2%). As such, there were social and environmental components of the homestay experience for the homestay operators to manage.

These suggested that the homestay service environment needed to be holistic in order to create the memorable and delightful tourist experience.

Table 1: Dimensions of Tourist Service Experience

Dimensions and Items (Total variance explained =64.1%)	Factpr Loadings
1. Culture (36.7%) 1. Fascinating traditional and customary practices.	0.57
2. Homestay cultural activities are very interesting.	0.57
3. Fascinated with the homestay architecture.	0.51
4. Enjoyed cultural activities organized by them.	0.54
5. Have opportunity to understand a new culture.	0.74
6. Enjoyed knowing the language of the people.	0.81
7. Have opportunity to learn their native language.	0.73
8. People of the homestay are special/unique.	0.52
9. Unique cultures for the homestay.	0.57
2. Guiding (6.8%) 10. Sufficient info. about the homestay before the trip.	0.67
11. Person in charge of the trip understands my needs.	0.72
12. Person who brings me there is friendly with me.	0.65
13. The person gives me individual attention.	0.71
14. The person is always willing to help me.	0.62
15. The person is knowledgeable about the homestay.	0.52
3. Accommodation (4.8%) 16. Enough bathroom/toilet to accommodate visitors.	0.53
17. Do not have to spend much for accommodation.	0.65
18. Sufficient electricity supply in the homestay.	0.68
19. Water supply is enough for visitor's use.	0.66
20. Can go to the homestay conveniently.	0.53
4. Services (3.3%) 21. Good telecommunication services.	0.71
22. Tour guiding services are provided.	0.75
23. Good homestay packages/programmes available.	0.63
5. Food & Beverages (2.9%) 24. There are many choices of food and drinks.	0.71
25. Can get exotic (special) local food in homestay.	0.76
26. Can taste foods that I have never eaten before.	0.75
27. Can taste drinks that I have never drunk before.	0.74
28. I enjoyed the food that they served.	0.53
6. Journey (2.7%) 29. The journey to the homestay is enjoyable.	0.67
30. Enjoyed activities along the journey to homestay.	0.68
31. The visit to the homestay is memorable.	0.66
7. Natural Environment (2.5%) 32. Good nature trail(s) is/ are found near homestay.	0.69
33. Serenity (quietness) surrounding of homestay.	0.68
34. Restful and relaxing atmosphere at homestay.	0.71
8. Accessibility (2.3%) 35. Location of the homestay is easily found.	0.71
36. Homestay is accessible by right mode of transport.	0.67
37. Road condition along the journey is satisfactory.	0.67
9. Cleanliness (2.2%) 38. Clean environment surrounding homestay area.	0.61
39. Guestroom cleanliness is acceptable.	0.57
40. Food and drinks served are hygienic.	0.61
41. Bathroom and toilets are clean.	0.53

A path diagram (Figure 1) was drawn and the measurement modeling was done using the AMOS software. The 9 dimensions indicated a satisfactory model fit and the indices (CFI=0.88, GFI=0.80, TLI=0.87, RMSEA=0.06) were considered acceptable.

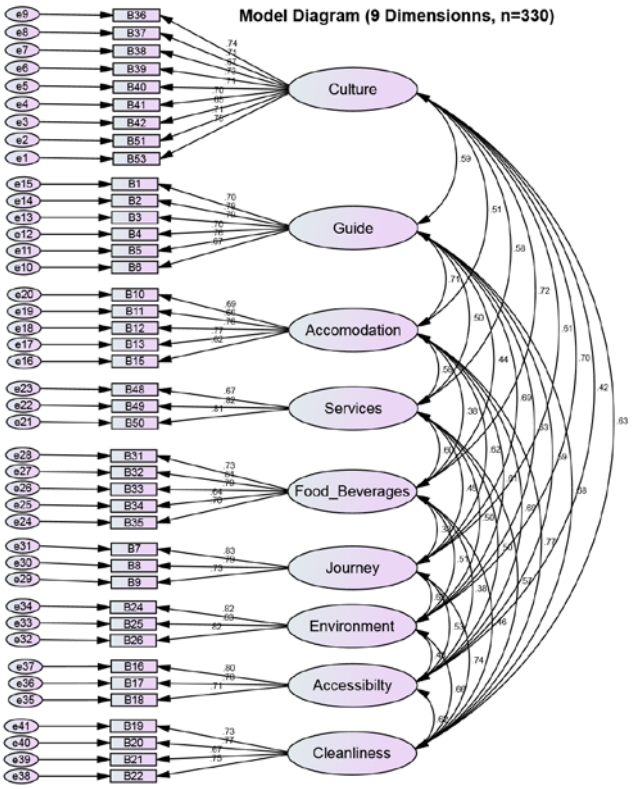

Fig. 1: Path Diagram for the Measurement Model

The 9 dimensions were significantly correlated among them and their correlation coefficients range from 0.38 to 0.72. These associations suggested satisfactory validity of the measure. The convergent and discriminant validities were exhibited. Besides, the overall construct also related significantly (at 5% level of significance) with the meaningful variables namely tourist satisfaction (path coefficient, 0.78) and behavioural intentions (0.24). The effect of tourist satisfaction on behavioral intentions was 0.71. This suggested an indirect effect (through tourist satisfaction) of tourist service experience on behavioural intentions.

The homestay programmes which could offer multi-dimensional service experience (social and environmental aspects, socio-environmental) for the visiting tourists should be managed and improved in terms of the various dimensions in order to please the tourists as well as for sustainable development which would benefit the multi-stakeholders. The social aspects would be very much people- and cultural-driven where human elements were essential. Training on human relations and cultural conservations would be essential to improve and sustain the competencies and authenticity which the local and foreign tourists treasure for the unique experiences. Besides, the components of service environment which were essentially tangibles and hence to a great extent could be carefully engineered and conserved, taking into consideration the human

factors too. For instance, the accommodation, natural environment, accessibility, and cleanliness aspects could be engineered. The green engineering can be instrumental to preserve, conserve and enhance the original and authentic natural environment and biodiversity. The natural trails, building architecture, cultural artifacts, road system and landscape were among the homestay destinations and journey aspects in which the civil, electronic and electrical, ICT and human-factor engineers could assist to improve and sustain. What the homestays have and operators do would be important in order to create delightful and authentic experiences. Ultimately, the tourists must be very satisfied as the findings indicated that the tourists who had had very good experiences with the homestays would then to be very satisfied, and thereafter would like to revisit or tell other people about the homestay programmes and destinations.

CONCLUSIONS

This empirical research suggested that tourist service experience of homestay programmes was multi-dimensional in nature. The homestay service environment indeed must be holistic and sustainable to create the memorable and delightful tourist experience. The socio-environmental aspects essentially required much attention from the multiple stakeholders for a more sustainable tourism development and improved quality of life for the homestay operators. The exploratory research suggested nine dimensions of experience for tourism marketing and management. Ideally, the homestay destinations should be a 'living habitat' though on a temporary basis. Future research can employ relevant quantitative techniques such as logistics regressions and Kansei Engineering to identify items which will lead to greater tourist satisfaction or loyalty. Besides, samples from different cultural settings from other parts of the world can be used to understand the situations more contextually for effective tourist relationship management.

ACKNOWLEDGEMENT

This research was financed by Ministry of Higher Education of Malaysia, under the Fundamental Research Grant Scheme (FRGS/1/2014/SS05/UiTM/02/5). The kind assistance from the administrative staff of Research Management Institute (UiTM Shah Alam) and UiTM Sarawak, Graduate Research Assistance and enumerators are much appreciated.

REFERENCES

[1] Bhuiyan, M.A.H., Siwar, C. & Ismail, S. M. (2013). Tourism development in Malaysia from the perspective of development plans. *Asian Social Science*, *9*(9), 11-18.

[2]Hair, J.F., Anderson, R, Tatham,R.L. & Black,W.C. (1995). *Multivariate Data Analysis with Readings*, 4th Edition, NJ: Prentice Hall International.

[3]Nunnally, J. C. & Bernstein, I. H. (1994). *Psychometric Theory*, 3rd ed. New York: McGraw-Hill, Inc.

[4]Voon, B.H. (2006). Linking a Service-Driven Market Orientation to Service Quality. *Managing Service Quality*, 16 (6), 595-619.

[5]Voon, B.H., Abdullah, F., Lee, N. & Kueh, K. (2014). Developing a HospiSE scale for hospital service excellence. International Journal of Quality & Reliability Management, 31 (3), 261-280.

[6]Gilmore, J. H. & Pine II, B. J. (2007). Authenticity – What Consumers Really Want, Boston: Harvard Business School.

[7]Zeithaml, V. & Bitner, M. (2000), *Services Marketing: Integrating Customer Focus Across the Firm*, Second Edition, The McGraw-Hill Companies, Inc., USA.

[8]Grönroos, C. (1982). *Strategic Management and Marketing in the Service Sector*, Marketing Science Institute, Cambridge, MA.

[9]Qin, H. & Prybutok, V.R. (2008). Determinants of customer-perceived service quality in fast-food restaurants and their relationship to customer satisfaction and behavioral intentions. *The Quality Management Journal*, 15(2), 35-50.

[10]McKenzie, R. (2000). *The Relationship-Based Enterprise – Powering Business Success Through Customer Relationship Management*, Singapore: McGraw Hill Ryerson Limited.

[11]Kim, S., Cha, J., Knutson, B. J. & Beck, J. A. (2011). Development and testing of the Consumer Experience Index (CEI). *Managing Service Quality*, 21(2) 112-132.

[12]Kim, W.G. & Moon, Y.J. (2009). Customers' cognitive, emotional, and actionable response to the servicescape: A test of the moderating effect of the restaurant type. *International Journal of Hospitality Management*, 28, 144-156.

[13]Qu, H. (1997). Determinant factors and choice intention for Chinese restaurant dining: A

Multivariate approach. *Journal of Restaurant & Foodservice Marketing*, 2(2), 35-49.

[14]Woo, G. K., Ng, C.Y.N & Kim. Y (2009). Influence of institutional DINESERV on customer satisfaction, return intention and word-of-mouth, *International Journal of Hospitality Management*, 28, 10-17.

[15]Soderlund, M. & Rosengren, S. (2007). Receiving word-of-mouth from the service customer: An emotion-based effectiveness assessment. *Journal of Retailing and Consumer Services*, 14, 123-136.

[16]Sureshchandar, G. S., Rajendran, C. & Anantharaman, R. N. (2001). A holistic model for total quality service. *International Journal of Service Industry Management*, 12 (4), 378-412.

[17]Voon, B.H., Jamil, H., Lee, N., Firdaus, A. & Kueh, K. (2012). Developing a service culture-value chain for hospitals. *IACSIT International Journal of Engineering and Technology*, 4(4), 354-357.

[18]Byrne, B. M. (2001). Structural EquationModeling with AMOS: Basic Concepts, Applications, and Programming. London: Lawrence Erlbaum Associates.

Second International Conference on Science, Engineering & Environment,
Osaka City, Japan, Nov.21-23, 2016, ISBN: 978-4-9905958-7-6 C3051

RESEARCH AND DEVELOPMENT OF INCULCATION PROCESS FOR FUTURE AGRICULTURAL RESEARCH OFFICER

Supasit Deeraksa[1] , Paisarn Worakham[1], Piyatida Panya[1]
[1]Faculty of Education, Rajabhat Mahasarakham University, Mahasarakham, Thailand

ABSTRACT

The purposes of this study were to study and to develop the process of agriculture wisdom holders and local philosophers in multi-cased studies. The samples were 2 agriculture wisdom holders and 2 local philosophers. The data collection was done through in-depth interview, documentary study and non-participatory observation. The developed of the inculcation process of agriculture wisdom holders and local philosophers was evaluated by the experts with focus group discussion method. The research findings were as follows:

In the study of inculcation process of agriculture wisdom holders and local philosophers, the researcher found that. They are all doing modern agriculture according to the sufficient economy concept, following the new theory of His Majestic the King as a guide to life and farming that rejects the use of chemicals but regardless of how the natural environment and essentially reduce expenses and reduce pollution from toxic chemicals. The process consisted of 5 steps which were Creative of understanding, Adjusting or modifying the way of thinking, Transferring the knowledge and experience, Field study at the farmland spot and practical performance and Summarizing the knowledge and assessment.

Keywords: Agriculture Wisdom Holders, Local Philosophers, Future Agricultural Research Officer

INTRODUCTION

At the present time the farmers have changed the method of working process into the new high technology for practical and management of their farm, but still not succeed in their career , instead being indebted , affecting that they have to sell the farm-land. Most of the farmer of the country being in poverty condition more than other vocations , therefore many people refuse to work as a farmer because this career always being poor , and so lonely no any agency to support. The new generation therefore interesting in working in other career, as to earn more salary or move income from the business , but not to work as the agriculturist. The tendency of number of the labors who work for agricultural systems has been declined at the present time , in the near future Thailand may facing the problem do not have enough man power or labor who want to work in the agricultural sector. The result from census survey in October 2013 found that total population who have a job 38.02 million , but have the worker who working in the agricultural sector only 12.85 million or 33.8% of all total work force, comparing to the statistic of October 2012 , found that the worker work in the agricultural sector has reduced by 2.02 million [4].

Therefore this research study apprehended the significant of the process , how to instill the technical academy for new generation farmer in the future , through the direct learning process , transferring the knowledge to the learner from the experience of the successful farmer , who have been working as the farmer until successful in sustainable career , living securely and produce safely products for the consumer and eco-friendly to all other living thing and organics leading to the development for food sustainable in the future.

To research and study the development process how to instill the Future Agricultural Research Officer

METHOD

This research study were using Qualitative Research, Case study , Field Research and Documentary Research. The researcher have selected purposive study for data collection in the field research sector , and using self interview and observation by the researcher. The case study about agriculture wisdom holders , two Teacher Suthi Nun PratchaPrit (How to modify the suitable technology) From Buri Ram province , and Mr. Lek Kud Wong Kaew (Agriculture by Agricultural system) From Sakon Nakhon province and local philosophers, two participants were sub-district Headman Adison Lao Sapan (Mix agricultural process) From Maha Sarakham province and Mr. Khumpan Lao Wong Si (Sustainable Agriculture) from Maha Sarakham province.

1. Researching Method

1.1 Documentary study and some other media materials , such as research papers , and printing materials.

1.2 Non-participant Observation , the researcher have observed the process of how the agriculture wisdom holders and local philosophers to instill the new generation by observing and keep record step by step and how they use the media

material , using observation record from and take a picture of the activities.

1.3 In-depth Interview , the researcher have interview the agriculture wisdom holders and local philosophers which considering that they were the key informants by using the informal interview method. [3].

2.Tool used for this research

Tool used were as follows

2.1 The researcher to study and gather and collect the significant document and record , observing the activities in the local community and in-deph interview for the key informants

2.2 Observation for using non-participant observation form prior to the observation in order to investigate the sign of how the teacher instill , and instruction.

2.3 Interview format using the in-depth interview with the participant for the key informants.

RESULTS

The result of research study on how to instill the Future Agricultural Research Officer from the Thai agricultural wisdom holders and the local philosophers from the community.

1.The result of case-study from teacher Kruba Suthinun pratchapruk (How to adjust of modify the suitable technology) at Buri Ram province.

The process for instill or training of teacher Kruba Suthinun which have been given the knowledge to the near by people and all over the region including the government sector personnel and private sector personnel. The majority of the text of the knowledge were about forestry emphasize the big tree such as Blackwood (Dalbergia cochinensis) Yang gurjun (Dipterocarpus alatus) Malabat ironwood (Hopea odorata) and Indian Oak (Barringtonia spp.). To conservation the natural resources and the environment , management and use proper technology , produce and transform the agricultural production for sustainable agriculture , develop Thai education under the basic rule of sufficiency economy such as careful agriculture process on 1 Rai farm land. The practical process for instill or training of the knowledge can be summarized as follows. 1. Compile the problems and the requirement of the student who need to be transfer the knowledge. 2. Change the way of thinking. 3. Give the example of suitable guideline for better life living. 4. Create co-learning lesson plan. 5. Transfer the knowledge and experience. 6. Practical performance on the real farmland. 7. Pilot study and practice. 8. Summarize the result of pilot study project and practical performance on the farmland. 9. Assessment and take the best knowledge for practical performance.

2. The result of case study with Mr. Lek Kud Wong Keaw (Agriculture by agricultural system) Sakon Nakhon province.

The process for instill the knowledge of Mr. Lek Kud Wong Keaw were emphasizing on the thinking system or process more than the text knowledge which means that we are all give the importance to the way how to think , once we know how to think step by step , then the knowledge will comes later on , because every one can conclude what they can get from the knowledge , and experience. The instill process from Mr. Lek to create the awareness about how oneself can survive , first to all one must have food then therefore emphasizing on producing agricultural products for life survival , reducing the expenditure , including for buying food , medicine , and others by planting enough vegetable and fruit for own consumption , produce or make material and tool or equipment for use by oneself eat the food that you plant , and plant every thing that you need to eat. The result of case study at Mr. Lek agriculture can be summarized as follows. 1. Inspiration of the awareness. 2. Adjust the way of thinking process. 3. Adapt and modify the suitable way of life , know how to save , and economize on spending. 4. Transferring the knowledge and experience by emphasizing on the way of good thinking process , more than the text knowledge. 5. Gain the knowledge from practical study in the farmland 6. Discussion summarized and take the best knowledge for practical performance.

3.The result of case study of Mr. Adisorn Lao Sapan (Mixed agricultural) Maha Sarakham province.

The instill or transferring knowledge of Mr. Adisorn LaoSapan were, that he will inquire the need of the learner in order to justify the objective of the learner and then explain the text of the knowledge briefly , then take the learner to study in the farmland , lecture and explain the detail step by step so the learner can understand all of the process of mixed agriculture and can be able to do by themselves , and then will divided the land for each student to practice. The process of instill can be summarized as follows. 1. Inquire the objective of the learner. 2. Exchange the knowledge and experience of mixed or combination agriculture , process , frog raising Turkey raising , Making fertilizer , and Mushroom planting. 3. Practical learning from the farmland. 4. Summarizing the knowledge. 5. Assessment and take the best knowledge for practical performance.

4.The result of case study at Mr. Khampan LaowongSi (Sustainable agriculture process) Maha Sarakham province.

The instill process of Mr. Kha-mpan Laowongsi, he stating that “Wishing all of you to use the Royal initiative project of our King to apply in your own farmland our Thai Farmer are very

lucky to live under His Royal highness the king's grace." Rising from the man who not even have the land for his own farming , but after modify and develop using the new theory for agricultural practice Mr. Khampan have a new life and prosperity no debt , his instill process can be summarized as follows. 1. Inquire the need of the learner. 2. Explain and exchange the knowledge and experience. 3. Study from agricultural farmland and practical performance. 4. Summarize the knowledge. 5. Be self confidence and strongly believe in agricultural career and Organic agriculture.

Table 1 Synthesis process form case studies

Case study / process	Suthinun pratchapruk	Lek Kud Wong Keaw	Adisorn Lao Sapan	Khampan LaowongSi	total
1. Compile the problems and Inspiration of the awareness	✓	✓	✓	✓	4
2. Change the way of thinking.	✓	✓	✓		3
3. Exchange the knowledge and experience			✓	✓	2
4. Adjust the way of thinking process		✓			1
5. Adapt and modify the suitable way of life		✓			1
6. Give the example of suitable guideline for better life living	✓				1
7. Create co-learning lesson plan	✓				1
8. Transfer the knowledge and experience.	✓	✓	✓		3
9. Practical performance on the farmland	✓	✓	✓	✓	4
10. Pilot study and practice.	✓				1
11. Summarize the result of pilot study	✓	✓	✓	✓	4
12. Assessment and take the best knowledge	✓	✓	✓		3
13. Be self confidence and strongly believe in agricultural				✓	1

The researcher have collect all the data from the field work survey and analyzed the process of how the teacher using Thai intelligence and local folk wisdom in agricultural practice of each teacher and summarized into 6 steps as follows 1.Summarizing for the requirement of the learner. 2. Adjust the way of thinking and the process of thinking system 3. transferring the knowledge. 4. Field study at the farmland and practical performance. 5.Summarige of the gained knowledge. 6. Assessment and take the best knowledge for practice

The result for data analysis and discussion with the expert group , the researcher have summarized 5 proposal steps and 12 sub-topic as the suggestion for developing the instill process to train the new generation academic Agriculturist as follows.

Step 1 Creative of understanding

To compile the problem and inquiry the need of the learner in order to resolve the problem together , and to find out from the learner what is the most requirement that the learner need to know in this step there were sub-topics to be discussion as follows:-

(1) To have a meeting for create understanding with self volunteer to receive the instill process and to make understanding for making decision to participate in instill process.

(2) Compile the problem and the requirement of the participants by questioning the need of participants , what is the problem in order to resolve problem to the directly need.

Step 2 Adjusting or modifying the way of thinking

To change the way of thinking concerning the agriculture knowledge by inspiration for the agricultural career awareness at this step need to give the challenge for the learner to think , by using the key informants knowledge for and analyzed in order to train how to use the imagination to analyze and identify the original root of the problem at this step have the sub topic as follows.

(3) Develop the capability by using group process and brain storming for finding out the positive aim , such as dividing into subgroup , plant , animal , fishery and mixed or combination agriculture in order to gain the knowledge precisely for each group and having the group leader for driving the activity.

(4) Develop the capability of the group leader or core leader to gain the knowledge and fully understand the development activity , and have the teacher as the group advisor.

Step 3 Transferring the knowledge and experience**.**

To transferring the knowledge and experience is the most importance step that need the advise from the teacher or the expert who have capability and experience in the agricultural field , to transferring the knowledge by lecture and retell the story and experience therefore the informers must have the acceptable knowledge , and understand the need or requirement of the learner , at this step divided into sub topics as follows:

(5) Specify the place for practical performance such as the farmland or agricultural in

the university campus or use the farmland of the teacher in the near by local area.

(6) To transferring the knowledge in the from of short term training , exhibition lecture discussion and questioning or using teaching aid media such as audio – vision equipments.

Step 4 Field study at the farmland spot and practical performance

(7) Field study at farmland spot after have gained the knowledge and understand the process from the teacher's experience the learner must have his own experience in the field study and do the actual practical performance.

(8) For the practical performance , each of the learner group and every one must participate in the activity step by step until proving that every one is capable for doing the new agricultural process in the reality.

Step 5 Summarizing the knowledge and assessment

(9) Exchange the knowledge within the group number who were interested in the same topic in order to built the understanding for development or the interesting subject.

(10) Presentation the result of the knowledge from learning process to all concern or all groups including the suggestion using appropriate technic for fully understanding and successful achievement.

(11) Analyzed and use the model for improve the process , for producing the agricultural product in the better quality.

(12) Assessment the changing behavior of the learner that haw much can be develop the process of working in agricultural production emphasizing on giving mental support and give cooperative help , maintain good relationship and assessment form the knowledge , attitude and skill.

SUMMARY AND DISCUSSION

The process of how to instill the agricultural knowledge by the agriculture wisdom holders and local philosophers total 4 expert were the process for performing the agricultural production base on the sufficiency theory which was initiated this new theory by His Royal Highness King Rama IV of Thailand , basically emphasize to produce the product for own consumption the left over can be given to the neighbor and friend , and after that the product can be sold in the local market, "plant any vegetable that need for consumption and eat what ever you plants", Try to be cooperate in group production for the agricultural product and expanding the marketing in order to can be able to become strong in self-efficiency and become happy family living with no debt, the people in community fully cooperate, the environment and ecological system were well balance , and full of biodiversity which consistent with the ecologist philosophy that give significant to the relation between the living thing and the environment both physical and biological , and by this agricultural practice process can built the community to become more stronger and bring the civilization and happiness to both mind and the body , of the community member.

CONCLUSION

The Inculcation Process for Future Agricultural Research Officer development is consistent with the findings of [5] have studied the form and process knowledge to the Thai profession whose wisdom 14 participants, [2] to study and develop the transmission process. knowledge, wisdom, teachers in rural Thailand agriculture. The study of teacher wisdom of Thailand 6 participants who find wisdom there is and [1] study common characters of wise community leaders with modern agriculture in northeastern. The transfer process is different. But the pattern transfer process knowledge in the profession. The match in four stages, namely the awareness of the importance of vocational training to the recipient happens to be broadcast. Joint planning teaching Course exercises And evaluate recipients relay which is consistent at each step

ACKNOWLEDGEMENTS

The study was supported by the Graduate School and Institute of Research and Development Rajabhat Mahasarakham University, Faculty of Education, Rajabhat Mahasarakham University, Office of Vocational Education Commission .

REFERENCES

[1] Pengpinit Thawadchai 2006**.** Common Characters of Wise Community Leaders with Modern Agriculture in Northeastern. Organization Humanity and Social Science Suan Dusit Rajabhat University

[2] Popoonsak Pongtorn. 2003. Development of the knowledge transmission process in rural areas of agriculture wisdom holder. Dissertation for the Degree of Doctor of Philosophy in Non-Formal Education Faculty of Education, Chulalongkorn University.

[3] Supang Chantavanich, 2010, Qualitative Research Method. Bangkok, Chulalongkorn University.

[4] The office of National Statistic. The results of the Labor Force Survey for the month. October , 2013. searched on December 23, 2013

[5] Yaipuak, Darunee. 1999. Local wisdom for the improvement of quality of life project. [Online]. Available from: http://www.accu.or.jp/litdbase/break/index.htm The Educational of Supervisory Unit, Non-Formal Education Department, Ministry of Education, Thailand.

Second International Conference on Science, Engineering & Environment,
Osaka City, Japan, Nov.21-23, 2016, ISBN: 978-4-9905958-7-6 C3051

MONITORING AIR QUALITY USING LICHENS IN CHELYABINSK, RUSSIAN FEDERATION

Anastasiya M. Kostryukova, Tatyana G. Krupnova and Irina V. Mashkova
Chemistry Department, South Ural State University, Russia

ABSTRACT

Air pollution in large cities is one of the most serious ecological problems, because emissions always go into the atmosphere. One of the specific methods of pollution monitoring is lichen indication. The aim of the study is to evaluate the quality of the atmospheric air of Chelyabinsk city (Russian Federation). The results were obtained from samples collected in June-July 2015. The trees for the lichen sampling were chosen from the areas with different pollution levels: relatively clean, moderately polluted, hardly polluted. For the purposes of the comparison lichens were measured in Ilmen reserve, as the protected relatively clean territory. Using the method of lichen indication mapping we identified an indicator species *Parmelia sulcate*. Based upon epiphytic lichen distribution in sampling areas we distinguished several zones of atmospheric pollution: polluted zone, relatively clean zone, the cleanest zone. Lichen biodiversity and their projective cover are stated to decrease as the anthropogenic load is increasing. In urban and anthropogenic environment lichen population density is declining more intensively than the number of species. Also we measured elemental composition of lichens by X-ray fluorescence (XRF) analysis. We have studied the presence of heavy metals. Zink oxide, chrome and mangan oxide rate in the samples from environmentally troubled areas near steel factories and the power plantis almost twice higher.

Keywords: Lichens, Monitoring Air Quality, Bioindication, X-Ray Fluorescence Analysis

INTRODUCTION

In urban ecosystems most of the pollutants are spread by air. It calls for air emission monitoring. Today lichen indication is a priority area of modern eco-toxicological and monitoring researches. It is one of the promising and most developed ways of eco-monitoring which lets assess the industrial impact on the environment (including urban ecosystems) on a reliable and cost-efficient basis [1], [2].

There are several advantages of using lichens as bioindicators. First, these objects let forecast the pollution level in time, assess the dynamics of air quality. Secondly, there are many indicator values to assess the environment on the basis of lichen population [1], [2]. That makes it possible to use lichens in large-scale mapping [3], [4].

For the last 15 years in many cities of the Russian Federation lichens have been studied in detail. Romanova and Sedelnikova [5] examined the lichen population of large and small cities of Siberia. Biazrov [3], Anishchenko and Azarchenkova (Safrankova) [4] investigated the lichens of the South and North-West of Russia. They revealed bioindicators and biotic diversity indicators, measured lichen indication indices and zoned the territory according to the air pollution level [3]–[6]. The substances increasing atmospheric acidity and speeding up oxidizing, such as sulfur dioxide (SO_2), nitrogen oxides (NO, NO_2), fluoro- (HF) and chloride hydrogen (HCl), ozone (O_3) are primarily known to have a destructive influence on lichens. Pollutants together with precipitation and dust penetrate into thallus from air. Among eco-substrate groups, epiphytic lichens are the most sensitive to the change of chemical substances concentration in air. Lichens are stated to accumulate heavy metals from precipitation 2–5 times faster than higher plants, with epiphytic lichens being more intensive in the process than soil lichens [7]–[10].

There is no data concerning the use of lichens as air quality indicators in South Ural (Russia). Today such studies are of special importance because many large industrial cities with an intensive traffic are situated on the territory of South Ural. Chelyabinsk, for example, is a large industrial city with a steelworks, three power stations and other industrial facilities. The present study contains an X-ray fluorescence analysis of lichen element composition in some sites of Chelyabinsk. Numerous studies shown the need to study regional geochemical background at evaluation of the effectiveness of the anthropogenic load [11]. That is why the Ilmen State Reserve (located near Chelyabinsk) was taken as the unpolluted control site.

The aim of the paper is to study the potential use of lichens as biomonitors of urban air quality as exemplified by Chelyabinsk.

METHODS

Methods of Sampling

The research methods included describing the structure of epiphytic lichens along the gradient "pollution source – background". Sampling sites of 20x20 m^2 were laid in the vegetation period of June – July 2015 on the territory of Chelyabinsk and the Ilmen State Reserve (the control site) (Fig.1). The territories under research varied in the degree of anthropogenic influence. We described the lichen synusiae from four aspects at the height of 1.0–1.5 m from the base of the tree trunks. All the epiphytic lichens met on the sampling trees were considered. Then the lichens were dried.

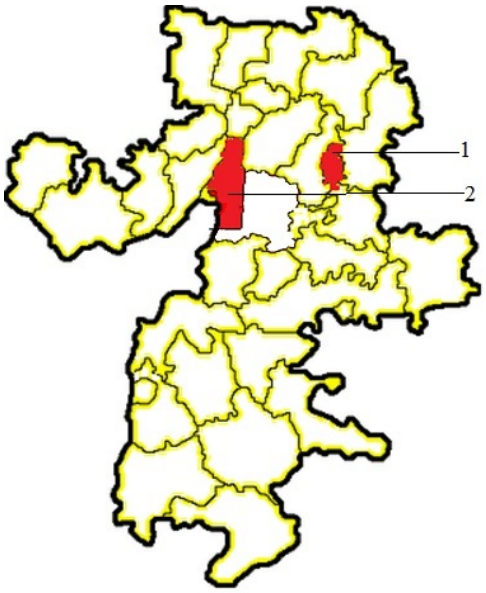

Fig. 1 Map of Chelyabinsk region:
1 – Chelyabinsk city, 2 – Ilmen State Reserve.

Methods to assess occurrence

The species activity was assessed on the basis of its occurrence on the sampling trees and its projective cover. A five-grade scale was used to measure each species activity: 5 – highly active (it is rich in frequency of occurrence on all the sampling trees, and covers the tree trunks and/or lower branches to 50 %); 4 – active (it occurs on most of the sampling trees, and covers the trees to 10 %); 3 – moderately active (its frequency of occurrence is 50–30 %, but it has a low level of cover (5–1 %); 2 – low active (its frequency of occurrence is 30–10 %, and it covers the trees to less than 1 %); 1 – not active (it rarely occurs (less than 10 % of trees), just small thallus, its projective cover approaches zero) [12].

X-ray fluorescence analysis

Air dried lichen samples were burnt in a muffle furnace at 550 °C. The lichen ash was ground in a mortar. The finely ground rock powder, mixed with a small amount of polyvinyl alcohol dissolved in water, was compressed using a hydraulic press into a pellet.

XRF patterns were registered in the lab of Center for Nanotechnology at South Ural State University. Rigaku SuperMini200 XRF Spectrometer was used for XRF analysis. The relative standard results deviation was not more than 5 %.

Site Characteristics

Chelyabinsk city is situated in forest steppe zone of South Ural. It is a large industrial city with a developed traffic network. To analyze the chemical composition of lichen thallus we selected average samples from the typical habitats within the urban ecosystems: Site 1 is a city pine forest; Site 2 is a city park; Site 3 is the territory of the steelworks; Site 4 is the territory of a transport hub in the city centre; Site 5 is the territory near a power station (Fig. 2).

Fig. 2 Map of Chelyabinsk city and location of the sampling stations (Site 1–5).

The city pine forest (Site 1) is a relict pine forest at the western part of Chelyabinsk. It stretches from North-East to South-West for about 5.5 km. Its width is about 2 km. The Victory Park (Site 2) is a city park and occupies more than 19 hectares. The Chelyabinsk steelworks (Site 3) is one of the largest steel manufacturers in Russia. Its area is more than 22 km^2. The transport hub (Site 4) in the city centre covers the city major avenue with adjusting highways. The territory of the power station (Site 5) is to the South-East of Chelyabinsk.

The Ilmen State Reserve is located on the eastern macroslope of South Ural. It's a part of the South Ural physiographic region of the Ural highlands. The Ilmen State Reserve is of an utmost importance as a gene bank preserving flora. It serves as a standard of undisturbed and relatively undisturbed vegetation communities of the South Ural pine and birch forests that are seriously damaged nearby. The Reserve is a refuge for many endemic and extinct plants and for rare and protected species. The scientific and production center of the South forestry in Ilmen State Reserve was Site 6. It was the control site

RESULTS AND DISCUSSION

Using the method of lichen indication mapping on the territory of the Ilmen State Reserve (Site 6) we identified an indicator species *Parmelia sulcate* [13]. To detect the chemical composition more than 300 samples of *Parmelia sulcate* were gathered and described. To map the zones of urban pollution we relied on the lichens idiosyncrasies to accumulate pollutants in thallus [14]–[16]. We found out *Parmelia sulcate* in all the sites. But we should admit that there are few lichens on the territory of the city (Site 3, Site 4, Site 5).

That species, at the same time, is dominant in epiphytic lichen population in the background zone (Site 6). It is rich in occurrence with the rate of 3–5. Based upon epiphytic lichen distribution in sampling areas we distinguished several zones of atmospheric pollution. The first (polluted) zone includes the territory near the steelworks (Site 3), the territory of the power station (Site 5) and the transport hub (Site 4). The second (relatively clean) is a park territory (Site 2). But as far as the park is located in the anthropogenic zone of the city, the values under research are close to the limits. The third (the cleanest) zone corresponds to the background territory (Site 6) and the city pine forest (Site 1).

Lichen biodiversity and their projective cover are stated to decrease as the anthropogenic load is increasing. In urban and anthropogenic environment lichen population density is declining more intensively than the number of species. For example, in the city pine forest and the city park lichen population density is rather high, but the average projective cover of lichen synusiae is essentially lower than on the background territory (the Ilmen State Reserve) (Fig. 3). In addition, the share of the trees without lichens is much bigger (64.2 %) in contrast to the background lichen communities of the Ilmen State Reserve where that value doesn't exceed 12 %.

a) b)

Fig. 3 Average projective cover of lichen synusiae in the city pine forest (a) and in the Ilmen State Reserve (b)

Within the city the share of the trees with lichens is definitely rich. The city pine forest has the largest number of the trees with lichens (82 %), the city park – 46 %. There are far fewer such trees in the buffer zone of the steelworks (27 %) and the adjusting territory of the power station (14 %). Lichens occurred there in small thallus on 1–2 trees of 10. Lichens were rarely found (10 % of trees). They are in a poor condition.

Some authors in their works insist not to overestimate the role of lichens as bioindicators. Byazorov says empirical indices and correlation with the concentration of some xenobiotics are locally important. He also notices that regularities set in some regions can't always work in others [2], [3], [6]. There isn't enough data about the impact of some elements where there are other elements in the environment. And there is little information about the pollutant transformation under the environmental factors. Some organic compounds may form from 16 to 20 transformation products some of which may be more toxic and harmful than the original substance [3]. For example, the engines of modern cars emit a lot of organic compounds such as benzene, toluene, phenol, which as a result of active chemical interactions can quickly turn into substances more toxic than the original**.**

To make the comparative analysis more reliable we used *Parmelia sulcate* as the species occurred in all the sites, as morphological and physiological properties of each species influence the accumulation of elements in lichen thallus. The ration analysis of oxides in mixed sampling of epiphytic lichens in summer showed that lichen accumulation of mangan, zink, cuprum and chrome might be related to the environmental load. The average rate of copper oxide and silver oxide in samples is small (Table 1). But cuprum and silver in lichen even in small concentrations are known to

make cell membrane more permeable and therefore they "push off" potassium more intensely than other metals. In fact the increase of cumulative percent of these oxides in samples leads to the decrease of potassium oxide rate.

Table 1 The content of oxide in the sol lichens

Oxide	Sites					
	1	2	3	4	5	6
MgO	0.94	2.26	3.12	2.13	2.79	1.6
Al_2O_3	8.21	17.52	10.67	14.51	16.43	9.6
SiO_2	16.70	31.89	28.53	27.13	19.54	16.34
P_2O_5	3.37	2.93	1.74	2.13	2.67	4.98
SO_3	3.66	3.58	7.04	3.29	5.28	4.15
Cl	0.72	0.48	1.34	0.71	1.30	0.78
K_2O	6.51	6.49	3.24	4.23	5.32	9.67
CaO	34.65	10.74	8.65	9.76	12.74	23.64
TiO_2	2.50	1.6	3.24	3.12	2.95	2.85
MnO	1.00	0.45	1.96	2.01	2.04	0.87
Fe_2O_3	18.46	20.33	25.56	26.41	24.45	23.10
ZnO	1.02	1.02	1.56	1.43	1.74	0.86
SrO	–	–	–	–	–	0.11
Ag_2O	0.51	0.33	0. 42	0. 31	–	0.41
CuO	–	0.33	0.51	0.49	0.47	0.63
CrO	1.70	–	2.10	2.11	2.14	0.36
ZrO_2	0.05	0.05	0.23	0.16	0.14	–
Y_2O_3	–	–	0.09	0.08	–	0.05

Zink oxide rate in the samples from environmentally troubled areas is almost twice higher (Fig. 4). For example, zink oxide rate of the background territory is 0.86 %, that rate in lichen samples gathered from the trees of the territory near the power station is 1.74 %. Chrome and mangan oxide in the anthropogenic sites is two and more times higher.

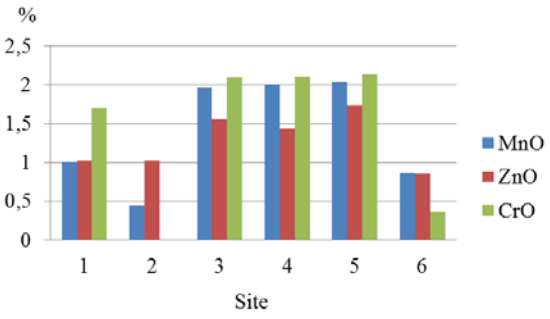

Fig. 4 The content of oxide (MnO, ZnO, CrO) in the sol lichens.

Three zones different in chrome and mangan rate are distinguished: relatively clean (to 0.9 %) – the background territory; moderately polluted (from 1.0 % to 1.9 %) – the city pine forest; significantly polluted (from 2.0 % to 2.9 %) – the territory of the steelworks (3), transport hub in the city centre (4), power station (5).

CONCLUSION

The study revealed the main regularities of the lichen distribution on the territory of Chelyabinsk. Environmental assessment of the territory of Chelyabinsk was conducted. With the increase of anthropogenic load there is a tendency towards the decrease of lichen species diversity and the amount of trees with lichens. The projective cover of lichen groups and the amount of trees with lichens are more informative, in comparison with species diversity.

The chemical lichen monitoring revealed a trustworthy difference between the rates of metal oxides in lichen thallus gathered on the territories of the Reserve and the city. To detect the degree of pollution chrome and copper oxide rates in *Parmelia sulcate* thallus may be used. The use of these oxides to give a similar characteristic of the territory pollution based on other lichen species considers revising.

ACKNOWLEDGEMENTS

The authors wish to thank D. Uchaev (ERC Nanotechnology, SUSU) for XRF quantification measurements.

REFERENCES

[1] Nimis PL, Scheidegger C, Wolseley PA, "Monitoring with lichens – monitoring lichens", NATO Science Series, IV. Earth and Environmental Sciences, Vol. 7, 2002, pp. 1–4.

[2] Byazrov LG, Maximova VF, Rukhadze EV, "Use of epiphytic lichens as indicators of air pollution degree in Moscow", Ecology and industry of Russia, Vol. 8, 2004, pp. 4–7.

[3] Biazrov LG, "Die Dynamik der Artendiversität epiphytischer Flechten im Nordbezirk von Moskau (Russland)", Archive for lichenology, Vol. 6, 2010, pp. 1–8.

[4] Anishchenko LN, Azarchenkova (Safrankova) EA, "Background monitoring of habitat by lichen indication method (as in protected areas of Nerusso-Desnyansky woodlands)", BSU Bulletin: Exact and Natural Sciences, Vol. 4, 2012, pp. 27–32.

[5] Romanova EV, Sedelnikova NV, "Lichens as bioindicators of air pollution in Novosibirsk urban agglomeration", Novosibirsk: Geo, 2010, pp. 5–49.

[6] Byazrov LG, Epiphytic lichens of Moscow: modern dynamics of species diversity, Moscow: KMK, 2009, pp. 3–112.

[7] Boutron CF, Patterson CC, "Relative levels of natural and anthropo-genic lead in recent

Antarctic snow", Journal of Geophysical Research, Vol. 92, 1987, pp. 8454–8464.
[8] De Bruin M, "Les indicateurs biologigues, l'analyse par activation neutronique, et leurs applications à l'étude de la pollution atmosphérique par les métaux lourds, AIEA Bulletin, Vol. 4, 1990, pp. 22–27.
[9] Nriagu JO, Pacyna JM, "Quantitative assessment of worldwide contamination of air, water and soils with trace metals", Nature, Vol. 333, 1988, pp. 134–139.
[10] Reimann C, Caritat P, Chemical elements in the environment, Berlin: Springer-Verlag, 1998, pp. 5–16.
[11] Dubrova SV, Podlipskiy II, Kurilenko VV, Siabato W, "Functional city zoning. Environmental assessment of eco-geological substance migration flows", Environmental Pollution, Vol. 197, 2015, pp. 165–172.
[12] Furbish CE, Geiser LH, Rector C, "Lichen-air quality pilot study for Klondike Gold Rush National Historical Park and the City of Skagway, Alaska, Natural resources management program, 2003, pp. 2–17.
[13] Shcherbina AG, Mashkova IV, "Air quality assessment with method of lichen indication monitoring in Ilmen State Reserve", Natural and Mathematical Sciences in the modern world, Vol. 36–37, 2015, pp. 173–177.
[14] Hauck M, "Ammonium and nitrate tolerance in lichens", Environmental Pollution, Vol. 158, 2010, pp. 1127–1133.
[15] Van Herk CM, "Mapping of ammonia pollution with epiphytic lichens in the Netherlands", Lichenologist, Vol. 31, 1999, pp. 9–20.
[16] Van Herk CM, Mathijssen-Spiekman EAM., de Zwart D, "Long distance nitrogen air pollution effects on lichens in Europe", Lichenologist, Vol. 35, 2003, pp. 347–359.

Second International Conference on Science, Engineering & Environment,
Osaka City, Japan, Nov.21-23, 2016, ISBN: 978-4-9905958-7-6 C3051

MECHANISM OF COAGULATION USING CHITOSAN FROM MYTILUS VIRDIS LINNEAUS SHELLS IN WATER TREATMENT

Sinardi[1], Prayatni Soewondo[2], Suprihanto Notodarmojo[3], Cynthia Radiman[4]
[1]Bandung Institute of Technology, Doctoral Program Environmental Engineering Department, Bandung 40132, Indonesia
Fajar University, Chemical Engineering Departement, Makassar, 90000, Indonesia
2,3Bandung Institute of Technology, Environmental Engineering Departement, Bandung 40132, Indonesia
4Bandung Institute of Technology, Chemistry Departement, Bandung 40132, Indonesia

sinardi@unifa.ac.id

ABSTRACT

Green mussel (*Mytilus viridis Linnaeus*) is one of the shells from marine source that can be used as chitosan. On the other side of drinking water treatment using synthetic coagulant such us aluminum sulphate ($Al_2 (SO_4)_3$) concerns about the residual aluminum in the water that contains inorganic compounds are carcinogenic so it is necessary to do research about potential use of chitosan as a coagulant. This study conducted on laboratory-scale use of chitosan from green mussel shells as a coagulant in coagulation-flocculation process using turbid water from Tirtawening in Bandung City, Indonesia. The purpose of this study was to determine the mechanism of coagulation-flocculation process based on the characteristics of chitosan. Preparation of chitosan with deproteination process done using a solution of NaOH 3.5% 10: 1 (v: w), stirring 2 hours 65^oC. Demineralization process using a solution of HCl 1 N 15: 1 (v: w), stirring 30 minutes 50 °C. Deacetylation process using a solution NaOH 60% 20:1 (v: w) stirred 60 minutes 120^oC produce chitosan with degree of deacetylation about 77.8% and molecular mass about $4{,}26x10^4$ g / mol. The degree of deacetylation of chitosan effect ability formation of flock and the molecules of mass of chitosan effect in binding colloids in turbid water into one and form a flock large. The results concluded that chitosan from green mussel shells can be used as a coagulant for turbidity removal in water treatment and use it safe for the environment and health because from natural compounds and biodegradable.

Keywords: Mytilus viridis Linnaeus, Chitosan, Degree of Deacetylation, Molecular of Mass, Coagulation-Flocculation, Turbid Water, Turbidity Removal

INTRODUCTION

Human consciousness about the importance of health led to the need for clean water increases. But the problem of clean water availability decreased mainly quality, the most common problem encountered is the turbidity of the water. Turbidity is caused by the presence of organic and inorganic materials are suspended and dissolved, as well as inorganic and organic materials in the form of plankton and other microorganisms contained in water. Turbidity in the water treatment process can be eliminated through the process of coagulation.

Coagulation is one process of the water treatment to improve the quality of water produced. Coagulation process aims to eliminate the solute to be precipitated by adding a chemical compound into the water resulting in the incorporation of particles that are difficult to settle and form a flock.

Until now, the polymer coagulant derived from synthetic are commonly used type of coagulant. In between the two types of the coagulant, the coagulant is a synthetic material that is widely used in water treatment processes, in addition to more easily obtained, from an economic point of relatively cheaper price. But the use of synthetic coagulant excess it undesirable effects on the environment and health as a coagulant of this type is not biodegradable. This is the basis of the researchers focused on the use of natural coagulants such as chitosan is a solution that can be used as a coagulant derived from natural materials [1].

The process of coagulation is the charge neutralization process by adding a coagulant or chemical, while coagulation is to destabilize the process of agglomeration of the particles to form a flock becomes larger and easier to settle [2]. With the addition of coagulant, the colloidal stability in disturbed water as coagulant will stick to the surface of colloidal and change their electrical charge to form aggregates which can be precipitated [3].

Chitosan is a chitin derivative obtained by deacetylation process, a cationic polymer which is biodegradable. Chitosan can substitute synthetic coagulants in water treatment with the advantages: (1) residual coagulant is not harmful to human health because it is an organic material, (2) generate sludge biodegradable, and (3) can be made using the waste

of fishery products [4].

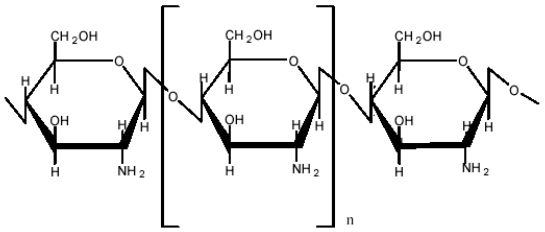

Figure1. Structure Molecule of Chitosan

Chitosan is a biopolymer obtained by deacetylation of chitin contained in some marine shells [5]. Amine groups (NH2) on chitosan (see Figure.1) is a strong nucleophile that can be used as a polyelectrolyte that has many functions and is more reactive than chitin.

MATERIAL AND METHODS

Chitosan

Chitosan was extracted from *Mytilus viridis linnaeus* shells prepared using Knorr method with some modifications [6]. Preparation of chitosan with deproteination process done using a solution of NaOH 3.5% 10: 1 (v: w), stirring 2 hours 65ºC. Demineralization process using a solution of HCl 1 N 15: 1 (v: w), stirring 30 minutes 50 °C. Deacetylation process using a solution NaOH 60% 20:1 (v: w) stirred 60 minutes 120ºC. Chitosan produced has characteristics of the degree of deacetylation was 77.80% and a molecular mass was $4{,}26x10^4$ g/mole.

Turbid Water

This study uses turbid water from the outlet unit PDAM Tirtawening in Bandung, Indonesia. The characterization of raw water can be seen in the Table.1 below.

Table 1 Physical and Chemical of Turbid Water

pH	Turbid	Conduct	TSS	TDS	OM	Fe	Mn
6.73	30.10	110.83	25	77.77	1	0.34	0.05

Total Suspended Solid
Total dissolved solids
Organic Matter
Turbidity, NTU; Conductivity, µS/cm; all concentrations are in mg/L.; pH were determined by the author

Dissolution Chitosan

Dissolution of chitosan following the method [7] of 1 g chitosan was dissolved in 100 mL of 1% acetic acid (v / v) to obtain 10 mg of chitosan in 1 mL of solution (1% w / v). Stirring chitosan solution using a magnetic stirrer for 6 hours to ensure perfect chitosan dissolved. With this dissolution, 100 ml of acetic acid solution 1% (v / v) then obtained 1000 mg / ml of chitosan in solution.

Jar Test

Research conducted in batches in a laboratory scale using jar test, which is also the operational simulation of conventional treatment processes.

1. Jar test use Flocculation SW1 Stuart Scientific, using a beaker containing 500 mL of turbid water.
2. Stirring rapidly performed at 100 rpm for 1 minute after the addition of coagulant, followed by slow mixing at 60 rpm for 10 minutes.
3. After the flocculation process is completed, flock had formed allowed to settle for 30 minutes, separated from the flock, turbid water and then analyze.

RESULTS AND DISCUSSION

Effect of the Chitosan Dosage

Chitosan coagulant dosage effect on the amount for turbidity removal that occur after the coagulation process, as seen in the results of tests conducted jar in Figure.2. Turbidity removal increased with increasing dosage of chitosan, but the addition of coagulant dosage showed excessive turbidity removal which does not different much even decline, this is due to the failure of flock formation and saturation of chitosan aside turbidity.

In addition to turbidity, pH is a very important parameter in the coagulation process, because it can affect the pH of the surface charge of the colloidal molecules, the charge of the functional groups of organic material contained in the charge of water and other components dissolved in water. At high pH (alkaline), colloid-containing organic compounds will be ionized due to the carboxyl groups of chitosan will lose a proton (due react with alkali), as well as the positive charge of coagulant required to neutralize the charge of colloids will also be reduced. As a result, the required dosage of coagulant will also increase at higher pH.

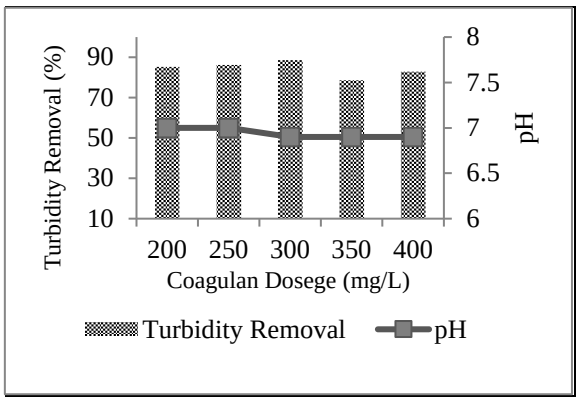

Figure2. Turbidity Removal using Chitosan

Provision for turbidity using chitosan as a coagulant optimum dose of 300 mg/L of 88.60% and pH 6.73 to 6.9 after coagulation. At higher coagulant dosage higher concentrations are 350 and 400 mg / L allowance for the lower turbidity, is due at the dose of chitosan as cationic polyelectrolyte becomes saturated. The result will damage the bridge between the particles so that not all of the colloidal particles can be deposited.

Mechanism of Coagulation

Mechanism of coagulation using chitosan in water treatment due to chitosan cannot react with water because of the hydrogen bonds that are formed are very weak. So that the OH and NH_2 owned makes chitosan is alkaline. The amine group attached to the C atom, while the primary hydroxyl groups attached directly to a carbon atom other and bonded to the secondary hydroxyl amine group.

Chitosan can be used as a coagulant that is more effective and efficient than the use of alum in the process of coagulation, evident from the reduced turbidity of river water with the use of chitosan in the chitosan concentration is low [8]. Coagulation process using chitosan flocculation can decrease inorganic and organic particles suspended and dissolved organics contained in water [9].

Mechanism of coagulation using chitosan was when the polymer molecules into contact with the colloidal particles, then some of chitosan groups adsorbed on the surface of the particle and the rest remain in solution. Furthermore, the particles will be attached to another part of the polymer chain which serves as a bridge that can confine the particles and form flocks larger so as to bring the particles together down and deposited polymer. In acidic conditions, the amino group ($-NH_2$) chitosan will catch H^+ from the environment so that the amino group protonated be $-NH_3^+$ and then chitosan acts as a salt that can be dissolved in water.

Associated with the mechanism of coagulation, colloidal chitosan can bind into flock by two methods, namely the charge neutralization and bridge colloid polymer [10]. Chitosan with a large molecular mass means having long-chain polymer colloids will bind together and form large flocks. NH_2 group in the chitosan will catch H^+ in water and form a group $-NH_3^+$. This group will neutralize the negative charge of colloid and polymer chain of chitosan will catch colloids into a single unit see Figure.3 below.

Chitosan is a cationic polyelectrolyte and long-chain polymer, has a large molecular mass and reactive because of the amine and hydroxyl groups which act as electron donors. Due to the properties of the regular chitosan interacts with the colloidal particles contained in the water through the bridge between flock particles (coagulation) [11] and [12]. To simplify the process of coagulation, the chitosan dissolved in advance by using acid to obtain a solution of chitosan. The mechanism is based on the properties of the chitosan-containing amine group which reacts with the acid when it will form a salt. Therefore it must be dissolved into the acidic chitosan.

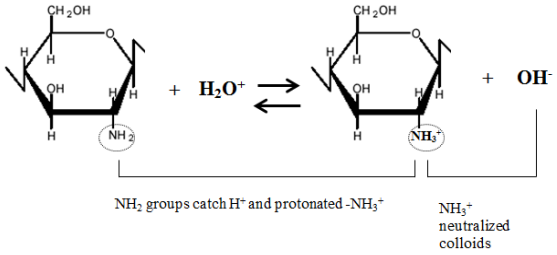

Figure3. Illustration Chitosan as a Coagulant

Amino groups of chitosan (NH_2) in a solution of making the chitosan is positively charged (indicated as a polyelectrolyte cationic) so attractive for flocculation and application of binding different that allow molecules binding different that allows the molecules bind to the surface of the negatively charged through the binding of ionic or hydrogen [13].

The mechanism of coagulation and flocculation of chitosan, beginning with the charge neutralization colloid charge neutralization in turbid water, amine containing a lone pair on the nitrogen atom, the amine is alkaline (*Bronsted-Lowry*) and nucleophiles character. Then the bridge is formed between the particles form a flock colloids, the chitosan polymer chain of chitosan increasingly charge (-) colloidal neutralized by NH_3^+ group see Figure 4. The chitosan polymer colloids catch into a single unit to form larger aggregates so easy to settle.

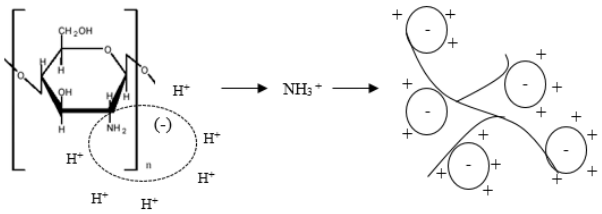

Figure 4. Illustration Coagulation and Flocculation Process Using Chitosan

SEM images in Figure.5 shows the surface of the slab-shaped chitosan large and stringy. While the surface of the flock formed has a solid surface and porosity smaller, it shows that during the process of coagulation merger colloidal particles which are then attached to the surface of chitosan. SEM on chitosan and flock that is formed can be known before the change of the surface structure of chitosan is used as a coagulant and after the coagulation process.

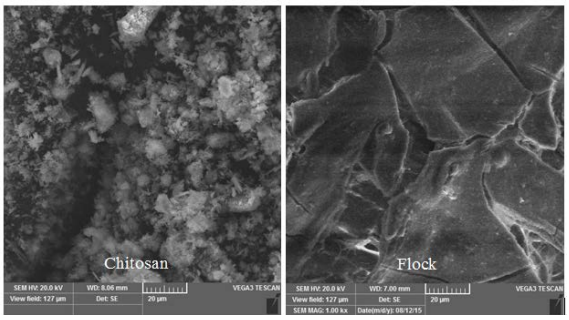

Figure5. *Scanning Electron Microscope* (SEM) of Chitosan and Flock Formed after Coagulation

Changes in the surface structure of chitosan and chitosan flock occurs because of the addition of the turbid water in water treatment caused colloidal particles will come closer together and the collisions between colloidal particles and alter its cargo into neutral, causing clumping and forming flock.

CONCLUSION

Chitosan from *Mytilus viridis linnaeus* shells can be used as a coagulant to substitute synthetic coagulant in water treatment because it has the ability for turbidity removal. The ability of chitosan aside turbidity because it has a large molecular mass so long chitosan polymer molecule chains that play a role in the neutralization of the charge of colloids and polymers as a bridge that has the ability to bind and precipitate colloids into flock.

ACKNOWLEDGEMENTS

The authors gratefully acknowledge the financial support received in the form of Dissertation Research Grant from Ministry of Research, Technology and Higher Education in Indonesia.

REFERENCES

[1] Yang, Z, Yabo Shang, Yaobo Lu, Yichun Chen, Xin Huang, Aimin Chen, Yuxiang Jiang, Wei Gu, Xiaozhi Qian, Hu Yang, dan Rongshi Cheng, Flocculation Properties of Biodegradable Amphoteric Chitosan-Basen Flocculants, Chemical Engineering Journal, 172, (2011) 287-295.

[2] Hammer, M. J, Water Supply & Polluti on Control 7th Edition, Pearson Prentice Hall, United States of America, 2005.

[3] Eckenfelder, W. J, Industrial Water Poluttion Control, Third edition,. Mc Graw-Hill Company, Singapore, 2000.

[4] Pan, J.R, Chihpin Huang, Shuchuan Chen, and Ying Chien Chung, Evaluation of a Modified Chitosan Biopolymer for Coagulantion of Colloidal Particles, Physicochemical and Engineering Aspects, 147, (1998) 359-364.

[5] Marganof. Potensi Limbah Udang Sebagai Penyerap Logam Berat (Timbal, Kadmium dan Tembaga) di Perairan. Information on http://rudict.topcities.com/pps702-71034/margonof.html

[6] Sinardi, Soewondo P, Notodarmojo S, and Radiman C, The Degree of Deacetylation Chitosan Various Marine Shells, International Journal of Applied Engineering Research, (2014) 18047-18051.

[7] Danwanichakul, P., Werathirachot, R., Kongkaew, C., and Loykulnat, S, Coagulation of Skim Natural Rubber Latex Using Chitosan or Polyacrylamide as an Alternative to Sulfuric Acid, European Journal of Scientific Research, Volume 62 No. 4, (2011) 537-547.

[8] Mu'minah, Aplikasi Kitosan Sebagai Koagulan untuk Penjernihan Air Keruh, Program Studi Kimia, FMIPA. Institut Teknologi Bandung. Indonesia, 2008.

[9] Renault, F, B. Sancey, P.M Badot, dan G. Crini, Chitosan for Coagulations/Flocculation Processes–An Eco-Friendly Approach, European Polymer Journal, Volume 45, Issue 5, (2008) 1337-1348.

[10] Tripathy, Tridiband De, and Bhudeb R, Flocculation: A New Way to Treat the Waste Water, Journal of Physical Sciences, Volume 10, (2006) 93-127.

[11] Chung GH, K. B, Physicochemical Properties of Chitin andChitosan Prepared from Lobster Shrimp Shell, Korean Journal Food Science Technology, 28, (1996) 870–876.

[12] Prashanth KVH and Tharanathan RN, Chitin/Chitosan: Modification and Their Unlimited Application Potential an Overview, Journal Food Science Technology, 18, (1997) 17-131.

[13] Hasan M.A, and Mohd Hafiz Puteh, Pre-Treatment of Palm Oil Mill Effluent (POME): Comparison Study Using Chitosan and Alum, Malaysian Journal of Civil Engineering, (2007) 19:2.

Second International Conference on Science, Engineering & Environment,
Osaka City, Japan, Nov.21-23, 2016, ISBN: 978-4-9905958-7-6 C3051

FEATURES AND ACTIVITIES FOR OVERCOMING THE CHALLENGES IN THE LANDCARE MOVEMENT IN AUSTRALIA: A MODEL OF COMMUNITY SUPPORT SYSTEM

Tomomi Maekawa

[1] Graduate School of Humanities and Social Sciences, Chiba University, Japan

ABSTRACT

It is recognised that environmental problems are best handled with the participation of all concerned citizens at the relevant level, but the development of effective models for promoting citizen participation to solve environmental issues remains a work in process. With the goal of suggesting such a model, this study focuses on the system of Landcare in Australia, a nation-wide movement of community-based natural resource management that has been tackling Australia's serious environmental problems. Through analysing the outcomes of in-field research in Australia, this study describes that the community support system of the Landcare movement in Australia has three characteristic elements: establishing a system and a spirit of multi-party partnership throughout the nation; securing coordinators who, with flexibility to adjust to each locale, support local groups; and maintaining a holistic support system from governments who respect the autonomy of local groups. Through the discussion, this study shows the strengths of the three elements such as the diversity of the financial sources and the challenges regarding the provision of financial and coordinating support to the communities. Also it shows that there are activities that local groups and their networks have carried out in the movement that aim to overcome these challenges.

Keywords: Landcare in Australia, Community-based Natural Resource Management, Voluntary Groups, Citizen Participation, Multi-party Partnership

INTRODUCTION

It is recognised that environmental problems are best handled with the participation of all concerned citizens at the relevant level [1]. However, the development of effective models for promoting citizen participation to solve environmental issues is still in its early stage. With the aim of suggesting such a community support system model, this study focuses on the system of the Landcare movement in Australia (here, referred to simply as Landcare).

Landcare is a nation-wide movement of community-based natural resource management born in Victoria in 1986. It has been tackling Australia's serious environmental problems, which have resulted from extensive deforestation and from weed and pest animal infestations begun with European settlement in 1788. Landcare promotes and supports local voluntary groups which are managed by the local people themselves [2][3]. Its effectiveness has been evaluated by the government [4] and research shows that participating in Landcare leads to significantly higher levels of awareness and concern for a range of environmental and social problems among landholders [5].

PURPOSE AND METHODOLOGY

The aim of this study is to suggest a community support system model that promotes citizen participation in solving environmental problems and to this end describes three main structural characteristics of Landcare. In order to achieve this aim, a model has been constructed by analysing the outcomes of in-field research carried out by the author in Australia, mainly in Victoria, with support from universities, other organisations and individuals from both Australia and Japan [6]-[9]. The in-field research in Australia was carried out through interviews with individuals, observation through participation and documentation analysis, during the periods 24th August to 6th September 2012 and from 1st June 2013 to 20th May 2014.

ANALYSIS AND DISCUSSION

Through analysing the outcomes of the author's in-field research, from the perspective of trying to identify the institutional structure, it was found that there were three main characteristic elements which comprise the structure of Landcare:

- Establishing a system and a spirit of multi-party partnership throughout the nation [6].
- Securing human resources who, with flexibility to adjust to each locale, act as coordinators supporting local groups [7][9].

- Maintaining a holistic support system from governments who respect the autonomy of local groups [8].

Establishing a System and a Spirit of Multi-Party Partnership

The first characteristic element of Landcare is establishing a system and a spirit of multi-party partnership across the nation. In this section I will summarise the findings of [6]. The basic unit of Landcare is each local voluntary group called a Landcare group, and there are six core related organisations which support and empower Landcare groups and one organisation which supports and connects overseas groups/activities to Landcare in Australia (See Table 1). This network of multi-party partnership works at four different levels.

Table 1 Core related organisations in Landcare (including Landcare groups and Landcare networks which are systems of networking among the Landcare groups)

Levels	Names of organisations
local	Landcare Groups
local/regional	Landcare Networks
regional	Catchment Management Authorities
state	Victorian Landcare Council
state	Farm Tree and Landcare Association
state	State Governments
national	Landcare Australia Limited
national	Australian Federal Government
international	Australian Landcare International

Core Organisations at Regional, State, National and International Levels

Ten Catchment Management Authorities (CMAs) function as delivery agents at the regional level in Victoria providing information and skilled staff members, allocating funds, and facilitating collaboration between individuals, community groups, local organisations, and others.

Three organisations function at state level. The Victorian Landcare Council (VLC) presents the interests of grassroots individuals and groups to state and federal governments, government agencies, local government and CMAs. It participates in developing government policy on natural resource management and building a stronger partnership between Landcare members and policy makers. Delegates of the Landcare groups, networks, and the staff supporting them make up the council. The Farm Tree and Landcare Association (FTLA) provides information, governance training and consultation to the groups and to individual members, and also since the 1990s has provided insurance packages to them in case of accident. Within the Victorian State Government Department of Environment and Primary Industries (DEPI) there is a team called the Victorian Landcare Team whose members work at regional or state level.

At the national level there are a further two organisations. Landcare Australia Limited (LAL) manages public awareness and sponsorship campaigns. It obtains corporate sponsorship funding for Landcare and similar groups associated with it, and raises awareness of the programs, brands and logos of Landcare across the nation. The Australian Federal Government invests in the 56 regional natural resource management (NRM) bodies across the nation, including CMAs, to support farmers and land managers and encourage conservation in local communities. This is carried out primarily through Regional Landcare Facilitators (RLFs) whose roles will be described later.

At the international level, Australian Landcare International (ALI) helps other countries or regions outside of Australia to learn from the Australian Landcare movement, and promotes cross-referencing and learning between different countries or regions.

Support from the Organisations and Coordinators

The seven identified core organisations and the people collectively called Landcare Coordinators or Landcare Facilitators (here, referred to simply as coordinators) support individuals, the Landcare groups and their activities in various ways by providing information, consultation, funds, volunteers, and know-how about how to access appropriate resources to care for the land.

For example, focusing on the state level, in Victoria, each CMA encourages landholders, community groups, and governments to address NRM issues through providing information, allocating funds, and through communication with local people, communities, organisations and governments. On the other hand, focusing on the national level, the National Landcare Programme (NLP) was launched, taking its lead from the state of Victoria, with the goal of achieving efficient, sustainable, and equitable management of natural resources throughout Australia. The 56 NRM bodies across the nation (including the CMAs) act as delivery agents at the regional level of the NLP. Each of them works with communities to identify and set local priorities for how funding is to be used. The coordinators at regional NRM bodies link individuals, community groups including Landcare groups and networks, and funding organisations at the regional level.

Securing Coordinators to Support Local Groups

Positions and Roles of Coordinators

The second characteristic element of Landcare is securing coordinators who support local groups including Landcare groups. In this section I will summarise the findings of [7] and [9]. There are six identified Coordinator positions working at four different levels (See Table 2).

Table 2 Identified coordinator positions

Names of positions	Levels
Local Landcare Facilitator (LLF)	local
Landcare Project Officer (LPO) / Project Officer / Project Manager	local
Regional Landcare Coordinator (RLC)	regional
Regional Landcare Facilitator (RLF)	regional
Victorian Landcare Team (VLT)*	state
National Landcare Facilitator (NLF)	national

*The VLT comprises the 10 RLCs, 2 theme based state-wide coordinators and the members of the relevant unit in the Victorian State Department of Environment and Primary Industries.

Local Landcare Facilitators (LLFs) and Landcare Project Officers/Project Officers/Project Managers (LPOs) who work at the local level help the Landcare groups and networks to concentrate on the on-ground work by assisting them with administration and other duties.

Regional Landcare Coordinators (RLCs) and Regional Landcare Facilitators (RLFs) who work at the regional level support Landcare networks or groups and similar associated groups by providing them with relevant information such as upcoming events, funding, forums, training for capacity building and allocating funding from the governments in the form of grants.

The members of the Victorian Landcare Team (VLT) who work at the regional and state levels manage the state-wide program of Landcare through allocating funds and by providing information where needed. They hold forums in each region, publish newsletters, and manage a website where people can access information related to Landcare in Victoria including contact numbers of coordinators.

The National Landcare Facilitator (NLF) who works at the national level plays an advisory role with a special focus on sustainable production in the primary industry sector and the engagement and participation of community groups in natural resource management programs. This role links Landcare in the six Australian states and two territories through communicating with RLFs based in 56 NRM bodies across Australia.

In short, at each level, coordinators have promoted the building of a network of partnership among the various stakeholders. Through the four levels of coordination, Landcare as a whole has a structure that enables individuals and groups who need information, volunteers, funding, and know-how to access these resources.

Motivating Local Groups to have Coordinators and Provide Training Programs

An initiative called the Victorian Local Landcare Facilitators Initiative motivates local groups to have coordinators. In this initiative, the roles and responsibilities of each local Landcare facilitator are defined in a way that is adapted to the circumstances and needs of the particular area, thus contributing to the empowerment of the local people. The Initiative (known as the Victorian Landcare Facilitator Program since 2015) supports Landcare groups and networks in Victoria by providing funds to 60 new LLFs, who are paid part-time coordinators, based on the recognition that "recruiting from within the local community means the facilitators will have a good understanding of the local area and issues and will be able to work more closely with their local groups" [10]. Funding can be used to cover the salary and operating costs of the new position.

It has become apparent that various skills such as "computer skills, sponsorship marketing, mapping and monitoring, project management, publicity and community education" are required of coordinators [11]. A one day training program entitled "Secrets to Successful Groups" which is held at a local hall provides coordinators with the opportunity to learn about the governance of groups or networks. The training is provided by the FTLA with support from the RLF in that area. The program covers topics such as "Effective Decision-Making", "Legal Duties of Committee Members" and "Volunteer Recruitment", and includes lectures by a staff member of the FTLA, a lawyer, and a specialist in community engagement and facilitation [12]. Through attending this program, participants acquire the basic knowledge needed for managing a group or a network, such as decision making, risk management, and how to get more people involved.

Maintaining a Holistic Support System from Governments

The third characteristic element of Landcare is maintaining a holistic support system from state and federal governments. In this section I will summarise the findings of [8]. There are four types of government support (See Fig.1).

With regard to informational support, the Victorian state government provides information related to Landcare through managing a website called the Victorian Landcare Gateway where people "can find news from Landcare groups and

networks, including up-coming volunteer activities and events, resources and toolkits for groups, information on grants and projects, as well as group and network contacts" [13] and through a magazine called *Victorian Landcare & Catchment Management*. At the national level, LAL provides information on its website which includes a National Landcare Directory.

As for financial support, in the state of Victoria, the state government provides funding in the form of Victorian Landcare Grants which are for "on-ground works that deliver on local, regional and State priorities, capacity building activities for land stewardship and on-ground change, projects that promote innovation through experimental trials and pilot programs, start-up funding and maintenance grants to ensure a strong Landcare base across the State, and opportunities to promote Landcare and increase membership and volunteer numbers" [13]. At the national level, the federal government provides funding through the National Landcare Program and also provides the possibility of tax deductions for landowners incurring capital expenditure for their property improvements.

Regarding technical support, in Victoria, the state government invests in RLCs, one based in each region in Victoria, and also, the federal government invests in RLFs, one based in each of 56 regional NRM bodies across Australia.

With regard to motivational support, the state government of Victoria provides the Victorian Landcare Awards (VLA), and the federal government provides State & Territory Landcare Awards (STLA) and National Landcare Awards (NLA). STLA including VLA are held "to acknowledge the success and achievements of community Landcarers, groups, networks, and organisations who have been working to protect and restore our environment" and the winners of some categories will go on to represent their state or territory at the NLA [14].

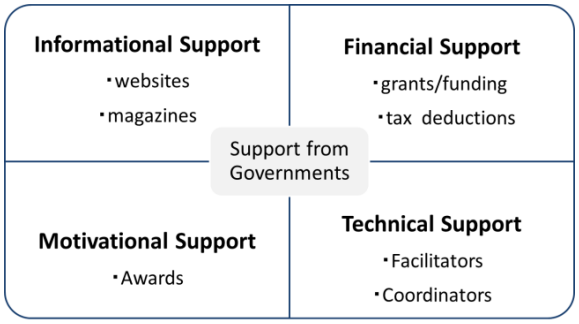

Fig.1 Four types of government support

Features and Challenges of Landcare and Addressing these Challenges

Features–Strengths of the Three Elements

Firstly, there are three strengths of the Landcare multi-party partnership structure. Continuous economic support towards local Landcare groups and their activities is ensured based on the diversity of the financial sources such as state and federal governments and LAL who provide or allocate grants to local groups and their activities. Because Landcare groups are basically self-funding, they won't immediately cease to function even if some of the financial support from governments or others is withdrawn. Due to the diversity of the financial sources in Landcare which result from its multi-party partnership structure its economic base is strong.

Also, the efficiency of solving environmental problems and managing natural resources from a government perspective is improved. It is more cost effective for governments to support and promote maintenance of the local environment by local groups at the local level, than to carry out the same activities using public expenditure [15].

Finally, the structure provides opportunities for companies, schools and individuals to contribute to improving or regenerating their own local environment. For example, Landcare has been regarded as a valuable activity for companies wishing to invest in the environmental sector. Furthermore, Landcare provides opportunities for in-field education about the local environment for local school children, and it also provides opportunities for older persons to connect with the community through Landcare groups enabling them to sustain social connectedness through working with others for their local environment.

Secondly, securing coordinators who support local groups in Landcare is a strength in that it is protecting and enhancing the local knowledge regarding the natural environment and culture which has been passed from one generation to the next and amongst individuals within each local community. As shown in the previous sections in this paper, the initiative called Victorian Local Landcare Facilitators Initiative (VLLFI) and the training program organised by FTLA support local Landcare groups and networks to employ and improve the skills of coordinators who are familiar with the local environment and community. Such initiatives and programs improve the management of the local groups and expand the range of their activities while protecting and enhancing the local knowledge in local communities.

Thirdly, support from the state and federal governments is a system strength in that it has been encouraging sustainable management and development of the local groups and networks holistically whilst maintaining their autonomy. Examples of government support include providing grants which promote and support the establishment

of new groups and networks, publishing magazines, managing websites, and funding coordinators who provide information related to NRM ranging from know-how regarding soil conservation to group management, which supports sustainable group management and the development of activities.

Challenges in the Three Elements

Firstly, there are two challenges regarding the structure of the multi-party partnership in Landcare. The budget allocated by governments to Landcare has declined due to changes in the economic situation and changes in government policy [15]. The decline of the budget does not immediately affect the local Landcare groups and their activities because they are basically self-funding. However, ultimately it affects the local activities which are supported by government grants and it also affects the employment of coordinators who are employed through funding from the governments.

Another challenge is the aging of the members of local Landcare groups and the limited number of younger participants. This is a shared challenge across the state of Victoria [16]. It is apparent Landcare needs to develop and implement a plan to foster the next generation, and encourage them to take over local group management and the planning and implementation of activities.

Secondly, there are also two challenges with regard to securing coordinators to support local Landcare groups. It is becoming increasingly difficult for local groups and networks to employ coordinators. With regard to this, Curtis and Sample (2010) point out that the Landcare groups and networks rely heavily on the work of coordinators in communicating with co-operators including governments, and also point out that most of the coordinators who are employed by Landcare groups and networks are funded through grants from governments [17]. Thus the decline in the budget provided by the governments to Landcare affects the employment of coordinators.

Another challenge is the excessive amount of work of coordinators and the unstable situation some of the coordinators find themselves in. The VLLFI (VLFP) stipulates that the role of coordinators is to help local groups become self-sustainable and also, that day to day administrative work for group management and activities are not the coordinator's role. However, their workload remains huge, especially regarding paperwork related to reports and fundraising. This makes it difficult for coordinators who are employed part-time to sustain their role due to limited work time and salary.

Thirdly, the challenge with regard to maintaining a holistic support system from state and federal governments is the tendency to depend on government support and to switch off the priority in government policy on NRM from the local perspective to wider perspectives such as regional, state or national. It has been pointed out that group management and the development of activities has been slowed down by such tendencies [18]. At meetings of the Victorian Landcare Council (VLC), the tendency to switch off the priority in government policy on NRM from the local perspective to a wider perspective was one of the topics of discussion [19].

Activities for Overcoming the Challenges

Activities for overcoming the challenges in the structure of the multi-party partnership in Landcare, local Landcare groups and networks include encouraging others to join the activities carried out by local groups, by putting more recreational activities rather than purely conservation or agricultural activities into tree planting programs or other field day events [6]. As for the recruitment of new members, especially younger people, by local groups, this is still in process, but the current members have been implementing plans to promote the activities of local Landcare groups in order to encourage others to join to compensate for the shortage of participants.

Also, the VLC holds meetings and discussions at which they share information about the situation in each region and suggest ideas for improvement through communication with the staff of CMAs and other local groups. The VLC has its own website and provides notes and other information regarding its meetings and the outcomes to interested people.

CONCLUSION

From the perspective of institutional structure, this study has described three main characteristic elements which comprise the structure of Landcare in Australia. It has been put forward as a model for a community support system which promotes the establishment of local voluntary groups which plan and implement activities for improving their local environment. The three characteristic elements are: establishing a system and a spirit of multi-party partnership throughout the nation; securing human resources who have the flexibility to adjust to each locale and function as coordinators supporting local groups; and maintaining a holistic support system from governments who respect the autonomy of local groups.

With regard to the three characteristic elements, this study has described the strengths of Landcare such as a diversity of financial sources within the system as a whole. At the same time, it showed there are challenges such as the broad and heavy workload with a limited budget for each coordinator, and the shift of the priority in NRM from local to wider perspectives. Also discussed is the establishment and

management of an organisation representing local community groups which enhances communication between grass-roots community groups and governments/other authorities with the intention of overcoming the challenges.

ACKNOWLEDGEMENTS

This work was greatly supported by Charles Sturt University Institute for Land, Water and Society, and Mr. Rob Youl and his family and colleagues at the Australian Landcare International, and the administrative officers at the relevant organisations. I also express my appreciation to the people who kindly helped with the in-field research in Australia, and for the support from the Secretariat for Promoting the Establishment of Landcare in Japan and from Kuwako Lab at the Tokyo Institute of Technology.

REFERENCES

[1] United Nations Department of Economic and Social Affairs, "Report of the United Nations Conference on Environment and Development (Rio de Janeiro, 3-14 June 1992)" [online], <http://www.un.org/documents/ga/conf151/aconf15126-1annex1.htm> (Accessed 8 June 2016).

[2] Campbell A, "Landcare－communities shaping the land and the future－", Allen & Unwin Pty Ltd, NSW, 1994, pp. 31-36.

[3] Youl R, Marriott S, and Nabben T, Landcare in Australia –founded on local action. SILC and Rob Youl Consulting Pty Ltd, Australia, 2006.

[4] The State of Victoria Department of Environment, Land, Water and Planning, <http://www.depi.vic.gov.au/environment-and-wildlife/community-programs/landcare> (Accessed 8 June 2016).

[5] Curtis A, "Landcare in Australia: Does it Make a Difference?", Journal of Environmental Management, 46, 1996, pp.119-137.

[6] Maekawa T, Seigel M, and Kuwako T, "A Study of the Educational Approach of the Australian Landcare Movement", International Journal of Affective Engineering, Vol.15, No.2 (Special Issue), 2016, pp.73-82.

[7] Maekawa T and Seigel M, "Fostering and Organizing a System of Human Resources to Encourage Local Groups to Care for the Land: A Study of an Australian Model with a View to Learning from this for the Benefit of Japanese Rural Areas", proceedings of the 4th Asian Cultural Landscape Association 2015 International Symposium on Agricultural Landscapes of Asia: Learning, Preserving, and Redefining, Indonesia, presented on 11 September 2015, pp.17-31.

[8] Maekawa T, "A Method of Partnership between Governments and Citizen's Community Groups for Achieving Environmental Sustainability in the Landcare Movement in Australia", International Journal of GEOMATE, Vol. 11, Issue. 24, accepted in 2016, pp.2284-2290.

[9] Maekawa T and Aron D, "Community Coordination for Addressing Local Environmental Challenges: Application of the Australian Landcare Model to Japan", Interdisciplinary Environmental Review, accepted in April 2016.

[10] The Hon Ryan Smith MP, Media release [online] Ready to recruit: 60 new Landcare facilitator positions now open, Tuesday 6 December 2011.

[11] Johnson M, Poussard H, and Youl R, "Landcare in Australia" Landcare: Local action-global progress, Catacutan D, Neely C, Johnson M, Poussard H, and Youl R, Eds. Nairobi: World Agroforestry Centre, 2009, p.20.

[12] Based on an observation and on the provided documents at the event "Secrets to Successful Groups" held at Yackandandah, 4 April 2014.

[13] Department of Environment and Primary Industries, the State of Victoria. <http://www.depi.vic.gov.au/environment-and-wildlife/community-programs/landcare/victorian-landcare-gateway> (Accessed 8 June 2016).

[14] The State of Victoria Department of Environment and Primary Industries, 2013 Victorian Landcare Awards Winners' Booklet. Melbourne: The State Government of Victoria Department of Environment and Primary Industries, August 2013, p2.

[15] Based on an interview with a member of the Victorian Landcare Team at Thurgoona, 12 May 2014.

[16] Based on an observation at the North East Landcare Forum held at Wodonga, 7 June 2013.

[17] Curtis A and Sample R, CBNRM in Victoria: Contributing to dialogue, learning and action. Institute for Land, Water and Society, Charles Sturt University, Albury, NSW, 2640, Report/ILWS, No.55, 2010, pp.52-53 and p57.

[18] Tennent R and Lockie S, "Vale Landcare: the rise and decline of community-based natural resource management in rural Australia", Journal of Environmental Planning and Management 56, no.4, 2013, pp.572-587.

[19] Based on an observation at annual meeting of VLC at Nhill, 8-10 November 2013; an observation at annual meeting of VLC at Ovens Valley, 17 and 18 May 2014.

Second International Conference on Science, Engineering & Environment,
Osaka City, Japan, Nov.21-23, 2016, ISBN: 978-4-9905958-7-6 C3051

DEVELOPING A PACKAGE OF LOCAL CAPITAL STOCKS MANAGEMENT FOR ACHIEVING ENVIRONMENTAL SUSTAINABILITY: A CASE OF ICHIHARA CITY

Tomomi Maekawa[1] and Hidefumi Kurasaka[2]
[1,2] Graduate School of Humanities and Social Sciences, Chiba University, Japan

ABSTRACT

It is necessary that capital stocks be maintained for achieving environmental sustainability, however, there is as yet no firmly established methodology for maintaining and managing capital stocks. In order to develop a methodology of capital stocks management, this study focuses on the developmental process of creating a methodology package that will assist city officials and others such as the staff of not-for-profit organisations in Japan to manage local capital stocks. The package has two main elements; providing access to a simulator which shows expected changes in local capital stocks in each city; and providing workshops to promote the sharing of knowledge and discussion among local students and people of other generations. Through the implementation of this package by the project members, it has been found that the package generated realisation within junior high school and high school students of expected changes to the cities, and encouraged a diversity of ideas among them. Through promoting the sharing of ideas, it has proved effective as a tool for generating suggestions regarding the management of capital stocks to be presented by participants at the workshops to the city mayor.

Keywords: Sustainable Resource Management, Local Capital Stocks Management, Participation, Simulator, Workshops

INTRODUCTION

It is recognised that there are four categories of capital stocks which need to be maintained for achieving sustainability of societies, including environmental sustainability [1][2]. These categories are "natural stock" such as agricultural land maintenance and fish stock maintenance, "material stock" such as architecture and recycling, "human stock" such as education and care, and "social stock" such as public service and community NPOs [3].

Focusing on the situation in Japan, especially since 2008 when the population of Japan began to decline [4], there are various challenges due to the population decline. Some of these challenges are the following: population decline and ageing, global warming and environmental degradation, ageing infrastructure, and disappearance of communities and decline of social connectedness [3]. To deal with these challenges, it is necessary to consider the particular context of each locality and also to respond to local needs, from the perspective of the subsidiarity principle which means that what can be dealt with by the basic administrative unit should be left to that unit, and a wider administrative unit should deal with other issues [2][5]. However, the basic administrative unit tends to lack the necessary information and human resources for dealing with the challenges mentioned above, and further, there is no firmly established holistic methodology that can be used for maintaining and managing these capital stocks at the level of the basic administrative unit: city, town, or village [2].

In order to assist city officials and others such as the staff of not-for-profit organisations with maintaining and managing the local capital stocks, the project called OPoSSuM (Open Project on Stock Sustainability Management), was launched in November 2014 [2].

PURPOSE AND METHODOLOGY

In this study, the authors, who are members of the management team of the project (Tomomi Maekawa joined in March 2016 and Hidefumi Kurasaka has also joined since the launch of the project), focus on the developmental process and the outcomes of the project OPoSSuM, which have been achieved during the period from November 2014 to June 2016.

The purpose of this study is to analyse the developmental process and the outcomes of the project and to identify the challenges for the future of the project with a view to improving the contents of the package. In order to achieve this purpose, the authors focus on a case study of the implementation of the package in Ichihara city, Chiba prefecture. The implementation was carried out on 19 and 20 August 2015, and on 24 March 2016.

The methodologies used in this study are documentation analysis on the project including materials such as the brochure and leaflet used for

carrying out the implementation in Ichihara city, and participatory observation through participating in the management team of the project as members.

ABOUT PROJECT OPoSSuM

In order to deal with the various challenges that Japan has been facing, mentioned in the first chapter of this paper, the project team of OPoSSuM (which is composed of researchers from several different universities and institutes) has been developing a package, which is intended to assist people such as city officials and the staff of not-for-profit organisations to maintain and manage local capital stocks in their areas [2]. In this chapter, we describe the contents of the package through analysis of the project's documents such as the brochure and the leaflet [3][6].

Designing a Package as an Approach

Based on the recognition that local capital stocks management should respond to local needs and that future generations are an important part of the community, the project team decided to develop a package with the following two elements.

The first is providing access to a simulator which shows expected changes in local capital stocks in each basic administrative unit—city, town or village —, which is named the "Future Simulator". And secondly, providing workshops to promote the sharing of knowledge and discussion between local students and people of other generations, which are named the "Future Workshops".

Developing the "Future Simulator"

The project team has been developing the "Future Simulator" in order to identify the challenges facing local capital stocks management in each basic administrative unit. The aim of the development of the "Future Simulator" is to predict the gaps generated between demand and supply for maintaining human capital stock such as childcare, education, medicine and care; between demand and supply of housing; and between revenue and expenditure of local authorities. These gaps are predicted based on the hypothesis that the trends existing in or around 2015 will continue until 2040.

For example, with regard to the industrial structure, the "Future Simulator" predicts the likely industrial structure in 2040 based on the long term population projection while assuming that the trends in the number of people employed by industry since 2000 will continue — It is estimated that the population in Japan in 2040 will have shrunk by about 15% compared to 2015 and the number of people who are employed will have decreased by 20%—. Regarding the other topics, it predicts the following changes: the supply and demand in childcare, education, medical and care services; the level of labour which is necessary to maintain the current level of cultivation; the amount of housing and number of households; and future revenue and expenditure.

Using the "Future Simulator", the project produces the "Future Card" which summarises what the "Future Simulator" shows. The project distributes a "Future Card" to each city/town/village which requests it from the project.

Developing the "Future Workshops"

The project team has also been developing a workshop method which it has named "Future Workshops". This encourages local people such as junior high school students, high school students and elderly persons to recognise the challenges in their own areas identified through the "Future Simulator", and to start thinking about and taking action towards solving the challenges.

At the "Future Workshops", the participants— mainly junior high school students and high school students — give policy recommendations to the current mayor, as future mayors of 2040. With a view to enhancing the understanding of the local area by the participants themselves, after a lecture on the results of the "Future Simulator" by the project members, the participants walk around key areas of the city/town/village which demonstrate the type of community, the local industrial structure, educational facilities, etc. Then, the participants are divided into several groups and through discussion within the groups work on generating policy recommendations.

Implementing the Package

Implementing the package involves three steps: lecturing on the results of the "Future Simulator" to the participants; leading the participants on a walk around key areas in the locality; and facilitating the discussion and generating policy recommendations among the participants. The 3 steps are carried out by the members of the project.

Step 1: Lecturing on the Results of the "Future Simulator"

Firstly, the participants learn about the status of the local capital stocks in their own area from the results of the "Future Simulation." This is carried out through listening to a lecture referring to the "Future Card" which is made and distributed by the project team.

Step 2: Leading Participants on a Walk around Key Areas in the Locality

Secondly, the participants walk around key areas in the locality while referring to a map which reflects the estimated local population in 2040. The project members ensure the safety of the student participants, and also enhance awareness in the participants about the expected changes in reality.

Step 3: Facilitating Discussion and Generating Policy Recommendations among Participants

Finally, with assistance from the facilitators (the project members), the participants, working in several groups, generate policy recommendations through exchanging ideas with the other members of their group. This workshop style ensures each participant gains new ideas and also clarifies his/her recognition of the challenges in the local area. Group discussion is facilitated by a series of guidelines (See Table 1) [6].

Table 1 "Future Workshops" Discussion Group Guidelines

Suggesting ideas to others	• Suggest as many ideas as possible, don't worry about their quality. • Unique ideas which might sound strange to others will be welcome. • Don't be critical of others' ideas. • Think holistically through seeing and listening to others' ideas.
Attitudes	• Try to show your agreement or sympathy to others by nodding or your facial expression. • Write down ideas in large characters and speak clearly when you make suggestions. • Keep calm and quiet when you have to concentrate on writing ideas.

IMPLEMENTATION

Implementation Targeting Younger Generations

In this section, we describe the process and outcomes of the implementation of the package in Ichihara city on 19 and 20 August 2015, based on the documentation and reports created by the project members. This implementation targeted the younger generation, that is, junior high school and high school students living in Ichihara city [7]. Through recruitment by advertising in the publicity of Ichihara city and by distributing flyers to the local junior high schools and high schools through the board of education of the city, 39 junior high school students and 1 high school student participated in the implementation [7].

Implementation—Step 1

In Step 1 the results of the "Future Simulation" were presented in a lecture to the participants at a hall in Ichihara city. Information presented regarding the results of the "Future Simulation" for Ichihara city included the following [6]:

- The population of the city will decline by about 20% by 2040 as compared to 2015.
- The number of workers in 2040 will shrink to about 75% of that in 2015.
- The number of people working in both the construction industry and agriculture in 2040 will decline to about 40% of that in 2015, and the number of people working in the areas of care and welfare will increase by about 10% in 2040 as compared to 2015.
- The population of school children in 2040 will decline to about 60% of that in 2015, and due to this, the number of schools in the southern area of the city will decline.
- The rate of abandoned farm land will be about 28% of the cultivated land in the city.
- The rate of vacant houses will be about 15% of the houses in the city.
- The number of households located far from public transport such as railways and bus services will amount to 8500 (7.5% of the total number of the households in the city).
- Landfills in the city will be filled to capacity in around 2026.
- Revenue of the city will amount to 640 billion yen and expenditure of the city will amount to 698 billion yen.

Implementation—Step 2

Fig.1 The participants at the Future Workshop on 19 and 20 August 2015 walking around the area near Jyousouushiku station. (Photo was taken by H. Kurasaka.)

The participants visited the following 3 key areas of the city including experiencing the local railway called Kominato railway; the area around Jyousouushiku station (See Fig.1); a community centre named Uchida Mirai Gakkou which is using a building of a closed local school; and Idemitsukousanchibaseiyujo, which produces about 40% of the total oil production of the Idemitsu group. The participants also listened to lectures given by the staff at Uchida Mirai Gakkou and at Idemitsukousanchibaseiyujo [6].

Implementation—Step 3

On the second day of the implementation the participants worked on generating policy recommendations through exchanging ideas with the other members of their groups. In each discussion group, the participants wrote their own ideas on small sticky notes which were then placed on a large blank sheet of paper. The sticky notes were then grouped according to categories suggested following discussion of what the students had seen, heard, and learnt at the lecture and after visiting the key areas of the city. The methodology used in this discussion was the *Jigsaw* method where the members are partly exchanged among the groups during discussion [7].

Finally, after completing the work on the blank sheets, the participants gave presentations regarding what they had generated through discussion in their groups to all the other participants and the observers including the mayor of the city (See Fig.2). The participants — local students — gave their policy recommendations, as future mayors, to the current mayor and exchanged comments. Some of the suggestions which were generated by the participants included:

- Growing seedlings via field learning at schools.
- Students/staff of local schools visiting elderly people and informing them of events which they can join in.
- Increasing the salaries of care workers and increasing the number of care facilities for elderly people.

Also the project team received comments from the participants after the implementation such as: "The most important thing is the relationships between people. I think interactions among people will grow Ichihara city as a city where people can talk together and cooperate with each other. I would like to talk with various people at another 'Future Workshop' in the future." [8].

Implementation Targeting Elderly Generations

In this section, we describe the process and outcomes of an implementation of the package in Ichihara city on 24 March 2016, through participatory observation and based on the documents created by the participants and the project members. This implementation targeted the elderly generation living in Ichihara city and comprised of 10 people aged over 65 years of age. They were recruited at a centre for elderly people who are willing to work. Step 2 of the implementation was omitted as the participants had enough knowledge of the local geography and situation.

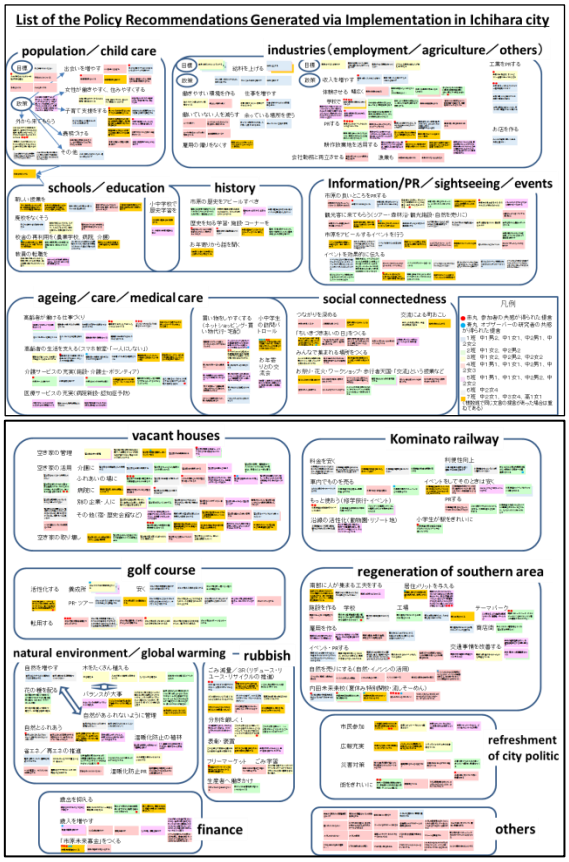

Fig.2 The list of policy recommendations generated at the Future Workshop on 19 and 20 August 2015. (The project team compiled this composite list from the recommendations of all the groups at the implementation. The original list was made by H. Kurasaka and was then translated by T. Maekawa.) The categories of the ideas are as follows: population/child care, industries (employment/agriculture/others), schools/education, history, information/PR /sightseeing/ events, ageing/care/medical care, social connectedness, vacant houses, Kominato railway, golf course, regeneration of southern area, natural environment/global warming, rubbish, refreshment of city politic, finance, and others.

Implementation—Step 1

As with the implementation in August 2015, the results of the "Future Simulation" were presented to the participants at a lecture in Ichihara city. Because the location was the same, the materials used were identical to those used at the previous implementation.

Implementation—Step 3

Fig.3 Participants at the Future Workshop on 24 March 2016 studying the completed blank sheet of the other group. (Photo taken by T. Maekawa.)

After the lecture on the results of the "Future Simulator", the participants divided into 2 groups of 5 and worked on generating policy recommendations through exchanging ideas with the members of their group. The discussion style was almost the same as the implementation in August 2015, but this time the participants studied the other group's recommendations after completing the work with the sticky notes, instead of applying the *Jigsaw* method (See Fig.3). Some of the suggestions which were generated from the participants were as follows (See Fig.4):

- Use local temples as venues for local people who wish to come together to learn.
- Provide education to people on classifying rubbish in order to promote reducing/reusing/ recycling.
- Establish volunteer groups for conservation of forests.
- Switch the way of caring for *Satoyama* from conservation to utilising livelihoods.

DISCUSSION

Findings from the Implementations

Impact of the Package to the Participants

The lists of policy recommendations based on the completed sticky note displays (See Fig.2) show the diversity of the ideas and suggestions generated through discussion. Also, the participants at the Future Workshop on 24 March 2016 realised that the two groups came up with ideas that were both similar and different, through being able to view both displays (See Fig.3).

Thus, through implementing the package in Ichihara city, it was found that the package generated a realisation within junior high school and high school students and also within elderly people of expected changes to the city, and encouraged a diversity of ideas among them.

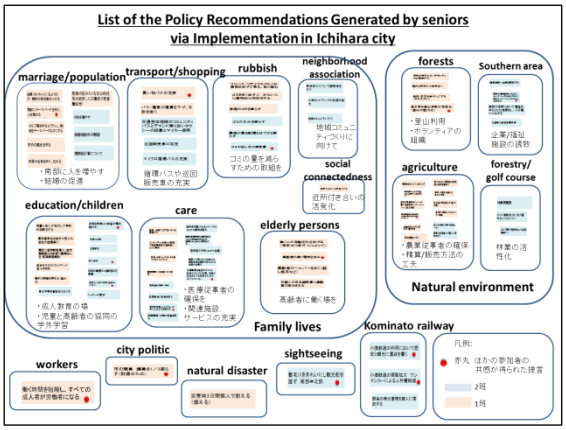

Fig.4 List of policy recommendations generated at the Future Workshop on 24 March 2016. (This list was compiled and translated by T. Maekawa on behalf of the project team and based on the recommendations made by the groups at the implementation.) The categories of the ideas are as follows: marriage/population, transport/shopping, rubbish, neighborhood association, social connectedness, education/children, care, elderly persons, forests, southern areas, agriculture, forestry/golf course, workers, city politic, natural disaster, sightseeing, and Kominato railway.

Difference in Areas of Interest of the Participants by their Generations

It was found that there were differences in the ideas generated by the younger participants and those of a more elderly generation. The differences appeared in some characteristic topics for each generation, and these indicated that the interests of each generation were different. For example, the younger generation suggested many ideas on topics such as child raising and ways of contributing to the society or community, while the elderly generation suggested many ideas on life-long learning and also on ways to conserve *Satoyama*, the word which expresses not only the natural environment but also

the traditional Japanese livelihoods that harmonise with the native ecosystems.

Challenges for Improving the Package

There are challenges for improving the quality of the program and the implementation of the package. These are as follows:

- Reflecting the estimated influence on the city/town/village of the temporary population decline which is caused when younger people move away to higher education.
- Designing and incorporating some new steps or other devices for promoting links among the participants at "Future Workshops" and also between the different generations.
- Establishing a system for fostering additional facilitators and other staff who can deliver the package, including training in facilitation skills.

CONCLUSION

Through analysing the developmental process and the outcomes of the package that the project has been developing, through using a case study of the implementation in Ichihara city, it has been found that the package generated realisation within junior high school and high school students and also within elderly people of expected changes to the cities/towns/villages, and encouraged a diversity of ideas among them. While the package needs additional development to improve its impact on the participants including building social connectedness among the participants at the workshops, through promoting the sharing of ideas it has proved effective as a tool for generating suggestions for managing local capital stocks (in this case in Ichihara city) which were able to be presented to the city mayor.

ACKNOWLEDGEMENTS

The project OPoSSuM obtained funding from the Japan Science and Technology Agency (JST) and the Research Institute of Science and Technology for Society (RISTEX) in 2014 under the 'designing and sustainable multi-generational, co-creational society' research and development area. The participants of this project are the following universities, institutes, and authorities: Chiba University, Shibaura Institute of Technology, National Institute for Environmental Studies, Yachiyo City, Ichihara City, Tateyama City, Chiba Prefecture. The principal investigator of this project is Professor Hidefumi Kurasaka, Chiba University.

REFERENCES

[1] Ekins P, "Sustainable Development", Environmental thought, ch.8, Edward A. Page and John Proops, Eds. Edward Edger publishing, 2003, pp. 144-172.

[2] Kurasaka H, Satoh S and Miyazaki F, "Houkoku/Katsudoushoukai: Chiiki stock management ni kansuru kenkyuu project OPoSSuM no gaiyou [Report/Introduction of activities: A Summary of 'OPoSSuM' ―the Research Project on Local Stocks Management]", Koukyoukenkyuu, Vol. 11, Issue. 1, Koukyoukenkyuu henshuuiinkai, Ed. Chiba: Koukyougakkai, 2015.

[3] Kurasaka Laboratory Graduate School of Humanities and Social Sciences Chiba University, Brochure of the project entitled "Open Project on Stock Sustainability Management", Kurasaka Laboratory Graduate School of Humanities and Social Sciences Chiba University, Ed. and publisher, 2016. Available at the homepage on the internet of the project, <http://opossum.jpn.org/english/> (Accessed on 22 June 2016).

[4] The National Institute of Population and Social Security Research "Trend of the Births, Deaths and their Rates (as of October 1 each year)' in 'Population Projection for Japan' (January 2012), Available at the homepage on the internet of the National Institute of Population and Social Security Research, <http://www.ipss.go.jp/index-e.asp> (Accessed on 22 June 2016).

[5] Kurasaka H, Kankyouseisakuron: kankyouseisakunorekishi oyobi gensoku to shuhou [Environmental Policy Studies ― History, Principles and Methodologies of Environmental Policy]. Tokyo: Shinzansha, 2014, pp. 170-171.

[6] Kurasaka Laboratory Graduate School of Humanities and Social Sciences Chiba University, Leaflet of the project entitled "Ichihara Mirai workshop, collaboration of Ichihara-shi and Chiba-daigaku OPoSSuM, 2015. 8. 19 Wed & 20 Thu" Kurasaka Laboratory Graduate School of Humanities and Social Sciences Chiba University, Ed. and publisher, 2015.

[7] Miyazaki F, "Ichihara Mirai workshop no jisshikekka ni tsuite [A Report on the Result of the Implementation of Ichihara Future Workshop]" Koukyoukenkyuu, Vol. 12, Issue. 1, Koukyoukenkyuu henshuuiinkai, Ed. Chiba: Koukyougakkai, 2016.

[8] Based on a comment from one of the participants at the implementation. Translated by T. Maekawa.

Second International Conference on Science, Engineering & Environment,
Osaka City, Japan, Nov.21-23, 2016, ISBN: 978-4-9905958-7-6 C3051

A PRELIMINARY STUDY OF THE UTILIZATION OF LIQUID SMOKE FROM PALM KERNEL SHELLS FOR ORGANIC MOUTHWASH

M. Faisal[1], Asri Gani[1] , Husni[2], Hiroyuki Daimon[3]
[1]Department of Chemical Engineering, Syiah Kuala University, Banda Aceh, Indonesia
[2]Department of Agro Technology, Syiah Kuala University, Banda Aceh, Indonesia
[3]Department of Environmental and Life Science, Toyohashi University of Technology, Toyohashi, Aichi, Japan

ABSTRACT

Palm kernel shells are a waste product of the palm oil industry. They have a high content of cellulose, hemicellulose, and lignin, all of which can be converted through a pyrolysis process into liquid smoke that contains the oxidized organic compounds ketones, aldehydes, phenols, and carboxylic acid groups with antimicrobial properties. The objective of this research is to study the potential use of grade 1 liquid smoke as organic mouthwash. This research considers liquid smoke's antimicrobial properties and focuses on analyzing its ability to inhibit the growth of streptococcus mutans living in the oral cavity. The liquid smoke used was produced by pyrolysis performed in temperatures of 340-420^{o}C. In order to obtain grade 1 liquid smoke, distillation was subsequently carried out at 190^{o}C. The ability of the produced liquid smoke to inhibit streptococcus mutans was then tested for its minimum inhibitory concentration and diameter of inhibitory region. Both minimum inhibitory concentration and diameter of inhibitory region tests were performed with a liquid smoke concentration of 0.005-0.1 mg/ml. Test results of the minimum inhibitory concentration showed that the liquid smoke possesses good antimicrobial properties against streptococcus mutans, while test results of the diameter of inhibitory region was medium at 6-9 mm. The highest diameter of inhibitory region was obtained from liquid smoke created from pyrolysis performed at 400^{o}C and a concentrate of 0.1 mg/ml.

Keywords: Palm Kernel Shells, Liquid Smoke, Streptococcus Mutans, Mouthwash

INTRODUCTION

Liquid smoke is a liquid created from smoke condensation during the pyrolysis process on wooden materials that have cellulose, hemicelluloses, and lignin. These three components are needed to create a high-quality batch of liquid smoke; furthermore, different compositions of these compounds alter the quality of the liquid smoke produced [1]-[3]. Palm kernel shells (PKS) contain 27.7% cellulose, 21.6% hemicelluloses, and 44% lignin [1].

Haji [4] studied the liquid smoke composition gained from PKS; his studies showed a liquid smoke yield of 52.02%. Another research was conducted by Kim et al.[5], and found that the liquid smoke composition produced in a temperature of 490^{o}C contained around 22.1% phenol, 5.46% acetic acid, and 20% comprises other compounds. This composition indicates that PKS have the potential to be developed into high-quality liquid smoke.

Liquid smoke possesses antibacterial and antioxidant properties that may be utilized in various fields, such as medical and food industries. Previous research found that it contains effective antibacterial and antioxidant properties which inhibit and kill bacteria [6]-[8]. Research on liquid smoke conducted in the medical field was carried out by Utami [9], where it was used to treat scabies in goats. Other research found that the antimicrobial and antioxidant properties came from its content of phenol [10]. Liquid smoke was used as a natural biopesticide to inhibit the growth of *colleototrichium capsici* in chili plants [11]. In pharmaceutical and cosmetic industries, it is used mostly as skin ointment and additional ingredients in cosmetics [7],[10].

Commercial mouthwash products commonly contain alcohol as their active ingredient, providing antibacterial properties while giving clean and fresh sensations to the users [12]. However, the alcohol content may cause negative effects; for example, the potential to cause cancer increases when the alcohol concentration is above 25% [13]. Therefore, there is a need to conduct studies on non-alcoholic mouthwashes. The antimicrobial compounds found in liquid smoke have the potential to be developed as organic mouthwash. These antimicrobial properties show promise in inhibiting the growth of bacteria living in oral cavities.

This research aims to study the potential use of liquid smoke as an organic mouthwash and focuses on analyzing its ability to inhibit *streptococcus mutans* living in the oral cavity.

METHODOLOGY

Samples of PKS were obtained from PTPN Cot Girek, North Aceh. Pyrolysis of PKS into liquid smoke was performed in a pyrolysis reactor, in batches exposed to temperatures of 340-420ºC. The reactor was composed of a form of stainless steel and was equipped with a temperature control. More detailed explanations into the procedures of creating liquid smoke may be found in previous research [14]. The smoke was condensed using a condensation unit made of stainless steel, resulting in a grade 3 liquid smoke, which subsequently was distilled to a grade 1 in a temperature of 190ºC. The chemical compounds were then identified using Pyro-GCMS (GCMS-QP2010, SHIMADZU) based on a method developed by Guillen and Ibargoitia [15],[16]. The antibacterial activity test was performed by determining the liquid smoke's minimum inhibitory concentration (MIC) value against streptococcus mutans, using the contact method on a nutrient broth (NB) medium. In addition, the diameter of inhibitory region (DIR) was also tested as a reference to compare the antimicrobial ability between substances [17]. MIC and DIR tests were performed upon the liquid smoke with concentration of 0.005-0.1 mg/ml.

RESULTS AND DISCUSSIONS

Composition of Compounds in the Liquid Smoke

The composition of liquid smoke is one parameter that determines the quality of that same liquid smoke. Liquid smoke commonly contains phenol, carboxylic acid, furan, lactone, and alcohol. Different raw materials will produce different compositions [11]. The analysis results of liquid smoke produced at 420ºC are shown in table 1. In addition to the materials used, the pyrolysis temperature also helps to determine the variety of chemical components. Liquid smoke produced from PKS at a temperature of 490ºC and with 0.64 mm samples contained 22.1% phenol and 5.46% acetic acid [5]. The liquid smoke produced in pyrolysis of a fruit stem at 500ºC contains around 12.42% w/w phenol and formaldehyde, as well as around 0.2-2.0% char [2].

Tabel 1 Composition of liquid smoke produced at 420ºC (after distillation)

No.	R. Time	Area	%	Name
1	2,864	8187797	0.16	Carbamic acid, monoammonium salt (CAS) Ammonium carbamate
2	3,289	3958610	0.08	2-Propanone (CAS) Acetone
3	5,639	9.5E+08	18.39	Formic acid, methyl ester (CAS) Methyl formate
4	6,144	2.9E+08	5.64	Hexanoic acid, 5-oxo-, methyl ester (CAS) METHYL 5-KETOHEXANOATE
5	8,005	2.4E+08	4.64	Acetic acid (CAS) Ethylic acid
6	9,425	1.9E+07	0.36	2-Furancarboxaldehyde (CAS) Furfural
7	9,872	1.8E+07	0.35	Butanoic acid (CAS) n-Butyric acid
8	10,108	2210756	0.04	Butanoic acid (CAS) n-Butyric acid
9	0.257	5458099	0.11	2-Pentanone, 5-(1,2-propadienyloxy)- (CAS) 5-PROPADIENYLOXY-2-PENTANONE
10	10,996	2.2E+07	0.43	2-Butenal, 2-ethenyl- (CAS) Crotonaldehyde, 2-vinyl-
11	11,549	5.8E+07	1.13	2(3H)-Furanone, dihydro- (CAS) Butyrolactone
12	12,419	8.5E+08	16.47	Benzenamine (CAS) Aniline
13	12,625	7.5E+08	14.57	2,4,6-Cycloheptatrien-1-one, 2-hydroxy- (CAS) Tropolone
14	13,260	2.1E+08	4.00	Phenol, 2-methyl- (CAS) o-Cresol
15	13,603	3.9E+08	7.53	Phenol, 2-methoxy- (CAS) Guaiacol
16	14,478	9.2E+07	1.80	Phenol, 2,4-dimethyl- (CAS) 2,4-Xylenol
17	14,810	9.6E+07	1.88	2-Methoxy-4-methylphenol
18	15,208	1.8E+07	0.36	Phenol, 2,6-dimethyl- (CAS) 1-Hydroxy-2,6-dimethylbenzene
19	15,477	4.3E+07	0.84	2-Propenoic acid, 2-methyl-, ethyl ester (CAS) Ethyl methacrylate
20	15,712	8.4E+07	1.64	2,5-Dimethoxytoluene
21	16,005	6.9E+07	1.34	3-Methoxy-pyrocatechol
22	16,513	1.1E+08	2.19	Phenol, 2,6-dimethoxy- (CAS) 2,6-Dimethoxyphenol
23	17,325	2.7E+07	0.52	Benzene, 1,2,3-trimethoxy- (CAS) 1,2,3-Trimethoxybenzene (CAS) Methylsyringol
24	17,692	6907259	0.13	1,3-Dithiolane, 2-(28-norurs-12-en-17-yl)- (CAS)
25	17,992	6284551	0.12	Benzene, 1,2,3-trimethoxy-5-methyl- (CAS) Toluene, 3,4,5-trimethoxy-

MIC Value of Liquid Smoke From PKS Against Streptococcus Mutans

Mouthwash is used in medicines to prevent caries caused by bacterial activity. Caries often lead to tooth cavities and thus the disturbance of health. The bacteria that play the main role in forming caries are streptococcus mutans, which decrease pH, which prevents tooth mineralization [18],[19].

Streptococcus mutans live in tooth and gum

surfaces and are the main bacteria behind caries [12]. The research conducted on germ-free animals showed that the plaque comprising streptococcus mutans leads to the formation of caries [20]. Streptococcus mutans living in the oral cavity produced acid from carbohydrate remains on tooth and gum surfaces. This research tested the MIC of liquid smoke against streptococcus mutans.

An MIC value refers to the minimum concentration of an antimicrobial substance that inhibits the growth of microorganisms overnight. MIC is widely used in laboratory analyses to study the resistance of certain bacteria against antimicrobial substances. This value indicates the lowest concentration of the antimicrobial substance in which bacteria can grow [21]. MIC is also frequently used to determine the in vitro activities of new antimicrobial substances. MIC values cannot be used as a direct comparison between the ability of one antimicrobial substance to another.

Table 2 shows that the growth of streptococcus mutans started to be inhibited at a concentration of 0.02 mg/ml. This means that the liquid smoke's MIC value against streptococcus mutans is 0.02 mg/ml.

Table 2 MIC values for different pyrolysis temperatures and liquid smoke concentrations

Liquid Smoke	MIC (mg/ml)		
Temperature	0.005	0.01	0.02
340°C	-	-	+
360°C	-	-	+
380°C	-	-	+
400°C	-	-	+
420°C	-	-	+

At a concentration of 0.005 mg/ml to 0.01 mg/ml, there was no inhibitory area seen around the paper disk after a drop of the liquid smoke. The preliminary study focused, from necessity, on these MIC values to see whether the bacteria were immune to a certain antimicrobial substance. Bacteria are categorized as sensitive to a substance if MIC value is below 8 mg/ml [22]. The MIC values in table 2 are the same at every temperature and indicate that the liquid smoke has good antimicrobial properties against streptococcus mutans residing in oral cavities, due to its active compounds: acetic acid and phenol.

The Antimicrobial Properties of Liquid Smoke from PKS Against Streptococcus Mutans

A substance's antimicrobial properties are categorized as low if its DIR is less than 5 mm, meaning that its inhibitory action is weak. A DIR value of 5-10 mm signifies medium antimicrobial properties, whereas 10-19 mm is considered strong and 20 mm or more is categorized as very strong [17]. Figure 1 shows the effects of various liquid smoke concentrations on DIR values against streptococcus mutans. As shown in the picture, DIR values and liquid smoke concentrations increase in parallel, in which DIR values of 6-9 mm signified that the liquid smoke possesses medium antimicrobial properties against streptococcus mutans at a concentration of 0.005-0.1 mg/ml.

The liquid smoke's DIR value is highly influenced by its phenol and acetic acid contents. Phenol and acetic acid influence a liquid smoke's antimicrobial ability, as demonstrated by the DIR at every temperature. The post-distillation phenol concentration produced in this research was approximately 9.88-15.8%. The liquid smoke produced at different temperatures contained different compositions of phenol and acetic acid. Phenol compound can inhibit the growth of bacterial population by extending its lag-phase proportionally inside a body or a product, whereas the speed of growth in its exponential phase remained the same except with a high concentration of phenol [23].

The above characteristics led to different DIR values for each liquid smoke concentration. The optimum condition in which to produce liquid smoke with effective antimicrobial activity against streptococcus mutans was achieved in pyrolysis conducted in a temperature of 400ºC, which produced a liquid smoke concentration of 0.02 mg/ml, resulting in phenol and acetic acid contents of 14.15% and 22.64%.

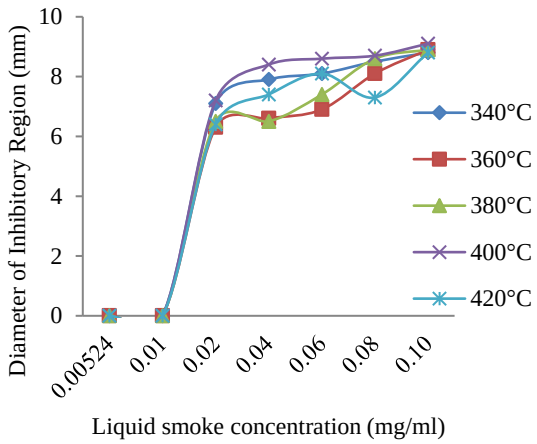

Fig. 1 The effect of liquid smoke concentration on the DIR against streptococcus mutans.

CONCLUSIONS

MIC and DIR tests showed that the liquid smoke has effective antimicrobial properties against streptococcus mutans. MIC values obtained were

0.02 mg/ml constant at every temperature, which indicates that the growth of streptococcus mutans started to be inhibited at a concentrate of 0.02 mg/ml. Therefore, the temperature at which the pyrolysis is performed has no significant influence on the MIC value. However, the pyrolysis temperature and the liquid smoke concentration significantly influenced DIR value, in which the DIR increase is parallel to the liquid smoke concentration. At 0.005-0.1 mg/ml of concentration, the DIR became approximately 6-9 mm, indicating that the liquid smoke's ability to act as an antimicrobial agent against streptococcus mutans has a medium value.

ACKNOWLEDGEMENTS

This work was supported by the Ministry of Research, Technology and Higher Education of Indonesia, under grand research of International Research Collaboration and Scientific Publication. The authors also thank Mr. Harita Cahyo for valuable discussion and help in the data analysis of this study.

REFERENCES

[1]. Abnisa F, Arami-Niya A, Daud WW, Sahu JN, "Characterization of bio oil and bio char from pyrolysis of palm wastes", Bioenerg. Res., Vol. 6, Jun 2013, pp. 830-840.

[2]. Abdullah N, Sulaiman F, Gerhauser H, **"**Characterisation of oil palm empty fruit bunches for fuel application", J. Phys. Sci., Vol. 22, No.1, Jan 2011, pp. 1-24.

[3]. Islam MN, Zailani R, Ani FN, "Pyrolytic oil from fluidised bed pyrolysis of oil palm shell and its characterisation", Renew. Energ., Vol.17, No.1, May 1999, pp. 73-84.

[4]. Haji AG, "Chemical composition of liquid smoke from pyrolysis of oil palm waste", JRKL, Vol. 9 , 2013, pp. 109-116.

[5]. Kim SJ, Jung SH, Kim JS, "Fast pyrolysis of palm kernel shells: influence of operation phenol and phenolic compounds", Bioresour. Technol., Vol. 101, Dec 2010, pp. 9294-9300.

[6]. Darmadi A, "Utilization of liquid smoke from sweet wood (Cinnamomum burmanni) for meat preservative", Thesis, Faculty of Science and Math., Andalas University, 2008.

[7]. Milly PJ, "Antimicrobial properties of liquid smoke fractions", Thesis, The Graduate Faculty Of The University Of Georgia, 2003.

[8]. Sulistiyowati B, Cahyono F, Swastawati, Identification of phenolate compounds and antioxydant activities for liquid smoke from bagasse and sugarcane skin (Sacharum Officinarum)", Chem info, 1 ,2013, pp. 362-363.

[9]. Utami ASJ, Dinata ANG, Guntoro S, "Utilization of liquid smoke as scabies medicine in goats," JITV, Vol. 19, No.2, 2014.

[10]. Mela E, Arkeman Y, Noor E, Achsani NA, " Potential products of coconut shell wood vinegar", Res. J Pharm. Bio. Chem. Sci., Vol 4, No.4, 2013, pp. 1480-1493.

[11]. Faisal M, Husni, Sriwati R, Chamzurni T, "Pyrolysis of palm kernel shell into liquid smoke: effect of pyrolysis temperature on liquid smoke products to inhibit colletotrichum capsici on chili", International Conference And Exhibition of Palm Oil: Jakarta, 2014, 26-28 Mei.

[12]. Nareswari A, "Differences in the effectiveness of mouthwashes without alcohol chorhexidine compared to alcoholic chlorhexidine in reducing the quantity of colonies of bacteria of the oral cavity", Thesis, Medicine Faculty, Sebelas Maret University, 2010.

[13]. Winn DM, Diehl SR, Brown LM, Harty LC, Bravo-Otero E, Fraumeni Jr JF, Kleinman DV, Hayes RB, "Mouthwash in the etiology of oral cancer in Puerto Rico", Cancer Causes Contr., Vol 12, No. 5 , Jun 2001, pp.419-429.

[14]. Lisa G, Suhendrayatna, Faisal M, Utilization of liquid smoke from palm oil shell for tofu preservative", Jurnal Teknik Kimia USU, Vol. 4, No.3, 2015, pp. 7-11.

[15]. Guillen MD, Ibargoitia ML, "Influence of the moisture content on the composition of the liquid smoke produced in the pyrolysis process of fagus sylvatica L. wood, ". J.Agri. Food Chem., Vol. 47, Oct. 1999, pp. 4126-4136.

[16]. Guillen MD, Ibargoitia ML, "New components with potential antioxidant and organoleptic properties, detected for the first time in liquid smoke flavoring preparations", J. Agri. Food Chem. Vol. 46, Apr. 1998, pp. 1276-1285.

[17]. Ningsih AP, Agustien A, "Anti bacterial test of extract viscous of *kepok* yellow banana plants (Musa paradisiaca Linn.) for Staphylococcus aureus and Escherichia coli,"J. Bio. UA, Vol. 2, No.3, Sep.2013, pp. 207-213.

[18]. Pradewa MR, "Dosage formulations of the mouthwash made from Gambir (Uncaria gambier Roxb)", Thesis, Agrotechnology Faculty, Fakultas Teknologi Pertanian, Bogor Agricultural Institute, 2008.

[19]. Marchetti E, Mummolo S, Di Mattia J, Casalena F, Di Martino S, Mattei A, Marzo G, "Efficacy of essential oil mouthwash with and without alcohol: a 3-day plaque accumulation model", Trials, Vol 12, No.1, Dec. 2011, pp. 262.

[20]. Angela A, "Primary prevention in children

with high caries risk", Dent.J., Vol. 38, Jul 2005, pp. 130-134.
[21]. Wiegand I, Hilpert K, Hancock RE, "Agar and broth dilution methods to determine the minimal inhibitory concentration (MIC) of antimicrobial substances," Nature Protocols, Vol. 3, Jan 2008, pp. 163-175.
[22]. Andrews JM, "Determination of minimum inhibitory concentrations", J. Antimicrob. Chemother., Vol. 48, Jul 2001, pp. 5-16.
[23]. Barylko N, Pikielna, "Contribution of smoke compounds to sensory bacteriostatic and antioxidative effect in smoked foods," Pure and Appl. Chem., 49, Jan 1978, pp 1667-1671.

Second International Conference on Science, Engineering & Environment
Osaka City, Japan, Nov. 21-23, 2016, ISBN: 978-4-9905958-7-6 C3051

ASSESSMENT OF OFF−FLAVOR TAP WATER DUE TO NUTRIENT AND RIVER FLOW MANAGEMENT PRACTICES IN THE UPPER KINOKAWA RIVER WATERSHED

Ryota Hino[1], Nobuyuki Egusa[2], Yasuhiro Wada[3], Masahide Ishizuka[4] and Tatemasa Hirata[5]
[1,2] Dept. of Environmental Systems, Wakayama University, Japan, [3] City Hall of Wakayama City, Japan,
[4] Dept. of Engineering, Kagawa University, Japan, [5] Dept. of Housou University, Japan

ABSTRACT

The off-flavor taste of tap water due to 2-methylisoborneol (2-MIB) is caused by blue-green algae. This is one of the water quality problems associated with high nutrient loads, such as those found in the Kinokawa River, with drains the southwestern part of the Kii peninsula in Japan. Water quality monitoring data showed that 2-MIB tended to increase when total phosphorus (TP) exceeded 0.02 mg/L. This study employed mass load and river water quality analyses coupled with water runoff analyses to examine ways of mitigating TP load in river water. In this study, we showed that (1) TP mass load could be reduced by approximately half if the industrial drainage volume standards defined in the Water Pollution Control Law were more stringent, (2) TP could be decreased by 41% in response to TP mass load reduction and by 5% in response to an increase in river flow, and (3) TP mass load reduction combined with an increase in river flow could reduce TP to less than 0.015 mg/L and prevent increases in 2-MIB in tap water.

Keywords: Kinokawa River; off-flavor tap water; total phosphorus; mass load analysis; river water quality analysis; distribution hydrological model

1. INTRODUCTION

In the Kinokawa River watershed (Fig. 1), off-flavor tap water due to 2-methylisoborneol (2-MIB) produced by blue-green algae has been a water quality problem since 2004 [1]. 2-MIB was first detected downstream from Hashimoto City (monitoring point (9) in Fig.1), and off-flavor tap water started to be reported upstream after 2006 (monitoring points (10) to (12)). Periphytic *Phormidium autumnale* is considered to be one of the causative organisms [2].

In research on the relationship between blue-green algae and nutrient concentrations, total nitrogen (TN) and total phosphorus (TP), along with the nitrogen phosphorus ratio (N/P ratio) are often used. For example, Yokoyama and Yamashita [3] showed that an increase in *Phormidium tenue*, a causative organism of 2-MIB, was markedly higher under high N/P ratio. Other research showed that the growth of blue-green algae remained strong under nitrogen limitation but was slower under phosphorus limitation [4]. Therefore, the control of nutrient concentrations in a watershed is considered to be one of the important strategies for solving the problem of off-flavor tap water.

In the Kinokawa River watershed, the total maximum daily loading is set in order to reduce COD, TN and TP inputs to the Seto Inland Sea. That is, control of TP in the Kinokawa River watershed is needed in order to solve the problem of off-flavor tap water and to reduce TP inflow to the Seto Inland Sea.

This study simulated changes in TP concentration upstream by using a numerical modeling and examined the control policy in place to decrease TP concentration. The study area is upstream from Ooyodo Town to Gojo City (Fig. 2) and the period of evaluation was from 2004 to 2006.

2. STUDY AREA

Points (1) - (12) in Fig. 1 are water quality monitoring points set by the Ministry of Land, Infrastructure, Transport and Tourism (MLIT) or Wakayama City. The Kinokawa River is about 136 km in length and has a watershed area of about 1,750 km^2. The river flows northwest and changes course to flow west-southwest into the Seto Inland Sea. There are 23 cities, towns and villages in Wakayama and Nara prefectures. The population is approximately 700,000, about half of which is in Wakayama City, located downstream from monitoring point (1) and reaching to the estuary (Fig. 1). Forest covers about 70% of the watershed, but the land use along the river changes.

The upper reaches of the river are covered by forest but paddy field and orchard gradually increase from Gojo City (monitoring point (10) in Fig. 1). In the estuary region of Wakayama City, residential area is the main land use.

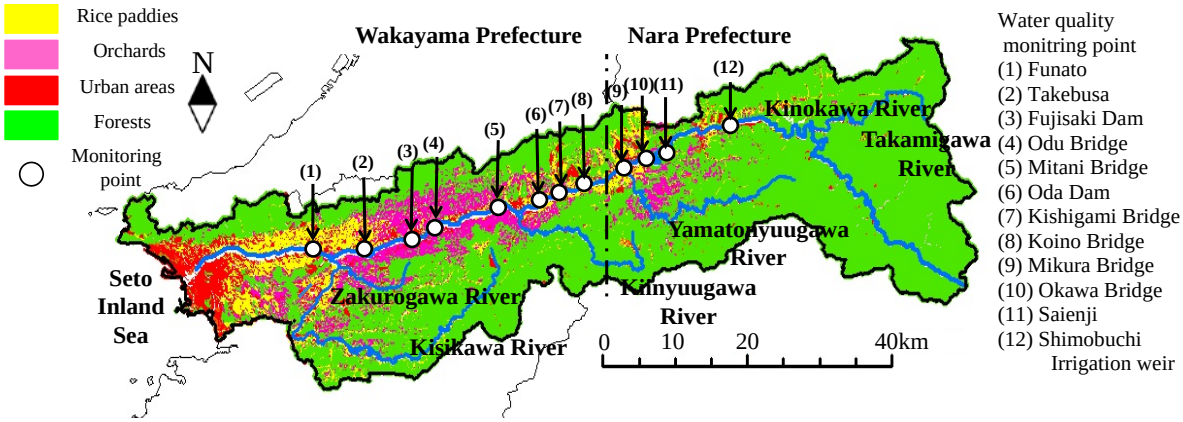

Fig. 1 Figure of land use of the Kinokawa River watershed
(The Ministry of Land Numerical land information in 1997)

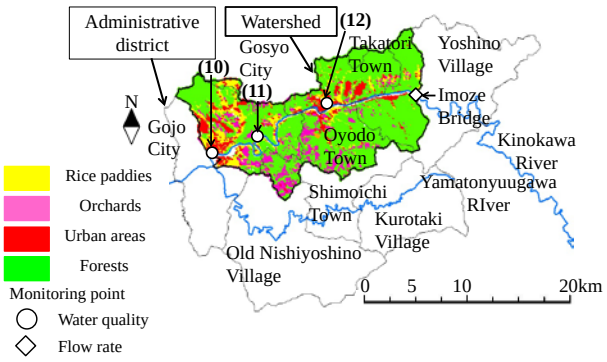

Fig. 2 Study area

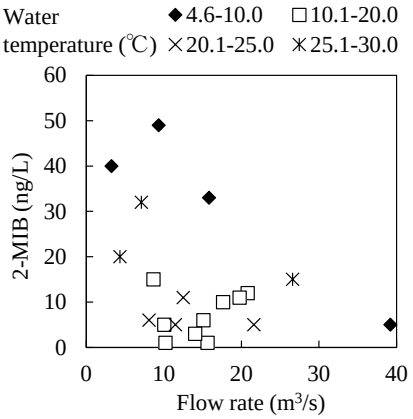

Fig. 3 Correlation chart (Flow rate, Water temperature, 2-MIB concentration in Okawa Bridge)

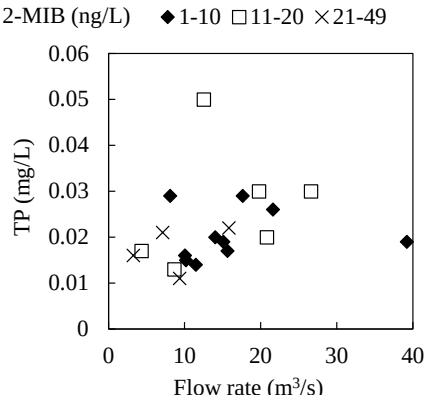

Fig. 4 Correlation chart (Flow rate, 2-MIB and TP concentration in Okawa Bridge)

In the study area shown in Fig. 2, the river is about 20 km in length and has a watershed area of about 220 km^2. The population is approximately 115,000, and about half live in Gojo City, which is located immediately downstream of monitoring point (10). Forest covers about 60% of the watershed in this region.

Fig. 3 and Fig. 4 show the relationship between 2-MIB and temperature and flow rate and between TP and water temperature and flow rate at the Okawa Bridge (monitoring point (10)). TP concentration was determined by the molybdenum blue method (potassium peroxodisulfate decomposition). 2-MIB concentration was assayed by these methods: gas chromatography mass spectrometry (GC-MS) of headspace gas in 2004, GC-MS of purge and trap samples from 2005 through 2006, and GC-MS of solid-phase extractions from 2007 through 2011. As shown in Fig. 3 and Fig. 4, the 2-MIB concentration tends to increase when the flow rate of the river is low and TP exceeds the eutrophication standard (0.02 mg/L, [3]).

3. STUDY METHOD

3.1 Summary

The models and analytical procedures employed in this study are as follows (Fig. 5).

<1> River flow rate and runoff rate of surface and subsurface water to the river are simulated by a distributed hydrological model.

<2> TP loading from point (discharge load) and non-point (runoff load) sources is simulated by a macro model using unit load ratios of TP along with the runoff rate of surface and subsurface water to the river.

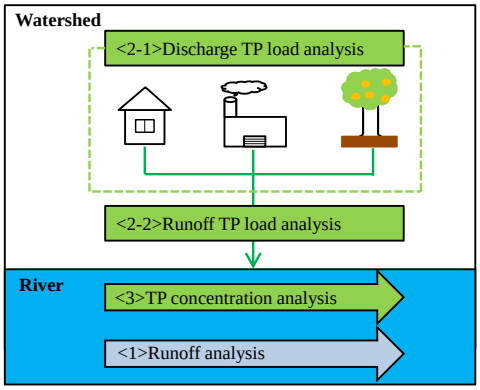

Fig. 5 Model conception diagram

<3> TP in the river is simulated by a one-dimensional steady state advection equation.

The study area was divided into 2 km × 2 km units (Fig. 6).

3.2 Runoff analysis using distributed hydrological model

The distributed hydrological model proposed by Ishizuka and Egusa [5] was used to calculate the river flow rate and the runoff rates of surface and subsurface water to the river (see Fig. 7).

This model consists of three sub models: surface water and river water runoff, subsurface water runoff, and rain water runoff with forest interception. In this study, the water intake rate from the weir (Shimobuchi irrigation weir in Fig. 6) was used for the river water runoff sub model.

The kinematic wave method was applied as the sub model for surface water and river water runoff.

Continuous equation

$$\frac{\partial h}{\partial t}+\frac{\partial q}{\partial x}-I=r_e \qquad (1)$$

Motion equation

(river channel)

$$q=\frac{\sqrt{\sin\theta}}{n}h^{\frac{5}{3}} \qquad (2)$$

(slope)

$$q=\begin{cases}\dfrac{k\cdot\sin\theta}{\gamma}h & (h<D)\\ \dfrac{k\cdot\sin\theta}{\gamma}h+\dfrac{\sqrt{\sin\theta}}{n}(h-D)^{\frac{5}{3}} & (h>D)\end{cases} \qquad (3)$$

Where, h: height of runoff (mm), q: flow rate per unit width (mm^3/s), t: time (s), I: water intake rate from the weir, r_e: effective rainfall intensity (mm/s), x: distance from the top of slope mesh (mm), θ: gradient of river channel or slope (degrees), n: roughness coefficient of Manning (mm$^{-1/3}$/s), k: coefficient of permeability (cm/s), and γ: effective porosity.

A two-cascade storage function method was applied as the sub model for subsurface water runoff.

Where, S_i: storage height of watershed (mm), t: time (s), r_i: inflow intensity (mm/h), Q_i: height of

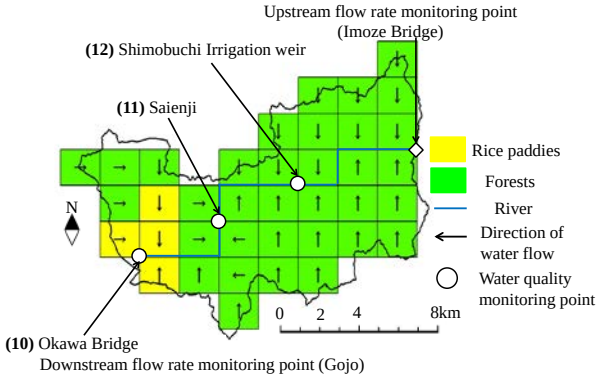

Fig. 6 Watershed mesh model (2km)

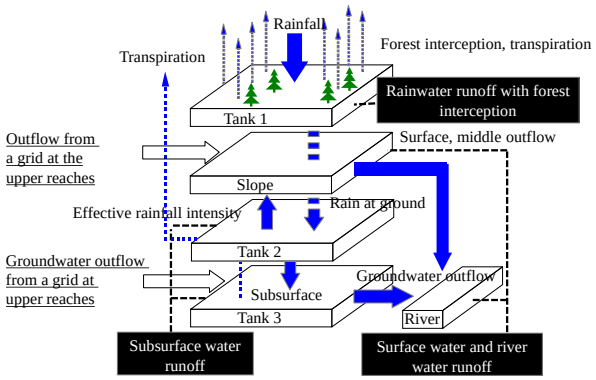

Fig. 7 Structure of the water sentence outflow model

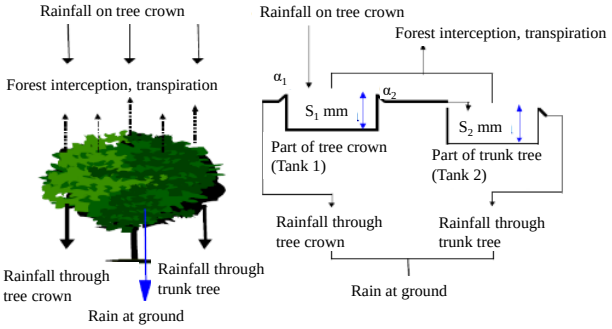

Fig. 8 Sub model for rain water runoff with forest interception

Continuous equation

$$\frac{dS_i}{dt}=r_i-Q_i \qquad (4)$$

Motion equation

$$S_i=K_i\cdot Q_i^{P_i} \qquad (5)$$

runoff (mm/h), K_i: storage parameter of watershed, P_i: model parameter, and i: tank number.

A tank model was applied as the sub model for rainwater runoff with forest interception (Fig. 8) [5].

3.3 Macro model using unit loading of TP and runoff rate of surface and subsurface water to the river

TP discharge load from point and non-point sources was simulated using unit load ratios. This method is useful for identifying the causes of changes in water quality or water pollution and has

Table 1 Load ratios of household wastewater and non-point sources

Source	TP load ratio	Unit
Household wastewater	1.3	g/(d・person)
Urban area	190	kg/(year・km^2)
Forest	34	kg/(year・km^2)
Rice paddy	165	kg/(year・km^2)
Vegetable farm	72	kg/(year・km^2)
Orchard	186	kg/(year・km^2)

Table 2 Load ratios of industrial wastewater

	Source	TP load ratio (g/(d・million yen))
9	Food	0.67
10	Drink, tabacco, livestock feed	0.14
11	Textiles (except for cloth)	1.12
12	Cloth, others	0.11
13	Food (except for furniture)	0.00
14	Furniture	9.04
15	Pulp, paper	0.01
16	Publication, printing	0.02
17	Chemicals	0.22
18	Oil, coal	0.00
19	Plastics	0.07
20	Rubber	0.08
21	Leather	0.20
22	Ceramic	0.20
23	Steel	0.03
24	Nonferrous metals	0.00
25	Metals	0.33
26	Machines	0.05
27	Electoric machines	0.12
28	Communication equipment	0.04
29	Electronic device	0.13
30	Transport equipment	0.23
31	Precision machine	0.00
32	Other	2.11

sometimes been used for the design of water basin-wide sewage treatment strategies in Japan [6]. Table 1 and Table 2 show the unit load ratios used in this study. Household and industrial wastewater, forests, orchards, rice paddies, vegetable farms and urban areas were considered to be the main sources, and most of the unit load ratios were obtained from published literature [7].

The unit load ratio for industrial wastewater was calculated using published literature and the value of the industrial shipment for Wakayama and Nara prefectures [7], [8].

The TP load ratio of the orchards was calculated by subtracting the production of each fruit crop from the amount of fertilizer applied to the orchards [9]. This was necessary because the discharge of phosphorous from the orchards is greatly dependent upon the type of fruit, the crop of fruit, and the amount of fertilizer applied, and it was therefore impossible to obtain the proper load ratio for orchards from previous literature.

Daily TP discharge load values from point sources were calculated by dividing the annual TP discharge load by 365.

On the other hand, daily TP runoff load from non-point sources was calculated by using the macro model [10].

Table 3 Self-purification coefficient

Self-purification coefficient (1/min)		
Age unit		0.022
2004	February 4	0.060
	August 18	0.008
2005	February 2	0.027
	August 3	0.022
2006	February 1	0.030
	July 12	0.028
	August 2	0.023
	December 6	0.034

$$DL_{i,j} = \sum_{n=1}^{2} k_{i,n} A_i Q_{j,n}^{a} \quad \textbf{(6)}$$

$$DL_{5,j} = \sum_{n=1}^{2} k_{5,n} A_5 Q_{j,n}^{a} M_{j,n}^{b} \quad \textbf{(7)}$$

Where, *DL*: daily TP runoff load (kg/day), subscript *i*: land use (*1*: urban area, *2*: rice paddy, *3*: vegetable farm, *4*: forest, *5*: orchard), *j*: time (1-365 days), *A*: land use area ratio, *R*: precipitation, *M*: amount of TP in orchard, *k*: model parameter.

3.4 One-dimensional steady state advection equation

The TP concentration in the river was calculated by using a one-dimensional steady state advection equation.

$$v\frac{dc}{dx} = -\lambda c + S \quad \textbf{(8)}$$

Where, *c*: TP concentration in river (mg/L), *v*: river flow velocity (m/min), λ: self-purification coefficient (1/min), *S*: TP runoff load calculated by the macro model (mg/(m^3・min)).

The river flow velocity was calculated by using river flow rate on a target day (14.1 m^3/s in 2004, 7.4 m^3/s in 2005, 13.5 m^3/s in 2006). The self-purification coefficient used in this study is shown in Table 3. The self-purification coefficient tends to show small in high runoff load and small river flow rate in this model. For example, in February, the ratio of river flow rate per runoff load is smaller than the others. It shows 0.038 m^3/kg in 2004, 0.077 m^3/kg in 2005, 0.073 m^3/kg in 2006. August is also the same and the ratio in 2004 is larger than the others. As a result, it is guessed that the self-purification coefficients of 2004 differed from the others.

4. RESULTS AND DISCUSSION

4.1 River flow rate

Fig. 9 shows the river flow rate at Okawa Bridge (monitoring point (10)). The simulated river flow rate (A) considers the water intake at the Simobuchi irrigation weir, while (B) does not consider the water

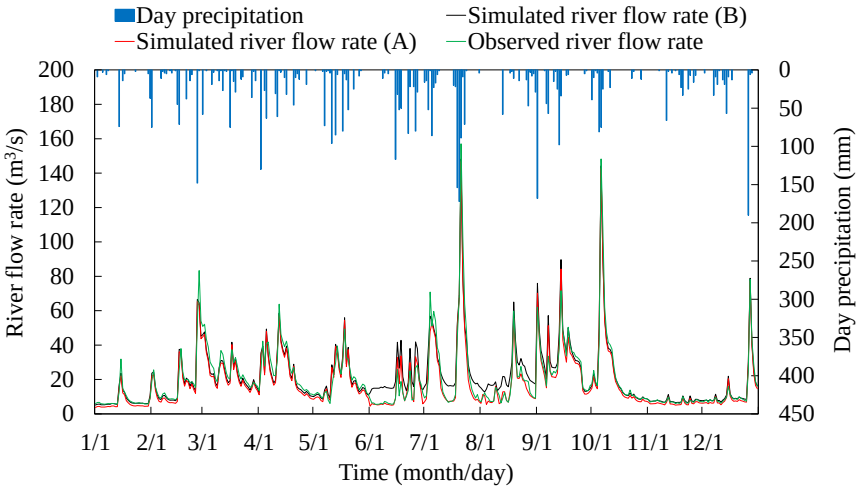

Fig. 9 River flow rate (Gojo in 2006)

Table 4 Simulated result (TP runoff load, river flow rate and TP concentration)

Year	Time	Load (kg/day)	River flow rate (m^3/day)	TP simulated (mg/L)	TP observed (mg/L)
2004	February 4	109.6	4.18	0.027	0.027
	August 18	109.6	16.92	0.014	0.014
2005	February 2	107.5	8.35	0.023	0.023
	August 3	107.5	11.14	0.020	0.020
2006	February 1	300.3	22.08	0.036	0.036
	July 12	123.7	9.40	0.023	0.023
	August 2	123.7	11.30	0.021	0.021
	December 6	123.7	6.25	0.028	0.028

intake.

Particularly in the period of irrigation (June to September), simulation result (A) better reflects the decrease in river flow rate than does simulation (B). Thus, simulation (A) was used in the distributed hydrological model.

4.2 TP runoff load and TP concentration

Table 4 shows the results of the river flow rate, TP runoff load and TP concentration at Okawa Bridge. The simulated TP concentration matches the monitoring point observations well. In addition, the simulation results show that TP tends to increase when river flow rate is low and/or TP runoff load is large. These results mean that the increase in TP concentration can be controlled by management of river flow rate and TP runoff load.

4.3 TP concentration control policy

In this section, the policy for reducing TP discharge load from point sources is examined because the loads from households and industry are much larger those from non-point sources. In the study area in 2006, the sewage system coverage was 22%. Combined type private sewage treatment tanks were used in 20% of the area, and single type private sewage treatment tanks were used in 23% of the area. The remaining 35% of the area had no sewage treatment. In this area, the switch to the sewage system is pushed forward by a Yoshinogawa River basin sewerage plan started from 1982. Therefore TP runoff load from households was calculated for sewage system coverage at 100%.

For industrial drainage, the Fifth Area-Wide Total Pollutant Load Control for water quality was applied from 2003 to industrial sites with drainage exceeding 50 m^3/d in the Kinokawa River watershed. However, most industrial sites in this area have drainage that is less than 50 m^3/d. In this simulation, TP runoff load from industry was calculated on the assumption that the Fifth Area-Wide Total Pollutant Load Control for water quality was applicable to all industrial sites. The simulation result shows that the TP runoff load would be reduced by 46.1%, with 42.8% from industry, 3.3% from households, respectively.

As a simulation of river flow rate, the control of water intake from the Shimobuchi irrigation weir was attempted. River flow rate increased approximately 30% when the amount of water intake was reduced 20% in the irrigation period.

Fig. 10 shows the result of the simulation. When the average TP runoff load and river flow rate are controlled, the TP concentration decreased 48%. The decrease achieved by TP runoff load control is 45%, but the effect of water intake control is only 3%. When focusing on the irrigation period, the TP concentration could decrease 46%. The effect of TP runoff load control is 41% and the effect of water intake is 5%. This result means that the TP runoff load control is effective in this study area. It should be noted that the TP concentration was below 0.02 mg/L, which is the eutrophication standard, except for on February 1.

The TP discharge load on February 1 was much larger than the others, and the effect of concentration reduction was only 22% and TP exceeded 0.02 mg/L because TP runoff loading from non-point sources was large due to rainfall. If the amount of fertilizer application and runoff load from forest can be reduced, the TP concentration on February 1 could

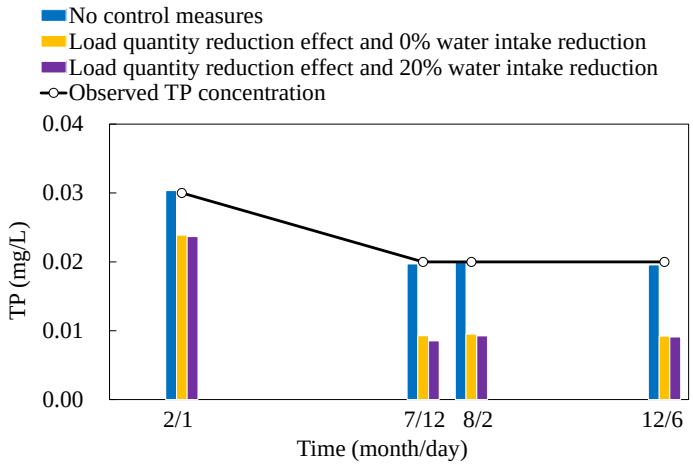

Fig. 10 Rise in river TP concentration suppressant effect result (2006)

be below 0.02 mg/L.

5. CONCLUSION

The results of this study can be summarized as follows:

1) The distributed hydrological model was applicable to this system.
2) The increase in TP can be controlled by management of river flow rate and TP runoff load by using a macro model and one-dimensional steady state advection equation.
3) The increase in TP can be controlled by management of river flow rate and TP runoff load.
4) When the average TP runoff load and river flow rate are controlled, the TP concentration could be decreased 46%. The TP runoff load control effect is 41% and water intake effect is 5% when focusing on the irrigation period.
5) TP mass load reduction combined with an increase in river flow could reduce TP to less than 0.015 mg/L and prevent increases in 2-MIB in tap water.

6. ACKNOWLEDGEMENTS

This study was funded in part by a Ministry of Education, Grant-in-Aid for Scientific Research (C), "Elucidation of nutrient runoff from fruit trees in agricultural catchment areas (representative: Nobuyuki Egusa)".

7. REFERENCES

[1] Kusube K., Okamoto M., Motooka S., Simizu T., Tozaki O., Wada Y., Tabita K. and Yano H., "The off-flavor of tap water outbreak example by *Phormidium tenue*", National Water Service Research Papers, Vol. 57, 2006, pp. 570-571 in Japanese.

[2] Ando N., Numata T., Ueda K. and Asano Y., "Outbreak and correspondence (III) of the off-flavor of tap water in Yoshinogawa, Nara", National Water Service Research Papers, Vol. 62, 2011, pp. 590-591 in Japanese.

[3] Yokoyama H. and Yamashita S., "Investigation of the factors of musty odor in a dam reservoir", Advances in River Engineering, Vol. 13, 2007, pp. 23-28 in Japanese with English abstract.

[4] Sato A. and Magara Y., "For tap water high quality by the alga obstacle security in waterworks", Gihodo, 1996, pp. 15-40 in Japanese.

[5] Ishizuka M. and Egusa N., "Runoff analysis using distributed hydrological model with irrigation water use model in the Kinokawa River", Annual Journal of Hydraulic Engineering, Vol. 52, 2008, pp. 391-396 in Japanese with English abstract.

[6] Okada M. and Peterson S.A., "Water Pollution Control Policy and Management", The Japanese Experience, Gyosei, 2000, pp. 220-235 in Japanese.

[7] Association of Japanese Sewer, "A sewer maintenance synthesis plan investigation guidance and commentary according to the watershed", 270 pp., 1999 in Japanese.

[8] Research and Statistics Department, "Economic and Industrial Policy Bureau, Ministry of Economy, Trade and Industry." Census of Manufacturers 2000 Report by Respective Industry, pp. 356-363, 2000 in Japanese.

[9] Hino, R., Egusa, N. and Hirata, T., "Primary considerations in calculation method of nutrient emission factors based on mass balance in orchard", Papers on Environmental Information Science, Vol. 25, 2011, pp. 269-274 in Japanese with English abstract.

[10] Ichigi, A., "Collection of underground waterway formula exercise programs, sixth water environment (exercise 6-15)", Japan Society of Civil Engineering, CD-ROM, 2002 in Japanese with English abstract

Second International Conference on Science, Engineering & Environment,
Osaka City, Japan, Nov.21-23, 2016, ISBN: 978-4-9905958-7-6 C3051

MICROCOSM EXPERIMENTS ON A COCONUT-FIBRE BIOFILM TREATMENT SYSTEM FOR EVALUATING WASTE WATER TREATMENT EFFICIENCIES

Naofumi Sato[1,2], W. N. K. Dharmarathne[3], Takeshi Saito[1], Hiroyasu Sato[4], and Norio Tanaka[1,5], and Ken Kawamoto[1,5]

[1] Graduate School of Science and Engineering, Saitama University, Japan
[2] EX Research Institute Ltd., Japan
[3] Faculty of Engineering & Built Environment, The University of Newcastle, Australia
[4] Graduate School of Frontier Sciences, The University of Tokyo, Japan
[5] International Institute for Resilient Society, Saitama University, Japan

ABSTRACT

In developing countries, it is needed to develop low-cost wastewater treatment systems. Utilizations of locally available biomass as biofilm support media for the wastewater treatment are increasing interests for applications. In this study, microcosm experiments on a coconut-fibre biofilm treatment system were carried out for evaluating wastewater treatment efficiencies in the laboratory using two wastewater, synthetic sewage and leachate, with different pollutant loads. A bundle of coconut-fibre was put inside the treatment tank with low density of a single bundle and high density of two bundles. The wastewater was firstly circulated in the system for 6 weeks (circulation stage) and then was discharged from the treatment tank for 7-24 weeks (treatment stage). Water quality parameters of effluents such as pH, DO, EC, BOD, COD, TC, and TN were measured at 1-week interval, and sedimented sludge in each treatment tank was collected to determine C and N contents. Results shows the circulation stage became more effective to reduce BOD and COD in synthetic sewage. For the synthetic leachate, on the other hand, effective reductions in BOD and COD were observed under both circulation and treatment stages. There was no effect on the fiber density on the reduction in TC and TN values for the synthetic sewage while HFD conditions became more effective to reduce TC and TN under the treatment stage for the synthetic leachate. The C and N consumptions in the microcosms were dependent on fibre-densities and pollutant loads of wastewater under both circulation and treatment stages. The C consumptions under treatment stage became around 2 times higher than those under circulation stage and the HFD conditions gave the highest C consumptions for both synthetic sewage and leachate.

Key words: sewage, leachate, coconut-fibre, biofilm treatment

INTRODUCTION

Water pollution can be defined as extensive presence of substances organisms dissolved or suspended in water causing serious health and environmental impacts. Especially, improper management and treatment of wastewater cause significant environmental degradation in developing countries. Even in Sri Lanka, the amount of sewage collected has been increasing with increase in the number of separate toilets since 1980's. But, most of the collected sewage has been directly discharged in vacant lands, forests, streams or excavated pits without any treatment ([1], [2]). Furthermore, a common practice of collected solid waste is open dumping without any leachate treatment. Thus, improper management and treatment of wastewater cause surface and groundwater pollution and trigger numerous resident complaints in Sri Lanka.

The utilization of local-available biomass resources as natural biofilm support media for the wastewater treatment is of an increasing interest for applications due to its low cost and low technology. Coconut-fiber biofilm treatment system (COTS), for example, has been introduced at some local authorities in Sri Lanka to treat the collected sewage and leachate at waste disposal sites [1]. It has been reported that COTS performed well for treating wastewater under the proper maintenance and operation. However, mechanism of wastewater treatment in COTS and quantitative analysis for designing and optimizing the system are not fully understood. In this study, we have carried out microcosm experiments in the laboratory using

both synthetic sewage and leachate for evaluating wastewater treatment efficiency in COTS.

MATERIALS AND METHODS

Coconut fiber

The fiber of coconut (*Cocos nucifera* L.) is rich in hard organic matters with high specific surface area and wetting ability ([3], [4]), it seems suitable for microorganisms adhesion and biofilm formation [5]. Coconut fiber is a waste by products from the coconut processing industries and is abundantly available in Sri Lanka.

Preparation of synthetic wastewater

The preparation of synthetic sewage in this study has been adapted based on measured data at Balangoda Urban Council in Sri Lanka and a reported data ([6], [7]]. The synthetic leachate was prepared to meet the following objectives: 1) to be more representative of real leachate in Sri Lanka, 2) the medium should be stable during the operation of experiment (2 week). The preparation of synthetic leachate in this study has been adapted from a previous study with some modifications ([8], [9]). Water qualities for supplied synthetic sewage and synthetic leachate were shown in Table 1.

Experiment apparatus

Experimental apparatus for the microcosm experiment consisted of a supply tank for synthetic sewage or synthetic leachate, a peristaltic pump, and a treatment tank (0.012-m^3 volume) with inlet and outlet valves (Fig. 1).

Table 1 Water qualities for supplied synthetic wastewater.

Wastewater		Synthetic sewage		Synthetic leachate	
Pollutant load		Low	High	Low	High
pH		8.2	7.6	8.1	7.8
DO	mg/L	5.0	2.9	0.2	0.1
EC	mS/m	564	1,336	710	1,790
BOD	mg/L	1,450	5,930	938	14,300
COD	mg/L	1,770	6,360	1,720	21,400
TC	mg/L	955	3,423	705	6,490
TOC	mg/L	529	3,018	406	5,570
TN	mg/L	736	2,590	640	691
TP	mg/L	258	703	780*	780*

*Calculated value from added K_2HPO_4 [3].

A bundle of coconut-fiber (~0.2 m length) was used as a biofilm support media. The bundle of coconut-fiber was put inside the treatment tank with two conditions: low fiber density (LFD; single bundle per a treatment tank) and high fiber density (HFD; two bundles per a treatment tank). As a control condition, a blank container without a coconut-fiber bundle was also used in the experiment. The synthetic sewage or synthetic leachate solution flowed into the treatment tank from the supply tank through the peristaltic pump at a rate of 870 cm^3/day (two-weeks retention time). Lightning with illumination intensity of 4,730 lux was maintained on the top of treatment tank for twelve hours per day and temperature was maintained at 20°C.

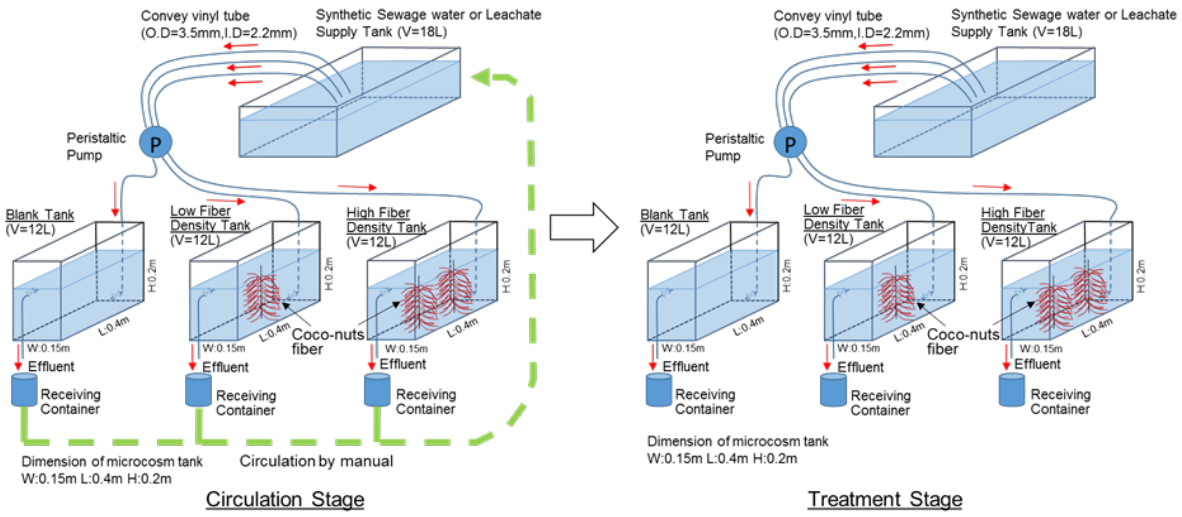

Fig. 1 Schematics of microcosm experiment.

Experiment procedures

The flow schedule of microcosm experiment was separated into two stages such as circulation stage and treatment stage (Fig. 1). For the circulation stage, a mixture of raw wastewater from a sewage treatment plant in Saitama City, Japan and synthetic wastewater (1 L of raw wastewater and 35 L of synthetic wastewater) was initially prepared and recycled through the microcosm system to accelerate biofouling to the bundle of coconut-fiber. The circulation period was set to be 42 days.

Water samples in the supply tank and treatment tanks were collected during the circulation stage on a weekly basis for analysis of basic water quality parameters such as Chemical Oxygen Demand (COD_Cr; hereafter just COD), Biological Oxygen Demand (BOD), Total Carbon (TC), pH, dissolved oxygen (DO), Oxidation Reduction Potential (ORP) and Electrical Conductivity (EC). After the completion of the circulation stage, water and sludge in the supply tank and treatment tank were removed. Carbon and nitrogen contents for the coir fiber and sludge settled at the bottom of the treatment tank were quantified using air-dried ground samples in an automatic CN-analyzer (FLASH 2000, Thermo Fisher Scientific, Inc.) .

For the following treatment stage, the microcosm system was first filled with the synthetic wastewater solution. Then, the synthetic sewage / synthetic leachate solution was supplied continuously from the supply tank. During the treatment stage, water quality parameters were measured at one week interval.

RESULTS AND DISCUSSION

Figure 2 shows variations in BOD and COD for the effluents under circulation and treatment stages. For both synthetic sewage and leachate, BOD and COD values decreased generally with time during the circulation stage. The decrease rates in BOD and COD at the low pollutant load conditions were greater than those for the high pollutant load conditions. There were no significant differences in BOD and COD variations between LFD and HFD conditions.

For the treatment stage, a different trend was observed between the synthetic sewage and leachate; i.e., measured BOD and COD values for the synthetic leachate became continuously low values during the treatment stage and reductions in BOD and COD at LFD and HFD conditions became higher compared to the control condition. For the synthetic waste water, on the other hand, the BOD and COD values increased gradually close to the concentrations of inflow solutions under the treatment stage and there was no difference among LFD, HFD, and control conditions. These results suggested that the BOD and COD removals under the treatment stage were more effective for the synthetic leachate in the microcosm experiments.

Figure 3 shows variations in TC and TN for the effluents under circulation and treatment stages. Some fluctuations in measured TC and TN values observed, however, not so much differences in measured TC and TN values observed between the circulation and treatment stages except for the syntheic leachate at the condition of low pollutant load. For the synthetic sewage, there was no effect on the fiber density on the reduction in TC and TN values. For the synthetic leachate, on the other hand, HFD conditions became more effective to reduce TC and TN especially under the treatment stage.

In order to clarify the removal efficiencies of C and N in the microcosm COTS, the consumption of C and N per unit volume of microcosm (unit volume of the treatment tank) per week [mg/L of microcosm/week] was calculated by using TC and TN values of inflow solutions and effluents, C and N contents for collected coir and sludge samples. An example of calculation sheet for C consumption under the circulation stage was shown in Table 2.

Table 3 summarizes the calculated C and N consumption values for the synthetic sewage and leachate at both conditions of high and low pollutant loads with different fiber densities. The C and N consumptions in the microcosm varied depending on both fibre-densities and pollutant loads of wastewater. The C and N consumptions in the microcosm became more effective at HFD conditions for both low and high pollutant loads of wastewater. For both synthetic sewage and leachate, the C consumptions under the treatment stage became around 2 times higher than those under the circulation stage except for the low pollutant load of synthetic sewage. The C consumptions for the synthetic leachate were greater than those for the synthetic sewage under both circulation and treatment stages; i.e., the C consumptions for the synthetic leachate became around 2-3 times higher than those for the synthetic sewage at low pollutant load conditions and became around 3-7 times higher than those for the synthetic sewage at high pollutant load conditions.

The N consumptions under the treatment stage became also higher than those under the circulation stage. The HFD gave the highest C consumption values among tested conditions and became around 1.8 and 1.5 times higher than those for blank

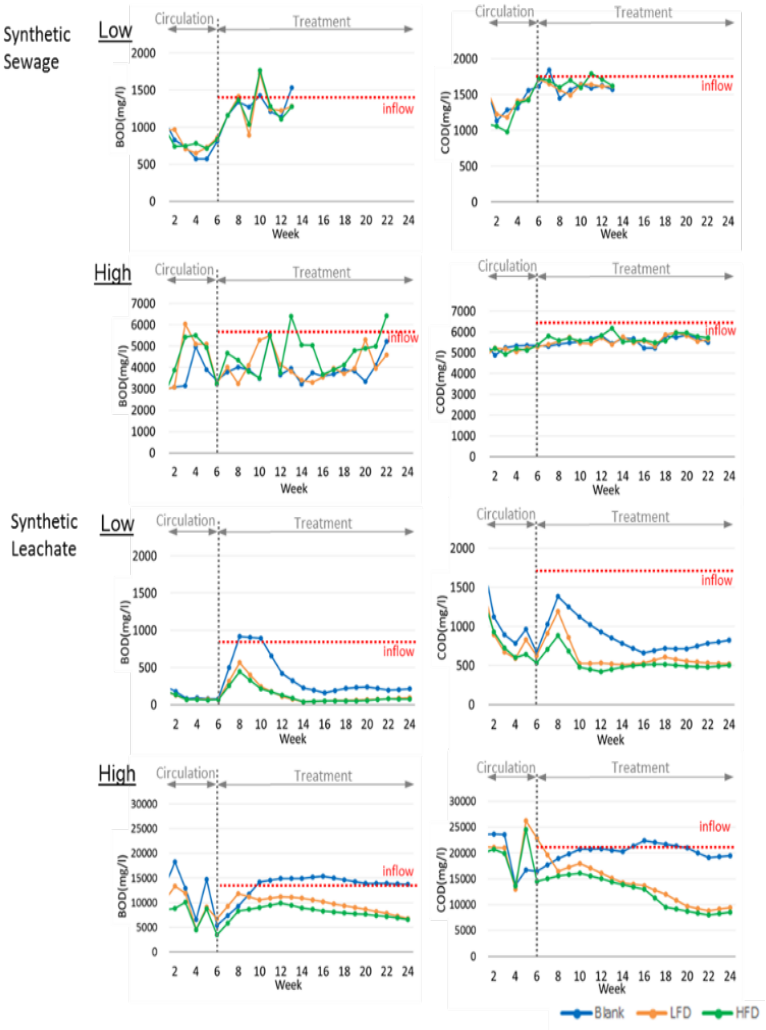

Fig. 2 Variations in BOD and COD of the effluents under circulation and treatment stages.

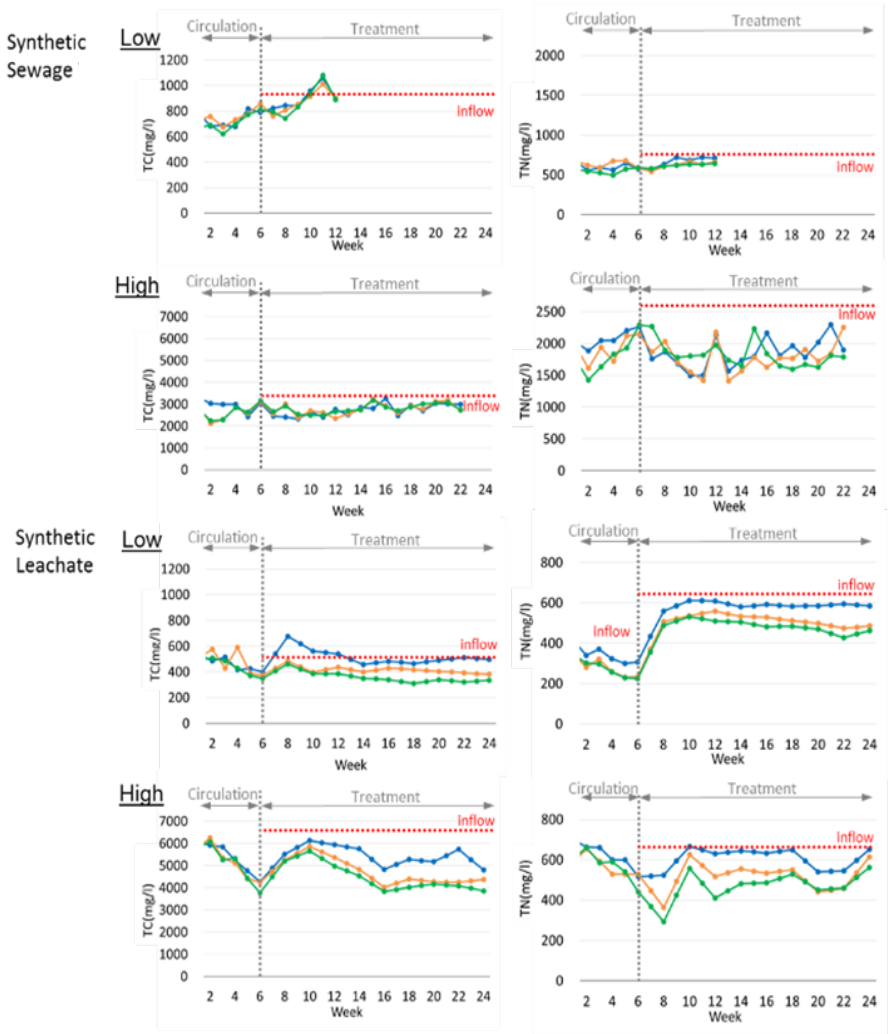

Fig. 3 Variations in TC and TN of the effluents under circulation and treatment stages.

Table 2 An example of calculation sheet for C consumption

No.	Parameter	HFD	LFD	BLANK
1	TC inflow (mg/l)	3424	3424	3424
2	TC outflow (after 42 days) mg/l	3161	3129	3062
3	Total C consumption (mg/l)	263	295	362
4	volume of leachate in circulation period (L)	12	12	12
5	Initial C in solution- final C in solution (g)	3.16	3.54	4.35
6	Accumulated Sludge mass (g)	17	18	11
7	C content in sludge (%)	7.13	8.36	5.50
8	C content in accumulated sludge (g)	1.21	1.51	0.61
9	Dry mass of coir fiber(g)	48.6	24.6	-
10	C content of coir fiber after the recirculation (%)	45.8	46.8	-
11	C content in raw coir fiber (%)	40.8	40.8	-
12	Accumulated C mass in coir fiber (g)	2.4	1.5	-
13	Total used C in recirculation phase for 42 days(g)	6.8	6.5	5.0
14	volume of microcosm tank (L)	12	12	12
15	C consumption (g/L of microcosm/day)	0.0135	0.0129	0.0098

Table 3 C and N consumptions for synthetic sewage and leachate.

Pollutant load.	Stage	Treatment tank	Synthetic sewage				Synthetic leachate			
			C		N		C		N	
			Consumption (mg/L of microcosm / week)	% in sludge	Consumption (mg/L of microcosm / week)	% in sludge	Consumption (mg/L of microcosm / week)	% in sludge	Consumption (mg/L of microcosm / week)	% in sludge
Low	Circulation	Blank	0.042	15.0	0.002	1.7	0.073	16.9	0.025	1.0
		LFD	0.053	16.8	0.002	2.5	0.095	20.4	0.038	1.5
		HFD	0.072	16.5	0.002	2.3	0.101	19.6	0.038	1.3
	Treatment	Blank	0.034	6.0	0.001	4.2	0.116	11.5	0.014	0.4
		LFD	0.055	9.2	0.004	4.7	0.170	13.0	0.063	0.4
		HFD	0.067	7.8	0.004	3.6	0.203	12.4	0.074	0.2
High	Circulation	Blank	0.069	5.5	0.005	1.6	0.482	13.3	0.037	1.0
		LFD	0.090	8.4	0.006	1.8	0.618	18.0	0.044	1.5
		HFD	0.095	7.1	0.004	1.5	0.691	17.0	0.056	1.3
	Treatment	Blank	0.223	3.7	0.021	1.6	0.865	20.9	0.089	0.9
		LFD	0.365	4.0	0.011	1.3	1.12	21.6	0.090	1.0
		HFD	0.371	5.3	0.025	1.8	1.30	20.0	0.088	0.7

(control) and LFD conditions. This implies that higher coir fiber condition contributed to the C consumption in the microcosm COTS. It is noted that the C % in sludge for LFD and HFD did not vary so much among tested conditions, indicating that the C removal in sludge did not directly contribute to the higher C consumption at HFD condition.

CONCLUSIONS

Based on the results from laboratory tests, it was revealed that the microcosm COTS contributed to reduce BOD and COD in the effluents and to remove C and N from both synthetic sewage and leachate. Further quantitative analyses will be done for evaluating wastewater treatment efficiencies of microcosm COTS.

ACKNOWLEDGEMENT

This study was partially supported by the SATREPS Project of the Japanese International cooperation Agency (JICA) and Japan Science and Technology agency (JST). We would like to acknowledge the Nishibori Treatment Plant, Saitama City, Saitama Prefecture, Japan, for providing us raw wastewater. We also acknowledge Mr. Takuya Ogiso, a former undergraduate student, Department of Civil and Environmental Engineering, Saitama University, for his dedicated effort on the laboratory tests.

REFERENCES

[1] Sato, N., K. Kawamoto, H. Sato, M. Lokuliyanaga, T. Koide, and N. Tanaka (2013). Utilization of a local-available biomass resource for wastewater treatment in Sri Lanka: Comparison between initial and current performance of coconut-fibre biofilm treatment system (COTS). Proceedings of Fourteenth International Waste Management and Landfill Symposium (Sardinia 2013), 181.

[2] Gunawardana, I.P.P., L.W. Galagedara, and S. De Silva (2011). Practical issues f partial onsite sanitation systems: Two case studies from Sri Lanka. Tropical Agricultural Research, 22(2): 144-153.

[3] Abad, M., P.Noguera, R.Puchades, A.Maquieira and V.Noguera (2002). Physico-chemical and chemical properties of some coconut coir dusts for use as a peat substitute for containerized ornamental plants. Bioresource Technology, 82: 241-245.

[4] Nam, T.H., S. Ogihara, N. H. Tung, and S. Kobayashi (2001). Effect of alkali treatment on interfacial and mechanical properties of coir fiber reinforced poly (butylene succinate) biodegradable composites. Composites: Part B. doi:10.1016/j.compositesb.2011.04.001.

[5] Picano, P.A., Vallero, G.V.M., Gianotti, P.E., Zaiat, M., Blundi, E.C. (2001). Influence of porosity and composition of supports on the methanogenic biofilm characteristics developed in a fixed bed anaerobic reactor. *Water Sci. Technol*. 44(4): 197-204.

[6] Crites, R. and G. Tchobanoglous (1998). Small and decentralized wastewater management systems, McGraw-Hill Science / Engineering/ Math, Page 944.

[7] Tanaka, N., A.K. Karunarathna, and K.B.S.N. Jindasa (2008). Effect of coconut coir-pith supplement on nitrogen and phosphate removal in subsurface flow wetlend microcosms. Chemistry and Ecology, 24(1): 15-22.

[8] Dharmarathne, N.K., N. Sato, K. Kawamoto, T. Koide, H. Sato, and N. Tanaka (2013). Evaluation of wastewater treatment efficiency using coconut fiber biofilm reactor system with synthetic leachate. Proceedings of International Conference on Engineering and Applied Science (ICEAS), 629-636.

[9] Jamie. F., R. VanGulck, and K. Rowe. (2004) Evolution of clog formation with time in columns permeated with synthetic landfill leachate. Journal of Contaminant Hydrology 75: 115– 139.

Second International Conference on Science, Engineering & Environment,
Osaka City, Japan, Nov.21-23, 2016, ISBN: 978-4-9905958-7-6 C3051

TEMPORAL VARIATIONS IN PERCHED WATER AND GROUNDWATER QUALITIES AT AN OPEN SOLID WASTE DUMPSITE IN SRI LANKA

Udayagee Kumarasinghe[1], Y. Inoue[1], T. Saito[1], M. Nagamori[2], Y. Sakamoto[3], M.I.M. Mowjood[4], K. Kawamoto[1,5]

[1]Graduate School of Science and Engineering, Saitama University, Japan
[2]Material Cycles and Waste Management Group, Centre for Environmental Science in Saitama, Japan
[3]Institute for Geo-Resources and Environment, Advanced Industrial Science and Technology, Japan
[4]Department of Agricultural Engineering, Faculty of Agriculture, University of Peradeniya, Sri Lanka
[5]International Institute for Resilient Society, Saitama University, Japan

ABSTRACT: Open dumping of municipal solid waste is a common practice in many developing countries which leads surface and groundwater contamination in the vicinity. In this study, a long-term monitoring was done at an abundant solid waste dumpsite to characterize the temporal variations of perched water and groundwater qualities underneath the dumped waste. The dumpsite located on a sloping bank of the Mahaweli River in Udapalatha Pradeshiya Sabha in Central Province of Sri Lanka. Dumpsite consisted of two sections: old section and new section used for waste dumping for 7 years (2003-2010) and 0.5 year (2011), respectively. Multiple boreholes were installed for each section and the water quality has been monitored for 2 years from May 2013-March 2015. Water quality parameters such as pH, EC, BOD, COD, TN, TP, major cations, anions, and heavy metals were measured monthly. Leachate Pollution Index (*LPI*) was calculated to quantify the leachate contamination potential. Results showed that the groundwater samples from both new and old sections exhibited relatively constant and low *LPI* during the monitored period, whereas the perched water samples from new section showed high *LPI* with fluctuations. No correlations were observed between water quality parameters and rainfall pattern. Perched water and groundwater persist as two independent bodies in this dumpsite. There were significant linear correlation between EC and major equivalent cations/anions, suggesting EC is a simple and convenient parameter to characterize the dumped waste condition.

Key words: Waste dumpsite, Open dumping, Groundwater, leachate pollution index (LPI).

1. INTRODUCTION

Open dumpsites are not designed lands for waste dumping; there are no landfill liners, leachate collection systems, final soil covers or leachate treatment mechanisms. This type of dumpsites requires minimum operational and maintenance costs, thus prevalent in developing countries from several decades [1]. Many groundwater contamination incidents have been reported at open dumpsites and their surroundings, caused by leachate generated as a result of waste degradation [2]. Since leachate consists of high concentrations of BOD, COD, TOC, cations, anions, xenobiotic compounds and heavy metals, there is a risk of soil and water pollution surrounded by dumping sites [3]. Absence of proper waste separation technique leads to elevated concentrations of heavy metals in the leachate [3]. Heavy metals may release by waste such as ceramics, electronic wastes, batteries, debris of motor mechanic industry etc. High concentrations of Cd, Hg, Ni, Mn, Cu and Pb have been reported form leachate collected at many open dumpsites [4]. Leachate generated at waste layers and rainwater drains downward by gravitational forces, stagnated at the bottom of the waste dump. This polluted water enters to groundwater aquifers through soil. The subsequent migration of leachate through the sides and/or bottom of the dumpsite into subsurface formations is a serious environmental pollution concern and it is a threat to public health and safety. In this context, groundwater pollution is by far the most significant concern arising from leachate migration.

The level of contamination is mostly depends on the severity of leachate quality at open dumpsites. Quality of leachate greatly varies with respect to the type of waste, age of the dumpsite, management practices at the dumpsites, climatic factors and etc. The resulted risk of soil and groundwater contamination can be minimized by applying field scale treatment mechanisms such as permeable reactive barriers. In order to do that, the leachate generated at open dumpsites should be well characterized and their variations should be properly understood [5].

Leachate Pollution Index *(LPI)* is a tool which developed for the leachate characterization with respective to the quality and severity of contamination. *LPI* quantitatively analyze the effect of organic pollutants, inorganic pollutants and heavy metals with the different sub-indices of *LPI* [6]. This might be successfully used for the implementation of

leachate treatment mechanisms and identification of groundwater pollution potential at open dumpsites. This study is focused assessment of water quality and its variability using *LPI* indices and identification of different categories of perched water and groundwater in the same dumpsite.

2. MATERIALS AND METHODS

2.1 Site selection and initiation of monitoring session

Fig. 1 shows the location of dumpsite and monitoring boreholes. The study area is an abandon open solid waste dumpsite located in Udapalatha Pradeshiya Sabha (07^0 80' 30.1" N and 80^0 34' 43.2" E) in central province, Sri Lanka. The dumpsite consisted with two sections. Old section was used for waste dumping for 7 years from 2003-2010 and new section was used for 0.5 year in 2011. Both old and new sections have a steep slope toward the right bank of the River Mahaweli. The waste dumping rate was approximately, 15-20 t/day in the operational period.

Groundwater and perched water monitoring wells were installed along the two transits of old and new sections using rotary boring. Perched water monitoring wells (PBH) were drilled up to original soil layer whereas groundwater monitoring wells (BH) were drilled up to the bed rock.

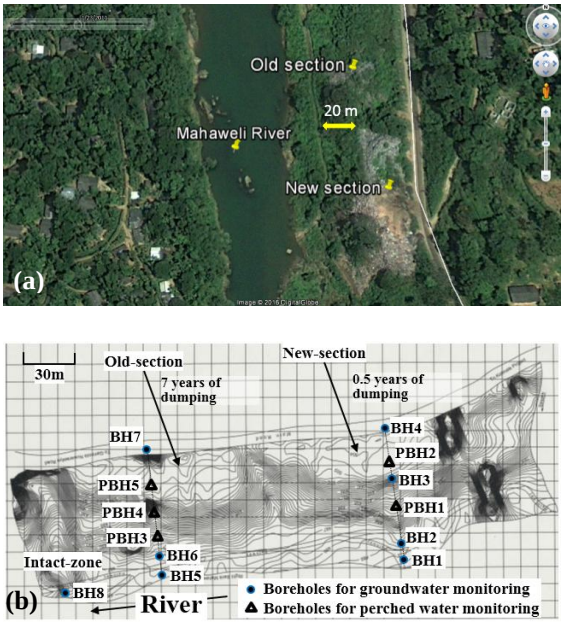

Figure 1: (a) Location of the dumpsite and (b) location of the monitoring borehols at the dumpsite (Source: 2015 Google Inc. 17-03-2011)

2.2 Monitoring the water quality

The dumpsite was monitored for a period of two years from May 2013 to March 2015 with one month interval. Perched water samples were collected from PBH wells, whereas groundwater samples were collected from BH wells, into clean 1L polypropylene bottles. Water remaining in the wells was removed by manual pumping before sampling. Water samples were analyzed for BOD_5, COD, TOC, Major cations/anions, and heavy metals. Onsite parameters were taken for pH, EC, water temperature. Standards methods were used to analyze BOD_5 (APHA 5210B) and COD (APHA 5220A). TOC analyzer (TOC-LCSH/TNM-L Shimadzu, Japan) was used to measure the TOC, IC and TN, after filtering samples through 0.45µm filter papers. HCO_3^- was calculated by DIC in samples. Anions; Cl^-, SO_4^{2-}, NO_3^- were analyzed with ion chromatography (HPLC-IC, SHIM-PACK IC-A3 Shimadzu, Japan). Cations; Na^+, K^+, Mg^{2+}, Ca^{2+} were analyzed with atomic absorption spectrophotometer AAS (AA-7000 Shimadzu Corporation, Japan) and NH_4^+ was analyzed with UV-Vis spectrophotometer (UV-2700 Shimadzu, Japan). Heavy metals; Fe, Ni, Cu, Zn, Pb were measured with AAS and As, Cr were analyzed with inductively coupled plasma mass spectrometry (ICPM-8500, Shimadzu, Japan).

Rainfall data were collected from a close by rain-gauge station to the dumpsite.

2.2 Leachate Pollution Index *(LPI)*

Sub-indices and overall *LPI* were used to evaluate perched water and groundwater contamination over the monitoring session. Sub-indices of *LPI; LPI* organic, *LPI* inorganic and *LPI* heavy metals were calculated according to the equation 1. Then the overall *LPI* was calculated by equation 2[7].

$$LPI = \frac{\sum_{i=1}^{n} W_i P_i}{\sum_{i=1}^{n} W_i} \qquad (1)$$

$$LPI_{overall} = 0.232\ LPI_{or} + 0.257\ LPI_{in} + 0.511\ LPI_{hm} \quad (2)$$

where *LPI* is the leachate pollution index, w_i is the weight for the i^{th} pollutant variable, p_i is the sub index score of the i^{th} pollutant variable and, n is the number of leachate pollutant variables used in calculating *LPI* [6,7].

3. RESULTS AND DISCUSSION

Table 1 illustrates the sub-indices and overall LPI calculated for perched water collected from PBH2 in June 2013. Using the data for different water quality parameters, sub-index values were calculated according to the weight factors [7]. Finally, the overall *LPI* was calculated.

Table 1: Sub-indices and $LPI_{overall}$ calculated for PBH2 for June 2013

Index	Parameter	Value mg/L	Sub-index (P_i)	Weight factor (w_i)	W_iP_i	*LPI*
LPI_{or}	BOD	11.0	5.02	0.061	0.3	9.3
	COD	333	13.5	0.062	0.8	
LPI_{in}	pH	7.10	5.00	0.055	0.3	
	TDS	3.20	9.00	0.05	0.5	
	TN	856	27.2	0.053	1.5	17
	NH_4^+-N	472	41.5	0.051	2.1	
	Cl^-	331	6.18	0.048	0.3	
LPI_{hm}	TotalFe	7.60	5.20	0.045	0.2	
	Cu	0.01	5.01	0.050	0.3	
	Zn	0.20	5.04	0.056	0.3	
	Pb	0.03	5.15	0.063	0.4	5.1
	Ni	0.06	5.14	0.052	0.4	
	As	0.01	5.01	0.061	0.3	
	Cr	0.04	5.09	0.064	0.3	
$LPI_{overall}$						9.3

Temporal variability of general water quality parameters, heavy metals, total nitrogen, total phosphate and *LPI* indices were compared with the temporal variability of rainfall and water temperature (Fig. 2). Temporal variability of perched water quality at new and old sections was evaluated by PBH2 and PBH4, respectively. BH2 and BH6 were used to evaluate groundwater quality variations at new and old sections. BOD, COD, TN, TP showed comparatively higher concentrations in perched water samples over the groundwater samples. Further the perched water collected from new section showed higher concentrations than the old section. EC of the perched water at new section showed high values; it is higher than 10 times that of perched water at old section and groundwater at both sections. Heavy metals (Cr, Pb) and pH of the both perched and groundwater samples showed similar values. The heavy metal concentrations were comparatively lower than few other studied dumpsites in Sri Lanka [10].

LPI_{in}, LPI_{or} and $LPI_{overall}$ calculated for PBH2 are 3 - 4 times higher from other perched water and groundwater samples. Perched water well at old section; PBH4 showed comparatively higher values than the groundwater in old section at the initial stage of the monitoring session. *LPI* indices calculated for the perched water at new section gradually decreased with the time and at the end of the monitoring session, reduced up to that of the perched water at old section. The gradual reduction of *LPI* indices over the time might govern by the dissolution factor, since the site is very sloppy. The contaminants might dissolve in the rain water and move towards the river. *LPI* indices calculated for groundwater is far below than that of the perched water. In addition, the fluctuation of $LPI_{overall}$ over the time is not prominent (fig.3a).

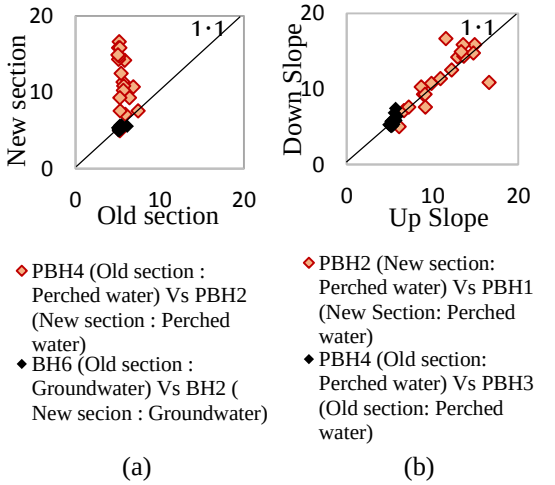

Figure 3: 1:1 Relationship between $LPI_{overall}$ in monitoring boreholes

As showed in fig. 3a, $LPI_{overall}$ calculated for perched water and groundwater behaves differently. $LPI_{overall}$ calculated for perched water scattered separately form that for the groundwater. This depicts that the perched water and groundwater persists as two independent water bodies in this site. This might be due to the steep slope (15m/50m) of the dumpsite and the different permeabilities of the waste and soil layers. Lower permeability of the soil may facilitate the development of the perched water aquifer between original soil layes and burried wastes. Thus the groundwater contamination at this dumpsite is comparatively lower. Similar phenomena was observed by [8], that development of a perched water aquifer in an open dumpsite in Chennai, India.

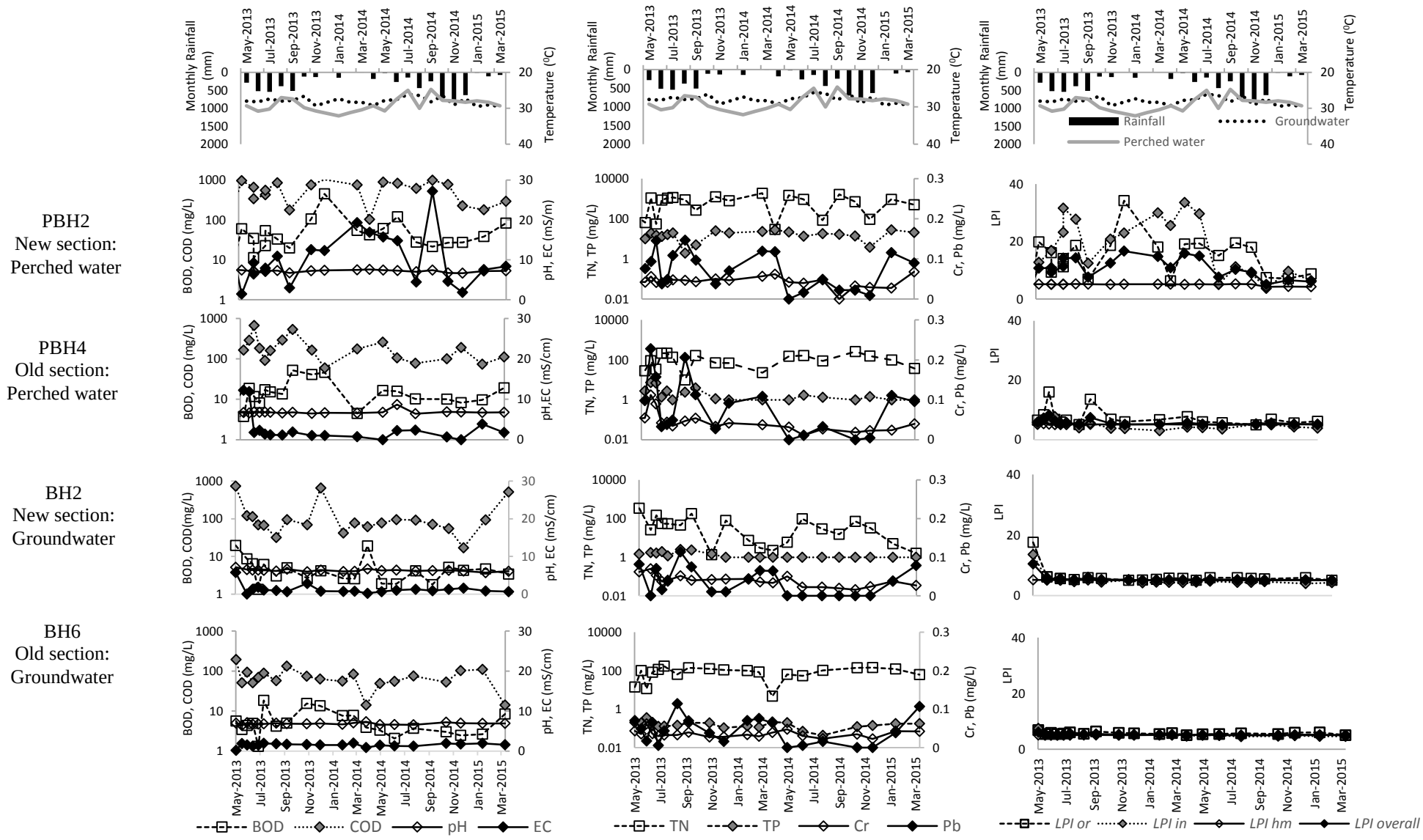

Figure 2: Temporal variability of meteriological parameters, water quality variables and leachate pollution indices of the monitoring borehols

The effect of the age of the dumpsite on the leachate quality is described in fig. 3b. 1:1 relationship develop for the perched water at new section (PBH2 vs. PBH1) and perched water at old section (PBH4 vs. PBH3), scattered separately. This revealed that perched water quality at new section significantly different from that of old section. Further the contamination level has been reduced with the aging. This might be due to dissolution and attenuation of the contaminants over the time. Same results were observed in Malaysia, which is a comparative study to differentiate $LPI_{overall}$ over the aging effect. It is found that the $LPI_{overall}$ calculated for old dumpsites are comparatively lower than that of new dumpsites [9]. Thus, when selecting leachate treatment facility, age factor should be considered.

The effect of rainfall on water quality parameters were analyzed separately for the perched water and groundwater. As illustrates in fig. 4, there is no correlation observed for both perched water and groundwater quality parameters with rainfall. Only BOD at perched water slowed slight correlation. Since the dumpsite is located at the wet zone Sri Lanka, the rainfall pattern is not significantly change over the time. Further no significant dry season could be observable. This might lead the lower correlation of water quality with the rainfall pattern. In another study, $LPI_{overall}$ has been calculated for leachate collected from different open dump sites located in different climatic regions in Sri Lanka. There was no significant difference found among the sites located at Wet, Intermediate and Dry zones. They have suggested, leachate quality in Sri Lanka depends on waste type rather climatic factors [10]. Thus, seasonal variations of the leachate treatment facilities might not be required, especially for the dumpsite located at the wet zone Sri Lanka.

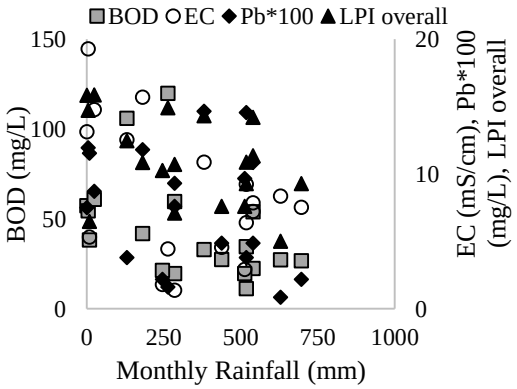

(a)

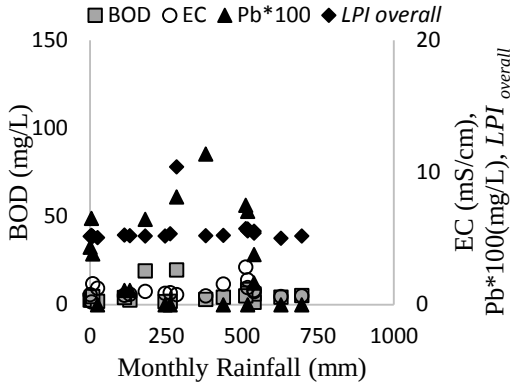

(b)

Figure 4: Rainfall Vs Major parameters of (a) PBH2 (Perched water : New section) and (b) BH2 (Groundwater : New section)

The dependency of EC on major equivalent anions and cations were evaluated using the same data. Fig. 5 (a) and (b) show the relationship developed for major equivalent cations and anions respectively.

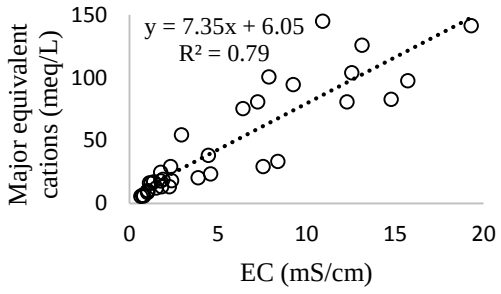

(a)

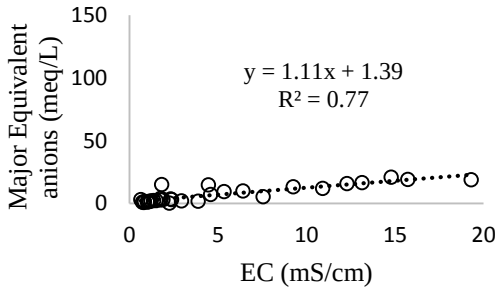

(b)

Figure 5: (a) Major Equivalent cations Vs EC and (b) Major Equivalent anions Vs EC

Both major equivalent cations and anions calculated for perched water, collected from both new and old sections highly correlate with the EC, with regression coefficient of 0.79 and 0.77, respectively for major equivalent cations and anions. Thus the concentrations of major equivalent cations and anions might describe by EC, which is an easy and portable measurement at the field level.

For the calculation of major anion NO_3^-, SO_4^{2-}, Cl^- and HCO_3^- were used. The source of this HCO_3^- might be solid waste or the rainwater. Further this HCO_3^- might not come with the geomorphological characters of the land, since the pH of the water is around neutral values [10].

For the calculation of major cations, Na^+, K^+, Mg^{2+}, Ca^{2+} and NH_4^+ were used. There might be an effect from the other missing cations such as Fe^{2+} and Mn^{2+}. Major cations found in perched water are Na^+, K^+, Mg^{2+}, Ca^{2+} and major anion is Cl^-. Similar result was found by a previous research which have been done for the leachate quality analysis in Sri Lanka [10]. Since the Sri Lankan municipal soils waste contains higher proportions of domestic waste, these ions release to leachate at the degradation process. Further Cl^- is highly mobile under all conditions. Thus it is a readily available ion and directly contribute for the EC.

4. CONCLUSIONS

Groundwater aquifer and local perched water aquifer persist as two different water bodies, in this particular dumpsite. Thus the groundwater contamination is less. The steep slope of the dumpsite might facilitate leachate to the bottom of the dumpsite than infiltration through soil.

Water quality parameters and rainfall has no correlation.

There were significant linear correlations between EC and major equivalent cations/anions, suggesting EC is a simple and convenient parameter to characterize the leachate and dumped waste conditions.

The risk of groundwater contamination is comparatively higher at the new dumpsites rather old dumpsites. Dissolution and attenuation processes reduce the contamination level with the time. Thus the leachate should be collected and treated before move into water bodies.

The toxicity of leachate, generated at the old dumpsites is lower than the new dumpsites. Thus leachate treatment mechanisms might be changed with respect to the age of the dumpsites.

LPI is an effective tool to characterize the leachate and select suitable treatment facility for the different groups of the leachate.

5. ACKNOWLEDGEMENT

This study was supported by the SATREPS Project of the Japanese International cooperation Agency (JICA) and Japan Science and Technology agency (JST).

6. REFERENCES

[1] Mahees, M.T.M, C. Sivayoganathan, B.F.A. Basnayaka. (2011). Consumption, Solid Waste Generation and Water Pollution in Pinga Oya Catchment area, Tropical Agricultural Research 22: 239-250.

[2] Christensen J.B., D.L. Jensen, C. Gron, Z. Filip, T.H. Christensen. (1998). Characterization of the dissolved organic carbon in landfill leachate-polluted groundwater. Water Resource, 32:125–135.

[3] Langler, G.J. (2004). Aquatic toxicity and environmental impact of landfill leachate. University of Brighton, 3–6

[4] Chen P. H. (1996). Assessment of leachates from sanitary landfills: Impact of age, rainfall, and treatment. Environ. Int., vol. 22, n. 2, 225-237.

[5] Esakku S., K. Palanivelu, Kurian Joseph. (2003). Workshop on Sustainable Landfill Management 3–5 December, 2003, Chennai, India, pp.139-145 139.

[6] Kumar D. and Alappat B. (2005a). Evaluating leachate contamination potential of landfill sites using leachate pollution index. Clean Technologies and Environmental Policy. vol. 7, n. 3, 190-197.

[7] Kumar D. and Alappat B. J. (2005b). Analysis of leachate pollution index and formulation of sub-leachate pollution indices. Waste Manage. Res., vol. 22, 230-239.

[8] Esakku S., K. Palanivelu, Kurian Joseph. (2003). Workshop on Sustainable Landfill Management 3–5 December, 2003, Chennai, India, pp.139-145 139.

[9] Muhammad U, A.A. Hamidi, M.S. Yusoff. (2010). Variability of Parameters Involved in Leachate Pollution Index and Determination of LPI from Four Landfills in Malaysia. Int. J. Chem Eng.

[10] Sewwandi, B.G.N., K. Takahiro, K. Kawamoto, S. Hamamoto, S. Asamoto and H. Sato. (2013). Evaluation of leachate contamination potential of municipal solid waste dumpsites in Sri Lanka using leachate pollution index. Sardinia, 14th international waste management and landfill symposium, Forte village resort, Italy, 30th October – 4th September 2013.

[11] Dergisi T.B. (2010).Morphology, Physico-Chemical Properties and Classification of Soils on Terraces of the Tigris River in the South-east Anatolia Region of TurkeyJ. OF AGRIC SCI 16:205-212.

Second International Conference on Science, Engineering & Environment,
Osaka City, Japan, Nov.21-23, 2016, ISBN: 978-4-9905958-7-6 C3051

EFFICIENCY OF PUBLIC TRANSPORTATION USING GNSS SYSTEM

Riza Putera[1], Anisa Santoso[2], Irene Sondang[3], Esty Suyanti[4], Garrin Nandhito[5] dan Okky Pratama[6]
[1,2,3,4] Urban Studies, Graduate Programe, Universitas Indonesia, Indonesia;
[5]Infomation Technology, Faculty of Engineering, Universitas Islam Negeri Syarif Hudayatulloh, Indonesia;
[6]Departement Of Geography, Faculty of Mathematic and Natural Science, Universitas Indonesia, Indonesia

ABSTRACT

Motor vehicles are one of the biggest air pollution contributor in the city. Pollution getting worse by poor public transport system in the city that caused lack of public services. In order to minimize the impact, so the focus not only by reducing the quantity of vehicles but also by managing the use of motor vehicles becomes more efficient. Through the GNSS system as precise navigation tool, the patterns of transport system can be estimated accurately by the length of trip, duration, number of vehicle that will be more efficient. This research will test a GNSS system that is applied to the public transportation system belongs to the campus as a miniature city transportation. Mode of transportation that will be tested in the form of yellow buses, patrol cars. The method used is quantitative experimental integrated with Geographic Information Systems (GIS). The results obtained are 1) GNSS systems can predict the patterns of the most efficient public transport trips, 2) the application of GNSS systems increased public services of transportation system.

Keywords: Pollution, GNSS, public transportation, spatial, GIS

INTRODUCTION

Urban dynamics and mobility has bad consequences such as environmental degradation that eventually matters to health issue [1], [2].

As a development country, cities in Indonesia deals with growth and environmental degradation at once. The condition in Jakarta, the capital city itself has been rated one of the worst polluted in Asia. It rated 43 from the World Health Organizations in their 2013 report. Research have also showed that around 58 percent of reported public health issues in Jakarta itself have been traced to ailing level of air quality in the city [3]. It needs a better solution in urban transportation if city want to increase the quality of environment and health.

The use of public transportation is the best answer for solving the urban transportation issues. However it does need to be re-examined whether it operate efficient or not in accordance to better impact not only for the services changes to urban residents but also for urban environment.

The role of technology in this sense becomes crucial as it not only facilitates these changes, but also makes managing issues such as mobility, distance to service distribution much faster and more effective [4]. The assumption is the more effective, the more satisfied of passengers and the lesser of pollution on the local environment, in the end the better of life quality at urban area. Hence, technology intervention could make mobility predictable precisely that impact to the punctuality and less pollute to the environment.

Nowadays the using of navigation technology is very common. GPS as one of Global Navigation Satellite System (GNSS) is known as the most popular navigation technology that used by public, particularly in Indonesia. The accessible and open source navigation system like Google Map, or even Waze is using GPS. However the open public GPS has limitation. GPS not to precise if we compare with the real location. In GPS operation, it is still 8-10 meters deviation if we compare map and real location. The measurements with real time kinetic (RTK) GNSS also become a solutions to predict the mobility. Based on the experimental study, measurements with RTK have much higher accuracy [5].

Therefore, Tokyo University developed GNSS-RTK using the QZSS satellite to make accurately navigation. It could predict the mobile location until only 2-3 cm deviation to the real condition [6]. This navigation system applied in Jakarta, Indonesia with cooperate with Multidiciplinary Graduate Study Universitas Indonesia. Due to the limitations coverage of the system, we like to explore this system to pinpoint the urgent urban issues which are transportation sector. In this research case, through technology methods like GNSS –RTK we like to know the mobility of public transport as depicted on the bus trip at campus.

METHODOLOGY

In order to expose the efficiency pattern of public transport, in this research we do several techniques of data collecting. Figure 1 shows the workflow of this research.

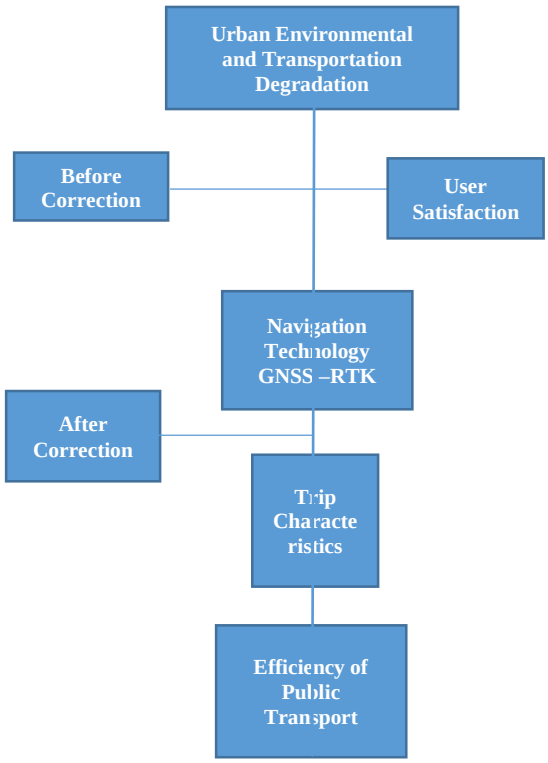

Fig.1 Workflow of the research.

Campus as city Minitiature

To test the mapping of transportation, Universitas Indoensia is chosen as a simulative miniature. With regards to contextual similarity, a chosen suitable city miniature should have similar characteristics to a city. Both need to be similar in terms of being a centre of resources while at the same time having society members as supplier of demands that require constant supply of resources. UI Campus in Depok is one of the widest campus in Indonesia, with 320 hectare consist of 25 % are built area and the other 75% are green area [7]. Figure 2 shows the campus area of Universitas Indonesia.

Since they have 11 faculties, the infrastructure and facilities in this campus are complete enough to meet the activities more than 3000 inhabitants in this campus.

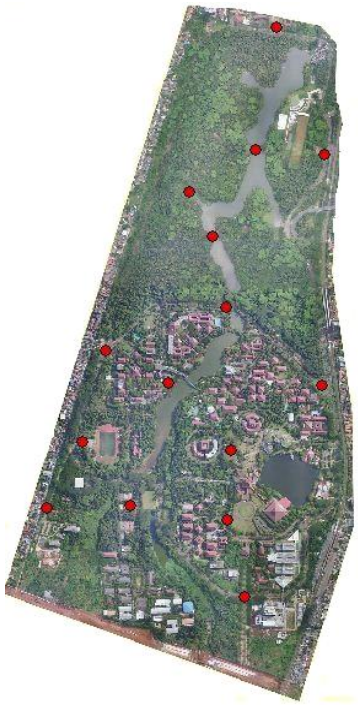

Fig 2. Universitas Indonesia

Based on that data, this UI campus could representative the city life. In particular of transportation sector, this campus has public transport namely is BIKUN stand for Bis Kuning or yellow busesin english.. In order to mobility inside the campus, this yellow bus is very important to support the movement from one faculty to others or another point of interest in campus. This particular distribution of landuse and infrastructure represents similar characteristics as that can be found in a big city. The premises therefore drives this research to utilise the frameworks of university campus as a simulated miniature for a city.

Integrating GNSS RTK and GIS

Device that we used as a Rover is *U-Blox EVK-M8T Evaluation Kit* (and *U-Center* as its supporting software). We attached U-Blox to the BIKUN along the tracking movement. This device produce .ubx data that contain the track movement from BIKUN.
After we got the .ubx data, we used *RTKLIB ver.2.4.2 p11* software to process the data. With *RTKCONV*, we converted the .ubx data into .obs data (observation from the rover). And then, we have to download the raw data (.T02) and navigation data (.P) from the *Trimble* base station as the correction data. But we have to convert the .T02 data with *Convert to RINEX* to get the observation data (.o).

With *RTKPOST*, we processed the observation data (.obs) from the rover, observation data (.o) from the base station, and navigation data (.P) with the

kinematic configuration to get the position data (.pos). This position data (.pos) is more accurate and precise. We can use and convert this data as needed, for example, excel extension (.xlsx), keyhole markup manguage (.kml), shapefile (.shp), etc.

Using Observation and Questionnaire

By doing observation and interview with questaionnaire, we like to complete the big picture of public transportation mechanism in UI campus. Statistical review is important to optimize the spatial data form the GNSS system.

An observation lead us to uncover the characteristic BIKUN trip. We have 4 variables to loof forward such as: number and location of bus stop, number passengers, headways, lay overtime.

In general, we observe the trip characteristic based on two time sequence; first is busy hour and the other is less busy hour. We assumed there are differences pattern in that two time sequence. So we divides into 6 time phase consist of : 1)Morning-busy hour : 07.00-09.00, 2)Morning-less busy hour 09.00-12.00, 3),Noon- less busy hour 12.00-14.00, 4)Noon –busy hour 14.00-16.00, 5) Evening-Busy Hour. 16.00-18.00, 6) Evening-Less Busy hour > 18.00.

Meanwhile the structural interview by questionnaire lead us to find out the user satisfactory about the BIKUN as public transportation in campus. We had random purposive sampling to 70 respondents that spread along the bus stop. We ask about 12 closed question to the BIKUN user. This structural open ended question become a benchmark for the user satisfactory

At the processing phase, we use descriptive statistic to expose the data. By using SPSS and Microsoft excel we did a modest statistic processing to describe a characteristic of BIKUN trip.

RESULT

This research are defining in two results consist of the spatial analysis and the characteristic of BIKUN trip pattern.

Spatial Analysis of Public Transport Mobility

The data show us that there is differences between before and after correction. Still, we divided the data collecting using GNSS RTK by two sequence of time: busy hour and less busy hour. Busy hour needs 33 minute for each trip compere with 22 minute in less busy hour.

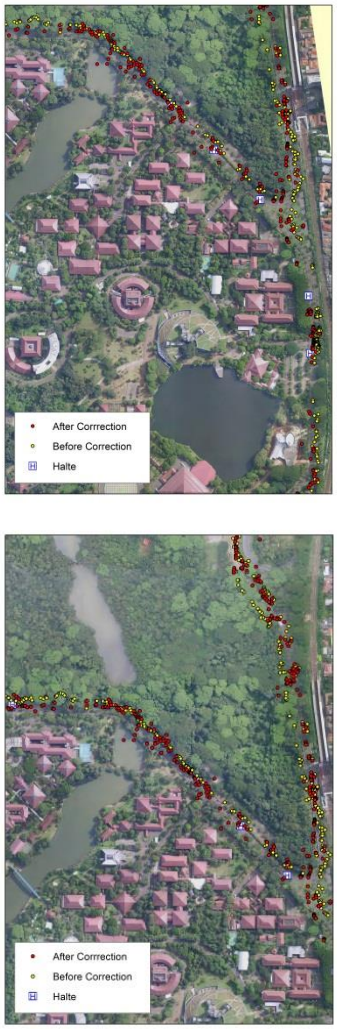

Fig 3. Mobility pattern of less busy hour (top) and busy hour (bottom).

Form the figure 3, the after correction dot which the red dot more precise at the road route, meanwhile the yellow ones is slightly away, too close to the vegetation edge.

Moreover, if we could see the spatial pattern of the real time kinematic result so we could know where the BIKUN/yellow busses slower the speed. The first red circle show us, the dot is pile up at one location, so it means the bus slower or even stopby. It is a bus stop namely Stasiun UI, which are the biggest bus stop at campus. Then, the second red circle show the dot also pile up, but there is bus stop surround it. It was the main gate of campus and ussualy has congestion on it.

If we compare the busy hour pattern and less busy hour pattern we could see, the pile up not much more than the less busy pattern.

BIKUN mobility could monitor by GNSS-RTK. It helps us to predict where the position of BIKUN at the real time. Real time Kinematic system with precisely makes us know whether the BIKUN has

obstacle or not. It predict from the speed of the BIKUN movements from one point to other points.

Limitation of this testing using GNSS-RTK is the skyview is disrupt with the vegetation cover. So it makes the signal and the track is sometimes on and off. From the survey we known that the skyview is very important to have the clearer signal and data, Basen on the map the dot is scrambled not to regularly. It is because the poor signal that stunted byt the vegetation cover likes leafes, tree branches and so on.

Estimated Pattern of Yellow Bus/BIKUN Trip as Public Transportation

The infrastructure to support public transport like BIKUN at campus UI already developed. Based on our data campus UI has 16 bus stop in each faculty and another point of interest (Figure 2).

To serve the mobility on campus, so Universitas Indonesia has 12 yellow bus. Hence the reason affordability with an area of campus is so large, the service of BIKUN comprises two routes the blue ones and the red ones. Actually, it still the same route but difference sequence of bus stop (Figure 2).

By our observation at 6 time phase, we found there is different between pattern busy hour and less busy hour, as shown in the figure 4. The average total number passengers in one day trip of BIKUN normally around 64 peoples in less busy hour and incrase 100 % to busy hour become 120 or even 160 peoples for each trip. Figure 5 below.

Fig 4. Number of total Average Passengers

Passenger numbers rose the most numerous in the Satsiun UI bus stop (123), followed by FT bus stop (84). From the data observation it seems that the most busy bus stop that stops the station UI, FT, and Pocin.

Average time stops at every stop on the red line is 17.5 seconds and 20:14 seconds unutuk blue line. The average time to stop the longest contained in pocin stop, both the blue line and the red line. The average time a round yellow bus trip is 28 minutes on the Red Line and 29 minutes to the blue line. The longest time there in the afternoon rush hour (note: the normal path).

Number of passengers we find out from the 16 bus stop, there are 2 biggest one which are stasiun UI and Pocin bus stop.

Table 1. Headways time (minutes).

Route	Busy Morning	Less Busy Morning	Less Busy Noon	Busy Noon	Busy Evening	Less Busy Evening	Average
Blue	**4**	**5**	**6**	**5**	**7**	**7**	**5.67**
Red	**4**	**6**	**5**	**5**	**5**	**3**	**4.67**

BIKUN time headways between the two most recently occurred at rush hour afternoon and evening hours for the blue route. The time headways between two bikun longest occurred in leisure hours in the morning to the blue route (table 1).

Table 2. Number of road barriers.

U-Turn	Speed Bump	Intersection
14	**21**	**11**
14	**18**	**8**

Barriers are most numerous along the gerbatama-station UI. Where in the path of the many vehicles that lined entrance to the UI campus. Plus a lot of vehicles dropping off passengers at the station UI or motorcycle-motorcycle line that was waiting for passengers at the station stops UI. The number of road barriers is shown in the table 2.

Meanwhile, base from our data collecting that show about user satisfaction. Overall the user is satisfy enough, but not too optimilize (Figure 5).

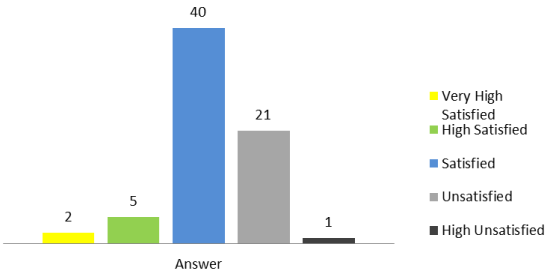

Fig 5. BIKUN service rank.

Moreover, if we talk about services, the waiting time is very important. The BIKUN arrival as public transport at campus less punctual and do not have regularly pattern. Based on the survey form the questionnaire, the respondents said more than 5 minutes to have the BIKUN in each bus stop (Figure 6). And it is ver time consuming. Actualy, the universities already have the bus schedule, but it seem blurry when in operational phase.

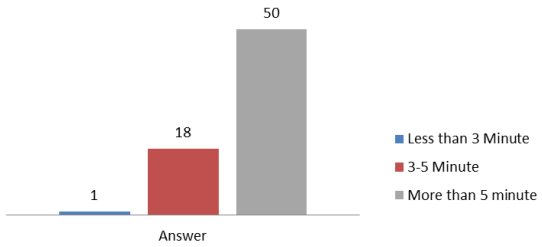

Fig 6. BIKUN time arrival.

CONCLUSION

The Multi –RTK could predict precisely the mobility of public transport, in this case is BIKUN moility at campus. However the skyveiw is very important to be considerd ones. The conclusion obtained are 1) GNSS systems can predict the patterns of the most efficient public transport trips, 2) the application of GNSS systems increased public services of transportation system.

REFERENCES

[1] Jiang, B., Zhang, T., & Sullivan, W. C. (2015). Healthy cities: mechanisms and research questions regarding the impacts of urban green landscapes on public health and well-being. Landscape Architecture Frontiers, 3(1), 24e35.
[2] Xu Liyan 2016).
[3] Haryanto, B., & Franklin, P. (2011). Air Pollution: A Tale of Two Countries. Reviews on Environmental Health, 26(1), 53-59.
[4]Graham, S., Cornford, J., & Marvin, S. (1996). The socio-economic benefits of a universal telephone network: A demand-side view of universal service. Telecommunications Policy, 20(1), 3-10.
[5] A. Kluga*, J. Kluga*, A. Bricis*, I. Mitrofanovs* Multiple Frequencies Precise GNSS RTK System Research in Dynamic Mode

Second International Conference on Science, Engineering & Environment,
Osaka City, Japan, Nov.21-23, 2016, ISBN: 978-4-9905958-7-6 C3051

THE INTEGRATION OF GIS AND GNSS SYSTEM FOR LAND UTILIZATION MONITORING

Komara Djaja[1], Riza Putera[1], Esty Suyanti[1], Irene Sondang[1], Garrin Nanditho[2] dan Akmal Fathu Rohman[3]
[1]Urban Studies, Graduate Programe, Universitas Indonesia, Indonesia;
[2]Infomation System, Faculty of Science and Technology, UIN Syarif Hidayatullah, Indonesia;
[3]Departement Of Geography, Faculty of Mathematic and Natural Science, Universitas Indonesia, Indonesia

ABSTRACT

Limited open space area requires accurate monitoring to avoid changes in land use that not suitable with city spatial planning. The difference between spatial planning and existing land utilization should be minimized. Currently, land utilization monitoring using GPS System and processed by GIS System but the result has a deviation from the existing land utilization. Within GNSS system as a new approach will correct the result of GPS become more precise map of land utilization. This research will test a GNSS system that is applied to the land utilization belongs to the campus as a miniature city land use. The land use will be divided as built up area and open space. The method used is quantitative experimental integrated with Geographic Information Systems (GIS). The results obtained are, 1) the difference of land utilization area with GPS system and GNSS system, 2) GNSS systems can get more accurate data than GPS. Base on the result, the conclusion is through GNSS and GIS system, landuse monitoring can be more effective because the highly precision of land area.

Keywords : GNSS, land utilization, monitoring, GIS, spatial planning

INTRODUCTION

The use of various tools to facilitate positioning for survey and mapping has been growing and has the speed and accuracy with a high degree of accuracy. One development of satellite-based technology is GNSS (Global Navigation Satellite System) which operates supported by several satellites and operated for 24 hours as a reference in positioning both in real time and post-processing.

GNSS (Global Navigation Satellite System) is a constellation of currently satellites such as GPS (Global Positioning System-USA), GLONASS (Russia), Galileo (Europe), BeiDou (China), and QZSS (Japan), that transmitting signals for navigation and positioning applications, anywhere on the surface of the earth.

Generally GNSS has been widely used by various groups to support the data processing models included in urban studies. Accuracy of measurement and data processing method in a study in urban becomes very important that the utilization of GNSS into one solution to increase the accuracy of the data. In studies in urban areas of signal problems become obstacles in determining the position and navigation signal propagation because of problems such as shadowing and multipath effects [1].

Satellite navigation tools such as the Global Positioning System (GPS), which is often used as a means of positioning has disadvantages signal if the area is covered with high-rise buildings and also have the imprecision in determining the position should be. Some experimental research in the field of urban trying to compare between the GPS to GNSS to see the level of accuracy to the two tools (Case Urban Canyon) [2]. Besides the accuracy in the application of the navigation system also depends on the availability of accurate references. At this time generally commercially available map accuracy rate of less,. The level of map accuracy standards used (for the metropolitan area) ranging between 5-20 meters [3].

In relation to the land utilization GNSS monitoring is also used to reconstruct the boundaries of plots of land. Utilization of GNSS-based technology Continuous Operating Reference System (CORS) can be applied to dynamic cadaster, geodetic framework that is as dynamic and has a homogeneous accuracy so it can be used as a reference in the connective point position changes and limit land parcels that have been measured [4]. This dynamic cadaster concept which is then tested at the University of Indonesia, located in Depok, West Java on land use / land cover. Land use / land cover will be given for making land utilization monitoring system. Land cover is an important factor in the analysis of the environment and spatial planning physically because it is a dynamic variable, which reflects the socio-economic interaction and regional environmental change [5].

Data retrieval land use / land cover done using GPS which is then corrected by taking the connective point using GNSS. Geo-data base and integration of satellite data is processed, and analyzed by technical Geographic Information System (GIS) to map the more accuracy and precision.

GNSS-RTK GNSS is using QZSS satellites developed by Tokyo University. University of Indonesia is one of the universities in Southeast Asia are getting antenna and Receiver GNSS RTK from Tokyo University's education and research activities base on navigation system.

METHODOLOGY

Mapping UI using Drone

Aerial image data was gathered between May 12th 2016 to May 14th by using Phantom 3. Image gathering was spread into 4 region in 333 hectares of Universitas Indonesia. The result was 1500 sets of image which merged using Agisoft. The result of merged image still show some area outside Universitas Indonesia region. Therefore, the image was cropped using ArcMap. The Final results was aerial image of Universitas Indonesia.

Imagery of Universitas Indonesia was acquired by drone. Consideration chosen drone to be process imagery mode is the resolution. All imagery must be taken in same weather characteristic. Because it can reduce sun exposure differentiation, so we can get same quality of imagery.

First process of imagery is study area orientation. It is useful to make flight track Because we choose drone on automatical mode. We can refer to google earth imagery for finding coordinate reference. From imagery we can get photos coordinates from default GPS system in drone.

Geometric Correction using GNSS Data and GPS Data

Default GPS system that included in drone has several weaknesses. Limit of accuration become a challenge for application aerial photos for mapping purposes, specially in detail mapping activity. GNSS is one of technology that has developed to fix this problem.

There are location bias in aerial image which influenced by GPS accuracy in the platform. Therefore, to increase the image accuracy, geometric correction was needed. This geometric correction could reduce bias value from the image. Some Ground Control Points (GCP) was needed in geometric correction to bind the true location so that they could reduce bias value. For high resolution image, it needs 9 to 15 minimum points which spread in the entire area of image. In this research, there are 15 GCPs, as shown in the figure 2. These points was obtained by using U-blox, a GNSS tools, by recording data from satellite. Duration of recording was around 30 minutes because the result was more accurate than 15-25 minutes recording.

Ground Control Points (GCP) was converted to excel Format that include coordinates of GCP. From recorded coordinates around 30 minutes must be combined into a single point. We can get more than 1000 unique coordinates. Simple statistic was used to measured average values from recorded coordinates.

Ground Control Points (GCP) must be distributed well (Fig 1.), it can affluence the accuration and precision of corretion. For synchronization between aerial image and GCP, choosed attractive spot is more better for reducing misinterpretation. Street lights, street cross section and tree are example o atratctive spots.

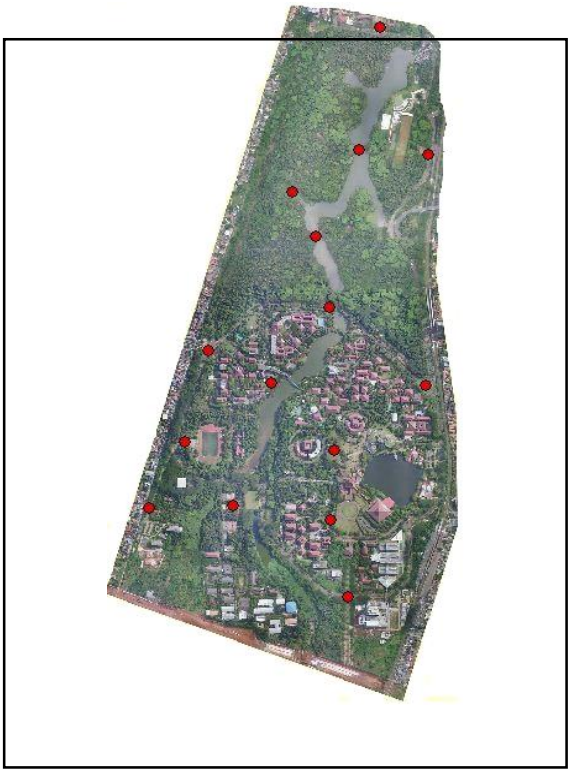

Fig 1. The locations of GCP

Result of correction process will show the differentiation between GNSS and GPS system. The accuration both GNSS and GPS can be estimated by correction process. It is important for measuring error in mapping process. RMSE value of geometric correction should be an indicator in correction process. Application for estimated RMSE is ArcMap, that can automatically measure RMSE error from GNSS and GPS.

The RMSE value of geometric correction should be concerned. A good RMSE value ranged between 0 - 1. If RMSE value was more than 1, then the geometric correction is not good enough and couldn't be used to further processing. The result of RMSE value in this research is o.o8, which was satisfy for further processiong.

Conversion Raster Data to Vector Data

From the result of aerial image that had corrected geometric can be a Base map for Interpretation land use change. Aerial image have raster format must be converted into vector format, so we can analysis easily. Vector data format is Shape File. Conversion was using manual digitization. Manual interpretation has several advantage, it can reduce error because the identic of spectral values.

Vector data features are acquired by following point, line, or polygon which identified manually (like forest of building) from aerial image in vector mode. The accuracy and spatial information of the features depend on the spatial resolution of the aerial image. Spatial resolution of the image is 0.83 meter, which should be able to map detailed scale up to 1:500.

However, manual digitation has some weakness. It required a lot of works and concentration. It also a tedious work, especially if there are a lot of features. Therefore, manual digitation is susceptible with human error. Furthermore, lots of buildings and features in Universitas Indonesia were covered by trees so that it makes feature identification harder.

Universitas Indonesia 2016

Result of digitization will be divided into 3 classes. Built up area, vegation area, water body. Bulit up can be classified into parking area, building and road and vegetation can be classified into konservation forest and park.

RESULT

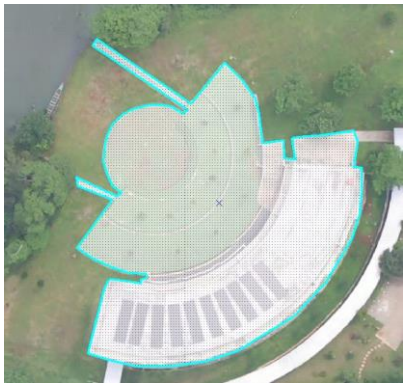

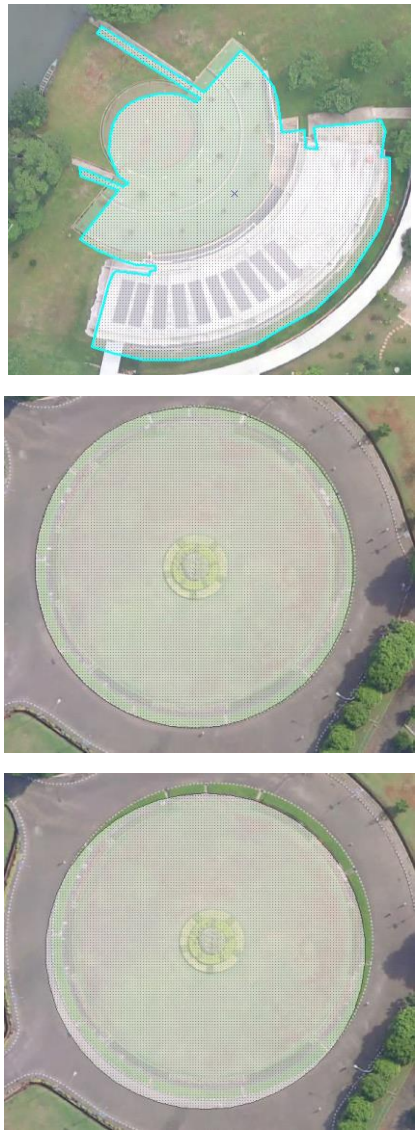

Figure 2. Comparison between corrected (top) and uncorrected (bottom) image

Figure above shows the comparison between geometrically uncorrected and correted aerial image using 15 distributed points of GCP, which coordinates was obtained from filed survey using Ublox and GNSS. Uncorrected image still used default coordinates, while corrected image utilized GNSS to determine coordinates. Hence, there are shift between object's location. The RMSE value of georecitified image is 0.08, which means

CONCLUSION

The difference of GPS System and GNSS System is the process of mapping. Several differences are the process of acquairing location coordinate and tools. So the coordinate result both GPS and GNSS are different. From RMS Error We can conclued if GNSS More Accurate than GPS.

Based on result of the research, GNSS System for land utilization mapping is more accurate than GPS

System. Because RMS error that estimated total error in land utilazaztion mapping is lower than GPS RMS error. Further for implemantation GNSS for land utilization specially for detail mapping is more better than GPS, because GNSS System can decrease potential error in mapping process

REFERENCES

[1] A. Bourdeau, M. Sahmoudi, J.-Y. Tourneret, "Tight Integration of GNSS and a 3D City Model for Robust Positioning in Urban Canyons", Conference Proceedings of the 25th International Technical Meeting of The Satellite Division of the Institute of Navigation (ION GNSS 2012), pp. 1263 – 1269

[2] Paul D. Grove, "Shadow Matching: A New GNSS Positioning Technique for Urban Canyons", The Journal Of Navigation, Volume 64, Issue 03, July 2011, pp. 417–430

[3] Rafael Toledo-Moreo, David Bétaille, and François Peyret, "Lane-Level Integrity Provision for Navigation and Map Matching With GNSS, Dead Reckoning, and Enhanced Maps", Journal of IEEE Transactions On Intelligent Transportation Systems, Issue 1, March 2010, pp.100-112.

[4] Kariyono, Eko Budi Wahyono, Tanjung Nugroho, "Rekonstruksi Batas Bidang Tanah Menggunakan Jaringan Referensi Satelit Pertanahan", Journal of Bhumi, Vol. 1, No. 1, May 2015, pp.99-112

[5] Marina-Ramona Rujoiu-Mare*; Bogdan-Andrei Mihai, "Mapping Land Cover Using Remote Sensing Data and GIS Techniques: A Case Study of Prahova Subcarpathians", Procedia Environmental Sciences , Vol 32, 2016, pp. 244 – 255

[6] O' Sullivan, Arthur. 2007. *Urban Economics: Sixth Edition*. Singapure: McGraw-Hill Companies.

[7] Sadyohuotmo, Mulyono. 2013. *Tata Guna Tanah dan Penyerasian Tata Ruang*. Yogyakarta.Pustaka Pelajar

[8] Sandy, I Made. 1986. Geografi Regional Indonesia.Jakarta. Departemen Geografi Universitas Indonesia :

[9] Scott, Allen. (2012). A World In Emerge. Cheltenham : Edward Elgar Publishing Limited

[10] Wiemwiel, Wim., Persky, Josepj J. (Ed.). (2002). *Suburban Sprawl : Private Decision adn Public Policy*. New York: M.E Sharpe

[11] Widiatmaka, Sarwono. 2007. *Evaluasi Kesesuaian Tanah dan Perencanaan Tata Guna Tanah*. Yogyakarta. Gadjah Mada University Press.

Second International Conference on Science, Engineering & Environment,
Osaka City, Japan, Nov.21-23, 2016, ISBN: 978-4-9905958-7-6 C3051

STUDY ON IMPLEMENTATION OF COMMUNITY-BASED SOLID WASTE MANAGEMENT AT GUNDIH, BUBUTAN DISTRICT, SURABAYA CITY, INDONESIA

Eddy S. Soedjono[1)], I Made Wahyu Wijaya[1),] Nurina Fitriani[1)], Premakumara Jagath Dickella Gamaralalage[2)]

[1)] Environmental Engineering Department, Institut Teknologi Sepuluh Nopember, Surabaya, Indonesia
[2)] Institute for Global Environmental Strategies, Kitakyusu, Japan

ABSTRACT: Gundih is one of the sub-district in Bubutan District in Surabaya City. The current solid waste generation in Gundih is 0,282 kg/person.day which is below the average of generation from residential area in Surabaya. Therefore, the purpose of the research is to get the knowledge, attitude, and awareness of community in Gundih about solid waste management, including 3R (reuse, reduce, and recycle) and waste bank. Questionnaires were used in this research and focused on people's knowledge, attitude, and awareness. The respondents were classified based on economic level and gender. The results shows that 93% of rich people knows waste separation while it is 79% for the poor. The results about awareness showed that 64% of rich people and 43% of poor people had conducted waste separation. Regarding recycling process, 43% of rich people knew about recycling and 64% of them had conducted recycling, poor community, however, only 14% were familiar with recycling and 36% had conducted the recycling. The existence of waste bank is already acknowledge in Gundih, 93% of all people know about it and become the member of waste bank. In terms of reuse activity, more than 50% respondents also stated that they always carry their own bag for shopping. Rich community in Gundih has more knowledge in solid waste management, perform better attitude and awareness than the poor.

Keywords: Community-based, 3R, composting, waste bank, solid waste management

1. INTRODUCTION

Rapid urban population and economic growth in a city contribute the increase of municipal solid waste generation. Surabaya is the capital city of Jawa Timur Province with second largest of population in Indonesia. Development of solid waste management has become one of challenging issues in Surabaya. Since 2005, Surabaya have started and implemented community based solid waste management (CBSWM) [1]. According to Agency of Cleansing and Gardening of Surabaya City, the amount of solid waste that is transported to Benowo Landfill was 1.300 tons/day [20]. In terms of waste composition, range of 60-70% of waste in Surabaya City belongs to biodegradable waste. According to Challcharoenwattana [2] Solid waste composition has also changed according to some stages of population. Less urbanized town produce mostly food waste while the more urbanized town has more diverse waste with high number of plastic and paper waste. High income community generate more solid waste than other community with low or middle of income.

Solid waste management in most developing countries are characterized by inefficient collecting methods, inadequate served area of collection system, inappropriate disposal system, and real operation and maintenance cost are never fully covered [3]. In order to reduce the amount of waste transported to landfill continuously, it needs a solid waste management which is supported by community based. Solid waste management need better approaches to be more efficient and effective. The stakeholder in solid waste management is an important part as it is widely claimed that participatory approaches in planning, action, and research can be one of the solutions [4]. In this research, community based include some activities about solid waste management, such as collection, separation, transportation, 3R, and disposal. Organic and inorganic waste will have economic potential or benefits for the community, if they are processed and managed properly [5]. Community-based solid waste management in waste collection and disposal have been recommended by many research to develop the management of solid waste in municipals [12]

Gundih Sub-district in Bubutan District, Surabaya City, is one of the community which becomes a pilot model in good environment management. The area of study is shown in figure 1. The previous research [6] has found the solid waste generation of Gundih is 0,282 kg/person.day. According to Indonesia National Standard [21], it is below the average of solid waste generation from residential. The practice of solid waste management in Gundih was very good. There was composting and recycle activity that conducted by the community. The separation of solid waste is still

going well and supported by separated bin.

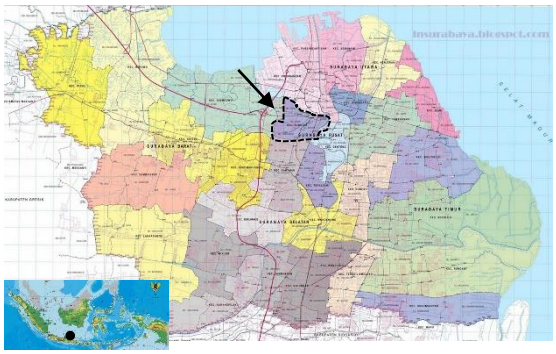

Fig. 1 Area of Bubutan District in Surabaya City

According to Tallei, et al [7], solid waste management practices in a community, tends to differ by gender. It stated that male members of community had higher awareness scores than the female, but on the other side female had better practices in solid waste management, cause in most household, female do most cleaning and sweeping activities. Different research [8] has been stated that females participate more actively in waste management then male. This study is in support with Adogu [9], who found that female is more aware and displayed better attitude than males in solid waste management. Women are the most potential segment of the society, most of their earnings are spent to livelihoods. They have an important role to bring a sustainable in their family [10]. The sustainability is influenced by selected technology, investment cost, operation cost, technical operation, community participation, and institutional management [22].

A study from Singhirunnsorn [11] stated that social status of community show the significant differences in attitude and behavior in solid waste management. The household income has a negative relation with the attitude. Socio-economic factor had a significant impact in determining the waste generation by each household. This factor had influence on littering behavior. Percentage of waste generation by household generally varied depending on area as well as economic status of the residence. This study observed that in high income area, people had more concern about solid waste management [13]. Solid waste generation depends on the economic level or income of the family or individual. An increase of economic growth is correlated positively with waste generation [14].

This research is purposed to know the knowledge, attitude, and awareness of community in Gundih about environment management. Scope of community in this study is classified into economic level (rich and poor community) and gender (male and female). A structured questionnaire will be used for all classified respondents.

2. METHODS

This study was carried out at Gundih Sub-District, Bubutan District, Surabaya City, Indonesia. The research was a descriptive survey of selected members of community in Gundih using well-structured questionnaire. The questionnaire were purposed to get the knowledge, attitude, and awareness of solid waste management. The respondents were classified based on economic level and gender.

The questionnaires were focused on 2 topics (Section A and B) that would describe the knowledge, attitude, and awareness of community. Section A consisted of questions to assess the knowledge of community about solid waste management including separation, recycling, waste bank, and composting. Section B consisted of questions to assess their attitude and awareness of solid waste management. Each completed questionnaire was reviewed for completeness. The questionnaire that has been answered, analyzed by calculating the percentage of responses from the respondents for each question. All percentage will be described based on the sight of female and male category and also poor and rich community

The research was conducted in three districts of Surabaya based on the density of community and their concern in environment. A total of 84 respondents have been interviewed for all districts. Bubutan District has been selected to represent the highest density of community and best concern on environment. Those respondents include rich and poor community and also male and female categories. Collecting data is carried out by door to door. All items will be presented in form of percentage graph.

3. RESULTS AND DISCUSSION

Knowledge about the negative impact of unmanaged solid waste to environment become very important for the community. The results show that 93% of both rich and poor community were familiar with the negative impacts of unmanaged solid waste. All males familiar with this issue, but only about 86% of females who know about it. Causing bad smell, obstructing the walkways, and polluting the river are the negative impact that most widely known by the respondents. Television become the most frequent source of information about those problem. In personal, community based group become the one of information's source. In term of city regulation about solid waste management, only about 50% from the rich community is familiar with the regulation, while 72% of poor community are never

heard about it. Only about 22% of female respondent stated that they are familiar with the regulation, but the half of the male also stated. Most of information about regulation obtained from television and community based group. The rich community will be easier to get some information from others media, such as internet.

Proper solid waste management will affect various aspects of the community, such as health, productivity, and economic level. Based on the results, 43% of rich community stated that properly solid waste management is very important, 29% stated it is important, and 28% stated that is enough important. From the poor community, 57% stated that is enough important. Male respondents stated that very important in 43% and only about 21% of female stated the same.

Solid waste collection system in Gundih is still using handcart with the service from house to house. Operational and maintenance cost of collecting system is obtained from the regularly payment of community members. Based on that case, this study also asked the opinion of community members about the reasonable fee for collection service per month. The results showed that from rich community, 28% agree to pay 1000-5000, 36% argue to pay 5000-10.000, and 36% stated that they are willing to pay more than 10.000. A half of poor people agree to pay 5000-10.000. The same percentage from male respondent showed that 36% agreed to 1000-5000 and 36% agreed to more than 10.000. A total of 57% of female respondents more agree to pay 5000-10.000. Only about 22% agreed to pay 1000-5000 and 21% agreed to more than 10.000. Generally, woman will more thinking about their household needs. This reason is in line with the previous research [10].

3.1 Implementation of 3R (Reuse, Reduce, Recycle)

3R is a strategy to manage solid waste generation into new resources, reducing pollution, and optimizing natural resource utilization [15]. The results showed that 79% of poor community has never heard about 3R. The rich community not showed best results, 36% stated that they are familiar with 3R and 36% stated the opposite. The male respondents performed 11% higher of percentage in knowing 3R than female which is only about 14%. Community information board has important role in spreading the information about 3R, it is evidenced by the high percentage of information sources according to the respondents. Previous study [24] stated that implementation strategic of 3R in solid waste management which is fully implemented is in order to decrease the cost, performance, and people's throw away culture that should be changed through awareness and practice.

Based on the action of 3R plan, solid waste management will serve a sustainable separation system at sources. It shows that all municipal solid waste is collected and transported to the disposal facility and support the social manner responsibility for environment [25].

3.2 Solid Waste Separation

Generally for the rich community, if the community is aware of the collection service and know that the worker is responsible, they will tend more likely to pay for the service than the service is impersonal [6]. The results showed that 93% of rich community is familiar with waste separation, while the poor community only about 79%. About 43% of rich community stated that solid waste separation is very important to be implemented, while only about 21% of poor community stated the same and 57% argue that it is enough important. The best result performed by male respondent, all of them very familiar with waste separation, and 43% of them agree that solid separation is very important to do. Female showed 71% in knowing about this activity, however only 21% of them stated that it is very important, 43% expressed to enough important. In this case, community information board is the most becoming the choice of all community besides television and relatives. Separating activity must be accompanied by the provision of solid waste storage. Unavailability of separation storage cause of solid waste remained mixed when it is collected.

Based on the solid waste management practice in separation activity showed that 64% of rich community separate their solid waste generation every time, 29% of them just separate 75% of their time. In other side, only about 43% of poor community separate their solid waste every time. The occurrence of separating activity is influenced by the availability of separated waste storage. In this case, providing some waste storages become an obstacle for poor community. Male respondents are more active in performing separation than female, about 64% of male do separation of their solid waste every time, while only about 43% do the same thing.

3.3 Solid Waste Recycling

Recycling of solid waste into new product with some process happen in small scale because it depends on the machinery and technology [15]. Accordance with the that statement, the result showed that rich community showed higher percentage in knowing recycling activity that is 43% than the poor community only about 14%. About half of rich community stated that recycling is important, however the poor community argue that it is enough important with 64% respondent.

Recycling activity depends on the machinery and technology, it cause the poor community do not prioritize in recycling. Male respondent showed that 36% are familiar with recycling, however the female only about 21%. Half of male respondent thought that recycling is very important to be implemented, while only 21% of female stated the same. According to Kumar [16], due to people's busy schedule in their daily life, they are only want to dispose their solid waste out the house. The lack of willingness to do recycling is caused by the low of awareness, responsiveness, time, and less information. Waste recycling from informal sector and local community can enhance the efficiency of recovering process, reduce the disposal cost, and avoid unnecessary disposal technology.

3.4 Waste Bank

Nowadays, waste bank is very familiar in some communities. Waste bank has been developed on the basis of public participation. The bank is operated by the local community members and opened regularly [11]. Same percentage of rich and poor community (93%) showed that waste bank is very familiar in Gundih. All male respondents stated that they are familiar with waste bank and 86% of female stated the same. Mostly, members of community in Gundih have joined become a member of waste bank. In high percentage, rich community showed that 93% of them become the member of waste bank in Gundih similar with that, 86% of poor community has become the member of waste bank. The same pattern also occurs in the male and female respondents. According to previous study [11], at the beginning of waste bank development, the members of waste bank officially get the credit on their account. Their solid waste that has been collected and remitted will be sold to recycling network seller whether formal or informal sector. Then the members will consequently receive money in exchange their solid waste.

4 CONCLUSION

Economic level and gender influence in community-based solid waste management in Gundih Sub-District. Rich community shows better performance in solid waste management activities. Their knowledge, attitude, and awareness were better than poor community. Male community has good results in applied community-based solid waste management in Gundih if compared to the female.

5 ACKNOWLEDGE

The research was supported by Institute for Global Environmental Strategies (IGES), Japan

6 REFERENCES

[1] DAI. "Comparative Assessment Community Based Solid Waste Management (CBSWM) Medan, Bandung, Subang, and Surabaya". 2006. Jakarta: Development Alternatives, Inc.

[2] Challcharoenwattana, A., Pharino, C. "Co-Benefits of Household Waste Recycling for Local Community's Sustainable Waste Management in Thailand". Journal Sustainability Vol 7, 2015, pp 7417-7437.

[3] Ahmadi, M., Hashim, H. S., Mohamed, A. F., Moharamnejad, N. "Toward Community-Based Waste Management: Tehran as a Case Example". Middle-East Journal of Scientific Research Vol. 15 (8), 2013, pp 1102-1107

[4] Okalebo, S. E., Opata, G. P., Mwasi, B. N. "An Analysis of the Household Solid Waste Generation Patterns and Prevailing Management Practice in Eldoret Town, Kenya". International Journal of Agriculture Policy and Research, Vol. 2 (2), 2014, pp. 076-089

[5] Tilaye, M., van Dijk, M. P. "Sustainable Solid Waste Collection in Addis Ababa: The User's Perspective". International Journal of Waste Resources, Vol. 4 (3), 2014.

[6] Tisna, A., Trihadiningrum, Y. "Study of Solid Waste Management System in Bubutan District, Surabaya City. Theses, Environmental Engineering, RSL 628.44 Ayu k. 2010

[7] Tallei, T. E., Iskandar, J., Runtuwene, S., Filho, W. L. "Local Community-Based Initiatives of Waste Management Activities on Bunaken Island in North Sulawesi, Indonesia". Research Journal of Environmental and Earth Science, Vol. 5 (12), 2013, pp. 737-743

[8] Agwu, M. O. "Issues and Challenges of Solid Waste Management Practice in Port-Harcourt City, Nigeria – A Behavioural Perspective". American Journal of Social and Management Science, Vol. 3 (2), 2012, pp. 83-92

[9] Otitoju, T. A. "Individual Attitude toward Recycling of Municipal Solid Waste in Lagos, Nigeria". American Journal of Engineering Research (AJER), Vol. 3, No. 7, 2014, pp. 78-88

[10] Adogu, P. O. U., Uwakwe, K. A., Egenti, N. B., Okwuoha, A. P., Nkwocha, I. B. "Assassment of Waste Management Practices Among Residents of Owerri Municipal Imo State Nigeria". Journal of Environmental Protection, Vol. 6, 2015, pp. 446-456

[11] Muhammad, M. N., Manu, H. I. "Gender Roles in Informal Solid Waste Management in Cities of Northern Nigeria: A Case Study of Kaduna Metropolis". Academic Research International, Vol. 4, No. 5, 2013, pp. 142-153

[12] Singhirunnsorn, W., Donlakorn, K., Kaewhanin, W. "Household Recycling Behaviors and Attitudes toward Waste Bank Project: Mahasarakham Municipality". Journal of Asian Behavioral Studies, Vol. 2 No. 6, 2012, pp. 35-47

[13] Chengula, A., Lucas, B. K., Mzula, A. "Assessing Awareness, Knowledge, Attitude and Practice of The Community Towards Solid Waste Disposal and Identifying the Threats and Extent of Bacteria in The Solid Waste Disposal Site in Morogoro Municipality in Tanzania". Journal of Biology, Agriculture, and Healthcare, Vol. 5 No.3, 2015, pp. 54-65

[14] Haider, A., Amber, A., Ammara, S., Mahrukh, K. S., Aisha, B. "Knowledge, Perception, and Attitude of Common People towards Solid Waste Management – A Case Study of Lahore, Pakistan". International Research Journal of Environment Sciences, Vol. 3 (3), 2015, pp. 100-107.

[15] Grover, P., Singh, P. "An Analysis Study of Effect of Family Income and Size on Per Capita Household Solid Waste Generation in Developing Countries". Review of Arts and Humanities, Vol. 3, No. 1, 2014, pp. 127-143

[16] Peprah, K., Amoah, S. T., Achana, G. T. W. "Assessing '3Rs' Model in Relation to Municipal Solid Waste Management in Wa, Ghana". World Environment, Vol. 5, No. 3, 2015, pp. 112-120.

[17] Kumar, M., Nandini, N. "Community Attitude, Perception and Willingness towards Solid Waste Management in Banglore City, Karnataka, India". International Journal of Environmental Sciences, Vol. 4, No. 1, 2013, pp. 87-95

[18] Jibril, J. J., Bin Sipan, I., Sapri, M., Shika, S. A., Isa, M., Abdullah, S. "3R's Critical Success Factor in Solid Waste Management System for Higher Educational Institutions". Procedia – Social and Behavioral Sciences 65, 2012, pp. 626-631.

[19] Chowdury, A. H., Muhammad, N., Ul Haque, M., R., Hossain, T. "Developing 3Rs (Reduce, Reuse, and Recycle) Strategy for Waste Management in the Urban Areas of Bangladesh: Socioeconomic and Climate Adoption Mitigation Option". IOSR Journal of Environmental Science, Toxicology and Food Technology, Vol. 8, No. 5, Ver. 1, 2014, pp. 09-18.

[20] Windi, Y. K., Rahariyani, L. D., Wijayanti, D., Rustamaji, E. "Assessing the Benefits of Super Depo as A Model of Integration of Waste Pickers in A Sustainable City Waste Management". International Journal of Environment and Ecological Engineering, Vol. 3, No. 1, 2016.

[21] Indonesia National Standard (SNI) No. 19-3694-1994. "Metode Pengambilan dan Pengukuran Contoh Timbulan dan Komposisi Sampah Perkotaan".

[22] Masduqi, A., Endah, N., E.S. Soedjono, Hadi, W. "Structural Equation Modelling for Assessing the Sustainability of Rural Water Supply System". Journal of Water Science and Technology. 2010.

Second International Conference on Science, Engineering & Environment,
Osaka City, Japan, Nov.21-23, 2016, ISBN: 978-4-9905958-7-6 C3051

A REVIEW ON IMPLEMENTATION OF SAFETY TRAINING AMONG STUDENTS IN SCHOOL

Nurul Husna Che Hassan[1], Ahmad Rasdan Ismail[1], Nor Kamilah Makhtar[2], Nik Anis Amanina Nik Ayub[1], Mohd Arifpin Mansor[3], Norhidayah Mat Sout[4]

[1]Faculty of Creative Technology and Heritage, University Malaysia Kelantan
Locked Bag 01, 16300 Bachok, Kelantan. Malaysia
[2]Institut Pendidikan Guru Kampus Kota Bharu,
Jalan Maktab, Pengkalan Chepa, 16109 Kota Bharu Kelantan, Malaysia
[3]Faculty of Technology Engineering, Universiti Malaysia Pahang,
Lebuhraya Tun Razak, 26300 Gambang, Malaysia
[4]Faculty of Mechanical Engineering, University Malaysia Pahang,
26600, Pekan Pahang Darul Makmur, Malaysia

ABSTRACT

This paper presents the review of safety implementation from several studies that focus on training program in school. A school is a strategic organization to develop young people of the country with the characteristics of society expects. Student, teacher and other staff in school expose with the variety of risk and hazard as they spend a lot of their time in schools. Therefore, training program regarding safety issue need to conduct in the school society to avoid any unplanned events occur that can bring harm to the people surrounding. The objective of occupational safety and health training is to equip students with necessary knowledge, information and also develop their ability so that they realize and know about the safety issue in school. Apart from that, training program need to include knowledge about the safety in educational environment to prevent accident and improve the safety in school. As conclusion, safety training has established support by organizations of school in improving safer work practice, then there remains limited empirical evaluation to determine specific impact on improvements in safety culture and safety performance in school.

Keywords: Safety, Health, Training, Students

INTRODUCTION

In recent years, safety has become a central issue which has been growing in the social context that increasing the concern for prevention of danger situations [2]. Certain safety conditions are being explored in entirely life scopes which are related to quality and welfare. One of the scopes for ensuring safety is from the educational activities in school. Children, young people, teachers and other staff spend most of their time in school. In Turkey, previous study reported that the period of students spend their daily in school is about 180 days of a year and 6 hours [9]. A school is considered as a place of work. In the Act, "place of work" means premises where persons work or premises used for the storage of plant and substance [20]. Thus, the probability of the risk and hazard occurred in school was higher. The risks and hazards that occur may negatively affect

their health and wellbeing. In order to prevent danger situations in schools, safety condition in school need to be considered in all of the aspects which are the school physical environment and the social environment [2].

Reference [9] stated that school safety means students and staff should feel themselves free in physically, psychologically and emotionally manners. The basic reason why schools exist is because of the students and their education. Therefore, school safety and student safety concepts are used interchangeably in literature. Safety schools provide a social and physical environment that effect appropriate behavior of students. The physical environment includes the way in which the building and the school's routines are managed to prevent problems [8].

Reference [4] clearly stated that, compared with older, young people are more vulnerable to accidents when entering any of the workplace. Another major studies were found that, although the schools are classed with a low-risk level, it is necessary to take preventive measures to prevent accident in school. Therefore, the community of school need to conduct safety program to prevent from unexpected situation occur in the workplace [7].

SAFETY TRAINING IN EDUCATION

Training is defined as the systematic of knowledge, skills and attitudes in order to develop the competencies for effective performance of the people in the work environment [25]. Reference [3] defined a safety program as the control of the working environment, equipment, processes, and the workers for the purpose of reducing accidental injuries in the workplace. Some studies have concluded that training in occupational health and safety (OHS) is important and need to be included in workplace-based learning (WPL). This training can be applied to the learning method as well as to the course content [11].

Several authors highlight the importance of close cooperation between school and work in order to deliver relevant and desired knowledge. The knowledge of teachers and experts in the workplace about the safety in school must higher and must be more willing to provide workplace-based learning (WPL) for pupils regarding the safety knowledge hence, the pupils will be aware of the safety issue at school [26]. Reference [28] identified the communication between pupil, teacher, and supervisor is the most successful way to reach training goals.

IMPLEMENTATION OF SAFETY TRAINING IN SCHOOL

Reference [5] points out that education and awareness strategies for preventing from injuries and accidents among young people especially students are widely described in the scientific literature. Safety training program is conducted regarding to the attitude or behavior of student that tend to contribute to the main cause of injury in school or workplace [16]. Training program also focus on ''safety culture'' among students which is directed a school education movement in other educational programs elsewhere in Canada and United States [23]. Previous research studies have revealed that most of the current occupational health and safety (OHS) training and awareness approach are based on a behavioral educational paradigm, which is oriented to ensure the student's attitude or behavior follow OHS rules [16]. Those approaches focus on the trainer role and unidirectional of knowledge exchanges from the trainer to the trainee.

Apart from that, with the strict application of educational and non-educational regulations are not enough, the prevention of risk and hazards in schools are requires to integrate the management of safety in the usual tasks in order to guarantee the protection of all the people in school [17].

Importance of effective safety training in school

Effective training involves changing cognition, attitudes and behaviors and consequently the way people conduct themselves at work [27]. According to some researchers, an important part of preparing people for the occupational processes is specially the education and training [24]. The increasing level of education reflects the improvement of education in schools [20]. The article proves the importance of education in field of respecting the safe work and the prevention of student's health in school [18].

Besides that, other study revealed that to develop and improve training in OHS education, headmasters could point out the importance of training including safety training for the students [1]. One way to improve the supervisors' role is by inform them about what students had been trained for at school about OHS, but they should also be given enough time to discuss the content of OHS with teachers.

Apart from that, according to researchers study, they noted that, the training need to include the knowledge about the safety in educational environment such as the school building which covers the all education activities and facilities. One of the buildings is laboratory which involving students who are conducting the practical work. During practical work, they involve with the chemical hazard [9]. Thus, laboratory safety can be stated as taking measures to risks that can be aroused while making experiments or possible failure of materials, devices, hardware. Therefore, both teachers and students should be informed about the possible hazards, and have the basic first aid ability. Reference [10] point out that the students who are trained for first-aid are more willing to take responsibility and to internalize safe attitudes.

Besides that, schools should have an emergency escape plan which is known by all students and staff. Evacuation procedures should be explained including procedures during lunch or at assemblies. In each floor or class, there has to be a fire alarm which is connected to early warning system. Fire drills can be practiced regularly as well as suddenly and should be considered indispensable for health and life safety. Reference [13] found that the knowledge of occupational health and safety hazards, legislation, standards for measurement of noise, lighting, indoor climate, chemicals in the workplace air, vibration etc. are needed.

Benefits of safety training implementation

Aside from providing specific courses in Occupational Health and Safety (OHS) at the beginning of the 3-year training programs, the teachers organize their teaching based on their own experiences and knowledge. The teaching is based on risk factors that are present in the workshops at school, where pupils have their practical training, or on the teacher's own experiences with accidents or incidents. In a review of 95 different methods of OHS training, some studies found that more implementation of training methods increased student's knowledge about OHS and were decrease the number of accidents and illnesses [6]. Therefore, safety training could be an effective way to improve the work environment as well as awareness of risks in

the work environment and thereby decrease the potential for accidents for students [1].

Reference [14] study found that the communication between students, teachers, and supervisors in the workplace is also an important part to achieve well-functioning training. The teachers normally visited the students at least once during the practice periods. Other study describes the importance of combining the rationales of education in OHS for the groups of pupils, schools, and workplace-based learning (WPL) companies to one common goal in order to make learning in OHS become more useful [12].

Some campaigns were carried out and focused on children's safety and health and preventing disease in children with a complete wellbeing support in school. Throughout these education, all individuals get fully benefit and advantage [22].

On the other hand, study by researcher point out that, the training activities was planned to make sure the employees have the appropriate attitudes, and also serve to keep their safety and health. Regular training is considered as a function to increase employees' knowledge, skills and performance and to protect their physical and spiritual health. Table 1 showed the overall issue of safety training in school among students.

Table1 Overall Issue of Safety Training in School among Students.

No	Author	Description
1	Reference [14]	The communication between organizations in school is important to develop well-functioning training.
2	Reference [21]	Fifty-percent of the school's heads agreed that it was necessary to improve the OSH status in their school.
3	Reference [19]	Training in OSH is becoming more important towards increasing the culture of job safety at work place, and to increase awareness among occupants
4	Reference [10]	Safety training need to include the knowledge about the safety in laboratory since it is involving students to expose with the chemical hazard.

CONCLUSION

Based on the reviews from many studies, it showed that the implementation of safety in schools is an essential aspect to increase the protection of all the students, teachers and staff from the risk and hazards in school environment. The whole school community plays an important role in school safety assurance. School must provide volunteers with the necessary information, training and supervision and consult with them on work health and safety matters. According to some studies, motivation and training that aimed to adhere the principles of safe work is very topical today [15]. The objective of occupational safety and health training is to equip students with necessary knowledge, information and develop their ability and skills [18]. It is very important during academic preparation of future teachers in order to educate them about OSH and provide them with all knowledge and information about the OSH topic. The majority of graduate students work as teacher at high schools, where they expose with the hazard and harm at school. Thus, they need to share their knowledge about safety

and health issues to the students. The education content, gained knowledge, abilities and skills should be useful in further study or every day's practice [18]. Therefore, systematic training programs prepared in the school are the right steps that lead the community to develop culture of safety and health in school.

REFERENCES

[1] Andersson I-M, Gunnarsson K, Moberg M, Rosén G. Knowledge and experiences of risks among pupils in vocational education. Saf Health Work 2014;5: 140-6.

[2] Anna Diaz Vicario. Safety Management in Catalonia's school. Social and Behavioral Sciences 46, 2012 : 3324 – 3328

[3] Anton TJ. Occupational Safety and Health Management, New York, McGraw-Hill, Second Edition. 1989

[4] Balany J, Adesina A, Kearny G, Richards S. Assessment of occupational health and safety hazard exposure among working college students. 2014;57:114-24.

[5] Burke, M.J., Sarpy, S.A., Smith-Crowe, K., Chan-Serafin, S., Salvador, R.O., Islam, G. Relative effectiveness of worker safety and health training methods. Am. J. Public Health 96 (2) ,2004: 315–324.

[6] Burke M.J, Sarpy SA, Smith-Crowne K, Chan-Serafin S, Salvador RO, Islam G. effectiveness of worker safety and health training methods. Am J Public Health 2006;96:315-24.

[7] Defensor del Pueblo Andaluz, 2003: Sevilla: Defensor del Pueblo Andaluz.

[8] Dwyer, Kevin, David Osher. *Safeguarding our children: An action guide*. Washington, DC: U.S. Department of Education and Justice, American Institute for Research. Isik, Halil. 2004: 32,164: 154 – 161.

[9] Erkan Tabancalia, Talha Bektas. Student safety in primary schools: A sample of Buyukcekmece county. Procedia Social and Behavioral Sciences 1, 2009: 281–284

[10] Ferika Ozer Saria. Effects of employee trainings on the occupational safety and health in accommodation sector. Procedia Social and Behavioral Sciences 1, 2009:1865–1870

[11] Holte KA, Kjestveit K. Young workers in the construction industry and initial OHS Training when entering work life. Work 2012;41:4137-41.

[12] Jorgensen CH. Connecting work and education: should learning be useful, correct or meaningful? Workplace Learn 2004;16:455-65.

[13] Karin Reinhold, Virve Siirak, Piia Tint. The Development of Higher Education In Occupational Health and Safety In Estonia and Selected EU Countries. Procedia - Social and Behavioral Sciences 143, 2014:52 – 56

[14] Kopsen S. How vocational teachers describe their vocational teacher identity. J Vocat Educ Train 2014;66:194-211.

[15] Kozik, T., & Feszterova, M. Dolezitost vzdelavania v oblasti bezpecnosti a ochrany zdravia pri práci. In. Edukacja - Technika -Informatyka : wybrane problemy edukacji technicznej i zawodowej. ISSN 2080-9069, Roc. 3, c. 2, 2011:1. cast, s. 115-120.

[16] Lavack, A.M., Magnuson, S.L., Deshpande, S., Basil, D.Z., Basil, M.D., Mintz, J.H. Enhancing occupational health and safety in young workers: the

role of social marketing. Int. J. Nonprof. Volunt. Sec. Market. 13 (3), 2008:193–204.

[17] Leger, L.; Young, I.; Blanchard, C. & Perry, M. Health promotion in schools. From evidence to action. France: UIPES.2010.

[18] Melania Feszterova. Implementation Of E - Learning In To OHS Education Procedia - Social and Behavioral Sciences 191.2015: 1275 – 1281

[19] Mustazar Mansur & Ho Shu Pengm . Effectiveness Of Occupational Safety And Health Training In Reducing Accidents At Work Place. Prosiding Perkem Iv, Jilid 2,2009: 293-324 Issn: 2231-962x

[20] NSKC. Promoting Child Safety to Prevent Unintentional Injury. *School Injury Fact Sheet Washington DC* [Online], 2004: Available: http://www.safekids.org. [Accessed 10th March 2015].\

[21] Nurul .A.H, Tengku M.A.Situational Analysis On Safety And Health In Primary School In Kota Bharu. Journal of Community Health, 2009: Vol 15 Number 2.

[22] Nutbeam, D. Health literacy as a public health goal: a challenge for contemporary health education and communication strategies into the 21th century. *Health Promotion International*, *1*5(3), 2000: 259-267.

[23] Power, N., Baqee, S. Constructing a 'culture of safety': an examination of the assumptions embedded in occupational safety and health curricula delivered to high school students and fish harvesters in Newfoundland and Labrador, Canada. Policy Pract. Heal. Saf. 8 (1), 2010: 5–23.

[24] Robson, L. S. ,Stephenson, C. M. , Schulte, P. A., et al. A systematic review of the effectiveness of occupational health and safety training. SCANDINAVIAN. JOURNAL OF WORK ENVIRONMENT & HEALTH, 2012: Vol. 38, Issue 3, 193-208.

[25] Salas, E. & Cannon-Bowers, J. The Science of Training: A Decade of Progress. *Annual Review of Psychology*, 52, 2001:471-499.

[26] Svensson L, Randle H, Bennich M. Organising workplace learning: an inter organizational perspective. J Eur Ind Train 2009;33:771-86.

[27] Tannenbaum, S. & Yukl, G. Training and Development in Work Organizations. *Annual Review of Psychology*, 43, 1992: 399-441.

[28] Winters A, Meijers F, Kuijpers M, Baert H. What are vocational training conversations about? Analysis of vocational training conversations in Dutch vocational education from a career learning perspective. J Vocat Educ Train 2009;61:247-66.

Second International Conference on Science, Engineering & Environment,
Osaka City, Japan, Nov.21-23, 2016, ISBN: 978-4-9905958-7-6 C3051

HEAVY METAL SPECIATION IN SEDIMENTS AND THE ASSOCIATED ECOLOGICAL RISK IN SAGULING LAKE WEST JAVA INDONESIA

Eka Wardhani[1,2], Suprihanto Notodarmojo[3] and Dwina Roosmini[4]
[1]Environmental Engineering Program ITB, Post-Graduate Academy, Bandung, Indonesia.[2]Department of Environmental Engineering, Itenas Bandung, Indonesia.
[3,4]Department of Environmental Engineering, ITB Bandung, Indonesia

ABSTRACT

The purpose of this study was to assess the chemical speciation of selected heavy metals (Cd, Cr, Cu, and Pb) in 12 surface sediments at Saguling Lake West Java Indonesia. A five-step sequential extraction technique was used to evaluate speciation heavy metals from Saguling Lake surface sediments. A risk assessment code (RAC) was applied to estimate the risk of heavy metals release in to the environment. The total mean value of heavy metals in surface sediment varied in the following descending order Cr>Cu>Cd>Pb. Based on the RAC value the sediments of Saguling Lake had been polluted by heavy metals, and they did pose medium ecological risk. The information on total metal concentrations in sediment was not sufficient for assessing the metal behavior in the environment, but metal speciation greatly determines the behaviors and toxicity of metals in the environment so it was more effective in estimating the environmental impact of contaminated sediments.

Keywords:Metals, Sediment, Speciation, Saguling

.

INTRODUCTION

Sediments are a significant storage compartment for metals that are released to the water column in rivers, lakes, and oceans. Because of their ability to sequester metals, sediments can describe water quality and record the effects of anthropogenic emissions [6].

It is well accepted that total metal content in sediments cannot predict the bioavailability and toxicity of that metal [4]. It is in fact the physicochemical forms of the metal that establish its possibility bioavailability and toxicity. Thus, the speciation and distribution study of metals in sediments has become one of the most important areas of environmental investigation [11],[16].

Metal speciation extremely determines the characters and toxicity of metals in the environment. Speciation indicates to the occurrence of a metal in a variant of chemical form. These forms may include free metal ions, metal complexes dissolved in solution and sorbed on solid surface, and metal species that have been co-precipitated in major metal solids or that occur in their own solid [10]. The speciation studies of metals in sediments not only conduct an showing of the current quality of the overlaying water but also provide important information on the transportation and fate of pollutants [5], [7], [14], [15].

Saguling lake was built on The Citarum River. The Citarum Watershed is home to the largest industrial area in West Java Province. Several economic activity are performed along Citarum River, including mining and agriculture. Futhermore, large amounts of untreated wastewater containing heavy metals from industrial sources have contributed to increased pollution of the lakes. The quality of water in the Saguling lake has been monitored since 1990 by the state agency for environmental control, there are no reports about heavy metals in sediment of the lake. There is insufficient information for an assessment of heavy metals distribution in the lake [9].

The objective of this study was to evaluate performance of the heavy metal speciation in sediments from Saguling Lake West Java Provinces, and to use the calculated risk assessment code (RAC) to assess the potential ecological risk associated with the heavy metals present. This work will provide the direct evidence needed by local environmental authorities to allow them to design and implement the measures necessary to improve lake water quality.

MATERIAL AND METHOD

Surface sediment were collected in November 2015 at twelve sampling sites around Saguling lake. The sampling sites in Saguling lake presented in TAble 1 and Figure 1. Surface sediment were collected using a Eickman Grab from the depth of 0-20 cm. The samples were packed by plastic spatula in plastic boxes and preserved at 4^{o}C until theirs transfer to the laboratory. In the laboratory, samples were dried, crushed, grind and sieve to fraction <1.5 mm.

Table 1 The location of sampling sites in Saguling lake

No. of the site	Latitude (N)	Longitude (E)	Location
1	06°56'29.8"	107°32'10.7"	Citarum River Nanjung section
2	06°54'58.9"	107°28'32.3"	Citarum River near Batujajar
3	06°53'13.5"	107°28'32.3"	Trash Boom Cihaur Village
4	06°53'13.4"	107°27'09.0"	Cimerang Village
5	06°53'13.0"	107°25'54.4"	Cihaur Estuary near Morocco Village
6	06°56'07.6"	107°27'25.5"	Cipantik Estuary
7	06°57'14.6"	107°26'03.8"	Ciminyak Estuary
8	06°56'14.9"	107°24'50.8"	Cijere Estuary
9	06°56'00.4"	107°22'22.4"	Cijambu Estuary
10	06°54'54.4"	107°22'26.3"	intake structure
11	06°51'49.8"	107°20'57.0"	trailrace
12	06°51'10.8"	107°20'58.0"	Bantar Caringin Village

Fig. 1 The location of sampling sites in Saguling Lake

Sequential extraction procedure of heavy metals

Sequential extraction was worked using a three stage modified procedure suggested by BCR plus the residual fraction [2]. The extraction steps took on in this study can be amply sum of as attends.

Step 1 (acid extractable/exchangeable fraction, F1): 40 mL of 0.11 M acetic acid was added to 1 g of sediment sample in a centrifuge tube and shaken for 16 h at room temperature. The concentrate was then separated from the solid residue by centrifugation and filtrate was separated by decantation as beforehand explained.

Step 2 (easily reducible fraction, F2): 40 mL of recently available hydroxyl ammonium chloride was added to the residue from step 1 in the centrifuge tube, and re-suspended by mechanical shaking for 16 h at room temperature. The separation of the extract collection of the supernatant, and cleansing of residues were the same as described in step 1.

Step 3 (oxidizable fraction, F3): The residue in step 2 was made twice with 10 mL of 8.8 M hydrogen peroxide. First 10 mL of hydrogen peroxide was added to the residue 2 in the centrifuge tube. The digestion was allowed to proceed at room temperature for 1 h with occasional manual shaking, attended by digestion at 85±2°C for another 1 h. During the digestion, the centrifuge tube was freely protected to avoid significant loss of hydrogen peroxide. Next, the centrifuge tube was disclose and heating was sequented until the volume reduced to about 2-3 mL. An additional 10 mL of hydrogen peroxide was added to the tube, covered, and digested with cover at 85±2°C for another hour. Heating was continued as before until the volume reduced to 2-3 mL. Finally, 50 mL of 1 M ammonium acetate was added to the cold mixture and shaken for 16 h at room temperature. The separation of the extract, collection of the supernatant, and rinsing of residues were the same as described in step 1.

Step 4 (residual fraction, F4): The residue from step 3 was digested using a compound of aqua regia. An internal check was performed on the products of the sequential extraction by comparing the total quantity of metal extracted by variant reagents during the sequential extraction procedure with the results of the total digestion.

The content of heavy metals (Cd, Cr, Cu, and Pb) was determined by Inductively coupled plasma mass spectrometry (ICP-MS).

RESULT AND DISCUSSION

Environmental Setting

The Saguling lake region is 4.710 Ha the water storage capacity is 730,5 million m^3. The surrounding area of Saguling Lake is hilly, while the river has many tributaries at this location. This makes the form of Saguling Lake very ragged or dendriform, with many extended bays. The lake area was previously densely populated by farmer resident with extensive agricultural lands. The catchment areas of the lake or the upper Citarum River basin are faced with high population tension. This is because more 50% of the population consists of farmers with a high annual growth rate (2.34% is the national average) [9].

Due to the high population density in the upper catchment of the lake, extensive agricultural land, soil erosion and the presence of industries, the lake water became polluted and eutrophic. The growth of aquatic weeds has been accelerated, with frequent blooms of *Microcystis* algae. The water is also contaminated by heavy metals, pesticides, etc. An extensive growth of water-hyacinth is maintained by fencing to reduce pollutant contents of water at inlets of the Citarum River [9]. Originally, the Saguling was planned for a single purpose lake to generate electricity. Later, considering the environmental problems of the area, the Saguling

was re-planned as a multipurpose lake such as raw water, fisheries, aquaculture, and tourism [9].

Phsyco-chemical characteristics of sediments

The phsyico-chemical characteristics of surface sediments were related with the speciation of heavy metals gives at Table 2. The pH is exactly influenced by many parameters, such as cation exchange capacity (CEC), clay content, redox conditions and others, being responsible for the solubility and mobility of metals and metalloids in soils and sediments [3]. The pH in sediments ranged from 6.1 to 7.0 and the average value is 6.4, explaining that the sediments were neutral and almost same value for all sampling location.

Table 1 Phsyico-chemical parameters of the Saguling lake surface sediments

No. of the site	pH	Sand	Silt	Clay
		%		
1	7.0	41.2	44.4	18.1
2	6.4	57.9	32.4	10.3
3	6.8	26.6	55.8	23.9
4	6.5	18.5	53.7	23.9
5	6.2	11.1	67.7	29.0
6	6.1	67.2	25.7	13.6
7	6.3	59.1	32.2	12.2
8	6.1	85.6	10.7	3.9
9	6.2	8.2	73.7	37.9
10	6.3	57.1	35.0	13.1
11	6.4	18.0	63.0	36.0
12	6.5	8.0	67.0	30.0

Sand content for the studied samples varies from 8.0-85.6% whereas silt and clay content varies from 10.7-73.7% and 3.9-37.8%, respectively. Sand, silt and clay value fluctuate from site 1 to 12. Site 8 had the highest value for sand, site 9 had the highest value for silt and site clay. Based on the analysis of the sediment type is silt-sand from site 1 and 2, site 7 and 10 are sand-silt, site 6 and 8 is sand, the last site 3,4,5,9,11, and 12 B is silt.

Total heavy metal concentrations

The concentrations of Cd, Cr, Cu, and Pb in surface sediment samples are shown in Table 3, Cd concentrations were greatest at site 2 at 29.2 mg/kg and lowest at site 11 at 12.9 mg/kg. The concentrations of Cr at site 8 is the highest with a value of 255.2 mg/kg, while lowest Cr concentration is at site 11 with a value of 93.4 mg/kg. The highest Cu concentration is at site 5 with a value of 96.3 mg/kg and the lowest Cu concentration is at site 11 with a value of 37.0 mg/kg.. The concentration of Pb were highest at site 5 at 29.0 mg/kg and lowest at site 11 at 5.5 mg/kg. In summary the contents of Cd, Cr, and Cu were conciderable higher than the standard level.

Table 3. Total heavy metals concentrations of the Saguling lake surface sediments

No. of the site	Total Concentration (mg/kg dry matter			
	Cd	Cr	Cu	Pb
1	25.6	236.3	66.2	12.1
2	29.2	236.3	75.5	28.7
3	22.6	214.0	87.8	23.2
4	27.3	233.9	69.5	22.3
5	26.9	253.8	96.3	29.0
6	25.1	224.0	90.9	26.0
7	22.3	177.6	82.7	26.1
8	22.4	255.2	85.8	17.8
9	22.5	187.3	84.1	25.8
10	26.9	210.7	91.3	22.4
11	12.9	93.4	37.0	5.5
12	15.6	123.9	45.2	9.9
Mean	23.3	203.9	76.0	20.7
Standard Deviation	4.8	50.7	14.5	7.7
Sample Variance	23.4	2,568	209.6	59.8
Minimum	12.9	93.4	45.2	5.5
Maximum	29.3	255.2	96.3	29.0
ANZECC ISQG-Low[a]	1.5	80	65	50
Average shale[b]	0.3	90	45	20

a: [1] b: [13]

Heavy metal speciations

In a natural, aerobic freshwater aquatic system with typical Cd-S-CO_2 concentrations, Cd^{2+} is the predominant species below pH 8, $CdCO_3^o$ is predominant from pH 8 to 10, and $Cd(OH)_2^o$ is dominant above pH 10. The solubility of Cd is minimum at pH 9.5 [8].

F1 concentrations ranged between 0.0-8.5 mg/kg with an average of 0.46 mg/kg. The highest concentration is in site 1 located Saguling lake inlet in the Citarum River Nanjung section, while the lowest concentration is in the site 11 located Saguling lake outlet. F2 concentrations ranged between 3.6-8.9 mg/kg with an average of 3.1 mg/kg. The highest concentration is in site 9 while the lowest concentration is in the site 12. F3 concentrations ranged between 0.0-4.1 mg/kg with an average of 0.8 mg/kg. The highest concentration is in site 11 while the lowest concentration is in the

site 1, 2, 4, 7, and 10. F4 concentrations ranged between 19.5-91.1 mg/kg with an average of 39.5 mg/kg. The highest concentration is in site 10 while the lowest concentration is in the site 7.

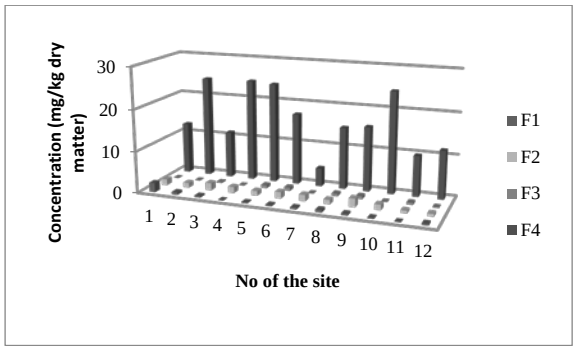

Fig. 2. Chemical peciation of Cd in twelve sediment samples from Saguling lake

Based on the average value of the concentration of the largest to the smallest fraction of the heavy metal Cd in Saguling lake is F4> F2> F1> F3 so it can be concluded that only a small fraction of heavy metals Cd which are mobile.

The speciation of Cd is generally considered to bedominated by dissolved forms except in cases where the concentration of suspended particulate matter is high such as “muddy” rivers and reservoirs and near-bottom benthic boundary layers, and underlying bottom sediments in river sand lakes [20].

Chromium (Cr)

Cr, as well as Zn, are the most abundant of the “heavy metals” with a concentration of about 69 mg/kg in the lithosphere. Cr occurs in nature mainly in the mineral chromite. The metallurgy industry uses the highest quality chromite ore whilst the lower-grade ore is used for refractory bricks in melting furnaces. Major atmospheric emissions are from the Cr alloy and metal producing industries. Cr^{6+} is a potent carcinogen and Cr^{3+} is an essential trace element [19].

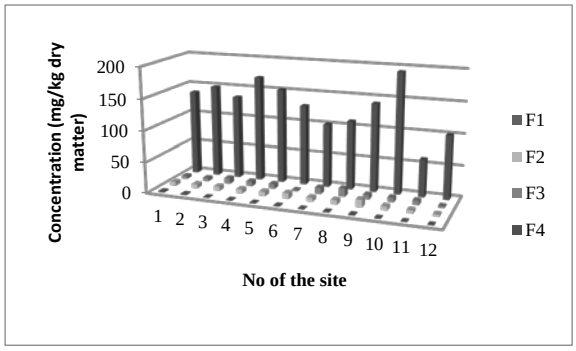

Fig. 3 Chemical peciation of Cr in twelve sediment samples from Saguling lake

The total content of Cr in Saguling lake surface sediment exceeds the standard base on Australian and New Zealand Environment and Conservation Council, 1997. Cr total concentration varied from 93.4-255.2 mg/kg. The minimum value of Cr is located in site 11 while the maximum value is located in site 8. The average value is 203.9 mg/kg, which is higher than the background value of word geochemical background value in average shale [13].

F1 concentrations ranged between 0.2-1.9 mg/kg with an average of 1.0 mg/kg. The highest concentration is in site 1 located Saguling lake inlet in the Citarum River Nanjung section, while the lowest concentration is in the site 12 located Saguling lake outlet. F2 concentrations ranged between 2.8-11.9 mg/kg with an average of 6.7 mg/kg. The highest concentration is in site 9 while the lowest concentration is in the site 12. F3 concentrations ranged between 2.5-13.44 mg//kg with an average of 7.1 mg/kg. The highest concentration is in site 8 while the lowest concentration is in the site 12. F4 concentrations ranged between 60.38-169.7 mg/kg with an average of 131.7 mg/kg. The highest concentration is in site 4 while the lowest concentration is in the site 11.

Based on the average value of the concentration of the largest to the smallest fraction of the heavy metal Cr in Saguling lake is F4> F3> F2> F1 so it can be concluded that only a small fraction of heavy metals Cr which are mobile.

Copper (Cu)

F1 concentrations ranged between 4.5-12.3 mg/kg with an average of 8.6 mg/kg. The highest concentration is in site 9, while the lowest concentration is in the site 12 located Saguling lake outlet. F2 concentrations ranged between 1.6-5.4 mg/kg with an average of 3.1 mg/kg. The highest concentration is in site 7 while the lowest concentration is in the site 12. F3 concentrations ranged between 7.2-30.0 mg//kg with an average of 20.5 mg/kg. The highest concentration is in site 3 while the lowest concentration is in the site 6. F4 concentrations ranged between 1.2-54.8 mg/kg with an average of 22.1 mg/kg. The highest concentration is in site 10 while the lowest concentration is in the site 4. Based on the average value of the concentration of the largest to the smallest fraction of the heavy metal Cu in Saguling lake is F4> F3> F1> F2 so it can be concluded that only a small fraction of heavy metals Cu which are mobile.

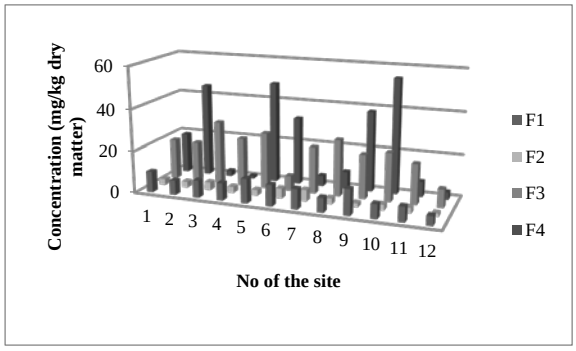

Fig. 4 Chemical peciation of Cr in twelve sediment samples from Saguling lake

Lead

F1 concentrations ranged between 0.0-1.5 mg/kg with an average of 0.1 mg/kg. The highest concentration is in site 1, while the concentration in other site are zero. F2 concentrations in all sampling point are zero. F3 concentrations almost zero in all sampling point except in site 6. F4 concentrations ranged between 3.4-23.3 mg/kg with an average of 12.3 mg/kg. The highest concentration is in site 5 while the lowest concentration is in the site 9.

Based on the average value of the concentration of the largest to the smallest fraction of the heavy metal Pb in Saguling lake is F4> F3> F1> F2 so it can be concluded that only a small fraction of heavy metals Pb which are mobile.

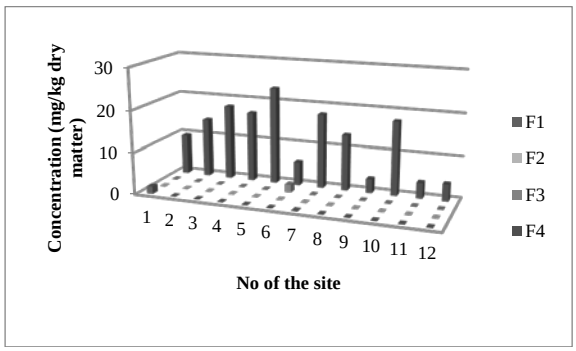

Fig. 5 Chemical peciation of Cr in twelve sediment samples from Saguling lake

The most important environmental sources for Pb are gasoline combustion (presently a minor source, but in the past 40 years a major contributor to Pb pollution), Cu-Zn-Pb smelting, battery factories, sewage sludge, coal combustion, and waste incineration [15].

risk assessment code (RAC)

Metals are bound to different sediment fractions, with the binding strength determining their bioavailability and the risk associated with their presence in aquatic systems. The risk assessment code (RAC) was determined based on the percentage of the total metal content that was found in the exchangeable and acid soluble fraction (F1). This fraction is considered to be the most unstable and reactive phase, which has greater potential for adverse effects on the aquatic environment compare to the other fractions [7]. When the percentage mobility is less than 1%, the sediment has no risk to the aquatic environment. Percentages of 1 < RAC < 10% may reflect low risk, 11 < RAC < 30% medium risk, and 31 < RAC < 50% high risk. A RAC percentage above 50% poses a very high risk and it is considered dangerous because metals are easily able to enter the food chain [7]. As can be seen from Table 4, sediment had no or low risks associated with Cd and Cr, which had RAC value below 10% in all of the samples, indicating that these metals were only slightly mobile in the lake sediment. All of the samples had low or medium risks (RAC values below 30%) associated with Cu. Pb pose a medium risk to the environment at site 1. The results suggested that Cd, Cr, Cu, and Pb, were not easily released by the sediments into the water and therefore that heavy metals wouldnot be likely to enter the food chain in the Saguling lake ecosystem.

Table 4. Risk assessment code (RAC) for heavy metals in surface sediment from Saguling lake

No. of the site	Heavy Metals			
	Cd	Cr	Cu	Pb
1	Low	No	Medium	Medium
2	Low	No	Low	No
3	Low	No	Low	No
4	No	No	Medium	No
5	No	No	Medium	No
6	Low	No	Medium	No
7	Low	No	Medium	No
8	Low	No	Low	No
9	Low	No	Medium	No
10	No	No	Low	No
11	No	No	Medium	No
12	Low	No	Low	No

RAC value can be used as illustration that Saguling lake surface sediments have been contaminated by heavy metals and should be planned recovery efforts of the heavy metal pollution before causing an adverse impact on public health.

CONCLUSION

Based on result in the surface sediment of Saguling lake demonstrated the existence of differences in the level of Cd, Cr, Cu, and Pb

concentration. The possible main source of the metal contamination in the sediment are municipal and industrial waste water discharge, agriculture runoff, and atmospheric input. Based on calculations with the RAC value sediment had low to medium risks associated with Cd, Cr, Cu, and Pb which had RAC value below 30% in all of the samples. Based on the average value of the concentration of the largest to the smallest fraction of the heavy metal Cd in Saguling lake is F4> F2> F1> F3, Cr in Saguling lake is F4> F3> F2> F1, Cu in Saguling lake is F4> F3> F1> F2, Pb in Saguling lake is F4> F3> F1> F2 so it can be concluded that only a small fraction of heavy metals Cd, Cr, Cu, and Cd which are mobile.

REFERENCES

[1] ANZECC (Australian and New Zealand Environment and Conservation Council) ANZECC Interim sediment quality guidelines report for the Environmental Research Institute of the Supervising Scientist, Sydney, Australia, 1997.

[2] Bo Luji, Wang Dejian, Zhabg Gang, Wang Can. "Heavy metal speciation in sediments and the associated ecological risk in rural river in Southern Jiangsu Province, China". Soil and Sediment Contamination, Vol 24 2015, pp 90-102.

[3] Camila V.A Santolin, Virginia S.T. Ciminelli, Clesia C. Nascentes, Claudia C. Windmoller; "Distribution and environmental impact evaluation of metals in sediments from the Doce River Basin, Brazil" Environmental Earth Science, 2015

[4] Chakraborty Parthasarathi, babu Raghunadh P.V, Sarma V.V, "A study of lead and cadmium speciation in some estuarine and coastal sediments" Chemical Geology Vol. 294-295 2012 . pp 217-225

[5] Cheng, Y., Hu, J., Luo, B., Xu, J.Z., "Geochemical processes controlling fate and transport of arsenic in acid mine drainage (AMD) and natural systems". Journal of Hazardous Materials Vol 165 2009 pp 13-26.

[6] Forstner U. Inorganic sediment chemistry and elemental speciation. In Sediments: Chemistry and Toxicity on In-Place Pollutants (eds. R. Baudo, J. P. Giesy, and H. Mantau). Lewis, 1990 pp. 61-105

[7] Gupta, A.K., Sinha, S., "Assessment of single extraction methods for the prediction of bioavailability of metals to Brassica juncea L. Czern. (var. Vaibhav) grown on tannery waste contaminated soil". Journal of Hazardous Materials 2007. Vol 149, 144-150.

[8] Hem J. D "Chemistry and occurrence of cadmium and zinc in surface water and ground water". Water Resour. Res.8, . 1972 661-679.

[9] Indonesia Power Unit Bisnis pembangkit Saguling, "Laporan Hasil Pemantauan Kualitas Air Waduk Saguling": Perusahaan Listrik Negara 2014.

[10] Kouassi, N.L.B., Yao. K.M., Trokourey A., Soro M.B., " Preliminary assessment of Cadium mobility in surface sediment of a tropical estuary". Bull. Chem. Soc. Ethiop, Vol, 28 (2), 2014 pp 245-254"

[11] Laing, G.D., De Vos, R., Vandecasteele, B., Lesage, E., Tack, F.M.G., Verloo, M.G., "Effect of salinity on heavy metal mobility and availability in intertidal sediments of the Scheldt estuary". Estuarine, Coastal and Shelf Science Vol 77, 2007 pp 589-602.

[12] Li Y.-H., Burkhardt L., and Teraoka H. "Desorption and coagulation of trace elements during estuarine mixing". Geochim. Cosmochim. Acta Vol 48, 1984 pp 1879-1884

[13] Turkerian, K.K and Wedepohl, K.H. "Distribution of the elements in soil mayor units of the earth's crust". Bull geol. Soc Am, Vol 72, 1961 pp 175-192

[14] Zhang, H., He, P., Shao, L.M.,. "Fate of heavy metals during municipal solid waste incineration in Shanghai". Journal of Hazardous Materials Vol 156, 2008 pp 365-373.

[15] Zhao, X., Dong, D., Hua, X., Dong, S.,."Investigation of the transport and fate of Pb, Cd, Cr (VI) and As (V) in soil zones derived from moderately contaminated farmland in Northeast, China". Journal of Hazardous Materials 170, 2009570-577.

[16] Zhong, A.P., Guo, S.H., Li, F.M., Li, G.K., Jiang, X.,. "Impact of anions on the heavy metals release from marine sediments. Journal of Environmental Sciences (China)" Vol 18 2006, pp 1216-1220.

Second International Conference on Science, Engineering & Environment,
Osaka City, Japan, Nov.21-23, 2016, ISBN: 978-4-9905958-7-6 C3051

EMISSION FACTORS OF BLACK CARBON (BC) FROM RICE STRAW OPEN BURNING SPECIFIC TO DISTRICT CIANJUR, WEST JAVA, INDONESIA.

Hafidawati[1], Puji Lestari[2] and Asep Sofyan[3]
[1,2,3]Civil and Environmental Engineering, ITB, Indonesia

ABSTRACT

Open burning of rice straw, common practice in Cianjur, West Java, to eliminate rice residues after harvesting. However, the common practice of post-harvest burning of rice straw emits particulate material , greenhouse gases, and short lived climate force to the atmosphere. Open burning of rice residues in the field releases a large amount of Black Carbon (BC). In this context, this work aims to determine rice straw burning emission factors for Black Carbon on particulate material smaller than 2.5 μm ($PM_{2.5}$) in the field open burning in Districts Cugenang, Cianjur, West Java, Indonesia. Samples of airborne particulate matter ($PM_{2.5}$) from open burning of rice straw were collected at seven locations in District Cugenang for eight varities of rice straw, from June through October 2015. The samples were collected using a minivol air sampler. Black carbon was analyzed using an EEL smoke stain reflectometer. Excess mixing ratios for CO_2, CO, BC in $PM_{2.5}$ were measured, allowing the estimation of their respective emission factors. Average estimated values for emission factors (g kg^{-1} of burned dry biomass) were 0.939 ±0.417 for BC in $PM_{2.5}$. These emission factors presented provide useful information for the development of local emission factors for Black Carbon from open burning of rice straw in Cianjur.

INTRODUCTION

Paddy is the most popular plants in Indonesia which is rapidly increasing annual production to meet domestic demand. Indonesia has a large population, 46% of which lives in rural areas.
Because of the large use of crop residues the burning of rice straw in the fields, this become important type of biomass burning open in Asia which is open combustion residues of rice on the ground. Intensive open burning activities generally take place during the dry season when stagnant atmospheric conditions [14]. It is releasing a number of aerosols cause atmospheric phenomena regional implications strong climate such as Atmospheric Brown Clouds [8].

Open burning of agricultural residue is one of the major source of aerosol emissions. Results of rice straw combustion emits types of particulate matter ($PM_{2.5}$) [3] the pollutant emissions from the combustion, such as BC in PM and CO, have contributed substantially to the regional environmental pollution problem [8]. Black Carbon (BC) contributes directly and indirectly to the earth's radiative balange change, and consequently, has impact on global warming as the second largest contributor after Carbon Dioxide (CO_2). Only a few studies on emissions of pollutants from open burning of waste is done post-harvest rice in Indonesia. Where one of the potential sources of emissions of pollutants BC in $PM_{2.5}$. Therefore, the main purpose of this study is: 1) To asses emission factor of Black Carbon from the burning rice straw in the filed open burning. 2) To investigated the characteristic Black Carbon emitted net burning smoke concentration from the burning of rice straw in the field open burning with different varieties in the Cianjur District. This study provides useful information on pollutant emission, which way lead to air quality management for both local and regional scales.

EXPERIMENTAL WORK

Corp residue collection

Burning straw experiments conducted in the District Cugenang, Cianjur on eight varieties of rice. Straw was collected from seven villages in the districs Cugenang Mekongga varieties collected from Sukamanah, ciherang and cintanur varieties collected from Giri Harja, hybrid varieties from the Babakan Imbangan, Inpari from Panumbangan, varieties inul and sarangue collected from Pangkalan Benjot, Varieties of Pandan wangi collected from Ranca Picung. Sampling was carried smoke from burning straw during the rice harvest in June-July 2015 by 8 field burning in rice harvested in Cianjur**.** Sampling location presented at Fig.1

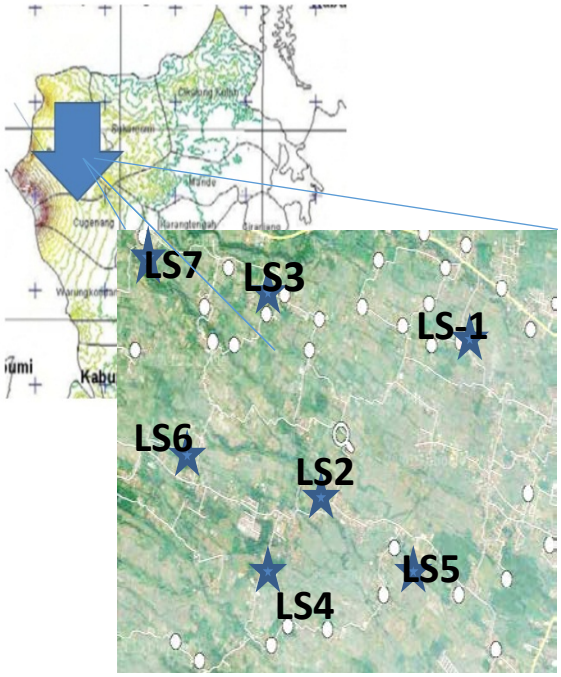

Fig.1 The location of Study Area

Processing Open Burning

Experimental field is the part that is harvested by farmers. Experiments in the field of combustion follow local practice of burning straw. Base on our survey at the seven villages in the Districts Cugenang shows that straw burning is done 4-10 days after the rice harvest in between the hours of 11:00-16:00. Each field experiments on rice varieties performed well every background sampling prior to combustion. Sampling background lasts for 1-2 hours. After completion of sampling the background conditions, the burning of rice straw begins to sample. Smoke sample measurement starts as soon as the fire becomes stable (smoldering) and continue until the fire stops.

Sampling of Black Carbon

Measurements of pollutants (BC, CO and CO_2) carried by air quality monitoring equipment comprising from minivol sampler, and CO and CO_2 analyzer.

Measurement of Black Carbon from field burning experiments was collected by two samplers minivol (Anderson 214 series) on the Teflon filter, collected by the flow rate of 5 $Lmin^{-1}$. Sampling equipments was placed at two points downwind in each experiment the combustion is at a distance of approximately 5 m from the edge downwind of the combustion field, to avoid damage from fire and heat. equipment is positioned at 1.5 m above the ground. Two minivol sampler located about 1-1.5 m from each other. At this distance, samplers considered close enough to capture the same piece of pollutants from smoke and far enough away to minimize disruption inlet flow. Figure of sampling equipment presented at fig.2.

Fig.2.Field Burning Sampling Equipment

All measurement in the field is also done recording meteorological conditions and CO and CO_2 over a period of combustion takes place in the field.

Parameters monitored meteorological conditions consist of wind speed, wind direction, temperature, pressure, and humidity. This parameter measurements carried out in order to see the influence of meteorological conditions on emissions and BC. Continuous data from CO/CO_2 analyzer is used to measure the concentration of gas near the fire, and this data is primarily used to determine the combustion deficiency. Both meter CO/CO_2 analizer at a height of 1.5 meter long stick close to the source of combustion.

Air quality monitoring is done before trial to get background ambient air concentrations and during open burning for measuring emissions from open burning of rice residue. Burning time from the start of combustion from the burning conditions (smoldering) until the fire dies. After burning, the ash and unburned straw collected for analyze the water content and to get dry mass to determine the fraction of combustion.

Black Carbon Analysis

Black carbon concentration level on Particulate Matter samples collected on filter media were analysed gravimetrically. To determined mass of Black carbon by an EEL Smoke Stain Reflectometer

(Model 43D, Diffusion Systems Ltd, London) at the Laboratory of air quality environmental engineering ITB.

Analysis of Black Carbon by optical methods, by comparing the transmission of light through a filter that contains suspended particles with the transmission of light through a filter that is still clean. It is possible to estimate Black Carbon (BC) concentrations in the atmosphere by simply measuring light absorption or reflectance.

Air is drawn through the filter and then the density of the particles retained on the filter was measured using a reflectometer. Particulate density can be converted using a calibration curve to obtain the mass concentration of Black Carbon.

Calculating Methods

The emission BC were measured in form of concentration (mg/m^3 BC). The concentrations of BC on $PM_{2.5}$ from the smoke emision were calculated as the following equation :

1). Calculation of carbon black weight per unit area of filter

$$\boldsymbol{BC = 4,37638\ x\ \{-ln(\bar{R})\} + 21,199} \qquad (1)$$

Where, BC is weight of black carbon per unit area of filter (mg / m^2). $\bar{R}$ is average reflectance samples.

2) .Calculation of carbon black mass

$$\boldsymbol{M = BC\ x\ A_{filter}} \qquad (2)$$

Where, M is mass of carbon black (g), A filter is ½ filter area (m^2).

Emission Factor Calculation

Emission factors (EF) for BC are calculated after analysis of the concentration of BC on $PM_{2.5}$. BC in the results obtained with the unit mg / m^3. The derivation of emission factors with direct method [9]. Emission factor from open burning of rice straw in the field was obtained by following equation.

$$EF = Ci/BR \qquad (3)$$

where, Ci is emission concentration of pollutant i (mg/m^3) and BR is burned rate (g/s). The units of BC, CO, and CO_2 concentration were changed from µg/m^3 and ppm to mg/m^3.

RESULT AND DISCUSSION

In this research, estimation of emission factor BC from open burning in the rice field is the target. Other pollutants ($PM_{2.5}$, CO_2, and CO) are also considered to investigate combustion characteristics and efficiency combustions (EC).

Emissions of BC from open burning of rice residues were measured in form of concentration (µg/m^3 BC) by real time monitored equipment. Emission factor of BC in form of gr/kg (dm). Emission factor from open burning of 8 varieties of rice straw results are presented in Table 1.

Table. 1 Emission factor of BC from Field Open Burning of Rice Straw.

.

Rice Straw Varieties	EF BC (g/kg)dm
Mekongga	0.55
Ciherang	0.41
Hibrida	0.63
Inpari	0.92
Cintanur	0.34
Inul	1.04
Sarangue	0.42
Pandan Wangi	0.86

Table 1 shows the average value of local emission factors for Black Carbon varied for each variety. Fluctuations in the value of emission factors among these varieties reflect variations in combustion conditions and other parameters including water content, surface soil moisture, biomass conditions and the meteorological conditions [10].

Differences of emissions factor from burning straw with different varieties influenced by the characteristics of the straw (moisture content, ash content, carbon content) and also influenced by the efficiency of combustion.

For this experiment, moisture content of the sarangue varieties (10,3%) was bigger level and lower ash content than other varieties. Based on this it can be explained that the lower the moisture content of the straw, the emission factor will be low. Conversely, if the high emission factors from burning the straw will be high [13]. Overall, BC Emission Factor correlated with the characteristics of the straw (moisture content, ash content, carbon content) and by the efficiency of combustion presented at Figure 3.

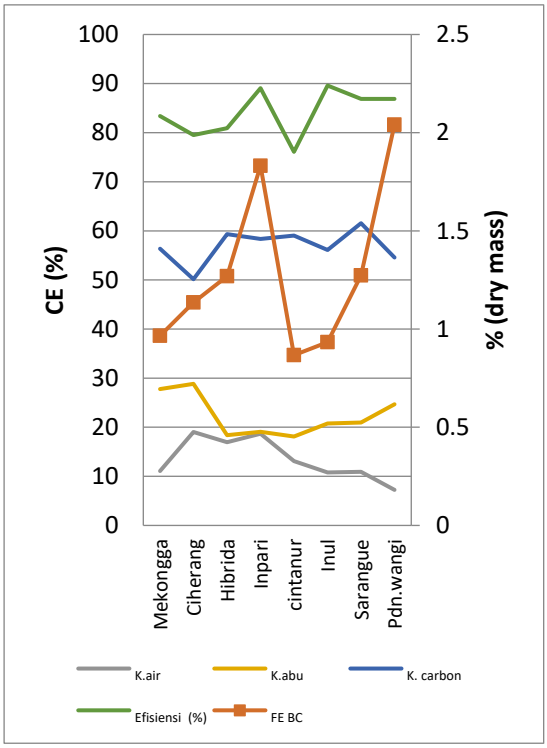

Fig 3. BC Emission Factors vs Characteristic rice straw.

Variations BC emission factors also influenced by the efficiency of combustion. Functions combustion efficiency in the field against BC in the $PM_{2.5}$ concentration is described by the linear regression equation y = -0.0813x+93.8 correlation value is negative (R^2 = 0.763).

Averaged value emission factors for BC from open burning straw without distinguishing varieties, in the district of Cianjur Cugenang can be compared with other studies. Comparison with some research can be seen in Table 2.

Table 2. Result and another research comparison.

Result	EF BC (g/kg) dm
Hayashi et. All (2005)	0.069 ±0.013
Andreas Merlet (2007)	0.47
Kanokkanjana (2011)	0.06 ±0.02
This research (2016)	0.939 ± 0,417

The Emission Factors reported in this study were much bigger than those of previous study [3], [6], [8], due to many factors as previously mentioned. This is expected because the characteristics of rice straw in Cianjur which has a higher carbon content (56.91%) when compared with the carbon content of the straw research [4] amounted to 35.4%.

Comparisons using inferential statistical analysis needs to be carried out using SPSS statistical 20. In this analysis the data inputted into the program is BC emission factor data from experiments in the field. Furthermore, the significance of the data is analyzed by comparing the average value using one-way ANOVA test (one way ANOVA) and t test-Two Sample at 95% confidence level. One-way ANOVA test is used to test the significance between varieties of the BC concentration. To answer the question whether the average value of the concentration of BC between varieties there are significant differences. The results of the analysis are summarized in Table 3.

Table 3. Resukt of the SPSS analysis

FE BC Lapangan	Anova (Tukey test)
MKGA(0.301)	A
CHRG (0.044)	A
CNTR (0.047)	A
SRNG (0.508)	A
INUL (0.056)	A
INPR (0.058)	A
PDNW(0.129)	B
HBRD(0.131)	B

Figures followed by the same letter in the same column are not significantly different according to Tukey test at 5% significance leve (α =95%).

CONCLUSIONS AND RECOMMENDATION

This study involved the assessment of Black Carbon Emission Factor in $PM_{2.5}$ from rice straw open burning in the field in District Cugenang, Cianjur, West Java Indonesia. Field experiments were conducted to quantify eight varieties rice straw, which is main fuel for combustion. The sample were collected using miniVol sampler and for Black carbon was measuremend using an EEL smoke stain reflectometer.

Result of BC emission factors for eight varieties Mekongga, Hibrida, Ciherang, Inpari, Cintanur, Sarangue, Inul, Pandan wangi was Emission Factor of BC from open burning of rice residues in the field is 0.939 ± 0.417 μg/m^3. Variations of this value is influenced by the efficiency of the combustion

simulation and the characteristics of the straw (moisture content, ash content, carbon content).

The results of this study presented provide useful information for the development of local emission factors for Black Carbon from open burning of rice straw in Cianjur. This research paved the way for a more accurate estimate of emissions that have an impact on air quality and climate impacts in Indonesia. Measurements of Emission factor for local sources should be conducted to provide a better estimate of amount of black carbon emission in all same typical rural areas in the country.

ACKNOWLEDGMENTS.

This research was supported by the ITB Research Grant 2016.

REFERENCES

[1] Anonymous, (2006). Manual EEL Smoke Stain Reflectometer.

[2] Akagi, S.K., Yokerson, R.J., Wiedinmyer, C., et al., (2010). Emission factors for open and domestic biomass burning for use in atmospheric models. Atmospheric Chemistry and Physics Discussion 10, 27.

[3] Andreae, M.O., Merlet, P., (2001). Emissions of trace gases and aerosols from biomass burning. Global Biogeochemical Cycles 15, 955-966.

[4] Christian, T.J., Kleiss, B., Yokelson, R.J., Holzinger, R., Crutzen, P.J., Hao, W.M., Saharjo, B.H., Ward, D.E., (2003). Comprehensive laboratory measurements of biomass-burning emissions: 1. Emissions from Indonesian, African, and other fuels. eophysical Research 108, 4719e4732.

[5] Garivait, S and Coauthors, (2013). Monitoring and Assessment of Biomass Open Burning in Agricultural Area/Lands in Thailand, Pollution Control Department, 60 pp.

[6] Hayashi, K., Ono,K., Kajiura,M., Sudo,S., Yonemuro,S., Fushimi,A. Saitoh,K., Fujitani, Y., and Tanabe, K. (2014). Trace gas and particle emission from open burning of three cereal crop residues: increase in residue moistness enhances emissions of carbon monoxide, methane, and particulate organic carbon. Atmospheric Environment Vol 95 pp 36-44.

[7] Hewitt, C..N. dan Andrea Jackson, (2003). Handbook of Atmosphere Science Principles and Applications. Blackwell Science Ltd.

[8] Indonesia Second National Communication Under The United Nation framework Convention on Climate Change (UNFCCC), (2010). Jakarta.

[9] Kanokkanjana, K., Cheewaphongphan,P., and Garivait,S (2011). " Black Carbon Emission from Paddy Field Open Burning in Thailand". 2nd International Conference on Environmental Science and Technology. IPCBEE vol.6, IACSIT Press, Singapore

[10] Kim Oanh, N.T., Thuy, L.B., Tipayarom, D., Manandhar, D.R. Manandhar, D.R., Pongkiatkul, P., Simpson C.D. (2011). Characterization of Particulate Matter Emission from Open Burning of Rice Straw. Atmospheric Environment 456 (2011) 483-502.

[11] Lemieux, P.M., Lutes,C.L., Santoianni,D.A. (2004). Emissions of organic air toxic from open burning ; a comprehensive review. Energy and Combustion Science 30 p 1-32.

[12] Munthe, K, K, J. (2011). Short Lived Climate Forcers- method development for emission inventories of Black Carbon Identifying gaps and reducing uncertainties. Swedish Environmental Research Institute.

[13] Ni, H., Han, Y., Cao., J., Huang, R and Li, H (2015): Emission characteristics of carbonaceous particles and traces gases from open burning of crop residues in China. Atmospheric Environment, xxx pp 1-4.

[14] Permadi, D,A. (2011), Assessment of biomass open burning emissions Indonesia and potential climate forcing impact. Atmospheric Environment Vol 28 pp 250-258

[15] Reid, et al., (2004). A review Biomass burning emissions, part II: Intensive Physical properties of biomass burning particles. Atmospheric Chemistry and Physics Discussion 4, 5135-5200.

[16] Tiparayom, D, Kim Oanh, N.T., (2007)." Effect from open rice straw burning emission on air quality in the Bangkok Metropolitan Region ". Journal of Science Asia 33 (3), 339-345

[17] Watson, J, Chow, Chen, Cample, (2011); *Particulate emission factors for mobile fossil fuel and biomass combustion sources*. Total environment. 109. Pp 2384-2396.

[18] Zhang, Y., Obrist, D., Zielinska, B., Gertler, A. (2013). Particulate emissions from different type of biomass burning. Atmospheric Environment Vol 72 pp 27-35.

Second International Conference on Science, Engineering & Environment,
Osaka City, Japan, Nov.21-23, 2016, ISBN: 978-4-9905958-7-6 C3051

EFFECT OF SLOPE ADJUSTMENT ON CURVE NUMBER USING GLOBAL DIGITAL ELEVATION DATA: NEW LOOK INTO SHARPLY-WILLIAMS AND HUANG METHODS

Abolghasem Akbari[1], Azizan Abu Samah[2] and Su Kong Ngien[1]
[1]Faculty of Civil Engineering & Earth Resources, University Malaysia Pahang (UMP), Malaysia
[2]The Institute of Ocean and Earth Sciences (IOES), University of Malaya, Malaysia

ABSTRACT

The Natural Resources Conservation Service Curve Number (NRCS-CN) method is highly recommended for runoff prediction in many climate conditions. The key parameters to obtain CN values are hydrologic soil groups and land use information with respect to soil moisture conditions. This method has been well documented and available in many popular rainfall-runoff models such as HEC-HMS, Mike, SWAT and many more. It is also easy to implement due to availability of required data in many countries. However, it is criticized in a way that NRCS-CN do not take into account the effect of terrain slope and drainage area. This study aimed to investigate the effect of slope on CN and the way that slope could change the domain of CN values in Kuantan River Basin (KRB), Malaysia. The Huang and Sharply-Williams methods were used to investigate the changes on CN values provided in National Handbook of Engineering. The Advanced Spaceborne Thermal Emission and Reflection Radiometer (ASTER) Global Digital Elevation Model (GDEM) version 2 was used to derive slope map with spatial resolution of 30 m for the study area. The study significantly enhanced the application of GIS tools and recent advances in earth observation technology in order to analyze hydrological process with respect to spatial dimension.

Keywords: ASTER-GDEM, GIS, Kuantan, NRCS-CN

INTRODUCTION

The Soil Conservation Service Curve Number (SCS-CN) methods is empirical equation which have been widely used in different studies. CN is an empirical parameter which is used for estimation of initial abstraction or infiltration from rainfall excess [1]-[3]. Regardless of some weaknesses, the CN approach provide some advantages such as ease of use and availability of data in many places. As result, the NRCS-CN method which originally intended for the study of agricultural land, became a fundamental part of hydrological practice and was adopted for application in different climate and conditions [1]. Moreover the CN method has been integrated into different hydrological models, including CREAMS [2], FEST [3, 4], EPIC [3], AGNPS [4], HEC-HMS [5] and SWAT [6]. There are many research articles and classical books in supporting and criticizing the CN method. Among them the works of Hawkins [7], [8], Hawkins et al. [7], Huang et al. [8, 9], Garen and Moore [8], Mishra et al. [9, 10] and Michel et al. [9] are notable. Review of literature shows that considerable attempted has been made for adjustment and adaptation of CN method for unaccented factors including drainage area [10], [11], soil moisture proxies [8, 10, 11, 32], slope [3, 10] and more recently Kakuturu et al. [10] investigated the effect of slope on estimation of CN values. The CN value have been adjusted for slope in Kuantan KRB [11] using Huang and Sharply-Williams. However, the effect of slope adjustment for CN did not investigated in respect to the spatial domain using available methods. The main objective of this research is to take another look into the effect of slope adjustment of CN with respect to the spatial variation of the terrain slope in KRB.

NRCS-CN approach

The traditional form of NRCS-CN equation is given by Eq. (1):

$$q = \begin{cases} 0 & \text{for } P \le I_a \\ \frac{(P-I_a)^2}{P-I_a+S} & \text{for } P > I_a \end{cases} \quad (1)$$

Where; q is direct runoff (mm), P is rainfall (mm), S is the potential maximum soil moisture retention after runoff begins (mm), I_a is the initial loss (mm), or the amount of water before runoff, such I_a as infiltration, or rainfall interception by vegetation originally, it has been assumed that $\frac{I_a}{S} = \lambda = 0.20$ [12], but more recent research [13] has shown that taking $\lambda = 0.05$ provide more accurate estimation for runoff. The potential maximum storage is obtained through the Eq. (2):

$$S = \frac{25400}{CN} - 254$$

Or

$$CN = \frac{25400}{254+S} \quad (2)$$

As the S range from zero to infinity, the CN can take value from 0 to 100 which is obtained from the NRCS standard tables. The larger value represent higher runoff potential and the lower value indicate low runoff potential.

Revised NRCS-CN method

Recent studies have shown $\lambda = 0.05$ provide a better prediction for runoff estimation. Details about the applied methodology and result from the work done by Woodward et al is referred to the reference [13].

RESEARCH MATERIALS

Location

The KRB located on East Coast of peninsular Malaysia was selected as case study (see Fig. 1).

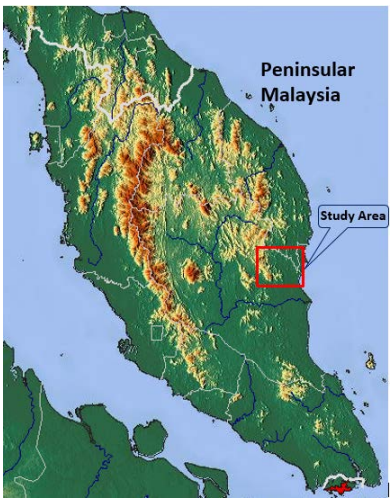

Fig. 1 Layout of the study area.

Data

Spatial data for this research including Hydrologic Soil Group (HSG) and Land Use (LU) maps were obtained from National Hydraulic Research Institute of Malaysia (NAHRIM) in vector format (ESRI shape file) projected in Kertau-RSO-Malaysia metric coordinate system. This dataset have been originally produced by Department of Agriculture (DOA) in Malaysia. According to DOA, the LU is representing the condition for 2013 and HSG have been generated in 2010. Main LU classes are forest (49%) and Palm (27%). The HSG map contains five HSG class including A&C, A&D, C&B, B and C. Predominate HSG in the study area are B, A&C, C&B with 56%, 15% and 15% respectively. The slope map was derived from the Advanced Spaceborne Thermal Emission and Reflection Radiometer (ASTER) Global Digital Elevation Model Version 2 (GDEM V2). It is freely available for download from NASA Re verb, LP DAAC Global Data Explorer, and J-space-systems ASTER-GDEM Page. The cell size of elevation data is 28×28 meter.

Software

The Integrated Land and Water Information System ILWIS 3.8 which is public domain raster-based GIS software was used for spatial data development and spatial analysis. ILWIS have high performance in geospatial analysis and image processing with friendly graphical user interface.

RESULT AND DISCUSSION

A two-dimensional table was created to combine and reclassify two raster maps including LU and HSG with class domain. Two-dimensional defines a value for each possible combination of input classes [14]. This automated processor used to generate CN map for the study area. Terrain slope of the study area was derived from ASTER-GDEM (See Fig. 2b).

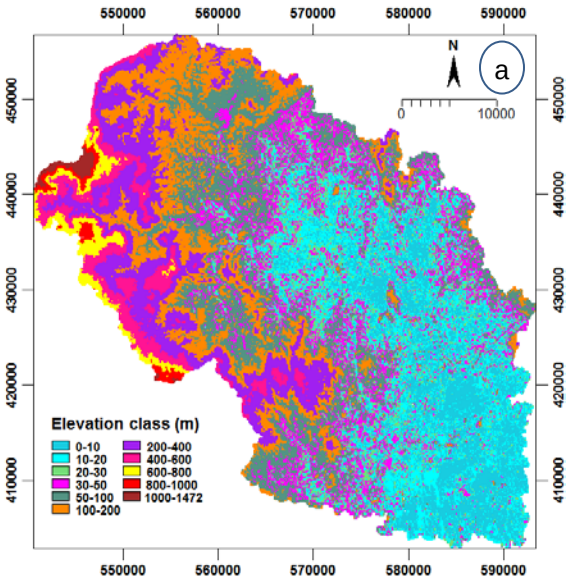

Fig. 2a Classified ASTER-GDEM of study area.

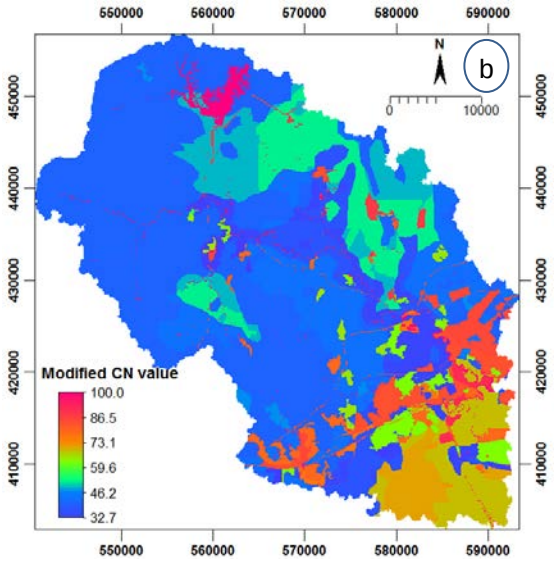

Fig. 2b Modified CN map of study area.

To obtain the modified CN map, transfer equation introduced by Woodward et al. [13] was employed. As it evident in Fig. 2.b, the CN values rage from 32.7 to 100 and predominate value change from 55 to 40 (39% area).

Slope adjustment of CN

It is recommended to adjust CN for slope because terrain slope can effect on runoff prediction by reduction in I_a [15], infiltration [16] and recession time of overland flow [17]. To perform this step, CN map was adjusted for slope using Sharply-Williams and Huang methods.

Sharply-Williams method

Slope adjustment was made based on the Sharply-Williams and Huang methods presented in Eq. (3) and Eq. (4). ILWIS GIS software was used for geospatial analysis and mapping.

$$\mathrm{CN_{SW}} = \frac{1}{3}(\mathrm{CN_w} - \mathrm{CN_m})(1 - 2e^{-13.86\alpha}) + \mathrm{CN_m} \quad (3)$$

Where, $\mathrm{CN_{SW}}$ is the slope adjusted CN by Sharply-Williams method, CN_w is CN for wet soil moisture condition. The $\mathrm{CN_m}$ represent CN for moderate soil moisture condition, α is terrain slope m/m.

$$\mathrm{CN_w} = \frac{100 * \mathrm{CN_m}}{43 + 0.57\mathrm{CN_m}} \quad (4)$$

It is noted that the CN values provided in TR55 represent the moderate soil moisture condition. Equation 4 is used to transfer $\mathrm{CN_m}$ into $\mathrm{CN_w}$ as it required by Sharply-Williams method. Slope-adjusted CN by Sharply-Williams is shown in Fig. 3a. The CN domain values have the range from 11.8 to 102.8.

Huang method

Huang [18] has introduced adjustment Eq. (5) for slope as shown in below:

$$\mathrm{CN_H} = \mathrm{CN_m} * \frac{322.79 + 15.63\alpha}{\alpha + 323.52} \quad (5)$$

Where; α is terrain slope m/m with respect to limited domain of 14-140%. It is believed that the Huang et al. method provide more reasonable adjustment for slope and therefore runoff prediction in the steep watersheds [18]. Slope-adjusted CN by Huang is shown in Fig. 3b. The CN domain values have the range from 17 to 104.6. To investigate the quantity of change on CN as result of slope adjustment in spatial domain, the difference between the adjusted and non-adjusted CN were calculated for both method using map calculation tools of ILWIS (See Fig. 4). The histogram generated from the two calculated maps shows the spatial distribution and relationship between the magnitude of changes in CN and number of pixels (See Fig. 5).

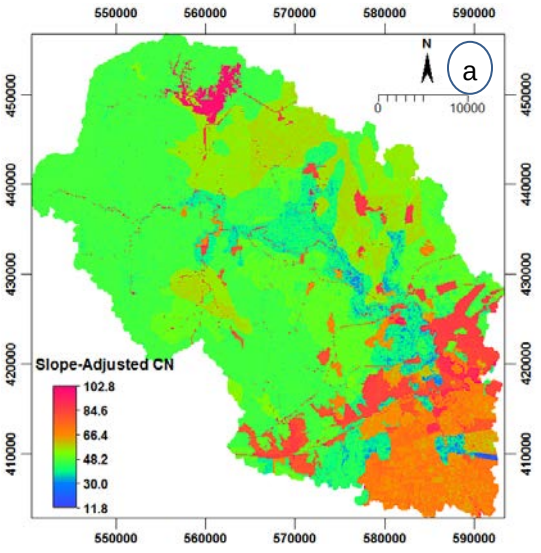

Fig. 3a Slope-adjusted CN by Sharply-Williams method.

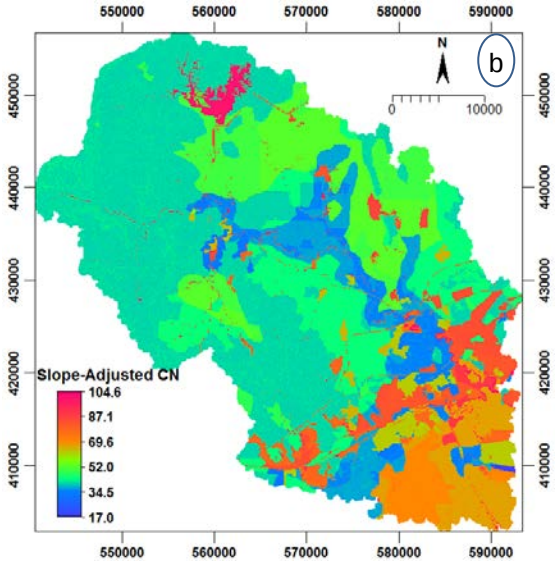

Fig. 3b Slope-adjusted CN by Huang method.

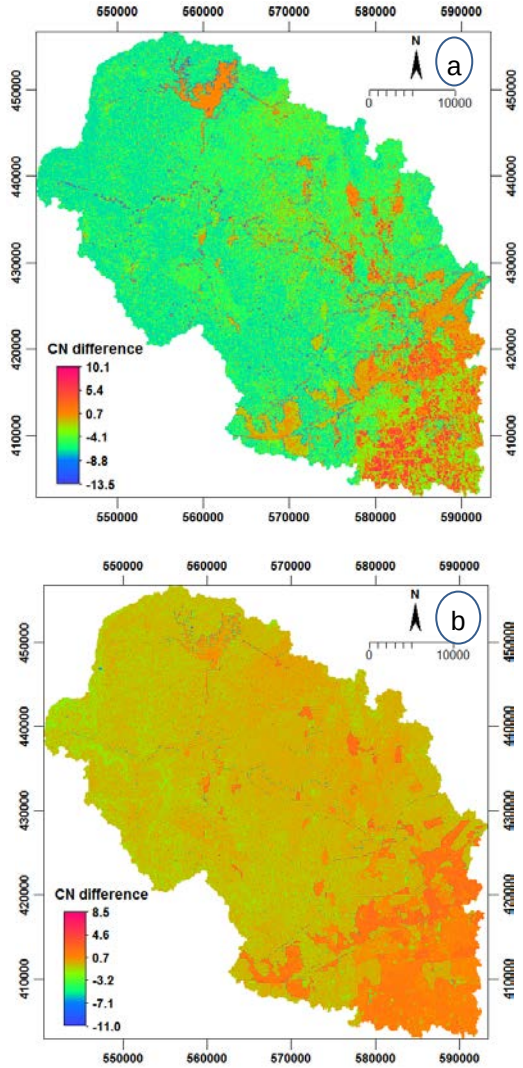

Fig. 4 Illustration of difference in slope-adjusted CN using a) Sharply-Williams and b) Huang, compare to none slope-adjusted CN

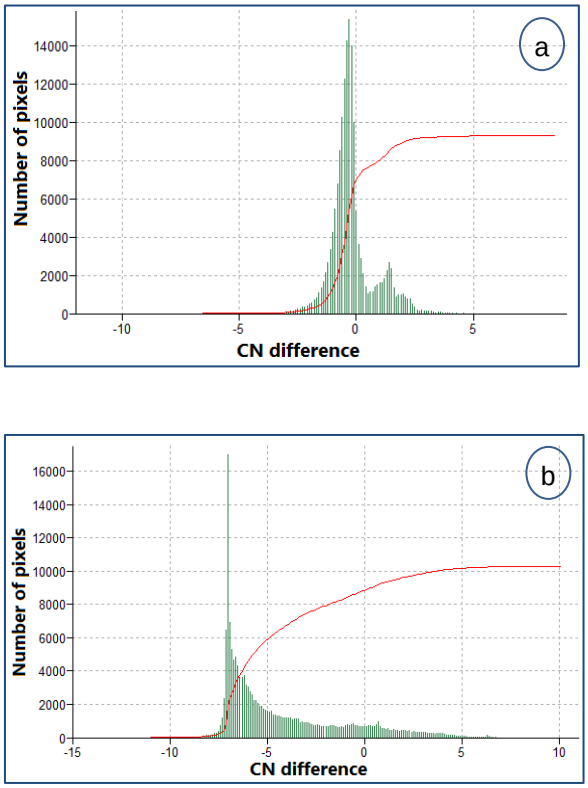

Fig. 5 Illustration of difference between the slope adjusted and non-adjusted CN for slope using a) Sharply-Williams and b) Huang method.

CONCLUSION

This study demonstrate the practical use of GIS tool in spatial analysis for hydrological process. It is evident from the result of this study that both method expanding the domain of CN to the lower and upper limits. It is also observed that both method have error in calculation of slope-adjusted CN at the upper domain as 102.8 and 104.5 are obtained from Sharply-Williams and Huang method respectively. It means stretching effect in both method do not limit with the maximum possible value for CN which is 100. In addition, the difference between the unjustified CN with slope-adjusted CNs, shows that both method tend to decrease the CN values (negative values) in the areas with the mild and flat slope while CN values are increased (positive values) in relatively high and steep areas. However, as illustrated in Fig. 6, in the same area Huang method significantly tend to increase the CN values in more number pixels compare to Sharply-Williams. This study can be further develop by performing in different river basins with more variety of terrain slope method.

ACKNOWLEDGMENT

The authors acknowledge the University Malaysia Pahang and the Institute of Ocean and Earth Sciences, University Malaya for supporting this research through the grant numbers RD150127 and IOES-2014B.

REFERENCES

[1] USDA, Urban Hydrology for Small Watersheds. United States Department of Agriculture, Natural Resources Conservation Service, Conservation Engineering Division: Washington DC, USA, 1986, pp. 164.
[2] Mahdavi, M., Applied Hydrology, vol.2, Tehran university, 2005.
[3] Alizadeh, A., Principles of applied hydrology, Astane Ghods: Mashhad, Iran. 2006 pp. 350.
[4] Miliani, F., G. Ravazzani, and M. Mancini, Adaptation of Precipitation Index for the Estimation of Antecedent Moisture Condition in Large Mountainous Basins. Journal of Hydrologic Engineering, Vol. 16(3), 2010, pp. 218-227.
[5] Knisel, W.G., CREAMS: A field-scale model for chemicals, runoff and erosion from agricultural management systems. USDA Conservation Research Report, 1980.
[6] Montaldo, N., G. Ravazzani, and M. Mancini, On the prediction of the Toce alpine basin floods with distributed hydrologic models. Hydrological processes, Vol.21 (5), 2007, pp. 608-621.
[7] Rabuffetti, D., et al., Verification of operational Quantitative Discharge Forecast (QDF) for a regional warning system–the AMPHORE case studies in the upper Po River. Natural Hazards and Earth System Science, Vol.8 (1), 2008, pp. 161-173.
[8] Sharpley, A.N. and J.R. Williams, EPIC-erosion/productivity impact calculator: 1. Model documentation. Technical Bulletin-United States Department of Agriculture, 1990 (1768 Pt 1).
[9] Young, R.A., et al., AGNPS: A nonpoint-source pollution model for evaluating agricultural watersheds. Journal of soil and water conservation, Vol.44 (2), 1989, pp.168-173.
[10] Feldman, A., Hydrologic Modeling System (HEC-HMS): Technical Reference Manual., U.S. Army Corps of Engineers: Washington DC, 2000, pp. 158.
[11] Neitsch, S., et al., Soil and water assessment tool theoretical documentation. Texas, USA, 2005.
[12] Hawkins, R.H., Runoff curve numbers with varying site moisture. Journal of the Irrigation and Drainage Division, Vol.104 (4): p. 389-398.
[13] Hawkins, R.H., Asymptotic determination of runoff curve numbers from data. Journal of Irrigation and Drainage Engineering, 1993. Vol.119 (2), 1978, pp. 334-345.
[14] Hawkins, R.H., et al., Curve Number Hydrology: State of the Practice, ed. R.H. Hawkins., Virginia, USA: American Society of Civil Engineers. 2009, pp.116.
[15] Huang, M., et al., A modification to the Soil Conservation Service curve number method for steep slopes in the Loess Plateau of China. Hydrological processes, Vol.20 (3), 2006, pp.579-589.
[16] Huang, M., et al., Use of soil moisture data and curve number method for estimating runoff in the Loess Plateau of China. Hydrological processes, Vol.21 (11), 2007, pp.1471-1481.
[17] Garen, D.C. and D.S. Moore, CURVE NUMBER HYDROLOGY IN WATER QUALITY MODELING: USES, ABUSES, AND FUTURE DIRECTIONS1. JAWRA Journal of the American Water Resources Association, Vol.41 (2), 2005, pp.377-388.
[18] Mishra, S., et al., A modified SCS-CN method: characterization and testing. Water Resources Management, Vol.17 (1), 2003, pp.37-68.
[19] Mishra, S., et al., SCS-CN-based modeling of sediment yield. Journal of Hydrology, Vol.324 (1), 2006, pp. 301-322.
[20] Michel, C., V. Andréassian, and C. Perrin, Soil Conservation Service Curve Number method: How to mend a wrong soil moisture accounting procedure? Water Resources Research, Vol.41 (2), 2005, pp.45-66.
[21] Simanton, J. and N. Sutter, Procedures for identifying parameters affecting storm runoff volumes in a semiarid environment. USDA, ARS. ARS-W, 1973. 1.
[22] Simanton, J., et al., Runoff curve number variation with drainage area, Walnut Gulch, Arizona. Transactions of the ASAE, Vol.39 (4), 1996, pp.1391-1394.
[23] Ponce, V.M. and R.H. Hawkins, Runoff curve number: Has it reached maturity? Journal of hydrologic engineering, Vol.1 (1), 1996, pp.11-19.
[24] Beck, H.E., et al., Improving curve number based storm runoff estimates using soil moisture proxies. Selected Topics in Applied Earth Observations and Remote Sensing, IEEE Journal of, Vol.2 (4), 2009, pp. 250-259.
[25] Kakuturu, S.P., et al., Runoff Curve Numbers for Simulated Highway Slopes under Different Slope, Soil-Turf, and Rainfall Conditions. Journal of Hydrologic Engineering, Vol.18 (3), 2013, pp. 299-306.

[26] Akbari, A. Slope adjustment of runoff curve number (CN) using Advanced Spaceborne Thermal Emission and Reflection Radiometer (ASTER) Global Digital Elevation Model (GDEM) for Kuantan River Basin. in SPIE Remote Sensing. International Society for Optics and Photonics. 2015, pp.76-98

[27] Woodward, D.E., et al. Runoff curve number method: examination of the initial abstraction ratio. in Proc. ASCE Conf. Proc., Philadelphia, PA. 2003.

[28] Schouwenburg, M., et al., Integrated Land and Water Information System (ILWIS), 52°North: The Netherlands, 2013, pp.90-105.

[29] Chaplot, V.A. and Y. Le Bissonnais, Runoff features for interrill erosion at different rainfall intensities, slope lengths, and gradients in an agricultural loessial hillslope. Soil Science Society of America Journal, Vol.67 (3), 2003, pp. 844-851.

[30] Philip, J., Hillslope infiltration: planar slopes. Water Resources Research, Vol.27 (1), 199, pp. 109-117.

[31] Evett, G.D., Length and slope effects on runoff from sodium dispersed compacted earth micro-catchments. Soil Science Society of America Journal, Vol.49, 1985, pp.734–738.

[32] Koichi Sumi et al. Effect of the Soil Moisture Distribution after Rainfall on Seismic Stability of Embankment Slope. Vol.8 (15), 2015, pp. 2088-2093

Second International Conference on Science, Engineering & Environment,
Osaka City, Japan, Nov.21-23, 2016, ISBN: 978-4-9905958-7-6 C3051

MT. GULUGOD BABOY: THE ASTONISHING 360 DEGREE ECOTOURISM OVERVIEW OF BATANGAS, PHILIPPINES

Ryan Joseph G. Calinao[1], July Aze V. Barcenas[2], Lilian R. Silang[3]
[1, 2] Instructor, [3]Dean, College of International Tourism and Hospitality Management
Lyceum of the Philippines University-Laguna,
The Republic of the Philippines

ABSTRACT

Tourism is the new propelling engine that gives the Philippines as one of the top destinations around the globe. From the (DOT) Department of Tourism's slogan: "*It's more fun in the Philippines*" featuring a seven thousand and a hundred seven islands going to the Southern Tagalog region's: "*All hear so near*" of Batangas Province. This study encompasses the proposed tourism development plan of Mabini, Batangas a town were a transverse peninsula can be found. Dubbed as Mt. Pinagbanderahan during the Japanese colonization renowned today as Mt. Gulugod Baboy or as the "*pig spine"*. This study features the top tourist destination and a natural wonder of Mabini, Batangas from resorts, white sand beaches, snorkeling, diving, kayaking, and mountaineering. This also features the Batangas Province's landscape up to the Municipality of Mabini where the center of the center of world's marine biodiversity in the world can be found. The master plan's main goal is to present a project that would promote a tourist destination site of five hundred twenty-one meters above sea level at Mt. Gulugod Baboy. More specifically to balance the environmental impact assessment on the proposed public-private partnership project in consideration of environmental and social issues.

Keywords: Philippine Tourism, Mt. Gulugod Baboy, Environmental Impact, Master Plan

INTRODUCTION

The history of tourism can be traced back thousands of years ago. Tourism has passed through different stages, from the world's first recorded international tourist, the geographer and historian Herodotus [5] going thru the Olympic games, the Grand Tour Era, the Jihad and the Crusades to define the segment of the history of tourism. Now Tourism is defined to be the new umbrella of the Hospitality industry together with the cruise line, food service, travel and lodging industry for in such tourist are the one who gives the new economic trail in the international market and in the Philippines also.

An Archipelagic Tourism, An Overview of the Philippines and Batangas.

Philippines, as the pearl of the orient seas is seated at the South East Asia which tourism is a vital industry. Philippine tourist arrivals represent a growth of 5.3 million as compared to the statistics of 11.5% from 2014 as compared to the average of 8.5% in the Asian region and 4% in the world. [10]

At the south of the Luzon island settles the land that endowed with destinations encompassing various natures-from usual to man-made, from conserved greatness of the bygone era to avant-garde constructions, from places where you can seek refuge to sites where one can be lavished with supreme Gourmet luxury and it is the Batangas Province.

Batangas is tagged as a premier tourist destination. What makes the area as such may be quite an effort to sum up because of the many things that contribute to Batangas being world-class. [11] Whatever the situation may be in visiting a place, the tourist finds way to Batangas. May it be for a spiritual trip, traditional, historic, scholastic, culinary adventure, or a beach vacation, the tourist gets a place to see in this progressive province.

Dubbed of its theme "it's all here, it's so near" Batangas promotes the greatest advantage of this is its proximity to the country's capital, Manila. Local and foreign tourists alike can traverse the province from various entry points. [11]

The heart of Batangas is the famous Taal volcano, known to be as the smallest volcano in the world surrounded by a lake and a volcano inside a volcano. Going further to the southern tip of Batangas, nineteen kilometers from Batangas City-the provincial hub of the province's economic activity, and a hundred twenty-seven kilometers from Manila is the center of the center of the world's marine biodiversity-the Municipality of Mabini. [5]

Mabini, Batangas: The seat of the center of the center of the world's marine biodiversity.

Mabini's geographical location and features (a long coastline, hilly terrain, and lack of rivers) have both positive and negative influences on its development. The long coastline and rich marine life provided livelihood opportunities, through small scale commercial and subsistence fishing, for people living in coastal barangays. Despite the hilly terrain and reliance on rain for irrigation, people farmed in uplands and gardened in their backyards producing

fruit, vegetables, and root crops primarily for local consumption, selling only part of the harvest in nearby communities.

The Mt. Gulugod Baboy: A Potential Ecotourism Site

Gulugod-Baboy is the universal term that describes the hills that traverse Calumpan Peninsula. Located in Southern Batangas, the point is more known for the diving resorts of Anilao, the birthplace of Philippine scuba diving. Since dive enthusiasts are also enthusiasts for anything outdoor activities, they began exploring the peaks, Gulugod Baboy became a trekking destination, and a popular sidetrip from a diving escapade to Anilao, or to the nearby El Sombrero island or Maricaban islands. [6] [9]

There is still a confusion regarding where the real "Gulugod-Baboy" is. From southeast to northwest from Barangay San Teodoro, Barangay Ligay up to Barangay Laurel, there are three peaks in the range. The first is 470 MASL (meters above sea level), the second is 485 MASL, and the third is 525 MASL. This third has a large, ancient tree as its landmark, and is known to mountaineers as the real Gulugod Baboy. However, locals say that this third peak is actually Mt. Pinagbanderahan, and the first peak is the Gulugod Baboy. The enthusiasts of Long Henson, father of itineraries, would remember that he wrote about a Mt. Pinagbanderahan in Mabini, Quezon. This may actually refer to Mabini, Batangas, and is actually one and the same as the Gulugod-Baboy known by the tourist. Thus, there are three peaks, from southeast to northwest and that is the Gulugod-Baboy, Gitna, and Pinagbanderahan. [9]

The View in Mt. Gulugod Baboy

Most directions have trails; indeed, there are many trails in the mountain which is both an advantage and a disadvantage. At its peaks, you can see, from east to west are the Janao Bay, Maricaban strait which bears El Sombrero and Maricaban islands, a distant, faint blue Mindoro, Verde Island from the southwest and Batangas Bay. The city and port of Batangas is visible on the west, following a farther Mt. Daguldul. To the north is Mt. Maculot, and even Mt. Batulao and the Tagaytay highlands. [9]

Review of Relevant Studies

There is a growing body of research concerned with the impacts of tourism and the perceptions of the community, although there is a void in the research on how to influence the tourism development and planning process of a destination which is needed to mitigate the negative impacts of tourism on the community. By designing the process necessary to develop and implement tourism development, the impacts and the contribution of tourism to the destination can, to an extent, be predicted.

As this study investigates tourism as an important tool of development in island destinations more particularly the Mt. Gulugod Baboy further known to be as Pinagbanderahan, the investigation of the tourism development and planning process is considered essential, since many island locations have seen tourism as a solution for underdevelopment problems. As a result, research that marries tourism with island community development is essential in order to explain how tourism can be used as a development tool. [3] [4]

In order for tourism to be used as a development tool for the island (Mt Gulugd Baboy) in Calumpan peninsula in Batangas, three issues should be considered:

1. *Commercial viability*. For the commercial sector to be viable, it is necessary to ensure its profitability through tourism spending and various incentives
2. *Place/environment* is the context of tourism and therefore its preservation should be ensured.
3. *The host population*. For tourism to be successful it has to be accepted by the residents who receive the benefits and the costs associated with tourism expansion.

The support for tourism can be measured by the perceptions of the local population which can dictate the extent of the host community's acceptability of tourism. The three groups of people who are important in tourism development are; (1.) business people, (2). the residents (3). the local authorities [4]

Mabini: A Prime Marine Biodiversity Hotbed

The area often referred to by outsiders as "Anilao" actually encompasses the municipalities of Bauan and Mabini in the Calumpan Peninsula as well as the island of Tingloy, which sits between the Maricaban and the Mindoro Straits. [5]

It is a place of extraordinary marine biodiversity. Recent studies by marine biologists Kent Carpenter and Victor Springer put Anilao in the waters of the Verde Island Passage between the provinces of Batangas and Mindoro, a corridor that has been labeled the "center of the center" of marine shore fish biodiversity because of IA DIVERS' HAVEN 32A school of Antiasis fish is a common sight in the coral reef of Beatrice in Tingloy. the Philippines' Mabini and Tingloy the number of species recorded in the area. A 2003 survey by coral taxonomist Douglas Fenner listed a total of 319 species and 74 genera of hard corals—25% more than the average number of corals found in the hotbed known as the

Coral Triangle, rich waters shared by the countries of Malaysia, Indonesia, and the Philippines. [5] [6]

In the middle and late 1970s, the underwater attractions of Balayan Bay were discovered by Manila-based scuba- divers, enthusiastic about their new-found sport. Camping was already a popular activity then, with guides leading hikers through yet undeveloped areas to set up campsites.

The earliest divers, however, came loaded with a lot more equipment, braving very rough roads with four-wheel- drive vehicles, lugging their own air tanks from Manila, and pitching tents to spend the night near the water, just to be able to dive and spearfish freely in what was then truly an underwater wilderness. "*It was really something else then,*" recalls Roberto "Abet" Napeñas, a former boatman and Batangas-based dive guide for 25 years now, whose father was a close friend of pioneering Anilao resort owner Danny Sarmiento. Sarmiento would establish the Aquaventure Reef Club, one of the first resorts in the peninsula. [6]

Gulugod Baboy- A Trekker's Experience

"Sensuous summit curves; Sea in perpetual tranquility; Vibrant tangerine sunset and glorious sunrise; Wild mushroom blossoms; Tantalizing breezes; Snaking silk fog"

"When it comes to romance, Mt. Gulugod Baboy looks like love, caressing, fresh, vibrato, mango-sweet. There is no question about it. This mountain is sensuous." -Insigne, 2011[9]

Located in Southern Batangas and just a bus ride away from Manila, this simple itinerary takes in Luzon's ideal weekend getaway. Just a short hop from the Philpan jump-off is the lovely coast of Anilao, which offers some of natures' most incredible diving sites – true to its title as the birthplace of Philippine scuba diving.

These beaches will lure you from the peaks of Mt. Gulugod-baboy, especially a view from the Pinagbanderahan, its highest peak, because from there you can see the Janao Bay, Maricaban strait which bears Sombrero and Maricaban Islands, hiding on the hazy bluish fog is the Mindoro straight. [9] [10]

The sun-drenched panoramic peaks of this lovely mountain is actually a triumvirate – (1) the "Gulugod Baboy" which means "pig's spine" – so named because of the contours of the hills; (2) "Gitna", the center peak and; (3) Pinagbanderahan, the historic peak where Japanese airmen crash landed and survived during World War II. [7]

Thus, upon taking such experiences of tourist and trekkers, Mt. Gulugod Baboy is a prime site that furnushly caters ecotourism and soon a pro-poor tourism adequate area. [9]

Environmental and Social Issues

Local communities comprise groups with different and potentially conflicting interest (see Figure .1). that is, not all groups want the same things.

The tourist industry seeks a healthy business environment with; (1). [7] Financial security, (2). A trained and responsible workforce (3). attractions of enough quality to ensure a steady flow of visitors-who stay longer and visit more often (4). significant return on investment (5). protection of the environment, (6). to motivate people to be more aware lastly (7). food, adequate and clean water, healthcare, rewarding work for equitable pay, education and recreation.

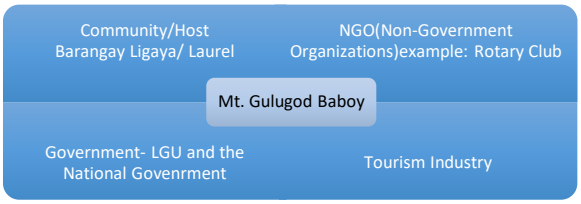

Figure 1. Matrix of Interest

Ecotourism and local communities of Gulugod Baboy

There are a number of reasons why local communities may consider ecotourism primer in Gulugod Baboy: (1). A desire to be part of strong growth in tourism generally and see the potential of catering for special-interest tourism more in trekkers and mountaineers in Calumpan Peninsula (2). An awareness of the high value of natural attraction in the locale (3). Empathy for conservation ideals and the need for sustainable tourism (4). A desire to responsibly rejuvenate and local tourist industry

One of the principles or elements of ecotourism is its ability to maximize the benefits of tourism, not only as far as income to a region but also the preservation of social infrastructure and biosphere conservation. [1]

The conflictual issue expressed by representative of host communities to tourism development generally fall into a number of interrelated categories; [4] (1). the lack of opportunities for involvement in decision-making relating to ecotourism (2). inadequate response from governments when administrative or legislative mechanisms (3). the need to established better tools for evaluating socio-cultural impacts. (4). impacts on community cohesion (5). the rapidity of the tourism development that in many cases significantly accelerates social change.

Access Conditions to Attractions

Tourism Infrastructures and Ecologic Entropy of Trekking in Gulugod Baboy and a prime ecotourism destination.

International tourism can be interpreted as a channel of globalization, which reveals its fundamental characteristics: polarization on a global

scale and the historicity of spatial disparities. Tourism is also one of the possible trajectories for the integration of places into global sphere. [1] [2] Tourism and heritage are often linked as showing the correlations with UNESCO's World heritage list and the number of international tourist visitors. The Center of the Center of the world's marine biodiversity is at the heart of Calumpan Peninsula, Mabini tourism had flourished in terms of ecotourism where diving is promoted. Mt. Gulugod Baboy is characterized with trifold magnificence accent; first an ecotourism site, secondly, a pro poor tourism that could be possibly help the people in the site and lastly, a youth involvement tourism or a trekking place for mountaineers.

Table 1. Transportation Summary from Manila to the Prime Site

Route/Mode of Transportation	Travel Time	Estimated Fare
• Manila to Batangas City Grand Terminal via Bus	2-2 ½ hours	Php120.00 or *$ 2.50*
• Grand Terminal to Anilao Port via Jeepney	45 minutes to 1 hour	Php 30.00 or less than *$1.00*
• Anilao Port to Philipan Dive Resort (Start of trail) via tricycle	~10-15 minutes	Php 60-100 or *$ 2.00*

Site Validation

Mabini: Dive and Trek Geographical location

Figure 2. Geographical Map of the Philippines [6]

It is only 127 kilometers or a 2½ hour drive from Manila, but it may well be one of the most accessible pieces of paradise on the Philippine archipelago. The municipality of Mabini in the province of Batangas is a place of golden sunsets, green hills and valleys, and calm blue waters embraced by a 32-kilometer stretch of rugged coastline.

Figure 3. Calumpan Peninsula (left) Location of Gulugod Baboy (right) [6]

With a land area of 4,296 hectares, Mabini dominates the Calumpan Peninsula, the strip of land dividing Balayan Bay in the west from Batangas Bay in the east. To the north is the town of Bauan, and on the south is Maricaban Strait, across which is the island municipality of Tingloy.

Identification of Existing & Potential Attractions

There are lots of existing natural attractions in Mabini, Batangas three of them are mountains which are the Mt. Gulugod Baboy in Barangay Ligaya and Laurel, Mt. Mailayen in Pulong Niyogan, and Mt. Panay in in Bagalangit. Matutungil Rock and Pagong Rock are some of the Rock Formations in San Jose and Solo respectively. Diving sites are prime tourist destinations in Mabini, namely Mato Pt., Batong Buhay, Chopper, Cathedral Rock, Mayumi, Eagle point and Casita Ysabel House Reef to name a few.

Figure 4. Mt. Gulugod Baboy (top) [12] and the Barrel sponges abound 90 feet deep in Mabini (bottom) [5]

Study of Visitor Market and Forecast of Visitor Arrival in Study Area

According to the tourism office of Municipality of Mabini, only few statistical data gathered by the researchers are available.

Diving: Around 40, 000 - 70, 000 tourists annually

Trekking: 6, 000 to 10, 000 tourists annually

In aforementioned data trekking put a best shot of 10, 0000 annually, thus, promoting Mt. Gulugod Baboy and putting necessary plans and development would be a big and long term project for the municipality. Handling tourism plans in the said site will cater a double visitor / trekkers around the southern coast of the Philippines and soon nation widely. [6]

Marketing Plans and Promotions Collaterals

Convention and Visitors Bureau

The sole purpose of a convention and visitor's bureau is to promote the community to attract visitors to a community. The vast majority of their promotions and marketing efforts are geared toward putting "heads in beds" or generating overnight conference, sports and leisure business.

Tourism Partners

A tourism partner within a community can be any organization or business that is involved in any way with visitors to one town. Attractions such as amusement parks, museums, zoos, botanical and water gardens as well as hotels, restaurants and other

businesses that cater to visitors are all considered as tourism partners

SWOT Analysis for Mt. Gulugod Baboy

Taking into account the background information on the site as well as the opinions from tourists, tour-operators, forest officials and local people, SWOT (Strengths, Weaknesses, Opportunities, Threats) [3] analysis has been done for ecotourism in Gulugod Baboy. In analysis of the Strengths, Weaknesses, Opportunities and Threats for each enterprise the following themes emerged:

Strengths: Mt. Gulugod Baboy is a new future established tourism destination with a variety of natural attractions like the triumvirate peaks. (1). Status of Biosphere Reserve and ecotourism for Mt. Gulugod Baboy (2). Good number of domestic and foreign tourists visiting this destination. (3). Unique culture of the local people. (4). Already existing natural tourism infrastructure.

Weaknesses: (1). Lack of coordination among locals, (2). Low involvement of locals in tourism, (3). Little incentive for the local people from tourism in terms of income generation.

Opportunities: (1). Social mobilization through SMERF- Social, Military, Education, Religious, and Fraternal groups, (2). Proper ecotourism package development involving local people in decision making and planning, and (3). Diversification of ecotourism products like stay in country boats, trail walks and likes.

Threats: (1). Migration of extremely poor landless people to Mt. Gulugod Baboy in search of job opportunities (2). Potential negative environmental impacts, (3). Pollution by sewage, dumping of the wastes. (4). Increase in biotic pressure due to increase in mass tourism, and (5). Lack of proper management causing negative impact on this fragile ecosystem.

Prioritization of Tourism Circuit

Most of tourist destinations in Mabini form a part of a larger tourist circuit with other destinations in the vicinity. Major tourist circuits are located in the Coastal area for diving. Diving circuit and trekking circuits are two major important circuits in the zone portraying Mabini as the center of the center for the world's marine biodiversity.

Diving Circuits

Mabini is known for its beaches and corals as centersas centers of the worlds world's marine biodiversity in the Philippines. Maintaining diverse species in innocuous and cleanliness at the place of site is of utmost importance to provide an enhanced experience and attract more tourists.

Trekking Circuits

Mabini has a large number of Mountain range which are treasured not only for their historical significance but also for their natural beauty and experiences. The Government of Mabini in coordination with DepEd and PTCAO-Provincial Tourism, Culture and the Arts Office -DOT, develop and conserve these ranges for realizing their tourism potential.

THE DETAILED RECOMMENDATIONS OF TOURIST ATTRACTION

Among other tourist attractions, the researchers recommend Mt. Gulugod Baboy to be the prime tourism attractions and to cultivate planning and development in accordance of the Municipal Planning and Development office criterion.

The recommendations are the following with EIA-Environmental Impact Assessment:

1. A whole new picnic grove near the peak (but not necessary in the site)
2. Construct a tourist center along the road of barangay Laurel and Ligaya
3. A viewing telescope/ observatory (Victoria Harbour in Hongkong)
4. A Zip line that will transverse the 3 hills of the Mt. Gulugod Baboy.

ESTIMATIONS OF DEVELOPMENT COST

Zipline Tower

(16 Square meter/ Floor)

₱ 20,000.00/ Square meter

₱1,600,000.00/ Tower

15% Markup: 720,000.00

Total Estimate for Zipline Tower: ***₱ 5,520,000.00*** or ***USD 115, 120.00***

List of materials:

- iBeam 0.20x30cm x 6 meters
- Rebars 12mm diameter at 10mm diameter
- Gravel ¾, White Sand, Cement, 2 inch Gi Pipe, schedule 40, 1 inch Gi Pipe schedule 40, 1"1, Tubular, Paint, Tiles, Cable Wire ½" diameter, (High Tension wire), Plywood ¾" thick.

Light House

(19.63 meter)

Light House	₱ 2,500,000.00
Parasol	100,000.00
Lamp Post	80,000.00
Solar Panel	60,000.00
15% Markup:	375,000.00
Total Estimate:	***₱ 3,115,000.00***

or ***USD 65, 000.00***

List of Materials:

- Tempered Glass
- Gravel ¾
- Cement
- Concrete
- Rebars 12mm diameter at 10 mm diameter

Light Bulb, Tiles, Paint, Steel Fence

Total of *Php 8, 635, 000.00* or *USD 180, 120.00*

Below are the Artist Sketch for the Proposed Tourism Development Plan of Mt. Gulugod Baboy

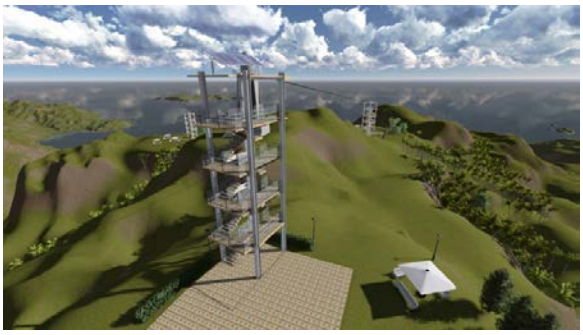

Figure 4. An Aerial View of the Triumvirate Peaks with 3 Zip Line towers that include 5 floors for each tower.

Figure 5. A View from the base of one of the Zip Line with picnic groves

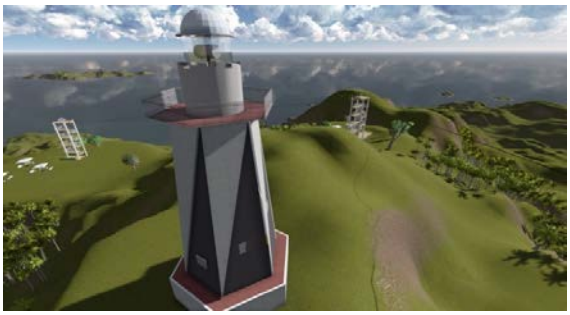

Figure 6. An Aerial view of the site with a Light House and an Observatory Telescope inside

FINANCING OPTIONS FOR TOURISM DEVELOPMENT

Options for tourism development funding are abundant which can be found at the national, provincial and local levels. Information is easily accessible if one takes the time to do the research and complete the application processes. The rewards are well worth the effort, but it takes time to see them come to completion.

1. National- Assistance for rural and agricultural areas is readily available formed by community taxes and infrastructures. Funds from the tourism master plan approved by the Philippine Congress and Senate and later signed by the President. The proposed budget disbursement will be coming from the joint project of the government and the private sector, thus, this will be called as PPP or the Public-Private Partnership.
2. Provincial and District Assistance – this will come from the budget allotted for the marketing and development of the PTCAO and together with the office of the congressman seated on the congress of the second district of Batangas of which Mabini is part of it.
3. Lastly, the Municipal government of Mabini, for the sustaining of the project one it has been propelled.

CONCLUSION

Aligning the Tourism master plan of the government and the proposed tourism development plan of the researchers would surely help the LGU of Mabini, Batangas and the province. Taking consideration of the EIA, a sustainable tourism program shall be proposed in order to achieve the common goal of the country as to be the top premier destination around the globe and prove its tag line as “It’s More Fun in the Philippines” and “Trekking: More Fun in Gulugod Baboy!”.

REFERENCES

[1] Arizona Hospitality Research and Resource Center, Northern Arizona University, 2007, pp1-3.
[2] Tourism Destination and Planning Development, University of Hawaii, Manoa, 2012.
[3] Massyn, Peter and Humphrey, Ed., Tourism Development Plan, Khomani San Community, March 15, 2010, pp. 56-60.
[4] Androitis K., (goo.gl/OUKth0) Chapters 1-10,
[5] Anilao Paying to Play: The Dive Fees of Mabini and Tingloy, by USAID and WWF, 2007
[6] State of the Coast of Batangas Province, Philippines, Partnerships with PEMSEA and UNDP, GEF, UNOPS, 2008
[7] Basa, Charito, De Guzman, Violeta and Villamil, Lorna., Migration, local development and governance in small towns: two examples from the Philippines, September 2009
[8] Henares, Ivan, Pinoy Mountaineer, (goo.gl/XXkeBh), 2007
[9] Directory of CRM Learning Destinations in the Philippines, League of Municipalities of the Philippines & WWF-Philippines, 2nd Edition 2009
[10] rappler.com (goo.gl/SdY88g), 2016
[11] http://www.batangasallheresonear.com, 2012-2015
[12] Magpantay, Ramon, DSLR Camera, 2016

Second International Conference on Science, Engineering & Environment,
Osaka City, Japan, Nov.21-23, 2016, ISBN: 978-4-9905958-7-6 C3051

A MODEL OF PARTICIPATION IN A WATER REHABILITATION PROJECT OF A LOCAL GOVERNMENT UNIT IN THE PHILIPPINES

[*]Gerby R. Muya[1], Merlita Medallon, Ph.D.[2], Nelson Tenorio, Ph.D.[3]

[1-3] Faculty, Lyceum of the Philippines University Laguna, Philippines

[*]Corresponding Author

ABSTRACT. To eradicate water pollution, a local government in the Philippines has implemented a water rehabilitation project called "Adopt-A-River Project. The project mobilized the local communities to preserve and maintain a clean and safe environment. Promoted through the use of communication media, Adopt-A-River Project has been implemented along the three main tributaries of the area. This study was designed to propose a model of participation considering the level of awareness and perception on the project and the level of participation of the 327 residents. Data were gathered using a validated researcher-made questionnaire with reliability index of 0.970 on perception items and 0.897 on level of participation. Data revealed that local group discussion (52%) is the most commonly used medium of communication in increasing awareness of the project. This is in addition to radio, television, newspaper and the internet. The use of different media resulted in the respondents being informed of the project which led to their involvement in decision-making and consultative role. The information about the project was disseminated using words that are simple and easy to understand. The project was accepted by the residents and participation was heightened. The perception level has an effect on the information level by 0.737. Path analysis using 14 variables showed a good fit with Chi-square = 0000 and GFI, NFI and CFI having values of 0.99 and RMSEA of 0.026. Significant predictors of participation are perception (p=.000) and awareness (p=.000).

Keywords: Awareness, Communication, Participation, Path Analysis, Water Rehabilitation

1. INTRODUCTION

Environmental problems are a global phenomenon. Every country is challenged to address environmental concerns to protect not only the current societal interests but also the welfare of the future generation. Thus, sustainability of environmental programs has been one of the major thrusts of every country in response to global environmental issues and the call of the United Nations towards attainment of sustainable development goals.

With the world being aware of the effects of global warming, projects concerning the preservation of our natural resources are taking place from different points of the world. One of these resources is rivers, which are the source of living of many plant and animal wildlife. Many projects concerning the health of rivers are being created and facilitated by the government and many local and private organizations. As these projects take place in their respective rivers, the facilitators of these projects request the locals to participate in order for these projects to be successful at the same time to help the rivers stay alive.

As rivers are a very important part in nation building, many projects have emerged in different countries in order to save endangered rivers—one of these river rehabilitation programs is the Adopt-a-River Project. In the Philippines, many of these are done in parts of our country where rivers cross to metropolitan areas like Manila, Cebu and Davao which all—all still goes to processes. Most of these are proven to be successful due to the community and stakeholders' efforts to maintain the project. Previous studies prove that these projects can help areas that have rivers in their territories; however, these would only work if the community are aware of the project [1].

In Calamba City, Province of Laguna, the local government unit has been implementing the Adopt-a-River project as part of its Rivers and Creeks Rehabilitation Program. It is a multisectoral partnership aimed at restoring the environmental quality of creeks and rivers in the city.

Launched in February 2011, adopt-a-river project hopes to bring in fruitful collaboration not just with the private sector but also with the communities in cleaning up their rivers and creeks.

The project is implemented in three communities, namely San Juan, San Cristobal, and Real.

Under the said project, each company that generates waste into the river shall adopt a portion of that river and be responsible for its cleanliness and rehabilitation. Companies, together with the schools, hospitals and commercial institutions, along San Juan River, the San Cristobal Rriver, and the Baranca de Sipit Creek in Real , shall be the private partners, while the barangay captains, Department of Education (DepEd), City Environment andNnatural Resource Office (CENRO), and the Office of the Mayor shall be the public counterpart. A total of 236 private sectors signed the memorandum of agreement with CENRO, which formalized the partnership in the context of Adopt-a-Rriver Project. On the other hand, the local government units are expected to provide guidance and technical assistance to all private partners or "the green partners". In addition, they are also responsible for dissemination of information material on the program.

Adopt-a-River project consists of seven components, namely Bantay Ilog, River Clean-up, River Restoration, Reforestation, River Campaigns, River Maintenance, Flood Protection Program, and Housing and Resettlement. The CENRO as the implementing agency is tasked to initiate the conduct of these components with the goal that the public and private sectors as partners will eventually initiate and sustain their own respective programs. CENRO has been implementing river clean-up drives every quarter of the year in the abovementioned communities.

Successful implementation of environmental, or development programs in general, is contextual. Essentially, participation and commitment of stakeholders is crucial ([2]–[4] Understanding the level of participation requires systematic analysis of the context within which a development project exists. Lovell (1992 in [2] suggests a number of factors such as population, employment, health literacy, among others that are associated with participation; however, Lovell stressed that these variables are not necessarily valid from country to country even when the needs appear similar. Along this line, this study aims to find out the factors associated to the level of participation of the community on Adopt-a-River project of a local government unit in the Philippines.

Specifically, it aims to determine the respondents' level of mass media exposure, their sources of information about the project, their level of awareness, perception, and participation in the project. This study further aims to present a model of participation in the context of a community in the Philippines in the hope that such model may be adopted in similar environmental projects.

2. LITERATURE REVIEW

When development scholars recognize the limitations of modernization paradigm which advocates top-down approach to development in the 1970s, they started to rethink how development can improve the standards and quality of life [5]. This rethinking calls for humane, egalitarian, and responsive communication theories and practices [6].Thus, the inclusion of participation in the development process.

Participation is a highly contested word. World Bank defines participation as " a process through which stakeholders influence and share control over development initiatives and the decisions and resources which affect them." Willis, (2006) on the other hand, views it as "an umbrella term to refer to the involvement of local people in development activities, often NGO-based." [7](2009) cited participatory communication as one of the major theories following modernization paradigm. He argued that participatory communication seeks to describe the power of individuals to change the world with an end goal of reaching positive development for all and better inter-cultural understanding. Dervin & Huesca [7],, in their meta-analysis of theoretical and empirical researches on participation, view the latter as being positive to successful development.

Participation varies in nature. [8] cites that participation can be classified according to the degree of participation in a continuum, according to the direction of communication flows, theoretical basis and objectives for which participation is being used. [9] enumerates four typologies of participation ranging from the lowest to the highest level. These are passive participation in which stakeholders participate by being informed about what is going to happen or has already happened, participation by consultation in which stakeholders participate by providing feedback to questions posed by outside researchers or experts, functional participation in which stakeholders take part in discussions and analysis of predetermined objectives set by the project, and empowered participation in which stakeholders are willing and able to be part of the process and participate in joint analysis, which leads to joint decision making about what should be achieved and how.

The benefits derived from involving the public in environmental programs have driven policymakers

to incorporate participation in national and international policy ([8], [10]–[12]. Thus, literature abounds with participation studies. While there is a growing concern for participation in development projects, previous studies support that involving the stakeholders does not happen in a vacuum. Factors such as demographic profile [13], [14]; media exposure [15]; quality of community members' life [16]; environmental values [17] and attitudes and motivation towards participation [18]. [19], on the other hand, found two variables that influence participation: "ownership variables" (personal interest and knowledge on the issue) and "ownership variables" (environmental strategies and belief in one's ability to succeed).

3. METHODOLOGY

Using the descriptive research design, the researchers administered a self-made instrument among 327 respondents from three communities in Calamba City, Philippines, where the three main tributaries are situated. The instrument is divided into four parts. The first part is the demographic profile; the second part elicits information about respondents' mass media exposure; the third gathers the level of awareness of and sources of information about the project, and the last part contains the statements on perception on the project. Data were analysed using frequency, percentage, mean and Chi-square using SPSS version 20. Structural equation modelling using path analysis was done to develop the participation model in the context of the said project.

4. RESULTS AND DISCUSSION

4.1 Respondents' Profile and Media Exposure

Respondents are comprised mostly of female (60.9 %). Their civil status is either separated (47.7%) or single (41.3%) and their age ranges from 18-47 years old. In terms of education, most of the respondents have reached elementary level. Only 17 out 327 respondents are college degree holders; however, most of them (76.5%) are employed.

Previous studies have shown that media exposure represents one variable that has association with planned behaviour change [15]; [20][21]. Thus, this study considers media exposure and its potential influence on environmental participation. Results revealed respondents are exposed to both traditional and new media. On a daily basis, they spent 30 minutes to 1 hour listening to radio (37.6%), reading the newspaper (56%) and surfing the Internet (61.5%) and 1-2 hours watching television (16.8%). It is worthy to note that most of them are exposed to the Internet among other forms of media.

4.2. Awareness of and Source of Information about Adopt-a-River Project

Respondents are only moderately aware (63.3%) of the Adopt-a-River Project. A significant number of respondents (82 or 25.1%) are unaware of the project. As to source of information about the project, group discussion serves as their main source, with 52% of the respondents citing it. Other sources of information are seminar (16.5%), television (7.3%) and radio (6.4%).

4.3. Perception on Adopt-a-River Project

Given an overall mean rating of 2.71 interpreted as "Agree", respondents apparently have favourable perception on the project. Specifically, respondents agreed with the message of the project (mean=2.89). They also agreed that the project's message is acceptable (mean=2.83) and understandable (mean=2.82) and that simple words were used to promote and implement the project (mean=2.72). Moreover, the project provided positive and useful learning to the residents (mean=2.72).

Table 1. Mean perception on the project

Statements	Mean	SD
1. I understand the message of the project.	2.82	0.93
2. The message of the project is acceptable.	2.83	0.92
3. I agree with the message of the program.	2.84	0.96
4. I easily comprehended the message of the project.	2.79	0.94
5. Simple words were used to promote and implement the project	2.72	0.95
6. The project offered opportunities to the citizen of the benefited community.	2.65	0.93
7. I have enough knowledge of the purpose of the project.	2.62	0.90
8. The project was continuously implemented in a way it's visible to the residents.	2.64	0.90
9. The project provided positive and useful learning for the residents.	2.72	0.91
10. The project used effective communication instruments in disseminating substantial information.	2.64	0.91
11. Timely and appropriate communication tools were used in the project.	2.69	0.94
12. Persuasive project design was used.	2.67	0.91
13. Information about the project was properly distributed.	2.69	0.92
14. The communication tools used in the project were sufficient and necessary.	2.60	0.94
Overall mean perception	2.71	0.78

Legend: 4-Strongly agree; 3-Agree, 2-Disagree, 1-Strongly disagree

4.4. Level of participation in the project

Anchored on Mefalopulos' typology, this study considers four levels of participation: Passive (Level 1), Participation by Consultation (Level 2), Functional Participation (Level 3), and Empowerment (Level 4 and 5). Results reveal that respondents have demonstrated different levels of participation in the project. However, in general they mostly showed passive participation. Respondents agreed that they were informed about the programs and regulations of Adopt-a-River (46.5%); however, they were not hindered or limited by the facilitators in their participation (45.9%). In contrast, respondents disagreed that they were part of the decision-making and implementation of Adopt-a-River, that were consulted by LGUs or facilitators about matters involving Adopt-a-River and that they are currently participating in Adopt-a-River.

Table 2. Level of participation

	Level 1		Level 2		Level 3		Level 4		Level 5	
Response	Freq	%	Freq	%	Freq	%	Freq	%	Freq	%
Strongly disagree	52	15.9	56	17.1	58	17.7	53	16.2	45	13.8
Disagree	75	22.9	126	38.5	123	37.6	102	31.2	95	29.1
Agree	152	46.5	116	35.5	117	35.8	134	41	150	45.9
Strongly agree	48	14.7	29	8.9	29	8.9	38	11.6	37	11.3
Mean	2.60		2.36		2.36		2.48		2.55	

Legend: 4-Strongly agree; 3-Agree, 2-Disagree;
1- Strongly disagree

4.5. Factors associated to participation level

All levels of participation are significantly correlated with level of awareness and level of perception (see Table 3). Passive participation is significantly correlated with the type of radio program exposed to and type of internet sites used. Likewise, participation by consultation and empowerment level are significantly correlated with type of TV program respondents are exposed to.

Table 3. Correlation between level of participation, awareness, perception, and length and type of media exposure

	level1	level2	level3	level4	level5	awareness	perception
awareness	-.326**	-.248**	-.205**	-.304**	-.287**	1	
perception	.625**	.512**	.475**	.486**	.485**	-.449**	1
Length of exposure to radio	0.002	-0.023	0.039	-0.007	0.068	-0.027	0.028
Length of exposure to TV	-0.062	0.004	-0.038	-0.058	0.054	-0.027	0.1
Length of exposure to newspaper	0.027	-0.006	-0.062	-0.06	0.032	-0.044	-0.009
Length of exposure to Internet	0.037	-0.022	0.06	-0.023	0.011	-0.006	0.055
Type of radio program	.171**	0.085	0.082	0.042	0.09	-.169**	.114*
Type of TV program	.140*	.129*	0.06	0.084	.121*	-0.1	.136*
Type of newspaper article	0.103	0.099	0.053	-0.01	0.083	-0.019	0.015
Type of sites used	.176**	0.058	0.043	-0.016	0.077	-0.07	.150**

**. Correlation is significant at the 0.01 level (2-tailed).

*. Correlation is significant at the 0.05 level (2-tailed).

Structural Equation Modelling using Path Analysis reveals the following model of participation.

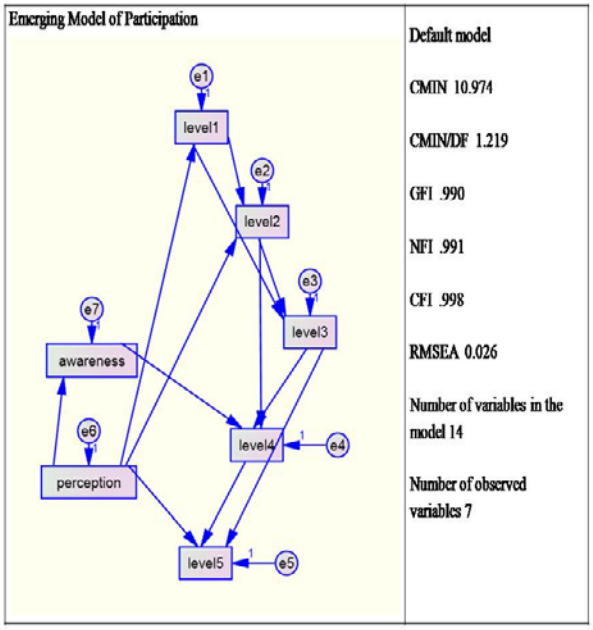

Fig. 1. Structural Equation Modelling Using Path Analysis

The emerging model shows a significant direct effect of perception on level 1 (.737), level 2 (.139) and level 5 (.183) participation, as well as on awareness (-.350). Level 1 participation has a significant effect on level 2 (.581) and level 3 (.271) participation. Level 2 participation has a significant effect on level 3 (.523) and level 4 (.434) participation. Level 3 participation has a significant effect on level 4 (.340) and level 5 (.230) participation. Level 4 participation has a significant effect on level 5 (.47) participation

5. CONCLUSION

In the context of this study, the local residents who took part in the study are mostly female, elementary graduates but employed. In terms of media exposure, they are light users of radio, television and Internet. Such exposure to media results in their awareness of the Adopt-a-River Project. However, their main source of information about the said project is group discussion. The Adopt-a-River Project was favourably perceived by the local residents. They agreed with the message of the project. They also agreed that the project's message is acceptable and understandable and that simple words were used to promote and implement the project. Moreover, the project provided positive and useful learning to the residents. While perception on the project is positive, results revealed that most local residents have passive participation in the project, suggesting that they were only informed of the programs and regulation, although some claimed that they were not hindered in their participation in the project. Path analysis showed that both awareness of and perception on the project are significant predictor of participation.

6. REFERENCES

[1] R. Bagherian, B. Samah, and A. Samah, "Factors influencing local people's participation in watershed management programs in Iran," *Am. J.*, 2009.

[2] G. M. Mathbor, "A Typology of Community Participation," *Eff. Community Particip. Coast. Dev.*, no. 1, p. 144, 2008.

[3] J. Maraga, J. Kibwage, and B. Oindo, "Factors determining community participation in afforestation projects in River Nyando basin, Kenya," *African J. Environ. Sci. Technol.*, vol. 4, no. 12, pp. 853–859, 2010.

[4] C. Cavalcanti, S. Engel, and A. Leibbrandt, "Social integration, participation, and community resource management," *J. Environ. Econ. Manage.*, vol. 65, no. 2, pp. 262–276, 2013.

[5] K. Willis, *Theories and Practices of Development - by Katie Willis*, vol. 172. 2006.

[6] K. G. Wilkins and B. Mody, "Reshaping development communication: Developing communication and communicating development," *Commun. Theory*, vol. 11, no. 4, p. 385, 2001.

[7] T. L. McPhail, *Development Communication: Reframing the Role of the Media*. 2009.

[8] M. S. Reed, "Stakeholder participation for environmental management: A literature review," *Biological Conservation*, vol. 141, no. 10. pp. 2417–2431, 2008.

[9] P. Mefalopulos, "Reflections on the Theory and Practice of Development Communication," in *Development Communication Sourcebook : Broadening the Boundaries of Communication*, 2008, pp. 37–79.

[10] L. S. Prokopy, "Determinants and Benefits of Household Level Participation in Rural Drinking Water Projects in India," *J. Dev. Stud.*, vol. 45, no. 4, pp. 471–495, 2009.

[11] N. Holman, "Community participation: Using social network analysis to improve developmental benefits," *Environ. Plan. C Gov. Policy*, vol. 26, no. 3, pp. 525–543, 2008.

[12] W. El Ansari and E. Andersson, "Beyond value? Measuring the costs and benefits of public participation," *J. Integr. Care*, vol. 19, no. 6, pp. 45–57, 2011.

[13] K. L. Granzin and J. E. Olsen, "Characterizing Participants in Activities Protecting the Environment: A Focus on Donating, Recycling, and Conservation Behaviors," *J. Public Policy Mark.*, vol. 10, no. 2, pp. 1–27, 1991.

[14] C. F. Clark, M. J. Kotchen, and M. R. Moore,

"Internal and external influences on pro-environmental behavior: Participation in a green electricity program," *J. Environ. Psychol.*, vol. 23, no. 3, pp. 237–246, 2003.

[15] D. Drew and D. Weaver, "Media Attention, Media Exposure, and Media Effects," *Journal. Mass Commun. Q.*, vol. 67, no. 4, pp. 740–748, 1990.

[16] S. A. Eshliki and M. Kaboudi, "Community Perception of Tourism Impacts and Their Participation in Tourism Planning: A Case Study of Ramsar, Iran," *Procedia - Soc. Behav. Sci.*, vol. 36, no. June 2011, pp. 333–341, 2012.

[17] A. L. Ahmad, S. A. Rahim, L. Pawanteh, and F. Ahmad, "The understanding of environmental citizenship among Malaysian youths: A study on perception and participation," *Asian Soc. Sci.*, vol. 8, no. 5, pp. 85–92, 2012.

[18] G. M. Hurtz and K. J. Williams, "Attitudinal and motivational antecedents of participation in voluntary employee development activities," *J. Appl. Psychol.*, vol. 94, no. 3, p. 635, 2009.

[19] H. R. Hungerford and T. L. Volk, "Changing Learner Behavior through Environmental Education," *Journal of Environmental Education*, vol. 21, no. 3. pp. 8–21, 1990.

[20] M. D. Slater, "Integrating application of media effects, persuasion, and behavior change theories to communication campaigns: A stages-of-change framework," *Health Commun.*, vol. 11, no. 4, pp. 335–354, 1999.

[21] I. K. A. Qader and Y. Zainuddin, "The influence of media exposure, safety and health concerns, and self-efficacy on environmental attitudes towards electronic green products," *Asian Acad. Manag. J.*, vol. 16, no. 2, pp. 167–186, 2011.

Second International Conference on Science, Engineering & Environment,
Osaka City, Japan, Nov.21-23, 2016, ISBN: 978-4-9905958-7-6 C3051

SINGLE ACID EXTRACTION OF HEAVY METAL IONS FROM CONTAMINATED SOILS

Hyo-il Jeon[1] and Seungkyung Park[1*]
[1]Korea University of Technology and Education, South Korea; * Corresponding Author

ABSTRACT

Early detection of heavy metal contaminations of soil and ground water has great importance for human health. In this study, single acid extraction methods have been tested and evaluated for the extraction of heavy metal ions for rapid and on-site soil sample preparations. Parametric studies have been performed including sample to acid volume ratio, extraction time, and acid concentration, and the performance of the proposed method has been compared with standard laboratory based protocol using soil samples spiked with target metal ions. The proposed protocol utilizing three different single acids (EDTA, HNO_3, HCl) has shown the comparable extraction efficiency over ~80% for heavy metal ions of major concerns, Pb, Hg, and As. Compared to standard method based on aqua regia digestion, single acid extraction provides reduced processing steps and reagent volume, possibly enabling the on-site processing of contaminated soils and analysis.

Keywords: Soil Analysis, Heavy metals, Ionic Extraction

INTRODUCTION

Heavy metal contaminations of soil and ground water have been one of major concern in the world due to their toxicity and numerous effects on human health [1]-[4]. Although conventional laboratory based detection methods are well established, rapid and on-site monitoring of soil contamination which is essential for preventing the environmental pollution in a very early stage is still limited[5]-[8]. Conventional analytical techniques are based on the large scale system involving time-consuming and serial processing of samples with hazardous materials, complicated instruments, central laboratories, and high skilled personnel are required [9]. Thus, the development of miniaturized procedures is crucial for on-site analysis.

Soil samples generally require sample pretreatment with efficient purification and extraction of target analytes before a specific analysis, and the preprocessing has been recognized as one of the most critical step for maximizing analytical accuracy. However, sample preprocessing usually involves labor-intensive and tedious process and has been the actual bottle neck of developing a rapid, automated and portable soil monitoring system [10], [11]. In this work, simplified extraction protocols for heavy metal detection from contaminated soils are presented. For the adaption in a syringe like miniaturized format, single acid based extraction methods have been designed and tested for the extraction of heavy metal ions of major concerns in South Korea, which are Hg, Pb, and As. Metal ions are extracted using acid solution first and filtered to remove any undesirable debris. In order to assess the performance of the proposed simplified and miniaturized preprocessing protocol, mock-up soil samples with known quantity of ions have been processed, and the comparison with the standard protocol has been made by measuring the ion concentration. The proposed protocol has shown the comparable extraction efficiency over 80% while the required processing steps and the reagent volume have been reduced significantly. Thus, the proposed method can be applied for on-site analysis of contaminated soils, enabling simplified and rapid analytical procedures.

MATERIALS AND EQUIPMENT

Two reference soils, CRM 109-03-002 (Korea Research Institute of Standards and Science, KRISS, South Korea) and BAM-U112a (Odlab, South Korea) were purchased and tested. Selected ion concentration in reference soils are shown in Table 1.

Table 1 Ion concentration in reference soils (mg/kg)

	Hg	Pb	As
KRISS-CRM	0.98	3945.3	1200
BAM-U112a	16.3	198	10.3

Ions of interest (Hg, Pb, As) were extracted and total concentrations of metal ions were analyzed by using inductively coupled plasma optical emission spectrometry (ICP-OES) and mercury analyzer. All test samples were filtered by filter paper (F1001, Chmlab) before the analysis. EP grade

Ethylenediaminetetraacetic acid (EDTA), Hydrochloric acid (HCl) and Nitric acid (HNO_3) were purchased (Daejung, South Korea). 18 MΩcm DI water was purified with a Pure Power System (Human corp., South Korea).

METHODS

Standard Method

For the comparison of the extraction efficiency with the standard extraction protocol, ES07000 from Korea Ministry of Environment was selected and applied, which is based on aqua regia digestion.

EDTA Extraction

1~4g of soil samples were mixed with 40 ml of 0.05M EDTA in a centrifuge tube and homogenized with tube shaker (Finepcr, South Korea) for 0.5~3 hours. After the extraction, samples were filtered through a filter paper, then collected.

HNO_3 Extraction

5~200 mg of soil samples were mixed with 5~50 ml of 10% and 50 % HNO_3 in a centrifuge tube, and were sonicated for 30 min at 35C (Hwashin, South Korea). Samples were then diluted with DI water and filtered through the filter paper and collected.

HCl Extraction

200 mg of soil samples were mixed with 10~40 ml of HCl in different concentrations from 1.7 % to 10 % in a centrifuge tube and homogenized with the tube shaker for 0.5~12 hours. If needed, sonication was applied at 60 C for 0.5~2 hours. Samples were then diluted with DI water and filtered through the filter paper and collected.

RESULTS AND DISCUSSION

Table 1 summarizes extraction efficiencies of different acids together with the results by standard method. For the extraction of Pb, most of acid extractions showed comparable efficiencies, while the extraction of Hg and As were achieved only for HNO_3 and HCl, respectively. Standard extraction efficiencies for Pb and Hg ions were appeared as over than 80% for both KRISS-CRM and BAM-U112a soils. For each acid, the protocol was empirically optimized and tested to achieve target efficiencies over 80% for future applications.

EDTA was first tested for the extraction of three ions. EDTA is the well-known chelating agent for soil washing method, and many studies have shown that EDTA is effective especially in removing Pb, while the efficiency can be affected by various parameters including acid concentrations and the acid to soil ratio [12]-[16]. The test results of Pb extraction with 0.05M EDTA also showed good efficiencies over 70% for BAM-U112a soils even within relatively short incubation time. However, the efficiency was lowered in the case of KRISS-CRM. To further examine the EDTA extraction efficiencies for KRISS-CRM, the effects of incubation time and acid to soil ratio were tested.

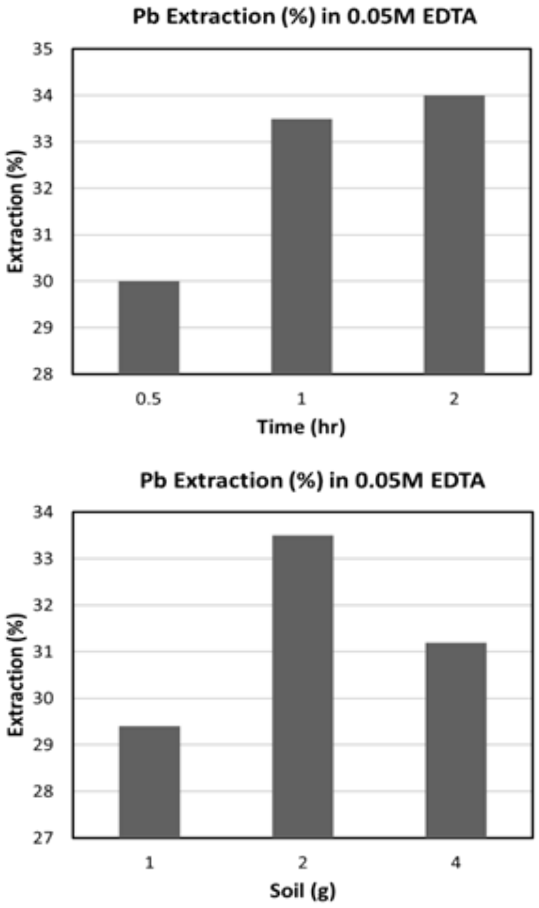

Fig. 1 Lead ion extraction efficiency in 0.05M EDTA as increased time (top) and soil mass (bottom).

Figure 1 shows the variation of Pb extraction efficiencies with different incubation time and soil mass in 0.05M EDTA. As seen on the figure, elongated incubation time increased the extraction efficiency, but the efficiency increase became saturated if incubated over 2 hours. Meanwhile, the test result of different soil amounts informs that the optimal acid to soil ratio exists. In this case, the incubation was performed for 1 hour for all cases in the consideration of assay time. Even the soil amount may further be optimized, it can be seen that the extraction efficiency is limited about 34%. The difference in extraction efficiencies for two soils may come from the labilities of ions in samples and the saturation due to the high Pb concentration in

Table 2 Acid extraction efficiency for heavy metal ions

Acid	Soil	Extraction	Efficiency	Remarks
0.05M EDTA	KRISS	40ml acid & 1-4g soil 0.5-3 hour	Pb 29-34%	Standard extraction (ES 07000)
	BAM	40ml acid & 1-4g soil 0.5-3 hour	Pb 70-107%	KRISS CRM . Pb 96-104% . Hg 90%
10% HNO_3	KRISS	5-50ml acid & 5-200mg soil 30 min sonication at 35C	Pb 33-42%	
	BAM	5-50ml acid & 5-200mg soil 30 min sonication at 35C	Pb 74-102%	BAM-U112a . Pb 77-95% . Hg 88-93% . As 107%
50% HNO_3	BAM	12ml acid, & 200mg soil 45 hour	Pb 75% Hg 87%	
1.7% HCl	BAM	40 ml acid & 0.2g soil 1 hour shaking	Pb 77% As 78%	
2.5% HCl	BAM	10ml acid+11.5% ethanol & 0.2g soil 90-120min sonication at 60C	Pb 75-83% Hg 33-38%	
10% HCl	BAM	40 ml acid & 0.2g soil 1-12hour shaking	Pb 76-91% As 78-136%	

KRISS-CRM. It can be observed that EDTA extraction can generally be optimized with longer incubation time before saturation and the proper sample and acid volumes. However, besides Pb, EDTA was inefficient or incapable for the extraction of Hg and As.

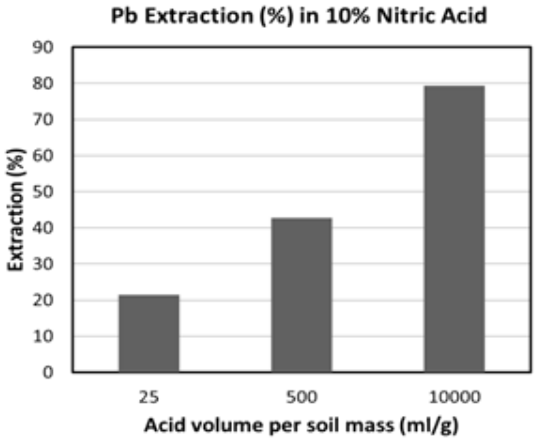

Fig. 2 Lead ion extraction efficiency in 10% nitric acid as increased acid volume per soil mass.

For the extraction of metal ions, nitric acid was tested. First, 10% HNO_3 extraction followed by 30 minutes sonication were performed based on the protocol [15]. The extraction efficiency of Pb ions was appeared as similar to the result of EDTA. Figure 2 shows the efficiency of lead ion extraction in 10% HNO_3. The extraction efficiency is rapidly increasing as the applied acid volume is getting larger. Unlike the laboratory based or large scale soil washing, acid volume should be minimized for field applications, and thus further increase of the acid volume was avoided. Instead, to increase the extraction efficiency and achieve the Hg extraction, acid of higher concentration was applied with elongated incubation time. On the application of 50% HNO_3, the increase in Hg extraction efficiency was achieved while the effect was negligible for Pb. However, Hg extraction over 80% was found to be challenging unless incubated over ~40 hours. Thus, additional complementary mechanism such as ultrasound, which is adequate for field application, will be necessary if reduced processing time is required [16].

HCl was tested with BAM-U112a especially focusing As ions. As KRISS-CRM contains high concentration, only BAM-U112a was tested for excluding saturation effect. 1.7% HCl with 1 hour shaking showed the good extraction efficiency close to 80%. Further increase in acid concentration was found to be ineffective, but the increase in incubation time showed more improved extraction of As ions. Hg extraction was also tested initially based on the protocol [17]. As expected, simple extration of Hg ions in HCl could not be achieved, but additional sonication steps at the elevated temperature (60C) provided significant increase in the extraction efficiency. Pb extraction in HCl also showed comparable efficiencies with other acids

regardless of the acid concentration.

CONCLUSIONS

As an alternative approach of standard extraction protocol based on aqua regia, single acid extraction methods have been tested and optimized. Single acid including EDTA, HNO_3, and HCl has shown comparable extraction efficiency compared to the standard protocol. Findings from the presented study can be summarized as follows:

- Single acid extraction of Pb and As ions can possibly be performed with the efficiencies over 78% through a simple incubation in 0.05M EDTA and 1.7% HCl, respectively, with optimized incubation time and acid volumes.

- Single acid extraction of Hg ions can possibly be performed by using 50% HNO_3 with the efficiency of 87%, but requires elongated incubation time more than 40 hours. Additional mechanism such as ultrasound is generally required to reduce the time.

In conclusion, the presented single extraction protocols provide simplicity of the sample preparation by bypassing the complicated procedure of the standard method with comparable ion recovery rates, thus, possibly allow the field applicable sample pre-processing. The developed protocol will be implemented to a field applicable analytical system and validated in our future study.

ACKNOWLEDGEMENTS

This subject is supported by Korea University of Technology and Education as “Professor‘s Education and Research Promotion fund 2014” and Korea Ministry of Environment (MOE) as “Geo-Advanced Innovative Action Project” (2015000540008).

REFERENCES

[1] Adriano DC. "Trace elements in the terrestrial environment" Springer Science & Business Media, 2001.

[2] Smith SR. "A critical review of the bioavailability and impacts of heavy metals in municipal solid waste composts compared to sewage sludge", Environment international, Vol. 35, 2009, pp.142-156.

[3] Nriagu JO. "A global assessment of natural sources of atmospheric trace metals", Nature, Vol. 338, 1989, pp.47-49.

[4] Wuana RA, Okieimen FE. "Heavy metals in contaminated soils: a review of sources, chemistry, risks and best available strategies for remediation", ISRN Ecology, 2011.

[5] Gleyzes C, Tellier S, Astruc M. "Fractionation studies of trace elements in contaminated soils and sediments: a review of sequential extraction procedures", TrAC Trends in Analytical Chemistry, Vol 21, 2002, pp.451-467.

[6] Tessier A, Campbell PGC, Bisson M. "Sequential extraction procedure for the speciation of particulate trace metals", Analytical chemistry, vol. 51, 1979, pp. 844-851.

[7] Quevauviller P. "Operationally defined extraction procedures for soil and sediment analysis I. Standardization", TrAC Trends in Analytical Chemistry, Vol. 17, 1998, pp.289-298.

[8] Sahuquillo A, Rigol A, Rauret G. "Overview of the use of leaching/extraction tests for risk assessment of trace metals in contaminated soils and sediments", TrAC Trends in Analytical Chemistry, Vol. 22, 2003, pp.152-159.

[9] Gu W, Zhou CY, Wong MK, Gan LM. "Orthogonal array design (OAD) for the optimization of mercury extraction from soils by dilute acid with microwave heating", Talanta, Vol. 46, 1998. pp.1019-1029.

[10] Park JH, Lamb D, Paneerselvam P, et al. "Role of organic amendments on enhanced bioremediation of heavy metal (loid) contaminated soils", Journal of hazardous materials, Vol. 185, 2011, pp.549-574.

[11] Pueyo M, Rauret G, Bacon JR, et al. "A new organic-rich soil reference material certified for its EDTA-and acetic acid-extractable contents of Cd, Cr, Cu, Ni, Pb and Zn, following collaboratively tested and harmonised procedures", Journal of Environmental Monitoring , Vol. 3, 2001, pp.238-242.

[12] Elliott HA, Brown GA. "Comparative evaluation of NTA and EDTA for extractive decontamination of Pb-polluted soils", Water, Air, and Soil Pollution, Vol. 45, 1989, pp.361-369.

[13] Elliott HA, Shastri NL. "Extractive Decontamination of Metal-Polluted Soils Using Oxalate", Water, Air, and Soil Pollution, Vol. 110, 1999, pp.335-346.

[14] Heil DM, Samani Z, Hanson AT, Rudd B. "Remediation of Lead Contaminated Soil by EDTA. I. Batch and Column Studies", Water, Air, and Soil Pollution, Vol. 113, 1999, pp.77-95.

[15] Katoh M, Masaki S, Sato T, “Single-Step Extraction to Determine Soluble Lead Levels in Soil”, Int. J. of GEOMATE, Vol. 3, 2012, pp.375-380.

[16] Moghal AAB, Al-Shamrani MA, Zahid WM, “HEAVY METAL DESORPTION STUDIES ON THE ARTIFICIALLY CONTAMINATED AL-QATIF SOIL”, Int. J. of GEOMATE, Vol. 8, 2015, pp.1323-1327.

[17] Ashley K. "Ultrasonic extraction and field-portable anodic stripping voltammetry of lead from environmental samples", Electroanalysis, Vol. 7, 1995, pp.1189-1192.

[18] De La Calle I, Cabaleiro N, Lavilla I, Bendicho C. "Ultrasound-assisted single extraction tests for rapid assessment of metal extractability from soils by total reflection X-ray fluorescence", Journal of hazardous materials, Vol. 260, pp.202-209.

[19] Han Y, Kingston HM, Boylan HM, et al. "Speciation of mercury in soil and sediment by selective solvent and acid extraction", Analytical and Bioanalytical Chemistry, Vol. 375, 2003, pp.428-436.

Second International Conference on Science, Engineering & Environment,
Osaka City, Japan, Nov.21-23, 2016, ISBN: 978-4-9905958-7-6 C3051

PHOTOCATALYTIC DEGRADATION OF FAMOTIDINE WITH DYE-SENSITIZED TiO_2 UNDER VISIBLE LIGHT

Md. Ashraful Islam Molla[1], Hideyuki Katsumata[1], Tohru Suzuki[2], Satoshi Kaneco[1,2]
[1]Department of Chemistry for Materials, Graduate School of Engineering, Mie University, Japan
[2] Mie Global Environment Center for Education & Research, Mie University, Japan

ABSTRACT

Photocatalytic degradation of Famotidine (FMT) by orange II (OII), bromophenol blue (BPB) and rhodamine B (RhB) sensitized TiO_2 has been investigated under LED light ($\lambda > 400$ nm). The photodegradation experiments were carried out at different periods of time using dye-sensitized 20 mg of TiO_2 and 30 mL of 5 mg/L of initial concentration of FMT at room temperature and at natural pH values of the solution. Dye-sensitization of 5 mg/L OII, BPB and RhB of TiO_2 enhanced its photoactivity in FMT degradation. The increased photoactivity of TiO_2-OII, TiO_2-BPB and TiO_2-RhB than bare TiO_2 under visible light illumination can be ascribed to the effect of dye-sensitized acting as electron transfer to the conduction band of the semiconductor (TiO_2). The photocatalytic activity, after sensitizing of TiO_2, enhances to about 1.7 times for TiO_2-OII, 2.0 times for TiO_2-BPB and 2.4 times for TiO_2-RhB. The kinetic behavior was described in terms of the Langmuir-Hinshelwood model. The possible mechanism of photodegradation under visible light was proposed.

Keywords: Photodegradation, Visible Light, TiO_2, Famotidine, Dye-sensitized

INTRODUCTION

In recent years, the presence of pharmaceuticals in the environment has become a serious cause for concern and the problem is continuing to grow with the on-going development of more potent and more metabolically resistant drugs [1]. Numerous studies have documented that both metabolized and non-metabolized pharmaceutical residues are speculated to have adverse effects on human health and the safety of ecosystems [2]-[4].

Famotidine (FMT, Fig. 1) is chemically 3-[({2-[(diaminomethylidene)amino]-1,3-thiazol-4-yl}methyl)sulfanyl]-*N'*–sulfamoylpropanimidamide. It is a histamine H_2-receptor antagonist used to treat peptic ulcers, gastroesophageal reflux, and conditions where the stomach produces an excess of acid [5],[6]. FMT is also used for treatment of Alzheimer's [7], and Parkinson's diseases [8]. In patients that use FMT, it has been documented that of the administered dose, between 65 and 70% of the parent compound is found unchanged in the urine [9]. This indicates that this drug is one of the many

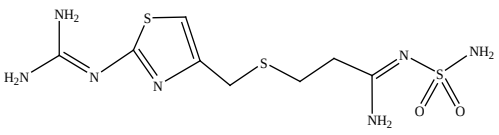

Fig. 1 Chemical structure of Famotidine.

compounds released into the environment on a day-to-day basis. FMT demonstrates excellent complicated properties which are due to the presence of amine, thiazole and thioether groups in its structure [10]. It creates stable complexes with palladium, copper, cobalt and nickel. Previous research reports have proved the stability of FMT in the environment and water bodies [11]. Taking the above-mentioned issues into account, one can argue that FMT should be considered as persistent contaminants in an aqueous environment which are frequently found in wastewater at various detectable concentrations. The frequent presence of these pharmaceuticals in wastewater underscores the necessity of removing them from water matrices before they are discharged into the environment.

A significant body of research has been devoted to tackling this issue, employing the use of advanced oxidation processes (AOPs). Of these AOP processes, those which use the photocatalyst TiO_2 are some of the most studied for pharmaceutical abatement.TiO_2 is an effective photocatalyst and is cheap, safe and regularly used in the pharmaceutical, food and cosmetic industries [12],[13]. TiO_2 can make use of only a small fraction of solar light for photodegradation. This problem can be solved only by extending the light absorption capacity of TiO_2 catalysts. Countless literature articles exist documenting its efficient degradation of a wide range of dyes, pesticides and pharmaceutical compounds [14],[15]. Most of these methods, however, are quite expensive and time-consuming. Dye-sensitization, on the other hand, is simpler methods that can extend TiO_2 activation to wavelengths longer than those corresponding to its band gap. Recent examples of titania sensitized with

visible light absorbing molecules include methylene blue, rhodamine B [16], and Chryosidine G [17]. In addition to these, macrocyclic sensitizing molecules such as phthalocyanines and porphyrins in their free [18] and metallated forms have also been applied [19],[20]. To the best of the authors' knowledge, the photocatalytic degradation of famotidine with dye-sensitized TiO_2 has not been studied yet under the visible light irradiation.

The dye-sensitization technique has been reported as an innovative technology that could play an important role in developing efficient and cost-effective semiconductor photocatalyst in the near future [21]. Dye sensitization begins with electron injection from the excited dye into the conduction band (CB) of TiO_2, followed by interfacial electron transfer [22]-[26]. The present study is intended to investigate the photocatalytic degradation of famotidine with dye (Orange II, Bromophenol blue and Rhodamine B) sensitized TiO_2 under the visible light irradiation.

EXPERIMENTAL

Materials

All reagents were of analytical grade and were used without further treatment. Famotidine, Orange II, Bromophenol blue and Rhodamine B used in this study was purchased from Nacalai Tesque Inc., Kyoto, Japan (grade >99%) and used to make standards and aqueous solutions for the photocatalytic reactions. Ultrapure water (18 MΩ) was prepared by an ultrapure water system (Advantec MFS Inc., Tokyo, Japan). TiO_2 powder (Degussa P25, 80%:20% anatase/rutile, purity 99.9%) was added to the solution to produce a given concentration of TiO_2 suspension. The detailed experimental conditions were shown in Table 1.

Table 1 Experimental conditions

Famotidine	:	5 mg/L (30 mL)
Temperature	:	Room temperature (25 ◦C)
Photocatalyst	:	P25 TiO_2 (20 mg)
Light source	:	LED lamp with cut filter (λ < 400 nm)
Sensitizer	:	OII, BPB and RhB (5 mg/L)
UV detection	:	276 nm and 486 nm
Illumination time	:	0 ~ 24 h
Analysis	:	HPLC, UV–visible spectro-photometer

Evaluation of Photocatalytic Activity

The photocatalytic activities of TiO_2, TiO_2-OII, TiO_2-BPB and TiO_2-RhB were evaluated by the degradation of famotidine under visible light irradiation at ambient temperature in air with magnetic stirring. Photocatalytic reactions were carried out in a Pyrex glass reactor. The catalyst powder (20 mg) was suspended in 30 mL of famotidine solutions with the concentration of 5 mg/L without adjustment of pH. The luminous intensity was measured by a UV radio meter (UVR-300, UD-400, 360-490, Iuchi Co., Osaka, Japan). The light intensity of the LED lamp was 2.4 mW/cm^2. Prior to light illumination, the catalyst suspension was dispersed by a magnetic stirrer for 30 min in the dark to achieve adsorption equilibrium. During irradiation, the catalyst was kept in suspension state by a magnetic stirrer. After the illumination, the photocatalyst was separated by the centrifugation. The amount of the remnant famotidine in the aqueous solution was measured using a high-performance liquid chromatograph (HPLC, JASCO Co., Tokyo, Japan), equipped with a JASCO UVIDEC-100-VI optical detector and a Chromspher 5 Poly C18 column (Chrompack, VARIAN Inc., California, USA). The elution was monitored at 276 nm. The eluent used was a mixed solvent of acetonitrile and water (1/1, v/v). The flow rate of the mobile phase was 1.5 ml/min. The concentration of BPB was measured by UV–vis spectrophotometer at a wavelength of 587 nm.

Calculation of Photocatalytic Efficiency

The degradation efficiency of pharmaceuticals in the reaction process was calculated using the following formula:

$$\text{Degradation efficiency} = \frac{C_t}{C_0}$$

where C_t is the concentration of famotidine at time t, and C_0 is the initial concentration of famotidine (5 mg/L) at the start of the reaction.

RESULTS AND DISCUSSION

Photocatalytic Efficiency of TiO_2-OII, TiO_2-BPB and TiO_2-RhB in Famotidine Degradation

The photocatalytic activity was evaluated by measuring the degradation of famotidine under visible light irradiation. Fig. 2 shows the degradation efficiency with reaction time in the presence of bare TiO_2, TiO_2-OII, TiO_2-BPB and TiO_2-RhB photocatalysts. The photodegradation of FMT on TiO_2-OII, TiO_2-BPB and TiO_2-RhB catalysts are about 60%, 74% and 85%, respectively, after 24 h irradiating by visible light. All dye sensitized TiO_2 samples are significantly better than P-25 TiO_2, which only achieves about 36% elimination of famotidine after 24 h under the same conditions. The improvement of the catalytic activities is due to the

sensitizing TiO_2 by OII, BPB and RhB respectively. TiO_2-RhB exhibited the highest activity of FMT elimination from water in 24 h.

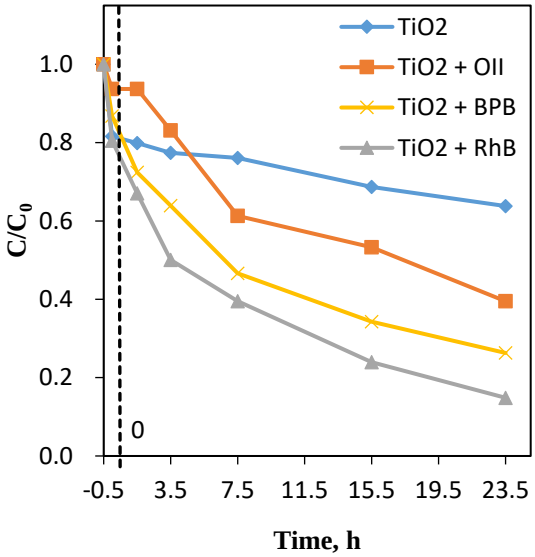

Fig. 2 Time courses of Famotidine concentration in the dispersions containing dye (OII, BPB and RhB) sensitized TiO_2 under $\lambda > 400$ nm radiation.

Photocatalytic Degradation of Sensitizer

The rate of degradation of sensitizer (OII, BPB and RhB) in the presence of FMT with TiO_2 was evaluated under visible light during reaction time. The amount of sensitizer used in these experiments is decreased with increasing time shown in Fig. 3.

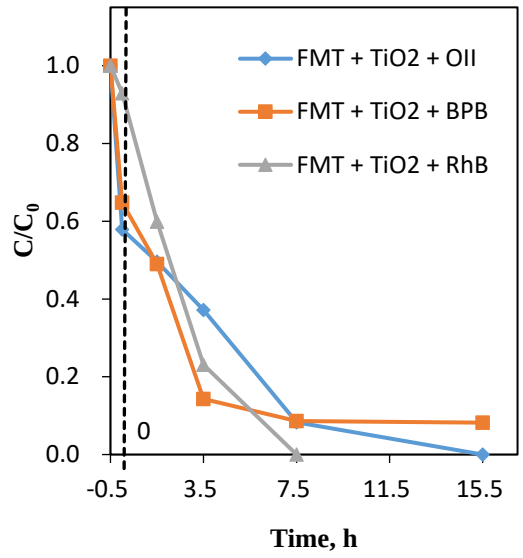

Fig. 3 Time courses of dye (OII, BPB and RhB) concentration in the dispersions containing famotidine with TiO_2 under $\lambda > 400$ nm radiation.

The degradation rate of OII and BPB were about 90% after 8 h irradiating by visible light while RhB was almost completely degraded under the same condition. Thus, the dye was firstly excited by absorbing visible light and then degraded through a self-sensitized mechanism.

Kinetic Analysis

The photocatalytic oxidation kinetics of many organic compounds has often been modeled with the Langmuir–Hinshelwood (L–H) equation, which also covers the adsorption properties of the substrate on the photocatalyst surface. This model was developed by Turchi and Ollis [27] and expressed as Eq. (1):

$$\mathbf{r_0} = -\frac{\mathbf{dC}}{\mathbf{dt}} = \frac{\boldsymbol{kKC_0}}{\mathbf{1+}\boldsymbol{KC_0}} \quad (1)$$

where r_0 is the degradation rate of the reactant, k is the reaction rate constant and K and C_0 are the adsorption equilibrium constant and concentration for the reactant, respectively. If the concentration of substrate is very low, i.e. $KC \ll 1$, the L–H equation (Eq. (1)) simplifies to a pseudo-first-order kinetic law (Eq. (2)) where k_{obs} is being the apparent pseudo-first-order rate constant.

$$-\frac{\mathbf{dC}}{\mathbf{dt}} = \boldsymbol{kKt} = \boldsymbol{k_{obs}t} \quad (2)$$

Integration of the above equation with the limit of $C = C_0$ at $t = 0$ with C_0 being the equilibrium concentration of the bulk solution gives the following equation:

$$-\mathbf{Ln}\frac{\mathbf{C}}{\mathbf{C_0}} = \boldsymbol{k_{obs}t} \quad (3)$$

The primary degradation reaction is estimated to follow a pseudo first- order kinetic law, according to Eq. (3). In order to confirm the speculation, $Ln(C/C_0)$ was plotted as a function of illumination time for famotidine shown in Fig. 4. Since the linear plots were observed as expected, the kinetics of famotidine in the TiO_2 suspension with dye solution followed the first-order degradation curve which was consistent to the L–H model resulting from the low coverage in the experimental concentration range (5 mg/L).

The values of rate constants have been determined from the slope and intercept of these plots. The rate constant for photodegradation of FMT using bare TiO_2 was found to be 0.011 min^{-1} whereas the rate constant were 0.039 min^{-1}, 0.065 min^{-1} and 0.083 min^{-1} for OII, BPB and RhB sensitized TiO_2 under visible light. During the photodegradation experiment, the substrate half-life $t_{1/2}$ of FMT was about 17 min for TiO_2-OII, 11 min for TiO_2-BPB and 8 min for TiO_2-RhB, respectively.

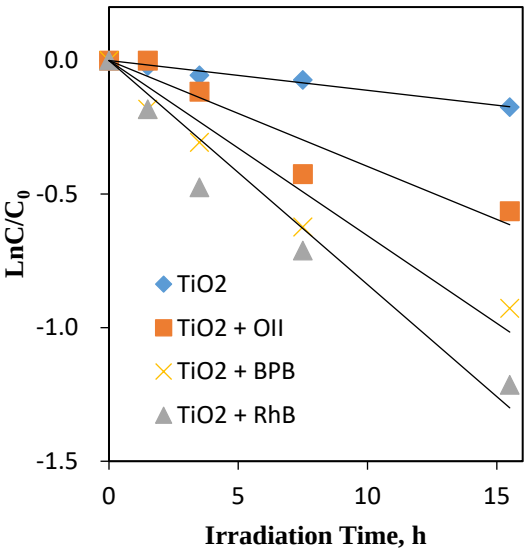

Fig. 4 Kinetic plot of Ln(C/C_0) versus irradiation time for famotidine.

Proposed Degradation Mechanisms

A number of mechanisms have been proposed by various authors, which include electron transfer/injection with subsequent formation of reactive oxygen species (ROS), or directly via a sensitizer-only generated singlet oxygen mechanism [28]-[30]. Both mechanisms are possible, and both would explain the observed sulfoxidation product, however, electron injection from the sensitizer directly into the conduction band of TiO_2 is generally the most accepted mechanism [12], [31]-[35].

TiO_2 cannot absorb visible light directly due to the band gap 3.2 eV [36], [37], but when a colored organic compound is present, a sensitized photocatalytic process is able to operate. Huang et al. reported dye sensitized photodegradation [39] which follows the radical mechanism. Park et al. also reported the dye-sensitization can be applied for the self-degradation of dyes [38]. In dye sensitized photocatalysis, a dye absorbing visible light excites an electron from the HOMO (highest occupied molecular orbital) of a dye to the LUMO (lowest unoccupied molecular orbital). The surface adsorbed dyes (OII, BPB and RhB) were excited by absorbing visible light and donate its electrons to the conduction band of TiO_2. As a result, the dyes are converted to a cationic radical, and the injected electron in the TiO_2 conduction band can reduce the surface-sorbed oxygen producing $O^{2\bullet-}$. The surface adsorbed FMT can undergo degradation by $O^{2\bullet-}$ and formed S-oxide of Famotidine. As soon as a FMT molecule degrade another FMT will adsorbed on TiO_2 surface and the photocatalytic cycle was continued.

$$\text{Dye} + h\nu \rightarrow \text{Dye}^* \quad (4)$$

$$\text{Dye}^* + TiO_2 \rightarrow \text{Dye}^{+\bullet} + TiO_2\,(e) \quad (5)$$

$$TiO_2\,(e) + O_2 \rightarrow TiO_2 + O_2^{-\bullet} \quad (6)$$

$$O_2^{-\bullet} + \text{Famotidine} \rightarrow \text{S-Oxide of Famotidine} \quad (7)$$

CONCLUSION

The investigation of photocatalytic ability indicated that OII–TiO_2, TiO_2-BPB and RhB–TiO_2 possessed higher photocatalytic activity than TiO_2 for the degradation of FMT under visible light irradiation. The photocatalytic activity, after sensitizing of bare TiO_2, enhances to about 1.7 times for TiO_2-OII, 2.0 times for TiO_2-BPB and 2.4 times for TiO_2-RhB. Dye molecules adsorbed onto TiO_2 semiconductors were excited under visible light irradiation and then injected electrons into the conduction band (CB) of TiO_2 particle. The electrons further react with O_2 adsorbed on the surface of semiconductors to produce $O_2^{-\bullet}$. The kinetics of FMT photodegradation was found to follow the pseudo-first order rate law and could be described in terms of Langmuir–Hinshelwood model.

ACKNOWLEDGEMENTS

The present research was partly supported by Grant-in-Aid for Scientific Research (C) 15K00602 from the Ministry of Education, Culture, Sports, Science, and Technology of Japan. All experiments were conducted at Mie University.

REFERENCES

[1] Khetan SK, collins TJ, Human pharmaceuticals in the aquatic environment: a challenge to green chemistry, Chem. Rev., Vol. 107, 2007, PP. 2319–2364.

[2] Verlicchi P, Al Aukidy M, Zambello E, Occurrence of pharmaceutical compounds in urban wastewater: removal, mass load and environmental risk after a secondary treatment-a review, Sci. Total Environ., Vol. 429, 2012, pp. 123–155.

[3] Khataee AR, Fathinia M, Joo SW, Simultaneous monitoring of photocatalysis of three pharmaceuticals by immobilized tio$_2$ nanoparticles: chemometric assessment, intermediates identification and ecotoxicological evaluation, Spectrochim. Acta Part A: Mol. Biomol. Spectrosc., Vol. 112, 2013, pp. 33–45.

[4] Nasuhoglu D, Rodayan A, Berk D, Yargeau V, Removal of the antibiotic levofloxacin (levo) in water by ozonation and TiO_2 photocatalysis, Chem. Eng. J., Vol. 189-190, 2012, pp. 41–46.

[5] Hassan MA, Salem MS, Sueliman MS, Najib N M, Characterization of famotidine polymorphic

forms, Int. J. Pharm., Vol. 149, 1997, pp. 227–232.

[6] Mady FM, Abou-Taleb AE, Khaled KA, Yamasaki K, Iohara D, Taguchi K, Anraku M, Hirayama F, Uekama K, Otagiri M, Evaluation of carboxymethyl-beta-cyclodextrin with acid function: improvement of chemical stability, oral bioavailability and bitter taste of famotidine, Int. J. Pharm., Vol. 397, 2010, pp. 1–8.

[7] Breitner JC, Welsh KA, Helms M.J, Gaskell PC, Gau BA, Roses AD, Pericak-Vance MA, Saunders AM, Delayed onset of Alzheimer's disease with nonsteroidal anti-inflammatory and histamine H_2 blocking drugs, Neurobiol. Aging, Vol. 16, 1995, pp. 523–527.

[8] Molinary SP, aminski R, Rocco AD, Yahr MD, The use of famotidine in treatment of Parkinson's disease: a pilot study, J. Neural Transm., Vol. 9, 1995, pp. 243–248.

[9] Lee KW, Kayser SR, Hongo RH, Tseng ZH, Scheinman MM, Famotidine and long QT syndrome, Am. J. Cardiol., Vol. 93, 2004, pp. 1325–1327.

[10] Murphy S, Saurel C, Morrissey A, Tobin J, Oelgemoller M, Nolan K, Photocatalytic activity of a porphyrin/TiO_2 composite in the degradation of pharmaceuticals, Appl. Catal. B: Environ., Vol. 119–120, 2012, pp. 156–165.

[11] Karpin´ska J, Sokoł A, Kobeszko M, Starczewska B, Czyzewska U, Hryniewicka M, Study on degradation process of famotidine hydrochloride in aqueous samples, Toxicol. Environ. Chem., Vol. 92, 2010, pp. 1409–1422.

[12] Linsebigler AL, Lu G, Yates JT, Photocatalysis on TiO_2 surfaces: principles, mechanisms, and selected results, Chem. Rev., Vol. 95, 1995, pp. 735–758.

[13] Chawengkijwanich C, Hayata Y, Development of TiO_2 powder-coated food packaging film and its ability to inactivate *Escherichia coli* in *vitro* and in actual tests, Int. J. Food Microbiol., Vol. 123, 2008, pp. 288–292.

[14] Lee BN, Liaw WD, Lou JC, Photocatalytic decolorization of methylene blue in aqueous TiO_2 suspension, Environ. Eng. Sci., Vol. 16, 1999, pp. 165–175.

[15] Coleman HM, Eggins BR, Byrne JA, Palmer FL, King E, Photocatalytic degradation of 17-β-oestradiol on immobilised TiO_2, Appl. Catal. B: Environ., Vol. 24, 2000, pp. 1–5.

[16] Chatterjee D, Mahata A, Visible light induced photodegradation of organic pollutants on dye adsorbed TiO_2 surface, J. Photochem. Photobiol. A: Chem., Vol. 153, 2002, pp. 199–204.

[17] Jiang D, Xu Y, Wu D, Sun Y, Visible-light responsive dye-modified TiO_2 photocatalyst, J. Solid State Chem., Vol. 181, 2008, pp. 593–602.

[18] Li D, Dong D, Sun S, Shi Z, Feng S, Photocatalytic degradation of acid chrome blue K with porphyrin-sensitized TiO_2 under visible light, J. Phys. Chem. C, Vol. 112, 2008, pp. 14878–14882.

[19] Sun Q, Xu Y, Sensitization of TiO_2 with aluminum phthalocyanine: factors influencing the efficiency for chlorophenol degradation in water under visible light, J. Phys. Chem. C, Vol. 113, 2009, pp. 12387–12394.

[20] Lu XF, Li J, Wang C, Duan MY, Luo Y, Yao GP, Wang JL, Enhanced photoactivity of CuPp-TiO_2 photocatalysts under visible light irradiation, Appl. Surf. Sci., Vol. 257, 2010, pp. 795–801.

[21] Ni M, Leung MKH, Leung DYC, Samathy K, A review and recent developments in photocatalytic water-splitting using TiO_2 for hydrogen production, Renew. Sustain. Energy Rev., Vol. 11, 2007, pp. 401-425.

[22] Ellingson RJ, Asbury JB, Ferrere S, Ghosh HN, Sprague JR, Lian T, Nozik AJ, Dynamics of electron injection in nanocrystalline titanium dioxide films sensitized with [Ru(4,4'-dicarboxy-2,2'-bipyridine)$_2$(NCS)$_2$] by infrared transient absorption, J. Phys. Chem. B, Vol. 102, 1998, pp. 6455-6458.

[23] Galoppini E, Linkers for anchoring sensitizers to semiconductor nanoparticles, Coord. Chem. Rev., Vol. 248, 2004, pp. 1283-1297.

[24] Gratzel M, Solar energy conversion by dye-sensitized photovoltaic cells, Inorg. Chem., Vol. 44, 2005, pp. 6841-6851.

[25] Duncan WR, Prezhdo OV, Theoretical studies of photoinduced electron transfer in dye-sensitized TiO_2, Annu. Rev. Phys. Chem., Vol. 58, 2007, pp. 143-184.

[26] Kim W, Tachikawa T, Majima T, Choi W, Photocatalysis of dye-sensitized TiO_2 nanoparticles with thin overcoat of Al_2O_3: enhanced activity for H_2 production and dechlorination of CCl_4, J. Phys. Chem. C, Vol. 113, 2009, pp. 10603-10609.

[27] Turchi CS, Ollis DF, Photocatalytic degradation of organic water contaminants: mechanisms involving hydroxyl radical attack, J. Catal., Vol. 122, 1990, pp. 178-192.

[28] Duan MY, Li J, Mele G, Wang C, Lu XF, Vasapollo G, Zhang FX, Photocatalytic activity of novel tin porphyrin/TiO_2 based composites, J. Phys. Chem. C, Vol. 114, 2010, pp. 7857–7862.

[29] Wang C, Yang G, Li J, Mele G, Slota R, Broda MA, Duan M, Vasapollo G, Zhang X, Zhang F, Novel *meso*-substituted porphyrins: Synthesis, characterization and photocatalytic activity of their TiO_2-based composites, Dyes Pigments, Vol. 80, 2009, pp. 321–328.

[30] Huang H, Gu X, Zhou J, Ji K, Liu H, Feng Y, Photocatalytic degradation of Rhodamine B on TiO_2 nanoparticles modified with porphyrin and iron-porphyrin, Catal. Commun., Vol. 11, 2009, pp. 58–61.
[31] Diaz-Uribe CE, Daza MC, Martinez F, Paez-Mozo EA, Guedes CLB, Di Mauro E, Visible light superoxide radical anion generation by tetra(4-carboxyphenyl)porphyrin/TiO_2: EPR characterization, J. Photochem. Photobiol. A: Chem., Vol. 215, 2010, pp. 172–178.
[32] Li W, Gandra N, Ellis ED, Courtney S, Li S, Butler E, Gao R, pH-responsive, TiO_2-attached porphyrin for singlet oxygen production in an aqueous solution, Appl. Mater. Interfaces, Vol. 1, 2009, pp. 1778–1784.
[33] Zhang J, Zhang L, Li X, Kang SZ, Mu J, Visible light photocatalytic activity of porphyrin tin(iv) sensitized TiO_2 nanoparticles for the degradation of 4-nitrophenol and methyl orange, J. Dispersion Sci. Technol. Vol. 32, 2011, pp. 943–947.
[34] Bonesi SM, Fagnoni M, Albini A, Photosensitized electron transfer oxidation of sulfides: a steady-state study, Eur. J. Org. Chem., Vol. 2008, 2008, pp. 2612–2620.
[35] Clennan EL, Persulfoxide: key intermediate in reactions of singlet oxygen with sulfides, Acc. Chem. Res., Vol. 34, 2001, pp. 875–884.
[36] Li H X, Bian ZF, Zhu J, Huo YN, Li H, Lu YF, Mesoporous Au/TiO_2 nanocomposites with enhanced photocatalytic activity, J. Am. Chem. Soc., Vol. 129, 2007, pp. 4538–4539.
[37] Subramanian V, Wolf EE, Kamat PV, Catalysis with TiO_2/Gold Nanocomposites. Effect of Metal Particle Size on the Fermi Level Equilibration, J. Am. Chem. Soc., Vol. 126, 2004, pp. 4943–4950.
[38] Hyunwoong P, Yiseul P, Wooyul K, Wonyong C, Surface modification of TiO_2 photocatalyst for environmental applications, J. Photochem. Photobiol. C: Photochem. Rev., Vol. 15, 2013, pp. 1– 20.

Second International Conference on Science, Engineering & Environment,
Osaka City, Japan, Nov.21-23, 2016, ISBN: 978-4-9905958-7-6 C3051

ENHANCED PHOTOCATALYTIC OXIDATION OF As(III) ON WO_3 NANO-PARTICLES WITH CuO CO-CATALYST

Abdus Samad[*,1], Hideyuki Katsumata[1], Tohru Suzuki[2] and Satoshi Kaneco[*,1, 2]
[1]Department of Chemistry for Materials, Graduate School of Engineering, Mie University, Japan
[2]Mie Global Environment Center for Education & Research, Mie University, Japan

ABSTRACT

WO_3 is one of the most extensively studied visible light active photocatalyst. However, low photocatalytic activity restricts its application. We explored the photocatalytic oxidation of As(III) over the WO_3 photocatalyst in the presence of CuO co-catalyst under visible light irradiation. It was found that CuO effectively promoted the photocatalytic activity of WO_3 for the oxidation of As(III). Optimized composition of CuO was found as 1% CuO coupled with WO_3. Photocatalytic performance was slightly higher at basic pH (pH 10) compared with both acidic (pH 3) and neutral pH (pH 7). The XPS study demonstrated that the oxidation state of copper in CuO remains unchanged after treatment. The oxidation rate of As(III) was suppressed remarkably in nitrogen environment. The reactive species scavenger results indicated that the photo-generated holes (h^+) play key role in As(III) oxidation while the effect of ·OH was found negligible. A possible mechanism for the enhancement of photocatalytic activity for the oxidation of As(III) has been proposed.

Keywords: Tungsten oxide, Cocatalyst, Visible light, Arsenic, Oxidation.

INTRODUCTION

Arsenic contamination is one of the most severe forms of water pollution due to its toxicity and ubiquitous presence on the earth's crust [1]. Primary forms of arsenic in water are arsenite [As(III)] and arsenate [As(V)]. As(III) is more toxic, highly mobile and difficult to remove from aqueous solution due to its poor affinity towards absorbents and coagulants. Therefore, the pre-oxidation of As(III) to As(V) is a crucial step for reducing the toxicity and enhancing the total arsenic removal efficiency from contaminated waters. Several methods have been developed for the oxidation of As(III) including photocatalysis [2], electrocatalysis [3], chemical process [4] and biological process [5]. Photocatalytic oxidation has been proven as an effective and environmentally acceptable green energy technique because of its high efficiency, no requirement for chemical oxidants and electrical energy, and applicability at a broad range of As(III) concentrations. Visible light active photocatalysts are actively sought for the better utilization of solar energy or indoor light [6], since visible light accounts for the major share of the solar spectrum (~42%) and artificial light sources. Due to small band gap (2.4-2.8 eV), strong absorption within the solar spectrum, high oxidation power of valence band (VB) holes and nontoxic nature, (WO_3) is an ideal candidate among the visible light active photocatalysts [7]. However, the low conduction band level of WO_3 restricts the conduction band electron to react with electron acceptors [8] which therefore increase the recombination of photo-generated electron–hole pairs leading to the lower photocatalytic activity.

One of the general approaches to improve the photocatalytic performance of WO_3 is to increase the efficiency of electron–hole separation by the coupling with suitable co-catalyst. The enhancement of photocatalytic activity of WO_3 by the use of appropriate co-catalyst has attracted extensive attention recently [9]. It has been reported that the loading of metal co-catalyst such as Pt, Ag, Pd and Au have significantly improved the visible light activity of WO_3 [10]. In spite of that, the high cost and resource constrain bottleneck the application of these precious metals as co-catalyst in large scale. As an alternative, metal oxides have been widely explored [11]. CuO can be an attractive co-catalyst because of easy to prepare, low cost and available in large quantity. Enhancement of photocatalytic activity under visible light with CuO has been cited in literature [12]. However, reported studies overwhelmingly focused on the degradation of dyes or oxidation of organic compounds. There is scarce literature on the oxidation of arsenic with WO_3. Kim and his research group studied the oxidation of As(III) under visible light with pristine WO_3 and explained the comprehensive mechanism of As(III) oxidation [13]. Kim and co-workers investigated the degradation/oxidation of six aquatic pollutant including As(III) with platinized WO_3 demonstrated the enhanced photocatalytic activity for As(III) oxidation as well as organic pollutant degradation [14]. Photocatalytic oxidation of As(III) on WO_3 has not been explored yet with CuO co-catalyst.

This work aims to investigate the photocatalytic oxidation of As(III) with WO_3 under visible light in the presence of CuO.

EXPERIMENTAL

Chemicals

All the chemicals and reagents were analytical grade of purity and used as received without further purification. WO_3 (particle size < 100 nm, surface area ~8.3 m^2/g) and CuO (particle size 33 nm, specific surface area 29 m^2/g) were purchased from Aldrich. Potassium arsenite ($KAsO_2$, 90%) and potassium arsenate (KH_2AsO_4, extra pure) were procured from Nakarai Tesque, Inc. and were used for the preparation of As(III) and As(V) stock solution, respectively. Ammonium molybdate ($(NH_4)_6Mo_7O_{24}\cdot 4H_2O$, 99%), L-ascorbic acid ($C_6H_8O_6$, 99%), antimony potassium tartrate ($C_4H_4KO_7Sb\cdot 1/2H_2O$, 99.8%), sulfuric acid (H_2SO_4, 98%), potassium permanganate ($KMnO_4$, 99.3%) were received from Nakarai Tesque, Inc. Ammonium oxalate monohydrate (Nachalai), Disodium ethylene diamine tetra acetate (EDTA-2Na, Chameleon), Isopropyl alcohol (IPA, Wako) and Tertiary butyl alcohol (TBA, Kanto) were used as reactive species scavengers.

Preparation of photocatalyst

Mechanical mixing method was used for the preparation of CuO/WO_3 photocatalyst mixture. The different weight ratios of CuO/WO_3 were prepared by mixing the estimated amount of WO_3 and CuO. The mixing was homogeneously performed with a mortar.

Photocatalytic oxidation experiment

A batch reactor of 50 mL cylindrical glass cell was used for performing photocalytic experiments. Catalyst loading for each experiment was 10 mg containing 30 mL of 10 mg L^{-1} As(III) solution. The pH of the suspension was adjusted to desired value with HCl or NaOH using micro volume. The reactor was positioned on the top of the magnetic stirrer for agitation. The suspension was then magnetically stirred for 30 min in the dark to get adsorption-desorption equilibrium between arsenic and photocatalyst prior to illumination. A UV cut filter was placed between light source and reactor to prevent the access of light below 400 nm. Next, the reaction mixture was irradiated with visible light. An ordinary incandescent light was used as visible light source providing irradiance with a peak wavelength at around 405 nm. During treatment, the arsenic solution was stirred magnetically to ensure a good contact of photocatalyst with arsenic species. A 0.20 μm Advantec membrane filter was used for the filtration of arsenic solution after treatment.

Concentration of As(V) was measured by UV-visible spectrophotometry using arseno–molybdate technique [15]. Total arsenic concentration was measured with a modified arseno–molybdate method [16]. The concentration of As(III) was determined from the difference between $[As]_{total}$ and [As(V)].

RESULTS AND DISCUSSION

Influence of CuO on the photocatalytic performance of WO_3

The effect of CuO on the photocatalytic activity of WO_3 was evaluated by the oxidation of As(III) under visible light irradiation. Fig. 1 illustrates the oxidation of As(III) over pristine WO_3, CuO, $1\%CuO/WO_3$ and $5\%CuO/WO_3$. Oxidation of As(III) was not perceived with pure CuO indicating that although being a *p*-type semiconductor with low band gap (1.7 eV), it cannot act as a photocatalyst alone. While As(III) could be oxidized with bare WO_3, its efficiency was low. About 55% of As(III) was oxidized to As(V) in 6 h of light irradiation. It is clear from the Fig. 1 that photocatalytic performance of WO_3 was remarkably enhanced with the incorporation of CuO. In the case of $1\%CuO/WO_3$, maximum oxidation yield was 90% in 6h irradiation. The photocatalytic performance of WO_3 was declined with the increase of percentage of CuO to 5%. Such a composition dependency of photocatalytic performance of WO_3 coupled with other semiconductor had been widely reported in previous studies [11].

The kinetics of photocatalytic oxidation of As(III) can be expressed by modified Langmuir–Hinshelwood kinetic model as shown in "Eq. (1)" [17].

$$-Ln(C/C_0) = kt \quad (1)$$

where C_0 (mg L^{-1}) is the initial concentration of As(III), C (mg L^{-1}) is the concentration of As(III) at the treatment time t, k (min^{-1}) represents the apparent first order rate constant and t is the treatment time (min). Table 1 shows the rate constant and the regression value (R^2) for the oxidation of As(III) with pure WO_3, $1\%CuO/WO_3$ and 5% CuO/WO_3. It can be inferred from the table that the As(III) oxidation rate constant with $1\%CuO/WO_3$ is 2.3 times higher than that with pure WO_3 demonstrating a significant improvement of arsenic oxidation performance with WO_3 in the presence of CuO co-catalyst.

Table 1 Rate constant and regression value for the oxidation of As(III).

Photocatalyst	Rate constant (min^{-1})	R^2
Pure WO_3	0.047	0.97
$1\%CuO/WO_3$	0.11	0.97

5%CuO/WO_3	0.084	0.92

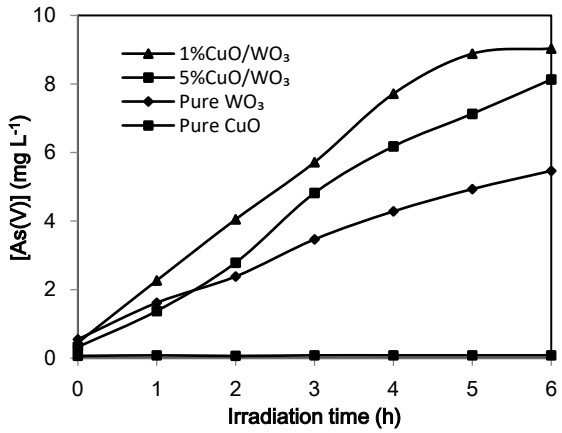

Fig. 1 Effect of CuO on the photocatalytic performance of WO_3 under visible light.

Effect of pH

The pH affects the surface condition of catalyst as well as the speciation of arsenic in aqueous solution. The effect of pH on the photocatalytic oxidation of As(III) on 1%CuO/WO_3 was investigated. Fig. 2 exhibits the effect of pH on the photocatalytic oxidation of As(III) 4 h irradiation. Oxidation efficiency was slightly increased at pH 3 than neutral pH and further improved at pH 10. This dependency of As(III) oxidation rate on pH is similar to the previous studies reported by Qin et al. [18] and Lee and Choi [19], although Lee and Choi found larger enhancement at basic pH. The valence band potential of WO_3 is +2.92 V_{NHE} [20] and the potential of As(V)/As(III) couple is +0.40 V_{NHE} denoting that photo-generated hole has enough thermodynamic potential to oxidize As(III) to As(V). At pH 10, the potential for As(V)/As(III) couple is less than -0.2 V [19]. The lowering of potential in alkaline solution may be contributed to increase the oxidation rate at high pH.

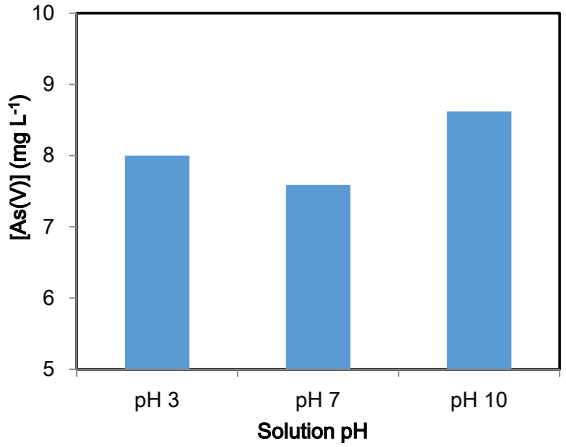

Fig. 2 Effect of pH on the photocatalytic oxidation of As(III) with 1%CuO/WO_3.

XPS analysis

To understand the change of catalyst during photocatalytic experiment, XPS spectra of pure WO_3 and 1%CuO/WO_3 before and after treatment was analyzed. Fig. 3 illustrates the narrow scan XPS spectra of Cu 2p. The peak of $2p_{3/2}$ of as prepared CuO/WO_3 was observed at 933 eV and $2p_{1/2}$ at 953 eV are corresponding to Cu(II). The Cu 2p spectra of CuO/WO_3 before and after treatment were almost similar implying that no change of catalyst occurred during reaction.

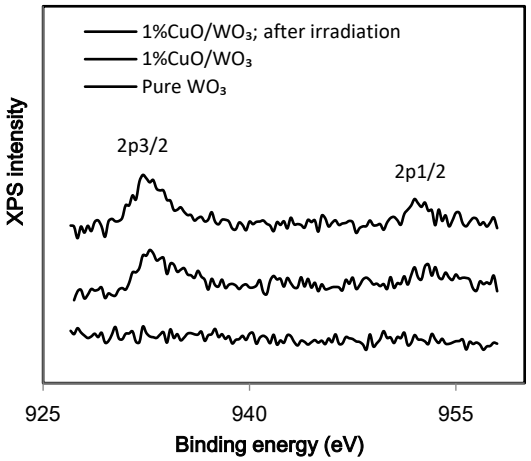

Fig. 3 XPS spectra of Cu 2p.

Effect of active species scavenger

Several possible species can be generated such as photo-generated hole, intermediates like ·OH and H_2O_2 when photocatalyst is irradiated under light energy. H_2O_2 does not play role for the oxidation of As(III) [13]. The role of active species was evaluated by using suitable quenching agents of high concentration (1000 mg L^{-1}). Ethylenediaminetetraacetic acid disodium salt (EDTA) and ammonium oxalate were used as hole scavenger, isopropyl alcohol and tert-butyl alcohol as hydroxyl radical scavenger. Results presented in Fig. 4 (a) reveals that the photocatalytic activity of CuO/WO_3 was markedly suppressed in the presence of both EDTA-2Na and ammonium oxalate. It is apparent from the figure that As(III) oxidation was inhibited more in the presence of EDTA-2Na than ammonium oxalate. The different hole scavenging efficiency was also reported in literature [21]. However, the oxidation rate was unaffected when reaction was performed with hydroxyl radical scavenger as illustrated in Fig. 4(b). These results infer that photo-generated holes play key role in the As(III) oxidation process.

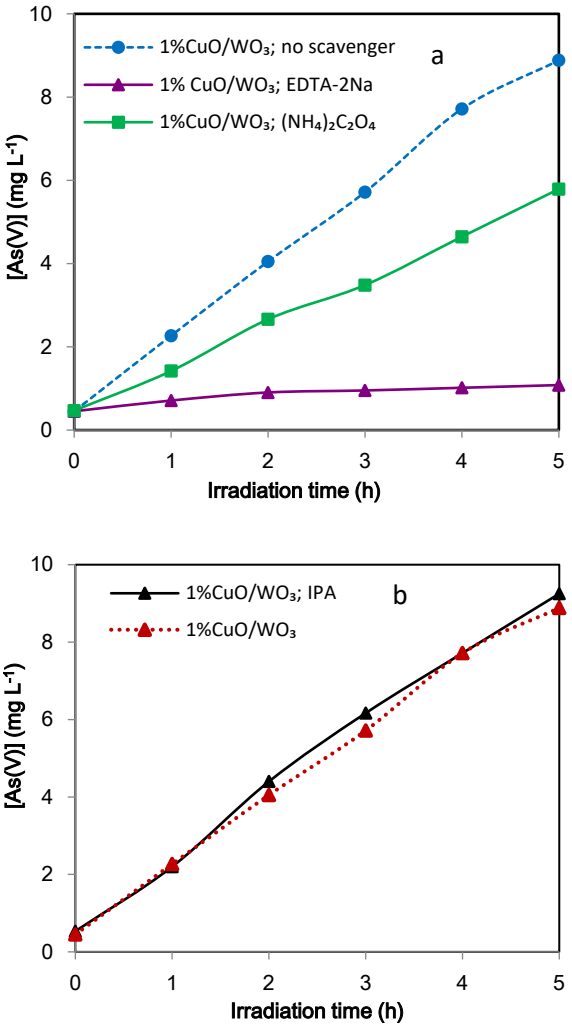

Fig. 4 Effect of (a) hole scavenger and (b) hydroxyl radical scavenger on the photocatalytic oxidation of As(III) under visible light.

Effect of dissolved oxygen

The effect of dissolved oxygen on the oxidation of As(III) was evaluated by conducting photocatalytic oxidation experiment in N_2 environment. As shown in Fig. 5, oxidation efficiency was decreased about 65-70% under N_2 compared to air equilibrated environment. This is indicative of the involvement of oxygen in the photocatalytic reaction.

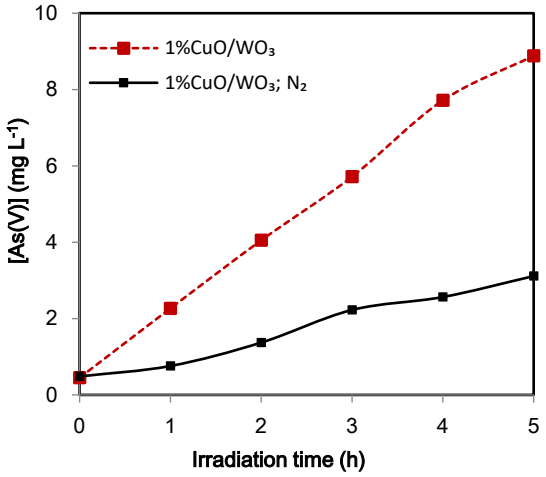

Fig. 5 Effect of dissolved oxygen on the photocatalytic oxidation of As(III).

Probable oxidation pathway

When the sample solution is irradiated under visible light, the electrons of WO_3 get excited and promoted to the conduction band causing the split of energy band as valence band hole and conduction band electron. The conduction band of WO_3 has a positive potential (*ca.* +0.22 V_{NHE}) and the reduction potential of O_2 is negative ($E^{\circ}(O_2/\cdot O_2^{-}) = -0.33$ V_{NHE} and $E^{\circ}(O_2/HO_2^{\cdot}) = -0.05$ V_{NHE}). Therefore, the reduction of O_2 by the conduction band electron on WO_3 surface is thermodynamically not favored. Consequently, pure WO_3 exhibits low photocatalytic activity because of the recombination of photoexcited electron and hole. However, in presence CuO, the separation of electron and hole is possible in two ways. As presented in Fig. 6, charge separation can be achieved either via Z-scheme mechanism (pattern 1) or by transferring conduction band electron of WO_3 to CuO as shown in pattern 2. When conduction band electron migrated to CuO, the copper in CuO get reduced from Cu(II) to Cu(I) [12]. The reduced Cu(I) is not further reduced to Cu(0). On the other hand, it regenerated to Cu(II) by dissolved oxygen in the reaction media. Although, the one-electron reduction of O_2 over WO_3 is thermodynamically restricted, it is highly probable that oxygen get reduced by multi electron transfer pathway ($E^{\circ}(O_2/H_2O_2) = +0.68$ V_{NHE}; $E^{\circ}(O_2/H_2O) = +1.23$ V_{NHE}) [20]. This process effectively suppressed electron/hole recombination and enhanced the efficiency of the charge separation. As(III) is then oxidized to As(V) by the photo-generated hole as illustrated in Fig. 6.

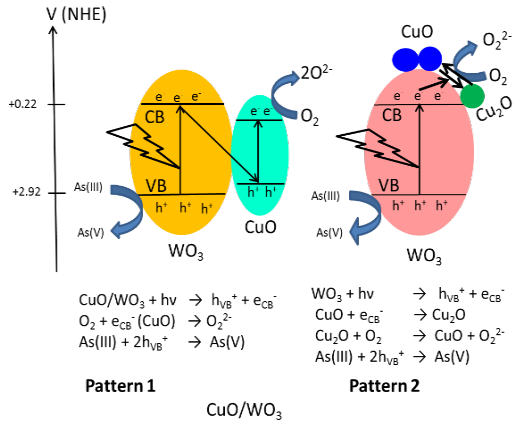

Fig. 6 Probable reaction pathway for the photocatalytic oxidation of As(III).

CONCLUSIONS

CuO significantly enhanced the photocatalytic performance of WO_3. Arsenic oxidation rate constant was 2.3 times higher in the presence of CuO co-catalyst. Oxidation efficiency was not changed remarkably in acidic or basic media although oxidation rate was higher at basic pH than acidic pH. Dissolved oxygen plays a significant role in oxidation process as oxidation rate was declined to 65-70% in N_2 environment. Arsenic was oxidized primarily by the photo-generated holes. This technique might be promising for As(III) oxidation as visible light can be used for photocatalytic reaction.

ACKNOWLEDGEMENT

The present research was partly supported by Grant-in-Aid for Scientific Research (C) 15K00602 from the Ministry of Education, Culture, Sports, Science, and Technology of Japan. All experiments were conducted at Mie University. Any opinions, findings, conclusions or recommendations expressed in this paper are those of the authors and do not necessarily reflect the view of the supporting organizations.

REFERENCES

[1] Kim D-H, Bokare AD, Koo MS, Choi W, "Heterogeneous catalytic oxidation of As(III) on nonferrous metal oxides in the presence of H_2O_2", Environ. Sci. Technol., Vol. 49, 2015, pp. 3506−3513.

[2] Vaiano V, Iervolino G, Sannino D, Rizzo L, Sarno G, Farina A, "Enhanced photocatalytic oxidation of arsenite to arsenate in water solutions by a new catalyst based on MoOx supported on TiO_2", Appl. Catal. B, Vol. 160–161, 2014, pp. 247–253.

[3] Kim J, Kwon D, Kim K, Hoffmann MR, "Electrochemical production of hydrogen coupled with the oxidation of arsenite", Environ. Sci. Technol., Vol. 48, 2014, pp. 2059–2066.

[4] Wang Z, Bush RT, Sullivan LA, Chen C, Liu J, "Selective oxidation of arsenite by peroxymonosulfate with high utilization efficiency of oxidant", Environ. Sci. Technol., Vol. 48, 2014, pp. 3978–3985.

[5] Xie W-Y, Su J-Q, Zhu Y-G, "Arsenite oxidation by the phyllosphere bacterial community associated with Wolffia Australiana", Environ. Sci. Technol., Vol. 48 (16), 2014, pp. 9668–9674.

[6] Kou J, Li Z, Yuan Y, Zhang H, Wang Y, Zou Z, "Visible-light-induced photocatalytic oxidation of polycyclic aromatic hydrocarbons over tantalum oxynitride photocatalysts", Environ. Sci. Technol., Vol. 43 (8), 2009, pp. 2919–2924.

[7] Kim H, Yoo H-Y, Hong S, Lee S, Lee S, Park B-S, Park H, Lee C, Lee J, "Effects of inorganic oxidants on kinetics and mechanisms of WO_3-mediated photocatalytic degradation", Appl. Catal. B, Vol. 162, 2015, pp. 515–523.

[8] Abe R, Sayama K, Sugihara H, "Development of new photocatalytic water splitting into H_2 and O_2 using two different semiconductor photocatalysts and a shuttle redox mediator IO_3^-/I^-", J. Phys. Chem. B, Vol. 109 (33), 2005, pp. 16052–16061.

[9] Villa K, Domènech X, García-Pérez UM, Peral J, "Photocatalytic hydrogen production under visible light by using a CdS/WO_3 composite", Catalysis Letters, Vol. 146 (1), 2016, pp. 100-108.

[10] Abe R, Takami H, Murakami N, Ohtani B, "Pristine simple oxides as visible light driven photocatalysts: highly efficient decomposition of organic compounds over platinum-loaded tungsten oxide", J. Am. Chem. Soc., Vol. 130 (25), 2008, pp. 7780–7781.

[11] Yan M, Wu Y, Zhu F, Hua Y, Shi W, "The fabrication of a novel Ag_3VO_4/WO_3 heterojunction with enhanced visible light efficiency in the photocatalytic degradation of TC", Phys. Chem. Chem. Phys., Vol. 18, 2016, pp. 3308-3315.

[12] Arai T, Horiguchi M, Yanagida M, Gunji T, Sugihara H, Sayama K, "Reaction mechanism and activity of WO_3-catalyzed photodegradation of organic substances promoted by a CuO cocatalyst", J. Phys. Chem. C, Vol. 113, 2009, pp. 6602–6609.

[13] Kim J, Moon G-H, Kim S, Kim J, "Photocatalytic oxidation mechanism of arsenite on tungsten trioxide under visible light", J. Photochem. Photobiol. A: Chem., Vol. 311, 2015, pp. 35–40.

[14] Lim G, Lee JH, Son JW, Lee HW, Kim J, "Oxidation behavior of tungsten in $H_2O_2^-$ and $Fe(NO_3)_3$-based aqueous slurries", J. Electrochem. Soc., Vol. 153 (5), 2006, pp. B169−B172.

[15] Tsang S, Phu F, Baum MM, Poskrebyshev GA, "Determination of phosphate/arsenate by a modified molybdenum blue method and reduction of arsenate by $S_2O_4^{2-}$", Talanta, Vol. 71 (4) 2007, pp. 1560-1568.

[16] Samad A, Furukawa M, Katsumata H, Suzuki T, Kaneco S, "Photocatalytic oxidation and simultaneous removal of arsenite with CuO/ZnO photocatalyst", J. Photochem. Photobiol. A: Chem., Vol. 325, 2016, pp. 97–103.

[17] Kumar KV, Porkodi K, Rocha F, "Langmuir–Hinshelwood kinetics - a theoretical study", Catal. Commun., Vol. 9, 2008, pp. 82–84.

[18] Qin Y, Li Y, Tian Z, Wu Y, Cui Y, "Efficiently visible-light driven photoelectrocatalytic oxidation of As(III) at low positive biasing using Pt/TiO_2 nanotube electrode", Nanoscale Res. Lett., Vol. 11 (1), 2016, pp. 32.

[19] Lee H, Coi H, "Photocatalytic oxidation of arsenite in TiO_2 suspension: Kinetics and mechanisms", Environ. Sci. Technol. Vol. 36, 2002, pp. 3872-3878.

[20] Bamwenda GR, Sayama K, Arakawa H, "The effect of selected reaction parameters on the photoproduction of oxygen and hydrogen from a WO_3–Fe^{2+}–Fe^{3+} aqueous suspension", J. Photochem. Photobiol. A., Vol. 122, 1999, pp. 175–183.

[21] Liu X, Wu X., Long Z, Zhang C, Ma Y, Hao X, Zhang H, Pan C, "Photodegradation of imidacloprid in aqueous solution by the metal-free catalyst graphitic carbon nitride using an energy-saving lamp", J. Agric. Food Chem., Vol. 63, 2015, pp. 4754−4760.

Second International Conference on Science, Engineering & Environment,
Osaka City, Japan, Nov.21-23, 2016, ISBN: 978-4-9905958-7-6 C3051

LASER LAND LEVELING FOR CROP YIELD AND WATER EFFICIENCY AT EASTERN REGION AFGHANISTAN

Shakerullah Hashimi[1], Homayoon Ganji[1], Masaaki Kondo[1], Ryoei Ito[1] and Takamitsu Kajisa[1]
[1]Graduate School of Bioresources, Mie University, 514-8507 Kurimamachiya-cho 1577, Tsu, Japan

ABSTRACT

The purpose of this study is to observe the impact of land layout improvement (LLI) and laser land leveling (LL leveling). LLI and LL leveling are undertaken through an important program by the Ministry of Agriculture Irrigation and Livestock of Afghanistan in five regions of the country. The poor farm layout in those areas, as well as the existence of uneven fields, unnecessary bunds, and ditches, are responsible for significant water losses at the farm level and yield reduction, thereby increasing water and labor demand. In addition, it is mandatory to apply irrigation at the highest levels of the fields, a practice leading to over-irrigation and the reduction of resources and yield. In the study area, the farm was separated into 29 small fields of less than 0.075 ha, attempting to form even and appropriately irrigated fields. The entire farm area was leveled, and the size of each field increased to 0.19 ha (6%). The number of fields dropped from 29 to 12, and the number of water inlets decreased from 39 to only 14. These reduction remind us the labor requirements decrease. By the measuring in two fields (Farm-A(leveled) and Farm-B(unleveled)), it is expected that water demand for wheat, corn, and eggplant will be reduced as 21%, 27%, and 17%, while the yield will be increased as 21%, 40%, and 38%. Furthermore, water productivity will be increased as 39%, 53%, and 37% for wheat, corn, and eggplant, respectively.

Keywords: Laser- land leveling, Land-layout improvement, Water saving, Yield increase, and Area increase

INTRODUCTION

One of the major challenges for the agricultural sector of Afghanistan is the high pressure on irrigation water [1]. Afghanistan economy mostly relies on agriculture, particularly on irrigated agriculture, while farmers still use traditional farming techniques with oxen providing the draught power. The farmers' knowledge of new irrigation technologies and cultural practices is insufficient. Consequently, the efficiency of the irrigation system is quite low (25%–30%), mainly due to high conveyance losses in traditional watercourse with earth canals, high operational losses in modern schemes with a lined conveyance canal, and high on-farm distribution losses (e.g., over irrigation, poorly leveled land) in both traditional and modern schemes. The productivity levels are low even by regional standards. About 20% of both traditional and modern irrigation systems require improvement of the on-farm water management in order to improve the low crop yield, or address water logging and Stalinization. In fact, the production potential of land under low and variable rainfall can be improved by promoting technology transfer [8-9].

Irrigated agriculture is the mainstay of food security and income for most of the rural population in Afghanistan. It accounts for more than half of the country's GDP, 70% of the total crop production, and provides a reliable and sustainable production base for many rural communities. The total cultivable area of Afghanistan is about eight million hectares, which is 12% of the total area of the country. Approximately 3.9 million ha of cultivated land exists in Afghanistan, of which 1.3 million ha is rainfed and 2.6 million ha irrigated. This irrigated area produces almost 85% of all agricultural productions [10]. Cropping intensity varies widely from system to system according to the scarcity of water versus land. It reaches 200% in the upper part of the irrigation schemes, whereas the lower parts, up to two-thirds of the command area, are kept fallow each year on a rotational basis. Flood damages to irrigated land are common, particularly in the large schemes supplied by rivers changing their course frequently due to their high sediment load and unfavorable geomorphological conditions [8-9].

In traditional as well as in modern irrigation schemes, the dominant irrigation method is basin/border irrigation for cereals and furrow irrigation for vegetables and grapes. Farmers usually lack knowledge about crop water requirements, and over-irrigation of crops is a common practice. Overall efficiency is only about 25%–30% for both modern and traditional irrigation schemes, resulting in water loss and low productivity [4].

Due to low water use efficiency and lack of input, crop yields are very low. At present, drought conditions have caused further reduction in crop yields, e.g., the average yield of wheat is 0.8 tons/ha today as opposed to about 1.1 tons/ha in 1978. The total area (irrigated and rainfed) for cereal crops is about 3.39 million ha. The total cereal production is 4.15 million tons, of which 2.65 million tons are dedicated only to wheat [8-9].

Traditional management practices of the irrigation supply and conveyance systems often contribute to the high water losses. On many farms, the low irrigation efficiency is further accentuated by farmers' traditional irrigation methods and practices, as well as inadequate land leveling [12]. Water shortage can be overcome by improving the water application efficiency at the field level [11]. Indeed, with normal application of water availability to the fields, the crop yields are reduced by 75%–85% on average, a percentage that varies widely amongst farms.

Furthermore, poor farm design and uneven fields are responsible for 30% of the water losses [8]. About 18 million acre-feet (MAF) of water are lost for irrigating uneven fields in Pakistan [2].

LL-leveling and agricultural technology transfer was implemented from 2008 to 2011 for wheat crops in the Kama district (Nangarhar and Balkh Province, Afghanistan). The maximum reported wheat yield was 6.18 tons/ha and the minimum was 4.01 tons/ha [7].

The present study is conducted at the irrigation demonstration site of the On-farm Water Management Project, at Bahrabad village, (Bihsud district, Nangarhar province; Fig 1). The objectives of this study are (i) to explore the impact of farm layout improvement, (ii) to investigate the agriculture benefits of laser land leveling, against the traditional unleveled field, and (iii) to increase water crop productivity.

MATERIALS AND METHODS

This study was conducted at the Irrigation demonstration site of the On-farm Water Management Project in Nangarhar Province in 2014. The province is located in the eastern part of Afghanistan (latitude 34.27° N and longitude 70.24° E), and the elevation is 570 m. The climate is sub-tropical, semi-arid, Mediterranean-type, with frost in the winter. Climatic data collected from Shishum Bagh Agricultural Research Farm indicates that the maximum annual temperature is 42 °C and the minimum is −2 °C. The annual precipitation varies from 178 mm to 324 mm. The rainy season starts from January and lasts until May, with few showers in the summer. The wind velocity is approximately 30 km/h. The maximum pressure of wind is observed in July and November. [5]

The field experiments consisted of two parts, the first part included Farm-A layout improvement, and the second part involved LL-leveling. The entire Farm-A was investigated before commencing on the actual experiment. Thus, permanent benchmarks were established.

After installing the benchmarks, the detailed survey of Farm-A started with the construction of a topographic map by total station theodolite (*TST*). Next, the features of Farm-A were indicated on the map, and detailed information was given about the slope, the elevations of the low and higher spots of the fields, the number and sizes of the fields, the quantities of water inlets, and the available water channels. In the same way, the main water channel and the secondary water channels were surveyed, and their profiles were prepared.

The water channels were designed for the earthen lining. In the next step, each single field in Farm-A was carefully studied and analyzed further in order to improve the farm's layout. With the new layout, the area size of each single field was expanded, and regular straight boundaries were established for all fields. In addition, water inlets and control structures were considered as suitable points for the installation of the farm's irrigation system. There were chosen according to the irrigation demand.

Then, the cut-and-fill soil ratio of low and high spots were calculated for each field and indicated in the site plan in order to facilitate field leveling for the machinery operators. The irrigation channels and the water inlets were adjusted based on the quantity required for the fields. Moreover, the water channels were earthen improved, and water inlets and a control structure were proposed to be constructed with break masonry. Subsequent layout improvement and water channels (contours, unwanted bunds, water inlets) of the field were removed.

In the next stage, we applied rough leveling and laser land leveling. To implement laser land leveling, the maximum difference in elevation between the different points in the land to be laser-leveled should not be more than 12–15 cm. In this case, however, most of the selected fields exhibited greater differences in elevations. Therefore, to solve this problem, another tractor was hired to plough and make the soil soft for leveling.

Laser land leveling is also called laser-guided land leveling or precision-custom farming laser land leveling, and it is a process applied for smoothing a land surface up to ±2 cm from its average elevation with the help of a laser-guided drag-bucket.

All the fields were laser leveled and the fields' sizes were increased to at least 0.19 ha. Thus, 12

Fig 1 The location of Farms A and B, in Nangarhar, Afghanistan (Source: Google map, 2016)

fields were established instead of 29 (Figures 2 and 3). All unnecessary water channels, undesired field boundaries, and ditches were removed, and new straight field bunds were established. After the Farm-A was laser-leveled, leveled fields in Farm-A were chosen to observe the impact of LL-leveling, and unleveled fields were selected in the adjacent Farm-B.

Overall, the leveled fields covered 2054 m^2, 2052 m^2, and 1924 m^2 for wheat, corn, and eggplant, respectively. On the other hand, the unleveled fields covered 1875 m^2, 2000 m^2, and 1680 m^2 for wheat, corn, and eggplant, respectively. Condition of crops without LL-leveling was considered equal.

The cutthroat flume was used to determine the water depth that was applied in the irrigation. The flume was installed in a uniform, straight, and vegetation free channel. The flume sides were entirely stopped with dirt to prevent water leakage from the sides and beneath the flume. The flume was installed at appropriate points to maintain free-flow conditions for easy calculation. Whenever the water flow became stable, constant readings were recorded; five to six readings were taken during irrigation. The duration of irrigation was recorded, and the area of the fields was measured by TST. Then, the depth of applied water was calculated for each irrigation line using the hydraulics formula given in Eq. 1.

Then, all crops were harvested manually from both the laser-leveled and the unleveled fields. The productions were weighed using a digital scale measurement device. The water productivities were computed using Eq. 1. The net crop harvested yields and the applied water volume $\boldsymbol{Q}$ was used for the calculation of water productivity. The harvested yield quantity for a single crop was recorded from the fields, and the irrigations applied were determined by the depth of water (mm) and later converted into volume.

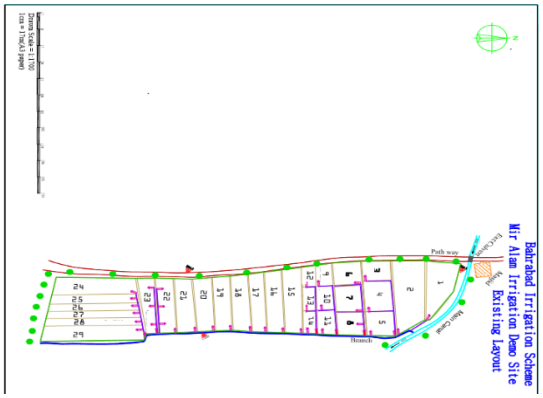

Fig. 2 Layout of Farm-A before improvement

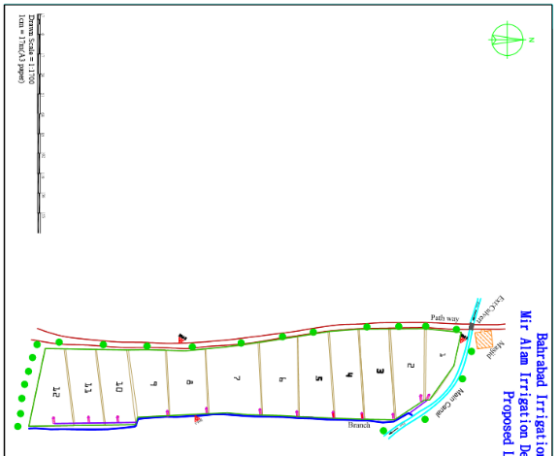

Fig. 3 Layout of Farm-A after improvement

$$D = QT/A \quad \text{[Eq. 1]}$$

where Q is the discharge (m^3/s), T is the irrigation duration in seconds, A is area of the field (m^2), and D is the applied depth (m).

$$WP = \text{yield}/Q \quad \text{[Eq. 2]}$$

where WP is the water productivity, yield is the total seasonal agricultural production (kg), and Q is the total seasonal irrigation water inflow (m^3).

RESULTS

Farm Design

The average area size of an unleveled (Farm-A) field was 752.41 m^2 (0.075 ha), as shown in the old farm layout (Fig. 2). After modification of the layout, the average area size of the new field enlarged to 1925 m^2 (0.19 ha). The number of fields dropped from 29 to 12, because several fields were unified. Moreover, the farm water channels were properly lined, and all unnecessary water channels and water inlets were removed. The number of water channels was reduced from 14 to 2. In addition, the number of water inlets dropped from 39 to 12. As a result, the cultivated area of the farm larger by about 6%, and the Farm-A rea expanded from 2.18 ha to 2.31 ha. (Table 1).

Table 1 Farm-A features before and after improvement

State	No. of fields	No. of water channels	No. of water inlets	Total Farm-A area (ha)	Total Farm-A area (%)	Average field area (m^2)
Before	29	14	39	2.18	100	752
After	12	2	12	2.31	106	1925
Impacted	17	12	27	0.13	6	1173

Crop Yield

The yield from the Farm-A was 4.4 tones/ha, whereas the harvested yield from the Farm-B fields was 3.5 tons/ha. The wheat yield from the Farm-A was almost 21% higher than that from Farm- B.

Similarly, after laser land leveling, the corn crop yield was 5.25 tons/ha from the Farm-A, whereas unleveled corn crop yield was 3.15 tons/ha from the Farm-B; thus, the corn yield larger by 40%. The Farm- A eggplant yield was 41 tons/ha and the Farm-B yield was 25.5 tons/ha. The eggplants yield in the Farm-Afield was about 38% higher than the Farm-B Eggplant yield. (Fig. 4)

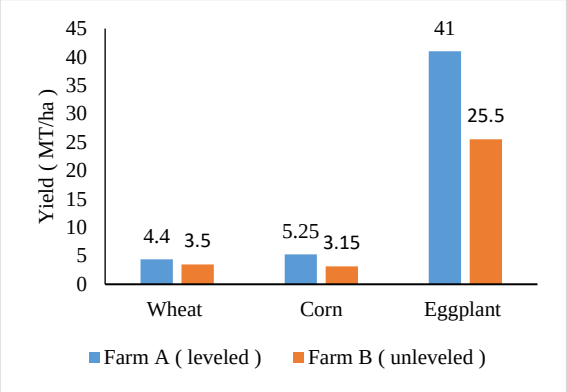

Fig. 4 The 2014 yields in metric tons (ha).

Water Depth

The Farm-A water depth (WD) was estimated at 420 mm, whereas, in the, Farm-B the applied water depth was 529 mm. The water demand for irrigation was smaller in the laser-leveled field by 21%, and the water depth lowered by 109 mm, which was different from the Farm-B for the wheat crop.

Furthermore, the total seasonal water applied depth for corn crop was 539 mm in the Farm- B, whereas it was 394 mm for the Farm-A. The water depth smaller by 27% in the Farm-A field and the water depth saved by 145 mm compared to the Farm-B. The maximum water depth for the eggplant crop was 1264 mm for the Farm-A, whereas it was 1052 mm for the Farm-B The eggplant water demand lowered by 17% in the Farm-A field and the water depth smaller by 213 mm (Fig. 5).

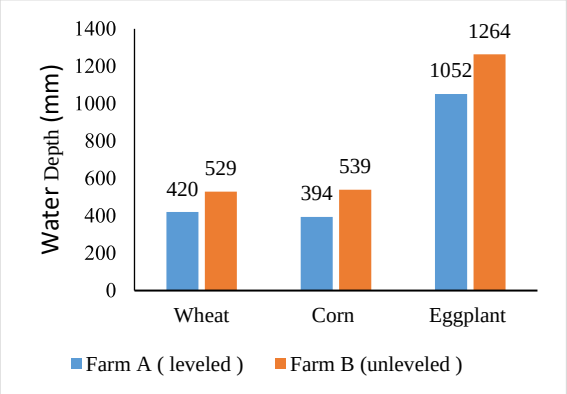

Fig. 5 Water depths for wheat, corn, and eggplant, in 2014.

Water Productivity

After laser land leveling, water productivity was analyzed for the three crops: wheat, corn, and eggplant. The water productivities for all three crops (wheat, corn, and eggplant) in the leveled fields were

compared with that of the unleveled fields.

The water productivities of unleveled field crops were 0.64 kg/m^3, 0.63 kg/m^3, and 2.33 kg/m^3 for wheat, corn, and eggplant, respectively. The laser-leveled fields' water productivities for wheat, corn, and eggplant were 1.05 kg/m^3, 1.33 kg/m^3, and 3.67 kg/m^3, respectively. (Table 2)

Table 2 Water productivity of Farm-A and Farm-B in (kg/m^3)

Crop	A (Leveled)		B (Unleveled)	
	Water Volume (m^3)	WP (kg/m^3)	Water Volume (m^3)	WP (kg/m^3)
Wheat	863	1.05	1009	0.64
Corn	808	1.33	1004.6	0.63
Eggplant	2148.1	3.67	2129.5	2.33

DISCUSSION

LL-leveling for crop yield and water efficiency

This study has led us the poor farm layout and the existence of uneven fields, unnecessary bunds, and ditches are responsible for water losses at the farm level; and yield reduction, thereby increasing water and labor demand. In addition, is mandatory to apply irrigation at the highest levels of the fields, a practices leading to over irrigation and reduction of resources and yields. The Farm-A had been separated into 29 small fields. the average area size of unleveled field 752 m^2 (0.075 ha) as depicted in the old farm layout (Fig. 2). But after modification of the layout the average area size of the new field expanded from 29 to 12, because of several fields were unified.

Moreover, the farm water channels were properly lined and all unwanted water channels and water inlets were removed. The number of water channels were dropped from 14 to 2. In addition, the number of water inlets fallen from 39 to 12. At the end, cultivated area of the farm larger about 6 % and the Farm-A area expanded from 2.18 ha to 2.31 ha. The land layout improvement should be a chance to use land and water resources more efficiently and effectively in those area.

Moreover, the yield from the Farm-A was 4.4 tons/ha. Whereas the yield from the Farm-B fields was 3.5 tons/ha. The wheat yield from the Farm-A about 21% higher than that from Farm-B. Equally, after LL-leveling the corn crop yield was 5.25 tons/ha in the Farm-A. While, corn crops yield from the Farm-B was 3.15 tons/ha. Thus, the corn crop yield larger by 40%. The Farm-A eggplant crop was 41 tons/ha and from the Farm-B was 25.5 tons/ha. The eggplant crop yield from the Farm-A was about 38 % higher than the Farm-B. The crops yield was shown higher from the Farm-A than the Farm-B. It should be mainly the merits of LL-leveling that provided land surface for homogenous water distribution, uniform soil moisture condition, constant seed germination, proper crop growth, stand & maturity, and productive utilization of nutrients (Fig. 4).

The Fig. 5 shows different between total applied depth of water for wheat, corn, and eggplant crops from the Farm-A and Farm-B. The total seasonal applied depth of water for each single crop were measured from the both the Farm-A and Farm-B. The Farm-A water depth was recorded at 420 mm, whereas, in the, Farm-B the applied water depth was 529 mm. The water requirement for irrigation was smaller in the laser-leveled field by 21%, and the water depth lowered by 109 mm, which was different from the Farm-B for the wheat crop.

Besides, the total seasonal water applied depth for corn crop was 539 mm in the Farm- B, whereas it was 394 mm for the Farm-A. The water depth smaller by 27% in the Farm-A field and the water depth saved by 145 mm compared to the Farm-B. The highest water depth applied for the eggplant crop was 1264 mm for the Farm-A, whereas it was 1052 mm for the Farm-B The eggplant water demand lowered by 17% in the Farm-A field and the water depth smaller by 213 mm (Fig. 5). The water demand reduction was probably due to the similar elevation of the fields' surfaces, the reduced lag in water consumption between the different parts in the fields or to the compaction of the land layers.

On other hand, in Farm-B, the water demand was higher due to the inhomogeneous elevation between the different parts of the fields, since a greater water volume was required for water to reach the highest levels of the fields. This also led to over-irrigation of the lower parts and under-irrigation of the higher points. As the total duration of irrigation in the laser-leveled fields decreased, the required labor for the irrigation system was also reduced.

In addition, as the total water depth requirement in Farm-A lowered after laser land leveling, so did the water demand for irrigation by 21%, 27%, and 17% for wheat, corn, and eggplant, respectively. The water volume used in the leveled fields (Farm-A) was 863 m^3/2054 m^2, 808 m^3/2052 m^2, and 2148.1 m^3/1924 m^2 for wheat, corn, and eggplant, respectively. However, the unleveled fields' (Farm-B) water volumes were 1009 m^3/1875, 1004.6 m^3 /2000 m^2, and 2129.5 m^3/1680 m^2, respectively. Consequently, the water productivities recorded higher after LL- leveling by 39%, 53%, and 37% for wheat, corn, and eggplant, respectively. LL-leveling limitations include a high initial cost and technical requirements, which are not met in the study area.

CONCLUSION

Given these points, LL-leveling and layout improvement resulted higher crops yields, enhanced water use efficiency and water productivity. Water application, labor requirements and irrigation problems are lowered after LL-leveling in the Farm-A in comparison with the Farm-B.

Applying a traditional farm layout adversely affects water productivity, land productivity, and labor requirements. The results of the present study indicate that with an appropriate farm layout improvement and LL-leveling, it is possible to conserve and use available water and other farm resources more efficiently and effectively. Moreover, such practices can higher crop production from per unit water and land. More importantly, it can expand the cultivable area, lower the labor requirements for irrigation operation, and lower weeds problems.

The improvements proposed in this study provide significant benefits for the traditional farm layout and unleveled fields. Therefore, it is recommended to concern should shift toward modifying the existing poor farm layout in order to mitigate water issues in a specific area.

Improving the traditional farm layout and applying LL- leveling should be the best options to resolve agriculture-related water management issues in central Asia. These methods can show us higher crop productions, enhanced water productivity, expand the cultivable area and thus the overall farm return, contributing to the rural economic of those areas.

ACKNOWLEDGEMENT

The authors would like to thank On-Farm Water Management Project, Afghanistan (OFWMP) for supporting this research.

REFERENCES

[1] Ali Azimi and David McCauley Afghanistan natural resources comprehensive need assessment final report. Page 9. (ADB).2002.

[2] Gill, M. Water for life. Proceeding of seminar on world food day. Directorate of Agriculture Information. Dept. Agric. Govt. Panjab, India.

[3] Hazart Hussain Khaurin. trees and bushes of Afghanistan, food and agriculture organization of the united nation (FAO). 2003. pp.9-13. 998

[4] National Development Strategy Article no.114 Afghan water law. 2005.

[5] Meteorological station of Shishum Bagh Agricultural Research Farm, Jalalabad city, Afghanistan. 2013-2014.

[6] Muhammad Asif, Manzoor Ahmad, Abdul Ghafoor and Zahoor Aslam. Wheat productivity, land and water use efficiency by treadational and lase land leveling techniques. Online J. Biol . Sci. 3(2): 141 to 146. 2003

[7] Prepared by New Mexico State University final report of Afghanistan water, agriculture and technology transfer. Page 13. 2011.
resource institute. Pakistan country series NO.

[8] Qureshi. A. S. Water Resources Management in Afghanistan: The Issues and Options. Pakistan country Series no.14.working paper 49. IWMI. 2002,

[9] Qureshi. A. S. Water resources management in Afghanistan. The issue and options. International water resource institute. Pakistan country series NO. 14 working paper 49. Colombo, Sir lanka. 2002

[10] Rout. B. Water management, livestock and the opium Economy. How the water flows: A typology of irrigation systems in Afghanistan Research and Evaluation Unit (AREU). Synthesis paper Series. Kabul, Afghanistan. 2008.

[11] Rana. M. A, Arshad. M. and Mausd. Effect of basin, furrow and rain gun sprinkler irrigation system on irrigation efficiencies, Nitrate-nitrogen leaching and yield of sunflower. Pakistan Journal of water resources. Volume. 10. No. 2. 2006

[12] Wolf. P and Stein. T. Improving on farm water management. A never ending challenge. Journal of Agriculture and Rural Development in the tropic sand and Sub tropic. Volume 104. No. 1: Pages 2003.

Second International Conference on Science, Engineering & Environment,
Osaka City, Japan, Nov.21-23, 2016, ISBN: 978-4-9905958-7-6 C3051

REMOVAL OF IRON (Fe) AND ZINC (Zn) IN TEXTILE WASTEWATER BY USING ACTIVATED CARBON FROM SUGARCANE BAGASSE

Izzatul Ashikin, Z.A[1], Mohd Adib, M.R.[2], Muhammad Amirza, A. R.[3]
[1,2,3] Department of Water and Environment, Faculty of Civil and Environmental Engineering,
Universiti Tun Hussein Onn Malaysia, Beg Berkunci 101, 86400, Parit Raja, Batu Pahat, Johor, Malaysia

ABSTRACT

Excessive release of heavy metals into environment due to textile industries has posed a great problem to the world. Heavy metal ions do not degrade, so it can give bad effect to human body and environment itself. Adsorption is one of the most effective techniques to remove heavy metals. Commercial activated carbon is the common adsorbent to remove heavy metals from wastewater but it is expensive material. The purpose of this study is to investigate the effectiveness of sugarcane bagasse as adsorbent for the removal of heavy metal in textile wastewater. The metal ions removal from textile wastewater was studied using batch method. The main parameters that influenced Fe and Zn adsorption on SBAC were contact time, adsorbent dosage and pH value. The sugarcane bagasse was modified using phosphoric acid before proceeds with batch studies. Next, the analysis was continued using different contact time in range of 30 minutes to 24hr. Besides that, the influences of adsorbent dosage also been studied in range of 0.6g to 6.0g. Then, for the pH parameter, the experiment was run using the value between 2 and 7. After that, contains of metals ions were analyzed using ICP-MS. For the contact time, the adsorption increased when the contact time increased and the optimum condition is achieved at 2hr. The research also gave similar results with the adsorbent dosage, where the adsorption of Fe and Zn increased with increasing of adsorbent because of greater surface area with optimum value at 4.0 g. The adsorption of Fe and Zn using SBAC was increased when the pH increased from 2 to 6 and the optimum condition at pH 5. As the conclusion, the optimum percentage removal of Fe, Zn was found to be more than 80%. It shows that SBAC is an attractive alternative adsorbent material for the metal ions removal in textile wastewater.
Keywords: Adsorption; Ferum; Zinc; Sugarcane bagasse; Activated carbon

INTRODUCTION

Wastewater from textile industries contains high load of contaminants, especially heavy metals, organic toxicants, and human pathogens. All heavy metals in textile wastewater represent a major environmental problem, and are a potential danger to human health when present on textiles. Therefore, the removal of heavy metal from wastewater has become one of the most imperative environmental issues [1]. Conventional textile wastewater treatment such as ion exchange, membrane technologies and adsorption on activated carbon are particularly costly and not economical [2].

In recent years, attention has been focused towards adsorption method from local agricultural wastes by transforming negative - valued to valuable material. Sugarcane bagasse is used as an alternative to replace raw material of producing expensive conventional activated carbon. Adsorption of textile wastewater before it is released into drains is seen to be brilliant idea in order to conserve our river. Adsorption is an effective method of lowering the concentration of dissolved dyes in the effluent resulting in colour removal and the process is one of the most efficient methods to remove organic and inorganic compound from effluent [3]. As we known, activated carbon has capability in removing heavy metal, pollutants from liquid and gas streams efficiently and it is the most commonly used and most successful adsorbent because of its extended surface area, micro porous structure, high adsorption capacity and high degree of reactivity [4]. Therefore, this research will explore the suitability of activated carbon from sugarcane bagasse as alternative and low cost medium approach to remove target heavy metals such as ferum and zinc from textile wastewater. Moreover, it is important to investigate optimum condition for heavy metal removal such as adsorbent dosage, contact time and pH.

MATERIALS AND METHOD

Sampling Location

The first step of an analytical procedure is sampling. The wastewater samples of this study were obtained from the garment manufacturing, fabric dyeing, finishing and foaming process. The textile wastewater examined in this study was collected from Syarikat Koon Fuat Industries Sdn. Bhd. Kawasan Perindustrian Tongkah Pecah, Jalan

Kapal, Batu Pahat, Johor. The samples are taken once a week and immediate preservation techniques are applied to avoid changes in nature of the sample. The experiment is carried out once a week.

Sample Handling

The fresh wastewater samples were collected from the effluent discharging drains originated from the textile wastewater treatment plan of the factory. Water samples were collected directly from the outlet by using 3liter bucket. Samples were placed in a high density polyethylene (HDPE) bottle. Before collecting the wastewater sample, the containers were washed thoroughly using distilled water. The samples were then placed in an ice-storage box containing ice packs to preserve and maintain their composition from degradation by microbes. All samples were collected between 9am to 12 pm., which is during the peak flow for dyeing process. After sample taken, keep samples cool with ice or if immediate analysis is not possible, refrigerated system with temperature 4oC to prevent decomposition. Preservation of sample were done accordance with the standard methods for the examination of water and wastewater, the dilution of nitric acid was used to maintain the textile wastewater in longer period [5].

Experimental Design

In the batch study, batch experiment is conducted to study the adsorption capability of activated carbon at different dosage, contact time and pH. Initial data percentage of heavy metal needed before conducting batch study. In the batch experiment, the reactor will be prepared by using 250ml conical flask which comprises of 100ml textile wastewater. The control experiments were set without adsorbent. The most effective size of the produced activated carbon by powdered activated carbon (PAC) where the size of particles is 63µm. The sample will be analyzed for metal ions removal and the experiment will be repeated using different dosage, contact time and pH to investigate the capability of media for heavy metal removal. Table 1 shows working range of ferum and zinc.

Table 1: Working range of ferum and zinc.

Heavy metal	Contact time	adsorbent dosage (g)	pH
Ferum	30min, 75min,1hr,<u>2hr</u>, 3hr,24hr	0.6,2.0,<u>4.0</u>, 6.0	2,3,4,5, <u>6</u>,7
Zinc	30min, 75min,1hr,<u>2hr</u>, 3hr,24hr	0.6,2.0,<u>4.0</u>, 6.0	2,3,4,<u>5</u>, 6,7

*underline indicates optimum condition

RESULTS AND DISCUSSION

Preliminary Study

In preliminary study, the raw textile wastewater was tested to determine the pollutant concentration in textile wastewater. Table 2 shows the pollutant concentration in raw textile wastewater samples. The results were compared with the Malaysia Environmental Quality (Sewage and Industrial Effluents) Regulations. The highlighted columns in the Table 2 shows that Fe and Zn concentration presented unsatisfactory values which is not in line with the standard. Therefore, in this study Iron (Fe) and Zinc (Zn) were choosing to analyze.

Table 2: heavy metal concentration in textile wastewater samples.

Date	**Zinc (Zn) (mg/L)**	**Iron (Fe) (mg/L)**
21/06/15	1.450	5.460
28/06/15	1.166	5.030
05/07/15	0.946	4.980
12/07/15	1.020	5.170
Standard B	**1.0**	**5.0**

Textile Wastewater Characteristics

Raw textile wastewater was characterized with the parameters such as pH, COD, BOD, TSS, Nitrate, Ammonia Nitrogen and two heavy metal namely Fe and Zn. Table 3 shows the characteristic of textile wastewater that analysed at Environmental Laboratory with following properties.

Table 3: Characteristics of textile wastewater before and after treatment process under optimum condition.

Parameters	**Before**	**After**
pH	5.6	6
Biochemical Oxygen Demand (mg/L)	97.8	28.71
Chemical Oxygen Demand (mg/L)	146.65	45.20
Total Suspended Solids (mg/L)	64.25	22.14
Ammonia Nitrogen (mg/L)	1.38	0.82
Nitrate (mg/L)	1.45	0.67
Iron (Fe) (mg/L)	5.42	0.62
Zinc (Zn) (mg/L)	1.16	0.12

All parameters unit in mg/L except pH

Batch Experiments

There are three (3) selected parameters to determine the effectiveness of the activated carbon by sugarcane bagasse. The parameters involved are effect on contact time, adsorbent dosage and pH. All experiments were carried out in Wastewater Laboratory for 4 months. Samples are taken from the batch experiment.

Effect of Contact Time on Removal Efficiency

In this experiment, the effect of contact time was studied over at agitation time of 30min, 75min, 2hr, 3hr and 24hr. 0.6g of Ac was shaken at 125rpm with 100ml of textile wastewater. Figure 1 shows the removal of Fe and Zn increased with increasing time, removal was significantly increased in the initial stages of the experiments and then becomes stable towards the end of the experiments. The maximum percentage metal ions removal approached equilibrium within 2hr with 78% and 85% for both Fe and Zn. This can be explained by the fact that initially, the rate of ion uptake was higher because all sites on the adsorbent were vacant and ion concentration was high, but decrease of adsorption sites reduced the uptake rate [6].

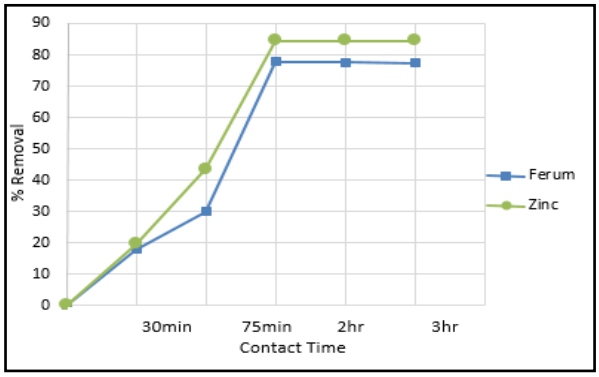

Figure 1: Effect of contact time to the removal efficiency of Fe and Zn.

Effect on adsorbent dosage

Adsorbent dosage was varied from 0.6 to 6.0g, contact time of 2hr, 125rpm shaking speed and at room temperature. The percentage removal efficiency of the of Fe and Zn usually improved on increasing adsorbent doses. This may occur due to the fact that the higher dose of adsorbents in the solution provides the greater availability of exchangeable sites for the ions [7]. The result as shown in figure 2 that the metal ions removal increased with the increased of adsorbent dosage. The maximum percentage removal of Fe and Zn was about 70% and 60% at the dosage of 4.0g. When the adsorbent dose increases, the number of active surface for adsorption will increase and this ultimately results in increase of the percentage of metal ions removal from the solution. The increasing in trend of removal of metal ions is due to the availability of greater active surface for adsorption. It was observed by raising the dose, the removal did not increase due to saturated adsorption site. This may be due to overlapping of adsorption sites as a result of overcrowding of adsorbent particles [8]. Hence 4.0g was chosen as the optimum adsorbent dosage for removal of Fe and Zn metal ions and for further investigation of work.

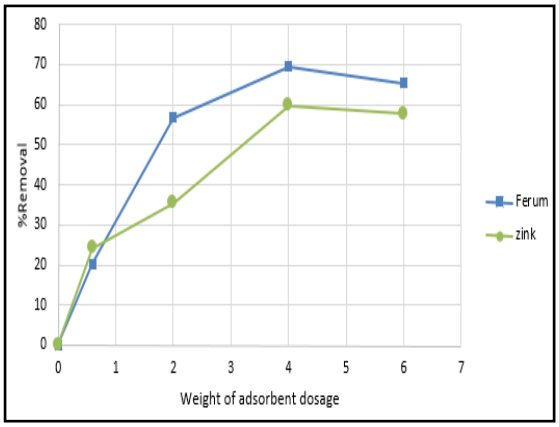

Figure 2: Effect of adsorbent dosage to the removal efficiency of Fe and Zn.

Effect on pH

The effect of pH was studied from a range 2 to 7 under the specific condition which contact time 2hr, 125 rpm shaking time speed, with 4.0g adsorbents used and at room temperature. Figure 3 shows the percentage removal efficiency increased steadily with increasing pH. The most adequate adsorption pH for Fe and Zn were 6 and 5, respectively. Many adsorption studies report pH 5.0 - 6.0 as the optimum pH for Fe and Zn adsorption by various adsorbents [9-10]. The increases in metal ions removal with increased pH can be explained by the fact that at low pH, metal ions had to compete with H+ ions for adsorption sites on the adsorbent surface, thus reducing attraction between surface and metal ions. So, the adsorbent become saturated and was inaccessible to metal cations [11].

Moreover, as the pH increased, this competition weakens and more metal ions were to replace H+ ions bound to adsorbent surface,

which results in a greater attraction between metal ions and adsorbent. According to Meena et al. (2003), precipitation of metal ion was occurred at pH values higher than 6.0. Thus, from the results it is clear that the pH of the metal especially pH 5 was taken as the optimum pH for the experiment.

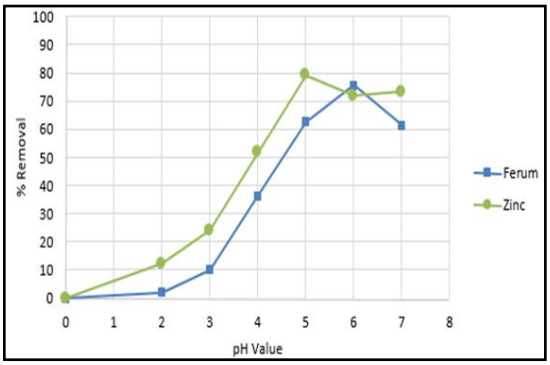

Figure 3: Effect of pH value to the removal efficiency of Fe and Zn.

Batch Reactor Performance

At the last stage of the laboratory experiment, the textile wastewater sample was repeatedly testing by using the optimum condition resulted from the batch experiment. According to table 4, the influent data shows that the average concentration of Fe and Zn were 5.455mg/l and 1.283mg/l, respectively. The high presence of heavy metals in the environment is a major concern because of their toxicity, threat to human life and the environment [13]. However, the level is still out of range of acceptable condition for discharge of industrial effluents of Standard B. After the treatment, the concentration of Fe and Zn achieved the compliance with the standard which is the Fe concentration which less than 5.0mg/l, and Zn concentration less than 1.0mg/l.

Table 4: Percentage removal of heavy metals from optimum condition

Parameters	Textile wastewater sample (mg/l)			Standard B
	Before	After	Percentage Removal (%)	
Fe	5.455	0.613	89	5.0mg/l
Zn	1.283	0.118	91	1.0mg/l

Characterization Studies

Scanning Electron Microscope was used to observe the pore structure of the activated carbon. Pores present in activated carbon act as the active sites, where adsorption take place. Figure 4 (a) and 4 (b) show comparison of the morphology of Ac before and after metal ions adsorption. The Ac revealed that the surface was highly porous in nature and this will increase the surface area for metal adsorption. The SBAC are characterized by having two regions, one being darker and the other being white. The white region is rich in inorganic material containing high proportion of calcium and phosphorus whereas the dark region is rich in protein because it has high proportion of carbon and oxygen [8]. Figure 4 (b) represents the micrograph of ferum and zinc loaded SBAC.

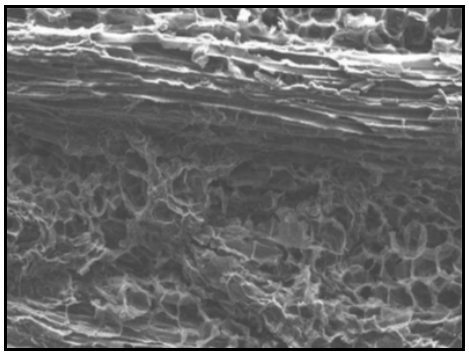

(a)

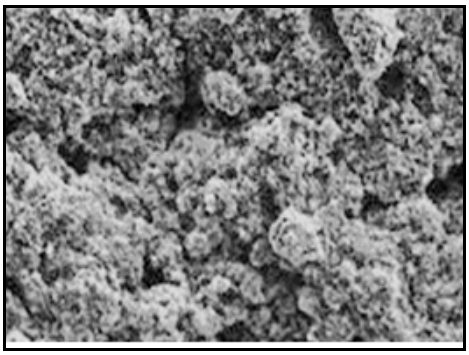

(b)

Figure 4: SEM of SBAC (a) before treatment and (b) after treatment.

Color Reduction on Using Activated Carbon

Color is commonly considered as a qualitative characteristic that can be used to assess the general condition of wastewater. Colour change can be observed in textile wastewater after adsorption process by SBAC. Figure 5 shows the colour removal before and after treatment with the optimum condition in the batch experiment.

Changes in colour of sample can be seen turn to clear during the optimum condition which is at contact time 2 hour, adsorbent dosage 4g and ph 5. This can be explained due to the characteristics of activated carbon which is very effective adsorbents. According to O'Neill et al. 2010, who indicates that effective adsorbents can adsorb all pollutant such as

heavy metal, pollutants from liquid and gas streams efficiently. Basically, SBAC it is the most commonly used and most successful adsorbent because of its extended surface area, micro porous structure, high adsorption capacity and high degree of reactivity

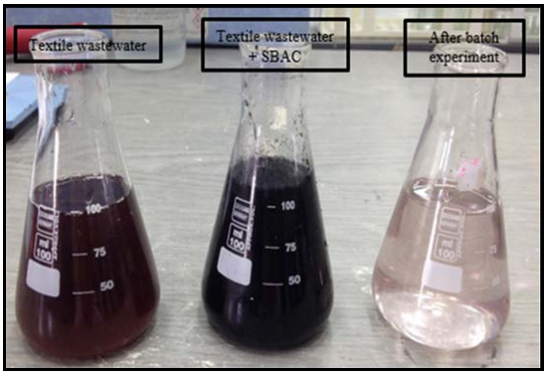

Figure 5: The color removal with the optimum condition in the batch experiment.

CONCLUSIONS

In general, the main objectives of the study are achieved. Based on this study, the parameter tested which are Fe and Zn show better quality after treatment. The key factors found to control the adsorption efficiency of the SBAC were adsorbent dose, contact time and pH. From the batch experimental studies that SBAC is the most efficient adsorbent for the removal of metal ions. It was proven that the SBAC had performed 60% up 85% removal in reducing heavy metals concentrations. This is due to the applicable of SBAC higher surface area provide the active surface for adsorption of metal ions.

Besides that, this study also demonstrated that SBAC could be alternative treatment for the textile wastewater in term of low cost effective and readily available compared to other material. The experiment results showed that maximum removal of Fe and Zn is 89% and 91% respectively at optimum condition. These experimental studies on adsorbents would be quite useful in developing an appropriate technology for the removal of heavy metal ions from contaminated textile effluents. Hence, it is necessary to remove these metals from textile effluents before discharging waste water into the environment.

RECOMMENDATIONS

There are few recommendations was suggested to improve the future study due to the heavy metals removal by using SBAC. Firstly, the apparatus used in the experiment must be ensured in good condition because the errors could be avoided during the experiment. Besides that, wastewater sample must be collected from different sources and places which high of metal ion concentration. This study must be continuing with adsorption isotherm mechanism where is to describe the distribution of metal ions between the solid phase (adsorbent) and liquid phase (solution) when equilibrium was reached. The Freundlich and Langmuir isotherm models should be used to describe the interaction between metal ions in solution and adsorbents.

ACKNOWLEDGEMENTS

We greatly acknowledge UTHM Laboratories for providing facilities, support and assistance throughout the project.

REFERENCES

[1] Cho, H., Oh, D. & Kim, K. (2005). *A study on removal characteristics of heavy metals from aqueous solution by fly ash*. J Hazard Mater,127(1-3),187–95.

[2] Arvanitoyannis, Barclay S., Buckley C., (1989). *Waste Minimization Guide for the Textile Industry: A Step Towards Cleaner Production*. The Pollution Research Group. University of Natal, Durban, South Africa.

[3] Malik, P.K., (2003). *Use of activated carbons prepared from sawdust and rice-husk for adsorption of acid dyes*: a case study of acid yellow 36, Dyes Pigments 56 pp. 239–249.

[4] Hao, O.J., Kim, H. & Chang, P.C., (2000). *Decolorization of wastewater*. Critical Reviews in Environmental Science and Technology, Vol.30, pp. 449-505.

[5] APHA, 2008. Standard method for the examination of water and wastewater, 21st ed. American Public Health Association, Washington, D.C.

[6] Annadurai, G., Juang, R.S. and Lee, D.J. *Adsorption of heavy metals from water using banana and orange peels.* Water Science and Technology Vol 47 No 1 pp 185–190. IWA Publishing 2002.

[7] Kannan, N., and Rengasamy, G. (2005). *Comparison of metal ion adsorption on various activated carbons*. Water Air Soil Pollut. 163 (2005) 185–201.

[8] Abbas, S.T., Mustafa, M., Al-Faize and Rah, A.Z. (2013). Adsorption of Pb^{2+} and Zn^{2+} ion from oil wells onto activated carbon produced from rice husk in batch adsorption process. *Journal Chemical Pham. Res.,5(4),*240-250.

[9] Rafatullah, M., Sulaiman, O., Hashim, R. and Ahmad, A. (2010). Adsorption of Iron(II) onto Different Adsorbents. *Journal*

of Dispersion Science and Technology, 31, 918-930.

[10] Chen, G., Fan, J., Liu, R., Zeng, G., Chen, A. and Zou, Z. (2012) Removal of Cd(II), Cu(II) and Zn(II) from Aqueous Solutions by Live Phanerochaete Chrysosporium. *Environmental Technology*, 33, 2653-2659.

[11] Horsfall, M. Jnr. And Spiff, A. I. (2004). Studies on the effect of pH onthe sorption of metal ions from aqueous solutions by caladiumbicolor biomass [online]. *Electronic J. Biotechnol. vol 7,* no 31. 16 December 2015.

[12] Meena, A. K., Mishra, G. K., Kumar, S., Rajagopal, C. and Nagar, P. N. (2003). Adsorption of Ni(II) and Zn (II) from aqueous solution by chemically treated activated carbon. *National Conference on Carbon.* Kanpur, pp 31140.

[13] Ademorati, C.M.A. (1996). *Environmental Chemistry and Toxicology.Pollution by Heavy metals*. Foludex press Ibadan. pp. 171-172.

Second International Conference on Science, Engineering & Environment,
Osaka City, Japan, Nov.21-23, 2016, ISBN: 978-4-9905958-7-6 C3051

REAL TIME REMOTE FISH POND MONITORING SYSTEM

Arnel M. Avelino, Leah Q. Santos ECE, April A. Clifford, John Nelson M. Decena, Joven B. Escares and Alfred Ray A. Sabale
Department of Engineering and Architecture, Lyceum of the Philippine University – Cavite, Philippines

ABSTRACT

This research is a real time remote monitoring system that notifies the person in charge of monitoring the water parameters in a fish pond via the designed webpage. The system measures the amount of dissolved oxygen and pH parameters of the monitored pond. The sensor reads the water quality parameters while the microcontroller converts the analog signal from the pH meter into digital signal, ready for transmission. The single board computer transmits the data to the database through Wifi communication standard and through a designed webpage; pond owners can observe, investigate and analyze the parameters being monitored. The website conveys the analyzed data in the form of a graphical representation and alerts the owner of the environmental conditions. Further application of this study includes monitoring of fishponds and fish pens remotely. Also, experimental evaluation of the battery performance, accuracy and data aggregation was presented. Results show that the system has great prospect and can be used to operate in real world environment for optimum monitoring of aquaculture environment.

Keywords: Aquaculture, Dissolved oxygen, pH, Fish pond, Monitoring system, Database, Webpage, Microcontroller, Single Board Computer (SBC)

INTRODUCTION

Aquaculture is the farming and husbandry of aquatic animals and plants to earn profit. It increases the production of fish and other useful food stuffs far above the level that can be produced naturally (Briones, 2012). It involves many species and farming practices in diverse ecosystems and most of the production comes from the farming of seaweed, milkfish, tilapia, shrimp, carp, oyster and mussel. It significantly contributes to the country's food security, employment and foreign exchange earnings. The global position of the Philippines in aquaculture production has fallen steadily from 4th place in 1985 to 12th place in 2015 (Gentiloni, 2006). As of now, the country contributes only a little over one percent of the global farmed fish production compared to five percent in the previous years.

A Philippine-Norway scientific study on Philippine aquaculture industry initially showed that some of the country's biggest aquaculture areas run the risk of being affected by recurrent fish kills if present culture practices are not improved. The study was launched early in year 2005, targeting three pilot aquaculture areas in Dagupan City and Bolinao, Pangasinan and Taal Lake in Batangas (Panorama Acuicola Magazine, 2005). According to this study, the incidence of fish kill will continue to be experienced not only because the rivers are very shallow but also because they are crowded with a big number of fish cages, pens and traps which results to overcrowding of fishes that leads to depletion of oxygen.

In Talisay, Batangas, there is an incident where hundreds of thousands of milk fish washed up dead at Taal Lake, alarming environmentalists and raising concerns over climate change issues. According to a local town agriculturist, the cause of the fish kill was a sudden climate change in the area. It is said that the common perception of fish death is linked to depletion of oxygen in water (Sinha, 2011). Almost 752.6 metric tons of fish died in Batangas after the oxygen level in water in Taal Lake lowered due to sudden change of temperature after the rainy season. It is estimated that 57,226,000Php worth of fish died (Raijin, 2011).

Milk fish aquaculture is one of the major revenue sources of Philippine economy. Therefore, this incident is a great loss to the country. With this, the group has come up with a solution. As the use of technology nowadays has been rapidly rising, the researchers have decided to use this in order to prevent fish kill for better aquaculture profitability. In this study, the researchers are planning to prevent the said phenomenon with the use of a prototype which will monitor the oxygen and pH level in the fishpond because according to studies, it sums up that the most critical parameters which affect this phenomenon are dissolved oxygen content of the water and its pH level (acidity or alkalinity).

Objective of the Study

This research aims to notify the person in charge of the monitoring system in the event where the parameters being monitored fall outside the acceptable range set for each sensor.

Specifically, the study aimed:

1) To design a monitoring system that reads the parameters such as dissolved oxygen and pH level that affects the aquatic life in the water to be tested;

2) To transfer the data gathered to a cloud storage using Single board computer and broadband modem;

3) To develop a webpage that will display the data from cloud storage and display the measurements from the monitoring system; and

4) To test and check the system in terms of accuracy and reliability.

Significance of the Study

This study is intended to provide a background to the phenomenon of fish kill and a system that monitor the factors that cause the said occurrence. Monitoring the vital parameters needed by the aquatic resources and to identify critical levels to be well prepared to this phenomenon is very important. It will be a great help in the aquaculture industry especially here in the Philippines. With the use of the fishpond monitoring system, fish kill can be monitored and the profit will be maximized.

Scope and Delimitation of the Study

In this study, the researchers focused more on the amount of dissolved oxygen and pH level needed by the fishes. This is because other factors affecting fish kill, such as temperature and salinity, are related with the depletion of oxygen in the bodies of water.

The system monitors only the amount of the DO and pH level in the water and notifies the user through the webpage whenever the amount of these parameters becomes critical. The webpage that was developed by the researchers is limited to only one monitoring system. It only displays the reading of the two sensors used in the system and notifies the user whenever it is in the critical level or when the level of the parameters stabilizes. This system only requires one sensor for each parameter (pH level and dissolved oxygen) and is designed to be used only in fresh water.

LITERATURE REVIEW

Fish kill is a sudden and unexpected mass mortality of wild or cultured fish. It can generate considerable public and media interest as they are often perceived to be the result of water pollution. There are parameters necessary for the health and growth of aquatic life forms which help them to fully absorb the nutrients they need in order to live. The most important parameters to be monitored and controlled in an aquaculture system are related to water quality, since they directly affect animal health, feed utilization, growth rates and carrying capacities. The primary water quality parameters include temperature, dissolved oxygen (DO), pH, ammonia, nitrites, nitrates, suspended solids, salinity, alkalinity, biochemical oxygen demand (BOD), and water flow rate (Fowler et al., 1994). It is said in their study that other parameters change slowly and tend to stay in range if proper flow rate is maintained. However, the most common parameters are dissolved oxygen and pH level.

Haron et al. (2009) stated that in most of the aquaculture industries, manual water quality monitoring is employed in order to assess the water quality of the pond. The monitoring activity includes inspection at the pond or conducting colorimetric test to ascertain the current water quality. This test requires a sample of the water to be taken from the pond and analysis will be conducted on the sample taken. The test is usually to measure ammonia level, pH level and dissolved oxygen (DO) level in water. The trained personnel have to take a few samples of the water and perform the required test. Each test usually takes between five and ten minutes to accomplish. Test will need to be repeated if samples used are spoiled or no longer usable. Thus, the process is time and cost consuming. In addition, aquaculture farms are normally spacious and humid making daily monitoring and inspecting of the ponds both expensive and time consuming.

Zhang discussed in their study that there are issues in manual monitoring of water quality in fishponds. He believed that the traditional artificial method of detection process which includes sampling, sample transportation and preservation is a waste of time, inefficient and difficult to objectively reflect variation rules and facts. It has been unable to meet current water quality monitoring needs (Zhang, Li, & Wang, 2011).

Additionally, transportation of samples may disturb their chemical properties (Klamath Hydroelectric Project, 2002). As data utility is affected in grab sampling by extended holding times before analysis, monitoring programs have shifted towards continuous measurements using in-site sensors (Lemos et al, 2007). Initially data loggers were used for in-site monitoring; however, they were limited by not providing data in real time as sites had to be visited to retrieve data. The expense of data loggers, infield reliability, calibration requirements and the need to extract data from them individually, prevent them from being used for a dense and long term deployment of sensors. Therefore, gathering of data back then were not real time and very inefficient (Zia et al, 2013).

Synthesis

Dissolved oxygen and pH level are the necessary to obtain the optimum condition for reproduction and growth of the aquatic life forms. Hence, it is very

important to monitor these parameters to know if the body of water is still healthy for the aquatic life forms in it. With the use of technology, monitoring these parameters will be easier for the monitoring team in an aquaculture industry.

Through this set of reviews, the group decided to create a monitoring system that detects the pH level and dissolved oxygen of water. The fish ponds need certain monitoring for it is one of the most important merchandise in the country. The measurement of the attribute chemicals of the water must be monitored not on a seasonal basis but must be done frequently. Given that the environmental and operational changes in natural trends, such as dissolve oxygen and pH change over time, it is necessary to understand how these parameters can affect aquaculture business.

METHODOLOGY

Research Design

The researchers used the experimental method where they designed, constructed and tested the prototype in terms of accuracy and reliability. The device was designed to monitor the DO level and pH level of the water and was tested at a fishpond located at BFAR – Batangas office for validation purposes. The sensors that were used in this research measured the parameters of water at a specific time and transmitted the data wirelessly to a webpage.

Sources of Data

The idea came from the researcher's wonder how would the system they are going to develop help solve problem of the country. The issue of fish kill got the attention of the researchers and from that, they have come up with a possible solution to prevent the phenomenon.

The researchers gathered data from different online sites from the internet, portable document format (PDF) files of published works related to the topic, news from online sites of different stations, patented works of other researchers that have been published online, and blogs and researches that focus about the main issue that the team wanted to resolve. Also, consultation has been a great help in data gathering to aid gain thoughts for the accomplishment of the scheme.

Data Gathering Procedures

1) Consultation

This is a method that was used to help the researchers answer their questions about the issue: significance of the study, factors to consider and innovation that can be done with the existing technology. This helped the proponents to conceptualize their work.

2) Reading News Articles

This gives them idea about fish kills, which greatly affects the Philippine economy for aquaculture business is considered to be one of the major revenues of the country. News articles presents the data regarding fish kills: where it happened, the estimated amount of money lost and possible causes of the incident.

3) Reading Blogs of Writers Related to the Issue

Some writers present their knowledge in their blog sites in the internet which is based on their interviews and, findings and explanations of the experts. It gives readers more information about the incidents that happened. This helps the researchers to further understand what really caused the incident, interconnect ideas and conclude from their own perspectives.

4) Review of Patented Works

Reviewing other published and patented works is a method used to compare and find new possibilities in improving existing technology. Through this, an idea was given to the researchers on how to improve the monitoring technology that is, using of cloud technology.

5) Reading Published Articles and Researches on the Internet

Internet is one of the major sources of information and knowledge as to date. Reading these articles gives the researchers deeper knowledge about the study. It gives them deeper understanding on why do fish kill happen and, the factors that are important and affect the aquatic life. This provides the researchers awareness about the important parameters that should be monitored to avoid fish kill.

Components Used

1) Single Board Computer

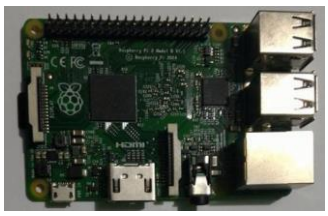

Figure 1. Raspberry Pi 2 Model B

The main feature of Raspberry Pi 2 Model B is that, it has a module power of 5V, 900MHz quad-core ARM Cortex-A7 CPU and 1GB RAM. This is used to

transfer data from the microcontroller to the database for future use.

2) Microcontroller

Figure 2. Gizduino v4.1

The main feature of Gizduino v4.1 is its module power of 5V and it uses ATmega168/168P microcontroller chip to which analog to digital conversion is possible. This is used to read the quantities from the meters and converts these quantities to parameter measurements. This also converts the analog signal from the pH meter into digital signal.

3) pH Meter Kit

Figure 3. pH Meter Kit

The main features of the meter used are the module power of 5V, measuring range from 0 to 14 pH, temperature rating of 0-60°C, ±0.1pH at 25°C accuracy, and a response time of less than 1 minute

4) Dissolved Oxygen (DO) Sensor

Figure 4. Dissolved Oxygen Meter Kit

This features a module power of 3.3V to 5V, measurement range from 0 to 20 mg/L (PPM), maximum temperature rating of 50°, maximum pressure rating of 690kPa, maximum depth rating of 60m, and a response time of 0.06 mg/L per second.

5) DC-to-DC Converter

Figure 5. KIS3R33S5V USB DC 7V-24V to 5V 3A Step Down Buck Module

The step down buck module has been used to regulate the 12VDC from the battery source to 5VDC to be used as the supply of the whole system. It has a maximum output current of 3A, 96% maximum conversion efficiency, ±0.5% load regulation and a voltage regulation of ± 2.5%.

Project Testing

1) Accuracy Test

The system that was used in the research was tested in terms of accuracy. The pH sensor used was calibrated and tested through solutions with known pH level to ensure accuracy in readings. The dissolve oxygen sensor did not have accuracy test due to the unavailability of solutions with constant dissolve oxygen level. Statistical methods were used in order to know the accuracy of the system.

2) Reliability Test

The said system was tested in terms of reliability as well. With the use of programs that were designed, the reading of the sensors was displayed in the prototype itself and the webpage. Here, reliability was tested by comparing the readings from the prototype developed by the researchers to the readings from the instruments that the Bureau of Fisheries and Aquatic Resources (BFAR) used in their sampling and measurements during water quality checking

RESULTS AND DISCUSSION

Results of Testing

1) Accuracy Testing

The results shown in table 1 are the data gathered during the testing. Five (5) samples were used to test the accuracy of the prototype that was developed. The group used pH 7.0 and pH 4.0 buffer solutions as two (2) of the samples for the reason that the two were used as the calibration points of the sensor, as recommended on the data sheet of the product. Vinegar and ammonia were used as the extremities of test for acidic and alkaline solution respectively due to the fact that the mentioned two are the most common household solutions that are available to be used. Lastly, the water with fish feed was used as the fifth solution to simulate the actual effect of fish feeds to the pH level of the water when not consumed by the fishes.

TABLE 1. *Results for Accuracy Test of pH Sensor*

Trial	Vinegar (pH 2.50)	Buffer Solution (pH 4.00)	Water w/ Fish Feeds (pH 5.00)	Buffer Solution (pH 7.00)	Ammonia (pH 9.60)
1	2.58	4.03	5.19	6.99	9.53
2	2.60	4.01	5.21	6.97	9.53
3	2.61	4.05	5.23	7.00	9.52
4	2.60	4.05	5.24	7.00	9.55
5	2.61	4.06	5.21	7.00	9.57

2.) Reliability Testing

The researchers had their prototype tested and compared with the instrument that the Bureau of Fisheries and Aquatic Resources use during their sampling and water quality check. The tests were gathered at an interval of one (1) hour each test. The comparative test results are as follows:

TABLE 2. *Results for Reliability Test of DO and pH Sensors*

TRIAL	DISSOLVED OXYGEN (mg/L)		POTENTIAL HYDROGEN	
	BFAR (YSI SONDE V6600)	LPU-CAVITE	BFAR (Pro DSS)	LPU-CAVITE
1	8.50	8.35	8.90	8.85
2	8.76	8.70	8.82	8.90
3	9.66	9.75	8.91	8.94
4	10.88	10.69	8.90	8.97
5	11.56	11.58	8.93	9.00

The battery used in the system as the source was also tested to know the expected battery life. The total current that was consumed by the system was measured in order to compute the expected battery life. As seen in Table 1 and 2, there are five trials in getting the total current.

TABLE 3. *Measured Total Current Consumed by the System*

TRIAL	I (mA)
1	214.1
2	206.2
3	239.2
4	215.0
5	216.3

Analysis and Interpretation of Data

Statistical methods were used in order to compute for the accuracy of the system. The equation shown below was used in order to compute for the mean of the data results from the conducted accuracy test for the system. As computed, the mean of the data gathered from the testing for pH sensor are the following:

$$\text{Mean} = \frac{\sum READING}{N}$$

TABLE 4. *Computed Mean of the Data Gathered from the Testing for pH Sensor*

SOLUTION	MEAN
Vinegar (pH 2.50)	2.60
Buffer Solution (pH 4.00)	4.04
Water w/ Fish Feeds (pH 5.00)	5.216
Buffer Solution (pH 7.00)	6.992
Ammonia (pH 9.60)	9.54

In computing for the accuracy of the system it is important to get the mean of the data gathered during testing. Using the formula below the computed accuracy for the pH sensor for each samples are the following:

$$A = 100 - \left|\frac{EXPECTED - MEASURED}{EXPECTED}\right| x100\%$$

TABLE 5. Computed Accuracy for the pH Sensor

SOLUTION	ACCURACY
Vinegar (pH 2.50)	96%
Buffer Solution (pH 4.00)	99%
Water w/ Fish Feeds (pH 5.00)	95.68%
Buffer Solution (pH 7.00)	99.886%
Ammonia (pH 9.60)	99.375%

In computing for the reliability of the developed system, statistical method was also used. To get the percentage error of the system, the formulae below were used. The computed percentage error per trial is shown in table 6.

TABLE 6. *Computed Percentage Error*

TRIAL	PERCENTAGE ERROR (%)	
	DISSOLVED OXYGEN	POTENTIAL HYDROGEN
1	1.7647	0.5618
2	0.6849	0.9070
3	0.9317	0.3367
4	1.7463	0.7865
5	0.1730	0.7839

CONCLUSION

The designed monitoring system was successful. It was able to read the dissolved oxygen contained in the test pond and was able to measure its pH level. Also, was able to store the data of the measured parameters to the cloud data storage for further analysis. The monitoring was easier with the help of the developed webpage, since this page has the ability to display the measured parameters in terms of numerical and graphical representation. In addition to this, based on the test results, it can be concluded that the system is accurate and reliable. It showed that the system developed can be a great help in monitoring fish pond, given its accuracy and reliability in association with the instruments that are being used by BFAR for their tests. The system limitation lies on the stability of the internet connection of both the prototype and user that is observing the fish pond. In conclusion to this, the system could maximize the profit of the aquaculture business owners by reducing the risk of having fish kills.

RECOMMENDATIONS

For the future researchers, the following are recommended to further improve the project.

The system can be modified by using parasitic supplies like solar panels to reduce the dependency of the whole system to a single supply to extend the duration expectancy of the battery that is being used.

They can also develop a mobile application that will add to the total feature of the system. With a mobile application that supports IOS and Android users, the future of monitoring can be handy and thoroughly accessible.

Also, the implementation of user / admin account for the system Enhancement of the system will accommodate many users and will access multiple monitoring systems with the use of a single webpage.

Lastly, early warning notification that broadcasts message through GSM to the personnel in charge in the monitoring system and the nearest concerned local government branch in case there is a sudden decrease in the level of the parameters being monitored can also be done.

REFERENCES

[1] Briones, M. R. (2012). Sustainability of aquaculture. Retrieved February 23, 2016, from https://www.bar.gov.ph/index.php/digest-home/digest-archives/97-2002-2nd-quarter/3310-apr-mar02-sustainability-of-aquaculture

[2] Fowler, P., Baird, D., Bucklin, R., Yerlan, S., Watson, C., & Chapman, F. (1994). Microcontrollers in recirculating aquaculture systems 1. Aquaculture, (April), 1–7.

[3] Haron, N., Mahamad, M., Aziz, I., & Mehat, M. (2009). Remote water quality monitoring system using wireless sensors. … , Hardware, Wireless and …, 148–154. Retrieved from http://www.wseas.us/e-library/conferences/2009/cambridge/EHAC/EHAC24.pd

[4] Klamath Hydroelectric Project. (2002). PacifiCorp Klamath Hydroelectric Project FERC No. 2082, (2082), 1–13.

[5] Lemos, S. G., Nogueira, A. R. A., Torre-Neto, A., Parra, A., & Alonso, J. (2007). Soil calcium and pH monitoring sensor system. Journal of Aquacultural and Food Chemistry, 55, 4658–4663.

[6] Panorama Acuicola Magazine. (2005). Study sees fishkill risk in Philippine Aquaculture Area - Panorama Acuícola Magazine. Retrieved February 23, 2016,from=http://www.panoramaacuicola.com/noticias/2005/10/21/study_sees_fishkill_risk_in_philippine_aquaculture_area.html

[7] Raijin. (2011). Fishkill in Batangas: A result of sudden change in temperature. Retrieved February 25, 2016, from http://philnews.ph/2011/05/30/fishkill-in-batangas-a-result-of-sudden-change-in-temperature/

[8] Sinha, S. (2011). A “sudden” climate change kills millions of fish in Philippines. Retrieved June 15, 2015, from http://www.ibtimes.com/sudden-climate-change-kills-millions-fish-philippines-photos-706854

[9] Zhang, M., Li, D., & Wang, L. (2011). Design and development of water quality monitoring system based on wireless sensor network in aquaculture, IFIP Advances in Information and Communication Technology, 347, 629–641.

[10] Zia, H., Harris, N. R., Merrett, G. V, Rivers, M., & Coles, N. (2013). The impact of agricultural activities on water quality : A case for collaborative catchment-scale management using integrated wireless sensor networks, 96, 126–138.

Second International Conference on Science, Engineering & Environment,
Osaka City, Japan, Nov.21-23, 2016, ISBN: 978-4-9905958-7-6 C3051

THE OPTIMIZATION OF RESERVOIR MANAGEMENT TO IMPROVE THE QUANTITY OF DRINKING WATER RESOURCES BY USING CONCEPTUAL MODEL (CASE STUDY: CITARUM CASCADE RESERVOIR, WEST JAVA, INDONESIA)

Lieza Corsita[1], Arwin Sabar[2] and Dyah Marganingrum[3]
[1]Faculty of civil engineering and planning, University of Science and Technology of Jayapura, Indonesia;
[2]Faculty of civil engineering and environmental, Institute of Technology of Bandung, Indonesia
3Research Center for Geotechnology-Indonesian Institute of Sciences, Indonesia

ABSTRACT

The Saguling reservoir, Cirata reservoir and Jatiluhur reservoir has formed a unified system called the Citarum Cascade. It was used to empower a Hydroelectric Power Plant. Jatiluhur reservoir is also be tapped as a source of drinking water, protecting the flooding, and irrigation. However, it is starting to lose some of its functions and deteriorating of environmental support system. The study aims to evaluate the characteristics of Citarum Cascade reservoirs condition, and also intended to develop an operational model for reservoir. This study used the Deterministic and Optimal Method. Analysis of hydrological data used the arithmetic method forecasts. The annual volume of reservoirs used Markov transition method and to predict the future discharge used discrete stochastic Markov and Continuous method. The calculation results on allocation of drinking water availability in the Citarum Cascade Reservoir is 59,02 m^3/sec. That is used as a drinking water supply for Jakarta City and surrounding area. The continuous inflow discharge forecasting method gave better calibration results than the Markov Discrete Method to calculate the inflow discharge of Citarum Cascade Reservoir. The biggest optimal reservoir management correlation value is 0,9 both for Saguling, Cirata, and Jatiluhur. It indicates that the continuous inflow discharge forecasting method suitable to develop Conceptual model for Citarum Cascade Reservoir.

Keywords: Optimization, Citarum Cascade Dam, Discrete Stochastic Method, Drinking Water Infrastructure

INTRODUCTION

Construction of dams in Indonesia has started with the development at Watershed Citarum downstream, namely Ir. H. Juanda or Jatiluhur in 1967. This reservoir has an area of 8,300-hectare of maximum puddle, with a maximum depth of 107 meters. Later, in 1985 and 1986 built Saguling and Cirata at the top Jatiluhur. They called the Citarum Cascade Reservoir (CCR). The third primary function of this reservoir is a power generation and flood control, but specifically, for Jatiluhur reservoir serves as a source of raw water for drinking water for Karawang area, Bekasi area, and Jakarta city. The climate change impact on the water resources infrastructure and their management can be a new challenge for the hydrologists and water resource managers. The Jatiluhur allocation capabilities and potential in the raw water flow needs to be examined. This study aims to review the hydrological aspects to give higher water demand for agricultural purposes, urban and industrial zones, along Kali Malang river. Besides a role in supplying drinking water areas of Jakarta, Citarum Cascade Reservoir, Jatiluhur reservoir also has primary function as Hydroelectric Power Plant. It is the central part of this system, also plays a role in flood control and irrigation as well. This study is needed because Jatiluhur reservoir began to decline and environmental capacity of its function [1]. Purpose of dam building will influence strategy of the operation determining. For example, a reservoir can be used to produce energy, irrigation, flood control and other purpose which using storage analytic varied and distribution arrangements of discharge to meet the needs in the downstream [2]-[4]. The condition of CCR operating has not reached the optimum condition that expected to be a balance in water storage and water discharge (release). This condition due to other factors inflows unevenness discharge each month and restrictions on physical

factors reservoirs, so many researches done so far to find a strategy reservoir operation of the CCR [2],[5]. The central component of research activities carrying out are as follows: 1) Assessment of physical environmental conditions and analysis hydrological regime of Citarum Cascade Reservoir, 2) analysis and evaluation of raw water allocation that needed for drinking water infrastructure proportionally in CCR, 3) Analysis of deterministic patterns to operate CCR, 4) Design of Conceptual models of optimal operational pattern CCR with deterministic methods and optimized using forecasts discharge in continuous model and discrete Markov.

STUDY AREA

Analysis of rainfall data is needed because the rain is an element of climate variability and as a determinant and limiting factor in planning in other sectors, in particular, infrastructure development of water resources [5]-[7]. Rainfall is primary source of water resources at any specified location, but the quantity of rain that it used depends on intensity, size, and rate of rain [4].[6],[8]. CCR is located in the watershed of Citarum River part of west Java Island, spread along the mainland West Java North Coast, Cikeas River, eastern border of Jakarta, and Cilalanang River in Indramayu. It owns building major dams, hydroelectric power, irrigation facilities and other supporting services [4]. Rainfall data analysis of CCR based on analysis of rainfall data observation posts scattered across from sub-watershed of Saguling, Cirata and Jatiluhur. To calculate the average rainfall of CCR watershed required hydrological analysis. The location of rainfall observation station in CCR is shown in Fig. 1, which distributed over seven stations in sub-watershed Jatiluhur, seven stations in sub-watershed Cirata and 18 stations in watershed of Saguling. The location of discharge inflow and outflow is showed by the notation Qin and Qout in each reservoir.

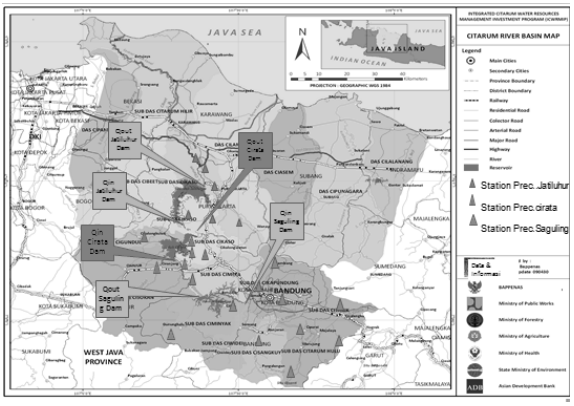

Fig. 1 Location of Citarum Cascade Reservoirs in Indonesia

FRAMEWORK AND METHODOLOGY

Data Collection

Historical data collected from different sources. Analysis of rainfall data in the watershed Saguling based on data analysis of rain 11 observation stations in the period 1986-2008 was almost evenly distributed in all parts of the watershed [5]. Rainfall data were used in the watershed Cirata and Jatiluhur is the monthly rainfall data from 1994 to 2011 year. Average rainfall value is determined using the method of arithmetic / algebra [9]. To obtained the complete of discharge data, the data is then made a statistical distribution, to analyze the probability of discharge data. It is intended to get the value of the maximum water discharge dry, normal and wet. This classification was used in the establishment of the class of the transition matrix of first order and the third order levels, and also to set the value of the arid and average discharge that used in the calculation of guidelines reservoir volume. Analyzes were carried out using theoretical distributions which are distributions Normal, Log-Normal, Gamma, Log-Person III and Gumbel. To decide the appropriate distribution then tested the goodness-of-fit.

Discharge Forecast

This study examines the forecasting models release by using continuous model approach and Markov stochastic model. Continuous discharge forecasting models have constituted the principle of statistical analysis of correlation and regression (multiple regression). Multiple regression was conduct by entering, which means all the variables included in the analysis. Multiple regression equations formulated as Eq. 1:

$$Y = a + b_1X_1 + b_2X_2 + ... b_nX_n + E \quad (1)$$

Where Y is the value of the independent variable; a is constant that is the value of Y when X = 0; b_n is the regression coefficient for -n; X_n is the value of the dependent variable to -n; and E is an error.

A correlation test was performed after the obtained regression equations to determine how strong the relationship between independent variables and the dependent variable (correlation coefficient = R). The value of R range between -1 and 1. For a value of R = -1 the relationship between independent variables and the dependent variable is adamant (perfect) just as the reverse direction. For R = one states that the relationship the independent variable and the dependent variable is an inflexible but related direction.

Conceptual Model

The principle of operation of the reservoir is to apply the theory of the mass balance to achieve optimal conditions for reservoir management. The method is also known as Hydraulic Budget states

that the stored water in the reservoirs from the beginning of the month t+1 is equal to saving water for the start of the month t. Then coupled with the input of water from the river during the month t, and minus the output of reservoirs and evaporation during month t [5],[6],[11]. In this study the operation of the management or operation of the reservoir reached by two ways: deterministic pattern of reservoir operation and optimal reservoir operation pattern [10],[11]. Referring to article number 45, Government Regulation No. 37 of 2010 on Dams, plan discharge was made in three classes, namely dry (0), normal (1) and wet (2). Third class design discharge is then used to determine the track of the guidelines : dry, normal and wet. The goal of optimization is to optimize the track of the reservoir to conform or approach the guidelines so that no water flow through the spillway. Scheme steps in the management of reservoir operation performed in this study in Fig. 2.

The central principle of simulating optimization of the conceptual model in the CCR is to define a physical problem with the equation where output is expected to approach the actual condition or the actual incident. Simulations performed on a monthly basis to test the model created through the scenario that is the first scenario that CCR as a single hydrological region from upstream to downstream, and the second scenario is the watershed CCR has a dynamic hydrological regime that consists of three sub-systems hydrologic region. The purpose or objective in reservoir optimization is based on the following functions [13] :

1. Minimize the risk of flooding in downstream::

$$f_1 \quad \min R \quad \max \frac{\sum(Q_{out} \leq Q_{max})}{T} \qquad (2)$$

2. Maximize water needs in downstream :

$$f_2 \quad \max Q_{am} \quad \max \frac{1}{N} \sum_{t-1}^{T} \cdot Q_{Rt} \Delta t \qquad (3)$$

3. Maximizing the propulsion Hydroelectric Turbine :

$$f_3 \quad max\, E \quad max \frac{1}{N} \sum_{t-1}^{T} P_t \Delta t \qquad (4)$$

A simulation of optimal reservoir management have differences in operation when compared with deterministic reservoir simulation in which the value of $S_{t+1guideline}$ and Q_{in-t} obtained from the model calculations. While $S_{(t)}$ at the beginning of the simulation following the actual trajectory of the guidelines that have $S_{(t)guidelines}$. By entering all variables into the equation then obtained Q_{out-t} calculation results. Then the value Q_{out-t}, $S_{(t)actual}$ and $Q_{(in)actual}$ added to the equation, the obtained value of $S_{(t+1)actual}$ used for the calculation of the next month. When determining Q_{out-T} and $S_{t+1actual}$ constraint should pay attention reservoirs and turbines. If the discharges incurred exceeded the maximum limit of the turbine, the turbine is used the maximum value, and the excess stock of water is the amount of water stored in reservoirs (St). If the value of the stock exceeds the maximum capacity of the reservoir, the water will flow excess stock as an additional discharge release (through the turbine). If after the addition of excess water from the reservoir and the amount Qout still exceeds the maximum capacity of the turbine there will be a runoff through the spillway.

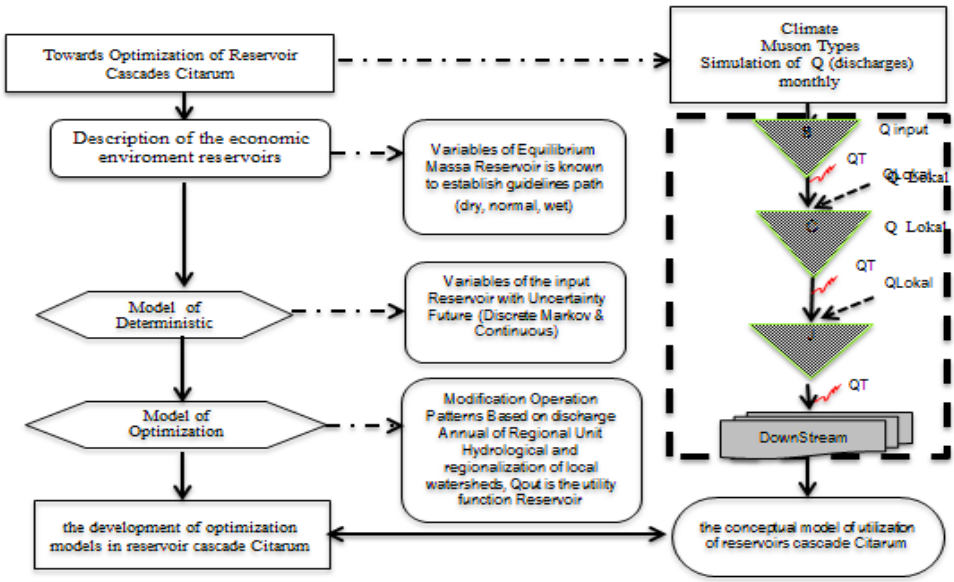

Fig. 2 Reservoir Operation Management Scheme in Conceptual Model

RESULTS AND DISCUSSION

Analysis discharge Allocation Plans for Raw Water in Citarum Cascade Reservoir

To provide the discharge plan in the flow at a particular time where the strong presence that exceeds or is equal to a value based on probability, and certain distributions that represent the flow characteristics. The amount of discharge of this plan has determined by the method of ranking, rational or statistical method approach. This study used a method Weibull (calculating the probability of 80% as R5 discharge plan, and 95% probability as R20 discharge plan). The discharge plans for raw water in the CCR become a constraint that must be considered in the easy pattern of reservoir operation and in order to guarantee the availability of raw water in the downstream. The allocation of drinking water providing in Saguling, Cirata and Jatiluhur are based on the design discharge R10 or R20 [10] which can be seen in Table 1 and Table 2. The allocation of water necessary to ensure the availability of drinking water discharge has used in downstream of the CCR. The result of the calculation of the distribution of water availability at CCR has a value of 97.95 m^3/sec proportionally; it use as a discharge of raw water for irrigation and drinking water at downstream (Jakarta and surrounding area).

Table 1 The Discharge Plan Calculation Results For Water Allocation In CCR

Location	Local Discharge / $Q\hat{R}5$ (m^3/sec)	Total water discharge (m^3/sec)
Saguling	46.92	46.92
Cirata	44.98	91.9
Jatiluhur	6.05	97.95

Table 2 The discharge plan calculation results for drinking water in CCR

Location	Local discharge / $Q\hat{R}20$ (m^3/sec)	Total drinking water discharge (m^3/sec)
Saguling	29,53	29,53
Cirata	28,51	58,04
Jatiluhur	0,98	59,02

A Continous Model

The concept of the continuous model is the correlation of spatial relationships between two or more random variables, variable discharge and rain. Debit incoming in Saguling (QS), Local Cirata (QLC) and Local Jatiluhur (QLJ) estimated by multivariate regression which Saguling discharge (QS_{t+1}), the discharge of local Cirata (QLC_{t+1}) and the discharge of local Jatiluhur (QLJ_{t+1}) as the dependent variable. The independent variables in the model of continuous discharge Saguling have measured in post-Nanjung (QN_{t+1}) and precipitation of rain 11 posts (P_{Xt}), while the independent variables consist of one post-Cirata local discharge and seven observation post-precipitation (P_{Xt}). The independent variable in Jatiluhur has assumed with one observation post local discharge and seven post-precipitation. Correlation value determination in the form of regression (R) on discharge models with historical discharge in reservoirs Saguling, local Cirata and Jatiluhur respectively 0.80, 0.85 and 0.73. The correlation value determination continuous model in the CCR higher than the discharge of stochastic Markov models, so that the main fundamental for the discharge forecasting to optimize simulation in CCR.

Discharge Classification Yearly Forecasts at CCR

Determination of the estimated yearly CCR class types using Markov transition has compiled the annual inflow of data series in three categories. The pattern of reservoir operations consists of the operating pattern of dry, normal and wet. Table 3 shows the results of the annual discharge classification using Markov various method which has indicates that each reservoir has the uniqueness and differences in the dimensions of space and time. Two approaches have been utilized to determine the guideline track. The first is CCR as a hydrological system from upstream to the downstream, and the second is the CCR as a dynamic hydrological system which has three sub hydrological unit system. So that the number of distinguished guidelines on subcascade system 1 (reservoir Saguling), subcascade system 2 (reservoir Cirata) and subcascade 3 (reservoir Jatiluhur). In this research, we found the number of directives track of each sub-system reservoir (PMiNj), and named it Arwin and Lieza guideline equation :

$$PMiNj \quad Mi^{Ni}$$

where N_i = 1 for subcascade system 1 (Saguling reservoir); N_i=2 for subcascade 2 (Cirata reservoir); N_i=3 for subcascade 3 (Jatiluhur reservoir), M_i = number of guidelines track (i = 3,5..n). The calculation in equation ten on the CCR produced the guidelines as a sub-track to Saguling cascade system 1 are a three-tracks, Cirata has nine tracks, and the Jatiluhur reservoir has 27 tracks. CCR optimization scenarios dynamically based on calculation yearly the discharge volume of each in every observation post. Annual volume calculation use as a base for predicting yearly class types to obtain the kind of year in the category of class dry, normal or wet

using Markov transition. Recapitulation years on the CCR class types are in Table 3.

Table 3 Determining The Classification Of The Type Of Year Based On The Annual Volume Of CCR

year	Saguling	Local Cirata	Local Jatiluhur
	Type of year		
1995	Normal	Normal	Wet
1996	Normal	Wet	Wet
1997	Dry	Normal	Wet
1998	Wet	Normal	Dry
1999	Normal	Normal	Normal
2000	Dry	Normal	Normal
2001	Wet	Wet	Dry
2002	Normal	Normal	Wet
2003	Wet	Wet	Wet
2004	Wet	Normal	Dry
2005	Wet	Wet	Dry
2006	Dry	Wet	Dry
2007	Wet	Normal	Normal
2008	Normal	Normal	Normal
2009	Dry	Normal	Normal
2010	Dry	Wet	Wet
2011	Normal	Normal	Wet

The Optimizing Simulation of CCR Conceptual Model

Simulations carried out monthly to test the model created by predetermined scenario. Scenario 1 used in simulation optimization where the yearly class type is the same on the each reservoir. For example, if used type of dry years on the Saguling, the type utilized in the same year in Cirata and Jatiluhur. The simulation results of the first scenario showed on Table 4 which the Continuous models, has produced the maximum R-value compared to the utilization of the discharge forecasts Stochastic Markov.

Table 4 A Summary Of The Correlation Value Of The Optimization Results In CCR With The First Scenario

No	Location	Discharge forecast model	R value
1	Saguling	Continous	0.9
		Markov	0.87
2	Cirata	Continous	0.88
		Markov	0.83
3	Jatiluhur	Continous	0.8
		Markov	0.76

The optimization of simulation scenario 2 using a continuous discharge forecasting, simulation results validation has done by making a comparison between the tracks guidelines with the actual tracks. Then computed using Spearman correlation test (R). The best scenario to get the value of the greatest relationship between tracks guidelines with actual tracks, and also, outcome Qout has fulfilled the needs on the downstream. Table 5 shows the correlation between the tracks guidelines (St guidelines) with the actual tracks (St_{actual}) of scenario 2, which uses continuous model forecasts discharge on the Cirata and Jatiluhur.

Table 5 A summary of the correlation value of the optimization results in CCR with the second scenario

No	Location	Type of year guideline	The discharge forecast model	R value
1	Cirata	2 (N-B)	continuous	0.9
2	Jatiluhur	2(N-B-X)	continuous	0.9

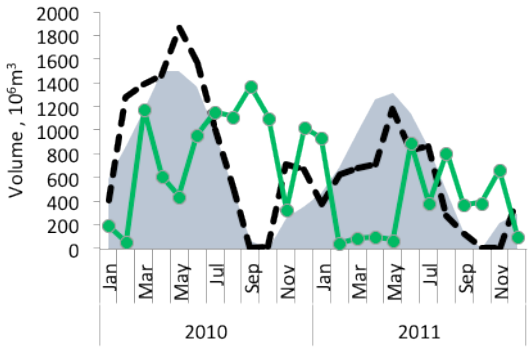

Fig 3 Simulation Optimization on Jatiluhur Reservoir in Years 2010-2011

The overall optimization simulation using two kinds of scenarios showed the greatest correlation value is in the scenario 2. It proves that the management of CCR as a single integrated system from upstream to the downstream dynamically, wherein each reservoir has its uniqueness, and the use of the various guidelines track has followed the local hydrological regime in each reservoir. The optimization of reservoir simulation using inflow discharge forecasts has raised through the rain-discharge correlation models which done in the

establishment of guidelines for efficient operation [5],[11]. The Jatiluhur simulation conducted in 2010 (Fig.3) shows that there is no runoff, which the value Q_{out} released are under the maximum stock of the discharge. When it compared with existing occurrence at the same time, it made a lot of runoff, so the conceptual model using two scenarios with continuous discharge forecasts is more applicable in the management of Citarum Cascade Reservoir.

CONCLUSIONS AND RECOMMENDATIONS

What allocation of raw water discharge for Citarum Cascade Reservoir to meet drinking water needs in downstream is proportional, it obtained the sequentially amount of water distribution for Saguling, Cirata and Jatiluhur respectively by 46.92 m^3/sec, 91.9 m^3/sec and 97.95 m^3/sec. The availability of drinking water allocations in the CCR was 59.02 m^3/sec that can use in the area of Jakarta and surrounding areas. The CCR management could optimally base on reservoir simulation approaches, a method of Markov Discrete and Continuous to forecast the discharge. The results showed that the method of Continuous give the R-value is better than discrete Markov method, in which the R value of discharge forecasting between historical was 0.9 for each reservoir. The simulation results showed that the first and second scenario provides optimum results in Saguling and Cirata. Thus, the second scenario simulation optimization of the CCR would prove the hypothesis, which states that the optimization management of CCR as an integrated system unit operation from upstream to the downstream if each reservoir treated as a unique sub hydrological system.

REFERENCES

[1] Corsita, Lieza., Arwin, Barti Setiani M and Indah Rachmatiah S.S., "Assesment Of The Water Quality of The Jatiluhur Reservoir, The downstream of Citarum Cascade River, Using Selected Physico-chemical Parameter ", J.Rekayasa Kimia dan Lingkungan, Vol.10 No 1, June. 2014, pp. 34-47,

[2] Navarro, Eugenio Molinna, Dennis Trolle, Silvia martinez Perez, Antonio Sastre Merlin, Erik Jeppesen," Hydrological and water quality impact assesment of mediterranean limno-reservoir under climate change and land use management scenarios", Journal of hydrology, Volume 509, 2014, pp. 354-366.

[3] Labadie, J.W, "Optimal Operation Of Multireservoir System : State Of The Art Review", Journal Of Water Resources Planning And Management, Vol.130 (2), 2004,pp 93-111.

[4] Hadihardaja, Iwan.K," Analisis Kehandalan Pengoperasian Optimal Waduk Kaskade Citarum Untuk Pemenuhan Kebutuhan Air Baku", J. Desain dan Konstruksi, Volume 5 No 1, 2006, pp.21-35.

[5] Marganingrum, Dyah., Dwina Roosmini, Pradono, Arwin, "Optimization of Reservoir Operation with Continue Model to Meet The Fresh Water Demand Rate and Face Hydrological Regime Change (Case Study: Saguling Reservoir-West Java, Indonesia)," Proceeding Environmental Technology and Management Conference, November 3-4, 2011, Bandung-Indonesia. Published by Faculty of Civil and Environmental Engineering Institut Teknologi Bandung – Indonesia, ISBN 978-979-98278-3-8, p: WRM 2: 1-15.

[6] Yin , Xin-An, Zhi-Feng Yang, Geoffrey E.Petts, G. Mathias Kondolf,"A Reservoir Operating Method For Riverine Ecosystem Protection, Reservoir Sedimentation Control and Water Supply ", Journal of Hydrology, Vol.512, 2014, pp. 379-387.

[7] Jothiprakash, V., R.B Magar, "Multi-time-step Ahead Daily and Hourly Intermittent Reservoir Inflow Prediction By Artificial Intelegent Technique Using Lumped and Distributed Data," Journal Of Hydrology, Vol. 450-451,2012, pp. 293-307.

[8] Kranz, N., Timo Menniken, dan Jochen Hinkel, "Climate Change Adaptation Strategies in The Mekong and Orange-Senqu basins : What Determines The State-of-Play?", Journal Enviromental Science & Policy,volume 13, 2010, pp. 648-659.

[9] Syariman, Petrus., Agus Heru, "Extreme Weather Impacts On Citarum Cascade Reservoir Operation Pattern, " Jurnal Tenik Hidraulik, Puslitbang Sumber Daya Air, Volume 2 No 1, 2011.

[10] Sabar, Arwin, "Tren global pembangunan infrastruktur sumber daya air yang berkelanjutan, Makalah Diskusi Pakar Perumusan Kebijakan Eco-Efficient Water Infrastructure Indonesia,"unpublished paper, Bappenas, Jakarta, 2009.

[11] Liu, Pan., Shenglian Guo, Xiaowei Xu dan Jionghong Chen, "Derivation Of Aggregation Based Joint Operating Rule Curves For Cascade Hydropower Reservoirs". Journal Water Resources Management, Vol. 25, 2011, pp 3177-3200.

[12] Zhou, Yanlai., dan Shenglian Guo, "Incorporating Ecological Requirement Into Multipurpose Reservoir Operating Rule Curves For Adaptation To Climate Change," Journal Of Hydrology, Vol 498, 2013, pp 153-164.

Second International Conference on Science, Engineering & Environment,
Osaka City, Japan, Nov.21-23, 2016, ISBN: 978-4-9905958-7-6 C3051

IMPACT OF RECYCLED WATER ON PLANTS BIOENERGETICS COMPONETS: CHALLENGES AND SOLUTION

Rafia Azmat*[1], Sumeira Moin[2], Ailyan Saleem[1], and Anum Khursheed[1] Tehseen Ahmed[1]and Mohsin Ali [1]

[1] ***Department of Chemistry, University of Karachi, Karachi, Pakistan***

[2]*Department of Botany, University of Karachi, Karachi, Pakistan*

[*]*Corresponding author's email: rafiasaeed200@yahoo.com*

ABSTRACT

A potential low-cost adsorbent surface was prepared from waste potato peels (PP) for the removal of Cu from the laboratory prepared contaminated water. The adsorption results were quite impressive which showed that the prepared potato peel surface (PPS) was affective for the adsorption of Cu metal from contaminated water. The effects of recycled water on the development and chemical formation of two plant species *Luffa acutangula* & *Vicia faba* were tested and proved that waste water can be safe and reuse in a better way for safety of vegetation. Physiological monitoring of plants showed that plant was well developed under irrigation of recycled water. There were almost similar growth rate in relation with that of plant height, weight and surface area of leaves when compared with the plants grown in regular tap water. The chief bioenergetics nutritious components like total carbohydrates, pigments and proteins were analyzed and found treated plants showed the same amount of contents like that of normal plants. Based on above investigation it was suggested that the PPS as an adsorbent can effectively be used as a future best technique for the control of industrial hazardous of metal contaminated wastewater followed the control the hazardous of polluted water on vegetation and ecosystem.

Keywords: Cu, Recycled Water, Adsorption, Contaminated Water.

INTRODUCTION

Contamination of metals due to discharge of industrial wastewater in soil and water, pressing more threats to these resources as well as to human health and living organisms [1]-[3]. As fresh water reservoirs are declining rapidly therefore, it's a need of time to develop the technologies which should use; for the treatment of contaminated water insisted of discharging into running streams. Among various water purifications and recycling technologies, adsorption is a fast, inexpensive and universal method. Wastewater irrigation enhances the heavy metal contents in soil and results excessive uptake of toxic trace metals in crop plants [4], [5]. Wastewater contains essential as well as non-essential metals which are toxic to plants however some essential metals may also became toxic to plants in excessive amount such as Cu^{2+}, Zn^{2+}, Mn^{2+}, Fe^{2+} and Ni^{2+}, and like the nonessential Cd^{2+} and Pb^{2+} metal ions affects the food quality and safety [6]-[8]. Heavy metal accumulation in plants depends on plant species and their ability to absorb metals. Toxic effects of metals have extensively been studied at the level of biochemical and physiological processes such as photosynthesis, transpiration and enzyme activity metal accumulation in tissue [9]-[11].

Copper plays a vital part in growth and development of plants. At cellular level, Cu has an essential role in signaling of transcription and protein trafficking machinery, oxidative phosphorylation and iron mobilization [12]. Absence and excess of copper both, inhibits the plant growth and impairs important cellular processes. Therefore, optimum copper concentration ensures a normal growth and development of plants [13]. At high concentration, copper was shown to inhibit plant growth by encumbering important cellular processes such as photosynthesis and respiration [14]. Excess copper concentrations generate the oxidative stress due to an increase in the levels of Reactive Oxygen Species (ROS) within subcellular compartments. ROS include the superoxide radical ($O^{2-\bullet}$), hydrogen peroxide (H_2O_2) and the hydroxyl radical ($^{\bullet}OH$), all of which affect mainly to lipids, proteins, carbohydrates and nucleic acids [15].Various scientists studied the effective removal of heavy metals from industrial waste water by different methods. There are many reported and established technologies for the recovery of metals from wastewater, which include chemical precipitation, flotation, adsorption, electrolytic recovery, membrane separation, ion exchange chromatography, etc. In which some are much expensive and require large amount of chemicals that ultimately put pressure of new pollution on the environment.

The aims and objective of this research based on integrated waste management via peels waste for removal of metal contaminates from wastewater in place of its reuse. Potato peels were selected for preparation of bio -sorbent surface to build as a cost effective eco-friendly technique. The recycled water

obtained by agitating the PPS with contaminated waste water to check to its impact on important contents of the edible plants *Luffa acutangula* & *Vicia faba*. The project highlights that bio-sorbant prepared from potato peel was effective for the metal removal without any further hazardous to environment.

MATERIAL AND METHOD

Preparation of Adsorbing Surface

Potato Peels were collected from a canteen of University of Karachi, Pakistan. The collected peels were washed in lab with tap water, followed to remove of all the dirt and inorganic material. The washed peels dried in sunshine for two days then they were placed in an oven at 105ºC for two hours so that all the moisture get evaporated and peels become crispy. The dried peels were grounded in a grinder and converted into the fine powder. The dried and grinded material was then placed in crucible and carbonized in a furnace at 500ºC for two hours. The carbonized material is now grinded in mortar and pastel, and preserved in air tight glass jar to avoid moisture absorption.

Water Treatment

Different concentration of Cu were prepared and mixed with 2g of potato peel charcoal. The reaction mixture was filter after placing 2h to magnetic stir. The clear solution was then tested for removal of Cu ion by treating with EDTA for complexion reaction. No blue colour complex indicates that all Cu (II) ions were adsorbed onto the prepared surface. The recycled water was used for irrigation of pots.

Irrigation of Plant

The two common edible plants (*Luffa acutangula* & *Vicia faba*) were selected for the practicing of recycled water and control plants were irrigated to the tap water. The plants were harvested after 60 days. Several analyses were taken into consideration, which included total carbohydrates, proteins and chlorophyll content.

Biochemical Analysis

Chlorophyll is extracted from the leaves of seedlings using 80% acetone and estimated by the method shown in [16] and while total proteins is estimated by the methods of [17] and total carbohydrates is estimated by [18].

RESULTS

The potato peels were selected for the preparation of bio-sorbant surface as a cost effective method for the removal of Cu. The dry peels were blazed and characterized via scanning electron microscope (SEM), to establish progressive changes in the surface during adsorption of Cu and presented in the Fig. 1 .It was clearly shown in Fig. 1 that it contain holes and porous structure. The results in Fig. 2 clearly indicate that Cu was attached on surface which showed that surface was effective for concentrating Cu on it. The effectiveness of surface for its reuse was monitored using EDTA by agitating the sorbed surface for ensuing i) To procure Cu from the surface to avoid further hazardous of Cu in ecosystem, ii) Recycling of surface for its reuse and iii) Surface efficiency. The SEM analysis of Fig. 1 showed that it is vacant when compared with Fig. 2 on which Cu was adsorbed while Fig. 3 showed desorbed surface for reuse. It was established that surface was effective for several times use which indicate that peels hazardous can also be managed through its proper investigation for its better utilization of biochemical compounds. Recycled water was obtained via this activated charcoal of potato peels through filtration after complete adsorption and used for irrigation of various vegetables. This technique described the integrated waste management of two types of waste like best use of vegetable peels simultaneously eliminating the metal from the contaminated water with less expenditures.

The growth parameters *Luffa acutangula* & *Vicia faba* were observed under normal and treated water for 30 days as they are most commonly used edible plants. The morphological growth parameters were monitored (Fig. 4-7) during cultivation period and found similar to that of normal plants. The surface area of two edible plants *Luffa acutangula* and *Vicia faba* were presented in Fig. (4-7) showed normal growth as compared to control plants (Table. 1). The leaf area, shoot root length, and weight of root and shoot found to be similar to that of control plants. The three important bioenergetics components like plants pigments, carbohydrates and proteins were checked to use the impact of recycled water on edible plants *Luffa acutangula* & *Vicia faba* as these three components are essential for human via food chain. The results of analyses these three contents pigment, carbohydrates and protein were tabulated in the Table. 1. This showed that pigments like chlorophyll a & b reaching to the normal plants followed by the same pattern in carotenoids and xanthophyll (Table.2). Moreover proteins, carbohydrate and other sugars of control and treated plants showed that these components are approximately similar (Table. 3) to that of plant grown in normal conditions.

TABLE 1 Biophysical parameters of *Visia faba* and *Luffa acutangula* in tap and treated water

Plants sample	Leaf area (cm^2)	Shoot length (cm)	Root length (cm)	Shoot weight (gm)	Root weight (gm)	Significance (p)
			Visia faba			
Control	9.061±0.120	7.112±0.269	7.487±0.525	0.472±0.007	0.090±0.006	0.000***
Treated	8.441±0.478	6.043±0.141	7.083±0.179	0.333±0.038	0.083±0.006	0.000***
			Luffa acutangula			
Control	59.881±0.604	12.053±0.143	8.581±0.476	5.110±0.111	0.332±0.021	0.000***
Treated	59.223±0.325	11.881±0.276	7.935±0.310	4.932±0.393	0.331±0.021	0.000***

Significance level = *P<0.05, **P<0.01 and ***P<0.001.

TABLE 2 Comparison of pigments of *Visia faba* and *Luffa acutangula* in tap and treated water

Plants sample	Chlorophyll(a) (mg/gm)	Chlorophyll(b) (mg/gm)	Cartenoids (mg/gm)	Xanthophyll (mg/gm)	Significance (p)
		Visia faba			
Control	0.846 ± 0.01	0.349 ± 0.055	0.355±0.004	0.011±0.003	0.000***
Treated	0.735±0.040	0.291±0.006	0.308±0.017	0.009±0.000	0.000***
		Luffa acutangula			
Control	1.728±0.037	0.9±0.016	0.742±0.047	0.025±0.000	0.000***
Treated	1.639±0.035	0.857±0.050	0.647±0.041	0.022±0.000	0.000***

Significance level = *P<0.05, **P<0.01 and ***P<0.001

TABLE 3 Biochemical parameters of *Visia faba* and *Luffa acutangula* in tap and treated water

Plants sample	Glucose (ug/mg)	Reducing sugar (ug/mg)	Sucrose (ug/mg)	Total soluble sugar (ug/mg)	Carbohydrate (ug/mg)	Protein (ug/mg)	Significance (p)
				Visia faba			
Control	1.739 ±0.044	0.328 ±0.035	8.18 ±0.174	7.067 ±0.158	1.26 ±0.007	0.506 ±0.015	0.000***
Treated	1.609 ±0.020	0.323 ±0.031	7.440 ±0.487	6.296 ±0.361	1.291 ±0.010	0.456 ±0.049	0.000***
				Luffa acutangula			
Control	3.590 ±0.519	0.496 ±0.015	14.356 ±0.404	8.231 ±0.062	1.231 ±0.005	1.606 ±0.016	0.000***
Treated	3.031 ±0.060	0.343 ±0.056	13.331 ±0.297	8.021 ±0.060	1.174 ±0.006	1.536 ±0.032	0.000***

Significance level = *P<0.05, **P<0.01 and ***P<0.001.

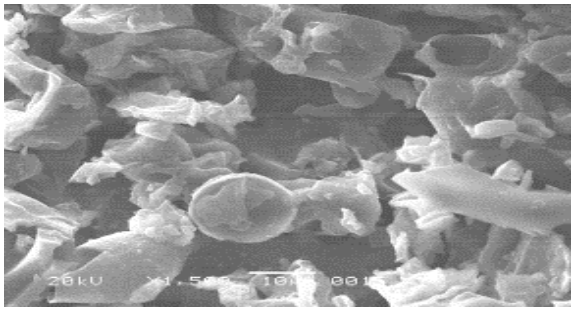

Fig. 1 Scanning electron microscopic of prepared potato peel surface showing porous surface

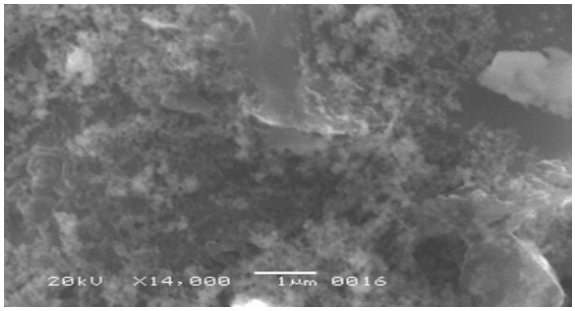

Fig. 2 Scanning electron microscopy of Cu adsorption on prepared potato peel surface

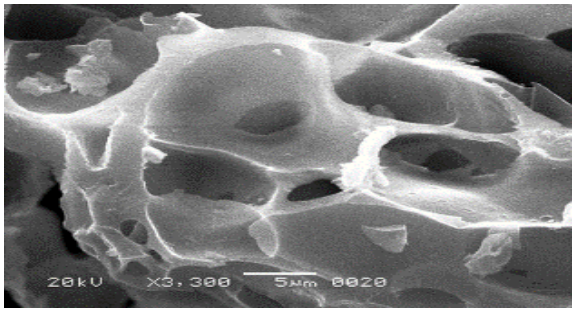

Fig. 3 Scanning Electron microscopy of desorbed surface for reuse

Fig. 4 Growth Rate of *Luffa acutangula* in regular Tap water

Fig. 5 Growth Rate of *Luffa acutangula* in recycled water

Fig. 6 Growth Rate of *Vicia faba* in regular Tap water

Fig. 7 Growth Rate of *Vicia faba* in recycled water

DISCUSSIONS

The recycled water on plant growth showed complete removal of contaminates and showed that the technique which was developed for deletion of heavy metal from contaminated water via potato peel charcoal surface was found effective at laboratory scale. Observation of plants on cultivated sites showed that the plants grown in recycled and normal water have approximately same growth rate which revealed that industrial waste water can be used effectively after its recycling for safe food chain [19]. Results disclosed that the both plants *Luffa acutangula* (Table. 1-3) and *Vicia faba* (Fig. 4-7) showed approximately normal biophysical and biochemical parameters in early stages of development which is vital for mature plant development as observed earlier by [20] and optimum growth conditions were established in treated wastewater. Moreover it was observed that the control plants (Fig. 5 & 6) was slightly increase in height as compared to treated plants (Table. 1) although they were grown under the same environmental conditions. It was experiential that the biochemical analysis of sugars, total carbohydrate, pigments and proteins which are important bioenergetics compounds were similar to the values of normal plants, as presented in Table. 2 & 3. The approximately normal values of pigment in treated plants compared with those of normal plants and values of literature [21]-[24] suggested that the photosynthetic apparatus may be particularly sensitive to damage from heavy metals and in recycled water their function was normal and safe from injury in treated waste water. The normal values of pigments lead the normal function of other processes of plant like glucose, reducing sugars, total soluble sugars, carbohydrate and proteins [14]. It was suggested that treatment of waste water by this technique is simple and cost effective and can easily be applied for waste water treatment at receiving sites before use in cultivation for healthy and safe food. The method which described here is an effective integrated management of both type of waste i-e domestic waste and industrial waste. Therefore it is recommended that more research should be undertaken for the removal of other metals

from laboratory prepared wastewater separately and in a mixture for the development of best cost effective waste water treatment technology. The current investigation established the facts that wastewater must be reused after elimination of contaminates for reducing the pollutants and preventing the soil resources [6]. Because pollutants soil is noxious to for cultivation of vegetables as vegetable easily extracted metals from soil due to their highest mobility as compared to macronutrients. Such type of plants from contaminated soil with high micronutrient and heavy metal content pose adverse effects on human health via consumption of various edible parts of these plants [13].

CONCLUSION

It is concluded from the above investigation that improper discharge of industrial effluent into fresh water reservoirs and its used in irrigation should be prohibited. Wastewater should be treated before discharging into main streams or in agriculture. The methods of recycling of wastewater through potato peel surface was found to be best and ecofriendly and cost effective which can be used for checking of heavy metal from wastewater for its its reuse as a potable water that also can be helpful in sharing the burden of declined fresh water resources of the world.

ACKNOWLEDGEMENT

Author is very thankful to DEAN faculty of Sciences to provide funds for this project

REFERENCES

[1] Singh KP, Mohan D, Sinha S, Dalwani R, “Impact assessment of treated/untreated wastewater toxicants discharged by sewage treatment plants on health, agricultural, and environmental quality in the wastewater disposal area”, Chemosphere, Vol. 55, Apr. 2004, pp. 227-255.

[2] Ahmad A, Ghufran R, Zularisam AW, “Phytosequestration of metals in selected plants growing on a contaminated Okhla industrial areas, Okhla, New Delhi, India”, Water, Air, & Soil Pollution, Vol. 217. May. 2011, pp. 255-266.

[3] Chopra AK, Pathak C, “Enrichment and translocation of heavy metals in soil and Spinacea oleracea grown in sugar mill effluent irrigated soil”, Sugar Tech, Vol. 77, Mar. 2013, pp. 77-83.

[4] Power JF, Dick WA, Kashmanian RM, Sims JT, Wright RJ, Dawson MD, Bezdicek D, “Land application of agricultural, industrial, and municipal by-products”, Soil Science Society of America Inc., 2000.

[5] Rattan RK, Datta SP, Chhonkar PK, Suribabu K, Singh AK, “ Long-term impact of irrigation with sewage effluents on heavy metal content in soils, crops and groundwater—a case study”, Agriculture, Ecosystems & Environment, Vol. 109, Sep. 2005, pp. 310-22.

[6] Muchuweti M, Birkett JW, Chinyanga E, Zvauya R, Scrimshaw MD, Lester JN, “Heavy metal content of vegetables irrigated with mixtures of wastewater and sewage sludge in Zimbabwe: implications for human health”, Agriculture, Ecosystems & Environment, Vol. 112, Jan. 2006, pp. 41-48.

[7] Broadley MR, Willey NJ, Wilkins JC, Baker AJ, Mead A, White PJ, “Phylogenetic variation in heavy metal accumulation in angiosperms”, New Phytologist, Vol. 152, Oct. 2001, pp. 09-27.

[8] Keser G, “Effects of irrigation with wastewater on the physiological properties and heavy metal content in Lepidium sativum L. and Eruca sativa (Mill.)”, Environmental Monitoring and Assessment, Vol. 185, Jul. 2013, pp. 6209-6217.

[9] Küpper H, Šetlík I, Spiller M, Küpper FC, Prášil O, “Heavy metal‐induced inhibition of photosynthesis: targets of in vivo heavy metal chlorophyll formation”, J. of Phycology, Vol. 38, Jun. 2002, pp. 429-441.

[10] Demirevska-Kepova K, Simova-Stoilova L, Stoyanova Z, Hölzer R, Feller U, “Biochemical changes in barley plants after excessive supply of copper and manganese”, Environmental and Experimental Botany, Vol. 52, Dec. 2004, pp. 253-266.

[11] Pandey SN, “Growth and biochemical changes in pulse seedlings irrigated with effluent from electroplating industry”, J. of Applied Bioscience, Vol. 34, 2008, pp. 79-82.

[12] Yruela I, “Copper in plants”, Brazilian J. of Plant Physiology, Vol. 17, Mar. 2005, pp. 145-56.

[13] Jain A, Poling MD, Smith AP, Nagarajan VK, Lahner B, Meagher RB, Raghothama KG, “Variations in the composition of gelling agents affect morphophysiological and molecular responses to deficiencies of phosphate and other nutrients”, Plant Physiology, Vol. 150, Jun. 2009, pp. 1033-1049.

[14] Fariduddin Q, Yusuf M, Hayat S, Ahmad A, “Effect of 28-homobrassinolide on antioxidant capacity and photosynthesis in Brassica juncea plants exposed to different levels of copper”, Environmental and Experimental Botany, Vol. 66, Sep. 2009, pp. 418-424.

[15] Mittler R, Zilinskas BA, “Purification and characterization of pea cytosolic ascorbate peroxidase”, Plant Physiology, Vol. 97, Nov. 1991, pp. 962-968.

[16] Maclachlan S, Zalik S, "Plastid structure, chlorophyll concentration, and free amino acid composition of a chlorophyll mutant of barley", Canadian J. of Botany, Vol. 41, Jul. 1963, pp. 1053-1062.

[17] Bradford MM, "A rapid and sensitive method for the quantitation of microgram quantities of protein utilizing the principle of protein-dye binding", Analytical Biochemistry, Vol. 72, May 1976, pp. 248-254.

[18] Yemm EW, Willis AJ, "The estimation of carbohydrates in plant extracts by anthrone", Biochemical J., Vol. 57, Jul. 1954, pp. 508-514.

[19] Azooz MM, Abou-Elhamd MF, Al-Fredan MA, "Biphasic effect of copper on growth, proline, lipid peroxidation and antioxidant enzyme activities of wheat (Triticum aestivum cv. Hasaawi) at early growing stage", Australian J. of Crop Science, Apr. 2012, pp. 688-694.

[20] Kosaric N, Nguyen HT, Bergougnou MA, "Growth of spirulina maxima algae in effluents from secondary waste‐water treatment plants", Biotechnology and Bioengineering, Vol. 16, Jul. 1974, pp. 881-896.

[21] Azmat R, Akhter H, "Changes in some biophysical and biochemical parameters of mungbean (Vigna radiata L) Wilczek grown on chromium-contaminated soil treated with solid tea wastage", Pakistan J. of Botany, Vol. 42, Oct. 2010, pp.3065-71.

[22] Azmat R, "The impact of siderophore secretion by pseudomonas stutzeri to chelating cu metal in solution culture", Pakistan J. of Botany, Vol. 46, Feb. 2014, pp. 383-387.

[23] Azmat R, Riaz S, "The inhibition of polymerization of glucose in carbohydrate under Cu stress in Vigna radiata", Pakistan J. of Botany, Vol. 44, Feb. 2012, pp. 95-98.

[24] Azmat R, Khan N, "Nitrogen metabolism as a bioindicator of Cu stress in Vigna radiate", Pakistan J. of Botany Vol. 43, Feb. 2011, pp. 515-520.

[25] Kimura S, "Journal paper title", J. of Computer Science, Vol. 1, Aug. 1987, pp. 23-49.

SEE-USQ 2017

Brisbane, Australia

Third International Conference on Science, Engineering & Environment

13-15 November 2017, Brisbane, Australia

Invitation to participate

- The "International Journal of GEOMATE" is a Scientific Journal of the GEOMATE International Society that encompasses a broad area in Geotechnique, Construction Materials and Environment.
- The key objective of this journal is to promote interdisciplinary research from various regions of the globe.
- The editorial board of the journal is comprised of extensively qualified researchers, academicians, scientists from Japan and other countries of the world.
- It is peer-reviewed Journal that is published quarterly till 2015 and now monthly. All articles published in this journal are available on line.
- Contributors may download the manuscript preparation template for submitting paper or contact to the Editors-in-Chief

[editor@geomatejournal.com].